Physics Abstracts

Science Abstracts Series A
July–December 1972

Subject Index part B

U. of ILL. LIBRARY
MAY 9 1973
CHICAGO CIRCLE

inspec
The Institution of Electrical Engineers

Physics Abstracts

Volume 75, part 2 July–December 1972

Subject Index part B

inspec
The Institution of Electrical Engineers

Physics Abstracts is published every two weeks by the Institution of Electrical Engineers in association with the American Institute of Physics. Twice-yearly subject and author indexes covering the period January–June and July–December are included in the subscription. Printed by Unwin Brothers Limited, Old Woking, Surrey, England. Second class postage paid in New York, NY 10001, USA.

© 1972: THE INSTITUTION OF ELECTRICAL ENGINEERS

CONTENTS

Title page	i	Subject index	S 1411
Contents list and explanation	ii	Yellow pages	SH 1

Six-monthly indexes

Cumulative indexes to Science Abstracts are published twice a year covering the period January-June and July-December. They comprise Author and Subject indexes and some specialised or 'small' indexes.

Author index

This lists in alphabetical order all authors of papers abstracted in the abstracts journal during the six months covered by the index, together with the title of the paper. Where there are co-authors of a paper the title of the paper is given only under the name of the first author. The serial number of the paper in the abstracts journal is in the form 2-12345, ie 1972—abstract no. 12345.

'Small' indexes

These are specialised indexes which allow the user to find quickly particular types of information which might be difficult to find using the subject or author indexes.

Bibliography index

In this index reference is made to articles which contain a significant list of references or bibliography on the subjects listed.

Book index

This gives details of books received and abstracted by the abstracts journal.

Patent and Report indexes

These give details of those reports or patents which have been abstracted in the abstracts journal during the past six months.

Conference index

This index lists conferences for which published proceedings have been received and abstracted. Reference is given to the individual papers and their serial numbers in the abstracts journal.

Subject index

The subject index provides an alphabetical subject key to the articles included in the abstracts journal. Some general guidance on its use is given below:

1. Look in the index for the name of the specific subject in which you are interested. In most cases this name will be a heading in the index and you will find relevant articles listed under it.

2. Occasionally you will be directed from the subject heading chosen to a different heading under which the relevant or additional articles are listed.

3. If you do not find the subject heading you first choose, try a more general heading.

4. If you have difficulty at any stage in determining the appropriate heading, consult the Classified List of Headings on the yellow pages at the end of the index. This gives for each broad subject area the headings used in the subject index. Choose the most appropriate and look them up in the index.

5. Each entry under the heading relates to an article appearing in the abstracts journal and gives the serial number of that article in the journal preceded by the last digit of the current year, eg 2—12345: ie Abstract number 12345 in the abstracts journal for 1972.

Metallography continued
  stainless steel, types 304 and 316 low-cycle fatigue behaviour at LMFBR operating temps. 2−60945
  steel, ε-carbide phase form. and struct. 2−43844
  steel, stability of FeC at 700°C 2−50944
  steel, transformer, hot rolling, effect of S content on recrystn. 2−47586
  steel, with high N content, formed by melting under high press. 2−50812
  steel, with high N content, formed by melting under high press., metallography 2−50812
  steel, X-ray 2−53892
  steel tempering, Ostwald ripening quantitative obs., grouping errors in data analysis 2−60942
  steels, stainless, phase state determ. method at rolling temps. 2−84091
  superplasticity obs. 2−56786
  television used as a visual aid for educational purposes 2−55350
  transition zone obs., contrast improvement using ZnSe vapour phase deposition 2−43780
  transmission electron microscopy, use of hydraulic-type tensile device 2−60743
  wear obs., scanning electron microscope technique 2−43741
  Al-Mn alloy, structural features of a plane strip obtained directly from melt by Stepanov method 2−50821
  Al alloy, multiphase, methods for investigation of microstructure and grain boundary sliding 2−80820
  Cd$_3$Mg, two-phase region, morphology, habit planes and orientation relns., metallographic obs. 2−61042
  Cu-Zn(40%) microduplex, superplasticity and cavitation study 2−80738
  Fe alloys and steel, trace nonferrous metals analysis, sample particle size effect 2−51476
  Fe green bodies, porous and sintered parts, polished metallographic specimen production 2−60933
  GaAs, grown from gas phase, cryst. morphology 2−56656
  GeTe−Bi solid soln., regions of existence at 250, 400, 500 and 600°C 2−53888
  Mo spray coatings, prepn. of polished sections and exam. of layers 2−64748
  Nb-O solid soln., form. of Nb$_4$O during decomp., annealing effects, 500-700°C 2−53902
  Ni, work hardened in tension, double texture, twinned growth influence 2−60985
  SiC-B alloy, phase composition rel. to press., 50-60 kbar 2−53996
  Ti-Al-V brazed foils, scanning e. microscope metallographic study 2−68158
  α-Ti, recrystallized, grain size distrib. obs. 2−56898
  U alloy, ion etching and scanning electron microscope obs. 2−56578
  Zn single crystal, oriented, surface morphology developed during sublimation 2−53558

Metallurgy
  see also Ageing; Metallography; Zone melting and refining
  autoradiography, techniques and applics. 2−76072
  concentrates, purification 2−83074
  defects in fusion welds rel. to basic metallurgy for non-destructive testing 2−53845
  field ion microscopy, development, applications to metallurgy, image form., construction operation 2−56643
  hot stage microscope applications 2−56838
  isostatic compression for metal forming including sheet metal 2−68128
  materials development and research 2−60940
  microscope and television system for educational purposes 2−55350
  nuclear materials sample preparation techniques 2−73906
  photoelectron spectroscopy, applications 2−53862
  physical, computational techniques, conf., Leeds, England, Jan. (1971) 2−58820
  physico-chemical, progress 1871-1971 2−47569
  planned casting production 2−77712
  powder, applic. to prod. of Co-based superalloys 2−43828
  powder, applic. to steel prep. and martensite ageing 2−43892
  powder, electrolytic prep. of Fe-Ni-Mo alloy 2−77725
  powder, high-speed pressing, occurrence of strong shock waves 2−43885
  powder, production of Fe-Ni-Mo, carbonyl method 2−68159
  powder, rolling mechanism in initial nonstationary period 2−50908
  powder, sintered compact production of TZM Mo alloy, solid state reactions 2−56906
  powder, spark isostatic pressing 2−68129
  powder, structural aspects of densification 2−56946
  powder metallurgy of high-temp. materials, conference, Tyrol, Austria, June 1971 2−53937
  powder metallurgy process for manufacture of dispersion strengthened Zircaloy-2 2−53917
  pressed metal-fibrous mats., radial thrust calc. 2−68150
  pressure effects, conf., Aviemore, Scotland, May (1972) 2−68127
  sample preparation by metallurgic methods, analysis of UF$_4$ 2−50810
  superalloys, thermal fatigue behaviour, effect of metallurgical variables 2−56879
  thermal and magnetothermal analysis methods 2−43762
  u.s. welding, electrical conductivity applications 2−45181
  vacuum melting and degassing, activated reactive evaporation 2−55336
  U, manufacture of metal and description of plant 2−83073
  UF$_4$, nuclear reactor fuel, description of production operations 2−83075
  UO$_2$, UO$_3$, nuclear reactor fuel, description of production operations 2−83075
  W rods doped with Al, K or Si, bubble-forming impurities, identification 2−80792

Metals
  see also Alloys; Metallography; Semiconductors; Semimetals
  Al oxide-Nb metal seals, by solder glass in system CaO-Al$_2$O$_4$-SiO$_2$-MgO 2−66377
  anharmonic, sound propagation in collision dominated regime 2−43965
  anharmonic, sound propagation in collision free regime 2−43966

Metals continued
  anisotropic, dislocation density determ. from second harmonic moments of oscillation 2−43628
  antiferromagnetic, particle scattering by coupled electromagnetic-magnon waves 2−84443
  b.c.c., brittle fracture, theory 2−43720
  b.c.c., disloc. distrib. in work hardening 2−60799
  b.c.c., dislocation struct. form. and strengthening mechanisms 2−43629
  b.c.c., neutron irrad., void form, and ordering, alloying and purity effects 2−53719
  b.c.c., swaged and drawn, deform. textures 2−53868
  bimetal, individual det. of residual and reactive internal stresses 2−43752
  bimetallic junction, e.m.f. generated by shock wave propag. 2−75010
  brittleness, role of impurities and cryst. struct. 2−43719
  bubble-raft grain boundary, order struct. and dislocations 2−53741
  bulk 1/f noise, exptl. evidence for existence 2−47938
  cavitation erosion, relax. hypothesis, proof of validity 2−71605
  ceramic seals, fast-neutron irradiation effect 2−63227
  ceramic-metal reaction welding, microscopic and macroscopic obs. 2−64785
  ceramic-metal systems, interfacial phenomena, chem. bonding 2−50861
  ceramic-metal systems, ion tunnelling 2−51183
  cermet, Fe-based, antifriction props. rel. to sintering in various protective atmospheres 2−77727
  cermet, Fe-based, effects of protective sintering atmos. on physiomech. props. 2−68166
  cermet, yield limit change regularities in compaction rolling 2−68126
  cermet. ZHGp1.5D2.5, effects of cooling after sintering on struct. and mech. properties 2−77722
  cermets, fatigue testing at elevated temperatures and aeronautical application 2−56870
  charging effects associated with surface plasmons, optical activity 2−68317
  chemisorption of atoms, theory, review 2−48329
  chemisorption of gas, thermodynamic and struct. aspects 2−50530
  close packed, Burgers vectors determ. using g.b=2 contrast in electron microscope 2−60792
  close-packed, relation between cohesive energy and Debye temperature 2−60697
  coating of materials, use of composite powders, new developments 2−61010
  coatings, high temp., deposition from fused salts and by ion plating 2−50860
  cold worked, press. induced thermal activation, tensile strength 2−43781
  cold-worked, nucleation of new grains in recrystallization 2−68134
  combustion rates of NH$_4$ClO$_4$, Ca(HClO$_4$)$_2$ and metal systems 2−61784
  contact behaviour between glass and metal in forming of hot viscous glass 2−56554
  corrosion, effect of deformation, autoclave for obs. 2−66375
  coupled helicon-magnon wave, neutron and electron scatt. 2−68314
  creep, complete description of process 2−52187
  creep, high temp., monograph 2−60871
  creep and sintering rate reduction by oxide dispersions 2−47512
  crystal chemistry of group IV elements 2−71360
  crystal growth macrosonic fields, dislocation structures 2−50590
  cubic, lattice statics of vacancy-screw disloc. interact. 2−56687
  d-band, clean and cesiated samples, photoemission verification of resonance formulation 2−84386
  damping capacity and dynamic modulus meas. under direct cyclic stresses 2−53861
  damping characteristics of certain steels, cast irons and other metals 2−69703
  data compilation, NBS Permuted Materials Index 2−68155
  deformation under axial loading, nonlinear memory type eqn. rel. to delayed yield 2−80734
  deformed polycrystalline, influence of hydrostatic pressure soaking on structural change X-ray study 2−84127
  dendrite formation on solid and mercury electrodes at limiting current 2−68795
  dendritic growth of spherical crysts. from highly supercooled liq. metals 2−60966
  deposits, optical consts. determ. by ellipsometry method 2−79379
  diamond-metal system, compaction during liq.-phase sintering 2−80829
  diffusion mechanisms, review 2−68044
  diffusion of gases, coeff. determ. from rate of change of elec. resist. 2−47452
  diffusion of He, migration and release after implantation 2−50639
  diffusion of hydrogen, by lattice expansion method 2−77606
  diffusion of hydrogen, quantum and classical theories 2−77605
  diffusion of hydrogen, review 2−77604
  diffusion of oxygen, from oxide film 2−71533
  Dirac monopole slowing down, calc. 2−79490
  dislocation line tension, effects of elastic anisotropy 2−74772
  dislocation loops and tetrahedra, annealing 2−53698
  dislocation structures, large angle specimen tilting device and stereoscopic obs. 2−82438
  dislocation substructure strengthening and mechanical-thermal treatment review 2−84099
  Doppler effect due to structural material for fast reactor systems 2−83104
  ductile fracture prediction under discrete loading 2−43728
  elastic constants, 2nd and 3rd order, calc. using pseudopotential methods 2−60836
  elastic property changes under pressure, u.s. meas. method 2−68060
  electrical cond, meas. by inductive method 2−49239
  electrical resist. var. with temp. reln. to interstitials and vacancies 2−68329
  electrode with one crystallographic plane only, prep. 2−48337
  electron beam welding, ions emission 2−68144
  electron field emission, effect of lattice potential 2−61457
  electron mean free path, skin depth temp. depend. 2−71829

Metals continued
electron microprobe analysis, correction for absorption and atomic number 2-65417
electron microscopy, electrolytic jet thinning apparatus, specimen holder design 2-67959
electronic structure of adsorbed atoms on metal substrate, inhomogeneous charge distribution 2-53589
embrittled, Auger spectrographic analysis of fracture surfaces 2-47541
entropy and heat of fusion, rel. to cryst. struct. 2-64506
epitaxial growth, electron microscope obs. 2-60727
extended dislocations, eigen frequency 2-60796
fatigue, high power ultrasonics, uses 2-50794
fatigue mechanism, scanning electron microscope obs. 2-56787
fatigue testing apparatus for use in controlled atmospheres 2-47565
fatigue testing apparatus for use in controlled atmospheres 2-47566
fatigue-crack propagation, review 2-64728
f.c.c., {001} surface, LEED expt. and theory 2-50428
f.c.c., grain boundary diffusion, computer calc. 2-50701
f.c.c., hexagonal Frank loop energy 2-50667
f.c.c., point detect-extended disloc. interaction, elastic modulus effect calc. 2-50652
f.c.c., simulation of rolling texture development 2-43813
f.c.c., stress relax. 2-71558
f.c.c., texture transition mechanism during rolling 2-47323
f.c.c., viscoplastic phenomena, stereographic models 2-60865
Fermi surface determination by angular correlation of annihilation photons, method description 2-61171
ferromagnet, hyperfine field, magnetization process, temp. depend. 2-48066
ferromagnetic, magnetiz. and hyperfine field temp. depend. comparison 2-54323
ferromagnetic reson., surface spin-wave mode 2-54486
fibre-reinforced, resist., calc. 2-50915
field emission microscopy, defects produced by method of exam. 2-56567
film, cond. e.p.r. line shapes, theory 2-81450
film, discontinuous, non-ohmic behaviour 2-57150
film, elastoresist., relax. phenomena and ionic diffusion 2-56765
film, fluctuation enhancement of mag. moment 2-81209
film, longitudinal and transverse strain coeff. of resistance 2-61218
film, morphological changes due to illumination during deposition 2-74620
film, on insulating substrate, heat transport, phonon emission, low temp. 2-54084
film, optical absorp. displaying quantum size effect 2-72314
film, optical constants., Vasickes theory, Murman-Forsterling theory, single refl. theory 2-48132
film, phonon generation in an electric field 2-54015
film, significance of electric field on growth 2-60634
film, surface impedance under anomalous skin effect conditions 2-51096
film deposition on alkali halides, multiply-twinned particles 2-47101
films, monocryst., orientational magneto-optic effect 2-61589
films, time taken for laser pulse to make hole 2-79255
foils, O and C impurities assay by meas. of proton energy spectra 2-50389
fractography by crack replication 2-47545
fracture, by superimposing stress waves generated by electron pulse techniques 2-56812
fracture due to force loading, fatigue, microfractographic characteristics 2-50730
galvanomagnetic effects in rectangular plate 2-59029
gas permeability of metals under non-isothermal conditions, digital computer calc. 2-60826
grain and particle size distrib. analysis, review 2-50817
grain boundary motion, in recovery and recrystn. 2-43785
grain boundary ordered struct., boundary dislocations, transmission electron microscopy 2-53651
grain boundary structure and segregation, conf., London, England [Nov 1971] 2-47606
h.c.p., stress relax. 2-71558
heat capacity at low temperature, review 2-47747
heavy, distribution in vicinity of industrial complex 2-65674
heavy ion radiation damage, 'in situ' expts. in electron microscope 2-74756
helicon reson., meas. by obs. of spatially decaying fields 2-80949
hexagonal, dislocations, undissociated, computer simulation of images 2-43632
hexagonal, stress corrosion cracking, fracture surface study 2-43737
hexagonal struct., orientation determ. by etch pit method 2-83923
imperfections, review 2-68012
interface with superfluid He, low temp. thermal cond. anomalies 2-54065
internal friction, automatic apparatus for high resolution meas. 2-68122
internal friction, negative reversing effect, elimination 2-53789
intraband transitions, collective plasmic excitations, magneto-optical obs. 2-72294
ion source, electron beam bombardment of metal surface 2-41934
ion sources 2-76463
irradiated, explanation of voids 2-80691
irradiated, explanation of voids 2-80690
irradiated, void formation 2-47361
lattice defect form. under radioactive irrad., review 2-47362
layers, dipolar interaction forces, effect on grains after thermic evaporation 2-64559
light pressure efficiency factor for spherical particles of metallic materials 2-45772
longitudinal spin relaxation, retardation effects 2-65190
Lorenz function, at high temps. 2-54124
magnetic cores, permeability freq. depend., Jordan's relations 2-61511
magnetic resonance 2-57384
magnetism in metallic fine particles, effect of discrete energy levels 2-81215
materials choosing for power and industrial applic., conf., Saclay, France (June 1970) 2-60971
mechanical forces caused by relativistic electron beams 2-57089

Metals continued
melt spreading over hard surfaces, kinetics 2-67814
melting of metallic conductors under action of large current impulses 2-77469
melts, thermodynamic props., determ. by e.m.f. meas. 2-77421
metal-electrolyte solution interface, electron photoemission 2-68496
metallographic production of phase pictures for hard metals coated with ZnSe 2-56918
micro-impurity conc. determ. by phys. methods, review 2-43646
molten, explosive interaction with water 2-73457
monovacancy formation energy, determ. from temp. depend. of positron annihilation 2-56689
needle-like microcrystals, adsorpt. induced strength reduction, ion emission microscope obs. 2-80729
neutron damage simulation by ion bombardment, void form. 2-53692
neutron damage simulation by ion bombardment, void form. 2-53693
neutron irad., displacement cascade, primary recoil energy depend., review 2-53691
neutron irrad., void form. 2-50641
neutron irrad., void form. and growth, theory 2-53701
n.m.r., fast magic-angle rot. technique 2-81480
nonideal axial ratios, analysis for close-packed hexagonal structures 2-71396
normal and superconducting, h.f. surface cond., contrib. of mag. field induced surface states 2-51083
notch toughness characterization, criteria and design of expts. 2-60922
nuclear materials, burning curve ignition, theory 2-46383
optical constant determ. by reflection method 2-78062
optical constants det., new method 2-61582
optical props., electronic transitions, opt. const. evaluation, review 2-72292
partial press. and evap. rate meas. by atomic reson. absorption 2-50406
particles, fine, electronic properties 2-61178
particulate, enhancement of electronic polarizability 2-72006
phonon spectra, electron-ion interaction higher order effects 2-47728
photoelectric emission, nonlinearity, optical field emission effects 2-48020
pitting, intergranular corrosion and stress-corrosion cracking, significance of protection potential 2-68787
plastic anisotropy, quantitative meas. method 2-60864
plastic deform., electron beam induced 2-47363
plastic deformation, review of 50 years' progress 2-68077
polycrystalline, very fine grain size, X-ray beam diffracted power obs. 2-56958
polycrystalline and monocrystalline sheet specimens, changes in misorientation during plastic deformation, X-ray study 2-84046
polygonized structure, heavily deformed, conditions of formation of recrystn. nuclei 2-56901
porous, ave. dimens. of pores 2-84147
positron annihilation, temp. depend., meas. of thermal expansion coeff. 2-81002
positron trapping obs. of defects, error sources 2-80676
powder, contact stresses, electron microscope obs. 2-56970
powder, hot pressing at different pressing rates and temps. 2-77697
powder, on the possibility of thermal explosion 2-61003
powders, e. microscopy study of adhesion and surface energy of contact zones 2-64789
pressurization, structural changes and effect on mech. characts. 2-68079
quenched, coagulation of excess vacancies, statistical mech. study 2-80658
radiation damage, atomic displacement cascades, computer simulation 2-53700
radiation damage, point defect stability, low-energy-recoil events and vibr. behaviour 2-53723
radiation-induced swelling implications in fast reactor design 2-49900
radiation-induced void form. 2-50638
radiation-induced voids, conf., Albany, USA [June 1971] 2-50637
reactor core materials characteriz. 2-59862
reflectivity, at high temperatures 2-44344
refractory, strength at elevated temp., vacuum technique obs. 2-77683
reversed creep deformation behaviour 2-77629
scanning electron microscopy, Lilienfeld radiation 2-79131
screw dislocation energy, band struct. energy contrib. 2-50669
secondary electron ejection, by metastable atoms, energy and ang. distribution of ejected electrons 2-48026
secondary ions from polycrystalline targets, energy distribution and mean energy, Ar^+ ion bombardment 2-61470
shear acoustic waves, electromagnetic excitation, influence of magnetoacoustic oscillations 2-71736
shear modulus near the melting point and internal pressure 2-80746
shock spallation, appl. of phonon theory of brittle fracture 2-80747
shock waves, effect on microstruct. and mech. props. 2-68073
skin effect influence on amplitude and phase of pulsed n.m.r. signals 2-83608
sliding of metal and hot viscous glass, mechanics of 2-56553
solidification, effects of shock, vibration and flow 2-80851
solubility of hydrogen and non-ideal soln. behaviour 2-77716
solute segregation and stresses generated around growing voids 2-53697
sound emission, impact forces, meas. device 2-80783
specific heat, influence of point defects at high temp. 2-54040
spheres, internal displacements meas. method 2-77644
spin-electromagnetic waves in ferromag. semicond. and metals, theory 2-81225
stacking fault energy and correl. with electronic struct. 2-43730
strain-hardened, plastic flow theory 2-43684
strength testing after saturation with gases in glow discharge 2-47564
strengthening, under variable stress, creep 2-53812
stress corrosion crack propagation, film rupture mechanism 2-43727
stress corrosion cracking, role of H environment 2-77654

Metals continued
- structural materials, irradiation induced volumetric swelling caused by void formation 2—74758
- surface, asperities, single and multiple, deform., profilometric obs. 2—50452
- surface, exo-emission detection using open counters 2—44187
- surface layer formation by anodic reaction within an electrolyte solution, thermodynamics 2—68781
- surface plasmons, collective mode excitation in electron and ion-solid scatt., theory 2—51087
- surface reconstruction due to chemisorption 2—50524
- surface roughness factor determ. method 2—47067
- surface struct., kinematic LEED intensities extraction from averaged data 2—43462
- surfaces covered by electropositive adsorbates, thermodynamic analysis 2—53588
- swelling data analysis using displacement rates from Lindhard model 2—52880
- in tension, under hydrostatic press., time depend. of fracture and creep 2—80728
- terrestrial planets, metal/silicate fractionation rel. to solar nebula 2—66166
- thermal cond., low temp., phonon spectrum 2—71754
- thermal conductivity, above and below melting point, laser pulse technique 2—54041
- thermal conductivity, accuracy 2—54067
- thermal conductivity, measurement in thermic non-stationary regime 2—47758
- thermal fatigue resistance of metals using fluidized beds 2—56877
- transition, thermal conductivity 2—71757
- tridimensional fibres for composites strengthening physical properties 2—71658
- vacancies, positron trapping rate, temp. depend. 2—80675
- vacancy annihilation in oxidation reactions in gases 2—53756
- vacancy clusters, point defect clusters, secondary defects, review 2—43619
- vapour, production of constant stream by control of electron emission 2—67890
- void and point defect agglomerate studies using h.v. electron microscopy 2—53695
- void form. due to quenching or irrad. 2—53696
- void form. on irrad., temp. effect 2—50642
- void nucleation and growth, computer simulation 2—53699
- void nucleation during high-energy irrad. 2—53703
- voids, gas containing, thermodynamics 2—50633
- voids, produced by irradiation, review 2—50635
- waves, finite amplitude in rods, subject to impact loading, Bell's parabolic law study 2—58901
- wear, methods of obs. and diagnostics 2—43754
- wear, stress effects 2—53851
- welding dissimilar metals with two electron beams 2—68145
- whiskers, tensile testing machine 2—43759
- work function, rel. to nonmetal to metal transition of adsorbed alkali metal layers 2—83870
- zonal melting, crystallization front shape 2—60718
- C content, dependence on metal monocarbide props. 2—56917
- Cu$_2$Te-Ag$_2$Te systems, regions of metallic, semimetallic and semiconducting behaviour 2—84323
- Fe cermet, highly porous, thermophysical properties 2—71651
- Fe cermets, thermal stability of sulphides of some metals 2—68164
- H content determination using an omegatron partial-pressure gauge 2—53866
- O/metal ratio in Pu/U oxide reactor fuels, gravimetric methods of study 2—74152
- O/metal ratios in Pu/U oxide reactor fuels, comparison of two determ. methods 2—74153
- O$_2$ content, spectrochemical determination, effect of heat 2—72590
- UO$_2$-Mo cermet, finely-dispersed, creep rate and particle growth 2—71650

liquid *see Liquid metals*

theory
- adsorbed film, plasmon excitations 2—47826
- adsorption of alkali atoms, theory or work function changes 2—48007
- alkali, binding energy, pseudopotential calc. 2—77832
- alkali, elec. resist., pseudopot. calc. 2—75052
- alkali, interband absorpt., plasmon sidebands 2—51334
- alkali, self-consistent screening calc. 2—77830
- alkali metals, anisotropic transport scatt. times 2—75014
- alkali metals and their liquid alloys, Knight shift and Pauli susceptibilities 2—72515
- alloy, concentrated strong scatt. disordered, elec. resist., temp. depend. 2—44049
- alloy, CPA approx. with random off-diagonal elements, Heisenberg ferromagnet 2—78004
- alloy, disordered binary, many site interactions and correlations 2—61138
- alloy, disordered binary, pair effects, multiple-scatt. formulation 2—75011
- alloy, electron charge transfer and electrochem. effects 2—64884
- alloy, substitutional, averaged electronic resolvent, approx. 2—64885
- alloys, coherent pseudopotential model 2—75025
- Auger emission, kinematic theory, dynamic theory 2—48010
- Auger spectrum, dynamical screening effects 2—44211
- b.c.c., nearly free electron model, surface states 2—57130
- bimetallic surface, adhesion bonding in terms of electronic struct. of combined metals 2—74652
- binary alloy, localized states 2—84252
- binding energy in pseudo-ion approx. 2—83883
- Brillouin scattering of light by long wavelength acoustic phonons in metals 2—54438
- brittle fracture surface energy from phonon freqs. 2—60902
- brittleness, arising from action of liquid metal, diffusional theory 2—71594
- bulk moduli calc. from methods of homogeneous deform. and long waves 2—47177
- capacitance, effect of anomalous field penetration 2—80953
- cathode, photoelec. emission, nonlinear effect due to optical field emission 2—44193

Metals continued
theory continued
- chemical forms, i.r. study when intruded in silica framework 2—72312
- coherent potential approximation, applic. to alloys and model systems 2—61141
- cohesive force conjugate to uniform expansion 2—67929
- correlation function of conduction electrons, influence of mag. field 2—77798
- creep process, model 2—47507
- crystal structure formation, electron effects 2—67982
- cyclotron resonance, Doppler-shifted, thin slabs, semi-classical approach 2—54120
- deformed, Knight shift due to contactless electron-nucleus interaction 2—44451
- degenerate electron gas magnetic props., Landau orbital ferromagnetic states 2—47823
- degenerate Fermi gas, high density, high freq. conductivity 2—57105
- degenerate Fermi systems, threshold anomaly 2—54432
- diamagnetism of free and Bloch electrons, many-body effects 2—68518
- Doppler-broadened annihilation radiation spectra, electron effective mass 2—61216
- elastic constants, Brugger-type, electrostatic contrib. 2—84057
- electron fluid, anisotropic, spin wave spectrum 2—57275
- electron gas, degenerate, specific heat 2—57102
- electron gas, exchange energy, Liberman approx. correction 2—68312
- electron gas, ground state, method of correlated basis functions 2—63044
- electron gas, localized modes of excitation in vicinity of an impurity 2—64902
- electron gas, longitudinal dielectric tensor in uniform magnetic field 2—75038
- electron gas, passage of a positron, energy loss 2—80967
- electron gas, positron correl. energy 2—57142
- electron gas, spin-up-spin-down pair distrib. function 2—71815
- electron liquid, positron vertex renormalization of effective electron-positron interaction 2—54115
- electron liquid, self-consistent pair correls. and dielec. response 2—61207
- electron liquid in metallic density range, correl. functions 2—54117
- electron transport, under external electric fields, magnetic fields and temp. gradients 2—47793
- electron-ion interaction pseudopot. model 2—77812
- electronic struct. of hydrogen 2—77822
- electronic structure and electron dynamics 2—61155
- f.c.c., irrad., elec. resist. of lattice defects 2—75045
- Fermi liquids, two-component, generalization of theory for zero-sound waves 2—71265
- Fermi surface, high pressure effects, review 2—57118
- Fermi surface parametrization 2—54103
- Fermi vels., point meas. by time-of-flight method 2—51075
- ferromagnet, anomalous spin-wave damping 2—72129
- ferromagnet, elementary spin excitations 2—44238
- ferromagnetic, anomalous Hall effect, contrib. of electron-electron collisions 2—57147
- ferromagnetic, cond. anisotropy, two-zone model of electron scatt. 2—71833
- field effect, rel. to field emission, ioniz. and capacitor capacitance 2—54206
- film, 1/f noise, physical process 2—68335
- film, anomalous skin effect 2—54121
- film, discontinuous, elec. props. rel. to strain 2—64908
- film, surface plasmon excitation by transmission of fast electrons 2—47828
- film, transport props., Halperns theory of size effects rel. to m.f.p. method 2—57149
- film, with adsorbed gas layer, demetallization phenomenon 2—47150
- films in magnetic field, microwave absorption peaks due to Doppler-shifted cyclotron resonances 2—80941
- Hall resistivity, formal expression using nonequilib. statistical operator 2—71776
- h.c.p., band struct. calc. by Kohn-Rostoker determinant method 2—80959
- h.c.p. and f.c.c., structs., atomic stacking order, dislocation theory 2—47422
- high temperature paramagnon modifications, in nearly mag. metals 2—71781
- homogeneous dynamical conductivity, jellium model 2—61220
- impurity config. of ionic and partly ionic impurities 2—71777
- indirect exchange and s-d model, dispersion and attenuation of spin waves, effect of e.m. wave 2—72132
- intermetallic compound, atomic vol. variation, pseudopotential theory 2—64774
- interzone transitions in b.c.c. pentavalent metals, detn. of freq. and intensities 2—80946
- ion emission, field evaporation theory, Mie potential 2—72101
- i.r. divergence, electron-phonon interaction 2—48167
- irradiated, void clusters, plasmon interaction 2—80677
- irradiated, void growth, interstitial and vacancy conc. rate theory eqns. 2—80661
- lattice dynamics, ang. force models 2—43945
- lattice dynamics, microscopic formulation, long-wavelength limit 2—84186
- liquid, elec. resist. near crit. point, calc. 2—67838
- liquid, elec. resist. near crit. point, calc. 2—61258
- liquid state, single-atomic metals 2—71152
- local model potentials, limitations and applics. 2—44026
- low energy ion refl., energy and angular distribs. 2—67895
- magnetic impurity, symmetric Anderson model and Mattis' model 2—75021
- magnetoplasma surface waves, dispersion relations 2—61206
- magnetoplasma surface waves 2—44042
- magnetoresistance, linear, and anisotropic quantum fluctuations 2—57141
- magnetoresistance, transverse, size effect 2—51095
- Mattheissen's rule deviations due to phonon spectrum changes 2—75046

Metals continued
theory continued
metal-H system, applied stress field effects, thermodynamic analysis 2−71640
model pseudopotential and energy wave number characteristics 2−75024
model structure factor for solid metals 2−61139
monovalent, high-temp. thermal resistivity and electron-phonon interaction 2−68258
muffin tin potentials, canonical density matrix 2−51071
muffin-tin potentials, non-spherically symmetric, KKR and APW methods 2−77811
narrow s-band, spectral moments for Hubbard model 2−75023
nearly-free-electron, core radius, binding energy and compressibility 2−47801
neutral atom model, ion-electron-ion interaction 2−68271
n.m.r., Bloch decay rel. to skin effect 2−78171
noble, electron-phonon coupling and pseudopots., mass enhancements 2−51069
noble, equation of state, based on elastic and cohesive props. 2−68063
noble, nearby-free-electron susceptibility 2−48034
noble, phase shift parametrization of Fermi surfaces 2−44030
nonferromagnetic, spin waves, quantum-mech. theory 2−75206
one dimensional disordered system, localization lengths 2−61176
one-dimensional system, Gor'kov-Eliashberg effect 2−57095
one-dimensional system, random disorder effect on interrupted strand model 2−47802
paramagnetic spin susceptibility, calc. for interacting electron gas 2−75207
paramagnetostriction, oscillatory magnetostriction, rel. to Fermi surface 2−54290
photoluminescence, two-band model 2−72439
piezothermoelectric effects in anisotropic media 2−51209
polyvalent metal, effect of Fermi surface shape on ideal resist. 2−75044
positron annihilation 2−54122
positron correl. energy in interacting electron gas, positron work function 2−84243
pseudopotential, general-model, for real-pot. approxs. 2−57116
rapidly convergent pseudopotentials, appl. to Li 2−75030
rare earth, single electron energies, many electron effects, renormalized atom scheme 2−64875
rare earth ions in metals, metal props. rel. to cryst. elec. field splitting 2−57315
refractory hard, hardness correlation with d-electron to atom ratio 2−47550
ribbon with surface macrostruct., thermal spectral radiation 2−72309
rigid neutral atom density, selfconsistent calc., auxiliary neutral atom model 2−71787
semimetal, sound and quantum waves, in strong mag. field 2−81008
Shockley surface states, model 2−71800
sound and quantum waves, in strong mag. field 2−81008
superconductivity, phenomenological model of electron-phonon interactions 2−57160
surface, embedded charges, self-consistent screening 2−47813
surface, image pot., static point charge interaction energy 2−61195
surface, scatt. of ions, dynamic screening effects 2−64892
surface energy, collective modes contribs. 2−56568
surface energy, plasmon theory 2−64893
surface state energies, analytical calc. for nearly free-electron metals 2−61196
surface state energies, exact and approx. calc. for nearly free electron metals 2−61197
transition, surface energy, plasmon theory 2−64894
two-band, acoustic plasmon phenomena 2−71814
two-band model, magnetic and excitonic instabilities 2−64881
X-ray Compton profiles 2−84255
X-ray emission spectra, core hole lifetime effects studied by nonequilibrium quantum statistical mechanics 2−48205
Ag, cond. electron optical mass 2−44029
Ag, total energy, pseudopot. theory 2−61137
Al, form factors, Harrison's pseudopotential 2−64877
Al, form factors, Harrison's pseudopotential 2−64877
Al, optical absorpt. peak temp. shift 2−54414
Au, total energy, pseudopot. theory 2−61137
Be, negative cond. electron contrib. to field gradient 2−68277
Cs-K alloy, Ashcroft's empty core model 2−74898
Cs-K(Rb) alloy, heat of soln., pseudo alloy atom model 2−74897
Cs-Rb alloy, Ashcroft's empty core model 2−74898
Cu-Au alloy, interpretation of press. depend. elastic consts. 2−74824
Cu-Cu$_3$Au alloy, Debye temp., elastic moduli, elec. resist., 4.2-293K 2−47752
Cu-Fe alloy, nearest neighbour atom distrib., Mossbauer spectra interpretation 2−74900
Cu, total energy, pseudopot. theory 2−61137
Fe-Pd-H alloy, Mossbauer spectrum interpretation 2−74953
H metallic phase, influence of expression for dielectric function in structure calcs. 2−77521
K-Cs, K-rb, pseudopotential theory and Vegard's rule 2−67992
K, interband opt. conductivity calcs. 2−68616
K, nearly-free-electron-model rel. to opt. consts. in 4-10.7 eV photon energy range 2−68593
LaSn$_3$ type compounds, band struct., impossibility of simple metal description 2−44032
Li, electron-electron interaction, conduction e.s.r. study 2−48288
Li, spin echo on cond. electrons 2−44314
Na, anomalous i.r. absorpt. and collective oscills. in small metal particles 2−65210
Na, electron-electron interaction, conduction e.s.r. study 2−48288
Na, interband opt. conductivity calcs. 2−68616
Na, metallic, Kohn-Sham self- consistent calc. of structure 2−60698
Na, metallic, Kohn-Sham self-consistent calc. of structure 2−60698
Na, nuclear contact densities for electrons 2−61569
V, renormalized-free-atom model, and electron momentum distrib. 2−68670

Metamagnetism
rare earth ionic cpds. with mag. dipole-dipole interaction, caloric and mag. obs. 2−68523
CeBi, struct., ordering 2−44291
CsNiF$_3$, one-dimens. behaviour 2−44241
ErB$_4$, ordering, 2-300K 2−81293
ErGa garnet, exchange parameters and spectroscopic tensor detn. 2−61557
ErNiAl, and mag.props. 2−72162
Fe-Co alloy, rel. to temp. depend. of mag. props. 2−51258
TbCu$_2$, mag. struct. and props. 2−44309
TmNiAl, and mag. props. 2−72162
YbB$_4$, ordering, 2-300K 2−81293
Zn$_{1-x}$Cu$_x$Cr$_2$Se$_4$, magnetization and susceptibility, 4.2-900 K 2−44311

Meteorites
see also Meteors
achondrites, Basaltic, X-ray diffraction and electron microprobe analysis of pigeonites 2−58533
age of Solar System, Moon rocks and stony meteorites 2−66190
Alfianello, shock metamorphism and dynamic deformation 2−44970
Allende, Frost's rule for number and mass of fragments 2−55155
Allende, white inclusion, ^{129}I and ^{244}Pu abundances 2−62718
Allende magnetic properties of individual chondrules 2−58537
analysis, use of ion microanalyzer 2−44504
asteroidal source, possibility 2−58531
ataxites, shock history investigations rel. to Ni-Fe alloys 2−75929
aubrites, new and old irradiations 2−44969
Bjurbole, magnetic properties of individual chondrules 2−58537
Bjurbole chondrules, ^{129}I-^{129}Xe dating by neutron irradiation 2−69174
Bruderheim chondritic, photometric and polarimetric properties 2−58538
carbonaceous chondrite, origin of organic matter 2−55156
Chainpur, magnetic properties of individual chondrules 2−58537
chondrite formation, fractionation events 2−75932
150 Kg chondrite of Keyes, Oklahoma, depth variations in cosmic ray spallation produced noble gases 2−58534
chondrites, ^{3}He production rate by solar protons 2−62721
chondrites, carbonaceous, magnetic memory 2−58532
chondrites, H-group, distribution of Ni, Ga, Ge and Ir in metal and silicate portions 2−62719
chondrites, magnetic hysteresis properties 2−58473
chondrites, recently fallen, noble gas analysis, ages 2−58535
chondrites, volatile trace elements by neutron activation analysis 2−62722
chondrule-like spherule preparation from supercooled molten oxide and silicate droplets 2−44581
composition of meteorites and terrestrial planets rel. to solar nebula 2−81939
cosmic spherules, constant influx rate during Quaternary, deep-sea cores 2−44971
cosmic spherules concentration in deep-sea Mn nodules from cores 2−75931
crater on Nyika Plateau between Zambia and Malawi, origin 2−51843
Denver, recently fallen, age 2−62720
detection panels on spacecraft 2−54983
dust in deep sea sediments 2−73101
Girgenti, mineralogical and chemical analysis of L-chondrite 2−75928
Gwarzo, recently fallen, age 2−62720
howardite origin, mixing model, supporting evidence 2−48785
impact, rel. to formation of lunar regolith glassy particles 2−73071
impact, simulation, release of energy 2−75924
impact detector, cactus micro-accelerometer 2−73100
Johnstown, analysis of bulk composition of hypersthene achondrite 2−44972
Kiffa, exposition age determ. by radioactive dating 2−55153
Kiffa, recently fallen, age 2−62720
L chondrites, evidence for Al-Ir abundance association 2−73099
Landes, inclusions, recrystallization textures and mineral compositions 2−51841
lunar fragmental material prod. by meteoroid impact 2−58467
lunar glass particles, micrometeorite craters, radial fracture zones and spall zones 2−51822
Mauritanian craters of explosive origin, gravity reconnaissance 2−51842
meteoroid impact flash analyzer 2−69176
meteroid breakup causing Martian doublet craters 2−69159
microtektites comparison with lunar glass spherules 2−62670
Murchison and Vigarano, olivines, Ca variations 2−51840
naming 2−51839
natural remanent magnetization, possibility of external mechanisms 2−48787
orbits rel. to cosmogenic radionuclides in stones 2−73097
origin hypotheses rel. to meteorite parent bodies 2−78514
PAWEL, laser microspectral analysis 2−48786
planetology congress (Montreal, September, 1972) 2−78499
Popigai basin, explosion crater 2−55154
preatmospheric dimensions from isotopes analysis 2−58530
Savonoski Crater, Alaska, possible meteorite impact structure 2−78296
Seoni chondrite, composition and evidence of recrystallization 2−75927
solar nebula, condensation 2−58443
spaced bumper systems, effects of material phase transformation effects 2−62413
St. Severin, proton spallation track registration in meteoritic whitlockite 2−58536
stones, elemental abundances for chondrites and achondrites 2−75930
superheavy elements, attempted characterization 2−44973
tektites, mag. susceptibility, 1050-4.2K 2−73073
tektites, search for ^{14}C 2−66189
tektites, vagabond 2−44968
Ucera, determ. of differential atmospheric heating using natural thermoluminescence 2−75926
Weston chondrite, complex irradiation history 2−73098

Meteorites continued
Wethersfield, recently fallen, age 2−62720
Al-Ir abundance association in L chondrites 2−73099
Fe, chemical classification, Ge conc. rel. to Ni, Ga and Ir 2−75925
Fe cosmic abundance rel. to Type I carbonaceous meteorites 2−69175
K distribution between metal and silicate 2−44582
Meteoroids *see Meteorites*
Meteorological instruments
see also Anemometers; Hygrometers; Ionosphere measuring apparatus
− 2−62141
aerospace instrumentation, conference Cranfield (1972) 2−62126
airborne ice nuclei generator, dynamic calibration 2−62193
anemometer, hot-wire, airborne, optimal choice of parameters for obs. of small scale atmos. turbulence 2−44680
anemometer, paired-Gill, algorithm for reducing errors based on response function 2−44679
aneroid pressure sensing element for radiosonde 2−72735
automatic stations, for network operation, remote regions 2−84756
for balloon and rocket expts. 2−72745
balloon shelters, wind tunnel investigation of shape 2−75517
ballooning services 2−72744
balloons, history, review 2−72743
cloud condensation nucleus counter, automatic 2−51580
cloud height lidar system semiconductor laser applic. 2−44684
computerized radar system with real- time display 2−75503
geostationary operational environmental satellite, state-of-the-art report 2−72746
ground based solution burner for cloud seeding and production of atmospheric tracer materials 2−62100
hygrometers, for horizontal soundings of troposphere and lower stratosphere, calibration techniques 2−57934
Integrated Environmental Detection and Ranging system, all solid state sensors for aviation use 2−57931
i.r. radiometers comparison with video satellite data 2−65632
i.r. system, application 2−84764
ITOS-1, 2nd generation operational meteorological satellite, design and orbital performance 2−48630
nephelometer, balloon-borne, for high altitude meas. of light scatt. 2−72805
Nimbus 4 temperature-humidity i.r. radiometer, 6.7 μm channel data 2−75487
numerical simulation of observing systems for tropical wind and reference pressure 2−54839
observing systems for GARP, simulation expts. 2−62105
ocean surface temp. meas., satellite microwave radiometer 2−78334
optical array spectrometer for liquid water content obs. 2−57975
pyrotechnic seeding devices, rain stimulation and hail suppresssion programs 2−62195
radar for obs. of snowfall rate 2−57974
radar hail detector, dual wavelength, performance evaluation 2−75494
radar installations, siting considerations 2−75496
radar raingauge accuracy rel. to drop size distribution and rainstorm type 2−75593
radar raingauge system for accurate precipitation measurements 2−75594
radio telemetering system for meteorological investigations 2−75520
radiotheodolite, obs. of ascent through cumulonimbus clouds during thunderstorm 2−62110
rain gauge, capacitor type, with d.c. output and improved flow characteristics 2−65650
rain gauge catch variation due to airflow disturbances around gauge 2−78246
reed switch anemometer, housing design 2−65709
scanning f.m.-c.w. radar sounder 2−75510
scanning radiometer, for orbiting satellite 2−84865
SKUA rocket sonde temp. sensor, corrections 2−44692
spectrometer, optical cloud particle, det. of cloud microstructure 2−48492
spherical balloon wind sensors, aerodynamic props. 2−57933
for storm basin characteristics det. 2−44716
stratospheric balloons, conference (Washington, USA, June 1971) 2−72742
temperature sensors, airborne, anal. of time responses 2−55815
thermal diffusion chambers, computation of steady-state supersaturations 2−62235
thermistor for use in atmos. boundary layer, radiation shield 2−51579
vertical wind measuring instrument 2−62109
wind and temp. flutuations meas. instrument attached to captive balloon 2−81663
Meteorology
1971, December, weather study 2−62106
1972, January, weather study 2−65642
AFGWC limited area meso-scale prediction model for weather forecasts 2−72753
air pollution meteorology rel. to pollution control 2−75489
air-sea interaction studies in Davis Strait 2−62121
aliasing with unequally spaced observations 2−51574
atmospheric attenuation compensation analysis rel. to radar meas. of rain rate 2−75501
atmospheric prediction models, filtered-equation, pressure-coordinate, numerical model 2−44678
atmospheric scalar fields, linear prediction analysis 2−72749
atmospheric soundings, relative merits of satellites and rockets 2−65639
balance initialization and data assimilation in primitive eqn. prediction models 2−62113
Barbados oceanographic and meteorological experiment of 1969 2−62057
baroclinic quasi-geostrophic model, numerical scheme 2−57932
Britain, effects on weather of polar low 2−75523
clear air scatter layers, meteorological structure meas. by ultra high resolution radar 2−75540
clear air turbulence, automated forecasting 2−72750
climatology, new zonal belt terminology 2−65630
cloud, clusters, over tropical north Atlantic Ocean, satellite study 2−65718
Meteorology continued
cloud cover estimates from satellites, effect of sensor spatial resolution, simulation study 2−48495
cloud field height determ. by ground photometric survey using two spherical mirrors 2−84852
cloud motion, and registering landmarks from satellite data by computer 2−48439
cloud seeding, single area expt. 2−51614
cloud seeding expts., analysis of effects and benefits 2−62202
cloud seeding expts. in Arizona, program anal. 2−62203
clouds, warm convective, modification by hygroscopic and hygrophilic materials 2−62208
clouds tracking from, ATS pictures man-computer system 2−48438
computation of meteorological elements for mesoscale processes 2−68876
convective activity at Bombay, effect of vertical wind structure 2−62178
counters photoelectric, for nuclei concentration determ. 2−62117
cumulonimbus convection, dry line of Northern India 2−68905
cumulus clouds, model of hygroscopic seeding 2−62204
cumulus clouds, numerical model, simulation of salt seeding 2−62206
cyclone, intermediate scale, numerical simulation of development in moist model atm. 2−84793
cyclones, extratropical, satellite radiometer meas. 2−54840
Cyprus, extreme weather conditions during April (1971) 2−54806
D/RADEX expt., echo predictability, constant elevation rel. to VIL radar data patterns 2−75498
D/RADEX project, digital radar expt. 2−75497
data analysis techniques 2−54811
data processing for weather radar 2−75506
dew point curves and diurnal temp., use in short-range forecasting 2−72763
digital surface-climate simulator, development and applications 2−65647
digitized weather radar data, computer processing techniques 2−75500
Doppler radar data interpretation 2−75509
dust haze preceding thunderstom, radar propagation characteristics 2−75512
dust storms, radiation fluxes during 2−48505
dynamic forecasting, satellite obs., retrieval of atmos. temp. profiles 2−48449
dynamic multiple cloud seeding expt. in Florida 2−62221
easterly wave development in tropical Atlantic, satellite study of air disturbance 2−54833
electric charge of small (1-40 μ) particles, effects of weather 2−78380
electric power demands rel. to variability in weather 2−65643
energy balance from scatt. and absorpt. obs. of atmos. aerosols 2−65780
EOLE, location and data collection 2−65651
European Centre for Medium-Term Weather Forecasting, cost and benefit anal., advantages 2−78338
field station for atmospheric electricity obs. 2−58002
flow over mountains, three-dimensional effects 2−84814
fog, warm, meteorological condits. for artificial dissipation 2−65719
fog dispersal at airports in US, potential economic benefits 2−72751
fog forecasting, and conductivity meas. 2−51582
forecast error, initial error and predictability 2−62114
forecasting, long-range, and inertia in the ocean and atmosphere 2−62123
forecasting, statistical interpolation, data assimilation 2−78345
forecasting methods and applications, multilinear regressions 2−72741
forecasting of cloud ceiling from forecast winds 2−65717
forecasting temp. for gas and electricity industries 2−75531
forecasting using sunspot cycle data 2−62791
forecasting yield of principal crops in India on basis of weather regression analysis 2−62108
frontogenesis, quasi-geostrophic versus non-geostrophic 2−44675
frontogenesis models, mathematical formulation and solution 2−44676
GARP weather forecasting rel. to atmospheric wave momentum flux 2−65678
Gauhati Airport, upper air mean dry bulb and dew point temp. profiles 2−72757
geostationary satellites, data collection 2−65652
giant cumulonimbus, potential vertical extent 2−57980
glossary of terms, book 2−54808
Great Lakes influence on weather 2−57935
Great Lakes Weather Modification Program, Lavoie model 2−62102
H. Johansen weather types probabilities of transition 2−48437
hail obs. using Doppler radar 2−75578
hail size distrib. and accumulation zones 2−84808
hailstorm with echo free region, radar obs. 2−75566
hailstorms, radar signal depolarization by hydrometeors 2−75493
halo phenomena, frontal rain 2−84853
ice phase seeding, cumulus clouds
Icelandic fjord weather phenomenon 2−75519
inadvertent weather modification, Los Angeles smog 2−51572
influences on ground-level pressure fluctuations and meas. chromatic acoustic-gravity waveforms in laterally inhomogeneous media 2−54809
i.r. data comparison with video satellite data 2−65632
Korat plateau, Thailand, weather and summer circulation 2−72752
Laredo air force base, Texas, terminal weather forecast reference file 2−72754
large scale movement of Saharan air outbreaks over northern equatorial Atlantic 2−54829
large scale processes, influence of Earths surface 2−48440
local climatologic variations det. from initial conditions of previous year 2−54804
long-range weather prediction, using proposed upper atmosphere laboratory 2−62293
mean frequency and variance of radar Dopple spectrum, uncertainties in coherent meas. 2−75507
meridian circulation unit from equatorial belt to polar front 2−72739

Meteorology continued

- mesoscale changes in atmos. due to convective band seeding 2−62103
- microseisms associated with cyclonic winds 2−48377
- monsoon period in S.W. India, rainfall and floods 2−62230
- morning glory, atmospheric hydraulic jump in Gulf of Carpentaria 2−51604
- mountain effects in weather forecasting, research aspects 2−65633
- national hurricane warning program 2−75492
- Navier-Stokes eqns., solns. for hydrocyclone with central air column 2−83454
- nocturnal temperature profiles for Edmonton, Alberta 2−48450
- northern Midwest USA, postglacial climatic change, fossil pollen spectra 2−75463
- numerical forecasting models, incorporation of steep mountain effects 2−84848
- numerical methods and computer applications 2−81695
- numerical models of atmosphere, vertical structure, Laguerre polynomials 2−65649
- numerical weather prediction, large scale, experimentation with imposed southern boundary 2−62115
- numerical weather prediction, reference level problem 2−48442
- numerical weather prediction and free oscillations of discrete stratified fluid 2−62112
- observational accuracy and sampling resolution in meteorological data 2−65644
- observatory sites, conditions and optical turbulence 2−51867
- operational subsynoptic advection model for short-period forecasting 2−65645
- orthogonal polynomial base functions for global analysis of data 2−62111
- Pasadena smog, aerometric factors affecting evolution 2−51573
- periodicities, biophysics, geophysics 2−52084
- perturbations, rel. to microseisms in small closed basins 2−48376
- planetary waves, energy and energy flux 2−44646
- planned weather modification, public survey 2−62101
- point or dot angels in winter and summer seasons 2−75513
- precipitation, primitive equation multilayer model for forecasting in N.E. coastal sections of USA 2−44724
- precipitation distribution rel. to wind direction, source areas of positive anomalies 2−62200
- precipitation from seeded convective storms, Ag fallout patterns 2−62220
- precipitation prediction, areal coverage in N.W. Utah 2−57976
- predictability with aid without random external forces 2−62163
- prediction model, performance of 1967 GFDL and improvements 2−65631
- premonsoon squall lines, Gauhati Airport, radar obs. 2−62167
- primitive equation barotropic model, applic. to precaution of movement of Western disturbances 2−51576
- probability score, scalar and vector partitions, two state situations 2−51577
- project Cloud Catcher, use of numerical cloud model 2−62209
- project Hailstop, seedability of supercell and multicellular hailstorms 2−62219
- project Snowman evaluation 2−62199
- radar, conference, (Champaign-Urbana, Ill., USA, Oct 1972) 2−75490
- radar and raingauge meas. of precipitation in Welsh hilly region 2−75589
- radar climatology of Gauhati airport and its neighbourhood 2−62228
- radar echo intensity and modified coeff. for weather radar eqn. 2−75508
- radar echo pattern, movement and evolution, from real time processing of radar signals 2−75499
- radar estimation of rainfall rate, improvement of accuracy 2−48494
- radar evaluation of artificial precipitation enhancement using computer 2−75585
- radar meteorology in Soviet Union during 1970, review 2−75488
- radar probing, obs. of electrodynamic ice models 2−44674
- radiation balance mapping 2−48506
- radio, tropospheric, refractivity gradient over Japan, obs. 2−65803
- radiometry limitations for meas. applications 2−81679
- radiosonde meas. comparison of Measural-Metox and Vaisala systems 2−72747
- rainfall anomalies in randomized seeding project 2−62222
- rainfall augmentation via warm rain process 2−62205
- rainfall events in convective storms, Z-R relationship for radar estimates 2−75571
- rainfall rate and drop size distributions, simultaneous meas. using radar and raingauges 2−75590
- randomized winter orographic cloud seeding expt. 2−62198
- Remote Automatic Meteorological Observing Station development 2−75515
- remote sensing buoy system 2−48432
- residual double-mass method studies 2−44670
- rocket data processor and results from 7 March 1970 solar eclipse 2−65648
- rotating fluid dynamics, ultrastable air bearing turntable 2−77232
- runoff producing rainfall, stochastic model for summer type storms 2−62119
- Santa Barbara aerial seeding program (1971-72) 2−65641
- satellites, reception 2−48443
- sea-atmosphere interaction, conference, Ft. Lauderdale, Fla., USA, (Dec. 1971) 2−65637
- serially correlated normally distributed rainfall durations generation 2−57982
- severe storm detection and prediction using digital radar data 2−75564
- severe storms, digital radar data applics. 2−75495
- severe weather events, radio noise obs. 2−84813
- Siberian Anticyclone, November 1967 to April 1968, periodicity in average daily strength 2−84851
- simulation expts. for observing systems for GARP 2−62105
- simultaneous FM CW radar and lidar obs. 2−75511
- snow hourly accumulation estimation from intensity or visibility obs. 2−51615
- solar radiation intensity and weather patterns 2−68878
- Southern Oscillation, its use in weather prediction 2−65646
- spectroscopical sounding of clouds 2−44731

Meteorology continued

- spelaeology, applic. to past climate obs. 2−62118
- squall line, Doppler velocity obs. 2−75561
- stability of climate, numerical expts., zonal averaged steady state equations 2−62096
- statistical test methods and effective number of independent sample values 2−54576
- stochastic dynamic prediction 2−48441
- storm, release of Li trace into cloud base, correlation with rainfall 2−57986
- storm basin, technical and regime characteristics 2−44716
- storm cell models from digital radar data 2−75563
- STORMFURY project, numerical expts. on artificial heating of eyewall 2−62187
- summer rainfall and temp., prediction for England and Wales from springtime anomalous atmospheric circulation 2−75518
- supersonic flight problems 2−78344
- surface wind fields and sea-level pressure, adjustment by variational matching 2−65705
- temperature forecasts by numerical method using centred time-differences, growth of random errors 2−62107
- terrestrial scintillation, meteorological influences 2−78378
- thermal pollution, general circulation model, possible climatic changes 2−75524
- thermal sounding from satellites problems 2−48453
- three dimensional model of front 2−75522
- Tornado funnel, force field required to maintain dynamics and shape 2−62186
- tornadoes, radar and Nimbus 4 i.r. obs. 2−75569
- tower network for urban meas. 2−75516
- trade-wind profile and shearing stress on tropical windward coast 2−44706
- tropical and hurricane, review 2−75491
- tropical cyclones Althea and Ada, radar estimation of max. wind speed 2−75570
- tropical depression analysis based on radar data 2−51578
- tropical hurricanes, unaccelerated drifting, eye effect and wind lengths 2−48484
- tropical prediction model, effects of parameterization of latent heating 2−51575
- tropical storm development conditions 2−62188
- tropical waves, satellite obs., intensity evaluation 2−57960
- troposphere, extreme highs, indices of energetic solar events 2−62125
- trowal, technique in frontal analysis 2−54807
- TWERLE, TIROS-N, Doppler systems 2−62116
- units, SI system, meteorological aspects 2−65638
- updating of variables, simple linear perturbation theory 2−44677
- upper atmos. wind and density obs. using v.h.f. radar 2−75618
- upper tropospheric frontogenesis, non-Boussinesq effects 2−68894
- urban growth area, micrometeorological observations, urban heat island 2−44685
- urban instrumentation 2−75514
- urban weather modifications, integrated cloud physics approach 2−54846
- vertical velocity distrib. in westerly disturbance determ. by numerical soln. of diabatic quasi-geostrophic omega eqn. 2−62131
- vertical water vapour flux, airborne measurements 2−78349
- visual flight rules and cloud clearance and visibility standards 2−68879
- warm core and coreless witners in polar regions, generation conditions 2−54805
- warm cumulus cloud modification expt., seeding using encapsulated urea 2−62207
- wavy air-water interface, energy and mass transfer through 2−72748
- weather and snow effects on VORTAC task 2 TACAN antenna 2−68880
- weather conditions, bearing of ^{90}Sr fallout 2−62286
- weather data radar system of IAS 2−75504
- weather forecasting, application of computer derived synoptic maps 2−62122
- weather forecasting, backward trajectory calculations rel. to advection process approximations 2−65636
- weather forecasting and analysis, conference, Portland, Ore., USA (1972) 2−62097
- weather forecasting using computer time-sharing 2−72736
- weather forecasting using hydrodynamic barrier flow 2−65635
- weather forecasts employing Eole satellite 2−68877
- weather forecasts using eight-level boundary layer physical-numerical model 2−65634
- weather modification, method of generating ice nuclei smoke particles 2−62099
- weather modification, pollution, turbulence and diffusion, conference (Rapid City, USA, June 1972) 2−62098
- weather modification expts., choice of exptal. unit and block system 2−65640
- weather predicting system, ultra long range 2−62124
- weather radar data files, survey of 1955-72 period 2−75502
- weather radar photographs computerized analysis 2−75505
- wind field, adjustment to geopotential data in primitive equations model 2−84796
- wind waves and swell, differential low of hydrometeorological characteristics distrib. 2−44636
- winter rainfall and temp. for England and Wales, foreshadowing 2−44681
- wintertime orographic randomized seeding project 2−62201

Meteors

- *see also Meteorites*
- ablation coefficient and maximum brightness of bright meteors 2−75923
- artificial, ablation obs. using Fe oxides 2−66188
- fading radio reflections from meteor tracks 2−81924
- flight and explosion, gas dynamics 2−81900
- Giacobinid meteor spectra from 1946 shower rel. to chemical compositions 2−78570
- Giacobinid shower, 1972 predictions 2−66186
- Glacobinid shower prediction, October (1972) 2−58528
- Global Radio Meteor Wind Studies Project 2−58036
- Lowicz 1935 meteoroid, fragmentation 2−51838

Meteors continued
  Lyrids meteor shower 1969, radiant position and meteor characteristics 2−58527
  mass and dynamics, statistics 2−75917
  meteoroids, effect of meteoric ion processes on radio obs. 2−69172
  micrometeoroid simulation on metal targets, Fe particles from Van de Graaff accelerator 2−66187
  orbit meas. in southern hemisphere using combined multi-station radar equipment of c.w. and pulse at 27 MHz 2−62717
  Orionid 1970 meteor shower, effect on optical properties of twilight sky 2−84781
  Quadrantid, sunrise effects on meteor region and radio echoes 2−44748
  Quadrantid meteor stream, 1970 and 1971 visual counts 2−44967
  Quadrantid stream, nodal retrogression 2−51837
  radar meteor wind measurements, drift in laser ionosphere 2−72870
  radio meteor echoes, decay time, effect of wind shear gradients 2−58529
  radio meteor velocity, mean-square error determination 2−58526
  radio observations, determ. of winds and turbulence of neutral atmosphere 2−48522
  radiolocation instruments 2−69173
  radiometeors, selectivity effect on distribution of orbital parameters 2−75922
  radiowave reflection from trails, detectability of radio meteors 2−73096
  research reviewed, structure and history of solar system 2−58524
  role in formation of sporadic E 2−72891
  short-period meteor orbits rel. to parent comet and perturbations of planets 2−58525
  winds obtained by radar meteor trails and chem. release methods, comparison 2−58037
Metrology *see Measurement; Mechanical measurement*
Mica
  Auger emission, relative intensities of lines 2−72081
  coexisting pairs from Central Alps, K-Ar ages 2−62001
  fission tracks stability rel. to water effects 2−67097
  fluorophlogopite, Ti and V impurities, colour of crystals explained by coordinations of Ti and V in mica structure 2−84562
  glass-ceramics, microstruct. and mech. props. 2−60999
  i.r. absorption spectra, in OH vibr. region, effect of Fe conc. 2−48168
  optical characts. for radiation receivers 2−55754
  surface conduction and surf. Hall coeff. dependence on temp. and mag. field 2−80541
  synthesis, hydrogen atmosphere, degree of reduction of Ti^{4+} and V^{5+} and coord. of Ti and V depend. on duration of crystn. 2−84562
  van der Waal's force between curved mica surfaces, meas. in range 1.5-130 nm 2−82169
  van der Waals dispersion forces 2−53104
  weathering, scanning electron microscope study of morphological aspects 2−56667
  Fe^{2+} ions, thermally modulated absorption 2−61637
  KAlSi$_3$O$_8$-Al$_2$O$_3$-SiO$_2$-H$_2$O system, muscovite melting to 30 kbars 2−61851
Micelle systems *see Colloids*
Microanalysis *see Chemical analysis*
Microhardness *see Hardness*
Micrometeorites *see Meteorites*
Micrometry
  see also Interferometry; Strain gauges; Thickness measurement
  stereo, three-dimensional object reconstruction in electron microscope 2−79118
Microphones
  see also Transducers
  for acoustic noise measurement, very low levels, method using principle of energy addition 2−66630
  capacitance, dynamic membrane deflections 2−41767
  capacitance-microphone static membrane deflections, nonlinear equations 2−73442
  capacitor-transducer array, for acoustic holography 2−69765
  differential, using electret transducer 2−41760
  dynamic response of suspended underwater hydrophone systems 2−41754
  electret, optimization of ridge backplate 2−41761
  gradient, performance in gas mask 2−41771
  miniature, using electrets 2−41759
  pressure gradient hydrophones, wide range calibration system 2−45518
Microphotometers *see Densitometry*
Microprobe analysis *see Electron probe analysis*
Micropulsations
  amplitude distribution patterns along meridional profile 2−72918
  correlated storm associated u.l.f. magnetic oscillations, simultaneous ground and satellite obs. 2−62392
  daytime irregular pulsation, relation to magnetospheric substorm 2−72914
  frequency dependence on geophysical parameters, $2\times10^{-3}<f<20\times10^{-3}$ Hz range, ATS-1 obs. 2−62390
  frequency drift of PDP type pulsations, due to protons motion under electric field in magnetosphere 2−48599
  geomagnetic, meas. by induction coils, digital computation of spectra by power spectral density method 2−62389
  high speed spectrum analyser, S-type hissa 2−72920
  induced by currents in ionosphere due to pulsating aurora 2−48572
  ionospheric micropulsations from finite source, ground signal rel. to Pc 1 disturbances 2−65960
  ionospheric propagation of oblique hydromagnetic plane waves at micropulsation frequencies 2−65959
  magnetospheric substorm Pi 1 micropulsations, ground-satellite correlations 2−62332
  magnetotelluric fields, spatial characteristics 2−58119
  magnetotelluric interpretation and field results in geologically complex areas 2−58120
  mid-latitude geomagnetic, octave-bandwidth analysis covering period range 16-24 secs 2−62388
  midlatitude, spatial characteristics 2−66009
  Pc1, recurrence period and carrier frequency pump obs. 2−62387
Micropulsations continued
  Pc3,4, diurnal variation of periods 2−44773
  Pc3, 25 mHz, diurnal variation of polarisation in horizontal plane 2−48600
  Pc 1 event (of April 7, 1971) 2−54931
  pc 1 event after 3 May 1967 storm, periodicity and formation mechanism 2−84924
  pc 1 hydromagnetic whistler diurnal effects rel. to early afternoon source model 2−84922
  Pc 1 occurrence, rel. to solar activity 2−58006
  Pc 4, observations at Tottori 2−78407
  Pc 5, storm associated events, obs. at synchronous equatorial orbit 2−66004
  Pcl propagated through ionospheric ducts, polarization 2−54930
  Pi2, development during substorms 2−81747
  pi 1 micropulsationa aub-class rel. to diurnal transit of neutral sheet 2−84921
  Pi 2, along meridian profile, pulsation spectra 2−81737
  Pi 2 and Pc 3, rel. to magnetotail field changes 2−66005
  polarization characteristics, effect of geoelectric structure 2−66010
  polarization properties of Pc1 micropulsations at low latitudes 2−72919
  polarization rel. to source rotation 2−72917
  quasiperiodic v.l.f. emissions, hydromagnetic modulations 2−72921
  spectral and polarization analysis, computer assisted, of obs. by ATS-1 2−62391
Microscopes
  see also Electron microscopes; Ion microscopes
  fluorescence, FLUOVAL, design and construction 2−59250
  focusing on surface, optical-photoelectric method 2−59244
  holographic, real time and double exposure for phase variation dynamics obs. 2−42148
  holographic interference, optical configuration and performance 2−73619
  hot stage, applications in glass, ceramic and metallurgy 2−56838
  lamp system design 2−42252
  optical, special aspects of development 2−59254
  optical projection, PAP-2, obs. of deformations of elastic sensing elements 2−45805
  photoelectric intensity, measurement of small displacements 2−55360
  polarizing, partially coherent image of opaque edge 2−42233
  resolution, two-point, rel. to condenser obstruction 2−76525
  scanned laser for photoluminescence obs. of semiconductor wafers 2−55706
  scanning, super resolution aperture 2−52464
  scanning acoustic, with visual picture of object 2−49163
  STANDARD KK08, reflected-light microscope 2−52468
  striae in glass, operation principles for observations 2−59253
  television microscopy 2−59266
  temperature-gradient microscope stage, aid in teaching solidification phenomena 2−58680
  TV, picture analysis, contrast increase with colour filters 2−76534
  zonal coma of semi-aplanat reflecting microscope, error in theory 2−82570
Microscopy
  see also Electron microscopy; Field ion microscopy
  annular source, two-point resolution in partially coherent light 2−66833
  automatic TV image analyzer, application to ceramics 2−56957
  β-brass, stress corrosion cracking obs. by optical microscopy 2−84132
  β-brass, stress corrosion cracking obs. by optical microscopy 2−84132
  ceramics, surface texture, reflective technique using metallographic microscope 2−80869
  colour contrast methods for living tissue obs. 2−76054
  colour television microscopy in biology and medicine 2−58613
  contact, epiobjective design 2−70004
  contact, OLK-2 adapters 2−70044
  education using visual aid televisions system 2−55350
  fluorescence with acridine orange, demonstration of tumour cells in cerebrospinal fluid 2−55256
  freezing of aqueous systems using temp. gradient microscope stage 2−74585
  graphite, artificial, anisotropic and isotropic, struct. characts., optical microscope exam. 2−53972
  graphite, high temp. fracture, opt. microscope obs. 2−56829
  graphite, highly oriented pyrolytic, effect of oxidation, optical microscope obs.. 2−56572
  high resolution microscopy of biological systems in high pressure chamber 2−85086
  holographic, time resolved differential 2−55715
  holographic interference microscopy of biological cells 2−62827
  holographic interferometry of small parts 2−55747
  i.r. transmission, utilizing high resolution video display, semiconductor crystal structure examination 2−71399
  magnetic moments of dust particles, microscopic determination 2−53456
  metal oxide structures, microanalysis 2−77540
  molecular, electron beam heating 2−66708
  molecular, scanning, for water 2−67465
  molecular beam, developments 2−67464
  Nomarski differential interference contrast microscopy, review 2−52467
  optical, interferometer systems, for refractive index, thickness and surface struct. obs. 2−55736
  optimal picture, from focusing by means of Fraunhofer diffraction 2−76533
  optimal visual magnification 2−63377
  phase-contrast and interference-contrast, for living cells in gynaecology 2−58612
  Pinus radiata, sample preparation 2−78640
  polymer testing machine for simultaneous study of structure and mechanical properties 2−53857
  polypropylene, effects of pre-melting conditions on spherulite structure 2−47066
  quantitative analysis of dislocation distribution, correspondence 2−68025
  quantitative analysis of dislocation distributions, comments 2−68024

Microscopy continued
refractive index measurement by interference microscopy and corrections for dispersion 2−70016
refractories, microstruct., optical microscopy obs. 2−56955
steel, martensitic, low-C Mn, effect of Sb on high temp. tempering, opt. microscopy 2−56905
techniques for improved resoln. of carbon and graphite samples 2−53637
tissue preparation for light and electron microscopy 2−78643
two point resolution in partial coherent light, microscopy 2−52457
Fe-Ta alloy, ductility enhancement using allotropic phase change opt. microscope obs. 2−57020
$(U,Pu)O_2$ microspheres and pellets, sol-gel derived, microstructure studied by optical microscopy 2−47610

Microstructure of crystals *see Crystal structure/microstructure; X-ray examination of materials/microstructure*

Microtomes *see Biological technique and instruments; Laboratory apparatus and technique; Microscopy*

Microtrons *see Particle accelerators*

Microwave spectra *see Spectra*

Microwave spectrometers *see Spectrometers, radiofrequency*

Microwave techniques and devices
acoustic surface wave attenuation due to gas loading 2−51009
acousto-optic modulators and deflectors 2−55709
airborne K_a-band microwave radiometric meas. mapping system 2−84779
anechoic chambers, optical design 2−49213
Arctic Sea ice, aircraft meas. of microwave emission 2−81632
atmosphere temp. meas., water vapour, isentropic analysis, winds, cloud free regions 2−84834
atmospheric O_2 temperature profiles, angular scan multi spectral measurements, radiometers 2−84826
atmospheric pressure level determ. by two-satellite microwave occultation method 2−84858
biophysical considerations and standards criteria 2−48874
bounded magnetoplasma, h.f. production and diagnostics 2−67661
cascade frequency multipliers, GaAs dividers, metal semiconductor barrier 2−84350
cavity excited in TM_{0n0} mode, diffusion-controlled gas breakdown meas. 2−50231
cavity resonators for plasma diagnostics 2−77284
circular helical conducting waveguide, excitation by electric, magnetic dipoles, e.m. wave diffraction 2−63194
complex permittivity meas., dynamic, high-temp. on microwave absorption heated samples 2−49237
conducting media impedance measurement, effects of e.m. wave front curvilinearity 2−49240
conductivity, microwave-induced anisotropy, for semiconductors in quantizing magnetic field 2−71893
correlometer for fast processes 2−55364
correlometer for precision meas. of time intervals having resolution of fractions of nanoseconds 2−55365
delay line, 600 MHz acousto-optical deflector 2−51296
dielectric characts. of low and high loss materials, 0° to 70°C., meas. 2−49235
dielectric props. of high or low loss materials, short-circuited waveguide meas., computer program 2−49236
diffraction loss due to spherical Earth, calc. 2−69830
diode switch, measurements of spin-lattice relaxation times 2−76421
direct detection noise meas. system using Schottky barrier diodes as envelope detectors, threshold 2−63212
discharge, low pressure 2−80268
Doppler radar study of clear air layer in lower troposphere 2−54834
double gap klystron, obs. of working range for ion beam bunching 2−45688
electronics, possible applic. of finite element calc. of propagation of elastic surface waves guided by ridges 2−76335
e.m. wave interaction with radially divergent electron beam 2−49327
e.p.r. absorption and dispersion signals, simultaneous meas. 2−55628
ferroelectric oscillatory system, effect of automatic temp. stabilization 2−44157
field perturbation by animals and apparatus 2−52004
gas fluidized bed density fluctuation detection by microwave beam 2−83505
Gunn diodes, GaAs epitaxial type, coaxial resonant cavity mounted, low temperature characteristics 2−71983
heating of high β hot electron plasmas 2−43139
heating processes of heterogeneous materials containing water, interaction of thermal, mechanical, e.m. parameters 2−54037
hologram radar system, design and operation 2−82535
holograms, optically reconstructed enhancement 2−59200
holographic interferometry, applications 2−79279
holographic reconstruction by electronic spatial frequency analysis 2−79278
holography, applications in modern aviation 2−82543
holography, resolution of defects 2−84171
holography, scanning technique 2−49403
homodyne microwave radar technique for flow meas. 2−60158
hot spot generation in lossy multilayer spheres, differential temp. rise obs. 2−49203
IMPATT oscillator, basic, phys. principles of operation 2−71971
interferometer, X-band, meas. of electron density in plasma 2−60257
interferometer analysis for plasma density meas. 2−46728
klystron, 50 kW, 2450 MHz, high efficiency 2−49329
Klystron bunching system for 5.5 MV Van de Graaff accelerator 2−52716
klystrons, axially symmetrical, analytic expressions for interaction gap electric fields 2−69880
Large Volume Microwave Plasma Generator 2−50211
layered structs., h.f. surface wave amplification, rel. to carrier density, drift vel. 2−65006
light modulation holography for large volume scenes 2−59202
line-of-sight propagation expt. for atmospheric turbulence resolution 2−68897
liquid crystals, by colour visualisation scanning 2−46977

Microwave techniques and devices continued
liquid-crystal hologram display for concealed weapon detection 2−69975
magnetron, c.w., dark current and electron energy spread obs. 2−49328
magnetron, natural oscillations of electron cloud 2−49326
magnetron amplifier frequency multiplying properties 2−59105
magnetron press. gauge on O VI-15, adsorption/desorption press. effects 2−58148
magnetron type ion source, radioactive isitope separation, high temperature techniques 2−82457
masers, resonator grating fabrication technology 2−41956
metal-to-metal point contact diode, i.r. generation by laser and microwave freq. mixing 2−69839
method for obs. of photoconductivity of photographic films 2−66867
microwave generation near electron cyclotron resonance 2−60265
microwave power symposium, Ottawa (1972) 2−49199
millimeter waveguide line attenuation, meas. by shuttle pulse method and pulse single reflection method 2−63192
molecules, barriers to internal rotation, relative intensity meas. of temp. on absorption lines 2−42943
nondestructive monitoring for optimization of in-service performance tests 2−60924
open resonator with axial corrugated metal rod, theory 2−49224
permittivity meas., modified infinite sample method 2−49238
plasma, capillary arc, Q-band propagation 2−60250
plasma diagnostic using resonant cavity 2−43169
plasma diagnostics, interference polarimeter-ellipsometer for resolution of ambiguity of meas. between rotation and ellipticity 2−83557
porous medium, drying with internal heat generation 2−45573
power measurement at microwave frequencies, waveguide, coaxial line techniques, book 2−52315
radio interferometer at K_u-band 2−55197
radiometer, theory and field tests for det. of sea ice thickness 2−44603
radiometry, applics. 2−48616
reflectometer system, electron density meas. in time varying plasma 2−74380
reflector antenna array, design 2−73156
remote passive sensing of ocean surface wind fields 2−44648
resonators with diffraction arrays, eigenmodes of periodic structure, waveguide damped resonance 2−63176
rodent phantom models, u.h.f. cavity exposure chamber, dosimetry 2−52003
spectrometer, design for chemical anal. 2−55626
SQUID freq. converter, resistive, design and h.f. response 2−44084
Stark microwave cavity spectrometer, Q-pulling effect, error compensation 2−66662
superconductive, constant-voltage steps in Josephson junctions, meas. technique 2−71878
teaching demonstration, standing waves by oblique incidence on mirror 2−41431
technique to extend lifetime and increase efficiency of flashlamps 2−63419
thioformaldehyde, generation and characterization from rotational spectrum, detection in space 2−44888
three-electrode system secondary electron resonance discharge, computer study of phase conditions of excitation 2−59107
transistors, employing evacuated capsule method for As diffusion into Si 2−71518
TWT, localized fields effect in cutoff intermediate section 2−59106
underwater sound source detection obs. 2−48425
water content of materials, nonresonant meas. method 2−49202
waveguide, beam, of rectangular symmetry, E- and H-wave superposition 2−63191
Al_2O_3 ceramics, microwave machining and piercing characteristics 2−53867
n- GaAs Gunn oscillators, hot electron microwave mobility 2−51139
H_2O FIR pulse excited laser output, effects of microwave power 2−59155
He arc plasma with superposition of h.v. pulse, interaction giving 2 to 40 GHz radiation 2−50212
InSb, n-type, electronic structure study by a microwave beat method 2−84246
$LiNbO_3$ single crystal longitudinal and shear hypersonic waves excitation 2−71741
n-Si, Faraday effect measurement 2−61591
Si X-band double-drift IMPATT diode fabrication by consecutive epitaxy 2−71976

Mie theory *see Scattering*

Milky way *see Galaxies/the Galaxy*

Mineralogy *see Minerals*

Minerals
see also Mica; Quartz; Ruby
absorption spectra meas. at high shock press., apparatus design 2−61828
activation analysis using NaI(Tl) shielded Ge(Li) detector system 2−72599
albite, plastically deformed, dislocation distrib. 2−81623
alkali feldspars, Na-K mixing, polymorphism 2−53675
alkali volcanic suite in Emperor Seamounts 2−57734
analysis, use of ion microanalyzer 2−44504
anorthite, Si-O and Al-O bond length parameters analysis 2−61850
Aouelloul crater glass, ^{26}Al content, rel. to Zli sandstone, formation theories 2−65584
apatite in Tatra Mountains, fission-track age determinations 2−72661
Apollo 12 soil samples, fragments of terra rock 2−69132
Apollo 14 lunar microbreccias, 14306 and 14055 specimens analysis 2−55120
Apollo 15 basalts, distinct cooling history 2−58452
armalcolite, synthetically prepared, comparison with lunar rock sample 2−44928
arsenates, near and i.r. spectra 2−72672
authigenic pyrite from Pacific deep-sea core, distribution and scanning electron microscope obs. 2−44579
basaltic rocks, high-velocity impact experiments 2−74851

Minerals continued
basaltic rocks, ion microprobe mass analyzer, microanalysis use 2−63297
basalts from Nunivak Island, ^{87}Sr/^{86}Sr ratios 2−57807
basalts of Barberton Mountain Land, Transvaal, silicate immiscibility 2−54672
basalts rel. to sea floor spreading, seismic wave vel. 2−72656
behierite, vibrational spectra, interpretation by factor group approx. calc. of force constants for BO_4 group 2−70728
beryl, anharmonicity of i.r. vibration modes, reflectivity obs. 2−51317
biotite, Mossbauer effect at ^{57}Fe nuclei 2−75266
blueschist belts, occurrence and mineralogic evolution 2−61956
bone content, measuring sites and methods 2−69262
boracite, reln. between elec. and mag. polarization, $T<64K$ 2−72104
borates, near and i.r. spectra 2−72672
bore mineral content of the radius, femoral neck and thoracic vertebrae 2−69356
breccia, lunar and terrestrial deform. substruct. 2−62688
British Tertiary Igneous Province, Skye lavas exam 2−62404
Burma, 12 biostratigraphic assemblage zones during late oligocene and early miocene times 2−48367
cahnite, vibrational spectra, interpretation by factor group approx., calc. of force constants for BO_4 group 2−70728
calc-alkaline rock suite in island arc of Lesser Antilles 2−65534
calcite, infrared dispersion parameters determination, comparison of three methods 2−57322
calcite emission polarization and rock discrimination 2−72692
California, Devil's Playground area of Mojave Desert, stratigraphy and tectonic framework of Mesozoic rocks 2−57739
carbonate crystals, natural rhombohedral, growth defects study by X-ray transmission topography 2−53732
celites, i.r. spectra and crystal structure 2−65254
Cenozoic basalts, southern Rocky Mountain region 2−57693
Chelmsford granite, crack growth and faulting in cylindrical specimens 2−75456
chlorapatite, hydrothermal growth 2−47234
chromian, petrologic implications of occurrence in Apollo-14 samples 2−73063
clay bearing rocks, resistance to weakening and disintegration resulting from drying and wetting cycle 2−54734
coesite, metastable growth in highly strained quartz 2−65579
composition and state in deep interior of Earth 2−72677
cookeite, in petalite, struct. determ. 2−81628
Debye-Huckel theory, appl. to clay minerals 2−83809
deep sea cristobalitic chert, ultramorphology 2−57843
diabase sills from Gila County, Arizona, palaeomagnetism of 1140 to 1150 million year samples 2−66021
dialogite, infrared dispersion parameters determination, comparison of three methods 2−57322
dickite, ground, negative surface charges 2−78235
dilatancy in rock under hydrostatic pressure 2−68860
diorite unjointed, effects of specimen size on mechanical properties 2−57820
dolomite, infrared dispersion parameters determination comparison of three methods 2−57322
dolomite, self-diffusion of C and O_2, obs. using isotopic exchange 2−68855
Earth resource rockets, first firing in Australia using Skylark 2−75640
elastic props. from u.s. and compression data 2−68848
enstatite, X-ray topographic studies of natural and deformed crystals 2−61970
equations of state and geophysical applications 2−72681
Ethiopia, lower Omo basin, late Cenozoic molloscan assemblages 2−75461
fayalite-forsterite solid solution between 900-1300°C at low pressures 2−65538
feldspar, axial growth of inclined en echelon cleavage cracks during compression 2−61972
feldspar, force field obs. 2−43955
feldspar megacrysts in basalt, K-Ar ages and origin 2−61992
ferric amphibole, pressure induced reduction 2−84721
ferromagnesian olivines, $(Fe_xMg_{1-x})_2SiO_4$, magn. transitions, comp. depend. 2−68987
ferromanganese nodules, thermomagnetic behaviour 2−58142
flint, u.s. light modulation and det. of photoelastic constants 2−70025
fluorite, natural X-ray topographic obs. 2−80669
fluorite, relative thermoluminesc. effects of α- and β-radiation 2−51379
forsterite, crystal synthesis, improvements in flux method 2−47265
forsterite with Mn impurity as e.p.r. field marker and intensity reference 2−66664
gabbros in equatorial Mid-Atlantic Ridge, rare earth element distrib. 2−54676
galena, mechanical strength as function of shallow tectonic temp. and pressure 2−61969
garnets, compression to 100 kbars 2−65581
Georgia marbles, shear strength, pressure dependence to 80 kbar 2−54741
Girgenti meteorite, mineralogical and chemical analysis of L-chondrite 2−75928
granite, precambrian, remanent magnetiz. obs. 2−62403
granite, stable sliding stick-slip transition, seismological implications 2−61941
granitic rocks in Cape Breton Island, Nova Scotia, radiometric dating 2−81592
grinding, change to props. 2−68148
Gulf of Mexico, Pleistocene paleoclimatology 2−75462
halides, near and i.r. spectra 2−72672
hercynitic spinel, petrologic implications of occurrence in Apollo-14 samples 2−73063
hydrothermal ore on floor of Indian Ocean 2−78291
Icelandic basalt, resistivity measurements 2−65562
igneous rocks, needle probe method of thermal conductivity det. 2−44592
igneous rocks, thermal conductivity estimation from mineral and chemical composition 2−44593

Minerals continued
igneous rocks from ophiolitic complexes, paleozoic ages 2−62002
igneous rocks from Rockall Plateau 2−54677
illite, microstructure and chemical comp. 2−84710
ilmenite-haematite solid solution, self-reversal and X-phase rel. to palaeomagnetic investigations 2−54960
ilmenites, from Mare Tranquillitatis, morphology, electron microscope obs. 2−44905
isomorphous proustite pyrargyrite series, vibrational spectra 2−44387
jade, toughness 2−50856
JOIDES basalts, compressional and shear wave velocities 2−57539
kaolinite ground, negative surface charges 2−78235
kernite, charge distribution from analysis of X-ray data 2−50560
kinoite, hydrogen atom positions and hydrogen bonds prediction 2−47312
landauite, Baumhauer type twins 2−71499
lapilli tuffs, primary fabrics use in strain determination of deformed volumetric rocks 2−57752
Laschamp and Olby basalts, mineralogical and palaeomagnetic properties rel. to geomagnetic field reversal 2−54945
Lawsonite, window for 50 cm liquid H_2 target 2−52670
Lewisian basement gneisses from Scotland, discordant zircon age patterns 2−61997
lherzolite inclusions and host basaltic rocks, ^{87}Sr/^{86}Sr geochemistry 2−57827
limestone, lightly loaded, stick-slip 2−72669
limestone rock, undergoing phase transitions, det. of velocity and attenuation of elastic waves 2−57594
Lower Devonian sandstone, strain rate effects on strength, deformation and fracture props. 2−54735
Lower Triassic rocks in central Nevada, fission track age 2−57927
lunar, Mg + Fe comp., rel. to parental liq. comp. 2−62676
lunar, shock melting and vaporization 2−51821
lunar and terrestrial calcic plagioclases, phase transforms. and exsolution 2−66162
lunar Apollo 14 and 15 samples, ^{40}Ar-^{39}Ar ages 2−62668
lunar basalt 14310 rel. to selective volatilization hypothesis 2−69136
lunar basalt rock 15085, comp. of tridymite and crystobalite 2−78486
lunar basaltic rocks, U-Th-Pb ages and Pb concentration obs. 2−44907
lunar basalts, rate of solidification rel. to Hawaiian lava lakes 2−66144
lunar breccias, Apollo-14 samples, geological implications 2−58460
lunar clastic materials, Apollo 14 samples, comp. characts. 2−58459
lunar igneous rocks, Apollo 15 samples, rare earth element analysis 2−62669
lunar olivine, temp. dependent Mg, Fe distribution 2−44908
lunar plagioclases, e.p.r., Ti^{3+}, Fe^{3+} and Mn^{2+} obs. 2−62686
lunar pyroxenes and olivines, polarized absorption spectra 2−51812
lunar regolith glassy particle formation, modelling 2−73071
lunar rock microcraters, classification of crater type and impact theory 2−81942
lunar rock samples, U-distribution in basaltic fragments 2−75849
lunar rocks, Apollo 15 samples, ^{40}Ar-^{39}Ar ages 2−62667
lunar rocks, breccias and fines, thermophysical props. 2−62661
lunar rocks, chondrules and ultramafic glasses 2−78483
lunar rocks, radiation induced e.p.r. signals 2−55123
lunar rocks and fines ferromagnetic and paramagnetic resonance spectra 2−62648
lunar soils, Rb-Sr isotope characts. of lunar soils 2−66139
lunar surface Breccias, theoretical reappraisal 2−62687
lunar surface exposed rocks, α-radioactivity obs., ^{210}Po activity obs. search 2−44910
lunar surface rocks and fines, i.r. and Raman spectra 2−62652
lunar terra materials, petrologic comparisons 2−78512
lunar zirkelites, U-bearing phase 2−44909
magnetic, in basalt samples. Mid Atlantic Ridge near 45°N, electron microscope obs. 2−61870
magnetite, magnetic and mineralogical changes associated with low-temp. oxidation 2−65571
magnetite dispersion, magnetic characteristics rel. to palaeomagnetism 2−58139
mantle, solid eqn. of state eval. scheme for h.p. phases 2−61981
Martian surface colour rel. to basaltic magnetic oxidation to red haematite 2−78546
melting temperatures in mantle, olivine, spinel and periclase melting curves 2−57481
merwinite, $Ca_3Mg[SiO_4]_2$, at. arrangement 2−78219
metabasic rocks, magnetic obs. 2−75639
metamorphosed belt-series sediments, discordant radiometric ages 2−61999
Mg_2SiO_4-Fe_2SiO_4 olivine transformed spinel system, equations of state det. using Birch's law 2−43504
mica and granite, weathering, scanning electron microscope study of morphological aspects 2−56667
microcline, shock deform. 2−61843
microcline perthite, K self-diffusion in 2−68859
montmorillonite, isolation moncrystalline particles, selected area electron diffraction patterns 2−68001
Moon, albedo and linear polarization rel. to optical properties of igneous rocks in i.r. range 2−75846
mudstones, resistance to weakening and disintegration resulting from drying and wetting cycle 2−54734
mushketovite, mag. props. rel. to ion content 2−51246
neutron activation analysis logging in mineral exploration programmes 2−57805
Nigeria, presence of metamorphic rocks of Kibaran age 2−65556
norite, post-failure stress strain path dependence 2−62009
oceanic basalt, brittle fracture 2−61971
olivine, dislocation mechanisms rel. to upper mantle flow 2−65533
olivine, electrical conductivity, rel. to lunar temperature profile 2−51806
olivine, electrical conductivity det. up to 1200°C and 7.5 kb 2−65580
olivine, Fe^{2+} ions, thermally modulated absorption 2−61637
olivine, pressure-induced elec. conductivity increase and red shift in absorption spectrum 2−54421

Minerals continued
- olivine electrical conductivity rel. to temperature profile of lunar interior 2−66142
- omphacite, plastically deformed, dislocation distrib. 2−81623
- palagonite formation in sea, structural analysis of basaltic glass failure 2−57753
- palygorskite colloid soln., stability, transient elec. light scatt. obs. 2−74567
- paragneisses, polymetamorphic and anatectic, zircon ages interpret. 2−61998
- particle track detector materials characteriz. 2−63714
- permeable inhomogeneous cylindrical conductor surrounded by thin shell, Turam response 2−72687
- perovskites, ordered, of type $Ba_2M^{2+}M^{6+}O_6$, vibrational spectra 2−81370
- petroleum exploration of sedimentary basins 2−44765
- phlogopite, annealing effect on etching figures of tracks produced by ^{252}Cf disintegration 2−71362
- phlogopite + enstatite, stability at high pressures, model of micas in upper mantle 2−78221
- phosphates, near and i.r. spectra 2−72672
- plagioclase, at. scatt. factor satellite intensities, reciprocal space distrib. 2−53678
- plagioclase feldspars, phase diagram 2−61849
- pliocene basalts, thermomagnetic obs. determ. of magma sources depth 2−78283
- pliocene volcanic rocks, K-Ar ages and K, Rb and Sr content 2−57809
- polycrystalline, optical diffraction, review of Raman theories 2−61594
- Precambrian rocks, Northern New Mexico, Rb-Sr geochronology 2−61995
- pseudoboehmites in dil. nitrate electrolytes, point of zero charge 2−75390
- pyrophyllite, mech. props., effect of firing temp. 2−50890
- pyroxene, lunar and terrestrial, microstruct. on cooling 2−62689
- pyroxenes in lunar soil samples rel. to telescopic spectral reflectivity measurements 2−78521
- pyrrhotite, mechanical strength as function of shallow tectonic temp. and pressure 2−61969
- quartz, emission polarization and rock discrimination 2−72692
- quartz sand and sandstone recognition by two-channel i.r. imagery 2−65438
- quartzite from Bonito Canyon, micromagnetometer investigations of remanent magnetism 2−72923
- radioactive waste treatment, use of local minerals 2−83158
- red sandstone, effect of heat treatment on magnetic minerals 2−81601
- red sediments, mag. mineralogy by coercivity spectrum analysis 2−51663
- residual elastic strains, reflecting crystal distortions 2−78299
- Rochelle salt, second order ferroelec. transitions, calorimetric exam. 2−77951
- rock, brittle, anal. of stresses associated with cracks 2−75457
- rock, brittle, complete stress-volumetric strain equation, up to strength failure 2−75455
- rock, percussive drilling, applic. of model 2−54737
- rock, percussive drilling, exptl. verification of mathematical theory 2−54736
- rock as composite material, effective elastic modulus calc. 2−56974
- rock deformation, volume changes at high pressure 2−62006
- rock discs and rings loaded in diametral compression, controlled failure 2−62011
- rock elasticity, effects of pressure 2−68849
- rock forming, Raman, resonance Raman and fluorescence spectra 2−42262
- rock fracture and flow, effect of triaxial stress system 2−72679
- rock fracture zone rel. to penetration of trapezoidal- shaped body 2−75425
- rock systems, Fe^{2+}-Fe^0-Si relations 2−61848
- rock-joint deformation, modelling 2−72668
- rocks, effect of stress gradient on brittle fracture initiation 2−72667
- rocks, effects of absorbing properties on results from steady state neutron method 2−54733
- rocks, elasticity in uniaxial strain 2−75454
- rocks, electric oven for studying mag. 2−73241
- rocks, fracture and flow 2−57822
- rocks, friction, model of fault behaviour 2−57728
- rocks, high-temp. rheology 2−57823
- rocks, indentation by rough wedge 2−57819
- rocks, Indian rel. to others, elastic wave velocity 2−75453
- rocks, internal friction, effects of temperature variation 2−65577
- rocks, mountain, seismoactive areas, electrical resistivity variation 2−65561
- rocks, pre-Caledonian, Mullet Peninsula, County Mayo, Ireland 2−61842
- rocks, similarity anal. of process of movement 2−62004
- rocks, static uniaxial deformation to 30 kb 2−62013
- rocks, stressed, elastic shock activity during injection of water 2−55510
- rocks, thermal stresses in spheres, model for grinding 2−62010
- rocks, yield condition and hardening rule 2−57818
- rocks and polycrystals, elasticity, mantle minerology 2−65569
- rocks in Idaho batholith, vertical distrib. of heat generation 2−65452
- rocksalt, epitaxy of Au, influence of interfacial amorphous C layers 2−77503
- rutile powder X-ray line profile analysis of particle size and strain 2−74831
- salt, Bryan field, sediment cored anticline 2−44584
- salt media, analysis of time-dependent deformations of openings 2−62012
- sandstone, specific resistivity 2−62015
- sandstone and shale, seismic signatures of sedimentation models 2−44557
- sandstones, Indian, resistivity obs. under dry and saturated conditions 2−75460
- sandstones and sand, book 2−84758
- sapphire, longitudinal elastic constants, third and fourth order, det. by shock compression 2−47567

Minerals continued
- sapphire, relationship between laser induced surface damage and surface plasmas 2−60266
- sapphire, wear behaviour sliding on steel 2−74867
- scapolite, antiphase domain structure 2−62014
- seismic properties of upper mantle rel. to its mineralogy 2−57695
- seismoelectric effects in rocks, borehole and lab. studies 2−54641
- Seoni meteorite, chondrite composition and evidence of recrystallization 2−75927
- shale samples, resistance to weakening and disintegration resulting from drying and wetting cycle 2−54734
- Siderite, infrared dispersion parameters determination, comparison of three methods 2−57322
- siderite, thermal decomposition from mag. props. and mossbauer effect 2−72666
- silicate rocks, spectral compositional imaging 2−65548
- siltstones, resistance to weakening and disintegration resulting from drying and wetting cycle 2−54734
- sinhalite, vibrational spectra, interpretation by factor group approx., calc. of force constants for BO_4 group 2−70728
- smithsonite, infrared dispersion parameters determination, comparison of three methods 2−57322
- snow-ball growth, theory 2−61961
- soil, microscopic study 2−65585
- Solenhofen limestone, creep testing at constant stress and constant force 2−62008
- Solenhofen limestone, effects of strain rate changes on strength and ductility 2−62007
- Solnhofen limestone, shear strength, pressure dependence to 80 kbar 2−54741
- South African kimberlite, $^{87}Sr/^{86}Sr$ abundance ratio in fresh specimens 2−75452
- southeastern California, petrography and statistical analysis of late Precambrian-Cambrian quartzites 2−57563
- sphalerite, e. microdiffraction exam. of microscopic impurity inclusions 2−71408
- sphalerite, mechanical strength as function of shallow tectonic temp. and pressure 2−61969
- spinel, pressure-induced elec. conductivity increase and red shift in absorption spectrum 2−54421
- spodiosite analogues, i.r. and Raman spectra 2−51318
- Staurolite, Fe^{2+} site distribution, Mossbauer spectrum 2−48143
- steatite, mech. props., effect of firing temp. 2−50890
- stishovite, u.s. vel. obs., rel. to upper mantle comp. 2−61980
- submarine basalts, excess Ar rel. to Earth-atmosphere evolution model 2−72689
- superheavy elements with atomic number 114, search in nature 2−82837
- surface hydrophilic character, determ. by N_2, Kr and H_2O adsorption 2−47155
- sylvite from W. Germany, K-Ca age determ. 2−81638
- talc, appl. as press. transmitting medium at low temp. 2−73248
- talc form sepiolite, Fourier analysis of line profiles 2−64627
- talenite, $Y_3[Si_3O_{10}](OH)$, cryst. struct. 2−71442
- Tennessee Sandstone, exptl. investigation of stick-slip 2−62089
- Tennessee Sandstone, influence of surface roughness and gouge on frictional sliding 2−65521
- ternary n + 3 phase multisystem, topological relationships 2−72693
- three variable closed array, nonuniform density of data points 2−81594
- time dependent crack growth, creep in rocks 2−65576
- titanomagnetite, effect of oxidation at low temp. on magnetic properties 2−54964
- titanomagnetite, Mossbauer determination of cation distribution, geological significance 2−54965
- titanomagnetite bearing rocks, piezomagnetic effects 2−68857
- titanomagnetite dispersion, magnetic characteristics rel. to palaeomagnetism 2−58139
- titanomagnetites, cation deficient, spontaneous magnetization curve and Curie points 2−72925
- titanomagnetities, effect of annealing on exchange anisotropy 2−72927
- topaz, surface structures of prism faces, development and growth mechanism 2−60702
- topaz, thermal and electron beam induced microstructural breakdown 2−60776
- tourmaline, isotropic e.s.r. line, rel. to impurity Fe^{3+} 2−75342
- transient e.m. response of conducting infinite cylinder, surveys for elongated ore deposits 2−44594
- transmission electron microscope obs., at high voltage 2−56631
- tremolite, natural, containing 0.15% Mn^{2+}, analysis of single crystal e.s.r. spectrum 2−68732
- Twin Sisters dunite intrusion, paleomagnetism and rock magnetism 2−58129
- ultrabasic lunar samples rel. to differentiation on Moon 2−85040
- ultramafic, nature of source material from He and Ar diffusion obs. 2−65583
- unsaturated rocks, dependence of compressional wave velocity on porosity 2−44555
- vanadates, near and i.r. spectra 2−72672
- vertebral bone mineral mass determ. by transmission obs. 2−69263
- vitrinite, carbonized, at various temps., hyperfine struct. obs. by e.p.r. 2−68731
- vivianite, Fe^{2+} ions, thermally modulated absorption 2−61637
- volcanic rocks, acid volcanism, phenocrysts, charnockites 2−84719
- Walvis ridge, volcanics, in situ rocks 2−81621
- weathering profiles, distinguishing modern from relict. 2−54580
- wolframites, i.r. spectra and crystal structure 2−65254
- wurstite, increase in remanent magnetization during heating 2−62407
- wustite, elastic consts., rel. to upper mantle comp. 2−61980
- yugawaralite, hydrogen atom positions and hydrogen bonds prediction 2−47312
- zenoliths from Tahiti, K-Ar ages 2−57808
- zeolite, adsorpt. of ethane and ethylene, effects of size, charge and conc. of exchange cation 2−74646
- zeolite, adsorption of water, molar heat, 90-300K 2−60694
- zeolite, cation-exchanged, Mossbauer effect of Fe^0-atoms 2−54390
- zeolite, with ultrafine channels, filling with liquid Hg and Ga 2−84153

Minerals continued
zircon U-Pb and whole rock Rb-Sr age lowering during metamorphism of Grenville Province 2−61996
Zli sandstone, ^{26}Al content rel. to Aouelloul crater glass 2−65584
zunyite, structural changes on heating 2−75451
Ag_3AsS_3, proustite, synthetic, low-temp. transform., spectral detect. 2−50930
Al_2MgO_4 spinel, lattice dynamics, elastic properties, seismic velocity and density profiles 2−72636
Al_2SiO_5, high and low pressure polymorphs thermal conductivity-density relationship 2−65582
C abundance in Apollo 11, 12 and 14 lunar samples 2−78513
C content of lunar basalt samples and related terrestrial rocks 2−58457
Ca-Fe olivines, X-ray diffraction study 2−47325
$Ca_5(PO_4)_3Cl$, chlorapatite, synthetic, monoclinic struct. 2−53656
Cu and Au, relation to tectonic features 2−57724
Cu and Zn, in presence of Fe, Ekco mineral analyser, radio-isotopic X-ray fluorescence 2−81643
Fe-rich, X-ray fluorescence anal. for Cu and Zn radioisotope detector-radiator assembly 2−61821
Fe, distribution in upper mantle 2−72675
Fe, Mg olivines, electrical conductivity in solid solutions rel. to planetary mantles 2−84292
Fe ore in South India, categorization of Precambrian 2−72628
$FeCO_3$, siderite, polycrystalline, elastic props. to 10 kbars 2−65573
Fe_2SiO_4 high and low pressure polymorphs, thermal conductivity-density relationship 2−65582
GeO_2, quartz and rutile type, thermal conductivity-density relationship 2−65582
$Hg_3Tl_4As_8Sb_2S_{20}$, vrbaite, cryst. struct. 2−53664
$KAlSi_3O_8$-Al_2O_3-SiO_2-H_2O system, muscovite melting to 30 kbars 2−61851
$MgCO_3$, magnesite, polycrystalline, elastic props. to 10 kbars 2−65573
MgO-FeO-SiO_2 system in mantle minerals, phase equilibria and elastic properties 2−57711
MgO lattice dynamics, elastic properties, seismic velocity and density profiles 2−72636
$Mg_5(O)(OH)_5[BO_3].nH_2O$, Wightmanite, octahedral 3 Å framework structure with pipe feature 2−72695
Mg_2SiO_4 spinel, lattice dynamics, elastic properties, seismic velocity and density profiles 2−72636
Mn crusts of Atlantis fracture zone 2−78230
Mn crusts of Atlantis Fracture Zone, mineralogy 2−61983
$MnCO_3$, rhodochrosite, polycrystalline, elastic props. to 10 kbars 2−65573
Ni olivine to Ni spinel, reaction rate of phase change, seismological implications 2−78270
Pb isotope ratios in conformable ores and oceanic rocks, evolutionary model 2−61991
$Pb(Mg_{1/3}Nb_{2/3})O_3$ formation processes in the solid state reaction 2−77560
$PbMnO_2OH$, quenselite, cryst. struct. 2−53677
S content of lunar basalt samples and related terrestrial rocks 2−58457
Sn in Burma, review 2−48366
U, preparation for X-ray fluorescence, pressed fused disc method 2−65586
U ore processing 2−61990
U well logging, pulsed neutron method 2−44598
W in Burma, review 2−48366
zeophyllite, crystal struct. determ. 2−77547

Minor planets *see Planets*

Mirages *see Atmospheric optics*

Mirrors
see also Telescopes/astronomical
— 2−70054
aberrations and design 2−70037
aspherical surface inspection using correction plates made by vacuum deposition of aspherizing layers 2−59262
astronomical mirror flexure, influence of cell deformation 2−48819
astronomical mirrors, method of determining thermal deformations 2−48820
catadioptric systems described 2−59218
confocal interference filter, imaging 2−66844
cored, holographic interferometric det. of vibratory mode shape patterns 2−52434
cube-corner reflector, treatment as linear operator 2−63371
cube-corner reflectors, testing method 2−66798
dichroic, interference filter to sharpen spectrophotometry 2−42279
electron mirror microscope, charge distribution in isolated layers 2−79128
exit slit for u.v. Ebert spectrometer 2−70085
image rotation devices, comparative survey. 2−66837
interferometric testing, computer generated holograms 2−82572
interferometric testing of flatness and sphericity 2−55757
light weight, elastic deformations 2−79392
light-weight, 1.8 m, design of fabrication and test mount 2−79428
metal polygon, automatic surface inspection device, lapping technique 2−79386
mirror-prism systems, three dimensional problems, anomalous property 2−59210
mounts for fabrication and test 2−79427
moving, scanning applics. 2−66799
multilayer, low loss reflection coatings using absorbing materials 2−42244
parabolic, off-axis corrector, design fabrication and testing 2−79426
plastic, manufacture by replica method 2−59261
reflection coefficient, measurement method 2−42181
reflection factor determination using a portable device, construction principles 2−45774
Schmidt mirror system, description 2−59218
solar energy conversion, large-scale concentration 2−73506
telescope, spaceborne, evaluation of real-time figure control system 2−81973
White Welsh four mirror system, imaging properties 2−45778
Al, u.v. refl. rel. to LiF and MgF_2 films overcoating 2−79370

Mixing *see Heat of solution; Solubility; Solutions*
Moderation *see Neutrons and antineutrons/moderation*
Moderators *see Nuclear reactors, fission/materials*
Modulation of light *see Light/modulation*
Modulation spectroscopy
see also Electroreflectance; Magnetoreflectance; Piezoreflectance; Thermoreflectance
ATR, use in surface chemistry 2−65360
interference spectrometer with selective modulation 2−42268
Lorentzian curve line parameters under conditions of combined modulation and saturation distortion 2−66661
microwave double reson. line intensities for pump freqs. far from reson. 2−79984
molecular beam mass spectrometry, i.r. laser modulated 2−81490
optical and first-derivative, surface elec. field effects 2−78089
reflectance, band struct. analysis, review 2−72298
saturation, improved technique using intermodulated fluorescence 2−67502
semiconductor, electro-transmission in visible and near i.r. 2−51323
white light source, modulation visibility meas. method 2−73675
Moire fringes *see Interference/light*
Moisture
see also Atmosphere/humidity; Humidity; Permeability, mechanical
— 2−66649
evaporation from wet surface, determ. of vapour flux in terms of humidity potential 2−83833
neutron meter response, effect of stones 2−54732
polymers as adhesives binders and hermetic sealers, investigation of moisture effects by electrical methods 2−53979
remote sensing of moisture of specular soils with multifrequency microwave radiometry 2−84778
solid-water system, n.m.r. obs. 2−48303
u.h.f. phase sensitive moisture gauge 2−52352
water content of materials, nonresonant microwave meas. 2−49202
SiO_2 and SiO films, dielec. props., moisture stability 2−72015
Molar volume *see Density*
Molecular beams
see also Particle velocity analysis
apparatus for crossed beams 2−68771
crossed, study of reactive scattering of atoms and molecules 2−44470
electric deflection analysis of reactive scattering expts. 2−65367
high pass mechanical velocity filter, transmission characteristics 2−42862
inert gas clusters, multiple ionization by electron impact 2−60287
LEED stainless steel assembly, H and N desorption 2−67922
low energy ion-molecule scattering apparatus 2−63302
mass spectrometry, i.r. laser modulated 2−81490
metastable state lifetimes measurement methods 2−46523
methyl iodide, reaction with K in crossed beams, energy dependence 2−68771
methyl radical + $Cl_2(Br_2)$ collisional reaction, molec. beam study 2−61779
microscope, scanning, for water 2−67465
microscopy, development for biological work 2−67464
rare earth di- and trifluorides, structure studies electric deflection of molecular beams 2−42905
reflection of e.m. waves by molecular beam using two-level medium as model of beam 2−82403
scattering by Ne absorbed layer on Ge, survival rel. to coverage 2−47159
scattering by W surface, effect of surface composition and cryst. orientation 2−47084
scattering by well defined surfaces 2−50422
slotted disk velocity selectors, design 2−59986
supersonic plane symmetrical, vel. distrib. and Mach no. 2−53302
system for transmission electron microscopy of nucleation 2−79113
time-of-flight chemical accelerator, for low centre-of-mass energy spreads 2−55937
time-of-flight spectrometer with shock tube coupled through molecular beam 2−71107
van der Waals apparatus, construction 2−67544
velocity distrib. function determ. by mechanical selection method 2−77055
velocity distrib. function meas. method 2−64106
velocity meas. by phase detection method 2−59985
Ar, laser, molecular-beam stabilized, 5145 Å 2−79185
Ar, produced by multichannel source, speed distrib. meas. 2−50018
$^{133}Cs^{23}Na$, molec. beam elec. resonance spectra, determination of molec. props. 2−64140
$D + H_2 \rightarrow HD + H$ molec. beam study 2−72546
GaAs-$Al_xGa_{1-x}As$ dielec. waveguide, fabrication by mol. beam epitaxy 2−80593
H, interaction with Pt and Mo surfaces, scatt., chemisorption 2−50461
H_2, interaction with Ne, Ar and ice surfaces at 4.2K 2−50539
HCN hypersonic beam, electric resonance spectrography 2−67478
I_2 molecular beam spectra excited by 5145 Å Ar ion laser 2−67486
$^{39}K^7Li$, $^{39}K^{23}Na$, molec. beam elec. resonance spectra, determination of molec. props. 2−64140
$K + CH_3I \rightarrow KI + CH_3$, translational energy depend., reaction cross-section 2−51432
Kcl crystal vaporization rate, effect of $MnCl_2$ mol. beam 2−71281
LiCl, hyperfine spectra in zero magnetic and low electric fields using new electric resonance molecular beam apparatus 2−46557
N_2, produced by multichannel source, speed distrib. meas. 2−50018
N_2O, reactive scatt. from clean and C covered Pt(100) surface 2−50547
O_2, modulated, oxidation of basal plane of pyrolytic graphite 2−51447
O_2, modulated, oxidation of prism plane of pyrolytic graphite 2−51448
Rb^7Li, $Rb^{23}Na$, molec. beam elec. resonance spectra, determination of molec. props. 2−64140
Molecular orbitals *see Molecules/electronic structure; Orbital calculation methods*
Molecular relaxation *see Molecules/relaxation*
Molecular spectra *see Spectra/inorganic molecules; Spectra/molecules; Spectra/organic molecules and substances*

Molecular structure *see Molecules/configuration and dimensions*
Molecular weight
biopolymer, flow dichroism spectra applic., review 2−53089
poly(dimethyl siloxane), in high shear rate region, relation between mol. wt. and viscosity 2−83374
polybenzimidazole, distribution determination by equilibrium sedimentation 2−61761
polyethylene, high density melt rheology 2−83371
polyethylene, high pressure, determination from gel permeation chromatography data 2−67530
polyethylene fractions, melt viscosity 2−83370
polymer, distribution in monodisperse polystyrene, thermal degradation, gel permeation chromatography 2−78186
polymer solutions, concentration depend. of steady state compliance 2−83373
polymers, narrow distribution, relation between mol. wt. and non Newtonian viscosity 2−83372
polypropylene melt, rel. to capillary flow props. 2−46885
polystyrene in N,N-dimethylformamide, intrinsic viscosity-molecular weight relationship 2−83359
polyvinyltriorganosilane solutions, relation between intrinsic viscosity and molecular weight studied by light scattering and viscometry 2−46997
proteins, by X-ray diffr., teaching techniques 2−82097
styrene-diene-styrene block copolymers, effect on mechanical properties 2−71584
Ni complexes, tetracoordinated trimethylphosphines Ni(II) 2−77091
Molecular weight determination
from osmotic pressure meas., numerical treatment of data 2−43343
photometric, using automated laser light-state photometer with single photon counting system 2−63307
polybutadiene, gel-permutation chromatography and viscometric techniques 2−43024
styrene-butadiene rubbers, gel-permutation chromatography and viscometric techniques 2−43024
Molecules
see also Kinetic theory, Polarisability; Spectra
autoionization, Rydberg electron, semiclassical theory 2−77032
collective anisotropic molecular reorientation applic. of Mori's method 2−50313
diatomic, dielectric model 2−70652
dynamic polarizability estimate using Tchebycheff theory and moment technique 2−74192
European Phys. Soc. conf., Wiesbaden, Germany (Oct. 1972) 2−76139
field ionization in mass spectrometer chamber, ion current and ion distrib. 2−49921
Green function techniques, reviews 2−49919
Hartree-Fock energy expectation value of Hamiltonian, direct minimization 2−70651
interstellar, abundances 2−51779
interstellar, formation by association reactions 2−44884
interstellar, formation via negative ions 2−58357
magnetic multipoles in uniform field, effect on 'pseudo-contact' chemical shift 2−64101
magnetic properties, determ. using energy spectrum and wave functions of anisotropic harmonic oscillator in magnetic field 2−76206
Me-OH(Me = Cr, Mn, Fe, Co, Ni, Cu, Zn), binding energy and electron density calc. 2−42867
models, computer simulation 2−46638
N 2-level, superradiant level shift 2−41964
on-line data bank for conversational retrieval 2−42723
optical birefringence expts., information obtainable from analysis of statistical nature of light 2−63308
optical properties second-order estimate using Tchebycheff theory and moment technique 2−74192
organic, ring shaped, having permanent magnetization, required conditions 2−77131
oxacarbocyanine, excimer and related emission at low temp. 2−66861
physics, recent advances, book 2−49914
quantum mechanical calc., integral transformations 2−56146
reduced rotation matrix elements, subprogram for calc. 2−66452
selenacarbocyanine, excimer and related emission at low temp. 2−66861
spin-coupled wave functions, review of general theory 2−49918
Sun, effects of molecules in solar phenomena 2−78584
superheavy, formation by heavy ion collisions 2−60112
symmetric top, theory of higher-order stark effect 2−42836
symmetry group O*, irreducible-tensor theory, V and W coeffs. 2−42830
tetrahedral, force constants by orbital release force field and Urey-Bradley force field 2−77077
thiacarbocyanine, excimer and related emission at low temp. 2−66861
van der Waal molecule, CsHg produced for first time 2−67545
variational wavefunctions, relativistic connection 2−70557
H_2O, second order props., perturbation theory 2−46541
I_2^+, spin-orbit coupling 2−70709
$Na_2Co(SO_4)_2$ assignments 2−83271
configuration and dimensions
see also Chemical structure; Crystal structure, atomic
π-electron molecule, geometry influence on excited state electron structure and transitions 2−52986
angles of very stable complexes, calc. 2−50000
atomic coordinates, as struct. parameters and angles of internal rotation 2−64102
bond-orbital approach to conform. energies determ. 2−53018
book, development of present day concepts, based on course for arts students 2−62954
bridge, coordination number 2, applic. of equations characterizing vibrational behaviour 2−59973
bridge, coordination number 2, derivation and verification of equations characterizing vibrational behaviour 2−59972
cluster and ring compounds, of main group and transition elements 2−52988
complex molecules in solution, structure and formation constant, determination from dielec. polarisation meas. 2−60486
conformational isomer detection using internal rot. effect on band contours in oscillation spectra 2−83239

Molecules continued
configuration and dimensions continued
coordination compounds of lanthanide elements, angular parameters of overlap integrals of f-orbitals 2−77034
crystallographic computation, mol. model generation and fitting 2−53647
diatomic, reduced matrix elements 2−46497
equilibrium configuration, refinement of molecular effective force fields and structures to complete force field and structure 2−46517
gases, polyatomic, program to predict phys. props. from mol. struct. 2−83698
inner coordinates, role of topological properties in the determ. of redundancy conditions 2−52960
LCAO methods for optimization of geometry 2−52987
many-electron wavefunctions expanded in spin-adapted antisymmetrized products, expectation values 2−74194
modelling, computer program 2−79990
network models, derivation of difference eqn., study of energy spectrum and dispersion curves 2−77520
permutational isomerization reactions, enumeration 2−42827
polyatomic, role of vibrational relaxations in formation of diffuse and complex configuration spectra 2−77045
polybutadiene, configurational fluctuations rel. to memory effects in proton spin-spin relaxation 2−46636
polystyrene, configurational and conformational effects on magnetic circular dichroism in atactic and isotactic solutions 2−43366
relative internuclear distances, determination by quantitative applic. of nuclear Overhauser effect 2−52989
shape models, description of Valence-Shell-Electron-Pair-Repulsion scheme and Walsh-Mulliken Diagrams 2−50016
steric hindrance effects on nonlinear responses to laser beams and self trapped filament diameters 2−42113
structural representations algorithm 2−64103
structure recognition automation from molecular spectra, by computer 2−79967
Walsh's rules, extension to more general systems 2−50017
X-ray analysis, organic and biological materials 2−42861
HF-HCN dimer, H-bonding and structure, prediction by ab initio molecular orbital methods 2−80005

configuration and dimensions, inorganic
acid hydrates, hydronium ion struct. and dynamics 2−84601
diatomic mol. Born-Oppenheimer approx. breakdown rel. to bond length determ. 2−56151
halogenosilane bis-pyridine and o-phenanthroline complexes, normal coord. analysis 2−77081
hydrates of ions Li^+, Na^+, Be^{2+}, F^-, Cl^-, calc. by CNDO/2 method, determ. of H bond strength 2−50053
magneto-optical, opt. behaviour of solids, review 2−72294
$NaHF_2$, neutron diffraction data refined, location of H, thermal motion and F-F distance 2−77087
rare earth di- and trifluorides, electric deflection of molecular beams 2−42905
surface roughness of crystals, effect of ion bombardment 2−74614
vibration effect on apparent bond lengths for isoelectronic series for diatomic molecules 2−56136
$[C_nO_n]^{-2}$ dianions, geometry, MINDO/2 wave function calcs. 2−70689
$AlBr_3(CH_3)_2O$, geometry of AlX_3-COC framework 2−42869
Al_2Cl_6, normal coordinate anal. 2−42945
$AlCl_3(CH_3)_2O$, geometry of AlX_3-COC framework 2−42869
BF_2, ab initio calc. of electronic struct. and geometry 2−83244
BH_n series, generalized valence bond approach 2−59991
$BH_3.CO$, conformation within framework of INDO approx. 2−46527
B_2O_3, apex angle in C_{2v}-'V' struct. 2−70683
BeB_2H_8, BeB_2D_8, BeB_2HD_7, structure determination from i.r. and Raman spectra 2−52994
$BeCl_2$, CNDO approx. 2−46529
BeF_2, CNDO approx. 2−46529
$BiCl_3$, and cryst. struct. 2−77553
CH, excited states, internuclear distance rel. to Rydberg and valence shell character 2−50056
CO_2^-, $^2A_1$ and $^2B_1$ states 2−42874
CO_2^+, branching ratios det. from photoelectron spectroscopy 2−50032
$CdCl_2$, adiabatic compressibility and sound propag. speed, reln. to molec. struct. 2−72564
Cl tetrahedral oxy-compounds, force constants and regularities of chemical bonding 2−70725
ClNCO, microwave spectrum, internucl. parameters 2−56165
ClO_2F_3, LCAO MO SCF calcs., configuration 2−80000
$CoCl_2$, adiabatic compressibility and sound propag. speed, reln. to molec. struct. 2−72564
Cu complex, bis (picolinato) bis (thiourea) Cu(II), X-ray analysis and Patterson-Fourier and least-squares methods 2−71446
Cu complex, bis (picolinato) bis (allylthiourea) Cu(II), X-ray analysis and Patterson-Fourier and least-squares methods 2−71446
Cu ion, influence of ethanol on first hydration shell, e.s.r. obs. 2−64123
$CuH_2SO_4.5H_2O$ isotope effects in structure, fractionation of O 2−47324
Eu chelates, comparison of Mossbauer resonant intensities used to determine structure differences 2−48142
$F_3P.BH_3$ and $F_2HP.BH_3$, preferred conformations, CNDO/2 calculations 2−53032
Fe complex, FeN_2 electronic and geometric structure 2−77073
Fe complexes, nitroprussides, Mossbauer spectra of ^{57}Fe 2−44352
Fe_2Cl_6, normal coordinate anal. 2−42945
GeF_2 microwave spectrum, determ. of equilibrium structure for three isotopic species 2−70698
GeH_3F, GeD_3F, structure determination from microwave spectrum 2−60001
H_2, excited states, internuclear distance rel. to Rydberg and valence shell character 2−50056
$(HF)_n$, bond lengths, microwave spectrum 2−56177
H_2O dimer, in CCl_4 soln., i.r. spectrum and structure 2−50043
HOF-H_2O mixed dimer, LCAO-MO-SCF calcs. of equilibrium structures and energies 2−67491

Molecules continued
  configuration and dimensions, inorganic continued
    $(HOF)_2$ dimer, LCAO-MO-SCF calcs. of equilibrium structures and energies 2−67491
    $H_2P_2O_6^{2-}$, C_{2v} configuration in $Na_2H_2P_2O_6$, C_{2h} configuration in $K_2H_2P_2O_6$ 2−83267
    $Hg(SCN)_2$, structure in crystalline form 2−50620
    K_3, K_3^+, equilibrium geometries, pseudo Hamiltonian model 2−56190
    KHF_2, neutron diffraction data refined, location of H, thermal motion and F-F distance 2−77087
    Li complex, Li^+-H_2O, config. determination from H_2O energy surface data 2−60010
    LiO, $X^2\pi$ and $A^2\Sigma^+$ state props. 2−60011
    Li_2O_2, ab initio molecular orbital study using Gaussian basis set 2−53022
    LiO_2H, ab initio molecular orbital study using Gaussian basis set 2−53022
    $MgCl_2$, adiabatic compressibility and sound propag. speed, reln. to molec. struct. 2−72564
    $MgCl_2$, CNDO approx. 2−46529
    MgF_2, a priori and semiempirical calculations of conformation 2−42908
    MgF_2, CNDO approx. 2−46529
    $Mn(CO)_4NO$ complex, trigonal bipyramidal structure predicted from i.r. spectra data 2−42909
    N_2, excited states, internuclear distance rel. to Rydberg and valence shell character 2−50056
    NCN_3, microwave spectrum obs. 2−60014
    NF_2, ab initio calc. of electronic struct. and geometry 2−83244
    NH_3-BF_3 complex, geometry 2−60016
    NH, excited states, internuclear distance rel. to Rydberg and valence shell character 2−50056
    NH_3, multi-config. self-consistent field wavefunction 2−67490
    NH_2CN, structural parameters, determ. from microwave spectra 2−77066
    NH_4HF_2, neutron diffraction data refined, location of H, thermal motion and F-F distance 2−77087
    NH_2OH-H_2O mixed dimer, LCAO-MO-SCF calcs. of equilibrium structures and energies 2−67491
    $(NH_2OH)_2$ dimer, LCAO-MO-SCF calcs. of equilibrium structures and energies 2−67491
    Na_3, Na_3^+, equilibrium geometries, pseudo Hamiltonian model 2−56190
    Ni complexes, tetracoordinated trimethylphosphines Ni(II) 2−77091
    $NiCl_2$, adiabatic compressibility and sound propag. speed, reln. to molec. struct. 2−72564
    O_3^- anion isolated in Ar matrix, determ. of valence angle and O-O bonds from vibrational spectra 2−70720
    P tetrahedral oxy-compounds, force constants and regularities of chemical bonding 2−70725
    PH_2-PF_2, conformational analysis using CNDO/2 approx. 2−70722
    PH_4 radical, CNDO calcs. of config. energies, optimum geom. 2−64154
    P_2H_4, gas phase electron diffraction determ. 2−42937
    $(PNX_2)_3$ ($X=$halogen), gas phase electron diffraction determination of bond lengths and angles 2−53036
    $^{31}P^{14}N$, internuclear distance, calc. from millimetre wave rotational spectrum 2−60029
    PrF_3, Raman matrix isolation spectra, investigation of matrix effects on molec. structure 2−60031
    Pt complex, bis(triphenylphosphine)(ethylene)platinum 2−43587
    S tetrahedral oxy-compounds, force constants and regularities of chemical bonding 2−70725
    SF_4O, S-O distance by microwave studies 2−70723
    SOF_2, microwave spectrum analysis 2−80036
    Sb complex, methyltrichloro(acetylacetonato)antimony(V) 2−42935
    SbF_5, trigonal bipyramidal shape of monomeric species, evidence from gas phase Raman spectrum 2−50067
    Si tetrahedral oxy-compounds, force constants and regularities of chemical bonding 2−70725
    SiH_2, ab initio calcs. for potential curves, description of geometry and electronic spectrum 2−46584
    Si_2H_6, gas phase electron diffraction determ. 2−42937
    Te(IV) penta- and hexacoordinate mixed halide anions 2−77094
    XeF_6, molecular geometry and electronic states, electronic isomerism 2−42940
    YO, $B^2\Sigma$-$X^2\Sigma$ system, electron transition moment variation with internucl. distance 2−56203

  configuration and dimensions, macromolecules
    biological, neutron diffraction methods 2−81994
    biopolymer, flow dichroism spectra applic., review 2−53089
    bond distances and angles, calc. by approximate molecular orbital method 2−70670
    cellulose, crystalline models, conformational terminology 2−43022
    chain molecules statistical determ. of possible conformation using computing methods 2−42860
    computer simulation of polymer conformation and conformational thermodynamics 2−70801
    dimensions determ. from transient scattering from absorbing solutions 2−50378
    DNA, λ phage, conformation changes rel. to u.v. irrad. 2−60093
    DNA, helix-coil transition 2−67526
    DNA hypochromism, sequence depend. using Hartree calcs. 2−80118
    ethylene-propylene copolymers, configurational statistics 2−70802
    (1→4)-linked galactans, configurational statistics, calc. of conformational energies, characteristic ratios 2−70804
    linear chain of r elements, geometrical structure and pair potential interactions 2−83342
    local configurational changes, probability, in chain macromolecules 2−80111
    n.m.r. data and their interpretation, book 2−83396
    nucleic acids, review 2−83383
    peptides, ab initio studies of H bonding, mutual orientation of peptide planes 2−46634
    peptides and oligopeptides, conform., influence of specific intramol. interactions 2−60095
    poly-γ-benzyl-L-glutamate, 220 MHz p.m.r. relaxation time at helix-coil transition 2−80112

Molecules continued
  configuration and dimensions, macromolecules continued
    poly-L-proline I chain, conform. depend. of vibr. modes 2−80113
    polybutadiene, structure study using ^{13}C n.m.r. 2−53091
    polyethylene, high pressure, molec. structure determination with gel permeation chromatography 2−67530
    polyethylene, static and kinetic friction over clean surfaces, transfer and structure 2−64738
    polyethylene, sulpho-chlorinated, optical anisotropy of statistical segment 2−44346
    polyethylene fractions, melt viscosity 2−83370
    polyethylene oxide supermolecules, electron microscope meas. of size and growth in solution 2−64204
    polyimide, aromatic, secondary dynamic dispersions 2−83366
    polyisoprene, configurational fluctuations rel. to memory effects in proton spin-spin relaxation 2−46636
    polymer chain, span calculation 2−50120
    polymers, fluorescence decay, evaluation of distribution of distances between energy donors and acceptors 2−74252
    polymers, liner random-flight chains, empirical probability density functions for radii of gyration 2−43020
    polypeptide chains, helix-coil transitions, thermodynamic parameters 2−60096
    polypeptide chains, random, conformation 2−43018
    polysaccharides, review 2−83383
    isotactic polystyrene in toluene temperature dependence of confirmation 2−74522
    polystyryl radicals, chain length dependence of coupling reactions 2−72556
    polyvinyl alcohol, configuration of polymer chains determ. by p.m.r. 2−60105
    proteins, atomic coordinates superimposition, math. procedure 2−83335
    proteins, review 2−83383
    PTFE, static and kinetic friction over clean surfaces, transfer and structure 2−64738
    radii of gyration, light scattering method for particles ≈100Å 2−50117
    Salmonella flagella, polymorphism, phenomenological theory 2−53088
    spiral polymers, interaction between recurring links between neighbouring loops in vibrational problem 2−77160
    tendon collagen, fractography 2−43016

  configuration and dimensions, organic
    β-(pyrazolyl-3)-L-alanine 2−47358
    acetone, coupling of motion between methyl groups studied by normal coordinate analysis using Urey-Bradley force field 2−56210
    acetyl bromide, zero-point average structures 2−77136
    acetyl chloride, zero-point average structures 2−77136
    acetylacetone, molecular geometry from gas phase electron diffraction 2−60045
    acrylic acids, substituted, and thin methyl esters, ^{13}C n.m.r. shieldings and molec. geometry 2−42950
    acrylonitrile-styrene copolymers, sequence distribution of acrylonitrile units from i.r. spectra 2−67528
    aliphatic nitro compounds, theoretical conformational analysis using Kitaigorodsky's mechanical model 2−83307
    n-alkanes, chain-length dependence of anisotropy and depolarization ratio, comparison with laser light scattering expts. 2−80083
    alkanes and derivatives, from polarization tensor 2−70736
    alkylaromatic radical cations, methylene h.f. splittings and methyl hydrogen splittings interpret. 2−60046
    allyl anion, bond angles and CC-distance determination by π-electron and all-valence electron method 2−53042
    amino acid, proton mag. resonance, chemical group assignments 2−46989
    amino acid conformation, determination by homonuclear INDOR spectroscopy 2−50078
    aniline derivatives, u.v. absorpt., temp. effect, conform. change 2−68812
    aniline-^{15}N and derivatives, amino group geometry 2−77137
    [14]annulene, molec. structure in crystal, three-dimensional X-ray study 2−64647
    N- aralkylpyridinium ions, conformational influences on intramolecular charge transfer transition 2−42955
    azolidones, i.r. absorpt. spectra rel. to H bonding and mol struct. 2−56216
    benzene, Dewar structure CNDO/2 calculation 2−60051
    benzenes, substituted, molecular orbital study of excited state geometry 2−50084
    benzvalene 2−77139
    biphenyls, conjugation and angle of twist, determination by Raman intensity investigation 2−50086
    1,3-butadiene, conformation in nematic mesophase 2−60053
    butadiene sulphone, configuration in isotropic and liquid crystal media 2−56222
    1,3-butadienes, 1-substituted and 1,4-disubstituted, electronic spectra, comparisons between geometric isomers 2−42965
    t-butyl chloride γ-irradiated, e.s.r. evidence for planarity of t-butyl radical 2−74288
    cantharidine, X-ray diffraction study, molecular bond lengths and conformation 2−68010
    carbonium ion struct., orbital calcs. 2−56223
    carbonium ions, CH bond lengths, MINDO/2 calc. 2−77112
    chemical structure search by molecular spectroscopy, on computer 2−79968
    chloralides, optically active, conformation 2−42971
    p-chlorobenzylidene-p-chloroaniline, conformation rel. to electronic structure, determination from solid-state reflection spectra 2−53051
    chloroethanes, conformational energies 2−42970
    α-chymotrypsin, conformationally dependent low-frequency motions from laser Raman spectra 2−56268
    croconic acid and derivatives, CNDO/2 calcs. 2−70760
    2-Cyanopyridines, microwave spectra, ring distortion 2−74295
    cycloalkanes, ring strain effects on stretching vibrations of methylene group 2−42972
    cyclobutane, CNDO/2 treatment with hybridization restictions 2−70762
    cyclobutanecarboxylic acid, dimer conformations 2−42973

Molecules continued
configuration and dimensions, organic continued
cyclobutanes, substituted, i.r. spectra-structure correlations 2−56227
cyclobutene, partially oriented in nematic phase, p.m.r. study of H-H distances and orientation parameters 2−83313
cycloheptane and cycloheptene derivatives, conformational equilibrium from ^{19}F n.m.r. 2−83288
cyclohexane, ring interconversion 2−42974
cyclopentadienylberyllium chloride, microwave spectrum analysis 2−70763
cyclopropanes, protonated, CH bond lengths, MINDO/2 calc. 2−77112
cyclopropylamine, SCF-LCAO-MO calculations of conformation 2−70786
dialkylureas, i.r. spectra, determ of molecular configurations from vibrational band assignments 2−70766
diazoaminobenzene(β modification) 2−71444
1.4-dibromo-butin, in liq. cryst., dipole-dipole interac. rel. to n.m.r. 2−46596
diethyl ether, mol. struct. at 128K 2−68011
2,3-dihydropyran i.r. spectra, hindered pseudorotation, estimation of barrier height for half-chair inversion 2−70764
dinitrobenzpyridines, tautomeric forms, rel. to photochromic transitions 2−48344
1,4-dioxene i.r. spectra, hindered pseudorotation, estimation of barrier height for half-chair inversion 2−70764
ehtylene, ground state geometry 2−56229
electron absorption spectra at u.v. and visible range for computer search system 2−79969
epoxybutyne, microwave spectrum, structure and dipole moment 2−80088
estrogenic steroids, elucidation from computer interpretation of mass spectra 2−84685
ethane-methyl radical system, theoretical critical configuration describing decomposition and recombination reaction 2−57420
ethyl thiocyanate, conformation from vibrational spectra data 2−42983
ethylbenzene, conformational structure correlation with semi-empirical LCAO calculations 2−60068
ethylene sulphone, structure determination from microwave rotational spectra 2−60065
ethylene trithiocarbonate in thermotropic nematic solvent, p.m.r. study 2−56230
fatty acids, normal, chemical structure from u.s. velocity obs. 2−56231
ferric haem, iron out-of- planarity and tetrapyrrole nitrogen nuclear spin state mixing 2−80101
fluorine containing σ-bonded molecules, MINDO/2 calc. 2−77111
o-, m-, p-fluorobenzaldehyde, stable conformer 2−83279
2-fluoropyridines, microwave spectra, ring distortion 2−74295
p-fluorotoluene, conform. depend. of long-range spin-spin coupling 2−64193
formic anhydride, electron diffraction examination of structure 2−60070
fulvene, microwave spectrum and struct., bond lengths and angles 2−80096
furan, n.m.r. study in liquid crystal of structural parameters 2−67514
furan-2, 5-dialdehyde partially oriented in nematic phase, n.m.r., conform. obs. 2−70769
2-furanaldehyde, conform., rot. isomerism, nematic-phase n.m.r. obs. 2−77147
haemoglobin, circular dichroism rel. to struct. modification during oxygen fixation 2−56264
heterocyclic, 5-membered saturated ring, spectral obs. 2−46589
homoallylic H-H coupling constants, conformational dependence 2−42856
hydrocarbon negative ions, CNDO calculations and reactions 2−64184
hydroxylamine, microwave spectra obs. 2−56234
4.5-iminophenanthrene unsymmetrical excimer in cyclohexane solution 2−46604
iminoxyl radicals, spatial struct., spin density propag. via bonds 2−80110
isothiocyanate, determ. of molecular dimensions and large amplitude vibration by electron diffraction 2−80080
Kekule structs. and topology 2−83222
maleic anhydride, structure determ. by gas-phase electron diffraction 2−42992
methanol in excited CO stretching state, microwave spectrum, torsion-vibration-rotation interaction 2−67517
2-methoxyethanol, minimum energy conformation from microwave spectrum 2−50098
methyl cellulose aqueous soln., viscoelastic props. 2−83380
methyl iodide, equilibrium structure determ. from rotation-vibration interaction constants from i.r. spectra 2−42995
methyl isothiocyanate, structure determ. by gas-phase electron diffraction 2−43001
methyl-substituted chloroaluminate ions, i.r. and Raman spectra, determ. of bonding and structure 2−77117
methylbromoform, microwave spectrum, disubstitution method for struct. determ. 2−56243
methylchloroform, and cryst. struct. at −60° and −145°C 2−53685
methylchlorosilyl radical, meas. of ^{29}Si coupling consts. effect of degree of CH$_3$ substitution on planar structure 2−56241
methylene chloride, in liq. cryst., dipole-dipole interac. rel. to n.m.r. 2−46596
methylenecyclopentane, structure 2−67516
monoalkylbenzenes, conformational structure 2−42953
monochloroamine, structure from microwave spectra data 2−46615
N-acetylphenylhydroxylamines, substituted, cis-trans conformational equilibrium, n.m.r. obs. 2−50074
neopentane, structure determ. by gas phase electron diffraction 2−70796
olefines, trisubstituted, regiospecific and stereoselective isomerization 2−77105
1,3,4-oxadiazoles, isotopic species, structure from microwave spectral data 2−43003
3-oxetanone, microwave rot. spectrum analysis 2−70787
phenol, investigation of molecular inversion 2−50109

Molecules continued
configuration and dimensions, organic continued
phenothiazines, MO calculations of conformational properties 2−60082
phosvitin, X-ray diffraction study 2−74298
plane aromatic, geometry in excited state, theory 2−70733
poly-γ-benzyl-L- glutamate solns., helix conform. model, rel. to i.r. elec. dichroism 2−60083
polybutadienes, sequence structure studies by ^{13}C−{^{1}H} Fourier transform n.m.r. 2−67529
polyurethane film forming materials, relationship between struct. and props. 2−83385
PPA nematic liquid crystals, order characterization 2−83777
propane, conform. depend. of vicinal ^{13}C−H spin-spin coupling const., INDO MO calcs. 2−77151
β- propioelectone, p.m.r. spectrum in thermotropic nematic solvents 2−50110
propiolic acid, microwave spectrum, conform. obs. 2−56256
proteins, determ. of quaternary structure 2−77158
proton- enhanced nuclear induction spectroscopy study of ^{13}C chemical shielding parameters 2−72524
pyrene unsymmetrical excimer in cyclohexane solution 2−46604
pyridine, quasiplanarity in first excited singlet state, demonstration by investigation of 2875 Å band system 2−46625
11-cis-retinal, p.m.r. calculation and conformation 2−77153
ring compounds, four-membered, puckering co-ordinates 2−42942
salicyl aldehyde, structure of H bond from microwave spectra 2−43008
semibullvalene, tricyclo[3,3,0,0$^{2.8}$]octa-3,6-diene, structure determ. in gas phase 2−77154
silyl isocyanate, determ. of molecular dimensions and large amplitude vibrations by electron diffraction 2−80080
spiropentane, structure determ. by gas phase electron diffraction 2−70796
cis- stilbene, steric conformational analysis 2−56258
trans-stilbene, steric conformational analysis 2−56258
sulphur diimide, through space coupling 2−64192
sultones and sultines, conformation 2−43009
tetracyanoquinodimethane and its mono- and di-valent anion, SCMO CI calcs., comparison with u.v. spectra 2−70791
tetramethylcyclobutane-1,3-dione, 2−77155
tetramethylenecyclobutane-d$_0$ (-d$_8$), meas. of Raman and i.r. spectra, symmetry assignments 2−70792
thiazanes, i.r. absorpt. spectra rel. to H-bonding and mol. struct. 2−56261
thioamides, conformational properties 2−43011
thiocarbonyl anion radical, e.s.r. studies of structure 2−53082
thiophene, n.m.r. study in liquid crystal of structural parameters 2−67514
thiosultanes, conformation 2−43009
toluene, conform. depend. of long-range spin-spin coupling 2−64193
trans-3,4-dimethyl-2,2,5,5-tetradeuteriocyclopentanone, vibrational assignment and conformational studies 2−64189
trans-3,4-dimethylcyclopentanone, vibrational assignment and conformational studies 2−64189
tri-tert-butylmethane, inferences combining electron diffraction spectroscopy, and molecular mechanics 2−77109
tri-tert-butylmethane, using gas phase electron diffraction 2−77108
tricyclopropylphosphine, structure determ. by gas phase electron diffraction 2−70796
trifluoroacetone, molecular geometry from gas phase electron diffraction 2−60045
trifluoroacetylacetone, molecular geometry from gas phase electron diffraction 2−60045
trimethyl silyl isocyanate, microwave spectrum analysis 2−80076
trimethylazidosilane, electron diffraction determ. 2−80109
tropolone, near u.v. spectrum rel. to molec. structure, rotational band contour analysis 2−53085
urea, changes in bond length and angles on protonation 2−60089
uridine and related structures, relationship of ^{13}C to vicinal ^{1}H coupling to torsion angle 2−43014
uronium ion, CNDO/2 calculations 2−60089
vinyl chloride, gas-phase electron diffraction study of structural parameters 2−67524
vinyl trifluoroacetate, i.r. and Raman spectra, vibrational assignment, depolarization ratios and configuration determ. 2−70797
vinyl-type radical in irrad. maleic acid matrix, e.s.r. obs. 2−64195
vinylcyclopropane and vinylcyclobutane, conform. preferences, group interactions 2−83291
xylenes, conform. depend. of long-range spin-spin coupling 2−64193
$(CH_3)_2XH_n$, ($X=C$, Si, N, P, O, S), equil. config., CNDO/2 calcs. 2−64182
Co(II) complex, paramag. shift of n.m.r. line due to outersphere coordination of solvent molecules 2−80106
1,1-dimethylcyclohexane, gas-phase struct., electron diffr. obs. 2−70765

dissociation
see also Heat of dissociation
acids, MO SCF calcs. of proton affinities 2−83220
alcohol ions, formed by charge exchange in in-line tandem mass spectrometer 2−64168
alkali chlorides, rates and mechanism 2−60021
alkali halides, mechanism 2−60020
alkane ions, formed by charge exchange in in-line tandem mass spectrometer 2−64168
angular distribution anisotropy of ions from dissociative attachment of electrons to molecules 2−59929
atmosphere, absorption cross sections, photodissociation 2−48548
atmospheric mols., dissoc. ioniz. processes 2−80057
benzene, Franck-Condon factors for predissoc. 2−80079
bromoacetylene, electronically excited, competition between photon emission and photodissociation 2−42969
carbonyl compounds, dissociative electron attachment 2−60055
chloroacetylene, electronically excited, competition between photon emission and photodissociation 2−42969
cyclobutanone (^{1}A$_2$, predissociation of and collisional energy transfer from vibronically selected species 2−48343

- **Molecules** continued
  - **dissociation** continued
    - diatomic, effect of VV transfer processes on rate of thermal dissociation 2−67456
    - diatomic, thermal dissociation 2−83235
    - diatomic mol., three-body recomb. and dissoc., Monte Carlo trajectory calcs. 2−64108
    - diatomic mol. thermal decomp. conjugate kinetic eqn. approach 2−78187
    - diatomic molecules, probability of dissociation 2−83416
    - diatomic mols., thermal decomp. in inert gas, diffusion theory approach 2−80059
    - diatomic oxides and sulfides, gaseous, bond energies and force constants, stabilities 2−64107
    - dynamic model of decomposition of excited molecules 2−78188
    - electron impact, linear momentum transfer effects 2−67460
    - ethylene, in induction-coupled Ar plasma jet 2−53062
    - formaldehyde, all-electron calc. of potential surfaces 2−42988
    - formaldehyde, all-electron calc. of potential surfaces 2−42987
    - formaldehyde, isotopic separation of H and D by photopredissociation 2−67438
    - hydrocarbon 40 keV $CH^+ \rightarrow C^+ + H$, $C + H^+C^+ + H^+ + e$, fragment kinetic energy meas. 2−70772
    - hydrocarbons CH_n^+, reactions with gas targets at 40-140 keV 2−64218
    - hydrocarbons of form CH_n^+, n=2, 3, 4, 5, dissociation, kinetic energy of H^+, H_2^+, H_3^+ fragments 2−70771
    - ideal gas, causing acoustic wave amplification 2−75369
    - ketone ions, formed by charge exchange in in-line tandem mass spectrometer 2−64168
    - Large Volume Microwave Plasma Generator 2−50211
    - methane, photodissociation cross-section meas., 555-1242 Å 2−51470
    - organic, photochemical dissociation, new formula in Bixon-Jortner model 2−72569
    - 2(2′-oxyphenyl)-benztriazole derivatives, dissoc. consts. in alcohol-borate buffer 2−83334
    - perfluoropropane, dissociative electron capture 2−60079
    - perfluoropropylene, dissociative electron capture 2−60079
    - photochemical, of large molecules theoretical results 2−81525
    - polyatomic, intramol. interactions and vibronic spectra, electronic rearrangments and four level scheme 2−67447
    - predissociation by rot. and long-range interactions 2−77041
    - in single heavy particle collisions, book 2−83419
    - s- tetracyanobenzene-benzene complex, ionic dissociation from excited Franck-Condon state 2−72579
    - toluene, photo fragmentation, obs. 2−70794
    - AgCl electron impact ionisation species, and dissociation energies 2−50021
    - Ar cluster fragmentation, detection with time-of-flight mass spectrometry 2−42870
    - Ar_2^+ afterglow, dissociative recomb. at elevated temp. 2−83262
    - Br_2, dissociation in presence of CO_2, shock tube investigation 2−67469
    - Br_2, outer vibr. turning pts. near dissoc. in $B(^3\Pi_{0u}{}^+)$ state 2−77082
    - Br_2, thermal decomp. in inert gas, diffusion theory approach 2−80059
    - CO, C^- and O^- production by dissociative resonance electron capture 2−83415
    - CO photoionization by soft X-rays, meas. of total and relative abundances of thermal energy ions and dissociation cross sections 2−80024
    - CO_2, by e capture, production of O^- 2−80026
    - CO_2, dissociative excitation of $CO(A^1\pi)$ system by electron impact 2−56164
    - CO_2, electron impact, dissociative excitation of vacuum u.v. emission features 2−50027
    - CO_2, electron impact, production of $CO(a^3\Pi)$ and other metastable fragments 2−64117
    - CO_2, electron impact dissociation, meas. of lifetime of a $^3\Pi$ state of CO 2−50028
    - CO_2, mass spectrometric study of dissociative electron attachment 2−42883
    - CO_2, photodissociative excitation, $CO(A^1\Pi)$ cross sections 2−56163
    - CO_2 electron impact dissociation, production of $CO(a^3\pi)$ and other metastable fragments 2−42884
    - CO_2 laser 2−76473
    - CO_2 photoionization by soft X-rays, meas. of total and relative abundances of thermal energy ions and dissociation cross sections 2−80024
    - CO_2^+, predissoc., photoelectron- photoion coincidence spectroscopy and photoion kinetic energy analysis 2−67470
    - Cl_2-Kr mixtures, shock tube heated, dissoc. relax. times 2−53244
    - Cl_2, outer vibr. turning pts. near dissoc. in $B(^3\Pi_{0u}{}^+)$ state 2−77082
    - Cl_2, thermal decomp. in inert gas, diffusion theory approach 2−80059
    - D_2, considered as Morse oscillator, DWBA theory for collision with Ar and He 2−43033
    - D_2 dissociative excitation, by electron impact, absolute meas. of 2S atom production 2−42889
    - D_2 vibrational level linewidths due to predissociation 2−79999
    - $Eu(NH_3)_6$, entropy of dissociation 2−61774
    - H_2, dissociative excitation of vacuum u.v. emission by electron impact, cross section meas. 2−42900
    - H_2, electron impact, linear momentum transfer effects 2−67460
    - H_2, miltiphoton dissoc., predissoc., autoionization 2−83263
    - H_2, model for dissoc. in elec. discharge 2−53007
    - H_2, multiphoton ioniz. and dissoc. due to 1.06 μm laser radiation 2−80051
    - H_2, vibrational level linewidths due to predissociation 2−79999
    - H_2 considered as Morse oscillator, DWBA theory for collision with Ar and He 2−43033
    - H_2 dissociative excitation, meas. of time-of-flight spectrum of metastable H(2S) atoms, evidence of predissociation 2−46551
    - H_2 electron impact dissociative excitation polarization free vacuum u.v. meas., obs. of Lyman α radiation 2−80120
    - H_2 in Ar importance of multiple quantum transitions 2−50035
    - H_2 pyrolysis on W filaments, atomization, e.s.r. obs. 2−72550
    - H_2^+, by impact on He, Ar, H_2, N_2 at 4-12 keV, meas. of cross sections for angular distribs. of H(2s) 2−70816
- **Molecules** continued
  - **dissociation** continued
    - HCl, thermal, in shock waves, density gradient meas. 2−44473
    - HD^+, collision induced by electron impact, effect of dipole moment studied using Born-Oppenheimer approx. 2−56173
    - H_2O, collision with metastable Ar, rotational excitation of $OH(A^2\Sigma^+, v'=0)$ 2−64215
    - H_2O, kinetic energy of dissociation 2−80028
    - H_2O vapour, electron impact cross sections, atmospheric applications 2−53019
    - H_2S, kinetic energy of dissociation 2−80028
    - H_2^+ + electron collisions, proton prod. cross sections, low energy 2−64132
    - $(HeH)^+$, by electron impact, distortion polarization of orbitals and asymmetry in forward-backward scattering fragments 2−56179
    - I_2-He mixture, interaction of dissoc. and vibr. relax. behind shock wave 2−77168
    - I_2, spontaneous predissoc. 2−70710
    - I_2, thermal decomp. in inert gas, diffusion theory approach 2−80059
    - Kr_2^+ dissociative recombination at elevated temperatures in Kr afterglow 2−70888
    - N_2, transistors to and predissociation of $C^2\Sigma_u{}^+$ state 2−80006
    - N_2 photoionization by soft X-rays, meas. of total and relative abundances of thermal energy ions and dissociation cross sections 2−80024
    - N_2^+, mechanism of electron-ion dissociative recombination in gas discharge 2−74272
    - NH_3 decomposition behind reflected shock waves, 2000-4500K, obs. of i.r. emission 2−48324
    - NO photoionization by soft X-rays, meas. of total and relative abundances of thermal energy ions and dissociation cross sections 2−80024
    - NO_2, photodissociation by pulsed laser light at 6943A 2−44490
    - NO_2, photolysis at high pressure, photodissociation rates 2−80010
    - N_2O unimolecular decomposition, study using wave-crossing model 2−67416
    - $N_2O^+ + N_2O \rightarrow NO^+N + N_2O$, $N_2O^+ + N_2O \rightarrow O^+ + N_2 + N_2O$, mass spectrometric study 2−51436
    - $N_2O + e^- \rightarrow N_2 + O^-$, regeneration of electrons, and attachment rate constant 2−74270
    - N_2 + Ar system, three-body recomb. and dissoc., Monte Carlo trajectory calcs. 2−64108
    - $N_2 + C^+$ reactive collisions, 3 to 100 eV, dissociative charge exchange cross sections 2−48322
    - Ne_2^+ afterglow, dissociative recomb. at elevated temp. 2−83262
    - O_2, collision with Ar, hot gas, rates of dissoc. excitation 2−83417
    - O_2, dissociative excitation of vacuum u.v. emission by electron impact, cross section meas. 2−42900
    - O_2 ion-pair production of O^+ and O^- by $He(2^12^3S)$ metastables 2−83260
    - O_2 photoionization by soft X-rays, meas. of total and relative abundances of thermal energy ions and dissociation cross sections 2−80024
    - $O_2 + C^+$ reactive collisions, 3 to 100 eV, dissociative charge exchange cross sections 2−48322
    - SO_2, attachment cross-sections by electron collision 2−60035
    - UO, UO_2, UO_3, electron impact ionization cross-sections and fragmentation 2−46588
    - $Yb(NH_3)_6$, entropy of dissociation 2−61774
  - **dissociation energies**
    - akali metal, diatomic, hetero- and homonuclear, theoretical ground state and excited state potential energy 2−42906
    - calculation by approximate molecular orbital method 2−70670
    - diatomic, estimation method 2−46549
    - diatomic mol., data compilation 2−56152
    - diatomic mols., extended-Huckel method calcs. 2−67443
    - kinetic energy release in unimolecular reactions, thermochemical aspects 2−75368
    - perfluoropropane, F-C_3F_7 bond dissociation 2−60079
    - Ar_2, spectroscopic dissociation energy for ground state 2−50022
    - Au_2, $XO_g{}^+$ state determ. 2−56155
    - $B_{10}H_{14}$, atomization energy, SCF study 2−64115
    - B_2H_6, atomization energy from minimum basis set and extended Slater orbital wave functions 2−64114
    - BaI, produced in Ba + HI reaction, determ. of lower bound for $D_0°$ 2−81494
    - $Be^{2+}He_2$ stability against dissoc., binding mechanism 2−80001
    - CaI, produced in Ca + HI reaction, determ. of lower bound for $D_0°$ 2−81494
    - Cs_2^+, formed during ionization of Cs vapour by method of space charge amplification 2−70603
    - CuCl gaseous mols., mass spectrometric study 2−83255
    - Cu_2Cl_2 gaseous mols., mass spectrometric study 2−83255
    - CuH, derivation from potential energy curves 2−59998
    - F_2, shock tube calorimeter studies 2−83253
    - F_2, vacuum u.v. absorption spectrum, determ. of dissociation energy and ionization potential 2−70696
    - GaBi, mass spectrometric determ. of dissociation energy 2−64126
    - GaH, potential energy curves 2−60000
    - K_3, K_3^+, pseudo Hamiltonian model 2−56190
    - KrF_2, linear symmetric config. 2−83251
    - LiO, $X^2\pi$ and $A^2\Sigma^+$ state props. 2−60011
    - $LuC_2(g)$, $LuC_4(g)$, rel. to investigations of Lu-C system vaporization 2−64518
    - Na_3, Na_3^+, pseudo Hamiltonian model 2−56190
    - O_2^-, optimized valence configurations method for binding energy of ground state, determ. of electron affinity of O_2 2−50019
    - P_2, ground state dissociation energy estimation 2−46581
    - S_2, ground state dissociation energy estimation 2−46581
    - SO, ground state dissociation energy estimation 2−46581
    - SeO, ground state dissociation energy estimation 2−46581
    - SrI, produced in Sr + HI reaction, determ. of lower bound for $D_0°$ 2−81494
    - SrO, from crossed beam expt. 2−80002
    - Te_2, ground state dissociation energy estimation 2−46581
    - TlH, potential energy curves 2−60000
  - **electron scattering**
    - benzenes, substituted, electron attachment and excitation processes 2−42949
    - carbonyls, electron attachment and excitation processes 2−42949

Molecules continued
electron scattering continued
diatomic, vibrational and rotational excitation within an electronic transition induced by positive ion or electron impact 2–42865
dipolar systems, low-energy scatt. cross sections 2–77170
double scattering effects in polyatomic molecules 2–42831
off electric dipole moments assoc. with vibrs. of target 2–80126
electronic collision frequency in ionospheric F-region, ground-based measurements 2–84913
frame transformations, formulations of Schroedinger equation appropriate to different ranges 2–50005
heterocyclic cpds., negative ion form. by electron interaction 2–80154
inelastic collisions of fast electrons studied in Bethe theory 2–42780
inner shell ionization, bremsstrahlung production, at 140 keV 2–42760
ionisation, secondary-electron-production cross sections 2–76963
ionization, differential cross-sections 2–56108
low-energy, resonance-type phenomena, extension of earlier review 2–74300
multiple scatt. effects in high energy collisions with polyatomic mols. 2–60107
naphthalene vapour, electron energy-loss spectroscopy 2–80131
nitrobenzene, excitation spectra by ion cyclotron resonance mass spectrometer 2–80135
nitromethane, excitation spectra by ion cyclotron resonance mass spectrometer 2–80135
photoelectron spectroscopy, electron- molecule interactions 2–83402
quantum electrodynamics of scattering phenomena involving bound states 2–55794
vacacancy cascades created, meas. of molecular spectra and lifetimes 2–42722
AgCl electron impact ionisation species, and dissociation energies 2–50021
CO, core excited resonances, electron transmission spectroscopic study 2–46547
CO, excitation of vacuum u.v. radiation, threshold studies 2–80141
CO, study of resonance phenomena associated with 10.04 eV Feshbach resonance 2–80147
CO, threshold electron impact spectrum, reson. struct. 2–70687
CO, threshold excitation spectrum meas. using trapped electron method, structure identification 2–80146
CO continuum, energy loss cross sections for 500 eV electrons 2–83410
CO_2, dissociative attachment production of O^- 2–80026
CO_2, dissociative excitation by electron impact of vacuum u.v. emission features 2–50027
CO_2, electron impact dissociation, meas. of lifetime of a $^3\Pi$ state of CO 2–50028
CO_2, mass spectrometric study of dissociative electron attachment 2–42883
CO_2 clusters, model for ionization cross section including energy losses inside cluster 2–80150
CO_2 dissociation, threshold-50 eV, production of CO($a^3\pi$) and other metastable fragments 2–42884
CsF, absolute differential and total cross sections 2–64214
D_2, core excited resonances, electron transmission spectroscopic study 2–46547
D_2 dissociative excitation, by electron impact, absolute meas. of 2S atom production 2–42889
H_2, core excited resonances, electron transmission spectroscopic study 2–46547
H_2, differential and total cross sections for elastic scattering, 30-912 eV, calc. in plane wave approx. 2–77167
H_2, dissociation by electron impact, linear momentum transfer effects 2–67460
H_2, vibrational correction to scattering intensity calc. using five term CI wavefunction 2–50036
H_2 clusters, model for ionization cross section including energy losses inside cluster 2–80150
H_2 collisions, differential and total cross section calcs. for models 2–64136
H_2 dissociative excitation, polarization free meas., obs. of Lyman α radiation 2–80120
H_2 vibrational excitation, application of theory for small-energy-transfer collisions in dominant long-ranged forces 2–70817
H_2^+, proton prod. by electron collision, Rundel's discussion 2–50041
HD^+, collision induced dissociation by electron impact, effect of dipole moment studied using Born-Oppenheimer approx. 2–56173
H_2O, electronic states of resultant H_2O^+ 2–42896
H_2O, small angle diffr., chemical binding energy detn. 2–64133
H_2O vapour, study of excitation, dissociation, ionization processes, atmospheric applications 2–53019
$H_2 + e^+$, 45-500 eV, cross sections for positronium-negative-ion formation by double electron capture 2–50044
H_2^+ + electron collisions, proton prod. cross sections, low energy 2–64132
$(HeH)^+$ dissociation by electron impact, distortion polarization of orbitals and asymmetry in forward-backward scattering fragments 2–56179
I_2 double scatt. investigated with Glauber theory 2–42831
N_2, core excited resonances, electron transmission spectroscopic study 2–46547
N_2, elastic, scatt. and excitation of first vibr. level 2–77161
N_2, elastic scatt., ang. distrib., cross sections 2–67494
N_2, elastic scatt., ang. distrib. 2–60018
N_2, elastic scatt. and nonresonant vibr. excitation 2–77162
N_2, electron impact, dissociative excitation of OI ($^5S^0$) 2–56106
N_2, excitation spectra by ion cyclotron resonance mass spectrometer 2–80135
N_2, impact excitation of electronic states 2–64148
N_2, slow electron impact, rotational level distrib. of N_2^+ 2–80053
N_2, test of Massey's method for calc. of static potential 2–70822
N_2, vibrational excitation by electron impact in 15-35 eV region, meas. of angular distrib. 2–56189
N_2 clusters, model for ionization cross section including energy losses inside cluster 2–80150

Molecules continued
electron scattering continued
N_2 electron impact excitation, emission cross section for second positive system bands 2–46564
N_2 low-energy scattering calc. using pseudo-potential method, determ. of cross sections 2–70819
N_2 vibrational excitation, application of theory of small-energy-transfer collisions in dominant long-ranged forces 2–70817
NO, core excited resonances, electron trnsmission spectroscopic study 2–46547
N_2O optical absorption and electron scattering spectra, obs. of resonant phenomena in B region at 6.8 eV 2–77061
$N_2(X^1\Sigma_g^+, v=0)$, energetic collisions, departure of $N_2^+(B_2\Sigma_u^+, v'=2$ and 3) vibrational populations from Franck-Condon predictions 2–50058
O_2, continuum, energy loss cross sections for 500 eV electrons 2–83410
O_2, core excited resonances, electron transmission spectroscopic study 2–46547
O_2, dissociative excitation of vacuum u.v. emission by electron impact, cross section meas. 2–42900
O_2, elastic scatt. and excitation of first vibr. level 2–77161
O_2, electron impact, dissociative excitation of OI ($^5S^0$) 2–56106
U_2 double scatt. investigated with Glauber theory 2–42831
UO, UO_2, UO_3, electron impact ionization cross-sections and fragmentation 2–46588

electronic structure
see also LCAO calculations
π-electron molecule, geometry influence on excited state structure and transitions 2–52986
π-electron systems, method of calc. orbital energies 2–50003
bond pair density analysis of wavefunctions 2–79977
book, development of present day concepts, based on course for arts students 2–62954
book, rigorous quantum mechanical results 2–83204
bound-state calcs. use of regional wavefunctions 2–49937
Brueckner orbitals determ. by iterative procedure 2–50006
charge distributions, semi-empirical MO method 2–42852
charge shifts in formation of covalent bonds 2–80034
closed shell systems, ground states calc. using Feynman diagrams 2–77052
complex molecules, effect of solvent on electronic vibrational spectra 2–74253
complex molecules in excited state, electronic terms. 2–79987
computing methods for determ. structure of small molecules, large molecules and macromolecules 2–42860
configuration interaction extent limitation, perturbation theory applic. 2–79974
configuration interaction rel. to method of electron correl. factors 2–79854
conjugated molecules, justification for π-electron approx. 2–79988
conjugated mols., complementarity condition and bond orders 2–70672
core level binding energy shifts for C, N, O, and S containing mols. 2–83224
core-level binding-energy shifts, relax. correction 2–67459
1,4-cyclohexadienes, 3,6 bridged, photoelectric assignment of states 2–77051
d orbitals, 5 equivalent, a continuum of sets 2–74193
delocalized orbitals, natural or inverted order discrimination, using photoelectric spectroscopy 2–77051
diabatic states, quasistationary electronic states, review 2–50015
diatomic, spin uncoupling and transformation of half-integral spin states 2–79983
diatomic, spin-spin and spin-other-orbit integrals 2–70669
diatomic molecules, static charge distributions generating exact potential curves 2–42826
diatomic two centre two-electron spin-spin and spin-orbit hybrid integrals 2–46516
effective configs. effect on radiative transition probabilities 2–64086
electron density matrix, cusp conditions as constraints 2–42858
energy levels in modified quantum statistical potentials 2–59881
energy properties, approximate molecular orbital method 2–70670
energy shift theory for calc. of excitation spectra 2–83228
excited electronic states, CI description effects 2–42989
excited states, extended Hartree-Fock theory 2–79971
four- and six-π-electron systems, configuration analysis and excited states properties 2–59980
geminals, diagrammatical method based on second quantization formalism, Wick's theorem, Feynman-like diagrams 2–56081
geminals, diagrammatical method calc. of overlap and energy mean value expressions for wavefunctions 2–52894
ground state, reduced partitioning procedure for configuration interaction studies 2–42703
ground state electron wave functions, symmetry properties of molecular orbitals calc. of vibrational potential functions 2–42847
Hartree-Fock perturbation theory of magnetic shielding and susceptibility developed using molecular orbital theory 2–42850
heavy-atom compounds, SCF-MO-LCAO method with quasi-relativistic approx. 2–67454
Hellmann-Feynman force integrals, three-centre, evaluation involving Slater-type orbitals 2–46499
icosahedral molecules, electronic states 2–64100
inner shell, chemical effects studied by photo-electron spectrometry 2–50014
interaction matrix elements among doubly excited configs. 2–70673
level crossing and level anticrossing in diatomic molecules 2–67449
linear, relative energies of electronic states, inapplicability of Hund's rules 2–56148
many-electron wavefunction, probabilistic interpretation of cluster function series development 2–70554
many-electron wavefunctions expanded in spin-adapted antisymmetrized products, expectation values 2–74194
method of strongly orthogonal geminals for determination of wavefunctions 2–70686
molecular integrals, investigation of auxiliary functions 2–50002
molecular orbital valency state and molecular orbital energies 2–42859

Molecules continued
  electronic structure continued
    multiconfiguration self-consistent field theory for localized orbitals, derivation of variational equations 2−52908
    N-atom, vibration-rotation energy operator including electron-nuclear interaction 2−77046
    natural orbitals, properties and uses, review 2−59880
    network model, energy states and dispersion waves 2−71773
    network models, derivation of difference eqn., study of energy spectrum and dispersion curves 2−77520
    one-electron integrals over Slater-type atomic orbitals and irregular solid spherical harmonics 2−42848
    orbital localization procedures and convergence problems 2−64098
    paramagnetic configuration interaction effects on spin-split states arising from inner orbital ionization 2−74271
    particle hole propagator, use of complete Pade approximant 2−79982
    perturbative configuration interaction using localized orbitals and numerical integration 2−52978
    polyatomic, importance of overlap densities in theory 2−52982
    polyatomic, intramol. interactions and vibronic spectra, electronic rearrangments and four level scheme 2−67447
    polyatomic, mechanisms for internal- conversion and line broadening processes 2−49989
    polyatomic mols., absorpt. and luminesc. relationship in four-level system of electronic states 2−64087
    quantum chemical semi-empirical theories, ab initio determ. of all parameters 2−70555
    quantum mechanical potential model of ESCA shifts, near equivalence with thermochemical model 2−72535
    Renner effect in four-atom molecules 2−52973
    resonant states in atomic collisions, determ. of wavefunctions and energies using finite-difference boundary value method 2−70616
    Rydberg excited states, basic formulas for one-electron perturbation calc. 2−67452
    SCF calcs. on large molecules using molecular fragments, construction of initial P-matrices 2−70667
    SCF perturbation theory and intermolecular interactions 2−42849
    Scheibe's rules for ionization potentials of first and higher excited states, atomic nature 2−50013
    semiempirical scaled molecular orbital theory (SESMO) 2−67457
    Serber-type spin eigenfunctions in terms of spin-adapted antisymmetrized products 2−74195
    Slater functions, electron- repulsion, spin-spin and spin-orbit integrals 2−79980
    Slater-type orbitals from 4s to 4f, approximate Gaussian expansions 2−77048
    small pi systems, perturbed excited state and complete configuration interaction wavefunctions 2−42853
    spectroscopic trends, estimation by perturbation method using Hellmann pseudopotentials 2−49997
    spectroscopy studies 2−83233
    spin densities, unrestricted Hartree-Fock calc. with orthogonalised atomic orbitals 2−67453
    symmetrical molecules, classification of vibronic energy levels with allowance for inversion levels 2−77035
    transition density matrices, suggested calculations 2−59882
    triatomics, effect of location of H atoms on order of energy levels 2−50017
    triplet state geometry studied by phosphorescence microwave double resonance spectroscopy 2−50010
    two-electron systems, cusp-satisfying orbitals effect on electron densities at nucleus 2−83208
    vibrationally induced stabilization of vertically excited states 2−77042
    vibronic coupling, matrix elements of position and momentum 2−79975
    vibronic intensity borrowing, comparison of Herzberg-Teller theory and mechanism based on nuclear momentum integrals 2−70659
    virtual electronic levels, review 2−59982
    wave function construction using cusped gaussian wave functions 2−49915
    wavefunctions, explicitly correlated, partially antisymmetric 2−42701
    Wigner-Witmer rules, elementary derivation 2−78732
    $X_3NO(X{=}F$, Cl or $CH_3)$, LCAO MO CNDO/2 study of NO bonds 2−42866
    $X_3PO(X{=}F$, Cl, or $CH_3)$, LCAO MO CNDO/2 study of PO bonds 2−42866
    containing X-N= group test of EH, IEH, CNDO/2 and MINDO/2 orbital calculation methods 2−52980
    H_2^+-like molecules, floating one-centre perturbation treatment 2−67455
    H_2^+, bound-state calcs. use of regional wavefunctions 2−49937
    ML_4 complexes, tetrahedral, tetragonally distorted, splitting of d^2-configuration in strong ligand fields of D_{2d} symmetry 2−80937
  electronic structure, inorganic
    — 2−67466
    akali metal, diatomic, hetero- and homonuclear, theoretical ground state and excited state potential energy 2−42906
    alkali metals, diatomic, SCF calcs. using Pariser-Parr-Pople type method of Pohl 2−80049
    co-ordination compounds, translation between MO and HL descriptions 2−52990
    diatomic, vibrational and rotational excitation within an electronic transition induced by positive ion or electron impact 2−42865
    hydrides, ab initio calcs. including electron correl. of lowest states 2−80011
    inert gas hydrides, realistic single-function potential models 2−50046
    O_2, self-consistent procedures for generalized valence bond wavefunctions 2−53012
    rare earth ions, effect of coordination polyhedra structure on 4f-shell energy level splitting 2−50051
    Slater basis set difference density maps, minimum and expanded, comparison 2−77088
    tetranuclear transition-metal systems determ. of relative energies by irreducible tensor method 2−80044
    transition metal complexes, extension of CNDO calcs. 2−83252
    transition metal complexes, revised INDO calc. of charge transfer spectra and sequence of metal and ligand orbitals 2−67472

Molecules continued
  electronic structure, inorganic continued
    transition metal compounds, parameterized self-consistent-field theory 2−46525
    transition metal coordination cpds., calc. by SSPMO LCAO method in p.p.d.p. approx. 2−50020
    transition metal halide complexes valence regions by X-ray photoelectron spectroscopy 2−83247
    $[C_nO_n]^{-2}$ dianions, MINDO/2 wave function calcs. 2−70689
    $[Mn(H_2O)_6]^{2+}$ complex, approx. SCF calc. with minimal basis set 2−56185
    AlO $^2\Sigma^+ - x^2\Sigma^2$ band system, calc. of Franck-Condon factors and r centroids using RKR potentials 2−70679
    As complex, Menshutkin's type, n.q.r. freq. shifts nature 2−83274
    Au_2, transition moment determ. using r-centroid values for band system 2−56155
    BF_2, ab initio calc. of electronic struct. and geometry 2−83244
    BH, self-consistent procedures for generalized valence band wavefunctions 2−53012
    BH_2, ab initio calcs. including electron correl. of lowest states 2−80011
    BH_n series, generalized valence bond approach 2−59991
    $B_{10}H_{14}$, SCF study 2−64115
    B_2H_6, comparison of properties from minimum basis set and extended Slater orbital wave functions 2−64114
    B_2H_6 Slater basis set difference density maps, minimum and expanded, comparison 2−77088
    BH_3.CO, within framework of INDO approx. 2−46527
    BN, variational calc. of $A^3\pi$ excited state configuration using McWeeny's SCF method 2−70681
    BaI, obs. of new band system in 4481-4300 Å region, study of electronic transitions, vibrational analysis 2−70685
    $BeCl_2$, CNDO approx. 2−46529
    $BeCl_2$, CNDO approx. 2−46529
    BeF_2, CNDO approx. 2−46529
    BeH_2, comparison of resonance, perfect pairing and MO wavefunctions 2−52995
    BeH_2, strongly orthogonal geminal wavefunctions for lowest singlet states 2−70686
    $Be^{2+}He_2$ ion-induced dipole clusters, stability against dissoc., binding mechanism 2−80001
    C_2, SCF-MO-CI calc. using atomic basis of contracted Gaussian lobe functions 2−64120
    CCL_4, Pariser-Pople and Wolfsberg-Helmholz calc. 2−83324
    CH, CI calcs. of potential curves for low lying excited electronic states $a^4\Sigma^-$, $A^2\Delta$, $B^2\Sigma^-$, determ. spectroscopic conts. 2−56160
    CH, excited states, Rydberg and valence shell character as functions of internuclear distance 2−50056
    CH, Rydberg levels, calc. and comparison with expt. 2−53001
    CH, upper limits of rotational states studied using potential energy functions of Morse and Hulburt-Hirschfelder 2−46543
    CH radical, ab initio valence bond treatment 2−50025
    CH^+, upper limits of rotational states studied using potential energy functions of Morse and Hulburt-Hirschfelder 2−46543
    CN, $a^2\Pi$ and $B^2\Sigma$ rotational states, level crossing 2−67449
    CN, calc. of Franck-Condon factors and R centroids for $B^2\Sigma \rightarrow A^2\Pi$ band system, validity of Morse potential 2−46535
    CO, intensity meas. of $d^3\Delta \rightarrow a^3\Pi$ emission system, determ. of relative electronic transition moments 2−80035
    CO electron impact threshold excitation spectrum meas. using trapped-electron method, structure identification 2−80146
    CO electron scattering, study of resonance phenomena associated with 10.04 eV Feshbach resonance 2−80147
    CO_2, semi-empirical analysis of electronic spectra and molecular structure 2−42891
    CS, new symmetry assignment to k state from LCAO MO SCF calcs. 2−70688
    CS_2, calc, of parallel component of shielding tensor and relationship to ^{13}C chemical shift 2−53000
    CS_2, MO LCAO-CNDO calc., comparison with X-ray absorption spectra 2−60034
    CdCN in Ar matrix, structure from e.p.r. 2−50072
    ClOF, localized orbital calc. of bonding 2−67498
    ClO_3F, photoelectron spectrum and ab initio SCF MO calcs. 2−46587
    ^{35}ClF, hyperfine structure constants in J=1, J=2 rotational states using molecular beam electric resonance spectroscopy 2−74261
    $Co(CN)_5^{3-}$, low spin square-pyramidal, SCCC calc. of orbital energy levels 2−46536
    $Cr(III)S_6$ trigonal systems, electronic structures and MCD spectra 2−59997
    CrO_4^{2-}, ground states, SCF-MO calcs. and X-ray spectroscopy 2−77095
    CrO_4^{2-}, valence region X-ray photoelectron spectra, energy spread of ioniz. pots. 2−80004
    Cu(II) complex, interpretation of u.v. spectrum using modified Pariser-Pople method 2−67471
    CuO, CNDO-II approx. SCF molecular orbital method, levels calc. 2−83252
    $F_3P.BH_3$ and $F_2HP.BH_3$, CNDO/2 calculations 2−53032
    Fe complex, FeN_2 electronic and geometric structure 2−77073
    FeH, ground and low-lying excited electronic states 2−67474
    H_2, excited states, Rydberg and valence shell character as functions of internuclear distance 2−50056
    H_2, ground state, mag. susceptibility, calc. upper and lower bounds 2−46524
    H_2, H_6 ring system, electron density and correlation in ground states, simple LCAO approx. 2−67476
    H_2, lowest $^1\Sigma^+$ states, adiabatic potential energies, frozen-core approximation 2−42898
    H_2, oscillator orbitals in CI calculations 2−59883
    H_2, upper limits of rotational states studied using potential energy functions of Morse and Hulburt-Hirschfelder 2−46543
    H_2, valence bond Aufbau principle for excited states 2−80008
    H_2 Brueckner orbitals applic. to ground state, determ. of one-electron operators 2−50006
    H_2 ground-state energy calc. by new transcorrelated method, comparison with variational method 2−64134
    H_2 hyperfine structure of N=1 rotational state of $^3\Pi_u$ electronic state 2−64137

Molecules continued
electronic structure, inorganic continued
H_2^+, charge shifts in formation of covalent bonds 2—80034
H_2^+, diamagnetic properties, variation-perturbation calculation 2—53008
H_2^+, diamagnetic properties, variation- perturbation calculation, effect of varying internuclear separation 2—53009
H_2^+, finite-difference soln. of united atom, one centre expansion of molecular wavefunctions 2—80048
H_2^+, floating one-centre perturbation treatment 2—67455
H_2^+, perturbation and perturbation-variation treatments of $1s_g$ and $2p_u$ states 2—53010
H_2^+, perturbed generalized eigenvalue equation 2—64128
H_2^+, spherical limit symmetry dilemma 2—42894
H_2^+, two-parameter wavefunctions for iso ground state 2—80032
H_2^+, upper limits of rotational states studied using potential energy functions of Morse and Hulburt-Hirschfelder 2—46543
H_3, self-consistent procedures for generalized valence band wavefunctions 2—53012
H_4, lowest $^1\Sigma_g^+$ state calc. 2—50039
HCN, minimal basis set LCGO calcs. 2—79989
HCN, semi-empirical analysis of electronic spectra and molecular structure 2—42891
HF-HCN dimer, H-bonding and structure, prediction by ab initio molecular orbital methods 2—80005
HF, calc. of magnetic shielding and spin-rotation constants associated with nuclei by molecular orbital theory 2—42850
HF, correlation energy calc. using linked cluster many body perturbation theory 2—67484
HNO_2, cis and trans isomer obs. 2—56172
HO_2 radical, stretching force const. interpret. 2—56174
H_2O, 13 basis function calc. based on selection of proper canonical orbitals 2—67477
H_2O, ab-initio bond-orbital calcs. 2—53018
H_2O, correl. energies by united-atom many-body perturbation procedure 2—67480
H_2O, correlation energy calc. using linked cluster many body perturbation theory 2—67484
H_2O, electrooptical parameters, H bond distortion 2—46548
H_2O, produced by electron bombardment of H_2O 2—42896
H_2O, self-consistent procedures for generalized valence bond wavefunctions 2—53012
H_2O, strongly orthogonal geminal wavefunctions for lowest singlet states 2—70686
H_2O, total nonrelativistic energy calc. using many-body perturbation theory 2—52914
$H_5O_2^+$, SCF-MO-LCGO calculations of properties of H-bond 2—56147
HOF-H_2O mixed dimer, LCAO-MO-SCF calcs. of equilibrium structures and energies 2—67491
$(HOF)_2$ dimer, LCAO-MO-SCF calcs. of equilibrium structures and energies 2—67491
HOO, nonempirical LCAO MO SCF and CI studies of low lying electronic state 2—50040
H_2S, MO LCAO-CNDO calc., comparison with X-ray absorption spectra 2—60034
He-H_2 system, population and natural spin orbital analyses 2—67540
He_2, energy barriers in excited states 2—56178
He_2, exchange and Coulomb energies, dependence on wave functions of interacting systems 2—56180
HeH, potential curves for ground state 2—74266
HeH^+, electron correl. influence on vibr. and rot. consts. 2—64139
HeH^+, ground state, calc. 2—46542
HeH^{++}, floating one-centre perturbation treatment 2—67455
HgCN in Ar matrix, structure from e.p.r. 2—50072
K complex, dipotassium cis-hexacyanobutenediide anion, rel. to crystal structure 2—53667
$K_3Fe(CN)_6$, model consistent with n.m.r. and Mossbauer data 2—54508
K_2SO_4, X-ray spectra, high-resolution sulphur Kβ emission, symmetry assignment 2—60007
KrF_2, ab initio calcs., bound pot. curve, bonding, electron correl. 2—83251
Li He, interaction potential, group function method 2—67487
Li_2, improved alternant molecular orbital function 2—56183
LiH, calc. of magnetic shielding and spin-rotation constants associated with nuclei by molecular orbital theory 2—42850
LiH, extended Hartree-Fock calculations using corresponding orbitals 2—53021
LiH, self-consistent procedures for generalized valence bond wavefunctions 2—53012
LuD, obs. of new electronic system in 4000-8000 Å region, determ. of molecular consts. 2—70711
LuF, new electronic spectrum obs. in 3000-8000 Å region, determ. of molecular constants 2—70712
LuH, obs. of new electronic system in 4000-8000 Å region, determ. of molecular consts. 2—70711
$MgCl_2$, CNDO approx. 2—46529
MgF_2, a priori and semiempirical calculations 2—42908
$Mn(CO)_5H$ and $Mn(CO)_5CH_3$ photoelectron spectra, ab initio SCF MO calcs. of electronic structure 2—70713
Mn(II) complex, tetrahalogenomangonates, structure obs. in diffuse reflectance and phosphorescence excitation spectra at 77K 2—67488
MnO_4^-, ground states, SCF-MO calcs. and X-ray spectroscopy 2—77095
MnO_4^-, valence region X-ray photoelectron spectra, energy spread of ioniz. pots. 2—80004
$MoXY_3$ C_{3v} ions, (X, Y=O, S, Se), assignments of electron charge transfer bands 2—80020
N_2, application of Auger electron spectroscopy to structure determ. 2—42756
N_2, calc. on ground state using various methods for soln. of SCF-LCAO-Mo eqns. 2—64099
N_2, electron density matrix, cusp conditions 2—42858
N_2, energy levels, analytic independent particle model 2—73254
N_2, excited states, Rydberg and valence shell character as functions of internuclear distance 2—50056
N_2, MO correlation diagram 2—50055
N_2, minimal basis set LCGO calcs. 2—79989
N_2, removal of core orbitals in valence only orbital calculation 2—49993
N_2, transistors to and predissociation of $C^2\Sigma_u^+$ state 2—80006
N_2 relative populations of $C^3\Pi_u$ and $B^2\Sigma_u^+$ states 2—80121
N_2 SCF-LCAO-MO wave function density-distribution analysis 2—80052
N_2 Slater basis set difference density maps, minimum and expanded, comparison 2—77088
NCNNN, microwave spectrum analysis and CNDO/2 calcs. 2—64142
NF_2, ab initio calc. of electronic struct. and geometry 2—83244
NH_3-BF_3 complex, valence electron density 2—60016
NH, excited states, Rydberg and valence shell character as functions of internuclear distance 2—50056
NH_2^+, low-lying electronic states, nonempirical CI study 2—53025
NH_3, ab-initio bond-orbital calcs. 2—53018
NH_3, correl. energies by united-atom many-body perturbation procedure 2—67480
NH_3, correlation energy calc. using linked cluster many body perturbation theory 2—67484
NH_3^+, Gaussian wavefunctions 2—42994
NH_2OH-H_2O mixed dimer, LCAO-MO-SCF calcs. of equilibrium structures and energies 2—67491
$(NH_2OH)_2$ dimer, LCAO-MO-SCF calcs. of equilibrium structures and energies 2—67491
NH_3 + HCl system, potential energy curves for proton motion, extended Huckel calculation 2—43040
NO, NO^+ configuration interaction studies, comparison with photoelectron spectra 2—83254
NO configuration interaction effects on spin-split states arising from inner orbital ionization 2—74271
NO configuration interaction effects on spin-split states arising from inner orbital ionization 2—74271
NO^- molecular constants determ. in laser photodetachment and photoelectron spectroscopy 2—53027
$(NO)_2$ dimer, low temperature electronic bands 2—67495
N_4S_4, electron delocalization, CNDO/2 calculation 2—77089
$N_4S_4F_4$, electron delocalization, CNDO/2 calculation 2—77089
Na_2 type diatomic molecule, application of model potential for valence electrons 2—77072
Ne_2, and positive ions produced in Ne-Ne^+ inelastic collisions, ab initio H.F. calcs. for different interatomic distances 2—49969
Ni complex, trigonal bipyramidal, computational errors in term energies 2—60025
O_2, determ. by laser photodetachment and photoelectron spectroscopy of O_2^- 2—53028
O_2, electron affinity determ. from binding energy of O_2^- by Hess cycle 2—50019
O_2, energy levels, analytic independent particle model 2—73254
O_2 pot. curves, for lowest three states, CI treatments 2—80012
O_3^- anion isolated in Ar matrix, obs. of electronic transition between 5100 and 3700 Å, presence of low-lying dissociative state 2—70720
OH, molecular constants from u.v. spectrum 2—64152
OPF_2 H, LCAO-MO-SCF calcs. valence-shell orbitals 2—83250
OsO_4, dipole transition moments determ. by LCAO-MO calcs. in terms of ligand mixing coeff. 2—42928
P_4, valence shell structure study using HeI photoelectron spectroscopy 2—46574
PF_2 H, LCAO-MO-SCF calcs. valence-shell orbitals 2—83250
PF_3, PF_5, semiempirical MO calc., pseudorotation in PF_5 2—53034
PH_2-PF_2, CNDO/2 approx. analysis 2—70722
PH_3, PH_5, semiempirical MO calc. 2—53034
PH_5, MO calc. for idealized geometries of D_{3h}, C_{4v} and C_s symmetries 2—53035
PH_5, nonempirical MO calc., intramolecular ligand exchange in phosphoranes 2—53033
PO emission spectrum, $C^2\Sigma$--$X^2\Pi_r$ transition and nature of C′ state 2—46573
P_4O_{10}, SCF calculations 2—60030
P_4O_6, SCF calculations 2—60030
Pb_2, new molecular constants for ground electronic state determ. from laser excited resonance fluorescence 2—42929
ReO_4^-, dipole transition moments determ. by LCAO-MO calcs. in terms of ligand mixing coeff. 2—42928
$ReXY_3$ C_{3v} ions, (X, Y=O, S, Se), assignments of electron charge transfer bands 2—80020
S_8 orthorhombic mol. orbital interpret. of valence X-ray emission 2—84488
SF_6, X-ray emission and absorption spectra determ. 2—56197
SF_6 optical spectra of gas and solid in extreme u.v. and soft X-ray region 2—42933
SO_2, MO LCAO-CNDO calc., comparison with X-ray absorption spectra 2—60034
SO_2, π^*-π (2350 Å) band system analysis 2—64155
SO_4^{2-}, localized orbital calc. of bonding 2—67498
$SOCl_2$, localized orbital calc. of bonding 2—67498
SO_2F_2, localized orbital calc. of bonding 2—67498
SO_2F_2, photoelectron spectrum and ab initio SCF MO calcs. 2—46587
^{33}S n.m.r. spectroscopy applic. 2—83290
ScO CNDO-II approx. SCF molecular orbital method, levels calc. 2—83252
SiH_2, ab initio calcs. for potential curves, description of geometry and electronic spectrum 2—46584
SiO, matrix elements of dipole moment of bands in the system $A^1\Pi$ to $X^1\Sigma^+$ 2—67500
TiO, CNDO-II approx. SCF molecular orbital method, levels calc. 2—83252
U complexes, insular uranyl complexes, equatorial ligation tests of coupling schemes 2—60037
V complex, trigonal bipyramidal, computational errors in term energies 2—60025
VO, CNDO-II approx. SCF molecular orbital method, levels calc. 2—83252
VO_4^{3-}, ground states, SCF-MO calcs. and X-ray spectroscopy 2—77095
VV charge transfer spectra 2—83268

Molecules continued
electronic structure, inorganic continued
W complex, hexamethyl tungsten, photoelectron spectrum and electronic struct. 2−64160
WO_4^{2-}, dipole transition moments determ. by LCAO-MO calcs. in terms of ligand mixing coeff. 2−42928
WXY_3 C_{3v} ions, (X, Y=O, S, Se), assignments of electron charge transfer bands 2−80020
XeF_6, electronic states and molecular geometry, electronic isomerism 2−42940
YO, $B^2\Sigma$-$X^2\Sigma$ system electron transition moment variation with internucl. distance and vibr. temp. 2−56203
Zn complexes, porphyrins, e.p.r. spectra, hyperfine structure 2−50071
ZnF_2, ab initio SCF study, determ. of Walsh diagram and molecular orbitals 2−70730
electronic structure, organic
2−67480
π-radicals in soln., ENDOR mechanisms for β-protons 2−71235
acenaphthene in stretched PVA sheets, polarized absorpt. spectra, electronic transitions 2−83276
acenaphthenequinone, LCAO-SCF-MO-CI calcs. for π-electron system 2−70784
acetaldehyde and complex, CNDO and INDO calcs. of atomic charges, band population, dipole moments 2−53043
acetophenone crystal, Zeeman splitting pattern obs., assignment of lowest triplet state 2−80061
acetylene, minimal basis set LCGO calcs. 2−79989
adenine, electrostatic potentials, MO LCAO GTO SCF calculation 2−60041
anthracene (-d_4), obs. and calc. of position dependent deuterium effect on triplet lifetime 2−70741
aromatic, intersystem- crossing process mechanism formulation 2−56206
aromatic carbonyl compounds, spin-orbit coupling effects in e.p.r. spectra of lowest triplet states 2−70756
azide ion, calc. of point-charge distrib. from quadrupole moments using SCF orbital wavefunctions 2−80086
azines, Stark effects and elec. dipole coupling of $n\pi^*$ and $\pi\pi^*$ states 2−77138
azines ^{14}N n.q.r., σ and π electron densities as function of CNN angle 2−80087
azobenzenes ^{14}N n.q.r., σ and π electron densities as function of CNN angle 2−80087
benzaldehyde, substituent and soluent effects on transitions 2−83319
benzaldehyde environmental effects on assignment and geometry of triplet state 2−61806
benzene, Dewar structure CNDO/2 calculation 2−60051
benzene, elec. field perturbation of A-B transition, in-plane polarisability 2−80068
benzene, mono-substutited derivatives, calc. of change densities and band order by Pariser-Parr-Pople method 2−46594
benzene, one-electron perturbation calc. of 3d electrons 2−67452
benzene, orbital energy calc. by Green's function method 2−50083
benzene ions, doublet energy levels, configuration interaction calculation 2−67507
benzene molecules, substituted, shift in lowest π-electron singlet excited state 2−70748
benzene mono-substituted derivatives, calc. of singlet energies, polarization direction, band intensities by Pariser-Parr-Pople method 2−46593
benzenes, dihydroxy- and diamino-substituted, u.v. spectra analysis 2−70749
benzenes, substituted, electronic correl. in excited states, singlet-triplet-excitation energy 2−56220
benzenes, substituted, lowest excited triplet state obs. by e.p.r. 2−60050
benzenes, substituted, lowest lying $\pi^* \leftarrow \pi$ transitions 2−67509
benzonitrile, CNDO/CI calcs. of lower electronic transitions 2−56221
benzophenone hydrazone, ^{14}N n.q.r., σ and π electron densities as function of CNN angle 2−80087
p- benzoquinone, electronic states and spectra 2−42961
benzylamine, ground and excited state frequencies 2−74286
biacetyl, ordering of lower electronic states, mechanism of radiationless $S \rightarrow T$ transitions 2−50085
bicyclo [1.1.1] pentane systems, ab initio SCF calcs. 2−70753
bicyclo[1.1.0]butane, ab initio SCF calculations 2−42963
bicyclo[1.1.0]pentane, ab initio SCF calculations 2−42963
biphenyl, ground and excited states, configuration interaction effect on energies and oscillator strengths 2−83316
o,o′-bridged biphenyl derivatives in frozen ethanol, determ. from e.s.r. spectra by fluorine labelling method 2−64170
borazane, internal rot. barrier and localized charge distribs. 2−64171
borazine, gaseous, 2000Å absorpt. system, analysis 2−80090
2- and 4-bromo-pyridine quadrupole hyperfine structure in rotational spectrum 2−70754
bromoethylene, photoelectron spectra, π interaction 2−77140
2-bromopropene, photoelectron spectra, π interaction 2−77140
trans-butadiene, application of Lowdin's orthogonal orbitals to π-electron calcs. 2−64172
butadiene, SCF and CI calcs. of electronic spectrum 2−80069
1,3-butudienes, substituted, electronic effect of geometric isomers 2−42965
carbene, one-electron perturbation calc. of 3d electrons 2−67452
carbonium ions, MINDO/2 calc. 2−77112
carboranes, orbital localization procedures and convergence problems 2−64098
charge transfer complexes, photoelectron energy spectra 2−64163
p-chlorobenzylidene- p-chloroaniline, as function of molec. conformation, determination from solid-state reflection spectra 2−53051
chloroform, electronic structure, dipole moments, n.m.r. and n.q.r. constants calc. 2−83324
cobaltocene, investigation by e.p.r., magnetic susceptibility meas., and optical spectrocopy 2−56226
complex conjugated mols., Huckel mol. orbital analysis, transfer matrix method applic. 2−77132
conjugated hydrocarbons, Huckel MO π resonance energies, σ structure 2−53068

Molecules continued
electronic structure, organic continued
conjugated molecules, calculation of ground and excited state potential surfaces 2−77130
conjugated molecules, comparison of various expansions in perturbation theory calculations 2−42855
conjugated nitriles, MMO LCAO investigation of influence on nitrile group i.r absorption band intensity 2−50104
coronene ion, electronic orbital angular momentum in ground state 2−80089
croconic acid and derivatives, CNDO/2 calcs. 2−70760
cumulene, long chains, unrestricted Hartree-Fock calculations 2−43023
cyanoacetylene initial orbital study by comparison of first Rydberg band in u.v. region with photoelectron spectrum 2−46600
cyclobutadiene, orbital energy calc. 2−50003
cyclohexanols, ^{13}C chem. shifts rel. to C electron densities from extended Huckel and Del Re theories 2−42948
cyclopentadiene, SPINDO calc. and photoelectron spectra 2−70761
cyclopentadienyl and pentadeuterio and pentachloro derivatives singlet-triplet separation, effect of vibronic interaction 2−50090
cyclopentadienyl cation, pi-electron states, projected states 2−83293
cyclopropane, photoelectron spectra, orbital structs. 2−64175
cyclopropanes, protonated, MINDO/2 calc. 2−77112
cyclopropene, orbital nature in electronic states 2−50091
cytochrome c, electron transfer between molecules obs. by pulsed Fourier transform n.m.r. 2−56267
cytosine, electrostatic potentials, MO LCAO GTO SCF calculation 2−60041
decacyclene SCF MO calc. of electronic spectrum in Pariser-Parr-Popl approx., comparison with exptl. data 2−42976
delocalized electron, energy spectrum in molecules with branched groups, coupled potential box model 2−70735
diazines, symmetric, $\pi \rightarrow \pi^*$ transitions, spectral and INDO orbital calcs. 2−53060
diazirine and difluorodiazirine, photoelectron spectra, orbital structs. 2−64175
p-dichlorobenzene, phosphorescence microwave double resonance studies of $^3\pi\pi^*$ state 2−60060
difluoromethane, ab initio SCF calculations and character of C-F bond 2−43000
2,3-dihydrofuran, microwave spectrum 12.4-40 GHz, Q- and R-branch assignments for ground and excited states of ring-puckering mode 2−42978
o-dimethoxybenzene, vibrational and electronic spectra 2−80081
1,4-dimethyl naphthalene, relationship of spin densities for monomer and dimer cations 2−60061
3,4-dimethylenecyclobutene, valence shell CNDO, INDO and CNDO-CI calculations 2−60063
dimethyloxalate, electronic state investigation using phosphorescence meas. 2−50106
α,ω- diphenyloctatetraene solutions in bibenzyl and n-paraffins, low-lying weak transition obs. in optical spectra 2−50121
DNA, electron correl. influence 2−77159
DNA base pairs, proton transitions in H bonds 2−80115
DNA bases, chem. shifts of inner-sheel electrons, CNDO/2 calcs. charge redistrib. effect 2−83345
energy levels, theoretical studies on position and ordering 2−67504
ethane, self-consistent procedures for generalized valence bond wavefunctions 2−53012
ethylene, $\pi\pi^*$ transition, electron correl. and Rydberg character 2−60064
ethylene, minimal basis set LCGO calcs. 2−79989
ethylene, multiconfig. wavefunctions for lowest $(\pi\pi^*)$ excited states 2−67512
ethylene, one-electron perturbation calc. of 3d electrons 2−67452
ethylene, orbital energy calc. 2−50003
ethylene, PCILON calculations 2−52978
ethylene V state, valence state description by config. interaction theory 2−64180
ethynylbenzene, CNDO/CI calcs. of lower electronic transitions 2−56221
flavins, excited states, luminescence and MO calculations 2−46605
fluorine containing σ-bonded molecules, MINDO/2 calc. 2−77111
fluorine containing compounds, calc. of second moments of electronic charge distrib. and quadrupole moments by CNDO/2D method 2−80085
fluoromethanes, molecular orbital valency state calculations 2−42859
fluoromethyl radicals, ab initio LCAO-SCF-MO-CI calculations 2−77148
fluoropyridine methyl derivatives, long-range spin-spin coupling consts., electron contribs. 2−77097
formaldehyde, all-electron nonempirical calc. of potential surfaces, dissociation into molecular products 2−42988
formaldehyde, all-electron nonempirical calc. of potential surfaces, dissociation into radical products 2−42987
formaldehyde, CI description of $^1(\pi \rightarrow \pi^*)$ excited state 2−42989
formaldehyde, PCILON calculations 2−52978
formaldehyde, semi-empirical analysis of electronic spectrum and molecular structure 2−42986
fragments of molecules, rel. to interaction processes 2−46590
fulvene, SPINDO calc. and photoelectron spectra 2−70761
furfural, calc. for rotational isomers 2−50096
D-glucose, ^{13}C chem. shifts rel. to C electron densities from extended Huckel and Del Re theories 2−42948
glycine, SCF calculations, example of peptide bond 2−56233
glycylglycine, SCF calculations, example of peptide bond 2−56233
glyoxal, LCAO-MO-SCF calc. determ of energy for cis-trans isomerization 2−53065
heterocyclics, six-membered with O and N, electron distribution, AVE CI SCF calculation 2−56204
hydrocarbon ions, closed shell, electronic absorption spectra calc. 2−42991
hydrocarbon negative ions, CNDO calculations 2−64184
hydrocarbons, π-electron approximation 2−50102
hydrocarbons, d-functions effect on orbital energies 2−80067
hydrocarbons, linear conjugated, lowest triplet excitations 2−77133
isoxazolinone-5, tautomeric equilibr. dipole moment, electronic spectrum calc. by semi-empirical MO methods 2−53070

Molecules continued
electronic structure, organic continued
ketene, MO study of low energy electronic states 2−60072
metallocenes, electron spectra, electronic configs. 2−64187
methane, ab-initio bond-orbital calcs. 2−53018
methane, analysis of formation in Hartree-Fock model 2−60074
methane, correlation energy calc. using linked cluster many body perturbation theory 2−67484
methane, electronic structure, dipole moments, n.m.r. and n.q.r. constants calc. 2−83324
methane, localized orbitals of ground state, pseudopot. calc. 2−80062
methane, minimal basis set LCGO calcs. 2−79989
methane, molecular orbital valency state calculations 2−42859
methane-d_1, i.r. spectrum, perturbation allowed transitions 2−77119
methyl and methylene chlorides, electronic structure, dipole moments, n.m.r. and n.q.r. constants calc. 2−83324
methyl fluoride, ab initio SCF calculations and character of C-F bond 2−43000
methyl radical, Gaussian wavefunctions 2−42994
methyl radicals, ab initio LCAO-SCF-MO-CI calculations 2−77148
3-methyl sydnone and related species, ab initio calculation of orbital energies 2−53080
methyl thiophenols, isomeric, excitation energies, oscillator strengths, transition moments, orbital calcs. 2−56239
methylamine, minimal basis set LCGO calcs. 2−79989
methylcyclohexanes, ^{13}C chem. shifts rel. to C electron densities from extended Huckel and Del Re theories 2−42948
methylene, low-lying electronic states, nonempirical CI study 2−53025
methylene, strongly orthogonal geminal wavefunctions for lowest singlet states 2−70686
methylenephosphorane, ab initio LCAO-MO-SCF study of bonding 2−56240
methylsilane, nonempirical calcs. 2−83292
naphthalene in stretched PVA sheets, polarized absorpt. spectra, electronic transitions 2−83276
naphthalene vapour, vacuum u.v. absorption spectrum, Rydberg series assigned 2−80064
α-naphthoquinone, LCAO-SCF-MO-CI calcs. for π-electron system 2−70784
nitrobenzene, and $-d_5$, electronic structure determ. using photoelectron spectroscopy 2−56251
nitromethane, and $-d_3$, electronic structure determ. using photoelectron spectroscopy 2−56251
1-nitronaphthalene, positions and assignments of electronic states 2−46619
nitroxide radicals, photoelectron spectra and mol. orbital calcs. 2−80073
norbornadiene, LCGO minimal basis calc. and ESCA obs. 2−70785
orbital studies, extended Gaussian-type basis, inclusion of second row elements 2−42941
oxalic acid, electronic state investigation using phosphorescence meas. 2−50106
oxyhaemoglobin and haem derivatives, SCC-EH-MO calc. on bonding and electric field gradient 2−60098
2(2′-oxyphenyl)-benztriazole derivatives, electronic absorpt. spectra analysis 2−83334
phenanthrenequinone, LCAO-SCF-MO-CI calcs. for π-electron system 2−70784
phenothiazines, MO calculations of conformational properties 2−60082
phosgene, interpretation of photoelectron spectra 2−43006
phosphonium ylide, ab initio LCAO-MO-SCF study of bonding 2−56240
pi hydrocarbon radicals, ^1H and ^{13}C hyperfine splitting, unrestricted Hartree-Fock calc. 2−67453
polyene chains doubly substituted, wavefunctions of local states 2−77129
polymer chain, two atoms per unit cell, local electronic states 2−83384
polyurethanes, H bond energy 2−83389
pyrazine, absorption spectrum in region of $n\pi^*$ transition, evidence for second electronic state 2−46624
pyridine, 2,4,6 tri-substituted, shift in lowest π-electron singlet excited state 2−70748
pyridine, free electron model 2−83304
pyridines, substituted, lowest excited triplet state obs. by e.p.r. 2−60050
pyridinium-pyridine system, H-bonded, extended Huckel calculation 2−70789
pyrrole-pyridine system, valence electron density distrib., extended Huckel calc. 2−43007
11-cis-retinal, PCILO calculation of p.m.r. in relation to molec. conformation 2−77153
rhodamine 6G, triplet state, absorpt. spectra obs. 2−46628
Rhodamine 6G monomers and associates, intramol. degradation processes of electron excitation energy 2−60485
ring mols., inflexible levels existence 2−77103
small molecules, structure determination from matrix isolation spectra 2−70708
trans-stilbene, energy levels calc. inc. steric effects 2−56259
cis-stilbene, energy levels calc. inc. steric effects 2−56259
sydnone, Pariser-Parr-Pople calcs. of energies of lower excited states 2−77128
sydnoneimine (cation), Pariser-Parr-Pople calcs. of energies of lower excited states 2−77128
1,2,4,5-tetrabromobenzene, o.d.m.r. and p.m.d.r. studies of $3\pi\pi^*$ state 2−60086
1,2,4,5-tetrachlorobenzene, o.d.m.r. and p.m.d.r. studies of $^3\pi\pi^*$ state 2−60086
s tetrazine, electronic structure obs. in electron impact energy loss spectrometer, ionization potential 2−70737
thioamides 2−43011
thiophosgene, interpretation of photoelectron spectra 2−43006
thymine, electrostatic potentials, MO LCAO GTO SCF calculation 2−60041
toluene, photoelectron spectrum and SPINDO calculation 2−70793
trifluoromethane, ab initio SCF calculations and character of C-F bond 2−43000

Molecules continued
electronic structure, organic continued
vinyl chloride, fragment calc. including polarization of σ-framework 2−83329
vinyl-type radical in irrad. maleic acid matrix, e.s.r. obs. 2−64195
zinc phthalocyanine, MO calculations 2−53086
Cu(II) ammine complexes, tetragonal, electronic spectra, symmetry-restricted covalence effects 2−80017
^{33}S n.m.r. spectroscopy applic. 2−83290
excitation
π-electron molecule, geometry influence on excited state electron structure and transitions 2−52986
(anthracene)-$(CH_2)_n$-(N, N-dimethylaniline) systems, intramol. electron donor-acceptor interactions 2−60047
acetylene, formation of metastable triplet state in Hg photosensitized reaction, obs. of biacetyl emission 2−51467
anharmonic oscillator-atom collision vibrational excitation cross-section 2−80124
aromatic acetylenes, reduced zero field splitting in EPR of photoexcited triplet state 2−68810
benzene, excited state relaxation, review 2−60052
benzene, with metastable Ar atoms produced in low power microwave discharge 2−70747
benzenes, substituted, electronic correl. in excited states, singlet-triplet-excitation energy 2−56220
benzenes, substituted, molecular orbital study of excited state geometry 2−50084
p- benzoquinone, electronic transitions involved in visible and near u.v. spectra 2−42961
c H_2, core excited resonances, electron transmission spectroscopic study 2−46547
carbonyl compounds, electron attachment and excitation processes 2−60055
collisional depolarization of excited states, effective lifetime rel. to correlated photons in cascade 2−74226
complex molecules in excited state, electronic terms. 2−79987
coumarins, H-bonding effects on excited $\pi\pi^*$ and $n\pi^*$ states 2−60057
covalent compounds, decrease in symmetry due to excitation obs. in X-ray emission spectra 2−70654
diatomic, rotational excitation, effect of generalized phase shift expansion terms on classical limit of gas transport coefficients 2−43030
diatomic, tunable Raman excitation and vibr. relax. 2−53023
diatomic, vibrational and rotational excitation within an electronic transition induced by positive ion or electron impact 2−42865
diatomic molecules, probability of vibr. excitation 2−83416
diatomic mols., electronic-vibr. energy transfer, vibr. distrib., i.r. fluoresc., Hg*-sensitized 2−59988
diatomic radicals from dissociative electron attachment in CO_2, conversion of electronic into vibrational excitation 2−42883
dimer composed of 2 biphenylene subunits, triplet exciton transfer study by e.s.r. 2−46509
2,4-dimethylpentyl-2*(-d_1*) vibrationally excited collisional de-excitation by H_2, D_2, CF_4 2−46648
dipolar system, pulsed excitation of polarized waves 2−70653
DNA, electron excitation energy long range migration 2−56265
dye lasers in rigid host medium, triplet state population control and utilization 2−69941
energy shift theory for calc. of excitation spectra 2−83228
ethylene, lowest excited singlet state prediction by time-depend. Hartree-Fock method 2−77040
ethylene in liquid and solid rare gas matrices intravalence and extravalence excitations 2−46603
Hartree-Fock calcs., time-dependent, of excitation energies 2−77040
hydrocarbons, linear conjugated, lowest triplet excitations 2−77133
ionization cross sections for electron and positrons, 0.1-2.7 MeV 2−70598
laser, recombinational, light enhancement by mol. ground state vibr. transitions 2−69897
mean energies, moment theory bounds rel. to passage of charged particles through matter 2−46496
metastable state lifetimes measurement by molec. beam methods 2−46523
metastable states, preparation by optical excitation 2−46503
metastables, production and detection 2−64050
methane, lowest ionization potential and transition energies, ab initio calc. 2−56244
NA, excited collision-induced rot. and vibr. transfer laser-induced fluoresc. obs. 2−83412
nonradiating excited complexes, props. 2−67531
nutation freq. transition between permanent states in r.f. field 2−42832
optically pumped system, diffusion coeff., and probing of excited species interaction 2−60106
Pariser-Parr-Pople model, self consistent polarization propagator calcs. 2−50012
phenanthrene, excited dimer luminescence of pairs of molecules 2−56253
phenazine, in rigid toluene glass matrix, spin polarization in photoexcitation of triplet state 2−68816
plane aromatic, geometry in excited state, theory 2−70733
polynuclear hydrocarbons, quenching of triplet excited states by O_2, possible effects of magnetic fields 2−50124
pyridazine vapour, single vibronic level fluoresc., excited states 2−80078
quinoline in durene mixed crystal, triplet-triplet absorption at 2K, obs. 2−50114
radiationless electron transitions, temp. depend., using Morse oscillator model, arbitrary values of Z 2−52965
reactive collisions, model 2−61766
resonance fluorescence, cross sections and quantum yields, general expressions 2−74251
resonant media, large coherent optical polarizations, prep. and detn. 2−41945
rhodamine B, xanthene dye vapours, optical and discharge excitation 2−42042
rotational excitations of three-particle systems 2−83236
selective laser photochem. reactions using predissoc. 2−68803
spiropyrans, 2 photon excitation of molecule under laser radiation 2−78208

Molecules continued
excitation continued
tetracyanoethylene as detector mol. in electron impact excitation 2−67687
transfer between identical luminescent molecules in solutions, effect produced by initial shock 2−50368
two-photon, of complex molecules, determ. of polarization limits of fluorescence 2−83237
two-photon absorption cross sections, method 2−41952
two-photon ionization, analysis using Laplace transformation theory 2−64029
universal function for ionization by structureless charged particles of arbitrary mass and charge 2−52925
Ar_2*, temp. dependence of vacuum u.v. emission spectra in gas and liquid phases 2−70680
BeI, electronic spectrum of first excited state 2−42872
C compounds, polyatomic negative ions, surface ionization 2−79928
CN red band system, shock tube determ. of electronic transition moment 2−77083
CO, by reson. absorpt., $A^1\Pi$ state 2−56159
CO, core excited resonances, electron transmission spectroscopic study 2−46547
CO, $\Delta v=1$ transitions, relative Einstein A coefficients 2−46531
CO, electron impact excitation of vacuum u.v. radiation, threshold studies 2−80141
CO, electronic-vibr. energy transfer, vibr. distrib., i.r. fluoresc., Hg*-sensitized 2−59988
CO, threshold electron impact spectrum, reson. struct. 2−70687
CO, totally inverted vibr. population, rel. to laser applic. 2−61777
CO, vibr. excitation by O + Cs reaction, chem. laser studies 2−72552
CO ($a^3\Pi$) quenching by $O(^3P)$, rate coeffs. 2−64213
CO electron impact threshold excitation spectrum meas. using trapped-electron method, structure identification 2−80146
CO electron scattering, study of resonance phenomena associated with 10.04 eV Feshbach resonance 2−80147
CO formed in O_2 + acetylene reaction, vibrational population distrib. 2−46532
CO ionization by electron impact, cross section for emission of comet-tail bands 2−46563
CO population by active nitrogen, rate coeffs. 2−70718
CO singlet and triplet state excitation by active N_2 2−70717
CO^+, radiative lifetimes of $A^2\Pi$ state 2−74259
CO_2, dissociative excitation of $CO(A^1\pi)$ system by electron impact 2−56164
CO_2, electron impact, dissociative excitation of vacuum u.v. emission features 2−50027
CO_2, near-resonant energy transfer to (00°1) vibr. level due to Hf collisions 2−53101
CO_2, photodissociative excitation, $CO(A^1\Pi)$ cross sections 2−56163
CO_2, solid, in extreme u.v. 2−44365
CO_2 laser, transversely excited atmospheric pressure, comparison of excitation methods 2−52412
CO_2 lower laser level relax. saturation 2−59992
CO_2 polyatomic mixtures, laser-excited vibrational fluorescence measurements 2−43035
$CO(a^3\Pi)$, lifetime meas. following electron impact dissociation of CO_2 2−50028
CS_2, u.v. absorpt. near N_2 laser wavelengths, excited states population 2−80014
D_2, core excited resonances, electron transmission spectroscopic study 2−46547
D_2, vibrationally excited, collisions with Na atoms excitation of D-line radiation 2−70627
D_2 dissociative excitation, by electron impact, absolute meas. of 2S atom production 2−42889
F + HCl → HF + Cl, effect of excess reagent vibr. excitation on reaction dynamics 2−84629
Gd^{3+} ions in solutions of complex compounds 2−71211
H_2-H^+ collisions, vibrational excitation, 15-1000 eV, semiclassical theory 2−80152
H_2, dissociative excitation of vacuum u.v. emission by electron impact, cross section meas. 2−42900
H_2, effects of rotational autoionization on angular distrib. of photoelectrons 2−50045
H_2, miltiphoton dissoc., predissoc., autoionization 2−83263
H_2, model potential for vibrational excitation by collision with Li^+ 2−43038
H_2, photoioniz. cross sections by Coulomb approx. method 2−70703
H_2, vibrational excitation by H^+ and e^- impact, cross section calc. 2−70817
H_2, vibrationally excited, collisions with Na atoms excitation of D-line radiation 2−70627
H_2 dissociative excitation, meas. of time-of-flight spectrum of metastable H(2S) atoms, evidence of predissociation 2−46551
H_2 electron impact dissociative excitation polarization free vacuum u.v. meas., obs. of Lyman α radiation 2−80120
H_2 vibrational excitation by Li^+, quantum mechanical studies 2−77171
HCl, selective laser excitation of high vibr. levels 2−53017
HCl, vibrational energy transfer, optical parametric oscillator pumped 2−80155
HCl, vibrational fluorescence, vibrational energy transfer from molecule to molecule 2−83256
H_2O vapour, electron impact cross sections, atmospheric applications 2−53019
H + H_2 vibr. excitation process, rate const. 2−67537
He_2, energy barriers in excited states 2−56178
$He_2(3p^3\pi)$, excitation transfer and quenching reactions 2−46552
I_2, fluorescence from vibrational levels excited by 6328 Å He/Ne laser 2−77085
I_2 vapour by Kr ion laser transitions assignment 2−80016
I_2 vapour excited by Ar ion laser, obs. of progressive change from resonance fluorescence to resonance Raman effect 2−56181
I_3^-, resonance Raman effect laser excited, vibration enhancement 2−80007
N_2-ar mixtures, rel. to relaxational absorpt. of sound 2−71116
N_2, autoionising levels, converging to $A^2\Pi_u$ and $B^2\Sigma_u{}^+$ limits 2−83403

Molecules continued
excitation continued
N_2, by electron impact, emission cross section for second positive system bands 2−46564
N_2, core excited resonances, electron transmission spectroscopic study 2−46547
N_2, elastic electron scatt. and nonresonant vibr. excitation 2−77162
N_2, elastic electron scatt. and excitation of first vibr. level 2−77161
N_2, electron impact excitation of electronic states 2−64148
N_2, electron impact excitation cross sections, ionospheric models 2−81724
N_2, electron swarm excitation of $C^3\pi_u$ level 2−60019
N_2, in high-frequency Ar + N_2 discharge, effective cross sections for excitation of $C^3\Pi u$ state 2−43041
N_2, rate constants for deactivation of $B^3\Pi_g$ and $A'^1\Sigma_u{}^-$ states 2−80125
N_2, transistors to and predissociation of $C^2\Sigma_u+$ state 2−80006
N_2, tunable Raman excitation and vibr. relax. 2−53023
N_2, vibrational excitation by electron impact in 15-35 eV region, meas. of angular distrib. 2−56189
N_2, vibrational excitation by e^-, cross section calc. 2−70817
N_2, vibrationally excited, collisions with Na atoms, excitation of D-line radiation 2−70627
N_2, vibrationally excited, reaction with O^+, cross section for formation of NO^+ 2−54530
N_2 excitation by fast electrons and spectrum in i.r. range 6500-11500 Angstroms rel. to auroral spectra 2−84874
N_2 i.r. emission spectra in auroral excitation conditions 2−84873
N_2 low-energy electron scattering, rotational excitation cross sections predicted using pseudo-potential model 2−70819
N_2 population by active nitrogen, rate coeffs. 2−70718
N_2 relative populations of $C^3\Pi_u$ and $B^2\Sigma_u{}^+$ states 2−80121
$N_2{}^+$, anomalous excitation in seeded Ar free plasma jet 2−42916
$N_2{}^+$ ionization by electron impact, cross section for emission of Meinel bands 2−46563
$N_2(A^3\Sigma_u{}^+)$ metastable, production of $N_2(C^3\Pi_u)$ and $N_2(C'^3\Pi_u)$ by mutual collisions 2−50132
NH_3, model potential for intramolecular inversion 2−42910
$NH_2(A^2A_1)$ produced by photolysis, collisional deactivation 2−50060
NO, core excited resonances, electron transmission spectroscopic study 2−46547
NO, Penning ionization by $Ar(^3P_1)$ 2−53041
NO_2, collisionally induced excitation, radiative lifetime 2−80015
N_2 + CO_2, high velocity mixing 2−83661
N_2*, vibrationally excited, quenching by O, determ. of rate coeff. 2−83400
NaK, laser-induced resonance fluorescence 2−64149
Ne-Br_2 mixtures, r.f. discharge spectrum, excitation mechanisms 2−71018
O_2, collision with Ar, hot gas, rates of vibr. excitation 2−83417
O_2, core excited resonances, electron transmission spectroscopic study 2−46547
O_2, dissociation excitation of vacuum u.v. emission by electron impact, cross section meas. 2−42900
O_2, elastic electron scatt. and excitation of frst vibr. level 2−77161
O_2, electron impact excitation cross sections, ionospheric models 2−81724
O_2, tunable Raman excitation and vibr. relax. 2−53023
O_2 excitation cross sections and intensity ratios in auroral conditions 2−84872
O_3, calculation on excited states 2−42924
OH, interstellar, interferometric obs. of $^2\pi_{3/2}$ $J=5/2$ microwave transition 2−75792
$OH(A^2\Sigma^+, v'=0)$, rotational excitation from dissoc. collision of H_2O with metastable Ar 2−64215
$OH(^2\Sigma^+)$ radicals, rotationally excited, formation in water vapour discharge 2−60027
$O_2{}^+(b^4\Sigma^-{}_g)$ collisional deactivation rates for O_2 and N_2 2−77172
$O_2(^1\delta_g)$, Penning ionization by $Ar(^3P_1)$ 2−53041
SO $A^3\Pi$-$X^3\Sigma^-$ band systems, oscillator strengths 2−56195
SeH-, photodetachment of electron determ. of electron affinity and spin-orbit coupling constant of SeH 2−46583
SiO, interstellar, detection of $J=2\rightarrow1$ rotational transition 2−58358
TiO β system, Einstein coeffs. and oscillator strengths of excited levels 2−60036
Xe_2*, temp. dependence of vacuum u.v. emission spectra in gas and liquid phases 2−70680

intermolecular mechanics
see also Association; Collision processes/molecules; Kinetic theory/gases; Liquids/structure; Liquids/theory; Solids/theory
acetonitrile, in trialkylphosphines and CCl_4, dipole-dipole interac., spectral study 2−46647
acetonitrile, interactions in liquid, i.r. spectra 2−83323
alkali ion + H_2O system, energy of hydration 2−68772
alkanes in cyclane solvents, orientated mol. interactions 2−50340
aniline in solution, ^{13}C spin-lattice relaxation and intermolecular interactions 2−80482
p-azoxyanisole, temp. dependence of intermolec. interactions in crystal ad nematic phases 2−50335
benzene, pure and isotropic mixed crystals, absorption spectroscopic study of isotope effects intermolecular interactions 2−81357
benzene-d_6 and mixed crysts. with benzene, isolated Na atom absorpt. spectra obs. 2−68653
benzene-methanol mixtures, interpretation of viscosity and density meas. in terms of intermolecular attractions 2−60450
biaxial liquid crystals, molecular field lattice model for repulsive interaction between platelike molecules 2−80445
binary gas mixture, asymptotic theory for steady source expansion 2−71108
binary mixtures of molecules interacting via Kihara potential, Percus-Yevick theory 2−67552
biological rate phenomena 2−81988
biphenyl crystal, lattice dynamics using 6-exp potential function 2−57043
caesium methanesulphonate, intermolecular coupling effects on crystal structure assignments from vibrational spectra 2−72375
carbon tetrachloride gas mixtures at high pressures, second cross virial coeffs. 2−43262
central potentials, effective including rotational correlation 2−46855

Molecules continued
intermolecular mechanics continued
chloroform, cryst. films, i.r. spectra in polarized light 2−84484
classical fluid, optimized cluster expansion, application to molecular liquids 2−67554
classical fluid, optimized cluster expansions, variational formulation of mean spherical model and hard sphere Percus-Yevick eqns. 2−67553
classical fluids, perturbation theory for repulsive forces 2−43044
collision induced electronic relax. dynamics 2−60110
crossed molecular beam apparatus for meas. of differential elastic or reactive cross section, determ. of intermolecular potentials 2−64211
degeneracy of spectra of linearized Boltzmann collision operated for Maxwellian molecules 2−46852
dense medium, thermodynamic functions in model of higher order 2−49036
diatomic, effective intermol. pots. from atom-atom pots 2−77366
diatomic mols., van der Waals interaction, expansion 2−67543
dynamics, computer simulation 2−46638
effective pair pots., density expansions 2−64210
equation of state data for parallel hard squares, comparison with two simple models 2−52105
ethylene gas, contributions of nonspherical and nonadditive molecular interactions to third virial coeff. 2−71110
exchange perturbation theories for interaction energies calc. 2−83421
exchange perturbation theory applic. to forces calc. 2−83420
excited species interaction obs. using diffusion of optically pumped mols. 2−60106
fibrin, elongated, films, dielectricity, viscoelasticity and piezoelectricity 2−85087
formamide crystals, ir. and Raman vibrational spectra 2−44395
Gaussian mixture, correlation functions 2−64205
Gaussian representations of charge overlap effects 2−43026
glory extrema in total scattering cross-section 2−49017
grain boundary struct. and energy, pairwise interactions, Morse, Lennard-Jones 6-12 and 4-7 pots. 2−56726
halide ion + H_2O system, energy of hydration 2−68772
Hellmann-Feynman and virial theorems in Xα method 2−70805
indole, fluoresc. in soln., interaction with methanol, kinetics 2−53069
interaction pot., determ. by elastic scatt. method 2−46643
interactions in liquids, study using oscillation spectra 2−77431
ion-neutral system, bonding energies 2−67532
Kihara intermolecular potential test using Ar 2−70811
large systems, selective long range dispersion forces 2−43031
lennard-Jones potentials from atom-diatomic molecule elastic scattering 2−56272
linear mols., effective intermol. potentials 2−64208
methanol, in trialkylphosphines and CCl_4, dipole-dipole interac., spectral study 2−46647
mica, van der Waals dispersion forces 2−53104
molecular crystals, calc. of small vibration spectra on basis of atom-atom representation of energy interaction 2−43947
molecular dynamics computer method for calc. of autocorrelation functions leading to transport coeffs. 2−82245
molecular-statistical treatment of diffusion consts. in liquids 2−74536
multicomponent solutions, intermolecular effects in n.m.r. studies 2−56520
multipole interaction effects on rotational energy exchange in molecular collisions 2−50269
olefins, activation energies for addition of O(^{3}P) 2−84621
organic compounds, van der Waals constant, relationship with molar refraction and molar volume 2−60119
oscillators in electromagnetic field, dispersion forces, semi-classical treatment 2−74302
phenol in solution, ^{13}C spin-lattice relaxation and intermolecular interactions 2−80482
polar, potential model 2−60114
polyatomic gas, contribution of nonspherical and nonadditive molecular interactions to third virial coeff. 2−71110
polymer dynamics 2−53090
polymers, effect of form of inelastic deformation 2−80119
potential constants determ. method 2−60111
potential determination, by inversion, from energy, depend. of total cross-section 2−64079
potential energy function determ. from gas viscosity meas. by new iterative method 2−64206
pyrazine, intermolecular effects on crystal spectra 2−78111
pyrene-perylene energy transfer, pressure dependence 2−60109
Pyrene-Pyrene system, dispersion forces calculation 2−60113
rare earth complexes, luminescence relaxation time, probabilities of inter- and intra-molecular energy transfer 2−54449
repulsive potentials 2−67379
SCF perturbation theory and intermolecular interactions 2−42849
short-range order in molecular liquids, 'perturbed crystal' model 2−64431
sodium methanesulphonate, intermolecular coupling effects on crystal structure assignments from vibrational spectra 2−72375
Stockmayer force constants for viscosity of polar gases 2−83716
tetramethylpyrazine, intermolecular effects on crystal spectra 2−78111
trifluoroethane and trifluoroethane-d_3, contribution to ^{19}F n.m.r. shielding 2−83308
Van der Waals forces, organic liquids, from u.s. velocity obs. 2−53429
van der Waals radii from known crystal structures 2−67970
water, molec. dynamics study of temp. effects on structure and kinetics 2−60417
Ar + Ar intermolecular potentials from differential scattering cross-sections 2−42782
BeF_2 melt, structure and motion, molecular dynamics calc. 2−74515
CO, matrix-isolated, i.r. obs. at cryogenic temps., interactions 2−68638
CO crystal, optical spectra of trapped atoms, intermolecular interactions of excited species 2−78096
CO_2 polyatomic mixtures, laser excited, rates for intermolecular energy transfer 2−43035

Molecules continued
intermolecular mechanics continued
CS_2 liquid, effects of intermolecular interactions on Raman spectrum 2−71205
D_2-Ne Van der Waals complexes in collision-induced fund. bands of deuterium, spectra 2−64127
DBr(I), matrix-isolated, i.r. obs. at cryogenic temps., interactions 2−68638
H_2-H_2 dispersion energy, basis set influence 2−67538
H_2-H_2 long range potential, analysis of SCF-Mo calcs. 2−64217
H_2-Ne Van der Waals complexes in collision-induced fund. bands of hydrogen, spectra 2−64127
H, perturbation theory of intermolec. forces in small overlap region 2−70812
H, perturbation theory of intermolec. forces in small overlap region 2−70813
HCl, vibrational energy transfer, optical parametric oscillator pumped 2−80155
H_2O, dissoc. collision with metastable Ar, rotational excitation of OH($A^2\Sigma^+$, $v'=0$) 2−64215
He-H_2 system, population and natural spin orbital analyses 2−67540
He-Kr mixtures, potentials obtained from temp. dependence of i.r. absorption spectrum 2−50131
He-Xe mixtures, potentials, obtained from temp. dependence of i.r. absorption spectrum 2−50131
He_2, attractive well, meas. by crossed beam differential elastic scatt. technique 2−50133
KH_2PO_4, molecular dynamics study and ferroelec.-antiferroelec. transitions by NMR and dielec. relax. 2−72032
$K + CH_3I \rightarrow KI + CH_3$, translational energy depend., reaction cross-section 2−51432
$LiBeF_3$ melt, structure and motion, molecular dynamics calc. 2−74515
LiF melt, structure and motion, molecular dynamics cals. 2−74515
N_2 crystal, optical spectra of trapped atoms, intermolecular interactions of excited species 2−78096
N_2 gas, contribution of nonspherical and nonadditive molecular interactions to third virial coeff. 2−71110
N_2 gas, kinetic theory of thermomagnetic torque 2−50271
$N_3{}^{2-}$ and $N_3{}^0$, molecular orbital calc. of isotropic hyperfine interactions 2−64144
$NH_3 + HCl$ system, potential energy curves for proton motion, extended Huckel calculation 2−43040
N_2O, excited on ν_3, vibr. energy transfer to CO and N_2, temp. depend. 2−60108
N_2 + Ar system, three-body recomb. and dissoc., Monte Carlo trajectory calcs. 2−64108

internal mechanics
(anthracene)-$(CH_2)_n$-(N, N-dimethylaniline) systems, intramol. electron donor-acceptor interactions 2−60047
acetone, coupling of motion between methyl groups studied by normal coordinate analysis using Urey-Bradley force field 2−56210
alkali halide molecule, ionic stabilization energy and Coulombic attraction 2−53030
alkali halides, modified form of Rittner's potential function 2−42904
alkali halides, potential curves from u.v. absorption cross section data 2−70738
alkali halides, potential energy curves 2−77076
anomalous energy minima in semiempirical CNDO/2 and INDO calcs. 2−83234
N- aralkylpyridinium ions, conformational influences on intramolecular charge transfer transition 2−42955
asymmetric rotor rot. spectra, internal rot.-quadrupole interaction 2−56143
azomethane, azomethane-d_6, calc. of internal rotational barrier of methyl group 2−42957
2-bromoethanol, normal coordinate analysis on rotational isomerism 2−42981
collision induced electronic relax. dynamics 2−60110
deformation vibrations, semiclassical electrostatic mode 2−50000
diatomic, atom-atom pot. and applic. in calc. gas props. 2−77366
diatomic, critical binding 2−46498
diatomic, dependence of rotational constant B_v on long-range internuclear potential 2−46505
diatomic molecules, static charge distributions generating exact potential curves 2−42826
dimer composed of 2 biphenylene subunits, triplet exciton transfer study by e.s.r. 2−46509
dipole moment, of symmetric systems, quantization of nuclear motion effects 2−77036
directions of normal vibrations of protons in a breaking H bond 2−67458
double minimum potentials, effect of introducing small amount of asymmetry 2−52975
energy properties, calculation by approximate molecular orbital method 2−70670
ethane, pot. surface using the MINDO/2 method 2−77126
ethanes, halogen substituted, vibr. spectra and barriers to internal rotation 2−50092
glyoxal, internal rotation determ. from molecular wave functions 2−53065
hexahalide anions of O_h symmetry, orbital valence force field 2−42903
hydrocarbon chains with (α-naphthyl)$-(CH_2)_j-$(α-naphthyl) struct., intramol. collision freq. 2−53067
inert gas hydrides, realistic single-function potential models 2−50046
intramolecular electronic relaxation, effect on optical line shape of large molecules 2−64088
macromolecules, models of interactomic force fields for analysis of vibrational spectra, Urey-Bradley model 2−43017
macromolecules in soln., polarized luminescence for investigation of intramolecular mobility 2−60090
methanol in excited CO stretching state, microwave spectrum, torsion-vibration-rotation interaction 2−67517
methyl cyanide, molec. force fields detn. by kinetic methods 2−70776
methyl isocyanide, molec. force fields detn. by kinetic methods 2−70776

- **Molecules** continued
  - **internal mechanics** continued
    - moment of inertia derivatives with respect to internal coords. calc. using general machine algorithm 2−52961
    - organic liquids, Wada's molecular compressibility from u.s. velocity obs. 2−53429
    - polyadenylic acids, intramolecular triplet-triplet energy transfer 2−51471
    - polyatomic, intramol. interactions and vibronic spectra, electronic rearrangments and four level scheme 2−67447
    - polyatomic, intramolecular interactions 2−77045
    - polyatomic, mechanisms for internal- conversion and line broadening processes 2−49989
    - polyatomic, non-crossing rule for potential energy surfaces 2−70668
    - polyethyleneoxalate, polyethylenesuccinate, intramolec. contributions to entropy and energy of fusion 2−46637
    - polymethylmethacrylates, intramolecular mobility in solutions, solvent effects 2−43337
    - porphyrins, influence of intramolecular spin-orbital perturbations on luminescence 2−53077
    - positronium, binding energy 2−64111
    - racemization of isoleucine rel. to fossil bone dating 2−65568
    - rare earth complexes, luminescence relaxation time, probabilities of inter- and intra-molecular energy transfer 2−54449
    - ring compounds, four-membered, puckering co-ordinates 2−42942
    - statistical total energy in multiple scattering formalism 2−42828
    - tetrahedral molecules and ions, force constants by orbital release force field and Urey-Bradley force field 2−77077
    - tetrapyrole, intramolecular transitions and energy, influence of structural factors 2−53078
    - trifluoroethane and trifluoroethane-d_3, contribution to ^{19}F n.m.r. shielding 2−83308
    - triplet exciton transfer study 2−46509
    - wormlike chains, statistical mechanics of asymptotic behaviour 2−74296
    - wormlike chains, stiff, with excluded volume, second virial coeff. 2−74297
    - Ar_3, binding energies, calc. for Lennard-Jones 12-6 pair potentials 2−60023
    - Au_2, true pot. energy curves and r-centroids 2−56155
    - BH_3NH_3, SCF calcs. of internal rotation barrier and its derivatives 2−42873
    - CH, CI calcs. of potential curves for low lying excited electronic states $a^4\Sigma^-$, $A^2\Delta$, $B^2\Sigma^-$, determ. spectroscopic conts. 2−56160
    - CN, true pot. energy curves, Morse r-centroids and Franck-Condon factors for $E^2\Sigma^+$-$X^2\Sigma^+$ band system 2−42880
    - CO_2 polyatomic mixtures, laser excited rates for intramolecular energy transfer 2−43035
    - CO_2^-, energy curves of $^2A_1$ and $^2B_1$ states 2−42874
    - CuH, potential energy curves, derivation of dissociation energy 2−59998
    - $D_3Co(CN)_6$, hydrogen bonds, potential energy wells 2−42895
    - GaH, potential energy curves 2−60000
    - $H_3Co(CN)_6$, hydrogen bonds, potential energy wells 2−42895
    - HF, HF^+, HF^-, pot. energy curves of ground states 2−60026
    - HeH_2^+, ab initio potential energy surface calcs., diatomics-in-mols. method 2−83246
    - hydrocarbon chains with (α-naphthyl)$-(CH_2)_j-$(α-naphthyl) struct., intramol. collision kinetics, e.s.r. obs. 2−56236
    - I_2, O_u^- repulsive potential curve determ. from obs. of magnetic quenching of fluorescence from vibrational levels 2−77085
    - Kr_3, binding energies, calc. for Lennard-Jones 12-6 pair potentials 2−60023
    - Li complex, Li^+-H_2O, energy surface of H_2O mol., config. determination 2−60010
    - Li He, interaction potential, group function method 2−67487
    - Mg_2, ground state pot. energy curve 2−60012
    - NCl_3, normal coordinate analysis, vibrational frequencies and force constants calc. 2−46567
    - NH_3 dipole moment, temp. depend. with allowance for internal motion 2−77036
    - Ne_2, ground state pot. curve, self-consistent-field α cluster calcs. 2−80003
    - Ne_3, binding energies, calc. for Lennard-Jones 12-6 pair potentials 2−60023
    - NeH, NeH^+, pot. energy curves of ground and excited states 2−60026
    - OH, pot. energy curves of ground states 2−60026
    - $^{31}P^{14}N$, Dunham potential constants, calc. from millimetre wave rotational spectrum 2−60029
    - $SOBr_2$, pot. energy consts. calc. 2−56169
    - $^{16}SO_2$, $^{18}SO_2$, second order anharmonic potential function 2−56201
    - $SbCl_6^-$, force constants determ. from frequency data using general valence, orbital valence and Urey- Bradley force fields 2−42934
    - SiH_3CN, molec. force fields detn. by kinetic methods 2−70776
    - TlH, potential energy curves 2−60000
    - Xe_3, binding energies, calc. for Lennard-Jones 12-6 pair potentials 2−60023
  - **moments**
    - acenaphthenequinone, elec. dipole moments due to π-electrons 2−70784
    - acetaldehyde and complex, CNDO and INDO calcs. of dipole moments 2−53043
    - acetophenone, 2-hydroxy-5-methyl derivative, dipole moment computation from permittivity and loss meas. in benzene solution at 37.4 GHz 2−60487
    - acetylene, minimal basis set LCGO calcs. 2−79989
    - alkyl acetates, dipole moments 2−60488
    - 2-aminopyridine, normal and deuterated, dipole moment from Stark effect meas. in microwave spectrum 2−50077
    - aromatic, magnetic anisotropy, comparison of theory and expt. 2−60049
    - benzene, CNDO calc. of dipole moment derivatives 2−50082
    - benzene derivatives, dipole moments calc. using CNDO and INDO methods 2−70750
    - benzonitrile, dipole moments and polarizabilities of lowest excited singlet states 2−67508
    - benzophenone, 2-hdyroxy-5-methyl derivative, dipole moment computation from permittivity and loss meas. in benzene solution at 37.4 GHz 2−60487

- **Molecules** continued
  - **moments** continued
    - benzophenone molecular crystal, dipole moments of lowest singlet and triplet $n\pi^*$ excited states 2−81136
    - benzoquinoline, 7,8- and 5,6-, dipole moments in ground and fluorescent states 2−74281
    - benzvalene, dipole 2−77139
    - bicyclo[2.1.1]hexan-5-one, microwave spectrum and dipole moment 2−42964
    - caprylophenone, 2-hydroxy-5-methyl derivative, dipole moment computation from permittivity and loss meas. in benzene solution at 37.4 GHz 2−60487
    - carbon tetrafluoride, octopole moments and dielec. second virial coeffs. 2−83294
    - chloralides, optically active, dipole moment. rel. to conformation determ. 2−42971
    - chloroacetylene, quadrupole and elec. dipole moments, Zeeman effect obs. 2−70758
    - chlorobenzene, dipole moments and polarizabilities of lowest excited singlet states 2−67508
    - chloroethanes, dipole moments calculations 2−42970
    - chloroform, electronic structure, dipole moments, n.m.r. and n.q.r. constants calc. 2−83324
    - conjugated molecules, comparison of expansions in calc. of elec. dipole π polarizability 2−42855
    - cyanamide, ab initio LCAO-MO-SCF calc. of dipole moment in semi-rigid model 2−64176
    - cyclopentadienylberyllium chloride, dipole moment 2−70763
    - diatomic, calc. of dipole moment in dielectric model 2−70652
    - dielectric properties of substances, tables 2−45631
    - 2,3- dihydrofuran, dipole moments of ground and excited states of ring-puckering mode determ. from microwave spectrum 2−42978
    - 3,4-dimethylenecyclobutene, valence shell CNDO, INDO and CNDO-CI calculations 2−60063
    - dimethylnitrosamine, microwave spectrum and dipole moment 2−80107
    - dimethylsulphide-d_6, elec. dipole moment sign 2−64177
    - 1,3-dioxane, microwave spectrum, dipole moment 2−64178
    - N,α-diphenylnitrones, substituted, dipole moment meas. 2−64179
    - dipole, intramolecular hydrogen bond effects 2−77127
    - dipole, of symmetric molecular systems, quantization of nuclear motion effects 2−77036
    - dipole moments of singlet and triplet excited states 2−77049
    - dipoles cross depolarization during adsorption on metal surfaces 2−50521
    - electron-vibrational dipole scatt. phenomena 2−80126
    - epoxybutyne, microwave spectrum, structure and dipole moment 2−80088
    - ethylene, minimal basis set LCGO calcs. 2−79989
    - ethylene sulphone, dipole moment determination from microwave rotational spectra 2−60065
    - fluorine containing compounds, calc. of second moments of electronic charge distrib. and quadrupole moments by CNDO/2D method 2−80085
    - o-, m-, p-fluorobenzaldehyde, dipole moments 2−83279
    - fulvene, dipole moment meas. 2−80096
    - furan, normal magneto-optical rot. dispersions, mag. moments 2−70770
    - cis-glyoxal, dipole moment determ. from microwave spectrum 2−93300
    - glyoxal calc. of dipole moment and electric field gradients at O and H nuclei from molecular wave functions 2−53065
    - Grad's thirteen moment approx., computer simulation 2−46638
    - heterocyclics, six-membered with O and N, dipole moment, AVE CI SCF calculation 2−56204
    - hexafluorobenzene, CNDO calc. of dipole moment derivatives 2−50082
    - isoxazolinone-5, tautomeric equilibr. dipole moment, electronic spectrum calc. by semi-empirical MO methods 2−53070
    - methane, calc. of octopole moments using semi-empirical wavefunctions 2−70701
    - methane, dipole moment due to centrifugal distortion, obs. of pure rotational spectrum 2−53072
    - methane, electronic structure, dipole moments, n.m.r. and n.q.r. constants calc. 2−83324
    - methane, minimal basis set LCGO calcs. 2−79989
    - methane, octopole moments and dielec. second virial coeffs. 2−83294
    - 2-methoxyethanol, dipole moment determination from microwave spectrum 2−50098
    - methyl chloride, electronic structure, dipole moments, n.m.r. and n.q.r. constants calc. 2−83324
    - methyl fluoride, nonlinear laser spectroscopy, elec. dipole moments 2−53063
    - methylamine, minimal basis set LCGO calcs. 2−79989
    - methylene chloride, electronic structure, dipole moments, n.m.r. and n.q.r. constants calc. 2−83324
    - methyleneimine, mol. transient, elec. dipole moment 2−64186
    - methylsilane, dipole moment 2−83292
    - 3- methylthiophene, dipole moment from microwave spectra 2−42997
    - myglobin in water, dipole moment 2−46976
    - myrisotophenone, 2-hydroxy-5-methyl derivative, dipole moment computation from permittivity and loss meas. in benzene solution at 37.4 GHz 2−60487
    - α-naphthoquinone, elec. dipole moments due to π-electrons 2−70784
    - NH_3, nuclear quadrupole moment of ^{14}N, vibrational and other corrections 2−60015
    - organic F containing σ-bonded molecules, MINDO/2 calc. of dipole moments 2−77111
    - organic nitroxide radicals, quadrupole splitting obs. by ENDOR in liquid crystals 2−50103
    - 3-oxetanone, dipole moment, Stark effect meas. 2−70787
    - trans 3-penten-1-yne, dipole moment, determination from microwave spectrm 2−50108
    - phenanthrenequinone, elec. dipole moments due to π-electrons 2−70784
    - phosphabenzene, microwave spectrum, dipole moment 2−56254

Molecules continued
- **moments** continued
  - polyatomic, calc. of dipole moment derivatives using Fock-Roothaan wave functions, intensities in i.r. spectra deduced 2−42921
  - polyatomic T_d molecules, effects of dipole moments on Stark effects and $\Delta J=0$ transitions 2−42844
  - propiolic acid, microwave spectrum, dipole moment obs. 2−56256
  - pyridine, normal magneto-optical rot. dispersions, mag. moments 2−70770
  - quadrupole, calculation method 2−52982
  - quadrupole, of various organic molecules from microwave Zeeman effect 2−70739
  - quark one-electron mol., dipole moment 2−52985
  - randomly coiling polypeptide chains, average dipole moments for hard-sphere models 2−64201
  - randomly coiling random copolymers, higher even moments for hard-sphere model 2−64202
  - sultones and sultines, dipole 2−43009
  - symmetric-top, dipolar absorption in microwave and far i.r. region 2−70655
  - thioformaldehyde obs. of high-field rotational Zeeman effect, quadupole moments determ. from g values and magnetic susceptibilities 2−43010
  - thiophene, dipole moment from microwave spectra 2−42997
  - thiosultones, dipole 2−43009
  - Au_2, electronic transition moment determ. using r-centroid values for band system 2−56155
  - BH, computation of force constants and dipole moment derivatives using Hartree-Fock 2−50052
  - BH_2 structure of transition dipole moment 2−80025
  - $B_{10}H_{14}$, dipole moment, SCF study 2−64115
  - BH_3NH_3, SCF calcs. of internal rotation barrier and its derivatives, determ. of dipole moment 2−42873
  - B_2O_3, dipole moment 2−70683
  - CCl_4, dipole moment, Pariser-Pople and Wolfsberg-Helmholz calc. 2−83324
  - CH_2 structure of transition dipole moment 2−80025
  - CN red band system, shock tube determ. of electronic transition moment 2−77083
  - CO, $a^3\Pi$ state, dipole moment from spectrum at 5 to 1000 MHz 2−50026
  - CO, intensity meas. of $d^3\Delta \rightarrow a^3\Pi$ emission system, determ. of relative electronic transition moments 2−80035
  - CO, vibrational matrix elements of quadrupole moment functions 2−64129
  - CO configuration interaction wavefunctions and dipole moment calc. 2−74258
  - CO^+, comet tail system, electronic transition moment 2−50029
  - CO^+, electronic transition moments for $A \rightarrow X$, $B \rightarrow X$, $B \rightarrow A$ transitions, abs. absorption cross sections 2−52998
  - $CO \rightarrow CO^+$ system, electronic transition moments for $A \leftarrow X$, $B \leftarrow X$ transitions, abs. absorption cross sections 2−52998
  - $CSCl_2$, dipole moment, i.r. spectra 2−46533
  - CSF_2, dipole moment, i.r. spectra 2−46533
  - 1-chloro-3,3,3-trifluoropropyne, microwave spectra analysis 2−70759
  - $^{133}Cs^{23}Na$, elec. dipole moment, determination from molec. beam elec. resonance spectra 2−64140
  - Cu^{2+} complexes, magnetic circular dichroism spectra of vibronically allowed d-d transitions 2−64124
  - D_2O, dipole moment determ. from Stark effect meas. on microwave transitions 2−80045
  - $F_3P.BH_3$ and $F_2HP.BH_3$, dipole, CNDO/2 calculations 2−53032
  - GeH_3F, GeD_3F, dipole moment determination from microwave spectrum 2−60001
  - H_2, vibrational matrix elements of quadrupole moment functions 2−64129
  - H_3^+, dipole moment derivative of electronic ground state $^1A_1$ 2−70705
  - HCN, minimal basis set LCGO calcs. 2−79989
  - HCNO, elec. dipole moment, iterative extended Huckel theory calc. 2−56187
  - HCP, dipole moments of $^1A''$ and $^3\Delta_1$ states 2−42897
  - HD^+, collision induced dissociation by electron impact, effect of dipole moment studied using Born-Oppenheimer approx. 2−56173
  - HDO, rotational dependence of dipole moment determ. from Stark effect meas. on microwave transitions 2−80045
  - H_2NCN, elec. dipole moment, iterative Huckel theory calc. 2−56187
  - HNCO, elec. dipole moment, iterative extended Huckel theory calc. 2−56187
  - HNNN, elec. dipole moment, iterative extended Huckel theroy calc. 2−56187
  - H_2O, calc. of octopole moments using semi-empirical wavefunctions 2−70701
  - HeH, dipole moment of ground molecular state as function of internuclear separation 2−74266
  - ICl, dipole moment by Stark effect meas. 2−42902
  - InCl, electric dipole moment, Stark effect measurement 2−46555
  - $^{39}K^7Li$, $^{39}K^{23}Na$, elec. dipole moment, determination from molec. beam elec. resonance spectra 2−64140
  - Li_2, computation of force constants and dipole moment derivatives using Hartree-Fock 2−50052
  - LiH, computation of force constants and dipole moment derivatives using Hartree-Fock 2−50052
  - $(LiNa)^+$, charged transfer, transition, dipole moment, cross sections of vibr. levels 2−60009
  - LiO, $X^2\pi$ and $A^2\Sigma^+$ state props. 2−60011
  - MoO_4^{2-}, LCAO MO calc. of dipole transition moment 2−77063
  - N_2, minimal basis set LCGO calcs. 2−79989
  - N_2, vibrational matrix elements of quadrupole moment functions 2−64129
  - NCN_3, dipole moment, microwave spectrum 2−60014
  - NCNNN, microwave spectrum analysis and CNDO/2 calcs. 2−64142
  - NH_2 structure of transition dipole moment 2−80025
  - NH_3, calc. of dipole moment derivatives using Fock-Roothaan wave functions, intensities in i.r. spectra deduced 2−42921
  - NH_3, force const., dipole moment derivatives by Hartree-Fock calculations 2−80029

Molecules continued
- **moments** continued
  - NH_3, interactions with foreign perturbers, press. induced shifts of $(J, K)=(12,12)$ inversion line 2−50061
  - NH_3 dipole moment, temp. depend. with allowance for internal motion 2−77036
  - NH_2CN, μ_a component of dipole moment, determ. from microwave spectra 2−77066
  - NNO, elec. dipole moment, iterative extended Huckel theory calc. 2−56187
  - NaLi, electric dipole moment and equilib. dipole moment, polarizabilities in electric resonance spectrum 2−53029
  - OCS, elec. dipole and mag. moments, determ. by mol. beam-electric resonance method 2−83245
  - OsO_4, dipole transition moments determ. by LCAO-MO calcs. in terms of ligand mixing coeff. 2−42928
  - P_4O_{10}, bond polarity 2−60030
  - Rb^7Li, $Rb^{23}Na$, elec. dipole moment, determination from molec. beam elec. resonance spectra 2−64140
  - ReO_4^-, dipole transition moments determ. by LCAO-MO calcs. in terms of ligand mixing coeff. 2−42928
  - RuO_4, LCAO MO calc. of dipole transition moment 2−77063
  - SiO, matrix elements of dipole moment of bands in the system $A^1\Pi$ to $X^1\Sigma^+$ 2−67500
  - TcO_4^-, LCAO MO calc. of dipole transition moment 2−77063
  - WO_4^{2-}, dipole transition moments determ. by LCAO-MO calcs. in terms of ligand mixing coeff. 2−42928
  - YO, $B^2\Sigma$-$X^2\Sigma$ system electron transition moment variation with internucl. distance and vibr. temp. 2−56203
- **nuclear coupling**
  - alkali halides, quadrupole coupling consts. 2−59989
  - alkanes, Del Re parameters, quadrupole and spin-spin coupling constants 2−67505
  - alkyl halides, Del Re parameters, quadrupole and spin-spin coupling constants 2−67505
  - aniline-^{15}N and derivatives, long-range spin-spin coupling consts. 2−77137
  - anisotropic hyperfine coupling tensor, derivation for molecule with one unpaired electron 2−59999
  - asymmetric rotor rot. spectra, internal rot.-quadrupole interaction 2−56143
  - azaaromatic radical anions, ^{14}N coupling consts. 2−70745
  - benzene derivatives, deuterated, meas. of quadrupole coupling const. and asymmetry parameter of ring deuterons 2−80082
  - biphenyls, bridged, long-range ^{13}C spin couplings 2−77134
  - 1,3-butadiene oriented in nematic mesophase, p.m.r. 2−60053
  - o- chloropyridine, quad. coupling consts. of ^{35}Cl 2−53052
  - coupling constants between directly bonded nuclei, Z dependence rel. to Fermi contact contribution 2−46522
  - cyclohexane, deuterated, meas. quadrupole coupling const. and asymmetry parameter of ring deuterons 2−80082
  - cyclopentadienylberyllium chloride, ^{35}Cl quadrupole coupling const. 2−70763
  - deuterated nitrogen compounds, ^{14}N quadrupole coupling constant 2−46618
  - dimethyl phosphite, neat and in dilute soln., effect of deuterium substitution on $^1J(^{31}P\text{-}H)$ 2−80104
  - 1,3-dimethylurea, ^{14}N NQR freqs., coupling consts., var. with temp. 2−83297
  - enynes, long-range spin-spin coupling consts. 2−67511
  - fluoroethanes, vicinal ^{19}F coupling consts., self-consistent perturbation theory calcs. 2−70767
  - fluoromethyl free radicals, ab initio calculations and α-F spin coupling parameters 2−77148
  - fluoropyridine methyl derivatives, long-range spin-spin coupling consts., electron contribs. 2−77097
  - fluorothiophenes, substituted, n.m.r. of ^1H and ^{19}F 2−46606
  - p-fluorotoluene, conform. depend. of long-range spin-spin coupling 2−64193
  - free radicals, hyperfine constants 2−42854
  - hemin, nuclear hyperfine interactions, Mossbauer studies 2−67527
  - homoallylic H-H coupling constants, conformational dependence 2−42856
  - bis-imidazole hemin, nuclear hyperfine interactions, Mossbauer studies 2−67527
  - inorganic radicals, calculation of hyperfine coupling constants 2−42863
  - isopropenyl system, ^{13}C-^{13}C coupling constants 2−56237
  - Karplus equation for vicinal coupling, functional form 2−83230
  - linear chains, alternate, coupled by indirect exchange interaction n.m.r. line shape 2−43019
  - methyl fluoride, anisotropy of spin-spin coupling 2−50099
  - methyl free radicals, ab initio calculations of hyperfine coupling 2−77148
  - methylchlorosilane microwave spectrum, quad. coupling consts. 2−64190
  - methylchlorosilyl radical, meas. of ^{29}Si coupling consts. effect of degree of CH_3 substitution on planar structure 2−56241
  - methyleneimine, mol. transient, quad. coupling consts. 2−64186
  - N-methylethylidenimine, quadrupole coupling consts. 2−64183
  - monochloroamine, quadrupole coupling constants from microwave spectra data 2−46615
  - naphthalene, deuterated, meas. of quadrupole coupling const. and asymmetry parameter of ring deuterons 2−80082
  - neopentane derivatives, substituent effects on $^4J_{hh}$, positional dependence 2−77107
  - NH_3, nuclear quadrupole moment of ^{14}N, vibrational and other corrections 2−60015
  - nitrobenzene, spin-spin couplings from ^{15}N to ring protons 2−77137
  - nitroxide radicals, ^{13}C coupling consts. 2−83295
  - 1,3,4-oxadiazoles, isotopic species, ^{14}N quadrupole coupling consts. from microwave spectral data 2−43003
  - 1-penten-3-yne, long-range spin-spin coupling consts. 2−67511
  - pi-electron molecules, proton-proton coupling constants 2−46521
  - propane, conform. depend. of vicinal $^{13}C-H$ spin-spin coupling const., INDO MO calcs. 2−77151
  - propane derivatives, substituent effects on $^4J_{hh}$, positional dependence 2−77107
  - pyrene, C-H satellite n.m.r. spectrum 2−46627

Molecules continued
nuclear coupling continued
pyridine, deuterated, meas. of quadrupole coupling const. and asymmetry parameter of ring deuterons 2−80082
11-cis-retinal, proton shifts calculation 2−77153
spin-spin coupling constants, double perturbation calculations using localized orbitals 2−46519
spin-spin interaction, exact quantum-mechanical theory 2−77031
1, 2, 4, 5-tetrabromobenzene, quad. coupling consts. of ^{79}Br and ^{81}Br 2−56260
tetramethylgermane, directly banded coupling constant between ^{73}Ge and ^{13}C 2−46522
tetramethylurea, ^{14}N NQR freqs., coupling consts., var. with temp. 2−83297
three-bond fragments, proton spin-spin coupling, Dirac vector model and variational treatments 2−77050
toluene, 1-^{13}C labelled, long-range C-C spin-spin coupling constants 2−77125
toluene, conform. depend. of long-range spin-spin coupling 2−64193
trifluoromethyl group containing compounds, long-range ^{19}F coupling constants 2−77113
trimethyl-lead radical, e.s.r. spectra, determ. of g tensors and hyperfine coupling 2−70795
trimethyl-tin radical, e.s.r. spectra, determ. of g tensors and hyperfine coupling 2−70795
1',3',3'-trimethylspiro- (indoline-2',3-thietane)-1,1-dioxide, long-range $^4J_{hh}$ couplings 2−67522
uridine and related structures, relationship of ^{13}C to vicinal ^{1}H coupling to torsion angle 2−43014
vinyl-type radical in irrad. maleic acid matrix, ^{13}C proton coupling 2−64195
o-xylene partially oriented in nematic phase, indirect spin-spin coupling consts. 2−77157
xylenes, conform. depend. of long-range spin-spin coupling 2−64193
B_2H_6, comparison of quadrupole coupling calc. using minimum basis set and extended Slater orbital wave functions 2−64114
C-C coupling in molecules with ^{13}C in natural abundance at each site 2−83287
^{13}C, long-range spin couplings 2−77134
1-chloro-3,3,3-trifluoropropyne, microwave spectra analysis 2−70759
ClCO, ClOO radicals, quadrupole coupling from e.s.r. spectra 2−50031
ClNCO, microwave spectrum, quad. coupling consts. 2−56165
CsI, quad. coupling consts. of ^{127}I 2−53003
^{133}Cs^{23}Na, quadrupole coupling const., determination from molec. beam elec. resonance spectra 2−64140
Cu complexes, Cu(II) bis(dithiocarbamate) and Cu(II) bis(diselenocarbamate), anisotropic hyperfine coupling tensors 2−59999
GeF_2 microwave spectrum, determ. of nuclear quadrupole coupling consts., and effect of centrifugal distortion 2−70698
GeH_3F,GeD_3F, ^{73}Ge quadrupole coupling constant, determination from microwave spectrum 2−60001
HD, spin-spin coupling const., perturbation calc. based on bare-nucleus pot. 2−70702
^{199}Hg-^{1}H, extended Huckel MO calculation 2−83223
ICl, rotational and quadrupole constants 2−42902
$^{127}I_2$,$^{129}I_2$, elec. quadrupole coupling rel. to hyperfine interactions in optical transitions 2−50050
^{39}K^{7}Li, ^{39}K^{23}Na, quadrupole coupling const., determination from molec. beam elec. resonance spectra 2−64140
^{14}N quadrupole coupling constants in organic liquids, determ. from n.m.r. linewidths 2−56523
$^{14}NH_3$ and $^{15}NH_3$ mol. beam h.f.s. data interpret. 2−83257
NaLi, nuclear electric quadrupole coupling consts. in electric resonance spectrum 2−53029
Rb^{7}Li, Rb^{23}Na, quadrupole coupling const., determination from molec. beam elec. resonance spectra 2−64140

relaxation
see also Acoustic wave propagation; Dielectric phenomena; Liquids/theory; Nuclear magnetic resonance and relaxation; Paramagnetic resonance and relaxation
2-amino-7-nitrofluorene/1,2-dichlorobenzene, special dye laser, solvent orientational relaxation 2−42040
anthracene (-d_4), obs. and calc. of position dependent deuterium effect on triplet lifetime 2−70741
aromatic and hetoroaromatic, meas. of fluorescence of phosphorescence quantum yields, study of radiative and radiationless transitions 2−53039
aromatic hydrocarbons, nonradiative decay of lowest triplet state 2−80074
aromatic hydrocarbons, vibrational coupling strengths for intramolec. non-radiative transitions 2−42954
aromatic mols., triplet deactivation parameters determ. 2−80075
atom-molecule collision, reactive, optical model for vibrational relaxation 2−65362
azobenzene and substituted derivatives in viscous solutions, meas. of structure relaxation using photodichroism 2−42959
azulene in gas phase, non-radiative decay time of S, singlet state determ. from quantum yield of radiative decays 2−42956
benzene, excited state relaxation, review 2−60052
benzene-chloroform weak complexes, radiationless decay of benzene triplet state, external deuterium isotope effect 2−84661
biacetyl, ordering of lower electronic states, mechanism of radiationless S→T transitions 2−50085
camphor in polar solvents, vibrational spectroscopy, separation of vibrational and rotational relaxation terms 2−70757
collision induced electronic relax. dynamics 2−60110
cyanine dyes, effect of energy gap between $^1S_2$ and nearest electron states on speed of radiationless deactivation processes 2−53054
diatomic, compilation of measured lifetimes 2−46502
diatomic, tunable Raman excitation and vibr. relax. 2−53023
1,4-diazabicyclo (2.2.2) octane and methyl analogue, struct. effects on photophys. processes 2−81512
1,1-difluoro-2, 2-dichloroethane, proton spin echo n.m.r. spectra, subspectral analysis 2−42977
p- dioxone, meas. of correlation functions of rotation-vibration bands, determ. of relaxation characteristics 2−56474

Molecules continued
relaxation continued
ethanol, ethanol-d_1, ethanol-He, microwave double resonance studies of collision-induced transitions 2−60118
final-state relax. corrections for core-level binding-energy shifts 2−67459
fluorescence decay, evaluation of distribution of distances between energy donors and acceptors 2−74252
fluorescence selfdepolarization, construction and analysis of models 2−70656
gasdynamic equations in presence of oscillatory relaxation 2−77364
intramolecular electronic, effect on optical line shape of large molecules 2−64088
laser, effect of rotational relaxation on form of impulse 2−49354
liquid, binary collision model of vibrational relaxation 2−53388
liquid, constants det. in dephasing time and lifetime of excited vibrational state 2−46958
liquids, rotational relaxation, inclusion of arbitrary reorientation angles 2−80138
macromolecules, chain, expression relaxation time 2−80111
macromolecules in absorbing solutions, from transient light scattering 2−50378
methane binary mixtures with He, Ar, Xe, ultrasonic absorption meas. of rotational relaxation 2−64219
$n\pi^*$ states in organic molecules, radiationless transitions 2−70732
nonradiative transition probabilities, consideration in statistical limit 2−42829
optical lineshapes, effects of vibrational relaxation 2−70658
organic, in gas phase, meas. of radiationless triplet-triplet energy transfer 2−53094
organic, radiationless transitions, Jortner-Stepanov model 2−80105
polyatomic, intramol. interactions and vibronic spectra, electronic rearrangments and four level scheme 2−67447
polyatomic, role of vibrational relaxations in formation of diffuse and complex configuration spectra 2−77045
polyethylmethacrylate, Brillouin scattering obs. 2−65284
polymers, with cooperative binding, Ising model 2−46635
polymethine dye, triplet state absorption and relaxation 2−77443
polymethylacrylate, Brillouin scattering obs. 2−65284
radiationless electron transitions, temp. depend., using Morse oscillator model, small Z 2−52964
radiationless electronic trans., using Morse oscillator model for small value of Z 2−52962
radiationless electronic transitions, using Morse oscillator model for arbitrary Z values 2−52963
radiationless transitions, perturbation description 2−42824
radiationless transitions, recurrence and irreversibility 2−42825
radiative and nonradiative, ultrafast reactions 2−79979
resonant state decay, nonsequential effects 2−56135
rhodamine B, 6G, vib. relaxation from optically excited state, new technique 2−83401
solid polymers under high pressure 2−74604
symmetrical top angular relaxation, finite collision rough sphere model for resistance in bath of atoms 2−70808
transient stimulated Raman scattering 2−41938
vibrational, anharmonic oscillators in nozzle flow 2−80142
Ar-N_2 system, rot. relax. time, classical trajectory calcs. 2−77165
Ar-N_2 system, rot. relax. time, GPS calc. 2−77164
BCl_3, i.r. double resonance 2−46526
CO_2:^{4}He, 300 to 600 K, vibrational relaxation times of 00°1 levels 2−42881
CO_2:N_2, 300 to 600 K, vibrational relaxation times of 00°1 levels 2−42881
CO_2-DF vibrational de-excitation on the basis of vibration-to-rotation energy transfer, 300-2000K 2−83406
CO_2-H halide mixtures, relaxation of asymmetric stretching vibration 2−43036
CO_2-H_2 mixtures, thermal relax. time 2−53099
CO, CO-Ar, CO-N_2 gas mixtures, vibrational relaxation rate in nozzle flow 2−80142
CO, vibr. relax. near 100K using discharge laser 2−80128
CO excited singlet state, vibr. relax. cross sections, fluoresc. obs. 2−56159
CO_2, 300 to 600 K, vibrational relaxation times of 00°1 levels 2−42881
CO_2, shock-heated, laser absorption meas. of vibrational relaxation of bending mode 2−56161
CO_2, thermal, of vibrations, period meas. by impact tube method 2−83398
CO_2, vibrational relaxation time in inert gas mixtures, meas. using acousto-optical effect 2−59995
CO_2 lower laser level relax. saturation 2−59992
CO_2 polyatomic mixtures, laser excited, vibrational relaxation 2−43035
CO_2−HF vibrational de-excitation on the basis of vibration-to-rotation energy transfer, 300-2000K 2−83406
CO + CO collision, vibrational transition probabilities, temp. dependence below 300K 2−60117
$Ce(NO_3)_3$, aqueous solution at 25°C, u.s. relaxation 2−53427
Cl_2-Kr mixtures, shock tube heated, dissoc. relax. times 2−53244
$Cl_2 + Cl_2$ collision, vibrational transition probabilities, temp. dependence below 300K 2−60117
D_2, compressed, thermal cond.-relax coupling, rel. to Rayleigh- Brillouin scatt. 2−56171
D_2, vibrational relaxation, studied by laser induced vibrational fluorescence technique 2−80134
DF, vibr. relax., catalytic efficiencies of NO 2−77163
H_2, charge density relax. during nucl. motion 2−60002
H_2, compressed, thermal cond.-relax. coupling, rel. to Rayleigh- Brillouin scatt. 2−56171
H_2, isotopic, rotational relaxation effects on sound absorption 2−46858
H_2, low-density, nuclear-spin relaxation at room temperature 2−70707
H_2, rot. relax. times, 140-450K 2−46550
H_2 in He and Ne, rotational relaxation, approx. soln. to Boltzmann eqn. 2−80137
H_2 inert gas binary mixtures, proton spin lattice relaxation times in 165-265K range 2−46645
HBr, mechanisms for vibrational relaxation 2−70704

Molecules continued
relaxation continued
HCl, mechanisms for vibrational relaxation 2−70704
HCl, vibrational fluorescence, vibrational energy transfer from molecule to molecule 2−83256
HD, compressed, thermal cond.-relax. coupling, rel. to Rayleigh- Brillouin scatt. 2−56171
HD, vibrational relaxation, studied by laser induced vibrational fluorescence technique 2−80134
HD in He and Ne, rotational relaxation, approx. soln. to Boltzmann eqn. 2−80137
HF, mechanisms for vibrational relaxation 2−70704
HF, vibr. relax., catalytic efficiencies of NO, H_2O, D_2O and HCl 2−77163
HF, vibrational relaxation measurements using combined shock tube and laser-induced fluorescence technique 2−53011
HF in He, rotational relaxation, approx. soln. to Boltzmann eqn. 2−80137
H_2-^{4}He system, thermal diffusion factor and quantum collision integrals, effect of inelastic collisions 2−56449
HI, mechanisms for vibrational relaxation 2−70704
H_2+H_2 reactive vibr. nonequil. effects 2−84627
I_2-He mixture, interaction of dissoc. and vibr. relax. behind shock wave 2−77168
I_2, magnetic quenching of fluorescence from vibrational levels in $B^3\Pi(O_u{}^+)$ state 2−77085
$La(NO_3)_3$, aqueous solution at 25°C, U.S. relaxation 2−53427
Li_2, charge density relax. during nucl. motion 2−60002
N_2-Na vibrational relaxation times in rapid expansion interpretation of Na line-reversal meas. 2−53102
N_2, anharmonic oscillator, time-dependent solutions for de-excitation rates 2−42913
N_2, microwave discharge, pink afterglow, vibrational relaxation 2−53255
N_2, tunable Raman excitation and vibr. relax. 2−53023
N_2, vibrational relaxation in collisions with $O(^3P)$ atoms 2−67416
NO $X^2\Pi$, rapid rate process meas. by kinetic spectroscopy during photolysis flash vibrational relaxation 2−54553
N_2O, thermal, of vibrations, period meas. by impact tube method 2−83398
N_2+N_2 collision, vibrational transition probabilities, temp. dependence below 300K 2−60117
O_2, collision with Ar, hot gas, rates of vibr. and dissoc. excitation, relax. eqn. 2−83417
O_2, tunable Raman excitation and vibr. relax. 2−53023
$O_2(^1\Delta_g)$ lifetime in solution, study of bimolecular loss processes 2−51464
O_2+O_2, collision, vibrational transition probabilities, temp. dependence below 300K 2−60117
$O_2\dagger+O(^3P)$ vibrational energy transfer, O_3 photolysis 2−51465
$Pr(NO_3)_3$, aqueous solution at 25°C, u.s. relaxation 2−53427
$Yb(NO_3)_3$, aqueous solution at 25°C, u.s. relaxation 2−53427
rotation
— 2−68583
— 2−67513
— 2−60028
acetonitrile, rotational diffusion in liquid, i.r. spectra 2−83323
acetonitrile, vibrational-rotational relaxation characteristics in liquid determ. from spectra 2−56474
acetyl bromide and chloride, barriers to internal rotation 2−77136
acetylene cryst., mol. motions, plastic behaviour 2−83881
acetylene-d_0, d_1, d_2, high resolution analysis of Raman-active fundamental bands 2−64166
acetylene-d_2 in CS_2 soln., ν_3 band profile analysis, temp. depend. 2−77135
adamantane, solid, proton spin-lattice relax. obs. 2−61563
adiabatic rapid passage spectra from slowly tumbling spin labels 2−83339
alkali halides produced in molecular beam reactions, determ. or rotational polarization and reprojection of angular momemtum 2−65367
alkylaromatic radical cations, e.s.r., methylene h.f. splitting interpret. 2−60046
n-alkylbenzenes, l.f. vibr. spectra interpret. rel. to rot. isomerism 2−56213
allyl chloride and bromide, rotational isomers 2−42952
2-aminopyridine, normal and deuterated, rotational constants from microwave spectra data 2−50077
asymmetric rotator, sum rules 2−42840
asymmetric rotor rot. consts., vibr. contrib. 2−56144
asymmetric rotor rot. spectra, internal rot.-quadrupole interaction 2−56143
asymmetric-top molecule in soln. effect of molecular shape and flexibility on γ-ray directional correlation for bound nucleus 2−51474
azabenzenes rot. mixing of excited electronic states 2−80099
1- azabicyclo[2.2.2]octane, torsional oscill. from microwave spectrum 2−42958
azulene, rotational microwave spectra of ground and vibrationally excited states 2−70744
benzene, solid, anisotropic nucl. spin relax. of ^{13}C 2−81310
benzenes, substituted, rotational analyses 2−67509
benzonitrile, vibrational-rotational relaxation characteristics in liquid determ. from spectra 2−56474
benzophenone, l.f. Raman spectrum, 300 and 30K, librational motions 2−81355
benzvalene, rotational transitions 2−77139
beryllium oxyacetate, polymorphism, -196°C to 286.7°C, pulsed n.m.r. investigation, study of molecular dynamics 2−57399
bicyclo[2.1.1]hexan-5-one, rotational constants of ground vibrational state 2−42964
bimolecular collisions, vibration-rotation Hamiltonian 2−46641
borazane, internal rot. barrier and localized charge distribs. 2−64171
2- and 4-bromo-pyridine quadrupole hyperfine structure in rotational spectrum 2−70754
bromoacetyl bromide, energy differences between rotational isomers by absolute i.r. intensity method 2−46598
d-camphor, solid, high press., n.m.r. obs. 2−51416
camphor, solid, molecular rotation at dielectric relaxation transition 2−61414

Molecules continued
rotation continued
camphor in polar solvents, vibrational spectroscopy, separation of vibrational and rotational relaxation terms 2−70757
carbamates, energy barriers to hindered rot. 2−60054
chloroacetyl chloride, energy differences between rotational isomers by absolute i.r. intensity method 2−46598
chloroform, liquid, calc. of orientation correlation functions from spectra 2−43363
o- chloropyridine, microwave spectrum, rot. consts. for vibr. ground state 2−53052
clathrate, possible transitions between rot. sublevels 2−54446
collision numbers, evaluation from thermal creep in gases 2−74484
collisional rotational energy transfer, acoustic meas. 2−64209
collisional rotational transitions 2−74301
collisions, rot. inelastic, exponential approxs. 2−56270
Coriolis, perturbations, in asymmetric top molecules, computer derivation 2−46508
crystal, neutron spectroscopy at high resolution 2−77607
cyanamide, analysis of microwave spectrum by rotation-inversion theory 2−80103
cyclohexane, cyclohexanol, cyclohexanone, liq., rot. correl. times 2−80446
cyclohexanol, crystalline, supercooled and plastic, dielec. relax. above glass temp. 2−81144
cyclopentanol, solid, unusual dielectric behaviour and molecular motion, dielectric and visual studies 2−57224
diatomic, calculation of vibration-rotation energies to sixth order of approximation 2−46512
diatomic, dependence of rotational constant B_v on long-range internuclear potential 2−46505
diatomic, perturbed by linear mols. with high moment of inertia, spectral line breadth 2−50011
diatomic, rotational excitation, effect of generalized phase shift expansion terms on classical limit of gas transport coefficients 2−43030
diatomic, spin uncoupling and transformation of half-integral spin states 2−79983
diatomic, vibr.-rot. spectrum in perturbation theory for Morse oscillator 2−67446
diatomic, vibration-rotation interaction effect on spectral line intensities, semiclassical treatment 2−70677
diatomic, vibrational and rotational excitation within an electronic transition induced by positive ion or electron impact 2−42865
diatomic gas in shock front and wake, relaxation equations for vibrational and rotational energy including transport processes and chemical reactions 2−52966
diatomic mol., multiplet struct. and centrifugal distortions, rot. energy levels 2−79991
diatomic mol., rot.-vibr. coupling and factorization method 2−64110
diatomic mol., vibr.-rot. intensities calc. by factorization method 2−64109
diatomic molecules, vibrational-rotational states, optimised calc. 2−56142
diatomic mols., vibr.-rot. interaction in diffusion theory of thermal decomp. 2−80059
diatomic species, split from 4-atom collision complex, rot. population distrib. 2−42864
dichloracetyl chloride, energy differences between rotational isomers by absolute i.r. intensity method 2−46598
1,4-dichloro-2-butyne, meas. of i.r. and Raman spectra, determ. of vibrational assignment, effect of internal rotation 2−53059
dichloromethane, rotational correlation times in liquid state from self-diffusion data 2−56472
diffusional model with variable collision distribution 2−74307
dimethyl ether, CH_3OCD_3, barrier to internal rotation 2−77144
N,N'-dimethyl-piperazine, ^{14}N quadrupole interaction, spin lattice relax., mol. motions 2−84603
dimethylnitrosamine, microwave spectrum analysis 2−80107
dimethylsulphide-d_6, rot. Zeeman effect 2−64177
1,3-dioxane, microwave spectrum analysis 2−64178
p-dioxane, vibrational-rotational relaxation characteristics in liquid determ. from spectra 2−56474
1,4-dioxane i.r. spectra, hindered pseudorotation, estimation of barrier height for half-chair inversion 2−70764
dipole molecule in fluid undergoing frequent collisions 2−74307
durene, hindered rotation in crystals by neutron transmission meas. 2−50999
equilibrium system, internal rot. effect on band contours in oscillation spectra 2−83239
1,2-ethane dithiol, Raman spectrum meas. in liquid and solid state, determ. of rotational isomerism 2−53061
ethanes, halogen substituted, vibr. spectra and barriers to internal rotation 2−50092
ethanol, ethanol-d_1, ethanol-He, microwave double resonance studies of collision-induced transitions 2−60118
ethanol, glassy, effect of dipole reorientation on trapped electron spectra, semicontinuum model 2−44495
ethyl alcohol, gauche, microwave rotational spectrum 2−80092
ethyl fluoride, barrier to internal rot., comparison with ethane 2−67513
ethylene, laser induced combination band luminescence, vibration-rotation energy transfer 2−60066
ethylene, rotational constants, determination from high resolution i.r. spectrum 2−50093
ethylene oxide, collision broadening of rot. lines by polar mols. 2−77115
ethylene sulphone, microwave rotational spectra, structure and dipole moment determination 2−60065
ethylene-d_2(-d_4), ground state rot. consts. 2−56229
ethylenes, methyl substituted, internal rotation barrier determination from Raman and i.r. spectra 2−60067
forbidden transitions between rotational levels of molecule, observational possibility 2−64104
2-furanaldehyde, conform., rot. isomerism, nematic-phase n.m.r. obs. 2−77147
furfural, electronic structure calc. for rotational isomers 2−50096
hexamethylbenzene, hindered rotation in crystals by neutron transmission meas. 2−50999
hindered, in various fields of cubic symmetry, Devonshire model 2−60564

Molecules continued
  rotation continued
    hydrocarbons, pair theorem and bipartite graph props. 2−53038
    hydrocarbons collisional rotational transitions 2−74301
    hydrogen halides, intensity of vibr.-rotation spectra, foreign gas density depend. 2−74263
    hydroxylamine, rot. consts., microwave spectra obs. 2−56234
    iminoxyl radical with ^{15}N isotope, reorientation models and e.s.r. lineshape 2−70773
    internal, rel. to atomic coordinates 2−64102
    inversion barriers, prediction by molecular orbital approximation 2−67445
    ketene, ground state rot. consts. 2−56238
    laser, effect of rotational relaxation on form of impulse 2−49354
    level crossing and level anticrossing in diatomic molecules 2−67449
    linear triatomic, K-type doubling in $^3\Pi$ electronic states 2−46510
    in liquids conditional fast rotational diffusion 2−60414
    in liquids relaxation, inclusion of arbitrary reorientation angles 2−80138
    macromolecule, fluorescence polarization dynamics 2−56266
    matrices in molecular theort, simple solution 2−77039
    methane, methane-d_4, in liquid Ar solutions, system dynamics investigation via collision induced far i.r. spectra 2−43372
    methane, microwave transitions in vibronic ground state 2−64096
    methane, of dissolved CH_3D, in liq. and plastic phases 2−80586
    methane, pure rotational spectrum arising from dipole moment due to centrifugal distortion 2−53072
    methane, studies on collision-broadened rotational lines in ν_4-fundamental 2−42999
    methane binary mixtures with He, Ar, Xe, ultrasonic absorption meas. of rotational relaxation 2−64219
    methane-d_1, i.r. spectrum, ground state constants, perturbation allowed transitions 2−77119
    methanol, barrier height in excited vibrational state, microwave spectrum obs. 2−56248
    methanol, isotopic, torsion-rotation spectra, moments of inertia, barrier heights, Kirtman perturbation constants 2−77124
    methanol and deuterated derivs., analysis of torsion-rotation spectra 2−67518
    methanol in excited CO stretching state, microwave spectrum, torsion-vibration-rotation interaction 2−67517
    methanol-d_4, microwave spectrum, torsion-vibration-rotation interactions 2−50100
    2-methoxyethanol, rotational constants, determination from microwave spectrum 2−50098
    methyl acetylene investigation of vibration-rotation bands in near infrared 2−70781
    methyl bromide, collision broadening of 0,0→1,0 rotational line by polar molecules 2−42996
    methyl bromide, isotopic splitting in pure rot. spectrum 2−70777
    methyl bromide collision broadening of o,o, rh 1.0 rot. line 2−83303
    methyl fluoride, nonlinear laser spectroscopy of i.r. vibr.-rot. system 2−53063
    methyl iodide, calc. of orientation correlation functions from spectra 2−43363
    methyl iodide, equilibrium structure determ. from rotation-vibration interaction constants from i.r. spectra 2−42995
    methyl iodide, i.r. spectra, fine structure 2−46611
    methyl iodide-d_3, consts. of vibrational states, i.r. spectra 2−46613
    methyl iodide-d_3, rotational fine structure of overtone and combination bands in vibrational spectrum 2−70782
    methyl isocyanide, rotational spectrum, hyperfine structure, high resolution meas. 2−56249
    methyl isocyanide of d_3-derivative, vibr.-rot. band analysis 2−70780
    methyl silane microwave spectrum, vibration-internal rotation- overall rotation interactions for symmetric-top molecules 2−70779
    methylammonium chlorides, solid, mol. and group motions, p.m.r. obs. 2−68750
    methylbromoform, microwave spectrum, rot. consts. 2−56243
    methylchloroform, librational motion, rel. to cryst. and mol. struct. at -60° and -145°C 2−53685
    methylchlorosilane, microwave spectrum obs. 2−64190
    methylene chloride, calc. of orientation correlation functions from spectra 2−43363
    methylene difluoride self-broadening of rotational lines meas. on double modulation microwave spectrograph 2−56242
    methyleneimine, mol. transient, microwave spectrum analysis 2−64186
    N- methylethylidenimine, microwave spectrum, internal rot. motions 2−64183
    3- methylthiophene, microwave spectrum, barrier height to internal rotation of methyl group 2−42997
    microwave absorption lines, barriers to internal rotation from relative intensity meas. of temp. 2−42943
    microwave double reson. line intensities for pump freqs. far from reson. 2−79984
    monochloroamine, rotational constants from microwave spectra data 2−46615
    myglobin in water, dielectric dispersion due to molecular rotation 2−46976
    N-atom, vibration-rotation energy operator including electron-nuclear interaction 2−77046
    NA, excited collision-induced rot. and vibr. transfer laser-induced fluoresc. obs. 2−83412
    near-symmetric rotor, Zeeman effect in doublet states 2−77064
    neopentane, plastic cryst., phase transitions cold neutron examination 2−50928
    neopentane, plastic crysts., mol. rot. motion 2−53513
    p-nitrobenzoic acid crystals, n.m.r. obs., rotational second moment at liquid nitrogen and room temp. 2−78167
    nitrosomethane, SCF-LCAO-MO calculations of barrier to internal rotation 2−70786
    1,3,4-oxadiazoles, isotopic species, centrifugal distortion consts. from microwave spectral data 2−43003
    trans 3-penten-1-yne, barrier to internal rotation, determination from microwave spectrum 2−50108
    periodic potential functions for pseudorotation and internal rotation, computer programme 2−64095
    phenylsilane, i.r. and Raman spectra 2−46623

Molecules continued
  rotation continued
    pivalic acid, plastic crystalline phase, Rayleigh and Brillouin scattering 2−44399
    polyatomic T_d, Stark effects and $\Delta J=0$ transitions 2−42844
    polyethylene glycol/water system, Mossbauer study of molecular motion at room temperature 2−72277
    polymers, low-temperature mechanical relaxation, assignment of molecular mechanisms 2−71557
    predissociation by rot. and long-range interactions 2−77041
    2-propanol, vibrational-rotational relaxation characteristics in liquid determ. from spectra 2−56474
    propiolic acid, microwave spectrum, hydroxyl group internal rot. 2−56256
    pyridine, rotational correlation times in liquid state from self- diffusion 2−56472
    reorientation, evaluation from Raman band shapes 2−59969
    reorientational correlation times, ratio for first and second rank spherical harmonics 2−56141
    rigid rotor, rotational excitation, classical results 2−50125
    rigid symmetric rotor, Stark perturbed energy levels 2−77028
    rotational excitations of three-particle systems 2−83236
    saturated molecules, Fourier component analysis of internal rotation potential functions 2−56208
    solid, random reorientation, influence of molecule symmetry 2−67880
    spectra, integral criterion of non-overlapping lines 2−56139
    spherical top mols., reorientation cross sections and spin-rot. consts. 2−56199
    spherical-top, rotational diffusion in liquids comment on paper by McClung (1969) 2−71178
    succinyl chloride, meas. of Raman spectrum in solid and liquid states, determ. of rotational isomerism 2−53079
    symmetric top mols., reorientation cross sections and spin-rot. consts. 2−56200
    symmetrical top angular relaxation, finite collision rough sphere model for resistance in bath of atoms 2−70808
    tetrahedral, Van Vleck perturbation theory applied to vibration-rotation interaction 2−42842
    tetrahedral mols., microwave transitions in vibronic ground state 2−64096
    tetrahedral mols., microwave transitions in vibronic ground state 2−64096
    tetroaldehyde, internal rot., effects on i.r. and electronic band contours 2−80093
    thioformaldehyde, microwave generation and characterization from rotational spectrum, detection in space 2−44888
    thioformaldehyde, obs. of high-field rotational Zeeman effect 2−43010
    trifluoro(trifluoromethyl)-silane, microwave spectrum and internal rot. barrier 2−83296
    trifluoroacetamide crystal, X-irradiated, analysis of internal rotation of CF_2CONH_2 radical obs. in e.s.r. spectrum 2−81526
    trifluoromethyl group, rotation barrier determ. from ^{19}F n.m.r. spectra 2−77113
    triglycine fluoroberylate, cryst., NH_3 group rot., rel. to e.p.r. 2−84575
    1,1,1-trimethoxyethane, rotational isomerism 2−43013
    trimethylsilylamides, study of rotational barriers 2−77110
    1,3,5trinitrobenzene charge transfer complex, cryst., mol. movements, proton mag. reson. 2−48308
    tropolone, near u.v. spectrum rel. to molec. structure, rotational band contour analysis 2−53085
    vibration-rotation interaction effect on molecular spectra 2−42841
    vibrational modes, rot. strengths 2−60040
    vibrational-rotational band, total band absorptance and absorption coefficient 2−56140
    vinylcyclopropane and vinylcyclobutane, internal rotation, ab initio MO description 2−83291
    XY_2 bent symmetrical, calculation of vibration-rotation energies to fourth order 2−46512
    o-xylene partially oriented in nematic phase, barrier to internal rot. 2−77157
    XYZ, bent molecule, vibration-rotation Hamiltonian 2−42843
    AlN, emission spectrum, rotational analyses and isotopic studies 2−42868
    Ar-N_2 collision, comparison of generalized phase shift with classical trajectory calcs. of rotational inelasticity 2−43032
    Ar-N_2 system, rot. relax. time, classical trajectory calcs. 2−77165
    Ar-N_2 system, rot. relax. time, GPS calc. 2−77164
    Ar_2, Van der Waals dimers, Raman spectra 2−80050
    AsF, near vacuum u.v. and near i.r., spectrum analysis 2−56154
    AsO radical, rot. analysis of $C^2\Delta$ and $D^2\Sigma^-$ states, C-state perturbations 2−74255
    AsS, $A/^2\pi_{3/2}-X^2\pi_{3/2}$ band system, vibrational analysis and rotational constants 2−77080
    B_2Cl_4 vapour, obs. of torsional mode in Raman spectrum excited by Kr laser 2−52993
    BH_3NH_3, SCF calcs. of internal rotation barrier and its derivatives 2−42873
    BaO, microwave rotational transition in short lived state obs. 2−67468
    BeH(D) λ doubling variation with rot. quantum no. 2−83261
    BeI, first excited state, rotational analysis 2−42872
    BiCl, rotational analysis of A-X band system 2−50024
    CH, oscillator strength of $A^2\Delta$-$X^2\Pi$ electron transition 2−59993
    CH, upper limits of rotational states studied using potential energy functions of Morse and Hulburt-Hirschfelder 2−46543
    CH, vibration-rotational levels determ. from potential curves and eqns. for motion of nuclei 2−56160
    CH^+, upper limits of rotational states studied using potential energy functions of Morse and Hulburt-Hirschfelder 2−46543
    $(CH_3)_2XH_n$, $(X=C$, Si, N, P, O, S), barriers to methyl rot., electronic origins, CNDO/2 calcs. 2−64182
    CN, $a^2\Pi$ and $B^2\Sigma$ rotational states, level crossing 2−67449
    CO_2-DF vibrational de-excitation on the basis of vibration-to-rotation energy transfer, 300-2000K 2−83406
    CO_2-H_2 mixtures, simultaneous vibr.-translation, vibr.-rot. and rot.-translation exchanges 2−53099

Molecules continued
rotation continued
CO, i.r. vibr.-rot. spectra, approx. calcs. of abs. coeffs., 300 and 1200 K 2−46534
CO, vibrational-rotational band, total band absorptance and absorption coefficient 2−56140
CO A $^1\Pi$ state, zero-field level crossing spectrosopy, obs. of fluorescence of resolved rotational features 2−70691
CO_2, i.r. vibr.-rot. spectra, approx. calcs. of abs. coeffs., 300 and 1200 K 2−46534
CO_2, laser source spectroscopy obs. of 00^01-$(10^00$-$02^00)_1$ band 2−74257
COS, centrifugal distortion and anharmonic potential constants 2−52997
CO_2-HF vibrational de-excitation on the basis of vibration-to-rotation energy transfer, 300-2000K 2−83406
CS, Hanle effect measurement of the lifetime of the $A^1\Pi$ vibration-rotation levels 2−42885
$^{13}C^{16}O$, $^{12}C^{18}O$, weak angstrom bands obs. 2−56157
1-chloro-3,3,3-trifluoropropyne, microwave spectra analysis 2−70759
ClNCO, microwave spectrum, rot. consts. 2−56165
ClO_2, $^2A_2 \leftarrow {}^2B_1$ transition, Zeeman effect 2−77064
ClO_2 adsorbed on CaX and NaX synthetic zeolites, preferred rotation 2−80579
^{35}ClF, hyperfine structure constants in $J=1$, $J=2$ rotational states using molecular beam electric resonance spectroscopy 2−74261
CsI, quadrupole h.f.s. on rot. transition 2−53003
CsI + Ar collisions, vibrational and rotational energy transfer, ballistic mechanism 2−67536
CuS, rot. consts. of (0,0) band in A-system 2−42887
D_2-He collisionally induced vibration, effect of rotational motion 2−80139
D_2-Ne Van der Waals complexes in collision-induced fund. bands of deuterium, spectra 2−64127
D_2, compressed, thermal cond.-relax, coupling, rel. to Rayleigh-Brillouin scatt. 2−56171
DBr, matrix-isolated, i.r. obs. at cryogenic temp., hindered rotation 2−68637
DOF, i.r. spectra, vibr.-rot. analysis 2−77062
1,2-dibromoethane, i.r. spectra study of medium effect on rotational equilibria 2−78109
2,3-dihydropyran i.r. spectra, hindered pseudorotation, estimation of barrier height for half-chair inversion 2−70764
$F_3P.BH_3$ and $F_2HP.BH_3$, barriers to internal rotation, CNDO/2 calculations 2−53032
FeO, absorption coeff. for i.r. vibration-rotation spectrum 2−42890
GaCl, hyperfine structure in spectrum 2−46540
GeF_2 microwave spectrum, effect of centrifugal distortion on rotational transitions, determ. rotational consts. in vibrational states 2−70698
GeH, multiplet struct. and centrifugal distortions, rot. energy levels 2−79991
GeH_3F, GeD_3F, rotational constant determination from microwave spectrum 2−60001
H_2-He collisionally induced vibration, effect of rotational motion 2−80139
H_2-Ne Van der Waals complexes in collision-induced fund. bands of hydrogen, spectra 2−64127
H_2, compressed, thermal cond.-relax. coupling, rel. to Rayleigh- Brillouin scatt. 2−56171
H_2, effects of rotational autoionization on angular distrib. of photoelectrons 2−50045
H_2, isotopic, rotational relaxation effects on sound absorption 2−46858
o-H_2, rot. relax., 170-300K, sound absorpt. meas. 2−80909
H_2, rot. relax. times, 140-450K 2−46550
H_2, rotational Raman lines, anisotropy of Dicke narrowing 2−42893
H_2, screening and polarization effects on vibration-rotation-props. 2−64130
o-H_2, solid, f.c.c. and h.c.p. phases, transitions between rot. states 2−64839
H_2, upper limits of rotational states studied using potential energy functions of Morse and Hulburt-Hirschfelder 2−46543
H_2, vibrational and rotational analysis of eight simple models 2−46549
H_2 hyperfine structure of $N=1$ rotational state of $^3\Pi_u$ electronic state 2−64137
H_2 in He and Ne, rotational relaxation, approx. soln. to Boltzmann eqn. 2−80137
H_2^+, upper limits of rotational states studied using potential energy functions of Morse and Hulburt-Hirschfelder 2−46543
HBr in condensed phases, first harmonic of vibration-rotation spectrum 2−53014
HBr in condensed phases, spectra of vibration rotation fundamental 2−53013
HBr in condensed phases, second harmonic of vibration rotation spectrum 2−53015
HCP, calc. of K-type doubling in $b^3\Pi$ electronic states 2−46510
HCl, in SF_6 solution, i.r. absorption bands, effect of vibration-rotation interaction 2−42841
HCl, population on vibr.-rot. levels during $NOCl + H_2$ reaction 2−53005
HCl in condensed phases, first harmonic of vibration-rotation spectrum 2−53014
HCl in condensed phases, spectra of vibration rotation fundamental 2−53013
HCl in condensed phases, second harmonic of vibration rotation spectrum 2−53015
HD, compressed, thermal cond.-relax. coupling, rel. to Rayleigh- Brillouin scatt. 2−56171
HD, rotational transitions in low-energy HD-He collisions 2−46644
HD in He and Ne, rotational relaxation, approx. soln. to Boltzmann eqn. 2−80137
HDO, rotational dependence of dipole moment determ. from Stark effect meas. on microwave transitions 2−80045
HF, anisotropic ultrahigh gain emission by optical pumping 2−50047
HF, perturbed by compressed gases, rot. line broadening 2−53006
HF, spin-rotation interactions 2−42907
HF, vibration-rotation level population during elementary act of $F + H_2$ reaction 2−66750

Molecules continued
rotation continued
HF in He, rotational relaxation, approx. soln. to Boltzmann eqn. 2−80137
H_2-^4He system, thermal diffusion factor and quantum collision integrals, effect of inelastic collisions 2−56449
HNO, rotational constants and centrifugal distortion 2−50034
H_2O, calculation of spectral intensities using vibrational rotational interaction data 2−74265
$H_2{}^{18}O$, rotational spectrum in ground vibrational state, study by submillimeter microwave spectroscopy 2−70706
H_2O_2 interpretation of barriers to internal rotation 2−83249
HOF, i.r. spectra, vibr.-rot. analysis 2−77062
HSSH, direct obs. of anomalous K doubling caused by centrifugal distortion 2−64131
HTO, microwave spectrum, rot. consts. of fund. state 2−83242
HTO, ν_1 and ν_3 levels determ. by i.r. spectrum, rot. consts. of fund. state 2−79997
HeH^+, electron correl. influence 2−64139
HfO, r-centroids for 12 band systems 2−77069
$HgAr^+$, analysis of u.v. emission spectrum 2−46553
$HgAr^+$, rotational energy levels, example of Hund's coupling case (c) 2−50048
HgH, quasibound vibr.-rot. levels obs. from orbiting resons. in Hg + Hg scatt. 2−77018
I_2, 5145Å excited anti-Stokes resonance Raman spectra, vibrational-rotational structure 2−77086
I_2, rot. Lande factors in $B^3\Pi_{0(\|)(u)}$ state 2−50049
I_2 levels excited by Kr ion laser, quantum nos. 2−80016
I_2 vapour, vibr.-Rot. struct. in reson. Raman effect 2−80037
ICl, coupling constants 2−42902
$^{127}I_2$, $^{129}I_2$, magnetic spin-rotation interaction rel. to hyperfine interactions in optical transitions 2−50050
IrO, band spectrum, 4200 to 6400 Å 2−77065
$La^{18}O$ emission spectrum at 5600 Å, determ. of rotational constants of $B-X$ band system 2−80019
Li complex, Li^+-H_2O, H_2O rotational energy 2−60010
LuH, electronic band systems analysis, 4200 and 5000 Å 2−74268
Mg_2, Franck-Condon factors in A-X system, rot. depend. 2−64141
N_2, active, vacuum u.v. emission, form. and removal of $N_2(a^1\Pi_g)$ 2−70716
N_2, c_n $^1\Pi_u$ and c_n' $^1\Sigma_u{}^+$ Rydberg states, high resolution studies 2−64145
N_2, consts. of lowest $^1\Sigma_g{}^+$ state 2−42915
N_2, distribution function at high vibrational temp. in electron beam fluorescence technique 2−56188
N_2, Gaydon- Herman green system, rot. analysis 2−64146
N_2, vibration-rotation interaction in calculated band strengths 2−46571
N_2 low-energy electron scattering, rotational excitation cross sections predicted using pseudo-potential model 2−70819
N_2 Raman rotational spectra, use of fixed path length etalon Fabry-Perot interferometer for meas. of wavelength of individual lines 2−74250
N_2^+, produced in slow electron ionization of N_2, rotational level distrib. 2−80053
NCN_3, microwave spectrum 2−60014
NCNNN, microwave spectrum analysis 2−64142
NH_3, inversion spectrum, rotational structure 2−80033
NH_3, transient-nutation effects in time-resolved i.r.-microwave double resonance 2−64147
NH_3 in Ne matrix, i.r. spectra obs. 2−72340
NH_3 spectral lines, collision-broadened by hydrogen, shapes and widths 2−67493
NH_4Cl, cryst. field hindering of ammonium ion, low temp. spin-lattice relax. 2−84447
NH_4ClO_4, solid, spin-rot. relax. for protons 2−54371
$(NH_4)_2S_2O_8$, hindered rotation in crystals by neutron transmission meas. 2−50999
$(NH_4)_2SiF_6$, hindered rotation in crystals by neutron transmission meas. 2−50999
NH_4SnCl_3, proton relax. of ammonium ion undergoing hindered rot., cross correl. effect 2−84448
$(NH_4)_2SnCl_6$, cryst. field hindering of ammonium ion, low temp. spin-lattice relax. 2−84447
NO, i.r. study of R(15/2) vibration- rotation transition 2−46561
NO, rotation-electronic spectrum 2−64166
NO_2, laser magnetic resonance at 311 and 337 μm 2−42912
N_2O band intensities and half-width of N-broadened lines rotational lines in ν_3 fundamental meas. near 4.5 μ 2−42923
$^{14}NH_3$ and $^{15}NH_3$, i.r. vibration-rotation spectra, 2-photon spectroscopy 2−42920
Na_2, electronically excited, meas. of collision-induced rotational energy transfer in $B^1\Pi_g$ state 2−56274
NaK, constants determ. from laser-induced resonance fluorescence 2−64149
$NaNH_2$, solid and molten, evidence for hindered rotation of NH_2- ion from laser Raman spectra 2−60022
No, i.r. vibr.-rot. absorpt. spectrum, nucl. hyperfine splitting 2−64143
O/heavy metal atom ratio meas. in unirradiated mixed Pu/U oxides reactor fuels 2−74154
O_2, molecular parameters 2−42927
O_2 Raman rotational spectra, use of fixed path length etalon Fabry-Perot interferometer for meas. of wavelength of individual lines 2−74250
O_2^- labile ions, stimulated emission during d.c. discharge 2−46793
O_2^+, spin-orbit coupling const. in $A^2\Pi_u$ state determ. from rotational term values of 1-7 and 0-8 bands 2−70721
O_3, rigid rotor upper state rotational constants 2−64153
OD, wavenumbers of $A^2\Sigma \rightarrow X^2\Pi$ (0, 0) and (1, 0) bands 2−67497
OH, OD free radicals, laser oscill. in pure rot. transitions 2−56192
OH, vibration-rotation interaction in calculated band strengths 2−46571
OH, wavenumbers of $A^2\Sigma \rightarrow X^2\Pi$ (0, 0) and (1, 0) bands 2−67497
OH emission spectra, intensity variations, vibrational and rotational temps. 2−46572
OH rot. temp. in nightglow 2−54882
OH rotational temp. meas. in Ar luminescent-arc discharge 2−43210

Molecules continued
rotation continued
$OH(A^2\Sigma^+, v'=0)$, rotational excitation from dissoc. collision of H_2O with metastable Ar 2−64215
$OH(A^2\Sigma^+)+Ar$, near resonant vibration-rotation energy transfer calc. of cross sections and rate consts. using IOS and DW approx. 2−70818
$OH(^2\Sigma^+)$ radicals, rotationally excited, formation in water vapour discharge 2−60027
PF_5, pseudorotation calc. using semiempirical MO methods 2−53034
PH_2, A^2A_1-X^2B_1 transition, analysis of bands 2−83241
PH_4 radical trapped in solid Kr, energy barrier to pseudorot. 2−64154
PO, analysis of some bands of β system 2−42931
PO, vibrational and rotational analysis of emission spectrum in 1850-2350 Å region, $C^2\Sigma$--$X^2\Pi_r$ transition 2−46573
PO γ-system, localization of rot. perturbations in first vibr. levels 2−79995
$P^{16}O$, and $P^{18}O$, rot. analyses and deperturbations of visible systems 2−79996
$^{31}P^{14}N$, millimetre wave rotational spectrum, molec. constants 2−60029
PbF, rotational analysis of (1,0), (0,0) and (0,1) bands of $B-X_2$ system 2−79994
Rb-Ar, Rb-Kr, Van der Waals molecules spin orbit interact. strength on vib.-rot. state, r.f. field obs. 2−56194
SF_6 reorientation in its clathrate deuterate, determ. of activation energy 2−72531
SF_4O, constants, S-O distance by microwave studies 2−70723
SH, second rotational level, Λ-doubling transition frequencies 2−46579
SO, $b^1\Sigma^+-X^3\Sigma^-$ transition, band structure 2−70724
SO_2, π^*-π (2350 Å) band system analysis 2−64155
SO_2, tunable-laser spectroscopy of vibr.-rot. band transitions 2−60033
$SOBr_2$, rot. distortion consts. 2−56169
$SO^{35}Cl^{37}Cl$, rot. spectrum analysis 2−60032
SOF_2, microwave spectrum and harmonic force field 2−80036
$^{18}SO_2$, vib.-rot. interaction consts. 2−56201
Sb_2, analysis of $B\rightarrow X$ system 2−50068
SiBr, emission spectrum, B-X system analysis 2−77060
SiI absorption spectra, 4200-4900 Å region, rotational analysis of new band system 2−70726
SiO, $A\rightarrow X$ band system, vibr.-rot. analysis 2−83248
SiO, interstellar, detection of $J=2\rightarrow1$ rotational transition 2−58358
SiO, transition probabilities for vibration- rotation bands 2−48696
SiO^+ electronic spectrum, vibr. and rot. anal. 2−77056
$^{28}SiH_3D$, ground state rotational constants determ. from high resolution i.r. spectra 2−64157
$^{28}SiH_4$, high resolution i.r. meas. on ν_3 vibr.-rot. band 2−80039
SnF, rotational structure and isotopic shift in (1,0) band of $(A-X)$ system 2−77093
SnH(D), multiplet struct. and centrifugal distortions, rot. energy levels 2−79991
T_2O, microwave spectrum, rot. consts. of fund. state 2−83242
TeS, gaseous, electronic spectrum, rot. struct. of bands 2−64158
ThO, r-centroids for 12 band systems 2−77069
TiO, u.v. bands, vibr.-rot. consts. 2−80042
vibration
3,3-bromomethyldiazirine, absorption spectra, vibrational analysis 2−50089
3,3-chloromethyldiazirine, absorption spectra, vibrational analysis 2−50089
⩽cis-]glyoxal, determ. by microwave spectrum 2−83300
— 2−60028
— 2−80950
— 2−64127
acenaphthene-d_{10}, i.r. spectra 2−60043
acenaphthene-h_{10}, i.r. spectra 2−60043
acenaphthylene, i.r. spectra 2−60043
acetic acid, O−H overtone bands and pot. energy curves 2−56211
acetone, coupling of motion between methyl groups studied by normal coordinate analysis using Urey-Bradley force field 2−56210
acetone ($-d_6$), polycrystalline, Raman spectra, assignment of methyl vibrations, determ. of torsional frequency splitting 2−72374
acetone oxime, vibrational assignment, torsional vibration 2−50073
acetonitrile, vibrational-rotational relaxation characteristics in liquid determ. from spectra 2−56474
acetyl fluoride vibrational spectra in-phase and out-of-phase stretches 2−83314
acetylene-d_0, d_1, d_2, high resolution analysis of Raman-active fundamental bands 2−64166
acetylene-d_2, assignment of spectrum near 18.6 μm 2−46592
acetylene-d_2 in CS_2 soln., ν_3 band profile analysis, temp. depend. 2−77135
acetylenic derivatives of Si, Ge, Pb, P, As, Sb, i.r. and Raman spectra vibr. assignment 2−56212
acridine and acridinium, i.r. and Raman spectra, vibr. assignment 2−60044
acrylonitrile-styrene copolymers, stretching mode of acrylonitrile units from i.r. spectra 2−67528
acyl peroxides, depend. of C−O−O−C chain vibrs. on mol. spatial struct. 2−83327
additive interatomic interaction model 2−77044
alkenoxyderivatives of silicon, frequencies and intensities of C=C vibrational bands 2−53045
alkyl isocyanates, integrated intensity of valence vibrations 2−74290
n-alkylbenzenes, l.f. vibr. spectra 2−56213
allyl chloride and bromide, rotational isomerism and vibrational spectra 2−42952
alternant molecules of finite length, calc. of frequencies by perturbation method 2−74254
amines, primary H bonding effects on stretching frequencies 2−83266
amino acids, high resolution laser Raman spectra, study of S-S vibrations 2−83337
o-, m-, p-aminobenzaldehydes, i.r. absorpt. and Raman spectra assignments 2−56214
Molecules continued
vibration continued
m- aminobenzotrifluoride, i.r. spectra, fund. vibr. assignment 2−56215
2-aminopyridine, normal and deuterated, assignment of microwave spectra 2−50077
anharmonic oscillator model, hypervirial and Hellmann-Feynman theorems 2−64093
anharmonic oscillator-atom collision vibrational excitation cross-section 2−80124
aniline vapour, vibrational analysis of absorption bands in resonance fluorescence spectra 2−70742
9,10-anthraquinone and 9,10-anthraquinone-d_8, planar vibrs. calc. 2−67506
aromatic acid halides, i.r. spectra, stretching frequencies 2−70743
aromatic hydrocarbons, vibrational coupling strengths for intramolec. non-radiative transitions 2−42954
aromatic mols., isotropic shifts of electronic origins and ring vibrs. 2−56207
aromatic mols., vibronic coupling in emission spectra revealed by crystal field distortion 2−75243
aryl isocyanates, integrated intensity of valence vibrations 2−74290
asymmetric rotor rot. consts., vibr. contrib. 2−56144
atom-molecule collision, reactive, optical model for vibrational relaxation 2−65362
1- azabicyclo[2.2.2]octane, torsional oscill. from microwave spectrum 2−42958
cis-azobenzene, IR and Raman spectra 2−53048
azomethane, azomethane-d_6, vibrational assignments from i.r. and Raman spectra 2−42957
cis-azoxybenzene, IR and Raman spectra 2−53048
trans-azoxybenzene and isotopic derivatives, i.r. and Raman spectra, vibr. assignment 2−56217
azulene, rotational microwave spectra of ground and vibrationally excited states 2−70744
azulene in frozen n-pentane, fundamental vibration in vibronic transitions in fluorescence spectrum 2−53046
azulene in frozen n-pentane, quasilinear vibrational structure of second electronic transition in absorption spectrum 2−50079
benzaldehyde vapour, active out-of-plane modes in $^1A''(n\pi^*)\leftarrow S_0$ 2−80097
benzene, calc. of relative strengths of vibrational structure lines of $^1A_{1g}\rightarrow{}^1B_{2u}$ band in absorption spectrum 2−42962
benzene, local mode model calc. Franck-Condon factors for predissoc. 2−80079
benzene, Urey-Bradley repulsive force const., quantum mech. estimation 2−83328
benzene, u.v. spectrum, vibrational structuring of magnetic circular dichroism 2−70751
benzene and benzene-CCl_4 charge transfer complexes, l.f. Raman spectra, assignments 2−81351
benzene chromium tricarbonyl-d_6, $-h_6$, Raman and i.r. spectra 2−70752
benzonitrile, vibrational-rotational relaxation characteristics in liquid determ. from spectra 2−56474
5,6- and 7,8- benzoquinoline trapped in n-paraffins at 77K, vibrational analysis of quasilinear luminescence spectra 2−50080
benzoyloxyimino-4 tetrahydroquinazolines and hexahydropyrimidines, i.r. absorpt. obs. 2−53049
bimolecular collisions, vibration-rotation Hamiltonian 2−46641
borazine, gaseous, 2000Å absorpt. system, analysis 2−80090
bridge, coordination number 2, applic. of equations characterizing vibrational behaviour 2−59973
bridge, coordination number 2, derivation and verification of equations characterizing vibrational behaviour 2−59972
bromoacetylene, electronically excited, competition between photon emission and photodissociation 2−42969
bromoanisole, o- and m-, vibration frequency assignment 2−74283
2-bromoethanol, normal coordinate analysis on rotational isomerism 2−42981
3,3-bromomethyl-d_3-diazirine, analysis of $\pi^*\leftarrow n$ transitions 2−50087
bromothiophene, vibrational analysis 2−60087
butadienetricarbonyliron vibrational spectra in gaseous, solution, liquid and solid phases, factor group analysis 2−70755
camphor in polar solvents, vibrational spectroscopy, separation of vibrational and rotational relaxation terms 2−70757
carbon tetrachloride, Raman spectra, force field 2−74289
carbonyl group, theory of valence vibration spectrum 2−60056
carboxylic acid hydrazides, valence oscillations of N-H group at i.r. spectra 2−42967
carboxylic acid salts, i.r. and Raman spectra, vibr. assignment 2−60085
Cartesian symmetry coords., automatic eval. 2−59968
3-chloro-1,2,5-thiadiazole, vibrational spectra 2−42968
chloroacetylene, electronically excited, competition between photon emission and photodissociation 2−42969
2-chloroethanol, normal coordinate analysis on rotational isomerism 2−42981
chloroform, cryst. films, i.r. spectra in polarized light 2−84484
chloroform, liquid, vibration-rotation bands, calc. of orientation correlation formation 2−43363
3,3-chloromethyl-d_3-diazirine, analysis of $\Pi^*\leftarrow n$ transitions 2−50087
chlorostyrenes, i.r. absorpt. bands, vibr. assignment 2−56225
chromates of divalent transition metal compounds, i.r. vibrational spectra, calc. of force constants 2−70678
α-chymotrypsin, conformationally dependent low-frequency motions from laser Raman spectra 2−56268
clathrates of $Ni(4\text{-methylpyridine})_4(NCS)_2$ complex study of splitting of out-of-plane CH vibration band by i.r. spectroscopy 2−53053
collision, inelastic, between structureless atom and harmonic model molecule, exact classical treatment of vibration- translation energy transfer 2−50127
complex molecules, effect of solvent on electronic vibrational spectra 2−74253
complexation, increase of vibrational atomic mean square cartesian displacements 2−70660
congruence method, convergence 2−59977

Molecules continued
vibration continued
Coriolis, perturbations, in asymmetric top molecules, computer derivation 2−46508
crotonaldehyde, vibrational spectra 2−67503
2-cyanoethanol, normal coordinate analysis on rotational isomerism 2−42981
cycloalkanes, stretching vibrations of methylene group and ring strain 2−42972
cyclobutanecarboxylic acid, vibrational spectra 2−42973
cyclopentadienyl and pentadeuterio and pentachloro derivatives, vibronic interaction effects 2−50090
cyclopentane-d_0 and -d_{10} cryst., vibr. assignment 2−84485
cyclopentene, Raman spectra, ring puckering vibrations 2−43005
cyclopentene, Raman spectrum, ring- puckering vibr. freqs. 2−60058
deformation vibrations, semiclassical electrostatic mode 2−50000
diacetyl, vibrational spectra 2−67503
dialkylureas, i.r. spectra, determ of molecular configurations from vibrational band assignments 2−70766
diatomic, calc. of ground-state force constant in dielectric model 2−70652
diatomic, calculation of vibration-rotation, energies to sixth order of approximation 2−46512
diatomic, dependence of rotational constant for vibrational levels near dissociation limit on long-range internuclear potential 2−46505
diatomic, effect of VV transfer processes on rate of thermal dissociation 2−67456
diatomic, electron-vibratory band, Ludenburg-Levy function analogue 2−70661
diatomic, tunable Raman excitation and vibr. relax. 2−53023
diatomic, vibr.-rot. spectrum in perturbation theory for Morse oscillator 2−67446
diatomic, vibration-rotation interaction effect on spectral line intensities, semiclassical treatment 2−70677
diatomic, vibrational and rotational excitation within an electronic transition induced by positive ion or electron impact 2−42865
diatomic gas in shock front and wake, relaxation equations for vibrational and rotational energy including transport processes chemical reactions 2−52966
diatomic mol., Born-Oppenheimer approx. breakdown rel. to force const. determ. 2−56151
diatomic mol., rot.-vibr. coupling and factorization method 2−64110
diatomic mol., vibr.-rot. intensities calc. by factorization method 2−64109
diatomic molecules, probability of vibrational state change 2−83416
diatomic molecules, vibrational-rotational states, optimised calc. 2−56142
diatomic mols., collisional vibr. transition probabilities calc. method 2−80122
diatomic mols., electronic-vibr. energy transfer, vibr. distrib., i.r. fluoresc., Hg*-sensitized 2−59988
diatomic mols., vibr.-rot. interaction in diffusion theory of thermal decomp. 2−80059
diatomic oscillator-atom collisions, influence of a attractive forces on quantum mechanical transition probabilities 2−77169
diatomic oxides and sulfides, gaseous, bond energies and force constants, stabilities 2−64107
diatomic species, split from 4-atom collision complex, vibr. population distrib. 2−42864
dibenzanthracenes, i.r. and Raman spectra interpret. 2−53055
2,6-dibromoaniline, fundamental frequencies 2−77145
p-dibromobenzene, vibr. analysis of 2800 Å band system 2−56228
1,4-dichloro-2-butyne, meas. of i.r. and Raman spectra, determ. of vibrational assignment, effect of internal rotation 2−53059
p-dichlorobenzene, phosphorescence microwave double resonance studies of $^3\pi\pi^*$ state 2−60060
dichloroethane, chem. activated, vibr. energy transfer probabilities, collisional deactivation 2−83409
dichloroethane-d_0 and -d_4, chem. activated, cascade deactivation and nonequil. kinetic isotope effects 2−83408
difluoromalonitrile, force consts. and pot. energy distrib. 2−70775
2,3-dihydrofuran, microwave spectrum 12.4-40 GHz, Q- and R-branch assignments for ground and excited states of ring-puckering mode 2−42978
2,5-dihydrofuran, Raman spectra, ring puckering vibrations 2−43005
dimer composed of 2 biphenylene subunits, low frequency torsional modes coupling monomer sites 2−46509
o-dimethoxybenzene, vibration mode assignments from Raman, i.r. and u.v. spectra 2−80081
dimethyl ether and deuterated compound, normal cond. analysis, determ. of mean amplitudes of vibration 2−53058
dimethyl selenide and deuterated compound, normal cond. analysis, determ. of mean amplitudes of vibration 2−53058
dimethyl sulfates vibrational, spectra, i.r. and Raman 2−83317
dimethyl sulphide and deuterated compound, normal cond. analysis, determ. of mean amplitudes of vibration 2−53058
1,1-dimethylhydrazine-monoborane, spectroscopic study, determ. of molecular structure, vibrational assignments 2−53057
dimethyliodoarsine, liq., normal modes of vibrs., freq. assignment 2−77141
dimethyloxalate, electronic states from absorption spectra 2−42980
2,4-dimethylpentyl-2*(-d_1*) vibrationally excited collisional de-excitation by H_2, D_2, CF_4 2−46648
2,5-dimethylphenol, vibr. assignments for obs. freqs. of i.r. spectrum 2−77101
dimethylphenols, 2,3, 2,5 and 3,5, u.v. spectra, vibrational analyses 2−74294
dimethylphenols, 2,4- and 2,6-, Raman and i.r. spectra 2−74293
2,3- and 3,5- dimethylphenols, Raman and i.r. spectra, assignment of obs. freqs. to modes of vibration 2−60059
dimethylselenone, vibrational analysis 2−77143
dimethylselenoxide, vibrational analysis 2−77142
1,3-dioxane, microwave spectrum analysis 2−64178
p-dioxane, vibrational-rotational relaxation characteristics in liquid determ. from spectra 2−56474
diphenyls, Raman and i.r. spectra 2−53056
disilyl methane and deuterated compound, normal cond. analysis, determ. of mean amplitudes of vibration 2−53058

Molecules continued
vibration continued
electron-vibrational dipole scatt. phenomena 2−80126
energy transfer process in collisions between diatomic mols. 2−50123
enzymes, high resolution laser Raman spectra, study of S-S vibrations 2−83337
equilibrium configuration, refinement of molecular effective force fields and structures to complete force field and structure 2−46517
equilibrium system, internal rot. effect on band contours in oscillation spectra 2−83239
ethane, force constant calc. using MINDO/2 potential surface 2−77126
ethane, potential functions calc. in terms of group valence force symmetry coordinates 2−42847
ethane derivatives, torsional oscill. freq. calcs. by atom-atom approach 2−42982
ethanes, halogen substituted, vibr. spectra and barriers to internal rotation 2−50092
ethyl thiocyanate, fundamental vibrations 2−42983
ethylamine, deuterated, Raman spectra analysed w.r.t. amino group vibration 2−46610
ethylene, Coriolis interactions, determination from high resolution i.r. spectrum 2−50093
ethylene, laser induced combination band luminescence, vibration-rotation energy transfer 2−60066
ethylene, normal coordinate analysis 2−70665
ethylene oxide (-d_4 oxide), i.r. and Raman spectra, assignment of normal vibrations and normal coordinate analysis 2−42984
ethylenediamine and deutero derivative, infrared, Raman vibrational spectra 2−77106
ethylenes, methyl substituted, torsional barrier determination from Raman and i.r. spectra 2−60067
expectation values, vibrational and vibrationally averaged structure 2−49999
ferrocene, electron spectrum, progressions in ν_4 2−64187
ferrocene, force const. calcs. 2−64181
ferrocene, symmetry coordinates, harmonic force field, and mean amplitudes 2−42985
fluoromethane, solid, i.r. absorpt. spectra, symmetrical and doubly degenerate modes 2−57356
fluoroperoxides, O-O stretching frequency identification by Raman obs. 2−56232
force const., matrices, prop. satisfying vibr. eqns. of two isotopic species 2−82219
force const. calc., approx. methods 2−64092
force const. solns. with singular jacobian, extremal nature 2−59965
force constant and normal coordinate calc. using fundamental oscillation frequencies on spectral data 2−52972
force constant calculation using generalized inverse matrix 2−59971
force constant solutions with singular jacobian extremal nature 2−49996
force constants, calc. by approximate molecular orbital method 2−70670
force constants, calc. by Green's function approach and L-matrix approx. method 2−49998
force constants, calculation from X-ray or electron diffraction data 2−77043
force constants, constraint for calc. using Green's function formalism 2−46506
force constants, improvement in Fletcher-Powell method of refinement 2−64121
force constants, quadratic, implication methods for determination 2−67450
force fields prediction using extended Huckel theory 2−79985
formaldehyde, all-electron calc. of potential surfaces 2−42987
formaldehyde, potential surfaces, all-electron nonempirical calc. 2−42988
formamides, deuterated, assignment of Raman spectra 2−50095
formic acid, O−H overtone bands and pot. energy curves 2−56211
formyl-2(3) furan and thiophene, valence vibr. band, splitting obs. 2−83283
Franck-Condon factor for o-v transitions, by Morse oscillator model 2−52962
Franck-Condon factor for radiationless transitions, using Morse oscillator model 2−52963
fringe shift and fringe slope band analysis procedures 2−49992
fulminic acid, u.v. absorpt. spectrum, gas phase, ground-excited state transition 2−80098
furan, solid phase, fund. vibrs. assignment from i.r. spectra 2−72355
furane derivatives, 2-substituted, fundamental frequencies 2−77146
group theoretical considerations 2−61069
group theory applic. and irreducible representations of a point group 2−64825
group V halides, Coriolis coupling constants 2−64122
group VI B metal carbonyls, cis-subst. derivatives, CO stretching spectra and force constants 2−80043
haloacetonitriles, normal co-ordinate calculations of force constants and normal vibrations 2−50097
halogenosilane bis-pyridine and o-phenanthroline complexes, vibr. spectra 2−77081
harmonic force constants, ab initio calc. using two-electron SCF wavefunctions 2−59967
harmonic system, consistency requirements for vibr. props. 2−74964
heterocyclic, 5-membered saturated ring, spectral transitions 2−46589
hexahalide anions of O_h symmetry, orbital valence force field 2−42903
hexamethylbenzene, absorption spectra, vibronic bands 2−51351
hexamethyldisiloxane, isotropic shifts in vibrational spectra by CD_3 substitution, force constant calc. 2−46632
hydrocarbons, aromatic, non-Born−Oppenheimer coupling and D effect on $T_1 \rightarrow S_0$ radiative transitions 2−43002
hydrogen halides, intensity of vibr.-rotation spectra, foreign gas density depend. 2−74263
inner coordinates, role of topological properties in the determ. of redundancy conditions 2−52960

Molecules continued
  vibration continued
    inverse vibrational problem, perturbation treatment of physical solution 2−59974
    1-iodoalkanes, obs. of vibrational structure in B, C, D, E bands of far u.v. spectra 2−74292
    ion-dipole collisions, computer plotter studies of vibrational effects, classical tunnelling 2−46467
    isocyanates, integrated intensity of valence vibrations 2−74290
    isoelectronic series for diatomic molecules, charge density and bond length changes 2−56136
    isothiocyanate, determ. of molecular dimensions and large amplitude vibration by electron diffraction 2−80080
    isotopic, force constants 2−46507
    isotopically substituted mols., mass effect on Coriolis coupling consts., perturbation theory 2−64094
    isotropically substituted molecules, effect of inaccurate assignments, by least squares method 2−46500
    ketene, ground state centrifugal distortion consts. 2−56238
    kinematic models of a force field 2−52976
    laser, effect of rotational relaxation and original degree of inversion on form of impulse 2−49354
    linear homopolymers and copolymers, analysis of vibrational spectra by Green's function method, effect of defects 2−43021
    linear molecules in nonpolar buffer gas, collisional broadening of rotational absorption spectrum 2−67535
    linear triatomic, anharmonic deformation vibrations and overlap integrals 2−59976
    linear triatomic, K-type doubling in $^3\Pi$ electronic states 2−46510
    liquid, binary collision model of vibrational relaxation 2−53388
    in liquids, direct measurement of vibrational lifetimes 2−42846
    long range force vibr. energy transfer and off-reson. transfer 2−64207
    M_2O_7 systems with C_{2v} symmetry, normal coordinate analysis 2−77079
    macromolecules, analysis of normal vibrations by digital computer, models of interactomic force field for analysis of vibrational spectra 2−43017
    malonitriles, normal coord. analysis, G matrix elements 2−70774
    mean amplitudes, calc. from experimentally observed frequencies, stepwise coupling method 2−59975
    mean amplitudes and correction coeffs., computation method 2−67444
    mean square amplitude matrix, low-temperature limit 2−59970
    mercury(I), (II) acetate compounds, vibrational spectra, stretching frequencies determ. 2−46608
    metastable isomeric nuclear levels, energy meas. by laser spectroscopy of mol. vibr. transitions 2−79713
    methane, 3.39 μm transition, laser freq. and wavelength meas., speed of light 2−78758
    methane, studies on collision-broadened rotational lines in ν_4-fundamental 2−42999
    methane, vibrational band of Raman spectra, use of pressure-scanned Fabry-Perot interferometer for high resolution 2−74250
    methane $^{12}CH_4$, interpretation of the F_2 sub-level of the $2\nu_3$ harmonic band 2−64188
    methane-d_3, force constants 2−67515
    methanol, barrier height in excited vibrational state, microwave spectrum obs. 2−56248
    methanol in excited CO stretching state, microwave spectrum, torsion-vibration-rotation interaction 2−67517
    methanol-d_4, microwave spectrum, torsion-vibration-rotation interactions 2−50100
    methyl acetylene investigation of vibration-rotation bands in near infrared 2−70781
    methyl chloride, Fermi resonance in system $2\nu_4$, $\nu_4+3\nu_6$ 2−70778
    methyl cyanide and isocyanide in solid Ar, matrix isolation studies 2−56246
    methyl fluoride, i.r. spectra analysis, general harmonic force field 2−77150
    methyl fluoride, laser excitation and equilibration of excited states 2−50101
    methyl fluoride, nonlinear laser spectroscopy of i.r. vibr.-rot. system 2−53063
    methyl group stretching and bending vibrs., substituent effect on i.r. absorpt. intensities 2−56245
    methyl iodide, equilibrium structure determ. from rotation-vibration interaction constants from i.r. spectra 2−42995
    methyl iodide, high-resolution i.r. spectra 2−46611
    methyl iodide, liquid, vibration-rotation bands, calc. of orientation correlation formation 2−43363
    methyl iodide crysts., harmonic vibr. freqs., harmonic intermol. pot. 2−81350
    methyl iodide-d_3, assignment of overtone and combination bands in vibrational spectrum 2−70782
    methyl iodide-d_3, i.r. spectra 2−46612
    methyl iodide-d_3, perpendicular bands ν_5 and ν_6, i.r. spectra 2−46613
    methyl isocyanide of d_3-derivative, vibr.-rot. band analysis 2−70780
    methyl radical, i.r. spectrum, study by rapid scan spectroscopy 2−83299
    methyl silane microwave spectrum, vibration-internal rotation- overall rotation interactions for symmetric-top molecules 2−70779
    methyl-2-propanol-1, vibrational spectra of OH groups 2−70740
    methyl-substituted chloroaluminate ions, stretching frequencies and force constants 2−77117
    methylamine, deuterated and partially deuterated, Raman and i.r. spectra analysed w.r.t. amino group vibrations 2−46610
    methylamine, force constant determination using ^{15}N isotope shifts in i.r. spectrum 2−60075
    methylchlorosilane microwave spectrum, centrifugal distortion consts. 2−64190
    3-methyldiazirine and 3-methyl-d_3- diazirine, electronic absorption spectra, vibrl. analysis 2−56250
    methylene chloride, liquid, vibration-rotation bands, calc. of orientation correlation formation 2−43363
    N-methylnitroamine, additive interatomic interaction model calculations 2−77044
    methylphenylsilanes, electronic-vibrational absorption spectra 2−50111

Molecules continued
  vibration continued
    methylpyridine, nonplanar vibrations, standard intensities and degrees of polarization of line widths 2−77152
    methylthiophene, in CS_2 solution, out-of-plane vibrations, i.r. band intensities 2−77120
    methyltrifluoride, -D, normal coordinate analysis 2−77123
    molecular cryst., harmonic freqs. of vibr., harmonic intermol. pot. 2−81349
    molecular crystal, neutron scatt. and vibrational spectra investigations 2−54012
    molecular crystals, electron-vibrational spectra, review 2−57345
    molecular crystals, vibronic spectra of absorption and luminescence, distortion of mirror symmetry 2−78108
    molecule, Raman resonance, effect of excitation freq. on overtone intensities 2−56182
    molybdates of divalent transition metal compounds, i.r. vibrational spectra, calc. of force constants 2−70678
    monhalogeno(methyl)germanes, i.r. and Raman spectra 2−46617
    monohalobenzene, monohalobenzene-d_5, calc. and interpretation of vibrational spectra 2−53066
    mononitro alcohols, vibrational spectra of OH groups 2−70740
    monophenyls, Raman and i.r. spectra 2−53056
    multiquantum vibrational-energy exchange, evaluation of S-matrix elements 2−70809
    MX_6 ions, force constants evaluated by orbital valence force field method 2−46511
    N-atom, vibration-rotation energy operator including electron-nuclear interaction 2−77046
    NA, excited collision-induced rot. and vibr. transfer laser-induced fluoresc. obs. 2−83412
    $NaHF_2$, neutron diffraction data refined, location of H, thermal motion and F-F distance 2−77087
    NH_3, nuclear quadrupole moment of ^{14}N, vibrational and other corrections 2−60015
    nitrobenzene, and $-d_5$, vibl. structure of photoelectron spectra 2−56251
    p-nitrobenzoic acid crystals, 17 bands, assignments to vibration modes 2−78167
    nitromethane, additive interatomic interaction model calculations 2−77044
    nitromethane, and -d_3, vibl. structure of photoelectron spectra 2−56251
    noncolinear collisions, inelastic pure vibrational transitions 2−70810
    oligopeptides, high resolution laser Raman spectra, study of S-S vibrations 2−83337
    optical absorption band shapes of Jahn-Teller systems with orbital doublet, path integration method 2−65198
    optical absorption band shapes of Jahn-Teller systems with orbital doublet, semiclassical approx. 2−65197
    optical activity of vibr. transitions, coupled oscillator model 2−60040
    optical lineshapes, effects of vibrational relaxation 2−70658
    organotin isocyanate, integrated intensity of valence vibrations 2−74290
    oscillator strengths, from self consistent propagator, Pariser-Parr-Pople model 2−50012
    oxalic acid, electronic states from absorption spectra 2−42980
    oxalic acid derivatives, vibrational spectra 2−67503
    3- oxetanone, microwave spectrum and ring-bending vibr. 2−70787
    pentafluorobenzoychloride, Raman spectra, frequency assignments 2−74285
    pentafluorostyrene in liquid phase, vibrational assignments from infrared and Raman spectra 2−50107
    pentafluorothiophenol, Raman and i.r. spectra, vibrational assignments assuming C_{2v} symmetry 2−60078
    perfluorocyclohexane, i.r. and Raman spectra 2−46620
    phenazine, assignment of i.r. and Raman spectra 2−46622
    phenyl derivatives, monosubstituted, application of Gordy's Rule 2−60081
    phenylsilane, electronic-vibrational absorption spectra 2−50111
    phenylsilane, i.r. and Raman spectra 2−46623
    phosphabenzene, microwave spectrum, l.f. vibr. assignments 2−56254
    phospholipid-water mixtures, vibrational spectra 2−43374
    poly-L-alanine in α- and β-forms, determ. of dispersion curves using Wilson's GF-matrix method 2−64203
    poly-L-proline I chain, normal modes and dispersion curves, conform. depend. 2−80113
    polyatomic, automization of symmetry calculations 2−64097
    polyatomic, intramol. interactions and vibronic spectra, electronic rearrangments and four level scheme 2−67447
    polyatomic, iteration method for calc. of vibrational frequency increments 2−77047
    polyatomic, normal coordinate analysis 2−70665
    polyatomic, role of vibrational relaxations in formation of diffuse and complex configuration spectra 2−77045
    polyatomic molecules, anharmonic and high amplitude vibrations, solution in exact natural vibrational coordinates 2−42845
    polyethylene, oriented samples assignment of laser-Raman spectrum for fundamental modes of vibration 2−70803
    polyethylene glycol/water system, Mossbauer study of molecular motion at room temperature 2−72277
    polypeptides, high resolution laser Raman spectra, study of S-S vibrations 2−83337
    polyphenyl derivatives, i.r. and Raman spectra, vibr. assignment 2−56255
    polystyrene, transverse torsional mode due to bulky phenyl side groups 2−71732
    population of levels excited by laser radiation, meas. method 2−79972
    potential functions calc. in terms of group valence force symmetry coordinates 2−42847
    prolate symmetric top mols., Coriolis constants from Raman band contours 2−70662
    propane, potential functions calc. in terms of group valence force symmetry coordinates 2−42847
    2-propanol, vibrational-rotational relaxation characteristics in liquid determ. from spectra 2−56474

Molecules continued
vibration continued
propylamine, deuterated, Raman spectra analysed w.r.t. amino group vibration 2−46610
pyrazine, vibronic coupling and Raman intensities 2−80066
pyridine, nonpolar vibrations, standard intensities and degrees of polarization of line widths 2−77152
pyridine, symmetry, from i.r. abs. spectra 2−46626
pyrroles, liq., i.r. and Raman spectra assignments 2−83306
quinoline, symmetry, from i.r. abs. spectra 2−46626
radiationless electron transitions, temp. depend., using Morse oscillator model, small Z 2−52964
radiationless electron transitions, temp. depend., using Morse oscillator model, arbitrary values of Z 2−52965
radiationless transitions, recurrence and irreversibility 2−42825
rare earth β-diketonate complexes, i.r. absorpt., vibr. modes 2−46577
rare-earth pyrosilicates, vibrational spectra 2−72322
relaxation of anharmonic oscillators in nozzle flow 2−80142
Renner effect in four-atom molecules 2−52973
1,4-selenoxan, fundamental frequenciesand force constants 2−83315
shock wave tail, relaxation, anti-Stokes Raman scattering obs. 2−52970
silyl isocyanate, determ. of molecular dimensions and large amplitude vibrations by electron diffraction 2−80080
solar Raman scattering, effect on distribution of molecules over vibrational levels 2−75940
spectra, effect of introducing small symmetry into symmetric double minimum potential 2−52975
spectral analysis of gases in metals using laser torch as light source 2−84701
spectroscopy, reorientation and vibrational relaxation as line broadening function 2−79981
spiral polymers, interaction between recurring links between neighbouring loops in vibrational problem 2−77160
substituted and perturbed molecules Green's function analysis determ. of molecular constants for XYZ type molecules 2−52974
sulphalane, doublet struct. of $\nu_{as}(SO_2)$ band 2−83331
symmetric hydrogen bonded complexes, proton pot. rel. to splitting of internal modes 2−70734
symmetrical molecules, classification of vibronic energy levels with allowance for inversion levels 2−77035
symmetry determ. using method of ascent in symmetry 2−56145
p-terphenyl, rigid mol., librational motion temp. factor 2−54025
1,2,4,5-tetrabromobenzene, o.d.m.r. and p.m.d.r. studies of $^3\pi\pi^*$ state 2−60086
1,2,4,5-tetrachlorobenzene, o.d.m.r. and p.m.d.r. studies of $^3\pi\pi^*$ state 2−60086
1,1,2,2-tetrafluorocyclopane-d_0, d_1 and d_2, i.r. and Raman spectra 2−46629
tetrafluoroethylene, i.r. spectrum 2−46630
tetrahedral, Van Vleck perturbation theory applied to vibration-rotation interaction 2−42842
tetrahedral molecules and ions, force constants by orbital release force field and Urey-Bradley force field 2−77077
tetrahedral oxoanions of main group elements, ν_1/ν_3 freq. ratio 2−52991
tetramethylcyclobutane-1,3-dione, out-of-plane ring vibration 2−77155
tetramethylenecyclobutane-d_0 (-d_8) mass of Raman and i.r. spectra, vibrational analysis 2−70792
thiazenes, i.r. absorpt. spectra, rel. to NH group valence vibrs. 2−56261
thiazyl fluoride, photoelectron spectra, vibr. analysis, comparison with LCAO calcs. 2−53083
thioamides, NH stretching vibrations 2−43011
thiophene, -D, in CS_2 solution, out-of-plane vibrations, i.r. band intensities 2−77120
thiophene, vibrational analysis 2−60087
1,4-thioselenan fundamental frequencies and force constants 2−83315
tolane, normal coordinate treatment 2−60088
trans-3,4-dimethyl-2,2,5,5-tetradeuteriocyclopentanone, vibrational assignment and conformational studies 2−64189
trans-3,4-dimethylcyclopentanone, vibrational assignment and conformational studies 2−64189
transition metal complex halides, modified orbital valence force field 2−70729
tri(trifluoromethyl) arsenic, phosphorus and antimony, i.r. and Raman spectra, vibr. assignment 2−56262
tri-tert-butylmethane, detailed structure and improvements in model force fields 2−77109
triallyl amine, vibrational spectra 2−43012
triatomic systems, generalised mean-square amplitudes and Coriolis coupling constants 2−59966
S-triazine triplet state at 3455 Å, Stark effect meas, vibronic origin of state 2−83280
1,1,1-trimethoxyethane, vibrational spectra and rotational isomerism 2−43013
trimethyl amine, normal coordinate analysis, determ. of mean amplitudes of vibration 2−53084
trimethyl silyl isocyanate, microwave spectrum analysis 2−80076
trimethylchlorosilane, isotropic shifts in vibrational spectra by CD_3 substitution, force constant calc. 2−46632
trimethylene oxide and deuterated analogues, i.r. band progressions and ring puckering vibr. 2−83277
trimethylene oxide and deuterated analogues, vapour phase Raman transitions and ring puckering vibr. 2−83278
trimethylene oxide deuterated analogs, far i.r. spectra and ring puckering vibr. 2−80094
trimethylene oxide deuterated analogues, Raman spectra and ring-puckering vibr. 2−80095
trimethyloxysilane, isotropic shifts in vibrational spectra by CD_3 substitution, force constant calc. 2−46632
vibration-rotation interaction effect on molecular spectra 2−42841
vibrational-rotational band, total band absorptance and absorption coefficient 2−56140
vibrationally induced stabilization of vertically excited states 2−77042

Molecules continued
vibration continued
vibronic coupling, matrix elements of position and momentum 2−79975
vibronic intensity borrowing, comparison of Herzberg-Teller theory and mechanism based on nuclear momentum integrals 2−70659
vibronic interactions in doubly degenerate electron states 2−49991
vinyl isocyanide, normal vibrs., pot. energy distrib., mean amplitudes 2−56263
vinyl trifluoroacetate, i.r. and Raman spectra, vibrational assignment, depolarization ratios and configuration determ. 2−70797
vinylsilane, vinylsilane-d_3, normal vibration analysis and force field 2−43015
water, Raman scattering 2−46566
XY_2 bent symmetrical, calculation of vibration-rotation energies to fourth order 2−46512
XY_2 type, nonlinear, compliance consts. 2−56138
XY_2 type, vibr. spectra freqs. and intensities calc. by method of partial oscillations 2−67448
XY_4 and XY_3 type mols., orbital valency force field, approx. to general valence force fields 2−70663
XY_4 and XY_3 type mols., unique force consts. calc. 2−70664
XY_4 isotopic substitutions, Green's function anal. of planar vibrs. 2−77029
XY_6 octahedral mol., normal vibration modes from group theoretical considerations 2−61068
XY_6 octahedral molecule, group theory applications 2−61067
XYZ, bent molecule, vibration-rotation Hamiltonian 2−42843
$[X_2O_7]^{n-}$ anions, vibr. spectra assignments 2−56153
$[C_nO_n]^{-2}$ dianions, squarate and croconate comparison 2−70689
$[PtCl_4]^{2-}$ type planar square complexes, absorpt. band lineshape, electron-vibr. interaction 2−80054
AgSb mol., visible emission spectrum, assignment 2−64113
Al complex, AlX_3-dimethyl sulphoxide coordination compound (X=Cl, Br), vibrational spectra 2−52992
$AlBr_3(CH_3)_2O$, force field compared with the derivatives $(CH_3)_2O$ and $AlBr_4^-$ 2−42869
$AlCl_3(CH_3)_2O$, force field compared with the derivatives $(CH_3)_2O$ and $AlCl_4^-$ 2−42869
AlM_gBO_4 vibrational spectra, interpretation by factor group approx. calc. of force constants for BO_4 group 2−70728
AlO $^2\Sigma^+ - x^2\Sigma^2$ band system, calc. of Franck-Condon factors and r centroids using RKR potentials 2−70679
AsF, near vacuum u.v. and near i.r., spectrum analysis 2−56154
AsF_3, ambiguities in harmonic force fields 2−50063
AsO radical, rot. analysis of $C^2\Delta$ and $D^2\Sigma^-$ states, C-state perturbations 2−74255
As_2O_7, systems, normal coordinate analysis using Urey-Bradley-Shimanouchi force field 2−77079
AsS, $A'^2\pi_{3/2} - X^2\pi_{3/2}$ band system, vibrational analysis and rotational constants 2−77080
Au_2, true pot. energy curves 2−56155
BF_3, ambiguities in harmonic force fields 2−50063
BF_3 i.r. spectra, obs. of l-type resonances in Q branches of ν_4 bands, determ. of cubic potential consts. 2−70682
BH, calc. of force constants by Hellmann-Feynman theorem 2−80055
BH, computation of force constants and dipole moment derivatives using Hartree-Fock 2−50052
B_2H_6, B_2D_6, potential function for ring puckering vibration 2−74256
$(BNH_2)_x$, mean-square amplitude of vibration detn. 2−80021
$B_3N_3H_6$, symmetry-forbidden $^1A_2'$-$^1A_1'$ transition analysis 2−70684
BO_2^-, in KBr, KCl crystal, molecular force constants meas. 2−42871
BaI, obs. of new band system in 4481-4300 Å region, study of electronic transitions, vibrational analysis 2−70685
BeB_2H_8, BeB_2D_8, BeB_3HD_7, i.r. and Raman spectra, frequency assignment 2−52994
BeH(D) λ doubling variation with rot. quantum no. 2−83261
BeO, radiative lifetimes of excited vibrational states 2−46528
Br_2, outer vibr. turning pts. near dissoc. in $B(^3\Pi_{0l}{}^+)$ state 2−77082
$BrNSF_2$ vibrational spectra, tentative assignment band shape and G-matrix elements calc. 2−70697
BrO_3^-, vibrational spectra and force constants 2−59996
CH, oscillator strength of $A^2\Delta$-$X^2\Pi$ electron transition 2−59993
CH, vibration-rotational levels determ. from potential curves and eqns. for motion of nuclei 2−56160
CO_2:^{4}He, 300 to 600 K, vibrational relaxation times of 00°1 levels 2−42881
CO_2:N_2, 300 to 600 K, vibrational relaxation times of 00°1 levels 2−42881
CO-COS collisions meas. of vibrational energy transfer on test of harmonic oscillator model 2−80140
CO_2-DF vibrational de-excitation on the basis of vibration-to-rotation energy transfer, 300-2000K 2−83406
CO_2-H-, halide mixtures, vibration-to-vibration energy transfer 2−43036
CO_2-H_2 mixtures, simultaneous vibr.-translation, vibr.-rot. and rot.-translation exchanges 2−53099
CO, CO-Ar, CO-N_2 gas mixtures, vibrational relaxation rate in nozzle flow 2−80142
CO, chemisorbed on W, vibr. freq., refl.-absorption i.r. spectra 2−47154
CO, $\Delta v=1$ transitions, relative Einstein A coefficients 2−46531
CO, electronic-vibr. energy transfer, vibr. distrib., i.r. fluoresc., Hg*-sensitized 2−59988
CO, i.r. vibr.-rot. spectra, approx. calcs. of abs. coeffs., 300 and 1200 K 2−46534
CO, isolated in solid Ne and Ar matrices, vibrational fluorescence laser excited low temp. study 2−59994
CO, lifetimes of vibrational levels determ. in zero-field level-crossing spectroscopy 2−70691
CO, totally inverted vibr. population, rel. to laser applic. 2−61777
CO, vibr. excitation by O+Cs reaction, chem. laser studies 2−72552
CO, vibr. relax. near 100K using discharge laser 2−80128
CO, vibrational-rotational band, total band absorptance and absorption coefficient 2−56140
CO, vibrational matrix elements of quadrupole moment functions 2−64129

Molecules continued
- **vibration** continued
  - CO crystal, α phase, librational motion by linear spin-wave theory 2−80588
  - CO excited singlet state, vibr. relax. cross sections, fluoresc. obs. 2−56159
  - CO formed in O_2 + acetylene reaction, vibrational population distrib. 2−46532
  - CO relax. measurement using transient stimulated raman scatt. 2−56150
  - CO^+, comet tail system, electronic transition moment 2−50029
  - CO^+, radiative lifetimes of $A^2\Pi$ state 2−74259
  - CO_2, 300 to 600 K, vibrational relaxation times of 00°1 levels 2−42881
  - CO_2, 9.33 and 10.18 μm transitions, laser freq. and wavelength meas., speed of light 2−78758
  - CO_2, general quartic force field, calc. using Parr-Brown anharmonic potential function 2−52999
  - CO_2, i.r. vibr.-rot. spectra, approx. calcs. of abs. coeffs., 300 and 1200 K 2−46534
  - CO_2, laser source spectroscopy obs. of 00^01-$(10^00$-$02^00)_1$ band 2−74257
  - CO_2, near-resonant energy transfer to (00°1) vibr. level due to Hf collisions 2−53101
  - CO_2, press.- induced absorpt., ν_1 band, density and temp. depend. of intensity, crit. phenomena 2−56158
  - CO_2, shock-heated, laser absorption meas. of vibrational relaxation of bending mode 2−56161
  - CO_2, stimulated Raman scatt., time meas. for vibr.-trans. energy transfer 2−64118
  - CO_2, thermal relaxation, meas. of period by impact tube method 2−83398
  - CO_2, vibrational relaxation time in inert gas mixtures, meas. using acousto-optical effect 2−59995
  - CO_2 lower laser level relax. saturation 2−59992
  - CO_2 polyatomic mixtures, laser-excited vibrational fluorescence measurements 2−43035
  - CO_2 solid (ν_1, $2\nu_2$) vibron-phonon infrared absorption band in temp. range 88-160 K 2−81347
  - CO_3^{2-} in complex structs. with bridge coord., plane vibr. freqs. 2−70690
  - COS, centrifugal distortion and anharmonic potential constants 2−52997
  - CO_2-HF vibrational de-excitation on the basis of vibration-to-rotation energy transfer, 300-2000K 2−83406
  - CO + CO collision, vibrational transition probabilities, temp. dependence below 300K 2−60117
  - CO + CO_2, N_2O, COS, shock-heated mixtures, vibrational energy transfer processes 2−53100
  - $CO_2 + N_2O$ collisions, vibr.-translation and vibr.-vibr. exchanges 2−43034
  - CO_2^-. energy curves of $^2A_1$ and $^2B_1$, states 2−42874
  - CS, Hanle effect measurement of the lifetime of the $A^1\Pi$ vibration-rotation levels 2−42885
  - CS_2, general quartic force field, calc. using Parr-Brown anharmonic potential function 2−52999
  - CS_2, u.v. absorpt. near N_2 laser wavelengths, excited states population 2−80014
  - C_3S_2, visible and near u.v. spectra, vibrational analysis 2−42877
  - $CSCl_2$, assignments from i.r. spectra 2−46533
  - CSF_2, assignments from i.r. spectra 2−46533
  - CU(II) complexes, six-coordinated, determ. of vibrational degrees of freedom associated with dynamic Jahn-Teller effect 2−53004
  - 1-chloro-3,3,3-trifluoropropyne, microwave spectra analysis 2−70759
  - Cl tetrahedral oxy-compounds, force constants and regularities of chemical bonding 2−70725
  - Cl_2, outer vibr. turning pts. near dissoc. in $B(^3\Pi_{0u}{}^+)$ state 2−77082
  - ClCN, general quartic force field, calc. using Parr-Brown anharmonic potential function 2−52999
  - Cl_2CNCl, i.r. and Raman spectra 2−70694
  - ClNCO, microwave spectrum, centrifugal distortion consts. 2−56165
  - $ClNSF_2$ vibrational spectra, tentative assignment band shape and G-matrix elements calc. 2−70697
  - ClO_3^-, vibrational spectra and force constants 2−59996
  - ClO_3F, force-constant ranges and improvement in Fletcher-Powell method of refinement 2−64121
  - ClO_3F, vibrational fine structure obs. in photoelectron spectrum 2−46587
  - $Cl_2 + Cl_2$ collision, vibrational transition probabilities, temp. dependence below 300K 2−60117
  - Co complex, trisethylenediamine cobalt(III) thiophosphate, i.r. spectra 2−46537
  - Co(II) complexes with N,N′-ethylenebis(acetylacetoneimine), i.r. spectra, normal coordinate analysis 2−70695
  - Co(III) triethylenediamine chloride, vibr. spectra analysis 2−72325
  - Cr(III) thiacyanate complex in dimethyl-sulfoxide, phosphorescence spectra 77-150 K 2−83269
  - Cr(III) triethylenediamine chloride, vibr. spectra analysis 2−72325
  - CrO_4^{2-}, resonance Raman spectra, analysis of ν_1 breathing mode 2−50054
  - CsI + Ar collisions, vibrational and rotational energy transfer, ballistic mechanism 2−67536
  - $CuCo_3.Cu(OH)_2$, vibr. freqs. assignment method 2−42886
  - Cu_3MX_4 (M = V,Nb,Ta; X = S,Se) 2−42888
  - D_2-He collisionally induced vibration, effect of rotational motion 2−80139
  - D_2-Ne Van der Waals complexes in collision-induced fund. bands of deuterium, spectra 2−64127
  - D_2, effect of collisions on Raman line profile 2−43039
  - D_2, vibrational relaxation, studied by laser induced vibrational fluorescence technique 2−80134
  - D_2, vibrationally excited, collisions with Na atoms excitation of D-line radiation 2−70627
  - D_2 considered as Morse oscillator. DWBA theory for collisional dissociation with Ar, He 2−43033
  - D_2 relax. measurement using transient stimulated raman scatt. 2−56150
  - D_2 vibrational level linewidths due to predissociation 2−79999

Molecules continued
- **vibration** continued
  - DF-CO_2, chemical laser, vibrational energy transfer and de-excitation 2−49366
  - DF, i.r. chemilum. quenching, vibr. energy transfer to CO_2 and HF 2−65371
  - DF, vibr. relax., catalytic efficiencies of NO 2−77163
  - DF chemical laser, vibrational energy transfer and de-excitation 2−49366
  - DOF, i.r. spectra, vibr.-rot. analysis 2−77062
  - F + HCl → HF + Cl, effect of excess reagent vibr. excitation on reaction dynamics 2−84629
  - $FNSF_2$ vibrational spectra, tentative assignment band shape and G-matrix elements calc. 2−70697
  - $Fe(CO)_5$, vibrational spectra of isotopic species, potential constants 2−67473
  - Fe(II) complexes, octahedral halogen-bridged, Ramn and far i.r. spectra 2−46558
  - FeO, absorption coeff. for i.r. vibration-rotation spectrum 2−42890
  - GeF_2, vacuum u.v. spectra, vibr. assignments 2−80040
  - GeF_2 microwave spectrum, effect of centrifugal distortion on rotational transitions, determ. rotational consts. in vibrational states 2−70698
  - GeH_2Br and GeHBr, fund. freqs. 2−61804
  - H_2-H^+ collisions, vibrational excitation, 15-1000 eV, semiclassical theory 2−80152
  - H_2-He collisionally induced vibration, effect of rotational motion 2−80139
  - H_2, coherently driven by light waves, obs. of anharmonic Raman scattering, determ. second order polarizability 2−42899
  - H_2, effect of collisions on Raman line profile 2−43039
  - H_2, force consts., Hartree-Fock wavefunction calcs. 2−60002
  - H_2, h.c.p., Raman spectrum, fund. and overtone vibr. transitions 2−61666
  - H_2, line profile of $Q_{01}(1)$ vibr. resonance in Dicke narrowing zone 2−56176
  - H_2, model potential for vibrational excitation by collision with Li^+ 2−43038
  - H_2, screening and polarization effects on vibration-rotation-props. 2−64130
  - o-H_2, solid, f.c.c. and h.c.p. phases, libron state density 2−64839
  - H_2, vibrational and rotational analysis of eight simple models 2−46549
  - H_2, vibrational correction to electron scattering intensity calc. using five term CI wavefunction 2−50036
  - H_2, vibrational excitation by H^+ and e^- impact, cross section calc. 2−70817
  - H_2, vibrational level linewidths due to predissociation 2−79999
  - H_2, vibrational matrix elements of quadrupole moment functions 2−64129
  - H_2, vibrationally excited collisions with Na atoms excitation of D-line radiation 2−70627
  - H_2 considered as Morse oscillator DWBA theory for collisional dissociation with Ar, He 2−43033
  - H_2 considered as Morse oscillator, DWBA theory for collisional dissociation with Ar, He 2−43033
  - H_2 relax. measurement using transient stimulated Raman scatt. 2−56150
  - H_2 vibrational excitation by Li^+, quantum mechanical studies 2−77171
  - H_2^+, nuclear motion, effect on wavefunctions in momentum space 2−46545
  - HBr, charge transfer reactions with Ar^+ and Kr^+, effect of resonance on vibr. distrib. 2−51424
  - HBr, mechanisms for vibrational relaxation 2−70704
  - HBr, vibr.-vibr. energy transfer and collisional pumping 2−80129
  - HBr in condensed phases, first harmonic of vibration-rotation spectrum 2−53014
  - HBr in condensed phases, second harmonic of vibration rotation spectrum 2−53015
  - HBr in condensed phases, spectra of vibration rotation fundamental 2−53013
  - HCN, general quartic force field, calc. using Parr-Brown anharmonic potential function 2−52999
  - HCP, calc. of K-type doubling in $b^3\Pi$ electronic states 2−46510
  - HCl, charge transfer reactions with Ar^+ and Kr^+, effect of resonance on vibr. distrib. 2−51424
  - HCl, in SF_6 solution, i.r. absorption bands, effect of vibration-rotation interaction 2−42841
  - HCl, mechanisms for vibrational relaxation 2−70704
  - HCl, population on vibr.-rot. levels during NOCl + H_2 reaction 2−53005
  - HCl, selective laser excitation of high vibr. levels 2−53017
  - HCl, vibrational energy transfer, optical parametric oscillator pumped 2−80155
  - HCl, vibrational fluorescence, vibrational energy transfer from molecule to molecule 2−83256
  - HCl in condensed phases, first harmonic of vibration-rotation spectrum 2−53014
  - HCl in condensed phases, second harmonic of vibration rotation spectrum 2−53015
  - HCl in condensed phases, spectra of vibration rotation fundamental 2−53013
  - HD, vibrational relaxation, studied by laser induced vibrational fluorescence technique 2−80134
  - HDO, structural model for effect of perchlorates on i.r. bands, assignment of stretching bands 2−53016
  - HF-CO_2, chemical laser, vibrational energy transfer and de-excitation 2−49366
  - HF, i.r. chemilum., quenching, vibr. energy transfer to CO_2 and HF 2−65371
  - HF, mechanisms for vibrational relaxation 2−70704
  - HF, relaxation measurements using combined shock tube and laser-induced fluorescence technique 2−53011
  - HF, vibr. relax., catalytic efficiencies of NO, H_2O, D_2O and HCl 2−77163
  - HF, vibration-rotation level population during elementary act of F + H_2 reaction 2−66750
  - HF chemical laser, vibrational energy transfer and de-excitation 2−49366
  - HF vib.-vib. energy transfer time, vib. fluorescence obs. 2−60005

Molecules continued
vibration continued
HF + F collisions, temp. dependence of vibrational energy transfer probability, 300 to 1500K 2−43037
HI, mechanisms for vibrational relaxation 2−70704
HNCS, u.v. spectrum analysis 2−56175
HO_2 radical, i.r. spectrum, stretching and deform. funds., force consts. 2−56174
H_2O, bond and angle change effect on stretching frequencies 2−83266
H_2O, calc. of force constants by Hellmann-Feynman theorem 2−80055
H_2O, calculation of spectral intensities using vibrational rotational interaction data 2−74265
H_2O dipole moment increase with deuteration for vibrational ground state, anharmonicity of bending vibration 2−80045
HOF, i.r. spectra, vibr.-rot. analysis 2−77062
H_2SO_4, force constants, normal coordinate treatment 2−74262
HTO, ν_1 and ν_3 levels determ. by i.r. spectrum, rot. consts. of fund. state 2−79997
$H + H_2$ vibr. excitation process, rate const. 2−67537
$H_2 + H_2$ reactive vibr. nonequil. effects 2−84627
HeH^+, electron correl. influence 2−64139
HeNe levels observed in vacuum u.v. absorption spectrum 2−77090
$HfBr_4(Cl_4)(I_4)$, orbital valence force field consts. 2−77075
Hg halides, bending in dioxane and benzene solutions, determination from i.r. and Raman spectra 2−64463
Hg_2, fluoresc., transitions between vibr. levels and ground state 2−53020
HgH, quasibound vibr.-rot. levels obs. from orbiting resons. in Hg + Hg scatt. 2−77018
I_2-He mixture, interaction of dissoc. and vibr. relax. behind shock wave 2−77168
I_2, 5145Å excited anti-Stokes resonance Raman spectra, vibrational-rotational structure 2−77086
I_2, magnetic quenching of fluorescence from vibrational levels in $B^3\Pi(O_u{}^+)$ state 2−77085
I_2 levels excited by Kr ion laser, quantum nos. 2−80016
I_2 vapour, vibr.-Rot. struct. in reson. Raman effect 2−80037
$I_3{}^-$, resonance Raman effect laser excited, vibration enhancement 2−80007
ICl, $J=2\leftarrow 1$ microwave spectra for $v=0$ and $v=1$ levels 2−42902
IF_7, nonrigid D_{5h} molecule, vibrational assignment from i.r. and Raman spectra 2−42901
$IO_3{}^-$, vibrational spectra and force constants 2−59996
$^{127}I_2$,$^{129}I_2$, vibrational energy in electronically excited state rel. to hyperfine interactions in optical transitions 2−50050
InF band systems, vibr. transition probabilities and r-centroids 2−60006
IrO, band spectrum, 4200 to 6400 Å 2−77065
K complex, pentacyanonitrosylchromate, i.r. spectrum, normal coordinate analysis for $[Cr(CN)_5NO]^{-3}$ anion 2−60008
KBr, inelastic collision with methanol, rel. to chemical kinetics 2−64220
$KFe(CrO_4)_2.2H_2O$, low temp. i.r. spectra 2−48175
KHF_2, neutron diffraction data refined, location of H, thermal motion and F-F distance 2−77087
Li_2, computation of force constants and dipole moment derivatives using Hartree-Fock 2−50052
Li_2, force consts., Hartree-Fock wavefunction calcs. 2−60002
LiH, calc. of force constants by Hellmann-Feynman theorem 2−80055
LiH, computation of force constants and dipole moment derivatives using Hartree-Fock 2−50052
$(LiNa)^+$, charged transfer, transition, dipole moment, cross sections of vibr. levels 2−60009
LiO. pot. curves for $X^2\pi$ and $A^2\Sigma$ states 2−60011
LuH, electronic band systems analysis, 4200 and 5000 Å 2−74268
MF_6, ions (M=P, As, Sb, Si, Be, Sn), determination and correction for nonactive frequencies 2−64125
$Mg(NH_3)_6Cl_2$ and $Mg(ND_3)_6Cl_2$, i.r. active vibr. freqs. assignment 2−77058
$Mn(CO)_4NO$ complex, i.r. spectra meas. in vapour phase and in solution, assignment of fundamental modes 2−42909
$MnF_6{}^{-2}$, molecular constants calc. 2−46559
$MnF_6{}^{2-}$, force constants and generalised mean amplitude of vibration calc. using seven parameter Urey-Bradley force 2−60013
Mn(I) complex, $K_5[Mn(CN)_6]$, vibr. spectra and force consts. 2−77074
Mn(II) complexes, octahedral halogen- bridged, Raman and far i.r. spectra 2−46558
MnO_4-, resonance Raman spectra, analysis of ν_1 breathing mode 2−50054
N_2-CO, vibration to vibration energy transfer, laser excited fluorescence obs. 2−67489
N_2-Na vibrational relaxation times in rapid expansion interpretation of Na line-reversal meas. 2−53102
N_2, active, vacuum u.v. emission, form. and removal of $N_2(a^1\Pi_g)$ 2−70716
N_2, active, vacuum u.v. emission from levels of forbidden B-X transition, $N_2(b'^3\Sigma_u{}^-)$ kinetic behaviour 2−70719
N_2, anharmonic oscillator, time-dependent solutions for de-excitation rates 2−42913
N_2, $B^3\Pi g$ state conc., reabsorption obs. 2−70715
N_2, elastic electron scatt. and nonresonant vibr. excitation 2−77162
N_2, elastic electron scatt. and excitation of first vibr. level 2−77161
N_2, excitation of vibrational $C^3\Pi u$, $v'=0-4$ levels in high frequency $Ar + N_2$ discharge 2−43041
N_2, microwave discharge, pink afterglow, vibrational relaxation 2−53255
N_2, Raman scattering 2−46566
N_2, tunable Raman excitation and vibr. relax. 2−53023
N_2, vibration-rotation interaction in calculated band strengths 2−46571
N_2, vibrational excitation by electron impact in 15-35 eV region, meas. of angular distrib. 2−56189
N_2, vibrational excitation by e^-, cross section calc. 2−70817
N_2, vibrational matrix elements of quadrupole moment functions 2−64129
N_2, vibrational relaxation in collisions with $O(^3P)$ atoms 2−67416

Molecules continued
vibration continued
N_2, vibrationally excited, collisions with Na atoms excitation of D-line radiation 2−70627
N_2, vibrationally excited, reaction with O^+, cross section for formation of NO^+ 2−54530
N_2 crystal, α phase, librational motion by linear spin-wave theory 2−80588
N_2 relative populations of $C^3\Pi_u$ and $B^2\Sigma_u{}^+$ states 2−80121
N_2 relax. measurement using transient stimulated raman scatt. 2−56150
$N_2{}^+$, mechanism of electron-ion dissociative recombination in gas discharge 2−74272
$N_2{}^+$ radiative lifetimes of a A^2PI_u vibr. levels 2−83257
$N_2{}^+(B_2\Sigma_u{}^+$, $v'=2$ and 3), departure of vibrational populations from Franck-Condon predictions for energetic electron-$N_2(X^1\Sigma_g{}^+$, $v=0)$ collisions 2−50058
$N_2{}^+B^2\Sigma$ products from Ne^+-N_2 collisions, vibrational distribution 2−56273
NCl_3, normal coordinate analysis, vibrational frequencies and force constants calc. 2−46567
NF_3, ambiguities in harmonic force fields 2−50063
NF_2SO_3F, spectra, C_s symmetry 2−42917
NH_3-ND_3 mixtures, liq., Raman spectra, vibr. freqs. assignment 2−77439
NH_3, force const., dipole moment derivatives by Hartree-Fock calculations 2−80029
NH_3, transient-nutation effects in time-resolved i.r.-microwave double resonance 2−64147
NH_4HF_2, neutron diffraction data refined, location of H, thermal motion and F-F distance 2−77087
$NH_3 + HCl$ system, potential energy curves for proton motion, extended Huckel calculation 2−43040
N_1(II) mandalate complex, i.r. spectrum 2−50065
NO-$\gamma(A^2\Sigma$-$X^2\Pi)$ system, oscillator strength of (0,0) band 2−50062
NO_{-3}, matrix-isolated, anharmonicity constants and harmonic frequencies from i.r. spectra 2−67492
NO, i.r. study of R(15/2) vibration- rotation transition 2−46561
NO $X^2\Pi$, rapid rate process meas. by kinetic spectroscopy during photolysis flash vibrational relaxation 2−54553
NO^- photodetachment spectrometry, identification of initial and final vibrational states 2−53027
$(NO)_2$ dimer, low temperature vibrational bands 2−67495
$NO_3{}^-$ in complex structs. with bridge coord., plane vibr. freqs. 2−70690
N_2O, excited on ν_3, vibr. energy transfer to CO and N_2, temp. depend. 2−60108
N_2O, forbidden character of 2000 Å transitions 2−56186
N_2O, general quartic force field, calc. using Parr-Brown anharmonic potential function 2−52999
N_2O, thermal relaxation, meas. of period by impact tube method 2−83398
N_2O, vibration bands when absorbed in cavities of zeolite NaA 2−46565
N_2O band intensities and half-width of N-broadened lines rotational lines in ν_3 fundamental meas. near 4.5 μ 2−42923
N_2O obs. weak diffuse vibrational bands in 6.8 eV B region 2−77061
$^{14}NH_3$ and $^{15}NH_3$, i.r. vibration-rotation spectra, 2-photon spectroscopy 2−42920
$N_2 + N_2$ collision, vibrational transition probabilities, temp. dependence below 300K 2−60117
$N_2 + O_2(HCl)$ collisions, vibr.-vibr. energy exchange 2−83407
$N_2{}^*$, vibrationally excited, quenching by O, determ. of rate coeff. 2−83400
$Na_2Cd(SO_4)_2.2H_2O$ vibrational frequencies assigned 2−83270
$Na_2Cd(SeO_2)_2.2H_2O$ vibrational frequencies assigned 2−83270
$Na_2Cr(SO_4)_2.2H_2O$ vibrational frequencies assigned 2−83270
$Na_2Cu(SO_4)_2.2H_2O$ vibrational frequencies assigned 2−83270
$NaFe(CrO_4)_2.2H_2O$, low temp. i.r. spectra 2−48175
$Na_2Fe(SO_4)_2$ assignments 2−83271
NaK, constants determ. from laser-induced resonance fluorescence 2−64149
NaLi, ground vibronic Stark coeff. in electric resonance spectrum 2−53029
$Na_2Mg(SO_4)_2$ assignments 2−83271
$Na_2Mn(SO_4)_2.2H_2O$ vibrational frequencies assigned 2−83270
$Na_2Mn(SeO_4)_2.2H_2O$ vibrational frequencies assigned 2−83270
$Na_2Ni(SO_4)_2$ assignments 2−83271
$Na_2Zn(SO_4)_2$ assignments 2−83271
$NbCl_6{}^-$, $NbBr_6{}^-$, Urey-Bradley force fields 2−42919
NbF_5, matrix isolated and gas phase, obs. of i.r. spectra, C_{4v} monomeric structure active frequencies 2−42918
NbO band systems, vibr. transition probabilities and r-centroids 2−60006
Ne_2 levels observed in vacuum u.v. absorption spectrum 2−77090
$NiF_6{}^{2-}$, force constants and generalised mean amplitude of vibration calc. using seven parameter Urey-Bradley force 2−60013
Ni(II) complexes, octahedral halogen-bridged, Raman and far i.r. spectra 2−46558
Ni(II) complexes with N,N′-ethylenebis(acetylacetoneimine), i.r. spectra, normal coordinate analysis 2−70695
No, i.r. vibr.-rot. absorpt. spectrum, nucl. hyperfine splitting 2−64143
O-H-O hypothetical linear mol., isotopic shift for large-amplitude vibrs. 2−83227
O_2, elastic electron scatt. and excitation of first vibr. level 2−77161
O_2, molecular parameters 2−42927
O_2, Raman scattering 2−46566
O_2, tunable Raman excitation and vibr. relax. 2−53023
O_2 relax. measurement using transient stimulated raman scatt. 2−56150
$O_2{}^-$ and $O_3{}^-$ ions Raman spectra in alkali metal superoxides and ozonides 2−81354
$O_2{}^-$ labile ions, stimulated emission during d.c. discharge 2−46793
$O_2{}^-$ laser photodetachment and photoelectron spectroscopy vibrational state analysis 2−53028
$O_3{}^-$ anion isolated in Ar matrix, vibrational and electronic spectra, 5100-3700 Å, determ of ν_3 2−70720
OCS, (01^10) vib. state, determ. of elec. and mag. moments 2−83245
OCS, forbidden character of 2000 Å transitions 2−56186

Molecules continued
  vibration continued
    OCS, general quartic force field, calc. using Parr-Brown anharmonic potential function 2−52999
    OH, vibration-rotation interaction in calculated band strengths 2−46571
    OH emission spectra, intensity variations, vibrational and rotational temps. 2−46572
    OH groups, dependence of torsional vibration frequency on H bond energy 2−42857
    $OH(A^2\Sigma^+) + Ar$, near resonant vibration-rotation energy transfer calc. of cross sections and rate consts. using IOS and DW approx. 2−70818
    $O_2 + O_2$ collision, vibrational transition probabilities, temp. dependence below 300K 2−60117
    $O_2^\dagger + O(^3P)$ vibrational energy transfer, O_3 photolysis 2−51465
    $Os_4O_4(CO)_{12}$, i.r. and Raman spectra, vibr. assignment, force consts. 2−56193
    P tetrahedral oxy-compounds, force constants and regularities of chemical bonding 2−70725
    PF_3, ambiguities in harmonic force fields 2−50063
    PH_5, E′ vibr. modes, ab initio obs. 2−80038
    PO, vibrational and rotational analysis of emission spectrum in 1850-2350 Å region, $C^2\Sigma$--$X^2\Pi_r$ transition 2−46573
    PO band systems, vibr. transition probabilities and r-centroids 2−60006
    PO γ-system, localization of rot. perturbations in first vibr. levels 2−79995
    P_2O_7 systems, normal coordinate analysis using Urey-Bradley-Shimanouchi force field 2−77079
    $POBr_3$, isolated in low-temperature matrix 2−44380
    Pb_2, new molecular constants for ground electronic state determ. from laser excited resonance fluorescence 2−42929
    Pd(II) complexes with N,N′-ethylenebis(acetylacetoneimine), i.r. spectra, normal coordinate analysis 2−70695
    Rb-Ar, Rb-Kr, Van der Waals molecules spin orbit interact. strength on vib.-rot. state, r.f. field obs. 2−56194
    ReF_7, Raman and i.r. spectra 2−46576
    Re(I) complex, $K_5[Re(CN)_6]$, vibr. spectra and force consts. 2−77074
    Rh(III) triethylenediamine chloride, vibr. spectra analysis 2−72325
    RuF_5 complexes with XeF_2, valence vibrations 2−74279
    Ru^aO_4, A=16, 18, Raman and i.r. spectra, determ. of anharmonicity corrections, Coriolis constants, force field 2−46578
    S tetrahedral oxy-compounds, force constants and regularities of chemical bonding 2−70725
    S_3, S_4, analysis of visible spectrum, correlation with photolysis reactions of S_3Cl_2 and S_4Cl_2 2−50069
    SF_4, vibrational spectra, solid phase 2−44381
    SO_2, ν_1 band, tunable laser spectroscopy 2−42938
    SO_2, tunable-laser spectroscopy of vibr.-rot. band transitions 2−60033
    $SOBr_2$, pot. energy consts., vibr. amplitudes, Corriolis coupling consts. 2−56169
    $SO^{35}Cl^{37}Cl$, centrifugal distortion consts. 2−60032
    SOF_2, microwave spectrum and harmonic force field 2−80036
    SOF_2, upper stage transitions in i.r. spectra 2−46580
    SO_2F_2, upper stage transitions in i.r. spectra 2−46580
    SO_2F_2, vibrational fine structure obs. in photoelectron spectrum 2−46587
    $SPCl_3$, valence force constants, polarizabilities 2−74276
    SPF_3, valence force constants, polarizabilities 2−74276
    $^{18}SO_2$, vib.-rot. interaction consts. 2−56201
    Sb_2, analysis of $B \rightarrow X$ system 2−50068
    $SbCl_6^-$, force constants determ. from frequency data using general valence, orbital valence and Urey- Bradley force fields 2−42934
    $SbCl_3(Br_3)$, freq., isotope effects 2−80022
    SeF_4 matrix isolated vibrational spectra, frequency assignments force constants 2−83265
    Si tetrahedral oxy-compounds, force constants and regularities of chemical bonding 2−70725
    $SiCl_4$, exact force field determ. from ^{35}Cl and ^{37}Cl isotope shift and analysis of vibrational spectra 2−42936
    SiF_2, vacuum u.v. spectra, vibr. assignments 2−80040
    SiI, absorption and emission spectra in 4200-4900 Å region, obs. of $A\ ^2\Sigma^+$-$X\ ^2\Pi_{1/2}$ transition, determ. of vibrational consts. 2−70726
    SiO, $A \rightarrow X$ band system, vibr.-rot. analysis 2−83248
    SiO, transition probabilities for vibration- rotation bands 2−48696
    SiO^+ electronic spectrum, vibr. and rot. anal. 2−77056
    $^{28}SiH_4$, high resolution i.r. meas. on ν_3 vibr.-rot. band 2−80039
    So_3F radical, and anion, normal coordinate analysis in Urey-Bradley force field 2−56198
    $TaCl_6^-$, $TaBr_6^-$, Urey-Bradley force fields 2−42919
    Tc(I) complex, $K_5[Tc(CN)_6]$, vibr. spectra and force consts. 2−77074
    TcO_3Cl, splitting of bands 2−77067
    TeF_4 matrix isolated vibrational spectra, frequency assignments force constants 2−83265
    Te(IV) penta- and hexacoordinate mixed halide anions 2−77094
    $TiBr_4(Cl_4)(I_4)$, orbital valence force field consts. 2−77075
    TiO, u.v. bands, vibr.-rot. consts. 2−80042
    TiO β system, Einstein coeffs. and oscillator strengths of excited levels 2−60036
    $TlFe(CrO_4)_2.2H_2O$, low temp. i.r. spectra 2−48175
    $(UO_2Cl_4)^{2-}$ and $(UO_2Br_4)^{2-}$ complexes, calculation of frequencies and normal vibrations 2−74278
    UO_2F_2, for i.r. spectrum determ. of frequencies of i.r. active bands 2−60038
    $(UO_2F_5)^{3-}$, frequencies and form of normal vibrations, interpretation of luminescence spectra 2−64159
    $UO_2(NO_3)_3$ crystals, anisotropy of i.r. absorption spectra 2−75308
    XY_5 model, mean amplitudes of vibration, polarizabilities 2−74275
    X_3Y_4, mixing of normal vibrations and isotropic freq. rules 2−56137
    XY_3Z_2, mixing of normal vibrations and isotropic freq. rules 2−56137
    XeF_2 complexes with RuF_5, valence vibrations 2−74279
    XeO_4, stretching freq., force consts., mean amplitudes, Coriolis coupling, bond order 2−52991
    XeO_4 i.r. and Raman spectra, determ. Corilis consts., isotopic freq. shift and force field 2−80023
    YO, $B^2\Sigma$-$X^2\Sigma$ system, electron transition moment variation with vibr. temp. 2−56203
    YO, $B^2\Sigma$-$X^2\Sigma$ system, Einstein coefficients and oscillator strengths 2−64161
    $Zn(py)_2X_2$ complexes, py=pyradine, X=halogen, band assignments from far i.r. and Raman spectra based on isotope shifts 2−70731
    $ZrBr_4(Cl_4)(I_4)$, orbital valence force field consts. 2−77075
Molecules, mesic and muonic
    muonic transfer from proton to deuteron, rate meas. 2−59960
    $\mu^+ + H_2 \rightarrow H^+ + \mu H$, differential cross section 2−67481
    $\mu^+ + H_2 \rightarrow \mu H + H^+$, total cross- section 2−67482
Mollier diagrams *see Thermodynamic properties*
Molybdenum
    adsorption of alkali metals, LEED and Auger spectroscopy obs. 2−50540
    adsorption of O_2, atomic and electronic processes 2−74649
    adsorption of O_2, Auger spectrum chem. shift 2−51223
    annealing, before and after neutron irradiation, physical mechanical properties 2−53730
    anode, with Cr, Fe, Co, Ni and Cu secondary anodes, K_α emission, primary and secondary excitation 2−61673
    arodic sectioning technique 2−60817
    chemical vapour deposition, for thermionic converters 2−53559
    controlled electrode surfaces, prebreakdown current in glow discharge 2−80370
    coverage of W single crystal surface rel. to work function change 2−54265
    creep, at high temp. and high stress 2−53817
    creep during hot pressing with and without addition of oxides 2−77694
    crystal, centred cubic, mean square displacement of atoms, simple calc. 2−57037
    crystal structure and mechanical properties, effect of B addition 2−56943
    defect obs., effects of voids on angular correlation of positron annihilation photons 2−71468
    deformed, Young's modulus and Poisson ratio, annealing time and temp. depend. 2−84054
    diffusion of Cr, bulk and boundary diffusion 2−53766
    electrical and thermal cond., 20 to 1200°C 2−47769
    electrical and thermal conductivity, high temp. 2−54130
    electrode, in vacuum, elec. breakdown rel. to electrode surface finish 2−75190
    electrode thermionic diodes for incore fuel elements 2−49270
    electron and hole free path lengths 2−47796
    electron irradiated at 4.2K, stage I recovery, resist. study 2−53718
    fibre, reinforced Cu composite, rolling and annealing characts., internal friction obs. 2−56987
    fibres, pressed part formation 2−53883
    filament reinforced nichrome, filament-matrix interface struct. 2−53966
    film, elec. cond. and Hall const., size effect 2−81030
    film, optical props., complex index obs. 2−56595
    foil, Au ion irrad., vacancy-type dislocation loop, prod. 2−43616
    free energies, interfacial meas. 2−80795
    fusion reactor blanket material, comparison with Nb and Nimonic alloy PE 16 2−83093
    ion irrad., void lattice obs. 2−53720
    ion irradiated, surface damage, LEED obs. 2−50468
    irradiated, void stability 2−50650
    lattice dynamics 2−84178
    linear dimensions variation under γ-ray irrad. 2−43607
    melting point as temp. secondary fixed point 2−53493
    metallographic examinations on spray coatings 2−64748
    microdeformation under dynamic loading, temp. and impurities influence 2−43696
    microhardness meas. by method of small penetration of indentor 2−47549
    monocrystal, electrical characteristics, thermionic emitter 2−54275
    neutron damage simulation by ion bombardment, void form. 2−53693
    neutron irrad., void form. and ordering, alloying and purity effects 2−53719
    neutron irradiated, correlation of void size and positron annihilation characteristics 2−71469
    neutron irradiated, stress induced ordering of stage I defects 2−64654
    neutron irradiated, void formation during annealing, electron microscope obs. 2−77575
    photoelectron energy distribution and photocurrent meas. 2−72093
    photoemission, changes due to exposure to CO, N_2 and O_2 2−51227
    plastic deformation, under compression, yield stress and slip 2−53806
    polycrystalline, role of impurity atmospheres, in brittle fracture 2−71587
    positron annihilation and band struct. 2−71824
    powder, sintering mechanism, mass transfer by diffusion-viscous flow 2−53941
    radiation generated during rapid deform. and rupture tribolum. 2−54482
    removal of C by heating with atmos. 2−64763
    room temp. ductility and intergranular cracking, after annealing 2−53875
    secondary electron emission anisotropy, raster method with modulation and deflection 2−81198
    secondary electron emission by keV K^+ ions, sharp threshold obs. 2−54282
    secondary electron spectrum, plasma satellites obs. 2−72099
    single crystals, emitter and collector work functions, modified Shelton measurement method 2−63234
    single crystals, influence of surf. states and Ti coatings on dislocat. struct. 2−83969
    single crystals, stress anal. for high temp.-creep and slip 2−84012
    solubility of H, 905-1521°C 2−50841
    spectral emissivity, 1000 to 2000K 2−64019
    sputter deposition and sputter removal from Cu, Al, Au and W, Auger spectroscopy 2−50520
    stationary cathodic arcing in vacuum 2−43221

Molybdenum continued
stopping power for 0.50-1.75 MeV protons meas. by backscattering method 2—64872
stopping power for 28 MeV α-particles 2—54099
sublimed collector coatings, additive diode operation 2—49278
superconducting, experimental obs. discussed in terms of band models 2—47832
surface, (100), Debye-Waller factor and thermal exp. coeff., LEED obs. 2—50992
surface, interaction with H beam scatt., chemisorption 2—50461
surface, proton and electron excited Auger electron spectra, composition detn. 2—50453
surface concentration, on types 316 and 304 stainless steel, Auger electron spectroscopy obs. 2—50442
surface electronic structure, positron annihilation study 2—54114
thermal expansion, to 2550°C 2—54061
thermionic converters, arc mode, influence of collector material work funct. 2—49281
thermionic emitters, CVD W coated, out of pile investigations 2—52370
thermophysical properties near melting point, electrical- explosion method 2—57066
thick target, energy loss of scatt. protons 2—80928
void form. on irrad., temp. effect 2—50642
void lattice theory, lattice spacing 2—56685
yield, surface orientation effects in single crysts. 2—74842
Al-9.5 wt.%Mg:Mo alloy, mech. props., fracture toughness, cracking effect of alloy in additions 47546 2—47546
Al_2O_3-Mo cemets, thermophysical characteristics in range 500-1300°K 2—43999
cathode, flashing effect, surface atom migration, field ion microscopy 2—53557
2-$^1/_4$ Cr-1 Mo steel, effect of carbon content on high temperature properties 2—60880
Er luminescence sensitizing, patent 2—82486
Mo:C film, supercond. transition temp. effect of C coating 2—54145
Mo:C film, supercond: transition temp., struct. 2—57169
Mo:^{57}Fe, impurity-host to host-host coupling const. ratio, Mossbauer study 2—84183
Mo/UO_2 thermionic conversion emitter-fuel system technology and test results 2—63251
Mo, angular distrib. of inelastically reflected electrons 2—80551
Mo^+, ion energy spectra from W-MO alloy sputtering 2—68263
Mo^{5+} e.p.r. in $SrTiO_3$ 2—48295
MoVIII, spectral anal., rel. to YV, ZrVI and NbVII 2—74217
in Ni alloy, effect on phase transforms. 2—43925
UO_2-Mo cermets, reactor behaviour 2—52883

Molybdenum compounds
— 2—61239
alloy, A15 type, low temp. sp. ht., supercond. transition temp. and cryst. order 2—61245
alloy, cellular struct. development during hydroextrusion 2—47642
alloy, strengthening by precip. of Ti and Zr carbides during ageing 2—47643
alloy, struct. changes during deform. 2—50839
alloy filament reinforced Ni-Cr base alloy, mech. props. 2—56988
complexes, polar and nonpolar in benzene and hexafluorobenzene, p.m.r. study of solvent induced shifts 2—83264
$^1/_2$Cr-Mo-V steels, high-strain fatigue properties 2—60948
digermanide, reaction hot pressing from Mo and Ge powders 2—61001
Mo-Ti(0.5%) alloy, transmission e. microscopy obs. of void superlattice after n. irradiation 2—64667
ternary sulphides, crystallographic instability 2—71691
Al-Mo, binary phase diagram, obs. 2—50955
Cr-Mo-Si system constitution diagram 2—50961
Cr-Mo-V steels, constitution diagrams for service lifetimes 2—60838
2$^1/_4$Cr-1Mo ferritic steel, high cycle fatigue properties at elevated temperatures 2—60951
Cu-Mo solid solns., binding energy of dislocations to impurities, internal friction obs. 2—43630
Fe-Mo alloys, nitrided, substitutional interstitial G.P. zones 2—80826
Fe-Mo solid solution, creep type, variation with applied stress 2—43703
Fe-(6 at.%)Mo alloy, precip. 43849 2—43849
Fe-MoC, quenched and tempered, microstruct., field ion microscopy obs. 2—47581
Fe-Ni-C-Mo-Cr alloy, tempering, effect on struct. and mech. props. 2—43853
Fe-Ni-Mo, powder metallurgy, carbonyl prod. method 2—68159
Fe-Ni-Mo alloy, dispersed, electrolytic deposition 2—77725
Fe-Ni-Mo alloys, cumulative thermal cycling behaviour, 300°C/hr. 2—60960
Mg/MoS_2 film/substrate system, curvilinear dislocations 2—80554
Mo-AlN-Al_2O_3 cermet, prep., microstruct., hardness, strength, density 2—43869
Mo-B system, phase diagram 2—50957
Mo-Cr-alloyed or unalloyed case hardened steel, residual stresses in carbonized layers for different thermal treatments 2—56931
Mo-Cu-Co cermet contact, elec. erosion characts. working surface struct., rel. to Co content 2—47659
Mo-Cu-Mn alloy, cold worked, heat treated, Young's modulus, rigidity, hardness, thermal expansion 2—47476
Mo-Fe alloy, precip. rel. to G.P. zone form., dislocations, vacancies 2—43851
Mo-H system, H solubility, 905-1521°C 2—50841
Mo-Hf, internal nitriding, high-temp. props. 2—60968
Mo-N, nitrogen solubility as a function of pressure and degassing kinetics 2—60967
Mo-Nb:Fe alloy, localized moments on Fe, Mossbauer obs. 2—48149
Mo-Nb alloy, elastic consts., 83-373K, effect of comp., Debye temp. 2—60845
Mo-Nb alloy, supercond. properties, u.s. technique, investigation 2—47862
Mo-Ni-TiC alloy, cermet, hardness, bending strength, wear resist. 2—47534
Mo-Pt, thermocouple, e.m.f. rel. to neutron irrad. 2—78940

Molybdenum compounds continued
Mo-Pt system, phase diagram, supercond. transition temp., conc. depend. 2—61246
Mo-Re film, A-15 struct., supercond. transition temp. 2—71867
Mo-34%Re, deform. struct., twin and disloc. microstruct. 2—43624
Mo-35%Re alloy, deform. twins, nucleation and growth 2—56720
Mo-34%Re alloy, effect of dislocation tangles on supercond. props. 2—57167
Mo-Ru alloy, microstruct., hardness and supercond. transition temp. 2—50840
Mo-Ru alloy, vapour deposited, struct., electron microscope obs. 2—60594
40 at% Mo-Tc alloy, crystal structure, X-ray obs., 4.2-298 K 2—80647
Mo-Ti, Mo-Ti-Zr alloys, radiation induced transformations in h.v. electron microscope 2—80874
Mo-Ti alloy, effect of deform. rate and temp. on ductility, mech. props. and struct. 2—47503
Mo-UO_2, W clad cermet fuel, behaviour under neutron irradiation 2—52882
Mo-W-Ti alloy, mech. and technological props. 2—47535
Mo-Zr alloy, vapour deposited, struct., electron microscope obs. 2—60594
Mo-1% Ti8% Al1% V alloy, accelerated stress-corrosion cracking in presence of hydrogen recombination poison 2—68107
Mo alloy TZM, sintered compact production, solid state reactions 2—56906
Mo complex, hexacarbonyl X-ray photoelectron spectra, multiple peak structure 2—46538
$Mo_{6-x}A_xS_6$ (A=Cu, Zn, Mg, Ag, Cd, Sn or Pb), high-temp. superconductors 2—51105
$MoAs_2$, Mo_2As_3, Mo_5As_4, growth by halogen chem. transport 2—67936
MoB_x, thermionic emission, rel. to electronic struct. 2—48017
$MoBr_3$, cryst. struct. refinement 2—47337
Mo_2C-TiC-Ni alloy, rupture strength and hardness rel. to microstruct. 2—47538
MoC, foil, stacking faults, twins 2—43641
Mo_2C, contact interaction with liquid Fe 2—77728
Mo_2C fibres, precipitation from austenite 2—77675
$Mo(CN)_8{}^{4-}$ ion, photoexcited, hydrated electrons formation 2—54555
MoCrCo alloy, total joint replacement, wear products in body 2—69292
$Mo_{1-x}M_xGa_4$, M=Nb, Ru, Mn, Fe, Co, exchange field on conduction electron spins due to paramagnetic impurities 2—77862
MoO_2 films, prepared by reactive sputtering 2—55335
MoO_2 phonon spectra rel. to VO_2. Raman spectra obs. 2—65277
MoO_3, ion bombardment enhanced elec. cond. 2—68408
MoO_3, ion impact effects on electrical conductivity 2—60779
MoO_3 film, a.c. elec. props. and I-V characts. under d.c. bias 2—68454
MoO_3 film, donor band and Schottky barrier obs. using dielectric relax. currents 2—68453
$MoO_4{}^{2-}$, LCAO MO calc. of dipole transition moment 2—77063
$MoO_{3-x}F_x$ 2—57146
$MoOS_3{}^{2-}$ amd alkali metal salts, i.r. and Raman spectra in aqueous solution 2—46560
$MoO_3 + SrCO_3 \rightarrow SrMoO_4 + CO_2$ reaction kinetics 2—54536
$MoO_3.2H_2O$, crystal structure from X-ray diffractometer data 2—56660
$MoO_3.2H_2O$, crystal structure, localization and refinement of H atom positions 2—43583
$Mo_{75}Os_{25-x}Fe_x$, supercond., compensation effect 2—64947
MoP_4, cryst. struct., synthesis, props. 2—53659
MoS_2, abrasiveness, role of impurities 2—47552
MoS_2, composite exciton absorpt. spectrum, optical phonon effects 2—44377
MoS_2, exciton mechanism for superconductivity, and nonequilibrium systems of excited excitons 2—71868
MoS_2, layer-type 2H-polytype, electronic band struct. 2—47914
MoS_2, layer semicond., magneto-optical interband absorp., energy band model 2—81333
MoS_2, rigid layer lattice vibrations and van der Waals bonding 2—84194
MoS_2 coating, applied to steel by detonation, heat and friction resist. 2—43744
MoS_2 film, sputtered, slip ring contact lubricant 2—56596
MoS_2 intercalation compound, struct., electron microscope and diffr. obs. 2—64643
MoS_2 layer struct., contact annealing effect on Hall data 2—54177
MoS_2 layer structures, a.c. conductivity in high and low frequency limit 2—81062
$MoS_4{}^{2-}$ and alkali metal salts, i.r. and Raman spectra in aqueous solution 2—46560
$MoS_2(Se_2)$, growth by direct vapour transport, and cryst. struct. 2—60707
$MoSe_2$, i.r. absorpt. spectra, transverse optic lattice vibr. freq. 2—78105
$MoSe_2$, stacking faults, anomalous X-ray line broadening obs. 2—60807
$MoSi_2$, formation on Si from Mo film 2—43861
Mo_5Si_3, diffusion of Si, oxide coating form., 1700°C 2—53769
$MoTe_2$, composite exciton absorpt. spectrum, optical phonon effects 2—44377
$MoTe_2$, growth by Br transport, and cryst. struct. 2—60707
$MoTe_2$, reflectivity, optical consts. Brillouin zone transitions 2—48162
$MoXY_3$ C_{3v} ions, (X, Y=O, S, Se), assignments, of electron charge transfer bands 2—80020
Nb-Mo-Fe alloy, discontinuous formation of localized moments, Mossbauer study 2—78076
Nb-Mo-N system, α solid soln., thermodynamic functions 2—43856
alpha-Nb-Mo-N ternary solid solution, equilibrium N concentration and thermodynamic behaviour 2—60983
Nb-Mo alloy, vapour deposited, struct., electron microscope obs. 2—60594
Nb-Mo alloy single crystals thermally activated deformation 2—80823
Nb-Mo alloys, elastic consts., anomalous temp. depend., rel. to Fermi surface features 2—47479

Molybdenum compounds continued
$Nb_{85}Mo_{15}$, supercond. energy gap field depend. from vortex entropy in low-field limit 2−57170
Ni-Cr-Mo alloy, porous material, physicomech., hydraulic, and corrosion props. 2−53977
Ni-Cr-Nb-W-Mo alloy, struct. and phase comp. 2−43941
Ni-Fe-Mo alloys, thin strips, magnetic properties and texture 2−68509
Ni-Mo alloy, porous material, physicomech., hydraulic, and corrosion props. 2−53977
Ni-Mo alloys, influence of V and Nb additions on ordering and isothermal transformations 2−71692
Ni-Mo system, interdiffusion coeffs., temp. and conc. depend. 2−56762
Ni_4Mo, internal friction study 2−43670
Pd-Mo system, interdiffusion coeffs., temp. and conc. depend. 2−56762
TZM alloy, arc casted, props. and applications 2−53825
Ta-7.3 at.%Mo alloy, oxidation, 950°C 2−72560
Ti-Al-Mo-V alloy, fatigue fracture behaviour in dry Ar environments 2−84118
Ti-Al-Mo-Zr alloy, ductility, influence of β-phase 2−50746
Ti-Mo alloy, anomalous resist, rel. to microstruct. 2−84297
Ti-Mo base β-alloy, ageing characs. rel. to tensile props. and microstruct. 2−50807
U-Mo alloy, stress corrosion cracking in humid aid, C content effects 2−53839
UO_2-Mo cermet, finely-dispersed, creep rate and particle growth 2−71650
W-Mo alloy, elec. and thermal cond., high temp. 2−54130
W-Mo alloy, sputtering, energy spectra of W^+ and Mo^+ ions 2−68263
(W, Mo)O_x, cryst. shear struct., electron microscope obs. 2−47352
Monitoring *see Radiation monitoring*
Monochromators
see also Filters, optical; Light sources; X-ray monochromators
cold neutrons, neutron spectrometer, slit package cross section Be filter, time of flight, wavelength resolution 2−82565
Czerny-Turner, without intermediate slit, aberration coma free 2−79438
double, compensation for coma and anamorphic effect 2−55773
double monochromator with two diffraction gratings 2−59285
grating, sine drive, cam and linkage design 2−55770
neutron, growth of suitable crysts. 2−47205
polarizing effects of 2−49452
Monolayers *see Adsorbed layers*
Monomers *see Molecules*
Monomolecular layers *see Adsorbed layers*
Monopoles, magnetic *see Magnetic monopoles*
Monte Carlo method *see Statistical analysis*
Moon
1019, September 16 eclipse from al-Biruni's solar data, det. of lunar acceleration 2−65427
1971, Feb. 10, total eclipse, obs. at 3.1 mm wavelength 2−44912
— 2−62702
accretion process, from geochemical and geophysical data 2−62662
accumulation by Earth, and lunar mass objects in early solar system 2−58445
accumulation on assumption that Moon is captured object 2−62655
albedo and linear polarization rel. to optical properties of igneous rocks in i.r. range 2−75846
albedo and temp. distribution at full moon 2−73065
amino acid abundance 2−57729
Apollo 11, 12 and 14 fines, Rn emanation meas. 2−62646
Apollo 11 and 12 fines, spectral reflectance and emittance 2−78518
Apollo 11 and 12 manned lunar landings, review of scientific results 2−44931
Apollo 12 soil samples, fragments of terra rock 2−69132
Apollo 14 active seismic experiment 2−55132
Apollo 14 microbreccias, 14306 and 14055 specimens analysis 2−55120
Apollo 14 samples, occurrence of chromian and hercynitic spinel, petrologic implications 2−73063
Apollo 14 seismic experiment 2−48764
Apollo 15 altimeter measurements, laser altimetry 2−62682
Apollo 15 lunar heat flow experiment 2−55135
Apollo 16, first report 2−62665
Apollo 16, more about it 2−62666
Apollo 16 soil 68501, trace element geochemistry 2−75851
Apollo II basalt flow sample, rate of solidification rel. to Hawaiian lava lakes 2−66144
Apollo lunar landing missions, landing site selection process 2−62644
Apollo lunar module exhaust gas, mass spectrometer analysis 2−58145
Apollo lunar seismic experiment, results from seismic station network 2−44922
Apollo lunar spacecraft, how it works 2−58455
Apollo samples, seismic and electrical props. 2−66158
Apollo spacecraft, equipment and instrumentation, review 2−51823
astronomical observatory, Apollo 16 2−45002
atmosphere, density and flux distributions of neutral gases 2−66156
atmosphere, upper limit determination by solar wind measurements 2−58470
basalt rock 15085, comp. of tridymite and crystobalite 2−78486
basaltic rocks, U-Th-Pb ages and Pb concentration obs. 2−44907
basaltic rocks and minerals, Mg+Fe comp., rel. to parental liq. comp. 2−62676
basalts, Apollo 15, distinct cooling history 2−58452
breccia, deform. substruct. obs. 2−62688
breccia and crystalline rocks, thermoremanent magnetization 2−51809
breccias, Apollo-14 samples, geological implications 2−58460
breccias and soils, possible origin of excess Fe 2−55127
brightness temps. in far i.r. for sunlit surface 2−73066
Brown's lunar theory, different methods of derivation of differentials 2−84938
calcic plagioclases, phase transforms. and exsolution 2−66162
Moon continued
centre of lunar mass, position determ. from photographic observations 2−75845
centre of mass position based on Lunar Orbiter-1 data 2−78523
chronology and evolution, unified treatment 2−62685
circular maria, mascons rel. to isostatic adjustment 2−69135
clastic materials, Apollo 14 samples, comp. characts. 2−58459
co-ordinates, literal expressions for first order terms 2−81922
colour information from space missions 2−81938
conductivity, models, compatibility with Apollo 12 magnetometer data 2−51803
conductivity profile and nonuniqueness of e.m. data inversion 2−75850
core material, thermoluminescence, temp. gradient obs. 2−62651
crater (6°N, 98°E), dedicated to Luis Enrique Erro 2−73062
crater development by fluidization 2−62674
crater diameters, depths and morphologies, the System of Lunar Craters, revision 2−44918
crater impact genesis rel. to geometric similitude of lunar and terrestrial craters 2−78510
crater laboratory simulation 2−44924
craters, origin studies using Mount Etna and Stromboli geologic and photoballistic obs. 2−81567
crust, velocity structure and props. 2−62663
crust rel. to Earth and Martian crusts, three-dimensional model 2−81917
density of interior 2−85036
density variations, large-scale, in interior 2−73064
Descartes region, evidence for Copernican age volcanism 2−66155
distance from Earth, measurement using sub-nanosecond laser pulse radar 2−85068
dust grains, micrometer-sized, Apollo and Luna 16 samples, obs. of ultrathin amorphous coatings 2−44929
dust grains with amorphous coatings, refl. spectra 2−85045
dust layers, effect of fluidization on polarization of reflected light 2−58453
dynamical properties and internal structures, review 2−51520
Earth-Moon distance measurements using lasers 2−44932
Earth-Moon system evolution rel. to satellite swarm accretion 2−58484
electrical conductivity, exptal det. 2−62664
electrical parameters and surface layer, thickness, r.f. interference depth sounding 2−55137
e.m. transfer function, investigation of differences 2−62683
equatorial region, i.r. and radar maps 2−62660
exploration geophysics role 2−55136
fayalite-forsterite solid solution between 900-1300°C at low pressures 2−65538
figure, based on laser altimetry obs. 2−62653
fines, Apollo 12 samples, thermal conductivity 2−51811
fines, Apollo 12 samples, thermal radiation props. 2−51815
fines, dumbbell shaped globules, mechanism of formation 2−44898
fines, ESR spectra, 'characteristic' resonance, lunar surface oxidation 2−58474
fines, total emittance as fn. of temp. 2−66152
flow of gases in granular media at low pressures, grain size matching that found at Apollo 12 landing site 2−56420
formation by modified fission process 2−62679
Fra Mauro breccias, form. modelling 2−62671
fragmental material prod. by meteoroid impact 2−58467
geodynamic and astronical research in France (CERGA) 2−62641
geomagnetic variations, lunar diurnal harmonic components 2−66013
glass, interferometric evidence for low temp. shock 2−55124
glass particles, micrometeorite craters, radial fracture zones and spall zones 2−51822
glass spherule comparison with microtektites 2−62670
gravity, Apollo 14 and 15 missions 2−55134
gravity anal., Apollo 15 S-band transponder expt. 2−62657
gravity anomaly det. using orbiting gravity gradiometer expt. 2−51813
gravity field expansion, coeffs. C_{20} and C_{22} 2−75852
gravity transverse expt. 2−62650
grazing occultation of ZC.3091, during eclipse 2−81927
heat flow, Apollo Lunar Surface Experiment Package 2−62656
h.f. e.m. response, transfer functions for tangential components of surface mag. field 2−66146
hypervelocity impacts on Earth and the Moon 2−66195
igneous rocks, Apollo 15 samples, rare earth element analysis 2−62669
igneous rocks, comparison of lunar sample with synthetically prepared armalcolite 2−44928
ilmenites, from Mare Tranquillitatis, morphology, electron microscope obs. 2−44905
impact produced plasma clouds, Apollo 14 lunar modules 2−66151
inner solar nebula, physical conditions 2−81948
intensity and colour variations across surface, high resolution scans 2−78520
interior, electrical conductivity, det. from magnetic field obs. 2−51810
internal constitution and evolution, models 2−62677
internal electromagnetic and thermal properties from surface mag. field meas. 2−55130
interplanetary magnetic field-Moon interaction, effect of boundary condition asymmetries 2−51816
known objects on lunar surface, list 2−55126
laser range meas. 2−55131
laser ranging expt., single photon detection and timing 2−48973
laser ranging expt. 2−44930
laser ranging expts. with decimeter accuracy 2−58447
lasers ranging experiment data, filtering 2−58448
lidar location of light reflector on Lunokhod-1 vehicle, distance measurements 2−69953
lineament azimuthal pattern, statistical study of Lunar Orbiter photographs and telescope observations 2−78509
lithification and metamorphism of breccias 2−85034
Littrow-Proclus area, Apollo 15 photographs, struct. geology and lunar grid 2−62673
lunar and terrestrial materials, ESCA study 2−48761
lunar composition rel. to early history of solar system 2−78501

Moon continued
lunar glasses, tektites, mag. suscep. 2−73073
lunar highlands, high albedo central region observations and model 2−78519
lunar influence on atmospheric ozone 2−48469
lunar ions, energy spectrum 2−58469
lunar motion, errors, numerical methods, lasers, Doppler effect 2−84939
lunar photon albedo from galactic and solar proton bombardment 2−66148
lunar regolith, model for Rn diffusion by random walk method 2−44921
lunar regolith and role of shock metamorphism 2−78511
lunar rilles rel. to Hawaiian volcanic features, lava tube formations 2−44919
lunar rock, transmission elec. microscopy obs. 2−56954
lunar rock microcraters, classification of crater type and impact theory 2−81942
lunar soil disturbance effect, rel. to changes in photometric function 2−44920
lunar soil samples rel. to telescopic spectral reflectivity measurements 2−78521
lunar theory, numerical isolation of flaws 2−81923
lunar variations in Peruvian electrojet, E-region electron-drift measurements 2−68955
lunar wake in solar wind flow, magnetic-field anomalies 2−69134
mag. field meas. by Apollo 15 subsatellite 2−55129
magnetic field, measurement by magnetometer on board Apollo 15 subsatellite 2−58472
magnetic field, satellite obs., remanent magnetization 2−62658
magnetic field variations, effect of sunspot cycle 2−75633
magnetic fields origin theories, review 2−51807
magnetic history, rock and subsatellite evidence 2−58466
magnetic susceptibility studies, review 2−52381
maria and mascons development, hypervolcanic flyby scars 2−62675
mass, gravitational field and moment of inertia determinations, Lunar Orbiter 2−44917
mass, refinement from obs. of artificial satellite motion 2−55139
moments of inertia, effect on chemical differentiation of outer layers 2−51805
moonquakes and lunar structure, Apollo 12 and 14 mission 2−55133
moonquakes recorded by Apollo short-period seismometers 2−58456
neutron stratigraphy 2−62647
nightside, energetic ion burst detection 2−66147
non-gravitational forces and acceleration of Moon's mean angular velocity 2−58477
nonisothermal scattering and absorptive medium, generalized Kirchhoff's law 2−75854
occultation, near elliptic bright stars 2−85063
occultation of PSR 1749-28, accurate radio position 2−66132
occultation of radio source Sgr A, obs. at 327 MHz 2−73046
occultation of single and double stars, catalogue of diffraction patterns 2−75701
offset core model rel. to centre of gravity, moment of inertia, mascons and maria 2−66160
olivine electrical conductivity rel. to temperature profile of lunar interior 2−66142
olivines, temp. dependent Mg, Fe distribution 2−44908
orbit, laser ranging data, trial solns. 2−58449
orbital elements soln. and derivation 2−62645
origin, evolution and present thermal state, review 2−85041
origin, joint formation with Earth 2−58444
origin and evolution of Earth-Moon system 2−73077
origin by tidal capture, geophysical consequences 2−73068
origin rel. to condensation of terrestrial planets 2−78524
paleocratering, post-Apollo data, review 2−85026
particle shadows, theoretical treatment 2−69131
penumbral eclipse, Sep. 25, 1969, photoelectric photometry 2−44906
petrogenesis, Sr isotope ages 2−62684
petrologic comparisons of lunar terra materials 2−78512
phase law and partial tides in H 2−58450
photographic degradation by atm., resolution enhancement by digital computer processing 2−76040
photometry in u.v. region using OAO-II Celescope experiment 2−81902
physical librations obs. using laser retroreflectors 2−51817
physical structure and evidence of core rel. to thermal models 2−78508
plagioclases, e.p.r., Ti^{3+}, Fe^{3+} and Mn^{2+} obs. 2−62686
planetology congress (Montreal, September, 1972) 2−78499
positions using 13-inch photographic equatorial refractor 2−66163
proto-Moon, form. times and initial temps. 2−62678
pyroxenes, microstruct. on cooling 2−62689
pyroxenes and olivines, polarized absorption spectra 2−51812
quakes, tidal cycles 2−58471
radio mapping, high resolution 2−75936
radiowave reflection, ultrashort, circularly polarized 2−55196
rare earth abundances and liquid type and solid type materials 2−55122
recurrence of lunar and solar eclipses 2−73102
regolith, noble gas variations with depth 2−58461
regolith evolution mechanisms from impact experiments and computer simulations 2−81943
regolith glassy particle formation, modelling 2−73071
remanent magnetization rel. to solar wind perturbations 2−66150
rock 12052, rim augite and core pigeonite, crystal structures 2−48762
rock 14310, whitelock and apatite, microprobe analysis 2−48760
rock from Fra Mauro formation, ^{244}Pu fission tracks obs. 2−69137
rock magnetism, effects of neutron irradiation on remanent magnetic properties of multidomain Fe 2−58458
rock magnetism, rel. between magnetism and temp. 2−51818
rock samples, Rb-Sr data rel. to 4.3 aeon pre-Imbrium event 2−55119
rock samples, remote-controlled boring and retieval by Luna 16 2−51802
rock type KREEP, form. time 2−58465
rocks, Apollo 14 and 15 samples, ^{40}Ar-^{39}Ar ages 2−62668

Moon continued
rocks, Apollo 15 samples, ^{40}Ar-^{39}Ar ages 2−62667
rocks, breccias and fines, thermophysical props. 2−62661
rocks, chondrules and ultramafic glasses 2−78483
rocks, radiation induced e.p.r. signals 2−55123
rocks, simultaneous meas. of u.s. vel. and compression 2−61982
rocks and fines, ferromagnetic and paramagnetic resonance spectra 2−62648
rocks and minerals, shock melting and vaporization 2−51821
rotational resonances and Cassini's laws 2−78498
rough surface, circular polarization of scattered light 2−63395
samples, magnetic hysteresis properties 2−58473
samples, thermoremanent magnetization and NRM 2−58440
satellite radio wave emission reflected energy spectrum 2−55600
seismic data, structure and composition of crust 2−55125
seismic Q and structure 2−62659
seismic ringing, experimental study 2−44926
seismic scattering, rel. to Earth 2−58475
seismic signals, experiments on u.s. signals in steel balls 2−44927
seismic waves on moon, duration, scattering and attenuation 2−73072
seismology, anal. of seismograms 2−51808
selective volatilization rel. to plagioclase-rich basalt (14310) 2−69136
selenodesic catalogues, mutual positions of centres, det. from hypsometric charts 2−55118
selenodetic catalogues, relative orientations rel. to Eulerian angles 2−81935
selenodetic nets of coordinates, relative deformations, comparison of catalogues 2−44916
single crystal samples, X-ray milliprobe for obs. 2−51481
soil, Apollo 14 and 15 samples, inorg. gas release obs. 2−62672
soil, mechanical properties, Luna-16 automatic spacecraft 2−55117
soil, physical properties, terrestrial analogues 2−75848
soil samples, L16/O78, nondestructive neutron activation analysis of Si and O$_2$ abundances 2−85043
solar and galactic cosmic rays, interaction with Moon 2−66149
solar wind, lunar wake in magnetohydrodynamic model, numerical calc. 2−58454
solar wind observations on lunar surface with Apollo-12 ALSEP 2−85057
space vehicles observations, reviews 2−66164
spectral reflectance ratios, computer generated colour image display 2−66877
spectral reflectivity properties, 0.3-1.1 μ 2−66153
spectrozonal map for area of surface 2−73070
spectrum features due to glasses in soil 2−58464
sphere of interaction rel. to Earth and Sun, restricted four body problem 2−68996
stratified rocks of Hadley Apennines, Apollo 15 obs. 2−75847
subsurface exploration with coherent radar 2−51814
subsurface temp. from thermal radiation 2−58451
suprathermal ion detection near surface 2−44913
surface, Apollo-16 geochemical X-ray fluorescence experiment 2−78497
surface, bistatic radar obs., Apollo 2−78495
surface, determ. of relative ages of areas from orbital photography 2−69133
surface, distribution of low angle impact craters and early history 2−73067
surface, post-sunset cooling behaviour 2−51804
surface Breccias, theoretical reappraisal 2−62687
surface brightness temp. as measured by Apollo 15 heat flow experiment 2−62681
surface comp. mapping using mid-i.r. spectroscopic remote sensing 2−58463
surface exposed rocks, α-radioactivity obs, ^{210}Po activity obs. search 2−44910
surface fields, thermal emission spectrum, wavelength depend. 2−58462
surface layer material, density, variations 2−55116
surface mag. meas. and interior properties 2−55128
surface rocks, d.c. electrical conductivity 2−51819
surface rocks and fines, i.r. and Raman 2−62652
surface topography, Earth based radar technique 2−62649
tectonic processes, relation between Earth and Moon, transient phenomena 2−48392
tectonism and Moonquakes 2−66159
telescopic spectral reflectivity rel. to four lunar spectral types and samples 2−78522
temperature profile, interior, olivine electrical conductivity obs. 2−51806
thermal charact., book 2−75853
thermal characteristics of surface layer 2−48763
thermal emission from a rough lunar surface, directionality 2−44915
thermal evolution of interior 2−51820
thermal history and lava filled craters 2−44923
thermal history and mare basalts rel. to terrestrial continental evolution 2−57449
thermal histroy and early magmatism 2−44911
tidal dynamics effects on O I5577 A nightglow 2−65891
tidal variations, O, component of geomag. lunar daily variation 2−44767
topographic features, colour boundaries 2−62654
transient events, correlation with perigee, observational bias 2−62680
transient events, correlation with perigee, source of observational bias 2−66157
transient phenomena, comparative anal. of obs. 2−44914
two-dimensional digital vidicon photometry in 0.38 to 1.1 micron range 2−78526
ultrabasic lunar samples rel. to differentiation on Moon 2−85040
umbral eclipse contact moments, accuracy determinations 2−58446
wake, interplanetary magnetic field anomaly production 2−62730
water, experiments and results 2−44925
winding and meandering furrows, origin 2−73069
zirkelites, U-bearing phase 2−44909
^{130}Ba(n,γ)^{131}Xe cross section rel. to origin of ^{131}Xe on the Moon 2−66143
C abundance in Apollo 11, 12 and 14 lunar samples 2−78513

Moon continued
C content of lunar basalt samples and related terrestrial rocks 2−58457
CH_4 and C_2H_6 in size-fractionated lunar fines in Apollo 12 and 14 samples 2−55121
^{14}C in rock 12002, depth profile 2−85035
Fe oxides, lunar surface, solar wind darkening 2−66154
H_2O vapours on lunar surface, Apollo 14 SIDE mass spectrometer analysis 2−58468
O_2 content of rock sample, neutron activation anal. 2−69138
Rb-Sr isotope characts. of soils 2−66139
^{222}Rn in lunar atmosphere rel. to ^{210}Po concentrations 2−66161
S content of lunar basalt samples and related terrestrial rocks 2−58457
U-distribution in basaltic fragments of five lunar rock samples 2−75849
Xe in lunar breccia, fission product from extinct ^{244}Pu 2−66145

Morphology, crystal *see Crystal morphology*

Morse potential *see Kinetic theory; Molecules/intermolecular mechanics*

Mosaic structure *see Crystal structure/microstructure*

Mossbauer effect
see also Gamma-rays/absorption; Nuclear excitation
— 2−67976
alkali borate glass containing Fe, struct. and magnetic props. 2−65230
alloy, mictomagnetic, rel. to mag. struct. model 2−65166
biotite, of ^{57}Fe, isomer shift and quadrupole splitting obs. 2−75266
chemical shift, determination of explicit value 2−61598
crystal, deformed, resonant absorption of X-rays 2−84474
crystal struct. damage on ion implantation, expt. 2−50631
diamond, of ^{57}Fe 2−48152
electron spin-Mossbauer double resonance 2−57334
excited nuclei, lifetime studies 2−46106
ferric amphibole, pressure induced reduction 2−84721
ferromagnet, freq.-modulation sidebands due to r.f. acoustic vibrs. 2−48141
ferrous metals, obs. of stresses and phases 2−51312
five line hyperfine split absorber spectra analysis 2−65227
glass, containing metal ions, structure obs. 2−64526
glass and supercooled liq., organic, mol. motion, Mossbauer scatt. obs. 2−61609
glasses and supercooled liquids, structure obs. 2−60583
group V_2-VI_3 semiconducting Sb compound, of ^{121}Sb and ^{125}Te nuclei 2−75274
group V-VI-VII semiconducting Sb compound, of ^{121}Sb and ^{125}Te nuclei 2−75274
haem derivatives, quadrupole splitting, SCC-EH-MO calculations 2−60098
hemin, nuclear hyperfine interactions 2−67527
hexaferrites, determ. of angle between spins of octahedral ions 2−84436
hyperfine spectra, temp. depend. line shape rel. to mag. orders 2−75263
illite, microstructure and chemical comp. 2−84710
bis-imidazole hemin, nuclear hyperfine interactions 2−67527
iron(II)formate-magnesium formate system, mixed crystn. obs. 2−56673
iron formate dihydrate, between 4.2 and 0.027K 2−54394
isomer shift, determination of explicit value 2−61598
isomer shift used in calc. of nuclear charge radius 2−76759
line broadening, many closely spaced internal fields 2−61601
line shape in coupled hyperfine interactions 2−75264
linear air track demonstration 2−62926
lineshape formula derivation and interference parameter 2−49721
liquid crystal, quenched nematic, alignment obs. 2−60425
magnetic anomalies caused by mag. order in spin system 2−72274
magnetic struct. investigation with polarized recoil-free γ-rays 2−44351
magnetically ordered crystals, kinematic theory including Rayleigh dispersion 2−68610
metal (h.c.p.):^{57}Fe, electric field gradient 2−80986
nuclear and electronic γ-ray scatt., interference rel. to polarization 2−54385
paramagnetic crystal, Mossbauer dispersion and nuclear Faraday effect 2−78073
permalloy, magnetic hyperfine field at ^{57}Fe 2−54386
phase transform, Debye-Waller anomaly, Mossbauer fraction 2−68211
photoelectron-conversion electron interference, effect of absorber thickness 2−55953
polyethylene glycol/water system, Mossbauer scattering study of molecular motion at room temperature 2−72277
polyisobutene Mossbauer scattering study of molecular motion in 90-310K range 2−72277
polytetrafluoroethylene, Mossbauer scattering study of molecular motion 2−72277
rare earth iron garnets, isomer shifts of ^{57}Fe 2−57333
rare earth iron garnets, mixed, easy magnetiz. direction 2−51314
rare earth materials, review of applics. to phys., chem. and metallurgy 2−51313
rare earth ortho-ferrite, substituted, mag. non equivalent states obs. 2−61602
rare-earth oxides, temp. spikes following Coulomb excitation, thermal after effects 2−71719
red beds, determination of components affecting rock magnetism 2−58141
resonant γ-ray nuclear Bragg reflection, azimuthal depend. elec. field determ. 2−81342
review, theory, expt., appls., 1970-71 2−52672
r.f. induced sidebands, quenching technique 2−51304
scattering, quadrupole diffr. peaks 2−48140
scattering probability in coupled hyperfine interactions 2−46107
scattering spectra, computer simulation 2−68609
semiconductor, III-V, transition metal doped, anomalous props. 2−68405
siderite, thermal decomposition kinetics 2−72666
single line, optimum absorber thickness, in presence of strong nonresonant absorption 2−59684

Mossbauer effect continued
spectra of complex structures, data processing by computer 2−61600
spectra of impurity atoms in crystals, correlation influence in diffusion 2−65228
spectral recording from scintillation counter by current method 2−59620
spectrometer, application to structural mechanics 2−55901
spectrometer, based on A1-256 analyzer 2−59630
spectrometer, multichannel, using multiwire proportional counters 2−42446
spectroscopy, backscatter detector 2−79659
Staurolite, Fe^{2+} site distribution, Mossbauer spectrum 2−48143
steel, retained austenite developed during surface grinding of carbon steel, exptl. obs. using conversion-electron scatt. 2−74880
tables and data for isotopes 2−63759
time-reversal expts., development of S-matrix formalism 2−46092
titanomagnetite, determination of cation distribution, geological significance 2−54965
zeolite, cation-exchanged, Fe^0-atom obs., Auger emission, e.f.g., Debye temp., f-factor 2−54390
γ-ray laser, based on crysts. of long lived nuclear isomers 2−66762
^{a}Os, A=188, 190, 192, comparison of IMPACT, PAC and Mossbauer effect meas. of g-factor, ferromagnetic host effects 2−42534
$Al_2Fe_3(SiO_4)_3$, almandite, garnet, elec. field gradient, internal mag. field, Mossbauer obs. 2−54388
Al_2O_3-Fe_2O_3 solid solns., impurity ion effects on spin relax. time of ferric ions 2−54368
As-Se-Ge-Sn glass, isomeric shift, quadrupole splitting, phase diagram 2−75267
AsI_3, $AsI_3.3S_8$, ^{129}I effects calc. of bond character 2−78071
Au-Sn alloy, Sn atom oscills., obs. 2−51308
Au-Yb dilute alloy, localized moments obs. 2−81210
AuCN, anomalously narrow linewidth in ^{197}Au 2−78074
AuFe alloy, reducing point charge model analysis 2−65229
B:Fe, crystallographic positions of Fe, isomer shifts 2−51305
β-B, rhombohedral of ^{57}Co and ^{57}Fe 2−61603
BI_3, ^{129}I effects calc. of bond character 2−78071
$Ba(Fe_{0.35}Al_{0.65})_2O_4$, disordered solid solution, blocking temps. of mag. random clusters 2−57309
Be-(1 wt.%)Fe alloy, precip. on thermal treatment, mechanism 2−50931
Bi-Sb alloy, 5-100% Sb, of ^{121}Sb, 80K 2−81345
$CaAl_{12-x}Fe_xO_{19}$ solid soln., $x \leqslant 4.8$, e.s.r. and Mossbauer obs., ferric ion positions 2−75268
$Ca_3Fe_{2-x}M_xGe_3O_{12}$, $M=Al^{3+}$, Ga^{3+}, Cr^{3+}, Sc^{3+}, In^{3+}, Mossbauer study of lattice 2−72278
$2CaO.Mn_xFe_{2-x}O_3(O \leqslant x \leqslant 0.5)$, temp. depend., meas. 2−43644
$Cd_3Fe_{2-x}M_xGe_3O_{12}$, $M=Al^{3+}$, Ga^{3+}, Cr^{3+}, Sc^{3+}, In^{3+}, Mossbauer study of lattice 2−72278
Co complex, $[Co(phen)_3](ClO_4)_2.2H_2O$ spin triplet states of Fe(II) 2−68806
Co complex, diarsine complexes, emission spectra, after effects of electron capture decay 2−65233
Co complex, diarsine complexes, absorption spectra, after effects of electron capture decay 2−65232
Co containing ^{57}Fe, contact charge density of conduction electrons 2−51307
$Co_xZn_{1-x}Fe_2O_4$, ferrite, Fe^{3+} spin fluctuations mag. hyperfine splitting, relax. effects, Mossbauer spectra 2−81287
$(Cr_{0.8}Fe_{0.2})(OH)_3$, thermal conversion to $(Cr_{0.8}Fe_{0.2})O_3$, Mossbauer parameters variation 2−72547
CrN_x, hexagonal, mag. props. obs. 2−54331
$CsCo(Cu)(Ni)Cl_3$, one-dimens. mag. obs. 2−72160
$CsFeF_4$, planar antiferromagnet 2−65180
Cu-Fe, distrib. of nearest neighbour atoms 2−74900
Cu-Ni:^{57}Fe, doublets, time-differential perturbed angular correlations 2−72275
Cu-1 at.%Fe alloy, obs. of precip. of Fe during ageing 2−77724
Cu_2FeSnS_4, mag. ordering obs. 2−75239
^{158}Dy, ^{160}Dy, low-temp. recoilless γ-ray emission decrease 2−67173
^{161}Dy, of 43.8 keV transition, obs. 2−63819
(Eu,Sm)Fe, and (Eu, Ho)Fe garnets, mixed, easy magnetiz. direction 2−51314
Eu chelates, comparison of resonant intensities used to determine structure differences 2−48142
Eu(III) complex, chelate, polymerization 2−51309
Eu(III) complexes, hexahalo, parameter determ. 2−51310
EuSe:Gd(La), ^{151}Eu hyperfine interactions, mag. struct. effect 2−48145
EuTe, Eu_3Te_4, Eu_4Te_7, Eu_3Te_7, Mossbauer spectra, sublattice covalent bonding, isomer shift, internal mag. field at Te nuclei 2−54389
^{151}Eu, after Coulomb excitation with 3.3 MeV α-particles 2−84473
^{151}Eu, effect of asymmetry parameter on unresolved quadrupole splitting of spectra 2−72279
^{153}Eu, isomer shifts of gamma transitions 2−59714
^{153}Eu, theoretical investigation of muonic and Mossbauer isomer shifts 2−42526
Fe-Cr dil. alloy, hyperfine field reduction and spin disturbance produced by solute 2−44354
Fe-Cr σ-phase, atomic distrib. and mag. props. study 2−44253
Fe-Ga alloys, magnetic props. 2−84416
Fe-Ga solid solns., of ^{57}Fe, lineshape effect on hyperfine fields 2−44353
Fe-Ni alloy, atom redistrib. on ageing 2−60981
Fe-Pd-H alloys 2−74953
Fe-Rh alloy, f.c.c., Neel temp. determ. 2−78072
β-Fe-Ti alloy, Fe diffusion coeff. determ. 2−77612
Fe-V σ-phase, atomic distrib. and mag. props. study 2−44253
Fe-12.3 at.%-Al, short-range order determination, heat treatment and cold rolling effects 2−51311
$(Fe,M)_2Mo_3O_8$, (M=Mg, Zn, Mn, Co, Ni), cryst. field interpretation 2−75270
Fe, ^{127}I mag. moment obs. 2−63812
Fe, electron spin density meas. by combined Mossbauer and electron spectroscopy technique 2−81343
Fe, high pressure obs. between 300-20K 2−72283
Fe, Mossbauer examination of internal mag. field variation with temp. and pressure 2−68330
Fe atoms in YuNDK24 alloy, exam. by nuclear γ reson. after thermomagnetic treatment 2−84471

Mossbauer effect continued
  Fe complex, aminoacid, measurement of Mossbauer spectra at temperatures 82 and 298K 2−57336
  Fe complex, diarsine complexes, absorption spectra, after effects of electron capture decay 2−65232
  Fe complex, diarsine complexes, emission spectra, after effects of electron capture decay 2−65233
  Fe complexes, $Fe^{II}Fe_2^{III}(CH_3COO)_6.O.X$, $X=5H_2O$, $py_{3.5}$, thermal electron transfer 2−72276
  Fe complexes, iron(II) naphthyridines, Mossbauer parameters and mag. moments 2−81340
  Fe complexes, nitroprussides, purity of samples tested by obs. of line widths in ^{57}Fe Mossbauer spectra 2−44352
  Fe film, corrosion products in $NaNO_2$ soln., internal conversion electrons study 2−72281
  Fe film, u.h.v. emission spectra, mag. behaviour rel. to particle size 2−72284
  Fe foil, high freq. mag. field effects 2−57332
  Fe thin films, Mossbauer spectra, 15-350 K, superparamagnetic fluctuations 2−68611
  $FeBO_3$, of ^{57}Fe, mag. field induced antiferromag. 2−54355
  $FeCl_3$ frozen aqueous solns., investigation of glass to crystal transformation at 200 K 2−72280
  $FeClO_4$ frozen solns., mag. props. of Fe^{3+} ion 2−78070
  $Fe(ClO_4)_2.6H_2O$, phase transition, Mossbauer spectra electric quadrupole interaction rel. to temp. and mag. field 2−75271
  $FeCl_3.6H_2O$, spontaneous magnetization, mag. ordering, mag. hyperfine fields, Mossbauer reson., $T<4.2$ K 2−75272
  $FeCr_2S_4$ spinel, quadrupole interaction, h.f.s., e.f.g., Debye model, Jahn-Teller effect 2−57331
  FeF_2, mag. hyperfine interactions of Fe^{2+} 2−61604
  Fe(II) complex, bis(thiosemicarbazide)iron(II) sulphate, large quadrupole splitting 2−61605
  Fe(II) salt solutions, frozen at normal pressure, spectra 2−78178
  Fe(IV) complex, paramagnetic hyperfine interactions in $t_{2g}{}^4$ config. of ^{57}Fe 2−84472
  $Fe_{3-x}Mg_xO_4$, ferrite-spinels, Mossbauer spectra and effect of admixture 2−72282
  FeN_x, hexagonal, mag. props. obs. 2−54331
  α-Fe_2O_3-β-FeOOH, disperse system, high surface area, Mossbauer obs. 2−68612
  $Fe_{0.95}O$, wustite, isomeric shift, mag. field, at 300, 223 and 80K 2−75269
  α-Fe_2O_3, haematite, of ^{119}Sn and ^{57}Fe, Morin transition obs. 2−65234
  Fe_2O_3, isomer shifts of ^{57}Fe 2−57333
  γ-Fe_2O_3, superparamagnetism obs. 2−48038
  γ-Fe_2O_3, vacancy distrib. over tetrahedral and octahedral sites 2−60786
  α-Fe_2O_3 microcrysts., chem. modification of quadrupole interaction 2−65231
  γ-FeOOH, lepidocrocite, crystal struct. and mag. props. at temp. of conversion to α-Fe_2O_3, hematite 2−57287
  β-FeOOH, thermal conversion to α-Fe_2O_3, Mossbauer parameters variation 2−72547
  $Fe_xPd_{80-x}P_{20}$ $(13\leqslant x\leqslant 44)$, amorphous alloys, of ^{57}Fe, mag. props. obs. 2−65114
  $Fe(Pd_xPt_{1-x})_3$, magnetic phase transitions obs. 2−48108
  FeS, hyperfine interactions obs. 2−48146
  FeS antiferromagnetic, determ. of spin arrangements, quadrupole interaction, internal magnetic field, chemical shift 2−81344
  Fe_3S_4, synthetic samples, magnetic properties 2−81338
  $FeSb_2$, Mossbauer spectra, quadrupole splitting, isomer shift, Debye temp., 6.4-540K 2−61606
  $Fe_{1\|6}Sb$, antiferromagnetism 2−84440
  $Fe_{3-x}Sc_xO_4$, electronic struct. of ions 2−48207
  $FeTiO_3$, below Neel temp. 2−57330
  ^{57}Fe, asymmetries in γ scatt., h.f.s., interference, vectorial relations 2−74025
  ^{57}Fe, calibration of isomer shift 2−46137
  ^{57}Fe, det. of electric field gradient parameters from Mossbauer spectra 2−54387
  ^{57}Fe, γ-ray diffr. by grating interpret. of amplitude modulation 2−46136
  ^{57}Fe, recoilless fraction and second-order Doppler shift, effect of pressure in some host lattices 2−61599
  ^{57}Fe in powdered absorbers, h.f.s. coupling and Mossbauer spectra parameters 2−75265
  Fe(II) complexes of 2-methyl-1, 10-phenanthroline, ^{57}Fe spectrum obs. from 298 K to 4.2K 2−51306
  Gd, $A=150$, 160, isomer shifts 2−70407
  $Gd_3Fe_{5-x}Al_xO_{12}$, cation distrib. detn. 2−48147
  ^{158}Gd, low-temp. recoilless γ-ray emission decrease 2−67173
  Ge-Se-Sn system glasses, chem. comp., struct. units 2−43452
  Ge, of ^{57}Fe 2−48152
  Hf, elec. quadrupole interaction of ^{181}Ta 2−61607
  Hf polycrystalline sample, influence of Zr on the quadrupole interaction of ^{181}Ta 2−84593
  ^{178}Hf 93.2 keV transition, isomer shift, shrinking of nucl. charge radius in rot. state 2−76804
  $Ho_xEr_{1-x}Fe_2$ system, spin orientation diagram obs. 2−72197
  HoPtSn and related intermetallics, isomer shift, Debye-Waller factors 2−50621
  IFe, meas. of magnetic moment of 57.6 keV state of ^{127}I, and hyperfine field 2−49747
  InSb:^{57}Co, doped by diffusion, diffusion and emission spectra obs. 2−65235
  $KAu(CN)_2$, anomalously narrow linewidth in ^{197}Au 2−78074
  $KAu(CN)_2$, elec. alignment of ^{197}Au 2−44356
  $KAu(CN)_2$, elec. hyperfine alignment of ^{197}Au 2−44355
  $K_3Co_{1-x}Fe_x(CN)_6$, Fe^{III} complex $3d(t_{2g})$ density distrib. detn. 2−68613
  $K_3Fe(CN_6)$, electronic structure model consistent with exptl. data 2−54508
  $KFeF_4$, antiferromag., critical behaviour 2−44301
  $KFeF_4$, planar antiferromagnet, isomer shift and quadrupole splitting obs. 2−78043
  Kr, solid, recoilless fractions calc. with central-force rigid-atom model 2−74974

Mossbauer effect continued
  $(LaCa)MnO_3$; ^{119}Sn, eff. mag. fields and transfer of spin density to electronic shells 2−72287
  $LaCoO_3$, high-spin-low spin equil. and localized-collective electron transition 2−54288
  $LaCrO_3$; ^{119}Sn, eff. mag. fields and transfer of spin density to electronic shells 2−72287
  $LiFe_2F_6$, electron hopping obs., 350-700K 2−71913
  Li_2WO_4, anhydrous, of ^{183}W, effective Debye temp. detn. 2−71720
  Mn_{1-x} Cr_xSb, of ^{121}Sb, hyperfine fields detn. 2−54514
  MnF_2, mag. hyperfine interactions of Fe^{2+} 2−61604
  MnN_x, hexagonal, mag. props. obs. 2−54331
  $Mn_{1-x}Zn_xFe_2O_4$, mag. order obs. 2−65168
  Mo:^{57}Fe;, impurity-host to host-host coupling const. ratio determ. 2−84183
  N_2, solid, of ^{57}Fe and ^{119}Sn, isomer shift obs. 2−48148
  $NH_4(^{57}Fe, Al)(SO_4)_2.12H_2O$, Mossbauer-electronic double resonance 2−57334
  Na-Sn silicate glasses, effect of Sn content on elec. props. 2−47055
  Nb-Mo:Fe alloy, localized moments on Fe, Mossbauer obs. 2−48149
  Nb-Mo-Fe alloy, discontinuous formation of localized moments, ^{57}Fe study 2−78076
  Nb, of ^{57}Fe, hydrogen conc. effects 2−78075
  Nb_3Sn, of ^{119}Sn, recoil-free fraction and Debye-Waller factors 2−44357
  Ni-Pd alloys of ^{61}Ni, hyperfine field interactions, conc. depend. 2−72285
  Ni-Pd(Pt) alloys, matrix and impurity cluster polarization 2−44358
  Ni-W alloy, conc. depend. of hyperfine field at ^{182}W 2−75273
  $NiFe_{0.8}Cr_{1.2}O_4$, ferrite, statistical angular spin configurations 2−72200
  $NiFe_{0.8}Cr_{1.2}O_4$, ferrite, structural transition at mag. transformation obs. 2−72201
  $Ni_xFe_{3-x}O_4$, Zeeman patterns of Fe^{2+} ions 2−54391
  $Ni_{1.2}Fe_{1.7}Sb_{0.1}O_4$, supertransferre d hyperfine fields and covalency at diamag. cations 2−48150
  $Ni_{1-x-y}Fe_x{}^{2+}Zn_yFe_2{}^{3+}O_4$ ferrite, spinel, Fe^{2+} cation distrib., i.r. spectra and Mossbauer obs. 2−72341
  Os, elec. quadrupole interaction of ^{181}Ta 2−61607
  Os isotopes, quadrupole moment obs. 2−63827
  PbI_2, isomer shifts and quadrupole coupling 2−68614
  Pr^{3+}, in crysts., rel. to validity of electronic shielding theory 2−81319
  PrO_2, of ^{141}Pr, hyperfine fields, effective and calculated 2−48151
  ^{141}Pr, isomer shifts between Pr^{4+} and Pr^{3+} compounds 2−48151
  ^{195}Pt, mag. moment, isomer shift, transitions 2−59719
  ^{239}Pu, recoilless resonance absorption of 57.3 keV γ-rays 2−74043
  $RbCaF_3$, isomer shift of ^{57}Fe at substitution sites 2−81339
  $RbFe(Ni)Cl_3$, one-dimens. mag. obs. 2−72160
  Re, elec. quadrupole interaction of ^{181}Ta 2−61607
  Ru, elec. quadrupole interaction of ^{181}Ta 2−61607
  Sb, Sb_2Te_3, Sb_2S_3, ^{119}Sn valence state obs. after ^{119}Sb decay 2−54392
  SbI_3, $SbI_3.3S_8$, ^{129}I effects calc. of bond character 2−78071
  Si, neutron irrad., lattice defects obs. 2−48153
  Si, of ^{57}Fe 2−48152
  Sm-Sn system intermetallics, correl. with electronic struct. 2−47573
  Sm ionic, semicond. and metallic cpds., isomer shifts 2−48154
  Sn-Pd sols, Mossbauer meas. in which core and stabilizing double layer distinguished 2−80491
  Sn, finely dispersed, determ. of oxidation degree, rel. to supercond. props. 2−61230
  Sn base dilute alloy, ^{119}Sn vibrations obs. 2−71721
  Sn halides, electronegativity correlations with ^{119}Sn Mossbauer shift 2−44360
  Sn halides, Mulliken electronegativities rel. to ^{119}Sn Mossbauer shifts 2−44359
  SnTe, oxidation and chem. stability obs. 2−44485
  ^{119}Sn, mag. moment of 89 keV excited state, deviation from Schmidt value, Mossbauer obs. 2−67169
  ^{119}Sn resonance Mossbauer detector with windowless electron multiplier 2−42471
  $SrO(6-x)Fe_2O_3xAl_2O_3$, influence of thermal history on Mossbauer spectra 2−48144
  Te, nuclear quadrupole diffr. of resonant γ-rays of ^{125}Te 2−57335
  Te hexahalides, ^{125}Te isomer shifts and quadrupole splittings 2−61608
  TiO_2:Fe^{3+}, hole trapping by surface ferric acceptor states, Mossbauer obs. 2−84236
  Tm^{3+}, in crysts., rel. to validity of electronic shielding theory 2−81319
  Tm_3Al_2, quadrupole coupling, EFG tensor 2−48155
  VN_x, hexagonal, mag. props. obs. 2−54331
  V_nO_{2n-1}, of ^{57}Fe, rel. to mag. ordering and metal-semicond transition 2−72286
  ^{186}W, scattering obs. with in-beam system 2−63685
  Xe:$^{57}Co \rightarrow {}^{57}Fe$, atomic states of Fe 2−46426
  $Y_{3-x}Ca_xFe_{5-x}Sn_xO_{12}$ garnet, noncolinear spin config., Mossbauer spectra obs. 2−54344
  $YFe_{1-x}Al_xO_3$, local mag. field at ^{57}Fe, effect of Fe^{3+} exchange linkages 2−72288
  $YFeO_3$; ^{119}Sn, eff. mag. fields and transfer of spin density to electronic shells 2−72287
  YIG, diamagnetically substituted, crit. region 2−78077
  YIG, electrostatic forces, elec. field gradient, mol. orbitals construct. 2−68615
  YIG, nucl. gamma reson. study of mag. anisotropy 2−81266
  Yb-Sn system intermetallics, correl. with electronic struct. 2−47573
  Yb, $A=170$, 172, 174, 176, isomer shifts 2−70407
  $YbPd_3$, of ^{170}Yb, mag. h.f. and cryst. fields, mag. ordering 2−54393
  Zn, large anisotropy prediction 2−80891
  ZnF_2, mag. hyperfine interactions of Fe^{2+} 2−61604
Motors *see Electrical machines*
Multiple stars
  32 Cygni, binary, atmospheric eclipse, preliminary analysis 2−55059
  ADS 15281, visual binary, orbital elements 2−58333
  ADS 16046, visual binary, orbital elements 2−58334

Multiple stars continued
ADS 16165, visual binary, orbital elements 2−58334
ADS 7334, magnetic Ap star, new orbit and mass 2−84982
ADS 7896, visual binary, orbital element determ. by Thiele-Innes method 2−73030
QS Agl, eclipsing binary, photoelectric observations 58335 2−58335
ο Andromedae shell star, eclipsing binary, 253 UBV photometry 2−73028
σ Aquilae, eclipsing variable, mean spectral type, rotational velocity and absolute visual magnitude of components51766 2−51766
ε Aur, eclipsing binary, light curve, secondary fluctuations 2−73026
LY Aur, eclipsing binary, UBV obs.62587 2−62587
AR Aurigae, eclipsing variable, mean spectral type, rotational velocity and absolute visual magnitude of components 2−51766
BD $+22^{0}$ 1679 and BD $+22^{0}$ 1680, two R5-stars, binary system possibility refuted by proper motion observations 2−48721
binaries, accretion disc model for X-ray sources 2−85014
binaries, close visual, use of electronic camera for photometric meas. 2−44876
binaries, detached close, obs. properties of models 2−44875
binaries, measurements made at Nice 2−58338
binaries, Mv(K) dependence on Fe/H ratio in late-type giants 2−73036
binaries, observations by grazing occultation, 1970 Feb. 2−66113
binaries, observations by grazing occultation, 1971 Oct. 2−66112
binaries, observations by grazing occultation, 1971 Sept. 2−66111
binaries, observations by grazing occultations, 1972 Feb. 2−66114
binaries, synthetic close, det. of elements 2−55064
binaries, X-ray spectra, and short period pulsations of Cen X-3 2−75776
binaries ADS41, 48 and BD + 31°3767 and Ross 413, parallaxes and proper motions 2−51768
binary, 8th series, obs. with 50 cm refractor at Nice 2−73031
binary, as X-ray sources, review of current theories 2−55102
binary, mass accretion by neutron star 2−58312
binary, synchronous rotating, oscillations by rotational and tidal perturbation 2−73013
binary, variable radio emission 2−58389
binary components with convective outer layers, mass loss 2−48716
binary double cepheid CE Cas, periods, photoelectric observations 2−75777
binary star model of compact galactic X-ray sources 2−58424
binary system containing dense object, pointless limits to gravitational radiation 2−58345
binary systems, distrib. of semimajor axes and eccentricities after rapid mass loss. 2−44877
44i Boo, eclipsing binary, rate of period changes, determ. using statistical method73025 2−73025
TZBootis, eclipsing variable, spectral classification determ. 2−81861
3C 225, fine structure, identification of components 2−58385
AS Cam, eclipsing binary, photometry 55039 2−55039
AScamelopardalis, eclipsing binary, spectroscopic study 2−84994
WYCancri, eclipsing variable, spectral classification determ. 2−81861
TW Cas, photoelectric light curves 2−73016
SX Cassiopeiae, analysis of giant binary system 2−69101
Cen X-3 system, X-ray flux and orbital elements 2−48758
SV Centauri, eclipsing and double lined spectroscopic binary, photometric and spectroscopic obs. 58347 2−58347
Centaurus X-3, reactivation of old neutron star by mass exchange in close binary 2−78479
EG Cep, eclipsing binary, photoelectric observations 58335 2−58335
AH and CW Cephei, eclipsing variables, mean spectral type, rotational velocity and absolute visual magnitude of components 51766 2−51766
14Cephei, spectroscopic binary, light variations 2−85000
close binaries, F-, G- and K-type components, transport mechanism in envelopes 2−78470
close binaries, uniformly rotating, stellar structure equations 2−55060
close binary systems, tidal evolution 2−84969
close binary systems, with intermediate initial mass ratio, evolution 2−66082
close binary systems Roche limits and Centaurus X-3 2−66138
contact binaries, mass flow and period changes 2−69104
contact binary systems, angular momentum loss 2−58348
α^2 CVn, binary, radial displacements for different elements 84965 2−84965
RS CVn, eclipsing binary, obs. of T Tauri-like star 2−44870
32 Cyg, 1971 eclipse, photoelectric observations 2−73027
32 Cygni, 1971 eclipse, UBV and spectrophotometric obs. 62588 2−62588
WWCygni, eclipsing binary, no pre-main-sequence contraction 2−84998
YCygni, eclipsing binary photoelectric obs., (1959-61) 2−75770
Y Cygni, improvement of spectroscopic orbit, masses and radii of binary components51764 2−51764
V1016 Cygni, symbiotic star, prominent i.r. excess84995 2−84995
SW Cygni, UBV photometry of ring 2−84999
FZ Del, eclipsing binary, photoelectric observations 58335 2−58335
dense double system, slow rotation 2−62491
double, aberration of components 2−73024
double, discovered at Nice with 50 cm refractor 2−58332
double, lunar occultation, catalogue of diffraction patterns 2−75701
double stars, discovered at Nice 50 cm refractor 2−58337
double stars, mean errors of average annual positions of 38 systems 2−48719
double stars, measurements with 38 cm equatorial refractor 2−58336
double stars, photographic meas. of separations and position angles of 111 objects 2−66107
double stars of equal components, spectral evidence of binary nature 2−55061
eccentric binary systems, det. of black holes 2−58350
eclipsing and visual binaries, mass-luminosity ratio 2−84968
eclipsing binaries, effect of time shift of secondary minimum 2−73035
eclipsing binaries, limb darkening problem 2−55063

Multiple stars continued
eclipsing binaries, parallaxes 2−73037
eclipsing binaries, rate of period changes, determ. using statistical method 2−73025
eclipsing binary system with extensive atmosphere, information available from monocolour brightness loss curves 2−48717
eruptive binaries, mechanisms and physical properties 2−51776
eruptive binaries, physical properties and outburst mechanisms 2−73034
formation by collapse of rotating gas 2−48733
four and five body systems, dynamics 2−58260
Galaxy and the distance scale, Woolley symposium, Herstmonceaux, Aug (1972) 2−69015
U Geminorum, eruptive binary, period variations 2−44883
HD 1273, possible astrometric spectroscopic binary, orbital elements 2−84989
HD 161227, double lined binary, spectral obs. 2−44880
HD 163181, peculiar spectroscopic eclipsing binary, N_2 enhanced, absorption line 2−73029
HD 175514, binary analysis of 1968 photoelectric light curve observations 2−51765
HD 208095, spectroscopic binary, light variations 2−85000
HD 217312, spectroscopic binary, light variations 2−85000
HD 27149, spectroscopic binary 2−58344
HD 49798, O-type subdwarf, spectroscopic binary, non-LTE anal. 2−66108
HD 77581, spectroscopic binary, B supergiant, in error box of Vela X-ray source 2−51770
HD 95363, spectroscopic binary, orbital elements 2−48715
AK Her, eclipsing binary, photoelectric observations 58335 2−58335
LS Her, eclipsing binary, photoelectric observations 58335 2−58335
AT Her, suspected eclipsing binary, photoelectric observations 2−58335
AKHerculis, eclipsing binary, photoelectric light curves 2−85001
88 Herculis, shell star, possible binary star 2−58318
88Herculis, spectroscopic binary? 2−73032
Herculis X-1, precessing binary pulsar model 2−81873
HO Telescopii, exclipsing binary, five colour photometry 2−78467
HR 4072, double lined binary Hg type, Am stars as companions, abundance anal. 2−58340
HR 4072 and chi Lupi binary Hg syndrome stars equivalent width meas. 2−69108
HR 6611, eclipsing binary, photoelectric obs. 2−75769
HR 7774, unresolved double lined binary, metallicism 2−66106
HZ 29, double white dwarf semidetached post cataclysmic nova? 2−55053
HZ-22, faint blue star, old evolved binary in Galactic halo 2−58343
IDS catalogue, proper motions of possible double and multiple systems 2−48718
SW Lac, eclipsing binary, rate of period changes, determ. using statistical method 2−73025
XY Leonis, W UMA-type eclipsing binary, period changes rel. to third mass55058 2−55058
17 Leporis, i.r. shell star? 2−55068
LR Cen, eclipsing binary, primary spectrum 2−58331
χ Lupi, double lined binary Hg star, orbital elements44852 2−44852
χ Lupi, double lined binary Hg type, Am stars as companions, abundance anal.58340 2−58340
LY Aur binary, u.v. photometry for OAO-2 2−75778
EW Lyr, eclipsing binary, photoelectric observations 58335 2−58335
TZ Lyrae, light variation and orbital elements 2−75753
β Lyrae, underluminosity and magnetic fields 2−58349
massive, fundamental data rel. to theoretical models 2−51726
AX Monocerotis, symbiotic stars, UBV obs. 84996 2−84996
U Ophiuchi, eclipsing variable, mean spectral type, rotational velocity and absolute visual magnitude of components 2−51766
δ Orionis, spectroscopic binary, apsidal motion, orbital elements 62584 2−62584
EQ Peg, double flare star, photometry and spectra48714 2−48714
AT Peg, eclipsing binary orbital elements, spectral obs. 66109 2−66109
UPegasi, photoelectric obs. 2−44873
AG Pegasi, symbiotic stars, UBV obs. 2−84996
U Pegasi close binary system, light curve variations 2−81864
periodic pulsating binary X-ray source in Hercules 2−75829
AG Persei, eclipsing variable, mean spectral type, rotational velocity and absolute visual magnitude of components 2−51766
AX Persei, symbiotic stars, UBV obs. 2−84996
pulsing X-ray binaries, models 2−69103
RX Puppis, symbiotic star, prominent i.r. excess 84995 2−84995
Ross 614, visual binary, orbit, mass ratio and absolute parallax 2−81822
Ross 986, parallax determination and possible binary orbital motion 2−69102
V505 Sagittarii, eclipsing binary system, UBV photoelectric observations 2−81821
β Sco, triple system, occultation by Jupiter 55142 2−55142
β Scorpii, occultation on 1971, May 13-14, by Jupiter and its satellite Io 44879 2−44879
β Scorpii, transit of Jupiter's system across the multiple star 44874 2−44874
β Scorpii C, evidence for duplicity from Io occultation 75864 2−75864
RY Scuti, symbiotic star, weak i.r. excess 2−84995
spectroscopic binaries, evolution of supergiants 2−62515
spectroscopic binaries, frequency among extreme high velocity dwarfs 2−75768
spectroscopic binaries, mass function distrib. det. 2−44881
spectroscopic binaries with circular orbits? 2−51774
spectroscopic visual binary in ADS 14893 triple system, orbital elements 2−75779
β Spropii, occultation by Jupiter62697 2−62697
RW Trianguli, eruptive binary, period variations 44883 2−44883
triple gravitational systems, evolution, termination of binary 2−58175
triple star systems, stability criteria 2−58169
triple systems, binary formation 2−51775

Multiple stars continued
- TX Cancri, close, light curves, period change, masses radii and luminosities 2−55069
- TX Cancri as test of theory of age zero contact binary systems 2−75763
- UX Ursae Majoris, eclipsing binary, photoelectric photometry of rapid variations81845 2−81845
- TYUrsae Majoris, eclipsing variable, photoelectric observations 2−81861
- UX Ursae Majoris, eruptive binary, period variations44883 2−44883
- W Ursae Majoris close binary system, light curve variations 2−81864
- V504 Sgr, eclipsing binary, UBV photometry 2−58342
- AG Vir., eclipsing binary, radial velocities, orbital elements 2−62586
- AH Vir, eclipsing binary, time of minimum light 2−66110
- AZVirginis, eclipsing variable, photoelectric observations and spectral classification determ. 2−81861
- VY Canis Major, obs. 2−55054
- W Ursae Majoris systems, explanation of hotter secondary 2−58341
- white dwarf non-radial pulsations in eclipsing binary systems 2−73018
- X-ray binary, 2U 1700-37, associated with O-type star HD 153919 2−75775

Muonic atoms *see Atoms, mesic and muonic*

Muonic molecules *see Molecules, mesic and muonic*

Muonium
- formation in slow collisions of positive mesons with H atoms 2−83217
- hyperfine internal corrections, use with corrections to H hyperfine structure for estimation of proton polarisability 2−83214
- hyperfine splitting in low-pressure Ar determ. from field independent Zeeman transitions 2−42822
- hyperfine structure interval at strong magnetic field, discussion of errors and theory of resonance line shape 2−42821
- production in η^0 decay, probability calculation 2−45948
- quadratic hyperfine pressure shift in inert gas atmospheres 2−77013
- two-particle procession in strong mag. fields, polarization changes 2−70649
- μ^+ depolarization in KCl, muoinium stage 2−80933

Muons
- *see also Cosmic rays/muons; Nuclear reactions and scattering due to/muons*
- anomalous gyromagnetic ratio, sixth-order contribution 2−63509
- anomalous magnetic moment, optimal lower bounds on hadronic contribution 2−76612
- anomalous magnetic moment, precise measurement in CERN muon storage ring 2−52563
- anomalous magnetic moments, quantum electrodynamics review 2−63471
- electron-muon mass doublet, lifetime of muon state 2−59422
- heuristic model, mass by general-relativistic considerations 2−45892
- magnetic moment, anomalous, hadronic contributions 2−45893
- magnetic moment, precision meas. 2−49512
- magnetic moment, weak contributions calc. in theory of weak and e.m. interactions 2−49510
- magnetic moment in finite theory of weak and e.m. interactions 2−66944
- mass difference rel. to electrons 2−76606
- mass origin from study of lepton inner structure 2−49502
- negative, use in therapeutic and diagnostic medicine 2−76084
- pair photoproduction, improved Weizsacker Williams method for calc. of energy-angle distrib. 2−66930
- telecommunications, using muon beams 2−82697
- ultrarelativistic, shielding, calc. of survival probability by Monte Carlo method 2−79845
- μ^-, range, 500 to 1500 MeV/c 2−76615
- μ^+, magnetic moment meas. from obs. of decay is uniform magnetic field, lifetime meas. 2−49511
- μ^+, range 500 to 1500 MeV/c 2−76615
- π-μ model, linear mass relationships 2−59526
- Cu, dipole relax. rate and diffusion coeff. 2−57090
- μ^+ depolarization in KCl, muoinium stage 2−80933
- **capture**
  - by complex nuclei, determ. of polarization of the emitted neutron 2−63868
  - light nuclei, partial capture rates, dependence on nuclear structure, derivation of μN coupling constants 2−55983
  - radioisotope prod. by stopped negative muons 2−82950
  - μ^-, by polarized proton target, diff. capture cross section detn. 2−55982
  - H_2 and other nuclei, multichannel recording system using computer 2−70296
- **decay**
  - higher-order corrections, renormalization of Weinburg's theory of interactions 2−79497
  - radiative corrections, intermediate vector-boson theory 2−45891
  - radiative corrections, i.r. divergences cancellation 2−63523
  - μ^+, determ. of mean lifetime and weak-interaction coupling constant G_μ 2−63522
  - μ^+, magnetic moment meas. from obs. of decay is uniform magnetic field, lifetime meas. 2−49511
- **detection, measurement**
  - identification using multiwire proportional counters 2−73934
  - ionization calorimeter for investigation of ultrahigh energy muons 2−73862
  - phototubes, testing device, design, for long-term stability 2−55896
  - μ^+, determ. of mean lifetime and weak-interaction coupling constant G_μ 2−63522
- **interactions**
  - e.m., effect on $K_l \to 2\mu$ decay 2−45939
  - inelastic, at low-momentum transfer, 6 and 12 GeV 2−63524
  - multiperipheral ladder model 2−70165
  - pair muoproduction, vacuum polarization corrections 2−63474
  - μ-d$\to$n,nν_μ, non-relativistic approx. using Primakoff weak interaction Hamiltonian 2−63525
  - μN, fireball production 2−76614
  - μN, intermediate boson production cross section calcs. 2−73832

Muons continued
- **interactions** continued
  - $\mu N \to \pi +$ anything, inclusive processes, 10.1 and 15.8 GeV/c 2−59430
  - μp, muonic pair production 2−49513
  - $\nu_\mu \mu$, upper limit for interaction constant 2−59416
  - H_2 and other nuclei, multichannel recording system using computer 2−70296
- **production**
  - lepton-triplet prod. in Coulom field 2−79500
  - massive muon pair production in hadron-hadron collisions 2−55878
  - muonic pair, in μp collisions 2−49513
  - pair creation via two-photon exchange in charged hadron collisions at very high energies 2−82698
  - pair creation via two-photon exchange in electron collisions QED investigation 2−82684
  - pair photoproduction in deep inelastic region, meas. of inclusive cross section 2−82696
  - pair-production in deep inelastic electroproduction, application to duality 2−59420
  - $e^+e^- \to \mu^+\mu^-$ meas. of muon polarization as test of weak-interaction models 2−73762
  - $K \to \mu^+\mu^-$, lower bound for CP nonconservation 2−73803
  - $K \to \mu\mu$, anomalous $K \to \pi\pi\gamma \to \mu\mu$ interaction 2−63585
  - $K_l{}^0 \to \mu^+\mu^-$, possibility of anomalous intermediate $\pi^0 \to 2\mu$, $3\pi \to 2\mu$ 2−63584
  - $\mu\mu$- pairs, possible bounds on production in super-high-energy hadron-hadron collisions 2−63537
  - $\mu^+\mu$- photoproduction obs. 2−66945
  - $\mu^+\mu^-$ electroproduction as test of algebra of bilocal operators 2−76582
  - $\nu_\mu N \to \mu^- W^+ N'$, μ^- production cross-sections, neutrino energy spectrum 2−76613
  - $pp \to \mu^+\mu^- +$ anything, calc. of cross section in parton model, comparison with expt. 2−70178
- **scattering**
  - elastic in an intense field, vacuum polarization corrections 2−63474
  - $e\mu$, invariant amplitudes and double dispersion relations 2−45884
  - μN inelastic scatt., high energy, vector-dominance model 2−82695
  - μp, inelastic at 12 GeV/c, meas. of differential cross section, comparison with p inelastic scattering 2−66946
  - μp possibility of anomalous interaction at low energies due to exchange of scalar meson 2−63526

Music *see Acoustics/musical*

Musical instruments
- bell tones, simulation with pipe-bells and keyboard sounds 2−63122
- bowed stringed, directional characteristics, effect on orchestral sound in concert halls 2−45521
- brass instrument design, theory of horns 2−41775
- cider bottle, reactance and decay of free oscillations 2−63124
- clarinet reed interaction with single resonance air column 2−41778
- electronic violin 2−41776
- flute and clarinet spectra, amplitude distortion 2−63125
- guitar, acoustical and hologram interferometric meas. of top plate vibrations 2−52244
- guitar, electronic amplification, effects equipment 2−76367
- guitar, tonal quality with various materials for belly and sides 2−63123
- kettledrum vibrations 2−41647
- organ pipes, attack transients analysis 2−82351
- pianos, electronic tuning device 2−45523
- tone build-up time measurements 2−41774
- treble viol, resonance of plates, obs. by hologram interferometry, design of improved instrument 2−45520
- viola with electronically simulated body resonances 2−41777
- wind, spectrum developments with playing level 2−41779

Navier-Stokes equations *see Flow; Hydrodynamics*

Nebulae
- *see also Planetary nebulae*
- Andromeda, estimate of frequency of novae 2−73023
- Andromeda, galactical sextruplet visual binary 2−75673
- Andromeda, nucleus, spiral structure and elliptical companion obs. at 1415 MHz 2−69031
- Bok globules, observations of formaldehyde and other molecules 2−58241
- Bok globules rel. to evolution of spherical protostars with masses 0.25 to 10 $M_\odot$, newly-formed stars 2−48694
- bright emission nebulae, near concentrations of high velocity gas 2−58239
- η Carinae nebula, Hα and NII profiles from high interferometric resolution observations 2−55024
- in Cassiopeia, investigation by Fabry-Perot interferometer 2−75695
- Coal Sack, southern, formaldehyde absorption 2−69042
- Crab, cosmic γ-ray obs. above 250 MeV 2−62628
- Crab, effect on cosmic ray acceleration 2−51693
- Crab, electron diffusion, energy distribution of relativistic electrons with synchrotron or Compton radiation 2−55083
- Crab, e.m. radiation rel. to neutron star models 2−75692
- Crab, energy balance, rotating neutron star theory 2−62471
- Crab, far i.r. flux meas. 2−55023
- Crab, interstellar circular polarization in that direction 2−69111
- Crab, interstellar reddening det. from obs. of S II lines 2−58247
- Crab, low energy X-ray survey 2−84952
- Crab, obs. of radial and tangential coronal broadening 1969-1971 2−62472
- Crab, pulsed X-radiation 2−55090
- Crab, radiation, elliptical polarization search 2−75724
- Crab, structure at 2.7 and 5 GHz 2−55022
- Crab interpretation of obs. of coronal broadening 1969-1971 2−62473
- Crab Nebula, detection of high energy γ-rays 2−58437
- Crab Nebula pulsar, VLBI obs. 2−75816
- Crab Nebula supernova explosion, Californian pictographic evidence 2−75760
- Crab Nebulae, appl. of rot. energy theory 2−85016
- dark, in Large Magellanic Cloud, positions, dimensions and photometric props. 2−62474
- differentially expanding, transfer of resonant line radiation 2−58250
- diffuse, dynamical effects of stellar mass loss 2−72984

Nebulae continued
- diffuse obs. of forbidden line of SIII at λ9532 2−58242
- dust clouds in the Large Magellanic Cloud 2−58248
- extreme Population I matter, noble gas abundance rel. to Sun 2−81838
- faint, associated with HB-21 radiosource interferometric obs. 2−81809
- filamentary, supernova remnants, spectrophotometric investigations 2−72985
- formaldehyde detection, 2cm isotropic background radiation absorption 2−75789
- galactic, temp. and density using forbidden line intensity ratios 2−51718
- gaseous, obs. of radio recombination lines 2−75694
- gaseous, pressure broadening of radio recombination lines 2−75693
- HBV 475, i.r. photometry 2−69126
- HD 87634, associated nova-like star 2−85005
- Herbig-Haro Object No. 1, spectrophotometric study 2−58246
- IC 410, linear filaments of diffuse nebulosity rel. to stellar winds 2−58363
- IC 4628, and RCW 113, evidence for origination from same gas cloud 2−62476
- inner solar nebula, physical conditions 2−81948
- internal dust, nonisotropic scattering 2−66067
- M8, M16, M17, M42, diffuse, obs. of forbidden line of SIII at λ 9532 2−58242
- M8 and association with NGC 6530 cluster 2−75772
- MHα 238-116, i.r. photometry 2−69126
- Mi, M17, He II 4686 Å intensity obs. and cosmic ray flux 2−58254
- in Milky Way, southern, atlas 75669 2−75669
- NGC 2261, cometary, spectrophotometry 2−58237
- NGC 2264, optical obs, of i.r. source 2−69044
- NGC 6164-5, surrounding peculiar O6f star (HD 148937) 2−66066
- NGC 6572, i.r. spectrum 2−58249
- non-spherical, ejecta from novae, spectral obs. 2−62573
- North America, for u.v. obs. by Apollo 16 from Moon 2−75699
- Nova Delphini 1967, high dispersion spectra during nebular stage 2−58240
- old hot subdwarfs, He abundance obs. 2−81859
- Ophiuchus cloud, interstellar molecules and dust and total-to-selective extinction ratio 2−75793
- Orion, 85α recombination line survey 2−81797
- Orion, far i.r. flux meas. 2−55023
- Orion, He II 4686 Å intensity obs. and cosmic ray flux 2−58254
- Orion, i.r. astronomy 2−73052
- Orion, microwave emission 2−69114
- Orion, optical and radio observations, intersteller absorption 2−72986
- Orion, radio emission in water vapour line 2−75823
- Orion, spectrophotometric obs. 2−84951
- Orion, total He abundance 2−58238
- Orion A, ^{15}N and U169.3 methanol line 2−66135
- Orion Nebula, 85α radio recombination line survey 2−58245
- Orion Nebula, λ4686 He II line intensity, reln. to cosmic ray flux 2−69043
- Orion nebula, i.r. sources rel. to evolution of spherical protostars with masses 0.25 to 10 $M_\odot$, newly-formed stars 2−48694
- Orion Nebula, observations of OII 3727 Angstroms forbidden line doublet 2−55021
- reflection and det. of albedo of interstellar particles 2−75794
- role of two-quantum photon-plasmon $2S_{1/2}-1S_{1/2}$ transition 2−79962
- Sagittarius B2, microwave emission 2−69114
- Sgr A and Sgr B2, ^{13}C isotope of formaldehyde absorption, and $^{12}C/^{13}C$ abundance ratio 2−48671
- Sharpless 157, diffuse nebula, exciting star and spectra of bright knot inside 2−55020
- solar, condensation, formation of chondrites 2−58443
- solar, evolution from proto-Sun stage to planet forming stages 2−78494
- solar system origin, nebular hypothesis 2−81926
- synchro-Compton radiation, polarisation 2−72983
- Vela, energy balance, rotating neutron star theory 2−62471
- W3 radio, 21cm, atomic H absorption profile, Cnα recombination line and radial velocity 2−44897
- Z-dependence of level intervals in $2s^22p^2$, $2s^22p^3$ and $2s^22p^4$ 2−73114
- He line spectra in gaseous nebulae, level populations 2−48672

Neel temperature *see Magnetic properties of substances*

Negatons *see Electrons*

Negatrons *see Electrons*

Nematic phase *see Liquid crystals*

Neodymium
- — 2−59166
- atom, hyperfine structure const., g_j values of $^5L_{4,5,6,7,8}$ atomic states 2−76990
- atomic absorption spectra computer program for calc. position and optical density of each band 2−46418
- $CaF_2.3Ca_3(PO_4)_2:Nd^{3+}$, local compensation of Nd^{3+} ionic charge 2−64681
- glass:Nd^{3+} laser, struct. of radiation 2−59170
- glass:Nd laser, damage mechanism and improvement of damage threshold 2−42050
- glass:Nd laser, set-up for plasma production 2−80294
- glass, Nd-activated, excitation of luminescence 2−78135
- glass-ceramic, Nd^{3+} doped, lasing threshold and efficiency 2−73589
- laser, single pulse, one mode, with frequency stabilization 2−76490
- laser, single-pulse, with cascaded multipliers and tunable frequency converter 2−59177
- laser, thermal distortion of laser resonance, study using pneumatic films 2−52429
- laser, with molecular crystals, second harmonic generation 2−82515
- laser frequency depend. of spatial synchronism of emission harmonics 2−76491
- in Li-Bi liquid alloy, solubility and heat of soln. 2−43334
- liquid laser, obs. of transverse modes 2−42033
- magnetic phase transitions, phenomenological theory 2−51279

Neodymium continued
- magnetoresistance, transverse and longit., at 1.38K, 4.2K, 13.96K and 20.4K 2−71836
- mass spectrometry of stable fission-product Nd as measure of burn-up of UO_2 reactor fuel 2−74182
- mixed oxide nuclear fuels, Nd-content and burn-up and isotopic distribution meas. 2−75401
- plasticity, strength, technological props. 2−47532
- $Ba_2ZnGe_2O_7:Nd^{3+}$, absorpt. and fluorescence spectra, Nd^{3+} stimulated emission and laser action 2−61705
- CaF_2-Nd^{3+}, energy level shifts at $oxygen^2$ compensated Nd sites 2−84229
- $Ca_5(PO_4)_3F:Nd^{3+}$, e.p.r. obs. crystal field at Ca^+ position 2−78161
- $CaWO_4:Nd^{3+}$, photon echoes, generation, detection, mag. field and temp. depend. 2−72251
- in Cr, O-enriched, solubility 2−43830
- glass:Nd laser, Q-switching a convex optical cavity 2−76467
- $LiGd(MoO_4)_2:Nd^{3+}$, laser, stimulated emission 2−69938
- Nd: glass, laser induced fluorescence line narrowing spectroscopy 2−48247
- Nd^{3+}: apatite lasers, properties and performance 2−42063
- Nd^{3+}: yttrofluorite crystals, time development of wide-band generation spectra in resonator with diffusion 2−42073
- Nd:CaLa silicate oxyapatite crystalline laser materials, pulsed and Q-swithced characteristics 2−42060
- $Nd:CaLaSi(PO_4)_2CaF_2$ laser material, temp. dependence of refractive index 2−49380
- $Nd:CaNb_2O_6$, cryst. growth and laser operation 2−50592
- $Nd^{3+}:CaO.2Al_2O_3$, stimulated emission cross section 2−54452
- Nd:glass, bis-(4-dimethylaminodithiobenzil)- Ni for Q-switching of i.r. laser 2−59175
- Nd:glass ion-ion energy transfer temp. depend., laser induced line narrowing obs. 2−65307
- Nd:glass laser, aqueous Cu(II) sulphate gel target to produce coherent X-rays 2−66765
- Nd:glass laser, cylindrical rod plano-convex cavity, mirror transmission 2−76492
- Nd:glass laser, mini face-pumped, free from thermal distortion 2−73582
- Nd:glass laser, picosec. electrical pulse generation by rectification in $LiTaO_3:Cu^{++}$ 2−79268
- Nd:glass laser, pulsed, beam parameter obs. using holographic interferometry 2−79218
- Nd:glass laser, single mode, with continuously variable pulse duration 2−42071
- Nd:glass laser, thermal lensing effects 2−63336
- Nd:glass laser frequency conversion to u.v. in range 216 to 234 nm 2−73604
- Nd:glass laser produced plasma, second harmonic generation 2−43146
- Nd^{3+}:glass laser, production of super-dense plasmas 2−77286
- Nd^{3+}:glass laser, set-up for obtaining a giant pulse by Q-factor modulation 2−76485
- $Nd^{3+}:POCl_3$-$ZrCl_4$ laser, line broadening of spectrum of Nd^{3+} ion in solution, stimulated emission cross section 2−42037
- Nd^{3+}:phosphate glasses, time development of wide-band generation spectra in resonator with diffusion 2−42073
- Nd^{3+}:YAG-YALO laser, hybrid operation at 1.064 μ 2−69939
- Nd:YAG, Q-switched laser, pumping CdSe i.r. parametric oscillator 2−42061
- Nd:YAG electro-optically Q-switched laser, multipulsing behaviour 2−59173
- Nd:YAG laser, CW pumped, output fluctuations 2−45751
- Nd:YAG laser, diode-pump-modulated, response to pump intensity sinusoidal modulation 2−52427
- Nd:YAG laser, harmonic mode locking 2−59172
- Nd:YAG laser, props. rel. to Nd:YALO, Nd:Yttralox, Nd:apatites 2−63338
- Nd:YAG laser, pulsed, organic dyes as filters 2−73588
- Nd:YAG laser, space qualified, design 2−69940
- Nd:YAG laser material, holographic interferometry meas. of thermal refractive index and expansion coefficients 2−59174
- Nd:YAG laser single freq. travelling wave, output 2−73581
- Nd:YAG lasers, bibliography 2−42065
- Nd:YAG new laser transitions $^4F_{3/2}$ to $^4I_{9/2}$ 2−42066
- Nd:YAG solid laser, pumping $LiIO_3$ internal parametric oscillator 2−45746
- Nd:YAG system for generation of controllable reproducible giant pulses 2−69925
- Nd^{3+}:YAG intracavity phase modulated laser separation of mode locked states 2−42048
- Nd^{3+}:YAG laser, effect of pressure in Xe and Kr arc lamps on pumping efficiency 2−42072
- Nd^{3+}:YAG laser, recirculating liquid N_2 system for cooling 2−63339
- Nd^{3+}:YAG laser target designators and range finders 2−42064
- Nd^{3+}:YAG solid laser, generation of subnanosecond 10 μ pulses 2−42068
- Nd:YALO laser material, holographic interferometry meas. of thermal refractive index and expansion coefficients 2−59174
- Nd:YAP solid laser, polarization and crystal direction effects 2−42067
- $Nd:YAlO_3$, laser, design, device parameter obs. 2−45752
- Nd:Yttralox ceramic, lasing threshold, loss coeff. 2−49381
- Nd-$CaWO_4$ laser, active Q switching technique for high power in single longitudinal mode 2−63337
- Nd-glass laser, production and meas. of pulses of several hundred picoseconds 2−59176
- Nd-glass thin film waveguide for amplification at 1.06 microns 2−42057
- Nd^{3+}-glass laser, giant light pulse generation for study of nonlinear optical effects 2−55685
- Nd^{3+}, analytical SCF wavefunctions for ground and some excited states, calc. of oscillator strengths for optical transitions 2−52915
- Nd^{3+}, in $Ba_2MgGe_2O_7$ glass and crystal matrices, luminesc. props. 2−72423
- Nd^{3+}, in glass, fluoresc. quenching by OH^- ions 2−54467
- Nd^{3+}, in $LaAlO_3$ laser cryst., luminescence and absorpt. spectra 2−75302

Neodymium continued

Nd^{3+}, in $LaCl_3$ and lanthanum ethyl sulphate, spin-lattice relax. at zero mag. field 2−65194
Nd^{3+}, optical spectra in oxidized CaF_2, Stark effect obs. 2−61702
Nd^{3+} in Nd_2O_2S, absorp. spectra and crystal field parameters 2−65263
Ne^{3+}, in YAG, random variation of the static crystalline field, e.s.r. line width obs. 2−44441
$POCl_3$:$ZrCl_4$:Nd^{3+} liquid laser, amplification of mode locked trains 2−59167
SrF_2:Nd, axial distrib. of impurities, neutron activation analysis 2−56744
YAG:Nd garnet, grown by Czochralski method, cryst. perfection rel. to melt comp. and rot. speed 2−67945
YAG:Nd^{3+} quasicontinuous laser, spectral characts. and oscill. dynamics 2−79216
$YAlO_3$:Nd^{3+}, high temp. phase instability 2−74958
Y_2SiO_5:Nd^{3+}, absorpt. and luminesc. spectra, and stimulated emission 2−78123

Neodymium compounds

Pockel cell Q-switched Nd:glass oscillator, amplified output, picosecond structure 2−42070
$CaSiO_3$-$NdSiO_5$ system, phase equilib. 2−47707
Dy-Nd alloys, struct., mag. and elec. props. 2−51237
Nd:glass lasers, pulsed mode-locked, evolution of high power picosecond pulses 2−42069
Nd-Th-Bi soln., mutual solubilities, 350-700°C 2−67809
$NdAg_2Si$, prep. and cryst. struct. 2−74735
$NdAlO_3$, Raman scatt. by localized electronic excitations and cryst. field model 2−72371
NdAs, crystalline electric field levels detn., neutron spectroscopy obs. 2−68585
$Nd(BO_2)_3$, cryst. struct., X-ray analysis 2−74738
$Nd(C_2H_5SO_4)_3.9H_2O$, relaxation processes measurement using a r.f. tunnel diode oscillator 2−68513
$NdCo_2$, dissolved hydrogen effect on elec. and mag. behaviour 2−48040
$NdCo_2$, mag. behaviour in ordering region 2−44280
$Nd_2Co_{1.7}$ intermetallic, cryst. struct. 2−47341
$Nd_2(Co_{1-x}Fe_x)_{17}$, lattice consts. 2−50626
$NdCrO_3$, anomalies in temp. depend. of spontaneous magnetiz. 2−72222
$NdCrO_3$, optical spectroscopy 2−84512
$NdFeO_3$, spontaneous magntiz., moment temp. depend., effective field 2−72221
NdGa, mag. props. 2−48079
NdGa, magnetization and susceptibility, temp. depend. 2−72170
$Nd_{1-x}Ho_xCo_3$, mag. moments, Curie temps., spin polarization effects 2−68535
Nd(III) complexes with N-donor ligands, solvent and complex formation defects on spectra 2−46569
$NdIn_3$ magnetic properties 2−72223
$Nd_2Mg_3(NO_3)_{12}.24H_2O$, spin-lattice relax., external mag. field depend., 1.5-2.0K 2−48115
$Nd_2(MoO_4)_3$, cryst. struct. 2−74736
$NdNi_2$, $NdAl_2$, $NdCo_2$, Laves phases, low temp. specific heat, cryst. field and exchange effect model 2−57067
$NdNi_3$, mag. struct. 2−48080
Nd_2NiO_4, monoclinic to tetragonal transform. 2−77750
Nd_2O_3, p- and n-type semiconductivity at varying pressure 2−44103
Nd_2O_3, vibr. spectra and space groups 2−51355
NdOBr(Cl), i.r. spectra, vibrs. assignments 2−57348
$Nd(OH)_3$, preparation from Nd_2O_3 in H_2O vapour 2−80598
Nd_2O_2S, absorp. spectra and crystal field parameters of Nd^{3+} ion 2−65263
NdP, crystalline electric field levels detn., neutron spectroscopy obs. 2−68585
NdP_5O_{14}, laser material, line widths/cross-sections and props. 2−73587
$Nd_{3-y}R_yR_xGa_{2-x}Ga_3O_{12}$ garnet, R=Yb, Tm, Er, Ho, Dy, mag. props., 1.6-300K 2−61485
$NdRu_2$, high press. phase transition 2−71689
NdS, domain struct., and temp. depend. of susceptibility 2−81307
Nd_3S_4, thermal and elec. cond., thermal e.m.f., 80−680 K, complex cond. band 2−80918
tris-$Nd_2(SO_4)_3$ diffuse reflectance spectrum, meas. of Slater-Condon, Racah, Lande, bonding and screening parameters, electronic energy states 2−61617
NdSb, crystalline electric field levels detn., neutron spectroscopy obs. 2−68585
NdSb, mag. struct. 2−44292
$POCl_3$-D_2O-Nd_2O_3 soln., lasing effect and prep. technique 2−45744

Neon

absorption tube in alternating magnetic field in laser cavity as frequency standard 2−78757
adsorbed layer on Ge, mol. beam scatt., survival rel. to coverage 2−47159
adsorption, on Cu and Ar plated Cu 2−47157
adsorption of H at 4.2K 2−50539
adsorption on solid Xe, energy spectrum calculation method 2−43499
afterglow plasma, diffusion cooling 2−56336
atom, 2p shell photoelectron angular distrib. parameter, 0-20 eV region above threshold 2−67405
atom, absolute cross sections for excitation by impact of 20-180 eV H^+, $H_2{}^+$, He 2−70628
atom, cascade effects in 2p level life time meas. 2−64032
atom, collision cross sections for 2p levels at 870K 2−42768
atom, collisions with H^+ at 4 keV, probability ratio for neutralization of H^+ to H(2p) or H(1s) 2−42802
atom, correlation energy calc. using linked cluster many body perturbation theory 2−67484
atom, elastic reson. energy 2−74230
atom, electron elastic scattering at 150 eV, absolute differential cross sections 2−59935
atom, electron impact excitation, 42-51 eV obs. of autoionizing $2s^22p^43s3l$ states and related Ne^- resonances 2−67402
atom, electron impact ioniz., slow electron obs. 2−64033
atom, electron scatt., reson. energy, bound-state calc. 2−59927
atom, excitation of 2p-3s lines in He-Ne mixture 2−42742

Neon continued

atom, inelastic scattering of He^+, differential cross sections 2−59956
atom, ionization in slow collisions with He and He^+, meas. of energy spectra and angular distribs. of ejected electron 2−56119
atom, Lande-factor of $2p_4$ level, meas. with He-Ne laser 2−63428
atom, mag. reson. line, press. shift, He-Ne laser obs. 2−64024
atom, metastable, deexcitation in collisions with gases, cross sections 2−64054
atom, outer s shell role in single ioniz. by electron impact 2−67399
atom, polarization of light emitted on de-excitation under H ion impact 2−42736
atom, pseudo particle state calc. of hyperpolarizability and third harmonic generation coeff. 2−79880
atom, scattering of K^+, 150-2350 eV, effective total cross section meas. 2−67415
atom, self-consistent symmetries, stability 2−76986
atom, similtaneous ionization and excitation by electron impact 2−49960
atom, Zeeman splitting in superradiance at 6143Å 2−46437
atom in ground state, importance of electronic correlations for calc. of X-ray and fast electron scattering 2−79882
atom line strengths and transition probabilities, obs. and theory 2−70590
atom scattering of inert gas and period II element ions in 8-25 keV range, comparison of exptl. and theoretical interatomic potentials 2−56118
atom-ion asymmetric collisions, electron promotion model 2−79899
atomic beam scatt. from (001) LiF surface, systematic trials study 2−74241
atomic beam scatt. from LiF surface, Lennard-Jones potential calc. 2−74240
atomic collisions, 10 to 75 keV, outer shell excitations 2−74238
atomic spectra, He as standard for unknown transition 2−59915
atoms, simultaneous ionization and excitation by electron impact 2−42754
breakdown, a.c., in cells with external electrodes 2−50234
crystalline, equilibrium vacancy formation and self-diffusion 2−71470
diffusion, in B_2O_3 glass, mass spectrometery obs. 2−53758
discharge, electron distrib. function, ioniz. waves influence 2−74430
discharge, h.f., re-ignition, influence of metastable states 2−43217
discharge, hot-probe investigation of spatial fine structure in plasma potential 2−60255
discharge, low current ioniz. wave theory 2−77312
discharge, narrow tube, freq. spectrum and dispersion relation of moving striations 2−64346
discharge in hollow cathode, effect of nonlinear absorption at 0.63 m wavelength 2−83641
discharge in magnetic field, optical pumping with multimode laser, saturation resonances by magnetic mode crossing 2−46436
gas, calc. of second virial coeff. viscosity, thermal diffusion factor using scattering potential of Siska 2−46863
gas, small-angle scattering of range of elements, meas. of inelastic energy losses 2−64045
glow discharge, p and s ionization waves, nonlinear interaction 2−71025
ionisation, Townsend primary coefficient, determination by luminous flux method 2−46790
ions, dipolar polarizability, variational calc. 2−74206
ions, multiply ionized, laser oscill. in Z-pinch discharge 2−49352
ions, scatt., multiple, by C and Ge foils 2−47781
isoelectronic sequence, electron impact excitation of ions, interpolation formulae 2−74244
isoelectronic series, energies of excited-state terms 2−74221
laser, fundamental characteristics and frequency stabilization 2−73571
laser, He-Ne, permeation of old laser to improve performance 2−42017
levels, population changes by 0.61 μm and 3.39 μm laser action 2−76483
liquid, electronic bubble states 2−43321
liquid, negative carrier mobility rel. to localized electrons 2−46916
liquid, thermodynamic properties determ. from sound velocity measurements 2−46950
liquid, three atom correlations 2−80447
liquid isotopes, shear viscosity 2−53406
low-pressure discharge, tail of electron, energy distribution function 2−50229
lunar atmosphere, density and flux distrib. 2−66156
metastable atoms, time-of-flight technique for detection 2−79878
molecule, ground state pot. curve, self-consistent-field α cluster calcs. 2−80003
multipole long range interaction coeffs. 2−64023
optical pumping with laser beam, nonlinear effects in weak magnetic field 2−46453
overlayer on Al or Sn film, depression supercond. transition temp. 2−61228
photoionization by X-rays, relative abundances of multiply charged ions 2−53245
pionic atom, strong interaction effects in 2p-1s transition 2−59964
plasma column, const. wavelength propagated oscills. 2−74389
plasma in Tokamak, electrical resistivity 2−64266
plasma produced by $^{10}B(n,\alpha)$ reaction 2−70887
pulsed n.m.r., of ^{21}Ne, solid and liquid state 2−65347
reaction rate constant for $Ne^+ + 2Ne \rightarrow Ne_2{}^+ + Ne$ 2−43226
shock wave downstream propagation in electrical shock tube with curved end wall 2−77356
solar atmosphere, density dependent ionization balance 2−66231
solar overabundance, accelerated by solar flares 2−76001
solid, anharmonic, interference effects in neutron inelastic scatt. 2−54023
solid, Debye temp., X-ray diffr. obs. 2−47753
solid, self-consistent local orbitals 2−75031
solid, use as Brewster polarizer 2−42211
spallogenic gas in Weston chondrite 2−73098
specific heat at constant volume and critical point determination 2−71113
submonolayer, on Ar coated grafoil, two phase system obs. 2−80582

Neon continued
- superradiant gas laser, field emission electron beam emission 2−42024
- third virial coeff. and nonadditivity 2−60367
- transition probabilities and collision induced transitions in excited levels 2−63995
- Ba-Ne collisions, excitation of metastable levels of Tl behind shock waves 2−79932
- H_2-Ne and D_2-Ne systems, conc. depend. of binary diffusion coeffs., 300K 2−64399
- He-Ne, in magnetic field, use for Zeeman spectroscopy 2−63428
- He-Ne 250 mW laser with Hg cathode 2−76482
- He-Ne colour TV laser display system wide screen and high definition, NHK Model 101C, 525 line 2−82506
- He-Ne glow discharge, average electron energy in positive column 2−60310
- He-Ne laser, 0.63 μ, radiation fluctuations, parasitic generation influence 2−45736
- He-Ne laser, coupling modulation charact. 2−49368
- He-Ne laser, gradual transition from single frequency to multifrequency 2−63328
- He-Ne laser, hysteresis, production by conversion from single to double frequency 2−73558
- He-Ne laser, impulse linear mag. field effect on generating power at $\lambda_{gen}=1.15$ μm 2−63329
- He-Ne laser, intensity correlation function, interferometry determ. 2−79200
- He-Ne laser, methane stabilized, frequency and wavelength det. at 3.39 microns, speed of light det. 2−42018
- He-Ne laser, output power, optimum tube diameter 2−59159
- He-Ne laser, output power intensity dips, use in Zeeman spectroscopy 2−66857
- He-Ne laser, transverse mag. field effect on radiated power 2−59161
- He-Ne laser, variation of longit. elec. field by internally modulated beam 2−49367
- He-Ne laser, with internal nonlinearly absorbing methane cell, 3.39μ freq. standard 2−59158
- He-Ne laser active element using external mirrors 2−49356
- He-Ne laser coupling to active rhodamine B doped polyurethane thin films 2−42055
- He-Ne laser frequency measurement rel. to speed of light determination 2−48974
- He-Ne laser mode selection and polarization control using dielectric plate 2−82474
- He-Ne laser open cavity, aerosol particle detection and size obs. 2−56528
- He-Ne laser output power rel. to electron temp. and density 2−45737
- ^{3}He-^{20}Ne, laser magnetic field effect at 3.39 μ on ring lasers 2−45734
- He + Ne laser, output-power fluctuations reduction 2−55692
- He + Ne lasers, automatic frequency control and frequency fluctuations of difference wave 2−55691
- Ne:NH_3, i.r. spectra, fine struct., rot. and inversion obs. 2−72340
- Ne-Ar pairs, retarded van der Waals pot. 2−67412
- Ne-Br_2 mixtures, r.f. discharge spectrum, excitation mechanisms 2−71018
- Ne-p-H_2, Ne-n-D_2 solutions, density obs., low temps. 2−57027
- Ne-He, streamers, in homogeneous fields induced by laserlight 2−74419
- Ne-He laser, atm. influence on wavelength, correction to laser interferometer 2−69957
- Ne-He laser, automatic optical bias control, p.c.m. communication 2−66797
- Ne-He laser, cathode glow discharge in transverse hollow cathode structure 2−79205
- Ne-He laser, effects of axial magnetic fields on mode intensity spectrum and output power 2−79208
- Ne-He laser, elimination of unwanted lasing at 640.1 nm 2−79183
- Ne-He laser, freq. and wavelength meas. 2−78758
- Ne-He laser, freq. stabilization using inverted Lamb dip and mode interaction effects 2−66753
- Ne-He laser, frequency stabilization by saturated absorption in I_2 vapour 2−66752
- Ne-He laser, single frequency operation and change to multifrequency 2−69909
- Ne-He laser, with dispersive cavity 2−49353
- Ne-He output powers, experimental values 2−59160
- Ne-Hg-Ar discharge, probe measurements in positive column 2−74425
- Ne-Kr, separation by ambipolar effusion, mass spectrometric obs. 2−74475
- Ne-N mixture, decaying plasma, collision processes 2−50189
- Ne^+-N_2 collisions, vibrational distribution of $N_2{}^+B^2\Sigma$ products 2−56273
- Ne-N_2, He-Ne mixtures, viscosity and binary diffusion coeff. meas. in temp. range 25 to 700°C 2−50278
- Ne-Ne pairs, retarded van der Waals pot. 2−67412
- Ne^+-Ne collisions, inelastic energy losses in electron transitions 2−64034
- Ne-Ne^+ inelastic collisions, ab initio H.F. calcs. for Ne_2, $Ne_2{}^+$, $Ne_2{}^{++}$ systems for different interatomic distances 2−49969
- Ne-O^+ close-encounter collisions, 50-200 keV, study of inner shell excitations 2−79914
- Ne-Xe discharge gyroscopic effect in constricted discharge 2−74410
- Ne- compound atom, ground state parameter eval. 2−52924
- Ne II, transition branching ratios 2−83194
- Ne IX in D plasma, meas. of depopulation of $2^3P_{0,1,2}$ triplet levels by electron collisions 2−79961
- Ne VIII solar spectral line, x.u.v., rocket measurements 2−55167
- Ne^+, angular and temp. depend. of Cu sputtering 2−51064
- Ne^+ beam, backscatt. by Ni surface, chain effect 2−77484
- Ne^+ beam scattering from C foil, foil lifetime, charge state distributions and beam scattering 2−52825
- Ne^+ ion scattering on Si (111) crystal surface, study of chemical reaction with bromine 2−50416
- Ne_2 absorption spectrum in vacuum u.v. region 2−77090
- $Ne_2{}^+$ afterglow, dissociative recomb. at elevated temp. 2−83262
- Ne_3, binding energies, calc. for Lennard-Jones 12-6 pair potentials 2−60023

Neon continued
- Ne^{8+}, obs. of 2 quantum processes 2−64279
- NeI, specific isotope shift of 1s-2p and 2p-2s lines, calc. 2−77007
- NeV, NeVI, NeVII, NeVIII, new spectral lines in 50-200 angstroms range 2−74220
- NeVII, experimental oscillator strengths, mean life meas. 2−64017
- ^{20}Ne-^{22}Ne mixture, freq. pulling between two spectral lines, calc. 2−46410
- ^{20}Ne laser, frequency stabilization 2−73552
- $Ne^+ + N_2$, K vacancy production, depend on relative Z of colliding atoms 2−74304
- $Ne^+ + WH_3$ K vacancy production, depend on relative Z of colliding atoms 2−74304
- Tl-Ne collisions, excitation of metastable levels of Tl behind shock waves 2−79932

Neon compounds
- He-Ne, laser LG 68 for building industry 2−66755
- He-Ne mixture, discharge, narrow tube, freq. spectrum and dispersion relation of moving striations 2−64346
- NeH, NeH^+, pot. energy curves of ground and excited states 2−60026

Neptune
- atmospheric temp. sounding 2−78539
- close approach to ν Scorpii, (1972) 2−73085
- construction of models rel. to new estimate of diameter 2−75907
- geometric albedo, calc. and obs. 2−58512
- masses, densities and moments of inertia 2−69142
- mathematical discovery, criterion for prediction 2−62707
- secular variations of asculating elements 2−62696

Neptunium
- atomic absorption spectra computer program for calc. position and optical density of each band 2−46418
- concentration determ. in irradiated fuel reprocessing solutions 2−74180
- covalent model for nature of 5f bonding 2−84396
- target, preparation using tilt-pour and injection casting techniques 2−73907
- targets, prep. techniques 2−73912
- ^{237}Np, hyperfine structure patterns A and B factors and nuclear magnetic moments 2−79938

Neptunium compounds
- $NpPd_3$, cubic and hexagonal phases, unit-cell and X-ray powder data 2−64644

Nernst effect *see Magnetothermal effects*

Nernst-Ettinghausen effect *see Magnetothermal effects*

Neumann algebra *see Algebra; Elementary particles; Field theory, quantum*

Neutrettos *see Neutrinos and antineutrinos*

Neutrinos and antineutrinos
- *see also Cosmic rays/neutrinos; Nuclear reactions and scattering due to/neutrinos*
- $\nu p \rightarrow \mu^+ n$, symmetry relations with $\nu p \rightarrow \mu^+ n$ 2−52557
- bremsstrahlung, electron-nucleus, ion-ion correlation effects 2−49785
- CERN beam facility, magnetic horn focussing device, remote handling system 2−70339
- e.m. and weak interactions in $l^- l^+ \rightarrow \nu\nu\gamma$ 2−76600
- emission onto neutron star 2−81852
- Fitzgerald-Lorentz contraction based on interactions with neutrino sea 2−82201
- forward inelastic scattering, scaling and infinite-momentum limit 2−66936
- four-component hypermass eqn. from quarternion mass generalization, application to unstable neutrinos 2−78791
- general relativity, neutrino field 2−69568
- in gravitational field, spherically symmetric 2−58727
- gravitational scatt. in one-graviton-exchange approx. 2−79499
- hadron production, isospin and SU(3) equalities 2−49484
- high-energy experiments, possible check of scheme with multiplications leptonic quantum numbers 2−76601
- inelastic interactions, low-q^2, comparison of exptl, results with PCAC hypothesis 2−59415
- inelastic scattering, sum rules, parastatistics 2−70158
- lepton-triplet prod. in Coulom field 2−79500
- neutrino-flip expts., meaning in relation to lepton inner structure 2−49502
- neutrino-photon interaction, effect on solar neutrino flux 2−85055
- nonzero rest mass, implications 2−45877
- pair production in weak and e.m. interactions, calc. of stellar energy-loss rates in Weinberg's theory 2−69071
- power spectrum of neutrino sea in Universe 2−72951
- production from collision dominated fluid in closed rotating cosmologies, determ. of collision time approx. 2−48648
- production of N* in harmonic-oscillator quark model 2−52647
- relativistic interacting particle system, asymptotic limit for speed of sound 2−66429
- rest mass 2−72953
- scattering, bounds on deep inelastic structure functions 2−55872
- scattering, current algebra sum rules and scale dimension of chiral symmetry breaking Hamiltonian 2−55818
- scattering, deep inelastic, on polarized targets, light-cone quark algebra 2−52584
- scattering, implications of quark-gluon lignt cone current algebra 2−42335
- scattering, inelastic, light-cone behaviour 2−82681
- scattering, polarization effects, locality 2−66937
- scattering, polarization effects, quark parton model 2−66938
- scattering processes, high energy, test for scalar-boson-mediated weak-interaction theories 2−82682
- scattering structure function, possible exchange degeneracy on light cone 2−55825
- solar neutrino, discrepancy between astrophysical predictions and terrestrial exptl. obs. 2−44979
- stellar reactions in supergiants and neutrino emission 2−51735
- weak interaction props. at high energy, review 2−59418
- γ-ν ang. correls. in muon capture 2−79778
- ν-lepton interaction and intermediate vector boson 2−55819
- ν_e rest mass, upper limit determ. from ^{3}H β-ray spectrum 2−73751
- $\nu_\mu + n(p) \rightarrow \nu_\mu + n(p) + \pi^0$, exptl. limit on neutral current 2−63508

Neutrinos and antineutrinos continued
$\nu_\mu + p \to \nu_\mu + p + \pi^0$, cross section calc. using Weinberg model 2–59417
$\nu d \to \mu$-pp quasi-elastic reaction, forward cross-section determ., relativistic effects, one-pion exchange contribs. 2–42334
νe (νe) scattering, weak interaction of photons 2–55817
νe and νe-, scattering anal. on assumption of ν- proton interaction 2–82680
νe and νe scattering, polarization effects 2–76602
νe forward scatt. amplitudes, sum rules 2–79498
ν_ee- scattering, search for reaction 2–45878
$\nu_\mu e \to \nu_\mu e$, amplitude of reaction in unified models, induced neutral current effects 2–70155
νl scattering, higher-order corrections, renormalization of Weinburg's theory of interactions 2–79497
$\nu_\mu \mu$ interaction, upper limit for interaction constant 2–59416
νN, Adler's sum rule for W_3 from time-space ETC 2–70154
νN, as test for algebra of bilocal operators 2–70109
νN, as test for algebra of bilocal operators 2–70109
νN, deep inelastic scattering, inequalities for structure function derived from quark parton model and quark model with neutral gluons 2–42329
νN, νN interactions, cross-sections calc. from 3 quark boson-nucleon model 2–45876
νN, pseudoscalar meson prod., generalized similarity relation and trilinear matrix elements 2–76724
νn scatt., structure function calc. in leading logarithm approx. to perturbation theory and massive g.e.d. Lagrangian 2–73752
νn scatt., structure function calc. in leading logarithm approx. to perturbation theory and massive g.e.d. Lagrangian 2–73752
νN scattering, determ. of sum rules from triplet quark model light-cone algebra of currents 2–76708
νN scattering, determ. of sum rules from triplet quark model light-cone algebra of currents 2–76708
νN scattering, dimension of symmetry breaking Hamiltonian 2–42336
νN scattering, operator product expansions and dimension of symmetry breaking Hamiltonian 2–55820
νN sum rules and low energy theorems 2–42337
$\nu N \to NX$, parton model predictions in Weinberg theory 2–45886
$\nu n \to \mu^- p$, symmetry relations with $\nu p \to \mu^+ n$ 2–52557
$\nu_\mu N \to \mu^- W^+ N'$, μ^- production cross-sections, neutrino energy spectrum 2–76613
$\nu_\mu n \to p\mu^-$, second class current limitations 2–52558
νp scatt., elastic, with strong W-boson interactions 2–79501
νp scatt., structure function calc. in leading logarithm approx. to perturbation theory and massive g.e.d. Lagrangian 2–73752
νp scatt., structure function calc. in leading logarithm approx. to perturbation theory and massive g.e.d. Lagrangian 2–73752
$\nu p \to \mu^+ \Lambda$, production cross-section for Λ 2–67061
$\nu p \to \mu^+ \Sigma^0$, production cross-section for Σ^0 2–67061
$\nu p \to \nu p$, amplitude of reaction in unified models, induced neutral current effects 2–70155
π production 2–45949
Neutron diffraction
biological molecules, structure 2–81994
Stern-Gerlach experiment, rel. to magnetic saturation determination of Co and Ni 2–54326
Al wires, pole figures to investigate cyclic textures 2–77700
Neutron diffraction crystallography
see also Crystal structure, atomic
charge density determ. in crystals desirability of absolute scale 2–77535
coherent neutron scattering amplitudes, table 2–53645
coherent scatt. amplitudes from powders 2–53654
converter screens, prod., for thermal neutrons 2–74713
cryomagnetic assembly for 2–66372
cryostat, 1-300K 2–73245
cubic and uniaxial compounds, ambiguity in powder diffr. magnetic lattice dimensions 2–54283
diffractometers provided by Australian Institute of Nuclear Science and Engineering at Lucas Heights 2–60746
ferromagnet, crit. depolarization of neutrons 2–81268
fine structure, limits on diffr. anal. 2–74697
fixed angle neutron diffractomer, resolution and intensity 2–47310
Fourier refinement methods 2–77531
high resolution spectroscopy applics. to mol. rots. and diffusion processes 2–77607
inelastic neutron scattering cross section, crystals with linear defects 2–50997
inelastic scattering, normalization of the resolution function 2–53644
integrated intensity of scattered neutron group, correction for dependence on scanning mode 2–47311
monochromator, growth of suitable crysts. 2–47205
monochromators, using curved Si crystals 2–79649
multiple scattering, perfect crystal, neutron wave field calc. 2–50614
order-disorder investigation 2–50991
rare earth metal isotope single cryst. growth 2–47225
spectrometer resolution function, computer programs 2–80609
spherical nature of coherent wave front 2–74744
Neutron diffraction examination of materials
alkali halides and sulphates, coherent scatt. amplitudes from powders 2–53654
amorphous solid, polymer chain conform. from small-angle scatt. 2–74600
antiferromagnet, impurity effects on excitation spectra 2–44282
antiferromagnetic- ferromagnetic transition point, fluctuations and scatt. of slow neutrons and e.m. waves 2–72207
benzene, liquid and solid, quasi-elastic scattering of cold neutrons, obs. of broadening 2–80451
diffusive motions in solids and liqs., quasielastic scatt., book 2–64456
durene, hindered rotation in crystals by neutron transmission meas. 2–50999
erOOH, monoclinic, mag. struct. 2–44296
ferromagnet, mag. dispersion phenomena 2–61488
ferromagnet, with weak antiferromagnetism, rel. to l-wave existence 2–78012
Neutron diffraction examination of materials continued
ferromagnetic mat., cold neutron diffr. by Bloch walls, nonelastic scatt. 2–51248
fuel irradiated 2–49884
germania, vitreous, structure obs. 2–53534
graphite, pyrolytic, lattice dynamics 2–43954
hexamethylbenzene, hindered rotation in crystals by neutron transmission meas. 2–50999
hydrocarbons, crystalline, intermolecular interaction potential from incoherent scattering of slow neutrons 2–47738
hydrogen containing compounds, crystal chemistry, review 2–74653
inelastic scatt. and diffl. cross sect. of slow neutrons by localized vibrations of interstitial atoms 2–71722
invars, crystal structure 2–68002
liquid crystal, neutron quasielastic scatt., incoherent cross-section 2–46924
low temperature studies, cryomagnetic assembly 2–66372
magnetic materials, mag. scatt. by neutrons on fluctuons 2–71151
magnetic scatt. in critical region, magnetization waves rel. to Brillouin-Mandelstam doublet 2–75214
metals, antiferromagnetic, neutron scattering cross section by electromagnetic-magnon waves 2–84443
methane, liquid, mol. motion 2–43324
methane-d_4, obs. of critical fluctuations at 27K phase transition 2–61040
molecular crysts. 2–48159
neopentane, phase transitions 2–50928
neopentane, plastic crysts., quasielastic scatt. rel. to mol. rot. motion 2–53513
neutron radiography, nondestructive testing technique, review 2–43765
nuclear pseudomagnetic reson. of neutron induced by r.f. field 2–84598
perdeuterobenzene, liquid and solid, quasi-elastic scattering of cold neutrons, obs. of broadening 2–80451
phonon freq. distrib. function determ. 2–50998
phonon polarization vectors meas. with triple-axis spectrometers 2–64838
plastic crystal, molecular rotation models 2–80590
polydomain ferromagnets, singularities of elastic and inelastic scattering of neutrons 2–81226
polystyrene soln., neutron small angle scatt., obs. 2–50341
quantum crystal, scatt. data interpretation 2–61060
rare earth metals, light, mag. props. 2–61517
rare earth-nickel intermetallics, mag. struct. 2–48080
silica, vitreous, structure obs. 2–53534
solutions, scatt. by fluctuons 2–71151
structure and dynamics of crystals, new exptl. methods 2–74706
superconductor, scattering spectral function and phonon modes, electron-phonon interactions 2–71861
tetra-acetylethane, crystal structure 2–43602
transition metal carbides, phonon anomalies 2–64836
transition metal/hydrogen systems, quasielastic scatt. obs. of diffusion process 2–77623
$[YCa_2][Zr_2](Fe_{2.75}Ge_{0.25})O_{12}$ garnet, mag. struct. 2–78038
Al-Mn dilute alloy, scatt. by spin fluctuations 2–61473
Al, liquid, meas. of structure factor 2–64435
Al, mag. scatt. of neutrons from dissolved Mn atoms 2–61474
Ar, liq., coherent- and incoherent-scatt. laws 2–67798
Ar, liquid, dynamics from first moments of coherent scattering function 2–46922
$BaFe_{12-x}Ti_xZn_xO_{19}$ ferrite, Ti-Zn cation distrib. effects on mag. props. 2–72195
$BaPrO_3$ and $BaTbO_3$, neutron diffr. and mag. susceptibility meas., mag. props. detn. 2–81217
Be, monocrystals, growth by Czochralski technique, obs. of cryst. perfection 2–47262
$Bi_4Ti_3O_{12}$, crystal struct. determ. 2–71425
$Ca_3Cr(GeO_4)_3$, mag. struct. and space group determ. 2–72145
CaF_2, dynamical struct. anal. 2–71723
$Ca(H_2AsO_4)_2$, cryst. struct. 2–67988
$Ca(Y)F_2$, containing excess anions, defect struct., neutron diffuse scatt. 2–77570
CeBi, mag. struct. 2–44291
$CeH_{2\pm x}$ system, nonstoichiometric, defect struct. and ordering 2–77755
CeSb, mag. struct. 2–44292
$Ce_{0.25}(Y,La)_{0.75}Al_2$, inelastic scatt. determination of cryst. field levels of Ce^{3+}, susceptibility calc. 2–72105
Ce_xY_{1-x} Sb, crystal field splitting of Ce^{3+} obs. 2–61570
Co, magnetic saturation determination using Stern-Gerlach experiment with neutrons 2–54326
Co_2MnSn, Heusler ferromag. alloy, magnetic struct. 2–48075
Cr-Re dil. alloys, single cryst., mag. struct. 2–61553
Cr-1.6%W alloy, phonon freqs. obs. 2–74973
Cr, antiferromagnet, obs. of Q-switch and polarization domains 2–65179
Cr_2O_3-Ti_2O_3 solid solution, mag. ordering study 2–48104
Cr_2O_3-V_2O_3 solid solution, mag. ordering study 2–48104
$Cr_{1-x}Te$, magnetic anisotropy with X=0.077 2–84415
CsCl, phonon-dispersion, neutron spectrometer study and shell model anal. 2–84192
$CsCoCl_3$, mag. struct. 2–72213
CsF, phonon dispersion relations determ. 2–64840
$CsH_3(SeO_3)_2$, struct. anal. 2–71428
$CsMnBr_3$, crystal perfection, mosaic spread obs. 2–47224
$CsNiF_3$, three dimensional mag. struct. 2–61556
Cu-Mn alloys, diffuse scattering peak between {100}, {110} positions due to γ-MnO_2, short range ordering 2–71644
$Cu_{0.5}Fe_{2.5}O_{4\pm x}$, spinel ferrite, neutron-diffraction study, with and without mag. field 2–61543
CuTe, liquid, structure 2–60421
D_2O liquid, atom pair correlation functions from neutron and X-ray diffraction 2–43323
Dy single cryst., depolariz. meas. near Curie point 2–51251
DySb, mag. struct. 2–44292
$DyVO_4$, refined cryst. struct. 2–60756
^{163}Dy production and crystal growth 2–74667
$ErAg_2$, magnetic structure, 297-1.5K 2–61551
$ErAl_2$ and $Er_xY_{1-x}Al_2$, mag. struct. obs. 2–81275

Neutron diffraction examination of materials continued
$ErAl_3$, mag struct. obs. 2−81275
$ErAu_2$, mag. struct. 2−72216
ErC_2, cryst. and mag. struct., 297-2K 2−72217
Fe-Co alloy equiatomic mag. scatt. form factors 2−44249
Fe-Pd alloys, f.c.c., mixed exchange interactions, neutron scatt. obs. 2−84421
Fe-Si solid solns., b.c.c., ordered atomic configs. 2−47326
Fe, critical and spin wave fluctuations 2−54309
Fe, small-angle magnon scatt. collapse 2−44242
Fe, spin-density asphericity, temp. depend. 2−44250
$FeCO_3$, Ising behaviour, magnon-phonon coupling 2−44297
FeF_2, scatt. struct. factor, nonlinearity effect 2−48107
Fe_2MoO_4, spinel, X-ray and neutron diffraction studies 2−84414
$Fe_{0.9}Nb_{1.1}O_4$ magnetic structure 2−65181
Fe_2O_3, produced from α-, β-, γ- and δ-FeOOH, mag. state 2−81292
FeOOH, α- and β-modifications, mag. state study 2−81292
Ga, liq., multiple scatt., effective scatt. factors 2−60422
Ge, phonon dispersion relations, homology with Si 2−84190
$Ge_{0.17}Te_{0.83}$, amorphous, radial distrib. functions 2−56548
o-H_2, solid, f.c.c. and h.c.p. phases, phonons, librons and rot. state 2−64839
He, liq., phonon dispersion underpress. 2−80510
He, superfluid, phonon emission and absorpt. due to rotons 2−64495
He II, emission and absorpt. of phonons by rotons 2−43425
^4He, b.c.c., scatt. function for inelastic scatt. 2−67867
^4He, h.c.p. and b.c.c. phases, single-particle scatt. phenomena 2−67866
^4He, solid, scatt. phenomena, review 2−80515
Hf-O system, near $HfO_{1/6}$, interstitial order-disorder transform. 2−68205
$HoAl_2$, mag. ordering obs. 2−75217
$HoAu_2$, mag. struct. 2−72218
$HoFe_3$, mag. struct. 2−51272
$HoVO_4$, refined cryst. struct. 2−60756
$HoZn_2$, mag. struct., ordering 2−68573
KD_2PO_4, soln. grown, space group determ. 2−60712
$KFeF_4$, antiferromag., critical behaviour 2−44301
$KFeF_4$, planar antiferromagnet, struct. in critical region obs. 2−78043
$K_3Hg(NO_2)_4NO_3$, crystal structure determ. by neutron diffraction 2−64639
K_2MnF_4, mag. struct. near crit. point 2−65182
$LiFe_2F_6$, mag. struct. 2−44302
$LiFe_2F_6$, trirutile, mag. structure obs. 2−65183
$LiFe_2F_6$, trirutile, mag. struct. 2−72220
$LiN_2H_5SO_4$, anomalous neutron scatt. and absence of ferroelectricity 2−84357
$MdPd_3$, mag. struct. obs. 2−54360
Mg-Mn ferrites, electronic struct. of Mn and Fe ions 2−47182
MgO, coherent neutron-scatt. amplitudes for ^{24}Mg, ^{25}Mg, ^{26}Mg isotopes 2−67995
MnB_2, mag. struct. 2−44306
MnF_2, critical scatt., spin fluctuations 2−54361
MnF_2, longit. scatt. behaviour below crit. temp. 2−54362
$MnFe_2O_4$, acoustic magnon dispersion 2−61544
MnO, spin wave dispersion relations detn. 2−61558
Mn_3Pd_5 phase, crystal and magnetic struct. 2−83960
$Mn_{1-x}Zn_xFe_2O_4$, mag. order obs. 2−65168
$(NH_4)_2S_2O_8$, hindered rotation in crystals by neutron transmission meas. 2−50999
$(NH_4)_2SiF_6$, hindered rotation in crystals by neutron transmission meas. 2−50999
NaN_3, rhombohedral, external vibration modes 2−43957
$NaNO_3$, crystal struct., order-disorder transforms, neutron diffraction obs., 20-290°C 2−77758
Nb-H system, phase diagram, 80-500 K 2−77756
Nb, 4.2K, superconducting, local magnetic field distributions 2−57155
NbD_x system, diffuse scatt. phenomena in α-phase, temp. depend. 2−77757
β-NbH, proton jump rate determ. 2−77614
NbH_x, diffusive motions of hydrogen 2−77615
NdSb, mag. struct. 2−44292
Ne, anharmonic crystal, interference effects in neutron inelastic scatt. 2−54023
NgH_x, vibr. and diffusive behaviour of hydrogen 2−77771
Ni, anisotropy of depolarization of neutron beams 2−61509
Ni, critical and spin wave fluctuations 2−54309
Ni, magnetic saturation determination using Stern-Gerlach experiment with neutrons 2−54326
Ni, near Curie temp., crit. depolarization of neutrons 2−81268
$NiCr_2O_4$ mag. struct. 2−84429
$NiFe_{0.8}Cr_{1.2}O_4$, ferrite, statistical angular spin configurations 2−72200
Ni_2MnSb, Ni_2MnSn, Heusler ferromag. alloys, magnetic struct. 2−48075
NiO, spin wave dispersion, inelastic scatt. study 2−81303
PbTe, transverse optic mode softening, Curie law temp. depend. 2−68230
Pd-Ag alloys, diffusive motions of hydrogen 2−77618
Pd, hydrogen diffusion, quasielastic scatt. obs. 2−83999
Pd_3Fe, lattice dynamics, 80K 2−43962
Pd_3Fe, spin wave dispersion relation 2−61503
Pr, f.c.c., singlet-ground-state ferromagnet, transition obs. 2−72152
Pr_3Tl, singlet-ground-state ferromagnet, transition obs. 2−72152
$RbFeCl_3$, crystal perfection, mosaic spread obs. 2−47224
$RbFeF_4$, two-dimens. antiferromag. ordering, and susceptibility obs. 2−54363
$RbMnF_3$, critical scatt., spin fluctuations 2−54361
$RbNiCl_3$, crystal perfection, mosaic spread obs. 2−47224
$RbNiCl_3$, mag. struct. 2−48111
$RbNiF_3$, ferrimagnet, spin waves obs. 2−65171
Si, Pendellosung fringe patterns, perfect crystals possess curved distortion 2−74744
Si, phonon dispersion relations, homology with Ge 2−84190
SiO_2, vitreous, struct., at. motions, neutron scatt. obs. 2−47061
SiO_2, vitreous, struct., random network theory validity 2−47054
^{154}Sm production and crystal growth 2−74667

Neutron diffraction examination of materials continued
^{170}Sm production and crystal growth 2−74667
$SrCoO_{2.5}$, mag. struct. obs. 2−81294
SrF_2:Dy, Tb, Nd, axial distrib. of impurities, neutron activation analysis 2−56744
SrF_2, phonon dispersion curves, harmonic vibr. props. 2−77760
$SrFeO_3$, mag. struct. obs. 2−81282
$SrTiO_3$, dynamics of structural transitions 2−65065
$SrTiO_3$, lattice dynamics, normal mode freqs., harmonic models 2−77761
TaC, phonon anomalies 2−64836
Ta_4D_3, stepwise phase transitions of order-disorder type obs. 2−74947
TaH_x, quasielastic scatt. obs. of hydrogen diffusion 2−77621
$TbAl_2$, mag. ordering obs. 2−75217
$TbCu_2$, mag. struct. and props. 2−44309
$Tb_2(MoO_4)_3$, ferroelec. phase transition obs. 2−65066
$TbVO_4$, refined cryst. struct. 2−60756
Te, liquid, structure, review 2−60423
ThCN, cryst. struct., X-ray and neutron powder diffr. 2−53681
Tl, phonon spectrum, supercond. tunnelling and neutron scatt. data, discrepancy 2−84189
TmSb, cryst. field effects in mag. form factor 2−81254
UAs-US system, magnetic phase diagram obs. 2−65188
$UAs_{1-x}S_x$ system, mag. phase diagram 2−44258
UPb_3, mag. struct. determ. 2−78041
US, cubic ferromagnet, mag. moment distrib. obs. 2−72171
US, mag. ordering, ordered mag. moment 2−84418
USe, mag. ordering, ordered mag. moments 2−84418
UTe, mag. ordering, ordered mag. moments 2−84418
VH_x, quasielastic scatt. obs. of hydrogen diffusion 2−77621
W, electron density distrib., neutron electron scatt. obs. 2−57138
YD_3, crystal struct. obs. 2−74752
$YbVO_4$, refined cryst. struct. 2−60756
Zr-O α solid solution, interstitial O atom arrangement 2−71443
Zr-O system, near $ZrO_{1/3}$, interstitial order-disorder transform. 2−68205
Neutron radiography *see Radiography*
Neutron sources *see Neutrons and antineutrons/production*
Neutron spectra
atmospheric equilibrium layers, energy spectrum 2−48455
benzene, liquid and solid, quasi-elastic scattering of cold neutrons, obs. of broadening 2−80451
cold sources containing liquid H obs. and Monte Carlo calc. of output 2−49859
continuous, of neutrons inelastically scattered from neutron weight nuclei at 14 MeV 2−70450
delayed neutrons from fission, energy spectra 2−46354
epithermal, in reactor lattices, spherical harmonics treatment 2−76901
fast power reaction blanket region characts. 2−79841
of fission products, mass-separated, structure studies using ^3He spectrometer 2−67150
fission source in water 2−83055
high power source, using $^{244}Cm + Be$, 4π angle yield 2−42440
intermediate system of C, B, Al, differential and integral measurements 2−70502
isobaric analogue resonances, survey of statistical neutron decay for nuclei in A=91-97 range 2−67131
isotopic source, using Be(α,n), line spectra meas 2−42439
kinetic energy, in delayed neutron emission 2−49855
methane, liquid and solid, suitability as slow neutron moderator 2−76897
neutron-gamma competition following (d,d′) reaction 2−46325
in nuclear reactor heavy-water-moderated coupled cores, static obs. 2−42628
perdeuterobenzene, liquid and solid, quasi-elastic scattering of cold neutrons, obs. of broadening 2−80451
photoneutron spectra, from 55 MeV bremsstrahlung 2−52796
pool type reactor, determ. of thermal neutron energy spectrum by activation foils 2−79832
reactor core with MTR type fuel elements 2−52842
resonance energy neutrons, space-energy distribution calculation 2−79827
resonance neutrons in reactor in kev region, measurement 2−46357
sea level flux determ., using knock-on protons 2−42433
slowing down in vicinity of strong scattering resonance 2−74133
space dependent, in lead and graphite crystalline prisms 2−70506
threshold reactions, maximization of desired activity against interfering activities 2−42616
(n,2n) fast neutron reactions, systematics of excitation functions 2−76849
Be, scattering, pseudo mode decay, anal. by inelastic scatt. expansion 2−83046
α-Be neutron sources 2−55928
$^9Be(p,n)^9B$, 17.8 MeV, determ. of width of excited state in ^9B from neutron spectra 2−52735
Bi, μ-capture reaction 2−59745
^{249}Bk spontaneous fission, average neutron yield 2−83026
^{12}C, pion capture, meas. of emitted neutron-charged particle final state 2−46300
$^{12}C(\mu,n)$, effects of giant resonance on energy spectra of emitted neutrons 2−46240
Ca, μ-capture reaction 2−59745
^{40}Ca muon capture, calculation 2−63903
Ca(μ^-,n), 2-13 MeV, meas. of neutron energy spectra, excitation of quasibound states of intermediate nucleus 2−52806
^{252}Cf, fission neutron spectrum from 0.002 to 1 MeV 2−46353
^{252}Cf, fission neutron spectra 2−46350
^{252}Cf, ternary fission, neutron energy spectrum 2−67338
^{252}Cf spontaneous fission, instantaneous neutron spectrum in low-energy region 2−83025
$(CoO)_{1.4}.P_2O_5$, glasses, antiferromag. interactions 2−75237
D_2O and CM-2 reactors, time-of-flight spectrum 2−63939
$(Fe_2O_3)_{0.79}.P_2O_5$, glasses, antiferromag. interactions 2−75237
^{55}Fe, level density determ. using evaporation neutrons in $^{55}Mn(p,n)^{55}Fe$ 2−63797
H_2O-moderated H_2O-cooled power reactor, differential fast spectra 2−63940
^2H, 120 MeV alpha bombardment, neutron energy spectra 2−67322

Neutron spectra continued
^{6}Li(p,n)^{6}Be, 17.8 MeV, determ. of width of excited state in ^{6}Be from neutron spectra 2−52735
NdP, NdAs, NdSb, crystalline electric field levels detn. 2−68585
^{16}O muon capture, calculation 2−63903
^{16}O(μ, n), effects of giant resonance on energy spectra of emitted neutrons 2−46240
O(μ^-,n), 2-13 MeV, meas. of neutron energy spectra, excitation of quasibound states of intermediate nucleus 2−52806
Pb, μ-capture reaction 2−59745
Pb(μ^-,n), 2-13 MeV, meas. of neutron energy spectra, excitation of quasibound states of intermediate nucleus 2−52806
Pu-Be, Po-Be sources, investigation of spectra at low energies, meas. of activation cross sections 2−67227
^{239}Pu, fission, β and γ residual powers 2−74128
^{239}Pu, fission neutron spectra 2−46350
^{32}S muon capture, calculation 2−63903
^{28}Si muon capture, calculation 2−63903
S(μ^-,n), 2-13 MeV, meas. of neutron energy spectra, excitation of quasibound states of intermediate nucleus 2−52806
Tl, μ-capture reaction 2−59745
U depleted in ^{235}U isotope, fast neutron spectra meas. and analysis 2−83057
^{235}U, fission, β and γ residual powers 2−74128
^{235}U, fission neutron spectra 2−46350
^{235}U fission, time-of-flight versus energy spectra 2−83031
ZrH$_x$, effect of H$_2$ chemical binding, using free gas and Nelkin-Rosenbluth models 2−56029

Neutron spectrometers
chopper monochromator, cold neutrons, time of flight, slit package cross section, Be filter, wavelength resolution 2−82565
cosmic ray spectrograph using recording channels with different τ 2−46022
fast neutrons, energy spectra of cyclotron produced neutron beams 2−52682
Geesthacht, error in meas. total cross section 2−52681
leakage type, design, for KEV range 2−70286
multiplicity counter, superheavy element search 2−52683
multisphere for spectrum of Pu-Be source 2−59878
neutron balance, proton recoil, time-of- flight, for fast reactor physics 2−76733
neutron energy, radiative capture cross-section, fission cross-section 2−82802
neutron-capture conversion electron spectrometer at HFR-ILL in Grenoble 2−67078
pyrolytic graphite neutron reflectivity and use as analyzer and higher order filter 2−55891
resolution function, computer programs 2−80609
time-of-flight for ultracold neutrons 2−55903
triple-axis, counting rate calc. method 2−63693
triple-axis, meas. of phonon polarization vectors 2−64838
^{3}He, obs. of delayed neutron emission of mass separated fission products 2−67150
^{3}He fast neutron, delayed neutron energy distrib. meas. 2−67194
^{3}He fast neutron, improved energy resolution considerations 2−67075
^{6}Li semiconductor sandwich, characteristics and performance 2−42448

Neutron transport theory
see also Neutrons and antineutrons/diffusion; Neutrons and antineutrons/moderation
2 group theory, half-range orthogonality theorem 2−49860
absorption during slowing down, correl. between Resonance and Greuling Goertzel Approx. 2−42608
adiabatic kinetics model parameters, applicability to LMFBR 2−83103
angular distrib. of thermal neutrons at surfaces of black and grey cylinders 2−83056
anisotropic scattered pulses, relaxation times in decay 2−74138
backscattering effects in wave propag. problem 2−42605
Boltzmann eqn. in slab geometry, spherical harmonics approximation, numerical computation 2−83042
cell diffusion coefficients, correction to earlier paper 2−42601
characteristics formulation of transport equation in complicated geometries 2−49870
consistent dipolar heterogeneous formulation, parameters calculated 2−59811
consistent dipolar heterogeneous formulation 2−56022
deceleration, lethargy probability distribution density calc. using integral representation of Dirac δ-function 2−46360
diffusion, steady-state solutions in two-group theory 2−83048
discrete ordinate eqn., effect of singularities on approximation in S_n methods 2−79825
discrete ordinate eqn. equivalent to P_l approx. 2−79824
distance to collision, Monte Carlo sampling with continuously varying cross-sections along flight paths 2−70508
eigenfunctions expansion method, pseudo mode calc. 2−52837
epithermal neutron spectra in reactor lattices, spherical harmonics treatment 2−76901
field in reactor core, hybrid computer solution 2−69628
first flight collision probability for finite cylinder, numerical calc. 2−83045
flux, reactor efficiency of absorbing element system 2−79828
flux distribution control in nuclear reactors 2−74144
flux perturbations due to absorbing materials in cosine flux gradient 2−83050
group collapsing problem in multigroup cross-sections 2−46365
heterogeneous media- cylindrical cell, effective diffusion coefficients 2−46362
in infinite absorbing non- multiplying medium initial condition for transport equation 2−67342
integral transform method for 2D and 3D neutron transport problems 2−70507
kinetics eqns. direct integral formulation 2−83097
kinetics optimization in zero reactivity method, application to coupled graphite-D$_2$O reactor 2−76907
LATREP lattice code accuracy 2−46244
lattice props., integral transform method for average transport props. 2−83058
lethargy-dependent age in perpendicular direction in slab lattices, Laplace transform 2−83059
linear, general theory of spherically symmetric boundary value problems 2−46361
moderation, analysis of pulsed neutron experiments in polycrystalline moderators 2−59812
monoenergetic burst decay in slabs, fund. mode calcs. 2−42604
Monte Carlo codes specification and testing 2−83061
multi-dimensional steady-state transport equations, soln. by Galerkin method 2−76896
multigroup cross sections, shielding factor generation for fast reactor analysis 2−49875
multigroup diffusion eqn., comparison of finite element and finite difference approxs. for numerical soln. 2−76900
multigroup diffusion theory, variation flux synthesis methods 2−83052
multigroup diffusion theory, variational flux synthesis methods 2−83051
multipoint P_3 method for transport equation solution 2−49867
neutronic calc. for blanket assembly by discrete ordinates and Monte-Carlo methods 2−46369
nodal equations, derivation from invariant imbedding theory 2−56023
in non-multiplying medium, initial value problem 2−67343
P_n and double P_n approximations to monoenergetic transport equation, modifications 2−49865
polycrystalline media, finite, analysis of total response of neutron waves 2−42603
pulsed problem, variational method 2−42606
pulsed thermal neutron theory 2−46364
reaction rate error estimation using functional analysis technique 2−70501
reactor kinetic eqns. space independent, new method of obtaining analytic solutions 2−49864
simplified spherical harmonics equations, Marshak conditions applicable in spherical geometry 2−56026
slab reactor, with moving boundaries, neutron distribution 2−56028
slowing down equation for infinite homogeneous monatomic medium, exact solution in analytical form 2−42602
slowing down in a cylindrical pile of finite height, solution for various types of source 2−46366
slowing down theory, time dependent phenomena 2−56027
slowing down time, by Pb and graphite moderators, space depend. multigroup theory 2−63945
spherical harmonic solns. of transport eqn. from discrete ordinate codes 2−76899
thermal flux determ., effective Cd cut-off energy 2−56021
thermal neutron spectra, double filter investigation technique 2−56025
thermal neutrons, albedo and Milne's problems 2−70503
thermal neutrons, problems solved by overlapping group techniques 2−83054
time-dependent equation, multigroup treatment 2−59810
time-dependent equation with nonhomogeneous boundary conditions, rigorous mathematical treatment 2−49869
time-moments, regular and adjoint, calculation and meaning 2−70505
transport equations, elementary solutions including anisotropic scattering 2−63944
two group diffusion equations, variational acceleration technique for iterative solution 2−59809
two-group existence and uniqueness of H-matrix 2−83049
wave, pulse propagation, cryst. media, effect of cold neutrons 2−83044
^{252}Cf thermal flux subcrit. multiplication 2−83062
D$_2$O, angular dependent leakage spectra 2−76906
U depleted in ^{235}U isotope, fast neutron spectra meas. and analysis 2−83057

Neutrons and antineutrons
see also Cosmic rays/neutrons; Nucleons and antinucleons
β-decay, application of model of Tanikawa et al in μ^-p resonances and duality in weak processes 2−70265
beam intensity estimation, biological and medical applications 2−76079
beta decay half life meas. 2−46006
bound trineutron search in natural Li bombardment by 19 MeV neutrons 2−63896
charge form factor study of octet dominance of baryon matrix elements, explanation of vanishing charge radius 2−67059
delayed neutron emission, β-strength functions and gross properties 2−49855
delayed neutrons, review of present status 2−83047
density modulation in nuclear reactor, comparison of modulated source and modulated poison methods 2−49862
dipole moment estimate from weak interaction theory 2−73801
distribution at large distances from source 2−63978
electric dipole moment, as bound state of mag. monopoles 2−45880
electric dipole moment estimate 2−73755
e.m. form factors, dipole behaviour 2−49588
e.m. form factors, dipole behaviour 2−76712
e.m. form factors, dipole behaviour 2−76711
e.m. form factors, from electron deuteron scattering meas. at squared four momentum transfers of 1.0 and 1.5 (GeV/c)^2 2−42418
energy spectrum in (n, n′) and (n, 2n) reactions at 14 MeV 2−67232
magnetic moment calc. using Markoffian model of hadrons 2−73773
metal, coupled helicon-magnon wave scattering 2−68314
parton structure anmuetron matter 2−69085
proton-neutron mass difference, finite contribution 2−49589
proton-neutron mass difference, investigation in configuration space 2−55875
proton-neutron mass difference and related topics, report 2−49590
radiography, nondestructive testing, technique and applications 2−52515
semiconductor, ferromagnetic, coupled helicon-magnon wave scattering 2−68314
thermal beam, focusing by reflective dispersion 2−67070
thermal neutron distributions meas. as surfaces of cylinders 2−56018

Neutrons and antineutrons continued
$n \to p\pi^-$ parity violating amplitude, presence of second-class currents 2−82656
νN scattering, deep inelastic, multiperipheral theory 2−59419
p-n mass difference, axial-vector massive, photons 2−70253
p-n mass difference, divergent contribution in Weinberg model 2−67048
pn bound state and mass of nucleon quark 2−73840
absorption
see also Nuclear excitation; Nuclear reactions and scattering due to/neutrons
burnt-up fuels, occurrence of high neutron dose rates 2−76915
displacement cross sections for stainless steel, Fe, Cr, Ni and Ta bases on Lindhard model 2−83053
flux perturbations due to absorbing materials in cosine flux gradient 2−83050
in heterogeneous lattices, intermediation resonance treatment by modified μ-method 2−79821
intermediate resonance calcs. for resonance absorber in absorber-moderator mixture, improved practical width 2−79820
reactor fuel elements, nondestructive meas. techniques 2−56040
shielding by two types of concrete 2−79846
during slowing down, correl. between Resonance and Greuling Goertzel Approx. 2−42608
spherical and cylindrical sources, calculation by computer code 2−42600
temperature sensing by neutron transmission 2−78942
ultracold neutrons, interference in transmission through thin layers 2−46358
^{252}Cf target in CM-2 reactor, effective cross-section 2−67341
^{253}Cf target in CM-2 reactor, effective cross-section 2−67341
by^{3}He, investigation of ^{3}He diffusion in liquid ^{4}He 2−64492
angular distributions
scattering, elastic, analysis yielding ang. distrib. data 2−82978
sea level spectrum, zenith and range distribs. 2−42433
Ag, Pr, Mo, Ge targets, bombardment by ^{12}C, ^{16}O, ^{22}Ne and ^{40}Ar ions 2−76886
^{10}B(d,n), $E_d=11.8$ MeV, neutron spectroscopy 2−67324
^{11}B(d,n), $E_d=11.8$ MeV, neutron spectroscopy 2−67324
^{9}Be(d,n)^{10}B, 650 keV, meas. of angular distrib. of neutrons, energy levels of ^{10}B 2−49830
^{9}Be(d,n)^{10}B, 650 keV, meas. of recoil proton tracks, angular distrib. of neutrons, determ. of Q-value spectrum 2−63913
^{12}C(d,n), $E_d=11.8$ MeV, neutron spectroscopy 2−67324
^{12}C(n,n$'\gamma$)^{12}C, improved statistics for angular correlation measurements 2−46273
^{13}C(^{3}He,n)^{15}O, meas. of neutron yield at 5.5 and 6.2 MeV 2−46316
Ca, distribution from μ^- capture 2−46356
^{55}Mn(α, nγ)^{58}Co, 10 MeV, meas. of n-γ angular correlations and lifetimes using Doppler-shift attenuation method 2−82890
^{14}N(d, n)^{15}O, 5.16 MeV, n polarization ang. distrib. meas., cross-section analyzed using optical model formalism 2−46318
S, distribution from μ^- capture 2−46356
capture *see Nuclear reactions and scattering due to/neutrons*
detection, measurement
see also Dosimetry; Neutron spectrometers
albedo-type personnel neutron dosimeter 2−73208
analysis methods, critical and exponential experiments, perturbation replacement and oscillation 2−76905
angular distrib. of thermal neutrons at surfaces of black and grey cylinders 2−83056
BWR, prompt/delayed neutronic response ratio meas. of self-powered vanadium detector 2−83111
coincidence counters, for nuclear safeguards applics. 2−49683
counter efficiency, gas radiator, isotopic flux 2−82799
delayed fission neutron spectrometry applic. to nucl. materials assay 2−67361
delayed neutron energy distrib. using high resolution spectrometry 2−67194
detectors, threshold activation, calibration with 14 MeV neutrons 2−79658
dosimeter, for use in nuclear reactors, preparations 2−49909
dosimeter prep. for reactors 2−74187
dosimeters, high temp. preparation methods 2−73949
dosimetry, personnel, integral methods, survey 2−85129
dosimetry, practical fast systems 2−69392
dosimetry obs. using CaF_2:Mn and ^{7}LiF thermoluminescent dosimeters 2−69382
dosimetry using solid-state detectors 2−69393
experimental channels of MR-reactor 2−42677
Fast Breeder Test Reactor, neutron spectrum and flux meas. 2−42634
fast neutrons, exposure estimation using direct counting ^{32}P in hair 2−85130
fast timing coincidence techniques applic. to reactions involving neutrons 2−59738
fission track dosimeter monitoring of neutron flux incident on Ge(Li) detector 2−74191
high resolution fast neutron spectrometry 2−67075
in-core meas., using self-powered neutron detectors 2−74185
multichannel recording system using computer 2−70296
neutron balance, null reactivity method for fast multiplying media and HTR lattices 2−76902
nondestructive techniques for absorpt. and fission rates meas. in fuel elements 2−56040
nuclear reactor stochastic two-group model including neutron and gamma detection 2−83095
oscillations in critical assemblies, small amounts of materials in thermal or fast reactors 2−76903
plasma focus, Thomson scattering and holographic interferometry 2−83583
precision monitoring from TD and DD reactions 2−70305
radiography, converter thickness for optimum intensity 2−73902
radiography, Gd-exposure neutron imaging, role of internal conversion electrons 2−59638
reactor, rel. to reactor parameter meas. 2−49908
resonance neutrons in reactor in kev region 2−46357
scintillation-pulse height analyser system, for 2-100 MeV neutrons 2−82817

Neutrons and antineutrons continued
detection, measurement continued
search for neutrons of solar origin using balloon borne detectors 2−73133
self-powered detector development 2−55922
shielding calc., prep. of group consts. 2−42693
therapy beams, dosimetry using $FeSO_4$ 2−69390
thermoluminescent dosimeters, responses in D^+ on Be neutron fields 2−69391
TRIGA research reactor, Heidelberg, neutron flux density measurements using gold foil activation, resonance probes 2−67346
upper atmos. and solar neutron search, large area detector for 2-100 MeV range 2−72818
Van de Graaff, fission and capture cross-sections, energy spectrum 2−76904
Au-foil, correction factors for β-ray self-absorption 2−76956
$^{10}BF_3$ detector, end window, multifilament use with time-of-flight spectrometer 2−59612
CaF_2:Mn dosimeter response 2−83161
CaF_2:Mn thermoluminescent γ-dosimeter, sensitivity to neutrons 2−82820
CaF_2, natural and Dy doped phosphors for thermoluminscent detection 2−83160
$CaSO_4$:Dy phosphor for thermoluminescent detection 2−83160
$CaSO_4$;Mn dosimeter response 2−83161
Ge(Li) detector, fast neutron flux meas. 2−63704
Li detection sensitivity 2−55909
LiF and natural fluorite, mixed field with 2−73948
LiF detector, thermoluminescent, for neutron and gamma radiation 2−52691
LiF dosimeter response 2−83161
LiI(Eu) crystal detector, meas. of fast- and thermal neutron fluxes 2−42461
Mn foil activation technique for ultra-cold neutrons 2−67084
Pd, neutron transmission measurement 2−74132
Rh, Ag and V direct discharge detectors for thermal and epithermal neutrons 2−52699
Si-Sb compressed composite, obs. of neutron energies in range 13-15 MeV 2−59633
Si photodiodes as dosimeters for fast neutrons 2−46057
diffusion
see also Neutron transport theory
active transmission line analog 2−49863
cavity containing media, cooling coeff. and transport correction derived 2−52836
cell diffusion coefficients, correction to earlier paper 2−42601
diffusion length, existence of minimum value 2−49866
energy modal synthesis appl. to fast reactor burnup anal. 2−83043
equation, solution by random walk technique 2−63938
graphite, diffusion length, depend. on temp. 2−76898
graphite-Bi mixture obs. on neutron diffusion lengths 2−49861
heterogeneous media- cylindrical cell, effective diffusion coefficients 2−46362
magnetic fields, effect on spin-orbit interactions 2−76895
multigroup theory, variation flux synthesis methods 2−83052
multigroup theory, variational flux synthesis method 2−83051
nodal equations, derivation from invariant imbedding theory 2−56023
in polarized proton reactor reflector 2−52835
pressurised water reactor, optimal control 2−59816
reactor core neutron flux distribution, on-line computer control 2−59814
two group equations, variational acceleration technique for iterative solution 2−59809
two-group transport equation, steady-state solutions 2−83048
Be, diffusion length, depend. on temp. 2−76898
Be, using subthermal pulsed neutrons 2−74135
C, using subthermal pulsed neutrons 2−74135
polycrystalline media, using subthermal pulsed neutrons 2−74135
effects
see also Nuclear reactions and scattering due to/neutrons
anthracene, lattice defects, effect on fluorescence 2−44411
anthracene, triplet exciton annihilation fluorescence changes induced by neutron radiation damage 2−84553
austenitic stainless steel, effect of neutron irradiation on tensile and creep-rupture ductility 2−77719
austenitic-steel, neutron-induced mechanical property changes, damage function analysis 2−77718
automatic irradiation apparatus for production of short-lived activities by (n,γ) reactions 2−79639
boronated graphite, irradiation-induced dimensional change 2−76949
brute fracture in structural materials 2−68099
ceramic and ceramic-metal seals 2−63227
Cherenkov radiation, induced, in mag. field, spectral distrib. intensity, theory 2−49500
Cherenkov radiation, induced, interac. with diff. polariz. 2−49501
core restraint system design effects of irradiation creep and swelling on structural materials 2−83124
embrittlement by reaction- produced He in structural mats. at high temps. 2−68100
fast neutron irradiation, strengthening of C fibres 2−71662
fast reactor control rods, performance modelling 2−76950
fission gas bubble re-solution, asymptotic behaviour 2−53690
fusion blanket materials, comparison of Nb, Mo and Nimonic alloy PE 16 2−83093
Gilsocarbon, characts. rel. to high temp. reactor design 2−52871
glasses containing La and Ce, optical stability 2−70071
graphite, and sp. ht., 0.6-5 K 2−57062
graphite, artificial, neutron irrad. effects on thermal conductivity 2−54073
graphite, damage obs. using improved high resoln. microscopy 2−53637
graphite, high temp. irrad. creep expt. in Dragon reactor 2−56802
graphite, interlayer props., effect of interstitial atoms, simple model 2−56605
graphite, irrad., sp. ht., 1.4-4.4 K, strong mag. field effects 2−57063
graphite, irrad., thermal cond., 50-1000°C 2−54075
graphite, irrad. at 715°C, dimens. stability 2−56047

Neutrons and antineutrons continued
effects continued
graphite, low temp. sp. ht. obs. rel. to heat treatment 2—54045
graphite, neutron irrad. at high-temp., mech. interactions among crystallites 2—56679
graphite, neutron irrad. damage, dose rate effects 2—53708
graphite, neutron irrad. defect struct., single cryst. 2—53709
graphite, nuclear, from coke mixtures, effects on pore size 2—59841
graphite, nuclear, nat. graphite filler, neutron irrad. behaviour rel. to comp. 2—56049
graphite, nuclear, strength distrib. functions, effect of high temp. fast neutron irrad. 2—53822
graphite, pyrolytic, highly oriented, high dose fast irrad. 2—57072
HTGR fuel block graphite, struct. and mech. strength on irrad. 2—56045
memory device, amorphous film, radiation effects 2—61365
metal, damage simulation by ion bombardment 2—53693
metal, damage simulation by ion bombardment 2—53692
metal, displacement cascade, primary recoil energy depend., review 2—53691
metal, irrad., void form. mechanisms 2—53696
metal, irrad., void formation 2—47361
metal, neutron irrad., void form. 2—50641
metal, pure and impure, irrad., void form., temp. effect 2—50642
metal, radiation- induced void form. 2—50638
metal, swelling data analysis using displacement rates from Lindhard model 2—52880
metal swelling implications in fast reactor design 2—49900
metallic materials, void form. and growth, theory 2—53701
metallic materials, void nucleation during high-energy irrad. 2—53703
metals under fast-neutron irradiation interrelation between swelling and irradiation creep 2—76941
moisture meter response to stony soils 2—54732
nuclear fuel, oxide, redistrib. during irrad. 2—52852
nuclear reactor structural mat., swelling, electron microscope obs. 2—59868
pulsed γ-neutron radiation, monkeys, brain blood flow, vascular resistance, blood pressure and heart rate obs. 2—69316
pyrocarbon, thermal diffusivity and conductivity fast neutron irrad. effects 2—54046
pyrocarbon coating, mech. props. 2—56771
α-quartz, fast neutron irradiated, Raman spectral line intensity changes 2—72373
radiation damage, including swelling, in fissile materials, book 2—70539
radiation damage data correl. using activation fluences and irrad. temp. 2—83131
radiation defect accumulation and annealing kinetics, testing apparatus 2—84062
radiation protection recommendations 2—70544
radiation-induced void growth, applied stress effects 2—53704
reactor absorber materials performance in HFIR control cylinders 2—83129
reactor cladding and struct. materials, irrad. induced void form. 2—49901
reactor fuel, irrad., neutron radiography obs. 2—52856
reactor fuel, simulation of fission damage 2—42676
reactor fuel element sheathing problems due to swelling 2—59866
reactor fuel elements, irrad., radiograph prod. and automatic meas. 2—42659
reactor fuel elements, post-irrad. radiographical exam. techniques 2—42660
reactor fuel particles, irrad., rupture stress 2—43772
reactor fuel pins, irrad., automated meas. of induced strain 2—42657
reactor materials, void formation studies, use of simulation with accelerators 2—76922
semiconductor, amorphous, radiation stability, effects of microstruct. 2—60567
space dependent energy spectra in lead and graphite crystalline primsms 2—70506
stainless steel, annealed type 316, effect of fast reactor radiation on creep behaviour 2—83123
stainless steel, types 304, 316 estimates of creep-fatigue interaction in irradiated and unirradiated samples 2—83121
stainless steel type 304, effect of irradiation on strain rate dependence of mechanical properties 2—83122
steel, austenitic stainless fast neutron induced swelling 2—63969
steel, ferritic, irrad. embrittlement 2—43854
steel, in-reactor, irradiation growth and creep behavior 2—46391
steel, low-alloy and low-C, irrad., radiation- and anneal-hardening 2—80681
steel, press. vessel material, time-depend. embrittlement phenomena 2—59849
steel, press. vessel type, radiation sensitivity, effect of impurities 2—53895
steel, reactor core material, swelling induced deform. problems 2—59863
steel, reactor core material, swelling induced problems, metallurgical parameters 2—59864
steel, sintered, swelling rel. to charact. for fuel element jackets 2—76951
steel, stainless, He prod. rel. to LMFBR development 2—49902
steel, stainless, in-reactor damage simulation by ion bombardment 2—53714
steel, stainless, irrad., cold work effects on void form. 2—50646
steel, stainless, irrad., fluence and temp. depend. of void form. 2—50647
steel, stainless, solution treated type 304, empirical representation of irradiation-induced swelling 2—43609
steel, stainless, void nucleation and growth during fast irrad. 2—50645
steel, stainless, void nucleation and growth obs. using h.v. electron microscope irrad. 2—53694
steel, stainless tube, fast neutron irrad. effect 2—83085
steel tube, stainless, type 304L, in-reactor creep 2—46382
steel/$UO_{2\pm x}$-$PuO_{2\pm x}$ cladding/fuel interface, reaction 2—52875
stilbene lattice defects, effect on fluorescence 2—44411
swelling in irrad. materials, theory 2—53702
therapy techniques and safety precautions 2—69259

Neutrons and antineutrons continued
effects continued
transient dislocation-point defect interaction effects 2—43634
transition metal borides, irradiation swelling 2—77790
void growth and nucleation in irradiated materials 2—47360
void swelling, semi-automatic length measurement 2—83092
zircaloy-2, -4, tensile props. rel. to neutron irrad. 2—80664
Zircaloy-2, corrosion in steam-water mixture under reactor radiations 2—51456
Zircaloy-2, irrad. and temp. effect on tensile and creep props. 2—43802
Zircaloy-4, irrad., deform. parameters, 300°C 2—50749
Ag, influence on bulk modulus and internal friction 2—77642
Al-Al_2O_3-Al, dielec. loss and conductivity variations 2—81114
Al-Li alloys, irrad., inert gas bubble effects on mech. props. 2—43688
Al-2.5 wt.%Mg alloy, neutron irrad., transmutation produced Mg_2Si precip. 56922 2—56922
Al-SiO_x-Al, dielec. loss and conductivity variations 2—81114
Al-li alloys behaviour of radiation produced gas atoms observed by ^3H autoradiography 2—44009
Al, damage effects on subsequent dislocation loop formation during electron irrad. 2—53733
Al, internal friction, comparison with values for annealed Al 2—60[illegible]50
Al, irrad., pt. defect clustering, low temp. electron microscope obs. 2—60783
Al, irrad., void annealing 2—53705
Al, irrad., void distrib., sturct. imperfections in fluence 2—53736
Al_2O_3, fast neutron irradiation, thermionic reactor design 2—53707
Al_2O_3 ceramic insulator, swelling in neutron irradiation 2—53706
Al_2O_3 coatings on BeO, effect on protective behaviour and crack form. 2—43870
As_2Se_2Te film switching and memory device 2—61373
B glass refractive index control by selective applic. of neutron irradiation 2—59226
B_4C, irrad. damage, electron microscope obs. 2—47369
B_4C, neutron radiation induced defects, transmission e. microscope obs. 2—67355
B_4C, thermal reactor irradiated, empirical He release 2—76954
B_4C irradiation in fast neutron spectra, meas. of pellet density, swelling, gas release, thermal conductivity 2—83116
B_4C neutron absorber in fast and thermal reactors, swelling gas release and structural integrity 2—83115
C-Si alloys, co-deposited, high-fluence irrad.-induced dimens. changes 2—53776
C, damage and thermal annealing, changes in electronic props. 2—57000
C, damage obs. using improved high resoln. microscopy 2—53637
C, effect on effective temperature factor 2—53655
C, isotropic, poorly crystalline, dimensional changes 2—76916
C, lampblack, graphitization 2—56995
C, neutron irrad. at high-temp., mech. interactions among crystallites 2—56679
C, poorly crystn. isotropic, fast neutron irrad. induced dimens. changes 2—56767
C, pyrolytic, annealing 2—56993
C, pyrolytic, irrad., thermal conductivity 2—57082
C and C-Si alloys, dimens. changes and creep 2—76917
C composite felt, neutron irrad., thermal expansion, 20-1000°C 2—54055
C fibre, irrad., mech. props. 2—43708
C fibre, tensile strength, fast neutron irrad. effects 2—80830
C fibre struct. 2—56991
C fibres, elec., mag. and thermal props. 2—56998
C fibres, property changes during fast neutron irradiation 2—53965
C products, graphitization effects on neutron irrad. induced dimensional changes 2—56996
C pyrolytic, impregnation with graphite, neutron irrad. stability 2—56997
CaO, F_a^+ centre formation, emission and absorp. band obs. 2—71522
CdS(Te), thermal neutron damage, photolum. and elec. resist. 2—48219
CdTe, radiation effects, carrier conc., Hall mobility, photocond. 2—47892
Cu-Al alloys, irrad. effect on lattice thermal cond. 2—51060
Cu-10at.%Al alloy, deformed, neutron irrad., dislocation strain fields, low temp. lattice thermal cond. obs. 71498 2—71498
Cu-Al(10 wt%), high fluence irrad. damage, electron microscope obs. 2—80686
Cu-(0.6 at.%)Cr alloy, irrad., precip.-hardening 2—43833
Cu-7at.%Ge alloy, deformed, neutron irrad., dislocation strain fields, low temp. lattice thermal cond. obs. 2—71498
Cu-Ni alloy, irrad., void formation, fluence effects 2—80687
Cu, cleared channels, correl. with surface slip steps 2—50761
Cu, deformed at 77K, irrad. effects on structure. and mech. props. 2—83968
Cu, high fluence irrad. damage, electron microscope obs. 2—80686
Cu, irrad., impurity atom effect on recovery, elec. resistivity obs. 2—60964
Cu, irrad., positron annihilation 2—75004
Cu, irrad., void formation, fluence effects 2—80687
Cu, irrad. temp. effect on defect aggregate size 2—53711
Cu_3Au, free vacancy no. determ. in fission-neutron displacement cascade 2—53712
Fe, fast neutron irrad. at 77K, softening and anneal hardening 2—80689
α-Fe, irrad., radiation- and anneal-hardening 2—80681
α-Fe, structure studies with transmission electron microscopy 2—60965
Fe, yield stress damage function for neutron irradiation, determ. using SAND II code for data analysis 2—79840
GaAs, electron and neutron irrad., i.r. absorpt. 2—72332
GaAs, irrad., i.r. absorpt. band obs. 2—48180
GaAs, Irrad., Tunnel assisted hopping via defect energy levels 2—51157
GaAs reactor irradiation effect on the optical transitions 2—83976
n-Ge, fast-neutron- compensated, model for amorphous semiconductors 2—68429

Neutrons and antineutrons continued
effects continued
p-Ge, irrad., resist., Hall coeff., 77K 2−47930
Ge, irrad. induced damaged region form. 2−47384
Ge reactor irradiation effect on the optical transitions 2−83976
LiF, irrad., defects, X-ray obs. 2−80660
LiF_4, annealing, rel. to small disloc. layer formation 2−71492
Mg, irrad., pt. defect clustering, low temp. electron microscope obs. 2−60783
Mg, irrad., struct. damage and annealing 2−80683
Mg, irrad. induced distortion and swelling, effects of alloying additions 2−60778
Mo, before and after neutron irradiation, physical mechanical properties 2−53730
Mo, irrad., stress induced ordering of stage I defects 2−64654
Mo, irrad., void form. and ordering, alloying and purity effects 2−53719
Mo, neutron irradiated, correlation of void size and positron annihilation characteristics 2−71469
Mo irrad., void formation during annealing, electron microscope obs. 2−77575
NaCl, irrad. induced dislocation pinning points 2−43638
Nb, diffusion of oxygen under irrad. 2−53768
Nb, irrad., annealing, resist. study 2−64766
Nb irrad., void form. and ordering, alloying and purity effects 2−53719
Ni, irrad., pt. defect clustering, low temp. electron microscope obs. 2−60783
Ni, irrad., void formation, fluence effects 2−80687
Ni alloys, irrad., void form. and swelling resist. 2−53721
Ni alloys, irrad., void form. and swelling resist. 2−53721
Ni and alloys, void nucleation and growth obs. using h.v. electron microscope irrad. 2−53694
Ni and alloys fast neutron induced swelling 2−63969
Pb-GaAs Schottky barrier tunnel junction, zero bias anomaly, irrad. effects 2−71960
Pt-Mo, thermocouple, e.m.f. rel. to neutron irrad. 2−78940
Se reactor irradiation effect on the optical transitions 2−83976
n-Si:Li, irrad. induced defects, impurity effects 2−47385
Si, fast neutron irrad., number of Frenkel defects, calc. 2−71458
Si, irrad., divacancy obs. 2−48194
Si, irrad., space-charge-limited current obs. of electron trapping 2−51168
Si, irrad., space charge limited currents, fitting expt. data, third side of Lampert triangle 2−84328
Si, irrad., traps-filled-limit region, third side of Lampert triangle 2−84329
Si, irrad. damage, Mossbauer effect obs. 2−48153
Si, irrad. damage, piezospectroscopic obs. 2−48193
Si, irrad. induced damaged region form. 2−47384
Si, irrad. induced defect clusters, edge absorpt. obs. 2−47389
Si, irrad. induced defect obs. 2−47937
Si, phonon boundary scatt., thermal cond. obs. 2−80917
Si, radiation damage, e.p.r. obs. 2−48282
Si, small spherical voids, electron diffr. contrast profile, calc. 2−77571
Si film, amorphous, thermal neutron effects on elec. and optical props. 2−60666
Si n-channel junction f.e.t. damage annealing 2−51181
α-SiC, irrad. effects on e.p.r. and i.r. absorpt. 2−48294
Si(Li) nuclear radiation detector, damage by thermal neutrons 2−76732
TiC, changes in microhardness, lattice parameters, electrical resistance following neutron irradiation 2−52848
$(U,Pu)O_2$ fuel, U-Pu redistrib., transport model 2−52853
$(U,Pu)O_2$ fuel pin, porosity and actinide redistrib., grain growth and desintering 2−56043
UO_2-PuO_2 mixed fuel irrad. performance in PRTR 2−59853
UO_2-PuO_2 mixed fuels, Pu and fission product redistrib. during irrad. 2−59852
UO_2, fission gas bubbles, nucleation and evolution, math. treatment 2−67358
UO_2, fission sintering and irrad. induced diffusion 2−52855
UO_2, irrad., fission gas bubble nucleation and gas migration 2−63971
UO_2 fuel, bubble re-soln. and creep 2−52862
UO_2 fuel rod, irrad., pore movement kinetics 2−52873
U_3Si, in-pile irrad. effects, electron microscopy and diffr. 2−47393
V, irrad., void form. and ordering, alloying and purity effects 2−53719
V, neutron irrad., activation volume rel. to dose and strain, interstitial impurity precip. 2−80663
V, neutron irrad., anneal and radiation hardening, tensile props. 2−80665
W, before and after neutron irradiation, physical mechanical properties 2−53730
W single crystal, density changes induced by neutron irradiation 2−52849
Y_2O_3, fast neutron irradiation, thermionic reactor design 2−53707
Zr-(2.5 wt.%) Nb press. tubes, heat-treated, embrittlement 2−50770
Zr, irrad., dislocation loops characteriz. 2−43639
Zr, irrad. effects on aqueous oxidation, 290°C 2−44486
Zr alloys, anisotropic creep behaviour under fast neutron flux 2−50756
Zr alloys, high-strength, response to fast irrad. 2−53920
interactions
– 2−59529
inclusive spectra, microscopic model 2−76713
Mylar, total neutron cross section, low energies 2−83060
neutron induced energy release, computer program NERMA 2−42599
photon absorption, space-time phenomenology 2−55811
thermal pulsed-neutron experiments on graphite system 2−74131
dn→pnn, unitary model for three-body collisions 2−82992
$\gamma \rightleftharpoons rp\pi^-$, in 33 resonance region, dispersion relation predictions 2−52550
$\gamma n \to \pi^0 n$, 450-800 MeV, differential cross- section meas. 2−45958
$\gamma n \to \pi n$, comparison with $\gamma p \to \pi^+ n$, π^-/π^+ ratios, dip test of isotensor current 2−49560
Neutrons and antineutrons continued
interactions continued
$\gamma n \rightleftharpoons p\pi$ in $\Delta(1236)$ resonance region, discrepancy between dispersion relation predictions and exptl. data 2−42324
K-n→$K^0\pi$-n, final state obs., 4.9 GeV/c 2−70222
K-n→π Σ-, 1850 to 2160 MeV, resonant states 2−59516
$K^-n \to K^-\pi^-p$, application of dual resonance model for $K^+K^-pn\pi^-$ system 2−76659
$K^-n \to K^0\pi^-$MM, final state obs., 4.9 GeV/c 2−70222
$K^-n \to \pi^-\Lambda$, partial wave analysis between 1.9 and 2.2 GeV 2−52600
$K^-n \to \pi^-\Lambda$ real process, use of FESR gives EXD residues with WSNZ 2−42351
K^+n, one and two prong interaction of K^+ on deuterium at 5.5 GeV/c, meas. of partial cross section 2−63595
$K^+n \to K^0p$, cross section deuced from observation of $K^+d \to K^0pp$ 2−49550
$K^+n \to K^0p$, cross section difference with $K^-p \to K^0n$, Regge analysis 2−76658
$K^+n \to K^+N^{*0} \to K^+\pi^-p$, 12 GeV/c, study of $p\pi^-$ mass enhancement 2−82742
$K^+n \to K^+\pi$-p analysis of $K\pi$ scattering 2−49558
$K^+n \to K^+\pi^-p$, application of dual resonance model for $K^+K^-pn\pi^-$ system 2−76659
Λn, Λn, 6 to 21 GeV/c, total cross sections 2−52645
nd total cross sections, 25-60 MeV 2−82982
nd total cross sections, 25-60 MeV 2−82982
nd→nnp, n-d initial-state interaction 2−82991
nn study in μ-d→nnν 2−63525
np charge- exchange reaction, model for pion-Pomeranchon Regge cut 2−52640
np non-coplanar bremsstrahlung obs. at 200 and 130 MeV, application to N-N interaction off-shell energy properties 2−79718
$np \to \gamma d$, E_n=300- 720 MeV, test of time reversal invariance 2−46007
$\nu_\mu + n \to \nu_\mu + n + \pi^0$, exptl. limit on neutral current 2−63508
$\nu n \to \mu^- p$, symmetry relations with $\nu p \to \mu^+ n$ 2−52557
$pn \to \kappa\kappa\pi$ at threshold, Veneziano model investigation 2−63552
$pn \to pp\pi^-$, 5.9 GeV/c, search for N*(1450) production, meas. of cross section 2−70257
$pn \to p\pi^-p$, cross section, 7 GeV/c, model fitting, $\Delta(1230)$ prod. 2−52638
$pn \to \pi^+\pi^-\pi^-$, 1.2 GeV, investigation using dual models 2−52636
π-n→π-ρ-p, 7 GeV/c, A_1 study 2−49584
π^-n, 40 GeV/c, determ. of charged and neutral particle multiplicity 2−76682
π^-n, 40 GeV/c, multiplicity distribution of charged particles produced 2−45960
$\pi^+n \to \omega p$, B meson exchange contribution 2−42387
$\pi^+n \to p\omega$, 13 GeV/c 2−70232
$\pi^+n \to \pi^0\pi^0p$, use with one-meson approx. to obtain $\pi\pi$ scattering cross-section 2−82764
$\pi N \to \rho N$, dynamical model for $P_{13}(1860)$ $Pp_{31}(1910)$ and $F_{35}(1890)$ resonances 2−49583
K-n, 4.91 GeV/c, prod. of K*-(890) and N*-(1236) 2−42372
moderation
see also Neutron transport theory
borated homogeneous water, effect on n collision rate of 1% change in boron 2−70501
burn-up dependent microflux-density distribs. in MTR fuel elements, transport calcs. 2−76914
cold sources containing liquid H obs. and Monte Carlo calc. of output 2−49859
epithermal neutron spectra in reactor lattices, spherical harmonics treatment 2−76901
flux discontinuities due to inelastic scattering of neutrons in non-absorbing medium 2−49858
generalized synthetic kernel for slowing down 2−74133
graphite moderator problems, conference, London (1972) 2−56052
in heterogeneous lattices, intermediation resonance treatment by modified μ-method 2−79821
infinite medium, generalized formulation of continuous slowing down 2−42607
intermediate resonance calcs. for resonance absorber in absorber-moderator mixture, improved practical width 2−79820
methane, slow neutron spectra, suitability as cold moderator 2−76897
numerical treatment of elastic slowing down 2−46363
polycrstalline media, using subthermal pulsed neutrons 2−74135
polycrystalline media, finite, analysis of total response of neutron waves 2−42603
polycrystalline moderators, transport theoretical analysis of pulsed neutron experiments 2−59812
slowing down eqn., solution by integral transform 2−74137
slowing down equation for infinite homogeneous monatomic medium, exact solution in analytical form 2−42602
slowing down in a cylindrical pile of finite height, solution for various types of source 2−46366
slowing down theory, time dependent phenomena 2−56027
slowing down time, by Pb and graphite moderators, space depend. multigroup theory 2−63945
small group model, for H_2O-Al core calc. 2−42609
streaming, effects anisotropic hole systems in moderator 2−52838
thermal-neutron radiography, using sealed-tube neutron generator and water moderator 2−42691
thermalization, synthetic scattering kernel 2−56017
three-layer barrier phenomena, spatial, ang. and energy distribs. of fast neutrons 2−70504
Be, low temperature, non-exponential decay of neutron pulses 2−56030
Be, using subthermal pulsed neutrons 2−74135
C, using subthermal pulsed neutrons 2−74135
^{252}Cf neutron sources, electronic assay by detection of thermalized neutrons in moderator 2−42597
D_2O and CM-2 reactors, time-of-flight spectrum 2−63939
$Pu(NO_3)_4$:Gd, Gd effect on criticality 2−56051
ZrH_x, effect of H_2 chemical binding on effective cross sections and n spectra, calc. 2−56029

Neutrons and antineutrons continued
- **polarization**
  - longitudinal, of emitted neutron in muon capture by complex nuclei 2−63868
  - methods, and applic. to nuclear and particle physics 2−76714
  - neutron spin echo, focusing effect 2−74136
  - scattering from natural carbon, polarization calc. from phase-shift analysis of cross neutrons 2−46274
  - in nd elastic scatt., P-wave interactions and tensor force effects 2−67060
  - nd scattering, simultaneous effect of P-wave interactions and tensor force 2−63666
  - pd scatt., production of high energy polarized neutrons 2−70264
  - A(n,n)A, elastic, A between 48 and 209, n polarization meas. 2−67239
  - ^{11}B(d,n), meas. of neutron polarization angular distrib. 2−63915
  - ^{40}Ca(d,n), meas. of neutron polarization angular distrib. 2−63915
  - ^{59}Co(n,γ)^{69}Co, interference effects in γ-ray emission after polarized neutron capture 2−79790
  - Cu, polarization meas. by associated particle method 2−70454
  - ^{2}H- neutron elastic scatt., three-body calc. with tensor force 2−42565
  - ^{2}H(d,n)^{3}He, 0.2 to 4 MeV 2−67323
  - ^{2}H(d,n)^{3}He, comparison with ^{2}H(d,p)^{3}H reaction 2−70473
  - ^{2}H(d,n)^{3}He, E_d=16-22 MeV, ang. distrib. 2−70472
  - ^{2}H(d,n)^{3}He, E_d=6-14 MeV, differential polarization ang. distrib. 2−70471
  - ^{2}H(γ,n), E_γ=7-30 MeV, differential polarization of photoneutrons 2−76828
  - ^{2}H(n,n)^{2}H, 35 MeV, n polarization meas. 2−67241
  - ^{3}H(p,n)^{3}He, 1.5-12 MeV, analyzing power polarization anomalous difference 2−49794
  - ^{3}H(p,n)^{3}He, polarization transfer 2−46257
  - ^{3}He(d,n)^{4}He, meas. of polarization for E_d=1.0 to 5.0 MeV 2−49829
  - ^{24}Mg(d,n), meas. of neutron polarization angular distrib. 2−63915
  - ^{14}N(d, n)^{15}O, 5.16 MeV, n polarization ang. distrib. meas., cross-section analyzed using optical model formalism 2−46318
  - ^{15}N(d,n_p)^{16}O, 4.83 MeV, meas. of polarization angular distribs. of ^{16}O states using time-of-flight method 2−70377
  - ^{16}O(d,n), E_d=3-4 MeV, cross sections and polarization, ^{17}F levels 2−83014
  - ^{28}Si(d,n), meas. of neutron polarization angular distrib. 2−63915
  - Zr, polarization meas. by associated particle method 2−70454
- **production**
  - 14 MeV high intensity pulse generation 2−79656
  - cold sources containing liquid H obs. and Monte Carlo calc. of output 2−49859
  - electron accelerators, medical applications 2−45035
  - electroproduction, Regge behaviour of scaling function 2−63511
  - exploding-wire discharges 2−67665
  - high power source, using ^{244}Cm+Be, spectra meas. 2−42440
  - high thermal flux reactor, Institut Laue-Langevin 2−46368
  - homogeneous flux in reactor beam tube 2−52639
  - ion getter pump and oil diffusion pump comparison 2−76720
  - isotopic source, using Be(α,n), n spectra meas. 2−42439
  - laser-induced yields from spherical targets 2−67339
  - monoenergetic beam, by resonance double scattering 2−79822
  - neutron generators, T, D impregnated targets, patent 2−82781
  - non-evaporation neutrons, prod. by 55 MeV bremsstrahlung, mechanism 2−52796
  - plane sources, electrostatic models 2−70500
  - polarized neutron source, 10 to 22 MeV, ^{2}H(d,n) applic. 2−70472
  - proton fragmentation, peripheral dynamics 2−79616
  - for radiographic inspection 2−73694
  - sources, based on ^{252}Cf 2−82795
  - thermal neutron flux standard facility, construction and calibration 2−63942
  - thermal neutron source, potential of laser-induced fusion device 2−56020
  - thermal-neutron radiography, using sealed-tube neutron generator and water moderator 2−42691
  - thick targets, bombardment by 46 MeV α-particles 2−76867
  - tubes, hydrogen generators 2−46035
  - yield dependence from ^{2}H(d,n) and ^{3}H(d,n) on irradiation time 2−55999
  - γd, cross section is resonance region determ. from total cross section and proton cross section 2−46020
  - pd scatt., production of high energy polarized neutrons 2−70264
  - Al(d,n) thick-target yields and total cross sections, 1-40 MeV 2−67333
  - Be(d,n) thick-target yields and total cross sections, 1-40 MeV 2−67333
  - C(d,n) thick-target yields and total cross sections, 1-40 MeV 2−67333
  - ^{252}Cf fission, development as source for neutron radiography 2−55890
  - ^{252}Cf medical neutron source, ion chamber dosimetry 2−69441
  - ^{252}Cf neutron sources, electronic assay by detection of thermalized neutrons in moderator 2−42597
  - ^{252}Cf spontaneous fission neutron source for medical implant therapy, dose tables and modified distribution system 2−69442
  - Cm, A=244, 246, 248, spontaneous fission, neutron yield 2−76888
  - D-T neutron generator, for fast neutron therapy 2−69246
  - ^{2}H(d,n)^{3}He, production of 90% polarized neutron beam for nuclear structure research 2−67130
  - Li(d,n) thick-target yields and total cross sections, 1-140 MeV 2−67333
  - from P by high energy bremsstrahlung beam 2−55980
  - ^{231}Pa target, capture cross sections 2−42575
  - Pu-Be, Po-Be sources, investigation of spectra at low energies, meas. of activation cross sections 2−67227
  - T-containing targets as high-yield generators 2−73923
  - T(d,n) gas target source, cancer therapy 2−69340
- **reflection**
  - parabolic mirror condensor system 2−55654
  - total refl., surface rougnness effects 2−63946
- **scattering**
  - angular distrib. analysis using cylindrical Bessel functions 2−82978

Neutrons and antineutrons continued
- **scattering** continued
  - anisotropic, inclusion in elementary solutions of neutron transport equation 2−63944
  - anisotropic scattered pulses, relaxation times in decay 2−74138
  - backscattering effects in wave propag. problem 2−42605
  - Bonner sphere counter, effects of scattered neutrons on calibration 2−79638
  - Compton scattering, evaluation of J=0 fixed pole 2−76721
  - cross-section in ferromag. semicond. and metals, theory 2−81225
  - crystal, gravitational waves detection, theory 2−52054
  - in crystals, investigation of order-disorder phenomena 2−50991
  - disadvantage factor in cell, effect of higher order anisotropy 2−63941
  - double differential cross section meas., Monte Carlo evaluation of multiple scatt. and resolution effects 2−56024
  - elastic, generalized synthetic kernel for slowing down 2−74133
  - hadron-neutron, shadow correction 2−42363
  - hydrogenous liquids for reacor moderation, slow neutron scatt. cross-section 2−70535
  - liquid, gravitational waves detection, theory 2−52054
  - magnetoordered crystals with small exchange constant, spin waves and scatt. proc. of neutrons and light 2−72209
  - molecular crystal, rel. to molec. vibration studies 2−54012
  - monoenergetic beam production by resonance double scattering 2−79822
  - multiple, in cold neutron scattering, Monte Carlo soln. 2−56019
  - multiple scattering of slow neutrons, estimation in CH_3OH 2−79826
  - np phase shifts, calc. of deuteron relativistic charge form factor 2−42427
  - one-dimensional structure, cross-section 2−74134
  - pyrolytic graphite neutron reflectivity and use as analyzer and higher order filter 2−55891
  - thermal, albedo and Milne's problems 2−70503
  - thermal, Monte Carlo treatment 2−63943
  - thermalization, synthetic scattering kernel 2−56017
  - two-dimensional structure, cross section 2−74134
  - water vapour mols., saturated and superheated, inelastic scatt. 2−67539
  - en structure function calc. in leading logarithm approx. to perturbation theory and massive g.e.d. Lagrangian 2−73752
  - $K^-n\to\Lambda\pi^-$, backward analysis of differential cross sections and polarization using trajectory parameters 2−70223
  - K^+n elastic scattering parameters studied in $K^+d\to K^+d$, $K^+d\to K^+pn$ and $K^+d\to K^0pp$ interactions 2−63577
  - $K^+n\to K^0p$, multiple scatt. model, duality breaking effects 2−63572
  - $K^+n\to K^0p$, total and differential cross sections inferred from K^+d data 2−70213
  - nd, elastic, polarization, P-wave interactions and tensor force effects 2−67060
  - nd, low energy elastic scatt., effective range approx. 2−63665
  - nd, SU(3) basis of representation for Faddeev eqns. for three particles 2−76722
  - nd cross sections, 3-nucleon problems, two-term nonlocal separable potentials 2−82845
  - nd S-wave scattering studied using N/D approximation 2−52081
  - nn, $^{1}S_0$ parameters from kinematically complete expt. on ^{2}H(n,2n)^{1}H 2−49805
  - nn scatt. length from ^{2}H(n,p)2n reaction obs. 2−76858
  - νn scatt., structure function calc. in leading logarithm approx. to perturbation theory and massive g.e.d. Lagrangian 2−73752
  - νn scatt., structure function calc. in leading logarithm approx. to perturbation theory and massive g.e.d. Lagrangian 2−73752
  - $\nu_\mu n\to p\mu^-$, second class current limitations 2−52558
  - Be, pseudo mode decay, anal. by inelastic scatt. expansion 2−83046
  - C, cross section 2−74134
  - Cu, neutron thermal effective cross-section meas. 2−59808
  - Fe-Ni quenched alloys, short-range order detn. in first and second coord. spheres 2−81199
  - H atoms in binary solutions of liquids, dependence of total neutron cross section on concentration of atom 2−79823
  - H_2O molecule, analytical improvement of Nelbin's formalism for slow neutrons 2−49868
  - ND_4Cl, first order phase transition 2−84150
  - nd, polarization, simultaneous effect of P-wave interactions and tensor force 2−63666
  - Pb-Bi alloy, neutron scattering law determ. 2−80931
  - Ta, neutron thermal effective cross section meas. 2−59808
  - ZrH_x, effect of H_2 chemical binding on effective cross section, calc. 2−56029
- **scattering, neutron-proton**
  - charge exchange, 8 to 29 GeV/c, differential cross sections 2−55879
  - charge exchange, π-exchange processes, elementary pion with transverse-momentum cutoff 2−42380
  - charge exchange, fixed poles, unitarity and duality 2−79533
  - elastic, modified Glauber theory 2−70260
  - inelastic at momentum 19.2 GeV/c, meas. of charged particle distrib. 2−67057
  - local $^{1}S_0$ potential, phase shifts calc. 2−82844
  - massive muon pair production, cross section at high energy 2−55878
  - phenomenological model based on pion exchange, data analysis 2−45999
  - small-angle, 24 MeV, differential cross-sections 2−73854

Newtonian fluids *see Fluids*

Nickel
- adsorbed K and Na layers, specular electron refl. 2−50544
- adsorption, of CO, preferential orientation, extended Huckel calc. 2−50546
- adsorption and condensation, on Si(111) surface, mass spectrometer obs. 2−50499
- adsorption enthalpy of hydrogen, cryst. orientation influence 2−60680
- adsorption of Hg, alloy formation 2−77489
- adsorption of O, thermal disorder, LEED pattern interpretation 2−60672
- adsorption of oxygen, He^+ backscatt. and LEED study 2−50543
- adsorption of Ti, surface band struct., X-ray appearance pot. obs. 2−47816
- alloying addition to WC-Co cemented carbides, effect on structure 2−43864

Nickel continued
atom, highly-ionized, far u.v. spectra, rel. to solar lines 2−83189
atom, K-shell and beta-decay, summing-energy spectrum meas. 2−46186
atomic central-field models for open shells, SCF calcs. 2−64025
Auger transitions, high-resolution meas., valence band density of states 2−81193
bombarded by C, N and O ions, 0.5-2 MeV, stopping power 2−47782
ceramic, refractory oxide particle growth, matrix density effects 2−68169
cermet, highly porous, gas permeability 2−56965
chemical classification of Fe meteorites, conc. rel. to Ge 2−75925
chemisorption of H_2 on (111) plane, flash desorption spectroscopy study 2−80568
chemisorption of O, S, Se, bonding, orbital electron energy spectra 2−48328
chondrites, H-group, distribution in metal and silicate portions 2−62719
coating, on Si_3N_4 whiskers, high temp. stability, gaseous environment effects 2−74640
coating of materials, use of composite powders, new developments 2−61010
composite, C fibre reinforced, prep., thermal expansion, high temp. deformation characts. 2−74919
coronal enhanced region 2−73150
critical and spin wave fluctuations, neutron scatt. 2−54309
Curie point, crit. depolarization of neutrons 2−81268
defects due to ultrasonic treatment, positron annihilation obs. 2−43612
deformed, angle and wave depend. of X-ray diffr. linewidth 2−43625
density at elevated temperatures exptl. results in liquid and solid phases 2−64505
desorption, of H_2, spatial distrib. obs. 2−50526
diamonds with Ni inclusions, determ. of Curie points for different coloured diamonds 2−81213
diffusion in Mg-Zr alloy, and precip. formation 2−47467
diffusion of H, quantum interpret. 2−71537
diffusion on Cu, 600 and 900°C 2−53761
diffusion width of wide-angle grain boundaries 2−47469
dislocation line tension, effects of elastic anisotropy 2−74772
dislocations, generation from grain boundaries 2−47418
dislocations and twinning in electrolytically obtained coatings, transmission electron microscopy 2−50519
dispersion, anomalous correction close A K-absorption edge 2−60764
dispersion strengthening effects on hydrogen susceptibility, deformation and fracture 2−74862
domain wall movement retardation, due to interaction with dislocations 2−68540
dumbbell interstitials, reorientation in deformed crystals 2−50655
dynamic strengthening singularities under infl. of shock waves 2−84075
effective magnetic field on ^{67}Zn 2−84404
electrical resist. behaviour in crit. region 2−57279
electrical resistivity due to dislocations, at low temps. 2−81033
electrolytic, anisotropic effects in magnetoelastic damping 2−54337
electrolytic, changes in internal energy associated with heating 2−43784
electrolytic deposition, cathodic impedance study 2−48339
electrolytic Matteucci effect, influence of cathodic H 2−48084
electron irrad., void form., effect of injected gas atoms 2−43613
electron irradiated, recovery of mag. after-effect and elec. resist. 2−64655
electron momentum distribution, from Doppler-broadened annihilation lineshapes 2−71782
emission line wavelengths, and solar far u.v. spectrum and forbidden line identity 2−42729
ferromagnetic, theory of magneto-optical effects 2−54380
ferromagnetic, tight binding method energy band calc. 2−47810
ferromagnetic after effect, at 55K after electron irrad. 2−78026
ferromagnetic host for $^{188,\ 190,\ 192}$Os g-factor meas., comparison of IMPACT, PAC and Mossbauer techniques 2−42534
field emission, electron spin polarization, band-structure calculation 2−44190
film, adsorption of H under ultra-high vacuum conditions, meas. of desorption spectrum 2−53590
film, adsorption of Xe, surface potential, photoelec. emission obs. 2−47163
film, amorphous, deposition and annealing, resist. study 2−77499
film, colour phenomena, exptl. obs. and mechanisms 2−59243
film, in Al-Al_2O_3-Ni supercond. junc., electron spin polariz. detn. 2−64958
film, magnetoresist., thickness depend. 2−51266
film, meas. of longitudinal Faraday effect 2−54379
film, on CaF_2, optical absorpt., polarization anisotropy rel. to thickness and orientation 2−57324
film, origins of stress interference obs. 2−43679
film, porous, magnetostriction, field depend. 2−72187
film, residual magnetization, susceptibility, anisotropy, Hall effect 2−48095
film, saturation magnetization, effect of H_2 adsorption 2−48094
film, single cryst., ripple magnetiz. effects in ferromag. resonance 2−65317
film, spontaneous magnetization rel. to Hall effect 2−48096
films, epitaxial, planar Hall effect 2−72186
films, intrinsic stress obs. by optical interference method 2−77649
films, monocryst., orientational magneto-optic effect 2−61589
films as opaque coatings for code modulating disks and grids 2−70047
foil, polarization of channelled deuterons 2−47784
fuel cell with oxygen/alkali gas diffusion electrodes, model 2−59043
high strain rate behaviour using split Hopkinson bar method 2−53796
hyperfine field at ^{181}Ta, perturbed ang. correl. study 2−65204
hyperfine field of ^{181}Ta, $\gamma-\gamma$ angular correl. obs. 2−44320
hyperfine magnetic field, at recoil implanted ^{41}K 2−65205
interfacial structure and energy using electron microscopy 2−56576

Nickel continued
internal demagnetizing factor, temp. and alternating field direction depend. 2−48074
internal friction in Ni containing H, effect of relax. and trapping of dislocations 2−53792
ion sources, laboratory, low intensity 2−55672
ions, multiply charged, hydrogenic transitions 2−67391
i.r. resonance, optical absorp. and magneto-optical absorp., exchange energy detn. 2−65264
isotopes, proton elastic scattering, phase analysis using computer 2−67214
itinerant ferromagnetism, intermediate-coupling theory 2−54301
Kerr and magneto-optical effect meas., electronic structure 2−72265
Kerr effect meas. for increasing accuracy of magneto-opt. parameters 2−84461
Kikuchi band defect and excess regions, calc. 2−60763
LEED, absolute intensity energy spectra, for (001) surface 2−50459
LEED, from (111) surface, averaged intensities 2−50460
low index surface, adsorped Pb layer, LEED obs. 2−60682
magnetic after-effect of hydrogen 2−78029
magnetic anisotropy, represented by lines of const. cryst. energy 2−78000
magnetic domain struct. after plastic deform. 2−44244
magnetic domain walls, 180°, tilted, struct. from Lorentz electron images 2−72151
magnetic moment, temp. depend., $T/T_c<0.5$ 2−65154
magnetic permeability calc. from optical spectra 2−65155
magnetic saturation, determination using Stern-Gerlach experiment with neutrons 2−54326
magnetic susceptibility, 0.6-6.0 kc, in critical region 2−78024
magnetization and magnetic susceptibility, 20-600°C 2−68546
magnetoelastic effects as function of elastic distortion 2−78028
melt spreading over graphite surfaces 2−67814
neutron beam depolarization, anisotropy 2−61509
neutron damage simulation by ion bombardment, void form. 2−53692
neutron damage simulation by ion bombardment, void form. 2−53693
neutron displacement cross sections, based on Lindhard model 2−83053
neutron irrad., pt. defect clustering, low temp. electron microscope obs. 2−60783
neutron irrad., void form. and growth, theory 2−53701
neutron irradiated, void formation, fluence effects 2−80687
Ni:H, hydrogenated, thermo-e.m.f., 3d band shape 2−72052
n.m.r., pulsed, in ⟨110⟩ single cryst., rel. to domain struct. 2−78173
oxidation, effect of cold work, examination 2−75382
oxidation, effects of surface preparation 2−72559
oxidation, mechanisms at low temp. for polycryst. Ni 2−72558
paramagnetic-ferromag. transition, rel. to inhomogeneous states 2−57283
particle sintering, obs. using new hot stage in scanning electron microscope 2−56641
permeation of hydrogen, surface effects 2−77608
photoelectron energy distribution, above and below Curie temp. 2−65108
plastically deformed, susceptibility and magnetization in strong fields 2−51259
point defect interactions with dislocations, high-voltage electron microscopy 2−56686
porous, creep kinetics, in acid and neutral media 2−43704
porous, transport props. depend. on porosity 2−77740
positron annihilation, appl. to struct. and props. determ. 2−47771
powder, mag. props., temp. depend. 2−51260
powder metallurgy, densification, structural aspects 2−56946
powders, monocrystalline, temp. depend. of rotational hysteresis 2−68508
recovery after 300 kbar shock wave loading 2−56794
reinforcement by Al_2O_3 fibres or whiskers, poor efficiency 2−47668
single crystal (100) films, magnetoelastic coefficients at room temp. 2−44264
sintering activator, role in W powder sintering 2−50899
solar photospheric abundance det. from spectrum synthesis 2−58554
solubility of U, low limit determ. from heterodiffusion coeffs. 2−43654
solute in liq. Sn, thermoelec. power 2−71227
stacking fault energy, low impurity conc. influence 2−43642
stacking fault propagation from a coherent twin boundary 2−80670
stopping power for 25-250 keV H ions 2−47774
stopping power for protons and deuterons at same velocity 2−54098
stopping powers for 30-90 MeV ^{238}U ions 2−47773
stopping powers for ^{4}He, ^{16}O, ^{35}Cl at 1 to 3 MeV 2−80921
substrate for Pb epitaxial film, azimuthal disorientation of elementary nuclei 2−47122
surface, (001), impurity segregation, work function and Auger electron spectroscopy obs. 2−53554
surface, (100), plasmon angular profiles, LEED obs. 2−51093
surface, (111), (00) LEED beam intensity at normal incidence 2−71308
surface, (111), charac. energy loss in Curie temp. region 2−51267
surface, backscatt. of Ne^+ 600 eV ions, chain effect 2−77484
surface, benzene and cyclohexane adsorp., LEED and mass spectrometer obs. 2−50545
surface, cleaned and oxidized, secondary ion yield 2−61471
surface, effect of disordered Na, K, Cs and Ba overlayers on specular electron refl. 2−60681
surface, electron energy loss spectra, function of surface impurity 2−47079
surface, multiple scatt. of low energy noble gas ions 2−50458
surface, N or S adsorbate-covered, electron energy loss spectra, elastic scatt. 2−84222
surface, reaction of O_2 and S, LEED obs. 2−78184
surface diffusion on W, coeff. determ., mass transfer method 2−50466
surface interplanar spacings, LEED, Bragg peak widths 2−77486
surface reconstruction on adsorption of O, S, Se, Madelung potential 2−47162

Nickel continued
surfaces, contamination during oxidation in fused SiO_2 reaction vessels 2−84102
swelling, fast neutron induced 2−63969
texture variation, during deform., recrystn., and ageing 2−50806
textures, produced by deform. and primary and secondary recrystn. 2−84070
u.s. attenuation, 5-134MHz, mag. contribution 2−77782
vacancy clusters after quenching, electron microscope obs. 2−64661
vacancy condensate prod. by laser irrad. 2−53726
valence band density of states, X-ray photoemission spectroscopy obs. 2−65104
void and point defect agglomerate studies using h.v. electron microscopy 2−53695
void form. on irrad., temp. effect 2−50642
void nucleation and growth obs. using h.v. electron microscope irrad. 2−53694
wire, recrystallization, cold worked, press. induced thermal activation 2−43781
work hardened in tension, double texture, twinned growth influence 2−60985
work hardened in tension, secondary recrystn. 2−60986
Co XVII, multiplet strengths for electric quadrupole transitions calc. using HF orbital wave functions 2−42728
Cu-Ni junction, e.m.f. generated by shock wave propag. 2−75010
Fe/Ni diffusion couples, atomic mobility in Kirkendall plane 2−53763
Ge:Ni, electron and hole capture rates, photomagnetoelec. and photocond. studies 2−75171
He migration and release after implantation 2−50639
NaF:Ni^{2+}, visible and i.r. absorpt., 300K and 80K 2−84490
Ni: ^{206}Bi, mag. hyperfine field at Bi 2−81251
Ni:As, hyperfine mag. fields at As, rel. to host mag. moments 2−78018
Ni:^{42}Ca, hyperfine fields, perturbed angular correlation studies, g-factor of 3.19 MeV 6^+ state in ^{42}Ca 2−72243
Ni:Pb, Bragg peaks, temp. effects 2−71310
Ni-Cr steels, weldability to C steels, gas pressure process 2−68146
Ni-Cu solid solution, X-ray determ. of composition profiles and diffusion generated subconstructure 2−74696
Ni-HfO_2 powders, effect of dispersion strengthening phase on thermal stability 2−77739
Ni-NbC, pseudobinary, phase equilib., phase diagram 2−68199
Ni-base superalloy, dispersion strengthened, rotating bending fatigue tests 2−56883
Ni-base superalloy, low-cycle fatigue with thermal and strain cycling 2−56880
Ni, Ni:Sn, plastically deformed, deviations from Matthiesen's rule 2−71837
Ni film on NaCl substrate, effect of annealing on dislocation struct. 2−80565
Ni II, theoretical investigation of $3d^84p+3d^74s4p+3d^85p$, $3d^84f$ levels 2−79874
Ni steels, 40N25, 60N20 and 80N15, amplitude-dependence of int. frict. 2−84076
Ni XXVII, highly ionized, X-ray spectra 2−52917
Ni^+ in $CsMgCl_3$, $CsMgBr_3$, interionic coupling effects on exchange spectra 2−84483
Ni^{2+}, in AgCl, thermal cond., relaxation time approx. analysis 2−51057
Ni^{2+}, in MgO, anharmonic interact. on spin-lattice relax. 2−65195
Ni^{2+}, in MgO, Brillouin spectra from microwave phonon bottleneck 2−65283
Ni^{2+}, in silicate glass, ligand field spectra and struct. 2−50409
Ni^{2+}, optical spectra in cubic lattices 2−44379
Ni^{2+} in MgF_2, impurity-ion spin-forbidden absorpt. enhancement by colour centres 2−78104
Ni^{2+} in MgO, grain boundary diffusion 2−50710
Ni^{2+} in MgO, Raman relax. modifications due to substitutional effects 2−48114
Ni^{2+} ions in alkali borate glasses, absorpt. anomalous, ligand field approach 2−75303
Ni^{2+} substitution in $RbMnF_3$, effect on e.p.r. linewidth and g-values 2−48292
$NiSiO_2$ cermet films, granular, microstruct. 2−50498
$^{28}Ni^+$ ion source, collimating system for mass spectrometer, with distributed ionization region 2−69883
^{61}Ni, hyperfine structure of $3d^84s^{23}F_2$ metastable state 2−46438
^{63}Ni, ultra-fast diffusion in α-Ti 2−64697
^{63}Ni, ultra-fast diffusion in α-Zr 2−64697
^{63}Ni contamination, thermoluminescent dosimetry obs. 2−62291
Si:Ni, photocond., thermal and field quenching by impurity electron capture 2−65088
SnO_2:Ni, e.p.r. of Fe^{3+} centre 2−84564

Nickel alloys
see also Nickel compounds
ageing, different volume disparity between precip. phase and matrix, X-ray obs. 2−71634
Al-Ni alloy, influence of short-range order on elec. and mag. resist. 2−71423
binary, optical obs. of indirect transitions from ground-state to impurity bands 2−71796
constantan-Fe(Ni) junction, e.m.f. generated by shock wave propag. 2−75010
creep behaviour, obs. 2−56920
dilute liquid, Ni in Cu, CuZn, Zn, ZnGa, Ga, GaGe, Ge, GeAs, As, mag. susceptibility 2−80485
dispersion hardened, role of grain size and shape in strengthening 2−71648
ferrites, iron rich, Hall mobility measurements, room temp. to 600°C, activated hopping process 2−81069
foil preparation, for electron microscopy, electrolytic jet thinning procedures 2−71415
grain growth, second max. and nonuniformity after deform. 2−83961
Hastelloy-X, neutron irrad., void form. and swelling resist. 2−53721
hot workability, Zr effect, boundary-phase plasticity 2−47645
Incoloy-800, neutron irrad., void form. and swelling resist. 2−53721
Inconel-625, neutron irrad., void form. and swelling resist. 2−53721

Nickel alloys continued
Invar, elastic consts. anomalous temp. depend. in ferromag. state 2−84053
Invar, mag. moment temp. depend., $T/T_c<0.5$ 2−65154
Invar, spontaneous magnetostriction, itinerant electron model interpret. 2−48085
Invar, thermal expansion, low temp., Fermi liquid props. 2−84217
invars, neutron diffraction study of crystal structure 2−68002
microstructure, implications for strength and alloy design 2−56945
nichrome, film, prod. by multiple sublimation, vacuum system, props. 2−47121
nichrome, Mo or W reinforced, filament-matrix interface struct. 2−53966
nichrome, W filament reinforced, microstruct. 2−53970
nichrome, W filament reinforced, struct. and props. 2−53967
nichrome thin films, sintering 2−68151
nimonic, ageing, solid soln. decomp. and volume change 2−50805
Nimonic, neutron damage simulation by ion bombardment, void form. 2−53692
Nimonic 90, tensile creep under transient stresses, elevated temp. 2−71575
Nimonic PE 16, as fusion reactor blanket material, comparison with Mo and Nb 2−83093
permalloy, film, on CaF_2, optical absorpt., polarization anisotropy rel. to thickness and orientation 2−57324
permalloy, magnetic hyperfine field at ^{57}Fe, Mossbauer spectra 2−54386
Permalloy field access bubble domain drive ccts., magnetostatic pot. wells, drive fields, meas. technique 2−73507
Permalloy film, appl. of networks method for electron probe anal. 2−61830
permalloy film, coercive force and anisotropy, influence of substrate 2−84411
Permalloy film, creep rel. to thickness 2−56806
Permalloy film, cross-tie walls, motion threshold field and behaviour at inhomogeneities 2−77994
Permalloy film, electrodeposited, mag. anisotropy and magnetostriction 2−57302
Permalloy film, ferromag. reson., mag. moment, thickness, magnetization pinning 2−61539
Permalloy film, oxidized, slow domain wall motion 2−54340
Permalloy film, oxidized antiferromag. surface layer, mag. after effect 2−44267
Permalloy film, spin waves, 0.8-16GHz, below saturation magnetization 2−78034
Permalloy films, domain boundary motion, effect of struct. factors 2−61526
Permalloy films, l.f. slip of domain boundaries 2−61528
Permalloy films, mag. anisotropy, annealing depend. 2−61525
Permalloy films, monocryst., orientational magneto- optic effect 2−61589
Permalloy films, stripe struct., magneto-optical obs. 2−61531
Permalloy films with supercrit. hysteresis loop, domain struct. 2−61532
Permalloy plated-wire memory, domain struct., electron microscope obs. 2−75231
Permalloy thin wires, Bitter pattern obs. 2−61535
permalloy-Mn film, exchange anisotropy, thermomag. recording 2−57286
Permalloy-SiO- Permalloy multilayer systems, stripe domain struct. 2−61530
phase analysis of alloys with high W content 2−57034
phase transformations, effect of Mo, Al and C 2−43925
pitting suppression in phase analysis 2−57423
reactor cladding and struct. materials, irrad. induced void form. 2−49901
silvers, fire-cracking mechanism 2−43794
stress-rupture data, relative abilities of time- temperature parameters to correlate and extrapolate data 2−47608
superalloy Mar-M200, yield, orientation and temp. depend. 2−56795
supermalloy, anomalous behaviour of antireson. transmission at 23.7 GHz 2−81442
swelling, fast neutron induced 2−63969
void nucleation and growth obs. using h.v. electron microscope irrad. 2−53694
Al-Cu-Mg-Ni, forged after quencing, forged treatment, creep strain mechanisms 2−43804
Au-Ni, dil., deviation from Matthiesen's rule, 0.5-60 K 2−77854
Co-Ni-Fe, ^{60}Co self-diffusion, Fe content effects 2−43659
Co-Ni-Sb system, intermetallic cpds., X-ray diffr. study 2−43940
Co-Ni-Ti system, decomp. and formation of modulated struct. in coherent phase zone of stability 2−57030
Cr-Ni-B system, isothermal section at 800°C 2−61044
Cr-Ni, structure of $K_{\beta 5}$ emission band, X-ray study 2−72378
Cr-Ni, tensile strength, stress rupture, hardness, alloying additions effect 2−74856
Cu-Al-Ni, damping characts. and causes 2−80776
Cu-Al-Ni, martensite memory, shape recovery effect 2−50935
Cu-Al-Ni, martensitic transform., interphase boundary shifting 2−43910
Cu-Al-Ni, shape memory effect 2−80844
Cu-Ni:^{57}Fe, Mossbauer doublets, time-differential perturbed angular correlations 2−72275
Cu-Ni:Mn, Cr, Al, struct. and props. with ageing and hardening 2−83954
Cu-(3o wt.%)Ni-0.3 wt.%)Be, cryst. struct. and morphology of age hardening precipitate phases 2−50934
Cu-Ni-Fe, intergranular fracture on spinodal decomp., mechanism 2−57012
Cu-Ni-Mg alloys eutectic mixtures constitution 2−84103
Cu-Ni-Mn, dilute soln., resist., magnetoresist., Z-100K, Kondo effect 2−47835
Cu-Ni-Mn, order-disorder transform., resist. and thermopower study 2−54001
Cu-Ni, d-band filling, X-ray spectra 2−47809
Cu-Ni, dil., vacancy-impurity complexes and positron annihilation 2−47398
Cu-Ni, elec. resist. behaviour in crit. region 2−57279
Cu-Ni, liquid, density, max. bubble pressure method 2−56488

Nickel alloys continued
- Cu-Ni, neutron irrad., void formation, fluence effects 2−80687
- Cu-Ni, surface composition after annealing and sputtering, Auger spectroscopy obs. 2−50440
- Cu-Ni, susceptibility in high intensity fields 2−65151
- Cu-Ni film, soft X-ray absorpt., band struct. interpretation 2−65286
- Cu-Ni(Cr), resistivity and magnetoresistance, Kondo effect 2−64913
- CuNi, dilute, optical absorptivity meas. at 4K, virtual-bound-state obs. 2−51337
- Fe-Al-Ni-Co-Ti, prod. by Magnicol process, reaction mechanisms 2−43834
- Fe-Co-Ni, coherent potential approx. calc. 2−71794
- Fe-Co-Ni, powder, highly disperse, effect of electrolytic prep. variables 2−68543
- Fe-Cr-Ni, plastic deform., low temp. 2−43693
- Fe-Cr-Ni system, phase boundary $\alpha+\gamma/\gamma$ determ. 2−84164
- Fe-Mg-Ni, austenite transform. 2−53991
- Fe-Mn-Ni system using semihard magnetic alloys 2−84407
- Fe-(30.3 wt.%)Ni, damping of oscillations during heating after martensitic transform.43791 2−43791
- Fe-Ni-Al-Cu, struct. and mag. props., alloying additive effects 2−43845
- Fe-Ni-Al, martensitic transformation, effect of dispersion particles 2−57015
- Fe-Ni-C-Mo-Cr, tempering, effect on struct. and mech. props. 2−43853
- Fe-Ni-C, deform.-induced martensitic reaction, kinetics 2−80833
- Fe-Ni-C, deform. martensite formation, effect on mech. props. 2−71684
- Fe-Ni-C, isothermal and athermal, deform. induced martensitic transform. 2−71685
- Fe-Ni-C, martensite, surface plastic deform., X-ray obs. 2−80769
- Fe-Ni-C, martensitic, microplastic deform. and isothermal transform. 2−43808
- Fe-Ni-C, martensitic, microplastic deform. and isothermal transform 2−43807
- Fe-Ni-C, quenching and hydrogenation effects on mechanical props. and brittleness 2−43723
- Fe-Ni-C, tempering, effect on struct. and mech. props. 2−43853
- Fe-Ni-Mn martensitic alloys, reversion behaviour 2−77747
- Fe-Ni-Mo, dispersed, electrolytic deposition 2−77725
- Fe-Ni-Mo, powder metallurgy, carbonyl prod. method 2−68159
- Fe-Ni-Nb-C, ageing, 700 and 800°C 2−47596
- Fe-Ni-Si, temper brittleness development, grain boundary adsorption of P, internal friction study 2−80767
- Fe-Ni-Ti-Al, solid soln. decomp. 2−56933
- Fe-Ni, atom redistrib. on ageing, Mossbauer obs. 2−60981
- Fe-Ni, deform. martensite obs. 2−43838
- Fe-Ni, diffusion of hydrogen, struct. influence 2−77611
- Fe-Ni, Fe-Ni-Co and Fe-Ni-Mo, cumulative thermal cycling behaviour, 300°C/hr. 2−60960
- Fe-Ni, ferromagnetic resonance line width, effect of Ni content after quenching or annealing 2−72174
- Fe-Ni, film, rotating mag. anisotropy, temp. depend. 2−57300
- Fe-Ni, Invar, elastic consts., anomalous temp. depend. 2−80751
- Fe-Ni, Invar, Hall and Nernst-Ettinghausen effect, 100-300°C 2−72164
- Fe-Ni, martensite, morphology and cryst. geometry, comp. effects 2−80771
- Fe-Ni, martensitic transformation study by internal friction during heat treatment 2−43916
- Fe-Ni, martensitic transform., interphase boundary shifting 2−43910
- Fe-Ni, para processes, high field susceptibility, conc. depend. 2−72114
- Fe-Ni, surface diff. and diff. of N and C along austenite/ferrite phase boundary 2−68052
- Fe-Ni, thermal stability of elastic modulus, contrib. of Invar anomaly and ΔE-effect 2−50724
- Fe-Ni, Young's and shear modulus anomalies, in Invar region, origin 2−77632
- Fe-Ni doped invar, f.c.c. lattice, main magnetic moment and effective magnetic field of ^{57}Fe 2−68533
- Fe-Ni film, crit. fields, effect of elastic stresses 2−51264
- Fe-Ni film, domain struct., influence of temp., elec. microscope obs. 2−72185
- Fe-Ni films, perpendicular anisotropy from galvanomag. meas. 2−61529
- Fe-Ni films, thermal evaporation prepn., detn. of lattice parameters and mag. props., 0-100% Ni 2−77496
- Fe-Ni magnon heat conduction and scattering processes 2−65142
- Fe-Ni melt in deep interior of Earth 2−72677
- Fe-Ni quenched alloys, short-range order detn. in first and second coord. spheres from n. scatt. 2−81199
- Fe-Ni single crystals, domain struct., Kerr effect obs. 2−78017
- Fe-30 wt.% Ni, surface martensite obs. 2−68196
- Fe 30% Ni, martensitic transform, plasticity 2−68197
- La-Ni system, 50-100 at.% Ni, phase equilib. and H_2 absorpt. 2−74934
- Mg-Cu-Ni, Laves phases, enthalpies of soln. and formation detn. 2−47692
- Mg-Zn-Ni, Laves phases, enthalpies of soln. and formation detn. 2−47692
- Mn-Permalloy film, coercivity, influence of driving field 2−81278
- Ni-Al-Cu-Mg-Mn-Fe-Si-Zr-Ti, D16T, recryst. and uncryst. struct., fracture under static and cyclic conditions 2−47527
- Ni-Al-W, γ' matrix, fatigue fracture 2−43716
- Ni-Al, flow-stress recovery 2−74888
- Ni-Al, high temp. deformed, flow-stress recovery 2−74889
- Ni-Al system, lattice parameters and density of β-NiAl and δ-Ni_2Al_3 phases 2−43938
- Ni-Al system, vacancy filling on high temp. compression 2−43939
- Ni-As dilute system, internal hyperfine mag. field determ. 2−44321
- Ni-Au, compositional changes, elec. diffr. critical voltage effect obs. 2−56944
- Ni-B electrolytic coatings, particle distrib., heat treatment effects 2−77730
- Ni-B system, phase diagram 2−50957
- Ni-B thin films, electrical conductivity 2−77860

Nickel alloys continued
- Ni-Be, extra spots in electron diffr. pattern, obs. during G.P. zone formation 2−77578
- Ni-Be, Fermi surface, electron scatt., de Haas-van Alphen and residual resist. obs. 2−71791
- Ni-C, saturated melt spreading over graphite surfaces 2−67814
- Ni-Co, coarse grained polycrystalline, Co self-diffusion at low temp. 2−47450
- Ni-Co, exchange consts. and saturation magnetiz. 2−44265
- Ni-Co, f.c.c., dislocation bands produced by electrolytic hydrogen charging 2−56713
- Ni-Co, thermo e.m.f. and Nernst-Ettingshausen effect, temp. depend. 2−72051
- Ni-Co alloys, diffn. of Co at temps. up to 1000°C 2−71538
- Ni-Co magnetic structure during electrodeposition in presence of magnetic field 2−77995
- Ni-Cr-Mo, porous material, physicomech., hydraulic, and corrosion props. 2−53977
- Ni-Cr-Nb-W-Mo, struct. and phase comp. 2−43941
- Ni-Cr-Ti, strengthening by precip. of intermetallic phases 2−43859
- Ni-Cr, hydrogenated, elec. resist. rel. to mag. field, localized moments 2−81034
- Ni-Cr, mag. props. temp. depend., deform. and annealing influence 2−44256
- Ni-Cr base, filament reinforced mech. props. 2−56988
- Ni-Cr lamellar composite alloy, fatigue deformation, crack propag., fracture energy 2−56821
- Ni-Cr steels, effect of Cu additive on tempering 2−60957
- Ni-Cr system, heat of disordering of Ni_2Cr 2−50954
- Ni-40%Cr alloy, effects of Al and Ti on age hardening 2−64767
- Ni-Cu-Al-Ti, age hardening, precip. 2−53878
- Ni-Cu-Fe, spinodal, interphase interfaces, interfacial dislocations 2−56719
- Ni-Cu-Mn, mag. props. 2−78025
- Ni-Cu, adsorption of CO and O_2 2−50536
- Ni-Cu, elec. resist. near Curie point, resist. anomaly 2−61225
- Ni-Cu, ferromag., density of states 2−54110
- Ni-Cu, grown by Bridgmans method, microstruct. 2−47322
- 40 at.% Ni-Cu, sp. ht. below 3K, effect of clusters and quenching 2−61103
- Ni-Cu, thermoelec. power rel. to Fermi surface shape and sample dimens. 2−68296
- Ni-Cu, X-ray appearance pot. spectra, density of states 2−61674
- Ni-Cu alloys single crystals, magnetostriction constants by optical lever method 2−65159
- Ni-Cu film, growth, struct., epitaxial temp. rel. to comp. 2−60654
- Ni-Cu plates for relay thin leaf springs, surface structure, mechanical properties 2−80862
- Ni-Fe/Fe-Co layers, permeability, intrinsic magnetization, coercivity, remanence 2−61536
- Ni-Fe-Al, martensite transform, effect of disperse particles 2−50942
- Ni-Fe-C, phase transform., martensite to austenite, rel. to heating rate 2−53985
- Ni-Fe-C martensitic, intercryst. mechanism, incompat form. 2−56815
- Ni-Fe-Cr based, γ'-hardened., electron irrad., void swelling 2−80684
- Ni-Fe-Mn, isothermal martensitic transform. rel. to mag. field 2−50937
- Ni-Fe-Mo alloys, thin strips, magnetic properties and texture 2−68509
- Ni-Fe-Nb, magnetic characteristics 2−57293
- Ni-Fe-W, mag. props., magnetostriction and elec. resistivity 2−48076
- Ni-(5wt.%)Fe-(5wt.%)W, powder composite, fracture micromechanism obs. 2−56947
- 81%Ni-Fe, Barkhausen effect, after heat treatment 2−78023
- Ni-Fe, dislocations, mobile, strain rate sensitivity and density 2−56711
- Ni-Fe, f.c.c., domain struct. after different annealing treatments, Kerr effect obs. 2−78016
- Ni-Fe, hardening at high strain rates, rel. to microstruct. changes 2−47593
- Ni-Fe, invar, areas of Fe conc., positron annihilation obs. 2−80524
- Ni-Fe, multilayer films, interaction energy 2−84403
- Ni-Fe, quenched, aged, toughness, ductility, inverse temp. depend. 2−47501
- Ni-Fe, spinwave dispersion coeff. in the Invar region, compositional depend. 2−48077
- Ni-Fe alloy (around 75-25), behaviour in neighbourhood of order-disorder transform. temp. 2−84137
- Ni-Fe alloys with f.c.c. structure, Curie temp. conc. depend. 2−68541
- Ni-Fe film, coercive force, field and freq. depend. 2−78033
- Ni-Fe film, electrodeposition, mag. props. optimization 2−61540
- Ni-Fe film, ripple spectrum, depend. on anisotropy, crystallite size, thickness and field 2−81279
- Ni-Fe films, domain wall creep effects of fields, film thickness 2−77993
- Ni-Fe films, mag. props. temp. depend. and transverse anisotropy 2−61538
- Ni-Fe films, polycryst., edge anisotropy 2−61527
- Ni-Fe powder compact, densification structural aspects 2−56946
- Ni-Fe sheets, heavily rolled, annealing textures, recryst. mechanism 2−74886
- Ni-Fe strip as sensor for two-dimensional magnetic field distributions 2−73508
- Ni-Fe system, Ni_3Fe ordered alloy, 4-s band struct., perturbation calc. 2−71801
- Ni-Fe(Pd) films, magnetoresist. anisotropy 2−44266
- Ni-Fe(18 wt%) electrodeposited film, hyper- crit. thickness, anisotropy fluctuations 2−84409
- Ni-Fe(50-50) alloy, mag. annealing effects 2−81241
- Ni-MC dispersion, M=refractory metal, prep. 2−74896
- Ni-Mn system, Ni_3Mn ordered alloy, 4-s band struct., perturbation calc. 2−71801
- Ni-Mo, Kerr effect magneto-optical effect meas., electronic structure 2−72265
- Ni-Mo, porous material, physicomech., hydraulic, and corrosion props. 2−53977

Nickel alloys continued

- Ni-Mo alloys, influence of V and Nb additions on ordering and isothermal transformations 2−71692
- Ni-Mo system, interdiffusion coeffs., temp. and conc. depend. 2−56762
- Ni-Mo$_2$C-TiC, rupture strength and hardness rel. to microstruct. 2−47538
- Ni-Ni$_3$Nb, directionally solidified eutectic alloy, slip and mech. twinning 2−56796
- Ni-P chemically deposited films, structure and elec. conductivity 2−77510
- Ni-P film, electroless deposited, growth and struct. 2−53566
- Ni-Pd-P-base, amorphous, containing Fe, resistivity temperature relationship, $T^{-1/2}$ singularity 2−44215
- Ni-Pd, magnetoresist., due to scatt. by spin fluctuations 2−48058
- Ni-Pd disordered, spin susceptibility calc. 2−65117
- Ni-Pd(Pt), matrix and impurity cluster polarization 2−44358
- Ni-Re and Ni-Fe, elimination of Barkhausen effect in electrodeposited films 2−72169
- Ni-Rh, disordered, spin susceptibility calc. 2−65117
- Ni-S solid solution, thermodynamic props. 2−50837
- Ni-Sb system, intermetallic cpds., X-ray diffr. study 2−43940
- Ni-Ti-Al-Cu-Fe-Co YuNDK42T8, homogenizing rel. to phase comp., mech. and mag. props. 2−47688
- Ni-(46 wt.%) Ti, martensite phase form., plastic deform. influence 2−43863
- Ni-TiC-Mo, cermet, hardness, bending strength, wear resist. 2−47534
- Ni-W, ^{182}W Mossbauer effect, rel. to saturation magnetization 2−75273
- Ni-Zn-Co ferrite film, anisotropy induced by thermomagnetic treatment 2−81228
- Ni-base heat- resistant alloys, carbide transformations during long-time ageing 2−71673
- Ni-be, deform., recrystn., and ageing, texture variation 2−50806
- Ni$_3$Al-Ni$_3$Nb eutectic, interface between two ordered lattices, elec. diffr. obs. 2−71647
- Ni$_3$Al-Ni$_3$Ta eutectic, directional solidification growth 2−47644
- Ni$_3$(Al,Ti), Ni-rich γ'-phase, solidification behaviour and γ-precip. 2−53904
- β-NiAl, ordered b.c.c. alloy, creep, transmission electron microscope obs. 2−56807
- Ni$_3$Al, hardness, effect of Cr, Ti or W alloying 2−43740
- Ni$_3$Al(Ga), band model approach to weak itinerant ferromag. 2−81245
- Ni$_2$(AlTi), Ni$_2$(AlNb), ordered ternary b.c.c. alloys, creep, transmission electron microscope obs. 2−56807
- Ni$_3$Cr, oxidation effects on mag. props. 2−54338
- NiFe films, e microprobe analysis 2−77509
- NiFe permalloy, film, oxidized, exchange anisotropy effects, hysteresis loop, 5-300 K 2−81230
- Ni$_3$Fe, long range order parameter 2−60984
- Ni$_3$(Mn,Co) and Ni$_3$(Mn,Fe), electron and hole mobility obs. 2−47837
- Ni$_2$MnSb, Ni$_2$MnSn, Heusler ferromag. alloys, atomic and mag. struct. 2−48075
- Ni$_4$Mo, internal friction study 2−43670
- Ni$_3$Nb phase in Inconel 718, cryst. struct. 2−77678
- Ni$_2$Si, solidification characts. 2−43924
- Ni$_{3\pm x}$Te$_2$, heat capacities and transition behaviour 2−57068
- NiTi, non-stoichiometric, elec. resist., comp. and temp. depend. 2−74885
- Ni$_2$V alloy, ordering transformation for wide range of subcritical temps. 2−74938
- Pd-Ni-H system, superconductivity, elec. resist. study 2−54135
- Pd-Ni, spin paramag. susceptibility, calc. 2−65125
- Permalloy-Mn bimetal film, mag. after-effect 2−81224
- Pt-Ni, spin paramag. susceptibility, calc. 2−65125
- Th-Ni system, 50-96% Ni, phase equilib., 1000-1500°C 2−74943
- Ti-Ni-Cu homogeneity range by electron microprobe X-ray analysis 2−43858
- Ti-Ni, near equiatomic, shape memory effect 2−77693
- Ti-Ni system, electron energy spectrum of equiatomic cpd., X-ray emission study 2−75316
- TiC$_{1-x}$N$_x$ in Ni binder, cermet hard alloy, prep. and props. 2−53945
- TiNi, unique property changes related to martensitic transformation 2−68200
- Y-Co-Ni pseudobinary compounds, magnetization minima 2−75223
- Y-Co-Ni system, CaCu$_5$-type phase stability 2−43944

Nickel compounds

see also Nickel alloys

- — 2−71693
- acetate tetrahydrate, sp. ht., 0.43-10.73 K 2−78040
- alloy and liquid Fe, thermodynamic study by electromagnetic levitation melting in inert atmosphere 2−67871
- Co-Ni-Cr-Ti alloy, quench-ageing behaviour, 700-900°C 2−68138
- ferrite, cation reordering, temp. depend. of cond. time variation obs. 2−75145
- magnetic phenomena of surface gas-solid interactions 2−84395
- 9Ni-4Co-0.30C, fracture mechanics of crack growth at elevated temperatures 2−56867
- Ni-base superalloys, thermal fatigue crack propagation under strain-temperature cycles 2−56868
- nickel superalloy, Rene' 77, thermal fatigue crack propagation testing 2−56878
- NiF$_2$.5HF.6H$_2$O, study of internal motion by meas. of temperature dependence of n.m.r. linewidth and second moments 2−65343
- non metallic, thermal decomposition, photostimulated exoelectron emission obs. 2−57408
- tutton salt, paramag. relax., mag. field and conc. depend. 2−54365
- Udimet 710, nickel-base superalloy, effect of mean stress on high-cycle fatigue at 1000°F 2−60950
- Al$_2$O$_3$-Ni(NO$_3$)$_2$.6H$_2$O system, effect of heating in oxidizing and reducing media 2−60992
- Cd$_3$As$_2$-NiAs eutectic, Nernst effect and thermal radiation detector fig. of merit 2−54246
- Cd$_3$As$_2$-NiAs eutectic, thermomag. props., rel. to device appl. 2−59064
- CoO-NiO solid solution, cryst. growth, for neutron monochromator appl. 2−47205

Nickel compounds continued

- Cr-Ni steels, austenitic, stabilisation of resistance to intercrystalline corrosion 2−65380
- Fe-Ni-Co alloys, dilatometric study of vol. exp. for fcc to bcc transformations 2−65146
- Fe-Ni alloys, magnetisation and magnetostriction in strong magnetic fields 2−68507
- Fe-Ni and Fe-Ni-C martensitic alloys, delayed fracture formation during cathodic charging under static stress 2−64731
- Fe-Ni carbonyl powders, phase composition 2−77726
- Fe-Ni superalloys, bend fatigue testing at elevated temperatures 2−56884
- (Fe,Ni)$_2$Mo$_3$O$_8$, Mossbauer effect 2−75270
- (Fe$_2$TiO$_4$)$_c$(NiFe$_2$O$_4$)$_{1-c}$, $O \leqslant C \leqslant 1$, binary solid solution, effect of comp., lattice parameter, saturation mag. moment and Curie temp. 2−83840
- Gd-Ni intermetallic compounds, paramagnetic resonance meas. of g_s values, study of exchange interactions 2−84568
- InSb-NiSb eutectic, thermomag. props., rel. to device appl. 2−59064
- N$_1$(II) mandalate complex, i.r. spectrum 2−50065
- Ni/D system, form. and decomp. equil. 2−77715
- Ni/Fe/H system, form. and decomp. equil. 2−77715
- Ni/H system, form. and decomp. equil. 2−77715
- Ni-C interstitial solid solution, sat. magnetiz. and high field suscept. 2−81249
- Ni-Co-Zn ferrite, h.f. magnetic props., temp. depend. 2−68723
- Ni-Ni hydroxide, sintered plate electrode, behaviour in lithiated electrolyte solution 2−84659
- Ni-Pd alloys, Mossbauer effect of ^{61}Ni, conc. depend., hyperfine field interactions 2−72285
- Ni-Zn ferrite powder, hot-pressing and densification 2−43893
- Ni-Zn ferrite powder, quality characterization 2−57312
- Ni-Zn ferrites, mag. losses in h.f. fields 2−84435
- Ni-base composite materials, superalloys with fibres obtained by direct solidification, props. 2−64793
- Ni complex, bipyramidal trigonal, computational errors in term energies 2−60025
- Ni complex, bis-(4-dimethylaminodithiobenzil)-Ni, Q-switching of Nd:glass i.r. laser 2−59175
- Ni complex, high-spin NiN$_3$O$_2$ chromophore, polarized single-cryst. electronic spectrum 2−57337
- Ni complex, Ni(C$_5$H$_5$)NO, bonds, SCF-MO calculations 2−50064
- Ni complex, Ni(CN)$_4^{2-}$, bonds, SCF-MO calculations 2−50064
- Ni complexes, carbonyls, Raman spectra 2−72363
- Ni complexes, tetracoordinated trimethylphosphines Ni(II), physicochemical properties 2−77091
- Ni II complexes, low-spin trigonal bipyramidal, electronic spectra, temp. dependence of lowest energy ligand field band 2−53031
- Ni II complexes, polarized crystal spectra, comparison with theoretical investigation of electronic spectra of trigonally distorted complexes 2−44372
- Ni olivine to Ni spinel, reaction rate of phase change, seismological implications 2−78270
- NiAl$_2$O$_4$, growth on sapphire, orientation relations 2−71333
- NiB, elec., thermal and mag. props. 2−51099
- NiB$_x$, rel. to elec. resist., 300-1200K 2−51100
- Ni$_3$B, electron structure, Ni X-ray K-emission obs. 2−72379
- NiBr$_2$, electronic absorpt. spectra, cryst. field parameters, phonon and magnon sidebands 2−51345
- Ni(CO)$_4$, E and F$_2$ type Raman contour bands 2−46585
- NiCl$_2$, adiabatic compressibility and sound propag. speed, reln. to molec. struct. 2−72564
- NiCl$_2$, electronic absorpt. spectra, cryst. field parameters, phonon and magnon sidebands 2−51345
- NiCl$_2$, in graphite, two dimens. paramag. transition to mag. ordered state 2−54320
- NiCl$_2$, X-ray Kβ emission and K absorpt. spectra 2−65287
- NiCl$_2$.2H$_2$O, crystallographic phase transition at 230 ± 20K 2−84143
- NiCl$_2$.6H$_2$O, proton spin-lattice relax. time, 1.12−4.18 K 2−78050
- NiCr$_x$Mn$_{2-x}$O$_4$, spinel, atomic and cation distrib., lattice distortion 2−74740
- NiCr$_2$O$_4$ mag. struct. determ. by representation anal. 2−84429
- NiF$_2$, covalency parameters 2−77057
- NiF$_6^{2-}$, force constants and generalised mean amplitude of vibration calc. using seven parameter Urey-Bradley force 2−60013
- NiF$_6^{4-}$, ave.-of-config. calc. of self-consistent- field electronic excitation energies 2−72240
- NiF$_6^{4-}$, ave.-of-config. interpret. rel. to 10Dq calc. 2−72239
- NiFe ferrites, freq. effect, torque obs. 2−44278
- Ni$_3$Fe, Kerr and magneto-optical effect meas., electronic structure 2−72265
- Ni$_2$Fe(CN)$_5$NO.2H$_2$O, i.r. spectra, cryst. chem. 2−78081
- NiFe$_{0.8}$Cr$_{1.2}$O$_4$, ferrite, statistical angular spin configurations 2−72200
- NiFe$_{0.8}$Cr$_{1.2}$O$_4$, ferrite, structural transition at mag. transformation, Mossbauer and X-ray obs. 2−72201
- NiFe$_2$O$_4$-Fe$_3$O$_4$-Fe$_2$TiO$_4$, ternary solid solution, effect of lattice parameter on solubility 2−83840
- NiFe$_2$O$_4$, cryst. growth rate variation with supersaturation in fluxed melts 2−47255
- NiFe$_2$O$_4$, crystal growth, from the flux systems PbO-V$_2$O$_5$ and Bi$_2$O$_3$-V$_s$O$_5$ 2−50589
- NiFe$_2$O$_4$, ferromag. relax. of parametric spin waves 2−72228
- NiFe$_2$O$_4$, magnetocryst. anisotropy, reson. fields, iodine additive effects 2−44279
- NiFe$_2$O$_4$, reson. phenomena at moving domain boundaries 2−72456
- NiFe$_2$O$_4$ films, ferromag. reson., etching effect 2−44431
- Ni$_x$Fe$_{3-x}$O$_4$, Mossbauer obs. of Fe^{2+} ions, Zeeman patterns 2−54391
- Ni$_{1.2}$Fe$_{1.7}$Sb$_{0.1}$O$_4$, supertransferre d hyperfine fields and covalency at diamag. cations 2−48150
- Ni$_{1-x-y}$Fe$_x^{2+}$Zn$_y$Fe$_2^{3+}$O$_4$ ferrite, spinel, Fe^{2+} cation distrib., i.r. spectra and Mossbauer obs. 2−72341
- NiH$_x$, energy band calcs., model obs. 2−61187
- Ni(II) complexes, octahedral, halogen- bridged, Raman and far i.r. spectra 2−46558
- Ni(II) complexes with N,N'-ethylenebis(acetylacetoneimine), i.r. spectra, normal coordinate analysis 2−70695
- NiMn$_2$O$_4$, i.r. absorpt. spectra, ionic ordering 2−72342

Nickel compounds continued
$Ni_{0.6}Mn_{2.4}O_4$, elec.-field-depend. cond. for hopping-type charge transport 2−81082
$NiMnZnO_4$, i.r. absorpt. spectra, ionic ordering 2−72342
Ni_3Mo, domain struct. formation 2−68021
Ni_4Mo, domain struct. formation 2−68021
$Ni(NH_3)_2.Ni(CN)_4.2C_6H_6$, mag. susceptibility, rel. to sp. ht., 1.2-4.2K 2−75241
$Ni(NO_3)_2,6NH_3$, order-disorder transitions, heat capacity obs. 2−61036
$Ni(NO_3)_26NH_3$, antiferromag. transition, susceptibility and specific heat obs. 2−65185
NiO:Li, electro-transmission in visible and near i.r., charge carrier obs. 2−51323
Ni_xO-Co_xO system, interdiffusion 2−50714
NiO, absorpt. of O_2, adsorbed species characterization by X-ray photoelectron spectroscopy 2−77516
NiO, antiferromag. ordering, exchange consts. calc. 2−61549
NiO, antiferromag. reson. 2−72463
NiO, Au contact resistance 2−61370
NiO, band struct., refl. and thermorefl. study 2−84505
NiO, bound polaron hopping 2−47899
NiO, dendritic growth from vapour phase 2−64592
NiO, diffusion of Cr, temp. depend. 2−50713
NiO, elastic constants and acoustic absorption coefficients 2−43971
NiO, experimental sintering kinetics, approx. equation 2−47652
NiO, f.c.c. cryst., antiferromag., magnons, light scatt., dispersion and absorpt. 2−61550
NiO, high temp. transport props. 2−84314
NiO, mag. insulator, exchange interactions, crystal field theory 2−68564
NiO, mag. superlattice X-ray diffr. peaks 2−44307
NiO, magnetocatalytic effects at Neel pt. 2−44480
NiO, photoexcited charge carrier drift and lifetime 2−68280
NiO, polycryst., self-diffusion of Ni, intercryst. diffusion 2−80721
NiO, positron lifetime spectra, rel. to cond. and nonstoichiometry 2−71825
NiO, spin wave dispersion, inelastic neutron scatt. study 2−81303
NiO, thermoreflectance, band transition assignment 2−44368
NiO, true work function, A constant, normal energy distribution 2−44192
NiO film, effect of surface preparation on Ni oxidation 2−72559
NiO film, mechanisms of low temp. oxid. of polycryst. Ni 2−72558
NiO films, optical consts., electrochem. deposition conditions depend. 2−61618
NiO on Ni, oxide growth and parabolic kinetics at high temps. 2−75383
$Ni_{1-x}O$, sintering, effect of O partial press. 2−61005
$Ni(OH)_2$, prep. from turbostratic hydroxide 2−47211
$Ni(OH)_2$ powder, crystallite struct. from X-ray diffr. profiles 2−74739
$Ni_2P_2O_7$, i.r. spectra and normal coordinate analysis 2−77079
$Ni_{1-x}S$:O(Se), mag. susceptibility conc. depend. rel. to cryst. chemistry 2−44255
NiS, hexagonal, heat capacity and metal-nonmetal transition 2−47754
NiS, metal- to-semimetal transition, stoichiometry and impurity effects 2−51280
NiS, thermal and elec. cond., thermoelec. power, Hall coeffs., 80−400 K, semicond.-semimetal transition 2−81097
NiS_2, conductivity and optical absorp. obs. 2−81020
NiS_2, semiconducting, band model, opt. absorpt. and elec. conductivity obs. 2−68417
$NiSO_4.6H_2O$ optical activity, calc. of rotatory strengths and dipole strengths associated with electronic transitions 2−57325
$NiSnCl_6.6H_2O$, susceptibility, magnetization and heat capacity, 0.35-4.2 K 2−78039
Ni_8Ta, quenched, microstruct. aspects, cry. orientation and grain boundaries during deformation 2−64709
$NiTiO_3$, crystal growth, from the flux systems PbO-V_2O_5 and Bi_2O_3-V_2O_5 2−50589
$(Ni_2TiO_4)_c(Fe_3O_4)_{1-c}$, $O \leqslant C \leqslant 1$, binary solid solution, effect of comp., lattice parameter, saturation mag. moment and Curie temp. 2−83840
Ni_2TiSn, Heusler alloy, paramag. props. 2−51255
Ni_2VSn, Heusler alloy, paramag. props. 2−51255
$NiWO_4$, flux growth 2−60717
$Ni_{1-x}Zn_xFe_2O_4$, high temp. enthalpy and specific heat 2−54049
$Ni_xZn_{1-x}Fe_2O_4$, thermal expansion coeffs. at Curie pt., conc. depend. 2−81281
Ni + NiO and NiS + NiO physical mixtures, electrical conduction rel. to planetary mantles 2−84292
Ti-Ni-H, intermetallic phase and absorption of hydrogen 2−71354
$ZnSO_4.7H_2O-NiSO_4.7H_2O-CoSO_4.7H_2O$, isomorphous relationships, distribution coeff. 2−74959

Night sky *see Airglow*

Nightglow *see Airglow*

Nilsson's model *see Nucleus/models*

Niobium
see also Superconducting materials/niobium
absorption spectra in rare gas matrix at 14 degrees K, 500 to 50000 cm^1 2−83178
adsorption, simultaneous of Cs and Ba, work function and thermal stability obs. 2−67923
adsorption and absorption of H, H solubility 2−50542
arodic sectioning technique 2−60817
cold worked, internal friction, vibr. freq., damping, β-process, 20-170°C 2−56778
cold-worked or neutron irradiated, annealing, resist. study 2−64766
creep during hot pressing with and without addition of oxides 2−77694
crystal, centred cubic, mean square displacement of atoms, simple calc. 2−57037
deformed, angle and wave depend. of X-ray diffr. linewidth 2−43625
deposition of Al, LEED and Auger spectroscopy obs., 22-1200°C 2−50484
desorption, of H_2, spatial distrib. obs. 2−50526
diffusion in Cu by an electrical-resistance method 2−53762

Niobium continued
diffusion of H, quantum interpret. 2−71537
diffusion of H and D, application to quantum theory 2−80718
diffusion of hydrogen, anelastic obs. 2−77616
diffusion of oxygen, under neutron irrad. 2−53768
diffusivity of H, low temp., determ. by Gorsky effect 2−80847
dislocation line tension, effects of elastic anisotropy 2−74772
electrical and thermal cond., 20 to 1200°C 2−47769
energy bands, Fong-Cohen pseudopotentials 2−84271
enthalpy, liquid and solid state 2−54038
evaluation for nuclear power systems 2−76938
fusion reactor blanket material, comparison with Mo and Nimonic alloy PE 16 2−83093
internal friction, Young's modulus, when in normal and supercond. states 2−77635
interstitial D site location by deuteron channelling 2−60811
ion backscattering, H^+, Ne^+ and Ar^+, energy and ang. distrib. 2−50467
magnetic susceptibility, 78-400 K 2−51238
melting point, normal spectral emittance at m.p., and electrical resistivity above 2650K 2−53487
Mossbauer spectrum of ^{57}Fe, hydrogen conc. effects 2−78075
multi-mechanical-thermal-treatments, role of oxygen and nitrogen solutes 2−64722
neutron damage simulation by ion bombardment, void form. 2−53693
neutron irrad., void form. and ordering, alloying and purity effects 2−53719
oxidation, stress effects on oxid. process, oxide wedge formation 2−43736
oxidation, stresses involved in oxid. process, annealing flexure obs. 2−43735
oxide growth in matrix 2−47468
paramagnetic susceptibility, infl. of plastic deform. 2−81216
permeation of hydrogen, surface effects 2−77608
photoactivation analysis in ores 2−65424
photoelectron energy distribution and photocurrent meas. 2−72093
polycrystalline wire, H_2 adsorption, u.h.v. technique 2−47161
recovery, cold-worked or irrad. samples, role of O and N impurities 2−47404
resistivity from 20°K to fusion temperature 2−81032
secondary standard, for ultrahigh vacuum, using equilib. pressure of H 2−78692
Snoek peaks, due to O and N, grain size effect 2−50736
steel, welded joints, crack formation in stress relieving annealing 2−64759
stressed, dislocation struct. form mechanism 2−71494
structure sensitive mech. props., review 2−43697
superconducting r.f. cavities in accelerators, meas. of surface condition 2−70337
thermionic converters, arc mode, influence of collector material work funct. 2−49281
thermionic fuel elements, Al_2O_3 ceramic to metal seal 2−53928
twinning energy, continuous nucleation theory 2−64588
X-ray K-absorption spectrum, fine struct. 2−68674
yield strength, meas. nder high pressure 2−60879
Nb:H, X-ray diffr. pattern, anomalous line broadening due to H 2−64642
Nb-H systems, phase transitions due to elastic interaction 2−77744
Nb-N, interstitial soln., mech. props. depend. on conc. and temp. 2−84009
Nb-O, interstitial soln., mech. props. depend. on conc. and temp. 2−84009
Nb-Ti-Zr alloy, Cu cladding bimetallic wire, solenoid, strong pulsed magnetic field 2−63255
Nb-W, CVD, variable spacing converter, thermionic performance 2−59053
Nb, superconducting point contacts, static and microwave properties 2−81054
Nb VII, spectral anal., configurations and levels determ. 2−74219
Nb^{2+}, in ZnO, dynamic Jahn-Teller effect, e.s.r. obs. 2−48284
NbVII, spectrum rel. to YV, MoVIII and ZrVI 2−74217
^{95}Nb-^{95}Zr accumulation in coastal sediments 2−62044
Nb + Zr + Ti and Nb + Ti alloys, properties of welded joints 2−61227

Niobium compounds
Al oxide-Nb metal seals, by solder glass in system CaO-Al_2O_4-SiO_2-MgO 2−66377
alloy, foil prep., for electron microscopy, electrolytic jet thinning procedures 2−71415
alloys, evaluation for nuclear power systems 2−76938
β-Nb-Al-Si alloys, superconducting critical temp. detn. 2−71869
Nb-Sn alloys, vacuum deposited, superconducting characteristics 2−68365
niobates, $M_4Nb_2O_9$ (M=Co, Mn), magneto- electric effect obs. 2−54359
system, plastic deformation, microhardness, emission electron microscopy 2−74843
CaO-Nb_2O_5-TiO_2-SiO_2 system, liquidus temps. 2−43436
Fe-Ni-Nb-C alloy, ageing, 700 and 800°C 2−47596
H-Nb system, equilibrium pressures, secondary standard for ultra high vacuum gauge calibration 2−78692
$LiNbO_3$ crystal, harmonic generator, patent 2−42171
Nb-40% Ti alloy, supercond., mag. irreversibility and microstruct. 2−47855
Nb-Al-Ge system, phase equilib. and supercond. props. 2−43936
Nb-Al alloy, supercond., heat treatments rel. to transition temp. 2−47589
Nb-Al system, diffusion in $NbAl_3$, Nb_2Al and Nb_3Al phases 2−74815
Nb-C, electron work function measurement, pulsing voltage procedure 2−63235
Nb-C thermionic emission constants and electron work function changes 2−54268
Nb-Ga system, constitution diagram 2−43937
Nb-H dil. solns., phase equil. and evolution kinetics of dil. solns. 2−53903
Nb-H foil, microcracks, transmission electron microscope obs. 2−68106

Niobium compounds continued
Nb-H solns., nondil., equil. press.- comp.-temp. relationships 2−50843
Nb-H system, H-dislocation interaction, cold work peak study 2−80841
Nb-H system, hydride precip. at sub-ambient temps. 2−47693
Nb-H system, phase diagram, 80-500 K 2−77756
Nb-Hf-B alloy, phase equilibria, at 1400°C, X-ray obs. 2−43912
Nb-Hf alloys, fracture morphology, transmission and scanning electron microscopy 2−56834
Nb-Mo:Fe alloy, localized moments on Fe, Mossbauer obs. 2−48149
Nb-Mo-Fe alloy, discontinuous formation of localized moments, Mossbauer study 2−78076
Nb-Mo-N system, α solid soln., thermodynamic functions 2−43856
alpha-Nb-Mo-N ternary solid solution, equilibrium N concentration and thermodynamic behaviour 2−60983
Nb-Mo alloy, elastic consts., 83-373K, effect of comp., Debye temp. 2−60845
Nb-Mo alloy, vapour deposited, struct., electron microscope obs. 2−60594
Nb-Mo alloy single crystals thermally activated deformation 2−80823
Nb-Mo alloys, elastic consts., anomalous temp. depend., rel. to Fermi surface features 2−47479
Nb-N alloy, nitride precip., prismatic loop generation 2−53994
Nb-O alloys with Zr and Hf additions, electron microscope obs. 2−43857
Nb-O solid soln., form. of Nb_4O during decomp., annealing effects, 500-700°C 2−53902
Nb-Pt alloy, strength, oxidation resist. 2−47533
Nb-Re alloy single crystals thermally activated deformation 2−80823
Nb-Sn sinter material, supercond., screening behaviour on addition of Cu, Ag or Au 2−75061
Nb-Ta alloy, superconductor, microwave surface resist. 2−54133
Nb-Ti alloy, mag. instabilities 2−64948
Nb-Ti and Nb-Ti-Zr alloys, supercond. wire, crit. current, mag. field intensity depend. 2−75062
9.5 wt %Nb-U alloy, gamma phase decomp., discontinuous precip., 450-600°C 2−80802
Nb-Zr-Ti alloy, supercond., struct. determ. 2−50842
Nb-(40 wt.%)Zr alloy, metallurgical variables influence on supercond. 2−47861
Nb-(25 wt.%)Zr wire, macroscopic quantum effect in meas. of current threshold57166 2−57166
Nb-Zr alloy, vapour deposited, struct., electron microscope obs. 2−60594
Nb-Zr alloys, internal friction peaks due to nitrogen impurity 2−60849
Nb-Zr alloys, superconducting point contacts, static and microwave properties 2−81054
Nb_3(Al-Ge) compound tapes, supercond., prep. and props. 2−64949
Nb_3Al, supercond. critical current variation, a.c. current obs. 2−61240
NbB_x, thermionic emission, rel. to electronic struct. 2−48017
NbC-X, X=Fe, Cr, Ni, Co, phase equilib., phase diagram 2−68199
NbC, hot working and strength improvement, NASA research 2−64801
NbC, solubility in austenitic steel 2−74902
NbC_{1-x}, vacancy short range order, calc. 2−83966
NbC_{1-x}, supercond. transition temp., rel. to band struct. determ. 2−81055
NbC_x, process for obtaining mat. in fluidized layer 2−68168
NbC_x, work function, correl. with surface recomb. of H atoms 2−50549
$NbCl_6^-$, $NbBr_6^-$, Urey-Bradley force fields 2−42919
NbD_x system, diffuse neutron scatt. phenomena in α-phase, temp. depend. 2−77757
NbF_5, matrix isolated and gas phase, obs. of i.r. spectra, C_{4v} monomeric structure active frequencies 2−42918
Nb_3Ga, annealed, supercond. transition temp. 2−43937
β-NbH, proton jump rate determ. by neutron scatt. and n.m.r. 2−77614
NbH_x, α-peak interpret., acoustical loss mechanism, kink generation on dislocations 2−77645
NbH_x, quasielastic neutron scatt., diffusive motions of hydrogen 2−77615
Nb_xH_y, impurity effects on stability 2−77729
Nb(38 at.%)Hf alloy, supercond., fluxoid pinning rel. to precipitate dispersion 2−44076
$Nb_{85}Mo_{15}$, supercond. energy gap field depend. from vortex entropy in low-field limit 2−57170
NbN, band struct., pseudopotential calc. 2−84253
NbN, bulk and films, lower crit. field meas. 2−54146
NbN, solubility in austenitic steel 2−74902
NbN film, crit. current anisotropies rel. to columnar structure 2−68366
NbN films, reactive high-vacuum codeposition and characteriz. 2−50497
NbN films, superconductive critical field 2−84310
NbN films prepared by d.c. sputtering, props. 2−84311
$NbN_{0.95}$, microhardness and thermal expansion, 80-300K 2−61112
Nb_2O_5-SiO_2-ZnO, ternary system, phase relations at liquidus and subsolidus temps. 2−68203
$Nb(O, F)_x$, cryst. shear struct., electron microscope obs. 2−47352
NbO band systems, vibr. transition probabilities and r-centroids 2−60006
NbO_2 and Nb_2O_5, X-ray K-absorpt. fine struct. 2−68674
NbO_x, in Nb-NbO_x-Al struct., varying surface barrier at NbO_x-Al interface obs. 2−68455
NbO_x, Nb_2O_5, oxidation of Nb, stresses involved in oxid, process, annealing flexure obs. 2−43735
Nb_2O_5, anodic oxide film, dielec. const. field depend., ellipsometric obs. 2−44150
Nb_2O_5, in m.i.m. struct., switching obs. 2−54223
Nb_2O_5, ion impact effects on electrical conductivity 2−60779
t- and h-Nb_2O_5, phase transformations under impact compression 2−61035
Nb_2O_5, thermal expansion, X-ray and dilatometric study 2−80803

Niobium compounds continued
Nb_2O_5 film, amorphous, conductivity and switching time obs. 2−61320
Nb_2O_5 film, r.f. sputtered, ionic instability, m.o.s. capacitance obs. 2−71995
$NbS_2(Se_2)$, supercond. transition temp., press. depend. 2−54147
$NbSe_2$-WSe_2 alloys, antifriction and elec. props., comp. depend. 2−68115
NbSe, organo intercalation compounds, electron microscope examination of lattice and superconductivity 2−53676
$NbSe_2$, 2H-type, Fermi surface 2−65002
$NbSe_2$, 2H polytype, cryst. struct. and mag. susceptibility 2−47339
$NbSe_2$, Auger electron spectroscopy investig. of adsorption anisotropy 2−60687
$NbSe_2$, lamellar superconductor, pressure effect on transition temp. 2−71860
$NbSe_2$, low-temp. cryst. modification and supercond. transition temp. 2−81052
$NbSe_2$, resist. anisotropy with press. 2−51116
$NbSe_2$, supercond., discontinuous flux flow 2−61241
$NbSe_2$, supercond. transition temp., press. depend., 1.5-6.5kbar 2−68346
$NbSe_2$, superconducting transition temp., pressure depend. to 140 kbar 2−68359
$NbSe_2$ intercalation compound, struct., electron microscope and diffr. obs. 2−64643
$NbSe_4$ and Nb_3Te_4, X-ray K-absorpt. fine struct. 2−68674
Nb_5Si_3, diffusion of Si, oxide coating form., 1700°C 2−53769
$NbSn_2$, supercond. transition temp. and crit. mag. field 2−75063
Nb_3Sn, elastic moduli and mag. susceptibility 2−51117
Nb_3Sn, high-T_c superconductor, tunnelling, phonon spectrum 2−81048
Nb_3Sn, Mossbauer recoil-free fraction and Debye-Waller factors 2−44357
Nb_3Sn, multifilamentary composite in ductile matrix, supercond. props. 2−51113
Nb_3Sn, phonon linewidths, Kohn anomaly 2−43951
Nb_3Sn, shear mode phonon spectra, Labbe-Friedel model 2−68229
Nb_3Sn, vapour deposited supercond., crit. current, effect of impurity gas additions 2−51109
$Nb_{1-x}Ta_x$ alloy, $0<x<0.25$, growth by electron beam float zoning 2−50599
$NbTe_2$, domain structure and dislocation config. 2−60804
$NbTe_2$ domain structure formation due to atomic displacements 2−68021
NbTi filaments, operating conditions for use as liquid He level sensors 2−66368
NbTi filaments of round composite superconductors, anisotropy of critical current density 2−71870
$Nb_{0.88}Ti_{0.12}N$ film, fluctuation broadening of supercond. transition 2−71850
NgH_x, vibr. and diffusive behaviour of hydrogen 2−77771
Ni-Cr-Nb-W-Mo alloy, struct. and phase comp. 2−43941
Ni-Fe-Nb alloy, magnetic characteristics 2−57293
Ni_3Nb phase in Inconel 718, cryst. struct. 2−77678
Ta-Nb alloys, superconducting, sp. ht. and mag. meas. 2−71875
$Ta_{0.96}Nb_{0.04}$ alloy, surface pinning of fluxoids 2−44064
Ti-Nb alloy, electronic struct., X-ray spectral study 2−44402
Ti-22at.%Nb alloy, ω-phase, electron diffr. obs. 2−53908
TiC-Nb cermet, hot pressing kinetics 2−56914
U-Nb alloy, stress corrosion cracking, metallic protective coating 2−53911
U-Nb and U-Nb-Zr alloys, low temp. oxidation 2−48334
$V_{1-x}Nb_xO_2$, metal-insulator transition, crystallographic and transport props. study 2−75101
$V_{1-x}Nb_xO_2$, metal-insulator transition, theory 2−75103
$V_{1-x}Nb_xO_2$, metal-insulator transition, mag. props. and n.m.r. studies 2−75102
$(W, Nb)O_x$, cryst. shear struct., electron microscope obs. 2−47352
WC-Nb cermet, hot pressing kinetics 2−56914
$W_xNb_{1-x}Se$, cryst. struct. 2−60767
Zr-(2.5 wt.%) Nb press. tubes, heat-treated, embrittlement 2−50770
Zr-(2.5 wt.%) Nb press. tubing, hydriding, orientation and effect on tensile props. 2−50849
Zr-(2.5wt.%)Nb press. tubes, irrad., metallurgical props.53913 2−53913
Zr-Nb alloy, strain rate depend. hardening 2−50847
Zr-Nb alloy, supercond. transition temp., constitution and microstruct. effects 2−51107
Zr-Nb alloys, phase transforms. 2−53999
Zr-(2.5 wt%)Nb press, tubes, texture development 50848 2−50848
ZrC-NbC, solid solution, creep in compression, temp. range 2600-3150 K 2−84033

Nitrogen
− 2−67388
absorption cross sections between 100 and 600 Å 2−80057
abundance in population II objects 2−69080
accelerated nuclei, autoactivation, application to radiology 2−69295
active, vacuum u.v. emission, absolute population rates of $N_2(a^1\Pi_g)$ and $CO(A^1\Pi)$ 2−70718
active, vacuum u.v. emission, excitation of singlet and triplet states of CO 2−70717
active, vacuum u.v. emission, form. and removal of $N_2(a^1\Pi_g)$ 2−70716
active, vacuum u.v. emission from levels of forbidden B-X transition, $N_2(B'^3{}_u^-)$ kinetic behaviour 2−70719
adlayer on Ni, electron energy loss spectra, electronic transition characts. 2−47079
adlayer on W, K shell total electron impact ionization cross sections, Auger spectra 2−64579
adsorbed on Ni(110), electron energy loss spectra, elastic scatt. 2−84222
adsorbed on Ti, photoemission energy level meas. 2−47166
adsorption and description on porous materials at liq. N_2 temps. 2−50541
adsorption on W, surface crystallography effects 2−47168
antiprotonic atoms, X-ray lines, strong-interaction effects 2−79965
arc, atm. cascade, electric field intensity and wall heat transfer meas. 2−46804
arc, cylindrical, radiative energy balance 2−67697

Nitrogen continued
arc plasma, disequilibrium effects 2—70898
arc plasma effect of reaction energies on radial temperature distribution 2—53261
atmospheric arc, determ. of thermal condition in asymptotic region using spectroscopy and equilibrium flow model 2—77317
atom, 1s-hole state, chemical effects on lifetime 2—70602
atom, beam-foil lifetime meas. of excited levels 2—79890
atom, doubly ionized by slow proton impact, Auger spectra, intense satellite lines 2—83195
atom, electronic struct., correl. energy 2—64021
atom, pulsed stimulated emission 2—79194
atomic, specific refractivities, dual frequency laser interferometry 2—79902
atomic $^4S_{3/2}$ g_j factor, by atomic-beam magnetic resonance technique 2—76984
atomic projectile interaction with Hg, pot. cross sections 2—77015
atoms adsorbed on W substrate, backscattering cross sections for K-shell ionization by electron impact 2—79919
breakdown, by 0.35μ picosecond laser pulse 2—60314
breakdown voltage estimation using empirical semi-empirical methods, pressures up to 7 atmospheres 2—56392
chemiluminescent reaction $N+O_2 \rightarrow NO+O$, overtone photon efficiency 2—57409
chemiluminescent reaction with Na 2—81492
chemisorption, on W, K shell ionization by electron impact 2—50553
counter-current flow with Hg in packed bed system, criteria for flooding 2—50294
D-region, theoretical models, ion pair production 2—78400
deficiency in Small Magellanic Cloud 2—44844
desorption from powder, rel. to surface area determ. 2—56969
desorption phenomena for stainless steel LEED and molec. beam assembly 2—67922
in diamond, irradiated, effect on annealing, optical absorp. obs. 2—71453
diatomic molecule, molecular vibration effect on apparent bond lengths 2—56136
diffusion in Fe, effective radii of diffusing particles, diffusion mechanisms 2—50709
diffusion in Fe, solid and liq. states 2—43661
diffusion in Fe-Ni along austenite/ferrite phase boundary 2—68052
discharge, h.f., re-ignition, influence of metastable states 2—43217
discharge, mechanism of spark breakdown 2—60318
discharge, positive ion drift velocities at high pressure 2—74411
discharge, thermalisation of spark channels 2—71046
doping level in Ta_2N film resistor, determ. by Seebeck effect 2—74793
electric arc, const. press. axial flow, local convection effects 2—74351
electric discharge, bremsstrahlung in strong electric field 2—80368
electron capture and losses of atoms and ions in air N_2 and O_2 2—70620
electron impact excitation cross sections, ionospheric models 2—81724
electron scatt., elastic, ang. distrib. 2—60018
electronegative gases, light emission in electron avalanches 2—74428
electrotransport in Gd 2—80716
equations of state representing all saturated state variables 2—53332
etch pitting of graphite 2—53553
fine-structure density shift 2—79964
gas, contributions of nonspherical and nonadditive molecular interactions to third virial coeff. 2—71110
gas, elec. breakdown due to large number of electrons 2—83709
gas, equilibrium pressure over GaN 2—47049
gas, influence on Mo photoemission 2—51227
gas, pulsed with 10.6 μm laser radiation, gas breakdown thresholds 2—83707
glow discharge, electron energy distrib., new probe technique 2—64348
image intensifier, nonlinear processes 2—42257
Io atmosphere, upper limits 2—75867
ion beam at 3.9 GeV, meas. of physical and radiobiological parameters 2—69425
ionizing gas breakdown waves in strong electric fields 2—80414
ionosphere, photoionization and photoabsorption cross sections calculations 2—78388
ions, 0.5-2 MeV, stopping powers in Cr, Fe, Co, Ni, Cu, Zn 2—47782
ions, multiply ionized, laser oscill. in Z-pinch discharge 2—49352
ions, range-energy relations in N_2 and air, 0.3-2.0 MeV 2—79917
isotopes, separation during photodissociation of NH_3 2—43198
laser, 3371 Å, with modified Blumlein excitation method 2—63331
laser, coaxial superradiant light source, emission props. at low repetition freq. 2—79203
laser, high power 2—59163
laser, pulsed molecular, wavelength meas. at low temp. 2—49370
laser, pumped by intense electron beam 2—73569
laser, transversely excited, spontaneous self-mode locking at 1.048 μm 2—73568
laser pulses, 337 nm, coherence props. and saturation broadening 2—73570
lasers, TEA, u.v., applic. to pulsed Raman spectroscopy of atmos. pollutants 2—42025
Lewis Rayleigh afterglow, excitation of Al and Cu atoms 2—77011
liquefied, maximum coefficient of heat transfer 2—83788
liquid, acoustic cavitation at 10 kHz 2—56464
liquid, acoustic nonlinearities parameters, temp. depend. 2—56501
liquid, cooling system for solid state lasers 2—63339
liquid, effective stimulated scatt. in u.v. and gain dispersion in 1.06-0.26 band 2—46956
liquid, film, boiling, heat transfer in plug stage, expt. 2—56546
liquid, level regulator 2—55328
liquid, stimulated thermal, Raman and Mandelstam-Brillouin scattering of light 2—46963
liquid, v.p. rel. to surface tension and surface curvature 2—46943
luminescence decay time, excited by α-particles 2—50057
microwave discharge, pink afterglow, vibrational relaxation 2—53255
microwave discharge, plasma sampling diagnostics 2—60258
mobility of K^+ in nitrogen, effect of clustering 2—67688

Nitrogen continued
molecular beam, produced by multichannel source, speed distrib. meas. 2—50018
molecular beam, scatt. from W surface 2—47084
molecular clusters, model for electron impact ionization cross section including energy losses inside cluster 2—80150
molecular collisions, vibrational transition probabilities, temp. dependence below 300K 2—60117
molecular collisions with Ar and Kr, Lennard-Jones potentials determ. 2—56272
molecule, $B^3\Pi g$ vibratory state conc., reabsorption obs. 2—70715
molecule, collisions with H atoms, electron loss cross sections 2—64216
molecule, core excited resonances, electron transmission spectroscopic investigation 2—46547
molecule, elastic electron scatt. and excitation of first vibr. level 2—77161
molecule, elastic electron scatt. and nonresonant vibr. excitation 2—77162
molecule, elastic scatt. of electrons, ang. distrib. 2—67494
molecule, electron impact excitation, emission cross section for second positive system bands 2—46564
molecule, energy levels, analytic independent particle model 2—73254
molecule, excitation of $C^3\pi_u$ level by electron swarm 2—60019
molecule, excited states, Rydberg and valence shell character as functions of internuclear distance 2—50056
molecule, minimal basis set LCGO calcs. 2—79989
molecule, MO correlation diagram 2—50055
molecule, reactive collision with C^+ at 3 to 100 eV, calculated cross sections for mass transfer, molecular and dissociative charge exchange reactions 2—48322
molecule, relative populations of $C^3\Pi_u$ and $B^2\Sigma_u{}^+$ states 2—80121
molecule, removal of core orbitals in valence only orbital calculation 2—49993
molecule, translational spectra due to overlap moments induced by collisions with He 2—50129
molecule, tunable Raman, excitation and vibr. relax. 2—53023
molecule, vibration to vibration energy transfer in N_2-CO 2—67489
molecule, vibrational matrix elements of quadrupole moment functions 2—64129
molecule, $X^1\Sigma_g{}^+$, v=0 state, energetic electron collisions, departure of $N_2{}^+(B_2\Sigma_u{}^+ m\ v'=2$ and 3) vibrational populations from Franck-Condon predictions 2—50058
molecules, quenching of Na D-doublet in flames of 1500-2500 K, temp. dependence of cross sections 2—46454
$10N_2+5O_2$+ propane mixtures shock and detonation speeds 2—83647
neutron radioactivation analysis in vivo of Ca, P, N and Cl in rat's organism 2—54575
nonequilibrium dissociation, effects on blunt body flows 2—77361
nuclei, geomagnetically trapped 2—65933
Pasadena smog, chemical states, photoelectron spectroscopy obs. 2—51602
photo-ion drift vel., diffusion coeffs. and temps. 2—64339
photoionization, by extreme u.v. radiation of laser produced plasma 2—53242
plasma, elec. field effects on rot. and vibr. temps. and excited level populations 2—74348
plasma, electrical and theraml conductivities 2—56335
plasma, h.p., spectra intensity, equil. radiation 2—60248
plasma, stationary microwave discharge at atmos. pressure 2—64293
plasma, thermal, collision cross section for momentum transfer 2—50194
plasma, thermal cond., 5000-18000 K 2—74350
pulsed discharge production in visible range, use for laser pumping 2—69890
quantitive det. in various matrices using nuclear track technique 2—48364
rotational temp. in rarefied supersonic flow in glowing-discharge 2—60311
rotational temp. meas. using Raman spectroscopy 2—46857
Scott thermomagnetic torque, temp. dependence 2—46861
solar overabundance, accelerated by solar flares 2—76001
solid, librational anharmonicity 2—47733
solid, Mossbauer effect of ^{57}Fe and ^{119}Sn, isomer shift obs. 2—48148
solid, n.q.r., slow beats in spin echo envelope 2—54518
spark breakdown at high pressure 2—71043
superradiant gas laser, field emission electron beam emission 2—42024
surface area meas. using N adsorption and Harkins and Jura isotherm 2—58686
temporal growth of ionization in long uniform field gaps 2—71029
thermal cond., 800-2000K meas. 2—71112
thermosphere, mass spectrometry, O/N_2 ratio 2—65824
thermospheric, longitudinal variations in density indicating magnetic control of polar heat input 2—65827
Townsend first ionization coeff. at low values of E/p 2—74405
Venus atmosphere, Venera entry probes and Mariner flyby 2—69164
vibrational energy transfer to CO_2 in thermosphere 2—58029
vibrational excitation electron energy transfer rates 2—72865
vibrationally excited, high velocity mixing with CO_2 2—83661
viscosity and second virial coeff., m-6-8 pot. analysis 2—77370
Ar-N binary mixtures, Percus-Yevick theory of radial distribution fns., thermodynamic props. and vapour-liquid equilibrium 2—67552
Ar-N_2 collision, comparison of generalized phase shift with classical trajectory calcs. of rotational inelasticity 2—43032
Ar-N_2 mixtures, heteronuclear associative ionization, formation of $ArN_2{}^+$ following 30 eV electron impact 2—51430
Ar-N_2 mixtures, u.s. absorpt., kinetic interpret. 2—71116
Ar-N_2 plasma in low power MHD generator, spectroscopic temp. detn. 2—46716
Ar-N_2 system, rot. relax. time, GPS calc. 2—77164
Ar-N_2 system, rot. relax. time, classical trajectory calcs. 2—77165
CO_2-N_2-H_2O arc-driven supersonic laser operating in gas-dynamic mode, numerical analysis 2—49359
CO_2-N_2 collisions, line broadening of CO_2 using laser source spectroscopy, application of Anderson Tsao and Curnutte theory 2—79993

Nitrogen continued

- CO_2-N_2 mixing laser, CW gasdynamic thermally excited and selectively pumped 2−63322
- CO_2 diffusion laser, interaction kinetics of diffusion mixing of CO_2 and N_2 2−73565
- CO_2 impurity in carbon dioxide isobaric sp. ht. at supercritical pressures, flow-type adiabatic calorimetry 2−83712
- $CO_2 + N_2 + He$, active medium in tuned prismatic resonator, selective properties 2−52411
- $C^+ + N_2$, K vacancy production probability depend. on relative Z numbers 2−74304
- $GaAs_{1-x}P_x$:N, photoluminescence, spontaneous and stimulated, from N A-line and NN pair, transitions 2−81414
- GaAsP(N), diode, light emitting, electrolum., N doping effects 2−81411
- GaP:N, localized vibr. modes due to N isotopes, i.r. absorp. obs. 2−68639
- GaP:N, Zeeman effect on bound exciton-complex 2−61693
- GaP:N(Bi), exciton binding to impurities, uniaxial stress effects 2−75108
- p-GaP(N), minority carrier lifetime, luminesc. decay obs. 2−48221
- $H_2/O_2/N_2$ flames, radical recomb. reactions, HO_2 participation 2−65373
- $H_2/O_2/N_2$ flames, with Cr and K additives, electron attachment and negative ion form. 2−72555
- $H_2/O_2/N_2$ mixtures, self-inflammation rates 2−81488
- H_2-N_2 and D_2-N_2 systems, conc. depend. of binary diffusion coeffs., 300K 2−64399
- H(2s)-N_2 charge-changing collisions, 20-120 keV, meas. of absolute cross sections 2−70638
- He-N mixture, decaying plasma, collision processes 2−50189
- N_2:CO_2:H_2O c.w. gas dynamic laser, unstable resonator calculations 2−82483
- N_2/O abundance ratio in thermosphere rel. to density- temperature phase delay 2−65816
- N_2-Ar-Hg discharge, electrodeless, r.f., electrical characteristics 2−71014
- N_2-Ar, rotational excitation of rigid rotor, classical results 2−50125
- N_2-Ar gas mixture, vibrational relaxation rate in nozzle flow 2−80142
- N_2-Ar mixture, viscosity, 25 to 500°C 2−80419
- N_2-CO_2-He deexcited plasmà, quantitative emission spectroscopy 2−79206
- N_2-CO transfer laser, low temp., energy exchange processes 2−69924
- N_2-CO_2 system, vibr. energy transfer, shock tube study 2−77166
- N_2-CO_2-^3He laser, high press., preionized in a reactor, performance 2−69916
- N_2-He-CO_2 TEA laser, double discharge trigger circuit 2−79199
- N_2-He-O_2-CO laser, CW operation in some CO lines below 5.0 μ 2−45726
- N_2-Hg two-phase system, propagation of pressure wave 2−71148
- N_2-Kr mixture, viscosity, 25 to 500°C 2−80419
- N_2-Na vibrational relaxation times in rapid expansion interpretation of Na line-reversal meas. 2−53102
- N_2-Ne mixtures, viscosity and binary diffusion coeff. meas. in temp. range 25 to 700°C 2−50278
- N_2-O_2 mixtures, ionization behind shock waves 2−77302
- N_2-methane mixture, cathode-directed streamer, secondary avalanche development 2−60298
- N, atmospheric, content variations at 100-250 km height, rel. to solar activity 2−48528
- N discharge, high-current pulsed, dependence on initial pressure and current 2−56387
- N discharge, motion of ionization front in microwave e.m. field 2−60238
- N I and N_2 lines in auroral u.v. spectrum 2−65897
- N III, electron impact ionization, calc. for $1s^22s^22p$ configuration 2−46451
- N III in O star spectra, spectrophotometric luminosity criteria 2−58290
- N III $\lambda\lambda$4640, 4097 emission lines in Of stars 2−55036
- N IV, V, VI, VII, atomic energy levels and multiplet tables 2−46434
- N VI in D plasma, meas. of depopulation of $2^3P_{0,1,2}$ triplet levels by electron collisions 2−79961
- N^+ ion beams, det. of metastable state population 2−59114
- N_2, anharmonic oscillator, time-dependent solutions for de-excitation rates 2−42913
- N_2, application of Auger electron spectroscopy to structure determ. 2−42756
- N_2, autoionising levels, converging to $A^2\Pi_u$ and $B^2\Sigma_u{}^+$ limits 2−83403
- N_2, bubble formation and removal in glass melts 2−56551
- N_2, c_n $^1\Pi_u$ and c_n' $^1\Sigma_u{}^+$ Rydberg states, high resolution studies 2−64145
- N_2, calc. on ground state using various methods for soln. of SCF-LCAO-Mo eqns. 2−64099
- N_2, distribution function at high vibrational temp. in electron beam fluorescence technique 2−56188
- N_2, electron density matrix, cusp conditions 2−42858
- N_2, electron impact, dissociative excitation of OI ($^5S^0$) 2−56106
- N_2, electron impact excitation spectra by ion cyclotron resonance mass spectrometer 2−80135
- N_2, electron impact excitation of electronic states 2−64148
- N_2, Gaydon- Herman green system, rot. analysis 2−64146
- N_2, in high-frequency $Ar + N_2$ discharge, effective cross sections for excitation of $C^3\Pi u$ state 2−43041
- N_2, new Rydberg bands in visible and identification of lowest $^1\Sigma_g{}^+$ Rydberg state 2−42915
- N_2, outflow under 4-12 kbar press. through small aperture nozzle 2−74474
- N_2, rate constants for deactivation of $B^3\Pi_g$ and $A'^1\Sigma_u{}^-$ states 2−80125
- N_2, reaction rates with U and U^+ 2−68766
- α-N_2, solid, isotopic mixture, n.q.r. freq. and linear shape 2−65356
- N_2, solid, model for lattice vibrs. 2−43959
- N_2, solid and liq., charge transport processes 2−77820
- N_2, transistors to and predissociation of $C^2\Sigma_u{}^+$ state 2−80006
- N_2, vibration-rotation interaction in calculated band strengths 2−46571

Nitrogen continued

- N_2, vibrational excitation by electron impact in 15-35 eV region, meas. of angular distrib. 2−56189
- N_2, vibrational excitation by e^-, cross section calc. 2−70817
- N_2, vibrational Raman scattering 2−46566
- N_2, vibrationally excited, collisions with Na atoms, excitation of D-line radiation 2−70627
- N_2, vibrationally excited, reaction with O^+. cross section for formation of NO^+ 2−54530
- N_2 and N^+ ion concentrations in ionospheric F_2-layer 2−72895
- N_2 collisional quenching of O(^{1}D) and vibrational relaxation, curve-crossing model 2−67416
- N_2 collisions with He(2s), meas. of electron capture cross sections 2−56123
- N_2 discharge, instationary, at high overvoltages 2−71005
- N_2 electron scattering, test of Massey's method for calc. of static potential 2−70822
- N_2 excitation by low energy proton bombardment rel. to atmospheric gases 2−84792
- N_2 gas, kinetic theory of thermomagnetic torque 2−50271
- N_2 i.r. emission spectra in auroral excitation conditions 2−84873
- N_2 ions, cross sections, prod. from N_2 by 16 to 600 eV electrons 2−83404
- α-N_2 librational modes, application of quantum mechanical lattice dynamics formalism 2−71709
- N_2 low-energy electron scattering, calc. using pseudo-potential method, determ. of cross sections 2−70819
- N_2 luminescence, energy dependence of collisional deactivation cross section 2−46646
- N_2 photoelectron spectra at 304 Å 2−80058
- N_2 photoionization by soft X-rays, meas. of total and relative abundances of thermal energy ions and dissociation cross sections 2−80024
- N_2 plasma, distribution function for free electrons 2−64263
- N_2 positive and $N_2{}^+$ band systems rel. to energy spectra of auroral electrons 2−54884
- N_2 pulsed laser with high repetition rate 2−59162
- N_2 Raman scattering cross sections and depolarization ratio 2−53026
- N_2 rotational Raman spectra, use of fixed path length etalon Fabry-Perot interferometer for meas. of wavelength of individual lines 2−74250
- N_2 SCF-LCAO-MO wave function density-distribution analysis 2−80052
- N_2 Slater basis set difference density maps, minimum and expanded, comparison 2−77088
- N_2 solid, emission spectra of trapped atoms, obs. of vibron- and phonon-induced dipole radiation of forbidden lines 2−78096
- N_2 spectrum in i.r. range 6500-11500 Angstroms rel. to auroral spectra 2−84874
- $N_2{}^+$, anomalous excitation in seeded Ar free plasma jet 2−42916
- $N_2{}^+$, emission produced by A→X transitions, meas. of lifetimes, cross section for excitation of Meinel bands 2−46563
- $N_2{}^+$, flux in higher atm. at middle latitudes 2−48526
- $N_2{}^+$, mechanism of electron-ion dissociative recombination in gas discharge 2−74272
- $N_2{}^+$, produced in slow electron ionization of N_2, rotational level distrib. 2−80053
- $N_2{}^+$ 4278Å intensity in auroral energy spectra rel. to precipitating electrons 2−65914
- $N_2{}^+$ radiative lifetimes of a A^2 PI_u vibr. levels 2−83257
- $N_2{}^+$ reactions, with H_2, CO_2, CH_4, N_2O, SO_2, O_2, C_2H_2, COS, NO and rate constants 2−51434
- $N_3{}^{2-}$ and $N_3{}^0$, molecular orbital calc. of isotropic hyperfine interactions 2−64144
- $N_4{}^+$ form. in swarm expts. and gas discharges 2−67685
- $N_4{}^+$ ions frequency in positive column of glow discharge 2−71023
- $N_2(A^3\Sigma_u{}^+)$ metastable, production of $N_2(C^3\Pi_u)$ and $N_2(C'^3\Pi_u)$ by mutual collisions 2−50132
- $N_2{}^+B^2\Sigma$ products from Ne^+-N_2 collisions, vibrational distribution 2−56273
- NI 5200 Å airglow observations at Arecibo using Hadamard photometer 2−72834
- NI allowed transitions in airglow and aurora 2−48547
- NI emission of 5200 Å in auroral arc event 2−72839
- NII, mean lives of excited levels, beam foil study 2−64020
- NII 6584 Angstroms forbidden line profile of η Carinae nebulae from high interferometric resolution observations 2−55024
- ^{13}N, in vivo metabolism meas. 2−69388
- ^{13}N, production and use in metabolic studies 2−69389
- $^{13}N_2$, use in clinical research 2−69387
- $^{14}N^+$ ion source, collimating system for mass spectrometer, with distributed ionization region 2−69883
- $N_2 + Ar$ system, three-body recomb. and dissoc., Monte Carlo trajectory calcs. 2−64108
- N + CN + organic gas reaction, C atoms obs. 2−61767
- N + NO, production of O(^{1}D) 2−51437
- $N_2 + O_2$ glow discharge, electron energy distrib., new probe technique 2−64348
- $N_2 + O_2$(HCl) collisions, vibr.-vibr. energy exchange 2−83407
- N_2 + methylene chloride chemiluminescent reaction, intensity variations of CN bands with temp. 2−83240
- $N_2{}^*$, vibrationally excited, quenching by O, determ. of rate coeff. 2−83400
- in Nb-Zr alloys, internal friction peak obs. 2−60849
- in Nb, cold-worked or irrad., role in recovery 2−47404
- inNb, Snoek peak, grain size effect 2−50736
- Ne-N mixture, decaying plasma, collision processes 2−50189
- $Ne^+ + N_2$, K vacancy production, depend on relative Z of colliding atoms 2−74304
- O ions, radiative lifetimes for u.v. transitions by pulse decay method 2−46413
- $O^+ + N_2 \rightarrow NO^+ + N$, ab initio calculation of potential energy curves 2−44468
- in Ta, interstitial effects on asymmetry of yield stress 2−74844

Nitrogen compounds

- — 2−68774
- acid hydrates, hydronium ion struct. and dynamics 2−84601
- molecules, free electron pairs in CNDO/2 wave functions 2−59981
- nitrate glasses, positron lifetimes, temp. depend., phase transitions influence 2−47772

Nitrogen compounds continued
nitrides, noncrystalline film prep. by sputtering 2−47114
NO absorption spectra in region 1890-1835 cm^{-1} with tunable spin flip Raman source 2−42264
$Ba+NO_2 \rightarrow BaO+NO$ crossed beam reactions, primitive product ang. distribs. 2−81493
CO_2-N_2O mixtures, competitive photolysis, 1633 Å 2−65389
Fe-N alloy, quench ageing and reversion 2−56903
Fe-V-N system, abnormal Snoek peak 2−47482
HNO_2, electronic struct., cis and trans isomer obs. 2−56172
He-N_2O system, binary diffusion coeffs. conc. depend. 2−67737
Li-B-N system, phase equilib., rel. to cubic BN growth 2−50970
NBr, $^1\Sigma^+$-$^3\Sigma^-$ system, Franck-Condon factors 2−53024
NCN_3, microwave spectrum, structure and dipole moment 2−60014
NCNNN, microwave spectrum rot. analysis, electronic struct., dipole moments 2−64142
NCl_2 in low temp. matrices, anisotropic e.s.r. spectra analysis 2−72571
NCl_3, normal coordinate analysis, vibrational frequencies and force constants calc. 2−46567
NF_2, calc. of g values 2−50066
NF_3 ambiguities in harmonic force fields 2−50063
NF_2SO_3F, vibration spectra, C_s symmetry 2−42917
NH, excited states, Rydberg and valence shell character as functions of internuclear distance 2−50056
NH_2-, evidence for hindered rotation from laser Raman spectra of solid and molten $NaNH_2$ 2−60022
NH_2, structure of transition dipole moment 2−80025
NH_2^+, low-lying electronic states, nonempirical CI study 2−53025
$NH_2(A^2A_1)$ produced by photolysis, collisional deactivation 2−50060
NH_2CN, microwave spectra, structural parameters 2−77066
$(NH_3)_2CS$ behaviour in electrolytic refining of Cu 2−75389
$(N_2H_5)_3CrF_6$, structure determination from X-ray 3-D film data 2−56661
NH_2OH-H_2O mixed dimer, LCAO-MO-SCF calcs. of equilibrium structures and energies 2−67491
$(NH_2OH)_2$ dimer, LCAO-MO-SCF calcs. of equilibrium structures and energies 2−67491
NNO, elec. dipole moment, iterative extended Huckel theroy calc. 2−56187
NO/O gas phase chemiluminescence intensity standard, absolute quantum yields 2−65372
N_2O-NH_3 population inversion in exothermal decomposition reactions on shock 2−73553
NO_2-N_2O_4-N_2-Al_2O_3, powder reactive nozzle flow 2−83660
$N^{16}O$-$N^{17}O$-$N^{18}O$ gaseous mixture, e.p.r. spectra 2−80031
NO-$\gamma(A^2\Sigma$-$X^2\Pi)$ system, oscillator strength of (0,0) band 2−50062
NO_{-3}, matrix-isolated, i.r. spectra, 4000-400 cm^{-1} region 2−67492
NO, atmospheric, content variations at 100-250 km height, rel. to solar activity 2−48528
NO, concentration determ. in water saturated N_2 using Raman effect 2−70714
NO, core excited resonances, electron transmission spectroscopic investigation 2−46547
NO, D-region, theoretical models, ion pair production 2−78400
NO, electron affinity determ. by laser photodetachment and photoelectron spectrometry on NO^- 2−53027
NO, high resolution i.r. spectroscopy using tunable PbSSe laser 2−42922
NO, i.r. absorption coeffs. 2−56156
NO, ionization of σ*2s orbital, configuration interaction effects on spin-split states arising from inner orbital ionization 2−74271
NO, ionosphere D-region, eddy diffusion coefficient 2−65970
NO, Martian atmosphere, minor constituents, Mariner borne i.r. spectrometer 2−69156
NO, mesospheric concentration during PCA 2−65666
NO, NO^+ configuration interaction studies, comparison with photoelectron spectra 2−83254
NO, obs. of Λ-doubling and Zeeman splitting in fundamental i.r. absorption band 2−46561
NO, Penning ionization by $Ar(^3P_1)$ 2−53041
NO, photoionization of small amounts in O_2, low temp. meas. of three-body electron attachment coeff. in O_2 2−53247
NO, positron annhilation 2−77070
NO atmospheric pollution in Los Angeles 2−57944
NO bonds in X_3NO compounds, CNDO/2 calculations 2−42866
NO gas, meas. of thermomagnetic force on thin disc in 30-35°C range 2−43264
NO molecule, Franck-Condon factors of Morse oscillator when $\Delta S>0$ 2−60017
NO molecule, rotation-electronic spectrum 2−64166
NO photoionization by soft X-rays, meas. of total and relative abundances of thermal energy ions and dissociation cross sections 2−80024
NO pollution monitor, laser device based on Zeeman modulation of absorption 2−61826
NO Raman scattering cross sections and depolarization ratio 2−53026
NO $X^2\Pi$, rapid rate process meas. by kinetic spectroscopy during photolysis flash vibrational relaxation 2−54553
NO^-, laser photodetachment and photoelectron spectrometry, determ. of molecular constants and electron affinity of NO 2−53027
NO^+ formation by reaction of O^+ and vibrationally excited N_2 in crossed molecular beams 2−54530
NO^+ ion concentrations in ionospheric F_2-layer 2−72895
NO_2-, NO_3-, reactions with HCl and HBr, rate const. meas. in flowing afterglow system 2−61775
NO_2, collisionally induced excitation, radiative lifetime 2−80015
NO_2, dynamics of electronic states excited by tunable dye laser 2−50059
NO_2, i.r. absorption coeffs. 2−56156
NO_2, interaction with Sn-Pb alloy, corrosion, humidity effects 2−65382
NO_2, laser magnetic resonance at 311 and 337 μm 2−42912
NO_2, light extinction, rel. to light scatt. by Los Angeles smog 2−51625
NO_2, Martian atmosphere, minor constituents, Mariner borne i.r. spectrometer 2−69156
NO_2, photodissociation by pulsed laser light at 6943A 2−44490

Nitrogen compounds continued
NO_2, photolysis at high pressure, photodissociation rates 2−80010
NO_2, positron annihilation 2−77070
NO_2, Raman, resonance Raman and fluorescence spectra 2−42262
NO_2, role in oxidation of SO_2, rel. to photolysis of atmospheric gaseous impurities 2−51586
NO_2, search for telluric lines in spectrum of star α Virginis (Spica) 2−51601
NO_2 aerosol, atmospheric, characterization and monitoring by fluorescence 2−81692
NO_2 and aerosol content of atmosphere rel. to brown colour of atmospheric haze 2−62264
NO_2 atmospheric pollution in Los Angeles 2−57944
NO_2 concentrations, remote sensing of ambient air quality and gaseous pollutant flow 2−84870
$(NO)_2$ dimer, low temperature vibrational and electronic bands 2−67495
NO_2 mol., inelastic photon scatt., of N_2, atmospheric pollutant monitoring 2−67496
NO_2 photometric measurements in atmosphere using Fabry-Perot filters 2−54827
NO_2^-, in alkali halides, harmonic band parameters, high temp. 2−54410
NO_2^-, vibr. absorpt. spectrum in CsCl(Br)(I) and CuCl 2−77769
NO_2^{2-}, calc. of g values 2−50066
NO_3^-, in alkali halides, harmonic band parameters, high temp. 2−54410
NO_3^-, vibr. absorpt. spectrum in CsCl(Br)(I) and CuCl 2−77769
NO_3^- in complex structs. with bridge coord., plane vibr. freqs. 2−70690
N_2O, adsorption on W, binding states, LEED obs. 2−64581
N_2O, calc. of rotational half-widths for air broadened absorption lines using Anderson-Tsao-Curnutte theory 2−53105
N_2O, collisional broadening of absorption lines 2−80056
N_2O, electrical breakdown at high voltages, mechanisms 2−71038
N_2O, excited on ν_3, vibr. energy transfer to CO and N_2, temp. depend. 2−60108
N_2O, forbidden character of 2000 Å transitions 2−56186
N_2O, general quartic force field, calc. using Parr-Brown anharmonic potential function 2−52999
N_2O, intermol. interaction pot., with N_2O, N_2, He, Ne, Ar, Kr and Xe 2−46643
N_2O, line parameters near 4.5 μm determ. from absorption spectra with Fabry-Perot interferometer 2−46568
N_2O, liquid/vapour equilibria of binary systems N_2O/N_2, N_2O/O_2, N_2O/methane 2−50402
N_2O, Martian atmosphere, minor constituents, Mariner borne i.r. spectrometer 2−69156
N_2O, matrix isolated i.r. spectrum, temp. depend. 2−74269
N_2O, parameter detn. of nonvalence interaction curve at 0°K 2−71440
N_2O, thermal relaxation of vibration, period determ. by impact tube method 2−83398
N_2O, vibration bands when absorbed in cavities of zeolite NaA 2−46565
N_2O band intensities and half-width of N-broadened lines rotational lines in ν_3 fundamental meas. near 4.5 μ 2−42923
N_2O compressed gas, meas. of microwave absorption at 9.75 GHz using resonant cavity technique 2−53339
N_2O decomposition, kinetic obs. using i.r. technique 2−82562
N_2O laser, cw operation assignment of laser lines using $^{14}NH_3$ absorption line 2−42026
N_2O molecular beam, reactive scatt. from clean and C covered Pt(100) surface 2−50547
N_2O optical absorption and electron scattering spectra, obs. of resonant phenomena in B region at 6.8 eV 2−77061
N_2O unimolecular decomposition, study using wave-crossing model 2−67416
N_2O_4, dissociated, stability of superheated liquid phase 2−47044
N_2O_4, dissociated, surface metastable states 2−47041
N_2O_4, liq., ioniz. enthalpy determ. from cond. and permittivity 2−84612
N_2O_4, liquid, convective heat exchange at precritical and supercritical pressures 2−46947
N_2O_4 nucleate boiling, criterial equation 2−45586
$NOCL+H_2$ reaction, vibr. energy distrib. of HCl mols. 2−53005
N_2O+CO_2, shock heated mixtures, vibrational energy transfer processes 2−53100
N_2O+CO_2 collisions, vibr.-translation and vibr.-vibr. exchanges 2−43034
$NO_2^- + Cl_2 \rightarrow Cl_2^- + NO_2$, thermal energy rate consts. 2−68774
$NO^+ + H_2O$ reactions in photoioniz. mass spectrometer 2−68775
NO + N, production of $O(^1D)$ 2−51437
$N_2O^+ + N_2O \rightarrow NO^+N + N_2O$, $N_2O^+ + N_2O \rightarrow O^+ + N_2 + N_2O$, mass spectrometric study 2−51436
$NO + O \rightarrow NO_2 + h\nu$, air-afterglow reaction mechanism 2−68773
$NO^+ + O^-$, mutual neutralization rates, ionospheric D-region 2−65969
$N_2O + e^- \rightarrow N_2 + O^-$, regeneration of electrons, and attachment rate constant 2−74270
NS, microwave spectra, transitions 2−76542
N_4S_4, electron delocalization, CNDO/2 calculation 2−77089
NSF, photoelectron spectrum 2−42946
$N_4S_4F_4$, electron delocalization, CNDO/2 calculation 2−77089
Nb-Mo-N system, α solid soln., thermodynamic functions 2−43856
alpha-Nb-Mo-N ternary solid solution, equilibrium N concentration and thermodynamic behaviour 2−60983
Nb-N alloy, nitride precip., prismatic loop generation 2−53994
No, i.r. vibr.-rot. absorpt. spectrum, nucl. hyperfine splitting 2−64143
$OH + NO_2 + Ar \rightarrow HNO_3 + Ar$ reaction rate const. determ. by u.v. fluorescent scatt. 2−81491
$SH^- + NO_2 \rightarrow NO_2^- + SH$, thermal energy rate consts. 2−68774
$S^- + NO_2 \rightarrow NO_2^- + S$, thermal energy rate consts. 2−68774
Ti-Zr-Al-N film, sputtered, struct., elec. resist. props 2−47130
UO_2-C-N_2 reaction kinetics, 1695°C, carbonitride form. 2−54537
V-N system, V_3N phase, electron microscope obs. 2−50978

ammonia
adsorption, activational, on synthetic Na-containing adsorbants, temp. and press. depend. 2−47160

Nitrogen compounds continued
ammonia continued
decomposition behind reflected shock waves, 2000-4500K, obs. of i.r. emission 2−48324
dielectric permeability of gas, static, variation in strong resonance field 2−77369
dipole moment, temp. depend. with allowance for internal motion 2−77036
enthalpies of solution and formation by direct solution calorimetry 2−77422
enthalpy of ionization of aqueous NH_3 by solution calorimetry 2−77423
hypersensitized IV-N photographic plates, photometric properties 2−82597
intramolecular inversion, model potential 2−42910
inversion spectra, rotational structure 2−80033
i.r. absorption in spectral band 0.8-2.5 microns 2−46562
i.r. spectrum, use for calibrating spectrometers 2−73681
i.r. vibration-rotation spectra of $^{14}NH_3$ and $^{15}NH_3$, 2-photon spectroscopy 2−42920
Jovian atmosphere absorption bands, obs. using Galilean satellite eclipse obs. 2−58490
Jupiter, variations over disk, spectrophotometric obs. at 1.5μ window 2−75876
Jupiter's atmosphere, aerosol layer of solid NH_3 rel. to optical properties and structure 2−58485
Martian atmosphere, minor constituents, Mariner borne i.r. spectrometer 2−69156
metal (K,Li,Na, Ca)-ammonia relaxation times and Overhauser enhancements for protons obs. 2−46988
metal-NHz solns., transport props. in the non-metal-metal transition range 2−80484
microwave line, transient Stark effects 2−42911
microwave spectrum, press. induced shifts of $(J,K)=(12,12)$ inversion line 2−50061
molecular vibr. levels population meas. method 2−79972
molecule, ab-initio bond-orbital calcs. 2−53018
molecule, CI expansion, large-scale method for coeffs. calc. 2−67451
molecule, correl. energies by united-atom many-body perturbation procedure 2−67480
molecule, correlation energy calc. using linked cluster many body perturbation theory 2−67484
molecule, multi-config. self-consistent field wavefunction 2−67490
molecule, nuclear quadrupole moment of ^{14}N, vibrational and other corrections 2−60015
molecules, intensities of i.r. spectra deduced from dipole moment derivatives calc. using Fock-Roothaan wave function 2−42921
molecules, two-step photodissociation and excitation by laser irrad. 2−72572
Raman spectra of polycrysts., metastable phase obs., lattice and internal modes 2−72370
self induced transparency at 10 μ extrapolation to CO_2 laser radiation atmospheric propagation 2−43268
solid, self-diffusion, rotating frame relaxation time 2−47451
spectral lines, collision-broadened by hydrogen, shapes and widths 2−67493
spin-rotation interaction, nucl. spin relax. obs. 2−56200
substituted ions, ^{14}N n.q.r. studies rel. to bonding 2−42914
transient-nutation effects in time- resolved i.r.-microwave double resonance 2−64147
Uranus, atmosphere model and NH_3 cloud layer 2−78558
$AgBrI:Br^-$, NH_3, cryst. morphology rel. to impurities 2−80648
CF_3+NH_3, Arrhenius parameters, kinetic isotope effects and tunneling corrections 2−81496
CH_3+NH_3, Arrhenius parameters, kinetic isotope effects and tunneling corrections 2−81496
$C^+ + NH_3$ K vacancy production probability depend. on relative Z numbers 2−74304
Cs-NH_3 solutions, velocity of 10 MHz waves on function of temp. and metal concentration, structural changes 2−43352
Li solutions, magnetic susceptibility in 1.5-296 K range 2−43389
ND_3, Raman spectra of polycrysts., metastable phase obs., lattice and internal modes 2−72370
NH_3-BF_3 complex, valence electron density 2−60016
NH_3-ND_3 mixtures, liq., Raman spectra, vibr. freqs. assignment 2−77439
NH_3-N_2O, population inversion in exothermal decomposition reactions on shock 2−73553
NH_3-Rb solutions, electrodeless method of det. conductivity 2−71226
NH_3, clinical feasibility of use in myocardial imaging 2−45030
NH_3, configuration diagram of solvated electron 2−71225
NH_3, force consts., dipole moment derivatives by Hartree-Fock calculations 2−80029
NH_3 photodissociation, separation of N and H isotopes 2−43198
$NH_3{}^+$, Gaussian wavefunctions 2−42994
$NH_3 + Cd(^3P_0) \rightarrow CdNH_3{}^*$ reaction kinetics, rate constant, excimer formation 2−81514
$NH_3 + HCl$ system, potential energy curves for proton motion, extended Huckel calculation 2−43040
NH_3...H-OH mol., hydrogen bonding 2−67475
$^{14}NH_3$, $^{15}NH_3$, inverse Lamb dip for i.r.-microwave two photon transitions 2−60024
$^{14}NH_3$ and $^{15}NH_3$ mol. beam h.f.s. data interpret. 2−83258
$^{15}NH_3$, $^{15}ND_3$, liquid, ^{15}N spin-lattice relaxation meas. 2−50371
Na/NH_3 frozen solution, supercond., libron induced interelectron interaction calc. 2−64941
in Ne matrix, i.r. spectra, fine struct., rot. and inversion obs. 2−72340
$Ne^+ + WH_3$ K vacancy production, depend on relative Z of colliding atoms 2−74304

ammonium compounds
alkali metal ammonia solns., solvation model 2−84614
carbamate, solid, i.r. spectra 2−84527
halides, spin-lattice relaxation of nuclear dipolar energy through dipole-dipole interaction 2−65191
metal-ammonia solutions, Hall coeff. and elec. cond. 2−46984

Nitrogen compounds continued
ammonium compounds continued
NH_4HSO_4, room temp. non-ferroelec. phase, structure; applic. of constrained refinement techniques 2−67999
oxalates, cryst. growth from aq. soln. 2−60714
p.m.r. lineshapes of ions undergoing quantum mech. tunnelling in solid state 2−81470
sodium tartrate, ferroelec. phase transition mechanism 2−81139
$Al_2(NH_4)_2(SO_4)_4.24H_2O$, cryst. growth 2−47202
$ND_4{}^+$ compounds, deuteron mag. reson., tunnelling effects 2−72512
$ND_4Al(SO_4)_2.12D_2O$, e.p.r. of Cr^{3+}, struct. phase transition obs. at 56K 2−84576
ND_4Br, two-phase region in lambda transition 2−44163
ND_4Cl, first order phase transition 2−84150
$(NH_4,RB)_2CuBr_4.2H_2O$, mag. interactions 2−65144
$(NH_4)_2,Cd_2(SO_4)_3$ ferroelec. phase transition temp. shift, permittivity, hydrostatic press. effects, 20-300K 2−77958
$NH_4Al(SO_4)_2:VO^{2+}$, polycrystalline, e.p.r. line shapes 2−61736
NH_4BF_4, cryst. struct. at 140K 2−60765
$(NH_4)_2BeF_4$-$(NH_4)_2SO_4$ concentration and temp. dependence of dielectric constant and spontaneous polarization 2−68471
$NH_4Br:Cu^{2+}$, e.p.r., covalency, core polarization 2−78154
NH_4Br, allotropic transform. kinetics 2−54008
NH_4Br, critical fluctuation enhanced Raman scatt. by phonons 2−43956
NH_4Br, l.f. soft vibrational modes under stress 2−71696
NH_4Br, order disorder transition, X-ray crit. scatt., obs. 2−47699
NH_4Br, phase transitions, Ising spin-phonon coupled system theory 2−47700
NH_4Br, two-phase region in lambda transition 2−44163
NH_4Br, X-ray diffr. pattern, diffuse rods 2−80893
$(NH_4)_2C_2O_4.H_2O$, meas of ratio of electroopt. const. to coeff. up to 20 MHz 2−72267
NH_4Cl-H_2O frozen solns., permittivity discontinuities at crit. pt. 2−53499
NH_4Cl, analysis of lattice vibrations in low-temp. ordered phase using rigid-molecule model 2−68219
NH_4Cl, dendritic growth under influence of electric fields 2−43486
NH_4Cl, ferromagnetic ordering mechanism 2−75215
NH_4Cl, low temp. spin relax. of hindered ions 2−84447
NH_4Cl, phase transitions, pseudospin and stochastic model description 2−43923
NH_4Cl, positron lifetimes, temp. depend., phase transitions influence 2−47772
NH_4Cl, proton spin-lattice relaxation and order-disorder transition 2−57401
NH_4Cl, spin-lattice relax. time of nucl. dipolar energy, temp. and orientation depend. 2−81314
NH_4Cl, system with disordered force constants, optical properties 2−43958
$NH_4Cl(Br)(I)$, ordered low temp. phases, cryst. field theory 2−74937
$NH_4Cl(I)$ aq. solns., elec. pots. generated on freezing at uniform rate, substrate effects 2−53495
NH_4ClO_4, a.c. elec. cond. 2−44155
NH_4ClO_4, $Ca(HClO_4)_2$ and metal mixture systems, rate of combustion 2−61784
NH_4ClO_4, proton transfer cond. 2−84361
NH_4ClO_4, solid, spin-rot. relax. for protons 2−54371
NH_4F, shock generation accompanying pressure-induced phase change, seismological implications 2−78268
NH_4F II, high pressure phase obtained at low temps., l.f. Raman spectrum 2−57360
$NH_4(^{57}Fe, Al)(SO_4)_2.12H_2O$, Mossbauer-electronic double resonance 2−57334
$(NH_4)_4Fe(CN)_6.H_2O$, ionic diffusion, Arrhenius activation energy, n.m.r. obs. 2−74814
β-$NH_4Fe(CrO_4)_2$, space group, lattice parameters 2−68000
$NH_4H_2AsO_4$ and $ND_4D_2AsO_4$, X-irradiated, identification of Slater configurations of $(AsO_4)^{4-}$ radical by ESR 2−81453
$NH_4H_2AsO_4$ antiferroelectric, EPR and ENDOR 2−68734
NH_4HCO_3, i.r. spectrum 2−84527
NH_4HF_2, neutron diffraction data refined, location of H, thermal motion and F-F distance 2−77087
$(NH_4)_2H_3IO_6$, antiferroelectric, n.m.r. level crossing expt. 2−61749
$(NH_4)_2HPO_4$, crystal structure by X-ray examination 2−56662
$NH_4H_2PO_4$, antiferroelectric, long-wavelength polarization fluctuations 2−78113
$NH_4H_2PO_4$, Pockels effect above 90°C 2−54381
$NH_4H_2PO_4$ parametric oscillator, pumped with tunable dye laser 2−42053
$NH_4H_2PO_4$ polarizers for lasers, modified Wallaston prism 2−42105
$NH_4H_2PO_4$ polishing, single lap apparatus 2−67893
NH_4HSO_4, γ-irrad., e.s.r. of $HNSO_3{}^-$ radical, ferroelec. transition mechanism, dielec. const. 2−84369
NH_4I-AgI compared to AgI-NaI in cloud seeding, hail suppression program 2−62194
NH_4I, p.m.r. intensity, nucl. spin value 2−84600
$(NH_4)_xK_{1-x}H_2PO_4$ epitaxial film, electro-optic waveguide 2−70058
$NH_4NH_2SO_3$, cryst. struct. 2−53671
NH_4NO_3, cryst. growth morphology at polymorphic transforms. 2−50945
NH_4NO_3, effect of deuteration on transition temperatures and energies between room temp. and melting point 2−50947
NH_4NO_3, phase IV, cryst. struct. 2−43584
NH_4NO_3, use in cloud seeding expt. 2−62208
NH_4NO_3 and ND_4NO_3, influence of sample listing on transition temps. of $II \rightarrow III$, $II \rightarrow IV$ and $IV \rightleftharpoons III$ transitions 2−50946
NH_4NO_3 phase II, permittivity measurements 2−65049
$5(NH_4)_2O.12WO_3.5H_2O$, polycrystalline, paramagnetic centres formed by γ irradiation 2−48349
NH_4PF_6, p.m.r. intensity, nucl. spin value 2−84600
$(NH_4)_3P_3O_9$, cryst. struct. and prep. 2−53668
$(NH_4)_2PO_3F.H_2O$, $(NH_4)_2PO_3F$ and NH_4LiPO_3F, space groups and lattice parameters 2−83951
$(NH_4)_2PO_3F.H_2O$, crystal structure from X-ray studies 2−56663
NH_4SCN, X-ray diffractometric refinement of struct. 2−71436
NH_4SH reflectivity studies rel. to structure of bodies in outer solar system 2−78525

Nitrogen compounds continued
ammonium compounds continued
$(NH_4)_2SO_4:VO^{2+}$ single crystal, ESR spectra 2−61731
$(NH_4)_2SO_4$, Brillouin spectra, elastic and photoelastic consts. 2−43665
$(NH_4)_2SO_4$, mascagnite, atmospheric aerosol constituent, optical consts. 2−57946
$(NH_4)_2SO_4$, paraelectric, ^{14}N quadrupole coupling 2−44456
$(NH_4)_2S_2O_8$, hindered rotation in crystals by neutron transmission meas. 2−50999
$(NH_4)_2SiF_6$, hindered rotation in crystals by neutron transmission meas. 2−50999
NH_4SnCl_3, proton relax. of ammonium ion undergoing hindered rot., cross correl. effect 2−84448
$(NH_4)_2SnCl_6$, low temp. spin relax. of hindered ions 2−84447
$(NH_4)_2U_2O_7$, precipitates, prep. of UO_2 pellets rel. to precip. conditions 2−80800
Na-NH_3, density of states, Mott g ratios, self consistence, significance in MNM transition 2−44033

Nobelium
No entries

Nobelium compounds
No entries

Noble gases *see Inert gases*

Noctilucent clouds *see Atmosphere/upper; Clouds*

Noise
analysis techniques, applic. to reactor problems 2−42684
boiling water reactor at Lingen, analysis of space dependent neutron flux density fluctuations by stochastic methods 2−79830
characteristics of FEU-86 photomultiplier 2−76461
computer generated holograms 2−82498
digital light deflectors characteristics 2−79388
distribution of optical receivers using avalanche photodiodes, laws governing 2−76529
Earth, structure beyond 20 secs., window for earthquakes 2−44551
electron micrographs reduction of noise by tilting a crystalline supporting film 2−59098
e.l.f., ionosphere, Q-type bursts, damping coefficients 2−78394
film grain, in holographic images, effect on memory performance 2−42140
geomagnetic, near L ~ 4, quiet-day power spectra 2−62384
hologram photoresists 2−49400
i.r. scanner, integrator, properties of output 2−76385
jet theory, using method of matched inner and outer expansions 2−77326
large quiescent collisionless h.f. discharge plasma, fluctuation level 2−56365
laser, quantum phase and quantum amplitude, above and below threshold 2−63314
laser microdensitometry of photographic film 2−59333
lasers, multimode oscillation buildup from quantum noise 2−63315
magnetic, in plasma sheet as meas. by Explorer 34 2−62325
model for video preamplifiers 2−66685
modulation, attenuation in n.m.r. spectrometer 2−76427
non-destructive testing of stressed materials, meas. of internal noise 2−60927
nuclear reactor noise anal., flash start technique 2−83084
nuclear reactors, monitoring for malfunctions 2−46394
optical, rate distortion fn., resolution 2−79306
optical coherent imaging, suppression 2−79307
in optical correlation effects 2−69963
optical heterodyne detection systems, S/N ratio 2−69951
photographic, photon fluctuations 2−73684
photographic quantum, rel. to granularity 2−73685
power reactor, determ. of dominant source 2−76918
pulse rate dependent, and counting losses in active processor with fast recovery 2−70303
reactor, means of failure detection in nuclear power reactors 2−79829
reactor noise analysis, statistical accuracy 2−70542
seismic, meas. in geothermal area 2−57499
seismic, short-period, phase velocity 2−44543
in seismic hydrophone arrays 2−44621
seismic noise reduction 2−61874
semiconductor laser, quantum noise, 80K and room temp. 2−45753
signal dependent, in optical transfer function meas. 2−79294
solar type III bursts, below 100 MHz, OGO 3 2−75964
thin phase holograms, noise effects of granularity 2−73610
transmission control and measurement in enclosed spaces 2−63135
white noise excitation of nonlinear structures 2−76347
γ-ray, meas. rel. to reactor parameter determination 2−49908
Ar discharge, temp. variation with mount style at 147 MHz 2−60304
acoustic
acoustic wave interaction with coherent light beam, phase fluctuations rel. to acoustic noise 2−73435
aero space vehicle, noise-induced structure vibrations 2−69714
aerodynamic, from circular jets 2−64387
aerodynamic, of obstacle placed in stream 2−46846
aerosound, source theory 2−46840
aircraft, Lloyd mirror effects 2−41824
aircraft, theory of excess jet noise 2−41819
aircraft carrier flight decks, effect of noise levels on humans 2−41825
aircraft noise, design and operation of continuous areawide monitoring system 2−45543
airfoil, nearwake props. leading to generation of vortex shedding sound 2−46844
annoyance, individual differences 2−45139
annoyance sensitivity scale 2−73223
annoyance susceptibility, in human subjects 2−55313
axial flow fans 2−41802
background, detection of sinusoids, as fn. of S/N ratio 2−45111
bang from sudden opening of pressure container with over critical pressure ratio 2−63132
blade interaction noise from lift fans 2−41806
broad-band, masking, effect on consonant confusions 2−45092
clackers, energy pathway 2−41753
in closed space, sound power level measurement of single source 2−82358

Noise continued
acoustic continued
combustion noise generation in burning fuel-air mixtures 2−55534
community level distribs., sampling errors 2−82354
control, conference, Lafayette USA (1971) 2−52249
critical masking interval, masking brief signal by noise 2−45110
cross correlograms, effects of dispersion 2−55517
deep sea hard-hat diving helmets, noise from gas flows 2−45542
detection and location in dispersive medium 2−55554
disc, pierced, nonlinear effect due to audio note of high intensity 2−45540
discrete tone radiation from supersonic jet 2−46841
in-ear meas., individual's exposure 2−45082
earphone enclosure for communication in noise, enhanced noise reduction 2−45083
effective perceived level, duration correction 2−73450
electrical machine, rot., magnetically induced noise 2−45655
evaluation in Algol-60 2−58930
facade walls, insulation from external noise with balconies and loggias 2−63137
fan, axial, primary sources 2−45536
fans, aeroacoistic tranfer function meas. and theoretical models 2−41821
fish, increase during breeding season 2−78919
fluid flow, cross correl. method 2−45533
Greater Vancouver, community survey 2−63134
grille in an airflow, detection of generated noise level 2−45529
hearing impairment and age relation 2−45140
hearing impairment caused in monkeys 2−45158
high rise buildings, due to external air flows 2−63136
high speed fans, from rotor/stator interactions 2−82355
high speed jets, turbulence in exhaust flow 2−77350
hydroacoustical cavitational noise spectra 2−43287
ideal homogeneous city, theory of steady-state urban noise 2−45528
impact, recurrent, impulse precision sound level meter for assessment of sound energy, limitations in use 2−41800
impact on floors, sound insulation 2−41808
impulse, exposure of guinea pigs, cochlear degeneration 2−45157
impulsive, chronic exposure of chimpanzees, bheavioural effects 2−45154
industrial, ear protection in factory environment 2−73218
industrial, hearing protectors, variation with noise spectra and with people 2−73217
industrial room models, noise propag. 2−45546
infrasonic, field meas. 2−52224
infrasonic, from aircraft, human discomfort evaluation, effects on brain alpha rhythm 2−69773
intermittent, h.f. and l.f., temporary threshold shift obs. 2−45098
jet, from small nozzle combinations 2−46845
jet aircraft takeoff, subjective annoyance 2−73222
jet noise, generalized theory 2−55552
jets, simple pressure source model 2−56429
jets perturbed by screens, near field pressure and hot wire meas. 2−41820
knee joint disease, acoustic pattern recognition 2−45047
knee joint disease, acoustical pattern-recognition 2−45047
large machines, nearfield measurements and sound power 2−41814
learning, masking level difference, gating from uncorrelated to correlated noise 2−66296
levels meas. from distant source 2−52248
l.f. sound, annoyance effects 2−69775
lined ducts, analysis, testing and design 2−41805
loudness calculations, ISO R-532 (Method B), optimal algorithms 2−73446
loudness discomfort levels for pure tones and noise 2−45125
loudness of transients, effect of rise time and repetition rate 2−45531
machine, as installed measurements 2−41817
machine noise, measurement errors, ISO recommendation 2−41815
machine noise, sound field near array of noise sources 2−41813
machines, measurement standards 2−41812
masking, tone detection, signal intensity and freq. 2−66302
masking of narrow bands of noise near h.f pure tones, combination band levels 2−82042
from mechanical equipment, noise source identification using real time analogue digital signal analyzer 2−69772
modal spectra in hard walled cylindrical ducts 2−41804
multiple pure tone broadband generation in high speed fans 2−41803
multitube multishroud supersonic jet noise suppressor 2−43233
noise radiation by plane arrays of incoherent sources 2−73449
noise rating assessment and dB(A) levels, computer compression 2−63133
on-line evaluation using minicomputer 2−58929
particle velocity components, spatial correlation fns. 2−69776
perceived noisiness, study of Doppler shift effects, computer analysis of data 2−66631
pitch, meas. 2−58641
propagation in corridors, insulation 2−41809
propeller vortex with boundary layer control 2−41822
reference source 2−45537
reverberant room measurements, integration time variance 2−45526
reverberant rooms, measurement 2−41810
sea ice cracking due to surface tension 2−65578
in semireverberant rooms, steady state reference sound sources 2−41816
separated flow noise, wall press. spectra and r.m.s. levels 2−45532
short tone pulses, pitch estimation, dependence in duration 2−69453
signature of aircraft in level flight, over hydrophone in sea 2−73423
signature of aircraft in level flight over hydrophone 2−44659
single number noise rating for $^1/_3$-octave band sound power levels 2−73447
snowmobiles, auditory temporary threshold shift measurements 2−45541
solid, random field, discrete levels sound amplification nonlinearity 2−68236
sonic boom signatures by bicharacteristic method 2−83668
sound power, qualification of reverberation rooms for det. 2−41795
sound power det. in reverberation rooms, effect of stationary and moving reflectors and sampling techniques 2−41811
sound power level of single noise source in closed space 2−82358
steady state measurements of power and absorption 2−41818

Noise continued
  acoustic continued
    stochastic transmission system diffusion function, white noise excitation 2−78915
    study offices, meas. for improving acoustic comfort 2−45556
    subsonic fan rotor alone noise, in-duct investigation 2−41807
    subsonic turbulent air jets, space correlations of fluctuating pressure 2−71076
    supersonic air ejectors, performance and noise characts. 2−46843
    supersonic jet, effects of nozzle plenum pressure fluctuations 2−69771
    supersonic Mach 1.5 cold model jet 2−41801
    turbojet exhaust noise, propagation at shear discontinuity between hot and cold regions 2−78921
    turbulent combustion generated, analytical results 2−69774
    underground workings, due to rail traffic, ballast and concrete supports comparison 2−45538
    vehicle noise, roadside large-display sound- level meter 2−45527
    very low levels, measurement method using principle of energy addition 2−66630
    wearable pocket noise dosimeter with digital readout 2−41826
    CdS acoustoelectric instability, scattering of light by sound 2−71728
    InSb microwave radiation, acoustoelectric amplification 2−54159
  electrical
    see also Cosmic radiation, radiofrequency; Sun/radiation, radiofrequency
    1/f, physical process for thin metallic films 2−68335
    1/f, variance fluctuations 2−51177
    anemometer, hot-wire, airborne, spectra 2−44680
    atmospheric radio noise meas. rel. to lightning flashes in India 2−84790
    atmospheric v.l.f. and e.l.f. noises observed by Alouette 2 satellite 2−81667
    bulk, 1/f, exptl. evidence for existence 2−47938
    circuit for on-line evaluation applic. to atmospheric turbulence and seeing conditions 2−45633
    counters, Geiger and proportional, mechanism for noise effects after filling 2−63694
    current, pickoff, elimination in tensiometry of rotating objects 2−76436
    current fluctuation in plasma, by freq. analysis method 2−53198
    currents, effect on measuring circuits of nuclear reactor conteol system 2−42636
    e.l.f. hiss, Ogo 4 satellite observations 2−65928
    e.p.r. spectrometer sensitivity calcs. 2−55627
    f.e.t., at long time constants 2−44136
    figure rating for marginal oscillators 2−45651
    filter distortion of spectral lines 2−52339
    immunity, scaling decade, trigger circuits, photography 2−82592
    LHR hiss rel. to magnetospheric and auroral activity 2−68953
    magnetosphere, upper-hybrid reson. noise obs. by IMP-6 AC-elec. fields exp. 2−65869
    metric continuum sources, active longitude persistence rel. to solar and interplanetary mag. fields 2−58545
    microwave, direct detection meas. system using Schottky barrier diodes as envelope detectors, threshold 2−63212
    microwave, standards, hot and cold, in Uk 2−78753
    optical signal detection in presence of nonuniform noise, pulse shape effect 2−59207
    photoelectronic image-brightness intensifier, multielectron noise and remanent gas pressure and composition 2−59273
    pulse shaping systems, relative performance 2−42474
    pyroelectric radiation detector noise sources 2−78944
    radio noise characteristics of auroral ionosphere 2−72840
    semiconductor, ambipolar diffusion noise spectrum, mag. field effects 2−61269
    semiconductor, inhomogeneous, universal mechanism of excess noise generation 2−75085
    semiconductor diode, p^+-n, terminal noise at high injection, theory 2−54218
    side window photomultiplier, with pulsing ns gate 2−66722
    sky-noise temp., at 11.75 and 17 GHz, in UK 2−72811
    spectroscopic data quality enhancement 2−59278
    superconductors, type II flux flow noise, study with pick-up coils 2−71862
    suppression by time exposure oscilloscope photography 2−45831
    thermal, automatic impedance measurements 2−73497
    thermal noise in Ge sensor used to meas. low temperatures 2−62889
    thermal noise standard WR15 2−78760
    thermometer, Josephson junction applics. 2−64956
    triglycine sulphate, dielec. const. near crit. point, thermal noise study 2−72040
    TV monitor picture of electron microscope image, modulation transfer 2−79081
    v.l.f. radio noise rel. to visible auroral arc emissions 2−65916
    $AgNa(NO_2)_2$, crit. slowing down of dielec. relax., thermal noise study 2−72029
    $Ba_xSr_{1-x}Nb_2O_6$, semicond., high 1/f noise anomaly 2−47888
    $BaTiO_3$, meas., confirmation of internal stress model of polycrystalline ferroelectric materials 2−44159
    CdF_2:Er^{3+} i.r. quantum counter, noise effects 2−59631
    CdSe-electrolyte blocking contact, photosensitivity and noise 2−72079
    CdSe, single crystals, l.f. noise, obs. 2−51136
    $CeMg_2(NO_3)_6$, powder, Johnson noise temp. rel. to 16Hz mag. temp., 2-20 mK 2−71897
    GaAs, 1/f noise due to free surface 2−81079
    $Hg_{1-x}Cd_xTe$, minority carrier shot noise current 2−54255
    In superconducting film 2−68348
    InSb, contact effect on microwave emission 2−47897
    InSb, electron-hole plasma in mag. field, carrier wave growth, noise meas. 2−61316
    n-InSb, l.f., electron plasma critical fluctuations, 4.5-12K 2−68319
    Pt film, discontinuous, current noise 2−68340
    Si photodiode operational amplifier combination, noise and frequency response 2−57214
    Sn superconducting film 2−68348

Noise abatement
    see also Absorption/acoustic waves
  airborne sound insulation in buildings, standardization of measuring techniques 2−52251
  aircraft noise, infrasonic, human discomfort evaluation, effects on brain alpha rhythm 2−69773
  attenuation in ducts with anisotropic lining, silencers 2−76376
  barriers on ground 2−55553
  community level distribs., sampling errors 2−82354
  conference, Lafayette USA (1971) 2−52249
  corridors, using absorbing and shielding baffles 2−41809
  enclosures and rubber suspensions applic. for noise minimization 2−45535
  impact noise on floors, sound insulation 2−41808
  motor vehicle, measurement procedures for regulation and monitoring 2−78929
  muffler element performance, effects of high-intensity sound 2−73448
  multitube multishroud supersonic jet noise suppressor 2−43233
  noise/vibration/shock control systems, design features 2−82364
  partition walls, porous absorber materials, influence of structural stiffness, attenuation on sound insulating efficiency 2−41827
  plastic for sound insulation 2−55551
  pollution, urban technology, conference, San Francisco (1972) 2−82029
  on Rhine cruise ship, due to damping material 2−45530
  rotor noise attenuation with leading edge serrations 2−41823
  sound insulation at l.f., two rooms coupled by panel 2−41831
  turbojet engine noise reduction 2−45510
  underground railway line, treatment of rolling stock and stations 2−45539

Nomenclature and symbols
    see also Units
  nuclear medicine, nomenclature for Fourier transforms of spread functions of imaging systems 2−76065

Nomograms
    see also Graphs
  acoustic wave velocity in solid media 2−64844
  Caucasian earthquakes, determination of K value 2−72646
  for charged particle energy loss determ. in absorber materials 2−56072
  coupled lenses double focusing calcs. 2−66716
  viscosity of immiscible liquid mixtures, continuous and dispersed phases 2−43392

Non-crystalline state *see Amorphous state; Vitreous state*

Non-Newtonian fluids
  bentonite-water suspensions, flow behaviour for time-dependent non-Newtonian fluid 2−60159
  Bingham type, laminar flow in square duct 2−83491
  boundary layer of non- Newtonian power-law fluids with arbitrary pressure gradients 2−60147
  bubble moving in liq., mass transfer, power law model 2−53374
  carboxymethyl cellulose, water soln., laminar flow, heat transfer 2−74498
  deformation velocity, relationship with strain, applications in lubrication 2−50162
  drop size in power law systems 2−46906
  fall of drops in non-Newtonian fluids 2−46905
  flow, economic optimization in laminar pipe flow 2−60143
  flow, in tube with sinusoidal deformation 2−53127
  flow around immersed rotating disc 2−83485
  flow from short tubes and nozzles 2−83489
  flow meas., pressure difference meters 2−83516
  flow rate obs. using orifices 2−83490
  heat transfer, non-isothermal laminar flow 2−83487
  laminar flow, fully developed, in vertical tube, buoyancy effects 2−70844
  laminar flow through circular pipes, heat transfer and hydrodynamics 2−60124
  liquid, convective mass transfer in circular tube, velocity and concentration fields 2−46883
  liquids, behaviour in spary 2−83500
  liquids, heat transfer in agitated vessels 2−74538
  liquids with solid suspension, viscosity 2−83822
  mass transfer from bubble using thin boundary layer approx. 2−53376
  models under conditions of complex hreological behaviour 2−82302
  poly(dimethyl siloxane), in high shear rate region, relation between mol. wt. and viscosity 2−83374
  polyethylene, high density, melt rheology 2−83371
  power-law, axisymmetrical laminar boundary layer flow along slender circular cylinders 2−67566
  rheological characterization in coaxial cylinder, applic. of rheogram template 2−53467
  Rivlin-Ericksen fluids, channel bounded by 2 flat parallel plates, axial press. gradient 2−83448
  second-order, oscillations near a sphere, calculation 2−56313
  solid particle-gas system, laminar flow 2−83821
  stability of plane Poiseuille flow to finite-amplitude perturbations 2−46666
  steady flow in entrance region of straight channel 2−83450
  suspension of drops in elec. field, stress system 2−83819
  suspensions in water, rheological model 2−83823
  time-dependent and time-independent thermodynamic approach to generalised rheological equations 2−67559
  torque on sphere inside rot. cylinder 2−83476
  turbulent flow in pipes, theory of heat transfer 2−46877
  turbulent heat transfer 2−50297
  two-dimensional flow in channel with rectangular cavities 2−67563
  visco-plastic medium, nonstationary shear flow 2−77235
  viscoelastic flow, in V-shaped duct, constitutive eqn. 2−43057
  viscoelastic fluids, unsteady flow through circular, coaxial circular ducts, press. function of time 2−83451
  viscosity, first normal stress difference prediction using Graessley molecular theory 2−83484
  viscosity and lubrication, teaching course 2−48969

Nonlinear optics
  absorption, three dimensional sequential information storage 2−73663

Nonlinear optics continued
absorption and optical breakdown of liquid laser attenuators 2−42119
alkali metal metavanadates, characteriz. 2−47261
analytic and numerical solns., comparison 2−82522
anisotropic dispersion of nonlinear susceptibility in four wave i.r. mixing 2−42107
anthracene, two-photon absorption 2−44410
benzene, second harmonic laser light scattering 2−43357
benzene, self-focusing effect on stimulated Raman scattering 2−77437
benzene derivative crysts., second harmonic generation and Miller's parameter 2−54377
biexciton theory, spectrum analysis 2−47817
birefringence, propagation through thermally distorted windows 2−82524
carbon tetrachloride, self-focusing effect on stimulated Raman scattering 2−77437
chalcopyrite semiconductors, review 2−48126
coherent optical pulse propagation, superradiance 2−41940
collisionless gases, transient orientational birefringence 2−43267
composite system factorization 2−73543
continuously tunable coherent source by beam mixing in ADP 2−45758
d-threonine, second harmonic generation 2−55711
diamond, three-wave mixing, resonant and resonant, interference 2−82507
dissipative behaviour, quantum mechanistic model 2−59120
dyes, semicolloidal solns., dispersion of intense light 2−50360
effects in liquids and solids excitation by psec. and nsec. u.v. pulses 2−43356
electron response in solid to X-rays 2−61576
ferroelectric, hydrogen-bonded, harmonic generation, tunnelling model 2−44326
ferroelectric crystal, second-harmonic scatt., domain shape effects 2−82508
film, waveguide, phase matching of nonlinear optical interactions 2−70012
gas lasers, stability of oscillation types with nonlinear selective losses 2−49355
glass, self-focusing rel. to electrostriction and Kerr effect, damage threshold 2−75249
glass, transparent, filamentary tracks formed by laser-beam self-focusing 2−65207
glasses, laser heating, internal focusing and defocusing 2−82526
harmonic generation, classical theory, practical generators based on CO$_2$ lasers 2−82505
harmonic generation, influence of third order nonlinearity 2−42167
harmonic generation due to electron retardation in presence of intensive light wave 2−66796
harmonic generation for obs. of dispersion in gases 2−71117
harmonics, spectral density calc., characteristic function 2−41986
heterodyning with noncritical angular alignment using pair of u.s. light modulators 2−79240
hexafluoroisopropanol, low dispersion liquid, enhanced nonresonant, optical four-photon parametric interaction 2−46957
holographic recording materials, nonlinear effects 2−49397
holography, quantization and other nonlinear distortions of transmittance 2−55718
hyper-Raman effect, polarization phenomena 2−46515
intense waves, focusing in ducts with parabolic, saturating nonlinearity 2−69838
i.r. to visible parametric upconversion in proustite 2−49388
i.r. upconverter, synchronously pulsed, conversion efficiency, peak power 2−79378
k three level system, coherent two photon propagation and self induced transparency of optical pulses 2−44330
Kerr effect self-focusing of picosecond laser pulses 2−52431
Kerr liq., spectral broadening of light filament, meas. with laser pulses 2−71204
Kerr liqs., optical filaments, pulse distortion, optical shock, dispersion effects 2−79234
laser, injection, large optical cavity heterojunction, transverse mode selection 2−59178
laser, optically pumped, reference frequency shift calc. 2−49341
laser, ring, radiation trapping rel. to mode competition and dispersion, Lamb eqns. 2−79182
laser beam, harmonic generation, change of axial intensity 2−66778
laser induced turbulence, spectral law of temp. fluctuations 2−82523
laser pulse in solid, two-dimensional thermal attenuation 2−75247
laser pulses, nonlinear responses and self trapped filament diameters, influence of steric interference 2−42113
laser self-focusing damage tracks, anatomy and thermal history 2−82501
laser surface damage and electric surface stress 2−59191
light modulation, LiNbO$_3$ applications 2−69988
liquid, low dispersive, enhanced optical four photon parametric interaction 2−79237
liquid, relaxation time determ. by laser probing 2−46958
liquids, nonlinear response to laser pulses, effect of steric effects and compressibility, rel. to diameters of self-trapped filaments 2−71200
lithium formate monohydrate, properties 2−48130
microwaves and short laser pulses, interaction in nonlinear medium 2−42128
mode-locked pulsed and c.w. lasers, production of intense light pulses, meas. of picosecond duration 2−76470
mode-locking and short pulse generation, bibliography 2−82469
multi-phonon processes, calc. using pseudo particle method 2−79880
multiatom multimode Hamiltonian, variational estimate of lowest eigenvalue 2−73538
N-soliton soln. for eqn. of nonlinear optics 2−82503
niobates, ABCNb$_2$O$_{15}$, A=Ca, Sr, Ba; B=Ca, Sr, Ba, C=Na, K, nonlinear optical props. 2−75251
nonlinear luminous interactions in electro-optical media excited by travelling circular modulating field 2−69995
optical bridge for mode-locked CO$_2$ laser assessment 2−73563

Nonlinear optics continued
optical parametric amplification and frequency conversion, coherency and efficiency 2−42168
optical parametric fluorescence, tuning in uniaxial crystals 2−82529
organic crystals, second harmonic generation of ruby laser radiation 2−68592
organic crystn. powders, second harmonic generation efficiencies, Nd laser irrad. 2−57319
organic liqs., thermal periodicity of filament form. and elastic lattice vibrs. 2−50359
parametric 4 photon exchange effect, spontaneous, theory 2−65236
parametric interactions, instabilities, numerical study 2−78780
parametric oscillator, behaviour 2−49344
phase and amplitude bunching in travelling wave interactions 2−42165
phase mismatch effects on pulse shapes in second harmonic generation 2−42166
phase modulation of coherent light, by liq. crysts. 2−42160
phenanthrene, two-photon absorption 2−44410
photoelastic parametric interactions in laser-pumped birefringent media 2−59121
picosecond, progress 2−42164
picosecond laser pulse investigations, reviews 2−63348
picosecond pulses, substructured and nonlinearly broadened, mode-locking characteristics 2−42121
piezoelectric, absolute signs of second harmonic generation coeffs. 2−44332
plane waves of const. amplitude in nonlinear dielectrics 2−76415
plasma in inhomogeneous electric field, parametric excitation of subharmonics, frequency division 2−70906
polar crystals, optical rectification by impurities 2−44327
polarization, symmetry properties of higher rank polar tensors, crystal symmetry 2−44331
polycrystals, polarization effects during transmission 2−81325
proustite, phase matched parametric upconversion, systems applications, review 2−79223
pulse chirping in self-induced transparency 2−59205
pulsed internal optical parametric oscillators, transient behaviour, model 2−79236
pumping coherence, effect on freq. conversion and parametric amplification 2−59125
quasi-c.w. parametric light generator for active Raman- scatt. spectroscopy 2−66853
random dispersive medium, electromagnetic wave propagation 2−73622
real time processing system 2−79425
refractive index tuning of phase matched second harmonic generation in optical waveguides 2−42111
resonance dispersion and Faraday rotation in self induced transparency 2−44324
resonant media, large coherent optical polarizations, prep. and detn. 2−41945
resonant or nonresonant theory, method of characteristics 2−41943
resonator, kinetics of single pulse production and second harmonic conversion efficiency 2−66739
resonator with inhomogeneous medium, equivalent parameters, quasi-geometric optics formulation 2−63316
rhodamine B, 6G, vib. relaxation from optically excited state, new technique 2−83401
ring laser with naturally active cell, radiation polarization 2−73557
ruby, phase relaxation and self induced transparency 2−42118
ruby cylinders, complex propagation constants 2−82528
ruby disk laser, optical distortion and depolarization effects 2−82489
ruby laser TE and TM modes generation and self- focusing 2−42074
sapphire, self focusing threshold enhancement with elliptical beams 2−61578
second harmonic and sum frequency generation from flashlamp pumped dye laser 2−73577
second harmonic generation; quantum effects 2−82502
second harmonic generation, applic. of generalized theory of diffraction 2−63368
second harmonic generation, microwave freq., by system of paramagnetic spins 2−61577
second harmonic generation, molecular crystals with Nd laser 2−82515
second harmonic generation and parametric oscillation, review in book 2−57318
second harmonic generation of twin frequency laser 2−42129
second harmonic of i.r. light, summed with fundamental and dye laser to give frequency tunable signal 2−73604
second order props. of solids, book contrib. 2−72250
self defocusing by Rb vapour 2−43273
self focusing, beam diameter limitation due to stimulated Raman scattering 2−42117
self focusing and self phase modulation in psec pulse oscillators 2−42054
self focusing in inhomogeneous nonlinear dielectric media 2−59206
self focusing threshold of gaussian elliptic beams 2−42116
self induced thermal lens effects on imaging or tracking systems viewing along same path, image quality degradation 2−49391
self induced transparency from coherent interaction with absorbing systems 2−44328
self induced transparency in semiconductors 2−44329
self trapping of short laser pulses in Kerr liquids 2−42112
self-focusing, statistically inhomogeneous nonlinear medium with weak regular inhomogeneity 2−78972
self-focusing of laser light, limiting diameters 2−67832
self-focussing, trapping, phase modulation of laser beam 2−79258
self-induced transparency and two-photon propagation in three-level system 2−82510
self-induced transparency of e.m. pulse, rot. of plane of polarization 2−52443
self-phase modulation electronic mechanism for production in liquids and solids 2−45770
semiconducting compounds, i.r. dispersion of second order elec. susceptibilities 2−61581
semiconductor, Miller's rule for susceptibilities, freq. depend. 2−51297
semiconductor, polycryst., laser-induced transmittance modulation 2−61575

Nonlinear optics continued
semiconductor, self-focusing mechanism, by energy depend. carrier scatt. 2−59179
shock waves in glass due to internal focusing of laser beam 2−42124
solid state and quantum electronics, book 2−57092
solutions illuminated by ruby laser, calc. of deviation from Beer-Lambert's law 2−81416
spectral intensity second harmonic growth with exciting radiation freq. half width growth 2−69994
spectroscopy, using tunable lasers 2−45820
steady state filament formation in self focusing 2−42114
stimulated Raman emission from bulk medium, theory of state of polarization of scattered radiation 2−63305
strontium formate and strontium formate dihydrate, phase matching 2−48124
sum frequency amplification, quantum theoretical treatment 2−69888
susceptibilities of optical materials 2−48125
tetrahedral crystal, second harmonic generation 2−78061
thermal image parametric upconversion, theory 2−69792
thermal lensing in solids, vector Kirchhoff approach 2−82525
transient self-focusing of light 2−42169
transient stimulated thermal scattering, frequency response 2−41939
transparent liquids and solids, avalanche ionization and limiting diameter of filaments by light pulses 2−77435
trifluorochloroethylene, absorption saturation and optical strength for CO_2 laser pulses 2−67523
triglycine sulphate, second-harmonic scatt., domain shape effects 2−82508
u.v. radiation generation, coherent, using Q-switched Nd:YAG laser 2−69956
vibrational Raman resonance nonlinear spectroscopy 2−42269
water anomalous frequency broadening of ruby laser beam by self modulation 2−43362
wideband parametric upconversion of i.r. waves to visible region using tunable dye laser 2−82511
$AgGaS_2$, absolute signs of second harmonic generation coeffs. 2−44332
$Al_xGa_{1-x}As$ solid solns., in heterostructs., optical and electronic channelling rel. to comp. 2−63341
$Ba_2NaNb_5O_{15}$, temp. of phase synchronization for two wave freq. addition 2−48128
$Ba_{0.5}Sr_{0.5}Nb_2O_6$, absolute signs of second harmonic generation coeffs. 2−44332
$Bi_xTi_yO_z$ cryst. props. 2−47231
CS_2, second harmonic laser light scattering 2−43357
$CaS_2O_6.4H_2O$, second harmonic generation 2−75248
$CaWO_4$:Nd^{3+}, photon echoes, generation, detection, mag. field and temp. depend. 2−72251
Cd-Ar vapour, phase-matched, vacuum u.v. radiation generation 2−79904
CdS, optical modulation due to moving acoustic domains, absorp. spectra obs. 2−54418
CdS semiconductors, dipole active exciton absorption, nonlinearity 2−44333
CdSe, singly resonant i.r. parametric oscillator 2−69903
CdSe(Te), absolute signs of second harmonic generation coeffs. 2−44332
CuCl, opt. susceptibility in exciton region from SHG and 2-photon luminesc. 2−54453
p-GaAs, absorpt. saturation intensity at 10.6 μm 2−79227
GaAs, submillimetre wave generation, by difference freq. mixing 2−49200
GaAs frequency mixing, 2 and 3 wave anisotropic interference 2−75250
GaP, two-photon spectra in k vector space, polariton obs. 2−71710
β-$Gd_2(MoO_4)_3$, second harmonic generation, pseudotetragonal symmetry effects 2−51298
p-Ge, absorpt. saturation intensity at 10.6 μm 2−79227
He, calc. of third harmonic generation coeff. using pseudo particle method 2−79880
InSb, magneto Raman scattering obs. 2−45730
n-InSb, microwave self-focusing, phenomenology 2−68591
InSb, model of nonlinear susceptibility, dispersion near band gap and second harmonic generation 2−44334
n-InSb, nonlinear optical susceptibility dispersion in mag. field, band model calc. 2−51299
InSb, nonlinearity dispersion near band gap 2−48127
InSb, resonant far-i.r. generation theory 2−61579
InSb, resonant nonlinearity due to cond. electron spins 2−65208
K, dispersion of cubic nonlinear susceptibility det. by self-focusing self-defocusing and self-modulation 2−42734
KH_2PO_4, excitation of natural and stimulated optical harmonics 2−61580
KH_2PO_4, trapping of parametrically amplified light waves 2−44335
KIO_3, symmetry props. rel. to use as nonlinear optical material 2−74733
$K_2S_2O_6$, second harmonic generation 2−75248
$LiIO_3$, noncollinearly phase matched second harmonic generation using Nd:YAG laser 2−79230
$LiIO_3$, tunable i.r. difference-frequency generation 2−63369
$LiNbO_3$, temp. of phase synchronization for two wave freq. addition 2−48128
$LiNbO_3$, third-order susceptibility, using tunable dye lasers 2−72252
$LiNbO_3$ crystal, harmonic generator, patent 2−42171
$LiNbO_3$ spontaneous parameteric scattering, idler absorption and dispersion 2−44337
$LiTaO_3$:Cu^{2+}, optical generation of intense picosec. electrical pulses 2−45768
$LiTaO_3$:Cu^{2+}, optical generation of picosecond electrical pulses 2−44336
N intensifier 2−42257
NH_3, self induced transparency at 10 μ, extrapolation to CO_2 laser radiation atmospheric propagation 2−43268
$NaNO_2$, elasto-optic consts. rel. to Brillouin scatt. at room temp. 2−48204
Nd:glass laser produced plasma, second harmonic generation 2−43146
Nd^{3+}-glass laser, giant light pulse generation for study of nonlinear optical effects 2−55685

Nonlinear optics continued
Ne, calc. of third harmonic generation coeff. using pseudo particle method 2−79880
Ne discharge in hollow cathode, effect of nonlinear absorption at 0.63 m wavelength 2−83641
$PbNb_4O_{11}$, absolute signs of second harmonic generation coeffs. 2−44332
$PbTiO_3$, absolute signs of second harmonic generation coeffs. 2−44332
Rb, resonance fluorescence 2−44328
$Rb_2S_2O_6$, second harmonic generation 2−75248
SF_6, saturation behaviour at high pressure and laser intensity 2−74277
p-Si, absorpt. saturation intensity at 10.6 μm 2−79227
SiC, absolute signs of second harmonic generation coeffs. 2−44332
$SrS_2O_6.4H_2O$, second harmonic generation 2−75248
β-$Tb_2(MoO_4)_3$, second harmonic generation, pseudotetragonal symmetry effects 2−51298
Te, second harmonic generation with CO_2 Q-switched laser, 290-370K 2−79238
Te, second harmonic generation phase matching, laser-induced change 2−44338
Tl_3AsSe_3, phase matchable i.r. nonlinear material 2−48129
$ZnGeP_2$, absolute signs of second harmonic generation coeffs. 2−44332
ZnTe, absolute signs of second harmonic generation coeffs. 2−44332

Novae
see also Stars
3C391 supernova remnant, continuum spectrum, effect of interstellar gas 2−58390
3C 391, supernova remnant, nature of low frequency absorption at 31.4 GHz 2−55085
3C 58, supernova remnant, brightness and polarization structures, obs. at 2.8 cm. 2−75757
Cephei 1971 spectrum 2−58319
chromospheric heating by radiation driven sound waves 2−69062
CNO abundances, hydrodynamic models of nova outburst 2−58315
Crab Nebula supernova explosion, Californian pictographic evidence 2−75760
Cygnus Loop, brightness and polarization meas. at 6-cm. wavelength 2−69017
Cygnus X-3, outburst of radio emission rel. to possible superrova precursor 2−73056
Delphini, metallic absorption lines before Dec. 1967 maximum 2−48707
filamentary, supernova remnants, spectrophotometric investigations 2−72985
frequency estimate, Andromeda Nebula and the Galaxy 2−73023
G296.8-0.3, supernova remnant, association with pulsar PSR 1154-62 2−55098
Galactic supernova remnants, supernova rate, galactic radio emission and pulsars 2−78452
HB 21 supernova remnant, obs. at 4170 MHz 2−55056
HD 87634, nova-like, associated with nebula 2−85005
HZ 29, double white dwarf semidetached post cataclysmic nova? 2−55053
IC 443, supernova remnant, brightness and polarization structures, obs. at 2.8 cm. 2−75757
IC 443 supernova remnant, obs. at 1.42 GHz 2−58328
IC 443 supernova remnant, obs. at 4170 MHz 2−55056
IM Normae, possible X-ray source 2−55052
NGC 5055, periodic light pulsations in supernova outburst 2−75761
NGC 5253, interstellar lines in supernova spectrum 2−81828
Nova Cephei 1971, spectrophotometry 2−62572
Nova Delphini 1967, high dispersion spectra during nebular stage 2−58240
Nova Delphini 1967, non-spherical ejecta, spectral obs. 2−62573
Nova Serpentis 1970, infrared spectrum 2−78454
Nova Serpentis 1970, non-spherical ejecta, spectral obs. 2−62573
Nova Vulpeculae 1968(i), non-spherical ejecta, spectral obs. 2−62573
pretelescopic, survey of novae and supernovae 2−73022
proper motions of N Her (1934) N Cyg (1920) N Aql (1918) N Aur (1891) and background stars 2−51758
remnants and variables, high speed photometry 2−44872
FH Serpentis 1970, velocity and spectrscopic obs.58330 2−58330
SN 1960 in NGC 4496, spectra interpretation after luminosity maximum 2−72998
spectra, formation coronal lines, heating in circumstellar envelope 2−75766
supernova 1968 in M83, photometry 2−62564
supernova event, 2U 1543-47, transient X-ray source, extragalactic origin 2−58420
supernova explosions, remaining ionization zones 2−81856
supernova explosions, supergiant evolution, Crab pulsar 2−62560
supernova in irregular galaxy NGC 5253, optical polarization 2−69091
supernova in NGC 5253, extragalactic Ca II absorption lines in spectrum 2−73015
supernova in NGC 5253, optical obs. 2−62574
supernova remnants, estimation of Hubble constants, radio obs. 2−81963
supernova remnants, galactic, absorption of 80 MHz emission by interstellar medium 2−69089
supernova remnants, galactic, distances, radio luminosity, function and distribution obs. 2−48705
supernova remnants, low energy X-ray survey 2−84952
supernova remnants, soft X-rays 2−58425
supernova remnants, spatial coincidences with X-ray sources 2−69128
supernova remnants as soft X-ray sources 2−44900
supernova remnants in Aquila, 2−20 keV X-rays search 2−75839
supernova remnants in Aquila, X-ray obs. 2−62569
supernova remnants in Large Magellanic Cloud 2−69090
supernovae, γ-ray flux 2−51792
supernovae, production as result of collapse following C exhaustion 2−48689
supernovae, rapid cosmic processes, morphology 2−81749

Novae continued
supernovae, source of universal X-ray background, observational evidence 2−58419
supernovae, synthesis of superheavy elements and termination of r-process 2−69093
supernovae, type I, in early stages of evolution, spectral interpretation 2−72998
supernovae, type I, spectra and Hubble constant 2−75765
supernovae, type I, spectra study 2−73011
supernovae, type II, absorption spectra 2−66100
supernovae cosmic ray interaction 2−66043
supernovae e.m. pulses, relativistic shock propagation 2−62567
supernovae remnants, acceleration of cosmic rays 2−62568
supernovae remnants, polarization and total power emission at 2700 MHz 2−58316
supernovae remnants at 11 c.m., high resolution obs. 2−75759
supernovae remnants at 80MHz, high resolution obs. 2−75758
supernovae remnants containing neutron star crustars radiating as soft X-ray black bodies 2−58433
type I supernovae, spectra of expansion envelope after maximum light 2−73021
type II supernova in M101, polarization measurements 2−73020
Vulpeculae 1968(1), photometric light curve 2−55051
Vulpeculae 1968 N. 1, photoelectric light curves 2−73010
w28, supernova remnant, brightness and polarization structures, obs. at 2.8 cm. 2−75757
w44, supernova remnant, brightness and polarization structures, obs. at 2.8 cm. 2−75757
W 44 supernova remnant, formaldehyde absorption 2−84983
white dwarf non-radial pulsations, oscillations rel. to dwarf novae and g-mode pulsations 2−73018

Novoids *see Novae*

Nuclear acoustic resonance
NaF, of ^{23}Na, spin-lattice relax., pulse method obs. 2−78170
RbMnF$_3$ antiferromagnetic, magnetoelastic theory of ^{19}F resonance and lattice imperfection 2−51412

Nuclear alignment *see Nuclear polarization*

Nuclear bombardment targets
accelerator, isotopic, prep. techniques 2−73962
actinide metal, preparation using tilt- pour and injection casting techniques 2−73907
actinides, electrodeposition methods of prep. 2−49618
actinides, electrodeposition methods of prep. for cross section obs. and accelerator bombardment 2−73919
alpha radioactive isotopes, preparation 2−49623
alpha-particle thickness gauge 2−41449
angular dependence of dose and hadron yields from targets in extracted proton beams 2−46254
chamber for charged particle induced X-ray fluorescence 2−73925
differential cross section for scattering of non-parallel non-uniform beam 2−52668
electrospraying and electrophoresis for layer preparation 2−73922
fabrication, sample assay 2−57440
foils, fabrication by rolling techniques 2−73910
foils, fabrication by rolling techniques 2−49621
gas, high density windowless 2−52671
geometrical corrections in coincidence meas. of nuclear reactions using gas target 2−63684
hydrocarbons, influence of mol. binding on alpha-particle stopping power 2−64869
inclusive production from nuclear targets 2−67202
ion damage distributions calc., computer program 2−79678
isotope, prep. by heavy ion sputtering 2−49622
isotopic, for accelerators, preparation 2−49702
isotopic, prep. by heavy ion sputtering 2−73911
material preparation using e.m. isotope separator 2−73918
material preparation using laboratory type isotope separator 2−73917
materials and preparation, conference (Gatlinburg, USA, Oct 1971) 2−73916
methanol-ethyleneglycol mixture, proton polariz. target 2−79677
neutron capture cross section meas. at 14 MeV and target geometry, application to nuclear targets 2−74094
Np ingots and disks, preparation using tilt-pour and injection casting techniques 2−73907
orientation using cryogenic apparatus of ^{3}He refrigerator and solenoid superconducting magnet 2−76736
preparation, conference (Gatlinburg USA, Oct 1971) 2−49617
preparation in e.m. isotope separator 2−49614
rotating, for radiational analysis of specimens cooled to liquid nitrogen temps., by elastic scattering 2−72597
stable and active, prep. techniques 2−73909
stable and active, techniques for preparation 2−49620
standard layer prep. by vacuum evaporation 2−73913
T impregnated, for neutron generators, patent 2−82781
thickness, and uniformity obs. using charged particles 2−73924
thickness and uniformity det. using α-particles 2−55897
thin self-supporting target, multiple layer and flat foil preparation 2−73921
γ-ray angular correlations, perturbation due to recoil nuclei, nucleus, solid interactions 2−68587
Al(d,n) thick-target yields and total cross sections, 1-40 MeV 2−67333
Am, isotopes, thin supported films, prep. techniques 2−73912
^{241}Am, powder, preparation and purification 2−73908
Be, dosimetry of neutron fields produced by d bombardment 2−67320
Be(d,n) thick-target yields and total cross sections, 1-40 MeV 2−67333
^{210m}Bi, preparation with low isotopic abundance 2−42444
C, evaporation production technique 2−49625
C thin film production using evaporation method 2−74629
^{14}C, self-supported, preparation techniques 2−49624
C(d,n) thick-target yields and total cross sections, 1-40 MeV 2−67333
^{252}Cf sources, effect of thin C and Au foil cover of fission fragment energy loss and spectrum parameter changes 2−42445
Cr, isotope, prep. of self-supporting metallic foils using electrodeposition 2−73920

Nuclear bombardment targets continued
Cr, isotopic, self-supporting foil, preparation by electrodeposition 2−49619
D impregnated, for neutron generators, patent 2−82781
H, 3 metre liquid target 2−59601
H, conical liquid target 2−59602
H track-sensitive target, use in studies of KN interactions 2−52669
H$_2$, liquid, 150 cm, for synchrophasotron 2−67072
H$_2$, liquid, 50 cm, with Lawsonite windows 2−52670
^{1}H, ^{2}H, ^{3}H, preparation techniques 2−49624
^{1}H liquid target system development, use of closed cycle refrigerator 2−46034
^{2}H liquid target system development, use of closed cycle refrigerator 2−46034
^{3}He, polarized, analysing power of ^{3}He(d,p)^{4}He reaction from 300 kev to 2.5 MeV 2−46312
Li(d,n) thick-target yields and total cross sections, 1-40 MeV 2−67333
Mo foils, fabrication by rolling techniques 2−73910
Np isotopes, thin supported films, prep. techniques 2−73912
^{237}Np, powder, preparation and purification 2−73908
Pu ingots and disks preparation using tilt-pour and injection casting techniques 2−73907
Pu isotopes, thin supported films, prep. techniques 2−73912
^{241}Pu, powder, preparation and purification 2−73908
Ra isotopes, thin supported films, prep. techniques 2−73912
T-containing, high-yield neutron generators 2−73923
U ingots and disks, preparation using tilt-pour and injection casting techniques 2−73907
U isotopes, thin supported films prep. techniques 2−73912
UF$_4$, sample prep. by metalluriginal methods 2−73906
Zr-^{3}H, calc. of ^{2}H-^{3}H neutron yield 2−42443

Nuclear decay schemes *see Radioactivity/decay schemes*

Nuclear decay theory
see also Beta decay theory; Nucleus/theory
α-decay, eqn. for compound state wavefunctions 2−52793
lifetime of compound nucleus meas. by shadow effect method, influence of exptl. conditions 2−67190
multinucleon wave function expression approach 2−59676
phenomenological causal model assuming interaction with neutrino sea 2−78434
weak processes, induced-tensor interaction 2−63728
α spontaneous emission from heavy radioactive nuclei 2−52773
p emission, beta-delayed, from heavy nuclei calc. of spectral shapes and intensities 2−46194
^{20}Ne, alpha-decay widths for ground state and other levels calc. using harmonic oscillator shell model wave functions 2−49761

Nuclear emulsions *see Nuclear track emulsions*

Nuclear energy level lifetimes *see Nucleus/energy level transitions*

Nuclear excitation
see also Isobaric analog states; Mossbauer effect; Nucleus/energy levels
— 2−70396
— 2−63817
(γ,n) reactions, photonenergy determ., threshold photoneutrons and photon doorways 2−46228
A=88 to 209, deformation parameters 2−42532
analogue state excitation by double charge exchange of pions, nuclear medium corrections 2−74103
channel correlation effects for fragmented analog states 2−46096
Colomb fission cross sections, nucl. forces influence 2−83033
compound nuclei, multiple-scatt. effects in mean lifetime expt. by blocking technique 2−63748
Coulomb, determ. of e.m. transition probabilities and lifetimes 2−82869
Coulomb, reorientation effect study in heavy-ion reactions 2−83023
Coulomb and nuclear excitation amplitudes, interference in inelastic scatt. 2−46304
Coulomb excitation by polarized particles and detn. of m.m. 2−70370
deformation energies, shell correction method 2−49720
doubly even nuclei, electroexcitation and electrodisintegration via 1p-1h continuum 2−52801
equations of motion approach to nuclear spectroscopy 2−82947
evaporation spectra analysis 2−52792
even-even nuclei, $125 \leqslant A \leqslant 188$ and $A \geqslant 224$, rotational and irrotational flow calc. 2−63782
even-odd nuclei, $91 \leqslant N \leqslant 113$, neutron capture, de-excitation 2−74003
fast neutron induced (n,p) and (n,α) reactions, systematics of excitation 2−59762
fission, excitation energy dependence of shell effects, review 2−59794
giant dipole and quadrupole states, excitation by protons 2−82937
giant dipole resonance, dynamic collective model 2−76774
giant resonance, isospin splitting 2−82948
heavy-ion induced reactions, excitation function and isomer ratios 2−76885
hole states, damping in giant dipole resonance 2−73983
intermediate structure in photon induced reactions 2−46227
isobaric analog resonances, form factor for stripping DWBA amplitude 2−63861
lifetimes of Coulomb-excited states meas. using plunger recoil distance technique 2−63756
light nuclei, study of scattering states, occurrence of narrow resonances at thresholds 2−73993
M1 and E2 excitation of levels with $K^{\pi}=1$, calc. of energy and reduced probabilities in random phase approx. 2−67136
mass fission asymmetry, depend. on compound excitation energy 2−46340
neutron capture giant resonances, failure of neutron valence model 2−46095
neutron resonance level distrib., non-statistical behaviour 2−67263
neutron resonance spectroscopy as a test of statistical theories 2−46074
neutron resonances, groupings of level spacing 2−67266
neutron states, single, available data compared with Woods-Saxon potential 2−67132
neutron widths distrib., exact no. of degree of freedom 2−67265

Nuclear excitation continued
- overlapping resonance, K-matrix formalism 2−52729
- p wave neutron capture at 25 keV in medium and heavy nuclei, structure of giant resonances 2−42567
- photonuclear reactions from correlated nucleon pairs 2−74060
- rare-earth nuclei, deformed, gamma and octupole states in Fermi liquid theory 2−46116
- residual nuclei, isomer ratios from low primary excitation 2−63754
- resonance energy estimating method, variational bounds formulation 2−46091
- resonance levels populated by (γ,γ'), props. 2−46103
- resonance parameters and the optical model 2−46217
- resonance reaction theory, bound and decay states 2−59737
- resonance theory, role of adjustable parameter Q_c 2−70426
- resonances; uncertainty in neutron strength function evaluation 2−63753
- resonances, ratio of average width to average spacing 2−42492
- spin current transitions in inelastic electro-excitation, matrix elements, using different vector potential decompositions 2−82839
- statistical theory of de-excitation, experimental contribution 2−59677
- two particle-two hole mixing in Hartree Fock calculations 2−42493
- vibrational levels, excitation by electrons in α-particle model 2−67134
- (n,2n) fast neutron reactions, systematics of excitation functions 2−76849
- (p, pn) reaction cross sections in light medium and heavy nuclei at high energies, calc. of excitation function 2−63875
- γ-ray laser, based on crysts. of long lived nuclear isomers 2−66762
- n resonance capture, radiation widths and non-statistical effects 2−67267
- n resonances, structure 2−67133
- ^{100}, low-lying states investigation via multiple Coulomb excitation 2−82910
- $^{204}(^{12}C,5n)^{211}Rn$, excitation function, cross sections, 50-200 MeV 2−74120
- ^{a}Fr, A=211-214, determ. of excitation functions in ^{12}C and ^{16}O reactions on ^{205}Tl, ^{209}Bi 2−74123
- ^{a}Pt, A=194, 195, 196, lifetimes of Coulomb-excited states meas. using plunger recoil distance technique 2−63756
- ^{221}Ac compound nucleus formed in $^{209}Bi+{}^{12}C$, $^{207}Pb+{}^{14}N$, $^{205}Tl+{}^{16}O$ reactions, yrast trapping study 2−46335
- ^{107}Ag, reactions with ^{20}Ne, ang. momentum limits, fusion excitation functions 2−59787
- ^{109}Ag lifetimes of Coulomb- excited states meas. using plunger recoil distance technique 2−63756
- ^{27}Al, ^{16}O and ^{20}Ne induced reactions, enhancement of direct processes at high ang. momenta 2−70482
- ^{27}Al, reactions with ^{16}O, ang. momentum limits, fusion excitation functions 2−59787
- $^{36}Ar(^{16}O,^{12}C)$, excitation of rot. bands in ^{40}Ca 2−83017
- ^{40}Ar, excited states observed in $^{40}Ar(\gamma,n_0)^{39}Ar$ reaction 2−46129
- ^{75}As, excitation functions for (d, 2n), (d, 4n), (d, 5n), (d, p), (d, p2n), (d, p3n), (d, 2p) reaction at 52 MeV 2−52824
- ^{75}As, neutron reson. level spacings, stat. distribs., deviations 2−67161
- $^{197}Au(d,2n)$, excitation function meas. between threshold and 12 MeV 2−49835
- $^{197}Au(d,p)$, excitation function meas. between threshold and 12 MeV 2−49835
- $^{197}Au(d,t)$, excitation function meas. between threshold and 12 MeV 2−49835
- $^{11}B(\alpha,t)^{12}C$, triton ang. distrib., 15-25 MeV, excitation functions 2−74112
- ^{9}Be, 1/2^{+} reson., coupled-channel calc. 2−76859
- ^{9}Be, 17.87 to 18.35 MeV, $^{6}Li(t,p)^{8}Li$ obs., low energy 2−63911
- $^{9}Be(^{3}He,\gamma\gamma)^{12}C$, 1.73-1.76 MeV, meas. of cross-section, search for $J^{\pi}=0$, T=2 resonance 2−82994
- $^{9}Be(^{3}He,\gamma\gamma)^{12}C$, 1.739 MeV, $J^{\pi}=0+$, T=2 reson. 2−70476
- $^{9}Be(^{3}He,\gamma\gamma)^{12}C$, T=2 reson. obs. 2−63914
- $^{9}Be(p,n)^{9}B$, excited-state-threshold reson. effects 2−79788
- $^{9}Be(p,p_0)^{9}Be$, excited-state-threshold reson. effects 2−79788
- ^{209}Bi analog resons., compound spreading widths 2−63835
- ^{243}Bk, excitation energy from $(\alpha,2n)$ reaction, time of flight obs. 2−76881
- ^{12}C-^{12}C scattering, nuclear molecular structure 2−49839
- ^{12}C, giant resonance, separation approximation in continuum shell model 2−59690
- ^{12}C, giant resons., $^{11}B(p,\gamma)^{12}C$ obs. 2−63772
- ^{12}C, μ^{-} capture, leading to specific final states, capture rate 2−74066
- $^{12}C(^{12}C,\alpha)^{20}Ne$, excitation functions 2−83022
- $^{12}C(^{16}O,^{16}O)^{12}C$, resonance like structure obs. with spin I=14 2−49837
- $^{12}C(\pi^{-},nn)$, study of excitation spectrum of residual nucleus 2−49816
- ^{40}Ca giant resonances in high-energy inelastic scatt. continuum 2−82967
- ^{48}Ca, elastic and inelastic proton scatt., isobaric analog states in ^{49}Sc 2−70390
- $Ca(\mu^{-},n)$, 2-13 MeV, meas. of neutron energy spectra, excitation of quasibound states of intermediate nucleus 2−52806
- ^{112}Cd lifetimes of Coulomb- excited states meas. using plunger recoil distance technique 2−63756
- $^{114}Cd(^{32}S,^{32}S\gamma)$ 50 MeV, determ. of sign of multiple Coulomb excitation interference term and static quadrupole moment 2−82893
- $^{114}Cd(^{3}He,\ ^{3}He)^{114}Cd$, interference between Coulomb and nuclear excitation amplitudes 2−46304
- $^{140}Ce(p,\ t)^{138}Ce$, $E_p=30.3$ MeV, strong and weak 0^{+} excitations 2−76847
- $^{142}Ce(p,\ t)^{140}Ce$, $E_p=30.3$ MeV, strong and weak 0^{+} excitations 2−76847
- ^{252}Cf, spontaneous fission, correlation between excitation energies of complementary fragments 2−46343
- ^{241}Cm, excitation energy from $(\alpha,2n)$ reaction, time of flight obs. 2−76881
- ^{50}Cr, octupole excitations 2−74022
- $^{133}Cs(^{20}Ne,4n)^{149}Nb$, excitation function, cross sections, 50-200 MeV 2−74120

Nuclear excitation continued
- ^{63}Cu, $^{65}Cu(\alpha,\alpha'\gamma\gamma)$ Coulomb excitation, 5.5, 7.0 MeV, meas. of angular distrib. and $\gamma\gamma$ angular correlations 2−63802
- $^{65}Cu(t,\ \alpha)$, $E_t=12$ MeV, excitation of ^{64}Ni, level struct. 2−76878
- $^{158}Dy(p,t)$, excited 0^{+} states population 2−63887
- $^{160}Dy(p,t)$, excited 0^{+} states population 2−63887
- $^{162}Dy(p,t)$, excited 0^{+} states population 2−63887
- ^{164}Dy, 4s-giant resonance, γ-ray spectra 2−67300
- Er, elastic and nucl. Raman scatt. of photons, giant dipole reson. 2−70431
- $^{164}Er(p,t)$, excited 0^{+} states population 2−63887
- ^{166}Er, ^{168}Er level calc. rel. to gamma oscillations in collective model for axially symmetric nuclei 2−52767
- $^{166}Er(p,t)$, excited 0^{+} states population 2−63887
- ^{151}Eu, neutron reson. spectroscopy, level population 2−63898
- ^{153}Eu, neutron reson. spectroscopy, level population 2−63898
- ^{18}F, excitation energy of fourth excited state 2−63777
- $^{19}F(d,\ \alpha)^{17}O$, 2.34 to 14.45 MeV, resonance structure in excitation function 2−67326
- $^{19}F(\gamma,xn)$, threshold −15MeV, meas. of giant resonance, obs. of fine structure 2−49783
- Fe, A=54, 56, 58, electroexciation of E2- and E3-transitions 2−70393
- ^{57}Fe, neutron resonances determ. from photoneutron cross-sections 2−46139
- ^{69}Ga, ^{71}Ga, Coulombic excitation of levels 2−52751
- ^{156}Gd, levels from ^{156}Eu decay, spins and parities 2−49751
- ^{158}Gd, levels from ^{158}Eu decay, spins and parities 2−49751
- $^{160}Gd(\gamma,n)$, 7-33 MeV, meas. of cross section, obs. of quadrupole resonance at 23.5 MeV 2−70436
- $^{160}Gd(\gamma,p)$, 7-33 MeV, meas. of cross section, obs. of quadrupole resonance at 23.5 MeV 2−70436
- $^{73}Ge(\alpha,\alpha'\gamma)$, Coulomb excitation, 2.6-4.0 MeV, test of quasiparticle-phonon coupling theories 2−74030
- $^{2}H(p,\gamma)^{3}He$, excitation function anomaly, $E_p=10-17.5$ MeV 2−59756
- ^{3}He broad reson. obs. in (p,α) and (p,2p) reactions 2−59760
- ^{4}He resonances in elastic deuteron-deuteron scattering 2−74104
- ^{174}Hf, role of K-quantum number in de-excitation following $Yb(\alpha,xn\gamma)^{174}Hf$ 2−46328
- ^{178}Hf, ^{180}Hf, J-depend. of level density from statistical props. of series of resonances 2−46171
- Hg isotopes, strongly deformed nuclei 2−46175
- $^{202}Hg(^{12}C,3n)^{211}Rn$, excitation function, cross sections, 50-200 MeV 2−74120
- ^{165}Ho, elastic and nucl. Raman scatt. of photons, giant dipole reson. 2−70431
- $^{41}K(\alpha,n)^{44}Sc$, excitation functions and isomer ratios calc. in stat. models 2−82997
- ^{86}Kr-^{87}Kr system, level structure investigated by inelastic proton scattering through isobaric analog resonances 2−46147
- $^{86}Kr(p,p)^{86}Kr$, 4.76-10.10 MeV, obs. of isobaric and analog resonances, study of core coupling in ^{87}Rb 2−46146
- ^{6}Li proton, elastic and inelastic scattering, 25-45 MeV, meas. of angular distrib. for excitation of excited states 2−55991
- ^{7}Li, Coulomb excitation of $^{1}._{2}{}^{-}$ state 2−76882
- $^{7}Li(\alpha,t)^{8}Be$, triton ang. distrib., 15-25 MeV, excitation functions 2−74112
- $\Lambda^{12}C\rightarrow{}^{1}H+\Lambda^{11}B$, unstable resonant state of ^{12}C obs. 2−79732
- Mn, excitation of 126 keV level by fast neutron scatt. 2−67245
- ^{94}Mo, low-lying states investigation via multiple Coulomb excitation 2−82910
- $^{96}Mo(p,xn)^{97-x}Tc$, $E_p=10$-80 MeV, excitation functions 2−74091
- ^{98}Mo, low-lying states investigation via multiple Coulomb excitation 2−82910
- $^{14}N(\pi^{-},nn)$ study of excitation spectrum of residual nucleus 2−49816
- ^{15}N giant dipole resonance, continuum shell model calc. 2−59691
- ^{21}Na, excited states, proton scatt. and radiative capture in ^{20}Ne obs. 2−55969
- ^{23}Na, reson. fluoresc. above 3 MeV, level struct. 2−74006
- ^{23}Na to 6.58 MeV, study using $^{26}Mg(p,\ \alpha'\gamma)^{23}Na$ and $^{23}Na(\alpha,\alpha'\gamma)^{23}Na$ 2−76789
- ^{90}Nb production by deuteron irradiation of Zr, determ. of excitation functions 2−74115
- ^{93}Nb, α-particle excitation 2−46152
- Nd(p,t) even isotopes, 5Z MeV , EXCITATION OF REMOVAL AND ADDITION TYPES OF QUADRUPOLE-PAIRING VIBRATIONAL STATES
- ^{20}Ne, second T=0 state obs. as compound nucleus in $^{19}F+p$ reactions 2−76785
- ^{60}Ni, giant reson. struct., low-lying collective states influence 2−74028
- ^{62}Ni, electroexcitation of E2- and E3-transitions 2−70393
- ^{16}O, compound-nuclear reson. at 14.8 MeV from $^{12}C(\alpha,\alpha_1\gamma_{4.43})^{12}C$ study 2−76869
- ^{16}O, fine structure of giant dipole resonance 2−46113
- ^{16}O, T=2 states, study by $^{14}N+d$ and $^{12}C+\alpha$ reactions 2−73999
- ^{16}O giant dipole reson., polarized proton capture reaction obs. 2−67149
- $^{16}O+{}^{12}C$ reaction, quasimolecular states, resonances in total reaction yield 2−74119
- $^{16}O(^{16}O,\ ^{12}C)^{20}Ne$, 17.5-30 MeV, cross-sections meas., possible $^{16}O+{}^{16}O$ quasimolecular resonance 2−52827
- $^{16}O(\pi^{-},nn)$, study of excitation spectrum of residual nucleus 2−49816
- $O(\mu^{-},n)$, 2-13 MeV, meas. of neutron energy spectra, excitation of quasibound states of intermediate nucleus 2−52806
- Os even-even isotopes, static quadrupole moments of first 2^{+} states, Coulomb excitation determ. 2−67177
- ^{186}Os level calc. rel. to gamma oscillations in collective model for axially symmetric nuclei 2−52767
- ^{188}Os, g-factors of several excited states determ. from perturbed angular correlation following ion implantation by Coulomb excitation 2−63829
- ^{192}Os, g-factors of several excited states determ. from perturbed angular correlation following ion implantation by Coulomb excitation 2−63829
- ^{32}P, first T=2 level analysis 2−63788
- Pb isotopes, excitation of low- lying octupole 2.6 MeV state by 14 MeV neutrons 2−67250

Nuclear excitation continued
^{206}Pb(n,n)^{206}Pb, particle vibration model of doorway states 2−46278
^{208}Pb, giant reson. struct., low-lying collective states influence 2−74028
^{208}Pb(n,n)^{208}Pb, particle vibration model of doorway states 2−46278
^{209}Pb giant reson. struct. from radiative neutron capture of ^{208}Pb 2−67307
Pb(μ^-,n), 2-13 MeV, meas. of neutron energy spectra, excitation of quasibound states of intermediate nucleus 2−52806
^{240}Pm, excitation energy from (α,2n) reaction, time of flight obs. 2−76881
^{141}Pr, neutron reson. level spacings, stat. distribs., deviations 2−67161
^{141}Pr(^{12}C,4n)^{149}Nb, excitation function, cross sections, 50-200 MeV 2−74120
^{141}Pr(p,γ)^{142}Nd, 6-17 MeV, isospin splitting of giant E1 excitations 2−82891
Pt, A=188, 190, 192, γ-ray spectra obs. lifetimes of isomeric states 2−70410
^{240}Pu, 35 s-wave resonances up to 500 eV 2−67312
Pu(p, 2n), excitation functions for prod. of fission isomers in Am isotopes 2−76894
Pu(t, 2n), excitation functions for prod. of fission isomers in Am isotopes 2−76894
Pu(t, 3n), excitation functions for prod. of fission isomers in Am isotopes 2−76894
^{226}Ra, total neutron cross section, below 1 eV, weak reson. level 2−67308
^{28}Si, possible nuclear molecule formation at 36.5 MeV in ^{16}O-^{12}C elastic scatt. 2−46122
^{28}Si octupole excitation of 29.5 MeV level by d inelastic scatt. 2−59776
^{30}Si, resonances obs. in α reactions on ^{26}Mg, spins, parties and widths 2−46123
^{152}Sm, Coulomb excitation including E2 and E4 interactions, third order perturbation treatment 2−70406
^{152}Sm, ground state rotational band excitation by electron scatt. 2−52764
^{152}Sm, neutron reson. spectroscopy, level population 2−63898
^{154}Sm, neutron reson. spectroscopy, level population 2−63898
S(μ^-,n), 2-13 MeV, meas. of neutron energy spectra, excitation of quasibound states of intermediate nucleus 2−52806
Sn(A=117, 119), Coulomb excitation using α-particle and ^{16}O projectiles 2−63810
^{181}Ta, ion bombardment, excited compound nuclei lifetime, $79<Z<89$, shadow effect obs. 2−76805
^{125}Te high-spin states and particle-core coupling 2−76781
Th (A=230,232), search for transitions to excited 0^+ states in (t,p) reactions 2−59785
^{230}Th, ^{232}Th, d and t induced fissions, obs. of subbarrier resonances 2−52834
^{203}Tl, muonic, first and higher level obs. 2−59961
^{203}Tl p-wave neutron reson. obs. by transmission meas. 2−76863
^{205}Tl levels deduced, resonance in ^{204}Hg(p, p)^{204}Hg 2−79767
^{205}Tl muonic, first and higher level obs. 2−59961
^{205}Tl p-wave neutron reson. obs. by transmission meas. 2−76863
^{169}Tm(n,γ), γ-ray spectra, study of resonances 2−46288
U(A=234,236,238), search for transitions to excited 0^+ states in (t,p) reactions 2−59785
^{235}U(α, 3n)^{236}Pu, 24.5-28 MeV, cross sections, fission isomer excitation functions 2−76880
^{238}U, elastic and nucl. Raman scatt. of photons, giant dipole reson. 2−70431
^{238}U, neutron resons., density and struct. 2−67185
^{182}W level calc. rel. to gamma oscillations in collective model for axially symmetric nuclei 2−52767
^{186}W, ion bombardment, excited compound nuclei lifetime, $79<Z<89$, shadow effect obs. 2−76805
^{88}Y production by deuteron irradiation of Zr, determ. of excitation functions 2−74115
^{174}Yb, 4s-giant resonance, γ-ray spectra 2−67300
^{90}Zr, giant reson. struct., low-lying collective states influence 2−74028

Nuclear explosions *see Explosions/nuclear*

Nuclear field theory *see Field theory, quantum*

Nuclear fission
see also Explosions/nuclear; Nuclear reactors, fission; Photofission
A=180-212, fission barriers and pot. energy surfaces 2−76890
barrier parameters from near-barrier fission and isomeric half-life data 2−46337
barriers, influence of axially asymmetric distortions 2−46339
barriers and odd-multipole shape distortions $84\leqslant Z\leqslant 120$ 2−70488
binary, double shell model 2−83038
charge polarization effects for liquid drop model of fissioning nuclei 2−79809
collective modes rel. to coupling terms in Hamiltonian 2−56007
Colomb fission cross sections, nucl. forces influence 2−83033
compound nuclei, direct type reactions, fission barrier value 2−70485
Coulomb interaction, Gaussian approximations 2−59664
double potential barrier, effect of deformation-dependent inertial parameter on penetration 2−79814
double spin isomers, kinetics of population 2−74124
droplet model, generalization of liquid drop model 2−82867
electron induced, second Born-Sinha approximation cross sections 2−79813
electron-induced cross-sections in first Born modified approximation 2−70494
even nuclei, correlation between properties of low-lying collective levels and fission process observables 2−42596
fragment anisotropies, fission widths and mass distrib. 2−46282
fragment ranges in U-Al alloys, UO_2, U_3O_8 2−83028
glass, Standard Reference Material, thermal stability of fission tracks 2−79686
heavy elements, reactions by protons $\leqslant$3GeV, spallation-fission competition 2−67218
heavy nuclei, by ions, direct fission 2−70493
heavy nuclei, review of Soviet work (1938 to 1971) 2−76887

Nuclear fission continued
heavy nuclei, total energy surfaces, single-particle model calculation 2−70489
isomer/prompt and neutron/prompt cross section ratios, stat. theory 2−83034
light elements, single-particle effects on fission probabilities 2−52829
mass fission asymmetry, depend. on compound excitation energy 2−46340
missed reson. levels in low-energy neutron cross sections 2−79815
models, fission barrier heights energy release and fragment energy partition processes, review 2−59799
neutron, active transmission line analog 2−49863
neutron cross sections, low energy, ambiguities in R-matrix parameters 2−67255
neutron induced, energy dependence of Γ/Γ_n, analysis using structure of single particle spectrum 2−49854
neutron reson. reactions, low-energy cross sections analysis, R-matrix parameters 2−76857
neutron-induced, conf., Bombay (1971) 2−59793
neutron-induced, low energy, prompt radiation emission 2−59797
nondestructive techniques for fission rates meas. in fuel elements 2−56040
nuclear energy and environment, XVIIth Nuclear Congress of Rome 2−59807
phase transitions, models 2−46338
positron induced, second Born-Sinha approximation cross sections 2−79813
positrons-induced cross-sections in first Born modified approximation 2−70494
potential energy surface evaluation by Strutinsky's method 2−52830
prompt gamma emission, review 2−59805
prompt neturon emission models 2−79816
radiation emission, review 2−59798
shell effects, excitation energy dependence, review 2−59794
source in infinite water, meas. of neutron spectrum 2−83055
space fissioning nuclei, new technique for detection and location 2−83039
spontaneous activities attributable to decay of possible super-heavy elements produced in seismology reactions 2−63781
superheavy elements, lowering of calc. barriers 2−49848
superheavy nuclei, half-lives calc. w.r.t. spontaneous fission 2−76816
symmetric, of superheavy nuclei and overabundance of rare earths in stellar systems 2−54998
ternary, in compound nuclear reactions 2−70484
thermal neutron induced, prompt neutron emission and associated fission energetics 2−70491
three fragment fission, review 2−63929
total fission width, distribution 2−59796
transplutonium elements, cross-sections for thermal fission and capture 2−76851
widths study using statistical assumption 2−46341
(d, p) reaction on fissioning nucleus, calc. of cross section for many-channel many level final states 2−74059
Am isotopes, fission isomer excitation functions 2−76894
^{242}Am^m isomeric fission, fission modes meas. using ^{242}Pu(d, 2n) reaction 2−70496
Au, recoil props. of rare earth nuclides 2−82971
^{249}Bk spontaneous fission, average neutron yield 2−83026
^{249}Cf, neutron induced, meas. of fragment angular distrib. 2−83035
^{252}Cf, development as source for neutron radiography 2−55890
^{252}Cf, fission rate, decay constant, profile and distribution determ. with solid state track detector 2−46060
^{252}Cf, long range α-particle emission 2−83037
^{252}Cf, neutron spectra 2−46350
^{252}Cf, spontaneous, instantaneous fission neutrons depend. on fragment mass 2−59790
^{252}Cf spontaneous, emission of ^{5}He obs. in correlation measurement 2−74125
^{252}Cf spontaneous 2−76889
^{252}Cf spontaneous fission, instantaneous neutron spectrum in low-energy region 2−83025
^{252}Cf triple fission, angular meas. of γ-radiation yield 2−49852
^{245}Cm, cross-sections for thermal fission and capture, resonance integral data 2−76851
^{245}Cm, thermal-neutron induced, determ. of mass yields 2−59791
Fm (A=252, 258, 264), symmetric and asymmetric fission probabilities from two-centre model 2−46342
Np (A=237, 238), by neutrons, relative yields of Xe isotopes 2−46346
^{237}Np, cross-sections by 20 eV to 7 MeV neutrons from nuclear explosive expt. 2−70492
^{237}Np, proton induced, 20-85 MeV, ^{134}Cs isomer obs. 2−63932
^{237}Np proton-induced, 20-85 MeV, meas. of nuclear charge dispersion 2−79812
^{208}Pb, single-particle effects on fission probabilities 2−52829
^{210}Po in ^{206}Pb(α,f) reaction, 29-46 MeV 2−67337
Pu(A=240, 242), scission configurations 2−49849
PuO_2 fuel neutron radiation characts. 2−83130
^{238}Pu, induced by 13.4-14.8 MeV neutrons, fragments angular anisotropy 2−52832
^{238}Pu cross section meas. using neutrons from underground nuclear explosion Persimmon 2−46347
^{239}Pu, ^{6}He and alpha-particle emission 2−76889
^{239}Pu, by neutron capture, contribution to burn up of plutonigen reactor fuel 2−74149
^{239}Pu, capture-to-fission cross section meas. 2−56011
^{239}Pu, effective delayed neutron fractions for two fast crit. assemblies 2−83105
^{239}Pu, fission rate, decay constant, profile and distribution determ. with solid state track detector 2−46060
^{239}Pu, induction by fast neutrons, β and γ residual powers 2−74128
^{239}Pu, neutron-induced, anomalous effect of neutron spectrum change on mass yields 2−74127
^{239}Pu, neutron induced autoradiography of bone 2−78660
^{239}Pu, neutron spectra 2−46350
^{239}Pu, relative fission cross section in low resonance region, measurement and normalization 2−56010

Nuclear fission continued

- ^{239}Pu, spontaneous, produced in ^{240}Pu(γ,n) reaction, meas. of excitation function 2−67210
- ^{239}Pu, subthermal-, thermal-, and reson.-neutron fission, long-range α-particle emission 2−83032
- ^{239}Pu, thermal neutron induced, kinetic energy distribution 2−70490
- ^{239}Pu, total fission activity, nondestructive absolute determination 2−42594
- ^{239}Pu fissioned by thermal neutrons, fission fragments β decay, inner bremsstrahlung, recoil radiation from 2−63843
- ^{240}Pu, 20 eV to 30 keV, neutron capture, fission, and total cross sections 2−82977
- ^{240}Pu, cross-section meas. 2−67312
- ^{240}Pu, lifetime estimates for asymmetric spontaneous fission including shell effects 2−42595
- ^{240}Pu isomer, identification of rotational band 2−74126
- ^{240}Pu neutron cross section data eval. 2−82986
- ^{242}Pu, neutrons below 1 keV, fission widths 2−67313
- ^{244}Pu fission tracks, evidence in lunar rock 3.95×10^9 years old 2−69137
- ^{240m}Pu spontaneously fissioning isomer, production probability in thermal neutron capture reactions 2−79818
- ^{181}Ta, He-ion induced at 41 and 65 MeV, radiochemical study of fission fragment mass distribution and total cross section 2−79810
- ^{230}Th, ^{232}Th, d and t induced, obs. of subbarrier resonances 2−52834
- ^{230}Th, neutron-induced fission rel. to determination of effective moment of inertia of ^{231}Th 2−59723
- ^{232}Th, induced by 13.4-14.8 MeV neutrons, fragments angular anisotropy 2−52832
- ^{235}U, effective delayed neutron fractions for two fast crit. assemblies 2−83105

products

- — 2−70498
- actinides, yields predicted by extrapolation of recommended values of fission product yields 2−46355
- chamber for isomeric fission modes meas. 2−49856
- in coated fuel particles, products distrib. determ. by ion sputtering 2−46390
- coupler fragments, evaporation 2−59802
- delayed neutron emission, β-strength functions and gross properties 2−49855
- delayed neutron emissions, applic. of gross theory of β-decay 2−46352
- delayed neutrons, exptl. data on precursors, total number of neutrons per fission, half-lives, yields, energy spectra 2−46354
- delayed neutrons, review of present status 2−83047
- FISP computer programme for generating fission product inventories for nuclear fuel 2−76955
- fissile nuclei, cross-sections for low energy neutrons, statistical analysis 2−67340
- fragment stopping in gases, kinetic energy deficit and energy distrib. width 2−63937
- fragment stopping in gases, range distrib. 2−63936
- fragment transport from fission sources by He-jet technique 2−73900
- fuel burn-up determ. by gamma and mass spectrometric methods 2−75408
- fuel burn-up monitoring and measurement methods, review 2−74188
- gas content of coated fuel particles 2−42664
- gas extracted from irrad. fuel pins, internal press. meas. 2−42666
- gas release from coated irrad. kernels 2−42665
- gas release from irrad. fuel pins, meas. methods 2−42667
- gas release in steady-state reactor operation, analytical method of calc. 2−46386
- high temperature gas-cooled, effects of transverse flow through graphite on fission product movement 2−42642
- high temperature reactor fuel cycle, burn-up determ. 2−74184
- high-altitude explosion, fission fragment localization method 2−51630
- ionization probabilities for K and L-shell daughter atoms 2−46351
- irradiated nuclear fuel, analysis for actinides and burn-up determ. 2−74183
- irradiated nuclear fuels, determ. of fission products by isotopic dilution 2−75400
- kinetic energy distribution in thermal neutron fission of ^{233}U and ^{239}Pu 2−70490
- mass and charge distribution, theory 2−59804
- mass distributions and related phenomena, review 2−59803
- mixed oxide nuclear fuels, burn-up and isotopic distribution meas. 2−75401
- neutron emission study using ^{3}He spectrometer, structure determ. 2−67150
- neutron spectra of ^{235}U, ^{239}Pu and ^{252}Cf 2−46350
- non-destructive burn-up determ. for spent fuel elements using heat output 2−74181
- nuclear fuel cycle, analytical methods, symposium (Vienna, Nov.-Dec. 1971) 2−74151
- photofission, single fragment kinetic energy spectra, fragment mass distribution and angular distribution 2−70495
- post-irradiation analysis of nuclear fuels for burn-up and heavy isotope content 2−75402
- prompt neutron emission and associated fission energetics resulting from thermal neutron induced fission 2−70491
- prompt neutrons, review 2−59805
- radioactive fallout from test, γ-ray spectra and fractionation effect 2−79819
- rare gas isotopes yields in 14 MeV fission of ^{233}U, ^{235}U, ^{238}U and ^{232}Th 2−59792
- in reactor fuel, contribution to post-shutdown heat release 2−79831
- release of gaseous products from high temperature fuel materials 2−52884
- specific activity calculation, algorithm 2−83027
- spontaneously fissioning isomers, search for production with 600 MeV protons on U, Th, Bi and Pb 2−79811
- transplutonium series, number of secondary neutrons, review 2−56012
- ^{a}Sn, A=123, 125, 128, cumulative yields from thermal-neutron induced fission of ^{235}U deduced from γ-ray intensities 2−46345
- ^{a}Xe, A=131, 132, 133, spin assignments and γ-ray multipole mixing ratios 2−46207

Nuclear fission continued

products continued

- Ac isotope production in ^{209}Bi + ^{12}C reaction, excitation function meas. 2−46349
- ^{242}Am^{m} isomeric fission, mass and kinetic energy distributions 2−70496
- ^{140}Ba cumulative formation in ^{237}Np proton induced fission, 20-85 MeV 2−79812
- ^{209}Bi, isomer ratios of ^{95}Nb product 2−63933
- ^{249}Cf, neutron induced, meas. of fragment angular distrib. 2−83035
- ^{252}Cf, ang. momentum of primary products formed in spontaneous fission 2−49850
- ^{252}Cf, β-spectrum of products and associated inner bremsstrahlung radiation 2−59806
- ^{252}Cf, fission neutron spectrum from 0.002 to 1 MeV 2−46353
- ^{252}Cf, gamma-neutron competition in de-excitation mechanism of fission fragments 2−56015
- ^{252}Cf, nucleon coupling effect in fragments 2−59790
- ^{252}Cf, search for π^0 production 2−46059
- ^{252}Cf, spontaneous fission, correlation between excitation energies of complementary fragments 2−46343
- ^{252}Cf, spontaneous fission ang. distrib. of α-particles 2−49851
- ^{252}Cf, ternary fission, neutron energy spectrum 2−67338
- ^{252}Cf, X-ray spectra of products rel. to charge parity 2−70497
- ^{252}Cf fission fragments energy loss in argon 2−59800
- ^{252}Cf neutron sources, electronic assay by detection of thermalized neutrons in moderator 2−42597
- ^{252}Cf spontaneous, emission of ^{5}He obs. in correlation measurement 2−74125
- Cm, A=244, 246, 248, spontaneous fission, neutron yield 2−76888
- ^{245}Cm, thermal-neutron induced, determ. of mass yields 2−59791
- Cs isotopes produced in ^{237}Np proton induced fission, 20-85 MeV, determ. of independent formation cross sections 2−79812
- ^{134}Cs isomer ratios in ^{237}Np fission with protons 2−63932
- ^{137}Cs in fission of ^{235}U and ^{239}Pu, contribution to burn up of plutonigen reactor fuel 2−74149
- ^{256}Fm, spontaneous, mass distribution 2−46344
- ^{134m}I, 3.8 min, from slow neutron fission of ^{235}U, identification and characterization 2−52759
- Kr isotopes, thermal neutron fission of ^{235}U, odd-even effect in element yield distribution 2−63935
- Np (A=237, 238), by neutrons, relative yields of Xe isotopes 2−46346
- from ^{239}Pu fissioned by thermal neutrons, inner bremsstrahlung, recoil radiation from β decay 2−63843
- ^{238}Pu, nuclear fission induced by 13.4-14.8 MeV neutrons, fragments angular anisotropy 2−52832
- ^{239}Pu, irrad., absolute yields 2−70499
- ^{239}Pu, neutron-induced, anomalous effect of neutron spectrum change on mass yields 2−74127
- ^{240}Pu, peak-to-peak ratio in fragment mass distrib. from spontaneous fission 2−42595
- ^{106}Ru in fission of ^{235}U and ^{239}Pu, contribution to burn up of plutonigen reactor fuel 2−74149
- ^{231}Th, highly deformed, nuclear spectroscopy 2−56014
- ^{232}Th, induced by 13.4-14.8 MeV neutrons, fragments angular anisotropy 2−52832
- ^{232}Th(n,f), isomer yield ratio of ^{115m}Cd and ^{115g}Cd 2−63808
- (U, Pu)O$_2$ mixed-oxide with initial addition of fission product elements, postirradiation obs. 2−76945
- from ^{235}U fissioned by thermal neutrons, inner bremsstrahlung, recoil radiation from β decay 2−63843
- UC fuel to simulate burn-up of 100000 MWd/t, thermodynamic study 2−67351
- inUO$_2$-PuO$_2$, mixed fuel, product migration due to irrad. 2−59852
- UO$_2$-PuO$_2$ fuels, simulated fission product transport 2−52867
- UO$_2$, simulation of gaseous fission products for nuclear fuels 2−79838
- UO$_2$ reactor fuel, burn-up meas. from mass spectrometry of stable fission-product Nd 2−74182
- ^{233}U, fast neutron bombardment, fission fragment distribution, yield and kinetic energy rel. to excitation energy 2−76893
- ^{233}U, product ang. distrib. anisotropy, neutron-induced fission from 0.4 to 2000 eV 2−59801
- ^{233}U, thermal neutron induced, determ. of nuclear charge distrib. in mass chain 132 2−52831
- ^{235}U, fragment range in Be, C, Al and Si 2−61125
- ^{235}U, irrad., absolute yields 2−70499
- ^{235}U, neutron induced, yields and energy spectra of light isotopes produced 2−49857
- ^{235}U, ranges of ^{99}Mo and ^{132}Te fragments in W 2−47786
- ^{235}U, thermal neutron induced, cumulative yield of 83-sec ^{136}I 2−63934
- ^{235}U, thermal neutron induced, determ. of nuclear charge distrib. in mass chain 132 2−52831
- ^{235}U, thermal neutron induced, meas. of mass and energy distrib. of fragments 2−79817
- ^{235}U fragment deceleration in light media 2−56013
- ^{235}U resonances, correl. between fission channel effects and fragment kinetic energies 2−67336
- ^{238}U, 450 MeV proton induced, mass yield distrib. and charge dispersion 2−46348
- ^{238}U, α-particle induced (E=25-120 MeV), distrib. of Cs isotopes produced 2−74130
- ^{238}U, fast-neutron fission, energy depend. of ν 2−56009
- ^{238}U, irrad., absolute yields 2−70499
- ^{238}U photofission product yields 2−74129
- ^{238}U(n,f), isomer yield ratio of ^{115m}Cd and ^{115g}Cd 2−63808
- Xe in lunar breccia, fission product from extinct ^{244}Pu 2−66145
- Xe isotopes, thermal neutron fission of ^{235}U, odd-even effect in element yield distribution 2−63935
- ^{95}Zr in fission of ^{235}U and ^{239}Pu, contribution to burn up of plutonigen reactor fuel 2−74149

uranium

- (U,Pu)C and (U,Pu)$_2$C$_3$, distribution coeffs. of U and Pu, microprobe analysis 2−67352
- binary and ternary fission, proton induced, cross sections 2−63931
- effective fission cross section ratio $\sigma^{235}/\sigma^{238}$, meas. by solid state track detects. 2−56008

Nuclear fission continued
uranium continued
missed reson. levels in low-energy neutron cross sections 2−79815
neutron activation analysis of rocks and cores 2−84690
recoil props. of rare earth nuclides 2−82971
in UO_2 clusters, fast fission ratios meas. 2−42671
UO_2 deposit thickness, effect on fission fragment double kinetic energy meas. 2−55895
^{233}U, ^{235}U, ^{6}He, ^{3}H emission spectra 2−76889
^{233}U, 14 MeV, rare gas isotopes yields 2−59792
^{233}U, fast neutron bombardment, fission fragment distribution, yield and kinetic energy rel. to excitation energy 2−76893
^{233}U, product ang. distrib. anisotropy, neutron-induced fission from 0.4 to 2000 eV 2−59801
^{233}U, thermal neutron induced, kinetic energy distribution 2−70490
^{233}U, thermal neutron induced, determ. of nuclear charge distrib. in mass chain 132 2−52831
$^{235}U/^{238}U$ rate ratios, determ. in CONSORT reactor 2−83094
^{235}U, 14 MeV, rare gas isotopes yields 2−59792
^{235}U, by neutron capture, contribution to burn up of plutonigen reactor fuel 2−74149
^{235}U, capture-to-fission cross section meas. 2−56011
^{235}U, cross-sections for low energy neutrons, statistical analysis 2−67340
^{235}U, enriched U in paraffin, homogeneous critical assemblies 2−70536
^{235}U, epithermal neutron induced fission, meas. of gamma-ray spectra 2−52820
^{235}U, Fermi age of emitted delayed neutrons 2−70498
^{235}U, fission rate, decay constant, profile and distribution determ. with solid state track detector 2−46060
^{235}U, fragment range in Be, C, Al and Si 2−61125
^{235}U, Ge isotopes identification 2−76814
^{235}U, induction by last neutrons, β and γ residual powers 2−74128
^{235}U, irrad., absolute yields 2−70499
^{235}U, neutron induced, yields and energy spectra of light isotopes produced 2−49857
^{235}U, neutron induced, yields of ^{128}Sb, ^{129}Sb, ^{130}Sb and ^{130}Sn 2−83036
^{235}U, neutron spectra 2−46350
^{235}U, ranges of ^{99}Mo and ^{132}Te fragments in W 2−47786
^{235}U, ratio of ternary to binary fission cross sections induced by resonance neutrons 2−83031
^{235}U, thermal-neutron-induced, emission of prompt. γ-rays 2−76892
^{235}U, thermal neutron induced cumulative yields of 40.1 min ^{123}Sn, 9.6 min ^{125}Sn, ^{128}Sn 2−46345
^{235}U, thermal neutron induced, meas. of mass and energy distrib. of fragments 2−79817
^{235}U, thermal neutron induced, determ. of nuclear charge distrib. in mass chain 132 2−52831
^{235}U, thermal neutron induced, independent yields of Kr and Xe isotopes, odd-even effect 2−63935
^{235}U, thermal neutron induced, cumulative yield of 83-sec ^{136}I 2−63934
^{235}U, thermal neutron induced, use of kinetic energy data to determ. barrier parameters for fusion of fragments 2−49847
^{235}U fissioned by thermal neutrons, fission fragements β decay, inner bremsstrahlung, recoil radiation from 2−63843
^{235}U fragment deceleration in light media 2−56013
^{235}U resonances, correl. between fission channel effects and fragment kinetic energies 2−67336
$^{235}U(\alpha, 3n)^{236}Pu$, 24.5-28 MeV, cross sections, fission isomer excitation functions 2−76880
^{236}U, fission isomeric state 2−59795
^{236}U, symmetric and asymmetric fission probabilities from two-centre model 2−46342
^{236}U fission isomer, search for conversion electrons 2−49853
$^{238}U/^{235}U$ fission cross section ratio, 1-5 MeV 2−83030
$^{238}U/^{235}U$ fission cross section ratio meas. in 2-3 MeV range using time-of-flight technique 2−83029
^{238}U, 14 MeV, rare gas isotopes yields 2−59792
^{238}U, 450 MeV proton induced, mass yield distrib. and charge dispersion 2−46348
^{238}U, α-particle induced (E=25-120 MeV), distrib. of Cs isotopes produced 2−74130
^{238}U, Colomb fission cross sections, nucl. forces influence 2−83033
^{238}U, fast-neutron fission, energy depend. of ν 2−56009
^{238}U, irrad., absolute yields 2−70499
^{238}U, long range α-particle emission 2−83037
^{238}U, n-and α-induced, lifetime determ. using shadow effect 2−76891
^{238}U, neutron-induced, blocking effect 2−63930
^{238}U, photofission cross sections near thresholds 2−83024
^{238}U, prompt and delayed, photofission 2−83039
^{238}U photofission, cross sections and angular distrib., obs. of band of rotation levels 2−83040
^{238}U photofission product yields 2−74129
^{238}U surrounded by water moderator, neutron multiplication expts. 2−42691
$^{238}U(n,f)$, isomer yield ratio of ^{115m}Cd and ^{115g}Cd 2−63808
Nuclear fission reactors *see Nuclear reactors, fission*
Nuclear forces
see also Field theory, quantum/meson field
− 2−70356
− 2−67117
A=180-212, fission barriers and pot. energy surfaces 2−76890
Alt-Grassberger Sandhas eqns., solution above three-particle break-up threshold using Yukawa potentials 2−70351
binding energy, continuum effects in Strutinsky calculations of shell corrections 2−52724
binding energy, relativistic Hartree-Fock approximation 2−42490
bond nature, state-of-the-art review 2−59665
charge symmetry breaking and nn scatt. 2−59663
charge symmetry violation rel. to $^{2}H(d,p)^{3}H$ and $^{2}H(d,n)^{3}He$ reactions 2−70473
closed-shell and one nucleon outside closed-shell nuclei, third-order corrections to energy 2−76776
Colomb fission cross sections depend. 2−83033
Coriolis anti-pairing rel. to A-depend. of crit. spin 2−82849

Nuclear forces continued
correlated wave functions and effective operators determ. using unitary separable approx. to two-body reaction matrix 2−63741
correlative basis in few nucleon problem 2−46081
Coulomb displacement energy, odd-even effects 2−76762
Coulomb energies in 1p shell 2−67122
Coulomb energy calc., relativistic corrections 2−46076
Coulomb interaction, Gaussian approximations 2−59664
Coulomb interference in half-shell two-nucleon t-matrix derived from Hamada Johnston potential 2−52722
Coulomb shifts and energies, isospin mixing, 1p shell calcs. 2−63739
coupled channel calculation method 2−55948
deformed doubly odd nuclei, effective neutron-proton interaction 2−70381
density- and momentum-dependent delta function interaction 2−70350
double-closed-shell nuclei, Hartree-Fock calcs. using modified delta interaction 2−63747
effective interaction in perturbation expansion form 2−73975
energy spectra Gaussian distrib. in *j* shell 2−67115
even-even nuclei, symmetry energy 2−79729
final state interactions, review 2−63487
finite nuclei, NN phase shift data rel. to solution of Bethe-Goldstone equation, applic. to ^{18}O and ^{18}F 2−46067
finite nuclei A=16−208, calc. of density dependent effective interactions using HF theory and local density approx. 2−79709
folded Yukawa singleparticle potential with two centres 2−70354
s,d)-Hartree-Fock calc. of simple effective interaction 2−49710
Hf odd isotopes, Coriolis coupling of N=6 states 2−79760
hypernuclei, light, binding energy, applic. of Garvey-Kelson mass formulas 2−46115
hypernuclei, p-shell props., Majorana forces influence 2−59685
hyperon-nucleon interaction in infinite matter, binding energy 2−73967
infinite and finite matter theory 2−63746
Jastrow method for nuclear matter, pair distribution function 2−76773
light nuclei, effective interactions as sum of Talmi integrals 2−76764
local density approx. calc. of elastic electron-^{4}He scatt. form factor 2−83004
local potentials, separable energy-dependent approx. of 2-body t-matrix 2−73969
magic nuclei, shell effects, self-consistent calc. 2−63783
many-particle matrix elements in seniority scheme, sum rules 2−55949
mirror nuclei, meson exchange corrections to β decay 2−42414
mirror nuclei residual n-p interaction derived from binding energy data 2−63731
momentum-dependent potential calcs. of single-particle energies 2−59673
morse type effective potential for Thomas- Fermi calcs. 2−52723
neutron stars, models 2−44864
neutron-deuteron elastic scattering above breakup threshold 2−63737
neutron-neutron scatt. length from $^{2}H(n,p)2n$ reaction obs. 2−76858
neutron-proton correlation effects in medium weight spherical nuclei 2−67123
neutron-proton local $^{1}S_0$ potential, phase shifts calc. 2−82844
non-local potential for single-particle properties of nuclei as function of A and Z 2−70349
nucleon-deuteron elastic scatt., variational scatt. 2−76767
nucleon-deuteron elastic scattering, perturbative calc. of spin observables 2−76768
nucleon-nucleon potential, off-shell effects studied in $^{2}H(p,2p)n$ reaction 2−63877
nucleon-nucleon potentials, saturation properties in nuclear matter 2−55947
nucleon-nucleon repulsion, short-range, and low energy three-nucleon parameters 2−46080
on- and off-shell T matrix, variational approach 2−73972
one-boson exchange potentials and relativistic nuclear matter calcs. 2−63744
optical potential, calc. of spin-orbit component from matter distribs. for spherical and deformed cases 2−70361
optical potential spin, isospin and spin-orbit dependence 2−46218
pairing correl., unified description 2−67116
pairing tendencies of T=1 and T=0 interactions 2−79719
parity violating potential, 2π exchange contribution to $\Delta T=1$ part 2−82852
particle-hole and particle-particle residual interaction effects on moments of inertia and gyromagnetic ratio 2−73988
potential energy surface structure and mass asymmetry in fission 2−46340
potential energy surfaces in two-centre shell model 2−63735
potential models, folding and deformed, for inelastic scatt. 2−46210
potential scattering, summation rules for rectangular pit, Gaussian, Yukawa and separable potentials 2−70355
potentials, phenomenological and meson theoretical, analysis of baryon-baryon scattering 2−49777
proton-proton bremsstrahlung calcs. at unequal angles in coplanar geometry 2−76769
rank-two separable potentials, trinucleon properties 2−76778
relativistic one-boson-exchange potential applied to two-nucleon data 2−76763
s-d shell, (44) and (60)+(06) interactions 2−70345
saturation of binding energies, sufficient conditions 2−46079
SCF theory, using relativistic form of generalized one Boson exchange potentials for NN force 2−70346
seniority number generalizations and binding energies 2−59666
single-particle potentials, nuclear rearrangement, (d, t) and (p, 2p) reactions discussed 2−73974
Skyrme's interaction, in asymptotic basis 2−73968
spherical nucleus, isobaric configuration 0^{+}-states, proton-neutron single particle potentials 2−76770
spherical Woods-Saxon potential well, asymptotic expansion for eigenvalue density 2−73330
spin-orbit potential, single particle, exchange part from N-N spin-orbit interaction 2−46082
T=1 interaction, non-pairing aspects, multipole character 2−70352
three and four nucleon systems, tensor forces 2−52732

Nuclear forces continued
three nucleon low-energy parameters in doublet spin-state, soln. of Skornyakov – Ter-Martirosyan eqns. 2 – 67118
three-body problem, Coulomb effects 2 – 67124
three-body problem, Faddeev – Lovelace equations in eikonal approximation 2 – 70348
three-body problem, potential harmonics 2 – 67119
three-body system, model for short-range correlation 2 – 46078
three-nucleon integral equations, Bateman method and algebraic solution 2 – 52733
three-nucleon problem, two-term nonlocal separable potentials 2 – 82845
three-nucleon problem with potential containing repulsive core 2 – 55954
three-nucleon system, calcs. using Reid and Gammel-Brueckner potentials 2 – 49723
three-nucleon systems, Faddeev eqns., bound-state wave functions 2 – 63738
three-parameter N-N soft-core central potential 2 – 73973
three-particle amplitude, Gilbert-Schmidt expansion 2 – 79728
tri-nucleon systems, effect of $\Delta(1236)$ resonance 2 – 49712
trinucleon bound state, properties from exact solution of Faddeev equations with realistic nuclear forces 2 – 46077
trinucleon energy using unitary pole approx. to Reid's soft core potential 2 – 49724
two-body matrix elements including bound states, Talmi-Moshinsky procedure 2 – 73966
two-body spin-orbit interaction in inelastic scattering 2 – 70430
two-body unobservable pot., observable many-body effects 2 – 63734
two-nucleon correl. depend. of forward deuteron emission in proton-nucleus collisions 2 – 59752
two-nucleon interaction in nuclear matter theory 2 – 73981
unitary pole approximation, quality of three-body wave function 2 – 49705
velocity-dependent in DWBA of inelastic nucleon scattering 2 – 74069
Woods-Saxon potential calc. and single neutron states in deformed nuclei 2 – 67132
$Z=59$ to 69, nucleon separation and pairing energies 2 – 52743
dd elastic scatt. rel. to channel spin nonconservation 2 – 59775
ΛN and ΛNN potentials in $^{3}_{\Lambda}$h, $^{4}_{\Lambda}$H and $^{4}_{\Lambda}$He 2 – 82876
ΛN interaction and hypernuclei 2 – 67139
Λp interaction, one boson exchange potential model including ΣN channel 2 – 82783
N-N effective interaction, RPA renormalization in HF basis 2 – 73971
N-N interaction, off energy shell properties studied by obs. of non-coplanar np bremsstrahlung 2 – 79718
N-N semirealistic interaction No. 2 of Saunier and Pearson used in light nuclei systematics 2 – 63733
n-p interaction in odd-odd nuclei, systematics 2 – 73970
N, nucleus scattering, low density expansion of optical model potential 2 – 76824
NN bremsstrahlung, Burnett-Kroll soft-proton theorem, application 2 – 82855
NN phase equivalent interactions, for ^{3}H calc. 2 – 76779
NN potential, nonlocal potential development 2 – 82856
nd 14 MeV elastic scattering, exact unitary model calcs., soln. of Faddeev eqns. 2 – 79800
nd scattering, low-energy S-matrix theory, construction of sum rules 2 – 76758
nd total cross sections, 25-60 MeV 2 – 82982
nn total cross sections, 25-60 MeV 2 – 82982
pp bremsstrahlung, cross section calcs. including relativistic corrections to Pauli-Schroedinger eqn. 2 – 67054
πN potential for use in low energy nuclear physics 2 – 63740
^{26}Al, effective neutron-proton interaction 2 – 70381
^{28}Al, effective neutron-proton interaction 2 – 70381
Ar($A=36$, 38), effective interactions in upper s-d shell 2 – 49737
^{8}Be nucleon-nucleon potential, α-particle cluster model 2 – 82880
^{209}Bi analog resons., compound spreading widths due to Coulomb interactions 2 – 63835
^{12}C, inelastic neutron scatt., E_n 7.48 MeV, spin-flip probability 2 – 82983
Cl ($A=36$,37), effective interactions in upper s-d shell 2 – 49737
^{34}Cl, effective neutron-proton interaction 2 – 70381
F($A=18$, 19, 20), effective interactions in s-d shell 2 – 49728
^{18}F, effective neutron-proton interaction 2 – 70381
^{20}F, effective neutron-proton interaction 2 – 70381
^{54}Fe, effective two-body interaction 2 – 70394
^{56}Fe, effective two-body interaction 2 – 70394
^{3}H, binding energy, reaction matrix approach 2 – 59687
^{3}H, ground state with realistic interactions 2 – 76777
^{3}H, off-shell variation of binding energy for exactly phase-equivalent separable potentials 2 – 55956
^{3}H magnetic moment, two-nucleon one-pion exchange contributions 2 – 67143
^{3}He, Coulomb energy, meson-exchange corrections, calc. using model for short-range correlation 2 – 46078
^{3}He magnetic moment, two-nucleon one-pion exchange contributions 2 – 67143
^{4}He, binding energy, reaction matrix approach 2 – 59687
^{4}He, ground state, effect of tensor force 2 – 73996
^{4}He, third-order corrections to binding energy 2 – 76776
^{5}He, third-order corrections to single-particle energies 2 – 76776
^{180}Hf, investigation of parity non-conserving force between nucleons by meas. of circular polarization of γ transitions 2 – 63840
^{180}Hf, parity admixture meas. 2 – 59726
^{166}Ho, residual interaction effect on rotational spectrum 2 – 46168
K($A=37$, 38), effective interactions in upper s-d shell 2 – 49737
^{41}K, circular polarization calc. for $7/2^- \rightarrow 3/2^+$ transition using $\Delta T=1$ parity violating potential 2 – 82852
^{6}Li, α-d clustering, rel. to ^{6}Li(p,pd)^{4}He cross sections 2 – 63879
NN spin-orbit interaction, use of K-harmonics method for splitting calcs. 2 – 67120
^{22}Na, effective neutron-proton interaction 2 – 70381
^{24}Na, effective neutron-proton interaction 2 – 70381
^{20}Ne, effective interactions in s-d shell 2 – 49728
^{56}Ni, effective two-body interaction 2 – 70394
^{58}Ni, effective two-body interaction 2 – 70394

Nuclear forces continued
O($A=18$, 19, 20), effective interactions in s-d shell 2 – 49728
^{16}O, off-shell effects in binding energy calcs. for set of phase-shift equivalent potentials 2 – 70376
^{16}O, third-order corrections to binding energy 2 – 76776
^{17}O, third-order corrections to single-particle energies 2 – 76776
^{30}P, effective neutron-proton interaction 2 – 70381
^{32}P, effective neutron-proton interaction 2 – 70381
^{208}Pb, effective particle-hole interaction from consistency relations 2 – 70414
^{36}S, effective interactions in upper s-d shell 2 – 49737
^{181}Ta, investigation of parity non-conserving force between nucleons by meas. of circular polarization of γ transitions 2 – 63840
^{181}Ta, parity admixture meas. 2 – 59726
^{159}Tb, investigation of parity non-conserving force between nucleons by meas. of circular polarization of γ transitions 2 – 63840
^{203}Tl, investigation of parity non-conserving force between nucleons by meas. of circular polarization of γ transitions 2 – 63840
^{203}Tl, parity admixture meas. 2 – 59726

Nuclear fusion
see also Explosions/nuclear; Nuclear reactors, fusion; Thermonuclear reactions
advances 2 – 42611
controlled, for space propulsion 2 – 51673
controlled, plasma diagnostic techniques 2 – 53213
controlled, present status of research, plasma confinement systems, reactor characteristics 2 – 63928
controlled fusion and heating by laser 2 – 70486
fragment fusion, determ. of barrier parameters in statistical model of nuclear fission 2 – 49847
high temp. plasma physics considerations, review 2 – 77287
laser applications 2 – 43175
laser compression of matter to super-high density, controlled fusion applications 2 – 70487
laser heating of plasma in focus-type system 2 – 77289
laser heating of plasma in focus-type system 2 – 77288
laser heating of solid deuterium and production of DD reactions 2 – 43140
laser-induced, potential as thermal neutron source 2 – 56020
plasma, two-temperature, laser heating 2 – 43116
plasma heating, averaged equations of hydrodynamic expansion and conduction-type heating fusion energy taken into consideration 2 – 77277
plasma heating and expansion in vacuo, optimum conditions for fusion yield 2 – 83558
plasma heating for spherical wave, fusion energy taken into consideration 2 – 77276
plasma research, book 2 – 60251
recovered energy, laser heating of plasma 2 – 64258
space propulsion rockets 2 – 48617
thermal effects in model of total fusion 2 – 46336
thermonuclear, controlled, progress and history of research 2 – 59789
thermonuclear combustion waves, existence conditions and propagation velocity in bounded plasma 2 – 64268
two-temperature plasma, conduction-type laser heating in spherically symmetric case 2 – 64259
D plasma estimation of Coulombian transparency as a function of temperature 2 – 42593
D_2 and H_2, controlled thermonuclear reactions, power generation 2 – 70930

Nuclear induction *see Nuclear magnetic resonance and relaxation*

Nuclear interactions *see Collision processes; Field theory, quantum/interactions; Elementary particles; Nuclear reactions and scattering*

Nuclear isomerism
see also Isomerism; Nucleus/energy levels
fission, isomer/prompt and neutron/prompt cross section ratios, stat. theory 2 – 83034
heavy-ion induced reactions, excitation function and isomer ratios 2 – 76885
Mossbauer isomer shift used in calc. of nuclear charge radius 2 – 76759
odd-proton $N=82$ nuclei, $J^{\pi}=11^{-}/2$(1) isomeric state 2 – 79756
residual nuclei, isomer ratios from low primary excitation 2 – 63754
$Z=69$-89 neutron deficient isotopes, search for γ-ray isomerism 2 – 55970
(n, γ) reactions, 25 keV, isomeric cross-section ratios 2 – 63897
^{113*}In (100 min) decay, internal conversion, M4, E5 character 2 – 74052
Am isotopes, fission isomer excitation functions 2 – 76894
^{210}At, evidence for 15^- and 11^+ isomeric states populated in ^{209}Bi(α, 3n) reaction 2 – 70415
^{197}Au(n,2n)^{196}Au, isomer cross-section ratios 2 – 63899
^{198}Au, new high-spin isomer and level struct. 2 – 82915
^{131}Ba, isomeric activity excitation by (n,2n) reaction at 14.8 MeV 2 – 82974
^{133}Ba, isomeric activity excitation by (n,2n) reaction at 14.8 MeV 2 – 82974
^{133}Ba, isomeric activity excitation by (n,2n) reaction at 14.8 MeV 2 – 82974
^{135}Ba, isomeric activity excitation by (n,2n) reaction at 14.8 MeV 2 – 82974
^{135}Ba, isomeric activity excitation by (n,2n) reaction at 14.8 MeV 2 – 82974
^{78}Br isomeric states, magnetic moment determ. 2 – 74029
^{81}Br isomeric states, magnetic moment determ. 2 – 74029
^{115}Cd, isomer yield ratios in neutron- induced reactions and fission 2 – 63808
^{116}Cd (n,γ), cross-sections and isomer ratios 2 – 59767
^{123}Cs, ^{122}Cs, levels found, β^+ decay of ^{122}Cs 2 – 74037
^{134}Cs isomer ratios in ^{237}Np fission with protons 2 – 63932
^{151}Eu (n,γ), cross-sections and isomer ratios 2 – 59767
^{57}Fe, calibration of Mossbauer isomer shift 2 – 46137
^{66}Ga isomeric states, magnetic moment determ. 2 – 74029
^{191}Ir(n,2n)^{190}Ir, isomer cross-section ratios 2 – 63899
^{41}K(α,n)^{44}Sc, excitation functions and isomer ratios calc. in stat. models 2 – 82997
^{177}Lu, nsec. isomeric transitions, (n,γ) reaction obs. 2 – 67176
^{91}Nb, isomeric 17/2 states 2 – 67162

Nuclear isomerism continued
^{95}Nb, isomer ratios of nuclear produced in ^{209}Bi fission 2−63933
^{134}Nd isomeric state excited in ^{118}Sn(^{20}Ne, 4n) reaction at 82-120 MeV 2−79745
^{206}Pb, g-factor of 12^{+} isomeric state and effective orbital g-factor of neutron 2−59720
^{111}Sn, ^{113}Sn, short-lived isomers obs. by pulse activation of enriched Cd isotopes using α-particles and ^{3}He beams 2−74036
^{93}Tc, isomeric 17/2 states 2−67162
^{235}U(α, 3n)^{236}Pu, 24.5-28 MeV, cross sections, fission isomer excitation functions 2−76880
^{236}U, fission isomeric state 2−59795
^{187}W, nsec. isomeric transitions, (n,γ) reaction obs. 2−67176
^{87}Y, isomer ratio, ^{89}Y (γ, 2n) reaction study 2−63754
^{87}Y, isomer ratios from ^{89}Y(p,p2n)^{87}Y, calc. based on statistical and cascade-evaporation theories 2−49730

Nuclear magnetic resonance and relaxation
see also ENDOR; INDOR; Knight shift; Molecules/nuclear coupling Nuclear acoustic resonance; Proton magnetic resonance; Spin-lattice relaxation; Spin-spin relaxation
220 MHz, review of applications 2−77030
— 2−59011
A_lB_k type spectra, structural properties 2−70676
acetoxime, ^{13}C chem. shifts, solvent and isotope effects 2−64165
acetylene, effects of deuterium substitution on π charge density and chemical shift 2−77096
acrylic acids, substituted, and their methyl esters, ^{13}C n.m.r., correlation of olefinic shieldings 2−42950
adamantane, mol. dynamics 2−81479
alkali borate and silicate glasses. ^{7}Li ionic motion obs. 2−64690
alkali bromides, gradient-elastic tensor, n.m.r. acoustic saturation study 2−44457
4-n-alkoxybenzylidene-4′-phenylazoanilene, nematic-spectra A phase transition, n.m.r. meas. on molecular orientation 2−53402
allene, ^{13}C chem. shifts 2−77102
by anisotropic spin-spin interaction 2−77038
antiferromagnet with easy axis anisotropy, freq. shift phenomena 2−81482
apparatus for n.m.r. spectrometers, patent 2−73491
atom, macroscopic optical coherence phenomena 2−59907
atoms and ions, 2-, 3- and 4-electron, Z^{-1} expansion for nuclear magnetic shielding constant 2−46460
p-azoxyanisole, strong collision relaxation in rotating frame 2−61747
benzene, mol. dynamics 2−81479
benzene, solid, anisotropic relax. of ^{13}C, chem. shielding 2−81310
benzene adsorbed on gel, n.m.r. 2−46614
benzenes, monosubstituted, partially oriented in nematic phase 2−77104
beryllium oxyacetate, polymorphism, -196°C to 286.7°C, pulsed n.m.r. investigation, study of molecular dynamics 2−57399
beryllium oxyacetate, spin lattice relax. of dipole-dipole reservoir and slow motion obs. 2−72525
biological rate phenomena molecular structure 2−81988
biphenyls, bridged, long-range ^{13}C spin couplings 2−77134
blood flowmeter for pulsatile flow, analysis 2−81981
2-, 3- bromothiophenes, meas. of proton spin-lattice relaxation times in 300-450°K range using spin-echo spectrometer 2−77116
butyne in solvents, adiabatic fast passage relaxation 2−71236
carbamates, energy barriers to hindered rot. 2−60054
carboxymioglobine aqueous soln., effect of hydration on relax. time 2−50373
chemical exchange, multi-site, principles of n.m.r. investigations 2−61763
chemical exchange induced relaxation, new method of treatment 2−64105
chloralides, optically active, molec. conformation determ. 2−42971
2-chlorocrylonitrile, spin relax., band shape studies 2−59983
chloroform, ^{13}C spin-lattice and spin-spin relaxation rates 2−56525
chloroform, n.m.r. and n.q.r. constants calc. by Pariser-Pople and Wolfsberg-Helmholz methods 2−83324
computer assistance in spectral analysis 2−52345
conference, Turku, Finland (Aug 1972) 2−81478
cyclobutene, partially oriented in nematic phase, p.m.r. study of H-H distances and orientation parameters 2−83313
cycloheptane and cycloheptene derivatives, conformational equilibrium from ^{19}F n.m.r. 2−83288
cyclopropylidene cycloalkanes, ^{13}C n.m.r. chemical shifts 2−42975
cytochrome c, electron transfer between molecules obs. by pulsed Fourier transform n.m.r. 2−56267
B-decachlorocarboranes, H bonding study 2−46602
deuteromethane, solid, proton mag. susceptibility 2−65351
1,1-difluoro-2, 2-dichloroethane, proton spin echo n.m.r. spectra, subspectral analysis 2−42977
N-dimethylaminoborane-d_2, ^{2}H n.m.r., quadrupole coupling constants 2−44461
dimethyldiacetylene in solvents, adiabatic fast passage relaxation 2−71236
1,1-dimethylhydrazine-monoborane, determ. of molecular structure, vibrational assignments 2−53057
dimethylphosphoryl halides, ^{31}P and ^{1}H spectra 2−46616
2,2-dimethylpropane in nematic liquid crystals, obs. of dipolar splitting in p.m.r. spectra 2−71238
dipolar interaction between non-equivalent nuclei, effect of Hamiltonian operators on spectral line width 2−72505
dipolar solids, decay of multiple spin echoes, theory 2−78172
dipolar solutes in benzene and fluorinated benzene, n.m.r. study of solvent induced shift effects on ^{1}H and ^{19}F 2−83311
dipolar spin-lattice relax. rates of quadrupole interacting spin system 2−84452
double resonance relaxation, techniques for solid state studies, review 2−61754
dynamically polarized spin system, autostabilization of reson. conditions 2−84583
electric effects, review 2−68728
emulsion, restricted diffusion, pulsed n.m.r. obs., droplet size distrib. 2−74573
ethylene, ^{13}C chem. shifts 2−77102
ethylene carbonate, solute in thermotropic nematic phase, p.m.r. study, comparison with lyotropic phase 2−83800

Nuclear magnetic resonance and relaxation continued
ethylene monothiocarbonate solute in thermotropic nematic phase, p.m.r. study, comparison with lyotropic phase 2−83800
exact quantum-mechanical treatment of spin nuclear system 2−77031
ferric haem, iron out-of- planarity and tetrapyrrole nitrogen nuclear spin state mixing 2−80101
ferrites, spin echo enhancement by double freq. pumping, mechanism 2−68740
ferroelectric, order-disorder type, temp. dependence of n.m.r. spectra second moment 2−81150
ferroelectric systems, spin-lattice relax. meas. by double reson., phase transition dynamics 2−84450
ferromagnet, spin echo phenomena 2−61488
flow measurement, n.m.r. technique, velocity distribution fn. 2−83757
fluid flow studies, pulsed field-gradient spin echo technique 2−56303
fluorobenzene-d_5 in liquid state, reorientation and angular momentum correlation times 2−80479
fluorothiophenes, substituted, spectra of ^{1}H and ^{19}F 2−46606
formaldehyde with Slater basis sets, ^{13}C and ^{17}O n.m.r. shielding constants, perturbed Hartree-Fock study 2−50094
formic acid, isotope effect and ^{13}C spin-lattice relax. 2−60069
Fourier spectroscopy, pulse and stochastic excitation controlled by computer 2−45627
free precession of magnetization in moving liquid and application to flowmetering 2−74502
furan molecule, in liquid crystal, determ. of structure parameters 2−67514
furan-2, 5-dialdehyde partially oriented in nematic phase, conform. obs. 2−70769
2-furanaldehyde, conform., rot. isomerism nematic-phase 2−77147
glass, aluminoborosilicate, B coordination number, heat treatment effects, obs. 2−64528
glass, atomic arrangements and chemical bonding obs. 2−54500
glass, chalcogenide, solid and liq., struct., n.m.r. and i.r. vibr. spectra obs. 2−60595
glycerine-water system, influence of free radicals and paramagnetic ions on viscosity 2−74530
glycerol, pulse n.m.r. meas. of self-diffusion 2−60453
glycerol, viscous, rotating frame relaxation 2−56526
halomethanes, chem. shifts correl. with K-shell electron binding energy shifts 2−56235
Heisenberg paramagnet, anisotropic, n.m.r. line shape calcs. using kinetic energy 2−72111
hexafluorobenzene, n.m.r. study of gas to infinite dilution chemical shifts 2−74291
high resolution techniques, pulse Fourier transform method 2−66669
hydrides, spin-lattice relax. times of diffusing hydrogen 2−54369
hydroazine alum, ferroelectric, rel. to phase transition 2−75357
hydrocarbons, ^{13}C chemical shifts determ. from INDO perturbation calc. of magnetic shielding consts. 2−64162
hydroxylamine alum, ferroelectric, rel. to phase transition 2−75357
ice, strong collision relaxation in rotating frame 2−61747
iminoxyl radicals, paramag. shifts, h.f.s., spin density propag., spatial struct. 2−80110
intensity error, second moment and line width for n.m.r. broad lines 2−82409
isopropenyl system, ^{13}C-^{13}C coupling constants 2−56237
lanthanide ions in solution, pseudocontact contribution to n.m.r. shifts 2−80481
line shape, molec. reorganization effects, calc. by permutation of indices 2−54524
linear chains, alternate, of inequivalent nuclei coupled by indirect exchange interaction, line shape 2−43019
linewidths, position-depend., in presence of hyperfine or electron-nucl. double interactions 2−48048
liquid crystal, struct. and dynamical processes determ. 2−83805
liquid metal, and electronic struct. 2−67842
liquid metals, rel. to hard- sphere interference functions, temp. dependence 2−67796
lithium ammonium tartrate, ferroelec. paraelec. transition phenomena 2−72527
lithium formate monohydrate, of ^{7}Li 2−54512
lock channel modification allowing obs. of variety of nuclei 2−63208
magnetic dipole and elec. quadrupole hyperfine interactions study by nuclear orientation with and without n.m.r. 2−63758
magnetic double resonance Overhauser and solid state effect in methods of high frequency spectroscopy 2−54516
magnetic flux density obs. in varying field 2−76443
magnetostatic echo analysis 2−57313
metal, Bloch decay rel. to skin effect 2−78171
metal, fast magic-angle rot. technique 2−81480
metal, skin effect influence on amplitude and phase of pulsed signals 2−84608
metal complexes, polar and nonpolar in benzene and hexafluorobenzene, p.m.r. study of solvent induced shifts 2−83264
metal/hydrogen systems, conf., Julich, Germany (Mar 1972) 2−77713
methane, adsorbed on gel, n.m.r. 2−46614
methane, n.m.r. and n.q.r. constants calc. by Pariser-Pople and Wolfsberg-Helmholz methods 2−83324
methane adsorbed on graphite, spin-lattice and spin-spin relax. 2−67925
methanes, deuterated, in nematic liquid crystals, obs. of dipolar splitting in p.m.r. spectra 2−71238
p-methoxybenzilidene p-n-butylaniline, nematic phase, n.m.r. meas. of anomalous alignment and domains 2−71161
4-methyl 2,6 ditertiarybutylphenol, proton dipole-dipole relax. rel. to quantum tunnelling 2−81472
methyl ammonium alum, ferroelectric, rel. to phase transition 2−75357
methyl and methylene chlorides, n.m.r. and n.q.r. constants calc. by Pariser-Pople and Wolfsberg-Helmholz methods 2−83324
microwave double resonance, signal saturation phenomena 2−63204
molecular crystals, reorientation and correlation functions 2−48302
molecular sieve, moisture content detn. 2−48303

Nuclear magnetic resonance and relaxation continued
molecule, linear elec. field effect on mag. screening const., variational calc. 2−77054
molecules containing sulphur, ^{33}S chem. shifts, electronic struct. investig. 2−83290
molecules in excited states, ODMR methods 2−46518
monoalkylbenzenes, rel. to conformational structure determination 2−42953
monomethylphosphoryl halides, ^{31}P and ^{1}H spectra 2−46616
multicomponent solutions, intermolecular effects, derivation of one-molecule density operator eqns. 2−56520
multiple field modulation, homonuclear stabilization of magnetic field 2−49230
N-acetylphenylhydroxylamines, substituted, cis-trans conformational equilibrium, n.m.r. obs. 2−50074
nematic liquid crystalline phase, proton spin-lattice relaxation 2−56524
neopentane derivatives, substituent effects on $^{4}J_{hh}$, positional dependence 2−77107
nicotinamide, its cations and related compounds, meas. of ^{13}C noise decoupled spectra, determ. of chemical shifts 2−83309
p-nitrobenzoic acid, n.m.r. at liquid nitrogen and room temps., i.r. spectra 2−78167
nitroxide radicals, ^{13}C coupling consts. 2−83295
nonmetallic diamag. cryst. with mag. impurity, spin diffusion and nucl. relax. 2−81313
nuclear magnetometer using stable oscillator 2−55649
off-resonance decoupled spectra, residual splittings 2−66673
optically pumped systems, obs. of wiggles phenomena 2−74487
organic compounds, characteristic ^{13}C chemical shifts 2−56209
organic compounds with ^{13}C in natural abundance at each site, C-C coupling determ. 2−83287
organic solids, ^{13}C chemical shielding parameters determ. using proton-enhanced nuclear induction spectroscopy 2−72524
organophosphorus esters, peak doubling, H bonding 2−70788
Overhauser effect, quantitative applic. to molec. structure determination 2−52989
oxamides and thio-oxamides, hydrogen bonding obs. 2−56252
pentaborane (9), effects of thermal decoupling on high-resolution ^{11}B n.m.r. spectrum 2−83801
perfluorocyclohexane plastic crystal, self- diffusion study by n.m.r. 2−50702
phase transition phenomena, struct. and mag., review 2−84599
phenoxyacetic acid derivatives, high-resolution spectra 2−53076
phthalazine, nematic phase 2−50324
poly(ester acrylates), NMR study of mol. motion 2−83391
poly(vinyl chloride)-rubber system, NMR analysis 2−83393
polyatomic mols., mol. orbital theories of chem. shifts 2−67461
polybutadiene, molec. structure study using ^{13}C n.m.r. 2−53091
polybutadienes, sequence structure studies by ^{13}C−{^{1}H} Fourier transform n.m.r. 2−67529
polycrystalline sample, central line form, quadrupole splitting theory 2−57395
polyisobutylene solns. obs. of spin-spin and spin-lattice n.m.r., relationship to viscosity 2−60513
polymer spectra, synthetic and biological, book 2−83396
polysulfones of monolefins, high resolution solution spectra 2−43390
polytetrafluoroethylene, irradiated and sintered, mol. chain entanglement obs. 2−65352
polyvinyl chloride, moisture content detn. 2−48303
porous glass desalination membrane, function of external salt concentration 2−56522
potassium hydrogen di-trifluoracetate, deuteron quadrupole coupling const. 2−72528
powder patterns, graphic analysis in the presence of quadrupole interactions 2−48300
propane derivatives, substituent effects on $^{4}J_{hh}$, positional dependence 2−77107
protons, magnetic field controller 2−82413
pseudomagnetic reson. of neutron induced by r.f. field 2−84598
pulse Fourier transform spectroscopy 2−66670
pulse method, applic. of spin temp. theory 2−61743
pulse n.m.r., technique for self-diffusion meas. in viscous liquids 2−60453
pulsed double resonance, solids, review 2−61755
pyrene ^{13}C-H satellite spectrum, calc. of coupling constants 2−46627
pyridine, its cations and related compounds, meas. of ^{13}C noise decoupled spectra, determ. of chemical shifts 2−83309
pyridine-borane-d$_3$, ^{2}H n.m.r., quadrupole coupling constants 2−44461
pyridines, monosubstituted, ^{14}N chemical shifts 2−56257
pyridinium salt, fused, rel. to specific conductance 2−72018
quantum mechanical calc. of n.m.r. spectra of AB spin system using analogue computer 2−66668
rare earth orthochromites, of ^{53}Cr, h.f.s., mag. props. 2−48307
rare spins in solids, high resolution reson. and differential relax. 2−81479
relaxation, effect of electron exchange interactions 2−65189
relaxation times, long, meas. by autogenerator 2−49229
review, literature from July 1969 to July 1971 2−52342
r.f. field effects, spin system quantization axis defn. 2−54502
rotating solids, Green's function method for lineshape 2−68741
ruby, investigation of instabilities in e.p.r. behaviour 2−44436
ruby, photon echo-nuclear double reson., Cr-Al interaction parameters 2−81474
self-diffusion obs. by pulsed gradient technique, current pulse generator 2−73502
silver trifluoroacetate, ^{19}F shielding tensors of trifluoromethyl group 2−68751
sixth moment of dipolar broadened line shapes, theory 2−65339
sixth moment of resonance line shape, theory 2−65340
solid, motionally narrowed n.m.r. spectrum, use second moment for studying kinetics of nuclear motion 2−84592
solid, with radioactive impurity, effects of relax. and r.f. field on impurity levels 2−75244
solid-water system, rel. to moisture detn. 2−48303
solids, method for calculating signals in n.m.r. pulse expts. 2−81476
solids without resonant nuclei, with sorbed gas, static susceptibility determ. 2−60671

Nuclear magnetic resonance and relaxation continued
spectra plotting, computer program 2−52344
spectral interpretation, applic. of K-nearest neighbour classification rule (pattern recognition) 2−66667
spectrometer, low-level for in situ magnetic field obs. at low temps. 2−63209
spectrometer, n.m.r. wide-line, applications and production details 2−55634
spectrometer, Varian HA-100, automatic lock holder 2−66671
spherical top mols., spin- lattice relax. obs. of spin-rot. interaction 2−56199
spin echo envelope, amplitudes of superhyperfine freq. 2−78168
spin echoes by inversion of mag. field gradient 2−63206
spin relax., band shape studies 2−59983
spin system, r.f. pulse response in presence of quadrupolar splitting 2−59019
spin systems, effects of strong time-dependent fields 2−59018
spin-1 nuclei perturbed by quadrupole coupling, calculation method 2−73490
spin-lattice relax. recovery laws and exptl. condition for exponential decay 2−84451
spin-lattice relaxation of system AB of slowly interconverting nuclei, exchange rate effect 2−46520
spin-spin relaxation, error compensation in Carr-Purcell spin echo expt. 2−59017
strongly coupled two-spin system relaxed by external catalyst, determ. of relaxation parameters by line-shape analysis 2−83231
superconducting A15 cpds., anomalies interpret. 2−77877
superconducting A15 cpds., spin relax., order parameter fluctuations influence 2−68355
symmetric top mols., spin- lattice relax. obs. of spin-rot. interaction 2−56200
TCNQ ditoluolchromium complex, electronic states localised characts. 2−72529
TCNQ salts, nuclear relaxation rate, role of disorder 2−64920
tetramethylammonium decaborate-d$_{10}$, ^{2}H n.m.r., quadrupole coupling constants 2−44461
thiophene molecule, in liquid crystal, determ. of structure parameters 2−67514
toluene, 1-^{13}C labelled, long-range C-C spin-spin coupling constants 2−77125
toluene, adiabatic fast passage relaxation 2−71236
transition metals, hydrogen diffusion obs. 2−77622
trifluoroethane and trifluoroethane-d$_3$, ^{19}F chemical shifts in gas phase 2−83308
trifluoromethyl group, parameters of individual fluorines 2−77113
trimethyl(phenylethynyl)-silane, ^{13}C Fourier transform n.m.r. study, detection of ^{19}Si-^{13}C spin-spin coupling, bonding 2−83312
trimethylsilyl amides, determination of activation parameters 2−77110
tropolone, of ^{13}C, tautomeric equil. 2−64194
π-tropyliumvanadium tricarbonyl, ^{51}V quadrupole relax., coupling const. 2−84453
Tutton salts, spin system dynamics obs. 2−84445
uridine and related structures, relationship of ^{13}C to vicinal ^{1}H coupling to torsion angle 2−43014
u.s. spin echoes, generation and detection 2−44312
vinyl polymers 2−60105
water dimer, hydrogen-bond shift 2−60003
o-xylene partially oriented in nematic phase, internal rot. barrier, spin-spin coupling 2−77157
YIG, nature of spin echo and obs. at 1.3 and 9.4 GHz 2−72522
Zeeman energy modification by non-resonating oscillation field in rot. frame 2−54501
zeolite/methane system, static mag. susceptibility determ. 2−60671
Ag$_2$O-B$_2$O$_3$ glass system, B sites obs. 2−65342
Al, diffusion, review 2−83992
Al, solid and liq., Knight shift, spin-lattice relax. obs. 2−54503
Al, temp. depend. of charge perturbation around 3d-transition metal impurities 2−44452
Al with transition metal impurities, temp. depend. of charge perturbation 2−48304
^{27}Al n.m.r. in Al film interlayered with transition metals 2−68743
^{28}Al, from beta decay asymmetry 2−42500
n-B$_9$H$_{15}$, resolution enhancement in partially relaxed Fourier transform ^{11}B n.m.r. 2−56521
B$_{10}$H$_{10}$D$_4$, B$_{10}$H$_4$D$_{10}$, ^{2}H n.m.r., quadrupole coupling constants 2−44461
^{10}BF$_3$, interference effects for spin-lattice and spin-spin relaxation 2−72506
BeO, of ^{9}Be, Stark shift of nuclear spin levels 2−44453
Bi$_4$Ge$_3$(Si$_3$)O$_{12}$ electro-optic crysts., quadrupole coupling consts. 2−84604
C, porous, adsorption of liquids, high resoln. obs. 2−53594
CCl$_4$ Pariser-Pople and Wolfsberg-Helmholz calc. 2−83324
CH$_4$ solid, spin isomer conversion, n.m.r. obs. 2−68749
^{13}C chem. shifts calc. using mol. orbital theory 2−77102
^{13}C relax. meas. under proton coupled and decoupled conditions 2−67462
CdFOH, ^{19}F and ^{1}H resonances 2−84591
CdS:Co^{2+}, spin-lattice relax., Orbach process Debye temp. 2−54367
Ce-V dilute alloy study of satellite lines, prediction of hyperfine field shifts 2−44454
CeAl$_x$, n.m.r. and magnetic susceptibilities 2−84594
Ce$_2$Mg$_3$(NO$_3$)$_{12}$.24H$_2$O, ^{14}N n.m.r. 2−48305
CeSn$_3$, absence of magnetic ordering obs. 2−84588
Cl$_2$, liq. and solid, spin lattice relax., temp. depend. 2−72507
^{38}Cl, from beta decay asymmetry 2−42500
Co-Cr dilute alloy study of satellite lines, prediction of hyperfine field shifts 2−44454
Co-Mn dilute alloy study of satellite lines, prediction of hyperfine field shifts 2−44454
Co film, effect of constitution and temp. 2−81471
CoF$_2$.5HF.6H$_2$O, study of internal motion by meas. of temperature dependence of n.m.r. linewidth and second moments 2−65343
Co(II) complex, paramag. shift due to outersphere coordination of solvent molecules 2−80106
Co$_3$S$_4$, of Co^{3+}, apparent hyperfine field 2−81475
CoSi, near-stoichiometric, comp. effects 2−68521

Nuclear magnetic resonance and relaxation continued
- ^{59}Co, in 2-phase Co, n.m.r. level inversion in 2000 Å films 2−68744
- $Cr_xMn_{1-x}Sb$, internal mag. fields obs. 2−54513
- Cs^+, free ions, involving photoionization, optical pumping and charge exchange 2−79897
- ^{133}Cs, superconducting solenoid magnetic field monitoring 2−66700
- $^{133}Cs^+$ ion, free, freq. shift due to charge exchange with Cs atom 2−79896
- Cu-Co dilute system, n.m.r. and double resonance studies of electron spin density near Co atom, obs. of satellite lines 2−75204
- Cu dil. alloys, elec. field gradients 2−51413
- Cu n.m.r. thermometer, pulsed 2−49185
- Cu nucl. spin-lattice relax. of Zeeman and spin-spin systems, 1 to 17 mK 2−68581
- Cu salts, chem. shifts of ^{63}Cu 2−44455
- $Cu(ClO_4)_2$ solutions in methaol and water, temp. and magnetic field dependence of nuclear spin relaxation 2−81452
- $CuSO_4$, moisture content detn. 2−48303
- $(DBNH)_3$, ^{2}H n.m.r., quadrupole coupling constants 2−44461
- D_2O ice, ^{2}H spin-lattice relaxation 2−61744
- Fe-Co dilute alloy, of ^{57}Fe, hyperfine field studies 2−65344
- Fe-Co very dilute alloy, 25 mK, spin-lattice relax. of ^{60}Co, field depend. 2−72232
- Fe-V alloy, Fe-rich, ^{57}Fe study 2−75355
- Fe, of ^{31}P, ^{75}As, ^{93}Nb, ^{121}Sb, ^{123}Sb, hyperfine fields detn. 2−75354
- Fe, of ^{74}As, mag. moment, internal field 2−76796
- Fe matrix, hyperfine fields at Al, P, Sc and Ta nuclei, spin echo obs. 2−72229
- $FeBO_3$, amplified n.m.r. signal from inside domains 2−68745
- $FeBO_3$, n.m.r. from ^{57}Fe, temp. depend. 2−72523
- Fe^{60}Co, single- passage resonance obs. by β-emission and spin-lattice relax. meas. 2−72508
- $(Fe_{1-x}Co_x)Si$ solid solns., moment form. obs. 2−44223
- FeF_3, transparent antiferromagnet, nuclear echo 2−54505
- FeMg garnet, ^{27}Al and ^{29}Si n.m.r. studies 2−65341
- Fe_3P, mag. struct. 2−44251
- FeSi-CoSi, system of ^{59}Co, itinerant ferromag. obs. 2−61745
- Ga, single cryst., elec. field gradient tensor determ. from high field spectra 2−57396
- $Ga_xAl_{1-x}As$, optical electron-nuclear reson. 2−61695
- $Ga(ClO_4)_3$ aqueous solns., relax. rates of ^{69}Ga and ^{71}Ga 2−77449
- $Ga_{1-x}Te_x$ alloy, liq., Knight shift, mag. relax., quadrupole relax., Fermi level 2−60512
- $GdAl_2$, mag. induced elec. field gradient, spin echo obs. 2−72509
- $GdCl_3$, low temp. cooperative behaviour obs. 2−72166
- $GdGa_xCu_{1-x}$, hyperfine field at nonmag. ions, rel. to electronic struct. 2−78020
- $GdIn_xAg_{1-x}$, hyperfine field at nonmag. ions, rel. to electronic struct. 2−78020
- $Gd_{1-x}La_xZn$, zero-field resonances, hyperfine field contribs. 2−72510
- $Gd_{1-x}Y_xZn$, n.m.r. zero field resonances, hyperfine field contribs. 2−72510
- $GdZn_xAg_{1-x}$, hyperfine field at nonmag. ions, rel. to electronic struct. 2−78020
- GeO_2-B_2O_3 glass, of ^{11}B 2−54506
- $Ge_{15}Te_{81}X_4$, X=Ga, P, As, switching glass, of ^{125}Te 2−61752
- H_2, solid, spin-lattice relax., temp. depend., 0.075-1.5K 2−68583
- H_2 inert gas binary mixtures, proton spin lattice relaxation times in 165-265K range 2−46645
- H_2 labile negative ion, assignation of cause of resonances in h.f.e.m. fields 2−74264
- H_2 solid, spin echoes obs., ortho H_2 conc. depend. 2−48306
- H_2O, adsorbed layer on silica, freezing process, linewidth obs. 2−53596
- H_2O on silica, self-diffusion obs. 2−60686
- ^{3}He-^{4}He solid mixture, anomalous n.m.r. data 2−43429
- ^{3}He, below 3 mK, magnetic phenomena 2−77460
- ^{3}He, solid, longit. and transverse relax. times, spectral density function 2−43433
- ^{3}He adsorbed monolayer on Vycor glass, config. and mobility obs, 2−80509
- ^{3}He liquid-solid mixture, interpretation of NMR and thermodynamic data below 3 mK, new liquid phase 2−80511
- ^{3}He monolayer film adsorbed on graphite, motional narrowing 2−64578
- Hf, solid, struct. refinement from ^{19}F n.m.r. data 2−71434
- HfV_2, quadrupole parameter anomaly 2−54507
- HgFOH, ^{19}F and ^{1}H resonances 2−84591
- In-Bi(Pb)(Tl) alloys, liq., longit. spin relax. of ^{115}In 2−50370
- ^{116}In, from beta decay asymmetry 2−42500
- $K_3Co(CN)_6$, of ^{59}Co, chemical shift interpretation 2−65345
- $K_3Co(CN)_6$, of ^{59}Co, chem. shift 2−54509
- K_2CuF_4, two-dimens. ferromagnet 2−81239
- $K_3Fe(CN_6)$, electronic structure model consistent with exptl. data 2−54508
- KH_2asO_4 ferroelectric, correlation with dielectric relaxation 2−57243
- K_2MnF_4, ^{19}F lineshift obs., hyperfine contrib., bonding, antiferromagnetism 2−54510
- KPF_6, solid, reorientation motions of PF_6^- ions 2−61562
- $La_{1-x}Gd_xAl_2$, spin-lattice relax. 2−54370
- $LaIn_3$, Knight shift and spin-lattice relax. 2−65346
- $La_2Mg_3(NO_3)_{12}.24H_2O$, spin system dynamics obs. 2−84445
- $LaPb_3$, ^{139}La Knight shift and spin-lattice relax., ^{207}Pb Knight shift 2−65346
- Li dil. alloys, spin relax. of ^{7}Li and translational diffusion 2−44317
- LiCl, gradient-elastic consts. determ. 2−77637
- $LiCuVO_4$, of ^{7}Li and ^{51}V, 77-413K 2−72511
- LiF, detection using Josephson junction magnetometer 2−66674
- $Li_{0.5}Fe_{2.5-x}Ga_xO_4$, supertransferred hyperfine fields at ^{69}Ga and ^{71}Ga 2−54511
- MgF_2, static electric quadrupole interaction of beta emitter ^{20}F produced by capture of polarized neutrons, n.m.r. obs. 2−75356
- α-Mn, antiferromagnet, of ^{55}Mn 2−61748
- Mn complex, $(CH_3)_4NMnCl_3$, direct process relaxation by spin waves in one dimensional antiferromagnet 2−51414
- MnAlGe, ferromagnetic 2−84586

Nuclear magnetic resonance and relaxation continued
- $MnBr_2.4H_2O$, antiferromagnetic, meas. of Br n.m.r. spectra down to 0.4K obs. of resonances in 10-90 MHz range 2−65175
- $Mn(CO)_5$-X_3M adducts, single crystals, ^{55}Mn broad-line n.m.r. at room temp. 2−68747
- $Mn_2(CO)_{10}$ single crystal, broadline n.m.r., quadrupole coupling and anisotropic chemical shift 2−57397
- $Mn_{1-x}Cr_xSb$, of ^{55}Mn, hyperfine fields detn. 2−54514
- MnSb, ferromag., internal mag. fields obs. 2−54513
- ND_4^+ compounds, of ^{2}H, tunnelling effects 2−72512
- $(NH_4,RB)_2CuBr_4.2H_2O$, mag. interactions 2−65144
- NH_4Cl, low temp. spin-lattice relax. times of hindered ions 2−84447
- NH_4Cl, spin-lattice relax. time of nucl. dipolar energy, temp. and orientation depend. 2−81314
- $(NH_4)_4Fe(CN)_6.H_2O$, obs. of ionic diffusion 2−74814
- $(NH_4)_2H_3IO_6$, antiferroelectric, level crossing expt. 2−61749
- ^{14}N linewidths in organic liquids, N nuclear quadrupole coupling consts. determ. 2−56523
- $^{15}NH_3$, $^{15}ND_3$, liquid, ^{15}N spin-lattice relaxation meas. 2−50371
- NaCl, vacancy-impurity complex, slow motion, press. effects, obs. 2−72514
- $NaClO_3$, steady state method, acoustically induced, quadrupole transitions 2−78166
- $NaNO_3$, of ^{23}Na, intensity variations under u.s. stimulating quadrupole transitions 2−81483
- Na_2O-B_2O_3 system, glassy and crystalline compounds, structural obs. 2−48301
- $NaPF_6$ in H_2O and D_2O solns., spin-lattice relaxation of ^{19}F, ^{31}P, ^{1}H, ^{2}H 2−50372
- Na_2PO_3F in H_2O and D_sO solns., spin-lattice relaxation of ^{19}F, ^{31}P, ^{1}H, ^{2}H 2−50372
- NaX zeolites with H_2O absorbed layer, meas. of proton magnetic relaxation 2−54515
- Ne, solid and liquid, pulsed n.m.r. of ^{21}Ne 2−65347
- Ni ⟨110⟩ single crysts., rel. to mag. domain struct. 2−78173
- $NiF_2.5HF.6H_2O$, study of internal motion by meas. of temperature dependence of n.m.r. linewidth and second moments 2−65343
- O_2 labile negative ion, assignation of cause of resonances in h.f.e.m. fields 2−74264
- PBr_3, gas phase and solvent chemical shifts, ^{31}P n.m.r. studies 2−46575
- $P_2Se_3-As_2Se_3$, semiconductor glasses, pseudobinary section, comp. depend. of width of spectral lines, second moment and chemical shift 2−84584
- PdH_x, Knight shifts of ^{105}Pd and proton lines 2−78174
- Pd_2MnSb, ferromagnet, hyperfine fields 2−61750
- $PrCl_3$, low temp. cooperative behaviour obs. 2−72166
- Pt/Al_2O_3 catalyst, butene adsorption, high resolution obs. 2−60683
- PtSi, spin-lattice relax., Knight shift obs. 2−65348
- RbBr(Cl), gradient-elastic consts. determ. 2−77637
- Rb_2CoF_4, of ^{87}Rb, antiferromag. transition obs. 2−44458
- $RbMnF_3$, of ^{19}F, 1.5 to 300K, spin-lattice and spin-spin relax. 2−48113
- $RbMnF_3$, spin-lattice and spin-spin relax. of ^{19}F and resonance of ^{87}Rb 2−72516
- $RbPF_6$, solid, reorientation motions of PF_6^- ions 2−61562
- $Re_2(CO)_{10}$ single crystal, broadline n.m.r., quadrupole coupling and anisotropic chemical shift 2−57397
- $ReMn(CO)_{10}$ single crystal, broadline n.m.r., quadrupole coupling and anisotropic chemical shift 2−57397
- SF_6 clathrate deuterate, ^{19}F spin-lattice relaxation meas. in 40-250 K range 2−72531
- Sb (A=120,124), n.m.r. meas. of ground state moment 2−49745
- Sc-H solid solution, Korringa product, diffusion parameters determ. 2−72517
- Se-Te alloy, liq., semicond., of ^{77}Se and ^{125}Te 2−61752
- Se, anisotropic chem. shift 2−44459
- SiO_2, water adsorption study 2−53597
- SmF_3, anomalous ^{19}F shift 2−84589
- SnH_4, solid, proton spin-lattice relax., phase transition obs. 2−48116
- $SrO.xB_2O_3$, glass and cpds., of ^{11}B, struct. 2−54504
- Te-Sn alloy, noncrystalline, at 1.3 K 2−61751
- Te, liquid, temp. depend. obs. rel. to electronic transport behaviour 2−71237
- Te, noncrystalline, at 1.3 K 2−61751
- TlCl, pulse n.m.r. investigation of vacancy and interstitial diffusion 2−71471
- $Tl_2SeAs_2Te_3$ chalcogenide semiconductor, liquid and glassy, of ^{205}Tl, struct. obs. 2−60420
- $Tl_{1-x}Te_x$ alloy, liq., Knight shift, mag. relax., quadrupole relax., Fermi level 2−60512
- Tm_3Al_2, quadrupole coupling, EFG tensor 2−48155
- $TmFeO_3$, spin reorientation study 2−44460
- σ-V-Co, of ^{51}V , quadrupole satellite intensity variation 2−72519
- V-Ge-Al alloy, Knight shift 2−57398
- V-H(D) systems, β- and δ-phase behaviour 2−78175
- V-Ru alloys, Knight shift, relax. rate and lineshape, temp. and mag. field depend. 2−61753
- $V_xCr_{1-x}B_2$, antiferromagnetic transition 2−72521
- $V_{1-x}Cr_xBe_2$, of ^{51}V and ^{9}Be, comp. depend. 2−72520
- $V_{1-x}Nb_xO_2$, metal-insulator transition obs. 2−75102
- $V_{1-x}Nb_xO_2$, metal-insulator transition, theory 2−75103
- WO_3-P_4O_{10}-V_2O_5 glass system, of ^{31}P 2−54495
- ^{131}Xe, natural, local magnetic field shift obs. 2−65349
- YIG:Cr^{3+},Cu^{2+} garnet, hyperfine interactions of Cr^{3+} and Cu^{2+} ions, n.m.r. obs. at 4.2 K 2−72504
- ZnFOH, ^{19}F and ^{1}H resonances 2−84591
- $ZnSiF_6.6H_2O$, n.m.r. study of internal motions 2−51415

measurement
- adiabatic fast passage relaxation in liquids 2−71236
- Andrew's second moment correction formula 2−55632
- autodyne spectrometer, attenuation of modulation noise 2−76427
- autogenerator, for meas. of long relax. times 2−49229
- chemically induced dynamic nuclear polarization in unmodified n.m.r. spectrometers 2−65388
- crystals, investigation of order-disorder phenomena 2−50991
- double nuclear resonant spectrometer, patent 2−78986
- Fourier transform p.m.r., modification 2−55631
- Fourier transform proton n.m.r. in aqueous solution 2−77448
- free precession technique, review 2−59020

- **Nuclear magnetic resonance and relaxation** continued
  - **measurement** continued
    - heteronuclear spin-spin interaction suppression using sweep generator 2–55630
    - high resolution spectra, calculation technique 2–76428
    - Josephson junction magnetometer fast detection method 2–66674
    - multiple, equivalence of perturbing fields for audio frequency magnetic field modulation, density matrix analysis 2–55636
    - Overhauser effect in suppression in ^{13}C meas. on mols. 2–67463
    - probe, crossed-coil, high sensitivity low-temp. meas. 2–82410
    - proton-enhanced nuclear induction spectroscopy 2–66676
    - pulse generator design 2–63207
    - pulse meas. in laboratory and rotating coordinate systems, equipment 2–59015
    - resonant helix and coil, Overhauser effects of benzene solution w. tanone free radical 2–66666
    - signal generator for polarization meas. of moving liquid 2–59014
    - signal pickups, using autodyne, sensitivity 2–76426
    - spectrometer, phase transient obs. 2–45628
    - spectrometer, R22, high resolution 2–41893
    - spectrometer, R-24, high resolution 2–41894
    - spectrometer, superconducting solenoid mag. field nonuniformity compensators 2–61250
    - spectrometer electromagnet current stabilizer 2–76424
    - spectrometer multiple pulse, low power 2–66675
    - spectrometer probe, for operation at v. low temps. 2–55635
    - spin echo technique, review 2–59020
    - spin-lattice relaxation time meas. with saturation recovery method using on-line computer 2–66672
    - stabilization system, steadiness under conditions of const. field modulation 2–78982
    - steady-state double reson. technique for low-abundance spin reson. detection 2–54520
    - strong field n.m.r. techniques 2–41895
    - T_1, effects of H_1 inhomogeneity 2–59016
    - two channel boxcar analogue integrator for pulsed n.m.r. relaxation time meas. 2–52343
    - uniform magnetic field of Helmholtz coil pair for n.m.r. signal detectors, living bodies 2–59013
    - ^{13}C, proton-decoupled, suppression of Overhauser effect 2–67463
    - ^{35}Cl in $CsNiCl_3$, magnetic struct. and props. determ. 2–72215
    - ^{133}Cs 2–72215
    - KH_2PO_4, molecular dynamics study and ferroelec.-antiferroelec. transitions 2–72032
    - Na borosilicate, glass, boron coordination 2–60586
    - $NaNd(WO_4)_2$, n.m.r. of ^{23}Na and mag. susceptibility detn. 4.2-300K 2–72513
    - ^{141}Pr-Tm intermetallic cpds., h.f. meas. at 4.2 degrees K 2–72518
    - ^{169}Tm-$M_{1(2)}$ intermetallic cpds., h.f. meas. at 4.2 degrees K 2–72518
    - Y-Ce alloys 2–65350
- **Nuclear matter** *see Nucleus/theory*
- **Nuclear orientation** *see Nuclear polarization*
- **Nuclear photoeffect** *see Gamma-rays/effects; Nuclear reactions and scattering due to/ photons*
- **Nuclear physics**
  - annual review of nuclear science, book 2–63725
  - Atomic Energy Canada, Physics Division progress report 2–67111
  - book, elementary treatment of basic ideas 2–82838
  - compilation and evaluation of data, neutron data, international organisation 2–76138
  - conference, Fribourg, Switzerland [Sept. 1972] 2–60563
  - conference, Jerusalem, Israel (May 1972) 2–70340
  - Conference, Netherlands Physical Society, Utrecht (1972) 2–49703
  - coupling constants, variation with time 2–59658
  - development at Radium Institute, USSR, (1922 to 1972) 2–76757
  - European Phys. Soc. conf., Wiesbaden, Germany (Oct. 1972) 2–76139
  - history, 2 discussion conferences 2–82085
  - information system, INIS, experience 2–66394
  - lepton nonconservation, review 2–46066
  - major problems of contemporary physics 2–42309
  - material prep. with isotope separator 2–49335
  - materials for nuclear obs. conference (Gatlinburg, USA, Oct 1971) 2–73916
  - matter at extremely high temp. and pressure 2–62912
  - meson factories, accelerators and experiments 2–82640
  - progress report of Atomic Energy of Canada 2–62910
  - reactors, neutron physics, assessment and conclusions 2–76926
  - research, computer and data processing applic. 2–79706
  - research materials, conference (Gatlinburg USA, Oct 1971) 2–49617
  - sample preparation in e.m. isotope separator 2–49614
  - SI units, reviews 2–49873
  - Springer Tracts in Modern Physics 2–82639
  - statistical props. of nuclei, conference, Albany, N.Y. (1971) 2–46065
  - superdense matter, condensed π^- phase 2–63727
  - superdense matter, condensed π^- phase 2–63726
  - superheavy elements with atomic number 114, search in nature 2–82837
  - textbook for final year undergraduate 2–62955
- **Nuclear polarization**
  - alkyl radical reaction products, chem. induced dynamic polarization 2–81540
  - chemical, and non-equilib. magnetization for reactions in mag. field 2–78203
  - chemically induced dynamic nuclear polarization in unmodified n.m.r. spectrometers 2–65388
  - chemically induced dynamic polarization in thin films 2–51461
  - cubic ordered magnet, radioactive nuclei orientation 2–68589
  - cyclohexane, nitroxide radical doped, plastic phase, spin diffusion 2–72526
  - di-t-butyl ketone, spin polarization during photolysis 2–51468
  - from exotic atoms 2–67439
  - high spin levels, degree of orientation, theory 2–42496
  - indirect interaction of nuclear spins through electrons in valence zones of semicond. 2–76760
  - magnetic dipole and elec. quadrupole hyperfine interactions study with and without n.m.r. 2–63758
- **Nuclear polarization** continued
  - mesic atom energy levels, nuclear polarization corrections 2–52958
  - metal-ammonia solutions, relaxation times and Overhauser enhancements for protons 2–46988
  - monopole core polarization 2–46069
  - optical potential, depolarization and tensor part of spin-spin term 2–82940
  - paramagnetic crystal, Mossbauer dispersion and nuclear Faraday effect 2–78073
  - rare earth nuclei implanted in Cu matrix, excitation by heavy ions, meas. of angular distrib. of de-exciting γ-rays 2–63927
  - resonant disorientation, modulation effects, theory 2–54375
  - semiconductor, optical detection of dynamic polarization 2–44323
  - standards, determ. using p polarization in ^{4}He(p, p)^{4}He 2–74072
  - SU_3 model consistency and core polarization effective charge 2–49709
  - Tutton salts, spin system dynamics obs. 2–84445
  - yttrium ethyl sulphate; Yb^{3+}, Dy^{3+}, proton polarization and relaxation by rotational cooling 2–48122
  - γ anisotropy, using Gorter-Rose method 2–42494
  - ^{12}C(μ^-, ν_μ)^{12}B, muon capture rate 2–74065
  - CaF_2:O, meas. of ^{19}F dynamic polarization, e.p.r. investigation 2–51295
  - ^{59}Co(n,γ)^{60}Co, final state spins determ. 2–67277
  - Fe:^{59}Fe, magnetic moment of ^{59}Fe, γ-ray anisotropies 2–84457
  - Fe:^{183}Re, orientation, magnetic hyperfine splitting constants 2–72245
  - Fe:^{184}Re, orientation, magnetic hyperfine splitting constants 2–72245
  - Fe, of ^{74}As, mag. moment, internal field 2–76796
  - Fe^{60}Co, single- passage resonance obs. by β-emission and spin-lattice relax. meas. 2–72508
  - H atoms in γ-irrad. aqueous solns., dynamic electron polarization 2–78204
  - ^{2}H(d, n)^{3}He, partially polarized neutron prod. for ^{12}C(n, n) elastic scatt. 2–76860
  - ^{3}He(^{3}He,^{3}He)^{3}He elastic scatt., 4-10 MeV, polarization analyzing power 2–82995
  - ^{3}He(^{3}He,^{3}He)^{3}He elastic scatt., 7-18 MeV, polarization analyzing power 2–82996
  - ^{3}He(α,α)^{3}He elastic scatt., 7-18 MeV, polarization analyzing power 2–82996
  - ^{3}He(α,α)^{3}He elastic scatt., 4-10 MeV, polarization analyzing power 2–82995
  - ^{4}He(p, p)^{4}He, 12 MeV, determ. of polarization standards 2–74072
  - ^{199}Hg, optical orientation of nuclear moments 2–76808
  - ^{201}Hg optical orientation of nuclear moments 2–76808
  - $La_2Mg_2(NO_3)_{12}$:Sm, dynamic proton polarization 2–68590
  - $La_2Mg_3(NO_3)_{12}.24H_2O$:Nd, spin diffusion processes in dynamic polarization 2–78049
  - $La_2Mg_3(NO_3)_{12}.24H_2O$, spin system dynamics obs. 2–84445
  - ^{54}Mn, γ radiation intensity pattern change oriented in $CoCl_2.6H_2O$ by spin flop transition 2–61552
  - ^{206}Pb, effective orbital g-factor of neutron 2–59720
  - ^{208}Pb muonic atom, effect of polarization on energies and relative intensities of transitions to and from 2s level 2–42823
  - ^{150}Sm, time-differential meas. of deorientation for recoils in vacuum 2–76802
  - ^{125}Te $11/2^-$ isomer, orientation in Fe, mag. moment obs. 2–76799
  - ^{203}Tl, mag. and elec. polarization 2–59961
  - ^{205}Tl, mag. and elec. polarization 2–59961
  - yttrium ethyl sulphate: Yb, nuclear spin refrigeration rel. to electron spin-spin interaction 2–72246
- **Nuclear power** *see Nuclear reactors, fission*
- **Nuclear quadrupole resonance**
  - acetonitrile, Stark effect on ^{14}N n.q.r. in asymmetric field gradient 2–44463
  - apparatus and high voltage cell 2–44463
  - azines ^{14}N n.q.r., σ and π electron densities as function of CNN angle 2–80087
  - azobenzenes ^{14}N n.q.r., σ and π electron densities as function of CNN angle 2–80087
  - benzophenone hydrazone, ^{14}N n.q.r., σ and π electron densities as function of CNN angle 2–80087
  - n-, tert-butylamine, obs. at liquid nitrogen temp., ionic character of N-H and N-C bonds 2–83310
  - chloroform, n.m.r. and n.q.r. constants calc. by Pariser-Pople and Wolfsberg-Helmholz methods 2–83324
  - chloropyridine, Stark effect on ^{14}N n.q.r. in asymmetric field gradient 2–44463
  - cyclohexane, deuterated, meas. of quadrupole coupling const. and asymmetry parameter of ring deuterons 2–80082
  - deuterated nitrogen compounds, obs. of ^{14}N resonances, determ. of π-, σ-electron densities 2–46618
  - 4,4′-dibromo-diphenylether, crystal structure study 2–64650
  - N,N′-dimethyl-piperazine, ^{14}N quadrupole interaction, spin lattice relax., mol. motions 2–84603
  - N-dimethylaminoborane-d_2, ^{2}H n.m.r., quadrupole coupling constants 2–44461
  - N-dimethylaminoborane-d_2, ^{2}H n.m.r., quadrupole coupling constants 2–44461
  - dimethylpyridine, Stark effect on ^{14}N n.q.r. in asymmetric field gradient 2–44463
  - 1,3-dimethylurea, ^{14}N, NQR freqs., coupling consts., var. with temp. 2–83297
  - dipolar interaction, calc. of second moment for arbitrary magnetic field directions and spin values 2–48310
  - electric effects, review 2–68728
  - ethylamine, ionic character of N-H, N-C bonds, determ. of temp. dependence of resonance frequencies 2–83310
  - Faraday effect technique 2–84606
  - ferroelectric, double reson. applic. to order-disorder studies 2–81481
  - frequency, direct numerical analysis of temp. dependence using Newton-Raphson approach 2–70675
  - group V double and triple chalcogens, of ^{75}As, ^{79}Br, ^{81}Br, ^{123}Sb, ^{127}Sb, ^{127}I, ^{209}Bi 2–48311
  - hexamethyl phosphoric triamide, temp. dependence of ^{14}N n.q.r. 2–48313

Nuclear quadrupole resonance continued
hexamethylenetetramine, Stark effect on ^{14}N n.q.r. in axially symmetric field gradient 2−61757
hexamethylphosphorus triamide, temp. dependence of ^{14}N n.q.r. 2−48313
hydrazine, ^{14}N nuclear relax. 2−72532
ice, of ^{17}O at 77 K, quadrupole coupling constants 2−75360
induction spectrometer, frequency swept, injection locked, with signal averaging 2−45629
p-iodoaniline, variation of frequencies with temp. 2−65357
o-iodophenol, variation of frequencies with temp. 2−65357
methane, n.m.r. and n.q.r. constants calc. by Pariser-Pople and Wolfsberg-Helmholz methods 2−83324
methyl chloride, n.m.r. and n.q.r. constants calc. by Pariser-Pople and Wolfsberg-Helmholz methods 2−83324
methylchloride, variation of Cl quadrupole coupling on deuteration 2−80091
methylene chloride, n.m.r. and n.q.r. constants calc. by Pariser-Pople and Wolfsberg-Helmholz methods 2−83324
methylpyridine, Stark effect on ^{14}N n.q.r. in asymmetric field gradient 2−44463
molecular crystals,^{14}N n.q.r. investigation of 50 compounds 2−68742
molecular crysts., two-freq. spin echo 2−84602
polymer, of dilute inert fillers as nondestructive probe 2−61758
n-, iso-propylamine, obs. at liquid nitrogen temp., ionic character of N-H and N-C bonds 2−83310
pyridine, Stark effect on ^{14}N n.q.r. in asymmetric field gradient 2−44463
pyridine-borane-d$_3$, ^{2}H n.m.r., quadrupole coupling constants 2−44461
rare earth trichlorides, hydrostatic press. coeffs. soft sphere model 2−54519
spin-lattice relax. times, double reson. meas. 2−81315
Stark effect, polarizability of single bonds 2−52984
temperature and thermal conductivity measurement, $KClO_3$, $RbClO_3$ 2−81477
tetramethylammonium decaborate-d$_{10}$, ^{2}H n.m.r., quadrupole coupling constants 2−44461
tetramethylurea, ^{14}N NQR freqs., coupling consts., var. with temp. 2−83297
triethylenediamine, Stark effect on ^{14}N n.q.r. in axially symmetric field gradient 2−61757
Zeeman effect, Hamiltonian, line splitting, mixed states 2−51418
$[PCl_4]^+[FeCl_4]^-$ frequencies, direct numerical analysis of temp. dependence using Newton-Raphson approach 2−70675
As complex, Menshutkin's type, freq. shifts nature 2−83274
As_2S_3, cryst. and amorphous state studies 2−84605
As_2S_3, vitreous, of ^{75}As, local struct. order obs. 2−57404
^{75}As, in α and β As_4S_4 2−84595
$B_{10}H_{10}D_4$, $B_{10}H_4D_{10}$, ^{2}H n.m.r., quadrupole coupling constants 2−44461
$BiCl_3$, of ^{209}Bi, temp. and press. depend. 2−78177
CCl_4 Pariser-Pople and Wolfsberg-Helmholz calc. 2−83324
Cl_2, liq. and solid, temp. depend. 2−72507
^{35}Cl in alkali and alkaline earth chlorates 2−44464
^{35}Cl in various compounds, study of bonding with B, C, N, P, and S 2−64112
Co(III) complexes, cis-$[Co(en)_2Cl_2]Cl.H_2O$ and cis-$[Co(en)_2Cl_2]NO_3$, ^{59}Co resonance frequencies, coupling consts. 2−75358
Cs_2PtCl_6, rotary lattice mode freq. over Brillouin zone, temp. depend. 2−77748
$(DBNH)_3$, ^{2}H n.m.r., quadrupole coupling constants 2−44461
Ge-Hf alloy, electric quadrupole interaction with ^{181}Ta 2−75359
$KClO_3$, of ^{39}K, ^{40}K and ^{41}K, detection using steady-state double reson. 2−54520
KIO_3, crystal struct. exam. and vibrat. struct. detn. 2−71435
$K_2Ir(Pd)(Pt)Cl_6$, incipient phase transitions 2−77748
K_2PtBr_6, of ^{79}Br, rotary lattice mode softening obs. 2−61756
$(La,Gd)Al_2$, dilute system, and mag. relax. obs., ordering onset 2−68754
$LiN_2H_5SO_4$, of ^{14}N, transition freqs. 2−68755
α-N_2, solid, isotopic mixture, reson. freq. and line shape 2−65356
N_2, solid, slow beats in spin echo envelope 2−54518
NH_3 ions, substituted, ^{14}N n.q.r. studies rel. to bonding 2−42914
^{14}N, Stark effect on n.q.r. in asymmetric field gradient 2−44463
^{14}N, Stark effect on n.q.r. in asymmetric field gradient 2−44462
^{14}N in solid N, teaching exercise in quantum mechanics 2−55353
$NaClO_3$, irrad., double reson. obs. of mag. dipolar interaction 2−72534
$NaClO_3$ of Cl, press. depend. to 20 kbar 2−51419
$NaICl_4.2H_2O$, resonance of Cl between 77 and 365°K 2−84590
Rb_2PtCl_6, rotary lattice mode freq. over Brillouin zone, temp. depend. 2−77748
2 $SbCl_3$ with naphthalene, temp. dependence of resonance frequencies 2−84587
Nuclear radius *see Nucleus/size*
Nuclear reactions and scattering
see also Chemical analysis/by nuclear reactions; Fallout; Nuclear bombardment targets; Nuclear excitation; Nuclear fission; Nuclear fusion; Nuclear spallation; Radioactivity; Stripping reactions; Thermonuclear reactions
— 2−70485
(particle, gamma) reaction, ang. distribution coeff. 2−52795
Adler-Adler resonance formalism for cross section, use in reactor physics calcs. 2−52790
amplitudes with positive imaginary part, lower bound problems for elastic cross-section 2−70137
antisymmetrization method for many nucleon systems 2−79777
bound-state Faddeev eqns., variational approach 2−46221
channel matrix inversion in R-matrix theory 2−55976
charge exchange reactions to unbound residual states, microscopic form factors 2−49778
cluster transfer reactions, DWBA treatment 2−42589
coherent reactions, multiple step production model 2−82945
coincidence meas. using gas target, geometrical corrections 2−63684
collective excitation, Thomas spin-orbit coupling, expansion in orbital ang. momentum transfer 2−82941
compound nuclear, role of γ-ray emission from unbound states 2−79804

Nuclear reactions and scattering continued
compound nuclear reactions, review 2−82100
compound nuclei, multiple-scatt. effects in mean lifetime expt. by blocking technique 2−63748
compound nucleus, dynamic deformation effects 2−70425
compound nucleus, ternary fission 2−70484
continuum shell-model approximation schemes, comparison 2−63855
continuum state production compound nucleus model 2−46219
correlations between partial widths of different channels 2−46216
Coulomb and nuclear excitation amplitudes, interference in inelastic scatt. 2−46304
Coulomb energy calc., relativistic corrections 2−46076
Coulomb interaction with absorption, inverse problem in complex λ-plane 2−82946
Coulomb production of hadrons, expression for integrated production cross section and calc. of Σ^0 lifetime 2−42550
coupled channel calculation method 2−55948
cross-section fluctuations as a function of energy 2−46215
currents, nuclear, global method of treatment 2−67113
Dalitz plots, evaluation 2−63854
deformed nuclei, two-nucleon transfer form factors 2−63860
in degenerate electron nuclear plasma 2−58256
diffraction dissociation of hadrons from nuclei, modification of Glauber theory 2−70428
diffraction scattering of charged particles, quantitate criteria for transfer and Fresnel scattering 2−63859
direct reaction, angular distribution of products and asymmetry 2−70424
direct reaction mechanisms in unified microscopic nuclear theory 2−46226
direct reactions, dependence of polarization effects on total ang. momentum of exchanged particle 2−46225
direct reactions, particle knocking out-polarization correl., meas. possibilities 2−49779
direct reactions, plane-wave matrix approach 2−82941
direct reactions, polarization phenomena using simple diagrams 2−46224
direct reactions to many-channel many-level final states, calc. of cross section 2−74059
doorway states, review 2−46220
DWA method, effect of adding an effective imaginary part 2−74081
DWBA, study using ^{6}Li(n, d)^{5}He ground state angular distrib. 2−70452
DWBA, use of Eckhart interactions 2−46223
DWBA coexistence model failures 2−74089
DWBA model for stripping to unbound states 2−46209
effective cross-sections using partial-wave analysis 2−46208
elastic and total cross sections for high energy scatt., nucl. density distrib. sensitivity 2−67203
elastic scattering, K-matrix expansion, phase shifts resonances and few-level approx. 2−42552
elon-nucleus collisions, where elon = any elementary particle, determ. of meson-nucleon cross sections 2−76648
equations of motion approach to nuclear spectroscopy 2−82947
Erickson fluctuations, use of weighting functions in Fourier analysis 2−52791
evaporation spectra analysis 2−52792
fast timing coincidence and n-γ ang. correl. techniques applic. 2−59738
final-state interactions, review 2−63487
folded Yukawa singleparticle potential with two centres 2−70354
forward dispersion relation for low- energy charged particle elastic scatt. 2−67205
generator-coordinate analysis 2−52828
Glauber series derivation from Feynman diagrams, generalization to nonzero scattering angles 2−74056
hadron production, coherent, in nuclear Coulomb field 2−52794
heavy ion elastic scatt., optical model analyses, absorptive potentials 2−79807
hodoscopic system for study of interactions in 1 MeV region 2−82805
inclusive production from nuclear targets 2−67202
inelastic scatt. folding and deformed potential models 2−46210
inelastic scattering, role of two-body spin-orbit interaction 2−70430
inelastic scattering Born approx. calcs. of probability of spin flip, explanation of backward- angle peak 2−79787
interaction time meas. and causality 2−58744
intermediate structures, generalization 2−63857
isobaric analogue resonances, survey of statistical neutron decay for nuclei in A = 91-97 range 2−67131
K-matrix method for nucl. scatt. reactions 2−82943
light nuclei, intranuclear cascade model taking into account changes in density of target 2−55977
light nuclei, sum rules for two-nucleon transfer 2−42553
local and nonlocal potentials; equivalence, S-matrix 2−82936
many-body Jastrow and Brueckner theories, subsidiary conditions 2−46071
models, review 2−46217
multinucleon wave function expression approach 2−59676
multiple at high energy in passage of charged particle beam through matter, possibility of mass separation 2−82429
nonlocal potential matrix elements from scatter phases 2−52079
nucleon-transfer from factors relative to microscopically specified core 2−46222
optical model parameters from elastic scattering and their correlations 2−49781
optical model resonance parameters 2−46217
optical potential, depolarization and tensor part of spin-spin term 2−82940
optical potential spin, isospin and spin-orbit dependence 2−46218
optical potentials, criteria for elimination of discrete ambiguities 2−67204
pion production in nucleus-nucleus collisions, study using current algebra 2−63862
potential model R-matrix theory, applic. to single and 2 channels 2−63858
pre-equilibrium statistical model and complex particle emission 2−76827
precompound emission, even-odd effects 2−46211

Nuclear reactions and scattering continued
primary particle energy effects on meson production parameters 2−74057
R-matrix theory, boundary condition parameter 2−67200
radionuclide production by charged particle bombardment, units and quantities 2−42554
reaction matrix parameters non- invariance of statistical distributions under changes in boundary conditions 2−67201
reactions, role of simple configurations, review 2−63732
rearrangement reactions, reduction to pair of two-particle problems 2−74053
relativistic kinematics of three body reaction, computer program 2−74054
resonance absorption, temp. dependent intermediate resonance integrals 2−55978
resonance reaction theories, survey 2−46213
resonance reaction theory, bound and decay states 2−59737
resonance scattering theory and structure of compound states 2−52793
resonance theory, role of adjustable parameter Q_c 2−70426
resonant, isobaric analogue resonances in spherical and collective nuclei 2−70367
resonant, Regge pole summation of partial wave series 2−76825
S-matrix derived from Lane-Robson theory, boundary condition constants 2−46212
Sasakawa theory of scattering, generalization and applications 2−59734
scattering T-matrix, eikonal expansion 2−70621
semi-leptonic weak interactions, analysis using electron scattering on basic, application to ^{16}O 2−76831
sequential-decay model validity, rescatt. corrections 2−63856
single nucleon transfer involving multi-shell target states, iso-spin centroids 2−59781
single nucleon transfer reactions, form factor calc. 2−70427
single-channel strength-function limit test 2−82942
stars, He burning processes 2−69086
stripping to unbound states DWBA model 2−46209
three momentum particle motion, generalized method of intermediate structure 2−55975
three-body, application of method of moments 2−73748
three-body scatt. amplitudes, inelastic effects of bound state break-up 2−82944
three-particle final-state reactions, triangle graphs and isospin violation 2−74055
three-particle scatt. amplitude, distorted wave method, second order terms 2−59735
transfer reactions to unbound states studied by diffraction model 2−49780
triplet production meas. near threshold, streamer chamber technique 2−76751
two-body interaction, potentials determ. from analysis of baryon-baryon scattering 2−49777
two-nucleon transfer, sum rules 2−79781
unitary parametrization, K-matrix behaviour 2−46214
unstable states, theoretical approach 2−42551
yields, statistical separation with various multiplicities, suppression of accelerator-beam intensity oscillations effects 2−59736
γ-rays, perturbed angular distribution following nuclear reactions 2−67206
NN scattering in nucleus-nucleus collisions, calc. of total cross-sections using Glauber's multiple scattering theory 2−70429
^{109}Ag(^{18}O, 5n)^{123}Cs positron decay and decay scheme of ^{123}Cs 2−74037
^{12}B, semileptonic weak interactions, cross-sections 2−74067
^{12}C, semileptonic weak interactions, cross-sections 2−74067
^{4}He, proton scattering, Majorana component in imaginary potential 2−46248
^{12}N, semileptonic weak interactions, cross-sections 2−74067
^{16}O, semi-leptonic weak and e.m. interactions 2−76831
^{16}O nucleon-transfer form factors relative to microscopically specified core 2−46222

chemical effects
see also Chemical effects of radiations/ionizing radiations
(n, γ) recoil copper in α copper phtalocyanine crystals, chemical state 2−72586
I_2, in aqueous CH_3I solns., (n, γ) reactions 2−81537

high energy ⩾1 GeV
cosmic ray inelastic interactions, 10^{11}-10^{12} eV, multiplicity depend. on energy 2−73885
emulsion-nuclei interactions with p at 22.6 GeV/c, velocity distrib. of secondary π meson 2−76840
photoemulsion exposure to 60 GeV pions, meas. of yield, spectrum, angular distrib. of ^{8}Li 2−52821
superheavy elements search 2−59893
d elastic and inelastic cross-sections on photoemulsion nuclei and proton stripping, 2.43 GeV/c 2−63909
Fe, interaction of cosmic ray μ, meas. of cascades with energies ⩾1 GeV using ionization calorimeter 2−73895
n interaction with paraffin nuclei >200 GeV, average multiplicity, azimuthal effect in ang. distrib. 2−74101
pπ- from interaction of 25-30 GeV/c neutrons with C 2−63670
π, 60 GeV, angular inclination of secondaries 2−74102
π interaction with paraffin nuclei >200 GeV, average multiplicity, azimuthal effect in ang. distrib. 2−74101
3π production cross-sections meas. in 15.1 GeV/c π reactions on various nuclei 2−49815
π production on various nuclei, 2 and 3 GeV 2−82951
π^{-}C, 40 GeV/c, multiplicity distribution of charged particles produced 2−45960
C, inelastic interac. with cosmic nucleons, 760-7600 GeV 2−42558
^{12}C-N high energy cosmic ray interaction, cf of optical and Glauber models 2−73892
Fe, estimate of photonuclear cross-section 2−73895
^{57}Fe-N high energy cosmic ray interaction, cf of optical and Glauber models 2−73892
LiH, target for 150-550 GeV cosmic ray nucleons, multiplicity of particles generated 2−74070
Pb, cosmic ray hadron interaction, 3-30 TeV 2−73889
^{208}Pb-N high energy cosmic ray interaction, cf of optical and Glauber models 2−73892

Nuclear reactions and scattering continued
high energy ⩾1 GeV continued
W, negative hyperon production by 24 GeV/c proton bombardment 2−42419

Nuclear reactions and scattering due to alpha-particles
^{2}H (α, αp)n, new impulse approx. reaction mechanism 2−79796
elastic and inelastic scattering on heavy nuclei, determ. of surface form from angular distrib. meas. 2−79765
elastic scattering, 166 MeV, meas. of angular distribs., differential cross sections, determ. of neutron radii 2−63904
medium and heavy nuclei, elastic scattering differential cross-sections near Coulomb barrier 2−70467
optical potentials, criteria for elimination of discrete ambiguities 2−67204
rare-earth compound nuclei formed in bombardment with 40 MeV α-particles of rare-earth targets, intensities of ground band transitions 2−49731
spin-orbit potential estimation 2−83006
thick targets, 46 MeV, generation of neutrons 2−76867
unnatural- parity amplitudes from exchange effects in local energy approximation 2−76835
(α,2α) three-particle final state reactions 2−49827
(α,2nγ) and (α,2nγ) reactions on ^{181}Ta, ^{175}Lu and ^{169}Tm, rotational bands and lifetimes of isomeric states 2−70409
(α,α) scattering amplitude determ. including angular-momentum matching of absorbed partial waves 2−49821
(α,xγ), γ-ray ang. distribs. of high-spin states, spin determ. method 2−79721
^{a}Cu(α,p), A=63, 65, 27.2 MeV, meas. of differential cross section, analysis of p angular distrib. in three nucleus stripping theory 2−49833
^{a}Sn(α, $\alpha'\gamma$) (A=117, 119), Coulomb excitation study 2−63810
^{241}Am(α,2n)^{243}Bk, excitation energy, spontaneous fissioning products, time-of-flight obs. 2−76881
^{40}Ar(α,n), E_n=6.3-8 MeV, states of ^{43}Ca 2−82897
^{40}Ar(α,n)^{43}Ca, 5.5-8 MeV, lifetimes of low-lying states of ^{43}Ca 2−74018
^{197}Au(α, αn), E_α=900 MeV cross-sections direct neutron emission mechanism
^{197}Au(α,n)^{200}Tl, neutron spectra analysis, level density of residual nucleus 2−63831
^{11}B(α,n)^{14}N, differential cross- section at 12-15 MeV 2−46314
^{11}B(α,t)^{12}C, triton ang. distrib., 15-25 MeV, excitation functions 2−74112
^{138}Ba, differential cross sections for elastic and inelastic scattering to low-lying states, 50 MeV 2−46305
Be(α,n), for isotopic n source, line spectra. meas. 2−42439
^{209}Bi(α, 3n)^{210}At, evidence for 15^- and 11^+ isomeric states in ^{210}At 2−70415
^{209}Bi(α, $\alpha'\gamma$), e.m. matrix elements of low-lying states near ^{208}Pb closed shell 2−76782
^{209}Bi(α,3n)^{210}At, g-factor of 0.8μs isomeric state at 2549 keV, in ^{210}At 2−49756
^{81}Br(α, $\alpha'\gamma$) 2.5-8.2 MeV, Coulomb excitation of low-lying levels, meas. of γ-ray energies, yields, angular distribs., Doppler broadening 2−74032
^{12}C, 880 MeV, cross-sections for production of ^{6}Li and ^{7}Li 2−74088
^{12}C, alpha-gamma ang. correlation studies 2−70477
^{12}C(α, ^{8}Be)^{8}Be, 15 to 18.96 MeV, search for 8^+ level in ^{16}O 2−79733
^{12}C(α,^{6}Li)^{10}B, ^{12}C(α,^{7}Be)^{9}Be, ang. distribution and cross sections of emitted heavy ions 2−49831
^{12}C(α, α)^{12}C, 4-13.3 MeV, spin and parity assignments, new O^+ level in ^{16}O 2−79735
^{12}C(α,$\alpha_1\gamma_{4.43}$)^{12}C, E_2=10.2-10.5 Mev, ang. correls. and 14.8 MeV level in ^{16}O 2−76869
Ca isotopes, anomalous backward alpha scatt. interpret. 2−83007
^{40}Ca(α,2p)^{42}Ca, mag. moment determ. for ^{42}Ca 2−59700
^{40}Ca(α,α)^{40}Ca, 29 MeV, calc. of α-cluster effects using L-independent optical potential 2−83013
^{44}Ca(α,pγ)^{47}Sc, mean lives of low-lying levels in ^{47}Sc determ. by Doppler-shift attenuation method with p-γ coincidences 2−74021
^{106}Cd(α.3n)^{107}Cd isotope identification 2−82886
^{108}Cd, ^{111}Cd(α, xnγ)$^{111m, 113m, 114m}$Sn, study of short- lived isomers in ^{111}Sn, ^{113}Sn 2−74036
^{35}Cl(α,p), 27.2 MeV, meas. of differential cross section, analysis of p angular distrib. in three nucleon stripping theory 2−49833
^{59}Co, study of excitation functions and average changes of recoil nuclei, comparison of exptl. and theoretical cross section 2−67316
^{59}Co(α,p), 42 MeV, particle emission probabilities 2−42587
^{50}Cr, inelastic scatt., ang. distribs., octupole excitations 2−74022
^{40}Cu(α,p)^{43}Sc, E_α=28.5 MeV, stripping rel. to knockout mechanism 2−76871
^{63}Cu, ^{65}Cu(α,$\alpha'\gamma\gamma$) Coulomb excitation, 5.5, 7.0 MeV, meas. of angular distrib. and $\gamma\gamma$ angular correlations 2−63802
^{65}Cu(α, αn), E_α=900 MeV cross-sections direct neutron emission mechanism 2−83010
^{162}Dy(α,α')^{162}Dy, Coulomb excitation quadrupole and hexadecapole, deforms. determ. 2−79752
^{164}Dy(α,α')^{164}Dy, Coulomb excitation quadrupole and hexadecapole, deforms. determ. 2−79752
^{166}Er(α,α')^{166}Er, Coulomb excitation quadrupole and hexadecapole, deforms. determ. 2−79752
^{168}Er(α,8n), production of high-spin states in ^{164}Yb, anomalous behaviour of nuclear moment of inertia at large rotational frequencies 2−42528
^{168}Er(α,α')^{168}Er, Coulomb excitation quadrupole and hexadecapole, deforms. determ. 2−79752
^{170}Er (α, 3n)^{171}Yb, 26-43 MeV, meas. of cross sections, population of rotational states 2−74040
^{170}Er(α,α')^{170}Er, Coulomb excitation, quadrupole and hexadecapole, deforms. determ. 2−79752
^{151}Eu(α, $\alpha'\gamma$), 30-90 MeV, Coulomb excitation studies of level struct. 2−76884
^{153}Eu(α, $\alpha'\gamma$), 30-90 MeV, Coulomb excitation studies of level struct. 2−76884
^{19}F(α,2α), ^{19}F (α,αt), α and triton clustering probabilities, PWIA analysis 2−59778

Nuclear reactions and scattering due to continued
alpha-particles continued
^{56}Fe(α,p), 27.2 MeV, meas. of differential cross section, analysis of p angular distrib. in three nucleon stripping theory 2−49833
^{158}Gd(α,α')^{158}Gd, Coulomb excitation quadrupole and hexadecapole, deforms. determ. 2−79752
^{160}Gd(α,α')^{160}Gd, Coulomb excitation quadrupole and hexadecapole, deforms. determ. 2−79752
Gd(γ t) energy levels of Tb odd isotopes 2−82916
^{73}Ge(α,$\alpha'\gamma$), Coulomb excitation, 2.6-4.0 MeV, test of quasiparticle-phonon coupling theories 2−74030
^{2}H, 120 MeV alpha bombardment, neutron energy spectra 2−67322
^{2}H(α,α^{1})d + (^{1}S$_0$)→n + p isospin impurity of ^{6}Li 4.57 MeV state 2−82879
^{2}H(α,t)^{3}He, two-mode finite-range DWBA analysis of mechanism 2−70475
^{3}He(α,α')^{3}He*, 115 MeV, continuum spectra analysis 2−67141
^{3}He(α,α)^{3}He elastic scatt., 7-18 MeV, polarization analyzing power 2−82996
^{3}He(α,α)^{3}He elastic scatt., 4-10 MeV, polarization analyzing power 2−82995
^{4}He + ^{4}He, direct solution of Hill-Wheeler equation 2−42583
^{4}He(α, $\alpha\gamma$)^{4}He, meas. of bremsstrahlung cross section 12.5-19.0 MeV 2−74105
^{4}He(α,α)^{4}He, 63, 69 and 77 MeV, potential construction 2−82946
^{4}He(α,α)^{4}He 30-70 MeV study of even-spin positive-parity levels in ^{8}Be by phase-shift 2−82878
^{165}Ho, scatt. from aligned target, optical model ambiguities 2−79798
^{165}Ho(α, 4nγ)^{165}Tm, 38 and 50 MeV, determ. of rotational bands by meas. of γ-γ coincidences 2−74039
^{115}In(α,p), 42 MeV, particle emission probabilities 2−42587
^{41}K(α,n)^{44}Sc, excitation functions and isomer ratios calc. in stat. models 2−82997
^{7}Li(α,t)^{8}Be, triton ang. distrib., 15-25 MeV, excitation functions 2−74112
^{24}Mg(α,α), meas. of differential cross sections between 22 and 28 MeV, optical-model and Hauser Feshbach analysis 2−49824
^{24}Mg(α,α)^{24}Mg, 20-23 MeV, compound nucleus effects in elastic scatt. 2−46303
^{24}Mg(α,p)^{27}Al, search for high-spin states in ^{27}Al in excitation range 4.8-8.0 MeV 2−42504
^{24}Mg(γ, γ'), E$_\alpha$ = 15.4 − 19.1 MeV, continuum region obs. 2−76872
^{26}Mg(α, n)^{29}Si, ^{26}Mg(α, α)^{26}Mg, ^{26}Mg(α, γ)^{30}Si, 2.5-4.3 MeV, study of resonances in ^{30}Si 2−46123
^{26}Mg(α,α), meas. of differential cross sections between 22 and 28 MeV, optical-model and Hauser Feshbach analysis 2−49824
^{55}Mn(α, nγ)^{58}Co, 10 MeV, meas. of n-γ angular correlations and lifetimes using Doppler-shift attenuation method 2−82890
Mo, A = 92, 94, 96, 98, 100, elastic and inelastic scatt., 30.87 MeV 2−63905
^{92}Mo(α,t)^{93}Tc, 41.5 MeV, ang. distribution meas. 2−46327
^{94}Mo, multiple Coulomb excitation, low-lying level props. 2−82910
^{96}Mo(α,t)^{97}Tc, 41.5 MeV, ang. distribution meas. 2−46327
^{98}Mo, multiple Coulomb excitation, low-lying level props. 2−82910
^{100}Mo, multiple Coulomb excitation, low-lying level props. 2−82910
^{14}N(α, γ)^{18}F, E$_\alpha$ = 1526 keV, transition strengths of analogue states 2−74000
^{14}N(α,d)^{16}O, ^{16}O energy levels up to 30 MeV 2−46317
^{93}Nb(α,α), Coulomb excitation of levels 2−46152
^{150}Nd (α, 2n) ^{152}Sm, ground state rotational bands in ^{152}Sm 2−59713
^{150}Nd (α, 4n) ^{150}Sm, ground state rotational bands in ^{150}Sm 2−59713
^{150}Nd(α, t)^{151}Pm, 25 MeV, meas. of cross section, determ. of level structure of ^{151}Pm 2−74038
^{22}Ne(α,nγ)^{25}Mg, excited states of ^{25}Mg obs. 2−59725
^{58}Ni, alpha-gamma ang. correlation studies 2−70477
^{58}Ni(α, αn), E$_\alpha$ = 900 MeV, cross sections direct neutron emission mechanism 2−83010
^{58}Ni(α, pγ) ^{61}Cu, compound statistical theory computation of cross-section for level population, γ-ray emission 2−79804
^{58}Ni(α, ppγ)^{60}Ni compound statistical theory computation of cross-section for level population, γ-ray emission 2−79804
^{58}Ni(α,α')^{58}Ni, high-lying states of ^{58}Ni 2−59784
^{58}Ni(α,p)^{61}Cu, ^{61}Cu level studies, transitions, spin assignments 2−59783
^{60}Ni(α,p)^{63}Cu, ^{63}Cu level studies, transitions, spin assignments 2−59783
^{62}Ni(α,p)^{65}Cu, ^{65}Cu level studies, transitions, spin assignments 2−59783
^{64}Ni(α,p)^{67}Cu, ^{67}Cu level studies, transitions, spin assignments 2−59783
^{16}O, elastic scatt., antisymmetrization method applic. 2−79777
^{16}O, inelastic excitation of 2$^-$(8.88 MeV) level, role of two-body spin-orbit interaction 2−70430
^{16}O(^{4}He,^{6}Li)^{14}N, ^{16}O(^{4}He,^{7}Li)^{13}N, ^{16}O(^{4}He,^{7}Be)^{13}C, ^{16}O(^{4}He,^{9}Be)^{11}C, ang. distribution and cross sections of emitted heavy ions 2−49831
^{18}O(α,nγ), level struct. of ^{21}Ne 2−55958
^{18}O(α,nγ)^{21}Ne, excited states of ^{21}Ne obs. 2−59696
^{31}P(α,p), 27.2 MeV, meas. of differential cross section, analysis of p angular distrib. in three nucleon stripping theory 2−49833
^{31}P(α,p)^{34}S, 3.25-5.5 MeV, obs. 2−46323
^{31}P(α,p)^{34}S, spin assignments for higher excited states of ^{34}S 2−52746
^{206}Pb(α,f), integral and differential cross-sections for ^{210}Po fission, 29-46 MeV 2−67337
^{208}Pb, investigation of nucleon distribution near surface 2−46150
^{208}Pb(α, α') cross sections, 65 MeV, strong multipole vibrs. in low-excitation region 2−76879
Pb(α,α) elastic scattering, incoming wave boundary condition calc. of cross section at incident energies near Coulomb barrier 2−42592
PuO$_2$ fuel neutron radiation characts. 2−83130
^{239}Pu(α,2n)^{241}Cm, excitation energy, spontaneous fissioning products, time-of-flight obs. 2−76881
Rb isotope yields 2−55988
^{104}Ru(α,3n)^{105}Pd, 26-43 MeV, γ-ray spectrum of excited states of ^{105}Pd 2−49744
^{32}S, scattering at 104 MeV, evidence for prolate shape of nucleus 2−46126
^{32}S(α,p)^{35}Cl, 10.0 MeV, meas. of mean lifetimes of levels in ^{35}Cl by Doppler-shift attenuation method 2−70386

Nuclear reactions and scattering due to continued
alpha-particles continued
^{34}S(α,γ)^{38}Ar, 3.6-4.8 MeV, meas. of cross sections, angular distributions and angular correlations ^{38}Ar levels deduced 2−63791
^{34}S(α,n)^{37}Ar, meas. of lifetimes of levels in ^{37}Ar below 3 MeV excitation by Doppler shift attenuation method 2−63790
Se isotopes, E$_2$ = 14.2 MeV, gamma ray transitions of odd Kr isotopes 2−79759
^{28}Si(α,α,γ)^{28}Si, 10-18 MeV, angular correlation studies for excitation of 1.78 MeV 2$^+$ state 2−63787
^{28}Si(α,α), meas. of differential cross sections between 22 and 28 MeV, optical-model and Hauser Feshbach analysis 2−49824
^{28}Si(α,p), 27.2 MeV, meas. of differential cross section, analysis of p angular distrib. in three nucleus stripping theory 2−49833
^{29}Si(α,p)^{32}P, 10.4-11.0 MeV, pγ angular correlation and Doppler-shift meas. 2−49735
^{30}Si(α,nγ)^{33}S, 6.0-9.5 MeV, study of ^{33}S levels up to 4.3 MeV excitation, analysis of γ-ray angular distribs. 2−70385
^{144}Sm, differential cross sections for elastic and inelastic scattering to low-lying states, 50 MeV 2−46305
^{144}Sm(α,n)^{147}Gd, high spin levels excited in ^{147}Gd, particle core coupling 2−49750
Sn, A = 116, 118, 120, 124 targets, 166 MeV, nuclear sizes 2−63809
^{112}Sn, ^{115}Sn(α, xnγ)$^{115m,\,117m}$Te, study of short-lived isomers in ^{115}Te, ^{117}Te 2−74036
^{116}Sn(α,p), 42 MeV, particle emission probabilities 2−42587
^{124}Sn(α,3nγ), E$_\alpha$ ≐ 26-37 MeV, particle-core coupling in ^{125}Te 2−76781
^{181}Ta(α,n)^{184}Re, neutron spectra analysis, level density of residual nucleus 2−63831
^{169}Tm (α, 2n)^{171}Lu, high spin rotational levels, γ-ray obs. 2−59717
^{169}Tm(α, 2n)^{171}Lu, 27 MeV, lifetime meas. and isomeric E1 transitions with ΔK = 0 in ^{171}Lu 2−63823
^{169}Tm(α, 2n)^{171}Lu, rel. to validity of rotor motor for ^{171}Lu 2−59718
^{235}U(α, 3n)^{236}Pu, 24.5-28 MeV, cross sections, fission isomer excitation functions 2−76880
^{238}U(α,2n)^{240}Pu, excitation energy, spontaneous fissioning products, time-of-flight obs. 2−76881
^{51}V(α, nγ)^{54}Mn, 7.1, 7.6 MeV, meas. of γ-ray spectra, determ. of ^{54}Mn level structure 2−79743
^{171}Yb(α,nγ)^{174}Hf, ^{172}Yb(α,nγ)^{174}Hf, role of K-quantum number in de-excitation of ^{174}Hf 2−46328
^{172}Yb(α,8n), production of high-spin states in ^{168}Hf, anomalous behaviour of nuclear moment of inertia at large rotational frequencies 2−42528
^{173}Yb(α,t)^{174}Lu, 28.5 MeV, determ. of levels in ^{174}Lu 2−82896
^{64}Zn, influence of nonlocality on inelastic scattering 2−46326
Zn(α,α'), A = 68, 70, 31 MeV, angular distributions 2−42581
^{90}Zr, investigation of nucleon distribution near surface 2−46150
^{90}Zr(α,α), angular distribs. and differential cross sections in angular range 4° − 150° at 40, 60, 80 and 100 MeV 2−49825
^{90}Zr(α,t)^{91}Nb, 41.5 MeV, ang. distribution meas. 2−46327

cosmic rays
see also Cosmic rays/effects and interactions
energies > a few hundred GeV, existence of large transverse momenta 2−73873
neutrino sea, interaction with nuclei, phenomenological causal model of nuclear decay 2−78434
μ interactions with Fe meas. of cascades with energies ⩾1 GeV using ionization calorimeter 2−73895

deuterons
breakup collisions, symmetrization effects in spectator momentum distribution 2−46309
breakup reaction, importance of Pauli mechanism 2−67318
Coulomb break-up of deuteron in field of nucleus, DWBA treatment 2−63907
internal wavefunction deform. by Coulomb field 2−63906
light nuclei, analysis of reactions with polarized deuterons 2−46307
mass number dependence of diffraction model parameters 2−42579
neutron stripping, relation of cross section with off-shell neutron scattering cross section 2−67319
with photoemulsion nuclei, 2.43 GeV/c elastic and inelastic cross-sections and proton stripping determ. 2−63909
photographic emulsions, inelastic collisions 2−55997
scattering at high energy, connection between model of opaque nucleus and Glauber model 2−70462
stripping form factors, Sturmian function applic. in calculations 2−46308
stripping on deformed nuclei, 2 step processes 2−63910
stripping reaction, DWBA validity and three-body model 2−59780
stripping reaction, polarization of protons 2−59779
stripping reaction, rel. to investigation of intermediate nuclear structure 2−70347
three-body scatt. amplitudes, inelastic effects of deuteron break-up 2−82944
transfer reactions, charge asymmetry deviation 2−67321
unnatural- parity amplitudes from exchange effects in local energy approximation 2−76835
(d, p), j-depend. in l = 3 transitions 2−76845
(d, p) reaction on fissioning nucleus, calc. of cross section for many-channel many level final states 2−74059
(d, t), single-particle potentials, nuclear rearrangement 2−73974
(d,p), three-body treatment in truncated model space 2−49819
(d,p), using formalism of Green's functions 2−83012
(d,p) Coulomb stripping reactions, analytic expression for proton polarization 2−46311
(d,p) reactions for spectroscopic information on nuclear structure of N = 83 nuclei 2−67170
(d,p) stripping reaction, three body model 2−49826
(d,p) stripping reactions on spherical and deformed nuclei, multistage effects 2−46306
(d,pγ), proton ang. distrib. from shape-studies of γ-ray spectra 2−79802
(d,pn) reaction, search for difference in deuteron breakup by heavy nuclei for closed-shell and non-closed-shell nuclei 2−52822
(N,d), Pade approximants 2−49823
^{a}Hg(d,d'), A = 204, 202, 201, 17 MeV, obs. of transitions up to 4.5 MeV excitation 2−46329

Nuclear reactions and scattering due to continued
deuterons continued
^{a}Hg(d,t), A=204, 202, 200, 198, 17 MeV, meas. of angular distrib., spectroscopic factors 2−46329
^{a}Hg(d,t), A=204, 202, 200, 198, 17 MeV, meas. of angular distrib., spectroscopic factors 2−46329
^{a}Nb(d,n) (A=91,97), study of single-particle proton states in Nb 2−70400
^{a}Ni(d,α)Co, A=58, 60, high resolution spectroscopy of ^{56,58}Co, DWBA analysis of angular distrib. 2−63800
^{a}Tc(d,n) (A=92,93,95,97), study of single-particle proton states in Tc 2−70400
^{27}Al, d absorption cross section, 25 GeV/c, Glauber theory calc. and comparison with expt. 2−70469
Al(d,n) thick-target yields and total cross sections, 1-40 MeV 2−67333
^{36}Ar(d, α)^{34}Cl, 19 MeV, level properties of ^{34}Cl up to 3.6 MeV., D.W.B.A. analysis 2−76877
^{75}As, excitation functions for (d, 2n), (d, 4n), (d, 5n), (d, p), (d, p2n), (d, p3n), (d, 2p) reaction at 52 MeV 2−52824
Au, scatt., low energy breakup phenomena 2−67317
^{197}Au(d,2n), excitation function meas. between threshold and 12 MeV 2−49835
^{197}Au(d,p), excitation function meas. between threshold and 12 MeV 2−49835
^{197}Au(d,t), excitation function meas. between threshold and 12 MeV 2−49835
^{10}B(d,n), E_d=11.8 MeV, neutron spectroscopy 2−67324
^{11}B(d,n), E_d=11.8 MeV, neutron spectroscopy 2−67324
^{11}B(d,n)^{12}C, polarized deuterons, reaction study at 900 keV 2−42584
^{11}B(d,n) meas. of neutron polarization angular distrib. 2−63915
Be, dosimetry of neutron fields produced 2−67320
^{9}Be, angular distribs. for scattering, neutron pick-up, neutron stripping reactions analysed using DWBA and optical model 2−49820
^{9}Be(d,n)^{10}B, 650 keV, meas. of angular distrib. of neutrons, energy levels of ^{10}B 2−49830
^{9}Be(d,n)^{10}B, 650 keV, meas. of recoil proton tracks, angular distrib. of neutrons, determ. of Q-value spectrum 2−63913
^{9}Be(d,p)^{10}Be, E_d=12 MeV, proton polarization for ground state and first excited state transitions 2−82998
Be(d,n) thick-target yields and total cross sections, 1-40 MeV 2−67333
^{79}Br, ^{81}Br(d, p)$^{80,\,82}$Br, 12 MeV meas. of cross sections, excitation of low-lying states of $^{80,\,82}$Br, DWBA analysis 2−74031
^{12}C, d absorption cross section, 25 GeV/c, Glauber theory calc. and comparison with expt. 2−70469
^{12}C(d,^{6}Li), 28 MeV, ang. distribution meas. and DWBA analysis 2−59782
^{12}C(d,^{7}Li)^{7}Be, angular distrib. meas. on test of Barshay- Temmer theorem 2−46259
^{12}C(d, α)^{10}B, 7.19-13.99 MeV, isospin forbidden reaction obs. 2−63916
^{12}C(d, d), 20-30MeV polarized beam, meas. of angular distribs., vector polarization, differential cross sections, optical model parameters 2−74106
^{12}C(d, p_0)^{13}C, polarized deuteron reaction 2−55998
^{12}C(d, p_1)^{13}C, polarized deuteron reaction 2−55998
^{12}C(d,d′)^{12}C*, isospin-mixing matrix element obs. 2−63771
^{12}C(d,d′)^{12}C$\rightarrow{}^{8}$Be + α, 9.6 MeV, meas. of angular correlation function of (d,α) coincidences, comparison with theory 2−49832
^{12}C(d,d), 1.6 to 2.7 MeV, tensor polarization of deuterons 2−42580
^{12}C(d,n), E_d=11.8 MeV, neutron spectroscopy 2−67324
^{12}C(d,n)^{13}N, weakly bound projectile model calcs. of spectroscopic factors 2−67325
^{13}C(d,n), E_d=11.8 MeV, neutron spectroscopy 2−67324
^{40}Ca(d,^{6}Li), 28 MeV, ang. distribution meas. and DWBA analysis 2−59782
^{40}Ca(d,n), meas. of neutron polarization angular distrib. 2−63915
^{41}Ca(d,p)^{42}Ca, E_d=12 MeV, $(1f_{7/2})^2$ multiplet of ^{42}Ca 2−67155
^{44}Ca(d,α)^{42}K, E_d=11 MeV, energy levels of ^{42}K 2−70380
C(d,n) thick-target yields and total cross sections, 1-40 MeV 2−67333
^{142}Cd(d, p), 12.6 MeV 2−67332
^{142}Ce(d, t), 12.6 MeV 2−67332
^{50}Cr, inelastic scatt., ang. distribs., octupole excitations 2−74022
^{50}Cr(d, p)^{51}Cr, 10 MeV, spin assignments based on ln=1 J-dependence in (d, p) reaction 2−63920
^{52}Cr, elastic scatt. of vector polarized deuterons, 11.9 MeV, optical pot. 2−70465
^{64}Cu, d absorption cross section, 25 GeV/c, Glauber theory calc. and comparison with expt. 2−70469
(d,^{6}Li), multistep reaction processes 2−63908
D(d,n)^{3}He, fast timing coincidence techniques applic. 2−59738
^{163}Dy(d, 2nγ), 13.5 MeV meas. of γ-ray spectra, deduced ^{163}Ho level scheme 2−63820
^{19}F(d,^{6}Li), 28 MeV, ang. distribution meas. and DWBA analysis 2−59782
^{19}F(d, α)^{17}O, 2.34 to 14.45 MeV, resonance structure in excitation function 2−67326
^{19}F(d,α)^{17}O, 3 MeV, meas. of α-particle angular distribs. 2−67151
^{19}F(d,p)^{20}F, 3 MeV, meas. of differential corrections and angular distrib. of proton groups 2−67151
^{19}F(d,p)^{20}F, E_d=16 MeV, nucl. struct. of ^{20}F 2−63917
^{19}F(d,pγ)^{20}F, p,γ ang. correl., low-lying states of ^{20}F 2−79801
^{57}Fe(d,α)^{55}Mn, 16 MeV, study of two-nucleon pick-up from spin-1/2 target, differential cross section meas. 2−63883
^{57}Fe(d,d′n), 19 MeV, neutron-gamma competition 2−46325
^{57}Fe(d,p)^{58}Fe, 7.0 MeV meas. of angular distrib., comparison with DWBA calcs., ^{58}Fe level structure deduced 2−42512
^{58}Fe(d,p)^{59}Fe, 10 MeV, meas. of angular-momentum transfer, study of ^{59}Fe level structure 2−63921
^{1}H(d, d)^{1}H, large angle scattering at 433, 362, 2.91 MeV, meas. of cross-section, neutron-exchange mechanism 2−82993
^{1}H(d,pn)^{1}H, calc. of amplitude for deuteron break-up, theory of proton-proton final state interaction 2−70470
^{2}H(d, ^{3}He)n, cross section meas., 1.96-6.2 MeV 2−74108
^{2}H(d, d), 6−11.5 MeV polarized beam, meas. of angular distribs. of analysing powers iT_{11}, T_{20}, T_{21}, T_{22} 2−74104
^{2}H(d, n)^{1}H, off-energy shell effects 2−74110

Nuclear reactions and scattering due to continued
deuterons continued
^{2}H(d, n)^{3}He, 10.0 and 11.5 MeV polarized beam, meas. of differential cross section and analysing powers 2−74109
^{2}H(d, n)^{3}He, partially polarized neutron prod. for ^{12}C(n, n) elastic scatt. 2−76860
^{2}H(d, p)^{3}H, 3.0-11.5 MeV polarized beam, meas. of differential cross section and analysing powers 2−74109
^{2}H(d,d), elastic scattering study using resonating-group method and imaginary potential 2−55996
^{2}H(d,d), rel. to channel spin nonconservation 2−59775
^{2}H(d,d)^{2}H, cross section meas, 1.96-6.2 MeV 2−74108
^{2}H(d,dpn), study at low bombarding energies 2−67221
^{2}H(d,n)^{3}He, 0.2 to 4 MeV, polarization of neutrons 2−67323
^{2}H(d,n)^{3}He, cross section meas., 1.96-6.2 MeV 2−74108
^{2}H(d,n)^{3}He, E_d=16-22 MeV, neutron polarization ang. distrib. 2−70472
^{2}H(d,n)^{3}He, E_d=6-14 MeV, neutron polarization ang. distrib. 2−70471
^{2}H(d,n)^{3}He, neutron yield rel. to irrad. time 2−55999
^{2}H(d,n)^{3}He, polarization, comparison with ^{2}H(d,p)^{3}H reaction 2−70473
^{2}H(d,n)^{3}He, production of 90% polarized neutron beam for nuclear structure research 2−67130
^{2}H(d,p)^{3}H, appl. to interstitial ^{2}H site location in Nb 2−60811
^{2}H(d,p)^{3}H, E_d=2-14 MeV, proton polarization, ang. distrib. 2−70473
^{2}H(d,p)^{3}He, cross section meas., 1.96-6.2 MeV 2−74108
^{2}H(d,pn)^{2}H, isospin conservation 2−49828
^{2}H(d,t)p, cross section meas., 1.96-6.2 MeV 2−74108
^{3}H(d,n)^{4}He, neutron generator, health physics problems associated with operation 2−58603
^{3}H(d,n)^{4}He, neutron yield rel. to irrad. time 2−55999
^{3}He(d,n)^{4}He, meas of neutron polarization for E_d=1.0 to 5.0 MeV 2−49829
^{3}He(d,p)^{4}He, 300 keV to 2.5 MeV, polarized target, analyzing power of the reaction 2−46312
^{3}He(d,t)2p, centre-of-mass energy 23.5 MeV, energy spectra studied in DWBA approximation 2−42582
^{177}Hf(d, t)^{176}Hf, nuclear structure of ^{176}Hf 2−63824
^{179}Hf(d, p)^{180}Hf, nuclear structure of ^{180}Hf 2−63824
^{39}K level structure, inelastic scattering of 12.8 MeV deuterons 2−46324
^{41}K(d,p)^{42}K, 6 MeV, spins of ^{42}K states determ. by γ-γ correlations 2−46131
^{139}La (d, p), correlation with (n, γ) reaction 2−59768
^{139}La(d,p)^{140}La and ^{139}La(n,γ)^{170}La, positive correlation 2−67293
^{139}La(d,t)^{138}La, 16 MeV, meas. of angular distrib. of tritons, Q-value, low-lying states in ^{138}La 2−52761
Li target, neutron straggling 2−76868
^{6}Li, d absorption cross section, 25 GeV/c, Glauber theory calc. and comparison with expt. 2−70469
^{6}Li(d,α′^{3}He)n, 52 MeV, excited states of ^{4}He 2−49725
^{6}Li(d,α′t)^{1}H, 52 MeV, excited states of ^{4}He 2−49725
^{6}Li(d,αd)^{2}H, 52 MeV, excited states of ^{4}He 2−49725
^{7}Li(d,α)^{5}He, detn. of first excited state of ^{5}He 2−63768
^{7}Li(d,α)^{5}He, E_d=0.45-2MeV, sequential mechanism 2−74111
^{7}Li(d,t)^{6}Li, two-mode finite-range DWBA analysis of mechanism 2−70475
Li(d,n) thick-target yields and total cross sections, 1-40 MeV 2−67333
^{175}Lu(d,t)^{174}Lu, 12 MeV, determ. of levels in ^{174}Lu 2−82896
^{176}Lu(d,p), correlations with (n,γ) reactions 2−70456
^{176}Lu(d,p)^{177}Lu, and ^{176}Lu(n,γ)^{177}Lu, positive correlation 2−67293
^{24}Mg, elastic and inelastic scatt. of 12 MeV polarized deuterons, vector analysing power 2−67327
^{24}Mg(d,n), meas. of neutron polarization angular distrib. 2−63915
^{25}Mg(d,α)^{23}Na, dependence of integrated cross sections on rotational states of ^{23}Na at 20.9 MeV 2−46322
^{25}Mg(d,d′n), 19 MeV, neutron-gamma competition 2−46325
^{92}Mo(d,pγ), coincidence obs. of ^{93}Mo γ-decay 2−63805
^{101}Mo spectroscopy by sub-Coulomb stripping 2−76797
Mo(d,t), producing isobaric analog states, hole strength variations 2−46151
^{14}N(d, n)^{15}O, 5.16 MeV, n polarization ang. distrib. meas., cross-section analyzed using optical model formalism 2−46318
^{15}N(d,n_p)^{16}O, 4.83 MeV, meas. of polarization angular distribs. of ^{16}O states using time-of-flight method 2−70377
^{15}N(d,p)^{16}N(unbound), parallelism between proton spectra and off-energy-shell n-^{15}N total cross section 2−42585
^{20}Ne(d, n)^{21}Na, 3.6-6 MeV, meas. of angular distribs., excitation energies, stripping patterns 2−74005
^{20}Ne(d,pγ)^{21}Ne, study using p-γ and γ-γ coincidence techniques, determ. of levels in ^{21}Ne 2−79762
^{21}Ne(d, d)^{21}Ne, deform. parameters of ^{21}Ne 2−76842
^{21}Ne(d, p)^{22}Ne, 3.3 and 3.6 MeV, cross-section meas., spectroscopic factors extracted 2−46321
^{21}Ne(d, p)^{22}Ne, spectroscopic factors of ^{22}Ne 2−76842
^{21}Ne(d,p)^{22}Ne, E_d=12 MeV, level struct. of ^{22}Ne 2−76787
^{61}Ni(d,d′), competition between neutron and gamma emission de-excitation process 2−70466
^{61}Ni(d,d′n), 19 MeV, neutron-gamma competition 2−46325
^{62}Ni(d,p)^{63}Ni, 4.45, 5.12 MeV., meas of absolute differential cross sections, determ. of spectroscopic factors, DWBA analysis 2−79794
^{16}O, Pauli breakup of deuterons 2−46320
^{16}O(d,^{6}Li), 28 MeV, ang. distribution meas. and DWBA analysis 2−59782
^{16}O(d,d)^{16}O, cross sections and vector and tensor analysing powers, study with polarized deuterons 2−46319
^{16}O(d,n), E_d=3-4 MeV, cross sections and polarization, ^{17}F levels 2−83014
^{16}O(d,p)^{17}O, cross sections and vector and tensor analysing powers, study with polarised deuterons 2−46319
^{18}O(d,n)^{19}F, E_d=4 MeV, excited level lifetimes meas. 2−52739
^{18}O(d,p)^{19}O, 3 MeV, meas. of absolute differential cross for proton groups, DWBA analysis 2−52740
^{31}P(d,p)^{32}P, 10 MeV, meas. of angular distribs., spectroscopic factors 2−49834

Nuclear reactions and scattering due to continued
  deuterons continued
    ^{208}Pb, d absorption cross section, 25 GeV/c, Glauber theory calc. and comparison with expt. 2−70469
    ^{208}Pb(d,p)^{207}Pb, polarized deuterons, vector analyzing power and differential cross section 2−67330
    ^{208}Pb(d,t)^{207}Pb, polarized deuterons, vector analyzing power and differential cross section 2−67330
    ^{240}ppu(d.p) and (d.t) reactions, single-particle assignments of levels in ^{241}Pu 2−82911
    ^{194}Pt(d,p), neutron and γ-ray yields from threshold region 2−67225
    ^{241}Pu(d.d^{1})^{241}Pu single-particle assignments of levels in ^{241}Pu 2−82911
    ^{242}Pu(d, 2n)^{242}Am^{m}, 22.7 MeV, meas. of fission modes of ^{242}Am^{m} isomeric fission 2−70496
    ^{242}Pu(d, d)^{242}Pu, 16 MeV, level study 2−46178
    ^{242}Pu(d.p) and (d.t) reactions, single-particle assignments of levels in ^{243}Pu 2−82911
    ^{34}S(d,pγ)^{35}S, γ-ray from first excited state of ^{35}S 2−74014
    ^{28}Si (d,d)^{28}Si, obs. of octupole excitation of 29.5 MeV level 2−59776
    ^{28}Si(d,n), meas. of neutron polarization angular distrib. 2−63915
    ^{28}Si(d,p)^{29}Si, DWBA analysis of data at 10 MeV 2−56000
    ^{28}Si(d,p)^{29}Si, Ej=10 MeV, energy levels of ^{29}Si 2−82887
    ^{29}Si(d,n)^{30}P, E_d=4 MeV, odd parities of ^{30}P levels 2−67328
    ^{144}Sm(d,t)^{143}Sm, E_d=12.1 and 13.1 MeV level scheme of ^{143}Sm 2−82989
    ^{116}Sn(d,p)^{117}Sn, 4.35-5.55 MeV, Coulomb stripping to states in ^{117}Sn 2−67331
    ^{119}Sn(d,d′n), 19 MeV, neutron-gamma competition 2−46325
    ^{122}Sn(d,p)^{123}Sn, 4.35-5.55 MeV, Coulomb stripping to states in ^{123}Sn 2−67331
    ^{124}Sn(d,p)^{125}Sn, 4.35-5.55 MeV, Coulomb stripping to states in ^{125}Sn 2−67331
    Sn(d, d)Sn, A=112, 118, 119, 124, 20 and 27 MeV, ang. distrib., optical model fits. 2−79803
    ^{88}Sr(a α)^{86}Rb E_d=17 MeV, hole states of ^{86}Rb 2−82909
    ^{88}Sr(d,np)^{88}Sr, differential and total cross-sections, consistent coupled channel Born approximation analysis 2−74114
    ^{88}Sr(d,p)^{89}Sr, differential and total cross-sections, consistent coupled channel Born approximation analysis 2−74114
    ^{232}Th (d,p) ^{233}Th, energy levels of ^{233}Th 2−59722
    ^{232}Th (d,t) ^{231}Th, energy levels of ^{231}Th 2−59722
    ^{232}Th(d, d)^{232}Th, 16 MeV, level study 2−46178
    ^{232}Th(d,p)^{233}Th, level scheme of ^{233}Th 2−63837
    ^{46}Ti(d, p)^{47}Ti, 5 MeV, study of spin-dependent reaction mechanism from pγ correlation 2−63919
    ^{46}Ti(d,α)^{44}Sc, 26.7 MeV, meas. of cross section, angular distribs. of excited levels, two-nucleon transfer analysis 2−70479
    ^{48}Ti, elastic scatt. of vector polarized deuterons, 11.9 MeV, optical pot. 2−70465
    ^{48}Ti(d,α)^{46}Sc, 26.7 MeV, meas. of cross section, angular distribs. of excited levels, two-nucleon transfer analysis 2−70479
    ^{49}Ti, elastic scatt. of vector polarized deuterons, 11.9 MeV, optical pot. 2−70465
    ^{50}Ti, elastic scatt. of vector polarized deuterons, 11.9 MeV, optical pot. 2−70465
    ^{238}U(d, d)^{238}U, 16 MeV, level study 2−46178
    ^{51}V, elastic scatt. of vector polarized deuterons, 11.9 MeV, optical pot. 2−70465
    ^{136}Xe(d,t), neutron-single hole state determ. 2−46157
    ^{90}Zr (d,α)^{88}Y, DWBA computer analysis 2−70480
    ^{90}Zr(d, 2n)^{90}Nb, ^{90}Zr(d, αn(^{88}Y, excitation functions, 9-27 MeV 2−74115
    ^{90}Zr(d, n)^{91}Nb, energy level properties in ^{91}Nb 2−63922
    ^{90}Zr(d,p)^{91}Zr, 7.5 MeV, high resolution, meas. of angular distrib. for transition 2−42588
    ^{90}Zr(d,p)^{91}Zr, polarized deuterons, vector analyzing power and differential cross section 2−67330
    ^{91}Zr(d,d′n), 19 MeV, neutron-gamma competition 2−46325
    ^{96}Zr(d, n)^{97}Nb, energy level properties in ^{97}Nb 2−63922
    Zr(d, xn)^{90}Nb, Zr(d, αxn)^{88}Y, excitation functions, 9-27 MeV 2−74115
    Zr(d,p)^{91}Zr, 16 MeV, obs. of new levels and doublets in ^{91}Zr 2−52754

  electrons
    bremsstrahlung, two-photon process, influence of polarization of electrons and γ-quanta 2−70149
    bremsstrahlung cross section in nuclear fields, formula including high-order Coulomb correction 2−42328
    charge density determ. for pairs of isotones 2−46104
    charge deposition in water from high energy electron beam 2−55984
    doubly even nuclei, electroexcitation and electrodisintegration via 1p-1h continuum 2−52801
    elastic scatt., dispersion corrections, applic. to scatt. off ^{40}Ca 2−46235
    elastic scatt., neutron charge form factor and spin-orbit interactions contrib. 2−82955
    e.m. multipole transitions, angular momentum recoupling 2−70437
    e.m. multipole transitions, angular momentum recoupling 2−70437
    excitation of vibrational levels in α-particle model 2−67134
    inelastic scattering, equations of motion approach 2−82947
    light nuclear shell structure, influence on inelastic high-energy scattering 2−63866
    light nuclei, spectroscopy by low energy (<70 MeV) inelastic electron scatt. 2−82882
    from magnetic dipole moments, calc. of cross-section and asymmetry function 2−63867
    multipole operation formation as an angular momentum recoupling problem 2−58757
    near forward, comparison of impulse approximation and absorption model 2−59744
    neutrino bremsstrahlung, ion-ion correlation effects 2−49785
    quasi-elastic scatt. in many-body field theory 2−52800
    scattering, present and future expts. at IKO 2−49784
    scattering, use for analysing semi-leptonic weak interactions in nuclei, application to ^{16}O 2−76831
    scattering at intermediate energies 2−82958
    scattering operators renormalization 2−79779

Nuclear reactions and scattering due to continued
  electrons continued
    spin current transitions in inelastic electro-excitation, matrix elements, using different vector potential decompositions 2−82839
    (e,e′p), short range correlation effects on proton angular distribs. 2−82952
    (e,e’p), quasielastic scatt., short-range correl. effects 2−76832
    ^{107}Ag electrodisintegration, 20 to 30 MeV, absolute cross-sections
    ^{27}Al, quasielastic 550−1150 MeV electron scatt. cross-section 2−76834
    ^{11}B, quasielastic 550−1150 MeV electron scatt. cross-section 2−76834
    ^{9}Be, scattering data rel. to charge radius determination 2−49726
    ^{9}Be elastic and inelastic scattering, extended Nilsson model and projected Hartree-Fock 2−82957
    ^{12}C, anomalous quasi-elastic cross section 2−74063
    ^{12}C, dispersion correlations to elastic scatt. 2−46237
    ^{12}C, elastic and inelastic scatt. form factors in Hartree-Fock approx. 2−82956
    ^{12}C, elastic scatt., symmetrized Fermi density distrib. appl. 2−76833
    ^{12}C, quasielastic 550−1150 MeV electron scatt. cross-section 2−76834
    ^{12}C, quasifree scattering, Born approx. calc. 2−49786
    ^{12}C, scattering data rel. to charge radius determination 2−49726
    ^{12}C electrodisintegration 20 to 20 MeV, absolute cross-sections 2−82954
    ^{12}C positron induced disintegration, 20 to 30 MeV absolute cross-sections 2−82954
    ^{12}C(e,e′p)^{11}B, quasi-free scattering and independent particle model 2−49787
    ^{40}Ca, Ee=150-497 MeV, charge distribs. determ. 2−52745
    ^{40}Ca, elastic scatt., dispersion corrections 2−46235
    ^{40}Ca, quasielastic 550−1150 MeV electron scatt. cross-section 2−76834
    ^{40}Ca scattering data as test of HF charge distributions 2−74016
    ^{48}Ca scattering data on test of HF charge distributions 2−74016
    ^{63}Cu, positron induced disintegration, 20 to 30 MeV, absolute cross-sections 2−82954
    ^{63}Cu, positron induced disintegration, 20 to 30 MeV, absolute cross-sections 2−82954
    ^{63}Cu electrodisintegration, 20 to 30 MeV, absolute cross-sections 2−82954
    ^{3}He, elastic cross-section meas. at high momentum transfer, determ. of form factors 2−76830
    ^{3}He, high energy scatt., large angles, two-photon exchange contrib. 2−74062
    ^{3}He(e,e′p)d, electrodisintegration, cross section, final state interaction depend 2−74064
    ^{4}He, elastic scatt., symmetrized Fermi density distrib. appl. 2−76833
    ^{4}He, elastic scatt. form factor in local density approx. 2−83004
    ^{4}He, high energy scatt., large angles, two-photon exchange contrib. 2−74062
    ^{4}He(e,d)e′^{2}H, ang. distrib., cross section, 36-50 MeV 2−63869
    ^{39}K, Ee=150-497 MeV, charge distribs., determ. 2−52745
    ^{39}K, quasielastic 550−1150 MeV electron scatt. cross-section 2−76834
    ^{6}Li, ^{7}Li elastic and inelastic scattering, extended Nilsson model and projected Hartree-Fock 2−82957
    ^{6}Li, elastic scatt., symmetrized Fermi density distrib. appl. 2−76833
    ^{6}Li, pion electroproduction at 1180 MeV 2−70439
    ^{6}Li, structure and properties from high energy electron scattering 2−52802
    ^{6}Li(e,d)^{4}He, born approx. calc. of deuteron cross section 2−59748
    Mg isotopes, elastic and inelastic scattering, extended Nilsson model and projected Hartree-Fock 2−82957
    ^{60}Ni(e,e), 225 MeV, determ. of cross-sections, charge density distrib. parameter 2−52803
    ^{16}O, dispersion corrections to elastic scatt. 2−46237
    ^{16}O, elastic scatt., symmetrized Fermi density distrib. appl. 2−76833
    ^{16}O(e,e)^{16}O, with short range correlations, study of third order terms 2−70438
    ^{18}O, scattering operators renormalization 2−79779
    ^{31}P(e,e)^{31}P, Ee=250- 400 MeV, charge distribs. determ. 2−52745
    ^{208}Pb scattering data on test of HF charge distributions 2−74016
    ^{208}Pb(e,e′), inelastic scattering at 124, 167 MeV, meas. of differential cross sections, investigation of ^{208}Pb low-lying states 2−63833
    ^{32}S, Ee=250-400 MeV, charge distribs. determ. 2−52745
    ^{132}Sm(e,e)^{152}Sm, cross-section for excitation of ground-state rotational band 2−52764
    ^{46}Ti, scatt. determ. of charge distrib., isotope no. depend. 2−67211
    ^{48}Ti, scatt. determ. of charge distrib., isotope no. depend. 2−67211
    ^{50}Ti, scatt. determ. of charge distrib., isotope no. depend. 2−67211
    Ti(e,e)Ti, (A=46, 48, 50), study of ground state distribs. 2−52749
    ^{64}Zn(e,e), 225 MeV, determ. of cross-sections, charge density distrib. parameter 2−52803
    ^{66}Zn(e,e), 225 MeV, determ. of cross-sections, charge density distrib. parameter 2−52803
    ^{90}Zr, giant multipole resonances, spin and parity 2−79776

  gamma-rays *see Nuclear reactions and scattering due to/photons*

  heavy ions *see Nuclear reactions and scattering due to/nuclei of* $Z>2$

  helium-3
    ^{12}C(^{3}He, p)^{14}N, 13.3 MeV, meas. of differential cross-section, comparison with distorted wave calcs. 2−83011
    ^{28}Si(^{3}He,n)^{30}S, 25 MeV, meas. of energy spectrum of neutrons, differential cross sections, orbital angular momentum transfers 2−46315
    optical potential, energy dependence 2−70468
    two-nucleon transfer reactions, noncentral effects 2−74107
    unnatural- parity amplitudes from exchange effects in local energy approximation 2−76835
    ^{a}Ni(^{3}He,n)Zn, A=58, 60, 62, 25 MeV, meas. of energy spectrum of neutrons, differential cross sections, orbital angular momentum transfers 2−46315
    ^{27}Al, large angle data in optical model analysis 2−46313
    ^{27}Al(^{3}He,n)^{29}P, 25 MeV, meas. of energy spectrum of neutrons, differential cross sections, orbital angular momentum transfers 2−46315

Nuclear reactions and scattering due to continued
helium-3 continued
^{27}Al(^{3}He,p)^{29}Si, 9-14 MeV, comparison of exptl. angular distribs. with two-nucleon transfer DWBA calcs. 2−70478
^{27}Al(^{3}He ^{3}He), 13 to 27 MeV angular distributions 2−83001
^{36}Ar(^{3}He,t)^{36}K, mass, decay props. and levels of ^{36}K 2−70387
^{40}Ar(τ,t)^{40}K, 35 and 18 MeV, contribution of single-nucleon transfer mechanism to cross section 2−79799
B(^{3}He,^{3}He), A=10,11,13 to 27 MeV angular distribution 2−83001
^{10}B(^{3}He, particle)^{13}N, 11-19 MeV, cross sections, levels of ^{13}N 2−76873
^{11}B(^{3}He,p)^{13}C, E_{3he}=4-12 MeV, proton ang. distribs., DWBA 2−52823
^{9}Be(^{3}He,^{3}He) 13 to 27 MeV angular distributions 2−83001
^{9}Be(^{3}He,$\gamma\gamma$)^{12}C, 1.73-1.76 MeV, meas. of cross-section, search for $J^\pi=0$, T=2 resonance 2−82994
^{9}Be(^{3}He,$\gamma\gamma$)^{12}C, 1.739 MeV, $J^\pi=0+$, T=2 reson. 2−70476
^{9}Be(^{3}He,$\gamma\gamma$)^{12}C, T=2 reson. obs. 2−63914
^{12}C(^{3}He,^{3}He), inelastic, spin-flip of ^{3}He 2−70464
^{12}C(^{3}He, n)^{14}O, 13.3 and 18.2 MeV, meas. of differential cross- section, comparison with distorted wave calcs. 2−83011
^{12}C(^{3}He,n)^{14}O, 25 MeV, meas. of energy spectrum of neutrons, differential cross sections, orbital angular momentum transfers 2−46315
^{12}C(^{3}He,p)^{14}N(p′)^{13}C$_{g.s.}$, 14 MeV, proton and γ-ray decay of T=0 level in ^{14}N 2−73997
^{12}C(^{3}He,p)^{15}N, 5 MeV, study of two-particle three-hole structure of negative-parity states in ^{15}N 2−70375
^{12}C(^{3}He,pγ)^{14}N, 14 MeV, proton and γ-ray decay of T=0 level in ^{14}N 2−73997
^{12}C(^{3}He,pγ)^{14}N, parity of first unbound state in ^{14}N 2−63773
^{13}C(^{3}He,n)^{15}O, 6 MeV, proton configurations and spectroscopic factors of ^{15}O levels deduced by DWBA analysis 2−67148
^{13}C(^{3}He,n)^{15}O, meas. of absolute differential cross section, angular distrib. of neutron yield, 5.5 and 6.2 MeV 2−46316
^{13}C(^{3}He,p)^{15} meas. of absolute differential cross section at 5 MeV and excitation functions from 3.5-6.0 MeV 2−63775
^{40}Ca(^{3}He,α)^{39}Ca, neutron pick-up in N=20 closed shell, 11 MeV, meas. of spectroscopic factors 2−42586
^{44}Ca/^{3}He,d) ^{45}Sc, 24 MeV, transition strength to $d_{3/2}$ hole state 2−82854
^{44}Ca(^{3}He,t)^{44}Sc, 25 MeV, level struct. of ^{44}Sc 2−74020
^{110}Cd, ^{111}Cd(^{3}He, xnγ)$^{115m,\,117m}$Te, study of short-lived isomers in ^{115}Te, ^{117m}Te 2−74036
^{114}Cd, inelastic scatt., form factor phase and shape 2−59777
^{114}Cd(^{3}He, ^{3}He)^{114}Cd, interference between Coulomb and nuclear excitation amplitudes 2−46304
^{37}Cl(^{3}He,α)^{36}Cl, neutron pick-up in N=20 closed shell, 11 MeV, meas. of spectroscopic factors 2−42586
Cr(^{3}He,p), even-even nuclei, 1^+ states investigation, 1f-2p shell model predictions 2−46130
^{50}Cr, inelastic scatt., ang. distribs., octupole excitations 2−74022
^{50}Cr(^{3}He,t) 70 MeV isobaric analog ground state obs. 2−83009
^{52}Cr, large angle data in optical model analysis 2−46313
Cu(^{3}He,p), even-even nuclei, 1^+ states investigation, 1f-2p shell model predictions 2−46130
Er(^{3}He, α), A=165, 167, 169, 25.5 MeV, positive-parity states 2−79747
Fe(^{3}He,p), even-even nuclei, 1^+ states investigation, 1f-2p shell model predictions 2−46130
^{54}Fe(^{3}He,n)^{56}Ni, gamma-ray transitions induced in ^{56}Ni 2−59701
^{54}Fe(^{3}He,p)^{56}Co, high resolution spectroscopy of ^{56}Co, DWBA analysis of angular distribs. 2−63800
^{56}Fe(^{3}He, ^{3}He) elastic scatt., 53.4 MeV, optical model analysis 2−67329
^{56}Fe(^{3}He,d)^{57}Co, meas. of angular distribs. of deuterons leading to levels in ^{57}Co 2−46138
^{56}Fe(^{3}He,dγ)^{57}Co, coincidences between d and γ used to obtain γ decay of levels in ^{57}Co 2−46138
^{57}Fe(^{3}He,d)^{58}Co, high resolution spectroscopy of ^{58}Co, DWBA analysis of angular distribs. 2−63800
Gd(^{3}He,d) energy levels of Tb odd isotopes 2−82916
^{2}H(^{3}He,dd)p, ^{2}H(^{3}He,dp)d, 26.8 MeV, meas. of absolute cross sections for coincidence detection, DWBA analysis 2−70474
(^{3}He,^{7}Be) cluster transfer reaction, DWBA treatment with finite-range interaction 2−42589
(^{3}He,^{3}H) scattering, complex effective interactions in microscopic descriptions 2−49822
^{3}He + ^{3}He, resonant energy depend. of neutrino-producing solar nuclear reactions 2−82990
^{3}He(^{3}He,^{3}He)^{3}He elastic scatt., 4-10 MeV, polarization analyzing power 2−82995
^{3}He(^{3}He,^{3}He)^{3}He elastic scatt., 7-18 MeV, polarization analyzing power 2−82996
^{3}He(^{3}He, α)2p, 6.9, 7.88, 9.11 MeV, differential spectra and angular distributions 2−79795
^{113}In(^{3}He,d)^{114}Sn, 37.7 MeV, proton particle-hole states of ^{114}Sn 2−74116
^{39}K(^{3}He, α)^{38}K, obs. of two-hole states 2−70388
^{39}K(^{3}He,α)^{38}K, 21.09 MeV, meas. of two-hole strengths in ^{38}K 2−42507
^{39}K(^{3}He,α)^{38}K, neutron pick-up in N=20 closed shell, 11 MeV, meas. of spectroscopic factors 2−42586
^{6}Li, elastic, inelastic and charge-exchange scatt., 24.6 and 27.0 MeV 2−70463
^{6}Li(^{3}He, ^{3}He)^{6}Li, 24.5 and 27.0 MeV cross section for scatt. to excited states of ^{16}Li meas. 2−46302
^{6}Li(^{3}He, αp)^{4}He, asymmetric proton yield meas., cf with Reimann, Martin and Vogt model 2−63912
^{6}Li(^{3}He, t)^{6}Be, 24.6 and 27.0 MeV, cross-section determ. 2−46302
^{7}Li(^{3}He,p)^{9}Be, ^{7}Li(^{3}He,t)^{7}Be, two-mode finite-range DWBA analysis of mechanism 2−70475
^{175}Lu(^{3}He,α)^{174}Lu, 24 MeV, determ. of levels in ^{174}Lu 2−82896
Mg(^{3}He,^{3}He), A=24,25,26, 13 to27 MeV angular distributions 2−83001
^{24}Mg(^{3}He,^{3}He), inelastic, spin-flip of ^{3}He 2−70464
^{24}Mg(^{3}He,p)^{26}Al, 18 MeV, level struct. of ^{26}Al 2−76876
Mo(^{3}He,d)Tc, A=92, 94, 96, unbound analog states in Tc isotopes 2−46180
^{92}Mo(^{3}He,d)^{93}Tc, isobaric analogue resonances in ^{93}Tc 2−49743

Nuclear reactions and scattering due to continued
helium-3 continued
^{92}Mo(^{3}He,d)^{93}Tc, spectroscopic factors 2−63861
^{92}Mo(^{3}He,xn), production of short-lived neutron deficient Ru isotopes 2−49768
^{94}Mo(^{3}He, ^{4}He)^{93}Mo, 16 MeV, meas. of cross section, angular distribs., DWBA analysis 2−70401
^{14}N(^{3}He, P$_5$)^{16}O*, 8.88 MeV, rectangular graphs 2−74113
^{14}N(^{3}He, p)^{16}O, 7.9-18.0 MeV, ang. distrib., compound nucleus formation, optical parameters 2−76875
^{15}N(^{3}He,n)^{17}F, missing state obs. in ^{17}F 2−46114
^{150}Nd(^{3}He, d)^{151}Pm, 24 MeV, meas. of cross section, determ. of level structure of ^{151}Pm 2−74038
^{20}Ne(^{3}He, ^{4}He)^{19}Ne, 18 MeV, meas. of excitation energies of states in ^{19}Ne, angular distrib. of ^{4}He 2−63780
^{20}Ne(^{3}He,d)^{21}Na, 16 MeV, analysis of emitted deuterons, search for missing $J^\pi=3/2^+$ level in ^{21}Na 2−79761
^{20}Ne(^{3}He,nγ)^{22}Mg, 4.3-11.5 MeV, angular correlation and coincidence meas., ^{22}Mg deduced levels 2−63784
^{58}Ni, ^{60}Ni(^{3}He, t), study of isobaric analogue states 0^+ and 2^+ in ^{58,60}Cu at 24.6 MeV 2−63918
^{58}Ni(^{3}He,^{3}He), inelastic, spin-flip of ^{3}He 2−70464
^{16}O(^{3}He, n)^{18}Ne, 10.3-18 keV, lifetimes of states in ^{18}Ne 2−76784
^{87}Rb(^{3}He, ^{4}He)^{86}Rb, 16 MeV, meas. of cross-section, identification of low-lying levels in ^{86}Rb 2−70397
^{32}S(^{3}He, n)^{34}Ar, 6.5-10 MeV, Doppler shift attenuation method for decay and lifetime of ^{34}Ar low-lying levels 2−74012
^{28}Si(^{3}He, n)^{30}S, 6.5-10 MeV, Doppler shift attenuation method for decay and lifetime of ^{30}S low-lying levels 2−74012
^{30}Si(^{3}He,pγ)^{32}P, first T=2 level analysis 2−63788
^{144}Sm, elastic and inelastic scatt. at 53.4 MeV, DWBA and SCA analysis 2−56002
^{114}Sn(^{3}He, 2nγ)^{115m}Te, study of short-lived isomers in ^{115}Te 2−74036
^{86}Sr(^{3}He, $\alpha\gamma$)^{85}Sr, 17 MeV meas. of $\alpha\gamma$ coincidences, mean lives of low lying levels in ^{85}Sr deduced 2−42514
Ti(^{3}He,p), even-even nuclei, 1^+ states investigation, 1f-2p shell model predictions 2−46130
^{46}Ti, ^{48}Ti(^{3}He, t), study of isobaric analogue states 0^+ and 2^+ in ^{46,48}V at 24.6 MeV 2−63918
^{49}Ti(^{3}He,d)^{50}V, ^{48}Ti(^{3}He,p)^{50}V, study of ^{50} levels 2−63796
^{169}Tm enriched with ^{170}Yb, production of neutron deficient Hf, Lu isotopes, 45-80 MeV 2−49771
^{173}Yb(^{3}He,d)^{174}Lu, 24 MeV, determ. of levels in ^{174}Lu 2−82896
^{64}Zn(^{3}He, 3n)^{64}Ge, ^{64}Ge decay studies 2−55963

hyperons
Σ-, capture in Ne-H mixture, relative rates compared with π- and K-capture 2−49817
^{2}H, relative capture rates for stopping π-, K-, Σ- 2−70460
^{4}He, Λ scatt., spin-orbit coupling using one-boson-exchange model 2−63900

mesons
see also Cosmic rays/effects and interactions
coherent production of Ω^- and Ξ hyperons, spin and parity 2−76725
complex nuclei, below 3 GeV, nonelastic interactions of pions 2−63871
photoemulsion exposure to 60 GeV pions, meas. of yield, spectrum, angular distrib. of ^{8}Li 2−52821
pion-nucleus total cross-sections, model dependence 2−74099
radiative muon capture, nonlocal Hamiltonian 2−42577
radiative pion absorpt. processes in complex nuclei 2−82987
stopped kaon nucl. γ-rays intensity and identification 2−59773
(K$^-$,γ) radiative capture processes, hyperons prod. 2−67315
(π, πN) reactions, final state interactions and charge dependence 2−42576
(π^+,p) reactions in meson factories at 68 MeV 2−82640
K$^-$-nucleus scatt. lengths determ. 2−59771
K-, capture in Ne-H mixture, relative rates compared with π- and Σ-capture 2−49817
K$^-$ capture data interpret. rel. to K$^-$N scatt. amplitudes 2−63901
K$^-$ interactions with emulsion nuclei, prod. of ^{8}He 2−79792
K$^-$ interactions with nuclear emulsion nuclei, existence of ^{8}He nucleus 2−52736
K$^-$ scattering direct interaction theory of production of hypernuclei 2−63761
$k^- + \text{nucleus} \to \pi^- + \text{charged particle} + \text{hypernucleus}$ 2−79732
π--light nuclei scatt., nucl. sigma terma, threshold behaviour 2−70242
π-nucleus, scatt., Coulomb flux corrections and total cross sections in Δ-reson. region 2−67314
π-nucleus interaction, πN potential for about 180 MeV 2−63740
π- capture, 600 MeV, identification of emitted charged particles 2−46293
π- capture in Ne-H mixture, relative rates compared with K- and Σ-capture 2−49817
π, 50 GeV/c, complex nuclei of nuclear emulsions, primary-energy estimation 2−76826
π, 60 GeV, angular inclination of secondaries 2−74102
π, elastic scattering on heavy nuclei using Glauber approx., corrections due to Coulomb scattering, nucleon correlations 2−46246
π double charge exchange, nuclear medium corrections in analogue state excitation 2−74103
π elastic scattering, influence of Fermi motion included in kisslinger optical potential description 2−49814
π interaction with paraffin nuclei >200 GeV, average multiplicity, azimuthal effect in ang. distrib. 2−74101
3π production cross-sections meas. at 15.1 GeV/c on various nuclei 2−49815
π scatt., Chew-Low approach 2−59770
π scattering at intermediate energies 2−82958
π scattering near 3,3 resonance, differential of total cross sections calc. by multiple-scattering theory 2−46291
π^- capture, energy spectra and emission probabilities of proton, deuteron and triton 2−79793
π^- reaction cross sections on range of nuclei, rel. to nuclear sizes 2−52726
π^- scatt. cross sections calc., 20 MeV to 10 GeV 2−63890
$\pi^\pm$ scatt., elastic to explore n-p distributions in nuclei 2−63745
$\pi \to A_1$ problem, multiparticle propagation through nucleus, non-classical effects 2−76865

Nuclear reactions and scattering due to continued

- **mesons** continued
  - π^-C, 40 GeV/c, multiplicity distribution of charged particles produced 2−45960
  - C, π- absorption from rest, obs. of α spectrum, p spectrum and secondary particles 2−63902
  - ^{12}C, forward scatt. amplitudes, $K_s{}^0$ regeneration amplitude 2−82737
  - ^{12}C, nuclear- Coulomb interference in $\pi+$ scattering 2−42578
  - ^{12}C, photon spectra from radiative absorption of pions 2−46296
  - ^{12}C, pion capture, meas. of emitted neutron-charged particle final state 2−46300
  - ^{12}C, π^- inelastic scatt. cross sections 2−59772
  - ^{12}C, π and K elastic scatt., cross sections analysis 2−82723
  - ^{12}C(π, πn)^{11}C, near 3-3 resonance, isospin invariance examination 2−46297
  - ^{12}C(π-,π-) 69.5, 80, 87.5 MeV, influence of Fermi motion included in Kisslinger optical potential description 2−49814
  - ^{12}C(π-,π-π-)^{12}N, 4 GeV, cross section obs. 2−46299
  - ^{12}C(π^-, nn)^{10}C, expressions for transition strength analysis of data 2−46298
  - ^{12}C(π^-,nn), study of excitation spectrum of residual nucleus 2−49816
  - ^{12}C(π^+, 2p), 70 MeV, differential cross section 2−70461
  - ^{40}Ca, photon spectra from radiative absorption of pions 2−46296
  - ^{19}F(π^-, π^-n)^{18}F, cross sections in 3-3 reson. region 2−59774
  - ^{1}H, radiative π capture, sign of π^0 decay amplitude 2−46295
  - ^{1}H, transmission regeneration of K^0 in momentum region 14 to 42 GeV/c 2−46294
  - ^{2}H, pion elastic scatt., accuracy of Glauber approx. in intermediate energy region 2−46292
  - ^{2}H, relative capture rates for stopping π-, K-, Σ- 2−70460
  - ^{2}H(π^+, p)p, 70 MeV, differential cross-section 2−70461
  - ^{4}He, photon spectra from radiative absorption of pions 2−46296
  - ^{4}He interaction with π^+, obs. in cloud chamber 2−52703
  - ^{4}He(π,π) scattering near 3,3 resonance, differential and total cross sections calc. by multiple-scattering theory 2−46291
  - ^{4}He($\pi^\pm$,$\pi^\pm$), analysis for information on pion charge form factor 2−63604
  - ^{6}He(π^-,π^-), 8 GeV/c, calc. of differential cross-section using Glauber's multiple scattering theory 2−74100
  - K^- irradiation of photonuclear emulsions, production of hypernuclei 2−76576
  - ^{6}Li(π^-, nn), pion absorption and structure of ^{6}Li 2−82988
  - ^{6}Li(π^-,d)^{4}H, search for ground and excited states of ^{4}H in three-body phase space energy distrib. for deuterons 2−52734
  - Li(π^+, 2p), A=6, 7, 70 MeV, differential cross section 2−70461
  - ^{24}Mg, photon spectra from radiative absorption of pions 2−46296
  - ^{14}N(π, πn)^{13}N, near 3-3 resonance, isospin invariance examination 2−46297
  - ^{14}N(π^-,nn), study of excitation spectrum of residual nucleus 2−49816
  - Ne pionic atom, 1s line width meas. in agreement with low-energy pion-nucleus interaction theories 2−59964
  - ^{16}O, elastic π- scatt. in (3,3) reson. region 2−76864
  - ^{16}O, photon spectra from radiative absorption of pions 2−46296
  - ^{16}O, π^- scattering, 250 MeV, γ spectra study 2−70459
  - ^{16}O, π^+ scatt., 270 MeV, optical models 2−76866
  - ^{16}O(π, πn)^{15}O, near 3-3 resonance, isospin invariance examination 2−46297
  - ^{16}O(π,π) scattering near 3,3 resonance, differential and total cross sections calc. by multiple-scattering theory 2−46291
  - ^{16}O(π^-,nn), study of excitation spectrum of residual nucleus 2−49816
  - ^{16}O(π^+, 2p), 70 MeV, differential cross section 2−70461
  - ^{31}P(π^-, π^-n)^{30}P, cross sections in 3-3 reson. region 2−59774
- **muons**
  - capture by complex nuclei, determ. of polarization of the emitted neutron 2−63868
  - capture on closed shell targets at intermediate energy 2−82958
  - capture rate, correction due to presence of muon wave function in nuclear matrix elements 2−52804
  - inelastic, at low-momentum transfer, 6 and 12 GeV 2−63524
  - light nuclei, partial capture rates, dependence on nuclear structure, derivation of μN coupling constants 2−55983
  - radioisotope prod. by stopped negative muons 2−82950
  - total capture rate, study using impulse and closure approximations 2−52808
  - Fe, interaction of cosmic ray μ, meas. of cascades with energies $\geqslant 1$ GeV using ionization calorimeter 2−73895
  - γ-ν ang. correls. in capture reactions 2−79778
  - Al-π interactions, 30-300 GeV, accelerator and cosmic ray obs. 2−73896
  - ^{11}B($\mu\nu$), impulse and closure approximation study of total muon capture rate and average neutrino momentum 2−52808
  - Bi, μ-capture, neutron spectra 2−59745
  - C-π interactions, 30-300 GeV, accelerator and cosmic ray obs. 2−73896
  - ^{12}C, μ^- capture, leading to specific final states, capture rate 2−74066
  - ^{12}C(μ,n), effects of giant resonance on energy spectra of emitted neutrons 2−46240
  - ^{12}C(μ^-, ν_μ)^{12}B, recoil nuclear polarization of ^{12}B 2−74065
  - Ca, ang. distrib. of neutrons from μ^- capture 2−46356
  - Ca, μ-capture, neutron spectra 2−59745
  - ^{40}Ca, neutron spectra following muon capture 2−63903
  - Ca(μ^-n), 2-13 MeV, meas. of neutron energy spectra, excitation of quasibound states of intermediate nucleus 2−52806
  - Cu(μ^-, e$^+$)Co reaction search 2−82935
  - Cu(μ^-,e$^+$) Co, search for raction 2−46301
  - ^{19}F, muon capture, partical transitions 2−52807
  - ^{1}H, polarized, capture of μ^- mesons, diff. capture cross section detn. 2−55982
  - ^{6}L(μ-,ν_μ)^{6}He, rate of reaction, impulse approximation treatment 2−59747
  - ^{139}La(μ^-, ν), probability of occurrence 2−46241
  - ^{24}Mg(μ^-,γ)^{24}Na, γ-ray, yield meas. following μ^- capture 2−63870
  - ^{16}O, nuetron spectra following muon capture 2−63903
  - ^{16}O, total capture rate calc. using closure approx. effect of 2p-2h ground state admixtures 2−46085

Nuclear reactions and scattering due to continued

- **muons** continued
  - ^{16}O(μ,n), effects of giant resonance on energy spectra of emitted neutrons 2−46240
  - O(μ^-,n), 2-13 MeV, meas. of neutron energy spectra, excitation of quasibound states of intermediate nucleus 2−52806
  - Pb, μ-capture, neutron spectra 2−59745
  - ^{208}Pb(μ^-, ν), probability of occurrence 2−46241
  - Pb(μ^-,n), 2-13 MeV, meas. of neutron energy spectra, excitation of quasibound states of intermediate nucleus 2−52806
  - S, ang. distrib. of neutrons from μ^- capture 2−46356
  - ^{32}S, neutron spectra following muon capture 2−63903
  - ^{28}Si, neutron spectra following muon capture 2−63903
  - ^{28}Si(μ^-,γ)^{28}Al, γ-ray, yield meas. following μ^- capture 2−63870
  - S(μ^-,n), 2-13 MeV, meas. of neutron energy spectra, excitation of quasibound states of intermediate nucleus 2−52806
  - Tl, μ-capture neutron spectra 2−59745
  - ^{203}Tl, muonic μ-capture γ-rays 2−59961
  - ^{205}Tl, muonic, μ-capture γ-rays 2−59961
- **neutrinos**
  - deep inelastic scattering, systematics 2−52805
  - lepton pair production 2−46239
  - scattering, deep inelastic lepton pair production 2−46236
  - ν processes, cross sections and spectra of resultant particles 2−46238
  - ^{12}C, cross-sections 2−74067
  - ^{37}Cl, absorpt. cross sections, rel. to solar neutrino absorpt. 2−67212
  - ^{37}Cl, solar neutrino capture rate 2−55960
  - ^{2}H(ν, μ-p)^{1}H, quasi-elastic reaction, impulse approx. 2−59746
- **neutrons**
  - *see also Nuclear fission*
  - 14.4 MeV activation cross-sections of some of the elements $76 \leqslant Z \leqslant 82$ 2−76862
  - A=27 to 209, 1.5 to 8 MeV, generalized parameters of spherical optical potential 2−67235
  - A=48-75, inelastic scattering at 14 MeV, meas. of continuous spectra, cross section 2−70450
  - activation capture cross section, mass number dependence at 14 MeV 2−46281
  - activation cross sections for Pu-Be and Pe-Be neutrons 2−67227
  - capture, neutron, non-statistical effects 2−46267
  - capture cross section meas. at 14 MeV and target geometry, application to nuclear targets 2−74094
  - capture studies using γ band-filter spectrometer 2−67077
  - circular polarization of gamma radiation in neutron capture 2−67226
  - cross section measurement and analysis technique, review 2−46282
  - cross section of 31 heavy elements meas., 2.7 keV 2−46269
  - cross sections, calc. using shell model level densities 2−67129
  - cross-sections, role of doorway states and intermediate structure 2−46268
  - deep S- and P-wave strength function minima, relation to variation of absorptive strengths of optical potential 2−67229
  - deformed doubly even nuclei, knock-on mechanism for (n,α) reactions induced by fast neutrons 2−42568
  - displacement cross sections for stainless steel, Fe, Cr, Ni and Ta bases on Lindhard model 2−83053
  - elastic scattering at 8 MeV, optical model analysis 2−49799
  - energy dependence of Γ/Γ_n, analysis using structure of single particle spectrum 2−49854
  - even-odd nuclei, $91 \leqslant N \leqslant 113$, neutron capture, de-excitation 2−74003
  - fissile nuclei, low-energy cross sections analysis, R-matrix parameters 2−76857
  - heavy elements, $76 \leqslant Z \leqslant 82$, activation cross-sections, 14.4 MeV 2−76862
  - high resolution fast neutron spectrometry 2−67075
  - inelastic, $24 \leqslant A \leqslant 209$, 2-4.5 MeV, cross-sections meas. 2−67237
  - low energy inelastic scatt., non-statistical effects 2−67240
  - low-energy cross-section analysis, ambiguities in R-matrix parameters 2−67255
  - moisture meter response to stony soils 2−54732
  - multiparameter cross-section experiments, satellite data acquisition 2−78862
  - multiple scattering correction in cold neutron exprts. 2−76852
  - multiple scattering in cold neutron scattering Monte Carlo soln. 2−56019
  - neutron resonance spectroscopy as a test of statistical theories 2−46074
  - neutron widths distrib., exact no. of degree of freedom 2−67265
  - nuclear struct. studies, conf., Budapest, Hungary, [Aug. 1972] 2−67114
  - nuclei- neutron high energy collisions, total cross-sections 2−74093
  - off-shell scattering, relation of total cross-section to neutron stripping reaction cross section 2−67319
  - optical model, semi-classical at 14 MeV 2−67238
  - optical model, volume integrals 2−67230
  - optical model for scattering, low density expansion 2−76824
  - optical model potential, search procedure for optimizing parameters 2−67236
  - oriented target nuclei, meas. of distrib. of γ radiation following polarized and unpolarized neutrons capture 2−49800
  - oriented targets, interaction with fast neutrons, cryogenic apparatus 2−76736
  - p wave neutron capture at 25 keV in medium and heavy nuclei, structure of giant resonances 2−42567
  - p-wave neutron strength function near mass 55 and 160, spherical optical model potential 2−67258
  - pulsed neutron gamma method for highly absorbing media 2−54728
  - radiative capture cross-section, fission cross section, neutral energy, time of flight measurement 2−82802
  - radiative capture of 14 MeV neutrons on 11 medium and heavy nuclei, γ spectra meas. 2−67261
  - radiative capture widths meas. 2−46095
  - radioactivation analysis in vivo of Ca, P, N and Cl in rat's organism 2−54575
  - rare earth isotopes, neutron resonance capture integral values 2−49811
  - rare- earth nuclei, deformed, 14 MeV (n,α) reactions, triangular diagram dominance 2−67253
  - reaction rate in homogeneous sphere, study in BC 2−63892

Nuclear reactions and scattering due to continued
neutrons continued
resonance activation integrals of nuclides of interest in neutron activation analysis 2−70451
resonance capture, radiation widths and non-statistical effects 2−67267
resonance level distrib., non-statistical behaviour 2−67263
resonance structure 2−67133
resonances, correlations between reduced partial alpha widths and neutron and radiative widths 2−46280
resonances, groupings of level spacing 2−67266
s-wave strength function, comparison of optical model and continuum shell-model results 2−52816
scattering of 11.1 MeV neutrons at backward angles, new technique for meas. of differential cross sections 2−67234
scattering of polarized neutrons, 3.2 MeV, from D(p,n)^{3}He, on 20 elements from Ti to Bi, optical-model analysis 2−49797
scintillation detector for (n,γ) cross section meas. 2−55911
spectroscopic factor determ., R-matrix theory 2−63858
spin dependence of strength function, analysis in terms of spin-spin term in optical potential 2−67260
strength function meas., evidence for complex Lane potential 2−67228
structure research using 90% polarized neutron beam produced in ^{2}H(d,n)^{3}He reaction 2−67130
textbook for 1st yr. graduate student 2−52815
thermal neutron capture, production probability of spontaneously fissioning isomer ^{240m}Pu 2−79818
threshold reactions, maximization of desired activity against interfering activities 2−42616
total cross- sections for various elements, fluctuation analysis 2−46270
total scatt. cross sections calc., 20 MeV to 10 GeV 2−63890
transplutonium elements, cross-sections for thermal fission and capture 2−76851
(n, 2n), 14 MeV, energy spectra of emitted neutrons 2−67232
(n, 2n), 14.7 MeV, evaluation of cross-sections 2−67231
(n, 2n), cross-section, γ-decay of unbound nuclear states 2−67219
(n, 2n) reactions on ^{45}Sc, ^{89}Y, ^{90}Zr, ^{93}Nb, ^{151}Eu, ^{169}Tm, ^{175}Lu, ^{197}Au, 13.7-15.0 MeV, meas. of cross sections 2−63893
(n, γ), 25 keV, isomeric cross-section ratios 2−63897
(n, γ), cross-section, γ-decay of unbound nuclear states 2−67219
(n, γ), deexcitation of $^1{}_{.2}{}^-$ [541] and $^1{}_{.2}{}^+$ [411] bands in ^{177}Lu 2−79749
(n, γ), nuclei with n=28, 82, phonon-particle doorway states 2−79789
(n, γ) recoil copper in α copper phtalocyanine crystals, chemical state 2−72586
(n, n′), 14 MeV, energy spectra of emitted neutrons 2−67232
(n, n′), cross-section, γ-decay of unbound nuclear states 2−67219
(n, p), cross-section, γ-decay of unbound nuclear states 2−67219
(n,2n), 14 MeV, A<50, spin cut-off factors 2−70391
(n,2n), calculation of energy spectra 2−42570
(n,2n) fast neutron reactions, systematics of excitation functions 2−76849
(n,α), 14 MeV obs. on various nuclei, pre-formation of alpha-particles 2−67285
(n,α), fast neutron induced, systematics of excitation function 2−59762
(n,α) cross- sections, 14-15 MeV, dependence on asymmetry factor (N−Z)/A 2−63889
(n,α) cross sections, shell effects, E_n=14 MeV 2−52817
(n,α) reactions, optical model determ. using method of average alpha widths of neutron resonances 2−67259
(n,^{3}He), medium and heavy mass region, 14.6 MeV, systematic trends in activation cross-sections 2−67254
(n,γ), exit states of compound nucleus, role in high-energy γ-ray emission 2−59763
(n,γ), radiative capture cross sections for 14 MeV neutrons mass depend. 2−67282
(n,γ), radiative capture mechanism, compound nucleus exit states model 2−67262
(n,γ), spin assignment of populated bound levels 2−67137
(n,γ), thermal neutron capture, absolute γ-ray efficiencies of Ge(Li) detectors 2−67256
(n,γ) cross-sections, (N-Z) dependence 2−70447
(n,γ) cross section systematics, 14 MeV 2−67264
(n,γ) reactions, meas. of circular γ-ray polarization for primary transitions 2−49801
(n,γ) reactions, production of short-lived activites, automatic irradiation apparatus with on-line meas. system 2−79639
(n,n′), calculation of energy spectra 2−42570
(n,p), fast neutron induced, systematics of excitation function 2−59762
(n,p) cross-sections, calc. by pre-equilibrium exciton model 2−82984
(n,p) cross sections, shell effects, E_n=14 MeV 2−52817
(n,p) reaction, cross sections for 14 MeV neutrons 2−59764
(n,p) reactions in meson factories 2−82640
(n,t), medium and heavy mass region, 14.6 MeV, systematic trends in activation cross-sections 2−67254
(n,t) reactions on Be, B, Fe, Ni, Cu, Zn with 14 MeV neutrons, determ. of cross sections by direct β-counting of tritium 2−67257
(n.2n) knock-out reaction amplitudes on heavy nuclei, calculation 2−42569
n interaction with paraffin nuclei >200 GeV, average multiplicity, azimuthal effect in ang. distrib. 2−74101
nd total cross sections, 25-60 MeV 2−82982
nn total cross sections, 25-60 MeV 2−82982
pπ- from interaction of 25-30 GeV/c neutrons with C 2−63670
^{a}Dy(n,α), A=160, 162, 164, 14 MeV, energy distrib. of α particles calc. using Feynman triangular diagram 2−42568
^{a}Er(n,α), A=166, 168, 14 MeV, energy distrib. of α particles calc. using Feynman triangular diagram 2−42568
^{a}Ge, A=70, 72, 74, 76, γ-ray spectra following thermal neutron capture 2−46286
^{a}Yb(n,p)^{a}Tm, A=172, 173, 174, meas. of activation cross sections at 14.5 MeV 2−79791
^{107}Ag(n,γ)^{108}Ag, study of level transitions in ^{108}Ag 2−52757

Nuclear reactions and scattering due to continued
neutrons continued
^{107}Ag(nα), 14 MeV, α-particle ang. distributions and energy spectra 2−42573
^{109}Ag(n,γ)^{110}Ag, study of E1 level transitions in ^{110}Ag 2−52757
Al, high resolution spectroscopy using R-matrix 2−46285
^{27}Al(n, n′γ), 0.8 to 13 MeV, γ-ray production cross-sections, channel dependent level widths and correlated intermediate structure 2−67244
^{27}Al(n,n)^{27}Al, inelastic, 0.8-9.0 MeV, cross-section for production of de-excitation γ-rays 2−67243
^{27}Al(n,p)^{27}Mg, E_n=14 MeV, cross section meas. by activation method 2−49802
^{27}Al(n,p)^{27}Mg, E_n=14.1 MeV, proton energy and ang. distribs. 2−82981
A(n,n)A, elastic, A between 48 and 209, n polarization meas. 2−67239
As, neutron reson. level spacings, stat. distribs., deviations 2−67161
^{75}As(n,2n), 14.1 MeV, meas. of cross section using activation method 2−49810
Au, Doppler effect studies in unresolved resonance region 2−67233
^{197}Au(n,2n)^{196}Au, isomer cross-section ratios 2−63899
^{197}Au(n,γ), γ-ray specta of resonances 2−67305
Au(n,γ), fast neutron capture γ-rays, intensity distribs., 5.5 MeV anomaly 2−67304
^{10}B(n, 2α)^{3}H, tritium generation in coolant moderator of PWR's 2−83107
^{10}B(n,α), noble- gas plasma produced by emitted heavy charged particles 2−70887
^{130}Ba(n,γ)^{131}Xe cross section rel. to origin of ^{131}Xe on the Moon 2−66143
^{131}Ba isomeric activity excitation by (n,2n) reaction at 14.8 MeV 2−82974
^{133}Ba, isomeric activity excitation by (n,2n) reaction at 14.8 MeV 2−82974
^{135}Ba, isomeric activity excitation by (n,2n) reaction at 14.8 MeV 2−82974
^{135}Ba, isomeric activity excitation by (n,2n) reaction at 14.8 MeV 2−82974
^{138}Ba(n,γ), 14 MeV radiative capture, mass depend. of direct- semi-direct theory calcs. 2−67270
^{138}Ba(n,γ)^{139}Ba, role of doorway states of 'phonon + particle' type 2−49809
Ba(n,γ), capture of 5-80 keV neutrons, γ spectra analysis 2−67286
^{9}Be, 1/2$^+$ reson., coupled-channel calc. 2−76859
C, angular distribs. for elastic scattering from natural target and inelastic scattering from ^{12}C, 3-7 MeV 2−46274
C, inelastic scattering, 7.5 MeV, spin-flip probability 2−70448
C recoil scintillations in Naton 136 plastic scintillator 2−63701
^{12}C, elastic scatt., microscopic approach, coupled channel calcs. 2−76855
^{12}C inelastic scatt., E_n = 7.48 MeV, spin-flip probability 2−82983
^{12}C(n, n)^{12}C elastic scatt. of partially polarized neutrons, asymmetry 2−76860
^{12}C(n,α)^{9}Be, 14.8 to 18.8 MeV, differential cross sections 2−42571
^{12}C(n,n′γ)^{12}C, improved statistics for angular correlation measurements 2−46273
^{12}C(n,n), elastic scattering of 11.1 MeV neutrons, optical model analysis 2−67234
^{12}C(n,n)^{12}C, below 4.43 MeV, comparison of Feshbach with R-matrix theory 2−46275
^{40}Ca(n, α_0)^{37}Ar, 13.9 MeV, absolute differential cross-sections by parallel plate avalanche counter telescope 2−70453
^{40}Ca(n,α) and (n,p) cross-sections obs., 5.85 MeV 2−76848
^{40}Ca(n,γ), 14 MeV radiative capture, mass depend. of direct- semi-direct theory calcs. 2−67270
^{40}Ca(n,γ)^{41}Ca, radiative capture, E_n=6-15 MeV, cross sections 2−67275
^{40}Ca(n,p)^{40}K, cross section fluctuations, 2.4 to 2.9 MeV 2−59766
^{113}Cd(n,γ)^{114}Cd, parity violation in neutron capture γ-rays 2−67289
^{116}Cd(n,2n)^{115}Cd, isomer yield ratio of ^{115m}Cd and ^{115g}Cd 2−63808
^{116}Cd(n,γ), cross-sections and isomer ratios 2−59767
Cd(n,γ), capture of 5-80 keV neutrons, γ spectra analysis 2−67286
^{140}Ce(n,γ)^{141}Ce, role of doorway states of 'phonon + particle' type 2−49809
^{252}Cf target in CM-2 reactor, effective absorption cross-section 2−67341
^{253}Cf target in CM-2 reactor, effective absorption cross-section 2−67341
Cl, high resolution spectroscopy using R-matrix 2−46285
^{37}Cl(n, γ)^{38}Cl, meas. of γ radiation, excitation energies for ^{38}Cl levels, Q-value 2−49808
^{37}Cl(n,γ)^{38}Cl, γ-ray spectra obs., correlation with E1 reduced intensities 2−67272
Cm isotopes, A=243-6, total cross sections, 0.01-30 eV 2−82976
^{245}Cm, cross-sections for thermal fission and capture, resonance integral data 2−76851
^{58}Co, capture cross-sections 2−74098
^{59}Co(n,γ) ^{60}Co, polarization, final state spins determ. 2−67277
^{59}Co(n,γ) ^{60}Co, polarized neutron capture, anisotropy of γ-rays 2−67276
^{59}Co(n,γ) ^{60}Co, thermal neutron capture, ang. distrib. of emitted γ-rays 2−67278
^{59}Co(n,γ)^{69}Co, interference effects in γ-ray emission after polarized neutron capture 2−79790
^{59}Co(n,p)^{59}Fe, 14.1 MeV, obs., deuteron elimination, comparison with statistical theory 2−67271
^{59}Co(n,p)^{59}Fe, E_n=14.1 MeV, proton energy and ang. distribs. 2−82981
Cr isotopes, meas. of total cross section, optical model analysis 2−46271
^{52}Cr(n,γ)^{53}Cr, role of doorway states of 'phonon + particle' type 2−49809
^{54}Cr(n,γ)^{55}Cr, thermal neutron capture, meas. of γ-ray spectra and level structure of ^{55}Cr 2−42510
Cr(n,γ) A=51, 53, circular polarization determ. of spin states 2−67158
Cs, mapping of correlation between neutron width and radiative capture 2−67292
Cs, neutron-capture cross-sections, 0.01 to 100 eV 2−59761

Nuclear reactions and scattering due to continued
neutrons continued
^{133}Cs(n,α), 14 MeV, α-particle ang. distributions and energy spectra 2−42573
Cu, scatt. cross section and polarization meas. by associated particle method 2−70454
Cu isotopes, meas. of total cross section, optical model analysis 2−46271
^{63}Cu(n,2n)^{62}Cu, En=14 MeV, cross section meas. by activation method 2−49802
^{63}Cu(nα), 14 MeV, α-particle ang. distributions and energy spectra 2−42573
^{65}Cu(n,2n)^{64}Cu, En=14 MeV, cross section meas. by activation method 2−49802
D(n,p)2n, meas. and pole diagram anal. of reaction cross section at 14.5 MeV 2−74096
Dy, neutron-capture cross-sections, 0.01 to 100 eV 2−59761
^{160}Dy(n,α), energy spectra E$_n$=18 MeV, knock-on mechanism 2−67298
^{162}Dy(n,α), energy spectra E$_n$=18 MeV, knock-on mechanism 2−67298
^{162}Dy(n,γ)^{163}Dy, direct capture and non-statistical effects 2−67299
^{163}Dy(n,γ)^{164}Dy, nonstatistical aspects in 4s giant resonance 2−67300
^{164}Dy, capture cross sections, 5−160 keV 2−82979
^{164}Dy(n,α), energy spectra E$_n$=18 MeV, knock-on mechanism 2−67298
^{167}Er neutron capture, mag. moments of ^{168}Er states 2−67175
^{151}Eu, reson. spectroscopy, level population 2−63898
^{151}Eu (n,γ), cross-sections and isomer ratios 2−59767
^{153}Eu, reson. spectroscopy, level population 2−63898
F, high resolution spectroscopy using R-matrix 2−46285
^{19}F, (n,α) cross-sections obs. 5.85 MeV 2−76848
^{19}F(n,2n)^{18}F, E$_n$=14 MeV, cross section meas. by activation method 2−49802
^{54}Fe, neutron pickup reaction, ^{53}Fe states calcs. 2−67159
^{54}Fe(n,γ)^{53}Fe, role of doorway states of 'phonon + particle' type 2−49809
^{54}Fe(n,pγ)^{54}Mn, level structure of ^{54}Mn 2−46133
^{55}Fe(n,γ), circular polarization determ. of spin states 2−67158
^{56}Fe, neutron inelastic scatt. excitation function of 3120 keV level 2−74024
^{56}Fe(n, n$'\gamma$), 0.8 to 13 MeV, γ-ray production cross-sections, channel dependent level widths and correlated intermediate structure 2−67244
^{56}Fe(n,n)^{56}Fe, inelastic, 0.8-9.0 MeV, cross-section for production of de-excitation γ-rays 2−67243
^{56}Fe(n,p), cross-sections for 14.4 MeV neutrons 2−46290
^{57}Fe(n,γ)^{58}Fe, interference of two spin components in thermal neutron capture state 2−49801
^{57}Fe(n,γ)^{58}Fe, meas. of circular γ-ray polarization for primary transitions, interference of spin components of capture state 2−42572
^{58}Fe(n,p), cross-sections for 14.4 MeV neutrons 2−46290
Fe(n,n)Fe, intermediate structure analysis based on doorway state picture 2−46276
^{69}Ga(n,2n), 14.1 MeV, meas. of cross section using activation method 2−49810
^{71}Ga(n,2n), 14.1 MeV, meas. of cross section using activation method 2−49810
Gd scattering, 1.5-3.5 MeV, meas. of angular distrib., comparison with spherical optical model, coupled-channels theory 2−67247
^{153}Gd(n,α), determ. of distrib. of total alpha-particle widths of neutron resonances 2−67297
^{155}Gd, correlations for equidistant neutron resonances 2−67296
^{160}Gd, capture cross sections, 5−160 keV 2−82979
^{160}Gd(n,2n), 14.1 MeV, meas. of cross section using activation method 2−49810
Ge(Li) total absorption spectrometer for (n, xγ) cross section meas. 2−46039
^{74}Ge, keV radiative capture cross section and reson. integral 2−76861
^{76}Ge, activation reson. integral 2−76861
^{1}H, scattering at 526 keV, meas. of total cross section by time of flight method 2−46272
^{1}H(n,γ)^{2}H, possible test for capture via $^{1}S_0 \rightarrow {}^{2}S_1$ transition 2−46283
^{2}H, analysis of low energy elastic scattering 2−55994
^{2}H, neutron scattering, Gilbert-Schmidt series for doublet and quartet length 2−79728
^{2}H, review of low energy scattering cross sections 2−55995
^{2}H, scattering, low-energy S-matrix theory 2−76758
^{2}H, short range internucleon repulsion and low energy three nucleon parameters 2−46080
^{2}H, three-body break-up, application of method of moments 2−73748
^{2}H, three-body calc. with tensor force for elastic scatt. 2−42565
^{2}H break-up reaction, cross-section calc. using separable potentials 2−63895
^{2}H(n, n)np, n-d initial-state interaction 2−82991
^{2}H(n, n)pn, unitary model for three-body collisions 2−82992
^{2}H(n, p)2n, 50 MeV, proton energy spectrum and neutron-neutron scatt. length 2−63894
^{2}H(n,2n)^{1}H, nn $^{1}S_0$ scattering parameters from kinematically complete expt. 2−49805
^{2}H(n,d)n, 152 MeV, elastic and inelastic differential cross sections 2−49798
^{2}H(n,n), effective range approx. 2−63665
^{2}H(n,n) 14 MeV elastic scattering, exact unitary model calcs., soln. of Faddeev eqns. 2−79800
^{2}H(n,n)^{2}H, 35 MeV, n polarization meas. 2−67241
^{2}H(n,p)2n, E$_n$=14 Mev, n-n scatt. length obs. 2−76858
^{2}H(n,p)2n reaction, cross section, diagram summation approximation technique 2−74097
^{3}H, coherent scattering amplitude 2−46284
^{3}H(n,n), meas. of differential elastic cross section at 14 MeV 2−67242
^{2}He(n,p)2n, 152 MeV, spectra of protons 2−49804
^{3}He elastic scattering of polarized neutrons at 21.9 MeV asymmetries meas. 2−42566
^{4}He (n, n) ^{4}He up to 20 MeV, R matrix formulation and phase shifts 2−76853

Nuclear reactions and scattering due to continued
neutrons continued
^{4}He(n, n)^{4}He, 0.55, 0.84, 1.16 and 1.33 MeV, cross-sectipns meas. 2−76854
^{177}Hf, correlations for equidistant neutron resonances 2−67296
^{177}Hf(n,α), determ. of distrib. of total alpha-particle widths of neutron resonances 2−67297
^{177}Hf(n,γ), spin dependence of average radiative widths 2−67302
^{177}Hf(n,γ)^{178}Hf, quantum no. influence on partial γ transitions 2−67303
Hg(n,γ), fast neutron capture γ-rays, intensity distribs., 5.5 MeV anomaly 2−67304
^{165}Ho, capture cross sections, 5−160 keV 2−82979
^{165}Ho target, total cross-section, resonance parameters and neutron width distributions 2−67301
^{165}Ho(n,nγ), differential cross sections and angular distributions of gamma rays 2−46159
I, mapping of correlation between neutron width and radiative capture 2−67292
^{127}I(n,α), 14 MeV, α-particle ang. distributions and energy spectra 2−42573
^{127}I(n,n$'\gamma$), 0.5 to 1.6 MeV, low-lying states of ^{127}I 2−49746
^{129}I- ^{129}Xe, radiation effects, dating of Bjurbole chondrules 2−69174
^{113}In(n, 2n), 13 to 18 MeV, cross-section 2−67246
^{113}In(n, n$'$), 13 to 18 MeV, cross-section 2−67246
^{115}In(n,γ)^{116}In, obs. of γ-rays in spin-assigned capture resonances 2−67290
^{115}In(n,γ)^{116}In, thermal neutron capture, γ-ray spectroscopy study of ^{116}In level scheme 2−67168
^{191}Ir(n,2n)^{190}Ir, isomer cross-section ratios 2−63899
K, high resolution spectroscopy using R-matrix 2−46285
^{39}K(n,γ)^{40}K, circular polarization of capture γ-radiation, spin assignment 2−67273
^{39}K(n,γ)^{40}K, interference of two spin components in thermal neutron capture state 2−49801
^{39}K(n,γ)^{40}K, meas. of circular γ-ray polarization for primary transitions, interference of spin components of capture state 2−42572
^{39}K(n,γ)^{40}K, thermal neutron capture, ^{40}K level scheme 2−67274
^{80}Kr(n,γ)^{81}Kr, reaction cross section, meas. using multifilament proportional counter 2−70455
^{83}Kr(n,γ)^{84}Kr, thermal neutrons, Q-value, energies and intensities of γ-radiation 2−49741
^{139}La, 1 eV to 0.26 MeV, angular distributions of scattered neutrons 2−67248
^{139}La (n, γ), meas. of γ-ray spectrum, correlation with (d, p) rection 2−59768
^{139}La(n,γ)^{140}La and ^{139}La(d,p)^{140}La, positive correlation 2−67293
Li natural target, search for bound trineutron produced by 19 MeV bombardment 2−63896
^{6}Li, total neutron cross section from 100 to 1500 keV 2−49806
^{6}Li(n, d)^{5}He, ground state angular distrib. rel. to DWBA 2−70452
^{7}Li, review of total and principal partial cross-sections in range 10 keV-15 MeV 2−74095
Lu, neutron-capture cross-sections, 0.01 to 100 eV 2−59761
^{175}Lu(n, e)^{176}Lu slow neutron capture, study of ^{176}Lu excited levels by obs. of conversion electron spectra 2−79744
^{175}Lu(n, γ)^{175}Lu slow neutron capture, study of ^{176}Lu excited levels by obs. of γ-ray spectra 2−79744
^{176}Lu, motion induced shifts in resonance absorptions 2−49812
^{176}Lu (n,γ), study of high-energy region of γ spectrum, search for correlations with (d,p) reactions 2−70456
^{176}Lu(n, γ)^{177}Lu, γ spectra, level scheme, transitions 2−59769
^{176}Lu(n,γ)^{177}Lu, nsec. isomeric transitions, γ-γ coincidence obs. 2−67176
^{176}Lu(n,γ)^{177}Lu and ^{176}Lu(d,p)^{177}Lu, positive correlation 2−67293
^{176}Lu(n,γ)^{177}Lu capture studies using γ band-filter spectrometer 2−67077
Mn, neutron-capture cross-sections, 0.01 to 100 eV 2−59761
Mn(n,n)Mn, cross-section for excitation of 126 keV level, meas. 2−67245
^{92}Mo(n,γ)^{93}Mo, γ-ray spectra meas., test of valency model 2−67283
Mo(n,γ), capture of 5-80 keV neutrons, γ spectra analysis 2−67286
^{14}N, meas. of γ-ray production cross sections at 4.2, 5.9 and 6.9 MeV for (n,n$'\gamma$), (n, $\alpha\gamma$) and (n,pγ) reactions 2−79507
^{14}N(n,α), ang. distrib., emulsion method 2−59765
^{14}N(n,α)^{11}B, 14.8 to 18.8 MeV, differential cross sections 2−42571
^{15}N scattering, parallelism between off-energy-shell total cross section and proton spectra from ^{15}N(d,p)^{16}N 2−42585
^{22}Na, capture cross-sections 2−74098
^{91}Nb, polarization effects in isospin-coupled reaction channels 2−63884
^{93}Nb, elastic and inelastic scattering in 1.0 to 5.0 energy range 2−42574
^{93}Nb(n,α), 14 MeV, α-particle ang. distributions and energy spectra 2−42573
^{93}Nb(n,γ), angular distribution of γ-rays in resonant neutron capture 2−67284
^{93}Nb(n,n$'\gamma$)^{93}Nb, de-excitation γ-rays, ^{93}Nb level scheme 2−67164
^{142}Nd(n,γ)^{143}Nd, role of doorway states of 'phonon + particle' type 2−49809
^{143}Nd(n,γ), γ-ray spectra from resonance neutron capture 2−67295
^{144}Nd(n,γ)^{145}Nd, thermal neutron capture, γ-ray spectroscopy study of ^{145}Nd 2−67172
^{58}Ni, inelastic scattering, calc. of optical-model potential in particle-vibration coupling picture 2−76850
^{58}Ni(n,p)^{58}Co, 14.1 MeV, obs., deuteron elimination, comparison with statistical theory 2−67271
^{58}Ni(n,p)^{58}Co, E$_n$=14.1 MeV, proton energy and ang. distribs. 2−82981
Ni(n,γ), capture of 4 to 90 keV neutrons, γ transitions 2−67279
Ni(n,γ) A=61, 63, circular polarization determ. of spin states 2−67158
^{16}O, backward scattering of 14.1 MeV neutrons, meas. of angular distrib. in 150°-180° range 2−76856
^{16}O(n,α), ang. distrib., emulsion method 2−59765
^{16}O(n,α) cross sections, R-matrix analysis with diffuse-edge pot. 2−67268
^{16}O(n,n), elastic scattering of 11.1 MeV neutrons, optical model analysis 2−67234

Nuclear reactions and scattering due to continued
neutrons continued
^{16}O(n,n) cross sections, R-matrix analysis with diffuse-edge pot. 2−67268
^{189}Os(n$_{th}$,γ)^{190}Os, meas. of γ-ray spectra, evidence for K=0 excited states 2−67179
^{31}P, inelastic scatt. cross section between 0.75 and 9.00 MeV 2−52818
^{31}P(n,n)^{31}P, inelastic, 0.8-9.0 MeV, cross-section for production of de-excitation γ-rays 2−67243
^{231}Pa for ^{232}U production 2−49813
Pb isotopes, excitation of low- lying octupole 2.6 MeV state by 14 MeV neutrons 2−67250
^{204}Pb(n, 2n), 13 to 18 MeV, cross-section 2−67246
^{204}Pb(n, n′), 13 to 18 MeV, cross-section 2−67246
^{206}Pb(n,n)^{206}Pb, particle vibration model of doorway states 2−46278
^{207}Pb, 13.3 to 17.1 MeV, resonant character of cross-section 2−67306
^{208}Pb(n,γ), 14 MeV radiative capture, mass depend. of direct- semi-direct theory calcs. 2−67270
^{208}Pb(n,γ)^{209}Pb, radiative capture, E$_n$=6-15 MeV, cross sections 2−67275
^{208}Pb(n,γ)^{209}Pb, radiative capture cross section, E$_n$=6.2-14.7, reson. struct. 2−67307
^{208}Pb(n,n)^{208}Pb, particle vibration model of doorway states 2−46278
Pb(n,n) Pb, 13.7 MeV A=206, 207, 208, obs., cf with optical model 2−67249
Pd, fast neutron cross sections meas., optical pot. 2−82980
^{105}Pd, neutron reson. spins determ. by γ-ray multiplicity method 2−67167
^{108}Pd(n,γ)^{109}Pd*, gamma-ray spectrum, resonance spin determ. 2−67288
Pr, neutron reson. level spacings, stat. distribs., deviations 2−67161
^{141}Pr, 1 eV to 0.26 MeV, angular distributions of scattered neutrons 2−67248
^{141}Pr(n,γ)^{142}Pr, test of valency neutron model 2−67294
^{141}Pr(n,nγ), differential cross sections and angular distributions of gamma rays 2−46159
^{239}Pu, capture-to-fission cross section meas. 2−56011
^{239}Pu(n,γ)^{240}Pu, 2keV neutron capture, γ-ray studies of ^{240}Pu 2−67187
^{239}Pu(n,γ)^{240}Pu, thermal neutron capture, γ-spectroscopy study of ^{240}Pu 2−67186
^{240}Pu, 20 eV to 30 keV, neutron capture, fission, and total cross sections 2−82977
^{240}Pu, neutron total and capture meas., 20 eV-30 keV 2−67312
^{240}Pu cross section data eval. 2−82986
^{241}Pu(n,γ)^{242}Pu, thermal neutron capture, γ-ray spectroscopy study of ^{242}Pu level structure 2−67188
^{242}Pu target, below 1 keV, resonance parameters 2−67313
^{226}Ra, total cross section, below 1 eV, weak reson. level 2−67308
^{226}Ra bombardment with 14.5 MeV neutron and neutrons of wide energy spectrum, search for decay isomers in 88, 89 range 2−70458
Rb isotope yields 2−55988
^{185}Re, ^{187}Re, obs. of slow neutron resonance in range 3-300 eV 2−70457
^{103}Rh(n,α), 14 MeV, α-particle ang. distributions and energy spectra 2−42573
Ru(A=99, 100, 101, 102, 104), En=1-1500 eV, total n cross section meas. 2−49803
^{102}Ru(n,γ)^{103}Ru, thermal neutron capture, ^{103}Ru level scheme obs. 2−67166
^{104}Ru(n$_{th}$,γ)^{105}Ru, thermal neutron capture, γ spectra, spin assignments of ^{105}Ru levels 2−67287
^{32}S(n, α_0)^{29}Si, 13.9 MeV, absolute differential cross-sections by parallel plate avalanche counter telescope 2−70453
^{32}S(n,n)^{32}S, inelastic, 0.8-9.0 MeV, cross-section for production of de-excitation γ-rays 2−67243
^{32}S(n,p)^{32}P, 14.1 MeV, obs., deuteron elimination, comparison with statistical theory 2−67271
^{32}S(n,p)^{32}P, E$_n$=14.1 MeV, proton energy and ang. distribs. 2−82981
^{32}S(n,p) and (n,α) cross-sections obs., 5.85 MeV 2−76848
^{34}S(n,γ)^{35}S, thermal neutron capture, meas. of γ-ray spectra, transition scheme for ^{35}S 2−49807
Sb, cross- sections for energy range 0.05-150eV, Doppler and crystal binding effects on resonance 2−46277
Sb, mapping of correlation between neutron width and radiative capture 2−67292
Sb, slow neutron resonances 2−82975
^{121}Sb, neutron reson. spins determ. by γ-ray multiplicity method 2−67167
^{123}Sb, neutron reson. spins determ. by γ-ray multiplicity method 2−67167
Sb(n,γ), A=121, 123, γ-ray spectra of resonances 2−67291
^{45}Sc(n,γ)^{46}Sc, γ spectroscopic obs. of ^{46}Sc level scheme 2−67156
^{77}Se(nγ)^{78}Se, thermal n, decay scheme for ^{78}Se 2−52779
Se(n,n)Se, cross-section structure 2−46279
Si, elastic and inelastic scattering, 7.5 MeV, spin-flip probability 2−70449
^{28}Si(n,γ), 14 MeV radiative capture, mass depend. of direct- semidirect theory calcs. 2−67270
^{29}Si, 1.5 to 2.0 MeV, cross-section 2−67152
^{29}Si(n,α) cross-sections obs., 5.85 MeV 2−76848
^{30}Si(n,γ)^{31}Si, thermal neutron capture, meas. of γ-ray spectra, transition scheme for ^{31}Si 2−49807
Si(n,γ), gamma-ray spectra meas., cross-sections for γ-transitions 2−67269
^{144}Sm(n,2n), 14.1 MeV, meas. of cross section using activation method 2−49810
^{147}Sm, correlations for equidistant neutron resonances 2−67296
^{147}Sm, neutron reson. spins determ. by γ-ray multiplicity method 2−67167
^{147}Sm(n, γ)^{148}Sm, spins of levels of ^{148}Sm 2−76801
^{147}Sm(n,α), determ. of distrib. of total alpha-particle widths of neutron resonances 2−67297
^{147}Sm(n,α)^{144}Nd, investigation of decay of ^{148}Sm resonance states 2−46287
^{149}Sm, correlations for equidistant neutron resonances 2−67296

Nuclear reactions and scattering due to continued
neutrons continued
^{149}Sm, neutron reson. spins determ. by γ-ray multiplicity method 2−67167
^{152}Sm, reson. spectroscopy, level population 2−63898
^{154}Sm, capture cross sections; 5−160 keV 2−82979
^{154}Sm, reson. spectroscopy, level population 2−63898
^{154}Sm(n,2n), 14.1 MeV, meas. of cross section using activation method 2−49810
S(n,γ), gamma-ray spectra meas., cross-sections for γ-transitions 2−67269
^{118}Sn(n,α)^{115}Cd, isomer yield ratio of ^{115m}Cd and ^{115g}Cd 2−63808
^{120}Sn scattering, 1.5-3.5 MeV, meas. of angular distrib., comparison with spherical optical model, coupled-channels theory 2−67247
Sn(n,γ), capture of 5-80 keV neutrons, γ spectra analysis 2−67286
Sr, A=86 to 88, capture cross sections for 3 to 600 keV neutrons 2−67281
^{88}Sr(n,γ), 14 MeV radiative capture, mass depend. of direct- semi-direct theory calcs. 2−67270
^{88}Sr(n,γ), radiative capture cross sections for 14 MeV neutrons mass depend. 2−67282
^{181}Ta(n,2n)^{180}Ta, E$_n$=14 MeV, cross section meas. by activation method 2−49802
Ta(n,γ), fast neutron capture γ-rays, intensity distribs., 5.5 MeV anomaly 2−67304
^{159}Tb(n,γ)^{160}Tb, level scheme and spin assignment of ^{160}Tb 2−67174
^{160}Tb level scheme from (n,e$^-$) reaction 2−67174
^{230}Th mixed with ^{232}Th, for ^{232}U production 2−49813
^{232}Th, inelastic neutron scatt., excited level struct. and decay schemes 2−67183
^{232}Th(n,γ)^{233}Th, level scheme of ^{233}Th 2−63837
Ti isotopes, meas. of total cross section, optical model analysis 2−46271
^{50}Ti(n,γ)^{51}Ti, role of doorway states of ‘phonon + particle’ type 2−49809
^{203}Tl p-wave neutron reson. obs. by transmission meas. 2−76863
^{205}Tl p-wave neutron reson. obs. by transmission meas. 2−76863
^{205}Tl(n,γ)^{206}Tl, anomalous 5.5 MeV γ-radiation 2−46289
Tl(n,γ), fast neutron capture γ-rays, intensity distribs., 5.5 MeV anomaly 2−67304
^{169}Tm target, total cross-section, resonance parameters and neutron width distributions 2−67301
^{169}Tm(n,γ), γ-ray spectra, study of resonances 2−46288
^{235}U, capture-to-fission cross section meas. 2−56011
^{235}U(n,γ)^{236}U, conversion electron spectrum, level struct. of ^{236}U 2−67309
^{235}U(n,γ)^{236}U, epithermal neutron capture, level structure of ^{236}U and spins of resonances determ. 2−52820
^{235}U(n,γ)^{236}U, thermal neutron interaction, meas. of G-ray spectra 2−67310
^{235}U(n,n), 1.5 to 2.3 MeV, differential cross-sections 2−67251
^{236}U, 140 to 770 eV, neutron widths and total cross-sections 2−67311
^{238}U, 1.13-2.37 MeV, inelastic scatt., cross section meas. 2−67252
^{238}U, inelastic neutron scatt., excited level struct. and decay schemes 2−67183
^{238}U, radiative capture, 1.2-4 MeV 2−82973
^{238}U(n,γ)^{239}U, neutron resons., density and struct. 2−67185
V, neutron-capture cross-sections, 0.01 to 100 eV 2−59761
^{182}W(N, γ)^{183}W rapid determ. of tungsten in rocks 2−61834
^{186}W(n,γ)^{187}W, nsec. isomeric transitions, γ-γ coincidence obs. 2−67176
^{170}Yb(n,γ)^{171}Yb, thermal neutrons, excited states in ^{171}Yb 2−46170
^{171}Yb, neutron reson. spins determ. by γ-ray multiplicity method 2−67167
^{173}Yb(n,γ)^{174}Yb, nonstatistical aspects in 4s giant resonance 2−67300
^{174}Yb(n,α)^{171}Er meas. of activation cross sections at 14.5 MeV 2−79791
^{176}Yb(n,α)^{173}Er meas. of activation cross sections at 14.5 MeV 2−79791
^{64}Zn(n,2n), calc. of excitation function in direct knockon model, and cross section for formation of combined nucleus 2−67280
Zr, scatt. cross section and polarization meas. by associated particle method 2−70454
^{91}Zr(n$_{th}$,γ)^{92}Zr, investigation of level structure in ^{92}Zr 2−67163
^{94}Zr(n,nγ), search for 2.37 MeV γ-rays 2−82985
Zr(n,γ), capture of 5-80 keV neutrons, γ spectra analysis 2−67286
nuclei of Z>2
see also Ions/scattering
(^{6}Li,d) cluster transfer reaction, DWBA treatment with finite- range interaction 2−42589
Coulomb dissociation of relativistic nucleus in field of heavy nucleus 2−49843
Coulomb excitation technique for meas. static and dynamic quadrupole moments of first excited states of ^{20,22}Ne 2−42537
heavy ion reactions, γ-spectroscopy determ. of e.m. matrix elements 2−83023
heavy ion scattering, finite size effects 2−76883
heavy ion scattering, intermediate structure in excitation functions of cross sections 2−49836
heavy-ion induced, excitation function and isomer ratios 2−76885
heavy-ion optical potential, influence of elastic transfer on imaginary part 2−79806
heavy-ion transfer reactions at energies well above Coulomb barrier, kinematical effects 2−49842
identical heavy ions scattering, generator-coordinate method 2−83015
interface phenomena, between compound nucleus processes and direct transfer effects 2−56003
multinucleon transfer reactions, surface nature and quasi-classical relative motion of nuclei 2−49844
neutrons precision monitoring from TD and DD reactions 2−70305
nucleus-nucleus interaction, investigation of particles at 90° in L system 2−52826
particle transfer, quantum mechanical treatment for heavy ions near Coulomb barrier in presence of Coulomb excitation 2−46330
proton-rich nuclei production, predicted limits for heavy ion compound nucleus mechanism 2−49840

Nuclear reactions and scattering due to continued
  nuclei of $Z>2$ continued
    rare earth nuclei implanted in Cu matrix, excitation by heavy ions, meas. of angular distrib. of de-exciting γ-rays 2−63927
    scattering, elastic and inelastic, semiclassical description above contents barrier 2−59786
    semiclassical transfer theory for neutron- and proton transfer, numerical investigation 2−63924
    synthesis of nuclei with excess of neutrons 2−63872
    two-nucleon transfer with heavy ions, DWBA calc. 2−83018
    ^{a}Cd(^{16}O,4n)^{126,128}Ba A=114, 116 lifetime measurements in ^{126,128}Ba 2−46154
    ^{a}Cr(nγ) (A=50,52), circular polarization meas. and spin assignment of ^{51}Cr and ^{53}Cr levels 2−52819
    ^{a}Mg(^{16}O, ^{12}C) (A=24,26), ang. distrib. meas. 2−63926
    ^{a}Ni(nγ,) (A=60,62), circular polarization meas. and spin assignment of ^{61}Ni and ^{63}Ni levels 2−52819
    ^{a}Sn(^{16}O, ^{16}O$'\Gamma$) (A=117, 119), Coulomb excitation study 2−63810
    ^{221}Ac compound nucleus formed in ^{209}Bi + ^{12}C, ^{207}Pb + ^{14}N, ^{205}Tl + ^{16}O reactions, yrast trapping study 2−46335
    Ag, ^{12}C, ^{16}O, ^{22}Ne and ^{40}Ar ion bombardment, inelastic interaction, neutron production, ang. distrib. 2−76886
    ^{107}Ag, with ^{20}Ne, ang. momentum limits, fusion excitation functions 2−59787
    ^{109}Ag(^{16}O, 3n)^{123}Cs, positron decay and decay scheme of ^{123}Cs 2−74037
    ^{109}Ag(^{18}O, 4n)^{123}Cs isomeric level and γ-transitions found 2−74037
    ^{109}Ag(^{84}Kr,xn), neutron-deficient Bi isotope prod. and α-decay 2−76822
    ^{27}Al, with ^{16}O, ang. momentum limits, fusion excitation functions 2−59787
    ^{27}Al ^{16}O and ^{20}Ne induced, enhancement of direct processes at high ang. momenta 2−70482
    ^{27}Al(^{16}O, ^{12}C), ang. distrib. meas. 2−63926
    ^{36}Ar(^{16}O,^{12}C), excitation of rot. bands in ^{40}Ca 2−83017
    ^{197}Au, recoil study of transfer reactions induced by ^{12}C, evidence for α and ^{8}Be transfers 2−56006
    ^{11}B, optical model analysis of ^{6}Li elastic scatt. 2−56004
    ^{11}B many-nuclear transfer reactions induced by ^{16}O, ^{19}F, finite DWBA calculations 2−56005
    ^{134}Ba, ^{16}O scatt., reorientation effect meas., static quadrupole moment 2−76800
    ^{136}Ba, ^{16}O scatt., reorientation effect meas., static quadrupole moment 2−76800
    ^{138}Ba, ^{16}O scatt., reorientation effect meas., static quadrupole moment 2−76800
    ^{209}Bi, recoil study of transfer reactions induced by ^{12}C, evidence for α and ^{8}Be transfers 2−56006
    ^{209}Bi(^{12}C,xn)$^{221-x}$Ac, 60-90 MeV, meas. of cross sections, reaction thresholds and excitation functions 2−74123
    ^{209}Bi(^{16}O, ^{16}O$'\gamma$), e.m. matrix elements of low-lying states near ^{208}Pb closed shell 2−76782
    ^{81}Br(^{16}O, ^{16}O$'\gamma$), 33 MeV, Coulomb excitation of low-lying levels, meas. of γ-ray energies, yields, angular distribs., Doppler broadening 2−74032
    (^{12}C, xn) reactions on nuclei with Z=63-83, 88 MeV, search for γ-ray isomerism in produced neutron deficient isotopes 2−55970
    C (A=12,13), optical model analysis of ^{6}Li elastic scatt. 2−56004
    ^{12}C-^{12}C scattering, nuclear molecular structure 2−49839
    ^{12}C, elastic scatt. of ^{16}O, possible formation of nuclear molecule in ^{28}Si at 36.5 MeV 2−46122
    ^{12}C, elastic scattering of ^{7}Li and ^{6}Li 2−42590
    ^{12}C, transfer reactions induced by ^{12}C, selective excitation of one-, two- and three-nucleon excitation 2−49845
    ^{12}C + ^{12}C elastic scattering, presence of quasi-molecular rotational bands 2−49838
    ^{12}C + ^{12}C $\rightarrow \alpha_1$ + ^{20}NC* $\rightarrow \alpha_2$ + ^{16}O g.s., high-spin states in ^{20}Ne and classification into rotational bands 2−49732
    ^{12}C(^{12}C, ^{8}Be)^{16}O, rotational bands of ^{16}O 2−42499
    ^{12}C(^{12}C,α)^{20}Ne, excitation functions 2−83022
    ^{12}C(^{16}O, ^{16}O) elastic scattering, analysis by Feynmann graph techniques 2−74117
    ^{12}C(^{16}O,^{16}O)^{12}C, resonance like structure obs. with spin I=14 2−49837
    ^{12}C(^{16}O,p)^{27}Al, search for high-spin states in ^{27}Al in excitation range 4.8-8.0 MeV 2−42504
    ^{12}C(^{6}Li, d)^{16}O mechanism, determ. of ^{16}O energy levels 2−83021
    ^{12}C(^{6}Li,d)^{16}O, angular distrib. of γ-rays meas. on function of bombarding energy 2−46332
    ^{12}C(^{6}Li,d)^{16}O stripping reaction, use of Eckhart interactions in DWBA 2−46223
    ^{12}C(^{7}Li,α)^{15}N, 28-38 MeV, triton transfer, excited states of ^{15}N 2−70481
    ^{13}C, elastic scatt. of ^{12}C, nucleon exchange 2−83019
    ^{14}C, elastic scatt. of ^{12}C and ^{13}C, nucleon exchange 2−83019
    Ca(^{16}O,^{16}O) elastic scattering, incoming wave boundary condition calc. of cross section at incident energies near Coulomb barrier 2−42592
    ^{40}Ca, backward-angle elastic scatt. of ^{16}O 2−74118
    ^{40}Ca, transfer reactions induced by ^{12}C, selective excitation of one-, two- and three-nucleon excitation 2−49845
    ^{40}Ca(^{6}Li,d)^{44}Ti, 32 MeV, angular distributions, cross-sections 2−70483
    ^{48}Ca, backward-angle elastic scatt. of ^{16}O 2−74118
    ^{114}Cd(^{32}S,^{32}Sγ) 50 MeV, determ. of sign of multiple Coulomb excitation interference term and static quadrupole moment 2−82893
    ^{133}Cs(^{20}Ne,4n)^{149}Tb, excitation function, 50-200 MeV cross-sections 2−74120
    Dy(^{40}Ar,xn)Po excitation function and isomer ratios 2−76885
    ^{151}Eu(^{35}Cl, ^{25}Cl$'\gamma$), 8-12 MeV, Coulomb excitation studies of level struct. 2−76884
    ^{153}Eu(^{35}Cl, ^{35}Cl$'\gamma$), 8-12 MeV, Coulomb excitation studies of level struct. 2−76884
    ^{19}F many-nuclear transfer reactions induced by ^{16}O, ^{19}F, finite DWBA calculations 2−56005
    ^{54}Fe(^{16}O, ^{12}C)^{58}Ni, reaction-mechanisms study in 1f-2p shell 2−67334
    ^{54}Fe(^{16}O, ^{12}C)^{58}Ni, analysis using generator-coordinate form factors 2−52828

Nuclear reactions and scattering due to continued
  nuclei of $Z>2$ continued
    ^{54}Fe(^{16}O, ^{14}C)^{56}Ni, 80 MeV two-nucleon stripping reaction, meas. of cross section, determ. of levels in ^{56}Ni 2−74121
    ^{54}Fe(^{16}O, ^{14}N)^{56}Co, 80 MeV two-nucleon stripping reaction, meas. of cross section, determ. of levels in ^{56}Co 2−74121
    ^{54}Fe(^{16}O,^{15}N)^{55}Co, E=104 MeV, j-assignments of final states 2−79805
    ^{54}Fe(^{16}O,^{15}N)^{55}Co, E=78 MeV, j-assignments of final states 2−79805
    ^{54}Fe(n,γ), circular polarization meas. and spin assignment of ^{55}Fe levels 2−52819
    ^{56}Fe, Coulomb excitation by ^{32}S ions, 60-70 MeV, meas. of static electric quadrupole moments 2−63795
    ^{56}Fe(^{32}S, ^{32}Sγ), 65 MeV, determ. static electric quadrupole moments of first excited states of ^{56}Fe 2−63799
    ^{154}Gd(^{35}Cl, ^{35}Cl^{1})^{154}Gd, 100 MeV, recoil distance meas., lifetimes 2−70405
    ^{155}Gd(^{40}Ar,xn), neutron-deficient Pb isotope prod. and α-decay 2−76822
    ^{156}Gd(^{35}Cl, ^{35}Cl^{1})^{156}Gd, 100 MeV, recoil distance meas., lifetimes 2−70405
    Ge, ^{12}C, ^{16}O, ^{22}Ne and ^{40}Ar ion bombardment, inelastic interaction, neutron production, ang. distrib. 2−76886
    ^{72}Ge, meas. of B(E2; $O_2^+ \rightarrow 2_1^+$) by Coulomb excitation with ^{16}O 2−46144
    ^{2}H(^{24}Mg, nγ)^{25}Al, population of 3/2^{+} 945 keV level in ^{25}Al, meas. of mean lifetime for γ-ray decay 2−79736
    ^{2}H(^{24}Mg, pγ)^{25}Mg, population of 3/2^{+} 975 keV level in ^{25}Mg, meas. of mean lifetime for γ-ray decay 2−79736
    ^{202}Hg(^{12}C,3n)^{211}Rn, excitation function, 50-200 MeV cross-sections 2−74120
    ^{204}Hg(^{12}C,5n)^{211}Rn, excitation function, 50-200 MeV cross-sections 2−74120
    ^{113}In(^{12}C, 3n)^{123}Cs, positron decay and decay scheme of ^{123}Cs 2−74037
    ^{115}In(^{12}C, 3n)^{124}Cs, excited levels and position decay 2−74037
    ^{115}In(12C, 4n)^{123}Cs, isomeric level and γ-transitions found 2−74037
    (^{7}Li,t) cluster transfer reaction, DWBA treatment with finite- range interaction 2−42589
    ^{6}Li, Coulomb breakup 2−46331
    ^{6}Li(^{35}Cl, d)^{39}K, 68 MeV, excited states of ^{39}Km lifetimes 2−76792
    ^{6}Li(^{6}Li, 2α)^{4}He direct process interpret 2-13 MeV 2−83020
    ^{6}Li(^{6}Li, α)2α, 2, 6 and 13 MeV, energy spectra fit 2−63925
    ^{7}Li(^{7}Li,2p)^{12}Be, ground state mass of ^{12}Be 2−70374
    ^{24}Mg(^{132}Xe,3−5n)$^{153-151}$Dy, compound nucleus production, identification of reaction products over energy of γ-transfer and fission semidecay periods 2−49846
    Mo, ^{12}C, ^{16}O, ^{22}Ne and ^{40}Ar ion bombardment, inelastic interaction, neutron production, ang. distrib. 2−76886
    Mo(^{18}O,^{16}O), DWBA calc. of two-nucleon transfer 2−83018
    ^{94}Mo, ^{16}O induced multiple Coulomb excitation, low-lying level props. 2−82910
    ^{98}Mo, ^{16}O induced multiple Coulomb excitation, low-lying level props. 2−82910
    ^{100}Mo^{16}O induced multiple Coulomb excitation, low-lying level props. 2−82910
    ^{15}N(^{6}Li, t)^{18}F, prefernetial excitation of odd-parity levels with three-particle one-hole structure 2−74001
    ^{15}N(^{7}Li,t)^{19}F, 15 MeV, finite range DWBA analysis, diff. cross section calc. using weak coupling model 2−42591
    Ne^{+} beam scattering from C foil, foil lifetime, charge state distributions and beam scattering 2−52825
    Ni, A=58,60, Coulomb excitation by ^{32}S ions, 60-70 MeV, meas. of static electric quadrupole moments 2−63795
    ^{58}Ni(^{16}O, ^{14}C)^{60}Zn, 80 MeV two-nucleon stripping reaction, meas. of cross section, determ. of levels in ^{60}Zn 2−74121
    ^{58}Ni(^{16}O, ^{14}N)^{60}Cu, 80 MeV two-nucleon stripping reaction, meas. of cross section, determ. of levels in ^{60}Cu 2−74121
    ^{58}Ni(^{6}Li,d) 38 MeV, meas. of angular distribs., cross sections, comparison with DWBA analysis 2−74122
    ^{62}Ni(^{12}C,^{11}B)^{65}Cu, E=78 MeV, j-assignments of final states 2−79805
    ^{62}Ni(^{16}O,^{15}N)^{65}Cu, E=104 MeV, j-assignments of final states 2−79805
    ^{64}Ni(^{6}Li,d) 38 MeV, meas. of angular distribs., cross sections, comparison with DWBA analysis 2−74122
    (^{16}O, ^{15}N), on fp shell target nuclei 2−49841
    ^{16}O-^{16}O elastic scattering above Coulomb barrier, generator-coordinate method 2−83015
    ^{16}O, transfer reactions induced by ^{12}C, selective excitations of one-, two- and three-nucleon excitation 2−49845
    ^{16}O + ^{12}C, quasimolecular states, resonances in total reaction yield 2−74119
    ^{16}O + ^{12}C system, study near Coulomb barrier, correlated resonances in excitation functions of α-particle and proton exit channels 2−79808
    ^{16}O + ^{16}O elastic scattering, presence of quasi-molecular rotational bands 2−49838
    ^{16}O(^{12}C, ^{8}Be)^{20}Ne, rotational bands of ^{20}Ne 2−42499
    ^{16}O(^{12}C, α)^{24}Mg*, triple correlation meas. to determine spin and parities of highly excited states in ^{24}Mg 2−74007
    ^{16}O(^{14}C,pn)^{28}Al, ^{16}O(^{14}C,p)^{29}Al, independence hypothesis tested 2−46334
    ^{16}O(^{16}O, ^{12}C)^{20}Ne, 17.5-30 MeV, cross-sections meas., possible ^{16}O + ^{16}O quasimolecular resonance 2−52827
    ^{16}O(^{16}O, ^{16}O) elastic scattering, calc. of adiabatic and angular-momentum dependent potential 2−63923
    ^{16}O(^{7}Li,t)^{20}Ne, 15 MeV, finite range DWBA analysis, diff. cross section calc. using weak coupling model 2−42591
    ^{18}O + ^{16}O elastic scattering in 13-33 MeV energy range 2−46333
    ^{18}O(^{12}C,pn)^{28}Al, ^{18}O(^{12}C,p)^{29}Al, independence hypothesis tested 2−46334
    ^{18}O(^{18}O,2p + n)^{33}Si, 50 MeV, exotic nucleus prod. in s-d shell 2−74013
    ^{18}O(^{19}F,2p)^{35}P, 42-46 MeV, ^{35}P identification and characteriz. 2−74014
    ^{18}O(^{7}Li,t)^{22}Ne, 12 MeV, rot. bands in ^{22}Ne 2−76788
    ^{a}Pb(^{16}O,4n)^{120,122}Xe, A=108, 110, lifetime measurements in ^{120,122}Xe 2−46154

Nuclear reactions and scattering due to continued
nuclei of $Z>2$ continued
^{208}Pb(^{12}C,^{11}B)^{209}Bi, $E=78$ MeV, j-assignments of final states 2−79805
^{208}Pb(^{16}O,^{15}N)^{209}Bi, $E=104$ MeV, j-assignments of final states 2−79805
^{208}Pb(^{7}Li, ^{6}Liγ)^{209}Pb, lifetimes and branching ratios of ^{209}Pb 2−76782
^{208}Pb(^{7}Li,^{7}Li*)^{208}Pb, Coulomb excitation of $^{1}._{2}{}^{-}$ state in ^{7}Li 2−76882
^{208}Pb(^{7}Li, $\alpha 2n\gamma$)^{209}Bi, lifetimes and branching ratios of ^{209}Bi 2−76782
^{208}Pb(^{7}Li,αn)^{210}Bi, mag. moments of 7^{-} and 5^{-} states in ^{210}Bi 2−67181
Pr, ^{12}C, ^{16}O, ^{22}Ne and ^{40}Ar ion bombardment, inelastic interaction, neutron production, ang. distrib. 2−76886
^{141}Pr(^{12}C,4n)^{149}Tb, excitation function, 50-200 MeV cross-sections 2−74120
^{32}S(^{12}C,α)^{40}Ca, 30 MeV, search for multihole-multiparticle states of ^{40}Ca 2−42508
^{28}Si(^{16}O, ^{12}C), ang. distrib. meas. 2−63926
^{152}Sm(^{35}Cl, ^{35}Cl^{1})^{152}Sn, 100 MeV, recoil distance meas., lifetimes 2−70405
^{118}Sn(^{20}Ne, 4n), 82-120 MeV, excitation of isomeric state in ^{134}Nd 2−79745
^{181}Ta, ion bombardment, excited compound nuclei lifetime, $79<Z<89$, shadow effect obs. 2−76805
^{159}Tb(^{40}Ar,xn), neutron-deficient Bi isotope prod. and α-decay 2−76822
^{128}Te(^{40}Ar, 4n)^{164}Yb, Doppler shift meas. on recoil nuclei, determ. of lifetime of rotational levels 2−79764
^{232}Th, ^{84}Kr induced, transfer reaction thresholds 2−59788
^{232}Th(^{22}Ne, ^{21}O)^{233}U 174 MeV, Q-value measurements, determ. of ground state mass of ^{21}O 2−70383
^{232}Th(^{22}Ne, ^{22}O)^{232}U 174 MeV Q-value measurements, determ. of ground state mass of ^{22}O 2−70383
^{48}Ti, Coulomb excitation by ^{32}S ions, 60-70 MeV, meas. of static electric quadrupole moments 2−63795
^{48}Ti(^{32}S, ^{32}Sγ), 60 MeV, determ. static electric quadrupole moments of first excited states of ^{48}Ti 2−63799
^{205}Tl(^{12}C,xn)$^{217-x}$Fr, 60-90 MeV, meas. of cross sections, reaction thresholds and excitation functions 2−74123
^{205}Tl(^{16}O,xn)$^{221-x}$Ac, 60-100 MeV, meas. of cross sections, reaction thresholds and excitation functions 2−74123
^{238}U bombardment with ^{136}Xe ions, production of Au isotopes, $A=194$, 196, 198, 199 2−67335
W, Coulomb dissociation of C at 10 GeV/nucleon, cross section behaviour 2−49843
W, Coulomb dissociation of O at 10 GeV/nucleon, cross section behaviour 2−49843
^{186}W, ion bombardment, excited compound nuclei lifetime, $79<Z<89$, shadow effect obs. 2−76805

nucleons
complex nuclei, below 3 GeV, nonelastic interactions 2−63871
cross section calcs., role of γ-decay of unbound nuclear states 2−79780
deformed nuclei, direct and semi-direct radiative capture 2−55985
inelastic scatt. by deformed nuclei, microscopic theory 2−82954
inelastic scattering, inclusion of velocity dependent forces in DWBA 2−74069
inelastic scattering at intermediate energies 2−82958
neutron activation prediction program system 2−63947
nonlocal optical potential with finite number of separable terms for elastic, inelastic and charge-exchange scattering 2−70440
nucleon-deuteron elastic scatt., variational scatt. 2−76767
nucleon-deuteron elastic scattering, perturbative calc. of spin observables 2−76768
nucleon-nucleus potential, Hartree-Fock approx. with Skyrme interaction 2−63891
pion production study using current algebra 2−63862
scattering, description in terms of nucleon-nucleon force and nucleon motions 2−42557
scattering amplitude, continuum-continuum interaction effect 2−59749
three-nucleon scattering calc., perturbation method 2−46242
unnatural- parity amplitudes from exchange effects in local energy approximation 2−76835
Watson multiple scattering theory for generation of first and second order optical potentials 2−74068
NN bremsstrahlung, Burnett-Kroll soft-proton theorem applic. 2−82855
C, inelastic interac. with cosmic nucleons, 760-7600 GeV 2−42558
^{12}C, high energy cosmic ray interaction, cf of optical and Glauber models 2−73892
^{57}Fe high energy cosmic ray interaction, cf of optical and Glauber models 2−73892
^{2}H, relativistic exchange scattering 2−49788
LiH, 150-550 GeV, cosmic ray expt., multiplicity of particles generated 2−74070
Nd elastic scatt., perturbative calc. of spin observables, tensor force 2−82960
^{208}Pb, high energy cosmic ray interaction, cf of optical and Glauber models 2−73892

photons
7 MeV, resonant elastic scattering 2−67208
(γ,n) reactions, photonenergy determ., threshold photoneutrons and photon doorways 2−46228
(gamma, particle) reaction, ang. distribution coeff. 2−52795
attenuation coefficient, meas. from 10 eV to 100 GeV 2−46243
Butler−Pearson model verification, max. photon energy 1140 MeV 2−55979
complex nuclei, 4.25 to 9.6 GeV, π^{0} production 2−42555
Compton scattered neutron capture gamma rays for photofission studies 2−52833
correlated nucleon pairs, photoexcitation, cross-section determ. 2−74060
Delbruck scatt., high-energy, from heavy nuclei 2−59740
dipole IAS in even-even nuclei, two classes of proton channels 2−59741

Nuclear reactions and scattering due to continued
photons continued
fermion pair and γ quantum, photoprod. on nuclei, polariz. phenomena 2−70147
intermediate structure in photon induced reactions 2−46227
lepton pair production, Born-approximation analysis taking account of form factors of e.m. multipole moments 2−49782
optical model, volume integrals 2−67230
pair production, screening effects at intermediate and high energies 2−83201
photometer, cross sections above 20 GeV, indirect determ. 2−67209
photoneutron data from monochromatic γ excitation calc. using bremsstrahlung photoneutron data 2−70432
photoneutron reaction, betatron bremsstrahlung application 2−46234
photoproduction of vector mesons on complex nuclei, determ. of strong interaction nuclear radii 2−70433
Raman scatt. by deformed nuclei in giant resonance region 2−82950
resonance levels, decay props. 2−46103
(γ,3π) reaction to test low-energy theorem for $\gamma\gamma\rightarrow\pi\pi\pi$, meas. of cross sections, energy and angular distribs. 2−76596
(γ,α) reactions in region $Z=22$-30, yields and ang. distribs. 2−59743
(γ,γ'), exit states of compound nucleus, role in high-energy γ-ray emission 2−59763
(γ,n), using 55 MeV bremsstrahlung, mech. of non-evaporation neutrons 2−52796
(γ,p), short range correlation effects on proton angular distribs. 2−82952
(γ,pπ^{-}) cross section eval. 2−76829
n production from P by high energy bremsstrahlung beam 2−55980
π production reactions on various nuclei, 2 and 3 GeV, π^{-}/π^{+} ratio meas. 2−82951
π production transparency calc. 2−59739
^{a}Sn(γ,p), $A=116$-118, 120, 122, 124, meas. of spectra and yeild curves, isobaric analog states 2−46233
Al target, angular distribution of photoneutrons 2−63864
^{27}Al (γ,γ'), transition strengths and decay properties of excited energy levels 2−52744
^{40}Ar(γ,n$_{0}$)^{39}Ar, excited state formation in ^{40}Ar 2−46129
^{11}B(γ,π^{+}), study of photoproduction in framework of impulse approximation 2−52798
^{12}C, continuum structure discussed in eigenchannel reaction theory 2−67147
^{12}C, photonuclear induced giant resonance, separation approximation in continuum shell model 2−59690
^{35}Cl (γ,γ'), transition strengths and decay properties of excited energy levels 2−52744
^{137}Cs, at 0.662 MeV, absolute differential scattering cross sections 2−46229
Cu target, angular distribution of photoneutrons 2−63864
Er, elastic and nucl. Raman scatt. cross sections, giant dipole reson. 2−70431
^{19}F(γ,γ'), transition strengths and decay properties of excited energy levels 2−52744
^{19}F(γ,xn), threshold −15 MeV, meas. of total photoneutron cross section 2−49783
Fe, estimate of photonuclear cross-section for energies $\geqslant 1$ GeV 2−73895
^{57}Fe(γ,n)^{56}Fe, ground state radiation width for resonances determ. 2−46139
^{160}Gd(γ,n), 7-33 MeV, meas. of cross section, obs. of quadrupole resonance at 23.5 MeV 2−70436
^{160}Gd(γ,p), 7-33 MeV, meas. of cross section, obs. of quadrupole resonance at 23.5 MeV 2−70436
^{1}H, total hadronic cross section in energy range 0.265 to 4.215 GeV 2−46230
^{2}H(γ, n)^{1}H in burnt-up reactor fuel, cause of high neutron dose rates 2−76915
^{2}H(γ,n), $E_{\gamma}=7$-30 MeV, differential polarization of photoneutrons 2−76828
^{3}He, two-body photodisintegration between 40 and 150 MeV 2−46231
^{4}He, cross-section for disintegration, effect of velocitydependent 2−83003
^{4}He γ p ^{3}H elec. dipole reactions, isospin mixing of excited states 2−83000
^{4}He(γ,d)^{2}H, photospallation process, ang. distrib., total cross sections 2−59742
^{4}He(γ,n)^{3}He, threshold to 34 MeV, cross-section calc. 2−52797
^{4}He(γ,p)^{3}H, threshold to 34 MeV, cross-section calc. 2−52797
^{4}He(γ,pπ^{-}) cross section around Δ(1236) 2−79493
^{165}Ho, elastic and nucl. Raman scatt. cross sections, giant dipole reson. 2−70431
^{39}K(γ,γ'), transition strengths and decay properties of excited energy levels 2−52744
^{139}La(γ,xn) meas. of photoneutron cross sections 8-24 MeV, by direct neutron detection 2−63865
^{6}Li(γ, np)^{4}He, 3.7 to 25 MeV, cross section calc. using dispersion theory methods 2−70434
Mo target, angular distribution of photoneutrons 2−63864
^{14}N, photoneutron cross sections, 15.5-29.5 MeV 2−70435
^{23}Na(γ,γ'), transition strengths and decay properties of excited energy levels 2−52744
Nb, photoactivation analysis in ores 2−65424
^{16}O, photodisintegration and intermediate structure 2−46232
^{16}O(γ, p$_{0}$)^{15}N, cross section calc. rel. to ^{15}N giant dipole resonance 2−59691
^{18}O(γ,p), cross section determ., 16.4-24.5 MeV 2−52799
^{31}P (γ,γ'), transition strengths and decay properties of excited energy levels 2−52744
Pb, scattering of 40 MeV-120 MeV photons, cross section for electron pair production 2−67207
Pb target, angular distribution of photoneutrons 2−63864
^{208}Pb(γ,N)^{207}Pb existence of giant M1 resonance in ^{208}Pb 2−82949
^{141}Pr, bremsstrahlung 100 to 300 MeV, ^{140}Nd yield values 2−42556
^{141}Pr(γ,π-2n)^{139}Nd, cross-sections of photopion prod. 2−55981
^{141}Pr(γ,π-n)^{140}Nd, cross-sections of photopion prod. 2−55981
^{141}Pr(γ,xn), meas. of photoneutron cross sections, 8-24 MeV, by direct neutron detection 2−63865

Nuclear reactions and scattering due to continued
photons continued
^{240}Pu(γ,n), meas. of excitation funtion leading to production of spontaneously fissing isomer ^{239}Pu 2−67210
^{32}S(γ,nγ'), influence of γ-cascade on population of low-lying levels of residual nucleus 2−42505
^{32}S(γ,pγ'), influence of γ-cascade on population of low-lying levels of residual nucleus 2−42505
^{29}Si(γ,n), doorway states and background cross sections 2−63863
^{144}Sm(γ, γ'), level scheme of ^{144}Sm 2−63816
^{144}Sm(γ,xn), production of Sm isotopes 2−46200
^{86}Sr, elastic and inelastic scattering, 12 MeV, meas. of cross sections and angular distribs. 2−74077
^{88}Sr resonance scattering, determ. of life-time of 2.734 MeV level from average cross section 2−49742
Ta, photoactivation analysis in ores 2−65424
Ti target, angular distribution of photoneutrons 2−63864
^{238}U, elastic and nucl. Raman scatt. cross sections, giant dipole reson. 2−70431
W target, angular distribution of photoneutrons 2−63864
Zn(γ,γ')(A=64,66,68), radiative widths of spin-1 levels 2−59692

protons
(p,d) reactions at 30 MeV, excitation of low-lying states in ^{140}Pr, ^{138}La, meas. of angular distrib 2−42564
angular dependence of dose and hadron yields from targets in extracted proton beams 2−46254
blocking effect technique for reaction time meas. 2−74058
coherent production of particles, energy dependence of cross-section 2−55990
complex nuclei of nuclear emulsions, 22.8 GeV/c, primary-energy estimation 2−76826
cross sections for 30 to 60 MeV protons on various elements 2−49792
Cu(p,π), 200-500 MeV, contributions of pions created in cascade mechanism to nuclear evaporation process 2−52813
deutron production in interactions of 670 MeV protons with various nuclei 2−82965
elastic scattering, extraction of nuclear forward-scattering amplitude 2−46245
elastic scattering at 180 MeV, optical model analysis 2−46249
elastic scattering for spectroscopic information on nuclear structure of N=83 nuclei 2−67170
elastic scattering on heavy nuclei using Glauber approx., corrections due to Coulomb scattering, nucleon correlations 2−46246
emulsion nuclei, 22.6 GeV/c, velocity distrib. of secondary π mesons 2−76840
energy transfer to electrons in fast proton collisions 2−55986
excitation of giant dipole and quadrupole states 2−82937
heavy elements, $\leqslant$3GeV, spallation-fission competition 2−67218
high energy, forward deuteron emission and nucl. correls. 2−59752
inelastic cross sections, 10^2 to 10^5 GeV proton-nucleus inelastic cross sections behaviour, 10^2 to 10^5 GeV 2−63678
isobaric analog states and applic. to nucl. spectroscopy 2−59754
isobars from spallation reaction for nuclear spectroscopy 2−63876
optical potential Becchetti-Greenlees used to fit ^{209}Bi(p, np)^{208}Bi 2−46266
p-nucleus interaction, experimental set up to study light nuclei production 2−55889
photonucleon cross section det. for separate residual nuclei states utilizing continuum γ sources 2−74061
pre-equilibrium statistical model and complex particle emission 2−76827
proton-nucleon interactions in emulsion, 14 GeV 2−74082
resonance reactions, high resolution on nuclei 40$\leqslant$A$\leqslant$64 2−46251
semiconductor telescope for detection of light recoiling nuclei in coherent elastic scattering expts. at high energy 2−46058
solar p-p reaction, interaction contributions 2−75934
spectra of fast deutrons produced by 670 MeV protons with various nuclei 2−82965
time reversal, validity tests, optimization 2−63750
two-nucleon transfer reactions on deformed nuclei, use of angular momentum projection technique 2−42561
(p, 2p), single-particle potentials, nuclear rearrangement 2−73974
(p, γ), cross-section, γ-decay of unbound nuclear states 2−67219
(p, n), cross-section, γ-decay of unbound nuclear states 2−67219
(p, n) transitions to analogue states, determ. of isovector coupling potential 2−82937
(p, pn) reaction cross sections in light medium and heavy nuclei at high energies, calc. of excitation function 2−63875
(p, t), on rare earth nuclei, two-neutron transfer 2−55989
(p, t) reaction, study of rare-earth K=0 bands 2−63885
(p,2p) reaction on nuclei in Ni region studied at incident energy of 17MeV 2−52822
(p,α), 40 MeV, obs. on various nuclei, pre-formation of alpha-particles 2−67285
(p,d), complex form factors in nucleon transfer reaction 2−49791
(p,γ), exit states of compound nucleus, role in high-energy γ-ray emission 2−59763
(p,γ) reactions, meas. of ion penetration profiles in solids 2−61122
(p,n) charge-exchange reaction, energy depend., coupled-channel calcs. 2−59759
(p,n) charge exchange reaction, qualitative studies of angular distribution 2−46253
(p,n) compound reactions, direction correlation coefficients of γ-decay 2−70369
(p,n) reactions in meson factories 2−82640
(p,p), calc. of double differential bremsstrahlung cross section in forward direction at 51.8 MeV 2−49789
(p,π^+) reactions in meson factories at 600 MeV and 185 MeV 2−82640
(p,t), complex form factors in nucleon transfer reaction 2−49791
(p,t), in N=50 region, systematics of L=0 transitions 2−79753
^{6}4(p,^{3}He)^{4}He, direct reaction mechanisms in unified microscopic nuclear theory 2−46226
^{a}Sn(p,xn), A=112, 114, production $^{110-114}$Sn, study of decay schemes 2−46191
^{27}Al, analysis of 20 GeV elastic scattering 2−42560
^{27}Al, high energy interactions, production of fast nuclides 2−74087
^{27}Al, intranuclear cascade calculations 2−46262
^{27}Al(p,γ)^{28}Si, γ-rays from reson. at E_p=612 keV 2−76844

Nuclear reactions and scattering due to continued
protons continued
Al(p,π), 200-500 MeV, contribution of pions created in cascade mechanism to nuclear evaporation process 2−52813
^{36}Ar(p,n) ^{36}K, E_p=15-30 MeV, excitation function for positron decay 2−76817
^{36}Ar(p,n)^{36}K, mass, decay props. and levels of ^{36}K 2−70387
^{75}As(p,d)^{74}As, energy levels in ^{74}As 2−52753
^{75}As(p,n)^{75}Se, internal conversion coeffs. of ^{75}Se 2−52752
Au, E = 28 GeV, recoil props. of rare earth nuclides 2−82971
^{197}Au, high energy interactions, production of light fast nuclides 2−74087
^{197}Au(p,n)^{197}Hg, neutron spectra analysis, level density of residual nucleus 2−63831
^{11}B(p, 3α), 2.65 MeV, effect of 3^- state of ^{12}C on separation energies of final state 2−79784
^{11}B(p,^{4}He)^{8}Be, cross sections, ang. distribs., reaction mech. 2−46255
^{11}B(p, α)^{8}Be*, α-particle ang. distrib., 2.9 MeV, detector arrangement 2−74086
^{11}B(p,γ)^{12}C, E_p=14-22 MeV, giant resons. in ^{12}C 2−63772
^{138}Ba, inelastic scattering at 3.0 MeV, meas. of differential cross sections 2−74079
^{138}Ba(p,d), neutron-single hole state determ. 2−46157
^{9}Be, analysis of 20 GeV elastic scattering 2−42560
^{9}Be, scattering at 19.3 GeV/c, applic. of Steenberg model 2−59750
^{9}Be(p,^{4}He)^{6}Li, cross sections, ang. distribs. for first 3 states, reaction mech. 2−46255
^{9}Be(p,α), E_p=3.56 MeV, population of ^{6}Li levels 2−82883
^{9}Be(p,γ)^{10}B, isospin impurity of 6.88 MeV state in ^{10}B 2−63770
^{9}Be(p,n)^{9}B, 17.8 MeV, determ. of width of excited state in ^{9}B from neutron spectra 2−52735
^{9}Be(p,n)^{9}B, excited-state-threshold reson. effects 2−79788
^{9}Be(p,p_0)^{9}Be, excited-state-threshold reson. effects 2−79788
^{9}Be(p,p)^{9}Be, excited states in ^{10}B near 10 MeV obs. 2−70378
^{9}Be(p,π^-)^{10}C, 600 MeV, cross-section for π^- production 2−67222
^{209}Bi(p, n)^{209}Po(p)^{208}Bi, 28, 35, 45 MeV, n ang. distrib. and n decay of isobaric analogue resonance obs. 2−46266
^{209}Bi(p,2p)^{208}Pb, obs. of T=23 double analogue states in ^{210}Po 2−70446
^{209}Bi(p,n), charge-exchange reaction, energy depend., coupled-channel calcs. 2−59759
^{209}Bi(p,n)^{209}Po, neutron spectra of analysis, level density of residual nucleus 2−63831
^{209}Bi(p,n)^{209}Po(IAS), 28, 35 and 45 MeV, angular distributions and excitation function 2−70446
^{209}Bi(p,np), excitation functions and energy dependence of reaction 2−67223
^{209}Bi(p,p$'$), proton decay of isobaric analogs of ground states 2−63888
^{12}C, 150, 600 MeV, cross-sections for production of ^{6}Li and ^{7}Li 2−74088
^{12}C, analysis of 20 GeV elastic scattering 2−42560
^{12}C, calc. for quasi-elastic (p,2p) scatt. at 460 MeV 2−46258
^{12}C, elastic and inelastic Glauber scatt. in alpha-particle model 2−59751
^{12}C, elastic scatt., cross sections analysis 2−82723
^{12}C, high energy interactions, production of light fast nuclides 2−74087
^{12}C, total cross-sections, 180-560 MeV 2−74071
^{12}C(p,^{6}Li)^{7}Be, differential cross section from 36-56.8 MeV angular distrib. and excitation functions meas., DWBA analysis 2−46259
^{12}C(p,2p), microscopic calcs. of cross sections in plane wave impulse approx., determ. of spectral function 2−55992
^{12}C(p,γ_0)^{13}N, 8.6-16.3 MeV, destructive interference 2−46250
^{12}C(p,p$'$3α), mechanism, cross sections, ^{8}Be and ^{9}B ground states, E_p=13 MeV 2−59757
^{12}C(p,pn)^{11}C cross-section at 7.6 GeV 2−82969
^{13}C, elastic scatt. phase shifts calc. 2−76855
^{13}C(p, γ)^{14}N, γ-decay of levels in ^{14}N 2−76780
^{40}Ca, calc. for quasi-elastic (p,2p) scatt. at 460 MeV 2−46258
^{40}Ca, inelastic scatt., 24.93-39.83 MeV, energy depend. 2−76838
^{40}Ca giant resonances in high-energy inelastic scatt. continuum 2−82967
^{40}Ca(p,2p)^{39}K, 460 MeV, ^{40}Ca energy level structure 2−46263
^{40}Ca(p,p$'$), e_p=8.7 MeV, lifetime of 3.74 MeV (3^-) state of ^{40}Ca 2−67154
^{40}Ca(p,p), 14.5 MeV, optical-model calcs., determ. of nuclear forward-scattering amplitude 2−46245
^{40}Ca(p,p)^{40}Ca, polarized protons, 2.3-2.8 MeV, meas. of proton polarization, determ. of angular momentum of ^{41}Sc excited states 2−52812
^{42}Ca(p, t)^{40}Ca, 41.7 MeV, failure of DWBA coexistence model 2−74089
^{42}Ca(p,t)^{40}Ca, 40 MeV, excitation of levels in ^{40}Ca 2−46264
^{44}Ca(p,γ)^{45}Sc, ^{45}Sc energy levels up to 3 MeV 2−42509
^{48}Ca, elastic and inelastic scatt., isobaric analog states in ^{49}Sc 2−70390
^{48}Ca, inelastic scatt., ang. distribs. excited states obs. 2−76839
^{48}Ca(p, p$'\gamma$), particle-γ angular correlation and lifetime studies of 4.61 and 5.15 MeV levels 2−82889
Ca(p, p)Ca, A=40, 44, 48, optical model determ. of r.m.s. radius 2−74076
Cd (p,t), A=112, 114, 116, anomalous two-phonon transitions in Cd 2−63806
^{106}Cd(p,p'), γ-ray multiplicity, comparison with direct reaction mechanisms 2−67224
^{116}Cd(p,p') γ-ray multiplicity, comparison with compound nucleus reaction mechanisms 2−67224
^{140}Ce(p, t)^{138}Ce, E_p=30.3 MeV, strong and weak 0^+ excitations 2−76847
^{140}Ce(p,d), neutron-single hole state determ. 2−46157
^{142}Ce(p, p_0), 9.5 to 12 MeV, isobaric analogue resonances 2−67332
^{142}Ce(p, p_1), 9.5 to 12 MeV, isobaric analogue resonances 2−67332
^{142}Ce(p, t)^{140}Ce, E_p=30.3 MeV, strong and weak 0^+ excitations 2−76847
^{35}Cl(p, γ)^{36}Ar, branching ratios, excitation energies, lifetimes of ^{36}Ar levels 2−79748
^{35}Cl(p,d)^{34}Cl, low-lying positive-parity states obs. 2−59698

Nuclear reactions and scattering due to continued
protons continued
^{35}Cl(p,γ)^{36}Ar, 0.8-2.3 MeV, obs. of γ decay of resonances, determ. of branching ratios, energies 2−52747
^{35}Cl(p,γ)^{36}Ar, J^{π}=6- bound state in ^{36}Ar 2−59699
^{36}Cl prod. cross sections, rel. to cosmic ray constancy 2−59753
^{37}Cl(p,d)^{36}Cl, low-lying positive-parity states obs. 2−59698
^{37}Cl(p,n)^{37}Ar, low-lying level props. of ^{37}Ar 2−55960
^{37}Cl(p,nγ)^{37}Ar, 3.25-5.90 MeV, meas. of γ-ray angular distribs. and mean lifetimes of levels in ^{37}Ar 2−74015
^{50}Cr, inelastic scatt., ang. distribs., octupole excitations 2−74022
^{50}Cr(p, pγ)^{50}Cr 7 MeV, γ-ray spectra, Doppler shift attenuation of lifetimes in ^{46}Ti 2−76794
^{52}Cr(p,p)^{52}Cr optical model determ. of r.m.s. radius 2−74076
^{54}Cr(p, d)^{53}Cr, j-depend. in l=3 transitions 2−76845
^{54}Cr(p, nγ)^{54}Mn, 2.0-3.9 MeV, meas. of excitation functions and angular distributions of gamma rays, determ. of ^{54}Mn level structure 2−79743
^{54}Cr(p,nγ)^{54}Mn, Ep=2.1-3.2 MeV, low lying levels of ^{54}Mn 2−46134
Cu, Ep=82-416 MeV, thin-target cross-sections for radionuclide prod. 2−82970
Cu isotopes, inelastic scatt. in unified model 2−63803
^{2}D, total cross-sections, 180-560 MeV 2−74071
D(p, 2p)n, cross-section, attenuation of quasifree scattering 2−74084
D(p,2p), Ep=39.5 MeV, destructive interference effects 2−79797
^{158}Dy(p,t), excited 0^{+} states population 2−63887
^{160}Dy(p,t), excited 0^{+} states population 2−63887
^{162}Dy(p,t), excited 0^{+} states population 2−63887
^{163}Dy(p, nγ) 6.7 MeV, 13.5 MeV, meas. of γ-ray spectra, deduced ^{163}Ho level scheme 2−63820
^{164}Er(p,t), excited 0^{+} states population 2−63887
^{166}Er(p,t), excited 0^{+} states population 2−63887
^{169}Er scattering, excitation of analogue resonances for study of ^{168}Er structure 2−46169
^{19}F isospin- forbidden reactions, second T=0 state of ^{20}Ne as compound reson. 2−76785
^{19}F(p,^{3}He)^{17}O, E_p=45 MeV, cross sections analysis, ^{17}O levels 2−82972
^{19}F(p,t)^{17}F, E_p=45 MeV, cross sections analysis, ^{17}F levels 2−82972
^{54}Fe(p,d)^{53}Fe, 52 MeV, spectroscopic factors determ. for ^{53}Fe 2−42563
^{54}Fe(p,γ)^{55}Co, isobaric analog state obs. 2−59754
^{54}Fe(p,γ)^{55}Co, γ-decay of analogue states of ^{55}Fe 2−46135
^{54}Fe(p,p$'\gamma$)^{54}Fe, E_p=10 MeV, spectroscopy of ^{54}Fe 2−76836
^{54}Fe(p,p)^{54}Fe optical model determ. of r.m.s. radius 2−74076
^{56}Fe(p,γ)^{57}Co, 1250-1685 keV, obs. or resonance states in ^{57}Co, isobaric analogs of states in ^{57}Fe 2−63882
^{57}Fe(p,t)^{55}Fe, 27 MeV, study of two-nucleon pick-up from spin-1/2 target, differential cross section meas. 2−63883
^{57}Fe(p,τ)^{55}Mn, 27 MeV, study of two-nucleon pick-up from spin-1/2 target, differential cross section meas. 2−63883
^{58}Fe(p, nγ)^{58}Co 3.9 MeV, meas. of nγ correlations and g-factors, determ. lifetimes and magnetic moment of ^{58}Co levels 2−79742
^{58}Fe(p, p)^{58}Fe, 2.65-3.11 MeV, ^{59}Co excited state analogue of 3/2- excited state in ^{59}Fe 2−46140
Gd(p, t), 18 MeV, l=o, l=2 transitions identified for levels of several isotopes 2−46163
Ge crystal, blocking of protons, effect on lifetime of compound nucleus fine structure 2−52811
^{70}Ge(p, p$'$)^{70}Ge, compound nucleus lifetime meas. by blocking technique, multiple scatt. effects 2−63748
^{70}Ge(p, p$'$)^{70}Ge, time meas. by blocking technique 2−74058
^{70}Ge(p,p)^{70}Ge, ^{71}As, isobaric analogue resonance evidence for intermediate structure 2−46143
^{70}Ge(p,p)^{70}Ge, 1.04 MeV, compound nucleus lifetime meas., crystal blocking technique 2−46252
^{72}Ge(p, p$'$)^{72}Ge, compound nucleus lifetime meas. by blocking technique, multiple scatt. effects 2−63748
^{72}Ge(p, p$'$)^{72}Ge, time meas. by blocking technique 2−74058
^{72}Ge(p,p)^{72}Ge, ^{73}As, isobaric analogue resonance evidence for intermediate structure 2−46143
^{72}Ge(p,p)^{72}Ge, 0.8 MeV, compound nucleus lifetime meas., crystal blocking technique 2−46252
^{73}Ge(p,n)^{73}As, internal conversion coeffs. of ^{73}As 2−52752
^{1}H, total cross-sections, 180-560 MeV 2−74071
^{2}H, elastic cross section and polarisation at 198 MeV 2−49790
^{2}H, spin structure of scattering, Glauber theory 2−59755
^{2}H, triple scattering meas. 2−46256
^{2}H scattering, optical model and DWBA calculation 2−52809
^{2}H(P, 2P)n, 20-60 MeV, rescattering effects, cross-sections obs. 2−63878
^{2}H(p, p)^{2}H, 600 MeV cross-section obs., p. polarization meas. cf with Watson and Glauber theory 2−63873
^{2}H(p, pn)n, 20-60 MeV, rescattering effects, cross-sections obs. 2−63878
^{2}H(p,2p)n, 155 MeV, high momentum transfers, meas. of cross sections, importance of off energy shell nucleon nucleon interaction 2−63877
^{2}H(p,2p)n, 51.8 MeV, study in coplanar symmetric geometry at forward angles 2−67220
^{2}H(p,2p)n and ^{2}H(p,pn)p, cross-sections for small momentum transfer, difference 2−74083
^{2}H(p,γ)^{3}He, excitation function anomaly, E_p=10−17.5 MeV 2−59756
^{2}H(p,n)p correlation spectra of cross-section calc. 2−83005
^{2}H(p,p), energy dependence of backward elastic scattering in range 360-670 MeV 2−67216
^{2}H(p,pn)^{1}H, meas. of nucleon-nucleon final state interaction as function of angular and energy variables 2−49793
^{2}H(p,pp)n, correlation spectra of cross-section calc. 2−83005
^{2}H(p,pp)n, p effective momentum distribution in deuteron determ. 2−46247
^{2}H(p,ppn), study at low bombarding energies 2−67221
^{3}H, elastic scatt. of polarized protons between 19 and 57 MeV, cross sections and asymmetries 2−42562
^{3}H(p,d)^{2}H, E_p=6.7-14.7 MeV, analyzing power ang. distrib., ^{2}H(d,p)^{3}H studies 2−70473

Nuclear reactions and scattering due to continued
protons continued
^{3}H(p,n)^{3}He, 1.5-12 MeV, analyzing power polarization anomalous difference 2−49794
^{3}H(p,n)^{3}He, 56.7 MeV, cross section meas. 2−42562
^{3}H(p,n)^{3}He, polarization and polarization transfer 2−46257
^{3}H(p,p), polarized proton beam, meas. of differential cross section, proton analyzing power at 19 and 30 MeV 2−63874
^{3}H(p,p)^{3}H, elastic scatt., E_p=9.4-14.7 MeV, analyzing powers, ang. distrib. 2−70441
^{3}He, elastic scatt., coupling const. for deuteron exchange 2−76870
^{3}He, elastic scatt., modified phase shift analysis 2−42559
^{3}He, elastic scatt. cross sections, S$'$- and D-state effects 2−42497
^{3}He broad reson. obs. in (p,α) and (p,2p) reactions 2−59760
^{3}He(p, 2p), 590 MeV, cross-section 2−74085
^{3}He(p, p)^{3}He, 600 MeV, cross-section obs., cf, with multiple-scattering theory of Watson and Glauber 2−63873
^{3}He(p, pd), 590 MeV, cross-section 2−74085
^{3}He(p,2p)^{2}H, meas. of nucleon-nucleon final state interaction as function of angular and energy variables 2−49793
^{3}He(p,p), polarized proton beam, meas. differential cross section, proton analyzing power at 30 MeV 2−63874
^{4}He, total cross-sections, 180-560 MeV 2−74071
^{4}He(p, p)^{4}He, 12 MeV, determ. of polarization standards 2−74072
^{4}He(p, p)^{4}He, 600 MeV, cross-section obs., p. polarization meas. 2−63873
^{4}He(p, p)^{4}He up to 20 MeV, R matrix formulation and phase shifts 2−76853
^{4}He(p,d)^{3}He*, 65 MeV, continuum spectra analysis 2−67141
^{4}He(p,p)He elastic scatt. below 50 MeV, forward dispersion relation 2−67205
^{204}Hg(p, p), elastic and inelastic resonant scattering, 12.5-14.2 MeV and 16.0-18.8 MeV, meas. of excitation functions, resonance parameters 2−74080
^{204}Hg(p, p) ^{204}Hg, 14-16.4 MeV, resonances in ^{205}Tl at 14.72 and 15.43 MeV 2−79767
H(p, p)H, 600 MeV, cross-section obs., cf with Livermore phase shifts 2−63873
^{115}In (p,p)^{115}In, analogue states of ^{116}In 2−67215
^{192}Ir(p,nnnn) ^{188}Pt, ^{191}Ir(p,nn)^{190}Pt study of levels of Pt 2−70410
^{193}Ir(p,2n)^{192}Pt, ^{193}Ir(p,4n)^{190}Pt, study of levels in Pt 2−70410
^{86}Kr, inelastic scattering through isobaric analog resonances, level structure of ^{86}Kr-^{87}Kr system 2−46147
^{86}Kr(p,p)^{86}Kr, 4.76-10.10 MeV, obs. of isobaric and analog resonances, study of core coupling in ^{87}Rb 2−46146
La molten, 600 MeV, production of very neutron-deficient isotopes of Cs, study using on-line isotope separator techniques 2−42545
^{6}Li, elastic and inelastic scattering, 25-45 MeV, meas. of angular distrib. for excitation of excited states 2−55991
^{6}Li(p,2p)^{5}He 100 MeV, angular correlation measurements 2−82966
^{6}Li(p,n)^{6}Be, 17.8 MeV, determ. of width of excited state in ^{6}Be from neutron spectra 2−52735
^{6}Li(p,pd)^{4}He, E_p=590 MeV, α-d clustering in ^{6}Li 2−63879
^{6}Li(p,pd)^{4}He, Treiman-Yang test for pole approx. at 19 MeV 2−63880
^{7}Li(p,2d)^{4}He, 45 MeV, study of reaction mechanisms 2−49795
^{7}Li(p,pt)^{4}He structure of ^{7}Li by cluster model 2−82964
^{24}Mg, microscopic coupled-channel study of inelastic scattering using projected HF wave functions 2−70443
^{24}Mg(p, p) elastic scatt. cross sections, E_p=100 MeV, optical model analysis 2−74074
^{24}Mg(p,γ)^{25}Al reaction, gamma decay of excited states of ^{25}Al 2−42503
^{24}Mg(p,p$_1'\gamma$)^{24}Mg, ^{25}Al excited state spins determ. 2−74009
^{26}Mg(p, $\alpha\gamma$)^{23}Na, level study of ^{23}Na 2−76789
^{26}Mg(p, t)^{24}Mg, 26 MeV, statistical-model explanation of levels in ^{24}Mg 2−63881
^{55}Mn(p,n)^{55}Fe, determ. of level density in ^{55}Fe 2−63797
^{92}Mo+p, conversion electron spectra by in-beam spectroscopy 2−82913
^{92}Mo(p,t)^{90}Mo, 39 MeV, meas. of angular distribs. of levels in ^{90}Mo 2−70398
^{92}Mo(p,xn), production of short-lived neutron deficient Tc isotopes 2−49768
^{94}Mo(p,p$'\gamma$)^{94}Mo, angular correlation obs., analog resonance in ^{95}Tc 2−74078
^{95}Mo(p,t)^{93}Mo, spin-parity assignment of 1.69 MeV level 2−74034
^{96}Mo(p,xn)$^{97-x}$Tc, E_p=10-80 MeV, excitation functions 2−74091
^{97}Mo(p,nγ)^{97}Tc, E_p=3−6 MeV, excited states in ^{97}Tc 2−67165
^{98}Mo, ^{100}Mo, inelastic scatt., E_p=14.7 MeV, ang. distrib. 2−79782
^{98}Mo, energy dependence of inelastic scatt. cross section, inbeam internal conversion electron studies 2−70417
Mo(p,d), producing isobaric analog states, hole strength variations 2−46151
^{14}N, inelastic scattering 17 MeV meas. of angular distribs., use of microscopic potential, weak coupling model 2−46260
^{14}N(p,2p)^{13}C, 46 MeV comparison of local and non-local t-matrix calc. of angular distrib. in distorted wave approx. 2−55993
^{14}N(p,γ)^{15}O, E_p=8.8 to 9.0 MeV, reson. struct. in ^{15}O 2−63774
^{14}N(p,p), 3 to 3.55 MeV, excited states of ^{15}O between 10 and 10.5 MeV 2−46112
^{15}N, inelastic scattering, 17 MeV meas. of angular distribs., use of microscopic potential, weak coupling model 2−46260
^{15}N(p,γ_0)^{16}O, polarized proton capture reaction, giant dipole reson. obs. 2−67149
^{15}N(p,n)^{15}O, meas. of threshold energy, ^{15}O deduced mass 2−55957
^{23}Na, 1.7-3.0 MeV proton bombardment, study of ^{24}Mg resonance states 2−70384
^{23}Na(α, $\alpha'\gamma$)^{23}Na, level study of ^{23}Na 2−76789
^{142}Nd(p,d), neutron-single hole state determ. 2−46157
Nd(p,t) even isotopes, 5Z MeV, excitation of removal and addition types of quadrupole-pairing vibrational states 2−82968
^{20}Ne, microscopic coupled-channel study of inelastic scattering using projected HF wave functions 2−70443
^{20}Ne, proton scatt. and radiative capture, excited states in ^{21}Na obs. 2−55969
^{20}Ne (p, γ)^{21}Na, 0.98-2.2 MeV, meas. of excitation energies, Q-value, determ of branching ratios 2−74005
^{20}Ne(p,γ)^{21}Na, meas. of γ-ray branching ratios and lifetimes, search for missing J^{π}=3/2^{+} level in ^{21}Na 2−79761

Nuclear reactions and scattering due to continued
protons continued
^{20}Ne(p,n)^{20}Na, 20 MeV, meas. of cross section, reduction of background influences associated with gas target 2−49796
^{21}Ne(p, d)^{20}Ne, spectroscopic factors of ^{20}Ne 2−76842
^{21}Ne(p, p)^{21}Ne, deform. parameters of ^{21}Ne 2−76842
^{22}Ne(p, γ)^{23}Na, γ-ray resonant absorpt., ^{23}Na level widths, Rutherford scatt. effect 2−76843
^{22}Ne(p,γ)^{23}Na, 1.2 to 3.0 MeV, obs. of resonances corresponding to excited states of ^{23}Na 2−49733
^{22}Ne(p,p$'\gamma$)^{22}Ne, 1.2 to 3.0 MeV, obs. of resonances corresponding to excited states of ^{23}Na 2−49733
^{22}Ne(p,t)^{20}Ne, E_p=39.8 MeV, transition to 2$^-$ rot. band in ^{20}Ne 2−79786
Ni (A=58,60,61,62,64), excitation functions and peak cross sections for energy range 5 to 56 MeV 2−59758
^{58}Ni(p, γ)^{59}Cu, study of $g_{9/2}$ isobaric analogue and anti-analogue states of ^{59}Cu, core structure 2−74027
^{58}Ni(p, nγ)^{58}Cu, 12.0-13.03 MeV, determ. of γ-ray decay modes of low-lying states of ^{58}Cu by n-γ and γ-γ coincidence techniques 2−74026
^{58}Ni(p, p)^{58}Ni, study of $g_{9/2}$ isobaric analogue and anti-analogue states of ^{59}Cu, core structure 2−74027
^{58}Ni(p,p$'$)^{58}Ni(2$^+$), 20 and 100 MeV, Born approx. calcs. of probability of spin flip, explanation of backward-angle peak 2−79787
^{58}Ni(p,p)^{58}Ni DWA cross-section calc. with imaginary part 2−74081
^{60}Ni(p,p'), γ-ray multiplicity, comparison with direct reaction mechanism 2−67224
^{64}Ni(p,nγ)^{64}Cu, 3.47-5.19 MeV, study of structure and γ-decay of levels excited near isobaric analogue resonances 2−67160
^{64}Ni(p,p$'$), 3-5 MeV, elastic and inelastic excitation of ^{65}Cu isobaric analogue resonance 2−63804
^{64}Ni(p,p'), γ-ray multiplicity, comparison with compound nucleus reaction mechanism 2−67224
^{14}O(p,p), E_p=65 MeV, ang. distribs., optical model 2−74073
^{16}O, 2$^-$ state, spin-flip mechanisms, core polarization exchange contribution 2−76841
^{16}O, calc. for quasi- elastic (p,2p) scatt. at 460 MeV 2−46258
^{16}O, E_p=135 and 550 MeV, radiochem. meas. of ^{10}Be and ^{7}Be form. cross sections 2−82961
^{16}O, total cross-sections, 180-560 MeV 2−74071
^{16}O(p,2p), microscopic calcs. of cross sections in plane wave impulse approx., determ. of spectral function 2−55992
^{16}O(p,2p)^{15}N, two step process in amplitude calc. 2−46261
^{16}O(p,p), 14.5 MeV, optical-model calcs., determ. of nuclear forward-scattering amplitude 2−46245
^{16}O(p,p), optical model calcs. with realistic nucleon-nucleon interaction 2−76837
^{17}O(p, γ)^{18}F, E_p=741 keV, transition strengths of analogue states 2−74000
^{17}O(p,p), E_p=65 MeV, ang. distribs., optical model 2−74073
^{17}O(p,p), optical model calcs. with realistic nucleon-nucleon interaction 2−76837
^{18}O(p, t)^{16}O, 41.7 MeV, failure of DWBA coexistence model 2−74089
^{18}O(p,p), E_p=65 MeV, ang. distribs., optical model 2−74073
^{18}O(p,p), optical model calcs. with realistic nucleon-nucleon interaction 2−76837
O(p, p)O, A=16, 17, 18, 65 MeV, angular distribs. 2−70442
(p,n), microscopic description in deformed potential model, core polarization knock out mechanism 2−67213
^{31}P(p, γ)^{32}S, E_p=1100-1600 keV, resonances 2−74090
^{31}P(p,p$'$), excited states at 185 MeV 2−46125
^{206}Pb(p,p$'$), proton decay of isobaric analogs of ground states 2−63888
^{206}Pb(p,p$'$)^{206}Pb*(2$_1$$^+$), and direct nuclear processes 2−59721
^{207}Pb(p,p$'$), proton decay of isobaric analogs of ground states 2−63888
^{208}Pb(p,n), charge-exchange reaction, energy depend., coupled-channel calcs. 2−59759
^{208}Pb(p,n)^{208}Bi, isobaric analogue state of ^{208}Pb ground state, population and decay 2−52770
^{208}Pb(p,np), excitation functions and energy dependence of reaction 2−67223
^{208}Pb(p,p$'$), proton decay of isobaric analogs of ground states 2−63888
^{208}Pb(p,p)^{208}Pb, elastic scatt., 8 to 14 MeV, optical model analysis 2−67217
^{208}Pb(p,p)^{208}Pb DWA cross-section calc. with imaginary part 2−74081
Pb(p,π), 200-500 MeV, contribution of pions created in cascade mechanism to nuclear evaporation process 2−52813
^{141}Pr(p, t)^{139}Pr, 40 MeV, collective effects 2−63886
^{141}Pr(p,γ)^{142}Nd, 6-17 MeV, isospin splitting of giant E1 excitations 2−82891
^{195}Pt(p,p$'$), neutron and γ-ray yields from threshold region 2−67225
Pu(p, 2n), excitation functions for prod. of fission isomers in Am isotopes 2−76894
Rb isotope yields 2−55988
^{29}S(p,γ)^{30}P, lifetimes of excited states in ^{30}P 2−49734
^{32}S(p,p$'$), excited states at 185 MeV 2−46125
^{32}S(p,p)^{32}S, ^{34}S(p,p)^{34}S, asymmetry in polarized p elastic and inelastic scatt., 24.5 MeV, optical model analysis 2−52810
^{32}S(p,p)^{33}Cl, polarized protons, 2.5-3.0 MeV, study of ^{33}Cl excited states, resonance parameters 2−67153
^{33}S(p,γ)^{34}Cl, 1058, 1098, 1121 keV, study of odd-parity spectrum of ^{34}Cl 2−46127
^{45}Sc(p, nγ)^{45}Ti, used to study levels in ^{45}Ti 2−46132
^{28}Si(p, p$'$)^{28}Si, time meas. by blocking technique 2−74058
^{28}Si(p, p) elastic scatt. cross sections, E_p=100 MeV, optical model analysis 2−74074
^{28}Si(p,p)^{28}Si polarized protons, 1.5-3.0 MeV, meas. of proton polarization, determ. of angular momentum of ^{29}P excited states 2−52812
Si(p, p), 5-15 MeV, analyzing power 2−74075
Sm (A=148, 154), coupled channel analysis of 12 MeV scattering 2−55987
Sm (p.t.) E_p-19 MeV, level assignments for even isotopes 2−82962
^{144}Sm, differential cross sections for elastic and inelastic scattering to low-lying states, 30 MeV 2−46305

Nuclear reactions and scattering due to continued
protons continued
^{144}Sm, inelastic scattering at 30 MeV, meas. of differential cross sections 2−74079
^{144}Sm(p,d), neutron-single hole state determ. 2−46157
^{154}Sm(p,t)^{152}Sm two-nucleon transfer reaction, use of angular momentum projection technique 2−42561
^{112}Sn(p, xn), decay of light Sb isotopes 2−76818
^{112}Sn(p,p'), γ-ray multiplicity, comparison with direct reaction mechanisms 2−67224
^{114}Sn(p, xn), decay of light Sb isotopes 2−76818
^{116}Sn(p,np$^\sim$) charge exchange reaction, qualitive studies of angular distribution 2−46253
^{119}Sn(p, n), 28 and 35 MeV, populating IAS, angular distribution meas. 2−70444
^{119}Sn(p,n) charge-exchange reaction, energy depend., coupled-channel calcs. 2−59759
^{119}Sn(p,np), excitation functions and energy dependence of reactions 2−67223
^{119}Sn(p,np), total cross section, excitation function 2−70444
^{120}Sn(p,p)^{120}Sn, DWA cross-section calc. with imaginary part 2−74081
^{122}Sn(p,p'), γ-ray multiplicity, comparison with compound nucleus reaction mechanism 2−67224
^{88}Sr(p,p$'\gamma$)^{88}Sr, polarization-analyzing power inequality 2−76846
^{181}Ta intranuclear cascade calculations 2−46262
^{159}Th(p, t)^{157}Tb, 30 MeV, collective and higher- order effects 2−74092
^{46}Ti(p, pγ)^{46}Ti, 7 MeV, γ-ray spectra, Doppler shift attenuation of lifetimes in ^{46}Ti 2−76794
^{48}Ti, elastic and inelastic scattering, meas. of differential crosssections, obs. of isobaric analogue resonances 2−79783
^{48}Ti(p,γ)^{49}V, g-factor 3/2$^-$ 153 keV state in ^{49}V 2−67157
^{49}Ti(p,n) ^{49}V 2.03 to 3.25 MeV energy levels 2−82898
^{50}Ti(p,p)^{50}Ti, optical model determ. of r.m.s. radius 2−74076
U, E = 28 GeV recoil props. of rare earth nuclides 2−82971
U, high energy, new isotope prod. obs. 2−82925
U (p, secondary reactions), 24 GeV, production cross-sections of super-heavy elements 2−70379
^{238}U, 12 and 28 GeV protons, search for actinides and super-heavy elements in secondary reactions 2−63781
^{51}V(p, γ)^{52}Cr, 1.567, 1.629 MeV, analogue resonances low lying levels of ^{52}V 2−74023
^{51}V(p,γ) up to 3.12 MeV, study of isobaric analogue states in ^{52}Cr 2−76795
^{51}V(p,n)^{51}Cr, obs. of 2.335 MeV isobaric analog resonance, study of excited states of ^{51}Cr 2−46265
^{51}V(p,n) up to 3.12 MeV, study of isobaric analogue states in ^{52}Cr 2−76795
^{51}V(p,nγ)^{51}Cr, 4.013, 5.016 MeV, study of excited states of ^{51}Cr 2−46265
^{51}V(p,nγ)^{51}Cr, ang. distrib. of ground state e.m. transitions, level spins, comparison with Hauser-Feshbach theory 2−79751
^{51}V(p,p)^{51}V, obs. of 2.335 MeV isobaric analog resonance 2−46265
^{51}V(p,p)^{51}V optical model determ. of r.m.s. radius 2−74076
W, 28 GeV protons, search for actinides and super-heavy elements in secondary reactions 2−63781
W, negative hyperon production by 24 GeV/c proton bombardment 2−42419
^{186}W(p,d), angular distributions, higher-order processes 2−79785
^{186}W(p,t)^{184}W, strong inelastic processes 2−52814
^{89}Y (p,p)^{89}Y, analogue states of ^{90}Y 2−67215
^{89}Y(p,nγ)^{89}Zr, ^{89}Zr transition rates 2−46149
^{89}Y(p,p2n)^{87}Y, isomer ratios, calc. based on statistical and cascade-evaporation theories 2−49730
^{172}Yb(p,d), angular distributions, higher-order processes 2−79785
^{91}Zn(p,np), excitation functions and energy dependence of reaction 2−67223
Zr (A=90, 96), energy dependence of inelastic scatt. cross section, inbeam internal conversion electron studies 2−70417
^{90}Zr, energy dependence of radiative capture cross section, inbeam internal conversion electron studies 2−70417
^{90}Zr, inelastic excitation of low lying levels by 61.2 MeV proton, role of two-body spin-orbit interaction 2−70430
^{90}Zr(p,nγ)^{90}Nb, 6.9-9.5 MeV, meas. of excitation functions for low-lying levels of ^{90}Nb and their γ decay 2−42515
^{90}Zr(p,p), 14.5 MeV, optical-model calcs., determ. of nuclear forward-scattering amplitude 2−46245
^{91}Zr, polarization effects in isospin-coupled reaction channels 2−63884
^{91}Zr(p, n), 28 MeV, populating IAS, angular distribution meas. 2−70444
^{91}Zr(p, np), total cross section, excitation functions 2−70444
^{91}Zr(p, t)^{89}Zr, 51.7 MeV, level determ. for ^{89}Zr 2−70445
^{91}Zr(p,n) charge-exchange reaction, energy depend., coupled-channel calcs. 2−59759
^{91}Zr(p,p')^{91}Zr, 20.4 MeV, obs. of new levels and doublets in ^{91}Zr 2−52754
^{96}Zr(p,p$'$e), rel. to meas. of first excited state lifetime of ^{96}Zr 2−59704

tritons
two-nucleon transfer reactions, noncentral effects 2−74107
two-nucleon transfer reactions on deformed nuclei, use of angular momentum projection technique 2−42561
unnatural- parity amplitudes from exchange effects in local energy approximation 2−76835
(t, p), on rare earth nuclei, two-neutron transfer 2−55989
(t,p) stripping reactions, repulsive core effects 2−49818
^{a}Th(t,p) (A=230,232), search for transitions to excited 0$^+$ states 2−59785
^{a}U(t,p) (A=234,236,238), search for transitions to excited 0$^+$ states 2−59785
^{9}Be(t,p)^{11}Be, investigations of ^{11}Be energy levels 2−59689
^{12}C(t, n)^{14}N, 8.0 MeV, meas. and comparison with double stripping theory 2−76874
^{65}Cu(t, α), E_t=12 MeV, excitation of ^{64}Ni, level struct. 2−76878
^{57}Fe(t,p)^{59}Fe, 12 MeV, meas. of angular-momentum transfer, study of ^{59}Fe level structure 2−63921
^{6}Li(t,p)^{8}Li, excitation function, ^{9}Be level obs. 2−63911

Nuclear reactions and scattering due to continued
  tritons continued
    Nd(t,p), (A=142, 144, 146, 148, 150) 13 MeV, angular distributions of protons, Q-values and spin and parity of states 2−42523
    ^{20}Ne(t, pγ)^{22}Ne, 3 MeV, p-γ ang. correl., spin assignments 2−79739
    ^{17}O(t,p)^{19}O, distorted-wave analysis of angular distribs., spin-parity assignments to states near 2.7 MeV excitation 2−79734
    ^{204}Pb(t,p)^{206}Pb, $E_t=6$ MeV, pairing vibr. states of ^{206}Pb 2−82900
    ^{208}Pb(t,p)^{210}Pb, 20 MeV, meas. of angular distribs., determ. of ^{210}Pb structure 2−82892
    ^{210}Po(t,α)^{209}Bi, 20 MeV, meas. of absolute cross sections, determ. of spectroscopic factors, study of particle-hole states 2−82894
    Pu(t, 2n), excitation functions for prod. of fission isomers in Am isotopes 2−76894
    Pu(t, 3n), excitation functions for prod. of fission isomers in Am isotopes 2−76894
    ^{36}S(t,α)^{35}P, $E_t=3.4$ MeV, ^{35}P identification and characteriz. 2−74014
    ^{152}Sm(t, α)^{151}Pm, 15 MeV, meas. of cross section, determ. of level structure of ^{151}Pm 2−74038
    ^{119}Sn(t, p)^{121}Sn, 13 MeV, ang. distrib transferred orbital momentum derived 2−76798
    ^{120}Sn(t, d)^{121}Sn 13 MeV, ang. distrib transferred orbital momentum derived 2−76798
    Zn(t,p), energy level studies 2−56001
  X-rays *see Nuclear reactions and scattering due to/photons*
Nuclear reactors, fission
  accident, field radiological monitoring system, optimum design principles 2−76957
  aseismic design of composite structures, earthquake response analysis and damping 2−59823
  aseismic design of reactor building, stress analysis and stiffness evaluation 2−59824
  ATR, effective booster rod 2−49881
  automation of power plant, discrete drive control systems 2−76910
  Beloyarsk power plant, strength investigation of fuel-channel structural elements 2−76909
  biological and occupational hygiene aspects 2−67345
  boiling light water reactors, pressure control system design, testing, computer simulation 2−46380
  Boreal array for determ. of B content in B-Al alloy samples 2−63976
  breeder, future energy solution 2−49876
  burn-out detectors by differential circuit method 2−63975
  BWR, development in Germany, review 2−63949
  BWR, prompt/delayed neutronic response ratio meas. of self-powered vanadium detector 2−83111
  CANDU, power, likely development to 2000 A.D. 2−42614
  candu system, Pickering reactor's success 2−83153
  channels and heat exchangers, stochastic identification and modelling of heat transfer 2−42647
  closed cycle water, waste disposal systems 2−56075
  codes of practice, asset or liability 2−56891
  compilation and evaluation of neutron data, international organisation 2−76138
  component design in HTR reactors using He coolant, conference, London (1972) 2−42617
  component design using creep data acquisition system 2−83120
  component testing for high quality production 2−76927
  computer program control system, CARONTE modular system, status, applications future developments 2−83071
  containment vessel, soil-structure interaction 2−61873
  control system, effect of noise currents on measuring circuits 2−42636
  control system design and modelling 2−59813
  cooling by He and CO_2, comparison 2−56032
  cooling of active zone, temp. distribution obs. 2−42637
  core heterogeneity, effect on transient pressure behaviour in high-energy excursion, simulation expt. 2−42640
  core measurement, calculational model for self-powered neutron detector 2−56071
  correlation methods for flow speed meas. 2−77230
  coupled cores, heavy-water-moderated, static obs. of critical heights, flux distrib. and neutron spectrum 2−42628
  creep machine for high flux applics. 2−46391
  critical assemblies and methods for bucklings and spectral indices meas. 2−76923
  critical facility of pulsed fast reactor 2−42631
  cross flow resist. in rod bundle cores 2−83133
  cylindrical concrete pressure vessel, prestressing by wedge winding method 2−76933
  delayed neutrons, review of present status 2−83047
  direct conversion of charged-particle energy from plugs using skew diaphragm system 2−70510
  dynamics and stability, influence of fluctuating fluid flow and heat transfer processes 2−42646
  dynamics of nuclear reactors, book 2−42612
  effective delayed neutron fractions for two fast crit. assemblies 2−83105
  environmental considerations of nuclear power 2−46367
  environmental radiation due to nucl. power prod., population dose 2−70548
  fast, kinetic parameters 2−76928
  fast, neutron spectrometry, neutron balance, proton recoil, time-of-flight 2−76733
  fast breeder, Na bond disruption by gas bubbles 2−49888
  fast breeder, operational, continuous reactivity monitoring, receiver 2−46393
  fast breeder reactor, French, commercial plant design 2−83139
  fast breeder reactors, commercial development 2−83141
  fast breeders, development trends in Europe 2−59819
  fast reactor analysis, shielding factor method of generating multigroup cross sections 2−49875
  fast reactor fuels burn-up determ. by Mo complex equilibria 2−79837
  FBIR, neutronic meas. 2−42634
  FFTF assembly, design and operation 2−63966
  FFTF instrumentation design and control system 2−63968
  flux distributions in flux trap type core, enriched U-light water assembly 2−74141
  frequency response deduced by pulsed neutron technique 2−46374

Nuclear reactors, fission continued
  frequency response meas., optimum binary signals 2−83108
  FRG, research react., void coeff., of reactivity expt. 2−49878
  fuel cladding using zircaloy 2−49893
  fuel element circulating system, temp. distribution along tube containing flowing fluid 2−52840
  fuel element heating channel, meas. of local void fraction at high pressure 2−49907
  fuel rod assembly, utilizing helical wire wrap spacer, forced flow interchannel mixing model 2−76931
  fuel rod assembly, utilizing helical wire wrap spacer, turbulent flow pressure drop model 2−76930
  gamma-heat in core, on-power meas. calorimetry 2−83079
  gas breeder, pin and coated particle fuel, safety studies, integrity of primary circuit, emergency coolant flow 2−83091
  gas release loop, improvements (1965 to 1970) 2−83087
  GCFR, review of several design and assessment studies, summary of performances 2−83090
  Germany, technical development 2−59820
  heat transfer and pressure drop performance of roughened surfaces 2−59872
  heavy water reactor systems, inverse kinetics analysis of power time trace data 2−42635
  high temperature gas-cooled reactors, effects of transverse flow through graphite on fission product movement 2−42642
  high thermal flux reactor, Institut Laue-Langevin 2−46368
  housing, concrete slab shear slip 2−59822
  HTGR, industrial development, reactor physics expts. benefits 2−83068
  HTR, conservation of He gas, safety, economic and resource utilization criteria, design considerations 2−42621
  HTR, fault conditions, available safeguards 2−42622
  HTR, He cooled, boiler plant, main design features 2−42687
  HTR, He cooled, circulator design 2−42689
  HTR, He cooled, components of THTR 300 heat transfer system 2−42688
  HTR, He cooled, core design, review 2−42623
  HTR, He cooled, thermal barrier systems design, waffle plate concept 2−42620
  HTR, He gas circulation experimental loops, maintenance of controlled atmospheres 2−42618
  HTR, on-load refuelling plant, design, development 2−42625
  HTR core design, graphite stack structure, assembling problems 2−42624
  in core thermionic reactors, applications to space and underwater technologies 2−49269
  in-pile calorimetry in Hungary, status report 2−63977
  ionisation chamber for controlling irradiation times in reactor pneumatic transport system 2−74189
  ionization chamber for γ-ray energy deposition meas. in nuclear reactors 2−42699
  kinetic parameters, amplitude calc. in Rossi α experiment 2−46392
  lasers, super power, appl. 2−56037
  lattice substitution, oscillation experiments with thermal and fast neutrons 2−76924
  liquid metal heat pipes, vapour transport limits 2−83128
  LMFBR, advantages of primary system flow control during reactor scram 2−56039
  low power, for on-line meas. of burn-up of irrad. fuel 2−42630
  marine PWR control and in-core instrumentation system design 2−79637
  mass transfer in small diameter packed beds 2−42656
  materials testing, furnace for use up to 2000°C 2−49905
  measuring equipment, French development 2−74186
  MHD electric power system, space applications 2−59050
  miniature goniometer for in-pile expts. 2−42682
  mirror reactors, electron heating effect on power balance 2−52839
  molten salt, containment and disposal of T produced 2−46378
  Monte Carlo reliability calculation, critical time step approach 2−56038
  N-zone absorbing rod, length of extrapolation 2−46389
  neutron and γ radiation shielding by two types of concrete 2−79846
  neutron balance, null reactivity method for fast multiplying media and HTR lattices 2−76902
  neutron beam intensity obs. 2−70541
  neutron converter and blanket simulation facility 2−79841
  neutron density modulation, comparison of modulated source and modulated poison methods 2−49862
  neutron flux and energy spectra obs., dosimeter prep. 2−74187
  neutron flux meas. techniques, review 2−82791
  neutron flux obs., dosimeter preparation 2−49909
  neutron measurements, oscillations in critical assemblies, small amounts of materials in thermal or fast reactors 2−76903
  neutron physics, assessment and conclusions 2−76926
  neutron selector phase stabilizer 2−70280
  neutron source for variable energy cyclotron, for simulation of fast reactor spectra 2−67110
  neutron streams obs. in exptal. channels 2−42677
  noise analysis techniques applics. to problems 2−42684
  noise level meas. in controllers, by ioniz. fission chambers, characts. 2−42678
  noise monitoring for malfunctions 2−46394
  nuclear irradiation studies, report 2−63954
  nuclear measurement techniques for lay-out and monitoring of reactor experiments 2−59870
  parameters, from neutron and gamma-ray noise meas. 2−49908
  peaceful uses of atomic energy, conference, Geneva (1972) 2−56033
  pebble bed type, shell thermal stress distrib. in loose-kernel spherical fuel element 2−49890
  piping systems design, safety, dynamic response to multi-inputs 2−70540
  planning of nuclear industry 2−56034
  power, health physics measures relating to radiation exposure of general public 2−55243
  power, hub/tip ratio rel. to cost 2−49871
  power and research reactors, release of ^{3}H to environment during operation 2−52890
  power plants, internal contamination risk, influence on monitoring programmes 2−58628
  power reactors, direct conversion methods, book 2−83145

Nuclear reactors, fission continued
power reactors, fault tree analysis 2—46372
power stations, environmental ^{14}C contamination 2—54871
power stations, radiological safety for general public, health physics aspects 2—55226
pressure vessels, approx. struct. analysis for non-homogeneous linear visco-elastic material 2—76333
prestressed concrete vessel, ultimate load anal. 2—70520
pulsed fast, physics design aspects 2—42619
pulsed fast reactor, Brookhaven, critical expts. 2—83110
pulsed reactors in Japan, present status and future plans 2—83088
PWR, ^{135}Xe and ^{149}Sm poisoning computation algorithm 2—63957
PWR, development in Germany, review 2—63948
radiation protection, ecology 2—49910
reactivity, time-variant, on-line determination using process computer 2—52886
reactivity and reactor stability, effects of voids 2—70511
reactivity meas. accuracy in dynamic expts. 2—70518
release of radioactive material to environment 2—70515
releases of radioactivity and heat from reactors in Canada, environmental effects 2—62292
safety, u.s. inspection equipment 2—59871
with slab geometry, space perturbation, error estimate by functional anal. technique 2—42613
SNR fast breeder, Na cooled, safety problems 2—59837
SNR project, Germany, present status 2—83140
SNR-300 fast breeder, safety systems 2—59836
SNR-300 prototype fast breeder reactor, Na cooled 2—59830
sodium cooled SNR300, aerosol behaviour under hypothetical accident 2—49877
solid electrolytes, applications to measure solubility and diffusion in nuclear materials 2—49904
space research, in France 2—68993
space time kinetics, computer code KSPACE 2—76934
spatially dependent, optimal control problem 2—63960
spherical fuel elements for HTR, pneumatic transport 2—49874
stability domain, analytic determ. of boundary 2—79836
sub-critical assemblies, kinetic parameters determ. 2—70517
subassembly ducts, prismatic shells with hexagonal cross section, vibration analysis 2—76932
subchannel flow and enthalpy distribution, at exit of typical fuel core geometry 2—76929
subcriticality degree from second moment of detector count rate 2—42633
thermal insulation at high temp. and pressure 2—63950
thermal neutron critical assemblies, equivalent sample method for analysis of oscillation of fissile materials 2—56070
thermal neutron distributions meas. as surfaces of cylinders 2—56018
thermoluminescence dosimetry 2—42696
thermonuclear, controlled, heat transfer obs. 2—42645
time series analysis applications, developments 2—42598
TRIGA research reactor, Heidelberg, neutron flux density measurements 2—67346
UTR-10 at Iowa State Univ., determ. of space-dependent frequency response by pulsed neutron technique 2—46374
vibration meas. in PWR-instrumentation 2—74142
water cooled and gas cooled, relative merits with view to future use in UK 2—59828
water-cooled, flow parameter meas. 2—42681
West Germany, review 2—59821
Gd application as burnable poison for light water reactors 2—59844
H$_2$O-moderated H$_2$O-cooled power reactor, differential fast neutron spectra 2—63940
^{131}I monitor for nuclear plants 2—67364
Na cooled fast breeder reactor, heat transfer problems 2—52843
Pt-Mo, thermocouple, e.m.f. rel. to neutron irrad. 2—78940
U, enrichment status in Europe 2—56016
UO$_2$ fuelled, characteristics, obs. 2—70519
^{235}U/^{238}U fission rate ratios, determ. in CONSORT reactor 2—83094

materials
absorber materials performance in HFIR control cylinders 2—83129
alloy, high temp., long cylindrical shell, creep collapse under external pressure at elevated temp. 2—76329
analysis of irradiated reactor fuels, isotopic dilution, α and γ spectrometry, properties of operating reactors 2—76925
analytical methods in nuclear fuel cycle, review 2—74161
anodic disgregation of HTGR spent fuel, electrolytical cell performance 2—83070
austenitic stainless steel, effect of neutron irradiation on tensile and creep-rupture ductility 2—77719
austenitic-steel, neutron-induced mechanical property changes, damage function analysis 2—77718
automatic control using spectrometer 2—49872
Beloyarsk power plant, strength investigation of fuel-channel structural elements 2—76909
bismuth oxide ceramics 2—83064
boronated graphite, irradiation-induced dimensional change 2—76949
Bugey fuel element sheathing, in-reactor behaviour 2—59865
burnt-up fuels, occurrence of high neutron dose rates 2—76915
burnup estimation, method using mass spectrometric data 2—42652
CANDU fuel 2—83152
ceramic, binderless granulation mechanism and sphere growth 2—47660
ceramic application of linear analysis to study of porosity using Cahn-Fullman relation 2—74147
ceramic fuel material in fast reactor environment 2—56058
ceramic fuels, radiation induced creep, effect on performance 2—46387
Charpy specimens, precracked, dynamic fracture toughness from impact hammer tests 2—71609
clad fissionable foil manufacture for ZPR obs. 2—74148
cladding and fuels, in-reactor creep obs. and effects 2—70538
cladding and struct. materials, irrad. induced void form. 2—49901
cladding and struct. materials, post-irrad. exam. by electron microscopy 2—42669
cladding from irrad. fuel pins, burst testing 2—43776
cluster-type fuel elements, rupture under low applied deform. 2—59867

Nuclear reactors, fission continued
materials continued
coated fuel particles, fission products distrib. determ. by ion sputtering 2—46390
coated irrad. kernels, fission gas release determ. method 2—42665
coated particle fuels, design for high-temp. gas-cooled reactor 2—52863
coated particle fuels, irrad., migration in temp. gradient 2—52866
components, non-destructive testing and quality control 2—84065
control during operation by solid-state chemical reactions 2—49880
coolant, modelling criteria for two-phase pressure drop 2—83150
coolant circuits, hydrodynamics, neutron fluctuations 2—76936
core cladding using Zr alloy, rel. to corrosion and hydrogen pick up dependent on coolant 2—49892
core components, radiation induced creep and swelling 2—74757
creep behavior, application to elevated temperature design criteria 2—83119
cylindrical oxide fuel elements, thermal radiation and mechanical analysis for unsteady state fuel restructuring in fast reactors 2—49887
defective fuel elements. behaviour 2—49897
dielectrics, inorganic, for reactor use, radiation induced changes 2—52851
effective cross sections ratios determ. from burnup data for Yankee Rowe 2—83126
fast breeder fuel, swelling, fission gas release and creep considerations 2—63972
fast reactor, sub-assemblies, voidage-induced bowing 2—59831
fast reactor control rods, performance modelling 2—76950
fast reactor safety and influence of PuO$_2$ particle size of mixed oxide fuels 2—76937
fission-gas behaviour under irradiation at high temperature 2—79835
fuel, 90% dense, fabrication for irrad. testing 2—53924
fuel, coated particle and ceramic filling and fission gas meas. techniques 2—42668
fuel, effects of fission spikes 2—56042
fuel, FISP computer programme for generating fission product inventories 2—76955
fuel, from M.A.N. centrifuges 2—59850
fuel, irrad., electron probe analysis 2—44510
fuel, irrad., neutron radiography obs. 2—52856
fuel, irrad. ceramic oxide, microstruct. charact. 2—59869
fuel, modelling behaviour during fast reactor accidents 2—52860
fuel, oxide, redistrib. during irrad. 2—52852
fuel, post-irrad. exam. using high resolution gamma spectrometry 2—42670
fuel, post-irrad. mech. tests 2—43775
fuel, post-shutdown heat release, analysis of decay contribution 2—79831
fuel, simulation of fission damage 2—42676
fuel, transport, procedures for accidents 2—73175
fuel and cladding interaction 2—49894
fuel and core component handling 2—63967
fuel and structural materials, IV international conference on nuclear energy, Geneva 1971 2—76908
fuel assemblies for gas cooled fast reactors 2—63963
fuel burn-up, on-line meas., low power reactor design 2—42630
fuel burn-up determ. by gamma and mass spectrometric methods 2—75408
fuel burn-up measurement methods, review 2—74188
fuel burnup prediction, spectrum-averaged cross sections, applic. to methods verification 2—59860
fuel claddings for LMFBRs, minimizing swelling and embrittlement 2—70537
fuel cycle, reference materials for accurate determ. of U, Pu and Th 2—74160
fuel cycle and relationship to production of raw material 2—56055
fuel element, electronic processing system for data from post-irradiation examination 2—52885
fuel element development for in-core thermionic reactor for space applications 2—49263
fuel element fabrication, Netherlands activities 2—70531
fuel element for mark III gas cooled reactor, manufacturing route 2—56066
fuel element of PHENIX reactor 2—56059
fuel element sheathing problems 2—59866
fuel element technology 2—56069
fuel elements, automatic handling and meas. 2—42658
fuel elements, electron microscope specimen prep. 2—42685
fuel elements, irrad., electron probe microanalysis 2—44511
fuel elements, irrad., radiograph prod. and automatic meas. 2—42659
fuel elements, nondestructive, techniques for neutron absorpt. and fission rates meas. 2—56040
fuel elements, post-irrad. radiographical exam. techniques 2—42660
fuel elements apparatus for studying radial migration of radioactive products 2—52847
fuel elements for high temp. gas cooled reactors 2—52872
fuel elements for high temp. reactors, production and irradiation testing 2—56064
fuel elements of MTR, determ. of burn-up dependent micro flux-density distrib. by transport calcs. 2—76914
fuel irradiated, non-destructive inspection using neutron radiography 2—49884
fuel materials, statistically designed program for sampling and chemical analysis 2—74156
fuel particle coatings, tensile strength meas. method 2—50790
fuel particles, coated, free volumes and gas content determ. 2—42664
fuel particles, irrad., rupture stress, meas. device 2—43772
fuel performance models, review 2—52857
fuel pin burst properties, evaluation of effect of intergranular attack 2—76942
fuel pins, associated pressure equalization in water-cooled system 2—42654
fuel pins, intergranular cladding attack 2—52865
fuel pins, irrad., automated meas. of induced strain 2—42657
fuel pins, irrad., eddy current testing 2—42661
fuel pins, irrad., fission gas release meas. 2—42667
fuel pins, irrad., microsegregation of Cs, obs. technique 2—43774
fuel pins, irrad., tritium meas. technique 2—42663
fuel pins for Mk III gas cooled system 2—56063

Nuclear reactors, fission continued
materials continued
fuel preparation 2−56068
fuel rod, with time varying heat transfer coeff., calc. of temp. transients 2−42615
fuel rod behaviour analysis using CYGRO-F computer code 2−76946
fuel rod bundle cores, subchannel thermal analysis 2−52878
fuel rod bundles, single and two phase pressure drops at 70 atm. 2−56054
fuel rod cladding, sintered Mg composites, anisotropy of properties of extruded and recrystallized products 2−46385
fuel rod cluster and coolant channel performance, heat transfer and fluid dynamics 2−42644
fuel rods, irrad., neutron radiography investigation 2−83098
fuel rods in parallel flow, computer program for determ. characteristics 2−63973
fuel supply and demand and fuel cycle services in W. Germany 2−56035
fuel technology, fabrication of oxides, swelling and compatibility of carbides, cladding 2−56060
fuel-clad interactions, diffusion expression 2−83146
fuels, advanced, anal. of U, Pu, C, O_2 and S for quality control and characterization 2−74176
fuels, non destructive analysis techniques 2−74174
fuels, total fissile content and isotopic anal. using γ-ray spectrometry 2−74175
fuels for HIGCR, chemical analysis techniques for control and evaluation 2−74168
gas bubbles in UO_2, comput. simulation of precipitation kinetics 2−64424
gas cooled, fuel management methods 2−42653
gas-cooled, fuelling grabheads 2−59848
Gilsocarbon, characts. rel. to high temp. reactor design 2−52871
graphite, artificial, neutron irrad. effects on thermal conductivity 2−54073
graphite, creep under neutron irrad. in Dragon reactor, high temp. 2−56802
graphite, high fluence neutron irrad. behaviour, two-phase model 2−56048
graphite, interlayer props., effect of interstitial atoms, simple model 2−56605
graphite, microscopy at high resolution, sample prep., technique improvement 2−53637
graphite, nat. graphite filler, neutron irrad. behaviour rel. to comp. 2−56049
graphite, neutron irrad., low temp. sp. ht. obs. rel. to heat treatment 2−54045
graphite, neutron irrad., sp. ht., 0.6-5 K 2−57062
graphite, neutron irrad., thermal cond., 50-1000°C 2−54075
graphite, neutron irrad. at 715°C, dimens. stability 2−56047
graphite, neutron irrad. at high-temp., mech. interactions among crystallites 2−56679
graphite, neutron irrad. damage, dose rate effects 2−53708
graphite, neutron irrad. defect struct., single cryst. 2−53709
graphite, oxidation in a reactor due to irradiation obs. 2−52850
graphite, POCO grade HPD-1, high temperature creep, comparison with polycrystalline graphite 2−77625
graphite, pyrolytic, highly oriented, high dose fast irrad. 2−57072
graphite, strength distrib. functions, effect of high temp. fast neutron irrad. 2−53822
graphite, thermal cond. at high temps., modulated electron beam technique 2−84210
graphite, thermal diffusivity, 650-2700K 2−54082
graphite, UO_2-dispersed, fission gas release, obs. 100-950°C, release mechanisms discussed 2−70534
graphite, X-irrad., dynamical mech. props. 2−53777
graphite core, calc. of thermal resistance between hexagonally arrayed channels 2−42651
graphite core element for NUGG reactor 2−56067
graphite fibre, reinforcement for composites for struct. applic. 2−56992
graphite moderator problems, conference, London (1972) 2−56052
graphite-Bi mixture obs. on neutron diffusion lengths 2−49861
graphite/CO_2 radiolytic reaction, effect of CO, 225-375°C 2−57434
graphites, isotropic and 'PCO' reactivity to oxygen 2−59843
graphites, reaction with hydrogen 2−59842
graphites from coke mixtures, props. and irrad. effects 2−59841
heat flux distribution and temp., computer program THISTLE 2−83149
heterogeneous lattices, intermediation resonance treatment by modified μ-method 2−79821
high temperature reactor fuel cycle, burn-up determ. 2−74184
HTGR fuel block graphite, struct. props. and mech. strength due to irradiation 2−56045
HTR, He quality control, gas circuit purification 2−42675
HTR, high temperature behaviour of steels, alloys in He and its impurities 2−42673
HTR, spherical fuel elements, reprocessing by continuous combustion method 2−49885
HTR fuel elements, visualization of heavy metals in, radiographic technique 2−67360
hydrogenous liquids for reacor moderation, slow neutron scatt. cross-section 2−70535
hydrostatic stress effects on void growth during irradiation, appl. to reactor core 2−76940
in-pile irrad. testing apparatus for internal friction and modulus of shear 2−84062
irradiated nuclear fuel, analysis for actinides and burn-up determ. 2−74183
irradiated nuclear fuels, determ. of fission products by isotopic dilution 2−75400
lattices intermediate resonance calcs. for resonance absorber in absorber-moderator mixture, improved practical width 2−79820
liquid coolant, explosive boiling studies for accident prevention 2−42686
loose-kernel spherical fuel element for pebble bed reactor, shell thermal stress distrib. 2−49890
magnox fuel element components prep. for quantitative metallography 2−43773

Nuclear reactors, fission continued
materials continued
Mark II gas cooled, fuel cycle performance 2−46381
mark III He cooled HTR, effects of coolant impurities 2−42672
metal, burning curve ignition, theory 2−46383
metal, He migration and release after implantation 2−50639
metal, neutron irrad., void form. 2−50641
metal, radiation- induced void form. 2−50638
metal, radiation-induced voids, conf., Albany, USA [June 1971] 2−50637
metal, void and point defect agglomerate studies using h.v. electron microscopy 2−53695
metal swelling implications in fast reactor design 2−49900
metallic cladding and structural materials, radiation induced creep, effect on performance 2−46387
metallic core materials characteriz. 2−59862
metals, voids as result of irradiation, review 2−50635
metals and alloys, irradiation induced volumetric swelling caused by void formation 2−74758
metals under fast-neutron irradiation interrelation between swelling and irradiation creep 2−76941
mixed oxide nuclear fuels, burn-up and isotopic distribution meas. 2−75401
mixed-oxide fuel elements, performance in 11 at.% burnup 2−76943
mixed-oxide fuel pins, F3A series unencapsulated, examination following irradiation in EBR-II 2−76947
moderator model, small group neutron, for H_2O-Al core calcs. 2−42609
neutron absorber rods, modelling of swelling and gas release 2−52861
neutron diffusion in cavity containing media, cooling coeff. and transport correction derived 2−52836
non-destructive burn-up determ. for spent fuel elements using heat output 2−74181
non-destructive burn-up determ. for spent fuel elements using heat output 2−74181
nondestructive assay using delayed fission neutron spectrometry 2−67361
nondestructive determination of fuel burn-up by high resolution gamma-ray spectroscopy 2−42441
nuclear fuel cycle, analytical methods, symposium (Vienna, Nov.-Dec. 1971) 2−74151
nuclear fuels containing Th, separation of U as UF_6 from mixtures of U/Th chlorides by hydrofluorination 2−49886
oxide fuel pin behaviour, COMETHE code 2−52859
oxide fuel struct. evolution, modelling using BEHAVE-2 code 2−52858
oxide fuels, irrad., oxygen distrib. 2−52869
pellet and vipac fuels comparison 2−49895
plutonigen fuel, contribution of ^{235}U and ^{239}Pu to burn-up 2−74149
polyphenylene oxide, irradiation resist. 2−79839
post-irradiation analysis of nuclear fuels for burn-up and heavy isotope content 2−75402
post-irradiation exam. of highly radioactive samples, density change meas. 2−42662
preservice and inservice inspections, design and metallurgical problems 2−52887
pressure vessel steels, time-depend. embrittlement phenomena 2−59849
prestressed concrete press. vessels, prospects for LWRS 2−83143
purification of concentrates 2−83074
pyrocarbon coated reactor fuels, anisotropy determination using scanning electron microscope 2−74145
pyrocarbon coating, neutron irrad. effects on mech. props. 2−56771
pyrocarbons, lattice thermal expansion perpendic. to layer planes, depend. on struct. props. 2−68252
pyrofoil tape, production and characterisation for reactor use 2−56050
radiation damage, including swelling, in fissile materials, book 2−70539
radiation damage data correl. using activation fluences and irrad. temp. 2−83131
radiation induced brittle fracture in structural materials 2−68099
radiation induced embrittlement by neutron reaction-produced He in structural mats. at high temps. 2−68100
radiation-induced void growth, applied stress effects 2−53704
reinforced concrete vessels present status and future trends 2−46388
release of gaseous fission products from high temperature fuel materials 2−52884
resin derived fuel, recent developments and irradiation obs. 2−56044
resonance energy neutrons, space-energy distribution calculation 2−79827
rod bundle type fuel elements design 2−49896
rod bundle-geometries with streamline coolant flow, variation of heat transfer 2−74146
rod fuel element, effect of surface roughness on heat transfer 2−76911
SCOT development of rig for out- of-pile testing of reactor fuel elements 2−59847
stainless steel, 20% cold-worked Type 316, fatigue- crack growth at elevated temps. 2−84141
stainless steel, annealed type 316, effect of fast reactor radiation on creep behaviour 2−83123
stainless steel, types 304, 316 estimates of creep-fatigue interaction in irradiated and unirradiated samples 2−83121
stainless steel cladding for fast reactor fuel elements, review of properties 2−59846
stainless steel type 304, effect of irradiation on strain rate dependence of mechanical properties 2−83122
steel, austenitic, stainless, grain boundary penetration by Cs-O solutions and caesium oxide, out-of-reactor study 2−67356
steel, austenitic stainless 2−81505
steel, ferritic, irrad. embrittlement 2−43854
steel, low-C and low-alloy, neutron irrad., radiation- and anneal-hardening 2−80681
steel, sintered, for fuel element jackets, processing and mech. characterization 2−76951
steel, stainless, ^{3}H diffusion, 25-222°C 2−47458
steel, stainless, deuteron generated void form., in-reactor damage simulation 2−53714

Nuclear reactors, fission continued
materials continued
steel, stainless, He prod. rel. to LMFBR development 2−49902
steel, stainless, irrad., cold work effects on void form. 2−50646
steel, stainless, irrad., fluence and temp. depend. of void form. 2−50647
steel, stainless, neutron induced swelling 2−63969
steel, stainless, proton irrad., swelling, displacement damage depend. 2−53716
steel, stainless, proton- and nickel-irrad., void form. 2−53715
steel, stainless, solution treated type 304, empirical representation of irradiation-induced swelling 2−43609
steel, stainless, suppression of void form. 2−50648
steel, stainless, void nucleation and growth during fast neutron irrad. 2−50645
steel, stainless tube, fast neutron irrad. effect 2−83085
steel, swelling induced deform. problems 2−59863
steel, swelling induced problems, metallurgical parameters 2−59864
steel, type 304 stainless, prediction of in-pile behaviour using SCIM, theory based computer code 2−76939
steel for fuel cladding and core structural components, nucleation of voids 2−71466
steel tube, stainless, type 304L, in-reactor creep 2−46382
steel/$UO_{2\pm x}$-$PuO_{2\pm x}$ cladding/fuel interface, reaction 2−52875
steels, austenitic, fatigue crack growth at high temperatures for types 304, 316, 321 and 348 2−56864
structural material of fast reactors, Doppler effect analysis 2−83104
structural materials aspects of LMFBR core restraint system design 2−83124
swelling data analysis using displacement rates from Lindhard model 2−52880
swelling in fast-neutron-irrad. materials, theory 2−53702
swelling under neutron irrad., electron microscope obs. 2−59868
thermal conductivity, measurement methods 2−49903
thermal pulsed-neutron experiments on graphite system 2−74131
thermionic reactors, alumina insulators, neutron damage reduction using hydrogenous moderators 2−63228
thermionic reactors, b.c.c. refractory metals, effects of fast neutron irradiation 2−63229
transition metal borides, neutron irradiation swelling 2−77790
tubular manufacture stiffened by convolutions, stress analysis 2−83066
two-phase fuel element, randomly dispersed discontinuous phase, temp. distrib. 2−49889
void formation, simulation expts. in fast reactor materials 2−59861
void formation studies, use of simulation with accelerators 2−76922
void swelling, semi-automatic length measurement 2−83092
water corrosion in nuclear installations 2−59845
zircaloy, in water cooled reactors, hydriding rel. to surface conditions 2−81502
Zircaloy cladding-fuel reaction 2−59853
Zircaloy tubing, mech. props., effect of oxygen and fabrication variables 2−53915
zircaloy-2, -4, tensile props. rel. to neutron irrad. 2−80664
Zircaloy-2, containing ZrH_x, fatigue, metallographic obs. 2−47649
Zircaloy-2, corrosion in steam-water mixture under neutron irrad. 2−51456
Zircaloy-2, dispersion strengthening with yttria 2−53917
Zircaloy-2, irrad. and temp. effect on tensile and creep props. 2−43802
Zircaloy-2, stress orientation and circumferential ductility, thermal cycling effect 2−53914
Zircaloy-4, deform. and fracture 2−50747
Zircaloy-4, neutron irrad., deform. parameters, 300°C 2−50749
Zircaloy-4 tubing, yield loci, effect of texture variations 2−50850
zonal configuration of fuel in fast reactors 2−76952
Al_2O_3 insulators for thermionic reactors, dielectric breakdown, 300 to 1200°K, mechanisms 2−65056
^{241}Am, irradiated, separation of ^{238}Pu and ^{242}Cm by solvent extraction using bis-(2-ethylhexyl) phosphoric acid 2−83086
B-Al alloys, determ. of B content, Boreal array 2−63976
B-stainless steel control rods, effect of B concentration gradient on thermal reactor performance 2−76948
B epoxy composites, irrad. in nuclear reactor, strength 2−80801
B_4C, neutron irrad. damage, electron microscope obs. 2−47369
B_4C, neutron radiation induced defects, transmission e. microscope obs. 2−67355
B_4C, thermal reactor irradiated, empirical He release 2−76954
B_4C irradiation in fast neutron spectra, meas. of pellet density, swelling, gas release, thermal conductivity 2−83116
B_4C neutron absorber in fast and thermal reactors, swelling gas release and structural integrity 2−83115
BeO, physical properties and electrical conductivity after neutron irradiation 2−52881
BeO insulators for thermionic reactors, dielectric breakdown, 300 to 1200°K, mechanisms 2−65056
C-Fe film, on heat-transfer surface, thickness, electron probe anal. determ. 2−44509
C, microscopy at high resolution, sample prep., technique improvement 2−53637
C, neutron irrad. at high-temp., mech. interactions among crystallites 2−56679
C, nuclear applications, Royal Aircraft Establishment review 2−43903
C, poorly crystalline isotropic, dimensional changes induced by neutron irradiation 2−76916
C, poorly crystn. isotropic, fast neutron irrad. induced dimens. changes 2−56767
C, pyrolytic, γ-irrad. stress-graphitized, dynamic mech. props. 2−53775
C and C-Si alloys, dimensional changes and creep during neutron irradiation 2−76917
C fibre, reinforcement for composites for struct. application 2−56992
C fibres, heat treated Rigilor AC, neutron irrad. behaviour 2−56998
C film, on heat-transfer surface, thickness, electron probe anal. determ. 2−44509
C products, graphitization effects on neutron irrad. induced dimensional changes 2−56996

Nuclear reactors, fission continued
materials continued
C pyrolytic, impregnation with graphite, neutron irrad. stability 2−56997
Cd-Mg poison rod, burn-up, expt. and theory 2−49879
Cu, neutron thermal effective cross-section meas. 2−59808
D_2O and CM-2 reactors, time-of-flight spectrum of neutrons 2−63939
Fe, yield stress damage function for neutron irradiation, determ. using SAND II code for data analysis 2−79840
αFe neutron irrad., radiation- and anneal-hardening 2−80681
Mg-Be fuel jacket, distrib. of U, track recording technique 2−42679
Mg-Zr alloy, Ni diffusion and precip. formation 2−47467
Mg, neutron irrad., distortion and swelling, effects of alloying additions 2−60778
Mg alloy cladding for fuel elements, composition, fabrication, properties, structure, development and use 2−83089
Mg composites, fuel cladding, corrosion in CO_2 2−57424
Mo-UO_2, W clad cermet fuel, behaviour under neutron irradiation 2−52882
Mo base alloys, properties under He high temperature conditions 2−42674
Na-Ar liquid gas system, influence of gas on nucleation in sinusoidal pressure field 2−46893
Na, flowing, nonisothermal, ^{60}Co transport processes, corrosion and deposition rates 2−67344
Na, liq., solubility of inert gases, 600 degrees C 2−56041
Na bond disruption by gas bubbles 2−49888
Na coolant corrosion and mass transfer analysis using ion probe mass spectrometer 2−83118
Na corrosion deposits, structure and effect on heat transfer coeffs. 2−83117
Nb, Nb alloys, evaluation for nuclear power systems 2−76938
Ni-Fe-Cr based alloy, γ'-hardened, electron irrad., void swelling 2−80684
Ni alloys, neutron irrad., void form. and swelling resist. 2−53721
Ni and alloys, neutron induced swelling 2−63969
Np concentration determ. in irradiated fuel reprocessing solutions 2−74180
^{239}Np fuel, contribution to post-shutdown heat release 2−79831
Pb/NaCl-UCl_3 molten metal/fused salt system, surface and interfacial energy 2−52874
Pb-Si alloys, cooling agent, neutron scale law determ. 2−80931
Pu/U oxide fabrication process, sampling and analysis 2−74157
Pu/U oxide fuels, gravimetric methods of studying O/metal ratio 2−74152
Pu/U oxides reactor fuel, comparison of two methods of determ. of O/metal ratios 2−74153
Pu/U oxides reactor fuel, determ. of Pu content by calorimetry 2−74164
Pu/U oxides reactor fuel, measurement O/heavy metal atom ratio 2−74154
Pu, expt. confirmation of burning curve ignition theory 2−46383
Pu, titration errors in chemical analysis 2−74166
δ-Pu, Young's modulus, elastic limit, dislocation interstitial interaction, meas. apparatus, 4-300 K 2−80739
Pu fuel development for fast and thermal reactors 2−56057
Pu fuel development lab. in Japan 2−70533
Pu fuel production plant and breeder projects 2−63962
Pu fuels, irradiated, determ. of Pu, Am, Cm and Pu valency in reprocessing 2−74178
Pu metal, reference specimens for determ. amount of Pu and impurities in reactor fuels 2−75399
Pu recycle prospects for LWR's 2−83138
Pu recycling in thermal reactors 2−56046
$Pu(NO_3)_4$:Gd, Gd effect on criticality 2−56051
PuO_2-UO_2 fuel rods, foil handling technique for meas. of lattice parameters 2−70532
PuO_2-UO_2 in FFTF driver assembly 2−63965
PuO_2-polystyrene homogeneous fuel, 50 H/Pu, critical experiments 2−56053
PuO_2, reference specimens for determ. of impurities in reactor fuels 2−74158
PuO_2, thermal cond., self-irrad. effects 2−54078
PuO_2 chlorination in melts of alkali metal chlorides, valent states 2−68776
PuO_2 enriched fuel rod lattices in light water, exptl. characteriz. 2−59858
PuO_2 enriched fuel rod lattices in light water, Pu-fueled system analysis 2−59859
PuO_2 enriched fuel rods, kinetic parameters in light water lattice 2−59851
PuO_2 fuel neutron radiation characts. 2−83130
PuO_2 fuels in HTGRs, space-energy-depend. problems 2−83127
PuO_2 nuclear reactor fuel, analysis of Pu content and impurities 2−74163
$Pu_xU_{1-x}O_2$, thermal cond., 673-1273K 2−54079
^{238}Pu, economic aspects and production 2−49899
$^{238}PuO_2$ fuel fabrication by hot pressing 2−53932
^{239}Pu contribution to total fission activity, non-destructive absolute determination 2−42594
^{239}Pu reactor fuel, detection and analysis of actinide contaminants 2−74179
^{240}Pu neutron cross section data eval. 2−82986
Ta, neutron thermal effective cross-section meas. 2−59808
Th/U fuel elements with known irradiation data, actinide composition studies 2−75403
Th cycle utilization in HTGR 2−56065
ThO_2, thermal diffusivity, 900-2550°C 2−54081
ThO_2 as heat source in thermionic conversion rel. to ^{228}Th radioactive decay simulations 2−52787
$Th_{1-x}U_xO_2$, thermal diffusivity, 650-2700K 2−54082
TiC, changes in microhardness, lattice parameters, electrical resistance following neutron irradiation 2−52848
Tl metal, as LWR fuel 2−42650
U/Pu oxide fuel, reference material for chemical specification analysis 2−74159
U-9.5 wt %Nb alloy, gamma phase decomp., discontinuous precip., 450-600°C 2−80802

Nuclear reactors, fission continued
materials continued
U-Mo alloy, stress corrosion cracking in humid air, C content effects 2-53839
U-Nb and U-Nb-Zr alloys, low temp. oxidation 2-48334
U-Pu-W-C system, phase relations 2-54011
U-Pu carbide fuel particles, preparation 2-56062
U-Sb alloys, liq., thermodynamic props., 1130°C 2-56497
(U, Pu)O_2 fuel rods, cladding plastic deformation and swelling rate 2-76944
(U, Pu)O_2 mixed-oxide with initial addition of fission product elements, postirradiation obs. 2-76945
(U,Pu)O_2 fuel, U-Pu redistrib., transport model 2-52853
(U,Pu)O_2 fuel pin, porosity and actinide redistrib., grain growth and desintering 2-56043
(U,Pu)O_2 microspheres and pellets, sol-gel derived, microstructure 2-47610
(U,Pu)O_{2-x}fuel irrad., oxygen redistrib. 2-52868
U, β phase, microstress behaviour during quenching cycles 2-77659
U, concentrates of metal 2-83072
U, expt. confirmation of burning curve ignition theory 2-46383
U, manufacture of metal and description of plant 2-83073
α-U, radiation-induced size changes 2-52845
U and Pu, automatic analysis in solutions 2-75411
U and Pu determ. in reprocessing of Rapsodie fuel using X-ray fluorescence 2-74173
U concentrates, safety in operations and processes 2-83154
U determination by liquid phase chromatography 2-74165
U enrichment, calc. of flow rate in cascade separator 2-83082
U enrichment, gas centrifuge method 2-70530
U III, prep. and absorption spectra in acid solutions 2-75367
U IV-U VI photosensitized electron exchange reaction in HCl kinetics 2-75365
U industry and fuel requirements in Portugal 2-56056
U isotope separation studies 2-63961
U oxides reactor fuels, O/U ratio determ. methods, review and comparisons 2-74155
U products, chemical analysis service of JEN for purification 2-83077
U products, control of manufacture 2-83078
U products, quality and specifications 2-83076
UC_2-ThC_2, UO_2, UO_2-ThO_2 coated fuels for GCR, chemical analysis techniques 2-74169
UC-UC_2 and UC_2 phases, U_2C_3 formation 2-47720
UC-UN, solid soln. formation mechanism 2-53910
UC-ZrC solid solns., diffusion props. 2-71541
UC, fuel, swelling and fission gas release obs. 2-52877
UC, kinetics of surface smoothing 2-53556
UC, oxidation in liq. Na with small O content 2-51452
UC, polycrystalline, high-temp. deformation and yielding 2-67348
UC, UC_2, U_2C_3 mag. susceptibility, after neutron irradiation, anomalous behaviour 2-84398
UC fuel to simulate burn-up of 100000 MWd/t, thermodynamic study 2-67351
UC_{1-x}, estimation of electrical resistivity increase due to C deficients 2-43874
UC_2, decomp. to U_2C_3 2-46384
UC_2 coated fuel, kernel migration in out-of-pile heating 2-83081
UC_x, fuel, fission gas swelling, external diametrical swelling, $T \leqslant 1900$°C 2-43614
UC_x, high temp. deform., proportional limit 2-53809
$UC_{1-x}N_x$, $0 \leqslant x \leqslant 1$, meas. of electrical resistivity and absolute Seebeck coeff. 2-44105
UF_4, description of production operations 2-83075
UF_6, spark source mass spectrometric anal. of trace elements 2-74172
UF_6 MHD units, thermal efficiency 2-63964
UN, elastic consts., 278K, u.s. determ. 2-53783
UN_x, fuel, fission gas swelling, external diametrical swelling, $T \leqslant 1900$°C 2-43614
UO_2-C-N_2 reaction kinetics, 1695°C, carbonitride form. 2-54537
UO_2-Mo cermet, finely-dispersed, creep rate and particle growth 2-71650
UO_2-Mo cermets, reactor behaviour 2-52883
UO_2-PuO_2, irradiated, gas release and swelling, 1260-1900°C 2-80662
UO_2-PuO_2, mixed fuel, control and behaviour of O/M, offgas and moisture during fabrication 2-53934
UO_2-PuO_2 fuel, temp. calc., use of GAPCON and HYBRID-SINTER programs 2-52854
UO_2-PuO_2 fuel rods, ratios of effective cross sections from burnup data 2-59856
UO_2-PuO_2 fuels, analysis techniques for process control, quality assurance and post-irradiation examination 2-74170
UO_2-PuO_2 fuels, chemical analysis techniques 2-74171
UO_2-PuO_2 fuels, determ. of non-metallic specification impurities 2-74177
UO_2-PuO_2 fuels, simulated fission product transport 2-52867
UO_2-PuO_2 mixed fuel, discrete PuO_2 particle behaviour during rapid power transients 2-59857
UO_2-PuO_2 mixed fuel, plastic flow and stress relax. 2-53808
UO_2-PuO_2 mixed fuel, radiation dose rates 2-59876
UO_2-PuO_2 mixed fuel, thermal creep, 1300-1700°C 2-53818
UO_2-PuO_2 mixed fuel irrad. performance in PRTR 2-59853
UO_2-PuO_2 mixed fuels, Pu and fission product redistrib. during irrad. 2-59852
UO_2-PuO_2 particulate fueled lattice, H_2O-moderated, neutron multiplication and relative reaction rates 2-59854
UO_2-PuO_2 thermal reactor fuel, defect performance 2-59855
UO_2-Zircaloy-2 contacts, thermal conductivity 2-42655
UO_{2-x}, thermodynamic props., 1600-1900°C 2-53935
UO_2, fission gas bubbles, nucleation and evolution, math. treatment 2-67358
UO_2, fission sintering and irrad. induced diffusion 2-52855
UO_2, irradiated, gas release and swelling, 1260-1900°C 2-80662
UO_2, lenticular pore migration, impurity effects 2-74150
UO_2, molten, for analysis of gross fuel movement 2-67353
UO_2, molten, stoichiometry change 2-53621
UO_2, neutron irrad., fission gas bubble nucleation and gas migration 2-63971

Nuclear reactors, fission continued
materials continued
UO_2, plastic deform., fracture, rel. to porosity 2-43699
UO_2, simulation of gaseous fission products for nuclear fuels 2-79838
UO_2, thermal diffusivity, 750-2700°C 2-54081
UO_2, thermal diffusivity, 650-2700K 2-54082
UO_2, UO_3, description of production operations 2-83075
UO_2 and UO_2/PuO_2 nuclear fuels, X-ray spectrometric obs. of impurities 2-74167
UO_2 clad fuel element swelling at high temp., factors 2-63250
UO_2 clusters, fast fission ratios meas. 2-42671
UO_2 coated fuel, kernel migration in out-of-pile heating 2-83081
UO_2 fuel, bubble re-soln. and creep 2-52862
UO_2 fuel coating failure analysis 2-52864
UO_2 fuel elements, Zircaloy-sheathed, circumferential strain obs. 2-52879
UO_2 fuel pellets technology 2-56061
UO_2 fuel pins, irrad. Zircaloy clad, internal free vol. and press. meas. 2-42666
UO_2 fuel rod, irrad., pore movement kinetics 2-52873
UO_2 fuelled reactor, characteristics, obs. 2-70519
UO_2 pellets, grain growth, long term obs. under annealing 2-49898
UO_2 pellets, prep. by sintering of $(NH_4)_2U_2O_7$ 2-80800
UO_2 properties 2-49891
UO_2 reactor fuel, burn-up meas. from mass spectrometry of stable fission-product Nd 2-74182
UO_2 single crystal, influence of stoichiometry on compression creep 2-67350
UO_2 unirradiated nuclear fuel, analytical methods for determ. of total U and impurities 2-74162
UO_2 vipac and pellet fuels, transient behaviour 2-63970
$UO_{2\pm x}$, redistribution of oxygen subject to temp. gradient 2-67359
UO_x, fuel, fission gas swelling, external diametrical swelling, $T \leqslant 1900$°C 2-43614
U_3Si, in-pile irrad. effects, electron microscopy and diffr. 2-47393
U_3Si, irradiated, effect of electropolishing on voids 2-67354
^{235}U, enriched U in paraffin, homogeneous critical assemblies 2-70536
^{235}U content of fuel assemblies, nondestructive assay 2-83132
^{235}U fuel element, meas. of surface contamination by fission fragments 2-52846
$^{238}U/^{235}U$ fission cross section ratio meas. in 2-3 MeV range using time-of-flight technique 2-83029
^{238}U-^{239}Pu mixture, mutual shielding effect related to prototype fast reactor MONJU 2-70547
^{239}U fuel, contribution to post-shutdown heat release 2-79831
Uo_2-PuO_2 mixed fuels, advanced characteriz. 2-52870
V, neutron irrad., activation volume rel. to dose and strain, interstitial impurity precip. 2-80663
V, neutron irrad., anneal and radiation hardening, tensile props. 2-80665
V alloys in contact with mixed oxide fuel, oxidation 2-83099
W single crystal, density changes induced by neutron irradiation 2-52849
Zr-(1.5wt.%)Cr-(0.1wt.%)Fe tubing, hydrided, mech. props. and struct. 2-53918
Zr-(2at.%)Cr-(0.16at.%)Fe alloy, precip. reactions rel. to corrosion resist. 2-53919
Zr-(2.5 wt.%) Nb press. tubes, heat-treated, embrittlement 2-50770
Zr-(2.5 wt.%) Nb press. tubing, hydriding, orientation and effect on tensile props. 2-50849
Zr-(2.5wt.%)Nb press. tubes, irrad., metallurgical props.53913 2-53913
Zr-Nb alloys, phase transforms. 2-53999
Zr-(2.5 wt%)Nb press, tubes, texture development 50848 2-50848
Zr-Y syst., H_2 diffusion through layers, calc. by eigenfunction method 2-50720
Zr-alloy pressure tubes rel. to tube irradiation programme 2-76953
α-Zr, bulk diffusion of ^{51}Cr 2-67357
Zr, neutron irrad. effects on aqueous oxidation, 290°C 2-44486
Zr alloy fuel element sheaths, F contamination, proton activation analysis 2-52876
Zr alloys, accelerated oxidation, significance of surface preparation 2-68786
Zr alloys, anisotropic creep behaviour under fast neutron flux 2-50756
Zr alloys, anisotropy of secondary in-reactor creep, relation to texture 2-67349
Zr alloys, conf., Montreal, Canada (Aug. 1971) 2-50815
Zr alloys, corrosion and hydriding behaviour in org. coolants 2-51454
Zr alloys, corrosion resist. in steam, 400 to 500°C 2-51457
Zr alloys, high-strength, creep and stress-rupture 2-53921
Zr alloys, high-strength, development 2-53920
Zr alloys, in-flux corrosion in pressurized water loop 2-51455
Zr alloys, strain-induced phase transforms., microstruct. exam. 2-54000
Zr and Zircaloy tubular materials, texture and anisotropy rel. to plastic deform. 2-53916
Zr and Zr-Nb alloy, strain rate depend. hardening 2-50847
operation
14th international ISA power instrumentation symposium, New York (1971) 2-46371
200/500 MW, thermal power levels, Monte Carlo analyses 2-70549
γ-ray spectra obs. in reactor room 2-63983
accident, health and medical physics procedures 2-73175
accident, radition dose obs. in vicinity 2-67370
acoustic diagnostics applics. 2-63974
adaptive control for nuclear power plant load changes 2-59815
adaptive control models 2-59817
automation of power plant, discrete drive control systems 2-76910
Beloyarsk atomic power station pumps, assessment of reliability 2-70543
Beloyarsk power reactor, reactivity meas. 2-42626
boiling water reactor at Lingen, analysis of space dependent neutron flux density fluctuations by stochastic methods 2-79830
Budapest Polytech. Univ. Training Reactor, model approach 2-83063
burn-up, of Cd-Mg rods, expt. and theory 2-49879

Nuclear reactors, fission continued
- **operation** continued
  - BWR core with NAIG critical assembly, critical expt. 2−67365
  - composite fuel annular bodies, fracture and elastic props. 2−71588
  - coolant temp. and flow vel. fluctuations., determ. of noise source 2−76918
  - core neutron flux distribution, on-line computer control 2−59814
  - critical condition, neutron production 2−63951
  - Dresden 2 reactor, operating experience from startup, maintenance and repairs 2−70526
  - EBR-II, exptal. LMFBR power plant 2−70529
  - Enrico Fermi Fast Breeder Reactor, experiences, maintenance and repairs 2−70527
  - Enrico Fermi FBR, 200 MWt operation 2−70522
  - erosion by small leaks in sodium water heat exchangers 2−59832
  - experimental fast reactor, MASURCA 2−59834
  - fast breeder, steam generator vessel pressures resulting from sodium-water reaction, computer analysis using SWEAR code 2−46377
  - fast breeder reactor, growth of single Na bubble, safety factors 2−74143
  - fast criticality facility control, d.c. channels 2−42632
  - fast reactor, HARMONIE neutron source 2−59833
  - FBR, burnup and power shift effects during long-term operation 2−83125
  - FBR's HTGR's and gas turbines strategy 2−42641
  - flux sensing system for wide power range 2−49906
  - fuel melting, peak burnups optimization 2−49882
  - fuel rod in vertical coolant tube, hydrodynamics, vibration and wear obs. 2−52844
  - gamma heating, calorimetric determ. in material testing reactor ESSOR 2−83065
  - heat release, meas. by calorimeters 2−42680
  - high temp. reactors, Cesar and Marius critical assemblies 2−59840
  - HORACE reactor II, light water moderated 2−52841
  - HTR, He cooled, assessment of fuelling systems, on- and off-load 2−42648
  - HTR, refuelling equipment, chute and rigid mast type 2−42649
  - in-core fuel management optimization by heurisitic learning technique 2−76919
  - ionization chamber calibration system 2−67362
  - LATREP lattice code accuracy 2−46244
  - light water power reactors, construction, operating experience in W. Germany 2−70521
  - light water power reactors, loss-of-coolant accidents 2−70523
  - liquid metal fast breeder reactor single subassembly accident, inertial contribution of fluid in plenum to rapid coolant-expulsion process 2−70524
  - local power meas. using gamma ray fluctuations 2−83102
  - LWR, prospects for Pu recycle 2−83138
  - Mark II gas cooled, fuel cycle performance 2−46381
  - maximum temp. in irradiated samples, in pile measurements, magnetic monitor 2−67363
  - Minerva atomic pile for neutron studies 2−59826
  - neutron and thermionic fuel elements studies on experimental EOLE reactor 2−59835
  - neutron flux distribution control 2−74144
  - nucleate and film boiling, heat transfer mechanisms 2−53510
  - optimization of fuel distribution 2−63955
  - pebble-bed once-through fuelling 500 MW reactor 2−42627
  - pool type reactor, determ. of thermal neutron energy spectrum by activation foils 2−79832
  - power, water cooled, air-water flow in bundle geometries, mixing rate meas. 2−53120
  - power reactors, failure detection by noise meas. 2−79829
  - power reactors, safety requirements 2−46379
  - power response determ. to sinusoidal reactivity input, small parameter expansion method 2−83067
  - power stations, radioactive safety 2−63982
  - pressurised water reactor, optimal control 2−59816
  - pressurized water reactor, emergency cooling of 37-rod cluster by heat radiation following accident 2−79834
  - pressurized water reactor one-point 4-group algorithm for computing nuclear fuel depletion 2−63956
  - products retention by solid-state chemical reactions 2−49880
  - prototype fast reactor MONJU, mutual shielding effect in ^{238}U-^{239}Pu mixture 2−70547
  - PWR, tritium generation in coolant moderator 2−83107
  - radiation dosimetry in WR-1, flux density determination 2−83159
  - radiation dosimetry in WR-1 nuclear reactor, calorimeter 2−46396
  - radiation protection instrumentation and applics. 2−70545
  - reactivity, void coeff., of FRG research reactor, expt. 2−49878
  - reactivity determination of weakly coupled two-core system 2−42629
  - reactor-physics and project studies 2−59825
  - reflected reactor, effectiveness of partially inserted control rods 2−63959
  - reflector, polarized proton, neutron diffusion 2−52835
  - reliability of nuclear reactor instrumentation 2−56036
  - repetitive-pulse operation, Hitachi Training Reactor, online data processing 2−46375
  - research and measurement reactors at Braunschweig, during 1971 2−76935
  - rod motion transients, computational model 2−83106
  - safety, radiation protection 2−67369
  - safety from seismic faults, siting on Californian coastal terraces 2−57562
  - secondary cct. components study and testing 2−63958
  - SEFOR, experiences, maintenance and repairs 2−70528
  - shielding, weight optimization using transmission matrix methods 2−76960
  - SLOWPOKE, lab. reactor for neutron irrad. 2−83148
  - stack, derivation of maximum permissible ^{41}Ar emission rate 2−70551
  - statistical optimization by modal analysis 2−42638
  - steady-state, analytical method for calc. of fission gas release 2−46386
  - temperature and power noise analyses 2−70525
  - testing and commissioning for large power plants 2−83136

Nuclear reactors, fission continued
- **operation** continued
  - thermal neutron spectrum in reactor core with MTR type fuel elements 2−52842
  - thermal reactor performance, effect of B concentration gradient on B-stainless steel control rods 2−76948
  - voiding initiation point and reactor safety 2−74139
  - water cooled power reactors, pressure-time histories in pressure suppression containments 2−79833
  - water-cooled, heat transfer 2−49883
  - water-moderated water-cooled, testing of thermal-emission converters 2−76912
  - zero energy mock-up of 100 MW(e) steam generating heavy water reactor 2−59839
  - ^{41}Ar release from Lowell Technological Institute reactor, environmental significance 2−59875
  - Na corrosion deposits, structure and effect on heat transfer coeffs. 2−83117
- **theory**
  - approximation techniques for the design of geometries for γ radiation scattering 2−79847
  - boiling-water reactor, stat. characts. near solid boundary 2−56031
  - boundary value problems in optically thick media, Lie series treatment 2−83112
  - Budapest Polytech. Univ. Training Reactor, model approach 2−83063
  - CIRENE system, design calc. and economic evaluations, optimization 2−59827
  - coolant heat transfer, multichannel calc., lumped model 2−83080
  - core thermal design, hot spot expectation 2−76921
  - coupled graphite-D_2O, neutron kinetics optimization in zero reactivity method 2−76907
  - critical, variational estimates of reactivity worths and reaction rate ratios 2−70513
  - critical heat flux, compensated-distortion fluid model 2−46370
  - dynamics, soln. of nonlinear space time problems using eigenfunction expansions 2−83101
  - efficiency, neutron flux, absorbing elements system 2−79828
  - elevated temperature design criteria based on time-dependent material deformation behaviour 2−83119
  - error estimation of eigenvalues in reactor theory problems 2−76913
  - fast and thermal reactor models linear stability using space-time kinetics 2−76920
  - fast critical expts., analysis by energy modal method 2−70512
  - fast power reactors, reactivity coefficients, calculation methods, book 2−83144
  - fast reactor burnup calc., use of energy modal synthesis 2−83043
  - fast reactor calculations, one- group method for neutron balances 2−70514
  - fuel rods adjacent to subassembly walls, laminar- and slug-flow heat transfer characts. 2−83114
  - gas cooled, heating/cooling channel perturbation dynamics 2−59818
  - graphite core, calc. of thermal resistance between hexagonally arrayed channels 2−42651
  - intermediate reactors, fuel enrichment distrib. and minimum crit. mass 2−83109
  - kinetic reactor equations with linear feedback, stability criterion 2−42639
  - LMFBR core restraint system design, structural materials aspects 2−83124
  - LMFBR dynamics, reactivity table model 2−83103
  - MICRETE 4, basic theory 2−46359
  - migration area defn. for presence of fission in epithermal region 2−70509
  - moderator model, small group neutron, for H_2O-Al core calcs. 2−42609
  - noise anal., flash start technique 2−83084
  - noise analysis, statistical accuracy 2−70542
  - point kinetics, direct integral formulation 2−83097
  - power reactors, use of signal coherence to detect anomalous behaviour 2−42683
  - rod motion transients, computational model 2−83106
  - shield design with graphical assistance 2−42694
  - slab reactor, with moving boundaries, neutron distribution 2−56028
  - space perturbation, error estimate by functional anal. technique 2−42613
  - stable periods, algorithms for precise meas. for use with real-time computer 2−74140
  - stochastic two-group model including neutron and gamma detection 2−83095
  - stress on pressure vessels of pressurized water reactors at start up 2−59829
  - thermal design, order statistics for determ. temp. limits 2−83083
  - thermohydrodynamics design, state-of-the-art 2−70516
  - threshold reactions, maximization of desired activity against interfering activities 2−42616
  - time-moments, regular and adjoint, calculation and meaning 2−70505
  - transient anal. space and energy-dependent neutronics 2−83135
  - transient flow in boiling channel, finite difference scheme 2−59838
  - transients, space dependent, closed-form analysis 2−83096
  - n field in reactor core, hybrid computer solution 2−69628
  - Cd cutoff energies, integral forms 2−83113
  - Fe, atomic displacement rate and displacement cross section 2−42643
  - U depleted in ^{235}U isotope, fast neutron spectra meas. and analysis 2−83057

Nuclear reactors, fusion
- atomic and cluster injection into D-T mirror fusion power system 2−64262
- blanket and magnet shield structure, design concept 2−83147
- blanket chemistry of D-T reactors 2−63953
- blanket materials, comparison of Nb, Mo and Nimonic alloy PE 16 2−83093
- breeding ratio, inventory and doubling time in D-T type 2−83134
- characteristics and technological problems 2−63928
- conditions for quasi steady development of self sustaining nuclear reactions 2−63952
- controlling plasma confinement 2−64280

Nuclear reactors, fusion continued
current status and engineering problems 2−83142
cyclotron radiation, yield coeff. in energy balance calcs. 2−83539
D-T reactor, thermal stability of spatially non-uniform plasma 2−80309
development as profitable energy source, prospects 2−42610
direct conversion concepts, book 2−83145
inverse Compton scattering as energy loss mechanism 2−83100
laser-triggered, use of very powerful beams which could be developed in the foreseeable future 2−63313
l.f. heating, engineering problems 2−46373
minimum-B mirror reactors, optimized magnetic field profiles and β-limitation 2−46751
neutron induced reaction rates 2−63892
neutronic calc. for blanket assembly by discrete ordinates and Monte-Carlo methods 2−46369
power needs and fusion energy 2−83137
pulsed, high-β, based on θ-pinch, design obs. 2−83613
research progress and prospects of controlled thermonuclear fusion 2−67347
review article 2−79842
Soviet high-flux reactors, design and technical features 2−79844
thermonuclear, feasibility, Tokamak expts. study 2−64283
toroidal, liquid Li as coolant, calc. of pumping power 2−46748
toroidal, neutral injection heating 2−46746
toroidal, use of liquid Li as coolant, stress limitations 2−46749
wall erosion due to sputtering 2−46376
D-T mixture, review of recent progress in mag. confinement 2−79843

Nuclear relaxation *see Nuclear magnetic resonance and relaxation*

Nuclear scattering *see Nuclear reactions and scattering*

Nuclear-solid interactions *see Mossbauer effect; Solids*

Nuclear spallation
cosmic rays, effect on chem. comp. 2−63677
isobars production and isolation for nuclear spectroscopy 2−63876
^{27}Al, intranuclear cascade calculations, proton-induced 2−46262
Au, recoil props. of rare earth nuclides produced by 28 GeV proton interactions 2−82971
^{209}Bi(^{12}C,xn), mass distrib. of fission fragments 2−46349
^{4}He(γ,d)^{2}H, photospallation process, ang. distrib., total cross sections 2−59742
^{181}Ta intranuclear cascade calculations, proton-induced 2−46262
U recoil props. of rare earth nuclides 2−82971

Nuclear structure
accelerator development for struct. research 2−59649
compound nucleus, phase difference of interfering states 2−52730
deformed heavy nuclei, densities calc. in model well of arbitrary shape 2−67112
density distrib. sensitivity to high energy nucl. scatt. 2−67203
dynamic structure of nuclear states; conference, Mount Tremblant, Canada (August 1972) 2−82862
energy-of-deformation calcs., Strutinsky model 2−82842
G-matrix equation, new treatment for projection operator 2−42488
generalized microscopical optimal model 2−52725
ground state energy in Brueckner and Jastrow theories 2−79711
Hartree-Fock method, Newton-Kantorovic procedure, consistent symmetry 2−70342
Hartree-Fock wavefunctions applic., cranked Hamiltonian concept 2−59682
high resolution fast neutron spectrometry 2−67075
infinite and finite matter theory 2−63746
intermediate, investigation using deuteron stripping reaction 2−70347
isobar configurations, construction, application and possible tests 2−82860
light nuclei, G-matrix elements for 1s, 1p, 1d and 2s shells 2−49714
light nuclei, orbital rearrangement effects due to removal of a proton 2−49716
linked cluster amplitude eqns. and energy variational principle 2−70343
local potentials, separable energy-dependent approx. of 2-body t-matrix 2−73969
microscopic nuclear theory, book 2−79731
multinucleon wave function expression approach 2−59676
neutron investigations using 90% polarized beam produced in ^{2}H(d,n)^{3}He reaction 2−67130
neutron rich light nuclei, stability relationships 2−82841
neutron studies, conf., Budapest, Hungary, [Aug. 1972] 2−67114
one and two body struct. defn. 2−59662
reduced width calculational method 2−70366
rotational motion, symmetry approach 2−49706
shell model, deviations in light, medium wt. nuclei 2−79725
shell structure study by inelastic high-energy electron scattering 2−63866
simple configurations, review of role 2−63732
T=1 interaction, non-pairing aspects, multipole character 2−70352
three resonantly interacting particle system, level spectrum 2−82230
transuranium and superheavy element props. 2−59893
tunable wavelength spectroscopy, high-resolution techniques 2−55777
weak coupling between modes of motion 2−63743
n-p distributions in nuclei, use of $\pi^{\pm}$ scatt. to study 2−63745
^{26}Al, K=3 rotational and members 2−63786
^{209}Bi isomer shift, nuclear structure depend. 2−70579
^{40}Ca, orbital rearrangement effects due to removal of a proton 2−49716
^{20}F, from ^{19}F(d,p)^{20}F reaction 2−63917
^{4}He, modified shell model wave function and binding energy 2−46109
^{6}Li, study by ^{6}Li(π^{-}, nn) reaction 2−82988
^{7}Li structure by reaction (p,pt) using cluster model 2−82964
^{14}N, configuration mixing calc. 2−52738
^{20}Ne, orbital rearrangement effects due to removal of a proton 2−49716
^{16}O, configuration mixing calc. 2−52738
^{16}O, orbital rearrangement effects due to removal of a proton 2−49716
^{16}O, photodisintegration and intermediate structure 2−46232
^{16}O, review of theory 2−52741

Nuclear structure continued
^{16}O, rigorous method for soln. of Hartree Fock equation 2−76761
^{207}Pb isomer shift, nuclear structure depend. 2−70579
^{87}Rb core coupling studied through isobaric analog resonances 2−46147
^{87}Rb core coupling studied through isobaric-analog resonances 2−46146
^{44}Ti, Hartree-Fock variation after projection method, test 2−74019

Nuclear track emulsions
cellulose nitrate as rapid neutron dosimeter material, cf with emulsions 2−63709
concealed image distrib., pulsed field effects 2−46061
dosimetry of heavy particle radiation, comparison with solid track detectors 2−46062
ion-sensitive plate response, depend. on ion struct. and comp. 2−83163
ionizing particle recording, effect of electric field 2−59642
photographic, primary energy determ. 2−73957
photographic emulsions, 2.43 GeV/c deuterons inelastic collisions with nuclei 2−55997
pile for detection of primary cosmic rays 10^{12}-10^{13} eV 2−73861
reduction reactions effects on threshold sensitivity 2−70317
relativistic particle identification with inclined tracks 2−79680
shortening of tracks in elec. field, 1.5-6.0 × 10^{4} V/cm 2−42476
d elastic and inelastic cross-sections on photoemulsion nuclei and proton stripping, 2.43 GeV/c 2−63909
AgBr, ionizing particle track formation, analog theory 2−81543
AgCl:Cd, crysts., nuclear particle track detectors, development and props. 2−79687
^{14}C dating method employing emulsion 2−75438

Nucleation
adsorbed layers, thick, rel. to heterogeneous nucleation 2−64577
alkali halide, growth from solution, comp. effect 2−74674
artificial stimulation of rain in Yugoslavia 2−44718
atmospheric aerosol, water and ice nucleating effectiveness 2−51613
atmospheric ice whiskers, growth, nuclei and crystal concentrations 2−84855
boiling and cavitating liquids, models 2−53503
cholesteryl derivatives, crystal nucleation in supercooled mesomorphic phases 2−77414
cloud and Aitken nuclei downwind of urban pollution sources 2−48466
cluster formation, statistical thermodynamics 2−43435
cold fog seeding at Oslo Airport 2−72793
contact nucleation, supercooled water, organic chemicals ice embryos 2−84828
crystal growth, surface nucleation theory 2−43507
crystallization operation, method of complete segregation 2−74690
droplet growth, kinetic theory 2−60551
electrolytic, probabilistic aspects 2−50474
epitaxial electrodeposition, two dimensional nucleation effect on electrocrystalliz. rate 2−71320
ethanol drops, homogeneous nucleation and growth in supersonic flow 2−80393
fatigue cracks, commencing at root of a notch, physical processes 2−56817
film, vapour deposited, kinetics, analytical formula 2−64562
film, vapour deposited, theory, capture number evaluation 2−64561
films, exptl. approach to well controlled studies 2−56583
films, LEED-Auger instrument and u.h. vac. electron microscope 2−74624
gas bubbles in liquid, applic. to gases dissolved in blood 2−45028
glass-ceramic, high quartz solid solution, fine grained crystallization rel. to nucleating agents 2−50411
glass-ceramic, viscosity changes 2−53923
heterogeneous, Fisher droplet model 2−71278
homogeneous, droplet approach 2−80520
homogeneous, external elec. field effects 2−47088
ice, det. of size distribution of natural and artificial nuclei 2−60529
ice, mechanism on AgI 2−62192
ice, obs. of ice crystal conc. in natural cap clouds 2−48488
ice clouds, heterogeneous nucleation rel. to AgI-bearing smoke activity curves 2−57971
ice crystal growth from vapour phase study of abrupt habit changes as function of temperature 2−54847
ice nuclei, rate of soln. in water drops, nucleation 2−75600
ice particle growth in atmosphere from vapour and cloud drop accretion 2−54849
In film, vapour deposited, rel. to thickness and substrate temp. 2−77512
ion induced nucleation phenomenon, role of small clusters 2−83812
kinetics, role of active centres 2−47089
liquid metals, supercooling, homogeneous nucleation study 2−71275
magnetic phase transitions, 1st order, determ. by computer simulation 2−78948
metal, cold-worked, nucleation of new grains in recrystallization 2−68134
metal film deposition on alkali halides, multiply-twinned particles 2−47101
nuclear reactor boiling, heat transfer mechanisms 2−53510
oxide formation during anodisation of Al 2−68798
piezoelectric semiconductor, moving acoustoelectric domain nucleation 2−68237
and pitting of underlying metals, relation to thermal treatments and oxidation of semiconducting surface film 2−57422
polar molecules, exhibiting an electric double layer at liquid surface, correction to class. homogeneous nucl. theory 2−50403
probabilistic aspects 2−50474
pyrrhotite, cryst. growth, use of deformed greigite as seed cryst. 2−60723
rare gases on graphite, molecular beam system and specimen holder for t.e.m. obs. 2−79113
Rochelle salt grown from soln., size distribution 2−67939
sodium phosphate melt, condensed, vitrifaction, effect of cooling rates 2−77479
stirred vessel cooling crystallizer, secondary nucleation 2−47281
supercooled water, crystallization 2−74588
theory, outline 2−47090
two-dimensional nucleus, shape stability 2−47280
vapour deposition, adatom capture and nuclei growth 2−50475

Nucleation continued
vapour deposition, computer simulation 2−50476
vapour deposition, role of active centres 2−47089
voids in irradiated stainless steel 2−71466
vtrifaction of condensed sodium phosphate melts, effect of cooling rates 2−77479
water, props. of clathrate-like cluster structures, theory 2−50404
water boiling at artificially active nuclei 2−50405
water drop freezing 2−47036
water vapour, heterogeneous 2−47047
Ag halogenides primary photochemical process 2−49455
AgI as contact or sublimation nucleus, electron microscope obs., cloud seeding 2−62190
β-AgI crystal shapes rel. to ice nucleation properties 2−64589
AgI in water drop, effects of diffusion and interfacial kinetics 2−60434
AgI particles, efficiency 2−48459
AgI particles in seeded hail, simple technique for locating in nucleus 2−65747
Al, growth from the melt, nucleation by Ti cpds. 2−47098
Al film, on KCl, rel. to epitaxy 2−67905
Au, on alkali halide, nuclei with five fold symmetry 2−47102
Au film, on KCl, rel. to epitaxy 2−67905
Au nucleation on an ionic crystal, diffusion mechanism 2−71534
Bi droplets, crystallization and nucleation 2−71382
Cd, bulk, and on W and Ge surfaces, mol. beam technique 2−50534
Co-P film, electroless deposition 2−53566
Co, magnetic domains, h.v. electron microscopy 2−84402
Cr, evaporated, condensation on NaCl 2−50488
Cu, oxide nucleation on (001) face, off angle effect 2−64566
Cu film, deposition on cold substrate, texture form., nucleation theory 2−50480
Cu film, lattice consts. of small nuclei, rel. to surface stress 2−60655
Cu foil recrystallization in a high voltage electron microscope 2−80825
GaP crystals grown by vapour transport, 780-935°C, thermodynamics, kinetics, rate of transport, nucleation and crystal size 2−71372
Ge single crystal, of Cd, by mol. beam technique, rel. to nucleation 2−47158
H_2O, clusters from vap. phase, Rayleigh scatt. obs. 2−64511
He superfluid vortices and turbulence as ultrasonic cavitation nucleation mechanism 2−43426
Hg droplets, crystallization and nucleation 2−71382
In, deposition on NaCl, island density 2−43480
In film, on Si substrate, mass spectrometer obs. 2−47117
KBr solution, containing Pb^{2+}, internal evolution of heat 2−47236
KCl:Ba, solid soln., decomposition due to homogenous and heterogeneous nucleation in two regions 2−80526
Li_2O-SiO_2 glass, phase separation and crystn., X-ray obs. 2−56560
Na-Ar liquid gas system, influence of gas on nucleation in sinusoidal pressure field 2−46893
$NaClO_3$, collision breeding of cryst. nuclei 2−50608
$NaClO_3$, growth from supersaturated soln., contact nucleation mechanism 2−50585
$NaClO_3$, rel. to cryst. growth rate from soln. 2−47240
$NaClO_3$ seeded solns., secondary nucleation 2−47283
Na_2O-SiO_2 glass, nucleation process in the metastable region 2−60584
Nb, continuous nucleation theory, twinning energy 2−64588
Ni-P film, electroless deposition 2−53566
Pb^+ ion gas-phase hydration, mass spectrometric obs. 2−80493
Pt film, lattice consts. of small nuclei, rel. to surface stress 2−60655
Se, amorphous, crystn., effect of alternating elec. field. 2−60565
Si growth from solution, 2-dimensional nucleation and corner growth 2−74684
Sn, deposition on NaCl, island density 2−43480
Sn film, vapour deposited, rel. to thickness and substrate temp. 2−77512
UO_2, fission gas bubbles, nucleation and evolution, math. treatment 2−67358

Nuclei with A$\leqslant$5
^{2}H (α, αp)n, new impulse approx. reaction mechanism 2−79796
G-matrix elements for 1s, 1p, 1d and 2s shells 2−49714
muon capture rate, correction due to presence of muon wave function in nuclear matrix elements 2−52804
spin cut-off factors from (n,2n) reactors at 14 MeV 2−70391
three nucleon bound state, convergence of generalized spherical harmonic emphasis 2−63765
three-nucleon problem with potential containing repulsive core 2−55954
three-nucleon system, Faddeev-Lovelace formulation, angular momentum decomposition 2−67144
tri-nucleon systems, effect of Δ(1236) resonance 2−49712
trinucleon, rank-two separable potentials 2−76778
α-Be, neutron spectra 2−55928
Be(α,n), for isotopic n source, line spectra. meas. 2−42439
^{13}C-H satellite n.m.r. spectrum, of coupling constants in pyrene 2−46627
^{2}D, proton total cross-sections, 180-560 MeV 2−74071
D(n,p)2n, meas. and pole diagram anal. of reaction cross section at 14.5 MeV 2−74096
D(p, 2p)n, cross-section, attenuation of quasifree scattering 2−74084
D(p,2p), Ep=39.5 MeV, destructive interference effects 2−79797
H, A=1,2,3, production in high energy proton interaction with ^{12}C, ^{27}Al and ^{197}Au 2−74087
H, spin lattice relaxation in β-tetramethylsilane, 77−174K 2−75242
H isotopes emitted following π- capture in nuclei, meas. of energy spectra, branching ratios 2−46293
H spin echo n.m.r. spectra of 1,1-difluoro-2, 2-dichloroethane, subspectral analysis 2−42977
H track-sensitive target, use in studies of KN interactions 2−52669
^{1}H, dynamic nuclear polarization in $La_2Mg_3(NO_3)_{12}$:Sm 2−68590
^{1}H, n.m.r. in Sc-H solid solution, Korringa product and diffusion parameters 2−72517
^{1}H, neutron scattering at 526 keV, meas. of total cross section by time of flight method 2−46272
^{1}H, p.m.r. of ice, review of recent investigations 2−61746
^{1}H, polarized, capture of μ^- mesons, diff. capture cross section detn. 2−55982

Nuclei with A$\leqslant$5 continued
^{1}H, proton total cross-sections, 180-560 MeV 2−74071
^{1}H, spin-lattice relaxation time, Na_2PO_3F and $NaPF_6$ solns. in H_2O 2−50372
^{1}H, total hadronic cross section of γ-rays in energy range 0.265 to 4.215 GeV 2−46230
^{1}H, transmission regeneration of K^0 in momentum region 14 to 42 GeV/c 2−46294
$^{1}H^+$ in metal-ammonia solutions, relaxation times and Overhauser enhancements 2−46988
^{1}H and ^{19}F n.m.r. spectra in substituted fluorothiophenes 2−46606
^{1}H n.m.r. spectra of monomethylphosphoryl halides, and dimethylphosphoryl halides 2−46616
^{1}H spin-lattice relax. in symmetric top mols. 2−56200
^{1}H(d, d)^{1}H, large angle scattering at 433, 362, 2.91 MeV, meas. of cross-section, neutron-exchange mechanism 2−82993
^{1}H(d,pn)^{1}H, calc. of amplitude for deuteron break-up, theory of proton-proton final state interaction 2−70470
^{1}H(n,γ)^{2}H, possible test for capture via $^{1}S_0 \rightarrow {}^{2}S_1$ transition 2−46283
^{2}H, 120 MeV alpha bombardment, neutron energy spectra 2−67322
^{2}H, analysis of low energy elastic neutron scattering 2−55994
^{2}H, neutron scattering, short-range internucleon repulsion and low energy three nucleon parameters 2−46080
^{2}H, pion elastic scatt., accuracy of Glauber approx. in intermediate energy region 2−46292
^{2}H, proton elastic scatt. and polarisation at 198 MeV 2−49790
^{2}H, proton scattering, optical model and DWBA calculation 2−52809
^{2}H, quadrupole moment calc. 2−67140
^{2}H, relative capture rates for stopping π-, K-, Σ- 2−70460
^{2}H, relativistic exchange scattering 2−49788
^{2}H, relativistic wave function 2−49722
^{2}H, review of low energy neutron scattering cross sections 2−55995
^{2}H, spin-lattice relaxation time, Na_2PO_3F and $NaPF_6$ solns. in D_2O 2−50372
^{2}H, spin structure of proton scatt., Glauber theory 2−59755
^{2}H, three-body calc. with tensor force for elastic scatt. 2−42565
^{2}H n.m.r., quadrupole coupling constants in boron deuterides 2−44461
^{2}H n.m.r. in lithium ammonium tartrate 2−72527
^{2}H proton scattering, triple scattering meas. 2−46256
^{2}H+n break-up reaction, cross-section calc. using separable potentials 2−63895
^{2}H(^{24}Mg, nγ)^{25}Al, population of 3/2$^+$ 945 keV level in ^{25}Al, meas. of mean lifetime for γ-ray decay 2−79736
^{2}H(^{24}Mg, pγ)^{25}Mg, population of 3/2$^+$ 975 keV level in ^{25}Mg, meas. of mean lifetime for γ-ray decay 2−79736
^{2}H(^{3}He,dd)p, ^{2}H(^{3}He,dp)d, 26.8 MeV, meas. of absolute cross sections for coincidence detection, DWBA analysis 2−70474
^{2}H(α,α^{1})d+($^{1}S_0$)$\rightarrow$n+p isospin impurity of ^{6}Li 4.57 MeV state 2−82879
^{2}H(α,t)^{3}He, two-mode finite-range DWBA analysis of mechanism 2−70475
^{2}H(d,^{3}He)n, cross section meas., 1.96-6.2 MeV 2−74108
^{2}H(d, d), 6−11.5 MeV polarized beam, meas. of angular distribs. of analysing powers iT_{11}, T_{20}, T_{21}, T_{22} 2−74104
^{2}H(d, n)^{1}H, off-energy shell effects 2−74110
^{2}H(d, n)^{3}He, 10.0 and 11.5 MeV polarized beam, meas. of differential cross section and analysing powers 2−74109
^{2}H(d, n)^{3}He, partially polarized neutron prod. for ^{12}C(n, n) elastic scatt. 2−76860
^{2}H(d, p)^{3}H, 3.0-11.5 MeV polarized beam, meas. of differential cross section and analysing powers 2−74109
^{2}H(d,d), elastic scattering study using resonating-group method and imaginary potential 2−55996
^{2}H(d,d), rel. to channel spin nonconservation 2−59775
^{2}H(d,d)^{2}H, cross section meas., 1.96-6.2 MeV 2−74108
^{2}H(d,dpn), study at low bombarding energies 2−67221
^{2}H(d,n)^{3}He, 0.2 to 4 MeV, polarization of neutrons 2−67323
^{2}H(d,n)^{3}He, cross section meas., 1.96-6.2 MeV 2−74108
^{2}H(d,n)^{3}He, E_d=16-22 MeV, neutron polarization ang. distrib. 2−70472
^{2}H(d,n)^{3}He, E_d=6-14 MeV, neutron polarization ang. distrib. 2−70471
^{2}H(d,n)^{3}He, neutron yield rel. to irrad. time 2−55999
^{2}H(d,n)^{3}He, polarization, comparison with ^{2}H(d,p)^{3}H reaction 2−70473
^{2}H(d,n)^{3}He, production of 90% polarized neutron beam for nuclear structure research 2−67130
^{2}H(d,p)^{3}H, E_d=2-14 MeV, proton polarization, ang. distrib. 2−70473
^{2}H(d,p)^{3}He, cross section meas., 1.96-6.2 MeV 2−74108
^{2}H(d,t)p, cross section meas., 1.96-6.2 MeV 2−74108
^{2}H(γ, n)^{1}H in burnt-up reactor fuel, cause of high neutron dose rates 2−76915
^{2}H(γ,n), E_γ=7-30 MeV, differential polarization of photoneutrons 2−76828
^{2}H(n, n)np, n-d initial-state interaction 2−82991
^{2}H(n, n)pn, unitary model for three-body collisions 2−82992
^{2}H(n, p)2n, 50 MeV, proton energy spectrum and neutron-neutron scatt. length 2−63894
^{2}H(n,2n)^{1}H, nn $^{1}S_0$ scattering parameters from kinematically complete expt. 2−49805
^{2}H(n,d)n, 152 MeV, elastic and inelastic differential cross sections 2−49798
^{2}H(n,n), effective range approx. 2−63665
^{2}H(n,n) 14 MeV elastic scattering, exact unitary model calcs., soln. of Faddeev eqns. 2−79800
^{2}H(n,n)^{2}H, 35 MeV, n polarization meas. 2−67241
^{2}H(n,p)2n reaction, cross section, diagram summation approximation technique 2−74097
^{2}H(ν, μ-p)^{1}H, quasi-elastic reaction, impulse approx. 2−59746
^{2}H(p, 2p)n, 20-60 MeV, rescattering effects, cross-sections obs. 2−63878
^{2}H(p, p)^{2}H, 600 MeV cross-section obs., p polarization meas. cf with Watson and Glauber theory 2−63873
^{2}H(p, pn)n, 20-60 MeV, rescattering effects, cross-sections obs. 2−63878

Nuclei with A$\leqslant$5 continued

^{2}H(p,2p)n, 155 MeV, high momentum transfers, meas. of cross sections, importance of off energy shell nucleon nucleon interaction 2 − 63877

^{2}H(p,2p)n, 51.8 MeV, study in coplanar symmetric geometry at forward angles 2 − 67220

^{2}H(p,2p)n and ^{2}H(p,pn)p, cross-sections for small momentum transfer, difference 2 − 74083

^{2}H(p,γ)^{3}He, excitation function anomaly, $E_p = 10 - 17.5$ MeV 2 − 59756

^{2}H(p,n)p correlation spectra of cross-section calc. 2 − 83005

^{2}H(p,p), energy dependence of backward elastic scattering in range 360-670 MeV 2 − 67216

^{2}H(p,pn)^{1}H, meas. of nucleon-nucleon final state interaction as function of angular and energy variables 2 − 49793

^{2}H(p,pp)n, correlation spectra of cross-section calc. 2 − 83005

^{2}H(p,pp)n, p effective momentum distribution in deuteron determ. 2 − 46247

^{2}H(p,ppn), study at low bombarding energies 2 − 67221

^{2}H(π^{+}, p)p, 70 MeV, differential cross section 2 − 70461

^{3}H, beta-decay investigations 2 − 67193

^{3}H, binding energy, charge radii and D-state probability, using Riihimaki potential 2 − 67142

^{3}H, binding energy, Faddeev approach with two-body local interactions 2 − 73994

^{3}H, binding energy, reaction matrix approach 2 − 59687

^{3}H, binding energy in ground state with realistic interactions 2 − 76777

^{3}H, coherent scattering amplitude of neutrons 2 − 46284

^{3}H, elastic scatt. of polarized protons between 19 and 57 MeV, cross sections and asymmetries 2 − 42562

^{3}H, estimation of relative role of penetration into critical organs through intact skin 2 − 55295

^{3}H, influence of irradiation on incorporation in hair and other tissues of rabbits and rats 2 − 55293

^{3}H, low energy three nucleon parameters and short-range repulsion 2 − 46080

^{3}H, mag. moment 2 − 59688

^{3}H, off-shell variation of binding energy for exactly phase-equivalent separable potentials 2 − 55956

^{3}H, Reid potential calc., of binding energy admixture probabilities and charge form factor 2 − 76779

^{3}H, shell-model analysis of Brueckner calcs. 2 − 63766

^{3}H, standard unit for radionuclide activity in gases 2 − 55971

^{3}H, two-nucleon one-pion exchange contributions 2 − 67143

^{3}H autoradiography, obs. of behaviour of gas atoms in neutron irradiated Al-Li alloys 2 − 44009

^{3}H β-activity meas. for determ. of cross-sections of (n,t) reactions with 14 MeV neutrons 2 − 67257

^{3}H β-ray spectrum, determ. of upper limit for electron-continuities rest mass 2 − 73751

^{3}H contamination of Ti ion-getter pump in neutron generator 2 − 58662

^{3}H exhalation analysis, design of acclimation room 2 − 58597

^{3}H labelled compounds production control of surface and internal contamination 2 − 58604

^{3}H magnetic moments, quark model approach 2 − 82877

^{3}H release to environment due to operation of research and power stations 2 − 52890

^{3}H(d,n)^{4}He, neutron generator, health physics problems associated with operation 2 − 58603

^{3}H(d,n)^{4}He, neutron yield rel. to irrad. time 2 − 55999

^{3}H(n,n), meas. of differential elastic cross section at 14 MeV 2 − 67242

^{3}H(p,d)^{2}H, $E_p = 6.7$-14.7 MeV, analyzing power ang. distrib., ^{2}H(d,p)^{3}H studies 2 − 70473

^{3}H(p,n)^{3}He, 1.5-12 MeV, analyzing power polarization anomalous difference 2 − 49794

^{3}H(p,n)^{3}He, 56.7 MeV, cross section meas. 2 − 42562

^{3}H(p,n)^{3}He, polarization and polarization transfer 2 − 46257

^{3}H(p,p), polarized proton beam, meas. of differential cross section, proton analyzing power at 19 and 30 MeV 2 − 63874

^{3}H(p,p)^{3}H, elastic scatt., $E_p = 9.4$-14.7 MeV, analyzing powers, ang. distrib. 2 − 70441

^{4}H, search for ground and excited states formed in ^{6}Li(π^{-}, d) reaction 2 − 52734

^{4}HE, binding energy, radius, Hartree- Fock calculations with Feshbach-Lomon potential 2 − 73995

He, A = 3,4, production in high energy proton interaction with ^{12}C, ^{27}Al and ^{197}Au 2 − 74087

^{2}He(n,p)2n, 152 MeV, spectra of protons 2 − 49804

^{3}He-^{4}He mixture, thermodynamic relationship between second sound velocity and osmotic pressure 2 − 64501

^{3}He, broad reson., ^{2}He(p,γ)^{3}He obs. 2 − 59756

^{3}He, charge form factor with Reid soft-core potential 2 − 63764

^{3}He, charge radii, using Riihimaki potential 2 − 67142

^{3}He, charge radius 2 − 63763

^{3}He, elastic proton scatt., coupling const. for deuteron exchange 2 − 76870

^{3}He, electromagnetic structure 2 − 70372

^{3}He, form factors and proton elastic scatt. cross sections, S′- and D-state effects 2 − 42497

^{3}He, high energy scatt., large angles, two-photon exchange contrib. 2 − 74062

^{3}He, mag. moment 2 − 59688

^{3}He, optical potential, energy dependence 2 − 70468

^{3}He, proton elastic scatt., modified phase shift analysis 2 − 42559

^{3}He, two-body photodisintegration between 40 and 150 MeV 2 − 46231

^{3}He broad reson. obs. in (p,α) and (p,2p) reactions 2 − 59760

^{3}He elastic electron scattering cross-section meas. at high momentum transfer, determ. of form factors 2 − 76830

^{3}He elastic scattering of polarized neutrons at 21.9 MeV asymmetries meas. 2 − 42566

^{3}He excited state search in ^{4}He(p,d) and ^{3}He(α,α') reactions 2 − 67141

^{3}He magnetic moment, two-nucleon one-pion exchange contributions 2 − 67143

^{3}He spectrometer, obs. of delayed neutron emission of mass separated fission products 2 − 67150

Nuclei with A$\leqslant$5 continued

^{3}He + ^{3}He system reson. existence rel. to solar neutrino flux 2 − 69188

^{3}He(^{3}He,^{3}He)^{3}He elastic scatt., 4-10 MeV, polarization analyzing power 2 − 82995

^{3}He(^{3}He,^{3}He)^{3}He elastic scatt., 7-18 MeV, polarization analyzing power 2 − 82996

^{3}He(^{3}He, α)2p, 6.9, 7.88, 9.11 MeV, differential spectra and angular distributions 2 − 79795

^{3}He(α,α')^{3}He*, 115 MeV, continuum spectra analysis 2 − 67141

^{3}He(α,α)^{3}He elastic scatt., 4-10 MeV, polarization analyzing power 2 − 82995

^{3}He(α,α)^{3}He elastic scatt., 7-18 MeV, polarization analyzing power 2 − 82996

^{3}He(d,n)^{4}He, meas of neutron polarization for $E_d = 1.0$ to 5.0 MeV 2 − 49829

^{3}He(d,p)^{4}He, 300 keV to 2.5 MeV, polarized target, analyzing power of the reaction 2 − 46312

^{3}He(d,t)2p, centre-of-mass energy 23.5 MeV, energy spectra studied in DWBA approximation 2 − 42582

^{3}He(e,e′p)d, electrodisintegration, cross section, final state interaction depend 2 − 74064

^{3}He(p, 2p), 590 MeV, cross-section 2 − 74085

^{3}He(p, p)^{3}He, 600 MeV, cross-section obs., cf. with multiple-scattering theory of Watson and Glauber 2 − 63873

^{3}He(p, pd), 590 MeV, cross-section 2 − 74085

^{3}He(p,2p)^{2}H, meas. of nucleon-nucleon final state interaction as function of angular and energy variables 2 − 49793

^{3}He(p,p), polarized proton beam, meas. differential cross section, proton analyzing power at 30 MeV 2 − 63874

^{4}He, binding energy, reaction matrix approach 2 − 59687

^{4}He, c.m. spuriosity effects on charge form factor 2 − 67145

^{4}He, elastic electron scatt., symmetrized Fermi density distrib. appl. 2 − 76833

^{4}He, elastic electron scatt. form factor in local density approx. 2 − 83004

^{4}He, excited states, study by reactions on ^{6}Li by deuterons at 52 MeV 2 − 49725

^{4}He, ground state, effect of tensor force 2 − 73996

^{4}He, high energy scatt., large angles, two-photon exchange contrib. 2 − 74062

^{4}He, Λ scatt., spin-orbit coupling using one-boson-exchange model 2 − 63900

^{4}He, modified shell model wave function and binding energy 2 − 46109

^{4}He, ohotodisintegration cross-section, effect of velocity-dependent potential 2 − 83003

^{4}He, photon spectra from radiative absorption of pions 2 − 46296

^{4}He, proton scattering, Majorana component in imaginary potential 2 − 46248

^{4}He, proton total cross-sections, 180-560 MeV 2 − 74071

^{4}He, shell-model analysis of Brueckner calcs. 2 − 63766

^{4}He, third-order corrections to binding energy 2 − 76776

^{4}He, variational calc. of binding energy and charge form factor fit 2 − 63767

^{4}He (n,n)^{4}He, up to 10 MeV, R matrix formulation and phase shifts 2 − 76853

^{4}He (p, p)^{4}He up to 20 MeV, R matrix formulation and phase shifts 2 − 76853

^{4}He excited states study via ^{2}H(d, p)^{3}H and ^{2}H(d, n)^{3}He reaction using polarized d beam 2 − 74109

^{4}He ground state energy bounds and convergence of perturbation expansions 2 − 79715

^{4}He interaction with π^{+}, obs. in cloud chamber 2 − 52703

^{4}He γ p ^{3}H elec. dipole reactions, isospin mixing of excited states 2 − 83000

^{4}He resonances in elastic deuteron-deuteron scattering 2 − 74104

^{4}He + ^{4}He scattering, direct solution of Hill-Wheeler equation 2 − 42583

^{4}He(α, $\alpha\gamma$)^{4}He, meas. of bremsstrahlung cross section 12.5-19.0 MeV 2 − 74105

^{4}He(α,α)^{4}He, 30-70 MeV, study of even-spin positive-parity levels in ^{8}Be by phase-shift analysis 2 − 82878

^{4}He(α,α)^{4}He, 63, 69 and 77 MeV, potential construction 2 − 82946

^{4}He(e,d)e′^{2}H, ang. distrib., cross section, 36-50 MeV 2 − 63869

^{4}He(γ,d)^{2}H, photospallation process, ang. distrib., total cross sections 2 − 59742

^{4}He(γ,n)^{3}H, threshold to 34 MeV, cross-section calc. 2 − 52797

^{4}He(γ,p)^{3}H, threshold to 34 MeV, cross-section calc. 2 − 52797

^{4}He(n, n)^{4}He, 0.55, 0.84, 1.16 and 1.33 MeV, cross-sectipns meas. 2 − 76854

^{4}He(p, p)^{4}He, 12 MeV, determ. of polarization standards 2 − 74072

^{4}He(p, p)^{4}He, 600 MeV, cross-section obs., p. polarization meas. 2 − 63873

^{4}He(p,d)^{3}He*, 65 MeV, continuum spectra analysis 2 − 67141

^{4}He(p,p)He elastic scatt. below 50 MeV, forward dispersion relation 2 − 67205

^{4}He(π,π), scattering near 3,3 resonance, differential and total cross sections calc. by multiple-scattering theory 2 − 46291

^{4}He($\pi^{\pm}$,$\pi^{\pm}$), analysis for information on pion charge form factor 2 − 63604

^{5}He, first excited state detn. from ^{7}Li(d,α)^{5}He at 1 MeV 2 − 63768

^{5}He, third-order corrections to single-particle energies 2 − 76776

^{5}He, two-centred cluster model calc. using supermultiplet scheme 2 − 55955

^{5}He emission in spontaneous fission of ^{252}Cf 2 − 74125

^{5}He ground state energy bounds and convergence of perturbation expansions 2 − 79715

^{6}He(π^{-},π^{-}), 8 GeV/c, calc. of differential cross-section using Glauber's multiple scattering theory 2 − 74100

H(p, p)H, 600 MeV, cross-section obs., cf with Livermore phase shifts 2 − 63873

^{131}I-triolein excretion test for steatorrhoea using unabsorbed radioactive marker 2 − 69267

LiH, target for 150-550 GeV cosmic ray nucleons, multiplicity of particles generated 2 − 74070

^{6}Li(p,2p)^{5}He 100 MeV, angular correlation measurements 2 − 82966

${}^{3}_{\Lambda}$H, binding energy, ΛN potential and Λp scatt. data 2 − 82876

${}^{4}_{\Lambda}$H, binding energy, effects of Λ-Σ coupling 2 − 74002

${}^{4}_{\Lambda}$He, binding energy, effects of Λ-Σ coupling 2 − 74002

Nuclei with $A \leqslant 5$ continued
- $^{4}_{\Lambda}$He, binding energy, ΛN potential and Λp scatt. data 2−82876
- $^{4}_{\Lambda}$h, binding energy, ΛN potential and Λp scatt. data 2−82876
- $^{5}_{\Lambda}$He, binding energy, effects of Λ-Σ coupling 2−74002

Nuclei with $6 \leqslant A \leqslant 19$
- 4n nuclei, HF calcs. of multipole deformations, static quadrupole moments, e.m. transitions 2−70364
- ^{11}B(d,n), meas. of neutron polarization angular distrib. 2−63915
- ^{14}N n.q.r., bonding studies in substituted NH$_3$ ions 2−42914
- — 2−67148
- — 2−59748
- A=18, 19, energy level data 2−59686
- A=19, $J^{\pi}=7/2^{+}$ and $11/2^{+}$, T=1/2 states 2−49729
- A=6 nuclei, vertex functions and coupling constants for virtual decay 2−63762
- G-matrix elements for 1s, 1p, 1d and 2s shells 2−49714
- muon capture, partial capture rates, dependence on nuclear structure, derivation of μN coupling constants 2−55983
- muon capture rate, correction due to presence of muon wave function in nuclear matrix elements 2−52804
- neutron rich light nuclei, stability relationships 2−82841
- polarization of α-clusters 2−73980
- spin cut-off factors from (n,2n) reactors at 14 MeV 2−70391
- surface density, light nuclei, in solids, determ. by charged particle beam, review 2−80556
- visual perception of accelerated N nuclei interacting with human retina 2−76112
- π- capture, 600 MeV, identification of emitted charged particles 2−46293
- ^{6}4(p,^{3}He)^{4}He, direct reaction mechanisms in unified microscopic nuclear theory 2−46226
- Al-N, Al-π interactions, 30-70 GeV accelerator obs., 100-300 GeV 2−73896
- B(^{3}He,^{3}He), A=10,11,13 to 27 MeV angular distributions 2−83001
- ^{9}B, determ. of width of excited state from neutron spectrum in ^{6}Li(p,n) 2−52735
- ^{9}B ground states in ^{12}C(p,p$'$3α) reaction mechanism 2−59757
- ^{10}B, excited states near 10 MeV, ^{9}Be(p,p)^{9}Be reaction obs. 2−70378
- ^{10}B, isospin impurity of 6.8 MeV state 2−63770
- ^{10}B energy levels determ. in ^{9}Be(d,n) reaction at 650 keV 2−49830
- ^{10}B states populated in ^{9}Be(d,n) reaction at 650 keV 2−63913
- ^{10}B*, T=0, $J^{\pi}=1^{+}$, limits on magnetic moment 2−79754
- ^{10}B(^{3}He, particle)^{13}N, 11-19 MeV, cross sections, levels of ^{13}N 2−76873
- ^{10}B(2155 keV) level, strength of β decay of ^{10}C 2−46185
- ^{10}B(d,n), $E_d=11.8$ MeV, neutron spectroscopy 2−67324
- ^{10}B(n, 2α)^{3}H, tritium generation in coolant moderator of PWR's 2−83107
- ^{10}B(n,α), noble- gas plasma produced by emitted heavy charged particles 2−70887
- ^{10}B(p,α)^{7}Be low-energy cross-sections, branching ratio 2−82963
- ^{11}B, high resolution n.m.r. spectrum of pentaborane (9), effects of thermal decoupling 2−83801
- ^{11}B, n.m.r. in Ag$_2$O-B$_2$O$_3$ glass system 2−65342
- ^{11}B, n.m.r. in GeO$_2$-B$_2$O$_3$ glass 2−54506
- ^{11}B, n.m.r. in SrO.xB$_2$O$_3$, struct. 2−54504
- ^{11}B, optical model analysis of ^{6}Li elastic scatt. 2−56004
- ^{11}B, quasielastic 550−1150 MeV electron scatt. cross-section 2−76834
- ^{11}B many-nuclear transfer reactions induced by ^{16}O, ^{19}F, finite DWBA calculations 2−56005
- ^{11}B partially relaxed transform n.m.r. in n-B$_9$H$_{15}$, resolution enhancement 2−56521
- ^{11}B(^{3}He,p)^{13}C, $E_{3he}=4$-12 MeV, proton ang. distribs., DWBA 2−52823
- ^{11}B(α,n)^{14}N, differential cross- section at 12-15 MeV 2−46314
- ^{11}B(α,t)^{12}C, triton ang. distrib., 15-25 MeV, excitation functions 2−74112
- ^{11}B(d,n), $E_d=11.8$ MeV, neutron spectroscopy 2−67324
- ^{11}B(d,n)^{12}C, polarized deuterons, reaction study at 900 keV 2−42584
- ^{11}B(γ,π^{+}), study of photoproduction in framework of impulse approximation 2−52798
- ^{11}B($\mu\nu$), impulse and closure approximation study of total muon capture rate and average neutrino momentum 2−52808
- ^{11}B(p, 3α), 2.65 MeV, effect of 3^{-} state of ^{12}C on separation energies of final state 2−79784
- ^{11}B(p,^{4}He)^{8}Be, cross sections, ang. distribs., reaction mech. 2−46255
- ^{11}B(p, α)^{8}Be*, α-particle ang. distrib., 2.9 MeV, detector arrangement 2−74086
- ^{11}B(p,γ)^{12}C, $E_p=14$-22 MeV, giant resons. in ^{12}C 2−63772
- ^{12}B, half-life determ. by Cerenkov counter and activation anal. 2−51488
- ^{12}B, semileptonic weak interactions, cross-sections 2−74067
- Be, π^{-} capture, energy spectra and emission probabilities of proton, deuteron and triton 2−79793
- ^{6}Be, determ. of width of excited state from neutron spectrum in ^{6}Li(p,n) 2−52735
- ^{6}Be breakup into 2 ^{3}He clusters, rel. to solar neutrino flux 2−69188
- ^{7}Be form. cross sections in ^{16}O by 135 and 550 MeV protons, radiochem. meas. 2−82961
- ^{7}Be→^{7}Li radiative electron capture transition to first excited state 2−46184
- ^{8}Be, α-cluster structure 2−83038
- ^{8}Be, α-particle cluster structure 2−82880
- ^{8}Be even-spin positive-parity levels in 15.35 MeV excitation region obs. in α-α elastic scattering 2−82878
- ^{8}Be ground states in ^{12}C(p,p$'$3α) reaction mechanism 2−59757
- ^{8}Be rotational states, properties of projected HF functions of ground state bands 2−73992
- ^{8}Be transfer processes in ^{12}C bombardment of ^{209}Bi, formation of partial fusion nucleus 2−74123
- ^{9}Be, $1/2^{+}$ reson., coupled-channel calc. 2−76859
- ^{9}Be, analysis of 20 GeV proton elastic scattering 2−42560
- ^{9}Be, charge radius from electron scattering data 2−49726
- ^{9}Be, dueteron-induced scattering, neutron pick-up, neutron stripping 2−49820
- ^{9}Be, formed during ^{7}Li(d,α)^{5}He, spin and parity assignment 2−74111
- ^{9}Be, n.m.r. in BeO, Stark shift of nuclear spin levels 2−44453

Nuclei with $6 \leqslant A \leqslant 19$ continued
- ^{9}Be, n.m.r. in V$_{1-x}$Cr$_x$Be$_2$ 2−72520
- ^{9}Be, proton induced reactions, excited states in ^{10}B near 10 MeV obs. 2−70378
- ^{9}Be, proton scattering of 19.3 GeV/c, applic. of Steenberg model 2−59750
- ^{9}Be electron elastic and inelastic scattering, extended Nilsson model and projected Hartree-Fock 2−82957
- ^{9}Be excitation, ^{6}Li(t,p)^{8}Li obs., low energy 2−63911
- ^{9}Be(^{3}He,^{3}HER) 13 to 27 MeV angular distributions 2−83001
- ^{9}Be(^{3}He,$\gamma\gamma$)^{12}C, 1.73-1.76 MeV, meas. of cross-section, search for $J^{\pi}=0$, T=2 resonance 2−82994
- ^{9}Be(^{3}He,$\gamma\gamma$)^{12}C, 1.739 MeV, $J^{\pi}=0+$, T=2 reson. 2−70476
- ^{9}Be(^{3}He,$\gamma\gamma$)^{12}C, T=2 reson. obs. 2−63914
- ^{9}Be(d,n)^{10}B, 650 keV, meas. of recoil proton tracks, angular distrib. of neutrons, determ. of Q-value spectrum 2−63913
- ^{9}Be(d,n)^{10}B, 650 keV, meas. of angular distrib. of neutrons, energy levels of ^{10}B 2−49830
- ^{9}Be(d,p)^{10}Be, $E_d=12$ MeV, proton polarization for ground state and first excited state transitions 2−82998
- ^{9}Be(p,^{4}He)^{6}Li, cross sections, ang. distribs. for first 3 states, reaction mech. 2−46255
- ^{9}Be(p,α), $E_p=3.56$ MeV, population of ^{6}Li levels 2−82883
- ^{9}Be(p,γ)^{10}B, isospin impurity of 6.88 MeV state in ^{10}B 2−63770
- ^{9}Be(p,n)^{9}B, 17.8 MeV, determ. of width of excited state in ^{9}B from neutron spectra 2−52735
- ^{9}Be(p,n)^{9}B, excited-state-threshold reson. effects 2−79788
- ^{9}Be(p,p$_0$)^{9}Be, excited-state-threshold reson. effects 2−79788
- ^{9}Be(p,π^{-})^{10}C, 600 MeV, cross-section for π^{-} production 2−67222
- ^{9}Be(t,p)^{11}Be, investigations of ^{11}Be energy levels 2−59689
- ^{10}Be, half-life meas. 2−63845
- ^{10}Be form. cross sections in ^{16}O by 135 and 550 MeV protons, radiochem. meas. 2−82961
- ^{11}Be, energy level investigations using ^{9}Be(t,p)^{11}Be reaction 2−59689
- ^{12}Be, ground state mass, reaction ^{7}Li(^{7}Li,2p)^{12}Be study 2−70374
- Be(d,n) thick-target yields and total cross sections 2−67333
- C, angular distrs. of neutrons for elastic scattering from natural target and inelastic scattering from ^{12}C, 3-7 MeV 2−46274
- C, Coulomb dissociation of W at 10 GeV/nucleon 2−49843
- C, inelastic interac. with cosmic nucleons, 760-7600 GeV 2−42558
- C, neutron inelastic scattering, 7.5 MeV, spin-flip probability 2−70448
- C, photonuclear reaction, Butler−Pearson model verification 2−55979
- C, π- absorption from rest, obs. of α spectrum, p spectrum and secondary particles 2−63902
- C,π^{-} capture, energy spectra and emission probabilities of proton, deuteron and triton 2−79793
- C (A=12,13), optical model analysis of ^{6}Li elastic scatt. 2−56004
- C recoil produced by neutrons in Naton 136 plastic scintillator 2−63701
- ^{9}C, β-delayed proton decay 2−63844
- ^{10}C→^{10}B(2155 keV) β branch strength 2−46185
- ^{11}C, production with 3 MeV Van de Graaff 2−70646
- ^{11}C 8.694 MeV level half-width 2−82963
- ^{11}C 8.694 MeV level half-width 2−82963
- ^{12}C/^{13}C ratio in atm. of Jupiter 2−66170
- ^{12}C-^{12}C scattering, nuclear molecular structure 2−49839
- ^{12}C-N high energy cosmic ray interaction, cf of optical and Glauber models 2−73892
- ^{12}C, alpha-gamma ang. correlation studies 2−70477
- ^{12}C, analysis of 20 GeV proton elastic scattering 2−42560
- ^{12}C, α-cluster model, effect of internal structure of α particle on binding energy 2−70357
- ^{12}C, α chain states study through decay widths 2−46110
- ^{12}C, calc. for quasi-elastic (p,2p) scatt. at 460 MeV 2−46258
- ^{12}C, charge radius from electron scattering data 2−49726
- ^{12}C, cluster model 2−70373
- ^{12}C, continuum structure discussed in eigenchannel reaction theory 2−67147
- ^{12}C, cross-sections for production of ^{6}Li and ^{7}Li by 150, 600 MeV protons and 800 MeV α-particles 2−74088
- ^{12}C, d absorption cross section, 25 GeV/c, Glauber theory calc. and comparison with expt. 2−70469
- ^{12}C, elastic and inelastic electron scatt. form factors in Hartree-Fock approx. 2−82956
- ^{12}C, elastic and inelastic Glauber scatt. of protons in alpha-particle model 2−59751
- ^{12}C, elastic electron scatt., dispersion corrections 2−46237
- ^{12}C, elastic electron scatt., symmetrized Fermi density distrib. appl. 2−76833
- ^{12}C, elastic hadron scatt. cross sections 2−82723
- ^{12}C, elastic scatt. of ^{16}O, possible formation of nuclear molecule in ^{28}Si at 36.5 MeV 2−46122
- ^{12}C, elastic scatt. of neutrons, elastic scatt., microscopic approach, coupled channel calcs. 2−76855
- ^{12}C, elastic scattering of ^{7}Li and ^{6}Li 2−42590
- ^{12}C, forward scatt. amplitudes, $K_s{}^{0}$ regeneration amplitude 2−82737
- ^{12}C, giant resonance, separation approximation in continuum shell model 2−59690
- ^{12}C, giant resons., ^{11}B(p,γ)^{12}C obs. 2−63772
- ^{12}C, high energy proton-nucleus interactions, production of light fast nuclides 2−74087
- ^{12}C, inelastic neutron scatt., E_n = 7.48 MeV, spin-flip probability 2−82983
- ^{12}C, isospin-mixing matrix element 2−63771
- ^{12}C, $J^{\pi}=0+$, T=2 reson. search in ^{9}Be(^{3}He, $\gamma\gamma$)^{12}C reaction 2−70476
- ^{12}C, μ^{-} capture, leading to specific final states, capture rate 2−74066
- ^{12}C, nuclear- Coulomb interference in π^{+} scattering 2−42578
- ^{12}C, photon spectra from radiative absorption of pions 2−46296
- ^{12}C, pion capture, meas. of emitted neutron-charged particle final state 2−46300
- ^{12}C, proton total cross-sections, 180-560 MeV 2−74071
- ^{12}C, π^{-} inelastic scatt. cross sections 2−59772
- ^{12}C, quasielastic 550−1150 MeV electron scatt. cross-section 2−76834
- ^{12}C, quasifree electron scattering, Born approx. calc. 2−49786

Nuclei with $6 \leqslant A \leqslant 19$ continued
^{12}C, semileptonic weak interactions, cross-sections 2−74067
^{12}C, transfer reactions induced by ^{12}C, selective excitation of one-, two- and three-nucleon excitation 2−49845
^{12}C electron and positrons induced disintegration, 20 to 30 MeV absolute cross-sections 2−82954
^{12}C electron scattering, anomalous quasi-elastic cross section 2−74063
^{12}C polarimeter for 20-30 MeV deuterons, calibration 2−52700
^{12}C quadrupole and octupole vibrations, form factors and transition densities of 4.34 and 9.64 MeV levels 2−82881
^{12}C rotational states, properties of projected HF functions of ground state bands 2−73992
^{12}C + ^{12}C, reaction, stellar reaction rate 2−51737
^{12}C + ^{12}C elastic scattering, presence of quasi molecular rotational bands 2−49838
$^{12}C + ^{12}C \rightarrow \alpha_1 + ^{20}NC^* \rightarrow \alpha_2 + ^{16}O$ g.s., high-spin states in ^{20}Ne and classification into rotational bonds 2−49732
^{12}C + ^{16}O reaction, stellar reaction rate 2−51737
^{12}C(^{12}C,α)^{20}Ne, excitation functions 2−83022
^{12}C(^{16}O, ^{16}O) elastic scattering, analysis by Feynmann graph techniques 2−74117
^{12}C(^{16}O,^{16}O)^{12}C, resonance like structure obs. with spin $I=14$ 2−49837
^{12}C(^{16}O,p)^{27}Al, search for high-spin states in ^{27}Al in excitation range 4.8-8.0 MeV 2−42504
^{12}C(^{3}He,^{3}He), inelastic scattering, spin-flip of ^{3}He 2−70464
^{12}C(^{3}He, n)^{14}O, 13.3 and 18.2 MeV, meas. of differential cross-section, comparison with distorted wave calcs. 2−83011
^{12}C(^{3}He, p)^{14}N, 13.3 MeV, meas. of differential cross-section, comparison with distorted wave calcs. 2−83011
^{12}C(^{3}He,n)^{14}O, 25 MeV, meas. of energy spectrum of neutrons, differential cross sections, orbital angular momentum transfers 2−46315
^{12}C(^{3}He,p)^{14}N(p′)^{13}C$_{g.s.}$ 14 MeV, proton and γ-ray decay of $T=0$ level in ^{14}N 2−73997
^{12}C(^{3}He,p)^{15}N, 5 MeV, study of two-particle three-hole structure of negative-parity states in ^{15}N 2−70375
^{12}C(^{3}He,pγ)^{14}N, 14 MeV, proton and γ-ray decay of $T=0$ level in ^{14}N 2−73997
^{12}C(^{3}He,pγ)^{14}N, parity of first unbound state in ^{14}N 2−63773
^{12}C(^{6}Li, d)^{16}O mechanism, determ. of ^{16}O energy levels 2−83021
^{12}C(^{6}Li,d)^{16}O, angular distrib. of γ-rays meas. on function of bombarding energy 2−46332
^{12}C(^{6}Li,d)^{16}O stripping reaction, use of Eckhart interactions in DWBA 2−46223
^{12}C(^{7}Li,α)^{15}N, 28-38 MeV, triton transfer, excited states of ^{15}N 2−70481
^{12}C(α, ^{8}Be)^{8}Be, 15 to 18.96 MeV, search for 8^+ level in ^{16}O 2−79733
^{12}C(α,^{6}Li)^{10}B, ^{12}C(α,^{7}Be)^{9}Be, ang. distribution and cross sections of emitted heavy ions 2−49831
^{12}C(α, α)^{12}C, 4-13.3 MeV, spin and parity assignments, new O^+ level in ^{16}O 2−79735
^{12}C(α,$\alpha_1\gamma_{4.43}$)^{12}C, $E_2=10.2$-10.5 Mev, ang. correls. and 14.8 MeV level in ^{16}O 2−76869
^{12}C(d,^{6}Li), 28 MeV, ang. distribution meas. and DWBA analysis 2−59782
^{12}C(d,^{7}Li)^{7}Be, angular distrib. meas. on test of Barshay- Temmer theorem 2−46259
^{12}C(d, α)^{10}B, 7.19-13.99 MeV, isospin forbidden reaction obs. 2−63916
^{12}C(d, d), 20-30MeV polarized beam, meas. of angular distribs., vector polarization, differential cross sections, optical model parameters 2−74106
^{12}C(d, p$_0$)^{13}C, polarized deuteron reaction 2−55998
^{12}C(d, p$_1$)^{13}C, polarized deuteron reaction 2−55998
^{12}C(d,d′)^{12}C*, isospin-mixing matrix element obs. 2−63771
$^{12}C(d,d')^{12}C \rightarrow ^8Be + \alpha$, 9.6 MeV, meas. of angular correlation function of (d,α) coincidences, comparison with theory 2−49832
^{12}C(d,d), 1.6 to 2.7 MeV, tensor polarization of deuterons 2−42580
^{12}C(d,n), $E_d=11.8$ MeV, neutron spectroscopy 2−67324
^{12}C(d,n)^{13}N, weakly bound projectile model calcs. of spectroscopic factors 2−67325
^{12}C(d,p)^{13}C, weakly bound projectile model calcs. of spectroscopic factors 2−67325
^{12}C(d,p)^{13}C, weakly bound projectile model calcs. of spectroscopic factors 2−67325
^{12}C(e,e′p)^{11}B, quasi-free scattering and independent particle model 2−49787
^{12}C(μ,n), effects of giant resonance on energy spectra of emitted neutrons 2−46240
^{12}C(μ^-, ν_μ)^{12}B, recoil nuclear polarization of ^{12}B 2−74065
^{12}C(n, n)^{12}C elastic scatt. of partially polarized neutrons, asymmetry 2−76860
^{12}C(n,α)^{9}Be, 14.8 to 18.8 MeV, differential cross sections 2−42571
^{12}C(n,n′γ)^{12}C, improved statistics for angular correlation measurements 2−46273
^{12}C(n,n), elastic scattering of 11.1 MeV neutrons, optical model analysis 2−67234
^{12}C(n,n)^{12}C, below 4.43 MeV, comparison of Feshbach with R-matrix theory 2−46275
^{12}C(p,^{6}Li)^{7}Be, differential cross section from 36-56.8 MeV angular distrib. and excitation functions meas., DWBA analysis 2−46259
^{12}C(p,2p), microscopic calcs. of cross sections in plane wave impulse approx., determ. of spectral function 2−55992
^{12}C(p,γ_0)^{13}N, 8.6-16.3 MeV, destructive interference 2−46250
^{12}C(p,p′3α), mechanism, cross sections, ^{8}Be and ^{9}B ground states, $E_p=13$ MeV 2−59757
^{12}C(p,pn)^{11}C cross-section at 7.6 GeV 2−82969
^{12}C(π,πn)^{11}C near 3-3 resonance, isospin invariance examination of reaction 2−46297
^{12}C(π-,π-) 69.5, 80, 87.5 MeV, influence of Fermi motion included in Kisslinger optical potential description 2−49814
^{12}C(π-,π-π-)^{12}N, 4 GeV, cross section obs. 2−46299
^{12}C(π^-, nn)^{10}C, expressions for transition strength analysis of data 2−46298
^{12}C(π^-,nn), study of excitation spectrum of residual nucleus 2−49816
^{12}C(π^+, 2p), 70 MeV, differential cross-section 2−70461

Nuclei with $6 \leqslant A \leqslant 19$ continued
^{12}C(t, n)^{14}N, 8.0 MeV, meas. and comparison with double stripping theory 2−76874
^{13}C-^{73}Ge directly bonded coupling constant in tetramethylgermane 2−46522
^{13}C, e.m. transitions from isobaric analogue states 2−46111
^{13}C, elastic scatt. of ^{12}C, nucleon exchange 2−83019
^{13}C, energy level, study from reaction ^{11}B(d,n)^{12}C at 900 keV 2−42584
^{13}C, n.m.r. long-range spin couplings 2−77134
^{13}C, positive parity bound states energies 2−76855
^{13}C, pulsed double resonance in solid adamantane, analogue Fourier transform spectroscopy 2−68752
^{13}C, spin and parity assignments made by phase- shift analysis of elastic scattering cross sections for neutrons on natural C targets 2−46274
^{13}C absolute determ. from $\sigma\|$ for CS$_2$ 2−53000
^{13}C chemical shielding parameters in organic solids determ. using proton enhanced nuclear induction spectroscopy 2−72524
^{13}C chemical shift in cyclopropylidene cycloalkanes 2−42975
^{13}C chemical shifts in hydrocarbons determ. from INDO perturbation calc. of magnetic shielding consts. 2−64162
^{13}C contact shift study of interaction between halogenated molecule and nitroxide radical 2−51440
^{13}C coupling consts. from NMR analysis of some nitroxide radicals 2−83295
^{13}C Fourier transform n.m.r. study of trimethyl(phenylethynyl)-silane, Si-C bonding 2−83312
^{13}C ground state and 3.09 MeV state spectroscopic factors determ. by weakly bound projectile model calcs. on ^{12}C(d,p) reaction 2−67325
^{13}C hyperfine splitting in e.s.r. spectra, linear dependence of spin polarization parameters 2−79986
^{13}C impurity in benzene crystal, impurity effect on i.r. exciton spectrum 2−80950
^{13}C in mols., suppression of Overhauser effect in n.m.r. 2−67463
^{13}C internucl. Overhauser effect, paramag. species influence 2−59984
^{13}C n.m.r., molec. structure study of polybutadiene 2−53091
^{13}C n.m.r. chem. shifts calc. using mol. orbital theory 2−77102
^{13}C n.m.r. chem. shifts for polyatomic mols., mol. orbital theories of n.m.r. shifts 2−67461
^{13}C n.m.r. in acetoxime, chem. shift 2−64165
^{13}C n.m.r. in tropolone 2−64194
^{13}C n.m.r. investigation of pyridine, nicotinamide, their cations and related compounds 2−83309
^{13}C relax. meas. under proton coupled and decoupled conditions 2−67462
^{13}C spin-lattice relax. in formic acid 2−60069
^{13}C spin relax. in solid benzene 2−81310
^{13}C−{^{1}H} Fourier transform n.m.r., sequence structures of polybutadienes 2−67529
^{13}C(^{3}He,n)^{15}O, meas. of absolute differential cross section, angular distrib. of neutron yield, 5.5 and 6.2 MeV 2−46316
^{13}C(^{3}He,p)^{15} meas. of absolute differential cross section at 5 MeV and excitation functions from 3.5-6.0 MeV 2−63775
^{13}C(d,n), $E_d=11.8$ MeV, neutron spectroscopy 2−67324
^{13}C(p, γ)^{14}N, γ-decay of levels in ^{14}N 2−76780
^{14}C, elastic scatt. of ^{12}C and ^{13}C, nucleon exchange 2−83019
^{14}C dating method employing emulsion 2−75438
^{14}C environmental contamination due to nuclear power stations 2−54871
^{14}C exhalation analysis, design of acclimation room 2−58597
^{14}C exhalation radiometry using CO$_2$-counter 2−58619
^{14}C labelled compounds, production control of surface and internal contamination 2−58604
^{14}CO$_2$ standard unit for radionuclide activity in gases 2−55971
C(d,n) thick-target yields and total cross sections 2−67333
F, neutron resonance spectroscopy using R-matrix 2−46285
F($A=18.19$), effective interactions in s-d shell 2−49728
^{17}F, missing state obs. using ^{15}N(^{3}He,n)^{17}F reaction 2−46114
^{17}F levels excited in ^{16}O(d,n) reaction at 3-4 MeV 2−83014
^{17}F levels excited in two-nucleon transfer reactions in ^{19}F 2−82972
^{18}F, adsorption on glass, Ti, Al surfaces 2−83877
^{18}F, Bethe-Goldstone equation, solution from NN phase shift data 2−46067
^{18}F, E2 transition strengths of analogue states 2−74000
^{18}F, effective neutron-proton interaction 2−70381
^{18}F, excitation energy of fourth excited state 2−63777
^{18}F, exptl. evidence for alpha-particle cluster states 2−82884
^{18}F, odd-parity levels with three-particle one-hole structure excited in ^{15}N(^{6}Li, t) reaction 2−74001
^{18}F, $T=0$ levels calc. using one-boson- exchange pots. 2−63778
^{18}F internal radiation dose, use in bone scanning 2−55274
^{18}F off-shell effects in shell model spectra 2−63779
^{19}F, (n,α) cross-sections obs., 5.85 MeV 2−76848
^{19}F, anomalous n.m.r. shift in SmF$_3$ 2−84589
^{19}F, dynamic polarization in CaF$_2$:O 2−51295
^{19}F, ENDOR in KZnF$_3$:V^{2+} 2−75353
^{19}F, e.m. transitions from isobaric analogue states 2−46111
^{19}F, excited state lifetimes 2−52739
^{19}F, mag. screening in tetrahedral and octahedral environments 2−48120
^{19}F, muon capture, partical transitions 2−52807
^{19}F, n.m.r., in RbMnF$_3$, spin-lattice and spin-spin relax. obs. 2−72516
^{19}F, n.m.r. in K$_2$MnF$_4$ planar antiferromagnet, hyperfine contribs. to lineshift obs. 2−54510
^{19}F, n.m.r. in solid HF 2−71434
^{19}F, spectroscopic factors for 4p-0h states from DWBA analysis of ^{15}N(^{7}Li,t) reaction 2−42591
^{19}F, spin-lattice relaxation time, Na$_2$PO$_3$F and NaPF$_6$ solns. in D$_2$O and H$_2$O 2−50372
^{19}F, spin coupling parameters in fluoromethyl radicals 2−77148
^{19}F, spin lattice relax. in BaF$_2$:Er in laboratory frame and rot. frame 2−68582
^{19}F, transitions strengths and decay properties, study by (γ,γ') reaction 2−52744
^{19}F, two-nucleon transfer reactions using 45 MeV protons 2−82972
^{19}F and ^{1}H n.m.r. spectra in substituted fluorothiophenes 2−46606

Nuclei with $6\leqslant A\leqslant 19$ continued
^{19}F isospin- forbidden reactions, second T=0 state of ^{20}Ne as compound reson. 2−76785
^{19}F lifetime meas. by recoil distance method 2−46120
^{19}F many-nuclear transfer reactions induced by ^{16}O, ^{19}F, finite DWBA calculation 2−56005
^{19}F n.m.r. in KPF_6 and $RbPF_6$ 2−61562
^{19}F n.m.r. in $RbMnF_3$ 2−48113
^{19}F n.m.r. parameters of individual fluorines of trifluoromethyl group 2−77113
^{19}F shielding tensors of trifluoromethyl group in silver trifluoroacetate 2−68751
^{19}F spin-lattice relax. in spherical top mols. 2−56199
^{19}F spin-lattice relax. in BaF_2: Eu^{2+} 2−44315
^{19}F spin-lattice relax. in symmetric top mols. 2−56200
^{19}F spin-lattice relaxation in sulphur hexafluoride clathrate deuterate 2−72531
^{19}F(α,2α), ^{19}F (α,αt), α and triton clustering probabilities, PWIA analysis 2−59778
^{19}F(d,^{6}Li), 28 MeV, ang. distribution meas. and DWBA analysis 2−59782
^{19}F(d, α)^{17}O, 2.34 to 14.45 MeV, resonance structure in excitation function 2−67326
^{19}F(d,α)^{17}O, 3 MeV, meas. of α-particle angular distribs. 2−67151
^{19}F(d,p)^{20}F, 3 MeV, meas. of differential corrections and angular distribs. of proton groups 2−67151
^{19}F(d,p)^{20}F, E_d=16 MeV, nucl. struct. of ^{20}F 2−63917
^{19}F(d,pγ)^{20}F, p,γ ang. correl., low-lying states of ^{20}F 2−79801
^{19}F(γ,xn), threshold −15 MeV, meas. of total photoneutron cross section 2−49783
^{19}F(n,2n)^{18}F, E_n=14 MeV, cross section meas. by activation method 2−49802
^{19}F(π^-, π^-n)^{18}F, cross sections in 3-3 reson. region 2−59774
^{1}H-^{13}C satellite n.m.r. spectrum, of coupling constants in pyrene 2−46627
^{8}He, evidence of production and subsequent disintegration in K^- interactions with nuclear emulsion nuclei 2−52736
^{8}He production in K^- interactions on emulsion nuclei 2−79792
^{6}L(μ-,ν_μ)^{6}He, rate of reaction, impulse approximation treatment 2−59747
Li, A=6, 7, cross-sections for production by 150, 600 MeV protons and 880 MeV α-particles on ^{12}C 2−74088
Li natural target, search for bound trineutron produced by 19 MeV neutron bombardment 2−63896
Li target, neutron straggling 2−76868
^{6}Li, ^{3}He elastic, inelastic and charge-exchange scatt., 24.6 and 27.0 MeV 2−70463
^{6}Li, ^{7}Li electron elastic and inelastic scattering, extended Nilsson model and projected Hartree-Fock 2−82957
^{6}Li, Coulomb breakup 2−46331
^{6}Li, d absorption cross section, 25 GeV/c, Glauber theory calc. and comparison with expt. 2−70469
^{6}Li, elastic electron scatt., symmetrized Fermi density distrib. appl. 2−76833
^{6}Li, meas of hyperfine structure of 2^2P term by level crossing technique 2−63769
^{6}Li, parity and isobaric spin violating decay of 3.56 MeV level 2−82883
^{6}Li, pion electroproduction at 1180 MeV 2−70439
^{6}Li, structure and properties from high energy electron scattering 2−52802
^{6}Li, T=0, $J^\pi=1^+$, limits on magnetic moments 2−79754
^{6}Li, total neutron cross section from 100 to 1500 keV 2−49806
^{6}Li, two-centred cluster model calc. using supermultiplet scheme 2−55955
^{6}Li high energy limit for ^{4}He-^{2}H and ^{3}He-^{3}H form factors and nodes of wavefunctions 2−67146
^{6}Li isospin impurity of 4.57 MeV state 2−82879
^{6}Li proton, elastic and inelastic scattering, 25-45 MeV, meas. of angular distrib. for excitation of excited states 2−55991
^{6}Li(^{35}Cl, d)^{39}K, 68 MeV, excited states of ^{39}Km lifetimes 2−76792
^{6}Li(^{3}He, ^{3}He)^{6}Li, 24.5 and 27.0 MeV cross section for scatt. to excited states of ^{16}Li meas. 2−46302
^{6}Li(^{3}He, αp)^{4}He, asymmetric proton yield meas., cf with Reimann, Martin and Vogt model 2−63912
^{6}Li(^{3}He, t)^{6}Be, 24.6 and 27.0 MeV, cross-section determ. 2−46302
^{6}Li(^{6}Li, 2α)^{4}He direct process interpret 2-13 MeV 2−83020
^{6}Li(^{6}Li, α)2α, 2, 6 and 13 MeV, energy spectra fit 2−63925
^{6}Li(γ, np)^{4}He, 3.7 to 25 MeV, cross section calc. using dispersion theory methods 2−70434
^{6}Li(n, d)^{5}He, ground state angular distrib. rel. to DWBA 2−70452
^{6}Li(p,2p)^{5}He 100 MeV, angular correlation measurements 2−82966
^{6}Li(p,n)^{6}Be, 17.8 MeV, determ. of width of excited state in ^{6}Be from neutron spectra 2−52735
^{6}Li(p,pd)^{4}He, E_p=590 MeV, α-d clustering in ^{6}Li 2−63879
^{6}Li(p,pd)^{4}He, Treiman-Yang test for pole approx. at 19 MeV 2−63880
^{6}Li(π^-, d)^{4}H, search for ground and excited states of ^{4}H in three-body phase space energy distrib. for deuterons 2−52734
^{6}Li(π^-, nn), pion absorption and structure of ^{6}Li 2−82988
^{6}Li(t,p)^{8}Li, excitation function, ^{9}Be level obs. 2−63911
^{7}Li, Coulomb excitation of $^{1}._{2}{}^{-}$ state 2−76882
^{7}Li, γ-rays from first excited state populated by ^{7}Be radiative electron capture transition 2−46184
^{7}Li, n.m.r. in $LiCuVO_4$ 2−72511
^{7}Li, n.m.r. in lithium formate monohydrate 2−54512
^{7}Li n.m.r. in lithium ammonium tartrate 2−72527
^{7}Li neutron scattering, review of total and principal partial cross-sections in range 10 keV-15 Mev 2−74095
^{7}Li spin relax. in dil. Li alloys 2−44317
^{7}Li(^{3}He,p)^{9}Be, ^{7}Li(^{3}He,t)^{7}Be, ^{7}Li(d,t)^{6}Li, two-mode finite-range DWBA analysis of mechanism 2−70475
^{7}Li(α,t)^{8}Be, triton ang. distrib., 15-25 MeV, excitation functions 2−74112
^{7}Li(d,α)^{5}He, detn. of first excited state of ^{5}He 2−63768
^{7}Li(d,α)^{5}He, E_d=0.45-2MeV, sequential mechanism 2−74111
^{7}Li(p,2d)^{4}He, 45 MeV, study of reaction mechanisms 2−49795
^{7}Li(p,pt)^{4}He structure of ^{7}Li by cluster model 2−82964
^{8}Li emission by heavy nuclei of photoemulsion exposed to 60 GeV pions 2−52821

Nuclei with $6\leqslant A\leqslant 19$ continued
Li(d,n) thick-target yields and total cross sections 2−67333
Li(π^+, 2p), A=6, 7, 70 MeV, differential cross section 2−70461
Λ^{12}C→^{1}H+Λ^{11}B, unstable resonant state of ^{12}C obs. 2−79732
^{12}N, semileptonic weak interactions, cross-sections 2−74067
^{12}N→^{12}C β decay to 4.44 MeV excited state, β-γ coincidence meas. 2−82927
^{13}N, 26, 28 and 32 MeV states from ^{10}B(^{3}He, particle) reactions 2−76873
^{13}N ground state spectroscopic factors determ. by weakly bound projectile model calcs. on ^{12}C(d,n) reaction 2−67325
^{14}N, core-excited 5^+ state identification 2−73997
^{14}N, first unbound state parity 2−63773
^{14}N, γ-decay of 8.06 and 5.69 MeV levels, isospin mixing 2−76780
^{14}N, level spectroscopy from ^{12}C(t, n)^{14}N study 2−76874
^{14}N, meas. of γ-ray production cross sections at 4.2, 5.9 and 6.9 MeV for (n,n′γ), (n, $\alpha\gamma$) and (n,pγ) reactions 2−79507
^{14}N, n.m.r. in $Ce_2Mg_3(NO_3)_{12}.24H_2O$ 2−48305
^{14}N, n.q.r., Stark effect 2−44463
^{14}N, n.q.r., Stark effect 2−44462
^{14}N, n.q.r. in hexamethylphosphorus triamide and hexamethyl phosphoric triamide, temp. dependence 2−48313
^{14}N, n.q.r. in hydrazine 2−72532
^{14}N, photoneutron cross sections, 15.5-29.5 MeV 2−70435
^{14}N, proton inelastic scattering, 17 MeV meas. of angular distribs., use of microscopic potential, weak coupling model 2−46260
^{14}N, spectroscopic factors of lower bound states determ. from ^{12}C(^{3}He, p) reaction 2−83011
^{14}N coupling consts. in azaaromatic radical anions 2−70745
^{14}N hyperfine tensor meas. in e.p.r. study of diphenylnitroxide in benzophenone 2−72474
^{14}N in 1,3-dimethylurea and tetramethylurea, NQR freq., coupling consts., var. with temp. 2−83297
^{14}N in solid N, teaching exercise in quantum mechanics 2−55353
^{14}N n.m.r., chemical shift in monosubstituted pyridines 2−56257
^{14}N n.q.r., Stark effect in axially symmetric field gradient in triethylenediamine and hexamethylenetetramine 2−61757
^{14}N n.q.r., σ and π electron densities as function of CNN angle in azines 2−80087
^{14}N n.q.r. and spin-lattice relax. in ferroelec. systems 2−81481
^{14}N n.q.r. in 50 molecular crystals 2−68742
^{14}N n.q.r. in $LiN_2H_5SO_4$ 2−68755
^{14}N quadrupole coupling in paraelectric $(NH_4)_2SO_4$ 2−44456
^{14}N quadrupole resonances of deuterated N compounds 2−46618
^{14}N(^{3}He, P_5)^{16}O*, 8.88 MeV, rectangular graphs 2−74113
^{14}N(^{3}He, p)^{16}O, 7.9-18.0 MeV, ang. distrib., compound nucleus formation, optical parameters 2−76875
^{14}N(α, γ)^{18}F, E_α=1526 keV, transition strengths of analogue states 2−74000
^{14}N(α,d)^{16}O, ^{16}O energy levels up to 30 MeV 2−46317
^{14}N(d, n)^{15}O, 5.16 MeV, n polarization ang. distrib. meas., cross-section analyzed using optical model formalism 2−46318
^{14}N(n,α), ang. distrib., emulsion method 2−59765
^{14}N(n,α)^{11}B, 14.8 to 18.8 MeV, differential cross sections 2−42571
^{14}N(p,2p)^{13}C, 46 MeV comparison of local and non-local t-matrix calc. of angular distrib. in distorted wave approx. 2−55993
^{14}N(p,γ)^{15}O, E_p=8.8 to 9.0 MeV, reson. struct. in ^{15}O 2−63774
^{14}N(p,p), 3 to 3.55 MeV, excited states of ^{15}O between 10 and 10.5 MeV 2−46112
^{14}N(π,πn)^{13}N, near 3-3 resonance, isospin invariance examination of reaction 2−46297
^{14}N(π^-,nn), study of excitation spectrum of residual nucleus 2−49816
^{15}N, proton inelastic scattering, 17 MeV meas. of angular distribs., use of microscopic potential, weak coupling model 2−46260
^{15}N, spin-lattice relaxation in $^{15}NH_3$ and $^{15}ND_3$ 2−50371
^{15}N, two-particle three-hole character of negative parity states studied using ^{13}C(^{3}He,p) reaction 2−63775
^{15}N, two-particle three-hole structure of negative parity states studied via ^{12}C(^{3}He,p) reaction 2−70375
^{15}N excited levels from ^{12}C(^{7}Li,α)^{15}N triton transfer reaction 2−70481
^{15}N giant dipole resonance, continuum shell model calc. 2−59691
^{15}N in organic compounds, spin-lattice relaxation, interaction mechanisms at high and low temperatures 2−57400
^{15}N in Orion A i.r. nebula 2−66135
^{15}N neutron scattering, parallelism between off-energy-shell total cross section and proton spectra from ^{15}N(d,p)^{16}N 2−42585
^{15}N(^{3}He,n)^{17}F, missing state obs. in ^{17}F 2−46114
^{15}N(^{6}Li, t)^{18}F, preferential excitation of odd-parity levels with three-particle one-hole structure 2−74001
^{15}N(^{7}Li,t)^{19}F, 15 MeV, finite range DWBA analysis, diff. cross section calc. using weak coupling model 2−42591
^{15}N(d,n_p)^{16}O, 4.83 MeV, meas. of polarization angular distribs. of ^{16}O states using time-of-flight method 2−70377
^{15}N(d,p)^{16}N(unbound), parallelism between proton spectra and off-energy-shell n-^{15}N total cross section 2−42585
^{15}N(p,γ_0)^{16}O, polarized proton capture reaction, giant dipole reson. obs. 2−67149
^{15}N(p,n)^{15}O, meas. of threshold energy, ^{15}O deduced mass 2−55957
^{17}N→^{17}O, energy distrib. of delayed neutrons 2−67194
Ne-H mixture, relative capture rates for slow π-,K-,Σ- 2−49817
^{18}Ne, Fermi β decay, mirror asymmetry 2−79772
^{18}Ne, lifetimes of 3376, 357 keV states 2−76784
^{19}Ne, excitation energies of states meas. in ^{20}Ne(^{3}He, ^{4}He) reaction up to 10.6 MeV 2−63780
^{19}Ne decay K electron capture/positron emission ratio 2−82926
^{20}Ne, second T=0 state obs. as compound nucleus in ^{19}F+p reactions 2−76785
^{20}Ne exptl. evidence for alpha-particle cluster states 2−82884
^{58}Ni(α, αn)E_α=900 MeV cross sections direct neutron emission mechanism 2−83010
O, Coulomb dissociation of W at 10 GeV/nucleon 2−49843
O(A=18,19), effective interactions in s-d shell 2−49728
^{14}O, half-life, beta decay coupling constant 2−74048
^{14}O, spectroscopic factors of lower bound states determ. from ^{12}C(^{3}He, n) reaction 2−83011
^{15}O, excited states between 10 and 10.5 MeV, study by ^{14}N(p,p) 2−46112

Nuclei with $6 \leqslant A \leqslant 19$ continued

^{15}O, proton configurations and spectroscopic factors from ^{13}C(^{3}He,n)^{15}O 2−67148

^{15}O, reson. struct., ^{14}N(p,γ)^{15}O obs. 2−63774

^{15}O and ^{15}N, identification of analogue states with corresponding theoretical negative-parity states 2−70375

^{15}O decay, K electron electron capture/positron emission ratio 2−82926

^{15}O levels populated in ^{12}C(^{3}He,n), determ. of spectroscopic factors using DWBA analysis 2−46316

^{15}O mass deduced from threshold energy meas. of ^{15}N(p,n)^{15}O 2−55957

^{16}O-^{16}O elastic scattering above Coulomb barrier, generator-coordinate method 2−83015

^{16}O, 8^{+} level, study by ^{12}C(α, ^{8}Be)^{8}Be reaction from 15 to 18.96 MeV 2−79733

^{16}O, α chain states study through decay widths 2−46110

^{16}O, backward scattering of 14.1 MeV neutrons, meas. of angular distrib. in 150°-180° range 2−76856

^{16}O, binding energy, radius, Hartree-Fock calculations with Feshbach-Lomon potential 2−73995

^{16}O, binding energy of first 0^{+} excited state, α-particle model 2−73998

^{16}O, c.m. spuriosity effects on charge form factor 2−67145

^{16}O, calc. for quasi- elastic (p,2p) scatt. at 460 MeV 2−46258

^{16}O, calc. of energy and saturating nuclear size using density- and momentum-dependent delta function interaction 2−70350

^{16}O, compound-nuclear reson. at 14.8 MeV from ^{12}C(α,$\alpha_1\gamma_{4.43}$)^{12}C study 2−76869

^{16}O, elastic α-particle scatt., antisymmetrization method applic. 2−79777

^{16}O, elastic electron scatt., symmetrized Fermi density distrib. appl. 2−76833

^{16}O, elastic electron scatt., dispersion corrections 2−46237

^{16}O, elastic π- scatt. in (3,3) reson. region 2−76864

^{16}O, fine structure of giant dipole resonance 2−46113

^{16}O, Hartree-Fock calcs. using modified delta interaction 2−63747

^{16}O, Hartree-Fock intrinsic states 2−63776

^{16}O, inelastic excitation of 2^{-} (8.88 MeV) level by α particles, role of two-body spin-orbit interaction 2−70430

^{16}O, inelastic nucleon scattering, excitation of abnormal parity states, dominance of spin flip mechanism 2−74069

^{16}O, level parameters and assignments, new O^{+} level at 15.17 MeV 2−79735

^{16}O, neutron spectra following muon capture 2−63903

^{16}O, off-shell effects in binding energy calcs. for set of phase-shift equivalent potentials 2−70376

^{16}O, orbital rearrangement effects due to removal of a proton 2−49716

^{16}O, Pauli breakup of deuterons 2−46320

^{16}O, photodisintegration and intermediate structure 2−46232

^{16}O, photon spectra from radiative absorption of pions 2−46296

^{16}O, proton bombardment, $E_p = 135$ and 550 MeV, radiochem. meas. of ^{10}Be and ^{7}Be form. cross sections 2−82961

^{16}O, proton inelastic scattering, core polarization exchange contribution 2−76841

^{16}O, proton total cross-sections, 180-560 MeV 2−74071

^{16}O, π^{-} scattering, 250 MeV, γ spectra study 2−70459

^{16}O, π^{+} scatt., 270 MeV, optical models 2−76866

^{16}O, rigorous method for soln. of Hartree Fock equation 2−76761

^{16}O, rotational bands, study by ^{12}C(^{12}C, ^{8}Be) reaction 2−42499

^{16}O, semi-leptonic weak and e.m. interactions 2−76831

^{16}O, shell-model analysis of Brueckner calcs. 2−63766

^{16}O, struct., review of theory 2−52741

^{16}O, $T = 2$ states, study by ^{14}N + d and ^{12}C + α reactions 2−73999

^{16}O, third-order corrections to binding energy 2−76776

^{16}O, total binding energy, relativistic Hartree-Fock approximation 2−42490

^{16}O, total muon-capture rate calc. using closure approx. effect of 2p-2h ground state admixtures 2−46085

^{16}O, transfer reactions induced by ^{12}C, selective excitation of one-, two- and three-nucleon excitation 2−49845

^{16}O calc. using generalized method of harmonic polynomials 2−79727

^{16}O energy levels, determ. by ^{12}C(^{6}Li, d)^{16}O mechanism 2−83021

^{16}O energy levels up to 30 MeV, ^{14}N(α,d)^{16}O reaction 2−46317

^{16}O giant dipole reson., polarized proton capture reaction obs. 2−67149

^{16}O ground state energy bounds and convergence of perturbation expansions 2−79715

^{16}O levels populated in ^{15}N(d,n$_p$) reaction at 4.83 MeV 2−70377

^{16}O nucleon-transfer form factors relative to microscopically specified core 2−46222

^{16}O odd-parity levels, transition rates and mean lifetimes, renormalized RPA calc. 2−82917

^{16}O rotational states, properties of projected HF functions of excited 8p-8h band 2−73992

^{16}O to ^{20}Ne region, exptl. evidence for alpha-particle cluster states 2−82884

^{16}O + ^{12}C reaction, quasimolecular states, resonances in total reaction yield 2−74119

^{16}O + ^{12}C system, reaction study near Coulomb barrier, correlated resonances in excitation functions of α-particle and proton exit channels 2−79808

^{16}O + ^{16}O elastic scattering, presence of quasi-molecular rotational bands 2−49838

^{16}O + ^{16}O reaction, stellar reaction rate 2−51737

^{16}O + ^{16}O stellar reactions at balanced power 2−51736

^{16}O(^{12}C, α)^{24}Mg*, triple correlation meas. to determine spin and parities of highly excited states in ^{24}Mg 2−74007

^{16}O(^{14}C,pn)^{28}Al, ^{16}O(^{14}C,p)^{29}Al, independence hypothesis tested 2−46334

^{16}O(^{16}O, ^{12}C)^{20}Ne, 17.5-30 MeV, cross-sections meas., possible ^{16}O + ^{16}O quasimolecular resonance 2−52827

^{16}O(^{16}O, ^{16}O) elastic scattering, calc. of adiabatic and angular-momentum dependent potential 2−63923

^{16}O(^{3}He, n)^{18}Ne, 10.3-18 keV, lifetimes of states in ^{18}Ne 2−76784

^{16}O(^{4}He.^{6}Li)^{14}N, ^{16}O(^{4}He,^{7}Li)^{13}N, ^{16}O(^{4}He,^{7}Be)^{13}C, ^{16}O(^{4}He,^{9}Be)^{11}C, ang. distribution and cross sections of emitted heavy ions 2−49831

Nuclei with $6 \leqslant A \leqslant 19$ continued

^{16}O(^{7}Li,t)^{20}Ne, 15 MeV, finite range DWBA analysis, diff. cross section calc. using weak coupling model 2−42591

^{16}O(d,^{6}Li), 28 MeV, ang. distribution meas. and DWBA analysis 2−59782

^{16}O(d,n), $E_d = 3$-4 MeV, cross sections and polarization, ^{17}F levels 2−83014

^{16}O(d,p)^{17}O, cross sections and vector and tensor analysing powers, study with polarised deuterons 2−46319

^{16}O(e,e)^{16}O, with short range correlations, study of third order terms 2−70438

^{16}O(γ, p$_0$)^{15}N, cross section calc. rel. to ^{15}N giant dipole resonance 2−59691

^{16}O(μ,n), effects of giant resonance on energy spectra of emitted neutrons 2−46240

^{16}O(n,α), ang. distribs., emulsion method 2−59765

^{16}O(n,α) cross sections, R-matrix analysis with diffuse-edge pot. 2−67268

^{16}O(n,n), elastic scattering of 11.1 MeV neutrons, optical model analysis 2−67234

^{16}O(n,n) cross sections, R-matrix analysis with diffuse-edge pot. 2−67268

^{16}O(p,2p), microscopic calcs. of cross sections in plane wave impulse approx., determ. of spectral function 2−55992

^{16}O(p,2p)^{15}N, two step process in amplitude calc. 2−46261

^{16}O(p,p), 14.5 MeV, optical-model calcs., determ. of nuclear forward-scattering amplitude 2−46245

^{16}O(p,p), $E_p = 65$ MeV, ang. distribs., optical model 2−74073

^{16}O(p,p), optical model calcs. with realistic nucleon-nucleon interaction 2−76837

^{16}O(π,π) scattering near 3,3 resonance differential and total cross sections calc. by multiple-scattering theory 2−46291

^{16}O(π,πn)^{15}O, near 3-3 resonance, isospin invariance examination of reaction 2−46297

^{16}O(π^{-},nn), study of excitation spectrum of residual nucleus 2−49816

^{16}O(π^{+}, 2p), 70 MeV, differential cross-section 2−70461

^{17}O, 4.55 MeV level width, ^{17}N β-decay obs. 2−67194

^{17}O, third-order corrections to single-particle energies 2−76776

^{17}O h.f.s. in e.s.r. spectra of Cu(II) hydroxyquinolinate complex in phthalimide crysts. 2−80071

^{17}O in ice, pure quadrupole reson. at 77 K, quadrupole coupling const. 2−75360

^{17}O levels excited in two-nucleon transfer reactions in ^{19}F 2−82972

^{17}O(p, γ)^{18}F, $E_p = 741$ keV, transition strengths of analogue states 2−74000

^{17}O(p,p), $E_p = 65$ MeV, ang. distribs., optical model 2−74073

^{17}O(p,p), optical model calcs. with realistic nucleon-nucleon interaction 2−76837

^{17}O(t,p)^{19}O, distorted-wave analysis of angular distribs., spin-parity assignments to states near 2.7 MeV excitation 2−79734

^{18}O, Bethe-Goldstone equation, solution from NN phase shift data 2−46067

^{18}O, electron scattering operators renormalization 2−79779

^{18}O, low-lying level spacing, shell model calculations 2−49727

^{18}O, off-shell effects in shell model spectra 2−63779

^{18}O + ^{16}O elastic scattering in 13-33 MeV energy range 2−46333

^{18}O(^{12}C,pn)^{28}Al, ^{18}O(^{12}C,p)^{29}Al, independence hypothesis tested 2−46334

^{18}O(^{18}O,2p + n)^{33}Si, 50 MeV, exotic nucleus prod. in s-d shell 2−74013

^{18}O(^{19}F,2p)^{35}P, 42-46 MeV, ^{35}P identification and characteriz. 2−74014

^{18}O(^{7}Li,t)^{22}Ne, 12 MeV, rot. bands in ^{22}Ne 2−76788

^{18}O(α,nγ), level struct. of ^{21}Ne 2−55958

^{18}O(α,nγ)^{21}Ne, excited states of ^{21}Ne obs. 2−59696

^{18}O(d,n)^{19}F, $E_d = 4$ MeV, excited level lifetimes meas. 2−52739

^{18}O(d,p)^{19}O, 3 MeV, meas. of absolute differential cross for proton groups, DWBA analysis 2−52740

^{18}O(γ,p), cross section determ., 16.4-24.5 MeV 2−52799

^{18}O(p, t)^{16}O, 41.7 MeV, failure of DWBA coexistence model 2−74089

^{18}O(p,p), $E_p = 65$ MeV, ang. distribs., optical model 2−74073

^{18}O(p,p), optical model calcs. with realistic nucleon-nucleon interaction 2−76837

^{18}O[2 +], mag. moment determination from hyperfine interactions in O^{7+} at 1.98 MeV 2−52906

^{19}O, orbital angular momentum and spectroscopic factors for levels populated in ^{18}O(d,p) reaction 2−52740

^{19}O, spin-parity assignments to levels near 2.7 MeV excitation determ. in ^{17}O(t,p) reaction 2−79734

^{19}O, study of energy spectrum and e.m. properties in framework of unified asymmetrical rotational models 2−52737

O($\mu -$,n), 2-13 MeV, meas. of neutron energy spectrum, excitation of quasibound states of intermediate nucleus 2−52806

O(p, p)O, $A = 16$, 17, 18, 65 MeV, angular distribs. 2−70442

Nuclei with $20 \leqslant A \leqslant 49$

4n nuclei up to ^{28}Si, HF calcs. of multipole deformations, static quadrupole moments, e.m. transitions 2−70364

^{22}Ne, static and dynamic quadrupole moments of first excited state determ. by projectile Coulomb excitation technique 2−42537

^{28}Si(^{3}He,n)^{30}S, 25 MeV, meas. of energy spectrum of neutrons, differential cross sections, orbital angular momentum transfers 2−46315

^{31}P(α,p)^{34}S, spin assignments for higher excited states of ^{34}S 2−52746

^{34}S, spin assignments for higher excited states using ^{31}P(α,p)^{34}S 2−52746

— 2−59725

— 2−59695

— 2−67244

— 2−67152

$A = 20$, energy level data 2−59686

$A = 48$, 49, inelastic scattering of 14 MeV neutrons 2−70450

A between 20 and 24, mixing of SU(3) symmetry, ds-shell model 2−82853

even-odd nuclei with $21 \leqslant A \leqslant 41$, p-level transition probabilities 2−59693

muon capture rate, correction due to presence of muon wave function in nuclear matrix elements 2−52804

Nuclei with $20\leqslant A\leqslant 49$ continued
quartet structs. in Ca, Cr, Fe, T, Zn 2−82840
spin cut-off factors from (n,2n) reactors at 14 MeV 2−70391
toroidal nuclei, deform. minima 2−82903
Z=59 to 69, nucleon separation, pairing and decay energies, atomic mass difference connections 2−52743
p resonance reactions on isotopes of Ar, Ca and Ti, review 2−46251
π- capture, 600 MeV, identification of emitted charged particles 2−46293
^{a}Mg(^{16}O, ^{12}C) (A=24,26), ang. distrib. meas. 2−63926
Al, neutron resonance spectroscopy using R-matrix 2−46285
Al, π^- capture, energy spectra and emission probabilities of proton, deuteron and triton 2−79793
^{24}Al→^{24}Mg, investigation of energy levels in ^{24}Mg 2−52774
^{25}Al, gamma decay of excited states, ^{24}Mg(p,γ)^{25}Al reaction 2−42503
^{25}Al, population of 3/2$^+$, 945 keV level in ^{2}H(^{24}Mg, nγ) reaction, meas. of mean lifetime for γ-ray decay 2−79736
^{25}Al excited state spins, ^{24}Mg(p,p$_1$'γ)^{24}Mg obs. 2−74009
^{26}Al, effective neutron-proton interaction 2−70381
^{26}Al, J=4 obtained for 2068.7 keV level, rotational structure evidence 2−63786
^{26}Al level struct. from ^{24}Mg(^{3}He,p) reaction 2−76876
^{27}Al, ^{16}O and ^{20}Ne induced reactions, enhancement of direct processes at high ang. momenta 2−70482
^{27}Al, analysis of 20 GeV proton elastic scattering 2−42560
^{27}Al, d absorption cross section, 25 GeV/c, Glauber theory calc. and comparison with expt. 2−70469
^{27}Al, high energy proton-nucleus interactions, production of light fast nuclides 2−74087
^{27}Al, intranuclear cascade calculations, proton-induced 2−46262
^{27}Al, large angle data in optical model analysis of helion elastic scattering 2−46313
^{27}Al, quasielastic 550−1150 MeV electron scatt. cross-section 2−76834
^{27}Al, reactions with ^{16}O, ang. momentum limits, fusion excitation functions 2−59787
^{27}Al, spin-lattice relax. in La$_{1-x}$Gd$_x$Al$_2$ 2−54370
^{27}Al, transition strengths and decay properties, study by (γ,γ') reaction 2−52744
^{27}Al high-spin states produced in ^{12}C(^{16}O,p) and ^{24}Mg(α,p) reactions, meas. of γ-ray branching ratios, p-γ angular correlation 2−42504
^{27}Al in MnAlGe ferromagnet. n.m.r. studies
^{27}Al n.m.r. in Al film interlayered with transition metals 2−68743
^{27}Al n.m.r. in FeMg garnet, quadrupole coupling const. 2−65341
^{27}Al n.m.r. in Tm$_3$Al$_2$ 2−48155
^{27}Al quadrupole interaction in ferromag. GdAl$_2$ 2−72509
^{27}Al(^{16}O, ^{12}C), ang. distrib. meas. 2−63926
^{27}Al(^{3}He,n)^{29}P, 25 MeV, meas. of energy spectrum of neutrons, differential crosssections, orbital angular momentum transfers 2−46315
^{27}Al(^{3}He,p)^{29}Si, 9-14 MeV, comparison of exptl. angular distribs. with two-nucleon transfer DWBA calcs. 2−70478
^{27}Al(^{3}He ^{3}He), 13 to 27 MeV angular distributions 2−83001
^{27}Al(n,n)^{27}Al, inelastic, 0.8-9.0 MeV, cross-section for production of de-excitation γ-rays 2−67243
^{27}Al(n,p)^{27}Mg, E_n=14 MeV, cross section meas. by activation method 2−49802
^{27}Al(n,p)^{27}Mg, E_n=14.1 MeV, proton energy and ang. distribs. 2−82981
^{27}Al(p,γ)^{28}Si, γ-rays from reson. at E_p=612 keV 2−76844
^{28}Al, beta decay asymmetry and n.m.r. 2−42500
^{28}Al, effective neutron-proton interaction 2−70381
^{28}Al, γ-γ ang.-correl. on low-lying levels, PAC determ. of 2$^+$ state moment 2−76790
Al(d,n) thick-target yields and total cross sections 2−67333
Al(p,π), 200-500 MeV, contribution of pions created in cascade mechanism to nuclear evaporation process 2−52813
Ar(A=36,38), effective interactions in upper s-d shell 2−49737
^{34}Ar, Fermi β decay, mirror asymmetry 2−79772
^{34}Ar, γ-decay and lifetime of low-lying states populated in ^{32}S(^{3}He, n) reaction 2−74012
^{36}Ar, branching ratios, excitation energies, lifetimes of levels, study by ^{35}Cl(p, γ) reaction 2−79748
^{36}Ar, bubble nuclei approach 2−82904
^{36}Ar, cluster model 2−70373
^{36}Ar, Hartree-Fock calcs. of bubble phenomena 2−82905
^{36}Ar, J^π=6- bound state, ^{35}Cl(p,γ) reaction study 2−59699
^{36}Ar 6$^-$ level obs. in ^{35}Cl(p,γ) reaction at 0.8-2.3 MeV following γ decay of 2231 keV resonance 2−52747
^{36}Ar γ transitions and levels from positron decay of ^{36}K 2−76817
^{36}Ar(^{16}O,^{12}C), excitation of rot. bands in ^{40}Ca 2−83017
^{36}Ar(3He,t)^{36}K, mass, decay props. and levels of ^{36}K 2−70387
^{36}Ar(d, α)^{34}Cl, 19 MeV, level properties of ^{34}Cl up to 3.6 MeV., D.W.B.A. analysis 2−76877
^{36}Ar(p,n) ^{36}K, E_p=15-30 MeV, excitation function for positron decay 2−76817
^{36}Ar(p,n)^{36}K, mass, decay props. and levels of ^{36}K 2−70387
^{37}Ar, lifetimes of levels below 3 MeV excitation populated by ^{34}S(α,n) meas. by Doppler shift attenuation method 2−63790
^{37}Ar, low-lying level props. 2−55960
^{37}Ar, mean lifetime of levels below 3.30 MeV excitation populated in ^{37}Cl(p,nγ) reaction 2−74015
^{37}Ar in expired air after low level neutron irradiation as measure of total body Ca content 2−69365
^{37}Ar lifetime meas. 2−63789
^{38}Ar, lifetime of lowest 5- state meas. by recoil-distance and Doppler-shift techniques 2−42506
^{38}Ar, transition strengths, branching ratios, spins and parities of levels populated in ^{34}S(α,γ) reaction 2−63791
^{40}Ar, excited states observed in ^{40}Ar(γ,n$_0$)^{39}Ar reaction 2−46129
^{40}Ar(α,n), E_n=6.3-8 MeV, states of ^{43}Ca 2−82897
^{40}Ar(α,n)^{43}Ca, 5.5-8 MeV, lifetimes of low-lying states of ^{43}Ca 2−74018
^{40}Ar(τ,t)^{40}K, 35 and 18 MeV, contribution of single-nucleon transfer mechanism to cross section 2−79799
^{41}Ar→^{41}K β-decay, study of nonconservation of P-parity in γ-decay of ^{41}K 2−49739
C-N, C-π interactions, 30-70 GeV accelerator obs., 100-300 GeV 2−73896

Nuclei with $20\leqslant A\leqslant 49$ continued
Ca, A=40, 44, 48, nuclear size, study by Ca(p,p) scattering at 10.8 to 16.3 MeV 2−49738
Ca, ang. distrib. of neutrons from μ^- capture 2−46356
Ca, even-even nuclei, 1$^+$ states investigation using (^{3}He,p) reactions, 1f-2p shell model predictions 2−46130
Ca, π^- capture, energy spectra and emission probabilities of proton, deuteron and triton 2−79793
Ca even isotopes, level spectra using self-consistent approxs. 2−76793
Ca isotopes, anomalous backward alpha scatt. interpret. 2−83007
Ca(A=39,41), core-particle coupled model of effective charge 2−46128
Ca(^{16}O,^{16}O), elastic scattering, incoming wave boundary condition calc. of cross section at incident energies near Coulomb barrier 2−42592
^{39}Ca, spectroscopic factors meas. in ^{40}Ca(^{3}He,α) neutron pick-up reaction 2−42586
^{40}Ca, backward-angle elastic scatt. of ^{16}O 2−74118
^{40}Ca, binding energy, radius, Hartree-Fock calculations with Feshbach-Lomon potential 2−73995
^{40}Ca, calc. for quasi-elastic (p,2p) scatt. at 460 MeV 2−46258
^{40}Ca, calc. of energy and saturating nuclear size using density- and momentum-dependent delta function interaction 2−70350
^{40}Ca, charge distribs., from electron scatt. 2−52745
^{40}Ca, elastic electron scatt., dispersion corrections 2−46235
^{40}Ca, ground state in closed-shell configuration 2−63792
^{40}Ca, HF charge distribution tested by electron scattering data 2−74016
^{40}Ca, levels excited in ^{42}Ca(p,t) reaction at 40 MeV 2−46264
^{40}Ca, neutron spectra following muon capture 2−63903
^{40}Ca, orbital rearrangement effects due to removal of a proton 2−49716
^{40}Ca, photon spectra from radiative absorption of pions 2−46296
^{40}Ca, proton inelastic scatt., 24.93-39.83 MeV, energy depend. 2−76838
^{40}Ca, quasielastic 550−1150 MeV electron scatt. cross-section 2−76834
^{40}Ca, rot. bands excitation 2−83017
^{40}Ca, search for multiparticle-multihole states in ^{32}S(^{12}C,α) reaction at 30 MeV 2−42508
^{40}Ca, transfer reactions induced by ^{12}C, selective excitation of one-, two- and three-nucleon excitation 2−49845
^{40}Ca elastic alpha scatt. energy depend. microscopic optical model 2−83008
^{40}Ca giant resonances in high-energy inelastic scatt. continuum 2−82967
^{40}Ca Hartree-Fock calcs. using modified delta interaction 2−63747
^{40}Ca muon capture, determ. of polarization of the emitted neutron 2−63868
^{40}Ca(^{3}He,α)^{39}Ca, neutron pick-up in N=20 closed shell, 11 MeV, meas. of spectroscopic factors 2−42586
^{40}Ca(^{6}Li,d)^{44}Ti, 32 MeV, angular distributions, cross-sections 2−70483
^{40}Ca(α,2p)^{42}Ca, mag. moment determ. for ^{42}Ca 2−59700
^{40}Ca(α,α)^{40}Ca, 29 MeV, calc. of α-cluster effects using L-independent optical potential 2−83013
^{40}Ca(d,^{6}Li), 28 MeV, and. distribution meas. and DWBA analysis 2−59782
^{40}Ca(d,n), meas. of neutron polarization angular distrib. 2−63915
^{40}Ca(n, α_0)^{37}Ar, 13.9 MeV, absolute differential cross-sections by parallel plate avalanche counter telescope 2−70453
^{40}Ca(n,α) and (n,p) cross-sections obs., 5.85 MeV 2−76848
^{40}Ca(n,γ), 14 MeV radiative capture, mass depend. of direct- semidirect theory calcs. 2−67270
^{40}Ca(n,γ)^{41}Ca, radiative capture, E_n=6-15 MeV, cross sections 2−67275
^{40}Ca(n,p)^{40}K, cross section fluctuations, 2.4 to 2.9 MeV 2−59766
^{40}Ca(p,2p)^{39}K, 460 MeV, ^{40}Ca energy level structure 2−46263
^{40}Ca(p,p'), e_p=8.7 MeV, lifetime of 3.74 MeV (3$^-$) state of ^{40}Ca 2−67154
^{40}Ca(p,p), 14.5 MeV, optical-model calcs., determ. of nuclear forward-scattering amplitude 2−46245
^{40}Ca(p,p)^{40}Ca, polarized proton, 2.3-2.8 MeV, meas. of proton polarization, determ. of angular momentum of ^{41}Sc excited states 2−52812
^{41}Ca, single-particle states and γ-ray transitions 2−67275
^{41}Ca, spin assignments, (d, pγ) reaction study at 3 MeV 2−63793
^{41}Ca(d,p)^{42}Ca, E_d=12 MeV, (1f$_{7/2}$)^2 multiplet of ^{42}Ca 2−67155
^{42}Ca, (1f$_{7/2}$)^2 multiplet, ^{41}Ca(d,p) obs. at E_d=12 MeV 2−67155
^{42}Ca, g-factor of 3.19 MeV 6$^+$ state 2−72243
^{42}Ca, low-lying level spacing, shell model calculations 2−49727
^{42}Ca, lowest 6$^+$ state, mag. moment, ^{40}Ca(α,2p) study 2−59700
^{42}Ca(p, t)^{40}Ca, 41.7 MeV, failure of DWBA coexistence model 2−74089
^{42}Ca(p,t)^{40}Ca, 40 MeV, excitation of levels in ^{40}Ca 2−46264
^{43}Ca level lifetimes from γ-ray Doppler-shift meas. 2−82897
^{43}Ca low-lying state lifetimes 2−74018
^{44}Ca/^{3}He,d) ^{45}Sc, 24 MeV, transition strength to d$_{3/2}$ hole state 2−82854
^{44}Ca, d$_{3/2}$ hole strength in ground state 2−82854
^{44}Ca(^{3}He,t)^{44}Sc, 25 MeV, level struct. of ^{44}Sc 2−74020
^{44}Ca(α,pγ)^{47}Sc, mean lives of low-lying levels in ^{47}Sc determ. by Doppler-shift attenuation method with p-γ coincidences 2−74021
^{44}Ca(d,α)^{42}K, E_d=11 MeV, energy levels of ^{42}K 2−70380
^{44}Ca(p,γ)^{45}Sc, ^{45}Sc energy levels up to 3 MeV 2−42509
^{45}Ca in solid Xe, β-decay, optical excitation of the daughter atoms Sc. 2−84244
^{48}Ca, backward-angle elastic scatt. of ^{16}O 2−74118
^{48}Ca, binding energy, radius, Hartree-Fock calculations with Feshbach-Lomon potential 2−73995
^{48}Ca, elastic and inelastic proton scatt., isobaric analog states in ^{49}Sc 2−70390
^{48}Ca, HF charge distribution tested by electron scattering data 2−74016
^{48}Ca, odd-parity levels, transition rates and mean lifetimes, renormalized RPA calc. 2−82917
^{48}Ca, proton inelastic scatt., ang. distribs. excited states obs. 2−76839
^{48}Ca Hartree-Fock calcs. using modified delta interaction 2−63747

Nuclei with $20 \leqslant A \leqslant 49$ continued
^{48}Ca(p, p′γ), particle-γ angular correlation and lifetime studies of 4.61 and 5.15 MeV levels 2−82889
Ca(μ^-,n), 2-13 MeV, meas. of neutron energy spectrum, excitation of quasibound states of intermediate nucleus 2−52806
Ca(p,p)Ca, A=40, 44, 48, cross-section meas., optical model determ. of r.m.s. radius 2−74076
^{38}Cd + CH_3Cl, H and halogen displacement factors, survival probability of products 2−84664
Cl, neutron resonance spectroscopy using R-matrix 2−46285
Cl (A=35, 37), optically detected ENDOR in excited triplet states of 8-chloroquinoline and paradichlorobenzene 2−46518
Cl (A=36,37), effective interactions in upper s-d shell 2−49737
^{33}Cl levels excited in ^{32}S(p,p) scattering, 2.5-3.0 MeV, spin and parity assignments 2−67153
^{34}Cl, effective neutron-proton interaction 2−70381
^{34}Cl, low-lying positive-parity states, (d,p) reaction and shell model obs. 2−59698
^{34}Cl, low-lying structure studied in modified vibrational unified model 2−46124
^{34}Cl, odd parity spectrum exptl. and theoretical study using ^{33}S(p,γ) reaction and six- particle shell-model calculations 2−46127
^{34}Cl, props. up to 3.6 MeV studied by ^{36}Ar(d, α)^{34}Cl 2−76877
^{35}Cl-^{23}Na spin system, rotating frame nuclear double resonance in NaCl 2−81473
^{35}Cl, mean lifetime, e.m. transition strengths of levels populated in ^{32}S(α,p) reaction 2−70386
^{35}Cl, n.m.r. and n.q.r. in liq. and solid Cl_2 2−72507
^{35}Cl, n.q.r. in alkali and alkaline earth chlorates 2−44464
^{35}Cl, populated in ^{34}P(α,p)^{34}S reaction 2−46323
^{35}Cl, transition strengths and decay properties, study by (γ,γ') reaction 2−52744
^{35}Cl n.q.r. and spin-lattice relax. in cubic antifluorite struct. cpds. 2−77748
^{35}Cl n.q.r. in rare earth trichlorides under hydrostatic press. 2−54519
^{35}Cl n.q.r. in various compounds, study of bonding with B, C, N, P, and S 2−64112
^{35}Cl quad. coupling consts. of o-chloropyridine 2−53052
^{35}Cl(α,p), 27.2 MeV, meas. of differential cross section, analysis of p angular distrib. in three nucleon stripping theory 2−49833
^{35}Cl(p, γ)^{36}Ar, branching ratios, excitation energies, lifetimes of ^{36}Ar levels 2−79748
^{35}Cl(p,d)^{34}Cl, low-lying positive-parity states obs. 2−59698
^{35}Cl(p,γ)^{36}Ar, 0.8-2.3 MeV, obs. of γ decay of resonances, determ. of branching ratios, energies 2−52747
^{35}Cl(p,γ)^{36}Ar, J^π=6- bound state in ^{36}Ar 2−59699
^{36}Cl, low-lying positive-parity states, (d,p) reaction and shell model obs. 2−59698
^{36}Cl, new levels populated in ^{37}Cl(^{3}He,α) neutron pick-up reaction, spectroscopic factors deduced 2−42586
^{36}Cl prod. from high energy protons, rel. to cosmic ray constancy 2−59753
^{37}Cl, n.m.r. and n.q.r. in liq. and solid Cl_2 2−72507
^{37}Cl, neutrino absorpt. cross sections, rel. to solar neutrino absorpt. 2−67212
^{37}Cl(^{3}He,α)^{36}K, neutron pick-up in N=20 closed shell, 11 MeV, meas. of spectroscopic factors 2−42586
^{37}Cl(n, γ)^{38}Cl, meas. of γ radiation, excitation energies for ^{38}Cl levels, Q-value 2−49808
^{37}Cl(n,γ)^{38}Cl, γ-ray spectra obs., correlation with E1 reduced intensities 2−67272
^{37}Cl(p,d)^{36}Cl, low-lying positive-parity states obs. 2−59698
^{37}Cl(p,n)^{37}Ar, low-lying level props. of ^{37}Ar 2−55960
^{37}Cl(p,nγ)^{37}Ar, 3.25-5.90 MeV, meas. of γ-ray angular distribs. and mean lifetimes of levels in ^{37}Ar 2−74015
^{38}Cl, beta decay asymmetry and n.m.r. 2−42500
^{38}Cl, excitation energies for levels populated in ^{37}Cl(n,γ) reaction 2−49808
^{38}Cl, mag. multipole props., effects of weak particle- hole admixtures 2−76791
^{40}Co, odd-parity levels, transition rates and mean lifetimes, renormalized RPA calc. 2−82917
^{47}Cr, mass, proton-rich nucleus in $1f_{7/2}$ shell 2−63794
^{40}Cu(α,p)^{43}Sc, E_α=28.5 MeV, stripping rel. to knockout mechanism 2−76871
^{20}F, effective interactions in s-d shell 2−49728
^{20}F, effective neutron-proton interaction 2−70381
^{20}F, γ-ray transitions of 1824, 1843 and 3176 keV levels 2−74004
^{20}F, structure, from ^{19}F(d,p)^{20}F reaction 2−63917
^{20}F β-emission, production by capture of polarized neutrons in MgF_2, static electric quadrupole interaction 2−75356
^{20}F levels excited in ^{19}F(d,p) reaction at 3 MeV, determ. of spectroscopic factors 2−67151
^{20}F low-lying states obs. from ^{19}F(d,pγ) ang. correl. 2−79801
^{59}Fe, magnetic moment 2−84457
K, neutron resonance spectroscopy using R-matrix 2−46285
K(A=37, 38), effective interactions in upper s-d shell 2−49737
^{36}K, mass, decay props. and levels from ^{36}Ar(p,n) and ^{36}Ar(^{3}He,t) reactions 2−70387
^{36}K → ^{36}Ar positron decay, excitation function, γ transitions 2−76817
^{38}K, new levels populated by ^{39}K(^{3}He,α) reaction at 21.09 MeV 2−42507
^{38}K, new levels populated in ^{39}K(^{3}He,α) neutron pick-up reaction, spectroscopic factors deduced 2−42586
^{38}K, two-hole states, obs. in ^{39}K(^{3}He, α) reaction 2−70388
^{39}K, charge distribs., from electron scatt. 2−52745
^{39}K, E2 calc. from hyperfine structure of 5p $^2P_{3/2}$ and 6p $^2P_{3/2}$ levels of K I spectra 2−46430
^{39}K, lifetimes of 2815 and 3598 keV levels 2−76792
^{39}K, low energy levels, examination by intermediate coupling model 2−55961
^{39}K, missing low lying states 2−52748
^{39}K, quasielastic 550−1150 MeV electron scatt. cross-section 2−76834
^{39}K, transition strengths and decay properties study by (γ,γ') reaction 2−52744
^{39}K level structure, inelastic scattering of 12.8 MeV deuterons 2−46324
^{39}K quadrupole reson. in $KClO_3$, steady-state double reson. obs. 2−54520

Nuclei with $20 \leqslant A \leqslant 49$ continued
^{39}K(^{3}He, α)^{38}K, obs. of two-hole states 2−70388
^{39}K(^{3}He,α)^{38}K, 21.09 MeV, meas. of two-hole strengths in ^{38}K 2−42507
^{39}K(^{3}He,α)^{38}K, neutron pick-up in N=20 closed shell, 11 MeV, meas. of spectroscopic factors 2−42586
^{39}K(n,γ)^{40}K, circular polarization of capture γ-radiation, spin assignment 2−67273
^{39}K(n,γ)^{40}K, interference of two spin components in thermal neutron capture state 2−49801
^{39}K(n,γ)^{40}K, meas. of circular γ-ray polarization for primary transitions, interference of spin components of capture state 2−42572
^{39}K(n,γ)^{40}K, thermal neutron capture, ^{40}K level scheme 2−67274
^{40}K, interference of two spin components of capture state in ^{39}K(n,γ) reaction 2−42572
^{40}K, spin assignment, (n,γ) reaction obs. 2−67273
^{40}K level scheme, ^{39}K(n,γ) obs. 2−67274
^{40}K mag. multipole props., effects of weak particle-hole admixtures 2−76791
^{40}K quadrupole reson. in $KClO_3$, steady-state double reson. obs. 2−54520
^{41}K, circular polarization calc. for 7/2-→$3/2^+$ transition using $\Delta T=1$ parity violating potential 2−82852
^{41}K, γ-decay nonconservation of P-parity studied by meas. of γ-transition circular polarization 2−49739
^{41}K, recoil implanted in Ni, hyperfine mag. field determ. 2−65205
^{41}K quadrupole reson. in $KClO_3$, steady-state double reson. obs. 2−54520
^{41}K(α,n)^{44}Sc, excitation functions and isomer ratios calc. in stat. models 2−82997
^{41}K(d,p)^{42}K, 6 MeV, spins of ^{42}K states determ. by γ-γ correlations 2−46131
^{42}K, energy levels, from ^{44}Ca(d,α)^{42}K reaction at 11 MeV 2−70380
^{42}K, spins of states determ. by γ-γ correlations in ^{41}K(d,p) reaction at 6 MeV 2−46131
^{43}K production for medical use 2−73173
^{48}K isotope obs. in proton reactions on U 2−82925
^{49}K isotope obs. in proton reactions on U 2−82925
^{140}La, contamination of monkeys by inhalation exposure, DTPA treatment 2−55259
Mg, A=24, 26 static quadrupole moment meas. via reorientation effect using Doppler-shift 2−74010
Mg isotopes, electron elastic and inelastic scattering, extended Nilsson model and projected Hartree-Fock 2−82957
Mg(^{3}He ^{3}He), A=24,25,26,13 to 27 MeV angular distributions 2−83001
^{22}Mg, Fermi β decay, mirror asymmetry 2−79772
^{22}Mg new states at 5006 ± 2 keV, 5317 ± 5 keV and 5837 ± 5 keV obs. in ^{20}Na(^{3}He,nγ) reaction 2−63784
^{24}Mg, elastic and inelastic scatt. of 12 MeV polarized deuterons, vector analysing power 2−67327
^{24}Mg, microscopic coupled-channel study of inelastic scattering using projected HF wave functions 2−70443
^{24}Mg, pairing vibrations, modified Tamm-Dancoff approximation 2−46100
^{24}Mg, photon spectra from radiative absorption of pions 2−46296
^{24}Mg, quasi-molecular rotational bands suggested by analysis of elastic ^{12}C + ^{12}C scattering 2−49838
^{24}Mg, resonance states, γ-ray decay props. 2−70384
^{24}Mg, SU(3) calculations 2−46121
^{24}Mg assignments to highly excited states from triple correlation meas. on ^{16}O(^{12}C, α)^{24}Mg* reaction 2−74007
^{24}Mg spectra, shell-model and Hartree-Fock calculations 2−74008
^{24}Mg(^{132}Xe,3−5n)$^{153-151}$Dy, compound nucleus production, identification of reaction products over energy of γ-transfer and fission semidecay periods 2−49846
^{24}Mg(^{3}He,^{3}He), inelastic scattering, spin-flip of ^{3}He 2−70464
^{24}Mg(^{3}He,p)^{26}Al, 18 MeV, level struct. of ^{26}Al 2−76876
^{24}Mg(α,α), meas. of differential cross sections between 27 and 28 MeV, optical-model and Hauser Feshbach analysis 2−49824
^{24}Mg(α,α)^{24}Mg, 20-23 MeV, compound nucleus effects in elastic scatt. 2−46303
^{24}Mg(α,p)^{27}Al, search for high- spin states in ^{27}Al in excitation range 4.8-8.0 MeV 2−42504
^{24}Mg(d,n), meas. of neutron polarization angular distrib. 2−63915
^{24}Mg(γ, γ'), E_α=15.4−19.1 MeV, continuum region obs. 2−76872
^{24}Mg(μ^-,γ)^{24}Na, γ-ray, yield meas. following μ^- capture 2−63870
^{24}Mg(p, p) elastic scatt. cross sections, E_p=100 MeV, optical model analysis 2−74074
^{24}Mg(p,γ)^{25}Al reaction, gamma decay of excited states of ^{25}Al 2−42503
^{24}Mg(p,$p_1'\gamma$)^{24}Mg, ^{25}Al excited state spins determ. 2−74009
^{25}Mg, population of $3/2^+$, 975 keV level in ^{2}H(^{24}Mg, pγ) reaction, meas. of mean lifetime for γ-ray decay 2−79736
^{25}Mg excited states, ^{22}Ne(α,nγ)^{25}Mg obs. 2−59725
^{25}Mg(d,α)^{23}Na, dependence of integrated cross sections on rotational states of ^{23}Na at 20.9 MeV 2−46322
^{25}Mg(d,d′n), 19 MeV, neutron-gamma competition 2−46325
^{26}Mg(α,α), meas. of differential cross sections between 22 and 28 MeV, optical-model and Hauser Feshbach analysis 2−49824
^{26}Mg(p, $\alpha\gamma$)^{23}Na, level study of ^{23}Na 2−76789
^{26}Mg(p, t)^{24}Mg, 26 MeV, statistical-model explanation of levels in ^{24}Mg 2−63881
^{27}Mg, level density parameters, nucl. temp. 2−82981
^{14}N structure, configuration mixing calc. 2−52738
^{20}Na, β^+-decay, anomalous fermi strength and minimum symmetry 2−59729
^{20}Na production in ^{20}Ne(p,n) reaction, method for reduction of background influences associated with gas target 2−49796
^{21}Na, excited states, proton scatt. and radiative capture in ^{20}Ne obs. 2−55969
^{21}Na, search for missing $J^\pi=3/2^+$ level using ^{20}Ne(^{3}He,d) and ^{20}Ne(p,γ) reactions 2−79761
^{21}Na energy level, investigation with ^{20}Ne(p, γ) and ^{20}Ne(d, n) reactions 2−74005
^{22}Na, e.m. transition probabilities, mean lives 2−63785
^{22}Na, effective neutron-proton interaction 2−70381
^{22}Na, higher-order matrix elements in hindered-allowed β-decays 2−82921
^{22}Na, neutron capture cross-sections 2−74098

Nuclei with $20 \leqslant A \leqslant 49$ continued
^{22}Na, practical angular momentum projection method in multishell Hartree-Fock calc. 2−46119
^{22}Na lifetime meas. by recoil distance method 2−46120
^{23}Na-^{35}Cl spin system, rotating frame nuclear double resonance in NaCl 2−81473
^{23}Na, 1.7-3.0 MeV proton bombardment, study of ^{24}Mg resonance states 2−70384
^{23}Na, dependence of integrated cross sections of ^{25}Mg(d,α)^{23}Na on rotational states at 20.9 MeV 2−46322
^{23}Na, excitation and levels to 6.58 MeV, spin, branching and elec. dipole strength of transitions 2−76789
^{23}Na, lowest lying $J\pi={}^{1}._{2}$ level prediction 2−46118
^{23}Na, n.m.r. in NaNO$_3$, intensity variations under u.s. stimulating quadrupole transitions 2−81483
^{23}Na, nuclear acoustic resonance in NaF 2−78170
^{23}Na, reson. fluoresc. above 3 MeV, level struct. 2−74006
^{23}Na, transition strengths and decay properties, study by (γ,γ') reaction 2−52744
^{23}Na in NaNd(WO$_4$)$_2$, n.m.r. and mag. susceptibility detn. 4.2-300K 2−72513
^{23}Na levels populated in ^{23}Ne β-decay, calcs. of ft-values using Nilsson model, and mixed states 2−79773
^{23}Na resonances corresponding to excited states observed in ^{22}Ne(p,γ) and ^{22}Ne(p,p$'\gamma$) reactions 2−49733
^{23}Na spin energy levels in NaClO$_3$, obs. 2−78166
^{23}Na(α, $\alpha'\gamma$)^{23}Na, level study of ^{23}Na 2−76789
^{24}Na, effective neutron-proton interaction 2−70381
^{24}Na, log ft values for second forbidden β-transitions 2−49762
^{32}Na isotope obs. in proton reaction on U, half-life meas. 2−82925
^{33}Na isotope obs. in proton reactions on U 2−82925
Ne-H mixture, relative capture rates for slow π-,K-,Σ- 2−49817
Ne, A=20, 22, static quadrupole moment meas. via reorientation effect using Doppler-shift 2−74010
^{20}Ne, ^{22}Ne shell model, quartet states and cluster model 2−82868
^{20}Ne, 0$^+$ states, spectroscopic strengths, α-particle widths 2−70382
^{20}Ne, alpha-decay widths for ground state and other levels calc. using harmonic oscillator shell model wave functions 2−49761
^{20}Ne, classification of high-spin states into rotational bands 2−49732
^{20}Ne, effective interactions in s-d shell 2−49728
^{20}Ne, excitation function for ^{12}C(^{12}C,α) leading to 2$^+$ state 2−83022
^{20}Ne, generator-coord. spectrum, T=0 levels 2−76786
^{20}Ne, ground and excited states, bounds on energy and wave functions 2−63751
^{20}Ne, low-lying even-parity levels, α-like spatial four-body correlations 2−46108
^{20}Ne, microscopic coupled-channel study of inelastic scattering using projected HF wave functions 2−70443
^{20}Ne, orbital rearrangement effects due to removal of a proton 2−49716
^{20}Ne, proton scatt. and radiative capture, excited states in ^{21}Na obs. 2−55969
^{20}Ne, rotational bands, study by ^{16}O(^{12}C, ^{8}Be) reaction 2−42499
^{20}Ne, spectroscopic factors from ^{21}Ne(p, d) obs. 2−76842
^{20}Ne, spectroscopic factors for 4p-0h states from DWBA analysis of ^{16}O(^{7}Li,t) reaction 2−42591
^{20}Ne, static and dynamic quadrupole moments of first excited state determ. by projectile Coulomb excitation technique 2−42537
^{20}Ne, transition to 2$^-$ rot. band in ^{22}Ne(p,t)^{20}Ne reaction 2−79786
^{20}Ne, two particle-two hole mixing in Hartree Fock calculations 2−42493
^{20}Ne rotational states, properties of projected HF functions of ground state bands 2−73992
^{20}Ne(^{3}He, ^{4}He)^{19}Ne, 18 MeV, meas. of excitation energies of states in ^{19}Ne, angular distrib. of ^{4}He 2−63780
^{20}Ne(^{3}He,d)^{21}Na, 16 MeV, analysis of emitted deuterons, search for missing $J^{\pi}=3/2^+$ level in ^{21}Na 2−79761
^{20}Ne(^{3}He,nγ)^{22}Mg, 4.3-11.5 MeV, angular correlation and coincidence meas., ^{22}Mg deduced levels 2−63784
^{20}Ne(d, n)^{21}Na, 3.6-6 MeV, meas. of angular distrib., excitation energies, stripping pattern 2−74005
^{20}Ne(d,pγ)^{21}Ne, study using p-γ and γ-γ coincidence techniques, determ. of levels in ^{21}Ne 2−79762
^{20}Ne(p, γ)^{21}Na, 0.98-2.2 MeV, meas. of excitation energies, Q-value, determ. of branching ratios 2−74005
^{20}Ne(p,n)^{20}Na, 20 MeV, meas. of cross section, reduction of background influences associated with gas target 2−49796
^{20}Ne(t, pγ)^{22}Ne, 3 MeV, p-γ ang. correl., spin assignments 2−79739
^{21}Ne, deform. parameters from (p, p) and (d, d) scatt. obs. 2−76842
^{21}Ne, level struct., ^{18}O(α,nγ) obs. 2−55958
^{21}Ne, levels up to 4.7 MeV excited in ^{20}Ne(d,pγ) reaction, comparison with Nilsson model calcs. 2−79762
^{21}Ne, lowest lying $J\pi={}^{1}._{2}$ level prediction 2−46118
^{21}Ne, pulsed n.m.r. in solid and liquid He 2−65347
^{21}Ne excited states obs. using ^{18}O(α,nγ) reaction 2−59696
^{21}Ne(d, d)^{21}Ne, deform. parameters of ^{21}Ne 2−76842
^{21}Ne(d, p)^{22}Ne, 3.3 and 3.6 MeV, cross-section meas., spectroscopic factors extracted 2−46321
^{21}Ne(d, p)^{22}Ne, spectroscopic factors of ^{22}Ne 2−76842
^{21}Ne(d,p)^{22}Ne, E_d=12 MeV, level struct. of ^{22}Ne 2−76787
^{21}Ne(p, d)^{20}Ne, spectroscopic factors of ^{20}Ne 2−76842
^{21}Ne(p, p)^{21}Ne, deform. parameters of ^{21}Ne 2−76842
^{22}Ne, e.m. transition probabilities, mean lives 2−63785
^{22}Ne, l_n=O and l_n=1 transfers associated with various levels 2−46321
^{22}Ne, lifetime meas. by recoil distance method 2−46120
^{22}Ne, spectroscopic factors from ^{21}Ne(d, p) obs. 2−76842
^{22}Ne level struct. by ^{21}Ne(d,p) reaction 2−76787
^{22}Ne rot. bands excited in ^{18}(^{7}Li,t)^{22}Ne 2−76788
^{22}Ne spin assignments following ^{20}Ne(t, pγ)^{22}Ne 2−79739
^{22}Ne(p, γ)^{23}Na, γ-ray resonant absorpt., ^{23}Na level widths, Rutherford scatt. effect 2−76843
^{22}Ne(p,γ)^{23}Na, 1.2 to 3.0 MeV, obs. of resonances corresponding to excited states of ^{23}Na 2−49733
^{22}Ne(p,p$'\gamma$)^{22}Ne, 1.2 to 3.0 MeV, obs. of resonances corresponding to excited states of ^{23}Na 2−49733
^{22}Ne(p,t)^{20}Ne, E_p=39.8 MeV, transition to 2$^-$ rot. band in ^{20}Ne 2−79786
^{23}Ne β-decay to levels in ^{23}Ne, meas. of γ radiation 2−79773

Nuclei with $20 \leqslant A \leqslant 49$ continued
^{58}Ni, ^{60}Ni(^{3}He, t), study of isobaric analogue states 0$^+$ and 2$^+$ in ^{58,60}Cu at 24.6 MeV 2−63918
^{16}O structure, configuration mixing calc. 2−52738
^{20}O, effective interactions in s-d shell 2−49728
^{21}O, ground state mass determ. from Q-value meas. of ^{232}Th(^{22}Ne, ^{21}O)^{233}U reaction 2−70383
^{22}O, ground state mass determ. from Q-value meas. of ^{232}Th(^{22}Ne, ^{22}O)^{232}U 2−70383
P, neutron production by incidence of high energy bremsstrahlung beam 2−55980
^{28}P→^{28}Si investigation of energy levels in ^{28}Si 2−52774
^{29}P, determ. of total angular momentum of excited states from ^{28}Si(p,p) elastic scattering 2−52812
^{30}P, e.m. transition probabilities, mean lives 2−63785
^{30}P, effective neutron-proton interaction 2−70381
^{30}P, lifetimes of excited states, in reaction ^{29}S(p,γ) 2−49734
^{30}P, low-lying structure studied in modified vibrational unified model 2−46124
^{30}P levels, odd parities, ^{29}Si(d,n)^{30}P reaction obs. 2−67328
^{30}P lifetime meas. by recoil distance method 2−46120
^{31}P, charge distribs., from electron scatt. 2−52745
^{31}P, e.m. transitions from isobaric analogue states 2−46111
^{31}P, excited states in (p,p$'$) reaction at 185 MeV 2−46125
^{31}P, inelastic neutron scatt. cross section between 0.75 and 9.00 MeV 2−52818
^{31}P, influence of γ-cascade on population of low-lying levels in ^{32}S(γ,p) reactions 2−42505
^{31}P, n.m.r. in Fe, hyperfine field detn. 2−75354
^{31}P, n.m.r. in P$_2$Se$_3$−As$_2$Se$_3$ semiconductor glasses, pseudobinary section comp. depend. 2−84584
^{31}P, n.m.r. in WO$_3$-P$_4$O$_{10}$-V$_2$O$_5$ glass system 2−54495
^{31}P, spin-lattice relaxation time, Na$_2$PO$_3$F and NaPF$_6$ solns. in D$_2$O and H$_2$O 2−50372
^{31}P, transition strengths and decay properties, study by (γ,γ') reaction 2−52744
^{31}P n.m.r., gas phase and solvent chemical shifts of PBr$_3$ 2−46575
^{31}P n.m.r. spectra of dimethylphosphoryl halides, and monomethylphosphoryl halides 2−46616
^{31}P spin-lattice relax. in symmetric top mols. 2−56200
^{31}P(α,p), 27.2 MeV, meas. of differential cross section, analysis of p angular distrib. in three nucleon stripping theory 2−49833
^{31}P(α,p)^{34}S, 3.25-5.5 MeV, obs. 2−46323
^{31}P(d,p)^{32}P, 10 MeV, meas. of angular distribs., spectroscopic factors 2−49834
^{31}P(n,n)^{31}P, inelastic, 0.8-9.0 MeV, cross-section for production of de-excitation γ-rays 2−67243
^{31}P(p, γ)^{32}S, E_p=1100-1600 keV, resonances 2−74090
^{31}P(π^-, π^-n)^{30}P, cross sections in 3-3 reson. region 2−59774
^{32}P, Cherenkov radiation from emitted electrons, applic. to detection of eye lesions 2−69459
^{32}P, decay modes and spins of states excited in ^{29}Si(α,p) reaction 2−49735
^{32}P, effective neutron-proton interaction 2−70381
^{32}P, first T=2 level analysis 2−63788
^{32}P, higher-order matrix elements in hindered-allowed β-decays 2−82921
^{32}P, internal irrad. source for inducing chemiluminesc. in luminol 2−48325
^{32}P, level density parameters, nucl. temp. 2−82981
^{32}P, spectroscopic factors deduced from angular distrib. meas. in ^{31}P(d.p) at 10 MeV 2−49834
^{32}P content in breast cancer, surface detection of diurnal variation 2−69266
^{32}P measurement in hair, exposure estimation method for fast neutrons 2−85130
^{33}P, half-life 2−52775
^{35}P, 48-sec. isotope, mass and decay 2−74014
^{35}P→^{35}S β-decay, ^{35}S level obs. and element assignment 2−74049
S, ang. distrib. of neutrons from μ^- capture 2−46356
S, π^- capture, energy spectra and emission probabilities of proton, deuteron and triton 2−79793
^{28}S, problems in structure studies 2−74011
^{30}S, γ-decay and lifetime of low-lying states populated in ^{28}Si(^{3}He, n) reaction 2−74012
^{31}S, influence of γ-cascade on population of low-lying levels in ^{32}S(γ,n) reaction 2−42505
^{32}S, charge distribs., from electron scatt. 2−52745
^{32}S, energies and branching ratios of bound levels, ^{31}P(p, γ) study 2−74090
^{32}S, energy and density of yrast levels considered in adiabatic potential calcs. on ^{16}O-^{16}O elastic scattering 2−63923
^{32}S, excited states in (p,p$'$) reaction at 185 MeV 2−46125
^{32}S, neutron spectra following muon capture 2−63903
^{32}S, prolate shape evidence from 104 MeV alpha scattering 2−46126
^{32}S, quasi-molecular rotational bands suggested by analysis of elastic ^{16}O + ^{16}O scattering 2−49838
^{32}S muon capture, determ. of polarization of the emitted neutron 2−63868
^{32}S spectra, shell-model and Hartree-Fock calculations 2−74008
^{32}S(^{12}C,α)^{40}Ca, 30 MeV, search for multihole-multiparticle states of ^{40}Ca 2−42508
^{32}S(^{3}He, n)^{34}Ar, 6.5-10 MeV, Doppler shift attenuation method for decay and lifetime of ^{34}Ar low-lying levels 2−74012
^{32}S(α,p)^{35}Cl, 10.0 MeV, meas. of mean lifetimes of levels in ^{35}Cl by Doppler-shift attenuation method 2−70386
^{32}S(γ,nγ'), influence of γ-cascade on population of low-lying levels of residual nucleus 2−42505
^{32}S(γ,pγ'), influence of γ-cascade on population of low-lying levels of residual nucleus 2−42505
^{32}S(n, α_0)^{29}Si, 13.9 MeV, absolute differential cross-sections by parallel plate avalanche counter telescope 2−70453
^{32}S(n,n)^{32}S, inelastic, 0.8-9.0 MeV, cross-section for production of de-excitation γ-rays 2−67243
^{32}S(n,p)^{32}P, 14.1 MeV, obs., deuteron elimination, comparison with statistical theory 2−67271
^{32}S(n,p)^{32}P, E_n=14.1 MeV, proton energy and ang. distribs. 2−82981
^{32}S(n,p) and (n,α) cross-sections obs., 5.85 MeV 2−76848

Nuclei with $20 \leqslant A \leqslant 49$ continued

^{32}S(p,p)^{32}S, ^{34}S(p,p)^{34}S, asymmetry in polarized p elastic and inelastic scatt., 24.5 MeV, optical model analysis 2−52810
^{32}S(p,p)^{33}Cl, polarized protons, 2.5-3.0 MeV, study of ^{33}Cl excited states, resonance parameters 2−67153
^{33}S low-lying levels up to 4.3 MeV excitation studied by ^{30}Si(α,nγ) reaction 2−70385
^{33}S n.m.r. spectroscopy applic. to electronic struct. of mols. 2−83290
^{33}S(p,γ)^{34}Cl, 1058, 1098, 1121 keV, study of odd-parity spectrum of ^{34}Cl 2−46127
^{34}S, lifetime of 5.69 MeV 5$^-$ level 2−49736
^{34}S(α,γ)^{38}Ar, 3.6-4.8 MeV, meas. of cross sections, angular distributions and angular correlations ^{38}Ar levels deduced 2−63791
^{34}S(α,n)^{37}Ar, meas. of lifetimes of levels in ^{37}Ar below 3 MeV excitation by Doppler shift attenuation method 2−63790
^{34}S(d,pγ)^{35}S, γ-ray from first excited state of ^{35}S 2−74014
^{34}S(n,γ)^{35}S, thermal neutron capture, meas. of γ-ray spectra transition scheme for ^{35}Si 2−49807
^{35}S, γ-transition scheme determ. from thermal neutron reaction ^{34}S(n,γ) 2−49807
^{35}S level scheme from ^{35}P β-decay obs. 2−74049
^{36}S, effective interactions in upper s-d shell 2−49737
^{36}S(t,α)^{35}P, E_t=3.4 MeV, ^{35}P identification and characteriz. 2−74014
^{41}Sc, determ. of total angular momentum of excited states from ^{40}Ca(p,p) elastic scattering 2−52812
^{42}Sc, transition rates between $(1f_{7/2})^2$ states 2−74017
^{42}Sc particle-particle nucleus, transformation properties of effective transition operator 2−82861
^{44}Sc, positron source for metal defect studies 2−80676
^{44}Sc level struct., ^{44}Ca(^{3}He,t) obs. 2−74020
^{44}Sc levels excited in ^{46}Ti(d,α) reaction at 26.7 MeV, two-nucleon transfer analysis 2−70479
^{45}Sc, energy of levels up to 3 MeV from ^{44}Ca(p,γ)^{45}Sc reaction 2−42509
^{45}Sc, n.m.r. in Sc-H solid solution, Korringa product and diffusion parameters 2−72517
^{45}Sc(n,γ)^{46}Sc, γ spectroscopic obs. of ^{46}Sc level scheme 2−67156
^{45}Sc(p, nγ)^{45}Ti, used to study levels in ^{45}Ti 2−46132
^{46}Sc, effect of hormones on retention in rats 2−55260
^{46}Sc level scheme, ^{45}Sc(n,γ) reaction obs. 2−67156
^{46}Sc levels excited in ^{46}Ti(d,α) reaction at 26.7 MeV, two-nucleon transfer analysis 2−70479
^{46}Sc source strength meas. using scintillation detectors and γ-γ coincidence, student expt. 2−78738
^{47}Sc, mean lives of low-lying levels determ. by Doppler-shift attenuation method with p-γ coincidences in ^{44}Ca(α,pγ) 2−74021
^{49}Sc, isobaric analog states study by elastic and inelastic proton scatt. from ^{48}Ca 2−70390
^{49}Sc M1 transition, analogue to antianalogue in $1f_{7/2}$ shell 2−82846
Si, neutron elastic and inelastic scattering, 7.5 MeV, spin-flip probability 2−70449
^{26}Si, Fermi β decay, mirror asymmetry 2−79772
^{28}Si, γ-ray decay of 15.22 MeV, T=2 state 2−59697
^{28}Si, neutron spectra following muon capture 2−63903
^{28}Si, possible nuclear molecule formation at 36.5 MeV in ^{16}O-^{12}C elastic scatt. 2−46122
^{28}Si, psec. lifetime of 9.699 MeV(5$^-$) level, delayed coincidence meas. 2−55959
^{28}Si, static quadrupole moment meas. via reorientation effect using Doppler-shift 2−74010
^{28}Si, two particle-two hole mixing in Hartree Fock calculations 2−42493
^{28}Si 612 keV reson. in ^{27}Al(p,γ) reaction 2−76844
^{28}Si muon capture, determ. of polarization of the emitted neutron 2−63868
^{28}Si octupole excitation of 29.5 MeV level by d inelastic scatt. 2−59776
^{28}Si spectra, shell-model and Hartree-Fock calculations 2−74008
^{28}Si(^{16}O, ^{12}C), ang. distrib. meas. 2−63926
^{28}Si(^{3}He, n)^{30}S, 6.5-10 MeV, Doppler shift attenuation method for decay and lifetime of ^{30}S low-lying levels 2−74012
^{28}Si(α,α,γ)^{28}Si, 10-18 MeV, angular correlation studies for excitation of 1.78 MeV 2$^+$ state 2−63787
^{28}Si(α,α), meas. of differential cross sections between 22 and 28 MeV, optical-model and Hauser Feshbach analysis 2−49824
^{28}Si(α,p), 27.2 MeV, meas. of differential cross section, analysis of p angular distrib. in three nucleon stripping theory 2−49833
^{28}Si(d,n), meas of neutron polarization angular distrib. 2−63915
^{28}Si(d,p)^{29}Si, DWBA analysis of data at 10 MeV 2−56000
^{28}Si(d,p)^{29}Si, Ej=10 MeV, energy levels of ^{29}Si 2−82887
^{28}Si(μ^-,γ)^{28}Al, γ-ray yield meas. following μ^- capture 2−63870
^{28}Si(n,γ), 14 MeV radiative capture, mass depend. of direct- semidirect theory calcs. 2−67270
^{28}Si(p, p$'$)^{28}Si, reaction time meas. by blocking technique 2−74058
^{28}Si(p, p) elastic scatt. cross sections, E_p=100 MeV, optical model analysis 2−74074
^{28}Si(p,p)^{28}Si, polarized protons, 1.5-3.0 MeV, meas. of proton polarization, determ. of angular momentum of ^{29}P excited states 2−52812
^{29}Si, Fourier transform n.m.r. spectroscopy, studies of organosilicon compounds 2−65355
^{29}Si, n.m.r., in PtSi 2−65348
^{29}Si, shell-model wave functions of ground and excited states tested in ^{27}Al(^{3}He,p)^{29}Si reaction 2−70478
^{29}Si energy levels from deuteron stripping obs. 2−82887
^{29}Si n.m.r. in FeMg garnet 2−65341
^{29}Si(α,p)^{32}P, 10.4-11.0 MeV, pγ angular correlation and Doppler-shift meas. 2−49735
^{29}Si(d,n)^{30}P, E_d=4 MeV, odd parities of ^{30}P levels 2−67328
^{29}Si(γ,n), doorway states and background cross sections 2−63863
^{29}Si(n,α) cross-sections obs., 5.85 MeV 2−76848
^{30}Si, resonances obs. in α reactions on ^{26}Mg, spins, parties and widths 2−46123
^{30}Si(^{3}He,pγ)^{32}P, first T=2 level analysis 2−63788
^{30}Si(α,nγ)^{33}S, 6.0-9.5 MeV, study of ^{33}S levels up to 4.3 MeV excitation, analysis of γ-ray angular distribs. 2−70385
^{30}Si(n,γ)^{31}Si, thermal neutron capture, meas. of γ-ray spectra, transition scheme for ^{31}Si 2−49807

Nuclei with $20 \leqslant A \leqslant 49$ continued

^{31}Si, γ-transition scheme determ. from thermal neutron reaction ^{30}Si(n,γ) 2−49807
^{33}Si, mass determ. in compound reactions 2−74013
Si(n,γ), gamma-ray spectra meas., cross-sections for γ-transitions 2−67269
Si(p, p), 5-15 MeV, analyzing power 2−74075
S(μ^-,n), 2-13 MeV, meas. of neutron energy spectrum, excitation of quasibound states of intermediate nucleus 2−52806
S(n,γ), gamma-ray spectra meas., cross-sections for γ-transitions 2−67269
Ti, (A=46, 48), ground state charge distribs., using Ti(e,e) 2−52749
Ti, angular distribution of photoneutrons 2−63864
Ti, even-even nuclei, 1$^+$ states investigation using (^{3}He,p) reactions, 1f-2p shell model predictions 2−46130
Ti even isotopes, static electric quadrupole moments of first excited states determ. from (^{32}S, ^{32}Sγ) reaction 2−63799
Ti isotopes, and Hartree Fock Bogoliubov approx. compared 2−46072
Ti isotopes, meas. of total cross section, optical model analysis 2−46271
^{43}Ti, mass, proton-rich nucleus in $1f_{7/2}$ shell 2−63794
^{44}Ti, Hartree-Fock variation after projection method, test 2−74019
^{45}Ti, decay modes, lifetimes and spins of low-lying levels 2−46132
^{46}Ti, ^{48}Ti(^{3}He, t), study of isobaric analogue states 0$^+$ and 2$^+$ in ^{46,48}V at 24.6 MeV 2−63918
^{46}Ti, Doppler shift lifetime meas. using p scatt. 2−76794
^{46}Ti, electron scatt. determ. of charge distrib., isotope no. depend. 2−67211
^{46}Ti(d, p)^{47}Ti, 5 MeV, study of spin-dependent reaction mechanism from pγ correlation 2−63919
^{46}Ti(d,α)^{44}Sc, 26.7 MeV, meas. of cross section, angular distribs. of excited levels, two-nucleon transfer analysis 2−70479
^{46}Ti(p, pγ)^{46}Ti, 7 MeV, γ-ray spectra, Dopper shift attenuation of lifetimes in ^{46}Ti 2−76794
^{47}Ti E2/M1 mixing ratios of γ-decays and population ratios determ. from pγ correlation meas. in ^{46}Ti(d, p) 2−63919
^{48}Ti, elastic and inelastic scattering of protons, meas. of spins, parities, widths and spacing of analogue resonances 2−79783
^{48}Ti, elastic scatt. of vector polarized deuterons, 11.9 MeV, optical pot. 2−70465
^{48}Ti, electron scatt. determ. of charge distrib., isotope no. depend. 2−67211
^{48}Ti(d,α)^{46}Sc, 26.7 MeV, meas. of cross section, angular distribs. of excited levels, two-nucleon transfer analysis 2−70479
^{48}Ti(p,γ)^{49}V, g-factor 3/2$^-$ 153 keV state in ^{49}V 2−67157
^{49}Ti, elastic scatt. of vector polarized deuterons, 11.9 MeV, optical pot. 2−70465
^{49}Ti(^{3}He,d)^{50}V, ^{48}Ti(^{3}He,p)^{50}V, study of ^{50} levels 2−63796
^{47}V, proton resonances, study by ^{46}Ti(p, p) and ^{46}Ti(p, p$_1$) reactions 2−70389
^{49}V, g-factor of 3/2$^-$ 153 keV state, ^{48}Ti(p,γ) obs. 2−67157
^{49}V, proton resonances, study by ^{48}Ti(p, p) and ^{48}Ti(p, p$_1$) reactions 2−70389
^{49}V energy levels, study by ^{49}Ti(p,n) reaction 2−28298
^{49}V isobaric analogue resonances obs. in elastic and inelastic scattering of proton on ^{48}Ti 2−79783
^{51}V(^{3}He,α)^{50}V, study of ^{50}V levels 2−63796

Nuclei with $50 \leqslant A \leqslant 89$

^{54}Mn, γ radiation intensity pattern change oriented in CoCl$_2$.6H$_2$O by spin flop transition 2−61552
^{59}Fe→^{59}Co β-decay, determ. of coincident intensity ratio for γ-rays and X-rays from K-electron conversion 2−79769
— 2−70396
— 2−67281
— 2−67244
A=50-75, inelastic scattering of 14 MeV neutrons 2−70450
A=57-81, nonschematic random-phase- approximation description of gamma vibrations 2−42511
A$\leqslant$80, muon capture rate, correction due to pressure of muon wave function in nuclear matrix elements 2−52804
cosmic rays with Z>75, propagation, r- process source 2−62447
Cu(p,π), 200-500 MeV, contributions of pions created in cascade mechanism to nuclear evaporation process 2−52813
deformation parameters 2−42532
magic, transitional and strongly deformed nuclei, proton scattering, systematics and fine structure of Coulomb displacement energies 2−46148
rare-earth compound nuclei formed in bombardment with 40 MeV α-particles of rare-earth targets, intensities of ground band transitions 2−49731
toroidal nuclei, deform. minima 2−82903
(n, γ) reactions, phonon-particle doorway states 2−79789
Fe, interaction of cosmic ray μ, meas. of cascades with energies $\geqslant$1 GeV using ionization calorimeter 2−73895
n activation of some cross-sections, $76 \leqslant Z \leqslant 82$ 2−76862
p resonance reactions on isotopes of Ti, Cr, Fe and Ni 2−46251
^{5}-7Co radionuclide prod., thin-target cross sections 2−82970
^{84} Kr standard unit for radionuclide activity in gases 2−55971
^{a}Co A=56, 58, high resolution spectroscopy using direct two nucleon transfer reactions 2−63800
^{a}Cr(n,γ), (A=50,52), circular polarization meas. and spin assignment of ^{51}Cr and ^{53}Cr levels 2−52819
^{a}Cu(A,p), A=63, 65, 27.2 MeV, meas. of differential cross section, analysis of p angular distrib. in three nucleon stripping theory 2−49833
^{a}Ge, A=70, 72, 74, 76, γ-ray spectra following thermal neutron capture 2−46286
^{a}Ni(^{3}He,n)Zn, A=58, 60, 62, 25 MeV, meas. of energy spectrum of neutrons, differential cross sections, orbital angular momentum transfers 2−46315
^{a}Ni(d,α)Co, A=58, 60, high resolution spectroscopy of ^{56,58}Co, DWBA analysis of angular distrib. 2−63800
^{a}Ni(nγ,) (A=60,62), circular polarization meas. and spin assignment of ^{61}Ni and ^{63}Ni levels 2−52819
^{a}Sr, A=89, 90, bone contamination by β emission, calc. of local and average doses 2−55265
A(n,n)A, elastic, A between 48 and 209, n polarization meas. 2−67239

Nuclei with $50\leqslant A\leqslant 89$ continued
^{57}As n.q.r. and spin-lattice relax. in ferroelec. systems 2−81481
^{71}As, of ^{71}Ge in ^{70}Ge(p,p)^{70}Ge, evidence for intermediate structure 2−46143
^{71}As→^{71}Ge, γ-spectrum analysis 2−63848
^{73}As, internal conversion coeffs. of low level transitions, using ^{75}As(p,n) 2−52752
^{73}As of ^{73}Ge in ^{72}Ge(p,p)^{73}Ge, evidence for intermediate structure 2−46143
^{74}As, decay to ^{74}Ge and ^{74}Se, energy level studies 2−49765
^{74}As n.m.r. and polarization in Fe, mag. moment 2−76796
^{75}As, excitation functions for (d, 2n), (d, 4n), (d, 5n), (d, p), (d, p2n), (d, p3n), (d, 2p) reaction at 52 MeV 2−52824
^{75}As, in α and β As$_4$S$_4$, nuclear quadrupole resonance 2−84595
^{75}As, low-lying levels interpret. rel. to core excitation model 2−42513
^{75}As, n.m.r. in Fe, hyperfine field detn. 2−75354
^{75}As, neutron reson. level spacings, stat. distribs., deviations 2−67161
^{75}As, nuclear quadrupole resonance in group V double and triple chalcogens 2−48311
^{75}As n.q.r. in vitreous As$_2$S$_3$ 2−57404
^{75}As(n,2n), 14.1 MeV, meas. of cross-section using activation method 2−49810
^{75}As(p,n)^{75}Se, internal conversion coeffs. of ^{75}Se 2−52752
^{81}As decay, partial scheme 2−76814
^{82}As decay, partial scheme 2−76814
Br n.m.r. spectra meas. in antiferromagnetic MnBr$_2$.4H$_2$O determ. of magnitude and orientations of internal mag. field 2−65175
^{77}Br used to determine capillary permeability in anterior tibial muscle 2−69359
^{78}Br, γ-ray spectrum, rel. to energy level determ. of ^{78}Se 2−74050
^{78}Br isomeric states, magnetic moment determ. 2−74029
^{79}Br, ^{81}Br(d, p)$^{80,\ 82}$Br, 12 MeV, meas. of cross sections, excitation of low-lying states of $^{80,\ 82}$Br, DWBA analysis 2−74031
^{79}Br, nuclear quadrupole resonance in group V double and triple chalcogens 2−48311
^{79}Br quad. coupling consts. of 1, 2, 4, 5-tetrabromobenzene 2−56260
^{80}Br, ^{82}Br, low-lying states populated in $^{79,\ 81}$Br(d, p) reactions 2−74031
^{80}Br + CH$_3$Br, H and halogen, displacement factors, survival probability of products 2−84664
^{81}Br, Coulomb excitation of low-lying levels by α-particles and ^{16}O ions, determ. of energies and spins 2−74032
^{81}Br, nuclear quadrupole resonance in group V double and triple chalcogens 2−48311
^{81}Br isomeric states, magnetic moment determ. 2−74029
^{81}Br quad. coupling consts. of 1, 2, 4, 5-tetrabromobenzene 2−56260
^{80g}Br, half-life determ. 2−70418
^{65}C(α, αn)E$_α$=900 MeV cross sections direct neutron emission mechanism 2−83010
Co, capture of polarized and unpolarized neutrons, determ. of spin of excited nuclei 2−49800
Co, π- capture, 600 MeV, identification of emitted charged particles 2−46293
^{54}Co hole-hole nucleus, transformation properties of effective transition operator 2−82861
^{54}Co→^{57}Fe in Xe, Mossbauer studies of ^{57}Fe atom 2−46426
^{55}Co, final states in (^{16}O,^{15}N) and (^{12}C,^{11}B) reactions, j-assignments 2−79805
^{56}Co, levels populated in ^{54}Fe(^{16}O, ^{14}N) two-nucleon stripping reaction at 80 MeV 2−74121
^{56}Co radionuclide prod., thin-target cross sections 2−82970
^{57}Co, half-life 2−52775
^{57}Co, Mossbauer effect, in InSb 2−65235
^{57}Co, Mossbauer effect in β-rhombohedral B 2−61603
^{57}Co, obs. of resonance states in ^{56}Fe(p,γ) reaction, isobaric analogs of states in ^{57}Fe 2−63882
^{57}Co, soft e.m. radiation detection using semiconductor spectrometer 2−70288
^{57}Co, unified model description, quadrupole vibrs. 2−63801
^{57}Co levels populated in ^{56}Fe(^{3}He,d) and ^{56}Fe(^{3}He,dγ) reactions 2−46138
^{58}Co, higher-order matrix elements in hindered-allowed β-decays 2−82921
^{58}Co, level density parameters, nucl. temp. 2−82981
^{58}Co, lifetimes of 111.5 keV and 53.2 keV levels and magnetic moment of 111.5 keV level determ. from ^{58}Fe(p, nγ) reaction 2−79742
^{58}Co, neutron capture cross-sections 2−74098
^{58}Co, probability of γ transitions, lifetimes of levels excited in ^{55}Mn(α, nγ) reaction 2−82890
^{58}Co radionuclide prod., thin-target cross sections 2−82970
^{59}Co, in 2-phase Co, n.m.r. level inversion in 2000 Å films 2−68744
^{59}Co, level density determination from alpha and proton induced reactions 2−63798
^{59}Co, n.m.r. in FeSi-CoSi system, intinerant ferromag. obs. 2−61745
^{59}Co, n.m.r. in K$_3$Co(CN)$_6$ 2−54509
^{59}Co, n.m.r. in K$_3$Co(CN)$_6$, chemical shift interpretation 2−65345
^{59}Co, n.q.r. in cis-[Co(en)$_2$Cl$_2$]Cl.H$_2$O and cis-[Co(en)$_2$Cl$_2$]NO$_3$ 2−75358
^{59}Co, of 3/2- excited state in ^{59}Fe, fine structure 2−46140
^{59}Co, spin assignments to levels at 1.01, 1.29 and 1.43 MeV populated in β-decay of ^{59}Fe 2−79769
^{59}Co, study of nuclear reactions caused by α-particles 2−67316
^{59}Co, unified model description, quadrupole vibrs. 2−63801
^{59}Co n.m.r. in (Fe$_{1-x}$Co$_x$)Si solid solns. 2−44223
^{59}Co(^{3}He,^{4}He)^{58}Co, high resolution spectroscopy of ^{58}Co, DWBA analysis of angular distribs. 2−63800
^{59}Co(α,p), 42 MeV, particle emission probabilities 2−42587
^{59}Co(n,γ) ^{60}Co, polarization, final state spins determ. 2−67277
^{59}Co(n,γ) ^{60}Co, polarized neutron capture, anisotropy of γ-rays 2−67276
^{59}Co(n,γ) ^{60}Co, thermal neutron capture, ang. distrib. of emitted γ-rays 2−67278

Nuclei with $50\leqslant A\leqslant 89$ continued
^{59}Co(n,γ)^{69}Co, interference effects in γ-ray emission after polarized neutron capture 2−79790
^{59}Co(n,p)^{59}Fe, 14.1 MeV, obs., deuteron elimination, comparison with statistical theory 2−67271
^{59}Co(n,p)^{59}Fe, E$_n$=14.1 MeV, proton energy and ang. distribs. 2−82981
^{60}Co, decay scheme 2−52777
^{60}Co, effect of hormones on retention in rats 2−55260
^{60}Co, final level spins determ. in ^{59}Co(n,γ) reaction 2−67277
^{60}Co, intensity ratio of 2158 keV and 2505 keV γ-rays 2−76811
^{60}Co, γ-ray irradiation of malignant lymphopathies, dose distribution 2−69412
^{60}Co, n.m.r. in Fe, single-passage resonance obs. by β-emission and spin-lattice relax. meas. 2−72508
^{60}Co, spin-lattice relax. in Fe-Co very dil. alloy 2−72232
^{60}Co, spin assignments, using γ-ray ang. distrib. from ^{59}Co(n,γ) reaction 2−67278
^{60}Co, spins of excited states, γ- transitions 2−67276
^{60}Co, teletherapy, skin doses 2−69417
^{60}Co Cathetron after-loading unit rel. to dose-rate effects 2−69331
^{60}Co in flowing nonisothermal Na, transport processes, corrosion and deposition rates 2−67344
^{60}Co γ-ray dosimetry in extended media, influence of size of CaF$_2$:Mn thermoluminescent dosimeter 2−67088
^{60}Co γ-rays, effect on luminescence of Tb^{3+} ions in crystals and glasses 2−84547
^{60}Co radiation therapy, compensation for large irregular fields 2−69395
^{60}Co radiation therapy, determ. of treatment time using computer 2−69317
^{60}Co radionuclide prod., thin-target cross sections 2−82970
^{60}Co source strength meas. using scintillation detectors and γ-γ coincidence, student expt. 2−78738
^{60}Co states, spin assignments following polarized neutron capture by ^{59}Co 2−79790
^{61}Co, unified model description, quadrupole vibrs. 2−63801
^{63}Co, unified model description, quadrupole vibrs. 2−63801
Cr, A=51, 53, spin determ. from (n,γ) circular polarization 2−67158
Cr, even-even nuclei, 1$^+$ states investigation using (^{3}He,p) reactions, 1f-2p shell model predictions 2−46130
Cr isotopes, meas. of total cross section, optical model analysis 2−46271
^{50}Cr, Doppler shift lifetime meas. using p scatt. 2−76794
^{50}Cr, octupole excitations 2−74022
^{50}Cr(^{3}He, t) 70 MeV, isobaric analog ground state obs. 2−83009
^{50}Cr(d, p)^{51}Cr, 10 MeV, spin assignments based on ln=1 J-dependence in (d, p) reaction 2−63920
^{50}Cr(p, pγ)^{50}Cr 7 MeV, γ-ray spectra, Doppler shift attenuation of lifetimes in ^{46}Ti 2−76794
^{51}Cr, ang. distrib. of ground state e.m. transitions, level spins 2−79751
^{51}Cr, excited states studied via (p,n) and (p,nγ) reactions on ^{51}V 2−46265
^{51}Cr radionuclide prod., thin-target cross sections 2−82970
^{51}Cr spin assignments based on ln=1 J-dependence in ^{50}Cr(d, p) reaction, calc. of spectroscopic factors 2−63920
^{52}Cr, elastic scatt. of vector polarized deuterons, 11.9 MeV, optical pot. 2−70465
^{52}Cr, large angle data in optical model analysis of helion elastic scattering 2−46313
^{52}Cr low-lying isobaric analogue states, study from (p,γ) and (p,n) reaction in ^{51}V 2−76795
^{52}Cr(n,γ)^{53}Cr, role of doorway states of 'phonon+particle' type 2−49809
^{52}Cr(p,p)^{52}Cr optical model determ. of r.m.s. radius 2−74076
^{53}Cr, intensities of E1-type γ-transitions from neutron capture states to lower p-levels 2−49809
^{53}Cr, spin assignments, (d, pγ) reaction study at 3 MeV 2−63793
^{53}Cr in SnO$_2$, ENDOR 2−48309
^{53}Cr n.m.r. in rare earth orthochromites 2−48307
^{54}Cr(n,γ)^{55}Cr, thermal neutron capture, meas. of γ-ray spectra and level structure of ^{55}Cr 2−42510
^{54}Cr(p, d)^{53}Cr, j-depend. in l=3 transitions 2−76845
^{54}Cr(p, nγ)^{54}Mn, 2.0-3.9 MeV, meas. of excitation functions and angular distributions of gamma rays, determ. of ^{54}Mn level structure 2−79743
^{54}Cr(p,nγ)^{54}Mn, Ep=2.1-3.2 MeV, low lying levels of ^{54}Mn 2−46134
^{55}Cr, γ-ray spectra and level structure from thermal neutron capture in ^{54}Cr 2−42510
Cu, angular distribution of photoneutrons 2−63864
Cu, proton bombardment, 82-416 MeV thin-target cross-sections for radionuclide prod. 2−82970
Cu, π$^-$ capture, energy spectra and emission probabilities of proton, deuteron and triton 2−79793
Cu, scatt. cross section and polarization meas. by associated particle method 2−70454
Cu isotopes, low-lying struct. and inelastic scatt. in unified model 2−63803
Cu isotopes, meas. of total cross section, optical model analysis 2−46271
Cu(A=60, 62) level density determination from alpha and proton induced reactions 2−63798
Cu(A=63, 65), level density determination from alpha and proton induced reactions 2−63798
^{58}Cu levels populated in ^{58}Ni(p, nγ), determ of lifetimes and decay modes of levels below 1.7 MeV 2−74026
^{59}Cu, core excitation of g$_{9/2}$ analogue and anti-analogue states 2−74027
^{60}Cu, levels populated in ^{58}Ni(^{16}O, ^{14}N) two-nucleon stripping reaction at 80 MeV 2−74121
^{60}Cu(II) β$^+$ decay, analysis of γ transitions between levels populated in ^{60}Ni 2−63846
^{61}Cu level studies, transitions, spin assignments, (α,p) reactions on Ni isotopes obs. 2−59783
^{63}Cu, ^{65}Cu, multipole admixtures of transitions between low-lying states, B(E2) and B(M1) transition rates following Coulomb excitation 2−63802

Nuclei with $50 \leqslant A \leqslant 89$ continued
^{63}Cu, ^{65}Cu($\alpha,\alpha'\gamma\gamma$) Coulomb excitation, 5.5, 7.0 MeV, meas. of angular distrib. and $\gamma\gamma$ angular correlations 2−63802
^{63}Cu, electron and positron induced disintegration, 20 to 30 MeV, absolute cross-sections 2−82954
^{63}Cu level studies, transitions, spin assignments, (α,p) reactions on Ni isotopes obs. 2−59783
^{63}Cu n.m.r. chem. shifts. in cuprous salts 2−44455
^{63}Cu(n,2n)^{62}Cu, En=14 MeV, cross section meas. by activation method 2−49802
^{63}Cu(n,d), 14 MeV, α-particle ang. distribution and energy spectra 2−42573
^{64}Cu, d absorption cross section, 25 GeV/c, Glauber theory calc. and comparison with expt. 2−70469
^{64}Cu life-time variation and chemical state of (n, γ) recoil copper in α copper phtalocyanine crystals 2−72586
^{65}Cu-^{63}Cu spin flip-flops, spin-lattice relax. 2−68581
^{65}Cu, elastic and inelastic widths of isobaric analogue states excited in ^{64}Ni(p,p'), spectroscopic factors deduced 2−63804
^{65}Cu, final states in (^{16}O,^{15}N) and (^{12}C,^{11}B) reactions, j-assignments 2−79805
^{65}Cu level studies, transitions, spin assignments, (α,p) reactions on Ni isotopes obs. 2−59783
^{65}Cu(n,2n)^{64}Cu, En=14 MeV, cross section meas. by activation method 2−49802
^{65}Cu(t, α), E_t=12 MeV, excitation of ^{64}Ni, level struct. 2−76878
^{67}Cu, half-life 2−52775
^{67}Cu level studies, transitions, spin assignments, (α,p) reactions on Ni isotopes obs. 2−59783
Cu(μ^-,e$^+$) Co, search for raction 2−46301
Fe, A=54, 56, 58, electroexcitation of E2- and E3-transitions 2−70393
Fe, estimate of photonuclear cross-section for energies $\geqslant$1 GeV 2−73895
Fe, even-even nuclei, 1$^+$ states investigation using (^{3}He,p) reactions, 1f-2p shell model predictions 2−46130
^{51}Fe, mass, proton-rich nucleus in 1f$_{7/2}$ shell 2−63794
^{53}Fe, transferred l-values and spectroscopic factors, ^{54}Fe(p,d) determ. 2−42563
^{53}Fe energy levels, extended space calcs. 2−67159
^{54}Fe, (^{16}O,^{15}N) and (^{12}C,^{11}B) induced reactions, j-assignments of final states 2−79805
^{54}Fe, Eo decay of 2561 keV O$^+$ level 2−82907
^{54}Fe, intensities of E1-type γ-transitions from neutron capture states to lower p-levels 2−49809
^{54}Fe, magnetic moment of 1.409 MeV 2$^+$ state 2−70392
^{54}Fe, neutron pickup reaction, ^{53}Fe states calcs. 2−67159
^{54}Fe, shell-model states, E2 transitions, effective two-body interaction 2−70394
^{54}Fe(^{16}O, ^{12}C)^{58}Ni, reaction-mechanisms study in 1f-2p shell 2−67334
^{54}Fe(^{16}O, ^{12}C)^{58}Ni, analysis using generator-coordinate form factors 2−52828
^{54}Fe(^{3}He,p)^{56}Co, high resolution spectroscopy of ^{56}Co, DWBA analysis of angular distribs. 2−63800
^{54}Fe(n,γ), circular polarization meas. and spin assignment of ^{55}Fe levels 2−52819
^{54}Fe(n,γ)^{55}Fe, role of doorway states of 'phonon+particle' type 2−49809
^{54}Fe(n,pγ)^{54}Mn, level structure of ^{54}Mn 2−46133
^{54}Fe(p,d)^{53}Fe, 52 MeV, spectroscopic factors determ. for ^{53}Fe 2−42563
^{54}Fe(p,γ)^{55}Co, isobaric analog state obs. 2−59754
^{54}Fe(p,γ)^{55}Co, γ-decay of analogue states of ^{55}Fe 2−46135
^{54}Fe(p,p'γ)^{54}Fe, E_p=10 MeV, spectroscopy of ^{54}Fe 2−76836
^{54}Fe(p,p)^{54}Fe optical model determ. of r.m.s. radius 2−74076
^{55}Fe, hole state lifetimes 2−55962
^{55}Fe, γ-decay of analogue states excited in ^{54}Fe(p,γ)^{55}Co reaction 2−46135
^{55}Fe, level density determ. using evaporation neutrons in ^{55}Mn(p,n)^{55}Fe 2−63797
^{55}Fe, orbital electron capture ratios in decay 2−49763
^{55}Fe, spin assignments, (d, pγ) reaction study at 3 MeV 2−63793
^{55}Fe, spin determ. from (n,γ) circular polarization 2−67158
^{55}Fe energy levels and spin-parity assignments determ. in ^{57}Fe(p,t) reaction at 27 MeV 2−63883
^{55}Fe radionuclide prod., thin-target cross sections 2−82970
^{56}Fe, Coulomb excitation by ^{32}S ions, 60-70 MeV, meas. of static electric quadrupole moments 2−63795
^{56}Fe, level density determination from alpha and proton induced reactions 2−63798
^{56}Fe, primary standard, for atomic masses 2−73282
^{56}Fe, shell-model states, E2 transitions, effective two-body interaction 2−70394
^{56}Fe, static electric quadrupole moments of first excited states determ. from ^{56}Fe(^{32}S, ^{32}Sγ) 2−63799
^{56}Fe 3120 keV level spin determ. 2−74024
^{56}Fe(^{3}He, ^{3}He) elastic scatt., 53.4 MeV, optical model analysis 2−67329
^{56}Fe(^{3}He,d)^{57}Co, meas. of angular distribs. of deuterons leading to levels in ^{57}Co 2−46138
^{56}Fe(^{3}He,dγ)^{57}Co, coincidences between d and γ used to obtain γ decay of levels in ^{57}Co 2−46138
^{56}Fe(α,p), 27.2 MeV, meas. of differential cross section, analysis of p angular distrib. in three nucleon stripping theory 2−49833
^{56}Fe(n,n)^{56}Fe, inelastic, 0.8-9.0 MeV, cross-section for production of de-excitation γ obs. 2−67243
^{56}Fe(n,p), cross- sections for 14.4 MeV neutrons 2−46290
^{56}Fe(p,γ)^{57}Co, 1250-1685 keV, obs. or resonance states in ^{57}Co, isobaric analogs of states in ^{57}Fe 2−63882
^{57}Fe-N high energy cosmic ray interaction, cf. of optical and Glauber models 2−73892
^{57}Fe, 122-14KeV cascade, ang. correl. obs. 2−70395
^{57}Fe, asymmetries in γ scatt., h.f.s., interference, vectorial relations 2−74025
^{57}Fe, calibration of Mossbauer isomer shift 2−46137
^{57}Fe, in hexagonal close-packed metals, electric field gradients 2−80986
^{57}Fe, meas. of differential cross sections for (p,t), (p,τ) and (d,α) two-nucleon pick-up reactions 2−63883

Nuclei with $50 \leqslant A \leqslant 89$ continued
^{57}Fe, Mossbauer effect, in neutron irrad. Si 2−48153
^{57}Fe, Mossbauer effect in biotite 2−75266
^{57}Fe, Mossbauer effect in β-rhombohedral B 2−61603
^{57}Fe, Mossbauer effect in Cu$_2$FeSnS$_4$ 2−75239
^{57}Fe, Mossbauer effect in Fe(Pd$_x$Pt$_{1-x}$)$_3$, magnetic phase transitions obs. 2−48108
^{57}Fe, Mossbauer effect in Ho$_x$Er$_{1-x}$Fe$_2$ system 2−72197
^{57}Fe, Mossbauer effect in NiFe$_{0.8}$Cr$_{1.2}$O$_4$ ferrite, structural transition at mag. transformation obs. 2−72201
^{57}Fe, Mossbauer effect in Nb-Mo(Fe) alloy 2−78076
^{57}Fe, Mossbauer effect in solid N$_2$, isomer shift obs. 2−48148
^{57}Fe, Mossbauer effect in V$_n$O$_{2n-1}$ 2−72286
^{57}Fe, Mossbauer effect in YFe$_{1-x}$Al$_x$O$_3$, local mag. field obs. 2−72288
^{57}Fe, Mossbauer effect obs. from 298 to 4.2K in Fe(II) complexes of 2-methyl-1, 10-phenanthroline 2−51306
^{57}Fe, Mossbauer recoilless fraction and second-order Doppler shift, effect of pressure in some host lattices 2−61599
^{57}Fe, n.m.r. in dil. Fe-Co alloy 2−65344
^{57}Fe, n.m.r. in Fe-V alloys 2−75355
^{57}Fe, n.m.r. in Li$_{0.5}$Fe$_{2.5}$O$_4$ 2−78169
^{57}Fe, neutron resonances determ. from photoneutron cross-sections 2−46139
^{57}Fe, size for 14.4 keV transition, obtained from Mossbauer effect in Xe 2−46426
^{57}Fe hyperfine mag. fields in Ni alloys 2−44358
^{57}Fe in Co metal, contact charge density of conduction electrons, internal conversion meas. 2−51307
^{57}Fe in permalloy, magnetic hyperfine field, Mossbauer spectra 2−54386
^{57}Fe in powdered absorbers, h.f.s. coupling and Mossbauer spectra parameters 2−75265
^{57}Fe in SnO$_2$, ENDOR 2−48309
^{57}Fe isomer shifts in Fe$_2$O$_3$ and rare earth iron garnets 2−57333
^{57}Fe Mossbauer effect, γ-ray diffr. by grating interpret. of amplitude modulation 2−46136
^{57}Fe Mossbauer effect in bis(thiosemicarbazide)iron(II) sulphate 2−61605
^{57}Fe Mossbauer effect in Fe-Ga solid solns. 2−44353
^{57}Fe Mossbauer effect in FeClO$_4$ frozen solns. 2−78070
^{57}Fe Mossbauer effect in Fe complexes nitroprussides 2−44352
^{57}Fe Mossbauer effect in FeBO$_3$ 2−54355
^{57}Fe Mossbauer effect in haematite 2−65234
^{57}Fe Mossbauer effect in Nb containing hydrogen additives 2−78075
^{57}Fe Mossbauer effect in RbCaF$_3$, isomer shift 2−81339
^{57}Fe Mossbauer effect in YIG 2−68615
^{57}Fe Mossbauer emission spectra in cobaltous complexes 2−68806
^{57}Fe size calc. from M1 transitions and Mossbauer isomer shift 2−76759
^{57}Fe(^{3}He,d)^{58}Co, high resolution spectroscopy of ^{58}Co, DWBA analysis of angular distribs. 2−63800
^{57}Fe(d,d'n) 19 MeV, neutron-gamma competition 2−46325
^{57}Fe(γ,n)^{56}Fe, ground state radiation width for resonances determ. 2−46139
^{57}Fe(n,γ)^{58}Fe, interference of two spin components in thermal neutron capture state 2−49801
^{57}Fe(n,γ)^{58}Fe, meas. of circular γ-ray polarization for primary transitions, interference of spin components of capture state 2−42572
^{57}Fe(t,p)^{59}Fe, 12 MeV, meas. of angular-momentum transfer, study of ^{59}Fe level structure 2−63921
^{58}Fe, interference of two spin components of capture state in ^{57}Fe(n,γ) reaction 2−42572
^{58}Fe(d,p)^{59}Fe, 10 MeV, meas. of angular-momentum transfer, study of ^{59}Fe level structure 2−63921
^{58}Fe(n,p), cross-sections for 14.4 MeV neutrons 2−46290
^{58}Fe(p, nγ)^{58}Co, 3.9 MeV, meas. of nγ correlations and g-factors, determ. lifetimes and magnetic moment of ^{58}Co levels 2−79742
^{58}Fe(p, p)^{58}Fe, 2.65-3.11 MeV, ^{59}Co excited state analogue of 3/2-excited state in ^{59}Fe 2−46140
^{59}Fe, level density parameters, nucl. temp. 2−82981
^{59}Fe absorption in man, whole-body counting 2−55282
^{59}Fe level structure studied in ^{57}Fe(t,p) and ^{58}Fe(d,p) reactions, evidence of rotational band structure 2−63921
^{59}Fe radionuclide prod., thin-target cross sections 2−82970
Fe(n,n)Fe, intermediate structure analysis based on doorway state picture 2−46276
Ga isotopes, odd-mass, struct. of low-lying states with particle-phonon coupling model 2−63839
^{64}Ga ground state, isospin impurity 2−79771
^{65}Ga, β-decay to ^{65}Zn 2−63847
^{65}Ga, disintegration to ^{65}Zn, level scheme, γ-ray spectrum 2−49764
^{66}Ga, first excited state, g-factor meas. by DPAD method 2−49740
^{66}Ga isomeric states, magnetic moment determ. 2−74029
^{67}Ga, ^{111}In and ^{75}Se in tumours, Ge(Li) detector for simultaneous meas. 2−73206
^{67}Ga for tumour localization 2−69297
^{69}Ga, ^{71}Ga, Coulombic excitation of levels 2−52751
^{69}Ga, ^{71}Ga, n.m.r. in Ga$_{1-x}$Te$_x$ liq. semicond. alloy 2−60512
^{69}Ga, Alaga model 2−46141
^{69}Ga, supertransferred hyperfine fields in lithium ferrite-gallates, n.m.r. obs. 2−54511
^{69}Ga relax. rates in Ga(ClO$_4$)$_3$ solns. 2−77449
^{69}Ga(n,2n), 14.1 MeV, meas. of cross-section using activation method 2−49810
^{71}Ga, supertransferred hyperfine fields in lithium ferrite- gallates, n.m.r. obs. 2−54511
^{71}Ga relax. rates in Ga(ClO$_4$)$_3$ solns. 2−77449
^{71}Ga shell model study of energy levels, transition probabilities, moments of ground state 2−46142
^{71}Ga(n,2n), 14.1 MeV, meas. of cross-section using activation method 2−49810
^{78}Ga, decay props. and nucl.-charge distrib. 2−76814
Ge, ^{12}C, ^{16}O, ^{22}Ne and ^{40}Ar ion bombardment, inelastic interaction, neutron production, ang. distrib. 2−76886
^{64}Ge, attempted separation and half-life meas. 2−49766
^{64}Ge, half-life, β-decay, abundance 2−55963
^{68}Ge, positron source for metal defect studies 2−80676
^{70}Ge(p, p')^{70}Ge, compound nucleus lifetime meas. by blocking technique, multiple scatt. effects 2−63748

Nuclei with 50⩽A⩽89 continued
^{70}Ge(p, p′)^{70}Ge, reaction time meas. by blocking technique 2−74058
^{70}Ge(p,p)^{70}Ge, ^{71}As, isobaric analogue resonance evidence for intermediate structure 2−46143
^{70}Ge(p,p)^{70}Ge, 1.04 MeV, compound nucleus lifetime meas., crystal blocking technique 2−46252
^{71}Ge excited states, ^{71}As decay obs. 2−63848
^{72}Ge, meas. of B(E2; $0_2^+ \to 2_1^+$) by Coulomb excitation with ^{16}O 2−46144
^{72}Ge(p, p′)^{72}Ge, compound nucleus lifetime meas. by blocking technique, multiple scatt. effects 2−63748
^{72}Ge(p, p′)^{72}Ge, reaction time meas. by blocking technique 2−74058
^{72}Ge(p,p)^{72}Ge, ^{73}As, isobaric analogue resonance evidence for intermediate structure 2−46143
^{72}Ge(p,p)^{72}Ge, 0.8 MeV, compound nucleus lifetime meas., crystal blocking technique 2−46252
^{73}Ge-^{13}C directly bonded coupling constant in tetramethlygermane 2−46522
^{73}Ge, γ-ray decay modes and reduced upward transition probabilities following Coulomb excitation, test of quasiparticle-phonon coupling theories 2−74030
^{73}Ge(p,n)^{73}As, internal conversion coeffs. of ^{73}As 2−52752
^{74}Ge, excited states, obs. from ^{74}As decay 2−49765
^{74}Ge, keV neutron radiative capture cross section and reson. integral 2−76861
^{76}Ge, neutron activation reson. integral 2−76861
^{79}Ge, decay props. and nucl.-charge distrib. 2−76814
^{80}Ge, decay props. and nucl.-charge distrib. 2−76814
^{81}Ge, decay props. and nucl.-charge distrib. 2−76814
^{82}Ge, decay props. and nucl.-charge distrib. 2−76814
^{83}Ge, decay props. and nucl.-charge distrib. 2−76814
^{84}Ge, decay props. and nucl.-charge distrib. 2−76814
^{2}H n.m.r., spin-lattice relaxation in D_2O ice 2−61744
^{50}K isotope obs. in proton reactions on U 2−82925
Kr, element yield distribution in thermal neutron fission of ^{235}U 2−63935
^{73}Kr→^{71}Se+p+e$^+$, beta-delayed proton emission obs. proton separation and electron capture energies 2−46187
^{79}Kr, γ-ray transitions, relative intensities and mixing parameters 2−79759
^{79}Kr, γ-ray transitions 2−79758
^{80}Kr(n,γ)^{81}Kr, reaction cross section, meas. using multifilament proportional counter 2−70455
^{81}Kr, γ-ray transitions, relative intensities and mixing parameters 2−79759
^{81}Kr, γ-ray transitions 2−79758
^{82}Kr, spins of excited states, γ-γ correlation study 2−46145
^{83}Kr, γ-ray transitions, relative intensities and mixing parameters 2−79759
^{83}Kr, γ-ray transitions 2−79758
^{84}Kr, energy of excited states, study of ^{83}Kr(n,γ) using thermal neutrons 2−49741
^{85}Kr, γ-ray transitions, relative intensities and mixing parameters 2−79759
^{85}Kr, γ-ray transitions 2−79758
^{86}Kr-^{87}Kr system, level structure investigated by inelastic proton scattering through isobaric analog resonances 2−46147
^{86}Kr(p,p)^{86}Kr, 4.76-10.10 MeV, obs. of isobaric analog resonances, study of core coupling in ^{87}Rb 2−46146
^{83m}Kr, internal conversion coeff. for 9.4 keV transition 2−82888
^{85m}Kr, ^{87}Kr, ^{88}Kr, fission gas release in irradiated UO_2 dispersed through graphite 2−70534
Mn, excitation of 126 keV level by fast neutron scatt. 2−67245
Mn, neutron-capture cross sections, 0.01 to 100 eV 2−59761
^{52}Mn radionuclide prod., thin-target cross sections 2−82970
^{54}Mn, level structure from ^{54}Fe(n,pγ)^{54}Mn reaction 2−46133
^{54}Mn, low lying levels, by ang. correlation study using ^{54}Cr(p,nγ) 2−46134
^{54}Mn level structure determ. from ^{54}Cr(p, nγ) and ^{51}V(α, nγ) reactions 2−79743
^{54}Mn radionuclide, meas. of activity in source 2−55974
^{54}Mn radionuclide prod., thin-target cross sections 2−82970
^{55}Mn, n.m.r. in α-Mn 2−61748
^{55}Mn, n.m.r. in Mn_{1-x} Cr_xSb, hyperfine fields detn. 2−54514
^{55}Mn energy levels and spin-parity assignments determ. in ^{57}Fe(p,τ) and ^{57}Fe(d,α) reactions at 27 MeV and 16 MeV 2−63883
^{55}Mn in activation foils, determ. of thermal neutron energy spectrum for pool type reactor 2−79832
^{55}Mn in MnAlGe ferromagnet. n.m.r. studies 2−84586
^{55}Mn single crystal broad-line n.m.r. of $Mn(CO)_5$-X_3M adducts 2−68747
^{55}Mn(α, nγ)^{58}Co, 10 MeV, meas. of n-γ angular correlations and lifetimes using Doppler-shift attenuation method 2−82890
^{55}Mn(p,n)^{55}Fe, determ. of level density in ^{55}Fe 2−63797
^{56}Mn, higher-order matrix elements in hindered-allowed β-decays 2−82921
^{58}Mn, half-life 2−46290
Mn(n,n)Mn, cross-section for excitation of 126 keV level, meas. 2−67245
Ni, A=58,60, Coulomb excitation by ^{32}S ions, 60-70 MeV, meas. of static electric quadrupole moments 2−63795
Ni, A=61, 63, spin determ. from (n,γ) circular polarization 2−67158
Ni (A=58,60,61,62,64), proton reactions, excitation functions and peak cross sections for energy range 5 to 56 MeV 2−59758
Ni even isotopes, level spectra using self-consistent approx. 2−76793
Ni isotopes, even-mass, low-lying level props. 2−63801
^{55}Ni, mass, proton-rich nucleus $1f_{7/2}$ shell 2−63794
^{56}Ni, gamma-ray transitions induced by ^{54}Fe(^{3}He,n)^{56}Ni, reaction 2−59701
^{56}Ni, levels populated in ^{54}Fe(^{16}O, ^{14}C) two-nucleon stripping reaction at 80 MeV 2−74121
^{56}Ni, shell-model states, E2 transitions, effective two-body interaction 2−70394
^{56}Ni radionuclide prod., thin-target cross sections 2−82970
^{58}Ni, alpha-gamma ang. correlation studies 2−70477
^{58}Ni, inelastic nucleon scattering, excitation of abnormal parity states, dominance of spin flip mechanism 2−74069

Nuclei with 50⩽A⩽89 continued
^{58}Ni, shell-model states, E2 transitions, effective two-body interaction 2−70394
^{58}Ni neutron inelastic scattering, calc. of optical-model potential in particle-vibration coupling picture 2−76850
^{58}Ni(^{3}He,^{3}He), inelastic scattering, spin-flip of ^{3}He 2−70464
^{58}Ni(^{6}Li,d) 38 MeV, meas. of angular distribs., cross sections, comparison with DWBA analysis 2−74122
^{58}Ni(α, pγ)^{61}Cu, compound statistical theory computation of cross-section for level population, γ-ray emission 2−79804
^{58}Ni(α, ppγ)^{60}Ni compound statistical theory computation of cross-section for level population, γ-ray emission 2−79804
^{58}Ni(α,α′)^{58}Ni, high-lying states of ^{58}Ni 2−59784
^{58}Ni(α,p)^{61}Cu, ^{61}Cu level studies, transitions, spin assignments 2−59783
^{58}Ni(n,p)^{58}Co, 14.1 MeV, obs., deuteron elimination, comparison with statistical theory 2−67271
^{58}Ni(n,p)^{58}Co, E_n=14.1 MeV, proton energy and ang. distribs. 2−82981
^{58}Ni(p, γ)^{59}Cu, study of $g_{9/2}$ isobaric analogue and anti-analogue states of ^{59}Cu, core structure 2−74027
^{58}Ni(p, nγ)^{58}Cu, 12.0-13.03 MeV, determ. of γ-ray decay modes of low-lying states of ^{58}Cu by n-γ and γ-γ coincidence techniques 2−74026
^{58}Ni(p, p)^{58}Ni, study of $g_{9/2}$ isobaric analogue and anti-analogue states of ^{59}Cu, core structure 2−74027
^{58}Ni(p,p′)^{58}Ni(2$^+$), 20 and 100 MeV, Born approx. calcs. of probability of spin flip, explanation of backward-angle peak 2−79787
^{58}Ni(p,p)^{58}Ni DWA cross-section calc. with imaginary part 2−74081
^{60}Ni, giant reson. struct., low-lying collective states influence 2−74028
^{60}Ni, intermediate states of dipole analogue resons. 2−59702
^{60}Ni, γ transitions of levels populated in β$^+$ decay of ^{60}Cu(II) 2−63846
^{60}Ni(α,p)^{63}Cu, ^{63}Cu level studies, transitions, spin assignments 2−59783
^{60}Ni(e,e), 225 MeV, determ. of cross-sections, charge density distrib. parameter 2−52803
^{60}Ni(*p,p′*), γ-ray multiplicity, comparison with direct reaction mechanism 2−67224
^{61}Ni, Mossbauer effect in Ni-Pd alloys, conc. depend. 2−72285
^{61}Ni hyperfine mag. fields in Ni alloys 2−44358
^{61}Ni(d,d′), competition between neutron and gamma emission deexcitation process 2−70466
^{61}Ni(d,d′n), 19 MeV, neutron-gamma competition 2−46325
^{62}Ni, (^{16}O,^{15}N) and (^{12}C,^{11}B) induced reactions, j-assignments of final states 2−79805
^{62}Ni, electroexcitation of E2- and E3-transitions 2−70393
^{62}Ni radionuclide prod., thin-target cross sections 2−82970
^{62}Ni(^{3}He,t), 70 MeV isobaric analog states obs. 2−83009
^{62}Ni(α,p)^{65}Cu, ^{65}Cu level studies, transitions, spin assignments 2−59783
^{62}Ni(d,p)^{63}Ni, 4.45, 5.12 MeV, meas. of absolute differential cross sections, determ. of spectroscopic factors, DWBA analysis 2−79794
^{63}Ni, disintegration rate by 4π counting 2−79672
^{63}Ni spectroscopic factors deduce from ^{62}Ni(d,p) reaction near Coulomb barrier, DWBA analysis 2−79794
^{64}Ni level struct. from ^{65}Cu(t, α) at 12 MeV 2−76878
^{64}Ni(^{6}Li,d) 38 MeV, meas. of angular distribs., cross sections, comparison with DWBA analysis 2−74122
^{64}Ni(α,p)^{67}Cu, ^{67}Cu level studies, transitions, spin assignments 2−59783
^{64}Ni(p,nγ)^{64}Cu, 3.47-5.19 MeV, study of structure and γ-decay of levels excited near isobaric analogue resonances 2−67160
^{64}Ni(p,p′), 3-5 MeV, elastic and inelastic excitation of ^{65}Cu isobaric analogue resonance 2−63804
^{64}Ni(*p,p′*), γ-ray multiplicity, comparison with compound nucleus reaction mechanism 2−67224
^{65}Ni, beta decay and K electrons from internal ionization, summing-energy spectrum 2−46186
Ni(n,γ), capture of 4 to 90 keV neutrons, γ transitions 2−67279
Rb isotope yields, in reactions with protons, neutrons and α-particles 2−55988
^{77}Rb production from nuclear spallation, identification and half life 2−63876
^{78}Rb, precision meas. of half-life, gamma transition energies 2−52778
^{78}Rb identification as source of 19 m activity following production of Rb and Sr isotopes 2−54563
^{83}Rb, half-life determ. 2−70419
^{83}Rb levels populated in decay of ^{83}Sr, direct evidence for 5.23 keV level 2−55964
^{85}Rb, lifetime of 517 keV level, application to calibration of nuclear timing systems 2−79750
^{86}Rb, identification of low-lying levels excited in ^{87}Rb(^{3}He,^{4}He) reaction at 16 MeV, distorted-wave analysis 2−70397
^{86}Rb hole states obs. using ^{88}Sr(d.α) ^{86}Rb reaction 2−82909
^{87}Rb, E2 moment from E2, interaction in $np^2P_{3/2}$ series of Rb I spectrum 2−46439
^{87}Rb, half-life redetermined 2−46189
^{87}Rb, isobaric analogue resonances, total and partial widths 2−59703
^{87}Rb, n.m.r. in $RbMnF_3$ 2−72516
^{87}Rb core coupling studied through isobaric-analog resonances 2−46146
^{87}Rb core coupling studied through isobaric analog resonances 2−46147
^{87}Rb n.m.r. in Rb_2CoF_4 2−44458
^{87}Rb n.q.r. and spin-lattice relax. in ferroelec. systems 2−81481
^{87}Rb(^{3}He, ^{4}He)^{86}Rb, 16 MeV, meas. of cross-section, identification of low-lying levels in ^{86}Rb 2−70397
Se isotopes, alpha-induced 2−79759
^{75}Se, ^{67}Ga and ^{111}In in tumours, Ge(Li) detector for simultaneous meas. 2−73206
^{75}Se, internal conversion coeffs. of transitions, low levels, using ^{71}As(p,n) 2−52752
^{75}Se, γ-γ cascade decade, meas. of hyperfine mag. fields at As in Fe, Co and Ni 2−78018
^{75}Se in selenourea, preparation 2−54527
^{77}Se, n.m.r. in Se-Te liq. semicond. alloy 2−61752

Nuclei with $50\leqslant A\leqslant 89$ continued
- ^{77}Se n.m.r. in trigonal Se, anisotropic chem. shift 2−44459
- ^{77}Se(nγ)^{78}Se, thermal n, decay scheme for ^{78}Se 2−52779
- ^{78}Se, decay scheme, from ^{77}Se(n,γ) using thermal n 2−52779
- ^{78}Se, energy levels, ^{78}Br decay study 2−74050
- ^{84}Se, bubble nuclei approach 2−82904
- Se(n,n)Se, cross-section structure 2−46279
- ^{83}Sr decay, meas. of low-energy electron spectrum, obs. of 5.23 keV transition assigned to ^{83}Rb 2−55964
- ^{85}Sr, ^{89}Sr, effect of hormones on retention in rats 2−55260
- ^{85}Sr, absorption through skin, influence of decontamination treatment on degree of internal contamination 2−55236
- ^{85}Sr, changes of passage and absorption in gastrointestinal tract of irradiated rats 2−55294
- ^{85}Sr, excitation energies and mean lives of low-lying levels populated by ^{86}Sr(^{3}He, $\alpha\gamma$) 2−42514
- ^{85}Sr, half-life 2−52775
- ^{85}Sr internal radiation dose, use in bone scanning 2−55274
- ^{85}Sr released to water basins, meas. of accumulation in bed sediment 2−57833
- ^{86}Sr ground and excited states obs. following elastic and inelastic proton scattering, deformation parameters 2−74077
- ^{86}Sr(^{3}He,$\alpha\gamma$)^{85}Sr, 17 MeV, meas. of $\alpha\gamma$ coincidences, mean lives of low lying levels in ^{85}Sr deduced 2−42514
- ^{88}Sr, lifetime of 2.734 MeV level determ. from average cross section for resonance scattering of γ-rays 2−49742
- ^{88}Sr(d,np)^{88}Sr, differential and total cross-sections, consistent coupled channel Born approximation analysis 2−74114
- ^{88}Sr(d,p)^{89}Sr, differential and total cross-sections, consistent coupled channel Born approximation analysis 2−74114
- ^{88}Sr(n, γ), 14 MeV radiative capture, mass depend. of direct- semi-direct theory calcs. 2−67270
- ^{88}Sr(n,γ), radiative capture cross sections for 14 MeV neutrons mass depend. 2−67282
- ^{88}Sr(p,p$'\gamma$)^{88}Sr, polarization-analyzing power inequality 2−76846
- ^{89}Sr, estimation of relative role of penetration into critical organs through intact skin 2−55295
- ^{89}Sr, half-life 2−52775
- ^{89}Sr and ^{90}Sr determination by liquid scintillation beta spectroscopy 2−85083
- ^{90}Sr-^{90}YTiO$_3$, thick cylindrical β-source, bremsstrahlung 2−67191
- ^{50}Ti, calc. of levels B(M1), B(M2), static moments 2−63799
- ^{50}Ti, elastic scatt. of vector polarized deuterons, 11.9 MeV, optical pot. 2−70465
- ^{50}Ti, electron scatt. determ. of charge distrib., isotope no. depend. 2−67211
- ^{50}Ti ground state charge distribs., using Ti(e,e) 2−52749
- ^{50}Ti(n,γ)^{51}Ti, role of doorway states of 'phonon + particle' type 2−49809
- ^{50}Ti(p,p)^{50}Ti, optical model determ. of r.m.s. radius 2−74076
- ^{51}Ti, intensities of E1-type γ-transitions from neutron capture states to lower p-levels 2−49809
- V, neutron-capture cross-sections, 0.01 to 100 eV 2−59761
- ^{50}V level study using ^{3}He reactions 2−63796
- ^{51}V, elastic scatt. of vector polarized deuterons, 11.9 MeV, optical pot. 2−70465
- ^{51}V, n.m.r. in LiCuVO$_4$ 2−72511
- ^{51}V, n.m.r. in σ-V-Co alloys, quadrupole satellite intensity variation 2−72519
- ^{51}V, n.m.r. in V$_{1-x}$Cr$_x$Be$_2$ 2−72520
- ^{51}V, proton resonances, study by ^{50}Ti(p, p) reaction 2−70389
- ^{51}V quadrupole moment obs. 2−61741
- ^{51}V quadrupole relax. in π-tropyliumvanadium tricarbonyl 2−84453
- ^{51}V(^{3}He,α)^{50}V, study of ^{50}V levels 2−63796
- ^{51}V(α, nγ)^{54}Mn, 7.1, 7.6 MeV, meas. of γ-ray spectra, determ. of ^{54}Mn level structure 2−79743
- ^{51}V(p,γ), ^{51}V(p,n) up to 3.12 MeV, study of isobaric analogue states in ^{52}Cr 2−76795
- ^{51}V(p,n)^{51}Cr, obs. of 2.335 MeV isobaric analog resonance, study of excited states of ^{51}Cr 2−46265
- ^{51}V(p,nγ)^{51}Cr, 4.013, 5.016 MeV, study of excited states of ^{51}Cr 2−46265
- ^{51}V(p,nγ)^{51}Cr, ang. distrib. of ground state e.m. transitions, level spins, comparison with Hauser-Feshbach theory 2−79751
- ^{51}V(p,p)^{51}V, obs. of 2.335 MeV isobaric analog resonance 2−46265
- ^{51}V(p,p)^{51}V optical model determ. of r.m.s. radius 2−74076
- ^{52}V, analogue resonances of low lying levels, study by ^{51}V(p, γ)^{52}Cr 2−74023
- ^{87}Y, isomer ratio, ^{89}Y (γ, 2n) reaction study 2−63754
- ^{87}Y, isomer ratios from ^{89}Y(p,p2n)^{87}Y, calc. based on statistical and cascade-evaporation theories 2−49730
- ^{88}Y, structure, computer analysis of ^{90}Zr (d,α)^{88}Y analysis 2−70480
- ^{88}Y production by deuteron irradiation of Zr, determ. of excitation functions 2−74115
- ^{89}Y, energy levels, model calcs 2−82906
- ^{89}Y, isobaric analog resons., proton inelastic scatt. 2−76846
- ^{89}Y, isobaric analogue resonances, total and partial widths 2−59703
- ^{89}Y (p,p)^{89}Y, analogue states of ^{90}Y 2−67215
- ^{89}Y(p,nγ)^{89}Zr, ^{89}Zr transition rates 2−46149
- ^{89}Y(p,p2n)^{87}Y, isomer ratios, calc. based on statistical and cascade-evaporation theories 2−49730
- ^{88m}Y, half-life decay times, int. conv. spectra and excitation functions detn. 2−67195
- Zn, A = 73, 74, decay characteristics, half-lives and Q-values 2−79746
- Zn(A = 64,66,68), radiative widths of spin-1 levels using γ-ray scatt. 2−59692
- ^{60}Zn, levels populated in ^{58}Ni(^{16}O, ^{14}C) two-nucleon stripping reaction at 80 MeV 2−74121
- ^{64}Zn, ^{65}Zn, applic. of theory of neutron-proton correlation effects 2−67123
- ^{64}Zn, influence of nonlocality on inelastic α-scattering 2−46326
- ^{64}Zn(^{3}He, 3n)^{64}Ge, ^{64}Ge decay studies 2−55963
- ^{64}Zn(e,e), 225 MeV, determ. of cross-sections, charge density distrib. parameter 2−52803
- ^{64}Zn(n,2n), calc. of excitation function in direct knockon model, and cross section for formation of combined nucleus 2−67280
- ^{65}Zn, effect of hormones on retention in rats 2−55260
- ^{65}Zn, level scheme, from β-decay of ^{65}Ga 2−63847
- ^{65}Zn radionuclide prod., thin-target cross sections 2−82970

Nuclei with $50\leqslant A\leqslant 89$ continued
- ^{65}Zn released to water basins, meas. of accumulation in bed sediment 2−57833
- ^{66}Zn(e,e), 225 MeV, determ. of cross-sections, charge density distrib. parameter 2−52803
- ^{67}Zn, lifetime of 184 keV level 2−76765
- Zn(α,α'), A = 68, 70, 31 MeV, angular distributions and excited states 2−42581
- Zn(t,p) reaction, energy level studies 2−56001
- ^{89}Zr, level scheme, ^{91}Zr(p, t) study 2−70445
- ^{89}Zr energy level transition rates from ^{89}Y(p,nγ)^{89}Zr reaction 2−46149

Nuclei with $90\leqslant A\leqslant 149$
- — 2−70402
- — 2−59705
- — 2−67248
- — 2−67248
- — 2−67246
- — 2−67184
- cosmic rays with Z > 75, propagation, r- process source 2−62447
- deformation parameters 2−42532
- fission fragment ranges in U-Al alloys, UO$_2$, U$_3$O$_8$ 2−83028
- fission products of uranium, behaviour in types of soil found in Czechoslovakia 2−57804
- isobaric analogue resonances, survey of statistical neutron decay for nuclei in A = 91-97 range 2−67131
- magic, transitional and strongly deformed nuclei, proton scattering, systematics and fine structure of Coulomb displacement energies 2−46148
- N = 50 region (p,t) reactions, systematics of L = 0 transitions 2−79753
- odd-proton N = 82 nuclei $11^-/2(1)\rightarrow 7^+/2(1)$ and $11^-/2(1)\rightarrow 5^+/2(1)$ transitions 2−79756
- rare earth isotopes, neutron resonance capture integral values 2−49811
- rare earth nuclei, K = 0 band study using (p, t) reactions 2−63885
- rare earth nuclei, prediction of singularities in ground state bands using Meissner effect 2−46117
- rare-earth even-even nuclie, excitation of collective states by radiationless muonic transitions 2−67171
- rare-earth nuclei, deformed, gamma and octupole states in Fermi liquid theory 2−46116
- rare-earth region, ground state deformations, investigation by Strutinsky renormalization method 2−70363
- virtual decay, vertex functions and coupling constants 2−63762
- (n, γ) reactions, phonon-particle doorway states 2−79789
- ^{113*}Tn (100 min) decay, internal conversion, M4, E5 character 2−74052
- $^{143(m+g)}$Sm, decay scheme 2−46200
- $^{93g+m}$Ru, produced by ^{92}Mo(^{3}He, xn), obs. of γ transitions 2−49768
- 1^{33b}a, isomeric activity excitation by (n,2n) reaction at 14.8 MeV 2−82974
- ^{a}Ba, A = 126, 128, produced by (^{16}O,4n) reactions, lifetime measurements 2−46154
- ^{a}Cd(^{16}O,4n)^{126,128}Ba A = 114, 116, lifetime measurements in ^{126,128}Ba 2−46154
- ^{a}Cs, A = 117-120, half-lives determ. using on-line isotope separator techniques 2−42545
- ^{a}Pb(^{16}O,4n)^{120,122}Xe, A = 108, 110, lifetime measurements in ^{120,122}Xe 2−46154
- ^{a}Sb, A = 110-114, meas. of half lives and decay schemes 2−46191
- ^{a}Sn, A = 123, 125, 128, cumulative yields from thermal-neutron induced fission of ^{235}U deduced from γ-ray intensities 2−46345
- ^{a}Sn, A = 129-132, half-lives determ. from X- and γ-ray emissions 2−46196
- ^{a}Sn(γ,p), A = 116-118, 120, 122, 124, meas. of spectra and yeild curves, isobaric analog states 2−46233
- ^{a}Sn(p,xn) A = 112, 114, production of $^{110-114}$Sn, study of decay schemes 2−46191
- ^{a}Xe, A = 120, 122, produced by (^{16}O,4n) reactions, lifetime measurements 2−46154
- ^{a}Xe A = 131, 132, 133, fission products, spin assignments and γ-ray multipole mixing ratios 2−46207
- Ac isotope production in ^{209}Bi + ^{12}C reaction, excitation function meas. 2−46349
- Ag, ^{12}C, ^{16}O, ^{22}Ne and ^{40}Ar ion bombardment, inelastic interactions, neutron production, ang. distrib. 2−76886
- Ag, n and p distrib. 2−82951
- Ag (A = 107, 109), solution of I = j-1 anomaly in Alaga model 2−46153
- ^{107}Ag, ^{109}Ag dipole moments of very short-lived states by recoil-into-gas method 2−70371
- ^{107}Ag, reactions with ^{20}Ne, ang. momentum limits, fusion excitation functions 2−59787
- ^{107}Ag electron and positron induced disintegration, 20 to 30 MeV, absolute cross-sections 2−82954
- ^{107}Ag(n,d), 14 MeV, α-particle ang. distribution and energy spectra 2−42573
- ^{107}Ag(n,γ)^{108}Ag, study of level transitions in ^{108}Ag 2−52757
- ^{108}Ag, E1 transition study using ^{107}Ag(n,γ)^{108}Ag reaction 2−52757
- ^{109}Ag lifetimes of Coulomb- excited states meas. using plunger recoil distance technique 2−63756
- ^{109}Ag(^{16}O, 3n)^{123}Cs, positron decay and decay scheme of ^{123}Cs 2−74037
- ^{109}Ag(^{18}O, 4n)^{123}Cs isomeric level and γ-transitions found 2−74037
- ^{109}Ag(^{18}O, 5n)^{123}Cs positron decay and decay scheme of ^{123}Cs 2−74037
- ^{109}Ag(^{84}Kr,xn), neutron- deficient Bi isotope prod. and α-decay 2−76822
- ^{109}Ag(n,γ)^{110}Ag, study of E1 level transitions in ^{110}Ag 2−52757
- ^{110}Ag, decay, study of γ transitions to elucidate low-spin excited states in ^{110}Cd 2−74035
- ^{110}Ag, E1 transition study using ^{109}Ag(n,γ)^{110}Ag 2−52757
- Al, angular distribution of photoneutrons 2−63864
- A(n,n)A, elastic, A between 48 and 209, n polarization meas. 2−67239
- ^{130}Ba(n,γ)^{131}Xe cross section rel. to origin of ^{131}Xe on the Moon 2−66143
- ^{131}Ba, energy level struct., unified model calcs. 2−42517

Nuclei with $90 \leqslant A \leqslant 149$ continued
^{131}Ba, isomeric activity excitation by (n,2n) reaction at 14.8 MeV 2−82974
^{133}Ba, isomeric activity excitation by (n,2n) reaction at 14.8 MeV 2−82974
^{134}Ba, ^{16}O scatt., reorientation effect meas., static quadrupole moment 2−76800
^{134}Ba, spin of 1643 keV state and multiple mixing ratios of γ transitions following β-decay of ^{134}Cs 2−70404
^{134}Ba levels populated in decay of ^{134}Cs 2−52781
^{135}Ba, isomeric activity excitation by (n,2n) reaction at 14.8 MeV 2−82974
^{135}Ba, test of applicability of core-excitation model 2−59710
^{136}Ba, ^{16}O scatt., reorientation effect meas., static quadrupole moment 2−76800
^{137}Ba, energy level struct., unified model calcs. 2−42517
^{137}Ba^{m} K-conversion lines meas. with Si(Li)-β-spectrometer in 4π geometry 2−63689
^{138}Ba, ^{16}O scatt., reorientation effect meas., static quadrupole moment 2−76800
^{138}Ba, differential cross sections for elastic and inelastic scattering of α particles to low-lying states 2−46305
^{138}Ba, energy spectra, effect of proton-neutron interactions 2−46157
^{138}Ba, inelastic proton scattering at 30 MeV, determ. differential cross sections, J^{π} assignments 2−74079
^{138}Ba, intensities of E1-type γ-transitions from neutron capture states to lower p-levels 2−49809
^{138}Ba γ-ray and conversion electron spectra, spin-parity assignments 2−46155
^{138}Ba(n, γ), 14 MeV radiative capture, mass depend. of direct- semi-direct theory calcs. 2−67270
^{138}Ba(n,γ)^{139}Ba, role of doorway states of 'phonon + particle' type 2−49809
^{139}Ba level scheme investigation in unified model calc. and particle core model 2−67170
^{140}Ba cumulative formation in ^{237}Np proton induced fission, 20-85 MeV 2−79812
Ba(n,γ), capture of 5-80 keV neutrons, γ spectra analysis 2−67286
^{96}Br→^{86}Kr decay, assignment of transitions, half-life determ. 2−46188
^{131}Ca, level scheme, transitions 2−42521
Cd, anomalous two-phonon transitions, study by Cd (p,t) reaction 2−63806
Cd, π^{-} capture, energy spectra and emission probabilities of proton, deuteron and triton 2−79793
^{106}Cd(α.3n)^{107}Cd isotope identification 2−82886
^{106}Cd(p,p'), γ-ray multiplicity comparison with direct reaction mechanisms 2−67224
^{107}Cd, study of levels populated in β^{+}/EC decay of ^{107}In by obs. of γ-ray spectra 2−82934
^{109}Cd, mass spectrometer meas. of charge state of ions 2−79884
^{110}Cd, g-factor expt. on first excited 2+ state 2−52742
^{110}Cd, low-spin states studied in decay of ^{110}Ag 2−74035
^{111}Cd, in In and In-Cd alloys, perturbed ang. correl. studies 2−75246
^{111}Cd quadrupole interaction in Ag, time-differential perturbed ang. correl. obs. 2−57316
^{112}Cd, low-spin states studied in decay of ^{110}Ag 2−74035
^{112}Cd lifetimes of Coulomb, excited states meas. using plunger recoil distance technique 2−63756
^{113}Cd spin-lattice relax. in CdS:Co^{2+} 2−54367
^{113}Cd(n,γ)^{114}Cd, parity violation in neutron capture γ-rays 2−67289
^{114}Cd, ^{3}He inelastic scatt., form factor phase and shape 2−59777
^{114}Cd(^{32}S,^{32}Sγ) 50 MeV, determ. of sign of multiple Coulomb excitation interference term and static quadrupole moment 2−82893
^{114}Cd(^{3}He, ^{3}He)^{114}Cd, interference between Coulomb and nuclear excitation amplitudes 2−46304
^{116}Cd (n,γ), cross- sections and isomer ratios 2−59767
^{116}Cd(n,2n)^{115}Cd, isomer yield ratio of ^{115m}Cd and ^{115g}Cd 2−63808
^{116}Cd(p,p'), γ-ray multiplicity comparison with compound nucleus reaction mechanisms 2−67224
^{117}Cd and ^{117}Cd^{m} decay, energy levels of ^{117}In 2−76819
^{15m}Cd, retention and elimination in man, meas. using whole body counting technique 2−55285
^{113m}Cd, 14.6±0.5 year half-life, decay data analyzed by least squares programme 2−46192
^{115m}Cd, decay to ^{115}In, internal conversion electrons 2−70420
Cd(n,γ), capture of 5-80 keV neutrons, γ spectra analysis 2−67286
^{132}Ce, yrast states, energies and spins, collective bands 2−79757
^{138}Ce, 0^{+} level struct. from ^{140}Ce(p, t) reaction 2−76847
^{138}Ce, bubble nuclei approach 2−82904
^{140}Ce, 0^{+} level struct. from ^{142}Ce(p, t) reaction 2−76847
^{140}Ce, 2412 keV level lifetime meas. 2−52762
^{140}Ce, angular correlation of γ-cascade 2−49748
^{140}Ce, distribution of E1 strength, preliminary obs. on ^{139}La(p,γ_0)^{140}Ce 2−82891
^{140}Ce, energy spectra, effect of proton-neutron interactions 2−46157
^{140}Ce, gyromagnetic ratio of 2083 keV 4^{+} state and $\gamma\nu$ ang. correlation 2−52763
^{140}Ce(n,γ)^{141}Ce, role of doorway states of 'phonon + particle' type 2−49809
^{140}Ce(p, t)^{138}Ce, E_p = 30.3 MeV, strong and weak 0^{+} excitations 2−76847
^{141}Ce, intensities of E1-type γ-transitions from neutron capture states to lower p-levels 2−49809
^{141}Ce, longitudinal polarization of β-particles 2−82933
^{141}Ce, mechanism of uptake in isolated perfused rat liver 2−55225
^{141}Ce level scheme investigation in unified model calc. and particle core model 2−67170
^{142}Ce(d, p), 12.6 MeV, reaction study 2−67332
^{142}Ce(d, t), 12.6 MeV, reaction study 2−67332
^{142}Ce(p, p$_0$), 9.5 to 12 MeV, isobaric analogue resonances 2−67332
^{142}Ce(p, p$_1$), 9.5 to 12 MeV, isobaric analogue resonances 2−67332
^{142}Ce(p, t)^{140}Ce, E_p = 30.3 MeV, strong and weak 0^{+} excitations 2−76847
^{144}Ce, biological half-life in human chest determ. from in vivo meas. following accidental inhalation 2−55233
^{144}Ce, effect of hormones on retention in rats 2−55260
^{144}Ce, influence of irradiation on incorporation in hair and other tissues of rabbits and rats 2−55293

Nuclei with $90 \leqslant A \leqslant 149$ continued
^{145}Ce, 3.0 min. γ-decay studied by method of separation, determ. of energies and relative intensities 2−42524
Cs, A = 132,134,136,137, distrib. of isotopes produced by α-particle induced fission of ^{238}U 2−74130
Cs, mapping of correlation between neutron width and radiative capture 2−67292
Cs, neutron-capture cross-sections, 0.01 to 100 eV 2−59761
Cs isotopes produced in ^{237}Np proton induced fission, 20-85 MeV, determ. of independent formation cross sections 2−79812
^{122}Cs, positron decay 2−74037
^{123}Cs, energy levels 2−74037
^{124}Cs, energy levels and positron decay 2−74037
^{129}Cs decay, γ-ray energy determ. 2−42546
^{131}Cs decay, double K-shell ionization 2−64028
^{131}Cs decay, gamma gamma directional correl. meas. 2−46197
^{132}Cs, comparative behaviour in males and females following oral administration 2−55292
^{133}Cs, internal conversion electron studies 2−70422
^{133}Cs, n.m.r. in free Cs^{+} ions 2−79897
^{133}Cs^{+} ion, free, n.m.r. freq. shift due to charge exchange with Cs atom 2−79896
^{133}Cs n.m.r., superconducting solenoid magnetic field monitoring 2−66700
^{133}Cs(^{20}Ne,4n)^{149}Nb, excitation function, cross sections, 50-200 MeV 2−74120
^{133}Cs(n,d), 14 MeV α-particle ang. distribution and energy spectra 2−42573
^{134}Cs, half-life 2−52775
^{134}Cs β-decay, meas. of directional correlations of ^{134}Ba γ-rays 2−70404
^{134}Cs isomer ratios in ^{237}Np fission with protons 2−63932
^{134}Cs released to water basins, meas. of accumulation in bed sediment 2−57833
^{134}Cs→^{134}Ba decay scheme study by meas. of γ-γ coincidences 2−52781
^{135}Cs, ^{137}Cs, ^{139}Cs, γ-ray and conversion electron spectra, spin-parity assignments 2−46155
^{137}Cs, absolute differential scattering cross sections for 0.662 MeV photons 2−46229
^{137}Cs, absorption through skin, influence of decontamination treatment on degree of internal contamination 2−55236
^{137}Cs, estimation of relative role of penetration into critical organs through intact skin 2−55295
^{137}Cs, internal bremsstrahlung spectrum of unique β-transition 2−82932
^{137}Cs, product of ^{235}U and ^{239}Pu fission, contribution to burn-up of plutonigen reactor fuel 2−74149
^{138}Cs levels populated in decay of ^{138}Xe, shell-model interpretation 2−82924
^{141}Cs, direct meas. of half-life and gamma-ray energies 2−76812
^{147}Gd, high spin levels excited in ^{144}Sm (α,n) reaction, particle core coupling 2−49750
I, mapping of correlation between neutron width and radiative capture 2−67292
I isotopes, internal contamination in isotope production heat laboratory, Budapest 2−58632
I radionuclides and precursors inhaled into human body, calc. of radiation dose to thyroid 2−55275
^{126}I, decay to ^{126}Te, ^{126}Xe, meas. of half-life and energies and intensities of γ-rays 2−52780
^{127}I, low-lying states, ^{127}I(n,n$'\gamma$) reaction study from 0.5 to 1.6 MeV 2−49746
^{127}I, mag. moment of 57.6 keV state, Mossbauer obs. 2−63812
^{127}I, meas. of magnetic moment of 57.6 keV state by Mossbauer effect in IFe 2−49747
^{127}I, nuclear quadrupole resonance in group V double and triple chalcogens 2−48311
^{127}I n.q.r. and spin-lattice relax. in ferroelec. systems 2−81481
^{127}I quad. coupling consts. of CsI 2−53003
^{127}I(n,d), 14 MeV, α-particle ang. distribution and energy spectra 2−42573
^{129}I- ^{129}Xe, radiation effects, dating of Bjurbole chondrules 2−69174
^{129}I, Mossbauer effect in AsI$_3$, SbI$_3$, BI$_3$, and sulphur complexes, bonding character 2−78071
^{129}I Mossbauer effect in quenched liq. cryst. 2−60425
^{131}I, estimation of permissible radiation dose to gonads and foetus 2−55280
^{131}I behaviour in types of soil found in Czechoslovakia 2−57804
^{131}I production laboratories, radiation monitoring and risk of internal contamination 2−58630
^{131}I production risks, routine thyroid monitoring 2−58631
^{131}I therapy and whole-body scanning in thyroid carcinoma 2−48883
^{136}I, 83 sec isomer, cumulative yield in thermal neutron induced ^{235}U fission 2−63934
^{134m}I, 3.8 min, from slow neutron fission of ^{235}U, identification and characterization 2−52759
In odd-A isotopes, A = 113-117, structure of low-lying states calc. in semi-microscopic model 2−63807
In odd mass isotopes, low energy props. 2−42516
^{107}In, β^{+}/EC decay, study of level scheme of ^{107}Cd by obs. of γ-rays 2−82934
^{111}In, ^{67}Ga and ^{75}Se in tumours, Ge(Li) detector for simultaneous meas. 2−73206
^{112}In, 1+ ground state, beta decay 2−42544
^{112}In, decay, study of γ transitions to elucidate low-spin excited states in ^{112}Cd 2−74035
^{113}In^{m} K-conversion lines meas. with Si(Li)-β-spectrometer in 4π geometry 2−63689
^{113}In(^{12}C, 3n)^{123}Cs, positron decay and decay scheme of ^{113}Cs 2−74037
^{113}In(^{3}He,d)^{114}Sn, 37.7 MeV, proton particle-hole states of ^{114}Sn 2−74116
^{113}In(n, n$'$), 13 to 18 MeV, cross-section 2−67246
^{115}In, from decay of ^{115m}Cd, internal conversion electrons 2−70420
^{115}In (p,p)^{115}In, analogue states of ^{116}In 2−67215
^{115}In in activation foils, determ. of thermal neutron energy spectrum for pool type reactor 2−79832
^{115}In(^{12}C, 3n)^{124}Cs, excited levels and positron decay 2−74037
^{115}In(^{12}C, 4n)^{123}Cs, isomeric level and γ-transitions found 2−74037

Nuclei with $90 \leqslant A \leqslant 149$ continued
^{115}In(α,p), 42 MeV, particle emission probabilities 2−42587
^{115}In(n,γ)^{116}In, obs. of γ-rays in spin-assigned capture resonances 2−67290
^{115}In(n,γ)^{116}In, thermal neutron capture, γ-ray spectroscopy study of ^{116}In level scheme 2−67168
^{116}In, beta decay asymmetry and n.m.r. 2−42500
^{116}In, isobaric analogue states, formation in ^{115}In (p,p), properties 2−67215
^{116}In γ-rays from neutron capture resonances in ^{116}In, determ. E1 and M1 strengths 2−67290
^{116}In level scheme of lower states and hole-particle structure study by thermal neutron capture γ-ray spectroscopy 2−67168
^{117}In level scheme from ^{117}Cd and ^{117}Cd^{m} decay 2−76819
^{124}In→^{124}Sn decay, E2-E1 transitions, energy levels 2−42520
^{192}Ir hairpin interstitial radiation therapy, dosimetric considerations 2−69424
Kr, element yield distribution in thermal neutron fission of ^{235}U 2−63935
^{86}Kr, levels fed in decay of ^{96}Br 2−46188
^{92}Kr, gamma ray study following beta decay 2−49767
^{92}Kr, γ-ray decay scheme 2−70399
La, odd-mass isotopes, decoupled Yrast states 2−63814
La molten, 600 MeV proton production of very neutron-deficient isotopes of Cs, study using on-line isotope separator techniques 2−42545
^{131}La→^{131}Ba and ^{132m}La→^{132}Ba decay, conversion electron data analysis 2−70421
^{135}La, angular correlations for 567-206, 664-206, 605-265 and 571-300 keV cascades 2−46156
^{137}La, dipole and quadrupole moments, optical determ. 2−63813
^{138}La, optical determ. of quadrupole moment 2−52760
^{138}La, shell model configuration interpretation of low-lying states populated in ^{139}La(d,t) reactions 2−52761
^{138}La decay obs. 2−46198
^{138}La low-lying levels excited in (p,d) reactions at 30 MeV, total angular momenta assignments 2−42564
^{139}La, correlation between (n, γ) and (n, p) reactions 2−59768
^{139}La, det. of total coeff. of internal γ-radiation conversion 2−59711
^{139}La, n.m.r., in LaPb$_3$ and LaIn$_3$ 2−65346
^{139}La, spin-lattice relax. in La$_{1-x}$GdAl$_2$ 2−54370
^{139}La(d,p)^{140}La and ^{139}La(n,γ)^{140}La, positive correlation 2−67293
^{139}La(d,t)^{138}La, 16 MeV, meas. of angular distrib. of tritons, Q-value, low-lying states in ^{138}La 2−52761
^{139}La(γ,xn) meas. of photoneutron cross sections 8-24 MeV, by direct neutron detection 2−63865
^{139}La(μ^-, ν), probability of occurrence 2−46241
^{139}La(n,γ)^{140}La and ^{139}La(d,p)^{140}La, positive correlation 2−67293
Mo, ^{12}C, ^{16}O, ^{22}Ne and ^{40}Ar ion bombardment, inelastic interaction, neutron production, ang. distrib. 2−76886
Mo, A=92, 94, 96, 98, 100, elastic and inelastic α-particle scatt., 30.87 MeV 2−63905
Mo, angular distribution of photoneutrons 2−63864
Mo isotopes, hole-strength variations in neutron pick-up reactions 2−46151
Mo(^{3}He,d)Tc, A=92, 94, 96, unbound analog states in Tc isotopes 2−46180
Mo(^{18}O,^{16}O), DWBA calc. of two-nucleon transfer 2−83018
^{90}Mo, angular distribs. and spin-parity assignments of levels populated in ^{92}Mo(p,t) reaction 2−70398
^{92}Mo, E2 transition rates, shell model calc. 2−67162
^{92}Mo, energy levels, model calcs 2−82906
^{92}Mo+p, conversion electron spectra by in-beam spectroscopy 2−82913
^{92}Mo(^{3}He,d)^{93}Tc, spectroscopic factors 2−63861
^{92}Mo(^{3}He,xn) and (p,xn) reactions, production of short-lived Ru and Tc isotopes 2−49768
^{92}Mo(α,t)^{93}Tc, 41.5 MeV, ang. distribution meas. 2−46327
^{92}Mo(d,pγ), coincidence obs. of ^{93}Mo γ-decay 2−63805
^{92}Mo(n,γ)^{93}Mo, γ-ray spectra meas., test of valency model 2−67283
^{92}Mo(p,t)^{90}Mo, 39 MeV, meas. of angular distribs. of levels in ^{90}Mo 2−70398
^{93}Mo, spin-parity assignment of 1.69 MeV level, j-value determination by spectroscopic factor ratios 2−74034
^{93}Mo γ-decay from ^{92}Mo(d,pγ) and ^{93}Tc β-decay 2−63805
^{93}Mo levels excited in ^{94}Mo(^{3}He, ^{4}He) reaction at 16 MeV, identification of 3 new levels 2−70401
^{94}Mo, low-lying states investigation via multiple Coulomb excitation 2−82910
^{94}Mo(^{3}He, ^{4}He)^{93}Mo, 16 MeV, meas. of cross section, angular distribs., DWBA analysis 2−70401
^{94}Mo(p,p$'\gamma$)^{94}Mo, angular correlation obs., analog resonance in ^{95}Tc 2−74078
^{95}Mo(p,t)^{93}Mo, spin-parity assignment of 1.69 MeV level 2−74034
^{96}Mo(α,t)^{97}Tc, 41.5 MeV, ang. distribution meas. 2−46327
^{96}Mo(p,xn)$^{97-x}$Tc, E_p=10-80 MeV, excitation functions 2−74091
^{97}Mo(p,nγ)^{97}Tc, E_p=3−6 MeV, excited states in ^{97}Tc 2−67165
^{98}Mo, ^{100}Mo, inelastic proton scatt., E_p=14.7 MeV, ang. distrib. 2−79782
^{98}Mo, proton scatt. and excitation studies using in-beam internal conversion electrons 2−70417
^{99}Mo fragment from neutron fission of ^{235}U, range in W 2−47786
^{100}Mo, low-lying states investigation via multiple Coulomb excitation 2−82910
^{100}Mo, low-lying states investigation via multiple Coulomb excitation 2−82910
^{101}Mo spectroscopy by sub-Coulomb stripping 2−76797
^{101}Mo→^{101}Tc decay, γ-ray spectra, energy levels of ^{101}Tc 2−74051
Mo(n,γ), capture of 5-80 keV neutrons, γ spectra analysis 2−67286
Nb, A=91,97, single particle proton states, reaction (d,n) study 2−70400
Nb(A=91, 97), level properties from ^{90}Zr(d, n) and ^{96}Zr(d, n) reactions 2−63922
^{90}Nb, γ-decay scheme studied using ^{90}Zr(p,nγ) reaction 2−42515
^{90}Nb production by deuteron irradiation of Zr, determ. of excitation functions 2−74115
^{91}Nb,^{93}Nb, isobaric analogue resonances, total and partial widths 2−59703
^{91}Nb, E2 transitions and isomeric 17/2 states 2−67162
^{91}Nb, ebergy levels, model calcs 2−82906

Nuclei with $90 \leqslant A \leqslant 149$ continued
^{91}Nb, structure of lower states 2−52755
^{91}Nb+n, polarization effects in isospin-coupled reaction channels 2−63884
^{93}Nb, α-particle excitation 2−46152
^{93}Nb, elastic and inelastic neutron scattering in 1.0 to 5.0 energy range 2−42574
^{93}Nb, n.m.r. in Fe, hyperfine field detn. 2−75354
^{93}Nb(n,d), 14 MeV, α-particle ang. distribution and energy spectra 2−42573
^{93}Nb(n,γ), angular distribution of γ-rays in resonant neutron capture 2−67284
^{93}Nb(n,n$'\gamma$)^{93}Nb, de-excitation γ-rays, ^{93}Nb level scheme 2−67164
^{95}Nb, isomer ratios of nuclear produced in ^{209}Bi fission 2−63933
^{97}Nb decay, γ-obs. 2−42543
Nd, even nuclei, magnetic moment of first (2^+) and second (4^+) states 2−42522
Nd neutron-deficient isotopes, spin values 2−82899
^{134}Nd isomeric state excited in ^{118}Sn(^{20}Ne, 4n) reaction at 82-120 MeV 2−79745
^{140}Nd→^{140}Pr, meas. of K-capture component of electron capture log β, energy of decay deduced 2−46199
^{142}Nd, energy spectra, effect of proton-neutron interactions 2−46157
^{142}Nd, isospin splitting of giant E1 excitation in ^{141}Pr(p,γ) reaction 2−82891
^{142}Nd(n,γ)^{143}Nd, role of doorway states of ‘phonon + particle’ type 2−49809
^{143}Nd, intensities of E1-type γ-transitions from neutron capture states to lower p-levels 2−49809
^{143}Nd, neutron resonance spin determinations from capture gamma ray meas. 2−49749
^{143}Nd level scheme investigation in unified model calc. and particle core model 2−67170
^{143}Nd(n,γ), γ-ray spectra from resonance neutron capture 2−67295
^{144}Nd, lifetime of 1314 keV level 2−63815
^{144}Nd, spin assignments, new excited states and transitions following ^{144}Pn→^{144}Nd 2−67196
^{144}Nd(n,γ)^{145}Nd, thermal neutron capture, γ-ray spectroscopy study of ^{145}Nd 2−67172
^{145}Nd, neutron resonance spin determinations from capture gamma ray meas. 2−49749
^{145}Nd low-lying excited states populated by thermal neutron capture 2−67172
Nd(p,t) even isotopes, 5Z MeV, excitation of removal and addition types of quadrupole-pairing vibrational states 2−82968
Nd(t,p) (A=142, 144, 146, 148) 13 MeV, angular distributions of protons, Q-values and spin and parity of states 2−42523
^{101}Pb, decay, internal conversion and γ-ray intensities 2−49770
Pd, fast neutron cross sections meas., optical pot. 2−82980
^{105}Pd, gamma ray spectrum in ^{104}Ru(α,3n) reaction, determ. of multipolarities 2−49744
^{105}Pd, neutron reson., spin determ. by γ-ray multiplicity method 2−67167
^{105}Pd, quadrupole coupling constants of $^3D_2$, $^3D_1$ and $^1D_2$ levels 2−52756
^{105}Pd n.m.r. in PdH$_x$, Knight shift 2−78174
^{106}Pd, g-factor expt. on first excited 2+ state 2−52742
^{108}Pd(n,γ)^{109}Pd*, gamma-ray spectrum, resonance spin determ. 2−67288
^{109}Pd, spin of 3/2 resonance determ. 2−67288
^{144}Pm, electron capture decay and ground state spin assignment 2−67196
^{144}Pm→^{144}Nd decay, triple coincidence meas., time spectra analysis 2−63815
^{147}Pm$_2$O$_3$, thick cylindrical β-source, bremsstrahlung 2−67191
^{147}Pm containing luminous paint, metabolism following inhalation by mice, removal of radioactive materials 2−55288
^{148}Pm, ground state struct. 2−42525
^{148}Pm decay, β-γ circular polarization correl. 2−42547
^{142m}Pm, half-life decay times, int. conv. spectra and excitation functions detn. 2−67195
Pr, ^{12}C, ^{16}O, ^{22}Ne and ^{40}Ar ion bombardment, inelastic interactions, neutron production, ang. distrib. 2−76886
Pr neutron-deficient isotopes, spin values 2−82899
^{135}Pr→^{135}Ce decay scheme, excited states of ^{135}Ce 2−52782
^{139}Pr γ-γ angular correlations for 114-708 and 114-738 keV cascades, lifetime of 822 keV level 2−46158
^{140}Pr low-lying levels excited in (p,d) reactions at 30 MeV, total angular momenta assignments 2−42564
^{141}Pr-Tm intermetallic cpds., h.f. n.m.r. at 4.2 degrees K 2−72518
^{141}Pr, high energy photonuclear reactions, residual activity and γ-ray scintillation spectroscopy 2−42556
^{141}Pr, K-shell internal conversion coeffs. meas. with X-ray scintillation spectrometer 2−79737
^{141}Pr, Mossbauer, scatt., isomer shifts between Pr^{4+} and Pr^{3+} compounds 2−48151
^{141}Pr, Mossbauer scatt., PrO$_2$, hyperfine fields 2−48151
^{141}Pr, neutron reson. level spacings, stat. distribs., deviations 2−67161
^{141}Pr(^{12}C,4n)^{149}Nb, excitation function, cross sections, 50-200 MeV 2−74120
^{141}Pr(γ,π-2n)^{139}Nd, cross-sections of photopion prod. 2−55981
^{141}Pr(γ,π-n)^{140}Nd, cross-sections of photopion prod. 2−55981
^{141}Pr(γ,xn), meas. of photoneutron cross sections, 8-24 MeV, by direct neutron detection 2−63865
^{141}Pr(n,γ)^{142}Pr, test of valency neutron model 2−67294
^{141}Pr(n,nγ), differential cross sections and angular distributions of gamma rays 2−46159
^{141}Pr(p, t)^{139}Pr, 40 MeV, collective effects 2−63886
^{141}Pr(p,γ)^{142}Nd, 6-17 MeV, isospin splitting of giant E1 excitations 2−82891
^{143}Pr→^{143}Nd, hindered $7/2^+ \rightarrow 3/2^-$ decay 2−63849
^{92}Rb, gamma ray study following beta decay 2−49767
^{92}Rb, γ-ray decay scheme 2−70399
^{99}Rh→^{99}Ru, new gamma-ray energy of 910.8 KeV 2−79740
^{101}Rh, levels with spin-parity assignments 2−49770
^{103}Rh dipole moments of very short-lived states by recoil-into-gas method 2−70371
^{103}Rh(n,d), 14 MeV, α-particle ang. distribution and energy spectra 2−42573

Nuclei with $90 \leqslant A \leqslant 149$ continued
Ru isotopes, potential energy surfaces in two-centre shell model 2−63735
Ru(A=99, 100, 101, 102, 104), En=1-1500 eV, total n cross section meas. 2−49803
^{92}Ru, 3.6 min produced by ^{92}Mo(^{3}He,xn), obs. of new weak γ transitions 2−49768
^{92}Ru, new neutron-deficient isotope, determ. of half-life and gamma-ray spectra 2−76813
^{92}Ru, separation and half-life meas. 2−49766
^{94}Ru, E2 transition rates, shell model calc. 2−67162
^{94}Ru, energy levels, model calcs 2−82906
^{99}Ru, level scheme, transitions using ^{99} Rh decay 2−79740
^{101}Ru level scheme from ^{101}Tc decay obs. 2−74051
^{102}Ru, g-factor expt. on first excited 2+ state 2−52742
^{102}Ru(n,γ)^{103}Ru, thermal neutron capture, ^{103}Ru level scheme obs. 2−67166
^{103}Ru level scheme, ^{102}Ru(n,γ) obs. 2−67166
^{104}Ru(α,3n)^{105}Pd, 26-43 MeV, γ-ray spectrum of excited states of ^{105}Pd 2−49744
^{104}Ru(n$_{th}$,γ)^{105}Ru, thermal neutron capture, γ spectra, spin assignments of ^{105}Ru levels 2−67287
^{105}Ru levels, spin assignments, ^{104}Ru thermal neutron capture obs. 2−67287
^{106}Ru, product of ^{235}U and ^{239}Pu fission, contribution to burn-up of plutonigen reactor fuel 2−74149
^{119}SN(p, np), total cross section excitation function 2−70444
Sb, A=122, 124, spin and parity of levels 2−67291
Sb, mapping of correlation between neutron width and radiative capture 2−67292
Sb, slow neutron resonances 2−82975
Sb(A=120,124), oriented in Fe, ground state moment from n.m.r. 2−49745
^{a}Sb, A=121, 123, nuclear electric quadrupole radiative transitions in InSb, explanation of microwave emission 2−44404
^{110}Sb→^{110}Sn decay scheme, spin and parity of ^{110}Sb 2−76818
^{111}Sb→^{111}Sn decay scheme, spin and parity of ^{111}Sb 2−76818
^{112}Sb→^{112}Sn decay scheme, spin and parity of ^{112}Sb 2−76818
^{113}Sb→^{113}Sn decay scheme, spin and parity of ^{113}Sb 2−76818
^{114}Sb→^{114}Sn decay scheme, spin and parity of ^{114}Sb, isomeric state 2−76818
^{117}Sb, isomeric level, g-factor 2−59708
^{119}Sb Mossbauer effect in Sb, Sb_2Te_3 and Sb_2S_3 2−54392
^{121}Sb, Mossbauer effect in Bi-Sb alloy 2−81345
^{121}Sb, Mossbauer effect in group V_2-VI_3 and group V-VI-VII semiconductor compounds 2−75274
^{121}Sb, Mossbauer effect in Mn_{1-x} Cr_xSb, hyperfine fields detn. 2−54514
^{121}Sb, n.m.r. in Fe, hyperfine field detn. 2−75354
^{121}Sb, neutron capture, reson. obs. 2−67167
^{121}Sb, neutron spectroscopy, cross- sections, Doppler and crystal binding effects on resonance 2−46277
^{121}Sb Mossbauer effect in $Ni_{1.2}Fe_{1.7}Sb_{0.1}O_4$ 2−48150
^{123}Sb, n.m.r. in Fe, hyperfine field detn. 2−75354
^{123}Sb, neutron capture, reson. obs. 2−67167
^{123}Sb, nuclear quadrupole resonance in group V double and triple chalcogens 2−48311
^{125}Sb→^{125}Te decay, $\gamma-\gamma$ directional correlation expts. concerning negative and positive parity levels 2−46195
^{127}Sb, nuclear quadrupole resonance in group V double and triple chalcogens 2−48311
^{128}Sb, charge and mass. distrib., half-life, yield from ^{235}U fission 2−83036
^{129}Sb, yield from ^{235}U fission, half-life 2−83036
^{130}Sb, charge and mass. distrib., half-life, yield from ^{235}U fission 2−83036
^{132}Sb proton-neutron-hole states populated in β-decay of ^{132}Sn 2−82923
^{134}Sb β-decay to two-proton and proton-neutron states in doubly closed shell ^{132}Sn region 2−82895
Sb(n,γ), A=121, 123, γ-ray spectra of resonances 2−67291
Sm, even nuclei, magnetic moment of first (2^+) and second (4^+) states 2−42522
^{140}Sm, decay scheme 2−46200
^{142}Sm, decay scheme 2−46200
^{144}Sm, differential cross sections for elastic and inelastic scattering of α particles and protons to low-lying states 2−46305
^{144}Sm, elastic and inelastic ^{3}He scatt. at 53.4 MeV, DWBA and Sca analysis 2−56002
^{144}Sm, energy spectra, effect of proton-neutron interactions 2−46157
^{144}Sm, inelastic proton scattering at 30 MeV, determ. differential cross sections, J^{π} assignments 2−74079
^{144}Sm, level scheme, study by (γ, γ') reaction 2−63816
^{144}Sm(d,t)^{143}Sm, E_d=12.1 and 13.1 MeV level scheme of ^{143}Sm 2−82989
^{144}Sm(n,2n), 14.1 MeV, meas. of cross-section using activation method 2−49810
^{147}Sm, correlations for equidistant neutron resonances 2−67296
^{147}Sm, neutron reson., spin determ. by γ-ray multiplicity method 2−67167
^{147}Sm(n, γ)^{148}Sm, spins of levels of ^{148}Sm 2−76801
^{147}Sm(n,α), determ. of distrib. of total alpha-particle widths of neutron resonances 2−67297
^{147}Sm(n,α)^{144}Nd, investigation of decay of ^{148}Sm resonance states 2−46287
^{148}Sm, proton scattering at 12 MeV, coupled channel analysis 2−55987
^{148}Sm levels, spin determ. 2−76801
^{148}Sm resonance states, investigation of α-decay using ^{147}Sm(n,α)^{144}Nd 2−46287
^{149}Sm, correlations for equidistant neutron resonances 2−67296
^{149}Sm, neutron reson., spin determ. by γ-ray multiplicity method 2−67167
^{149}Sm, PWR poisoning computation algorithm 2−63957
^{141m}Sm, decay scheme 2−46200
Sm(p,t.)E_p-19 MeV level assignments for even isotopes 2−82962
Sn, A=116, 118, 120, 124, nuclear sizes by 166 MeV α-particle scattering 2−63809
Sn isotopes, even, static quadrupole moments and anharmonicity parameters 2−59706

Nuclei with $90 \leqslant A \leqslant 149$ continued
Sn(A=117, 119), Coulomb excitation using α-particle and ^{16}O projectiles 2−63810
^{107}Sn isotope identification in ^{106}Cd(α.3n) reaction 2−82886
^{111}Sn, ^{113}Sn, short-lived isomers obs. by pulse activation of enriched Cd isotopes using α-particles and ^{3}He beams 2−74036
^{112}Sn(p, xn), decay of light Sb isotopes 2−76818
^{112}Sn(p,p'), γ-ray multiplicity comparison with direct reaction mechanisms 2−67224
^{113}Sn, half-life 2−52775
^{114}Sn, photoproton spectra, calc. and comparison with expt. 2−59741
^{114}Sn(p, xn), decay of light Sb isotopes 2−76818
^{116}Sn(α,p), 42 MeV, particle emission probabilities 2−42587
^{116}Sn(d,p)^{117}Sn, 4.35-5.55 MeV, Coulomb stripping to states in ^{117}Sn 2−67331
^{116}Sn(p,np~) charge exchange reaction, qualitive studies of angular distribution 2−46253
^{117}Sn, levels populated in Coulomb (d,p) stripping 2−67331
^{117}Sn, lifetime of 158.6 keV level 2−76765
^{118}Sn(^{20}Ne, 4n), 82-120 MeV, excitation of isomeric state in ^{134}Nd 2−79745
^{118}Sn(n,α)^{115}Cd, isomer yield ratio of ^{115m}Cd and ^{115g}Cd 2−63808
^{119}Sn, mag. moment of 89 keV excited state, deviation from Schmidt value, Mossbauer obs. 2−67169
^{119}Sn, Mossbauer effect in Cu_2FeSnS_4 2−75239
^{119}Sn, Mossbauer effect in Sn dilute alloy, nuclei vibration obs. 2−71721
^{119}Sn, Mossbauer effect in solid N_2, isomer shift obs. 2−48148
^{119}Sn Mossbauer effect in haematite 2−65234
^{119}Sn Mossbauer effect in HoPtSn and related intermetallics 2−50621
^{119}Sn Mossbauer recoil-free fraction in Nb_3Sn 2−44357
^{119}Sn n.m.r. in $CeSn_3$, absence of magnetic ordering obs. 2−84588
^{119}Sn resonance Mossbauer detector with windowless electron multiplier 2−42471
^{119}Sn size calc. from M1 transitions and Mossbauer isomer shift 2−76759
^{119}Sn(d,d′n), 19 MeV, neutron-gamma competition 2−46325
^{119}Sn(p, n), 28 and 35 MeV, populating IAS, angular distribution meas. 2−70444
^{119}Sn(p,np), excitation functions and energy dependence of reactions 2−67223
^{119}Sn(t, p)^{121}Sn, 13 MeV, ang. distrib. transferred orbital momentum derived 2−76798
^{120}Sn neutron scattering, 1.5-3.5 MeV, meas. of angular distribs., comparison with spherical optical model, coupled-channels theory 2−67247
^{120}Sn(^{16}O,^{4}n), yrast states in ^{132}Ce 2−79757
^{120}Sn(p,p)^{120}Sn, DWA cross-section calc. with imaginary part 2−74081
^{120}Sn(t, d)^{121}Sn 13 MeV, ang. distrib. transferred orbital momentum derived 2−76798
^{121}Sn, 1 and 3 quasiparticle states, core-particle discription of low-lying levels 2−76798
^{122}Sn(d,p)^{123}Sn, 4.35-5.55 MeV, Coulomb stripping to states in ^{123}Sn 2−67331
^{122}Sn(p,p'), γ-ray multiplicity, comparison with compound nucleus reaction mechanism 2−67224
^{123}Sn, levels populated in Coulomb (d,p) stripping 2−67331
^{124}Sn, energy levels and transitions, ^{124}In decay obs. 2−42520
^{124}Sn, photoproton spectra, calc. and comparison with expt. 2−59741
^{124}Sn(α,3nγ), E_{α}=26-37 MeV, particle-core coupling in ^{125}Te 2−76781
^{124}Sn(d,p)^{125}Sn, 4.35-5.55 MeV, Coulomb stripping to states in ^{125}Sn 2−67331
^{125}Sn, levels populated in Coulomb (d,p) stripping 2−67331
^{129}Sn isomers, half-lives 2−83036
^{130}Sn, yield from ^{235}U fission, half-life 2−83036
^{132}Sn doubly closed shell nucleus, β-decay to proton-neutron-hole states in ^{132}Sb 2−82923
^{132}Sn doubly closed shell region, two-proton and proton-neutron states populated in ^{134}Sb beta decay 2−82895
^{117m}Sn, g-factor, halflife, M4-transition 2−63811
Sn(d, d)Sn, A=112, 118, 119, 124, 20 and 27 MeV, ang. distrib., optical model fits. 2−79803
Sn(n,γ), capture of 5-80 keV neutrons, γ spectra analysis 2−67286
^{90}Sr, estimation of permissible radiation dose to gonads and foetus 2−55280
^{90}Sr, internal contamination in isotope production heat laboratory, Budapest 2−58632
^{90}Sr concentration in human bones, ratio of spongious/compact bone in relation to age and time 2−58594
^{90}Sr fallout, bearing on weather conditions 2−62286
^{90}Sr nasopharyngeal applicator, photographic determ. of dose rate distribution 2−69435
^{90}Sr nasopharyngeal applicators, dose distributions 2−69436
^{90}Sr sealed sources, accidental contamination during handling 2−55234
^{92}Sr, gamma ray study following beta decay 2−49767
^{92}Sr, γ-ray decay scheme 2−70399
Tc (A=92,93,95,97), single particle proton states, reaction (d,n) study 2−70400
Tc isotopes, unbound analogue states, stripping reaction study 2−46180
^{91}Tc, 3.2 min produced in ^{92}Mo(p,xn), obs. of γ transitions 2−49768
^{92}Tc, growth and decay of gamma-rays obs. following decay of ^{92}Ru neutron-deficient isotope 2−76813
^{93}Tc,^{97}Tc, isobaric analogue resonances, total and partial widths 2−59703
^{93}Tc, E2 transitions and isomeric 17/2 states 2−67162
^{93}Tc, energy levels, model calcs 2−82906
^{93}Tc, isobaric analogue resonances, (^{3}He,d) population 2−49743
^{93}Tc, structure of lower states 2−52755
^{93}Tc β-decay, coincidence obs. of ^{93}Mo γ-decay 2−63805
^{95}Tc, $^{5}\cdot_{2}{}^{+}$(g.s.) analog in ^{94}(Mo(p,p′γ)^{94}Mo 2−74078
^{97}Tc excited states, ^{97}Me(p,nγ)^{97}Tc obs. 2−67165
^{99}Tc, effect of high hydrostatic pressure (100 kbar) on decay constant 2−46190
^{101}Tc, low-energy transitions, ^{101}Mo β decay obs. 2−59705

Nuclei with 90$\leqslant$A$\leqslant$149 continued
^{101}Tc level scheme from ^{101}Mo decay obs. 2-74051
^{101}Tc$\rightarrow$^{101}Ru decay, γ-ray spectra, energy levels of ^{101}Ru 2-74051
^{99m}Tc, γ-emitter, fully automated γ imager for obs. 2-69283
^{99m}Tc decay, obs. of weak γ transition of 322 keV, determ. energy and intensity ratio to 140 keV transition 2-49769
^{99m}Tc polyphosphate, internal radiation dose, use in bone scanning 2-55274
^{99m}Tc thyroidal uptake, area and profile scanning 2-69360
Te isotopes, even, static quadrupole moments and anharmonicity parameters 2-59706
^{115}Te, ^{117}Te, short-lived isomers obs. by pulse activation of enriched Sn isotopes using α-particles and ^{3}He beams 2-74036
^{121}Te, energy level struct., unified model calcs. 2-42517
^{122}Te, neutron proton mass deform. of first excited 2^+ state 2-42518
^{123}Te, energy level struct., unified model calcs. 2-42517
^{124}Te, energy level transitions, multipole mixing ratios 2-42519
^{125}Te, energy level struct., unified model calcs. 2-42517
^{125}Te, γ-γ ang. correlation of cascade and g-factor of 462 keV $5/2^+$ level 2-52758
^{125}Te, lifetime of 321 keV(9/2-) state 2-59709
^{125}Te, magnetic moment, internal perturbed angular correlation method 2-79766
^{125}Te, Mossbauer effect in group V_2-VI_3 and group V-VI-VII semiconductor compounds 2-75274
^{125}Te, n.m.r. in $Ga_{1-x}Te_x$ and $Tl_{1-x}Te_x$ liq. semicond. alloys 2-60512
^{125}Te, n.m.r. in noncrystalline Te and Te-Sn alloys at 1.3 K 2-61751
^{125}Te, n.m.r. in Se-Te liq. semicond. alloy and $Ge_{15}Te_{81}X_4$ glass, X=Ga, P, As 2-61752
^{125}Te, nuclear quadrupole diffr. of resonant γ-rays in Te cryst. 2-57335
^{125}Te, study of positive of negative parity states populated in decay of ^{125}Sb 2-46195
^{125}Te $11/2^-$ isomer, orientation in Fe, mag. moment obs. 2-76799
^{125}Te high-spin states and particle-core coupling 2-76781
^{125}Te Mossbauer isomer shifts in Te hexahalides 2-61608
^{126}Te, levels populated in ^{126}I decay 2-52780
^{128}Te(^{40}Ar, 4n)^{164}Yb, Doppler shift meas. on recoil nuclei, determ. of lifetime of rotational levels 2-79764
^{132}Te, fragment from neutron fission of ^{235}U, range in W 2-47786
^{238}U(n,f), isomer yield ratio of ^{115m}Cd and ^{115g}Cd 2-63808
Xe, element yield distribution in thermal neutron fission of ^{235}U 2-63935
Xe in lunar breccia, fission product from extinct ^{244}Pu 2-66145
Xe isotopes, relative yields from neutron induced fission of ^{237}Np, ^{238}Np 2-46346
Xe$\rightarrow$Te+p+e^+, statistical calculation of p intensities, branching ratios to final levels and approx. spectral shapes 2-46194
^{115}Xe and neighbouring region, shell-model calc. of β^+ strength 2-82922
^{115}Xe$\rightarrow$^{114}Te(709 keV state), coincidences between γ-rays and β-delayed protons 2-46193
^{117}Xe$\rightarrow$^{116}Te(679 keV state) coincidences between γ-rays and β-delayed protons 2-46193
^{126}Xe levels populated in ^{126}I decay 2-52780
^{129}Xe, formed from ^{129}Cs decay, energy levels 2-42546
^{131}Xe, n.m.r., local mag. field shift obs. 2-65349
^{131}Xe origin on the Moon 2-66143
^{133}Xe, ^{135}Xe, ^{136}Xe, γ-ray and conversion electron spectra, spin-parity assignments 2-46155
^{133}Xe, ^{135}Xe, ^{138}Xe, fission gas release in irradiated UO_2 dispersed through graphite 2-70534
^{133}Xe, low-lying levels, core-excitation model applic. 2-70403
^{133}Xe, radioactive, nonlinear relation between inhaled activity and whole-body activity, retention in man and rat 2-55289
^{133}Xe standard unit for radionuclide activity in gases 2-55971
^{133}Xe used to determine rates of clearance in anterior tibial muscle 2-69359
^{135}Xe, PWR poisoning, computation algorithm 2-63957
^{136}Xe, energy spectra, effect of proton-neutron interactions 2-46157
^{137}Xe level scheme investigation in unified model calc. and particle core model 2-67170
^{138}Xe fission product, β- and γ-decay study using ARIEL on-line isotope separator, meas. of internal conversion and Auger L spectra 2-82924
^{90}Y, analogue states, formation in ^{89}Y (p,p), properties 2-67215
^{90}Y, internal bremsstrahlung spectrum, contrib. of detour transitions 2-42542
^{90}Y determination by liquid scintillation beta spectroscopy 2-85083
^{171}Yb, neutron capture, reson. obs. 2-67167
^{90}Zn, lifetime of excited 0^+ state, configuration mixing 2-74033
^{91}Zn(p,np), excitation functions and energy dependence of reaction 2-67223
Zr, scatt. cross section and polarization meas. by associated particle method 2-70454
Zr (A=90, 96), proton scatt. and capture studies using in-beam internal conversion electrons 2-70417
^{90}Zr, E2 transition rates, shell model calc. 2-67162
^{90}Zr, energy levels, model calcs 2-82906
^{90}Zr, giant multipole resonances by inelastic electron scattering 2-79776
^{90}Zr, giant reson. struct., low-lying collective states influence 2-74028
^{90}Zr, Hartree-Fock calcs. using modified delta interaction 2-63747
^{90}Zr, inelastic excitation of low-lying levels by 61.2 MeV protons, role of two-body spin-orbit interaction 2-70430
^{90}Zr, intermediate states of dipole analogue resons. 2-59702
^{90}Zr, nucleus distribution near surface from α-particle scatt. 2-46150
^{90}Zr (d,α)^{88}Y, DWBA computer analysis 2-70480
^{90}Zr(^{3}He,t), 70 MeV isobaric analog ground state obs. 2-83009
^{90}Zr(α,α), angular distribs. and differential cross sections in angular range 4°-150° at 40, 60, 80 and 100 MeV 2-49825
^{90}Zr(α,t)^{91}Nb, 41.5 MeV, ang. distribution meas. 2-46327
^{90}Zr(d, 2n)^{90}Nb, ^{90}Zr(d, αn(^{88}Y, excitation functions, 9-27 MeV 2-74115
^{90}Zr(d, n)^{91}Nb, energy level properties in ^{91}Nb 2-63922

Nuclei with 90$\leqslant$A$\leqslant$149 continued
^{90}Zr(d,p)^{91}Zr, 7.5 MeV, high resolution, meas. of angular distrib. for transition 2-42588
^{90}Zr(d,p)^{91}Zr, polarized deuterons, vector analyzing power and differential cross section 2-67330
^{90}Zr(p,nγ)^{90}Nb, 6.9-9.5 MeV, meas. of excitation functions for low-lying levels of ^{90}Nb and their γ-decay 2-42515
^{90}Zr(p,p), 14.5 MeV, optical- model calcs., determ. of nuclear forward-scattering amplitude 2-46245
^{91}Zr, new levels below 6.5 MeV excitation populated in ^{90}Zr(d,p) reaction 2-42588
^{91}Zr, obs. of new levels and doublets in (d,p), (p,p′), (p,d) high resolution reactions 2-52754
^{91}Zr+p, polarization effects in isospin-coupled reaction channels 2-63884
^{91}Zr(d,d′n) 19 MeV, neutron-gamma competition 2-46325
^{91}Zr(n_{th},γ)^{92}Zr, investigation of level structure in ^{92}Zr 2-67163
^{91}Zr(p, n), 28 MeV, populating IAS, angular distribution meas. 2-70444
^{91}Zr(p, np), total cross section, excitation functions 2-70444
^{91}Zr(p, t)^{89}Zr, 51.7 MeV, level determ. for ^{89}Zr 2-70445
^{91}Zr(p,n) charge-exchange reaction, coupled-channel calcs. 2-59759
^{91}Zr(p,p')^{91}Zr, 20.4 MeV, obs. of new levels and doublets in ^{91}Zr 2-52754
^{92}Zr, low-lying level spacing, shell model calculations 2-49727
^{92}Zr level structure determ. using (n_{th}, γ) reaction 2-67163
^{92}Zr(p,d)^{91}Zr, 22.0 MeV, obs. of new levels and doublets in ^{91}Zr 2-52754
^{92}Zr(p,d)^{91}Zr, 22.0 MeV, obs. of new levels and doublets in ^{91}Zr 2-52754
^{94}Zr(n,nγ), search for 2.37 MeV γ-rays 2-82985
^{95}Zr, product of ^{235}U and ^{239}Pu fission, contribution to burn-up of plutonigen reactor fuel 2-74149
^{96}Zr, first excited state lifetime, meas. using ^{96}Zr(p,p′e) reaction 2-59704
^{96}Zr(d, n)^{97}Nb, energy level properties in ^{97}Nb 2-63922
^{97}Zr decay, γ-ray obs. 2-42543
Zr(d,p)^{91}Zr, 16 MeV, obs. of new levels and doublets in ^{91}Zr 2-52754
Zr(n,γ), capture of 5-80 keV neutrons, γ spectra analysis 2-67286

Nuclei with 150$\leqslant$A
^{209}Bi, recoil study of transfer reactions induced by ^{12}C, evidence for α and ^{8}Be transfers 2-56006
^{250}104, secondary minimum in bubble degree of freedom 2-82904
— 2-67251
— 2-67189
— 2-70411
— 2-70414
— 2-70498
— 2-70406
— 2-67311
— 2-63834
— 2-63817
— 2-59732
α-decay of even-even nuclei 174$\leqslant$A$\leqslant$232, absolute probabilities and superfluidity 2-82931
actinide even-even nuclei, excitation of collective states by radiationless muonic transitions 2-67171
actinides, alpha decay and pairing vibrations 2-42540
actinides, production in secondary reactions induced by GeV protons on W and ^{238}U 2-63781
and deformed nuclei, 179$\leqslant$A$\leqslant$185, irrotational states 2-52769
cosmic rays with Z>75, propagation, r- process source 2-62447
decay isomers in Z=88, 89 region produced by neutron bombardment of ^{226}Ra 2-70458
deformation parameters 2-42532
deformed nuclei with odd protons, 153$\leqslant$A$\leqslant$177, irrotational excited states 2-55965
fission barriers and pot. energy surfaces for 180$\leqslant$A$\leqslant$212 2-76890
heavy elements, reactions by protons $\leqslant$3GeV, spallation-fission competition 2-67218
Hf odd isotopes, Coriolis coupling of N=6 states 2-79760
magic, transitional and strongly deformed nuclei, proton scattering, systematics and fine structure of Coulomb displacement energies 2-46148
odd-mass nuclei with simple configs., core polarization and mesonic current effects 2-82902
optical potential Becchetti-Greenlees used to fit ^{209}Bi(p, np)^{208}Bi 2-46266
rare earth isotopes, neutron resonance capture integral values 2-49811
rare earth nuclei, K=0 band study using (p, t) reactions 2-63885
rare-earth even-even nuclie, excitation of collective states by radiationless muonic transitions 2-67171
rare-earth region, ground state deformations, investigation by Strutinsky renormalization method 2-70363
super-heavy elements, possible production in secondary reactions induced by GeV protons on W and ^{238}U 2-63781
superheavy, evidence for previous existence in solar system 2-62643
superheavy, production cross-sections in U (p, secondary reactions) 2-70379
superheavy, radii and binding energies using Hartree-Fock calculations 2-63838
superheavy element det. using X- and gamma-ray astronomy 2-51687
superheavy elements, synthesis by r-process in supernovae 2-69093
superheavy nuclei, half-lives calc. w.r.t spontaneous fission, α- and β-decay 2-76816
superheavy nuclei, long-lived, theoretical stability regions esp. Z=114 2-79763
toroidal nuclei, deform. minima 2-82903
transitional odd-A nuclei amplitudes of quadrupole electric transitions by projection method 2-42501
transuranium and superheavy element props. 2-59893
^{241} Am, soft e.m. radiation detection using semiconductor spectrometer 2-70288
^{a}Dy(n,α), A=160, 162, 164, 14 MeV, energy distrib. of α-particles calc. using Feynman triangular diagram 2-42568

Nuclei with 150$\leqslant$A continued
^{a}Er(n,α), A=166, 168, 14 MeV, energy distrib. of α particles calc. using Feynman triangular diagram 2−42568
^{a}Eu$\rightarrow$^{a}Gd, A=156, 158, obs. of band mixing in ^{156,158}Gd 2−52766
^{a}Fr, A=211-214, determ. of excitation functions in ^{12}C and ^{16}O reactions on ^{205}Tl, ^{209}Bi 2−74123
^{a}Hg(d,d′), A=204, 202, 201, 17 MeV, obs. of transitions up to 4.5 MeV excitation 2−46329
^{a}Hg(d,p), A=204, 202, 200, 198, 17 MeV, meas. of angular distrib., spectroscopic factors 2−46329
^{a}Hg(d,t), A=204, 202, 200, 198, 17 MeV, meas. of angular distrib., spectroscopic factors 2−46329
^{a}Ho, A=164m, 164g, decay to ^{164}Dy, ^{164}Er meas. of energies and relative intensities of γ-rays and X-rays 2−52785
^{a}Os, A=188, 190, 192, comparison of IMPACT, PAC and Mossbauer effect meas. of g-factor, ferromagnetic host effects 2−42534
^{a}Pt, A=194, 195, 196, lifetimes of Coulomb- excited states meas. using plunger recoil distance technique 2−63756
^{a}Th(t,p) (A=230,232), search for transitions to excited o^{+} states 2−59785
^{a}U(t,p) (A=234,236,238), search for transitions to excited 0^{+} states 2−59785
^{a}Yb(n,p)^{a}Tm, A=172, 173, 174, meas. of activation cross sections at 14.5 MeV 2−79791
^{217}Ac, lifetime by in-beam α-spectroscopy 2−67199
^{221}Ac compound nucleus formed in ^{209}Bi + ^{12}C, ^{207}Pb + ^{14}N, ^{205}Tl + ^{16}O reactions, yrast trapping study 2−46335
^{223}Ac form. on bombardment of ^{232}Th by ^{84}Kr 2−59788
^{224}Ac form. on bombardment of ^{232}Th by ^{84}Kr 2−59788
Am isotopes, fission isomer excitation functions 2−76894
^{240}Am$\rightarrow$^{240}Pu electron capture decay, determ. of half-life and spin-parity assignment of ground-state 2−79770
^{241}Am, biological action of compounds as function of dose, routes and character of intake 2−55281
^{241}Am, estimation of permissible radiation dose to gonads and foetus 2−55280
^{241}Am, estimation of relative role of penetration into critical organs through intact skin 2−55295
^{241}Am, half-life determ. from metal sample using adiabatic microcalorimetric method 2−52789
^{241}Am, insoluble, treatment of wound contamination 2−58592
^{241}Am, irradiated, separation of ^{238}Pu and ^{242}Cm by solvent extraction using bis-(2-ethylhexyl) phosphoric acid 2−83086
^{241}Am sealed sources, accidental contamination during handling 2−55234
^{241}Am target, power preparation and purification 2−73908
^{241}Am(α,2n)^{243}Bk, excitation energy, spontaneous fissioning products, time-of-flight obs. 2−76881
^{242}Am^{m} isomeric fission, fission modes meas. using ^{242}Pu(d, 2n) reaction 2−70496
^{243}Am, L X-ray spectra, γ-transition multipolarity, coincidence obs. 2−74042
A(n,n)A, elastic, A between 48 and 209, n polarization meas. 2−67239
^{210}At, evidence for 15^{-} and 11+ isomeric states populated in ^{209}Bi(α, 3n) reaction 2−70415
^{210}At, g-factor of 0.3μs isomeric state at 2549 keV, study by ^{209}Bi(α,3n) reaction 2−49756
^{211}At, configurational mixing and effective charge 2−52771
^{211}At, energy levels from electron capture decay of ^{211}Rn 2−49775
^{211}At, half-life of 3/2^{-} level at 1116 keV, E2 rates 2−49757
^{211}At, low-lying states, shell-model calcs., effects of ^{208}Pb core vibrs. 2−67182
Au, deuteron, scatt., low energy breakup phenomena 2−67317
Au, recoil props. of rare earth nuclides produced by 28 GeV proton interactions 2−82971
Au isotopes, A=194, 196, 198, 199, produced by bombarding ^{238}U with ^{136}Xe ions 2−67335
Au neutron Doppler effect studies in unresolved resonance region 2−67233
^{197}Au,*77 keV transition, internal conversion process 2−55968
^{197}Au, anomalously narrow Mossbauer linewidth 2−78074
^{197}Au, high energy proton-nucleus interaetions, production of light fast nuclides 2−74087
^{197}Au, recoil study of transfer reactions induced by ^{12}C, evidence for α and ^{8}Be transfers 2−56006
^{197}Au Mossbauer effect in KAu(CN)$_2$ 2−44355
^{197}Au Mossbauer effect in KAu(CN)$_2$, elec. alignment 2−44356
^{197}Au(α,αn)E$_{\alpha}$=900 MeV cross sections, direct neutron emission mechanism 2−83010
^{197}Au(α,n)^{200}Tl, neutron spectra analysis, level density of residual nucleus 2−63831
^{197}Au(d,2n), excitation function meas. between threshold and 12 MeV 2−49835
^{197}Au(d,p), excitation function meas. between threshold and 12 MeV 2−49835
^{197}Au(d,t), excitation function meas. between threshold and 12 MeV 2−49835
^{197}Au(n,2n)^{196}Au, isomer cross-section ratios 2−63899
^{197}Au(n,γ), γ-ray specta of resonances 2−67305
^{197}Au(p.n)^{197}Hg, neutron spectra analysis, level density of residual nucleus 2−63831
^{198}Au, new high-spin isomer and level struct. 2−82915
^{198}Au, spin and parity of levels 2−67305
^{198}Au beta spectral shape, precision analysis 2−67198
^{200}Au, beta-decay 2−79774
^{201}Au$\rightarrow$^{201}Hg decay, low-lying levels of ^{201}Hg 2−63832
Au(n,γ), fast neutron capture, γ-rays, intensity distribs., 5.5 MeV anomaly 2−67304
Bi, search for spontaneously fissioning isomers produced with 600 MeV protons 2−79811
Bi neutron-deficient isotopes, α-decay parameters 2−76822
^{198}Bi$\rightarrow$^{198}Pb, ^{200}Bi$\rightarrow$^{200}Pb, γ-ray and conversion electron spectra 2−46174
^{205}Bi$\rightarrow$^{205}Pb decay, level scheme of ^{205}Pb 2−82928
^{206}Bi conversion-electron spectra, study of level structure of ^{206}Pb 2−70413
^{207}Bi electron capture-to-positron ratio 2−82930
^{208}Bi, spreading widths of 1^{-} particle-hole state 2−76810
^{209}Bi, charge distribution, comparison with ^{208}Pb 2−46177

Nuclei with 150$\leqslant$A continued
^{209}Bi, E1 radiative widths of isobaric analog states 2−76809
^{209}Bi, e.m. matrix elements of low-lying states 2−76782
^{209}Bi, isomer ratios of ^{95}Nb product 2−63933
^{209}Bi, multiplet energy levels calc. using single-particle and 3^{-} phonon coupling 2−42538
^{209}Bi, nuclear quadrupole resonance in group V double and triple chalcogens 2−48311
^{209}Bi, particle-hole states studied in ^{210}Po(t,α) reaction at 20 MeV 2−82894
^{209}Bi, proton decay of isobaric analogs of ground states 2−63888
^{209}Bi,final states in (^{16}O,^{15}N) and (^{12}C,^{11}B) reactions, j-assignments 2−79805
^{209}Bi analog resons., compound spreading widths 2−63835
^{209}Bi antianalogue states, calc. of compound spreading width of analogue resonance 2−42539
^{209}Bi n.q.r. in BiCl$_3$ crysts. 2−78177
^{209}Bi(^{12}C,xn)$^{221-x}$Ac, 60-90 MeV, meas. of cross sections, reaction thresholds and excitation functions 2−74123
^{209}Bi(α, 3n)^{210}At, evidence for 15^{-} and 11^{+} isomeric states in ^{210}At 2−70415
^{209}Bi(p, n)^{209}Po(p)^{208}Bi, 28, 35, 45 MeV, n ang. distrib. and n decay of isobaric analogue resonance obs. 2−46266
^{209}Bi(p,2p)^{208}Pb, obs. of T=23 double analogue states in ^{210}Po 2−70446
^{209}Bi(p,n)^{209}Po, neutron spectra of analysis, level density of residual nucleus 2−63831
^{209}Bi(p,n)^{209}Po(IAS), 28, 35 and 45 MeV, angular distributions and excitation function 2−70446
^{209}Bi(p,n) charge-exchange reaction, coupled-channel calcs. 2−59759
^{209}Bi(p,np), excitation functions and energy dependence of reaction 2−67223
^{210}Bi, mag. moments of 7^{-} and 5^{-} states 2−67181
^{204m}Bi, half-life decay times, int. conv. spectrum and excitation functions, detn. 2−67195
^{206m}Bi, half-life decay times, int. conv. spectrum and excitation functions, detn. 2−67195
^{210m}Bi target, preparation with low isotopic abundance 2−42444
^{243}Bk, excitation energy from (α,2n) reaction, time of flight obs. 2−76881
^{249}Bk spontaneous fission, average neutron yield 2−83026
^{249}Cf, L X-ray spectra, γ-transition multipolarity, coincidence obs. 2−74042
^{249}Cf fission, neutron induced, meas. of fragment angular distrib. 2−83035
^{249}Cf$\rightarrow$^{245}Cm, γ decay, obs. of γ-γ coincidences, determ. total conversion coeff. of 54.7 and 66.7 keV transitions in first rotational band 2−52772
^{249}Cf$\rightarrow$^{245}Cm, γ decay, obs. of γ-γ coincidences, determ. total conversion coeff. of 54.7 and 66.7 keV transitions in first rotational band 2−52772
^{252}Cf, ang. momentum of primary products formed in spontaneous fission 2−49850
^{252}Cf, α-decay, rel. to fluoresc. yield determ. for Cm L$_2$subshell 2−79924
^{252}Cf, β-spectrum of fission products and associated inner bremsstrahlung radiation 2−59806
^{252}Cf, disintegration track etch figures in phlogopite, effect of annealing 2−71362
^{252}Cf, fission-neutron spectra 2−46350
^{252}Cf, fission, X-ray spectra of products rel. to charge parity 2−70497
^{252}Cf, fission neutron spectrum from 0.002 to 1 MeV 2−46353
^{252}Cf, fission rate, decay constant, profile and distribution determ. with solid state track detector 2−46060
^{252}Cf, gamma-neutron competition in de-excitation mechanism of fission fragments 2−56015
^{252}Cf, implantable, calc. neutron dose rates 2−66287
^{252}Cf, spontaneous fission, search for π^0 production 2−46059
^{252}Cf, spontaneous fission, correlation between excitation energies of complementary fragments 2−46343
^{252}Cf, spontaneous fission 2−76889
^{252}Cf, spontaneous fission ang. distrib. of α-particles 2−49851
^{252}Cf, ternary fission, neutron energy spectrum 2−67338
^{252}Cf brachytherapy program, dosimetry and radiation protection 2−69381
^{252}Cf fission, development as source for neutron radiography 2−55890
^{252}Cf fission, long range α-particle emission 2−83037
^{252}Cf fission fragments energy loss in argon 2−59800
^{252}Cf medical neutron source, ion chamber dosimetry 2−69441
^{252}Cf neutron sources, electronic assay by detection of thermalized neutrons in moderator 2−42597
^{252}Cf sources, effect of thin C and Au foil cover of fission fragment energy loss and spectrum parameter changes 2−42445
^{252}Cf spontaneous, emission of ^{5}He obs. in correlation measurement 2−74125
^{252}Cf spontaneous fission, instantaneous fission neutrons depend. on fragment mass 2−59790
^{252}Cf spontaneous fission, instantaneous neutron spectrum in low-energy region 2−83025
^{252}Cf spontaneous fission neutron source for medical implant therapy, dose tables and modified distribution system 2−69442
^{252}Cf target in CM-2 reactor, effective neutron absorption cross-section 2−67341
^{252}Cf therapeutic sources, absorbed dose and linear energy transfer distributions 2−45039
^{252}Cf thermal flux subcrit. multiplication 2−83062
^{252}Cf triple fission, angular meas. of γ-radiation yield 2−49852
^{253}Cf target in CM-2 reactor, effective neutron absorption cross-section 2−67341
Cm, A=244, 246, 248, spontaneous fission, neutron yield 2−76888
Cm isotopes, A=243-6, total neutron cross sections, 0.01-30 eV 2−82976
^{241}Cm, excitation energy from (α,2n) reaction, time of flight obs. 2−76881
^{244}Cm + Be neutron source, high power 2−42440

Nuclei with $150 \leqslant A$ continued
^{245}Cm, cross-sections for thermal fission and capture, resonance integral data 2−76851
^{245}Cm, groundstate rotational band, γ branching and total conversion coeffs. of intraband transitions 2−52772
^{245}Cm, half-lives of 388 keV and 55 keV levels 2−49759
^{245}Cm, thermal neutron induced fission, determ. of mass yields 2−59791
Dy, neutron-capture cross-sections, 0.01 to 100 eV 2−59761
Dy(^{40}Ar,xn)Po excitation function and isomer ratios 2−76885
^{153}Dy→^{153}Tb and ^{155}Dy→^{153}Tb decay, conversion electron data analysis 2−70421
^{155}Dy level scheme, ^{155}Ho decay obs. 2−59716
^{158}Dy, ^{160}Dy, Mossbauer spectra, decrease in recoilless γ-ray emission 2−67173
^{158}Dy(p,t), excited 0^+ states population 2−63887
^{160}Dy, ^{158}Dy, one parameter model with EXP for energy ratios of YRAST levels to high spin 2−73984
^{160}Dy, 2^+-2^+ transition of 879 KeV, e-γ directional correlation 2−42527
^{160}Dy, mean lifetimes of high energy levels 2−46165
^{160}Dy(n,α), energy spectra, E_n=18 MeV, knock-on mechanism 2−67298
^{160}Dy(p,t), excited 0^+ states population 2−63887
^{161}Dy, Mossbauer effect of 43.8 keV transition 2−63819
^{162}Dy, quadrupole and hexadecapole deforms. 2−79752
^{162}Dy(n,α), energy spectra, E_n=18 MeV, knock-on mechanism 2−67298
^{162}Dy(n,γ)^{163}Dy, direct capture and non-statistical effects 2−67299
^{162}Dy(p,t), excited 0^+ states population 2−63887
^{163}Dy, isotope preparation and crystal growth techniques 2−56613
^{163}Dy(d, 2nγ) 13.5 MeV, meas. of γ-ray spectra, deduced ^{163}Ho level scheme 2−63820
^{163}Dy(n,γ)^{164}Dy, nonstatistical aspects in 4s giant resonance 2−67300
^{163}Dy(p, nγ) 6.7 MeV, meas. of γ-ray spectra, deduced ^{163}Ho level scheme 2−63820
^{164}Dy, 4s-giant resonance, γ-ray spectra 2−67300
^{164}Dy, neutron capture cross sections, 5−160 keV 2−82979
^{164}Dy, quadrupole and hexadecapole deforms. 2−79752
^{164}Dy in activation foils, determ. of thermal neutron energy spectrum for pool type reactor 2−79832
^{164}Dy levels populated in decays of ^{164m,g}Ho 2−52785
^{164}Dy(n,α), energy spectra, E_n=18 MeV, knock-on mechanism 2−67298
^{165}Dy→^{165}Ho, β-transitions calcs. using model of non-axial odd nucleus 2−55973
Er, A=165, 167, 169, positive-parity states by (^{3}He, α) reaction 2−79747
Er, elastic and nucl. Raman scatt. of photons, giant dipole reson. 2−70431
^{158}Er, moment of inertia of high-spin rotational states 2−63818
^{158}Er→^{158}Ho and ^{161}Er→^{161}Ho decay, conversion electron data analysis 2−70421
^{161}Er, ^{163}Er, hyperfine interaction consts. and nuclear moments meas. using atomic beam magnetic resonance method 2−79741
^{161}Er→^{161}Ho decay, level scheme of ^{161}Ho 2−76815
^{162}Er, one-parameter model with EXP for energy ratios of YRAST levels to high spin 2−73984
^{163}Er electron capture decay γ-radiation, determ. level scheme of ^{163}Ho 2−63820
^{164}Er levels populated in decays of ^{164m,g}Ho 2−52785
^{164}Er(p,t), excited 0^+ states population 2−63887
^{165}Er, level det. from ^{165}Tm decay 2−63821
^{166}Er, ^{168}Er level calc. rel. to gamma oscillations in collective model for axially symmetric nuclei 2−52767
^{166}Er, in La and Y ethylsulphates, crystal orientation effect on γγ angular correlation 2−78053
^{166}Er, quadrupole and hexadecapole deforms. 2−79752
^{166}Er(p,t), excited 0^+ states population 2−63887
^{167}Er neutron capture, mag. moments of ^{168}Er states 2−67175
^{168}Er, quadrupole and hexadecapole deforms. 2−79752
^{168}Er states excited by neutron capture, mag. moments 2−67175
^{168}Er structure studied through formation and decay of isobaric analogues of ^{169}Er 2−46169
^{168}Er(α,8n), production of high-spin states in ^{164}Yb, anomalous behaviour of nuclear moment of inertia at large rotational frequencies 2−42528
^{169}Er formation and decay of isobaric analogues used to study structure of ^{168}Er 2−46169
^{170}Er, isotope preparation and crystal growth techniques 2−56613
^{170}Er, quadrupole and hexadecapole deforms. 2−79752
^{170}Er(α, 3n)^{171}Yb, 26-43 MeV, meas. of cross sections, population of rotational states 2−74040
^{173}Er, 1.4 min beta decay 2−46202
^{185}Er decay, double K-shell ionization 2−64028
^{151}Eu, Coulomb excitation level struct. 2−76884
^{151}Eu, Mossbauer effect after Coulomb excitation with 3.3 MeV α-particles 2−84473
^{151}Eu, Mossbauer effect in EuSe:Gd(La), hyperfine interactions 2−48145
^{151}Eu, neutron reson. spectroscopy, level population 2−63898
^{151}Eu (n,γ), cross-sections and isomer ratios 2−59767
^{151}Eu in activation foils, determ. of thermal neutron energy spectrum for pool type reactor 2−79832
^{151}Eu Mossbauer spectra, effect of asymmetry parameter on unresolved quadrupole splitting 2−72279
^{151}Eu spin-spin relax. in EuO 2−72230
^{152}Eu, decay to ^{152}Sm, monoenergetic positon line and positon distributions 2−52783
^{152}Eu, mechanism of uptake in isolated perfused rat liver 2−55225
^{153}Eu, Coulomb excitation, level struct. 2−76884
^{153}Eu, muonic and Mossbauer isomer shifts of gamma transitions 2−59714
^{153}Eu, neutron reson. spectroscopy, level population 2−63898
^{153}Eu, theoretical investigation of muonic and Mossbauer isomer shifts 2−42526
^{153}Eu spin-spin relax. in EuO 2−72230
^{155}Eu→^{155}Gd, as source of X-radiation for subshell fluoresc. yield meas. on Gd 2−70581

Nuclei with $150 \leqslant A$ continued
^{156}Eu→^{156}Gd, decay scheme, from single and γ-γ coincidence meas. 2−49751
^{158}Eu→^{158}Gd, decay scheme, from single and γ-γ coincidence meas. 2−49751
^{152m}Eu→^{152}Sm decay, level scheme 2−59730
Fm (A=252, 258, 264), symmetric and asymmetric fission probabilities from two-centre model 2−46342
^{256}Fm, spontaneous fission, mass distribution 2−46344
^{214}Fr isomeric ratio determ. in ^{12}C and ^{16}O reactions on ^{205}Tl, ^{209}Bi 2−74123
^{227}Fr isotope obs. in proton reactions on U 2−82925
^{228}Fr isotope obs. in proton reactions on U 2−82925
Gd, A=158, 160, isomer shifts, Mossbauer effect study 2−70407
Gd isotopes, level study using (p, t) reaction 2−46163
Gd neutron scattering, 1.5-3.5 MeV, meas. of angular distrib., comparison with spherical optical model, coupled-channels theory 2−67247
Gd(^{3}He,d) energy levels of Tb odd isotopes 2−82916
^{151}Gd, meas. of angular γ-γ correlations and multipolarities of transitions 2−46160
^{152}Gd, 1053 keV state O^+ excited identified 2−46163
^{152}Gd level scheme, ^{152m}Eu decay obs. 2−59730
^{154}Gd, 123 keV transition, internal conversion coeffs. and particle parameter meas. 2−46161
^{154}Gd, internal conversion electron studies 2−70422
^{154}Gd, γ-transitions, angular correlation measurements 2−82919
^{154}Gd, level scheme from ^{154}Tb decay 2−52784
^{154}Gd, time differential perturbed ang. correlation studies in liquid environment at different temp. 2−60511
^{154}Gd(^{35}Cl, ^{35}Cl$'$)^{154}Gd, 100 MeV, recoil distance meas., lifetimes 2−70405
^{155}Gd, correlations for equidistant neutron resonances 2−67296
^{155}Gd, half-life obs. using two dimensional analyzer and computer, γ-γ coincidence method 2−59715
^{155}Gd(^{40}Ar,xn), neutron-deficient Pb isotope prod. and α-decay 2−76822
^{155}Gd(n,α), determ. of distrib. of total alpha-particle widths of neutron resonances 2−67297
^{156}Gd, K-conversion coeffs., γ-ray intensities, level transitions, spin and parity assignments 2−46162
^{156}Gd, level struct., rot.-vibr. interac., from ^{156}Eu decay 2−49751
^{156}Gd, meas. of energies and intensities of γ-rays depopulating low spin levels of β- and γ-vibrational bands 2−52766
^{156}Gd(^{35}Cl, ^{35}Cl$'$)^{156}Gd, 100 MeV, recoil distance meas., lifetimes 2−70405
^{158}Gd, level struct., rot-vibr. interac., from ^{158}Eu decay 2−49751
^{158}Gd, meas. of energies and intensities of γ-rays depopulating low spin levels of γ-vibrational bands 2−52766
^{158}Gd, Mossbauer spectra, decrease in recoilless γ-ray emission 2−67173
^{158}Gd, quadrupole and hexadecapole deforms. 2−79752
^{160}Gd, neutron capture cross sections, 5−160 keV 2−82979
^{160}Gd, neutron irrad., radiation characts. of ^{157}Sm 2−76820
^{160}Gd, quadrupole and hexadecapole deforms. 2−79752
^{160}Gd(γ,n), 7-33 MeV, meas. of cross section, obs. of quadrupole resonance at 23.5 MeV 2−70436
^{160}Gd(γ,p), 7-33 MeV, meas. of cross section, obs. of quadrupole resonance at 23.5 MeV 2−70436
^{160}Gd(n,2n), 14.1 MeV, meas. of cross section using activation method 2−49810
Gd(γ t) energy levels of Tb odd isotopes 2−82916
Gd(p, t), 18 MeV, l=o, l=2 transitions identified for levels of several isotopes 2−46163
^{161}H level scheme from ^{161}Er decay 2−76815
Hf neutron deficient isotopes studied in ^{167}Hf-^{167}Lu-^{167}Yb decay chain 2−49771
^{168}Hf, high-spin states produced in (α,8n) reactions, anomalous behaviour of nuclear moment of inertia at large rotational frequencies 2−42528
^{173}Hf, Δk=1 retarded E1 transition 2−49753
^{173}Hf→^{173}Lu, obs. of isomeric E1 transitions with ΔK=0 and lifetimes of states in ^{173}Lu 2−63823
^{174}Hf, role of K-quantum number in de-excitation following Yb(α,xnγ)^{174}Hf 2−46328
^{176}Hf, nuclear structure, single-neutron-transfer-reaction study 2−63824
^{176}Hf mixing of 2-proton and 2-neutron bands 2−52768
^{177}Hf, 113 keV transition, relative internal conversion electron intensities 2−63825
^{177}Hf, correlations for equidistant neutron resonances 2−67296
^{177}Hf, internal conversion coefficients for E1 transitions with energies 71.6, 208.3, 321.3 keV 2−49754
^{177}Hf(n,α), determ. of distrib. of total alpha-particle widths of neutron resonances 2−67297
^{177}Hf(n,γ), spin dependence of average radiative widths 2−67302
^{177}Hf(n,γ)^{178}Hf, quantum no. influence on partial γ transitions 2−67303
^{178}Hf, ^{180}Hf, J-depend. of level density from statistical props. of series of resonances 2−46171
^{178}Hf, low lying energy levels 2−42531
^{178}Hf, quantum no. influence on partial γ transitions from ^{177}Hf(n,γ) reaction 2−67303
^{178}Hf 93.2 keV transition, Mossbauer isomer shift, shrinking of nucl. charge radius in rot. state 2−76804
^{178}Hf γ-ray intensities and branchings follwing ^{178}Ta decay 2−76803
^{180}Hf, investigation of parity non-conserving force between nucleons by meas. of circular polarization of γ-transitions 2−63840
^{180}Hf, nuclear structure, single-neutron-transfer-reaction study 2−63824
^{180}Hf, parity admixture in nuclear forces 2−59726
^{180}Hf, two-particle level from ^{180}Lu decay 2−52786
^{180}Hf 57 keV gamma transition, parity-violating and normal multipole mixing ratios 2−46172
^{177m}Hf and ^{178m}Hf, decay obs. using γ-ray spectroscopy by He jet recoil transport method 2−70290
Hg isotopes, strongly deformed nuclei 2−46175
Hg→Pt+p+e^+, statistical calculation of p intensities, branching ratios to final levels and approx. spectral shapes 2−46194

Nuclei with 150$\leqslant$A continued
^{181}Hg→^{180}Pt(158 keV state) coincidences between γ-rays and β-delayed protons 2−46193
^{193}Hg, magnetic oment by optical pumping 2−70412
^{197}Hg, level density parameters 2−63831
^{198}Hg, K-shell internal conversion coeffs. meas. with X-ray scintillation spectrometer 2−79737
^{199}Hg-^{1}H coupling constants, semiempirical MO calc. 2−83223
^{199}Hg, optical orientation of nuclear moments 2−76808
^{199}Hg nuclear shielding consts. in organomercury compounds, heteronuclear double magnetic resonance studies 2−57403
^{200}Hg, bubble nuclei approach 2−82904
^{200}Hg, Hartree-Fock calcs. of bubble phenomena 2−82905
^{200}Hg, spin and parity of 1515.2 and 1972.5 keV levels 2−79774
^{201}Hg, low-lying levels from decay of ^{201}Au 2−63832
^{201}Hg optical orientation of nuclear moments 2−76808
^{202}Hg(^{12}C,3n)^{211}Rn, excitation function, 50-200 MeV cross-sections 2−74120
^{203}Hg, nuclear matrix elements in first-forbidden beta-decay 2−46204
^{204}Hg(^{12}C,5n)^{211}Rn, excitation function, 50-200 MeV cross-sections 2−74120
^{204}Hg(p, p), elastic and inelastic resonant scattering, 12.5-14.2 MeV and 16.0-18.8 MeV, meas. of excitation functions, resonance parameters 2−74080
^{204}Hg(p, p) ^{204}Hg, 14-16.4 MeV, resonances in ^{205}Tl at 14.72 and 15.43 MeV 2−79767
^{205}Hg, single-particle fragments 2−46176
^{193m}Hg, magnetic moment by optical pumping 2−70412
^{195m}Hg, magnetic moment by optical pumping 2−70412
^{197m}Hg, magnetic moment by optical pumping 2−70412
Hg(n,γ), fast neutron capture, γ-rays intensity distribs., 5.5 MeV anomaly 2−67304
^{155}Ho→^{155}Dy decay, level scheme for ^{155}Dy 2−59716
^{158}Ho, ^{161}Ho, levels and transitions, conversion electron spectra obs. 2−70421
^{163}Ho, rotational bands and fast E1 transitions investigated by in-beam and decay spectroscopic methods 2−63820
^{164}Ho beta and electron capture, gamma and X-ray meas. 2−46201
^{165}Ho, α-particle scatt. from aligned target, optical model abiguities 2−79798
^{165}Ho, elastic and nucl. Raman scatt. of photons, giant dipole reson. 2−70431
^{165}Ho, hyperfine structure of ground state $^{4}I_{15/2}$ 2−46166
^{165}Ho, magnetic dipole moment, direct meas. by atomic beam magnetic resonance method 2−46167
^{165}Ho, neutron capture cross sections, 5−160 keV 2−82979
^{165}Ho, neutron width distributions, total cross-section, resonance parameters 2−67301
^{165}Ho, nonrotational states, calc. 2−70408
^{165}Ho(α, 4nγ)^{165}Tm, 38 and 50 MeV, determ. of rotational bands by meas. of γ-γ coincidences 2−74039
^{165}Ho(n,nγ), differential cross sections and angular distributions of gamma rays 2−46159
^{166}Ho, residual interaction effect on rotational spectrum 2−46168
^{191}Ir, energy level struct. unified model calcs. 2−42536
^{191}Ir low-lying states, ang. correl. meas., electron conversion coeffs. spin assignments, multipolarities of de-exciting transitions 2−76806
^{191}Ir(n,2n)^{190}Ir, isomer cross-section ratios 2−63899
^{192}Ir, half life 2−52775
^{192}Ir decay, γ-ray spectrum, K-shell internal conversion coeffs. 2−70423
^{192}Ir sealed sources, accidental contamination during handling 2−55234
^{192}Ir wire, contamination hazard in handling 2−69319
^{192}Ir(p,nnnn)^{188}Pt, ^{191}Ir(p,nn)^{190}Pt study of levels of Pt 2−70410
^{193}Ir, energy level struct., unified model calcs. 2−42536
^{193}Ir, level scheme, transitions, spin-parity assignments 2−46173
^{193}Ir(p,2n)^{192}Pt, ^{193}Ir(p,4n)^{190}Pt, study of levels in Pt 2−70410
^{194}Ir→^{194}Pt decay, half-life meas. 2−59732
Lu, neutron-capture cross-sections, 0.01 to 100 eV 2−59761
Lu neutron deficient isotopes studied in ^{167}Hf-^{167}Lu^{167}Yb decay chain 2−49771
^{167}Lu, ground state spin meas. with atomic-beam magnetic resonance method, comparison with Nilsson model value 2−42529
^{169}Lu, ^{171}Lu, rotational bands and lifetimes of isomeric states, ^{169}Tm(α,4nγ) and ^{169}Tm(α,2nγ) study 2−70409
^{170}Lu→^{170}Yb decay, energy levels of ^{170}Yb 2−76821
^{171}Lu, ^{173}Lu, obs. of isomeric E1 transitions with $\Delta K=0$ and lifetime meas. 2−63823
^{171}Lu, high spin rotational levels, ^{169}Tm(α, 2n)^{171}Lu obs. 2−59717
^{171}Lu, validity of rotor model, ^{169}Tm (α, 2n)^{171}Lu obs. 2−59718
^{174}Lu states populated in single-particle transfer reactions, obs. of Coriolis coupling 2−82896
^{175}Lu(^{3}He,α)^{174}Lu, 24 MeV, determ. of levels in ^{174}Lu 2−82896
^{175}Lu(α, 2nγ)^{177}Ta, rotational bands and lifetimes of isomeric states in ^{175}Ta 2−70409
^{175}Lu(α,4nγ)^{175}Ta, rotational bands and lifetimes of isomeric states in ^{175}Ta 2−70409
^{175}Lu(d,t)^{174}Lu, 12 MeV, determ. of levels in ^{174}Lu 2−82896
^{175}Lu(n, e)^{176}Lu slow neutron capture, study of ^{176}Lu excited levels by obs. of conversion electron spectra 2−79744
^{175}Lu(n, γ)^{176}Lu slow neutron capture, study of ^{176}Lu excited levels by obs. of γ-ray spectra 2−79744
^{176}Lu, correlation between (n,γ) and (d,p) reactions 2−70456
^{176}Lu, motion induced shifts in neutron resonance absorptions 2−49812
^{176}Lu in activation foils, determ. of thermal neutron energy spectrum for pool type reactor 2−79832
^{176}Lu levels populated in ^{176}Lu(n, γ) and ^{175}Lu(n, e) reactions, study of rotational bands 2−79744
^{176}Lu(d,p)^{177}Lu and ^{176}Lu(n,γ)^{177}Lu, positive correlation 2−67293
^{176}Lu(n, γ)^{177}Lu, γ spectra, level scheme, transitions 2−59769
^{176}Lu(n,γ)^{177}Lu, nsec. isomeric transitions, γ-γ coincidence obs. 2−67176
^{176}Lu(n,γ)^{177}Lu and ^{176}Lu(d,p)^{177}Lu, positive correlation 2−67293
^{176}Lu(n,γ)^{177}Lu capture studies using γ band-filter spectrometer 2−67077

Nuclei with 150$\leqslant$A continued
^{177}Lu, deexcitation of $^{1}._{2}^{-}$ [541] and $^{1}._{2}^{+}$ [411] bands, reaction (n, γ) study 2−79749
^{177}Lu, level scheme, transitions, ^{176}Lu(n, γ) reaction obs. 2−59769
^{177}Lu, nsec. isomeric transitions, (n,γ) reaction obs. 2−67176
^{177}Lu→^{177}Hf, β-transitions calcs. using model of non-axial odd nucleus 2−55973
^{180}Lu, β- decay and half life 2−52786
Mg isotope during, rel. to properties of low lying levels of even mass Pt nuclei 2−49755
^{237}Nb, fission cross-sections by 20 eV to 7 MeV neutrons from nuclear explosive expt. 2−70492
Nd, even nuclei, magnetic moment of first (2^+) and second (4^+) states 2−42522
^{150}Nd(^{3}He, d)^{151}Pm, 24 MeV, meas. of cross section, determ. of level structure of ^{151}Pm 2−74038
^{150}Nd(α, t)^{151}Pm, 25 MeV, meas. of cross section, determ. of level structure of ^{151}Pm 2−74038
^{150}Nd(t,p), 13 MeV, angular distributions of protons, Q-values and spin and parity of states 2−42523
^{237}Nd, lifetime of 60 keV level, application to calibration of nuclear timing systems 2−79750
Nd(p,t) even isotopes, 5Z MeV, excitation of removal and addition types of quadrupole-pairing vibrational states 2−82968
Np (A=237,238), neutron induced fission, relative yields of Xe isotopes 2−46346
^{232}Np, decay schemes determ. by gamma spectroscopy 2−82929
^{235}Np, L-subshell fluorescence, Coster-Kronig yields 2−82918
^{236}Np long-lived isomer, determ. of partial negation half-life from growth of ^{235}Pu daughter 2−52788
^{237}Np, biological action of compounds as function of dose, routes and character of intake 2−55281
^{237}Np, mag. dipole moment determ. from h.f.s. in atomic spectrum 2−79938
^{237}Np fission, proton induced, 20-85 MeV, ^{134}Cs isomer obs. 2−63932
^{237}Np fission fragment registration for fast neutron personnel monitoring 2−79676
^{237}Np proton induced fission, 20-85 MeV, meas. of nuclear charge dispersion 2−79812
^{237}Np target, powder, preparation and purification 2−73908
^{239}Np, polarized in ZrFe$_2$, γ-decay to levels of ^{239}Pu 2−46207
^{239}Np fuel, contribution to post-shutdown heat release 2−79831
Os, A=184, 186, 188, 190, 192, static quadrupole moments of first 2^+ states 2−63826
Os even-even isotopes, static quadrupole moments of first 2^+ states, Coulomb excitation determ. 2−67177
Os N=108 deformed shell, effect on nuclear properties 2−55950
^{170}Os, alpha decay props. 2−49772
^{171}Os, alpha decay props. 2−49772
^{185}Os electron capture populated from electron capture decay of ^{185}Os 2−67178
^{186}Os, quadrupole moment, Mossbauer obs. 2−63827
^{186}Os level calc. rel. to gamma oscillations in collective model for axially symmetric nuclei 2−52767
^{187}Os, level structure investigation via ^{187}Ir decay 2−55966
^{188}Os, g-factors of several excited states determ. from perturbed angular correlation following ion implantation by Coulomb excitation 2−63829
^{188}Os, quadrupole moment, Mossbauer obs. 2−63827
^{189}Os, quadrupole moment, Mossbauer obs. 2−63827
^{189}Os(n_{th},γ)^{190}Os, meas. of γ-ray spectra, evidence for K=0 excited states 2−67179
^{190}Os, evidence for K=0 excited states studied by ^{189}Os(n_{th},γ) reaction 2−67179
^{190}Os, quadrupole moment, Mossbauer obs. 2−63827
^{192}Os, g-factors of several excited states determ. from perturbed angular correlation following ion implantation by Coulomb excitation 2−63829
^{193}Os→^{193}Ir, +β, energies and intensities of internal conversion lines 2−46173
^{191m}Os, K conversion coefficient near threshold 2−42535
PU (A=240, 242), fissioning, scission configurations 2−49849
^{230}Pa→^{230}Th decay meas. of γ and electron singles-spectra and γ-γ coincidences, study of bands in ^{230}Th 2−70416
^{231}Pa, ^{232}U production by neutron reaction 2−49813
^{231}Pa target capture cross section of slow neutrons 2−42575
Pb, angular distribution of photoneutrons 2−63864
Pb, cosmic ray hadron interaction, 3-30 TeV 2−73889
Pb, n and p distrib. 2−82951
Pb, photonuclear reaction, Butler−Pearson model verification 2−55979
Pb, π- capture, 600 MeV, identification of emitted charged particles 2−46293
Pb, π^- capture, energy spectra and emission probabilities of proton, deuteron and triton 2−79793
Pb, scattering of 40 MeV-120 MeV photons, cross section for electron pair production 2−67207
Pb, search for spontaneously fissioning isomers produced with 600 MeV protons 2−79811
Pb (A=202m, 204m), decay schemes of even-even isomers 2−49773
Pb isotopes, excitation of low- lying octupole 2.6 MeV state by 14 MeV neutrons 2−67250
Pb isotopes, pairing vibrations, modified Tamm-Dancoff approximation 2−46100
Pb neutron-deficient isotopes, α-decay parameters 2−76822
^{198}Pb, ^{200}Pb, level props. studied from ^{198}Bi, ^{200}Bi decay 2−46174
^{203}Pb, carrier-free, for tracer obs. 2−69268
^{203}Pb, kinetics of retention and distribution in young rats meas. with scintillation counter 2−55284
^{204}Pb, $4^+ \rightarrow 0^+$ cross-over transition 2−67180
^{204}Pb, e.m. matrix elements of low-lying states 2−76782
^{204}Pb(n, 2n), 13 to 18 MeV, cross-section 2−67246
^{204}Pb(n, n′), 13 to 18 MeV, cross-section 2−67246
^{204}Pb(t,p)^{206}Pb, E_t=6 MeV, pairing vibr. states of ^{206}Pb 2−82900
^{205}Pb level scheme populated by ^{205}Bi decay 2−82928
^{206}Pb, e.m. matrix elements of low-lying states 2−76782
^{206}Pb, g-factor of 12^+ isomeric state and effective orbital g-factor of neutron 2−59720

Nuclei with $150 \leqslant A$ continued
^{206}Pb, lifetime of O_2^+ state 2−74041
^{206}Pb, proton decay of isobaric analogs of ground states 2−63888
^{206}Pb, three-phonon monopole and quadrupole pairing vibr. states 2−82900
^{206}Pb levels populated in decay of ^{206}Bi, determ. of γ-multipolarities 2−70413
^{206}Pb(α,f), integral and differential cross-sections for ^{210}Po fission, 29-46 MeV 2−67337
^{206}Pb(n,n)^{206}Pb, particle vibration model of doorway states 2−46278
^{206}Pb(p,p$'$)^{206}Pb*(2_1^+), and direct nuclear processes 2−59721
^{207}Pb, 13.3 to 17.1 MeV neutrons, resonant character of cross-section 2−67306
^{207}Pb, E1 radiative widths of isobaric analog states 2−76809
^{207}Pb, e.m. matrix elements of low-lying states 2−76782
^{207}Pb, n.m.r., in LaPb$_3$ 2−65346
^{207}Pb, proton decay of isobaric analogs of ground states 2−63888
^{207}Pb hyperfine splitting in lead acetate hydrate e.p.r. spectra 2−75347
^{208}Pb-N high energy cosmic ray interaction, cf of optical and Glauber models 2−73892
^{208}Pb, (^{16}O,^{15}N) and (^{12}C,^{11}B) induced reactions, j-assignments of final states 2−79805
^{208}Pb, charge distribution, comparison with ^{209}Bi 2−46177
^{208}Pb, d absorption cross section, 25 GeV/c, Glauber theory calc. and comparison with expt. 2−70469
^{208}Pb, e.m. matrix elements of low-lying states 2−76782
^{208}Pb, giant reson. struct., low-lying collective states influence 2−74028
^{208}Pb, HF charge distribution tested by electron scattering data 2−74016
^{208}Pb, Hartree-Fock calcs. using modified delta interaction 2−63747
^{208}Pb, nucleon distribution near surface from α-particle scatt. 2−46150
^{208}Pb, odd- and even-parity levels, transition rates and mean lifetimes, renormalized RPA calc. 2−82917
^{208}Pb, proton decay of isobaric analogs of ground states 2−63888
^{208}Pb, single-particle effects on fission probabilities 2−52829
^{208}Pb, spreading widths for 1^- particle-hole state 2−76810
^{208}Pb core vibr. effects on shell-model calcs. for ^{211}At and ^{211}Pb 2−67182
^{208}Pb region, mag. dipole transitions 2−82901
^{208}Pb transition probability and transition charge density, investigation using inelastic electron scattering 2−63833
^{208}Pb(^{7}Li,^{7}Li*)^{208}Pb, Coulomb excitation of $^{1}{}_{\cdot 2}^{-}$ state in ^{7}Li 2−76882
^{208}Pb(^{7}Li,αn)^{210}Bi, mag. moments of 7^- and 5^- states in ^{210}Bi 2−67181
^{208}Pb(α, α') cross sections, 65 MeV, strong multipole vibrs. in low-excitation region 2−76879
^{208}Pb(d,p)^{207}Pb, polarized deuterons, vector analyzing power and differential cross section 2−67330
^{208}Pb(d,t)^{207}Pb, polarized deuterons, vector analyzing power and differential cross section 2−67330
^{208}Pb(μ^-, ν), probability of occurrence 2−46241
^{208}Pb(n, γ), 14 MeV radiative capture, mass depend. of direct- semi-direct theory calcs. 2−67270
^{208}Pb(n,γ)^{209}Pb, radiative capture, E_n=6-15 MeV, cross sections 2−67275
^{208}Pb(n,γ)^{209}Pb, radiative capture cross section, E_n=6.2-14.7, reson. struct. 2−67307
^{208}Pb(n,n)^{208}Pb, particle vibration model of doorway states 2−46278
^{208}Pb(p,n)^{208}Bi, isobaric analogue state of ^{208}Pb ground state, population and decay 2−52770
^{208}Pb(p,n) charge-exchange reaction, coupled-channel calcs. 2−59759
^{208}Pb(p,np), excitation functions and energy dependence of reaction 2−67223
^{208}Pb(p,p)^{208}Pb, elastic scatt., 8 to 14 MeV, optical model analysis 2−67217
^{208}Pb(p,p)^{208}Pb., DWA cross-section calc. with imaginary part 2−74081
^{208}Pb(t,p)^{210}Pb, 20 MeV, meas. of angular distribs., determ. of ^{210}Pb structure 2−82892
^{209}Pb, e.m. matrix elements of low-lying states 2−76782
^{209}Pb, first forbidden beta decay 2−46205
^{209}Pb, single-particle states and γ-ray transitions 2−67275
^{209}Pb giant reson. struct. from radiative neutron capture of ^{208}Pb 2−67307
^{210}Pb, in area of Roumania with increased natural background, meas. of absorption levels in population 2−58633
^{210}Pb, influence of irradiation in incorporation in hair and other tissues of rabbits and rats 2−55293
^{210}Pb, low-lying level spacing, shell model calculations 2−49727
^{210}Pb, theoretical and exptl. structure investigation, use of ^{208}Pb(t,p) reaction 2−82892
^{211}Pb low-lying states, shell-model calcs., effects of ^{208}Pb core vibrs. 2−67182
Pb(α,α) elastic scattering, incoming wave boundary condition calc. of cross section at incident energies near Coulomb barrier 2−42592
Pb(μ^-,n), 2-13 MeV, meas. of neutron energy spectrum, excitation of quasibound states of intermediate nucleus 2−52806
Pb(n,n) Pb, 13.7 MeV A=206, 207, 208, obs., cf with optical model 2−67249
Pb(p,π), 200-500 MeV, contribution of pions created in cascade mechanism to nuclear evaporation process 2−52813
^{147}Pm, g-factor of 91keV state, meas. using 319 to 91 keV gamma cascade 2−59712
^{151}Pm, structure determ. from ^{150}Nd(^{3}He, d), ^{150}Nd(α, t) and ^{152}Sm(t, α) reactions Coriolis coupling calcs. 2−74038
^{240}Pm, excitation energy from (α,2n) reaction, time of flight obs. 2−76881
Po-Be neutron sources, investigation of spectra at low energies, meas. of activation cross sections 2−67227
^{203}Po, decay scheme, transition multipolarities 2−49774
^{205}Po, decay scheme, transition multipolarities 2−49774
^{209}Po, level density parameters 2−63831
^{210}Po, energy level study using ^{210}At→^{210}Po electron capture decay 2−63836

Nuclei with $150 \leqslant A$ continued
^{210}Po, kinetics of metabolism in body after radionuclide intake through skin and determ. of contamination levels 2−55283
^{210}Po, lunar soil, search for α-activity 2−44910
^{210}Po, T=23 double analogue states, obs. in ^{209}Bi(p,2p)^{208}Pb reaction 2−70446
^{210}Po concentrations rel. to ^{222}Rn in lunar atmosphere 2−66161
^{210}Po fission in ^{206}Pb(α,f) reaction, 29-46 MeV 2−67337
^{210}Po(t,α)^{209}Bi, 20 MeV, meas. of absolute cross sections, determ. of spectroscopic factors, study of particle-hole states 2−82894
Pt, A=188, 190, 192, excited level observation, excitations, γ-ray anisotropies 2−70410
Pt, even mass nuclei $182 \leqslant A \leqslant 192$, low- lying level properties from Hg isotope decay data 2−49755
^{159}Pt size calc. from Mossbauer isomer shift and isomer transition 2−76759
^{194}Pt, e.m. props., excited states lifetimes, quadrupole transition probabilities 2−76807
^{194}Pt(d,p), neutron and γ-ray yields from threshold region 2−67225
^{195}Pt, g-factors of 211 and 240 keV states 2−63830
^{195}Pt, n.m.r., in PtSi 2−65348
^{195}Pt Mossbauer effect obs. 2−59719
^{195}Pt(p,p$'$), neutron and γ-ray yields from threshold region 2−67225
^{196}Pt, e.m. props., excited states lifetimes; quadrupole transition probabilities 2−76807
Pu-Be neutron sources, investigation of spectra at low energies, meas. of activation cross sections 2−67227
Pu contaminated wound, assessment and treatment 2−58593
^{238}Pu, economic aspects and production as reactor fuel 2−49899
^{238}Pu, fission induced by 13.4-14.8 MeV neutrons, fragments angular anisotropy 2−52832
^{238}Pu fission cross section meas. using neutrons from underground nuclear explosion Persimmon 2−46347
^{238}Pu(d, d)^{238}Pu, 16 MeV, level study 2−46178
^{239}Pu, asymmetry of E1 and M1 γ transitions, multipole mixing ratios 2−46207
^{239}Pu, biological action of compounds as function of dose, routes and character of intake 2−55281
^{239}Pu, capture-to-fission cross section meas. 2−56011
^{239}Pu, determ. of quantity in living human organism from rate of elimination 2−55301
^{239}Pu, effective delayed neutron fractions for two fast crit. assemblies 2−83105
^{239}Pu, estimation of relative role of penetration into critical organs through intact skin 2−55295
^{239}Pu, fission-neutron spectra 2−46350
^{239}Pu, fission, thermal neutron induced, kinetic energy distribution 2−70490
^{239}Pu, fission emission ^{6}He, ^{4}He spectra 2−76889
^{239}Pu, fission fragments from fission by thermal neutrons, inner bremsstrahlung, recoil radiation from β decay 2−63843
^{239}Pu, fission rate, decay constant, profile and distribution determ. with solid state track detector 2−46060
^{239}Pu, higher order spacing distributions 2−67184
^{239}Pu, in vivo meas. in man, comparison of different counting equipments 2−58617
^{239}Pu, influence of irradiation on incorporation in hair and other tissues of rabbits and rats 2−55293
^{239}Pu, insoluble, treatment of wound contamination 2−58592
^{239}Pu, irrad., absolute fission yields 2−70499
^{239}Pu, levels populated by electron capture decay of ^{239}Am 2−46179
^{239}Pu, low lying energy levels 2−42531
^{239}Pu, Mossbauer effect 2−74043
^{239}Pu, neutron-induced, anomalous effect of neutron spectrum change on mass yields 2−74127
^{239}Pu, relative fission cross section in low resonance region, measurement and normalization 2−56010
^{239}Pu, subthermal-, thermal-, and reson.-neutron fission, long-range α-particle emission 2−83032
^{239}Pu absolute meas. of α-activity by low- geometry method 2−63853
^{239}Pu contribution to total fission activity, non-destructive absolute determination 2−42594
^{239}Pu fission, contribution to burn-up of plutonigen reactor fuel 2−74149
^{239}Pu spontaneously fissing, produced in ^{240}Pu(γ,n) reaction, meas. of excitation function 2−67210
^{239}Pu(α,2n)^{241}Cm, excitation energy, spontaneous fissioning products, time-of-flight obs. 2−76881
^{239}Pu(n,γ)^{240}Pu, 2keV neutron capture, γ-ray studies of ^{240}Pu 2−67187
^{239}Pu(n,γ)^{240}Pu, thermal neutron capture, γ-spectroscopy study of ^{240}Pu 2−67186
^{240}Pu, 20 eV to 30 keV, neutron capture, fission, and total cross sections 2−82977
^{240}Pu, alpha particle emission energy meas. 2−76823
^{240}Pu, average widths of E1 and M1 radiative transitions from neutron capture states 2−67187
^{240}Pu, levels populated in electron capture decay of ^{240}Am, spin-parity assignments and γ-multipolarities 2−79770
^{240}Pu, lifetime estimates for asymmetric spontaneous fission including shell effects 2−42595
^{240}Pu, neutron total, capture and fission cross-section meas. 2−67312
^{240}Pu, obs. of γ transitions of levels populated by thermal neutron capture in ^{239}Pu 2−67186
^{240}Pu fission isomer, identification of rotational band 2−74126
^{240}Pu neutron cross section data eval. 2−82986
^{240}Pu(N,γ)^{241}Pu single-particle assignments of levels in ^{241}Pu 2−82911
^{240}Pu(d.p) and (d.t) reactions, single-particle assignments of levels in ^{241}Pu 2−82911
^{240}Pu(γ.n), meas. of excitation function leading to production of spontaneously fissing isomer ^{239}Pu 2−67210
^{241}Pu levels, single-particle assignments, reaction-spectroscopy obs. 2−82911
^{241}Pu target, power preparation and purification 2−73908
^{241}Pu(d.d$'$)^{241}Pu single-particle assignments of levels in ^{241}Pu 2−82911

Nuclei with 150$\leqslant$A continued
^{241}Pu(n,γ)^{242}Pu, thermal neutron capture, γ-ray spectroscopy study of ^{242}Pu level structure 2−67188
^{242}Pu, ground state rotational and octupole-vibrational states, B(E2), B(E3) reduced transition probabilities 2−46178
^{242}Pu, neutron capture below 1 keV, resonance parameters 2−67313
^{242}Pu octupole bands study by thermal neutron capture γ-ray spectroscopy 2−67188
^{242}Pu(d, 2n)^{242}Am^{m}, 22.7 MeV, meas. of fission modes of ^{242}Am^{m} isomeric fission 2−70496
^{242}Pu(d, d)^{242}Pu, 16 MeV, level study 2−46178
^{242}Pu(d.p) and (d.t) reactions, single-particle assignments of levels in ^{243}Pu 2−82911
^{243}Pu levels, single-particle assignments, reaction-spectroscopy obs. 2−82911
^{244}Pu fission tracks, evidence in lunar rock 3.95 × 10^{9} years old 2−69137
^{240m}Pu spontaneously fissioning isomer, production probability in thermal neutron capture reactions 2−79818
Pu(p, 2n), excitation functions for prod. of fission isomers in Am isotopes 2−76894
Pu(t, 2n), excitation functions for prod. of fission isomers in Am isotopes 2−76894
Pu(t, 3n), excitation functions for prod. of fission isomers in Am isotopes 2−76894
Ra daughters, lung cancer risk in relation to long-term exposure 2−55231
^{216}Ra, lifetime by in-beam α-spectroscopy 2−67199
^{223}Ra levels determ. by α-γ coincidence and directional correlation studies on ^{227}Th decay 2−49776
^{223}Ra levels populated in decay of ^{227}Th 2−63852
^{224}Ra, ^{226}Ra, analysis of γ spectra in non-equilibrium with decay products, application to retention in mice 2−58615
^{224}Ra, ^{226}Ra, kinetics and decay products in mice, dose-effect relation 2−55279
^{224}Ra α decay, study of hyperfine interactions when implanted in Fe, Al, Cd, Bi, α-γ correlation meas. 2−81341
^{226}Ra, influence of irradiation on incorporation in hair and other tissues of rabbits and rats 2−55293
^{226}Ra, late effects induced in mice, meas. of total activities, determ. of death causes 2−55232
^{226}Ra, time course of distribution in some bones of mice 2−55286
^{226}Ra, total neutron cross section, below 1 eV, weak reson. level 2−67308
^{226}Ra bombardment with 14.5 MeV neutron and neutrons of wide energy spectrum, search for decay isomers in 88, 89 range 2−70458
^{214m}Ra, produced in (^{12}C, xn) reactions, meas. of half-life 2−55970
Re, (A = 182, 182m), ground state structure and moments of inertia, Nilsson model 2−46164
Re, obs. of slow neutron resonances in range 3-300 eV, shape analyses based on Breit-Wigner single level formula 2−70457
^{181}Re, ^{183}Re, rotational bands and lifetimes of isomeric states, ^{181}Ta(α,4nγ) and ^{181}Ta(α,2nγ) study 2−70409
^{184}Re, level density parameters 2−63831
^{185}Re, multipole mixing ratios of γ-transiions from levels populated in ^{185}Os electron capture decay 2−67178
^{187}Re 72-134 keV cascade, ang. correl. coeff. 2−82885
^{188}Re, level scheme 2−63828
^{190}Re, implications of allowed unhindered 3 min-β decay 2−46203
Rn steady-state turbulent diffusion in atm. 2−65669
Rn(A = 220, 222) activity and potential alpha energy in different air atmospheres 2−56078
^{211}Rn, electron capture decay to ^{211}At, energy levels 2−49775
^{220}Rn α decay, study of hyperfine interactions when implanted in Fe, Al, Cd, Bi, α-γ correlation meas. 2−81341
^{222}Rn- and ^{220}Rn-daughters, inhaled α-energy rel. to absorbed 2−82019
^{222}Rn, ^{220}Rn, and daughters, radiation dose to inhabitants of radon-spa from air contamination 2−58014
^{222}Rn, atmospheric, vertical distrib. up to 6 km 2−51594
^{222}Rn, determ. of concentration in hot spring water using scintillation chamber 2−61833
^{222}Rn and ^{220}Rn exhalation from ground, technique for meas. 2−65565
^{222}Rn and daughter ions, vertical profiles in air layer adjacent to ground 2−54870
^{222}Rn and daughter products, dependence of chromosomal aberrations in peripheral blood lymphocytes on inhaled internal dose 2−55272
^{222}Rn and daughters, detection of α-decay particles by triacetate cellulose foils for exposure evaluation 2−58618
^{222}Rn and daughters, dose to epithelium and upper respiratory tract 2−82020
^{222}Rn daughter ions, relative concentrations in air 2−65668
^{222}Rn exhalation analysis, design of acclimation room 2−58597
^{222}Rn in lunar atmosphere rel. to ^{210}Po concentrations 2−66161
^{222}Rn inhalation in rats, meas. of body accumulation of ^{210}Po, ^{210}Pb and increase of activity with time 2−55287
^{222}Rn short-lived daughters, recommendation of maximum permissible intake by inhalation 2−55270
^{222}Rn short-lived daughters, maximum permissible doses by inhalation in mines and radon spas 2−55271
Sm, even nuclei, magnetic moment of first (2^{+}) and second (4^{+}) states 2−42522
^{132}Sm(e,e)^{152}Sm, cross-section for excitation of ground-state rotational band 2−52764
^{150}Sm, ground state rotational bands, reaction ^{150}Nd (α, 4n) ^{150}Sm study 2−59713
^{150}Sm, proton scattering at 12 MeV, coupled channel analysis 2−55987
^{150}Sm, time-differential meas. of deorientation for recoils in vacuum 2−76802
^{152}Sm, ground state rotational bands, reaction ^{150}Nd (α, 2n) ^{152}Sm study 2−59713
^{152}Sm, ground state rotational band excitation by electron scatt. 2−52764
^{152}Sm, lifetimes of 121.78 and 366.5 keV levels 2−76783
^{152}Sm, neutron reson. spectroscopy, level population 2−63898
^{152}Sm, static hyperfine interactions at free atoms 2−70560
^{152}Sm level scheme, ^{152m}Eu decay obs. 2−59730

Nuclei with 150$\leqslant$A continued
^{152}Sm(^{35}Cl, ^{35}Cl^{1})^{152}Sm, 100 MeV, recoil distance meas., lifetimes 2−70405
^{152}Sm(t, α)^{151}Pm, 15 MeV, meas. of cross section, determ. of level structure of ^{151}Pm 2−74038
^{153}Sm, effective g$_{s}$ factor determ. by internal conversion processes 2−52765
^{154}Sm, isotope preparation and crystal growth techniques 2−56613
^{154}Sm, neutron capture cross sections, 5−160 keV 2−82979
^{154}Sm, neutron reson. spectroscopy, level population 2−63898
^{154}Sm(n,2n), 14.1 MeV, meas. of cross-section using activation method 2−49810
^{154}Sm(p,t)^{152}Sm two-nucleon transfer reaction, use of angular momentum projection technique 2−42561
^{157}Sm, from ^{160}Gd radioactivity, half-life, γ-ray energy, maximum β^{-}-ray energy 2−76820
Sm(p,t.) E$_{p}$-19 MeV level assignments for even isotopes 2−82962
^{119}Sn(p,n) charge-exchange reaction, coupled-channel calcs. 2−59759
^{132}Sn half-life determ. following production in thermal neutron fission of $^{235,\ 233}$U 2−52831
Ta, analogue states, study by ^{178}Hf(p,p) reaction at 11.2 to 12.6 MeV 2−42532
^{175}Ta, ^{177}Ta, rotational bands and lifetimes of isomeric states, ^{175}Lu(α,4nγ) and ^{175}(α,2nγ) study 2−70409
^{177}Ta, partial transition probabilities 2−42530
^{178}Ta→^{178}Hf decay, γ-ray intensities and branchings in ^{178}Hf 2−76803
^{181}Ta, He-ion induced fission at 41 and 65 MeV, radiochemical study of fission fragment mass distribution and total cross section 2−79810
^{181}Ta, in hexagonal transition metals, quadrupole interaction, Mossbauer obs. 2−61607
^{181}Ta, in Ni, hyperfine field, $\gamma-\gamma$ angular correl. obs. 2−44320
^{181}Ta, in Ni lattice, hyperfine field, perturbed ang. correl. study 2−65204
^{181}Ta, internal conversion electron studies 2−70422
^{181}Ta, investigation of parity non-conserving force between nucleons by meas. of circular polarization of γ-transitions 2−63840
^{181}Ta, ion bombardment, excited compound nuclei lifetime, 79 < Z < 89, shadow effect obs. 2−76805
^{181}Ta, parity admixture in nuclear forces 2−59726
^{181}Ta, time differential perturbed γ-γ angular correlation in frozen HfF$_{4}$ in dilute HF, temp. dependence 2−81321
^{181}Ta in Ge-Hf alloys, electric quadrupole interaction 2−75359
^{181}Ta intranuclear cascade calculations, proton-induced 2−46262
^{181}Ta quadrupole coupling in octocoordinated Hf(IV) complexes, perturbed ang. correl. obs. 2−61571
^{181}Ta quadrupole interaction in hafnium oxychloride 2−78057
^{181}Ta(α, 2nγ)^{183}Re, rotational bands and lifetimes of isomeric states in ^{183}Re 2−70409
^{181}Ta(α, 4nγ)^{181}Re, rotational bands and lifetimes of isomeric states in ^{181}Re 2−70409
^{181}Ta(α,n)^{184}Re, neutron spectra analysis, level density of residual nucleus 2−63831
^{181}Ta(n,2n)^{180}Ta, E$_{n}$ = 14 MeV, cross section meas. by activation method 2−49802
^{182}Ta, β- decay, population of K$^{\pi}$ = 2- octupole vibration band in ^{182}W 2−42533
^{182}Ta, ground state structure and moments of inertia, Nilsson model 2−46164
^{182}Ta, higher-order matrix elements in hindered-allowed β-decays 2−82921
^{203}Ta, investigation of parity non-conserving force between nucleons by meas. of circular polarization of γ-transitions 2−63840
Ta(n,γ), fast neutron capture γ-rays, intensity distribs., 5.5 MeV anomaly 2−67304
Tb A = 155,157,159,161, levels excited in (^{3}He,d) and (α,t) reactions on Gd 2−82916
^{153}Tb, ^{155}Tb, levels and transitions, conversion electron spectra obs. 2−70421
^{154}Tb→^{154}Gd, decay, γ-ray, conversion electron and γ-γ coincidence spectra 2−52784
^{156}Tb→^{156}Gd, study of levels in ^{156}Gd 2−46162
^{157}Tb, population of collective states and higher-order effects in ^{159}Tb(p, t) reaction 2−74092
^{159}Tb, investigation of parity non-conserving force between nucleons by meas. of circular polarization of γ-transitions 2−63840
^{159}Tb(^{40}Ar,xn), neutron-deficient Bi isotope prod. and α-decay 2−76822
^{159}Tb(n,γ)^{160}Tb, level scheme and spin assignment of ^{160}Tb 2−67174
^{160}Tb, ground state structure and moments of inertia, Nilsson model 2−46164
^{160}Tb, level scheme and spin assignment, (n,γ) and (n,e^{-}) reaction obs. 2−67174
^{160}Tb decay, 2^{+}-2^{+} transition of 879 keV in ^{160}Dy, e-γ directional correlation 2−42527
Th, search for spontaneously fissioning isomers produced with 600 MeV protons 2−79811
Th and daughters in body following spinal injection determ. of quantitative location 2−58626
Th daughter products, rel. to alpha spectroscopy, applic. to nuclear chemistry teaching 2−62931
^{159}Th(p, t)^{157}Tb, 30 MeV, collective and higher-order effects 2−74092
^{225}Th form. on bombardment of ^{232}Th by ^{84}Kr 2−59788
^{226}Th form. on bombardment of ^{232}Th by ^{84}Kr 2−59788
^{227}Th, L X-ray spectra, γ-transition multipolarity, coincidence obs. 2−74042
^{227}Th decay, α-γ coincidence and directional correlation studies 2−63852
^{227}Th→^{223}Ra decay, α-γ coincidence and directional correlation studies 2−49776
^{228}Th radioactive decay simulations rel. to use of ThO$_{2}$ as thermionic conversion heat source 2−52787
^{230}Th, ^{232}Th, d and t induced fissions, obs. of subbarrier resonances 2−52834
^{230}Th levels populated in decay of ^{230}Pa 2−70416
^{230}Th mixed with ^{232}Th, ^{232}U production by neutron reaction 2−49813

Nuclei with 150≤A continued
^{231}Th, energy levels, (d,t) reaction obs. 2−59722
^{231}Th, highly deformed, effective moment of inertia, determination from neutron-induced fission of ^{230}Th 2−59723
^{231}Th, highly deformed, nuclear spectroscopy 2−56014
^{232}Th, ^{84}Kr induced transfer reactions, threshold obs. 2−59788
^{232}Th, fission induced by 13.4-14.8 MeV neutrons, fragments angular anisotropy 2−52832
^{232}Th, ground state rotational and octupole-vibrational states, B(E2), B(E3) reduced transition probabilities 2−46178
^{232}Th, inelastic neutron scatt., excited level struct. and decay schemes 2−67183
^{232}Th, level structures and decay schemes 2−59724
^{232}Th, low lying energy levels 2−42531
^{232}Th, photofission cross sections near threshold 2−83024
^{232}Th (d,p) ^{233}Th, energy levels of ^{233}Th 2−59722
^{232}Th fission, 14 MeV, rare gas isotopes yields 2−59792
^{232}Th photofission, cross sections and angular distribs., obs. of band of rotational levels 2−83040
^{232}Th prompt and delayed photofission 2−83039
^{232}Th(^{22}Ne, ^{21}O)^{233}U 174 MeV Q-value measurements, determ. of ground state mass of ^{21}O 2−70383
^{232}Th(^{22}Ne, ^{22}O)^{233}U 174 MeV Q-value measurements, determ. of ground state mass of ^{22}O 2−70383
^{232}Th(d, d)^{232}Th, 16 MeV, level study 2−46178
^{232}Th(d,p)^{233}Th, level scheme of ^{233}Th 2−63837
^{232}Th(d,t)^{231}Th, energy levels of ^{231}Th 2−59722
^{232}Th(n,f), isomer yield ratio of ^{115m}Cd and ^{115g}Cd 2−63808
^{232}Th(n,γ)^{233}Th, level scheme of ^{233}Th 2−63837
^{233}Th, energy levels, (d,p) reaction obs. 2−59722
^{233}Th, level scheme, neutron capture and (d,p) reaction obs. 2−63837
^{189}Tl isotope, search for and energy levels 2−55967
^{200}Tl, level density parameters 2−63831
^{203}Tl, K-shell internal conversion coeffs. meas. with X-ray scintillation spectrometer 2−79737
^{203}Tl, muonic X-rays, nucl. γ-rays and μ-capture γ-rays analysis 2−59961
^{203}Tl, parity admixture in nuclear forces 2−59726
^{203}Tl p-wave neutron reson. obs. by transmission meas. 2−76863
^{204}Tl, β-decay, internal bremsstrahlung spectral distrib. 2−42549
^{204}Tl, K-shell internal ionization accompanying β-decay, obs. 2−63850
^{204}Tl$_2$O$_3$, thick cylindrical β-source, bremsstrahlung 2−67191
^{205}Tl, levels populated in inelastic proton scattering on ^{204}Hg, study of isobaric analogue strength 2−74080
^{205}Tl, muonic X-rays, nucl. γ-rays and μ-capture γ-rays analysis 2−59961
^{205}Tl, n.m.r. in Tl$_{1-x}$Te$_x$ liq. semicond. alloy 2−60512
^{205}Tl, n.m.r. in Tl$_2$SeAs$_2$Te$_3$ liquid and glassy semicond., struct. obs. 2−60420
^{205}Tl levels deduced, resonance in ^{204}Hg(p, p)^{204}Hg 2−79767
^{205}Tl p-wave neutron reson. obs. by transmission meas. 2−76863
^{205}Tl(^{12}C,xn)$^{217-x}$Fr, 60-90 MeV, meas. of cross sections, reaction thresholds and excitation functions 2−74123
^{205}Tl(^{16}O,xn)$^{221-x}$Ac, 60-100 MeV, meas. of cross sections, reaction thresholds and excitation functions 2−74123
^{205}Tl(n,γ)^{206}Tl, anomalous 5.5 MeV γ-radiation 2−46289
^{206}Tl β-decay, meas. of half-life, spectral shape and nuclear matrix elements 2−63851
Tl(n,γ), fast neutron capture, γ-rays intensity distribs., 5.5 MeV anomaly 2−67304
^{165}Tm, level det. of ^{165}Er from decay 2−63821
^{165}Tm, rotational bands determ. by γ-γ coincidences in ^{165}Ho(α, 4nγ) reaction 2−74039
^{169}Tm, neutron width distributions, total cross-section, resonance parameters 2−67301
^{169}Tm, penetration effects in internal conversion of·transitions 2−63822
^{169}Tm enriched with^{170}Yb, production of neutron deficient Hf, Lu isotopes by 45-80 MeV ^{3}He bombardment 2−49771
^{169}Tm perturbed ang. correl. in YFe garnet and Ag-Yb dil. alloys 2−72247
^{169}TmM$_{1(2)}$ intermetallic cpds., h.f. n.m.r. at 4.2 degrees K 2−72518
^{169}Tm(α, 2n)^{171}Lu, 27 MeV, lifetime meas. and isomeric E1 transitions with $\Delta K=0$ in ^{171}Lu 2−63823
^{169}Tm(α, 2n)^{171}Lu, high spin rotational levels, γ-ray obs. 2−59717
^{169}Tm(α, 2n)^{171}Lu, rel. to validity of rotor motor for ^{171}Lu 2−59718
^{169}Tm(α, 2nγ)^{171}Lu, rotational bands and lifetimes of isomeric states in ^{171}Lu 2−70409
^{169}Tm(α, 4nγ)^{169}Lu, rotational bands and lifetimes of isomeric states in ^{169}Lu 2−70409
^{169}Tm(n,γ), γ-ray spectra, study of resonances 2−46288
^{170}Tm, structure of low-lying rotational bands 2−49752
^{170}Tm decay, first forbidden beta matrix elements 2−42548
^{171}Tm, penetration effects in internal conversion of transitions 2−63822
U, proton reactions, 24 GeV, new isotope prod. obs. 2−82925
U, recoil props. of rare earth nuclides produced by 28 GeV proton interactions 2−82971
U, search for spontaneously fissioning isomers produced with 600 MeV protons 2−79811
U (A=235, 238), effective fission cross section ratio, meas. by solid state track detects. 2−56008
U (p, secondary reactions), 24 GeV, production cross-sections of super-heavy elements 2−70379
U and fission products, use of polyaminopolyalkylphosphonic acids as effective ligands for binding and elimination from body 2−55258
U assay in rocks using ^{140}La line 2−84690
U depleted in ^{235}U isotope, fast neutron spectra meas. and analysis 2−83057
U deposition in human organs by chronic exposure, mathematical model 2−55278
^{232}U, alpha particle emission energy meas. 2−76823
^{233}U, ^{235}U, fission emission ^{6}He, ^{3}H spectra 2−76889
^{233}U, fast neutron bombardment, fission fragment distribution, yield and kinetic energy rel. to excitation energy 2−76893
^{233}U, fission, thermal neutron induced, kinetic energy distribution 2−70490

Nuclei with 150≤A continued
^{233}U, neutron-induced fission from 0.4 to 2000 eV, product ang. distrib. anisotropy 2−59801
^{233}U, thermal neutron induced, determ. of nuclear charge distrib. in mass chain 132 2−52831
^{233}U fission, 14 MeV, rare gas isotopes yields 2−59792
^{235}U/^{238}U fission rate ratios, determ. in CONSORT reactor 2−83094
^{235}U, ^{235}U+Cd, ^{235}U+^{10}B, ^{237}Np, ^{238}U, and ^{32}S, threshold neutron counters, radiation characteristics 2−42472
^{235}U, capture-to-fission cross section meas. 2−56011
^{235}U, effective delayed neutron fractions for two fast crit. assemblies 2−83105
^{235}U, enriched U in paraffin, homogeneous critical assemblies 2−70536
^{235}U, fission-neutron spectra 2−46350
^{235}U, fission by fast neutrons, β and γ residual powers 2−74128
^{235}U, fission by fast neutrons, β and γ residual powers 2−74128
^{235}U, fission fragment range in Be, C, Al and Si 2−61125
^{235}U, fission fragments from fission by thermal neutrons, inner bremsstrahlung, recoil radiation from β decay 2−63843
^{235}U, fission rate, decay constant, profile and distribution determ. with solid state track detector 2−46060
^{235}U, level scheme and distribution of single-particle strength in excited states 2−49758
^{235}U, neutron induced, yields of ^{128}Sb, ^{129}Sb, ^{130}Sb and ^{130}Sn 2−83036
^{235}U, ratio of ternary to binary fission cross sections induced by resonance neutrons 2−83031
^{235}U, thermal-neutron-induced fission, emission of prompt. γ-rays 2−76892
^{235}U, thermal-neutron fission, odd-even effect in element yield distribution 2−63935
^{235}U, thermal neutron induced fission, cumulative yield of 83-sec ^{136}I 2−63934
^{235}U, thermal neutron induced fission, meas. of mass and energy distrib. of fragments 2−79817
^{235}U content of fuel assemblies, nondestructive assay 2−83132
^{235}U epithermal neutron induced fission, meas. of gamma- ray spectra 2−52820
^{235}U fission, 14 MeV, rare gas isotopes yields 2−59792
^{235}U fission, contribution to burn-up of plutonigen reactor fuel 2−74149
^{235}U fission, Ge isotopes identification 2−76814
^{235}U fission, thermal neutron induced, cumulative yields of 40.1 min ^{123}Sn, 9.6 min ^{125}Sn, ^{128}Sn 2−46345
^{235}U fission, thermal neutron induced, use of kinetic energy data to determ. barrier parameters for fusion of fragments 2−49847
^{235}U fission, thermal neutron induced, use of kinetic energy data to determ. barrier parameters for fusion of fragments 2−49847
^{235}U fission fragment deceleration in light media 2−56013
^{235}U resonances, correl. between fission channel effects and fragment kinetic energies 2−67336
^{235}U(α, 3n)^{236}Pu, 24.5-28 MeV, cross sections, fission isomer excitation functions 2−76880
^{235}U(n,γ)^{236}U, conversion electron spectrum, level struct. of ^{236}U 2−67309
^{235}U(n,γ)^{236}U, epithermal neutron capture, level structure of ^{236}U and spins of resonances determ. 2−52820
^{235}U(n,γ)^{236}U, thermal neutron interaction, meas. of G-ray spectra 2−67310
^{236}U, fission isomeric state 2−59795
^{236}U, half-life and specific activity 2−46206
^{236}U, symmetric and asymmetric fission probabilities from two-centre model 2−46342
^{236}U fission isomer, search for conversion electrons 2−49853
^{236}U level struct., thermal neutron capture in ^{236}U obs. 2−67309
^{236}U level structure determ. from ^{235}U(n,γ) reaction 2−52820
^{238}U/^{235}U fission cross section ratio, 1-5 MeV 2−83030
^{238}U/^{235}U fission cross section ratio meas. in 2-3 MeV range using time-of-flight technique 2−83029
^{238}U, 450 MeV proton induced, mass yield distrib. and charge dispersion 2−46348
^{238}U, α-particle induced fission (E=25-120 MeV), distrib. of Cs isotopes produced 2−74130
^{238}U, Colomb fission cross sections depend. 2−83033
^{238}U, elastic and nucl. Raman scatt. of photons, giant dipole reson. 2−70431
^{238}U, fast-neutron fission, energy depend. of ν 2−56009
^{238}U, ground state rotational and octupole-vibrational states, B(E2), B(E3) reduced transition probabilities 2−46178
^{238}U, in area of Roumania with increased natural background, meas. of absorption levels in population 2−58633
^{238}U, inelastic neutron scatt., excited level struct. and decay schemes 2−67183
^{238}U, inelastic neutron scatt., 1.13-2.37 MeV, cross section meas. 2−67252
^{238}U, level structures and decay schemes 2−59724
^{238}U, n-and α-induced, lifetime determ. using shadow effect 2−76891
^{238}U, neutron-induced fission, blocking effect 2−63930
^{238}U, photofission cross sections near thresholds 2−83024
^{238}U, secondary reactions induced by 12 and 28 GeV protons, search for actinides and super-heavy elements 2−63781
^{238}U bombardment with ^{136}Xe ions, production of Au isotopes, A=194, 196, 198, 199 2−67335
^{238}U fission, 14 MeV, rare gas isotopes yields 2−59792
^{238}U fission, long range α-particle emission 2−83037
^{238}U fuel, contribution to post-shutdown heat release 2−79831
^{238}U neutrons, radiative capture, 1.2-4 MeV 2−82973
^{238}U photofission, cross sections and angular distrib., obs. of band of rotation levels 2−83040
^{238}U photofission product yields 2−74129
^{238}U prompt and delayed photofission 2−83039
^{238}U surrounded by water moderator, neutron multiplication expts. 2−42691
^{238}U(α,2n)^{240}Pu, excitation energy, spontaneous fissioning products, time-of-flight obs. 2−76881
^{238}U(n,f), isomer yield ratio of ^{115m}Cd and ^{115g}Cd 2−63808
^{238}U(n,γ)^{239}U, neutron resons., density and struct. 2−67185

Nuclei with $150 \leqslant A$ continued
^{239}U neutron resons., density and struct. 2−67185
^{235m}U decay rate perturbation by implantation in transition metals 2−79755
W, angular distribution of photoneutrons 2−63864
W, Coulomb dissociation of C and O at 10 GeV/nucleon 2−49843
W, secondary reactions induced by 28 GeV protons, search for actinides and super-heavy elements 2−63781
W N=108 deformed shell, effect on nucleus properties 2−55950
^{182}W, 3^-, 1374 keV level, mag. moment 2−79738
^{182}W, e.m. properties of $K^\pi = 2$- octupole band populated in β- decay of ^{182}Ta 2−42533
^{182}W, Mossbauer effect in Ni-W alloy 2−75273
^{182}W level calc. rel. to gamma oscillations in collective model for axially symmetric nuclei 2−52767
^{182}W(N, γ)^{183}W rapid determ. of tungsten in rocks 2−61834
^{183}W, Mossbauer effect in anhydrous Li_2WO_4, effective Debye temp. detn. 2−71720
^{186}W, ion bombardment, excited compound nuclei lifetime, $79 < Z < 89$, shadow effect obs. 2−76805
^{186}W(n,γ)^{187}W, nsec. isomeric transitions, γ-γ coincidence obs. 2−67176
^{186}W(p,d), angular distributions, higher-order processes 2−79785
^{186}W(p,t)^{184}W, strong inelastic processes 2−52814
^{187}W, nsec. isomeric transitions, (n,γ) reaction obs. 2−67176
^{188}W→^{188}Re, forbidden $0^+ \rightarrow 0^+$ β transition, quantitative interpretation 2−59731
Yb, A=170, 172, 174, 176, isomer shifts, Mossbauer effect study 2−70407
^{162}Yb, half-life and γ-ray spectra 2−67197
^{164}Yb, high-spin states produced in (α,8n) reactions, anomalous behaviour of nuclear moment of inertia at large rotational frequencies 2−42528
^{164}Yb lifetime of rotational levels meas. by Doppler shift method on recoil nuclei in ^{128}Te(^{40}Ar, 4n) 2−79764
^{166}Yb, moment of inertia of high-spin rotational states 2−63818
^{168}Yb, one-parameter model with EXP for energy ratios of YRAST levels to high spin 2−73984
^{169}Yb, decay, energies and intensities of γ-rays,total internal conversion coeff. for 20.7 keV transition 2−79768
^{170}Yb level scheme from β-decay of ^{170}Lu 2−76821
^{170}Yb Mossbauer effect in $YbPd_3$ 2−54393
^{170}Yb(n,γ)^{171}Yb, thermal neutrons, excited states in ^{171}Yb 2−46170
^{171}Yb, excited states, in thermal neutron capture by ^{170}Yb 2−46170
^{171}Yb(α,nγ)^{174}Hf, ^{172}Yb(α,nnγ)^{174}Hf, role of K quantum number in de-excitation of ^{174}Hf 2−46328
^{172}Yb(α,8n), production of high-spin states in ^{168}Hf, anomalous behaviour of nuclear moment of inertia at large rotational frequencies 2−42528
^{172}Yb(p,d), angular distributions, higher-order processes 2−79785
^{173}Yb(^{3}He,d)^{174}Lu, 24 MeV, determ. of levels in ^{174}Lu 2−82896
^{173}Yb(α,t)^{174}Lu, 28.5 MeV, determ. of levels in ^{174}Lu 2−82896
^{173}Yb(n,γ)^{174}Yb, nonstatistical aspects in 4s giant resonance 2−67300
^{174}Yb, 4s-giant resonance, γ-ray spectra 2−67300
^{174}Yb, secondary minimum in bubble degree of freedom 2−82904
^{174}Yb(n,α)^{171}Er meas. of activation cross sections at 14.5 MeV 2−79791
^{175}Yb, mechanism of uptake in isolated perfused rat liver 2−55225
^{176}Yb(n,α)^{173}Er meas. of activation cross sections at 14.5 MeV 2−79791
Nucleic acids *see Macromolecules*
Nucleons and antinucleons
see also Cosmic rays/nucleons; Neutrons and antineutrons; Nuclear reactions and scattering due to/nucleons; Protons and antiprotons
anomalous magnetic moment, derivation of Drell-Hearn sum rule from light-cone current commutators 2−73841
axial vector and magnetic moment form factors of nucleon 2−67043
bound-state nature, rel. to fixed poles in Compton amplitudes 2−66928
charge form factor determ. using $ep \rightarrow en\pi^+$ process 2−42405
electromagnetic excitations in relativistic quark model 2−55870
e.m. form factors in perturbation theory, field-theoretical model 2−79608
e.m. structure, mean radius of mass distrib. 2−52631
e.m. structure function, Regge depression from duality applic. to virtual photon nucleon scattering 2−42406
excited nucleons in superdense neutron star matter, energy shifts 2−58313
form factor estimation from dispersion model for $\pi^- p \rightarrow e^+ e^- n$, 275 MeV 2−63602
form factor t-dependence 2−59557
form factors, asymptotic behaviour, solution of Bethe-Salpeter eqn. 2−79606
form factors, scaling, information on Z_2 and Drell-Yan-West relation 2−55869
form factors in field theory on homogeneous space of Poincare groups 2−63650
isovector axial form factor in electroproduction at threshold 2−79509
lepton-nucleon inelastic structure functions, scaling, Greens functions of currents 2−70150
mass of nucleon quark, pn bound state 2−73840
meson nucleon sigma terms, theoretical estimate 2 -63571
parton structure, evidence in muon-pair photo-production expts. in deep inelastic region 2 82696
parton structure 2· 69085
physical bound state nature and scaling properties in deep inelastic eN scattering 2−45991
physical nucleon, bound-state model 2−67044
polarization in pion photoproduction, review 2−45959
resonances, possible existence of I=5/2 resonances 2−82785
structure and chiral symmetry 2−76707
subnuclear particles, highly charged, theory 2−59559
$eN \rightarrow e\gamma +$ anything, SU(4) bilocal current algebra 2−73756
γNN electromagnetic vertices, conformal invariance and Bjorken scaling 2−79495
KNΛ, KNΣ coupling consts., upper bounds 2−76652
NN bound system, possible levels in pd→n(NN) 2−46005
NNπ form factor and Goldberger-Treiman relation 2−59558
πN coupling constant determ. from π photoproduction 2−45951
Nucleons and antinucleons continued
Nd elastic scatt., perturbative calc. of spin observables, tensor force 2−82960
antinucleons
No entries
interactions
— 2−59499
baryon resonance, electroproduction, form factors 2−55881
hyperon-nucleon, exact SU(3) symmetry and unitarity of S-matrix 2−79622
with hyperons, review of theoretical concepts and exptl. knowledge 2−59587
with massive vector meson I-spin triplet, low-energy theorems 2−76697
meson-nucleon coupling, parity-violating, meson-dominance model 2−73833
meson-nucleon cross sections, determ. from elon-nucleus collisions 2−76648
meson-nucleon dynamics, Ward identity for axial current, Wilson expansions and commutators 2−49461
model, $SU(2)_l \times Y_l$ gauge theory 2−66934
photoproduction in resonance region, multichannel analysis 2−66927
photoproduction of charged pions, absorptive corrections 2−42385
unstable particle photoproduction, cross-section, effect of coupling of unstable particle to continuum 2−63498
vector meson, photoprod. differential cross-sections, quark model 2−55864
vector meson photoproduction, and nucleon Compton scatt. amplitude, quark model 2−55865
Yang-Mills field interacting with nucleons, Feynman rules 2−73735
ΔN total cross section estimation from final state Δ production on nuclei 2−42425
eN, as test for algebra of bilocal operators 2−70109
eN, intermediate boson production cross section calcs. 2−73832
eN, parton description of forward peak as function of photon mass 2−79505
eN, vector meson dominance model 2−59406
$e^- N \rightarrow e^- +$ anything electroproduction, parton dual resonance model 2−66931
$eN \rightarrow e +$ soft pion + anything, SU(4) bilocal current algebra 2−73756
γN, ps. meson production, scale dimension of chiral symmetry breaking Hamiltonian 2−49540
γN, single-pion photoproduction via s- channel resonances in model of higher baryon couplings 2−45955
γN, vector meson dominance model 2−59406
$\gamma N \rightarrow \Lambda(\Sigma)K$, photoproduction near the threshold, amplitudes and cross-sections 2−66929
$\gamma N \rightarrow N\pi^+\pi^-$, nonrelativistic solvable model 2−79575
$\gamma N \rightarrow N\pi\pi$, generalized Watson theorem, interdependence of reactions 2−63501
$\gamma N \rightarrow$0-B, s-channel transformation matrices for helicity and invariant amplitudes calc. using computer language REDUCE 2−55812
$\gamma N \rightarrow \eta N$, Regge-pole Regge-cut analysis 2−63500
$\gamma N \rightarrow \pi^0 N$, Regge-pole Regge-cut analysis 2−63500
$\gamma N \rightarrow \pi^+\pi$-$\Delta$, e.m. ρ^0-ω interference effect 2−59402
$\gamma N \rightarrow \pi N$, baryon Regge pole exchange model 2−52623
$\gamma N \rightarrow \pi N$, sum rules and Veneziano model 2−82670
KN, 2-5 GeV/c, review including polarization, R parameter data, cross sections 2−52602
KN, 2-5 GeV/c, review including polarization, R parameter data, cross sections 2−52602
KN, partial wave analyses, multichannel scatt. 2−73806
KN, study using track sensitive targets 2−52669
KN charge exchange reactions, effects of correction to real part of Regge amplitudes 2−59472
KN parametrizations below 2 GeV/c 2−52601
KN production of 2^+ and 1^+ mesons studied in $U(6,6) \otimes O(3,1)$ peripheral absorption model 2−55863
$KN \rightarrow \pi\Lambda$, 1.54 to 2.15 GeV, duality and role of daughter resonances 2−79568
$KN \rightarrow \pi\Lambda$, energy independent coupled channel phase shift analysis 2−79563
$KN \rightarrow \pi\Sigma$, energy independent coupled channel phase shift analysis 2−79563
$KN \rightarrow \pi\Sigma$, Λ, strangeness-exchange interactions at high-energy, cross-section and polarization 2−76650
$KN \rightarrow \pi\Sigma$, new Regge absorption model fits to polarization and cross section data 2−73794
$KN \rightarrow \pi[\Sigma,\Lambda]$, hypercharge exchange reaction, amplitude analysis 2−42389
$KN \rightarrow \pi\pi\Lambda$, usefulness of meas. of Λ-polarization 2−63667
K^+N, 0.6-1.5 GeV/c, phase shift analysis of I=0 and I=1 states 2−76660
$K^0{}_l N$, cross-sections and ang. distrib., compilation of 13 papers 2−82749
ΛN potential, two-pion exchange 2−59588
μN, fireball production 2−76614
μN, intermediate boson production cross section calcs. 2−73832
$\mu N \rightarrow \pi +$ anything, inclusive processes, 10.1 and 15.8 GeV/c 2−59430
$Np \rightarrow \Delta X$, new cross-section relations 2−63545
$N\rho \rightarrow N^*\pi$, pion-gauge conditions 2−52632
νN, as test for algebra of bilocal operators 2−70109
νN, as test for algebra of bilocal operators 2−70109
νN, νN interactions, cross-sections calc. from 3 quark boson-nucleon model 2−45876
νN, pseudoscalar meson prod., generalized similarity relation and trilinear matrix elements 2−76724
$\nu N \rightarrow NX$, parton model predictions in Weinberg theory 2−45886
$\nu_\mu N \rightarrow \mu^- W^+ N'$, μ^- production cross-sections, neutrino energy spectrum 2−76613
pN asymmetry of angular distrib., momentum spectra, distrib. of 4-dimensional transfer 2−73819
$pN \rightarrow NNKK$, total cross- sections, model with single kaon exchange 2−76719
$pN \rightarrow \pi^+\pi$-π-, isospin and grand ang. momentum analyses 2−59563
$\pi^- A \rightarrow V^0 A'$, obs. of polarized V^0 mesons interaction with nucleons 2−70233
πN, secondaries momentum characteristics at 60 GeV 2−76672

Nucleons and antinucleons continued
interactions continued
πN, short range P-wave interaction, comparison with high energy backward Regge models 2−70234
πN asymmetry of angular distrib., momentum spectra, distrib. of 4-dimensional transfer 2−73819
πN charge-exchange forward scattering, invariant amplitudes 2−79579
πN charge exchange cross-sections, calc. using new Regge absorption model 2−73794
πN charge exchange reactions, effects of correction to real part of Regge amplitudes 2−59472
πN chiral invariant, matrix superpropagator 2−73820
πN coupling const., derivations from pion photoproduction data 2−79573
πN coupling constants, radiative corrections 2−49565
πN cross-section through extrapolation of deep inelastic electroproduction and photoproduction data 2−67021
πN form factor, corrections to Goldberger-Treiman relation 2−59530
πN multiplicity of secondary particles, 5-5.10^4 GeV, analysis of models and data 2−82763
πN potential for use in low energy nuclear physics 2−63740
πN production of 2^+ and 1^+ mesons studied in U(6,6)⊗O(3,1) peripheral absorption model 2−55863
πN resonance dynamics, review 2−46015
$\pi^-N\to\pi^-\pi^-\pi^+N$, 60 GeV/c, photoemulsion study 2−73818
$\pi^-N\to\pi^-\pi^-\pi^+N$ and $\pi^-N\to\pi^-\pi^-\pi^-\pi^+\pi^+N$, coherent interactions with photoemulsion nuclei at 17 GeV 2−45961
$\pi^-N\to\pi^-\pi^0\pi^0N$, photoemulsion study 2−73818
$\pi N\to A_1N$, t-channel helicity conservation and $A_1\rho\pi$ coupling 2−59554
πN→KΣ, Λ, strangeness-exchange interactions at high-energy, cross-section and polarization 2−76650
πN→KΣ, new Regge absorption model fits to polarization and cross section data 2−73794
πN→K[Σ,Λ], hypercharge exchange reaction, amplitude analysis 2−42389
πN→KπΛ, usefulness of meas. of Λ-polarization 2−63667
πN→V + N′, differential cross section and density matrices determ. in model of higher baryon couplings 2−45983
πN→ω(N,Δ), isolation of isotopic symmetry possible due to ρ^0-ω mixing 2−63615
πN→πΔ(1236), study of baryon decays involving two partial waves, test for basic violation of $SU(6)_w$ 2−63642
πN→πΣ(Λ), PCAC prediction of Σ(Λ) production cross sections and polarization phenomena 2−52644
πN→ππN, results of combining conformal invariance and chiral symmetry 2−63612
πN→ρN, baryon Regge pole exchange model 2−52623
πN→ρN, dual amplitudes 2−67020
πN→ρπN, dual resonance model for A_1 production 2−63613
πN; inclusive spectra, microscopic model 2−76713
ΞN, estimate of cross section for ΛΛ production 2−49598
$K\text{-}N\to\pi\text{-}\pi\text{-}\pi^+\Lambda$, 4.9 GeV/c, cross sections meas. 2−42371
$K\text{-}N\to\pi\text{-}\pi\text{-}\pi^+\Sigma^0$, 4.9 GeV/c, cross sections meas. 2−42371
$K\text{-}N\to\pi\text{-}\pi\text{-}\pi^0\Lambda$, 4.9 GeV/c, cross sections meas. 2−42371
interactions, nucleon-nucleon
annihilation processes, conf., Chexbres, Switzerland [Mar. 1972] 2−59560
baryon-antibaryon pairs ane quarks, production, modified peripheral model 2−82711
bremsstrahlung, Burnett-Kroll soft-proton theorum applic. 2−82855
finite nuclei, phase shift data rel. to solution of Bethe-Goldstone equation, applic. to ^{18}O and ^{18}F 2−46067
inclusive spectra, microscopic model 2−76713
Lagrangian field theory 2−45992
meson factory expts. at low energy 2−82640
Monte Carlo simulation at high and ultrahigh energies 2−73893
multiplicity of secondary particles, 5-5.10^4 GeV, analysis of models and data 2−82763
nucleus, single-particle spin-orbit potential following from spin-orbit interaction 2−59670
three-nucleon problem, two-term nonlocal separable potentials 2−82845
NN annihilation at rest in statistical bootstrap model including resonance production 2−82703
NN annihilation into pions, possibility of determining spin for resonances in direct channel 2−73843
NN annihilation processes, gross features 2−59562
NN annihilation processes, models 2−59561
NN→NN + nπ, uncorrelated jet model 2−70173
NN→3π, duality and final-state-interaction approach 2−52634
NN→3π, isospin and grand ang. momentum analyses 2−59563
interactions, pion-nucleon *see Pions/interactions, pion-nucleon*
scattering
amplitude, unitary approx. computation using linear σ model 2−52633
charge exchange, model for relationship of fixed pole to shielding cut 2−49571
electron scattering, elastic and inelastic, relation between form factors 2−70162
inelastic, of polarized nucleons from polarized leptons, threshold relations determ. 2−63507
lepton-nucleon, deep inelastic scatt., recent developments 2−76583
lepton-nucleon deep inelastic, form factors of nucleon 2−67043
lepton-nucleon scatt. linked by sum rule to baryon mass splitting D/F ratio 2−70153
lepton-nucleon scattering, parton model predictions in Weinberg theory 2−45886
meson-nucleon backward scattering extrapolations to baryon pole, rel. to coupling constant 2−76702
meson-nucleon in Eckmann model 2−76570
structure functions of inelastic lepton-nucleon scattering, light-cone approach to scaling-limit inequalities 2−66935
virtual Compton effect, fixed pole in amplitude 2−45873
eN, deep-inelastic, breaking of scaling behaviour in multi-triplet quark models 2−66949
eN, deep inelastic, parton model and ratio $\nu W_2^n/\nu W_2^p$ 2−70251
eN, deep inelastic expts., comparison with high-order Feynman diagram model for hadrons 2−42347

Nucleons and antinucleons continued
scattering continued
eN, deep inelastic region, partons, virtual photon mass parameters 2−70167
eN, deep inelastic region, role of one-pion exchange 2−45888
eN, deep inelastic scattering and geometric duality, virtual photon nucleon scatt. 2−42406
eN, determ. of sum rules from triplet quark model light-cone algebra of currents 2−76708
eN, inelastic scatt., proton data analysis 2−79506
eN deep inelastic, inequalities for structure function derived from quark parton model and quark model with neutral gluons 2−42329
eN deep inelastic, interpretation of exptl. data in proton model, Regge pole analysis 2−59427
eN deep inelastic scaling properties and bound state nature of physical nucleon 2−45991
eN inclusive electroproduction in target fragmentation region, consequences of light-cone dominance 2−79607
eN inelastic, connection between structure function of eN→eγ + anything and N→e + anything using Fritzch- Gell-Mann algebra 2−42340
eN inelastic, vector dominance and n/n ratio 2−82687
eN inelastic electroproduction, possible relation between prominent resonances and limiting scaling data 2−76608
eN inelastic structure functions, field theoretic models 2−66941
eN scaling of structure functions and compositeness 2−55823
γN, deep inelastic, scattering amplitude, scaling and Regge behaviour on Feynman diagram model 2−45872
γN→γ′ + anything, comparison between bilocal algebra on the light cone and parton model calcs. of structure functions 2−49498
KN, absorption model construction 2−63651
KN, amplitudes analysis in intermediate energy region 2−63596
KN, amplitudes analysis in intermediate energy region 2−63596
KN, calc. of magnitude of nucleon expectation value of σ commutator 2−63598
KN, chiral symmetry braking 2−49554
KN, consequences of local duality, specific solution in exact SU(3) limit 2−67012
KN, elastic and charge exchange, phenomenological analysis, Regge contributions 2−42400
KN, modified dispersion relation, constant scattering length parametrization 2−49557
KN, sum rules for elastic scatt. amplitudes, threshold behaviour 2−70242
KN, sum rules for elastic scatt. amplitudes, threshold behaviour 2−70242
KN, urbaryon rearrangement and reson. correl. 2−63563
KN, urbaryon rearrangement and reson. correl. 2−63563
KN inelastic channels below 3 GeV/c, review 2−52611
KN total cross sections, resonance and background contributions, 1-4 GeV/c 2−76646
KN→KN, energy independent coupled channel phase shift analysis 2−79563
KN→K*(890)N, Regge pole ρ_{10} production, unnatural parity exchange 2−49586
K^+N, below 2 GeV/c, review of I=0 state 2−52610
K^+N, I=0 state, phase shift analyses 0.6-1.5 GeV/c 2−49556
ΛN, two-channel separable potentials to represent low-energy S-wave interaction 2−46012
ΛN two-channel ${}^3S_1$-${}^3D_1$ separable potential 2−55880
ΛN two-channel separable potentials, restrictions 2−46010
μN inelastic scatt., high energy, vector-dominance model 2−82695
NN, amplitude spin structure, partial analysis at high energy using Regge pole classification 2−45993
Nd, elastic scatt., polarization calc. 2−67046
nd, spin structure in cross-section defect 2−82771
νN, Adler's sum rule for W_3 from time-space ETC 2−70154
νN, deep inelastic, inequalities for structure function derived from quark parton model and quark model with neutral gluons 2−42329
νN, deep inelastic, multiperipheral theory 2−59419
νN, determ. of sum rules from triplet quark model light-cone algebra of currents 2−76708
νN, determ. of sum rules from triplet quark model light-cone algebra of currents 2−76708
νN, dimension of symmetry breaking Hamiltonian 2−42336
νN scattering, operator product expansions and dimension of symmetry breaking Hamiltonian 2−55820
νN sum rules and low energy theorems 2−42337
π N low energy theorems, current algebra description 2−59525
πN, absorptive separable potential construction 2−59536
πN, amplitude analysis at 6 GeV/c 2−49570
πN, analyticity of forward scattering amplitude, test, determ. of πN coupling constant 2−73822
πN, backward amplitudes, dual absorptive model 2−79580
πN, below 1 GeV/c, isospin mixing as source of enhanced isospin violation 2−52620
πN, Coulomb interference data, amplitude analysis 2−63622
πN, dispersion relations, soln. by Pade approximant method 2−49569
πN, dual geometrical model 2−67031
πN, dual Regge cut amplitudes 2−55856
πN, dynamic model for 33-phase shift 2−63626
πN, eikonal model for Regge cuts 2−59538
πN, elastic, four-vectors and helicity amplitudes 2−63625
πN, elastic and charge exchange, phenomenological analysis, Regge contributions 2−42400
πN, elastic phase-shift analysis, removal of ambiguities 2−63555
πN, fixed-u finite energy sum rule calcs. using realistic spectral functions 2−63627
πN, forward charge exchange, finite energy sum rules and Regge cuts 2−59537
πN, G_{39}-resonance, evidence 2−70239
πN, isospin bounds and zeros of scattering amplitudes 2−76665
πN, multiple scattering model and slope of Pomeranchuk trajectory 2−42396
πN, N and Δ exchanges, separation and deduction of amplitude zeros 2−59508
πN, peripheral partial wave amplitudes from two pion exchange 2−42397
πN, Regge pole residues, optimized FESR 2−66980

Nucleons and antinucleons continued
scattering continued
πN, relativistic Regge-cut model for invariant functions 2−76667
πN, s-channel helicity amplitudes, structure determ. as function of momentum transfer and energy 2−82760
πN, sigma term value reviewed 2−45929
πN, strong shrinkage of $d\sigma/dt$ at $|t|=(1\text{-}3)\ (GeV/c)^2$ 2−70241
πN, sum rules for elastic scatt. amplitudes, threshold behaviour 2−70242
πN, σ term, validity of extrapolation procedure of Cheng and Dashen 2−79590
πN, urbaryon rearrangement and reson. correl. 2−63563
πN 6 GeV/c, enhanced absorption model, and impact parameter space 2−45974
πN at high-energy, linear trajectory fits in simple Regge model 2−63623
πN change-exchange, fixed-t dispersion relations and polarization 2−63624
πN charge-exchange at 6 GeV/c, structure of partial wave amplitudes 2−59533
πN charge exchange, applications of unitarized finite energy sum rules 2−45921
πN charge exchange, strong suppression of Regge-Regge cuts 2−59493
πN charge exchange polarization and violation of Pomeranchuk theorem 2−45976
πN conservation of s-channel helicity for pomeron exchange and flip dominance for ρ- exchange studied in ABFST multiperipheral model 2−42398
πN cross sections, optimal extrapolation 2−76668
πN forward scattering amplitude, duality and high-energy limit 2−76664
πN forward scattering data, consistency with analyticity and crossing 2−76666
πN helicity amplitudes calc. for isospin $I=0$ and $I=1$ states at 6 GeV/c and for $I=0$ exchange at 16 GeV/c 2−55857
πN $I_t=0$ scattering amplitude at 6 GeV/c, properties of pomeron term 2−70240
πN low-energy parameters evaluation using finite-energy and current algebra sum rules in quark model 2−63529
πN low energy theorem from source dynamics 2−59542
πN P-wave scattering amplitudes and their S-matrix calculations 2−45975
πN polarization, relative magnitude and phase of amplitudes depend. 2−59535
πN Regge pole exchange, multiple, consequence of crossing symmetry 2−79576
πN Regge pole model with explicit quark spin applied to meson and baryon exchange 2−49572
πN resonances, introduction of effective mass and effective width 2−63561
πN S-wave analysis, low energy ambiguities of $\pi\pi$ isospin-zero S-wave on comparison 2−55861
πN scatt., Pomeron-exchange amplitude and cross sections due to resons. 2−52619
πN scatt. amplitudes determ. using rot. parameters 2−82752
πN scattering length, sum rule derivation using broken scale invariance and mass-dispersion relations 2−66911
πN short range P-wave, comparison with backward Regge models 2−79578
πN sigma term, new determ. including off shell effects 2−76662
πN static model for elastic scattering, possible improvements 2−42399
πN total cross sections, resonance and background contributions, 1-4 GeV/c 2−76646
$\pi N \to A_1N$, helicity conservation 2−45973
$\pi N \to \omega N(\Delta)$, dual amplitudes and relations between coupling consts. 2−76684
$\pi N \to \pi\Delta$, theoretical analysis concerning resonance coupling 2−59534

scattering, nucleon-nucleon
absorption model construction 2−63651
amplitude determ. using Pade approx. 2−73291
amplitude spin structure, partial analysis at high energy using Regge pole classification 2−45993
elastic, damped pseudoscalar- and vector-meson model 2−76709
elastic one-boson exchange model with amplitudes constructed from Veneziano functions 2−45994
Kantor amplitudes below 500 MeV 2−73842
low energy scatt. amplitude helicity struct. 2−70250
low-energy, one-boson exchange model using relativistic Blankenbecler-Sugar eqn. 2−67047
Regge cuts from inclusiive finite mass sum rules 2−67045
Regge cuts of pp and A_2A_2, sum rule calcs. 2−63652
Regge- like behaviour of scatt. amplitudes at low energy 2−55873
S-scattering, numerical stability test 2−46003
scattering length calc. using Pade approximants and Yukawa theory 2−76706
urbaryon rearrangement and reson. correl. 2−63563
π diffractive production, application of model for case of simple fluctuations 2−76632

scattering, pion-nucleon *see Pions/scattering, pion-nucleon*

Nucleus
see also Elements/origin; Hypernuclei; Radioactivity; Scattering, particles
charge density determ. for pairs of isotones by electron scatt. 2−46104
mass quadrupole density, information from study of pionic and kaonic atoms 2−49713
threshold of disintegration in degenerate electron neutron gas and eqn. of state of superdense matter 2−58255
^{58}Co, neutron capture cross-sections 2−74098
^{3}He, electromagnetic structure 2−70372
^{6}Li, structure study by ^{6}Li(π^-, nn) reaction 2−82988
^{22}Na, neutron capture cross-sections 2−74098

electric moment
see also Molecules/nuclear coupling
— 2−70406

Nucleus continued
electric moment continued
A=8-28 4n nuclei, HF calcs. of static quadrupole moments using projection before variation procedure 2−70364
deformation effects on elastic quadrupole transitions and quadrupole moments of first excited 2^+ states, rigid symmetric rotator model 2−79726
deformed even-even, influence of spin and quadrupole interactions on properties of state with $K^\pi=1^+$ 2−67136
even-even nuclei of p-f shell, quadrupole moments of first excited states, BE2 values, variation of shape and deformation 2−79716
light nucleides, quadrupole moments 2−52731
magnetic dipole and elec. quadrupole hyperfine interactions study by nuclear orientation with and without n.m.r. 2−63758
quadrupole, of high spin states in collective nucleus model 2−59675
quadrupole moment mean values for high spin states in asymmetric top model 2−67138
(s,d)shell nuclei, α-type, of intrinsic quadrupole moments 2−49710
transitional odd-A nuclei, quadrupole moment by projection method 2−42501
^{75}As, static moments of ground state, core excitation model description 2−42513
^{134}Ba, static quadrupole moment of first 2^+ state 2−76800
^{136}Ba, static quadrupole moment of first 2^+ state 2−76800
^{138}Ba, static quadrupole moment of first 2^+ state 2−76800
Cd, anomalous two-phonon transitions, study by Cd (p,t) reaction 2−63806
^{114}Cd, multiple Coulomb interference effects on quadrupole moment 2−59707
^{114}Cd, static quadrupole moment of first 2^+ state determ. from ^{114}Cd(^{32}S,^{32}Sγ) reaction 2−82893
^{161}Er, ^{163}Er, hyperfine interaction consts. and nuclear moments meas. using atomic beam magnetic resonance method 2−79741
^{20}F quadrupole coupling const., method of meas. by obs. of n.m.r. of neutron irradiated MgF_2 crystals 2−75356
^{56}Fe, Coulomb excitation by ^{32}S ions, 60-70 MeV, meas. of static electric quadrupole moments 2−63795
^{56}Fe, static electric quadrupole moments of first excited states determ. from ^{56}Fe(^{32}S, ^{32}Sγ) 2−63799
^{154}Gd, quadrupole interaction with liquid environment, estimation from time differential perturbed ang. correlation studies 2−60511
^{2}H, quadrupole moment calc. 2−67140
^{173}Hf, $\Delta k=1$ retarded E1 transition 2−49753
^{39}K, E2 calc. from hyperfine structure of 5p $^2P_{3/2}$ and 6p $^2P_{3/2}$ levels of K I spectra 2−46430
^{137}La, quadrupole moment, optical determ. 2−63813
^{138}La, optical determ. of quadrupole moment 2−52760
^{7}Li, ground state quadrupole moment 2−76882
Mg, A=24, 26 static quadrupole moment meas. via reorientation effect using Doppler-shift 2−74010
^{23}Na, transition strengths of $J^\pi={}^1/_2{}^-$, ${}^3/_2{}^-$ and ${}^3/_2{}^-$ levels 2−76789
Ne, A=20, 22, static quadrupole moment meas. via reorientation effect using Doppler-shift 2−74010
^{20}Ne, static and dynamic quadrupole moments of first excited state determ. by projectile Coulomb excitation technique 2−42537
^{22}Ne, static and dynamic quadrupole moments of first excited state determ. by projectile Coulomb excitation technique 2−42537
Ni, A=58,60, Coulomb excitation by ^{32}S ions, 60-70 MeV, meas. of static electric quadrupole moments 2−63795
Os, A=184, 186, 188, 190, 192, static quadrupole moments of first 2^+ states 2−63826
Os even-even isotopes, static quadrupole moments of first 2^+ states, Coulomb excitation determ. 2−67177
^{186}Os, quadrupole moment, Mossbauer obs. 2−63827
^{188}Os, quadrupole moment, Mossbauer obs. 2−63827
^{189}Os, quadrupole moment, Mossbauer obs. 2−63827
^{190}Os, quadrupole moment, Mossbauer obs. 2−63827
^{105}Pd, quadrupole coupling constants of $^3D_2$, $^3D_1$ and $^1D_2$ levels 2−52756
^{87}Rb, E2 moment from E2, interaction in $np^2P_{3/2}$ series of Rb I spectrum 2−46439
^{28}Si, static quadrupole moment meas. via reorientation effect using Doppler-effect 2−74010
Sn isotopes, even, static quadrupole moments and anharmonicity parameters 2−59706
Te isotopes, even, static quadrupole moments and anharmonicity parameters 2−59706
Ti, (A=46, 48, 50), ground state charge distribs., using Ti(e,e) 2−52749
Ti even isotopes, static electric quadrupole moments of first excited states determ. from (^{32}S, ^{32}Sγ) reaction 2−63799
^{48}Ti, Coulomb excitation by ^{32}S ions, 60-70 MeV, meas. of static electric quadrupole moments 2−63795
^{48}Ti, Coulomb excitation by ^{32}S ions, 60-70 MeV, meas. of static electric quadrupole moments 2−63795

energy level transitions
^{23}Na, spin, branching and mixing ratio 2−76789
— 2−59785
— 2−59725
— 2−59705
— 2−70406
A=8-28 4n nuclei, HF calcs. of e.m. transitions using projection before variation procedure 2−70364
angular correlations, static and time-dependent perturbations 2−59661
cascade E2, of high spin states in collective nucleus model 2−59675
closed shell nuclei, radiative widths of E1 and M1 resons. 2−70368
compound nucleus, exit states role in high-energy γ-ray emission 2−59763
deformation effects on elastic quadrupole transitions and quadrupole moments of first excited 2^+ states, rigid symmetric rotator model 2−79726
direction correlation coefficients in compound nuclear reactions 2−70369
1-3 directional correlations with mixed unobserved transitions and parity 2−73963
E1 internal conversion, study based on Saxon-Woods potential 2−49719
E2, probability in SU(3) scheme 2−59680
E2 intensities, effect of rotation and intrinsic motion 2−83236

Nucleus continued
energy level transitions continued
E2 transition probabilities for high spin states in asymmetric top model 2−67138
electric, generation of matrix elements from vector potential 2−46102
from electron spectrometry, low energy, book 2−41925
e.m. matrix elements determ. from γ-spectroscopy with heavy ions 2−83023
e.m. transition probabilities and lifetimes determ. by Coulomb excitation method 2−82869
even even nucleides, rotational spectra of ground state bands in spin region $I<30$, phenomenological descriptions 2−49718
even-even nuclei, E2 transition probabilities from 2^+ state of 2γ-vibr. band 2−42502
even-even nuclei of p-f shell, quadrupole moments of first excited states, BE2 values, variation of shape and deformation 2−79716
even-odd nuclei, $91\leqslant N\leqslant 113$, neutron capture, de-excitation 2−74003
even-odd nuclei with $21\leqslant A\leqslant 41$, p-level transition probabilities 2−59693
gamma ray angular correlations perturbation by stochastic Gaussian-Markov process 2−55946
hypernuclei of mass 4, obs. of γ-rays from excited states, consequences for Λ-N interactions 2−76775
isomeric, half life determ. using fast pneumatic tube system for transport of sample 2−79634
$L=0$ transition systematics from (p,t) reactions in $N=50$ region 2−79753
lifetimes of Coulomb- excited states meas. using plunger recoil distance technique 2−63756
lifetimes of levels, apparatus for meas. 10^{-9}-10^{-12} sec 2−82794
lifetimes of levels populated and depopulated by $\gamma-\gamma$ cascade 2−76765
light nuclei, spectroscopy by low energy (<70 MeV) inelastic electron scatt. 2−82882
M1 transition, analogue to antianalogue in $1f_{7/2}$ shell 2−82846
M1 used in calc. of nuclear charge radius 2−76759
M1-intranuclear conversion analysed on basis of Saxon-Woods potential 2−46089
mixing ratio determ. from meas. of γ-ray linear polarization correlation, graphical method 2−70365
Mossbauer line shape in coupled hyperfine interactions 2−75264
multishell Hartree-Fock calculations, practical angular momentum projection method, applic. to ^{22}Na 2−46119
neutron resonances, correlations between reduced partial alpha widths and neutron and radiative widths 2−46280
odd-proton $N=82$ nuclei $11^-/2(1)\rightarrow 7^+/2(1)$ and $11^-/2(1)\rightarrow 5^+/2(1)$ transitions 2−79756
p-shell hypernuclei, spectra based on numerical fitting to B_Λ data 2−63760
parity nonconserving interactions, circular polarization of gamma-rays 2−42495
rare-earth compound nuclei formed in bombardment with 40 MeV α-particles of rare-earth targets, intensities of ground band transitions 2−49731
renormalization rate induced by 2p-2h ground-state admixtures 2−46085
resonance levels populated by (γ,γ'), props. 2−46103
single-closed-shell nuclei, relations among magnetic moments and M1 rates 2−67135
spin current transitions in inelastic electro-excitation, matrix elements, using different vector potential decompositions 2−82839
time reversal, validity tests, optimization 2−63750
transitional odd-A nuclei amplitudes of quadrupole electric transitions by projection method 2−42501
unbound states in nucleon-induced reactions, γ-decay 2−79780
-1-6O, odd-parity levels, transition rates and mean lifetimes, renormalized RPA calc. 2−82917
^{98} Mo, low-lying states investigation via multiple Coulomb excitation 2−82910
^{113*}Tn (100 min) decay, internal conversion, M4, E5 character 2−74052
^{a}Ba, $A=126$, 128, produced by (^{16}O,4n) reactions, lifetime measurements 2−46154
^{a}Co $A=56$, 58, high resolution spectroscopy using direct two nucleon transfer reactions 2−63800
^{a}Xe, $A=120$, 122, produced by (^{16}O,4n) reactions, lifetime measurements 2−46154
^{a}Xe $A=131$, 132, 133, fission products, spin assignments and γ-ray multipole mixing ratios 2−46207
^{108}Ag, E1 transition study using ^{107}Ag(n,γ)^{108}Ag reaction 2−52757
^{109}Ag lifetimes of Coulomb-excited states meas. using plunger recoil distance technique 2−63756
^{110}Ag, E1 transition study using ^{109}Ag(n,γ)^{110}Ag 2−52757
^{108m}Ag, 30 keV isomeric transition, K-conversion coeff. 2−70402
^{25}Al, gamma decay of excited states, ^{24}Mg(p,γ)^{25}Al reaction 2−42503
^{25}Al, population of $3/2^+$, 945 keV level in ^{2}H(^{24}Mg, nγ) reaction, meas. of mean lifetime for γ-ray decay 2−79736
^{27}Al, transition strengths and decay properties, study by (γ,γ') reaction 2−52744
^{27}Al high-spin states produced in ^{12}C(^{16}O,p) and ^{24}Mg(α,p) reactions, meas. of γ-ray branching ratio, p-γ angular correlation 2−42504
^{243}Am, L X-ray spectra, γ-transition multipolarity, coincidence obs. 2−74042
^{34}Ar γ-decay and lifetime of low-lying states populated in ^{32}S(^{3}He, n) reaction 2−74012
^{36}Ar, branching ratios, excitation energies, lifetimes of levels, study by ^{35}Cl(p, γ) reaction 2−79748
^{36}Ar, lifetimes of bound states and resonances in ^{35}Cl(p,γ) reaction determ. from γ-ray angular distribs. 2−52747
^{36}Ar γ transitions and levels from positron decay of ^{36}K 2−76817
^{37}Ar, lifetimes of levels below 3 MeV excitation populated by ^{34}S(α,n) meas. by Doppler shift attenuation method 2−63790
^{37}Ar, low-lying levels, decay to ground state, γ transitions 2−55960
^{37}Ar, mean lifetime of levels below 3.30 MeV excitation populated in ^{37}Cl(p,nγ) reaction 2−74015
^{37}Ar lifetime meas. 2−63789

Nucleus continued
energy level transitions continued
^{38}Ar, lifetime of lowest 5- state meas. by recoil-distance and Doppler-shift techniques 2−42506
^{38}Ar, meas. of transition strengths and branching ratios of levels populated in ^{34}S(α,γ) reaction 2−63791
^{73}As, internal conversion coeffs. of low level transitions, using ^{75}As(p,n) 2−52752
^{74}As, γ energies and intensities from decay to ^{74}Ge and ^{74}Se 2−49765
^{75}As, M1 and E2 transition rates, core excitation model description 2−42513
^{210}At, half-lives of isomeric states populated in ^{209}Bi(α, 3n) reaction 2−70415
^{211}At, half-life of $3/2^-$ level at 1116 keV, E2 rates 2−49757
^{211}At, reduced transition probabilities for E2 transitions 2−67182
^{197}Au, 77 keV transition, internal conversion process 2−55968
Ba, elec. dipole transitions following p-wave neutron capture 2−67286
^{134}Ba, multipole mixing ratios of γ-transitions following β-decay of ^{134}Cs 2−70404
^{134}Ba, reduced transition probability of first 2^+ state 2−76800
^{136}Ba, reduced transition probability of first 2^+ state 2−76800
^{138}Ba, intensities of E1-type γ-transitions from neutron capture states to lower p-levels 2−49809
^{138}Ba, reduced transition probability of first 2^+ state 2−76800
^{139}Ba level scheme investigation in unified model calc. and particle core model 2−67170
^{208}Bi, spreading widths of 1^- particle-hole state 2−76810
^{209}Bi, E1 radiative widths of isobaric analog states 2−76809
^{209}Bi, e.m. matrix elements of low-lying states 2−76782
^{80}Br, ^{82}Br, transition strengths of low-lying states populated in ^{79,81}Br(d, p) reactions 2−74031
^{81}Br, Coulomb excitation of low-lying levels by α-particles and ^{16}O ions determ. of B(E2), B(M1) transition probabilities, half-lives 2−74032
^{12}C, photon spectra from radiative absorption of pions 2−46296
^{12}C quadrupole and octupole vibrations, form factors and transition densities of 4.34 and 9.64 MeV levels 2−82881
^{13}C, e.m. transitions of isobaric analogue states 2−46111
^{40}Ca, lifetime of 3.74 MeV (3^-) state 2−67154
^{40}Ca, odd-parity levels, transition rates and mean lifetimes, renormalized RPA calc. 2−82917
^{40}Ca, photon spectra from radiative absorption of pions 2−46296
^{41}Ca, γ-ray transitions to neutron single-particle states 2−67275
^{43}Ca level lifetimes from γ-ray Doppler-shift meas. 2−82897
^{43}Ca low-lying state lifetimes 2−74018
^{48}Ca, odd.parity levels, transition rates and mean lifetimes, renormalized RPA calc. 2−82917
^{48}Ca(p, p'γ), particle-γ angular correlation and lifetime studies of 4.61 and 5.15 MeV levels 2−82889
^{131}Ca, relative intensities 2−42521
Cd, elec. dipole transitions following p-wave neutron capture 2−67286
^{112}Cd lifetimes of Coulomb-excited states meas. using plunger recoil distance technique 2−63756
^{140}Ce, 2412 keV level lifetime meas. 2−52762
^{140}Ce, angular correlation of γ-cascade 2−49748
^{140}Ce, γ-γ ang. correlation meas. of 329 to 487 to 1596 keV cascade 2−52763
^{141}Ce, intensities of E1-type γ-transitions from neutron capture states to lower p-levels 2−49809
^{141}Ce level scheme investigation in unified model calc. and particle core model 2−67170
^{145}Ce, 3.0 min. γ-decay studied by method of separation, determ. of energies and relative intensities 2−42524
^{249}Cf, L X-ray spectra, γ-transition multipolarity, coincidence obs. 2−74042
^{34}Cl, odd parity spectrum exptl. and theoretical study using ^{33}S(p,γ) reaction and six- particle shell-model calculations 2−46127
^{35}Cl, lifetimes of low-lying excited states 2−82908
^{35}Cl, mean lifetime, e.m. transition strengths of levels populated in ^{32}S(α,p) reaction 2−70386
^{35}Cl, transition strengths and decay properties, study by (γ,γ') reaction 2−52744
^{37}Cl, lifetimes of low-lying excited states 2−82908
^{38}Cl, E1 reduced intensities, correlation with γ-ray spectra 2−67272
^{38}Cl, mag. multipole props., effects of weak particle-hole admixtures 2−76791
^{245}Cm, groundstate rotational band, γ branching and total conversion coeffs. of intraband transitions 2−52772
^{245}Cm, half-lives of 388 keV and 55 keV levels 2−49759
^{54}Co hole-hole nucleus, transformation properties of effective transition operator 2−82861
^{55}Co, analogue state of ^{55}Fe, γ-decay in ^{54}Fe(p,γ)^{55}Co 2−46135
^{57}Co, γ decay of levels populated in ^{56}Fe(^{3}He,dγ) reaction 2−46138
^{58}Co, lifetimes of 53.2 keV and 111.5 keV levels populated in ^{58}Fe(p, nγ) reaction 2−79742
^{58}Co, probability of γ transitions, lifetimes of levels excited in ^{55}Mn(α, nγ) reaction 2−82890
^{59}Co, M1 and E2 characters of transitions between levels populated in ^{59}Fe β-decay 2−79769
^{60}Co γ-transitions, polarized neutron capture in ^{59}Co 2−67276
^{50}Cr 3^- states transition rates 2−74022
^{50}Cr lifetimes of 9 states by Doppler shift attenuation method 2−76794
^{51}Cr, ang. distrib. of ground state e.m. transitions 2−79751
^{51}Cr, angular distirb. of γ-rays from transitions from excited states populated in (p,n) and (p,nγ) reactions on ^{51}V 2−46265
^{51}Cr spin assignments based on ln=1 J-dependence in ^{50}Cr(d, p) reaction, calc. of spectroscopic factors 2−63920
^{53}Cr, intensities of E1-type γ-transitions from neutron capture states to lower p-levels 2−49809
^{54}Cr(p, d)^{53}Cr, j-depend. in l=3 transitions 2−76845
^{123}Cs obtained in ^{115}In(^{12}C, 4n) and ^{109}Ag(^{18}O, 4n) reactions 2−74037
^{131}Cs decay, gamma gamma directional correl. meas. 2−46197
^{58}Cu levels populated in ^{58}Ni(p, nγ), determ. of lifetimes and decay modes of levels below 1.7 MeV 2−74026
^{61}Cu, L=1 and ground state transitions, (α,p) reactions on Ni isotopes obs. 2−59783

Nucleus continued
energy level transitions continued
^{63}Cu, ^{65}Cu, multipole admixtures of transitions between low-lying states, B(E2) and B(M1) transition rates following Coulomb excitation 2—63802
^{63}Cu, L=1 and ground state transitions, (α,p) reactions on Ni isotopes obs. 2—59783
^{64}Cu, γ-transitions of levels excited in ^{64}Ni(p,nγ) reactions near isobaric analogue resonances 2—67160
^{65}Cu, L=1 and ground state transitions, (α,p) reactions on Ni isotopes obs. 2—59783
^{67}Cu, L=1 and ground state transitions, (α,p) reactions on Ni isotopes obs. 2—59783
^{160}Dy, 2^+-2^+ transition of 879 KeV, e-γ directional correlation 2—42527
^{160}Dy, mean lifetimes of high energy levels 2—46165
^{161}Dy, Mossbauer effect of 43.8 keV transition 2—63819
^{162}Dy, elec. quadrupole and hexadecapole transition matrix elements 2—79752
^{164}Dy, elec. quadrupole and hexadecapole transition matrix elements 2—79752
^{161}Er, ^{163}Er, hyperfine interaction consts. and nuclear moments meas. using atomic beam magnetic resonance method 2—79741
^{166}Er, elec. quadrupole and hexadecapole transition matrix elements 2—79752
^{168}Er, elec. quadrupole and hexadecapole transition matrix elements 2—79752
^{169}Er formation and decay of isobaric analogues used to study structure of ^{168}Er 2—46169
^{170}Er, elec. quadrupole and hexadecapole transition matrix elements 2—79752
^{153}Eu, E1 transition from ground state to 97.43 keV level 2—76884
^{153}Eu, muonic and Mossbauer isomer shifts of gamma transitions 2—59714
^{18}F, E2 transition strengths of analogue states 2—74000
^{18}F, γ-ray transition to first excited state 2—63777
^{19}F, e.m. transitions of isobaric analogue states 2—46111
^{19}F, excited state lifetimes 2—52739
^{19}F, transition strengths and decay properties, study by (γ,γ') reaction 2—52744
^{19}F lifetime meas. by recoil distance method 2—46120
^{20}F, γ-ray multipole mixing ratios from DWBA analysis of ^{19}F(d,pγ) 2—79801
^{20}F, γ-ray transitions of 1824, 1843 and 3176 keV levels 2—74004
Fe, A=54, 56, 58, electroexcitation of E2- and E3-transitions 2—70393
^{53}Fe, transferred l-values and spectroscopic factors, ^{54}Fe(p,d) determ. 2—42563
^{54}Fe, E2 transition rates 2—70394
^{54}Fe, intensities of E1-type γ-transitions from neutron capture states to lower p-levels 2—49809
^{54}Fe, M1 and E1 transition strengths, multipole mixing ratios 2—76836
^{55}Fe, hole state lifetimes 2—55962
^{56}Fe, E2 transition rates 2—70394
^{57}Fe, 122-14KeV cascade, ang. correl. obs. 2—70395
^{57}Fe(d,p)^{58}Fe, 7.0 MeV, meas. of angular distrib., comparison with DWBA calcs., ^{58}Fe level structure deduced 2—42512
^{58}Fe levels deduced from ^{57}Fe(d,p) reactions at 7.0 MeV determ. of spectroscopic strengths 2—42512
^{65}Ga, γ-ray spectrum, level scheme 2—49764
^{69}Ga, Alaga model 2—46141
^{71}Ga shell model study of energy levels, transition probabilities, moments of ground state 2—46142
Gd isotopes, l=o, l=2 transitions identified 2—46163
^{151}Gd, meas. of angular γ-γ correlations and multipolarities of transitions 2—46160
^{154}Gd, 123 keV transition, internal conversion coeffs. and particle parameter meas. 2—46161
^{154}Gd, angular correlation measurements 2—82919
^{154}Gd lifetimes meas. by Doppler-shift recoil-distance method 2—70405
^{155}Gd, half-life obs. using two dimensional analyzer and computer, γ-γ coincidence method 2—59715
^{156}Gd, conversion electron intensities and γ-ray intensities obtained 2—46162
^{156}Gd, from ^{156}Eu decay, level scheme 2—49751
^{156}Gd, meas. of energies and intensities of γ-rays depopulating low spin levels of β- and γ-irradiated bands 2—52766
^{156}Gd lifetimes meas. by Doppler-shift recoil-distance method 2—70405
^{158}Gd, elec. quadrupole and hexadecapole transition matrix elements 2—79752
^{158}Gd, from ^{158}Eu decay, level scheme 2—49751
^{158}Gd, meas. of energies and intensities of γ-rays depopulating low spin levels of γ-vibrational band 2—52766
^{160}Gd, elec. quadrupole and hexadecapole transition matrix elements 2—79752
^{64}Ge, half-life meas. 2—55963
^{72}Ge, meas. of B(E2; $O_2{}^+ \rightarrow 2_1{}^+$) by Coulomb excitation with ^{16}O 2—46144
^{73}Ge, γ-ray decay modes and reduced upward transition probabilities following Coulomb excitation, test of quasiparticle-phonon coupling theories 2—74030
^{4}He, photon spectra from radiative absorption of pions 2—46296
^{173}Hf, Δk=1 retarded E1 transition 2—49753
^{177}Hf, 113 keV transition, relative internal conversion electron intensities 2—63825
^{177}Hf, internal conversion coefficients for E1 transitions with energies 71.6, 208.3, 321.3 keV 2—49754
^{178}Hf, quantum no. influence on partial γ transitions from ^{177}Hf(n,γ) reaction 2—67303
^{178}Hf 93.2 keV transition, Mossbauer isomer shift, shrinking of nucl. charge radius in rot. state 2—76804
^{178}Hf γ-ray intensities and branchings follwing ^{178}Ta decay 2—76803
^{180}Hf, investigation of parity non-conserving force between nucleons by meas. of circular polarization of γ-transitions 2—63840
^{180}Hf 57 keV gamma transition, parity-violating and normal multipole mixing ratios 2—46172

Nucleus continued
energy level transitions continued
Hg, transitions of levels populated in deuteron induced reactions on even-even isotopes of Hg 2—46329
^{198}Hg, K-shell internal conversion coeffs. meas. with X-ray scintillation spectrometer 2—79737
^{158}Ho, ^{161}Ho, conversion- electron transitions 2—70421
^{163}Ho, rotational bands and fast E1 transitions determ. by meas. of single γ-ray and conversion electron spectra 2—63820
^{165}Ho, between Zeeman levels in ground state, rel. to magnetic dipole moment meas. 2—46167
^{165}Ho, transition probabilities, calc. 2—70408
^{165}Ho (n,nγ), new gamma-ray transitions 2—46159
^{116}In γ-rays from neutron capture resonances in ^{116}In, determ. E1 and M1 strengths 2—67290
^{191}Ir, multipolarities of de-exciting transitions 2—76806
^{193}Ir, 66 transitions, energies and intensities from ^{193}Os decay 2—46173
^{38}K, two-hole strengths determ. using ^{39}K(^{3}He,α) reaction at 21.09 MeV 2—42507
^{39}K, lifetimes of 2815 and 3598 keV levels 2—76792
^{39}K, transition strengths and decay properties, study by (γ,γ') reaction 2—52744
^{40}K, γ-transitions, spin values and mixing ratios 2—67274
^{40}K 4.36 MeV transition, ^{39}K(n,γ) reaction, circular polarization 2—67273
^{40}K mag. multipole props., effects of weak particle-hole admixtures 2—76791
^{41}K, circular polarization calc. for $7/2^- \rightarrow 3/2^+$ transition using ΔT=1 parity violating potential 2—82852
^{41}K, γ-decay nonconservation of P-parity studied by meas. of γ-transition circular polarization 2—49739
^{42}K, mixing ratios and population parameters determ. by γ-γ correlations in ^{41}K(d,p) reaction at 6 MeV 2—46131
^{79}Kr, γ-ray transition energies and intensities, ang. distrib., γ-γ coincidences 2—79758
^{79}Kr, γ-ray transitions, relative intensities and mixing parameters 2—79759
^{81}Kr, γ-ray transition energies and intensities, ang. distrib., γ-γ coincidences 2—79758
^{81}Kr, γ-ray transitions, relative intensities and mixing parameters 2—79759
^{83}Kr, γ-ray transition energies and intensities, ang. distrib., γ-γ coincidences 2—79758
^{83}Kr, γ-ray transitions, relative intensities and mixing parameters 2—79759
^{85}Kr, γ-ray transition energies and intensities, ang. distrib., γ-γ coincidences 2—79758
^{85}Kr, γ-ray transitions, relative intensities and mixing parameters 2—79759
^{92}Kr, gamma ray study following beta decay 2—49767
^{83m}Kr, conversion coeff. for 9.4 keV transition 2—82888
^{135}La, angular correlations for 567-206, 664-206, 605-265 and 571-300 keV cascades 2—46156
^{139}La, det. of total coeff. of internal γ-radiation conversion 2—59711
^{6}Li, parity and isobaric spin violating decay of 3.56 MeV level 2—82883
^{7}Li, E2 transition 2—76882
^{7}Li, γ-rays from first excited state populated by ^{7}Be radiative electron capture transition 2—46184
^{169}Lu, ^{171}Lu, rotational bands and lifetimes of isomeric states, ^{169}Tm(α, 4nγ) and ^{169}Tm(α, 2nγ) study 2—70409
^{171}Lu, ^{173}Lu, obs. of isomeric E1 transitions with ΔK=0 and lifetime meas. 2—63823
^{177}Lu, deexcitation of $^{1}.{}_{2}{}^{-}$ [541] and $^{1}.{}_{2}{}^{+}$ [411] bands, reaction (n, γ) study 2—79749
^{177}Lu, level scheme fitting, ^{176}Lu(n, γ) reaction obs. 2—59769
^{177}Lu, nsec. isomeric transitions, (n,γ) reaction obs. 2—67176
^{22}Mg, mean life of 1247 keV state determ. using Doppler shift attenuation method in ^{20}Ne(^{3}He,nγ) reaction 2—63784
^{24}Mg, photon spectra from radiative absorption of pions 2—46296
^{24}Mg, resonance states, γ-ray decay props. 2—70384
^{25}Mg, population of $3/2^+$, 975 keV level in ^{2}H(^{24}Mg, pγ) reaction, meas. of mean lifetime for γ-ray decay 2—79736
^{54}Mn, in ^{54}Fe(n,pγ)^{54}Mn reaction 2—46133
Mo, elec. dipole transitions following p-wave neutron capture 2—67286
^{92}Mo, E2 transition rates, shell model calc. 2—67162
^{93}Mo γ-decay from ^{92}Mo(d,pγ) and ^{93}Tc β-decay 2—63805
^{94}Mo, $2^+ \rightarrow 0^+$ γ-rays, following inelastic p scatt. 2—74078
^{94}Mo, low-lying states investigation via multiple Coulomb excitation 2—82910
^{98}Mo, lifetime of 0^+, 0.736 MeV state, inbeam internal conversion electron studies 2—70417
^{14}N, γ-decay of 8.06 and 5.69 MeV levels, isospin mixing 2—76780
^{14}N, life-times of lowest excited states populated in neutron-induced reactions, γ-ray angular distrib. meas. 2—79507
^{15}N, γ-ray decay, lifetime determ. by Doppler shift attenuation method using ^{12}C(^{3}He,p) reaction 2—70375
^{21}Na, meas. of γ-ray branching ratios and lifetimes in ^{20}Ne(p,γ) reaction 2—79761
^{22}Na, e.m. transition probabilities, mean lives 2—63785
^{22}Na lifetime meas. by recoil distance method 2—46120
^{23}Na, γ-decay of levels populated in β-decay of ^{23}Ne 2—79773
^{23}Na, transition strengths and decay properties, study by (γ,γ') reaction 2—52744
^{90}Nb, γ-decay scheme studied using ^{90}Zr(p,nγ) reaction 2—42515
^{91}Nb, E2 transition rates, shell model calc. 2—67162
^{93}Nb decays, (n,n'γ) reaction obs. 2—67164
^{134}Nd E1 and M2 transitions from isomeric state excited in ^{118}Sn(^{20}Ne, 4n) reaction 2—79745
^{142}Nd, isospin splitting of giant E1 excitation in ^{141}Pr(p,γ) reaction 2—82891
^{143}Nd, intensities of E1-type γ-transitions from neutron capture states to lower p-levels 2—49809
^{143}Nd level scheme investigation in unified model calc. and particle core model 2—67170
^{144}Nd, 5 new transitions obs. 2—67196
^{144}Nd, lifetime of 1314 keV level 2—63815

Nucleus continued
energy level transitions continued
^{145}Nd, decay characteristics of low-lying excited states populated by thermal neutron capture 2−67172
^{237}Nd, lifetime of 60 keV level, application to calibration of nuclear timing systems 2−79750
^{18}Ne, lifetimes of 3376, 357 keV states 2−76784
^{20}Ne, static and dynamic quadrupole moments of first excited state determ. by projectile Coulomb excitation technique 2−42537
^{20}Ne, transition to 2^- rot. band in ^{22}Ne(p,t)^{20}Ne reaction 2−79786
^{21}Ne, meas. of γ-ray branching ratios using ^{20}Ne(d,pγ) reaction 2−79762
^{21}Ne excited states obs. using ^{18}O(α,nγ) reaction 2−59696
^{22}Ne, e.m. transition probabilities, mean lives 2−63785
^{22}Ne, static and dynamic quadrupole moments of first excited state determ. by projectile Coulomb excitation technique 2−42537
^{22}Ne lifetime meas. by recoil distance method 2−46120
Ni, γ transitions from 4 to 90 keV neutron capture 2−67279
^{56}Ni, E2 transition rates 2−70394
^{56}Ni, gamma-ray transitions induced by ^{54}Fe(^{3}He,n)^{56}Ni reaction 2−59701
^{58}Ni, E2 transition rates 2−70394
^{60}Ni, γ transitions of levels populated in β^+ decay of ^{60}Cu(II) 2−63846
^{61}Ni, excited by (d,d′) scatt., competition between gamma emission and neutron decay de-excitation process 2−70466
^{62}Ni, electroexcitation of E2- and E3-transitions 2−70393
^{63}Ni spectroscopic factors deduced from ^{62}Ni(d,p) reaction near Coulomb barrier, DWBA analysis 2−79794
^{16}O, photon spectra from radiative absorption of pions 2−46296
^{19}O, study of energy spectrum and e.m. properties in framework of unified asymmetrical rotational models 2−52737
^{190}Os, depopulations of 1115 keV level and their reduced transition probabilities 2−67179
^{30}P, e.m. transition probabilities, mean lives 2−63785
^{30}P, lifetimes of excited states, in reaction ^{29}S(p,γ) 2−49734
^{30}P lifetime meas. by recoil distance method 2−46120
^{31}P, e.m. transitions of isobaric analogue states 2−46111
^{31}P, influence of γ-cascade on population of low-lying levels in ^{32}S(γ,p) reactions 2−42505
^{31}P, transition strengths and decay properties, study by (γ,γ') reaction 2−52744
^{31}P(p,p′), excited states at 185 MeV 2−46125
^{32}P, decay modes of first 15 excited states and lifetimes of levels below 3.5 MeV excited in ^{29}Si(α,p) reaction 2−49735
^{32}P, γ-decay scheme of first T=2 level 2−63788
^{198}Pb half-life of 1822 keV level 2−46174
^{200}Pb, half-lives of 1908 and 2153 keV levels 2−46174
^{204}Pb, $4^+ \rightarrow 0^+$ cross-over transition 2−67180
^{204}Pb, e.m. matrix elements of low-lying states 2−76782
^{206}Pb, e.m. matrix elements of low-lying states 2−76782
^{206}Pb, lifetime of $O_2{}^+$ state 2−74041
^{206}Pb levels populated in decay of ^{206}Bi, determ. of γ-multipolarities 2−70413
^{207}Pb, E1 radiative widths of isobaric analog states 2−76809
^{207}Pb, e.m. matrix elements of low-lying states 2−76782
^{208}Pb, e.m. matrix elements of low-lying states 2−76782
^{208}Pb, odd- and even-parity levels, transition rates and mean lifetimes, renormalized RPA calc. 2−82917
^{208}Pb, spreading widths of 1^- particle-hole state 2−76810
^{208}Pb region, mag. dipole transitions 2−82901
^{208}Pb transition probability and transition charge density, investigation using inelastic electron scattering 2−63833
^{208}Pb(γ,N)^{207}Pb existence of giant M1 resonance in ^{208}Pb 2−82949
^{209}Pb, e.m. matrix elements of low-lying states 2−76782
^{209}Pb, γ-ray transitions to neutron single-particle states 2−67275
^{210}Pb, transitions from levels populated in ^{208}Pb(t,p), structure determ. 2−82892
^{105}Pd, gamma ray spectrum in ^{104}Ru(α,3n) reaction, determ. of multipolarities 2−49744
^{147}Pm, 319 to 91 keV gamma cascade rel. to meas. of g-factor of 91 keV state 2−59712
^{210}Po, investigations using ^{210}At→^{210}Po electron capture decay 2−63836
^{139}Pr γ-γ angular correlations for 114-708 and 114-738 keV cascades, lifetime of 822 keV level 2−46158
^{141}Pr, K-shell internal conversion coeffs. meas. with X-ray scintillation spectrometer 2−79737
^{141}Pr (n,nγ), new gamma-ray transitions 2−46159
Pt, A=188, 190, 192, mixing ratios of transitions, γ-ray anisotropies, observation 2−70410
Pt, even mass nuclei $182 \leqslant A \leqslant 192$, low- lying level properties from Hg isotope decay data 2−49755
^{a}Pt, A=194, 195, 196, lifetimes of Coulomb-excited states meas. using plunger recoil distance technique 2−63756
^{194}Pt, e.m. props., excited states lifetimes, quadrupole transition probabilities 2−76807
^{194}Pt γ-ray spectra following ^{194}Ir decay 2−59732
^{195}Pt Mossbauer effect obs. 2−59719
^{196}Pt, e.m. props., excited states lifetimes, quadrupole transition probabilities 2−76807
^{239}Pu, asymmetry of E1 and M1γtransitions, multipole mixing ratios 2−46207
^{239}Pu, Mossbauer effect 2−74043
^{239}Pu obs. M1 multipolarity of 124.42 keV transition 2−46179
^{240}Pu, average widths of E1 and M1 radiative transitions from neutron capture states 2−67187
^{240}Pu, E2 nature of γ-ray transitions between levels populated in electron capture decay of ^{240}Am 2−79770
^{240}Pu, obs. of γ transitions of levels populated by thermal neutron capture in ^{239}Pu 2−67186
^{242}Pu, relative reduced transition probabilities B(E2), B(E3) 2−46178
^{85}Rb, lifetime of 517 keV level, application to calibration of nuclear timing systems 2−79750
^{92}Rb, gamma ray study following beta decay 2−49767
^{181}Re, ^{183}Re, rotational bands and lifetimes of isomeric states, ^{181}Ta(α, 4nγ) and ^{181}Ta(α, 2nγ) study 2−70409
^{185}Re, multipole mixing ratios of γ-transitions from levels populated in ^{185}Os electron capture decay 2−67178

Nucleus continued
energy level transitions continued
^{187}Re 72-134 keV cascade, ang. correl. coeff. 2−82885
^{94}Ru, E2 transition rates, shell model calc. 2−67162
^{99}Ru, cascade transitions, half-life of 89.4 keV level 2−79740
^{30}S, γ-decay and lifetime of low-lying states populated in ^{28}Si(^{3}He, n) reaction 2−74012
^{31}S, influence of γ-cascade on population of low-lying levels in ^{32}S(γ,n) reaction 2−42505
^{32}S(p,p′), excited states at 185 MeV 2−46125
^{34}S, lifetime of 5.69 MeV 5^- level 2−49736
^{35}S, γ-transition scheme determ. from thermal neutron reaction ^{34}S(n,γ) 2−49807
^{132}Sb, γ-transitions of levels populated in β-decay of ^{132}Sn, determ. of B(M1) values 2−82923
^{42}Sc, transition rates between $(1f_{7/2})^2$ states 2−74017
^{42}Sc particle-particle nucleus, transformation properties of effective transition operator 2−82861
^{45}Sc, levels between 1.05 and 3 MeV, ^{44}Ca(p,γ)^{45}Sc reaction 2−42509
^{46}Sc level scheme, multipole mixing ratios 2−67156
^{47}Sc, mean lives of low-lying levels determ. by Doppler-shift attenuation method with p-γ coincidences in ^{44}Ca(α,pγ) 2−74021
^{49}Sc M1 transition, analogue to antianalogue in $1f_{7/2}$ shell 2−82846
^{75}Se, internal conversion coeffs. of low level transitions, using ^{75}As(p,n) 2−52752
^{78}Se, low lying levels, from ^{77}Se(n,γ) using thermal n 2−52779
^{28}Si, γ-ray decay of 15.22 MeV, T=2 state 2−59697
^{28}Si, psec. lifetime of 9.699 MeV(5^-) level, delayed coincidence meas. 2−55959
^{28}Si 612 keV reson. in ^{27}Al(p,γ) reaction 2−76844
^{29}Si, DWBA analysis of data from ^{28}Si(d,p)^{29}Si reaction at 10 MeV 2−56000
^{30}Si, resonances obs. in α reactions on ^{26}Mg, spins, parties and widths 2−46123
^{31}Si, γ-transition scheme determ. from thermal neutron reaction ^{30}Si(n,γ) 2−49807
^{144}Sm, level scheme, study by (γ, γ') reaction 2−63816
^{150}Sm, time-differential meas. of deorientation for recoils in vacuum 2−76802
^{152}Sm, lifetimes of 121.78 and 366.5 keV levels 2−76783
^{152}Sm, static hyperfine interactions at free atoms 2−70560
^{152}Sm lifetimes meas. by Doppler-shift recoil-distance method 2−70405
^{153}Sm, effective g_r factor determ. by internal conversion processes 2−52765
Sn, elec. dipole transitions following p-wave neutron capture 2−67286
Sn(A=117, 119), B(E2) and B(M1) transition probabilities and mean lives for Coulomb excited states 2−63810
^{107}Sn isotope identification in ^{106}Cd(α.3n) reaction 2−82886
^{117}Sn, lifetime of 158.6 keV level 2−76765
^{124}Sn, E2-E1 transitions, ^{124}In decay obs. 2−42520
^{132}Sn doubly closed shell region, γ-decay of states populated in β-decay of ^{134}Sb to two proton and p-n states 2−82895
^{117m}Sn, halflife, 158.6 keV level, M4-transition 2−63811
^{85}Sr, excitation energies and mean lives of low-lying levels populated by ^{86}Sr(^{3}He, $\alpha\gamma$) 2−42514
^{88}Sr, lifetime of 2.734 MeV level determ. from average cross section for resonance scattering of γ-rays 2−49742
^{92}Sr, gamma ray study following beta decay 2−49767
^{92}Sr, gamma ray study following beta decay 2−49767
Ta, life-time of excited states produced in ion irradiation of ^{181}Ta 2−76805
^{175}Ta, ^{177}Ta, rotational bands and lifetimes of isomeric states, ^{175}Lu(α, 4nγ) and ^{175}(α, 2nγ) study 2−70409
^{177}Ta, partial transition probabilities 2−42530
^{181}Ta, investigation of parity non-conserving force between nucleons by meas. of circular polarization of γ-transitions 2−63840
^{203}Ta, investigation of parity non-conserving force between nucleons by meas. of circular polarization of γ-transitions 2−63840
^{153}Tb, ^{155}Tb, conversion-electron transitions 2−70421
^{159}Tb, investigation of parity non-conserving force between nucleons by meas. of circular polarization of γ-transitions 2−63840
^{93}Tc, E2 transition rates, shell model calc. 2−67162
^{97}Tc, excited state transitions, γ-ray ob 2−67165
^{124}Te, multipole mixing ratios 2−42519
^{125}Te, γ-γ ang. correlation of 171 to 427 keV cascade 2−52758
^{125}Te, lifetime of 321 keV(9/2-) state 2−59709
^{227}Th, L X-ray spectra, γ-transition multipolarity, coincidence obs. 2−74042
^{232}Th, decay γ-rays, inelastic neutron scatt. obs. 2−67183
^{232}Th, level structures and decay schemes 2−59724
^{232}Th, relative reduced transition probabilities B(E2), B(E3) 2−46178
^{45}Ti, mean lifetimes of levels meas. 2−46132
^{46}Ti, lifetimes of 9 states by Dopper shift attenuation method 2−76794
^{47}Ti, E2/M1 mixing ratios of γ-decays and population ratios determ. from pγ correlation meas. in ^{46}Ti(d, p) 2−63919
^{51}Ti, intensities of E1-type γ-transitions from neutron capture states to lower p-levels 2−49809
^{203}Tl, E2/M1 mixing ratios, muonic X-rays, nucl. and μ-capture γ-rays analysis 2−59961
^{203}Tl, K-shell internal conversion coeffs. meas. with X-ray scintillation spectrometer 2−79737
^{205}Tl, E2/M1 mixing ratios, muonic X-rays, nucl. and μ-capture γ-rays analysis 2−59961
^{169}Tm, penetration effects in internal conversion of transitions 2−63822
^{171}Tm, penetration effects in internal conversion of transitions 2−63822
^{235}U, level scheme and distribution of single-particle strength in excited states 2−49758
^{238}U, decay γ-rays, inelastic neutron scatt. obs. 2−67183
^{238}U, level structures and decay schemes 2−59724
^{238}U, relative reduced transition probabilities B(E2), B(E3) 2−46178
^{235m}U decay rate perturbation by implantation in transition metals 2−79755

Nucleus continued
energy level transitions continued
^{50}V neutron-proton pair transfer with zero angular momentum 2−63796
W, life-time of excited states produced in ion irradiation of ^{186}W 2−76805
^{182}W, e.m. properties of $K^{\pi}=2$- octupole band populated in β- decay of ^{182}Ta 2−42533
^{187}W, nsec. isomeric transitions, (n,γ) reaction obs. 2−67176
^{137}Xe level scheme investigation in unified model calc. and particle core model 2−67170
^{138}Xe fission product, β- and γ-decay study using ARIEL on-line isotope separator, meas. of internal conversion and Auger L spectra 2−82924
^{90}Y, internal bremsstrahlung spectrum, contrib. of detour transitions 2−42542
^{162}Yb, γ-ray spectra 2−67197
^{164}Yb lifetime of rotational levels meas. by Doppler shift method on recoil nuclei in ^{128}Te(^{40}Ar, 4n) 2−79764
^{170}Yb, γ-ray transitions, from β-decay of ^{170}Lu 2−76821
^{171}Yb, E2/M1 amplitude mixing ratios of levels populated in ^{170}Er(α, 3n) reaction 2−74040
^{67}Zn, lifetime of 184 keV level 2−76765
^{90}Zn, lifetime of excited 0^{+} state, configuration mixing 2−74033
Zr, elec. dipole transitions following p-wave neutron capture 2−67286
^{89}Zr transition rates, ^{89}Y(p,nγ)^{89}Zr reaction 2−46149
^{90}Zr, E2 transition rates, shell model calc. 2−67162
^{91}Zr, spectroscopic factors, summed strengths determ. by ^{90}Zr(d,p) reaction 2−42588
^{92}Zr level structure determ. using (n_{th},γ) reaction 2−67163
^{96}Zr, first excited state lifetime, meas. using ^{96}Zr(p,p′e) reaction 2−59704
energy levels
see also Nuclear structure; Radioactivity/decay schemes
— 2−59725
— 2−67148
A=14, 15, wave functions of non-normal parity states 2−42498
A=18, 19, 20, compilation of data 2−59686
A=19, $J^{\pi}=7/2^{+}$ and $11/2^{+}$, T=1/2 states 2−49729
A=48-75, temperature and level density parameter determ. following inelastic scattering of 14 MeV neutrons 2−70450
A=57-81, nonschematic random-phase- approximation description of gamma vibrations 2−42511
A=8-28 4n nuclei, HF calcs. of multipole deformations using projection before variation procedure 2−70364
actinide even-even nuclei, excitation of collective states by radiationless muonic transitions 2−67171
actinides, pairing vibrational states 2−42540
analogue state excitation by double charge exchange of pions, nuclear medium corrections 2−74103
and deformed nuclei, $179 \leqslant A \leqslant 185$, irrotational states 2−52769
anharmonic collective oscillations, theory 2−55951
bound and virtual levels determ. using summation rules for various potentials 2−70355
complex nuclei, parametric representation of single-frequency states 2−52728
compound nuclei with A=130-200, level density 2−59694
compound nucleus, phase difference of interfering states 2−52730
Coriolis anti-pairing transition of ground state rotational band, simplified microscopic model 2−73986
Davydov model analyzed 2−46083
deformation effects on elastic quadrupole transitions and quadrupole moments of first excited 2^{+} states, rigid symmetric rotator model 2−79726
deformation of doubly odd nuclei, force range and mixture effects 2−70381
deformed even-even, influence of spin and quadrupole interactions on properties of state with $K^{\pi}=1^{+}$ 2−67136
deformed nuclei with odd protons, $153 \leqslant A \leqslant 177$, irrotational excited states 2−55965
deformed shell structure 2−73979
densities, methods of determ. 2−46099
density of particle-hole excited states in shell model 2−67128
even nuclei, correlation between properties of low-lying collective levels and fission process observables 2−42596
even nuclei, one-parameter model with EXP for energy ratios of YRAST levels to high spin 2−73984
even-even deformed nuclei, rotational motion at large angular momentum 2−73987
even-even nuclei, ground state bands in shape fluctuation model 2−70359
even-even nuclei of p-f shell, quadrupole moments of first excited states, BE2 values, variation of shape and deformation 2−79716
excited level density calc. using supercond. theory 2−59681
excited nuclei, Mossbauer experiments on lifetime studies 2−46106
excited state lifetime determ. using cyclotron ion beam 2−70311
fission products, mass-separated, structure studies using delayed neutron spectrometry 2−67150
fractional parentage coefficients with isotopic spin, degenerate states separation 2−76771
Gamow states of square-well plus square-barrier model, expectation value of r^{2} 2−73978
ground and excited states, bounds on energy and wave functions 2−63751
ground state energy, many fermion, correction to 2-hole line approximation eqns. 2−63752
ground state radii, elastic and inelastic electron scattering meas. 2−82957
Hf odd isotopes, Coriolis coupling of N=6 states 2−79760
high spin levels, degree of orientation, theory 2−42496
hypernuclei excited states 2−67139
level density distribution theory 2−46098
level density theories, a survey 2−46097
light nuclei, study of scattering states, occurrence of narrow resonances at thresholds 2−73993
low-lying levels of light nuclei, alpha-particle model studies 2−67126

Nucleus continued
energy levels continued
magic, transitional and strongly deformed nuclei, proton scattering, systematics and fine structure of Coulomb displacement energies 2−46148
Meissner effect in spherical nuclei and K-isomers of deformed nuclei 2−46101
metastable isomeric nuclear levels, energy meas. by laser spectroscopy of mol. vibr. transitions 2−79713
multinucleon wave function expression approach 2−59676
multishell Hartree-Fock calculations, practical angular momentum projection method, applic. to ^{22}Na 2−46119
neutron level spacing distributions, statistical description 2−46075
neutron resonance level distrib., non-statistical behaviour 2−67263
neutron resonance spectroscopy as a test of statistical theories 2−46074
neutron resonances, groupings of level spacing 2−67266
neutron states, single, available data compared with Woods-Saxon potential 2−67132
odd-a deformed nuclei, $153 \leqslant a \leqslant 177$, excited states, equilibrium deformation effect on energy and structure 2−63817
odd-A nuclei, alpha intensities to rotational bands 2−49760
odd-even nuclei, variable moment of inertia description of bands 2−73985
odd-mass rare-earth, nonadiabatic treatment of rotation bands 2−49717
odd-odd and even-even spherical nuclei splitting of multiplet of $[j_{1}^{\pm 1}; j_{2}^{\pm 1}]$ configuration 2−55952
odd-proton N=82 nuclei, $J^{\pi}=11^{-}/2(1)$ isomeric state 2−79756
pairing vibrations, modified Tamm- Dancoff approximation 2−46100
particle-hole states density in Fermi gas model, spin depend. 2−59674
rare earth nuclei, prediction of singularities in ground state bands using Meissner effect 2−46117
rare-earth even-even nuclei, excitation of collective states by radiationless muonic transitions 2−67171
reduced width calculational method 2−70366
rotating nuclei, band structure at high angular momenta 2−59679
rotational states, phenomenological description 2−73990
rotational states, stability condition determ. using procedure of Hartree-Fock-Bogoliubov method 2−63755
shape deformed nuclei, importance of quadrupole pairing field in $J^{\pi}=0^{+}$ vibrations 2−59678
shell corrections, parameterization of numerical state density calc. 2−46090
shell model level densities, applics. to neutron cross section calcs. 2−67129
(s,d)-shell nuclei, α-type, Hartree-Fock calc. of ground state energy 2−49710
single-particle energy calcs. using momentum-depend. pot. 2−59673
spacing distribution, widths calc. 2−46094
spacings, correlation functions and statistics 2−46073
spectra, features not covered by present models, survey 2−79725
spectroscopic factors determ. by dispersion relations 2−67127
structure of compound states and resonance scattering theory 2−52793
superheavy nuclei, single particle level densities 2−67189
symmetries and distrib., general simplicities in complicated systems 2−82865
three resonantly interacting particle system, level spectrum 2−82230
total internal conversion coefficients meas. using Ge(Li) detector 2−73982
U(3(A-1)) scheme model, calc. of nuclear deformation 2−67125
vibrational, excitation by electrons in α-particle model 2−67134
widths of levels, mean, statistical model calc. between A=16 and A=116 2−46093
^{a}Co A=56, 58, high resolution spectroscopy using direct two nucleon transfer reactions 2−63800
Ag (A=107, 109), solution of I=j-1 anomaly in Alaga model 2−46153
^{25}Al excited state spins, ^{24}Mg(p,$p_{1}'\gamma$)^{24}Mg obs. 2−74009
^{26}Al level struct. from ^{24}Mg(^{3}He,p) reaction 2−76876
^{27}Al, channel dependent widths and correlated intermediate structure, reaction ^{27}A(n, n′γ) study 2−67244
^{27}Al, shell-model wave function of ground state tested in ^{27}Al(^{3}He,p)^{29}Si reaction 2−70478
^{28}Al, γ-γ ang.-correl. on low-lying levels, PAC determ. of 2^{+} state moment 2−76790
Ar(A=36, 38), effective interactions in upper s-d shell 2−49737
^{36}Ar, $J^{\pi}=6$- bound state, ^{35}Cl(p,γ) reaction study 2−59699
^{36}Ar 6^{-} level obs. in ^{35}Cl(p,γ) reaction at 0.8-2.3 MeV following γ decay of 2231 keV resonance 2−52747
^{37}Ar, low-lying level props., excitation energies 2−55960
^{40}Ar, excited states observed in ^{40}Ar(γ,n_{0})^{39}Ar reaction 2−46129
^{74}As, from ^{75}As(p,d)^{74}As reaction 2−52753
^{75}As, low-lying levels interpret. rel. to core excitation model 2−42513
^{75}As, low-lying negative parity states, core-excitation calculations 2−70396
^{75}As, neutron reson. level spacings, stat. distribs., deviations 2−67161
^{210}At, evidence for 15^{-} and 11^{+} isomeric states populated in ^{209}Bi(α, 3n) reaction 2−70415
^{211}At, configurational mixing and effective charge 2−52771
^{211}At, electron capture decay of ^{211}Rn 2−49775
^{211}At, low-lying states, shell-model calcs., effects of ^{208}Pb core vibrs. 2−67182
^{9}B, determ. of width of excited state from neutron spectrum in ^{9}Be(p,n) 2−52735
^{9}B ground states in ^{12}C(p,p′3α) reaction mechanism 2−59757
^{10}B, excited states near 10 MeV, ^{9}Be(p,p)^{9}Be reaction obs. 2−70378
^{10}B, isospin impurity of 6.8 MeV state 2−63770
^{10}B levels determ. in ^{9}Be(d,n) reaction at 650 keV 2−49830
^{10}B states populated in ^{9}Be(d,n) reaction at 650 keV 2−63913
^{131}Ba, unified model calcs. 2−42517
^{134}Ba levels populated in decay of ^{134}Cs 2−52781
^{135}Ba, low-lying energy levels evaluated on basis of centre of gravity theorem 2−59710
^{137}Ba, unified model calcs. 2−42517

Nucleus continued
- **energy levels** continued
  - ^{138}Ba, determ. by inelastic proton scattering at 30 MeV 2−74079
  - ^{138}Ba, differential cross sections for elastic and inelastic scattering of α particles to low-lying states 2−46305
  - ^{138}Ba, neutron-single hole states, proton-neutron interaction effects 2−46157
  - ^{139}Ba level scheme investigation in unified model calc. and particle core model 2−67170
  - ^{6}Be, determ. of width of excited state from neutron spectrum in ^{6}Li(p,n) 2−52735
  - ^{8}Be, rotational spectrum, calc. using α-particle cluster model 2−82880
  - ^{8}Be even-spin positive-parity levels in 15.35 MeV excitation region obs. in α-α elastic scattering 2−82878
  - ^{8}Be ground states in ^{12}C(p,p$'$3α) reaction mechanism 2−59757
  - ^{8}Be rotational states, properties of projected HF functions of ground state bands 2−73992
  - ^{9}Be, 1/2^{+} reson., coupled-channel calc. 2−76859
  - ^{11}Be, investigations using ^{9}Be(t,p)^{11}Be reaction 2−59689
  - ^{209}Bi, final states in (^{16}O,^{15}N) and (^{12}C,^{11}B) reactions, j-assignments 2−79805
  - ^{209}Bi, multiplet energy levels calc. using single-particle and 3^{-} phonon coupling 2−42538
  - ^{209}Bi, particle-hole states studied in ^{210}Po(t,α) reaction at 20 MeV 2−82894
  - ^{209}Bi antianalogue states, calc. of compound spreading width of analogue resonance 2−42539
  - ^{80}Br, ^{82}Br, low-lying states populated in $^{79,\,81}$Br(d, p) reactions 2−74031
  - ^{12}C, α chain states study through decay widths 2−46110
  - ^{12}C, giant resons., ^{11}B(p,γ)^{12}C obs. 2−63772
  - ^{12}C, isospin-mixing matrix element 2−63771
  - ^{12}C, $J^{\pi}=0+$, T=2 reson. search in ^{9}Be(^{3}He, $\gamma\gamma$)^{12}C reaction 2−70476
  - ^{12}C quadrupole and octupole vibrations, form factors and transition densities of 4.34 and 9.64 MeV levels 2−82881
  - ^{12}C rotational states, properties of projected HF functions of ground state bands 2−73992
  - ^{13}C, positive parity bound states energies 2−76855
  - ^{13}C, study from reaction ^{11}B(d,n)^{12}C at 900 keV 2−42584
  - ^{13}C ground state and 3.09 MeV state spectroscopic factors determ. by weakly bound projectile model calcs. on ^{12}C(d,p) reaction 2−67325
  - Ca, even-even nuclei, 1^{+} states investigation using (^{3}He,p) reactions 1f-2p shell model predictions 2−46130
  - Ca even isotopes, level spectra using self-consistent approxs. 2−76793
  - ^{40}Ca, ground state in closed-shell configuration 2−63792
  - ^{40}Ca, levels excited in ^{42}Ca(p,t) reaction at 40 MeV 2−46264
  - ^{40}Ca, rot. bands excitation 2−83017
  - ^{40}Ca, search for multiparticle-multihole states in ^{32}S(^{12}C,α) reaction at 30 MeV 2−42508
  - ^{40}Ca level struct., proton inelastic scatt., 24.93-39.83 MeV, energy depend. 2−76838
  - ^{40}Ca(p,2p)^{39}K, 460 MeV, ^{40}Ca energy level structure 2−46263
  - ^{41}Ca, neutron single-particle states 2−67275
  - ^{42}Ca, (1f$_{7/2}$)^{2} multiplet, ^{41}Ca(d,p) obs. at E_d=12 MeV 2−67155
  - ^{42}Ca, low-lying level spacing, shell-model calculations 2−49727
  - ^{44}Ca, d$_{3/2}$ hole strength in ground state 2−82854
  - ^{48}Ca, proton inelastic scatt., ang. distribs. excited states obs. 2−76839
  - ^{131}Ca, level scheme 2−42521
  - ^{107}Cd, study of levels populated in β^{+}/EC decay of ^{107}In by obs. of γ-ray spectra 2−82934
  - ^{110}Cd, low-spin states studied in decay of ^{110}Ag 2−74035
  - ^{112}Cd, low-spin states studied in decay of ^{110}Ag 2−74035
  - ^{132}Ce, yrast states, energies and spins, collective bands 2−79757
  - ^{138}Ce, 0^{+} level struct. from ^{140}Ce(p, t) reaction 2−76847
  - ^{140}Ce, 0^{+} level struct. from ^{142}Ce(p, t) reaction 2−76847
  - ^{140}Ce, neutron-single hole states, proton-neutron interaction effects 2−46157
  - ^{141}Ce level scheme investigation in unified model calc. and particle core model 2−67170
  - Cl (A=36, 37), effective interactions in upper s-d shell 2−49737
  - ^{33}Cl levels excited in ^{32}S(p,p) scattering, 2.5-3.0 MeV 2−67153
  - ^{34}Cl, low-lying positive-parity states, (d,p) reaction and shell model obs. 2−59698
  - ^{34}Cl, low-lying structure studied in modified vibrational unified model 2−46124
  - ^{34}Cl, props. up to 3.6 MeV studied by ^{36}Ar(d, α)^{34}Cl 2−76877
  - ^{35}Cl, branching ratios, excitation energies of levels populated in ^{32}S(α,p) reaction 2−70386
  - ^{35}Cl, populated in ^{34}P(α,p)^{34}S reaction 2−46323
  - ^{36}Cl, low-lying positive-parity states, (d,p) reaction and shell model obs. 2−59698
  - ^{36}Cl, new levels populated in ^{37}Cl(^{3}He,α) neutron pick-up reaction, spectroscopic factors deduced 2−42586
  - ^{38}Cl, excitation energies for levels populated in ^{37}Cl(n,γ) reaction 2−49808
  - ^{55}Co, final states in (^{16}O,^{15}N) and (^{12}C,^{11}B) reactions, j-assignments 2−79805
  - ^{56}Co, levels populated in ^{54}Fe(^{16}O, ^{14}N) two-nucleon stripping reaction at 80 MeV 2−74121
  - ^{57}Co, obs. of resonance states in ^{56}Fe(p,γ) reaction, isobaric analogs of states in ^{57}Fe 2−63882
  - ^{57}Co, unified model description quadrupole vibrs. 2−63801
  - ^{57}Co levels populated in ^{56}Fe(^{3}He,d) and ^{56}Fe(^{3}He,dγ) reactions 2−46138
  - ^{58}Co, level density parameters, nucl. temp. 2−82981
  - ^{59}Co, level density determination from alpha and proton induced reactions 2−63798
  - ^{59}Co, unified model description quadrupole vibrs. 2−63801
  - ^{61}Co unified model description, quadrupole vibrs. 2−63801
  - ^{63}Co, unified model description, quadrupole vibrs. 2−63801
  - Cr, even-even nuclei, 1^{+} states investigation using (^{3}He,p) reactions 1f-2p shell model predictions 2−46130
  - ^{50}Cr, 3^{-} states evidence from inelastic scatt. of protons, deuterons, ^{3}He and ^{4}He 2−74022
  - ^{51}Cr, excited states studied via (p,n) and (p.nγ) reactions on ^{51}V 2−46265

Nucleus continued
- **energy levels** continued
  - ^{55}Cr levels populated by thermal neutron capture in ^{54}Cr 2−42510
  - ^{124}Cs, obs. in ^{115}In(^{12}C, 3n)^{124}Cs 2−74037
  - ^{138}Cs levels populated in decay of ^{138}Xe, shell-model interpretation 2−82924
  - Cu isotopes, low-lying struct. in unified model 2−63803
  - Cu(A=60, 62), level density determination from alpha and proton induced reactions 2−63798
  - Cu(A=63, 65), level density determination from alpha and proton induced reactions 2−63798
  - ^{58}Cu levels populated in ^{58}Ni(p, nγ), determ. of spins and energies of levels below 1.7 MeV 2−74026
  - ^{60}Cu, levels populated in ^{58}Ni(^{16}O, ^{14}N) two-nucleon stripping reaction at 80 MeV 2−74121
  - ^{61}Cu, levels excited in ^{58}Ni(α,p) 2−59783
  - ^{63}Cu, levels excited in ^{60}Ni(α,p) 2−59783
  - ^{64}Cu, structure of levels excited in ^{64}Ni(p,nγ) reactions near isobaric analogue resonances 2−67160
  - ^{65}Cu, elastic and inelastic widths of isobaric analogue states excited in ^{64}Ni(p,p$'$), spectroscopic factors deduced 2−63804
  - ^{65}Cu, final states in (^{16}O,^{15}N) and (^{12}C,^{11}B) reactions, j-assignments 2−79805
  - ^{65}Cu, levels excited in ^{62}Ni(α,p) 2−59783
  - ^{67}Cu, levels excited in ^{64}Ni(α,p) 2−59783
  - ^{155}Dy level scheme, ^{155}Ho decay obs. 2−59716
  - ^{164}Dy levels populated in decays of ^{164m,g}Ho 2−52785
  - ^{153}E level struct., Coulomb excitation obs. 2−76884
  - ^{164}Er levels populated in decays of ^{164m,g}Ho 2−52785
  - ^{165}Er, level det. from ^{165}Tm decay 2−63821
  - ^{166}Er, ^{168}Er level calc. rel. to gamma oscillations in collective model for axially symmetric nuclei 2−52767
  - ^{168}Er structure studied through formation and decay of isobaric analogues of ^{169}Er 2−46169
  - ^{151}Eu, neutron reson. spectroscopy, level population 2−63898
  - ^{151}Eu level struct., Coulomb excitation obs. 2−76884
  - ^{153}Eu, neutron reson. spectroscopy, level population 2−63898
  - F (A=18, 19, 20), effective interactions in s-d shell 2−49728
  - ^{17}F, missing state obs. using ^{15}N(^{3}He,n)^{17}F reaction 2−46114
  - ^{17}F levels excited in ^{16}O(d,n) reaction at 3-4 MeV 2−83014
  - ^{17}F levels excited in two-nucleon transfer reactions in ^{19}F 2−82972
  - ^{18}F, exptl. evidence for alpha-particle cluster states 2−82884
  - ^{18}F, odd-parity levels with three- particle one hole structure excited in ^{15}N(^{6}Li, t) reaction 2−74001
  - ^{18}F, T=0 levels calc. using one-boson- exchange pots. 2−63778
  - ^{18}F off-shell effects in shell and model spectra 2−63779
  - ^{19}F, spectroscopic factors for 4p-0h states from DWBA analysis of ^{15}N(^{7}Li,t) reaction 2−42591
  - ^{20}F levels excited in ^{19}F(d,p) reaction at 3 MeV, determ. of spectroscopic factors 2−67151
  - Fe, even-even nuclei, 1^{+} states investigation using (^{3}He,p) reactions 1f-2p shell model predictions 2−46130
  - ^{53}Fe, extended space calcs. 2−67159
  - ^{53}Fe, transferred l-values and spectroscopic factors, ^{54}Fe(p,d) determ. 2−42563
  - ^{54}Fe, shell-model states 2−70394
  - ^{55}Fe, hole state lifetimes 2−55962
  - ^{55}Fe, level density determ. using evaporation neutrons in ^{55}Mn(p,n)^{55}Fe 2−63797
  - ^{55}Fe, level scheme determ. in ^{57}Fe(p,t) two-nucleon pick-up reaction at 27 MeV 2−63883
  - ^{56}Fe, channel dependent widths and correlated intermediate structure, reaction ^{56}Fe(n, n$'\gamma'$ study 2−67244
  - ^{56}Fe, level density determination from alpha and proton induced reactions 2−63798
  - ^{56}Fe, shell-model states 2−70394
  - ^{58}Fe levels deduced from ^{57}Fe(d,p) reactions at 7.0 MeV, determ. of spectroscopic strengths 2−42512
  - ^{59}Fe, level density parameters, nucl. temp. 2−82981
  - ^{59}Fe level structure studied in ^{57}Fe(t,p) and ^{58}Fe(d,p) reactions, evidence of rotational band structure 2−63921
  - Ga isotopes, odd-mass, struct. of low-lying states with particle-phonon coupling model 2−63839
  - ^{69}Ga, ^{71}Ga, Coulombic excitation of levels 2−52751
  - ^{71}Ga shell model study of energy levels, transition probabilities, moments of ground state 2−46142
  - ^{147}Gd, high spin levels excited in ^{144}Sm (α,n) reaction, particle core coupling 2−49750
  - ^{152}Gd, 1053 keV state O^{+} excited identified 2−46163
  - ^{152}Gd level scheme, ^{152m}Eu decay obs. 2−59730
  - ^{154}Gd, level scheme from ^{154}Tb decay 2−52784
  - ^{156}Gd, level struct., rot.-vibr. interac., from ^{156}Eu decay 2−49751
  - ^{158}Gd, level struct., rot-vibr. interac., from ^{158}Eu decay 2−49751
  - ^{71}Ge excited states, ^{71}As decay obs. 2−63848
  - ^{74}Ge, excited states, obs. from ^{74}As decay 2−49765
  - ^{3}H, Reid potential calc., of binding energy admixture probabilities and charge form factor 2−76779
  - ^{3}H, shell-model analysis of Brueckner calcs. 2−63766
  - ^{4}H, search for ground and excited states formed in ^{6}Li(π^{-}, d) reaction 2−52734
  - ^{161}H level scheme from ^{161}Er decay 2−76815
  - ^{3}He, broad reson., ^{2}He(p,γ)^{3}He obs. 2−59756
  - ^{3}He excited state search in ^{4}He(p,d) and ^{3}He(α,α') reactions 2−67141
  - ^{4}He, excited states, study by reactions on ^{6}Li by deuterons at 52 MeV 2−49725
  - ^{4}He, shell-model analysis of Brueckner calcs. 2−63766
  - ^{4}He excited states study via ^{2}H(d, p)^{3}H and ^{2}H(d, n)^{3}He reactions using polarized d beam 2−74109
  - ^{5}He, first excited state detn. from ^{7}Li(d,α)^{5}He at 1 MeV 2−63768
  - ^{168}Hf, high-spin states produced in (α,8n) reactions, anomalous behaviour of nuclear moment of inertia at large rotational frequencies 2−42528
  - ^{176}Hf, single-neutron-transfer-reaction study 2−63824
  - ^{176}Hf mixing of 2-proton and 2-neutron bands 2−52768
  - ^{178}Hf, ^{180}Hf, J-depend. of level density from statistical props. of series of resonances 2−46171
  - ^{178}Hf, low lying level obs., vibr.-rot. interaction 2−42531
  - ^{178}Hf first rot. state, shrinking of nucl. charge radius 2−76804
  - ^{180}Hf, single-neutron-transfer-reaction study 2−63824

Nucleus continued
energy levels continued
^{180}Hf, two-particle, from ^{180}Lu decay 2−52786
Hg, levels populated in deuteron induced reactions on even-even isotopes of Hg 2−46329
^{197}Hg, level density parameters 2−63831
^{201}Hg, low-lying levels from decay of ^{201}Au 2−63832
^{205}Hg, single-particle fragments 2−46176
^{158}Ho, ^{161}Ho, level scheme, conversion electron spectra obs. 2−70421
^{163}Ho level scheme including rotational bands, investigation using in-beam and decay spectroscopic methods 2−63820
^{165}Ho, hyperfine structure of ground state $^{4}I_{15/2}$ 2−46166
^{165}Ho, nonrotational states, calc. 2−70408
^{166}Ho, residual interaction effect on rotational spectrum 2−46168
^{127}I, low-lying states, ^{127}I(n,n$'\gamma$) reaction study from 0.5 to 1.6 MeV 2−49746
^{134}I, from decay of ^{134m}I formed in slow neutron fission of ^{235}U, identification and characterization 2−52759
In odd-A isotopes, A=113-117, structure of low-lying states calc. in semi-microscopic model 2−63807
In odd mass isotopes, low energy props. 2−42516
^{115}In, from decay of ^{115m}Cd, internal conversion electrons 2−70420
^{116}In level scheme for lower states and hole-particle structure study by thermal neutron capture γ-ray spectroscopy 2−67168
^{117}In level scheme from ^{117}Cd and ^{117}Cd^{m} decay 2−76819
^{191}Ir, ang. correl. meas. 2−76806
^{191}Ir, unified model calcs. 2−42536
^{193}Ir, level scheme deduced from ^{193}Os decay 2−46173
^{193}Ir, unified model calcs. 2−42536
K(A=37, 38), effective interactions in upper s-d shell 2−49737
^{36}K, from ^{36}Ar(p,n) and ^{36}Ar(^{3}He,t) reactions 2−70387
^{38}K, new levels populated by ^{39}K(^{3}He,α) reaction at 21.09 MeV 2−42507
^{38}K, new levels populated in ^{39}K (^{3}He,α) neutron pick-up reaction, spectroscopic factors deduced 2−42586
^{38}K, two-hole states, obs. in ^{39}K(^{3}He, α) reaction 2−70388
^{39}K, low lying levels, examination by intermediate coupling model 2−55961
^{39}K, missing low lying states 2−52748
^{39}K level structure, inelastic scattering of 12.8 MeV deuterons 2−46324
^{40}K level scheme, ^{39}K(n,γ) obs. 2−67274
^{42}K, from ^{44}Ca(d,α)^{42}K reaction at 11 MeV 2−70380
^{84}Kr, excited states, study by ^{83}Kr(n,γ) using thermal neutrons 2−49741
^{86}Kr-^{87}Kr system, level structure investigated by inelastic proton scattering through isobaric analog resonances 2−46147
^{86}Kr levels fed in decay of ^{96}Br 2−46188
^{92}Kr, γ-ray decay 2−70399
La, odd-mass isotopes, decoupled Yrast states 2−63814
^{135}La, quantum characteristics of some levels 2−46156
^{138}La, shell model configuration interpretation of low-lying states populated in ^{139}La(d,t) reactions 2−52761
^{138}La low-lying levels excited in (p,d) reactions at 30 MeV, total angular momenta assignments 2−42564
^{6}Li, meas of hyperfine structure of 2^{2}P term by level crossing technique 2−63769
^{167}Lu, ground state spin meas. with atomic-beam magnetic resonance method, comparison with Nilsson model value 2−42529
^{169}Lu, ^{171}Lu, rotational bands and lifetimes of isomeric states, ^{169}Tm(α, 4nγ) and ^{169}Tm(α, 2nγ) study 2−70409
^{171}Lu, high spin rotational levels, ^{169}Tm(α, 2n)^{171}Lu obs. 2−59717
^{174}Lu states populated in single-particle transfer reactions, obs. of Coriolis coupling 2−82896
^{176}Lu levels populated in ^{175}Lu(n, γ) and ^{175}Lu(n, e) reactions, study of rotational bands 2−79744
^{177}Lu, level scheme, ^{176}Lu(n, γ) reaction obs. 2−59769
^{22}Mg new states at 5006 ± 2 keV, 5317 ± 5 keV and 5837 ± 5 keV obs. in ^{20}Na(^{3}He,nγ) reaction 2−63784
^{24}Mg, investigation using ^{24}Al→^{24}Mg beta decay 2−52774
^{24}Mg, o^{+}, 2^{+} and 4^{+} members of ground state rotational band in coupled-channel treatment of inelastic proton scattering 2−70443
^{24}Mg, pairing vibrations, modified Tamm-Dancoff approximation 2−46100
^{24}Mg, quasi-molecular rotational bands suggested by analysis of elastic ^{12}C + ^{12}C scattering 2−49838
^{24}Mg, shell-model and Hartree-Fock calculations 2−74008
^{24}Mg, statistical-model explanation, reaction ^{26}Mg(p, t) study at 26 MeV 2−63881
^{27}Mg, level density parameters, nucl. temp. 2−82981
Mn, excitation of 126 keV level by fast neutron scatt. 2−67245
^{54}Mn, low lying levels, by ang. correlation study using ^{54}Cr(p,nγ) 2−46134
^{54}Mn level structure determ. from ^{54}Cr(p, nγ) and ^{51}V(α, nγ) reactions 2−79743
^{55}Mn level scheme determ. in ^{57}Fe(p,τ) and ^{57}Fe(d,α) two-nucleon pick-up reactions at 27 MeV and 16 MeV 2−63883
^{90}Mo, angular distribs. of levels populated in ^{92}Mo(p,t) reaction 2−70398
^{92}Mo, model calcs 2−82906
^{93}Mo levels excited in ^{94}Mo(^{3}He, ^{4}He) reaction at 16 MeV, identification of 3 new levels 2−70401
^{94}Mo, low-lying states investigation via multiple Coulomb excitation 2−82910
^{98}Mo, low-lying states investigation via multiple Coulomb excitation 2−82910
^{101}Mo spectroscopy by sub-Coulomb stripping 2−76797
^{13}N, 26, 28 and 32 MeV states from ^{10}B(^{3}He, particle) reactions 2−76873
^{13}N ground state spectroscopic factors determ. by weakly bound projectile model calcs. on ^{12}C(d,n) reaction 2−67325
^{14}N, core-excited 5^{+} state identification 2−73997
^{14}N, level spectroscopy from ^{12}C(t, n)^{14}N study 2−76874
^{14}N, spectroscopic factors of lower bound states determ. from ^{12}C(^{3}He, p) reaction 2−83011
^{15}N, two-particle three-hole structure of negative parity states studied via ^{12}C(^{3}He,p) reaction 2−70375
^{15}N, two-particle three-hole character of negative parity states studied using ^{13}C(^{3}He,p) reaction 2−63775

Nucleus continued
energy levels continued
^{15}N excited levels from ^{12}C(^{7}Li,α)^{15}N triton transfer reaction 2−70481
^{21}Na, excited states, proton scatt. and radiative capture in ^{20}Ne obs. 2−55969
^{21}Na, investigation with ^{20}Ne(p, γ) and ^{20}Ne(d, n) reactions 2−74005
^{21}Na, search for missing $J^{\pi}=3/2^{+}$ level using ^{20}Ne(^{3}He,d) and ^{20}Ne(p,γ) reactions 2−79761
^{22}Na, practical angular momentum projection method in multishell Hartree-Fock calc. 2−46119
^{23}Na, dependence of integrated cross sections of ^{25}Mg(d,α)^{23}Na on rotational states at 20.9 MeV 2−46322
^{23}Na, lowest lying $J\pi={}^{1}._{2}$ level prediction 2−46118
^{23}Na, reson. fluoresc. above 3 MeV, level struct. 2−74006
^{23}Na levels populated in ^{23}Ne β-decay, calcs. of ft-values using Nilsson model, and mixed states 2−79773
^{23}Na resonances corresponding to excited states observed in ^{22}Ne(p,γ) and ^{22}Ne(p,p$'\gamma$) reactions 2−49733
^{23}Na to 6.58 MeV, study using ^{26}Mg(p, $\alpha'\gamma$)^{23}Na and ^{23}Na(α, $\alpha'\gamma$)^{23}Na 2−76789
Nb, A=91,97, single particle proton states, reaction (d,n) study 2−70400
Nb(A=91, 97), level properties from ^{90}Zr(d, n) and ^{96}Zr(d, n) reactions 2−63922
^{90}Nb, low-lying levels populated in ^{90}Zr(p,nγ) reaction 2−42515
^{91}Nb, structure of lower states 2−52755
^{93}Nb, α-particle excitation 2−46152
^{93}Nb, elastic and inelastic neutron scattering in 1.0 to 5.0 energy range 2−42574
^{93}Nb level scheme, (n,n$'\gamma$) reaction obs. 2−67164
^{20}Nc, low-lying even-parity, α-like spatial four-body correlations 2−46108
Nd, A=142, 146, 148, higher order spacing distributions 2−67184
^{134}Nd isomeric state excited in ^{118}Sn(^{20}Ne, 4n) reaction at 82-120 MeV 2−79745
^{142}Nd, neutron-single hole states; proton-neutron interaction effects 2−46157
^{143}Nd level scheme investigation in unified model calc. and particle core model 2−67170
^{144}Nd, 2 new excited states, obs. 2−67196
^{145}Nd low-lying excited states populated by thermal neutron capture 2−67172
Nd(p,t) evev isotopes, 5Z MeV, excitation of removal and addition types of quadrupole-pairing vibrational states 2−82968
^{19}Ne, excitation energies of states meas. in ^{20}Ne(^{3}He, ^{4}He) reaction up to 10.6 MeV 2−63780
^{20}Ne, ^{22}Ne shell model, quartet states and cluster model 2−82868
^{20}Ne, 0^{+} states, spectroscopic strengths, α-particle widths 2−70382
^{20}Ne, classification of high-spin states into rotational bands 2−49732
^{20}Ne, effective interactions in s-d shell 2−49728
^{20}Ne, excitation function for ^{12}C(^{12}C,α) leading to 2^{+} state 2−83022
^{20}Ne, generator-coord. spectrum, T=0 levels 2−76786
^{20}Ne, ground and excited states, bounds on energy and wave functions 2−63751
^{20}Ne, O^{+}, 2^{+} and 4^{+} members of ground state rotational band in coupled-channel treatment of inelastic proton scattering 2−70443
^{20}Ne, rotational bands, destruction of alpha-cluster and shell-model states 2−59695
^{20}Ne, rotational bands, study by ^{16}O(^{12}C, ^{8}Be) reaction 2−42499
^{20}Ne, second T=0 state obs. as compound nucleus in ^{19}F + p reactions 2−76785
^{20}Ne, spectroscopic factors from ^{21}Ne(p, d) obs. 2−76842
^{20}Ne, spectroscopic factors for 4p-oh states from DWBA analysis of ^{16}O(^{7}Li,t) reaction 2−42591
^{20}Ne, static and dynamic quadrupole moments of first excited state determ. by projectile Coulomb excitation technique 2−42537
^{20}Ne rotational states, properties of projected HF functions of ground state bands 2−73992
^{21}Ne, deform. parameters from (p, p) and (d, d) scatt. obs. 2−76842
^{21}Ne, level struct., ^{18}O(α,nγ) obs. 2−55958
^{21}Ne, levels up to 4.7 MeV excited in ^{20}Ne(d,pγ) reaction, comparison with Nilsson model calcs. 2−79762
^{21}Ne, lowest lying $J\pi={}^{1}._{2}$ level prediction 2−46118
^{21}Ne excited states obs. using ^{18}O(α,nγ) reaction 2−59696
^{22}Ne, l_{n}=O and l_{n}=1 transfers associated with various levels 2−46321
^{22}Ne, spectroscopic factors from ^{21}Ne(d, p) obs. 2−76842
^{22}Ne, static and dynamic quadrupole moments of first excited state determ. by projectile Coulomb excitation technique 2−42537
^{22}Ne level struct. by ^{21}Ne(d,p) reaction 2−76787
^{22}Ne rot. bands excited in ^{18}(^{7}Li,t)^{22}Ne 2−76788
Ni even isotopes, level spectra using self-consistent approx. 2−76793
Ni isotopes, even-mass, low-lying level props. 2−63801
^{56}Ni, levels populated in ^{54}Fe(^{16}O, ^{14}C), two-nucleon stripping reaction at 80 MeV 2−74121
^{56}Ni, shell-model states 2−70394
^{58}Ni, high-lying states, ^{58}Ni(α,α')^{58}Ni obs. 2−59784
^{58}Ni, shell-model states 2−70394
^{60}Ni, giant reson. struct., low-lying collective states influence 2−74028
^{64}Ni level struct. from ^{65}Cu(t, α) at 12 MeV 2−76878
^{232}Np decay scheme and level struct. 2−82929
O(A=18, 19, 20), effective interactions in s-d shell 2−49728
^{14}O, spectroscopic factors of lower bound states determ. from ^{12}C(^{3}He, n) reaction 2−83011
^{15}O, excited states between 10 and 10.5 MeV, study by ^{14}N(p,p) 2−46112
^{15}O, reson. struct., ^{14}N(p,γ)^{15}O obs. 2−63774
^{15}O levels populated in ^{12}C(^{3}He,n), determ. of spectroscopic factors using DWBA analysis 2−46316
^{16}O, ^{14}N(α,d)^{16}O at 30 MeV 2−46317
^{16}O, 8^{+} level, study by ^{12}C(α, ^{8}Be)^{8}Be reaction from 15 to 18.96 MeV 2−79733
^{16}O, α chain states study through decay widths 2−46110
^{16}O, binding energy of first 0^{+} excited state, α-particle model 2−73998

ucleus continued
energy levels continued
^{16}O, compound-nuclear reson. at 14.8 MeV from ^{12}C(α,α γ)^{12}C study 2−[illegible]
^{16}O, determ. by ^{12}C(^{6}Li, d)^{16}O mechanism 2−83021
^{16}O, Hartree-Fock intrinsic states 2−63776
^{16}O, inelastic excitation of 2⁻ (8.88 MeV) level by α particles, role of two-body spin-orbit interaction 2−70430
^{16}O, new 0⁺ level at 15.17 MeV refined level parameters using ^{12}C(α,α)^{12}C 2−79735
^{16}O, rotational bands, study by ^{12}C(^{12}C, ^{8}Be) reaction 2−42499
^{16}O, shell-model analysis of Brueckner calcs. 2−63766
^{16}O, T=2 states, study by [illegible]N + d and [illegible]C + α reactions 2−73999
^{16}O giant dipole reson., polarized proton capture reaction obs 2−67149
^{16}O levels populated in ^{14}N(d,n$_γ$) reaction at 4.83 MeV 2−70377
^{16}O rotational states, properties of projected HF functions of excited 8p-8h band 2−73992
^{16}O to ^{20}Ne region, exptl. evidence for alpha-particle cluster states 2−82884
^{17}O, 4.55 MeV level width, ^{17}N β-decay obs. 2−67194
^{17}O levels excited in two-nucleon transfer reactions in ^{19}F 2−82972
^{18}O, low-lying level spacing, shell-model calculations 2−49727
^{18}O, off-shell effects in shell and model spectra 2−63779
^{19}O, orbital angular momentum and spectroscopic factors for levels populated in ^{18}O(d,p) reaction 2−52740
^{19}O, study of energy spectrum and e.m. properties in framework of unified asymmetrical rotational models 2−52737
^{186}Os level calc. rel. to gamma oscillations in collective model for axially symmetric nuclei 2−52767
^{187}Os, level structure investigation via ^{187}Ir decay 2−55966
^{190}Os, evidence for K=0 excited states studied by ^{190}Os(n,n'γ) reaction 2−67179
^{29}P, determ. of total angular momentum of excited states from ^{28}Si(p,p) elastic scattering 2−52812
^{30}P, low-lying structure studied in modified vibrational unified model 2−46124
^{32}P, first T=2 level analysis 2−63788
^{32}P, level density parameters, nucl. temp. 2−82981
^{32}P, spectroscopic factors deduced from angular distrib. meas. in ^{31}P(d,p) at 10 MeV 2−49834
Pb isotopes, pairing vibrations, modified Tamm-Dancoff approximation 2−46100
^{200}Pb, ^{202}Pb, level energies determ. from ^{200}Bi, ^{202}Bi decay 2−46174
^{205}Pb level scheme populated by ^{205}Bi decay 2−82925
^{206}Pb, compound particle-core coupled states, [illegible] study 2−59721
^{206}Pb, g-factor of 12⁺ isomeric state and effective orbital g-factor of neutron 2−59720
^{206}Pb, three-phonon monopole and quadrupole pairing vibr. states 2−82900
^{206}Pb levels populated in decay of ^{206}Bi 2−70413
^{208}Pb, giant reson. struct., low-lying collective states influence 2−74028
^{208}Pb, strong multipole vibrs. in low- excitation region 2−76879
^{208}Pb low-lying states, investigation using inelastic electron scattering 2−63833
^{209}Pb, neutron single-particle states 2−67275
^{209}Pb giant reson. struct. from radiative neutron capture of ^{208}Pb 2−67307
^{210}Pb, low-lying level spacing, shell model calculations 2−49727
^{210}Pb, theoretical and exptl. structure investigation, use of ^{208}Pb(t,p) reaction 2−82892
^{210}Pb low-lying states, shell-model calcs., effects of ^{208}Pb core vibrs. 2−67182
^{105}Pd, quadrupole coupling constants of $^3D_2$, $^3D_1$ and $^1D_2$ levels 2−52756
[illegible]Pd, quasi-vibrational levels occupied in ^{104}Ru(α,3n) reaction 2−49744
^{146}Pm, ground state struct. 2−42525
^{151}Pm, structure determ. from ^{150}Nd(^{3}He, d), ^{150}Nd(α, t) and ^{152}Sm(t, α) reactions Coriolis coupling calcs. 2−74038
^{210}Po, level density parameters 2−63831
^{210}Po, investigations using ^{210}At→^{210}Po electron capture decay 2−63836
[illegible]Pt low-lying levels excited in (p,d) reactions at 30 MeV, total angular momenta assignments 2−42564
[illegible]Pt, neutron reson. level spacings, stat. distribs., deviations 2−67161
Pt, A=188, 190, 192, study using bombardment of Ir 2−79416
Pt, even mass nuclei 182≤A≤192, low- lying level properties from Hg isotope decay data 2−49755
^{239}Pu, higher order spacing distributions 2−67184
[illegible]Pu, low-lying level obs., vibr.-rot. interaction 2−42531
[illegible]Pu populated by electron capture decay of [illegible]Am 2−46179
[illegible]Pu fission isomer, identification of rotational band 2−74126
[illegible]Pu levels, single-particle assignments, reaction-spectroscopy obs 2−82911
[illegible]Pu, ground state rotational, octupole-vibrational states identified 2−46178
^{240}Pu octupole bands study by thermal neutron capture γ-ray spectroscopy 2−67188
[illegible]Pu levels, single-particle assignments, reaction-spectroscopy obs. 2−82911
^{223}Ra levels determ. by α-γ coincidence and directional correlation studies on ^{227}Th decay 2−49776
^{223}Ra levels populated in decay of ^{227}Th 2−63852
^{85}Rb levels populated in decay of ^{85}Sr, direct evidence for 5.23 keV level 2−55964
[illegible]Rb, identification of low-lying levels excited in ^{87}Rb(^{3}He, ^{4}He) reaction at 16 MeV, distorted-wave analysis 2−70397
[illegible]Rb hole states obs. using ^{88}Sr(d,α)^{86}Rb reaction 2−82909
[illegible]Rb, γ-ray decay 2−70399
Re, obs. of slow neutron resonances in range 3-300 eV, shape analyses based on Breit-Wigner single level formula 2−76457
Re, A=182, 182m, ground state structure and moments of inertia, Nilsson model 2−46164
[illegible]Re, [illegible]Re, rotational bands and lifetimes of isomeric states, ^{181}Ta(α, 4n) and [illegible]Ta(α, 2nγ) study 2−70409
[illegible]Re, level density parameters 2−63831

Nucleus continued
energy levels continued
[illegible]Ru level scheme 2−63929
[illegible]Ru model calc. 2−82906
[illegible]Ru level scheme established, new cascade transitions using ^{99}Rh decay 2−7970
^{101}Ru level scheme from ^{101}Tc decay obs. 2−74051
^{103}Ru level scheme, ^{102}Ru(n,γ) obs. 2−67166
^{32}S, energies and branching ratios of bound levels, ^{31}P(p, γ) study 2−74090
[illegible]S, energy and density of yrast levels considered in adiabatic potential calcs. in ^{16}O-^{16}O elastic scattering 2−63923
[illegible]S, quasi-molecular rotational bands suggested by analysis of elastic ^{16}O + ^{16}O scattering 2−49738
[illegible]S, shell-model and Hartree-Fock calculations 2−74008
[illegible]S low-lying levels up to 4.3 MeV excitation studied by ^{30}Si(α,nγ) reaction 2−7885
[illegible]S, spin assigments for higher excited states using ^{31}P(α,p)^{34}S 2−52745
[illegible]S level scheme from [illegible]P β-decay obs. 2−74049
[illegible]S, effective interactions in upper s-d shell 2−49737
Sb, level spacings and strength functions of slow neutron resonances 2−[illegible]
[illegible]Sb, isomeric level, g-factor 2−59708
[illegible]Sb, 6.24 eV level, neutron resonance obs. 2−46277
[illegible]Sb proton-neutron hole states populated in β-decay of [illegible]Sn 2−[illegible]
[illegible]Sc determ. of total angular momentum of excited states from [illegible]Ca(p,p) elastic scattering 2−52812
[illegible]Sc level scheme [illegible] obs. 2−74020
[illegible]Sc levels excited in [illegible] reaction at 26.y MeV, two-nucleon transfer analysis 2−70479
^{46}Sc level scheme, ^{45}Sc(n,γ) reaction obs. 2−67156
^{46}Sc levels excited in [illegible] reaction at 26.7 MeV, two-nucleon transfer analysis 2−70479
[illegible]Se, from γ-ray spectrum of [illegible]Br 2−74050
[illegible]Si, angular correlation studies for α-particle excitation of 1.78 MeV 2⁺ state 2−[illegible]
[illegible]Si, investigation using [illegible]P→[illegible]Si beta decay 2−52774
[illegible]Si, shell-model and Hartree-Fock calculations 2−74008
[illegible]Si, [illegible] doorway states, [illegible] single particle fragments 2−67152
[illegible]Si, shell-model wave functions of ground and excited states tested in [illegible] reaction 2−[illegible]
[illegible]Si, level struct. from deuteron stripping obs. 2−82887
[illegible]Si spin, parity and partial widths determ. form α reactions on Mg 2−[illegible]
Sm isotopes, even, level assignments from (p,t) reactions 2−82962
[illegible]Sm level scheme from [illegible] studies 2−82989
[illegible]Sm determ. by inelastic proton scattering at 30 MeV 2−74079
[illegible]Sm differential cross sections for elastic and inelastic scattering of α particles and relation to low-lying states 2−46305
[illegible]Sm, neutron single hole states, proton-neutron interaction effects 2−[illegible]
[illegible]Sm ground state rotational bands, reaction ^{150}Nd (α, 4n) ^{150}Sm study 2−52[illegible]
[illegible]Sm ground state rotational bands, reaction ^{150}Nd (α, 2n) ^{152}Sm study 2−52[illegible]
[illegible]Sm neutron-capture spectroscopy, level population 2−63898
[illegible]Sm level scheme, [illegible]Eu decay obs. 2−59730
[illegible]Sm neutron-capture spectroscopy, level population 2−63898
Sn, A=[illegible], [illegible] Coulomb excited level energies 2−63810
[illegible]Sn isotope identification in [illegible]Cd(α,3n) reaction 2−82886
[illegible]Sn, proton single hole states, study by [illegible]In(^{3}He, d)^{114}Sn at 37.7 MeV 2−[illegible]
[illegible]Sn levels populated in Coulomb (d,p) stripping 2−67331
[illegible]Sn [illegible] and quasi-particle states, core-particle discription of low-lying levels 2−[illegible]
[illegible]Sn levels populated in Coulomb (d,p) stripping 2−67331
[illegible]Sn [illegible] decay obs. 2−42520
[illegible]Sn levels populated in Coulomb (d,p) stripping 2−67331
[illegible]Sn doubly closed shell region, two-proton and proton-neutron states populated in [illegible] beta decay 2−82895
[illegible]Sr ground and excited states obs. following elastic and inelastic proton scattering, deformation parameters 2−74077
[illegible]Sr γ-ray decay 2−70399
[illegible]Ta, [illegible]Ta, rotational bands and lifetimes of isomeric states, ^{175}Lu(α, 4n) and [illegible] study 2−70409
[illegible]Ta, ground state structure and moments of inertia, Nilsson model 2−46164
Tb A=155, 57, 159, 161, levels excited in (^{3}He,d) and (α,t) reactions on Gd 2−82916
[illegible]Tb, [illegible]Tb level scheme, conversion electron spectra obs. 2−[illegible]
[illegible]Tb population of collective states and higher-order effects in [illegible] 2−74092
[illegible]Tb, ground state structure and moments of inertia, Nilsson model 2−46164
[illegible]Tb level scheme from (n,γ) reactions 2−67174
Tc, A=92, [illegible], 97, single particle proton states, reaction (d,n) study 2−[illegible]
[illegible]Tc model calc. 2−82906
[illegible]Tc structure of lower states 2−52755
[illegible]Tc [illegible](p,nγ)[illegible]Tc obs. 2−67165
[illegible]Tc level scheme from [illegible]Mo decay obs. 2−74051
[illegible]Te [illegible] states 2−42517
[illegible]Te [illegible] mass deform. of first excited 2⁺ state 2−[illegible]
[illegible]Te [illegible] states 2−42517
[illegible]Te [illegible] of negative parity states populated in decay of [illegible]
[illegible]Te [illegible] states 2−42517
[illegible]Te [illegible] and particle-core coupling 2−76781
[illegible]Te [illegible] I decay 2−52780
[illegible]Th levels populated in decay of ^{230}Pa 2−70416
[illegible]Th [illegible] obs. 2−59722
[illegible]Th [illegible] struct., neutron inelastic scatt. obs. 2−67183
[illegible]Th ground state rotational, octupole-vibrational states identified 2−[illegible]
[illegible]Th level features and decay schemes 2−59724
[illegible]Th, low-lying level obs., vibr.-rot. interaction 2−42531

Nucleus continued
energy levels continued
^{233}Th, (d,p) reaction obs. 2−59722
^{233}Th, level scheme, neutron capture and (d,p) reaction obs. 2−63837
Ti, (A=46, 48, 50), ground state charge distribs., using Ti(e,e) 2−52749
Ti, even-even nuclei, 1$^+$ states investigation using He,p) reactions 1f-2p shell model predictions 2−46130
^{44}Ti, Hartree-Fock variation after projection method test 2−74019
^{48}Ti, elastic and inelastic scattering of protons, meas. spins, parities, widths and spacing of analogue resonances 2−7[illegible]3
^{189}Tl isotope, search for and energy levels 2−55[illegible]
^{200}Tl, level density parameters 2−63831
^{203}Tl, muonic, excitation of first and higher levels [illegible]−59961
^{205}Tl, levels populated in inelastic proton scattering on ^{204}Hg, study of isobaric analogue strength 2−74080
^{205}Tl, muonic, excitation of first and higher levels [illegible]−59961
^{205}Tl levels deduced, resonance in ^{204}Hg(p, p)^{204}Hg 2−79767
^{165}Tm, rotational bands determ. by γ-γ coincidences in ^{165}Ho(α, 4nγ) reaction 2−74039
^{170}Tm, structure of low-lying rotational bands 2−[illegible]752
^{236}U level struct., thermal neutron capture in ^{236}U [illegible]. 2−67309
^{236}U level structure determ. from ^{235}U(n,γ) reaction 2−52820
^{238}U, excited level struct., neutron inelastic scatt. [illegible]. 2−67183
^{238}U, ground state rotational, octupole-vibrational states identified 2−46178
^{238}U, level structures and decay schemes 2−5972[illegible]
^{239}U neutron resons., density and struct. 2−6718[illegible]
^{49}V, g-factor of 3/2$^-$ 153 keV state, ^{48}Ti(p,γ) obs. 2−67157
^{49}V study by ^{49}Ti(p.n) reaction from 2.03 to 3.25 MeV 2−82898
^{182}W, e.m. properties of K$^\pi$=2- octupole band populated in β- decay of ^{182}Ta 2−42533
^{182}W level calc. rel. to gamma oscillations in collective model for axially symmetric nuclei 2−52767
^{126}Xe levels populated in ^{126}I decay 2−52780
^{129}Xe, formed from ^{129}Cs decay 2−42546
^{133}Xe, low-lying, core-excitation model applic. 2−[illegible]0403
^{136}Xe, neutron-single hole states, proton-neutron interaction effects 2−46157
^{137}Xe level scheme investigation in unified model calc. and particle core model 2−67170
^{88}Y, structure, computer analysis of ^{90}Zr (d,α)^{88}Y analysis 2−70480
^{89}Y model calcs. 2−82906
^{164}Yb, high-spin states produced in (α,8n) reactions, anomalous behaviour of nuclear moment of inertia at large rotational frequencies 2−42528
^{169}Yb, energies and intensities of γ-rays, total internal conversion coeff. for 20.7 keV transition 2−79768
^{170}Yb level scheme from β-decay of ^{170}Lu 2−768[illegible]
^{171}Yb, excited states, in thermal neutron capture by Yb 2−46170
^{171}Yb, rotational states populated in ^{170}Er(α, 3n) reaction, Coriolis interaction 2−74040
^{171}Yb, rotational states populated in ^{170}Er(α, 3n) reaction, Coriolis interaction 2−74040
Zn isotopes, from Zn(t,p) investigations 2−56001
Zn(A=64,66,68), radiative widths of spin-1 levels using γ-ray scatt. 2−59692
^{60}Zn, levels populated in ^{58}Ni(^{16}O, ^{14}C) two-nucleon stripping reaction at 80 MeV 2−74121
^{65}Zn, from β-decay of ^{65}Ga 2−63847
Zn(α,α'), A=68, 70, 31 MeV, angular distribution and excited states 2−42581
^{89}Zr, ^{91}Zr(p, t) study 2−70445
^{90}Zr, giant reson. struct., low-lying collective states influence 2−74028
^{90}Zr, inelastic excitation of low lying levels by 61.2 MeV proton, role of two-body spin-orbit interaction 2−70430
^{90}Zr, model calcs 2−82906
^{91}Zr, new levels below 6.5 MeV excitation populated in ^{90}Zr(d,p) reaction 2−42588
^{91}Zr, obs. of new levels and doublets in (d,p), (p,p$'$), [illegible] high resolution reactions 2−52754
^{92}Zr, low-lying level spacing, shell model calculation 2−49727
^{92}Zr level structure determ. using (n$_{th}$,γ) reaction 2 67163
excitation *see Nuclear excitation*
magnetic moment
see also Gyromagnetic ratio; Molecules/nuclear cooling; Nuclear magnetic resonance and relaxation
beam spot size changes due to second order effects in first order achromatic beam transport system 2−73958
closed electron drift accelerator, effect of magnetic field 2−73961
Coulomb excitation by polarized particles and detn. of m.m. 2−70370
dipole moments of very short-lived states by recoil-into-gas method 2−70371
electron beam, 100 GeV, separation from other particles by synchrotron radiation 2−73959
electron scatt. from magnetic dipole moments, calc. of cross-section and asymmetry function 2−63867
excited nuclei, determination from hyperfine interactions in highly ionized atoms 2−52906
light nuclei, quasiparticle spin-orbit interaction effect A=11 to 65 2−73991
magnetic dipole and elec. quadrupole hyperfine interactions study by nuclear orientation with and without n.m.r. 2−6[illegible]8
nuclear spin-lattice relaxation due to the orbital interaction 2−84585
odd-mass nuclei with simple configs., core polarization and mesonic current effects 2−82902
orbital g-factor, change due to exchange currents, rel. to E1 sum rule for photoabsorption 2−63757
rigid movable sphere, motion when struck by plane or spherical acoustical waves 2−73402
single-closed-shell nuclei, relations among magnetic moments and M1 rates 2−67135
n resonance, calc. 2−67133
Os, A=188, 190, 192, comparison of IMPACT, PAC and Mossbauer effect meas. of g-factor, ferromagnetic host effects 2−42534
^{107}Ag, ^{109}Ag dipole moments of very short-lived state by recoil-into-gas method 2−70371

Nucleus continued
magnetic moment continued
^{28}Al, γ-γ ang.-correl. on low-lying levels, PAC determ. of 2$^+$ stat moment 2−76790
^{74}As, n.m.r. and polarization in Fe obs. 2−76796
^{210}At, g-factor of 0.3μs isomeric state at 2549 keV, study by ^{209}Bi(α,3n) reaction 2−49756
^{10}B*, T=0, J$^\pi$=1$^+$, limits on magnetic moment 2−79754
^{210}Bi, of 7$^-$ and 5$^-$ states 2−67181
^{78}Br isomeric states, g-factor meas. by time differential methods and stroboscopic obs. 2−74029
^{81}Br isomeric states, g-factor meas. by time differential methods and stroboscopic obs. 2−74029
^{42}Ca, lowest 6$^+$ state, ^{40}Ca(α,2p) study 2−59700
^{110}Cd, g-factor expt. on first excited 2+ state 2−52742
^{140}Ce, gyromagnetic ratio of 2083 keV 4$^+$ state 2−52763
^{38}Cl, mag. multipole props., effects of weak particle- hole admixtures 2−76791
^{58}Co, moment of 111.5 keV level populated in ^{58}Fe(p, nγ) reaction 2−79742
^{161}Er, ^{163}Er, hyperfine interaction consts. and nuclear moments meas using atomic beam magnetic resonance method 2−79741
^{168}Er states excited by neutron capture 2−67175
^{18}F, T=0, J$^\pi$=1$^+$, limits on magnetic moments 2−79754
^{54}Fe, 1.409 MeV 2$^+$ state 2−70392
^{59}Fe, γ-ray anisotropies 2−84457
^{66}Ga, first excited state, meas. by DPAD method 2−49740
^{66}Ga isomeric states, g-factor meas. by time differential methods an stroboscopic obs. 2−74029
^{154}Gd, dipole interaction with liquid environment, estimation from tim differential perturbed ang. correlation studies 2−60511
^{3}H, isovector and isoscalar parts 2−59688
^{3}H, meson-exchange corrections, calc. using model for short-range correlation 2−46078
^{3}H, quark model approach 2−82877
^{3}H, two-nucleon one-pion exchange contributions 2−67143
^{3}H quark model approach 2−82877
^{3}He, isovector and isoscalar parts 2−59688
^{3}He, meson-exchange corrections, calc. using model for short-rang correlation 2−46078
^{3}He, two-nucleon one-pion exchange contributions 2−67143
^{193}Hg, determination by optical pumping technique 2−70412
^{193m}Hg, determination by optical pumping technique 2−70412
^{195m}Hg, determination by optical pumping technique 2−70412
^{197m}Hg, determination by optical pumping technique 2−70412
^{165}Ho, dipole moment, direct meas. by atomic beam magnetic resonance method 2−46167
^{127}I, 57.8 keV state, Mossbauer obs. 2−63812
^{127}I, meas. of magnetic moment of 57.6 keV state by Mossbauer effect in IFe 2−49747
^{40}K, mag. multiple props., effects of weak particle- hole admixtures 2−76791
^{137}La, dipole moment, optical determ. 2−63813
^{6}Li, T=0, J$^\pi$=1$^+$, limits on magnetic moments 2−79754
Nd, even nuclei, first (2$^+$) and second (4$^+$) states 2−42522
^{237}Np, determ. from h.f.s. in atomic spectrum 2−79938
^{18}O[2+], determination from hyperfine interactions in O^{7+} at 1.98 MeV 2−52906
^{188}Os, g-factors of several excited states determ. from perturbed angular correlation following ion implantation by Coulomb excitation 2−63829
^{192}Os, g-factors of several excited states determ. from perturbed angular correlation following ion implantation by Coulomb excitation 2−63829
^{208}Pb region, mag. dipole transitions 2−82901
^{106}Pd, g-factor expt. on first excited 2+ state 2−52742
^{147}Pm, g-factor of 91keV state, meas. using 319 to 91 keV gamma cascade 2−59712
^{195}Pt Mossbauer effect obs. 2−59719
^{103}Rh dipole moments of very short-lived states by recoil-into-gas method 2−70371
^{102}Ru, g-factor expt. on first excited 2+ state 2−52742
Sb(A=120,124), oriented in Fe, ground state moment from n.m.r. 2−49745
Sm, even nuclei, first (2$^+$) and second (4$^+$) states 2−42522
^{119}Sn, of 89 keV excited state, deviation from Schmidt value, Mossbauer obs. 2−67169
^{125}Te, internal perturbed angular correlation method 2−79766
^{125}Te, of 462, 5/2$^+$ level, computed using Kisslinger-Sorensen model 2−52758
^{125}Te 11/2$^-$ isomer, orientation obs. 2−76799
^{51}V quadrupole moment obs. 2−61741
^{182}W, 3$^-$, 1374 keV level 2−79738
magnetic resonance *see Nuclear magnetic resonance and relaxatio*
models
alpha-cluster model effect of internal structure of α particle 2−70357
alpha-particle, analysis of Glauber scatt. of protons on ^{12}C 2−5975
alpha-particle models, classical and unified, light nuclei 2−67126
alpha-particle structure, of light self-conjugate 4n nuclei in ground state 2−63742
asymmetric rotor models, best- parameter search 2−46083
binary clustering, ref. to fission 2−83038
Bohr-Mottelson theory, classical model of collective motions 2−70360
Bohr-Mottleson collective equation, derivation from many body problem Hamiltonian 2−46087
cluster description of light nuclei using supermultiplet scheme 2−55955
cluster model, simplified calculations 2−59667
cluster model applied to ^{12}C, ^{36}Ar 2−70373
collective model equations, derivation from many particle Schrodinger equation 2−59668
collective motions, symmetry-conserving theories 2−73977
collective nucleus, E2-transitions and quadrupole moments of high spin states 2−59675
continuum shell model, separation approx., applic. to 12C giant resonance 2−59690
continuum shell-model approximation schemes, comparison 2−63855

Nucleus continued
models continued
core excitation model, applicability to low-lying levels of ^{133}Xe 2−70403
core excitation model description of ^{75}As low- lying levels 2−42513
core-excitation, applicability to ^{135}Ba 2−59710
core-particle coupled model of effective charge 2−46128
droplet, generalization of liquid drop model 2−82867
dynamic collective model, of giant dipole resonance 2−76774
exactly solvable, application of hole line expansion 2−82850
Fermi gas, particle-hole states density, spin depend. 2−59674
Fermi liquid model for gamma and octupole vibrations in deformed nuclei 2−46116
Fermi-liquids drop, oscillations rel. to giant resonance in medium and heavy nuclei 2−46086
fission, barrier heights, energy release and fragment energy partition processes, review 2−59799
Gamow states of square-well plus square-barrier model, expectation value of r^2 2−73978
generalized microscopical approach for explaining nuclear structure 2−52725
Glauber, of the inelastic interaction of cosmic-ray nucleons with nuclei 2−73892
intermediate coupling model calc. for ^{39}K low lying levels 2−55961
linked cluster eqn. Brueckner-Bethe theory 2−79708
liquid drop model of fissioning nuclei, charge polarization effects 2−79809
microscopic model analysis of elastic alpha scatt. from 40 ca 2−83008
Nilsson model, rel. to excited states in ^{21}Na 2−55969
Nilsson model Hamiltonian, matrix elements 2−79722
opaque and Glauber models correction for case of deuteron-nucleus scattering 2−70462
optical, calc. of spin-orbit component from matter distrib. for spherical and deformed cases 2−70361
optical, of n and p scatt., volume integrals 2−67230
optical, of the inelastic interaction of cosmic-ray nucleons with nuclei 2−73892
optical fit for Sn(d, d)Sn data, 20 and 17 MeV 2−79803
optical model analysis of differential cross sections for elastic α-particle scattering from ^{90}Zr 2−49825
optical model analysis of heavy ion scatt., absorptive potentials 2−79807
particle-hole, study of transition rate renormalization induced by 2p-2h ground-state admixtures 2−46085
particle-phonon coupling model study of level struct. of Ga isotopes 2−63839
potential energy surfaces in two-centre shell model 2−63735
pre-equilibrium exciton model, analysis of total (n,p) cross sections around 14 MeV 2−82984
quartet structs. in medium-wt nuclei 2−82840
rotor model validity for ^{171}Lu, ^{169}Tm(α, 2n) reaction obs. 2−59718
RPA, renormalized, calc. of e.m. transitions in ^{16}O, ^{40}Ca, ^{48}Ca, and ^{208}Pb 2−82917
RPA method with angular momentum projection 2−79730
shape fluctuation model, ground state bands in even-even nuclei 2−70359
shell, density of particle-hole excited states 2−67128
shell, modified, wave function for and binding energy of ^{4}He 2−46109
shell, single-particle, history 2−69523
ds- shell, SU(3) symmetry mixing 2−82853
shell model, deviations in light, medium wt. nuclei 2−79725
shell model, state-of-the-art review 2−59669
shell model calcs. of masses 2−70362
shell model description of inelastic electron scattering spectra 2−63866
shell model for nuclear charge densities 2−46104
shell model level densities, applics. to neutron cross section calcs. 2−67129
shell structure for deformed nuclear shapes 2−73979
shell-model analysis for Brueckner calcs. in light nuclei 2−63766
shell-model analysis of Λ binding energies for p-shell hypernuclei 2−63760
single nucleon models when NN interaction has hard core 2−76772
single particle, rel. to collective motions 2−52719
spurious states in shell-model calculations, removal by projection techniques 2−49708
statistical, of de-exciting nucleus 2−59677
Strutinsky model, energy-of-deformation calcs. 2−82842
SU$_3$ model consistency and core polarization effective charge 2−49709
three-body cluster energy calc. 2−82858
U(3(A-1)) scheme, calc. of nuclear deformation 2−67125
unified model calcs. of odd neutron isotopes 2−42517
valency model, test using neutron capture in ^{92}Mo 2−67283
valency neutron model, test in ^{141}Pr(n,γ)^{142}Pr 2−67294
variable moment of inertia models in framework of Generator Coordinate Method 2−82870
variable moment-of-inertia model, applic. to odd-even nuclei 2−73989
variational principle, general formulation 2−73976
weak coupling between modes of motion 2−63743
α-particle model of Brink, α-cluster polarization, spherical cluster stability 2−73980
^{36}Ar, cluster model 2−70373
^{8}Be, α-cluster structure 2−83038
^{12}C, cluster model 2−70373
Ca, even-even nuclei, 1$^+$ states investigation using (^{3}He,p) reactions, 1f-2p shell model predictions 2−46130
^{40}Ca(α,α)^{40}Ca, 29 MeV, calc. of α-cluster effects using L-independent optical potential 2−83013
Cr, even-even nuclei, 1$^+$ states investigation using (^{3}He,p) reactions, 1f-2p shell model predictions 2−46130
Fe, even-even nuclei 1$^+$ states investigation using (^{3}He,p) reactions, 1f-2p shell model predictions 2−46130
^{71}Ga shell model study of energy levels, transition probabilities, moments of ground state 2−46142
^{5}He, two-centred cluster model calc. using supermultiplet scheme 2−55955

Nucleus continued
models continued
^{6}Li, two-centred cluster model calc. using supermultiplet scheme 2−55955
^{171}Lu, validity of the rotor model, ^{169}Tm(α, 2n)^{171}Lu obs. 2−59718
^{20}Ne, ^{22}Ne shell model, quartet states and cluster model 2−82868
^{16}O, α-particle model, binding energy of first 0$^+$ excited state 2−73998
^{30}P, low-lying structure studied in modified vibrational unified model 2−46124
Re (A=182, 182m), ground state structure and moments of inertia, Nilsson model 2−46164
Sn(d, d)Sn, A=112, 118, 119, 124, 20 and 27 MeV, ang. distrib., optical model fits. 2−79803
^{182}Ta, ground state structure and moments of inertia, Nilsson model 2−46164
^{160}Tb, ground state structure and moments of inertia, Nilsson model 2−46164
Ti, even-even nuclei, 1$^+$ states investigation using (^{3}He,p) reactions, 1f-2p shell model predictions 2−46130
size
— 2−63817
— 2−59678
bubble nuclei stability phenomena 2−82904
Ca, A=40, 44, 48, optical model determ. of r.m.s. radius 2−74076
core renormalization Coulomb energy differences 2−82847
critical charge, calculation method 2−46105
deformation energies, shell correction method 2−49720
deformed shapes, evidence for shell structure 2−73979
derivation from high-energy π^- reaction cross sections 2−52726
double-closed-shell nuclei, Hartree-Fock calcs. using modified delta interaction 2−63747
exotic nuclei, preparation, stability, use of Garson-Kelson mass relation 2−79724
fission barriers and odd-multipole shape distortions $84\leqslant Z\leqslant 120$ 2−70488
heavy nucleus surface form, determ. from angular distribs. of elastic and inelastic α-particle scattering 2−79765
mass, shell correction method 2−49720
mass calc. in shell model 2−70362
mass number dependence of diffraction model parameters for deuterons 2−42579
Mossbauer isomer shift and M1 transition used to determ. 2−76759
muon capture rate, correction due to presence of muon wave function in nuclear matrix elements 2−52804
N=108 deformed shell, effect on nuclear properties 2−55950
octupole deformation, nuclei beyond ^{208}Pb 2−63834
on-shell and off-shell uncertainties of nuclear-matter properties 2−55947
potential-energy surfaces, calc. using Strutinsky and alternative procedures 2−82843
radii of neutron matter distrib. in nuclei determ. from α-particle elastic scattering expts. 2−63904
radius parameters determ. from semi-classical model of n scatt. 2−67238
rare-earth region, ground state deformations, investigation by Strutinsky renormalization method 2−70363
superheavy nuclei radii using Hartree-Fock calculations 2−63838
toroidal nuclei, deform. minima 2−82903
Z=59 to 69, mass difference connections 2−52743
Ag, n and p distrib. 2−82951
^{36}Ar, Hartree-Fock calcs. of bubble phenomena 2−82905
^{9}Be, charge radius from electron scattering data 2−49726
^{12}Be, ground state mass, reaction ^{7}Li(^{7}Li,2p)^{12}Be study 2−70374
^{209}Bi, charge distribution, comparison with ^{209}Bi 2−46177
^{12}C, charge radius from electron scattering data 2−49726
Ca, A=40, 44, 48, study by Ca(p,p) scattering at 10.8 to 16.3 MeV 2−49738
^{40}Ca, calc. of energy and saturating nuclear size using density- and momentum-dependent delta function interaction 2−70350
^{40}Ca, radius, Hartree-Fock calculations with Feshbach- Lomon potential 2−73995
^{48}Ca, radius, Hartree-Fock calculations with Feshbach-Lomon potential 2−73995
^{47}Cr, mass, proton-rich nucleus in 1f$_{7/2}$ shell 2−63794
^{52}Cr, optical model determ. of r.m.s. radius 2−74076
^{162}Dy, quadrupole and hexadecapole deforms. 2−79752
^{164}Dy, quadrupole and hexadecapole deforms. 2−79752
^{166}Er, quadrupole and hexadecapole deforms. 2−79752
^{168}Er, quadrupole and hexadecapole deforms. 2−79752
^{170}Er, quadrupole and hexadecapole deforms. 2−79752
^{51}Fe, mass, proton-rich nucleus in 1f$_{7/2}$ shell 2−63794
^{54}Fe, optical model determ. of r.m.s. radius 2−74076
^{57}Fe, for 14.4 keV transition, obtained from Mossbauer effect in Xe 2−46426
^{57}Fe calc. from M1 transitions and Mossbauer isomer shift 2−76759
^{158}Gd, quadrupole and hexadecapole deforms. 2−79752
^{160}Gd, quadrupole and hexadecapole deforms. 2−79752
^{78}Ge, nucl.-charge distrib. 2−76814
^{79}Ge, nucl.-charge distrib. 2−76814
^{80}Ge, nucl.-charge distrib. 2−76814
^{81}Ge, nucl.-charge distrib. 2−76814
^{82}Ge, nucl.-charge distrib. 2−76814
^{83}Ge, nucl.-charge distrib. 2−76814
^{84}Ge, nucl.-charge distrib. 2−76814
^{3}H, charge radii, using Riihimaki potential 2−67142
^{3}He, charge and magnetic radii, S- and D-state effects 2−42497
^{3}He, charge radii, using Riihimaki potential 2−67142
^{3}He, charge radius 2−63763
^{4}He, radius, Hartree-Fock calculations with Feshbach-Lomon potential 2−73995
^{178}Hf first rot. state, shrinking of nucl. charge radius 2−76804
Hg isotopes, strongly deformed nuclei 2−46175
^{200}Hg, Hartree-Fock calcs. of bubble phenomena 2−82905
^{36}K, mass excess determ. from ^{36}Ar(p,n) and ^{36}Ar(^{3}He,t) reactions 2−70387
^{39}K and ^{40}Ca isotones, charge distribs., from electron scatt. 2−52745
^{6}Li, r.m.s. charge radius, determ. in photodisintegration calc. 2−70434
^{55}Ni, mass, proton-rich nucleus 1f$_{7/2}$ shell 2−63794

Nucleus continued
size continued
^{60}Ni(e,e), 225 MeV, determ. of cross-sections, charge density distrib. parameter 2−52803
^{15}O mass deduced from threshold energy meas. of ^{15}N(p,n)^{15}O 2−55957
^{16}O, calc. of energy and saturating nuclear size using density- and momentum-dependent delta function interaction 2−70350
^{16}O, radius, Hartree-Fock calculations with Feshbach- Lomon potential 2−73995
^{21}O, ground state mass determ. from Q-value meas. of ^{232}Th(^{22}Ne, ^{21}O)^{233}U reaction 2−70383
^{22}O, ground state mass determ. from Q-value meas. of ^{232}Th(^{22}Ne, ^{22}O)^{232}U 2−70383
Os N=108 deformed shell, effect on nuclear properties 2−55950
^{31}P and ^{32}S isotones, charge distribs., from electron scatt. 2−52745
^{35}P, 48-sec. isotope, mass 2−74014
Pb, n and p distrib. 2−82951
^{208}Pb, charge distribution, comparison with ^{209}Bi 2−46177
^{208}Pb, nucleon distribution near surface from α-particle scatt. 2−46150
^{195}Pt calc. from M1 transitions and Mossbauer isomer shift 2−76759
^{32}S, prolate shape evidence from 104 MeV alpha scattering 2−46126
^{128}Sb, charge and mass distrib. 2−83036
^{130}Sb, charge and mass distrib. 2−83036
^{33}Si, mass determ. in compound reactions 2−74013
Sn, A=116, 118, 120, 124 targets, study by 166 MeV α-particle scattering 2−63809
^{119}Sn, calc. from M1 transitions and Mossbauer isomer shift 2−76759
^{122}Te, neutron proton mass deform. of first excited 2^{+} state 2−42518
^{43}Ti, mass, proton-rich nucleus in $1f_{7/2}$ shell 2−63794
^{51}Ti, optical model determ. of r.m.s. radius 2−74076
^{203}Tl, muonic, size parameters 2−59961
^{205}Tl, muonic, size parameters 2−59961
^{51}V, optical model determ. of r.m.s. radius 2−74076
W N=108 deformed shell, effect on nuclear properties 2−55950
^{64}Zn(e,e), 225 MeV, determ. of cross-sections, charge density distrib. parameter 2−52803
^{66}Zn(e,e), 225 MeV determ. of cross-sections, charge density distrib. parameter 2−52803
^{90}Zr, nucleus distribution near surface from α-particle scatt. 2−46150

spin and parity
see also Gyromagnetic ratio; Molecules/nuclear coupling
— 2−59725
A=14, 15, wave functions of non-normal parity states 2−42498
A<50, spin cut-off factors from (n,2n) reactions at 14 MeV 2−70391
bound levels populated by (n,γ) reactions, method of spin assignment 2−67137
channel spin nonconservation, rel. to d-d elastic scatt. 2−59775
compound nucleus, phase difference of interfering states 2−52730
critical spin, A-dependence estimation from Coriolis anti-pairing 2−82849
deformed even-even, influence of spin and quadrupole interactions on properties of state with $K^{\pi}=1^{+}$ 2−67136
even nuclei, one-parameter model with EXP for energy ratios of YRAST levels to high spin 2−73984
even rare-earths calcs. of moments of inertia and g_r factors including residual p-h and p-p interaction 2−73988
even-even nuclei, $125 \leqslant A \leqslant 188$ and $A \geqslant 224$, rotational and irrotational flow calc. 2−63782
excitation of abnormal parity states by inelastic nucleon scattering, DWBA 2−74069
giant resonance, isospin splitting 2−82948
high spin states, probabilities of E2 transitions and meas. value of quadrupole moments in asymmetric top model 2−67138
high-spin states excited in (α,xγ) reactions, spin determ. from γ-ray ang. distrib. 2−79721
indirect interaction of nuclear spins through electrons in valence zones of semicond. 2−76760
K-quantum number, role in the de-excitation of compound nucleus 2−46328
light nuclei, A=11 to 65, mag. moment rel. to quasiparticle spin-orbit interaction 2−73991
light nuclei, use of K-harmonics method for spin- orbit splitting calcs. 2−67120
Meissner effect, nuclear prediction of singularities in ground-state bands of deformed nuclei 2−46117
moment of inertia, Hartree-Fock wavefunctions applic., cranked Hamiltonian concept 2−59682
moment of inertia calc. using cranking model 2−59681
neutron-nucleus spin-spin interaction and neutron strength functions 2−67260
nonconserving interactions, circular polarization of gamma-rays 2−42495
odd-even nuclei, application of variable moment of inertia model 2−73989
odd-odd and even-even spherical nuclei splitting of multiplet of $[j_1^{\pm 1}; j_2^{\pm 1}]$ configuration 2−55952
optical potential, depolarization and tensor part of spin-spin term 2−82940
optical potential spin, isospin and spin-orbit dependence 2−46218
selection rules in inelastic scattering, role of two-body spin-orbit interaction 2−70430
spin ($J \leqslant 10$) determ. from meas. of γ-ray linear polarization correlation, graphical method 2−70365
spin assignments to excited states made by measuring circular γ-ray polarization for transition in (n,γ) reactions 2−49801
spin flip in inelastic scattering possible explanation of observed backward-angle peak 2−79787
spin of levels excited by neutron capture is oriented target nuclei 2−49800
spin-isospin strength distrib. in final nucleus of radiative pion absorpt. processes in complex nuclei 2−82987
spin-spin interaction in nuclear system, exact quantum-mechanical theory 2−77031

Nucleus continued
spin and parity continued
Thomas-Fermi statistical method generalization to include spin-orbit interaction 2−42489
^{a}Cr (A=51,53), spin assignment using ^{b}Cr(n,γ) (B=50,52) 2−52819
^{a}Ni (A=61,63), spin assignment using ^{b}Ni(n,γ) (B=60,62) 2−52819
^{a}Xe A=131, 132, 133, fission products, spin assignments and γ-ray multipole mixing ratios 2−46207
^{221}Ac compound nucleus formed in ^{209}Bi + ^{12}C, ^{207}Pb + ^{14}N, ^{205}Tl + ^{16}O reactions, yrast trapping study 2−46335
^{25}Al excited state spins, ^{24}Mg(p,$p_1'\gamma$)^{24}Mg obs. 2−74009
^{26}Al, J=4 obtained for 2068.7 keV level, rotational structure evidence 2−63786
^{26}Al level struct. from ^{24}Mg(^{3}He,p) reaction 2−76876
^{27}Al high-spin states produced in ^{12}C(^{16}O,p) and ^{24}Mg(α,p) reactions, meas. of γ-ray branching ratio, p-γ angular correlation 2−42504
^{240}Am assignment to ground state based on log ft value meas. in electron capture decay 2−79770
^{36}Ar 6^{-} level obs. in ^{35}Cl(p,γ) reaction at 0.8-2.3 MeV following γ decay of 2231 keV resonance 2−52747
^{37}Ar, assignments to 3.171 MeV and 3.185 MeV levels populated in ^{37}Cl(p,nγ) reaction 2−74015
^{37}Ar assignments to levels below 3 MeV excitation determ. from lifetime and γ-ray angular distrib. meas. 2−63790
^{38}Ar, assignments to levels populated in ^{34}S(α,γ) reaction 2−63791
^{210}At, evidence for 15^{-} and 11^{+} isomeric states populated in ^{209}Bi(α, 3n) reaction 2−70415
^{211}At, configurational mixing and effective charge 2−52771
^{198}Au levels 2−67305
^{10}B, isospin impurity of 6.8 MeV state 2−63770
^{134}Ba, spin of 1643 keV state populated in β-decay of ^{134}Cs 2−70404
^{138}Ba, assignments verified by DWBA analysis of differential cross sections for elastic and inelastic scattering of α particles 2−46305
^{138}Ba, γ-ray and conversion electron spectra, spin-parity assignments 2−46155
^{138}Ba assignments to levels populated by inelastic proton scattering at 30 MeV 2−74079
^{9}Be, formed during ^{7}Li(d,α)^{5}He 2−74111
^{209}Bi, spin-dipole mode coupling with dipole oscillations 2−76809
^{81}Br, Coulomb excitation of low-lying levels by α-particles and ^{16}O ions, determ. of energies and spins 2−74032
^{12}C, isospin-mixing matrix element 2−63771
^{12}C(d, α)^{10}B, 7.19-13.99 MeV, isospin forbidden reaction obs. 2−63916
^{13}C, assignments made by phase-shift analysis of elastic scattering cross sections for neutrons on natural C targets 2−46274
^{41}Ca, spin assignments, (d, pγ) reaction study at 3 MeV 2−63793
^{43}Ca levels, spin values 2−82897
^{48}Ca, assignments to 4.61 and 5.15 MeV levels excited by inelastic proton scattering 2−82889
^{110}Cd, low-spin states studied in decay of ^{110}Ag 2−74035
^{112}Cd, low-spin states studied in decay of ^{110}Ag 2−74035
^{132}Ce, yrast states, energies and spins, collective bands 2−79757
^{33}Cl, assignments to levels excited in ^{32}S(p,p) scattering, 2.5-3.0 MeV 2−67153
^{34}Cl, odd parity spectrum exptl. and theoretical study using ^{33}S(p,γ) reaction and six- particle shell-model calculations 2−46127
^{34}Cl assignments for 1^{+} states 2−76877
^{37}Cl, low-lying level assignments 2−55960
^{57}Co, assignments to levels populated in ^{56}Fe(p,γ) reaction 2−63882
^{58}Co, assignments to levels excited in ^{55}Mn(α, nγ) reaction 2−82890
^{59}Co, spin assignments to levels at 1.01, 1.29 and 1.43 MeV populated in β-decay of ^{59}Fe 2−79769
^{60}Co, final level spins determ. in ^{59}Co(n,γ) reaction 2−67277
^{60}Co, spin assignments, using γ-ray ang. distrib. from ^{59}Co(n,γ) reaction 2−67278
^{60}Co excited state spins determ. by polarized neutron capture in ^{59}Co 2−67276
^{60}Co states, spin assignments following polarized neutron capture by ^{59}Co 2−79790
Cr, A=51, 53, spin determ. from (n,γ) circular polarization 2−67158
^{51}Cr, level spins determ. 2−79751
^{51}Cr, spin assignments to levels populated in (p,n) and (p,nγ) reactions on ^{51}V 2−46265
^{51}Cr spin assignments based on ln=1 J-dependence in ^{50}Cr(d, p) reaction 2−63920
^{53}Cr, spin assignments, (d, pγ) reaction study at 3 MeV 2−63793
^{131}Cs decay, gamma gamma directional correl. meas. 2−46197
^{135}Cs, ^{137}Cs, ^{139}Cs, γ-ray and conversion electron spectra, spin-parity assignments 2−46155
^{58}Cu levels populated in ^{58}Ni(p, nγ), determ. of spins and energies of levels below 1.7 MeV 2−74026
^{61}Cu levels spin assignments using DWBA curves from (α,p) reactions on Ni isotopes 2−59783
^{63}Cu levels spin assignments using DWBA curves from (α,p) reactions on Ni isotopes 2−59783
^{65}Cu levels spin assignments using DWBA curves from (α,p) reactions on Ni isotopes 2−59783
^{65}Cu spins of isobaric analogue states excited in ^{64}Ni(p,p′) reaction 2−63804
^{67}Cu levels spin assignments using DWBA curves from (α,p) reactions on Ni isotopes 2−59783
^{153}E level struct., Coulomb excitation obs. 2−76884
Er, A=165, 167, 169, positive-parity states by (^{3}He, α) reaction 2−79747
^{158}Er, moment of inertia of high-spin rotational states 2−63818
^{161}Er, ^{163}Er, hyperfine interaction consts. and nuclear moments meas. using atomic beam magnetic resonance method 2−79741
^{151}Eu level struct., Coulomb excitation obs. 2−76884
^{18}F, odd-parity levels with three- particle one hole structure excited in ^{15}N(^{6}Li, t) reaction 2−74001
^{20}F low-lying states obs. from ^{19}F(d,pγ) ang. correl. 2−79801
Fe, spin assignment using ^{54}Fe(n,γ) 2−52819
^{54}Fe levels, spin assignments 2−76836
^{55}Fe, spin assignments, (d, pγ) reaction study at 3 MeV 2−63793
^{55}Fe, spin determ. from (n,γ) circular polarization 2−67158

Nucleus continued
spin and parity continued
^{55}Fe assignments determ. in ^{57}Fe(p,t) two-nucleon pick-up reaction at 27 MeV 2–63883
^{56}Fe 3120 keV level spin determ. 2–74024
^{58}Fe, interference of two spin components of capture state in ^{57}Fe(n,γ) reaction 2–42572
^{59}Fe spin assignments made from comparison of angular-momentum transfer in ^{57}Fe(t,p) and ^{58}Fe(d,p) reactions 2–63921
^{147}Gd, high spin levels excited in ^{144}Sm (α,n) reaction, particle core coupling 2–49750
^{151}Gd, spin of excited states determ. from γ-γ angular correlation 2–46160
^{156}Gd, level assignments 2–46162
^{156}Gd, of excited states, from ^{156}Eu decay 2–49751
^{158}Gd, of excited states, from ^{158}Eu decay 2–49751
^{74}Ge, excited states, obs. from ^{74}As decay 2–49765
^{4}He isospin mixing in excited states rel. to (γ,n) and (γ,p) reactions 2–83000
^{168}Hf, high-spin states produced in (α,8n) reactions, anomalous behaviour of nuclear moment of inertia at large rotational frequencies 2–42528
^{174}Hf, role of K-quantum number in de- excitation following Yb(α,xnγ)^{174}Hf 2–46328
^{178}Hf, ^{180}Hf, J-depend. of level density from statistical props. of series of resonances 2–46171
^{180}Hf, investigation of parity non-conserving force between nucleons by meas. of circular polarization of γ transition 2–63840
^{180}Hf, parity admixtures in nuclear forces 2–59726
^{180}Hf 57 keV gamma transition, parity-violating and normal multipole mixing ratios 2–46172
^{200}Hg, 1515.2 and 1972.5 keV levels 2–79774
^{165}Ho(n,nγ), differential cross sections and angular distributions of gamma rays 2–46159
^{117}In level scheme from ^{117}Cd and ^{117}Cd^{m} decay 2–76819
^{191}Ir, level assignments 2–76806
^{193}Ir, assignments 2–46173
^{40}K, interference of two spin components of capture state in ^{39}K(n,γ) reaction 2–42572
^{40}K, spin assignment, (n,γ) reaction obs. 2–67273
^{41}K, γ-decay nonconservation of P-parity studied by meas. of γ-transition circular polarization 2–49739
^{42}K, spins of states determ. by γ-γ correlations in ^{41}K(d,p) reaction at 6 MeV 2–46131
^{79}Kr, low-lying state spin determ. 2–79759
^{81}Kr, low-lying state spin determ. 2–79759
^{82}Kr, γ-γ correlation study 2–46145
^{83}Kr, low-lying state spin determ. 2–79759
^{85}Kr, low-lying state spin determ. 2–79759
^{86}Kr, assignments to levels fed in decay of ^{96}Br 2–46188
^{137}La, spin=7/2 obs. 2–63813
^{6}Li, parity and isobaric spin violating decay of 3.56 MeV level 2–82883
^{6}Li isospin impurity of 4.75 MeV state 2–82879
^{167}Lu, ground state spin meas. with atomic-beam magnetic resonance method, comparison with Nilsson model value 2–42529
^{24}Mg assignments to highly excited states from triple correlation meas. on ^{16}O(^{12}C, α)^{24}Mg* reaction 2–74007
^{54}Mn, assigments to levels populated in ^{54}Cr(p, nγ) and ^{51}V(α, nγ) reactions 2–79743
^{54}Mn, level structure from ^{54}Fe(n,pγ)^{54}Mn reaction 2–46133
^{54}Mn, of low lying levels, using ^{54}Cr(p,nγ) 2–46134
^{55}Mn assignments determ. in ^{57}Fe(p,τ) and ^{57}Fe(d,α) two- nucleon pick-up reactions at 27 MeV and 16 MeV 2–63883
^{90}Mo assignments for levels populated in ^{92}Mo(p,t) reaction 2–70398
^{93}Mo, 1.69 MeV level, j-value determination by spectroscopic factor ratios near closed shells 2–74034
^{93}mo, assignments to levels excited in ^{94}Mo(^{3}He, ^{4}He) reaction at 16 MeV 2–70401
^{14}N, first unbound state parity 2–63773
^{14}N, γ-decay of 8.06 and 5.69 MeV levels, isospin mixing 2–76780
^{15}N, two-particle three-hole character of negative parity states studied using ^{13}C(^{3}He,p) reaction 2–63775
^{15}N, two-particle three-hole structure of negative parity states studied via ^{12}C(^{3}He,p) reaction 2–70375
^{23}Na, level transitions and level assignments 2–76789
^{23}Na, lowest lying $J\pi={}^{1}\!\cdot_{2}$ level prediction 2–46118
^{93}Nb levels, assignments from (n,n'γ) reaction 2–67164
^{142}Nd, isospin splitting of giant E1 excitation in ^{141}Pr(p,γ) reaction 2–82891
^{143}Nd, neutron resonance spin determinations from capture gamma ray meas. 2–49749
^{144}Nd, high state assignments 2–67196
^{145}Nd, neutron resonance spin determinations from capture gamma ray meas. 2–49749
Nd(t,p), (A=142, 144, 146, 148, 150) 13 MeV, angular distributions and Q-values 2–42523
^{20}Ne, classification of high-spin states into rotational bands 2–49732
^{21}Ne, level struct., ^{18}O(α,nγ) obs. 2–55958
^{21}Ne, lowest lying $J\pi={}^{1}\!\cdot_{2}$ level prediction 2–46118
^{21}Ne excited states obs. using ^{18}O(α,nγ) reaction 2–59696
^{22}Ne, level assignments following ^{20}Ne(t, pγ)^{22}Ne 2–79739
^{22}Ne rot. bands excited in ^{18}(^{7}Li,t)^{22}Ne 2–76788
Ni, A=61, 63, spin determ. from (n,γ) circular polarization 2–67158
^{56}Ni, from ^{54}Fe(^{3}He,n)^{56}Ni reactions 2–59701
^{15}O, assignment to 10.4 66 MeV excitation state populated in ^{12}C(^{3}He,n) reaction 2–46316
^{16}O, 8^{+} level, study by ^{12}C(α, ^{8}Be)^{8}Be reaction from 15 to 18.96 MeV 2–79733
^{16}O, level assignments from ^{12}C(α, α)^{12}C 2–79735
^{19}O, assignments to levels near 2.7 MeV excitation determ. in ^{17}O(t,p) reaction 2–79734
^{30}P levels, odd parities, ^{29}Si(d,n)^{30}P reaction obs. 2–67328
^{31}P(p,p'), excited states at 185 MeV 2–46125
^{32}P, spin assignments of levels populated in ^{31}P(d,p) reaction at 10 MeV 2–49834
^{32}P, spins of five states populated in ^{29}Si(α,p) reaction 2–49735
^{35}P ground state spin-parity 2–74014
^{198}Pb, ^{200}Pb, level assignments from ^{198}Bi, ^{200}Bi decay 2–46174
^{206}Pb, assignments to levels populated in ^{206}Bi decay 2–70413
^{207}Pb, spin-dipole mode coupling with dipole oscillations 2–76809
^{105}Pd, assignments to levels populated in ^{104}Ru(α,3n) reaction 2–49744
^{105}Pd, neutron reson., spin determ. by γ-ray multiplicity method 2–67167
^{109}Pd, spin of 3/2 resonance determ. 2–67288
^{144}Pm, ground state upon assignment 2–67196
^{210}Po, assignment using ^{210}At$\rightarrow$^{210}Po electron capture decay 2–63836
Pr neutron-deficient isotopes spin values 2–82899
^{139}Pr, assignment to 852 keV excited state 2–46158
^{141}Pr(n,nγ), differential cross sections and angular distributions of gamma rays 2–46159
Pt, even mass nuclei 182$\leqslant$A$\leqslant$192, low- lying level properties from Hg isotope decay data 2–49755
^{239}Pu, parity mixing of hindered E1 γ transitions 2–46207
^{240}Pu, assignment to two-quasi-particle configuration state populated in electron capture decay of ^{240}Am 2–79770
^{86}Rb hole states obs. using ^{88}Sr(d α)^{86}Rb reaction 2–82909
Re (A=182, 182m), ground state structure and moments of inertia, Nilsson model 2–46164
^{185}Re, spin 1/2^{+} assignment to 879 keV level populated from electron capture decay of ^{185}Os 2–67178
^{105}Ru levels, spin assignments, ^{104}Ru thermal neutron capture obs. 2–67287
^{32}S(p,p'), excited states at 185 MeV 2–46125
^{34}S, spin assignments for higher excited states using ^{31}P(α,p)^{34}S 2–52746
^{35}S level scheme from ^{35}P β-decay obs. 2–74049
Sb, A=122, 124, levels 2–67291
^{110}Sb, from decay obs. following Sn(p, xn) reactions 2–76818
^{111}Sb, from decay obs. following Sn(p, xn) reactions 2–76818
^{112}Sb, from decay obs. following Sn(p, xn) reactions 2–76818
^{113}Sb, from decay obs. following Sn(p, xn) reactions 2–76818
^{114}Sb, from decay obs. following Sn(p, xn) reactions 2–76818
^{44}Sc level struct., ^{44}Ca(^{3}He,t) obs. 2–74020
^{45}Sc, levels between 1.05 and 3 MeV, ^{44}Ca(p,γ)^{45}Sc reaction 2–42509
^{46}Sc low-excited states, spin values 2–67156
^{49}Sc, isobaric analog states study by elastic and inelastic proton scatt. from ^{48}Ca 2–70390
^{28}Si 612 keV reson. in ^{27}Al(p,γ) reaction 2–76844
^{29}Si, DWBA analysis of data from ^{28}Si(d,p)^{29}Si reaction at 10 MeV 2–56000
^{30}Si, resonances obs. in α reactions on ^{26}Mg, spins, parties and widths 2–46123
^{144}Sm, assignments, verified by DWBA analysis of differential cross sections for elastic and inelastic scattering of α and p 2–46305
^{144}Sm assignments to levels populated by inelastic proton scattering at 30 MeV 2–74079
^{147}Sm, neutron reson., spin determ. by γ-ray multiplicity method 2–67167
^{148}Sm levels, spin determ. 2–76801
^{149}Sm, neutron reson., spin determ. by γ-ray multiplicity method 2–67167
Sn(A=117, 119), spins of Coulomb excited states 2–63810
^{132}Sn doubly closed shell region, assignments to two-proton and proton-neutron states populated in ^{134}Sb beta decay 2–82895
^{181}Ta, investigation of parity non-conserving force between nucleons by meas. of circular polarization of γ-transitions 2–63840
^{181}Ta, parity admixtures in nuclear forces 2–59726
^{182}Ta, ground state structure and moments of inertia, Nilsson model 2–46164
^{159}Tb, investigation of parity non-conserving force between nucleons by meas. of circular polarization of γ transitions 2–63840
^{160}Tb, ground state structure and moments of inertia, Nilsson model 2–46164
^{160}Tb levels, spin assignments, (n,γ) and (n,e^{-}) reaction obs. 2–67174
^{101}Tc, low-lying positive-parity states, ^{101}Mo β decay obs. 2–59705
^{125}Te, study of positive of negative parity states populated in decay of ^{125}Sb 2–46195
^{231}Th, highly deformed, effective moment of inertia, determination from neutron-induced fission of ^{230}Th 2–59723
^{45}Ti, assignments to 40, 1353 and 1468 keV levels 2–46132
^{48}Ti, elastic and inelastic scattering of protons, meas. of spins, parities, widths and spacing of analogue resonances 2–79783
^{203}Tl, investigation of parity non-conserving force between nucleons by meas. of circular polarization of γ-transitions 2–63840
^{203}Tl, parity admixtures in nuclear forces 2–59726
^{170}Tm, structure of low-lying rotational bands 2–49752
^{236}U spins of resonances produced in epithermal neutron capture by ^{235}U 2–52820
^{50}V, level assignments, ^{3}He reaction study 2–63796
^{133}Xe, ^{135}Xe, ^{136}Xe, γ-ray and conversion electron spectra, spin-parity assignments 2–46155
^{164}Yb, high-spin states produced in (α,8n) reactions, anomalous behaviour of nuclear moment of inertia at large rotational frequencies 2–42528
^{166}Yb, moment of inertia of high-spin rotational states 2–63818
^{170}Yb level scheme from β-decay of ^{170}Lu 2–76821
Zn isotopes, from Zn(t,p) investigations 2–56001
Zn(A=64,66,68), radiative widths of spin-1 levels using γ-ray scatt. 2–59692
^{90}Zr, giant multipole resonances by inelastic electron scattering 2–79776
^{92}Zr spins of levels populated in (n$_{th}$,γ) reaction 2–67163
theory
see also BCS theory; Nuclear forces; Nuclear structure
A=59, 60 nuclei, validity of pseudo SU(3) 2–52750
Alt-Grassberger Sandhas eqns., solution above three-particle break-up threshold using Yukawa potentials 2–70351
angular correlations, static and time-dependent perturbations 2–59661
anharmonic oscillator, centre-of- mass motion 2–73965

Nucleus continued
theory continued
anharmonic vibrations, collective momentum and collective Hamiltonians 2−82874
average one-body operators with fixed angular momentum and seniority 2−82848
BCS and Hartree Fock Bogoliubov approx. compared 2−46072
Bethe-Goldstone equation, solution in finite nuclei from NN phase shift data, applic. to ^{18}O and ^{18}F 2−46067
boson expansions and Hartree-Bogoliubov theory 2−63736
Brueckner-Bethe theory, relation to equations for linked clusters 2−79708
bubble nuclei stability phenomena 2−82904
charge and current distribs. meas. using exotic atoms with large overlap orbitals 2−77027
cluster expansion renormalization 2−79720
collective motion, description in terms of boson expansion technique 2−70358
collective motion, description of monopole degree of freedom 2−82864
collective motions, symmetry-conserving theories 2−73977
collective potential energy surface, effect of spurious motion 2−70356
collective rotation in particle index space 2−70344
conserving approximations, aaplication to calc. of effective particle-hole interaction 2−73964
continuum shell-model approximation schemes, comparison 2−63855
core renomalization, Coulomb energy differences 2−82847
Coriolis anti-pairing transition of ground state rotational band, simplified microscopic model 2−73986
correlated wave functions and effective operators determ. using unitary separable approx. to two-body reaction matrix 2−63741
Coulomb displacement energy, odd even effect 2−70341
Coulomb energies in 1p shell 2−67122
Coulomb interference in half-shell two-nucleon t-matrix derived from Hamada Johnston potential 2−52722
coupled channel calculation method 2−55948
coupling constants, variation with time 2−59658
currents, nuclear, global method of treatment 2−67113
density- and momentum-dependent delta function interaction 2−70350
density-matrix expansion for effective nuclear Hamiltonian 2−46088
effective interaction in perturbation expansion form 2−73975
energy bounds and convergence of perturbation expansions 2−79715
energy spectra Gaussian distrib. in *j* shell 2−67115
equations of motion approach to nuclear spectroscopy 2−82947
even-even deformed nuclei, rotational motion at large angular momentum 2−73987
even-even nuclei, symmetry energy 2−79729
excited nuclei, pairing fluctuations in nuclear gap parameter, absence of second order phase transition 2−49715
extended uniformly charged nucleus, hydrogenic wave function 2−49704
finite nuclei $A=16-208$, calc. of density dependent effective interactions using HF theory and local density approx. 2−79709
fissioning nuclei, double potential barrier, effect of deformation-dependent inertial parameter on penetration 2−79814
folded diagrams, soln. of model-space eigenvalue problem 2−82866
fractional parentage coefficients with isotopic spin, degenerate states separation 2−76771
gamma ray angular correlations perturbation by stochastic Gaussian-Markov process 2−55946
Gamow states of square-well plus square-barrier model, expectation value of r^2 2−73978
Glauber theory, modification for diffraction dissociation of hadrons in nuclei 2−70428
ground state binding energy of s-d shell nuclei, calc. using Strutinsky model 2−82875
ground state energy in Brueckner and Jastrow theories 2−79711
harmonic polynomials, generalized method 2−79727
Hartree-Fock theory and collective motion for nuclear states 2−82863
hole states, damping in giant dipole resonance 2−73983
infinite and finite matter theory 2−63746
isobar configurations, construction, application and possible tests 2−82860
Jastrow method for nuclear matter, pair distribution function 2−76773
Jastrow-type correlated wave function, expansion procedures 2−59659
level spacings, correlation functions and statistics 2−46073
light nuclei, $4\leqslant A\leqslant 41$ unrestricted HF approx. calcs. of ground state properties 2−63733
light nuclei, α-like spatial four-body correlations 2−46108
light nuclei, G-matrix elements for 1s, 1p, 1d and 2s shells 2−49714
light nuclei, use of K-harmonics method for spin- orbit splitting calcs. 2−67120
light nuclei ($A\leqslant 6$), vertex functions and coupling constants for virtual decay 2−63762
liquid drop model of fissioning nuclei, charge polarization effects 2−79809
local density approximation, spurious centre of mass effect 2−59671
M1-intranuclear conversion analysed on basis of Saxon-Woods potential 2−46089
many body problem, Hartree Fock method generalization incorporating 2 body correlations 2−63730
many-body Jastrow and Brueckner theories, subsidiary conditions 2−46071
many-body problem, collective motions and single particle models 2−52719
many-particle config., moments of energy spectra, reduction relations 2−59660
many-particle matrix elements in seniority scheme, sum rules 2−55949
many-quasiparticle subspaces, extension of spectral distrib. method 2−63749
matter, comparison of reaction-matrix and Jastrow methods 2−79714
matter, ground state of fermion system, model wave junction of BCS type 2−63043

Nucleus continued
theory continued
matter, role of gas-liquid phase transition 2−73981
matter distribs. calc. of spin-orbit component of optical model for spherical and deformed cases 2−70361
Meldner's realistic single-particle Hamiltonian, fast and accurate solutions 2−49711
microscopic, book on theory of nuclear structure 2−79731
morse type effective potential for Thomas- Fermi calcs. 2−52723
multineutrons, criteria for existence 2−46070
neutron charge form factor contrib. to elastic electron scatt. from nuclei 2−82955
neutron star internal structure in density region 3.1×10^{11}-2×10^{15} g/cm^3, study using new nuclear matter energy model 2−69087
neutron-proton correlation effects in medium weight spherical nuclei 2−67123
non-adiabatic TDHF eqns. of large amplitude, new cranking model for solution 2−82871
non-Hermitian Hamiltonians, decaying states and perturbation theory 2−63729
non-local potential for single-particle properties of nuclei as function of A and Z 2−70349
nuclear matter, unitary model approach for tensor correlations 2−59672
odd superfluid nuclei, use of number-projected BCS model to improve IGE method 2−49707
odd-even nuclei, application of variable moment of inertia model 2−73989
odd-mass nuclei, decoupled Yrast states 2−63814
off-shell two-body T-matrix and separable potential, Noyes-Kowalski approximation 2−70353
on- and off-shell T matrix, variational approach 2−73972
one-particle, one-hole nuclei, core excitations by six-point Green function 2−79712
pairing, generalized pairing, new derivation 2−46068
pairing correl., unified description 2−67116
pairing tendencies of T=1 and T=0 interactions 2−79719
pairing vibrations, modified Tamm-Dancoff approximation 2−46100
projection-operator in G-matrix eqn. 2−79717
properties in relation to nucleon structure 2−76766
quasi-particle subspaces, applications of spectral distribs. method 2−82873
quasiboson operator, generating function method 2−52720
reduced rotation matrix elements, subprogram for calc. 2−66452
reduced width calculational method 2−70366
relativistic nuclear matter calcs., deficiency of one-boson exchange potentials 2−63744
rotation matrices, simple solution 2−77039
rotational states, phenomenological description 2−73990
rotational states, stability condition determ. using procedure of Hartree-Fock-Bogoliubov method 2−63755
RPA method with angular momentum projection 2−79730
saturation properties in nuclear matter of six realistic nucleon-nucleon potentials 2−55947
SCF theory, using relativistic form of generalized one Boson exchange potentials for NN force 2−70346
separable potentials and Coulomb interactions 2−67117
shell corrections, parameterization of numerical state density calc. 2−46090
shell stabilizing effects and neutron level spacing distributions 2−46075
single nucleon models when NN interaction has hard core 2−76772
soft multipole radiation and charge-current distribution 2−59683
spherical nuclei, HF calcs. in local density approx., saturation properties 2−79710
spherical Woods-Saxon potential well, asymptotic expansion for eigenvalue density 2−73330
spurious states in shell-model calculations, removal by projection techniques 2−49708
Strutinsky's method of calc. shell corrections to expressions for nuclear energy 2−52727
superconducting nuclei, number conserving quasi- particle correlations 2−79707
superheavy nuclei, long-lived, theoretical stability regions esp. Z=114 2−79763
symmetries and distrib., general simplicities in complicated systems 2−82865
Talmi integrals and effective interaction, contrib. of central, spin-orbit and tensor forces 2−76764
Talmi-Moshinsky transformation brackets of unequal-mass particles 2−46084
Thomas-Fermi statistical method generalization to include spin-orbit interaction 2−42489
three nucleon bound state, convergence of generalized spherical harmonic emphasis 2−63765
three nucleon low-energy parameters in doublet spin-state, soln. of Skornyakov−Ter-Martirosyan eqns. 2−67118
three-body cluster energy calc. 2−82858
three-body problem, Faddeev−Lovelace equations in eikonal approximation 2−70348
three-body problem, potential harmonics 2−67119
three-nucleon bound state from Faddeev equations with realistic potential 2−63763
three-nucleon problem with potential containing repulsive core 2−55954
three-nucleon system, calcs. using Reid and Gammel-Brueckner potentials 2−49723
three-nucleon system, Faddeev-Lovelace formulation, angular momentum decomposition 2−67144
three-nucleon systems, Faddeev eqns., bound-state wave functions 2−63738
three-parameter N-N soft-core central potential 2−73973
three-particle amplitude, Gilbert-Schmidt expansion 2−79728
toroidal nuclei, deform. minima 2−82903
transformation properties of effective transition operator for particle-particle and hole-hole nuclei 2−82861
tri-nucleon systems, effect of $\Delta(1236)$ resonance 2−49712
trinucleon bound state, properties from exact solution of Faddeev equations with realistic nuclear forces 2−46077

Nucleus continued
- **theory** continued
  - trinucleon energy using unitary pole approx. to Reid's soft core potential 2−49724
  - two interacting particles in potential hole, possibility of bineutron existence 2−67121
  - two-body interaction, expansion coefficients of many-particle matrix elements 2−52721
  - two-body matrix elements including bound states, Talmi-Moshinsky procedure 2−73966
  - two-body random Hamiltonian ensembles, properties 2−82872
  - unitary pole approximation, quality of three-body wave function 2−49705
  - variational principle, general formulation 2−73976
  - weak interaction and currents of second kind 2−52718
  - weak processes, induced-tensor interaction 2−63728
  - NN spin-orbit interaction, single-particle spin-orbit potential 2−59670
  - ^{36}Ar, Hartree-Fock calcs. of bubble phenomena 2−82905
  - ^{135}Ba, test of applicability of core-excitation model 2−59710
  - ^{8}Be, α-particle cluster structure 2−82880
  - ^{12}C, continuum structure discussed in eigenchannel reaction theory 2−67147
  - ^{40}Ca, HF charge distribution tested by electron scattering data 2−74016
  - ^{42}Ca, shell-model calculations, low-lying level spacing 2−49727
  - ^{48}Ca, HF charge distribution tested by electron scattering data 2−74016
  - ^{2}H, relativistic wave function 2−49722
  - ^{3}He form factors, S'- and D-state effects 2−42497
  - ^{4}He, ground state, tensor force formalism 2−73996
  - ^{200}Hg, Hartree-Fock calcs. of bubble phenomena 2−82905
  - ^{24}Mg, SU(3) calculations 2−46121
  - ^{16}O, off-shell effects in binding energy calcs. for set of phase-shift equivalent potentials 2−70376
  - ^{18}O, shell-model calculations, low-lying level spacing 2−49727
  - ^{19}O, study of energy spectrum and e.m. properties in framework of unified asymmetrical rotational models 2−52737
  - ^{208}Pb, HF charge distribution tested by electron scattering data 2−74016
  - ^{210}Pb, shell-model calculations, low-lying level spacing 2−49727
  - ^{28}S, problems in structure studies 2−74011
  - ^{92}Zr, shell-model calculations, low-lying level spacing 2−49727

Oceanography
- *see also Liquid waves; Seawater*
- acoustic communication channel, model capacity 2−49157
- acoustic current meter 2−54772
- acoustic propagation, velocity profiles in geometrical acoustics 2−44653
- acoustic propagation in uniformly moving ocean channel with depth-dependent sound speed 2−57839
- acoustic ray propagation in channel with depth variable sound speed and current 2−62029
- acoustic transmission into basin with bigradient sound speed profile 2−44654
- acoustic wave generation, normal mode, vertical array of projectors in shallow water 2−44660
- acoustics, intensity range relations 2−72715
- air mass transformation experiment, East China Sea 2−62164
- air-sea interaction studies in Davis Strait 2−62121
- air-sea interface, unified model for heat and gas exchange 2−62069
- Alaskan tsunami (1964), characteristics at Pacific tide stations 2−62059
- albedo of sea surface 2−78318
- Alboran Sea, evidence for rigid plate separation 2−54752
- Alboran Sea, statistical analysis of bottom topography 2−51551
- Antarctic, structure and circulation of deep water 2−81596
- Antarctic Circumpolar Current, Kerguelen-Gaussberg Ridge effect 2−54783
- anticyclonic vortex trapped above seamount, mechanism for generation 2−44627
- Arabian Sea during southwest monsoon season, stratification and circulation 2−62026
- Arctic, internal wave spectra, temp. profile study 2−62039
- Arctic and Antarctic investigations during the Soviet Regime 2−62049
- Arctic Sea ice, aircraft meas. of microwave emission 2−81632
- Arctic SOFAR propagation, effect of ice layer 2−41787
- Atlantic, sea-air interaction, quantitative aspects 2−54759
- Atlantic currents, role in directing of hurricanes 2−44635
- Atlantic Ocean, equatorial countercurrent, velocity structure 2−54770
- Atlantic Ocean, heat flow profiles 2−51534
- Atlantic Ocean, surface temperature nonuniformities 2−44642
- Atlantic Ocean, western boundary undercurrent caused by subsidence due to contraction of cooling lithosphere 2−72649
- Atlantic Ocean floor, geomorphological aspects 2−72684
- Atlantic Ocean thermocline statistics 2−54760
- Atlantic thermolcine, tritium penetration, exchange coeffs., advection rules 2−72705
- Aves Ridge in Caribbean Basin, petrogenesis of oceanic granites 2−62023
- axially symmetric submarine daylight field 2−57892
- Baffin Bay, heat flow obs. 2−68869
- Baltic Sea, light scattering, intensity fluctuations 2−48419
- Baltic sea water, influence of suspended matter on transparency 2−78329
- Barbados oceanographic and meteorological experiment of 1969 2−62057
- baroclinic ocean currents, comparison of different methods of calc. 2−44617
- Bay of Bengal, prediction model for storm surges 2−75482
- Bay of Bengal, storm surges rel. to dynamics and storm-tide tables 2−75483
- beach dynamics as function of prevailing wind direction and speed 2−57852
- beam transmittance in turbid waters of Biscayne Bay, time series study 2−57893
- Beaufort Sea, southern, warm water intrusion 2−57884

Oceanography continued
- benthic front in South Pacific, salinity-temperature-depth soundings 2−75465
- benthic inspection using ship towed sensor vehicles 2−72724
- Bermuda slope, temp. and salinity microstructure rel. to mean flow pattern 2−84752
- Bermudan main thermodine; temperature fluctuation spectrum 2−81597
- biogenic opal solution rate in seawater 2−72710
- bistatic backscattering, of l.f. underwater sound, from ocean surface 2−75479
- Black Sea, late Pleistocene and Holocene history 2−65451
- Black Sea, O_2-H_2O balance 2−44645
- Black Sea floor, heat flow 2−54738
- Black Sea temp. fields and salinity rel. to statistical structure analysis 2−81612
- Black Sea tsunami energy, and wave field charts 2−48421
- Block Island Sound, seasonal variation in temperature and salinity 2−57872
- bottom topography effects on circulation, currents over a ridge 2−51540
- bottom topography effects on circulation, two layer model 2−51541
- bottom topography influence on circulation, barotropic model 2−51539
- boundary currents in rot. β-plane water tunnel 2−53353
- BPV-type current recorders, dispersion in current velocity meas. 2−62054
- breaking waves, air entrainment 2−57924
- breakwaters and transportable wave barriers, review 2−54747
- cabbeling instability analysis 2−57919
- calcareous marine sediments, isoelectric racemization, kinetics and mechanism 2−48417
- Cannikin nuclear explosion, long period water wave meas. 2−62068
- Cape Farewell, Greenland, new mid-ocean channel 2−57914
- Cape Hatteras, power spectra of temp. and salinity fluctuations in slope water 2−57858
- Caribbean basement basalt, compressional or extensional tectonics 2−62064
- Caribbean Sea, tidal currents 2−54751
- Caribbean Sea, western, Lagrangian current and hydrographic meas. 2−62070
- Caribbean water masses 2−54750
- Caspian Sea oil field areas, maximum wave parameters computation 2−54762
- channel with horizontal and vertical sound-speed gradients, reflected/refracted ray propagation 2−57841
- Chesapeake Bay, mixing model of fluoride distribution 2−65610
- circulation and wind driven currents in two-link barotropic ocean 2−51537
- Clipperton Fracture Zone, eastward-flowing bottom currents 2−44612
- coastal boundary layer in Lake Ontario, spring regime 2−62035
- coastal currents, stability, formation of gyres 2−51546
- coastal currents of Great Lakes, complex diffusion processes 2−62038
- coastal dynamics, problems 2−62052
- coastal upwelling, beta-plane model 2−54782
- coastal upwelling numerical model 2−62032
- coastal upwelling region, automated NH_3 determ. 2−72708
- coastal waters, sound-speed dispersion and fluctuations 2−44661
- coastal zone, variable mag. field induced by geomag. field 2−48596
- coastline under hurricane action, computer simulation 2−57875
- collection and processing of data from instrumental measurements 2−62047
- collection and processing of data from instrumental measurements 2−62047
- colour determination through scattering atm. 2−65587
- colour meas. from spacecraft in noon orbit rel. to Earth resources studies 2−84773
- computer simulation of ocean currents rel. to two fluid media model 2−78320
- conduction signalling 2−81630
- conference, Brighton, England, (1972) 2−62058
- contemporary trends originating with the floating marine research institute 2−62046
- continental margin of NW Indian Ocean, probable extension 2−54765
- continental slope, current struct. 2−57920
- continuously stratified ocean, internal waves 2−51556
- continuously stratified ocean, steady coastal upwelling 2−62033
- coral growth rate using ^{228}Ra and ^{210}Pb 2−62025
- cosmic spherules concentration in deep-sea Mn nodules from cores 2−75931
- current and wind obs. over continental shelf 2−65612
- current meas. east of Barbados 2−65618
- current sensors using quartz crystals, for use in deep sea 2−44668
- currents, variations, recent data 2−62048
- currents, wind driven, stationary, theory in two layer ocean 2−44618
- currents and density fields in oceans with arbitrary bottom relief 2−68867
- currents in subarctic frontal zone in NW Pacific Ocean, computation 2−54756
- cyclonic eddy obs. S.E. of Cape Hatteras 2−62077
- daylight field, axially symmetric submarine 2−65607
- deep current obs. near 36°N, 70°W 2−62081
- deep ocean drill sites, heat flow 2−54777
- deep Pacific Ocean cores, susceptibility stratigraphy and paleomagnetism 2−44763
- deep scattering layers in Gulf of Mexico response to total solar eclipse 2−48416
- deep sea anomalies and salt domes 2−57926
- deep sea channels, near bottom currents, transport of suspended materials 2−65595
- deep sea chert, origin 2−62065
- deep sea cores, mago properties and mineralogy 2−62024
- deep sea cristobalitic chert, ultramorphology 2−57843
- Deep Sea Drilling Project, biostratigraphy 2−62066
- deep sea sediments rel. to cosmic dust 2−73101
- deep submergence windows 2−84765

Oceanography continued
Deep Western Boundary Current, flow, in western equatorial Pacific 2−57864
Denmark Strait, bottomside sea ice features, statistical analysis 2−57885
Devon Island, small Arctic catchment, annual hydrological regime 2−51532
diffusion in the sea, use of tracers, dependence of eddy diffusion coefficients on scale of phenomena 2−44630
diffusion process, application to dispersion of pollutants 2−44631
dissipative two-layer model, anomalous baroclinic response 2−54781
disturbed water surface, brightness, statistical characts. 2−48418
diurnal effect at Pt. Mugu, Calif., from wave gauge data 2−57866
diurnal variation in visually-observed breaking waves 2−57867
Drake Passage, sealevel slope rel. to press. and wind half-yearly oscills. 2−72709
Earth-atmosphere-ocean system, intransitive model 2−44518
East African coast, current reversal with onset of southwest monsoon 2−65617
eastern equatorial Pacific, heat flow and bottom water temperature tectonic interpretation 2−48374
Eastern Indian Ocean, thermal anomalies 2−65626
eastern Mediterranean Sea, thermal frontal zones 2−65599
Eastern Pacific Ocean, diurnal and seasonal variations in acoustic volume scattering meas. 2−62030
eddy currents in sea of finite depth, modelling 2−44639
eddy stability criteria 2−62079
edge and geostrophic waves, current shear effect 2−54791
Ekmans non-linear boundary layer in deep sea, theory 2−51538
e.m., conduction and magnetic induction techniques, review 2−81629
e.m. reflection properties of smooth brackish water, direct det. $10^8-4\times10^9$ Hz 2−72694
e.m. water-current velocity meter, oceanographic applications 2−71138
energy exchange between internal waves of finite amplitude and simple steady shear flow 2−43292
energy spectra of random field of internal waves 2−54773
engineering in ocean environment, conference, San Diego, USA (1971) 2−48426
ent. inment. turbulent diffusion across density interface in ocean model 2−84706
Equatorial Countercurrent, model 2−57908
equatorial currents driven by eastern wind, nonlinear theory 2−68866
equatorial dynamics of deep homogeneous ocean 2−54745
estuaries, partially stratified, mass transport mechanisms 2−51535
estuaries, shallow barricaded, variable-boundary tidal circulation model 2−57873
estuarine circulation, wind effects 2−57868
eustatic sea level change, postglacial rebound 2−75448
evaporation at air-liquid interface, wind tunnel study using isotopic techniques 2−56544
evaporative heat losses from water bodies 2−77475
fetches, short, distribution of wave heights in sea 2−62053
fjord-like estuary, bottom-water flushing obs. 2−57871
floor underthrusting and Indonesian Island Arc form. 2−57490
Florida current, bottom boundary layer, expt. study 2−62036
Florida current, neighbour diffusivity rel. to lateral shear 2−72706
Florida Current off Cuba, drogue meas. of downstream acceleration 2−62073
Florida Current western boundary region, cyclonic spin-off eddies 2−62075
Florida Straits, barotropic long waves 2−54793
Florida Straits, synoptic current profiling 2−62074
flow direction, speed and temp. meas. using thermistor and laser techniques 2−54775
fluxgate magnetometer for geomagnetic variations in shallow seas 2−69851
free convection onset in upper layer 2−72713
freezing of sea water, interferometry meas. of convection currents 2−65601
gamma ray anti-Compton spectrometer for marine environmental radionuclide analysis 2−82806
geochemical ocean sections (Geosecs) program, 1970-1 period 2−75412
geodesy, role in ocean physics 2−54610
geodetic positioning data, location of underwater acoustic transponders 2−62088
Geodyne model underwater sensor unit 2−72720
geomorphological development and post-Pleistocene sea level changes in Northumberland straits 2−72660
Geosecs II, North Atlantic Ocean salinity, temperature and o-profiles 2−75413
gravity anomalies over ocean ridges 2−57473
gravity eave field interaction with mean vel. and buoyancy field 2−54788
gravity wavefield, random, nonlinear dispersion relation 2−54784
gravity waves, internal standing, breaking mechanism, in atmos. and ocean 2−72776
gravity waves, linear low-pass filter development 2−57903
gravity waves, nonlinear, phase and group vel. 2−54786
gravity waves, scatt. by irregular bottom 2−54787
gravity waves, weakly nonlinear surface and internal, interaction 2−54789
Great Lakes, concentration-time model for ^{90}Sr 2−65615
Great Lakes, numerical study of effect on winter cyclones 2−62175
Great Lakes hydrodynamics, modified sigma equations' approach to numerical modeling 2−65597
Gulf of California, identification of water masses by physical-chemical relations 2−57879
Gulf of California and Revilla Gigedo islands, thermohaline struct. and baroclinic flow 2−65623
Gulf of Mexico, subsurface features, three dimensional method 2−57659
Gulf of Mexico, western, upper watermass form. 2−62072
Gulf Stream, enhanced transport mechanism 2−54778
Gulf Stream, entrainment of shelf water 2−65614

Oceanography continued
Gulf Stream meandering rel. to baroclinic instability in simple two-layer model 2−81610
hardness of sea floor in nearshore waters 2−65619
heat transfer and thermal struct., near air- water interface 2−65625
heat transfer to/from atmosphere, comparison of total static energy classification with energy flux classification 2−54815
high sea-levels, in upper Pleistocene in mid-north Mediterranean 2−62018
hydrodynamical and biochemical state variables, evolution equation for mathematical modelling of sea pollution 2−44632
hydrodynamics, conference Liege, Belgium (1971) 2−44625
hydrographic surveys, remote-controlled, high-speed system 2−72730
hydrologic parameters, seasonal and year-to-year variations 2−54758
hydrothermal percolation at ridge-crest and oceanic crust form. 2−57495
ice cover, air drag coefficients and roughness length 2−65566
ice floes, radar obs. of drift 2−78331
iceberg drift observations 2−57882
iceberg trajectories, computed and observed, comparison 2−57881
in core thermionic reactors, applications to space and underwater technologies 2−49269
Indian Ocean currents, vertical structure meas. 2−54757
induction currents due to electrojet 2−54913
inert gas profiles in east equatorial and southeast Pacific 2−65603
inertia in ocean and atmosphere and long-range forecasting 2−62123
inertia-gravity wave propag. during geostrophic adjustment, variable Coriolis parameter 2−54790
inertial oscillations in Mediterranean, vertical structure of motion determined 2−44628
instrument recovery methods 2−48427
instrumental system for multichannel recording of data 2−51566
inter-tropical convergence zone, seasonal variations, interacting atmosphere and ocean model 2−72734
internal gravity waves, effects of microstructure of ocean density fields 2−75478
internal gravity waves, refl. by small density variations 2−60397
internal tides at continental slope of Norway 2−57876
internal wave generation by travelling atmospheric disturbances 2−51554
internal waves, caused by periodic fluctuations of atmospheric pressure 2−51558
internal waves, space-time scales 2−54746
internal waves, wavenumber-freq. spectrum 2−57905
internal waves caused by periodic wind fluctuations 2−51559
International Ice Patrol, processing of digital data logger STD tapes 2−57883
Ionian Sea, surface temp., temporal and spatial variability 2−72704
irregular wind induced waves, review, prediction methods 2−44641
islands, circular, as resonators of long-wave energy 2−48424
Jervis Bay, N.S.W. calc. of longitudinal free oscillations by Galerkin method 2−75480
jet discharging horizontally into lake or river, heat transfer, diffusion and mixing 2−78304
Kelvin wave attenuation along nearly straight coastlines 2−44624
Kelvin waves, large amplitude, generation and propag. in shallow layer 2−54792
Kelvin waves on oceanic boundaries, effects of continental shelf and coastlines 2−78319
Labrador Sea, heat flow obs. 2−68869
Labrador Sea, Mesozoic rocks from dredging operations 2−54753
Lake Biwa-ko, seiche, numerical expt. 2−78316
lake coastal boundary layers for finite vertical Ekman numbers 2−57909
Lake Erie, wind-driven currents 2−65609
Lake Michigan, air-water interaction study 2−65691
Lake Ontario, coastal boundary layer in summer-fall regime 2−65622
Lake Ontario, net radiation meas. rel. to land surface albedo 2−65588
Lake Superior, sound attenuation frequency range 500 to 10000 Hz 2−44663
lakes cyclonic flow and thermal bar circulation 2−44606
laplace's tidal eqns. and tidal friction, computer solns. 2−84712
large stratified lakes, response to wind stress 2−62031
lateral convection in Atlantic Ocean 2−78325
latitudinally varying bottom topography effects on wind driven ocean circulation 2−54774
Lau Basin, sediment accumulation, volcanic deposits 2−44610
Lesser Antilles passages, current meas. 2−65596
Levantine intermediate water, flow, salinity 2−72707
l.f. sound propagation in offshore shelf zone under conditions of varying depth 2−72719
light propagation under water, radiance distribution 2−65590
light scattering by ocean particles, multi- component models 2−57894
light sources for deep ocean waters, Cd and Zn vapour arc lamps 2−49442
linear waves, generalized dispersion relation 2−54785
lineated magnetic anomalies near sea floor rel. to geomagnetic chronology of Gilbert epoch 2−58125
Little Creek Harbour, circulation as defined by physical and chemical parameters 2−57870
Loch Ness, velocity gradient meas. using free fall probe 2−48415
logarithmic layer on offshore seabed, determination of roughness and depths 2−72718
Lomonosov Current in Gulf of Guinea, velocity, temp. and salinity fields 2−57846
longshore current generation, wave height relationship 2−54795
magnetotelluric soundings in sea by difference arrangements 2−72714
major oceanic currents and water masses, use of selected indicator organisms 2−57902
mantle plume activity on ocean crust 2−57897
marine archeology, applic. of parametric sonar 2−41781
marine deposits, Mg content and crystal habits in ancient carbonates 2−54754
marine exploration, GULFREX computer systems 2−54798

Oceanography continued
marine frequency soundings, apparent resistivity curves in wave zone 2−72700
marine frequency soundings, problems with transmitting-measuring systems 2−72701
marine pillow basalt, magnetic changes rel. to sea floor weathering 2−54966
marine sediments, electrical resistivity meas. system for porosity determination 2−75481
marine sediments classification 2−62067
marine seismic refraction system using single ship for shooting, recoverable sonobuoys 2−68843
Mediterranean, deep-water formation by convective mixing 2−54761
Mediterranean Sea, thermistor buoy obs. of surface response to wind and sea state 2−57922
meridional geostrophic transport across South Pacific Ocean 2−57865
mesoscale double diffusivity effect 2−57856
mesoscale structure of velocity field, est. of statistical characteristics 2−51553
microseism generation by atmospheric coupling through ocean 2−72654
microseisms associated with cyclonic winds 2−48377
microstructure, billow turbulence and vertical mixing, thermoclines 2−44609
microstructure obs. using high speed digitizer 2−72728
microwave brightness temp. of natural sea ice and salt water ice 2−84777
Mid-Atlantic Ridge sediments, age studies 2−44611
mid-oceanic frontal passage in near surface current meas. 2−65600
mirror sonar with 30° sector coverage, experimental equipment 2−69769
Mississippi River Delta, vertical mixing periodicity in laterally expanding river effluent 2−57869
mixing in deep stratified ocean 2−78224
MnO$_2$ deposition, pressure effects 2−54620
moored temp. spectra, Doppler shift in frequency of inertial waves 2−81598
multidiscipline ocean research programs, status report 2−57900
multiple surface reflection in linear gradient medium 2−44623
N. Atlantic deep sea sediments, Cd distrib. 2−81618
natural underwater light field, dependence of radiance fluctuations on statistical characteristics of rough sea surface 2−44616
nearshore circulation and meandering currents 2−65613
nearshore currents due to momentum transfer from shoaling waves 2−54794
nepheloid layer characteriz., correl. between light scatt. and suspended material analysis 2−57913
nepheloid layers, light scattering rel. to suspended matter 2−68870
noise signature of aircraft in level flight over hydrophone 2−44659
nonlinear wave radiation in surf zone, qualitative aspects 2−68865
North American Basin, convergence zone propagation 2−44657
North Atlantic, anticyclonic and cyclonic eddies 2−62078
North Atlantic, Geosecs II meas. of total Co$_2$, dissolved O$_2$, ^{13}C and ^{18}O 2−75470
North Atlantic, internal waves and turbulence 2−62040
North Atlantic basin, currents and density fields rel. to bottom relief 2−68867
North Atlantic deep sea sediments, Eocene and Neocomian, paleocirculation, formation and origin 2−62062
North Atlantic Ocean, vertical velocity calc. from function of total flows and level surface 2−51557
North Pacific, horizontal and vertical distributions of radionuclides 2−65598
North Pacific, intermediate high salinity layer formation 2−57848
North West Passage, marine seismic exploration 2−54647
north-west Africa, variability of oceanographic observations off coast 2−65589
northern California, pelagic tidal height 2−68868
northern Skye and Little Minch, negative gravity anomaly rel. to deep sedimentary basin 2−54596
Northwest Pacific, shallow depth explosions, long range detection 2−72702
Norwegian Sea, thermal condits., influence of N. Atlantic current 2−44640
ocean energy budget rel. to mean annual global radiation budget 2−65445
ocean waves, deep, spectra, meas., review 2−64416
ocean-atmosphere system, albedo calc. from cloudiness data 2−51581
Oceanic Magnetized Layer, limits and estimates of props. from near-bottom meas. 2−54776
oceanic Rossby waves, transient, Reynolds stress and lateral eddy viscosity 2−57859
oceanization, isostasy, sea floor spreading 2−78332
oceanology (conference, Brighton March 1972) 2−72722
offshore floating structures and wave motion analysis 2−72733
offshore refraction, field and data processing techniques 2−54665
offshore tidal stream, residual flow 2−62037
oil pollution, remote sensing by u.v. fluorescence 2−84771
open channel surges and bores, numerical simulation 2−43277
optical heterodyne detection systems, S/N ratio 2−69951
optical meas. of seawater using two-detector integrating system 2−72699
optical turbulence in sea 2−84766
Pacific, regionalised, Rayleigh wave phase vel. variations 2−57656
Pacific catastrophy and ocean floor convergence considerations 2−57489
Pacific equatorial undercurrent as revealed by inert gas profiles 2−57895
Pacific Ocean, currents and stationary circulation 2−51542
Pacific Ocean, deep, pressure depend. of high- frequency sound attenuation 2−44662
Pacific Ocean, eastern, subsurface Northern Equatorial Countercurrent 2−62082
Pacific Ocean floor, near-bottom mag. lineations 2−54712
Pacific polar front interaction with atmospheric circulation 2−54771
partial differential eqn., third order, for ocean currents near equator 2−84707

Oceanography continued
penetration of density interface by heavy vortex rings 2−77214
periodic wind driven currents, theory 2−51545
periodicity in whitecaps 2−81620
Philippine Sea, deep sound-scattering layers 2−57849
photography, exposure control method 2−82599
physical fields obs. using adaptive measurements 2−51561
phytoplankton, vertical distribution in Gulf of Aden, patterns rel. to oceanographic conditions 2−57853
planetary waves, energy and energy flux 2−44646
pollution and international law 2−78333
pressure sensor, quartz crystal, for use on deep ocean floor 2−44667
pyranometers, Eppley model 6-90, sensitivity stability 2−63144
quasi-geostrophic flow, generalized potential vorticity equation 2−57857
quasihomogeneous marine media, kinetic energy distrib., in vertical oscillations 2−81591
radar meas. of waves and tides 2−48430
radar properties of non-Rayleigh sea clutter 2−41880
radar returns from sea ice, data interpretation 2−48431
radar wave propagation and sea evaporation effects 2−65629
radiative transfer in atmosphere-ocean system, Monte Carlo calcs. of radiance 2−65628
radiative transfer in atmosphere-ocean system, Monte Carlo calcs. of the flux 2−65627
radioisotopic power generators, appl. 2−49301
radiometry limitations for meas. applications 2−81679
Red Sea hot brines, electrical resistivity probings of marine sediments 2−72729
remote sensing buoy system 2−48432
remote sensing of Earth resources and environment, seminar (Palo Alto, USA, Nov. 1971) 2−84767
remote sensing with radar, applications 2−44649
remote spectroscopy from high altitude, effect of atmospheric back-scatter on reflection spectra 2−84774
response of ocean model to inertial impulses 2−84751
reversing tidal current, statistics of vel. field 2−78324
Reykjanes ridge crest, bottom topography, chart construction 2−51552
Rossby wave behaviour in mean current, model 2−54780
Rossby waves, forced l.f., model 2−54779
Rossby waves, scatt. by semiinfinite barrier 2−62041
rotating fluid dynamics, ultrastable air bearing turntable 2−77232
rough sea surface, acoustic field reflection 2−57837
salinity and temperature structure obs. with variable depth towed body 2−72723
salt fingers, finite amplitude 2−62083
sampling filter for drawing interstitial water from sediments 2−62086
Saragasso Sea, western, cyclonic eddy, satellite obs. 2−62076
Sargasso Sea, trace element profiles from Geosecs II test station 2−75471
satellite-tracked IRLS buoy for ocean-current measurement, development and testing 2−54748
sea bed topography, fine structure using side scan sonar 2−68873
sea brightness temperatures at microwave frequencies, geometrical optics theory 2−44652
sea floor spreading and basalts behind Mariana Island arc 2−51533
sea floor spreading magnetic anomalies in Central North Atlantic Ocean 2−57898
sea foam emissivity at microwave freq. 2−65602
sea ice open channels as ion sources 2−81669
sea ice research, important problems from marine expeditions 2−62050
sea level at southern California, decadal fluctuation 2−81635
Sea of Azov, Dynamics of stationary currents 2−78328
sea surface as random filter for underwater sound waves 2−57838
sea surface cooling, evaporation, radiation and heat transfer 2−65593
sea surface in Block Island Sound, remote sensing by underwater acoustics 2−57886
sea surface roughness rel. to wind profile development 2−44707
sea surface temp., estimation from space 2−78231
sea surface temp. nonuniformity, automatic recording device 2−44644
sea surface temp. obs. by i.r. sensing, factors affecting accuracy 2−44651
sea surface waves, wind driven, exptal det. of phase velocities of spectral components 2−44619
sea temp. obs. by i.r. radiometry 2−44650
sea tidal effects on daily geomag. variations 2−84926
sea water, integral light scattering coeff. rel. to scattering coeff. in fixed direction 2−51564
sea wave generation by turbulent wind 2−44608
sea waves, microwave emissivity calculation 2−72712
sea waves, wind induced, microscale fluctuations 2−68871
sea-atmosphere interaction, conference, Ft. Lauderdale, Fla., USA, (Dec. 1971) 2−65637
sea-level, eustatic changes, rel. to vertical crustal movements 2−57775
seamount reflections from CANNIKIN underground explosion 2−44664
second-order scattering from sea, 10 m-radar observations of Doppler continuum 2−81634
sediment cloud below Mediterranean outflow 2−81616
sedimentation rates, diffusion, reaction importance to deep sea drilling cores 2−62063
sediments, dating by gamma ray spectrometry 2−57854
seismic arrays, horizontal and vertical 2−81605
seismic exploration radio refraction buoy 2−57662
seismic hydrophone arrays for sea bed profiling, effects of noise 2−44621
seismic reflection data processing 2−48428
seismic reflections from inhomogeneous layers with gradually changing velocity 2−54764
self-contained recording system for measuring electric field at ocean floor 2−68862
semicircular bay, wave induced longshore currents 2−65591
sensors, inductively coupled, design of power transfer system 2−72725

Oceanography continued
shallow sea, calc. of stationary wind-driven currents 2−51544
shallow water, primary frequency microseisms, theoretical model 2−48389
shallow-water spectra 2−65608
sheeted thermocline, internal waves 2−46897
shelf seiches at La Parguera, Puerto Rico, semi-monthly periodicity 2−57878
Skagerrak, long-term variations of subsurface temperatures 2−48413
small-scale Langmuir circulations, growth characts. 2−65604
solar broadband irradiance attenuation 2−62019
solar radiation, multiple scattering calc. in atm.−ocean system 2−65756
sonar signal processing, off-line digital techniques 2−57901
sound absorption in sea water, multistate dissociation 2−48434
sound field in interbedded liq.-solid half space, integral soln. 2−82366
sound propagated in deep water and shallow water geometries, spatial coherence 2−44655
sound scattering by planktonic animals small rel. to sound wavelength 2−78330
sound transmission from deep to shallow water 2−44658
sound transmission in isospeed ocean channel with depth dependent current 2−44622
source to detector ranges, traveltime of multiply reflected sound waves 2−44614
South Atlantic, dissolved O_2 distrib. 2−65594
South Pacific Ocean, water circulation 2−78327
stationary coastal currents, automodel solutions of non-linear problems 2−51548
stationary surges and ebbs off sloping coast, non-linear theory 2−51547
Stokes waves, nonlinear, phys. props. 2−54786
Straits of Florida, high resolution current profiling 2−44613
Straits of Gibraltar, current meas. 2−48422
stratified bay, three-dimensional circulation under variable wind-stress 2−44633
stratified ocean, coastal upwelling 2−57907
stratified ocean, vertical structure of planetary waves 2−51560
subarctic front in N.W. Pacific Ocean, thermohaline structure 2−57847
submarine biological objects, acoustic characteristics of fish species 2−69763
sun reflection zone obs. using satellite aerial photographs 2−48433
Sun-glitter pattern rel. to sea roughness and surface wind measurements from spacecraft 2−84772
surface and form-drag hypotheses for Langmuir streaks 2−62085
surface layer genesis, evaporation and microconvection 2−78323
surface slope water, hydrographic station obs. 2−62080
surface temp. determ. by multispectral technique using Nimbus 2 data 2−65621
surface temp. field det. from satellite obs. 2−44638
surface temp. meas., satellite microwave radiometer 2−78334
surface temp. meas. with satellite microwave radiometer 2−72721
surface temperature, remote sensing from NOAA-I satellite, atmospheric effects 2−57888
surface temperature fluctuations, radiation thermometer meas. 2−57890
surface temperatures derived from direct readout i.r. data via APT satellite receiver 2−57887
surface topography using space systems 2−54614
surface water temp. and ice regimes of Georgian Bay 2−57862
surface waves resonant interaction with internal gravity wave 2−44620
surface waves wind driven, exptal det. of phase velocities of spectral components 2−44619
surface wind fields, remote passive microwave sensing 2−44648
surge, crest and hollow distrib. 2−54743
survey operations, use of real-time satellite infrared data 2−57889
suspension flows in Riga Bay, meas. of velocity and density 2−84755
SW Indian Ocean, year-to-year variability in water movement 2−78322
swell-wave-tide u.s. analysis, industrial equipment 2−72731
tectonics of ocean-floor metamorphism 2−57710
temperature and current velocity meters, self- contained integrating systems 2−72732
temperature and salinity, vertical microstructure in San Diego trough, obs. 2−62021
temperature conductivity-depth survey equipment 2−72727
temperature fluctuations at air-water interface caused by surface waves 2−65616
temperature gradient, fine structure of vertical component for San Diego Trough, Florida Current and central Pacific 2−68864
temperature meas. real time constant and salinity determ. reliability in ocean using temperature-conductivity probe 2−81611
temperature non-uniformities at great depths 2−51565
thermal balance of mid ocean ridge and sea floor spreading 2−48398
thermal plumes, model for predicting temps. 2−78305
thermal waves in nearshore environment 2−48429
thermo-hydrodynamical model of ocean circulation 2−62027
thermocline, composite spectrum of temp. fluctuations 2−57923
thermocline, fine struct. and mixing 2−57917
thermocline formation in tropical zone, nonlinear boundary value problems 2−51549
thermocline microstruct., shear obs. 2−57918
thermohaline convection, numerical simulation 2−57916
tidal delay due to inland seas and harbors 2−44615
tidal flow, resistance law 2−48420
tidal gravity profiles, trans-US and trans- Europe link 2−54602
tidal loading, global calcs. 2−57844
tidal obs. near amphidrome 2−57912
tidal resonance in Bay of Fundy/Gulf of Maine system 2−68872
tidal sensitivity measurements, borehole tiltmeter 2−72703
tides, effect on secular deceleration of Earth's rotation 2−78240
tides, Laplaces eqns., ideal liquid on smooth rotating sphere 2−72711
tides, triggering of volcanic eruptions from Mt. Stromboli, Italy 2−78321

Oceanography continued
tides and polar motions 2−57861
tides and storm surges, numerical solution of three dimensional hydrodynamical eqns. 2−44634
topographic Rossby waves, exptl. models of double Kelvin and continental shelf waves 2−44626
transverse circulation, near coast, anal. 2−62034
trapped shallow water waves for continuous bottom topographies 2−72698
tropical Atlantic, temperature variations in upper active layers 2−62028
tsunami, nonlinear effects in propagation 2−51555
tsunami amplitude est. as function of earthquake surface wave magnitude 2−62061
tsunami generation following Alaska-Aleutian earthquakes 2−61911
tsunami wave generation, propagation and open- sea characteristics, model 2−62060
tsunamis, amplitude patterns from submarine earthquakes 2−65611
turbidity currents problem in lithodynamics 2−57845
turbidity in estuaries, spectrophotometric techniques 2−54797
turbulent equations of general ocean circulation 2−57836
turbulent heat and mass transfer from large body of water 2−57891
turbulent motion, basic eqn. for turbulent mixing of substance in sea, use of eddy diffusivity tensor 2−44629
two layer model of equatorial currents taking into account nonlinear accelerations 2−51543
two-dimensional free oscillations of natural basins, reson. iteration method 2−65620
underwater bioluminograph for meas. of bioluminescence potentials of luminous organisms 2−54749
underwater communication using magnetic loop transmitter-receiver 2−81631
underwater explosions, total pressure waves, apparent transmission gain 2−41713
underwater illumination, statistical characteristics rel. to sea roughness 2−81609
underwater loudspeaker, small size, high efficiency 2−41770
underwater sound, surface backscatt. coeff. calc. from measured data 2−66625
underwater sound generator using boomer class of seismic sources 2−57661
underwater sound sources, detection by microwave radiation obs. 2−48425
upper ocean response to variable winds 2−57921
upwelling, large-scale, off northwestern Mexico 2−65624
upwelling layers in wind-driven ocean 2−78237
u.s. wave backscatter from rough water surface 2−68861
velocity microstructure, free fall probe for determining velocity and density gradients 2−48415
vertical crustal movements along U.S. east coast, sea level measurements 2−57759
vertical turbulent exchange, effect of water stability 2−44637
vertical velocity of water surface, registration using e.m. induction method 2−72717
vertically stratified water columns, gravitational potential energy 2−57860
viscous-dominated bottom boundary currents, thin jet flow down inclined plane 2−57910
volume reverberation, mathematical model 2−44665
volume reverberation simulation 2−44666
water circulation in polar-regions associated with peculiarities of beta effect 2−54755
water exchange between Caribbean Sea and Atlantic Ocean through Northern Passages 2−51550
water quality survey vessel 2−72726
water samples, meas. of T content using gas proportional counter 2−82808
water temp. and salinity anomalies, spatial correlation functions 2−51562
wave breaking, wave generation by wind and momentum conversion to steady currents 2−78335
wave breaking on submarine bar 2−57874
wave characteristics in coastal area 2−44643
wave data management 2−75484
wave field generated by variable wind in local storm area 2−54744
wave generation, relation to wind flow 2−78336
wave generation and propagation in one-dimensional linear dispersive systems, application to oceanography 2−83725
wave generation theories, invalidity 2−54796
wave height measurement with nanosecond radar 2−44647
wave height variation around vertical cylinders 2−57880
wave periodicities at surface of cohesionless medium and fluid, time-dimensional parameter 2−54766
wave propagation across continental shelf 2−57842
wave set-up on coral reefs 2−65606
wave-pressure pickups with hydraulic filters 2−54767
waves, energy transfer from wind 2−78315
waves, long nonlinear internal and quasi-steady lee, generation mechanism 2−57911
West Greenland Sea, acoustic meas. 2−44656
western Mediterranean Sea, inertial oscillations, circularly polarized currents 2−48414
western Mediterranean sea, microbial activity and organic material 2−68863
western tropical Atlantic in Winter, thermohaline water structure 2−78326
whitecap, spray and capillary wave obs. 2−62084
wind stress fluctuations in continuously stratified ocean, quasi-geostrophic response 2−57906
wind waves, frequency spectra of inner and outer structure at different development stages 2−81613
wind waves and swell, differential low of hydrometeorological characteristics distrib. 2−44636
wind-disturbed water, curvature distrib. 2−57925
wind-driven inshore currents, trajectories 2−57877
WKB approximation, turning points and meas. of phase vel. 2−57840
Woodlark Basin, sea-floor spreading evidence 2−57904
World Ocean, constituents of chemical balance 2−62051
World Ocean level increase in 20th century, reasons 2−57855

Oceanography continued
Yacatan Strait, deep current obs. 2−62071
Zubov's vertical winter circulation scheme, computer analysis 2−62055
B exchange between sea and atmosphere 2−57851
Ba abundance profiles in Pacific and Mediterranean sea water 2−75467
Ba concentrations at Geosecs I and III 2−75468
Ba profiles in southwest Pacific from Geosecs III station near Tonga 2−75466
^{7}Be concentrations in Atlantic Geosecs II water column rel. to oceanic circulation 2−75475
Ca and Mg distribution in tropical Atlantic 2−54763
^{3}H abundance profile in Atlantic Ocean from Geosecs test cruise station 2−75474
^{3}He excess in Atlantic Ocean 2−75473
Mn and Cu microquantities det. in marine suspensions 2−54768
O_2 minimum layer depth and surface of no motion 2−57850
$^{18}O/^{16}O$ ratio, ocean isotope evolution and growth, model 2−84749
^{18}O concentration, reef corals, temp. dependence 2−65592
^{228}Ra profile at Geosecs II in North Atlantic 2−75477
Si and trace elements in seawater, in-situ analysis using synthetic fibres 2−75469
Sr abundance profiles in Pacific and Mediterranean sea water 2−75467
Sr distributions in seawater profiles at Geosecs I and II test stations 2−75472
^{90}Sr in seawater from Geosecs II, shipboard analysis techniques 2−75476
T levels in rivers and coastal sea water 2−62042
Octet theory *see SU(n) rules*
Omegatrons *see Leak detection; Mass spectrometers; Vacuum technique*
Onsager relations *see Statistical mechanics; Thermodynamics*
Optical activity *see Optical rotation*
Optical communication *see Laser beams/applications*
Optical constants
see also Absorption/light; Reflectivity
activated glass, thermo-optic constants 2−59276
barium behenate molec. film, ellipsometric study of optical constants and refractive index detn. 2−78064
barium margarate molec. film, ellipsometric study of optical constants and refractive index detn. 2−78064
crystal, evaluation from excitonic spectra 2−72317
determination from meas. of relative derivative of reflectance with angle of incidence 2−55730
determination from reflection spectra 2−42189
disperse systems, effect on dependence of relaxation coefficients on particle size 2−53461
evaporated films, properties in e.u.v. 2−48133
film, ellipsometry, calc. method 2−44339
film, meas., ellipsometric method 2−47095
film, metallic, Vasiceks theory, Murman-Forsterling theory, single refl. theory 2−48132
frequency depend., classical calc. 2−73632
group III-V compounds, amorphous, static electronic dielectric constant 2−51300
group VI chalcogenides, layer semicond., transmission obs. 2−81334
Lifshitz-Van der Waals constant calcs. 2−53457
lunar surface rocks and fines 2−62652
metal, evaluation from spectral obs., review 2−72292
metal, liq., ellipsometry obs. 2−43359
metal deposits, ellipsometry method 2−79379
metallic conductors, optical cond. and dielec. const., phenomenological model 2−75253
metals, det., new method 2−61582
molecular optical anisotropy dispersion obs. 2−63394
powder, Kubelka-Munk diffuse reflectance remission function rel. to fund. optical parameters 2−79329
semiconductor, degenerate, dielec. func. rel. to free carrier absorp., quantum theory 2−51329
semiconductor, disturbed internal reflection method, electronic props. detn. 2−72253
semiconductor, evaluation from spectral obs., review 2−72291
semiconductors, group III−V cpds. pressure depend. of dielectric constant 2−72297
water, optical absorption in vacuum u.v. 2−50361
Ag, cond. electron optical mass 2−44029
Ag film, dielectric const. changes, piezoreflectivity obs. 2−54382
$AgGaS_2$, det. from i.r. reflectivity 2−44364
AgI, optical constants of thin films in exciton band region, meas. 2−65209
Al, absolute values of ε_1 and ε_2 2−48134
As_2Se_3, amorphous films, determination from reflectivity spectra 2−61620
Au evaporated films, variation with time 2−75254
Bi:Te deposits, determ. in 15-70μ region 2−75255
C, turbostratic film, conductivity and dielec. consts. 2−78080
C glass, refl. meas., 0-82 eV 2−61584
Ca, absolute values of ε_1 and ε_2 2−48134
$CdGeP_2$, change in constants for change from crystalline to vitreous states 2−72299
Co, mag. permeability calc. from spectral meas. 2−65155
Cs, liquid and solid, 0.3 to 2.5 μ region, dependence on temp. 2−68596
Cu-Ni alloys, meas. of refractive index and absorption coeff. in visible and ultraviolet spectral regions 2−81330
CuAu, Cu_3Au, Kramers Kronig relations used to determine optical constants changes due to ordering 2−72303
CuO film, wavelength depend., transmittance obs. 2−48135
Fe, mag. permeability calc. from spectral meas. 2−65155
GaAs, dielec. function, freq.- and wave-vector-depend., calc. 2−84262
GaSe, anisotropy near band edge 2−48178
Ge, amorphous film, effect of void struct. on optical dielec. consts. 2−78063
Ge, dielec. function, freq.- and wave-vector-depend., calc. 2−84262
a-Ge film, u.v. dielectric consts., reflectance obs. 2−61586

Optical constants continued
H_2O, in the vacuum u.v. from reflectances 2−43361
Hg, surface-induced vectorial props. 2−77436
HgS, cinnabar, refl. spectra obs. 2−61615
In, absolute values of ε_1 and ε_2 2−48134
K, determ. in 4-10.7 eV proton energy range 2−68593
K, optical props. and surface plasmon states 2−71819
K anomalous infra-red absorption and collective oscillations in small metal particles 2−65210
Li, 2-3.8 eV, meas. by excitation of nonradiative surface plasmons 2−75256
Li, absolute values of ε_1 and ε_2 2−48134
$LiNbO_3$, third order nonlinear susceptibility, using tunable dye lasers 2−72252
Mn ferrite, Kerr effect and optical consts., magnetooptical reson. in visible 2−81337
Mo film, complex index obs. 2−56595
$MoTe_2$, reflectivity spectra obs. 2−48162
N atomic, specific refractivities, dual frequency laser interferometry 2−79902
Na, anomalous infra-red absorption and collective oscillations in small metal particles 2−65210
Na, optical props. and surface plasmon states 2−71819
NaCl aqueous solns., I.R. 2−50362
$NaNO_3$, optical props. in vacuum u.v. region 2−84487
Ni, mag. permeability calc. from spectral meas. 2−65155
NiO films, electrochem. deposition conditions depend. 2−61618
O atomic, specific refractivities, dual frequency laser interferometry 2−79902
Os film, in v.u.v. from 300 to 2000 Å 2−81336
Pb, absolute values of ε_1 and ε_2 2−48134
$PbBr_2$ thin film, Kramers-Kronig analysis in 2-10 eV region, 4.2K 2−57321
$Pb_{1-x}Sn_xTe$, refl. meas., Kramers-Kronig analysis 2−48165
$Pb_{1-x}Sn_xTe$, dielec. const., i.r. plasma refl. study 2−84504
$Pb_{1-x}Sn_xTe$, reflectivity spectra obs. 2−48164
PbTe, refl. meas., Kramers-Kronig analysis 2−48165
Pt film, for u.v. reflectance obs. 2−61653
SbSI, far i.r. reflectivity, complex dielec. const. deriv., soft mode in paraelec. phase 2−61619
Se, amorphous films, determination from reflectivity spectra 2−61620
Si, irrad. with 400 eV ions, surface damage, change in optical consts., ellipsometric obs. 2−47081
Si, surface oxide layer influence 2−51325
SnTe, refl. meas., Kramers-Kronig analysis 2−48165
Ti(0001) single crystal and polycrystalline, obs. as function of temp. 2−44341
TlBr, electron energy loss spectra obs. 2−61129
TlCl, electron energy loss spectra obs. 2−61129
TlI, electron energy loss spectra obs. 2−61129
WSe_2, optical response in excitonic region 2−44383
W(110) single crystal and polycrystalline, obs. as function of temp. 2−44341
ZnSe, dielec. function, freq.- and wave-vector-depend., calc. 2−84262
Optical dispersion *see Dispersion, optical*
Optical fibres *see Fibres/optical*
Optical films *see Films/liquid; Films, solid/optical properties*
Optical filters *see Filters, optical*
Optical images
see also Aberrations, optical; Holography; Resolving power, optics
− 2−70009
active optical transmission, incoherent linear method 2−42185
all reflective linear image space scanner 2−79390
analysis by multiplex coding 2−42183
apodisation for coherent imagery of extended objects, application to semi-transparent phase edges 2−76526
calculation of object corresponding to given diffraction image 2−42204
coherent, noise suppression 2−79307
computer generated kinoform filters for image production 2−79313
condenser systems, dispositive plane, light intensity distribution calc. 2−59217
confocal interference filter, imaging 2−66844
controllable edge sharpening for time sequential imaging devices 2−42182
correlation coeff. det. by intensity transmission of images 2−42180
Culgoora solar magnetograph, image motion due to vibr. 2−85071
degraded, linear unbiased restoration at low light levels 2−79304
depth of focus increasing by two step image processing 2−79384
detectability on photoelectric surface 2−79455
detection and location of point images in sampled optical systems 2−79423
detection by human observers, display signal-to-noise ratio requirements 2−82066
difference between images detection 2−76527
diffraction images of partially coherent phase discs with variable phase plates 2−76519
dye-forming imaging system in viscous media, long exposure density reversal 2−66868
Earth Resources Technology Satellite data digital image processing 2−81641
electro-optical rectifier for transformation of photographic images 2−59301
by electron microscope and stimulated Compton scattering 2−82451
electron microscope channelling patterns, meas. of image contrast changes 2−83944
electron microscope images Fourier analysis 2−79160
electron microscopy three dimensional image reconstruction by object illumination from discrete set of directions 2−79159
estimation, objective and subjective evaluation 2−82548
evaluation and photographic emulsion 2−59307
evaluation using target recognition 2−66807
formation in γ-Ruticon by electrostatic deformation of elastic layer 2−79415
formation using antenna properties of optical heterodyne receivers 2−79300

Optical images continued
  formed by glancing incidence telescopes, polarization effects 2−79305
  ghosting of distant objects in twin-glazed windows, environmental effects 2−70005
  hologram imagery by ray-tracing method 2−69896
  holographic, accuracy 2−63350
  holographic, magnification properties 2−42146
  holographic, structure produced by nonlinear distortions during recording, spatial filtering 2−59201
  holographic image-deblurring filter, high-resolution extended-range, realization method 2−45766
  holography, associative reproduction of pictures by optical correlation 2−79242
  holography, position calc. 2−45761
  holography, projective transformations 2−69971
  homothetic, interference between two superposed images 2−63383
  imaging apertures, circular and rectangular, three dimens. intensity impulse responses 2−79298
  imaging systems and detective quantum efficiency, primary parameters 2−59267
  incoherent sources, off-axis Fresnel zone plate as coded aperture 2−70021
  large variation phase objects, quantitative visualization 2−55728
  laser speckle patterns, wavelength diversity technique for speckle size reduction 2−66774
  many conjugate zoom systems 2−59212
  merit function, correlation with subjective image judgments 2−63439
  microscopy, optimal magnification 2−63377
  MTF estimation for imaging system from edge response 2−49420
  multicolour spatial frequency analysis by optical multiplexing 2−42186
  multiple image storage system, spatial filtering process 2−79288
  multiple imaging using various types of simple phase gratings 2−66802
  multiple storage system, spatial filtering process 2−79288
  multiplexing using random diffuser 2−63366
  optical data processor, coherent and noncoherent, space invariance conditions 2−79368
  partially coherent, of opaque edge, with polarizing microscope 2−42233
  $Pb_xLa_{1-x}(Zr, Ti)O_3$ ceramics for selectively erasable image storage and display 2−79454
  photographic, electronic transfer 2−76553
  photographic, restoration, superresolution of diffraction blurred impulses 2−73691
  photographic diazosulphonate imaging 2−59308
  photographic relief, linear transformation of density image 2−79303
  processing, coherent method of variance obs. 2−55722
  processing systems using Woodward functions 2−79422
  quality assessment, diffraction pattern analysis 2−79407
  quality degradation of imaging or tracking systems viewing along same path as laser beam inducing thermal lens effects 2−49391
  quality determ. using mean square error criterion 2−79301
  quality of photogrammetric camera systems 2−59337
  radiographic, quality assessment 2−59346
  reconstruction of complex image function from electrons micrographs 2−79157
  recording on magnetic plate 2−52469
  reflected-shadow method for constrained zone study of cracks in birefringent media 2−68101
  reflection caustics of conic sections 2−79312
  restoration, resolution, rate distortion fn. 2−79306
  rotation devices, comparative survey. 2−66837
  from satellites, atmospherically degraded, restoration 2−79308
  scattered objects image transformation in holography 2−59195
  space variant enhancement and restoration, coordinate transformations 2−79302
  target edge response viewed through atmospheric turbulence over water 2−81648
  three dimensional display techniques, holography, stereoscopy 2−82580
  three-dimensional image reconstruction rel. to information theory 2−66803
  transfer characteristics, carrier frequency photography 2−42287
  transfer props. of interferometrically produced fibre optics structure, ray anal. 2−73666
  transmission of spatial frequencies by nonisoplanar devices 2−66806
  two-dimensional objects using u.s. light diffraction 2−45790
  weak, detection with photon counting techniques 2−66732
  White Welsh four mirror system, imaging properties 2−45778
  zone plates, third order and chromatic aberrations 2−59227
  $Bi_{12}SiO_{20}$ electro-optic image modulator, sensitivity and resolution 2−79417
  $Bi_{12}SiO_{20}$ electro-optic image modulator for optical processing 2−79416
  n-InSe, rapid recomb. centres, during laser beam excitation 2−72063
Optical instrument testing
  afocal systems, workshop instrument using m.t.f. criterion 2−55758
  glass safety lenses, drop-ball testing 2−42228
  interferometry, roughness and scratch determination 2−73638
  long focus systems, common path interferometer 2−73637
  reflecting and refracting elements, application of computer generated holograms 2−82572
  service life determ. rel. to trouble-free operation 2−59263
  simple lenses, convex elliptical, parabolic and hyperbolic surfaces, quality control technique 2−63375
  surface inspection, automatic, metal polygon mirror, lapping technique 2−79386
Optical instruments
  Some instruments are listed separately, e.g. Refractometers
  — 2−66837
  — 2−70053
  acousto-optic and electro-optic modulators, developments 2−73657
  advances in meas. 2−55751
  aerosol particle counters, coincidence and cross-channel sensitivity 2−43403
  all reflective linear image space scanner 2−79390
  anamorphic optics, manufacture 2−70054

Optical instruments continued
  angle sensing system 2−70030
  angular displacement meter, accuracy analysis 2−63404
  anomaloscope, transformation of arbitrary data to CIE system of specifications 2−66347
  2nd order aspherical surfaces, rel. between angular and linear tolerances in manufacture 2−70055
  black body radiometer, self-calibrating, for use in u.v., i.r. and visible 2−66638
  catadioptric system, using reflecting curved cone 2−63408
  circular table 800, for exact angle obs. and production of precise graduations 2−55753
  computer-based electrooptical system for measuring wave induced sand concentrations 2−68874
  concave aspheric surfaces fabrication 2−79393
  conference (San Francisco, Oct 1972) 2−79287
  contact endoscope with surrounding light used as source and simultaneous lighting and optical system 2−52465
  correcting lens design for printing colour kinescope screens for colour TV 2−70051
  c.r.t. optical film recorder with optical feedback exposure control 2−42223
  depth of scratches on inside of tubes, meas. by luminous section method 2−70052
  design 2−70096
  design and aberrations, tutorial 2−42179
  design and aberrations, tutorial 2−59248
  design and aberrations, tutorial 2−52447
  design and aberrations 2−73626
  design for laser systems using phase holograms 2−69965
  dichrometer, linear and circular, near i.r. 10000-1750 cm^{-1} range 2−79374
  Differential II, for measuring light scatt. of individual particles 2−47000
  diffractomter, laser light source 2−63405
  digital light beam deflector, 20-stage, design and performance 2−66826
  for displacement monitoring of u.s. welding equipment probes 2−69755
  electro-optic circular scan deflectors 2−66830
  electro-optical light modulator, use with nonlaser light sources 2−76528
  electro-optical shutter for Q-switching lasers emitting unpolarized radiation 2−69959
  electro-optical spatial light modulator for optical data processing, two dimensional, adaptive, online 2−79418
  electronic correlator for photoelectric correlation obs. 2−73662
  ellipsoidal mirror system for increasing gain in Raman scattering 2−79414
  ellipsometer, new alignment method 2−59247
  ellipsometer with oscillographic presentation of pattern 2−66834
  enlarger, condenser type, design and aberrations 2−66829
  evaporograph, influence of absorbant on sensibility 2−55756
  Fabry Perot modulator for space use 2−72945
  focusing screens, meas. of modulation transfer functions 2−70039
  Fourier transform techniques in optical metrology 2−45793
  glare characteristics in visible region 2−66824
  glass spectacle lenses with back surface vinyl membrane, fracturing and safety properties 2−70066
  glass windows, thin hemispherical, construction for nuclear and optical expts. 2−82573
  gloss power measuring device, based on Schulz-Methke principle 2−63411
  gyrostabilized sights for use in firing control and observation from moving vehicles 2−52466
  Hewlett Packard 3721A correlator, for stellar optical energy meas. 2−69196
  holographic interferometer and fringe analyser, study of supersonic flow in wind tunnels 2−46836
  holographic microscope, real time and double exposure for phase variation dynamics obs. 2−42148
  integrating sphere, transmittance measurements 2−66840
  interference, for inspecting optical flats 2−59232
  interferometric fan trace plotter for evaluation of lens systems 2−79420
  i.r. dichroism meas. in polyethylene during elongation 2−83354
  i.r. reflectivity meas. at low temps. and high magnetic field 2−82569
  i.r. thin film filters rel. to developments in optical equipment 2−73667
  Kerr cell, multiple refl., for liq. birefringence obs. 2−76524
  large pupil systems, visual aberrations 2−66801
  laser beam optical quality improvement device, patent 2−82549
  lens assembly system, mini computer controlled 2−79399
  light trapping cell for Raman spectra meas. 2−79380
  luminance meter, optical systems for defining, viewing and measuring fields 2−70034
  many-photon absorpt. in crystals and their applications, review 2−75282
  metal clad dielec. waveguide, mode selective props., attenuation, phase consts. 2−78964
  microdensitometer, multiple sine-slit, eval. of m.t.f. of photographic emulsions 2−45807
  moire analysis using profile projection with adjustable screen grids in image plane 2−59265
  multiple beam interference refractometer and comparator 2−45787
  noise characteristics of digital light deflectors 2−79388
  ocular fundus reflectometer 2−66312
  off-axis Fresnel zone plate as coded aperture for imaging incoherent sources 2−70021
  OLK-2 adapters for contact microscopy 2−70044
  particle size analyzer, comments 2−55750
  particle size spectrometer, electro-optical technique, meas. from aircraft 2−82579
  periodic arrays inspection by intensity spatial filtering 2−79424
  with periodic instrument function, method of determ. real contour parameters from observed contour 2−66836
  phase fluctuations meas. with strioscopic appliance 2−48512
  phase object visualization by Hilbert transformation 2−42232
  phosphoroscopes, disc, for phosphorescence decay meas. 2−79440

- **Optical instruments** continued
  - photoelectric, effects of nonuniform energy absorption in compensator plate on accuracy 2−70050
  - polymer crystallization rate, obs. by depolarized light intensity method 2−47065
  - probe for displacement meas. 2−79394
  - projector, modified, for evaluation of interferograms 2−66832
  - radiance meter, optical systems for defining, viewing and measuring fields 2−70034
  - real time processing system employing nonlinear optics 2−79425
  - real time wave front meas. system for display of surface quality and lens performance 2−79398
  - receivers using avalanche photodiodes, laws governing noise distrib. 2−76529
  - reflectance, absolute meas. in range 0.3-12 μ 2−55755
  - reflectance and transmittance measuring, calibration 2−66827
  - reflection meter, RCO type for measuring reflection ratio of flat, curved surfaces 2−66828
  - reflectometer, automated, for u.h.v. obs. 2−79409
  - reflectometer, single beam single optical path for continuous meas. 2−49435
  - refractometer, one-dimensional focusing critical angle, for mass transfer obs. 2−55760
  - relative reflectance meas. using sliding mirrors and single beam reflectometer 2−82568
  - reprographic and photomechanical equipment 2−49436
  - review of work performed by Honeywell Corporation 2−79366
  - ruling engine, 750 mm, for producing large gratings and echelles 2−42221
  - γ- Ruticon, image formation mechanism 79415 2−79415
  - scan interferometry, interference meas. on moved faces 2−63401
  - scanner, 600 MHz acousto-optical deflector 2−51296
  - for scattered light obs. in upper atmosphere 2−48513
  - screens, ground-glass, modulation transfer functions 2−70032
  - semiautomatic scanning, film information, automatic readout, dissector monitoring device 2−82566
  - sensitometer with high range of non-selective modulation 2−70040
  - shutter, fast magnetokinetic 2−59249
  - sighting devices for armoured fighting vehicles, optical transfer function applics. to testing 2−66831
  - space vehicle contaminant material optical constants det. by quartz microbalance and reflectometer 2−78418
  - spectroprojector SPP-2 2−70087
  - stack polarizers, quarter-wave, radiant transmittance obs. 2−79411
  - strain measurement, optical correlation methods 2−82141
  - super-polished reflectors with low scatter, applics. 2−79429
  - surfaces, ionic polishing, computer controlled system 2−79434
  - thickness monitor for thin film vacuum deposition control 2−47094
  - time division demultiplexer for twenty four channels using sinusoidal polarization switches 2−49434
  - t.w. electro-optic modulators, performance 2−73661
  - unseeded supersonic airflow meas. using a laser anemometer 2−83682
  - visibility meter and modality and Disability Glare Factor meas. 2−51973
  - wavelength converter, i.r. region, antiStokes mechanism, heterojunction structure 2−66848
  - Westinghouse Electric Corporation products, review 2−42222
  - zone plate disk sensor combinations, chromatic properties 2−79432
  - zoom autocollimator for centring optical surfaces 2−79397
  - Ag halides, thermolum. and photocond., trap levels, meas. apparatus and technique 2−79389
  - $Bi_{12}SiO_{20}$ electro-optic image modulator, sensitivity and resolution 2−79417
  - $Bi_{12}SiO_{20}$ electro-optic image modulator for optical processing 2−79416
  - $NH_4H_2PO_4$ polarizers for lasers, modified Wallaston prism 2−42105
  - Ni films as opaque coatings for code modulating disks and grids 2−70047
  - Pb Mo acousto-optic deflector 2−79419
  - TeO_2 acoustooptic light deflector 2−45804
  - TeO_2 acoustooptic light deflector with 1000 spot capacity and 40 microsecond retrace time 2−51016
- **Optical materials**
  - *see also Filters, optical*
  - activated glass, thermo-optic constants 2−59276
  - cathodochromic sodalite, storage and display applications 2−63423
  - cement, UF-235, new preparation method 2−59255
  - ceramics, transparent, cryst., optical applications, prep. 2−60988
  - coatings, detection of laser induced damage 2−63415
  - component blanks, precision blocking 2−59264
  - concave aspheric surfaces, machine for fabrication 2−79393
  - correction of optical elements by selective deposition by Glacier process 2−79395
  - dielectric thin films, spot size dependence of laser induced damage thresholds 2−48123
  - dielectrics, transparent, laser surface damage thresholds rel. to Fresnel reflections 2−79228
  - films, photoelectric thickness measurement 2−59225
  - glass:Nd, phase separation degree, rel. to optical props. 2−57372
  - glass, abrasion, microindentation hardness, max. fracture velocity 2−56550
  - glass, homogeneity 2−42224
  - glass, laser damage rel. to surface film 2−82504
  - glass, optical finishing by ion-beam sputtering machining 2−82571
  - glass, optical grade, relative intensities of Rayleigh and Brillouin scatt. 2−57364
  - glass, self-focusing rel. to electrostriction and Kerr effect, damage threshold 2−75249
  - glass, transparent, filamentary tracks formed by laser-beam self-focusing 2−65207
  - glass melt, striae solubility 2−59260
  - glass-ceramic, Nd^{3+} doped, lasing threshold and efficiency 2−73589
  - glasses, refractive index determination, non-immersion method 2−70048
  - glasses containing La and Ce, radiation and optical stability 2−70071
  - hard dielectric film waveguides, dispersion and loss meas. 2−42238
- **Optical materials** continued
  - holographic storage media, recyclable, performance parameters, review 2−63361
  - for holography, high resolution photomaterials 2−66790
  - interference coatings, multilayer, optical monitoring 2−79408
  - i.r. thin film filters rel. to developments in optical equipment 2−73667
  - layers with imposed spectral characts., control and preparation 2−63418
  - low loss, glasses, absorption measurement, using laser beam 2−63407
  - methylene blue dye film waveguides, absorption 2−63416
  - mica, optical characts. for radiation receivers 2−55754
  - monomolecular layers for study of light emission 2−55765
  - multipole radiation in optically uniaxial media 2−52311
  - nonlinear optical susceptibility det. 2−48125
  - plastic, mixed polymers of diethylene glycol-bis-allyl carbonate and isophthalic acid diallyl ester, with controlled refraction and dispersion 2−55752
  - PMMA, γ-irrad., absorpt. spectrum, optical density increment, u.v. filter 2−72357
  - polishing and quality evaluation of Fabry-Perot interferometer surfaces 2−76509
  - polymethylmetacrylate, volumetrical damage due to laser 2−76541
  - proustite, phase matched parametric upconversion, systems applications 2−79223
  - quartz, synthetic, loss at 1.06 μ, related to fibre optic appl. 2−48136
  - quartz optical contacts, hardening by heat treatment 2−59252
  - reflection coating, deterioration by intermetallic diffusion, protection method 2−55764
  - ruby boules, quality estimation from e.p.r. line widths 2−54493
  - sapphire, ion beam polished, increased laser surface damage threshold obs. 2−57317
  - semitransparent, thermophysical props. at high temps. 2−54069
  - silicate glasses K-8, F-5, volumetrical damage due to lasers 2−76541
  - space radiation effects on transmittance meas., simulated 2−49440
  - structural relations between racemic and optically active cryst. structures 2−53626
  - surfaces, holographic interferometric anal. of contamination 2−45809
  - thermoplastic photoconductor media for holographic recording 2−63360
  - thin film coatings, Multilayer Automatic Coater for deposition 2−73659
  - thin films, refractive indexes and thickness determ. from X-ray specular reflection data 2−53563
  - transparent objects, study by spatial frequency modulation of carrier wave 2−45806
  - two-dimensional thermal attenuation of laser pulse in solid 2−75247
  - window for spacecraft, characteristics, structure, testing and thermal effects 2−79391
  - Yttralox ceramic, Th-doped, processing 2−50900
  - Yttralox ceramic characteriz. as laser material 2−49381
  - $AgGaS_2$, as suitable mixing material for far i.r. generation 2−44364
  - Al_2O_3, translucent alumina prep. and characteriz. 2−50863
  - $Bi_4Ge_3(Si_3)O_{12}$ electro-optic crysts., quadrupole coupling consts. 2−84604
  - CaF_2 plates, plug cutting 2−45182
  - $CaNb_2O_6$:Nd, cryst. growth for laser applic. 2−50592
  - CdTe, optical grade cryst. prod. by directional solidification 2−50607
  - KIO_3, symmetry props. rel. to use as nonlinear optical material 2−74733
  - La flint glass, Bragg diffraction rel. to acousto-optic applications 2−66839
  - LiF films on Al, thickness monitoring by reflectance meas. using 1216 Å line of H 2−55733
  - $LiNbO_3$, directional dispersion and assignment of optical phonons 2−77764
  - $LiNbO_3$ single domain crystals, growth by pulling method in h.f. induction furnace, properties, applications 2−77528
  - $LiTaO_3$, self-induced thermal effects on light extinction 2−72254
  - MgF_2, X-ray structural study of texture of KO-1 ceramic 2−70042
  - MgF_2 films on Al, thickness monitoring by reflectance meas. using 1216 Å line of H 2−55733
  - MgO film, evaporated, refr. index and absorpt., 0.22-8μ 2−79369
  - $Na_2ZrSiO_5:Eu^{3+}$, cryst. struct. and luminesc. 2−72414
  - Re evaporated film, reflectance in v.u.v. from 300-2000 Å 2−44345
  - SiO_2, fused, development of new variety 2−70046
  - $ThO_2:Y_2O_3$ ceramic, high optical quality, powder prep. and processing technique 2−77736
  - Tl_3AsS_4, optoacoustic props. 2−61597
  - Tl_3AsS_4 acousto-optic crystal, props. 2−76530
  - Tl_3AsSe_3, nonlinear, optical props. 2−42243
  - Tl_3AsSe_3, phase matchable i.r. nonlinear material 2−48129
  - W evaporated film, reflectance in v.u.v. from 300-2000 Å 2−44345
  - $YAlO_3:Nd^{3+}$, high temp. phase instability 2−74958
  - $Y_2SiO_5:Nd^{3+}$, absorpt. and luminesc. spectra, and stimulated emission 2−78123
  - ZnS(Se), chem. vapour deposition of transparent polycrysts. 2−50578
- **Optical mode, crystals** *see Crystals/lattice mechanics*
- **Optical model** *see Nucleus/models*
- **Optical properties of substances**
  - *see also Optical constants; Optical materials*
  - 8/65/35 PLZT fine grained ferroelec. ceramic, dielec. and optical fatigue effects 2−77953
  - amorphous, intrinsic props., book contrib. 2−72293
  - D L azidophenilacetic acid, use of optical activity to control resolution and determ. optical purity 2−54523
  - calcite, infrared dispersion parameters determination from reflectivity, Kramers-Kronig relations and damped oscillator theory 2−57322
  - carbon tetrachloride, liquid in vac. u.v. 2−50363
  - ceramics, transparent, cryst., optical applications, prep. 2−60988
  - chalcopyrite semiconductors, review 2−48126
  - cholesteric liquid crystal and uses for testing materials 2−60931

Optical properties of substances continued

collisionless gases, transient orientational birefringence 2−43267
condensed matter, book contrib. 2−72249
crystal, excitonic region of spectrum, book contrib. 2−72317
cyclohexane, liquid in vac. u.v. 2−50363
density, continuous-flow ultraviolet microdensitometer 2−56504
dialogite, infrared dispersion parameters determination from reflectivity, Kramers-Kronig relations and damped oscillator theory 2−57322
dielectric thin film waveguides, TE_0 and TM_0 modes spectral props., coupling 2−78969
dolomite, infrared dispersion parameters determination from reflectivity, Kramers-Kronig relations and damped oscillator theory 2−57322
dolomite, infrared dispersion parameters determination from reflectivity, Kramers-Kronig relations and damped oscillator theory 2−57322
epoxide resin Epidian 2, short-term props. 2−47672
fused quartz, ion-bombarded, refractive index and optical loss variations 2−50688
gas, plane-parallel layer, radiative flux and flux divergence of Lorentz line 2−43271
gases, molecular band model formulation for large variation in temperature along optical path 2−43269
glasses and liqs., superbroadening of ultrashort pulse spectrum 2−43368
hexafluoroisopropanol, enhanced nonresonant, optical four-photon parametric interaction 2−46957
n-hexane, liquid in vac. u.v. 2−50363
igneous rocks rel. to albedo and linear polarization of lunar surface 2−75846
liquid crystal, nematic, acoustic modulation of light 2−59241
liquid crystal, nematic film polarimetry and interferometry studies 2−43329
liquid crystal, nematic mechanochromatic effects 2−84463
lithium formate monohydrate, nonlinear optical crystal 2−48130
metal, book contrib. 2−72292
molecules in solution organic dye two-photon absorption profile, apparatus 2−66734
optical pumping use for study of solids 2−64007
plastic, mixed polymers of diethylene glycol-bis-allyl carbonate and isophthalic acid diallyl ester, with controlled refraction and dispersion 2−55752
poly(glycol methocrylate), photoelastic effect in molecular 3d networks, optical anisotropy, thermodynamic rigidity 2−44347
polyethylene, sulpho- chlorinated, anisotropy of statistical segment 2−44346
polymer fracture surface layer, optical thickness determ. 2−70013
reflected-shadow method for constrained zone study of cracks in birefringent media 2−68101
semiconductor, amorphous, reversible elec. and optical memory effects 2−57185
semiconductor, amorphous 2−61573
semiconductor, book contrib. 2−72291
siderite, infrared dispersion parameters determination from reflectivity, Kramers-Kronig relations and dampled oscillator theory 2−57322
smithsonite, infrared dispersion parameters determination from reflectivity, Kramers-Kronig relations and damped oscillator theory 2−57322
solids, book 2−72248
spectrophotometers, SF-10 and SF-14, automatic recording of optical characteristics variations of sample 2−59289
Al_2O_3-Cr_2O_3 system, sub- solidous phase equilib. rel. to sample prep. for opt. studies 2−53983
Ar, freq. depend. of light distortion 2−50273
Ar singly ionized, specific refractivity 2−79903
As-Se-Ge glass film, amorphous to crystalline state conversion by light irradiation 2−75077
Au-Zn dilute alloys, optical and piezo- optical properties from reflectivity measurements 2−68621
$Ba_2NaNb_5O_{15}$, characterization, vibr. props. 2−72364
$BaTiO_3$, recent research 2−61412
Bi-Sb solid soln., thermomagnetogalvanic props. 2−54245
$CaCO_3$, optical strength and damage caused by laser radiation 2−72273
Cs optical constants in liquid and solid, 0.3 to 2.5 μ region, dependence on temp. 2−68596
CuAu, Cu_3Au, effect of ordering using reflectance measurements 2−72303
Ge, determination from electron energy loss function via Kramers Kronig dispersion relations 2−71769
InBr(I), type I and II crysts. 2−64638
Ir, meas. in range 15-0.302 μm at 77 and 295 K 2−81359
K, interband opt. conductivity calcs. 2−68616
K, opt. conductivity in 4-10.7 eV photon energy range 2−68593
K, optical props. and surface plasmon states 2−71819
K, vapour, reson. nonlinear susceptibility dispersion 2−43272
K anomalous infra-red absorption and collective oscillations in small metal particles 2−65210
Kr pulsed discharge, as function of discharge conditions 2−43212
$LiNbO_3$ spontaneous parameteric scattering, idler absorption and dispersion 2−44337
$LiTaO_3:Cu^{2+}$, optical generation of picosecond electrical pulses 2−44336
MgO crysts. growth by chem. vapour deposition 2−47223
Na, anomalous infra-red absorption and collective oscillations in small metal particles 2−65210
Na, interband opt. conductivity calcs. 2−68616
Na, optical props. and surface plasmon states 2−71819
NaCl, laser induced breakdown 2−54376
$NiSO_4.6H_2O$ optical activity, calc. of rotatory strengths and dipole strengths associated with electronic transitions 2−57325
Si, determination from electron energy loss function via Kramers Kronig dispersion relations 2−71769
SiO_2CaO-Al_2O_3 glass, stratification, liquation, opalescence 2−56564
TiO_2 hydrosol, turbidity and refractive index 2−74574
Tl_3AsS_3, nonlinear optical material 2−42243
Tl_3AsS_4, single crystal, transparency, refractive index, optoacoustic props. 2−48137
Tl_3AsSe_3, phase matchable i.r. nonlinear material 2−48129
$Tl_2Cd_2(SO_4)_3$ ferroelectric Langbeinite 2−51199
Tm orthoferrite, Faraday effect, periodic stripe struct. 2−54384
Xe, freq. depend. of light distortion 2−50273
Xe plasma pulsed discharge 2−74381
YIG, photomechanical effect 2−81332

Optical pumping

alkali atoms, excited $^2P_{3/2}$ state, nuclear spin in optical pumping with D_2-light 2−74227
alkali halides, F-centre pumping, spin mixing 2−53750
alkali halides, pumping cycle dynamics of F-centres 2−53749
atomic spectroscopy use and optical study of solids 2−64007
Bloch equations, solution method 2−69841
clathrate, laser action utilizing rot. transitions, speculation 2−54446
coherence, effect on freq. conversion and parametric amplification 2−59125
continuous-wave lasers based on ionic crystals, high-current arc discharge 2−55703
cylindrical ruby rods in elliptical condenser, energy distribution 2−42059
2,5-diphenyloxazol, anthryl derivatives, dependence of threshold of generation on pumping polarization 2−53450
dye laser, efficiency, pump parameter and triplet lifetime depend., calcs. 2−69927
dye laser, N_2-laser pumped, simultaneous two- wavelength selection technique 2−79186
dye laser, u.v., by Nd:YAG laser 2−52426
dye laser, vortex confined discharge laser soln. 2−49371
ethanol solution, anthracene added, induced loss during flashtube pumping 2−76488
evanescent field pumped dye laser with dye on surface of waveguide 2−42056
evanescent-field-pumped dye laser, pumping scheme using waveguide mode 2−79184
face-pumped solid-host laser, concept and implementation 2−42047
flashlamp for solutions of organic dyes 2−76466
focal length of pump induced lenses in laser media meas. 2−41959
gas lasers, high-pressure, simple model for fast transverse discharges 2−52416
hot electron population inversion, in crossed elec. and mag. fields, theory 2−75007
ions, for meas. of r.f. spectra, obs. of hyperfine structure, g-values, nuclear magnetic moments 2−77009
lamp power supply control circuit 2−45648
laser, reference frequency shift calc. 2−49341
linear water cooled ablating-wall flashlamp pumped dye laser for study of upper atmospheric composition 2−73580
magnon oscillation generation, threshold values 2−54306
methyl fluoride laser, by CO_2 TEA laser 2−42028
mode locked, of KDP parametric light amplification and oscillation 2−42052
molecular vibr. levels population meas. method 2−79972
molecule, diffusion coeff. and probing of excited species interaction 2−60106
multimode laser beam, saturation resonances by magnetic mode crossing 2−41955
pulsed high power laser, single mode TEM_{00q} operation 2−82472
pumped systems, n.m.r., obs. of wiggles phenomena 2−74487
quantum counter up-conversion, 10-μ, in rare earth doped crysts. 2−45704
Raman scattering, polariton, in the vicinity of phonon resonance, fluctuation−dissipation theory 2−84496
rare earth and actinide ions in single crysts., two-photon absorpt. and stimulated emission 2−48225
rhodamine 6G laser, pumped by pinched discharge, energy characteristics 2−42046
rhodamine 6G laser emission field characteristics, thermo-optical distortion 2−52424
rhodamine 6J laser, dynamic compensation of thermo-optical distortion 2−73579
rhodamine 6J lasing, effect of transverse pumping distribution, on thermal-optical distortion 2−49376
rhodamine B solution in methanol, anti-Stokes fluorescence in organic dye solutions 2−43378
semiconductor, many-valley, n-type, effects on conductivity 2−57204
semiconductor, optically pumped, instability in strong mag. field 2−71889
semiconductor lasers, absorption saturation 2−49383
short cavity tunable dye laser, longitudinal excitation by N_2 laser 2−66757
for soft X-ray lasers 2−41960
solid state pumping source for Nd YAG lasers with integrated focusing optics 2−69943
spin memory, rel. to optical techniques in e.p.r. 2−61729
super radiant light source produced by electron beam pumping of CdS crystal 2−79215
superluminal motion in inverted media 2−82608
system using double plane parallel lamps, efficiency 2−45705
tetraphenylbutadene liquid and solid solutions, dependence of threshold of generation on pumping polarization 2−53450
transient stimulated Raman scattering, molecular relaxation and dispersion 2−41938
two-level atom, modified Bloch equations 2−67396
vapour, relaxation at cell walls, Franzen's approx. 2−76995
wideband parametric upconversion of i.r. waves to visible region using tunable dye laser 2−82511
YIG, d.c. magnetization produced by parallel pumping 2−72203
Zeeman scanning of optically pumped vapour for determ. h.f.s. 2−46429
$Ba_2NaNb_5O_{14}$, fluorescence, tunable, stimulated parametric, induced by picosecond pump pulses 2−69889
CO_2, atmospheric pressure laser, using HBr laser 2−55689
CdS, slow traps, optically pumped differential absorption apparatus 2−68427
of CdSe i.r. parametric oscillator, by Q-switched Nd:YAG laser 2−42061

Optical pumping continued
- Cs-Rb differential Stark shift investigated using optically pumped atomic light modulation oscillators 2−46424
- Cs, influence of modulation of crossbeam on amplitude of r.f. field 2−52934
- Cs, transverse relaxation time 2−83191
- Cs atoms, effect of transverse pumping 2−70605
- Cs^+, free ions, rel. to n.m.r. 2−79897
- ^{133}Cs, phase destruction detection of ground state hyperfine transitions and population inversion with GaAs lasers 2−70599
- $^{133}Cs^+$ ion, free, n.m.r. freq. shift due to charge exchange with Cs atom 2−79896
- GaSe, under two-photon excitation, stimulated emission 2−72405
- H_2, tunable stimulated Raman emission by dye laser 2−77078
- HBr chemical laser, using CO_2 and N_2O 2−42015
- HCl, parametric oscillator pumped, vibrational energy transfer 2−80155
- HF laser rate eqns., closed-form soln. 2−82479
- HF low-pressure gas sample, laser-induced line narrowing spectroscopy 2−45819
- He-CO_2 laser, chemical, pulsed, output pulse obs., pumping mechanism 2−73561
- Hg spectral lamp in u.h.p. cavity resonator, optical pumping 2−73550
- ^{193}Hg, nuclear magnetic moment determination 2−70412
- ^{193m}Hg, nuclear magnetic moment determination 2−70412
- ^{195m}Hg, nuclear magnetic moment determination 2−70412
- ^{197m}Hg, nuclear magnetic moment determination 2−70412
- I population inversion processes 2−55693
- I_2 vapour, by Kr ion laser, transitions assignment 2−80016
- of $LiIO_3$ internal parametric oscillator, by Nd:YAG laser 2−45746
- Mg_2, matrix-isolated, absorpt. peaks 3540-3700, absence of optical pumping 2−80041
- N_2-CO transfer laser, low temp., energy exchange processes 2−69924
- N_2, ionized, pulsed discharge production in visible range, use for laser pumping 2−69890
- N_2 laser, pumped by intense electron beam 2−73569
- Na atom, obs. of maser transitions between Paschen-Back levels of ground state 2−52935
- Nd^{3+}:YAG, effect of pressure in Xe and Kr arc lamps on pumping efficiency 2−42072
- Ne, cascade effects in 2p level life time meas. 2−64032
- Ne atom excited with laser beam, nonlinear effects in weak magnetic field 2−46453
- Ne gas discharge in magnetic field, saturation resonances by magnetic mode crossing with multimode laser 2−46436
- Ne levels, population changes by 0.61 μm and 3.39 μm laser action 2−76483
- O_2, ionized, pulsed discharge production in visible range, use for laser pumping 2−69890
- OH interstellar molecule, pumping by polarized i.r. radiation, maser emission 2−81851
- Pb polarized metastable states, obs. of optical-pumping Zeeman resonances 2−42785
- Rb-Ar, Rb-Kr, Van der Waals molecules, rel. to action of r.f. field 2−56194
- Rb-electron-exchange optical pumping expts., determ. of temperature dependence of cross sections 2−70615
- Rb, coherently excited, spontaneous decay 2−67403
- Rb gas cell type atomic oscillator 2−77008
- Rb magnetometer, vector, operation and performance 2−73511
- ^{87}Rb spectral source, hyperfine structure of D_1 line 2−73670
- ZnI, Hanle effect obs. of $4s4p\,^3P_1$ and $4s5s\,^3S_1$ levels 2−74232

Optical quantum generators *see Lasers*

Optical rotation
- *see also Magneto-optical effects; Optical constants; Polarimeters; Polarization/light*
- camphor carbonyl, rot. force of $n \rightarrow \pi^*$ transition 2−60071
- chloralides, optically active, molecular conformation 2−42971
- cholesteric liquid crystals in isotropic phase, pretransitional increase in optical rotation 2−80434
- cholesteric solns. with helically arranged mols., induced optical activity 2−53394
- circular dichroism, semi- classical theory, time-dependent Schrodinger equation 2−52460
- crystals, electro-optical activity from piezomagnetic tensor 2−72258
- furan, normal magneto-optical rot. dispersions, mag. moments 2−70770
- ketone-tetracyanoethylene system, optical activity inducement in charge transfer band 2−60071
- liquid crystal, cholesteric, rel. to rapid conical-helical perturb., a.c.-d.c. technique obs. 2−71217
- macromolecules, rot. dispersion rel. to conform. transitions determ. 2−83383
- l-menthol in nematic solvent, optical activity and circular dichroism 2−80442
- molecular vibr. transitions, i.r. activity, coupled oscillator model 2−60040
- optically inactive crystals, opt. rotat. induced by crossed elec. and mag. fields 2−78066
- pyridine, normal magneto-optical rot. dispersions, mag. moments 2−70770
- quartz, gyrotropy and asymmetric electro-optic props., two beam refraction obs. 2−72269
- racemic mixtures, optical activity rel. to polarization dependence of multipole absorption probability 2−49994
- superimposed birefringence and optical activity of medium polariscope investigation 2−66835
- transition layer effects in gyrotropic and nongyrotropic media 2−69820
- $CdGeAs_2(P_2)$, i.r. birefringence, 2-10μ 2−72261
- $CdSiAs_2$, i.r. 2−72261
- α-HgS, synthetic, rotatory power and Faraday effect 2−75258
- $Hg_3Te_2Cl_2$, 5000-7000Å 2−71374
- $NiSO_4.6H_2O$ optical activity, calc. of rotatory strengths and dipole strengths associated with electronic transitions 2−57325
- $Pb_5Ge_3O_{11}$ single crystal, ferroelec. optical rotation domains 2−44164
- Te, rotatory power, theory, k.p perturbation calc. 2−81018

Optical rotation continued
- $ZnGeP_2$, i.r. 2−72261

Optical systems
- *see also Aberrations, optical; Lenses; Optical images; Optical instruments; Optical materials; Resolving power, optics*
- — 2−66837
- aberration effect on design, teaching 2−76506
- aberrations caused by decentring, summing 2−59215
- aerosol particle counter, response curve, aperture effect 2−67852
- air jet flow observation of fluidics by optical methods 2−73653
- alignment and straightness meas., two-aperture method 2−70035
- alignment of planes and straight lines in space 2−70006
- all-metal, ultra-light-weight, for space vehicles 2−73658
- analytical ultracentrifuge, alignment of schlieren and interference systems 2−61819
- angle sensing system 2−70030
- anisotropic waveguides, optical propagation, applications of electrooptic effect to guided wave modulation 2−63410
- automatic lens design, desensitizing model 2−79406
- bench, apparatus for making x and y adjustments 2−41436
- bilinear transformation of polarization 2−73646
- Cassegrainian, stellar photometer, for 1300-2000 Å range 2−69050
- catadioptric system, using reflecting curved cone 2−63408
- catadioptric systems described 2−59218
- colour correction of systems operating in visible light 2−59257
- compensator, artificial hologram 2−76503
- computer output microfilm 2−59295
- concentric, third-order aberrations, object plane positions 2−59259
- for continuous monitoring of haemolysis in flow system 2−51883
- control using laser interferometer 2−42127
- Delano diagram, application to optical design 2−79402
- design, applications of automatic mathematical correction methods 2−45803
- design and aberrations, tutorial 2−49410
- design and aberrations, tutorial 2−49411
- design and aberrations, tutorial 2−42178
- design and aberrations, tutorial 2−52446
- design and aberrations, tutorial 2−59211
- design and aberrations, tutorial 2−63382
- design and aberrations, tutorial 2−45775
- design and aberrations 2−73626
- design by computer, curvilinear bicubic spline fit interpolation scheme 2−79404
- diffused mixed single crystal waveguides on II-VI compound substrates 2−42240
- directional coupler made from multilayered glass films 2−42237
- with electron-optical brightness intensifiers investigation of edge image characteristics 2−82576
- electrooptical processing of phased array antenna data 2−42226
- electrophotographic apparatus, requirements of optical systems 2−73696
- ellipsoidal and plane mirror for increasing gain in Raman scattering 2−79414
- embossed integrated optical structures fabrication 2−42230
- enlarger, condenser type, design and aberrations 2−66829
- evaluation, systematization, estimation of images 2−82548
- fabrication and test mount for 1.8 m light weight mirror, design 2−79428
- fibre array for radial distrib. of light intensity obs. for particle size anal. 2−70057
- geometrical transfer function, correction term 2−63376
- Hamiltonian, with discrete axial symmetry 2−45779
- illumination distrib. produced by system in arbitrary plane, computer program 2−59258
- image conversion from i.r. to visible region 2−42255
- image quality, effect of linear and sinusoidal motion 2−63403
- image sampling and reconstruction, electro-optical systems 2−59242
- imaging, performance degradation, mirror mounting systems for fabrication and testing 2−79427
- imaging and detective quantum efficiency, primary parameters 2−59267
- imaging apertures, circular and rectangular, three dimens. intensity impulse responses 2−79298
- imaging spectral radiometer, optical design for Earth resources applications 2−84775
- incohrent optical correlation system for integration of functions of one variable 2−55441
- i.r. systems, applications 2−84764
- kinoform, linear array, generation, random number generator 2−79283
- large aperture, testing using Twyman Green interferometer 2−63402
- laser photography, in hyperballistics range 2−82578
- laser pulse duration meas. using optical bridge 2−73563
- lens design, LASL, improved speed 2−79405
- linear, analogy with two port elec. ccts. 2−79367
- linear optical data processors used with coherent or incoherent light 2−79293
- luminance subtraction, birefringent prism arrangements 2−66805
- mirrored surfaces, method of measuring reflection coefficients 2−42181
- multicolour spatial frequency analysis by optical multiplexing 2−42186
- off-axis corrector for parabolic mirror 2−79426
- optical data processor, coherent and noncoherent, space invariance conditions 2−79368
- optical surface microtopography measurement and/or automatic focusing 2−73655
- phase holograms as optical elements 2−42143
- photoelectric for monitoring thickness of optical films 2−59225
- plane symmetric, aberration coeffs. determ. 2−73627
- polarization-mapping props. in Poincare sphere representation 2−73631
- profile technique for inspection of surface profiles 2−70049
- pupil scan aberration analyser 2−76531
- radiographic screen-film system, truncation errors in calc. MTF from line spread function 2−42234
- resolution of circular aperture focusing system, nonuniform coherent illumination 2−59246
- resonators, low loss, modes and losses, diffr. formulas 2−79375
- sampled, detection and location of point images 2−79423

Optical systems continued
scanning detection system, spatial filter applications 2−42245
scanning with light beams produced by decentered spherical surfaces 2−59245
single-beam u.v. gas and liq. analyzer 2−61827
space bandwidth product of multichannel coherent processors 2−79291
super-polished reflectors with low scatter, applics. 2−79429
superresolving for holography 2−76501
teaching, design rel. to aberrations 2−73630
thin film waveguides, absorption 2−63416
thin film waveguides, propagation characteristics 2−55762
three dimensional displays, holographic, stereoscopic techniques 2−82580
three dimensional sequential information storage, nonlinear absorption 2−73663
three-reflection-grating, for linear displacement meas. 2−59256
tilted plane optical processor for data from synthetic aperture radars 2−66828
transfer function determ. using incoherent Fourier transform technique 2−66804
two-lens systems of reversed Ramsden and reversed Huygenian types, primary aberration 2−63373
unitary matrix description, exptl. polariscope investigation 2−66835
unusual image distortion, use of spline aspheric surfaces 2−79403
viewing and measuring fields in luminance/radiance meters 2−70034
Wadsworth mounting, three-dimensional theory 2−63389
waveguides, electrically induced migration of ions in glass plates 2−42229
White Welsh four mirror system, imaging properties 2−45778
without symmetries, Lagrangian aberration coeffs. 2−79297
GaAs epitaxial films, light beam guidance and control 2−42236
ZnO single crystal waveguides, visible range, properties, technology 2−52463
Optical waveguides *see Electromagnetic wave propagation/guided waves*
Optics
see also Aberrations, optical; Atmospheric optics; Lenses; Mirrors, etc.; Optical images; Quantum optics
abridged supporting block set for optical expts. 2−78737
amplitude fluctuation correlation in angle spaced beams 2−79318
beam width-divergence product, maximization 2−79290
birefringent polymer films on substrates for integrated optics 2−80592
character recognition, characteristic extraction 2−42227
coherent method of variance obs., applic. to image processing 2−55722
conference, Jerusalem, Israel (May 1972) 2−70340
conference (San Francisco, Oct 1972) 2−79287
coupling between optical waveguides 2−79400
course for engineers and scientists, book 2−69992
data processor, patent 2−69996
diffusion pump oil on Au mirrors, ellipsometric meas., simulation of space effects on optical surfaces 2−79431
Du Pont's progress 2−69990
frequency and velocity 2−69997
gas lens, effect of initial section, constant heat flow 2−79333
Hamilton's principle and ray optics 2−52445
inked traced curves analysis, coherent optical processing 2−79286
integrated, progress review 2−49437
integrated, status report 2−63406
light frequency division in case of demultiplication resonance 2−63379
lighting technology, reviews 2−70067
location of optical axis of aspheric surfaces 2−79396
measurement and computation by light rays 2−63409
microwave anechoic chambers design 2−49213
nonequilibrium optical field, temperature 2−69991
optoacoustic processing of large time-bandwidth signals 2−45771
physical, geometrical, relationship, application of covariant Hamilton's principle 2−63172
projection system, description 2−66875
review of work performed by Honeywell Corporation 2−79366
signal detection in presence of nonuniform noise, pulse shape effect 2−59207
small-angle multiple scatt. in iconal approx. 2−73621
speckling in diffraction and image field of rough objects, statistical functions for linear systems 2−52455
standard of light, NBS, luminous emissivity, effect of ceramic spectral emissivity variations 2−45808
Stokes parameters, significance and transformation equations 2−45780
time dilation and Doppler effect in space optics 2−79433
geometrical
anamorphic lens attachments for wide- screen cinematographic systems 2−52509
angle sensing system 2−70030
caustics, method for crack tip stress singularity calc. 2−52161
compensator, artificial hologram 2−76503
diffraction theory of moving conducting strip at h.f. 2−78960
e.m. field, correlation tensors, light-ray approximation 2−73625
e.m. propagation in nonuniform media, approximation to series soln. 2−58987
Gaussian beam optics rel. to conventional optics 2−79296
inhomogeneous media in y-y diagram 2−79311
optical design and aberrations, part XXVIII 2−69999
plane light wave propagation in randomly inhomogeneous medium, Markov's approximation 2−55726
ray diagrams for virtual objects 2−70007
ray optics, principles and applications 2−69821
ray tracing in cylindrical gradient index media 2−42177
sagittal ray correction method for reduction of primary aberration 2−55729
scanning with moving mirrors 2−66799
spatial intensity distribution of light beam in weakly inhomogeneous medium 2−79310
systems without symmetries, Lagrangian aberration coeffs. 2−79297
theory of rough-surface emission and scattering 2−44652
total aberration formula, skew rays optical aberration 2−76505

Optics continued
geometrical continued
zoom lenses, optical design and aberrations, tutorial series 2−52448
nonlinear *see Nonlinear optics*
Orbital calculation methods
see also LCAO calculations
13 basis function calc. for water molecule based on selection of proper canonical orbitals 2−67477
ab initio calcs., using Gaussian basis set of geometries of Li_2O_2 and LiO_2H 2−53022
ab initio SCF calcs. of electronic structure of ZnF_2, determ. of Walsh diagram 2−70730
ab initio SCF MO calcs. of electronic structure of $Mn(CO)_5H$ and $Mn(CO)_5CH_3$ 2−70713
all-valence-electron molecular orbital theory, bond order-bond length relationship 2−46513
allyl anion, bond angles and CC-distance determination by π-electron and all-valence electron method 2−53042
AMO function for Li_2 molecule 2−56183
angular parameters of overlap integrals of f-orbitals 2−77034
approximate molecular orbital method for energy properties 2−70670
APW method, quasi-self-consistent, calc. of energy band structure of VC 2−51082
atom, d-shell computational tools and calculations, bibliography 2−49924
atomic, simultaneous eigenfunctions of $\mathfrak{L}^2$ and $\mathfrak{S}^2$ by direct diagonalization 2−74196
Aufbau valence bond principle for molecular excited states 2−80008
Brueckner orbitals of molecular and atomic systems determ. by iterative procedure 2−50006
chemisorption and catalysis, orbital symmetry rules for surface sites prediction 2−51441
CI expansion, large-scale method for coeffs. calc. 2−67451
Clementi SCF orbitals, fitting orbitals of a cusped gaussian basis 2−49916
CNDO, extend Huckel Pariser-Parr-Pople Huckel-ω calcs. of tautomeric equilib. of isoxazolinone-5 2−53070
CNDO, INDO calcs. of electronic structure of acetaldehyde and complex 2−53043
CNDO and IEHT wavefunctions in calculation of quadrupole moments 2−52982
CNDO calcs. of doublet splitting of mols. 2−67442
CNDO calculations extended to transition metal complexes 2−83252
CNDO method for mols. with second row atoms, invariance 2−83225
CNDO/2, appl. to electron delocalization in N_4S_4 and $N_4S_4F_4$ 2−77089
CNDO/2 and INDO semiempirical calcs., anomalous energy minima 2−83234
CNDO/2 localized wavefunctions of molecules containing N atoms, free electron pairs 2−59981
CNDO/2 SCF calcs. of proton affinities of acids 2−83220
CNDO/2D calcs. of second moments of electronic charge distrib. and molecular quadrupole moments in fluorine containing organic compounds 2−80085
CNDO/CI calcs. of lower electronic transitions of benzonitrile and ethynylbenzene 2−56221
co-ordination compounds, translation between MO and HL descriptions 2−52990
concerted chem. reactions, correl. diagrams using orbital symmetry from exact wavefunctions 2−72539
configuration interaction, reduced partitioning procedure for atomic and molecular ground state studies 2−42703
configuration interaction wavefunctions for calc. of molecular elec. dipole moment 2−74258
Coulomb and hybrid integrals over Slater-transform-Preuss functions 2−42702
cusped gaussian wave functions for second row atoms and Kr 2−49917
cyclopentadienyl cation, unrestricted Hartree Fock treatment 2−83293
cyclopropene, orbital nature in electronic states 2−50091
cyclopropylketones, electronic transitions by MO methods 2−77122
d orbitals, 5 equivalent, a continuum of sets 2−74193
density matrix values in configuration space, computation 2−52897
diatomic mols., energy calcs. with extended-Huckel method 2−67443
doubly degenerate band, electron correlation 2−84425
electron propagation moment conserving decoupling techniques 2−79982
extended Huckel procedure for calculating ^{199}Hg-^{1}H coupling constants 2−83223
F-centre molecular-orbital model for excited conditions of Li atom 2−68041
first-row atoms, B to Ne, ground state orbital approx. using cusped gaussian wave functions 2−49916
Fourier transform of two-centre Slater orbital products 2−52895
Gaussian atomic orbitals, property- optimized 2−46401
generalized valence bond approach to BH_n series 2−59991
GI(SOGI) spin-coupling optimized calcs. of reaction surface for $H_2+D_2\to 2HD$ 2−48323
GIAO calcs. of n.m.r. chem. shifts 2−67461
Green function techniques, review 2−49919
halogenated molecule-nitroxide radical interaction, ^{13}C constant shift and MO studies 2−51440
Hartree-Fock, unrestricted method 2−43023
Hellmann-Feynman force integrals, three-centre, evaluation involving Slater-type orbitals 2−46499
Huckel, iterative extended method 2−43007
Huckel analysis of complex conjugated mols., transfer matrix method applic. 2−77132
hydrocarbons, d-functions effect on orbital energies 2−80067
INDO and MINDO/2 crystal orbital study of polyacetylene, polyethylene, polyglycine 2−44035
INDO geometry optimized H_2O_2 barriers, analysis 2−83249
INDO orbital studies of $n\to\pi^*$ transitions in symmetric diazines 2−53060
INDO perturbation theory of magnetic shielding constants, determ. of ^{13}C chemical shifts 2−64162

Orbital calculation methods continued
interaction matrix elements among doubly excited configs. 2-70673
IOC-ω technique, detailed analysis 2-46397
large molecules, Hartree-Fock model, numerical computation with dynamical basis set 2-83232
linked cluster many body theory for calc. of correlation energies of 10-electron systems 2-67484
localization procedures and convergence problems 2-64098
localized molec. orbitals, review 2-50008
localized orbitals for methane, NH_3 and h_2O mols. 2-53018
Lowdin's orthogonal orbitals, application to π-electron calcs. 2-64172
maximal overlap method subject to additional condition 2-77033
maximum overlap method with additional condition, to calc. polarizability of LiH mol. 2-83273
3-methyl sydnone and related species, ab initio calculation of orbital energies 2-53080
MINDO, for photoelectron spectra interpret. 2-67501
MINDO/2 calc. of ground states of σ-bonded F containing cpds. 2-77111
MINDO/2 calc. of potential surface for ethane 2-77126
MINDO/2 improved version, applic. to carbonium ions and protonated cyclopropanes 2-77112
molecular, for prediction of rotation and inversion barriers 2-67445
molecular hamiltonians, choice of gauge 2-50004
molecular integrals, investigation of auxiliary functions 2-50002
molecular orbital theory of magnetic shielding and susceptibility 2-42850
molecular orbital valency state and molecular orbital energies 2-42859
molecular quantum mechanical calc., integral transformations 2-56146
molecular wave function construction using cusped gaussian wave functions 2-49915
molecular wave functions, calc. and applic. to atomic and molec. processes, review 2-50007
molecules containing X-N= group, test of EH, IEH, CNDO/2 and MINDO/2 methods 2-52980
molecules-in-molecules method, four- and six-π-electron system calculations 2-59980
multicentre quantum chem. integrals and matrix elements, computation method 2-79848
multiconfiguration self-consistent field theory for localized orbitals, derivation of variational equations 2-52908
n-electron problem and matrices representing symmetric groups 2-52896
natural orbitals, properties and uses, review 2-59880
natural orbitals, variational principle 2-59879
network model for mols. and solids 2-71773
non-orthogonal orbitals, valence bond calc. and matrix elements between two tableau functions 2-67372
non-orthogonal radial orbitals, in complex electronic configurations of atom 2-42711
nuclear spin-spin coupling constants, double perturbation calculations using localized orbitals 2-46519
orbit-orbit integrals for diatomic molecules, evaluation of integrand 2-49988
orbital valence force field used to calc. force constants 2-46511
orthonormal space orbitals, construction of spin-adapted antisymmetrized products 2-74194
oscillator orbitals in CI calculations on two-electron systems 2-59883
parameterized self-consistent-field theory for transition metal compounds 2-46525
Pariser-Parr-Pople calcs. of electronic correl. in excited states of substituted benzenes 2-56220
Pariser-Parr-Pople model, self consistent polarization propagation calcs. 2-50012
Pariser-Parr-Pople SCF-MO calcs. of electronic struct. of isomeric methyl thiophenols 2-56239
PCILON, perturbative configuration interaction using localized orbitals and numerical integration 2-52978
perturbative configuration interaction with localized orbitals (PCILO), appl. to 11-cis-retinal 2-77153
perturbed molecular orbital discussion of ambiguities in use and generalized Huckel rule 2-50001
polarization propagator approx., self-consistent, as random phase method 2-46495
polarized orbital approximations for atomic electron scatt. 2-64039
pseudopotential SCF calculations for atoms 2-59904
quantum chemical semi-empirical theories, ab initio determ. of all parameters 2-70555
reduced density matrix variational principle, effectiveness of symmetry and Pauli condition on 1 matrix 2-46514
resonance integral-bond length relationship 2-50009
Roothaan-Hartree-Fock, selection of proper canonical orbitals for particular applications 2-67373
Rydberg excited states, basic formulas for one-electron perturbation calc. 2-67452
SCF calcs. of internal rotation barrier and its derivatives in BH_3NH_3 2-42873
SCF calcs. on diatomic alkali metal molecules, Pariser-Parr-Pople type method of Pohl 2-80049
SCF calcs. on large molecules using molecular fragments, construction of initial P-matrices 2-70667
SCF extended Gaussian-type basis for organic molecules, inclusion of second row elements 2-42941
SCF field molecular wave functions, approximations 2-42851
SCF many-shell method of McWeeny for calc. of $A^3\pi$ state of BN 2-70681
SCF MO ab initio calcs. of electronic structure of SO_2F_2 and ClO_3F 2-46587
SCF MO LCGO calcs. on mutual orientation of peptide planes in linearly H bonded peptides 2-46634
SCF open shell, simplified method 2-83229
SCF Pariser-Parr-Pople method for calc. electronic structure spectra of mono-substituted benzene derivatives 2-46594
SCF perturbation theory and intermolecular interactions 2-42849
SCF theory, eigenspace manipulation 2-67371

Orbital calculation methods continued
SCF wavefunctions for calc. of point-charge distrib. of azide ion 2-80086
SCF-LCAO-MO wave function density-distribution analysis 2-80052
SCF-MO calcs. for H_2-H_2 interactions at large internuclear separations 2-64217
SCF-MO-CI calc. of C_2 mol. 2-64120
SCMO CI calcs. of tetracyanoquinodimethane and its mono- and divalent anion 2-70791
second row atoms, use of cusped gaussian wave functions 2-49917
self-consistent procedures for generalized valence bond wavefunctions 2-53012
self-consistent-field α cluster calcs. for ground state Ne_2 mol. 2-80003
semi-empirical CNDO/2, INDO and MINDO/2 approach to electronic struct. of nitrous acids 2-56172
semi-empirical MO method, molecular charge distributions 2-42852
semiempirical scaled molecular orbital theory (SESMO) 2-67457
single-site theory of transport in systems with randomly distributed scatterers 2-80979
Slater functions, electron- repulsion, spin-spin and spin-orbit integrals 2-79980
Slater-type atomic orbitals, molecular one-electron integrals 2-42848
Slater-type orbitals from 4s to 4f, approximate Gaussian expansions 2-77048
small pi systems, perturbed excited state and complete configuration interaction wavefunctions 2-42853
spin-coupled wave functions, review of general theory 2-49918
SPINDO calc. of electronic structs. of cyclopentadiene and fulvene 2-70761
SPINDO calc. of photoelectron spectra of hydrocarbons 2-77114
strongly orthogonal geminal wavefunctions 2-70686
symmetry in self-consistent field theory of localized MO 2-59979
term symbols, group theoretical determination 2-52981
tetrahedral molecules and ions, force constants by orbital release force field and Urey-Bradley force field 2-77077
toluene, SPINDO calculation of electronic structure 2-70793
transformation props. of antisymmetric spin eigenfunctions under linear mixing of orbitals 2-70556
transition metal complexes, revised INDO calc. of charge transfer spectra and sequence of metal and ligand orbitals 2-67472
two particle correlations, evaluation of an integral 2-59898
valence orbital only method, removal of core orbitals 2-49993
vibrational force fields prediction using extended Huckel theory 2-79985
vinylcyclopropane and vinylcyclobutane, internal rotation, ab initio MO description 2-83291
wavefunctions, explicitly correlated, partially antisymmetric 2-42701
π-electron approx., justification from Hartree-Fock method 2-79988
Ag, clusters, calc. of electronic props. 2-81026
BF_2, ab initio calc. of electronic struct. and geometry, gaussian base set 2-83244
Be atoms in small aggregates Hartree-Fock calculation of electron states 2-80978
CO configuration interaction wavefunctions and dipole moment calc. 2-74258
Cd, clusters, calc. of electronic props. 2-81026
$Co(CN)_5^{3-}$, low spin square-pyramidal, SCCC calc. of orbital energy levels 2-46536
F^-, stability of self-consistent symmetries 2-76986
H_2, gaussian functions rel. to Slater orbitals 2-83243
Kr, use of cusped gaussian wave functions 2-49917
LCGO-SCF-MO method, mixed Gaussian basis, for ab initio calcs. 2-59978
Li atoms in small aggregates Hartree-Fock calculation of electron states 2-80978
N_2 SCF-LCAO-MO wave function density-distribution analysis 2-80052
N_3^{2-} and N_3^0, molecular orbital calc. of isotropic hyperfine interactions 2-64144
NF_2, ab initio calc. of electronic struct. and geometry, gaussian base set 2-83244
Ne, stability of self-consistent symmetries 2-76986
$Ni(C_5H_5)NO$, SCF-MO calculations, bonds 2-50064
$Ni(CN)_4^{2-}$, SCF-MO calculations, bonds 2-50064
O^-, stability of self-consistent symmetries 2-76986
Pb, clusters, calc. of electronic props. 2-81026
SiH_2, ab initio calcs. for potential curves, description of geometry and electronic spectrum 2-46584

Orbitals *see LCAO calculations*

Order-disorder changes
alloy, effect on channelling 2-44004
Bragg line sidebands, model of structure periodically modulated in three dimensions 2-50615
β-brass obs. in thermopower near order-disorder phase 2-84371
cooperative phenomena in compressible Ising model, pressure effects, double interaction model 2-45297
crystals lattice mechanics, position, orientation, magnetic disorder, experimental techniques 2-50991
dicalcium lead propionate, proton spin-lattice relax. time anomaly 2-65196
ferroelectric, nucl. double reson. studies 2-81481
ferroelectric, order-disorder transform., dynamic wave-vector-depend. susceptibility 2-81151
ferroelectric, order-disorder type, temp. dependence of n.m.r. spectra second moment 2-81150
ferroelectric phase transition dynamics, spin- lattice relax. meas. by double reson. 2-84450
ferroelectrics, temp. depend. of complex dielec. const. related to fluctuational ordering 2-84365
graphite, ordering, effect of Zr and Si additives 2-50829
Hubbard model, disordered four point, thermodynamic properties 2-81300
ice:KOH, dielec. dispersion and phase transition 2-72014
Landau theory, nematic-isotropic transition comparison with mag. crit. behaviour 2-53401

Order-disorder changes continued
magnetic transitions, sound propag. phenomena 2−54026
melting process interpret. at h.p. 2−56541
mixed crystal growth, influence of phase transitions 2−50816
percolation processes rel. to cooperative phenomena 2−55425
solid solution, X-ray diff. and model of rigid atoms in closed-packed arrangement 2−77768
solid solution, X-ray diffr. and model of interatomic force equil. 2−74965
steel, martensite, ordering temp. 2−57026
transition element oxide glasses, amorphous antiferromagnets, absence of ordering 2−81301
transition metal carbides and nitrides, (Gp IV and V), nonstoichiometry effects 2−61029
transmission electron microscope obs. 2−56631
1,2,3-trichloro-4,5,6-trimethybenzene, and struct. determ. at 298K, X-ray obs. 2−56674
1,2,3-trichloro-4,5,6-trimethylbenzene, and orientational order, ht. capacity obs. 2−57070
1,2,3-trichloro-4,5,6-trimethylbenzene, and structure determ. at 173K, X-ray obs. 2−56675
Vanadium Permendur, rel. to dimens. stability 2−43994
$AuCu_3$, effect of ordering on lattice heat capacities 2−57060
$BaTiO_3$ Raman cross sections, temp. dependence 2−84514
Bi_2Te_2Se, 7.5 MeV proton irrad. induced disorder, X-ray obs. 2−64653
Cd_3Mg, two-phase region, morphology, habit planes and orientation relns., metallographic obs. 2−61042
$CeH_{2\|x}$ system, nonstoichiometric, neutron diffr. obs. 2−77755
CsCl-phases, disorder parameter, graphical representation 2−80843
Cu-Au disordered alloys, correlation phenomena 2−64815
Cu-Ni-Mn alloy, 540°C, resist. and thermopower study 2−54001
Cu-Pd alloy, effect on band struct., absorpt. study 2−84237
CuAu, Cu_3Au, effect of ordering on optical properties, reflectance measurements 2−72303
Cu_3Au, influence on low temp. electronic sp. ht. 2−47750
Fe-Al system, β-solid solns., sp. ht. obs. 2−54002
Fe-Si solid solns., b.c.c., ordered atomic configs. 2−47326
Fe_xO, non-stoichiometric, magnetite-wustite boundary 2−84067
H_2 solid, ortho-enriched, fundamental i.r. absorption band meas. above and below order-disorder phase transition 2−81346
^3He, solid, λ transition to ordered antiferromag. phase 2−56537
Hf-O system, near $HfO_{1/6}$, neutron diffr. study 2−68205
KPF_6, solid, reorientation motions of PF_6^- ions 2−61562
$LiO_2(5-2t)Fe_2O_3tCr_2O_3$ ferrite, crystallographic struct., influence of heat treatment 2−57021
ND_4Cl, first order phase transition 2−84150
NH_4Br, microscopic theory, Ising spin-phonon coupled system 2−47700
NH_4Br, X-ray crit. scatt. obs. 2−47699
NH_4CL, lambda transition study by meas. of proton spin-lattice relaxation 2−57401
$NaNO_2$, ferroelec. order- disorder transition 2−61432
$NaNO_3$, crystal struct., order-disorder transforms, neutron diffraction obs., 20-290°C 2−77758
$NaNO_3$, X-ray diffr. obs. 2−65048
NaO_2, obs. at 230K from susceptibility meas. 2−65116
Ni-Cr system, heat of disordering of Ni_2Cr 2−50954
Ni_4Mo, rel. to dislocation generation, internal friction study 2−43670
$Ni(NO_3)_2,6NH_3$, heat capacity obs. 2−61036
$RbPF_6$, solid, reorientation motions of PF_6^- ions 2−61562
$SrTiO_3$ Raman cross sections, temp. dependence 2−84514
Ta_4D_3, stepwise phase transitions, neutron diffr. obs. 2−74947
V-C alloys, ordering effects on struct. comp. depend. 2−71378
VC_x, elec. resist. and enthalpy changes 2−54004
Zr-O system, near $ZrO_{1/3}$, neutron diffr. study 2−68205
Ordered structure *see Crystals/structure; Solids/structure*
Organic compounds
see also Free radicals; Macromolecules; Plastics; Polymers; Waxes
3,3-bromomethyldiazirine, absorption spectra, vibrational analysis 2−50089
3,3-chloromethyldiazirine, absorption spectra, vibrational analysis 2−50089
— 2−63709
— 2−67807
— 2−67513
— 2−67501
— 2−67519
— 2−72041
— 2−71447
π-radicals in soln., ENDOR mechanisms for β-protons 2−71235
(anthracene)-$(CH_2)_n$-(N, N-dimethylaniline) systems, intramol. electron donor-acceptor interactions 2−60047
β-(pyrazolyl-3)-L-alanine, crystal and molecular structure 2−47358
acenaphthene in stretched PVA sheets, polarized absorpt. spectra, electronic transitions 2−83276
acenaphthene-d_{10}, vibrational spectra 2−60043
acenaphthene-h_{10}, d_{10}, u.v. absorption spectra 2−74282
acenaphthene-h_{10}, vibrational spectra 2−60043
acenaphthenequinone, near-u.v. and visible absorpt. spectra and electronic struct. 2−70784
acenaphthylene, vibrational spectra 2−60043
acetaldehyde and complex, CNDO and INDO calcs. of dipole moments and electronic structure 2−53043
acetate ion, heat of protonation, 20°C 2−48314
acetates, u.s. velocity, det. of molecular parameters 2−53429
acetic acid, aqueous solution, u.s. absorption from 15-85 MHz 2−74542
acetic acid, O−H overtone bands and pot. energy curves 2−56211
acetic acid etchant, crystal impurity sensitive, cause of neg. etching action 2−67934
acetic acid in benzene solution, deuterated and non- deuterated, dielectric relaxation 2−71219
acetic acid/acetone mixtures, H bond formation causing ultrasonic relaxation, two state model 2−43322
acetic acid/water, viscosity-pressure behaviour 2−60449
acetone, coupling of motion between methyl groups studied by normal coordinate analysis using Urey-Bradley force field 2−56210
acetone, inverse Raman effect 2−71206
Organic compounds continued
acetone (-d_6), polycrystalline, Raman spectra, assignment of methyl vibrations, determ. of torsional frequency splitting 2−72374
acetone drops, heat transfer from small diameter channel in film boiling temp. range 2−53379
acetone metastable ions, determ. of lifetimes by field ionization mass spectrometry 2−46789
acetone oxime, obs. 70-4000 cm^{-1}, vibrational behaviour 2−50073
acetone-cyclohexane, solution properties at 25°C 2−53408
acetone-d_5, D chem. shifts meas. by ^1H-{^2H} INDOR 2−42947
acetone-methanol, solution properties at 25°C 2−53408
acetone-water, (CCl_4) mixtures, binary film condensation, effects of forced flow and variable properties 2−77411
acetone-water liquid system, relationship between self-diffusion and inter-diffusion coeffs. 2−50350
acetonitrile, in trialkylphosphines and CCl_4 , intermol. interac., spectral study 2−46647
acetonitrile, i.r. spectra of liquid, rotational diffusion and intermolecular interactions 2−83323
acetonitrile, Stark effect on ^{14}N n.q.r. 2−44463
acetonitrile-chloroform mixtures, complex form., solid phase, i.r. absorpt. obs. 2−60042
acetophenone, 2-hydroxy-5-methyl derivative, dielec. relaxation and dipole moment determination 2−60487
acetophenone crystal, Zeeman splitting pattern obs., assignment of lowest triplet state 2−80061
acetoxime, ^{13}C n.m.r., chem. shift, solvent and isotope effects 2−64165
9-CN, 10-acetoxy anthracene dimers, thermal behaviour and monomerization kinetics in the solid state 2−57436
acetyl bromide, zero-point average structures 2−77136
acetyl chloride, zero-point average structures 2−77136
acetyl fluoride, i.r. spectra of gas and solid, Raman spectra og liquid 2−83314
acetylacetone, molecular geometry from gas phase electron diffraction 2−60045
acetylcholine release by olivocochlear bundles on electrical stimulation 2−45166
acetylene, aerosol, produced by X-irrad. 2−46999
acetylene, conjugation reaction centre model of anionic polymerization 2−44481
acetylene, effects of deuterium substitution on n.m.r. parameters 2−77096
acetylene, formation of metastable triplet state in Hg photosensitized reaction, obs. of biacetyl emission 2−51467
acetylene, minimal basis set LCGO calcs. 2−79989
acetylene, photoionization products, rate coeffs. for reactions 2−51435
acetylene, vacuum u.v. spectra in solid carbon tetrafluoride 2−49957
acetylene + O reaction, totally inverted vibr. population of CO 2−61777
acetylene cryst., mol. motions, plastic behaviour 2−83881
acetylene derivatives, liq. crysts., synthesis and props. 2−46929
acetylene dicarboxylic acid dihydrate crystal, irradiated, free radicals, e.s.r. 2−75348
acetylene reaction with C^+, behaviour of cross section as function of incident energy, 2-100 eV 2−57416
acetylene-air flames, impingement heat transfer rates 2−52288
acetylene-d_0, d_1, d_2, high resolution analysis of Raman-active fundamental bands 2−64166
acetylene-d_2, vibrational assignment of spectrum near 18.6 μm 2−46592
acetylene-d_2 in CS_2 soln., ν_3 band profile analysis, temp. depend. 2−77135
acetylene-oxygen mixture, shock and detonation waves, local vel. meas. by Schlieren interferometry 2−63138
acetylene-oxygen-nitrogen mixtures, divergent spherical detonation propag. speed 2−52258
acetylenic derivatives of Si, Ge, Pb, P, As, Sb, i.r. and Raman spectra vibr. assignment 2−56212
acids, MO SCF calcs. of proton affinities 2−83220
acridine, molecular crysts., melting point rel. to intensity of incident u.v. radiation 2−50399
acridine and acridinium, i.r. and Raman spectra, vibr. assignment 2−60044
acridine red, two-photon absorption cross sections using psec laser pulses 2−61808
acrylic acids, substituted, and their methyl esters, ^{13}C n.m.r., correlation of olefinic shieldings 2−42950
acrylonitrile butadiene styrene, Poisson's ratio and temp. dependence of tensile props., stress analysis 2−53784
acyl peroxides, depend. of C−O−O−C chain vibrs. on mol. spatial struct., IR spectroscopic study 2−83327
adamantane, free radicals in high energy irrad., e.s.r. obs. 2−54562
adamantane, mol. dynamics, n.m.r. of rare spins 2−81479
adamantane, solid, ^{13}C pulsed double resonance analogue Fourier transform spectroscopy 2−68752
adamantane, solid, mol. rot., proton spin-lattice relax. obs. 2−61563
adenine, 1s binding energy calc. for C and N atoms using perturbational model 2−77156
adenine, molecular electrostatic potentials, MO LCAO GTO SCF calculation 2−60041
adsorption at electrodes, in double layer 2−84646
L-alanine, irradiated, unstable radical CH_3CHR, temp. dependence of ESR spectrum 2−68818
alcohol, thin films, flow and stability on rotating horizontal disc 2−43309
alcohol in heptane solns., dielec. relax. times, permittivities, loss tangent, rel. to comp. and temp. at 9.3477 GHz 2−74555
alcohol ions, formed by charge exchange in in-line tandem mass spectrometer, dissociation 2−64168
alcohol solns. with nonpolar solvents, dielec. dispersion behaviour 2−80487
alcohol-tetraalkylphosphorus salt, spectroscopic study of H-bond strength 2−53044
alcohols, compressional study through pseudo-Gruneisen parameters 2−83789
alcohols, ionization potential and proton- acceptor props. of H bonds 2−50076

Organic compounds continued
- alcohols, straight-chain, nonlinear dielec. effect, significant struct. theory 2−46970
- alcohols in n-heptane soln., dielectric behaviour and assoc. 2−84611
- aliphatic alcohols, far i.r. spectra, group frequencies 2−50075
- aliphatic hydrocarbons, μ- depolarization, molec. wt. and temp. dependence 2−64083
- aliphatic nitro compounds, theoretical conformational analysis using Kitaigorodsky's mechanical model 2−83307
- alkane ions, formed by charge exchange in in-line tandem mass spectrometer, dissociation 2−64168
- alkane monoiodide solutions, X-ray diffraction study, quasiliquid crystal form 2−50318
- alkanes, calculations using Del Re parameters 2−67505
- n-alkanes, chain-length dependence of anisotropy and depolarization ratio, comparison with laser light scattering expts. 2−80083
- n alkanes, from n pentane-n decane, relative permittivity as function of pressure and temperature 2−43384
- alkanes, halogen substituted branched chain, obs. of far u.v. spectra, conjugative effects 2−80100
- alkanes, x-ray excited fluorescence, lifetime meas. 2−42951
- alkanes and derivatives, bonds, polarization tensor study 2−70736
- alkanes in cyclane solvents, orientated mol. interactions 2−50340
- alkenoxyderivatives of silicon, frequencies and intensities of C=C vibrational bands 2−53045
- p- alkoxy-p′-acyloxyazoxybenzenes, homologous, nematic mesomorphic behaviour 2−80453
- alkoxyazoxybenzenes, Raman spectra 2−81386
- p-n-alkoxybenzoic acid, periodic oriented oscillations of domain struct. in alt. elec. fields 2−71159
- 4-n-alkoxybenzylidene-4′-phenylazoanilene, nematic-spectra A phase transition, n.m.r. meas. on molecular orientation 2−53402
- alkyl acetates, dielec. relax. in aromatic and aliphatic solvents at microwave freqs. 2−60488
- alkyl benzenes, pulsed radiolysis, spectra of transitory species 2−57435
- alkyl halides, calculations using Del Re parameters 2−67505
- alkyl iodide photodissociation laser, criterion for quenching 2−79201
- alkyl iodides, X-ray photoelectron spectra, comparison of valence shell and core ionization potentials 2−64167
- alkyl isocyanates, integrated intensity of valence vibrations 2−74290
- alkyl radical reaction products, chem. induced dynamic nucl. polarization 2−81540
- alkylaromatic radical cations, methylene h.f. splittings and methyl hydrogen splittings, e.s.r. 2−60046
- p,p′-di-n-alkylazobenzenes, melting point and dielectric constants, determination and explanation 2−56484
- p,p′-di-n-alkylazoxybenzenes, melting point and dielectric constants, determination and explanation 2−56484
- n-alkylbenzenes, l.f. vibr. spectra 2−56213
- allene, ^{13}C chem. shifts 2−77102
- allyl anion, bond angles and CC-distance determination by π-electron and all-valence electron method 2−53042
- allyl bromide, rotational isomerism and vibrational spectra 2−42952
- allyl chloride, rotational isomerism and vibrational spectra 2−42952
- amides, positron lifetimes, intensity of orthopositronium component 2−71228
- amines, primary, molecular stretching frequency band angle change effect 2−83266
- amines, protonated, in aqueous solns., i.r. investig. of polarizable hydrogen bonds and pKa depend. 2−68652
- amino acid, proton mag. resonance chemical group assignment and chemical shifts 2−46989
- amino acid conformation, determination by homonuclear INDOR spectroscopy 2−50078
- α-amino acid crystals, e.p.r. of VO^{2+} impurity ions 2−84566
- amino acids, γ-irrad., effect of cryst. struct. on stability, yield, and shape of e.s.r. spectra 2−81536
- amino acids, geochemistry and cosmochemistry 2−57729
- amino and γ-irradiated crysts., study of u.v.-induced free radical conversion using EPR 2−84667
- α-amino isobutyric acid, p.m.r. study of line widths and second moments 2−68748
- 2-amino-7-nitrofluorene/1,2- dichlorobenzene, dye laser action 2−45742
- 2-amino-7-nitrofluorene/1,2-dichlorobenzene, special dye laser, solvent orientational relaxation 2−42040
- amino-compounds, liquids, ultrasonic velocity 2−53428
- 3-amino-N-methylphthalimide exiplexes with acetone, pyridine and dimethyl formamide, luminesc. 2−64169
- 3-aminobenzaldehyde, in aprotic solvent, chemilum. on ozonization 2−54538
- o-, m-, p-aminobenzaldehydes, vibr. spectra 2−56214
- m- aminobenzotrifluoride, i.r. spectra, fund. vibr. assignment 2−56215
- 2-aminopyridine, normal and deuterated, microwave spectrum studies 2−50077
- ammonium carbamate, solid, i.r. spectra 2−84527
- ammonium citrate, i.r. spectra, 700 to 4000 cm^{-1} 2−72356
- ammonium oxalate, triboluminesc. intensity obs. rel. to elastic const. detn. 2−51396
- ammonium oxalates, cryst. growth from aq. soln. 2−60714
- ammonium thiocyanate and ammonium thiocyanate-d_4 far i.r. and Raman spectra of polycrystalline samples 2−48201
- aniline binary mixtures, ultrasonic velocity and free length and collision factor theories 2−53424
- aniline derivatives, u.v. absorpt., temp. effect, conform. change 2−68812
- aniline in solution, ^{13}C spin-lattice relaxation and intermolecular interactions 2−80482
- aniline vapour, vibrational analysis of absorption bands in resonance fluorescence spectra 2−70742
- aniline-^{15}N and derivatives, long-range spin-spin coupling consts. 2−77137
- aniline-cyclohexane opalescent mixture, r.f. cond. 2−71230
- anils, thermotropic liquid crystals, transition temps. and mesophase identification 2−50326
- anisaldazine, nematic liq. cryst., mol. theory, stability, thermodynamic conditions 2−46930

Organic compounds continued
- anisaldazine liquid crystal, Raman scattering by Ar laser 2−60476
- [14]annulene, crystal and molec. structure, three-dimensional X-ray study 2−64647
- anthracene, auto-association of frozen solns,., fluorescence 2−54558
- anthracene, auto-association of frozen solns., absorption spectra 2−54557
- anthracene, deuterated, isotope effect in carrier mobility 2−47906
- anthracene, dye-sensitized, delayed fluorescence, magnetic hyperfine modulation 2−65309
- anthracene, electron transfer to $[Fe(CN)_6]^{3-}$ and O_2 in aq. soln. 2−61805
- anthracene, electron-hole interactions 2−80982
- anthracene, evolution of space charge limited currents 2−75105
- anthracene, excitonic sounding method for measuring charge density gradient 2−47907
- anthracene, fluoresc. quenching by CCl_4 wavelength effects 2−68694
- anthracene, fluorescence, effect of neutron induced crystal defects 2−44411
- anthracene, freq. depend. cond. in single cryst. with monopolar injection 2−64993
- anthracene, gas phase, sensitized anti-Stokes delayed annihilation fluoresc. 2−74284
- anthracene, mag. field effect on prompt fluoresc., singlet exciton fission obs. 2−81521
- anthracene, meso-substituted, obs. of laser emission in 4100-4400 Å range at low temp. 2−45745
- anthracene, molecular crysts., melting point rel. to intensity of incident u.v. radiation 2−50399
- anthracene, photoelectron spectra and ionization potentials 2−60048
- anthracene, radiation induced fluorescence in cyclohexane and benzene solutions, yields of excited singlet and triplet states 2−53447
- anthracene, radiation induced fluorescence in cyclohexane solution 2−53446
- anthracene, Raman scatt. of light, polarization effects 2−65275
- anthracene, singlet exciton collision fluorescence decay following laser stimulation 2−78144
- anthracene, tetracene-doped, singlet-exciton energy transfer, generalized random walk model 2−84270
- anthracene, transient photoinjection current meas. 2−57200
- anthracene, triplet exciton annihilation fluorescence changes induced by neutron radiation damage 2−84553
- anthracene, two-photon absorption, blue fluorescence as function of incident laser energy 2−44410
- anthracene, two-photon excitation fluoresc. polarization 2−60039
- anthracene (-d_4), obs. and calc. of position dependent deuterium effect on triplet lifetime 2−70741
- anthracene addition to ethanol solns., triplet-triplet transfer 2−76488
- anthracene and 9-methyl-anthracene in ethanol as actinometer for u.v. region of impulse lamps 2−51462
- anthracene compounds, fluorescence quenching of rhodamine solutions 2−43380
- anthracene crystal, hot carrier injection rel. to field depend. of photocurrents 2−75189
- anthracene crystal, luminescence of surface exciton states 2−54461
- anthracene crystal, reflection and luminescence spectra, evidence for surface states 2−44408
- anthracene crystal growth from melt effect on detect concentration 2−83904
- anthracene crystals, calculation of light reabsorption 2−61715
- anthracene crystals and molecules in solution, two-photon absorption spectra meas. using dye lasers 2−72354
- anthracene crystals and solutions, fluorescence quenching under intense excitation 2−54471
- anthracene crysts., carrier-exciton interactions, delayed fluoresc. quenching 2−65308
- anthracene derivatives in toluene, monomeric and exomeric fluorescence, concentration quenching 2−53445
- 9-CNanthracene dimers, thermal behaviour and monomerization kinetics in the solid state 2−57436
- anthracene diode, double injection electrolum., and carrier injection props. of C fibres 2−75338
- anthracene dyes in alcohol soln., fluoresc. correl. with photochem. activity 2−77432
- anthracene films and crystals current/voltage charact. rel. to thickness, temperature and light emission 2−57201
- anthracene monocrystals, eximeric emission from mechanically worked surfaces 2−65298
- anthracene single crystal irradiated by electron beam, hole trap 2−51126
- 9,10-anthraquinone and 9,10-anthraquinone-d_8, planar vibrs. calc. 2−67506
- anthrone, refinement of crystal structure 2−77566
- Araldites, polycrystalline specimens, edge effect in elastic wave velocities and moduli 2−60854
- N- aralkylpyridinium ions, conformational influences on intramolecular charge transfer transition 2−42955
- aromatic acetylenes, reduced zero field splitting in EPR of photoexcited triplet state 2−68810
- aromatic acid halides, i.r. spectra, stretching frequencies 2−70743
- aromatic alcohols, luminescence properties in solution, quantum yields of free radicals 2−71212
- aromatic carbonyl compounds, spin-orbit coupling effects in e.p.r. spectra of lowest triplet states 2−70756
- aromatic carbonyl mols., host and substitution effects on lowest excited triplet states, PMDR obs. 2−56205
- aromatic hydrocarbon aliphatic amine systems, exciplex formation studies by time resolved fluorescence 2−68691
- aromatic hydrocarbons, anisotropic polarizability eval. using optical meas. 2−80108
- aromatic hydrocarbons, nonradiative decay of lowest triplet state 2−80074
- aromatic hydrocarbons, vibrational coupling strengths for intramolec. non-radiative transitions 2−42954
- aromatic hydrocarbons fluorescence quenching by carbon tetrachloride, wavelength effects and complex formation 2−78205
- aromatic ion radical crystals, electrostatic energy calc. 2−51073

Organic compounds continued
aromatic ketones, semi-empirical calcs. of zero-field splitting parameters of lowest triplet states 2−80102
aromatic molecules, magnetic anisotropy, comparison of theory and expt. 2−60049
aromatic molecules adsorbed on MgO surface, photoactivation by u.v. radiation 2−78206
aromatic molecules in complexes with hydrogen bonds, luminescence, quenching of triplet state 2−54462
aromatic mols., absorpt. and luminesc. relationship in four-level system of electronic states 2−64087
aromatic mols., intersystem-crossing process mechanism formulation 2−56206
aromatic mols., isotropic shifts of electronic origins and ring vibrs. 2−56207
aromatic mols., triplet deactivation parameters determ. 2−80075
aromatic mols., vibronic coupling in emission spectra revealed by crystal field distortion 2−75243
aryl isocyanates, integrated intensity of valence vibrations 2−74290
2-(N-arylamino)-6-naphthalene sulphonates, fluoresc. emission and quenching analysis 2−80077
in atmosphere over Hawaii 2−62153
azaaromatic radical anions, ^{14}N coupling consts. 2−70745
azabenzenes rot. mixing of excited electronic states 2−80099
1- azabicyclo[2.2.2]octane, torsional oscill. from microwave spectrum 2−42958
azide ion, calc. of point-charge distrib. from quadrupole moments using SCF orbital wavefunctions 2−80086
D L azidophenilacetic acid, use of optical activity to control resolution and determ. optical purity 2−54523
azines, non radiative coupling of phosphorescent state into ground state 2−70732
azines, Stark effects and elec. dipole coupling of $n\pi^*$ and $\pi\pi^*$ states 2−77138
azines ^{14}N n.q.r., σ and π electron densities as function of CNN angle 2−80087
cis-azobenzene, IR and Raman spectra 2−53048
azobenzene, liquid crystalline behaviour rel. to molecular struct. 2−60428
azobenzene and substituted derivatives, reversible orientational photodichroism and photoisomerization in viscous solutions 2−42959
azobenzenes ^{14}N n.q.r., σ and π electron densities as function of CNN angle 2−80087
azobisisobutyronitrile u.v. irradiated in polycrystalline state, e.s.r. spectrum 2−75394
azolidones, i.r. absorpt. spectra rel. to H bonding and mol struct. 2−56216
azomethane, azomethane-d$_6$, vibrational assignments and structure from i.r. and Raman spectra 2−42957
azomethines with fluorine-containing substituents, luminescence 2−75326
p-azoxyanisole, dielectric anisotropy of liquid crystal produced by magnetic field 2−50336
p-azoxyanisole, mol. conformations in nematic and isotropic states, Raman spectra 2−81382
p-azoxyanisole, nematic, temp. depend. of orientational order 2−56481
p-azoxyanisole, nematic liq., cryst., mol. theory, stability, thermodynamic conditions 2−46930
p-azoxyanisole, nematic liquid crystal, thermal cond., interfacial effect 2−50323
p-azoxyanisole, nematic phase, elastic constants, calc. based on lattice model 2−50325
p-azoxyanisole, n.m.r., strong collision relaxation in rotating frame 2−61747
n-azoxyanisole, polarization of i.r. spectra in liq. cryst. and solid states 2−82588
p-azoxyanisole, temp. dependence of intermolec. interactions in crystal ad nematic phases 2−50335
4,4′-azoxyanisole liquid crystals, Raman scattering by Ar laser 2−60476
p,p′-azoxyanisole liquid crystals, thermal conductivity in magnetic fields 2−67828
p-azoxyanisole liquid crystals ultrasonic absorption and viscosity anisotropy in oriented crystals 2−50334
p-azoxyanisole nematic liquid crystal in Poiseuille flow, apparent viscosity calc. by continuum theory 2−50337
cis-azoxybenzene, IR and Raman spectra 2−53048
azoxybenzene, liquid crystalline behaviour rel. to molecular struct. 2−60428
trans-azoxybenzene and isotopic derivatives, i.r. and Raman spectra, vibr. assignment 2−56217
p-azoxyphenetole, nematic liq. cryst., mol. theory, stability, thermodynamic conditions 2−46930
p-azoxyphenetole, oriented nematic phase, cylindrical atom distrib., X-ray scatt. 2−80441
p-azoxyphenetole liquid crystals ultrasonic absorption and viscosity anisotropy in oriented crystals 2−50334
p-azozyanisole, nematic and isotropic, proton spin-lattice relax. 2−64440
azulene, isotopic species, vibrationally excited states, far i.r. spectra 2−70746
azulene, rotational microwave spectra of ground and vibrationally excited states 2−70744
azulene in frozen n-pentane, quasilinear structure of fluorescence spectra 2−53046
azulene in frozen n-pentane, quasilinear vibrational structure of second electronic transition in absorption spectrum 2−50079
azulene in gas phase, laser excited emission of two lowest singlet states 2−42956
barium behenate, built-up films dielec. constant study 2−77948
barium behenate molec. film, ellipsometric study of optical constants and refractive index detn. 2−78064
barium margarate, built-up films dielec. constant study 2−77948
barium margarate molec. film, ellipsometric study of optical constants and refractive index detn. 2−78064
barium palmitate, built-up films dielec. constant study 2−77948
BDPA film, vapour deposition and props. 2−56598
benzaldehyde, substituent and soluent effects on transitions 2−83319

Organic compounds continued
benzaldehyde environmental effects on assignment and geometry of triplet state 2−61806
benzaldehyde vapour, active out-of-plane modes in $^1A''(n\pi^*)\leftarrow S_0$ 2−80097
benzene, ^{13}C relax. meas. under proton coupled and decoupled conditions 2−67462
benzene, $^1B_{2u}\rightarrow{}^1A_{1g}$ emission in Ar afterglow 2−70747
benzene, absolute delay in Cotton-Mouton effect 2−43364
benzene, adsorp. on Ni surface, LEED and mass spectrometer obs. 2−50545
benzene, aerosol, produced by X-irrad. 2−46999
benzene, calc. of relative strengths of vibrational structure lines of $^1A_{1g}\rightarrow{}^1B_{2u}$ band in absorption spectrum 2−42962
benzene, CNDO calc. of dipole moment derivatives 2−50082
benzene, Dewar structure CNDO/2 calculation 2−60051
benzene, elec. field perturbation of A-B transition, in-plane polarisability 2−80068
benzene, excited state relaxation, review 2−60052
benzene, forced combination diffusion in laser resonator 2−41976
benzene, Franck-Condon factors for predissoc. 2−80079
benzene, heat of mixing with xylene 2−77426
benzene, inverse Raman effect 2−71206
benzene, i.r. dispersion study of absolute integrated absorption intensity 2−64464
benzene, liq., stimulated Raman scatt., rel. to limiting diameters of self-focusing 2−67832
benzene, liquid, meas. of absorption spectra in u.v. region in room temp. to freezing point range 2−71208
benzene, liquid and solid, optical generation of charge carriers via excitons 2−57259
benzene, liquid and solid, quasi-elastic scattering of cold neutrons, obs. of broadening 2−80451
benzene, luminescence properties in solution, quantum yields of free radicals 2−71212
benzene, mol. dynamics, n.m.r. of rare spins 2−81479
benzene, nonlinear U(u) Hugoniot below 15kb 2−53390
benzene, one-electron perturbation calc. of 3d electrons 2−67452
benzene, orbital energy calc. by Green's function method 2−50083
benzene, pure and isotropic mixed crystals, absorption spectroscopic study of isotope effects intermolecular interactions 2−81357
benzene, second harmonic laser light scattering 2−43357
benzene, self-focusing effect on stimulated Raman scattering 2−77437
benzene, solid, anisotropic nucl. spin relax. of ^{13}C 2−81310
benzene, solid and liquid, electron and hole mobilities 2−51146
benzene, solvent induced shift effects of nonpolar and polar metal complex solutes 2−83264
benzene, substituted, molecular polarizability values, calc. 2−46425
benzene, Urey-Bradley repulsive force const., quantum mech. estimation 2−83328
benzene, u.s. attenuation meas. in 600-900 MHz range using Brillouin scattering techniques 2−71198
benzene, u.v. spectrum, vibrational structuring of magnetic circular dichroism 2−70751
benzene + cyclohexane system, vapour pressure meas. using all-glass-mercury static equilibrium still 2−53511
benzene + O(^{3}P), rate constant meas. 2−61778
benzene adsorbed on gel, n.m.r. 2−46614
benzene and benzene plus cyclohexane, dilution piezometer meas. at 298.15K of excess compressibility 2−67823
benzene and benzene-CCl$_4$ charge transfer complexes, l.f. Raman spectra, assignments 2−81351
benzene and cyclohexane simultaneous adsorption on charcoal 2−68779
benzene and fluorinated benzenes, solvent induced shift effects on ^{1}H and ^{19}F nuclei of dipolar solutes 2−83311
benzene and halogenated derivatives, det. of molecular parameters 2−53429
benzene and hexadeuterobenzene impurity, absorption spectra and exciton-phonon interaction 2−71717
benzene and n-paraffin mixture, luminescence at 77 K 2−51378
benzene chromium tricarbonyl-d$_6$, -h$_6$, Raman and i.r. spectra 2−70752
benzene crystal, impurity effect on i.r. exciton spectrum 2−80950
benzene D_{2h}^{15}, Raman line strengths of lattice vibrations 2−44394
benzene derivative crysts., second harmonic generation and Miller's parameter 2−54377
benzene derivatives, deuterated, meas. of quadrupole coupling const. and asymmetry parameter of ring deuterons 2−80082
benzene derivatives, dipole moments calc. using CNDO and INDO methods 2−70750
benzene flash desorption and decomp. from clean or contaminated W polycryst. 2−84624
benzene in cyclohexane matrix, sensitivity of pseudo-Jahn-Teller distortion to host lattice 2−80952
benzene ions, doublet energy levels, configuration interaction calculation 2−67507
benzene lenses at air-water interface, with translational and rotational symmetry 2−74510
benzene molecule, ^{13}C shift of a_{2u} vibration mode 2−80950
benzene molecules, substituted, shift in lowest π-electron singlet excited state 2−70748
benzene mono- and disubstituted derivatives, sound propagation rel. to H bonding analysis 2−56502
benzene mono-substituted derivatives, calc. of singlet energies, polarization direction, band intensities by Pariser-Parr-Pople method 2−46593
benzene mono-substituted derivatives, electronic structure and spectra calc. by Pariser-Parr-Pople method 2−46594
benzene pi-electron system, propagation calcs. in Pariser-Parr-Pople model 2−50012
benzene single crystal, assignment of i.r. active exciton components 2−51316
benzene single crystal, first $\pi^*\leftarrow\pi$ transition in polarized light 2−57354
benzene solution w. tanone free radical, resonant helix and coil 2−66666
benzene triplet yield in dil. cyclohexane soln., temp. depend. 2−57429

Organic compounds continued
benzene vapour, fluorescence lifetime and quenching 2−83285
benzene vapour, u.s. excited shift in u.v. absorption band, sound velocity dispersion curve obs. 2−56218
benzene-chloroform weak complexes, radiationless decay of benzene triplet state, external deuterium isotope effect 2−84661
benzene-cyclohexane system, acoustical properties on saturation line 2−71199
benzene-d_6, on phosphorescence characts. 2−84678
benzene-d_6 and mixed crysts. with benzene, isolated Na atom absorpt. spectra, interactions 2−68653
benzene-methanol mixtures, viscosity and density meas. in temp. range 10°-50°C 2−60450
benzene-nitroalkane solns., total intensity Rayleigh scatt. and depolarization at 546 nm and 30°C 2−64444
benzene-phenol mixture, cond., applied voltage, comp. and temp. depend. 2−60508
benzenes, dihydroxy- and diamino-substituted, electronic absorpt. spectra and struct. 2−70749
benzenes, fluorinated, X-ray photoelectron spectra, binding energy shifts 2−83289
benzenes, methylated and fluorinated, fluoresc. decay times and rates of first excited singlet states 2−53050
benzenes, methylated and fluorinated, fluoresc. quenching by singlet energy transfer, mechanisms 2−56219
benzenes, monosubstituted, partially oriented in nematic phase, n.m.r. 2−77104
benzenes, substituted, electron attachment and excitation processes 2−42949
benzenes, substituted, electronic correl. in excited states, singlet-triplet-excitation energy 2−56220
benzenes, substituted, electronic structs. of lowest excited triplet states 2−60050
benzenes, substituted, high resolution electronic spectra, rotational analyses and Stark effects 2−67509
benzenes, substituted, molecular orbital study of excited state geometry 2−50084
benzol crystal with impurities, low-temperature spectral investigations of formation of local exciton states 2−54464
benzonitrile, CNDO/CI calcs. of lower electronic transitions 2−56221
3,4-benzophenanthrene, bimolecular fluorescence quenching, interaction between excited molecules in solution 2−56506
benzophennone molecular crystal, polarizabilities and dipole moments for lowest singlet and triplet $n\pi^*$ excited states 2−81136
benzophenone:diphenylnitroxide, anisotropic e.p.r. study, meas. of ^{14}N hyperfine tensors and g tensors 2−72474
benzophenone, 2-hydroxy-5-methyl derivative, dielec. relaxation and dipole moment determination 2−60487
benzophenone, cryst., triplet exciton and phosphoresc., low temp. 2−61718
benzophenone, kinetics of quenching and quantum emission in relation to energy of exciting laser pulse 2−54463
benzophenone, l.f. Raman spectrum, 300 and 30K, librational motions 2−81355
benzophenone, prompt and delayed fluorescence 2−50081
benzophenone crysts., phosphorescence, temp. depend., T→S emission 2−65312
benzophenone hydrazone, ^{14}N n.q.r., σ and π electron densities as function of CNN angle 2−80087
benzopurpurine, molecular dimensions from light scattering in absorbing suspensions 2−50378
benzoquinoline, 7,8- and 5,6-, dipole moments in ground and fluorescent states 2−74281
5,6- and 7,8- benzoquinoline trapped in n-paraffins at 77K, vibrational analysis of quasilinear luminescence spectra 2−50080
p-benzoquinone, electronic conduction mechanism, molecular orbital energies 2−75015
p- benzoquinone, electronic states and spectra 2−42961
benzoxazolyl-substituted aromatic hydrocarbons, fluorescence 2−57375
benzoyl peroxide, reaction with diphenyl amine and tetraphenyl hydrazine, reaction rate consts., chemilum. 2−78191
benzoylacetonate anions, fragment calc. 2−83325
benzoyloxyimino-4 tetrahydroquinazolines and hexahydropyrimidines, i.r. absorpt. and n.m.r. 2−53049
1,12-benzperylene fluorescent thin films for α particle detection 2−73939
benzvalene, microwave spectrum and dipole moment 2−77139
benzyl, kinetics of quenching and quantum emission in relation to energy of exciting laser pulse 2−54463
benzyl benzoate, complex dielectric constant in microwave region 2−71220
benzyl chloride vapour, photolysis in presence of ethane or n-butane 2−65390
benzyl formate, complex dielectric constant in microwave region 2−71220
benzylamine, complex dielectric constants by microwave absorption 2−74553
benzylamine, near u.v. absorption spectrum 2−74286
benzylbromide, complex dielectric constants by microwave absorption 2−74553
benzylchloride, complex dielectric constants by microwave absorption 2−74553
benzylcyanide, complex dielectric constants by microwave absorption 2−74553
benzylidene anilines, terminally substituted, liquid crystalline properties, synthesis 2−83767
beryllium oxyacetate, polymorphism, -196°C to 286.7°C, pulsed n.m.r. investigation, study of molecular dynamics 2−57399
beryllium oxyacetate, spin-lattice relax. of dipole-dipole reservoir and slow motion, n.m.r. obs. 2−72525
biacetyl, ordering of lower electronic states, mechanism of radiationless S→T transitions 2−50085
biacetyl, triplet-singlet emission analysis 2−72574
bicyclo [1.1.1] pentane systems, ab initio SCF calcs. of electronic struct. 2−70753
bicyclo[1.1.0]butane, electronic structure 2−42963
bicyclo[1.1.0]pentane, electronic structure 2−42963

Organic compounds continued
bicyclo[2.1.1]hexan-5-one, microwave spectrum and dipole moment 2−42964
5,5′- biisoxasole, twinning, Weissenberg photographs 2−83964
binary mixtures, surface tension at 15°C 2−53410
biphenyl, influence of chloro substitution on electronic spectra 2−46595
biphenyl, singlet, and triplet electronic spectra 2−83316
biphenyl crystal, lattice dynamics using 6-exp potential function 2−57043
biphenyl derivatives in dibenzofuran single crystal, e.s.r. spectra of triplet state 2−64170
o,o′-bridged biphenyl derivatives in dibenzofuran single crystal, e.s.r. spectra of triplet state 2−64170
biphenylene, photoelectron spectra and ionization potentials 2−60048
biphenyls, bridged, long-range ^{13}C spin couplings 2−77134
biphenyls, conjugation and angle of twist, determination by Raman intensity investigation 2−50086
2,2′-bipyridinetetracarbonylchromium -molybdenum and -wolfram, luminescence spectra 2−68689
bis(2-imino-4-amino-4-methyl-pentane)nickel II bromide, X-ray detn. of cryst. struct. 2−71445
bis(picolinato)bis(allylthiourea)Cu(II), X-ray analysis and Patterson-Fourier and least-squares methods 2−71446
bis(picolinato)bis(thiourea)Cu(II), X-ray analysis and Patterson-Fourier and least-squares methods 2−71446
bis-(N-methylsalicylaldiminata)-copper, spin $^1/_2$ system, non Lorentzian e.s.r. line shape obs. 2−65329
borazane, internal rot. barrier and localized charge distribs. 2−64171
borazine, gaseous, 2000Å absorpt. system, vibronic analysis, electronic transition 2−80090
2- and 4-bromo-pyridine quadrupole hyperfine structure in rotational spectrum 2−70754
bromoacetyl bromide, energy differences between rotational isomers by absolute i.r. intensity method 2−46598
bromoacetylene, electronically excited, competition between photon emission and photodissociation 2−42969
bromoalkanes in cyclohexane soln., dielec. relax. 2−71221
bromoanisole, o- and m-, vibration frequency assignment 2−74283
2-bromoethanol, normal coordinate analysis on rotational isomerism 2−42981
bromoethylene, photoelectron spectra, π interaction 2−77140
bromoform, polycryst., combination scattering spectra 2−57339
bromomethane, pulse radiolysis, electron disappearance 2−61816
3,3-bromomethyl-d_3-diazirine vibrational analysis of $\pi^* \leftarrow n$ transitions 2−50087
bromonaphthalenes, microwave dielectric props. in solutions 2−43381
2-bromopropene, photoelectron spectra, π interaction 2−77140
bromothiophene, high resolution photoelectron spectra 2−60087
2-, 3- bromothiophenes, meas. of proton spin-lattice relaxation times in 300-450°K range using spin-echo spectrometer 2−77116
trans-butadiene, application of Lowdin's orthogonal orbitals to π-electron calcs. 2−64172
butadiene, pi-electron system, propagation calcs. in Pariser-Parr-Pople model 2−50012
butadiene, SCF and CI calcs. of electronic spectrum 2−80069
1,3-butadiene oriented in nematic mesophase p.m.r. 2−60053
butadiene sulphone, p.m.r. in isotropic and liquid crystal media 2−56222
1,3-butadienes, 1-substituted and 1,4-disubstituted, electronic spectra, comparisons between geometric isomers 2−42965
butadienetricarbonyliron vibrational spectra in gaseous, solution, liquid and solid phases, factor group analysis 2−70755
butanol, meas. of isothermal piezo-optic coeff. 2−50364
butenes, adsorption on Pt/Al_2O_3 catalyst, high resolution n.m.r. obs. 2−60683
butyl alcohol, chemical aspects of shock initiation 2−83724
butyl alcohol aqueous solutions, light scattering and phase transitions 2−74547
t-butyl chloride γ-irradiated, e.s.r. evidence for planarity of t-butyl radical 2−74288
butyl hydroperoxides, H bonding, effect of solvent, i.r. spectra study 2−46964
t- butyl ion-molecule reactions, charge recombination rate coeff. and absolute rate constants 2−68820
n-butyl-α-naphthalenide$^-$ + n-butyl-α-naphthyl→exchange, comparison with intramol. collisions 2−56236
n-butyl-α-naphthalenide$^-$ + n-butyl-α-naphthyl→exchange, rel. to intramol. collisions 2−53067
n-, tert-butylamine n.q.r meas. at liquid nitrogen temps. ionic character of N-H, N-C bonds 2−83310
tert-butylbenzene, conformational structure, i.r. and n.m.r. spectra 2−42953
tert-butylperoxy radical, prep. and e.s.r. spectrum 2−65391
butyne in solvents, n.m.r. adiabatic fast passage relaxation 2−71236
caesium methanesulphonate meas. of Raman and i.r. spectra, correlation with crystal structure 2−72375
calcium stearate lubricant monolayers, shear strength 2−53383
d-camphor, molecular rotation at high press., n.m.r. obs. 2−51416
camphor, solid, molecular rotation at dielectric relaxation transition 2−61414
camphor carbonyl, rot. force of $n \rightarrow \pi^*$ transition 2−60071
camphor in polar solvents, vibrational spectroscopy study of molecular dynamics 2−70757
cantharidine, X-ray diffraction study, molecular bond lengths and conformation 2−68010
caprylophenone, 2-hydroxy-5-methyl derivative, dielec. relaxation and dipole moment determination 2−60487
carbamates, energy barriers to hindered rot. 2−60054
carbazyl, recrystallised samples, e.s.r. line width and exchange narrowing 2−65330
carbene, one-electron perturbation calc. of 3d electrons 2−67452
carbene anthronylidene, e.p.r. spectrum 2−44496
carbohydrate, automatic spectrophotometry in sea water 2−61824
carbon tetrachloride, choice design and performance 2−82075
carbon tetrachloride, comparison of neutron diffraction data with perturbed crystal model of short-range order 2−64431

Organic compounds continued
carbon tetrachloride, enthalpy of transition and heat capac. for metastable fcc to stable rhombohedral transform. 2−77754
carbon tetrachloride, Kerr effect induced by fluctuational statistical processes 2−46955
carbon tetrachloride, Martian atmosphere, minor constituents, Mariner borne i.r. spectrometer 2−69156
carbon tetrachloride, optical props. of liquid in vac. u.v. 2−50363
carbon tetrachloride, Raman spectra, force field 2−74289
carbon tetrachloride, rate const. prediction for reaction with excited Kr atoms 2−80145
carbon tetrachloride, self-focusing effect on stimulated Raman scattering 2−77437
carbon tetrachloride, settling process of unstable dispersed droplets 2−80435
carbon tetrachloride, transport coeffs., density depend., rel. to hard sphere fluid model 2−74525
carbon tetrachloride, u.s. velocity, det. of molecular parameters 2−53429
carbon tetrachloride + K reaction, dependence of reactivity on internal and translational energy 2−75374
carbon tetrachloride and mixtures with cyclohexane collision-induced light scatt. 2−71202
carbon tetrachloride-cyclohexane, liquid system, relationship between self-diffusion and inter-diffusion coeffs. 2−50350
carbon tetrachloride-gas mixtures at high pressures, second cross virial coeffs. determ. from solubilities 2−43262
carbon tetrachloride-He system, surface tension, 1-71 atm., room temp. 2−64453
carbon tetrafluoride, E and F_2 type Raman contour bands 2−46585
carbon tetrafluoride, fluorescence surrounding CO_2 laser induced sparks 2−74440
carbon tetrafluoride, nucl. spin relax. obs. of spin-rot. interaction 2−56199
carbon tetrafluoride, octopole moments and dielec. second virial coeffs. 2−83294
carbon tetrafluoride, Percus-Yevick and Lennard-Jones (7-28) potential calc., comparsion with exptl. data 2−43259
carbon tetrafluoride, solid, vacuum u.v. spectroscopy of Wannier impurity states, conduction band data 2−49957
carbonium ion struct., orbital calcs. 2−56223
carbonyl compounds, electron attachment and excitation processes 2−60055
carbonyl group, theory of valence vibration spectrum 2−60056
carbonyls, electron attachment and excitation processes 2−42949
carboranes, orbital localization procedures and convergence problems 2−64098
carboxylic acid hydrazides, valance oscillations of N-H group at i.r. spectra 2−42967
carboxylic acid salts, i.r. and Raman spectra, vibr. assignment 2−60085
carboxylic acid series, u.s. velocity dispersion 2−71192
carboxylic acids, alkoxy substituted, intramol. hydrogen bonding effect on i.r. bands 2−67510
carboxylic acids, virial expansion, convergence for assoc. gas 2−83711
carboxymethyl cellulose, water soln., laminar flow, heat transfer 2−74498
carboxymethyl-cellulose dil. solns., viscosity in absence of neutral electrolytes 2−50343
carboxymioglobine aqueous soln., effect of hydration on relax. time from n.m.r. meas. 2−50373
β-carotene, elec. cond., photocond., and optical absorpt. 2−72072
β-carotene, Raman, resonance Raman and fluorescence spectra 2−42262
β-carotene film, solid, gas adsorption effect on absorpt. spectra 2−57355
β-carotene glass, photocond. transients 2−48003
β-carotene glass, photoconduction 2−48002
castor oil, speed of sound meas., 0−40°C, 1 atmosphere−110 MPa 2−76375
cellulose, cryst. state, effect of moisture 2−83962
cellulose, crystalline models, conformational terminology 2−43022
cellulose acetate, H detection by neutron radiography 2−65408
cellulose acetate membrane porosity rel. to intrusion cell formation 2−53420
cellulose and modified cellulose, study of fine structure using electron microscope 2−64624
cellulose triacetate, γ- or u.v. irradiated, e.s.r. obs. of radicals formed 2−44494
cerium dipicolinate: Ce^{3+}, e.p.r. obs. 2−72487
cerium ethyl sulphate, heat capacity, demagnetiz. and susceptibility meas. below 1K 2−68551
cerium ethyl sulphate, low temp. calorimetry 2−44229
cesium citrate, proton irradiation, 660 MeV production of radioactive Sb and Te, annealing effects 2−68817
cetyl alcohol for fog modification 2−65743
cetyltrimethylammonium bromide, velocity profile in turbulent pipe flow 2−53350
charge transfer complexes, photoelectron energy spectra 2−64163
chemisorbed mols. on silica; surface-chlorosilane interactions 2−84643
chiral cpds., vibr. spectra and polymorphism 2−44396
chloracetylene, electronically excited, competition between photon emission and photodissociation 2−42969
chloralides, optically active, molecular conformation 2−42971
chloramphenicol palmitate insoluble monolayer leakage across movable barriers, radiotracer detection method 2−53416
p-chloranil, electronic conduction mechanism, molecular orbital energies 2−75015
p- chloranil, Frenkel exciton dissociation at Al interface, photocurrent obs. 2−51085
3-chloro-1,2,5-thiadiazole, i.r. and Raman spectra 2−42968
6-chloro-1-hexanol, variation of complex dielectric const. with frequency in 300 MHz-24 GHz region at −42° and +20°C 2−64468
chloroacetyl chloride, energy differences between rotational isomers by absolute i.r. intensity method 2−46598
chloroacetylene, mol. g-value, mag. susceptibility anisotropy, quadrupole and elec. dipole moments 2−70758
2-chloroacrylonitrile, nucl. spin relax. 2−59983

Organic compounds continued
p-chloroaniline D_{2h}^{16}, Raman line strengths of lattice vibrations 2−44394
chlorobenzene, absolute delay in Cotton- Mouton effect 2−43364
chlorobenzene, dipole moments and polarizabilities of lowest excited singlet states 2−67508
chlorobenzene, rate of fall of drops in water column subjected to sinusoidal pulsations 2−46904
chlorobenzene, u.s. excited shift in u.v. absorption curve and sound velocity dispersion curve 2−56224
chlorobenzol-n-butanol system, microwave absorpt. and complexing 2−67810
p-chlorobenzylidene-p-chloroaniline, molec. conformation and electronic structure from solid state reflection spectra 2−53051
chlorocyclobutane, low frequency Raman spectra 2−74287
chloroethanes, dipole moments and conformational energies 2−42970
2-chloroethanol, normal coordinate analysis on rotational isomerism 2−42981
chloroform, ^{13}C spin-lattice and spin-spin relaxation rates 2−56525
chloroform, absolute delay in Cotton-Mouton effect 2−43364
chloroform, cryst. films, i.r. spectra, polarization depend. components assignments, vibrs. 2−84484
chloroform, cryst. films, i.r. spectra, polarization depend. components assignments, vibrs. 2−84484
chloroform, electronic structure, dipole moments, n.m.r. and n.q.r. constants calc. 2−83324
chloroform, liq., ang. autocorrel. function determ. from Raman spectra 2−71213
chloroform, liquid, calc. of orientation correlation functions from spectra 2−43363
chloroform, nonlinear U(u) Hugoniot below 15kb 2−53390
chloroform, polycryst., combination scattering spectra 2−57339
chloromethane, pulse radiolysis, electron disappearance 2−61816
3,3-chloromethyl-d_3-diazirine, vibrational analysis of $\pi^* \leftarrow n$ transitions 2−50087
1-chloronaphthalene, liquid, complete polarization study of two-photon absorption 2−43371
chloronaphthalenes, microwave dielectric props. in solutions 2−43381
chlorophyll, Raman, resonance Raman and fluorescence spectra 2−42262
chlorophyll, sensitizing action on ZnO/O absorbed layers to corona discharge 2−44176
chlorophyll charge transfer complexes crystn., exciton character of e.p.r. signal 2−48298
chlorophyll-a microcrystal suspension, photoelectric response 2−51469
o- chloropyridine, microwave spectrum, quad. coupling consts. 2−53052
chloropyridine, Stark effect on ^{14}N n.q.r. 2−44463
8-chloroquinoline, optically detected e.s.r. and ENDOR spectra of excited triplet states 2−46518
p-chlorostyrene, electronic absorption spectrum in 2961-2743 Å range, assignment of bonds 2−64173
chlorostyrene, ortho and meta, electronic absorption spectra 2−46597
chlorostyrenes, i.r. absorpt. bands, vibr. assignment 2−56225
chlorparaffin/paraffin-white oil, viscosity-pressure behaviour 2−60449
cholesteric mesophases, normal stress effects 2−83770
cholesteric solns. with helically arranged mols., circular dichroism 2−53394
cholesteryl derivatives, crystal nucleation in supercooled mesomorphic phases 2−77414
cholesteryl esters, effect of substituent groups on mesophase transition temp. and range 2−80452
choline salicylate, effects on AC cochlear potential of guinea pigs 2−45163
chromocene, mag. reson. props., zero-field splitting and g-values 2−64174
chrysene, dielectric tensor components derived from energy loss spectra 2−81138
chrysene, X-irradiated, e.s.r. examination to investigate stable free radicals formed 2−57393
clathrate, possible transitions between rot. sublevels 2−54446
clathrates of $Ni(4\text{-methylpyridine})_4(NCS)_2$ complex study of splitting of out-of-plane CH vibration band by i.r. spectroscopy 2−53053
cobaltocene, electronic structure and dynamic Jahn-Teller effect from e.p.r. and optical studies 2−56226
colchicine, excited states multiplicity of absorpt. and emission 2−65392
complex conjugated mols., Huckel mol. orbital analysis, transfer matrix method applic. 2−77132
complex fluorocarbon, in neutralizer cell, angular spreading of low energy charged particle beams 2−79697
complex mols., two-photon excitation fluoresc. polarization 2−60039
conjugated hydrocarbons, Huckel MO π resonance energies, σ structure 2−53068
copper formate, low dimensional antiferromagnet, thermal conductivity meas. 2−51062
copper formate tetrahydrate, thermal cond., magnon contrib. 2−72226
αcopper phtalocyanine crystals, ^{64}Cu life-time variations and chemical state of (n, γ) recoil copper 2−72586
copper stearate, spreading to produce monomolecular layers 2−71177
copper-phthalocyanine, reduced radiation damage in electron microscopy 2−80635
coronene, bimolecular fluorescence quenching, interaction between excited molecules in solution 2−56506
coronene, in n-nonane, fluoresc. 77K, complex struct. of doublets 2−78145
coronene, radiation damage occuring in electron microscope 2−43617
coronene (III) in crystalline solutions of isooctane and CCl_4, spectra and temperature dependence of phosphorescence 2−51377
coronene ions, magnetic circular dichroism and electronic orbital ang. mom. of ground state 2−80089

Organic compounds continued
  coumarins, H-bonding effects on excited $\pi\pi^*$ and $n\pi^*$ states 2−60057
  coumarins, in conc. H_2SO_4, protonated complexes, i.r. spectra, 1400-1800 cm^{-1} 2−46599
  coupled molecular aggregates, exciton theory of excited electronic states 2−68301
  cresyl violet and rhodamine B pulsed dye laser, spectral properties 2−42041
  cresyl violet dye, laser and spectral props. 2−73578
  critical volume prediction, new correlation using parachor 2−50397
  croconic acid and derivatives, struct. and electronic props., CNDO/2 calcs. 2−70760
  crotonaldehyde, vibrational spectra 2−67503
  cryptocyanine illuminated by ruby laser, calc. of deviation from Beer-Lambert's law 2−81416
  cryptocyanine Q-switches in ruby lasers, photochemical decomposition due to light source 2−49378
  cryptocyanine solns., fluoresc. quantum yield, 140−300K 2−77441
  cumene, conformational structure, i.r. and n.m.r. spectra 2−42953
  cumene hydroperoxides, H bonding, effect of solvent, i.r. spectra study 2−46964
  c.w. rhodamine 6G dye laser, passive mode locking 2−42043
  cyanamide, ab initio LCAO-MO-SCF calc. of dipole moment in semi-rigid model 2−64176
  cyanamide, analysis of microwave spectrum by rotation-inversion theory 2−80103
  cyanine dye, monolayer on AgBr, spectral sensitization 2−81551
  cyanine dyes, adsorbed, external photoelec. yield and ioniz. energy 2−48025
  cyanine dyes, luminescence of solid films 2−75327
  cyanine dyes, regularities in radiating transitions from second excited singlet state, polarization characteristics of absorption and fluorescence bands 2−53054
  cyanine dyes, sensitization of photographic emulsions for blue exposure at 77 K 2−66866
  cyano group long-range shielding effects 2−77098
  cyanoacetohydrazide, X-irradiated, obs. of e.s.r. spectrum of RNHNH type radical 2−81530
  cyanoacetylene, vacuum u.v. spectrum, calc. of ionization potential 2−46600
  Cyanoacetylurea, X and gamma irradiated, radical formation 2−51473
  2-cyanoethanol, normal coordinate analysis on rotational isomerism 2−42981
  2-Cyanopyridines, microwave spectra, ring distortion 2−74295
  cyanuric acid, X-ray diffr. data, two-centre formalisms in least-squares refinement 2−83813
  cycloalkanes, stretching vibrations of methylene group and ring strain 2−42972
  cyclobutadiene, orbital energy calc. 2−50003
  cyclobutane, CNDO/2 treatment with hybridization restictions 2−70762
  cyclobutanecarboxylic acid, vibrational spectra 2−42973
  cyclobutanes, substituted, i.r. spectra-structure correlations 2−56227
  cyclobutanone, vacuum u.v. photochem. 2−68813
  cyclobutanone ($^1A_2$), fluorescence excitation, photodecomposition, of first excited singlet 2−48343
  cyclobutene, partially oriented in nematic phase, p.m.r. study of H-H distances and orientation parameters 2−83313
  cycloheptane derivatives, conformational equilibrium from ^{19}F n.m.r. 2−83288
  cycloheptene derivatives, conformational equilibrium from ^{19}F n.m.r. 2−83288
  1,4-cyclohexadienes, 3,6 bridged, photoelectric assignment of states 2−77051
  cyclohexane, adsorp. on Ni surface, LEED and mass spectrometer obs. 2−50545
  cyclohexane, cyclohexanol, cyclohexanone, liq., rot. correl. times and self-diffusion coeffs. 2−80446
  cyclohexane, deuterated, meas. quadrupole coupling const. and asymmetry parameter of ring deuterons 2−80082
  cyclohexane, inverse Raman effect 2−71206
  cyclohexane, nitroxide radical doped, plastic phase, dynamic polarization and spin-lattice relax. 2−72526
  cyclohexane, nonlinear U(u) Hugoniot below 15kb 2−53390
  cyclohexane, optical props. of liquid in vac. u.v. 2−50363
  cyclohexane, ring interconversion 2−42974
  cyclohexane, v.p. rel. to surface tension and surface curvature 2−46943
  cyclohexane and benzene, simultaneous adsorption on charcoal 2−68779
  cyclohexane and benzene plus cyclohexane, dilution piezometer meas. at 298.15K of excess compressibility 2−67823
  cyclohexane and mixtures with CCl_4, collision-induced light scatt. 2−71202
  cyclohexane solns., psec. pulse radiolysis 2−81519
  cyclohexanol, polar liquid, microwave Kerr effect, Kerr const. 2−80470
  cyclohexanols, ^{13}C chem. shifts rel. to C electron densities from extended Huckel and Del Re theories 2−42948
  cyclohexyl hydroperoxide, in bases, H bonding, from i.v. spectra 2−46601
  cyclopentadiene, electronic struct., SPINDO calc. and photoelectron spectra 2−70761
  cyclopentadiene, negative ion formation and negative ion-molecule reactions 2−46986
  cyclopentadienyl and pentadeuterio and pentachloro derivatives, vibronic interaction effects 2−50090
  cyclopentadienyl cation, pi-electron states, projected states 2−83293
  cyclopentadienylberyllium chloride, microwave spectrum analysis 2−70763
  cyclopentane-d_0 and -d_{10} cryst., vibr. assignment 2−84485
  cyclopentanol, solid, unusual dielectric behaviour and molecular motion, dielectric and visual studies 2−57224
  cyclopentanone, microwave- optical double reson. of triplet state 2−80065
  cyclopentanone, transient effects in microwave optical double resonance 2−81524

Organic compounds continued
  cyclopentene, Raman spectra, ring puckering vibrations 2−43005
  cyclopentene, Raman spectrum, ring- puckering vibr. freqs. 2−60058
  cyclopropane, photoelectron spectra, orbital structs. 2−64175
  cyclopropene, orbital nature in electronic states 2−50091
  cyclopropylamine, SCF-LCAO-MO calculations of conformation 2−70786
  cyclopropylidene cycloalkanes, ^{13}C n.m.r. chemical shifts 2−42975
  cyclopropylketones, u.v. spectra, electronic transitions 2−77122
  cysteine hydrochloride monochydrate, u.v. and γ-irrad., radical recomb., mag. reson. obs. 2−72575
  cystine dihydrochloride, e.s.r. centre formation by monochromatic u.v. radiation 2−61811
  cytochrome c, magnetic circular dichroism 2−50118
  cytosine, molecular electrostatic potentials, MO LCAO GTO SCF calculation 2−60041
  d-threonine, second harmonic generation 2−55711
  B-decachlorocarboranes, H bonding, i.r. spectr. study 2−46602
  decacyclene, absorption spectra meas., comparison with LCAO SCF MO calc. in Pariser-Parr-Popl approx. 2−42976
  n-decane, metastable ions 2−59884
  deuterated nitrogen compounds, ^{14}N quadrupole resonances, determ. of π-, σ-electron densities 2−46618
  deuterochlorofrom, comparison of neutron diffraction data with perturbed crystal model of short-range order 2−64431
  deuteromethane, solid, proton mag. susceptibility 2−65351
  p,p′-di-n-butyl azoxybenzene, nematic, instabilities in elec. fields, domains and reorientation 2−56477
  4,4′-di-n-heptyloxyazoxybenzene, nematic phase, anomalous alignment due to elec. fields 2−77412
  1,2:5,6-di-O-isopropylidene-α-D-allofuranose-3d, D chem. shifts meas. by ^1H-{^2H} INDOR 2−42947
  di-t-butyl ketone, nuclear spin polarization during photolysis 2−51468
  diacetyl, vibrational spectra 2−67503
  dialkylureas, i.r. spectra, determ of molecular configurations from vibrational band assignments 2−70766
  1,4-diazabicyclo (2.2.2) octane and methyl analogue, struct. effects on photophys. processes 2−81512
  diazines, symmetric, spectra of $n \rightarrow \pi^*$ transitions, INDO orbital calcs. 2−53060
  diazirine and difluorodiazirine, photoelectron spectra, orbital structs. 2−64175
  diazoaminobenzene(β modification), cryst. and molec. struct. 2−71444
  diazosulphonate photographic imaging 2−59308
  dibenzanthracenes, vibr. and electronic spectra 2−53055
  dibenzofuran excimer emission 2−46967
  dibenzo[a,e,]cyclooctatetraene, spectral discrepancies rel. to synthesis 2−77099
  1,4-dibromo-butin, in liq. cryst., proton mag. res. spectra, effect of solvent 2−46596
  4,4′-dibromo-diphenyl ether, crystal structure by n.q.r. and temp. variation of frequencies 2−64650
  1,4dibromo-naphthalene, e.s.r. of triplet excitons, optical detection 2−81522
  2,6-dibromoaniline, i.r. and Raman spectra 2−77145
  dibromobenzene:naphthalene in T_1 state, phosphorescence spectra, study of external spin-orbit coupling mechanism 2−72427
  p-dibromobenzene, coupling of optical phonons to $T_1 \leftarrow S_0$ transition 2−81362
  p-dibromobenzene, vibr. analysis of 2800 Å band system 2−56228
  1,4-dibromonaphthalene, triplet exciton diffusion 2−48252
  dibromonaphthalene in n-hexane solvent, deviations from C_{2v} symmetry studied by phosphorescence microwave double resonance spectroscopy 2−50010
  1,4-dibromonapthalene, triplet exciton state band structure, properties of real linear chain 2−47820
  4,4′-dibutoxyazoxybenzene, liquid crystal, p.m.r. obs. 2−50338
  dibutyl phthalate, aerosol generation in flow reactor, exptl. 2−50386
  dibutyl phthalate, aerosol generation in flow reactor, theory 2−50387
  dicalcium lead propionate, spin-lattice relax. near crit. point 2−65196
  dicalcium strontium propionate, ferroelectric 180° domain struct., electron mirror microscope obs. 2−65060
  dichloracetyl chloride, energy differences between rotational isomers by absolute i.r. intensity method 2−46598
  2,2,-dichlorethanol, weakly coupled three-spin system, relaxation effects 2−50116
  1,4-dichloro-2-butyne, meas. of i.r. and Raman spectra, determ. of vibrational assignment, effect of internal rotation 2−53059
  α,ω-dichloroalkanes, dielec. relax., rel. to intramol. cooperative phenomena 2−60489
  p-dichlorobenzene, phosphorescence microwave double resonance studies of $^3\pi\pi^*$ state 2−60060
  dichlorobenzophenone crystal, optical and electric field effects in singlet and triplet states 2−44385
  dichlorobis (pryidine)-copper, spin $^1/_2$ system, non Lorentzian e.s.r. line shape obs. 2−65329
  dichlorodifluoromethane, fluorescence surrounding CO_2 laser induced sparks 2−74440
  dichloroethane, chem. activated, vibr. energy transfer probabilities, collisional deactivation 2−83409
  dichloroethane-d_0 and -d_4, chem. activated, cascade deactivation and nonequil. kinetic isotope effects 2−83408
  dichlorofluoramine, heat content, heat capacity, entropy, free energy determ. from spectroscopic data 2−60372
  dichloromethane, self-diffusion coeffs., freezing to boiling point, rotational correlation times 2−56472
  2-dichloromethyl-4-(4-bromobenzyl)-5-(4-bromophenyl)-6- hydroxypyrimidine, X-ray obs. 2−64649
  2-dichloromethyl-4-(4-chlorobenzyl)-5-(4- chlorophenyl)-6-hydroxypyrimidine, crystallographic props., X-ray obs. 2−64648
  2,2-dichloropropane, heat capacity detn. by adiabatic calorimeter 2−76406
  diepoxy-cyclohexane, crystal structure 2−43598
  diethyl 4,4′-azoxydibenzoate liquid crystal, p.m.r. obs. 2−50338

Organic compounds continued
- diethyl ether, cryst. and mol. struct. at 128K 2−68011
- diethyl ether, liq., correl. factor determ. 2−53387
- diethyl ether-methyl chloride mixtures, thermal conductivity measurement 2−53337
- 1,1′- diethyl-2,2′-cyanine, adsorbed on Ag halide emulsion grains, J-aggregates props. 2−81027
- diethylamine phosphor activated by TlCl, luminescence, excitation and emission spectra after exposure to u.v. radiation 2−54484
- 7-diethylamine-4-methylcomarin laser, coaxial 11 MW, 6.8J flashlamp pumped, performance 2−82476
- diffusion pump oil on Au mirrors, ellipsometric meas., simulation of space effects on optical surfaces 2−79431
- 1,1-difluoro-2, 2-dichloroethane, proton spin echo n.m.r. spectra, subspectral analysis 2−42977
- 1,1-difluoroalkyl radical, solution e.s.r. spectra, asymmetric linewidth effects in presence of resolved second order splittings 2−56519
- 2,3-difluoroaniline, u.v. absorption spectrum, vapour phase 2−77100
- difluorochloromethane, bubble evaporation, influence of pressure 2−73244
- difluorocyanamide gas heat content, heat capacity, entropy and free energy calc. 2−71114
- difluorodichloromethane, passive Q-switching of CO_2 laser 2−45725
- difluoroethylene, molecular g-values from Zeeman effect 2−70739
- difluoromalonitrile, force consts. and pot. energy distrib. 2−70775
- difluoromethane, molecular g-values from Zeeman effect 2−70739
- difluoromethane, partial double-bond character of C-F bond 2−43000
- p-dihalogenobenzenes, Raman spectra, Davydov splitting, temp. and state of aggregation influence 2−68666
- 2,3-dihydro-1,4-benzoxazepin-5(4H)-ones, X-ray powder patterns 2−56672
- 2,3-dihydrofuran, microwave spectrum 12.4-40 GHz, Q- and R-branch assignments for ground and excited states of ring-puckering mode 2−42978
- 2,5-dihydrofuran, Raman spectra, ring puckering vibrations 2−43005
- 2,3-dihydropyran i.r. spectra, hindered pseudorotation, estimation of barrier height for half-chair inversion 2−70764
- 2,5- dihydropyrrole, Raman spectra, ring-puckering transitions 2−80084
- diiodomethane, nonlinear U(u) Hugoniot below 15kb 2−53390
- 2,4-diisopropyl-3-methylthiazolium bromide, structure determinations for the geometry of the thiazolium ring 2−56668
- β-diketones, phosphorescence spectra rel. to triplet state studies 2−60062
- dimer composed of 2 biphenylene subunits, triplet exciton transfer study by e.s.r. 2−46509
- o-dimethoxybenzene, vibrational and electronic spectra 2−80081
- dimethyl ether, CH_3OCD_3, barrier to internal rotation 2−77144
- dimethyl ether, gas, solubility in liqs. 2−53405
- dimethyl ether, u.v. photolysis at 1470 Å 2−81527
- dimethyl ether and deuterated compound, normal cond. analysis, determ. of mean amplitudes of vibration 2−53058
- 1,4-dimethyl naphthalene, relationship of spin densities for monomer and dimer cations 2−60061
- dimethyl phosphite, neat and in dilute soln., effect of deuterium substitution on $^1J(^{31}P\text{-}H)$ 2−80104
- dimethyl selenide and deuterated compound, normal cond. analysis, determ. of mean amplitudes of vibration 2−53058
- dimethyl siloxane fluids, photoinjection from metal-free phthalocyanine film 2−56512
- dimethyl sulfates vibrational, spectra, i.r. and Raman 2−83317
- dimethyl sulphide and deuterated compound, normal cond. analysis, determ. of mean amplitudes of vibration 2−53058
- dimethyl sulphoxide, pulse radiolysis, transient species 2−68819
- 2.5-dimethyl-2, 5-hexamediol tetrahydrate, water-hydrocarbon layer crystal structure 2−50629
- N,N′-dimethyl-piperazine, ^{14}N quadrupole interaction, spin lattice relax., mol. motions 2−84603
- N-dimethylaminoborane-d_2, ^2H n.m.r., quadrupole coupling constants 2−44461
- 4-N-dimethylaminopyridine, EPA solution, flash photolysis, triplet-triplet absorption 2−74548
- 9,10-dimethylanthracene, gas phase, sensitized anti-Stokes delayed annihilation fluoresc. 2−74284
- 2,3-dimethylaquinoxaline, polarization of triplet-triplet absorption spectrum 2−42979
- dimethyldiacetylene in solvents, n.m.r. adiabatic fast passage relaxation 2−71236
- 3,4-dimethylenecyclobutene, valence shell CNDO, INDO and CNDO-CI calculations 2−60063
- 1,1-dimethylhydrazine-monoborane, spectroscopic study, determ. of molecular structure, vibrational assignments 2−53057
- dimethyliodoarsine, liq., i.r. and Raman spectra 2−77141
- dimethylnitrosamine, microwave spectrum and dipole moment 2−80107
- dimethyloxalate, electronic state investigation using phosphorescence meas. 2−50106
- dimethyloxalate, electronic states from absorption spectra 2−42980
- 2,4-dimethylpentyl-2*(-d_1*) vibrationally excited collisional de-excitation by H_2, D_2, CF_4 2−46648
- 2,5-dimethylphenol, i.r. spectrum 2−77101
- dimethylphenols, 2,3, 2,5 and 3,5, u.v. spectra, vibrational analyses 2−74294
- dimethylphenols, 2,4- and 2,6-, Raman and i.r. spectra 2−74293
- 2,3- and 3,5- dimethylphenols, Raman and i.r. spectra, assignment of obs. freqs. to modes of vibration 2−60059
- dimethylphosphoryl halides, ^{31}P and ^1H n.m.r. spectra 2−46616
- 2,2-dimethylpropane in nematic liquid crystals, obs. of dipolar splitting in p.m.r. spectra 2−71238
- dimethylpyridine, Stark effect on ^{14}N n.q.r. 2−44463
- dimethylselenone, vibrational analysis 2−77143
- dimethylselenoxide, vibrational analysis 2−77142
- dimethylsulphide-d_6, rot. Zeeman effect 2−64177
- dimethylsulphoxide-d_5, D chem. shifts meas. by ^1H-{^2H} INDOR 2−42947

Organic compounds continued
- 1,3-dimethylurea, ^{14}N NQR freqs., coupling consts. var. with temp. 2−83297
- dinitrobenzpyridines, photochromic transitions and relative stability of tautomers 2−48344
- dinitrobenzyl pyridine photochromism, photoequilibrium and decay mechanism 2−68814
- dioxan mixtures with halogens and related molecules, v.l.f. far i.r. spectra 2−83322
- 1,3-dioxane, microwave spectrum, rot. consts. of vibr. states, dipole moment 2−64178
- dioxane based scintillation fluid, chemiluminescence 2−52687
- 1,4-dioxene i.r. spectra, hindered pseudorotation, estimation of barrier height for half-chair inversion 2−70764
- dipeptides, γ-irrad, effect of cryst. struct. on stability, yield, and shape of e.s.r. spectra 2−81536
- 2,5-diphenloxazole, radiation induced fluorescence in cyclohexane and benzene solutions, yields of excited singlet and triplet states 2−53447
- diphenyl, migration of triplet excitons and nonlinear- effects 2−54474
- diphenyl acetylene, photoelectron spectra and ionization potentials 2−60048
- diphenyl amine, reaction with benzoyl peroxide, reaction rate consts., chemilum. 2−78191
- diphenyl crystal, fluorescence and electron excitation energy migration 2−72425
- diphenyl mols., vibrational spectra 2−53056
- diphenylamine, two-photon fluorescence patterns, absorption cross sections and picosecond relaxation times 2−43379
- diphenylamine systems, effect of H bonding on i.r. spectra 2−74280
- 9,10-diphenylanthracene, gas phase, sensitized anti-Stokes delayed annihilation fluoresc. 2−74284
- diphenylanthracene, rotational diffusion in poly-γ-benzyl-L-glutamate solutions 2−60451
- 9, 10-diphenylanthracene photoperoxidation, quantum yield and intersystem crossing 2−72576
- diphenylene sulphide (V) in crystalline solutions of isooctane and CCl_4, spectra and temperature dependence of phosphorescece 2−51377
- N,α-diphenylnitrones, substituted, dipole moment meas. 2−64179
- 2,5-diphenyloxazol, anthryl derivatives, liquid and solid solutions, dependence of threshold of luminescence generation on pumping polarization 2−53450
- 2,5-diphenyloxazole-1,3 and derivatives eximeric fluorescence 2−53075
- diphenylpolyene film, elec. cond. temp. depend. 2−84338
- diphenylsilane, spin-lattice relaxation and Overhauser effect, ^{29}Si Fourier transform n.m.r. studies 2−65355
- dipolar solutes in benzene and fluorinated benzene, n.m.r. study of solvent induced shift effects on ^1H and ^{19}F 2−83311
- 4,4′-dipropoxyazoxybenzene, liquid crystal p.m.r. obs. 2−50338
- disilyl methane and deuterated compound, normal cond. analysis, determ. of mean amplitudes of vibration 2−53058
- disodium fluorescein, two-photon absorption cross sections using psec laser pulses 2−61808
- distyryldurene derivatives synthesis as wavelength shifters in plastic scintillators 2−61703
- divinyl-benzene, pressure carboniz., prep. of C precursor 2−56983
- dl-alanine, aqueous solutions, measurement of u.s. velocities using conventional flaw detector 2−60467
- DL-serine, X-ray irradiated, 153 to 340K, free radicals by ESR and ENDOR 2−75350
- DNA, aqueous solutions, u.s. absorption 2−80116
- DODCI, two-photon absorption cross sections using psec laser pulses 2−61808
- donor-acceptor crystals, electrostatic binding energy by Ewald's method and charge transfer in lattices 2−67928
- DPPD, excited, electron transfer to oxygen mols., contact ion-pair and dissociated ion-radicals form. 2−68811
- DPPH dil. benzene solns., proton spin-lattice relax. times 2−42960
- DPPH film, vapour deposition and props. 2−56598
- DPPH-benzene, electron energy band model applic. 2−68299
- durene, hindered rotation in crystals by neutron transmission meas. 2−50999
- durene, phonon spectrum, Raman scatt. obs. 2−54022
- dye aggregates on AgBr, struct. and spectra 2−80557
- dye filters, for visible and i.r. region methods of production and properties 2−55745
- dye fluorescence, quenching by absorption from excited singlet state 2−79970
- dye laser, CW mode-locked, intracavity pumped, wavelength tuning 2−73576
- dye laser, performance enhancement by chem. quenching of triplet state 2−63334
- dye laser, short cavity tunable, longitudinal excitation by N_2 laser 2−66757
- dye lasers, CW, tunable, use in atomic beam deflection 2−73624
- dye lasers, thermal resonator effects 2−79204
- dye lasers in rigid host medium, triplet state population control and utilization 2−69941
- dye molecules in solid lipid layers, effect of electric field on absorption spectrum 2−68801
- dye solution, effects of emission from Xe impulse lamp 2−53378
- dye solutions, absorption and fluorescence spectra in far anti-Stokes region 2−74546
- dye solutions, frequency of electronic transitions, determ. method 2−50367
- dyes: Eu^{3+}, Tb^{3+}, solid and liquid solution luminescence quenching due to dipole-dipole transfer of energy from ions 2−54460
- dyes, flashlamp for pumping 2−76466
- dyes, luminescence, selective light quenching 2−53074
- dyes, polarization of stimulated emission 2−49375
- dyes as active filters for Nd:YAG laser output power 2−73588
- dysprosium ethyl sulphate, caloric and mag. obs. 2−68523
- electrical insulation and dielectric phenomena, conference, Williamsburg (1971) 2−57222
- electronic spectra of trapped electrons 2−81516
- enynes, long-range spin-spin coupling consts. 2−67511
- epoxy resin polymerization in elec. field. electret form 2−47991

Organic compounds continued
epoxy-diamine networks, glass transition temp. determ. using torsion pendulum 2−71287
epoxybutyne, microwave spectrum, structure and dipole moment 2−80088
erbium ethyl sulphate, caloric and mag. obs. 2−68523
erbium ethyl sulphate, low temp. calorimetry 2−44229
erythrosin molecule in alcohol and isopropanol solvents, dynamics of ultrafast decay processes 2−43367
estradiol-urea complex., struct. determ. by two-dimens. struct. invariants 2−53686
estrogenic steroids, structure elucidation from computer interpretation of mass spectra 2−84685
ethambutol hydrochloride causing visual loss and recovery of retinal sensitivity 2−82069
ethane, adsorption on zeolites, effects of size, charge and conc. of exchange cations 2−74646
ethane, barrier to internal rot., comparison with ethyl fluoride 2−67513
ethane, bond lengths in ground state 2−46513
ethane, pot. surface using the MINDO/2 method 2−77126
ethane, potential functions calc. in terms of group valence force symmetry coordinates 2−42847
ethane, saturated absorption heterodyne spectroscopy 2−46609
ethane, self-consistent procedures for generalized valence bond wavefunctions 2−53012
ethane, thermal energy charge transfer reactions with rare gas ions 2−83399
ethane, vapour pressure, 80 to 135K 2−60559
ethane adsorption onto (100) face of W crystal 2−74642
ethane derivatives, torsional oscill. freq. calcs. by atom-atom approach 2−42982
1,2-ethane dithiol, Raman spectrum meas. in liquid and solid state, determ. of rotational isomerism 2−53061
ethane reaction with C^+, behaviour of cross section as function of incident energy, 2-100 eV 2−57416
ethane translational spectra due to overlap moments induced by collisions with He 2−50129
ethane-methyl radical system, theoretical critical configuration describing decomposition and recombination reaction 2−57420
ethanes, halogen substituted, vibr. spectra and barriers to internal rotation 2−50092
ethanol, ethanol-d_1, ethanol-He, microwave double resonance studies of collision-induced transitions 2−60118
ethanol, glassy, effect of dipole reorientation on trapped electron spectra, semicontinuum model 2−44495
ethanol, meas. of isothermal piezo-optic coeff. 2−50364
ethanol, pressure effects on reaction rates of solvated electrons 2−61812
ethanol, semicontinuum model applied to pressure effects 2−61807
ethanol, vitreous transition, fluoresc. depolarization obs. in soln. 2−60602
ethanol drops, homogeneous nucleation and growth in supersonic flow 2−80393
ethanol glass, electron trapping and solvation at 4K, optical absorption and e.s.r. meas. 2−61810
ethanol glass, trapped electrons produced by biphotonic photoioniz. rel. to delayed emission of indole ring 2−54559
ethanol glasses, free radical photoproduction, e.s.r. study 2−81509
ethanol solution, addition of anthracene, effect of triplet-triplet transfer on lasing threshold 2−76488
ethoxybenzylidene-p'-n-butylaniline: 1-menthol (racemic menthol), liquid crystals, optical storage effects 2−43365
p-ethoxybenzylidene-p-n-butylaniline, proton spin-lattice relaxation in nematic phase 2−56524
p-ethoxyphenylazo phenylheptanoate, proton spin-lattice relaxation in nematic phase 2−56524
ethyl acetate-water interface, effect of heats of solution on Marangoni convection 2−77381
ethyl alcohol, dehydrated, hydrostatic effect in obs. of ultrasound velocity in critical region 2−43354
ethyl alcohol, explosive boiling, overheating, nuclear reactor coolants 2−42686
ethyl alcohol, gauche, microwave rotational spectrum 2−80092
ethyl alcohol counterflow diffusion flame in transverse electric field, optical study of temperature profiles 2−83703
ethyl benzoate, complex dielectric constant ion microwave region 2−71220
ethyl bromide and chloride, pulse radiolysis, electron disappearance 2−61816
ethyl esters of some carboxylic acids, temp. variation of u.s. velocity 2−74486
ethyl isocyanate, emission spectra in high frequency discharge 2−42990
ethyl nitrate, and propyl nitrate, chemical aspects of shock initiation 2−83724
ethyl pyridines, substituted, electronic spectra 2−53071
ethyl thiocyanate, i.r. and Raman spectra, vibrational assignment and conformation 2−42983
ethylacrylate, dielec. props. in microwave region 2−60491
ethylamine, deuterated, Raman spectra analysed w.r.t. amino group vibrations 2−46610
ethylamine, effect of deuterium substitution on vapour pressure 2−43450
ethylamine, n.q.r meas. at liquid nitrogen temps. obs. of phase transition, ionic character of N-H, N-C bonds 2−83310
ethylamine phosphor activated by TLCl, luminescence, excitation and emission spectra after exposure to u.v. radiation 2−54484
ethylbenzene, conformational structure, i.r. and n.m.r. spectra 2−42953
ethylbenzene, conformational structure correlation with semi-empirical LCAO calculations 2−60068
ethylbromide-Ar mixture in multiwire chamber 2−70291
ethylene, ^{13}C chem. shifts 2−77102
ethylene, $\pi\pi^*$ transition, electron correl. and Rydberg character 2−60064
ethylene, adsorption and decomposition on W surface 2−50552
ethylene, adsorption on zeolites, effects of size, charge and conc. of exchange cations 2−74646
ethylene, dissociation in induction-coupled Ar plasma jet 2−53062

Organic compounds continued
ethylene, high resolution i.r. spectrum, determination of rotational constants and Coriolis interactions 2−50093
ethylene, ion-mol. reaction studies with quadrupole ion storage trap 2−83405
ethylene, i.r. absorption coeffs. 2−56156
ethylene, laser induced combination band luminescence, vibration-rotation energy transfer 2−60066
ethylene, lowest excited singlet state prediction by time-depend. Hartree-Fock method 2−77040
ethylene, minimal basis set LCGO calcs. 2−79989
ethylene, multiconfig. wavefunctions for lowest ($\pi\pi^*$) excited states 2−67512
ethylene, normal coordinate analysis of vibrational spectrum 2−70665
ethylene, one-electron perturbation calc. of 3d electrons 2−67452
ethylene, orbital energy calc. 2−50003
ethylene, perturbative configuration interaction calculations 2−52978
ethylene, photoionization products, rate coeffs. for reactions 2−51435
ethylene, pi-electron system, propagation calcs. in Pariser-Parr-Pople model 2−50012
ethylene and D_2 mixed adsorption on polycrystalline W 2−44484
ethylene carbonate, solute in thermotropic nematic phase, p.m.r. study, comparison with lyotropic phase 2−83800
ethylene gas, contributions of nonspherical and nonadditive molecular interactions to third virial coeff. 2−71110
ethylene glycol, Debye effect and relax. time distrib. 2−46971
ethylene in liquid and solid rare gas matrices intravalence and extravalence excitations 2−46603
ethylene monothiocarbonate, solute in thermotropic nematic phase, p.m.r. study, comparison with lyotropic phase 2−83800
ethylene oxide, collision broadening of rot. lines by polar mols. 2−77115
ethylene oxide (-d_4 oxide), i.r. and Raman spectra, assignment of normal vibrations and normal coordinate analysis 2−42984
ethylene reaction with C^+, behaviour of cross section as function of incident energy, 2-100 eV 2−57416
ethylene sulphone, microwave rotational spectra, structure and dipole moment determination 2−60065
ethylene trithiocarbonate in thermotropic nematic solvent, p.m.r. spectrum 2−56230
ethylene V state, valence state description by config. interaction theory 2−64180
ethylene-d_2(-d_4), and ethylene geometry 2−56229
ethylenediamine, crystal structure determ. 2−43599
ethylenediamine and deutero derivative, infrared, Raman vibrational spectra 2−77106
ethylenes, methyl substituted, torsional and internal rotation barrier determination from Raman and i.r. spectra 2−60067
ethylmethacrylate, dielec. props. in microwave region 2−60491
ethynylbenzene, CNDO/CI calcs. of lower electronic transitions 2−56221
europium benzoylacetonate, e.p.r. of Gd^{3+}, cryst. field symmetry 2−81469
europium dibenzoylmethide chelate, electronic transitions, spectroscopic obs. 2−65239
europium dibenzoylmethide chelate with ethanolamine, luminesc. props. 2−65310
fatty acids, molecular depression of surface tension on dissolution in water 2−71172
fatty acids, normal, u.s. velocity obs. and chemical structure det. 2−56231
ferric haem, iron out-of- planarity and tetrapyrrole nitrogen nuclear spin state mixing 2−80101
ferrocene, force const. calcs. 2−64181
ferrocene, symmetry coordinates, harmonic force field, and mean amplitudes 2−42985
ferrocenoylacetonate anions, fragment calc. 2−83325
ferrocyanide in glasses produced by freezing NaOH-H_2O solutions, photoelectron emission spectra 2−44210
fibres, optical waveguides, essential thickness calc. 2−83860
film, thin, charact. energy losses by slow electrons at 77K 2−84669
flavins, molecular luminescence, excited states 2−46605
fluoranthene, bimolecular fluorescence quenching, interaction between excited molecules in solution 2−56506
fluoranthene, fluorescence quenching due to exciton-exciton interaction, determ. of rate const. and exciton migration rate 2−81426
fluoranthene crystal, purity determ. by spectral depend. of fluorescence lifetime 2−84536
fluorcarbon/paraffin-white oil, viscosity-pressure behaviour 2−60449
fluorescein solns. luminance, rel. to contact lens practice 2−55318
fluorescence of solns., temp. depend. of non- radiative, deactivation processes 2−80070
fluorescence spectra fine structure obs., solvent selection for laser excitation conditions 2−68693
fluorinated ethylene propylene encapsulated N/P Si solar cell, effect of simulated micrometeoribid exposure 2−52380
fluorine containing σ-bonded molecules, MINDO/2 calc. 2−77111
fluorine containing compounds, calc. of second moments of electronic charge distrib. and quadrupole moments by CNDO/2D method 2−80085
o-, m-, p-fluorobenzaldehyde, dipole moments and conforms. 2−83279
fluorobenzene, exciton states characts., spectroscopic obs. 2−77807
fluorobenzene-d_5 in liquid state, reorientation and angular momentum correlation times by NMR 2−80479
fluorocyclobutane, low frequency Raman spectra 2−74287
fluoroethanes, vicinal ^{19}F coupling consts., self-consistent perturbation theory calcs. 2−70767
fluoroform, nucl. spin relax. obs. of spin-rot. interaction 2−56200
fluoromethane, solid, i.r. absorpt. spectra, vibr. modes 2−57356
fluoromethanes, molecular orbital valency state calculations 2−42859
fluoroperoxides, O-O stretching frequency identification by Raman obs. 2−56232

Organic compounds continued
fluoropyridine methyl derivatives, long-range spin-spin coupling consts., electron contribs. 2−77097
2-fluoropyridines, microwave spectra, ring distortion 2−74295
fluorothiophenes, substituted, n.m.r. of ^{1}H and ^{19}F 2−46606
p-fluorotoluene, conform. depend. of long-range spin-spin coupling 2−64193
formadlehyde absorption of W33 2−81869
formaldehyde, ^{13}C isotope in Sgr A and SgR B2, absorption spectrum and ^{12}C/^{13}C abundance ratio 2−48671
formaldehyde, absorption in the direction of Bok globules 2−58241
formaldehyde, all-electron nonempirical calc. of potential surfaces, dissociation into radical products 2−42987
formaldehyde, all-electron nonempirical calc. of potential surfaces, dissociation into molecular products 2−42988
formaldehyde, bond lengths in ground state 2−46513
formaldehyde, CI description of $^{1}(\pi\rightarrow\pi^*)$ excited state 2−42989
formaldehyde, double resonance of 3.5 μm He-Xe laser radiation 2−46607
formaldehyde, far i.r. laser emission in large gas-laser tube 2−45740
formaldehyde, interstellar, in direction of Cygnus X-3, 6 cm. obs. 2−81849
formaldehyde, isotopic separation of H and D by photopredissociation 2−67438
formaldehyde, perturbative configuration interaction calculations 2−52978
formaldehyde, semi-empirical analysis of electronic spectrum and molecular structure 2−42986
formaldehyde + H, abs. rate constant, investigation using formaldehyde photolysis 2−54539
formaldehyde absorption in southern Coal Sack 2−69042
formaldehyde absorption in W 44 supernova remnant 2−84983
formaldehyde in dark nebulae, 2 cm isotropic background radiation absorption 2−75789
formaldehyde with Slater basis sets, magnetic susceptibility and ^{17}O and ^{13}C n.m.r. shielding constants 2−50094
formamide crystals, vibration spectra 2−44395
formamides, deuterated, vibrational assignment of Raman spectra 2−50095
formic acid, emission spectra in high frequency discharge 2−42990
formic acid, isotope effect and ^{13}C spin-lattice relax. 2−60069
formic acid, O−H overtone bands and pot. energy curves 2−56211
formic anhydride, electron diffraction examination of structure 2−60070
formyl-2(3) furan and thiophene, valence vibr. band, splitting obs. 2−83283
freon, explosive boiling, overheating, nuclear reactor coolants 2−42686
freon, u.s. transmission intensity variation with time at 22 kHz at atmos. and excess pressure 2−52232
Freon 113-water system, direct contact heat transfer in stratified flow with similtaneous interfacial boiling 2−50285
freon 11, 113 droplet splattering on hot surface, heat transfer rates 2−55575
Freon 11, condensation, heat transfer, finned tubes 2−82248
Freon 12, influence of curvature on post burnout heat transfer up to supercritical pressures 2−77223
freon-113, meas. of local heat transfer during boiling on nonisothermal surface 2−64516
freons, boiling heat transfer, smooth tubes, finned tubes 2−82249
freons, Raman spectroscopy 2−80418
fulminic acid, u.v. absorpt. spectrum, gas phase, ground-excited state transition 2−80098
fulvene, electronic struct., SPINDO calc. and photoelectron spectra 2−70761
fulvene, microwave spectrum and struct., bond lengths and angles 2−80096
furan, 1s binding energy for C atom 2−77156
furan, interstellar, 6 cm search 2−48725
furan, n.m.r. study in liquid crystal of structural parameters 2−67514
furan, normal magneto-optical rot. dispersions, mag. moments 2−70770
furan, solid phase, fund. vibrs. assignment from i.r. spectra 2−72355
furan quinone pigments, DFC and DF, photoinjection and photoemission, energy levels 2−54256
furan-2, 5-dialdehyde partially oriented in nematic phase, n.m.r., conform. obs. 2−70769
furan-quinone pigment, DFC, charge transport props. 2−51219
2-furanaldehyde, conform., rot. isomerism, nematic-phase n.m.r. obs. 2−77147
furane derivatives, 2-substituted, i.r. and Raman spectra 2−77146
furazan, u.v. absorpt., non-planar state obs. and barrier to planarity 2−70768
furfural, electronic structure calc. for rotational isomers 2−50096
furocoumarins, in conc. H_2SO_4, protonated complexes, i.r. spectra, 1400-1800 cm^{-1} 2−46599
galvinoxyl radical, g-factor, solvent effects 2−53064
gas discharges, organic reactions leading to polymer deposits 2−74408
gas phase molecule collisions, meas. of radiationless triplet-triplet energy transfer 2−53094
gelatin, stress frozen, photoelastic analysis for gravity stresses 2−41628
gelatine in photographic layers, mechanical properties and means of modification 2−52508
germanium (IV)-mandelic acid coordinated cpds., i.r. spectra 2−83332
glass and supercooled liq., mol. motion, Mossbauer scatt. obs. 2−61609
D-glucose, ^{13}C chem. shifts rel. to C electron densities from extended Huckel and Del Re theories 2−42948
glycerin, velocity of ultrasound, as function of temperature and pressure 2−71193
glycerine, rotating annulus, isothermal motion of O_2 bubbles 2−46912
glycerine solutions, wave inception in falling film 2−50287
glycerine-water system, influence of free radicals and paramagnetic ions on viscosity 2−74530

Organic compounds continued
glycerol, meas. of diffusion const. of pyrene molecules in triplet state from -17 to +15°C 2−68804
glycerol, pulse n.m.r. meas. of self-diffusion 2−60453
glycerol, viscous, rotating frame proton spin relaxation 2−56526
glycerol-water mixture, heat transfer on boiling in trapezoidal channel 2−60556
glycine, aqueous solutions, measurement of u.s. velocities using conventional flaw detector 2−60467
glycine, SCF calculations, example of peptide bond 2−56233
glycine silver(I) nitrate, ferroelec., cryst. struct. 2−47356
glycolaldehyde, molecular g-values from Zeeman effect 2−70739
glycylglycine, SCF calculations, example of peptide bond 2−56233
glyoxal, LCAO-MO-SCF calc. determ of energy for cis-trans isomerization 2−53065
cis-glyoxal, microwave spectrum in range 18-40 GHz 2−83300
trans-glyoxal $^{3}A_u$ mols., laser induced phosphorescence 2−48345
haloacetonitriles, normal co-ordinate calculations of force constants and normal vibrations 2−50097
halobenzenes, hypersonic velocity and absorpt. 2−77429
halobenzenes, significant struct. theory applic. 2−83778
halogen-carbon compounds, meas. of molecular stopping cross sections of α particles, 0.3-2.0 MeV 2−70820
halogenated molecule-nitroxide radical interaction, ^{13}C constant shift and MO studies 2−51440
halomethanes, K-shell electron binding energy and n.m.r. chem. shifts correl. 2−56235
n-heptane, heat capacity detn. by adiabatic calorimeter 2−76406
n-heptane, isobaric heat capacity along boundary curve 2−64458
heptane, u.s. velocity, det. of molecular parameters 2−53429
n-heptane in n-hexadecane, effect of temp. gradient on diffusion coeff. 2−77418
6-heptyloxy−5-iodo−2-naphthoic acid quenched nematic, alignment obs. 2−60425
heterocyclic, 5-membered saturated ring, combination scatt. spectra 2−46591
heterocyclic, 5-membered saturated ring, struct. and symmetry 2−46589
heterocyclic compound, saturated five membered, diamag. suscept., temp. variation 2−71232
heterocyclic cpds., negative ion form. by electron interaction 2−80154
heterocyclic five membered ring compounds, solns. i.r. absorpt. spectra 2−83284
heterocyclics, six-membered with O and N, AVE CI SCF calculation 2−56204
hexachlorobenzene, triplet state geometry at 1.6 K, PMDR obs. 2−81517
hexachloroethane, γ-irrad., thermolum. and e.s.r. 2−48259
hexafluorobenzene, CNDO calc. of dipole moment derivatives 2−50082
hexafluorobenzene, n.m.r. study of gas to infinite dilution chemical shifts 2−74291
hexafluorobenzene solvent induced shift effects of nonpolar and polar metal complex solutes 2−83264
hexafluoroisopropanol, low dispersion liquid, enhanced nonresonant, optical four-photon parametric interaction 2−46957
hexahydrotriphenylene (II) in crystalline solutions of isooctane and CCl_4, spectra and temperature dependence of phosphorescence 2−51377
hexamethyl phosphoric triamide, temp. dependence of ^{14}N n.q.r. 2−48313
hexamethylbenzene, absorption spectra, vibronic bands 2−51351
hexamethylbenzene, hindered rotation in crystals by neutron transmission meas. 2−50999
hexamethyldisiloxane, isotopic shifts in vibrational spectra by CD_3 substitution, force constant calc. 2−46632
hexamethylenetetramine, Start effect on ^{14}N n.q.r. in axially symmetric field gradient 2−61757
hexamethylenetetramine, X-ray scattering and interpretation of the thermal scattering power 2−53632
hexamethylphosphorus triamide, temp. dependence of ^{14}N n.q.r. 2−48313
hexane, charge carriers apparent mobilities 2−74556
n-hexane, electrically stressed, prebreakdown processes 2−60490
n-hexane, isobaric heat capacity along boundary curve 2−64458
n- hexane, nonlinear U(u) Hugoniot below 15kb 2−53390
n- hexane, optical props. of liquid in vac. u.v. 2−50363
hexane, u.s. velocity, det. of molecular parameters 2−53429
n-hexane and nitrobenzene liquid system, nonlocal shear viscosity and mode-mode coupling near consolute point 2−64445
n-hexane-nitrobenzene critical mixtures, Brillouin scattering investigation by interferometric technique 2−46965
p-n-hexyloxybenzylidene-p′-aminobenzonitrile, temp. depend of flow alignment 2−50339
high temperature contact nucleation, supercooled water, organic chemicals, ice embryos 2−84828
higher alkanes, meas. of acoustic nonlinearity parameter 2−71197
hydrazil, recrystallised samples, e.s.r. line width and exchange narrowing 2−65330
hydrazine, n.q.r., ^{14}N nuclear relax. 2−72532
hydrazine alum, ferroelectric, n.m.r. rel. to phase transitions 2−75357
hydrocarbon, electronic conduction 2−56511
hydrocarbon, photoinjection from metal-free phthalocyanine film 2−56512
hydrocarbon 40 keV $CH^+ \rightarrow C^+ + H$, $C + H^+ C^+ + H^+ + e$, fragment kinetic energy meas. 2−70772
hydrocarbon chains with (α-naphthyl)$-(CH_2)_j-$(α-naphthyl) struct., intramol. collision freq. 2−53067
hydrocarbon ions, closed shell, electronic absorption spectra calc. 2−42991
hydrocarbon negative ions, CNDO calculations and reactions 2−64184
hydrocarbons, ^{13}C chemical shifts determ. from INDO perturbation calc. of magnetic shielding consts. 2−64162
hydrocarbons, aromatic, non-Born−Oppenheimer coupling and D effect on $T_1 \rightarrow S_0$ radiative transitions 2−43002
hydrocarbons, atmospheric pollution in Los Angeles 2−57944
hydrocarbons, band length-resonance integral relationship 2−50009

Organic compounds continued
  hydrocarbons, conversion by high-temp. fuel cells with ceramic electrolytes 2−59041
  hydrocarbons, crystalline, intermolecular interaction potential from incoherent scattering of slow neutrons 2−47738
  hydrocarbons, d-functions effect on orbital energies 2−80067
  hydrocarbons, electron structure in π-electron approximations 2−50102
  hydrocarbons, fluorescence surrounding CO_2 laser induced sparks 2−74440
  hydrocarbons, influence of mol. binding on alpha-particle stopping power 2−64869
  hydrocarbons, interpretation of photoelectron spectra using SPINDO calc. 2−77114
  hydrocarbons, linear conjugated, lowest triplet excitations 2−77133
  hydrocarbons, Raman spectroscopy 2−80418
  hydrocarbons, rot., pair theorem and bipartite graph props. 2−53038
  hydrocarbons, solid, anomalous annihilation of positrons 2−68264
  hydrocarbons, vibr. force fields prediction using extended Huckel theory 2−79985
  hydrocarbons $CH_n{}^+$, reactions with gas targets at 40-140 keV 2−64218
  hydrocarbons collisional rotational transitions 2−74301
  hydrocarbons liquid, localized electron theory 2−67840
  hydrocarbons of form $CH_n{}^+$, $n=2, 3, 4, 5$, dissociation, kinetic energy of H^+, $H_2{}^+$, $H_3{}^+$ fragments 2−70771
  hydrogenous liquids for reacor moderation, slow neutron scatt. cross-section 2−70535
  1 and 2hydronaphthyl radicals in naphthalene single crystals, e.p.r. study 2−54499
  hydroquinone, intermediate products of pulse photolysis 2−75391
  hydroquinone developers, salt effects 2−59312
  o-hydroxyacetophenone, microwave dielectric props. in solutions 2−43381
  2-hydroxyethyl methacrylate networks in dry and swollen states, effect of crosslinking density and dilution 2−56782
  hydroxylamine alum, ferroelectric, n.m.r. rel. to phase transitions 2−75357
  hydroxylamine molecule, microwave spectra 2−56234
  9-hydroxymethylphenanthrene, photolytic dissociation cis syn dimer, fluorescence 2−56253
  hypotaurocyamine, crystal structure 2−43600
  imidazole, interstellar, 6 cm search 2−48725
  imidazole radical produced by γ-irradiation of single crystals, ENDOR determ. of hyperfine tensors for protons in H bonds 2−65394
  4.5-iminophenanthrene unsymmetrical excimer in cyclohexane solution 2−46604
  iminoxyl radical with ^{15}N isotope, mol. reorientation character effect on e.s.r. lineshape 2−70773
  iminoxyl radicals, n.m.r. spectra interpret. 2−80110
  impure crysts., spectra, temp. broadening and shift of phonon-free lines 2−61613
  indole, fluoresc. in soln., interaction with methanol, kinetics 2−53069
  indole and derivatives in aqueous salt solns., effect of adding salt on deactivation of excited state 2−77442
  indolizine and azaindolizines, photophys. props. 2−68815
  insulating materials, corona rel. to partial discharges phenomena 2−71006
  interdigital electro-optic thin film modulator using nitrobenzene 2−79376
  interstellar, chemistry 2−78476
  intramolecular hydrogen bond effects on mol. dipole moments 2−77127
  Io atmosphere, upper limits 2−75867
  iodo-alkenes, branched chain, for u.v. spectra, effect of fluorine substitution and conjugative effects 2−80100
  iodoacetylene, far-u.v. spectrum, band assignments, electronic transitions 2−80072
  1-iodoalkanes, far u.v. spectra, obs. of Rydberg series leading to one of first two ionization potentials 2−74292
  p-iodoaniline, variation of n.q.r. frequencies with temp. 2−65357
  2- iododibenzoyl peroxides, conservative twinning, topotaxy 2−77525
  o-iodophenol, variation of n.q.r. frequencies with temp. 2−65357
  ionic salt mesophases, struct. behaviour 2−71158
  i.r. absorption bands, temp. dependence of half-band widths 2−71207
  iron(II)formate-magnesium formate system, mixed crystn., Mossbauer obs. 2−56673
  iron citrate, crystal hydrate and local heat build up in process of destruction of thin layers 2−73455
  iron formate dihydrate, Mossbauer effect, between 4.2 and 0.027K 2−54394
  isobutyric acid-water mixture near critical point, temperature dependence of electrical resistance 2−80525
  isobutyric acid-water solns., supercrit., elec. cond. and viscosity 2−53453
  isobutyric acid-water solution, Rayleigh linewidth in critical region rel. to Kawasaki-Einstein-Stokes formula and dynamical scaling 2−46933
  isocyanates, integrated intensity of valence vibrations 2−74290
  isoleucine racemization in calcareous marine sediments kinetics and mechanism 2−48417
  isopropenyl system, ^{13}C-^{13}C coupling constants 2−56237
  isopropyl nitrate, effect of confinement on detonation 2−80422
  isoquinoline, photoelectron spectra, perfluoro effect 2−70790
  isothiazole and derivatives, photoelectron and mass spectra obs. of ioniz. pots. 2−83305
  isothiocyanate, determ. of molecular dimensions and large amplitude vibration by electron diffraction 2−80080
  isoxazolinone-5, tautomeric equilibr. dipole moment, electronic spectrum calc. by semi-empirical MO methods 2−53070
  kerosene, ambient medium for photopotential of CdS 2−68482
  kerosene with suspension of SiO_2 and diatomite, mechanical behaviour during shearing in electric field 2−60531
  Kerr effect, isotropic phase of some nematogenic compounds, investigation, temperature dependence and relaxation times 2−53430
  ketene, ground state rot. and centrifugal distortion consts. 2−56238
  ketene, MO study of low energy electronic states 2−60072

Organic compounds continued
  ketone energy transfer to rare earth ions, mechanism 2−60482
  ketone ions, formed by charge exchange in in-line tandem mass spectrometer, dissociation 2−64168
  ketone-tetracyanoethylene system; optical activity inducement in charge transfer band 2−60071
  ketones, aliphatic, in benzene, dielec. absorpt. of microwaves, dielec. props. 2−60509
  α-lactose monohydrate, failure props. 2−43889
  lanthanide ethyl sulphate:Gd^{3+}, host lattice effects on e.p.r. spectra 2−48299
  lanthanum ethyl sulphate:Dy^{3+}, crystal field energy levels and Zeeman spectra 2−80951
  lanthanum ethyl sulphate, spin-lattice relax. at zero mag. field of Nd^{3+} and Er^{3+} 2−65194
  lanthanum ethylsulphate, e.p.r. of Gd^{3+} in single crystals below 40G 2−51405
  large molecules, photochemical dissociation, new formula in Bixon-Jortner model 2−72569
  laser dyes, design criteria 2−42031
  laser dyes in solid matrices, photobleaching 2−55704
  lead acetate hydrate, X-irradiated, Pb^+ and PbH^+ identification, e.p.r., g-factors, hyperfine splitting 2−75347
  light-atom struct., absolute configs. and $\Delta f''$ values determ. 2−47355
  liquid, thermal periodicity of filament form. and elastic lattice vibrs. 2−50359
  liquid crystal, cholesteric mixtures, shear-induced struct. changes, refl. spectra obs. 2−64438
  liquid laser based on Rhodamine 6J for spectrochemical analysis 2−84702
  liquids, hydrated-electron reactions, specific rate determ. by pulse radiolysis 2−78210
  liquids, thermal cond., molecular structure depend., Debye model, incremental method, paraffin series 2−80468
  lithium acetate, elastic consts. meas. by Brillouin effect 2−50732
  lithium acetate dihydrate, i.r. and Raman spectra, temp. dependence 2−72376
  lithium ammonium tartrate, n.m.r., ferroelec. paraelec. transition phenomena 2−72527
  lithium citrate tetrahydrate, i.r. spectrum in mull and KBr matrix, assignment 2−60073
  lithium formate monohydrate, n.m.r. of ^7Li 2−54512
  lithium formate monohydrate, nonlinear optical crystal, linear and nonlinear optical props. 2−48130
  luminol oxidation liquid phase phase chemiluminescence intensity/standard, absolute quantum yields 2−65372
  luminol-alkali-^{32}P system, internal irrad. induced chemiluminesc. 2−48325
  luminophores in solvents of different polarities, activation energies of radiationless transitions 2−53443
  2,6-lutidine-water, diffusion and viscosity obs. 2−46941
  2,6-lutidine-water light scatt. and shear viscosity studies in critical region 2−50344
  magnesium phthalocyanine film, impurity level energies from photoemission and cond. obs. 2−81028
  maleic acid, irrad., electron trapping centre obs. in single cryst. 2−78211
  maleic anhydride, molec. structure determ. by gas-phase electron diffraction 2−42992
  malonamide, X and gamma irradiated, radical formation 2−51473
  malonamide, X-irradiated, confirmation of σ-radical, e.s.r. spectra obs. 2−64185
  malonic acid, irradiated, electron spin-lattice and cross relaxation 2−44442
  malonitriles, normal coord. analysis, G matrix elements 2−70774
  manganese formate, mag. phase transitions 2−44293
  manganese formate dihydrate, mag. diagram of state, spin-flop transition 2−68577
  manganese pentacarbonyl adducts, single crystals, ^{55}Mn broad-line n.m.r. at room temp. 2−68747
  manganocene, mag. reson. props., zero-field splitting and g-values 2−64174
  MBBA, Kerr const. temp. depend. near isotropic-liq. cryst. transition 2−77430
  MBBA, nematic, alignment kinetics in mag. fields, viscosity coeff. 2−53400
  MBBA, nematic liquid crystals, proton spin-lattice relaxation mechanisms 2−84596
  MBBA, nonsingular model for screw disclinations 2−56482
  MBBA, small angle X-ray scatt. near nematic-isotropic transition temp. 2−43328
  MBBA liq. cryst., dynamic scatt. in hydrodynamic regime, relax. time 2−77438
  MBBA liquid crystals ultrasonic absorption and viscosity anisotropy in oriented crystals 2−50334
  l-menthol, helical twisting power in nematic solvent 2−80442
  mercuric cyanide.tetrahydrofuran addition compound, development of {111} habit 2−60706
  mercury(I), (II) acetate compounds, vibrational spectra, stretching frequencies determ. 2−46608
  mercury picramate, cryst. data, orthorhombic cell dimens. 2−74754
  metallocenes, electron spectra, electronic configs. 2−64187
  metalorganic, in epitaxial growth of semicond. films 2−47091
  methabetellurol and isotopic species, vibr., infrared and Raman spectra 2−83301
  methane, $^{13}C/^{12}C$ ratio detn., mass spectrometry obs. 2−48355
  methane, ab-initio bond-orbital calcs. 2−53018
  methane, absorption line profile using laser tuned by magnetic field 2−60076
  methane, activated chemisorption on Rh surfaces 2−80577
  methane, adsorbed on gel, n.m.r. 2−46614
  methane, adsorpt. on W, field ion microscopy obs. imaging props. 2−64583
  methane, analysis of Kuiper bands of Uranus 2−62709
  methane, atmospheric, concentration between 44 and 62 kms altitude 2−65667
  methane, atmospheric conc. correl. with airborne continental dust 2−62158
  methane, bond lengths in ground state 2−46513

Organic compounds continued
methane, calc. of half-widths of rotational lines in ν_3-band using Anderson-Tsao-Curnutte theory 2−53105
methane, calc. of octopole moments using semi-empirical wavefunctions 2−70701
methane, compressed liquid, eqn. of state 2−80448
methane, correl. energies by united-atom many-body perturbation procedure 2−67480
methane, correlation energy calc. using linked cluster many body perturbation theory 2−67484
methane, dipolar polarizability, variational calc. 2−80060
methane, electronic structure, dipole moments, n.m.r. and n.q.r. constants calc. 2−83324
methane, gas, eqn. of state, from unit-compressibility line 2−53330
methane, in Jovian visible clouds, spectral obs. 2−75875
methane, ion-mol. reaction studies with quadrupole ion storage trap 2−83405
methane, ionization cross sections for high- energy electrons and positrons, comparison with CD_4 2−70598
methane, i.r. absorption coeffs. 2−56156
methane, Jovian atmosphere absorption bands, obs. using Galilean satellite eclipse obs. 2−58490
methane, laser radiation absorption behind shock wave front 2−64396
methane, liquid, mol. motion, neutron scatt. cross section 2−43324
methane, localized mol. orbitals of ground state, pseudopot. calc. 2−80062
methane, lowest ionization potential and transition energies, ab initio calc. 2−56244
methane, mass spectra, observation of isotope effects 2−83321
methane, methane-d_4 solutions in liquid Ar, collision induced far i.r. spectra, system. dynamics investigation 2−43372
methane, microwave transitions in vibronic ground state 2−64096
methane, minimal basis set LCGO calcs. 2−79989
methane, mol. rot. of dissolved CH_3D, in liq. and plastic phases 2−80586
methane, molecular absorptions, laser freq. and wavelength meas., speed of light 2−78758
methane, molecular orbital valency state calculations 2−42859
methane, octopole moments and dielec. second virial coeffs. 2−83294
methane, photodissociation cross-section meas., 555-1242 Å 2−51470
methane, photoionization products, rate coeffs. for reactions 2−51435
methane, projectile ion thermal energy charge transfer reactions, reson. effects 2−80132
methane, pure rotational spectrum arising from dipole moment due to centrifugal distortion 2−53072
methane, Raman scattering cross sections and depolarization ratio 2−53026
methane, saturated absorption heterodyne spectroscopy 2−46609
methane, scattering of Na, K, meas. of velocity dependence and total cross section, study of glory undulations 2−70821
methane, shocked, 3.39 μ resonance line absorption 2−83275
methane, singly deuterated, obs. in atmosphere of Jupiter 2−51826
methane, slow neutron spectra, suitability as cold moderator 2−76897
methane, solid, γ-irrad., spin species conversion by paramag. impurities 2−84446
methane, solid, second transition due to spin isomerisation, obs. by optical birefringence 2−64814
methane, solid, static dielectric const. at low temp. and high pressure 2−81146
methane, studies on collision-broadened rotational lines in ν_4-fundamental 2−42999
methane, temp. dependence of Scott thermomagnetic torque 2−46861
methane, thermal energy charge transfer reactions with rare gas ions 2−83399
methane, transient saturated molecular absorption 2−43274
methane, translational spectra due to overlap moments induced by collisions with He 2−50129
methane, vibrational band of Raman spectra, use of pressure-scanned Fabry-Perot interferometer for high resolution 2−74250
methane $^{12}CH_4$, interpretation of the F_2 sub-level of the $2\nu_3$ harmonic band 2−64188
methane absorption at 3.39 μ, effect of pressure and temp. on half-width studied using He-Ne laser 2−42998
methane adsorbed layer, on graphite, formation stages 2−47152
methane adsorbed on graphite, spin-lattice and spin-spin relax. 2−67925
methane adsorbed on MgO, microdynamics, n.m.r. relax. obs. 2−83875
methane adsorption on to (100) face of W crystal 2−74642
methane binary mixtures with He, Ar, Xe, ultrasonic absorption meas. of rotational relaxation 2−64219
methane cloud layer in atmosphere model for Uranus 2−78558
methane in atmosphere of Jupiter, computation of transmission profiles in ν_4 band 2−48769
methane liquid, acoustic nonlinearities parameters, temp. depend. 2−56501
methane molecule, electronic structure, analysis of formation in Hartree-Fock model 2−60074
methane spectral line equivalent widths in Jovian atmosphere rel. to absorption line formation models 2−78535
methane stabilized He-Ne laser, frequency and wavelength det. at 3.39 microns, speed of light calc. 2−42018
methane with ^{13}C in atm. of Jupiter 2−66170
methane-^{13}C, identification in Jovian atm. 2−75883
methane-Ar-Kr and methane-Ar-H_2 mixtures, mean ionization energy 2−60290
methane-d_1, i.r. spectrum, ground state constants, perturbation allowed transitions 2−77119
methane-d_1, resonances and doublings in i.r. spectrum 2−77118
methane-d_3, force constants and i.r. spectrum 2−67515
methane-d_4, critical fluctuations at 27K phase transition, neutron scatt. obs. 2−61040
methane-d_4 + silane ion molecule reactions, hydride ion transfer and isotope effects 2−68778

Organic compounds continued
methane-deuterated, abundance in Jupiter 2−75885
methane-N_2 mixture, cathode-directed streamer, secondary avalanche development 2−60298
methanes, deuterated, in nematic liquid crystals, obs. of dipolar splitting in p.m.r. spectra 2−71238
methanes, solid, orientational ordering, quantum mech. theory 2−61039
methanol, barrier height in excited vibrational state, microwave spectrum obs. 2−56248
methanol, gain meas. of stimulated Raman scattering using tunable dye laser 2−43375
methanol, in trialkylphosphines and CCl_4, intermol. interac., spectral study 2−46647
methanol, isotopic, torsion-rotation spectra, moments of inertia, barrier heights, Kirtman perturbation constants 2−77124
methanol, scattering of Na, meas. of velocity dependence and total cross section, study of glory undulations 2−70821
methanol, solvated electron spectra, semicontinuum model applied to pressure effects 2−61807
methanol adsorption in Si and Ge 2−56601
methanol and deuterated derivs., analysis of torsion-rotation spectra 2−67518
methanol drops, heat transfer from small diameter channel in film boiling temp. range 2−53379
methanol glass at 77K, matrix ENDOR linewidths of trapped electrons 2−57402
methanol in excited CO stretching state, microwave spectrum, torsion-vibration-rotation interaction 2−67517
methanol U169.3 line in Orion A i.r. nebula 2−66135
methanol ultrasonic waves thermal excitation by laser beams interference 2−41737
methanol-air mixtures, thermal explosion, boundary of flame propagation region 2−75378
methanol-cyclohexane, solution properties at 25 to 50°C 2−53408
methanol-cyclohexane critical mixture, simultaneous meas. of viscosity and light scattering 2−71169
methanol-cyclohexane-acetone, solution properties at 25°C 2−53408
methanol-d_4, microwave spectrum, torsion-vibration-rotation interactions 2−50100
methanol-ethyleneglycol mixture, dynamic polariz. of protons 2−79677
methanol-hexane solution, reflection coeff. rel. to surface layer thickness meas. 2−60474
methanol-potassium bromide vibrationally excited, inelastic scatt. 2−64220
methanol-water mixtures, binary film condensation, effects of forced flow and variable properties 2−77411
methoxy benzylidene butyl aniline, nematic, bend oscillations in dielectric electrohydrodynamical instability 2−46931
p-methoxy benzylidene p-n butylaniline, liq. cryst., nematic-isotropic liq. phase transition, sp. ht. obs. 2−74523
p-methoxybenzilidene p-n-butylaniline, nematic phase, anomalous alignment and domains 2−71161
p-methoxybenzylidene p-n butylaniline, dynamical behaviour above nematic-isotropic transition from spin-lattice relaxation 2−71160
p′-methoxybenzylidene-p-n-butylanilene, temp. depend of flow alignment 2−50339
p-methoxybenzylidene-p-n-butylaniline, nematic phase electric const. 2−60427
N-p-methoxybenzylidine-p-butylaniline, nematic liquid crystal, temp. dependence of anisotropic u.s. propagation 2−46953
2-methoxyethanol, microwave spectrum, minimum energy conformation and molec. properties 2−50098
m-, p- methoxyphenyl thioethers, u.v. absorpt., steric interactions 2−56247
4-methyl 2,6 ditertiarybutylphenol, proton dipole-dipole relax. rel. to quantum tunnelling 2−81472
methyl acetate, thermal conductivity meas. at various temps. and pressures 2−60373
methyl acetylene investigation of vibration-rotation bands in near infrared 2−70781
methyl alcohol, hydrostatic effect in obs. of ultrasound velocity in critical region 2−43354
methyl alcohol, inverse Raman effect 2−71206
methyl alcohol, saturated absorption heterodyne spectroscopy 2−46609
methyl ammonium alum, ferroelectric, n.m.r. rel. to phase transitions 2−75357
methyl and methylene chlorides, electronic structure, dipole moments, n.m.r. and n.q.r. constants calc. 2−83324
methyl benzoate, complex dielectric constant in microwave region 2−71220
methyl bromide, isotopic splitting in pure rot. spectrum 2−70777
methyl bromide, pressure broadening, Stark and double-resonance spectroscopy 2−42993
methyl bromide collision broading of o,o, rh 1.0 rot. lines 2−83303
methyl chloride, Fermi resonance in system $2\nu_4$, $\nu_4 + 3\nu_6$ 2−70778
methyl chloride, gas, solubility in liqs. 2−53405
methyl chloride, scattering of Na, meas. of velocity dependence and total cross sections, study of glory undulations 2−70821
methyl chloride + ^{38}Cl, H and halogen displacement factors, survival probability of products 2−84664
methyl chloroform, crystal and mol. structure at −60° and −145°C 2−53685
methyl cyanide, molec. force fields detn. by kinetic methods 2−70776
methyl cyanide and isocyanide in solid Ar, matrix isolation studies 2−56246
methyl ethyl ketone-heptane-toluene system, free-energy and chemical potentials 2−78181
methyl fluoride, anisotropy of spin-spin coupling 2−50099
methyl fluoride, i.r. spectra analysis, general harmonic force field 2−77150
methyl fluoride, laser excitation and equilibration of excited vibrational states 2−50101
methyl fluoride, nonlinear laser spectroscopy, elec. dipole moments 2−53063
methyl fluoride, nucl. spin relax. obs. of spin-rot. interaction 2−56200

Organic compounds continued
methyl fluoride, partial double-bond character of C-F bond 2−43000
methyl fluoride laser, 10W at 496 microns 2−42029
methyl fluoride laser, methyl fluoride, ten watts at 496 microns, pumped by CO_2 TEA laser 2−42028
methyl formate, molecular g-values from Zeeman effect 2−70739
methyl group stretching and bending vibrs., substituent effect on i.r. absorpt. intensities 2−56245
methyl halides, saturated absorption heterodyne spectroscopy 2−46609
methyl iodide, ν_4 band, spectroscopic consts. detn. 2−60077
methyl iodide, calc. of orientation correlation functions from spectra 2−43363
methyl iodide, equilibrium structure determ. from rotation-vibration interaction constants from i.r. spectra 2−42995
methyl iodide, high-resolution i.r. spectra 2−46611
methyl iodide, reaction with K in crossed beams, energy dependence 2−68771
methyl iodide, reactive scattering of Rb, determ. of potential and cross sections 2−72553
methyl iodide, vacuum u.v. spectra in solid carbon tetrafluoride 2−49957
methyl iodide + K → KI + methyl radical, interpretation of product ang. and energy distribution using direct interaction model 2−57412
methyl iodide + K → KI + methyl radical, translational energy depend., reaction cross-section 2−51432
methyl iodide crysts., harmonic vibr. freqs., harmonic intermol. pot. 2−81350
methyl iodide fixation by silver zeolites 2−84640
methyl iodide-d_3, assignment of overtone and combination bands in vibrational spectrum 2−70782
methyl iodide-d_3, perpendicular bands ν_5 and ν_6, i.r. spectra 2−46613
methyl iodide-d_3 isolated in Ar matrix, i.r. spectra 2−46612
methyl isocyanide, molec. force fields detn. by kinetic methods 2−70776
methyl isocyanide, rotational spectrum, hyperfine structure, high resolution meas. 2−56249
methyl isocyanide, RRKM theory, decomposition of hot-atom substitution products 2−51428
methyl isocyanide of d_3-derivative, vibr.-rot. band analysis 2−70780
methyl isothiocyanate, molecular structure determ. by gas-phase electron diffraction 2−43001
methyl malonic acid, tunnelling sidebands of methyl group hyperfine structure, e.s.r. obs. 2−57389
methyl mercaptan adsorption in Si and Ge 2−56601
methyl nitrite isomers, i.r. spectra 2−77149
methyl palmitate insoluble monolayer leakage across movable barriers, radiotracer detection method 2−53416
methyl pyrazines, absorption spectrum in region of $n\pi^*$ transition, evidence for second electronic state 2−46624
methyl pyridines, substituted, electronic spectra 2−53071
methyl radical, Gaussian wavefunctions 2−42994
methyl radical, vibrational frequency assignments, study by rapid scan spectroscopy 2−83299
methyl radical + $Cl_2(Br_2)$ collisional reaction, molec. beam study 2−61779
methyl silane microwave spectrum, vibration-internal rotation- overall rotation interactions for symmetric-top molecules 2−70779
methyl sulphite isomers, i.r. spectra 2−77149
3-methyl sydnone and related species, ab initio calculation of orbital energies 2−53080
methyl thiophenols, isomeric, electronic struct. and spectra 2−56239
methyl-2-propanol-1, vibrational spectra of OH groups 2−70740
N-methyl-4-brom benzamide, cryst. struct., X-ray obs. 2−64651
3-methyl-pentane molecular liquid, Rayleigh scattering, influence of temperature on collisional wing 2−80471
methyl-substituted chloroaluminate ions, i.r. and Raman spectra, determ. of bonding and structure 2−77117
methylacrylate, dielec. props. in microwave region 2−60491
methylamine, deuterated and partially deuterated, Raman and i.r. spectra analysed w.r.t. amino group vibrations 2−46610
methylamine, effect of deuterium substitution on vapour pressure 2−43450
methylamine, force constant determination using ^{15}N isotope shifts in i.r. spectrum 2−60075
methylamine, minimal basis set LCGO calcs. 2−79989
methylammonium chlorides, solid, mol. and group motions, p.m.r. obs. 2−68750
N-methylaniline, dissolved, low temp. i.r. study of self-association by H bonds 2−54540
9-methylanthracene, molecular crysts., melting point rel. to intensity of incident u.v. radiation 2−50399
methylbromide + ^{80}Br, H and halogen displacement factors, survival probability of products 2−84664
methylbromoform, microwave spectrum, disubstitution method for struct. determ. 2−56243
2-methylbutanol-2 solutions, dielec. polarization 2−46975
methylchloride, variation of Cl quadrupole coupling on deuteration 2−80091
methylchlorosilane, microwave spectrum, rot., centrifugal distortion and nucl. coupling consts. 2−64190
methylchlorosilyl radical, meas. of ^{29}Si coupling consts. effect of degree of CH_3 substitution on planar structure 2−56241
methylcyclobutane, low frequency Raman spectra 2−74287
methylcyclohexanes, ^{13}C chem. shifts rel. to C electron densities from extended Huckel and Del Re theories 2−42948
3-methyldiazirine and 3-methyl-d_3- diazirine, electronic absorption spectra 2−56250
methylene, low-lying electronic states, nonempirical CI study 2−53025
methylene, strongly orthogonal geminal wavefunctions for lowest singlet states 2−70686
10-methylene anthrone, polarizations of low energy $S_n \leftarrow S_0$ transitions 2−60080
methylene blue dye film waveguides, optical absorption 2−63416
methylene chloride, calc. of orientation correlation functions from spectra 2−43363
methylene chloride, in liq. cryst., proton mag. res. spectra, effect of solvent 2−46596

Organic compounds continued
methylene chloride + N_2 chemiluminescent reaction, intensity variations of CN bands with temp. 2−83240
methylene difluoride self-broadening of rotational lines meas. on double modulation microwave spectrograph 2−56242
methylenecyclopentane, microwave spectrum 2−67516
methyleneimine, mol. transient, microwave spectrum analysis 2−64186
methylenephosphorane, ab initio LCAO-MO-SCF study of bonding 2−56240
N- methylethylidenimine, microwave spectrum, internal rot. motions 2−64183
3-methylhexane, solvated electrons, time dependent behaviour, 77K, detector response time <1600 nm 2−75001
3-methylhexane, solvated electrons, time dependent behaviour, 77K, detector response time effect <1600 n.m. 2−75002
methylmercury systems, ^{199}Hg-^{1}H coupling constants, semiempirical MO calc. 2−83223
methylmethacrylate, dielec. props. in microwave region 2−60491
1-methylnaphthalene, activated by oxazoles and oxadiazoles, scintillation, conc. depend., role of triplet mols. 2−48237
1-methylnaphthalene, excimer-monomer equil., deactivation processes, temp. effects 2−71214
α-methylnaphthalene, liquid, specular reflection spectrum, obs. of excitons 2−80474
N-methylnitroamine, normal vibrations, additive interatomic interaction model calculations 2−77044
methylphenylsilanes, electronic-vibrational absorption spectra 2−50111
methylpyridine, nonplanar vibrations, standard intensities and degrees of polarization of line widths 2−77152
methylpyridine, Stark effect on ^{14}N n.q.r. 2−44463
methylsilane, electronic struct., dipole moment 2−83292
2-methyltetrahydrofuran glass at 77K, matrix ENDOR linewidth of trapped electrons 2−57402
3- methylthiopene, microwave spectrum, barrier height to internal rotation of methyl group and dipole moment 2−42997
methylthiophene, in CS_2 solution, out-of-plane vibrations, i.r. band intensities 2−77120
methyltrifluoride, -D, normal coordinate analysis using vibrational data 2−77123
4-methylumbelliferone, acidified solutions, influence of excitation intensity on laser spectra 2−77433
methyne radical, circumstellar molecules of Pleiades 2−58354
mixed vacancy square planar complexes, elec. and mag. props., review 2−61140
molecular cryst., biexciton spectra 2−57338
molecular cryst., electron spin echoes in photo-excited triplet states in zero field 2−54556
molecular cryst., excitonic polarons, band narrowing and band shifts 2−44039
molecular cryst., impurity one-phonon spectra, mirror symmetry breakdown 2−65271
molecular cryst., low symmetry, quantitative simulation of ENDOR 2−65354
molecular cryst., optical electron spin polarization in excited triplet states 2−81466
molecular crystals, single exciton decay into triplet excitons 2−71811
molecular crystals with Nd laser, second harmonic generation 2−82515
molecular crysts., dilute mixed, multicomponent cluster states, Frenkel excitons 2−84228
molecular crysts., local elec. field and charge-carrier mobilities 2−81129
molecular fragments, electronic struct. and interaction processes 2−46590
molecular radiationless transitions, Jortner-Stepanov model 2−80105
molecular vibr. transitions, i.r. activity, coupled oscillator model 2−60040
molecules containing sulphur, ^{33}S n.m.r. obs. of electronic struct. 2−83290
molecules in interstellar clouds 2−75788
molecules in solution dye, two-photon absorption profile, apparatus 2−66734
mono-alkyl benzenes in rigid hydrocarbon glasses, triplet emission 2−81515
monoalkylbenzenes, conformational structure, vibrational and n.m.r. spectra 2−42953
monochloroamine, molec. structure and quadrupole coupling constants from microwave spectra data 2−46615
monohalobenzene, monohalobenzene-d_5, calc. and interpretation of vibrational spectra 2−53066
monohalogeno(methyl)germanes, i.r. and Raman spectra 2−46617
monomers, μ^- depolarization 2−64084
monomethylphosphoryl halides, ^{31}P and ^{1}H n.m.r. spectra 2−46616
mononitro alcohols, vibrational spectra of OH groups 2−70740
monophenyl mols., vibrational spectra 2−53056
multiple scattering of slow neutrons estimation 2−79826
myristic acid monolayers on water, surface diffusion 2−71179
myristophenone, 2-hdyroxy-5-methyl derivative, dielec. relaxation and dipole moment determination 2−60487
N-acetylphenylhydroxylamines, substituted, cis-trans conformational equilibrium, n.m.r. obs. 2−50074
n-alkanes, liquid transport properties and theorem of corresponding states 2−83342
N-methylphenazinium 7,7,8,8-tetracyanoquinodimethanide, lattice energy, Ewald's method 2−67931
naphthalene, anthracene- and tetracene-doped, singlet-exciton energy transfer, generalized random walk model 2−84270
naphthalene, appearance of nonsingular surfaces on equilibrium form 2−50561
naphthalene, deuterated, meas. of quadrupole coupling const. and asymmetry parameter of ring deuterons 2−80082
naphthalene, electron-hole interactions 2−80982
naphthalene, enthalpy of sublimation, calorimetric detn. 2−77477
naphthalene, impurity centre conc. and distrib., exciton scatt. theory calc. 2−81436
naphthalene, migration of excitation energy between impurity molecules studied by polarization method 2−54465

Organic compounds continued
naphthalene, persistent internal polarization temp. and electric field dependence 2−75138
naphthalene, radiation induced fluorescence in cyclohexane and benzene solutions, excited states, effect of singlet state quenchers 2−53448
naphthalene, radiation induced fluorescence in cyclohexane and benzene solutions, yields of excited singlet and triplet states 2−53447
naphthalene, radiation-induced formation of excited states in cyclohexane solution, effect of electron scavengers 2−53449
naphthalene, Raman spectra, exciton splittings and normal modes, heavily doped isotopic mixed crystal method 2−57362
naphthalene, spherical single cryst., polarization luminesc. rel. to impurity molecule orientation 2−75328
naphthalene, triplet exciton diffusion 2−48252
naphthalene compressed pellets, electrical conductivity, 1 kc/s to 100 Mc/s range 2−61415
naphthalene crystals, trap density calc. using space charge limited theory 2−84325
naphthalene crystals, X-ray irradiated, annealing, behaviour of colour centre and e.s.r. spectrum 2−80711
naphthalene crysts., exciton states 2−84228
naphthalene crysts., surface energy, cleavage method 2−80543
naphthalene disc rotating in uniform forced stream, laminar mass transfer 2−73465
naphthalene in 1,4-dibromobenzene, PMDR obs., heavy atom perturbation effects 2−67519
naphthalene in stretched PVA sheets, polarized absorpt. spectra, electronic transitions 2−83276
naphthalene ion in low bulk dielec. const. media, e.s.r. linewidth, conc. depend. 2−67841
naphthalene isotopic mixed crystals, Raman phonon spectra, exciton model and amalgamation limit 2−57363
naphthalene on metal-substituted type-X zeolites, luminesc. and adsorption characts. 2−80585
naphthalene Rydberg spectrum, analysis of antiresonances 2−70783
naphthalene thermoelectrets, X-ray diffraction structural studies 2−65075
naphthalene vapour, electron energy-loss spectroscopy 2−80131
naphthalene vapour, vacuum u.v. absorption spectrum, Rydberg series assigned 2−80064
naphthalene with indol impurity, spectra of local excitons 2−54466
naphthalene-d_8, heavy-atom effect on phosphorescence characts. 2−84678
naphthalene-d_8 phosphorescence, comparison of matrix emission spectra with frozen solution spectra in cyclohexene hosts 2−72428
α-naphthol in pure and mixed crysts., electronic singlet-singlet absorpt. spectra 2−65395
1-naphthol velocity profile in turbulent pipe flow 2−53350
α-naphthoquinone, near. u.v. and visible absorpt. spectra and electronic struct. 2−70784
naphthoquinone diazide resists photodecomposition 2−61802
α-naphthylamine compressed pellets, electrical conductivity, 1 kc/s to 100 Mc/s range 2−61415
1,5-naphthyridine, optical detection of e.s.r. in the triplet state 2−57394
napthalene, radiation induced fluorescence in cyclohexane solution 2−53446
natural gas, welding torch flame, temp. distrib. 2−69484
natural-gas-O_2 flames, impingement heat transfer rates 2−52288
nematic liquid crystal, instabilities under a.c. fields, special effects near cut-off freq. 2−56478
nematic-smectic C phase transition, periodic free surface disclination obs. 2−60432
nematogenic azobenzene derivatives, anomalous melting behaviour at solid-nematic transition 2−56483
neopentane, molecular structure determ. by gas phase electron diffraction 2−70796
neopentane, phase transitions, cold neutron examination 2−50928
neopentane, plastic crysts., mol. rot. motion 2−53513
neopentane derivatives, substituent effects on $^4J_{hh}$, positional dependence 2−77107
neopentane metastable ions, determ. of lifetimes by field ionization mass spectromety 2−46789
neopentane-d_{12}-alkane mixtures, gas phase pulse radiolysis 2−68820
nickel (II) oxalate complexes, structure resolution on basis of infrared and magnetic susceptibility meas. 2−61659
nickel acetate tetrahydrate, sp. ht., 0.43-10.73 K 2−78040
nickel sodium triacetylacetonate- dioxane-benzene, paramagnetic cross-relaxation study 2−65122
nicotinamide, its cations and related compounds, ^{13}C chemical shifts determ. for n.m.r. investigation 2−83309
nitrile group, MMO LCAO investigation of conjugated nitrile structure influence on i.r. absorption band intensity 2−50104
nitro-compounds, liquids, ultrasonic velocity 2−53428
nitroalkane-benzene solns., total intensity Rayleigh scatt. and depolarization at 546 nm and 30°C 2−64444
m-nitroaniline, crystal structure rel. to linear electro-optic props. 2−72271
p-nitroaniline single crystals, near i.r. study of hydrogen bonding 2−78110
nitrobenzene, and $-d_5$, electronic structure determ. using photoelectron spectroscopy 2−56251
nitrobenzene, chemical aspects of shock initiation 2−83724
nitrobenzene, chemisorption on Ge, effect on surface recomb. 2−71938
nitrobenzene, electron impact excitation spectra by ion cyclotron resonance mass spectrometer 2−80135
nitrobenzene, Kerr effect, meas. of absolute phase delay using polarization interferometer 2−42197
nitrobenzene, negative ion spectra, electron energy and press. range 2−84680
nitrobenzene, spin-spin couplings from ^{15}N to ring protons 2−77137
nitrobenzene, u.s. velocity, det. of molecular parameters 2−53429
nitrobenzene and n-hexane liquid system, nonlocal shear viscosity and mode-mode coupling near consolute point 2−64445
nitrobenzene-hexane, solution, reflection coeff. rel. to surface layer thickness meas. 2−60474
nitrobenzene-n-hexane, crit. mixture, light scatt. intensity and correlation length 2−80473

Organic compounds continued
nitrobenzene-n-hexane binary mixture near critical point, dispersion of u.s. waves 2−71196
nitrobenzene-n-hexane critical mixtures, Brillouin scattering investigation by interferometric technique 2−46965
nitrobenzene-n-hexane opalescent mixture, r.f. cond. 2−71230
p-nitrobenzoic acid, n.m.r. at liquid nitrogen and room temps., i.r. spectra 2−78167
nitrocellulose, solid state self focusing optical waveguide 2−63412
nitrocyclopropane, microwave spectrum 2−70786
nitroethylene, negative ion formation, mass spectrometric study 2−57432
nitrogen compounds, ^{14}N n.m.r. linewidths in liquid phase 2−56523
nitromethane, and $-d_3$, electronic structure determ. using photoelectron spectroscopy 2−56251
nitromethane, chemical aspects of shock initiation 2−83724
nitromethane, divergent cylindrical detonation 2−83722
nitromethane, effect of confinement on detonation 2−80422
nitromethane, electron impact excitation spectra by ion cyclotron resonance mass spectrometer 2−80135
nitromethane, normal vibrations, additive interatomic interaction model calculations 2−77044
1-nitronaphthalene, electronic spectra and intramolec. energy transfer 2−46619
nitrosomethane, SCF-LCAO-MO calculations of barrier to internal rotation 2−70786
nitroxide radical solns. electron-electron double resonance, relation to spin relaxation 2−71234
nitroxide radicals, photoelectron spectra and mol. orbital calcs. 2−80073
nitroxide radicals, quadrupole splitting obs. by ENDOR in liquid crystals 2−50103
non-electrolytes, binary solutions, viscosity measurements 2−46940
2-4-nonadienic acid, nematic liq. cryst., mol. theory, stability, thermodynamic conditions 2−46930
n-nonane:coronene, fluoresc., 77K, complex struct. of doublets 2−78145
nonpolar liquids, electron dynamics 2−81531
nonpolar solvents, meas. of i.r. absorption spectra in water solutions 2−46932
norbornadiene, electronic struct., LCGO minimal basis calc. and ESCA obs. 2−70785
norbornadiene, norbornylene and norbornane, plastic crysts., struct. 2−43601
31-norcycloartonal, liq. cryst., prep. from a triterpene 2−46936
nucleotides, spectrophotometry of very small volumes using TLC method 2−75410
octamethylcyclotetrasiloxane, spin-lattice relaxation and Overhauser effect, ^{29}Si Fourier transform n.m.r. studies 2−65355
n-octane, isobaric heat capacity along boundary curve 2−64458
oil deformation of velocity profile in turbulent boundary layer 2−74492
oils, viscosity index, repeatability and reproducibility 2−60448
olefines, trisubstituted, regiospecific and stereoselective isomerization 2−77105
olefins, activation energies for addition of O(^{3}P) 2−84621
olefins, chem. reactions with O atoms, product obs. 2−68763
organoluminor solution, obs. of stimulated emission by exciplexes 2−67836
organomercury compounds, heteronuclear double magnetic resonance studies of ^{199}Hg nuclear shielding consts. 2−57403
organometallic, $Ir(CO_3)Br$, thermoelec. analysis of elec. cond. 2−72055
organometallic, $K_2Pt(CN)_4Cl_{0.3}.xH_2O$, thermoelec. analysis of elec. cond. 2−72055
organometallic, use for incorporating metals into resins for composites 2−50923
organophosphorus esters, n.m.r. spectra, peak doubling, H bonding 2−70788
organosilicon film, r.f. plasma polymerization 2−43484
organotin isocyanate, integrated intensity of valence vibrations 2−74290
orthooxyazomethynes molecules, luminescence and radiationless transitions 2−53047
orthophenylene diamine dihydrochloride, structure study by X-rays 2−71449
ovalene in condensed media at room and liquid N temp. obs. of two-level emission as function of pressure 2−50105
oxacarbocyanine, excimer and related emission at low temp. 2−66861
1,3,4-oxadiazoles, isotopic species, microwave spectra, structure, ^{14}N quadrupole coupling and rotational consts. 2−43003
oxalic acid, crystal growth, habit rel. to solution supersaturation 2−74685
oxalic acid, electronic state investigation using phosphorescence meas. 2−50106
oxalic acid, electronic states from absorption spectra 2−42980
oxalic acid derivatives, vibrational spectra 2−67503
oxamides and thio-oxamides, hydrogen bonding obs. 2−56252
3- oxetanone, microwave spectrum and ring-bending vibr. 2−70787
2(2′-oxyphenyl)-benztriazole derivatives, electronic absorpt. spectra analysis 2−83334
oxypyrrol radical, ELDOR spectra, obs. of multiple quantum transitions 2−73489
p-chloranil, hot carrier injection rel. to field depend. of photocurrents 2−75189
p-methoxybenzylidene-p′-amino phenyl acetate, nematic, dynamic scatt. life, current density effects 2−71203
palladium benzoylacetonate, VO^{2+} doped, e.p.r., ^{51}V quadrupole moment obs. 2−61741
paradichlorobenzene, optically detected e.s.r. and ENDOR spectra of excited triplet states 2−46518
paraffin crysts., spectra, temp. broadening and shift of phonon-free lines 2−61613
paraffin film, i.r. holograms using pulsed high power lasers 2−55713
paraffin hydrocarbons, absorption spectrum in vacuum u.v., comparison with photoelectron and electron loss spectra 2−43004
n-paraffin-aromatic hydrocarbon system, radiative and non-radiative processes 2−61719

Organic compounds continued
in paraffins, broadening and shift of non-phonic lines in spectra in lower Debye temp. range 2−72296
paraffins, liq., two-phonon absorpt. processes 2−74550
paraterphenyl laser, laser-pumped, u.v. output characts. 2−52426
Pasadena smog, carbon content 2−51603
pentaborane (9), effects of thermal decoupling on high-resolution ^{11}B n.m.r. spectrum 2−83801
pentachloronitrobenzene, molecular packing, partial structure determination 2−53684
pentaerythritol, high temp. phase, u.s. velocity 2−57049
pentaerythritol, molecular crystal, thermal expansion, X-ray obs. 2−74995
pentafluorobenzoylchloride, vibrational spectra 2−74285
pentafluorostyrene in liquid phase, vibrational assignments from infrared and Raman spectra 2−50107
pentafluorothiophenol, Raman and i.r. spectra, vibrational assignments assuming C_{2v} symmetry 2−60078
n-pentane, isobaric heat capacity along boundary curve 2−64458
n-pentane, magnetic quenching of positronium 2−53384
n-pentane-cyclopentane binary solution, height and temperature variations in scattering power near critical point of vaporization 2−43373
2,3-pentanedione, photolysis, fluorescence and phosphorescence yields 2−54560
2,3-pentanedione, photolysis emission and deactivation of excited states 2−54561
pentanol, meas. of isothermal piezo-optic coeff. 2−50364
trans 3-penten-1-yne, barrier to internal rotation and dipole moment, determination from microwave spectrum 2−50108
1-penten-3-yne, long-range spin-spin coupling consts. 2−67511
perchloroethylene, u.s. transmission intensity variation with time at 22 kHz at atmos. and excess pressure 2−52232
perdeuterobenzene, liquid and solid, quasi-elastic scattering of cold neutrons, obs. of broadening 2−80451
perfluorocyclohexane, i.r. and Raman spectra 2−46620
perfluorocyclohexane plastic crystal, self- diffusion study by n.m.r. 2−50702
perfluoropropane, dissociative electron capture 2−60079
perfluoropropylene, dissociative electron capture 2−60079
perylene, electron transfer to $[Fe(CN)_6]^{3-}$ and O_2 in aq. soln. 2−61805
perylene radical cation in H_2SO_4 or HSO_3F, solvation shell relaxation and ion-electron recombination 2−46934
phenanthrene, dielectric tensor components derived from energy loss spectra 2−81138
phenanthrene, energy of free electron conduction band, flash photoconducwivity determination 2−44177
phenanthrene, excited dimer luminescence of pairs of molecules 2−56253
phenanthrene, photoelectron spectra and ionization potentials 2−60048
phenanthrene, polarized absorpt. edge and exciton-photon interaction 2−44386
phenanthrene, two-photon absorption, blue fluorescence as function of incident laser energy 2−44410
phenanthrene-naphthacene thin layer, u.v excited sensitized luminesc. 2−48251
phenanthrenequinone, near-u.v. and visible absorpt. spectra and electronic struct. 2−70784
phenanthrenes, aryl substituted, triplet-triplet absorpt. analysis 2−65396
phenazine, in rigid toluene glass matrix, spin polarization in photoexcitation of triplet state 2−68816
phenazine, vibrational assignment of i.r. and Raman spectra 2−46622
phenol, investigation of molecular inversion 2−50109
phenol formaldehyde resin, thermal degraded, a.c. and d.c. cond. 2−47903
phenol in solution, ^{13}C spin-lattice relaxation and intermolecular interactions 2−80482
phenol-triethylamine complexes, H-bond polarity, effect of permittivity of medium 2−46621
phenolic nitrated polynuclear compounds and oligo nuclear compounds u.v. spectra comparison 2−83320
phenothiazines, MO calculations of conformational properties 2−60082
phenoxyacetic acid derivatives, high-resolution n.m.r. 2−53076
α- phenyl o- cresol, crystn., growth rate vs. temp. 2−50606
phenyl derivatives, monosubstituted, application of Gordy's Rule 2−60081
phenyl radical, photoionization, determ. of heat formation and ionization potential 2−67520
N-phenyl-α-naphthylamin in n-heptane-n-butanol mixtures, spectra and local effective dielectric constant 2−56149
N-phenyl-β-naphthylamin in n-heptane-n-butanol mixtures, spectra and local effective dielectric constant 2−56149
phenylacetylene systems, effect of H bonding on i.r. spectra 2−74280
2-phenylbutane, conformational structure, i.r. and n.m.r. spectra 2−42953
phenylcyclopropanes and phenylethanes, emission spectra, 77K 2−84663
α-phenylethylamine, circular dichroism obs. in Raman spectra 2−64191
3-phenylpentane, conformational structure, i.r. and n.m.r. spectra 2−42953
phenylsilane, electronic-vibrational absorption spectra 2−50111
phenylsilane, i.r. and Raman spectra, normal vibrations and free rotation 2−46623
phosgene, high resolution photoelectron spectra 2−43006
phosphabenzene, microwave spectrum, dipole moment and l.f. vibr. states 2−56254
phospholipid-water mixtures, i.r. and Raman spectra 2−43374
phosphonium ylide, ab initio LCAO-MO-SCF study of bonding 2−56240
phthalaldehyde, polarizations of low energy $S_n \leftarrow S_0$ transitions 2−60080
phthalazine, nematic phase, n.m.r. spectra 2−50324
phthalic acid, methylsubstituted, u.v. spectra, obs. of bathochromic shift of short wave bands 2−83330

Organic compounds continued
phthalimide derivatives, luminescence, selective light quenching 2−53074
phthalimide derivatives, two-photon excitation fluoresc. polarization 2−60039
phthalimide derivatives, vapour phase, of fluorescence on frequency of emitted light 2−53073
phthalimide solution, double-band generation, fluorescence spectra 2−43377
phthalimides and other dyes, bathochromic luminescence in alcoholic solutions and polymer matrices 2−77440
phthalocyanine and derivatives, fluoresc. and photocond. 2−72426
phthalocyanine solns., absorpt. from excited singlet states 2−84677
pi hydrocarbon radicals, ^{1}H and ^{13}C hyperfine splitting, unrestricted Hartree-Fock calc. 2−67453
picene, triplet-triplet absorption spectrum 3750 to 15800 Å region 2−83281
piperylenes, mag. field effects on photosensitized reactions 2−65397
pivalic acid, plastic, Brillouin spectra, mol. symmetry effects 2−57366
pivalic acid, plastic crystalline phase, Rayleigh and Brillouin scattering 2−44399
polar liquids, far-i.r. and microwave absorpt., theory 2−77434
polar substances in n-pentane, solid soln. struct., dielec. meas. 2−72016
poly-γ-benzyl-L-glutamate solns., i.r. elec. dichroism 2−60083
poly-γ-methyl-L-glutamate in soln., spin-lattice relaxation time meas. 2−66672
poly-N-vinylcarbazole complexed with trinitrofluorenone film, bulk recomb. of charge carriers 2−72073
poly-N-vinylcarbazole films, doped, spectral response and sensitometric curves, positive and negative modes 2−66884
polyacrylamide aqueous soln., pulsation velocity in turbulent boundary layers 2−74491
polyaminopolyalkylphosphonic acids as effective ligands for binding and eliminating U and fission products from body 2−55258
polyene chains doubly substituted, wavefunctions of local states 2−77129
polyethylene, deuterated, prod. of CD_2 plasma by irrad. with plasma 2−80269
polyethylene, lattice vibration dispersion curves 2−71718
polyethylene doped with I, h.f. Gunn domains 2−57202
polyethylene terephthalate, electret, characterization 2−65076
polyisobutylene in decaline, flow in concentric cylinders, rheo-optical analysis 2−56457
polymethine cyanide dye, saturable props. rel. to variable ultrafast photographic shutter 2−49405
polymethine cyanine dyes, bleaching kinetics 2−42039
polymethyl siloxanes, velocity of ultrasound, as function of temperature and pressure 2−71193
polymethylene dyes resonant stimulated combination dispersion of laser pulses 2−49377
polymethylmethacrylate, Monte Carlo simulation of energy dissipation of electron beam 2−62826
polynuclear hydrocarbons, quenching of triplet excited states by O_2, possible effects of magnetic fields 2−50124
polyphenyl derivatives, i.r. and Raman spectra, vibr. assignment 2−56255
polytetrafluoroethylene, irradiated and sintered, mol. chain entanglement, n.m.r. obs. 2−65352
porphyrins, luminescence, influence of nitromolecular spin-orbital perturbations 2−53077
positron annihilation, appl. to struct. and props. determ. 2−47771
potassium biphthalate, lattice consts. and space group 2−47357
potassium carbamate, solid, i.r. spectra 2−84527
potassium hydrogen di-trifluoracetate, deuteron quadrupole coupling const. 2−72528
potassium oxalates cryst. growth from aq. soln. 2−60714
PPA nematic liquid crystals, order characterization 2−83777
praseodymium tartrate complexes, i.r. circular dichroism 2−67521
primary alcohols, excess u.s. absorption, evaluated from relaxation time and relaxing compressibility 2−74541
propane, combustion, heat release in multistage reaction 2−58146
propane, conform. depend. of vicinal $^{13}C-H$ spin-spin coupling const., INDO MO calcs. 2−77151
propane, potential functions calc. in terms of group valence force symmetry coordinates 2−42847
propane, thermal energy charge transfer reactions with rare gas ions 2−83399
propane $+ 5O_2 + 10N_2$ mixtures, shock and detonation speeds 2−83647
propane adsorption onto (100) face of W crystal 2−74642
propane derivatives, substituent effects on $^{4}J_{MM}$, positional dependence 2−77107
propane flame, cold, math. model 2−61781
propane-air mixture, turbulent flow, burning stability 2−67702
propane-oxygen-nitrogen mixtures, divergent spherical detonation propag. speed 2−52258
propanol, meas. of isothermal piezo-optic coeff. 2−50364
n-propanol is cascade electro-osmotic cell 2−66678
propanol-water mixtures, binary film condensation, effects of forced flow and variable properties 2−77411
β-propiolactone, structure investigation, p.m.r. spectrum in thermotropic nematic solvents 2−50110
propiolic acid, microwave spectrum, conform. and dipole moment 2−56256
propionitrile-chloroform mixtures, complex forms, solid phase, i.r. absorpt. obs. 2−60042
propylamine, deuterated, Raman spectra analysed w.r.t. amino group vibrations 2−46610
propylamine, effect of deuterium substitution on vapour pressure 2−43450
n-, iso-propylamine n.q.r meas. at liquid nitrogen temps., ionic character of N-H, N-C bonds 2−83310
propylene, addition of $O(^3P)$ atoms by flash photolysis, absolute rate constants 2−44492
propynal, laser-excited fluorescence, collision-induced radiationless transitions 2−83298

Organic compounds continued
purine aqueous solutions, i.r. spectra study of formation of strong polarizable H bonds with increasing protonation 2−50112
pyrazine, absorption spectrum in region of $n\pi^*$ transition, evidence for second electronic state 2−46624
pyrazine, optically detected e.s.r. spectra in triplet $n\pi^*$ state 2−46518
pyrazine, polarized single-crystal absorption spectra 2−78111
pyrazine, vibronic coupling and Raman intensities 2−80066
pyrazine electronic transition, mechanisms of vibronic intensity borrowing 2−70659
pyrazine vapour, pressure dependence of fluorescence and phosphorescence, obs. of long fluorescence lifetime 2−50113
pyrazine-d$_4$, spin-lattice relaxation and Zeeman effects in triplet state 2−60084
pyrazine-h$_4$, -d$_4$, in benzene, fluorescence and phosphorescence spectra at 4.2 K 2−77121
pyrene, ^{13}C-H satellite n.m.r. spectrum, calc. of coupling constants 2−46627
pyrene, character of nonlinear luminescence quenching in temperature range 77-373 K 2−54442
pyrene, Davydov splitting of first triplet state 2−61660
pyrene, photoelectret effect 2−81131
pyrene, radiation induced fluorescence in cyclohexane and benzene solutions, excited states, effect of singlet state quenchers 2−53448
pyrene, radiation induced fluorescence in cyclohexane and bezene solutions, yields of excited singlet and triplet states 2−53447
pyrene, radiation induced fluorescence in cyclohexane solution 2−53446
pyrene, temp. depend. of nonlinear luminesc. quenching 2−44409
pyrene crystal, calc. of Davydov splitting 2−51352
pyrene electronic transition, mechanisms of vibronic intensity borrowing 2−70659
pyrene meas. of diffusion const. in triplet state in glycerol from -17°C to +15°C 2−68804
pyrene solutions, fluorescence quenching under intense excitation 2−54471
pyrene solutions, fluorescence under pulsed excitation 2−60483
pyrene unsymmetrical excimer in cyclohexane solution 2−46604
pyrene-d-10, temperature dependent saturation meas. in photo-excited triplet state 2−84567
pyrene-perylene energy transfer, pressure dependence 2−60109
Pyrene-Pyrene system, dispersion forces calculation 2−60113
pyridazine vapour, single vibronic level fluoresc., excited states 2−80078
pyridine, 1s binding energy for N atom 2−77156
pyridine, 2,4,6 tri-substituted, shift in lowest π-electron singlet excited state 2−70748
pyridine, deuterated, meas. of quadrupole coupling const. and asymmetry parameter of ring deuterons 2−80082
pyridine, free electron model 2−83304
pyridine, in organic and inorganic solvents, complex formation, i.r. spectra, mol. vibr. 2−46626
pyridine, its cations and related compounds, ^{13}C chemical shifts determ. from n.m.r. investigation 2−83309
pyridine, molecular g-values from Zeeman effect 2−70739
pyridine, nonpolar vibrations, standard intensities and degrees of polarization of line widths 2−77152
pyridine, normal magneto-optical rot. dispersions, mag. moments 2−70770
pyridine, quasiplanarity in first excited singlet state, demonstration by investigation of 2875 Å band system 2−46625
pyridine, self-diffusion coeffs., freezing to boiling point, rotational correlation times 2−56472
pyridine, Stark effect on ^{14}N n.q.r. 2−44463
pyridine solutions, stimulated Raman spectra, effect of intermolecular interaction 2−60477
pyridine-borane, ^{2}H n.m.r., quadrupole coupling constants 2−44461
pyridines, monosubstituted, chemical shift in ^{14}N n.m.r. 2−56257
pyridines, substituted, electronic structs. of lowest excited triplet states, e.p.r. obs. 2−60050
pyridinium salt, fused, specific cond. and n.m.r. spectra 2−72018
pyridinium-pyridine system, H-bonded, extended Huckel calculation 2−70789
pyrimidine crystals, absorption and emission spectra at 4.2K 2−44412
pyrimidine nucleosides, electronic spectra from circular dichroism data 2−74299
pyrrole, 1s binding energy calc. for C and N atoms using perturbational model 2−77156
pyrrole-pyridine system, valence electron density distrib., extended Huckel calc. 2−43007
pyrroles, liq., vibr. spectra 2−83306
pyrrone moulding, dynamic modulus determ. from stress relax. data 2−43667
quinoline, in organic and inorganic solvents, complex formation, i.r. spectra, mol. vibr. 2−46626
quinoline, photoelectron spectra, perfluoro effect 2−70790
quinoline in durene mixed crystal, triplet-triplet absorption at 2K, obs. 2−50114
quinoline molecular liquid, Rayleigh scattering, influence of temperature on collisional wing 2−80471
quinolinium (TCNQ)$_2^-$, electron localization 2−44110
rare earth ethyl sulphate: Gd^{3+}, e.s.r. obs. at room temp. and 77K 2−75349
rare earth ethyl sulphates, paramag. relax., interactions contrib. to sp. ht. 2−57314
reserpine, fluoresc. detection reaction, sensitivity increase by Th ion addition 2−71215
resin-ZnO electrophotographic coating for positive charging 2−63452
11-cis-retinal, p.m.r. calculation in relation to molec. conformation 2−77153
rhodamin B molecules in cadmium arachidate multilayers in thin capacitors, electrochromic spectra 2−68802
rhodamine 6G, increased resistance to photodegradation in cooled solid matrices 2−57430
rhodamine 6G, triplet state, absorpt. spectra obs. 2−46628
rhodamine 6G, two-photon fluorescence patterns, absorption cross sections and picosecond relaxation times 2−43379

Organic compounds continued
rhodamine 6G amorphous film, carrier trapping, thermostimulated cond. study 2−54180
rhodamine 6G and B, and cresyl violet, picosecond dye laser pulses, frequency tunable 2−42045
rhodamine 6G and B, two-photon absorption cross sections using psec laser pulses 2−61808
rhodamine 6G CW dye laser, passive mode locking, stable output, 5900-6100Å 2−79189
Rhodamine 6G dye laser, efficiency, pump parameter and triplet lifetime depend., calcs. 2−69927
rhodamine 6G dye laser, flashlamp pumped, second harmonic and sum frequency generation 2−73577
rhodamine 6G dye laser, transistory absorption meas. and stimulated emission 2−42044
Rhodamine 6G excited mols., luminesc. and absorpt. 2−60484
rhodamine 6G fluorescent dye laser, principle and design 2−59165
rhodamine 6G laser, coaxial 11 MW, 6.8J flashlamp pumped, performance 2−82476
rhodamine 6G laser, pumped by pinched discharge, energy characteristics 2−42046
rhodamine 6G laser emission field characteristics, thermo-optical distortion 2−52424
Rhodamine 6G monomers and associates, intramol. degradation processes of electron excitation energy 2−60485
rhodamine 6J, intermediate products of pulse photolysis 2−75391
rhodamine 6J in liquid laser, energy parameters of generation, effect of excitation 2−42034
rhodamine 6J laser, dynamic compensation of thermo- optical distortion 2−73579
rhodamine 6J lasers, excitation by pulsed lamps of different types 2−69930
rhodamine 6J lasing, effect of transverse pumping distribution, on thermal-optical distortion 2−49376
rhodamine B, 6G, vib. relaxation from optically excited state, new technique 2−83401
rhodamine B, in aqueous soln., absorb. and fluoresc. excitation spectra 2−64465
rhodamine B, xanthene dye vapours, optical and discharge excitation 2−42042
rhodamine B and cresyl violet pulsed dye laser, spectral properties 2−42041
rhodamine B doped polyurethane film ring laser, light amplification and coupling 2−42055
rhodamine B solution in methanol, anti-Stokes fluorescence in organic dye solutions 2−43378
rhodamine B-rhodamine 6J mixed solution, laser generation characteristics 2−52425
rhodamine laser, use of organic dye light converters 2−69929
rhodamine solutions, fluorescence quenching by anthracene compounds 2−43380
rhodamine solutions, u.v. absorption spectra in 220 to 400 nm region 2−64466
ring mols., inflexible levels existence 2−77103
rubidium trihydroselenite, struct. detn. using diffraction data 2−71450
rubin, electron irrad., phosphoresc. 2−72429
s-triazine isotopic mixed crystal, variable trap problem 2−75043
salicyl aldehyde, structure of H bond from microwave spectra 2−43008
salicylideneaniline, coherent optical props. as hologram recording medium 2−82530
samarium ethylsulphate, e.p.r. of Gd^{3+} in single crystals below 40G 2−51405
saturated molecules, Fourier component analysis of internal rotation potential functions 2−56208
Schiff base, liquid crystalline behaviour rel. to molecular struct. 2−60428
scintillators, frequencies of molecular electronic transitions, for u.v. lasers 2−76484
second harmonic generation efficiencies, Nd laser irrad. 2−57319
second harmonic generation of ruby laser radiation by organic crystals 2−68592
selenacarbocyanine, excimer and related emission at low temp. 2−66861
selenourea-^{75}Se, preparation 2−54527
1.4-selenoxan i.r. spectra in vapour, liquid and crystal states, Raman spectra of liquid and solid 2−83315
semibullvalene, tricyclo[3,3,0,0^{2,8}]octa- 3,6-diene, structure determ. in gas phase 2−77154
semiconductor, amorphous, elec. cond., press. depend., random field model 2−44108
silane, thermal energy charge transfer reactions with rare gas ions 2−83399
silane-methane mixtures, determ. of relative and absolute rate constants for ion-molecule reaction 2−68777
silicate with complex cation, 4[Cu(NH$_2$CH$_2$CH$_2$NH$_2$)$_2$)$_2$]. Si$_8$O$_{20}$. 38H$_2$O, 3-D Patterson synthesis 2−74753
silicone liquids thermal breakdown under pulsed h.f. fields 2−56513
silicone resin hardening by electron beams and electron beam resists for microimaging 2−59297
silver trifluoroacetate, ^{19}F shielding tensors of trifluoromethyl group 2−68751
silyl isocyanate, determ. of molecular dimensions and large amplitude vibration by electron diffraction 2−80080
sodium ammonium tartrate, ferroelec. phase transition mechanism 2−81139
sodium carbamate, solid, i.r. spectra 2−84527
sodium citrate pentahydrate, i.r. spectra, 700 to 4000 cm^{-1} 2−72356
sodium methanesulphonate meas. of Raman and i.r. spectra, correlation with crystal structure 2−72375
sodium methylammonium tungstovanadate, VO^{2+} doped, e.p.r., ^{51}V quadrupole moment obs. 2−61741
sodium *n*-butyrate and isovalerate mesophases, struct. behaviour 2−71158
sodium oxalate, monohydrate, crystal struct. by method of rhombs 2−74755
sodium salicylate fluorescent thin films for α particle detection 2−73939

Organic compounds continued
sodium tartrate, triboluminesc. intensity obs. rel. to elastic const. detn. 2−51396
solid, d.c. cond. mechanism 2−47904
solid, density of states in bandgap 2−47916
spin labelled fatty acids in oriented lecithin bilayers, moment analysis of e.p.r. spectra 2−80063
spiropentane, energy nonrandomized decomposition initiated by recoil T substitution reactions 2−81533
spiropentane, molecular structure determ. by gas phase electron diffraction 2−70796
spiropyrans, 2 photon excitation of molecule under laser radiation 2−78208
squalane, spin-lattice relaxation rates meas., cf. with viscoelastic relaxation 2−46987
squalane containing biphenyl, variation of thermoluminescence with concentration 2−46969
squalene spin-lattice relaxation rates meas., cf. with viscoelastic relaxation 2−46987
stearic acid films, high-field transient behaviour of dielec. props. 2−77950
stearic acid insoluble monolayer leakage across movable barriers, radiotracer detection method 2−53416
stearic acid monolayers on water, surface diffusion 2−71179
stilbene, elec. cond. in weak and strong elec. fields 2−77901
trans-stilbene, electronic absorp. spectra calc. 2−56259
cis-stilbene, electronic absorp. spectra calc. 2−56259
stilbene, fluorescence, effect on neutron induced crystal defects 2−44411
trans-stilbene, steric conformational analysis 2−56258
trans-stilbene, triplet exciton diffusion 2−48252
stilbenes, mag. field effects on photosensitized reactions 2−65397
stimulated Raman parameters for different types of substances, exptl. and theoretical substances 2−42944
strontium formate, i.r. and Raman spectra 2−61661
strontium formate and strontium formate dihydrate, phase matchable optical nonlinearity 2−48124
substrate role in det. crystallinity of organic thin films 2−77533
succinic acid, ESR studies on radical conversions 2−81528
succinyl chloride, meas. of Raman spectrum in solid and liquid states, determ. of rotational isomerism 2−53079
sucrose aqueous soln., freezing using temp. gradient microscope stage 2−74585
sugar, triboluminesc. intensity obs. rel. to elastic const. detn. 2−51396
sugarcane wax electrets, heterocharge mechanism 2−75157
sulphalane, doublet struct. of $\nu_{as}(SO_2)$ band 2−83331
sulphur diimide, through space coupling 2−64192
sulphuryl molecules, photoelectron spectra 2−64156
sultones and sultines, dipole moments and conformation 2−43009
sydnone, Pariser-Parr-Pople calcs. of electronic structure 2−77128
sydnoneimine (cation) Pariser-Parr-Pople calcs. of electronic structure 2−77128
symmetric hydrogen bonded complexes, proton pot. rel. to splitting of internal modes 2−70734
tartaric acid, triboluminesc. intensity obs. rel. to elastic const. detn. 2−51396
tartaric acid in ethanol, etchant for alums 2−74662
TCNQ complex, elec. cond., thermally assisted hopping mechanism 2−68409
TCNQ complexes, hopping cond. 2−44109
TCNQ complexes, quasi-one-dimensional disordered systems, Mott transition, susceptibility obs. 2−84238
TCNQ complexes, with quinolinium and triethylammonium, i.r. spectra, vibronic effects 2−81387
TCNQ cpds., low temp. sp. ht., ionic binding contrib. 2−54052
TCNQ ditoluolchromium complex, electronic states localised characts., n.m.r. 2−72529
TCNQ quaternary ammonium salts, paramag. 2−84399
TCNQ salts, e.s.r. dipolar split line obs. of excitons 2−61742
TCNQ salts, role of disorder rel. to electronic props. 2−64920
TCQN complexes, elec. and mag. props., review 2−61140
p-terphenyl, rigid mol., librational motion temp. factor 2−54025
tetra-acetylethane, crystal structure determ. by neutron diffraction 2−43602
1,2,4,5-tetrabromobenzene, o.d.m.r. and p.m.d.r. studies of $^3\pi\pi^*$ state 2−60086
1, 2, 4, 5-tetrabromobenzene, phosphorescent triplet state props., ODMR and PMDR obs. 2−56260
tetracene, carrier drift mobility meas. 2−47905
tetracene, e.p.r. of triplet excitons, spin polarization and singlet exciton fission role 2−81448
tetracene, e.p.r. of triplet excitons, spin polarization and singlet exciton fission role 2−81449
tetracene, photovolt. current, anomalous temp. depend. 2−72075
tetracene crystals, temp. depend. of charge carrier mobility 2−81075
tetracene crysts., fluoresc., exponential decay time, singlet fission 2−54472
tetracene films, investigation high and low conductivity stable states and switching 2−54181
tetracene in soln., auto-associated species identification 2−81520
1,2,4,5-tetrachlorobenzene, o.d.m.r. and p.m.d.r. studies of $^3\pi\pi^*$ state 2−60086
tetrachlorobenzene in durene, hole burning in optically detected zero-field spectrum using EEDOR 2−84561
1,2,4,5-tetrachlorobenzene in durene, zero-field parameter signs from MODR spectra 2−65398
tetracyano-polymethine anions, far i.r. and laser Raman spectra 2−53081
s-tetracyanobenzene complexes, electronic spectra in phosphorescent state 2−72578
s-tetracyanobenzene complexes formation of phosphorescent state from excited Franck-Condon state 2−72577
1,2,4,5-tetracyanobenzene- durene complex, fluorescence quenching due to exciton-exciton interaction, determ. of rate const. and exciton migration rate 2−81426
s- tetracyanobenzene-benzene complex, ionic dissociation from excited Franck-Condon state 2−72579
tetracyanoethylene, negative-ion form. by electron bombardment 2−67687

Organic compounds continued
tetracyanoquinodimethane and its mono- and di-valent anion, u.v. spectra, comparison with SCMO CI calcs. 2−70791
tetraethoxysilane, dielectric film growth by low temperature oxidation 2−60636
1,1,2,2-tetrafluorocyclopane-d_0, d_1 and d_2, i.r. and Raman spectra, vibrational assignments 2−46629
tetrafluoroethylene oxide i.r. spectrum and vibrational assignments 2−46630
tetramethyl-para-phenylene-diamine in solution, photoionization, role of energy of excess electron state 2−74557
tetramethylammonium cadmium chloride crystal structure using X-ray analysis 2−56651
tetramethylammonium decaborate-d_{10}, ^{2}H n.m.r., quadrupole coupling constants 2−44461
tetramethylammonium manganese chloride, low-temp. transitions 2−72530
tetramethylammonium manganese chloride, susceptibility in fields of 250Oe, 10kOe and 50kOe 2−72227
tetramethylcyclobutane-1,3-dione, vibrational spectra 2−77155
tetramethylenecyclobutane-d_0 (-d_8), meas. of Raman and i.r. spectra, symmetry assignments 2−70792
tetramethylgermane, directly banded coupling constant between ^{73}Ge and ^{13}C 2−46522
5,5,11,11-tetramethylhexadecane, spin-lattice relaxation rates meas., cf. with viscoelastic relaxation 2−46987
tetramethylpyrazine, polarized single-crystal absorption spectra 2−78111
β-tetramethylsilane, 77−174K, p spin-lattice relaxation 77−174K 2−75242
tetramethylsiloxane, spin-lattice relaxation and Overhauser effect, ^{29}Si Fourier transform n.m.r. studies 2−65355
tetramethylurea, ^{14}N, NQR freqs., coupling consts., var. with temp. 2−83297
5,12,6,11-tetraoxytetracene crystals, photoconductivity 2−48001
tetraphenyl hydrazine reaction with benzoyl peroxide, reaction rate consts., chemilum. 2−78191
tetraphenyl tin and isomorphs, defect struct. determ. 2−53731
tetraphenylbutadene liquid and solid solutions, dependence of threshold of luminescence generation on pumping polarization 2−53450
tetrapyrole, intramolecular transitions and energy, influence of structural factors 2−53078
s tetrazine, electronic structure obs. in electron impact energy loss spectrometer, ionization potential 2−70737
tetroaldehyde, internal rot., effects on i.r. and electronic band contours 2−80093
thiacarbocyanine, excimer and related emission at low temp. 2−66861
thiacarbocyanine dyes with different substituents in meso position, absorption and luminescence spectra 2−61701
thianthrene complexes in solution, fluorescence study, enthalpies 2−84637
thiazanes, i.r. absorpt. spectra rel. to H-bonding and mol. struct. 2−56261
thiazyl fluoride, photoelectron spectra, vibr. analysis, comparison with LCAO calcs. 2−53083
thioamides, heterocyclic, H-bonding, formation of cyclic dimers 2−83318
thioamides, i.r. spectra in region of NH stretching frequency 2−43011
thiocarbonyl anion radical, e.s.r. studies of structure 2−53082
thioformaldehyde, microwave generation and characterization from rotational spectrum, detection in space 2−44888
thioformaldehyde, obs. of high-field rotational Zeeman effect, molecular quadrupole moments determ. from g values and magnetic susceptibilities 2−43010
thioformaldehyde, pyrolysis products of dimethyldisulphide, photoelectron spectrum 2−72538
thionyl molecules, photoelectron spectra 2−64156
thiophene, -D, in CS_2 solution, out-of-plane vibrations, i.r. band intensities 2−77120
thiophene, dipole moment from microwave spectra 2−42997
thiophene, high resolution photoelectron spectra 2−60087
thiophene, n.m.r. study in liquid crystal of structural parameters 2−67514
thiophosgene, high resolution photoelectron spectra 2−43006
1.4-thioselenan i.r. spectra in vapour, liquid and crystal states, Raman spectra of liquid and solid 2−83315
thiosultones, dipole moments and conformation 2−43009
thiourea, grown by evaporation, defect struct., X-ray topography obs. 2−74769
thiourea, paraelec. and ferroelec. phases, i.r. absorpt. 2−75309
thiourea, Raman spectra above and below 169K, librational modes 2−75314
thulium ethyl sulphate, spin-lattice relax. of rare earth ions 2−78051
thulium ethyl sulphate, splitting of $p_{3/2}$ core levels of Tm^{3+} due to crystal field 2−44318
thyamine, radiation abstraction of H atoms, analysis by e.s.r. spectroscopy 2−72585
thymine, 1s binding energy calc. for C and N atoms using perturbational model 2−77156
thymine, molecular electrostatic potentials, MO LCAO GTO SCF calculations 2−60041
TMPD in hydrocarbon glass, rigid matrix photoioniz., anion form., bleaching kinetics 2−81511
tolane, vibration, normal coordinate treatment 2−60088
toluene, 1-^{13}C labelled, long-range C-C spin-spin coupling constants 2−77125
toluene, absolute delay in Cotton-Mouton effect 2−43364
toluene, conform. depend. of long-range spin-spin coupling 2−64193
toluene, conformational structure, i.r. and n.m.r. spectra 2−42953
toluene, electronic structure photoelectron spectrum and SPINDO calculation 2−70793
toluene, Fe suspended particles, magnetization, temp. depend. 2−77450
toluene, liq., stimulated Raman scatt., rel. to limiting diameters of self-focusing 2−67832

Organic compounds continued
toluene, luminescence properties in solution, quantum yields of free radicals 2−71212
toluene, n.m.r. adiabatic fast passage relaxation 2−71236
toluene, photo fragmentation, obs. 2−70794
toluene, u.s. velocity, det. of molecular parameters 2−53429
toluene and polymeric solutions of derivatives of oxazoles and oxadiazoles, stimulated emission 2−59164
toluene based scintillation fluid 2−52687
toluquinone single cryst., excitonic and zero-field splittings of first triplet state 2−78209
trans-3,4-dimethyl-2,2,5,5-tetradeuteriocyclopentanone, vibrational assignment and conformational studies 2−64189
trans-3,4-dimethylcyclopentanone, vibrational assignment and conformational studies 2−64189
transformer oil, electric strength, for use in h.v. pulse generators 2−65055
tri(trifluoromethyl) arsenic, phosphorus and antimony, i.r. and Raman spectra, vibr. assignment 2−56262
tri-o-cresylphosphate, polar liquid, microwave Kerr effect, Kerr const. 2−80470
tri-tert-butylmethane, detailed structure and improvements in model force fields 2−77109
tri-tert-butylmethane, determination of structure using gas phase electron diffraction 2−77108
triallyl amine, vibrational spectra and rotational isomerism 2−43012
triaryl 1,3,5-trivinylbenzene derivatives, i.r. spectral band obs. 2−83333
s-triazine absorption spectra, obs. of Jahn-Teller distortion in lowest excited singlet state 2−46631
triazine dyes in aqueous soln. determ. of quantum yield for intercombination conversion using triplet-triplet transfer 2−84676
S-triazine triplet state at 3455 Å, Stark effect meas, vibronic origin of state 2−83280
1,2,4-triazole radical produced by γ-irradiation of single crystals, ENDOR determ. of hyperfine tensors for protons in H bonds 2−65394
1,2,3-trichloro-4,5,6-trimethylbenzene, heat capacity determination by adiabatic calorimetry, 30-300K 2−57070
1,2,3-trichloro-4,5,6-trimethylbenzene, order-disorder orientation change structure determination at 298K from X-ray data 2−56674
1,2,3-trichloro- 4,5,6-trimethylbenzene, order-disorder orientation change, structure determination at 173K from X-ray data 2−56675
1,1,2-trichloroethane, weakly coupled three-spin system, relaxation effects 2−50116
tricyclopropylphosphine, molecular structure determ. by gas phase electron diffraction 2−70796
triethyl boron, chemiluminescent reaction with O, fluorescent enhancement of BO_2 band 2−44475
triethylamine phosphor activated by TlCl, luminescence, excitation and emission spectra after exposure to u.v. radiation 2−54484
triethylamine-water critical mixture, simultaneous meas. of viscosity and light scattering 2−71169
triethylammonium(tetracyanoquinodimethan)$_2$ TEA(TCNQ)$_2$, elec. cond., anisotropy 2−75016
triethylammonium-(TCNQ)$_2$ elec. cond., 77-355K, and metal-insulator transition 2−68410
triethylenediamine, Start effect on ^{14}N n.q.r. in axially symmetric field gradient 2−61757
trifluoro(trifluoromethyl)-silane, microwave spectrum and internal rot. barrier 2−83296
trifluoroacetamide, X-irradiated, analysis of internal rotation of CF_2CONH_2 radical obs. in e.s.r. spectrum 2−81526
trifluoroacetone, molecular geometry from gas phase electron diffraction 2−60045
trifluoroacetylacetone, molecular geometry from gas phase electron diffraction 2−60045
trifluorochloroethylene, absorption saturation and optical strength for CO_2 laser pulses 2−67523
trifluoroethane and trifluoroethane-d$_3$, ^{19}F chemical shifts in gas phase 2−83308
trifluoromethane, partial double-bond character of C-F bond 2−43000
trifluoromethyl group, n.m.r. parameters of individual fluorines 2−77113
triglycine fluoroberylate: Cu^{2+}, spin Hamiltonian parameter and hyperfine struct., e.p.r. obs. 2−51409
triglycine fluoroberylate:Cu^{2+}, e.p.r. spectra, applic. of rhombic spin Hamiltonian formalism 2−51410
triglycine fluoroberylate, Cu^{2+} aggregate e.p.r. spectrum, h.p. and temp. influence 2−84575
triglycine fluoroberyllate, thermal expansion in ferroelec. transition region 2−71751
triglycine selenate, thermal and elastic props., deuteration effects 2−72042
triglycine sulphate, absorpt. spectra, photoemission, band struct., ionic cond. 2−77932
triglycine sulphate, coercive force, freq., amplitude and temp. depend. 2−47988
triglycine sulphate, dielec. const. near crit. point, thermal noise study 2−72040
triglycine sulphate, effect of growth rate on defect struct. and dielec. props. 2−47987
triglycine sulphate, electron microscope examination of fine structure of irradiated crystals 2−65067
triglycine sulphate, ferroelec., temp. depend. of dielec. props. in far i.r. 2−61435
triglycine sulphate, ferroelec. phase transition dynamics, spin-lattice relax. meas. by double reson. 2−84450
triglycine sulphate, ferroelectric, electromech. coupling near T_c 2−68475
triglycine sulphate, L-alanine doped, induced growth anisotropy 2−53608
triglycine sulphate, multi-domain single crystal, dielec. relaxation 2−61434
triglycine sulphate, pyroelectric, heat diffusion and heat sink problems for pyroelec. detectors 2−77960
triglycine sulphate, pyroelectric coeff. determ. 2−65072
triglycine sulphate, reshaping of ferroelec. domains after heat treatment 2−54234

Organic compounds continued
triglycine sulphate, second-harmonic scatt., domain shape effects 2−82508
triglycine sulphate, surface potential variation, observation with scanning electron microscope 2−81157
triglycine sulphate, thermal and elastic props., deuteration effects 2−72042
triglycine sulphate, thermal cond. near Curie point 2−44002
triglycine sulphate, vanadyl-doped, domain struct. changes, e.p.r. obs. 2−77937
triglycine sulphate pyroelectric detector, laser study of nucleation sites 2−44165
triglycinefluoroberylate cryst., l.f. Raman spectra, effect of temp. 2−51357
triglycineselenate cryst., l.f. Raman spectra, −115 to 36°C 2−51357
triglycinesulphate, ferroelec., critical thickness and thermodynamic stability 2−61425
triglycinesulphate cryst., l.f. Raman spectra, effect of temp. 2−51357
trimesitylboron$^-$, liquid and rigid medium ESR spectrum 2−50115
1,1,1-trimethoxyethane, vibrational spectra and rotational isomerism 2−43013
trimethyl(phenylethynyl)-silane, ^{13}C Fourier transform n.m.r. study, detection of ^{19}Si-^{13}C spin-spin coupling, bonding 2−83312
trimethyl amine, normal coordinate analysis, determ. of mean amplitudes of vibration 2−53084
trimethyl phosphite, γ-irradiated, e.s.r. spectrum of radicals 2−81534
trimethyl silyl isocyanate, microwave spectrum analysis 2−80076
trimethyl-lead radical, e.s.r. spectra, determ. of g tensors and hyperfine coupling 2−70795
trimethylazidosilane, electron diffraction determ. of molecular structure 2−80109
trimethylchlorosilane, isotopic shifts in vibrational spectra by CD_3 substitution, force constant calc. 2−46632
trimethylene oxide and deuterated analogues, i.r. band progressions and ring puckering vibr. 2−83277
trimethylene oxide and deuterated analogues, vapour phase Raman transitions and ring puckering vibr. 2−83278
trimethylene oxide deuterated analogs, far i.r. spectra and ring puckering vibr. 2−80094
trimethylene oxide deuterated analogues, Raman spectra and ring-puckering vibr. 2−80095
trimethyleneimine, 1-d-, Raman spectra, ring-puckering transitions 2−80084
trimethylmethane, scattering of Na, meas. of velocity dependence and total cross sections, study of glory undulations 2−70821
trimethyloxysilane, isotopic shifts in vibrational spectra by CD_3 substitution, force constant calc. 2−46632
trimethylsilyl amides, study of rotational barriers 2−77110
1',3',3'-trimethylspiro- (indoline-2',3-thietane)-1,1-dioxide, long-range $^4J_{hh}$ couplings 2−67522
2,3,4-trimethylthiazolium bromide, structure determinations for the geometry of the thiazolium ring 2−56668
1,3,5 trinitrobenzene charge transfer complexes, mol. movements, proton mag. reson. 2−48308
trinitrofluorenone-poly(N-vinylcarbazole), photogeneration efficiency, field depend. 2−65399
trinitrotoluene, negative ion spectra, electron energy range 2−84680
triphenylamine in alkane, ion recombination fluorescence, viscosity dependent rate 2−46968
triphenylamine light-induced conversion to excited triplet state of 11,12-dihydrocarbazole 2−57431
triphenylene (I) in crystalline solutions of isooctane and CCl_4, spectra and temperature dependence of phosphorescence 2−51377
triphenylenes, aryl substituted, triplet-triplet absorpt. analysis 2−65396
triphenylmethane, exciton splitting in electronic spectra 2−81523
triphenylmethane dyes in films of poly(methylmethacrylate), photochemistry 2−65387
tris(2,2′-bipyridine)osmium(II) complex, singlet triplet charge transfer absorption spectrum 2−68632
tris-(hydroxymethyl)-aminomethane, heats of protonation and dissolution, 20°C 2−48314
tristearin, polymorphism, positron annihilation study 2−60773
tropolone, near u.v. spectrum rel. to molec. structure, rotational band contour analysis 2−53085
tropolone, n.m.r. of ^{13}C, tautomeric equil. 2−64194
π-tropyliumvanadium tricarbonyl, ^{51}V quadrupole relax., coupling const. 2−84453
2-4-undecadienic acid, nematic liq. cryst., mol. theory, stability, thermodynamic conditions 2−46930
urea, changes in bond length and angles on protonation 2−60089
urea, encapsulated, use in cloud seeding expt. 2−62207
urea, fog dispersal from airport by airborne hygroscopic particle seeding 2−65720
urea, use in cloud seeding expt. 2−62208
uridine and related structures, relationship of ^{13}C to vicinal ^1H coupling to torsion angle 2−43014
uronium ion, CNDO/2 calculations of structure 2−60089
van der Waals constant, relationship with molar refraction and molar volume 2−60119
vanadium(urea)$_6$ $(ClO_4)_3$ and (urea)$_6I_3$, near i.r. sharp line luminesc. 2−81409
vapour, diffusion in glassy polymers 2−83362
vapour press. rel. to surface tension and surface curvature 2−46943
vinyl chloride, fragment calc. including polarization of σ-framework 2−83329
vinyl chloride, gas-phase electron diffraction study of structural parameters 2−67524
vinyl isocyanide, normal vibrs. 2−56263
vinyl trifluoroacetate, i.r. and Raman spectra, vibrational assignment, depolarization ratios and configuration determ. 2−70797
vinyl-type radical in irrad. maleic acid matrix, e.s.r., geom. and electronic struct. 2−64195
vinylcyclopropane and vinylcyclobutane, conform. preferences, group interactions 2−83291
vinylsilane, vinylsilane-d$_3$, normal vibration analysis and force field 2−43015

Organic compounds continued
water-ethanol liq. layer, heated from below, temp. field oscills. due to thermal diffusion 2−67821
white oil based scintillators, efficiency obs. 2−55912
Wurster's blue perchlorate, electrostatic binding energy using Ewald's method 2−67927
xanthene dye laser, effect of triplet levels on energy characteristics when pumped with mode-locked laser 2−66759
xanthene dyes in aqueous soln. determ. of quantum yield for intercombination conversion using triplet-triplet transfer 2−84676
xylene, heat of mixing with benzene 2−77426
xylene, inverse Raman effect 2−71206
p-xylene, relative intensities of vibr.-struct. lines in absorpt. spectrum 2−67525
o-xylene partially oriented in nematic phase, internal rot. barrier, spin-spin coupling 2−77157
xylenes, conform. depend. of long-range spin-spin coupling 2−64193
ytterbium ethylsulphate, magnetic and thermal props. 2−51241
yttrium ethyl sulphate:Gd^{3+}, host lattice effects on e.p.r. spectra, lanthanide behaviour 2−48299
yttrium ethyl sulphate:Yb^{3+}, phonon field contrib. to g shift 2−68586
yttrium ethyl sulphate; Yb^{3+}, Dy^{3+}, proton polarization and relaxation by rotational cooling 2−48122
zinc acetate study of X-ray K absorption edge of Zn atom 2−70595
zinc phthalocyanine, MO calculations 2−53086
zinc porphin, polarized sharp line absorption spectra 2−64196
Ag-naphthalene-Ag structures, electronic conduction in dark 2−57199
B-epoxy laminated omposite plates, holographic stress analysis 2−78895
CH, oscillator strength of $A^2\Delta$-$X^2\Pi$ electron transition 2−59993
CH_4 solid, spin isomer conversion, n.m.r. obs. 2−68749
C_4H_8 isomers ionisation efficiency at 123.6 nm 2−83302
CH_3I, mol. cryst., exciton spectrum in presence of Fermi reson., exciton absorpt. 2−68311
$(CH_3)_2XH_n$, (X=C, Si, N, P, O, S), barriers to methyl rot., electronic origins, CNDO/2 calcs. 2−64182
^{13}C characteristic n.m.r. chemical shifts 2−56209
^{13}C chemical shielding parameters determ. using proton-enhanced nuclear induction spectroscopy 2−72524
^{14}C labelled vapours, self-diffusion through polymer membrane, obs. using radio tracer technique 2−71180
1-chloro-3,3,3-trifluoropropyne, microwave spectra analysis 2−70759
Co(II) complex, paramag. shift of n.m.r. line due to outersphere coordination of solvent molecules 2−80106
1,2-dibromoethane, i.r. spectra study of medium effect on rotational equilibria 2−78109
1,1-dimethylcyclohexane, gas-phase mol. struct. 2−70765
6α-fluorocortisol, struct. determ. by two- dimens. struct. invariants 2−53686
^{67}Ga-citrate and scintillation camera in detection of liver tumours, computer scintigraphy 2−73198
guanidinium aluminium sulphate hexahydrate, optical and interferom. studies of cleavages and etch patterns 2−64670
H_2-phthalocyanine in 1-chloronaphthalene, solutions, fluorescence decay curves meas. by single-photon method 2−68695
Ho^{3+} in yttrium ethyl sulphate, spin-lattice relaxation rate measurement using electron paramagnetic resonance techniques 2−68584
hydrocarbon chains with (α-naphthyl)$-(CH_2)_j-$(α-naphthyl) struct., intramol. collision kinetics, e.s.r. obs. 2−56236
^{131}I rose bengal imaging, differential diagnosis of jaundiced patients 2−58611
Li_2O_2 geometry, ab initio molecular orbital study using Gaussian basis set 2−53022
LiO_2H geometry, ab initio molecular orbital study using Gaussian basis set 2−53022
^{15}N spin-lattice relaxation, interaction mechanisms at high and low temperatures 2−57400
NaCl 2−81409
$Na_3[Ce(C_7H_3NO_4)_3].15H_2O$, mag. and thermometric props. in 2-20 mK range 2−82079
$NbSe_2$/organo intercalation compounds, electron microscope examination of lattice and superconductivity 2−53676
Ni hexamethylenedithiocarbamate with M-S bonds, X-ray struct. study 2−71448
TaS_2/organic intercalation compounds, electron microscope examination of lattice and superconductivity 2−53676
tertiary butyl chloride, absorption spectra, concentration dependence, obs. 2−50088
yttrium ethyl sulphate: Yb, nuclear spin refrigeration rel. to electron spin-spin interaction 2−72246
Organometallic compounds *see Organic compounds*
Orthicons *see Electron tubes*
Oscillations
see also Electromagnetic oscillations; Liquid oscillations; Piezoelectric oscillations; Vibrations
aerofoil section, aerodynamic force by Mach-Zehnder interferometer 2−77358
anisotropic elastic cylinder, torsional oscillations in mag. field 2−52206
antisymmetric, nonlinear dynamo waves for solar cycles 2−73134
axisymmetric inertial, of rotating fluid 2−74342
bubbles, non-spherical oscil., stability 2−53372
bubbles, nonspherical 2−43305
charged drop, relaxation and damping, EHD stability 2−80227
chromospheric, in Hα plage 2−78606
circular plate, variable thickness, clamped and free 2−69706
coherent, transverse, frequency determ. in electronic model of ring cyclotron 2−70332
continuous medium, self-oscillatory motion due to loss of stability during stationary mode 2−63092
convective plane parallel flow in vertical slot, oscillatory instability 2−83472
correlation technique for transient response of hysterically damped system to stationary random excitations 2−55500
corrugated cylinder rotating in incompressible viscous fluid 2−64249
Oscillations continued
cylinder in fluid, oscillatory damping 2−45473
cylinder in stationary fluid, jet like flow 2−43100
damped, measurement, time average holographic interferometry 2−63094
damping element characteristic, determ. method 2−69690
dipole gas, polarization oscills. 2−80415
dispersive media, oscillatory solitary waves 2−52047
displacements of metal during mag. pulse treatment 2−76360
disturbance due to point source in layered half space 2−75421
Earth, earthquakes, nonlinear effects 2−81584
Earth, laterally heterogeneous, toroidal free oscillations 2−51500
Earth's core, hydromagnetic oscillations rel. to geomagnetic secular variation 2−62378
Earth's free oscillations for order numbers higher than 50 from earthquakes 2−84704
Earth model consistent with free oscillation and surface wave data 2−84726
elastic sphere, horizontal heterogeneity effects on torsional oscillation 2−76354
elastic-gravitational, of laterally heterogeneous Earth 2−78286
elastically nonlinear body, forced longit. oscillations 2−78901
electric welding arc, conduction, acoustic vibration effect 2−71050
electromechanical filters, flexural waves, thin blades 2−52355
electron beam, effect on freq. shift of axial oscillations in cyclotron 2−70330
electron beam in synchrotron, meas. of freq. 2−59652
electron gas, unstable, population and oscillations of two level system 2−63266
ferrimagnetic solids 2−44272
forced, mechanical system for teaching demonstrations 2−62937
forced harmonic torsional of inertialess finite rigid cylinder clamped in circular borehole 2−69702
fourth order nonlinear oscillations, normal forms 2−49084
free, Sun, possible stimulation by solar flares 2−66227
free movement of and viscous fluid 2−77195
free oscillations of laterally heterogeneous spherical Earth model, variations of density and elastic moduli 2−51493
free stream flow which oscillates without reversing, two- dimensional boundary layer 2−80172
free torsional, of inhomogeneous sphere, equation of motion 2−44544
frequency response testing, spectrally shaped transient forcing function 2−73396
frequency-time analysis of oscillations rel. to seismic waves 2−84703
galvanomagnetic phenomena, longitudinal, in thin wires, oscillations of resistances 2−68328
gas, thermally driven, heat balance, acoustic streaming 2−80358
gas bubble in liquid, acoustically forced 2−64423
gas discharge, longitudinal mag. field effects 2−80363
harmonic causing one-dimensional propag. of small disturbances in radiating gray gas 2−80404
Helmholtz eqns., approx. reduction, for nonuniform media 2−82319
high-frequency, of second-order fluids near a sphere, calculation 2−56313
horizontally oscillating liquid with beds of dense particles, study of transitions between flow regimes 2−83741
hydroelastic stability of flat panel in fluid flow, influence of free surface 2−46701
hypersonic flow past wedge, effects of upstream unsteadiness 2−74466
inertial effects in motion driven by hydrodynamic fluctuations 2−70827
instantaneous and finite-duration pulses, influence on oscillations of time-measuring mechanisms 2−73284
isotropic defect in anharmonic crystal, local oscillations 2−71473
Lamb waves in presence of realistic temp. and dissipation distribs. 2−65688
large flexural, of thin beams 2−66598
l.f. electrical, demonstration 2−73265
liquid core of Earth, dynamics 2−84724
mass measurement by measuring frequencies of natural oscillations of body 2−66406
mass-spring system, 2nd order extension of Lienard's graphical construction 2−78870
natural oscillation magnitudes from dynamic response by harmonic excitation in one configuration 2−52202
non-linear, stochastic instability 2−66574
non-radial, stars, tidal perturbations 2−73013
nonlinear, theory, applied methods 2−76341
nonlinear self-oscillatory systems, determ. of dynamic characteristics 2−82294
nonlinear syst., appl. of averaging method, energy losses 2−49085
parametric and forced, nonlinear elastic systems, obs. using method of averages 2−76339
parametric eqns., general class 2−45438
pendulum type, infinitesimal stability and instability 2−49052
plane-parallel layer motion 2−67607
quasi-biennial cycle of tropical stratosphere 2−84798
radial oscillations of gas cavity in compressible fluid rel. to underwater detonation of TNT 2−60174
Rivlin-Ericksen fluid, oscillations by rotating sphere about fixed diameter 2−60155
rod, homogeneous, dynamic boundary effect, abridged problems formulation 2−78902
rod/spring/block system, impulse driven, mech. self-oscillation 2−78867
rotating fluid in thin spherical shell, trapped oscillations 2−83474
sandwich beams, flexural vibrations, eigenvalue boundary problems 2−69707
self induced in open water channel with slotted walls 2−80432
self-excited, waterfall, stabilization 2−80423
shock computations, self-adjusting hybrid schemes 2−55560
simple harmonic motion, a teaching example 2−55445
simple linear oscillator, stationariness, filtration, periodic nonstationary random process 2−73406
solar, five-minute, spatial properties 2−73105
solar atmosphere, velocity 2−73106

Oscillations continued
solar atmospheric five minute oscillations, horizontal propag. 2−81946
sphere in viscous fluid, high frequency oscillations 2−70866
spherical pendulum, resonance in small oscillations 2−58831
stability of coaxial rotating jet and vortex of different densities 2−74336
stability of horizontal two component fluid with positive vertical temp. gradient 2−70831
stability of liquid interfaces in porous media 2−71131
stability of nonlinear oscillations of elastic rod 2−73399
symmetric body, in rotating viscous fluid, effect of Coriolis force 2−46679
torsional, optical measurement using mechano-optic polarization modulator 2−70036
torsional spring subjected to sinusoidal oscillations, heat generation 2−55501
trapped in slightly viscous rotating fluid trapped oscillations 2−67582
tube in cross flow, influence of Coulombic damping on susceptibility to vibr. damage 2−53112
tuning fork, excitation of self-oscillation 2−58887
vibrational relaxation of anharmonic oscillators 2−66422
viscoelastic Maxwell fluid, oscillatory motion in annular channel under periodic pressure gradient 2−74343
water drops, freely suspended 2−64427
Bi liquid-solid interface, damping by magnetic field 2−71303
Fe-(30.3 wt.%)Ni alloy, damping of oscillations during heating after martensitic transform. 2−43791
W, cryst., damping of elastic oscillations, orientation depend. 2−43671

Oscillators
classical non linear, dynamic susceptibility 2−73287
in electromagnetic field, dispersion forces, semi-classical treatment 2−74302
ferroelectric, effect of automatic temp. stabilization 2−44157
Hamiltonian system, stability of periodic orbits in regions exhibiting stochastic behaviour 2−41525
Josephson junction applics. 2−64956
light, independent calibration of Cherenkov spectrometer 2−59624
lumped two-frequency parametric oscillators, stationary regime analysis 2−82499
marginal, low level tracking, for in situ mag. field obs. at low temps. 2−63209
microwave, frequency variable semiconductor oscillator 2−73479
noise figure rating for marginal oscillators 2−45651
nonlinear classical electrical, e.p.r. and n.m.r. detection in operation region far from sinusoidal 2−59011
nonlinear spring mass systems, stop function response taking into account static deflection 2−49091
optical parametric, behaviour 2−49344
optical parametric oscillator, using CdSe, i.r. operation 2−69903
oscillogyro, dynamical characteristics 2−78871
parametric, instability region in spectral density distribution 2−58986
parametric, phase matched in GaAs thin-film waveguides, operation 2−73483
PKW marginal oscillator, performance improvement 2−73500
Pockel cell Q-switched Nd:glass oscillator, amplified output, picosecond structure 2−42070
radiotelescope 25W 378 MHz local oscillator 2−81959
RC and transistorized, with mixed feedback, analysis 2−59033
self-excited, with non-linear capacitance, parametric nature of synchronization 2−55637
superconductive lumped parameter circuit, temp. dependence 2−63216
synchronization, pseudo-indirect technique 2−55638
TEM_{00} mode HF chemical laser oscillator 2−49348
tunnel diode, r.f. design for use in susceptibility measurement and relaxation processes 2−68513
waveguide gas lasers 2−41987
CO_2 TEA, oscillator amplifier laser, 2 GW peak power generation 2−41994
GaAs, high resistivity, characteristic operation 2−44137
$LiIO_3$ pulsed doubly resonant parametric oscillator, spectral and other props. 2−73586
$LiNbO_3$, parametric, rapidly tunable dye-laser pumped 2−73547
Rb frequency generator, phase tuned, r.m.s. fluctuations in standard frequency 2−82122
ZnO acoustoelectric device, high and low field resistivity, uniaxial press. effect 2−63119

Oscillistor effect *see Semiconductors*
Oscillistors *see Semiconducting devices*
Oscillographs *see Electrical measurement*
Oseen method *see Flow; Hydrodynamics*

Osmium
electric quadrupole interaction of ^{181}Ta, Mossbauer obs. 2−61607
films, evaporated, reflectance and optical constants in v.u.v. from 300 to 2000 Å 2−81336
inFe, hyperfine field, anomalous temp. depend. 2−48121

Osmium compounds
pyrochlores, $M_2Os_2O_7$, (M=Ln,Bi,Pb,Tl), struct. and props. 2−60987
$Mo_{75}Os_{25-x}Fe_x$, supercond., compensation effect 2−64947
Os-Pt alloy, low field Hall coeffs. at 4.2K and 300K, two band model 2−61188
OsO_4, dipole transition moments determ. by LCAO-MO calcs. in terms of ligand mixing coeff. 2−42928
$Os_4O_4(CO)_{12}$, i.r. and Raman spectra, vibr. assignment, force consts. 2−56193
Th-Os-Ir system, comp. range of stability of $ThOs_2$-ThIr phase 2−50976

Osmosis
^{3}He-^{4}He solns., osmotic press. along phase separation curve near absolute zero 2−80500
a.c. electroosmosis 2−72562
electro osmosis, layered porous systems, filtration 2−83783
membranes, preselective, ion and water movements, equilib. props. 2−60460

Osmosis continued
osmometer, design for foil swelling pressure meas. 2−53417
osmotic pressure data, numerical treatment 2−43343
poly(trans-2,5-dimethylpiperazine fumaramide) films, reverse osmosis props. 2−83786
polymer-binary solvent system, osmotic and sorption equilibria 2−75375
polymer-binary solvent system, osmotic equilibrium 2−75376
polymer-solvent system, second osmotic virial coefficient, interdependence of enthalpic entropic contributions 2−50353
porous partitions, capillary osmosis 2−46902
salt free polydisperse polyelectrolyte, possible source of error 2−56492
tissues, induced by gases, obs. of peak water displacement 2−45024
water and solute, flow in extracellular channels 2−46879
^{3}He-^{4}He dil. mixtures, osmotic press. 2−47005
^{3}He-^{4}He dil. mixtures, osmotic press. thermometry 2−45184
^{3}He-^{4}He dilute mixtures, osmotic press., 20-400 mK 2−73242
^{3}He-^{4}He saturated mixtures, osmotic press. below 300 mK 2−43423

Overhauser effect *see INDOR*

Oxidation
— 2−67901
3-aminobenzaldehyde, in aprotic solvent, chemilum. on ozonization 2−54538
anodic, of binary compounds of transition elements in H_2SO_4 2−61790
anodic oxidation etching technique, for Al and Al-Cu alloy cast morphology determ. 2−47602
cytochrome c, electron transfer between molecules obs. by pulsed Fourier transform n.m.r. 2−56267
development, non exposed grains, reactivity, fogging metallic silver 2−84672
9, 10-diphenylanthracene photoperoxidation, quantum yield and intersystem crossing 2−72576
DPPD, excited, electron transfer to oxygen mols., contact ion-pair and dissociated ion-radicals form. 2−68811
electropolishing soln., necessary characteristic for universal application 2−80547
fatigue, high temperature phenomenological mechanisms 2−56818
graphite, effect of adsorbed $POCl_3$ on oxidation 2−68783
graphite, electrothermal, rel. to crystallite size 2−57001
graphite, high temp. reaction obs. by molecular beam and mass spectrometer 2−48332
graphite, highly oriented pyrolytic, effects on basal and edge surfaces 2−56572
graphite, isotropic nuclear and 'Poco', reactivity 2−59843
graphite, pyrolytic, effects on surface structures 2−60620
graphite in reactor, due to irradiation 2−52850
graphite powder, fine-disperse, effects on pressing ability 2−77737
luminol in liquid phase and NO in gas phase, chemiluminescent intensity standards 2−65372
luminophores activated with Eu^{2+}, rel. to luminesc. 2−54483
magnetite, low-temp., magnetic and mineralogical changes 2−65571
metal, vacancy annihilation in oxidation reactions in gases 2−53756
metal powder, destruction of oxide layers by spark isostatic pressing 2−68129
methanol-air mixtures, thermal explosion, boundary of flame propagation region 2−75378
noble metals, thin oxide formation in aqueous electrolyte solutions with anodic current, reaction kinetics 2−68784
polypropylene photooxidation, surfaces changes, i.r. spectroscopic and electron microscopic studies 2−51472
pyrolytic graphite basal plane, reaction with modulated O_2 beam, study of surface chemistry 2−51447
pyrolytic graphite prism plane, reaction with modulated O_2 beam, double diffusion effect on reactivity meas. 2−51448
range pair counting method application to combustion chamber exhaust gases 2−57421
rare earth metal ions, electron transfer reactions and oxidation potential in aqueous soln., pulse radiolysis study 2−61815
reduction reactions effects on threshold sensitivity of nuclear photographic emulsions 2−70317
Si, thermal oxidation, stacking fault generation, impurity effects 2−60809
solid, internal and precipitation phenomena 2−68187
solid surfaces, conference, Boston Mass., USA, Oct. (1971) 2−47070
steel, surface oxidation during annealing, obs. 2−67899
steel/$UO_{2\pm x}$-$PuO_{2\pm x}$ cladding/fuel interface 2−52875
tetraethoxysilane, dielectric film growth by low temperature oxidation 2−60636
thin film atomic oxygen sensors 2−65403
titanomagnetite, low temp., effect on magnetic properties 2−54964
Verneuil furnace, oxidation-reduction potential of environment, thermodynamic calc. 2−60705
wustite, and reduction in H_2O vapour and H_2 mixtures, kinetics and mechanism 2−75381
wustite, reduction, crystal diminution 2−75380
Zircaloy-2, in steam-water mixture under reactor radiations 2−51456
Ag-Zn-Al alloy, transition from internal to external oxidation 2−48331
Al, adsorption of O_2, work function changes obs. 2−77517
Al, growth of α-Al_2O_3 whiskers 2−74637
Al, in moist H_2 atm., α-Al_2O_3 tab growth 2−43508
Al, influence on lubricated friction of steel 2−53844
Al, oxide formation mechanism rel. to nucleation and electrochemical transport processes 2−68798
Al film, effect on supercond. transition temp. 2−71845
Al film, LEED obs. 2−51445
Al powder, oxide film rel. to sintering props. 2−43888
Al ribbon, rel. to thermal spectral radiation 2−61629
Al_2O_3-$Ni(NO_3)_2.6H_2O$ system, effect of heating in oxidizing and reducing media 2−60992
Al_2O_3 film, growth by plasma anodization 2−43477
Ba, reaction kinetics, photoemission spectra of chemisorbed levels 2−51446
C fibre-reinforced composite, effects on mech. strength 2−53951
CO, catalytic oxidation on Pt surface 2−78185
CO, in shock waves, catalytic effect of $Fe(CO)_5$ 2−57417

Oxidation continued
CO catalytic oxidation, on Pt(110) surface, Auger spectroscopy obs. 2−51443
porous Cd electrodes, passivation in KOH solution 2−84656
Ce, u.v. photoelectron spectroscopy obs. 2−72557
Co-Cr alloys, effect of scale porosity, second- phase oxides and doping 2−75379
β-Co, diffusion of O and Si, 1000-1300°C, internal oxidation studies 2−74811
Cu-Al crystals, internal oxidation, comments 2−65377
Cu-Mn alloys, γ-MnO_2 weak diffraction line at centre of diffuse neutron scattering peak due to 2−71644
Cu-Zn alloys, tarnish film formation, electrometric study 2−68785
Cu, internal oxidation at low pressures, comments 2−65376
Cu, nucleation and growth of oxide, Rheads scheme 2−51449
Cu, oxide nucleation on (001) face, off angle effect 2−64566
Cu, protected by Si_3N_4 reactively sputtered film 2−43481
Cu, residual resistivity, high-temp. oxidation influence 2−71832
Cu film, condensed in presence of residual gases 2−71328
Er, oxide film form. 2−50491
Er film, f.c.c. struct. and oxidation, HEED obs. 2−50490
Fe-Al-Cr alloys, effect of zirconium 2−60935
Fe-Mn alloy, kinetics of manganeseo-wustite scale formation 2−48333
Fe alloys, partitioning of transition metals in oxide scales, chem. diffusion model 2−78197
α-Fe_2O_3 (haematite) from oxidation of basaltic magnetite rel. to surface colour of Mars 2−78546
Fe_2O_3 and Fe_3O_4, morphological and struct. changes during reduction 2−50881
Fe + O_2, fast flow reactor for kinetic obs. 2−48318
GaAs, controlled sectioning by anodic oxidation and removal of oxide layer 2−64544
H_2-air mixtures, thermal explosion, boundary of flame propagation region 2−75378
$La_{1-x}Sr_xCrO_3$, volatile oxidation kinetics for optimum material characteriz. 2−50885
Li chemistry in upper atmosphere 2−58030
Mg composites, surface oxide film growth mechanism 2−57424
Mn-Zn ferrite powders, calcination and effects in crack reduction on core production 2−68163
MoC in H_2SO_4, corrosion rate meas. 2−61790
$MoSi_2$ in H_2SO_4, corrosion rate meas. 2−61790
Mo_5Si_3, oxide coating form, Si diffusion, at 1700°C 2−53769
NO in gas phase and luminol in liquid phase, chemiluminescence intensity standards 2−65372
N_2O molecular beam, reactive scatt. from clean and C covered Pt(100) surface 2−50547
Na_2SO_4, volatile oxidation kinetics, 1173 to 1473K 2−50891
Na + O_2 fast flow reactor for kinetic obs. 2−48318
Nb, oxide growth in matrix 2−47468
Nb, stress effects on oxid. process, oxide wedge formation 2−43736
Nb, stresses involved in oxid. process, annealing flexure obs. 2−43735
Nb_5Si_3, oxide coating form., Si diffusion, at 1700°C 2−53769
Ni-Co, alloy, f.c.c., dislocation bands produced by electrolytic hydrogen charging 2−56713
Ni, effect of cold work, examination 2−75382
Ni, effects of surface preparation 2−72559
Ni, polycryst., mechanism of low temp. oxid. 2−72558
Ni surfaces, contamination during oxidation in fused SiO_2 reaction vessels 2−84102
Ni_3Cr alloy, effects on mag. props. 2−54338
NiO on Ni, oxide growth and parabolic kinetics at high temps. 2−75383
Pb evaporated layers, by low energy O_2^+ bombardment 2−61791
PrO_x-ZrO_2 ternary system, phase relationships, oxygen press. effect 2−47694
Pt-Nb alloy, oxidation resist. 2−47533
Pt-Re alloy, oxidation resist. 2−47533
Pt-Ta alloy, oxidation resist. 2−47533
Pt-Ti alloy, oxidation resist. 2−47533
Pt-W alloy, oxidation resist. 2−47533
Pt, interaction with O_2, thermodynamic props. of volatile products, obs. method 2−65378
Pt, interactions with O_2 2−51450
β-Pu, hot stage X-ray diffr., microtopography and thermogravimetric obs. 2−54544
Pu, in moist O_2-N_2 mixture 2−54545
Pu, retardation by PuO, surface film form. 2−51451
Re, interactions with O_2 2−51450
SO_2, rel. to photolysis of atmospheric gaseous impurities 2−51586
Si-Ge alloy, oxide layer etched away reoxidation, production of MOS transistors 2−75132
Si, kinetics of thermal growth of ultra thin layers of SiO_2 2−71337
Si, SiO_2 film growth by tetraethoxysilane oxidation 2−47126
Si wafer, device-processed, generation of stacking faults and dislocation loops 2−51179
Si wafer, surface defect generation on reoxidation in H_2O vapour during B diffusion 2−64672
SiC, strength oxidation resist. 2−60882
SiO_2/Si interface, surface-state density, obs. 2−65041
SiO_2 formation over Au layer on Si substrates 2−67911
Sn, finely dispersed, effect on supercond. transition temp. 2−61230
SnTe, Mossbauer obs. 2−44485
Sr, reaction kinetics, photoemission spectra of chemisorbed levels 2−51446
Sr, u.v. photoelectron spectroscopy obs. 2−72557
TZM alloy, arc casted, oxidation resist. 2−53825
Ta-7.3 at.%Mo alloy, 950°C 72560 2−72560
TaC in H_2SO_4, corrosion rate meas. 2−61790
$TaSi_2$ in H_2SO_4, corrosion rate meas. 2−61790
Ta_5Si_3, oxide coating form, Si diffusion, at 1700°C 2−53769
Th, photon appearance potential spectroscopy on O_2 exposure 2−54441
Ti, anodic oxide film formation, p-i-n junction 2−47138
Ti, diffusional saturation with O_2, residual stresses introduced 2−56949
U-Nb and U-Nb-Zr alloys, low temp. 2−48334
UC, in liq. Na with small O content 2−51452

Oxidation continued
UO_2-PuO_2 thermal reactor fuel, defect performance 2−59855
$UO_{2\pm x}$, controlled atmosphere, x-ray study of equilibria 2−44487
V alloys in contact with mixed oxide nucl. fuel 2−83099
W film, on SiGe, interface reactions, effects of p- or n-type substrates, ion backscattering analysis 2−71951
W oxide form. at 1000 K, LEED obs. 2−78196
WC in H_2SO_4, corrosion rate meas. 2−61790
WSi_2 in H_2SO_4, corrosion rate meas. 2−61790
W_5Si_3, oxide coating form, Si diffusion, at 1700°C 2−53769
Zr-(2.5wt.%)Nb press. tubes, irrad. effects 2−53913
α-Zr, diffusion of oxygen, coeff. variations 2−71543
Zr, neutron irrad. effects on aqueous oxidation, 290°C 2−44486
Zr, short-time O_2 exposure, 440-850°C, kinetics 2−51453
Zr alloys, accelerated oxidation, significance of surface preparation 2−68786
Zr alloys, in-flux behaviour in pressurized water loop 2−51455

Oxide cathodes *see Cathodes/oxide*

Oxygen
in (^1D) state production in N + NO reaction 2−51437
absorbed layer on ZnO, sensitizing action of chlorophyll to corono discharge 2−44176
absorption cross sections between 100 and 600 Å 2−80057
absorption on (111) face of Ge single crystals 2−80583
absorption rate into blood under turbulent conditions 2−73166
abundance in population II horizontal branch stars HD 86986, HD 109995, HD 161817 2−66095
abundance in powdered lunar soil samples, L17/O78, nondestructive neutron activation analysis 2−8530
accelerated nuclei, autoactivation, application to radiology 2−69295
acetylene-oxygen mixture, shock and detonation waves, local vel. meas. by Schlieren interferometry 2−63138
adlayer on W, K shell total electron impact ionization cross sections, Auger spectra 2−64579
adsorbed layers on NiO and CuO, species characterization by X-ray photoelectron spectroscopy 2−77516
adsorbed on Ag, e.p.r. obs. 2−50531
adsorbed on NaI, effect on X-ray, u.v. and visible spectra 2−81399
adsorbed on Ni, He^+ backscatt. and LEED study 2−50543
adsorbed on Ti, photoemission energy level meas. 2−47166
adsorbed on W, LEED and work function obs. 2−47169
adsorption, on W single crystal plane, field emission microscope obs. 2−64580
adsorption and O-Cs co-adsorption of W single crystal surface rel. to work function change 2−54266
adsorption lifetime and desorption energy on W as function of coverage 2−47171
adsorption on Ag, slow irreversible processes, work function depend., LEED pattern changes 2−60675
adsorption on Al, obs. of interactions by work function changes 2−77517
adsorption on Cu-Ni alloy 2−50536
adsorption on MgO, obs. of ESR signal, charge transfer effects 2−47139
adsorption on Mo, Auger spectrum chem. shift 2−51223
adsorption on Ni, surface reconstruction, Madelung potential 2−47162
adsorption on Ni, thermal disorder, LEED pattern interpretation 2−60672
adsorption on Si, comments on expts. 2−47165
adsorption on Si 2−47164
adsorption on W, low coverage, at 78K, field ion microscopy 2−64584
adsorption on W, thermionic electron emission and work function obs. 2−47172
adsorption on W and Mo single crysts., atomic and electronic processes 2−74649
adsorption on W surface, inhibition of reactions with H 2−71344
adsorption on Y, Auger spectrum chem. shift 2−51223
airglow emission at 6300 Å, during geomagnetic storms 2−48540
antiprotonic atoms, X-ray lines, strong-interaction effects 2−79965
atmosphere, transmission function in 0.76 microns O_2 band 2−44732
atmospheric, det. of temp. profile from meas. of microwave emission 2−65658
atmospheric, nighttime number density from stellar occultation data 2−58034
atmospheric concentration in 70-95 km region 2−48463
atmospheric O_2, attenuation of 4.3 mm waves 2−68914
atom, 1s-hole state, chemical effects on lifetime 2−70602
atom, calc. of electron affinity using symmetry-adapted pair correlations 2−42709
atom, chem. reactions with ethylene and propylene, products obs. in high-intensity mol. beams 2−68763
atom, effective lifetime in pulsating aurora 2−81704
atom, electron collisions, close-coupling calculations 2−42766
atom, electron scatt. cross section calcs. using polarized orbital close coupling theory 2−64043
atom, Lamb shift meas. for n=2 state of $^{16}O^{7+}$ 2−49975
atom, lifetime of $2p^33s^5S$ metastable state 2−42737
atom, meas of Lamb shift in $^{16}O^{7+}$ 2−49976
atom, metastable ^1D, deactivation in upper atmospheric conditions 2−65814
atom adsorbed on W surface, backscattering cross sections for K-shell ionization by electron impact 2−79919
atom excitation to S^1 state during aurora borealis 2−44745
atomic, 5577 Å emission intensity, nocturnal and semiannual variations 2−65889
atomic, chemiluminescent reaction with triethyl boron, fluorescent enhancement of BO_2 band 2−44475
atomic, Li-like, spectra of autoionization electrons 2−49953
atomic, nightglow, 5577 photometric observations 2−48545
atomic, quenching of $O(^1S)$ by $O(^3P)$ 2−49970
atomic, specific refractivities, dual frequency laser interferometry 2−79902
atomic, thin film sensors for upper atmosphere 2−65403
atomic beam system for obs. of mass spectrometer response in upper atmos. 2−64058
atomic ions, excited states effect on ionospheric F-layer recomb. 2−62375

Oxygen continued
atoms, charge-changing cross sections in collisions with I ions, 5-25 MeV 2−70623
atoms, quenching of vibrationally excited N_2* 2−83400
aurora, ^{1}S-level excitation by delayed processes 2−81705
auroral zone, 1.2 μ O_2 i.r. band intensity 2−58067
blast flow rate, industrial systems, compensation differential manometers 2−56415
in blood, fibre optic catheter for obs. 2−51897
chemical analysis by metastable ion detection 2−65402
chemiluminescent reaction $N + O_2 \rightarrow NO + O$, overtone photon efficiency 2−57409
chemisorbed on Si(111) surface, electron bombardment surface ion desorption study 2−71351
chemisorbed on W, mass spectrometric obs. of desorption 2−48327
chemisorption, on CdS, CdSe, and PbI_2, induced conductivity changes 2−47886
chemisorption, on W, K shell ionization by electron impact 2−50553
chemisorption on Ag, rel. to surface struct. LEED and secondary electron spectroscopy 2−51442
chemisorption on Cu (110) and (100) faces 2−60678
chemisorption on metal, thermodynamic and struct. aspects 2−50530
chemisorption on Ni, bonding, orbital electron energy spectra 2−48328
chemisorption on W(100) surface, work function 2−83878
concentration cells, e.m.f. meas. 2−66681
consumption during exercise, radiotelemetry obs. 2−85099
D-region, theoretical models, ion pair production 2−78400
desorption and adsorption on W, SIMS, EID, flash-filament obs. 2−47170
detection of mol. O_2 on Mars 2−85047
diffusion, moving-boundary problem for oxygen in absorbing medium 2−83997
diffusion, SiO_2-K_2O and SiO_2-Na_2O systems 2−53772
diffusion coeffs. in polypropylene and polyethylene, radiothermoluminescence method 2−84004
diffusion in α-Zr, coeff. variations 2−71543
diffusion in β-Co, internal oxidation studies 2−74811
diffusion in blood and plasma 2−51886
diffusion in Fe, effective radii of diffusing particles, diffusion mechanisms 2−50709
diffusion in Fe, solid and liq. states 2−43661
diffusion in Nb, under neutron irrad. 2−53768
diffusion into metal from oxide film and diffusive motion in metal 2−71533
diffusional saturation of Ti, residual stresses introduced 2−56949
discharge, ion form. mechanism 2−83637
discharge, mechanism of spark breakdown 2−60318
dissolved, distrib. in South Atlantic 2−65594
dissolved in liq. Ag, effect on surface tension 2−43340
ear, tunnel of Corti, availability, meas. by microelectrode 2−66307
electron capture and losses of atoms and ions in air N_2 and O_2 2−70620
electron impact excitation cross sections, ionospheric models 2−81724
electrotransport in Gd 2−80716
etch pitting of graphite 2−53553
gas, absorption into turbulent distilled water 2−50298
gas, elec. breakdown due to large number of electrons 2−83709
gas, influence on Mo photoemission 2−51227
hyperbaric oxygen toxicity in central nervous system, changes in electrical activity of brain as criterion 2−62866
impurity in metal foils, assay by meas. of proton energy spectra 2−50389
in metals, spectrochemical determination, effect of heat 2−72590
interactions on Re and Pt 2−51450
interstellar, abundance det. from u.v. stellar spectra 2−58359
ion collisions with atoms with $13 \leqslant Z \leqslant 79$ at 7.5 to 40 MeV, characteristic X-ray production 2−70629
ion density in topside ionosphere 2−58074
ionosphere, photoionization and photoabsorption cross sections calculations 2−78388
ionospheric sunrise, time variation of O_3, metastable O_2, O densities 2−72881
ions, 0.5-2 MeV, stopping powers in Cr, Fe, Co, Ni, Cu, Zn 2−47782
leak source for vacuum system, using $Zr_{0.85}Ca_{0.5}O_{1.85}$ 2−85174
liquid, acoustic nonlinearities parameters, temp. depend. 2−56501
liquid, stimulated thermal, Raman and Mandelstam-Brillouin scattering of light 2−46963
lunar sample content, neutron, activation anal. 2−69138
massive stars, He burning, advanced evolution, ^{16}O nucleosynthesis 2−66086
molecular beams, reaction with graphite, mass spectrometer obs. 2−48332
molecular collisions, vibrational transition probabilities, temp. dependence below 300K 2−60117
molecular collisions with Ar and Kr, Lennard-Jones potentials determ. 2−56272
molecular parameters 2−42927
molecule, collisional reaction with Ba, laser-induced fluorescence meas. of product internal state distribution 2−61770
molecule, collisions with H atoms, electron loss cross sections 2−64216
molecule, core excited resonances, electron transmission spectroscopic investigation 2−46547
molecule, elastic electron scatt. and excitation of first vibr. level 2−77161
molecule, energy levels, analytic independent particle model 2−73254
molecule, pot. curves for lowest three states, CI treatments 2−80012
molecule, reactive collision with C^+ at 3 to 100 eV, calculated cross sections for mass transfer, molecular and dissociative charge exchange reactions 2−48322
molecule, spin-orbit contribution to zero-field splitting 2−42925
molecule, tunable Raman, excitation and vibr. relax. 2−53023
molecule, u.v. photolysis, optical emission from $O(^1D)$ and $O_2(b^1\Sigma_g)$ 2−61801
natural-gas-O_2 flames, impingement heat transfer rates 2−52288
5577 A nightglow and lunar semidiurnal variation 2−65891

Oxygen continued
North Atlantic Ocean, salinity, temperautre and o-profiles 2−75413
innuclear fuels, chemical anal. 2−74176
nuclei, geomagnetically trapped 2−65933
O_2 and O_3 absorption in atmosphere of solar radiation in 2150 Å region 2−65766
ocean, minimum layer depth and surface of no motion 2−57850
photo-ion drift vel., diffusion coeffs. and temps. 2−64339
photodissociation rates in mesosphere in lower thermosphere 2−65830
plasma, e.m. absorption, 50-70 MHz 2−74368
in polystyrene, contact charge transfer complexing 2−72580
pulsed discharge production in visible range, use for laser pumping 2−69890
pumping effect of W cathodes, rel. to ionization gauges and mass spectrometers 2−48943
pumping effect of W cathodes, rel. to ionization gauges and mass spectrometers 2−48943
quenching of $CO(a^3\Pi)$, rate coeffs. 2−64213
reaction with S on Ni surface 2−78184
self-diffusion in dolomite, obs. using isotopic exchange 2−68855
solar atmosphere, density dependent ionization balance 2−66231
solar flares, 1971, January and September, composition and energy spectra of heavy nuclei, 0.5 to 40 MeV per nucleon 2−58556
solubility in Cu single cryst., 350-1000°C 2−56926
solubility in organic electrolytes, rel. to air electrode feasibility for energy conversion 2−84652
solubility in UN, 1600-1900°C 2−71649
solubility of Ce, Pr, and Nd in O-enriched Cr 2−43830
sorption on CeO_2, e.s.r. study 2−47156
in steel, stainless, effect on microstruct. and props. 2−53899
stratosphere, O_3 concentrations rel. to photodissociation of O_2 by solar radiation 2−84837
surface reaction, with Ge, LEED and conductivity obs. 2−50448
thermionic converters Cs_2O-Cs soln. as source of Cs and O_2 2−49280
thermosphere, mass spectrometry, O/N_2 and O/O_2 ratios 2−65824
thermosphere, molecular densities, from Ariel 3 measurements 2−51631
thermospheric abundance variation, 6300Å twilight airglow obs. 2−58055
thermospheric densities, meas. with rocket-borne open-source mass spectrometers 2−68929
transfer across gas-liquid fluidized beds 2−67547
Van der Waals forces for systems involving non-spherical atoms 2−63998
vibrational excitation and electronic excitation electron energy transfer 2−72865
vibrational relaxation, transient stimulated Raman scatt., obs. 2−56150
viscosity and second virial coeff., m-6-8 pot. analysis 2−77370
viscosity and thermal conductivity coeffs. calc. using modified Enskog theory over wide temp. and density range 2−64227
Al film, effect on electromigration 2−50703
Ar-O_2 system, solid, lattice mechanics, Raman spectra and luminesc. sideband obs. 2−75310
inAr, solid, mol. oxygen luminesc: and excitation spectra at 4.2K 2−48215
CS_2-O_2 chem. laser, c.w. overtone bands 2−49360
CS_2-O_2 CW chem. laser, reactions producing vibrationally excited CO 2−79202
CaF_2 crystal growth, removal by CoF_2 scavenger 2−50568
Cs-O_2 sources in systems for thermionic converters 2−63222
p-GaP:Cu,O, bound exciton luminesc., emission and excitation spectra 2−78131
GaP:O p-n junction, deep double electron O trap transitions, photocapacitance obs. 2−75013
n-GaP:Te,Zn,O, electrolum., mean electron conc., influence of Te content 2−57381
GaP:Zn, O, light emitting diode, efficiency shift under forward bias 2−75181
p-GaP:Zn,O, donor electron capture cross sections, rel. to quantum efficiency limits 2−68681
GaP:Zn,O, luminesc. time response rel. to multiple trapping at Zn-O impurity centres, 4-120K 2−61696
p-GaP:Zn,O, photolum. efficiency and kinetics of Zn-O complex formation 2−51368
p-GaP:Zn,O, recomb. of electrons bound to deep neutral donors and acceptors 2−68682
p-GaP(Zn,O), minority carrier lifetime, luminesc. decay obs. 2−48221
n-Ge:O, γ-irrad., Hall mobility, anisotropy 2−54196
$H_2/O_2/N_2$ flames, radical recomb. reactions, HO_2 participation 2−65373
$H_2/O_2/N_2$ flames, with Cr and K additives, electron attachment and negative ion form. 2−72555
$H_2/O_2/N_2$ mixtures, self-inflammation rates 2−81488
$H_2 + O_2$ on Cu surface, mechanism 2−54531
K-O_2, spin exchange scatt. obs. 2−67541
$NO + O \rightarrow NO_2 + h\nu$, air-afterglow reaction mechanism 2−68773
$N_2 + O_2$ collisions, vibr.-vibr. energy exchange 2−83407
in Nb, cold-worked or irrad., role in recovery 2−47404
inNb, Snoek peak, grain size effect 2−50736
O_2/H_2 combustion, shock-induced 2−83651
O/N_2, O/O_2 abundance ratios in thermosphere rel. to density-temperature phase delay 2−65816
O/U ratio meas. in U oxides reactor fuels, review and comparisons 2−74155
O/heavy metal atom ratio meas. in unirradiated mixed Pu/U oxides reactor fuels 2−74154
O/metal ratio in Pu/U oxide reactor fuels, gravimetric methods of study 2−74152
O/metal ratios in Pu/U oxide reactor fuels, comparison of two determ. methods 2−74153
O_2-Ar mixture, excitation by low energy proton bombardment rel. to atmospheric gases 2−84792
O_2-Ar mixture, spectra by proton bombardment 2−74235
O_2-CO gas mixtures ionization 2−60288
O^{5+}-Ca collisions, observation of Kα hypersatellites 2−64046

Oxygen continued
O_2-CmO_x, phase reactions during isobaric thermogravimetric analysis 2–74927
O-Cs layers, on GaAs and $InAs_{0.4}P_{0.6}$ cathodes, thickness rel. to photoemission 2–75194
O_2-H_2 mixtures, ioniz., non-attaching gas behaviour of oxygen 2–53246
O_2-H_2O system, formation and decomposition of water cluster ions 2–57414
O_2-H_2S balance in water of Black Sea 2–44645
O_2-He high pressure medium, speech intelligibility 2–73212
O_2^+-He collisions, vibrational excitation of diatomic Morse- oscillator 2–70806
O_2-N_2-He-CO laser Cw operation in some CO lines below 5.0 μ 2–45726
O_2-N_2 mixtures, ionization behind shock waves 2–77302
O^+-Ne close-encounter collisions, 50-200 keV, study of inner shell excitations 2–79914
O_2-Pt system, thermal cond., accommodation effect 2–67734
O, Martian airglow, u.v. spectral obs. 2–66178
O, thermospheric, longitudinal variations in density indicating magnetic control of polar heat input 2–65827
O, upper atmosphere, concentration, semiannual variations 2–48529
O concentrations, atmospheric, from incoherent-scatter and satellite-drag data 2–65826
O I 1304 and 1356 Angstroms lines intensity rel. to O concentrations in upper atmosphere 2–78567
O I lines in auroral u.v. spectrum 2–65897
O I reson. lines in far-u.v. spectrum of Venus 2–58515
O II, 3p and 3p′ level radiative lifetimes 2–76985
O II, mean lives and g values of beam-foil excited levels, suppression of optical cascading effects 2–79910
O IV-Vi, lifetime determ. in u.v., beam foil technique 2–56096
O IV, electron impact ionization, calc. for $1s^22s^22p$ configuration 2–46451
O ions, radiative lifetimes for u.v. transitions by pulse decay method 2–46413
O layer in upper atmos., estimates of height and concentration 2–48527
O λ6300 and λ5577 spectral line profiles, from twilight and nightglow, det. of neutral temp. in ionospheric F_2 and E-regions 2–65973
O nightglow emission at 5577 Angstroms during 1958-67 period above Ashkhabad 2–84881
O nighttime 6300 Angstroms airglow emission at magnetic equator rel. to ionospheric anomaly 2–84880
O photoionization, by soft X-rays, meas. of total and relative abundances of thermal energy ions and dissociation cross section 2–80024
O red emission, auroral, energy release in upper atm. during geomag. disturbances 2–81717
O VI solar spectral line, x.u.v., rocket measurements 2–55167
O VII in D plasma, meas. of depopulation of $2^3P_{0,1,2}$ triplet levels by electron collisions 2–79961
O^-, O_2^-, O_3^- ions, mobilities and ion-mol. reaction rates 2–53248
O^-, self-consistent symmetries, stability 2–76986
O^- formation from CO by electron impact 2–83415
O^- production in dissociative electron capture by CO_2 2–80026
O^+, dependence of calculated production rates on solar activity 2–48464
O^+, O^- ion-pair production from O_2 by He metastable states 2–83260
O^+, polar wind distributions, model 2–81698
O^+ $(^4S) + N_{2(v)}(^1\Sigma)$ crossed molecular beams, cross section for formation of NO^+ 2–54530
O^+ beam interacting with surface, obs. of mass spectrum 2–79849
O^+ ion beam, optical spectra Zeeman splitting 2–70577
O^+ ion concentrations in ionospheric F_2-layer 2–72895
O^+ ion distribution and vertical motions in lower part of F-region 2–72894
O_2, bubble formation and removal in glass melts 2–56551
O_2, collision induced transitions causing airglow 2–65887
O_2, dissociative excitation of vacuum u.v. emission by electron impact, cross section meas. 2–42900
O_2, electron affinity determ. from binding energy of O_2^- by Hess cycle 2–50019
O_2, electronic energy transfer from $^{32}O_2(a^1\Delta_g)$ to $^{36}O_2(X^3S_g$-), meas. of rate constant 2–53103
O_2, fine struct. parameters of $B_3\Sigma_u^-$ state 2–64150
O_2, H_2, Cl_2, subsonic flow, photochemical initiation of combustion 2–84660
O_2, impact line shift in 0.762 μ band 2–77092
O_2, ionization extrapolated ranges for Ar ions, 0.3-1.0 MeV 2–79917
O_2, laser magnetic resonance lines obs. 2–74274
O_2, low energy electron attachment at v. high gas density 2–50222
O_2, O_2-Ar, and O_2-N_2 mixtures, meas. of microwave absorption in 48-81 GHz region using Fabry-Perot interferometer 2–74273
O_2, quenching of triplet excited states of polynuclear hydrocarbons, possible effects of magnetic fields 2–50124
O_2, radiative transfer, 100 to 1000 K, Planck mean absorption coeff., total emissivity 2–76391
O_2, self-consistent procedures for generalized valence bond wavefunctions 2–53012
O_2, solid, model for lattice vibrs. 2–43959
O_2, solid and liq., charge transport processes 2–77820
O_2 7620 Angstroms A-band observations of Mars during and after 1971 dust storm 2–78549
O_2 7635 Angstroms band observations in atmospheres of Mars and Venus 2–78548
O_2 A-band absorption lines at different pressures, equivalent widths 2–46570
O_2 A-band at 7620 Å, detection in Martian atmosphere 2–69157
O_2 absorption cross-section rel. to H Lyman-α determinations of upper atmospheric pressure, density and scale height 2–65817
O_2 atmospheric microwave emission, radiometric ground-based observations 2–68928
O_2 collisions with He(2s), meas. of electron capture cross sections 2–56123

Oxygen continued
O_2 dissolved in seawater, and ^{18}O profiles in dissolved O_2 at Geosecs II in North Atlantic Ocean 2–75470
O_2 doped spherical laser plasmas, high intensity X-ray spectra and stimulated emission 2–74378
O_2 effect of VV transfer processes on rate of thermal dissociation 2–67456
O_2 emission in night glow of Martian atmosphere, height of emitting layer 2–55145
O_2 excitation cross sections and intensity ratios in auroral conditions 2–84872
O_2 gas, meas. of thermomagnetic force on thin disc in 30-35°C range 2–43264
O_2 gas flow condensation in boundary layer 2–77354
O_2 in solar sunspot spectrum, 4900-6441 Angstrom range 2–62743
O_2 labile negative ion, electronic and nuclear magnetic resonances 2–74264
O_2 luminescence, energy dependence of collisional deactivation cross section 2–46646
O_2 Martian abundance upper limits and mixing ratio with CO_2 from photoelectric spectra 2–78550
O_2 photoelectron spectra at 304 Å 2–80058
O_2 Raman scattering cross sections and depolarization ratio 2–53026
O_2 rotational Raman spectra, use of fixed path length etalon Fabry-Perot interferometer for meas. of wavelength of individual lines 2–74250
pO_2 telemetry system for obs. during exercise 2–82011
O_2 three-body electron attachment coeff., low temp. meas. 2–53247
O_2 vibrational Raman scattering 2–46566
O_2^-, laser photodetachment and photoelectron spectroscopy determ. of structure of O_2^- and electron affinity of O_2 2–53028
O_2^- chemisorbed on thermally activated MgO powders, e.s.r. obs. 2–56602
O_2^- ion, in synthetic sodalite, photolum. spectra, 4.2-300 K, fine struct., multiband spectra 2–81422
O_2^- labile ions, stimulated emission during d.c. discharge 2–46793
O^{2+}, lateral diffusion in O_2 2–43204
O_2^+, low energy, bombardment of Pb, oxide formation 2–61791
O_2^+, O_2^+ formation and loss in Kr-O_2 afterglow plasmas, possible ionospheric implications 2–70889
O_2^+, spin-orbit coupling const. in $A^2\Pi_u$ state determ. from rotational term values of 1-7 and 0-8 bands 2–70721
$O_{2(3)}^-$ ions in alkali metal superoxides and ozonides, Raman spectra 2–81354
O_3, atmospheric, trace material obs. program in atmosphere 2–62152
O_3^- anion isolated in Ar matrix, vibrational and electronic spectra, 5100-3700 Å, determ of v_3 2–70720
O_3^- anions in Ar matrix, spectrum and struct. 2–56191
O_4- anions in Ar matrix, spectrum and struct. 2–56191
O^{7+}, hyperfine interaction of $^{18}O[2+]$ at 1.98 MeV 2–52906
$O(^1D)$ quenching in collisions with N_2, curve-crossing model 2–67416
$O(^1D) + O_3 \rightarrow 2O_2\dagger$, $2O(^3P) + O_2$ energy distribution of products, ozone u.v. photolysis 2–84668
$O_2(^1\Delta_g)$ altitude profile at night 2–72837
$O_2(^1\Delta_g)$ and $O_2(^1\Sigma_g)$ chem. excitation in auroras 2–58060
$O_2(^1\Delta_g)$ lifetime in solution, study of bimolecular loss processes 2–51464
$O_2(^1\Delta_g)$ twilight emission, altitude profile 2–58054
$O_2(^1\Delta_g) + O_3$ reaction rates 2–57413
OI 1304 Å emission obs. by Mariner 9 2–58505
OI 5577 Å airglow observations at Toronto using Hadamard photometer 2–72834
OI 5577 Å line emission at auroral zone latitude rel. to O concentrations 2–84890
OI 6300 Angstroms airglow emission, predawn enhancement above Abastumani 2–84883
OI $(^5S^0)$, dissociative excitation, absolute cross sections and radiative lifetime 2–56106
OI (6300 Å) emission, global mapping 2–62337
OI (6300 Å) emission, post sunset enhancement 2–62342
OI (6300 Å) emission, pre-dawn enhancement 2–62341
OI (6300 Å) night airglow, equatorial anomaly 2–62340
OI (6300 Å) night airglow, low latitude phenomena 2–62339
OI allowed transitions in airglow and aurora 2–48547
OI emission at 6300 and 5577 Å in auroral arc event 2–72839
OI solar u.v. line anal., statistical equilibrium and radiative transfer equations 2–51847
OII 3727 Anstroms forbidden line doublet, observations in Orion Nebula 2–55021
$O(^3P)$ addition to simple olefins, activation energies 2–84621
$O(^3P)$ atoms, addition to propylene by flash photolysis, absolute rate constants 2–44492
$O(^3P) + CO \rightarrow CO_2$, rate coeffs., meas., 250-370K 2–51438
$O(^3P)$ + benzene, rate constant meas. 2–61778
O^1S atoms in pulsating aurora, method for estimating indirect process in production 2–84888
$O(^1S)$ deactivation by CO_2, O_2, N_2, Ar, temp. depend. 2–79871
^{15}O, in vivo metabolism meas. 2–69388
^{15}O, production and use in metabolic studies 2–69389
$^{15}O_2$, use in clinical research 2–69387
^{16}O ion beam bombardment of NaI(Tl) at intermed. velocities, track-account theory 2–70316
$^{18}O/^{16}O$ abundance ratio in Amery Ice Shelf, Antarctica, evidence for bottom freezing 2–68852
$^{18}O/^{16}O$ ratio, ocean isotope evolution and growth, model 2–84749
^{18}O concentration, reef corals, temp. dependence 2–65592
^{18}O in atmospheric precipitation, model 2–62240
$O^+ + CO \rightarrow CO^+ + O$, apparent charge transfer reaction, meas. of cross section from threshold to 100 eV 2–80133
$O + CS \rightarrow CO\dagger + S$, chem. laser studies of initial vibr. distrib. of CO 2–72552
$O^+ + N_2 \rightarrow NO^+ + N$, ab initio calculation of potential energy curves 2–44468
$O_2 + N_2$ glow discharge, electron energy distrib., new probe technique 2–64348
O_2 + Na(K) reaction in Ar matrix, Raman spectra of products 2–61776

Oxygen continued
- $O + O_3$ reaction, rate constant and rate expression direct determination in flow system 2–61769
- $O^- + O_2^+$, $O^- + Na^+$, $O^- + NO^+$, mutual neutralization rates, ionospheric D-region 2–65969
- $O_2^+ + O^-$, mutual neutralization rates, ionospheric D-region 2–65969
- $O_2\dagger + O(^3P)$ vibrational energy transfer, O_3 photolysis 2–51465
- $O_2 + Xe^+ \rightarrow Xe + O_2^+$, charge transfer cross sections of $^2P_{3/2}$ and $^2P_{1/2}$ ions 2–70625
- $5O_2 + 10N_2$ + propane mixtures shock and detonation speeds 2–83647
- O + acetylene totally inverted vibr. population of CO 2–61777
- $O(2^1D_2)$, electronically excited, kinetic study by time-resolved atomic absorption spectroscopy in vacuum u.v. 2–83168
- $O_2^+(b^4\Sigma^-_g)$ collisional deactivation rates for O_2 and N_2 2–77172
- $O_2(^1\delta_g)$, Penning ionization by $Ar(^3P_1)$ 2–53041
- Si:Ge, O, C, low temp. electron irrad. damage, i.r. obs. 2–48192
- Si:O, lattice damage due to ion implantation, e.p.r. obs. 2–60780
- inSi, i.r. and activation analysis 2–71502
- in Ta-W-Hf alloy, effect on tensile props. 2–43862
- $U + O_2 \rightarrow UO_2^+ + e$ chemi-ionization, determ. probability of occurrence 2–68766
- $U^+ + O_2(N_2) \rightarrow UO^+ + O$, determ. of reaction rate from thermal energy to 5 eV using drift mobility-tube-mass spectrometer 2–68766
- W:O, grain boundary segregation, field run microscopy obs. 2–53746
- (ZnO-MgO):Fe,O photoconductor transient effect, shallow trap obs. 2–84377

Oxygen compounds
- $A^IB^{III}O_2$ with rhombohedral α-$NaFeO_2$ structure, Raman and i.r. spectra 2–72321
- magnetic phenomena of surface gas-solid interactions 2–84395
- metal oxide structures, microanalysis 2–77540
- metal oxides, elec. cond., characts., classification 2–57106
- metal oxides, reduction by fuels, mechanisms 2–44478
- OH radiosource W3, variability in 1665 MHz spectrum 2–58413
- oxides, complex, flux growth 2–60717
- oxides, high temp. coatings, deposition from fused salts and by ion plating 2–50860
- ClOO radical in Venusian atm., structure and stability 2–78559
- Cu-P-O system phase relations 2–50962
- Eu-Fe-O system, phase relations and cpd. formation 2–47710
- Fe-Cu-O system, equilib. phase diagram detn. 2–64818
- Fe-Mg-O system, activities, calc. by Darken's method 2–43815
- Fe-Mn-O system, activities, calc. by Darken's method 2–43815
- Hf-O system, near $HfO_{1/6}$, interstitial order-disorder transform. 2–68205
- Nb-O alloys with Zr and Hf additions, electron microscope obs. 2–43857
- Nb-O solid soln., form. of Nb_4O during decomp., annealing effects, 500-700°C 2–53902
- OBF, infrared matrix isolation spectrum 2–64151
- OCS, (01^10) vib. state, determ. of elec. and mag. moments 2–83245
- OCS, forbidden character of 2000 Å transitions 2–56186
- OCS, general quartic force field, calc. using Parr-Brown anharmonic potential function 2–52999
- OD, wavenumbers of $A^2\Sigma \rightarrow X^2\Pi$ (0, 0) and (1, 0) bands 2–67497
- OD^- ion, diffusion in fluorapatite 2–77609
- OF free radical, Raman spectra 2–51466
- OH-, in RbCl, Arrhenius relax., dielec. susceptibility study 2–65050
- OH-, reorientation rate in RbBr, calc. from phonon spectra 2–61080
- OH, interstellar, in direction of Cygnus X-3, 18 cm. obs. 2–81849
- OH, interstellar, interferometric obs. of $^2\pi_{3/2}$ $J = 5/2$ microwave transition 2–75792
- OH, mirowave spectra, transitions 2–76542
- OH, molecular constants from u.v. spectrum 2–64152
- OH, nightglow emission, intensity ratio bet. (5,1) and (9,4) bands 2–72836
- OH, OD free radicals, laser oscill. in pure rot. transitions 2–56192
- OH, on quartz, refl. spectra obs. 2–48163
- OH, pot. energy curves of ground states 2–60026
- OH, vibration-rotation interaction in calculated band strengths 2–46571
- OH, wavenumbers of $A^2\Sigma \rightarrow X^2\Pi$ (0, 0) and (1, 0) bands 2–67497
- $OH + NO_2 + Ar \rightarrow HNO_3 + Ar$ reaction rate const. determ. by u.v. fluorescent scatt. 2–81491
- OH abundance between interstellar clouds, upper limits in high-latitude directions 2–81817
- OH airglow at 2.2 μ rel. to possibility of ground- based observations of zodiacal light 2–65886
- OH astrophysical masers, parametric down conversion 2–62590
- OH emission, auroral, energy release in upper atm. during geomag. disturbances 2–81717
- OH emission spectra, intensity variations, vibrational and rotational temps. 2–46572
- OH groups, dependence of torsional vibration frequency on H bond energy 2–42857
- OH i.r. emission from NML Cygnus 2–55045
- OH i.r. sources V Mic, R Hor and VX Sgr, correlation of i.r. colour with velocity separation of emission peaks 2–48755
- OH i.r. stars, maser emission at 1612 MHz 2–81830
- OH in atmosphere, meas. of small relative concentrations using high-power frequency-controlled dye laser 2–42109
- OH in Hoffman i.r. sources 2–81870
- OH in interstellar medium, amplified spontaneous emission 2–55075
- OH interstellar molecule, pumping by polarized i.r. radiation, maser emission 2–81851
- OH maser, at HII region boundaries, gain parameters 2–69047
- OH nightglow emissions, spectrophotometric study 2–48546
- OH radiation from interstellar medium, models 2–62592
- OH radicals formed from water of crystallization, role of H-bonding 2–81495
- OH radiosources, classification 2–44894
- OH reactions with H_2, D_2 and CO, pulsed vacuum u.v. obs. using reson. fluoresc. 2–84665
- OH rot. temp. in nightglow 2–54882
- OH rotational temp. meas. in Ar luminescent-arc discharge 2–43210

Oxygen compounds continued
- OH stars, emission spectra rel. to laser and maser mechanisms 2–51754
- OH^-, in glass, quenching of rare earth fluoresc. 2–54467
- OH^-, in KCl, X-irrad., conc. effect on F-centre formation 2–47449
- OH^- in alkali halides, tunnelling levels, low temp., thermal cond. obs. 2–71758
- OH^- influence on water diffusion in KCl crysts. 2–60831
- OH^- ion, in RbBr and RbI, paraelastic alignment 2–61596
- $OH(A^2\Sigma^+, v'=0)$, rotational excitation from dissoc. collision of H_2O with metastable Ar 2–64215
- $OH(A^2\Sigma^+) + Ar$, near resonant vibration-rotation energy transfer calc. of cross sections and rate consts. using IOS and DW approx. 2–70818
- $OH(^2\Sigma^+)$ radicals, rotationally excited, formation in water vapour discharge 2–60027
- $OH(X^2\Pi)$ formed in atomic collision, determ. of wavefunctions and energies using finite-difference boundary value method 2–70616
- Ta-O system, high temp. solid solubility limit and phase studies 2–50975
- Ti-V-O and Ti-V-Al-O solid solutions, charact. temp. and elasticity modulus 2–50844
- U-O system, oxidation equilib. study 2–44487
- Zr-O alloy, strain-ageing, internal friction and electron microscope obs. 2–47599
- Zr-O α solid solution, cryst. struct., neutron and X-ray diffr. obs. 2–71443
- Zr-O dil. alloys, internal friction peaks 2–50737
- Zr-O system, near $ZrO_{1/3}$, interstitial order-disorder transform. 2–68205

Ozone
- 9.6 μm band in atmospheric spectra, elimination of cloud effects 2–65662
- absorption in Martian north polar region 2–75896
- atmosphere, biological screen, history of life 2–78348
- atmospheric, absorption of radio waves 2–48518
- atmospheric, distrib. effects on transmittance 2–65771
- atmospheric, effect on radiative equilibrium 2–62262
- atmospheric, measurements, 1969, April, May and June 2–78351
- atmospheric, nighttime number density from stellar occultation data 2–58034
- atmospheric, power spectrum analysis during summer season, periodicities 2–51598
- atmospheric, total content and distribution obs. using satellite 2–48456
- atmospheric, total content correl. with ionospheric D-region radio wave 2–78399
- atmospheric, vertical sounding with Nimbus IV i.r. spectrometer expt. 2–48452
- atmospheric absorption of solar radiation rel. to radiation budget of stratosphere 2–65663
- atmospheric content, Dobson spectrophotometer and filter ozonometer obs. 2–48468
- atmospheric content det. using satellite horizon obs. in 1042 cm^{-1} band 2–48458
- atmospheric content using astronomical multi-colour extinction measurements 2–54858
- atmospheric data, lunar influences 2–48469
- atmospheric extinction measurements, departures from Rayleigh scattering rel. to O_3 absorption 2–54860
- Dobson spectrophotometer, circuit modification 2–75539
- excited states, calculation 2–42924
- Martian atmosphere, minor constituents, Mariner borne i.r. spectrometer 2–69156
- mesospheric abundance, seasonal changes inferred from twilight $O_2(^1\Delta_g)$ emission 2–57951
- mesospheric content during solar proton event 2–84803
- photolysis, $O_2\dagger + O(^3P)$ vibrational energy transfer 2–51465
- photolysis by u.v. radiation, $O(^1D)$ reactions 2–72573
- spectrum, analysis of $(\nu_1 + \nu_2 + \nu_3)$ combination band 2–64153
- stratosphere, O_3 concentrations rel. to dissociation of H compounds and N oxides 2–84837
- tropospheric distrib., measurements aboard airliners 2–57950
- urban atmosphere, meas. 2–62144
- O_3^-, calc. of g values 2–50066
- O_3^-, in drift tube, photodetachment cross section 2–42926
- $O(^1D) + O_3 \rightarrow 2O_2\dagger$, $2O(^3P) + O_2$ energy distribution of products, ozone u.v. photolysis 2–84668

Ozonosphere *see Atmosphere*

p-n junctions *see Semiconducting devices/junctions*

P-V-T relations *see Equations of state*

Pair creation *see Electron pairs; and under individual particles, e.g. Mesons*

Palaeomagnetism *see Rock magnetism*

Palladium
- atom, e.u.v. spectra, energy levels 2–64001
- inAuGa$_2$, effect on Fermi surface 2–51078
- band struct. and density of states, pseudopot. calcs. 2–47811
- colloid particles, struct. depend. on electrolytic deposition parameters 2–83818
- diffusion of H, at elevated press. 2–77620
- diffusion of H, coeff. meas. by electrochem. methods 2–77602
- diffusion of H, quantum interpret. 2–71537
- diffusion of hydrogen, equil. and kinetic isotope effects 2–77619
- diffusion of hydrogen, jump model, neutron quasielastic scatt. obs. 2–83999
- electrodeposition of powder, from chloride solutions 2–68799
- electron phonon enhancement factor, from specific heat data 2–64932
- epitaxy by vapour deposition, low temp. 2–53575
- film, low-energy electron beam transmission, orientation depend. 2–47787
- film deposition by sputtering, temp. rise as a function of applied power 2–67913
- neutron transmission measurement 2–74132
- solubility of hydrogen, rel. to Fermi level position and clustering 2–77716
- thermal expansion, and elec. cond., 77-300K, effect of paramagnons 2–61226

Palladium continued
- thin oxide formation in aqueous electrolyte solutions passing anodic current, reaction kinetics 2−68784
- He migration and release after implantation 2−50639
- Pd:Er^{3+}, e.s.r., exchange coupling const. and hyperfine splitting obs. 2−61732
- Pd:Gd^{3+}, paramag. resonance, resolved fine structure 2−68733
- Pd-Ag powder, soln.-precip. sintering in presence of reactive glass 2−80878
- Pd-H and Pd 24% Ag-H foils, electron microscope examination 2−56948
- Pd^{2+}, activator in CaS:Bi, Pd, thermoluminesc. 2−54475
- Sn-Pd sols, Mossbauer meas. in which core and stabilizing double layer distinguished 2−80491
- Ti(Pd)Ag passivated contacts, use with Si solar cells 2−59057

Palladium compounds
- alloyed with nonmag. impurities, magnetoresist., carrier scatt. 2−61152
- benzoylacetonate, VO^{2+} doped, e.p.r., ^{51}V quadrupole moment obs. 2−61741
- hydrides, clustering model rel. to sp. ht. anomalies 2−77716
- Ag-Pd-H system, phase diagram 2−74953
- AgPd system, density of states, X-ray photoemission obs. 2−61179
- Au-Pd alloy, short-range order formation, resistivity obs. 2−74894
- Ce$_x$La$_{1-x}$Pd$_3$ alloy, Kondo effect, elec. resistivity and heat capacity 2−51098
- CeRh$_x$Pd$_x$ alloys electronic state, magnetic susceptibility and lattice spacings 2−81317
- Cr-Pd, structure of K$_{\beta 5}$ emission band, X-ray study 2−72378
- Cu-Pd alloy, disordered and ordered, band struct., optical absorpt. study 2−84237
- Cu-Pd alloys, influence of domain size and ordering on mech. props. and elec. resist. 2−68506
- Fe-Pd-H system, phase diagram and Mossbauer spectrum 2−74953
- Fe-Pd alloys, f.c.c., mixed exchange interactions, neutron scatt. obs. 2−84421
- Fe$_x$Pd$_{80-x}$P$_{20}$ ($13 \leqslant x \leqslant 44$), amorphous alloy, magnetic properties study from Mossbauer effect of ^{57}Fe 2−65114
- Mn$_3$Pd$_5$ phase, crystal and magnetic struct. 2−83960
- Ni-Pd-P-base, amorphous, containing Fe, resistivity temperature relationship, T$^{-1/2}$ singularity 2−44215
- Ni-Pd alloys, matrix and impurity cluster polarization 2−44358
- Ni-Pd alloys, Mossbauer effect of ^{61}Ni, conc. depend., hyperfine field interactions 2−72285
- Ni-Pd disordered alloy, spin susceptibility calc. 2−65117
- Ni-Pd films, magnetoresist. anisotropy 2−44266
- Pd/Ag/H system, form. and decomp. equil. 2−77715
- Pd/Pt/H system, form. and decomp. equil. 2−77715
- Pd/Rh/H system, form. and decomp. equil. 2−77715
- Pd-Ag alloy, low field Hall coeffs. at 4.2K and 300K 2−61188
- Pd-Ag alloys, diffusion of H, coeff. meas. by electrochem. methods 2−77602
- Pd-Ag alloys, diffusive motions of hydrogen 2−77618
- Pd-Ag alloys, solubility and electromigration of H$_2$ and D$_2$ 2−83990
- Pd-Ag alloys, solubility of hydrogen, rel. to Fermi level position and clustering 2−77716
- Pd-Co(Fe)(Mn) dil. alloys, mag. ordering obs. 2−81246
- Pd-Fe alloy, powder remag. mechanism, hysteresis characts. 2−48097
- Pd-Fe dil. alloy, elec. resist. behaviour in crit. region 2−57279
- Pd-H system, isotope equilib., 77K 2−68154
- Pd-H system, superconductivity, elec. resist. study 2−54135
- Pd-H systems, phase transition due to elastic interaction 2−77744
- Pd-Mn dil. alloys, giant moment of Mn 2−44257
- Pd-Mo system, interdiffusion coeffs., temp. and conc. depend. 2−56762
- Pd-Ni-H system, superconductivity, elec. resist. study 2−54135
- Pd-Ni alloy, magnetoresist., due to scatt. by spin fluctuations 2−48058
- Pd-Ni(Pt) alloy, spin paramag. susceptibility, calc. 2−65125
- Pd-Pt alloy, low field Hall coeffs. at 4.2K and 300K, two band model 2−61188
- Pd-Rh alloy, low field Hall coeff. at 4.2K and 300K. 2−61188
- Pd-Rh alloys, solubility of hydrogen, rel. to Fermi level position and clustering 2−77716
- Pd-Ru alloy, low field Hall coeff. at 4.2K and 300K 2−61188
- Pd-V system, diffusion processes, phase obs. 2−53770
- Pd-rare earth dil. alloys, magnetiz., susceptibility, moments 2−44224
- Pd-rare earth intermetallic compound, electrical resistivity obs. 2−51102
- Pd complex, Pd(II)-bis-biguanide perchlorate, crystal structure, preliminary data 2−50625
- Pd complexes, magnetic susceptibility of new complexes, Gouy method 2−77979
- Pd II complexes, low-spin trigonal bipyramidal, electronic spectra, temp. dependence of lowest energy ligand field band 2−53031
- Pd$_5$B$_2$, Pd$_3$B, specific resistance and thermal e.m.f. 2−72054
- PdCr$_3$N, crystallographic parameters and struct. transforms. 2−60759
- Pd$_{0.775}$Cu$_{0.06}$Si$_{0.165}$ glassy alloy, electronic and lattice contribs. to sp. ht., excess, 2-18K 2−80916
- Pd$_3$Fe, lattice dynamics, 80K 2−43962
- Pd$_3$Fe spin wave dispersion relation, neutron scatt. obs. 2−61503
- β-PdH, internal friction, temp. depend., peak interpret., 4-200 K 2−77646
- PdH$_x$, energy band calcs., model obs. 2−61187
- PdH$_x$, Knight shifts of ^{105}Pd and proton n.m.r. lines 2−78174
- Pd(II) complexes with N,N′-ethylenebis(acetylacetoneimine), i.r. spectra, normal coordinate analysis 2−70695
- PdRhNi alloy, spin fluctuation resistivity 2−64916
- Pd$_2$Si, formation on Si from Pd film 2−43861
- Pd$_{0.775}$Si$_{0.165}$Cu$_{0.06}$ glass, soft transverse phonon obs. 2−54021
- PdTe$_2$, refl., 1-12.5 eV, rel. to band struct. calc. 2−48161
- Pt-Pd disordered alloy, spin susceptibility calc. 2−65117
- Rh-Pd, disordered alloy, spin susceptibility calc. 2−65117

Paper
- No entries

Paraelectric materials *see Dielectric properties of substances*

Paraelectric resonance
- ion-lattice interaction of noncentral ions in cubic crystals 2−72236
- KCl:Li, generation and detection of 55 GHz phonons 2−84191
- KCl:Li$^+$, of impurity noncentral ion in vicinity of an A-centre 2−78176

Paramagnetic resonance and relaxation
- *see also Acoustic paramagnetic resonance; ENDOR; Lasers; Masers; Spin-lattice relaxation; Spin-spin relaxation*
- 5(NH$_4$)$_2$O.12WO$_3$.5H$_2$O, polycrystalline, centres formed by γ irradiation 2−48349
- acetylene dicarboxylic acid dihydrate crystal, irradiated, free radicals 2−75348
- adamantane, free radicals in high energy irrad. 2−54562
- L-alanine, irradiated, unstable radical CH$_3$CHR, temp. dependence of ESR spectrum 2−68818
- alkali borate glass, X-irrad., hole and electron centres obs. 2−54489
- alkali halide-alkali borate glass hole and electron centres, and halogen atom obs. 2−54489
- alkali halides, F-centre relaxed-excited state detection 2−53749
- alkali halides, irrad. paramag. centre obs., h.f.s., many-electron wavefunction calc. 2−81467
- alkali halides, rare earth doped, Z-centres, optical absorpt. and e.p.r. at 77K 2−71526
- alkylaromatic radical cations, methylene h.f. splittings and methyl hydrogen splittings 2−60046
- alloy, mictomagnetic, rel. to mag. struct. model 2−65166
- amino acid γ-irradiated crysts., study of u.v.-induced free radical conversion 2−84667
- α-amino acid crystals, e.p.r. of VO^{2+} impurity ions 2−84566
- amino acids, γ-irrad., effect of cryst. struct. on stability, yield and shape of spectra 2−81536
- anthracene, electron irradiated, rel. to hole traps 2−51126
- antiferromagnet, linewidth and zero field relaxation time, crit. point anomalies 2−78159
- antiferromagnet with dipolar interaction, linewidth near crit. point 2−75341
- aqueous solutions, identification of H$_3$O radical 2−72583
- aromatic acetylenes, reduced zero field splitting in EPR of photoexcited triplet state 2−68810
- aromatic carbonyl compounds, spin-orbit coupling effects in e.p.r. spectra of lowest triplet states 2−70756
- aromatic ketones, semi-empirical calcs. of zero-field splitting parameters of lowest triplet states 2−80102
- aromatic molecules adsorbed on MgO surface, photoactivation by u.v. radiation, e.p.r. spectra 2−78206
- arsenates, H-bonded ferroelectrics 2−68734
- BDPA film, organic free radical, vapour deposited 2−56598
- benzene solution w. tanone free radical, resonant helix and coil 2−66666
- benzenes, substituted, electronic structs. of lowest excited triplet states 2−60050
- benzophenone:diphenylnitroxide, anisotropic e.p.r. study, meas. of ^{14}N hyperfine tensors and g tensors 2−72474
- biphenyl derivatives in dibenzofuran single crystal, e.s.r. spectra of triplet state 2−64170
- o,o′-bridged biphenyl derivatives in frozen ethanol, e.s.r. spectra, determ. electronic structure 2−64170
- bis-(N-methylsalicylaldiminata)-copper, spin $^1/_2$ system, non Lorentzian line shape obs. 2−65329
- borate glasses, struct. changes 2−54496
- borophosphate glasses, radiation colour centres 2−44444
- butatrienyl radicals isolated in Ar matrices 2−83286
- t-butyl chloride γ-irradiated, e.s.r. evidence for planarity of t-butyl radical 2−74288
- tert-butylperoxy radical, ^{17}O hyperfine coupling consts. 2−65391
- carbazyl, recrystallised samples, e.s.r. line width and exchange narrowing 2−65330
- carbene anthronylidene, e.p.r. spectrum 2−44496
- cellulose triacetate, γ- or u.v. irradiated, e.s.r. obs. of radicals formed 2−44494
- cerium dipicolinate: Ce^{3+}, g-values and g-axes 2−72487
- chalcogenide glass, Mn^{2+}-, Fe^{3+}-, or Gd^{3+}-doped, fine struct. 2−72476
- chlorophyll charge transfer complexes, crystn., exciton character of signal 2−48298
- 8-chloroquinoline, triplet $\pi\pi^*$ state, optically detected spectra 2−46518
- chromocene, zero-field splitting and g-values 2−64174
- chrysene, X-irradiated, e.s.r. examination to investigate stable free radicals formed 2−57393
- cobaltocene, e.p.r. investigation of electronic structure 2−56226
- cross-relaxation between paramagnetic ions in crystals 2−68578
- cross-relaxation in $s=1$ paramagnets, temp. dependence, application of theory to dipolar systems 2−65119
- Cu:Mn, giant e.s.r. transmission through one-sided and two-sided ion implanted Cu foil 2−84569
- cyanoacetohydrazide, X-irradiated, obs. of e.s.r. spectrum of RNHNH type radical 2−81530
- cyclopentanone, microwave- optical double reson. of triplet state 2−80065
- cysteine hydrochloride monohydrate, irrad., radical recomb. study 2−72575
- cystine dihydrochloride, e.s.r. centre formation by monochromatic u.v. radiation 2−61811
- diamond:B, e.p.r. of free and bound holes 2−81458
- 1,4dibromo-naphthalene, of triplet excitons, optical detection 2−81522
- dichlorobis (pyridine)-copper, spin $^1/_2$ system, non Lorentzian line shape obs. 2−65329
- 1,1-difluoroalkyl radical, solution spectra, asymmetric line-width effects in presence of resolved second order splittings 2−56519
- dimer composed of 2 biphenylene subunits, triplet exciton transfer study by e.s.r. 2−46509
- dipeptides., γ-irrad., effect of cryst. struct. on stability, yield and shape of spectra 2−81536
- disordered system, line shape calc. 2−72466
- DL-serine, X-ray irradiated, 153 to 340K, free radicals 2−75350
- DNA radical transfer with protein in DPA 2−60094
- DPPH film, organic free radical, vapour deposited 2−56598

Paramagnetic resonance and relaxation continued
elastomers, detection of free radicals during mechanical testing at low temperatures 2−60886
electric effects, review 2−68728
electron double paramagnetic resonance spectroscopy, multiple quantum transitions 2−73489
electron spin echo envelope, amplitudes of superhyperfine freq. 2−78168
electron-spin polarization, generated by radical-pair mechanism, calc. of limiting polarization 2−54543
e.p.r. and mag. circular dichroism spectrometer 2−78983
e.s.r. spectra, analogue computing system for gaussian and lorentzian simulation 2−45782
e.s.r. spectrometer, fast-sampling, time resolved for photoflash expts. with gases 2−66663
e.s.r. spectrum of u.v. irradiated azobisisobutyronitrile in polycrystalline state 2−75394
ethanol, glassy, effect of dipole reorientation on trapped electron spectra, semicontinuum model 2−44495
ethanol glass, e.s.r. meas. of electron trapping and solvation at 4K 2−61810
ethanol glasses, free radical photoproduction, e.s.r. study 2−81509
europium benzoylacetonate, of Gd^{3+}, cryst. field symmetry 2−81469
exchange interaction meas. technique 2−61730
F-centres, calc. rel. to electronic struct., review 2−56746
Fermi liquids, two component, study of spin waves and their excitation 2−81000
flavoproteins, analysis of in vivo and in vitro e.s.r. spectra of intrinsic spin label ^{2}H-flavin 2−83338
forsterite, of Gd^{3+} and Fe^{3+}, location of droping ions detn. 2−47265
glass, borate, of X-ray induced Ti centres 2−44450
glass, relation to structure 2−54488
glass Ti, e.p.r. centre obs. of hyperfine structure 2−84571
graphite irradiated with heavy ions 2−78152
group II-VI compound, of group IV ion, theory 2−51399
hexachloroethane, γ-irrad., thermolum. and e.s.r. 2−48259
hydrazil, recrystallised samples, e.s.r. line width and exchange narrowing 2−65330
hydrocarbon chains with (α-naphthyl)−$(CH_2)_j$−(α-naphthyl) struct., intramol. collision freq. 2−53067
hydrocarbon chains with (α-naphthyl)−$(CH_2)_j$−(α-naphthyl) struct., intramol. collision kinetics 2−56236
1 and 2hydronaphthyl radicals in naphthalene single crystals, e.p.r. study 2−54499
hyperfine coupling consts. for S=1/2 system, determ. of relative signs through e.p.r., ENDOR, double ENDOR 2−70674
iminoxyl radical with ^{15}N isotope, mol. reorientation character effect on lineshape 2−70773
ion, with orbital ang. momentum, e.p.r. studies of interactions in insulators, review 2−65112
ion-electron recombination in solutions, solvation shell relaxation 2−46934
Karplus-Fraenkel eqn. for ^{13}C hyperfine splitting, linear dependence of spin polarization parameters 2−79986
Kubo Anderson theory using Monte Carlo calc., ESR line shapes 2−73486
lanthanide ethyl sulphate: Gd^{3+}, host lattice effects on e.p.r. spectra 2−48299
lanthanum ethylsulphate, e.p.r. of Gd^{3+} in single crystals below 40G 2−51405
lead acetate hydrate, X-irradiated, Pb$^+$ and PbH^{2+} identification g-factors, ^{207}Pb hyperfine splitting 2−75347
lineshape, effect of coupled coherent and incoherent motion of triplet excitons 2−65320
liquid crystal, nematic phase, degree of order detn. 2−50333
liquid crystal, struct. and dynamical processes determ. 2−83805
lunar fines 'characteristic' resonance, lunar surface oxidation 2−58474
lunar plagioclases, Ti^{3+}, Fe^{3+} and Mn^{2+} obs. 2−62686
lunar rocks, radiation induced e.p.r. signals 2−55123
lunar rocks and fines 2−62648
magnetic alloy, dil., theory 2−78160
magnetic alloy, dilute crystal field effects on line breadth and splitting 2−51401
magnetic field measurement, using e.p.r. magnetometer 2−76441
maleic acid, irrad., electron trapping centre obs. in single cryst. 2−78211
malonamide, X-irradiated, confirmation of σ-radical, e.s.r. spectra obs. 2−64185
malonic acid, irradiated, electron spin-lattice and cross relaxation 2−44442
manganocene, zero-field splitting and g-values 2−64174
metal, conduction e.s.r. 2−57384
metal film, cond. e.p.r. line shapes, theory 2−81450
methyl malonic acid, tunnelling sidebands of methyl group hyperfine structure 2−57389
molecular crystals, irradiated, e.s.r. study of diffusion processes 2−80722
multilevel systems, e.p.r. and stationary ENDOR dynamics, state diff. of populations, elec. simulat. 2−84572
naphthalene crystals, X-ray irradiated, annealing, behaviour of colour centre and e.s.r. spectrum 2−80711
naphthalene ion in low bulk dielec. const. media, linewidth, conc. depend. 2−67841
1,5-naphthyridine, optical detection of e.s.r. in the triplet state 2−57394
nickel sodium triacetylacetonate-dioxane-benzene 2−65122
nitroxide radical solns. electron-electron double resonance, relation to spin relaxation 2−71234
noncrystalline solids, ELDOR, theoretical and exptl. spectra, molecular dynamics 2−65353
optical electron spin polarization in excited triplet states 2−81466
optical techniques, reviews 2−61729
orthorhombic symmetry spin hamiltonian eigenvalues 2−81316
palladium benzoylacetonate, VO^{2+} doped, ^{51}V quadrupole moment obs. 2−61741
paradichlorobenzene, triplet ππ* state, optically detected spectra 2−46518

Paramagnetic resonance and relaxation continued
phenazine, in rigid toluene glass matrix, spin polarization in photoexcitation of triplet state 2−68816
phenylphosphinic acid and salts, X-irradiation, e.s.r. spectrum study of radical formation 2−72584
pi hydrocarbon radicals, ^{1}H and ^{13}C hyperfine splitting, unrestricted Hartree-Fock calc. 2−67453
poly(methyl methacrylate), radiation produced free radicals 2−84671
poly(vinyl chloride), electron and γ-irrad. at 77K, e.s.r. 2−83360
poly-4-methylpentone-1, irradiated, e.s.r. of radical pairs 2−75395
polyethylene, application to study of degradation due to partial discharges 2−74606
polymer, e.s.r. detection of free radical formation during fluorination 2−61771
polyphenylacetylene, also electrical conductivity 2−51127
polyurethane, mechanically induced bond rupture, e.p.r. 2−43711
powder, lineshape calc. 2−65319
propargyl radicals isolated in Ar matrices 2−83286
pulsed e.p.r., review 2−59012
pyrazine, triplet nπ* state, optically detected spectra 2−46518
pyrene-d-10, temperature dependent saturation meas. in photo-excited triplet state 2−84567
pyridines, substituted, electronic structs. of lowest excited triplet states 2−60050
quartz, neutron-irrad., spin relax. rate depend. on static mag. field 2−57391
rare earth ethyl sulphate: Gd^{3+}, obs. at room temp. and 77K 2−75349
rare earth ethyl sulphates, Faraday rot. obs. of relax., interactions contrib. to sp. ht. 2−57314
rare earth insulators: Gd^{3+}, isotropic exchange interaction obs. 2−72487
rare earth-Co Laves phase, $LnCo_2$, correl. with mag. props. 2−81276
rare earth-Ni Laves phase, $LnNi_2$ 2−81277
recrystallized free radical powder, PAC, meas. of line shapes, line widths, g factors of e.s.r. spectra 2−81484
relaxation rel. to phys. processes characteriz. 2−84454
review, transition metal ions in liqs., equilibria of systs. 2−54569
r.f. field effects, spin system quantization axis defn. 2−54502
rubber, free radicals formed during tensile testing at low temp., e.p.r. 2−43710
ruby, influence of lattice defects on e.p.r. line shapes 2−72468
ruby, instabilities near centre of allowed transitions 2−44436
ruby boules, quality estimation from e.p.r. line widths 2−54493
S-state ion, covalency effects 2−48272
samarium ethylsulphate, e.p.r. of Gd^{3+} in single crystals below 40G 2−51405
semiconductor, group II-VI cpds., radiation damage obs. 2−47366
semiconductor, III-V, transition metal doped, anomalous props. 2−68405
semiconductor surface states, correlation with Hubbard model 2−51154
semiconductors, II-VI, deep Cu impurity, dynamical Jahn-Teller interaction 2−80954
signal detection, method using nonlinear classical oscillator operating far from sinusoidal region 2−59011
site assignment of Fe^{3+} in low symmetry crystals 2−44439
sodium methylammonium tungstovanadate, VO^{2+} doped, ^{51}V quadrupole moment obs. 2−61741
spectrum analysis, appl. of tensor operators 2−78156
spin echo, excitation by sound 2−54490
spin labelled fatty acids in oriented lecithin bilayers, moment analysis 2−80063
spin relaxation function, integrodifferential equation governing time behaviour 2−61560
spin system, S=1, reson. shift due to exchange interaction 2−72465
spin-lattice relaxation time, calc. with allowance for spin-spin interaction 2−81312
spin-packet width and spin-lattice relax. time determ. from saturation curves for rapid transit 2−77053
styrene-butadiene block copolymers, mechanically induced bond rupture, e.p.r. 2−43711
succinic acid, ESR studies on radical conversions 2−81528
TCNQ quaternary ammonium salts, triplet paramag. 2−84399
TCNQ salts, dipolar split lines, exciton obs. 2−61742
tetracene, of triplet excitons, spin polarization and singlet exciton fission role 2−81448
tetracene, of triplet excitons, spin polarization and singlet exciton fission role. 2−81449
tetrachlorobenzene in durene, hole burning in optically detected zero-field spectrum using EEDOR 2−84561
thiocarbonyl anion radical, e.s.r. studies of structure 2−53082
thyamine, radiation abstraction of H atoms, analysis by e.s.r. spectroscopy 2−72585
tourmaline, isotropic line, rel. to impurity Fe^{3+} 2−75342
transition metal ions, core polarization, semiempirical law 2−84577
tremolite, natural, containing 0.15% Mn^{2+}, analysis of single crystal e.s.r. spectrum 2−68732
trifluoroacetamide, X-irradiated, analysis of internal rotation of CF_2CONH_2 radical obs. in e.s.r. spectrum 2−81526
triglycine fluorberylate:Cu^{2+}, spin Hamiltonian parameters and hyperfine struct. 2−51409
triglycine fluoroberylate:Cu^{2+}, applic. of rhombic spin Hamiltonian formalism 2−51410
triglycine fluoroberylate, Cu^{2+} aggregate spectrum, h.p. and temp. influence 2−84575
triglycine sulphate, vanadyl-doped, domain struct. changes, obs. 2−77937
trimesitylboron$^-$, liquid and rigid medium ESR spectrum 2−50115
trimethyl phosphite, γ-irradiated, e.s.r. spectrum of radicals 2−81534
trimethyl-lead radical, e.s.r. spectra, determ. of g tensors and hyperfine coupling 2−70795
trimethyl-tin radical, e.s.r. spectra, determ. of g tensors and hyperfine coupling 2−70795
triplet exciton spin systems, Heisenberg exchange 2−68729
triplet spectra, hyperfine anomaly from nuclear spin-forbidden transition, abs. sign determination of zero- field splitting constant 2−57388

Paramagnetic resonance and relaxation continued
Tutton sals, spin system dynamics obs. 2–84445
vinyl radicals isolated in Ar matrices 2–83286
vinyl-type radical in irrad. maleic acid matrix, geom. and electronic struct. 2–64195
yttrium ethyl sulphate:Gd^{3+}, host lattice effects on e.p.r. spectra, lanthanide behaviour 2–48299
zeolite, Y-type, e.p.r. study of Cu^{2+} pairs 2–75343
Ag-Er alloy, dilute, exchange interactions with cond. electrons obs. 2–72467
Ag complex, Ag di-isopropyldithiocarbamate, evidence for spin-spin and spin-orbit interaction 2–44443
Ag halogenides, structure of electronic defects in primary photochemical process 2–49455
α-Al_2O_3:Fe, α-Al_2O_3, Ti and α-Al_2O_3(Fe,Ti), polarized and high resolution UV, visible and IR spectra, e.s.r. spectra 2–78082
Al_2O_3:Ti^{3+}, corundum, g-value calc., Jahn-Teller theory 2–65331
Al_2O_3:V, rel. to phonon scatt. study 2–68214
Al_2O_3-Fe_2O_3 solid solution, mag. interactions, obs. 2–75351
α-Al_2O_3, of Fe^{3+} ions, forbidden transitions 2–78158
As_2Se_3-As_2Te_3(Tl_2Se) (Sb_2Se_3)(As_2S_3) glass, comp. and annealing temp. effects 2–61734
As_xSey glasses, spin conc. and signal intensity 2–65332
Au-Gd alloy, dilute, exchange interactions with cond. electrons obs. 2–72467
BN, hexagonal, due to paramag. centres 2–74804
BN, hexagonal, paramag. centre identification 2–72430
BS, 4K, g tensors, hyperfine structure const. 2–80030
$BaBr_2$, F-centre spectra 2–51336
$BaCl_2$, F-centre spectra 2–51336
BaF_2, linear elec. field effects for Ce^{3+}-F^- tetragonal sites 2–48285
BaF_2, of Mn^{2+}, spin Hamiltonian parameters 2–54497
BaF_2, trigonal Gd^{3+} centres produced by hydrolysis reaction 2–84582
BaO, sites of cubic symmetry, g values 2–54491
$BaSO_4$:MnO_4^{2-}-, anisotropic g and hyperfine tensors deduced from e.s.r. spectra 2–48274
BeO, γ-irrad. induced effects 2–44445
Be_2SiO_4:Cr_2O_3, of Cr^{5+}, 77K and 4.2K, 9.5GHz 2–72477
$Bi_2Mg_3(NO_3)_{12}$.24 H_2O, e.p.r. of Gd^{3+} in single crystals below 40G 2–51405
C, graphitized film, anisotropy of g-value 2–78153
C black family, P33, 4.2-300 K, pheonom. model 2–57390
$CaAl_{12-x}Fe_xO_{19}$ solid soln., $x \leqslant 4.8$, e.s.r. and Mossbauer obs., ferric ion positions 2–75268
CaF_2:Gd^{3+}, second order spin-lattice coeffs., temp. depend. 2–80890
CaF_2:O, meas. of ^{19}F dynamic polarization, e.p.r. investigation 2–51295
CaF_2, linear elec. field effects for Ce^{3+}-F^- tetragonal sites 2–48285
CaF_2, low symmetry complexes involving hydride ions paired with rare earth ions 2–47434
CaF_2, of Mn^{2+}, spin Hamiltonian parameters 2–54497
CaF_2, signals from paramagnetic centres following intense γ-irradiation 2–84529
CaO:Ce^{3+}, sites of cubic symmetry, g values 2–54491
CaO:Fe^{2+}, energy of first excited electronic levels 2–72478
CaO:Fe^{3+}, obs. 2–48275
CaO:Li^+,Na^+, of Mn^{4+} ions, spin Hamiltonian parameters detn. 2–51402
CaO, excited states of F centres, optical detection 2–44437
$Ca(OH)_2$:Mn^{2+}, 4.2–800 K, vibronic effects 2–78163
$Ca_5(PO_4)_3Cl$:Mn^{2+}, site substitution by Mn, field parameters 2–72479
$Ca_5(PO_4)_3F$:Nd^{3+}, e.p.r. obs. crystal field at Ca^+ position 2–78161
CaS:Fe^{3+}, obs. 2–48275
CaSe:Fe^{3+}, obs. 2–48275
$CaWO_4$:Eu^{2+}, elec. field effect 2–48287
CdCN in Ar matrix, chemical bonding 2–50072
$CdCl_2$ crystals, impurity ion spectra at 5 eV, effect of X-, γ-radiation 2–84475
CdF_2:Er^{3+}, C_{2v} local-site symmetry 2–78164
CdF_2:Gd^{3+}, second order spin-lattice coeffs., temp. depend. 2–80890
CdF_2:Mn^{2+}, obs. of hyperfine and superhyperfine splittings in e.p.r. spectra 2–48276
CdF_2, of Mn^{2+}, spin Hamiltonian parameters 2–54497
$CdIn_2S_4$, intrinsic and Co^{2+} doped, effect of S vacancies 2–68735
CdS, paramag. surface centre density meas. 2–65334
CdS hexagonal, Gd^{3+} centres at sites of axial symmetry 2–65333
CdS ligand hyperfine interaction of Ti^{2+} on sites with trigonal symmetry C_{3v} 2–80977
$CdS_{1-x}Se_x$:Mn, Mn^{2+} conc. determ. 2–72481
$CdS_{1-x}Se_x$:Mn^{2+}, hyperfine interaction const., temp. and comp. depend. 2–81456
CdSe, paramag. surface centre density meas. 2–65334
CdSe ligand hyperfine interaction of Ti^{2+} on sites with trigonal symmetry C_{3v} 2–80977
$Cd_{1-x}Zn_xS$:Mn, Mn^{2+} conc. determ. 2–72481
$Cd_{1-x}Zn_xS$:Mn^{2+}, hyperfine interaction const., temp. and comp. depend. 2–81456
$Ce_2Mg_3(NO_3)_{12}.24H_2O$, paramag. relax at liq. He temps. 2–68736
CeO_2, oxygen sorption study 2–47156
CeO_2, u.v. irradiated, hole centre obs. 2–65322
ClCO, ClOO radicals, g-factor and h.f.s. tensors and nuclear quadrupole coupling constants 2–50031
Co rare earth Laves phase, type RCo_2 2–51403
Co(III) dithiocarbamates: Mn^{3+}, e.s.r. spectra 2–48281
Cr complex, di-μ- hydroxotetraglycinatodichromium(III), zero-field splitting, domination by Zeeman interaction 2–80645
Cr_2O_3-Ti_2O_3 solid solution, mag. ordering study 2–48104
Cr_2O_3-V_2O_3 solid solution, mag. ordering study 2–48104
Cr_2O_3, e.p.r. spectra below Neel temp. 2–54492
Cs alums, interpretation of Ti^{3+} e.s.r. spectra 2–81445
Cs_2HfCl_6, of Yb^{3+} in octahedral cryst. field 2–72482
CsHg, free paramanetic van der Waal molecule produced 2–67545
$CsMnF_3$, Neel pt. phenomena 2–68726
$Cs_2SO_4.Cr_2(SO_4)_3.24H_2O$ alum., paramag. spin-lattice relax. times of Cr^{3+} 2–84444

Paramagnetic resonance and relaxation continued
$Cs_2[CuCl_4]^{2-}$, covalency and excited 4p states effects on 3d ground states of Cu^{2+} 2–84578
Cu-Mn dilute alloy, thin film 2–44446
Cu complex, copper picolinate, effect of host lattice on coupling parameters 2–81455
Cu complex copper hydroxyquinolinate effect of host lattice on coupling parameters 2–81455
Cu complexes in solutions, study of metal-ligand bonding, magnetic susceptibility and moment of Cu(II) ion 2–64473
Cu ion, influence of ethanol on first hydration shell obs. 2–64123
Cu^{2+} complex ion, tetragonal, ligand contribution to spin-spin anisotropic hyperfine interaction 2–56168
Cu^{2+} tetragonal complexes, covalency effects in anisotropic h.f.s. 2–84580
CuCl, electrolytic coloration study 2–83985
CuCl with point defects associated with impurities 2–75290
$Cu(ClO_4)_2$ solutins in methanol and water, temp. and magnetic field dependence of electrons in relaxation 2–81452
$CuCs_2(SO_4)_2.6H_2O$, electron spin- lattice relax. of Zeeman and interaction systems 2–68580
Cu(II) bis(di-n-butyldiselenocarbamate):Ni e.p.r. spectra of single crystal, polycrystalline sample, frozen soln. 2–48277
Cu(II) complex, bis- diethyldithiophosphate, hyperfine couplings of ^{33}S 2–81446
Cu(II) complex, bis(O,O′-di-iso-propyl- dithiophosphato) copper(II), s.h.f. splitting 2–81510
Cu(II) complex, diammine-(o-phthalato) Cu(II), interaction between coupled ion pairs 2–65335
Cu(II) complex, hydroxyquinolinate, in phthalimide crysts., ^{17}O h.f.s. 2–80071
Cu(II) complex of tetraethylthiuramdisulphide, single crystal e.s.r. study, determ. of Cu sites 2–72483
Cu(II) complexes, chromophore trans-CuN_2S_2, e.s.r. investigation of covalent bonding 2–46539
Cu(II) complexes, six- coordinated, temperature dependence of e.s.r. spectra determ. from dynamic Jahn-Teller effect 2–53004
Cu(II) zeolites, meas. of enhancement of proton resonance line on saturation of e.p.r. at liquid He temp. 2–54517
$Cu(NO_3)_2$, mag. field and conc. depend. of paramag. relax. 2–54365
CuO-SeO_2 system phases, anomalous behaviour 2–84573
D_3O, matrix stabilised, comparison of e.s.r. spectra with INDO calculations 2–42892
EuB_6, demagnetizing effects, g-factor and linewidths 2–84565
EuB_6, exchange interaction obs. 2–81468
EuTe, critical phenomena in resonances near Neel temp. 2–61728
EuTe, linewidth near crit. point 2–75341
Fe(III) complexes with oxyacids, low temperature photolysis 2–75393
Ga surfaces, heat-treated in various atmospheres 2–72488
GaP:Ge, linewidth and g-value 2–72484
GaP:Mn,S, Mn-S nearest neighbour complex obs. 2–75344
GaP:Sn, under uniaxial stress 2–84570
Gd-Ni intermetallic compounds, meas. of g_s values, study of exchange interactions 2–84568
Gd, magnetic interactions 2–75352
Gd^{3+}, in single crysts., review 2–72485
GdAg, exchange interaction deduced 2–51404
GdB_6, exchange interaction obs. 2–81468
GdB_6, polycrystalline, e.p.r. spectrum at 9.16 Ghz, using reflection type cavity spectrometer 2–72486
GdCu, exchange interaction deduced 2–51404
Gd(III) complexes in dimethylformamide solution, electron spin relaxation 2–64474
$Gd_2(SO_4)_3.8H_2O$ longit. relax. times meas. 2–84455
$Gd_xY_{1-x}Ag$, of Gd, g-shift and linewidths 2–81462
Ge:P, electron irrad., bombardment induced interstitial P obs. 2–48279
n-Ge:P(As), resist. decrease due to donor spin reson. 2–81106
Ge-Mn-Te alloy, degenerate, molecular field model and bottleneck effect 2–48273
n-Ge, resist. rel. to donor spin reson., spin energy transfer model, 4K 2–68434
GeO_2:V^{4+}, g and A tensors, orbital mixing parameter, radial average, core polarization 2–72503
H, gaseous, spin- relaxation effects on spectrum 2–79950
H atoms in γ-irrad. aqueous solns., dynamic electron polarization 2–78204
H_2 labile negative ion, assignation of cause of resonances in h.f.e.m. fields 2–74264
H_2 pyrolysis on W filaments, atomization 2–72550
H_3O, matrix stabilised, comparison of e.s.r. spectra with INDO calculations 2–42892
$HfSiO_4$ host, spectra of Er^{3+}, Yb^{3+} and Ge^{3+} 2–48278
HgCN in Ar matrix, chemical bonding 2–50072
HgTe, magnetoabsorpt. of i.r. and submillimetric waves rel. to mag. field, band struct. 2–68294
Ho^{3+} in yttrium ethyl sulphate, spin-lattice relaxation 2–68584
$InSiO_4$ host, spectra of Er^{3+}, Yb^{3+} and Gd^{3+} 2–48278
Ir:Dy (Er), localized moment cond. electron exchange interaction 2–68737
KCL, H-centre prod. by u.v. photodestruction of U_2-centres, optical and e.s.r. obs. 2–77599
KCl:Ag, obs. of colour centre form. 2–80713
KCl:Br, $BrCl^-$–V_k centre 2–81461
KCl:(Li^+,Br-), $H_a(Li^+)$-type BrCl- centre, obs. 2–60825
KCl:(Li^+,I-), $H_a(Li^+)$-type ICl- centre, obs. 2–60825
KCl:Li^+, reorientation motions of H_a-centre 2–43648
KCl, F′ to F centre conversion obs. 2–71529
$K_3Co_{1-x}Fe_x(CN)_6$, Fe^{III} complex $3d(t_{2g})$ density distrib. detn. 2–68613
K_2CrO_4 irradiated at ambiant temp., e.s.r. spectroscopy study of paramagnetic centres 2–48280
K_2CuF_4, two dimensional ferromagnet temp. and frequency dependence of the e.s.r. line width 2–84563
KH_2AsO_4, X-irradiated in ferroelectric phase at 4.2 and 77 K, e.p.r. study of AsO_4^{4-} centre 2–72469
KH_2AsO_4 and Kd_2AsO_4 ferroelectrics 2–68734

Paramagnetic resonance and relaxation continued
KH_2AsO_4 and Kd_2AsO_4, X-irradiated, identification of Slater configurations of $(AsO_4)^{4-}$ radical 2−81453
KH_2PO_4-KH_2AsO_4 ferroelectric 2−68734
KI, relaxed-excited state of F-centre, wave function determ. 2−68738
$K_3Ir^{III}(CN)_6$, electron irradiated in KCl single crystals, ligand hyperfine structure in $Ir^{II}(CN)_5$ species 2−61735
$KMnF_3$, $KMnF_3$:Mg, temperature dependence of e.p.r. line width, room to liquid nitrogen temp., effect near Neel temp. 2−44440
K_2MnF_4, above Neel temp. 2−72489
K_2MnF_4, quadratic layer antiferromagnet, linewidth temp. depend. 2−75345
$KMnO_4$, γ-irrad., $MnO_4{}^{2-}$ obs. 2−68809
KN_3, u.v. irrad., spectra, correl. with optical absorpt. bands 2−75299
β-KNO_3:Mn^{2+}, phonon sidebands 2−72490
K_2O-SiO_2 glass, irrad., nature of hole centres 2−65336
K_2SO_4:Tl^{2+}, mag. props., g-factor, hyperfine interaction 2−72470
KX-K_2O-B_2O_3 glass, (X=F,Cl,Br,I,O), X-irrad., colour centres 2−81463
K_2ZnF_4:Mn^{2+}, spin Hamiltonian parameters detn. 2−65323
$KZnF_3$:V^{2+}, hyperfine interactions 2−75353
$LaAlO_3$, static and dynamic crit. phenomena near struct. phase transitions 2−81465
$La_2Mg_3(NO_3)_{12}.24H_2O$:$Ce^{3+}$,$Pr^{3+}$, spin-phonon interaction 2−44316
$La_2Mg_3(NO_3)_{12}.24H_2O$, spin system dynamics obs. 2−84445
$La_2Mn_3(NO_3)_{12}.24H_2O$, paramag. relax. at liq. He temps. 2−68736
La_2O_2S:Gd^{3+}, angular variation 2−72491
Li, spin diffusion and electron- electron interaction studies 2−48288
Li, spin echo on cond. electrons 2−44314
Li alloy, liq., semicond., spin flip processes 2−60510
$LiAl_5O_8$:Fe^{3+}, e.s.r. spectra of ordered and disordered phases 2−48253
LiF:Mn^{2+}, low-field X-band e.p.r. transitions 2−72492
$LiNbO_3$: Fe^{3+}, Hamiltonian parameters detn. 2−65324
$LiNbO_3$:Mn^{2+} ferroelectric, e.s.r. studies of crystal field parameters 2−81451
Mg:Gd, dil. mag. alloy, exchange narrowing of fine structure 2−72496
Mg-Er alloy, dilute, exchange interactions with cond. electrons obs. 2−72467
Mg-Mn alloy, relaxation bottleneck theory applied 2−44438
$MgAl_2O_4$ spinel, cation disorder obs. 2−65325
MgO:Cr^+, γ irrad., g-factor, cubic field splitting and hyperfine const. obs. 2−75346
MgO:Fe^{3+}, mag. circ. dichroism-ESR double resonance obs. of charge transfer bands 2−72339
MgO:V^{3+}, effect of random static strains on line shape, model 2−72495
MgO, adsorption of chlorine and oxygen obs. of ESR signal, charge transfer effects 2−47139
MgO, $F^+ \rightleftharpoons F$ centre conversion obs. 2−68043
MgO, linewidth of iron group ions, temp. depend. 2−48289
MgO, of adsorbed COS- and CS_2-, g-tensor shifts 2−72494
MgO, radiation-induced $[Na]^0$ centres 2−43651
MgO powders, of chemisorbed $O_2{}^-$ species, adsorption site identification 2−56602
MgO surface, $V_{oh}{}^*$ trapped hole centre obs. 2−81447
2 $MgO.5SiO_2.2Al_2O_3.nCr_2O_3$ glass due to Cr_2O_3 additions, e.s.r. obs. 2−83850
Mg_2Si, powdered and doped, 2-300K 2−65337
$MgWO_4$:Fe^{3+}, elec. field effect 2−48286
Mn, phosphate glass, mag. props. and structure obs. 2−57292
Mn (II) complex, tris(octamethylpyrophosphoramide) manganese(II) perchlorate, h.f. splitting parameter 2−81513
Mn_3As_2, MnAs, Mn_2Sb, e.s.r. and thermomagnetic meas. rel. to determination of Lande factor 2−51411
$MnAu_2$, spiral phase, microwave absorpt. peaks interpret. 2−44429
MnF_2, linewidth, crit. point anomaly, role of anisotropy 2−78165
$Mn_xMg_{1-x}Al_2O_4$ spinel, spin Hamiltonian analysis 2−48290
$Mn(NH_4)_2(SO_4)_2.6H_2$ longit. relax. times meas. 2−84455
NCl_2 in low temp. matrices, anisotropic spectra analysis 2−72571
$ND_4Al(SO_4)_2.12D_2O$, struct. phase transition obs. at 56K 2−84576
$NH_4Al(SO_4)_2$:VO^{2+}, polycrystalline, e.p.r. line shapes 2−61736
NH_4Br:Cu^{2+}, h.f.s., covalency, core polarization 2−78154
$NH_4({}^{57}Fe, Al)(SO_4)_2.12H_2O$, Mossbauer-electronic double resonance 2−57334
$NH_4H_2AsO_4$ and $ND_4D_2AsO_4$, X-irradiated, identification of Slater configurations of $(AsO_4)^{4-}$ radical 2−81453
$NH_4H_2AsO_4$ antiferroelectric 2−68734
NH_4HSO_4, γ-irrad., of $HNSO_3{}^-$ radical, ferroelec. transition mechanism 2−84369
$(NH_4)_2SO_4$:VO^{2+} single crystal, spin Hamiltonian parameters 2−61731
$N^{16}O$-$N^{17}O$-$N^{18}O$ gaseous mixture, isotopic effects 2−80031
Na, spin diffusion and electron-electron interaction studies 2−48288
Na, valence electron magnetic moment, rel. to free electron moment 2−42744
$NaAlSi_3O_8$:Fe^{3+}, site assignment of Fe^{3+} based on fourth-order spin Hamiltonian constants 2−44439
NaCl:Mn^{2+}, diffusion coeff. of Mn^{2+} 2−50700
$NaClO_3$, ClO_3 centres formed by low temp. X-irradiation, e.s.r. study 2−51407
$NaClO_3$, irrad., double reson. obs. of mag. dipolar interaction 2−72534
Ni tutton salt, mag. field and conc. depend. of paramag. relax. 2−54365
O_2-, chemisorbed layer on Ag 2−50531
O_2 labile negative ion, assignation of cause of resonances in h.f.e.m. fields 2−74264
OH radicals formed from water of crystallization, role of H-bonding 2−81495
PCl_2 in low temp. matrices, anisotropic spectra analysis 2−72571
PH_4 radical trapped in solid Kr, h.f.s., config. energies, internal tunnelling 2−64154
P_2O_5-B_2O_3-Cs_2O glass, of Cu(II) paramag. centres, struct. 2−48291
$PbBr_2(Cl_2)$, u.v. irrad., pairs and colloidal centres obs. 2−44448

Paramagnetic resonance and relaxation continued
$PbMoO_4$:Cu, Gd site occupancies of dopant and trace impurity 2−68739
α-$Pb(N_3)_2$:Mn^{2+}, spin Hamiltonian parameters and linewidth temp. dependence 2−44447
PbS, paramag. surface centre density meas. 2−65334
PbTe, paramag. surface centre density meas. 2−65334
Pd:^{163}Dy, hyperfine splitting, consts., e.s.r. 2−72497
Pd:^{167}Er, hyperfine splitting, consts., e.s.r., nuclear quadruiple interaction effects 2−72497
Pd:Er^{3+}, exchange coupling const. and hyperfine splitting obs. 2−61732
Pd:Gd^{3+} single crystal, resolved fine structure 2−68733
Rb-electron collisions, meas. of e.s.r. linewidth and shift in resonance frequency 2−70615
RbH_2AsO_4 ferroelectric 2−68734
$RbMnF_3$, impure exchange-coupled, substitutions effect on linewidth and g-values 2−48292
$RbMnF_3$, temperature dependence of e.p.r. line width, room to liquid nitrogen temp., effect near Neel temp. 2−44440
Rb_2MnF_4, quadratic layer antiferromagnet, linewidth temp. depend. 2−75345
ScS, e.s.r. in solid Ar and He matrices 2−46582
n-Si:Li, irrad. induced defects and impurity effects 2−47385
Si:O, lattice damage due to ion implantation, e.p.r. obs. 2−60780
Si:P, heavily doped, linewidth, temp. depend. 2−72500
Si:P, intermediate region of impurity cond., effect on resist. 2−72498
Si:P, shallow trapped donor electrons, spin echo decay 2−72499
n-Si, degenerate, two band model applied 2−48273
Si, fast neutron radiation damage obs. 2−48282
Si, hyperfine structure of the e.s.r. spectrum of A centre 2−81005
Si, irradiated, multiple vacancy centres obs. 2−48283
n-Si, resist. rel. to donor spin reson., spin energy transfer model, 4K 2−68434
Si film, amorphous, characteriz. as function of decreasing spin conc. 2−78162
α-SiC, neutron and alpha-particle irrad. effects 2−48294
SiO_2, fused, of transition metal ions struct. obs. 2−65338
SiO_2, obs. of E'_s dangling bonds and CO_2 adsorbed radicals 2−71352
SiO_2, silica, mechanically crushed, paramag. centres obs. 2−67888
$SiTiO_3$, critical asymmetry in local fluctuations for $T \rightarrow T_c{}^-$ 2−72472
n-Si;Li, irrad., Li-defect interaction obs. 2−48293
SnO_2:Ni, signal due to Fe^{3+} centre 2−84564
SnO_2, e.p.r. meas. on Cr^{3+} and Fe^{3+} 2−48309
Sr fluorophosphate, Mn^{2+} doped, optical excitation and fluoresc. spectra of Mn^{2+} 2−81421
$SrCl_2$:Cm^{3+}, e.p.r. investigations of zero-field splittings 2−44449
$SrCl_2$:${}^{151}Eu^{2+}$, ${}^{153}Eu^{2+}$, hyperfine interactions, temp. dependence 2−72471
$SrCl_2$:Ti^{2+}, e.p.r. investigation, obs. of double quantum transitions, determ. of spin- Hamiltonian parameters 2−81454
$SrCl_2$, of Ag^{2+}, conform. instability in hexagonal sites 2−84579
$SrCl_2$, U_2-centre obs. 2−71531
SrF_2: Gd^{3+}, Ce^{3+}, Ce^{3+} codopant effect on Gd^{3+} e.p.r. spectrum at room temp. 2−61737
SrF_2:$Cm^{3+}(Am^{2+})$, e.p.r. investigations of zero-field splittings 2−44449
SrF_2, linear elec. field effects for Ce^{3+}-F^- tetragonal sites 2−48285
SrF_2, of Mn^{2+}, spin Hamiltonian parameters 2−54497
SrF_2, trigonal Gd^{3+} centres produced by hydrolysis reaction 2−84582
SrO, radiation-induced $[Na]^0$ centres 2−43651
SrO, sites of cubic symmetry, g values 2−54491
$SrTiO_3$, antiferrodistortive transition, fluctuation phenomena 2−84574
$SrTiO_3$, of Mo^{5+}, dynamic Jahn-Teller effect 2−48295
$SrTiO_3$, predicted divergence, near structural transition above T_c 2−65065
$SrTiO_3$, static and dynamic crit. phenomena near struct. phase transitions 2−81465
TbO_2, Tb^{4+} e.p.r., comparison with computer-calculated spectrum 2−54494
TeO_2, amorphous and cryst., electronic bonding of Cu^{2+} 2−72501
ThO_2:Cm^{3+}, e.p.r. investigations of zero-field splittings 2−44449
ThO_2, absorpt. spectrum of monovalent iron 2−48296
ThO_2, spin-lattice relax. of Fe^+ amd hyperfine splitting of Gd^{3+}, Debye temp. obs. 2−84581
TiO_2:Fe^{3+}, substitutional and charge compensated impurity in anatase, temp. depend. 2−68730
TiO_2:Fe^{3+} spin- lattice relaxation mechanism 2−81459
TiO_2:Li,V,Cr,Mn,Fe, transition metal impurity levels determ. 2−44117
TiO_2, anatase, g-tensor for Ti(III), parametric obs. 2−61739
TiO_2, of interstitial V^{4+}, thermal treatment effects 2−61738
TlN_3:Mn^{2+}, spin Hamiltonian parameters, temp. depend. 2−72502
$UO_2(NO_3)_2.6H_2O$:VO^{2+}, hindered motion obs., single crysts. 2−57392
V_2O_5-Fe_2O_3 system, of Fe^{3+} 2−48297
V_2O_5-P_2O_5 glass, e.s.r. line intensity vs. temp. 2−44310
VO^{2+} impurity ions in α-amino acid crystals 2−84566
WO_3-P_4O_{10}-V_2O_5 glass system, magnetic props. obs. 2−54495
Y garnets, magneto-elastic bonding of Fe^{3+} and Cr^{3+} ions 2−65321
YAG:Nd^{3+}, line width, random variation of static crystalline field 2−44441
YAl_2:Gd, paramagnetic resonance meas., 5-70K, temp. and impurity depend. 2−65327
$YAsO_4$:Yb^{3+}, pair interaction and relax., e.p.r. obs. 2−65326
YCo_2, Laves phase, correl. with mag. props. 2−81276
YNi_2, Laves phase 2−81277
YS, e.s.r. in solid Ar and He matrices 2−46582
$Y_{1-w}Th_wAl_2$, paramagnetic resonance meas., 5-70K, temp. and impurity depend. 2−65327
Zn complex, 2,6-pyridinedicarboxylate, Cu-doped, mag. parameters 2−78155
Zn complexes, porphyrins, e.p.r. spectra, hyperfine structure 2−50071
ZnO:Cu^{2+} e.s.r. line width, doping and temp. depend., spin-lattice relaxation mechanism 7-17 K 2−65328

Paramagnetic resonance and relaxation continued
$ZnO:Nb^{2+}$, dynamic Jahn-Teller effect obs. 2−48284
ZnO thermal control coating pigment, u.v. irrad., defects 2−81460
ZnSe, paramag. surface centre density meas. 2−65334
$ZnWO_4:Co^{2+}$, epr spectrum and interpretation 2−81457
$ZnWO_4:Cr^{3+}$, impurity conc. determ. 2−78157
$ZnWO_4:Cr^{3+}$, temp. variation of line splitting by external electric field 2−72473
$ZnWO_4:Fe^{3+}$, elec. field effect 2−48286
ZrO_2, Y_2O_3-stabilized, current blackening effects, defect struct. obs. 2−61740
$ZrSiO_4$ host, spectra of Er^{3+}, Yb^{3+} and Ge^{3+} 2−48278
$Zr_{1-x}Ti_x(Hf_x)Zn_2$, itinerant ferromag. obs. 2−72173
measurement
absorption and dispersion signals, simultaneous meas. 2−55628
adiabatic rapid passage spectra from slowly tumbling spin labels 2−83339
data analysis using programmable calculator 2−84565
double integration of spectra in presence of base line drift, numerical method 2−52341
e.p.r. spectroscopy, specimen orientation instrument 2−73487
fluorophlogopite, Ti and V impurities, e.p.r. and optical absorption spectra, levels of Ti^{2+} and Ti^{3+} ions 2−84562
glass, nontransparent quartz, colour changes investigated by e.p.r. and elec. cond. meas. 2−84482
mag. field intensity marker pickup circuit based on automatic pen recorder of RE-1301 radio spectrometer 2−59009
magnetometer, sensitivity improvement 2−69852
Mossbauer- electronic double resonance 2−57334
recording e.s.r. spectra in digital form by remote computer 2−59010
resonant helix and coil, Overhauser effects of benzene solution w. tanone free radical 2−66666
spectra, simultaneous recording in X and K bands 2−41892
spectrometer, broadband low-field 2−78985
spectrometer, sensitivity calcs., noise performance 2−55627
spectrometer with automatic balanced bridge 2−66665
spectroscopy meas. and data processing development 2−73488
spin-lattice relaxation times, adaptive method 2−55633
temperature control device, 4.2-100 K 2−76425
vitrinite, carbonized, at various temps., hyperfine struct. obs. 2−68731
Al_2O_3, α-phase polycrystalline, e.p.r. study γ, n in-pile radiation of effects 2−80667
$CaWO_4:Er^{3+}$, compensation of the excess charge during activation of scheelites with rare-earth ions 2−72480
$CaWO_4:Tb^{3+}$ compensation of the excess charge during activation of scheelites with rare-earth ions 2−72480
$La_3In:Gd$, supercond. metal 2−72475
$LiVO_3:Mn^{2+}$, e.p.r. at 9.3 and 36.9 GHz 2−72493
Mg_2SiO_4 with Mn impurity, preparation and calibration as field marker and intensity reference 2−66664
$Mn(NO_3)_2$ aqueous solutions, e.s.r. 2−71233
Paramagnetism
see also Magnetic properties of substances/paramagnetic
Curie-Weiss law for narrow-band electrons 2−44221
disordered system, low temp. thermodynamics, van Vleck like paramag. 2−69614
doubly degenerate band, electron correlation 2−84425
electrons interacting with paramagnetic impurities, kinetic equations 2−77816
Heisenberg paramagnet, anisotropic, n.m.r. line shape calcs. using kinetic theory 2−72111
Hubbard model, ground state energy 2−54291
magnetothermodynamic props. of paramagnetic ions in axial crystal fields 2−44220
maser, push-pull, inversion ratios, comparison with three-level devices, magnetic field intensities 2−82467
metals, containing Sm, susceptibility theory 2−65126
Mossbauer hyperfine spectra, temp. depend. line shape rel. to mag. orders 2−75263
nonferromagnetic metal, spin waves, quantum-mech. theory 2−75206
optokinetic, via optoelectrical effect, theoret. expressions, applic. to stars 2−66656
orbital susceptibility of interacting electron gas 2−65120
Pauli spin, applied to lower crit. field meas. in NbN 2−54146
second harmonic generation, microwave freq., by system of paramagnetic spins 2−61577
semiconductor, magnetic polaron props. 2−47880
spin and orbital susceptibilities of nearly free electrons in spatially varying field 2−61493
spin polarized case, local exchange-correlation potential 2−57266
spin-phonon system, energy spectrum of elementary excitations 2−65118
van Vleck, excitation spectrum 2−61479
Parametric amplifiers *see Amplifiers*
Parent *see Nucleus; Radioactivity*
Parity
see also individual particles, e.g. Mesons/spin and parity
divergence of weak parity-nonconserving NNP amplitude, pion-pole dominance 2−82662
doublets, elimination in residue functions, Reggeized baryon exchange theory 2−79605
multipole for arbitrary spin, generalized using ALGOL 2−42315
violation in neutron capture γ-rays 2−67289
ρ_{10} production in $KN \rightarrow K^*(890)N$, unnatural parity exchange 2−49586
^{252}Cf, fission, X-ray spectra of products rel. to charge parity 2−70497
Particle accelerators
see also Ion beams
300 GeV program, CERN annual report 2−67109
beam current integration using digital multimeter 2−49613
beam flatness for medical dosimetry, computer-aided evaluation 2−67103
chemical, time-of-flight for low centre-of-mass energy spreads 2−55937
coherent phase oscillations, separatrix, beam voltage, particle current, detuning, cavity resonator 2−82828

Particle accelerators continued
collective ion acceleration by intense relativistic electron rings 2−55942
construction, appl. of Al 2−67102
dose estimates outside shielding, CERN intersecting storage rings, Moyer method 2−59877
electron, particle energy control 2−52712
electron, relativistic beam interaction with axial and convergent magnetic guide fields 2−70320
electron cyclotron resonance plasma accelerators as ion beam source 2−60253
electron pre-accelerator, high potential for use with magnetic β-ray spectrometer 2−79693
electron ring, axial oscillations, instability 2−67107
electron ring, model of radiation losses 2−42481
electron ring, selg-consistent Vlasov description of relativistic equilibria 2−82830
electron ring field in resonator 2−79703
electrostatic, electronic load appearance in accelerator tubes 2−70323
Fermi stochastic particle acceleration mechanism 2−52710
H_{111} mode in cylindrical cavity in axial mag. field 2−63718
high current ion accelerator, optimization 2−79704
interactive beam design program with Monte Carlo capabilities 2−82831
ISR, elementary particle physics experimentation 2−79699
ISR, running-in behaviour and phenomena 2−79698
macroparticles, rail gun at A.N.U., description, results, plans 2−82829
mag. dipole radiation 2−55936
in meson factories, experiments 2−82640
microtron, stability limits of phase oscillations 2−79695
neutron production for medical applications 2−45035
omegatron, influence of non-uniform r.f. field on ion trajectories, harmonic peaks 2−59650
proton, high-energy, muon shielding, calc. 2−46063
radiation problems estimation by calc. of hadronic cascade in matter 2−59643
radiation protection instrumentation and applics. 2−70545
radiation therapy facility at NAL 2−69320
relativistic particle interaction with free e.m. waves in presence of helical magnet 2−52709
reverse beam plant, computer-aided control 2−52707
shielding, patent 2−82835
testing, improving vacuum conditions 2−78708
tube fabrication, centrifugal casting method 2−70318
O_2 ion beam, from Bevatron, depth dose characteristic 2−69404
accessories
see also Storage rings
auxiliary cyclotron beam monitor using proton reactions with Cu 2−70334
beam extractor, compensated current channel isochronons cyclotron 2−63720
beam monitor, Si surface barrier detector 2−63723
beam transporting system design, ion optics principles utilization 2−55945
biperiodic deflectors, theory of $\pi/2$-mode 2−70336
camera with Kerr cell shutter, 10 picosecond time resolution 2−42291
corona stabilizer for Van de Graaf accelerators 2−76754
debuncher, determ. of injection efficiency in synchrophasotron 2−70333
electron beam energy analyzer, on-line 2−63724
electron scattering facility, 100 MeV, at University of Glasgow 2−55943
electron synchrotron, dosage of accelerated beam intensity, accessory control device 2−52713
fast cycling pulsed h.v. power supply for bunch transfer between proton synchrotron 2−42487
grounded monitor for high voltage accelerators 2−63721
high β insertions for use with 1000 GeV superconducting extension of European synchrotron 2−42486
high β insertions with application to 1000 GeV supercon. extension of European accelerator 2−59656
hollow current conducting plate of septum magnets for beam extraction, construction 2−70335
Klystron bunching system for 5.5 MV Van de Graaff accelerator 2−52716
magnet for 176 cm 3 sector focused cyclotron, model and mag. field obs. 2−79705
magnetic horn focussing device, CERN neutrino beam facility, remote handling system 2−70339
magnets for radiation resistant system 2−82832
matched insertions in low periodicity lattices 2−59657
model beam analyzing magnet, field inhomogeneities measurement 2−63722
neutron source for variable energy cyclotron, for simulation of fast reactor spectra 2−67110
passive magnetic shield, beam extractor on isochronous cyclotron 2−63717
phase acceptance of alternating gradient quadrupole doublet with quadrupoles of different apertures 2−45679
pulsed magnet power supply for fast cycling synchrotrons 2−49697
pulsed quadrupole magnets, peak field meas. by peak to d.c. comparison method 2−55647
quadrupolar magnetic lens using spiral focusing 2−42485
radiation area monitoring system, digital, multiplexing 2−49698
ratio circuit for plotting dose distribution in radiation field of 8 MV linear accelerator 2−59653
r.f. regulator for Saturne synchrotron's 20 MeV proton linac injector 2−49701
secondary emission monitor of accelerated electron beam position, design and sensitivity 2−55944
superconducting resonant cavities, low phase velocity, magnetic and electric field meas. 2−49700
superconducting r.f. cavities, electron loading 2−59655
superconducting r.f. cavities, surface condition of Nb 2−70337
tagged photon-electron beam facility for NAL, design 2−52717
tank circuit, energy stabilization 2−59654
target material preparation using e.m. isotope separator 2−73918

Particle accelerators continued
accessories continued
targets, isotopic, prep. techniques 2−73962
targets, isotopic, preparation 2−49702
Van de Graaff 2−59644
H_2 target, liquid, 150 cm, for synchrophasotron 2−67072
betatrons
beam flattening in moving field therapy with electrons 2−69438
bremsstrahlung, applications to physical research 2−46234
electron energy spread, in cylindrically symmetrical mag. field, equation 2−79690
transients accompanying infection of dense beams into compressor 2−59651
cyclotrons
automated radiation therapy, synchrocyclotron sterotaxis 2−69315
auxiliary beam monitor using proton reactions with Cu 2−70334
beam energy obs., time of flight method 2−42484
beam properties of Eindhoven AVF cyclotron, method of measurement 2−49695
beam space charge, effect on freq. shift of axial oscillations 2−70330
beam transport system, measurements and calculations on Eindhoven AVF cyclotron 2−49696
biomedical applics., selection of size 2−69272
Cracow U-120, properties of α-beam using ion optics principles 2−55945
Cyclo-Graaff system, 38 MeV, developments for nucl. struct. applic. 2−59649
fast neutron beams, energy spectra by neutron spectrometer 2−52682
Hamburg isochronous, meas. of charge distribution in external beam individual pulses 2−79691
IPCR, T ion acceleration, 13-24 MeV 2−70328
isochronons, compensated current channel for beam extraction 2−63720
isochronous, compact, particle extraction 2−67106
isochronous, passive magnetic shield, for beam extractor 2−63717
microtron, 11-25 MeV, basic characteristics and design features 2−76752
microtron, as neutron source for activation analysis 2−52708
microtron, measurement of injector cathode losses 2−79702
orbits, design study using computer programs 2−76753
oscillating electron ion source characts. 2−50216
ring, electronic model, frequencies of coherent transverse oscillations 2−70332
sector focused, 176 cm, mag. field obs. of 107 cm model magnet 2−79705
synchrocyclotron, r.f. system, deuteron acceleration modifications, obs. 2−63719
synchrocyclotron, space charge field approx. for different beam forms 2−42482
^{3}He-^{4}He mixture, study of specific heat near gas- liquid critical point 2−71255
T contamination of workers 2−73189
linear
4 MeV, reliability record and safety features 2−67105
A-bomb radiation simulation, biological effects 2−59648
application to gamma radiography non-destructive testing 2−70325
clinical electron accelerator, Mitsubishi model ML-15M II, for cancer treatment 2−69236
electron, automatic freq. control against temp. change 2−55940
electron, beam defocusing due to filament mag. fields in electron guns 2−49691
electron, collective effect, design, operation and performance 2−79700
electron, compact tube 2−59646
electron, for undergraduates, cheap 2−78723
electron, mark-space ratio reduction 2−70327
electron, methods for increasing limiting current 2−59645
electron, radiotherapy, dose distrib., stability, contamination 2−69377
electron, travelling-wave, Q-value effect on performance 2−59647
electrostatic generator, charge collection, theory 2−52711
emittance meas. of intense low-energy proton beams, critical study 2−79692
focussing calcs. for intensely bunched charged particles 2−55938
heavy ion, electrostatic tandem arrangement, straight acceleration tube, patent 2−82836
helical structures, field distrib., power losses and parameter optimization 2−70326
injection conditions effects on transverse instability of beam 2−73960
ion, suitable Nb superconducting helix resonator 2−70321
MEL, 8 MV, ratio circuit for plotting dose distribution in radiation field 2−59653
microtron, for radiation therapy 2−69276
Pelletron, 14 UD, developments for nucl. struct. applic. 2−59649
radiation from electron bunches interacting with iris loaded waveguide 2−79020
radiotherapy applics., history, principles and developments 2−69273
r.f. cavity structure study and application to ion linear accelerators 2−46064
r.f. regulator for Saturne synchrotron's 20 MeV proton linac injector 2−49701
stabilization of field patterns in drift tube linacs 2−49694
structures, voltage standing wave ratio obs. using photographic method 2−70324
Tandem, developments for nucl. struct. applic. 2−59649
tandem Van de Graaff, improved beam energy resolution by using associated beam to generate correction signals 2−49693
transverse instability in linear accel. resonator 2−82834
travelling-wave voltage standing wave ratio vs. freq. 2−49692
Van de Graaf, corona stabilizer 2−76754
Van de Graaff, 5.5 MV, Klystron bunching system 2−52716
Van de Graaff, beam characteristics, meas. 2−70322
Van de Graaff, neutron measurements, fission and capture cross-sections, energy spectrum 2−76904
Van de Graaff 5 MeV ion accelerator 2−67104
Van de Graaff 8 MeV tandem proton accelerator at C.I.S.E. 2−55939
Van de Graaff accelerator and accessories 2−59644

Particle accelerators continued
linear continued
Van de Graaff generator, applic. to sterilisation of throw-away medical articles 2−85119
synchrotrons
bunch transfer using fast cycling pulsed h.v. power supply 2−42487
CERN, low-momentum antiproton production 2−42417
electron, dosage of accelerated beam intensity, accessory control device 2−52713
electron beam, meas. of freq. of coherent oscills. 2−59652
electron motion at output, nonlinear resonance of betatron oscill. obs. 2−70329
high β insertions with application to 1000 GeV supercon. extension of European accelerator 2−59656
high B insertions for use with 1000 GeV superconducting extension of European synchrotron accelerator 2−42486
magnet with Fe yoke saturation and error fields, computer obs. 2−73518
Nimrod proton accelerator, operation and development 2−67108
NINA, additional projects 2−52715
ondulator, electron accel. 2−52714
orbits, design study using computer programs 2−76753
phase vibrations of electrons in synchrotrons, effect of synch. rad. 2−79689
proton, CERN, low energy separated beam for stopped K and p 2−42483
proton, supercond. magnet design 2−45670
pulsed magnet power supply for fast cycling synchrotrons 2−49697
radiation field, spatial-time correlation 2−55941
Saturne, preservation of proton polarization 2−70331
synchrophasotron, efficiency of injection using debuncher 2−70333
vertical polarization rotation of circulating electron beam into horizontal plane by imperfection resonance excitation 2−76756
Ar ions, 1.17×10^{10} eV, in Princeton Accelerator 2−79701
$InBr_2$, heterogeneous equilib. 750-1050 K, enthalpy, entropy of evaporation, boiling point 2−74593
Particle beams
accelerator, interactive beam design program with Monte Carlo capabilities 2−82831
accelerator, use in improving evacuation rate in vacuum systems 2−78708
charged, analysis of internal structure of nonlaminar beams 2−49317
charged, computer simulation 2−79696
charged, formation in current carrying plasma 2−70893
charged, intensity obs. using inductive method 2−69864
charged particle stream, transverse instabilities growth rates 2−66704
current distribution and geometry analysis using rotating probe 2−52388
current integration using digital multimeter 2−49613
cyclotron, Eindhoven AVF, method of measuring beam properties 2−49695
cyclotron, energy obs., time of flight method 2−42484
debuncher, determ. of injection efficiency in synchrophasotron 2−70333
deuteron storage rings, use to generate 14 MeV high intensity pulses 2−79656
deuterons, angular spreading in neutralizer cell 2−79697
dispersion of high energy charged particle beam in matter, multiple nuclear scattering effects, possibility of mass separation 2−82429
extraction from compact isochronous cyclotron 2−67106
extraction from ring accelerator, construction of hollow current conducting plate of septum magnets 2−70335
fast neutron beams, energy spectra by neutron spectrometer 2−52682
generating functions for single fields of Siemens Gammatron 1 and Gammatron 3 2−69301
instability, nonlinear stabilization by plasma oscills. 2−74388
modulated, interference effects 2−49316
neutron, research reactor, intensity obs. 2−70541
neutron 14 MeV high intensity pulse generation 2−79656
neutron beam intensity estimation, biological and medical applications 2−76079
neutron parabolic mirror condensor system 2−55654
neutron source for variable energy cyclotron, for simulation of fast reactor spectra 2−67110
photon, in Van de Graaf accelerator, characteristics meas. 2−70322
photons, relativistic, transit through strong mag. field 2−81897
positive beams, 25-70 GeV/s pulse, from internal target in accelerator 2−42480
protons, angular spreading in neutralizer cell 2−79697
pulse counting apparatus 2−82811
spot size changes due to second order effects in first order achromatic beam transport system 2−73958
synchrotron instability of modulated beam of charged particles 2−78777
temperature distrib. in presence of excited structure 2−84225
transport system, measurements and calculations on Eindhoven AVF cyclotron 2−49696
n, thermal, focusing by reflective dispersion 2−67070
p beams, colliding, calibration or cross-sections 2−45997
π^-, radiotherapy, Los Alamos Meson Physics Facility 2−69342
π^- beams, radiotherapy, biomedical facilities 2−69341
N accelerated nuclei, autoactivation, application to radiology 2−69295
O accelerated nuclei, autoactivation, application to radiology 2−69295
Particle detectors
see also Bubble chambers; Cloud chambers; Counters; Ionization chambers; Nuclear track emulsions; Particle track visualization — 2−70307
angular distribution attenuation coeffs. comparison for detectors of arbitrary geometry 2−73914
for balloon and rocket expts. 2−72745
change distrib. in external beam of Hamburg isochronous cyclotron 2−79691
charge coupled devices, rel. to position sensitive particle detection 2−49611
charged particle position sensing preserving energy resolution in semiconductor detector 2−49647
cosmic ray meas. by Intercosmos 3, PG-1 apparatus 2−81650

Particle detectors continued
counters Coulter principle operation, patent 2−73947
curved channel multipliers, origin of background counting rate 2−63699
cylindrical plate electrostatic analyzer, geometric factor 2−59629
by deflection of e.m. waves by excitation train 2−59603
digital multimeter for beam current integration 2−49613
e.m. shower detector with high rejection power against pions 2−49612
equilibrium charge distributions of light ions in He, meas. with position sensitive open electron multiplier 2−52698
Faraday cup to measure kA/cm² electron beam distributions 2−82792
gamma emitting radioisotope camera using liquid Xe for medical use 2−55249
geometrical corrections in coincidence meas. of nuclear reactions using gas target 2−63684
glass, effect of mass and energy on track diameters 2−79681
gravitational radiation detector, insensitivity to cosmic ray showers 2−46059
heavy ion detector, over biased thin surface barrier detectors 2−63705
identifier, stopping range in solid state detectors 2−73927
ion beam monitor for nanoampere currents 2−73537
magnetostrictive chambers for beam monitoring and event reconstruction 2−42450
metals and ferrites use of generation of u.s. waves, spin waves, and Cherenkov radiation 2−73941
miniature photomultiplier, for scintillation and space use 2−49680
multiwre structures rel. to recent progress in large detector systems 2−49637
n-p(n-i-p) detectors, space charge layer polarization during irrad. 2−65023
neutral, thermocouple system 2−59628
neutron, self powered, in-core meas. 2−74185
neutron, self-powered detector development 2−55922
neutron, self-powered for reactor core meas., calculational model 2−56071
neutron, U or Th doped fission track detector 2−52706
neutron coincidence, for nuclear safeguards applics. 2−49683
neutron dosimeters, high temp. 2−49684
neutron dosimeters, high temp. preparation methods 2−73949
neutrons in range 2-100 MeV, for upper atmosphere obs. and solar neutron search 2−72818
neutrons precision monitoring from TD and DD reactions 2−70305
nuclear interactions, 1 MeV region, a hodoscopic system 2−82805
nuclear reactor flux sensing system for wide power range 2−49906
parallel plate available counter telescope for (n, α) reactions 2−70453
photographic emulsion, effect of electric fields on ionizing particle recording 2−59642
polarity cross correlation, improved computer method 2−73904
positron camera, multicrystal, for use with radionuclides, medical applications 2−55248
prompt/delayed neutronic response ratio meas. of self-powered vanadium detector 2−83111
proportion counter, position sensitive, particle identification 2−63696
protons, satellite instrument for obs. in energy range 0.1 MeV to 6 MeV 2−65923
radiation monitor capable of simultaneous meas. of direction and intensity 2−52664
radioisotope detector-radiator assembly in X-ray fluorescence anal. for Cu and Zn in Fe-rich minerals 2−61821
recent advances in high-energy particle detectors, review 2−49610
scattering chamber, for nuclear reactions 2−79635
scintillation-pulse height analyser system, for 2-100 MeV neutrons 2−82817
secondary electron emission from KCl films applic. 2−72098
semiconductor stopping detector for proton energies to 300 MeV, advantages of laminated detector 2−46041
solid state, prolonged etching factor rel. to track detection 2−46031
solid-state α-particle track detectors in reactor experiments 2−63715
spiral channel multiplier as electron detector, current and counting characteristics 2−76745
streamer chambers, 7 ft., bank of four, performance obs. 2−42479
threshold neutron counters, radiation characteristics 2−42472
timing walk and time resolution estimation by least squares fitting technique 2−52665
X-ray calorimeters, array, development 2−63708
X-ray transition radiation for charged particle detection in 300 GeV region 2−73903
n threshold activation, calibration with 14 MeV neutrons 2−79658
Be-Cu electron multiplier dynodes, cleaning and activation 2−82793
^{12}C polarimeter for 20-30 MeV deuterons, calibration 2−52700
Ge p-n junction, γ-ray detector, space charge region polarization, impurity centre charge exchange 2−65026
Ge(Li), coaxial, gamma ray camera for medical use, computerised display 2−51936
Ge(Li) coaxial detector, local efficiency variations 2−70301
Li-glass scintillator tip for detection of secondary electrons in electron microscopes, long life 2−82430
LiI(Eu) crystal detector, meas. of fast- and thermal neutron fluxes 2−42461
Mn foils, ultra-cold neutron detection by activation 2−67084
Rh, Ag and V direct discharge detectors for thermal and epithermal neutrons 2−52699
Si-Sb compressed composite, obs. of neutron energies in range 13-15 MeV 2−59633
Si, surface barrier for neutron dosimetry 2−69393
Si surface barrier detector for large angle scattering electron spectrometer, 20 to 50 keV energy range 2−79679
^{119}Sn resonance Mossbauer detector with windowless electron multiplier 2−42471
T, gas counting tube 2−70306
TlCl(Be,I) scintillator as a total absorption shower cascade detector 2−49646
^{235}U, ^{235}U + Cd, ^{235}U + ^{10}B, ^{237}Np, ^{238}U, and ^{32}S, threshold neutron counters, radiation characteristics 2−42472

Particle focusing *see Particle optics*

Particle optics
see also Electron optics; Ion optics
beam spot size changes due to second order effects in first order achromatic beam transport system 2−73958
bunching by speed modulation using n gaps 2−63683
charged particle trajectory, in time- varying laplacian field, calc. 2−59079
Cherenkov effect is alternating electric field in dielectric media 2−69822
electrostatic hexapole lens, third-order transfer matrix 2−59078
imaging system for diagnostic radiography using pulse compression techniques 2−51930
multipole components in quadrupole end fields caused by longitudinal field components and sag of probe arm, distortions in analysis 2−55656
multipole elements for correcting image aberrations 2−73520
neutron parabolic mirror condensor system 2−55654
particle spectrometers, trajectories in toroidal condenser to third order approx. 2−76447
phase acceptance of alternating gradient quadrupole doublet with quadrupoles of different apertures 2−45679
prismatic uniform-field astigmatic spectrometer, ray tracing of charged-particle trajectories 2−73521
proton beam separation in CERN Proton Synchrotron 2−42483
n, thermal, focusing by reflective dispersion 2−67070

Particle range *see Energy loss of particles*

Particle size
see also Surface measurement
absolute determination 2−52031
aerosol, distrib. analysis of aerodynamic size and mass by spiral centrifuge 2−50382
aerosol, distribution, informational entropy appl. 2−67851
aerosol, particle size distrib., determ. using Boltzmann's charge distrib. law 2−71244
aerosol beam focusing and spectrometry 2−85158
aerosol filter collection efficiency, total mat theory 2−56530
aerosol size distribution, determination from multistage sampler data 2−53465
aerosol size distribution from spectral attenuation meas. 2−56529
aerosol spectral impactor, size distribution meas. 2−64488
aerosols, Brownian coagulation, self-preserving particle size distrib. 2−50384
aerosols, det. using open cavity of He-Ne gas laser 2−56528
aerosols, polydisperse, submicron, size distribution determ. by response matrix method 2−74568
aerosols, stratospheric 2−62156
analysis, optical fibre, array for radial distrib. of light intensity obs. 2−70057
analysis using automated laser light-state photometer with single photon counting system 2−63307
analyzer, comments 2−55750
atmosphere, optical spatial filtering for detection of shape 2−48462
atmosphere, suspended particulates, size distribution 2−65677
atmospheric aerosol, condensational growth and particle size distrib. 2−48461
atmospheric aerosol, particle size distrib., photometric obs. 2−75538
atmospheric aerosols, radioactive, nuclepore and golden membrane filters for meas. 2−84819
atomized droplets, determination from photographs of atomization process in convective gas stream 2−46908
centrifugal particle size and analysis, size distrib. integrals soln. 2−74563
centrifugal sedimentation particle size analysis method, uncertainties, deviations from Stokes law 2−68170
ceramics, strength/grain size effects 2−68092
cloud nuclei, det. by means of Nucleopore filters 2−48489
Coulter type counter, lower limit for off axis particles 2−46994
disperse system turbidity spectrum, determ. of size and refractive index of particles 2−43399
disperse systems, determ. by sequential X-ray fluorescence 2−64485
electrolyte, proportional to voltage pulse meas. 2−44489
emulsion size distribs., meas. by electrolytic reduction 2−80499
grain diameter, true volume calculation 2−67977
grain size determ. in polycrystals, factors influencing diffraction patterns 2−60733
grained solid, grains/unit volume, determ. from theory of stochastic processes 2−43877
graphite, artificial, anisotropic and isotropic, struct. distrib. 2−53972
graphite, electrothermal, and crystallite size 2−57001
gravimetric sedimentation method particle-size distribution of dust 2−78754
ice nuclei, natural and artificial, size distribution det. 2−60529
labelled aerosols, specific radioactivity measurements rel. to particle size 2−53464
latex distribution meas. using electron microscopy 2−43405
light scattering, data inversion information theory 2−64476
Los Angeles smog, light scatt., correlation with size distrib. and vol. concentration 2−51624
Los Angeles smog, Minnesota aerosol analyzing system obs. 2−51588
Lovelace aerosol particle separator, design and performance 2−64483
magnetic oxide powders, sub-micron range, distribution measurement, electron microscope technique 2−71654
Mars simulation samples, size classification 2−69160
metal system, grain and particle size distrib. analysis, review 2−50817
optical particle counters, coincidence and cross- channel sensitivity 2−43403
organic aerosol, produced by X-irrad. 2−46999
Pasadena smog, mass and size distrib., Minnesota aerosol analyzing system obs. 2−51589
Pasadena smog, rel. to chemical composition 2−51603
Pasadena smog, rel. to chemical composition 2−51602
polydisperse crystal suspensions obeying McCabe's ΔL law, growth calc. 2−77524
polymer latex, particle size analysis, angular light scattering data 2−43411

Particle size continued
polymers, X-ray diffraction profiles, applic. of variance analysis 2−64602
polystyrene latex, freeze-etched, electron microscope study 2−60522
powder, effect on diffusion models for initial sintering 2−50904
powder analysis by Sartorius sedimentation balance, correct end-weight determ. 2−43881
rain drop size distribution and rainstorm type rel. to radar raingauge accuracy 2−75593
rain drop size distribution determ. by radar, errors rel. to vertical air motion 2−75592
rain drop size distributions using 35 GHz Doppler radar 2−75591
rainfall rate and drop size distributions, simultaneous meas. using radar and raingauges 2−75590
satellite droplets formed by liquid atomization by rotating disk 2−60404
seeding aerosol, X-ray diffr. method 2−62246
seeding aerosols, computer program 2−60528
silica 'roseki' refractories, particle size distrib., effect on packing props. 2−64786
Skylab contamination ground test, particle size distribution and velocities 2−78416
suspension, Coulter counter instrument settings, calc. 2−50380
suspension methods in Coulter counter analysis 2−64480
X-ray diffraction profiles, application of Wilson's variance-range analysis 2−64601
Ag, in glass matrix, effect on optical props. 2−54412
AgI, nucleating ability 2−48459
Al_2O_3 ceramic, fine grain, Cr_2O_3 additions effect 2−50867
C fibres, size effects on radial distribution analysis, influence of atomic bonding 2−64630
CaF_2, effect of calcining temp. 2−61004
CdSb:Ag pressed powders, effect on elec. cond. 2−64906
2 at.%Co-Cu alloy, superparamag. relax. time rel. to Co precip. particle size 2−48067
Cr, coarse-grain melted, failure mode and ductility transition temperature 2−68098
Cu powder, distrib. determ. 2−43891
Fe alloys and steel, trace nonferrous metals analysis, sample particle size effect 2−51476
Fe film, effects on mag. behaviour, u.h.v. Mossbauer emission spectra 2−72284
LiF thermoluminescent dosimetry grade 100 powder incorporated in silicone rubber, dependence of energy response on grain size 2−68702
$Li_{0.93}Na_{0.07}Fe_5O_8$, effect of sintering conditions 2−64790
Pd colloid, depend. on electrolytic deposition parameters 2−83818
Sn, finely dispersed, effect on supercond. transition temp. 2−61230
TiB_2 powder, effect on sintering kinetics 2−61006
TiT_x, size spectrum, T contamination determ. during neutron generator target replacement 2−83155
W, coarse-grain melted, failure mode and ductility transition temperature 2−68098
Zn condensed particles, determ. using time discrete sampling apparatus 2−77454
ZnO powder, size distrib. data processing, computer appl. 2−53942

Particle spectrometers
see also Alpha-particle spectrometers, etc.
— 2−70282
Auger, combined with LEED system 2−76739
Auger electron, using concentric hemispheres, design and construction 2−74610
automated lead, for nuclear fuel control 2−49872
automatic spark chamber with sonic and magnetostrictive readout 2−67101
correction of single photon or particle timing meas. for multiparticle events 2−46030
displayed at 1972 Physics Exhibition 2−55899
electron, resolution improvement using semiconductor detector ladder 2−49631
electron distortion of differentiated deflection analyser current 2−45685
electron microscope with prism spectrometer for selected area electron spectrometry 2−79095
electron spectroscope, patent 2−82816
electron spectroscopy for chemical analysis, electron spectroscopy, e.s. energy analyser 2−68829
electrons, retarding potential diff. and retarded energy 2−67074
electrostatic parallel plate spectrograph for relativistic particles, optical props. 2−63691
electrostatic particle guide for time-of- flight spectroscopy of low energy ions 2−52402
electrostatic sector, cylindrical, for energy analysis 2−69870
identifier, stopping range in solid state detectors 2−73927
ion optics and double focusing 270° magnetic analyzer 2−52677
isobars from spallation reaction for nuclear spectroscopy 2−63876
mag. automated spectrograph MARS, geometrical characteristics 2−52674
magnetic, with large gap using multiwire proportional chamber system 2−79666
magnetic β-ray, construction of high potential electron preaccelerator 2−79693
magnetic detection of heavy ions in focal plane by resistive-wire proportional transmission counter 2−79640
2π magnetic spectrometer for study of K^+ decays 2−73931
MARS, operation and elements 2−52675
MARS, spectrograph data storage and analysis 2−52676
modulated electron beam, for ionization cross-section meas. 2−76456
Mossbauer, in-beam system for use in backscattering geometry 2−63685
multiparticle, wide aperture, with spark chambers, analysis of systems and use in particle spectroscopy 2−76737
multiparticle for very high intensity charged particle beams, analysis of $ep \rightarrow epn\pi$ final-states 2−76738
neutron monochromators, using curved Si crystals 2−79649
neutron selector phase stabilizer for pulsed reactor 2−70280
neutron-capture conversion electron spectrometer at HFR-ILL in Grenoble 2−67078
optical cloud, det. of cloud microstructure 2−48492

Particle spectrometers continued
optimum open aperture fraction for chopper 2−73928
photoelectron, energy spectra obs. 2−63692
photon, using scattering 2−49629
prismatic uniform-field astigmatic, ray tracing of trajectories 2−73521
pulse height, lifetime correction 2−59606
retarding field analyser, electrostatic 2−46040
scintillation counter combined with spark chamber, high aperture ratio 2−59621
semiconductor, for proton energies to 300 MeV, laminated stopping detector 2−46041
semiconductor detectors, for use in 80 MeV range 2−49626
soft e.m. radiation, with resolution of 550 eV 2−70288
split field, employing multiwire proportional chamber, at CERN, intersecting storage rings 2−76740
time-of-flight, three body final state reactions 2−63686
time-of-flight apparatus for (n,x) reactions using isochronous cyclotron 2−79636
trajectories in toroidal condenser to third order approx. 2−76447
two-crystal, dependence of luminescence yield of scintillated crystals on radiation energy 2−59604
pp annihilation, for investigation of heavy meson spectra 2−73926
for ^{14}C and tritium, energy spectra, comparison of chemiluminescence and phosphorescence 2−59605
Ge counter, γ-compensated, as α and β particle spectrometer 2−52696
Ge(Li), pileup rejector for pulse spectrometry 2−79657
Ge(Li), use of single escape peak 2−46036
Ge(Li) counters for detection and energy det. of high energy protons 2−46055
Ge(Li) detector coincidence system for simultaneous spectroscopy of charge 1 and 2 particles, 1 to 60 MeV 2−49633
NaI(Tl) total absorption spectrometer, properties and applications 2−49630

Particle symmetry *see Elementary particles/symmetry*

Particle track visualization
see also Bubble chambers; Cloud chambers; Luminescence chambers; Nuclear track emulsions; Spark chambers
aerosol aspiration study by photographing particle tracks under flash illuminations 2−43404
automatic scanner for photographic plates 2−79685
bubble chamber, computerised 2−79688
cellulose triacetate as track imaging detector of alpha-particles 2−82827
cloud chambers, automated analysis of tracks, counting individual droplets 2−67098
cylindrical wide gap and streamer chamber, construction, operation and response 2−42478
dosimetry of heavy particle radiation, nuclear emulsions and solid track detectors 2−46062
electronic counting and projection of etched tracks in solid state track detectors 2−49690
energetic heavy nuclei identification with solid dielec. track detectors 2−63714
glass, Standard Reference Material, thermal stability of fission tracks 2−79686
Hough Powell device, track detection program 2−76747
Hough Powell device for meas. of Big European Bubble Chamber pictures 2−76749
liquid argon combined with spark chamber 2−73955
location of particle along length of Ne flash tube 2−70314
meteorite, St. Severin, proton spallation track registration in meteoritic whitlockite 2−58536
multi-terminal interactive graphics, system using small computer 2−79683
neutrons, U or Th doped fission track detector 2−52706
optical image recognition systems, computer applications 2−79684
phlogopite, annealing effect on etching figures of tracks produced by ^{252}Cf disintegration 2−71362
plastic detectors, actual precision, automatic meas. 2−63713
protons in cellulose nitrate, monoenergetic 2−42477
relativistic particles in nucl. emulsions, inclined track obs. 2−79680
RFK-5 photographic camera used in start-stop mode 2−70312
scintillating crystals, random and heavy channelled ions at intermed. vels., track-account theory 2−70316
solid state detectors, determ. of fission rate, decay constant, profile and distribution of ^{252}Cf, ^{239}Pu and ^{235}U 2−46060
solid-state α detectors in reactor experiments 2−63715
stereophotography in track devices, correction of external orientation elements of photogrammetric cameras 2−59639
streamer chamber in SKM-200 installation, 2 m model 2−59640
streamer chambers, 7 ft., bank of four, performance obs. 2−42479
U distrib. in Mg-Be fuel jacket, technique 2−42679

Particle tracks
see also Energy loss of particles
fission tracks in mica and volcanic glass, stability rel. to water effects 2−67097
glass detectors, effect of mass and energy on track diameters 2−79681
images matching from three views in bubble chamber 2−55931
nuclear, quantitative elemental obs. 2−48364
particle detector, solid states, prolonged etching factor rel. to track detection 2−46031
shortening, in emulsion, in elec. fields of $1.5\text{-}6.0 \times 10^4$ V/cm 2−42476
α particles on triacetate-cellulose foils, use for detection and measurement of ^{222}Rn and daughters 2−58618
e^+ beam traversing heavy liquid bubble chamber, momentum estimation 2−52704
γ rays produced in K^+ high energy instructions with nuclei in heavy liquid bubble chamber, momentum estimation 2−52704

Particle velocity analysis
see also Alpha-particle spectrometers; Beta-ray spectrometers; Energy loss of particles; Ion velocity; Mass spectrometers
air, electron velocity distribution function in r.f. discharges 2−77262
by deflection of e.m. waves by excitation train 2−59603
desorption of molecules from surface following recombination of atoms, vel. distrib., model 2−47148

Particle velocity analysis continued
  motion in vertical shear flow with density stratification 2−43397
  semiconductor stopping detector for proton energies to 300 MeV, advantages of laminated detector 2−46041
  theta-pinch, toroidal energy and mass analysis of emitted neutral particles 2−80278
  Ar, molecular beam, produced by multichannel source, speed distrib. meas. 2−50018
  N_2, molecular beam, produced by multichannel source, speed distrib. meas. 2−50018
Particles *see Elementary particles; Energy loss of particles; Scattering, particles; and under individual particles, e.g. Protons and antiprotons*
Paschen-Back effect *see Spectra*
Patterson diagrams *see X-ray crystallography/calculation methods*
Peierls-Nabarro force *see Crystal imperfections/dislocations; Internal friction*
Peltier effect *see Thermoelectricity*
Pendellosung fringes *see X-ray crystallography*
Pendulums
  Askania borehole tiltmeter, ball calibration 2−54599
  compound, anal. of forces at pivot bearing 2−45345
  compound, motion in artificial satellite 2−66489
  Foucault, role of constraining force, teaching 2−48967
  Foucault's, and Earth's rotation 2−54582
  inverted, almost periodic and stochastic base motion, stability analysis by method of averaging 2−45342
  oscillation, infinitesimal stabiity and instability 2−49052
  simulation by analogue computer 2−73347
  single harmonic motion, damped period 2−49050
  spherical, resonance in small oscillations 2−58831
Periodic system
  see also Elements
  approximate symmetry, modified Aufbau procedure 2−46402
  doping element in semiconductors, position in table, heat treatment 2−84321
  global group struct. 2−59894
  heavy end extension 2−59893
  model Hamiltonian, rel. to building up of many- electron ground states 2−59892
  n + l filling rule and focussing potentials 2−79927
  new systematic table of the elements 2−57405
Permalloy *see Iron alloys; Nickel alloys*
Permeability, magnetic *see Magnetic properties of substances; Magnetization process*
Permeability, mechanical
  see also Diffusion in solids
  coatings, permeability of the H_2O vapour, measurement technique 2−80757
  fissured media models, streaming potentials 2−57702
  gas permeability of metals under non-isothermal conditions, digital computer calc. 2−60826
  glass-forming oxides, He migration 2−50707
  polystyrene, foamed, of H_2O vapour, rel. to structure 2−43412
  steel, stainless, hydrogen permeation, surface effects 2−77608
  C pyrolytic, impregnation with graphite, neutron irrad. stability, He permeability 2−56997
  Cu, hydrogen permeation, surface effects 2−77608
  Fe, hydrogen permeation, surface effects 2−77608
  Nb, hydrogen permeation, surface effects 2−77608
  Ni, hydrogen permeation, surface effects 2−77608
  Pt, hydrogen permeation, surface effects 2−77608
  TiO_2-SiO_2 glass, of He 2−50718
Permittivity
  2,3-dimethylbutane, crystalline, meas. from 4K to melting point 2−81144
  acetone-cyclohexane, meas. at 25°C 2−53408
  acetone-methanol, meas. at 25°C 2−53408
  acetophenone, 2-hydroxy-5-methyl derivative, meas. in benzene solution at 37.4 GHz, calc. of dielec. relaxation and dipole moment 2−60487
  acrylates, microwave region, 30-70°C 2−60491
  alcohol in heptane solns., dielec. relax. times, permittivities, loss tangent, rel. to comp. and temp. at 9.3477 GHz 2−74555
  alcohol solns. with nonpolar solvents, dielec. dispersion behaviour 2−80487
  alcohols in n-heptane soln., microwave absorpt.obs. 2−84611
  n alkanes, from n pentane-n decane, relative permittivity as function of pressure and temperature 2−43384
  p,p′-di-n-alkylazobenzenes, melting point and dielectric constants, determination and explanation 2−56484
  p,p′-di-n-alkylazoxybenzenes, melting point and dielectric constants, determination and explanation 2−56484
  amorphous semiconductor, photodielec. effect, rel. to trapping 2−61443
  anisotropic mat. dielec. constant determ. using electron microscopy 2−56635
  Antarctic ice sheet using v.l.f. band 2−54731
  anthraquinone-pyrometallic anhydride polymer 2−81143
  barium behenate, built-up films dielec. constant study 2−77948
  barium margarate, built-up films dielec. constant study 2−77948
  barium palmitate, built-up films dielec. constant study 2−77948
  benzophenone, 2-hydroxy-5-methyl derivative, meas. in benzene solution at 37.4 GHz, calc. of dielec. relaxation and dipole moment 2−60487
  benzyl benzoate, complex dielectric constant in microwave region 2−71220
  benzyl formate, complex dielectric constant in microwave region 2−71220
  benzylamine, complex dielectric constants by microwave absorption 2−74553
  benzylbromide, complex dielectric constants by microwave absorption 2−74553
  benzylchloride, complex dielectric constants by microwave absorption 2−74553
  benzylcyanide, complex dielectric constants by microwave absorption 2−74553
  camphor, solid, molecular rotation at dielectric relaxation transition 2−61414

Permittivity continued
  caprylophenone, 2-hdyroxy-5-methyl derivative, meas. in benzene solution at 37.4 GHz, calc. of dielec. relaxation and dipole moment 2−60487
  ceramic matrix, chemically reacted, for fibre reinforced composites 2−56972
  6-chloro-1-hexanol, variation of complex dielectric const. with frequency in 300 MHz-24 GHz region at −42° and +20°C 2−64468
  clay, meas. method eliminating contact phenomena 2−72009
  Cole-Cole eqn., causality 2−59024
  collagen, effect of adsorbed water 2−47908
  complex, meas. method, patent 2−82424
  crystals, measurement, investigation of order-disorder phenomena 2−50991
  cyclohexanol, crystalline, meas. from 4K to melting point 2−81144
  dielectric absorpt. spectrum in Debye regions, decomp. unicity 2−41468
  dielectric constant, complex, classical calc. 2−73632
  dipole gases, calc. 2−80415
  electron plasma, static dielec. const. in presence of strong e.m. wave 2−77843
  emulsion with cond. dispersed phase, dipolar type Debye relax. 2−43408
  epoxy resins, rel. to effect of fillers and plasticizers on molecular mobility 2−47062
  ethyl benzoate, complex dielectric constant in microwave region 2−71220
  exchange polarized electron gas, dielectric const. 2−77842
  ferroelectric, order-disorder type 2−72027
  ferroelectric materials, permittivity and pyroelec. coeff. from pyroelec. response to step radiation signals 2−81126
  ferroelectric solid solution, thermodynamic theory 2−61424
  ferrorelectrics, frequency and temperature dependence near Curie point 2−84365
  film, chalcogenide, amorphous, dielec. const., elec. cond., struct. features 2−61309
  fluid, rigid-dipole, existence of dielectric constant 2−74306
  H, solid normal, 4.2-13.1K 2−77934
  ice:KOH, temp. depend., rel. to phase transition 2−72014
  ice, cubic, dielectric correlation factor 2−81137
  ice, evolution in premelting stage 2−53497
  ice, low temp. meas., rel. to lattice vibrs. 2−82414
  ice, microwave dielectric const. 2−81134
  ionic cryst., dielec. props., model interpret. 2−43952
  liquid, hydrogen-bonded, nonlinear dielec. effect, significant struct. theory 2−46970
  liquid, meas. using automated coaxial line system 2−64470
  liquid cryst., cholesteric, dielec. loss and const., function of temp. and freq. 2−71229
  liquid crystal, relax. and EHD instabilities 2−53395
  liquid crystals, nematic, angular depend. studies of dielec. anisotropy 2−80459
  liquids, method for precise obs. in wide frequency range 2−46973
  low m.p. solids between 320 and 77,2k 2−59028
  low temperature dielec. cell design 2−82414
  lunar surface rocks and fines 2−62652
  maximum absorpt. freq. eval. expression 2−57176
  measurement at audio frequencies, elimination of contact phenomena 2−72009
  metallic conductors, phenomenological model 2−75253
  methane, solid, static dielectric const. at low temp. and high pressure 2−81146
  methanol-cyclohexane, meas. from 25 to 50°C 2−53408
  methanol-cyclohexane-acetone, meas. at 25°C 2−53408
  methyl benzoate, complex dielectric constant in microwave region 2−71220
  microwave absorption heated samples, dynamic high-temp. complex permittivity meas. 2−49237
  microwave meas., modified infinite sample method 2−49238
  myristophenone, 2-hydroxy-5-methyl derivative, meas. in benzene solution at 37.4 GHz, calc. of dielec. relaxation and dipole moment 2−60487
  non-linear dielectric loss (imaginary part of susceptibility) at high elec. fields 2−77944
  nonpolar fluids, mol. model approach 2−83803
  organic solvent, effect on H-bond polarity of phenol-triethylamine complexes 2−46621
  plane-laminated medium, cumulative distribution of dielectric constant 2−75486
  polar molecules in non-polar solvents, dilute solution, theory of dielectric constant 2−74551
  polar substances in n-pentane, rel. to solid soln. struct. 2−72016
  polymer, meas. using coaxial resonators 2−81133
  polymer, static dielec. permittivity calc. method 2−47972
  powder and bulk materials, correl. over range of permitt. and packing fraction 2−61411
  quartz, X-cut, strain dependence by shock compression obs. 2−51207
  rocks, complex dielectric permittivity meas. method 2−54718
  saline aqueous frozen solns., permittivity obs. of cooperative phenomena 2−75139
  semiconductor, AB type, third moment of imaginary part of dielectric const. 2−68461
  semiconductor with contacting bands, dielec. function, transverse and longit., RPA approx. 2−77941
  semiconductor with contacting bands, transversal dielec. function in mag. field, RPA approx. 2−77942
  semiconductors, group III−v, pressure depend. of dielectric constant 2−72297
  semiconductors, photodielectric effect, instrument for obs. 2−77907
  solid, static dielectric const., accurate determ. 2−72011
  solid state plasma, including effects of diffusion 2−75039
  solutions with high specific electrical conductivity 2−71218
  spectrometer for complex permittivity meas. using unbalanced a.c. bridge and chart recorder 2−82419
  static, of pentanol isomers, pressure dependence 2−56510
  static dielec. const., press., temp. and freq. depends., meas. technique 2−65046
  stratified media, parallel, anisotropic and homogeneous, equivalent permittivity tensor calc. 2−80483

Permittivity continued
thin films, dielectric constant, determination by contactless method 2-57225
time domain technique for meas. in biological substances 2-81985
triglycine sulphate, near crit. point, thermal noise study 2-72040
trisiloxane film, electron beam polymerized 2-47909
water, static dielec. const. to high temps. and press. from Mean Spherical Model 2-83793
YIG sphere under parallel pumping condits., anisotropy of above-threshold susceptibility 2-72140
$Al-Al_2O_3-Al$ 2-81114
$Al-SiO_x-Al$ 2-81114
As_2S_3 and As_4Se_4 films, rel to a.c. cond. 2-68392
As_2Se_3 film, rel. to a.c. cond. 2-68392
$Ba_2Bi^{5+}Bi^{3+}O_6$, phase transition obs. 2-75150
BaF_2, l.f. dielec. consts., press. and temp. derivatives 2-51189
$BaO-B_2O_3-Fe_2O_3$ glass, microstruct. effects 2-65113
$Ba_{1-x}Sr_xTiO_3$, flux-grown, temp. dependence in range 4.2 to 600K 2-47966
$Ba_xSr_{1-x}ZrO_3$ ceramics, high-permittivity, temp. coeff. 2-51190
$BaTiO_3$, dielec. const. changes after electron or gamma irrad., X-ray study 2-65047
$BaTiO_3$, rel. to dynamic fatigue, ageing of switching props. 2-72031
$BaTiO_3$ ceramic, sintering parameter effects 2-57241
$BaTiO_3$ single crystals influence of the amplitude of free vibrations on the permittivity 2-81154
$BaTi_{1-x}^{4+}Ti_x^{3+}O_{3-x}F_x$ solid solution 2-47705
Bi:Te deposits, static constants 2-75255
Bi, thin films, in Ku-band, meas. 2-47975
Bi_2WO_6, temp. depend. 2-47263
CaF_2, l.f. dielec. consts., press. and temp. derivatives 2-51189
$Ca(Zr,Ti)O_3$ ceramics, high-permittivity, temp. coeff. 2-51190
$CdGeP_2$, high-freq. and static dielectric const. detn. from reflection spectra 2-72299
$(CoO)_{1.4}.P_2O_5$, glasses, antiferromag. interactions 2-75237
$CsPbCl_3$, rel. to press. depend. of cubic-tetragonal transition temp. 2-71676
α-CuI solid electrolyte, 2-40 GHz 2-83989
F, compressed gaseous and liquid, meas. of dielectric const. and molar polarizability 2-67736
$(Fe_2O_3)_{0.79}.P_2O_5$, glasses, antiferromag. interactions 2-75237
Ga_2Se_3, i.r. refl. spectra at 290K, phonon freqs. and dielec. consts. 2-75279
$Gd_2(MoO_4)_3$ diffracted light obs. from domain wall 2-84467
Ge_3N_4 film, vapour deposited on Ge 2-54224
H_2O, structure in complex part of dielectric constant 2-43361
InSe single crystals reflection and absorption in the i.r. region 2-81395
K, dielectric const. determ. in 4-10.7 eV photon energy range 2-68593
KBr(Cl), l.f. dielec. consts., press. and temp. derivatives 2-51188
KCN, temp. depend., anomalies at transition points 2-75141
$KCl-H_2O$ frozen solns., discontinuities at crit. pt. 2-53499
KCl, OH^- substituted, paraelectric centres with low zero field splitting 2-75147
$KH_{2(1-x)}D_{2x}PO_4$, rel. to comp. depend. of ferroelec. props. 2-54236
$KH_{2(1-x)}D_{2x}PO_4$, study in ferroelectric and paraelectric phases 2-84364
KH_2PO_4, rel. to proton tunnelling, 130-280K 2-77945
KH_2PO_4 and KD_2PO_4, dielec. consts., 300-500K, phase transition obs. 2-71688
$KNbO_3$, under biasing conditions 2-61430
$KTa_xNb_{1-x}O_3$, pyroelectric detectors, characteristics 2-73460
$KTaO_3$, paraelec., press. depend. of static dielec. const. 2-44161
$KTaO_3$, three terminal meas. and rel. to point defect models 2-47967
LiF, l.f. dielec. consts., press. and temp. derivatives 2-51188
$LiGaO_2$, rel. to electromech. coupling factor and reson. freq. 2-51206
$LiIO_3$, near and far i.r. investigations for α and β crystals 2-84511
$Li(N_2H_5)SO_4$ dielectric const., 6 to 5.10^6 Hz, 20 to 200°C 2-77931
$LiNbO_3$, dispersion of elastic waves and permittivity along trigonal axis 2-72033
Li_2SO_4, polycryst. pellet, radio and microwave freqs. 2-61413
$LiTaO_3$ single crystal, temp. dependence 2-72008
$MgO-SiO_2-Al_2O_3$, pressure sintered specimens, phase composition and dielectric constants 2-57226
Mn ferrite, elec. permittivity tensor from Kerr effect and optical consts. 2-81337
$(NH_4)_2BeF_4-(NH_4)_2SO_4$ concentration and temp. dependence of dielectric constant and spontaneous polarization 2-68471
$(NH_4)_2Cd_2(SO_4)_3$, press. to 1400 bar, 20-300K 2-77958
NH_4Cl-H_2O frozen solns., discontinuities at crit. pt. 2-53499
NH_4HSO_4, γ-irrad., ferroelec. transition phenomena 2-84369
NH_4NO_3 phase II, 9.52 GHz, room temp. to 125°C 2-65049
N_2O_4, liq., ioniz. enthalpy determ. 2-84612
NaBr(Cl)(F), l.f. dielec. consts., press. and temp. derivatives 2-51188
$NaBrO_3$, optical phonon spectrum by laser Raman spectroscopy 2-84495
NaCl, static dielec. const., anharmonic contribs. 2-50996
$NaNbO_3$, dielec. const. changes after electron or gamma irrad., X-ray study 2-65047
$NaNd(WO_4)_2$, n.m.r. of ^{23}Na and mag. susceptibility detn. 4.2-300K 2-72513
$NaTh_2(PO_4)_3$, temp. depend. 2-54237
Nb_2O_5, on Nb, ellipsometric obs. of field depend. 2-44150
Ni-Zn ferrite powder, quality characterization 2-57312
O_2, compressed gaseous and liquid, meas. between 100 and 300K and 55 and 154K, calc. of Clausius-Mosotti function 2-50274
$PbTiO_3$, dielec. const. changes after electron or gamma irrad., X-ray study 2-65047
$Pb(Zr,Ti)O_3$ type, static dielec. const. and dissipation factor, nonlinear field depend. 2-72035
$PbZrO_3$, dielec. cond. changes after electron or gamma irrad., X- ray study 2-65047
RbBr, high temp. dielectric constants meas. by standing wave technique 2-47968

Permittivity continued
RbCl, high temp. dielectric consts. meas. by standing wave technique 2-47968
RbH_2PO_4, dielec. consts., 300-500K, phase transition obs. 2-71688
RbI, high temp. dielectric consts. meas. by standing wave technique 2-47968
$SbSI:Sb_2S_3$, prep., spontaneous polarization, dielec. permittivity, photocurrent, dark current rel. to phase transition, −50-50°C 2-75143
SbSI, ferroelec. semicond., rel. to temp. depend. of photoelec. e.m.f. 2-72078
SbSI, ferroelectric, one dimensional mech. stress effect on phase transition obs. 2-75155
Se film, rel. to a.c. cond. 2-68392
Si, amorphous, cryst. polytypes, imaginary part of energy depend. dielec. const. 2-71946
Si_3N_4, film, reactivity sputtered onto Cu substrate 2-43481
SiO films, investigation of anomalous behaviour 2-44149
SiO_2, r.f. sputtered, temp. coeff. of capacitance 2-61407
Sr vanadates, dielec. const. and loss tangent 2-43589
$SrCl_2:K^+(Na^+)$, dielec. const., dopant conc. depend. 2-47969
SrF_2, l.f. dielec. consts., press. and temp. derivatives 2-51189
$SrTiO_3$, anomalous reson. in permittivity on cooling in elec. field 2-77935
$SrTiO_3$, dielec. const. changes after electron or gamma irrad., X-ray study 2-65047
$Sr(Zr,Ti)O_3$ ceramics, high-permittivity, temp. coeff. 2-51190
Ta_2O_5, anodic oxide film on Ta, ellipsometric obs. of field depend. 2-44150
TiO_2, reduced, mag. impurity effects 2-47902
triglycine sulphate single crystal, effect of growth rate 2-47987
V_2O_3, real and imaginary part of dielec. const. from refl. spectra 2-81407
W_2O_5, anodic oxide film on W, ellipsometric obs. of field depend. 2-44150

Perturbation theory
analysis of buoyancy effects on forced-convection flow and heat transfer 2-74319
anharmonic oscillator, density matrix 2-76216
anisotropic cubic crystals, elastic displacement field of point defects 2-80697
anomalies in quantum electrodynamics, review 2-63472
antiferromagnets, two-magnon Raman scatt., temp. depend., calc. 2-81304
atomic structure calcs., polarized core approx. 2-70565
axial vector current and PCAC in σ-model, explicit opera construction in perturbation theory 2-76579
axiomatic field theory, perturbation expansions 2-59376
Bjorken, Johnson and Low theorem, equal-time commutators 2-63478
bound eigenstates of electron in exponential cosine screened Coulomb potential 2-69597
Brueckner-Goldstone many-body theory, applic. to He photoionization calc. 2-46493
Brueckner-Goldstone many-body theory, use of multiple basis sets for atomic problems 2-46445
celestial mechanics, Lindelof's method 2-81782
classical fluids, theory for repulsive forces 2-43044
classical gas, dynamical correlation function, first order perturbation calculation 2-43258
commutator techniques, application to calcs. on two-electron ions 2-69593
conformal invariance validity derivation of Ward identities 2-49466
conjugated molecules, comparison of various expansions in perturbation theory calculations 2-42855
continued-fraction method application to Mathieu eqn. and anharmonic oscillator eqn. 2-73326
crystals with point defects, influence of small perturbations on resonance vibrational states 2-74761
diatomic mols., collisional vibr. transition probabilities calc. method 2-80122
distribution function of mixed hard spheres, perturbation calc. 2-78941
electrodynamics in strong magnetic field, phenomena studied by perturbation formalism 2-63265
exchange perturbation theories for mol. interaction energies calc. 2-83421
exchange perturbation theory applic. to intermol. forces calc. 2-83420
exchange perturbations, optimization of treatment 2-49004
fermion systems, ground state, invariant cones and uniqueness 2-76558
Feynman atomic diagrams with simple denominators, summation in perturbation series 2-67381
first approximation, calc. energy levels of optical electron of ionic core 2-46420
first order, for quasi-energy and wave functions of quantum syst. 2-45271
fluid, corresponding state theories 2-53107
fluid viscosity coeffs. eval. method 2-77213
hamiltonian dynamical system, perturbations in action-angle variables 2-82289
Hartree-Fock, exact derivation of single excitation model 2-49009
Hartree-Fock scheme applic. to polarizability calcs. of 12- and 18-electron systems 2-79929
homogeneous interactions in quantum field theories 2-76567
improved systematic procedure for calculating vibration-rotation energies of molecules 2-46512
light-cone commutators 2-73776
linear systems, variational estimates and generalized perturbation theory for ratios of linear and bilinear functionals 2-58702
many-body, calc. of correlation energy of C atom and H_2O molecule 2-52914
modified perturbation expansion generalization for density matrix in path-integral formalism 2-78821
molecules, alternant, calculation of vibration frequencies 2-74254
molecules, radiationless transitions 2-42824
non-normalizable eigenvectors 2-41510
non-separable systems, multidimensional WKB perturbation, classical limit 2-82221
nonlinear dispersive wave problems, multiphase modes 2-52037

Perturbation theory continued
nonlinear oscillators, synchronously tuned coupled and autonomous 2−82225
nonlocal potential matrix elements from scatter phases 2−52079
oil and water simultaneous flow through cracked porous medium of small inclination, finger-imbibition phenomenon 2−53358
oscillating charge, in inhomogeneous medium, radiation 2−41917
oscillators, weakly coupled 2−45444
$P(\varphi)_2$ model, vacuum energy shift and Wightman functions 2−82607
plasma, ion oscillation modes, automodulation 2−70938
polymer chain, local electronic states using method of local perturbations 2−83384
pressure derivatives calculation, of elastic constants in alkali metals 2−60839
QED of particles of spin $\leqslant 1$, perturbation theory of two particle states 2−66902
Rayleigh-Schrodinger, generalized equations 2−52071
Rayleigh-Schrodinger single perturbation theory, for degenerate level with two perturbations, second-order energy 2−69592
Rayleigh-Schroedinger, calc. of ground state energies of He and Be through second order 2−64072
rubberlike slightly compressible circular cylinders, finite torsion 2−76321
Rydberg excited states, basic formulas for one-electron perturbation calc. 2−67452
S-matrix, for electromagnetic corrections in strong interactions and field-theoretic self-energy calculations 2−52518
SCF perturbation theory and intermolecular interactions · 2−42849
Schrodinger eqn. with odd perturbation, eigenvalues 2−82222
Schrodinger equation, perturbation by potentials with small support 2−66445
second order, calc. of infinite sum of intermediate conditions 2−49010
second-order, with exact zeroth-order Hamiltonian 2−76212
self-interacting fermion systems, perturbation theory for grand canonical Gibbs states 2−45328
singular perturbation methods in nonlinear acoustics 2−41684
singular perturbations, asymptotics, Feynman path integrals, evaluation 2−41511
soft-pion theorems, factor ordering problems 2−45272
spectroscopic trends, estimation by perturbation method using Hellmann pseudopotentials 2−49997
stationary, ambiguities, teaching paper 2−73325
symmetric top molecules, theory of higher- order Stark effect 2−42836
tetrahedral molecules, Van Vleck theory applied to vibration-rotation interaction 2−42842
tidal, non-radial oscillations of star 2−73013
time-dependent, review 2−58759
tunnelling, general theory and appl. to static impurity case 2−68275
variation-perturbation calculation of diamagnetic properties of H_2^+ molecule ion 2−53009
variation-perturbation calculation of diamagnetic props. of H_2^+ molecule ion 2−53008
vector-meson dominance 2−82709
virial expansion for non-ideal reference system, compared with perturbation theory 2−45298
water, gravity waves, nonlinear modulation 2−71144
weakly bound states 2−78828
Wigner-Weisskopf, applic. to spontaneous decay in time dependent external field 2−41514
Wigner-Weisskopf, decay of positronium system 2−73765
N e.m. form factors, field-theoretical model 2−79608
FeH, electronic states, many-body perturbation theory approach to approx. HF calc. 2−67474
H_2^+-like molecules, floating one-centre perturbation treatment 2−67455
H, perturbation theory of intermolec. forces in small overlap region 2−70813
H, perturbation theory of intermolec. forces in small overlap region 2−70812
H_2^+, perturbation and perturbation-variation treatments of $1s_g$ and $2p_u$ states 2−53010

pH *see Electrochemistry*

Phase-contrast microscopy *see Microscopy*

Phase diagrams *see Phase equilibrium; Phase transformations*

Phase equilibrium
see also Solubility; Solutions
— 2−66479
σ phases melting points and compositions 2−80799
alkali metal ammonia solns., solvation model 2−84614
alloy, binary, isothermal reaction stage influence on cpd. growth by diffusion 2−64686
alloy, binary, vaporization, condensation and solidification diagrams 2−53509
benzene lenses at air-water interface, with translational and rotational symmetry 2−74510
C16-type compounds and pseudobinary alloys, stability and competitive structs. 2−50851
characteristic temperatures of matter on the saturation line 2−71270
charged Bose gas, density-temp. diagram 2−78851
cholesteryl derivatives, phase diagrams for binary mixtures 2−77414
complex reaction problem calculation by computer 2−74580
data prediction for multi-components distillation column design 2−75361
diagrams, teaching aid 2−48964
diagrams, temp. vs. comp., and press. vs. temp., correl. 2−71699
differential thermal analysis, interpretation of anomalous peak shape 2−57438
garnet film, product phase control in chem. vapour deposition 2−71321
gas mixtures at high pressures rel. to planetary interior structure 2−83843
geological systems, multicomponent, REACTION program 2−61847
glasses, phase separation, X-ray study under different collimation conditions 2−71285
graphite-SiO_2 system, diagram determ. 2−43930
heterogeneous mixture, partial thermodynamic functions 2−41538

Phase equilibrium continued
III-V compound, quasi-binary phase diagram, solid solution excess free energy 2−74948
interphase interfaces, strain fields, epitaxial dislocations, steps, electron diffr. contrast 2−56625
ionic substances, establishment of empirical rules governing polymorphism 2−68191
ketone/alkane binary mixtures, isothermal vapour-liquid equilibria 2−74590
liquid-vapour penetrable sphere and related models 2−80523
liquid/vapour equilibria of binary systems N_2O/N_2, N_2O/O_2, N_2O/methane 2−50402
metal/hydrogen systems, h.p. thermodynamics 2−77715
multicomponent vapour-liquid equilibrium data computation 2−74589
plagioclase feldspars, phase diagram 2−61849
rare earth hexaborides, stability 2−50965
rare earth orthoferrites, phase relationships in R_2O_3-Fe_2O_3 melts 2−50601
rare earth tetraborides, thermal stability 2−53995
semiconductor, tetrahedral, temp.-pressure phase diagram, scaling theroy calc. from optical spectra 2−80528
steel, austenitic manganese, struct. stability 2−43848
steel, critical pts., additive effects 2−47686
steel, high-alloy, suppression of pitting in phase analysis 2−57423
steel, kinetics of isothermal coalescence of dispersed phase 2−47611
steel, low-C martensiti, austenite stability 2−50834
steel, phosphide eutectic classification 2−47633
steel, stability of FeC at 700°C 2−50944
surface phases determined from stepwise adsorption isotherms 2−77518
ternary $n+3$ phase multisystem, topological relationships 2−72693
thermodynamic treatment of chemical equilibrium 2−44465
transition metal binary alloys, low-temp, sp. Lt. parameters γ and θ_d, inverse scaling, rel. to phase stability 2−68248
tricritical points, geometric predictions of scaling 2−64503
vapour-liquid, general correlations 2−84610
vapour-liquid, in binary systems, derivation of new equilibrium correlations 2−71277
vapour-liquid, multicomponent separation calculations, modified Newton's method 2−68756
vapour-liquid equilibria of binary mixtures of molecules interacting via Kihara potential, Percus-Yevick theory 2−67552
Ag-Pd-H system, diagram 2−74953
Ag_2S, phase II existence region determ. from electronic props. 2−47703
Al-Cr, solid solution, high supersaturated, range extension in equilibrium diagram when cooled 2−43824
Al-Ge alloys, rapidly solidified, constitution 2−43929
Al-Mg alloy, kinetics of isothermal coalescence of dispersed phase 2−47611
Al-Mn, solid solution, high supersaturated, range extension in equilibrium diagram when cooled 2−43824
Al-Mo, binary phase diagram, obs. 2−50955
Al-Zn solid solution, miscibility gap, resist. study 2−50826
Al_2O_3-Cr_2O_3 phase diagram and ideal soln. behaviour 2−50852
Al_2O_3-Cr_2O_3 system, sub-solidus phase equilibria 2−53983
Al_2O_3-$Ni(NO_3)_2.6H_2O$ system, effect of heating in oxidizing and reducing media 2−60992
Al_2O_3-ZrO_2-SiO_2 fused grain refractories, rebonded, characteriz. 2−53926
Ar, Monte Carlo calculations along solid-vapour coexistence curve 2−57055
As-Se-Ge-Sn glass, phase diagram, Mossbauer effect, isomeric shift, quadrupole splitting 2−75267
Au-Zn alloy, β' phase, liquidus and solidus temps. 2−80838
B binary alloys, diagram, review 2−50957
B_2O_3-Li_2O-H_2O system borate hydrates 2−47181
BP-P system, h.p. equil. 2−50956
Ba silicates, solidus and liquidus temps. 2−54006
$Ba_4SrNb_{10}O_{30}$, solidification structs. 2−47654
$BaTiO_3$-$BaGeO_3$ system 2−84105
Bi-Pb alloy, thermal expansion meas. applicability of rule of mixtures in two phase region 2−60975
Bi-Sb alloys, pressure-temp.-comp. diagrams 2−68192
Bi-Sn alloy, thermal expansion meas. applicability of rule of mixtures in two phase region 2−60975
Bi_2Se_3-Bi_2Te_2S solid soln., phase diagram 2−57028
Ca-Si system, existence of silicides 2−71700
CaO-Nb_2O_5-TiO_2-SiO_2 system, liquidus temps. 2−43436
$CaO.Al_2O_3$-Al_2O-CaF_2 solid soln., phase diagram 2−57029
CaSi system, temp. vs. comp. and press. vs. temp. diagrams, correl. 2−71699
$CaSiO_3$-$NdSiO_5$ system 2−47707
Cd-Ge-As-Se glass-forming melt, liq.-liq. immiscibility 2−56561
Cd-S system, rel. to liquid phase epitaxy of CdS 2−47104
Cd_3As_2-2CdTe system, diagram 2−47708
Cd_3Mg, two-phase region, morphology, habit planes and orientation relns., metallographic obs. 2−61042
Cd_3P_2-2CdSe system, diagram 2−47708
CdSe, solid-gas phase equilibria and thermodynamic props. 2−71368
CdTe-CdSe system, phase diagram, rel. to cryst. growth technique selection 2−47702
CdTe, rel. to cryst. growth and props. 2−50593
Ce binary alloys, isomorphic transform. theory, stable constitution diagram 2−50960
Ce binary alloys, isomorphic transform. theory, metastable constitution diagram 2−50959
Ce_2Se_3-GeS_2 system, diagram, intermediate cpd. formation 2−61043
CmO_x-O_2, phase reactions during isobaric thermogravimetric analysis 2−74927
Co-Mn-Al system, decomp. studies 2−64816
Co-Ni-Sb system, X-ray diffr. study 2−43940
Co-Ni-Ti system, decomp. and formation of modulated struct. in coherent phase zone of stability 2−57030
$Co(PO_3)_2$-C_5PO_3, phase diagrams, invariant points solid soln. 2−74950
$Co(PO_3)_2$-$NaPO_3$, phase diagrams, invariant points solid soln. 2−74950

Phase equilibrium continued
- Cr-Ga alloy, phase diagram, intermetallic cpds. 2−64817
- Cr-I system, phase diagram and phase identification 2−71701
- Cr-Mo-Si system constitution diagram 2−50961
- Cr-Ni-B system, existence of ternary compounds 2−61044
- Cr-V alloy system, melting equil. diagram 2−47709
- CsCl-KCl and CsCl-KCl-NaCl systems, diagram 2−43932
- CsCl-NaCl and CsCl-KCl-NaCl systems, diagram 2−43932
- $CsNO_2$, phase diagrams, cryst. struct., to 40 kbar 2−74951
- Cu-As system, phases, struct., homogeneity rangers 2−74731
- Cu-Mn-Al alloy, interphase interfaces, interfacial dislocations 2−56719
- Cu-Ni-Fe alloy, interphase interfaces, interfacial dislocations 2−56719
- Cu-P-O system phase relations 2−50962
- Cu-P system, constitution diagram determ. 2−61045
- Cu-Sn system, electrodeposited, phase diagram 2−84085
- Cu-Zn-Mn system, phase diagram 2−50963
- $CuFe_2O_4-CuGa_2O_4$ system, phase diagram 2−71702
- $CuO-Al_2O_3$ solid soln., form. of $CuAl_2O_4$ phase at 890°C, stability 2−74899
- $Cu_2O-Al_2O_3$ solid soln., form. of $Cu_2Al_2O_4$ phase at 930°C, stability 2−74899
- Cu_2S-CuCl melt, phase diagram rel. to elec. and structural props. 2−46983
- Cu_xS, differential thermal analysis of the Cu-S system, 30-500°C 2−84138
- Dy-Au alloy system, phase diagram, intermetallic form. 2−50973
- Dy_2O_3-BaO solid soln., phase diagram 2−54005
- $Dy_2O_3-WO_3$, solid soln., phase equilib., transform., phase diagram, densities, m.p. 2−57013
- Er-B system, temp.-comp. phase diagram 2−50964
- ErB_6, form. and stability 2−50965
- Eu-Fe-O system, phase relations and cpd. formation 2−47710
- Eu-W-O, subsolidus phase relations and cryst. chem., phase diagram 2−74952
- Fe-Cr-Co system, phase boundary $\alpha+\gamma/\gamma$ determ. 2−84164
- Fe-Cr-Mn alloy, α-γ phase equilib., effect of transition metal additions 2−47687
- Fe-Cr-Mn system, phase boundary $\alpha+\gamma/\gamma$ determ. 2−84164
- Fe-Cr-Ni system, phase boundary $\alpha+\gamma/\gamma$ determ. 2−84164
- Fe-Cr system, computed low temp. equilib. 2−50966
- Fe-Cu-O system, equilib. phase diagram detn. 2−64818
- $Fe-Fe_3C$-Si, phase diagram, white cast iron and carbon equivalent 2−74954
- Fe-Ga-Sb and Fe-Sb systems, rel. to mag. props. 2−64821
- Fe-Ge α' solid solution, precipitation behaviour 2−64819
- Fe-Ge system, rel. to mag. props. 2−64821
- Fe-Ni carbonyl powders, phase composition 2−77726
- Fe-Pd-H system, diagram, X-ray and Mossbauer determ. 2−74953
- Fe-Sn-C system, formation and stability range of ternary cpds. 2−43933
- Fe-Sn system, phase boundaries of γ-loop 2−47712
- Fe-V-C system, phase diagram, pseudo-binary section at 0.5 wt-%V 2−47711
- $Fe_2O_3-B_2O_3$, rel. to applic. to $FeBo_3$ crystal growth 2−50594
- Fe_2O_3-FeO-$Li_{0.5}Fe_{0.5}O$, coexisting phases equilibrium and thermodynamics, 900-1200°C 2−74931
- $FeS-FeCl_2$ melt, phase diagram rel. to elec. and structural props. 2−46983
- $Fe_2SiO_4-Mn_2SiO_4$ phase diagram and ideal soln. behaviour 2−50852
- Ga-As-Te system, GaAs-Te polythermal section determ. 2−61047
- Ga-As-Zn system, GaAs-Zn polythermal section determ. 2−61046
- Ga-Sb system, solid and liq. states, rel. to mag. props. 2−64820
- $Ga_{1-x}Al_xAs$, pseudobinary system, solidus boundary, thermodynamic analysis 2−50968
- $GaAs-As_2Te_3$ system, diagram 2−47713
- GaAs-Si, amphoteric impurity distrib. equilib. calc. 2−83981
- GaAs-Sn quasi-binary system, phase diagram 2−43934
- GaSb-GaAs system, phase diagram, thermodynamic analysis 2−44086
- $Ga_2Te_3-As_2Te_3$ system, diagram 2−47713
- Ga_2Te_3-Cu system diagram 2−47715
- Gd-B system, temp.-comp. phase diagram 2−50969
- $Gd_2O_3-GeO_2$ system, phase diagram obtained by high temp. microscopy, microstructural and X-ray phase anal. 2−84097
- Ge-Sb system, diagram incorporating metastable GeSb 2−47329
- Ge-Sr system, stoichiometric cpd. formation 2−47714
- HFC-Re system, determ. of solubility relations and phase diagram of eutectic type 2−84096
- $^3He-^4He$ mixture, diagram of state singularities due to hydrostatic effect 2−43414
- Hf-Nb-B alloy, at 1400°C, X-ray obs. 2−43912
- Hg-chalcogenides, solid-liquid phase equilibrium and physico-chemical properties 2−68759
- In-Ga-As-Cl-H system, rel. to vapour growth of $In_xGa_{1-x}As$ 2−47222
- In-Ga-P-Cl-H system, rel. to vapour growth of $In_xGa_{1-x}P$ 2−50576
- $InBr_2$, heterogeneous equilib. 750-1050 K, enthalpy, entropy of evaporation, boiling point 2−74593
- $In_xGa_{1-x}P$ ternary phase diagram and band gap energy obs. 2−74949
- InP-GaP system, component distrib. coeffs. and phase diagram 2−47716
- $In_2Se_3-Sb_2Te_3$ system, diagram, intermediate cpd. formation 2−61048
- In_2Te_3-Cu system, diagram 2−47715
- $KMnF_3-ErF_3$ system, diagram, existence of $KMnEr_3F_{12}$ 2−50622
- $KPO_3-Sr(PO_3)_2$ system, phase diagram 2−43935
- $K_2WO_4-In_2(WO_4)_3$ solid soln., phase diagrams 2−57033
- La-Ni system, 50-100 at.% Ni, intermetallic cpds. 2−74934
- Li-B-N system, rel. to cubic BN growth 2−50970
- $Li_2MoO_4-Cr_2(MoO_4)_3$ solid soln., phase diagrams 2−57033
- Li_2O-SiO_2 glass, phase separation and crystn., X-ray obs. 2−56560
- $Li_2SO_4-Cs_2SO_4(Na_2SO_4)(Rb_2SO_4)$ systems, phase diagrams 2−80527
- $Li_2WO_4-Li_4WO_5$ system, $Li_6W_2O_9$ phase existence 2−54007
- Lu-H(D) system, α-phase characts. 2−77749
- $MgAl_2O_4-Al_2O_3$ system, liquidus- solidus determ. 2−50971
- $MgO-B_2O_3$, system, phase relations, quenching method 2−57031
- $MgO-B_2O_3$ system, obs. using thermobalance 2−73283
- $MgO-Cr_2O_3-CuO(Cu_2O)$ system, phase diagram 2−43931

Phase equilibrium continued
- Mn-Ga alloys, rel. to internal friction 2−50735
- Mn-Zn ferrite powders, comp. effects on technological props. 2−68163
- Mn-Zn system, X-ray and magnetic obs. 2−57032
- Mo-Pt system, rel. to conc. depend. of supercond. transition temp. 2−61246
- Mo ternary sulphides, crystallographic instability 2−71691
- N_2, det. from equations of state representing all saturated state variables 2−53332
- N_2O_4, dissociated, stable states of liquid and gas near phase transition 2−47041
- N_2O_4, stability of superheated liquid phase 2−47044
- Na_2-CaO-MgO-SiO_2 glass, in glass forming region 2−57023
- Na-K, eutectic, liquidus curves from conformal solution theory 2−83842
- Na-β-Al_2O_3 phases formation and area of existence 2−84066
- $NaNbO_3-BaTiO_3-BaNb_2O_6$ system, tungsten bronze field 2−72034
- Na_2O-SiO_2 glass, immiscibility temp., effect of small additions of Al_2O_3 and Ga_2O_3 2−53539
- Na_2S_x, molten, phase diagram, open circuit voltage obs. 2−71185
- $Na_2WO_4-Y_2(WO_4)_3$ solid soln., phase diagram 2−74955
- Nb-Al-Ge system, phase equilib. and supercond. props. 2−43936
- Nb-Fe system, plastic deformation, microhardness, melting, emission electron microscopy 2−74843
- Nb-Ga system, constitution diagram 2−43937
- Nb-H dil. solns., equil. press. and ideal behaviour 2−50843
- Nb-H solns., nondil., equil. press.- comp.-temp. relationships 2−50843
- Nb-H system, phase diagram, 80-500 K 2−77756
- Nb-Sn-Cu(Ag)(Au), supercond., rel. to shielding behaviour 2−75061
- NbC-X, X=Fe, Cr, Ni, Co, pseudobinary, and phase diagrams 2−68199
- NbD_x system, diffuse neutron scatt. phenomena in α-phase, temp. depend. 2−77757
- Ne submonolayer, on Ar coated grafoil, two phase system obs. 2−80582
- Ni-Cr-Nb-W-Mo alloy, struct. and phase comp. 2−43941
- Ni-Sb system, X-ray diffr. study 2−43940
- Ni alloys, suppression of pitting in phase analysis 2−57423
- Ni alloys with high W content, phase analysis 2−57034
- $P_2O_5-LaF_3-RF_2$, R=Ba, Mg, triangular diagrams, crystn. and vitrification regions 2−57035
- Pb-Ge-As-Se glass-forming melt, liq.-liq. immiscibility 2−56561
- $(Pb,La)(Zr,Ti)O_3$, diagram 2−56968
- $PbBr_2-PbCl_2$ phase diagram and ideal soln. behaviour 2−50852
- $PbFe_{2/3}W_{1/3}O_3-PbTiO_3$ solid solution, diagram, antiferromag., ferromag., paramag., ferroelec., and paraelec. regions 2−81229
- PbTe-GeTe system, diagram 2−84108
- PbTe-PbSe system, phase diagram, rel. to cryst. growth technique selection 2−47702
- PbTe-UTe system, diagram 2−47717
- PrO_x-ZrO_2 ternary system, phase relationships, oxygen press. effect 2−47694
- PrP_{1-x}, phase diagram, homogeneity region, limits of existance, 400-1000°C 2−74956
- $Pu(MoO_4)_2-Na_2MoO_4(Li_2MoO_4)$ system, scheelite phase obs. 2−71694
- $Rb_2BeF_4-Na_2BeF_4$, phase diagram, struct. of phases 2−74957
- $Rb_2MoO_4-Al_2(MoO_4)_3$ solid soln., phase diagrams 2−57033
- $RbNO_2$, phase diagrams, cryst. struct., to 40 kbar 2−74951
- Re-Al(Si)-B systems, diagram, X-ray study 2−64822
- $Sb_2Se_3-SbI_3$ system, phase diagram 2−43942
- Sc_2O_3-MgO solid soln., phase diagram, defects, disintegration, decomp. precip. 2−74906
- Si-C system, solid soln. formation, X-ray obs. 2−50972
- $SiO_2-B_2O_3-Na_2O-Al_2O_3$ system, comp. fluctuation and phase decomp. 2−53543
- $SiO_2-Si_3N_4$ film, phase composition, by spectrophotometry 2−47086
- Sm-Au alloy system, phase diagram, intermetallic form. 2−50973
- Sm-Sn system, relative stability of intermetallics 2−47573
- Sn-Bi-As system, Sn_4As_3-Bi-SnAs subsystem 2−74942
- SnO_2-TiO_2 system, two-phase region studies 2−50974
- SnTe-UTe system, diagram 2−47717
- $SrAl_2SiO_8-BaAl_2SiO_8$ solid soln., isomorphism, phase diagram 2−54009
- Ta-Cr-B alloy, at 1400°C, X-ray obs. 2−43912
- Ta-O system, high temp. solid solubility limit and phase studies 2−50975
- Te-As system, vapour press. of Te_2, As_4, and As_2 over molten As_2Te_3 2−47046
- Th-Ir system, 66-83%Ir 2−50976
- Th-Ni system, 50-96% Ni, 1000-1500°C 2−74943
- $ThN-ThO_2$-Th system, phase behaviour 2−50977
- $ThO_2-Ln_2O_3$ systems, diagram, 1250-2100°C 2−47718
- $ThOs_2-ThIr_2$ system, comp. range of stability C15 phase 2−50976
- Ti-C-N-O solid soln., phase diagram, form. of carbonitrides and oxycarbides 2−54010
- Ti-Ce-S system, diagram and alloy struct. 2−43943
- TiN-VN particles, nitriding and annealing effects 2−68202
- $TiO_2-Cr_2O_3$ system, solid solubility of $Ti_2Cr_2O_7$ 2−47719
- TiO_2-SnO_2 solid soln., extent of miscibility gap region 2−77732
- U-O system, oxidation equilib., x-ray study 2−44487
- U-Pu-W-C system, X-ray diffr. and metallography study 2−54011
- UC-UN system, solid soln. formation mechanism 2−53910
- UO_2/W system, eutectic structs., influence of growth parameters 2−53969
- VO_2-NbO_2, system, rel. to metal-insulator transition 2−75101
- WSe_2-NbSe_2 system, intermediate cpds., cryst. struct. 2−60767
- YCo_5-YFe_5 pseudobinary system, $CaCu_5$-type phase stability 2−43944
- YCo_5-YNi_5 pseudobinary system, $CaCu_5$-type phase stability 2−43944
- $Y_2O_3-Al_2O_3$ system, high temp. phase instability of $YAlO_3$ 2−74958
- Y_2O_3-BaO solid soln., phase diagram 2−54005
- Yb-Sn system, relative stability of intermetallics 2−47573
- Yb_2O_3-BaO solid soln., phase diagram 2−54005

Phase equilibrium continued
Zn-Cd-Te system, phase diagram, rel. to cryst. growth technique selection 2−47702
ZnO-Nb_2O_5-SiO_2, ternary system, phase relations at liquidus and subsolidus temps, 2−68203
ZnO-TeO_2, exptl. study 2−64504
$ZnSO_4.7H_2O-NiSO_4.7H_2O-CoSO_4.7H_2O$, isomorphous relationships, distribution coeff. 2−74959
Zr-C-N-O solid soln., phase diagram, form. of carbonitrides and oxycarbides 2−54010
ZrC-W solid soln., interactions, isothermal sections struct. at 2200 and 2600°C 2−74911
ZrO_2-Y_2O_3 system, phase diagram above 2000°C 2−61049
ZrO_2-Yb_2O_3 and ZrO_2-Yb_2O_3-Y_2O_3 systems, solid soln. formation kinetics 2−47721
ZrO_2, calcia-stabilized, destabilization by ZrB_2 2−50902
$ZrSiO_4$-TiO_2 system, 1050-1600°C 2−47722

Phase flow *see Flow/two-phase*

Phase meters *see Electrical measurement*

Phase transformations
Used for structural transitions only
4-n-alkoxybenzylidene-4′-phenylazoanilene, nematic-spectra A phase transition, n.m.r. meas. on molecular orientation 2−53402
anils, thermotropic liquid crystals, transition temps. and mesophase identification 2−50326
antiferromagnets, domain structure as result of two phases in coexistence 2−81306
binary mixture, hydrostatic effect near critical point 2−60537
binary mixtures, holographic investigation of critical phenomena 2−71269
binary-liquid phase transition, critical viscosity and diffusion 2−53407
Biot's variational principle for Stefan problem with constant heat flux 2−43437
β- brass type alloys, quenched, structure and microstructure 2−84106
butyl alcohol aqueous solutions 2−74547
cholesteric liquid crystals in isotropic phase, pretransitional increase in optical rotation 2−80434
cholesteryl esters, effect of substituent groups on mesophase transition temp. and range 2−80452
critical exponents and interactions 2−60540
critical phenomena, conf., New York, USA (June 1970) 2−52102
decoupled-mode dynamic scaling theory 2−52103
diagrams and multiple valued free energy 2−78947
differential thermal analysis, interpretation of anomalous peak shape 2−57438
disperse syst., of vapour, study by microwave abs. 2−56543
dynamical spherical model 2−52104
ethylamines, n.q.r. meas. at liquid nitrogen temp., obs. of phase transition at 184K 2−83310
ferroelectric transitions by exciton-phonon interactions 2−81153
field theory, Feynman graphs screening solution 2−78848
freezing transition in Kirkwood Monroe theory 2−53494
gas-liquid, role in nuclear matter theory 2−73981
gas-liquid critical point region, gravity effects, analysis by linear model parametric eqn. of state 2−47040
gases and solids, F-ensemble and quantum mech. calc. 2−45321
in hadron matter 2−59432
idealised Ising model, 1st, 2nd order transitions, computer simulation 2−78948
interstellar matter, spiral arm density wave, star formation 2−62591
Ising lattice, cubic, correl. functions near crit. temp. 2−78840
Kirkwood-Alder transition, evidence for existence in colloidal system 2−67874
Landau theory for tricritical systems, validity estimate by Ginzburg criterion 2−63040
laws of thermodynamics 2−45566
linear stability analysis of interface in isothermal phase transform. with conc. dependent diff. coeff. 2−68181
liquid crystal, theory 2−50322
liquid crystal film, second order, size effects 2−83869
liquid crystal homologous series, isotropic-nematic transition temp., alkyl chain length depend. 2−74518
liquid crystals, cholesteric nematic transition, ultrasonic investigation 2−80456
liquid crystals, cholesterol, form. of both cholesteric and smectic mesophases 2−80457
liquid crystals, lophenol, fatty acid esters, form. of smectic mesophase 2−80457
liquid-glass transition, bond-lattice model, configurational excitations in condensed matter 2−50408
liquid-solid, lattice theory, Lennard-Jones and $1/r^{12}$ system 2−77468
liquid-solid transition, mol. dynamics simulation 2−56540
liquid-vapour, in water cooled column, effect of axial dispersions in gas, liquid phases on mass transfer efficiency 2−67875
liquid-vapour, Wilson theory of critical point 2−64510
metal/hydrogen systems, due to elastic ineraction 2−77744
model systems, Peierl's arguments and thermodynamic limits 2−58798
Monte Carlo method application to calc. of equilibrium properties 2−82245
motion of interface on plate with variable heat fluxes 2−63147
nematic-isotropic transition in liquid crystals with biaxial phases 2−80445
nematic-smectic A phase transition, n.m.r. meas. on molecular orientation 2−53402
nematic-smectic C phase transition, periodic free surface disclination obs. 2−60432
non-equilibrium, chemical reaction models 2−51422
non-equilibrium thermodynamic considerations 2−63037
nuclear fission models, phase transitions 2−46338
order-parameter correlations within screening approximation 2−63036
phospholipid-water mixtures 2−43374
pulsed ultrasonic studies 2−58927
quantum kinetics, near 0K 2−78857
random cluster model 2−49030
random system, critical conc. against interaction range 2−52089

Phase transformations continued
salt systems binary and ternary, simultaneous recording of electrical conductivity and DTA 2−78179
second-order transitions, universality, scale factor for correl. length 2−63029
solids with U_s-u_p linear relationship, melting line determ. 2−80518
spaced bumper systems, projectile target transforms., effect on system performance 2−62413
statistical mechanical models 2−58799
steroids, influence of ring unsaturation position on type and formation of mesophase 2−80458
Tisza theory, equilibrium thermodynamics of critical points 2−41536
tricritical exponents and scaling fields for two-component systems 2−63035
tricritical point, Landau theory 2−55430
triterpenes, influence of ring unsaturation position on type and formation of mesophase 2−80458
Yang-Lee theory, extension to two variables 2−78947
Ar fluid around critical point, density fluctuations in microscopic volumes 2−56539
As_2Te_3-As_2Se_3 glass, DTA obs. 2−61299
CaO-CaF_2 system liquidus line determ. by the capillary method 2−84683
Cd-Si-As system, glass-forming region determ. by differential thermal analysis 2−74599
CdS, retaining metastable phases by quenching under pressure 2−84152
Cr-Ti compounds 2−80798
Cr interfacial free energies meas. 2−80795
Cu-Ni-Mg alloys eutectic mixtures constitution 2−84103
Fe-Zn alloy, phase diagram, obs. of Fe rich side 2−50967
Fe(II) salt solutions, frozen at normal pressure 2−78178
GaAs-GaP pseudobinary, phase diagram, solidus boundary 2−83841
GaAs-GaP pseudobinary solidus boundary 2−83841
H-bonded solvents, lattice models 2−41526
^{3}He-^{4}He mixtures, Landau theory test 2−63040
^{3}He fluid near critical point, meas. of thermal relaxation times 2−80514
^{3}He liquid-solid mixture, interpretation of NMR and thermodynamic data below 3 mK, new liquid phase 2−80511
$In_xGa_{1-x}As$ prep. and props. rel. to electroluminescent diodes 2−68708
LiCl-$UCl_{3(4)}$ systems, binary and ternary, melting point diags. 2−67873
Mg_2Sn, retaining metastable phases by quenching under pressure 2−84152
Mo interfacial free energies meas. 2−80795
Na-K, eutectic, liquidus curves from conformal solution theory 2−83842
Nb-H systems, due to elastic interaction 2−77744
NbC-X, X=Fe, Cr, Ni, Co, pseudobinary, phase diagrams 2−68199
Nh_4Br, l.f. soft vibrational modes under stress 2−71696
Pd-H systems, due to elastic interaction 2−77744
SF_6 liquid-vapour, interferometric meas. of isotherms in critical region 2−80519
SnTe-GeTe alloys, retaining metastable phases by quenching under pressure 2−84152
SnTe, retaining metastable phases by quenching under pressure 2−84152
Ta-H systems, due to elastic interaction 2−77744
TeAsGeS glass, DTA structural obs. 2−61329
Ti alloys, radiation induced transformations in h.v. electron microscope 2−80874
V-H systems, due to elastic interaction 2−77744
V_2O_5 bronzes, electrical conductivity in solid and liquid state 2−84339
W interfacial free energies meas. 2−80795
Xe, afterflow, electron temp. lowering by diffusion cooling 2−70882
Zn-Ti alloys, effect of comp. and cooling rate on microstructure and eutectic 2−80818

solid-state
see also Ageing; Order-disorder changes
2,3-dimethylbutane, dielec. relax. below glass temp. by trans-gauche transform. 2−81144
— 2−71693
$A^{II}B^{IV}C^V_2$, polymorphic transitions and changes of the forbidden zone width 2−80947
adamantane, press. induced transition, hysteresis 2−61563
alkali metal superoxides and ozonides, effect of Raman spectra 2−81354
alloy, binary one-dimens., theory 2−50980
alloy, supersaturated solid soln. decomp., review 2−43928
antiferromagnetic-ferromag. transform., mag. moment oscill., mag. dipole radiation 2−78007
athermal martensitic morphology, arrow-like formations 2−67980
austenite, C content of small regions and transformation mechanism of Mo_2C fibres 2−77675
austenite, static recrystalliz. between intervals of hot working 2−47575
austenite to martensite transform., effects of hydrogen 2−74923
beryllium oxyacetate, polymorphism, -196°C to 286.7°C, pulsed n.m.r. investigation, study of molecular dynamics 2−57399
carbon tetrachloride, enthalpy of transition and heat capac. for metastable fcc to stable rhombohedral transform. 2−77754
ceramics, texture and phases in spark plugs, e. probe anal. and X-ray diffr. study 2−71390
composite materials, oriented, prep. from solid phase 2−74918
Debye-Waller anomaly, Mossbauer fraction 2−68211
diamond graphitization at zero pressure and at high pressure 2−47677
displacive type, sound propag. phenomena 2−54026
domains, interface geometry, contrast effects, electron microscope and diffr. obs. 2−56718
Earth's upper mantle, role of exptal., physical acoustics 2−57450
elastic constants and the ΔE effect 2−77664
epoxy-diamine networks, glass transition temp. determ. using torsion pendulum 2−71287
ferroelastic, with temp. independent elastic compliance in prototypic phase 2−72026

- **Phase transformations** continued
  - **solid-state** continued
    - ferroelectric, displacive type, lattice modes, polarization correlation 2–81127
    - ferroelectric, sixteen vertex lattice model 2–65058
    - ferroelectric domain structures, phase transition, scanning electron microscope 2–57240
    - ferroelectric solid solution, thermodynamic theory 2–61424
    - ferroic crystals and ceramics, coupled props. 2–57238
    - first order displacive phase transition, soft heat diffusion mode 2–61028
    - glass, laser irrad., electron microscope obs. 2–60588
    - graphite-diamond transition, diffusional mechanism in strong elec. field 2–47706
    - group ABO_3 perovskites, theory of rotation of BO_6 octahedra 2–65065
    - heterophase systems, phase nucleation, internal stress relax., coherent loss, thermodynamics 2–60859
    - hydrazine alum, ferroelectric, n.m.r. obs. 2–75357
    - hydroxylamine alum, ferroelectric, n.m.r. obs. 2–75357
    - interface between two isotropic phases, stress fields and strain energies of dislocations 2–80668
    - ionic substances, establishment of empirical rules governing polymorphism 2–68191
    - $KDHPO_4$ ferroelectric transition, molecular field approx. study 2–65062
    - Landau theory, microscopic formulation 2–58776
    - langbeinites, Landau theory 2–61423
    - limestone rock, effect on velocity and attenuation of elastic waves 2–57594
    - liquid crystal, study of propag. of hypersonic waves near cholesteric-isotropic transition 2–80454
    - liquid crystals, induced circular dichroism method for determ. of chirality of cholesteric mesophase 2–80460
    - low temp. physics, conf., Freudenstadt, Germany (Apr. 1972) 2–45183
    - lunar and terrestrial calcic plagioclases, electron microscope obs. 2–66162
    - martensite, soft phonon modes and propagation velocity 2–53982
    - martensite formation, abnormal cryst. lattice 2–68186
    - martensite-austenite lattices, orientation relationships, application of statistical methods 2–43532
    - martensitic, Burgers and Bogers-Burgers mechanisms 2–68182
    - martensitic, concept of habit plane and phenomenological theories 2–68196
    - martensitic, cryst. habit, phenomenological theory 2–68183
    - martensitic, crystallographic theories 2–64805
    - martensitic, interphase boundary shifting 2–43910
    - martensitic, kinetics of nucleation and growth 2–47675
    - martensitic, strain-induced nucleation mechanism 2–68184
    - martensitic, stress-induced, and shape-memory effect 2–68185
    - martensitic particle, growth path, radial growth and thickening kinetics 2–43907
    - martensitic transform. activation by stimulated emission of phonons 2–43909
    - massive reaction interfaces, solidification analogy approach 2–74924
    - metastable state lifetime, effect of quantum fluctuations 2–84154
    - metastable system, influence of constant homogeneous elec. field 2–71668
    - methane, second transition due to spin isomerisation, obs. by optical birefringence 2–64814
    - methane, static dielectric const. at low temp. and high pressure 2–81146
    - methane-d_4, critical fluctuations at 27K transition, neutron scatt. obs. 2–61040
    - methanes, orientational ordering, quantum mech. theory 2–61039
    - methyl ammonium alum, ferroelectric, n.m.r. obs. 2–75357
    - MgO-Fe_2O_3-CaO-Al_2O_3-SiO_2, during heating, change in thermal, X-ray and electrical resistance characts. 2–83839
    - mixed crystal growth, order-disorder charges 2–50816
    - molecular crystal, polymorphic, orientation of lattices and interfaces 2–84109
    - neopentane, cold neutron examination 2–50928
    - nitrate glasses, influence on positron lifetimes 2–47772
    - n.m.r. and spin-lattice relax. applicability 2–84599
    - noble metal alloy, β-brass type, lattice vibrs. rel. to martensite struct. 2–56930
    - nonsteady state diffusionless phase transition in a binary system, comput. simulation 2–71671
    - O_r^3 type crystals, symmetry types associated with phase transitions of second kind 2–47701
    - order-parameter correlations within screening approximation 2–63036
    - organic glasses, influence of annealing on thermal behaviour in glass transition region 2–71744
    - pearlite electron diffraction patterns, orientation determinations using computer 2–68188
    - perovskite nitrides, reversible transforms. 2–60759
    - perovskite type crystal, self consistent lattice dynamical theory 2–77767
    - poly(1,4-phenylene ether), transitions and relax. of phenomena, 100-800K 2–83355
    - polyethylene, bulk modulus and density in 30 kbar, glass transition temp. press. coeff. 2–83352
    - polymorphic transitions of the elements and system of structural types 2–71397
    - polystyrene, β transition 2–60615
    - polystyrene polyvinyl methyl ether mixtures, thermally induced phase separation 2–61041
    - polytetrafluoroethylene, cryst. struct. at high press., transition at 4.5kbar 2–83849
    - pulsed ultrasonic studies 2–58927
    - pyrophyllite, effect of firing temp. 2–50890
    - rare earth Co compounds, with $CaCu_5$ struct., stability 2–80796
    - rare earth compounds, $LnRu_2$ and $LnOs_2$, high press. effects 2–71689
    - rare earth cpds., Jahn-Teller induced transitions 2–64806
    - rare earth monochalcogenides, press. induced electronic collapse and struct. changes 2–68297

- **Phase transformations** continued
  - **solid-state** continued
    - rare earth monochalcogenides, press. induced transforms. 2–50948
    - rare earth orthoferrites, possibility of intermediate state existence for first order phase transformation 2–81291
    - rare earth oxide film, martensitic transform 2–50949
    - rare earth titanates, $Ln_2Ti_2O_7$ type, press.-induced transform. 2–47344
    - rare earth vanadates, arsenates and phosphates, low temp., Jahn-Teller effect 2–77746
    - rare earth vanadates, cooperative Jahn-Teller distortions 2–43926
    - rare-earth elements, related forms of coordination polyhedra from icosahedron, polymorphic 2–84094
    - relativistic statistical mechanics with e.m. interactions 2–70876
    - selenides, mol. transform. rel. to elec. resist. 2–47900
    - self-consistent phonon and mean-field approxs. 2–64829
    - Shubrikov point groups 2–84006
    - silicate glasses, oxides influence 2–53525
    - sound propag. phenomena in critical region 2–54027
    - spinodal, transmission electron microscope obs. 2–56631
    - stability limits, characterization for ternary systems using Gibbs triangle for isothermal contours 2–64803
    - stability limits for ternary regular system as functions of three binary interaction parameters 2–64804
    - steatite, effect of firing temp. 2–50890
    - steel, 18-8 stainless, α- martensite induced by plastic deform. at high hydrostatic pressure 2–56936
    - steel, $\alpha \to \gamma$, singularities, rel. to initial state 2–80764
    - steel, AISI type 310, transformation characteristics for ferrite, sigma phase and carbides, e. microscope study 2–68189
    - steel, AISI type 310, transformation characteristics for ferrite, sigma phase and carbides, e. microscope study 2–68189
    - steel, austenitic, isothermal pearlitic transform. kinetics, plastic deform. effect 2–50939
    - steel, carbide form. during low temp. isothermal tempering 2–43842
    - steel, cementite, Ostwald ripening, alloying additions effects 2–50936
    - steel, critical pts., additive effects 2–47686
    - steel, during laser beam heating, effect of original struct. 2–53990
    - steel, eutectoid carbon, upper bainite and isothermal pearlite transform., effect of austenitizing cond. 2–50941
    - steel, ferritic-austenitic transform., stored deform. energy influence 2–43918
    - steel, high C, low temp. tempering, retained austenite, X-ray obs. 2–74883
    - steel, high Ni, austenite stabilization rel. to reverse transformation 2–74930
    - steel, high-speed W-Mo, effects of Co 2–53992
    - steel, kinetics of isothermal coalescence of dispersed phase 2–47611
    - steel, low-C, hot-rolled, quenched, effects on microstruct. and mech. props. 2–57017
    - steel, low-C low-alloy, fine struct. and phase comp. at elevated temps. 2–53898
    - steel, low-C low-alloy pipe, formation of abnormal struct. 2–53897
    - steel, α- martensite decomp., second stage, X-ray obs. 2–50938
    - steel, martensite form., mechanism and kinetics 2–43917
    - steel, martensite transform. study using X-ray camera and He cryostat 2–43546
    - steel, martensitic stainless, ageing 2–53989
    - steel, of austenite, isothermal phase diagrams 2–47690
    - steel, pearlitic, deform. influence on lowering of critical pts. 2–53986
    - steel, peritectic transformation 2–61034
    - steel, plastically deformed, austenite form., kinetics and morphology 2–57014
    - steel, quenched, effect of cooling rate 2–47587
    - steel, rel. to effect of heat treatment on mech. props. 2–53842
    - steel, retained austenite developed during surface grinding of carbon steel, exptl. obs. 2–74880
    - steel, stainless, effect of explosive load 2–43836
    - steel, stainless, proton irrad., austenite-ferrite transform. 2–53716
    - steel, stainless 18-8, martensitic at fracture surface, cryogenic temps. 2–56939
    - steel, structural, austenite grain growth 2–53988
    - steel, structural, austenite phase, obs. using high-speed dilatometer 2–57008
    - steel, tempering, transform. of retained austenite 2–47689
    - steel 34KhN3GSV, plastic deformation effects on kinetics of bainitic transf. 2–84077
    - steels, stainless, phase state determ. method at rolling temps. 2–84091
    - structural relations and possible transformation mechanisms rel. to topological variation of crystal coordination 2–53599
    - superconducting A15 cpds., anomalies interpret. 2–77877
    - symmetry props. of transform. twins 2–77522
    - tantalates with potassium tungstate bronze structures 2–71422
    - s- tetracyanobenzene-benzene complex, ionic dissociation from excited Franck-Condon state 2–72579
    - thermionic emission electron microscopy applic. 2–57016
    - Ti alloy VT14, phase transf. during heating and cooling 2–68201
    - Ti-Mo binary alloys, phase separation processes in beta phase during aging 2–80816
    - topaz, thermal and electron beam induced 2–60776
    - tristearin, polymorphism, positron annihilation study 2–60773
    - two-fluid model, heat diffusion mode 2–84185
    - unit for obs. up to 40 kbar in 2 to 400 K range 2–78691
    - zunyite, structural changes on heating 2–75451
    - Ag-15% Ge alloy, splat-cooled, martensitic transformation of structure 2–56921
    - β-Ag-Al alloys, splat quenched, martensitic transform 2–71672
    - Ag-Ge alloy, laser irrad., metastable phase formation 2–50929
    - Ag-Zn(41 at%) alloy, deform. induced martensite, X-ray diffr. obs. 2–80846
    - Ag_3AsS_3, proustite, synthetic, low-temp. transform., spectral detect. 2–50930
    - $AgNO_3$, cryst. growth morphology at polymorphic transforms. 2–50945
    - $AgNa(NO_2)_2$, ferroelectric transition, hydrostatic pressure effects 2–61426
    - Ag_2Se, polymorphic, X-ray obs. 2–64809

Phase transformations continued
  solid-state continued
    Ag_2Se thin films, effect of heat treatment on properties, phase transformation temp. determ. from electrical resistance variation 2−53570
    Al-Ge alloys, microstruct. and metastable phases, detn. 2−71675
    Al-Mg-Li alloy, 01420, ageing, phase comp. changes 2−47594
    Al-Mg-Zn alloy, decomp., influence of Zn 2−43911
    Al-Mg alloy, kinetics of isothermal coalescence of dispersed phase 2−47611
    Al-Mo, binary phase diagram, obs. 2−50955
    α-Al_2O_3, polymorphic transform. under electron irrad., thermodifferential analysis 2−47681
    α-Al_2O_3 formation, in presence of AlF_3 2−47704
    $AlPO_4$, partial volume determination for glassy and crystalline states of glass-ceramics 2−56562
    As-Se-Ge-Sn glass, phase diagram, Mossbauer effect, isomeric shift, quadrupole splitting 2−75267
    As, high press. polymorphic transform., and supercond. phase 2−44058
    Au-47.5 at.%Cd alloy, elastic and anelastic props. near cubic-orthorhombic phase transform. 2−77643
    B, rhombohedral, $\alpha \to \beta$ transform., electron diffr. study 2−47680
    BN, hexagonal to cubic transform., synthesis at high press. 2−83903
    B_2O_3-MgO, relations determined by quenching 2−74936
    $Ba_2Bi^{5+}Bi^{3+}O_6$, dielectric const. and loss obs. 2−75150
    BaF_2-YF_3, phase relations 2−74922
    $BaTiO_3$:Y and reduced single crystal, phase transition effects on d.c. conductivity 2−68468
    $BaTiO_3$, domain interactions 2−61427
    Baf_2-TiO_2 system, $baTi_{1-x}{}^{4+}Ti_x{}^{3+}O_{3-x}F_x$ formation and props. 2−47705
    BeO, crystallographic transition study using DTA 2−64808
    Bi-In(Sn)(Tl) alloys, induced high press. phases, X-ray and specific volume studies 2−74926
    Bi-Sb alloys, pressure-temp.-comp. diagrams 2−68192
    Bi, high press. polymorphic transform., and supercond. phase 2−44058
    Bi, polymorphic transitions, under pressure, strain gauge obs. of volume changes 2−47678
    Bi polymorph III modification at 42 kbar and 20°C, volume change 2−74925
    Bi_2O_3, transform. deform. 2−50932
    Bi_2Se_3-Bi_2Te_2S solid soln., phase diagram 2−57028
    C film, amorphous, graphitization by light pulses 2−61030
    C film, graphitization under light pulse irrad. 2−57002
    $CaO.Al_2O_3$-Al_2O-CaF_2 solid soln., phase diagram 2−57029
    $CdCu_{1.5}Ga_{0.5}$, Laves phases, enthalpies of soln. and formation detn. 2−47692
    $CdGeP_2$, $CdGeAs_2$, sphalerite-chalcopyrite transition, struct. of phases, microhardness 2−57025
    $CdGeP_2$, crystal lattice disorder, effects on vibr. spectrum and optical states 2−72299
    CdI, polytypes, phase transform. 250−280°C 2−77745
    CdS, kinetics of high pressure polymorphic transitions from wurtzite to rock salt structure 2−61031
    CdS, polymorphic transform. under electron irrad., thermodifferential analysis 2−47681
    $CdSnAs_2$, sphalerite-chalcopyrite transition, struct. of phases, microhardness 2−57025
    CdTe, kinetics of high pressure polymorphic transitions from zinc blende to rock salt structure 2−61031
    Ce, $\alpha - \gamma$ transform., mean field approx. 2−57119
    Ce, $\gamma \rightleftharpoons \alpha$ transform., critical point determ. 2−57009
    Ce alloy, γ phase stability rel. to mag. ordering 2−68571
    Ce binary alloys, isomorphic transform. theory, stable constitution diagram 2−50960
    Ce binary alloys, isomorphic transform. theory, metastable constitution diagram 2−50959
    Ce_2O_3-ZrO_2, quenching between 1350 and 1900°C 2−74935
    CmO_x-O_2, phase reactions during isobaric thermogravimetric analysis 2−74927
    Co-Ti alloy, solid soln. decomp. 2−56933
    Co-base alloys, microstruct. obs. of phase transformations, photoemission e. micro. obs. 2−68193
    Co alloy, h.c.p.→f.c.c. transform., enthalpy, transform. temp. 2−43913
    Co whiskers, martensitic transformations, constitution and dislocation structure 2−71340
    $Co(PO_3)_2$-C_5PO_3, phase diagrams, invariant points solid soln. 2−74950
    $Co(PO_3)_2$-$NaPO_3$, phase diagrams, invariant points solid soln. 2−74950
    Co_2Si, rel. to solidification characts. 2−43924
    Co_2Si, rel. to solidification characts. 2−43924
    Cr-Ga alloy, phase diagram, intermetallic cpds. 2−64817
    CrH_x, electrodeposited, f.c.c., h.c.p.→b.c.c. transform., heating time and temp. effects 2−47682
    CsCl, B2⇋B1 transition kinetics 2−53984
    CsCl, effects of KCl and NaCl additions 2−43932
    CsCl B2 type struct., transform. twinning, inhomogeneous shear model, comments 2−61032
    CsCl B2 type struct., transform. twinning, inhomogeneous shear model, reply to comments 2−64810
    $CsFeF_4$, ferroelastic effect, spontaneous lattice strain 2−71571
    Cs_2GeF_6, press.-induced transform. 2−71677
    $CsNO_2$, phase diagrams, cryst. struct., to 40 kbar 2−74951
    $CsPbCl_3$, cubic-tetragonal transition temp., press. depend. 2−71676
    Cs_2ZrCl_6, press.-induced transform. 2−71677
    Cu-Al-Ni alloy, martensite memory, shape recovery effect 2−50935
    Cu-Al-Ni alloy, shape memory effect 2−80844
    Cu-Al-Ni(Mn) alloys, martensitic, interphase boundary shifting 2−43910
    Cu-Al, two-phase struct. formation 2−71678
    Cu-Al alloy, two-phase struct. formation 2−71678
    Cu-Al tempered martensite, long period superlattice phases 2−43914
    Cu-Be-Ag and Cu-Be-Ti, decomposition of solid solns., phase transformations 2−68194
    Cu-Se, extension of equilibrium diagram 2−64812
    Cu-Sn alloy, electrolytically deposited on steel 08kp 2−47683

Phase transformations continued
  solid-state continued
    Cu-Sn alloy, γ phase decomposition at lower temps. 2−71679
    Cu-Sn alloys, martensitic, interphase boundary shifting 2−43910
    Cu-Zn alloy martensite memory, shape recovery effect 2−50935
    Cu alloys, determ. of intermetallic phases, thermodynamic investigation 2−80811
    Cu surface, phase transitions in two dimensional adsorbed layer of S ions 2−50535
    $Cu_{64}In_{36}$, phase bundles and homogeneity detn. 2−71680
    $Cu_4Mn_2Te_4$, X-ray and mag. studies 2−84442
    CuO, thermal e.m.f. temp. depend. during dissociation, 960-1330K 2−57251
    Cu_xS, differential thermal analysis of the Cu-S system, 30-500°C 2−84138
    Cu_2Se, $\alpha \to \beta$, X-ray obs. 2−64811
    Cu(15.1 at.%)Sn alloy, β_1 phase stabilization mechanism 2−47684
    DcSe, kinetics of high pressure polymorphic transitions from wurtzite to rock salt structure 2−61031
    $DyAsO_4$, Jahn-Teller induced trans., 34K, study by Raman scatt. 2−48198
    Dy_2O_3-BaO solid soln., phase diagram 2−54005
    Dy_2O_3-WO_3, solid soln., phase equilib., transform., phase diagram, densities, m.p. 2−57013
    $DyVO_4$, elastic consts. anomalous behaviour at Jahn-Teller induced phase transition 2−84038
    $DyVO_4$, Jahn-Teller induced trans., 14K, study by Raman scatt. 2−48198
    $DyVO_4$, Jahn-Teller phase transitions, acoustic mode anomalies 2−71681
    $DyVO_4$, quadratic-orthorhombic transition 2−43915
    $DyVO_4$, uniaxial stress in co-operative Jahn-Teller distortion, theory 2−51292
    Eu-W-O, subsolidus phase relations and cryst. chem., phase diagram 2−74952
    Fe-30% Ni alloy, martensitic transform. plasticity 2−68197
    Fe-Al-C alloy, martensite, X-ray diffr. obs. 2−80766
    Fe-Al-C alloys, influence of ordering and martensitic transformations during quenching 2−84073
    Fe-C, Fe-C-X alloys, thermionic emission electron microscopy applic. 2−57016
    Fe-(0.11 wt.%)C alloy, austenite grain size effects on Widmanstatten start temp. of proeutectoid ferrite reaction 2−68195
    Fe-Co-Ni-Ti-Al-Cu alloy, YuNDK42T8, phase comp. rel. to homogenizing 2−47688
    Fe-Co(Ni)-Ti-Al alloy, solid soln., decomp. 2−56933
    Fe-Cr-Mn alloy, α-γ transform., Gibbs free energy 2−47687
    Fe-Mg-Ni alloy, austenite transform. 2−53991
    Fe-Mn-C alloy, orientation relationship of the (225) martensitic transform. 2−74928
    Fe-Mn alloys, $\gamma \rightleftharpoons \varepsilon$ transformations, austenite stabilisation, effect of interstitials and substitutional atoms 2−71682
    Fe-Mn and Fe-Mn-C alloys, martensitic transformations and temp. conc. boundaries 2−71683
    Fe-(30.3 wt.%)Ni alloy, strain relax. and damping of oscillations 2−43791
    Fe-Ni-Al, martensite transform, effect of disperse particles 2−50942
    Fe-Ni-Al alloy, martensitic, effect of dispersion particles 2−57015
    Fe-Ni-C alloy, deform.-induced martensitic reaction, kinetics 2−80833
    Fe-Ni-C alloy, deform. martensite formation, effect on mech. props. 2−71684
    Fe-Ni-C alloy, isothermal and athermal, deform. induced martensitic transform. 2−71685
    Fe-Ni-C alloy, martensite to austenite, rel. to heating rate 2−53985
    Fe-Ni-C alloy, martensitic microplastic deform. and isothermal transform. 2−43807
    Fe-Ni-C alloy, martensitic, microplastic deform. and isothermal transform. 2−43808
    Fe-Ni-Co alloys, dilatometric study of vol. exp. for fcc to bcc transformations 2−65146
    Fe-Ni-Mn alloy, isothermal martensitic transform. rel. to mag. field 2−50937
    Fe-Ni-Mn martensitic alloys, reversion behaviour 2−77747
    Fe-Ni, diffusion of N and C along austenite/ferrite phase boundary 2−68052
    Fe-Ni alloy martensitic transformation study by internal friction due to heat treatment 2−43916
    Fe-Ni alloys, martensitic, interphase boundary shifting 2−43910
    Fe-30 wt.% Ni, surface martensite obs. 2−68196
    Fe-Si alloy, phase stability and high temp. elastic consts. 2−71546
    Fe-Ta alloy, ductility enhancement using allotropic phase change 2−57020
    Fe-V-C steel, fibrous VC_x occurrence during transform. 2−61033
    Fe-Zn alloy, phase diagram, obs. of Fe rich side 2−50967
    Fe-Zn system, influence of ultrasonic strains on diffusion growth of various phases 2−43655
    Fe, α-γ-α transform, dilatometric behaviour 2−53987
    Fe, bcc-hcp, high pressure Mossbauer effect obs., 300-20K 2−72283
    Fe, cast, bainite growth kinetics 2−43920
    Fe, effect on diffusion of C, O, H, N and S 2−43661
    Fe alloy, martensitic 2−50943
    Fe plates, collisions, shock wave propag., hardening by explosion 2−80725
    $FeCl_3$ frozen aqueous soln., Mossbauer spectra, investigation of glass to crystal transformation at 200 K 2−72280
    $Fe(ClO_4)_2.6H_2O$, Mossbauer spectra electric quadrupole interaction rel. to temp. and mag. field 2−75271
    $FeSi_2$, $\alpha \rightleftharpoons \beta$ transition mechanism 2−43919
    $FeSi_2$, high temp. phase, stability 2−47685
    Fe_2Ti, elec. resist. thermo-hysteresis rel. to martensitic transform., 4.2−1200K 2−71834
    Ga, superconducting transition, anisotropy in length change of single crystals 2−71846
    GaSe, exciton absorpt. peak shift and phase change induced by hydrostatic press. 2−72330
    $GdCo_5$, powder, coercive force rel. to sintering temp., decomp. stability 2−68511
    GdIG, high temp. high press. phase formation 2−57024

Phase transformations continued
solid-state continued
$Gd(MoO_4)_3$, rel. to ferroelec. domains and condensed soft mode 2−68470
$Gd_2(MoO_4)_3$, ferroelec., ferroelastic, elastic constants and soft optic modes 2−65061
Ge, Au and Sb impurities, absorption and movement of melted zone in the solid phase 2−83892
Ge covalent-metallic phase transition under pressure, theory 2−83886
Ge film, amorphous, crystalline transform. rel. to thickness and environment 2−67882
GeSe thin film, amorphous polycrystalline phase transformation, radial distrib. of atoms 2−71686
GeTe, thin film, amorphous polycrystalline phase transformation, radial distrib. of atoms 2−71686
H, molecular into metallic atomic at high density 2−43501
HfB_2-ZrN alloy, annealing, resist. and microhardness study 2−47638
HfV_2, lattice transition, supercond., cryst. struct., alloying effects 2−71865
In, transition in properties at 170K 2−68198
KCN, rel. to anomalies in temp. depend. of permittivity 2−75141
KCl:Ba, solid-soln., transformation in two temp. regions of decomposition 2−80526
KCl-NaCl mixed single crystals, phase separation during heat treatment 2−74884
$KH_{2(1-x)}D_{2x}PO_4$, ferroelec. to paraelectric, study of dielec. and thermal props. 2−84364
KH_2PO_4 and KD_2PO_4, high temp. transitions 2−71688
$K_2Ir(Pd)(Pt)Cl_6$, incipient transitions, n.q.r. obs. 2−77748
$KMnF_3$, superstructure arising from transition 2−74933
KNO_3, aragonite- to calcite-type, surface effects 2−74932
KNO_3, cryst. growth morphology at polymorphic transforms. 2−50945
K_2PtBr_6, rotary lattice mode softening, n.q.r. obs. 2−61756
K_2WO_4-$In_2(WO_4)_3$ solid soln., phase diagrams 2−57033
$LaAlO_3$, static and dynamic crit. phenomena, e.p.r. obs. 2−81465
$LiAlO_2$, partial volume determination for glassy and crystalline states of glass-ceramics 2−56562
$LiAlSiO_4$-SiO_2, partial volume determination for glassy and crystalline states 2−56562
Li_2MoO_4-$Cr_2(MoO_4)_3$ solid soln., phase diagrams 2−57033
Li_4SiO_4-Zn_2SiO_4-Mg_2SiO_4-SiO_2 glass, phase equilibria and crystallization 2−64520
Lu-H(D) system, α-phase characts. 2−77749
Mg-Cu-Ni, Mg-Zn-Ni, Laves phases, enthalpies of soln, and formation detn. 2−47692
Mg-Th and Mg-Th-Zr systems, e. microscopy exam. of precipitation 2−71690
$MgAl_2O_4$, partial volume determination for glassy and crystalline states of glass-ceramics 2−56562
MgCuGa, Laves phases, enthalpies of soln. and formation detn. 2−47692
$MgHPO_4.3H_2O$, newberyite, thermal transform 20-900°C 2−57022
MgO-B_2O_3, relations determined by quenching 2−74936
$MgO.Al_2O_3.SiO_2$ glass-ceramic, ZrO_2 nucleated 2−47691
$Mg_2P_2O_7$, α/β transitions 2−77079
$MgSiF_6.6H_2O$, at 25°C, cryst. struct. of low temp. form 2−67996
mischmetal-Mg alloys, dilute, metallographic study of phase transformations 2−80794
Mn-Al alloy, mag. props., effect of $\varepsilon \rightarrow \tau$ transform. 2−57280
MnAs whiskers, phase boundary motion at coupled lattice- and spin-disorder transition, resist study 2−78021
MnBi films, Ti-substitution effect 2−51265
$Mn_xFe_{3-x}O_4$, rel. to Jahn-Teller domains 2−43922
Mo alloy, struct. changes during deform. 2−50839
Mo ternary sulphides, crystallographic instability 2−71691
$ND_4Al(SO_4)_2.12D_2O$, 56K transition, Cr^{3+} e.p.r. obs. 2−84576
NH_4Br, allotropic transform. kinetics 2−54008
NH_4Br, critical fluctuation enhanced Raman scatt. by phonons 2−43956
NH_4Br, X-ray diffr. pattern near T_c, diffuse rods 2−80893
NH_4Br and ND_4Br, two-phase region in lambda transition 2−44163
NH_4Cl, influence on positron lifetimes 2−47772
NH_4Cl, pseudospin and stochastic model description 2−43923
$NH_4Cl(Br)(I)$, ordered low temp. phases, cryst. field theory 2−74937
NH_4F, pressure-induced, seismological implications of generated shock wave 2−78268
NH_4NO_3, effect of deuteration on transition temperatures and energies between room temp. and melting point 2−50947
NH_4NO_3 and ND_4NO_3, influence of sample listing on transition temps. of $II \rightarrow III$, $II \rightarrow IV$ and $IV \rightleftharpoons III$ transitions 2−50946
NH_4NO_3 cryst. growth morphology at polymorphic transforms. 2−50945
Na-β-Al_2O_3 phases formation and area of existence 2−84066
γ-Na_2BeF_4, high temp. orthorhombic-monoclinic transition 2−61109
$NaClO_3$ ferroelectric, relation to phonon structure 2−61431
$NaNbO_3$, 575°C, rel. to soft phonon modes 2−80649
NaO_2, pyrite- marcasite transformation at 200K, obs. using susceptibility meas. 2−65116
Na_2WO_4-$Y_2(WO_4)_3$ solid soln., phase diagram 2−74955
Nb-H system, athermal martensitic transform. 2−47693
NbD_x system, diffuse neutron scatt. phenomena in α-phase, temp. depend. 2−77757
t- and h-Nb_2O_5, phase transformations under impact compression 2−61035
Nb_3Sn-type compounds, cubic to tetragonal, lattice dynamical calc. 2−84187
Nb_3Sn, elastic moduli behaviour around cubic-tetragronal transform. 2−51117
Nd_2NiO_4, monoclinic to tetragonal 2−77750
Ni-Fe alloy (around 75-25), behaviour in neighbourhood of order-disorder transform. temp. 2−84137
Ni-Mo alloys, influence of V and Nb additions on ordering and isothermal transformations 2−71692
Ni-P chemically deposited films, structure in relation to elec. conductivity 2−77510

Phase transformations continued
solid-state continued
Ni-(46 wt.%) Ti alloy, martensite phase form., plastic deform. influence 43863 2−43863
Ni-base heat- resistant alloys, carbide transformations during long-time ageing 2−71673
Ni alloy, effect of Mo, Al, and C 2−43925
Ni olivine to Ni spinel, reaction rate of phase change, seismological implications 2−78270
$NiCl_2.2H_2O$, crystallographic phase transition at 230 ± 20K 2−84143
$NiFe_{0.8}Cr_{1.2}O_4$, ferrite, structural transition at mag. transformation, Mossbauer and X-ray obs. 2−72201
$Ni_2P_2O_7$, α/β transitions 2−77079
Ni_2Si, rel. to solidification characts. 2−43924
$Ni_{3\pm x}Te_2$, heat capacities and transition behaviour 2−57068
Ni_2V alloy, ordering transformation for wide range of subcritical temps. 2−74938
$NpPd_3$, cubic and hexagonal phases, unit-cell and X-ray powder data 2−64644
O_2 in polystyrene, contact charge transfer complexing 2−72580
P_2O_5-LaF_3-RF_2, R = Ba, Mg, triangular diagrams, crystn. and vitrification regions 2−57035
PbF_2, and thermal expansion 2−84216
$Pb_{1-x}Ge_xTe$, transform. temp., comp. depend 2−84108
$Pb_{1-3x/2}La_xZr_{0.65}Ti_{0.35}O_3$, comp. depend. 2−57245
Pb_3O_4, quadratic-orthorhombic transition, low temp. 2−74939
$PbTiO_2$, β-PbO_2 phase formation after neutron irrad. 2−65047
$PbTiO_3$, plate-like growth and exam. of domain struct. 2−71398
$Pb(Zr,Ti)O_3$, thermodynamic theory of morphotropic phase transition 2−75153
PrP_{1-x}, phase diagram, homogeneity region, limits of existance, 400-1000°C 2−74956
Rb_2BeF_4-Na_2BeF_4, phase diagram, struct. of phases 2−74957
RbBr, hysteresis under hydrostatic pressure 2−74940
RbCl, hysteresis under hydrostatic pressure 2−74940
$RbFeF_4$, ferroelastic effect, spontaneous lattice strain 2−71571
RbH_2PO_4, ferroelectric, sound velocity obs, effect of deuteration 2−74979
RbH_2PO_4, high temp. transitions 2−71688
$RbH_3(SeO_3)_2$, improper ferroelec. phase transition, group theoretical analysis 2−51197
RbI, hysteresis under hydrostatic pressure 2−74940
Rb_2MoO_4-$Al_2(MoO_4)_3$ solid soln., phase diagrams 2−57033
$RbNO_2$, phase diagrams, cryst. struct., to 40 kbar 2−74951
Rb_2SiF_6, press.-induced transform. 2−71677
ReO_2, polymorphic transition, electron microscope obs. 2−47695
SF_4, low temperature films, vibrational spectra 2−44381
Sb, high press. polymorphic transform., and supercond. phase 2−44058
Sb_2S_3, allotropic transform. 2−54160
SbSI:Sb_2S_3, prep., spontaneous polarization, dielec. permittivity, photocurrent, dark current rel. to phase transition, −50-50°C 2−75143
SbSI, ferroelec. p-T phase diagram rel. to critical point 2−72038
SbSI, ferroelectric, one dimensional stress effects, permittivity obs. 2−75155
SbSI, illum. and rate of cooling depend. 2−47986
ScF-TlF solid soln., phases, fusion diagram 2−53997
Sc_2O_3-MgO solid soln., phase diagram, defects, disintegration, decomp. precip. 2−74906
Si-N-O, free energies of form. of α and β silicon nitride and silicon oxynitride, 1200-1350°C 2−61037
Si covalent-metallic phase transition under pressure, theory 2−83886
SiC-B alloy, phase composition rel. to press., 50-60 kbar 2−53996
SiC, α-β polymorphic transformation 2−74941
SiC 2H, low temp. obs. and mechanics 2−71695
SiO_2, partial volume determination for glassy and crystalline states of glass-ceramics 2−56562
SiO_2, quartz-coesite transition, effect of shear 2−77751
$SiTiO_3$, second-order, critical asymmetry in local fluctuations for $T \rightarrow T_c^-$ 2−72472
$SmCo_5$, powder, coercive force rel. to sintering temp., decomposition stability 2−68511
Sn covalent-metallic phase transition under pressure, theory 2−83886
Sn thermodynamics, determ. by obs. of Pb-Sn alloy 2−50950
$SnCl_2.2H_2O$ and $2D_2O$, anomalous behaviour of sp ht 2−84212
SnH_4, proton spin-lattice relax. obs. 2−48116
$SrAl_2SiO_8$-$BaAl_2SiO_8$ solid soln., isomorphism, phase diagram 2−54009
$SrTiO_3$, antiferrodistortive transition, fluctuation phenomena, e.p.r. obs. 2−84574
$SrTiO_3$, cubic-tetragonal rel. to wavelength modulated absorp. spectra 2−51348
$SrTiO_3$, l.f. soft vibrational modes under stress 2−71696
$SrTiO_3$, static and dynamic crit. phenomena, e.p.r. obs. 2−81465
Ta_4D_3, stepwise phase transitions, neutron diffr. obs. 2−74947
Ta + Co, Laves phases and thermodynamic props., solid-electrolyte galvanic cell studies 2−77424
$TbAsO_4$, crystallographic distortion at $T < 26K$, transition, X-ray diffr. obs. 2−84142
$TbAsO_4$, magnetically controllable transition 2−78045
TbIG, high temp. high press. phase formation 2−57024
$Tb_2(MoO_4)_3$, ferroelectric phase transition, neutron scatt. obs. 2−65066
$TbPO_4$, rel. to low temp. sp. ht. anomalies 2−78046
$TbVO_4$, elastic consts. anomalous behaviour at Jahn-Teller induced phase transition 2−84038
$TbVO_4$, Jahn-Teller induced trans., 34K, study by Raman scatt. 2−48198
$TbVO_4$, Jahn-Teller phase transitions, acoustic mode anomalies 2−71681
$TbVO_4$, quadratic-orthorhombic transition 2−43915
Tc-40 at% Mo alloy, struct., X-ray obs., 4.2-298 K 80647 2−80647
Tc, struct., X-ray obs., 4.2-298 K 2−80647
$TeVO_4$, polymorphic transform. at 650°C 2−74748
Th-Ce, alloy, critical region, elec. resistivity obs. 2−50951
Ti-C-N-O solid soln., phase diagram, form. of carbonitrides and oxycarbides 2−54010
Ti-Ni alloy, near equiatomic, shape memory effect 2−77693
Ti-Ta alloys, martensitic, precip. reactions 2−47697

Phase transformations continued
solid-state continued
Ti-Ta alloys, martensitic transform. 2−47696
Ti, alpha and beta phase stabilizers, segregation 2−64807
Ti, prep. technique for single crysts. 2−77526
Ti alloy, martensitic transform., under isothermal conditions 2−43927
Ti alloy, orthorhombic martensites 2−71697
Ti alloys, $\beta\rightarrow\omega$ transform. 2−68204
TiN-MgO solid soln., solid phase interaction, diffusion of Ti, 1700-2000 K 2−53907
TiNi, martensitic, unique property changes 2−68200
Tip$_4$O$_7$, metal-insulator transitions, charge localization, crystallographic evidence 2−44087
TlN$_3$. low temp. phase transformation, i.r. absorption and Raman scatt. study 2−74944
Tl$_2$XO$_4$, X=Se, Cr, Mo, thermal props. 2−53680
TmAsO$_4$, heat capacity, near Jahn-Teller transition, evidence of low-lying excited state 2−61105
TmAs(V)O$_4$, Jahn Teller induced transitions 2−54436
Tm$_2$Si$_2$O$_7$, press. effect on $\beta\rightarrow\alpha$ transform. 2−71698
TmVO$_4$, optical obs. spectrum obs. of cooperative Jahn-Teller transition 2−65269
U, multiquenched rods, $\alpha\rightarrow\beta$, microstress behaviour 2−77659
UC-UC$_2$ and UC$_2$ phases, U$_2$C$_3$ formation 2−47720
UO$_2$(OH)$_2$, $\beta\rightarrow\alpha$ transform., transition temp. and mechanism 2−74945
V-C, low C alloys, -phase nucleation, stacking fault role 2−71378
V-H system, low temp., electron microscope obs. 2−53998
V$_x$H$_y$(D$_y$), ordering transitions at low temps. 2−77752
VO$_2$, twinned crystal to tetragonal phase, X-ray obs. 2−47698
V$_4$O$_7$, metal-insulator transitions, charge localization, crystallographic evidence 2−44087
V$_3$Si, martensitic phase transform, in mag. fields 2−77869
YIG, high temp. high press. phase formation 2−57024
Y$_2$O$_3$-BaO solid soln., phase diagram 2−54005
Yb-Al system eutectic transformations 2−80797
Yb films, f.c.c.-h.c.p. transform. 2−50952
Yb$_2$O$_3$-BaO solid soln., phase diagram 2−54005
ZnAl$_2$O$_4$, partial volume determination for glassy and crystalline states of glass-ceramics 2−56562
ZnGeAs$_2$, ZnGeP$_2$, sphalerite-chalcopyrite transition, struct. of phases, microhardness 2−57025
ZnO-Nb$_2$O$_5$-SiO$_2$, ternary system, phase relations at liquidus and subsolidus temps, 2−68203
ZnSiAs$_2$, sphalerite-chalcopyrite transition, struct. of phases, microhardness 2−57025
ZnSnAs$_2$, ZnSnP$_2$, sphalerite-chalcopyrite transition, struct. of phases, microhardness 2−57025
Zr-C-N-O solid soln., phase diagram, form. of carbonitrides and oxycarbides 2−54010
Zr-Co alloy system, paramagnetic behaviour in non stoichiometric composition of the Laves phase compound 2−81220
Zr-Cr alloys, thermodynamic props. 2−74912
Zr-Nb alloy, rel. to supercond. transition temp. 2−51107
Zr-Nb alloys, α and ω phase form. and segregation mechanisms 2−53999
Zr alloys, $\beta\rightarrow\omega$ transform. 2−68204
Zr alloys, strain-induced transforms., microstruct. exam. 2−54000
Zr containing refractories, influence of gaseous medium 2−84095
ZrO$_2$-Ce$_2$O$_3$, quenching between 1350 and 1900°C 2−74935
ZrO$_2$-Y$_2$O$_3$ system, tetragonal-cubic, X-ray exam., determ. of lattice parameters of two phases 2−84098
ZrO$_2$, calcia stabilized, thermal stress induced microstruct. modifications 2−50901
ZrO$_2$, martensitic transform. struct. 2−50953
ZrO$_2$, monoclinic-tetragonal inversion, effects of detonation shock wave 2−74946
ZrO$_2$, monoclinic-tetragonal transform., isothermal kinetics, burst phenomena, 850-1000°C 2−77753

Phase transitions *see Phase transformations*

Phonographs *see Sound reproduction*

Phonon bottleneck *see Crystals/lattice mechanics*

Phonon drag *see Crystal electron states/transport processes; Crystals/lattice mechanics*

Phonon-electron interactions *see Crystal electron states/transport processes; Crystals/lattice mechanics; Electron-phonon interactions*

Phonons
see also Crystals/lattice mechanics
— 2−61081
— 2−65266
— 2−72462
— 2−72367
acoustic in metal, theory of Brillouin scattering of light 2−54438
alkali halide, higher anharmonic contribs. to diffuse X-ray scatt. 2−61059
alkali halide, u.s. wave absorp., relax. theory 2−68233
alkali metals, optical absorpt., phonon effects 2−61628
anharmonic crystals, frequencies and widths 2−68207
anharmonic crystals, frequencies and widths 2−68208
anthracene, rel. to polarization effects in Raman scatt. 2−65275
benzene and hexadeuterobenzene impurity, absorption spectra and exciton-phonon interaction 2−71717
biphonon bound state contrib. to nonlinear polarizability 2−84197
bone, low temp., thermal cond., phonon mean free path, hydroxyapatite crystallite struct. 2−61115
boson echo technique for studying phonon interactions 2−84177
Boson system interacting, struct. functions, two-phonon backflow 2−45323
coherent states elementary excitations and order phenomena 2−77762
cristobalite, α, β, fundamental optical modes from 77K to 538K 2−81364
cross exchange diagrams rel. to energy-momentum relation for optical polarons 2−64900
crystal states, symmetry labelling, orientation depend. 2−61134
crystals, effects of external force gradients on i.r. and Raman activity of long wavelength optical phonons 2−84513

Phonons continued
cubic crysts., localized polariton modes, continuum approx., variational approach 2−80885
p-dibromobenzene, coupling of optical phonons to $T_1 \leftarrow S_0$ transition 2−81362
dielectric cryst., light scatt. by entropy fluctuations, phonon transport theory 2−81327
dielectric film, surface phonons and electron energy losses, metal contact influence 2−47829
dielectric thin layers and plates, thermal cond. and Poiseuille flow of phonons 2−61058
dislocation motion in a crystal, two dimensional lattice and Lorentz force 2−83972
disordered force constant systems, optical properties 2−43958
dispersion relations, accurate determ. by neutron scattering, correction to integrated intensity 2−47311
electron-hole-phonon quasiparticle bound states in strong mag. fields 2−68302
elementary excitations, book 2−71806
exciton-phonon bound. state, calc. 2−64831
ferroelectric phase transitions by exciton-phonon interactions 2−81153
ferromagnet, Heisenberg model, spin-lattice interactions 2−61497
ferromagnet, phonon polarization operator in Ising model 2−81265
fluoranthene, fluorescence quenching, determ. of phonon freq. for transport of excitons through exciton-phonon coupling 2−81426
fluorite-type crystals, doped spin- phonon interaction 2−72235
Franck-Condon displacements, effects on mobility edge and energy gap in disordered materials 2−54014
frequency distrib. function determ. by neutron scatt. 2−50998
gas atom scatt. by surface, one-phonon quantum theory 2−50423
glass, low temp. thermal cond., elec. and mag. field depend. 2−51056
graphite, mean free path, calc. from thermal diffusivity 2−54082
graphite, pyrolytic, mean free path from thermal diffusivity obs. 2−54066
group III-V compound, amorphous, density of states, Raman scatt. obs. 2−61664
hadronic, application of representation to determ. of inelastic excitation function of proton 2−70170
heat diffusion mode of structural phase transition by two-fluid model 2−84185
III-V compounds, dominant second order dipole moment contribution two two-phonon sidebands in i.r. absorption 2−75284
inelastic surface scatt. transition matrix for bound state interactions 2−83854
insulating crystal with paramagnetic impurities, spin-phonon modes, change in thermal cond. 2−71706
interface between solids, nonelectronic thermal cond. at low temp. 2−43998
ionic crystal, realistic models for surface phonons 2−50988
ionic crystal lattice, energies and polarizations in strong static magnetic field 2−43946
Ising model spin-phonon interaction, effect of lattice vibrations on phase transitions 2−68524
Kapitiza resist., phonon attenuation effects, acoustic mismatch model 2−67853
Kapitza resist., phonon absorpt. 2−54072
Kapitza resistance, phonon scatt., effects, transfer hamiltonian approach 2−56533
mag. ordering effect on exciton-phonon process compared to absorption in Y-Fe garnets 2−81392
magnetically ordered crystal, long wavelength optical phonons, morphic effects 2−72359
magnon-phonon interaction, microscopic theory of Raman scatt. modifications caused by mag. ordering 2−72360
martensite, soft phonon modes and propagation velocity 2−53982
maser effect in ferrous alloys and martensitic transform. activation 2−43909
metal, brittle fracture surface energy from phonon freqs. 2−60902
metal, dispersion curves and calc. of binding energy in pseudo-ion approx. 2−83883
metal, liq., phonon drag association with Tl diffusion 2−46945
metal, low temp. thermal cond. calc. and phonon spectrum 2−71754
metal, Matthiessen's rule deviations due to phonon spectrum changes 2−75046
metal, shock spallation, appl. of phonon theory of brittle fracture 2−80747
metal, simple, phonon spectra, electron-ion interaction higher order effects 2−47728
metal films, fast electron energy loss in phonon spectral range, phonon excitation 2−47828
metallic glass, softening of long-wavelength transverse acoustic phonons 2−54021
microwave bottleneck, rel. to optical techniques in e.p.r., obs. by Brillouin scattering 2−61729
molecular cryst., impurity one-phonon spectra, mirror symmetry breakdown 2−65271
molecular crystal, determination of general coupling parameters from classical theory of stimulated Stokes generation 2−51315
molecular crystals, effect of resonance interaction and exciton-phonon coupling on absorpt. band intensities 2−81373
molecular crystals, rel. to polarization effects in Raman scatt. 2−65275
molecular crysts., spectra 2−48159
multiphonon quantum theory of adatom desorption 2−50523
naphthalene isotopic mixed crystals, Raman phonon spectra, exciton model and amalgamation limit 2−57363
neutron spectroscopy at high resolution 2−77607
optical phonon spectra of single crystals 2−68656
organic semiconductors with narrow conductivity zones, electron-phonon interaction 2−77810
paraffins, liq., two-phonon absorpt. processes 2−74550
paramagnetic crystals, ion-phonon interactions, review 2−48117
phase transitions in self-consistent phonon and mean-field approxs. 2−64829
phonon generation in metal films in an electric field 2−54015
phonon spectra of crystal with imperfections of stacking fault type 2−68209

Phonons continued
phonon- impurity centre-exciton bound states, theory of dielec. modes 2−68303
phonon-roton spectrum of superfluid He, derivation of Pitaevskii singularity at end point 2−71261
photon-phonon interactions in solids, review 2−72318
photon-roton spectrum of superfluid He, application of equation-of-motion method 2−71260
pivalic acid, plastic crystalline phase, velocity and lifetime rel. to mol. reorientation 2−44399
plastic, stimulated Brillouin scatt., phonon lifetime and gain determ. 2−68668
polar, Raman scattering, quantitative formulation 2−68655
polariton eigenfreqs. and eigenvectors, small wave vector case 2−64833
polariton formalism of hyper Raman scattering 2−72361
polariton phase matching in enhanced Raman scattering 2−42108
polariton Raman scattering, anisotropy effect 2−44388
polyethylene, localized and resonance modes below 700 cm^{-1}, due to kinks and folds, calc. 2−61153
polyethylmethacrylate, hypersonic phonon waves, Brillouin scattering 2−65284
polyglycine, extended form, density of phonon states for two-dimensional lattice 2−68210
polymethylacrylate, hypersonic phonon waves, Brillouin scattering 2−65284
quantum cryst., low temp. localized single particle formalism 2−61061
Raman oscillators, stationary, molecular crystals, polariton theory 2−65273
Raman oscillators molecular crystals, polariton theory of stimulated Raman scatt. 2−65272
Raman scattering, polariton, in the vicinity of phonon resonance, fluctuation−dissipation theory 2−84496
rare earth:YLF solid laser, energy transfer and phonon interactions 2−42058
rare earth garnets, LnAlG and LnGaG, phonon cond. 2−77786
rare earth metals, with helical spin struct., magnon- phonon interaction 2−75225
rare earth oxide systems, far-i.r. spectra, phonon excitation 2−51346
rare gas crystal, Brillouin scatt. from transverse phonons 2−84509
Rochelle salt, thermal cond., Curie pt. phenomena 2−44001
semiconductor, coupled electron-phonon system evolution in strong elec. field 2−61291
semiconductor, degenerate, rel. to free carrier absorp., quantum theory 2−51329
semiconductor, II-VI, phonon scatt. by Fe^{2+} impurities 2−84213
semiconductor, III-V, hot electron magnetophonon reson., theory 2−68386
semiconductor, nonpolar, longitudinal magnetoresist., magnetophonon struct. 2−84327
semiconductor, polar, coupled optical phonon-magnetoplasmon surface waves 2−68377
semiconductor, polar, electron-hole interaction, effective mass eqn., optical phonon effects 2−68306
semiconductor, polar, electron-hole interaction, optical phonon interactions 2−68305
semiconductor, polar, exciton-phonon interactions, Urbach's rule 2−44369
semiconductor, Raman scatt. from coupled LO-phonon-plasmon modes, theory 2−68663
semiconductor, transport processes, magnetophonon spectroscopy study 2−68385
semiconductors, cubic, stress dependence of the Raman frequencies and elastic constants 2−84497
spin-phonon interaction effect of lattice vibration on magnetic phase transformation 2−68524
superconducting phonon spectra, determ. by computer from tunnelling effect 2−81056
superconducting tunnel junction phonon bremsstrahlung, modulation 2−47732
superconductor, neutron scatt. spectral function reln. 2−71861
superconductor, phonon generation 2−47735
surface, inelastic scatt. of low energy electrons by one phonon processes, theory 2−50986
surface, role in energy exchange during atom- cryst. collisions 2−80537
surface phonons and gas surface interactions 2−50522
surface phonons and magnons, review 2−50985
surface-optical, coupling with surface plasmons in semi-infinite medium 2−47827
teflon, thermal conductivity, 0.17 to 4.0 K, dislocation scattering 2−71762
1,2,4,5-tetracyanobenzene-durene complex, fluorescence quenching, determ. of phonon freq. for transport of excitons through exciton-phonon coupling 2−81426
thermal and electrical conduction, effect of hydrodynamic excitation 2−71775
three phonon processes in acoustoelectric interaction 2−84181
transfer phenomena in electron-phonon system in strong mag. field at low temp. 2−57100
uniaxial crystal, oblique polaritons, freq. dispersion 2−77770
u.s. spin echoes, generation and detection 2−44312
vibrational edge modes, long wave acoustic phonons at edge 2−61063
vibrational spectra of isotropically disordered crystals 2−64828
X-ray Brillouin scattering investigations 2−47725
$\gamma N \rightarrow 0$-B, s-channel transformation matrices for helicity and invariant amplitudes calc. using computer language REDUCE 2−55812
Ag, dispersion curve, pseudopotential calc. 2−57039
Ag, u.s. attenuation, Gruneisen mode and const., phonon viscosity and thermoelastic effects 2−68234
$AgCl:Ni^{2+}$, scattering rel. to thermal cond., relaxation time approx. analysis 2−51057
AgCl, pure and doped, thermal cond., transverse phonon contrib. 2−77789
Al-Al_2O_3 granular films, superconducting, sp. ht. obs., density of states enhancement 2−77878
Al, phonon-dislocation interactions 2−50671

Phonons continued
Al film, surface phonon spectrum, rel. to overlayer effects on supercond. props. 2−61228
AlN:Mn, phonon structure obs. in luminescence spectrum 2−75319
AlN, interaction with electron transitions, cathodoluminescence 2−75336
Al_2O_3:V, before and after γ-irrad., phonon scatt., thermal cond. study 2−68214
$Al_2O_3:V^{3+}$, ground state study using phonon generation in Sn 2−47735
$Al_3O_3:V^{3+}$, phonon scatt, using superconducting tunnel junction source obs. 2−47732
$Ar:O_2$ crystal, phonon sideband in luminesc. spectra at 4.2K 2−48215
Au, spectrum, lattice dynamics 2−61074
Au, u.s. attenuation, Gruneisen mode and const., phonon viscosity and thermoelastic effects 2−68234
$BaTiO_3$, Raman scatt. line shape of soft E polariton mode 2−78112
$BuF_2:Sm^{2+}$, sideband fluoresc. theory 2−65304
CO_2 solid (ν_1, $2\nu_2$) vibron-phonon infrared absorption band in temp. range 88-160 K 2−81347
CaF_2, coloured, zero-phonon lines 2−53752
CaF_2, coloured, zero-phonon lines 2−53751
CaO, dispersion, three body force shell model 2−68216
$Ca(OH)_2:Mn^{2+}$, e.p.r., 4.2−800 K, vibronic effects 2−78163
Cd, spectrum and umklapp processes rel. to thermal cond. calc. 2−51058
$Cd_xHg_{1-x}Te$ mixed crysts., reststrahlen spectra, transverse optic modes 2−44366
CdO microcrystals, coupled surface phonon-surface plasmon modes, i.r. absorpt. 2−84263
$CdS:Co^{2+}$, lattice thermal cond., phonon-reson. scatt. 2−47763
CdS, fast electron excitation, phonon assisted exciton recombination 2−48240
CdS, optical modulation by acoustic phonon flux 2−61088
CdS, polariton-phonon interaction and effect on exciton absorption bands 2−80999
CdS, resonance Raman scattering by turnable dye laser 2−84486
CdS, two-phonon sidebands in i.r. absorption due to third order potential 2−75284
CdS crystallites, Raman scattering from surface modes 2−75311
CdS polariton emission 2−48218
CdS(Se), phonon-exciton interaction, rel. to spontaneous and stimulated emission, 2-100K 2−68677
$CdS_{1-x}Se_x$, reson. Raman effect 2−72365
CdS_xSe_{1-x} mixed crystal, study of lattice dynamics, phonon-phonon interactions by Raman spectra 2−51353
$CdTe:Fe^{2+}$, phonon conductivity 2−64864
CoO, paramag., phonon dispersion relations, three body force shell model 2−68222
Cr-W alloy, dilute, phonon freqs. and widths rel. to force const. changes 2−68223
Cr-1.6%W alloy, phonon freqs., neutron scatt. obs. 2−74973
Cr, magnon-phonon interaction 2−48109
CrO_2, spectra rel. to VO_2, Raman spectra obs. 2−65277
$Cr(ur)_6I_3$ and deuterated complex, luminescence low temp. spectra, obs. of ^2E level splitting, zero-phonon transitions 2−51290
CsCl, phonon-dispersion, neutron spectrometer study and shell model anal. 2−84192
CsCl, single effective phonon frequencies of U band 2−47446
CsF, phonon dispersion relations, neutron scatt. study 2−64840
$CsMnF_3$, perovskite, polarised i.r. refl. spectra, phonon dielec. dispersion 2−51319
$CsPbCl_3$, far i.r. refl. spectra, Kramers- Kronig analysis, optical lattice vibrs. 2−72300
Cu-Al alloys, neutron irrad. defect-phonon scatt., lattice thermal cond. 2−51060
Cu, dispersion curve, pseudopotential calc. 2−57039
Cu, nonlinearity constant D and hypersonic attenuation, temp. depend. 2−47744
Cu, scattering of quasiparticle excitations by thermal phonons in symmetry zones of Fermi surface 2−44020
Cu, u.s. attenuation, Gruneisen mode and const., phonon viscosity and thermoelastic effects 2−68234
CuCl, rel. to Raman spectra interpretation 2−65278
Cu_2O, double phonon processes, i.r. absorp. and light scattering obs. 2−61636
Cu_2O, exciton luminesc. spectra, ortho- and para-exciton interactions, optical phonon freq. 2−57133
^{63}Cu crystals, phonon model of sp. ht., anharmonicity manifestations in exptl. data 2−64855
$DyAsVO_4$, spectra at 12K, Jahn Teller phase trans., Raman scatt. study 2−48198
$DyVO_4$, Jahn-Teller phase transitions, acoustic mode anomalies 2−71681
$DyVO_4$, spectra at 14K, Jahn Teller phase trans., Raman scatt. study 2−48198
$FeCO_3$, Ising behaviour, magnon-phonon coupling 2−44297
FeF_2, magnon-phonon interactions, coupling, spin Hamiltonian 2−80886
FeF_2, magnon-phonon interaction 2−44298
$Ga_{1-x}Al_xAs$ semiconductor alloys tunnelling characteristics due to phonon interactions 2−71981
GaAs, dispersion of Brillouin scatt. cross section for fast TA phonons 2−61670
GaAs, exciton-phonon coupling, optical absorp. obs. 2−61642
GaAs, strain induced phonon line broadening observed by surface reflection Raman scattering 2−83858
GaAs and $GaAs_{1-x}P_x$, multiphonon Raman scatt. 2−68659
$GaAs_{1-x}P_x$ semiconductor alloys tunnelling characteristics due to phonon interactions 2−71981
GaP, phonon damping func. freq. depend., polariton Raman scatt. obs. 2−61076
GaP, polariton dispersion and damping temp. depend. from k vector space non-linear spectra 2−71710
GaP, two phonon Raman spectra 2−48156
GaSb, heavily doped, phonon scatt., thermal cond. obs. 2−47765
Ga_2Se_3, i.r. refl. spectra at 290K, phonon freqs. and dielec. consts. 2−75279
p-Ge:Cu, hole recomb. via phonon emission 2−51214

Phonons continued
Ge:Cu, hole recomb. via phonon emission 2−51215
Ge:Sb, electron irrad., phonon scatt. and induced energy levels 2−47766
Ge:Sb, phonon propag. characts. 2−47735
Ge, amorphous, density of states, Raman scatt. obs. 2−61664
Ge, dispersion curves and specific heats, angular force model 2−74969
Ge, dispersion relations, thermal neutron spectrometry, homology with Si 2−84190
Ge, electron spectroscopy of amorphous film at energy losses below 1 eV 2−80934
Ge, lifetimes 2−71725
n-Ge, light modulation by non-equilib. optical phonons in pulsed elec. fields 2−78069
n-Ge, phonon-assisted, tunnelling, impurity dependence 2−54195
Ge, thermal cond., three phonon resist., second upper bound 2−71759
Ge, three-phonon scatt. strengths and Ziman limit of thermal resist. 2−75000
Ge amorphous, obs. of electron tunnelling between metal electrodes, determ. tunnelling phonon density of states 2−44125
α-HIO$_3$, Fermi resonance in Raman scatt. of light by polaritons 2−84493
He/metallic layer/He bath system, energy flux calc. 2−47010
He/metallic layer/He bath system, energy flux eval. 2−53474
He, liq., phonon-like excitations and roton spectrum 2−77461
He, liq., phonon dispersion underpress. 2−80510
He, liquid, acoustic multiple beam scattering 2−83832
He, superfluid, phonon emission and absorpt. due to rotons 2−64495
He II, emission and absorpt. of phonons by rotons 2−43425
He II, h.f. u.s. attenuation, press. depend. of phonon dispersion 2−47025
He II, long-wavelength phonon dispersion 2−60534
He II, phonon emission rate of rotons 2−47011
He II, phonon spectrum, thermodynamic evidence against quadratic term 2−77456
He II, thermal phonons, finite life, effect of nonlinear spectrum 2−60536
He liquid-solid interface, reflection of phonons 2−74576
^{4}He, liquid, dispersion and contribution to heat capacity 2−47001
^{4}He, solid, hypersonic phonons 2−43432
^{4}He, superfluid, phonon spectrum, self-energy 2−71258
HgTe, reststrahlen spectra, transverse optical modes 2−44366
Ho, dispersion relations, lattice dynamics, non-central force model 2−74970
Ho, paramag., spin-phonon interaction via modulation of exchange interaction 2−68522
In$_{1-x}$Ga$_x$P semiconductor alloys tunnelling characteristics due to phonon interactions 2−71981
InP, second order Raman spectrum and phonon frequencies detn. 2−81367
InSb, acoustic dispersion relns., meas. by heat pulse technique using supercond. bolometer 2−80911
InSb, magnetophonon mass change in drifting hot carriers 2−68389
InSb, n-type, effective mass of conduction electrons det. from magnetophonon effect, undergad. expt. 2−65009
InSb, reson. Raman scatt. near E$_1$ transition 2−68661
n-InSb, surface plasmon-phonon interaction 2−71930
n-InSb, thermal-equilib. distrib., rel. to amplified acoustic flux source 2−68242
InSe, exciton-phonon interaction, absorption edge obs. 2−84518
InSe single crystals reflection and absorption in the i.r. region 2−81395
K, Umklapp processes, contrib. to elec. resist. 2−84293
KBr:SH$^-$(SD$^-$), rel. to i.r. spectra interpretation 2−84491
KCl:Li, generation and detection of 55 GHz phonons, paraelec. reson. study 2−84191
KCl:NaCl, symmetry of far i.r. resonant-pair mode 2−84507
KCl:SH$^-$(SD$^-$), rel. to i.r. spectra interpretation 2−84491
KCl, thermal cond., temp. depend., role of longitudinal and transverse phonons 2−84214
KI:SH$^-$(SD$^-$), rel. to i.r. spectra interpretation 2−84491
KI-SH-, sideband struct. in i.r. absirot. spectrum 2−48185
KN$_3$, i.r. absorpt., selection rules and internal ± internal and internal ± external mode absorpts. 2−72336
β-KNO$_3$:Mn^{2+}, e.p.r., phonon sidebands 2−72490
Kr, liquid longitudinal phonons, law of corresponding states 2−71156
La film superconducting, phonon structure in tunnelling density of states 2−75059
Li, b.c.c., phonon freqs., from Krasko-Gurskii model 2−68227
Li, Umklapp processes, contrib. to elec. resist. 2−84293
Li thermal expansion coefficient and Gruneisen parameter, lattice dynamical calculation 2−84179
LiAl$_5$O$_8$:Fe^{3+}, ordered and disordered, phosphorescence and excitation spectra, zero-phonon transition, fine structure 2−48253
LiD, dispersion, three body force shell model 2−68217
LiF, isotope-induced one-phonon i.r. absorpt. 2−78103
LiF, slow transverse, dynamic scattering by mobile dislocations, 0.04 to 0.8°K 2−68218
LiF, surface, scatt. of He atoms, one-phonon transitions 2−50451
LiF, surface phonons on (001) face, calc. using shell model 2−68226
LiIO$_3$, polariton dispersion, light scatt. associated with photons 2−68617
LiNbO$_3$, directional dispersion and assignment of optical phonons 2−77764
LiNbO$_3$, polariton frequencies, third-order optical nonlinear susceptibility 2−72252
LiNbO$_3$, Raman scattering and obs. of polaritons by photographic method 2−81374
LiNbO$_3$, X-cut, microwave phonon attenuation, hypersonic attenuation obs., temp. effects 2−68225
LiNbO$_3$ polariton eigenfreqs. and eigenvectors, small wave vector case 2−64833
LiIO$_3$, oblique polaritons, freq. dispersion 2−77770
(M,Cr)(ur)$_6$(ClO$_4$)$_3$, M=Al, Ga, low temp. spectra, obs. of ^{2}E level splitting, zero-phonon transitions 2−51290

Phonons continued
(M,Cr)(ur)$_6$I$_3$, M=Al, Ga, low temp. spectra, obs. of ^{2}E level splitting, zero-phonon transitions 2−51290
Mg freqs. from Krasko and Gurshii model potential 2−74976
MgMoO$_4$, i.r. reflection bands, shifts of polar phonon frequencies 2−81352
MgO:Cr^{3+}, phonon sideband of R line 2−48187
MgO:Fe^{2+}, phonon conductivity 2−64864
MgO, dispersion, crystal dynamics calc. 2−61077
MnO, dispersion props., three body force shell model 2−61078
MoO$_2$, spectra rel. to VO$_2$, Raman spectra obs. 2−65277
MoS$_2$, composite exciton absorpt. spectrum, optical phonon effects 2−44377
MoSe$_2$, i.r. absorpt. spectra, transverse optic lattice vibr. freq. 2−78105
MoTe$_2$, composite exciton absorpt. spectrum, optical phonon effects 2−44377
N$_2$ solid, obs. of phonon induced dipole radiation in emission spectrum, cooperative effects 2−78096
NH$_4$Br, order-disorder transition, X-ray diffuse scatt. obs. 2−47699
NH$_4$Br, phase transitions, Ising spin-phonon coupled system theory 2−47700
NH$_4$Cl disordered force constant systems, optical properties 2−43958
NH$_4$H$_2$PO$_4$, antiferroelectric, long-wavelength polarization fluctuations 2−78113
Na, Umklapp processes, contrib. to elec. resist. 2−84293
NaBrO$_3$, optical phonon spectrum by laser Raman spectroscopy 2−84495
NaCl:Ag$^+$, rel. to Raman scatt. and far i.r. absorpt. calc. 2−84508
NaCl, dislocation-phonon interaction, 70-300K 2−83975
NaCl, thermal cond., temp. depend., role of longitudinal and transverse phonons 2−84214
NaCl, two-phonon Raman scattering and phonon-phonon interaction, nonlinear shell model 2−81368
NaCl crystals containing colour centres, flow stress spectroscopy 2−81396
NaClO$_3$, ferroelectric phase transition, relation to phonon structure 2−61431
NaF, intrinsic anharmonic phonon-phonon interactions, second sound, low temp. thermal cond. obs. 2−68228
NaN$_3$ dispersion curves 2−43957
NaNbO$_3$, rel. to anisotropic diffuse X-ray scatt. and phase transitions 2−71715
Nb, supercond., thermal cond. 2−47767
NbN type cpds., RY, R=Ti, Zr, Hf, V, Nb, Ta, Y=C, N, O, rel. to supercond. transition temp. 2−61247
Nb$_3$Sn, shear mode phonon spectra, Labbe-Friedel model 2−68229
Ne, anharmonic crystal, interference effects in neutron inelastic scatt. 2−54023
NiBr$_2$(Cl$_2$), electric absorpt. spectra, phonon sidebands 2−51345
Pb-In dil. alloy, phonon spectra, tunnelling obs. 2−47865
Pb-In dilute alloy, supercond., phonon spectra detn., elec. tunnelling obs. 2−54142
Pb-In superconducting alloy, hydrostatic pressure effect on phonon spectra, tunnelling obs. 2−64936
Pb, phonon excitation spectra, junc. tunnelling obs., effects of material props. 2−68360
PbTe, transverse optic mode softening, Curie law temp. depend. 2−68230
Rb, Umklapp processes, contrib. to elec. resist. 2−84293
RbBr, reorientation rates of OH- defects, calc. from phonon spectra 2−61080
RbCl, surface phonon branch distrib., shell model 2−47734
RbCl dispersion relations, shell model calc. 2−61079
RbF, surface phonon branch distrib., shell model 2−47734
SbSI, critical light scatt. phenomena 2−61612
Si:In, localized modes in extrinsic photocond. 2−51216
Si, dispersion relations, thermal neutron spectrometry, homology with Ge 2−84190
Si, electron spectroscopy of amorphous film at energy losses below 1 eV 2−80934
Si, energy assignments, multiphonon Raman spectra obs. 2−68221
Si, γ-irrad., vibronic spectra, temp. depend. 2−48262
Si, low field electroabsorpt., split-off exciton and phonon-depend. lineshape 2−72349
Si, neutron irrad., boundary scatt., thermal cond. obs. 2−80917
Si, phonon frequencies calc. 2−47933
Si, two phonon Raman spectra 2−48156
Si (111) surface, low energy electron spectroscopy obs. 2−50987
n-SiC, Raman scatt., electronic transition-phonon interference 2−51356
SiC, Raman scatt. from coupled LO-phonon-plasmon modes 2−68663
SiC, struct. and energies from tunnelling characts. of p-n junctions 2−57042
SiO$_2$, vitreous, low temp. thermal cond., elec. and mag. field depend. 2−51056
SiO$_2$ thin layer, energy and scatt. parameter from hot electron energy loss obs. 2−81061
Sn-Sn supercond. tunnelling junction, on Si, in liq. He, phonon emission 2−84304
Sn, phonon excitation spectra, junc. tunnelling obs., effects of material props. 2−68360
Sn film, surface phonon spectrum, rel. to overlayer effects on supercond. props. 2−61228
SrF$_2$, coloured, zero-phonon lines 2−53752
SrF$_2$, coloured, zero-phonon lines 2−53751
SrF$_2$, dispersion curves, harmonic vibr. props. 2−77760
SrTiO$_3$, lattice dynamics, normal mode freqs., harmonic models 2−77761
SrTiO$_3$, phonon assisted transitions in differential optical spectra 2−72307
SrTiO$_3$, rel. to fundamental absorpt. edge, 6-300K 2−78107
TaC$_x$, phonon spectrum dependence on stoichiometry 2−68349
Tb, meachnism for mixing of acoustic magnons and optic phonons propagating along c axis 2−75227
Tb films, phonon emission at 15 GHz, dynamic magnetoelastic coupling obs. 2−68562

Phonons continued
- $Tb_2(MoO_4)_3$, low freq. phonon dispersion rel. to ferroelectric phase transition, neutron scatt. obs. 2−65066
- $TbVO_4$, 34K, Jahn Teller phase trans., Raman scatt. study 2−48198
- $TbVO_4$, Jahn-Teller phase transitions, acoustic mode anomalies 2−71681
- Te, amorphous, vibrational density of states, Raman spectra obs. 2−65281
- Te, extraordinary phonon Raman scatt. and reson. enhancement 2−84492
- $Th_{1-x}U_xO_2$, mean free path, calc. from thermal diffusivity 2−54082
- Tl, phonon spectrum, supercond. tunnelling and neutron scatt. data, discrepancy 2−84189
- $TmAs(V)O_4$, Jahn Teller induced phase transitions, Raman scatt. obs. 2−54436
- UO_2, mean free path, calc. from thermal diffusivity 2−54082
- V^{3+} complexes, trigonally distorted octahedral, lattice-ion interactions in the ligand field theory 2−81205
- V_3Au, origin of cryst. order effect on supercond. T_c 2−64952
- V_3Au, supercond. transition temp. rel. to ordering, rel. to phonons and electronic density of states 2−84308
- VO_2, phonon softening, rel. to metal-insulator transition 2−51152
- W-He, energy accommodation coeffs. for one-phonon inelastic scatt. 2−50528
- Xe, liquid longitudinal phonons, law of corresponding states 2−71156
- Y_2O_3, phonon-assisted energy transfer between Ln^{3+} ions 2−48234
- YVO_4, Raman scatt. 2−48203
- $Zn_xCd_{1-x}Se$ solid solution, Raman scatt. obs. 2−64837
- $Zn_xCd_{1-x}Te$ solid solution, phonon freq. detn. from reflection spectra 2−72308
- ZnO, Fuchs Kliewer surface modes, low energy electron spectroscopy obs. 2−50987
- ZnO, resonance Raman scatttering by turnable dye laser 2−84486
- ZnO, two-phonon sidebands in i.r. absorption due to third order potential 2−75284
- ZnS:Be, i.r. lattice absorption spectra, localized mode sidebands obs. 2−72385
- ZnS:Co with stacking faults, piezospectroscopic effect on group of zero-phonon lines associated with centres 2−44384
- ZnS polytypes, Raman scatt. obs. 2−61084
- $ZnSiF_6.6H_2O$ spin-lattice relax. of Cu^{2+} phonon assisted tunnelling contrib. 2−84456
- $ZnSiP_2$, optical phonons, polaritons, mode freqs., strengths, damping factors 2−61621

Phosphorescence
- (polystyrene + naphthalene), sensitized triplet quencher phosphorescence, study of photoprotective efficiency 2−72581
- aromatic and heteroaromatic molecules, meas. of quantum yields, study of radiative and radiationless transitons 2−53039
- aromatic carbonyl molecules, π-π* triplet state, steady state and transient phosphorescence microwave double resonance studies 2−42966
- aromatic carbonyl mols., host and substitution effects on lowest excited triplet states, PMDR obs. 2−56205
- aromatic ketones, semi-empirical calcs. of zero-field splitting parameters of lowest triplet states 2−80102
- aromatic mols., triplet deactivation parameters determ. 2−80075
- averaging response using pulsed microwaves 2−60084
- benzene-chloroform weak complexes, radiationless decay of benzene triplet state, external deuterium isotope effect 2−84661
- benzene-d_6, heavy-atom effect 2−84678
- benzophenone, cryst., low temp., triplet exciton obs. 2−61718
- benzophenone crysts., temp. depend., T→S emission 2−65312
- 5,6- and 7,8- benzoquinoline trapped in n-paraffins at 77K, vibrational analysis of quasilinear spectra 2−50080
- biacetyl, in formation of metastable triplet state of acetylene in Hg photosensitized reaction 2−51467
- biphenyl, influence of chloro substitution 2−46595
- build-up in complex formation, effect on nonradiation transitions 2−78207
- coronene (III) in crystalline solutions of isooctane and CCl_4, 77K-melting point 2−51377
- cyclopentanone, transient effects in microwave optical double resonance 2−81524
- decay meas. using disc phosphoroscopes 2−79440
- 1,4dibromo-naphthalene, e.s.r. of triplet excitons, optical detection 2−81522
- dibromobenzene:naphthalene in T_1 state, study of external spin-orbit coupling mechanism 2−72427
- 1,4-dibromonaphthalene, study of triplet exciton state band structure 2−47820
- p-dichlorobenzene, phosphorescence microwave double resonance studies of $^3\pi\pi^*$ state 2−60060
- β-diketones, triplet state studies 2−60062
- dimethyloxalate, electric state investigation using phosphorescence meas. 2−50106
- diphenyl, sensitization by triplet excitons, nonlinear dependence on exciting illumination 2−54474
- diphenylene sulphide (V) in crystalline solutions of isooctane and CCL_4, 77K-melting point 2−51377
- DNA, decay rate, 4.2 to 160K 2−65393
- electron-donor acceptor complexes formation of phosphorescent state from excited Franck-Condon state 2−72577
- flavins, excited states 2−46605
- trans-glyoxal ^3A_u mols., laser induced phosphorescence 2−48345
- hexachlorobenzene, triplet state geometry at 1.6 K, PMDR obs. 2−81517
- hexahydrotriphenylene (II) in crystalline solutions of isooctane and CCl_4, 77K-melting point 2−51377
- hydrocarbons, aromatic, non-Born−Oppenheimer coupling and D effect on $T_1 \rightarrow S_0$ radiative transitions 2−43002
- mixed ligand metal chelates, abs. and emission spectra, lifetimes and quantum yields 2−68630
- molecular cryst., intermol. electronic relax. pathways, determ. by photon echoes 2−68696
- molecular triplet state geometry studied by phosphorescence microwave double resonance spectroscopy 2−50010
- mono-alkyl benzenes in rigid hydrocarbon glasses, triplet emission 2−81515

Phosphorescence continued
- nπ* states in organic molecules reasons for variable luminescent behaviour 2−70732
- naphthalene in 1,4-dibromobenzene, PMDR obs., heavy atom perturbation effects 2−67519
- naphthalene-d_8, comparison of matrix emission spectra with frozen solution spectra in cyclohexane hosts 2−72428
- naphthalene-d_8, heavy-atom effect 2−84678
- 1,5-naphthyridine, optical detection of e.s.r. in the triplet state 2−57394
- optical electron spin polarization in excited triplet states 2−81466
- oxalic acid, electronic state investigations using phosphorescence meas. 2−50106
- n-paraffin-aromatic hydrocarbon system, radiative and non-radiative processes 2−61719
- 2,3-pentanedione, photolysis emission and deactivation of excited states 2−54561
- 2,3-pentanedione, yield on photolysis 2−54560
- phenanthrene, excited dimer phosphorescence of pairs of molecules 2−56253
- phenylcyclopropanes and phenylethanes, emission spectra, 77K 2−84663
- poly(styrene co-vinylnaphthalene), sensitized triplet quencher phosphorescence, study of photoprotective efficiency 2−72581
- powder luminophore, elec. field influence 2−48214
- pyrazine vapour, pressure dependence of collisionally induced relaxation 2−50113
- pyrazine-d_4, triplet state, in low temperature matrix in magnetic field 2−60084
- pyrazine-h_4, -d_4, in benzene, 4.2 K, Frank-Condon patterns 2−77121
- pyrimidine-benzene mixed crystals, spectra at 4.2K 2−44412
- quinoxaline in 1,4-dibromobenzene, PMDR obs., heavy atom perturbation effects 2−67519
- rare earth ion-aromatic acid complexes, rare consts. for intramol. energy transfer 2−72305
- rubin, electron irrad., Cr content effects 2−72429
- 1, 2, 4, 5-tetrabromobenzene, triplet state props., ODMR and PMDR obs. 2−56260
- tetrachlorobenzene in durene, hole burning in optically detected zero-field spectrum using EEDOR 2−84561
- s-tetracyanobenzene complexes, electronic spectra in phosphorescent state 2−72578
- s-tetracyanobenzene complexes formation of phosphorescent state from excited Franck-Condon state 2−72577
- triphenylene (I) in crystalline solutions of isooctane and CCl_4, 77K-melting point 2−51377
- ^{14}C energy spectra comparison with chemiluminescence 2−59605
- CaS:Bi:Fe phosphors, emission characteristics, role of S^{2-} and Cl^- determ. by Fe^{3+} impurity 2−65311
- CaS phosphors, self activated emission, study of trap depths and nature of trapping centres 2−54473
- Cr(III) thiacyanate complex in dumethyl-sulfoxide, phosphorescence spectra 77-150 K 2−83269
- ^3H energy spectra comparison with chemiluminescence 2−59605
- $LiAl_5O_8:Fe^{3+}$, ordered and disordered, phosphorescence and excitation spectra, zero-phonon transition, fine structure 2−48253
- Mn(II) complex, tetrahalogenomangonates, structure obs. in excitation spectra at 77K 2−67488
- SrS:Mn, Zr phosphors decay study 2−75330
- SrS phosphors activated by Zr, Sn, Pb and Th, decay 2−65314

Phosphors *see Luminescence; Luminescent devices*

Phosphorus
- − 2−71945
- − 2−72499
- − 2−72498
- anomalous diffusion, in Si 2−50694
- diffusion, in fluorapatite 2−77609
- diffusion, in Si, impurity profile kink form. mechanism 2−56742
- diffusion in Si, coeff. determ. by Boltzmann-Matano method 2−71540
- diffusion in Si, enhancement by proton irrad., dose rate effects 2−80707
- in α-Fe-Zn solid solution, effect on precip. 2−80855
- hyperfine field, in Fe matrix, spin echo obs. 2−72229
- implantation in Si, channelling and anomalous diffusion effects on charge carrier distrib. 2−47432
- low concentration diffusion in Si, under sealed tube conditions 2−74792
- neutron radioactivation analysis in vivo of Ca, P, N and Cl in rat's organism 2−54575
- surface impurity on Si, Auger electron signals as function of coverage 2−47080
- surface impurity on Th, bulk to surface equilib. 2−50465
- Fe-Ni-Si alloy, temper brittleness development, grain boundary adsorption of P, internal friction study 2−80767
- Ge:P, electron irrad., bombardment induced interstitial P, e.p.r. obs. 2−48279
- Ge:P, heavily doped, temp. depend. of resist. 2−71940
- n-Ge:P, resist. decrease due to donor spin reson. 2−81106
- $KBr:PO_2$, recombination luminescence, F-centre accumulation during β-irradiation 2−78136
- P_2, ground state dissociation energy estimation 2−46581
- P_4, valence shell structure study using HeI photoelectron spectroscopy 2−46574
- ^{32}P, Cherenkov radiation from emitted electrons, applic. to detection of eye lesions 2−69459
- ^{32}P content in breast cancer, surface detection of diurnal variation 2−69266
- Si:P, absorpt. due to transitions to cond. band edge region 2−72347
- Si:P, cond. band deform. potential const. from piezospectrocopy of donors 2−68438
- Si:P, electron drag rel. to impurity centre photoionization, photo-e.m.f. 2−65089
- Si:P, epitaxial, doping during growth 2−47431
- Si:P, ground state wavefunctions of shallow donor electrons, Fermi contact consts. 2−71950
- Si:P, heavily doped, e.s.r. linewidth, temp. depend. 2−72500
- Si:P, heavily doped, temp. depend. of resist. 2−71940
- Si:P, implantation damage annealing, resist. and electron microscope study 2−64678

Phosphorus continued
Si:P, implanted, annealing characts. 2−77594
Si:P, implanted, carrier density and mobility, depth distrib. 2−80993
Si:P, Knoop hardness and hardness anisotropy, impurity conc. effects 2−71604
Si:P, phonon and electric field influence on extrinsic photocond. 2−81179
Si:P, spin susceptibility of impurity band electrons, correl. effects 2−68520
Si:P impurity enhanced diffusion 2−50693
Si, surface state density distrib. rel. to diffusion induced disloc. near junc. formed by P diffusion 2−44038

Phosphorus compounds
− 2−60028
phosphate minerals and rocks, visible and near i.r spectra 2−72672
pyrophosphates (P_2O_7 systems), normal coordinate analysis 2−77079
tetrahedral oxy-compounds, force constants and regularities of chemical bonding 2−70725
$[PCl_4]^+[FeCl_4]$ nuclear quadrupole resonance frequencies, direct numerical analysis of temp. dependence using Newton-Raphson approach 2−70675
BP-P system, h.p. phase equil. 2−50956
Co-P film, electroless deposited, growth and struct. 2−53566
Cu-P-O system phase relations 2−50962
Cu-P system, constitution diagram determ. 2−61045
Cu-(7wt.%)P alloy, superplastic behaviour 2−74838
$55Fe-45P_2O_5$ glass, a.c. and d.c. characteristics, correlation with structure 2−81142
Fe_2O_3-P_2O_5 glass, forming range and mag. suscept. 2−54354
$Fe_xPd_{80-x}P_{20}$ ($13 \leqslant x \leqslant 44$), amorphous alloy, magnetic properties study from Mossbauer effect of ^{57}Fe 2−65114
Na_2O-P_2O_5, glass, containing metal ion impurities, u.v. transparency 2−65225
Ni-P chemically deposited films, structure and elec. conductivity 2−77510
Ni-P film, electroless deposited, growth and struct. 2−53566
Ni-Pd-P-base, amorphous, containing Fe, resistivity temperature relationship, $T^{-1/2}$ singularity 2−44215
OPF_2 H, LCAO-MO-SCF calcs. valence-shell orbitals 2−83250
P-Co film, mag. hysteresis characts. rel. to heat treatment conditions 2−48091
PBr_3, gas phase and solvent chemical shifts, ^{31}P n.m.r. studies 2−46575
PCl_2 in low temp. matrices, anisotropic e.s.r. spectra analysis 2−72571
PF_2 H, LCAO-MO-SCF calcs., valence-shell orbitals 2−83250
PF_3, ambiguities in harmonic force fields 2−50063
PF_3,PF_5, electronic structure, semiempirical MO calc., pseudorotation in PF_5 2−53034
PH_2-PF_2, conformational analysis and electronic struct. 2−70722
PH_2, A^2A_1-X^2B_1 transition, rotational analysis of bands 2−83241
PH_3, absorption in extreme u.v. 2−46586
PH_3, nucl. spin-relax. obs. of spin-rot. interaction 2−56200
PH_3, PH_5, electronic structure, semiempirical MO calc. 2−53034
PH_3, r.f./i.r. double resonance of ν_2 transition 2−42930
PH_4 radical trapped in solid Kr, e.s.r. obs. 2−64154
PH_5, E′ vibr. modes, ab initio obs. 2−80038
PH_5, electronic structure, MO calc. for idealized geometries of D_{3h}, C_{4v} and C_s symmetries 2−53035
PH_5, electronic structure and bonding, nonempirical MO calc., intramolecular ligand exchange in phosphoranes 2−53033
P_2H_4, molecular structure determ. by electron diffraction 2−42937
PH_4Cl, vibrational spectra and modes 2−72362
$(PNX_2)_3$ (X=halogen), gas phase electron diffraction determination of bond lengths and angles 2−53036
P_2O_5-B_2O_3-Cs_2O glass, struct., e.p.r. obs. of Cu(II) paramag. centres 2−48291
P_2O_5-Cr_2O_3-Al_2O_3, coating, radiative capacity rel. to struct., 600-2000K 2−57087
P_2O_5-Cr_2O_3-Al_2O_3 ceramic coating on steel, props. 2−56960
P_2O_5-LaF_3-RF_2, R=Ba, Mg, triangular diagrams, crystn. and vitrification regions 2−57035
P_2O_5-V_2O_5 glass, struct., elec. resist., thermal expansion, rel. to comp. 2−60601
PO, analysis of some bands of β system 2−42931
PO band systems, vibr. transition probabilities and r-centroids 2−60006
PO bonds in X_3PO compounds, CNDO/2 calculations 2−42866
PO emission spectrum, $C^2\Sigma$--$X^2\Pi_r$ transition and nature of C′ state 2−46573
PO γ-system, localization of rot. perturbations in first vibr. levels 2−79995
PO_4^{3-} in KBr and CsI, i.r. absorpt. 2−54424
$P^{16}O$, and $P^{18}O$, rot. analyses and deperturbations of visible systems 2−79996
P_4O_{10} SCF calculations 2−60030
P_4O_6 SCF calculations 2−60030
$POBr_3$, vibrational spectra and crystal structure 2−44380
$POCl_3$:$ZrCl_4$:Nd^{3+} liquid laser, amplification of mode locked trains 2−59167
$POCl_3$-D_2O-Nd_2O_3 soln., lasing effect and prep. technique 2−45744
$POCl_3$-$ZrCl_4$:Nd liquid laser, Q-switching parameters and energy scaling 2−59166
$POCl_3$ adsorbed, effect on oxidation of graphite 2−68783
$POCl_3$ solns., electrolum. of trivalent rare earth ions, emission mechanism 2−46966
$P_2Se_3-As_2Se_3$ pseudobinary section, semiconductor glasses, n.m.r. of ^{31}P, comp. depend. of width of spectral lines, second moment and chemical shift 2−84584
WO_3-P_4O_{10}-V_2O_5, elec. cond. and mag. resonances 2−54495

Photochemistry
see also Photochromism; Photographic process
9-CN, 10-acetoxy anthracene dimers, thermal behaviour and monomerization kinetics in the solid state 2−57436
acetylene, formation of metastable triplet state in Hg photosensitized reaction, obs. of biacetyl emission 2−51467
acetylene, photoionization products, rate coeffs. for reactions 2−51435
acridine red, two-photon absorption cross sections using psec laser pulses 2−61808

Photochemistry continued
airglow continuum, processes responsible for emission 2−65887
aniline derivatives, u.v. absorpt., temp. effect, conform. change 2−68812
anthracene, auto-association of frozen solns,., fluorescence 2−54558
anthracene, auto-association of frozen solns., absorption spectra 2−54557
anthracene, electron transfer to $[Fe(CN)_6]^{3-}$ and O_2 in aq. soln. 2−61805
anthracene, mag. field effect on prompt fluoresc., singlet exciton fission obs. 2−81521
anthracene and 9-methyl-anthracene in ethanol as actinometer for u.v. region of impulse lamps 2−51462
9-CNanthracene dimers, thermal behaviour and monomerization kinetics in the solid state 2−57436
anthracene dyes in alcohol soln., fluoresc. correl. with photochem. activity 2−77432
aromatic acetylenes, reduced zero field splitting in EPR of photoexcited triplet state 2−68810
aromatic hydrocarbons fluorescence quenching by carbon tetrachloride, wavelength effects and complex formation 2−78205
aromatic molecules adsorbed on MgO surface, photoactivation by u.v. radiation 2−78206
atmosphere, photolysis of gaseous impurities, neutral ultrafine particle production 2−51586
azobisisobutyronitrile u.v. irradiated in polycrystalline state, e.s.r. spectrum 2−75394
benzaldehyde environmental effects on assignment and geometry of triplet state 2−61806
benzene, Franck-Condon factors for predissoc. 2−80079
benzene triplet yield in dil. cyclohexane soln., temp. depend. 2−57429
benzene-chloroform weak complexes, radiationless decay of benzene triplet state, external deuterium isotope effect 2−84661
benzene-d_6, heavy atom effects on phosphorescence characts. 2−84678
benzophenone molecular crystal, polarizabilities and dipole moments for lowest singlet and triplet $n\pi^*$ excited states 2−81136
benzyl chloride vapour, photolysis in presence of ethane or n-butane 2−65390
biacetyl, triplet-singlet emission analysis 2−72574
binary gas medium, photochem. wave propag. 2−81539
bromoacetylene, electronically excited, competition between photon emission and photodissociation 2−42969
tert-butylperoxy radical, prep. and e.s.r. spectrum 2−65391
carbene anthronylidene, e.p.r. spectrum, u.v. irradiation of diazoanthrone 2−44496
chemically induced dynamic polarization in thin films 2−51461
chloroacetylene, electronically excited, competition between photon emission and photodissociation 2−42969
chlorophyll-a microcrystal suspension, photoelectric response 2−51469
colchicine, excited states multiplicity of absorpt. and emission 2−65392
complex formation, effect on nonradiative transitions 2−78207
cryptocyanine Q-swithces for ruby laser, photochemical decomposition due to light source 2−49378
cyanometalate complexes in aqueous solns. photoelectron emission spectroscopy 2−68808
cyclobutanone, vacuum u.v. photodecomp., quantum yields 2−68813
cyclobutanone ($^1A_2$), fluorescence excitation, photodecomposition, of first excited singlet 2−48343
cyclopentanone, microwave- optical double reson. of triplet state 2−80065
cyclopentanone, transient effects in microwave optical double resonance 2−81524
cysteine hydrochloride monochydrate, u.v. and γ-irrad., radical recomb., mag. reson. obs. 2−72575
decomposition of large molecules theoretical results 2−81525
detergent solutions, dye aggregation 2−78202
di-t-butyl ketone, nuclear spin polarization during photolysis 2−51468
1,4-diazabicyclo (2.2.2) octane and methyl analogue, struct. effects on photophys. processes 2−81512
1,4dibromo-naphthalene, e.s.r. of triplet excitons, optical detection 2−81522
p-dichlorobenzene, phosphorescence microwave double resonance studies of $^3\pi\pi^*$ state 2−60060
diffusion constants of triplet states, modification of Avakian-Merrifield method 2−68800
β-diketones, phosphorescence spectra rel. to triplet state studies 2−60062
dimethyl ether, u.v. photolysis at 1470 Å 2−81527
dinitrobenzyl pyridine photochromism, photoequilibrium and decay mechanism 2−68814
9, 10-diphenylanthracene photoperoxidation, quantum yield and intersystem crossing 2−72576
disodium fluorescein, two-photon absorption cross sections using psec laser pulses 2−61808
dissociation reactions, formal theory, Bixon-Jortner model 2−72569
DNA, phosphoresc. decay rate, 4.2 to 160K 2−65393
DODCI, two-photon absorption cross sections using psec laser pulses 2−61808
DPPD, excited, electron transfer to oxygen mols., contact ion-pair and dissociated ion-radicals form. 2−68811
dynamic nuclear polarization, chemically induced, in unmodified n.m.r. spectrometers 2−65388
electron transfer processes, nonradiative deactivation 2−48346
ethanol glass, trapped electrons produced by biphotonic photoioniz. rel. to delayed emission of indole ring 2−54559
ethylene, photoionization products, rate coeffs. for reactions 2−51435
flash photolysis, thermal actinometer construct. 2−81518
flash-photolysis of explosive reactions, decoupling of physical and chemical mechanisms 2−81486
formaldehyde photolysis, calculation of potential surface 2−42988
formaldehyde photolysis, H atom production, abs. rate constant for H+ formaldehyde reaction 2−54539

Photochemistry continued
free radical production in ethanol glasses, e.s.r. studies 2−81509
Gaevachrome film type 6.00 and 6.05, rel. to physicochemical processing methods 2−52502
gas photocells irradiated with pulsed light, molecular ions mobility 2−81529
gas reactions, e.s.r. system for obs. 2−66663
glycerol, meas. of diffusion const. of pyrene molecules in triplet state from -17 to + 15°C 2−68804
trans-glyoxal ^3A_u mols., laser induced phosphorescence, photochemical quenching 2−48345
hexachlorobenzene, triplet state geometry at 1.6 K, PMDR obs. 2−81517
hydroquinone solutions, intermediate products of pulse photolysis 2−75391
9-hydroxymethylphenanthrene, photolytic dissociation cis syn dimer, fluorescence 2−56253
ice, KF and NH_4F doped and irradiated, role of F- in increased colouring 2−60823
imidazole radical produced by γ-irradiation of single crystals, ENDOR determ. of hyperfine tensors for protons in H bonds 2−65394
indolizine and azaindolizines, fluoresc. quantum yields, lifetimes, energy gaps influence 2−68815
initiation of combustion in subsonic flow 2−84660
lower troposphere, steady state model 2−54823
Martian atom., chem. dynamic model 2−85046
methane, photodissociation cross-section meas., 555-1242 Å 2−51470
methane, photoionization products, rate coeffs. for reactions 2−51435
mono-alkyl benzenes in rigid hydrocarbon glasses, triplet emission 2−81515
multiphoton absorption cross sections, exptl., determ. of correction factor for distrib. of laser intensity 2−49990
naphthalene-d_8, heavy-atom effect on phosphorescence characts. 2−84678
α-naphthol in pure and mixed crysts., electronic singlet-singlet absorpt. spectra 2−65395
naphthoquinone diazide resists photodecomposition 2−61802
nonpolar liquids, electron dynamics 2−81531
optical electron spin polarization in excited triplet states 2−81466
organic mol. cryst., electron spin echoes in photo-excited triplet states in zero field 2−54556
organic semiconductors, gas reactions, photoelectric detection method 2−72570
2,3-pentanedione, photolysis, fluorescence and phosphorescence yields 2−54560
2,3-pentanedione, photolysis emission and deactivation of excited states 2−54561
perylene, electron transfer to $[Fe(CN)_6]^{3-}$ and O_2 in aq. soln. 2−61805
phenanthrenes, aryl substituted, triplet-triplet absorpt. analysis 2−65396
phenazine, in rigid toluene glass matrix, spin polarization in photoexcitation of triplet state 2−68816
phenylcyclopropanes and phenylethanes, emission spectra, 77K 2−84663
photoresists, negative working, continuous tone photographic materials modes 2−81508
phthalocyanine solns., absorpt. from excited singlet states 2−84677
piperylenes, mag. field effects on photosensitized reactions 2−65397
poly(1-vinylnaphthalene) and copolymers, excimer formation, fluorescence obs. 2−54564
poly(2-vinylnaphthalene), excimer formation, fluorescence obs. 2−54564
poly-N-vinylcarbazole (acid-doped): o-dinitrobenzene charge transfer complex films, photoelectronic properties 2−78212
polyadenylic acids, influence of triplet energy trapping on decay kinetics of delayed fluorescence produced by triplet-triplet annihilation 2−51471
polymers, role of photophysical processes 2−54554
polymethine, saturably absorbing dye solns., photostability 2−61809
polypropylene photooxidation, surfaces changes, i.r. spectroscopic and electron microscopic studies 2−51472
polystyrene, excimer formation, fluorescence obs. 2−54564
propylene, addition of $O(^3P)$ atoms by flash photolysis, absolute rate constants 2−44492
pulse photolysis apparatus for rapid flow processes 2−75391
pyrene-d-10, temperature dependent saturation meas. in photo-excited triplet state 2−84567
quantum yield for intercombination conversion, determ. using triplet-triplet transfer 2−84676
quinoline in durene mixed crystal, triplet-triplet absorption at 2K, obs. 2−50114
rare earth ion-aromatic acid complexes, rare consts. for intramol. energy transfer 2−72305
reactions, reversible energy transfer, analysis of transient and steady-state kinetics 2−50128
relaxation of excess electrons in polar solvent produced by photoionization 2−72568
rhodamine 6G, increased resistance to photodegradation in cooled solid matrices 2−57430
rhodamine 6G and B, two-photon absorption cross sections using psec laser pulses 2−61808
rhodamine 6J solutions, intermediate products of pulse photolysis 2−75391
selective laser photochem. reactions using predissoc. of mols. 2−68803
solutions illuminated by ruby laser, calc. of deviation from Beer-Lambert's law 2−81416
stilbenes, mag. field effects on photosensitized reactions 2−65397
stratosphere, O_3 concentrations rel. to photodissociation of O_2 by solar radiation 2−84837
tetracene, e.p.r. of triplet excitons, spin polarization and singlet exciton fission role 2−81449
tetracene, e.p.r. of triplet excitons, spin polarization and singlet exciton fission role 2−81448
tetracene in soln., auto-associated species identification 2−81520

Photochemistry continued
tetrachlorobenzene in durene, hole burning in optically detected zero-field spectrum using EEDOR 2−84561
1,2,4,5-tetrachlorobenzene in durene, zero-field parameter signs from MODR spectra 2−65398
s-tetracyanobenzene complexes, electronic spectra in phosphorescent state 2−72578
s-tetracyanobenzene complexes formation of phosphorescent state from excited Franck-Condon state 2−72577
three-photon phenomena for randomly oriented molecules, polarization dependence 2−67441
TMPD in hydrocarbon glass, rigid matrix photoioniz., anion form., bleaching kinetics 2−81511
S-triazine triplet state at 3455 Å, Stark effect meas, vibronic origin of state 2−83280
1,2,4-triazole radical produced by γ-irradiation of single crystals, ENDOR determ. of hyperfine tensors for protons in H bonds 2−65394
trinitrofluorenone-poly(N-vinylcarbazole), photogeneration efficiency, field depend. 2−65399
triphenylamine light-induced conversion to excited triplet state of 11,12-dihydrocarbazole 2−57431
triphenylenes, aryl substituted, triplet-triplet absorpt. analysis 2−65396
triphenylmethane, exciton splitting in electronic spectra 2−81523
triphenylmethane dyes in films of poly(methylmethacrylate) 2−65387
vinylnaphthalene polymers and copolymers with styrene and methyl methacrylate, triplet depletion 2−68805
1-vinylpyrene and poly(1-vinylpyrene), spectroscopic behaviour 2−65400
water, electrochemical photolysis at semiconductor electrode 2−57428
Ag halides, photochemically dyed, absorption spectra 2−75392
Ag halides, review of properties of holes 2−66863
Ag halogenides, nucleation structure and primary photochemical process 2−49455
AgBr, chemical sensitization by doping, electronic mechanisms 2−81545
AgBr, chemical sensitization rel. to spectral sensitization 2−81550
AgBr, emulsion, Ag formation in single emulsion grains 2−81546
AgBr reduction sensitization, effect of electron and positive hole traps 2−66862
$(AgBr + AgCl(5\%):C^{5+}(N^{5+})(O^{6+})(S^{6+})$, high energy implantations, Doppler broadening of positron annihilation photons meas. with Ge(Li) detector 2−71507
$AgCl:C^{5+}(N^{5+})(O^{6+})(S^{6+})$, high energy implantations, Doppler broadening of positron annihilation photons meas. with Ge(Li) detectors 2−71507
AgCl photolysis, temp. depend., 77-400K 2−61803
$Ar:OF_2$, laser photo-detachment of OF and Raman spectra 2−51466
As_2S_3/Ag system, transformation rate temp. depend., ht. treatment and ageing effects 2−57433
$As_2S_3(Se_3)$ cryst., photodecomp. 2−51463
CO_2-N_2O mixtures, competitive photolysis, 1633 Å 2−65389
CO fourth positive chemilum. excitation and quenching due to reactions involving C_2O 2−84628
CO_2, u.v. photolysis, optical emission from $O(^1D)$ and $O_2(b^1\Sigma_g)$ 2−61801
CO_2 photolysis at 1460Å and 1500 to 1670Å, CO quantum yield 2−69141
$(C_3O_2)n$ polymer, photolytic examination rel. to its colouring properties on surface of Mars 2−78542
$Cd(^3P_0) + NH_3 \rightarrow CdNH_3{}^*$ reaction kinetics, rate constant, excimer formation 2−81514
CdS:Cu, optoelectronic effects, photochem. effects 2−65000
Co complex, $[Co(phen)_3](ClO_4)_2.2H_2O$, spin triplet states of Fe(II) in Mossbauer spectra 2−68806
Er^{3+} ions in silicate glass, photoinduced absorption spectra 2−75291
F photolytic atom sources for chem. lasers 2−68807
Fe(III) complexes with oxyacids, low temperature photolysis, e.p.r. spectra 2−75393
GeH_3Br, u.v. photolysis and i.r. spectra of matrix-isolated products 2−61804
I laser, energy transfer obs. 2−55693
I laser, kinetic processes 2−52440
I recombination to I_2 in Ar, using flash photolysis 2−80009
KCl, flash light excitation, F-centre transformations, absorpt. spectra obs. 2−43649
$KMnO_4$, γ-irrad., e.s.r. of $MnO_4{}^{2-}$ 2−68809
$Mo(CN)_8{}^{4-}$ ion, photoexcited, hydrated electrons formation 2−54555
NCl_2 in low temp. matrices, anisotropic e.s.r. spectra analysis 2−72571
NH_3 molecules, two-step photodissociation and excitation by laser irrad. 2−72572
$NH_2(A^2A_1)$ produced by photolysis, collisional deactivation 2−50060
NO $X^2\Pi$, rapid rate process meas. by kinetic spectroscopy during photolysis flash vibrational relaxation 2−54553
NO_2, photodissociation by pulsed laser light at 6943A 2−44490
NO_2, photolysis at high pressure, photodissociation rates 2−80010
O_2, u.v. photolysis, optical emission from $O(^1D)$ and $O_2(b^1\Sigma_g)$ 2−61801
O_3, $O_2\dagger + O(^3P)$ vibrational energy transfer 2−51465
O_3 photolysis by u.v. radiation $O(^1D)$ reactions 2−72573
$O(^1D) + O_3 \rightarrow 2O_2\dagger, 2O(^3P) + O_2$ energy distribution of products, ozone u.v. photolysis 2−84668
$O_2(^1\Delta_g)$ lifetime in solution, study of bimolecular loss processes 2−51464
OH reactions with H_2, D_2 and CO, pulsed vacuum u.v. obs. using reson. fluoresc. 2−84665
OH + NO + M reaction, flash photochemical study using reson. fluoresc. detect. of OH 2−84666
$O(2^1D_2)$, electronically excited, kinetic study by time-resolved atomic absorption spectroscopy in vacuum u.v. 2−83168
PCl_2 in low temp. matrices, anisotropic e.s.r. spectra analysis 2−72571
$PbBr_2$ pressed discs, u.v. irrad., photodecomposition 2−44491
S_3Cl_2, S_4Cl_2, photolysis reactions, correlation with vibrational analysis of S_3 and S_4 visible spectra 2−50069

Photochemistry continued
TiO_2, anatase non porous particles, photoreduction under u.v. irrad. 2−48342
Photochromism
dinitrobenzpyridines, photochromic transitions and relative stability of tautomers 2−48344
dye molecules in solid lipid layers, effect of electric field on absorption spectrum 2−68801
rhodamin B molecules in cadmium arachidate multilayers in thin capacitors, electrochromic spectra 2−68802
spiropyrans, 2 photon excitation of molecule under laser radiation 2−78208
CaF_2 crystals, erase-mode optical recording characteristics 2−63422
CaF_2 crystals, La doped, application as recording medium for holographic interferometry 2−66789
$CaTiO_3$ crystals, erase-mode optical recording characteristics 2−63422
$SrTiO_3$ crystals, erase-mode optical recording characteristics 2−63422
Photoconducting devices
− 2−65031
Apollo fine sun sensor electrooptical system 2−81960
avalanche photodiodes, temp. dependence and stabilization 2−68485
calibration, arbitrary light spectra 2−82140
diffused PIN non-guard-ring photodiodes noise in dark and illuminated 2−57214
diode, light emitting, efficiency, carrier diffusion length, absorpt., auto-photovoltaic meas. 2−61451
ferroelectric/photoconductor memory device, switching and remanence 2−47982
gas photocells irradiated with pulsed light, molecular ions mobility 2−81529
heterojunction photodetectors, interface region struct. rel. to energy band profile 2−44181
heterojunction photodetectors, review 2−44180
junction, p-n, directly polarized, photoresist. effect 2−48006
metal-semicond. photodiodes, quantum yield inversion region effects 2−81116
m.i.s. photodetectors 2−77929
m.i.s.i.m. structs., light detect. by charge accumulation obs. 2−65095
Nimbus limb radiometer electrooptical system 2−81960
organic, inorganic, speed criterion, critical exposure, initial potential, cascade development 2−84376
photocells, relative spectral sensitivity 2−44183
photodiodes and phototransistors as detection devices for multichannel emission spectrometry 2−68486
in photometers 2−70026
photoresistors dosimetric characteristics, nuclear radiation detectors 2−82800
phototransistor, overcompensated semiconductor, mechanisms of decreased differential photosensitivity 2−75129
Schottky diodes, hole diffusion contrib. to photocurrent, temp. depend. 2−44178
semiinsulator long diode, S-type current-voltage characts. when illum., photosensitivity 2−65094
short-circuit current freq. response meas. principle 2−75179
Shottky barrier photodiodes, noise in dark and illuminated 2−57214
Skylab multispectral scanner electrooptical system 2−81960
thermoplastic media for holographic recording 2−63360
u.v. detector, response to solar radiation rel. to altitude 2−81962
$Al_xGa_{1-x}As$-GaAs heterojunctions, elec. props., photoresponse, graded gap model, laser operation 2−81117
Au−n-GaP, surface barrier diode, photosensitivity, 1.4-5.2 eV spectral range 2−75182
CdS, photoresistors, FSK-type, response to low-intensity modulated radiation 2−61452
CdS film prep. and characteriz. 2−53571
CdSe-CdS film photoresistor, role of activating powder 2−65096
CdSe-electrolyte blocking contact, photosensitivity and noise 2−72079
Cu_2S-CdS heterojunction, prep. and props. 2−72056
Cu_xS-CdS photovoltaic cell, model 2−54261
GaAs:Cr p-i-n diode, nonadditive photocond. under combined excitation conditions 2−72080
GaAs, Si-doped, infrared light emitting diode 2−65030
n-GaAs diodes, high-resist., hole accumulation at cathode 2−54220
GaAs green light emitting diodes, phosphor-coated 2−65028
GaAs light emitting diodes, optical fluctuations 2−75180
GaAs photodiode, feasibility of epitaxial production on single crystal strip of Ge 2−54260
GaAs with anti-Stokes luminors, in i.r. band 2−77967
$GaAs_{1-x}P_x$ light emitting diodes, fabrication processes and performance characteristics 2−65029
GaAsP(N), diode, light emitting, electrolum., N doping effects 2−81411
GaP:Zn, O, light emitting diode, efficiency shift under forward bias 2−75181
Ge:Hg photoresistor, heterodyne detection at high freq. 2−69986
Ge-Si heterojunction position sensitive photocell 2−44182
Ge detecting head for YAG laser 2−66761
$Pb_{1-y}Sn_ySe$, i.r. sensitive thin films, properties 2−64999
$Pb_{1-x}Sn_xTe$, i.r. sensitive thin films, properties 2−64999
$Pb_{1-x}Sn_xTe$, photodiode, prep. and props. 2−75183
Se and Si photocells, effects of polarization on performance 2−44185
Si p-n junction, spectral characts., effect of strong elec. fields 2−75184
Si photodiode operational amplifier combination, noise and frequency response 2−57214
Si photoelectric solar cells, crystals obtained by Stepanov method 2−45660
ZnCdS evaporated layers as photoresistors in u.v. 2−44179
$ZnSe_xTe_{1-x}$ p-n junction diodes, struct., props., electron microscope and cathodolum. obs., 77-300K 2−81118
Photoconductivity
see also Photoconducting devices
alkali halide, lattice distortion produced by edge disloc., photoconductivity spectra obs. 2−74777
anthracene, hot carrier injection rel. to field depend. 2−75189
Photoconductivity continued
anthracene, sensitized photoconductivity, magnetic hyperfine modulation 2−65309
anthracene crystal, dye adsorbed on surface, rel. to sensitized delayed fluorescence 2−81169
anthracene single crystal irradiated by electron beam, hole trap 2−51126
benzene, liquid and solid, optical generation of charge carriers via excitons 2−57259
β-carotene, wavelength and illum. intensity depend. 2−72072
β-carotene glass, transients, space charge and photovoltaic effects 2−48003
CdSe photoconductive films, field quenching 2−77964
chalcogenide, amorphous, review 2−61445
chalcogenide alloy, amorphous, model 2−61446
cyanine dyes, adsorbed, external photoelec. yield and ioniz. energy 2−48025
diamond, spectra rel. to electron irrad. 2−77962
electrostatic potentials across space charge layer in an illuminated photoconductor 2−51211
EuO, ferromag. semicond., Redfield technique detn. of Hall mobility of photoelectrons 2−81060
furan quinone pigments, DFC and DF, photoinjection and photoemission, energy levels 2−54256
furan-quinone pigment, DFC, charge transport props. 2−51219
minority carrier lifetime meas. method 2−75179
molecular crystal, exciton induced contact limited photocurrent, field depend. 2−77968
molecular crystal-metal interface, Frenkel exciton dissociation obs. 2−51085
molecular crysts., bibliography 2−48159
nematic liquid crystal, transient response caused by low freq. voltage pulse 2−53398
nematic liquid crystals, laser induced, drift mobility detn. 2−53398
organic semiconductors, gas reactions, photoelectric detection method 2−72570
p-chloranil, hot carrier injection rel. to field depend. 2−75189
phenanthrene, energy of free electron conduction band, flash photoconducwivity determination 2−44177
photoelectron energy, rel. to charges in media with dielectric function 2−57103
phthalocyanine, negative charge carrier injection into hydrocarbon and dimethyl siloxane fluids 2−56512
phthalocyanine and derivatives, fluoresc. and photocond. 2−72426
plasma injected into photoconductor, basis of new photocond. mode 2−54250
poly-N-vinylcarbazole complexed with trinitrofluorenone film, bulk recomb. of charge carriers 2−72073
polyethylene, anomalous photo-induced current transients 2−54257
polymer, photocurrent depend. on ambient condition, wavelength and temp. 2−48004
polyvinyl chloride films, pulsed photoconductivity, obs. of transient photocurrents with oscillations 2−72074
polyvinylcarbazole, dye sensitized film, photoinduced voltage decay 2−81165
pyrene, photoelectret effect 2−81131
rhodamine 6G amorphous film, carrier traps, photocurrent relax. study 2−54180
semiconductor, amorphous, photocond. response characts., obs. with photocond. ccts. 2−84375
semiconductor, amorphous, steady state theory 2−61447
semiconductor, conf., Warsaw, Poland, July (1972) 2−68384
semiconductor, high resistivity, meas. of dark current using electron beam contact 2−75166
semiconductor, high-resist. compensated, impurity photocond. kinetics 2−72058
semiconductor film, rel. to kinetics of small charge currents and carrier lifetime determ. 2−81088
semiconductor plate for microwave antenna near field amplitude-phase meas. 2−55624
semiconductors, negative photoconductivity 2−81174
semiconductors, photoconduction, anisotropy in persistent internal polarization 2−81176
semiconductors and insulators, amorphous, basic equations 2−61290
semiconductors multi-valley, discontinuities in lux-ampere characts. 2−71895
semiconductors with multi-level impurities, theory and obs. 2−54251
spin dependent, study by resonant methods 2−71778
5,12,6,11-tetaoxytetracene crystals 2−48001
transient photoinjection current in anthracene 2−57200
trinitrofluorenone-poly(N-vinylcarbazole), photogeneration efficiency, field depend. 2−65399
trisiloxane film, electron beam polymerized 2−47909
V-I characteristic 2−44171
Ag halides, thermolum. and photocond., trap levels, meas. apparatus and technique 2−79389
AgBr, rel. to sensitizing dye 2−81550
AgBr crystals, obs. of primary photographic process using transient photocharge obs. 2−66864
AgBr photographic films, obs. at 77 K with microwave methods 2−66867
AgCl, photographic coating, with adsorbed sensitizing and desensitizing dyes, photocurrents 2−81183
Ag_2S epitaxial thin films, spectral sensitivity of photocurrent 2−53567
As-S-Te vitreous semiconductor, γ-ray induced 2−54252
As-Se-Te vitreous semiconductor, γ-ray induced 2−54252
As_2S_3, vitreous, transient rel. to Fermi level analysis of localized states distrib. 2−47913
As_2Se_3 film, amorphous, charge transport study 2−68393
As_2Se_3 films, amorphous, dark discharges 2−49458
$As_2Se_3(Te_3)$ film, amorphous, trap-limited processes 2−61325
$3As_2Se_3.2Sb_2Se_3$ films, amorphous, spectral response, transport mechanism 2−54187
As_2Te_3, glassy, rel. to electronic props. 2−61297
As_2Te_2Se, amorphous semicond., thermalization in energy band tails 2−61685
BiI_3, effect of adsorption 2−47993

Photoconductivity continued
$CaWO_4$ following low temp. X-irradiation, photoconductivity 2−81175
β-carotene glass, response curves, rise and decay times 2−48002
$CdBr_2$-Pb crystals, temp. depend. of recombinat. luminesc. and photocond. 2−72049
CdF_2, high purity, semiconducting, spectrum interpreted in terms of band structure 2−84378
$Cd_{0.20}Hg_{0.80}Te$, photocond. oscillations in a magnetic field and photomagnetic effects 2−75169
$CdIn_2S_4$ single crystal, photocurrent oscillations 2−75170
CdS:Ag(Al), field quenching, influence of doping 2−54170
CdS:Cu, trapping parameters, photocond. response, i.r. quenching, photochem. effects 2−65000
CdS-$Cu_{2-x}Te$ heterojunctions, photoelements, spectral response curves and current-voltage characteristics 2−44184
CdS, anisotropy 2−72060
CdS, effects of 10 MeV electron irradiation 2−57254
CdS, photoconducting, acoustoelec. current, theory and expt. 2−54171
CdS, photosensitivity, luminesc. intensity, rel. to donor-acceptor photothermal dissociation 2−72393
CdS, photosensitivity rel. to elec. field 2−75167
CdS, prep. by reactive sputtering, photocond. props. 2−65082
CdS, with Ag, Cu, and In impurities, spectral characts. 2−72059
CdS crystal with insulated barriers, a.c. 2−68478
CdS film, gain in through thickness operation 2−44173
CdS film, photorectification in longitudinal quasi unipolar photocond. with non uniform illumination 2−81172
CdS film, prolonged relax. of dark current after illumination 2−81173
CdS film, sputter-deposited, characteriz. 2−53571
CdS films, shift in lux-ampere and I-V characts. due to photoelectret effect 2−81170
CdS films produced by r.f. sputtering in Ar, effects of sputtering conditions on photoconductive characteristics 2−68479
CdS phosphor, Schon-Klasens model interpret. 2−51213
CdS photoconductor, transverse surface wave depth penetration 2−84206
CdS(Se), hole photoemission into S, 2.11-3.54 eV 2−84265
CdS_xSe_{1-x} selective photoresistors for visible region 2−44172
CdS(Se)(Te) films, a.c. photocond. on excitation with intensity-modulated light, trapping levels 2−57255
p-CdSb, conductivity anisotropy effects 2−57257
CdSe:Cu, a.c. photocond. in negative photocond. region 2−65081
CdSe, eff. of real growth on elec. and photoelec. props. 2−71419
CdSe, memory and photocond., 77 and 300K 2−75168
CdSe, undamped oscill. in photocurrent 2−54253
CdSe film, photoelectronic props. 2−51212
CdSe films, energy spectrum and nature of trapping centres detn. by induced impurity photocond. method 2−71501
CdSe laser crystal, electron beam excited 2−77965
$CdSe_xTe_{1-x}$, n-type solid soln. photoelec. props. and recombination diagram 2−72061
$CdSi_xGe_{1-x}As$, glassy, spectral distrib., rel. to band struct. determ. 2−61448
$CdSnP_2$, spectra in extrinsic (impurity) range, and effects of doping 2−57256
p-CdTe, annealing effect on conductivity and photoconductivity, obs. 2−61263
n-CdTe, bending producing 60° dislocations, effect on conductivity and photoconductivity 2−61264
p-CdTe, film, mechanism 2−48217
CdTe, radiation effects of neutrons and electrons 2−47892
CuCl(Br)(I) layer, on Ag or Cu, light sensitivity spectra 2−77966
Cu_2O, near i.r., influence of annealing 2−47994
Cu_2O, near i.r., rel. to band scheme 2−54420
Cu_2O, spectral depend., oscills., up to 180 K 2−77963
Cu_2S-CdTe film heterojunction, voltage depend. 2−81123
Eu_3SiO_5, narrow band near absorpt. 2−48173
GaAs:Cr, energy spectrum of deep levels 2−71927
GaAs:Cr, instability of recomb. radiation and photocurrent 2−84540
GaAs:Cu, behaviour in strong elec. field 2−71904
p-GaAs, 300-77 K, λ=0.5-1 μ, surface effects 2−54254
GaAs, many-photon absorp., carrier generation obs. 2−84519
n-GaAs, negative, when illuminated with impurity absorbed light, recomb. mechanism 2−65083
GaAs, photothermal ionization of shallow donors 2−81177
GaAs, two-photon conductivity with nanosec. and picosec. light pulses 2−47995
GaAs epitaxial film, substrate orientation effects 2−47436
β-Ga_2S_3, kinetics 2−84532
GaSb, temp. depend., thermal ioniz. obs. 2−48179
p-GaSb, undoped, acceptor states and excitons 2−61708
Ge:As, comparison with i.r. absorpt. spectrum 2−68642
p-Ge:Au electron capture coeff., excess free carrier distrib., surface recomb. effects 2−81164
Ge:Au obs. and theory of multi-level impurities effects 2−54251
Ge:Cu, recomb. cross section for holes at singly ionized impurity 2−51215
p-Ge:Cu thermalization time of hot photoexcited holes 2−51214
Ge:Ni, electron and hole capture rates determ. 2−75171
Ge:Sb, monochromatic submillimeter radiation 2−81180
p-Ge-n-CdS_xSe_{1-x} epitaxial heterojunction 2−77924
Ge, amorphous, rel. to transport model 2−61352
Ge, d.c. and microwave, metal-insulator transition obs. 2−77829
p-Ge, nonspherical band cubic semicond., anisotropic photon drag effect 2−75165
Ge, photocond. spectra, donor excited states, Zeeman effect obs. 2−75172
p-Ge, radiation defect annihilation centre obs. 2−83978
n-Ge, rel. to laser generated carrier mobility, transient behaviour 2−47925
Ge, Surface excitation by Nd laser pulse, surface transport props. obs. 2−84379
Ge, wide range of band bending near surface 2−72062
$Hg_{1-x}Cd_xTe$, sweep out of minority carrier holes 2−54255
HgS, hole photoemission into S, 2.11-3.54 eV 2−84265
In-Te system, film, band gap determ. for In_2Te_3 phase 2−60662
InP, excitonic recomb. and photocond. 2−72410

Photoconductivity continued
n-InP, high resistivity, i.r. quenching 2−75173
n-InSb, anomalous microwave photocond. in strong mag. field 2−47896
InSb, effect of light and X-rays at 77K 2−47996
p-InSb, nonspherical band cubic semicond., anisotropic photon drag effect 2−75165
n-InSe, laser irrad., rel. to band struct. and carrier recomb. 2−72063
KBr, multiphoton conductivity, optical gap assignment 2−65084
KCl, gamma- irradiated, high temp. dependence of electron Hall mobility 2−44174
La_2O_2S:Eu, correlation with luminesc. 2−72064
LiH crystal, Mg-activated, photocond. excitation spectra meas. 2−77799
low mobility material, transient photocurrents, Monte Carlo calc. 2−61444
MnS, room temp. spectrum 2−68480
Pb, photocurrent temperature dependence due to superconducting energy gap, 2.5 to 12°K 2−68354
PbO, autocompensated, inversion of the sign of conductivity 2−44175
PbS, spectral depend., quantum yield of internal photoelec. effect and impact ioniz. 2−72065
PbS layers, photocond. mechanism, elec. cond. and Hall effect obs. 2−81166
$Pb_{0.8}Sn_{0.2}Te$, epitaxial film 2−65085
PbTe, epitaxial film 2−65085
RbCl, F_a(Li) centre, a.c. photocond. study 2−71530
SbSI:Sb_2S_3, prep., spontaneous polarization, dielec. permittivity, photocurrent, dark current rel. to phase transition, −50-50°C 2−75143
SbSI, paraelec. region, voltage-current characts., illumination effects 2−81163
SbSI, semicond. ferroelec., trapping levels, thermally stimulated photocurrents obs. 2−75154
$Sb_{1-x}Se_x$ film, amorphous, photocond. spectral response rel. to comp. 2−81167
Sb_2Se_3 film, amorphous, transport props. 2−61323
Se, compressed, photocurrent obs. of crystn. 2−64533
Se, hole photoemission into S, 2.11-3.54 eV 2−84265
Se, kinematics of deep trapping, rel. to photogeneration 2−61344
Se film, vitreous, trap-limited processes 2−61325
Se photocell, temperature dependence of relative spectral sensitivity 2−44186
Si:Ag, deep impurity properties, and thermally stimulated current obs. 2−61363
Si:B implanted, rel. to nature and characs. of defects 2−44126
Si:In, spectral depend. of extrinsic photocond. 2−51216
Si:Ni thermal and field quenching by impurity electron capture 2−65088
Si:P, electron drag rel. to impurity centre photoionization, photo-e.m.f. 2−65089
Si:P, phonon and electric field influence on extrinsic photocond. 2−81179
Si-SiO_2 interface, photoemission from Si to SiO_2 during laser irrad., photocurrents 2−81119
p-Si, electron irrad., low temp. spectra 2−47999
Si, neutron irrad., divacancy obs. 2−48194
n-Si, radiation induced defects obs. 2−72066
Si, rel. to surface states 2−47932
Si, spectral and field depend., electrostatic nonequilib. photopinch, photocarrier surface trapping 2−65086
Si, spectral and field depend., under different bulk and surface recomb. characts. 2−65087
Si, wide range of band bending near surface 2−72062
p-Si (001) inversion layer, continuously voltage tuneable line absorp. in surface quantization 2−47997
Si film, amorphous, rel. to band struct. 2−61655
Si film, epitaxial film, nonequilibrium carrier lifetime obs. 2−84331
Si intrinsic, spectral depend. 2−47998
Si photocell, temperature dependence of relative spectral sensitivity 2−44186
Si surface, spin-depend. recomb. of photocreated excess carriers 2−51217
SiO_2, photoinjection over interface barrier, exponential charging profiles effect on photocurrent 2−54226
SnSSe, room temp. and 77K, 300-2000 nm 2−67937
$SnS_2(Se_2)$, room temp. and 77K, 300-2000 nm 2−67937
Te, CO_2 laser induced photoeffects 2−81178
TiO_2 amorphous film, rel. to band struct. 2−72068
TlI, influence of polymorphic transitions 2−75174
Tl_2Se_3-As_2Te_3, vitreous, photoresponse 2−72067
Xe solid, energy gap, at 135K 2−72069
$(Y_2O_3)_3(Fe_2O_3)_5$ ferrite garnet, 280-800 nm 2−84380
$ZnAs_2$, rel. to band struct. detn. 2−51326
$Zn_xCd_{1-x}S$:Cu, Cl temp. and i.r. quenching of luminescence and photocond. 2−84543
ZnCdS-Cu, Mn powder crystallophosphors, interaction of electrolum. and photocond. during switching 2−68710
$Zn_2In_2S_5$ single crystal, decay kinetics 2−75175
ZnO:Li, light scatt., and photoconductivity, anisotropic 2−75317
ZnO/O absorbed layers, sensitizing action by chlorophyll to corono discharge 2−44176
(ZnO-MgO):Fe,O transient effect, space charge current flow 2−84377
ZnO, photovoltage inversion effect, surface states continuous spectrum 2−48000
ZnO, polycrystalline study of spectral, chemical sensitization centres of internal photo-effect, optical extinction method 2−75176
ZnO suspension and film, photocurrent obs. 2−51218
ZnP_2, rel. to band struct. detn. 2−51326
ZnS:Cu:Co,(O), existence of negative thermally stimulated current and transient effect 2−68481
ZnS:Ni,O, spectral response interpret. 2−57258
ZnS, many-photon absorp., carrier generation obs. 2−84519
ZnS, two-photon photocond., linear behaviour 2−72070
ZnS, two photon photocond. 2−61450
ZnS phosphor, Schon-Klasens model interpret. 2−51213
ZnS single crystal, homogeneous, and u.v. electroluminescence 2−68712

- **Photoconductivity** continued
  - ZnSe, many-photon absorp., carrier generation obs. 2−84519
  - ZnSe (Cu, Ga), epitaxial thin films, photoluminescent, oscillations of photocurrent 2−78147
  - n-ZnSe(Cu,Ga) film, photolum., photocurrent oscills., 80-220K, luminesc. field quenching 2−81168
  - p-ZnTe, high photosensitivity 2−72071
- **Photodisintegration** *see Deuterons/photodisintegration; Nuclear reactions and scattering due to/photons*
- **Photodissociation** *see Photochemistry*
- **Photoeffect, nuclear** *see Gamma-rays/effects; Nuclear reactions and scattering due to/ photons*
- **Photoelasticity**
  - *see also Double refraction/mechanical; Piezo-optical effects*
  - analysis using polarization holography 2−82148
  - anisotropic media, determ. from Brillouin scatt. 2−78114
  - Brillouin scatt. as consts. meas. method 2−50731
  - coating, full field isopachic generation 2−60938
  - composite, fibre-reinforced, shrinkage stresses near discontinuity, photothermoelasticity study 2−71659
  - composite and polycrystalline solids, calc. of average photoelastic tensor 2−61593
  - cracks, photoelastic detn. of mixed mode stress intensity factors 2−69650
  - dielectric cryst., light scatt. by entropy fluctuations, phonon transport theory 2−81327
  - double diffraction parameters, determination 2−82331
  - flint, u.s. light modulation and det. of photoelastic constants 2−70025
  - frozen-stress technique applied to oblique holes in thick plates and cylinders 2−69676
  - gelatin, stress frozen, analysis for gravity stresses 2−41628
  - holographic, simultaneous determination of isopachic and isochromatic fringe patterns for dynamic loadings 2−66551
  - holographic interferometric technique for meas. of absolute retardation 2−41623
  - holographic interferometry, surface displacement components of deformed body 2−66552
  - holography and interferometry, physical explanation in terms of warped-wavefront 2−52438
  - hyperelastic dielectric, dynamical theory 2−66602
  - hypoelastic dielectric, birefringence in simple shear 2−45417
  - hypoelastic dielectric, constitutive equations 2−45416
  - orthotropic, analysis of residual stresses in filament wound composite material rings 2−41601
  - parametric interactions in laser-pumped birefringent media 2−59121
  - poly(glycol methocrylate), photoelastic effect in molecular 3d networks, optical anisotropy, thermodynamic rigidity 2−44347
  - poly(methyl methacrylate), cross-linking effect on thermomech. and thermooptical behaviour 2−83390
  - polycarbonate, yield locus, characterization tests for photoelastoplastic material 2−43778
  - polyethylene, sulpho- chlorinated, anisotropy of statistical segment 2−44346
  - polyisobutylene in decaline, flow in concentric cylinders 2−56457
  - polyurethan rubber, dynamic stress analysis 2−41613
  - scattered light, use in stress anal. 2−66519
  - scattering of light from a non-alkali alumino silicate glass 2−65226
  - stress analysis 2−58876
  - for stress analysis in spot welded joints 2−68143
  - three dimensional characteristic methods 2−79334
  - As_2S_3, amorphous, dispersion of photoelastic consts., one-oscillation model 2−54383
  - $CaCO_3$, Brillouin scatt. study 2−78114
  - Ge cryst., at 13 MHz u.s., modulation of 10.6 mkm radiation 2−49201
  - $(NH_4)_2SO_4$, consts. determ. from Brillouin spectra 2−43665
- **Photoelectrets** *see Electrets; Photography*
- **Photoelectric cells** *see Photoconducting devices; Photoconductivity; Photoelectricity; Photovoltaic effects*
- **Photoelectric effect, atomic** *see Atoms*
- **Photoelectric emission** *see Electron emission/photoelectric*
- **Photoelectricity**
  - *see also Electron emission/photoelectric; Photoconductivity; Photovoltaic effects*
  - — 2−57253
  - amorphous semiconductor, photodielec. effect, rel. to trapping 2−61443
  - image detectability on photoelectric surface 2−79455
  - photocathode sensitivity enhancement by multiple internal total reflection 2−44197
  - photoelectric effects, rel. to charges in media with dielectric function 2−57103
  - semiconductor, III-V, transition metal doped, anomalous props. 2−68405
  - semiconductor, nonlinear forward drift of electrons in a laser beam 2−57252
  - solar cells, honeycomb absorbers on collecting base surface, absorption efficiency 2−41909
  - $Al-Al_2O_3-Al$ structure, photosensitive tunnelling conductance 2−54222
  - BiI_3, non isothermal relax. of photoelectret state 2−57247
  - BiI_3, photopolariz., localized states and electron-hole processes obs. 2−61706
  - CdS cell, electronic fringe counter for interferometric applications 2−42198
  - CdS m.o.s. system, amplification of pulse photoelectric current 2−44146
  - $n-CdS-p-Cu_2S$, photosensitivity 2−71955
  - Cu_2O, photomemory effects in elec. conduction 2−75091
  - GaAs-CdS heterojunction, isotypic, photosensitive props. 2−71956
  - Ge, thermophotoelec. effect due to hot carriers, 300 and 77K 2−72057
  - Se, amorphous layers, charge and trap concs. 2−84374
  - n-Si:Zn, photoelectronic props. of Zn centres, Zn^{2-} energy level, centre density 2−61449
  - $Si-SiO_2$ interface, effects of illumination on electrical properties 2−44147
- **Photoelectricity** continued
  - Si, spectral and field depend., electrostatic nonequilib. photopinch, photocarrier surface trapping 2−65086
  - Si, spectral and field depend., under different bulk and surface recomb. characts. 2−65087
  - Si solar cells, performance improvement using passivated Ti(Pd)Ag contacts 2−59057
  - $Si_{1-x}Ge_x$ solid soln., film, photoelec. props. 2−65090
  - $TlInSe_2$:Cu,Sn, cryst. and film, photosensitivity, optical absorpt., dark cond., forbidden band width 2−57197
  - ZnO, photovoltage inversion effect, surface states continuous spectrum 2−48000
- **Photoelectromagnetic effects**
  - semiconductor, photomagnetoelec. circulating current, spectral distrib. determ. 2−68483
  - $Cd_{0.20}Hg_{0.80}Te$, photocond. oscillations in a mag. field 2−75169
  - p- CdSb, transverse Dember effect, conductivity anisotropy effects 2−57257
  - CdTe film, with anomalously high photovolt. 2−75178
  - GaSb, in quantizing mag. field 2−68484
  - Ge:Ni, electron and hole capture rates determ. 2−75171
  - Ge, oscillatory spectral distrib., rel. to direct interband transitions 2−65093
  - Si:In, ion implanted, photoelectromag. effect rel. to dose and annealing 2−72077
  - YIG, light-induced Bloch wall pinning 2−48060
  - YIG(Si), reversible, microscopic theory 2−54259
  - ZnS-CdS, evaporated layers, mosaic heterojunction photo-emf 2−77970
- **Photofission**
  - betatron bremsstrahlung application 2−46234
  - Compton scattered neutron capture gamma rays for photofission studies 2−52833
  - intermediate energy, review 2−70495
  - prompt and delayed, basis of Strutinsky double barrier model, exptl. results 2−83039
  - ^{232}Th, cross sections and angular distrib., obs. of band of rotational levels 2−83040
  - ^{232}Th, prompt and delayed, exptl. results 2−83039
  - ^{232}Th cross section near threshold 2−83024
  - ^{238}U, cross sections and angular distrib., obs. of band of rotation levels 2−83040
  - ^{238}U, cross sections near thresholds 2−83024
  - ^{238}U, prompt and delayed, exptl. results 2−83039
  - ^{238}U photofission product yields 2−74129
- **Photographic light sources** *see Light sources; Photography*
- **Photographic materials**
  - *see also Nuclear track emulsions*
  - colour film for new one-step photography, picture automatically developed within minutes of exposure 2−66876
  - colour prints, optimum peak wavelengths and breadths of cyan magenta and yellow 2−63444
  - conference on unconventional photographic systems, Washington (1971) 2−42285
  - crowded emulsions, renewal theory rel. to statistical mechanics of monolayers 2−73683
  - cyanine dyes, luminescence of solid films 2−75327
  - dye components, spectral absorption curve matching, maximum error minimization algorithm 2−66858
  - dye-forming imaging system in viscous media, long exposure density reversal 2−66868
  - dyes in colour film, stability of selective grays 2−63443
  - electronographic emulsion, characteristic curve 2−42442
  - electrophotographic developers, electrical properties 2−70100
  - electrophotography, light sensitive materials, processing, review 2−70099
  - emulsion, cross-section, photomicrograph 2−55779
  - emulsion, model, simulated detective quantum efficiency 2−63440
  - emulsion, m.t.f. evaluation using multiple-sine-slit microdensitometer 2−45807
  - emulsion, used as holographic memory, effect of film grain noise on performance 2−42140
  - emulsion coating, kinetics of swelling 2−59319
  - emulsion coatings, photovoltaic effects 2−81182
  - emulsion design and image evaluation 2−59307
  - emulsion size distribs., meas. by electrolytic reduction 2−80499
  - emulsions, bleaching technique and application to holography 2−55712
  - emulsions, effect of electric fields on ionizing particle recording 2−59642
  - emulsions, effect of thickness on diffraction efficiency of recorded amplitude holograms 2−42141
  - emulsions, effects of u.s. radiation, formation of impurity centres, mechanisms 2−70094
  - emulsions, electric field effect as function of exposure conditions 2−72464
  - emulsions, sensitization by cyanine dyes for blue exposures at 77 K 2−66866
  - film, as input mechanism for coherent optical data recording, characteristics 2−66859
  - film, image, quality assessment, diffraction pattern analysis 2−79407
  - film, precise wash, calc. 2−49456
  - film graininess, density, colour films, black and white films 2−82595
  - film graininess and density, critical relationship 2−59306
  - films, apparatus for meas. of internal stress and strain, temp. and humidity dependence 2−52497
  - films, detective quantum efficiency 2−82598
  - furan quinone pigments, DFC and DF, photoinjection and photoemission, energy levels 2−54256
  - furan-quinone pigment, DFC, charge transport props. 2−51219
  - gelatin, relief capacity for acid dyes 2−70092
  - gelatine in photographic layers, mechanical properties and means of modification 2−52508
  - hologram, electron micrographs of cross sections 2−66784
  - holographic photomaterials, high resolution 2−66790
  - holographic recording materials 2−55716

Photographic materials continued
holographic recording medium, 3d character of photosensitive materials 2—42145
for holography, light scattering 2—63438
for holography, modulation transfer for 2—82527
liquid toner formulations and pH interactions, settling rates, acid number and surface activity 2—59323
Lithpet, electrosensitive film 2—76552
modulation function meas. for electron sensitive films 2—79154
modulation transfer function, by contact slit imaging 2—73688
multilevel grains, detective quantum efficiency and ideal photographic detector 2—63441
organic photoconductors and electrophotographic contact printing 2—59322
oxacarbocyanine, excimer and related emission at low temp. 2—66861
photopolymer hologram recording films for real time image formation without processing 2—69968
photoresists, negative working, continuous tone photographic materials modes 2—81508
polyethyleneglycol developers, active properties 2—52504
polyvinylcarbazole, dye sensitized, electrophotographic response 2—59325
polyvinylcarbazole, dye sensitized film, photoinduced voltage decay 2—81165
processing latitude of 3M 7842 and 7969 dry Ag films 2—59309
radiographic film detail evaluation, significance of light density 2—73695
reproduction of high resolution photography 2—59335
response to He-Cd laser radiation 2—59310
response to Q switched ruby laser energy 2—84679
rifled picture screens, optical parameters 2—76554
selenacarbocyanine, excimer and related emission at low temp. 2—66861
semiconductor-dielectric electrophotographic system, use in long-wave semicond. photography 2—70090
spectral plates, blackening distribution under various development conditions 2—59286
thiacarbocyanine, excimer and related emission at low temp. 2—66861
Ag conc. under variable exposure for latex, nitrocellulose, polyvinyl butyryl rel. to optical density 2—52500
Ag due bleach colour copy materials 2—59320
Ag halide, adsorpt. states of gelatin and photographic stabilizers 2—80584
Ag halide emulsions, modified electron transfer mechanism for spectral sensitization 2—59321
Ag halides, grains, photographic sensitizing and desensitizing by electron traps 2—81023
Ag halides, initial chem. development reaction 2—81547
Ag halides, photochemically dyed, absorption spectra 2—75392
Ag halides, physics and chem., conf., Montreal, Canada, Aug. (1972) 2—81541
Ag halides, review of properties of holes 2—66863
Ag halides, thermolum. and photocond., trap levels, meas. apparatus and technique 2—79389
Ag halogenides, nucleation structure and primary photochemical process 2—49455
Ag in photographic products, precision routine analysis 2—59332
AgBr, chemical sensitization by doping, electronic mechanisms 2—81545
AgBr, emulsion, Ag formation in single emulsion grains 2—81546
AgBr, emulsions and crysts., red luminesc. at 77K, electron-hole recomb. 2—81438
AgBr, photographic sensitivity, impurity effects 2—81544
AgBr emulsion, latent image centres displacement 2—80723
AgBr films, photoconductivity obs. at 77 K with microwave methods 2—66867
AgBr monodisperse emulsions, completely exposed, development, fixing rate measurements 2—66870
AgBr monodisperse photographic emulsions, r.m.s. granularity 2—66869
AgBrI, emulsion coatings, luminesc. spectra at 77K 2—81437
AgCl, coating, with adsorbed sensitizing and desensitizing dyes, photocurrents 2—81183
As_2Se_3 films, amorphous, dark discharges 2—49458
$LiNbO_3$, doped, as erasable optical recording medium 2—73612
NH_4 hypersensitized IV-N plates, photometric properties 2—82597
Se-polyvinylcarbazole multi-layer photoreceptor for electrophotography 2—59293
ZnO-resin electrophotographic coating for positive charging 2—63452

sensitivity
AgBr layers, electric fields, polarity, fog, speed 2—84674
black and white motion picture films 2—66873
colour photographic papers, spectral characteristics and effects of ageing 2—52505
cyanine dyes, adsorbed, external photoelec. yield and ioniz. energy 2—48025
emulsion, h.f. electric field control of sensitivity during exposure 2—52506
emulsion sensitometry evaluator 2—59331
film comparison with electronic devices 2—73697
films, frequency contrast characteristics measurement 2—70093
Gaevachrome film type 6.00 and 6.05, rel. to physicochemical processing methods 2—52502
granularity and quantum noise 2—73685
holograms recorded with pulsed, continuous sources exposure characteristics 2—69983
latent image formation rel. to sensitizing dyes 2—81548
non exposed grains, development, fogging, reactivity 2—84672
nuclear emulsions, reduction reactions effects on threshold sensitivity 2—70317
photon fluctuations and noise in emulsions 2—73684
photoplates, increased light sensitivity by preliminary hypersensitization, effect on spectral analysis 2—84675
poly-N-vinylcarbazole films, doped, spectral response and sensitometric curves, positive and negative modes 2—66884
resolving power determination, projection and interferometer methods 2—70095

Photographic materials continued
sensitivity continued
resolving properties and effects of variation of photosensitive parameters, application to photo-teleprinting 2—52507
solar Fraunhofer spectrum lines, photographic factors influencing intensities and line widths 2—48791
spectral properties of photo-protective glasses sensitized by AgCl and AgBr 2—52503
spectrally sensitized emulsions, effect of temperature 2—66865
xerography, sensitivity limitations 2—59324
Ag halide, spectral sensitization by trapping of dye mobile positive holes 2—81552
AgBr, coating, spectrally sensitized low intensity desensitization effect 2—81549
AgBr, heat of absorption of S sensitizers 2—73686
AgBr, photocond., photographic sensitivity, effect of sensitizing dyes 2—81550
AgBr, spectral sensitization by cyanine dye monolayer 2—81551
AgBr emulsions, low-intensity reciprocity curves, hole trapping mechanism 2—66871
AgBr emulsions, quantum sensitivity, absorption coefficient 2—59303
AgBr grain emulsions, spectrally sensitized, effect of temperature 2—66865
AgBr grains, effects of metal ions on photographic and emission processes 2—59305
AgBr phase holograms, dye induced desensitization to Ar laser light 2—42132
AgBr reduction sensitization, effect of electron and positive hole traps 2—66862
AgCl, heat of adsorption of S sensitizers 2—73686
Ag_2S, heat of adsorption of S sensitizers 2—73686
S sensitization mechanism 2—59304
Se thin films, recording of 10.6 μm laser radiation 2—69960
ZnO, polycrystalline study of spectral, chemical sensitization centres of internal photo-effect, optical extinction method 2—75176
ZnO Electrofax layers, effect of emission on print quality 2—66883

Photographic process
see also Photochemistry
Air Force needs for novel recording and reproduction processes 2—59296
cinematography, film printing, step printer for 16 mm film, pulse controlled 2—70089
colour, printing and processing 2—82591
colour negative printing system 2—59336
critical exposure, Se photoconductors, speed criterion, initial potential, cascade development 2—84376
development, non exposed grains, fogging, reactivity, metallic silver, oxidation 2—84672
development, redox potential, catalysis, filamentary silver 2—84673
diazosulphonate imaging 2—59308
electrophotographic contact printing based on organic photoconductors 2—59322
film production techniques, positive/negative/reversal systems 2—42286
fixing, Ag complexation by S_2O_3-, SCN- 2—59314
image transfer by ions at atmospheric press. 2—79453
latent image formation rel. to sensitizing dyes 2—81548
solar activity macrostructure distribution 2—69191
Ag due bleach colour copy materials 2—59320
Ag halides, grains, photographic sensitizing and desensitizing by electron traps 2—81023
Ag halides, physics and chem., conf., Montreal, Canada, Aug. (1972) 2—81541
AgBr, coating, spectrally sensitized low intensity desensitization effect 2—81549
AgBr, emulsion, Ag formation in single emulsion grains 2—81546
AgBr, nuclear track emulsion, track formatin, analog theory 2—81543
AgBr, photographic sensitivity, impurity effects 2—81544
in AgBr crystals, obs. using transient photocharge obs. 2—66864
AgBr emulsion, latent image centres displacement 2—80723
H_2, photoactive agent in emission from freshly treated surfaces 2—81538
H_2O_2, photoactive agent in emission from freshly treated surfaces 2—81538
H_2O_2 decomposition on Ag particles and heterogeneous catalysis of image forming vesicular reaction products 2—59315

development
colour, video colour analyser 2—76550
colour film processing, high speed 2—42288
colour negative processing system 2—59318
electrophotography, materials, review 2—70099
holograms recorded in photoresist 2—42137
hydroquinone developers, salt effects 2—59312
induction time, application of corrosion model 2—63442
monobath for Tri-X film 2—59317
polyethyleneglycol developers, active properties 2—52504
processing latitude of 3M 7842 and 7969 dry Ag films 2—59309
self threading microfilm camera and processor system monobath processor system 2—59330
solar Fraunhofer spectrum lines, photographic factors influencing intensities and line widths 2—48791
spectral plates, blackening distribution under various development conditions 2—59286
superadditive black and white developing agents 2—59316
Ag dye-bleach processing, printing 2—73687
Ag halides, initial chem. development reaction 2—81547
AgBr, sol, conversion to AgI; kinetics, turbidimetric obs. 2—81542
AgBr development and Ag filament growth rates and emulsion thickness 2—59313
AgBr monodisperse emulsions, completely exposed, development, fixing rate measurements 2—66870

Photography
see also Cameras; Cinematography; Lenses/photographic; Radiography
aerial photography, automatic exposure control rel. to seeing conditions 2—82602
Air Force needs for novel recording and reproduction processes 2—59296

Photography continued
- automatic plate scanner for nucl. expts. 2–79685
- automatic terrain classification from aerial photography 2–84769
- camera-attachment to SL-11 styloscope and ST-7-stylometer 2–49457
- cameras quantitative determination of stray light 2–59327
- carrier frequency, image transfer characteristics 2–42287
- chronophotographic analyser control 2–67708
- composite, screens for, description 2–70096
- computer output microfilm optical system 2–59295
- conference, San Francisco (1972) 2–59294
- detail determ. by scanning electron microdensitometry 2–81553
- difference between images detection 2–76527
- electro-optical rectifier for transformation of photographic images 2–59301
- electron beam resists, hardening of silicone resins by electron beam 2–59297
- electrophotographic apparatus, requirements of optical systems 2–73696
- electrophotographic ZnO-resin coating for positive charging 2–63452
- electrophotography, history, review 2–70099
- enlarger, condenser type, design and aberrations 2–66829
- etching technique to improve S/N ratio in photographic phase holograms 2–79245
- exposure det. for multispectral photographic systems 2–59302
- frequency contrast characteristics and limiting function calc. for reproduction system 2–52498
- holographic emulsion diffraction efficiency determ. using latent image technique 2–66786
- holography, scattering reduction technique 2–42149
- illumination, strobe lighting for action-stopping problems 2–59326
- image converter camera control by giant pulse laser 2–73672
- image detectability on photoelectric surface 2–79455
- image intensifiers and radiodiagnostics 2–70070
- image multiplexing using random diffuser 2–63366
- image processing, coherent method of variance obs. 2–55722
- image quality assessment, diffraction pattern analysis 2–79407
- image restoration, superresolution of diffraction blurred impulses 2–73691
- image transfer, electronic equipment 2–76553
- image transfer by ions at atmospheric press. 2–79453
- incandescent lighting for, colour temperature improvements using glass filters 2–73669
- i.r. photomicrography using liquid crystal 2–52501
- laser, applic. to aerospace tests 2–46848
- light sources, colour rendering index 2–82596
- long-wavelength semiconductor, use of semicond.-dielec. electrophotographic system 2–70090
- negative i.r. process, Gudden-Pohl effect quenching 2–51393
- noise in hologram photoresist 2–49400
- optical density meas. of hidden photographic image 2–52499
- optical merit function, correlation with subjective image judgments 2–63439
- optical quality relief images, linear transformation of sensitivity image 2–79303
- oscilloscope photographs information digitizing 2–48934
- oscilloscope photographs information digitizing 2–48934
- $Pb_xLa_{1-x}(Zr, Ti)O_3$ ceramics for selectively erasable image storage and display 2–79454
- photogrammetry, stereo pair scanning electron micrograph meas. conversion to real 3D data 2–43563
- photogrammetry and mapping appls. of holography 2–84780
- photographic films, electric field effect as function of exposure conditions 2–72464
- projection screens, description 2–66875
- γ- Ruticon, image formation mechanism 79415 2–79415
- satellite, i.r. data, sea ice location, image enhancement techniques 2–65574
- semiconductor p-n junction photographic system, resolving power enhancement in magnetic field 2–75123
- sensitometric technique for simultaneous recording of density wedge and high contrast resolution targets 2–59334
- from spacecraft, window characteristics, structure, testing and thermal effects 2–79391
- spatial filtering and correlation unit for processing of electron micrographs 2–42241
- stability of selective gray in subtractive colour photography, computer simulation 2–59311
- standard printing colour identification system for geodesy mapping and charting 2–59298
- standard printing screen system for mapping, charting and geodesy 2–59299
- storage vidicon electrophotographic spectrum imager for visible spectrum 2–59345
- swellometer for meas. of emulsion swelling after wetting 2–59338
- thermo-electrophotographic device 2–66882
- three dimensional map display with stereo-orthophoto 2–51491
- unconventional systems, conference, Washington (1971) 2–42285
- underwater, exposure control method 2–82599
- unitized multiplex for processing photographic images of planetary objects 2–78634
- upper-level precession, consid. of optimum precession angle 2–64607
- video processing film converter 2–59300
- xerography, sensitivity limitations 2–59324
- NaI, V_k polaron, temp. dependence of jump frequency and diffusion constant 2–71813
- Se photoconductors, speed criterion, critical exposure, initial potential, cascade development 2–84376
- ZnO Electrofax layers, effect of emission on print quality 2–66883

applications
- absorbed exit dose from patient radiation exposure, film techniques 2–69413
- acoustic reflex of animal's middle ear using high speed photography 2–45829
- AFU-75 camera, observations of satellite Pageos 2–62817
- airborne thermal scanner, intermittent film advance in camera 2–70091
- astrophotography, aerial cartography, new developments 2–66881

Photography continued
applications continued
- autoradiography techniques 2–76072
- carrier frequency photography using random diffuser 2–73692
- cassette, two film, one w. high-pressure X-ray camera 2–66872
- cloud and air discharges, stepped leader observation using high speed rotating camera 2–65791
- cloud motion meas. from geostationary satellite spin scan camera pictures 2–65716
- Comet Bennett 1969i 2–73095
- data processor, u.s. light diffractors, high speed printer 2–76116
- displacement, by double exposure laser photographs 2–52032
- dynamic vascular scintiphotography of liver, ^{75}Se and ^{67}Ga as imaging agents 2–58609
- Earth resources satellite mission planning, orbital photography 2–65510
- Earth resources using aerospace photography 2–61853
- electron microscope, ZEISS EM 10, high-resolution 2–79084
- eye, disease documentation 2–85138
- fault displacement meas. by optical parallax 2–54683
- filming, optical sound tracks on super-8-films, test film 2–59341
- flames, velocity and size of particle measurement 2–66879
- fluidic logic study by optical visualization of attached flow 2–73664
- fluidized bed gas distrib. obs. 2–83504
- fundus oculi obs. using retinophot 2–45830
- ground motions of initial ejection phase of underground explosions, X-ray photography 2–78931
- hyperballistics, laser optical system 2–82578
- ignition kernel development obs., high speed shadow photographic and oscillographic technique 2–63451
- lightning studies, stationary cameras 2–65790
- lightning studies in northern Poland, rotating cameras 2–65788
- lightning studies near east coast of South America, rotating camera 2–65787
- lightning studies using stationary cameras 2–65789
- linear accelerator structures, voltage standing wave ratio obs. 2–70324
- obs. of liquid jet interaction with free liquid surface, generation of unsteady oscillatory two phase flow 2–43285
- liquid-liquid dispersion, drop size measurements 2–71240
- Lithoconic Brownie on Mariner IX orbiting Mars 2–58476
- live white blood cells obs. 2–62832
- liver tumour detection with ^{67}Ga-citrate and scintillation camera, computer scintigraphy 2–73198
- Mars landing sites, photogrammetric mapping 2–55144
- medical diagnosis techniques, review 2–76075
- medical obs., lighting, posing and background requirements 2–76069
- medicine, capabilities in terms of human-performance 2–76070
- medicine, conference (Newton, Mass., USA, July 1972) 2–76068
- microelectronics, photomask production facility 2–66880
- Moon, determ. of relative ages of areas from orbital photography 2–69133
- multiband, remote sensing 2–44534
- multiband cameras for space missions, review of recent developments 2–82600
- ocean floor microrelief obs. 2–72683
- particle movement in flow system using scattered light at low levels of intensity 2–50376
- pelvimetry, fluoroscopic polaroid technique for dose reduction 2–69446
- photomacrography, LUMINARS and TESSOVAR 2–52512
- photometry, image splitter prism 2–48830
- photopolymer hologram recording films for real time image formation without processing 2–69968
- plasma focus, high speed photography 2–53205
- radiation therapy, use of radiologic films 2–69416
- read only holographic memory system 2–59203
- reconnaissance of soils and rocks, aerial colour obs. 2–44535
- regional agricultural survey using small- scale aerial and space photography 2–42293
- resource management using aerial photography 2–59344
- satellite obs. without using time recording arrangement 2–54981
- scaling decade, noise immunity, potential coupling 2–82592
- Schlieren techniques, high current arc investigations 2–64360
- scintillation camera and portal circulation evaluation in medicine 2–73199
- seasonal charge revealed by time lapse photography 2–59343
- obs. of shrinkage of metalloceramic materials during sintering 2–63450
- small particles in motion, technique 2–73693
- space research, geology 2–84750
- spark chamber film, photographic variables optimization for automatic meas. 2–59641
- stereo mensuration system for extracting 3D data from stereo film chips 2–59342
- stereo-photography, photogrammetric eval., obs. of three dimensional disturbances in boundary layer along concave wall 2–74495
- stereophotography in track devices, correction of external orientation elements of photogrammetric cameras 2–59639
- time exposure oscilloscope photography, noise suppression 2–45831
- transparent objects, study by spatial frequency modulation of carrier wave 2–45806
- urban blight detection, using i.r. colour photographs 2–82030
- X-ray scattering, recording, pinhole system efficiency comparison 2–73690
- $LiNbO_3$ obs. of ordinary polaritons 2–81374

colour
- aerial, reconnaissance of soils and rocks 2–44535
- binder refractive index, multilayer colour prints, reflection density 2–82594
- colour addition through lens 2–59340
- film processing, high speed 2–42288
- fluorescence, of fundus oculi, using retinophot 2–45830
- Gaevachrome film type 6.00 and 6.05, rel. to physicochemical processing methods 2–52502
- gelatin coatings, relief capacity for acid photographic dyes 2–70092
- i.r., use in detecting urban blight 2–82030
- lenses, flare meas. 2–63449

Photography continued
- **colour** continued
  - lunar spectral reflectance ratios, computer generation colour image display 2−66877
  - mask characts. in photomechanical process, computation 2−63445
  - negative processing system 2−59318
  - one-step, new camera, film process allowing sequential exposures at 1.5 second intervals, immediate hard copy 2−66876
  - printing and processing 2−82591
  - prints, optimum peak wavelengths and breadths of cyan magenta and yellow 2−63444
  - reproduction methods 2−42292
  - spectral absorption curve matching, maximum error minimization algorithm 2−66858
  - stability of selective grays 2−63443
  - subtractive, metameric colour matching, dye system, Lambert-Beer law 2−66878
  - three-colour, processing principles 2−59339
  - Ag dye-bleach processing, printing 2−73687
  - Ag sound tracks, in colour reversal film 2−76551
- **high-speed**
  - acoustic reflex of animal's middle ear using high speed photography 2−45829
  - fluidized bed gas distrib. obs. 2−83504
  - laser technique, model freezing 2−76556
  - relativistically moving objects, apparently rotated image 2−55778
  - shadow photographic and oscillographic technique for ignition kernel development 2−63451
  - stop-action photos using frequency-doubled four-level laser illumination 2−55781
  - variable ultrafast shutter, based on saturable props. of polymethane cyanide dyes 2−49405

Photoionization
- — 2−67400
- absorption of i.r. laser beam in plasma 2−43147
- acetylene, photoionization products, rate coeffs. for reactions 2−51435
- angular distribution of photofragments, parity-unfavoured transitions 2−79908
- angular distributions of secondary electrons in dipole approximation, relation between photon and charged particle impact 2−52931
- angular momentum transfer in theory of angular distributions 2−49965
- anthracene, photoelectron spectra and ionization potentials 2−60048
- atmospheric mols., dissoc. ioniz. processes 2−80057
- atom, by low-energy photons in intense laser fields 2−52927
- atom, multiphoton ioniz. by circularly and linearly polarized light 2−83182
- atom, polarization effects in high-order multiphoton ioniz. 2−79906
- atomic system, multiphonon ioniz., circular versus linear polarization 2−56105
- atoms, angular distribution of Auger electrons following photoionization 2−52939
- atoms, intermediate and high Z, analytical formula of K-shell photoeffect 2−79885
- atoms, study of electron spin polarization 2−42763
- biphenylene, photoelectron spectra and ionization potentials 2−60048
- bromothiophene, high resolution photoelectron spectra 2−60087
- cross section, reproduced from dipole oscillator strength distribution 2−76968
- diphenyl acetylene, photoelectron spectra and ionization potentials 2−60048
- elements with $Z<Z<30$, $Z=36$, calc. of partial cross section for photon energies threshold ∼300 keV 2−77010
- ethanol glass, trapped electrons produced by biphotonic photoioniz. rel. to delayed emission of indole ring 2−54559
- ethylene, photoionization products, rate coeffs. for reactions 2−51435
- F-region of ionosphere, photo-electron energy distrib. and its variation with sunspot activity 2−65984
- inert gas atoms, interference effect from $ns^2np^6 \rightarrow ns^2np^5\varepsilon d$ transition 2−67401
- inert gases, ang. distrib. of photoelectrons with many-electron correls. 2−49958
- ionosphere, photodetachment rates of negative ions, sunrise 2−72882
- linear mols., cross sections in valence electron approx., photoelectron spectra intensities 2−79976
- methane, photoionization products, rate coeffs. for reactions 2−51435
- nonpolar liquids, electron dynamics 2−81531
- one-electron atoms, multiphoton ioniz. with circularly polarized light 2−67421
- phenanthrene, photoelectron spectra and ionization potentials 2−60048
- phenyl radical, determ. of heat formation and ionization potential 2−67520
- photodetachment, cross-sections and electron affinities 2−64035
- quasifree electron production in polar solvent, obs. of ultrafast relaxation 2−72568
- tetramethyl-para-phenylene-diamine in solution, role of energy of excess electron state 2−74557
- thiophene, high resolution photoelectron spectra 2−60087
- TMPD in hydrocarbon glass, rigid matrix photoioniz., anion form., bleaching kinetics 2−81511
- toluene, photo fragmentation, obs. 2−70794
- CH, diatomic, calc. of Hartree-Fock photoionization cross section using many body perturbation theory 2−80018
- CaI, absolute absorption cross-sections at 1886.5, 1765.1 Å 2−76971
- Cs, excited-state cross sections 2−59922
- Cs atom, three-quantum photoionization 2−70604
- Cs vapour, by method of space charge amplification 2−70603
- Cs vapour, study of electron spin polarization 2−42763
- Cs^+, free ions, rel. to n.m.r. 2−79897
- H ground-state atom, multiphoton ionization in semiclassical treatment of intense e.m. field 2−79960
- H^-, photodetachment, variational calculation 2−46448
- H_2, cross section calc. 2−50037

Photoionization continued
- H_2, effects of rotational autoionization on angular distrib. of photoelectrons 2−50045
- H_2, multiphoton ioniz. and dissoc. due to 1.06 μm laser radiation 2−80051
- H_2, temp. depend. of multiphoton ionization 2−60004
- H_2 mols., excited, cross sections determ. 2−70703
- He, Brueckner-Goldstone many-body perturbation calc. 2−46493
- He, double, Roths threshold law 2−79956
- He, triplet metastable state, cross-section 2−79957
- $He + h\nu = He^+(n=2) + e$, simultaneous ionization and excitation, 100-200 eV, meas. of cross section ratio 2−56131
- K, pseudopotential calculation of cross-section 2−46448
- Li, pseudopotential calculation of cross-section 2−46448
- Li transitions, model pot. calcs. 2−76976
- Mg, cross-sections, excited by tunable u.v. lasers 2−43200
- $NO^+ + H_2O$ reactions in photoioniz. mass spectrometer 2−68775
- N_2^*, vibrationally excited, detection and study of quenching by O 2−83400
- Na, pseudopotential calculation of cross-section 2−46448
- O_3^-, in drift tube, photodetachment cross section 2−42926
- SeH-, photodetachment of electron determ. of electron affinity and spin-orbit coupling constant of SeH 2−46583
- Si:Zn, many-band pseudopotential calc. of photoioniz. 2−61357
- **gases**
  - air, by extreme u.v. radiation of laser produced plasma 2−53242
  - computer simulation rel. to streamer growth and breakdown 2−53257
  - impurity gas in inert gas, shock wave precursor shape and intensity 2−56381
  - intergalactic medium, by hot white dwarfs 2−81791
  - laser plasma, prod. by photoionization with u.v. light 2−79193
  - measurement methods including plasma arc spectroscopy 2−77301
  - multiphoton ionization, role of excited states 2−46446
  - NGC 4151 Seyfert galaxy and quasi-stellar objects 2−69024
  - phosgene, high resolution photoelectron spectra 2−43006
  - thiophosgene, high resolution photoelectron spectra 2−43006
  - Ar, by X-rays, relative abundances of multiply charged ions 2−53245
  - Ar, photo-ion drift vel., diffusion coeffs. and temps. 2−64339
  - Ar, pulsed with 10.6 μm laser radiation, gas breakdown thresholds 2−83707
  - Ba cloud experiments rel. to mechanism of photoionization and radiative transfer problem in freely expanding gaseous clouds 2−46791
  - CO, by soft X-rays, meas. of total and relative abundances of thermal energy ions and dissociation cross section 2−80024
  - CO_2 by soft X-rays, meas. of total and relative abundances of thermal energy ions and dissociation cross section 2−80024
  - Cs vapour, two step photoionization 2−64036
  - H_2, pulsed with 10.6 μm laser radiation, gas breakdown thresholds 2−83707
  - He, by extreme u.v. radiation of laser produced plasma 2−53242
  - He, pulsed with 10.6 μm laser radiation, gas breakdown thresholds 2−83707
  - Kr, by X-rays, relative abundances of multiply charged ions 2−53245
  - N, photo-ion drift vel., diffusion coeffs. and temps. 2−64339
  - N_2, by extreme u.v. radiation of laser produced plasma 2−53242
  - N_2, by soft X-rays, meas. of total and relative abundances of thermal energy ions and dissociation cross section 2−80024
  - N_2, ionizing gas breakdown waves in strong electric fields 2−80414
  - N_2, pulsed with 10.6 μm laser radiation, gas breakdown thresholds 2−83707
  - NO, by soft X-rays, meas. of total and relative abundances of thermal energy ions and dissociation cross section 2−80024
  - NO small amounts in O_2, low temp. meas. of three-body electron attachment coeff. in O_2 2−53247
  - Ne, by X-rays, relative abundances of multiply charged ions 2−53245
  - O, photo-ion drift vel., diffusion coeffs. and temps. 2−64339
  - O_2, by soft X-rays, meas. of total and relative abundances of thermal energy ions and dissociation cross section 2−80024
  - SF_6, photoabsorpt. cross sections in soft and ultrasoft X-ray range in ioniz. threshold region 2−67499

Photolysis *see Photochemistry*

Photomagnetic effects *see Photoelectromagnetic effects*

Photomagnetoelectric effects *see Photoelectromagnetic effects*

Photometers
- *see also Spectrophotometers*
- chopper improvement for use in i.r. photometry 2−85067
- differential monochromatic, for optical density meas. of hidden photographic image 2−52499
- glare, automatic, for obs. of glare characteristics of lenses and instruments 2−66824
- goniophotometer, design and characterization 2−79365
- heterojunction, interface region struct. rel. to energy band profile 2−44181
- heterojunction, reviews 2−44180
- illuminance measurement 2−45797
- laser light-scatt., automated, for particle size analysis 2−63307
- light scattering, using photographic film 2−73650
- low light TV system for astronomy applications 2−85070
- MF-4 microphotometer, program control system for two- coordinate frame motion 2−45798
- microphotometer digital readout system 2−52353
- microphotometer for transient local chemilum. meas. in combustion regions 2−61780
- for multiple scattering obs. in synthetic foggy atmos. 2−64478
- night sky, portable 2−69199
- use in optical information treatment engineering 2−42220
- with photoconductive cells 2−70026
- photoelectrets as memory photon detectors 2−42219
- photoelectric, automatic, with fast digital recording system 2−45005
- photon detectors, conference Varna (1971) 2−41954
- photon detectors conference Varna Bulgaria (1971) 2−42218
- for polymer solution light scatt. wavelength depend. obs. 2−64447
- reflection filter, 'Irtran-1' for 20μ atmospheric window 2−73163
- rocket borne, containing tilting filter channels for dayglow meas. 2−81646

Photometers continued
slit diaphragm type, errors 2−73648
standardization and calibration 2−63432
stellar, with Cassegrainian optical system, for 1300-2000 Å range 2−69050
synchronous, 3-colour, with sampling circuit 2−45799
two-photon absorpt. profile meas. for organic dye solutions 2−66734
zone plate disk sensor combinations, chromatic properties 2−79432

Photometry
see also Brightness; Densitometry; Illumination; Spectrophotometry
actinometer for flash photolysis 2−81518
applied to lighting industry, usefulness, equipment, cost, data 2−79360
asteroids, shape, orientation of rotation axis, photometric observations 2−58517
celestial light sources, low intensity, surface photometry from space vehicle 2−45003
cloud field height determ. by ground photometric survey using two spherical mirrors 2−83852
in Debye ring, photometry of X-ray patterns 2−42217
developments 2−49432
elliptical galaxies, multiple systems 2−69040
error, instrumental, in meas. of quasiharmonic signals 2−45800
filters, low temp., for 20 μ atmospheric window 2−63399
flame, effects of rate of entry and compos. of soln. 2−48358
flame photometry, book on laboratory practice 2−48359
light measurement techniques, apparatus 2−45797
light scattering, data inversion information theory 2−64476
measuring methods 2−79363
meteorite, Bruderheim chondritic, photometric properties 2−58538
optimum radiation flux detection by zone plate disc sensor combinations 2−79364
photoelectric scanning system for obs. of auto-ionization resonance structures of BaI 2−79943
photographic, image splitter prism 2−48830
photon coincidence, ang. correction to absolute photometric calibration 2−66733
photon counting, conditions for optimum use of photomultipliers 2−45699
photon pile up corrections in study of time varying light sources 2−82558
planetary observations using two-dimensional digital vidicon photometry in 0.38 to 1.1 micron range 2−78526
quantum statistical theory of photodetection 2−41953
rotating analyzer method for meas. depolarization of light scattered by gases 2−64395
short duration lights, calibration devices 2−76523
solar soft X-radiation, with broad band detectors, for signal-energy conversion function 2−73117
Stromgren, of weak G-band stars 2−75730
sun coronal lines, 5303Å and 6374Å, reduced intensities 2−73110
third order reaction rate consts. using Lyman alpha photometry 2−84625
TV microphotometry of photographic stellar images 2−76045
UBV, electrographic, of jet in 3C 273 2−44899
UBV, open clusters, slit spectra 2−84955
UBV, van Wijk sequence obs. in Large Magellanic Cloud 2−69033
UBV photometry at Bologna astronomical observatory 2−51869
UBV-Hβ, southern open clusters, galactic structure 2−84954
Van Cittert-Zernike theorem and Lambert's law 2−73649
NH_4 hypersensitized IV-N photographic plates 2−82597

light sources
for enlarger, condenser type, design and aberrations 2−66829

Photomultipliers
ceramic envelope, design and performance 2−49679
channel, parallel plate, dependence of gain on plate separation 2−41932
channel electron multipliers, saturation current rel. to applied voltage, space charge saturation 2−74609
circuits and systems, (conference, Washington USA, March 1972) 2−49644
control by clamping cross-bar grid 2−49330
curved channel multipliers, origin of background counting rate 2−63699
differential photometric position sensors, accuracy improvement by parallel substitution method 2−59110
electron multipliers performance in field ion microscope atom probes 2−66723
FEU-28 and -62, threshold characteristics 2−59109
FEU-30, transit effect 2−55670
FEU-85, time and threshold characteristics 2−76460
FEU-86, noise characteristics 2−76461
high current operation of 1P28 tube 2−73534
housing, photomultiplier housing, liquid N_2 cooled for use with side window tubes 2−52399
magnetic electron multipliers with continuous lead-silicate glass emitters 2−59104
meas. of luminous radiations in proportional counters 2−46033
microchannel plate imaging detectors, characteristics and performance 2−49322
miniature, for scintillation and space use 2−49680
negative electron affinity materials, review 2−49676
open channel, performance in satellite instrument 2−45690
parallel plate, properties and development, review 2−49323
photocathode, bialkali and trialkali, thermionic emission 2−61459
photocathodes, distrib. of relative sensitivity 2−49682
photoelectron coincidence number, modulation influence 2−52398
photoelectronic channel, output signal variation, pulse amplifier, stabilization 2−82804
photon counting photometry, conditions for optimum use 2−45699
photon counting system without amplifier for low radiation levels 2−52407
polarization effects on performance 2−44185
pulsed blocking with semiconductor device 2−59108
Quantacon-Foto-Multiplier, for increased sensitivity of flame emission instruments 2−66854
radiation current and optimal dimensions of entry chamber in γ-fields 2−76462
withS11 photocathode, temp. effect 2−41933

Photomultipliers continued
side window, pulsing ns gate, noise level in low light conditions 2−66722
signal amplitudes and thermionic noise distribution 2−55669
single electron response amplitude spectra, wavelength dependence 2−49681
slow response, threshold sensitivity to pulsed and harmonic signals 2−59111
small ion current detection, Daly-type detector 2−45689
spiral channel multiplier as electron detector, current and counting characteristics 2−76745
technological developments, review 2−69881
testing device, design, for long-term stability 2−55896
time resolution, transit time differences effect 2−52400
time-of-flight of electrons obs. 2−76459
transit time differences, influence on photomultiplier time resolution 2−49331
venetian blind type, response 2−73535
$AgPO_3-X^{n+}(PO_3)_n$, $X^{n+}=Mg^{2+}$, Ca^{2+}, Sr^{2+}, Ba^{2+}, Pb^{2+}, Al^{3+} use for multichannel image convertors and amp. 2−68501
GaP(Cs) dynodes, electron optics and time broadening 2−49677
GaP(Cs) dynodes, performance and characteristics 2−49678
Pb-silicate glass emitters for magnetic electron multipliers 2−59104
Si transmissive mode field emission array photoemitter, photosensitivity 2−81187
^{119}Sn resonance Mossbauer detector with windowless electron multiplier 2−42471

Photons
see also Cosmic rays/photons; Gamma-rays; Nuclear reactions and scattering due to/photons; X-rays
absorbed fractions for photon emitters within the body 2−55268
absorption by electron in high magnetic fields 2−52306
axial-vector massive, rel. to p-n mass difference 2−70253
binary signal demodulation photon count statistics 2−41947
central classical fields, creation and annihilation of spin pairs by photons and gravitons 2−82178
clipped intensity correl. meas. method 2−82462
coherent two photon propagation and self induced transparency of optical pulses in K three level system 2−44330
coincidence, ang. correction to absolute photometric calibration 2−66733
cooperative processes, correlated fluctuations in equil. and steady-state systems 2−78841
correlation method for lifetime meas. of excited states in multilevel atoms 2−42743
count distrib. of photoelectrons emitted in partially coherent Gaussian light 2−55674
counting, exact solution near laser threshold 2−41949
counting, improved spectrophotometric technique 2−63367
counting, pulse amplifier and discriminator 2−59124
counting, statistical method for recording regularities in radiant luminescence 2−63310
counting, thermoluminescence dosimetry 2−49340
counting apparatus for kinetic and spectral obs. 2−45703
counting individual quanta, working characteristics of dissector in operating mode 2−55675
counting procedure during short time interval 2−55676
counting system for single photons in automated photometer for particle size analysis 2−63307
counting system using static Gray-scale mask 2−49338
counting system without amplifier for low radiation levels 2−52407
counting technique for detection of weak optical images 2−66732
detectors, conference Varna (1971) 2−41954
drag detection, based on effect of radiation pressure on mobile charge carriers in semiconductor 2−76465
effective path length for cloud layer 2−72791
emission of radiation by charged particles reflected from solid surfaces 2−54397
Gaussian fields, sequential photon counting statistics and maximum likelihood estimation techniques 2−79266
glass:Nd laser, meas. of start photon number 2−52428
impulse flux density, Maxwell-Minkowski and De Broglie- Geheniau tensors 2−59123
impulse in anisotropic medium, linear and ang. recoils of cryst. 2−52406
impulse in dielectric, paradox soln. 2−52405
inclusive yields from high-energy bremsstrahlung on H target 2−76595
interaction with anisotropic refractive medium, energy calc. 2−45701
interference, single-photon double-slit, teaching demonstration 2−48959
large mass, amplitude asymptotic of virtual $\gamma\gamma$ scatt. 2−82675
laser, Compton collisions with high-energy electrons 2−52435
mass, limits 2−82106
metagalactic opacity to photons of 10^{17} eV 2−84940
multiple scatt., small-angle, in iconal approx. 2−73621
nonequilibrium optical field, temperature 2−69991
one-photon transition probabilities, composite system factorization 2−73543
parametric 4 photon exchange effect, spontaneous, theory 2−65236
phase modulated fields, statistical props. 2−45698
photocount statistics, probability distrib. of optical field emission counts 2−82459
photocount statistics of transient laser light 2−66777
photon-graviton vertex, e.m. corrections 2−82207
picosecond light pulses, statistical properties using two-photon absorbing semiconductors 2−41950
polarimeter counter, for astronomy, design and fabrication 2−76048
quantum counter up-conversion, 10-μ, in rare earth doped crysts. 2−45704
quantum statistical theory of photodetection 2−41953
real and virtual, duality and scaling 2−59401
real and virtual in weak leptonic processes at high energies 2−42344
rest mass, absorption of longitudinal electric waves in interstellar space 2−62595
rest mass, comments 2−78794
rest mass, determ. by meas. of hydromagnetic waves in plasma 2−52547
rest mass, of wave quanta 2−78795

Photons continued
rest mass, rel. to dispersion of longitudinal electric waves in interstellar space 2−55073
rest mass and dissipation of magnetic fields in Galaxy 2−75674
scaled photon-counting fluctuations, one-bit correlation 2−73542
single photon detection and timing, lunar laser ranging experiment 2−48973
single photon techniques for obs. of optical waveforms from radiative decays 2−49339
size and scaling model for lepton pair production 2−82688
stability, theoretical investigation of decay probability and detectability 2−63496
statistics of scattered light, analysis of generalized birefringence expts. 2−63308
stimulated absorpt. or emission by atomic beam 2−45700
structure function determ. in deep inelastic process e-$\gamma \rightarrow$e-nπ^+nπ- 2−63514
time measurement in partially coherent light 2−49337
two photon absorption by a crystal in elec. field 2−65243
two-photon absorption cross sections, method 2−41952
two-photon exchange effects in deep inelastic electroproduction 2−73759
two-photon propagation in three-level system 2−82510
two-photon superradiance 2−45702
vertex function of virtual photon interactions with scalar field 2−76565
virtual, in dual reson. model 2−76607
virtual heavy, pairs production at CERN ISR predictions 2−63505
virtual photon, role in hadron electroproduction in ep scatt., Regge behaviour 2−70171
virtual photon mass, effect on transverse momentum distributions in inclusive processes 2−49515
virtual photon mass parameters 2−70167
$\gamma \rightarrow 3\pi$, low-energy theorem relating to $\pi^0 \rightarrow 2\gamma$, derivation using anomalous Uland identities 2−52548
γNN electromagnetic vertices, conformal invariance and Bjorken scaling 2−79495
$\gamma\pi\pi$ electromagnetic vertices, conformal invariance and Bjorken scaling 2−79495
pp$\rightarrow\gamma$X, scaling of inclusive γ spectra at ISR energies and thermodynamic model 2−79612
pp$\rightarrow\gamma$X γs due to $\pi^\pm$ as well as π° decay 2−82755
p-Te, photon drag detector for CO_2 laser 2−79170
YAG:Nd laser, meas. of start photon number 2−52428
interactions
absorption by nucleons, space-time phenomenology 2−55811
atom-atom-photon collisions, excitation mechanisms 2−83174
atomic beam deflection and broadening by recoils due to photon absorption or emission 2−70619
atoms near reson., soln. for this interacting system 2−76979
Cabibbo-Radicati sum rule, high energy contrib. calc. 2−79539
collision of laser beam with bremsstrahlung beam, determ. of intense-field mass shift of electron 2−66904
with electron spin, in presence of static magnetic field 2−52551
with hadrons, analytic equivalence of Gupta- Bleuler formalism and S-matrix formalism 2−52578
with hadrons, theoretical aspects, conference, Hamburg July 1971 2−59404
hadrons pair production cross section for γ, 265-4215 MeV in hydrogen and deuterium 2−63497
helicity conservation, s-channel, Pomeron coupling 2−70142
helicity conservation, s-channel, Pomeron coupling 2−70141
inelastic photon-photon interactions and galactic redshift anomalies 2−48643
i.r. divergence of incident photons 2−49495
meson reson. photoproduction in backward direction cross sections prediction 2−63644
neutral mesons, spin determ. from coherent photoprod. on spin-O nuclei obs. 2−82767
neutrino-photon interaction, effect on solar neutrino flux 2−85055
pair production rate in electrodynamics in strong magnetic field 2−63265
phenomenological consequences of proton models for photon processes, effect of vector-meson dominance 2−66923
photon-hadron, high energy photoprod. processes, hadronic nature of photon 2−82677
photon-hadron, high energy pseudoscalar meson production models, review 2−59504
photon-hadron, Int. Summer Inst., Hamburg (1971) 2−59405
photoproduction, comparison of angular decay distribs. in three quark models 2−55813
photoproduction, connection with electroproduction examined from consideration of duality 2−59401
photoproduction, isospin and SU(3) equalities 2−49484
photoproduction in resonance region, multichannel analysis 2−66927
photoproduction of lepton pairs, improved Weizsacker Williams method for calc. of energy-angle distrib. 2−66930
photoproduction of pions near P_{33}(1236) reson., multipole analysis 2−67016
photoproduction of vector and axial vector resonances in broken nonlinear chiral $SU_3 \times SU_3$ dynamics 2−59547
photoproduction on hadrons, test of $\Delta I \leqslant 1$ rule 2−63499
photoproduction processes, backward, tests of $\Delta I \leqslant 1$ 2−42327
photoproduction processes, high-energy quasi-inclusive, multi-Regge model applic. 2−52575
positronium, splitting of ground state from photon exchange 2−42346
tachyon monopoles, searches in photoproduction reactions at 1 MeV, detection by emitted Cherenkov radiation 2−82638
two-photon particle production, application of Veizsacker-Williams approx. 2−66924
U-spin scalar interaction, predictions from extension of Odorico's bootstrap 2−73836
unstable particle production cross-section, effect of coupling of unstable particle to continuum 2−63498
vector meson, photoprod. differential cross-sections, quark model 2−55864
vector meson photoproduction, $\rho\omega$ mixing phenomena 2−59552

Photons continued
interactions continued
vector meson photoproduction, and nucleon Compton scatt. amplitude, quark model 2−55865
vector meson photoproduction on hadrons, test of vector meson dominance model 2−82674
vector mesons production, quark model predictions for angular decay distributions in inclusive processes 2−52624
virtual, analogy with hadron reactions 2−70187
virtual photon-hadron, vanishing longitudinal cross sections and operator Schwinger terms 2−59458
virtual scalar, single particle distribution 2−70143
$\alpha\gamma \rightarrow p\pi^-$(ppn) cross section around Δ(1236) 2−79493
d photodisintegration differential cross-sections and polarization of photonucleons 2−63672
η photoproduction, Virasoro model 2−70205
$\eta\gamma\gamma$, $\eta'\gamma\gamma$ vertices, investigation using electron-positron storage rings 2−49497
$\eta\gamma\gamma$, $\eta'\gamma\gamma$ vertices, investigation using electron- positron storage rings 2−49496
$\gamma \rightarrow 3\pi$, coherent production, low-energy theorems relating to $\pi \rightarrow 2\gamma$, $2\gamma \rightarrow 3\pi$ processes, anomalous Ward identities 2−63502
γ+d, ρ meson production, Glauber-model formalism 2−63638
γ+p$\rightarrow$n+pi$^+$(p+π^0), asymmetry meas. in range 400 to 900 MeV 2−59527
$\gamma \rightleftarrows$ rpπ^-, in 33 resonance region, dispersion relation predictions 2−52550
γd, 240 to 400 MeV, π^-/π^+ production ratio 2−67017
γd, charged pion production, Khuri Treiman formalism applied 2−42386
γd, coherent production of π^0 by polarized γ-rays, asymmetry ratio 2−70229
γd, photoproduction of ρ^0 and ω at 4.3 GeV, determ. of direct vector meson photon coupling 2−49579
γd, $\pi^\pm$ production, π^-/π^+ ratio 2−49559
γd, total cross section for hadron production in 0.265-4.215 GeV region 2−46020
γd$\rightarrow\Delta\Delta$, electromagnetic props. of Δ(1236) 2−82784
γd$\rightarrow\pi^0$d, differential cross section, coherent photoprod. of π^0 obs. 2−82671
γd$\rightarrow\rho^0$d cross sections interpret., coherent photoprod. of ρ 2−82676
$\gamma\gamma \rightarrow 3\pi$, coherent production, low-energy theorems relating to $\pi \rightarrow 2\gamma$, $\gamma \rightarrow 3\pi$ processes, anomalous Ward identities 2−63502
$\gamma\gamma \rightarrow (2n+1)\pi^0$, effective Lagrangian model 2−55853
$\gamma\gamma \rightarrow n\pi^+n\pi^-$, effective Lagrangian model 2−55853
$\gamma\gamma \rightarrow n\pi^+n\pi^-\pi^0$, effective Lagrangian model 2−55853
$\gamma\gamma \rightarrow \pi^+\pi$-, cross section determination using additive quark model 2−59410
$\gamma\gamma \rightarrow \pi^+\pi^-$, cross-section calc. with strong interaction correction 2−82669
$\gamma\gamma \rightarrow \pi\pi$, amplitude calc. using π radius and polarizability 2−63503
$\gamma\gamma \rightarrow \pi\pi$, $\gamma\gamma \rightarrow 3\pi$, $\gamma\pi \rightarrow \pi\pi$, structure of observable amplitudes 2−52549
$\gamma\gamma \rightarrow \pi\pi\eta$, amplitude calc. 2−63576
$\gamma\gamma \rightarrow \pi\pi\pi$, test of low-energy theorem using Z(γ,3π)Z reaction 2−76596
γN, ps. meson production, scale dimension of chiral symmetry breaking Hamiltonian 2−49540
γN, single-pion photoproduction via s- channel resonances in model of higher baryon couplings 2−45955
γN, vector meson dominance model 2−59406
γN$\rightarrow\Lambda(\Sigma)$K, photoproduction near the threshold, amplitudes and cross-sections 2−66929
γN$\rightarrow$N$\pi^+\pi^-$, nonrelativistic solvable model 2−79575
γN$\rightarrow$N$\pi\pi$, generalized Watson theorem, interdependence of reactions 2−63501
γN$\rightarrow\eta$N, Regge-pole Regge-cut analysis 2−63500
γn$\rightarrow\pi^-$p, γp$\rightarrow\pi^+$n, π^-/π^+ ratios, dip test of isotensor current 2−49560
γN$\rightarrow\pi^0$N, Regge-pole Regge-cut analysis 2−63500
γn$\rightarrow\pi^0$n, 450-800 MeV, differential cross- section meas. 2−45958
γn$\rightarrow\pi^0$n, differential cross-section explained by nonsense wrong signature zeros 2−59529
γN$\rightarrow\pi^+\pi$-Δ, e.m. ρ^0-ω interference effect 2−59402
γN$\rightarrow\pi$N, baryon Regge pole exchange model 2−52623
γN$\rightarrow\pi$N, sum rules and Veneziano model 2−82670
γn$\rightleftharpoons$pπ in Δ(1236) resonance region, discrepancy between dispersion relation predictions and exptl. data 2−42324
γp, asymmetry for π^+ production from polarized protons between 300 and 900 MeV at 90° 2−59528
γp, inclusive photoproduction and factorization 2−49562
γp, production of $A_1{}^0$, axial vector meson 2−66925
γp, π^+ production, isotensor contribution 2−67017
γp, π^+ production at 0.66 to 7.4 GeV/c 2−63610
γp, vector meson photoproduction, review of diffraction dissociation models 2−59551
γp, vector meson prod., triple-Regge formulae 2−79494
γp charged and neutral double π production cross-sections in γ-energy range 600-900 MeV 2−73815
γp$\rightarrow$K$^+\Lambda$, K*-K** absorbed exchanged, F/D ratio 2−70210
γp$\rightarrow$K$^+\Lambda$ photoproduction below 2.2 GeV c.m. energy, analysis of resonance contribs., radiative widths, stray baryonic states 2−82673
γp$\rightarrow$K$^+\Sigma$, K*-K** absorbed exchanged, F/D ratio 2−70210
γp$\rightarrow$K$^+\Sigma^0$, strong cut Reggeized absorption model 2−70144
γp$\rightarrow$V°p, Regge pole model 2−67035
γp$\rightarrow\eta$p, differential cross-section explained by nonsense wrong signature zeros 2−59529
γp$\rightarrow\kappa^+\Lambda$, 5 GeV, recoil polarization in K$^+\Lambda$ 2−66926
γp$\rightarrow$p$\pi^+\pi^-$, 4-6 GeV, ρ^0 prod. obs. 2−79492
γp$\rightarrow\pi$- + anything, investigation with polarized photons at 2.8, 4.7 and 9.3 GeV 2−45871
γp$\rightarrow\pi^-$+ anything inclusive process comparison of π^- distributions for k+,p and pp collisions 2−67052
γp$\rightarrow\pi^-$+ anything, inclusive reaction in photon fragmentation region, vector meson dominance model 2−79613
γp$\rightarrow\pi^0$p, differential cross- section explained by nonsense wrong signature zeros 2−59529
γp$\rightarrow\pi^0$p, in third resonance region 850-1250 MeV, recoil proton polarization 2−46004

Photons continued
- **interactions** continued
  - $\gamma p \to \pi^0 p$, $\gamma d \to \pi^0 p(n_s)$, 400 to 800 MeV, comparison of cross sections 2−42383
  - $\gamma p \to \pi^+ n$, 220-425 MeV, angular distrib. of pions between 15° and 180°, differential cross sections 2−52613
  - $\gamma p \to \pi^+ n$, data analysis by phenomenological model based on pion exchange 2−45999
  - $\gamma p \to \pi^+ n$, photoproduction in backward direction 0.7-8 GeV, comparison with Regge-pole analyses 2−63607
  - $\gamma p \to \pi^+ \pi^+ \pi^- \pi^- p$, linearly polarized 9.3 GeV photons, observation of four-pion vector meso state of mass = 1.5 GeVn0482668
  - $\gamma p \to \rho^0 p$, density spin matrix elements in Gottfried Jackson frame 2−70142
  - $\gamma p \to \rho V^0$, photoproduction of neutral vector meson studied in Regge pole model with cuts 2−49577
  - $\gamma p \to \rho' p$, 9.3 GeV, photoproduction of new vector meson $J^p = 1^-$ 2−76695
  - $\gamma \rho$, inclusive photoproduction cross sections for $\pi^\pm$, Λ predicted via factorisation 2−59403
  - $\mu^+ \mu^-$ photoproduction obs. 2−66945
  - N* photoproduction, review 2−46016
  - ν-photon, rel. to anal. of νe and νe scatt. 2−82680
  - νe (νe) scattering, weak interaction 2−55817
  - π- production in resonance region, polarized photons from 0.8 to 2.2 GeV 2−45956
  - π- production in resonance region, polarized photons from 0.8 to 2.2 GeV 2−45956
  - π photoprod., energy-independ. multipole analysis 2−67014
  - π photoproduction, determ. of πN coupling constant 2−45951
  - π photoproduction, kinematics of coupling of Regge poles to photons 2−63605
  - π photoproduction, method of evaluation of t-channel singularities 2−63504
  - π photoproduction, nonlocal theory 2−55854
  - π photoproduction, review of N polarization 2−45959
  - π photoproduction, Watson theorem, extension to double pion photo processes 2−67018
  - π photoproduction data, use in determ. of pion-nucleon coupling const. 2−79573
  - π photoproduction near threshold, current algebra description 2−59525
  - π photoproduction on hadrons at low and high energies 2−82674
  - π^0 photoprod., cut contribs. in dual cut model 2−55852
  - π^0 production in resonance region, polarized photons from 0.8 to 2.2 GeV 2−45956
  - $\pi^0 \gamma\gamma$ vertex, investigation using electron-positron storage rings 2−49496
  - $\pi^0 \gamma\gamma$ vertex, investigation using electron-positron storage rings 2−49497
  - πN cross section through extrapolation of deep inelastic photoproduction data 2−67021
  - $\gamma p \to K^+ \Lambda$, evidence for stray baryonic states 2−52646
  - NY, absorptive corrections in photoproduction of charged pions 2−42385
- **polarization**
  - atomic cascade, polarization correlations of emitted photons, exptl. limitations to validity of semiclassical radiation theories 2−46415
  - linear polarization coeffs., graphical representation 2−70365
  - ^{148}Pm decay, β-γ circular polarization correl. 2−42547
- **scattering**
  - bremsstrahlung, photoelectric effect, Compton effect, energy backscattering coeff., simulation 2−80926
  - Compton, corrections to vector meson dominance, estimation using light cone expansion 2−42326
  - Compton, light core approach to fixed poles 2−59409
  - Compton forward scatt. amplitudes, sum rules 2−79498
  - differential albedo measurement 2−76959
  - inverse Compton scattering as energy loss mechanism in CTR 2−83100
  - photo-photon and photon-particle, general relativity and quantum field theories 2−66433
  - photon-lepton, fourth-order Compton amplitude in Weinberg model, Drell-Hearn sum rule 2−59408
  - photon-photon amplitude in gauge theories, convergence 2−70145
  - photoproduction of vector mesons in Pomeron exchange reaction, s-channel helicity conservation 2−76694
  - spectroscopic technique 2−49629
  - virtual, bounds on deep inelastic structure functions 2−55872
  - e-$\gamma \to e$-$n\pi^+ n\pi^-$ deep inelastic process, calc. of differential cross section and photon structure functions 2−63514
  - $e\gamma$, inclusive soft pion production 2−42384
  - $e\gamma$ Compton scattering, calc. of spectral forms for invariant amplitudes to order e^4 2−76597
  - $e\gamma$ Compton scattering, polarized target, calc. of differential cross section to order e^6 and left-right asymmetry 2−76598
  - $\gamma^* \gamma^* \to$ hadrons, parton-antiparton contributions 2−59407
  - $\gamma^* \gamma^* \to$ hadrons off-mass shell behaviour of amplitude, scaling relation 2−45870
  - $\gamma\gamma$, forward scatt. amplitudes, positivity restrictions on imaginary part 2−70146
  - $\gamma\gamma$ forward scattering amplitude in multiperipheral ABFST model, asymptotic behaviour 2−79496
  - γN, deep inelastic, scattering amplitude, scaling and Regge behaviour on Feynman diagram model 2−45872
  - $\gamma N \to \gamma +$ anything, comparison between bilocal algebra on the light cone and parton model calcs. of structure functions 2−49498
  - γp, forward Compton scatt., cross section analysis 2−52553
  - $\gamma p \to 0^\circ p$, 'elastic' photoproduction at 8.5 GeV, determ. of cross sections 2−49580
  - $\gamma p \to \rho^\circ p$, 'elastic' photoproduction at 8.5 GeV, determ. of cross sections 2−49580
  - μ pair photoproduction in deep inelastic region meas. of inclusive cross -section 2−82696
  - ρ^0 photoproduction, forward slope, application of dual-absorptive model 2−73837

Photonuclear reactions *see Nuclear reactions and scattering due to/photons*

Photophoresis
- No entries

Photoproduction *see Gamma-rays/effects; Nuclear reactions and scattering due to/ photons; Photons/interactions*

Photoresistors *see Photoconducting devices; Semiconducting devices*

Photosphere
- abundances, spectrum synthesis 2−69192
- active regions, vel. field 2−62790
- activity, variation of geomagnetic K_p index 2−75992
- activity centres, early stages of development from photoheliograms 2−48804
- exploding granules, simulation model 2−75979
- faculae, and oblateness obs. 2−75977
- faculae, excess solar oblateness 2−51856
- faculae, interferometric obs. of small continuum features 2−81958
- faculae, relation to solar oblateness 2−51855
- filament disintegration and associated activities 2−55177
- fluctuations, radial veloc., coherence and phase spectra 2−75950
- force-free mag. field, non-linearity of dynamical behaviour 2−78582
- granulation, interferometric obs. of small continuum features 2−81958
- line formation, mean depth in a magnetic field 2−73112
- line profiles, line broadening by macroturbulence 2−75741
- magnetic field distrib. and He-D_3 spectroheliograms 2−73103
- magnetic field latitude distrib. rel. to temp. distrib. 2−75976
- magnetic field network, effect on spatial structure of corona 2−78604
- magnetic field variations flare generation 2−76009
- magnetic fields, flare-associated, real-time anal. 2−75980
- magnetic fields, meas. 2−62789
- magnetic fields, rel. to chromospheric features 2−66234
- microturbulence and macroturbulence, velocity spectrum 2−75982
- origin of spicules rel. to granulation perturbations and photospheric veins 2−75978
- photosphere-chromosphere transition region, brightness temperature minimum 2−62802
- polarization of light near solar limb 2−66223
- pole equator temp. differences 2−55162
- powerspectrum, 5-minute photospheric resonance oscillations 2−55178
- quiescent prominences 2−73145
- solar short period oscillations, velocity field at disk centre 2−55176
- solar-oblateness signal fluctuation rel. to density fluctuations above radiative zone 2−62788
- spectra, new lines obs. during total eclipse, 3600-6650 Å region 2−73115
- structure, CO fundamental lines 2−76003
- temperature variation with latitude 2−58555
- thermal oscill. for CO line 2−66224
- transport of cosmic rays in corona rel. to photospheric granular cell boundaries 2−44984
- umbral model atm. derived from i.r. obs. 2−78607
- velocity field in and around sunspots 2−75981
- Ag abundance det. from spectrum synthesis 2−58554
- Cr abundance det. from spectrum synthesis 2−58554
- Er abundance det. from spectrum synthesis 2−58554
- Fe I, first order analysis of variations of limb darkening and shapes for Fraunhofer lines 2−66199
- Fe I ionization and excitation equilibrium 2−66230
- Lu abundance det. from spectrum synthesis 2−58554
- MgI b_1 λ5183.6 line, residual intensity fluctuation measurements in wings 2−48793
- Ni abundance det. from spectrum synthesis 2−58554
- Th abundance det. from spectrum synthesis 2−58554
- Yb abundance det. from spectrum synthesis 2−58554

Photovoltaic effects
- β-carotene glass, resulting in photocond. transients 2−48003
- diode, light emitting, efficiency, carrier diffusion length, absorpt., auto-photovoltaic meas. 2−61451
- ice, photogalvanic effect, geophysical implications 2−54258
- liquid crystal, nematic 2−71223
- m.i.s. struct., surface-state density determ. by photovoltage meas. 2−44144
- m.i.s. structure, surface-state density determ. by photovoltage meas. 2−44143
- photographic emulsion coatings 2−81182
- protein and α-tocopherol membranes, induced potential 2−85089
- radio photovoltaic power conversion systems, efficiency and power limits 2−49255
- semiconductor, amorphous, contact and surface photovoltage, surface props. and chemisorption obs. 2−77969
- semiconductor epitaxial layer, minority carrier diffusion length determ., anal. 2−75177
- ternary group III-V semiconductor, composition from surface photovoltage obs. 2−51220
- tetracene, photovolt. current, anomalous temp. depend. 2−72075
- thermophotovoltaic radionuclide battery, model 2−49294
- CdS-Cu_2S, photovoltaic cell, props., doping effects 2−65092
- CdS, photopotential, surface effect of ambient kerosene instead of air 2−68482
- CdTe film, anomalously high photovoltage, and photomag. effect 2−75178
- CdTe layers and solar cells 2−41907
- Cu_2S-CdS heterojunction, photocapacitance effects 2−51221
- Cu_2S-CdTe, film heterojunction, and photocond. 2−81123
- p-GaAs, 300-77 K, $\lambda = 0.5$-1 μ, surface effects 2−54254
- GaAs, selective photoetching, surface photovoltaic effect 2−71364
- Ge thermophotovoltaic cell efficiency rel. to Er_2O_3 radiator performance 2−66693
- $Ge_{16}As_{35}Te_{28}S_{21}$, amorphous, semiconductor-metal contact 2−61374
- p^+-GaAs-nZnSe, diodes 2−53573
- PbS quantum yield of internal photoelec. effect and impact ioniz. 2−72065
- SbSI, ferroelec. semicond., temp. depend. of photoelec. e.m.f. 2−72078
- Si, amorphous, electronic struct. obs. 2−61454
- Si amorphous-crystalline junction, high photovoltages obs. 2−48005
- Si p-n diode, γ-irrad., impurity effects obs. 2−61358
- Si solar cells, effects of storage temperature on contacts 2−41908

Photovoltaic effects continued
SnO$_2$-CdS-Au, polarized memory device, photovoltage obs. 2−61381
Te, CO$_2$ laser induced photoeffects 2−81178
ZnO suspension and film, photovoltage obs. 2−51218
ZnS:Cl film, photovolt, polarity reversal by excess Zn 2−51222
ZnS, vapour phase grown crystal, rel. to perfection 2−47227
Physical chemistry
acids, MO SCF calcs. of proton affinities 2−83220
book, recent advances in chemical physics 2−61760
computer programs for laboratory expts., classroom problems 2−82101
data bank development of physical properties, with user access subroutine 2−75362
hydrated electron struct. and electron affinity of water 2−80013
multiple stationary state struct. 2−57406
pattern recognition applied to interpretation of chemical data 2−78182
phase equilibria data prediction for multi-components distillation column design 2−75361
plasma, in combustion MHD generator, chemical equilibrium, obs. 2−80257
polaron viewpoint of solvated electrons 2−78180
recrystallized free radical powder, PAC, meas. of line shapes, line widths, g factors of e.s.r. spectra 2−81484
S sensitization mechanism and photography 2−59304
B compounds, conference in Prague, 21-25 June 1971 2−51421
Fe cermet, highly porous, thermophysical properties 2−71651
Hg-chalcogenides, solid-liquid phase equilibrium and physico-chemical properties 2−68759
Physical effects of radiations
see also Under individual radiations. e.g. Neutrons and antineutrons/ effects
alkali halide crysts., u.v. and electron irradiation effects, decoration techniques 2−80607
analysis of irradiated reactor fuels, isotopic dilution, α and γ spectrometry, properties of operating reactors 2−76925
b.c.c. lattice, ejection of atoms, computer simulation 2−71763
b.c.c. lattice, void stability 2−50650
b.c.c. refractory metals for thermionic nuclear reactors, fast neutron irradiation damage 2−63229
carbons irradiated by neutrons and graphitisation, electronic props. change 2−68137
creep, measurement by neutron radiography 2−82593
creep meas. of irradiated specimens by neutron radiography 2−71621
crystal defects, vacancy-impurity complex, kinetics of formation and annealing 2−80693
crystal growth 2−74665
damage in accelerators, prototype radiation-resistant magnets 2−82832
defect clusters, transmission electron microscopy 2−50640
diamond, radiation damage, review 2−47371
diamond, vacancies, theory 2−47364
dielectrics, inorganic, changes in conductivity 2−52851
dielectrics, transparent, laser surface damage thresholds rel. to Fresnel reflections 2−79228
dimensional changes in graphite moderator, HTR reactor 2−42624
DNA, λ phage, conformation changes rel. to u.v. irrad. 2−60093
electron beam-induced radiation damage in polymers, effect on electron microscope image 2−80700
film, surface oxide, electromech., photomech. and conc. effects 2−51155
glass, laser damage rel. to surface film 2−82504
glass, photochromic, containing AgCl, u.v. irrad. effects on darkening 2−78065
graphite, Gilsocarbon, irrad. behaviour 2−56994
graphite in a reactor, oxidation obs. 2−52850
graphite-epoxy composites, radiation effects on mech. props. 2−64795
hardening of structural materials, review of developments in understanding 2−43803
heavy ion radiation damage of metals, 'in situ' expts. in electron microscope 2−74756
high energy particles, passage through thick layer, calc, using Monte Carlo method 2−42692
hydrogen-bonded glasses, Compton electrons generated by pulse radiolysis, Frohlich polaron model for trapping 2−44040
hydrostatic stress effects on void growth during irradiation, appl. to reactor core 2−76940
ice, KF and NH$_4$F doped and irradiated, role of F- in increased colouring 2−60823
incore thermionic reactor emitters, irradiation tests 2−52368
interstitial production in crystals, review 2−77577
ion-bombarded targets, ion damage distributions calc., computer program 2−79678
ionic crystals multistage formation of irradiation-induced F-centres 2−78087
lasers self-destruction, more resistant materials and components 2−55702
lunar rocks, e.p.r. signals 2−55123
metal, atomic displacement cascades, computer simulation 2−53700
metal, f.c.c., irrad., elec. resist. of defects 2−75045
metal, irrad., explanation of voids 2−80690
metal, irrad., explanation of voids 2−80691
metal, radiation-induced voids, conf., Albany, USA [June 1971] 2−50637
metal, void nucleation and growth, computer simulation 2−53699
metal, void production, review 2−50635
metal crystals growth in macrosonic fields, dislocation structures 2−50590
metal irradiated, void growth, interstitial and vacancy conc. rate theory eqns. 2−80661
metals and alloys, lattice defect form. under radioactive irrad., review 2−47362
metals and alloys, volumetric swelling caused by void formation 2−74758
3-methylhexane, solvated electrons, time dependent behaviour, 77K, detector response time effect <1600 n.m. 2−75002
Physical effects of radiations continued
3-methylhexane, solvated electrons, time dependent behaviour, 77K, detector response time <1600 nm 2−75001
mixed-oxide fuel pins, F3A series unencapsulated, examination following irradiation in EBR-II 2−76947
Mo-Ti(0.5%) alloy, transmission e. microscopy obs. of void superlattice after n. irradiation 2−64667
molecular crysts., melting point rel. to intensity of incident u.v. radiation 2−50399
n-p(n-i-p) nuclear particle detectors, space charge layer polarization during irradiation 2−65023
neutron irradiation of uranium carbides, effect on mag. susceptibility 2−84398
particle beam interaction with crystal structure channelling and shadow theories 2−84225
particle solid interactions, conference, Split, Yugoslavia (1972) 2−60291
plastic, ABS, light ageing behaviour, test method 2−50793
polyethylene, surface, anomalous low friction for steel-polymer friction by helium atom irradiation 2−56837
polymer, irrad., proton spin-lattice relax. times 2−84449
polymers, radiation-induced creep, relationship with radiation-induced electrical conductivity 2−47517
polypropylene, surface, anomalous low friction for steel-polymer friction by helium atom irradiation 2−56837
polystyrene structure changes by u.v. rad., reln. to polydispersity of polymer 2−64652
polyvinyltoluene, degradation by u.v. light, plastic scintillation counters 2−76731
quartz, radiation-induced diffusion of alkali ions and protons and formation of colour centres 2−71532
radiation damage, conf., Sydney, Australia [Feb. 1972] 2−43603
reactor fuel elements for high temp. reactors 2−56064
Reactor Radiation Division of NBS annual report 2−67367
ruby laser radiation, fracture of nonlinear crystals 2−79254
semiconductor, conf., Albany, (1970) 2−47877
semiconductor, conf. opening address Albany, (1970) 2−47878
semiconductor, group II-VI cpds., radiation induced and growth defect obs. 2−47372
semiconductor, group III-V cpds., radiation damage, review 2−47365
semiconductor, simulation of transient space-charge flow under ionizing radiation 2−71954
semiconductor, strong light irrad., optical cooling of conduction electrons 2−81004
solid, destruction by heavy ionizing particles, electronic subsystem excitation 2−68014
sonic boom startle, field study in West Germany 2−85137
sonic discontinuities in a radiative gas, growth and decay of waves for second and third order compatibility 2−56442
space radiation effects on selected optical materials, simulated 2−49440
structural materials, creep and growth effects 2−74757
thermionic converters, effects on lifetime failure and degradation 2−52364
transition metal borides, neutron irradiation swelling 2−77790
triple thermionic diodes 2−49271
water resistivity, applic. in dosimetry 2−69402
window response to sonic boom, acoustic coupling of rooms 2−45562
AgBr, positron lifetime, illumination effects, at 300 and 77 K 2−77808
AgCl, positron lifetime, illumination effects, at 300 and 77 K 2−77808
Al-4%Cu alloy, influence of precipitates on cavity formation for irrad. by fast neutrons 67984 2−67984
Al$_2$O$_3$, α-phase polycrystalline, e.p.r. study γ, n in-pile radiation of effects 2−80667
Al$_2$O$_3$ ceramics for thermionic reactor insulators, neutron induced swelling as function of neutron energy 2−63228
AmO$_2$, thermal cond., self-irrad. effects 2−54078
As-Se-Ge glass film, amorphous to crystalline state conversion by light irradiation 2−75077
B epoxy composites, irrad. in nuclear reactor, strength 2−80801
BaTiO$_3$, dielec. const. changes after electron or gamma irrad. 2−65047
C fibres, radiation effects on mech. props. based on 'sheath' and 'core' model of fibre structure 2−64702
C film, amorphous, graphitization by light pulses 2−61030
C film, graphitization under light pulse irrad. 2−57002
C film, rad. resist., diamond-like props. characterization 2−56588
CaF$_2$ centres of C$_{4v}$ symmetry containing trivalent rare earth-interstitial hydride in pairs, rel. to u.v. irrad. 2−83984
CdCr$_2$Se$_4$, mag. permeability rel. to illum., photoferromag. effect 2−54324
CdS:Yb^{3+}, emission spectrum at 10 K, before and after e irrad. 2−75339
CdTe, photoplastic behaviour 2−50742
Fe, multidomain, neutron irradiation effects on remanent magnetism rel. to magnetization of lunar samples 2−58458
α-Fe, neutron irradiation, structure studies 2−60965
Fe in fast reactors, atomic displacement rate and displacement cross section 2−42643
GaAs single crystal, work function, effect of light at low temps. 2−75188
Ga$_2$Te$_3$, semicond., stability due to stoichiometric vacancies 2−71906
Ge, low temp. irrad. and annealing, review 2−47375
p-Ge, radiation defect annihilation centre, photocond. obs. 2−83978
Ge alloy and drift transistors, modification of parameters during exposure 2−75133
InSb, photocond. rel. to light irrad., at 77K 2−47996
In$_2$Te$_3$, semicond., stability due to stoichiometric vacancies 2−71906
KCL, H-centre prod. by u.v. photodestruction of U$_2$-centres, optical and e.s.r. obs. 2−77599
KN$_3$, u.v. irrad., absorpt. bands identification 2−75299
K$_2$O-SiO$_2$ glass, irrad., nature of hole centres, e.p.r. obs. 2−65336
LiF, radiation-induced thermally activated depolarization 2−72007
LiF, radiation colloids, elec. microscope obs. 2−74760

Physical effects of radiations continued
MgF$_2$, F- and H-centre production, radiation damage process 2−56747
MgO, F$^+ \rightleftharpoons$F centre conversion obs. 2−68043
Mo, irrad., void stability 2−50650
NaCl, quenched, X-irrad., cry. lattice defects and near surface props. 2−71477
NaNO$_3$, thermoluminesc. glow curves, intensity as function of radiation dose 2−48257
NaNbO$_3$, dielec. const. changes after electron or gamma irrad. 2−65047
Nb, supercond., critical current rel. to radiation induced defects 2−81053
PbBr$_2$(Cl$_2$), u.v. irrad., e.p.r. and luminesc. obs. of centres 2−44448
PbTiO$_3$, dielec. const. changes after electron or gamma irrad. 2−65047
PbZrO$_3$, dielec. const. changes after electron or gamma irrad. 2−65047
PuO$_2$, thermal cond., self-irrad. effects 2−54078
SbSI, Seignette semicond., thermal currents induced by light 2−72039
SbSi, naturally polarized crysts., photodomain effect on illumination 2−77940
Si, irrad. defects, concepts and correlations 2−47387
Si, multiple vacancy centres, e.p.r. obs. 2−48283
Si, recombination centre parameters of irradiated p-n junctions, determ. 2−61382
Si, vacancies, theory 2−47364
Si p-n junction, reactor irrad., broadening of Zn and Ga impurity profiles 2−84355
Si(Li) detectors, radiation- damaged, i.r. response meas. 2−49657
Si(Li) detectors, radiation damage effects of electrons, protons and neutrons 2−49659
SiO$_2$, radiation damage, valence bond approx. model 2−80656
SrTiO$_3$, dielec. const. changes after electron or gamma irrad. 2−65047
(U, Pu)O$_2$ mixed-oxide, postirradiation obs. of microstructure changes 2−76945
α-U, radiation-induced size changes 2−52845
UO$_2$-PuO$_2$, irradiated, gas release and swelling, 1260-1900°C 2−80662
UO$_2$, irradiated, gas release and swelling, 1260-1900°C 2−80662
W, stress induced growth irradiated at low temp. 2−60781
ZnO thermal control coating pigment, u.v. irrad., e.s.r. of defects 2−81460
ZrO$_2$ amorphous, radiation induced thermal effects 2−64522

Physics
see also Biographies; History; Nuclear physics; Teaching
A-level course, digital computer applications 2−41442
Advanced level course lasting few months 2−82103
for biology and medicine, book 2−45208
book, modern physics topics 2−69520
comparability of scientific theories 2−41423
computer impact on scientific research in Europe 2−82087
course, humanistic approach 2−78721
course, non-mathematical, for non-scientists 2−78717
course covering war, peace, science and technology 2−62919
current development areas, review 2−62911
in developing countries 2−82090
Doppler effect, simple experiment 2−82108
education, integrated course in physics and mathematics for A level biology and arts students 2−41430
education in Ghana 2−62920
European physical society, origin and evolution 2−82089
guidelines for reporting numerical data and experimental procedures 2−76137
individualized instruction course (without lectures) 2−73257
information retrieval course for undergraduate 2−76141
Keller method of physics teaching, evaluation 2−62924
matter, extremal states under ultrahigh pressure or temperature, review 2−55342
medical, course based on hospital field experience 2−55346
microphysics, logic 2−73256
models involving analogies, interpretation 2−41425
non-destructive testing course 2−45204
Norwegian Physical Society meeting, (June 1971) 2−78713
Nuffield A level physics, background for students entering university 2−41428
Nuffield O-level course, conceptual demands 2−76143
Nuffield physical science course, background in physics which students entering university will have 2−41429
photon, limits on mass 2−82106
physical theories, construction of model 2−76136
problems of current interest 2−82086
relationship to acoustics 2−41685
replacement of theories under preservation of a given feature 2−41424
research, computer applications 2−41422
review course of theoretical physics at student level, book 2−82116
science policy in USA, need for radical changes 2−73259
scientific explanation, Aristotelean theory 2−82092
scientific theorizing, received view 2−82091
sensible physics, based upon sense impressions 2−82111
similarity, dimensional analysis of equations 2−82161
solid state, conference, Jerusalem, Israel (May 1972) 2−70340
solid state, neutron, theoretical, nuclear, maths. and computation, progress report of Atomic Energy of Canada 2−62910
solid state, teaching programme in secondary schools in Hungary 2−73258
spontaneous self-regulating systems, foundations 2−73333
statistical methods in experimental physics, books 2−45337
structure of matter, conf., Christchurch, New Zealand (July 1971) 2−58677
teaching, computer applications 2−41441
teaching, computer based methods 2−41440
teaching, evaluation of nonlecture technique 2−55345
teaching in schools and transition to universities 2−62921
textbook, American college for the non-physicist 2−45209
time series analysis applications, developments 2−42598
topological aspects, global approach 2−62968

Physics continued
undergraduate courses, in engineering eduction 2−55344
university, educational influences of technology 2−69524
I$_2$ vapour absorption spectrum, teaching to sixth form students 2−76147

Physics fundamentals
see also Cosmology; Elementary particles; Field theory, classical; Field theory, quantum; Indeterminacy; Mechanics; Parity; Probability; Quantum theory; Relativity; Thermodynamics; Units
2e/h measurement by a.c. Josephson effect 2−69532
aether theory, determ. of fine struct. const. 2−82203
causality violation in the motion of high spin particles in an e.m. field 2−82664
de Broglies book 'Research on quantum theory', translation into english of the first chapter 2−62996
elementary matter, new theory 2−55433
Faraday as natural philosopher, book 2−41427
foundations of physics, book 2−62913
Galilean particles and principle of correspondance 2−58676
homological foundation for scale problems, comment on paper by Atkin and Bastin, quantum logic framework 2−73313
hydrodynamics and heat transfer views of Predvoditelev 2−67548
Kelvin equation, review 2−53512
laws and theories, phenomenological symmetry 2−45202
macroscopic linear laws, conditions for derivation from microscopic law 2−49025
matter at extremely high temp. and pressure 2−62912
meaning changes, criteria in theoretical physics 2−62914
models involving analogies, interpretation 2−41425
philosophy, relevance to physics 2−62915
physical quantities, mathematical theory of units and dimensions 2−62956
principle of symmetry, foundations and applics. 2−82095
quantum logic and ordering of propositions 2−41488
reality in physics, a classroom dialogue 2−78718
school physics, concepts 2−55343
structure of space 2−73252
variational principles and invariance theory 2−62967

Physiology
see also Biological technique and instruments; Blood; Hearing; Vision
abnormal pulmonary circulatory dynamics, simulation 2−48862
alpha activity, change in freq. following eye opening and closure 2−78672
alveolar bone mineral content, in vivo measurement, monoenergetic attenuation technique 2−69314
alveolar ducts, gas diffusion model 2−48865
animals, visual pattern analysis 2−85140
biopotential meter, meas. of electrical activity of nerve cells 2−69240
bone mineral content, in vivo measurement, scanning radiology 2−69313
flow measurement, n.m.r. technique, velocity distribution fn. 2−83757
heartbeat as masker of l.f. noise 2−82051
human being rel. to light atmospheric ions 2−58585
human body, effects of long terms of weightlessness in Soyuz 9 2−62424
metabolism of cobalt by normal human male, retention data from disometry 2−58589
mice, bioelectric activity in immobilized muscle 2−81997
muscular contraction, phenomenological eqns. of biological motility 2−73170
nasal air flow, simplified nonlinear model, computational requirements 2−48863
nerve membrane, functional mechanism 2−58579
neural mechanisms of perception of real and apparent movement 2−51984
neural mechanisms of perception of real and apparent movement 2−51985
orthostatic tolerance modification with periodic lower body negative pressure 2−62829
pulmonary extravascular diffusion, distributed parameter model 2−48864
rabbits, phrenic neurons activity, effect of increased respiratory resistances 2−81996
skeletal health, computer assessment, scanning of radiographic image 2−69375
spatio-temporal characteristics of visual system, retina, analogue simulation 2−85139
telemetry for physiological data collection during exercise 2−82004
CoCrMo alloy, total joint replacement, wear products in body 2−69292
Ti bioimplant interfaces, biological aspects 2−69293

Piezo-optical effects
butanol, meas. of isothermal piezo-optic coeff. 2−50364
ethanol, meas. of isothermal piezo-optic coeff. 2−50364
infrared circular dichroism meas. instrument 2−67521
pentanol, meas. of isothermal piezo-optic coeff. 2−50364
propanol, meas. of isothermal piezo-optic coeff. 2−50364
Ag evaporated film, 4500-2150 Å, piezotransmission, rel. to electron states 2−81366
Ag film, piezoreflectivity, dielectric const. changes 2−54382
As$_2$S$_3$, amorphous, piezobirefringence freq. depend., one-oscillator model 2−54383
Au-Zn dilute alloys, optical and piezo- optical properties from reflectivity measurements 2−68621
γ-CuI thin films at 77K in fundamental absorption band region 2−48172
GaSb, piezoemission, stress effects on impurity and bound exciton lines 2−48179
Mg$_2$SiO$_4$, forsterite, press. depend. of refr. index 2−44350
Si:P(As) radiation-induced infrared absorption bands, piezospectroscopic studies 2−68650
Si, cond. band. deform. potential const. from piezospectroscopy of donors 2−68438
Si, wavelength modulated reflectivity spectrum in 3.4 eV region, piezo-optical evidence for λ transitions 2−75280
ZnS:Co with stacking faults, piezospectroscopic effect on group of zero-phonon lines associated with centres 2−44384

Piezoelectric oscillations
crystal plate h.f. vibration, two-dimensional eqns. 2−59025
disc vibrator, equivalent constants for double resonance 2−76365
extensional, for piezoelectric plates 2−45493
inverted mesa structure, mechanical response 2−52223
piezoceramic disk, equivalent circuit for radial vibrations 2−66617
in piezometric differential well, nonlinear system of differential equations, solution 2−76366
piezotransducers, photoelectric stabilized interferometer for amplitude-frequency response obs. 2−76515
quartz, X cut resonators, linear and nonlinear coeffs. 2−84362
quartz plates, coupled vibrs. freq. temp. depend. 2−61437
semiconductor, elastomagnetic waves, coupled e.m. and lattice oscills. 2−64848
thickness-twist trapped energy mode in piezoceramic plate, exact resonant frequencies 2−45494
transducer, bar vibrating in compressional mode, response calc. 2−63118
$BaTiO_3$, piezoeffect rel. to semicond. props. and work function 2−77959
$BaTiO_3$ single crystals influence of the amplitude of free vibrations on the permittivity 2−81154
$Bi_{12}GeO_{20}$, propagation of Bleustein-mode piezoelectric surface wave 2−61095
CdS, piezoelec. semicond., sound amplification threshold field nonmonotonic cond. depend., 5-120 MHz 2−77783
$LiNbO_3$, propagation of Rayleigh-mode piezoelectric surface wave 2−61095

Piezoelectricity
see also Electrostriction; Piezoresistance
84362
anisotropic media, piezothermoelec. effects 2−51209
CdS, boson echos obs. 2−65071
ceramics $PbTiO_3$, $BaTiO_3$, ZnO, CdS, Pb(Ti, Zr)O_3, flexural modes 2−84205
composite magnetostrictive phase, piezolec. phase, magnetoelec. prod. prop. 2−47664
composite transducer, mechanical response in thermal field 2−41756
constants, ultrasonic method of determ. 2−65069
crystal class 6m2, standard choice of axes 2−68474
crystalline powders, tester, description 2−59031
dielectric plate, pure bending 2−65068
elastic surface waves, waveform distortion meas. with electrostatic probe 2−49170
e.m. waves transformation from acoustic waves by piezoelectric plate 2−65070
ferroelectric, electrooptic materials 2−45641
ferroelectric, influence on transverse acoustic wave reflection at domain boundaries 2−74982
ferroelectric ceramic, transparent, grain size and porosity effects 2−57244
fibrin elongated, films, dielectricity and viscoelasticity 2−85087
film surface wave transducers, coupling factor, capacitance and phase velocity 2−49111
group III-V cpd., semicond., review 2−77774
group III-V cpd. semicond., review 2−77774
linear theory, nonlinear electroelastic interactions 2−51200
microwave acoustic surface wave attenuation due to gas loading 2−51009
mirror electron microscopy, image contrast formation 2−84368
multilayered anisotropic media, dispersion charact. calc. by computer 2−81130
nematic liquid crystals, molecular statistical appraoch in one-dimensional model 2−46972
noncentrosymmetrical crystals third order tensors for all symmetry elements 2−68473
piezoceramic bimorph infinitely extended, mixed boundary value problem 2−72043
piezoelastic bodies, dynamic problems for bounded bodies 2−76288
piezoresistive acceleration-integration system, for velocity obs. 2−45221
polaron, simultaneous strong and weak coupling 2−84268
polypeptides, oriented, and polymero, oriented and polarized, description 2−61436
polyvinylidene fluoride film, far i.r. spectral investigations of structural conformations rel. to piezoelectric props. 2−61438
proteins, possible relation to bioelectrical phenomena 2−61436
PZT-5, surface wave velocity depend. on degree of poling 2−51202
quartz, X-cut, strain dependence of longitudinal piezoelectric, elastic and dielectric constants det. by shock compression 2−51207
semiconductor, acoustoelec. effects at large sound intensities 2−61098
semiconductor, C_{6v} class cryst., interaction of transverse u.s. waves with charge carriers 2−54030
semiconductor, fluctuating elec. field and Franz-Keldysh effect inside acoustoelec. domains 2−54033
semiconductor, narrow propagating domains of acoustic flux, prod. method 2−43978
semiconductor, u.s. second harmonic generation 2−51039
semiconductor, u.s. second harmonic generation in mag. field 2−68239
semiconductor, u.s. wave propagation, effect of weak inhomogeneity in carrier density 2−74984
semiconductors, acoustoelectronic effects at large acoustic intensities 2−80915
semiconductors, impurity diffusion coefficients, ultrasonic meas. method 2−50691
semiconductors, waveguide effect of surface domains 2−54029
space charge effects on attenuation symmetry of u.s. amplification by piezoelectric semiconductors 2−51031
stacked crystals, transmission-line analogues 2−47989
stimulated sound scattering, by elec. field oscills. in piezoelec. cryst. 2−74981
surface acoustic wave correlation echo, generation from coupling to charge carriers 2−57045
surface acoustic wave guidance by $(\Delta v/v)$ guidance structures 2−51010
surface acoustic wave steering and switching by nonlinear mixing in anisotropic media 2−51011

Piezoelectricity continued
surface acoustic waves and applications 2−43973
surface elastic wave, rel. to charge storage of acoustic r.f. signals 2−61085
surface wave convolution in piezoelectric materials, nonlinear interaction 2−51001
surface wave transducers, apodized wideband, wavefront distortion meas. by electric probe 2−49138
three phonon processes in acoustoelectric interaction 2−84181
transducer, film on interdigital electrode structure, impedance and capacity for Rayleigh and SV modes 2−49151
transducer, mechanical response to current flowing in semiconducting boundary layer having polarization gradient 2−54239
transducer, mechanical response under influence of body force 2−69749
transducer, point source simulation in h.f. acoustical system 2−52242
transducer, surface acoustic waves, grating array 2−49153
transducer, using Yb for in-situ field meas. 2−61943
transducers, source detector system 2−41757
triglycine sulphate, ferroelectric, electromech. coupling near T_c 2−68475
ultrasonic bulk waves, scanned, surface excitation 2−51201
U.S devices, h.f., review in book 2−57046
$BaTiO_3$, piezoeffect rel. to semicond. props. and work function 2−77959
$BaTiO_3$ single crystals influence of the amplitude of free vibrations on the permittivity 2−81154
$Bi_{12}GeO_{20}$, piezoelectric constant meas. 2−51203
CdS-$LiNbO_3$, convolution and correlation by nonlinear interactions between sonic induced space charge and field waves 2−51015
CdS photoconductor, transverse surface wave depth penetration 2−84206
CdS transducer deposition, parameters controlling device usefulness 2−67906
CdSe, thin film transducer, operation characteristics and anomalous behaviour 2−77922
n-GaAs:O, stiffening of active bulk modes and increase in velocity of 30 MHz shear wave 2−51204
GaAs, i.r. radiation modulation at piezoresonance 2−57329
GaAs, piezoelectric amplification of acoustic waves abrupt decrease in gain at quantum limit 2−51033
$Gd_2(MoO_4)_3$ piezoelectric d_{36} coefficient 2−81149
$La_2Ti_2O_7$, paraelec. crystal 2−51205
$LiGaO_2$, rel. to electromech. coupling factor and reson. freq. 2−51206
$LiIO_3$, elastic surface wave props. and device applics. 2−77778
$LiNbO_3$-Si layered structure, transverse acoustoelectric effect obs. using capacity probes 2−51038
$LiNbO_3$, acoustic convolution and correl., nonlinearity parameters 2−51014
$LiNbO_3$, shear wave excitation by interdigital transducer operated at surface-wave centre freq. 2−51008
YZ $LiNbO_3$ reflection of elastic surface waves from periodic arrays 2−51022
$LiTaO_3$ single crystal, temp. dependence 2−72008
$NaNO_2$, rel. to Brillouin scatt. at room temp. 2−48204
$Pb_{1-x}La_x(Zr_yTi_z)_{1-x/4}O_3$ ceramic, radial mode coupling factors det. with large Poissons ratio variations 2−51195
$Pb_{1-3x/2}La_xZr_{0.65}Ti_{0.35}O_3$ 2−57245
$Pb(Mn_xNb_{1-x})O_3$ perovskites, synthesis and characteriz. 2−50893
$Pb(Zr,Ti)O_3$-Si-$LiNbO_3$, convolution and correlation by nonlinear interactions between sonic induced space charge and field waves 2−51015
$Pb(Zr,Ti)O_3$, rel. to thermodynamic theory of morphotropic phase transition 2−75153
SbSI, boson echos obs. 2−65071
SbSI, ferroelec., resonance method obs. 2−54240
Si:B, shear deform. pot. consts. of B acceptors ground state, piezospectroscopy obs. 2−75306
Si-$LiNbO_3$, convolution and correlation by nonlinear interactions between sonic induced space charge and field waves 2−51015
Si-PZT coupled system, acoustic surface wave convolution by 14.5 MHz Bleustein-Gulyaev waves 2−71742
Te, semicond., dislocations 2−60805
ZnO/Al_2O_3, heteroepitaxial layer structure, surface acoustic props. rel. to delay line behaviour 2−68235
ZnO, epitaxial layers on Al_2O_3, surface wave acoustic props. 2−51020
ZnO film surface acoustic wave transducers, coupling constants and film thickness 2−49152

Piezomagneto-optical effects *see Magneto-optical effects*

Piezoreflectance
No entries

Piezoresistance
see also Piezoelectricity
band struct. analysis, review 2−72298
Ag evaporated film, 4500-2150 Å, rel. to electron states 2−81366
As single crystals, with light polarized in basal plane 2−75262
Bi single crystal, obs. and rel. to optical interband transitions 2−65213
C film, amorphous, temp. depend. 2−61302
Ca semimetal, temp. and uniaxial stress dependence obs. 2−71840
Cu, a.c. modulated, symmetry breaking effects of shear stress 2−47789
Sb single crystal, obs. and rel. to optical interband transitions 2−65213
p-Si:Be, temp. and doping depend., gauge factor 2−54198
n-Si:P, 4.2, 77 and 300K 2−71945
p-Si inversion layer, band structure detn. 2−51171
Te film, on glass, rel. to temp. coeff. of cond. 2−75099
Yb semimetal, temp. and uniaxial stress dependence obs. 2−71840
ZnS, exciton, exciton states exchange splitting by stacking faults 2−81391

Piles, nuclear fission *see Nuclear reactors, fission*

Pinch effect *see Discharges, electric; Plasma/confinement; Semiconducting materials*

Pions
— 2−59454

Pions continued
charge form factor study by analysis of $\pi^{\pm}$ elastic scattering on ^{4}He 2−63604
charge radius determ. from form factor, contribution of ρ and ρ' vector mesons 2−76663
dual pion model, physical states and pomeron poles 2−70227
dual pion model and chiral symmetry breaking 2−73813
elementary pion with transverse-momentum cutoff, π-exchange processes, np considered 2−42380
e.m. form factor, duality 2−59524
e.m. form factor, sum rules 2−79498
e.m. form factor analytic properties rel. to optimal lower bounds on hadronic contrib. to muon magnetic moment 2−76612
e.m. form factor and charge radius, new constraints derived using Chou-Yang model 2−70224
e.m. mass difference calc. in gravity-modified quantum electrodynamics 2−42381
e.m. polarizability using low-energy technique 2−42388
exchange and cosmic-ray nucleon cascade 2−63681
exchange contribution to two and quasi two body reactions 2−73779
exchange process, model for inclusive processes 2−59442
factorizable dual model based on a coupling of dual spin fields with $J_2=-^1{}_2$ and $J_s=-1$ 2−42379
form factor, Bethe-Salpeter model 2−63601
form factor, electromagnetic, unitarization in smoothed Veneziano model 2−55850
form factor, possible heavy vector meson 2−70226
form factor, Veneziano-like represent. 2−79594
form factor estimation from dispersion model for $\pi^-p \to e^+e^-n$, 275 MeV 2−63602
form factor parametrization 2−67013
form factors, information from absence of zeros 2−63600
gas Cherenkov counter with large aperture for distinguishing between pions kaons and protons 2−76742
high energy interactions, zero pion mass limit 2−63603
in-flight beam flux monitor using proportional counters 2−55908
isomultiplet, dynamic chiral symmetry and cancellation of divergences in mass differences 2−52628
low energy theorems, current algebra description 2−59525
mass relations, pion-muon model 2−79555
momentum spectra, transverse and longitudinal, in pd reactions at 3.5 GeV/c 2−49591
negative, use in therapeutic and diagnostic medicine 2−76084
one-pion exchange role in deep inelastic eN scattering 2−45888
pionization particles, angular distrib. of multiplicity in hadron collisions, scaling law 2−42352
polarizability, derivation from $\pi \to e\nu\gamma$ data 2−63503
$A_1\rho\pi$ coupling constants, determination using collinear dispersion relations 2−63639
$\gamma\pi\pi$ electromagnetic vertices, conformal invariance and Bjorken scaling 2−79495
ΛN potential, two-pion exchange 2−59588
NNπ form factor and Goldberger-Treiman relation 2−59558
π-μ model, linear mass relationships 2−59526
π^- phase, condensed, in neutron-star matter 2−63726
π^- phase, condensed, in superdense nucl. matter 2−63727
$\pi^{\pm}$ e.m. form factors and inelastic structure function meas. using NAL and ISR 2−73812
πN coupling constant determ. from π photoproduction 2−45951
$\rho\pi\pi$ coupling constants, determination using collinear dispersion relations 2−63639

decay
$(\eta \to \gamma\gamma)/(\pi^0 \to \gamma\gamma)$ decay width ratio, SU(3) prediction 2−79553
$pp \to \gamma X$ γs due to $\pi^{\pm}$ as well as π° decay 2−82755
π^0, decay amplitude sign in radiative π capture by ^{1}H 2−46295
π^0 momentum spectra, deriv. from photon momentum spectra 2−79592
$\pi^0 \to 2\gamma$, anomalies in low energy theorems, nonperturbative evaluation 2−45856
$\pi^0 \to 2\gamma$, low-energy theorem relating to $\gamma \to 3\pi$, derivation using anomalous Uland identities 2−52548
$\pi^0 \to 2\mu$, $3\pi \to 2\mu$ anomalous intermediates in $K_l{}^0 \to \mu^+\mu^-$ 2−63584
$\pi^0 \to e^+e$-, $\pi^0 \to \gamma e^+e$-, rate evaluation in baryon loop model 2−45930
$\pi^0 \to \gamma +$ positronium, probability calculation 2−45948
$\pi^0 \to \gamma e^+e$-, calc. of radiative corrections over whole range of Dalitz plot 2−45947
$\pi^0 \to \gamma\gamma$, derivation of Adler's low-energy theorem using quark-loop dynamics 2−73770
$\pi^0 \to \gamma\gamma$, triangle anomaly, second-order radiative corrections 2−79589
$\pi^0 \to \gamma\gamma$ current algebra and the triangle approx. 2−63637
$\pi^0 \to \gamma\gamma\gamma\gamma$, decay rate calc. to α^4, branching ratios 2−79591
π^+, mean life time meas. 2−73814
$\pi \to A_1$, multiparticle propagation through nucleus, non-classical effects 2−76865
$\pi \to e\nu\gamma$, data used to derive polarizability of π 2−63503
$\pi \to l\nu_l\gamma$, form factors, Q^2 depend 2−76669
$\pi\pi\gamma \to \mu\mu$ anomalous intermediate in $K \to \mu\mu$ 2−63585

interactions
— 2−66934
energy depend. of spectra, calc. by bootstrap model 2−82751
with massive vector meson I-spin triplet, low-energy theorems 2−76697
SU(2) × SU(2) breaking and effective Lagrangian 2−82603
$e\pi \to e +$ anything, deep-inelastic PCAC, soft pion method 2−73758
$\gamma\pi \to \pi\pi$, structure of observable amplitudes 2−52549
$\omega\rho\pi$ nonrenormalizable, ladder approximation for vertex function 2−52627
$p\pi \rightleftharpoons \gamma n$ in $\Delta(1236)$ resonance region, discrepancy between dispersion relation predictions and exptl. data 2−42324
π^- beams, radiotherapy, biomedical facilities 2−69341
π^- beams, radiotherapy, Los Alamos Meson Physics Facility 2−69342
π^- condensation in neutron star rel. to cooling, independent particle model 2−75751
$\pi \to 2\gamma$, coherent production, low-energy theorems relating to $\gamma \to 3\pi$, $2\gamma \to 3\pi$ processes, anomalous Ward identities 2−63502
ΠN charge exchange, suppression of Regge-Regge cuts 2−59499
π^-d, 7 GeV/c, search for multipion resonances and validity of spectator model 2−67019

Pions continued
interactions continued
π^+d, 7 GeV/c, two pion final states 2−45957
π^+d, coherent A_2 production 2−59555
$\pi^{\pm}d$, total cross sections in momentum region 15 to 60 GeV/c, Glauber correction 2−45968
$\pi^{-}\,^3\mathrm{He} \to \pi^+(3n)$, resonances in three- nucleon system at low energies 2−42424
π-K^+, 2.45 GeV/c, meson and baryon reson. prod. 2−42403
$\pi K \to \omega K$, finite-energy sum rules 2−63635
$\pi K \to \varphi K$, finite-energy sum rules 2−63635
π-$n \to \pi$-ρ-p, 7 GeV/c, A_1 study 2−49584
π^-n, 40 GeV/c, determ. of charged and neutral particle multiplicity 2−76682
π^-n, 40 GeV/c, multiplicity distribution of charged particles produced 2−45960
$\pi^+n \to \omega p$, B meson exchange contribution 2−42387
$\pi^+n \to p\omega$, 13 GeV/c 2−70232
$\pi^+n \to \pi^0\pi^0p$, use with one-meson approx. to obtain $\pi\pi$ scattering cross-section 2−82764
$\pi^-p \to n\pi^+\pi^-$, 3.1 to 3.6 GeV/c, ang. distrib. meas. 2−67029

interactions, pion-nucleon
asymmetry of angular distrib., momentum spectra, distrib. of 4-dimensional transfer 2−73819
baryon-antibaryon pairs and quarks, production, modified peripheral model 2−82711
charge exchange cross-section, calc. using nes Regge absorption model 2−73794
charge exchange reactions, effects of correction to real part of Regge amplitudes 2−59472
charge-exchange forward scattering, invariant amplitudes 2−79579
chiral invariant, matrix superpropagator 2−73820
Coulomb interference data, amplitude analysis 2−63622
coupling const., derivations from pion photoproduction data 2−79573
coupling constants, radiative corrections 2−49565
cross-section through extrapolation of deep inelastic electroproduction and photoproduction data 2−67021
effective Lagrangian, nonuniqueness in chiral SU(2)⊗SU(2) symmetry 2−45845
form factor, corrections to Goldberger-Treiman relation 2−59530
inclusive spectra, microscopic model 2−76713
Monte Carlo simulation at high and ultrahigh energies 2−73893
multiplicity of secondary particles, 5-5.10^4 GeV, analysis of models and data 2−82763
P-wave interaction, short range, comparison with high energy backward Regge models 2−70234
potential for use in low energy nuclear physics 2−63740
resonance dynamics, review 2−46015
secondaries momentum characteristics at 60 GeV 2−76672
static model, existence of solns, charged scalar methods 2−79574
transverse momentum in interactions at high energy 2−79597
N* review 2−46016
N_{33}*, effective range formulae, energy bands 2−49602
production of 2^+ and 1^+ mesons studied in U(6,6)⊗O(3,1) peripheral absorption model 2−55863
$\pi^-A \to V^0A'$, obs. of polarized V^0 mesons interaction with nucleons 2−70233
$\pi^-N \to \pi^-\pi^-\pi^+N$, 60 GeV/c, photoemulsion study 2−73818
$\pi^-N \to \pi^-\pi^-\pi^+N$ and $\pi^-N \to \pi^-\pi^-\pi^-\pi^+\pi^+N$, coherent interactions with photoemulsion nuclei at 17 GeV 2−45961
$\pi^-N \to \pi^-\pi^0\pi^0N$, photoemulsion study 2−73818
$\pi N \to A_1N$, t-channel helicity conservation and $A_1\rho\pi$ coupling 2−59554
$\pi N \to K\Sigma$, Λ, strangeness-exchange interactions at high-energy, cross-section and polarization 2−76650
$\pi N \to K\Sigma$, new Regge absorption model fits to polarization and cross section data 2−73794
$\pi N \to K[\Sigma,\Lambda]$, hypercharge exchange reaction, amplitude analysis 2−42389
$\pi N \to K\pi\Lambda$, usefulness of meas. of Λ-polarization 2−63667
$\pi N \to V + N'$, differential cross section and density matrices determ. in model of higher baryon couplings 2−45983
$\pi N \to (\pi\pi)\Delta$, moment analysis for $\pi\pi$ phase shifts 2−67022
$\pi N \to (\pi\pi)N$, moment analysis for $\pi\pi$ phase shifts 2−67022
$\pi N \to \omega(N,\Delta)$, isolation of isotopic symmetry possible due to ρ^0-ω mixing 2−63615
$\pi N \to \pi\Delta(1236)$, study of baryon decays involving two partial waves, test for basic violation of $SU(6)_w$ 2−63642
$\pi N \to \pi\Sigma(\Lambda)$, PCAC prediction of $\Sigma(\Lambda)$ production cross sections and polarization phenomena 2−52644
$\pi N \to \pi\pi N$, results of combining conformal invariance and chiral symmetry 2−63612
$\pi N \to \rho N$, baryon Regge pole exchange model 2−52623
$\pi N \to \rho N$, dual amplitudes 2−67020
$\pi N \to \rho N$, dynamical model for $P_{13}(1860)$ $Pp_{31}(1910)$ and $F_{35}(1890)$ resonances 2−49583
$\pi N \to \rho\pi N$, dual resonance model for A_1 production 2−63613

interactions, pion-pion
diffraction peak, nonlinear duality calculation of width 2−82762
effective Lagrangian, nonuniqueness in chiral SU(2)⊗SU(2) symmetry 2−45845
even partial-wave phase shifts, meas. in $ee \to ee\pi\pi$ colliding beam expts. 2−63608
Veneziano model interpret. of low energy final state interaction 2−55855
$\pi^+p \to 3\pi^+2\pi^-p$, 8 GeV/c, ABFST model with dual amplitudes 2−82750
$\pi^-\pi^+ \to pp$ cross-section compared with that for $pp \to \pi^+\pi^-$ 2−45965

interactions, pion-proton
asymmetry of pion distrib. in high-energy interaction 2−45967
in free H_2, determ. of fraction of interaction in heavy liquid bubble chamber 2−70313
meson factory expts. at low energy 2−82640
p_t limited phase space predictions 2−55831
peripheral dynamics for limiting fragmentation 2−79586
total cross-section, relation to slope of diffraction cone 2−66964
transverse momentum in interactions at high energy 2−79597
A_1 diffraction production 2−82768

Pions continued
interactions, pion-proton continued
$p\pi^- \to pX^-$, 25 and 40 GeV/c, scaling and estimate of triple-Pomeranchukon coupling 2-76715
$p\pi^- \to pX^-$, 25 and 40 GeV/c, scaling and estimate of triple- Pomeranchukan coupling 2-73846
$p\pi \to p$ + anything, finite-energy sum rules, Reggeon-particle scattering amplitudes 2-73849
π-p, 2.45 GeV/c, meson and baryon reson. prod. 2-42403
π-p, comparison of multiperipheral model with inclusive data 2-49552
π-p, study of two-body strange-particle final states at 4.5 GeV/c and 6 GeV/c, meas. of differential cross sections 2-79599
π-p charge exchange, differential cross sections, evidence for tachyonic resonances 2-63546
$\pi\text{-}p \to K^0{}_s K\text{-}p$, 20.3 GeV/c, study of production and decay of A_2 resonance 2-63641
$\pi\text{-}p \to K^{*0}\Lambda$, 3.9 GeV/c, amplitude structure determ. from decay correlations 2-42391
$\pi\text{-}p \to \eta\varphi$, 1.8 GeV/c, decay mode $\varphi \to \eta\gamma$ obs. 2-63643
$\pi\text{-}p \to n\pi^0$ meas. of differential cross section at 317, 452, 491 MeV/c using $n\gamma$ coincidence method 2-63617
$\pi\text{-}p \to n\pi^+\pi\text{-}$, 2.77 GeV/c, parametrization of nonevasive exchange processes and background contribs. 2-76680
$\pi\text{-}p \to n\pi^+\pi\text{-} + (1, 2, 3, 4, 5)\pi^0$, 5 GeV/c, partial cross sections and ang. and momentum distributions 2-52617
$\pi\text{-}p \to \pi\text{-}\ pX^0$, 13.4 GeV/c, natural meson production meas., π°, ρ^0, ω^0, D° 2-52616
$\pi\text{-}p \to \pi\text{-}\pi^+ n$, 8 GeV/c, meas. of production and decay angular distributions of ρ^0, f^0, and $\pi^+\pi\text{-}$ mass distrib. 2-79600
$\pi\text{-}p \to \pi\pi N$ events from hydrogen bubble chambers, selective compilation 2-42395
$\pi\text{-}p \to \rho\text{-}p \to \pi\text{-}\pi^0 p$, 2.77 GeV/c, spin density matrix elements computed analysis of ρ polarization 2-63646
$\pi\text{-}p \to \rho n \to \pi^+\pi\text{-}n$, 2.77 GeV/c, spin density matrix elements computed, analysis of ρ polarization 2-63646
π^-p, 13.1 GeV/c, study of reactions with two charged final state particles 2-63620
π^-p, 16 GeV/c, obs. of central emission of pions, search for symmetry system 2-73816
π^-p, 1.69 GeV/c, production of $Y_0^*(1405)$, $Y_1^*(1385)^\circ$, meas. of width, mass, spin, parity of resonance 2-46018
π^-p, 25 GeV/c, single and double π prod. processes 2-45969
π^-p, 3.8 GeV/c, obs. of $X^0 \to \gamma\gamma$ 2-67037
π^-p, 40 GeV/c, determ. of charged and neutral particle multiplicity 2-76682
π^-p, 40 GeV/c, multiplicity distribution of charged particles produced 2-45960
π^-p, 7 GeV/c, four- and five-body final state interactions 2-67026
π^-p, intrinsic props. of η, S^0, ρ, ω, X^0, φ and $A_2{}^0$ mesons 2-73835
π^-p, two-particle correls., 60 GeV/c 2-63614
$\pi^-p \to B^-p$, cross-section, OMEA model, rel. to B-meson spin parity 2-76698
$\pi^-p \to K^+Y^{*-}(1385)$, final-state-interaction contributions to exotic forward peak 2-63618
$\pi^-p \to K^{*0}\Lambda$, meas. of joint density-matrix elements, study of vector-meson production with hypercharge exchange 2-82743
$\pi^-p \to K^{*0}\Lambda$, polarization and unnatural parity exchange 2-42376
$\pi^-p \to M^0 n$, 2.4 GeV/c, $M^0(940)$ and $\delta^0(963)$ obs. 2-76693
$\pi^-p \to M^0 n$, 2.4 GeV/c, neutral meson detection 2-70207
$\pi^-p \to X^-p$, boson missing-mass spectrum struct. 2-76679
$\pi^-p \to (MM)^-p$, 8, 11, 13.5, 16 GeV, meas. of missing mass spectra, evidence for triple factorizability of cross sections 2-76678
$\pi^-p \to (mm)^-p$, 8 GeV/c missing mass spectrum in R region 2-73821
$\pi^-p \to (pp)n$, 18.8 GeV/c, obs. 2-45965
$\pi^-p \to (\pi^0\pi^0)n$, production of neutral resonances that decay to $\pi^0\pi^0$ at Serpukhov energies 2-76683
$\pi^-p \to e^+e^-n$, dispersion model, use for calc. of N, π form factors 2-63602
$\pi^-p \to \eta^0 n$, partial differential cross section at large momentum transfer and incident pion momenta 3.67 and 4.38 GeV/c 2-63575
$\pi^-p \to \eta n$, applic. of symmetry point sum rules 2-49566
$\pi^-p \to$ missing mass + n, meson mass spectrum near $X^0(958)$ 2-42402
$\pi^-p \to nX^0$ near threshold, meson mass spectrum 2-76676
$\pi^-p \to n$ + (missing-mass), missing-mass spectrum near 960 MeV 2-76675
$\pi^-p \to n$ + neutral boson, search for decay mode $\omega \to \eta\gamma$ 2-79603
$\pi^-p \to \omega^0 n$, 3.65, 4.5, 5.5 GeV/c, study of ω^0 spin-density matrix 2-52625
$\pi^-p \to \omega^0 n$, 3.65, 4.5 and 5.5 GeV/c, differential cross section 2-67027
$\pi^-p \to pX^-$, 25, 40 GeV/c, missing mass spectra 2-49568
$\pi^-p \to p\pi^+\pi^-\pi^-$, spin-parity analysis of A_3 ($f\pi$) resonance 2-49581
$\pi^-p \to p\pi^+\pi^-\pi^-\pi^0$, decay properties of $\rho(1.71)$ resonance 2-49582
$\pi^-p \to \pi^-\pi^-\pi^+p$, 40 GeV/c, A_1 and A_2 prod. 2-76699
$\pi^-p \to \pi^-\pi^0 p$, $p_{\pi-} = 4.45$ GeV/c, elastic $\pi^-\pi^0$ scatt. cross section 2-76681
$\pi^-p \to \pi^-\pi^+n$, 17.2 GeV/c, $\pi\pi$ phase-shift analysis 2-76673
$\pi^-p \to \pi^-\pi^+n$, 4 GeV/c, determ. of isoscalar S-wave $\pi\pi$ phase shift with absorption modified one pion exchange model 2-63609
$\pi^-p \to \pi^0 n$, charge exchange at Serpukhov energies 2-76683
$\pi^-p \to \pi^0 n$, charge exchange differential cross sections at 3.67 and 4.83 GeV/c and intermediate momentum transfers 2-63619
$\pi^-p \to \pi^0 n$ (ηn), properties of polarization in forward direction determ. using Regge amplitudes 2-70237
$\pi^-p \to \pi^0 n$ charge exchange, momentum dependence of differential cross section at 180° in 1.8-6.0 GeV/c range 2-82758
$\pi^-p \to \pi^0\pi^0 n$, exptl. study at 447 MeV, cross sections and missing mass spectrum 2-49567
$\pi^-p \to \pi^0\pi^0 n$, use with one-meson approx. to obtain $\pi\pi$ scattering cross-section 2-82764
$\pi^-p \to \pi^+\pi^-n$, 15GeV/c, model amplitude analysis 2-67023
$\pi^-p \to \pi^+\pi^-n$, one pion exchange model developed using Veneziano five point function 2-52618
$\pi^-p \to \pi^+\pi^-\pi^-p$, 11-40 GeV, A_3 enhancement, non-resonant behaviour 2-76677
$\pi^-p \to \rho^-p$, 3.25 GeV/c, comparison between exptl. data and prediction of absorptive model 2-67024
$\pi^-p \to \rho^0 n$, 3.25 GeV/c, comparison between exptl. data and prediction of absorptive model 2-67024
$\pi^-p \to \rho^0 n$, appl. Reggezied OPEA model 2-76645
$\pi^0 p \to \rho^0 p$ differential cross- section explained by nonsense wrong signature zeros 2-59529
π^+p, 12-28 GeV, correlations between produced π^- particles 2-55832
π^+p, 4.1 GeV/c, analysis of 2-pronged events 2-63621
π^+p, 5 GeV/c, evidence for double diffractive dissociation 2-59531
π^+p, 5.45 GeV/c, production properties of $A_1{}^+$ 2-73838
π^+p, 8 and 16 GeV/c, obs. of central emission of pions, search for symmetry system 2-73816
π^+p, 895, 945, 995, 1040 MeV/c, cross sections and resonance fractions for two single pion production channels 2-42390
π^+p, correlation parameters for π^- production calc. from multiplicity distrib. 2-49592
π^+p, ω production at 2.67 and 2.30 BeV/c, differential cross sections, decay density matrix elements 2-45987
π^+p, π^- energy spectra, analysis for beam momenta of 8 and 16 GeV/c 2-52614
π^+p, single-particle and two-particle inclusive reactions at 7 GeV/c 2-45944
$\pi^+p \to K^+K^-\Delta^{++}$, 7.1 GeV/c, $\pi\pi$ phase shifts 2-76674
$\pi^+p \to K^+\Sigma^+$, 1.11 GeV/c, polarisation 2-42394
$\pi^+p \to K^+\Sigma^+$, calc. of $N^{*3/2}$ partial widths and branching ratios 2-70268
$\pi^+p \to K^+\Sigma^+$, differential cross sections near 0° at 3,5,7 GeV/c 2-70238
$\pi^+p \to K^+Y^{*+}(1385)$, differential cross sections near 0° at 3,5,7 GeV/c 2-70238
$\pi^+p \to (\pi^+\pi^-)\Lambda^{++}$, 13 GeV/c, phase shift analysis of $\pi^+\pi^-$ scattering in mass range 0.6-1.4 GeV 2-73826
$\pi^+p \to \eta\Delta^{++}$, local duality and dips 2-52615
$\pi^+p \to \kappa^+\Sigma^+$, 2 and 4 GeV/c, meas. of polarization in backward direction 2-76686
$\pi^+p \to \pi^-\pi^-X$, 18.5 GeV/c, two- particle inclusive distrib. and correlation functions 2-82707
$\pi^+p \to \pi^-\pi^-X$, evidence for factorization 2-63616
$\pi^+p \to \pi^0\Delta^{++}$, local duality and dips 2-52615
$\pi^+p \to \pi^+\pi^-\Delta^{++}$, 7.1 GeV/c, $\pi\pi$ phase shifts 2-76674
$\pi^+p \to \pi^+\pi^-\Delta^{++}$, model moments 2-73824
$\pi^+p \to \pi^+\pi^+\pi\text{-}p$, 13.1 GeV/c, spin-parity analysis of low-mass 3π system 2-45962
$\pi^+p \to \pi^+\pi^+\pi^-p$, 8 and 16 GeV/c, separation of production mechanisms by longitudinal phase space analysis 2-70235
$\pi^+p \to \pi^+\rho^0 n$, 7 GeV/c, A_1 study 2-49584
$\pi^+p \to \pi^\pm$ + anything, $\pi^-p \to \pi^-$ + anything, 3.7 to 18.5 GeV/c, energy dependence of inclusive distributions 2-42392
$\pi^+p \to \rho^0{}_{1236}{}^{++}$, near threshold, chiral SU(2) × SU(2) dynamics 2-67025
$\pi^+p \to \rho^+p$, 2.67 GeV/c, isoscalar exchange 2-45964
$\pi^\pm p$, $\Delta(1236)$ production, application of Regge-pole model 2-73856
$\pi^\pm p$ total cross-sections, empirical scaling behaviour 2-73778
$\pi^\pm p$ total cross section from 0.4-0.9 GeV/c meas. using transmission method 2-63611
$\pi^\pm p$ total cross sections, 0.4 to 0.9 GeV/c 2-79598
$\pi^\pm p \to A_1{}^\pm p$ at small momentum transfer, eikonal Regge model 2-45966
$\pi^\pm p \to \rho^\pm p$, 15 GeV/c, spark chamber meas. 2-79584
$\pi^\pm p \to \rho N$ rho production reactions at 16 GeV/c, study of exchange mechanisms 2-70236
$\pi p \to K^-\pi^+\pi^-$ 16 GeV/c s-channel and t-channel helicity conservation tested 2-82753
$\pi p \to K^*Kp$, obs. of F_1 (1540) kinematic enhancement, Reggeized Deck model, link with resonance 2-63633
$\pi p \to \Lambda(\Sigma)K$, inelastic reactions, complex moments analysis considering j-plane branching 2-76661
$\pi p \to p\pi^+\pi^-$, 16 GeV/c s-channel and t-channel helicity conservation tested 2-82753
$\pi p \to \pi\pi^+\pi^-$ 16 GeV/c s-channel and t-channel helicity conservation tested 2-82753
$\pi p \to \rho N$, pion exchange, 6 GeV/c 2-59532
$\pi\text{-}p \to n\gamma$, 370 and 332 MeV, meas. of diff. cross sections 2-42393
$\pi\text{-}p \to p\pi^+\pi\text{-}\pi\text{-}$, 20 GeV/c, production of N^{*++} (1236), ρ^0, f^0, A enhancement in 3π mass spectrum 2-45963
π^-p collisions, high multiplicity pion production 2-67028
$\pi^\pm p$, total cross sections in momentum region 15 to 60 GeV/c, Glauber correction 2-45968

production
asymmetry of distrib. in high energy πp and Kp interactions 2-45967
average multiplicities, proton proton interactions 2-59566
Bose distribution in p-p collisions at 12-30 GeV/c, determ. of scaling behaviour 2-76717
central emission in π^+p, π^-p, K^-p reactions, search for symmetry system 2-73816
charged, from γd interaction, Khuri Treiman formalism applied 2-42386
charged particle prod. at 90° in centre of mass in pp collisions 2-82773
electroproduction, charged pions, pseudovector pion-nucleon coupling 2-45952
electroproduction, form factor 2-70225
electroproduction, inclusive pion distributions 2-70231
emulsion-nuclei interactions with p at 22.6 GeV/c, velocity distrib. of secondary π meson 2-76840
factorization hypothesis in 'central' region 2-63542
in inclusive processes, multiperipheral model approach 2-79525
inclusive soft pion production, $e\gamma$ scattering 2-42384
inclusive two pion production, rapidity correlations, study by multiperipheral- thermodynamic model 2-49563
intersecting storage rings data at CERN 2-73853
longitudinal momentum distrib., derivation from quark- boson hadron model 2-66956
momentum distribs. in 19 GeV/c pp collisions with and without strange-particle production 2-73847

Pions continued
production continued
nonlocal theory of single pion photoproduction 2−55854
in nuclear collisions, study using current algebra 2−63862
pair production, e.m. form factor, inelastic contribs. 2−42382
in photonuclear reactions, nuclear transparency calcs. 2−59739
photoproduction, determ. of πN coupling constant 2−45951
photoproduction, kinematics of coupling of Regge poles to photons 2−63605
photoproduction, method of evaluation of t-channel singularities 2−63504
photoproduction, on protons and deuterons at 400 to 800 MeV, comparison of cross sections 2−42383
photoproduction, review of N polarization 2−45959
photoproduction, Watson theorem, extension to double pion photo processes 2−67018
photoproduction by γ-γ reactions, effective Lagrangian model 2−55853
photoproduction of charged and neutral pairs in energy range 600-900 MeV meas. of cross-sections 2−73815
photoproduction off nucleons, sum rules and Veneziano model 2−82670
photoproduction on deuterium, π^-/π^+ ratios, dip test of isotensor current 2−49560
photoproduction on deuterons by polarized gamma-rays, coherent, asymmetry 2−70229
photoproduction on nuclei 2 and 3 GeV 2−82951
photoproduction on protons near $P_{33}(1236)$ reson., multipole analysis 2−67016
photoproduction on quasi-free nucleons in nuclei 2−76829
photoproduction on quasifree nucleon in ^4He 2−79493
in proton interactions in nuclei at 24 GeV/c 2−63606
ratios at 21, 31, 45, 53 GeV in centre of mass 2−49564
scale invariance at high energies tested using cosmic ray primary nucleon and sea level muon intensities 2−49607
secondary, due to cosmic rays $>10^{12}$ eV, ang. distrib. and multiplicity 2−73899
single, in π^+p interactions at 895, 945, 995, 1040 MeV/c, cross sections and resonance fraction for $\pi^+\pi^0p$ and $\pi^+\pi^+n$ channels 2−42390
single-particle prod., dual-model analysis at intermediate energies 2−79526
e^+e^-, study of amplitudes for production of two and four charged pions by photons in low-energy region 2−52612
e^+e^- annihilation, validity of vector-meson dominance model 2−70230
$e^+e^-\to3\pi$, high energy limit in Feynman graph framework 2−76603
$e^+e^-\to\pi^+\pi^-\pi^0\pi^0$, 990 MeV, cross section meas. at Orsay Storage Ring 2−66943
ep deep inelastic scattering, light-cone analyis of soft-pion production 2−45954
$\eta\pi$ mass spectrum in $\pi^-p\to\eta\pi^-p$ at 6 GeV/c 2−76670
γd, 240 to 400 MeV, π^-/π^+ ratio 2−67017
$\gamma\gamma\to\pi^+\pi^-$, cross-section calc. with strong interaction correction 2−82669
$\gamma\gamma\to\pi\pi\pi$, test of low-energy theorem using $Z(\gamma,3\pi)Z$ reaction 2−76596
γn, calculation from π^+ photoproduction on protons 2−67017
γN, single-pion photoproduction via s- channel resonances in model of higher baryon couplings 2−45955
$\gamma N\to N\pi^+\pi^-$, nonrelativistic solvable model 2−79575
$\gamma n\to\pi^0n$, 450-800 MeV, differential cross- section meas. 2−45958
$\gamma n\to\pi^0n$ differential cross- section explained by nonsense wrong signature zeros 2−59529
$\gamma N\to\pi N$, baryon Regge pole exchange model 2−52623
γp, isotensor contribution 2−67017
$\gamma p\to\pi^0p$ differential cross-section explained by nonsense wrong signature zeros 2−59529
K/π ratio in single particle inclusive processes at cosmic ray energies 2−67051
$K\to\mu\mu$, anomalous $K\to\pi\pi\gamma\to\mu\bar{\mu}$ interaction 2−63585
$K_s^0\to\pi^+\pi^-/K^0\to\pi^0\pi^0$, branching ratio meas. 2−52594
$\mu N\to\pi+$anything, inclusive processes, 10.1 and 15.8 GeV/c 2−59430
$NN\to NN+n\pi$, uncorrelated jet model 2−70173
np charge- exchange reaction, model for pion-Pomeranchon Regge cut 2−52640
ν interaction 2−45949
p/π- diffractive excitation model adjustment of relative renormalization 2−82756
pN interactions with emulsion nuclei, 20-70 GeV, coherent π production cross-section 2−73844
pp collision processes, hydrodynamical model scaling law 2−82774
pp interaction, cross-section energy depend. in simple peripheral model 2−79596
$pp\to X^0\pi^0\to n\pi^+\pi$-$\pi^0$, n=3.4, 6.94 GeV/c obs. X^0 3.1, 3.4, and 3.6 2−63645
$pp\to6\pi$, 2.5 GeV/c, ω, ρ production resonance production 2−79615
$pp\to n\pi$ limiting behaviour of single particle distributions 2−59440
$pp\to\omega^0\pi^+\pi^-$, analysis of $I=0\pi^+\pi^-$ system 2−79602
$pp\to\pi^-\pi^-+$ anything, exptl. investigation of two-body correlations 2−42412
$pp\to\pi^+\pi^-$ cross- section compared with that for $\pi^+\pi^+\to pp$ 2−45965
$pp\to\pi^\pm+$anything 28.5 GeV, single-particle inclusive pion spectrum 2−45950
π^+/π-, diffractive excitation model adjustment of relative normalization 2−82756
π-π even partial-wave phase shifts, meas. in $ee\to ee\pi\pi$ colliding beam expts. 2−63608
π-, polarized photons from 0.8 to 2.2 GeV in resonance region 2−45956
π- photoprod., energy-independ. multipole analysis 2−67014
3π production cross-sections meas. in 15.1 GeV/c π reactions on various nuclei 2−49815
π^-, cross sections in inclusive photoproduction 2−49562
π^-, inclusive pp interactions from 13 to 28 GeV/c 2−67050
π^- i pp and π^+p collisions, correlation parameters calc. from multiplicity distrib. 2−49592

Pions continued
production continued
π^- in K^+p, π^+p and pp inclusive expts., 12-28 GeV, investigation of correlations 2−55832
π^- inclusive distrib. in γp, K^+p and pp collisions 2−67052
π^- inclusive reactions, factorization in central region 2−70228
π^- produced in high-energy pp collisions, two particle correlations 2−82780
π^0, analysis of $p+d\to{}^3He+X^0$ reaction 2−42411
π^0, by bremsstrahlung interaction with H at high-energy, spectrum determ. from inclusive photon yields 2−76595
π^0, photoproduction from complex nuclei from 4.25 to 9.6 GeV 2−42555
π^0, polarized photons from 0.8 to 2.2 GeV in resonance region 2−45956
π^0, π^+, photoproduction by linearly polarised gamma rays in range 400 to 900 MeV, asymmetry meas. 2−59527
π^0, search in spontaneous fission of ^{252}Cf 2−46059
π^0 electroprod. in second reson. region 2−67015
π^0 electroproduction at first resonance at momentum transfers $q^2=0.6$, 1.0 and 1.56 GeV^2 2−73817
π^0 in pp collisions at ISR energies, angular distrib. determ. from γ-ray data 2−49561
π^0 photoprod., cut contribs. in dual cut model 2−55852
π^0 photoprod. from deuteron in first reson. region 2−82671
π^+, asymmetry for photoproduction from polarized protons between 300 and 900 MeV at 90° 2−59528
π^+, cross sections in inclusive photoproduction 2−49562
π^+, polarized photons from 0.8 to 2.2 GeV in resonance region 2−45956
π^+ beam, 25-70 GeV/s pulse, from internal target in accelerator 2−42480
π^+ inclusive electroproduction, hypothesis of limiting fragmentation 2−79502
π^+ photoprod., energy-independ. multipole analysis 2−67014
π^+ photoproduction on protons in backward direction, 0.7-8 GeV, comparison with Regge-pole analysis 2−63607
π^+ photoproduction on protons, 220-425 MeV, meas. of angular distrib. between 15° and 180° 2−52613
π^+ photoproduction on protons obs., 0.66 to 7.4 GeV/c 2−63610
$\pi^\pm$, photoproduction on deuteron, π^-/π^+ ratio 2−49559
$\pi^\pm$, ratios at 21, 31, 45, 53 GeV in centre of mass 2−49564
$\pi\pm$ electroproduction, obs. of coincidences of electrons with forward produced pions 2−49503
$\pi^\pm$ inclusive spectra in pp collisions, quantitative Regge expressions with scaling 2−45953
$\pi^\pm$ photoproduction near proton fragmentation region, inclusive cross section predicted via factorisation 2−59403
π^o electroproduction in resonance region, dispersion relation calculation 2−55851
π° by high energy cosmic rays π and N (>1 TeV) 2−73888
$\pi^0\gamma\gamma$ vertex, investigation using electron- positron storage rings 2−49496
$\pi^0\gamma\gamma$ vertex, investigation using electron- positron storage rings 2−49497
$\pi^-N\to\pi^-\pi^-\pi^+N$, 60 GeV/c, photoemulsion study 2−73818
$\pi^-N\to\pi^-\pi^0\pi^0N$, photoemulsion study 2−73818
$\pi N\to\pi\pi N$, results of combining conformal invariance and chiral symmetry 2−63612
πp interaction, cross-section energy depend. in simple peripheral model 2−79596
$\pi^-p\to\pi^-\pi^+n$, 4 GeV/c, determ. of isoscalar S-wave $\pi\pi$ phase shift with absorption modified one pion exchange model 2−63609
$\pi^-p\to\pi^+\pi^-n$, 15GeV/c, model amplitude analysis 2−67023
$\pi^+p\to\pi^+\pi^+\pi$-p, 13.1 GeV/c, spin-parity analysis of low-mass 3π system 2−45962
$\pi\pi$ phase shifts in moment analysis of $\pi N\to(\pi\pi)N$ and $\pi N\to\pi\pi)\Delta$ 2−67022
$^{11}B(\gamma,\pi^+)$, study of photoproduction in framework of impulse approximation 2−52798
$^9Be(p,\pi^-)^{10}C$, 600 MeV, cross-section 2−67222
K-/π- diffractive excitation model, adjustment of relative normalization 2−82756
K-p interactions, 5.5 GeV/c single pion production 2−49551
^6Li, pion electroproduction at 1180 MeV 2−70439
π^0 photoprod., energy-independ. multipole analysis 2−67014
$\pi^\pm$, absorptive corrections in photoproduction 2−42385
π^-p collisions, high multiplicity production 2−67028

scattering
Compton, low-energy theorem and threshold identity, arguments for fixed pole 2−76671
$K\pi$ phase shifts, cross section and moment extrapolations to π pole 2−73824
lengths, modified current algebra in broken chiral symmetry 2−73736
$A_1\pi\to\pi\pi$, applic. of crossing symmetric dual amplitude with geometrical structure 2−59474
$K\pi$, analysis in $K^+n\to K^+\pi$-p reaction 2−49558
$K\pi$, calc. of consts. and parameters pade approx. 2−79556
$K\pi$, off-shell scatt., effects from linear dynamical zeros 2−73825
$K\pi$, phase-shift solutions in model satisfying analyticity, crossing symmetry and approx. unitarity 2−67032
$K\pi$, saturation of commutator matrix element, local approx. 2−49544
$K\pi$, sharp changes in behaviour of $\langle Y_1{}^0\rangle$ moment 2−45971
$K\pi$ angular distribs. obs. in $K^+p\to K^+\pi^-\pi^+p$ and $K^+p\to K^0\pi^0\pi^+p$ reactions from 3-13 GeV/c 2−42378
$K\pi$ elastic scattering cross-section in $I=3/2$ state studied using K^-d interaction at 5.5 GeV/c 2−63594
$K\pi$ phase shifts, duality structure 2−59543
$K\pi$ S-wave amplitude and 'up-down' ambiguity 2−59556
$K^+\pi^-\to K^0\pi^+\pi^-$, cross section determ. using Chew-Low extrapolation method 2−49555
$\pi^\pm$ e.m. form factors and inelastic structure function meas. using NAL and ISR 2−73812
πA_1-πA_1, analysis using hard-pion constraints of current algebra and current conservation in the Veneziano model 2−63632
π-^{12}C elastic scatt., cross sections analysis 2−82723
πd, elastic, in πN resonance region, use of Glauber formulas incorporating Fermi motion 2−45972

Pions continued
scattering continued
πd, generalised Glauber formula with recoil 2−59487
πd scattering length, formula obtained by summing infinite series of nonrelativistic Feynman graphs 2−45970
$\pi\Delta$, static model for elastic scattering, possible improvements 2−42399
$\pi\Delta\rightarrow\omega\Delta$, dual amplitudes and relations between coupling consts. 2−76684
$\pi\eta\rightarrow\pi\eta,\pi\rho$, t-channel Regge amplitudes for local duality 2−63552
πK, bootstrap calc. of K* using effective potential method 2−45989
πK, low-energy, compatibility between current algebra and unitarity constraints 2−67030
πK, low energy, inverse amplitude dispersion relations 2−82733
πK(s=0,T=1/2) phase shift for simple bound on $K\rightarrow\pi\mu(e)\nu$ decay parameters 2−82744
$\pi\Lambda$, sum rules for elastic scatt. amplitudes, threshold behaviour 2−70242
πN, peripheral partial wave amplitudes from two pion exchange 2−42397
πN charge exchange, strong suppression of Regge-Regge cuts 2−59493
$\pi\Sigma$, sum rules for elastic scatt. amplitudes, threshold behaviour 2−70242

scattering, pion-nucleon
6 GeV/c, enhanced absorption model, and impact parameter space 2−45974
σ term, validity of extrapolation procedure of Cheng and Dashen 2−79590
absorption model construction 2−63651
absorptive separable potential construction 2−59536
amplitude analysis at 6 GeV/c 2−49570
amplitude determ. using Pade approx. 2−73291
amplitudes determ. using rot. parameters 2−82752
analyticity of forward scattering amplitude, test, determ. of πN coupling constant 2−73822
backward amplitudes, dual absorptive model 2−79580
change-exchange, fixed-t dispersion relations and polarization 2−63624
charge exchange, application of unitarized finite energy sum rules 2−45921
charge exchange polarization and violation of Pomeranchuk theorem 2−45976
charge-exchange at 6 GeV/c, structure of partial wave amplitudes 2−59533
conservation of s-channel helicity for pomeron exchange and flip dominance for ρ-exchange studied in ABFST multiperipheral model 2−42398
cross sections, optimal extrapolation 2−76668
dispersion relations, soln. by Pade approximant method 2−49569
dual geometrical model applic. to elastic and charge exchange scatt. 2−67031
dual Regge cut amplitudes 2−55856
dynamic model for 33-phase shift 2−63626
elastic, four-vectors and helicity amplitudes 2−63625
elastic and charge exchange, phenomenological analysis, Regge contributions 2−42400
fixed-u finite energy sum rule calcs. using realistic spectral functions 2−63627
forward charge-exchange finite energy sum rules and Regge cuts 2−59537
forward scattering amplitude, duality and high-energy limit 2−76664
forward scattering data, consistency with analyticity and crossing 2−76666
helicity amplitudes calc. for isospin I=0 and I=1 states at 6 GeV/c and for I=0 exchange at 16 GeV/c 2−55857
high-energy, linear trajectory fits in simple Regge model 2−63623
I_t=0 scattering amplitude at 6 GeV/c, properties of pomeron term 2−70240
inelastic phase-shift analysis, removal of ambiguities 2−63555
isospin bounds and zeros of scattering amplitudes 2−76665
isospin mixing as source of enhanced isospin violation below 1 GeV/c 2−52620
low energy theorem from pion source dynamics 2−59542
low energy theorems, current algebra description 2−59525
low-energy parameters evaluation using finite-energy and current algebra sum rules in quark model 2−63529
multiple scattering model and slope of Pomeranchuk trajectory 2−42396
narrow-resonance approx. calcs. using gauge-field theory of fermions 2−82623
P-wave scattering amplitudes and their S-matrix calculations 2−45975
polarization, relative magnitude and phase of amplitudes depend. 2−59535
Pomeron-exchange amplitude and cross sections due to resons. 2−52619
Regge cuts, eikonal model 2−59538
Regge pole exchange, multiple, consequence of crossing symmetry 2−79576
Regge pole model with explicit quark spin applied to meson and baryon exchange 2−49572
Regge pole residues, optimised FESR 2−66980
relativistic Regge-cut model for invariant functions 2−76667
resonances, introduction of effective mass and effective width 2−63561
s-channel helicity amplitudes, structure determ. as function of momentum transfer and energy 2−82760
S-wave analysis, low energy ambiguities of $\pi\pi$ isospin-zero S-wave on comparison 2−55861
short range P-wave, comparison with backward Regge models 2−79578
sigma term, new determ. including off shell effects 2−76662
sigma term value 2−45929
static model for elastic scattering, possible improvements 2−42399
strong shrinkage of $d\sigma/dt$ at $|t|$=(1-3) (GeV/c)^2 2−70241
sum rule derivation for scattering length using broken scale invariance and mass-dispersion relations 2−66911
sum rules for elastic scatt. amplitudes, threshold behaviour 2−70242

Pions continued
scattering, pion-nucleon continued
total cross sections, resonance and background contributions, 1-4 GeV/c 2−76646
urbaryon rearrangement and reson. correl. 2−63563
G_{39}-resonance, evidence 2−70239
N and Δ exchanges, separation and deduction of amplitude zeros 2−59508
πN charge exchange, model for relationship of fixed pole to shielding cut 2−49571
$\pi N\rightarrow A_1N$, helicity conservation 2−45973
$\pi N\rightarrow\omega N(\Delta)$, dual amplitudes and relations between coupling consts. 2−76684
$\pi N\rightarrow\pi\Delta$, theoretical analysis concerning resonance coupling 2−59534

scattering, pion-pion
980 MeV, Odorico zeros of scattering data 2−49575
amplitude determ. using Pade approx. 2−73291
amplitude on mass shell and σ- commutator term 2−55862
asymptotic, new constraints derived using Chou-Yang model 2−70224
Bethe-Salpeter calc. using mesh-point inversion of the energy analytic kernel 2−82624
broken scale invariance low-energy theorems, I=0 $\pi\pi$ s wave 2−76689
chiral invariance and effective range expansion 2−79587
continuous moment sum rules, estimation of Regge parameters of exchanged trajectories 2−55859
crossing conditions and ρ meson existence 2−76688
diffraction peak, nonlinear duality calculation of width 2−82762
dual scattering amplitudes incorporating unitarity 2−63562
elastic, analysis using hard-pion constraints of current algebra and current conservation in Veneziano model 2−63632
forward scatt. amplitudes, sum rules 2−79498
high energy bounds, derivation from low energy data 2−59398
I=0 and I=1 partial waves in low energy scatt. 2−79577
inequality, restrictive, improved 2−70243
intermediate-energy bootstrap dynamics based on average nonlinear duality 2−66986
isospin-zero S-wave, low-energy ambiguities compared with πN S-wave analysis 2−55861
length, nonlinear model, chiral symmetry breaking, W-parity, octet dominance 2−73739
low energy, inverse amplitude dispersion relations 2−82733
low-energy, quasilinear models and rigorous constraints below threshold 2−70246
low-energy parameters determ. from current algebra, unitarity corrections 2−55860
off-shell scatt., effects from linear dynamical zeros 2−73825
partial wave ambiguities, analyticity props. 2−79581
partial wave amplitudes below threshold, constraints from crossing symmetry, positivity and analyticity 2−67033
phase shift parametrization 2−67013
phase shifts, cross section and moment extrapolations to π pole 2−73824
phase shifts, duality structure 2−59543
phase-shift solutions in model satisfying analyticity, crossing symmetry and approx. unitarity 2−67032
phenomenology below 1100 MeV 2−73827
physical-region sum rules derived from crossing symmetry and Regge high-energy behaviour 2−70245
resonances, introduction of effective mass and effective width 2−63561
review of current activity on this and related processes 2−82766
review of various models 2−45978
s and p wave inverse amplitudes, solns., existence of resonance predicted 2−73829
s and p waves, new inequalities 2−73828
s partial-wave amplitude, upper bound in unphysical region 2−70244
S-wave amplitude, summary of published papers and new expts. 2−59556
S-wave phase shifts 2−79570
s-wave phase shifts in $\pi^-p\rightarrow\pi^0\pi^0n$ reaction at 8 GeV/c 2−79588
S-wave scattering length, W-parity, octet dominance and breaking of chiral symmetry 2−66909
scattering lengths calc. using weak form of pion-pole dominance, comparison with Weinberg calc. 2−63631
total cross sections, 300 GeV, Froissart bound 2−82757
$\langle Y_1{}^0\rangle$, sharp changes in behaviour 2−45971
$\pi^0\pi^0$ general crossing symmetric amplitude, best positivity and analyticity inequalities 2−49576
$\pi^+p\rightarrow{}^+p$, 1.55-1.84 GeV/c high-statistics study, obs. of dip structures 2−82754
$\pi^0\pi^0$ partial waves, enlargement of domains of Mandelstan triangle 2−49574
$\pi^0\pi^0$ S-wave amplitude improved constraints 2−45977
$\pi^+\pi^-$ ang. distrib., unique set of $\delta_0{}^0$ 2−76687
$\pi^+\pi^-$ in $\pi^+p\rightarrow(\pi^+\pi^-)\Delta^{++}$ reaction at 13 GeV/c, phase shift analysis in mass range 0.6-1.4 GeV 2−73826
$\pi^+\pi^-\rightarrow\pi^0\pi^0$ charge exchange reaction, cross-section obtained from $\pi^-p\rightarrow\pi^0\pi^0n$ and $\pi^+n\rightarrow\pi^0\pi^0p$ 2−82764
$\pi\pi\rightarrow N\bar{N}$, lower bounds on scatt. amplitudes 2−52622
$\pi\pi\rightarrow N\bar{N}$ helicity amplitudes at T=0, phenomenological J-plane singularities 2−42401
$\pi\pi\rightarrow\pi A_1$, analysis using hard-pion constraints of current algebra and current conservation in Veneziano model 2−63632
$\rho\rho$ P triple-Regge vertex calc. from two-body scattering data assuming duality and f-coupled Pomeron 2−55842
$\pi^0\pi^0$, constraints on d-wave 2−49573

scattering, pion-proton
backward elastic, fluctuations, dips and duality 2−82759
elastic, slope parameter of diffraction peak 2−79611
inelastic collisions, prong-number distrib. 2−79617
nonshrinking diffraction peak due to fixed pomeron 2−45923
polarization, interpretation in terms of optical model 2−67056
radiative scatt. near Δ(1236) reson. 2−76685
spin rotation meas. at high energies, apparatus 2−73901
A_1 diffraction production 2−82768
$\pi^-\rightarrow\pi^0n$, multiple scatt. model, duality breaking effects 2−63572

- **Pions** continued
  - **scattering, pion-proton** continued
    - π-p, elastic, meas. of differential cross-section near 180° from 2.15 to 6 GeV/c 2−63629
    - π-p elastic backward Regge pole analysis 2−63630
    - $\pi\text{-}p\rightarrow k\gamma+n$, (k=2-4), pseudoscalar and vector meson obs. 2−70202
    - π^-p, differential cross-section, electromagnetic form factors in parton model 2−73811
    - π^-p, differential cross sections, unitarization and OBE contrib. 2−76638
    - π^-p, elastic charge exchange scatt., s-channel helicity amplitude 2−59520
    - π^-p, elastic scatt. cross section at 2.29 GeV/c 2−59541
    - π^-p charge-exchange reactions, kinematic variable 2−79595
    - π^-p forward elastic scattering near 1 GeV/c, meas. of differential cross section 2−73823
    - $\pi^-p\rightarrow K^0\Lambda$, 1400-2000 MeV, new phenomenological analysis 2−52621
    - $\pi^-p\rightarrow K^0\Lambda^0$ backward high energy, prediction of polarization sign 2−63628
    - $\pi^-p\rightarrow P^-p$, elastic, phenomenological use of Callan-Symanzik eqn., obs of scaling law 2−66922
    - $\pi^-p\rightarrow\eta n$, multiple scatt. model, duality breaking effects 2−63572
    - $\pi^-p\rightarrow\eta\pi^-p$, 6 GeV/c, study of $\eta\pi$ mass spectrum, D-wave Breit-Wigner analysis 2−76670
    - $\pi^-p\rightarrow\pi^-p$, 1400-2000 MeV, new phenomenological analysis 2−52621
    - $\pi^-p\rightarrow\pi^-p\pi^0$, 1400-2000 MeV, new phenomenological analysis 2−52621
    - $\pi^-p\rightarrow\pi^-\pi^-\pi^+p$, A_1 and A_2 prod. mechanisms, 7 GeV/c 2−55867
    - $\pi^-p\rightarrow\pi^-\pi^0\pi^0p$, A_1 and A_2 prod. mechanisms, 7 GeV/c 2−55867
    - $\pi^-p\rightarrow\pi^-\pi^+n$, 1400-2000 MeV, new phenomenological analysis 2−52621
    - $\pi^-p\rightarrow\pi^-\pi n$, 17.2 GeV/c, amplitude analysis, A_2 and absrobed pion exchange 2−79583
    - $\pi^-p\rightarrow\pi^0n$ amplitudes, estimate in terms of direct-channel resonances and dual absorptive requirements 2−82761
    - $\pi^-p\rightarrow\pi^0\pi^0n$, 8 GeV/c, $\pi\pi$ phase shifts 2−79588
    - $\pi^-p\rightarrow\pi^+\pi^-n$, 15 GeV/c, ρ prod., vector dominance and ρ-ω interference 2−82765
    - π^+p, backward elastic scatt. at 6GeV/c, polarization parameter meas. 2−55858
    - π^+p, differential cross-section, electromagnetic form factors in parton model 2−73811
    - π^+p backward scattering, simplified Regge analysis 2−79593
    - π^+p differential cross-sections, G_{39}-resonance 2−70239
    - π^+p elastic scattering, 2 and 4 GeV/c, meas. of polarization in backward direction 2−76686
    - $\pi^+p\rightarrow K^+\Sigma^+$, multiple scatt. model, duality breaking effects 2−63572
    - $\pi^\pm p$, backward elastic, relation to quantitative Regge expressions for $\pi^\pm$, K^+ inclusive spectra 2−45953
    - $\pi^\pm p$, elastic, at 6 and 16 GeV/c, meas. of spin rotation parameters 2−59539
    - $\pi^\pm p$, elastic scatt., Pomeron and f exchange amplitudes 2−59540
    - $\pi^\pm p\rightarrow(\pi^\pm\pi^+\pi^-)p$, interference between exchanges, 16 GeV/c 2−79585
    - $\pi^\pm p\rightarrow\pi^\pm(\pi^+\pi^-p)$, interference between exchanges, 16 GeV/c 2−79585
    - $\pi p\rightarrow\pi\pi^+n$, absorptive corrections 2−79582
- **Pitch detection** *see Acoustical measurement; Hearing*
- **Plages** *see Sun*
- **Planetary atmospheres**
  - absorption cross sections of relevant molecules between 100 and 600 Å 2−80057
  - absorption line profiles and equivalent widths in spectra from two model atmospheres 2−81930
  - aeronomy of CO_2 atmospheres rel. to Mars and Venus 2−73075
  - angular momentum, variance analysis 2−55032
  - boundary layer, baroclinic effects on resistance law 2−84784
  - circulation, global characteristics, effects of dissipation 2−73076
  - cloudy, spectral line formulation, application to Jupiter and Venus 2−62710
  - collision integrals for dissociated atms. 2−62692
  - Cytherean, CO_2 emission behaviour 2−77303
  - cytherian, conditions meas. by microwave interferometry 2−51829
  - Cytherian, propagation, Venera-7 spaceprobe data 2−55151
  - earth, travelling wave components estimated 2−62120
  - Earth evolution, prediction of runaway greenhouse effect 2−73083
  - exosphere, model, with flux continuity at base 2−58540
  - far u.v. emission spectra and features of Venus rel. to Mars 2−78566
  - hydrodynamic motions in stratified convective zones 2−78455
  - invariant imbedding and Chandrasekhar's planetary problem of radiative transfer 2−58479
  - Jovian, absorption bands, obs. using Galilean satellite eclipse obs. 2−58490
  - Jovian, clouds, greenhouse effect 2−44944
  - Jovian, clouds, semi-transparent, radiative transfer props. in thermal i.r. 2−65737
  - Jovian, D/H ratio 2−66172
  - Jovian, hypothetical chemical and spectroscopic activity of GeH_4 2−44942
  - Jovian, occultation of Jupiter by β Scorpii 2−62697
  - Jovian, parameter det. from obs. of occultation of β Scorpii 2−55142
  - Jovian, vertically inhomogeneous scattering models 2−58489
  - Jovian atmosphere Turbopause Probe and experiments 2−75644
  - Jovian cloud system, models 2−44943
  - Jovian entry probe rel. to atmospheric measurements 2−75642
  - Jovian inhomogeneous atmospheric models with two cloud layers 2−78540
  - Jovian magnetosphere, X-ray survey 2−66173
  - Jovian planets, temp. sounding 2−78539
  - Jovian visible clouds, structure determ. from methane and H_2 quadru- - pole lines 2−75875
  - Jupiter, ^{13}C methane identification and $^{12}C/^{13}C$ ratio 2−75883
  - Jupiter, absorption line formation models rel. to observations of methane equivalent widths 2−78535
  - Jupiter, aerosol distrib. determ. from satellite eclipse obs. 2−75877
- **Planetary atmospheres** continued
  - Jupiter, aerosol layer of solid NH_3 rel. to optical properties and structure 2−58485
  - Jupiter, application of atomic collision processes to study of composition 2−44941
  - Jupiter, atmospheric entry probe missions, scientific objectives 2−75871
  - Jupiter, basic optical scattering props., obs. using occultation expts. 2−75878
  - Jupiter, computation of transmission profiles in ν_4 band of methane 2−48769
  - Jupiter, decametric radio emission as indicator of high velocity fluxes and shock waves in solar wind 2−48801
  - Jupiter, estimation of ^{13}C methane and $^{12}C/^{13}C$ 2−66170
  - Jupiter, hydrogen, model 2−85048
  - Jupiter, i.r. spectrum and radiative props. of clouds 2−75884
  - Jupiter, minor constituents, u.v. spectroscopy from Orbiting Astronomical Observatory 2−69140
  - Jupiter, model, thermal radio emission 2−75882
  - Jupiter, obs. by occultation of β Scorpii 2−75863
  - Jupiter, obs. of singly deuterated methane in 4- to 5-micron spectrum 2−51826
  - Jupiter, occultation of β Sco, flashing phenomena 2−66171
  - Jupiter, photometric characteristics of regions of disk in 0.33-0.48 microns region 2−58486
  - Jupiter, physical props. from 1971 eclipse of Galilean satellites 2−75860
  - Jupiter, Physicochemical and meteorological explanation 2−44940
  - Jupiter, upper atmosphere thermal structure with convective heat transfer 2−44939
  - Jupiter's Red Spot, isodensity and photometric profiles for 1971 2−69149
  - Jupiter ionospheric winds and radiation belt, meas. of dawn-dusk potential differences, average wind velocity 2−62695
  - Kuiper bands of Uranus rel. to laboratory spectra of methane 2−62709
  - line shape and band structure effects on temperatures 2−78516
  - low temp. condensation accretion process rel. to planetary formation 2−44903
  - lunar, upper limit determination by solar wind measurements 2−58470
  - Mars, aerosol emission and transmission effects on i.r. spectra 2−78547
  - Mars, baroclinic instability, effect of topography 2−85037
  - Mars, bistatic radar occultation experiment rel. to spherical symmetry of model atmosphere and ionosphere 2−48776
  - Mars, chem. dynamic model 2−85046
  - Mars, discrete white clouds, diurnal and seasonal behaviour 2−69152
  - Mars, electron temp. in ionosphere 2−55146
  - Mars, evolution, prediction of runaway greenhouse effect 2−73083
  - Mars, minor constituents, Mariner borne i.r. spectrometer 2−69156
  - Mars, minor constituents, u.v. spectroscopy from Orbiting Astronomical Observatory 2−69140
  - Mars, O_2 7620 Angstroms A-band observations during and after 1971 dust storm 2−78549
  - Mars, O_2 emission in night glow of Martian atmosphere, height of emitting layer 2−55145
  - Mars, radiative transfer, use of dimensionless parameter 2−44946
  - Mars, radiative transfer by CO_2 2−65770
  - Mars, thermal probing by spectral dependence of thermal radiation 2−75906
  - Mars, thermal structure from Mariner 9 i.r. spectroscopy expt. 2−75898
  - Mars upper atm. structure, temp. and composition 2−75894
  - Martian, CO_2^+, CO and O airglow, u.v. spectral obs. 2−66178
  - Martian, CO_2 emission behaviour 2−77303
  - Martian, determ. of water vapour and minor constituents using i.r. spectral data 2−78541
  - Martian, effect of dust on temperature 2−48775
  - Martian, implications of $CO(A^1\pi)$ dissociative excitation by electron impact of CO_2 2−56164
  - Martian, Mariner 1969 obs., review 2−44954
  - Martian, Mariner 9 radio occultation meas. 2−58504
  - Martian, mid i.r. remote sensing of composition 2−58492
  - Martian, obs. using Mariner 9 radio occultation data. 2−75902
  - Martian, OI 1304 Å emission, Mariner 9 obs. 2−58505
  - Martian, possible composition as H_2O 2−66183
  - Martian, sterilization probability for small particles 2−62701
  - Martian, thermal struct. 2−58503
  - Martian, wind generation mechanisms 2−58506
  - Martian atmosphere, u.v. spectroscopy from Mariner 9 in 1100-3500 Angstroms region 2−75893
  - Martian atmosphere-polar cap, numerical simulation of radiative-conductive heating 2−69150
  - martian atmospheric structure meas. during Viking lander entry phase 2−75891
  - Martian exosphere, H_2O and CO_2 outgassing role in evolution 2−58507
  - Martian exosphere, He loss, thermal and non- thermal loss mechanisms 2−58509
  - Martian ground-atmosphere thermal boundary layer structure, transient variation 2−66175
  - Martian ionosphere, model, two-freq. bistatic-radar occultation expt., spherical symmetry departures influence 2−58510
  - Martian i.r. emission spectra, 5-50 μ range 2−75897
  - Martian north polar region, O_3 absorption 2−75896
  - Martian thermosphere, emission spectrum and altitude depend., response to solar activity 2−58502
  - Martian thermosphere comp. maintenace by large-scale circulation 2−58508
  - Martian upper atmosphere, CO Cameron band emission, electron impact dissociation of CO_2 2−64117
  - mass spectrometer experiment during Planetary Atmosphere Experiments Test 2−75533
  - Mercury, unipolar interaction with solar wind, steady state bow shock problem 2−44955
  - model, homogeneous and inhomogeneous, synthetic absorption profiles 2−66165

Planetary atmospheres continued
momentum and heat transports, non-geostrophic baroclinic stability 2−58481
multiple scattering of photons rel. to absorption lines, probability distribution 2−78529
nonisothermal scattering and absorptive medium, generalized Kirchhoff's law 2−75854
outer planet atmospheres analysis using ionization threshold spectrometer 2−76962
phase equilibria in gas mixtures at high pressures rel. to planetary interior structures 2−83843
Planetary Atmosphere Experiments Test Project, mission and spacecraft 2−75652
Planetary Atmosphere Experiments Test Project, re-entry vehicle dynamics, effects on atmospheric data 2−75528
Planetary Atmosphere Experiments Test Project, shock layer radiometry of re-entry vehicle in PAET project 2−75534
Planetary Atmosphere Experiments Test Project, terrestrial atmospheric structure meas. 2−75855
radiative transfer, conf., August 1972, Colorado 2−62248
radiative transfer with three-term phase function 2−58442
radiative-dynamical model for static stability of rotating atmospheres 2−58480
Saturn, methane bands, rel. to Titan 2−81906
Saturn, minor constituents, u.v. spectroscopy from Orbiting Astronomical Observatory 2−69140
Saturn, model, thermal radio emission 2−75882
Saturn, photometric characteristics of regions of disk in 0.33-0.48 microns region 2−58486
Saturn atmospheric investigations using Jupiter turbopause probe 2−78557
scattering of light in planetary atmospheres with refraction 2−81925
simulation of diffuse reflectivity from cloudy atmosphere 2−44933
use in spacecraft transfer from high elliptic to circular orbits 2−48634
spectral line formation, analytic scattering diagrams for computation 2−44936
stability of thin non-rotating Hadley circulations 2−66167
steady neutral planetary boundary layer forced by horizontally non uniform flow 2−62642
stratified Rayleigh structure, absorption lines, numerical model 2−73078
temperature distributions from reflected sunlight analysis 2−62711
temperature gradient detection by spectroscopic analysis 2−78561
temperature wave propagation in non-grey radiative fluid 2−65656
thermodynamic parameters from spacecraft descending by parachute 2−73074
Titan, composition 2−69163
Titan, polarization obs., evidence for optically thick atm. 2−81907
Uranus, microwave absorption of H_2 2−55150
Venus, above cloud deck, radiative transfer, study of diurnal variations in atmospheric temperature profiles 2−44946
Venus, cloud cover, circulation obs. 2−58513
Venus, CO_2 8710 Å line profile meas. rel. to several atmospheric models 2−78560
Venus, composition, Venera entry probes and Mariner flyby 2−69164
Venus, Hg clouds 2−75915
Venus, meas. of line shape parameters for HCl and HF in CO_2 atmosphere 2−42879
Venus, minor constituents, u.v. spectroscopy from Orbiting Astronomical Observatory 2−69140
Venus, model of lower atm. based on high resolution radio obs. 2−75914
Venus, phase anomaly, refraction effects 2−73089
Venus, Planetary Explorer probe studies of Venus' atmosphere 2−75643
Venus, radiative transfer by CO_2 2−65770
Venus, structure and stability of ClOO radical 2−78559
Venus, temp. and pressure distribution to surface, Venera-7 meas. 2−51831
Venus, temperature profiles, thermal equilibrium 2−85030
Venus, thermosphere comp. maintenance by large-scale circulation 2−58508
Venus, u.v. observations during 1969 W. elongation, features and atmospheric rotation 2−44961
Venus, Venera 4, 5 and 6 probes obs. 2−44964
Venus, water vapour evolution 2−44958
Venus absorption in lower atmosphere of Venus 2−48780
Venus clouds, dirty HCl model 2−44963
Venus clouds of HCl contain dissolved Fe compounds 2−58514
Venus halo effect during 1970 inferior conjunction, photometric obs. 2−44960
Venusian atmosphere, turbulence characteristics of atmosphere from Mariner V S-band occultation data 2−78568
Venusian mesosphere, radiative equilibrium, temp. profile 2−66185
vertically propagating planetary waves, effect of i.r. radiative transfer and frictional dissipation 2−65684
Viking entry mass spectrometer rel. to obs. of martian upper atmosphere 2−75653
viscous flow, two-dimensional, exact statistics with random dorcing 2−83464
CO_2 photolysis at 1460Å and 1500 to 1670Å, CO quantum yield 2−69141
(C_3O_2)n polymer production in Martian atmosphere and colouring of surface, laboratory studies 2−78542
H-He plasmas, thermodynamic properties for stagnation shock layer of spacecraft entering atmosphere of Jupiter 2−46718
H_2, Rayleigh and Raman scattering 2−58512
H_2, validity of Dicke approximation for computing collision narrowed profiles of quadrupole lines 2−75856
H_2 dominated, exospheric temp. of 2-component diffusive equilibrium model 2−44935
H_2O 8200 Angstroms band in Martian atmosphere, ground based photoelectric observations during Mariner 9 mission 2−78551
H_2O 8200 Angstroms band studies in Martian atmosphere with gound-based Varo image tube 2−78552
O_2 7635 Angstroms band observations rel. to atmospheric compositions of Mars and Venus 2−78548

Planetary atmospheres continued
O_2 A-band at 7620 Å, detection in Martian atmosphere 2−69157
O_2 Martian abundance upper limits and mixing ratio with CO_2 from photoelectric spectra 2−78550

Planetary nebulae
see also Galaxies; HI regions; HII regions; Nebulae
Bowen fluorescence mechanism, He II Lα radiation 2−58235
catalogue of radio observations of total fluxes, morphology and spectra 2−44845
chromospheric heating by radiation driven sound waves 2−69062
condensations in young planetary nebulae, life spans 2−78449
designations 2−44846
distances det. from stellar spectra 2−58236
evaluation of nuclei, mechanism for shell ejection 2−62470
extreme Population I matter, noble gas abundance rel. to Sun 2−81838
He 2-53, 100 micron flux density 2−55087
interstellar H_2 and H and He fluxes from planetary nebulae 2−78448
i.r. spectra prediction 2−51716
Kant and Laplace's nebular hypothesis 2−48670
with molecular anisotropy, soln. of auxilliary equation of radiative transfer 2−62690
motions and distances, statistical investigations 2−51717
in NGC 2818, open cluster62585 2−62585
NGC 7662, numerical model 2−62468
observation at 1.65-3.4 microns 2−51715
Owl, NGC 3587, isophotal contours in H_α light and hydrogen structure 2−72979
planetary nebulae formation analysis 2−72981
plasma arcs and loops, trapping in cosmic atm. 2−78577
radiation, elliptical polarization search 2−75724
radio flux, interferometric obs. 2−62469
in Small Magellanic Cloud, N II 6584/Hα line intensity ratio44844 2−44844
spatial and kinematic parameters of binebulous, centric and annular nebulae 2−44843
spatial spectroscopic diagnostic using synthetic approach 2−69041
spatial spectroscopic diagnostics, analytical approach using inverse integral equations 2−72982
C IV emission lines, polarization 2−48669
C IV ion, emission spectrum with different excitation conditions 2−48668
H-rich material ejection from white dwarfs computer calc. 2−72980

Planets
see also Asteroids; Jupiter; Mars; Mercury, planet; Neptune; Planetary atmospheres; Saturn; Solar system; Uranus; Venus
Bode's law and missing planet 2−81928
colour information from space missions 2−81938
condensation of terrestrial planets rel. to origin of Moon 2−78524
cosmogeny, solar nebula, low temp. condensation accretion process rel. to planetary formation 2−44903
creep, law which accounts for damping 2−58482
critical inclinations and eccentricities in N-planet problems 2−85033
dynamical properties and internal structures, review 2−51520
electrical conduction in physical and chemical mixtures rel. to planetary mantles 2−84292
emitted radiation and albedo simulator 2−78517
evolution from dust 2−69144
formation and volcanic activity 2−66169
formation from solar nebula 2−66168
giant, determination of H_2/He mixing ratio 2−62693
gravitational potential and derivatives for non-spherical body 2−54607
Hansen's planetary theory, computer implementation 2−62694
inhomogeneous planetary accretion hypothesis, cosmogony implications 2−44934
interplanetary flight trajectories, single impulse, energy optimum characteristics, variation 2−51668
lunar thermal history rel. to tectonic activity of Mars and Venus 2−57449
major, satellite topography 2−78491
Mars, Mariner 9 photographs results 2−48772
mass, influence on position of Laplace plane 2−55140
mass and angular momentum transmission from satellite or planetary system to primary 2−48759
metal/silicate fractionation of terrestrial planets rel. to solar nebula 2−66166
motion of ecliptic determ. for reciprocal planetary masses 2−81904
natural satellites, review of physical properties 2−78530
numerical relationship between orbits, applic. to obs. of Earth's gravitational field 2−85042
occultations of stars 2−48768
occultations of stars by planets, satellites and asteroids, predictions and observations 2−78515
orbital elements soln. and derivation 2−62645
origin and early development rel. to primitive solar nebula 2−78500
outer planet satellites, eclipse light curve calcs. 2−81908
perihelion advance calc. by field approach to gravitation 2−48765
perihelion motion from new gravitational theory 2−62977
phase equilibria in gas mixtures at high pressures rel. to planetary interior structures 2−83843
planetary sciences, symposia (Hawaii, USA, March 1972) 2−75841
planetology congress (Montreal, September, 1972) 2−78499
polar asymmetry 2−69146
polariscope program for obs. in 0.2-0.3 μm range 2−72988
pole of the ecliptic, position from improved values of reciprocal planetary masses 2−58172
positions using 13-inch photographic equatorial refractor 2−66163
potential development of smooth, dense rotating body rel. to planets 2−81757
radar astrometry techniques 2−76043
radiometry at 350 and 700 microns, extinction and temperature meas. 2−78527
radiowave reflection, ultrashort, circularly polarized 2−55196
resonance struct. bi-stable oscillation modes, rel. to solar activity 2−73079
satellites of outer planets, physico-chemical models 2−78532
satellites of outer planets, review of spectrophotometric observations 2−78531

Planets continued
short-period meteor orbits rel. to parent comet and perturbations of planets 2—58525
single close encounters in three-body problem rel. to planetary problem 2—81759
space vehicles observations, reviews 2—66164
structure, single static zone planet, general relativity 2—69143
surface, albedo and illuminance surrounded by purely scattering inhomogeneous atmosphere 2—48766
surface simulation studies, characteristics of microstructures 2—58483
terrestrial planets, structure and composition rel. to solar nebula 2—81939
three-body problem, new form of differential equations of relative motion of planets 2—81756
tidal effects of planets rel. to solar activity during 200 year period 2—75984
Titius-Bode law of planetary distances 2—48952
trans-Pluto, search based on periodic comets with large aphelion distances, orbit determination 2—69139
trans-Plutonian, Hypothetical, effect on Halley's comet, orbit and mass 2—44937
trans-Plutonian planet, search to 15.5 mag. with negative results 2—78533
two-dimensional digital vidicon photometry in 0.38 to 1.1 micron range 2—78526
unitized multiplex for processing photographic images of planetary objects 2—78634
unmanned exploration employing nuclear reactor power systems 2—66032

Plasma
see also Discharges, electric; Electrons; Ions; Space charge; Thermonuclear reactions
acceleration in conical induction source 2—67653
anisotropic, dielec. response function calc. 2—60240
arc, d.c., column, frequency-rotation function, in approx. by rigid conductor 2—60221
arc, d.c., rise time to stationary arc 2—60222
arc, d.c. free-burning, up to 2160A, plasma velocity distrib. meas. 2—60320
arc, effect of reaction energies on radial temperature distribution 2—53261
arc, in curved discharge tube, computer simulation 2—53173
atomic and cluster injection into D-T mirror fusion power system 2—64262
atomic level populations, distribution function 2—77269
book on plasma as fourth state of matter 2—53174
capillary, radiation and conductivity 2—70895
cathode flare, velocity of expansion during pulse breakdown of vacuum gaps 2—83636
classical, pair correl. function, screening effects, short distance behaviour 2—67621
classical convergent kinetic equation 2—70876
combustion products, conductivity Hall parameter and turbulence 2—64265
computational models, comparison, including superparticle, waterbag 2—80255
conduction heating and hydrodynamic expansion, derivation of joint equations 2—64258
cosmic, proposed use for spacecraft propulsion 2—51672
dense classical plasma, Balescu-Guernsey-Lenard eqn. extended 2—64261
discharge, positive column, stead-state theory in mag. field, finite cylinder separable solns. 2—50225
dispersion relation for Cerenkov radiation of moving test particle in magnetoplasma 2—80250
effective electron temp. from self- radiation in bunch discharge 2—60208
electric arc, chemical reaction effects on characteristics 2—50237
electron, formation of slot between inner and outer belts 2—62350
electron, meas. of properties across Earth's bow shock obs. from lunar orbit 2—62313
electron impact broadening of isolated spectral lines of heavy elements 2—60244
electron temp., meas. by electrostatic probe, plasma resist. effects 2—60260
European Phys. Soc. conf., Wiesbaden, Germany (Oct. 1972) 2—76139
flow, recombining, population inversion of atomic C 2—46452
flow in ionospheric trough regions, thermalization of colliding ion streams 2—65946
free flowing unipolar gas, electric field distribution in phase plane 2—64365
fugacity expansions, quantum statistical, for partially ionized plasma in equilibrium 2—43114
gas discharges, conference, London (1972) 2—70990
gravitational, non-Markovian time evolution, weakly oscillatory relax. process. 2—68999
guiding-centre, finite-orbit effects studied using simple model of gyroscopic fluid 2—56312
heating, Fermi stochastic particle, acceleration mechanism 2—52710
heating, magnetic field enhanced in CO_2 laser produced plasma 2—70929
heating and expansion, with internal heat sources 2—43300
heating by relativistic cyclotron resonance 2—70905
heating processes, role of nonlinear processes 2—80327
high temperature, continuum emission in vacuum u.v. 2—53196
homogeneous spheroid, elec. multipole moments, quasistatic calc. method 2—74357
hot dilute plasma using Debye approximation 2—46717
inductance, influence of cooling gas layer on geometric sizes, calc. 2—64340
interplanetary, rel. to small diameter radiosources scintillation spectra 2—58408
interstellar, dispersion of longitudinal electric waves rel. to photon rest mass 2—55073
ion and electron energy distributions in stellarator diverter 2—70890
ion and velocity structure in laser produced plasma 2—80272
ion-acoustic line profiles, Coulomb-collision corrected 2—67642
kinetic eqns. for chemically reacting plasma 2—70875

Plasma continued
laser heating, averaged equations of hydrodynamic expansion and conduction-type heating, case of spherical symmetry 2—77277
laser heating for spherical wave, fusion energy carbon into consideration 2—77276
laser produced, spectral analysis of backscattered light 2—56355
laser-produced, energy spectrum multiply charged ions 2—80253
magnetic pulse, anomalous penetration 2—80248
magneto-active, statistical mechanics 2—52113
magnetospheric, l.f. impedance obs. 2—48533
magnetospheric motion during sudden commencement on February 15th, 1967, analysis of ground magnetograms 2—62307
magnetospheric sheet, magnetic noise, Explorer 24 obs. 2—62325
Mars, exprts. on Mars 2 and 3 probes 2—78554
non-isothermic, dissociation and exchange reaction 2—50185
nonlinear heat transfer problems, analytic solns. 2—56329
nonlinear interactions in anisotropic plasma 2—46772
nonmagnetized, ion heating via turbulent ion acoustic waves 2—53178
nuclear reactions in degenerate electron nuclear plasma 2—58256
numerical simulation, basic interactions in real and numerical phasmas 2—53175
numerical simulation of processes, especially fusion, review 2—80254
numerical simulation with finite size particles, verification of theory 2—46712
one-component, short range order onset, theory 2—56327
particle correlation function and enlarged Bogoliubov hypothesis 2—50186
particle-in-cell model, elec. resist., computer simulation, review 2—80256
particle-in-cell plasma simulation 2—67620
permalloy films, thin, influence of plasma and cathode sputtering on struct. elec. and mag. props. 2—84410
plasmoids in solar corona, radio obs. 2—62806
2-quantum processes obs. in neon 2—64279
quasilinear theory reformulation allowing for resonant diffusion 2—80238
Rayleigh's problem in collisionless plasma 2—80252
relativistic, particle correlation function and enlarged Bogoliubov hypothesis 2—50186
solar corona gyro-synchrotron radiation, temperature effects 2—81950
spectra, pressure broadening, unified quantum statistical formulation 2—67382
spectra determ. of radial distribution of intensity of lines 2—60239
spectral intensities, their interpretation 2—74370
spectrochemical trace analysis in arc plasmas, use of external magnetic fields 2—51477
spectroscopy, single-spike laser-generated plasmas, rel. to spectrochemical analysis 2—60241
stationary rotating incompressible, with minimal internal energy loss 2—43113
statistical mechanics of totally neutral plasma, application of effective potential method 2—64257
Stokes line generation during laser irrad. due to Compton effect 2—74369
stratified, with tensor cond., elec. field periodic struct. 2—83542
superdense matter, vector plasma model, superluminal sound propagation 2—70874
temp. distribution, effect of electron density alteration 2—46726
temperature distribution, heated by relativistic electron beams 2—53183
thermal decay of mag. confined fully ionized arc plasma 2—67625
thermal plasma densities in magnetosphere, digital sonograms of hydromagnetic whistlers 2—48535
thermodynamic functions of nonthermal radiating systems 2—58943
thermonuclear, high power laser interaction with small particles 2—70879
trace element analysis in arc plasma, spectral line intensity depend. on magnetic field 2—48356
transit time heating, stochastic e.m. fields 2—70880
turbulent, spectra interpret. by Blokhintsev theory 2—64061
two-dimensional, canonical partition function stability 2—46715
two-temperature, conduction-type laser heating in spherically symmetric case 2—64259
Vlasov equation, difference scheme for numerical solution 2—53176
in weak u.h.f. electric and constant magnetic field, quasi- linear theory 2—56326
Al, laser produced, IV spectra, line identification 2—74212
Ar-N_2, spectroscopic temp. detn. rel. to MHD generator parameters 2—46716
Ar, continuous radiation, h.p. 2—43117
Ar, continuous radiation, influence of lowering of ioniz. energy 2—70911
Ar, high-pressure thermal, use as high-radiance standard 2—46713
Ar, LTE rel. to critical electron density 2—67632
Ar, laser perturbed, transient light emissions 2—80231
Ar, stabilized arc, near thermodynamic equilibrium, stationary and relaxational props. 2—60223
Ar discharge, hollow cathode, electron temp. and density profiles 2—77307
Ar discharge, hollow cathode, excitation mechanisms, electron and ion temp. and density 2—77308
Ar low-voltage spark discharge, space and time distribution of temperature 2—70881
Ar rise and fall in temperature traced using Lorenz method, calc. of thermal excitation functions 2—52911
Ba, laser-generated, spectral line parameters 2—67643
Ba cloud released in magnetosphere, balloon meas. of ionospheric electric fields and precipitating particles 2—62365
Ba ion cloud expt. in magnetosphere, analysis of optical data obtained by NASA 2—62299
Ba ion cloud released at 31000 km, analysis of resonance scattering of solar radiation 2—62303
Ba ion cloud released in magnetosphere, initial expansion phase investigated using computer model 2—62305
Ba ion cloud striations, acceleration to ambient magnetospheric plasma velocity 2—62301

Plasma continued
CO$_2$, atmospheric pressure, 6500 to 9500 K, emission capacity in visible spectral range 2—43155
CO$_2$, elec. discharge laser gas mixture, energy conversion, plasma kinetic processes 2—59151
CO$_2$ laser, optical investigation of plasma composition and mechanims of laser action for various systems 2—49361
Ca II, Stark broadening and shift of lines 2—60245
Cs, electron emission of W cathode rel. to temp. and current density 2—75191
Cs, partially ionized, impedance determ. 2—56343
Cs, thermodynamic props. 2—56328
D, infinite, estimation of Coulombian transparency as a function of temperature 2—42593
D, seeded with He-like ion, determ. of electron density from meas. of depopulation of $2^3P_{0,1,2}$ levels by electron impact 2—79961
D electron density determination, spatial and temporal 2—67624
Fe XXV and Fe XXVI, high temp. obs. in minute plasma pts. 2—53179
Fe XXVI, highly ionized, X-ray spectra 2—52917
H-He plasmas, thermodynamic properties for stagnation shock layer of spacecraft entering atmosphere of Jupiter 2—46718
H, dense, Lyman-α line asymmetry 2—70635
H, expanding, population inversion of excited atomic levels 2—46709
H, in plasma, line broadening, quasistatic and impact approx. 2—52948
H, population inversion 2—49973
H, positive column, population density and local thermal equilib. of excited atoms 2—43128
H, Stark broadened Lyman-α lines, electronic shifts 2—64059
H, Stark broadening of Balmer lines 2—64278
H line electron broadening, boundary of quasistatic region 2—77022
He$^+$/Ar$^+$ simultaneous ion heating in linear turbulent-heating expts., mass dependence 2—80288
He, cryogenic, electron-ion recomb. coeff. 2—77264
He, Stark profiles of forbidden and allowed transitions in dense, laser produced plasma 2—42805
He thermal, absorption and emission line shaped for Stark Broadened He II resonance line 2—79952
LiI, emission spectrum, line profiles, electron density 2—60247
N$_2$, elec. field effects on rot. and vibr. temps. and excited level populations 2—74348
N$_2$, h.p., spectral intensity, equil. radiation 2—60248
NaNbO$_3$-BaTiO$_3$-BaNb$_2$O$_6$ system, tungsten bronze field, lattice parameters and Curie point 2—72034
Ne in Tokamak, electrical resistivity 2—64266
Ni XXVII, highly ionized, X-ray spectra 2—52917
paired correlation function, integral equations 2—60207
Xe spectral lines, Stark coeffs. determ. 2—67393

collision processes
Appleton magneto-ionic eqns., quasi-longitudinal and quasi-transverse approximations for large Z 2—50190
in arc generator, with external axial anodic mag. field 2—71002
charged particle loss processes in arc plasma 2—67681
chemical reactions in steady state nonisothermal low pressure plasma, statistical model 2—57411
composite medium, effect of collisions with neutral atoms on dynamic stability 2—56379
Compton radiation from relativistic particles, depression of power spectrum 2—80228
counterstreaming magnetized, laminar interactions described theoretically and by computer simulation 2—43125
D-T plasma to thermonuclear temps., by ion-ion collisions due to laser radiation 2—64289
damping of plasma lines, numerical computations of linewidths and intensities 2—43143
damping of transverse waves 2—80357
decay in electrically conducting cylinder in longitudinal magnetic field 2—70916
dynamic shielding effects in partially ionized gases 2—43124
electron beam heating of non-uniform plasma with and without magnetic field, quasi-linear theory 2—46714
electron beam-plasma interaction beyond linear stage 2—67628
electron-heavy particle collisional relax. in strong radiation field 2—53182
e.m. instability, applic. to interplanetary matter and bow shock problems 2—60213
equilibrium with thermal energy, steady-state Vlasov-Maxwell equations 2—82832
estimated turbulent heating by cross- field current, effective ion collision frequency estimated 2—43194
Harris instability with collisions, numerical simulation 2—70968
heating in solar flares, by high energy electrons and non-thermal X-ray emission 2—81951
highly ionized plasma, numerical solution of one-dimensional afterglow decay 2—70894
hot magnetoplasma, dispersion curves calc. 2—50192
interaction processes in weakly turbulent collision free Vlasov plasma 2—43123
ion wave propagation, perpendicular longitudinal, effects of collisions 2—56370
ion-electron and charged particle-neutral, rel. to power transfer near lower hybrid reson. 2—53194
linear pinches, interaction with intense relativistic electron beams 2—83608
magnetoplasma, total energy loss of test charge 2—46725
metastable atom density in afterglow plasmas in neon 2—67629
momentum transfer interaction of laser produced plasma with low pressure background 2—80246
nonlinear interaction of small cold beam with plasma 2—56337
parametric instability, collision effect on threshold energy level 2—53233
Rosenbluth-post convective loss-cone instability, scatt. calc. using slab model 2—53184
scattering function of soft collisional plasma 2—50191
self-consistent Vlasov description of relativistic equilibria 2—82830
spectral line broadening, study by two-particle self-energy expansion 2—56091
stopping power, for fast electrons and positrons 2—46723

Plasma continued
collision processes continued
strong correl. systems, collision terms 2—46724
thermonuclear reaction initiation by high current electron beams 2—46722
toroidal modes, resonant scattering of trapped ions 2—70918
toroidal vortices in pulsed plasma 2—83587
effect on transverse e.m. wave propagation near electron gyrofrequency harmonics, wavelengths $<$ electron gyro-radius 2—46734
two-temperature plasma in chemical reaction equilibrium 2—43126
weakly ionized, theory of spherical probe 2—80296
weakly ionized medium, influence on nonlinear effects rel. to e.m. wave propag. 2—46733
Ar, backscattering of electrons, Monte Carlo simulation 2—70892
Ar, electron-neutral collision freq. near Ramsauer minimum 2—74354
Ar$^+$ laser plasma, population inversion, collisional radiative calc. 2—79197
Cs, thermionic diode, model improvements 2—49277
H, axially symmetric free expansion of non-equilibrium plasma 2—77270
H, observed discrepancies in central region of Hβ profile at low electron densities 2—70631
He$^+$-He^{2+}-e, calc. of collisional-radiative volume recombination and ionization coefficients 2—50193
He-N mixture, decaying plasma 2—50189
He, collisional-radiative ionization and recombination coefficients, influence of atom-atom collisions 2—67630
He, electron-ion recombination, production by laser 2—67631
He with 0.01% H, observed discrepancies in central region of Hβ profile at low electron densities 2—70631
Kr-O$_2$ afterglow, formation and loss of O$_2^+$ and O$_4^+$ ions 2—70889
Kr afterglow exptl. meas. of dissociative recombination at elevated temperatures 2—70888
Kr ions, three-body conversion to mol. ions 2—83188
N$_2$, cross section for momentum transfer 2—50194
Ne-N mixture, decaying plasma 2—50189
Xe ions, three-body conversion to mol. ions 2—83188

confinement
see also Stellarators
θ pinch, fast, properties of large diameter pinch at low densities 2—83579
θ pinch, fast, shock heating of low density plasma 2—83578
θ pinch, hard core, two dimensional obs. of spiral structure associated with initial breakdown 2—83576
θ pinch, linear, ISAR II, energy balance 2—83575
θ pinch, straight, modelling 2—83577
θ pinch, three metre, helical field expts. 2—64282
θ pinch with multipole cusp field, initial phase 2—83574
θ-pinch, anomalous resistivity in initial stages 2—80244
θ-pinch, caulked cusp torus field 2—83599
θ-pinch, CO$_2$ laser heating 2—83606
θ-pinch, conical, collinear plasmoid meas. and results 2—67651
θ-pinch, interferometric diagnostics 2—50201
θ-pinch, pulsed high-β fusion reactor, design study 2—83613
θ-pinch, two stage heating 2—83581
θ-pinch, ultrahigh mag. field, parametric obs. 2—83612
θ-pinch impulsing circuit parameters simulation and optimization 2—83611
accumulation in electrostatic potential well created by electron space discharge 2—46755
astron, neutralized E layer, stability of tearing mode 2—80286
astron E layer, precession 2—70915
Astron-type E layer, magnetic compression 2—56356
axisymmetric torus, neoclassical diffusion in intermediate region 2—50187
belt pinch, MHD stability 2—83601
Bennett pinch, hydromagnetic stability conditions 2—83619
Bohm-Langmuir criterion and boundary conditions for electric field 2—70917
book on plasma as fourth state of matter 2—53174
bounded magnetoplasma, h.f. production and diagnostics 2—67661
cosmic atm., trapping of condensed arcs and loops 2—78577
current-carrying, free boundary solution 2—64281
decay in electrically conducting cylinder in longitudinal magnetic field 2—70916
Divertor type source, scatt. centre estimation 2—46745
electron runaway in slow toroidal θ-Z pinch LT1 2—53202
electrostatic, plasma in an electron beam potential well 2—74404
electrostatic instabilities caused by ion beam heating 2—43187
elliptical torus, neoclassical diffusion 2—67645
expansion of toroidal equilibrium with finite periodicity length and 1=0,1 fields 2—83567
fast pinch, review of experiments in UK (1956-1972) 2—53200
first toroidal pinch, electron beam injection, low pressure operation 2—83598
flute instabilities, loss-cone single resonant, nonlinear stabilization 2—70966
flute mode stability in presence of nonuniform elec. fields 2—60281
focus, highly localized X-ray source 2—83585
focus, vortex breakdown condition 2—83586
focus device, meas. of beta 2—83591
fusion reactor, control 2—64280
fusion reactor blanket and magnet shield structure, design concept 2—83147
fusion research, book 2—60251
heating by electron beam in mirror trap, oscill. spectra 2—56368
helical equilibrium toroidal θ pinch, image current problems 2—83605
helical field, dispersion relations for const. oxide components 2—83552
h.f. heating in closed mag. trap 2—43156
high β fusion plasmas, formation by intense relativistic electron beams 2—83607
high density θ pinch, heating on transverse irradiation by pulsed CO$_2$ laser 2—50200
high temp., using high power laser power production 2—70930
high temperature, prospects for development of fusion reactors 2—42610

Plasma continued
confinement continued
high-β compact torus, stability obs. 2−83566
high-β plasma, remote feedback stabilization 2−70969
high-β reversed field discharges with extended lifetimes 2−83563
hot electron, anal. by electron cyclotron plugging 2−80284
hot electron plasma, produced by mirror θ pinch, instability 2−70961
hot electron plasma, transverse instabilities in cylindrical resonator 2−74402
inhomogeneous sheath, moving, kinetic theory of e.m. wave reflection 2−74366
injection techniques in toroidal Alcator 2−67647
injector-diverter, purification of H plasmoids by mag. field 2−80298
ions, in pressure of electrostatic potential and r.f. electron plugs in mirror trap 2−74372
kink modes and feedback control, energy considerations 2−67648
laser scattering from high density low temp. plasmas 2−67623
linear and toroidal high-β pinch, MHD instabilities near Kruskal-Shafranov limit 2−83546
linear pinch device, non-thermal process 2−83609
linear pinches, interaction with intense relativistic electron beams 2−83608
linear screw pinch, standing wave magnetic fields, stabilization expts. 2−83604
magnetic mirror, electron trapping due to enhanced fluctuations 2−80283
magnetic mirror, trapping of high-current relativistic electron beam 2−63270
MHD equilibria in sharply curved axisymmetric devices 2−56357
minimum-B mirror devices, stable equilibria computation, computer program 2−67652
mirror fields, stabilized by quadrupole and quadrupole-cusp fields 2−70913
mirror machines, controlled thermonuclear reactor, heat transfer obs. 2−42645
mirror machines, superadiabaticity 2−64287
mirror plasma, 2-dimensional criterion for distinguishing absolute instability 2−80307
negative θ pinch, instabilities and artificial resistivity 2−83573
nuclear fusion control systems, magnetic configurations 2−63928
optimized magnetic field profiles and β-limitation of minimum-B mirror reactors 2−46751
particle motion in magnetic mirrors with high-frequency electric field fluctuations 2−83554
Z-pinch, 100 kV, source of u.v. radiation for plasma production 2−74386
θ pinch, axial plasma flow and end loss obs. 2−50202
θ-pinch, controlled thermonuclear reactor, heat transfer obs. 2−42645
pinch, paramag. instability of $m=1$ mode in dynamic stabilization 2−77281
Q-pinch, toroidal, ISAR T 1, dynamical phase obs. 2−83562
pinch configuration, computation of growth rate of instabilities 2−83570
pinch discharges, heating and energy losses 2−83564
θ and Z pinches, high β phase plasma research 2−43158
poloidal Heliotron magnetic field, plasma equilib. 2−70912
pulsed high β Tokamac like system, rectangular chamber cross section 2−83602
pulsed high-β plasmas, conference (Garching, Germany, July 1972) 2−83560
Q-machine, single ended, antenna resonances and excitation of ion Bernstein modes 2−80323
Q-pinch, bumpy, stability of two-dimensional MHD equilibria 2−83550
Q-pinch torus, Scylac 5-meter, helical equilibria 2−83561
r.f., in open-ended toroidal quadrupole, computer simulation 2−53199
r.f. of low density plasma electric quadrupole mode plateau and luminosity obs. 2−74371
rotating e.m. field interaction with plasma in constant magnetic field, compression to column 2−50199
Schrodinger like equations for nonadiabatic escape of charged particles 2−56359
screw pinch like configurations, toroidal confinement of high-β plasma 2−53201
Scyllac, 5 m, linear θ pinch, column behaviour 2−83572
sheath conversion current, Langmuir probe meas. 2−56361
solar wind, closed mag. structures assoc. with interplanetary shock waves 2−66219
stabilization using external feedback 2−70877
steady-state linear multipole (SLIM-1) 2−67646
stellarator, convective motions due to trapped particles in field 2−43162
streaming plasma interaction w. mag. mirror 2−64286
thermonuclear fusion, progress and history of research 2−59789
thermonuclear fusion conditions, supersonic flow, high power electron beam 2−70914
theta pinch, with azimuthal mag. field, small-scale drift instability turbulence 2−67644
theta pinch column, MHD feedback stability 2−83603
theta pinch discharge, investigation of relation between compression, relaxation and end losses by two-dimensional m.h.d. computer programme 2−43160
theta-pinch, rotational disturbances 2−83621
theta-pinch, toroidal energy and mass analysis of emitted neutral particles 2−80278
theta-pinch gun operation 2−74373
time, as function of electron density and temp. studied in levitated spherator FM-1 2−80287
Tokamak, controlled thermonuclear reactor, heat transfer obs. 2−42645
Tokamak, localized collisionless trapped particle modes 2−43196
Tokamak, major radius oscill., theory 2−70936
Tokamak, MHD and tearing instabilities 2−70962
tokamak, neoclassical diffusion of finite β plasma 2−60210
Tokamak, neoclassical transport in banana/plateau region 2−70919
Tokamak, plasma properties 2−43161

Plasma continued
confinement continued
Tokamak configuration, particle diffusion under influence of slow magnetic compression wave 2−80275
Tokamak experiments, state-of-the-art 2−64283
Tokamak systems, particle diffusion and energy balance equations 2−53203
Tokamak type apparatus, field distrib. near gap formed by sectionalized shells 2−64288
toriodal belt pinch, ISAR IV, stability 2−83594
toroidal, decay, influence of external circuit 2−83596
toroidal, effects of plasma flow 2−64285
toroidal, electron fluctuations and thermal energy transport 2−80249
toroidal, magnetic system, current sustaining expt. 2−46747
toroidal, resistive plasma with flow, viscosity and thermal conductivity effects on containment 2−46756
toroidal belt pinch, MHD equilibria 2−83595
toroidal current carrying plasma column, equilib. displacement, instabilities 2−83622
toroidal current-carrying column, suppression of instability by feedback 2−77290
toroidal equilibria, local hydromagnetic, without symmetry 2−80273
toroidal equilibria, stationary, at finite beta 2−80274
toroidal fusion reactor, liquid Li coolant, calc. of pumping power 2−46748
toroidal fusion reactor, use of liquid Li as coolant, stress limitations 2−46749
toroidal geometry ion and electron transit time magnetic pumping 2−80242
toroidal inclusion, 2 dimens. heat flow 2−53177
toroidal modes, resonant scattering of trapped ions 2−70918
toroidal plasma, with helical mag. field, stationary equilib. and diffusion 2−77278
toroidal reactors, neutral injection heating 2−46746
toroidal system, virtual casing principle in calc. containing magnetic field 2−80277
toroidal systems, specific mag. inductance 2−83568
toroidal vortices in pulsed plasma 2−83587
toroidal Z-θ pinch at Padova, ionization heating and diffusion 2−83571
toroidality, influence on magnetic configuration with helical magnetic axis 2−64284
toroidally symmetric cusp, particle loss 2−43157
torsatron without toroidal field coils, configuration $l=2$ 2−46754
transverse velocity shear instabilities in Q-machine plasma 2−64333
trapped-ion instability in low-aspect ratio limit 2−50218
Troesch's two-point boundary value problem, solution by combination of techniques 2−83553
vortices, ball lightning, mechanism of formation, laser analogue 2−81665
Z-pinch, adiabatic contraction 2−83588
Z-pinch, dynamic, charged-particle acceleration mechanism, exptl. verification 2−67649
Z-pinch, high pressure confinement, losses 2−83600
Z-pinch, low pressure high voltage, formative phase 2−67650
Z-pinch, noncylindrical profiles, holographic interferometry 2−83597
z-pinch, toroidal, axisymmetric MHD equilibria and stability 2−83549
z-pinch, toroidal, shock heated, MHD stable mag. profiles 2−83565
Z-pinch discharge, characs. of plasma compression 2−43159
Ar, dynamics of inverse pinch 2−56358
D-T fusion reactor review of recent progress in mag. confinement 2−79843
D, θ pinches, sheath formation and ion heating in low density h.v. pinch 2−83580

devices
see also Plasma diodes; Stellarators
— 2−60296
accelerator, impulse, appl. of high voltage spectroscopy 2−46768
accelerator with closed electron drift and extended acceleration zone 2−64291
accelerators, use in gas dynamics and ionosphere simulation 2−77280
arc spectroscopy for photoionization meas. 2−77301
coaxial accelerator, luminous front 2−80281
coaxial deflagration gun, characteristics 2−83610
coaxial gun, r.f. plasma heating 2−64273
coaxial plasma accelerator, shocked layer 2−80285
conical induction source, plasma acceleration 2−67653
current multiplier 2−70921
cylindrical plasma capacitor, resonant props. in crossed fields 2−64290
d.c. jet generator, cathode sleeve, double arc phenomena 2−56400
display panel, a.c. breakdown mechanism 2−50234
Divertor type source, scatt. centre estimation 2−46745
double plasma device, beam and wave obs. 2−83556
electron cyclotron resonance plasma accelerators as source of ion beams 2−60253
e.m. waves amplitude modulation by acoustic waves in dispersive plasma 2−80251
emitter, for creation of plasma flow 2−53240
focus, 1 kJ expt., filament structure 2−83592
focus, current sheet collapse 2−80282
focus, dense, instabilities and turbulent heating 2−83589
focus, flow in a pulsed mag. compressor 2−83593
focus, highly localized X-ray source 2−83585
focus, investigation of high energy deuterons 2−83582
focus, meas. of beta 2−83591
focus, megajoule expt. project 2−83590
focus, neutron meas., Thomson scattering and holographic interferometry 2−83583
focus, vortex breakdown condition 2−83586
focus expt. rel. to two-dimensional MHD code 2−83584
fusion reactors, engineering problems of l.f. heating 2−46373
glass sphere production from quartz, by processing through plasma stream 2−56971
gun focus, high speed photography 2−53205
high current ion accelerator, optimization 2−79704

- **Plasma** continued
  - **devices** continued
    - injector for transverse injection into linear stellarator like magnetic field 2−80289
    - injector for transverse injection into linear stellarator like field 2−43163
    - injector-diverter, purification of H plasmoids by mag. field 2−80298
    - ISAR II linear θ pinch, energy balance 2−83575
    - J × B type plasma gun, closed magnetic trap expt. 2−70920
    - jet, Langmuir probe meas., saturation current behaviour 2−56361
    - jet generator with cathode sleeve 2−53206
    - jets, d.c., arc constriction 2−74374
    - levitated spherator FM-1, confinement times and particle loss 2−80287
    - magnetic de Laval nozzle, characteristic flow parameters of stationary supersonic Cs plasma flow 2−50203
    - magnetron diode, potential distribution effect on critical mag. field 2−60300
    - MHD equilibria in sharply curved axisymmetric devices 2−56357
    - MHD generator, combustion gas plasma, heat transfer, obs. 2−80300
    - MHD machines with liquid metal and plasma secondary, design and operation 2−52359
    - minimum-B mirror devices, stable equilibria computation, computer program 2−67652
    - minimum-B mirror reactors, optimized magnetic field profiles and β-limitation 2−46751
    - mirror machine, distribution function near loss cone 2−46752
    - mirror machines, superadiabaticity 2−64287
    - mirror reactors, electron heating effect on power balance 2−52839
    - mirror trap, ion confinement in presence of electrostatic potential and r.f. electron plugs 2−74372
    - nuclear fusion research, review 2−42611
    - θ pinch, axial plasma flow and end loss obs. 2−50202
    - plane plasma capacitor in crossed fields electron and ion densities and velocities 2−64304
    - plasmatron with diffusor-type arc channel 2−60264
    - pulsed ablation accelerator, electron density measurement 2−80297
    - pulsed ablation accelerator, monochromaticity 2−67654
    - pulsed high-β fusion reactor, based on θ-pinch, design obs. 2−83613
    - Q-machine, ideal, nonexistence of electrostatically driven ion acoustic waves and Landau damping 2−67671
    - Q-machine, influence of cathodes on flute instability 2−43191
    - radioactive (tritium) ignitors for plasma limiters 2−50204
    - r.f. torch, effects of pulsed magnetic field 2−70923
    - Scyllac, 5 m, linear θ pinch, column behaviour 2−83572
    - shock tube, electric discharge, as plasma flow source for MHD expts. 2−60252
    - spherator, supported, magnetic field errors 2−50205
    - stellarator diverter, ion and electron energy distributions 2−70890
    - thermonuclear reactor, yield coeff. of cyclotron radiation in energy balance calcs. 2−83539
    - theta-pinch gun operation 2−74373
    - Tokamak, major radius oscill., theory 2−70936
    - Tokamak, MHD and tearing instabilities 2−70975
    - Tokamak, plasma properties 2−43161
    - Tokamak systems, particle diffusion and energy balance equations 2−53203
    - Tokamak type apparatus, field distrib. near gap formed by sectionalized shells 2−64288
    - Tokamaks, skin effect and suppression in large devices 2−46753
    - torch, air, 20kW, induction and applications 2−46757
    - torch, with flame of oblong cross section 2−70922
    - toroidal θ-Z pinch LT1, electron runaway 2−53202
    - toroidal Z-θ pinch at Padova, ionization heating and diffusion 2−83571
    - toroidally symmetric cusp, particle loss 2−43157
    - Tuman-2, effect of transverse magnetic field 2−80295
    - twin plasma jet, welding and hardfacing of steel 2−68147
    - CO_2 laser, plasmotron excitation by plasma jet injection 2−69917
    - D_2 coaxial focus gun, current sheath obs. 2−80271
    - H atom injector for fast atom bunches 2−53204
    - H^- source, pulsed duoplasmatron 2−79169
  - **diagnostics**
    - *see also Langmuir probes*
    - α-particle probing of current distribution in axisymmetric plasma column 2−46763
    - θ-pinch, using laser interferometer 2−50201
    - absorbing optically-non-thin plasma calc. of temperature profile using extension of lightness-emissivity method 2−46761
    - afterglow electron density and temp. determ. by single Langmuir probe technique 2−53211
    - afterglow plasma, method based on potential meas. around embedded high freq. antenna 2−74375
    - antenna behaviour as function of frequency of excitation, summary 2−80291
    - antennas, characteristics as functions of frequency 2−80290
    - astrophysical phenomena interpret. 2−78432
    - Axicon-scanned Fabry-Perot spectrometer, non-homogeneity brightness of fringes 2−60262
    - bounded magnetoplasma, h.f. production and diagnostics 2−67661
    - bremsstrahlung photon emission rate from Maxwellian plasma to det. electron temp. 2−46764
    - cascaded arc, electron temp. and density meas. using scattered laser light 2−53260
    - charged particle flux, by l.f. modulated floating double probe 2−80279
    - coaxial generator system Cogen III 2−67660
    - collective phenomena, laser scatt. use as probe 2−56350
    - collisionless, density determ., probe theory 2−46759
    - confinement time as function of electron density and temp. studied in levitated spherator FM-1 2−80287
    - contact pot. between emitting electrode and probe 2−74376
    - cylindrical plasma capacitor, resonant props. in crossed fields 2−64290
    - d.c. glow discharge used for sputtering 2−50230
    - density, temp., fixed-bias floating double probe techniques 2−60259

- **Plasma** continued
  - **diagnostics** continued
    - density determ., calibration procedure to correct for effects of dielectric containers 2−67655
    - density meas., analysis of microwave interferometer 2−46728
    - detection props. of plasma in l.f. field 2−64305
    - discharge, low pressure 2−80268
    - double beam interferometric method of obs. of axisymmetric configs. 2−43170
    - drift-beam instability, of plasma-ion beam system in longitudinal mag. field 2−80345
    - dual mag. probe system for phase meas. in thermal induction media 2−50208
    - electroacoustic resonances measurement, broadband short pulse technique 2−43173
    - electron density, from intensity calibration using high temp. continuum emission in vacuum u.v. 2−53196
    - electron density, interferometric obs., circuit for direct registration 2−67658
    - electron density, laser interferometer with harmonically matched cavities 2−66811
    - electron density, rel. to voltage pulse profile of pulsed ioniz. chamber 2−52686
    - electron density, surrounding atmospheric re-entry body, simulation 2−72931
    - electron density distrib. from bending of laser beam 2−67657
    - electron density in collisionless flows, obs. using positively biased electrostatic probes 2−77282
    - electron density in laser-produced gas breakdown, interferometric holography 2−83559
    - electron density meas. using direct reading microwave interferometer 2−60257
    - electron density meas. with microwave reflectometer system 2−74380
    - electron energy distrib., second derivative Langmuir probe 2−67656
    - electron temp. and density meas. by laser radiation scattering in Tuman-2 2−70925
    - electron temp. meas. by electrostatic probe rel. to plasma resist. 2−60260
    - e.m. shock tube, probe meas. of press. and mag. field, bow shock effects 2−77291
    - emission coeff. calc. using exptal. intensity profiles 2−74377
    - energy distribution of electrons in positive column, influence of probe size and temperature 2−60256
    - Faraday rotation probe for magnetic flux density meas. 2−77279
    - floating probe method for study of l.f. oscillations 2−64298
    - flow characteristics in arc channel 2−64294
    - flowing transient plasma, Lecher wire microwave probe 2−77283
    - fluctuations, digital spectral analysis 2−70926
    - focus, 1 kJ expt., filament structure 2−83592
    - focus device, investigation of high energy deuterons 2−83582
    - focus device, meas. of beta 2−83591
    - focus device flow in a pulsed mag. compressor 2−83593
    - force-free collinear plasmoids produced by a conical theta pinch 2−67651
    - frequency analysis method, for current fluctuation in plasma 2−53198
    - geostationary operational environmental satellite, state-of-the-art report 2−72746
    - glow discharge plasmas, electron energy analysis 2−74379
    - glow discharges, diode sputtering system, obs. 2−53214
    - high current arc investigations, application of Schlieren techniques 2−64360
    - holographic recorder for transient and high speed events 2−76494
    - inverse problem density determ. from time record of reflected wave arising from S function electric field 2−46711
    - ion boundary layers on probes 2−56338
    - ion density and plama potential from Langmuir probe data 2−43174
    - ion energy distribution resulting from turbulent heating 2−70927
    - ion energy transverse to magnetic field, meas. methods 2−53212
    - ion temp., using high power a.c. probe 2−50210
    - ion temperature, laser produced plasma 2−43167
    - ion temperature in θ-pinch deuterium plasma, laser-beam-scattering meas., evidence for thermonuclear reaction 2−56364
    - ionosphere, D-region, double-probe technique 2−58086
    - ionospheric and magnetospheric altitudes 2−78397
    - i.r. techniques for high temp. 2−82562
    - jet, Langmuir probe meas., saturation current behaviour 2−56361
    - Langmuir probe and r.f. capacitance probe, electron density meas. 2−50209
    - Langmuir probe I-V characteristics, in afterglow plasma, technique for recording 2−64299
    - laser, use of very powerful beams which could be developed in the foreseeable future 2−63313
    - laser light scatt. technique 2−70924
    - light scatt., ion-acoustic line profiles determ. 2−67642
    - line oscillator strengths of spectral lines which are not optically thin 2−60242
    - local potential substitution for exchange operator 2−73332
    - magnetic field direction, spatial meas. 2−64302
    - magnetic field meas. using light scatt. 2−64301
    - magnetic probe, with nanosecond response time 2−46760
    - magnetoactive plasma, possibility of using induced wave scatt. 2−80347
    - magnetosheath structure obs. by 3 ALSEP/SIDE plasma detectors on lunar surface 2−62315
    - magnetospheric plasma circulation speed meas. using quadripole probe on spacecraft 2−84871
    - magnetospheric substorms, sheet variations 2−81710
    - mass spectroscopic det. of parameters in laser microplasmas 2−83551
    - by microwave cavity resonators 2−77284
    - microwave interference polarimeter-ellipsometer for resolution of ambiguity of meas. between rotation and ellipticity 2−83557
    - microwave plasmas, electron density, calc. 2−77271
    - microwave Q-band propagation on capillary arc plasma as diagnostic method 2−60250
    - microwave resonant cavity meas. of electron density 2−43169
    - multicomponent systems, disc-stabilized d.c. arc and solution nebulization device 2−64300

Plasma continued
diagnostics continued
negatively biased conical probes in supersonic flow, current drawn and det. of ion density 2−46758
neutral pressure obs., fast pressure gauge 2−56363
neutron meas., Thomson scattering and holographic interferometry in focus expt. 2−83583
non-thermal process in linear pinch device 2−83609
nonideal low-temp. plasma, electrical conductivity and metallization 2−64295
optically thick non-thermal, use of escape factors to compute atomic number densities 2−43166
optimum collection of scattered light, optical system 2−56360
particle concentr., in impulse accel., using high voltage spectroscopy 2−46768
pinch discharges, electron density and temp. obs. 2−83564
plane plasma capacitor in crossed fields electron and ion densities and velocities 2−64304
potential determ., i.f. noise in probe circuit 2−64306
potential in positive column of low-pressure discharge 2−60254
probe, impedance characteristics, spherical probe, isotropic plasma 2−46766
probe for detection of ion reflected from shock wave 2−60226
probeless technique for detecting ion waves 2−74396
pulsed X-ray obs. of shock waves in Cs plasma 2−64297
pyrometry, secondary radiation standard with $\lambda=640.2$ nm 2−45585
Q-pinch torus, Scylac 5-meter, helical equilibria 2−83561
radial temperature distribution measurement, Ar plasma jet 2−46767
r.f. discharge, electrostatic probe props. 2−50207
sampling diagnostics using ion kinetic energy distributions 2−60258
sheath capacitance obs. using tunnel diode oscillator 2−56362
solar wind, spatial disturbances of plasma parameters 2−73130
spectral temperature measurements, with applic. 2−43171
spectroscopic study and energy balance of pulsed toroidal discharge 2−53216
spectroscopic temperature determination Ar-N_2 plasma in low power MHD generator 2−46716
spherical Langmuir probe, classical theory 2−64303
stimulated emission contributions to a cathodic cavity plasma 2−82477
techniques applicable for controlled thermonuclear fusion 2−53213
temperature measurement, optical methods for plasma in MHD generator ducts and combustion chambers 2−43172
thermionic caesium convertor, by spectrographic method 2−59055
transient phenomena analysis using pulsed laser and liq. cryst. detector 2−53208
transport phenomena det. from e.m. waves interactions in turbulent plasma 2−70886
velocity meas. using Doppler effect 2−64296
wave-particle interactions, metho of obs. particle distribution function evolution 2−46765
weakly ionized, theory of spherical probe 2−80296
X-ray bandpass filter for nanosecond resolution of spectra 2−67659
X-ray emission meas. of laser produced plasmas 2−43165
X-ray flash tube applic. 2−85181
X-ray source, highly localized, focus expt. 2−83585
Ar, electrodeless discharge, high pressure, conc. of charged particles from line spectra 2−46423
Ar, low density, hypersonic, effect of angle of incidence on probe response 2−77285
Ar, pulsed plasma, containing 1-2% H_2, temp. from spectral meas. 2−49941
Ar, slightly ionized, electron energy distrib. and swarm parameters 2−70891
Ar, stabilized arc, cylindrical, emission line profile 2−64307
Ar, temp. determination in arc discharge 2−58971
Ar, with polydispersed Ti, thermophysical processes, investigation 2−46762
Ar arc discharge at 950 atm. 2−67662
Ar discharge, flowing, radial and axial characteristics 2−70896
Ar discharge, high current, pulsed, electron density obs. in early stages 2−60261
Ar discharge, motion of ionization front in microwave e.m. field 2−60238
Ar electron thermal conductivity, temperature dependence 2−60263
Ar ion laser, electron temp., meas. using Al double probe system 2−74349
Ar plasma, electrical conductivity using average- gradient and tuned-circuit-Q method 2−56386
Ar plasma impedance, waveguide probe meas., effects of e.m. wave-front curvilinearity 2−49240
Ar^+, wave interaction phenomena obs. on interaction with transverse mag. field 2−77268
Ar + H_2, stabilized arc, cylindrical, emission line profile 2−64307
C, d.c. arc, in ext. mag. field, electron temp., calc. from line intensities 2−50238
CO_2-TEA laser produced plasma, interferometric obs. 2−64310
CO_2 gas laser, with N_2 and He mixtures, temp. meas. from R-branch bands of N_2 2−46769
Cs, collisional, space pot. oscills., hot-probe meas. 2−67677
Cs, elec. cond., 1000-10000 K and 130-350 atm. 2−80292
Cs, forbidden line transitions, thermionic diode 2−60237
Cs, ion temps. determ. using probe with cold collector grid 2−74356
Cs, ionized vapour, electron density determ. from spectral line mixing 2−46792
Cs, low voltage and discharge, excitation and ionization processes 2−53265
Cs, thermionic energy convertors, probe measurements, space craft power source 2−54991
Cs ion beam, neutral atom rate meas. 2−53207
D_2, focused, X-ray fine structure in coaxial accelerator 2−80270
H, ion energy distribution resulting from turbulent heating 2−70927
H plasma, time-resolved diagnostics 2−53209
H plasmoids, purification by mag. field in injector-diverter 2−80298
H pulsed discharge, maximum electron conc. 2−67692
He discharge, hot-probe investigation of spatial fine structure in plasma potential 2−60255
K plasma, using laser, selective excitation spectroscopy 2−70928

Plasma continued
diagnostics continued
Kr electron thermal conductivity temperature dependence 2−60263
Li, laser produced, ion energy, retarding potential probe obs. 2−43168
N, dependence of high-current pulsed discharge on initial pressure and current 2−56387
N, electrical and thermal conductivities 2−56335
N discharge, motion of ionization front in microwave e.m. field 2−60238
N_2, collision cross section for momentum transfer 2−50194
N_2, distribution function for free electrons 2−64263
N_2, stationary microwave discharge at atmos. pressure 2−64293
N_2 arc, disequilibrium effects 2−70898
$Na_{2x}Sr_{1-x}Pb(OH)_6$, nonstoichiometric, struct. 2−71437
$Na_2Zn[PO_4](OH)$, cryst. struct. determ. 2−71439
Ne discharge, hot-probe investigation of spatial fine structure in plasma potential 2−60255
O_2 doped spherical laser plasmas, high intensity X-ray spectra and stimulated emission 2−74378
Rb-NH_3 solutions, electrodeless method of det. conductivity 2−71226
Xe, continuum absorption coefficient 2−60243
Xe, electrical conductivity det. 2−56341
Xe, electrodeless discharge, high pressure, conc. of charged particles from line spectra 2−46423
Xe electron thermal conductivity temperature dependence 2−60263
Xe pulsed discharge, basic parameters, optical and electrical props. 2−74381
Xe pulsed discharge, meas. of plasma temp. 2−56388

electromagnetic waves
absorption in hybrid resonance region 2−46736
absorption of extraordinary wave in bounded magnetoactive plasma 2−70907
alpha-effect calc. rel. to gyromotion of electrons and ions 2−60214
amplitude modulation by acoustic waves in dispersive plasma 2−80251
anomalous absorption computer simulations 2−83532
attenuation of communicating signal to reentering spacecraft 2−43137
bi-Maxwellian, numerical solution of dispersion equation Newton's method, stability 2−80330
bounded plasma, transverse elec. to transverse mag. partial transform in polarization 2−83540
breakdown thresholds and heating of CO_2 laser produced plasma in magnetic field 2−43134
bremsstrahlung instability, induced by electron streaming 2−67680
characteristics with TEA CO_2 laser and wavelength scaling law 2−43150
cold magnetoactive plasma, low-freq. potential oscills. in field of e.m. wave 2−80349
Compton radiation from relativistic particles, depression of power spectrum 2−80228
conductive liner, cumulation of plane field at relativistic initial velocities 2−43138
coupled e.m. and electron acoustic waves in warm stratified plasma 2−70901
Crab pulsar region 2−62610
cyclotron harmonic waves, instability 2−46741
cyclotron heating in magnetic trap, asymptotic particle distribution function 2−74365
cyclotron waves, dispersion 2−67673
cyclotron-harmonic waves, 10.6 μm laser scatt. 2−56350
direct and cross polarized backscatter power from turbulent plasma 2−74363
dispersive medium with moving density profile, pulse propagation 2−43142
Einstein-de Sitter cosmology, coupled to radiation at nonrelativistic temperature, e.m. wave absorption 2−68997
Einstein-De Sitter cosmology, coupled to radiation at relativistic temperature, e.m. wave absorption 2−68998
electron bremsstrahlung in strong mag. field, rel. to X-ray pulsars 2−78478
electron capture, in wave field excited by ion beam 2−70951
electron cyclotron resonance plasma produced by Lisitano coil 2−43178
electron density distrib. from bending of laser beam 2−67657
electron frequency greater than wave frequency, TE_0 mode 2−76420
electron plasma, static dielec. const. in presence of strong e.m. wave 2−77843
electrostatic instability of hot electron plasma in h.f. field 2−74395
emission processes in magnetoactive plasma, theory of solar bursts 2−69185
energy recovery from stream by decelerating wave 2−67640
energy transport and photon rest mass phenomena 2−83535
excitation in a degenerate plasma for quantizing magnetic field 2−67637
excitation in a solid by electron beam 2−71817
excitation of e.m. wave in plasma by beam of phased oscillations 2−80234
extraordinary wave absorption, weak inhomogeneous plasma in region of hybrid resonance with oblique incidence 2−56353
flows with radiant energy absorption and thermonuclear reaction behind shock wave 2−70909
free-free radiation from relativistic plasma with anisotropic electron energy distribution 2−67622
frequency division in plasma located in inhomogeneous electric field 2−70906
gain mechanism in homogeneous plasma 2−46738
galaxies and quasars, activity, syncrotron radiation 2−58193
generalized ion Bernstein mode near lower hybrid frequency, high β effect 2−60274
heating by r.f. power absorpt., coaxial electron gun 2−64273
helicon wave radial structure depend. on electron inertia, dispersion 2−68376
h.f. fields interactions in linear installations, tank circuits 2−60229
h.f. oscillations control 2−56377
homogeneous spheroid, diffr. problem, elec. multipole moments calc. 2−74357
hot magnetoplasma with collisions, dispersion curves calc. 2−50192

Plasma continued
- **electromagnetic waves** continued
  - hypersonic flow of ionized gas around blunt ended bodies and leading radiation 2–77347
  - impedance characteristics, spherical probe, isotropic plasma 2–46766
  - incoherent scattering from high temp. plasma 2–64276
  - incoherently reflected waves spectrum, interface influence 2–56347
  - inhomogeneous gyrotropic warm plasmas 2–56349
  - inhomogeneous warm, with static pressure gradients, coupled electromagnetic and electron-acoustic waves 2–60231
  - interplanetary plasma, monochromatic radio waves 2–55601
  - ion cyclotron harmonic waves, propag. bandwidths 2–64272
  - ion heating by geometrical Landau damping 2–67638
  - ion heating by microwave power modulation at l.f. 2–67664
  - ionosphere, electron cyclotron resonance, nf_h, frequency shifts 2–51647
  - ionosphere, electron resonances, topside sounder obs. 2–81727
  - ionospheric plasma resonances, time durations rel. to latitude, altitude and ratio of electron plasma and cyclotron frequencies 2–48573
  - i.r., inverse bremsstrahlung and photoionization absorption 2–43147
  - i.r. laser heating of dense electric arc plasma 2–43148
  - isotropic turbulence, radiative transport analysis 2–64274
  - kinetic theory of e.m. field fluctuations in anisotropic plasma half-space 2–80235
  - kinetic theory of plane wave scattering from cylinder 2–83537
  - Landau and collisional damping of plasma lines, numerical computations of linewidths and intensities 2–43143
  - laser created from solid target, parametric dependence of temp. 2–43149
  - laser heating of D-T plasma by ion-ion collisions 2–64289
  - lasers, nonlinear interactions 2–43153
  - l.f. radiation from relativistic electrons in magnetoplasma and U shaped type IV solar bursts 2–75959
  - light scattering in dense cold plasma 2–60246
  - linear transformation and absorption, review 2–56352
  - loop antenna, in isotropic compressible plasma, radiation impedances, calc. 2–52336
  - magnetic field direction, spatial meas. by microwave method 2–64302
  - magnetoactive, nonlinear interaction 2–46735
  - magnetoactive plasma, induced wave scatt. 2–80347
  - magnetoactive plasma, parametric excitation of nonelectrostatic instabilities 2–70972
  - magnetoionic media, waves on cond. infinite cylinder 2–55621
  - magnetoplasma, collisional, total energy loss of test charge 2–46725
  - magnetoplasma, collisionless linear damping 2–53193
  - magnetoplasma, propagation constant along infinitely long conducting wire 2–83533
  - magnetoplasma, propagation of v.l.f. waves 2–50197
  - magnetoplasma, three-fluid, wave eqn. 2–49228
  - magnetoplasma, warm, v.l.f. electric dipole radiation characts. 2–74364
  - magnetoplasma, weakly ionized warm, e.m. wave propagation determ. of refractive index 2–53189
  - magnetoplasma containing negative ions, right-hand circularly polarized wave propagation, thermal effects 2–80229
  - magnetosphere, e.l.f. hiss between 1 and 1000 Hz, detection by triaxial search coil magnetometers 2–62331
  - microwave cavity, sustained plasma 2–60234
  - microwave discharge, mag. field stabilized 2–64271
  - microwave generation near electron cyclotron resonance 2–60265
  - microwave heating for steady state high β hot electron plasmas 2–43139
  - microwave nonlinear excitation, instability 2–56354
  - microwave Q-band propagation on capillary arc plasma 2–60250
  - microwaves reflection in laboratory plasma 2–53192
  - modelling of dispersive propagation of symmetric magnetic waves 2–83534
  - modulation, by alternating mag. field in gas-discharge plasma 2–77266
  - moving e.m. sources in gyromagnetic plasma, dipoles 2–53195
  - moving sinusoidal stratified turbulent medium 2–83536
  - negative absorption of light 2–70910
  - nonequilibrium energy constants associated with large amplitude electron whistlers 2–50196
  - nonlinear, production by oscillatory electric dipole in spherical cavity 2–60227
  - nonlinear collisional excitation of longitudinal plasma waves 2–53232
  - nonlinear effects in r.f. plasma 2–60236
  - nonlinear effects in weakly ionized medium, collisions influence 2–46733
  - nonlinear instability of Bernstein modes pumped by e.m. wave 2–70965
  - nonuniform magnetized, description to all orders in electron and ion temperatures using operator method 2–50198
  - oblique incidence on dielectric bounding infinite plasma 2–60249
  - one-dimensional Maxwellian medium, simulation of excited monochromatic wave evolution 2–46732
  - opaque, nonlinear interaction with strong e.m. wave, volume ion-acoustic oscills. excitation 2–70941
  - optical transitions stimulated by plasma turbulence 2–43145
  - optically dense, passage of powerful laser emission 2–43154
  - ordinary mode instability for counter streaming plasmas with anisotropic temperatures and growth rates 2–43141
  - parametric excitation, stability analysis 2–60233
  - plane e.m. wave incidence on moving jump of ionized gas density 2–80232
  - power absorption in uniform plasma, neo-classical theory of Landau damping 2–80242
  - power transfer near lower hybrid reson., ion and electron press. effects 2–53194
  - propagation in plasma with fluctuations 2–64277
  - propagation in plasma with sheared magnetic field 2–80233
  - pulse compression, time-domain method 2–63200
  - pulse distortion in anisotropic system 2–53190
  - Q-device plasma, enhanced absorption due to parametric decay instability 2–70970

Plasma continued
- **electromagnetic waves** continued
  - quasi static approx., validity 2–55597
  - quasi-monochromatic wave momentum 2–74361
  - radiation from uniformly moving charge in time dependent magnetoactive plasma 2–53180
  - radiation from warm-slab-covered magnetic line source 2–60228
  - radiation resistance of cylindrical antenna in ionized magnetoplasma 2–41890
  - radiowave scattering from random electron density fluctuations in cold magnetoplasma 2–63201
  - ray tracing in anisotropic absorbing medium 2–80240
  - reflection, kinetic theory, moving inhomogeneous plasma sheath 2–74366
  - reflection coeffs. for random half-space and slab 2–64275
  - reflection from turbulent plasma, radiative transfer methods 2–80236
  - reflection on moving front of ionization 2–46737
  - relativistic cyclotron resonance heating 2–70905
  - relativistic Vlasov plasma, self-consistent e.m. waves 2–70904
  - resonance cone structure, warm plasma effects 2–67639
  - resonance radiation effects on Cs discharge 2–70908
  - resonant absorption, amplitude limitations and impedance of plasma capacitance 2–60235
  - restricted plasma, longitudinal wave excitation by relativistic electron beam injection 2–80348
  - r.f. energy transport to lower hybrid resonance 2–74362
  - rotating e.m. field interaction with plasma in constant magnetic field, compression to column 2–50199
  - scattering by conducting wedge 2–77273
  - scattering by hydrodynamically turbulent systems 2–46860
  - scattering by underdense plasmas, role of turbulence intermittency 2–50195
  - scattering causing attenuation, phenomenological model 2–46740
  - scattering from ion acoustic waves in Hg positive column 2–74387
  - scattering from moving cylindrical electron beam, velocity dependent scattering 2–52327
  - scattering in flat waveguide with magnetoactive plasma due to electron charge fluctuations 2–77275
  - self-focusing 2–70902
  - signal transmission through ionized media, distortion, obs. 2–45626
  - singularities in electric field 2–80237
  - sinusoidally space-time periodic plasma, uniaxial plasma 2–52318
  - slightly nonstationary plasma, general case 2–46743
  - solar flares comparison, X-ray spectra and microwave emission 2–76000
  - solar plasma heating, type II meter bursts 2–75963
  - space-time periodic media, wave-vector diagram 2–53191
  - ST tekomak plasma, second-harmonic generation at upper hybrid layer by extraordinary incident wave at 34-6 GHz 2–83541
  - stimulated v.u.v. and soft X-ray emission from optical transitions of multiionized atoms in high current density discharges 2–41961
  - stratified turbulent magnetized plasma, e.m. wave reflection, transmission 2–77274
  - surface, on metal-air boundary, light radiation with aid of roughness 2–75040
  - surface adsorption of extraordinary wave with specular reflection of particles at boundary 2–83544
  - synchrotron instability on e.m. waves, decay process stabilization 2–83617
  - temporal e.m. echoes oblique to external magnetic fields 2–60230
  - Thomson scattering, influence of radiation statistics 2–56348
  - transient wave in anisotropic plasmas, steepest descent evaluation of integral 2–56351
  - transition radiation from boundary 2–80230
  - transmission and reflection, e.m. wave incident normally on plasma half-space 2–46739
  - transparency, induced wave barriers 2–53219
  - transport phenomena det. from e.m. waves interactions in turbulent plasma 2–70886
  - transverse propagation in magnetoactive plasma near electron gyrofrequency harmonics, wavelengths < electron gyro-radius, effects of collisions 2–46734
  - travelling and standing waves for inductive plasma acceleration 2–43144
  - Tuman-2, microwave heating in upper hybrid range 2–74367
  - turbulent plasma scattering theories, criticism 2–46742
  - turbulently heated plasma, microwave radiation spectrum 2–60232
  - velocity of wave packet; calc. by saddle point method 2–80239
  - wave-wave interactions, lagrangian studies 2–43184
  - waveguide filled with compressible magneto plasma, excitation 2–52331
  - weakly ionized magnetoplasmas, incoherent scattering of light from charge density fluctuations 2–77267
  - weakly-turbulent plasma, kinetic equations by multiple scattering theory 2–70903
  - X-ray emission from laser plasma from high Z target 2–43151
  - Ar, high pressure, radiation capacity det. 2–64260
  - Ar discharge, motion of ionization front in microwave e.m. field 2–60238
  - Cs, forbidden line transitions, thermionic diode 2–60237
  - Cs, reson. absorpt. produced, radial distrib. of electron density 2–46727
  - Cs, s.h.f. emission 2–67641
  - H-He, absorption coefficients of i.r. radiation, photoionization and inverse bremsstrahlung 2–46744
  - H, continuum emission in visible and u.v. 2–80247
  - ^{2}H solid, heating by laser pulse 2–43152
  - Hg, s.h.f. emission 2–67641
  - N discharge, motion of ionization front in microwave e.m. field 2–60238
  - Nd:glass laser produced plasma, second harmonic generation 2–43146
  - O, absorption, 50-70 MHz 2–74368
- **magnetohydrodynamics**
  - *see also Magnetohydrodynamic waves*
  - — 2–60275
  - — 2–60279
  - Alfven waves, excitation in high β-plasma 2–64324
  - Alfven waves, nonlinear dissipation in cosmic plasmas 2–75784

Plasma continued
magnetohydrodynamics continued
Alfven waves in inhomogeneous mag. fields 2−64252
alpha-effect calc. rel. to gyromotion of electrons and ions 2−60214
axisymmetric toroidal equilibria and their stability 2−83549
belt pinch, stability 2−83601
book on plasma as fourth state of matter 2−53174
bounded layer, transverse mag. waves, h.f. pot. effects 2−56340
cloud, dynamic form. of strations 2−60218
conductive liner, cumulation of e.m. plane field at relativistic initial velocities 2−43138
crossed field accelerator, circulating currents 2−56339
current and heat dissipation, channel with undulating electrodes 2−53186
current through magnetic neutral point, expts. 2−64255
current-carrying, free boundary solution 2−64281
cylindrical MGD shock in nongravitating system 2−53185
density fluctuations, dependence on electrical field controlled by metal ends 2−43127
electric fields in MHD channels for anisotropic non uniform conductivity 2−60217
electrostatic instabilities driven by currents perpendicular to external magnetic field 2−46784
electrostatic ionic-cyclotron oscills., excitation by transverse current 2−46783
electrothermal instability, two-point correlation description 2−80266
e.m. wave propagation, wave eqn. 2−49228
equilibria, helically symmetric 2−83547
equilibria in sharply curved axisymmetric devices 2−56357
equilibrium configurations of Vlasov plasmas with current component along external magnetic field 2−60215
Faraday ring currents in low-pressure ring-shaped duct with radial mag. field 2−60219
flow of perfectly conducting fluid, multiplicity theorem 2−50173
flow pinch in coaxial plasma device, flow process energy balance 2−83538
focus, vortex breakdown condition 2−83586
focus device, meas. of beta 2−83591
focus expt., megajoule project 2−83590
focus expt. rel. to two-dimensional MHD code 2−83584
galaxies and quasars, activity, eruptive instability 2−58193
gas-particle, nonequilibrium ionization phenomena, calc. 2−80261
geomagnetic tail, flow meas. by spin-modulation method 2−62324
guiding-centre, finite-orbit effects studied using simple model of gyroscopic fluid 2−56312
Hall effect in plasma flow in travelling magnetic field 2−60216
hierarchy of eqns. for turbulent magnetized plasma 2−43132
hydromagnetic waves obs. in magnetosheath by 3 ALSEP/SIDE plasma detectors on lunar surface 2−62315
ideal, spectrum of eigenmodes of linearized equations of motion 2−83548
inert gases, parameters for nonequilibrium generator 2−59049
instabilities, near Kruskal-Shafranov limit in linear and toroidal high-β pinch 2−83546
instability of current carrying plasma in Tokamak 2−70975
ionization instabilities in nonlinear regime 2−80264
ionization instability control by feedback 2−80263
isotope separation, plasma centrifuge 2−70648
long wave oscillations, in m=1 mode in plasma pinch 2−77281
magnetic field annihilation 2−43129
magnetic field det. in vacuum for two dimensional MHD equilibria 2−64264
magneto-acoustic waves interactions with shock waves 2−60224
magnetoacoustic disturbances produced by arbitrary expansion of conducting sphere 2−46771
magnetoplasma, weakly ionized warm, e.m. wave propagation determ. of refractive index 2−53189
magnetosphere, generation of large scale electric field 2−65862
nonlinear waves, ergodic behaviour in cold collisionless system 2−80304
numerical methods and computational problems in MHD 2−80267
photon rest mass, determ. by meas. of hydromagnetic waves in plasma 2−52547
relativistic, infinite conductivity 2−74345
relativistic, isometric motion, vel. field, vorticity tensor, four vector mag. field invariance 2−67634
resistance free magnetosonic shocks, upper critical conditions 2−80324
resonant three wave interactions, application of hierarchy for turbulent magnetized plasma 2−43133
r.f. torch, effects of pulsed magnetic field 2−70923
shock tube, electric discharge, as plasma flow source for MHD expts. 2−60252
shock waves, low β perpendicular, exptl. study of turbulent resistivity 2−53187
shock waves slightly oblique in magnetized plasma 2−70899
solar wind, local density fluctuations, correlation with oblique nonlinear MHD waves 2−62784
solar wind, rotational discontinuities closed system of hydrodynamic equations 2−48800
solar wind, spherically symmetric outflow 2−48799
solar wind plasma interaction with magnetic field 2−72907
solutions representing dipole field immersed in plasma 2−43130
striations in transverse mag. field 2−64326
theta pinch column, MHD feedback stability 2−83603
theta pinch discharge, investigation of relation between compression, relaxation and end losses by two-dimensional m.h.d. computer programme 2−43160
theta-pinch, with azimuthal mag. field, small-scale drift instability turbulence 2−67644
threshold of ionization instability in unbounded low temp. plasma, dispersion relation 2−46788
Tokamak, MHD and tearing instabilities 2−70962
toroidal belt pinch, of equilibria 2−83595
toroidal equilibria, local hydromagnetic, without symmetry 2−80273
toroidal vortices in pulsed plasma 2−83587
turbulence, nonlinear analysis 2−80258
two dimensional flow, elec. properties, calc. 2−80260
two-dimensional equilibria, stability 2−83550

Plasma continued
magnetohydrodynamics continued
unsteady flow, near accelerated plate, effect of Hall currents 2−43131
z-pinch, toroidal, shock heated, MHD stable mag. profiles 2−83565
Ar, propagation of non-axisymmetric Alfven waves 2−53231
Ar$^+$, shock generated, interaction with transverse mag. field 2−77268
CO_2 laser, ionization instabilities and discharge characteristics 2−79207
Cs seeded Ar, stability 2−80262
H, ionized, upper bound of longitudinal wave frequency 2−74347
He-Cs gas, two-dimensional calc. of ionization fluctuations 2−80265
He ion motion in magnetic field in presence of induced electric field 2−70959
n-InSb magnetoresistance meas. 2−46729
measurement technique *see Plasma/diagnostics*
oscillations
see also Magnetohydrodynamic waves;
83531
Alfven waves, excitation in high β-plasma 2−64324
Alfven waves, m=1, propagation in high beta plasma 2−83630
Alfven waves, non-axisymmetric, propagation in Ar plasma 2−53231
alpha-effect calc. rel. to gyromotion of electrons and ions 2−60214
amplitude oscillation-linear Landau damping transition, Vlasov eqn., asymptotic method 2−53225
arc, magnetized, h.f. oscills., obs. using h.f. Stark effect 2−70942
astron, neutralized E layer, stability of tearing mode 2−80286
beam discharges, ion heating rel. to oscills., lower hybrid reson. region 2−67669
beam-current-density fluctuations along electron stream 2−50213
beam-plasma discharge, hot electron prod. 2−53236
beam-plasma instability in finite length system, computer simulation 2−80321
beam-plasma system, control using external h.f. signal 2−56377
beam-plasma system, nonlinear interaction of waves excited 2−74355
beam-plasma system, satellite generation of unstable wave 2−60282
beam-plasma system, turbulent-like spectrum of ion waves 2−64316
beat heating, by excitation of longit. waves by reson. with difference freqs. 2−67672
Bernstein mode pumped by e.m. wave, nonlinear instability 2−70965
Bernstein modes, application of weak inhomogeneity formalism 2−56373
Bernstein waves, inhomogeneous magnetoplasma, parametric excitation 2−53222
bounded systems, beam-plasma interaction, excitation of fields 2−80310
Cherenkov emission in presence of finite amplitude wave 2−64311
circularly polarized, in homogeneous plasma computer model 2−43181
coherent waves individual linear damping effects on nonlinear instability 2−60269
cold magnetized plasma, nonlinear interaction of plasma waves 2−46782
cold magnetoactive plasma, low-freq. potential oscills. in field of e.m. wave 2−80349
collisionless, damping of finite-amplitude electron waves 2−77293
collisionless ion-acoustic shocks, beam generated 2−46775
collisionless wave-particle interactions perpendicular to magnetic field 2−53237
column, major radius oscill., theory 2−70936
type I comet tails 2−73094
convectively unstable random ionization waves 2−60309
coupling, summary 2−80338
coupling due to magnetic field induced pressure anomalies in beam plasma system 2−43180
coupling of intense oscillations computer simulation 2−83532
current driven instabilities, linear theory 2−74391
current-driven drift wave instability in sheared mag. field 2−70964
cyclotron oscillations, unstable, development in inhomogeneous magnetic field 2−80328
cyclotron waves, dispersion 2−67673
cylindrical plasma, nonlocal drift wave propag. 2−64312
damping in electron beam modulation by l.f. signal 2−50215
decay in L-1 stellarator, nonstationary phenomena 2−67670
dispersion relations for bi-Maxwellian plasma, numerical solution 2−80330
dispersive waves, slightly ionized nonequilibrium plasma 2−70948
double plasma device, beam and wave obs. 2−83556
drift instabilities in collisionless inhomogeneous plasma 2−64329
drift wave, radial propagation in uniform mag. field 2−43188
drift wave growth, effect of mag. shear on temporal damping 2−70946
drift-beam instability, of plasma-ion beam system in longitudinal mag. field 2−80345
drift-dissipative instability development, plasma diffusion 2−60284
drift-dissipative instability in confined plasma 2−70949
echoes, Landau damping 2−53229
electron acoustic waves coupled to e.m. waves in warm stratified plasma 2−70901
electron beam plasma interaction, obs. Brownian motion model 2−67628
electron gas in positive column, non-hydrodynamic props., reson. behaviour 2−74420
electron-ion oscillation discharge, potl. distrib., temp. and density detn. 2−64319
electrons, upstream of Earth's bow shock 2−65846
electrostatic current-driven cross-field instability, asymptotic behaviour 2−83633
electrostatic instabilities driven by currents perpendicular to external magnetic field 2−46784
electrostatic instabilities in collisionless plasma driven by electric field perp. to magnetic field 2−83631
electrostatic instability of hot electron plasma in h.f. field 2−74395
electrostatic ionic-cyclotron oscills., excitation by transverse current 2−46783

- **Plasma** continued
  - **oscillations** continued
    - electrostatic l.f. waves, negative press. effect 2−46773
    - electrostatic longitudinal waves in homogeneous plasma, time of flight studies 2−53230
    - electrostatic waves in Vlasov plasma undergoing $E \times B$ and gradient B drifts 2−60272
    - electrostatic waves radiated from waveguide to inhomogeneous plasma 2−74362
    - e.m. waves amplitude modulation by acoustic waves in dispersive plasma 2−80251
    - excitation by relativistic electron beam 2−53228
    - excitation by relativistic electron beam 2−64338
    - excitation of e.m. wave in plasma by beam of phased oscillations 2−80234
    - excitation of nanosecond electron waves on positive columns 2−60271
    - excited by modulated electron beam in mirror machine, nonlinear effects 2−50217
    - fast wave damping, at second harmonic of ion cyclotron freq. 2−56369
    - finite amplitude obliquely propagating waves, reson., particle trapping and Landau damping 2−83626
    - finite amplitude obliquely propagating waves, resonance, particle trapping and Landau damping 2−80317
    - floating probe, l.f. oscillation meas. 2−64298
    - frequency spectra kinetics, plasma-beam discharge 2−70952
    - generalized ion Bernstein mode near lower hybrid frequency, high β effect 2−60274
    - generation of osc. by beam-plasma interaction 2−70945
    - glow discharge, random striations in positive column 2−46799
    - heating by electron beam in mirror trap, oscill. spectra 2−56368
    - helicon wave radial structure depend. on electron inertia, dispersion 2−68376
    - h.f. electrostatic wave instability, induced by electron beam 2−53239
    - h.f. exciting current, measurement of perturbed electron current 2−70955
    - hot plasma, surface waves 2−53227
    - hydrodynamics current driven instability in electrodeless induction discharge 2−80356
    - inert gas, kinetics of oscillation deactivation, rel. to spontaneous radiation 2−77298
    - inertial forces effect under glow discharge 2−64321
    - instabilities and turbulence, summary 2−80334
    - instability of nonlinear longitudinal oscillations of magnetoactive plasma 2−74398
    - interaction of two monochromatic Langmuir waves, induced scattering 2−80303
    - interaction processes in weakly turbulent collision free Vlasov plasma 2−43123
    - ion acceleration by electron beam- plasma interaction in a mirror machine 2−50214
    - ion acoustic wave, in collisionless plasma, trapped in instabilities 2−64323
    - ion acoustic wave, nonlinear, Kortweg-de Vries eqn., derivation including ion Landau damping 2−70940
    - ion acoustic wave, radially propagating in Hg positive column, microwave scatt. obs. 2−74387
    - ion acoustic waves, electron beam excited, effect of beam modulation 2−70963
    - ion acoustic waves, mode coupling 2−67682
    - ion acoustic waves, optical line modulation 2−70956
    - ion acoustic waves, trapped ion instabilities 2−64313
    - ion acoustic waves and Landau damping electrostatically driven in ideal Q-machine 2−67671
    - ion Bernstein modes, excitation, antenna resonances 2−80323
    - ion cyclotron wave exciter, loading resist., directivities, rel. to plasma density 2−60268
    - ion heating via turbulent ion acoustic waves 2−53178
    - ion oscillation, excitation by electron beam 2−80343
    - ion oscillation modes, automodulation, perturbation theory 2−70938
    - ion wave lifetimes in unstable and turbulent plasmas 2−80308
    - ion wave limiting amplitude, computer simulation 2−83532
    - ion wave propagation, perpendicular longitudinal, effects of collisions 2−56370
    - ion-acoustic, beam-plasma system, instability control 2−74403
    - ion-acoustic collisionless shocks in Q-machine 2−77272
    - ion-acoustic wave and pseudowave generation, computer simulation 2−80320
    - ion-acoustic waves, effect of time- varying mag. field 2−67674
    - ion-acoustic waves, h.f. modulation 2−80318
    - ion-acoustic waves, stability mechanism, nonlinear frequency shift 2−46774
    - ion-acoustic waves in collisionless system, nonlinear coupling 2−80319
    - ionization relaxation, direct absorpt. effect of transverse quanta of plasma oscills. 2−77296
    - ionosphere, electron resonances, topside sounder obs. 2−81727
    - ionosphere, topside, reson. obs. on rocket- borne advanced radio sounder 2−62372
    - ionospheric plasma resonances, time durations rel. to latitude, altitude and ratio of electron plasma and cyclotron frequencies 2−48573
    - ionospheric response to v.l.f. ion-acoustic waves rel. to sudden geomagnetic storms 2−83614
    - ionospheric transient responses, resonance spikes of topside sounders 2−81728
    - ionospheric wave phenomena, rel. to electron temp. determ. 2−62355
    - isotropic turbulence radiative transport analysis 2−64274
    - kinetic equations, strong plasma turbulence 2−53221
    - kink modes and feedback control, energy considerations 2−67648
    - Korteweg-de Vries equation, exact N-soliton soln. 2−43120
    - Lagrangian theory for nonlinear wave packets in collisionless plasma 2−43182
    - Landau's dispersion equation, asymptotic soln. 2−56374
    - Landau wave propag. in hot electron system 2−64317
    - large amplitude, solar radio bursts, Rayleigh and Raman scattering 2−75961
    - large amplitude electrostatic waves, role of trapped particles, computer simulation 2−80316
    - launching selectivity in electron waves on bounded plasmas 2−60277
    - l.f., in laser capillary discharge tube, due to moving striations 2−77314
    - l.f., in weakly ionized plasma of h.f. discharge in presence of magnetic field 2−77294
    - l.f. e.s. waves, produced by ion acoustic turbulence 2−70971
    - l.f. ionization-recombination, frequency and damping in bounded low density plasma 2−80352
    - l.f. of diffusion constricted discharge 2−74394
    - linear and nonlinear coupling of waves 2−80337
    - linear damping of interacting waves and explosive instability 2−70960
    - long wave ion cyclotron and ion acoustic, spontaneous excitation 2−64315
    - longitudinal plasma wave, wave vector in direction of electron stream, two stream electrostatic instability 2−80311
    - longitudinal waves, nonlinear collisional excitation by interacting e.m. waves 2−53232
    - longitudinal waves, physical mechanism of Landau damping 2−46779
    - longwave ion acoustic, in weakly ionized plasma 2−60278
    - Lorentz fully ionized, generation of third harmonic current density by h.f. electric field 2−43135
    - loss-cone flute instabilities, single, resonant, nonlinear stabilization 2−70966
    - loss-cone flute modes, nonlinear evolution 2−64335
    - macroscopic and microscopic density fluctuations, wave propagation 2−64277
    - magnetized column, l.f. grid excitation 2−43185
    - magnetized plasma, Fresnel-like interference and ion wave decay 2−70939
    - magneto-acoustic, in column in Tokamak TO-1 2−53220
    - magneto-acoustic waves interactions with shock waves 2−60224
    - magnetoacoustic disturbances produced by arbitrary expansion of conducting sphere 2−46771
    - magnetoactive plasma, induced wave scatt. 2−80347
    - magnetoplasma column, transverse Kelvin- Helmholtz turbulence 2−70933
    - magnetoplasma waves in strongly curved configurations 2−70953
    - magnetosphere, upper-hybrid reson. noise obs. by IMP-6 AC-elec. fields exp. 2−65869
    - magnetotail, resonant interaction of electrostatic wave with electrons in current sheet 2−72826
    - MHD, long wave, in $m=1$ mode in plasma pinch 2−77281
    - modified ordinary wave in presence of contrastreaming beams, macroscopic model and stability 2−46780
    - monochromatic wave, excitation by cold electron beam 2−46778
    - non acoustic instability in collisionless shocks 2−77299
    - nonlinear, collisionless system 2−46777
    - nonlinear cold plasma waves, stability 2−80305
    - nonlinear collisionless interaction between electron and ion modes in inhomogeneous magnetoactive plasmas 2−74396
    - nonlinear development at modulated electron beam interaction 2−70934
    - nonlinear evolution of firehose unstable Alfven waves 2−60273
    - nonlinear interaction between three waves, 1st initially absent. 2−83620
    - nonlinear interaction between waves, plasma with random inhomogeneities 2−80346
    - nonlinear interaction of small cold beam with plasma 2−56337
    - nonlinear interaction with MHD waves 2−46772
    - nonlinear ion acoustic waves in plasma, calc. of recurrence time using Korteweg-de Vries eqn. 2−83623
    - nonlinear longit., spatial dispersion effect on stability 2−43192
    - nonlinear magnetosonic waves in turbulent plasma 2−60275
    - nonlinear magnetosonic waves in turbulent system with finite conductivity 2−67668
    - nonlinear mechanics of unstable systems 2−83627
    - nonlinear MHD waves, ergodic behaviour in cold collisionless system 2−80304
    - nonlinear mode coupling linearly unstable and stable waves, obs. of relaxation oscillations 2−83624
    - nonlinear motions and trapping of particles in quasi-monochromatic wave 2−43183
    - nonlinear oscillations near boundary of breaking 2−83616
    - nonlinear plasma wave kinetics 2−70937
    - nonlinear scattering, cyclotron harmonic plasma waves 2−64322
    - nonlinear space charge waves in plasma sheath 2−74393
    - nonlinear stabilization of particle beam in stabilities 2−74388
    - nonlinear wave modulation, collisionless plasma 2−53223
    - nonlinear wave modulation, Landau damping effects 2−53224
    - nonlinear waves in multicomponent plasma with weak dissipation 2−80350
    - nonuniform magnetized, description to all orders in electron and ion temperatures using operator method 2−50198
    - numerical simulation of plasma echoes 2−70954
    - opaque, nonlinear interaction with strong e.m. wave, volume ion-acoustic oscills. excitation 2−70941
    - pair distribution function damped oscills. in one-component plasma 2−56327
    - parametric coexcitation of ion acoustic waves, h.f. electric field 2−67684
    - parametric instabilities in mag. field and dispersion relation for longitudinal waves in h.f. electric field 2−46785
    - Penning discharge plasma, l.f. oscills. under cyclotron ion source conditions 2−50216
    - perpendicular collisionless shock wave instability 2−77300
    - photon rest mass, determ. by meas. of hydromagnetic waves in plasma 2−52547
    - positive and negative ion beams, nonlinear effects 2−80344
    - potential, excitation by electron beam 2−64318
    - potential due to point charge oscillating in magnitude 2−64267
    - quasi-longitudinal mode near lower hybrid resonance, spatial and temporal damping 2−60276
    - quasilinear eqns. derivation 2−43115
    - quasilinear theory, experimental tests 2−67683

Plasma continued
oscillations continued
quasiparticle conservation in weakly turbulent plasmas 2−56372
radially bounded plasma, Landau attenuation, calc. 2−70950
radially oscillating coherent plasma of electron-positron pairs, props. rel. to pulsars 2−62615
resistance, anomalous, rel. to Bernstein modes buildup 2−56342
resistance free magnetosonic shocks, upper critical conditions 2−80324
resonances and Bernstein-mode electrostatic waves, summary 2−80332
resonances in collisionless heating by transit time magnetic pumping 2−64314
resonant three wave interactions, application of hierarchy for turbulent magnetized plasma 2−43133
restricted plasma, longitudinal wave excitation by relativistic electron beam injection 2−80348
r.f. collisional, growth rate and frequency dispersion characteristics of drift waves 2−53226
sawtooth solitary and turbulent waves in weakly ionized plasma 2−80312
scattering of beam of plasma waves by acoustic turbulence and type III solar radio bursts 2−62753
second harmonic generation using nonlinear interaction between electron beam and collisionless plasma 2−56367
sideband growth in nonlinear Landau wave-particle interaction and distortion of electron velocity distrib. 2−60270
soliton propagation in two stream plasma 2−46781
spatial ballistic wave echoes, props. 2−80314
stability of monochromatic wave against induced scattering 2−74392
standing striations as solns. of Pekarek equation 2−70986
stationary solitary snoidal and sinusoidal ion acoustic waves in Maxwellian plasma 2−74390
stationary turbulence, mechanism 2−77295
stimulated emission contributions to a cathodic cavity plasma 2−82477
strong turbulence and resonant diffusion 2−70943
Sun, type III radio bursts rel. to neutralization and stabilization of particle streams in corona 2−48798
surface wave propagation along boundary between two magnetoactive plasmas 2−80354
surface waves in cylindrical waveguide, kinetic theory 2−80353
symmetry properties of nonlinear responses 2−80329
synchrotron instability on Langmuir waves, nonlinear stabilization 2−83617
theta-pinch, rotational disturbances 2−83621
third order plasma echo, structure 2−80313
toroidal current carrying plasma column, equilib. displacement, instabilities 2−83622
transition from amplitude oscill. to linear Landau damping 2−83545
transport processed, higher harmonics, circularly polarized magnetic field, higher harmonics 2−74352
transverse waves, collisional damping 2−80357
turbulence, probabilistic models 2−56371
turbulence, stimulation of optical transitions 2−43145
turbulence, theories and expts. 2−80333
turbulence in solar atmosphere 2−62801
turbulent plasma theory, book 2−83625
two stream instability, attenuation, summary 2−80341
unstable potential oscillations in isothermal plasma in strong magnetic field 2−80306
virtual plasma wave echoes 2−46776
wave attenuation, collisions, absorption and coupling review 2−80340
wave coupling at collisionless plasma discontinuity 2−83615
wave excitation, review 2−80335
wave excitation, summary 2−80336
wave growth in strongly turbulent plasma 2−70944
wave kinetic equation for homogeneous plasma, systematic derivation 2−64256
wave propag., nonlinear processes 2−77297
wave propagation in magnetized plasma near lower hybrid resonance 2−67675
wave-particle interactions, metho of obs. particle distribution function evolution 2−46765
wave-wave interactions, lagrangian studies 2−43184
waves, excitation by two laser beams 2−70947
waves, experimental simulation in transmission line 2−73263
waves and resonances, conference (St. Johns, Newfoundland, July 1971) 2−80331
waves and resonances excitation in non-uniform high-β MHD plasmas 2−83629
waves in coaxial plasma cylinder 2−70957
weak cold beam-plasma system, nonlinear wave-particle interactions 2−53238
weakly turbulent plasma, nonlinear interactions, quantum mech. 2−43186
Ar, e.f. waves, mode-coupling 2−70958
Cs, collisional, space pot. oscills., hot-probe meas. 2−67677
Cs, rel. to s.h.f. emission 2−67641
Cs vapour, peculiarities of photoresonance perturbation relaxation in low-temp. discharge plasma 2−64320
He-Cs non-equilibrium plasma in mag. field 2−60267
He arc with superposition of h.v. pulse, interaction giving 2 to 40 GHz radiation 2−50212
He ion motion in magnetic field in presence of induced electric field 2−70959
Hg, ion sound wave parametrically excited in Tonks-Dattner resonance, radial pattern obs. 2−70932
Hg, parametric excitation of lower hybrid modes 2−70935
Hg, rel. to s.h.f. emission 2−67641
K magnetoplasma, effect of collective interactions on resistivity 2−70897
Ne, bounded, const. wavelength propagated oscills. 2−74389
Ne, p and s ionization waves, nonlinear interaction 2−71025

production
bounded magnetoplasma, h.f. production and diagnostics 2−67661
coaxial plasma accelerator, shocked layer 2−80285
dense column, high density,low electron temp., from hollow cathode arc discharge 2−74384

Plasma continued
production continued
explosion of polymer fibres, high ion energy prod. and neutron yield 2−67665
fusion by laser driven flame propagation in solid DT targets 2−64308
heating of laser-produced sphere, fusion yield optimum conditions 2−83558
high β fusion plasmas, formation by intense relativistic electron beams 2−83607
high temp., and containment, using high power laser, power production 2−70930
high temperature, laser radiation use 2−70931
high temperature, rel. to fusion, review 2−77287
hot electron, by Lisitano coil, multiply charged ion source 2−63303
hot electron, generated by high current electron beam 2−53217
ion heating by microwave power modulation at l.f. 2−67664
jet generator, pulsed injector and conical electrode geometry 2−64292
large quiescent collisionless h.f. discharge 2−56365
Large Volume Microwave Plasma Generator 2−50211
laser, fusion prospects 2−43175
laser, X-ray emission meas. 2−43165
by laser beams 2−74382
laser created from solid target, parametric dependence of temp. 2−43149
laser heating in focus-type system and heat of nucl. fusion 2−77288
laser heating in focus-type system and heat of nucl. fusion 2−77289
laser induced, momentum transfer and plasma formation above a surface, high powered CO_2 laser 2−67663
laser interaction, rel. to population inversion 2−49973
laser irrad. of D_2 pellet, parameter instabilities 2−67679
laser irradiation of polyethylene foil, determ. of ion and velocity structure 2−80272
laser plasma, ion energy spectrum, rel. to accel. and recombination effects 2−53215
laser plasma, prod. by photoionization with u.v. light 2−79193
laser prod. plasma, fusion, review of conditions, expt. work, prospects 2−80299
laser produced, breakdown thresholds and heating in magnetic field 2−43134
laser produced, ion energies 2−74385
laser setup, for high temp. heating of solid target 2−80294
laser-produced, obs. of nonlinear excitation of waves in meas. of X-radiation and scattered light 2−56366
linear screw-pinch discharge properties 2−46750
Lisitano coil, electron cyclotron resonance plasma 2−43178
microplasma generated by laser beam impact, far-u.v. source 2−70088
microwave generation near electron cyclotron resonance 2−60265
Moon, impact produced, Apollo 14 lunar models 2−66151
Penning source, formation position of ions, dependence on mag. field 2−53262
plasmatron, powerful light erosion 2−53218
plasmatron with diffusor-type arc channel 2−60264
pulsed toroidal discharge, energy balance and spectroscopic study 2−53216
reflected energy from nsec laser produced plasma 2−43177
sapphire, relationship between laser induced surface damage and surface plasmas 2−60266
byslotted cylindrical microwave cavity, electron temp. 2−74383
source for use in prep. of Si films 2−67912
super-dense, Nd^{3+}:glass laser induced 2−77286
superdense, high-temp. laser heating, radiation energy feeding problem 2−67667
thermonuclear hot spot expansion and energy production 2−64309
u.v. radiation source, 100 kVZ-pinch with Xe gas 2−74386
for X-ray flash tube 2−76134
Ar breakdown, threshold conditions at superhigh- pressure produced by Q-switched lasers 2−64355
Ba, photoionisation of intense atomic beam in metastable states 2−83197
CD_2, laser produced, irrad. of deuterated polyethylene by nanosecond and picosecond pulses 2−80269
CO_2-TEA laser, interferometric obs. 2−64310
Co_2 laser induced, magnetic field enhanced heating 2−70929
Cs, by reson. absorpt., contrib. of dissociative recomb. 2−67666
D, high temp., by laser heating of special gas target 2−80293
^{2}H, solid, heating by laser pulse and production of DD reactions 2−43140
^{2}H, solid, heating by laser pulse 2−43152
^{2}H, solid target, wavelength dependence of laser light absorption 2−43176
^{2}H laser heated pellets, decoupling of corona and core 2−46770
^{2}H plasma laser generation and heating to thermonuclear temps. 2−43179

shock waves
blast waves generation, by pulsed electric discharges 2−74360
bounded plasma, electron-plasma-wave shocks 2−64269
coaxial plasma accelerator, shocked layer 2−80285
collisionless, in cold plasma 2−74359
collisionless ion-acoustic shocks, beam generated 2−46775
collisionless magnetized plasma, slightly oblique waves 2−70899
collisionless plasma flow, strong mag. field, discontinuities 2−46731
cylindrical MGD shock in nongravitating system 2−53185
discharge, plasma focus type, obs. of second compression 2−56344
e.m. shock tube, probe meas. of press. and mag. field, bow shock effects 2−77291
generation by exploding current sheath 2−53188
gun focus, high speed photography 2−53205
heating of low density plasma in fast theta pinch 2−83578
interstellar HI region, strong polarization shocks 2−48735
ion acoustic, in collisionless plasma 2−64270
ion acoustic solitons in two-component system 2−56346
ion heating of high-β plasma 2−80280
ion thermalization in strong high-beta shocks 2−83632
ion-acoustic collisionless shocks in Q-machine 2−77272
laser solid surface interaction studies, shock wave propagation 2−43136

Plasma continued
shock waves continued
laser spark, decaying, plasma fireball, subsonic radiation front, shock wave 2−67636
magnetized low-β plasma, influence of reflected ions on magnetic structure of collisionless shock front 2−60226
magneto-acoustic waves interactions with shock waves 2−60224
magnetosonic, resistance free, upper critical conditions 2−80324
non acoustic instability in collisionless shocks 2−77299
nonisothermal plasma, turbulent heating by collisionless shock wave 2−56345
nonlinear magnetosonic waves in turbulent plasma 2−60275
oblique hydromagnetic shocks, instability of whistler structure 2−80326
perpendicular collisionless shock wave instability 2−77300
perpendicular MHD, low β, exptl. study of turbulent resistivity 2−53187
pulsed high-β plasmas, conference (Garching, Germany, July 1972) 2−83560
pulsed X-ray obs. of shock waves in Cs plasma 2−64297
solitary waves in two ion beam magnetized plasma 2−60225
thermonuclear combustion waves, existence conditions and propagation velocity in bounded plasma 2−64268
Ar, freejet, nonequilibrium effects, shock wave formation 2−70900
Ar^+, formation in interaction of plasma with transverse mag. field 2−77268
H-He plasmas, thermodynamic properties for stagnation shock layer of spacecraft entering atmosphere of Jupiter 2−46718
stability
θ-pinch, caulked cusp torus field 2−83599
astron, neutralized E layer, stability of tearing mode 2−80286
asynchronous excitation of instability 2−60280
auroral instability and dumping of particles 2−54883
with axial current, surrounded by cold gas with pressure gradient 2−80355
beam-plasma discharge, hot electron prod. 2−53236
beam-plasma instability, satellite modes 2−60282
beam-plasma instability during intense heating 2−43121
beam-plasma instability in finite length system, computer simulation 2−80321
beam-plasma interaction in bounded geometry, temp. effects 2−80301
beam-plasma system, dissipative instability, nonlinear theory 2−64338
beam-plasma system, instability control 2−74403
beam-plasma system, instability suppression by modulation of electron beam 2−70963
belt pinch, MHD 2−83601
Bennett pinch, hydromagnetic stability conditions 2−83619
bremsstrahlung instability, induced by electron streaming 2−67680
capillary discharge with evaporating wall 2−56385
charged particle mass rot. around axis, relative equil. 2−72946
coherent waves individual linear damping effects on nonlinear instability 2−60269
colliding plasmas, e.m. instability, applic. to interplanetary matter and bow shock problems 2−60213
colliding plasmas, ion motion and return currents 2−56376
collisional drift instability, effects of parallel wavelength 2−64332
collisionless plasma flow, strong mag. field, discontinuities 2−46731
collisionless wave-particle interactions perpendicular to magnetic field 2−53237
conditions for quasi steady development of self sustaining nuclear reactions 2−63952
convectively unstable random ionization waves 2−60309
counterstreaming ion instability for arbitrary angles 2−80315
coupling effect of three wave interaction on development of explosive instability 2−56378
current driven, linear theory 2−74391
current-driven drift wave instability in sheared mag. field 2−70964
cyclotron harmonic waves, instability 2−46741
D-T reactor, thermal stability of spatially non-uniform plasma 2−80309
diode, high-current field-emission instability during initial stages of breakdown 2−49325
dissipative instability due to supersonic motion of ions rel. to neutrals 2−74399
drift instabilities in collisionless inhomogeneous plasma 2−64329
drift instability in presence of nonuniform radial elec. fields 2−74397
drift wave, radial propagation in uniform mag. field 2−43188
drift wave growth, effect of mag. shear on temporal damping 2−70946
drift-beam instability, of plasma-ion beam system in longitudinal mag. field 2−80345
drift-dissipative instability development, plasma diffusion 2−60284
drift-dissipative instability in confined plasma 2−70949
dynamic, of composite medium, Larmor radius and collisional effects 2−56379
electric field induced, causing plasma heating, computer simulation 2−64334
electron clouds magnetically confined, equilibria and stability 2−74404
electron cyclotron drift instability and turbulence 2−46787
electrostatic current-driven cross-field instability, asymptotic behaviour 2−83633
electrostatic instabilities driven by currents perpendicular to external magnetic field 2−46784
electrostatic instabilities in collisionless plasma driven by electric field perp. to magnetic field 2−83631
electrostatic instabilities in confined plasma heated by high energy ion beams 2−43187
electrostatic instability of hot electron plasma in h.f. field 2−74395
electrothermal instability with effects of electron thermal conduction and wall boundaries 2−80359
equatorial ionosphere above Thumba, rocket meas. of ionization irregularities and plasma instabilities 2−84901
equatorial sporadic E, plasma instabilities 2−54901
equilibrium configurations of Vlasov plasmas with current component along external magnetic field 2−60215
equilibrium in configurations with helical magnetic axis with allowance for toroidality 2−64328
expansion of toroidal equilibrium with finite periodicity length and l=0,1 fields 2−83567
explosive instability, role of linear damping 2−70960
explosively unstable systems, time evolution 2−77292
external feedback stabilization 2−70877
finite-sized radiating system, onset of instability, metastable states 2−60285
flow, creation by plasma emitter 2−53240
flute, in Q-machine, influence of cathodes 2−43191
flute modes, in presence of nonuniform elec. fields 2−60281
focus, dense, instabilities and turbulent heating 2−83589
gravitational instability and frictional effects with neutrals 2−66073
growth rate of instabilities, computation for general pinch configuration 2−83570
guiding-centre, finite-orbit effects studied using simple model of gyroscopic fluid 2−56312
Hall system, combined Rayleigh and Kelvin instability 2−60279
Harris instability in two dimensions, numerical simulation 2−64331
Harris instability with collisions, numerical simulation 2−70968
helical field, dispersion relations for const. oxide components 2−83552
helical hydromagnetic instability, suppression in toroidal column by feedback 2−77290
helical instability and hysteresis in magnetized plasma 2−80342
helically symmetric MHD equilibria 2−83547
h.f. electrostatic wave instability, induced by electron beam 2−53239
high-β compact torus 2−83566
high-β plasma, remote feedback stabilization 2−70969
high-β plasmas, Vlasov-fluid model 2−83628
high-β plasmas, Vlasov-fluid model for studying gross stability 2−43193
highly force free relativistic electron beam equilibrium 2−80322
hot electron plasma, produced by mirror θ pinch, instability 2−70961
hot electron plasma, transverse instabilities in cylindrical resonator 2−74402
hydrodynamics current driven instability in electrodeless induction discharge 2−80356
inhomogeneous high β plasma, against Alfven waves 2−64324
inhomogeneous two stream plasma with water bag model 2−50219
instabilities, linear to nonlinear saturation evolution, rel. to Landau amplitude equation 2−64325
instabilities and turbulence, summary 2−80334
instability due to Doppler effects of multiloop electron stream interaction with plasma 2−74400
instability in negative θ pinch, artificial resistivity 2−83573
instability of inhomogeneous streams with nonuniform velocity profile 2−80339
instability of nonlinear longitudinal oscillations of magnetoactive plasma 2−74398
ion Bernstein modes, excitation, antenna resonances 2−80323
ion viscosity effects, for finite pressure plasma 2−80351
ion wave lifetimes, Boxcar integrator study in unstable conditions 2−80308
ion-acoustic instability, nonlinear saturation 2−64337
ion-acoustic instability of collisional plasma with nonstationary equilibrium 2−64336
ion-acoustic wave and pseudowave generation, computer simulation 2−80320
ion-acoustic waves, h.f. modulation 2−80318
ion-acoustic waves, stability mechanism, nonlinear frequency shift 2−46774
ion-acoustic waves in collisionless system, nonlinear coupling 2−80319
ion-sound instability, three-dimens. current-driven, computer simulation 2−53234
ionization equilibrium and stability of quantum plasma 2−64327
ionization instabilities in nonlinear regime 2−80264
ionization instability, inhomogeneity scale taking into account heat conduction 2−43189
ionization instability control by feedback 2−80263
ionosphere, electron temperature gradient instability 2−65956
ionosphere purely growing parametric instability 2−65957
isothermal plasma, unstable potential oscillations 2−80306
Kelvin Helmholtz instability, passive feedback stabilization 2−43197
kink modes and feedback control, energy considerations 2−67648
large amplitude electrostatic waves, role of trapped particles, computer simulation 2−80316
laser induced anomalous heating 2−56375
laser-produced, obs. of nonlinear excitation of waves in meas. of X-radiation and scattered light 2−56366
l.f. instability, near electron cyclotron resonance frequency 2−70973
l.f. instability of plasma in weak s.h.f. electric field, quasilinear theory 2−70974
linear screw pinch, standing wave magnetic fields 2−83604
linear screw-pinch discharge properties 2−46750
longitudinal plasma wave, wave vector in direction of electron stream, two stream electrostatic instability 2−80311
longwave instability caused by inhomogeneous ion beams in dense magnetized plasma 2−74401
loss-cone flute instabilities, single, resonant, nonlinear stabilization 2−70966
loss-cone flute modes, nonlinear evolution 2−64335
magnetoactive plasma, parametric excitation of nonelectrostatic instabilities 2−70972
magnetosphere, cyclotron instability, causing v.l.f. emission 2−81706
magnetospheric substorm expansive phase triggering 2−65870
MHD, subjected to electrothermal instability, two-point correlation description 2−80266
MHD and tearing instabilities in Tokamak 2−70975
MHD instabilities, near Kruskal-Shafranov limit in linear and toroidal high-β pinch 2−83546
mirror plasma, 2-dimensional criterion for distinguishing absolute instability 2−80307

Plasma continued
stability continued
mirror-confined, geomag. field, electrostatic instabilities 2−65866
mirror-confined plasma trapped near equator in geomagnetic field, electrostatic instabilities 2−62333
modified two stream instability, e.m. and finite β_e effects 2−53235
monochromatic waves, against induced scattering 2−74392
non acoustic instability in collisionless shocks 2−77299
non-viscous system, stationary motion stability 2−70878
nonisothermal plasma, turbulent heating by collisionless shock wave 2−56345
nonlinear cold plasma waves 2−80305
nonlinear electron cyclotron drift instability 2−64330
nonlinear instability of Bernstein modes pumped by e.m. wave 2−70965
nonlinear interaction between waves, plasma with random inhomogeneities 2−80346
nonlinear longit. oscillations, spatial dispersion effect on stability 2−43192
nonlinear mechanics of unstable systems 2−83627
nonlinear mode coupling linearly unstable and stable waves, obs. of relaxation oscillations 2−83624
nonlinear parametric interactions, instabilities, numerical study 2−78780
nonlinear theory of density fluctuations in turbulence plasma 2−56380
nonlinear wave-wave interacting systems with well- defined phase description, bounds for solution 2−45241
ordinary mode e.m. instability for counter streaming plasmas with anisotropic temperatures and growth rates 2−43141
oscillations excited by modulated electron beam in mirror-machine, nonlinear effects 2−50217
paramagnetic instability of m=1 mode in dynamic stabilization of pinch 2−77281
parametric instabilities, three-wave, in weakly homogeneous media 2−67679
parametric instabilities and anomalous heating near lower hybrid freq. 2−80325
parametric instabilities for excitation of cold plasma by e. beam 2−64318
parametric instabilities in mag. field and dispersion relation for longitudinal waves in h.f. electric field 2−46785
parametric instability, collision effect on threshold energy level 2−53233
parametric instability obs. near lower hybrid-resonance frequency 2−80327
particle motion in magnetic mirrors with high-frequency electric field fluctuations 2−83554
perpendicular collisionless shock wave instability 2−77300
plasmapause, Cerenkov instability and v.l.f. emissions 2−72827
plasmapause, wave-particle interactions, instabilities 2−62329
positive and negative ion beams, nonlinear effects 2−80344
pulsed high-β plasmas, conference (Garching, Germany, July 1972) 2−83560
Q-device plasma, parametric decay instability, enhanced absorption of electromagnetic waves and effective collisions frequency 2−70970
Q-pinch torus, Scylac 5-meter, helical equilibria 2−83561
radio aurora, caused by plasma instabilities 2−48555
Rayleigh-Taylor instability, astrophysical relevance 2−67676
resistance, anomalous, rel. to Bernstein modes buildup 2−56342
resistive instabilities 2−46786
r.f. collisional, growth rate and frequency dispersion characteristics of drift waves 2−53226
sawtooth solitary and turbulent waves in weakly ionized plasma 2−80312
spatially separated beams, finite thickness, two-stream instability in quasi-hydrodynamic approximation 2−43190
stellerator, finite β, 1=2 2−83569
striations in transverse mag. field 2−64326
superheat instability in a fully ionized current-carrying plasma, exptl. obs. 2−67678
synchrotron instability of Langmuir waves, nonlinear stabilization 2−83617
thermal instability of rotating plasma, Finite Larmor radius and Hall effects 2−70967
theta pinch column, MHD feedback stability 2−83603
theta-pinch, with azimuthal mag. field, small-scale drift instability turbulence 2−67644
threshold of ionization instability in unbounded low temp. plasma, dispersion relation 2−46788
Tokamak, MHD and tearing instabilities 2−70962
toroidal belt pinch, ISAR IV 2−83594
toroidal belt pinch, MHD equilibria 2−83595
toroidal current carrying plasma column, equilib. displacement, instabilities 2−83622
toroidal equilibria, local hydromagnetic, without symmetry 2−80273
toroidal equilibria, stationary, at finite beta 2−80274
transverse velocity shear instabilities in magnetically confined plasma 2−64333
trapped ion instabilities, ion acoustic wave, in collisionless plasma 2−64323
trapped ion instabilities in ion acoustic waves 2−64313
trapped particle instability, localization 2−43196
trapped-ion instability in low-aspect ratio limit 2−50218
turbulent heating by cross-field current, high- temperature limit 2−43194
turbulently heated plasma, rel. to microwave radiation spectrum 2−60232
two stream instability, attenuation, summary 2−80341
two-dimensional MHD equilibria 2−83550
two-ion-beam instability, meas. of self- stabilisation by micro turbulent ion heating 2−43195
two-stream instability, nonlinear limitation in beam-plasma system 2−74393
waves, nonlinear, in dispersive media, stationary solutions and stability 2−82153
weak cold beam-plasma system, nonlinear wave-particle interactions 2−53238
weak turbulence caused by electrostatic ion cyclotron instability, dispersion characts. 2−67681

Plasma continued
stability continued
in weak u.h.f. electric and constant magnetic field, quasi- linear theory 2−56326
whistler instability in anisotropic plasma, simulation 2−60283
z-pinch, toroidal, axisymmetric MHD equilibria and stability 2−83549
Ba cloud released in magnetosphere, instability mechanism for formation of striations 2−62302
CO_2 MHD laser, ionization instabilities and discharge characteristics 2−79207
Cs, collisional, space pot. oscills., hot-probe meas. 2−67677
Cs seeded Ar, nonequilibrium MHD 2−80262
He-Cs non-equilibrium plasma in mag. field 2−60267
Li, also spectroscopic discharge properties 2−53197

transport processes
θ-pinch, anomalous resistivity in initial stages 2−80244
accumulation in electrostatic potential well created by electron space discharge 2−46755
air, electrical conductivity and total radiant power 8000 to 12500 K 2−71061
air, electron velocity distribution function in r.f. discharges 2−77262
alkali metals, elec. cond. rel. to electron collision cross sections determ. 2−83186
anomalous current penetration, mechanism 2−46721
astron E layer, precession 2−70915
astrophysical phenomena interpret. 2−78432
axially decaying collisional plasma, anomalous diffusion 2−70884
between two plasmas in relative motion, momentum exchange acceleration caused by turbulence 2−50188
Boltzmann eqn. soln. for non Lorentzian system 2−80241
boundary fluctuations with longitudinal current 2−70883
circularly polarized magnetic field, higher harmonics 2−74352
collisionless flow over conducting sphere rel. to spacecraft wakes 2−83543
collisionless momentum-transfer interaction between ions in laser-produced system 2−67627
combustion, elec. conductivity meas., apparatus 2−80259
combustion gas plasma, in elec. fields, heat transfer, obs. 2−80300
computer investigation of nonlinear and turbulent phenomena 2−83532
current carrying, charge beam formation 2−70893
diffusion, neo-classical in banana regime 2−80243
diffusion, spectral dependence in magnetic field 2−46720
diffusion in toroidal Z-θ pinch at Padova 2−83571
diffusion waves induced by high intensity sources, laser heating 2−83699
discharge, self-sustained, form., electron-ion recomb. influence, nonlinear eigenvalue problem 2−56384
drift-dissipative instability development, plasma diffusion 2−60284
dynamic shielding effects in partially ionized gases 2−43124
electric arc, const. press. axial flow, local convection effects 2−74351
electron beam, high intensity, stability of 2−83618
electron drift velocity effect on life-time of ion waves 2−80308
electron gas of d.c. discharge, non-hydrodynamic props., reson. behaviour 2−74420
electron mean energy between parallel plates in Ar, variation of steady state value 2−43201
electron vel. distribution determination from polarization of free-free bremsstrahlung 2−56332
elliptical torus, neoclassical diffusion 2−67645
F-region 2−48590
flow, polarization interaction in transverse magnetic field 2−56334
flow pinch in coaxial plasma device, flow process energy balance 2−83538
flowing, steady-state diffusion controlled, effect of nonuniformity of applied h.f. electric field 2−67635
Green-Kubo formalism and linear relationships among coeffs. 2−70885
heat flow, two-dimensional, at toroidal inclusion 2−53177
heavy component contribution in partially ionized gases 2−43122
inhomogeneous, continuum eigenmodes 2−46710
injection of dense electron beam and motion along magnetic field 2−74358
ion acceleration at plasma boundaries, soln. of Poisson's equation 2−77263
ion diffusion coeffs. in gas mixtures at arbitrary field strengths, comp. depend. 2−77265
ionosphere, topside plasma flow inside and outside of plasmasphere 2−58095
isotropic turbulence radiative transport analysis 2−64274
jetstreams, numerical simulation 2−85027
kinetic theory and non-equilibrium aspects 2−83701
Korteweg-de Vries equation, exact N-soliton soln. 2−43120
laser produced, heat cond., Fourier's theory, applicability 2−80245
local electron heating, calc. of ionospheric energy flux from daylight to dark side 2−54904
mean energy, mobility and atom bremsstrahlung of electrons 2−43118
MHD, subjected to electrothermal instability, two-point correlation description 2−80266
multi-charge ions in impulse discharge, meas. of velocity of each component in plasma 2−50223
neoclassical diffusion in axisymmetric torus in intermediate region 2−50187
neoclassical diffusion of finite β tokamak plasma 2−60210
neoclassical theory 2−43119
neoclassical theory in Tokamaks in banana/plateau regimes 2−70919
non-viscous system, stationary motion and rate of entropy prod. 2−70878
Penning discharge ion source for plasma diffusion studies 2−52401
proportional counter, gas-filled, fluctuations in energy loss of 66 and 100 MeV protons 2−49634
radial response during intense heating 2−43121
resonant diffusion and strong turbulence 2−70943
r.f. energy transport to lower hybrid resonance 2−74362
seeded combustion plasma, flow parameter variations, obs. 2−80257

Plasma continued
 transport processes continued
  self-consistent rotating electron system, minimum-energy state 2−67619
  stagnation point heat transfer, heat pipe calorimetry 2−43164
  stellarator confined plasma viscosity damping of convective cells 2−80276
  subsonic motion in continuous laser light, thermal expansion, plasma extinction 2−74353
  supersonic ion flow, exptl. evidence in low pressure plasma 2−53181
  thermal induction media, dual mag. probe system for phase meas. 2−50208
  thermally ionized, heat transfer to wires, rel. to ionization 2−56330
  three-dimensional magnetized equil. system, transverse diffusion and cond. coeffs. 2−56333
  Tokamak configuration, particle diffusion under influence of slow magnetic compression wave 2−80275
  Tokamak systems, particle diffusion and energy balance equations 2−53203
  toroidal, azimuthal electric fields effects and kinetic theory for collision dominated regime 2−46719
  toroidal, electron fluctuations and thermal energy transport 2−80249
  turbulent plasma, det. from e.m. waves interactions 2−70886
  wave kinetic equation for homogeneous plasma, systematic derivation 2−64256
  weakly ionised, average electron density height profile 2−75630
  weakly nonideal in shock tube, electrical conductivity 2−60220
  AgNa(NO$_2$)$_2$, hysteresis loop in quasi-static elec. field 2−72030
  Ar, flowing, anode heat transfer at elevated temp. 2−67626
  Ar afterglow, diffusion cooling 2−56336
  Ar discharge, motion of ionization front in microwave e.m. field 2−60238
  Ba-Cs filled thermionic converter, ignited mode 2−49285
  Ba seeded, momentum transfer from ambient magnetospheric plasma, NASA/MPE cloud expt. 2−62300
  Cs, dense strongly nonideal, elec. cond., 1000-10000 K and 130-350 atm 2−80292
  Cs, near-thermal equilibrium, energy loss of traversing Cs ions beam 2−43112
  He, heavy charged particles produced by ^{10}B(n,α) reaction, slowing down 2−70887
  Hg afterglow, transition from free-fall to ambipolar diffusion 2−60212
  K magnetoplasma, anomalous resistivity 2−70897
  Kr afterglow, diffusion cooling 2−56336
  Kr multi-charge ions in impulse discharge, meas. of velocity of each component in plasma 2−50223
  N, electrical and thermal conductivities 2−56335
  N discharge, motion of ionization front in microwave e.m. field 2−60238
  N$_2$, thermal cond., 5000-18000 K 2−74350
  Na diffusion in d.c. arc plasma, obs. using intensity distrib. of emitted light 2−60211
  Ne, heavy charged particles produced by ^{10}B(n,α) reaction, slowing down 2−70887
  Ne afterglow, diffusion cooling 2−56336
  Xe multi-charge ions in impulse discharge, meas. of velocity of each component in plasma 2−50223
Plasma diodes
  calorelectric converter, thermionic principles 2−52367
  nonlinear current oscillations, rel. to high cathode temperature, low Cs pressure and Coulomb collisions 2−52365
  short discharge, thermionic energy conversion, physical properties 2−52366
  Cs, collisionless, current oscillations 2−63220
  Cs, thermionic convertors 2−59054
Plasma guns *see Plasma/devices*
Plasma in solids *see Crystal electron states/plasma; Electron gas; Semiconductors; Solids*
Plasma jets *see Plasma/devices*
Plasma sheath *see Plasma confinement*
Plasma thermocouples *see Electricity/direct conversion; Plasma/devices*
Plasma torches *see Plasma/devices*
Plasma waves *see Plasma/oscillations*
Plasmoids *see Plasma*
Plasmons *see Crystal electron states/plasma*
Plastic deformation
  see also Slip
  − 2−61721
  − 2−56919
  albite, microstructure and dislocation distrib. obs. 2−81623
  alloys, body centred cubic, theory of solid solution hardening 2−77691
  anisotropic work hardening materials, elasto plastic analysis 2−76265
  arches, clamped circular, buckling under point load 2−58873
  asymmetric buckling of spherical caps under uniform step pressures 2−45424
  austenitic-steel, neutron-induced mechanical property changes, damage function analysis 2−77718
  ball indentation analysis, elastic-plastic soln., finite element method 2−66496
  Bauschinger effect, kinematical strain hardening 2−55453
  b.c.c. lattice, accommodation of deform. twins by screw dislocations 2−74782
  b.c.c. lattice, screw dislocation; motion under stress at 0 K, computer simulation 2−71484
  b.c.c. metals, disloc. distrib. factors affecting flow stress 2−60799
  bend endurance testing unit for thin flat samples 2−56853
  bisphenol-A-polycarbonate, compression yield stress rel. to mech. loss peak 2−47506
  α-brass, containing SiO$_2$ particles, dislocation generation 2−56708
  $\alpha+\beta$ brass, superplasticity 2−64714
  breccia, lunar and terrestrial minerals, substruct. obs. 2−62688
Plastic deformation continued
  buckling, critical points and stability boundary determination 2−52151
  buckling, finite, of fibre reinforced columns 2−41570
  buckling, prebuckling and postbuckling, geometrical nonlinear analysis by finite elements method 2−52149
  buckling, soln. to paradox 2−69678
  buckling analysis for axially compressed flat plates, struct. sections and stiffened plates 2−69682
  buckling and vibration analysis for stiffened orthotropic shells of revolution 2−69693
  buckling of beams and plates on two unattached foundations 2−66534
  buckling of circular cylindrical shell in axial compression, SS4 boundary conditions 2−69677
  buckling of inelastic cylindrical shells, axial impact 2−76259
  buckling of infinite sheet with one-sided constraint 2−45386
  buckling of rectangular plates 2−63081
  buckling of shallow spherical caps and truncated hemispheres under axisymmetric loads 2−41574
  buckling stresses of axially compressed cylinders with localized or random axisymmetric imperfections, asymptotic formulae 2−45377
  ceramic, dislocation motion role 2−47493
  cermet, yield limit change regularities in compaction rolling 2−68126
  cermet. ZHGp1.5D2.5, effect of cooling rate after sintering 2−77722
  circular and ring plates, extension deformed, limiting equilibrium 2−63085
  clays, yield and failure 2−76268
  Coconino Sandstone, Luders bands and cataclasis 2−57763
  compressed circular plates, load carrying capacity 2−66492
  compression of short cylinders with radial expansion constraint 2−76306
  continuous heteroplastic medium, eqn. of state 2−76296
  at crack tip, stably growing 2−84014
  creep collapse of a cylindrical shell, effect of time-varying external pressure 2−41575
  creep fatigue at high temps., low cycle, deformation 2−56886
  crippling and buckling of corrugated ring stiffened cylinders 2−58852
  critical buckling load and deflection of beams, det. by three unknowns method 2−41580
  critical buckling loads of anisotropic shallow shells 2−41659
  crystalline solids, pore growth and mechanism during plastic deform. 2−80653
  crystals, stress effects on initial deformation, accumulation of dislocations 2−80696
  cubic crysts., screw dislocation motion at finite temp. under const. stress 2−60793
  deformation mechanism maps, plastic flow 2−50759
  deformation studies using a combination (synenergy) method of X-ray line profile topography and trans. e. microsc. 2−82432
  diamond, deform. twinning and twinning plane identification 2−50684
  diamond, framesite, microstructural aspects 2−50877
  diamond, intersecting twins 2−80692
  disclinations, geometrical structure of crystals 2−74766
  disclinations, relation between continuous and discrete 2−76267
  dynamic, ideal viscoplasticity, dislocation flux idealization 2−49076
  dynamic, internal structural changes, thermodynamic theory of viscoplasticity 2−78892
  dynamically loaded rigid plastic continua, lower bounds on deformations 2−41576
  elastic cylinder, Somigliani type dislocations 2−52159
  elastic plastic, generalised theory for thin membrane shells 2−45414
  elastic viscoplastic medium, propagation of two dimensional strong discontinuity waves 2−76255
  elastic-plastic buckling, variational method 2−78891
  elastic-plastic shells of revolution, finite element large deflection anal. 2−78875
  elastic-plastic solids, rolling resistances 2−41630
  elasto-plastic plates, finite element analysis 2−76254
  elasto-plastic plates, nonlinear analysis 2−73389
  elasto-plasticity, general variational theorem for rate problem 2−45418
  elastoplastic thick-walled cylinder, incremental stress analysis method 2−55469
  electron channelling pattern obs., selected area, in scanning electron microscopy 2−56638
  electron emission microscope examination 2−43779
  electron microscope determ, applic. of high voltage metallography 2−56632
  electron microscope obs., applic. of high voltage EM thick foil specimens 2−56785
  elliptic opening in elastoplastic body, stress conc.
  equivalence of F^{e}F^p and F^{p}F^e 2−49075
  expansion adiabats of solids 2−53801
  extrusion, flow function analysis of visioplasticity data 2−66560
  fatigue deformation and fracture under cyclic and steady loads 2−56816
  feldspar, axial growth of inclined en echelon cleavage cracks 2−61972
  fibre composites, plane-strain model 2−43898
  film, metal, discontinuous, elec. props. rel. to strain 2−64908
  finite deformation of elastic- plastic solids 2−76304
  finite elastic-plastic deflections in circular plates, numerical analysis 2−41629
  finite theory including second order effects 2−76258
  flat specimen with circular hole, polycrystalline metal, and stress analysis 2−45420
  galena, as function of shallow tectonic temp. and pressure 2−61969
  graphite, POCO grade HPD-1, high temperature creep, comparison with polycrystalline graphite 2−77625
  greigite, rel. to appl. as seed for pyrrhotite cryst. growth 2−60723
  hardening of plastic materials 2−80863
  hardness, general class for elasto-plastic deformations 2−63068
  high pressure effects on single crysts. 2−68080

Plastic deformation continued
  high-strain-rate investigations, stress/strain characts., review 2−47489
  hollow circular disk with heated stamps on external surface, stress relief through creep 2−66558
  hot workability, review 2−50795
  ice, associated activation volume 2−64698
  ice, columnar grained, two-dimens. behaviour 2−64732
  imperfection sensitivity of wide integrally stiffened panel under compression 2−76305
  impulsively loaded, uniformly expanding ring of elastic-perfectly plastic material 2−41631
  indentation of elastic-perfectly-plastic half- space by a hard sphere 2−47498
  interstitial, role of impurities in low temp. softening 2−47495
  kinetics, and low-cycle creep fatigue testing, method and equipment 2−56874
  laminated arch under mech. and thermal action 2−76324
  lherzolite Massif of Lanzo 2−54681
  line defect, dislocation and disclination contents 2−74774
  Luders band growth, rate-determininng process 2−74775
  Luders front geometry, application of continuum dislocation theory 2−52144
  magnesia, polycrystalline, deformation in compression, 1100-1750°C 2−68167
  magnetoelastic buckling of beams and thin plates of magnetically soft material 2−66554
  martensitic transformation, strain-induced nucleation mechanism 2−68184
  martensitic transformation plasticity, rel. to shape-memory effect 2−68185
  maximum, at point of ultimate failure of metal, due to torsion 2−56842
  metal, b.c.c., dislocation struct. form. and strengthening mechanisms 2−43629
  metal, electron beam induced 2−47363
  metal, f.c.c., simulation of rolling texture development 2−43813
  metal, f.c.c., viscoplastic phenomena, stereographic models 2−60865
  metal, in tension, under hydrostatic press., time depend. of fracture and creep 2−80728
  metal, polygonized struct., heavily deformed, conditions of formation of recrystn. nuclei 2−56901
  metal, pressurization, structural changes and effect on mech. characts. 2−68079
  metal, recovery, effect of impurity atoms on grain boundary motion 2−43785
  metal transition bands 2−68135
  metal under axial loading, nonlinear memory type eqn. rel. to delayed yield 2−80734
  metallic crystals, review of 50 years' progress 2−68077
  metallic materials, det. of reduction in area 2−43753
  metals, effect on high temp. aqueous corrosion, autoclave for obs. 2−66375
  metals, emission electron microscopic obs. 2−79115
  metals, polycrystalline and monocrystalline sheet specimens, changes in misorientation, X-ray method 2−84046
  microhardness tester attachment for meas. of deformation of wire in coiling 2−82129
  mild steel, spark machined and mechanically sectioned, deformation layers 2−74879
  mild steel plates, during automatic welding 2−69481
  multimode buckling, postcritical behaviour of discrete conservative systems 2−76243
  non-linear solutions, second order effects in plastic shear 2−58878
  nondestructive testing for brazed metal to ceramic bond, acoustic emission behaviour 2−74833
  nonpiezoelectric conductor, u.s. generation by deform. interaction with carriers 2−64841
  nonuniform bodies, convergence of method of uniform linear approx. 2−63084
  norite, post-failure stress strain path dependence 2−62009
  nuclear reactor housing, concrete slab shear slip 2−59822
  nylon 6 monofilament, model for deform. and fracture from creep and birefringence obs. 2−84022
  nylon 6 monofilament, model for deform. and fracture from creep and birefringence obs. 2−84021
  nylon-epoxide adhesive 2−47673
  omphacite, microstructure and dislocation distrib. obs. 2−81623
  pastes and polymers, instability at shear strength limit 2−68085
  plane strain of plastic material, effects of anisotropy and hydrostatic stress 2−69656
  plastic distortion and disclinations, semi-microscopic 2−76263
  plastics, deformation to fracture, review 2−60863
  plastics, dimensioning of cyclically and multiaxially stressed structures 2−64711
  plates, circular, flat, creep rel. to geometry changes during deform. 2−66555
  plates, limit analysis, simple loading problem involving complex exact solution 2−55460
  polyamides, real stress diagram classification, uniaxial extension 2−56780
  polycarbonate, longitudinal crazing in cyclic deform. 2−53840
  polycarbonate, strain softening and yield processes, moire-grid anal. 2−84084
  polycrystalline metals, slow elastic plastic deformation with micro stresses 2−76260
  polycrystals, Hill's stress rate 2−71564
  polyethylene, injection moulded specimens, crystallite orientation determ. by X-ray diffraction 2−64797
  polyethylene filled with randomly oriented glass fibres, stress-strain curve 2−77690
  polyethylene terephthalate films, influence of liq. media 2−50750
  polyimide, hydrostatic press. effect on mech. behaviour 2−83347
  polymer, isotropic, longitudinal crazing in cyclic deform. 2−53840
  polymer, yield criteria, press. effects 2−68094
  polymer cryst., morphology influence 2−60860
  polymeric rod, influence of cold working on tensile strength under tensile straining 2−80810

Plastic deformation continued
  polymers, crystalline, tensile stress-strain relations, generalized equation formulation 2−56783
  polymers, high, extrusion in solid state 2−84051
  polymethyl methacrylate, longitudinal crazing in cyclic deform. 2−53840
  polymethylmethacrylate, birefringence 2−51301
  polypropylene, quenched and annealed samples, wide-angle X-ray scattering in neck region 2−71572
  polystyrene, craze yielding and stress-strain characts. of crazes 2−64736
  polyvinylchloride, drawn samples, molec. orientation determ. by broad line p.m.r. 2−51417
  porous solids, theory 2−52189
  Portevin-Le Chatelier effect, and density and activation entropy of moving dislocations 2−80748
  portland cement paste, effects on microstructure 2−60995
  post yield fracture mechanics, crack model for high and low strength materials 2−64727
  postbuckling anal. of magnetoelastic beam 2−45381
  postbuckling behaviour of imperfection sensitive structures in plastic range 2−45422
  prismatic rods, automatic solution of elastoplastic twisting problem 2−82328
  PVC, yield stress in hexane and hexane/toluene environments 2−50779
  pyrrhotite, as function of shallow tectonic temp. and pressure 2−61969
  quartz, synthetic, yield and strain hardening, dislocation structs. 2−56797
  quartz in prograde metamorphic sequence, rel. to preferred orientation 2−57766
  random buckling behaviour, axially loaded cylindrical shells 2−41587
  ratcheting under cyclic axial strain with torsional stress 2−56876
  Reiner fluid, yield value 2−76264
  relaxation behaviour during supercond. transition 2−71843
  review of development of concepts 2−68078
  rigid thick walled spherical shells under hydrostatic pressure 2−78897
  rock salt crystal, uniform press. effects 2−56793
  rocks, fracture and flow 2−57822
  rocks, in uniaxial strain 2−75454
  rocks, indentation by rough wedge 2−57819
  rocks, volume changes at high pressure 2−62006
  rubber, styrene-butadiene, molecular orientation during stretching 2−56549
  sandwich shells of revolution, large elastic plastic deflections 2−76266
  semiconductors, strain, crystal defects 2−75076
  shallow circular arches, effect of initial imperfections on buckling load 2−66556
  shallow notched bar, three point loading, slip line field relations 2−41632
  shallow shell, dynamic snap-through under impulsive loading 2−45361
  sheet drawing, effect of friction 2−60913
  shock waves effects on yielding and permanent property changes 2−68072
  Shubrikov point groups 2−84006
  simple materials, non equilibrium thermodynamic theory, single integral entropic functional 2−76257
  slip concept, macrohomogeneous model of continuum 2−77640
  snap through buckling response of curved plates using discrete elements 2−45395
  Solenhofen limestone, creep testing at constant stress and constant force 2−62008
  Solenhofen limestone, effects of strain rate changes on strength and ductility 2−62007
  Solenhofen Limestone, Luders bands and cataclasis 2−57763
  sphalerite, as function of shallow tectonic temp. and pressure 2−61969
  spherical shell compressed between rigid plates, axisymmetric postbuckling and nonsymmetric buckling 2−45376
  stainless steel, type 304, passivity 2−78195
  stainless steel cladding on (U, Pu)O_2 fuel rods 2−76944
  steel, 18-8 stainless, flow stress, effect of high hydrostatic pressure 2−56936
  steel, annealed low C, at high strain rates 2−71565
  steel, annealed low carbon, cyclic stress-strain relation 2−84124
  steel, austenitic, effect on isothermal pearlitic transform. kinetics 2−50939
  steel, austenitic, plastic props. after strengthening by ageing 2−53876
  steel, austenitic, substruct., effect of deform. temp. during thermomech. treatment 2−80770
  steel, austenitic stainless, in acid agressive media, rel. to corrosion 2−68790
  steel, ball bearing, rolling fatigue life, retained austenite effects 2−64764
  steel, carbon, strain energy during rotatory bending fatigue, effect of pearlite patches 2−84125
  steel, deformed, austenite form., kinetics and morphology 2−57014
  steel, ductile-brittle transition, deform. mode influence 2−43694
  steel, eutectoid, mech. props. effect of directional growth of pearlite and rolling 2−47529
  steel, fatigue behaviour under reverse bending 2−50769
  steel, heat treated, cyclic strain softening at various hydrostatic pressures 2−68142
  steel, hot-worked, degree of deform., rel. to recrystn. 2−53873
  steel, Kh18N10T, fine structure changes for degree of deformation in creep 2−83956
  steel, low alloy, recrystallization during repeated deformation cycle 2−64778
  steel, low-C, dynamic strain aged, work softening 2−80837
  steel, low-C, martensite, surface deform., X-ray obs. 2−80769
  steel, low-C, plastic instability 2−43695
  steel, low-c, yielding and fatigue reln. under static and dynamic loading 2−84023
  steel, maraging, plane strain fracture toughness tests 2−60979

Plastic deformation continued

- steel, maraging with 18%Ni, flow behaviour 2−84068
- steel, mild, Bauschinger effect and discontinuous yielding 2−64716
- steel, mild, effect of high energy ultrasonic waves 2−77673
- steel, mild, resulting activation enthalpies for Luders band propagation and strain hardening 2−80814
- steel, mild, strain profile of propagating Luders front 2−47494
- steel, multilayer, rel. to strength 2−53824
- steel, quenched, tempered, resist. to plastic deform. and cold brittle failure 2−47502
- steel, sintered, for fuel element jackets, processing and mech. characterization 2−76951
- steel, slip lines 2−80831
- steel, spheroidization of cementite at subcritical temp. 2−43840
- steel, stainless, effect of explosive load 2−43836
- steel, stainless tube, fast neutron irrad. effect 2−83085
- steel 34KhN3GSV, plastic deformation effects on kinetics of bainitic transf. 2−84077
- steel pipes, Bauschinger effect on initial yield stress for design tests 2−60867
- steel thick-walled cylinders, microstrain obs. under internal pressure up to 6 kbar 2−68156
- stretched circular plates, load carrying capacity 2−66492
- structural elements of complex shape, limit analysis and plastic design 2−78888
- structural plastics, rupture machine for testing 2−43756
- structures, relationship between plastic and creep deformation 2−76261
- tensile testing device, usable from room temp. to −150°C in electron microscope 2−71613
- thermal ratcheting, review 2−56875
- thermoplastic films, local deformation of free emulsion surface 2−73235
- thin circular plate of variable thickness, buckling under uniform compression 2−63066
- thin walled tube, theory of plastic instability 2−43682
- time dependent materials, plastic behaviour 2−76256
- titania, room-temp. strengths for various biaxial stress states 2−77677
- torsion of hollow cylinder, anisotropy theory 2−47497
- transmission electron microscopy, use of hydraulic-type tensile device 2−60743
- transmission electron microscopy obs. straining holder using piezoelectric effect 2−79107
- tubes subject to explosive detonation as a function of the properties of the surrounding medium 2−60866
- twinning law, and applic. to reciprocal lattice 2−67932
- unit for determining the elastic limit in pure bending under the action of surface and corrosion active media 2−85156
- vibration creep, machine for testing, constructional foam plastics 2−56847
- volume dilatation caused by dislocations 2−50660
- yield criteria and Bauschinger effect for plastic solid 2−47496
- yield criterion, derivation considering couple-stresses 2−76278
- yield surfaces at elevated temps. 2−71563
- yielding, high pressure effects, crystn. and amorphous materials 2−68081
- Zircaloy-4, ductility transition, slip band form. 2−50747
- Zircaloy-4 tubing, yield loci, effect of texture variations 2−50850
- Ag-Si alloy, deformed by tension and rolling, X-ray diffr. 2−80845
- Ag-Zn(41 at%) alloy, deform. induced martensite, X-ray diffr. obs. 2−80846
- Ag alloys, soln. hardening, stress equivalence 2−80834
- Ag dispersion hardened, recryst. temp. rel. to particle vol. fraction, separation deform. 2−56900
- AgCl, polycryst., dislocation dynamics, thermally, activated deform., flow stress, 77-400K 2−77589
- Al-B and failure under transverse loading 2−84110
- Al-Cu-Mg-Mn alloy, mosaic angle and dislocation density, tensile deform. depend. 2−80772
- Al-Cu-Mg alloy, oversaturated solid soln. state, mech. props. rel. to strain rate and temp. 2−56547
- Al-Mg alloy, dislocation network form. during hot deform. 2−56712
- Al-(N at.%) Mg, N=10, 8, alloy, and age hardening 2−47612
- Al-(3 at.%)Mg alloy, high temp., dislocation dragging, lattice rotation 2−74835
- Al-Zn-Mg-Cu alloy, tensile deform. and high temp. creep rel. to microstruct. 2−56800
- Al-1% Mg alloy, creep deformation, electron microscopic obs. 2−80753
- 6Al-4V-Ti, surface embrittlement charact. during diffusion bonding 2−68160
- Al, 7075, laser shock-induced yield strength change 2−68075
- Al, deformed, dislocation arrangement in surface layer, electron microscope obs. 2−43465
- Al, deformed by rolling, positron interaction with defects 2−71460
- Al, dislocation multiplication mechanism 2−80679
- Al, ductility rel. to strain rate, −196 to 400°C 2−74834
- Al, effect of dislocations on substruct. strengthening 2−50763
- Al, heavily deformed, conditions of formation of recrsytn. nuclei 2−56901
- Al, high purity, and dil. alloys, review 2−68076
- Al, high voltage electron microscope obs. on thick foils 2−56785
- Al, lateral rolling, dislocation struct. and fracture 2−74837
- Al, mobile dislocation density and velocity, room temp. 2−43690
- Al, mobile dislocation density and velocity, room temp. 2−43689
- Al, plane shock structs., strain rate functions 2−60800
- Al, projectile penetration forces and yield behaviour 2−53803
- Al, radiation generated during rapid deform. and rupture, tribolum. 2−54482
- Al, recrystn., electron microscope obs. 2−80859
- Al, recrystn. nuclei formed by Rowland transform. 2−43822
- Al, resistivity changes in vicinity of grain boundaries 2−53744
- Al, strain rate role in dislocation substruct. form. 2−47499
- Al, stress effect on resist./strain relation 2−64700
- Al, uniaxial compression effects on Fermi surface third zone obs. 2−71790
- Al, water-quenched, effect on yield stress 2−50799
- Al alloy, two-phase, dislocation struct. 2−56789
- Al alloys, evaluation of irregularity of resistance 2−53802

Plastic deformation continued

- Al bar, annealed, containing a circumferential semicircular notch 2−77689
- 1100 Al corners in field surface under biaxial zig zag loading 2−43686
- Al dislocation loop struct. rel. to deform. method 2−77574
- Al non-isoaxial bicrystal, tensile deformation, effect of twist boundaries 2−50741
- Al non-isoaxial bicrystal, tensile deformation, effect of tilt boundaries 2−50740
- Al single crystal, anodic coating influence on slip 2−71576
- Al single crystal, rolling texture development and deformation banding tendency 2−56788
- Al single crystals, cavitation in liquid oxygen, plastic deformation in metal surface layers 2−71306
- Al single crystals, substruct. changes during high-temp. deform. in creep 2−84078
- Al_2O_3:Ti, precip. hardening kinetics 2−50872
- α-Al_2O_3, 1650-2000°C, thermoactive parameters, temp. and stress depend. 2−53804
- Al_2O_3, ceramic, microstruct. rel. to deform. processes 2−60993
- α-Al_2O_3, deformation memory 2−71566
- Al_2O_3, in hot-pressing 2−77735
- Al_2O_3, porous polycrystalline, compressive creep 2−47513
- Al_2O_3, sapphire, role in fracture 2−50762
- Al_2O_3 based refractories, stress-strain behaviour in torsion test 2−43687
- $Al_2(SiO_3)_3$, room-temp. strengths for various biaxial stress states 2−77677
- Ar cryst., ideal tensile and shear strength criteria 2−77630
- $BaFe_{12}O_{19}$, deform. texture 2−56962
- Be, anisotropy of deform. after programmed loading 2−80775
- Be, increase of microplastic deform. resist. by thermocyclic treatment 2−53871
- Be, obs. by synergy of TEM, selected area X-ray topography and line profile analysis 2−56791
- BeO high pressure effects on single crysts. and polycrystalline mat. 2−68082
- Bi, radiation generated during rapid deform. and rupture, tribolum. 2−54482
- Bi_2O_3, transform. deform. 2−50932
- C-graphite matrix composites, effects of microstruct. 2−61015
- CdTe:Li, self-compensation and interaction of Li with defects 2−75107
- CdTe, photoplastic behaviour 2−50742
- Co, single crystals, review 2−84008
- Cr, coarse-grain melted, non-propagating microcracks 2−68098
- Cr, deformed at 77, 213, and 293K, recovery resist. study 2−53805
- $CsFeF_4$, ferroelastic effect, spontaneous lattice strain 2−71571
- CsI, rel. to secondary slip generated by point load 2−74849
- Cu-Al-Fe bronze, superplastically deformed, textures and anisotropic flow 2−43831
- Cu-Al-Ni alloy, martensite memory, shape recovery effect 2−50935
- Cu-Al alloy, exoemission kinetics and hardness depend. on strain or elongation 2−74836
- Cu-10at.%Al alloy, neutron irrad., dislocation strain fields, low temp. lattice thermal cond. obs. 2−71498
- Cu-7at.%Ge alloy, neutron irrad., dislocation strain fields, low temp. lattice thermal cond. obs. 2−71498
- Cu-(7wt.%)P alloy, superplastic behaviour 2−74838
- Cu-Si single crystal, tensile deform. 2−50743
- Cu-X alloy, X=Mg,Cd,Zr,Cr,Ag, weakening resist. rel. to deform., heating time and temp. 2−50764
- Cu-Zn alloy, martensite memory, shape recovery effect 2−50935
- Cu-Zn system, influence on diffusion processes during electron irrad. 2−47456
- Cu-7.5 at.%Al alloy, deformed in tension, dislocations, etch pit obs. 2−64664
- Cu, Burgers vector rel. to external geometry at initial deform. stage 2−50673
- Cu, creep deform. under bending stress 2−80836
- Cu, deformation potentials for shear strain, determ. of strain-induced shifts of energy levels 2−80976
- Cu, deformed, exo-emission rel. to surface struct. 2−77975
- Cu, deformed, positron annihilation, annealing temp. depend. 2−54123
- Cu, deformed, specific dislocation energy determ. 2−53734
- Cu, deformed at 77K, neutron irrad. effects on struct. and mech. props. 2−83968
- Cu, influence on positron annihilation ang. correl. 2−51063
- Cu, initial disloc. density effects on disloc. multiplication and work hardening characs. 2−64665
- Cu, Mo fibre reinforced, rolling behaviour, internal friction obs. 2−56987
- Cu, polycrystalline, effects on elec. resistivity 2−47834
- Cu, radiation generated during rapid deform. and rupture, tribolum. 2−54482
- Cu, single crystals deformed in tension, effect of strain rate upon hardening 2−84160
- Cu, strain hardened polycrystalline, mechanisms 2−77679
- Cu, yield stress, rel. to fatigue hardening 2−53724
- Cu alloys, soln. hardening, stress equivalence 2−80834
- OFHC Cu corners in yield surface under biaxial zig zag loading 2−43686
- Cu single crystal, yield behaviour, disloc. density and cryst. size effects 2−56792
- Cu single crystals, mech. twinning during elongation or torsion at 78 K and room temp. 2−74783
- Cu trichites, Luders band form. 2−47321
- Cu wire specimens, plastic deformation and static lattice distortion, X-ray diffraction determinations 2−53890
- Fe-30% Ni alloy, martensitic transform. plasticity 2−68197
- Fe-C alloy, recovery of internal friction after strain ageing 2−47481
- Fe-Co-V alloy, tensile tests, and brittleness 2−60868
- Fe-Cr-Ni, low temp. deform. characts. 2−43693
- Fe-Cu alloy, dispersion strengthening model, slip dislocation precipitate interaction 2−50744
- Fe-Mn alloy, b.c.c., shock deformed, flow stress and elec. resistivity recovery 2−56912

Plastic deformation continued
Fe-Ni-C alloy, deform.-induced martensitic reaction, kinetics 2–80833
Fe-Ni-C alloy, deform. martensite formation, effect on mech. props. 2–71684
Fe-Ni-C alloy, isothermal and athermal, deform. induced martensitic transform. 2–71685
Fe-Ni-C alloy, martensite, surface deform., X-ray obs. 2–80769
Fe-Ni-C alloy, martensitic, microplastic deform. and isothermal transform. 2–43808
Fe-Ni-C alloy, martensitic microplastic deform. and isothermal transform. 2–43807
Fe-Ni alloy, dislocations, mobile, strain rate sensitivity and density 2–56711
Fe-Ni alloy, hardening at high strain rates, rel. to microstruct. changes 2–47593
Fe-Ni alloys, deform. martensite obs. 2–43838
Fe-Si, high voltage electron microscope obs. on thick foils 2–56785
Fe-Si, yield stress, influence of microstruct. 2–80778
Fe-Si single crystal, slip and hardening, effect of dimensional factors 2–71568
Fe-Si single crystals deformed by tensile forces, slip polygonization 2–84060
Fe-Zn system ultrasonic strain, effect on diffusion growth of various phases 2–43655
Fe, Armco, influence on electronic struct. 2–75028
Fe, deformed, defects, resist. study 2–80740
α-Fe, deformed, nature of debris loops 2–74778
Fe, high voltage electron microscope obs. on thick foils 2–56785
Fe, single crystals, effect of impurity concentration on type of deformation at 77K 2–64713
α-Fe and low C steels, effect of deformation temp. on changes of the mech. props. 2–84159
Fe foil, extended in electron microscope, cell formation obs. 2–71487
Fe foil, polycryst., struct. parameters, small-angle X-ray scatt. obs. 2–71567
Fe single crystal, H induced plastic strain, divergent X-ray beam obs. 2–64715
Fe solid solns., serrated yielding between 500 and 775 K 2–74839
Fe_3Al, compression induced mag. anisotropy and superlattice dislocations 2–61516
Ga, big unidirectional abrasion and rolling, surface struct. 2–83856
Gd, mag. permeability rel. to plastic deform. and recrystn. 2–81234
Ge, creep, and stress effects 2–84040
Ge, electron irrad., asymmetric damage regions, elec. props. obs. 2–74759
p-H_2, polycrystalline parahydrogen and n-D_2, comparison and influence of zero energy 2–71569
In, rolled, influence of twinning on texture 2–80774
KBr, computation of electronic structure of colour centres and electronic polarization fields 2–71520
KCl:Ba, solid soln., effect on two temp. regions of decomposition 2–80526
KCl-KBr solid solution, internal stress at Luders band front 2–84043
KCl, F-centre colouring, γ-ray induced, strain effects 2–71528
KCl whiskers, slightly deformed, etch pit distrib. 2–71490
LiF, radiation colloids, elec. microscope obs. 2–74760
Mg, plane strain extrusions, yield anisotropy and texture control 2–80848
Mg alloy, superplastic, internal stresses 2–74841
Mg alloys, soln. hardening, stress equivalence 2–80834
Mg substitutional soln. hardening 2–43855
MgO:V^{3+}. strain effects on e.p.r. for strongly coupled ions 2–72495
MgO, during cleavage fracture 2–71570
MgO, self climb of dislocation loops 2–80672
$MgZn_2$, deformed by u.s. vibrs., dislocation behaviour 2–64666
Mo-35%Re alloy, deform. twins, nucleation and growth 56720 2–56720
Mo-Ru alloy, α, β and σ phases 2–50840
Mo-Ti alloy, effect of deform. rate and temp. on ductility, mech. props. and struct. 2–47503
Mo, deformed, Young's modulus and Poisson ratio, annealing time and temp. depend. 2–84054
Mo, microdeform. under dynamic loading, temp. and impurities influence 2–43696
Mo, under compression, yield stress and slip 2–53806
Mo alloy, cellular struct. development during hydroextrusion 2–47642
Mo alloy, struct. changes during deform. 2–50839
Mo radiation generated during rapid deform. and rupture, tribolum. 2–54482
Mo single crysts., surface orientation effects on yield 2–74842
$MoSe_2$, stacking faults, anomalous X-ray line broadening obs. 2–60807
NaCl, deformed, dislocation arrangement and glide 2–53807
NaCl, ideal tensile and shear strength criteria 2–77630
NaCl, γ-irrad., effect on F-aggregate colour centres, optical absorp. obs. 2–53755
Nb-Mo alloy single crystals thermally activated deformation 2–80823
Nb-Re alloy single crystals thermally activated deformation 2–80823
Nb-Zr-Ti alloy, supercond., struct. after cold deform. 2–50842
Nb, stressed, dislocation struct. form. mechanism 2–71494
Nb, struct. sensitive mech. props., review 2–43697
Nb, supercond., surface pinning by defects, expt. evidence 2–77866
Nb, yield strength, meas. under high pressure 2–60879
Nb single crystals, paramagnetic susceptibility, infl. of plastic deform. 2–81216
$NbFe_2$, Laves phase, yield stress, microhardness, temp. depend., electron microscopy 2–74843
Ni/C fibre composite, high temp. deformation characts. 2–74919
Ni-Al alloy, high temp. deformed, flow-stress recovery 2–74889
Ni-Be alloy, texture variation 2–50806
Ni-Cr alloys, effect on mag. props. 2–44256
Ni-Ni_3Nb, directionally solidified eutectic alloy, mode behaviour 2–56796
Ni-ThO_2, dispersion strengthening effects on hydrogen susceptibility, deformation and fracture 2–74862

Plastic deformation continued
Ni-ThO_2, dispersion strengthening effects on hydrogen susceptibility, deformation and fracture 2–74862
Ni-(46 wt.%) Ti, effect on struct. evolution 43863 2–43863
Ni, deformed, susceptibility and magnetization in strong fields 2–51259
Ni, disloc. generation from grain boundaries 2–47418
Ni, mag. domain struct. after plastic deform. 2–44244
Ni, Ni:Sn, deviations from Matthiesen's rule on deform. 2–71837
Ni, recovery after 300 kbar shock wave loading 2–56794
Ni, texture variation 2–50806
Ni, textures produced by deform. 2–84070
Ni alloy, transmission electron microscope obs. rel. to strength 2–56945
Ni base superalloy Mar-M200, yield, orientation and temp. depend. 2–56795
Ni steels, 40N25, 60N20 and 80N15, amplitude-dependence of int. frict. 2–84076
Ni_8Ta, quenched, microstruct. aspects, cry. orientation and grain boundaries 2–64709
Pb-Bi-Sn eutectic, superplasticity 2–80839
Pb-Sb alloy, influence on precip. mechanism 2–80858
Pb-Sn alloy, superplastically deformed, const. stress creep and strain rate tensile tests 2–47504
PbS(Se)(Te), carrier conc. effect 2–50784
$RbFeF_4$, ferroelastic effect, spontaneous lattice strain 2–71571
Se film, rolling texture, X-ray and elec. resist. study 2–64574
Si, epitaxial film, lattice resolution e. microscopy obs. of struct. of twin boundaries, faults and dislocats. 2–74779
Si slice, spontaneous change in radius of curvature 2–68083
Sn-Pb alloy stainless steel fibre reinforced, fracture behaviour 2–50921
Sn, superconducting, effect on u.s. attenuation 2–51106
Sn, white, effect of elastic anisotropy 2–80726
steel, low C, changes of dislocation arrangement during fatigue process 2–84162
Ta-N, interstitial effects on asymmetry of yield stress 2–74844
Ta, deform. mechanism, orientation depend., 4.2-450K 2–50679
TaC_{1-x}, dislocation splitting and C-diffusion-assisted glide 2–60869
Ti-Al-Mo-Zr alloy, ductility, influence of β-phase 2–50746
Ti-Al alloy, cold-worked, X-ray diffr. study 2–80860
Ti-(13 wt.%)V-(11 wt.%)Cr-(3 wt.%)Al, deformation substructures rel. to strengthening56950 2–56950
α-Ti, cyclic work softening 2–80835
Ti, deformation kinetics for {1010}{1120} slip in single crystals below 0.4 T_m 2–64720
Ti, dislocation struct. effects in strain-, grain size– and interstitial solute hardening 2–56714
Ti, zone refined, thermal and athermal flow stress components 2–56798
Ti alloys, peculiarities in planar stress state 2–43698
Ti in shear, meas. using torsional split Hopkinson pressure-far and pneumatic-mechanical torsion testing machine 2–53797
U alloy, effects on microstruct., ion etching and scanning electron microscope obs. 2–56578
UC, polycrystalline, high-temp. deformation and yielding 2–67348
UC_x, high temp. deform., proportional limit 2–53809
UO_2, rel. to porosity 2–43699
V, yield behaviour, effect of pre-strain 2–80752
W, coarse-grain melted, non-propagating microcracks 2–68098
W, swaged and drawn, deform. textures 2–53868
W filament, rel. to appl. to composite reinforcement 2–53970
WC-Co cermet, electron microscope obs. 2–47505
WC-Co hard metal, X-ray stress meas. at carbide phase 2–74910
Y alloy, −95 to 796°C 2–68084
Zn-Al eutectic alloy, room-temp. deform. characts. rel. to superplasticity 2–43701
Zn-0.1%Cd single crystal, slip lines, elec. microscope obs. 2–47421
Zn, α-Al_2O_3, deformation memory 2–71566
Zn, activated vol. in dislocation structure 2–43700
Zn, ductility, in presence of Hg, effect of surface layer defects 2–74830
Zn single crystals, cavitation in liquid oxygen, plastic deformation in metal surface layers 2–71306
α-Zr, ductile void growth, unloading effects 2–50778
α-Zr, grain size depend. 2–50748
Zr alloys, high-strength, development 2–53920
Zr and Zircaloy tubular materials, rel. to texture, anisotropy and hardening 2–53916

Plastic flow
see also Rheology
alloy, ductile fracture prediction under discrete loading 2–43728
austenitic stainless steel, effect of neutron irradiation on tensile and creep-rupture ductility 2–77719
$\alpha+\beta$ brass, superplasticity 2–64714
composite, Ni-Cr base alloy, Mo alloy or W filament reinforced 2–56988
with Coulomb friction, equilib. method and upper bound theorem in plane problems 2–45419
deformation mechanism maps 2–50759
dislocation first contribution to the flow stress 2–83974
dislocation pile up interactions 2–50666
ductility, intermetallic compounds of copper, obs. 2–50782
ductility exhaustion model for prediction of thermal fatigue and creep interaction 2–60896
fibre composites, plane-strain model 2–43898
inextensible planes, spatial flows of incompressible media 2–45355
isotropic plastic solids, geometric instabilities under uniaxial compression 2–66513
in matrix of plane strain laminar composite at incipient fracture 2–55475
metal, b.c.c., ductile-brittle transition, theory 2–43720
metal, brittle fracture, ductile-brittle transition 2–43730
metal, characteriz. for reactor core applic. 2–59862
metal, ductile fracture prediction under discrete loading 2–43728
metal, role in brittleness 2–43719
metal, strain-hardened, theory 2–43684
metal under axial loading, nonlinear memory type eqn. rel. to delayed yield 2–80734
microflow, strain release method of obs. 2–50789

Plastic flow continued
nylon-epoxide adhesive 2−47673
oxide fuel struct. evolution, modelling using BEHAVE-2 code 2−52858
Portevin-Le Chatelier effect, mathematical solutions for tensile specimen 2−73354
rigid thick walled spherical shells under hydrostatic pressure 2−78897
rock deformation, volume changes at high pressure 2−62006
rocks in Earth, effect of triaxial stress system 2−72679
rubber, yielding due to crazing 2−43710
sandwich shells of revolution, large elastic plastic deflections 2−76266
softened media theory, stress/strain relations 2−80735
Solenhofen limestone, effect of strain rate changes 2−62007
steel, 18-8 stainless, flow stress, effect of high hydrostatic pressure 2−56936
steel, C, effect of structures on mech. props. at dynamic loading 2−84161
steel, ductile-brittle transition, theory 2−43720
steel, ductile-to-brittle transition, influence of cold rolling and heat treatment 2−80777
steel, ductility, hot impact tension testing 2−60978
steel, effect of isothermal treatment 2−53874
steel, effect of rare earth alloying 2−53900
steel, low-alloy, effect of Ce addition 2−53831
steel, low-C, plastic instability 2−43695
steel, slip lines 2−80831
steel alloys, high strain rate effect on ductility 2−60877
steel targets, effect on ballistic behaviour 2−60980
stress meas. using torosional split Hopkinson bar 2−68124
Ziraloy-2, circumferential ductility, thermal cycling effect 2−53914
Zircaloy tubing, effect of oxygen and fabrication variables 2−53915
Zircaloy-2, irrad. and temp. effect on tensile and creep props. 2−43802
AgCl, polycryst., dislocation dynamics, thermally, activated deform., flow stress, 77-400K 2−77589
Al-Li alloys, neutron irrad., inert gas bubble effects 2−43688
Al, ductility rel. to strain rate, −196 to 400°C 2−74834
Al, rel. to mobile dislocation density and velocity 2−43689
Al intergranular flow study, role of imperfections 2−43643
Al1-5% Mg, serrated flow study −50 to 150°C 2−43706
BeO, rel. to initial stage sintering mechanism 2−47662
CdTe, photoplastic behaviour 2−50742
Cr, coarse-grain melted, ductility transition temperature 2−68098
Cr, ductile-brittle transition, effect of rare-earth metals 2−43691
Cu-Al-Fe bronze, superplastically deformed 2−43831
Cu-Al alloys, mechanical properties and ductility as a function of temperatures 2−64776
Cu-Co alloy f.c.c. single crystals, effect of coherent precip. on yield stress 2−50798
Cu, grain topography in early stage 2−47500
Cu whiskers, ductility determ. 2−56810
Cu_3Au alloy, flow stress temp. depend. 2−43692
Fe-Al-Cr alloys, effect of zirconium on ductility 2−60935
Fe-Ni-C alloy, quenching and hydrogenation effects 2−43723
Fe-Ta alloy, ductility enhancement using allotropic phase change 2−57020
Fe, strain ageing and length of yield plateau 2−71624
Fe, zone-refined, hydrogen effects on ductility 2−43725
Fe single crystal, latent hardening with 110 extension axis 2−43799
In, flow stress meas. in normal and superconducting state 2−47857
KCl, γ-irrad. at liq. N_2 temp., hardening, H_a band obs. 2−53754
Mg-(10.8 at.%)Y alloy, thermomech. treatment for increased ductility and high strength 2−47588
Mo, ductility, effect of B addition 2−56943
Mo, polycrystalline, role of impurity atmospheres in brittle fracture 2−71587
Mo, room temp. ductility and intergranular cracking, after annealing 2−53875
Mo alloy, ductile-to-brittle transition, rel. to struct. changes during deform. 2−50839
NaCl crystals containing colour centres, flow stress spectroscopy 2−81396
Ni-Al alloy, flow-stress recovery 2−74888
Ni-Al alloy, high temp. deformed, flow-stress recovery 2−74889
Ni alloys, Zr effect on hot workability and boundary-phase plasticity 2−47645
Ni_8Ta, quenched, discontinuous plastic flow during tension and compression testing 2−64709
Pb-Bi-Sn eutectic, superplasticity 2−80839
Pb-Sn alloy, superplastically deformed, const. stress creep and strain rate tensile tests 2−47504
Si_3N_4, at fracture surface at high temps. 2−60907
Ti-Al-Mo-Zr alloy, ductility, influence of β-phase 2−50746
Ti, zone refined, thermal and athermal flow stress components 2−56798
U, superplastic behaviour under tensile stress and temp. cycles 2−47516
UC, polycrystalline, high-temp. deformation and yielding 2−67348
UO_2-PuO_2 mixed fuel, ductility and stress relax. 2−53808
W, coarse-grain melted, ductility transition temperature 2−68098
W, wire, nonsag, ductility, ruthenium effect 2−43683
Zn, ductility, presence of Hg, effect of surface layer defects 2−74830
Zn superplastic behaviour under tensile stress and temp. cycles 2−47516
Zr-(1.5wt.%)Cr-(0.1wt.%)Fe tubing, heat-treated and hydrided 2−53918
Zr-Sn alloys, solute strengthening at high temps. 2−50846
Zr alloy, ductile processes, rel. to stress corrosion cracking 2−43737

Plasticity
see also Viscoelasticity
adiabatic plastic bands, formation in thin tube submitted to dynamic torsion 2−69679
alpha-constant stiffness method for analysis of nonlinear problems 2−58850
anisotropic, maximum shear stress hypothesis 2−41633
anisotropy in linear transverse strains, calc. 2−64712

Plasticity continued
annular disk, stresses and strains due to radial temperature variation 2−69680
biological membranes, plasticity, nonstatic model 2−81989
circular and ring plates, extension deformed, limiting equilibrium 2−63085
constrained minimisation problems 2−76331
continuum mechanics, role of thermodynamics 2−52191
coupling of plastic waves, rel. to yield condition 2−49079
Cu-Zn(40%) microduplex, metallographic study of superplasticity 2−80738
deformation, dynamic, ideal viscoplasticity, dislocation flux idealization 2−49076
dynamic traction tests 2−66559
elastic relaxation and stress-strain relation which characterizes Schofield-Scott-Blair media 2−52186
elastic stress analysis, by numerical iterative procedure applic. 2−73388
elastic viscoplastic medium, propagation of two dimensional strong discontinuity waves 2−76255
elastic-plastic buckling, variational method 2−78891
elastic-plastic constitutive models 2−69635
elastic-plastic systems, shakedown theorem under dynamic loadings 2−66511
elastic/plastic compressed plate, buckling stress, yield surface 2−76301
elasto-plasticity, general variational theorem for rate problem 2−45418
elastoplastic material, eqn. of state 2−82300
elastoplastic wave propag. in bar for nonlinear stress/strain case 2−82345
extremum principles for rigid plastic dynamic loading problems 2−69681
extrusion, flow function analysis of visioplasticity data 2−66560
filament reinforced materials, plastic limit behaviour and failure 2−84086
finite, problem of minimum principles 2−76286
heteroplastic medium, equation of state 2−82301
idealized elastoplastic column, effect of external load nonconservativeness of stability 2−82330
impulsively loaded, uniformly expanding ring of elastic-perfectly plastic material, transient and final deformation 2−41631
inadmissible discontinuities 2−76307
incompressible continuous media, pure shear concept 2−76328
kinetics, and low-cycle creep fatigue testing, method and equipment 2−56874
metal, anisotropy, quantitative meas. method 2−60864
metal forming processes, tensile creep 2−76262
metal working, mechanics 2−71635
metal working mechanics 2−71635
metal-ceramic materials, technique for determ. 2−68161
metallography, mechanisms 2−56786
microplasticity, strain release method of obs. 2−50789
nonlinear solid mechanics, thermodynamic foundations 2−56766
nonuniform bodies, convergence of method of uniform linear approx. 2−63084
notched specimens, fatigue strength estimation method 2−73390
orthotropic grids with fixed supports, plastic design 2−49078
plane stress in plastic structures, finite element approach to optimal design 2−63082
plastic potential theory applied to viscoplasticity 2−55476
plastomechanics, potential notion 2−74832
plates, elastic-plastic and eccentrically stiffened, finite element analyses 2−66561
plates or tubes, plastic instability and growth of grooves and patches 2−55474
polycarbonate, yield locus, charactization tests for photoelastoplastic material 2−43778
polycrystals, Hill's stress rate 2−71564
polymethylmethacrylate, tensile creep behaviour and fracture mechanics, liquid environment 2−53819
porous solids, theory 2−52189
porous solids fluid saturated, single constitutive theory 2−68179
refractory carbides, nitrides and borides, NASA research 2−64801
rigid body insertion under press. into strengthened medium 2−63083
rigid body under const. contact force, model 2−78769
rotating cylinders, collapse speeds 2−55473
shell, steady-state creep pot. construct. 2−76330
shell, strongly buckling, crit. loads for loss of stability, asymptotic method 2−82323
shells, dynamic plastic behaviour 2−55472
simple materials, non equilibrium thermodynamic theory, single integral entropic functional 2−76257
steel, annealed low carbon, cyclic stress-strain relation 2−84124
steel, effect of cyclic bending, at 20 and −60°C 2−84080
steel, low carbon deep drawing sheet, method for determ. plastic anisotropy 2−64710
steel, Mn-Cr-B spring, tempering behaviour 2−77688
steel, structural, ductility rel. to inclusion elongation 2−43713
steel alloys, high strain rate effect on ductility 2−60877
strains associated with torsion of noncircular bars 2−45423
structural elements of complex shape, limit analysis and plastic design 2−78888
structures, relationship between plastic and creep deformation 2−76261
superplasticity, interface reaction controlled diffusion creep 2−50752
theories rel. to fracture theories, phenomenological approach 2−76317
thermoplastics, long term strength, ductile failure, brittle failure 2−43718
thin walled tube, theory of plastic instability 2−43682
tubes, under uniform pressure and steady temp., thermo-elastic-plastic transition 2−49083
visco-plastic medium, nonstationary shear flow 2−77235
viscoplasticity, nonlinear solid mechanics, thermodynamic foundations 2−56766
viscoplasticity, thermodynamic theory, for small deformations 2−78892

Plasticity continued
waves, with discontinuous loading conditions, hodograph transformation 2−66609
Cr, coarse-grain melted, ductility transition temperature 2−68098
Cr, polycrystalline tensile failure, crack propagation and nucleation 2−84041
Cu-Al alloy, b.c.c., superplasticity 2−50745
Cu-Al alloys, mechanical properties and ductility as a function of temperatures 2−64776
Cu-Zn alloy, b.c.c., superplasticity 2−50745
Fe-Ni alloy, quenched, aged, toughness, ductility, inverse temp. depend 2−47501
LiF:Mg, stress-relaxation curve analysis, temp. range 300−800K 2−74840
Mo-Ti alloy, ductility, effect of deform. rate and temp. 2−47503
Mo, polycrystalline, role of impurity atmospheres in brittle fracture 2−71587
Nd, technological props. 2−47532
Sn, white, elastic and plastic anisotropy 2−80726
α-Ti, torsional and longitudinal plastic waves 2−77638
Ti alloys, b.c.c., superplasticity 2−50745
UO_2, polycryst., 1400-2100°C 2−53810
W, coarse-grain melted, ductility transition temperature 2−68098

Plastics
see also Polymers
ABS, light ageing behaviour, test method 2−50793
ageing, testing of, colorimetric aspects 2−47671
antistatic agent, recovery processes, ellipsometry obs. 2−65073
beams, glass and carbon fibre reinforced, dynamic moduli and loss factors 2−47487
coating of materials, use of composite materials, new developments 2−61010
constructional form, machine for testing vibration creep and vibration strength 2−56847
copolymers, A-B type, domain formation mechanisms 2−57419
crack tip profile, static fatigue and stress corrosion 2−53521
cylinder, contact stresses, elastohydrodynamic lubrication 2−47559
deformation of hardening material 2−80863
deformation to fracture, review 2−60863
dimensioning of cyclically and multiaxially stressed structures 2−64711
distyryldurene derivatives synthesis as wavelength shifters in plastic scintillators 2−61703
epoxide resin Epidian 2, short-term mech. and optical props. 2−47672
epoxy resins (Epon 828), cyclic fatigue stress behaviour 2−64798
fatigue, effect of frequency and loading history on behaviour 2−64823
fibre reinforced, stress distrib. in brittle matrix surrounding woven or crimped fibres 2−71657
fluorescent, for obtaining visible emission from u.v. light sources 2−63421
glass, porosity influence on tensile strength 2−47522
glass-reinforced plastics, behaviour in water under high stress 2−84083
holographic testing of industrial plastic pipe products 2−79282
Lucite, isentropic compression 2−52010
mirror manufacture by replica method 2−59261
mixed polymers of diethylene glycol-bis-allyl carbonate and isophthalic acid diallyl ester, with controlled optical refraction and dispersion 2−55752
molding using high powered ultrasonics 2−50412
mylar, thermal conductivity between 0.05 and 0.5K 2−47759
Mylar, total neutron cross section, low energies 2−83060
nylon 6 monofilament, model for deform. and fracture from creep and birefringence obs. 2−84021
nylon 6 monofilament, model for deform. and fracture from creep and birefringence obs. 2−84022
particle track detector materials characteriz. 2−63714
perspex, characteristics of cubical thermo-electrets 2−61439
Perspex, stimulated Brillouin scatt., elastic const. variations with press. 2−47480
perspex magnetoelectrets, effect of forming magnetic field on dielectric behaviour 2−65074
Perspex sheet, orientated, axial and transverse thermal expansion, 0-30°C 2−64862
perspex strips, interaction between two collinear assymetric cracks 2−68109
plates, laminated orthotropic layers, analysis by finite element displacement 2−68057
plexiglass, P, S and Rayleigh waves 2−41674
plexiglass plate cracks, interferometric determination of opening and edge sliding mode stress-intensity factors 2−47544
poly(methyl methacrylate), hydrogen bonding influence on stress crazing and cracking 2−60908
poly(vinyl chloride), hydrogen bonding influence on stress crazing and cracking 2−60908
polyester resins, (Paraplex P43), cyclic fatigue stress behaviour 2−64798
polyethylene, linear, anomalous internal friction at low temps. 2−84107
polyethylene, low density, Monte Carlo simulation of struct. 2−83344
polyethylene filled with randomly oriented glass fibres, stress-strain curve 2−77690
polyethylene films, changes in crystal orientation with time following stretching 2−83381
polyethylene fractions, melt viscosity 2−83370
polyethylmethacrylate, stimulated Brillouin scatt. 2−68668
polymethylmethacrylate, stimulated Brillouin scatt. 2−68668
polypropylene, effects of cooling rate from melt on struct., strength and fracture 2−56908
polypropylene window proportional counter, for soft cosmic X-ray obs. 2−70271
polystyrene, foamed, thermal cond., H_2O vapour permeability, mech. props. 2−43412
polysulphone, hydrogen bonding influence on stress crazing and cracking 2−60908
polytetrafluoroethylene, surface, wetting angle of D_2O at boiling point, 10-770 Torr 2−74533

Plastics continued
polyvinyl acetate in toluene, u.s. absorpt. and dielec. dispersion 2−83376
polyvinyl chloride, fatigue crack propag. mechanism, comparison with polypropylene and ABS blend polymer 2−71601
polyvinyl chloride, processing effect on morphology for plasticised and unplasticised 2−57003
PVA, uniaxially stretched film, mechanical anisotropy 2−83365
PVC, stress cracking and crazing in hexane and hexane/toluene environments 2−50779
PVC(SR_{11}) electrets, thermal current meas. 2−44167
PVC thermoelectret behaviour under different humidity conditions 2−81145
resins, heat deflection temp. meas. with automatic apparatus 2−52293
rheology of high density polyethylene 2−83371
rings, fixture for testing by pulsed external pressure 2−53858
Rockwell α hardness ASTM D 785 and ball indentation hardness DIN 53456, conversion formula 2−57004
sound insulation sheets 2−55551
spatial gradients rel. to struct., props. and uses 2−61026
stimulated Brillouin scatt., phonon lifetime and gain determ. 2−68668
structural, testing under long term static load 2−53981
structural rupture machine for testing 2−43756
teflon, appl. as press. transmitting medium at low temp. 2−73248
test methods handbook 2−53865
thermal diffusivity measurement method 2−78935
thermo-plastics, long-period rupture strength and time welding factors 2−53880
thermoplastics, long term strength, ductile failure, brittle failure 2−43718
thermoplastics, testing by cyclic application of heated fluid 2−53980
unidirectional C-fibre reinforced, shear strength and modulus 2−74921
u.s. wave velocity as function of temp. 2−57048
viscoelastic behaviour, nonlinear, of polyethylene films 2−83375
viscoelastic theory of time-hardening media 2−77706
C-fibre reinforced, interlaminar-shear fatigue props. 2−71656

Platinum
adsorption, of Ba, field emission microscope work function obs. 2−67924
adsorption of H Rel. to promoted evap., field ion microscopy obs. 2−50548
adsorption of noble gases, accommodation coeffs., 80-450K 2−56603
atom, determ. of shell-wise photoelectric cross-sections at 100 and 279 keV by indirect method 2−49925
chemisorption of H_2, adsorpt. and desorpt. kinetics 2−77514
desorption, of H_2, spatial distrib. obs. 2−50526
diffusion in Cu, 750-1075°C 2−56756
electrode on alkali-containing glass, model of electrode ‘polarization’ by d.c. potential applic. 2−81141
electron phonon enhancement factor, from specific heat data 2−64932
epitaxy by vapour deposition, low temp. 2−53575
filament in CCl_4, electroconvection, purity depend. 2−52278
film, cond., rel. to temp., 77-573 K, adsorpt. effects 2−64917
film, discontinuous, current noise 2−68340
film, for u.v. reflectance 2−61653
film, lattice consts. of small nuclei, rel. to surface stress 2−60655
film, significance of electric field on growth 2−60634
film, vapour deposited on W, field ion microscopy, 78K 2−50500
fuel cell with oxygen/alkali gas diffusion electrodes, model 2−59043
gaseous, spectra rel to matrix isolated atoms in Ar matrix 2−52902
interaction with O_2, thermodynamic props. of volatile products, obs. method 2−65378
interactions with O_2 2−51450
ion sources, laboratory, low intensity 2−55672
optical interband absorption, 0.265-7 μ 2−81358
permeation of hydrogen, surface effects 2−77608
radiation damage, proton, deuteron and He-ion, energy depend. 2−50643
resistance thermometer, effects of static mag. field at 77 K 2−49186
specific heat, pulsed electron beam measurement 2−54039
spectra, 3064.71 Å line, effect of ext. mag. field on intensity 2−49954
stopping power for protons and deuterons at same velocity 2−54098
surface, (100), clean and C covered, reactive scatt. of N_2O molecular beam 2−50547
surface, (110), catalytic oxidation of CO, Auger spectroscopy obs. 2−51443
surface, catalytic oxidation of CO 2−78185
surface, detection of Ag monolayers using tracers 2−71302
surface, interaction with H beam scatt., chemisorption 2−50461
thin oxide formation in aqueous electrolyte solutions passing anodic current, reaction kinetics 2−68784
trace elements analysis by spark source mass spectroscopy 2−61823
vacancy conc. rel. to press., quenching effects, excess resist. obs. 2−60788
wetting by silicate glass, contact angle meas. 2−53371
wetting by silicates, effect of oxides 2−67782
Pt/Al_2O_3 catalyst, butene adsorption, high resolution n.m.r. obs. 2−60683
Pt/Pt-Rh movable-junction stationary-lead thermocouple 2−45602
Pt/Pt-10%Rh thermocouple method for control and measurement of wire temps. in preparatory anneals 2−45603
Pt/SiO cermet films, elec. resist. in a.c. 2−75095
Pt-O_2(CO_2)(Ar)(SO_2) system, thermal cond., accommodation effect 2−67734
Pt-Si contacts, solid-solid reactions 2−50715
Pt-W strain gauge, temp. dependence of gauge factor and magnetoresistance 2−68121
Pt black, low temperature sintering mechanism 2−43894
Pt island films on insulators magnetoresistance 2−84298

Platinum compounds
— 2−61239

Platinum compounds continued
$[PtCl_4]^{2-}$ type planar square complexes, absorpt. band lineshape, electron-vibr. interaction 2−80054
Cr-Pt, structure of $K_{\beta 5}$ emission band, X-ray study 2−72378
Ir-Pt alloy, chemisorbed CO, i.r. spectra 2−68645
Mo-Pt system, phase diagram, supercond. transition temp., conc. depend. 2−61246
Ni-Pt alloys, matrix and impurity cluster polarization 2−44358
Pd/Pt/H system, form. and decomp. equil. 2−77715
Pd-Pt alloy, spin paramag. susceptibility, calc. 2−65125
Pt-Au alloy, low field Hall coeffs. at 4.2K and 300K, two band model 2−61188
Pt-Co alloy, electrodeposited, mag. props., dispersity, struct. 2−44268
Pt-Co dil. alloys, nucl. sp. ht., low temp. 2−43986
Pt-Co dilute alloy, disappearance of giant mag. moments 2−81211
Pt-Ir alloy, low field Hall coeffs. at 4.2K and 300K, two band models 2−61188
Pt-Mo, thermocouple, e.m.f. rel. to neutron irrad. 2−78940
Pt-Nb alloy, strength, resist. to oxidation 2−47533
Pt-Ni alloy, spin paramag. susceptibility, calc. 2−65125
Pt-Os alloy, low field Hall coeffs. at 4.2K and 300K, two band model 2−61188
Pt-Pd alloy, low field Hall coeffs. at 4.2K and 300K, two band model 2−61188
Pt-Pd disordered alloy, spin susceptibility calc. 2−65117
Pt-Re alloy, strength, resist. to oxidation 2−47533
Pt-Ta alloy, strength, resist. to oxidation 2−47533
Pt-Ti alloy, strength, resist. to oxidation 2−47533
Pt-W alloy, strength, resist. to oxidation 2−47533
Pt cermet cathodes, electron microscope study of thermal activation 2−81506
Pt complex, bis(triphenylphosphine)(ethylene)platinum, crystal and molecular structure 2−43587
Pt complex, $K[PtCl_3NH_3].H_2O$, vibr. spectra 2−48183
Pt II complexes, low-spin trigonal bipyramidal, electronic spectra, temp. dependence of lowest energy ligand field band 2−53031
$PtCr_3N$, crystallographic parameters and struct. transforms. 2−60759
$PtGa_2$, single cryst. growth and prep. 2−50600
PtSi, nuclear resonance and susceptibility 2−65348
PtSi film on single crystal Si substrate, thermal stability 2−71334

Pleochroism
alkali halides, mag. circular dichroism of F-centre absorpt. band 2−53750
azobenzene and substituted derivatives, reversible orientational photodichroism and photoisomerization in viscous solutions 2−42959
trans-azoxybenzene and isotopic derivatives, i.r. dichroism 2−56217
benzene, u.v. spectrum, vibrational structuring of magnetic circular dichroism 2−70751
biaxial crystals., diachroism rel. to Faraday rotation, transform. matrix 2−72259
biopolymer, flow dichroism spectra applic. to molec. studies, review 2−53089
cholesteric solns. with helically arranged mols., circular dichroism 2−53394
circular dichroism, semi- classical theory, time-dependent Schrodinger equation 2−52460
complex molecules in solid solutions, with two-photon excitation, dichroism of two-photon light absorption 2−42837
coronene ions, magnetic circular dichroism meas. 2−80089
cubic cryst., linear dichroism due to stress induced mixing of electronic states of anisotropic centres 2−84462
cytochrome c, magnetic circular dichroism 2−50118
dichroism, i.r., spectroscopic meas. technique for elongated polymers 2−84465
haemoglobin, circular dichroism rel. to struct. modification during oxygen fixation 2−56264
hemoprotein derivatives, circular dichroism in visible region, nonlinear iron-ligand bonds 2−64197
infrared circular dichroism meas. instrument 2−67521
liquid crystals, induced circular dichroism method for determ. of chirality of cholesteric mesophase 2—80460
macromolecules, circular dichroism rel. to conform. transitions determ. 2—83383
l-menthol in nematic solvent, optical activity and circular dichroism 2—80442
α-phenylethylamine, circular dichroism obs. in Roman spectra 2—64191
poly-γ-benzyl-L-glutamate solas., i.r. elec. dichroism. 2—60083
polyethylene, amorphous crosslinked, dichroism study 2—84466
polyethylene, high speed elongation, i.r. dichroism, meas. apparatus 2—83354
polypeptides, α-helical, in soln., oriented circular dichroism spectrum 2– 80117
polystyrene solutions, atactic and isotactic, configurational and conformational effects on magnetic circular dichroism 2– 43366
praseodymium tartrate complexes, i.r. circular dichroism 2– 67521
pyrazine, dichroic ratios from crystal spectra 2– 78111
pyrimidine nucleosides, electronic spectra from circular dichroism data 2– 74299
suspension of oriented particles, dichroism determ. from polarizability coeffs. 2– 56532
tetramethylpyrazine, dichroic ratios from crystal spectra 2– 78111
AgCl emulsion microcrystals dichroism, spectral reversal 2– 84470
$CaF_2:Dy^{3+}$, magnetic circular dichroism rel. to detection of giant spin relaxation times 2– 44313
CaF_2, dichroism and F_2-centres 2– 53751
CaO, Jahn-Teller coupling in excited level of F^+ centre, uniaxial stress effects 2– 68635
$Cr(III)S_6$ trigonal systems, electronic structures and MCD spectra 2– 59997
$Cs_2ZrCl_6:Ir^{4+}$, high resolution magnetic circular dichroism spectra 2– 57342
Cs_2ZrCl_6, mag. circular dichroism spectra analysis 2– 75289
Cu^{2+} complexes, magnetic circular dichroism spectra of vibronically allowed d-d transitions 2– 64124
$Fe(CN)_5(OH_2)^{2-}$ -$Fe_2(CN)_{10}^{4-}$ equilibrium mixture in aqueous solution, study by magnetic circular dichroism 2– 71231
Fe(III) complexes, magnetic circular dichroism of d-d transition, ligand field theory analysis 2– 48176

Pleochroism continued
$KBr:Tl^+$, circular dichroism and Jahn Teller effect 2−68606
KCl:Na M_a centres, photodichroic, information storage 2−49399
KCl, F-centre g_{orb} factor determ. by mag. circular dichroism 2−77596
$KNiF_3$, stress-induced and mag. linear dichroism 2−81329
$MgO:Co^{2+}$, i.r. magnetic circular dichroism, study of first ^2E_g excited state 2−81365
$MgO:Fe^{3+}$, mag. circ. dichroism obs. of charge transfer bands 2−72339
MgO:V optical absorption and magnetic circular dichroism of impurity 2−68646
MnF_2, zero field circular dichroism, uniaxial stress depend. 2−44376
Si, neutron irrad. damage, piezospectroscopic obs. 2−48193
SmSe film, absorpt. spectra, resolution using mag. circular dichroism 2−81324
SmTe film, absorpt. spectra, resolution using mag. circular dischroism 2−81324
$SrCl_2$, mag. circular dichroism on F-centre absorpt. band, $g_{orbital}$ factor 2−74805
SrF_2, dichroism and F_2-centres 2−53751
YIG:Si, magnetiz. switching by i.r. irrad., linear dichroism obs. 2−68599
YIG:Si, photoinduced dichroism, model 2−72260
YIG(Si), linear dichroism, rel. to reversible photoelectromagnetic effects microscopic theory 2−54259

Plexiglas *see Plastics*

Pluto
accurate positions during 1969-70 period 2−69161
interior structure, models for various mass and radius 2−69162
linear polarization meas. 2−75909
occultations of stars 2−48768
spectrophotometry in 1972, 3400 to 5700 A 2−75908

Plutonium
(U,Pu)C and $(U,Pu)_2C_3$, distribution coeffs. of U and Pu, microprobe analysis 2−67352
artificial heart, ^{238}Pu as fuel 2−51909
atomic electron binding energies 2−46179
automatic analysis in solutions 2−75411
biological damage, interactions with cells and tissues 2−78659
burning curve ignition, expt. confirmation of theory 2−46383
covalent model for nature of 5f bonding 2−84396
diffusion, of Cu 2−71539
excretion equation evaluation, simplified method 2−62860
fuel production plant and breeder projects 2−63962
mixed oxide nuclear fuels, Pu-content and burn-up and isotopic distribution meas. 2−75401
nuclear fuel cycle, reference materials for accurate determ. of U, Pu and Th 2−74160
innuclear fuels, chemical anal. 2−74176
nuclear fuels irradiated, determ. of Pu, Am, Cm and Pu valency in reprocessing 2−74178
nuclear targets, electrodeposition methods of prep. for cross section obs. and accelerator bombardment 2−73919
oxidation, in moist O_2-N_2 mixture 2−54545
oxidation, of β-phase, hot stage X-ray diffr., microtopography, and thermogravimetric obs. 2−54544
oxidation, retardation by PuO surface film form. 2−51451
pacemakers, design and fabrication of Pu 238 sources 2−51910
pacemakers, radiation protection, plutonium 238, biological dose 2−51948
radioisotope fuelled batteries, plutonium 238 and strontium 90 2−49303
in Rapsodie fuel reprocessing, determ. using X-ray fluorescence 2−74173
reactor fuel development for fast and thermal development 2−56057
reactor fuel development lab. in Japan 2−70533
recycling in thermal reactors 2−56046
soil, seawater, coral and biological samples, Pu content in biological samples, separation and anal. 2−62045
systematic burden, manual and computer evaluation 2−78664
targets, prep. techniques 2−73912
titration errors in chemical analysis 2−74166
Pu- HNO_3 solns., radiolytic generation of H_2 and O_2 during storage 2−48350
Pu-Be source, neutron spectrum det. using multisphere spectrometer 2−59878
δ-Pu, Young's modulus, elastic limit, dislocation interstitial interaction, meas. apparatus, 4-300 K 2−80739
Pu metal, reference specimens for determ. amount of Pu and impurities in reactor fuels 2−75399
Pu^{3+} effect of core polarization on f-f interactions 2−52929
Pu^{3+} ions in cubic site, J-mixing effect on g-values of Γ_7 ground state 2−48119
^{238}Pu, for nuclear powered artificial hearts, potential availability, encapsulation, USAEC development programme 2−51915
^{238}Pu, production based on neutron irradiation of Np 2−49987
^{238}Pu for artificial heart system 2−49246
^{238}Pu for cardiac pacemakers 2−49249
^{238}Pu sealed for cardiac pacemakers, safety studies 2−51905
^{239}Pu, neutron induced autoradiography of bone 2−78660
^{239}Pu late phase lung clearance in vivo det. 2−58588
^{239}Pu reactor fuel, detection and analysis of actinide contaminants 2−74179
^{240}Pu, self-diffusion under hydrostatic pressure 2−64695

Plutonium compounds
mixed-oxide fuel elements, performance in 11 at.% burnup 2−76943
mixed-oxide fuel pins, F3A series unencapsulated, examination following irradiation in EBR-II 2−76947
Ce-Pu alloy, isomorphic transforms. 2−50959
Pu/U oxide fabrication process, sampling and analysis 2−74157
Pu/U oxide fuel, reference material for chemical specification analysis 2−74159
Pu/U oxide fuels, gravimetric methods of studying O/metal ratio 2−74152
Pu/U oxides reactor fuel, comparison of two methods of determ. of O/metal ratios 2−74153

Plutonium compounds continued
- Pu/U oxides reactor fuel, determ. of Pu content by calorimetry 2−74164
- Pu/U oxides reactor fuel, measurement of O/heavy metal atom ratio 2−74154
- Pu-U carbide nuclear fuel particles, preparation 2−56062
- $PuCl_4$, contaminative behaviour on protein film 2−78648
- $Pu(MoO_4)_2$-$Na_2MoO_4(Li_2MoO_4)$ system, existence of scheelite phases 2−71694
- $Pu(NO_3)_4$:Gd, Gd effect on criticality 2−56051
- PuO_2/UO_2 nuclear fuels, X-ray spectrometric obs. of impurities 2−74167
- PuO_2-UO_2, irradiated, gas release and swelling, 1260-1900°C 2−80662
- PuO_2-UO_2 fuel rods, foil handling technique for meas. of lattice parameters 2−70532
- PuO_2-UO_2 fuels, analysis techniques for process control, quality assurance and post-irradiation examination 2−74170
- PuO_2-UO_2 fuels, chemical analysis techniques 2−74171
- PuO_2-UO_2 fuels, determ. of non-metallic specification impurities 2−74177
- PuO_2-UO_2 in FFTF driver fuel assembly 2−63965
- PuO_2-polystyrene homogeneous fuel, 50 H/Pu, critical experiments 2−56053
- PuO_2, particle size effects on fast reactor safety 2−76937
- PuO_2, reference specimens for determ. of impurities in reactor fuels 2−74158
- PuO_2, thermal cond., self-irrad. effects 2−54078
- PuO_2 chlorination in melts of alkali metal chlorides, valent states 2−68776
- PuO_2 enriched fuel rod lattices in light water, exptl. characteriz. 2−59858
- PuO_2 enriched fuel rod lattices in light water, Pu-fueled system analysis 2−59859
- PuO_2 enriched fuel rods, kinetic parameters in light water lattice 2−59851
- PuO_2 fuel neutron radiation characts. 2−83130
- PuO_2 fuels in HTGRs, space-energy-depend. problems 2−83127
- PuO_2 nuclear reactor fuel, analysis of Pu content and impurities 2−74163
- $Pu_xU_{1-x}O_2$, thermal cond., 673-1273K 2−54079
- $^{238}PuO_2$ fuel fabrication by hot pressing 2−53932
- U-Pu-W-C system, phase relations 2−54011
- (U-Pu)C, two-phase mixed carbides, quantitative analysis by X-rays 2−64626
- $(U$-$Pu)_2C_3$, two-phase mixed carbides, quantitative analysis by X-rays 2−64626
- $(U, Pu)O_2$ fuel rods, cladding plastic deformation and swelling rate 2−76944
- $(U, Pu)O_2$ mixed-oxide with initial addition of fission product elements, postirradiation obs. 2−76945
- $(U,Pu)O_2$ fuel, U-Pu redistrib., transport model 2−52853
- $(U,Pu)O_2$ fuel pin, porosity and actinide redistrib., grain growth and desintering 2−56043
- $(U,Pu)O_2$ microspheres and pellets, sol-gel derived, microstructure 2−47610
- $(U,Pu)O_{2-x}$fuel irrad., oxygen redistrib. 2−52868
- $UO_{2\pm x}$-$PuO_{2\pm x}$/steel fuel/cladding interface, reaction 2−52875
- UO_2-PuO_2, mixed fuel, control and behaviour of O/M, offgas and moisture during fabrication 2−53934
- UO_2-PuO_2 fuel, temp. calc., use of GAPCON and HYBRID-SINTER programs 2−52854
- UO_2-PuO_2 fuel rods, ratios of effective cross sections from burnup data 2−59856
- UO_2-PuO_2 fuels, simulated fission product transport 2−52867
- UO_2-PuO_2 mixed fuel, discrete PuO_2 particle behaviour during rapid power transients 2−59857
- UO_2-PuO_2 mixed fuel, plastic flow and stress relax. 2−53808
- UO_2-PuO_2 mixed fuel, radiation dose rates 2−59876
- UO_2-PuO_2 mixed fuel, thermal creep, 1300-1700°C 2−53818
- UO_2-PuO_2 mixed fuel irrad. performance in PRTR 2−59853
- UO_2-PuO_2 mixed fuels, Pu and fission product redistrib. during irrad. 2−59852
- UO_2-PuO_2 particulate fueled lattice, H_2O-moderated, neutron multiplication and relative reaction rates 2−59854
- UO_2-PuO_2 thermal reactor fuel, defect performance 2−59855
- Uo_2-PuO_2 mixed fuels, advanced characteriz. 2−52870

Pockels effect *see Electro-optical effects*

Point defects *see Crystal imperfections*

Point groups *see Crystal structure, atomic*

Poiseuille flow *see Flow; Hydrodynamics*

Poisson ratio *see Elastic constants*

Polar cap absorption *see Electromagnetic wave propagation/ionosphere*

Polar cap flow *see Airglow*

Polarimeters
- *see also Ellipsometry*
- Compton γ-ray polarimeters, relative peak efficiencies 2−76743
- Compton symmetrical two-crystal for meas. of γ-ray linear polarization 2−79641
- interferometric, for microwave Voigt-type effect obs. in semiconductors 2−65215
- molecular structure of matter review of instruments 2−59240
- ORD-UV-5 spectropolarimeter, spectral range broadening to 2.3 microns 2−59281
- photoelectric, automatic, with fast digital recording system 2−45005
- photon counting, for astronomy, design and fabrication 2−76048
- photopolarimeter, computer control system 2−45007
- plasma diagnostics, microwave interference polarimeter-ellipsometer for resolution of ambiguity of meas. between rotation and ellipticity 2−83557
- polariscope investigation of optical systems described by a unitary matrix 2−66835
- pulsed laser Kerr system, for electro-optical fringe pattern obs. of transient electrical parameters 2−55744
- X-ray, graphite crystal, for stellar X-ray astronomy 2−62640
- X-ray, Thompson, scattering, celestial, design 2−51795
- ^{12}C polarimeter for 20-30 MeV deuterons, calibration 2−52700

Polarimeters continued
- Cu-Ni alloys, meas. of optical constants in visible and ultraviolet spectral regions 2−81330

Polarisability
- actinides, elec. dipole polarisabilities 2−59917
- aromatic hydrocarbons, anisotropic polarizability eval. using optical meas. 2−80108
- atom, freq. depend., rel. to Van der Waals forces 2−63998
- atom, in polyatomic molecules, applic. of Silberstein model 2−52983
- atomic, dipole oscillator strength distribution 2−76968
- atomic, effect on low-energy free-free radiative transitions 2−59901
- atomic, relation with interaction energy for a quantum mech. system 2−76979
- atomic and molecular estimate using Tchebycheff theory and moment technique 2−74192
- atomic dipole polarizabilities, coupled multiconfig. SCF method 2−64005
- atomic systems, many electron, elec. dipole polarizabilities using Hartree-Fock scheme 2−79929
- atoms, analytic multipole polarizabilities of ground and excited states, Coulomb approximation 2−46403
- atoms, energy interactions in $3d^n4s^0$ and $3d^n4s^2$ configuration excited states 2−76965
- benzene, elec. field perturbation of A-B transition, in-plane polarisability 2−80068
- benzene, substituted, molecular values, calc. 2−46425
- benzonitrile, dipole moments and polarizabilities of lowest excited singlet states 2−67508
- benzophennone molecular crystal, polarizabilities and dipole moments for lowest singlet and triplet $n\pi^*$ excited states 2−81136
- chlorobenzene, dipole moments and polarizabilities of lowest excited singlet states 2−67508
- conjugated molecules, comparison of expansions in calc. of elec. dipole π polarizability 2−42855
- dust particles, influence of polarizability on oscillatory behaviour in a.c. fields 2−49311
- rel. to gas atom-cryst. surface potentials 2−50450
- Hartree-Fock calculation for p^n excited states, B to Br atoms 2−76964
- heavy atoms and positive ions, calc. using semiempirical model for electrons 2−70570
- hydrogen bonds, extremely high polarizability 2−56147
- hydrogen-like atom, calc. of frequency-dependent dipole and quadrupole polarizability using method of Steiner 2−70632
- hyper-Raman effect, polarization phenomena 2−46515
- inert gases, linear polarizability at ruby laser freqs. 2−52909
- liquids, polar, solvated electron states 2−50308
- macropolarizability operator rel. to light scatt. in dipole approx. 2−79978
- metal particle, minute, enhancement of electronic polarizability 2−72006
- metallic system, one-dimens., Gor'kov- Eliashberg effect 2−57095
- methane, dipolar polarizability, variational calc. 2−80060
- molecular dynamic polarizability, time-depend. Hartree-Fock theory 2−77040
- nonlinear, calc. using pseudo particle method 2−79880
- polyatomic molecules, applic. of Silberstein model, determination of atom polarizabilities 2−52983
- rare earth metals, elec. dipole polarisabilities 2−59917
- single bonds, Stark effect on nuclear quadrupole resonance 2−52984
- solid, bound state contrib. to nonlinear polarizability from quasiparticle interaction 2−84197
- static electric, sign in relativistic quantum theory 2−78823
- thin film transistors, polarizability of bias-temperature drifted species 2−47946
- two-electron system, atomic and ionic dipolar polarizabilities, variational calc. 2−46471
- two-level system, representation as linear oscillator 2−49927
- variational bounds for imaginary frequency polarizability and dispersion interaction constant 2−52943
- weakly polarizable liquids, macroscopic electromagnetic field, spatial localization of equivalent forces 2−77252
- π, derivation from $\pi \rightarrow e\nu\gamma$ data 2−63503
- π, e.m. polarizability using low-energy technique 2−42388
- ρ, estimation from $\alpha^2 \ln\alpha^1$ recoil correction to H hyperfine structure and muonium hyperfine internal corrections 2−83214
- C, dipole polarizabilities, coupled multiconfig. SCF method 2−64005
- ^{113}Cs, Stark effect investigation of third excited $^2p_{3/2}$ levels in first spectrum, tensor polarizability determ. 2−70591
- D_2, temp. dependence 2−46546
- H_2, temp. dependence 2−46546
- H_2 coherently driven by light waves, obs. of anharmonic Raman scattering, determ. second order polarizability 2−42899
- HF, anisotropy from Stark coefficient 2−42907
- H_2O molecule, elec. dipole polarizability, perturbation theory calc. 2−46541
- H + H interaction, higher multipole coeffs. determ. from dynamic multipole polarizabilities 2−59945
- He, calc. of hyperpolarizability using pseudo particle method 2−79880
- He, ground state wavefunctions calc. 2−83211
- He, transition dipole polarizabilities 2−77025
- He ions, dipolar polarizability, variational calc. 2−74206
- He isoelectronic sequence, dynamic polarizabilities and mean excitation potentials 2−77026
- Kr, alignment depolarization cross- sections due to collisions 2−42751
- Li transitions, model pot. calcs. 2−76976
- LiH mol., using max. overlap method with additional condition 2−83273
- Na, 3 $^2P_{1/2}$ and 3 $^2P_{3/2}$ levels, Stark effect study 2−74218
- Ne, calc. of hyperpolarizability using pseudo particle method 2−79880
- Ne, ions, dipolar polarizability, variational calc. 2−74206
- Pr^{3+}, in crysts., quadrupole polarizability calc. 2−81319
- ^{87}Rb, Stark effect investigation of third excited $^2P_{3/2}$ levels in first spectrum, tensor polarizability determ. 2−70591
- $SPCl_3$, valence force constants 2−74276

Polarisability continued
SPF$_3$, valence force constants 2−74276
Tm^{3+}, in crysts., quadrupole polarizability calc. 2−81319
XY$_5$ molecular model, mean amplitudes of vibration 2−74275

Polarization
3 58, supernova remnant, obs. at 2.8 cm. 2−75757
A$_1$B$_2$ crystal, fluorite struct., dielec. props., theoretical analysis 2−72003
a.c. electrodes, in neurological recording, signal distortion 2−51895
alkali halide crystals, inertial force effects 2−54238
alkanes and derivatives, bonds, polarization tensor study 2−70736
antiferroelectric, rel. to equation of state 2−84360
atom characteristic of X radiation excited by electron impact, polarization determ. 2−76975
atomic line radiation, electron impact excited, variation with scattering angle 2−46457
auroral electrojet, idealized model 2−65901
boracite, reln. between elec. and mag. polarization, $T<64K$ 2−72104
3C 138, circular polarization of compact radiosource 2−58403
3C 273, circular polarization obs. 2−58405
circular, compact radiosources, search at 9 mm wavelength 2−62604
circular, of solar active regions, 2800 MHz and 13,500 MHz obs. 2−75987
circulating electron beam in synchrotron vertical polarization rotation into horizontal plane by imperfection resonance excitation 2−76756
Crab Nebula, structure at 2.7 and 5 GHz 2−55022
CTA 102, circular polarization of compact radiosource 2−58403
Cyg X-3, 8 GHz emission during radio flare, absence of linear polarization 2−81886
Cyg X-3 flare, limits to circular polarization at 2695 MHz 2−85019
Cyg X-3 radio outburst 2−85023
D$_1$ and D$_2$ radiation, destroyed by magnetic resonance, use as detection of mag. resonance 2−56443
dielectric, in inorganic glasses, empirical relation with electrical conduction 2−57188
dielectric, time depend. polarization and current after voltage applic. 2−47965
dielectric loss theory and orientation mechanism in external elec. field 2−77933
dielectrics, shock induced, effects of non-uniform dynamic loading of test piece 2−76382
2,3-dimethylquinoxaline, triplet absorption spectrum 2−42979
dipole gases, polarization oscills. 2−80415
direct and cross polarized radar backscatter power from turbulent plasma 2−74363
direct nuclear reactions, dependence on total ang. momentum of exchanged particle 2−46225
direct nuclear reactions, simple diagram representation 2−46224
Earth's electric field, near Upper Rhine Graben 2−57789
EAS emission, polarization at 6 MHz 2−70274
electrons, radiative polarization in storage rings 2−70338
e.m. wave reflected from ionosphere, polarization of mean field 2−72860
excitation master equation to multi-shell-model of polarization quenching to fluorescence, applic. 2−78142
extragalactic radio sources and quasars at 49 and 73 cms 2−58412
extragalactic radiosources, structure at 2695 and 8085 MHz 2−58402
ferroelectric film, critical thickness and thermodynamic stability 2−61425
ferroelectric solid solution, thermodynamic theory 2−61424
ferroelectric solid solutions, first-order phase transition characts. 2−65057
ferroelectrics, appearance explained by soft mode model based on lattice dynamics 2−81152
ferroelectrics, frequency and temperature dependence near Curie point considering polarization fluctuations 2−84365
ferromagnet, associated magnetoelastic waves, dispersion laws and polarization 2−57294
ferromagnet, phonon polarization operator in Ising model 2−81265
ferromagnetic film, polarization of domain boundaries of Neel type 2−57297
free-free polarization; plasma electron vel. distribution determination 2−56332
galactic background radiation, North Polar Spur, reduction of linear polarization at 1415 MHz 2−58387
Galactic spurs, survey at 1415 MHz 2−84950
gamma-rays, parity nonconserving interactions 2−42495
geomagnetic micropulsations, effect of geoelectric structure 2−66010
geomagnetic pulsations, rel. to source rotation 2−72917
gravitational synchrotron radiation, analysis in terms of Stokes parameters 2−72958
IC443, supernova remnant, obs. at 2.8 cm. 2−75757
ice, ferroelec., polariz. and depolariz. current obs. at low temp. 2−57242
inclusive reactions, effects 2−59446
limiting, rel. to Maxwell's equation solution 2−45606
linear, HI regions, galactic spurs, measurement antenna radiation patterns 2−85060
liquid, n.m.r. signal generator for monitoring changes 2−59014
magnetic structures, exchange interaction of electric and magnetic polarizations 2−81212
magnetoplasma, circularly polarized waves, dispersion 2−80229
2-methylbutanol-2 solutions, dielec. polarization 2−46975
10-methylene anthrone, polarizations of low energy $S_n \leftarrow S_0$ transitions 2−60080
mixed conductors, polarization measurement methods 2−68464
molecular crysts., local elec. field and charge-carrier mobilities 2−81129
Mossbauer spectra, nuclear and electronic γ-ray scatt., interference rel. to polarization 2−54385
muonium two-particle procession in strong mag. fields, polarization changes 2−70649
n-p(n-i-p) nuclear particle detectors, space charge layer polarization during irradiation 2−65023
naphthalene, persistent internal polarization temp. and electric field dependence 2−75138
NGC 1068, circular polarization obs. 2−58405
NGC 4051, circular polarization obs. 2−58405

Polarization continued
NGC 4151, circular polarization obs. 2−58405
nonlinear, gas laser with saturable absorber 2−41983
NRAO 140, circular polarization of compact radio source 2−58403
nuclear reactions, particle knocking-out polarization correl., meas. possibilities 2−49779
OJ 287, circular polarization obs. 2−58405
OJ 287, flux density and polarization variation at 8 GHz 2−75811
optically active mols., discrimination energy calc. 2−80127
optically inactive crystals, opt. rotat. induced by crossed elec. and mag. fields 2−78066
P1127-14, circular polarization of compact radiosource 2−58403
Pc3 micropulsations, 25 mHz, diurnal variation in horizontal plane 2−48600
Pcl micropulsations propagated through ionospheric ducts 2−54930
phonons, in ionic crystal lattice in strong static magnetic field 2−43946
phthalaldehyde, polarizations of low energy $S_n \leftarrow S_0$ transitions 2−60080
picene, triplet-triplet absorption spectrum 3750 to 15800 Å region 2−83281
Pioneer IV, solar occultation, transformation of signal polarization angle to plane of ecliptic 2−44999
plasma effects on injection of dense electron beam 2−74358
plasma waves, circular, in homogeneous plasma computer model 2−43181
poly(methyl methacrylate) thermoelectrets, thermodepolarization currents 2−83348
polyethylene, under static electric field, positron lifetime study 2−61409
polyethylene terephthalate, electrect, atmosphere effects 2−65076
polymer, dielec. depolarization spectra, thermal treatment effect 2−47974
polymer, insulating, conf., Bratislava, Czechoslovakia [May 1972] 2−47962
polymer, insulating, rel. to slow surface states 2−47971
polymer, linear chain, spontaneous polarization and pyroelec. coeff. 2−72045
polymer, thermostimulated depolarizing currents and thermoelectret effect 2−47973
polyvinylidene fluoride electret. depolarization current and surface potential decay 2−51208
propagator, self-consistent, particle-hole, as modified random phase method 2−46495
pulsar CP 1133, characteristics of subpulses 2−55095
pyrene, photoelectret effect 2−81131
quasars, with appreciable red shift 2−58376
radio sources, circular polarization meas. at 1.4 and 5 GHz 2−55096
radio sources, meas. at 9.55 mm wavelength 2−55082
radio-wave reflection from inhomogeneous ionosphere, determ. of polarization using Stokes parameter 2−94904
radiosources, 21 cm., 3C 270 and 3C 452 2−58380
radiosources, linear, obs. at 7.2 cm 2−66133
radiosources with appreciable red shift 2−58376
rainfall crosspolarisation of linearly and circularly polarised waves at microwaves 2−48514
resonant media, large coherent optical polarizations, prep. and detn. 2−41945
rocks, physical-and-mathematical model of non-linear phenomenon 2−57779
Saturn, polar scattering effect hemispherical circular 2−75912
seismic S waves, use in investigating focal mechanisms 2−61880
solar active regions at 3.8 cm 2−78599
solar type III radio bursts at 23.5 and 30 MHz, relative polarization 2−81953
solar X-ray flares 2−73121
solar X-ray meas. of Intercosmos-4 rel. to OSO-5 meas. 2−78591
spatially dispersive medium, of excitons, generalized extinction theory 2−68304
sum-frequency amplitudes formulae for propagation of e.m. waves from nonlinear multilayer film 2−58989
symmetrical objects, zero polarization bases of one-position scattering matrix 2−55617
synchro-Compton radiation, polarisation 2−72983
synchrotron radiation, electron dynamic effects, expt. 2−42339
synchrotron radiation, from 800 MeV electrons 2−45879
thermoelectret behaviour under different humidity conditions 2−81145
transmission intensities of dielectric coated gratings for MM waves, effects of polarization 2−69827
triglycine sulphate pyroelectric detector, laser study of nucleation sites 2−44165
VRO 42.22.01, circular polarization of compact radiosource 2−58403
w28, supernova remnant, obs. at 2.8 cm. 2−75757
w44, supernova remnant, obs. at 2.8 cm. 2−75757
X-ray diffraction of crystals, polarisation phenomena 2−83911
X-ray examination and Olekhnovich polarization factor for mosaic crystals, comment 2−53633
d photodisintegration differential cross-sections and polarization of photonucleons 2−63672
γ-rays, meas. by detection of angular correlation in pair production 2−79645
γ-rays, meas. using symmetrical two-crystal Compton polarimeter 2−79641
μ^- depolarization in aliphatic hydrocarbons, molec. wt. and temp. dependence 2−64083
μ^- depolarization in monomers and polymers 2−64084
$\pi^- p \rightarrow \pi^0 n$ (ηn), properties of polarization in forward direction determ. using Regge amplitudes 2−70237
AgNa(NO$_2$)$_2$, ferroelec., spontaneous polariz., pyroelec. obs. 2−54235
AgNa(NO$_2$)$_2$, in quasi-static elec. field, reversal of spontaneous polarization 2−72030
BaTiO$_3$, residual, rel. to dynamic fatigue, ageing of switching props. 2−72031
BaTiO$_3$ film, domain struct., stroboscopic electron microscope obs. 2−75149
C IV emission lines in planetary nebulae 2−48669

Polarization continued
CaF_2, rare earth doped, interstitial dipole relax., thermal depolarization obs. 2−60790
Cr, antiferromagnetic, domains obs. with neutron diffraction topography 2−65179
GaAs p-si-n structure, electroabsorption, polarization effects 2−70666
Ge electrode, rel. to equilibrium and nonequilibrium effect near semiconductor-electrolyte boundary 2−61798
Ge p-n junction, γ-ray detector, space charge region polarization, impurity centre charge exchange 2−65026
$^3He + {}^3He$ interaction pots. rel. to atomic- mass polarization effect 2−67434
$^4He + {}^4He$ interaction pots. rel. to atomic-mass polarization effect 2−67434
KH_2AsO_4, ferroelec., n.m.r. line anomalies due to polarization fluctuations 2−57243
KH_2AsO_4 and KD_2AsO_4, ferroelec., spontaneous polarization 2−47985
LiF, radiation-induced thermally activated depolarization 2−72007
$LiTaO_3:Cu^{2+}$, rel. to optical generation of intense picosec. electrical pulses 2−45768
$LiTaO_3$ single crystal, ferroelec. spontaneous polarization, temp. depend. 2−72008
$NaNO_2$, ferroelec., modulation of millimeter wave absorp. by polariz. reversal 2−48212
$NaNO_2$, polarization in reversal of applied field, 10^{-2} to 10^7 V/cm.sec 2−65064
Ni, foil, of channelled deuterons 2−47784
$PbBr_2$, elec. cond. in cell arrangement, space charge effects, elec. polarization 2−61420
$PbBr_2$, electronic cond., hole cond., elec. polarization 2−61419
$SbSI:Sb_2S_3$, prep., spontaneous polarization, dielec. permittivity, photocurrent, dark current rel. to phase transition, −50-50°C 2−75143
SbSI, ferroelec. semicond., trapping levels, effect of photopolariz. and spontaneous polariz. 2−75154
Si electrode, rel. to equilibrium and nonequilibrium effect near semiconductor-electrolyte boundary 2−61798
$SrTiO_3$, inertial force effects 2−54238
ZnO, decay of pyroelectrically induced polarization charges 2−54241

light
see also Double refraction; Optical rotation; Photoelasticity; Polarimeters
— 2−67436
n-alkane gases, meas. of anisotropy and depolarization ratio by photon counting of scattered laser light 2−80083
anisotropic media, light propag., evolution of ellipse of polarization 2−79322
anthracene, reson. Raman scatt. 2−65275
atom, linear and circular polarization effects in high-order multiphoton ioniz. 2−79906
D L azidophenilacetic acid, use of optical activity to control resolution and determ. optical purity 2−54523
benzene single crystal, i.r. spectrum, assignment of exciton components 2−51316
bilinear transformation by optical system 2−73646
bilinear transformation of optical polarization transducer 2−73645
birefringent laser polarizer, high efficiency 2−82556
Brillouin scattering in acoustically active crystals, calc. of polarization of scattered light relative to incident laser light 2−68667
3C 273, circular polarization of u.v. 2−81794
calibration of grating spectrometer 2−63430
1-chloronaphthalene, liquid, complete polarization study of two-photon absorption 2−43371
cholesteric liquid crystal, effect of a magnetic field on the optical transmission 2−84468
circular, aligned interstellar grains 2−69110
circular, interstellar, early type stars 2−73002
circular, light scattered from rough surfaces 2−63395
Comet Tago-Sato-Kosaka radiation, search for elliptical polarization 2−75724
complex molecules, two-photon excitation, determ. of polarization limits of fluorescence 2−83237
controllable dispersion interference-polarization filter, design method 2−66845
counting statistics of partially polarized chaotic light 2−69993
Crab Nebula radiation, search for elliptical polarization 2−75724
day glow, intensity and polarization, measurements made during 1965 total solar eclipse 2−72832
Deimos, obs. in blue light 2−58493
depolarization of laser light scattered from turbid water 2−64486
depolarization using scrambler plate 2−66821
diffraction of parallel and perpendicular polarized wave by echelette grating 2−49422
diffuse interstellar absorption feature, λ4430, polarization obs. 2−44854
in digital light deflector 2−79388
distribution transformation, synthesis of a field with angular depend. of exp (j2θ) 2−76521
distribution transformation, synthesis of circular symmetry 2−76522
dyes, organic, stimulated emission 2−49375
effects in images formed by glancing incidence telescopes 2−79305
ellipsometer with oscillographic presentation of pattern 2−66834
emitted by surface plasmons on metal, due to roughness 2−75040
Faraday rotation probe for plasma magnetic flux density meas. 2−77279
film polarizers, single wavelength 2−79381
galactic radiation, search for elliptical polarization 2−75724
in gas lasers 2−59139
grid polarisers for near i.r., fabrication method 2−52470
holographic subtraction with circularly polarized light 2−79247
holography, photoelastic analysis 2−82148
impurity luminescence, rel. to nuclear spin 2−44405
interferometer using mechanical modulation of polarized light, mass. of absolute phase delay in Kerr effect 2−42197
interferometric spectropolarimetry determ. by Fourier spectroscopy technique 2−79436
intrinsic polarization in atmosphere of supergiant stars 2−62545
IRC + 10216 in optical and i.r. regions 2−58280

Polarization continued
light continued
laser beam separation into two circularly polarized beams, total refl. 2−52430
laser beams, longitudinal displacements near total reflection, photon mass and new exptl. results 2−45759
linear, Hα emission line in halo of M82 2−58194
linearly, depolarization resulting from inhomogeneous dielectric heating of plane-parallel KH_2PO_4 crystal plates 2−42184
liquid, fine structure in depolarized light scatt., use in calc. of stress-optical coeff. 2−50358
macromolecules in soln., polarized luminescence for investigation of intramolecular mobility 2−60090
Mars, circular polarization spectrum 2−81910
mechano-optic polarization modulator, using reflection attraction grating 2−70036
microscope, partially coherent image of opaque edge 2−42233
Moire fringe patterns formed by polarization gratings 2−49429
molecular crystals, reson. Raman scatt. 2−65275
monochromators, polarizing effects 2−49452
Moon, albedo and linear polarization rel. to optical properties of igneous rocks in i.r. range 2−75846
NGC 1068, circular polarization of u.v. 2−81794
NGC 4151, circular polarization of u.v. 2−81794
NML Cyg, in optical and i.r. regions 2−58280
NML Tau in optical and i.r. regions 2−58280
OB stars, southern 2−62524
OJ 287, circular polarization of u.v. 2−81794
XPer, variable star 2−44869
permalloy, film, on CaF_2, rel. to thickness and orientation 2−57324
photospheric, near solar limb 2−66223
planetary nebulae radiation, search for elliptical polarization 2−75724
Pluto, linear meas. 2−75909
polar crystals, optical rectification by impurities 2−44327
polarization junction laser 2−69944
poly-γ-benzyl-L-glutamate, local viscosity of conc. solns. meas. by fluorescence depolarization 2−60451
polycrystals, effects during transmission 2−81325
polystyrene, structure in glassy state determ. by fluorescence depolarization 2−60615
quantized longitudinal and transverse shifts associated with total internal reflection 2−42213
quartz and calcite emission polarization and rock discrimination 2−72692
quasars, Seyfert galaxies, BL Lac and OJ 287 optical circular polarization, search 2−75800
radially polarized mode generation by laser oscillation, expt. 2−69901
random rough dielectric surface, depolarization props. 2−79309
effects on reflectance factor meas. 2−70010
reflected from lunar dust layers, effect of fluidization 2−58453
reflected u.v. at large angles of incidence 2−66855
reflection, by transparent film-absorbing substrate system 2−73644
reflection, polarization rotated, for travelling wave light intensity modulator 2−42158
reflection and transmission of partially polarized light by dielectric plates 2−42188
reflection nebulae radiation, search for elliptical polarization 2−75724
ring laser, polarising effect of decrease of competition by outer waves 2−63318
ring laser, polarization characteristics of opposite direction travelling waves, He-Ne plasma tube 2−45735
ring laser with naturally active cell, radiation polarization 2−73557
rotating interferometer for Sagnac effect meas. 2−79358
ruby disk laser, depolarization effects 2−82489
scattered radiation from diffr. grating, ellipsometric obs. 2−44343
o Sco, bright star, circular polarization, interstellar origin 51750 2−51750
Sco X-1, search for optical circular polarization 2−73001
self-synchronized laser, using polarization modulating cells and polarization beam splitter in optical cavity, patent 2−66795
simple gases, depolarized light scattering, contrib. of many-body effects 2−53338
specific refractivities, atomic O and N, dual frequency laser interferometer 2−79902
splitting of states, Goos-Hanchen and Imbert effects 2−76514
stack polarizers, quarter-wave, radiant transmittance obs. 2−79411
starlight, elliptical polarization search 2−75724
stimulated Raman emission from bulk medium, theory of state of polarization of scattered radiation 2−63305
supernova in irregular galaxy NGC 5253, optical polarization 2−69091
thin film polarizers, single wavelength, analytic solution 2−59239
three-level gas laser, effect of polarization pulling, determ. of degree of anisotropy 2−66741
three-photon phenomena for randomly oriented molecules, polarization dependence 2−67441
Titan, evidence for optically thick atm. 2−81907
total internal refl., transverse shift, quantization, circular polarization 2−70011
transfer matrices, consequences of non-commutability 2−79331
twilight, circular polarization of scattered light 2−68911
twilight sky, atmospheric scattering rel. to meas. of light polarization 2−81657
VY CMa in optical and i.r. regions 2−58280
white dwarf G195-19, circular polarization and ephemeris 2−55035
X.U.V., use of highly anisotropic materials as polarizers 2−42211
Zeeman laser with strong x-y anisotropies 2−52414
zinc porphin, polarized sharp line absorption spectra 2−64196
zodiacal light, circular polarization measurement 2−73108
$Al_xGa_{1-x}As-GaAs-Al_xGa_{1-x}As$ heterojunction laser, radiation spectral distrib. and polarization 2−63342
Ar singly ionized, specific refractivity 2−79903
As_2S_3 crystals, massive and thin film, effect on self-absorption edges 2−84479
Cd, magnetic depolarization of fluorescence lines, Hanle effect 2−79860
Co, mag. permeability calc. from spectral meas. 2−65155

Polarization continued
  light continued
    Cr^{3+} in $LiNbO_3$ and $LiTaO_3$, optical excitation causing macroscopic polarization 2−48138
    $CsCrCl_3$, single crystal polarized absorption spectra, ligand field interpretation 2−81363
    $CsMgCl_3$:$CsCrCl_3$, single crystal polarized absorption spectra, ligand field interpretation 2−81363
    Fe, mag. permeability calc. from spectral meas. 2−65155
    GaAs laser double heterostruct., threshold current rel. to press., light polarization flip 2−69949
    H_2O clouds, depolarization for monostatic Lidar 2−78377
    He-Ne laser, control by dielectric plate 2−82474
    KCl(Br)(I), Ag^- centres, polarization and decay time of luminesc. 2−80710
    KH_2PO_4 commutator, crystal plates showing Pockels effect, limitations to angular field 2−45796
    K_2SO_4, laser Raman spectra, lattice vibration modes 2−72368
    $LiNbO_4$ crystal cuts with low half wave voltage 2−42170
    Nd:YAP solid laser, polarization and crystal direction effects 2−42067
    Ni, mag. permeability calc. from spectral meas. 2−65155
    Ni film, on CaF_2, rel. to thickness and orientation 2−57324
Polarography *see Chemical analysis/electrochemical*
Polarons *see Crystal electron states/polarons*
Polishing *see Surface structure*
Polonium
  No entries
Polonium compounds
  No entries
Polyelectrolytes *see Electrochemistry; Polymers; Solutions*
Polymerization
  acetylene, conjugation reaction centre model of anionic polymerization 2−44481
  cyclohexene and formic acid, free radical form of polyester 2−83351
  divinyl-benzene, rel. to prep. of C precursor 2−56983
  epoxy resin, in elec. field. electret form 2−47991
  2-hydroxyethyl methacrylate networks in dry and swollen states, effect of crosslinking density and dilution 2−56782
  isothermal calorimeter design 2−82386
  organosilicon film, r.f. plasma polymerization 2−43484
  polyester resins, unsaturated, crosslinked with styrene, structure, Raman spectroscopy 2−44482
  polyfluoroalkoxyphosphazenes, dilute solution characterization 2−44483
  polystyrene, terminal group 2−51444
  semiconductor, amorphous, rel. to reversible optical effects, laser induced 2−60569
  C precursor, glassy, prep. under pressure from organometallic complexes 2−61014
  Eu(III) complex, chelate, Mossbauer obs. 2−51309
  GeO_2 network, depolymerization in presence of two cations 2−53535
  S, liq., equil. parameters, calc. method 2−57418
  Se, liq., equil. parameters, calc. method 2−57418
Polymers
  see also Plastics
  (polystyrene + naphthalene), sensitized triplet quencher phosphorescence, study of photoprotective efficiency 2−72581
  ABA block copolymer films, light scattering from anisotropic regions 2−44325
  ABS blend, fatigue crack propag. mechanism comparison with PVC 2−71601
  adhesion to solids, breakdown rel. to radio emission parameters 2−52314
  adhesives, binders and hermetic sealers, investigation of moisture effects by electrical methods 2−53979
  L-alanine randomly coiling random copolymers, higher even moments for hard-sphere model 2−64202
  amorphous, cell model partition function for thermodynamic calc. 2−43457
  amorphous, creep recovery, influence of volume change 2−56809
  amorphous state linear polymers, estimating specific heat 2−61106
  amylose triacetate, single crystal growth, morphological features 2−83346
  anthraquinone-mellitic anhydride, dielec. relax., permittivity, a.c. and d.c. cond. 2−81143
  antifriction self-lubricating heat-resisting materials 2−43745
  aqueous solutions, surface viscosity meas. using new double-ring rotational-torsional surface viscometer 2−83781
  band struct., energy band derivatives computation 2−57129
  biopolymers, flow dichroism spectra applic. to molec. studies, review 2−53089
  birefringent polymer films on substrates for integrated optics 2−80592
  bisphenol-A-polycarbonate, compression yield stress rel. to mech. loss peak 2−47506
  butadiene-styrene copolymer, nonlinear viscoelastic behaviour under constant strain rates 2−50733
  cellulose, crystalline models, conformational terminology 2−43022
  cellulose, precipitated, crystal morphology 2−83349
  cellulose and similar fibrous materials, dielectric constant and crystallinity 2−61408
  cellulose hydrate film, mech. props. rel. to mol. orientation, sound vel. obs. 2−47536
  cellulose triacetate as track imaging detector of alpha-particles 2−82827
  ceramic tile bodies, effect of polymer impregnation on physical and mech. props. 2−80759
  chain, span calculation 2−50120
  chain form. in amorphous solid from small-angle neutron scatt. 2−74600
  chain of rigid rods, vel. distrib. function 2−60100
  chains, two atoms per unit cell, local electronic states 2−83384
  chemical transformations, conf., Bratislava, Czechoslovakia (1971) 2−54533
  chlorinated polyethylene supramolecular structures, morphology and light dispersion 2−50413
Polymers continued
  composite, fibre-reinforced resin., metal incorporation using organometallics 2−50923
  computer simulation of conformation and conformational thermodynamics 2−70801
  concentration dependence of steady state compliance for polymer solutions 2−83373
  conductivity and diffusion rel. to mechanical strain 2−57232
  confined circular chain, matrix method for entropy 2−60099
  constitutive equations for nonlinear viscoelasticity 2−82316
  contact angle meas. of Hg on thin films, scanning electron microscope obs. 2−46942
  copolymers, A-B type, domain formation mechanisms 2−57419
  copolymers, amorphous blocks cast from soln., domain struct. 2−83848
  creep, radiation induced, relationship with radiation- induced electric conductivity 2−47517
  creep and long-term strength, stems for testing 2−71611
  crosslinked epoxy, effect of free volume on electrical conductivity 2−57233
  cryogenic loss peaks, assignment of molecular mechanisms 2−71557
  crystal, Debye-Waller factor, thermal fluctuations, valency angle stiffness 2−74972
  crystal growth, fractionation effects 2−81501
  crystal lattice vibrs., antiparallel chain sheet structs. 2−80884
  crystalline, π-electron spectrum, effect of stochastic bond defects 2−47812
  crystalline, anisotropy of dielectric relaxation for dipolar orientation change 2−75140
  crystalline, mech. props., morphology influence 2−60860
  crystalline, two-compound model 2−77480
  crystallization, mol. phenomena study by computer simulation 2−47192
  crystallization, quartz dilatometer applic. to obs. of Avrami parameters 2−56565
  crystallization, single cryst. form. from soln. 2−60710
  crystallization in temperature gradient field with controlled crystal growth, method of study 2−74603
  crystallization rate, obs. by depolarized light intensity method 2−47065
  crystallization rate by depolarized light intensity method 2−56566
  cumulene, long chains, unrestricted Hartree-Fock calculations of electronic structure 2−43023
  deformation, instability at shear strength limit 2−68085
  dielectric depolarization spectra, thermal treatment effect 2−47974
  dielectric properties, thermally stimulated current and voltage techniques 2−72004
  dielectric relaxation, meas. and mechanism 2−61416
  dielectrics, meas. using coaxial resonators 2−81133
  dilute semi-crystalline, elastic model 2−60840
  dilute solution, time-dependent elongational viscosity calc. using elastic dumbbell model 2−71171
  dilute solutions, drag-reducing, degradation 2−53351
  dilute solutions, dumbbell theory 2−63075
  dilute solutions, flowing in curved pipe, det. of normal stress coefficients 2−60385
  α,ω- diphenyloctatetraene solutions in bibenzyl and n-paraffins, low-lying weak transition obs. in optical spectra 2−50121
  dispersions, secondary dynamic, of aromatic polyimide 2−83366
  drag reducing, influence on turbulence in viscous sublayer 2−46880
  drag reducing and turbulent flow 2−77373
  drawn, mech. anisotropy represent. as spherical tensors 2−77627
  elastic deform., diffr. obs. 2−43749
  electric properties, mol. mechanism 2−57143
  electrical insulation and dielectric phenomena, conference, Williamsburg (1971) 2−57222
  electrical properties, book contrib. 2−47960
  electron beam-induced radiation damage, effect on electron microscope image 2−80700
  electron diffraction pattern of beam-sensitive specimens, cooling effects 2−79140
  electron irradiated, elec. cond., temp. amd electron dose effect 2−84316
  elongated, spectroscopic technique to meas. i.r. dichroism, stress and strain 2−84465
  epoxy, glass fibre reinforced, fatigue crack damage, vibr. testing 2−60921
  epoxy, graphite fibre reinforced 2−61021
  epoxy matrix with graphite particles as fatigue damage indicator 2−53971
  epoxy resins, correl. of supermol. struct. stability with electrophys. props. 2−83394
  epoxy resins, molecular mobility, effect of fillers and plasticizers, dielec. study 2−47062
  epoxy-diamine networks, glass transition temp. determ. using torsion pendulum 2−71287
  ESCA, appl. to nitroso rubbers 2−83350
  ethylene-carbon monoxide copolymer, anisotropy of relaxation for dipolar orientation change 2−75140
  ethylene-propylene copolymers, configurational statistics 2−70802
  ethylene-vinyl acetate copolymers, liquid lattice type absorption for far i.r. and millimetre waves 2−53437
  exoelectronemission 2−77974
  extrusion of polymer melts, computer aided rheology measurements and processing 2−64400
  fading memory materials, non-isothermal treatment 2−68056
  failure under stress 2−53829
  fatigue-crack propagation, review 2−64728
  film, adhesion mechanism with Al vacuum deposited film 2−43476
  film, dielec. breakdown 2−47980
  film, electromechanical model for capacitance effects 2−57228
  film, geminate recombination of charge carriers 2−57187
  film, internal struct. of single hole breakdown 2−47981
  film, mech. props. rel. to mol. orientation, sound vel. obs. 2−47536
  film, V. thin tensile, rupture and elongation props. 2−60887
  films, dynamic light scattering study 2−83382
  films, electrical conductivity, use as dielectric layers in m.i.m. structures 2−83859

Polymers continued
films, optical characterization 2−56599
films solvent-cast, dielectric relaxation rel. to residual solvent and crystallinity effect 2−57227
flow, elongational of chain of 100 segments, calc. of intrinsic birefringence 2−46870
fracture surface layer, optical thickness determ. 2−70013
friction coeff., three section single-contact roller machine for det. 2−56850
functional integrals and polymer statistics, review 2−60102
furfuryl methacrylate, thermomechanical props. 2−50751
(1→4)-linked galactans, configurational statistics, calc. of conformational energies, characteristic ratios 2−70804
gas discharges, organic reactions leading to polymer deposits 2−74408
glass, environmental crazing mechanics and mechanism 2−64735
glass temperature and expansion coefficients relationship 2−60604
glassy, crazing in alcohols and hydrocarbons 2−83357
glassy, diffusion of organic vapours 2−83362
glassy, fracture mechanisms 2−60889
glow layers, electron microscopy study of formation 2−53564
glycine randomly coiling random copolymers, hard-sphere model 2−60103
glycine randomly coiling random copolymers, higher even moments for hard-sphere model 2−64202
holographic recording materials, nonlinear effects 2−49397
h.v. electron microscopy of crystalline polymers 2−79139
poly(2-hydroxyethyl methacrylate networks in dry and swollen states, effect of crosslinking density and dilution 2−56782
immiscible polymers, interface theory 2−60441
impact fracture of polymeric substances 2−84052
impregnated porous ceramic, strength rel. to temp. 2−43899
insulating, normalized relax. spectrum construc. in log/log coords. 2−47972
insulating, polarization and cond., conf., Bratislava, Czechoslovakia [May 1972] 2−47962
insulating, surface states and polarization 2−47971
insulator thin film synthesis and deposition for Josephson tunnelling applics. 2−71877
ionic, dilute solution viscoelasticity, charged bead-spring models 2−53366
isotactic polystyrene from isotactic-atactic blends, effect of noncrystallizable components on crystallization kinetics 2−71294
isotropic, longitudinal crazing 2−53840
latex, Ag conc. under variable exposure, rel. to optical density 2−52500
latex, particle size analysis, angular light scattering data 2−43411
ligand-polymer complexes, exciton theory of excited electronic states 2−68301
light scattering, method of calc. for anisotropic elliptical objects 2−72289
linear chain, spontaneous polarization and pyroelec. coeff. 2−72045
linear chains, excluded-volume effect 2−64198
linear high, extended chain cryst. habits 2−60609
linear homopolymers and copolymers, analysis of vibrational spectra by Green's function method, effect of defects 2−43021
linear random-flight chains, empirical probability density functions for radii or gyration 2−43020
liquid viscosity, pressure and temp. effects 2−60443
mechanical anisotropy, glass-fibre filled films 2−84131
melts, flow, nonlinear thermodynamics 2−83748
melts, non-isothermal flow in round tubes 2−83749
membrane, self-diffusion through of organic vapours, obs. using radio tracer technique 2−71180
methyl cellulose aqueous soln., viscoelastic props. 2−83380
methyl methacrylate, thermomechanical props. 2−50751
mol. wt. and non Newtonian viscosity, relation, in narrow distribution polymers 2−83372
molecular dynamics 2−53090
morphological struct., annealing and temp. effect 2−60611
morphology, symposium, Prague, Czechoslovakia, (Aug-Sep 1971) 2−60608
morphology of amorphous materials, annealing and mech. treatment effects 2−60610
muonic atom interactions, μ^- depolarization 2−64084
Mylar, elec. cond., pulsed X-ray irrad. induced 2−65091
network, viscoelasticity, Mooney's mol. theory, effect of chain dimens. 2−83356
network theory for nonlinear viscoelasticity for conc. polymer systems 2−83377
nitrocellulose, Ag conc. under variable exposure, rel. to optical density 2−52500
n.m.r. data and their interpretation, book 2−83396
n.q.r. of dilute inert fillers as nondestructive probe 2−61758
nylon, preferred orientation 2−60751
nylon, solution- grown crystals, combined wide-angle and low-angle X-ray diffraction patterns 2−50630
nylon 66, monofilament, effect of torsion on uniaxial bond rupture 2−60858
nylon 66, relax., thermodepolarization current study 2−77938
nylon 66, space charge relaxation and Maxwell-Wagner effect 2−65051
nylon 66 fibres, adsorption of polyacrylic acids, model compounds and vapours, rel. to textile size applic. 2−60696
nylon 66 fibres, drawn, effect of high-temperature annealing on structure and morphology 2−74602
nylon 66 powder, adsorption of polyacrylic acids and model compounds, rel. to textile size applic. 2−60695
nylon 6, 6-6, 12, crystallization rate by depolarized light intensity method 2−56566
nylon 6, crystallization from melt, X-ray diffraction study of α and γ forms 2−74605
nylon 6, effect of anisotropy, orientation and water on relaxation behaviour from 4.2 to 300 K 2−71559
nylon 6, glass fibre reinforced, dynamic viscoelasticity temp. depend., two-phase blend system model applic. 2−71556
nylon 6 fibre, reaction rate model of fracture 2−74854
nylon 6-6 rod, cold extrusion drawing, mechanical props. by tension and compression tests 2−80810

Polymers continued
nylon-6, structure property, relationship from viscoelastic analysis 2−56775
optical plastic, mixed polymers of diethylene glycol- bis-allyl carbonate and isophthalic acid diallyl ester, with controlled refraction and dispersion 2−55752
organosilicon film, r.f. plasma polymerization 2−43484
osmotic virial coeff. of polymer-solvent system, interdepend. of enthalpic and entropic contribs. 2−50353
oxazole and oxadiazole derivs., solutions, stimulated emission 2−59164
particle size, X-ray diffraction profiles, applic. of variance analysis 2−64602
particle size and X-ray diffraction profiles, application of Wilson's variance-range analysis 2−64601
perfluropolyether as vacuum pump fluid resistant to electron induced polymerization 2−58664
phenyl containing anthracene, conformal depolarization of luminescence, dependence on polymer chemical structure 2−53444
photochemistry, role of photophysical processes 2−54554
photocurrent depend. on ambient condition, wavelength and temp. 2−48004
photopolymer hologram recording films for real time image formation without processing 2−69968
plane-polygonal, translational diffusion coeff., applic. of modified Oseen tensor 2−64200
plasmodium actin, obs. by quasielastic scattering of laser light 2−60606
plastic deformation and extrusion of high polymers in solid state 2−84051
plastic yielding, high pressure effects, crystn. and amorphous materials 2−68081
PMMA, γ-irrad., absorpt. spectrum, optical density increment, u.v. filter 2−72357
PMMA, irrad., proton spin-lattice relax. times 2−84449
PMMA, thermostimulated depolarizing currents and thermoelectret effect 2−47973
poly(1,4-phenylene ether), transitions and relax. of phenomena, 100-800K 2−83355
poly(1-vinylnaphthalene) and copolymers excimer formation, fluorescence obs. 2−54564
poly(2,6-diphenyl-p-phenylene-oxide), molecular motion study by meas. of Young's modulus and mechanical damping 2−74819
poly(2-vinylnaphthalene), excimer formation, fluorescence obs. 2−54564
poly(4-chlorostyrene,4-methylstyrene)copolymers dielectric properties 2−68462
poly(4-methylpentene-1), curved crystal formation 2−80529
poly(dimethyl siloxane), in high shear rate region, relation between mol. wt. and viscosity 2−83374
poly(ester acrylates), NMR study of mol. motion 2−83391
poly(ethyl methacrylate)/poly(n-butyl acrylate) 2−64490
poly(ethylene oxide), cryst. from soln., melting behaviour 2−83361
poly(ethylene oxide), crystn. of high mol. wt. fractions from dil. soln. in ethanol 2−64538
poly(ethylene terephthalate), growth rate of spherulites 2−64595
poly(ethylene terephthalate) light scattering study of spherulite evolution from rodlike nuclei in early stages of crystallization 2−64535
poly(ethylene terephthalate) superheating and reorganization on melting 2−71271
poly(ethyleneterephthalate) multiple endotherm melting behaviour due to recrystallization, relation to morphology 2−71291
poly(glycol methocrylate), photoelastic effect in molecular 3d networks, optical anisotropy, thermodynamic rigidity 2−44347
poly(hexamethylene sebacamide) (nylon 610), effects of melting on dielectric relaxation 2−44151
poly(methyl methacrylate), cross-linking effect on thermomech. and thermooptical behaviour 2−83390
poly(methyl methacrylate), effect of free radicals on u.v. absorpt. 2−84671
poly(methyl methacrylate) thermoelectrets, thermodepolarization currents 2−83348
poly(styrene co-vinylnaphthalene), sensitized triplet quencher phosphorescence, study of photoprotective efficiency 2−72581
poly(trans-2,5-dimethylpiperazine fumaramide) films, reverse osmosis props. 2−83786
poly(vinyl chloride), electron and γ-irrad. at 77K, e.s.r. 2−83360
poly(vinyl chloride)-rubber system, phys. props. 2−83393
poly(vinyl cinnamate), hydrodynamic, optical props. 2−83388
poly(vinylidene chloride), effect of heat treatment on morphology and structure powder 2−71293
poly 2,6-dimethylphenylene oxide, growth and unit cell dimensions of single crystals 2−60774
poly γ-benzyl L-glutamate, growth stages in epitaxial crystallisation 2−60605
poly N-vinylcarbazole, investigation of trap structure by thermally stimulated currents 2−54182
poly sodium acrylate, shear stress and normal stress meas. on moderately concentrated solutions under steady shear flow 2−60395
poly-4-methylpentone-1, irradiated, e.s.r. of radical pairs 2−75395
poly-4-vinylpyridine in solution, hydrodynamic and optical props. 2−60452
poly-γ-benzyl-L-glutamate, 220 MHz p.m.r. relaxation time at helix-coil transition 2−80112
poly-γ-benzyl-L-glutamate conc. solns., local viscosity meas. by rotational diffusion of diphenylanthracene 2−60451
poly-L-alanine, sp. ht., low temp., one-, two- and three dimens. models 2−47755
poly-L-alanine in α- and β-forms, determ. of dispersion curves using Wilson's GF-matrix method 2−64203
poly-L-proline I chain, normal modes and dispersion curves, conform. depend. 2−80113
poly-N-methyllaurolactam, fully methylated nylon 12, crystallinity 2−83846
poly-N-vinylcarbazole (acid-doped): o-dinitrobenzene charge transfer complex films, photoelectronic properties 2−78212
polyacetylene, INDO, MINDO/2 orbital calcs. of band structure and charge distrib. 2−44035
polyacrylamide, drag-reducing effect on gas-liquid slug flow 2−83424

Polymers continued
- polyacrylamide solutions, force obs. with Weissenberg rheogoniometer, effect of changes of surface tension and contact angle 2—64455
- polyacrylic acids, adsorption on nylon 66 fibres rel. to textile size applic. 2—60696
- polyacrylic acids, on nylon 66 powder rel. to textile size applic. 2—60695
- polyacrylonitrile, effect of heat treatment on morphology and structure of crystals powders and fibres 2—71293
- polyadenylic acids, influence of triplet energy trapping on decay kinetics of delayed fluorescence produced by triplet-triplet annihilation 2—51471
- polyamides, chain-folded lamellar crystals, structure analysis, X-ray diffraction study 2—47359
- polyamides, real stress diagram classification, uniaxial extension 2—56780
- polyazophenylenes, semiconducting, conductivity 2—44118
- polybutadiene, configurational fluctuations rel. to memory effects in proton spin-spin relaxation 2—46636
- cis-polybutadiene, cross-linked in swollen state, elastic and thermoelastic behavior 2—60835
- polybutadiene, extension and compression behaviour 2—43681
- polybutadiene, molec. structure study using ^{13}C n.m.r. 2—53091
- polybutadiene, molecular weight and long-chain branching determination 2—43024
- polybutadiene/polystyrene latex IPN's, synthesis and dynamic mech. props. 2—64490
- polybutadienes, narrow distribution, viscoelastic properties and capillary flow 2—60394
- polybutadienes, sequence structure studies by ^{13}C$-\{^{1}$H$\}$ Fourier transform n.m.r. 2—67529
- poly(n-butyl acrylate) lightly crosslinked network, dynamic mechanical behaviour in rubberlike region 2—71544
- poly(n-butyl methacrylate) lightly crosslinked network, dynamic mechanical behaviour in rubberlike region 2—71544
- poly-n-butylmethacrylate, effects of equilibrium vapour sorption on tensile creep 2—50758
- polycaprolactam, intermolecular reactions, effect of form of inelastic deformation 2—80119
- polycaprolactam, stressed, mechanism of submicrocrack generation 2—74858
- polycaprolactum polyethyleneimine graft copolymers, mech. props. as a function of av. mol. wt. 2—64799
- polycarbonate, cold extrusion and cold drawing, mechanical props. by tension and compression tests 2—80810
- polycarbonate, irrad., proton spin-lattice relax. times 2—84449
- polycarbonate, strain softening and yield processes, moire-grid anal. 2—84084
- polycarbonate, yield locus, characterization tests for photoelastoplastic material 2—43778
- polycarbonate films as dosimeter for 10-100 Mrad range 2—42700
- polycarbonate longitudinal crazing 2—53840
- trans-polychloroprene, cryst., mech. props., morphology influence 2—60860
- polychloroprene, gel fracture rate, crystallinity effects 2—47483
- polychloroprene-rubber, recrystalliz. and reorganization processes, calorimetric obs. 2—71289
- polydimethylsiloxanes, viscoelastic constants determ. using layered waveguide technique 2—64755
- polydimethylsiloxanes in n-heptane-tetralin mixtures, surface tension calcs. and expts. 2—74535
- polydisperse, undiluted, stress relaxation after steady-state shear flow 2—64482
- polydisperse methyl acrylate-methyl methacrylate copolymer latexes, turbidity spectrum, determ of size and refractive index of particles 2—43399
- polyelectrolyte solutions, Gibbs adsorption equation 2—83874
- polyenes and related molecules, origin of low-lying forbidden transition 2—50119
- polyester, glass fabric reinforced, fatigue crack damage, vibr. testing 2—60921
- polyester, glass fibre-reinforced, fracture energy determ. 2—50780
- polyester, glass- or C-fibre reinforced, work of fracture 2—74863
- polyester resin, steel wire reinforced, fracture toughness 2—47528
- polyester resins, unsaturated, crosslinked with styrene, structure, Raman spectroscopy 2—44482
- polyethene terephthalate, oriented, anisotropy of mechanical and dielectric relaxation 2—60856
- polyethlene insulators, treeing breakdown, voltage and temp. dependence obs. 2—72023
- polyethylene, ^{18}F adsorption on surface, time depend curve 2—83877
- polyethylene, ageing under natural atmos. condit. i.r. spectroscopy study 2—64800
- polyethylene, amorphous crosslinked, stress-dichroism studies 2—84466
- polyethylene, anomalous photo-induced current transients 2—54257
- polyethylene, bulk modulus and density in 30 kbar, glass transition temp. press. coeff. 2—83352
- polyethylene, combined tension-torsion creep testing 2—71619
- polyethylene, crack growth under tensile creep conditions 2—47548
- polyethylene, creep, stress level and temp. effect 2—47518
- polyethylene, crystallite size and lattice distortion, nitration effects 2—60612
- polyethylene, crystn. and elec. cond. 2—71290
- polyethylene, crystn. at high press., kinetic model 2—83358
- polyethylene, crysts., slip traces, dislocation motion 2—83847
- polyethylene, crytallization and melting under high pressure 2—50414
- polyethylene, degradation due to partial discharges, examination using electron paramagnetic resonance 2—74606
- polyethylene, direct obs. of screw dislocations 2—43640
- polyethylene, electric strength, for use in h.v. pulse generators 2—65055
- polyethylene, electron irrad., traps, thermally stimulated current obs. 2—83363
- polyethylene, electrostatic charging after contact with metals 2—72005
- polyethylene, film, I doped, elec. cond., form of current transients 2—64994

Polymers continued
- polyethylene, high density, cold extrusion and cold drawing, mechanical props. by tension and compression tests 2—80810
- polyethylene, high density, static and kinetic friction over clean surfaces, transfer and molecular structure 2—64738
- polyethylene, high pressure, molec. structure determination with gel permeation chromatography 2—67530
- polyethylene, high speed elongation, i.r. dichroism, meas. apparatus 2—83354
- polyethylene, INDO, MINDO/2 orbital calcs. of band structure and charge distrib. 2—44035
- polyethylene, injection moulded specimens, crystallite orientation determ. by X-ray diffraction 2—64797
- polyethylene, interatomic distances determination from radial distribution function 2—64605
- polyethylene, irrad., proton spin-lattice relax. times 2—84449
- polyethylene, laser-Raman spectrum of different samples, sensitivity to crystallinity and impurities 2—44397
- polyethylene, lattice vibration dispersion curves 2—71718
- polyethylene, linear, affine deformation during stretching and transformation to original state 2—64703
- polyethylene, localized and resonance modes below 700 cm^{-1}, due to kinks and folds, calc. 2—61153
- polyethylene, low mol. wt. crysts., interfacial free energy 2—60633
- polyethylene, low-density, determ. of diffusion coeffs. of O$_2$ by radiothermoluminescence method 2—84004
- polyethylene, melting behaviour of sample crystallized in pressure capillary viscometer 2—60546
- polyethylene, molten, flow through parallel slit, flow birefringence obs. 2—71142
- polyethylene, oriented, struct. effect of annealing under high press. 2—83395
- polyethylene, oriented samples assignment of laser-Raman spectrum for fundamental modes of vibration 2—70803
- polyethylene, positron annihilation 2—68265
- polyethylene, rigidity and limiting strength, comparative estimates 2—47475
- polyethylene, spherulitic, cryst., mech. props., morphology influence 2—60860
- polyethylene, stressed, mechanism of submicrocrack generation 2—74858
- polyethylene, sulpho-chlorinated, optical anisotropy of statistical segment 2—44346
- polyethylene, surface charge decay 2—51193
- polyethylene, terephthalate, morphology 2—60610
- polyethylene, X-ray diffraction relaxation 2—43674
- polyethylene crystallization at high temp. and pressure, birefringence obs. 2—47064
- polyethylene films formed by evaporation and deposition in vacuum, crystal morphology 2—50516
- polyethylene foil, degradations induced by ion bombardment and partial discharges 2—44148
- polyethylene glycol/water system, Mossbauer study of molecular motion at room temperature 2—72277
- polyethylene melt, low-density, branched rubber like liquid theory rel. to stress growth data for elongation 2—58871
- polyethylene melts, thermal motion obs. from solid specimen spectra 2—80536
- polyethylene melts, time dependent stress, review of viscoelastic theory 2—64708
- polyethylene oxide, data used to compute end interfacial free energy 2—71274
- polyethylene oxide, effect of addition to blood on flow 2—48850
- polyethylene oxide, mechanical damping index obs. with torsional braid analyser 2—71547
- polyethylene oxide fractions, crystallization isotherms 2—74601
- polyethylene oxide supermolecules, electron microscope meas. of size and growth in solution 2—64204
- polyethylene spherulites, origin of contrast effects in electron microscopy 2—60782
- polyethylene surface, anomalous low friction for steel- polymer friction by helium atom irradiation 2—56837
- polyethylene terephthalate, crystallinity effects on dielec. props. 2—61410
- polyethylene terephthalate, crystallization rate by depolarized light intensity method 2—56566
- polyethylene terephthalate, electret, characterization 2—65076
- polyethylene terephthalate, fiber texture sample crystallite orientation distribution, test of refinement procedure 2—80534
- polyethylene terephthalate, non-linear viscoelastic behaviour 2—56777
- polyethylene terephthalate, stressed, crack propag. in presence of org. liqs. 2—50781
- polyethylene terephthalate, structural characterization of mechanical properties 2—50721
- polyethylene terephthalate, study of spherulite growth during crystalliz. 2—43455
- polyethylene terephthalate film, stress relaxations, dielec. and dynamic mechanical obs. 2—56779
- polyethylene terephthalate films, mech. props., influence of liq. media 2—50750
- polyethylene terephthalate films, observations of optical irregularities 2—52452
- polyethylene thermoelectrets, heterocharge and depolarization current 2—72047
- polyethylene under static electric field, positron lifetime study of polarization 2—61409
- polyethylene with n-paraffin and nylon 6, true tensile stress-strain relations for plastic deformation 2—56783
- polyethylene-GaAs system, use in long-wave semicond. photography 2—70090
- polyethyleneoxalate, polyethylenesuccinate, intramolec. contributions to entropy and energy of fusion 2—46637
- polyethylenes, chlorinated, differential scanning calorimetry 2—50400
- polyethylenes, linear, melt blended with atactic polystyrenes, microstructure 2—67848
- polyethyleneterephthalate fibres, determ. of degree of crystallinity by X-ray methods 2—74607
- polyethyleneterphthalate, positron annihilation 2—68265

Polymers continued
polyethylmethacrylate, Brillouin scattering and hypersonic phonon waves 2−65284
polyethylmethacrylate, stimulated scattering, hypersonic vel. meas. 2−68669
polyfluoroalkoxyphosphazenes, dilute solution characterization 2−44483
polyfluoroethylene, filler content influence on phys. props. 2−47553
polyglycine, INDO, MINDO/2 orbital calcs. of band structure and charge distrib. 2−44035
polyimide, hydrostatic press. effect on mech. behaviour 2−83347
polyimide films, uniaxially drawn, orientation studied by IR spectroscopy and X-ray diffraction analysis 2−43677
polyimide moulding, dynamic modulus determ. from stress relax. data 2−43667
polyisobutene Mossbauer scattering study of molecular motion in 90-310k range 2−72277
polyisobutylene, deform., instability at shear strength limit 2−68085
polyisobutylene solns. obs. of spin-spin and spin-lattice n.m.r., relationship to viscosity 2−60513
polyisobutylenes in n-heptane-tetralin mixtures, surface tension calcs. and expts. 2−74535
polyisoprene, configurational fluctuations rel. to memory effects in proton spin-spin relaxation 2−46636
cis-polyisoprene, cryst., mech. props., morphology influence 2−60860
trans-1,4-polyisoprene, equilib. melting temp. of two crystalline modifications 2−71292
polyisoprene, extension and compression behaviour 2−43681
cis-1,4-polyisoprene, linear, nonlinear viscoelastic behaviour under constant strain rates 2−50734
polyisoprenes, narrow distribution, viscoelastic properties and capillary flow 2−60394
polyisoprenes, relaxation modulus, influence of entanglements 2−47484
polymer, ionic cond. temp. depend., struct. factors influence 2−72019
polymer films amorphous and crystalline, electrical conductivity in strong electric fields 2−84340
polymer-binary solvent system, occurrence and character of inversion in preferential sorption 2−75375
polymer-binary solvent system, occurrence of maxima and minima in curve of total sorption 2−75376
polymerized solid, motion of polymer molecules 2−70800
polymethacrylate, Brillouin scattering and hypersonic phonon waves 2−65284
polymethine, saturably absorbing dye solns., photostability 2−61809
polymethine dyes, stimulated fluorescence depend. on exciting illumination 2−77443
polymethyl methacrylate, epoxy formulations, u.s. dispersion, acoustic characterization 2−80905
polymethyl methacrylate, fracture, relaxation effects 2−80821
polymethyl methacrylate, internal flaws, crack nuclei density 2−64537
polymethyl methacrylate, longitudinal crazing 2−53840
polymethyl methacrylate, oriented, relax. rate depend. on struct. transform. 2−47485
polymethyl methacrylate in soln. containing solid phase, mech. destruction 2−47560
polymethylacrylate filters for visivle and i.r. region methods of production and properties 2−55745
polymethylmetacrylate, volumetrical damage due to laser 2−76541
polymethylmethacrylate, dilatational response 2−64707
polymethylmethacrylate, electrostatic charging after contact with metals 2−72005
polymethylmethacrylate, plastically deformed, birefringence 2−51301
polymethylmethacrylate, positron annihilation 2−68265
polymethylmethacrylate, scintillation counter 2−59617
polymethylmethacrylate, stimulated scattering, hypersonic vel. meas. 2−68669
polymethylmethacrylate, temp. dependence of u.s. absorption in conc. solns. in 9 to 900 MHz range 2−60472
polymethylmethacrylate, tensile creep behaviour and fracture mechanics, liquid environment 2−53819
polymethylmethacrylate, thermoelectret props. 2−75156
polymethylmethacrylate insulators, treeing breakdown, voltage and temp. dependence obs. 2−72023
polymethylmethacrylates, intramolecular mobility in solutions, solvent effects 2−43337
polymethylphenylsiloxanes, internal stresses 2−71562
polymethylsiloxanes, internal stresses 2−71562
polyolefins, variation in sound velocity rel. to deformation 2−80750
polyoxymethylene, dielec. absorption, analysis of anisotropy due to defects 2−61417
polyoxymethylene, temperature dependence of overgrowth thickens on NaCl 2−43485
polyoxymethylene dioxide thin films, structure studies using small angle polarized light scattering 2−84526
polypentene, struct. characteriz., dielec. relax. 2−60613
polypeptides, α-helical, in soln., oriented circular dichroism spectrum 2−80117
polypeptides and polymero, piezoelectric properties 2−61436
polyphenylacetylene, electrical conductivity and ESR absorption 2−51127
polyphenylene, fluorescence spectra, energy transfer mechanism 2−71209
polyphenylene oxide, irradiation resist., uses in reactor expts. 2−79839
polyphenylsiloxane, internal stresses 2−71562
polypropionic acid solutions, absorption spectra, energy transfer mechanism 2−71209
polypropylene, crystallinity effects on dielec. props. 2−61410
polypropylene, crystn. on solid surfaces, electron-microscopic study 2−83392
polypropylene, drawn and annealed, determ. of crystallite size from breadth of equatorial X-ray reflections 2−71288
polypropylene, effects of cooling rate from melt on struct., strength and fracture 2−56908

Polymers continued
polypropylene, effects of pre-melting conditions on isothermal crystallization 2−47066
polypropylene, fatigue crack propag. mechamism comparison with PVC 2−71601
polypropylene, hydrostatically extruded, tensile and compressive yield strengths 2−43709
polypropylene, irradiated formation of γ-form crystals from melt 2−60614
polypropylene, large- and small-spherulite, determ. of diffusion coeffs. of O_2 by radiothermoluminescence method 2−84004
polypropylene, quenched and annealed samples, wide-angle X-ray scattering in neck region 2−71572
polypropylene, stressed, mechanism of submicrocrack generation 2−74858
polypropylene, surface, anomalous low friction for steel-polymer friction by helium atom irradiation 2−56837
polypropylene, surface changes during photooxidation, i.r. spectroscopic and electron microscopic studies 2−51472
polypropylene, T-die film, mechanical props. and mol. orientation 2−47537
polypropylene, transcrystalline growth at an internal surface 2−74608
polypropylene melt, end corrections in capillary flow with positive exit pressure 2−64408
polypropylene melt, mol. wt. dependence of capillary flow props. 2−46885
polypropylene sandwich mouldings, deflection during bending, stress function solns. 2−43663
polypropylene thermoelectrets, heterocharge and depolarization current 2−72047
polysaccharides, configurational statistics 2−70804
polystyrene, absorpt. spectra of O_2, contact charge transfer complexing 2−72580
polystyrene, ang. distrib. of scattered electrons, elec. field effect 2−47068
polystyrene, atactic, morphology 2−60610
polystyrene, craze yielding and stress-strain characts. of crazes 2−64736
polystyrene, crazing in sample containing two rubber balls, model for ABS plastics 2−60909
polystyrene, diffusion in ethyl acetate ethyl alcohol mixtures 2−60458
polystyrene, effect of solvents on cryogenic dynamic mechanical properties 2−74820
polystyrene, example of three-dimensional damped Debye lattice 2−60104
polystyrene, excimer formation, fluorescence obs. 2−54564
polystyrene, isotactic, crystallization from solution , i.r. spectra 2−43456
polystyrene, isotactic, melting behaviour 2−47034
polystyrene, low-angle X-ray scattering from crazes and fracture surfaces 2−74855
polystyrene, mobility study of solvent mols. by dielec. relax. 2−83387
polystyrene, polymerization, terminal group study 2−51444
polystyrene, positron annihilation 2−68265
polystyrene, sheared, flow in capillaries, concept of molecular migration 2−50293
polystyrene, structure in glassy state determ. by fluorescence depolarization 2−60615
polystyrene, temp. dependence of u.s. absorption in conc. solns. in 9 to 900 MHz range 2−60472
polystyrene, transport properties from 1°K to 300°K 2−71732
polystyrene films, passage of transient currents along surface 2−72001
polystyrene in alcohol suspensions, ultrasonic relaxation 2−53462
polystyrene in cyclohexane soln., conc. fluctuation dynamics near critical pt. 2−46996
polystyrene in N,N-dimethylformamide, intrinsic viscosity-molecular weight relationship 2−83359
isotactic polystyrene in toluene temperature dependence of confirmation 2−74522
polystyrene latex, freeze-etched, electron microscope study of particle size 2−60522
polystyrene latexes, multiple scattering of light, determ. of coeffs. of scattering and absorption 2−43400
polystyrene lattices, surface conductance, comparison of theory and expt. 2−60521
polystyrene melts, time dependent stress, review of viscoelastic theory 2−64708
polystyrene polyvinyl methyl ether mixtures, thermally induced phase separation 2−61041
polystyrene slabs, finite, electron depth-dose distrib. meas. 2−61130
polystyrene soln., neutron small angle scatt., obs. 2−50341
polystyrene solns., u.s. absorpt., relax. freqs. 2−80114
polystyrene solution, viscoelastic constants determ. using layered waveguide technique 2−64755
polystyrene solution and latex, nonlinear viscoelasticity 2−83368
polystyrene solutions, atactic and isotactic, configurational and conformational effects on magnetic circular dichroism 2−43366
polystyrene sphere solution, light scatt. 2−73541
polystyrene spheres suspended in water, Rayleigh scatt. 2−50381
polystyrene structure changes by u.v. rad., reln. to polydispersity of polymer 2−64652
polystyrene with paraterphenyl, luminescent spectra, energy transfer of electronic excitation 2−71216
polystyrene-anisole solution, temp. depend. of spin-lattice relaxation obs., study of molecular mobility 2−60514
polystyrene-poly(2,6-dimethylphenylene oxide) freeze dried blends, viscoelastic response, rheological compatibility 2−83353
polystyrenes, adsorption on SiO_2, competitive effects 2−60684
polystyrenes, atactic, melt blended with linear polyethylenes, microstructure 2−67848
polystyrenes, star-shaped, concentrated solutions, viscoelastic props. 2−83369
polystyryl radicals, chain length dependence of coupling reactions 2−72556

Polymers continued
polysulfones of monolefins, high resolution solution spectra 2−43390
polytetrafluorethylene, low temp. lattice bands in far i.r. 2−81353
polytetrafluorethylene, shock compression, acoustic velocity behind stress wave front 2−77781
polytetrafluoroethylene, cryst. struct. at high press., transition at 4.5kbar 2−83849
polytetrafluoroethylene, cyclic loading effect on morphology 2−60870
polytetrafluoroethylene, elec. cond., pulsed X-ray irrad. induced 2−65091
polytetrafluoroethylene, emulsion-grade, studies of morphology of ribbons and rods 2−71295
polytetrafluoroethylene, irradiated and sintered, mol. chain entanglement, n.m.r. obs. 2−65352
polytetrafluoroethylene, Mossbauer scattering study of molecular motion 2−72277
polythene, elec. cond., pulsed X-ray irrad. induced 2−65091
polythene, irreversible local breakdown and electric stress, reln. 2−68466
polythene catheters, heparinization method 2−69291
polyurethane, mechanically induced bond rupture, e.p.r. 2−43711
polyurethane, porous, shock response, Hugoniot elastic limits, model 2−61024
polyurethane, rhodamine B doped, film ring laser, light amplification and coupling 2−42055
polyurethane block, meas. of stress and birefringence relaxation 2−74850
polyurethane expanded foam, mechanical and acoustic properties 2−69727
polyurethane film forming materials, relationship between struct. and props. 2−83385
polyurethane foam, highly absorbing sample, measurements in reverberation room 2−63114
polyurethanes, influence of urethane groups on thermodynamic, kinetic props. 2−83389
polyurethanes, ir spectra, OH and NH absorption bands 2−53092
polyvinyl alcohol, configuration of polymer chains determ. by p.m.r. 2−60105
polyvinyl alcohol-water mixtures, conductance meas., internal viscosity estimation 2−50345
polyvinyl butyryl, Ag conc. under variable exposure, rel. to optical density 2−52500
polyvinyl chloride, electrical response to i.r., preparation and use as sensor 2−47990
polyvinyl chloride, moisture content detn., n.m.r. obs. 2−48303
polyvinyl chloride, processing effect on morphology for plasticised and unplasticised 2−57003
polyvinyl chloride, wide mol. wt. range, struct. formation, conformational comp. 2−83386
polyvinyl chloride films, pulsed photoconductivity, obs. of transient photocurrents with oscillations 2−72074
polyvinyl fluoride, thermally stimulated elec. conductivity and thermoelectric effect 2−64995
polyvinylalcohol films, irradiated by ^{60}Co γ-rays, trapped radicals in u.v. and visible absorption spectra 2−57437
polyvinylcarbazole, carrier drift mobility meas. 2−47905
polyvinylcarbazole, dye sensitized, electrophotographic response 2−59325
polyvinylcarbazole, dye sensitized film, photoinduced voltage decay 2−81165
polyvinylcarbazole, viscosity dependence on shear rate, rotating viscometer meas. 2−60446
polyvinylcarbazole-Se multi-layer photoreceptor for electrophotography 2−59293
polyvinylchloride, drawn samples, molec. orientation determ. by broad line p.m.r. 2−51417
polyvinylchloride, positron annihilation 2−68265
polyvinylchloride-nitrile butadiene rubber system, dielectric props. 2−75144
polyvinylidene fluoride electret. depolarization current and surface potential decay 2−51208
polyvinylidene fluoride film, far i.r. spectral investigations of structural conformations rel. to piezoelectric props. 2−61438
polyvinyltoluene, plastic scintillation counters, effects of degradation by u.v. light 2−76731
polyvinyltriorganosilane solutions, relation between intrinsic viscosity and molecular weight studied by light scattering and viscometry 2−46997
polywater, existence and structure 2−53386
pressure effects on elastic modulus, yield strength and deformation 2−68094
PTFE, static and kinetic friction over clean surfaces, transfer and molecular structure 2−64738
PTFE, transfer in sliding. occurrence of thin film 2−53820
PVC, charged with carbon black, negative differential resist. 2−81064
PVC filters, for visible and i.r. region methods of production and properties 2−55745
PVC-filler composites, influence of fillers on dynamic mechanical props. 2−64792
PVP aqueous soln., freezing using temp. gradient microscope stage 2−74585
random flight, confined in cubical box, spatial average density distrib. 2−60101
randomly coiling polypeptide chains, average dipole moments for hard-sphere models 2−64201
randomly crosslinked, with Schulz-Zimm primary distributions, gel permeation chromatography and intrinsic viscosity analysis 2−61818
relaxation mechanism of cooperative binding, Ising model 2−46635
relaxation stresses, rigid dynamometer for obs. 2−43757
replica modulation by surface electrical and magnetic fields 2−64539
rheology, conference, Nagoya, Japan, Oct. (1971) 2−82315
rheoviscometer study of polymer solutions rel. to rheological properties and changes during two-phase separation 2−60392
ring electrets, electric field, state selection of masers 2−78955

Polymers continued
rodlike, translational diffusion coeff., applic. of modified Oseen tensor 2−64199
rubber like materials, thermomech. behaviour, Valanis- Landel strain energy function 2−82312
rubbers stress and temp. effects on molecular ordering 2−60873
Saran, effect of heat treatment on morphology and structure of powder 2−71293
SCF theory, polymer excluded volume problem 2−56269
semiconducting, Co chelate, of dihydroxyquinones, mag. moment and elec. resist. meas. 2−80815
Separan AP-30 solutions, laminar and turbulent entry flow 2−46884
seroalbumin polysaccharide complexes, u.s. spectrometric study of formation 2−73171
shavings, apparatus for surface area measurement 2−50471
silicone, extension and compression behaviour 2−43681
solid, jump motion of chain segments, neutron spectroscopy at high resolution 2−77607
solid, relaxation phenomena under high pressure 2−74604
solution, having draining effect, normal stress effect 2−71164
solution, light scatt. wavelength depend. 2−64447
in solution, refr. index increments, conc. depend. 2−60520
solution, simultaneous obs. of viscosity and surface tension 2−64452
solution, thermodynamic prop. depend. on mol. props. 2−60438
solution thermodynamics, free vol. role 2−60436
solutions, anomalous readings in Pitot tubes 2−53360
solutions, atomization by grooved-core nozzle, mean drop size 2−50377
solutions, dependence of threshold of luminescence generation on pumping polarization 2−53450
solutions, dil., excluded vol. effects and binary cluster integrals 2−60440
solutions, dil., thermodynamic interactions, virial coeffs. 2−60437
solutions, dilute, laser velocimeter obs. of Reynolds stress and turbulence 2−71128
solutions, dilute, mutual diffusivity of liq. solutes, conc. depend. 2−53411
solutions, free energy constitutive equation from dumbbell model 2−67811
solutions, interaction thermodynamics, symposium, Prague, Czechoslovakia (Aug-Sep 1971) 2−60435
solutions, laminar and turbulent entry flow 2−46884
solutions, relax. processes, from meas. of u.s. abs. 2−46954
solutions, suitability of eqns. for viscosity correlation over entire concentration range 2−60444
solutions, surface tension of three-component mixtures 2−74535
solutions, thermodynamics as functions of pressure and temp. 2−64446
solutions, ultrasound attenuation, frequency behaviour 2−56503
solutions and melts, rheological equations 2−63076
sorption systems, mol. clustering and segregation 2−60439
spatial gradients rel. to struct., props. and uses 2−61026
specific heat and enthalpy, automatic adiabatic calorimeter for meas. in temp. range −180 to +270°C 2−63165
spiral, interaction between recurring links between neighbouring loops in vibrational problem 2−77160
stability criteria for study of thermoresistant structural adhesives 2−57006
structural characterization using laser-excited Raman spectroscopy 2−83343
styrene, thermomechanical props. 2−50751
styrene-butadiene block copolymers, mechanically induced bond rupture, e.p.r. 2−43711
styrene-butadiene-styrene block copolymer cast from organic solvents, time-temperature superposition 2−74829
styrene-diene-styrene block copolymers, mechanical properties 2−71584
submicroscopic crack formation, under load, X-ray scatt. obs. 2−68108
supermolecular struct. form in thin layers 2−60637
surface wave propagation in monolayers of soluble polymers using Moire fringes 2−73445
surfaces, humidity effect 2−57223
Teflon, cementing at low temps. 2−85168
Teflon, electron irrad., traps, thermally stimulated current obs. 2−83363
teflon, thermal conductivity, 0.17 to 4.0 K, dislocation scattering 2−71762
teflon, working medium, pulsed ablation accelerator plasma, electron density measurement 2−80297
temperature-time superposition principle applic. 2−47063
tension-torsion creep testing, apparatus and results 2−71619
testing machine for simultaneous study of structure and mechanical properties 2−53857
thermal degradation, gel permeation chromatography, monodisperse polystyrene 2−78186
thin films and sheeting, dynamic puncture resist. determ. 2−60920
trapping phenomena and carrier injection in m.i.s. structures 2−71991
trinitrofluorenone-poly(N-vinylcarbazole), photogeneration efficiency, field depend. 2−65399
trisiloxane film, electron beam polymerized, physical and electrical props. 2−47909
turbulent friction, effect of addition to water in free flow in tubes 2−53361
two-phase viscoelastic composite, improved bounds for real and imaginary parts of complex moduli 2−56776
uniaxially and biaxially drawn, directional props. of compliance consts. 2−77628
u.s. absorption in conc. solns., 9-900 MHz, 20°C effect of conc. 2−46954
vinyl chloride-acetate copolymer, wear resist. and frictional props. 2−47561
vinylnaphthalene polymers and copolymers with styrene and methyl methacrylate, triplet depletion 2−68805
vinylparaterphenyl with styrene, luminescent spectra, energy transfer of electronic excitation 2−71216
1-vinylpyrene and poly(1-vinylpyrene), photophys. processes, spectroscopic behaviour 2−65400
viscoelasticity, non elastic, review of recent expt. aspects 2−83364

Polymers continued
- viscoelasticity of undiluted linear narrow molecular weight distrib. samples in terminal zone 2−83336
- $(C_3O_2)n$ polymer production in Martian atmosphere and colouring of surface, laboratory studies 2−78542
- Hg contact, electric field effect 2−57236
- SF_4, oligomers in solid state 2−44381

Polymorphism
- *see also Crystal structure*
- — 2−67966
- alkali feldspars, and Na-K mixing 2−53675
- beryllium oxyacetate - 196°C to 286.7°C, pulsed n.m.r. investigation, study of molecular dynamics 2−57399
- chiral cpds., effect on external vibrs. 2−44396
- elements, atomic coordination valency 2−80591
- ionic substances, predictability, empirical rules 2−68191
- lanthanide niobates, Ln_3NbO_7 type 2−47346
- liquid crystal, smectic, D and E modifications, X-ray diffr. obs. 2−50327
- methylchloromethane compounds, crystal and mol. structure of methyl chloroform at −60° and −145°C 2−53685
- molecular crystal, transition, orientation of lattices and interfaces 2−84109
- phase boundary model, mol. mechanism 2−47679
- trans-1,4-polyisoprene, equilib. melting temp. of two crystalline modifications 2−71292
- pyroxene, lunar and terrestrial minerals, transformation on cooling 2−62689
- rare earth-zirconium alloys, form. of metastable low temp. allotropic solid solns. 2−47646
- rare-earth elements, transformations, related forms of coordination polyhedra from icosahedron 2−84094
- Salmonella flagella, phenomenological theory 2−53088
- tristearin, positron annihilation study 2−60773
- $AgNO_3$, cryst. growth morphology at polymorphic transforms. 2−50945
- Ag_2Se, X-ray obs. 2−64809
- α-Al_2O_3, transformation under electron irradiation, thermodifferential analysis 2−47681
- As, high press. polymorphic transform., and supercond. phase 2−44058
- Bi, high press. polymorphic transform., and supercond. phase 2−44058
- Bi polymorph III modification at 42 kbar and 20°C, volume change 2−74925
- C, chaoite formation, and new form obs. 2−56650
- C, laser beam irrad., chaoite formation in craters 2−56574
- CdI, polytypes, phase transform. 250−280°C 2−77745
- CdI_2, growth characts., stacking faults distrib. and stability, polytypism 2−74781
- CdS, kinetics of high pressure polymorphic transitions from wurtzite to rock salt structure 2−61031
- CdS, transformation under electron irradiation, thermodifferential analysis 2−47681
- CdS single crystals, polytypic growth, electron microscope study 2−60769
- CdSe, kinetics of high pressure transitions from wurtzite to rock salt structure 2−61031
- CdTe, kinetics of high pressure polymorphic transitions from zinc blende to rock salt structure 2−61031
- $CsLn(MoO_4)_2$, synthesis, crystalliz. and polymorph. transformation 2−71392
- Cu, high purity, polygonization on recrystn. 2−68136
- Fe, high purity, polygonization on recrystn. 2−68136
- $FeSi_2$, rel. to high temp. phase stability 2−47685
- Ge, amorphous and crystalline, electronic struct. calc. 2−68431
- Ge III, Raman scattering from phonons 2−72372
- GeO_2, polymorph crystal growth, solution top-seeding 2−50583
- HgS single crystals, polytypic growth, electron microscope study 2−60769
- $K_4Fe(CN)_6.3H_2O$, ferroelectric, proton mag. resonance obs. 2−74655
- KNO_3 cryst. growth morphology at polymorphic transforms. 2−50945
- Mg_2SiO_4, computer simulated crystal structures, observed and hypothetical 2−47335
- NH_4Br, allotropic transform. kinetics 2−54008
- NH_4NO_3 cryst. growth morphology at polymorphic transforms. 2−50945
- Nd_2NiO_4, monoclinic to tetragonal transform. 2−77750
- ReO_2, transition, electron microscope obs. 2−47695
- Sb, high press. polymorphic transform., and supercond. phase 2−44058
- Sb_2O_3, valentinite and senarmontite polymorphs, crystalliz. under hydrothermal cond. 2−74683
- Si III, Raman scattering from phonons 2−72372
- SiC, α-β polymorphic transformation 2−74941
- TaS_2, 1S and 2S polytypes, cryst. growth and props. 2−47226
- $TeVO_4$, polymorphic transform. at 650°C 2−74748
- TlI, influence on photoconductivity 2−75174
- $VOPO_4$, β allotropic form obs. 2−50627
- Zn-In-S system polytypes, vapour growth 2−50579
- $Zn_xCd_{1-x}Se$ solid solution, rel. to Raman scatt. obs. of phonons 2−64837
- ZnS, hollow crystals, growth by pulling sealed tube method, X-ray obs. of polytypical struct. 2−43527
- ZnS, new polytypes of 28L family 2−68009
- ZnS, polytypes, high-order, identification and reliability of results 2−56670
- ZnS, polytypic ordering, X-ray obs. 2−47213
- ZnS, Raman scatt. obs. 2−61084
- ZnS, vapour phase growth, polytype form mechanisms 2−47227
- ZnS single crystals, polytypic growth, electron microscope study 2−60769

Polynomials *see Algebra; Functions*

Polytypism *see Polymorphism*

Pomeranchuk poles and trajectories
- — 2−59480
- amplitudes, explicit, compatible with t channel unitarity 2−45917

Pomeranchuk poles and trajectories continued
- Compton amplitudes, fixed poles and Pomeranchukon coupling 2−49537
- coupling in helicity flip transitions, spin structure at high-energy multiple scattering 2−73791
- diffraction dissociation, inclusive bootstrap constraints 2−59475
- dual absorptive model, helicity conserving and nonconserving pomeron exchange amplitudes 2−59467
- dual pion model, physical states and pomeron poles 2−70227
- elastic diffraction peaks, 'Pomeranchuk' theorem 2−66984
- exchange degeneracy and duality in generalized interference model 2−73792
- fixed pomeron in nonshrinking πp diffraction peak 2−45923
- fixed-pole Pomeron shielding-cut mechanism, diffr. scatt. asymptotic behaviour 2−52588
- fixed-pole Pomeron with shielding branch-cuts 2−59489
- Gribov's triple-Pomeranchukon vertex and inclusive reactions 2−66969
- helicity conservation in vector meson interactions, s-channel Pomeron coupling 2−70142
- helicity conservation in vector meson interactions, s-channel, Pomeron coupling 2−70141
- hypercharge-exchange reactions, octet Pomeranchukon component and absorption 2−79547
- modification due to piecewise-analytic scattering amplitude of indefinite-metric quantum field theory 2−63457
- moving pomeron trajectory in Regge eikonal model 2−73793
- multi-pomeron selection rules 2−66983
- multiperipheral dynamics, diffractive dissociation 2−73790
- multiperipheral model used to study effect of Pomeron exchange 2−63540
- nonlinearity of trajectory, relation to intercept below 1 2−79550
- photoproduction of vector mesons in Pomeron exchange reaction, s-channel helicity conservation 2−76694
- Pomeranchon Regge trajectory, decoupling 2−82726
- Pomeranchukon-pole couplings, general consequences of Regge theory 2−66985
- Pomeron exchange, simple description for high energy elastic scatt. 2−59494
- pomeron exchange in πN scattering, s-channel helicity conservation studied in ABFST multiperipheral model 2−42398
- pomeron exchange in spin-o and spin-s transitions, inclusion of s-channel vertices 2−59545
- pomeron term in $I_t=0$ πN amplitude at 6 GeV/c, helicity-nonflip description 2−70240
- Pomeron two component theory validity 2−52585
- residue at $t=0$, calcs. using intermediate-energy bootstrap dynamics based on average nonlinear duality 2−66986
- scalar boson scattering, complex Pomeranchukon singularities and asymptotic behaviour 2−49539
- singularity diffractive-multiperipheral model, relation to inclusive expts. 2−45907
- triple Pomeran vertex, eigenvalue integral equation 2−82724
- triple pomeranchukon vertex, consequence of vanishing at zero mass 2−59495
- triple-pomeron vertex estimation of associated parameter η_p assuming finite-energy sum rule for pomeron-proton scattering 2−42364
- two-Pomeranchukon cut, relation to diffraction inclusive processes 2−66987
- Veneziano model, dual Pomeron compatibility with unitarity and absence of ghosts 2−59491
- $ep \to ep +$ anything, t and q^2 dependence, triple-Regge formalism application 2−73757
- $K^-p \to K^-\pi^-\Delta^{++}(1236)$, 8.25 GeV/c, CLA model, Pomeron and K^* exchange 2−55847
- K^+p, Pomeron exchange amplitude and existence of Z^* 2−70212
- np charge- exchange reaction, model for pion-Pomeranchon Regge cut 2−52640
- pp elastic scatt. 20 and 200 GeV, slope break and Pomeron periphery 2−79614
- pp elastic slope parameter break, quantitative explanation given by Pomeron periphery 2−59570
- $p\pi^- \to pX^-$, 25 and 40 GeV/c, scaling and estimate of triple-Pomeranchukon coupling 2−76715
- $p\pi^- \to pX^-$, 25 and 40 GeV/c, scaling and estimate of triple- Pomeranchukan coupling 2−73846
- πN charge exchange polarization and violation of Pomeranchuk theorem 2−45976
- πN scatt., 6 GeV/c, Pomeron t-depend. predicted 2−45974
- πN scatt., Pomeron-exchange amplitude and cross sections due to resons. 2−52619
- πN scattering, multiple scattering model and slope of Pomeranchuk trajectory 2−42396
- $\pi^\pm p$, elastic scatt., Pomeron amplitudes 2−59540
- $\rho\rho P$ triple-Regge vertex calc. from two-body scattering data assuming duality and f-coupled Pomeron 2−55842

Pomeranchuk rule *see Elementary particles/scattering*

Population inversion *see Lasers; Masers; Optical pumping*

Porosity *see Porous materials*

Porous materials
- *see also Permeability, mechanical; Surface measurement*
- acoustical wave propagation, theory 2−55522
- adsorption, mech. effects, field theory 2−60670
- adsorption and desorption of N_2 gas at liq. N_2 temps. 2−50541
- alluvial soils, simulation mathematical models for water tables 2−84714
- box, convective flow when saturated with fluid 2−56308
- bronze powder, spherical particles, porosity rel. to sintering kinetics determ. 2−43890
- capillary, phase transf. of vapour, study by microwave abs. 2−56543
- cavity formation and damage during breakdown of ionic crystals 2−72022
- cellulose acetate membrane porosity rel. to intrusion cell formation 2−53420
- ceramic, polymer impregnated, strength rel. to temp. 2−43899
- ceramic, polymer-reinforced, strengthening 2−47521
- ceramic, transparent, elec. and optical props., grain size and porosity effects 2−57244

Porous materials continued
ceramic nuclear materials, application of linear analysis to study of porosity using Cahn-Fullman relation 2−74147
Coconino sandstone, fracture under confining pressure, effects of pore-fluid chemistry, temperature 2−68858
composite porous fibre material, strength rel. to porosity 2−43707
Cu, elimination of pores by hydrostatic pressures and density increase at 20 kbar 2−71626
diffusion of gas into material and viscous loss 2−80394
drying with internal heat generation by microwave 2−45573
elastic wave velocities, press. depend. 2−54635
ferrite memory cores, fracture stress, porosity depend. 2−84431
filtering fluid in porous medium, equations of behaviour, using thermodynamics principles 2−50286
filtration, models 2−74499
finite capillary body of arbitrary geometry, temperature and moisture distributions 2−66649
fluid saturated, single constitutive theory 2−68179
fluid-filled, energy and mass transfer, non-equilib. thermodynamics 2−50137
fluidised beds, liquid solid, local porosity fluctuations, study by elec. conductance meas. 2−77178
fuel cell electrodes, wetproofed, electrolyte stabilization 2−45657
glass, counterdiffusion of adsorbed hydrocarbons 2−60685
glass, freezing point lowering of water 2−80880
glass filters, separation of solid and liquid components of a mixture 2−80786
glass plastics, porosity influence on tensile strength 2−47522
graphite, artificial, anisotropic and isotropic, struct. distrib. 2−53972
graphite, effect on thermodynamic props. and kinetic parameters during evaporation 2−56545
graphite, high temp. thermal cond. meas. 2−54074
graphite, isotropic, Young's modulus porosity depend. up to 1800°C 2−56772
graphite, nuclear, from coke mixtures, pore size, neutron irrad. 2−59841
graphite, nuclear, high fluence neutron irrad. behaviour, two-phase model 2−56048
graphite, POCO grade HPD-1, high temperature creep, comparison of pore size with polycrystalline graphites 2−77625
graphite, pore network effects on neutron irrad. behaviour at high temps. 2−56679
graphite, thermal and elec. cond., elastic consts., porosity effects 2−50926
graphite from isotruxene carbons, porosity 2−61023
hydraulic conductivity, pore struct. modelling 2−67765
images of pores, collection of secondary electrons 2−80606
indentation of a consolidating half-space 2−78236
infinite flat plate, unsteady flow under time-dependent suction 2−50159
isotropic homogeneous, reciprocity theorem in quasistationary case 2−71663
layers, air-flow resistance meas. 2−56405
liquid flow through, soil physics, theoretical mechanics 2−77383
marine sediments, electrical resistivity meas. system for porosity determination 2−75481
metal, ave. dimens. of pores 2−84147
moisture transfer in porous elastic solids, stress development 2−46889
mullite, press.-sintered, porosity depend. of mech. props. 2−50722
mullite, Young's modulus rel. to porosity 2−43906
non-isomeric pores and gas filled cavities, coagulation 2−53976
packed beds, non-uniform porosity causing flow maldistribution 2−46665
plane strain consolidation in saturated clays, finite element method 2−76314
plasticity and deformation theories 2−52189
polyurethane, shock response, Hugoniot elastic limits, model 2−61024
pore analysis, method for direct obs. 2−77743
pore size and shape distrib. from porosimetric hysteresis curves 2−43882
pore structure analysis, t-method, applic. to circularly cylindrical pores 2−53975
pore structure analysis, t-method, applic. to slit- shaped pores 2−50925
porosity meas. by γ-ray absorpt., optimum conditions calcs. 2−68180
rigid spherically shaped particles, random packing density 2−80791
rocks, freeze-thawing of water in pores 2−75446
rocks, static uniaxial deformation to 30 kb 2−62013
sandy pay zones, pore space structure changes under pressure 2−53799
saturated, elastic wave absorption and velocity calc. using Frenkel-Biot theory 2−82343
scanning electron microscope applications 2−56956
siliconized coating on steel, porosity rel. to holding time and C content 2−47635
soil, electro osmosis, filtration 2−83783
sorption isotherms shapes and kinetics 2−47140
sound absorbers, quasihomogeneous absorber theory rel. to Rayleigh theory 2−55528
steel, sintered, mechanical behaviour, model to explain behaviour of elastic moduli 2−84128
structure, infiltration of epoxy mixture 2−80819
terrestrial and lunar rocks, simultaneous meas. of u.s. vel. and compression 2−61982
thermodynamic model for materials with vacuous pores, sound press. and vel. 2−50924
volume diffusion controlled pore shrinkage during final stage sintering 2−50854
wet, near f.p., transient simultaneous measuring method for thermal prop. determ. 2−74989
zeolite, with ultrafine channels, filling with liquid Hg and Ga 2−84153
Al, high purity, porosity formation 2−62896
Al_2O_3, polycrystalline, compressive creep 2−47513
Al_2O_3, porous compact, grain growth 2−43905
γ-Al_2O_3, specific surface area meas. 2−64548

Porous materials continued
Al_2O_3 bicrysts., porosity distrib. and pore growth on grain boundaries 2−60991
C-C composites, porsity and mech. props, nondestructive testing 2−61016
C, glassy, vol. fraction and pore size, X-ray small-angle scatt. obs. 2−53530
C, lampblack, pore spectrum rel. to graphitization obs. 2−56995
C, multiple X-ray small-angle scatt. 2−53978
C composite, chem vap. deposited felts, compressed, porosity effects on mech. props. 2−61018
C fibre, microporosity 2−53952
C fibrous structures, pyrolytic C infiltration 2−53957
C products, graphitization effects on neutron irrad. induced dimensional changes 2−56996
Ca_3SiO_5, hydrated, pore structure, temp. effects 2−71664
Cd, with Sb or Bi impurity, pore formation on annealing 2−71665
Co, dry wear behaviour, rubbed against mild steel 2−60911
$CoAl_2O_4$, porosity effect on elastic moduli 2−50729
CoO-MgO solid solns., porosity effect on elastic moduli 2−50729
Cu, internal porosity removal on sintering, effects of hydrostatic pressure 2−68130
Cu, shock response, Hugoniot elastic limits, model 2−61024
Fe, shock response, Hugoniot elastic limits, model 2−61024
Fe green bodies, porous and sintered parts, polished metallographic specimen production 2−60933
Fe_2O_3, density changes and pore distribution during heat treatment 2−68140
KCl film, energy distrib. of transmitted secondary electrons 2−81190
MgF_2, hot pressed, porosity effects on temp. depend. of elec. cond. 2−47898
NaCl, dynamic compression porosity effect 2−53800
NaCl, explosion of spherical charge, shock wave parameters 2−58936
Ni-Cr-Mo alloy, physicomechanical, hydraulic and corrosion props. 2−53977
Ni-Fe, powder compact, struct. charact., pore structure 2−56946
Ni-Mo alloy, physicomechanical, hydraulic and corrosion props. 2−53977
Ni, creep kinetics, in acid and neutral media 2−43704
Ni, powder compact, struct. charact., pore structure 2−56946
Ni, transport props. depend. on porosity 2−77740
Ni cermet, highly porous, gas permeability 2−56965
Ni film, magnetostriction, field depend. 2−72187
Pb, with Ag impurity, pore formation on annealing 2−71665
Sb-Sn alloy, peritectic crystn., pore form. 2−53906
Si_3N_4-Cr_2O_3 refractories, porosity and effects on impact strength 2−68162
$(U,Pu)O_2$ fuel pin, porosity and actinide redistrib., grain growth and desintering 2−56043
UO_2, lenticular pore migration, impurity effects 2−74150
UO_2, plastic deform., fracture, rel. to porosity 2−43699
UO_2 fuel rod, irrad., pore movement kinetics 2−52873
UO_2 pellets obs. under long term annealing, absence of porosity 2−49898
UO_2 sintered bodies, open pore distrib. 2−61025
W, CVD films, formation of pores, interdiffusion in emitters of thermionic converters 2−53560
W, shock response, Hugoniot elastic limits, model 2−61024
W, sintered, porosity influence on phys. and mech. props. 2−84145
YIG, polycryst., spin wave transit time, limitation by pores 2−75232
Zr containing refractories, influence of Cr_2O_3 contest on apparent porosity 2−84095
ZrC-NbC, solid solution, creep meas. in compression, temp. range 2600-3150 K 2−84033

Porterin-LeChatelier effect *see Stress/strain relations*

Positive column *see Discharges, electric*

Positive ray sources *see Ion sources*

Positive rays *see Chemical analysis/by mass spectrometry; Ion beams*

Positons *see Positrons*

Positronium
amides, intensity of orthopositronium component 2−71228
annihilation, in molecular liquids and solids 2−43311
atom, in NaCl type ionic cryst., lifetime and binding energy rel. to ion charges and lattice energy 2−77793
coupling of three or more positroniums, relativistic model, derivation of S-matrix elements 2−49508
fine structure, $\alpha^2 \ln\alpha^{-1}$ correction 2−42346
fine-structure interval of ground state 2−79964
formation in H, He by elastic positron scattering 2−42800
in ice, mag. quenching of o-positronium 2−77849
magnetic amplification in KCl colour centres 2−68039
metals, lifetime 2−54122
molecule model, binding energy 2−64111
negative-ion formation by double electron capture in H_2 by positrons 2−50044
ortho-positronium, pick-off quenching rate in liquid mixtures 2−64448
in n-pentane magnetic quenching, determ. of overlap density at 36, 54 and 76°C 2−53384
production in π^0 and η^0 decay, probability calculation 2−45948
spontaneous decay in time-dependent external field 2−73765
KCl-KBr solid solutions positronium formation 2−80988

Positrons
see also Electron pairs; and Electrons, which include both negative and positive electrons when the differences between them are of no special significance
annihilation, fundamental ideas, measurement techniques and annihilation radiation, review 2−59428
annihilation in AgCl and AgBr at extended defects 2−81024
annihilation in metals 2−54122
backscattering from Au surface coated with MgO, as conversion method 2−64078
beam traversing heavy liquid bubble chamber, momentum estimation 2−52704
focussing and selection, geometrical ray tracing for astigmatic sector spectrograph 2−52673
lifetime spectra analysis using FORTRAN program 2−52561

Positrons continued
  lifetimes in amides 2−71228
  metal, pitrons correl. energy in interacting electron gas, positron work function 2−84243
  metal, temp. depend. of position annihilation 2−81002
  polyethylene under static electric field, lifetimes, rel. to polariz. 2−61409
  scattering, elastic, by H atoms, optical potential method calc. 2−46421
  single-quantum annihilations by screened K- and L-shell electrons 2−76981
  trapped in solid state defects, response rel. to trap features 2−71459
  e^+e^-, annihilation, hadrons production, consequences of energy-momentum conservation 2−73764
  $e^+e^- \rightarrow$hadrons, oscillations in total cross section 2−63520
  μ pair creation via two-photon exchange in electron collisions, QED investigation 2−82624
  Al-(1.7 at.%) Zn, vacancy-impurity binding energy, positron-annihilation study 2−53727
  Al, deformed by rolling, positron interaction with defects 2−71460
  Al, positron and dislocation binding 2−83977
  Ar, elastic scattering cross sections 2−70644
  Cd, angular distributions using positron wavefunctions with proper crystal symmetry 2−80942
  Cu, angular distributions using positron wavefunctions with proper crystal symmetry 2−80942
  $e^+e^- \rightarrow \pi^0\gamma$, bound for cross section 2−45882
  Xe, elastic scattering cross sections 2−70644
  Zn, angular distributions using positron wavefunctions with proper crystal symmetry 2−80942

Potassium
  adsorbed layer, on Ni (001), specular electron refl. 2−50544
  adsorbed layer, on W(100), surface plasmon losses 2−64903
  adsorption on Mo, LEED and Auger spectroscopy obs. 2−50540
  anomalous infra-red absorption and collective oscillations in small metal particles 2−65210
  atom, cascade-decoupling meas. of excited S-state hyperfine structures 2−52922
  atom, elastic electron scatt., differential cross-section calc. 2−79883
  atom, electron scattering, differential and direct differential elastic scattering cross-sections 2−64040
  atom, scattering from methane, meas. of velocity dependence and total cross section, study of glory undulations 2−70821
  atom, spectrum in premixed H_2-O_2-N_2 flame, emission noise spectrum 2−49952
  atom, superthermal, angular scattering by I_2 2−42787
  atom, variations in relative intensities of lines in 4p-3d transition in i.r. region using hollow-cathode discharge 2−70585
  atomic, natural lifetimes and hyperfine structure for ^{39}K in 5p $^2P_{3/2}$ and 6p $^2P_{3/2}$ levels by resonant light scattering of K I spectra 2−46430
  atoms, photoionization, pseudopotential calculation of cross-section 2−46448
  atoms, polarized, differential cross-sections for elastic scattering of low energy electrons 2−46459
  atoms, reaction with methyl iodide in crossed beams, energy dependence 2−68771
  atoms, scattering by inert gases, total cross section meas. 2−83192
  boiling, forced convective controlling heat transfer and fluid flow mechanisms 2−71280
  deficiency, effects on cochlear potentials and cation content in endolymph 2−45165
  disordered overlayers, on Ni(001), specular electron refl. 2−60681
  drill core scanning by gamma ray spectrometry 2−78293
  duality, theorem and high-field linear magnetoresistance, geometrical effects 2−81031
  Earths core content, and distribution meteorites 2−44582
  electrical resistivity, contribution of Umklapp processes 2−84293
  electrical resistivity, temp. and volume depend., 20K-m.p. 2−84296
  environmental ions, microsensitivity enhancement of cochlear hair cells 2−66306
  film elec conductivity calc., electron-phonon scatt., soln. of Boltzmann eqn. 2−71830
  induced torque, non-saturating anisotropy 2−48036
  ions, reduced mobility in gases, apparent pressure dependence 2−56448
  liquid, determ. of pseudo-Gruneisen parameters 2−74540
  liquid, effective pair pots. 2−50317
  liquid, electron spectrum, calc. by cell method 2−83797
  liquid, self-diffusion, 97 to 284°C, capillary method 2−67817
  liquid, structure factor, expt. and theoretical 2−50314
  lunar soils, isotope characts. 2−66139
  magnetoplasma, anomalous resistivity 2−70897
  optical conductivity, interband, calcs. 2−68616
  optical constants in 4-10.7 eV photon energy range 2−68593
  optical props. and surface plasmon states 2−71819
  plasma diagnostics, laser obs. using selective excitation spectroscopy 2−70928
  pliocene volcanic rock content det. 2−57809
  r.f. size effect, calc. 2−71835
  self-diffusion in microcline perthite 2−68859
  self-diffusion in Na_2O-K_2O-SiO_2 glass, rel. to internal friction 2−50712
  thermal resist., low-temp., electron-phonon umklapp processes 2−51061
  thermoelectric power rel. to Fermi surface shape and sample dimens. effects 2−68296
  three level system, coherent two photon propagation and self induced transparency of optical pulses 2−44330
  u.s. shear waves, electromagnetic generation and attenuation 2−71729
  vapour, dispersion of cubic nonlinear susceptibility det. by self-focusing self-defocusing and self-modulation 2−42734
  vapour, multiphoton resonant processes under laser irradiation 2−42750
  vapour, reson. nonlinear susceptibility dispersion 2−43272
  vapour, three-photon excitation and ionization using dye laser beam 2−74215
  vapour, two-photon self-induced transparency of different-frequency optical short pulses 2−79248

Potassium continued
  β-Al_2O_3, K, and Ka-K substituted, mech. behaviour 2−56770
  Ar-K plasma, heat flow meas. to electrodes 2−60209
  CdF_2:Er^{3+}, K^+, correlated e.p.r. and optical study 2−78164
  in $H_2/O_2/N_2$ flames, electron attachment and negative ion form. 2−72555
  K/Ar data rel. to origin of feldspar megacrysts in alkali basalt 2−54729
  K/Ar radioactive dating, rift volcanics in S. Kenya 2−61993
  K-Ar ages of zenoliths from Tahiti 2−57808
  K-Ar dating, origin of Hawaiian Ridge 2−57725
  K^+-Ar collision, scatt. cross section, ion inelastic energy loss and u.v. emission 2−79925
  K^+-He(Ne,Ar) scattering, 150-2350 eV, effective total cross section meas. 2−67415
  K-K collisions, broadening of principal series lines 2−56117
  K-O_2, spin exchange scatt. obs. 2−67541
  K-ammonia solution, relaxation times and Overhauser enhancements for protons obs. 2−46988
  K^+, in CsBr, i.r. absorp. 2−61635
  K^+, ion migration in glass, from K^+ ion-exchanged layer under reverse electric field 2−75388
  K^+, mobility in He II, ion-roton scatt. cross sections 2−67863
  K^+, self-diffusion in K_2O-SrO-SiO_2 glass 2−53765
  K^+ energy spectra, laser-produced ions 2−52921
  K^+ ion transport of red blood cells of rats, comparison with Cs^+ by kinetic tracer model 2−55257
  K^+ ions elastic scatt. from diatomic mols., 150-4000 eV 2−80149
  K^+ mobility in N, effect of clustering 2−67688
  K_3, K_3^+ dissociation energies and equilibrium geometries, pseudo Hamiltonian model 2−56190
  K^+−Ar scatt., potentials derivation from intermediate and strong field mobility data 2−79912
  ^{42}K, blood-tissue transport in dog gracilis muscle 2−62822
  ^{43}K, myocardial uptake and clearance characteristics rel. to ^{129}Cs 2−66260
  K + molecule, atomic beam, reaction cross- sections meas. 2−51433
  K + CCl_4 reaction, dependence of reactivity on internal and translational energy 2−75374
  K + $CH_3I \rightarrow KI + CH_3$, translational energy depend., reaction cross-section 2−51432
  K + HBr molecular beam expts., rotational polarization of reaction products and reprojection of angular momentum 2−65367
  K + I_2 reaction, exoergic, product state distrib. and temp. concept 2−68761
  K + I_2 reaction, exoergic, product state distrib. and temp. concept 2−68761
  K + O_2 reaction in Ar matrix, Raman spectra of products 2−61776
  K + SF_6 reaction, dependence of reactivity on internal and translational energy 2−75374
  K + $SnCl_4$ reaction, dependence of reactivity on internal and translational energy 2−75374
  K + methyl iodide → KI + methyl radical, interpretation of product ang. and energy distribution using direct interaction model 2−57412
  Na^+-K^+ ion exchange, in Na borosilicate glass 2−53537
  $PbCl_2$:K^+, defects, ionic cond. and dielec. loss study 2−47402
  Si:K, doped surface layers, donor props. and diffusion 2−65019
  Si:K, elec. props., impurity atomic radius effects 2−71948

Potassium compounds
  − 2−71359
  − 2−72367
  alums, etching with ethanolic tartaric acid solns. 2−74662
  carbamate, solid, i.r. spectra 2−84527
  complex, pentacyanonitrosylchromate, i.r. spectrum, normal coordinate analysis for $[Cr(CN)_5NO]^{-3}$ anion 2−60008
  feldspar, force field obs. 2−43955
  $KDHPO_4$ ferroelectric transition, molecular field approx. study 2−65062
  KI:Tl, total emission spectra and energy transfer from excitons to activator 2−61710
  microcline, shock deform. 2−61843
  oxalates, cryst. growth from aq. soln. 2−60714
  $Ba_2KNb_5O_{15}$, Ta-substitution influence on crystallographic and dielec. props. 2−47315
  Cs-K alloy, ashcroft's empty core model 2−74898
  Cs-K alloy, heat of soln., pseudo alloy atom model 2−74897
  Hg-K melt, electrotransfer and elec. resist. 2−56517
  K-Cs, K-Rb alloys, pseudopotential theory and Vegard's rule 2−67992
  K-Cs alloys, liq., elec. resist., temp. depend. 2−64471
  K-Cs alloys, molten, electric transport, electrical resistance and density of electron states 2−60497
  K-Hg alloys, liq., zero wave vector partial struct. factors 2−43318
  K-NH_3 solution, Hall coeff. and elec. cond., 203-243K 2−46984
  K-Na eutectic, liquidus curves from conformal solution theory 2−83842
  K complex, dipotassium cis-hexacyanobutenediide, crystal structure and anion electronic structure 2−53667
  K complex, $K_2Pt(CN)_4Br_{0.3}.xH_2O$, electron localization 2−44110
  KAg_4I_5, thermoelectric power 2−77961
  $K_4As_2O_7$, i.r. spectra and normal coordinate analysis 2−77079
  $KAu(CN)_2$, anomalously narrow Mossbauer linewidth in ^{197}Au 2−78074
  $KAu(CN)_2$, elec. hyperfine alignment of ^{197}Au 2−44355
  $KAu(CN)_2$, Mossbauer effect, elec. alignment of ^{197}Au 2−44356
  $KBe_2(BO_3)F_2$, synthesis and physicochemical props. 2−47210
  KBr-KI solid solution single crystals, elastic consts. and Debye temp., u.s. pulse method obs. 2−71550
  KCN, permittivity, temp. depend., anomalies at transition points 2−75141
  KCN, single cryst. growth 2−67944
  KCO_3 molten, production of C-H-O fuels for high temp. fuel cells 2−59042
  $K_2CO_3 + 2PbSiO_3$ subsolidus reaction, kinetics and mechanism 2−60996
  $K_2CO_3 + 2(4PbO.SiO_2)$ reaction, kinetics and mechanism 2−50884
  KCl:Na, non-cubic Ag- centres in mixed crystals 2−44370
  KCl:Pb^{2+}, electrolytically coloured, T-centre struct. 2−64679
  KCl:SO_4^{2-}, anion vacancy trapping, i.r. absorpt. study 2−43620
  KCl, voltametric behaviour of γ-irradiated soln. 2−84662

Potassium compounds continued
KCl light scattering spectrum, charge induced anisotropy model 2−53432
$KClO_3$, molten, Raman spectra 2−74545
$KClO_3$, molten and aqueous, vibr. spectra 2−80475
$KClO_3$, n.q.r. of ^{39}K, ^{40}K and ^{41}K, detection using steady-state double reson. 2−54520
$KClO_3$ II, lattice constants, meas. using powder diffraction 2−47332
$K_3Co(CN)_6$, n.m.r. of ^{59}Co, chem. shift 2−54509
$K_3Co(CN)_6$, n.m.r. of ^{59}Co, chemical shift interpretation 2−65345
$K_3Co_{1-x}Fe_x(CN)_6$, Fe^{III} complex $3d(t_{2g})$ density distrib., Mossbauer and e.p.r. obs. 2−68613
K_xCrF_3, cryst. struct. 2−60760
K_2CrO_4 irradiated at ambiant temp., e.s.r. spectroscopy study of paramagnetic centres 2−48280
K_2CrO_4 struct. redeterm., effect of electrostatic crystal forces on observed bond lengths 2−77550
K_2CsSb photocathode, thermionic emission 2−61459
$KCuF_3$, low dimensional antiferromagnet, thermal conductivity meas. 2−51062
$KCuF_3$, one dimensional antiferromagnet, anomalous thermal cond. 2−71760
$KCuF_3$, stacking disorder, X-ray diffr. obs. 2−77569
K_2CuF_4, two-dimens. ferromagnet, mag. props. and sp. ht. 2−81239
K_2CuF_4, two dimensional ferromagnet temp. and frequency dependence of the e.s.r line width 2−84563
KD_2AsO_4, ferroelec. transitions, thermodynamic props. 2−47985
KDP, cooled, heating by 337 μm laser radiation 2−63347
KD_2PO_4, electro-optic light valve device, image storage and processing 2−66847
KD_2PO_4, growth and etching in solns. containing acetate ions 2−60712
KD_2PO_4, high temp. phase transitions 2−71688
KD_2PO_4, monoclinic, cryst. struct., X-ray obs. 2−64640
KD_2PO_4, u.s. stress wave interaction with domain walls 2−71740
KD_2PO_4 Raman scattering from crystals and solutions, anomalous temperature dependence of low frequency lines 2−48200
KF-BeF_2 glass, stratification effects on comp. depend. of elasticity modulus 2−47478
KF, ionicity, dispersion, and optical spectra 2−44374
KF, Raman spectra, phonon modes 2−48196
KF Hartree-Fock band structure 2−61172
$K_3Fe(CN)_6$, electronic structure model consistent with n.m.r. and Mossbauer data 2−54508
$K_3Fe(CN)_6$ in KCl solution in water, mass transfer in flowing electrolyte with quasi porous electrode 2−68794
$K_4Fe(CN)_6$ in aqueous solns. photoelectron emission spectroscopy 2−68808
$K_4Fe(CN)_6.3H_2O$, anomalous spin-lattice relax. by quasi-spin waves 2−75152
$K_4Fe(CN)_6.3H_2O$, ferroelectric, twinning and polymorphism, p.m.r. obs. 2−74655
$KFe(CrO_4).2H_2O$, space group, lattice parameters 2−67991
$KFe(CrO_4)_2.2H_2O$, low temp. i.r. vibr. spectra 2−48175
$KFeF_4$, antiferromag., critical behaviour, neutron and Mossbauer obs. 2−44301
$KFeF_4$, planar antiferromagnet, neutron scatt. and Mossbauer obs. 2−78043
K_xFeF_3, mag. props. and cryst. struct. 2−48071
$K_{0.2}FeF_{2.8}O_{0.2}$, mag. props. and cryst. struct. 2−48071
$K_2Ge(IO_3)_6$ crystal struct. determ. 2−77549
KH_2AsO_4, ferroelec. phase transition dynamics, spin-lattice relax. meas. by double reson. 2−84450
KH_2AsO_4, ferroelec. transitions, thermodynamic props. 2−47985
KH_2AsO_4, n.m.r. and dielectric relaxation correlation 2−57243
KH_2AsO_4, X-irradiated in ferroelectric phase at 4.2 and 77 K, e.p.r. and ENDOR study of AsO_4^{4-} centre 2−72469
KH_2AsO_4 and KD_2AsO_4 ferroelectrics, EPR and ENDOR 2−68734
KH_2AsO_4 and KD_2AsO_4, X-irradiated, identification of Slater configurations of $(AsO_4)^{4-}$ radical by ESR 2−81453
KH_2AsO_4 Raman scattering from crystals and solutions, anomalous temperature dependence of low frequency lines 2−48200
$KH_{2(1-x)}D_{2x}PO_4$, Curie const., comp. depend. 2−54236
$KH_{2(1-x)}D_{2x}PO_4$, study of dielec. and thermal props. in ferroelec. and paraelectric phases 2−84364
KHF_2, ionic cond., a.c. study, 50Hz-20kHz 2−68465
KHF_2, neutron diffraction data refined, location of H, thermal motion and F-F distance 2−77087
$K_2H(IO)_3)_2Cl$, cryst. struct., X-ray obs. 2−53665
KH_2PO_4-KH_2AsO_4 mixed ferroelectric, EPR and ENDOR 2−68734
KH_2PO_4, dense domain structure at ferroelectric transition, stress-induced birefringence 2−75260
KH_2PO_4, electro-optical effect, calc. from light wave intensity reduction 2−65222
KH_2PO_4, excitation of natural and stimulated optical harmonics 2−61580
KH_2PO_4, ferroelec., Raman scatt., oscillatory intensity behaviour with temperature 2−65280
KH_2PO_4, ferroelectric mode, proton-phonon coupling effects, Raman spectra obs. 2−65279
KH_2PO_4, high temp. phase transitions 2−71688
KH_2PO_4, light scatt. by elastic waves and rot. of polarisation plane 2−72358
KH_2PO_4, mode interactions 2−55680
KH_2PO_4, molecular dynamics study and ferroelec.-antiferroelec. transitions by NMR and dielec. relax. 2−72032
KH_2PO_4, parametric light amplification and oscillation, with mode locked pump 2−42052
KH_2PO_4, permittivity rel. to proton tunnelling, 130-280K 2−77945
KH_2PO_4, plane-parallel crystals, depolarization of linearly polarized light due to inhomogeneous dielectric heating in 2−42184
KH_2PO_4, polishing, single lap apparatus 2−67893
KH_2PO_4, soln. growth by gradual addition of reactant 2−47238
KH_2PO_4, transition order experiments 2−81155
KH_2PO_4, trapping of parametrically amplified light waves 2−44335
KH_2PO_4, z cut and electrode configuration effects on control voltage for switching electro-optical shutter 2−69894
KH_2PO_4 crystal as wide angle i.r. to visible image conversion system by pumping 2−45815
KH_2PO_4 nonlinear crystal, fracture by ruby laser radiation 2−79254

Potassium compounds continued
KH_2PO_4 polarization commutator, limitations to angular field 2−45796
KH_2PO_4 Raman scattering from crystals and solutions, anomalous temperature dependence of low frequency lines 2−48200
$KH_5(PO_4)_2$, hydrogen atom positions and hydrogen bonds prediction 2−47312
$K_2H_2P_2O_6$, $K_2H_2P_2O_6.3H_2O$, i.r. spectra C_2h configuration of $H_2P_2O_6^{2-}$ 2−83267
$K_3Hg(NO_2)_4NO_3$, crystal structure determ. by neutron diffraction 2−64639
$KI:Cu$, anomalous transmission spectra, 300-450 nm 2−72337
$KI:Cu$, antiresonance phenomena in transmission spectra 2−54423
$KI:K$, additively coloured, colloidal absorption bands 2−47448
$KI:KOH$, tunnelling levels, low temp., thermal cond. obs. 2−71758
$KI:SH^-(SD^-)$, i.r. spectra expt. and interpretation 2−84491
$KI:Tl$, host-sensitized luminesc., elec. field effects 2−81419
$KI:Tl$, recomb. and capture probabilities of F-centre electrons 2−84285
$KI:Tl$ covalency, overlap calcs. absorption spectra 2−61643
KI-$KCl:Tl$, intracentre luminesc. 2−81425
KI-SH-, phonon sideband struct. in i.r. absorpt. spectrum 2−48185
KI, Ag^- centres, polarization and decay time of luminesc. 2−80710
KI, coherent neutron scatt. amplitudes from powders 2−53654
KI, diffusion coeff. of self-trapped holes and migration to thallium centres 2−68709
KI, fast recomb. luminesc. transition lifetimes 2−54450
KI, harmonic band parameters of NO_2^- and NO_3^-, high temp. 2−54410
KI, ionicity, dispersion, and optical spectra 2−44374
KI, local and gap modes due to substitutional impurity 2−47731
KI, magneto-reflectance of first exciton 2−51322
KI, phonon modes of Ag^+ 2−50994
KI, photoemission from colour centres, in ultra high vac. 2−48023
KI, positron lifetime spectra, temp. depend. 2−75003
KI, relaxed-excited state of F-centre, wave function determ. 2−68738
KI, resonant phonon modes of Au^+ 2−54018
KI, solution grown, movement of solvent inclusions by centrifugation 2−47465
KI, sputtering, positive ion ejection patterns 2−44008
KI evaporated films, optical absorption spectra 1700-2500 Å, obs. of fine structure in exciton bands 2−44375
KI films, slow electron impact, luminescence excitation and characteristic energy losses 2−81417
KI solution, solubility of AgI particles in, significance to cloud seeding 2−51595
KIO_3, crystal struct. exam. and vibrat. struct. detn. by i.r. spectroscopy and n.q.r. 2−71435
KIO_3, symmetry props. rel. to use as nonlinear optical material 2−74733
$K_3IR^{III}(CN)_6$, electron irradiated in KCl single crystals, e.s.r. studies of ligand hyperfine structure in $Ir^{II}(CN)_5$ species 2−61735
$KI.PbI_2.2H_2O$, luminescence, absorption and emission spectra 2−54456
K_2IrCl_6, incipient phase transitions 2−77748
K_2MgCl_4, molten, ion clusters, Raman spectrum interpret. 2−67797
$KMgF_3$:$^{53}Cr^+$, ENDOR of $^{53}Cr^+$, hyperfine const., covalency depend. 2−68753
$KMgF_3$-$KMnF_3$ mixed crysts., electron irrad., single defect involving F-centre, prod. mechanism 2−68040
$K_4Mn(CN)_6$ in aqueous solns. photoelectron emission spectroscopy 2−68808
$KMnCl_3.2H_2O$, antiferromag., mag. phase boundaries, anisotropy, exchange fields 2−68574
$K(Mn_{1-c}Co_c)F_3$, antiferromagnetic, critical condition for magnon localization found for all impurity concentrations 2−44284
$KMn_{1-x}Co_xF_3$, spin waves theory and coherent potl. approx. applic. to mag. excitations 2−78044
$KMnF_3$, antiferromagnet, anomalous thermal cond. 2−71761
$KMnF_3$, canted antiferromagnet, resonance behaviour 2−84556
$KMnF_3$, doped, impurity effects on mag. excitation spectra 2−44282
$KMnF_3$, growth by Czochralski method, dislocation density determ. 2−53605
$KMnF_3$, $KMnF_3$:Mg, temperature dependence of e.p.r. line width, room to liquid nitrogen temp., effect near Neel temp. 2−44440
$KMnF_3$, mag. susceptibility anomalies interpret., magnetoelastic effects 2−54356
$KMnF_3$, specific heat, 70-210K, anomalies and phase transitions 2−71747
$KMnF_3$, superstructure arising from phase transition 2−74933
K_2MnF_4, e.s.r. above Neel temp. 2−72489
K_2MnF_4, mag. struct. near crit. point, neutron scatt. study 2−65182
K_2MnF_4, planar antiferromagnet, hyperfine contribs. to ^{19}F n.m.r. lineshift 2−54510
K_2MnF_4, quadratic layer antiferromagnet, e.p.r. linewidth temp. depend. 2−75345
$KMnF_3ErF_3$ system, phase diagram, existence of $KMnEr_3F_{12}$ 2−50622
$KMnLn_3F_{12}$ and $KMYb_3F_{12}(M=Mg, Zn, Ni, Co)$, cryst. struct. 2−50622
$KMnO_4$, γ-irrad., e.s.r. of MnO_4^{2-} 2−68809
$K_4Mo(CN)_8$ in aqueous solns., photoelectron emission spectroscopy 2−68808
$K_{0.3}MoO_3$, blue phase, semicond. to metal transition, elec. cond. 2−61151
KN_3, i.r. absorpt., selection rules and internal ± internal and internal ± external mode absorpts. 2−72336
KN_3, Raman active librational modes, anharmonic self energy shift 2−71726
KN_3, u.v. irrad., absorpt. bands identification 2−75299
β-KNO_3:Mn^{2+}, e.p.r., phonon sidebands 2−72490
KNO_3, aragonite- to calcite-type transform., surface effects 2−74932
KNO_3, cryst. growth morphology at polymorphic transforms. 2−50945
KNO_3, elec. bicond. phenomena 2−61319
KNO_3, molten, interdiffusion coeff. of Ag^+ 2−65383
KNO_3, precip. of bivalent metal nitrates, solid soln. form. 2−56942
$KNbO_3$, dielec. const. under biasing conditions 2−61430
$KNbO_3$, ferroelec., mech. switching of domain walls 2−44160

Potassium compounds continued
  $KNbO_3$, ferroelec., surface charge layers, obs. by AF electrolum. 2−75151
  $KNbO_3$, ferroelectric domain investigations using pseudocubic {001} cleavage planes 2−61429
  $KNbO_3$, ferroelectric single crystals, deformation and stress relaxation behaviour 2−80743
  $KNbO_3$, Raman and i.r. spectra, vibr. freqs. assignment 2−84476
  $K_{0.5}Nd_{0.5}TiO_3$, perovskite, prep., mag. susceptibility, cryst. field effects, 2-600K 2−54294
  $KNiF_3$, antiferromagnet, four-magnon excitation in Raman scatt. 2−54433
  $KNiF_3$, Neel point determ., elastic, magneto-optical and heat capacity meas. 2−72219
  $KNiF_3$, semiempirical LCAO-MO treatment of $[NiF_6]^{4-}$ cluster 2−65200
  $KNiF_3$, stress-induced and mag. linear dichroism 2−81329
  K_2O-KX-B_2O_3 glass, (X=F,I,O), X-irrad., colour centres, e.p.r. obs. 2−81463
  K_2O-$2SiO_2$ and Li_2O-K_2O-$4SiO_2$ glass, static longitudinal modulus, u.s. determ. 2−56773
  K_2O-SiO_2 glass, cond. and dielec. relax. as function of thermal history 2−54229
  K_2O-SiO_2 glass, irrad., nature of hole centres, e.p.r. obs. 2−65336
  K_2O-SrO-SiO_2, interdiffusion coeffs. matrix 2−80724
  K_2O-SrO-SiO_2 glass, cation self-diffusion coeffs. 2−53765
  KO_2, magnetic properties, obs. of structural and magnetic transitions 2−65116
  $KO_{2(3)}$, Raman spectra, O_2^- O_3^- ion props., solid-solid transition effects 2−81354
  KOH, in ice, dielec. dispersion and phase transition 2−72014
  $xK_2O(1-x)SiO_2$ glass, u.s. vel. and absorpt., meas. apparatus, 0−300K 2−74983
  K_2OsBr_6 Raman spectra, obs. of dynamic Jahn-Teller effects, and quenching by charge transfer and spin-orbit coupling 2−72369
  K_2OsCl_6, Raman spectra obs. of dynamic Jahn-Teller effects and quenching by charge transfer and spin-orbit coupling 2−72369
  KPF_6, solid, reorientation motions of PF_6^- ions 2−61562
  KPO_3-$Sr(PO_3)_2$ system, phase diagram 2−43935
  $K_3P_3O_9$, cryst. struct. and prep. 2−53668
  K_2PO_3F, space groups and lattice parameters 2−83951
  K_2PdCl_6, incipient phase transitions 2−77748
  K_2PtBr_6, rotary lattice mode softening, n.q.r. obs. 2−61756
  $K_2Pt(CN)_4Br_{0.3} \times 2.3H_2O$, one-dimensional conductivity, defect effects 2−68339
  $K_2Pt(CN)_4Br_{0.3} \times 3H_2O$, magnetic susceptibility 2−84401
  $K_2Pt(CN)_4Br_{0.30}.3H_2O$, one-dimens. cond. as two-dimens. problem 2−51142
  $K_2Pt(CN)_4Cl_{0.3}.n(H_2O)$, one-dimensional, low temp. sp. ht. 2−71746
  $K_2Pt(CN)_4Cl_{0.3}.xH_2O$, organometallic, thermoelec. analysis of elec. cond. 2−72055
  K_2PtCl_6, incipient phase transitions 2−77748
  $K_2Pt(N)_4Br_{0.3}.3H_2O$, quasi one dimensional conductor, anisotropic thermopower 2−64915
  $K_{1-x}Rb_xI$, susceptibility and lattice const., comp. depend. 2−54289
  K_2ReCl_6, X-ray L_{III} absorption discontinuity, splitting and edge structure 2−61676
  $KReO_4$, X-ray L_{III} absorption discontinuity, splitting and edge structure 2−61676
  $K_4Ru(CN)_6$ in aqueous solns., photoelectron emission spectroscopy 2−68808
  K_2SO_4:Tl^{2+}, g-factor, hyperfine interact., e.p.r. obs. 2−72470
  K_2SO_4, aqueous soln. resist. in electrolytic cell, geom. parameters depend. 2−78200
  K_2SO_4, coherent neutron scatt. amplitudes from powders 2−53654
  K_2SO_4, laser Raman spectra, lattice vibration modes 2−72368
  K_2SO_4, liq., u.s. vel. 2−53426
  K_2SO_4, nucleation and growth in fluidized bed crystallizer 2−47282
  K_2SO_4, X-ray spectra, high-resolution sulphur $K\beta$ emission, symmetry assignment 2−60007
  β-K_2SO_4 struct. redeterm., effect of electrostatic crystal forces on observed bond lengths 2−77550
  $K_2S_2O_6$, second harmonic generation 2−75248
  $K_2SO_4(c) \rightarrow 2K^+(g) + SO_4^{2-}(g)$, Madelung parameter and electrostatic energy charge, calc. based on Evald Bertaut method 2−47179
  $KSbSe_2(S_2)$, cryst. growth, Bridgman method 2−47273
  $K_2SiF_6.Na_2SiF_6$, occurrence, prep., cryst. data 2−74734
  $K_2Si_2Pb_2O_7$, product of $K_2Co_2 + 2PbSiO_3$, subsolidus reaction microstruct. 2−60996
  $KTa_xNb_{1-x}O_3$, cond. band edge splitting and lattice dynamics 2−54425
  $KTa_xNb_{1-x}O_3$, l.f. zone boundary lattice vibr. modes, Debye-Waller factor anisotropy 2−80902
  $KTa_xNb_{1-x}O_3$, absorpt. edge splitting, paraelec. and ferroelec. phases 2−48184
  $KTa_xNb_{1-x}O_3$, pyroelectric detectors, characteristics 2−73460
  $KTaO_3$, elec. props. and defect struct. 2−47967
  $KTaO_3$, paraelec., press. depend. of static dielec. const. 2−44161
  $KTaO_3$, Urbach's tail behaviour, unified mechanism 2−54430
  $K_5(UO_2)F_9$, struct. of binucl. $(UO_2)_2F_9^{5-}$ ion 2−83953
  KVO_3, cryst. growth and characteriz. 2−47261
  $K_4W(CN)_8$ in aqueous soln., photoelectron emission spectroscopy 2−68808
  K_2WO_4-$In_2(WO_4)_3$ solid soln., phase diagram 2−57033
  KX:PO_2^-, X=halide, photoluminescence, singlet-triplet transitions in PO_2^-, low temp. study 2−54455
  K_2ZnF_4:Mn^{2+}, e.s.r., spin Hamiltonian parameters detn. 2−65323
  $KZnF_3$:V^{2+}, e.p.r. and ^{19}F ENDOR study 2−75353
  $KZnF_3$, elastic consts., u.s. vel. meas. 2−84007
  $K_2Zn_2Mo_3O_{12}$, monoclinic, cryst. struct. 2−77555
  $K_5[Au_5(CN)_{10}I_2].2H_2O$, crystal struct. determ. 2−77544
  $K[PtCl_3NH_3].H_2O$, vibr. spectra 2−48183
  $LiNO_3$-KNO_3, molten mixtures, electrical conductivity, temp. dependence 2−53452
  MnF_2, doped, impurity effects on mag. excitation spectra 2−44282
  $MnKH(SO_4)_2.2H_2O$, Zeeman decomp. of visible absorpt. lines 2−54427
  $(NH_4)_xK_{1-x}H_2PO_4$ epitaxial film, electro-optic waveguide 2−70058
  Na-K alloys, liq., zero wave vector partial struct. factors 2−43318

Potassium compounds continued
  $NaClO_3$, irrad., radiation damage, Raman spectra obs. 2−57361
  Na_2O-K_2O-SiO_2 glass, Na and K self diffusion, rel. to internal friction 2−50712
  RBO_2, evaporation, mass spectrometer obs. 2−64512
  SiO_2-Al_2O_3-Na_2O-K_2O-CaO-MgO glass, viscosity-temp. relations 2−67883
  SiO-K_2O system, binary interdiffusion coeffs. and O_2 self-diffusion 2−53772
  $Sr_2KNb_5O_{15}$, Ta-substitution influence on crystallographic and dielec. props. 2−47315
  $Sr_{2-x}K_{1+x}Nb_5O_{15-x}F_x$, synthesis, struct. and ferroelec. props. 2−51198

potassium bromide
  coherent neutron scatt. amplitudes from powders 2−53654
  colour centre, transient formation under pulsed electron beam 2−53753
  colour centres, electron microscope obs. in cathode luminescence mode 2−80708
  colour centres, electronic struct. calc. and electronic polarization fields 2−71520
  crystals u.v. irrad. and colour centre prod. from exciton decay 2−71527
  dielectric consts., l.f., press. and temp. derivatives 2−51188
  electron density anisotropy and effective charge, positron and photon annihilation obs. 2−54100
  evaporated films, optical absorption spectra 1700-2500 Å, obs. of fine structure in exciton bands 2−44375
  F-centre hyperfine interactions, press. depend., ENDOR study 2−83986
  F-centres, excited, emission mechanisms 2−80709
  film, dielectric response, i.r. reflectivity obs. 2−72304
  harmonic band parameters of NO_2^- and NO_3^-, high temp. 2−54410
  ion bombardment, mass spectrometer obs. of sputtering and ion emission 2−71765
  ionic cond., press. depend. 2−44154
  ionicity, dispersion, and optical spectra 2−44374
  lattice dynamics, resonant phonon modes of Au^+ 2−54018
  limiting optical frequency, temp. variation calc. 2−72311
  luminescence, fast recomb. transition lifetimes 2−54450
  luminescence, hot, from vibrational transitions of OH^- molecular ion 2−57369
  mass transport along grain boundary pipe lines 2−56759
  mass transport along grain boundary pipelines, comments 2−56760
  methanol-potassium bromide vibrationally excited, inelastic scatt. 2−64220
  molecular CO^{2-}_3 centre, i.r. spectra 2−71350
  multiphonon i.r. absorption spectra, effects of melting 2−68220
  multiphoton conductivity, optical gap assignment 2−65084
  phonon energies at Van Hove crit. pts. 2−71712
  phonon modes of Ag^+ 2−50994
  point defects displacement field, X-ray scatt. 2−60787
  pure and doped, hardness, yield strength, Young's modulus 2−56835
  R_2 centre, analysis of absorp. struct. 2−51342
  solid solution, cryst. growth, for neutron monochromator appl. 2−47205
  solubility and mobility of He, permeation, gas release and ion implantation studies 2−84002
  solution, containing Pb^{2+}, nucleation and crystn., evolution of heat 2−47236
  sputtering, positive ion ejection patterns 2−44008
  X-ray diffuse scattering, higher anharmonic contribs. 2−61059
  KBr:Ag^-, polarization and decay time of luminesc. of Ag^- centres 2−80710
  KBr:Na, F_b centres, absorpt. and emission study 2−64682
  KBr:PO_2, recombination luminescence, F-centre accumulation during β-irradiation 2−78136
  KBr:$PO_4^{3-}(SiO_4^{4-})$, i.r. absorpt. 2−54424
  KBr:$SH^-(SD^-)$, rel. to i.r. spectra interpretation 2−84491
  KBr:Tl, ionisation of Tl^{2+} centres by interstitial halogen atoms 2−81001
  KBr:Tl^+, magneto-optical obs. of Jahn-Teller effect 2−68606
  KBr-KCl, mixed cryst., proton dechannelling, lattice distortion effects 2−47785
  KBr-KCl mixed crystal, with and without colour centres, spectra 2−74801
  KBr-K_2O-B_2O_3 glass, X-irrad., e.p.r. obs. of Br^0 2−81463
  KCl-KBr solid solution, internal stress at Luders band front 2−84043
  KCl-KBr solid solutions positronium formation 2−80988

potassium chloride
  absorption band spectra obs. of quasimetallic centres 2−72338
  absorption spectra, flash light excitation, F-centre behaviour 2−43649
  aqueous soln., freezing using temp. gradient microscope stage 2−74585
  Auger spectra using spectrometer with concentric hemispheres 2−74610
  channelling pattern recording using radioactive recoil atoms 2−54088
  cleavage of single crystal, dependence on cooling velocity 2−84122
  coherent neutron scatt. amplitudes from powders 2−53654
  colour centres, electron microscope obs. in cathode luminescence mode 2−80708
  colour centres, electronic struct. calc. and electronic polarization fields 2−71520
  colour centres, magnetic amplification of positronium effect 2−68039
  conduction, high-field current transients, electron hopping and localized levels 2−68425
  crystal growth, Czochralski method, diameter control, laser appl. 2−60715
  crystal growth, from soln., evidence for spiral mechanism 2−50586
  crystal growth, from soln., in presence of Pb^{2+} 2−47237
  defect pairs, intrinsic and extrinsic, association energies 2−80651
  dielectric consts., l.f., press. and temp. derivatives 2−51188
  diffusion coeff. of self- trapped holes and migration to thallium centres 2−68709
  diffusion of ion-implanted ^{85}Kr, effects of channeling, radiation damage and divalent doping 2−68053

Potassium compounds continued
potassium chloride continued
diffusion of water mols., influence of OH$^-$ ions 2−60831
dislocation formation during Czochalski growth, functional dependence 2−53616
F′-centre to F-centre conversion, ENDOR obs. 2−71529
F-centre, relaxed excited state, dynamical Jahn-Teller effect 2−43647
F-centre, thermal aggregation mechanisms 2−64683
F-centre colouring, γ-ray induced, strain effects 2−71528
F-centre g_{orb} factor determ. by mag. circular dichroism and Faraday effect 2−77596
F-centre hyperfine interactions, press. depend., ENDOR study 2−83986
F-centres, excited, emission mechanisms 2−80709
F-centres, thermal transform. into colloids, dislocation induced precip. 2−71525
film, controllable secondary electron films, controllable emission, applic. to particle detectors 2−72098
film, form. by vapour deposition, elec. field effects 2−64570
film, porous, energy distrib. of transmitted secondary electrons 2−81190
gamma-irradiated, high temp. dependence of electron Hall mobility 2−44174
Gruneisen constant at absolute zero 2−61113
H-centre prod. by u.v. photodestruction of U$_2$-centres, optical and e.s.r. obs. 2−77599
harmonic band parameters of NO$_2^-$ and NO$_3^-$, high temp. 2−54410
Hartree-Fock band structure 2−61172
heat of dissolution, in water, 20°C 2−48314
in high concentration ice, dielectric dispersion 2−75142
ionic Brillouin effect, theory 2−84502
ionic cond., press. depend. 2−44154
ionic melt, microstructure, computer generated configurations 2−43319
ionicity, dispersion, and optical spectra 2−44374
lattice dynamics, resonant phonon modes of Au$^+$ 2−54018
limiting optical frequency, temp. variation calc. 2−72311
local and gap modes due to substitutional impurity 2−47731
localized modes for H$^-$ centre, calc. 2−74963
localized one-electron states for crystal with divalent activator 2−84287
luminescence, hot, from vibrational transitions of OH$^-$ molecular ion 2−57369
M centre triplet state, quadrupole interactions, ENDOR obs. 2−72533
migration of water drops, under various driving forces 2−47466
molecular CO^{2}-$_3$ centre, i.r. spectra 2−71350
paraelectric centres, low zero field splitting, caused by OH$^-$ substitution 2−75147
phonon modes of Ag$^+$ 2−50994
photoemission, in ultra high vac., from colour centres 2−48023
position capture by colour centres, tempering effect 2−54092
pure and doped, hardness, yield strength, Young's modulus 2−56835
R$_2$ centre, analysis of absorp. struct. 2−51342
radiation hardening, γ-irrad. at LNT, H$_a$ band obs. 2−53754
reflection spectra in vacuum u.v., investigation using synchrotron radiation 2−44367
single crystals, pure and doped, extent of perfection 2−60822
sputtering, positive ion ejection patterns 2−44008
Stark effect of M- and N-centres 2−61624
surface, polygonization, produced by electron bombardment and illumination 2−50457
sylvite from W. Germany, K-Ca age determ. 2−81638
thermal conductivity, temp. depend., role of longitudinal and transverse phonons 2−84214
two-electron U-centres, point-ion models 2−83987
u.s. waves, phonon absorp., relax. theory 2−68233
vaporization rate of crystal surface, effect of MnCl$_2$ mol. beam 2−71281
whiskers, growth on KCl crysts., and struct. 2−67914
whiskers, slightly deformed, etch pit distrib. 2−71490
X-ray diffuse scattering, higher anharmonic contribs. 2−61059
μ^+ meson depolarization, muonium stage 2−80933
CsCl-KCl and CsCl-KCl-NaCl systems, M.P. AND phase transform. 2−43932
KBr-KCl mixed crystal, with and without colour centres, spectra 2−74801
KCL:Tl, electron pulse irrad., colour centre formation 2−71524
KCl:Ag, colour centre form. by X-ray irrad., e.p.r. and optical obs. 2−80713
KCl:Ag, thermostimulated electron emission, retarding field depend. 2−54274
KCl:Ag$^-$, polarization and decay time of luminesc. of Ag$^-$ centres 2−80710
KCl:Ba, solid soln. two temperature regions of decomposition 2−80526
KCl:Br-, with low Br- conc., optical absorpt., 77K 2−65259
KCl:Br, BrCl$^-$−V$_k$ centre, e.s.r. 2−81461
KCl:Ca^{2+}, positron annihilation, temp. and mag. field effects 2−77850
KCl:Co(CN)$_6^{3-}$, vibr. and electronic props. 2−54413
KCl:Eu^{2+}(Yb^{2+}) (Sm^{2+}), impurity-vacancy dipole relax. and aggregation, and X-ray effects 2−83982
KCl:In, thermostimulated electron emission, retarding field depend 2−54274
KCl:In(Tl), ionisation of In^{2+} and Tl^{2+} centers by interstitial halogen atoms 2−81001
KCl:KI films, slow electron impact, luminescence excitation and characteristic energy losses 2−81417
KCl:KOH, tunnelling levels, low temp., thermal cond. obs. 2−71758
KCl:(Li$^+$,Br-), H$_a$(Li$^+$)-type BrCl- centre, e.p.r. obs. 2−60825
KCl:(Li$^+$,I-), H$_a$(Li$^+$)-type ICl- centre e.p.r. obs. 2−60825
KCl:Li, generation and detection of 55 GHz phonons, paraelec. reson. study 2−84191
KCl:Li$^+$, ENDOR of A-centre electrons rel. to external elec. field 2−78176
KCl:Li$^+$, reorientation motions of H$_a$-centre 2−43648

Potassium compounds continued
potassium chloride continued
KCl:Na, F$_b$ centres, absorpt. and emission study 2−64682
KCl:Na impurity effects on colorability 2−77595
KCl:Na M$_a$ centres, information storage using photodichroic effect 2−49399
KCl:Na$^+$, X-ray irrad., hole centres, conversion and struct., optical absorpt. 2−84523
KCl:NaCl, symmetry of far i.r. resonant-pair mode 2−84507
KCl:OH$^-$, X-irrad., temp. effect on F-centre formation 2−47449
KCl:Pb, polarized luminesc. and dipolar relax. of Pb-vacancy complexes 2−72424
KCl:Pb, rapidly grown from melt, thermal stress defect model 2−50649
KCl:Pb^{2+}, grown from soln., inhomogeneous impurity distrib., spectrophotometric obs. 2−74796
KCl:Sn, M^{2+} (M=Mg,Ca,Ba,Zn,Cd), luminescence studies 2−65294
KCl:Sr, X-ray induced defects, thermal annealing, absorp. and luminesc. obs. 2−64684
KCl:Tl, luminesc. excitation spectra near fundamental absorpt. 2−48244
KCl:Tl, room temperature absorption and thermal glow 2−75333
KCl-H$_2$O frozen solns., permittivity discontinuities at crit. pt. 2−53499
KCl-KBr, mixed cryst., proton dechannelling, lattice distortion effects 2−47785
KCl-KBr solid solution, cryst. growth, for neutron monochromator appl. 2−47205
KCl-KBr solid solution, internal stress at Luders band front 2−84043
KCl-KBr solid solutions positronium formation 2−80988
KCl-KI:Tl, intracentre luminesc. 2−81425
KCl-K$_2$O-B$_2$O$_3$ glass, X-irrad., e.p.r. obs. of Cl^0 2−81463
KCl-NaCl mixed single crystals, phase separation during heat treatment 2−74884
KCl-NaCl solid solns., supersaturated, decomp. 2−43921
KCl, sylvite, thermal oscillation freqs., 295, 80 and 5K 2−64835
KCl.SnCl$_2$.H$_2$O, luminescence, absorption and emission spectra 2−54456
2 KCl.SnCl$_2$.2H$_2$O, luminescence, absorption and emission spectra 2−54456
K$_x$Rb$_{1-x}$Cl solid solutions, linear thermal expansion coefficients and lattice parameters 2−64861
Kcl:SH$^-$(SD$^-$), i.r. spectra, expt. and interpretation 2−84491
NaCl-KCl mixed crystal, with and without colour centres, spectra 2−74801

Potential energy, gaseous molecules *see Molecules/intermolecular mechanics*

Potential energy, single molecules *see Molecules/internal mechanics; Molecules/vibration*

Potentiometers *see Electrical measurement*

Powder diffraction cameras *see X-ray crystallography/apparatus*

Powder metallurgy *see Metallurgy; Sintering*

Powders
see also Granular structure; Particle size; Sintering; Surface measurement
alumina from vapour-deposited powders, reactive hot pressing 2−68171
bronze, spherical particles, sintering kinetics 2−43890
centrifugal sedimentation particle size analysis method, uncertainties, deviations from Stokes law 2−68170
ceramic, binderless granulation mechanism and sphere growth 2−47660
combustion in gas stream, mathematical model 2−61782
composite, use for coatings, new development 2−61010
compressed, pellets, i.r. refl. spectra rel. to struct. 2−68620
crystalline, piezoelectricity meas. apparatus 2−59031
diamond powder, oxygen chemisorption, kinetics 2−65374
dispersing and disaggregating method, rel. to quantitative SEM and optical microscopic studies 2−43884
e.p.r. lineshape calc. 2−65319
fine particles, sample prep. for scanning electron microscopy 2−50905
flowmeter 2−56302
fluidization, bottom restrained countercurrent, of binary particle mixtures 2−80193
fluidization column, solid flow pattern induced by single bubbles 2−80188
fluidized, horiz. vel., stat. meas. using piezoelec. prop. 2−43883
fluidized bed, gas, limiting factors in heat transfer 2−80190
fluidized bed, solids motion caused by a bubble 2−80191
fluidized bed, three phase, caused by size distribution of gas bubbles 2−80192
fluidized beds, liquid, mixing processes 2−80189
friability, comparison device 2−53939
friction, cohesion, elec. cond., effect of temp. and press. 2−43880
gas distributors design, and prediction of bubble size in large gas-solids fluidized beds 2−80186
glass, sintering, modelling of Fra Mauro breccias form. 2−62671
graphite, electrothermal, crystallite size 2−57001
graphite, fine-disperse, effects of oxidation on pressing ability 2−77737
Kubelka-Munk diffuse reflectance remission function rel. to fund. optical parameters 2−79329
α-lactose monohydrate, failure props. 2−43889
layer, finely dispersed, vibration effects 2−43393
luminophore grains, in dielec. medium, equiluminesc. curve 2−48213
magnetic oxides, sub-micron range, particle size distribution measurement, electron microscopy 2−71654
magnetic powder testing, comparison of use of a.c. and d.c. produced magnetic fields 2−59067
metal, contact stresses, electron microscope obs. 2−56970
metal, high-speed pressing, occurrence of strong shock waves 2−43885
metal, on the possibility of thermal explosion 2−61003
metal, rolling mechanism in initial nonstationary period 2−50908
metal, spark isostatic pressing 2−68129

Powders continued
metal-powder formation at metal-electrolyte interfaces, determ. of potential barriers and eqns. of tunnelling limiting current 2—57426
metallurgy, production of Fe-Ni-Mo, carbonyl method 2—68159
metallurgy, structural aspects of densification 2—56946
metals, e. microscopy study of adhesion and surface energy of contact zones 2—64789
mixing for spectral anal., applic. of ultrasound 2—65406
n.m.r. patterns, graphic analysis in the presence of quadrupole interactions 2—48300
particle ejection and entrainment from gas-fluidized beds 2—77177
particle size analysis by Sartorius sedimentation balance, correct end-weight determ. 2—43881
particle size and size distribution effect on the behaviour of gas-fluidized beds 2—80187
particle size distribution, effect on packing props. in high silica 'roseki' refractories 2—64786
permittivity, correl. between powder and bulk over range of permittivity and packing fraction 2—61411
pore size and shape distrib. from porosimetric hysteresis curves 2—43882
powder metallurgy of high-temp. materials, conference, Tyrol, Austria, June 1971 2—53937
pressure distribution in powders, theory 2—84129
pressure distribution in powders filled in a conical vessel, theory 2—84130
quartz, glassy sphere production from particles by processing through plasma stream 2—56971
rigid spherically shaped particles, random packing density 2—80791
scanning electron microscope exam. techniques 2—43565
sintering, combined, initial kinetic eqn. analysis 2—50903
sintering, initial, diffusion models, effect of particle size distrib. 2—50904
sintering, role of dislocations 2—61002
sintering under isostatic press. 2—50859
spherical particles, quasi-liquid flow, pressure loss equation 2—60139
spheroidal, sintering kinetics 2—50907
spout diameter prediction in the spouted lead technique 2—77176
statistically heterogeneous mixture, coordination of particles 2—43878
surface area, meas. by nitrogen desorption, apparatus 2—56969
thermal conductivity meas. using probe and bridge circuit 2—64863
volume diffusion controlled pore shrinkage during final stage sintering 2—50854
X-ray diffr., intensity rel. to granularity 2—74700
Yttralox ceramic, Th-doped, processing 2—50900
Ag, compaction process 2—50909
Al_2O_3, thermal diffusivity and cond. simultaneous meas. by flash method 2—43996
Al_2O_3 particles in flames, i.r. emission and temperature measurements 2—73468
^{241}Am target, prep. and purification 2—73908
B_4C, neutron irrad. damage, electron microscope obs. 2—47369
BeO, initial stage sintering mechanism 2—47662
C black, tinting strength 2—75281
$CaCO_3$, failure props. 2—43889
CaF_2, sintering activity, effect of calcination 2—61004
CdS:Cu phosphors, a.c. electroluminesc. characts. 2—44420
CdS:Cu phosphors, d.c. electroluminesc. characts. 2—44419
CdSb:Ag pressed powders, elec. cond. detn. 2—64906
Cu, drying, effect of temp. and ambient 2—80828
Cu, particle size distrib. determ. 2—43891
Cu, vibr. packing, inertial loading effect 2—50911
Eu_3SiO_5 synthesis by chem. transport 2—48173
Fe-Co-Ni alloy powder, highly disperse, effect of electrolytic prep. variables on mag. props. 2—68543
Fe-Ni carbonyl, phase composition 2—77726
Fe, fine, sintering 2—61000
Ge surfaces, heat-treated in various atmospheres, e.s.r. obs. 2—72488
$Li_{0.93}Na_{0.07}Fe_5O_8$, sintering, effect of conditions on density and particle size 2—64790
$MgAl_2O_4$ spinel, densification kinetics 2—50889
MgO refractories, effect of stress on grain growth 2—74915
Mn-Zn ferrite powders, comp. effects on technological props. 2—68163
Mo digermanide, reaction hot pressing from Mo and Ge powders 2—61001
Ni-B coatings, particle distrib., heat treatment effects 2—77730
Ni-(5wt.%)Fe-(5wt.%)W, powder composite, fracture micromechanism obs. 2—56947
Ni-Fe compact, structural aspects of densification 2—56946
Ni-HfO_2, effect of dispersion strengthening phase on thermal stability 2—77739
Ni-Zn ferrite, hot-pressing and densification 2—43893
Ni-Zn ferrite, mag. quality characterization 2—57312
Ni, mag. props., temp. depend. 2—51260
Ni, structural aspects of densification 2—56946
Ni powders, monocrystalline, temp. depend. of rotational hysteresis 2—68508
$Ni_{1-x}O$, sintering, effect of O partial press. 2—61005
^{237}Np target, prep. and purification 2—73908
Pt black, low temperature sintering, mechanism 2—43894
^{241}Pu, target, prep. and purification 2—73908
Sn, finely dispersed, supercond. crit. temp., particle size and oxidation effects 2—61230
TiB_2, sintering kinetics, particle size effects 2—61006
TiN, prod. using s.h.f. discharge 2—43896
TiO_2 compact, abrupt shrinkage on sintering, SEM obs. 2—43895
UO_2 pellets, prep. by sintering of $(NH_4)_2U_2O_7$ 2—80800
W, explosive compaction of powders by direct method, survey 2—61008
W, powder metallurgical, pure, doped and thoriated material, high temp. creep in wires 2—61007
W, sintering activation by Ni and Fe, mechanism 2—50899
W, with Ni additive, sintering, modified model 2—43897
ZnCdS-Cu, Mn powder crystallophosphors, interaction of electrolum. and photocond. during switching 2—68710
ZnO, particle size distrib. data processing, computer appl. 2—53942

Praseodymium
electrical resistance, anomaly near Neel temp. 2—51281
energy band calculations with combined basis function method 2—80991
f.c.c., singlet-ground-state ferromagnet, mag. excitons 2—72153
f.c.c., singlet-ground-state ferromagnet, neutron scatt. obs. 2—72152
magnetic properties and crystal field effects 2—75205
magnetic properties in magnetic fields 2—65121
magnetic-ground-state props. of single crysts. 2—48078
yield spectroscopy, fine struct. of 4d excitations 2—61675
$CaF_2:Pr^{3+}$, energy levels of tetragonally sited Pr^{3+} 2—80989
$CaF_2:Pr^{3+}$, linear dichroism due to stress induced mixing of electronic states of anisotropic centres 2—84462
in Cr, O-enriched, solubility 2—43830
$La_2Mg_3(NO_3)_2.24H_2O:Ce^{3+},Pr^{3+}$, spin-phonon interaction, e.p.r. obs. 2—44316
Pd: ^{167}Er, ^{63}Dy, hyperfine splitting, consts., e.s.r. 2—72497
Pr^{3+}, analytical SCF wavefunctions for ground and some excited states, calc. of oscillator strength for optical transitions 2—52915
Pr^{3+}, electronic shielding in crysts., variational and outward integration calc. 2—81319
Pr^{3+} effect of core polarization on f-f interactions 2—52929
Pr^{3+} impurity in Al_2O_3-Fe_2O_3 system, effects on spin relax. time of ferric ions 2—54368
Pr^{3+} in $Y_2O_2S:Eu^{3+}$, sensitization of luminesc. 2—51371
Pr_3Tl and $(Pr_{1-x}La_x)_3Tl$, induced-moment system, ferromagnetism 2—72154
^{141}Pr, h.f. n.m.r. at 4.2 degrees K 2—72518

Praseodymium compounds
oxides, higher, cryst. growth and struct. 2—47243
tartrate complexes, i.r. circular dichroism 2—67521
Co-Pr-Sm alloys, 10000 Oe B-coercive force magnet, props. optimization 2—44247
Pr-Cr_2O_3 glasses, absorption spectra 2—75286
Pr-Th alloys, h.f. n.m.r. at 4.2 degrees K 2—72518
Pr-γ alloy, h.f. n.m.r. at 4.2 degrees K 2—72518
Pr complex, tris(2,2,6,6-tetramethyl-3,5-heptadionato-) praeseodymium dimer, magnetic susceptibility down to 4.2 K 2—61481
$PrAg_2Si$, prep. and cryst. struct. 2—74735
PrB_6, nonstoichiometry 2—47183
$PrCl_3$, low temp. cooperative behaviour, n.m.r. obs. 2—72166
$PrCo_2$, dissolved hydrogen effect on elec. and mag. behaviour 2—48040
$PrCo_5$, permanent mag. 2—52385
$PrCo_5$ magnets, sintering with Sm-Co additive 2—50797
$Pr_2Co_{1.7}$, intermetallic, cryst. struct. 2—47341
$Pr_2(Co_{1-x}Fe_x)_{17}$, lattice consts. 2—50626
$PrCu_2$, cooperative nuclear magnetic order below 54 mK 2—51282
$PrCu_2$, spontaneous mag. order, 54 mK 2—44225
PrF_3, Raman matrix isolation spectra, investigation of matrix effects on molec. structure 2—60031
PrF_4, thermal decomp., elec. deflection study 2—51431
PrGa, magnetization and susceptibility, temp. depend. 2—72170
PrH_2, paramag. behaviour, sensitivity to hydrogen conc. 2—77986
$PrIn_3$ magnetic properties 2—72223
$Pr_2(MoO_4)_3$, cryst. struct. 2—74736
$PrNi_3$, mag. struct. 2—48080
PrO_x-ZrO_2 ternary system, phase relationships, oxygen press. effect 2—47694
PrO_2, Mossbauer scatt. of ^{141}Pr, hyperfine fields detn. 2—48151
Pr_6O_{11}, far-i.r. spectra, phonon excitation 2—51346
PrP_{1-x}, phase diagram, homogeneity region, limits of existance, 400-1000°C 2—74956
$PrRu_2(Os_2)$, struct., high press. effects 2—71689
$Pr_2(SO_4)_3.8H_2O$, spin-lattice relax. of rare earth ions 2—78051
PrTe, press. induced electronic collapse and struct. changes 2—68297
PrTe, press. induced struct. and electronic transform. 2—50948
Pr_3Tl-La_3Tl, induced moment system, superconductivity and mag. props. in paramagnetic region 2—72115
Pr_3Tl, singlet-ground-state ferromagnet, neutron scatt. obs. 2—72152
Pr_3Tl, singlet-ground-state ferromagnet, mag. excitons 2—72153
Pr_3X, (X=Al, Ga, In, Tl, Sn, Pb), supercond. and mag. props. 2—61244
$Pr_2Zn_{3c}Mg_{3(1-c)}(NO_3)_{12}.24H_2O$, satellite lines, field perturbation energy 2—72345
$Pr_2Zn_{3c}Mg_{3(1-c)}(NO_3)_{12}.24H_2O$, satellite lines, Zeeman effect, field perturbation 2—72344
$(Sm_{1-x}Pr_x)Co_5$, $0<x<1$, alloys, saturation magnetization, anisotropy field, coercive force 2—68510

Precipitation
see also Atmosphere/precipitation
aerosol sampling lines, transmission efficiency rel. to deposition 2—60526
Al-Mg alloy, rel. to intergranular corrosion susceptibility 2—71646
alloy, coarsening of precipitates, cumulative distrib. functions 2—47603
alloy, coherent phase formation, interfacial and strain energy effects, review 2—57007
alloy, grain boundary precip. coarsening, cumulative size distrib. function 2—47604
alloy, ternary, solidification behaviour, microsegregation and precip. mechanism 2—56915
alloy, two-phase, effects of coherency strain fields on dislocations struct. 2—56702
alloys, with different volume disparity between precip. phase and matrix, ageing, X-ray obs. 2—71634
coherent precipitate, parallel plate- shaped, strain energy influence on arrangement 2—71670
coherent precipitates in elastically anisotropic mats., diffraction constant 2—80671
colloids, gravitational deposition from laminar channel flow 2—83814
convective cloud, numerical simulation formation of long-lasting cloud 2—84815
crystalline ceramics 2—84063
electron microscope obs., applic. of high voltage metallography 2—56632
electrostatic techniques in cloud seeding 2—62191

Precipitation continued
eutectoid decomp., lamellar eutectoid growth, stepwise growth model 2−50814
gel, aqueous, effect of freeze/thaw treatment 2−83807
inert gas bubbles in solids, computer simulation of precipitation kinetics 2−64424
interfacial stress, at incoherent particles during coarsening 2−53798
metal, solute segregation around growing voids 2−53697
mischmetal-Mg alloys, dilute, metallographic obs. of eutectoid reaction 2−80794
pyroxene, lunar and terrestrial minerals, spinodal mechanism 2−62689
review 2−68187
solid solution composition changes from lattice parameters 2−61027
from solution, size distrib. effects 2−46992
spinodal decomposition, diffuse interface expansion, higher derivative terms 2−56951
spinodal decomposition, mean field pair interaction theory 2−56952
steel, 18-8 stainless, carbide precip. rel. to creep rupture strength 2−77684
steel, 38KhNVA, of structurally free ferrite during tempering 2−47689
steel, γ'-phase precip., influence of quenching temp. 2−80768
steel, austenitic, $Cr_{23}C_6$ precip., effect of Ni 2−47622
steel, austenitic, of VC during ageing, strengthening 2−47636
steel, austenitic Cr-Ni, rel. to intergranular corrosion susceptibility 2−71646
steel, austenitic stainless, at twin boundaries 2−43850
steel, austenitic stainless, containing delta ferrite, segregation and homogenisation 2−43847
steel, austenitic stainless, segregation and effects of B 2−47623
steel, austenitic vanadium nitrogen type, fine precipitates struct. 2−53893
steel, fully heat treated low alloy, effects of sulphide morphology as impact properties 2−56908
steel, high-C martensitic, tempering, carbide precip. 2−64762
steel, high-C martensitic, tempering, carbide precip. 2−64761
steel, low-C, hot-rolled, quenched transformation effects on microstruct. 2−57017
steel, low-C low-alloy, fine struct. and phase comp. at elevated temps. 2−53898
steel, low-C martensitic, ageing 2−50834
steel, martensitic, effect of lath boundary precip. on fracture toughness 2−57018
steel, martensitic, fracture mechanism, incompat form. at grain boundaries 2−56815
steel, martensitic, low-C Mn, effect of Sb on high temp. tempering, cementite coarsening 2−56905
steel, martensitic stainless, ageing 2−53989
steel, microalloyed, KODUR 60, of plane carbides of Ti and Nb 2−47631
steel, quenched, effect of cooling rate 2−47587
steel, quenched, quench-aged, fatigue behaviour rel. to microstruct. instability 2−50768
steel, stabilized recovery-induced substruct., formation for improved creep resistivity 2−56913
steel, stainless, characteriz. for fast breeder reactors 2−50648
steel, transformer, precip. at grain boundaries, rel. to coercive force 2−47632
steel. low-C, low-alloy, of AlN 2−50833
steel tempering, Ostwald ripening obs., grouping errors in data analysis 2−60942
superalloys, precipitation hardened, study of submicroscopic particles using extraction replica electron microscopy 2−80817
Ti-Mo binary alloys, phase separation processes in beta phase during aging 2−80816
weld metal, toughness below 0°C, effect of metallurgically conditioned inhomogeneities 2−74890
Ag-Cu alloy, 7.5 wt% Cu, discontinuous precip. kinetics, 200-500°C 2−80856
Ag-Mn-Al alloy, high coercivity, struct. of ferromag. precip. 2−43821
Al-Ag alloy, pre-precip., elec. resist. and Hall coeff. variations 2−77692
Al-Ag alloy, precipitation process study 2−84133
Al-Ag system, discontinuous reactions and ternary component influence 2−71674
Al-2.5 wt.%Mg alloy, neutron irrad., of Mg_2Si, transmutation produced 56922 2−56922
Al-1.2 wt%Mg_2Si alloy, two-step ageing behaviour 2−64765
Al-Cu-Mn alloy, heat treatment, homogenization, precip. 2−43786
Al-Cu alloy, film, second phase particle form., rel. to bulk alloy props. 2−47099
Al-4%Cu alloy, rel. to effects of additional elements on ageing 2−56910
Al-Fe alloy, microhardness rel. to precip. of Fe and annealing out of lattice defects 2−50828
Al-Fe alloy, of Fe 2−50827
Al-Mg-Si alloy, during ageing, structure of metastable precipitates 2−56909
Al-Mg and Al-Mg-Zn alloys, preprecip. zone obs. 2−53885
Al-9%Mg alloy, effects of additional elements on ageing 2−50801
Al-Si dilute alloy film, of Si, resist. study 2−50825
Al-Zn-Mg alloy, precipitate free zone, elec. microscope obs. 2−56902
Al_2O_3:Ti, precip. hardening kinetics 2−50872
α-Fe-Sn solid soln., supersaturated, precip. of FeSn by dislocations, effect of third component on morphology and kinetics 2−80812
$BaSO_4$, crystal growth kinetics and mechanisms 2−51420
$BaTiO_3$:F, prep. by precip. from $TiCl_4$ and $Ba(NO_3)_2$ aq. solns. 2−74675
Be-(1 wt.%)Fe alloy, thermal treatment, Mossbauer obs., mechanism 2−50931
Be bronze, hardened, cold worked, press. induced thermal activation 2−43781
Co-Cr-C alloy, effect of $Cr_{23}C_6$ precip. on strengthening 2−57011
Co-Cr-C solid soln., activity and solubility of C, 950-1200°C 2−56925
Co-Ti alloy, solid soln. decomp. 2−56933
Co alloy, dispersion hardened 2−50831

Precipitation continued
Cu-1 at.%Fe alloy, of Fe during ageing, Mossbauer obs. 77724 2−77724
Cu-Co alloy f.c.c. single crystals, effect of coherent precip. on work-hardening 2−50798
Cu-Cr alloy, dispersoid struct. precipitated by tempering 2−43832
Cu-(0.6 at.%)Cr alloy, precip.-hardening, neutron irrad. effect 2−43833
Cu-(30 wt.%)Ni-0.3 wt.%)Be alloy, age hardening precipitate phases, struct. and morphology 2−50934
Cu-Ni-Fe alloy, intergranular fracture on spinodal decomp., mechanism 2−57012
Cu-Zr-Cr alloy, specific heat and resistivity obs. 2−50933
Cu, of Fe_3O_4 impurities, effect on residual resist. 2−71832
Cu(15.1 at.%)Sn alloy, β_1 phase stabilization mechanism47684 2−47684
Fe-Au alloy, rel. to G.P. zone form., dislocations, vacancies 2−43851
Fe-1%C-0.5%As alloy, anomalous precip., resistivity, internal friction and elec. microscope obs. 2−50940
Fe-C-W alloy, of eutectic carbide, and microsegregation obs. 2−74929
Fe-C alloy, carbide precip. rel. to quench ageing and reversion 2−56903
Fe-(0.11 wt.%)C alloy, austenite grain size effects on Widmanstatten start temp. of proeutectoid ferrite reaction 2−68195
Fe-Co(Ni)-Ti-Al alloy, solid soln. decomp. 2−56933
Fe-Ge α' solid solution, of ε phase 2−64819
Fe-Mn alloy, field ion microscopy exam. comparing orientation to ferrite α and iron nitride 2−64777
Fe-Mo alloy, rel. to G.P. zone form., dislocations, vacancies 2−43851
Fe-Mo alloys, nitrided, substitutional interstitial G.P. zones 2−80826
Fe-(6 at.%)Mo alloy, electron microscope analysis43849 2−43849
Fe-N alloy, carbide preip. rel. to quench ageing and reversion 2−56903
Fe-Ni-Al alloy, effect of dispersion particles on martensitic transformation 2−57015
Fe-Ni-C-Mo-Cr alloy, during tempering 2−43853
Fe-Ni-C alloy, during tempering 2−43853
Fe-Ni-C alloy, martensitic, fracture mechanism; incompat form. at grain boundaries 2−56815
Fe-Ni-Co-Mo, maraging alloy, coherent precip. electron microscope obs. 2−57019
Fe-Ni-Nb-C alloy, ageing, 700 and 800°C 2−47596
Fe-Ta alloy, ductility enhancement using allotropic phase change 2−57020
Fe-Ti-Si alloy, during age hardening 2−43806
Fe-V-C steel, fibrous VC_x occurrence after transformation, precipitate morphology 2−61033
α-Fe-Zn solid solution, effect of P additive 2−80855
Fe, cast, of spheroidal graphite during annealing 2−47584
Fe, cast, rel. to bainite growth kinetics 2−43920
Fe, cast, spheroidal graphite, segragations rel. to microstruct. 2−50836
Fe, nitrided zone refined, $Fe_{16}N_2$ precip. rel. to ductile-brittle transition 2−47629
Fe_3C condensed films, carbide grain growth 2−56932
Fe_2O_3 and Fe_3O_4, morphological and struct. changes during reduction 2−50881
GaAs, selective photoetching obs. of precipitates 2−71364
Ga_2O_3, coprecip. during liquid phase epitaxy of GaP 2−50609
GaSb:Te, segregation coeff. of Te 2−74798
Ge, of Cu, vacancy effects 2−64659
In_2S_3-Ag_2S solid soln., coprecip. diagram 2−53901
KCl, F-centres, thermal transform. with colloids, dislocation induced precip. 2−71525
KNO_3, of bivalent metal nitrates, solid soln. form. 2−56942
Mg-Th, Mg-Th-Mn, Mg-Mn, Mg-Zr alloys, elec. microscope obs. 2−53993
Mg-Th and Mg-Th-Zr systems, e. microscopy exam. 2−71690
Mg-Zr alloy, on diffusion of Ni, 350-500°C 2−47467
Mg alloys, internal hydride form., kinetics and equilibria 2−47639
MgO-Al_2O_3-ZrO_2-SiO_2 glass, complex particle growth, small-angle X-ray scatt. obs. 2−67887
Mg_2Si-Al alloy, supersaturated solid soln., clustering mechanism 2−50822
Mn-Ga alloys, rel. to internal friction 2−50735
Mo-Ru alloy, of intermetallic cpd. 2−50840
Mo alloy, of Ti and Zr carbides, strengthening during ageing 2−47643
NaCl:Cd^{2+}, dissolution of precipitates study 2−83844
Nb-H system, hydride precip. at sub-ambient temps. 2−47693
Nb-N alloy, of nitride, prismatic loop generation 2−53994
Nb-O alloys with Zr and Hf additions, electron microscope obs. 2−43857
Nb-Zr-Ti alloy, supercond., after cold deform. and low temp. annealing 2−50842
Nb-(40 wt.%)Zr alloy, metallurgical variables influence on supercond. 2−47861
Nb(38 at.%)Hf alloy, precipitate dispersion, rel. to supercond. fluxoid pinning 2−44076
Ni-Cr-Ti alloys, strengthening by precip. of intermetallic phases 2−43859
Ni-40%Cr alloy, containing Al and Ti, precip. hardening 2−64767
Ni-Cu-Al-Ti alloy, during age hardening 2−53878
Ni alloy, transmission electron microscope obs. rel. to strength 2−56945
Ni ceramic, refractory oxide particle growth, matrix density effects 2−68169
$Ni_3(Al,Ti)$, Ni-rich γ'-phase, solidification behaviour and γ-precip. 2−53904
Pb-Sb alloy, mechanism, hardness, resist. and microscopy studies 2−80858
Sc_2O_3-MgO solid soln., super saturated, deposition of Sc_2O_3 2−74906
Si-Ge alloy thermocouples, of dopants 2−51210
SiO_2-Al_2O_3-K_2O-Na_2O glasses, formation of leucite and thermal expansion 2−74994

Precipitation continued
Sn-Bi-As system, Sn_4As_3-Bi-SnAs subsystem, primary phase of precip. 2−74942
Ta-W-Hf alloy, rel. to effects of O contamination on tensile props. 2−43862
TaC-Co alloy, oversaturated, microstructure 2−64775
Ti-Mo alloy, ω-phase precip., rel. to resist. anomalies 2−84297
Ti-Ta alloys, martensitic, precip. reactions 2−47697
α-Ti, hydride precip., resistometric obs. 2−64813
TiC-Co alloy, oversaturated, microstructure 2−64775
U-9.5 wt %Nb alloy, gamma phase decomp., discontinuous precip., 450-600°C 2−80802
UC-UN system, rel. to solid soln. formation 2−53910
V-N system, V_3N precip., electron microscope obs. 2−50978
V, neutron irrad., activation volume rel. to dose and strain, interstitial impurity precip. 2−80663
VC_x:B, and dislocation struct., electron microscope obs. 2−61038
WC-Co alloy, oversaturated, microstruct. and reaction behaviour 2−64775
WC-Co cemented carbide, of Co_3W, internal friction recovery obs. 2−68070
Yb-Al system eutectic transformations 2−80797
Zn-Cd alloy, microsegregation of Cd during growth, partition coefficient 2−47648
Zr-(2at.%)Cr-(0.16at.%)Fe alloy, precip. reactions rel. to corrosion resist. 2−53919
Zr-(2.5 wt.%) Nb press. tubing, hydriding, orientation and effect on tensile props. 2−50849

Pressure
see also Atmospheric pressure and density; High pressure phenomena and effects; Radiation pressure; Vapour pressure
distribution on yawed wedge interacting with oblique shock waves 2−69689
distribution over yawed wedge surface, interaction with shock wave 2−76380
elastic half-space, pressure of strip block 2−63057
flow, laminar, through rotating vertical cylinder, vel., friction loss, press. gradient 2−67714
fluids, pressure effect at arbitrary Knudsen numbers 2−74312
hydraulic, of liquid on cylindrical shell during hydraulic shock 2−83743
Lockhart and Martinelli flow model, calculation of pressure drop and hold up 2−56455
organic dye solution, impulse pressure formation by emission from Xe impulse lamp 2−53378
powder, filled in a conical vessel, theory of pressure distrib. 2−84130
powder, theory of pressure distribution 2−84129
regulator with pneumatic electric control, for vapour in cryostat 2−69487
subsonic turbulent air jets, fluctuations, space correlations of 2−71076

Pressure measurement
see also Manometers; Vacuum gauges; Vapour pressure measurement
aerodynamic, below liquid wave crests, measurement method 2−67780
aneroid sensing element for radiosonde 2−72735
atmospheric pressure level determ. by two-satellite microwave occultation method 2−84858
bluff body flows, influence of taper 2−80212
contactless vacuum thermal transducers 2−58695
deadweight free piston gauge with electromagnetic equilibrium 2−69492
deep ocean floor, quartz crystal sensor 2−44667
direction-insensitive static head sensor, wind-induced pressure in ambient air stream 2−82131
electrostatic feedback transducer for meas. of low differential pressure 2−58697
gas-liquid two-phase flow, pressure drop 2−70845
gases, average pressure measurement 2−53268
gases, micro-scale for meas. over eight decades 2−66411
gauge, damping device 2−76164
gauge utilizing static dielec. const. press. depend. 2−65046
Geodyne model underwater sensor unit 2−72720
heat transfer and pressure drop performance of roughed surfaces used in nuclear reactors 2−59872
hypersonic flow, low-density, surface meas. 2−83665
insert earphone pressure response in real ears and Zwislocki couplers 2−48899
intracranial, using modified pressure transducer 2−69296
intracranial pressure wave detection with ultrasound 2−69304
intraoral air pressures associated with stop consonants in various phonetic environments 2−45058
lip and tongue pressure patterns during syllable production 2−45057
liquids and gases, manometers 2−66410
luminescence method for high pressures 2−58658
near magnetized plasma, fast pressure gauge 2−56363
magnetron press. gauge on O VI-15, adsorption/desorption press. effects 2−58148
manganin pressure transducers, influence of high pressure H_2 on electrical resistance, compared with Au-Cr alloy 2−76122
metal, liq., equilib. thermodynamic states, at high temp. and press. 2−46949
meter for viscous resin obs. at high temps. 2−45224
noninvasive pressure pulse recorder, clinical applications 2−69264
ocean microstructure obs. using high speed digitizer 2−72728
osmometer, design for foil swelling pressure meas. 2−53417
partial, of O_2, ZnO thin film sensor 2−41454
piston cylinder apparatus, high pressures and high temps. 2−76163
pitot pressure interpretation in compressible two phase flow 2−50141
quartz bourdon tube gauges, absolute pressure level effects on sensitivity 2−45225
reactor fuel pins, irrad., internal press., meas. technique 2−42666
sea waves, wind induced, microscale fluctuations 2−68871
semiconductor transducer, patent 2−82138
shock wave in water under impulse heavy current 2−73452
shock wave pressures meas. in solid bodies, manganin pressure gauge 2−62894

Pressure measurement continued
sinusoidal calibration of pressure transducer 2−66412
small pressure change rates, variometers 2−55370
for solids weighing, in two-phase flow, hydrotransportline 2−46700
static, errors rel. to protruding pressure taps 2−67740
transducer, differential 2−45227
transducer, laser beam testing of temp. change effects 2−73286
transducers, laser technique for study of thermal transients on performance characteristics 2−66413
ultrahigh vacuum, master instruments, total and partial pressures 2−58663
vibration-frequency transducers, errors resulting from elastic imperfections in their materials 2−58696
Er-H system, gas pressure standard 2−52016
F_2 pressure change monitor for HF chemical laser 2−82509

Primary cells *see Electric cells*

Prisms, optical
biprism, for use in white light Fourier hologram synthesis 2−79241
birefringent, for luminance subtraction 2−66805
image splitter prism for photographic photometry 2−48830
for laser beam angular divergence det. 2−42161
mirror-prism systems, three dimensional problems, anomalous property 2−59210
rotational, alignment 2−70033
vision field loss treatment with cemented prisms 2−55322
modified Wollaston prism, $NH_4H_2PO_4$, for laser beam polarizers 2−42105
$PbMg_{1/3}Nb_{2/3}O_3$ crystals, change in refractive index as function of electric field strength, use of prisms as light beam deflectors 2−42215

Probability
see also Random processes; Statistical analysis
distribution function, shear fluctuations, stochastic process, mean wind profile, aeroapace vehicles 2−83465
field stars, simulation in numerical experiments 2−69105
Gaussian unitary and orthogonal ensembles, eigenvalues of random matrix 2−58801
generating functions and Laplace transforms in applied theory 2−45229
modularity of decision effects, symmetry of physical probability 2−82158
molecular transmission probability of complex systems, computation 2−82268
noncommutative, generalization to von Neumann algebras 2−41486
nuclear reactor noise anal., flash start technique 2−83084
one minute rainfall, coefficient of variation, geographical distribution 2−84824
quantum mechanics and statistical theories probabilistic concepts 2−63000
random walk, continuous, method of characteristic event 2−76227
real symmetric matrices class, eigenvalue distrib. 2−58791
Steck's determinantal expressions for probabilities in Kolmogorov and Smirnov tests, simple proofs 2−82243
transmission, resistance concept in molecular flow 2−60344
Na_2MoO_4-$Pu(MoO_4)_2$ system, existence of scheelite phases 2−71694

Probes
see also Plasma/diagnostics
binary gas mixture composition meas. 2−56401
capacitance, appl. in gas fluidized beds 2−50906
comets and asteroids, trajectories of spacecraft 2−58522
contact, for skin temp. obs. 2−69233
core-sampling, electrical probe properties, analysis 2−44519
discharge lamp, meas. of positive column field and electrode falls 2−71010
double appl. to distilled water electrical characts., isothermal plasma model 2−74554
double-probe technique for plasma diagnostics in lower ionosphere 2−58086
EHD, under floating pot., perturbation analysis 2−64223
electrochemical reactions, proposed use of electrode potential control of ZnO green luminescence 2−61717
electrode, for leader channel of long air gap discharge investigation 2−70992
electron, acceleration potential det. 2−63290
electron optical microprobe system, axially asymmetric elements 2−63280
electron temp., for obs. in ionosphere 2−44753
electrostatic, cylindrical, effect of angle of incidence on response at supersonic speeds 2−77285
electrostatic, elastic surface wave meas. 2−63093
electrostatic, obs. of electron density of hollow cathode Ar discharge 2−70988
electrostatic, positively biased, obs. of electron density in collisionless flows 2−77282
electrostatic, r.f. plasma diagnostics 2−50207
electrostatic cloud droplet probe, airflow pattern and droplet trajectories 2−57981
electrostatic surface wave probe, waveform distortion meas. 2−49170
Elmiskop 101, small probe techniques 2−79041
e.m. shock tube, probe meas. of press. and mag. field, bow shock effects 2−77291
energy distribution of electrons in positive column, influence of probe size and temperature 2−60256
Faraday rotation, for plasma magnetic flux density meas. 2−77279
flames, oscillating, probe measurements 2−82356
ion boundary layers 2−56338
Kelvin, u.h.v., guarded for contact potential differences obs. 2−45647
laser interferometer for θ-pinch plasma 2−50201
Lecher wire microwave interferometer, flowing transient plasma 2−77283
liquid crystal temperature sensitive elements for semiconductor investig. 2−69804
magnetic, Ge diode, for transistorized gaussmeter 2−55643
magnetic, with nanosecond response time, plasma diagnostics 2−46760
magnetospheric plasma circulation speed meas. using quadripole probe on spacecraft 2−84871

Probes continued
- microprobe, for increased sensitivity in impulse evaporation method in flame atomic absorption spectroscopy 2–54570
- microprobe analyzer for magnetic thin films 2–66702
- needle type solid state detectors for in vivo meas. of tracer activity 2–66275
- needle-shaped semiconductor detectors, regional distribution and transport of labelled compounds 2–66276
- negatively biased, conical, in supersonic flow, current drawn and det. of ion plasma density 2–46758
- n.m.r., crossed-coil, high sensitivity low-temp meas. 2–82410
- n.m.r. spectrometer, for operation at v. low temps. 2–55635
- noncontacting magnetic pick up, for meas. of pitch of solenoid 2–78994
- optical for displacement meas. 2–79394
- plasma, collisionless, density determ., theory 2–46759
- plasma, contact pot. between emitting electrode and probe 2–74376
- plasma, detection of ion reflected from shock wave 2–60226
- plasma, floating probe method for study of l.f. oscillations 2–64298
- plasma, impedance characteristics, spherical probe, isotropic plasma 2–46766
- plasma, ion temp. meas. with high power a.c. probe 2–50210
- plasma diagnostic using a l.f modulated floating double probe 2–80279
- plasma diagnostics, dual mag. probe system for phase meas. 2–50208
- plasma immersion probe measurements of electron work function 2–54263
- plasma potential determ., i.f. noise in probe circuit 2–64306
- pressure, submersible, obs. below water wave crests 2–67780
- rake, h.f., for inflight intake airflow distortion obs. 2–48637
- r.f., for ionospheric electron density meas. 2–48574
- r.f., surgical brain, heat transfer analysis 2–51899
- r.f. capacitance, comparison with Langmuir probes, for electron density meas. 2–50209
- scanning transmission electron microscope, size and current 2–59101
- sheathed thermo-electric, mechanical, electrical and dynamic properties and applics. 2–73470
- spherical, dense weakly ionized plasma 2–80296
- spherical aberration correction in electron microprobe by non axially symmetric elements 2–81560
- subsonic flows, characteristics of a cylindrical probe, mach 0.3 to 0.79 2–83683
- temperature fluctuations in turbulent wakes, thin film resistance thermometer 2–77330
- thermocouple, for hot gas temperature measurement, up to 1600°C 2–73471
- u.s., multiple array 2–69760
- u.s., standardization, factors affecting performance 2–69759
- waveguide conductivity media impedance measurement effects of e.m. wave front curvilinearity 2–49240
- X-ray milliprobe for small lunar single crystals 2–51481
- yaw characteristics of Preston tubes 2–43042
- Ar ion laser, electron temp., meas. using Al double probe system 2–74349
- CdTe, biomedical, efficiency, resolution and absorption 2–51891
- CdTe, miniature, medical 2–69271
- Cs, thermionic energy convertors, probe measurements, space craft power source 2–54991
- Cs plasma, collisional, space pot. oscills., hot-probe meas. 2–67677
- Kr afterglow, meas. of electron densities of plasma slice using double probe detectors 2–70888
- Si, rel. to CdTe, for γ-counting efficiency 2–69271
- Si(Li) miniaturized detector for β and γ meas. in superficial and deep parts of living tissue 2–55252
- Si(Li) semiconductor probe for semi-microscanning device 2–55250
- W wire, rotating, for analysis of spatial current distrib. in particle beam 2–52388

Procopiu effect *see Films, solid; Magnetoelectric effects; Magnetomechanical effects*

Programming *see Calculating apparatus/digital computer programmes*

Projectiles *see Ballistics*

Projectors, optical
- colour telecine projectors, connection between subtractive and colorimetric colour coordinates 2–66825
- modified measuring, for evaluation of interferograms 2–66832

Promethium
- in HR 465, identification 51741 2–51741
- HR 465 variable star content 2–51727
- Pm^{3+}: LaCl$_3$, absorption spectrum in 12000 to 28000 cm^{-1} range 2–81405
- Pm:YAG laser, radiative transition probabilities rel. to Nd:YAG 2–59186
- Pm II, spectal anal. in 3100 to 10000 Å region 2–79945
- Pm II in HR 465, peculiar A star, comments 2–66081
- Pm II in HR 465, peculiar A star 2–62501
- ^{147}Pm, contamination, thermoluminescent dosimetry obs. 2–62291

Promethium compounds
- Pr(NO$_3$)$_3$, aqueous solution at 25°C, u.s. relaxation 2–53427

Prominences, solar *see Sun/prominences*

Propagation *see Acoustic wave propagation; Electromagnetic wave propagation*

Propagators *see Field theory, quantum; Quantum electrodynamics*

Proportional counters *see Counters/proportional*

Prospecting *see Geophysical prospecting*

Protactinium
- Pr:Fe, elec. conductivity variation 0.3-300K, high temp. Neel points at different field intensities 2–68567

Protactinium compounds
- No entries

Proteins
- amino acids, high resolution laser Raman spectra, study of S-S vibrations 2–83337
- atomic coordinates superimposition, math. procedure 2–83335
- bovine serum albumin, cryst., Raman spectra, water content depend. 2–60092

Proteins continued
- α-chymotrypsin, conformationally dependent low-frequency motions from laser Raman spectra 2–56268
- collagen, elec. props., effect of adsorbed water 2–47908
- collagen, fracture of rat tail tendon 2–43016
- contaminative behaviour of PuCl$_4$ 2–78648
- cytochrome c, electron transfer between molecules obs. by pulsed Fourier transform n.m.r. 2–56267
- DNA natural and synthetic, denaturation 2–60097
- enzymes, high resolution laser Raman spectra study of S-S vibrations 2–83337
- fibrin, elongated, films, dielectricity, viscoelasticity and piezoelectricity 2–85087
- flavoproteins, analysis of in vivo and in vitro e.s.r. spectra of intrinsic spin label ^{2}H-flavin 2–83338
- haemoglobin, circular dichroism rel. to struct. modification during oxygen fixation 2–56264
- hemin, nuclear hyperfine interactions, Mossbauer studies 2–67527
- hemoprotein derivatives, circular dichroism in visible region, nonlinear iron-ligand bonds 2–64197
- bis-imidazole hemin, nuclear hyperfine interactions, Mossbauer studies 2–67527
- molecular wt. by X-ray diffr., teaching techniques 2–82097
- muscle proteins, dynamic props., effect of Ca^{2+}, quasielastic light scatt. study 2–70798
- myglobin in water, dielectric dispersion and dipole moment 2–46976
- myoglobin, high pressure optical cell for spectral obs. 2–45825
- natural, struct., review 2–83383
- oligopeptides, high resolution laser Raman spectra, study of S-S vibrations 2–83337
- oxyhaemoglobin and haem derivatives, SCC-EH-MO calc. on bonding and electric field gradient 2–60098
- peptides, ab initio studies of H bonding, mutual orientation of peptide planes 2–46634
- peptides and oligopeptides, conform., influence of specific intramol. interactions 2–60095
- phosvitin, X-ray diffraction study 2–74298
- piezoelectric properties 2–61436
- polyglycine, extended form, calc. of two-dimensional lattice vibrations 2–68210
- polyglycine I, cryst. struct., model 2–53687
- polypeptide chains, helix-coil transitions, thermodynamic parameters 2–60096
- polypeptide chains, random, conformation 2–43018
- polypeptides, high resolution laser Raman spectra, study of S.S vibrations 2–83337
- radical transfer with DNA in DPA, e.s.r. obs. 2–60094
- structure analysis by X-ray crystallography, role of computers in collection and processing of data 2–83340
- X-ray determ. of quaternary structure 2–77158
- ^{3}H labelled, liquid scintillation assay in rabbit lens 2–42457

Proton magnetic resonance
- acid hydrates, hydronium ion struct. and dynamics 2–84601
- amino acid, chemical group assignment and chemical shifts 2–46989
- α-amino isobutyric acid, p.m.r. study of line widths and second moments 2–68748
- ammonium salts, lineshapes of ions undergoing quantum mech. tunnelling in solid state 2–81470
- aniline-^{15}N and derivatives, long-range spin-spin coupling consts. 2–77137
- aqueous solns. of transition metal ions, field shift obs. 2–74558
- 4,4′-azoxydibenzoate, liquid crystal obs. 2–50338
- benzoyloxyimino-4 tetrahydroquinazolines and hexahydropyrimidines, four proton system obs. 2–53049
- 1,3-butadiene oriented in nematic mesophase 2–60053
- butadiene sulphone in isotropic and liquid crystal media 2–56222
- d-camphor, molecular rotation at high press., obs. 2–51416
- cyclohexane, nitroxide radical doped, plastic phase, spin diffusion 2–72526
- cysteine hydrochloride monohydrate, irrad., radical recomb. study 2–72575
- 1,4-dibromo-2 butin, in liq. cryst., effect of solvent 2–46596
- 4,4′-dibutoxyazoxybenzene, liquid crystal obs. 2–50338
- dicalcium lead propionate, spin-lattice relax. near crit. point 2–65196
- dichloromethane, liquid, τ_2 determ. rel. to rotation correlation times 2–56472
- 4,4′-dipropoxyazoxybenzene liquid crystal obs. 2–50338
- ethylene trithiocarbonate in thermotropic nematic solvent 2–56230
- fluoropyridine methyl derivatives, long-range spin-spin coupling consts., electron contribs. 2–77097
- Fourier transform p.m.r., modification 2–55631
- Fourier transform proton n.m.r. in aqueous solution 2–77448
- gaseous mixtures, spin-spin relax. times, density depend. 2–79973
- ice, review of recent investigations 2–61746
- liquid crystal, intermol. and intramol. contribs. to proton spin-lattice relax. 2–64440
- lithium ammonium tartrate, ferroelec. paraelec. transition phenomena 2–72527
- methane, solid, γ-irrad., spin species conversion by paramag. impurities 2–84446
- methane adsorbed on MgO, relax. obs. of microdynamics 2–83875
- methylammonium chlorides, solid, mol. and group motions 2–68750
- methylene chloride, in liq. cryst., effect of solvent, dipole interaction 2–46596
- 1-penten-3-yne, long-range spin-spin coupling consts. 2–67511
- poly-γ-benzyl-L-glutamate, 220 MHz p.m.r. relaxation time at helix-coil transition 2–80112
- polyatomic mols., mol. orbital theories of chem. shifts 2–67461
- polybutadiene, memory effects in proton spin-spin relaxation 2–46636
- polyisoprene, memory effects in proton spin-spin relaxation 2–46636
- polymer, irrad., spin-lattice relax. times 2–84449
- polyvinyl alcohol, probe for configuration of polymer chains 2–60105
- polyvinylchloride, drawn samples, molec. orientation determ. by broad line p.m.r. 2–51417
- β-propiolactone, structure investigation 2–50110

- **Proton magnetic resonance** continued
  - pyridine, liquid, τ_2 determ. rel. to rotation correlation times 2−56472
  - 11-cis-retinal, PCILO calculation in relation to molec. conformation 2−77153
  - tetramethylammonium manganese chloride, low-temp. transitions 2−72530
  - 1,3,5 trinitrobenzene, charge transfer complexes, mol. movement, spin-lattice relax. 2−48308
  - CdFOH, ^{19}F and ^{1}H resonances 2−84591
  - in H bonded solids, proton migration study, review 2−83998
  - HgFOH, ^{19}F and ^{1}H resonances 2−84591
  - $K_4Fe(CN)_6.3H_2O$, ferroelectric, twinning and polymorphism obs. 2−74655
  - $La_2Mg_3(NO_3)_{12}.24H_2O$:Nd, spin diffusion props. from spin heat bath relax. time 2−78049
  - NH_4I, low temp. intensity, nucl. spin value 2−84600
  - NH_4PF_6, low temp. intensity, nucl. spin value 2−84600
  - NH_4SnCl_3, spin-lattice relax. of ammonium ion undergoing hindered rot., cross correl. effect 2−84448
  - $(NH_4)_2SnCl_6$, low temp. spin-lattice relax. times of hindered ions 2−84447
  - β-NbH, proton jump rate determ. 2−77614
  - PdH_x, Knight shifts of reson. lines 2−78174
  - Ti hydrides, ternary and binary, temp. and freq. depend. of proton spin relax. 2−78052
  - ZnFOH, ^{19}F and ^{1}H resonances 2−84591
- **Proton spectra**
  - dipole IAS in even-even nuclei, two classes of proton channels 2−59741
  - pp collisions, diffraction excitation model analysis 2−73850
  - Sun, obs. from widely separated spacecraft 2−75970
  - (p,2p) reaction on nuclei in Ni region studied at incident energy of 17MeV 2−52822
  - ^{e}Sn(γ,p), A=116-118, 120, 122, 124, meas. of spectra and yeild curves, isobaric analog states 2−46233
  - C, π- absorption from rest, obs. of α spectrum, p spectrum and secondary particles 2−63902
  - ^{9}C, β-delayed proton decay 2−63844
- **Protonium** *see Protons and antiprotons*
- **Protonosphere** *see Atmosphere/upper*
- **Protons and antiprotons**
  - *see also Cosmic rays/protons; Nuclear reactions and scattering due to/protons; Nucleons and antinucleons*
  - channelling, stopping power, position depend. 2−44014
  - charge form factor determ. from nonlinear σ model at large momentum transfer, calc. of charge radius 2−76707
  - composite model, correlation effects and quantization 2−79511
  - dechannelling in Ge, Lindhard's multiple scatt. 2−47788
  - dechannelling in KCl-KBr mixed cryst., lattice distortion effects 2−47785
  - dechannelling in Si, Lindhard's multiple scatt. 2−47788
  - divergence of e.m. mass shift, relation to choice of scaling variable of e.m. structure function 2−70252
  - e.m. form factor, parton model 2−59564
  - e.m. form factor, rel. to inelastic p-p scatt. 2−55877
  - e.m. form factors, dipole behaviour 2−76712
  - e.m. form factors, dipole behaviour 2−76711
  - e.m. form factors, dipole behaviour 2−49588
  - fluxes $\gtrsim$30 keV obs. upstream from bow shock and in magnetosheath 2−62314
  - fluxes with ISIS-1 and 2 at mid-latitudes, association with plasmapause and SAR arcs 2−62327
  - form factors, scale relative 2−55874
  - in magnetosphere, diffusion by turbulent electrostatic oscillations 2−68940
  - metal, thick target, energy loss of protons scatt. by Pb, Ta, Yb, Ce, W, Ag and Mo 2−80928
  - physical proton, bound-state model 2−67044
  - probes of magnetospheric particle gradients, meas. using scanning proton telescope 2−62312
  - proton beam, angular spreading in neutralizer cell 2−79697
  - proton-neutron mass difference, finite contribution 2−49589
  - proton-neutron mass difference, investigation in configuration space 2−55875
  - proton-neutron mass difference and related topics, report 2−49590
  - protonium, strong-interaction energy shift as possible test of matter-antimatter separation 2−42416
  - radiography using 160 MeV protons 2−73204
  - radius, by general relativity 2−76200
  - Si:B, ion implanted, lattice disorder distributions, channelling effect analysis 2−68036
  - stopping power in Al, Ni, Cu, Rh, Ag, Pt, Au at 7.2 MeV and 14.4 MeV 2−54098
  - total cross-sections and diffraction con slope 2−82775
  - p-n mass difference, axial-vector massive, photons 2−70253
  - p-n mass difference, divergent contribution in Weinberg model 2−67048
  - $p \rightarrow p + t^0$, limits on negative energy tachyon emission rate 2−45254
  - Ge, electron scattering in planar dechannelling 2−61128
  - Si, channel-to-random transition meas. on single crystal overlaid with amorphous layer 2−61127
  - Si, electron scattering in planar dechannelling 2−61128
  - Si, energy spectra of back-scattered protons, variations 2−54093
  - **absorption**
    - fluctuations in energy loss of 66 and 100 MeV protons 2−49634
    - Al thin absorbers, loss of protons 2−80924
    - Cu thin absorbers, loss of protons 2−80924
  - **angular distribution**
    - cosmic ray primary produced in nuclear emulsion 2−49608
    - (d,pγ) reaction, from shape-studies of γ-ray spectra 2−79802
    - (e,e′p) reactions, short range correlation effects on proton angular distribs. 2−82952
    - (γ,p) reactions, short range correlation effects on proton angular distribs. 2−82952
    - ^{e}Cu(α,p), A=63, 65, 27.2 MeV, meas. of differential cross section, analysis of p angular distrib. in three nucleon stripping theory 2−49833
    - ^{27}Al(^{3}He,p)^{29}Si, 9-14 MeV, comparison of exptl. angular distribs. with two-nucleon transfer DWBA calcs. 2−70478

- **Protons and antiprotons** continued
  - **angular distribution** continued
    - ^{27}Al(n,p)^{27}Mg, E_n=14.1 MeV, proton energy and ang. distribs. 2−82981
    - ^{11}B(^{3}He,p)^{13}C, E_{3he}=4-12 MeV, DWBA anal. 2−52823
    - ^{48}Ca(p, p′γ), particle-γ angular correlation and lifetime studies of 4.61 and 5.15 MeV levels 2−82889
    - ^{35}Cl(α,p), 27.2 MeV, meas. of differential cross section, analysis of p angular distrib. in three nucleon stripping theory 2−49833
    - ^{59}Co(n,p)^{59}Fe, E_n=14.1 MeV, proton energy and ang. distribs. 2−82981
    - ^{19}F(d,p)^{20}F, 3 MeV, meas. of differential corrections and angular distrib. of proton groups 2−67151
    - ^{19}F(d,pγ)^{20}F, p,γ ang. correl., low-lying states of ^{20}F 2−79801
    - ^{56}Fe(α,p), 27.2 MeV, meas. of differential cross section, analysis of p angular distrib. in three nucleon stripping theory 2−49833
    - ^{6}Li proton, elastic and inelastic scattering, 25-45 MeV, meas. of angular distrib. for excitation of excited states 2−55991
    - ^{98}Mo, ^{100}Mo, inelastically scatt. protons, E_p=14.7 MeV 2−79782
    - ^{14}N(^{3}He, p)^{16}O, 7.9-18.0 MeV, ang. distrib., compound nucleus formation, optical parameters 2−76875
    - ^{20}Ne(t, pγ)^{22}Ne, 3 MeV, p-γ ang. correl., spin assignments 2−79739
    - ^{58}Ni(n,p)^{58}Co, E_n=14.1 MeV, proton energy and ang. distribs. 2−82981
    - ^{31}P(α,p), 27.2 MeV, meas. of differential cross section, analysis of p angular distrib. in three nucleon stripping theory 2−49833
    - ^{31}P(d,p)^{32}P, 10 MeV, meas. of angular distribs., spectroscopic factors 2−49834
    - ^{208}Pb(t,p)^{210}Pb, 20 MeV, meas. of angular distribs., determ. of ^{210}Pb structure 2−82892
    - ^{32}S(n,p)^{32}P, E_n=14.1 MeV, proton energy and ang. distribs. 2−82981
    - ^{28}Si(α,p), 27.2 MeV, meas. of differential cross section, analysis of p angular distrib. in three nucleon stripping theory 2−49833
  - **antiprotons**
    - atom, X-ray transition yields, strong interaction effects 2−79966
    - charged particle prod. at 90° in centre of mass in pp collisions 2−82773
    - features and interactions 2−63662
    - low-momentum, production at CERN proton synchrotron 2−42417
    - magnetic moment from fine-structure splitting study of Pb′ and U atoms 2−59573
    - production in proton interactions in nuclei at 24 GeV/c 2−63606
    - wide-angle production, CERN intersecting storage rings data 2−73853
    - pn bound state and mass of nucleon quark 2−73840
  - **detection, measurement**
    - change distrib. in external beam of Hamburg isochronous cyclotron 2−79691
    - gas Cherenkov counter with large aperture for distinguishing between pions kaons and protons 2−76742
    - low-energy beam, critical study of emittance meas. 2−79692
    - monochromatic method for meas. of 665 MeV proton energy by Vavilov Cherenkov radiation 2−73940
    - NE 230 and NE 231 liquid scintillators, response to deuterons and protons 2−79653
    - photonucleon cross section det. for separate residual nuclei states utilizing continuum γ sources 2−74061
    - satellite instrument for obs. in energy range 0.1 MeV to 6 MeV 2−65923
    - stopping detector for proton energies to 300 MeV, advantages of laminated detector 2−46041
    - Ge(Li) counters for detection and energy det. of high energy protons 2−46055
    - LiF thermoluminescent dosimeter response 2−85135
    - $NaNbO_3$, anisotropic diffuse X-ray scatt. and phase transitions 2−71715
  - **effects**
    - alkali halides, proton dechannelling obs. of incident beam damage 2−43606
    - atomic Coulomb excitation by heavy charged particles 2−79911
    - cesium citrate, proton irradiation, 660 MeV production of radioactive Sb and Te, annealing effects 2−68817
    - excitation of atmospheric gases by low energy proton bombardment 2−84792
    - film surface density meas. by proton excited X-rays, Fredholm expression 2−80542
    - graphite, production of electron spin centers, e.s.r. obs. 2−78152
    - steel, 304L stainless, surface characterization by proton induced X-rays 2−50832
    - steel, stainless, irrad., swelling, displacement damage depend. 2−53716
    - thin target, fast particle damage production, theory 2−50636
    - tissue equivalent gas, ionization 2−51918
    - Ag, radiation damage, energy depend. 2−50643
    - Al_2O_3, Al Kβ X-ray spectra, molecular struct. obs. 2−81381
    - Au, radiation damage, energy depend. 2−50643
    - $BaTiO_3$, proton channelling, above and below ferroelec. Curie temp. 2−65059
    - Bi_2Te_2Se, irrad. induced disorder, X-ray obs. 2−64653
    - CaF_2, density change and absorption band growth 2−71454
    - CaF_2, mechanism of intrinsic radiational defect formation 2−56680
    - CaF_2, proton irrad., elec cond. 300-800K, anion vacancy cond. mechanism 2−57230
    - $CsCO_3$, proton irradiation, 660 MeV production of radioactive Sb and Te, annealing effects 2−68817
    - Cs_2CrO_4, proton irradiation, 660 MeV, producing of radioactive Sb and Te, annealing effects 2−68817
    - $CsNO_3$, proton irradiation, 660 MeV, production of radioactive Sb and Te, annealing effects 2−68817
    - Cs_2SO_4, proton irradiation, 660 MeV, production of radioactive Sb and Te, annealing effects 2−68817
    - GaAs, irrad., absorpt. spectra 2−48177
    - n-GaAs, optical waveguiding by proton implantation 2−66841
    - GaAs p-n junction, insulation by proton irradiation 2−84353
    - Ge, radiation defect form. and annealing 2−47383
    - LiF, irrad., surface damage monitoring using (p,α) reaction 2−43610
    - Mo surface, Auger electron spectra obs. surface composition detn. 2−50453

Protons and antiprotons continued
effects continued
$Pb_{0.76}Sn_{0.24}Te$ thin films, p-type to n-type conversion 2−64999
Pt, radiation damage, energy depend. 2−50643
Si, irrad., enhanced diffusion of Sb and P, dose rate effects 2−80707
Si pn junction, deep centre spatial distrib. from capacitance meas. 2−68443
n-Si proton bombardment induced shallow donors, elec. props. 2−61355
Si surface barrier detector, radiation damage from 2 MeV protons 2−46056
Ti, bombarded, X-ray Kα and Kβ spectra 2−57368
Ti, X-ray de-excitation 2−57367

interactions
see also Nuclear reactions and scattering due to/protons
→ 2−73809
− 2−59529
annihilation spectrometer for investigation of heavy meson spectra 2−73926
diffraction cone slope, effect of cut contribution 2−82776
energy transfer to electrons in fast proton collisions 2−55986
inclusive photon yields from high-energy bremsstrahlung on H target 2−76595
inclusive spectra, microscopic model 2−76713
photoproduction of pions near $P_{33}(1236)$ reson., multipole analysis 2−67016
$dp \to {}^3H\ (mm)^+$, 2.8 to 3.8 GeV/c, high statistics missing mass spectroscopy 2−76727
$dp \to {}^3He\ (mm)^0$, 2.8 to 3.8 GeV/c, high statistics missing mass spectroscopy 2−76727
ep, vector meson prod., triple-Regge formulae 2−79494
e^-p, coincidence π^0 electroprod. in second reson. region 2−67015
$e^-p \to e +$ anything, analytic continuation of scaling function gives asymptotic scaling function for $e^+e^- \to p +$ anything 2−45890
$ep \to e'X(e'AX)$, applic. of dual parton model 2−63512
$ep \to e\mu^+\mu^-X$, test of algebra of bilocal operators 2−76582
$ep \to ep\pi^o$, dispersion relation calc. of π^o production in resonance region 2−55851
$ep \to e\pi^+ +$ anything, inclusive pion distributions 2−70231
$\gamma + p \to n + pi^+(p + \pi^0)$, asymmetry meas. in range 400 to 900 MeV 2−59527
γp, asymmetry for π^+ production from polarized protons between 300 and 900 MeV at 90° 2−59528
γp, inclusive photoproduction and factorization 2−49562
γp, production of $A_1{}^0$, axial vector meson 2−66925
γp, π^+ production, isotensor contribution 2−67017
γp, π^+ production at 0.66 to 7.4 GeV/c 2−63610
γp, vector meson photoproduction, review of diffraction dissociation models 2−59551
γp, vector meson prod., triple-Regge formulae 2−79494
γp charged and neutral double π production cross-sections in γ-energy range 600-900 MeV 2−73815
$\gamma p \to K^+\Lambda$, K*-K** absorbed exchanged, F/D ratio 2−70210
$\gamma p \to K^+\Lambda$ photoproduction below 2.2 GeV c.m. energy, analysis of resonance contribs., radiative widths, stray baryonic states 2−82673
$\gamma p \to K^+\Sigma$, K*-K** absorbed exchanged, F/D ratio 2−70210
$\gamma p \to K^+\Sigma^0$, strong cut Reggeized absorption model 2−70144
$\gamma p \to V^o p$, Regge pole model 2−67035
$\gamma p \to \kappa^+\Lambda$, 5 GeV, recoil polarization in $K^+\Lambda$ 2−66926
$\gamma p \to p\pi^+\pi^-$, 4-6 GeV, ρ^0 prod. obs. 2−79492
$\gamma p \to \pi$- + anything, investigation with polarized photons at 2.8, 4.7 and 9.3 GeV 2−45871
$\gamma p \to \pi^- +$ anything inclusive process comparison of π^- distributions for k^+p and pp collisions 2−67052
$\gamma p \to \pi^- +$ anything, inclusive reaction in photon fragmentation region, vector meson dominance model 2−79613
$\gamma p \to \pi^0 p$, 400 to 800 MeV, cross section comparison with $\gamma d \to \pi^0 p(n_s)$ 2−42383
$\gamma p \to \pi^0 p$, differential cross- section explained by nonsense wrong signature zeros 2−59529
$\gamma p \to \pi^0 p$, in third resonance region 850-1250 MeV, recoil proton polarization 2−46004
$\gamma p \to \pi^+ n$, 220-425 MeV, angular distrib. of pions between 15° and 180°, differential cross sections 2−52613
$\gamma p \to \pi^+ n$, comparison with $\gamma n \to \pi^- p$, π^-/π^+ ratios, dip test of isotensor current 2−49560
$\gamma p \to \pi^+ n$, data analysis by phenomenological model based on pion exchange 2−45999
$\gamma p \to \pi^+ n$, photoproduction in backward direction 0.7-8 GeV, comparison with Regge-pole analyses 2−63607
$\gamma p \to \pi^+\pi^+\pi^-\pi^- p$, linearly polarized 9.3 GeV photons, observation of four-pion vector meson state of mass = 1.5 GeV 2−82672
$\gamma p \to \rho^0 p$, density spin matrix elements in Gottfried Jackson frame 2−70142
$\gamma p \to \rho V^0$, photoproduction of neutral vector meson studied in Regge pole model with cuts 2−49577
$\gamma p \to \rho' p$, 9.3 GeV, photoproduction of new vector meson $J^p = 1^-$ 2−76695
$\gamma\rho$, inclusive photoproduction cross sections for $\pi^\pm$, Λ predicted via factorisation 2−59403
$K^\pm\ p \to cX$ inclusive reaction spectra, calc. by urbaryon rearrangement 2−82700
$K^+(K^-)p \to K^0(K^0) +$ anything, inclusive spectra calc. according to thermodynamic model 2−59517
K-p, 5.5 GeV/c, elastic scatt. and single-pion production 2−49551
K-p charge exchange, differential cross sections, evidence for tachyonic resonances 2−63546
K-p → $K^0 n$, 1700-2100 MeV c.m. energies, meas. of cross sections, angular distribs., polarizations 2−79572
K-p → $K^+\Xi$-, consequences of exchange degeneracy with respect to polarization 2−49548
k-p → $\Lambda\eta$, 1.25-1.85 GeV/c, duality 2−73810
k-p → $\Lambda\pi$, 1.25-1.85 GeV/c, duality 2−73810
K-p → $\Lambda\pi^0$, 1700-2100 MeV c.m. energies, meas. of cross sections, angular distribs., polarizations 2−79572
K-p → Ξ-$K^0\pi^+$, investigated at 2.18 GeV/c 2−45942
K-p → $\pi^\pm\Sigma^\mp$, 1.73 to 2.11 GeV, partial wave analysis 2−45943
Kp, high-energy asymmetry of pion distrib. in high- energy interactions 2−45967

Protons and antiprotons continued
interactions continued
K^-p, 10 GeV/c, obs. of central emission of pions, search for symmetry system 2−73816
K^-p, 3.9 and 4.6 GeV/c, study of production and decay of nonstrange mesons 2−66994
K^-p, 3.95 GeV/c, f and f′ production 2−79604
K^-p, 8.25 GeV/c, average transverse momentum of pions from final states 2−79566
K^-p, existence of M(953) meson 2−73831
K^-p, quasi-two body and multiple body reactions at 10 GeV/c, Ω and Ξ production, review of recent results 2−42377
K^-p experiments of Vienna Bubble Chamber Group at 10 GeV/c, 8.25 GeV/c, 16.6 GeV/c 2−76577
$K^-p \to K^-\pi^-\Delta^{++}(1236)$, 8.25 GeV/c, CLA model, Pomeron and K* exchange 2−55847
$K^-p \to K^-\pi^+n$, 3.9 and 4.6 GeV/c, study of interference effects of K*(890) and K*(1420) resonances with background 2−63647
$K^-p \to K^-\pi^+\pi^-$ 10 GeV/c, s-channel and t-channel helicity conservation tested 2−82753
$K^-p \to K^0n$, cross section difference with $K^+n \to K^0p$, Regge analysis 2−76658
$K^-p \to K^0p +$ anything, 10 GeV/c, correlations between longitudinal momenta of p and E^0 2−63659
$K^-p \to K^0\pi^-p$, 3.95 GeV/c, meas. of differential cross sections and density matrix elements for production of $K^{*-}(890)$ p and $K^{*-}(1400)p$ final states 2−70221
$K^-p \to K^{*-}p$, 10.9, 13.4, 15.9 GeV/c, meas. of differential cross sections, K^{*-} spectrum 2−49585
$K^-p \to K^{*-}\pi^+n$, U(6,6) symmetry and generalized Veneziano model 2−67010
$K^-p \to K^*(890)\pi N$, 10 GeV/c, isospin analysis, diffractive dissociation 2−82735
$K^-p \to \Lambda\eta'$, 2.2 GeV/c, η^1 parameters determ. 2−76692
$K^-p \to \Lambda\omega$, exchange mechanisms, 3.95 GeV/c 2−63592
$K^-p \to \Lambda\omega$, quasi-two body reaction, 1.26-1.84 GeV/c, partial wave analysis 2−52599
$K^-p \to \Lambda\varphi$, exchange mechanisms, 3.95 GeV/c 2−63592
$K^-p \to NK^*(890)$, quasi-two body reaction, 1.26-1.84 GeV/c, partial wave analysis 2−52599
$K^-p \to \Sigma^0\varphi$, exchange mechanisms, 3.95 GeV/c 2−63592
$K^-p \to \Sigma^0\rho$, exchange mechanisms, 3.95 GeV/c 2−63592
$K^-p \to \Sigma(1385)\pi$, quasi-two body reaction, 1.26-1.84 GeV/c, partial wave analysis 2−52599
$K^-p \to (\omega,\varphi)\Lambda$, meas. of joint density-matrrix elements, study of vector-meson production with hypercharge exchange 2−82743
$K^-p \to (\omega,\varphi)\Lambda$, polarization and unnatural parity exchange 2−42376
$K^-p \to \eta\Lambda$, 3.95 GeV/c, meas. of cross section, angular distributions and Λ polarizations 2−59518
$K^-p \to \eta'(958)\Lambda$, 3.95 GeV/c, meas. of cross section, angular distributions and Λ polarizations 2−59518
$K^-p \to \omega\Lambda$, 1915-2168 MeV, partial wave analysis, resonance formation 2−70220
$K^-p \to pK^-\pi^+\pi^-$, study of resonance production in two- and three-particle systems at 10 GeV/c, analysis of spin structure 2−76657
$K^-p \to pK^0\pi^+\pi^-\pi^-(\pi^0)$, 10 GeV/c, study of resonance production and three-body states 2−73808
$K^-p \to p\pi^+\pi^-$ 10 GeV/c, s-channel and t-channel helicity conservation tested 2−82753
$K^-p \to \pi^-Y^{*+}(1385)$, amplitude analysis of reaction 2−70211
$K^-p \to \pi^+\pi^-\pi^-$, 10 GeV/c, s-channel and t-channel helicity conservation tested 2−82753
$K^0p \to Q^0p$, 4 to 12 GeV/c, Q-enhancement phenomena 2−67034
$K^0p \to Q^0p$, 4 to 12GeV/c, Q-enhancement phenomena 2−67034
K^+p, 10 GeV/c, production cross section for Ξ^+, Ξ-, Ω^+ 2−63668
K^+p, 12-28 GeV, correlations between produced π^- particles 2−55832
K^+p, 12 GeV/c, investigation of low mass $K\pi\pi$ systems 2−59519
K^+p, backward produced Q obs. 2−79562
K^+p, comparison of multiperipheral model with inclusive data 2−49552
K^+p, inclusive $\pi^-\pi^-$ production, rapidity correlations 2−49563
K^+p, p_t limited phase space predictions 2−55831
K^+p, relation between GGLP effect and particle pair mass distribution 2−49549
K^+p, resonances produced in bubble chamber 2−45941
K^+p, search for weakly decaying $S = +2$ exotic meson 2−59549
K^+p, systematic methods analysis 2−63593
$K^+p \to K^0 +$ anything, momentum spectrum of K^0 2−79560
$K^+p \to K^0\pi^0\Delta^{++}$, 3-13 GeV/c, analysis of observed $K\pi$ scattering 2−42378
$K^+p \to K^0\pi^+\pi^-\pi^+p$, 5 and 8.25 GeV/c, analysis of $K\pi$ inelastic scattering 2−49555
$K^+p \to K^0\pi^+\pi^0p$, 5-12.7 GeV/c, longitudinal phase space analysis 2−73807
$K^+p \to K^+\pi^+n$, application of dual resonance model for $K^+K^-pn\pi^-$ system 2−76659
$K^+p \to K^+\pi^+\pi^-p$, 5-12.7 GeV/c, longitudinal phase space analysis 2−73807
$K^+p \to K + n$ charged + anything neutral, Feynman gas model 2−82704
$K^+p \to pK^+\omega$, momentum transfer and ang. decay spectra 2−63591
$K^+p \to pK^+\varphi$, momentum transfer and ang. decay spectra 2−63591
$K^+p \to \pi^- +$ anything inclusive process comparison of $\pi-$ distributions for γp and pp collisions 2−67052
$K^\pm p$ total cross-section, relation to slope of diffraction cone 2−66964
$K^\pm p$ total cross-sections, empirical scaling behaviour 2−73778
Λp, Λp, 6 to 21 GeV/c, total cross sections 2−52645
Λp, one boson exchange potential model including ΣN channel 2−82783
μp, muonic pair production 2−49513
np charge- exchange reaction, model for pion-Pomeranchon Regge cut 2−52640
np non-coplanar bremsstrahlung obs. at 200 and 130 MeV, application to N-N interaction off-shell energy properties 2−79718
$Np \to \Delta X$, new cross-section relations 2−63545
$np \to \gamma d$, $E_n = 300$- 720 MeV, test of time reversal invariance 2−46007

Protons and antiprotons continued
interactions continued
$\nu_\mu + p \to \nu_\mu + p + \pi^0$, cross section calc. using Weinberg model 2−59417
$\nu_\mu + p \to \nu_\mu + p + \pi^0$, exptl. limit on neutral current 2−63508
$\nu p \to \mu^+ \Lambda$, production cross-section for Λ 2−67061
$\nu p \to \mu^+ \Sigma^0$, production cross-section for Σ^0 2−67061
$\nu p \to \mu^+ n$, symmetry relations with $\nu p \to \mu^+ n$ 2−52557
p annihilations, dual model applic. 2−59577
PP, 23.2-52.7 GeV, charged particle prod. at 90° in centre of mass 2−82773
p−p, 40 GeV/c, determ. of charged and neutral particle multiplicity 2−76682
pd, 3.5 GeV/c, transverse and longitudinal momentum spectra of resultant pions 2−49591
pd, Impulse Approx. validity 2−59582
pd, p annihilation and study of pn bound states with detn. of nonzero orbital momenta 2−70262
pd annihilations, low energy phenomena 2−59586
$pd \to {}^3He + X^0$, study of missing mass spectra, 2 GeV protons 2−42410
$pd \to n(NN)$, bound states of (NN) system 2−46005
$pd \to p_s pn\pi^+\pi^-$, 5.55 GeV/c, meas. of cross section for pn reaction and production of $\Delta n\pi^+$ and $\Delta p\pi^+$ final states 2−63663
$pd \to \pi\Delta X$, new cross-section relations 2−63545
pN asymmetry of angular distrib., momentum spectra, distrib. of 4-dimensional transfer 2−73819
pN interactions with emulsion nuclei, 20-70 GeV, coherent π production cross-section 2−73844
$pN \to NNKK$, total cross- sections, model with single kaon exchange 2−76719
$pn \to 3\pi$, Moffat's model applic. 2−55843
$pn \to \kappa\kappa\pi$ at threshold, Veneziano model investigation 2−63552
$pn \to pp\pi^-$, 5.9 GeV/c, search for N*(1450) production, meas. of cross section 2−70257
$pn \to p\pi^- p$, cross section, 7 GeV/c, model fitting, $\Delta(1230)$ prod. 2−52638
$pN \to \pi^+\pi^-\pi^-$, isospin and grand ang. momentum analyses 2−59563
$pn \to \pi^+\pi^-\pi^-$, 1.2 GeV, investigation using dual models 2−52636
pp, 19 GeV/c, comparison of π momentum distribs. with and without strange-particle production 2−73847
pp, inclusive, high energy, correl. effects 2−79619
pp, multi-pion producing, cross section energy depend. in simple peripheral model 2−79596
pp annihilation, 1.6 to 2.2 GeV/c, final states containing $K_1{}^0$ meson 2−49596
pp annihilation, obs. of $\rho\omega$ interference at 2.32 GeV/c 2−70261
pp annihilation at 1.2 GeV/c, production of KK and $KK\pi$ resonances 2−73839
pp annihilation at rest, determination of $X^0(960)$ meson spin and parity 2−45981
$pp \to \gamma X$, scaling of inclusive γ spectra at ISR energies and thermodynamic model 2−79612
$p\pi^- \to pX^-$, 25 and 40 GeV/c, scaling and estimate of triple- Pomeranchukan coupling 2−73846
$p\pi^- \to pX^-$, 25 and 40 GeV/c, scaling and estimate of triple-Pomeranchukon coupling 2−76715
$p\pi \to p +$ anything, finite-energy sum rules, Reggeon-particle scattering amplitudes 2−73849
$p\pi \rightleftharpoons \gamma n$ in $\Delta(1236)$ resonance region, discrepancy between dispersion relation predictions and exptl. data 2−42324
π prod. processes, hydrodynamical model, scaling law 2−82774
π-p, comparison of multiperipheral model with inclusive data 2−49552
π-p, study of two-body strange-particle final states at 4.5 GeV/c and 6 GeV/c, meas. of differential cross sections 2−79599
π-p charge exchange, differential cross sections, evidence for tachyonic resonances 2−63546
$\pi\text{-}p \to K^0{}_s K\text{-}p$, 20.3 GeV/c, study of production and decay of A_2 resonance 2−63641
$\pi\text{-}p \to K^{*o}\Lambda$, 3.9 GeV/c, amplitude structure determ. from decay correlations 2−42391
$\pi\text{-}p \to \eta\varphi$, 1.8 GeV/c, decay mode $\varphi \to \eta\gamma$ obs. 2−63643
$\pi\text{-}p \to k\gamma + n$, (k=2-4), pseudoscalar and vector meson obs. 2−70202
$\pi\text{-}p \to n\pi^0$ meas. of differential cross section at 317, 452, 491 MeV/c using $n\gamma$ coincidence method 2−63617
$\pi\text{-}p \to n\pi^+\pi^-$, 2.77 GeV/c, parametrization of nonevasive exchange processes and background contribs. 2−76680
$\pi\text{-}p \to n\pi^+\pi^- + (1, 2, 3, 4, 5)\pi^0$, 5 GeV/c, partial cross sections and ang. and momentum distributions 2−52617
$\pi\text{-}p \to \pi^- pX^0$, 13.4 GeV/c, natural meson production meas., π°, ρ^0, ω^0, D° 2−52616
$\pi\text{-}p \to \pi^-\pi^+ n$, 8 GeV/c, meas. of production and decay angular distributions of ρ^0, f^0, and $\pi^+\pi^-$ mass distrib. 2−79600
$\pi\text{-}p \to \pi\pi N$ events from hydrogen bubble chambers, selective compilation 2−42395
$\pi\text{-}p \to \rho\text{-}p \to \pi^-\pi^0 p$, 2.77 GeV/c, spin density matrix elements computed analysis of ρ polarization 2−63646
$\pi\text{-}p \to \rho n \to \pi^+\pi^- n$, 2.77 GeV/c, spin density matrix elements computed, analysis of ρ polarization 2−63646
πp, meson factory expts. at low energy 2−82640
πp, multi-pion producing, cross section energy depend. in single peripheral model 2−79596
πp, peripheral dynamics for limiting fragmentation 2−79586
πp high-energy asymmetry of pion distrib. 2−45967
π^-p, 13.1 GeV/c, study of reactions with two charged final state particles 2−63620
π^-p, 16 GeV/c, obs. of central emission of pions, search for symmetry system 2−73816
π^-p, 1.69 GeV/c, production of $Y_0{}^*(1405)$, $Y_1{}^*(1385)^\circ$, meas. of width, mass, spin, parity of resonance 2−46018
π^-p, 25 GeV/c, single and double π prod. processes 2−45969
π^-p, 3.8 GeV/c, obs. of $X^0 \to \gamma\gamma$ 2−67037
π^-p, 40 GeV/c, multiplicity distribution of charged particles produced 2−45960
π^-p, 7 GeV/c, four- and five-body final state interactions 2−67026
π^-p, intrinsic props. of η, S^0, ρ, ω, X^0, φ and $A_2{}^0$ mesons 2−73835
π^-p, two-particle correls., 60 GeV/c 2−63614

Protons and antiprotons continued
interactions continued
π^-p charge exchange, differential cross sections, evidence for tachyonic resonances 2−63546
$\pi^- p \to B^- p$, cross-section, OMEA model, rel. to B-meson spin parity 2−76698
$\pi^- p \to K^+ Y^{*-}(1385)$, final-state-interaction contributions to exotic forward peak 2−63618
$\pi^- p \to K^{*0}\Lambda$, meas. of joint density-matrix elements, study of vector-meson production with hypercharge exchange 2−82743
$\pi^- p \to K^{*0}\Lambda$, polarization and unnatural parity exchange 2−42376
$\pi^- p \to M^0 n$, 2.4 GeV/c, $M^0(940)$ and $\delta^0(963)$ obs. 2−76693
$\pi^- p \to M^0 n$, 2.4 GeV/c, neutral meson detection 2−70207
$\pi^- p \to X^- p$, boson missing-mass spectrum struct. 2−76679
$\pi^- p \to (MM)^- p$, 8, 11, 13.5, 16 GeV, meas. of missing mass spectra, evidence for triple factorizability of cross sections 2−76678
$\pi^- p \to (mm)^- p$, 8 GeV/c missing mass spectrum in R region 2−73821
$\pi^- p \to (pp)n$, 18.8 GeV/c, obs. 2−45965
$\pi^- p \to (\pi^0\pi^0)n$, production of neutral resonances that decay to $\pi^0\pi^0$ at Serpukhov energies 2−76683
$\pi^- p \to e^+e^- n$, dispersion model, use for calc. of N, π form factors 2−63602
$\pi^- p \to \eta^0 n$, partial differential cross section at large momentum transfer and incident pion momenta 3.67 and 4.38 GeV/c 2−63575
$\pi^- p \to \eta n$, applic. of symmetry point sum rules 2−49566
$\pi^- p \to \eta\pi^- p$, 6 GeV/c, study of $\eta\pi$ mass spectrum, D-wave Breit-Wigner analysis 2−76670
$\pi^- p \to$ missing mass + n, meson mass spectrum near $X^0(958)$ 2−42402
$\pi^- p \to nX^0$ near threshold, meson mass spectrum 2−76676
$\pi^- p \to n +$ (missing-mass), missing-mass spectrum near 960 MeV 2−76675
$\pi^- p \to n +$ neutral boson, search for decay mode $\omega \to \eta\gamma$ 2−79603
$\pi^- p \to n\pi^+\pi^-$, 3.1 to 3.6 GeV/c, ang. distrib. meas. 2−67029
$\pi^- p \to \omega^0 n$, 3.65, 4.5, 5.5 GeV/c, study of ω^0 spin-density matrix 2−52625
$\pi^- p \to \omega^0 n$, 3.65, 4.5 and 5.5 GeV/c, differential cross section 2−67027
$\pi - p \to pX^-$, 25, 40 GeV/c, missing mass spectra 2−49568
$\pi^- p \to p\pi^+\pi^-\pi^-$, spin-parity analysis of A_3 ($f\pi$) resonance 2−49581
$\pi^- p \to p\pi^+\pi^-\pi^-\pi^0$, decay properties of $\rho(1.71)$ resonance 2−49582
$\pi^- p \to \pi^-\pi^-\pi^+ p$, 40 GeV/c, A_1 and A_2 prod. 2−76699
$\pi^- p \to \pi^-\pi^0 p$, $p_{\pi-} = 4.45$ GeV/c, elastic $\pi^-\pi^0$ scatt. cross section 2−76681
$\pi^- p \to \pi^-\pi^+ n$, 17.2 GeV/c, $\pi\pi$ phase-shift analysis 2−76673
$\pi^- p \to \pi^-\pi^+ n$, 4 GeV/c, determ. of isoscalar S-wave $\pi\pi$ phase shift with absorption modified one pion exchange model 2−63609
$\pi^- p \to \pi^-\pi n$, 17.2 GeV/c, amplitude analysis, A_2 and absrobed pion exchange 2−79583
$\pi^- p \to \pi^0 n$, charge exchange at Serpukhov energies 2−76683
$\pi^- p \to \pi^0 n$, charge exchange differential cross sections at 3.67 and 4.83 GeV/c and intermediate momentum transfers 2−63619
$\pi^- p \to \pi^0 n$ (ηn), properties of polarization in forward direction determ. using Regge amplitudes 2−70237
$\pi^- p \to \pi^0 n$ charge exchange, momentum dependence of differential cross section at 180° in 1.8-6.0 GeV/c range 2−82758
$\pi^- p \to \pi^0\pi^0 n$, exptl. study at 447 MeV, cross sections and missing mass spectrum 2−49567
$\pi^- p \to \pi^0\pi^0 n$, use with one-meson approx. to obtain $\pi\pi$ scattering cross-section 2−82764
$\pi^- p \to \pi^+\pi^- n$, 15GeV/c, model amplitude analysis 2−67023
$\pi^- p \to \pi^+\pi^- n$, one pion exchange model developed using Veneziano five point function 2−52618
$\pi^- p \to \pi^+\pi^-\pi^- p$, 11-40 GeV, A_3 enhancement, non-resonant behaviour 2−76677
$\pi^- p \to \rho^- p$, 3.25 GeV/c, comparison between exptl. data and prediction of absorptive metal 2−67024
$\pi^- p \to \rho^0 n$, 3.25 GeV/c, conparison between exptl. data and prediction of absorptive model 2−67024
$\pi^- p \to \rho^0 n$, appl. Reggezied OPEA model 2−76645
$\pi^0 p \to \rho^0 p$ differential cross- section explained by nonsense wrong signature zeros 2−59529
π^+p, 12-28 GeV, correlations between produced π^- particles 2−55832
π^+p, 4.1 GeV/c, analysis of 2-pronged events 2−63621
π^+p, 5 GeV/c, evidence for double diffractive dissociation 2−59531
π^+p, 5.45 GeV/c, production properties of $A_1{}^+$ 2−73838
π^+p, 8 and 16 GeV/c, obs. of central emission of pions, search for symmetry system 2−73816
π^+p, 895, 945, 995, 1040 MeV/c, cross sections and resonance fractions for two single pion production channels 2−42390
π^+p, correlation parameters for π^- production calc. from multiplicity distrib. 2−49592
π^+p, ω production at 2.67 and 2.30 BeV/c, differential cross sections, decay density matrix elements 2−45987
π^+p, π^- energy spectra, analysis for beam momenta of 8 and 16 GeV/c 2−52614
π^+p, single-particle and two-particle inclusive reactions at 7 GeV/c 2−45944
$\pi^+ p \to K^+K^-\Delta^{++}$, 7.1 GeV/c, $\pi\pi$ phase shifts 2−76674
$\pi^+ p \to K^+\Sigma^+$, 1.11 GeV/c, polarisation 2−42394
$\pi^+ p \to K^+\Sigma^+$, calc. of $N^{*3/2}$ partial widths and branching ratios 2−70268
$\pi^+ p \to K^+\Sigma^+$, differential cross sections near 0° at 3,5,7, GeV/c 2−70238
$\pi^+ p \to K^+ Y^{*+}(1385)$, differential cross sections near 0° at 3,5,7 GeV/c 2−70238
$\pi^+ p \to 3\pi^+ 2\pi^- p$, 8 GeV/c, ABFST model with dual amplitudes 2−82750
$\pi^+ p \to (\pi^+\pi^-)\Lambda^{++}$, 13 GeV/c, phase shift analysis of $\pi^+\pi^-$ scattering in mass range 0.6-1.4 GeV 2−73826
$\pi^+ p \to \eta\Delta^{++}$, local duality and dips 2−52615
$\pi^+ p \to \kappa^+\Sigma^+$, 2 and 4 GeV/c, meas. of polarization in backward direction 2−76686
$\pi^+ p \to \pi^-\pi^- X$, 18.5 GeV/c, two- particle inclusive distrib. and correlation functions 2−82707
$\pi^+ p \to \pi^-\pi^- X$, evidence for factorization 2−63616
$\pi^+ p \to \pi^0\Delta^{++}$, local duality and dips 2−52615
$\pi^+ p \to \pi^+\pi^-\Delta^{++}$, 7.1 GeV/c, $\pi\pi$ phase shifts 2−76674

Protons and antiprotons continued
interactions continued
$\pi^+p\to\pi^+\pi^-\Delta^{++}$, model moments 2−73824
$\pi^+p\to\pi^+\pi^+\pi$-p, 13.1 GeV/c, spin-parity analysis of low-mass 3π system 2−45962
$\pi^+p\to\pi^+\pi^+\pi^-p$, 8 and 16 GeV/c, separation of production mechanisms by longitudinal phase space analysis 2−70235
$\pi^+p\to\pi^+\rho^0n$, 7 GeV/c, A_1 study 2−49584
$\pi^+p\to\pi^\pm$ + anything, $\pi^-p\to\pi^-$ + anything, 3.7 to 18.5 GeV/c, energy dependence of inclusive distributions 2−42392
$\pi^+p\to\rho^0{}_{1236}{}^{++}$, near threshold, chiral SU(2) × SU(2) dynamics 2−67025
$\pi^+p\to\rho^+p$, 2.67 GeV/c, isoscalar exchange 2−45964
$\pi^\pm p$, Δ(1236) production, application of Regge-pole model 2−73856
$\pi^\pm p$, p_t limited phase space predictions 2−55831
$\pi^\pm p$, total cross sections in momentum region 15 to 60 GeV/c, Glauber correction 2−45968
$\pi^\pm p$ total cross-section, relation to slope of diffraction cone 2−66964
$\pi^\pm p$ total cross-sections, empirical scaling behaviour 2−73778
$\pi^\pm p$ total cross section from 0.4-0.9 GeV/c meas. using transmission method 2−63611
$\pi^\pm p$ total cross sections, 0.4 to 0.9 GeV/c 2−79598
$\pi^\pm p\to A_1{}^\pm p$ at small momentum transfer, eikonal Regge model 2−45966
$\pi^\pm p\to\rho^\pm p$, 15 GeV/c, spark chamber meas. 2−79584
$\pi^\pm p\to\rho N$ rho production reactions at 16 GeV/c, study of exchange mechanisms 2−70236
$\pi p\to K^-\pi^+\pi^-$ 16 GeV/c s-channel and t-channel helicity conservation tested 2−82753
$\pi p\to K^*Kp$, obs. of F_1 (1540) kinematic enhancement, Reggeized Deck model, link with resonance 2−63633
$\pi p\to\Lambda(\Sigma)K$, inelastic reactions, complex moments analysis considering j-plane branching 2−76661
$\pi p\to p\pi^+\pi^-$ 16 GeV/c s-channel and t-channel helicity conservation tested 2−82753
$\pi p\to\pi\pi^+\pi^-$ 16 GeV/c s-channel and t-channel helicity conservation tested 2−82753
$\pi p\to\rho N$, pion exchange, 6 GeV/c 2−59532
Σ^-p total cross sections at 19 GeV 2−79625
T-region reson. studies in annihilation expts. 2−59571
U-meson existence search 2−59567
$\gamma p\to K^+\Lambda$, evidence for stray baryonic states 2−52646
K^+p, one and two prong interaction of K^+ on deuterium at 5.5 GeV/c, meas. of partial cross sections 2−63595
K^+p, single-particle and two-particle inclusive reactions at 12.7 GeV/c 2−45944
π-p$\to n\gamma$, 370 and 332 MeV, meas. of diff. cross sections 2−42393
π-p$\to p\pi^+\pi$-π-, 20 GeV/c, production of N^{*++} (1236), ρ^0, f^0, A enhancement in 3π mass spectrum 2−45963
$\pi-p$ collisions, high multiplicity pion production 2−67028

interactions, proton-proton
200 GeV/c, charged particle multiplicities, fragmentation model 2−73848
angular distrib. of charged particles produced in collisions at ISR energies between 30° and 90° 2−49593
average pion multiplicities, high energy interactions 2−59566
Bose distribution of π and K, 12-30 GeV/c, determ. of scaling behaviour 2−76717
charged-particle multiplicity distribs., 200 GeV 2−67049
colliding beam experiments, survey of experiments at CERN 2−42409
colliding beam physics, review 2−76718
correlation parameters for π^- production calc. from multiplicity distrib. 2−49592
cosmic ray expt. properties between 100 and 1000 GeV 2−55876
fragmentation into neutrons, peripheral dynamics 2−79616
inclusive, 13 to 28 GeV/c, two-particle correlations 2−67050
inclusive, at high energy, explanation of correlation data using Feynman Wilson two-component picture 2−82780
inclusive collisions, invariant pion spectrum, non-diffractive region 2−82714
inclusive cross-section and asymptotic behaviour 2−59565
inclusive process comparison of π^- distributions for γp and K^+p collisions 2−67052
inclusive proton spectra in diffraction excitation model 2−73850
inclusive reactions, diffraction model, leading-particle and momentum conservation effects 2−70179
inclusive spectra in thermodynamical model 2−76716
neutral strange particle production from 24.9 and 28.6 GeV/c interactions 2−67053
p_t limited phase space predictions 2−55831
production of charged particles, angular distribution, collisions at CERN ISR 2−63658
secondary particle angular distrib., coherent π production 2−73844
spectra for fast π^+, π-, K^+ secondaries represented in Reggeized forms with scaling 2−45953
thermodynamic model for proton spectra, pion spectra and scaling behaviour 2−70255
total cross-section, relation to slope of diffraction cone 2−66964
two-particle correls., 60 GeV/c 2−63614
$K^-p\to K\pi N$, 10 GeV/c, isospin analysis, diffractive dissociation 2−82735
pp, 12-28 GeV, correlations between produced π^- particles 2−55832
pp, obs. of direct channel T and U meson formation using Rutgers Annihilation Spectrometer 2−76700
pp annihilation, ang. momentum analysis using Zemach tensors and helicity amplitudes 2−59579
pp annihilation, broad resons., methods of analysis 2−59583
pp annihilation at rest, initial ang. momentum state 2−59576
pp annihilation at rest 2−76647
pp annihilations, final states analysis, methods 2−59584
pp annihilations, final state analysis, resons. 2−59585
pp annihilations, low energy phenomena 2−59586
pp annihilations into two charged particles near centre-of-mass energy 2200MeV 2−42415
pp total cross-section, relation to slope of diffraction cone 2−66964
pp total cross-sections, empirical scaling behaviour 2−73778
pp total cross-sections empirical scaling behaviour 2−73778
$pp\to\Delta^{++}(1236)\Delta^{++}(1236)$, Regge eikonal model calc. 2−70256
$pp\to\Delta\Delta\to p\pi^-p\pi^+$, angular correlation theory 2−45863

Protons and antiprotons continued
interactions, proton-proton continued
$pp\to K_1{}^0K_1{}^0\omega^0$, direct S-channel effects in T-meson region 2−59575
$pp\to K^-K^+$ 5 GeV/c, differential cross-sections 2−79620
$pp\to KK$, low momentum, cross-section distrib. 2−59574
$pp\to K$ + anything, fireball like structure 2−67051
$pp\to K^*K\pi$, obs. of F_1 (1540) resonance, link with kinematic enhancement 2−63633
$pp\to X^0\pi^0\to n\pi^+\pi$-$\pi^0$, n = 3.4, 6.94 GeV/c obs. X^0 3.1, 3.4, and 3.6 2−63645
$pp\to X$ + anything ($X=\pi^\pm, K^\pm$, p), triplet Regge graph study 2−63656
$pp\to 2\pi^+2\pi$- annihilation process, 3.6 GeV/c, multi-peripheral model including reson. 2−59578
$pp\to 2\pi^+2\pi$-π^0, annihiliation, Isobar model analysis 2−59581
$pp\to 3\pi^+3\pi$- annihilation with isobaric amplitude, model analysis 2−59572
$pp\to 3\pi^+3\pi^-\pi^0$, study of η^0 production at 700 MeV/c, evidence for decays of D- and E-mesons into $\delta\pi$ 2−63640
$pp\to 6\pi$, 2.5 GeV/c, ω, ρ production resonance production 2−79615
$pp\to de^+v$, meson exchange corrections, usog W.K. Cheng method 2−42414
$pp\to d\pi^+$, $pp\to d\rho^+$, 10 to 24 GeV, differential cross sections and angular distributions 2−45995
$pp\to\gamma X$ γs due to $\pi^\pm$ as well as π° decay 2−82755
$pp\to k_1{}^0k_1{}^0\omega^0$, direct s-channel effects in T meson region 2−67039
$pp\to\mu^+\mu^-$ + anything, calc. of cross section in parton model, comparison with expt. 2−70178
$pp\to nX$, one-pion exchange model comparison with cosmic ray nucleon propagation through atmosphere 2−63681
$pp\to n$ + anything, pion exchange model 2−59442
$pp\to nn$, data analysis by phenomenological model based on pion exchange 2−45999
$pp\to n\pi$ limiting behaviour of single particle distributions 2−59440
$pp\to\omega^0\pi^+\pi^-$, evidence for $\omega\pi^\pm$ resonances 2−79602
$pp\to\omega\pi^+\pi$- annihilation, final state interpret. 2−59580
$pp\to pN^*(1688)$ 5.5 GeV/c, U(6,6)⊗O(3,1) peripheral absorption model study 2−55882
$pp\to p$ + anything, determination of triple Reggeon vertices 2−49594
$pp\to p$ + anything, finite-energy sum rules, Reggeon-particle scattering amplitudes 2−73849
$pp\to pn\pi^+$, 19 GeV/c, analysis of data using mechanism of kinetic coupling between momentum transfers 2−63488
$pp\to pn\pi^+$, 19 GeV/c, low mass $n\pi^+$ system studied by double-peripheral dynamics 2−49526
$pp\to ppe^+e^-$, for calibrating cross-sections in colliding p beams 2−45997
$pp\to pp\pi$-π^+, multi-Regge models analysis, 13.1 GeV/c 2−63655
$pp\to pp\pi^0$ 6.6 GeV/c, cross-sections for production of isotopic spin-$^1{}_{\cdot 2}$ and $^3{}_{\cdot 2}$ πN systems 2−76710
$pp\to pp\pi^+\pi^-$, 19 GeV/c, study of $p\pi^+\pi^-$ enhancements at 1500 and 1700 MeV 2−49599
$pp\to pp\pi^+\pi^-X^0$, 19 GeV/c, effective mass enhancement in $p\pi^-X^0$ system, Δ(2850) prod. 2−63654
$pp\to p\pi^+n$, 6.6 GeV/c, cross-sections for production of isotopic spin-$^1{}_{\cdot 2}$ and $^3{}_{\cdot 2}$ πN systems 2−76710
$pp\to p\pi^+n$, 6.6 GeV/c meas. of $|T_z|=3/2$ Δ(1238) production total and differential cross sections 2−67062
$pp\to p\pi^+\pi$-π^0p, 6.6 GeV/c meas. of $|T_2|=3/2$ Δ(1238) production toal and differential cross sections 2−67062
$pp\to p\pi^+\pi-p$, 6.6 GeV/c, meas. of $|T_z|=3/2$ Δ(1238) production total and differential cross sections 2−67062
$pp\to p\pi^+\pi^-\pi^+n$, 6.6 GeV/c meas. of $|T_2|=3/2$ Δ(1238) production total and differential cross sections 2−67062
$pp\to\pi^-\pi^-X$, evidence for factorization 2−63616
$pp\to\pi^-\pi^-$ + anything, exptl. investigation of two-body correlations 2−42412
$pp\to\pi^-\pi^+$, 2.3 GeV/c, comparison of data with other two meson states 2−63657
$pp\to\pi^-\pi^+$, 5 GeV/c, differential cross-sections 2−79620
$pp\to\pi^+\pi^-$ annihilation processes, integrated and local absolute bounds 2−67058
$pp\to\pi^+\pi^-$ cross- section compared with that for $\pi^+\pi^+\to pp$ 2−45965
$pp\to\pi^+\pi^0\pi$-, isospin and grand ang. momentum analyses 2−59563
$pp\to\pi^+\rho^-$, 5 GeV/c, differential cross-section 2−79621
$pp\to\pi^\pm$ + anything 28.5 GeV, single-particle inclusive pion spectrum 2−45950
$pp\to\pi$ + anything, fireball like structure 2−67051
π production, longitudinal momentum distrib., derivation from quark-boson hadron model 2−66956
π° production at ISR energies, angular distrib. determ. from γ-ray data 2−49561
$pp\to\pi^+\pi^+\pi^-\pi^-$, 3.6 GeV/c, analysis in terms of multiperipheral model including resonances 2−73845

magnetic moment
μ_p/μ_n meas. using ion cyclotron resonance technique 2−70254
Markoffian model of hadrons, moment calc. from solution of Kolmogorov's eqn. 2−73773

polarization
acceleration in Saturne, preservation of proton polarization 2−70331
beam production and applic. 2−73536
deuteron stripping reaction 2−59779
elastic scattering of polarized protons on ^{32}S, calc. of polarization map in 2.5-3.0 MeV range using resonance parameters 2−67153
methanol-ethyleneglycol mixture, dynamic polariz. of protons 2−79677
methods, and applic. to nuclear and particle physics 2−76714
polarisability estimation from $\alpha^2\ln\alpha^1$ recoil correction to H hyperfine structure and muonium hyperfine internal corrections 2−83214
$\gamma p\to\pi^0p$, in third resonance region 850-1250 MeV, recoil proton polarization 2−46004
pp polarization structure, differences in theory and expt. explained by exotic peripheral resonances 2−67056
pp scattering, 47.5 MeV, spin correlation parameters, A_{yy} and A_{xx} 2−79610
$^9Be(d,p)^{10}Be$, $E_d=12$ MeV, proton polarization for ground state and first excited state transitions 2−82998

- **Protons and antiprotons** continued
  - **polarization** continued
    - ^{40}Ca(p,p)^{40}Ca, polarized protons, 2.3-2.8 MeV, meas. of proton polarization, determ. of angular momentum of ^{41}Sc excited states 2−52812
    - (d,p) Colomb stripping reactions, analytic expression 2−46311
    - ^{2}H, proton elastic scattering, polarisation at 198 MeV 2−49790
    - ^{2}H(d,p)^{3}H, E_d=2-14 MeV, determ. via ^{3}H(p,d)^{2}H reaction 2−70473
    - ^{2}H(p, p)^{2}H, 600 MeV cross-section obs., p polarization meas. cf with Watson and Glauber theory 2−63873
    - ^{3}H(p,n)^{3}He, polarization and polarization transfer 2−46257
    - ^{3}H(p,p), polarized proton beam, meas. of differential cross section, proton analyzing power at 19 and 30 MeV 2−63874
    - ^{3}H(p,p)^{3}H, elastic scatt., E_p=9.4-14.7 MeV, analyzing powers, ang. distrib. 2−70441
    - ^{4}He(p, p)^{4}He, 600 MeV, cross-section obs., p. polarization meas. 2−63873
    - ^{28}Si(p,p)^{28}Si, polarized protons, 1.5-3.0 MeV, meas. of proton polarization, determ. of angular momentum of ^{29}P excited states 2−52812
    - ^{88}Sr(p,p$'\gamma$)^{88}Sr, polarization-analyzing power inequality 2−76846
  - **production**
    - charged particle prod. at 90° in centre of mass in pp collisions 2−82773
    - electroproduction, obs. of coincidences of electrons with forward and backward produced protons 2−49503
    - electroproduction, Regge behaviour of scaling function 2−63511
    - polarized beam production 2−73536
    - proton, high intensity, with low energy spread 2−73522
    - source, high intensity, with low energy 2−73522
    - K$^+$/p, diffractive excitation model, adjustment of relative normalization 2−82756
    - p/π- diffractive excitation model, adjustment of relative normalization 2−82756
    - P, in proton interactions in nuclei at 24 GeV/c 2−63606
    - p, low-momentum, at CERN proton synchrotron 2−42417
    - p,p, ratios at 21, 31, 45, 53 GeV in centre of mass 2−49564
    - $\pi^-\pi^+\to$pp cross-section compared with that for pp$\to\pi^+\pi^-$ 2−45965
  - **scattering**
    - — 2−59523
    - Compton effect, differential cross section meas. in $\Delta(1236)$ resonance region 2−63653
    - ep, spin dependent deep inelastic, light cone analysis 2−55826
    - fixed-pole Pomeron shielding-cut mechanism, diffr. scatt. asymptotic behaviour 2−52588
    - inelastic excitation function, calc. using hadronic phonon representation 2−70170
    - np phase shifts, calc. of deuteron relativistic charge form factor 2−42427
    - partons in proton, charge distributions and scaling in deep inelastic scattering 2−45916
    - structure function calc. in leading logarithm approx. to perturbation theory and massive g.e.d. Lagrangian 2−73752
    - sum rules, finite energy related to light-cone commutator of currents 2−63557
    - two-body calc. of $\rho\rho$ P triple-Regge vertex assuming duality and f-coupled Pomeron 2−55842
    - ep, and single particle distribs. due to virtual phonon in dual reson. model 2−76607
    - ep, Callan-Gross sum rule, rederivation from light-cone commutator 2−45889
    - ep, cross-sections longitudinal and transverse determ., magnetic dipole transition form factor 2−45887
    - ep, deep inelastic, massive quantum electrodynamics 2−42341
    - ep, deep inelastic, perturbation theory, connection with e$^+$e$^-$ annihilation 2−52562
    - ep, deep inelastic, two-photon exchange effects 2−73759
    - ep, elastic, large angle, parity violation 2−45885
    - ep, hadron, electroproduction distribution, one photon exchange part, Regge behaviour 2−70171
    - ep, inelastic, comparison of differential crosssection data with μp meas at 12 GeV/c 2−66946
    - ep, inelastic, generalized vector dominance, model 2−49505
    - ep, inelastic, nature of scale-invariance breaking term determ. from DGS representation 2−59425
    - ep, parton model, scaling behaviour 2−52560
    - ep, radiative corrections to cross-section for small angle scattering when detecting recoil protons 2−66942
    - ep, structure functions, non-scaling corrections 2−49504
    - ep, super-eikonal model, calc. of νW_2 structure function 2−63516
    - ep cross section data, rel. to scale relation for proton form factors 2−55874
    - ep deep inelastic, light-cone analysis of soft-pion production 2−45954
    - ep deep inelastic electroproduction, meas. of inclusive hadron momentum distributions 2−73777
    - ep elastic, phenomenological use of Callan-Symanzik eqn., obs. of scaling law 2−66922
    - ep exclusive scattering, Bjorken limit, scaling behaviour 2−42342
    - ep inelastic, test for duality in current amplitudes 2−42343
    - ep sum rule connecting resonance region of virtual Compton amplitude to deep inelastic region 2−70161
    - e$^-$p, inelastic structure functions in gluon model 2−63513
    - e$^-$p, virtual Compton scatt., off forward direction, scaling limit 2−63510
    - ep$\to$ep + anything, t and q^2 dependence, triple-Regge formalism application 2−73757
    - ep$\to$epρ°, yield of p + ρ° rel. to other hadron final states 2−63517
    - ep$\to$eπ^+ + anything, inclusive electroproduction 2−79502
    - ep$\to$eπnπ, study of multiparticle final states using spectrometer with spark chambers 2−76738
    - γp, forward Compton scatt., cross section analysis 2−52553
    - γp$\to\varphi^\circ$p, 'elastic' photoproduction at 8.5 GeV, determ. of cross sections 2−49580
    - γp$\to\rho^\circ$p, 'elastic' photoproduction of 8.5 GeV determ. of cross sections 2−49580
    - K-p backward elastic, 1.2-2.5 GeV/c, cross section analysis by resonance and Reggeized baryon exchange 2−63599
    - Kp, Chou Yang model for high energy diffraction slopes 2−49488
    - Kp, transition regeneration amplitude meas., 14-42 GeV 2−79609

- **Protons and antiprotons** continued
  - **scattering** continued
    - Kp dispersion relations, model independent calculation 2−79569
    - Kp interaction scaling radius hypothesis, comparison with data for 6-14 GeV/c 2−73788
    - Kp polarization, interpretation in terms of optical model 2−67056
    - K$^-$p, charge exchange cross section at 1.8 GeV/c 2−59521
    - K$^-$p, differential cross sections, unitarization and OBE contrib. 2−76638
    - K$^-$p, elastic scattering, 10 GeV/c, review of recent results 2−42377
    - K$^-$p$\to$K^{0}n, multiple scatt. model, duality breaking effects 2−63572
    - K$^-$p$\to\pi^-\Sigma^+$ multiple scatt. model, duality breaking effects 2−63572
    - K$^+$p, 2.11 to 2.72 GeV/c, elastic channel analysis 2−49553
    - K$^+$p, backward dispersion relations 2−45946
    - K$^+$p, backward elastic, relation to quantitative Regge expressions for $\pi^\pm$, K$^+$ inclusive spectra 2−45953
    - K$^+$p, below 1.3 GeV/c, dispersion relations 2−55848
    - K$^+$p, below 2.5 GeV/c, diffractive and elastic interactions 2−49541
    - K$^+$p, elastic, 0.9-1.9 GeV/c, meas. of differential cross section in computer expt. 2−52607
    - K$^+$p, elastic, 430-940 MeV/c, meas. of differential cross sections 2−52606
    - K$^+$p, elastic, below 1.3 GeV/c, partial-wave dispersion relation analysis 2−52609
    - K$^+$p, elastic, below 2 GeV/c, review of regions below and above 0.9 GeV/c, partial wave analysis 2−52604
    - K$^+$p, elastic, threshold 2.5 MeV/c, application of Cutcofsky-Deo method 2−52605
    - K$^+$p, partial wave dispersion relations, role of ε exchange 2−63597
    - K$^+$p, Pomeron exchange amplitude and existence of Z^* 2−70212
    - K$^+$p backward dispersion relations 2−45945
    - K$^+$p backward dispersion relations 2−52608
    - K$^+$p elastic, in range 0.9 to 1.9 GeV/c, meas. of differential cross sections 2−55849
    - K$^\pm$p, elastic, total cross sections 2−59522
    - K$^\pm$p, elastic charge exchange scatt., s-channel helicity amplitudes 2−59520
    - K$^\pm$p, large angle contribution of direct channel resonances 2−42366
    - K$^\pm$p, Regge fit with Veneziano residues 2−52603
    - Λp and binding energy of $^3_\Lambda$H, $^4_\Lambda$H and $^4_\Lambda$He 2−82876
    - μp, inelastic at 12 GeV/c meas. of differential cross section, comparison with p inelastic scattering 2−66946
    - μp possibility of anomalous interaction at low energies due to exchang of scalar meson 2−63526
    - np, charge exchange, 8 to 29 GeV/c, differential cross sections 2−55879
    - np, local $^1S_0$ potential, phase shifts calc. 2−82844
    - np charge exchange, π-exchange processes, elementary pion with transverse-momentum cutoff 2−42380
    - np$\to$pn, data analysis by phenomenological model based on pion exchange 2−45999
    - νp, elastic, with strong W-boson interactions 2−79501
    - νp scatt., structure function calc. in leading logarithm approx. to perturbation theory and massive g.e.d. Lagrangian 2−73752
    - νp scatt., structure function calc. in leading logarithm approx. to perturbation theory and massive g.e.d. Lagrangian 2−73752
    - νp$\to\nu$p, amplitude of reaction in unified models, induced neutral current effects 2−70155
    - p-^{12}C elastic scatt., cross sections analysis 2−82723
    - pd, elastic, investigation in diffraction cone region at energy 10 to 70 GeV 2−52635
    - pd, production of high energy polarized neutrons 2−70264
    - pd, spin structure in Glauber theory 2−59755
    - pd near- backward elastic scattering at high energies calc. of second order correction to first order baryon exchange formula 2−63661
    - pn, charge exchange, fixed poles, unitarity and duality 2−79533
    - pn, elastic, modified Glauber theory 2−70260
    - pn, small-angle, 24 MeV, differential cross-sections 2−73854
    - pn high energy collisions, cross section for massive muon pair production 2−55878
    - Pn inelastic at momentum 19.2 GeV/c, meas. of charged particle distrib. 2−67057
    - π-p, apparatus for spin rotation meas. at high energies 2−73901
    - π-p, elastic, meas. of differential cross-section near 180° from 2.15 to 6 GeV/c 2−63629
    - π-p elastic backward Regge pole analysis 2−63630
    - πP, elastic, slope parameter of diffraction peak 2−79611
    - πp, inelastic collisions, prong-number distrib. 2−79617
    - πp, nonshrinking diffraction peak due to fixed pomeron 2−45923
    - πp backward elastic, fluctuations, dips and duality 2−82759
    - πp polarization, interpretation in terms of optical model 2−67056
    - πp radiative scatt. near $\Delta(1236)$ reson. 2−76685
    - πp up to lab momentum of 3 GeV/c, calc. of partial-wave amplitudes with large angular momentum 2−42397
    - π^-p, differential cross-section, electromagnetic form factors in parton model 2−73811
    - π^-p, differential cross sections, unitarization and OBE contrib. 2−76638
    - π^-p, elastic charge exchange scatt., s-channel helicity amplitude 2−59520
    - π^-p, elastic scatt. cross section at 2.29 GeV/c 2−59541
    - π^-p charge-exchange reactions, kinematic variable 2−79595
    - π^-p forward elastic scattering near 1 GeV/c, meas. of differential cross section 2−73823
    - π^-p$\to$K$^0\Lambda$, 1400-2000 MeV, new phenomenological analysis 2−52621
    - π^-p$\to$K$^0\Lambda^0$ backward high energy, prediction of polarization sign 2−63628
    - π^-p$\to$P$^-$p, elastic, phenomenological use of Callan-Symanzik eqn., obs of scaling law 2−66922
    - π^-p$\to\eta$n, multiple scatt. model, duality breaking effects 2−63572
    - π^-p$\to\pi^-$p, 1400-2000 MeV, new phenomenological analysis 2−52621
    - π^-p$\to\pi^-$pπ^0, 1400-2000 MeV, new phenomenological analysis 2−52621
    - π^-p$\to\pi^-\pi^+$n, 1400-2000 MeV, new phenomenological analysis 2−52621
    - π^-p$\to\pi^0$n, multiple scatt. model, duality breaking effects 2−63572
    - π^-p$\to\pi^0$n amplitudes, estimate in terms of direct-channel resonances and dual absorptive requirements 2−82761

Protons and antiprotons continued
scattering continued
$\pi^-p \to \pi^0\pi^0n$, 8 GeV/c, $\pi\pi$ phase shifts 2−79588
$\pi^-p \to \pi^+\pi^-n$, 15 GeV/c, ρ prod., vector dominance and ρ-ω interference 2−82765
π^+p, backward elastic scatt. at 6GeV/c, polarization parameter meas. 2−55858
π^+p, differential cross-section, electromagnetic form factors in parton model 2−73811
π^+p backward scattering, simplified Regge analysis 2−79593
π^+p differential cross-sections, G_{39}-resonance 2−70239
π^+p elastic scattering, 2 and 4 GeV/c, meas. of polarization in backward direction 2−76686
$\pi^+p \to {}^+p$, 1.55-1.84 GeV/c high-statistics study, obs. of dip structures 2−82754
$\pi^+p \to K^+\Sigma^+$, multiple scatt. model, duality breaking effects 2−63572
$\pi^\pm p$, backward elastic, relation to quantitative Regge expressions for $\pi^\pm$, K^+ inclusive spectra 2−45953
$\pi^\pm p$, elastic, at 6 and 16 GeV/c, meas. of spin rotation parameters 2−59539
$\pi^\pm p$, elastic scatt., Pomeron and f exchange amplitudes 2−59540
$\pi^\pm p \to (\pi^\pm\pi^+\pi^-)p$, interference between exchanges, 16 GeV/c 2−79585
$\pi^\pm p \to \pi^\pm(\pi^+\pi^-p)$, interference between exchanges, 16 GeV/c 2−79585
$\pi p \to \pi\pi^+n$, absorptive corrections 2−79582
ep, inelastic, at small four- momentum transfers, test of finite-energy sum rules 2−45883
In_2S vapour, thermodynamic functions, electronic and i.r. spectra, heats of sublimation and formation, 273-2000 K 2−74485
Ni isotopes, phase analysis for elastic scattering using computer 2−67214

scattering, proton-proton
analytic continuation of forward amplitude, interactive determ. 2−59396
break in elastic slope parameter, peripheral pomeron component 2−79614
bremsstrahlung calcs. including relativistic corrections to Pauli-Schroedinger eqn. 2−67054
bremsstrahlung cross-section at low energy 2−73851
bremsstrahlung production at 51.8 MeV 2−45996
CERN data in 1000 GeV region reproduced by weak-cut-type Regge models 2−63660
coherent droplet model including Yukawa interaction term 2−70258
cross-section slope parameter depend. on Mandelstamm variables, 10-1000 GeV 2−82778
differential cross sections, unitarization and OBE contrib. 2−76638
diffraction cone slope, effect of cut contribution 2−82776
diffraction model involving hypothetical isobar of variable mass. 2−79618
diffraction slopes, high energy, Chou-Yang model 2−49488
elastic, 1.1 to 1.7 FeV/c Coulomb interference region, differential cross-sections 2−82777
elastic, CERN ISR expts. 2−79699
elastic, in Coulomb and nucl. interference region, 8 to 70 GeV 2−59569
elastic, modified Glauber theory 2−70260
elastic, phenomenological use of Callan-Symanzik eqn., obs. of scaling law 2−66922
elastic, slope parameter of diffraction peak 2−79611
elastic, small-angle, at very high energies, $460\ GeV^2 < s < 2900\ GeV^2$ 2−49595
elastic, urbaryon rearrangement diagram 2−70259
elastic high energy, strong interaction proton for factor 2−59568
elastic scatt., model description of cross sections 2−82779
elastic slope parameter break, quantitative explanation given by Pomeron periphery 2−59570
elastic small angle, 9 to 70 GeV/c, forward scatt. amplitude 2−42413
fixed-pole Pomeron with shielding branch-cuts 2−59489
forward spin-independent amplitudes, theoretical model- independent determ. of real parts and zeros 2−70263
inelastic, differential cross section rel. to e.m. form factor 2−55877
inelastic collisions, prong-number distrib. 2−79617
interaction scaling radius hypothesis, comparison with data for 6-14 GeV/c 2−73788
large angle contribution of direct channel resonances 2−42366
multiperipheral bootstrap model, exptl. consequences 2−79541
multiple quark scattering analysis 2−52637
nonshrinking diffraction peak due to fixed pomeron 2−45923
overlap function analysis at ISR energies 2−73852
parity violating analyzing power 2−82772
phase-shift analysis, experiments below 10 MeV suggested 2−46000
polarization structure, differences in theory and expt. explained by exotic peripheral resonances 2−67056
quasi-potential and eikonal approximation to high energy scattering 2−70193
quasifree, investigated in ${}^2H(p,pp)n$ reaction 2−46247
quasipotential amplitude, Argand diagrams 2−45998
spin correlation parameters, A_{yy} and A_{xx}, at 47.5 MeV 2−79610
total cross-sections and diffraction cone slope 2−82775
transverse momentum dependence, connection with q^2 behaviour studied in parton model 2−42407
pp, quasipotential amplitude, Argand diagrams 2−45998
pp, study of Λ,Σ, hyperon antihyperon yields by absorbed Regge pole model with exchange degeneracy 2−42408
pp backward scattering and s-channel resonances, upper limit to pp coupling of S(1929) meson 2−63664
pp elastic scattering slope parameter of diffraction peak 2−79611
Pp forward spin-independent amplitudes, theoretical model-independent determ. of real parts and zeros 2−70263
pp large angle contribution of direct channel resonances 2−42366
$pp \to nn$, 230 MeV, total and differential cross sections 2−46001
$pp \to pN^*$, calc. using modified shell-model wave functions 2−49600
$pp \to pX$, estimation of η_p associated with triple-pomeron vertex assuming finite energy sum rule 2−42364
$pP \to pp$, 230 MeV, total and differential cross sections 2−46001

Protons and antiprotons continued
scattering proton-deuteron
elastic, real part of amplitude at 70 GeV 2−46002
elastic scatt., phase shift analysis, 2.0 to 3.8 MeV 2−67055
$p + d \to {}^3He + X^0$, analysis of π^0, η^0 and ω^0 production 2−42411

Pseudopotential methods
alkali metals, binding energy calc. 2−77832
alkali metals, elec. resist. calcs. 2−75052
alloys, coherent pseudopotential model, appl. to Ag-Au system 2−75025
band structure, relativistic pseudopotential method 2−61175
band structure computation 2−84227
chemisorbed atoms on metals, pseudopot. for calc. of transition rates 2−43492
elastic constants, determination for simple metals 2−60836
electrical resistance, specific, of liquid metals, accuracy of integral 2−80477
Fong-Cohen, for transition metals 2−84271
interzone transitions in b.c.c. pentavalent metals, detn. of freq. and intensities 2−80946
liquid metal, specific elec. resist. calc. 2−80478
liquid metal applications, review 2−50311
localized mol. orbital calc. for methane 2−80062
metal, binding energy in pseudo-ion approx. 2−83883
metal, general-model pseudopot. for real-pot. approxs. 2−57116
metal, model pseudopotential and energy wave number characts. 2−75024
noble metals, electron-phonon coupling and mass enhancement obs. 2−51069
rapidly convergent pseudopotentials, appl. to Li 2−75030
semiconductor, III-V, band gap, temp. depend., calc. 2−68415
spectroscopic trends, estimation by perturbation method using Hellmann pseudopotentials 2−49997
Al, energy and struct. calcs, effect of statistical exchange approx. 2−80960
Ge covalent-metallic phase transition under pressure, theory 2−83886
K, interband opt. conductivity calcs. 2−68616
Mg, energy and struct. calcs., effect of statistical exchange approx. 2−80960
Na, interband opt. conductivity calcs. 2−68616
NbN, band struct. calc. 2−84253
Si:Zn, many-band pseudopotential calc. of photoioniz. 2−61357
Si covalent-metallic phase transition under pressure, theory 2−83886
Sn covalent-metallic phase transition under pressure, theory 2−83886

Pulsars
0950+08 and 1133+16, flux density spectra 2−75808
— 2−62602
astrophysical aspects of highly collapsed bodies 2−78460
atmospheres, ground state binding energies and bound free cross sections for atoms 2−58407
Cen X-3 optical identification with WRA 795 2−75828
Centaurus X-3, reactivation of old neutron star by mass exchange in close binary 2−78479
computer programs for mechanism causing pulsations 2−84932
cooling rates for superfluid neutron stars 2−66127
cosmic ray acceleration, theory rel. to obs. 2−51693
cosmic ray interaction 2−66043
cosmic ray source, rel. to explanation of anisotropies 2−72961
CP 0808, 0834, 0950, 1133, short term intensity variation in 70-115 MHz frequency range 2−81896
CP 0808, long-term intensity variations at 81.5 and 151 MHz 2−55089
CP 0834, long-term intensity variations at 81.5 and 151 MHz 2−55089
CP 1133, amplitude and polarization characteristics of subpulses 2−55095
CP 1133, Cherenkov light registration from extensive air showers 2−51791
CP 1919, long term intensity variations at 81.5 and 151 MHz 2−55089
Crab, γ-ray obs. with scintillation detectors 2−62631
Crab, as energy source in nebula 2−62471
Crab, e.m. wave propagation in surrounding area 2−62610
Crab, Faraday rotation of radiowaves by solar corona 2−66236
Crab, second speed up 2−58414
Crab, supernova explosions, supergiant evolution 2−62560
Crab, upper limit on gravitational flux reaching earth, laser interferometer expt. 2−81894
Crab nebula, pulsed X-radiation 2−55090
Crab Nebula, VLBI obs. 2−75816
in Crab Nebula, X-ray source 62597 2−62597
discovery, radiosource survey at Molonglo 2−48750
distances, period luminosity function 2−48743
dynamic spectrum, interstellar inhomogeneities effect 2−58370
electromagnetic field, special relativistic treatment 2−58386
e.m. fields, rotating, classification 2−58415
emission mechanism, formation of neutron star spots 2−55050
evolution of stable states of matter, review 2−55034
Galactic supernova remnants 2−78452
gamma-ray flux emission, cause 2−51792
geometrical radiation models 2−58395
gravitational radiation, detection on Earth 2−62439
Herculis X-1, precessing binary pulsar model 2−81873
induced radiation pressure, plasma dynamics 2−62603
isolated, upper mass limit 2−44893
magnetic neutron star atmospheres 2−44865
magnetosphere, self-consistent model of closed field lines 2−55084
maser theory 2−58394
microquakes and macroquakes in neutron stars 2−55048
Molonglo Cross, pulsar declinations and periods 2−48749
MP 1055, parameters, discovery in Molonglo radio survey 2−48750
MP 1700, parameters, discovery in Molonglo radio survey 2−48750
neutron stars, densities 2−69085
Np 0532, detection of high energy γ-rays, after spin up 2−58437
NP 0532, height distribution of giant pulses 2−58392
NP 0532, occultations by Sun, density of corona 2−51863
NP 0532, pulse height distribution 2−51789

Pulsars continued
- NP 0532, transfer equations for high energy electrons and photons and mag. fields 2−81897
- observation, new method based on detection of v.l.f. e.m. radiation associated with period 2−73041
- phase residuals 2−48746
- physics, book 2−73050
- physics of, neutron rich nuclei in Fermi gas 2−79723
- plasma phenomena in high energy, astrophysics 2−78432
- production as result of collapse following C exhaustion 2−48689
- properties rel. to radially oscillating coherent plasma of electron-positron pairs 2−62615
- PSR 0301 + 19, improved measurements of periods and pulse shapes at 408 MHz 2−48753
- PSR 0329 + 54, interstellar scintillation pattern 2−66130
- PSR 0329 + 54, interstellar scintillation pattern 2−58393
- PSR 0833-45, search for optical identification 2−75817
- PSR 0833-45, search for optical object 2−66128
- PSR 1112 + 50, improved measurements of periods and pulse shapes at 408 MHz 2−48753
- PSR 1154-62 possible association with radiosource G296.8-0.3 supernova remnant 2−55098
- PSR 1541 + 09, improved measurements of periods and pulse shapes at 408 MHz 2−48753
- PSR 1556-44, parameters, discovery in Molonglo radio survey 2−48750
- PSR 1749-28, accurate position from lunar occultations 2−66132
- PSR 2154 + 40, improved measurements of periods and pulse shapes at 408 MHz 2−48753
- pulse broadening due to mutliple scattering in interstellar medium 2−48752
- radiation from flares near magnetic poles 2−44901
- radiation mechanisms of pulsar models 2−73044
- radiation model involving relativistic beaming of rotating light source 2−58410
- radio emission, nature 2−85012
- radio intensity fluctuations and subpulse structure 2−78484
- relaxation, rel. to liquid He II relaxation at rotation acceleration in spherical vessel 2−81893
- rotating magnetic field, Hamiltonian anal. of charged particle motion 2−62613
- rotational energy theory for slowly rot. stars 2−85016
- search techniques using a computer 2−81976
- short term intensity variation in 70-115 MHz frequency range 2−81896
- Sun, quasiperiodic pulsations, d.m. wavelengths 2−75966
- survey of exptl. data and construction of theoretical models 2−44891
- tangential injection of relativistic particles into wave zone 2−58396
- Vela, search for optical object 2−66128
- Vela, speedups due to corequakes in solid core 2−55099
- Vela as energy source in nebula 2−62471
- wave zone, injection of relativistic particles by stellar wind 2−58381
- X-ray, pulsed radiation, considerations as bremsstrahlung radiation from hot plasma 2−78478
- X-ray pulsations of long-period in NPO527 region, search 2−75838
- X-ray radiation from neutron stars in pulsars 2−73006
- H I emission lines at 21 cm 2−48744
- He pulsating star, instability strip for $2M_\odot$ model 2−48709

Pulse generators *see Circuits*

Pulse-height analysers *see Counting circuits*

Pumps
- *see also Vacuum pumps*
- Beloyarsk atomic power station pumps, assessment of reliability 2−70543
- liquid flow generators for use with flow calorimeters 2−83736

Purkinje effect *see Vision*

Pyroelectricity
- dosimetry applic. 2−70308
- ferroelectric materials, permittivity and pyroelec. coeff. from pyroelec. response to step radiation signals 2−81126
- i.r. detectors, review 2−69793
- i.r. thermometer with pyroelectric detector 2−55590
- polymer, linear chain, spontaneous polarization and pyroelec. coeff. 2−72045
- polyvinyl chloride, electrical response to i.r., preparation and use as sensor 2−47990
- pyroelectric detectors voltage response rel. to thermal diffusivity 2−81135
- radiation detectors, noise sources 2−78944
- sinusoidally modulated heat flow in multilayer and pyroelectric effect 2−52275
- triglycine sulphate, heat diffusion and heat sink problems for pyroelec. detectors 2−77960
- triglycine sulphate, technique for coeff. determ. 2−65072
- triglycine sulphate detector, laser study of nucleation sites 2−44165
- $AgNa(NO_2)_2$, ferroelec., spontaneous polariz. obs. 2−54235
- KIO_3, rel. to nonlinear optical props. 2−74733
- Li_2SO_4, technique for coeff. determ. 2−65072
- $LiTaO_3$, subnanosecond detector, for use with pulse lasers 2−82466
- $Pb_5Ge_3O_{11}$, pyroelectric properties 2−57246
- $PbTiO_3$, pyroelectric i.r. detector 2−55572
- $Pb(Zr, Ti)O_3$, heat diffusion and heat sink problems for pyroelec. detectors 2−77960
- Tl_3AsSe_3, pyroelec. coeff. detn. 2−72044
- ZnO, decay of pyroelectrically induced polarization charges 2−54241

Pyrolysis *see Chemical reactions*

Pyrometers
- amplifier with photovaristor modulator for pyrometric instruments 2−69846
- colour, calibrations equipment 2−52297
- high temps., precise meas. apparatus 2−52291
- pyroelectric detectors voltage response rel. to thermal diffusivity 2−81135
- radiation thermometry, physical basis 2−55585
- ratio, two-colour pyrometer, construction 2−52298
- review 2−76386
- thermodynamic, temp. of flue gases 2−58971
- Pt, of Guyton de Morveau, design 2−69522

Q-switching
- cryptocyanine, photochemical decomposition due to light source 2−49378
- electro-optical shutter for lasers emitting unpolarized radiation 2−69959
- fast gas switch for laser output pulse charact. 2−69952
- frequency and spatial shift, in laser emission 2−42126
- junction diode laser, fabrication, patent 2−82487
- junction laser, effect of impurity gradients 2−59180
- laser-plasma for X-ray flash tube 2−76134
- lasers, high-power, simultaneous passive mode locking and Q-switching using optical Kerr effect 2−66737
- lasers, multimode oscillation buildup from quantum noise 2−63315
- molecular lasers, sequential technique 2−55686
- noninstantaneous of laser resonator for single pulse lasing 2−69902
- passive, CO_2 laser near 9.2μ, using difluorodichloromethane 2−45725
- passive shutter for periodically operating laser 2−59192
- Pockel cell Nd:glass oscillator, amplified output, picosecond structure 2−42070
- pulsed lasers synchronisation of Q switched pairs 2−69905
- ruby laser, intracavity modulation with frequency close to difference frequency of neighbouring axial modes 2−59171
- semiconductor injection lasers, self Q-switching with nonuniform pumping 2−42080
- semiconductor lasers, coupled to photovoltaic nonlinear absorber, self-Q-switching 2−63340
- transient stimulated thermal scattering, frequency response 2−41939
- CO_2 laser, active gas cell for Q-modulation 2−76481
- CO_2 laser, by rotating mirror, Doppler effect mechanism 2−59150
- CO_2 laser, single-mode, Doppler Q-switching by rot. mirror 2−69914
- CO_2 laser pulse time modulation Q-switch, patent 2−69931
- CO_2 laser with variable pulse delay 2−66746
- Cr, antiferromagnetic, domains obs. with neutron diffraction topography 2−65179
- Cs vapour discharge, for synchronizing mode-locked laser pulse trains in the external events 2−73546
- KH_2PO_4, z cut and electrode configuration effects on control voltage 2−69894
- Nd:glass i.r. laser, use of bis-(4-dimethylaminodithiobenzil)-Ni 2−59175
- Nd:glass laser, in convex optical cavity 2−76467
- Nd:$POCl_3$-$ZrCl_4$ liquid laser, parameters and energy scaling 2−59166
- Nd:YAG electro-optically Q-switched laser, multipulsing behaviour 2−59173
- Nd:YAG laser system for generation of controllable reproducible giant pulses 2−69925
- Nd-$CaWO_4$ laser, high power in single longitudinal mode using Pockels cell 2−63337
- Nd^{3+}-glass laser using toluene and benzene for giant pulse generation for study of nonlinear optics 2−55685
- Rb vapour discharge, for synchronizing mode-locked laser pulse trains with external events 2−73546

Quadrupole crystal field interactions *see Crystals/hyperfine field interactions*

Quadrupole moments, molecular *see Molecules/moments*

Quadrupole moments, nuclear *see Nucleus/electric moment*

Quanticule theory (of chemical binding) *see Bonds*

Quantization *see Field theory, quantum/quantization; Quantum theory/quantization*

Quantum chemistry
- atomic and molecular electronic structure, book 2−83204
- co-ordination compounds, translation between MO and HL descriptions 2−52990
- E184, superheavy element, calcs. on influence of quantum electrodynamical effects on chemistry 2−49929
- electron transferr, nonadiabatic effects 2−81504
- group theory, symmetrized powers of irreducible representations 2−52046
- molecular quantum mechanical calc., integral transformations 2−56146
- multicentre integrals and matrix elements, computation method 2−79848
- n-electron problem and matrices representing symmetric groups 2−52896
- pair theorem, rel. to bipartite graph props. 2−53038
- reaction rates formulation 2−61765
- reactive scattering calculations, exact method 2−69602
- semi-empirical theories, ab initio determ. of all parameters 2−70555
- thermochemical model of ESCA shifts, near equivalence of quantum mechanical potential model 2−72535
- transformation props. of antisymmetric spin eigenfunctions under linear mixing of orbitals 2−70556

Quantum counters *see Photons; Radiation detectors*

Quantum electrodynamics
- *see also Electrodynamics; Electromagnetism*
- anomalous moments, magnetic and quadrupole, interaction with e.m. field 2−82664
- bound electron g-factor, nuclear mass. correction 2−67386
- bound state, Lamb shift, theory and computation 2−64009
- Callan-Symanzik equations, correction with mass divergence theorems 2−49472
- rel. to classical theory, soft quanta approach 2−55793
- Dirac electron, in electromagnetic and uniform magnetic fields 2−55801
- discrete symmetries, e.m. field transformations, space inversion, time reversal 2−76574
- E184, superheavy element, calcs. on influence of quantum electrodynamical effects on chemistry 2−49929
- effective field equations for one-electron multiphoton stationary states 2−52534
- electron scattering, in gravitational field of rotating source, polarization effects, calc. 2−55381
- electron self-energy in a magnetic field 2−59374
- electron undergoing synchrotron radiation, second-order correction to first-order transition rates 2−82617

Quantum electrodynamics continued
electron wave functions in strong e.m. field, quantized dimensions 2–82219
electron-graviton vertex, low-energy e.m. corrections determ. using Feynmann graphs 2–76559
electron-positron colliding beams applics. for high q^2-values 2–76609
electrons interacting with cavities, radiation calc. 2–76414
e.m. field, generalized multipolar decomp., space-time multipolar sources 2–52530
e.m. field pot., multipolar represent. 2–45853
e.m. form factor, study of asymptotic behaviour by functional methods 2–79468
exotic atoms with small overlap orbitals, test 2–77027
finite, possible origin from weak interactions 2–52532
finite theory for spin zero boson case 2–66901
finite theory in eighth order, eigenvalue condition 2–79460
form factor in eikonal approx., determ. of bound state poles of two interacting particles 2–42304
fundamental bound systems, anomalous magnetic moments, high energy expts., comparison of theory and expt-., review 2–63471
gauge-invariant regularization, second- order vacuum polarization 2–52531
gravity modified, infinity suppression 2–55797
Gupta-Bleuler formalism for photon-hadron interactions, analytic equivalence of S-matrix formalism 2–52578
Gupta-Bleuler formalism with scalar fermions in massless Yang-Mills theory 2–73725
hadron, application of variant of Stuckelberg formalism for massive gauge fields 2–42305
heavy atom, configuration-space Hamiltonian constructed from QED, correction to Briet interaction 2–42719
high order processes, application of general method for evaluation of Feynmann graphs 2–73731
high spins in external fields, analogy with classical motion of point particles 2–55658
high-energy scatt. in φ^3 theory, eikonal approx. breakdown 2–59477
inductive contrib. to retarded interatomic pot. energy 2–79889
infinite momentum QED, applic. to high energy scattering 2–63473
in infinite-momentum frame 2–66896
intense-field mass shift of electron determ. from vacuum polarization on mass shell 2–66904
i.r. catastrophe, Bloch-Nordsieck model 2–76573
Jost and Schroers theorem 2–66900
Klein-Gordon and Dirac eqns. for motion of charged particle in transverse e.m. plane wave field 2–63262
Lyttleton-Bondi, charge paths as geodesics of Einstein connection 2–55795
many body problem, charged particle interactions 2–79462
mass spectrum, in pure Coulomb field, approx. 2–49471
massive, e^-p inelastic structure functions in gluon model 2–63513
massive spin 2 charged particle in external e.m. field, anomalous behaviour 2–55796
multipole expansion of retarded interatomic dispersion energy 2–49935
muonic atoms, higher-order vacuum polarization corrections 2–52959
non-local, form factor choice 2–59375
nonlocal generalization 2–52529
nonrelativistic particle spin rotation probability in nonuniform mag. field 2–73727
particles of spin $\leqslant 1$, perturbation theory of two particle states 2–66902
perturbation theory and renormalization in infinite momentum frame 2–82616
perturbation theory anomalies, review 2–63472
pion e.m. mass difference calc. in presence of scalar gravity 2–42381
radiative corrections in framework of Pade method 2–73726
renormalization group and series expansion of high-energy Green's function 2–55798
review for college lectures 2–73253
scalar, calculations of Z_3^{-1} to fourth order 2–66898
scattering high energy and relativistic eikonal propagators 2–63469
scattering phenomena involving bound states of particles 2–55794
Schwinger's proper-time method and eikonal approx. for electrons Green's function in plane-wave field 2–82618
self-consistent theory and correspondence with quantum mechanics 2–55433
short-distance behaviour and eigenvalue condition for fine-struct. const. 2–55800
spectrum generating current including spin-orbit and Lamb shift 2–59943
spin particle, relativistic diffusion 2–52063
spin-3/2 field in presence of interactions, quantisation 2–82618
spin-zero, fourth-order charge renormalization 2–66899
superluminal motion in inverted media 2–82608
synthesis with classical electrodynamics 2–78766
two-level system, coherently excited, spontaneous decay 2–67403
two-particle systems, relativistic dynamical algebras 2–52533
Uehling effect for atomic s-level shifts 2–70120
vacuum, k-dependent Lagrangian and dispersion relation 2–63470
vacuum polarization calculations without resorting to regularization 2–55802
vacuum polarization corrections to elastic electron and muon scattering in intense field, and pair electro- and muoproduction 2–63474
vacuum polarization due to self-coupling of Yang-Mills field 2–55799
vacuum polarization rel. to metal-insulator transition and force between two excitons 2–47818
vector approach to Ward-Takahashi relations derivation of massive Yang-Mills theory 2–63463
vertex function and ladder approx. calc. of electron dipole magnetic moment 2–73755
wave mechanical approach to magnetic electron lenses 2–79055
Wheeler-Feynman theory, extension to relativistic domain, emission processes 2–52525
e magnetic dipole moment, in ladder approx. 2–45880
ee^+ annihilation for experimental tests 2–82609

Quantum electrodynamics continued
e^+e^- annihilation, cross section meas. at 1.0 GeV, test for validity of quantum electrodynamics 2–63521
e^+e^- collisions, 1400-2400 MeV expts. at ADONE storage ring, confirmation of predictions 2–73761
e^+e^- production in vacuum under electric field 2–82632
ep deep inelastic scattering in massive QED 2–42341
μ pair creation via two-photon exchange in electron collisions, QED investigation 2–82684
H, ground-state energy, u.v. convergence of e.m. correction 2–42795
He atom, fine structure splitting of deepest triplet P state, quantum-electrodynamical corrections 2–42810
Hg muonic atom, energies of 5g to 4f X-rays, higher order vacuum polarization corrections 2–59962
^{203}Tl, muonic atom, energies of 5g to 4f X-rays, higher order vacuum polarization corrections 2–59962

Quantum electronics *see Lasers; Masers; Photons; Quantum optics*

Quantum field theory *see Field theory, quantum*

Quantum fluids
λ transitions for mixtures, special thermodynamic relations for Curie and Neel points 2–52107
λ transitions in mixtures, revised thermodynamic relations 2–52106
class one space-time, perfect fluid distributions 2–76183
electron liquid, self-consistent pair correls. and dielec. response 2–61207
feedback model 2–41531
fluctuations, higher order moment functions 2–78846
gas, physical adsorption in submonolayer region, significant structure theory 2–67917
ideal gas, statistical mechanics 2–45311
ideal gases, special class, fundamental properties 2–62944
imperfect gas, equation of state 2–45326
master equation, continuum thermodynamic limit 2–58802
ordered phase, point and planar singularities 2–78831
phase transitions, field theory, Feynman graphs screening solution 2–78848
roton trapping by vortex line 2–63039
superconducting neutron star matter, thermodynamic crit. field 2–73008
thermal equil., functional integration applic. 2–58800

boson systems
δ-function interaction model, one-dimensional, exact results for ground state energy of fermion- boson mixture 2–45320
Bogolyubov-Tyablikov transoformation, unitary operator form 2–55434
Bose condensation of photons, shock wave struct. in radiation spectrum 2–78856
Bose-Einstein and Fermi-Dirac systems supporting normal superfluid and superconducting components, unified theory 2–66476
charged Bose gas, density-temp. diagram 2–78851
charged Bose gas, excitation spectrum, Jastrow theory versus correlated basis functions 2–41545
charged Bose gas, properties in a magnetic field 2–73338
condensed, superfluidity, microscopic theory 2–45322
coupled system with phase coupling as model for Josephson effect 2–61231
critical phenomena, scaling theory for finite size effects 2–45303
ensemble density matrices, diagonal N-representability 2–66475
exact boson representation of spin operators, thermodynamical function evaluation 2–64882
excitation spectrum for bosons interacting via two-body potential, high-density calcs. 2–63042
ideal relativistic gases, thermodynamics 2–45325
imperfect gas, thermodynamic limit 2–78833
interacting, struct. functions, two-phonon backflow 2–45323
interacting Bose gas, moments of dynamic form factors for excited states generated by densities and currents 2–69623
light scatt. by rotating ground glass with surface inhomogeneities, statistical props. 2–79326
multiplicative renormalization group, critical behaviour in $d=4-\varepsilon$ dimensions 2–69622
para-Bose operators, irreducible represents. 2–63041
perfect gas, Einstein condensation 2–45327
spinless, strongly interacting, statistical thermodynamic, surface energy and tension 2–82267
superconductivity, boson method, application to study of Josephson effect 2–54136
superconductor, magnetization curve calc. for V at 0K 2–61233
superfluid, density determ. 2–58805
superfluid density determ. 2–41541
variationa wave function for ground state 2–45324
weakly interacting Bose gas, transverse waves 2–41546
weakly interacting gas, Bogoliubov-Zubarev description 2–49040
H_2 liquid, superfluidity 2–53470

fermion systems
δ-function interaction model, one-dimensional, exact results for ground state energy of fermion-boson mixture, equilib. thermodynamics of fermions 2–45320
anisotropic Fermi liquids, models 2–69624
Bogolyubov-Tyablikov transoformation, unitary operator form 2–55434
Bose-Einstein and Fermi-Dirac systems supporting normal superfluid and superconducting components, unified theory 2–66476
condensated gas, gapless excitations 2–58808
degenerate Fermi systems, threshold anomaly 2–54432
degenerate gas, equilibrium number density of unstable particles 2–73339
ensemble density matrices, diagonal N-representability 2–66475
Fermi liquid, two component, study of paramag. reson. and excitation of spin waves 2–81000
Fermi liquids, two-component, generalization of theory for zero-sound waves 2–71265
free fermion model equivalence to XY model ground state 2–45330
gas, dilute, infinite volume limit of Green's function 2–76233
Green function interpretation of Brueckner theory 2–78855
ideal relativistic gases, thermodynamics 2–45325
interacting, Green's function eqns. of motion as Feynman diagrams partial sums 2–52110

Quantum fluids continued
fermion systems continued
interacting electron model, eigenstates, free energy, diagonalization 2–58806
interacting gas, quantum condensation, thermodynamic limit and dimensionality 2–52111
Invar, thermal expansion, low temp., Fermi liquid props. 2–84217
Kando Hamiltonian, pseudo-fermion Hamiltonian representation 2–73340
Lee model with Fermi coupling, explicit solution in low sectors 2–52524
many-electron wavefunction, probabilistic interpretation of cluster function series development 2–70554
neutron matter, crystallization 2–55049
neutron rich nuclei, physics of pulsars 2–79723
nuclear many-body theories, subsidiary conditions 2–46071
nuclear matter theory, role of gas-liquid phase transitions 2–73981
rare-earth nuclei, deformed, gamma and octupole states in Fermi liquid theory 2–46116
self-interacting, perturbation theory for grand canonical Gibbs states 2–45328
sum rules and Landau theory of Fermi liquids 2–45331
superfluid ground-state model 2–63043
superfluid props., Ginzburg-Landau eqn. for ${}^3P_2$ pairing 2–76234
thermodynamic functions for fermions with gravostatic and electrostatic interactions 2–82244
thermodynamic Green's functions, approximation by Ritz variational method 2–58807
variational many body function with correlations between fermions of opposite spin 2–76232
Quantum generators *see Lasers; Masers*
Quantum mechanics *see Quantum theory*
Quantum optics
– 2–59122
aeroscopic wave function, coherence 2–41941
amplification of sterically hindered pulse in isotropic medium 2–73539
atom-field correls. role in coherent interactions 2–41946
Bloch equations, solution method 2–69841
chaotic and coherent radiation, superposed, simulation using h.f. signal processor 2–49406
clipped intensity correl. meas. method 2–82462
coherent optical pulse propagation, superradiance, nonlinear reactions 2–41940
coherent pulses, propagation in inhomogeneously broadened medium 2–41942
coherent states of radiation field, properties 2–76498
composite system factorization 2–73543
dissipative behaviour, quantum mechanistic model 2–59120
electroluminescent devices, apparatus for obs. of quantum efficiency 2–55759
electronics Raman's contributions, review 2–59277
Fresnel evanescent wave, Zeeman spectrum and mag. reson. 2–63306
Gaussian fields, sequential photon counting statistics and maximum likelihood estimation techniques 2–79266
harmonic generation, influence of third order nonlinearity 2–42167
heating kinetics of light-diffusing layer from radiant heat exchange calc. 2–82465
interaction between radiation and quantum systems with relaxing sublevels 2–41944
interaction of external radiation with a medium inside a cavity 2–66727
interaction of intense laser radiation with H atom, time-dependent approach 2–79955
interstellar OH, amplified spontaneous emission 2–55075
i.r. to visible parametric upconversion in proustite 2–49388
laser beam X-ray mixing, parametric conversion and nonlinear X-ray scattering 2–41937
laser linewidth due to quantum phase and quantum amplitude noise above and below threshold 2–49396
lasers, conference (Montreal 1972) 2–41957
light signal amplification in metal- $SiO_2(TiO_2)$-Si-$SiO_2(TiO_2)$-metal structures 2–45694
multiatom multimode Hamiltonian, variational estimate of lowest eigenvalue 2–73538
multiatom systems, radiative cooperative effects, Green's function applic. 2–66729
multiple coherence of e.m. fields 2–49336
nonlinear oscillator interaction with radiation field 2–64006
nonlinear parametric interactions, instabilities, numerical study 2–78780
optical field, coherence and fluctuation props. 2–82463
optical fields, coherence and fluctuation props. 2–82464
optimum array photocounting receivers rel. to aperture integration types for log normally distributed irradiance 2–79173
parametric oscillator, behaviour 2–49344
phase modulated fields, statistical props. 2–45698
photon counting apparatus for kinetic and spectral obs. 2–45703
quasi-monochromatic beam, interaction with free electrons 2–41936
radiating two-level systems, quantum-mech. saturation in reson. fluoresc. 2–66731
radiation field unpolarized states 2–52404
review of work performed by Honeywell Corporation 2–79366
scaled photon-counting fluctuations, one-bit correlation 2–73542
solid state and quantum electronics, book 2–57092
spectral distrib. of amplified spontaneous emission, rel. to interstellar media 2–45695
spectral line contour of optical transition at resonance with strong field on adjacent transition 2–49343
spontaneous emission by excited system, interference between different channels 2–79886
stimulated absorpt. or emission of photons by atomic beam 2–45700
stimulated elastic scattering, effect of coherence 2–42205
sum frequency amplification, quantum theoretical treatment 2–69888
three field mode model, statistical props., quantum theory 2–45696
transient stimulated Raman scattering, molecular relaxation and dispersion 2–41938
transient stimulated thermal scattering, frequency response 2–41939

Quantum optics continued
two-level atom, spontaneous emission analysis in rot. wave approx. 2–82461
two-level atom, spontaneous emission analysis in rot. wave approx. 2–82460
two-level atom in intense multimode radiation field, excited states population 2–66730
two-level system, coherently excited, spontaneous decay 2–67403
two-level system, obs. of Rayleigh and harmonic lines in scattering spectrum of intense light 2–49938
two-photon self-induced transparency of different-frequency optical short pulses in K vapour 2–79248
two-photon superradiance 2–45702
$LiIO_3$, tunable i.r. difference-frequency generation 2–63369
Quantum statistics *see Statistical mechanics/quantum*
Quantum theory
see also Electron theory; Elementary particles; Field theory, quantum
alkali metal crystals, quantum mechanical study 2–64585
angular momentum coherent states 2–55412
angular momentum exchange between small particles and light 2–62596
anharmonic oscillator, density matrix 2–76216
anharmonic oscillator, energy levels 2–69594
anharmonic oscillator with polynomial self-interaction 2–63015
atom, damped two-level 2–42708
atom-surface scattering, inelastic 2–46465
atomic collisions, inelastic, classical picture and semiclassical formulation for derivation of eqns. 2–56111
atomic collisions, inelastic, semiclassical theory, momentum-space formulation derivation of classical trajectory equations 2–52945
Balslev-Combes theorem, extension using quadratic form techniques 2–49005
Bohr model of atom, classical derivation from Rutherford model 2–58742
Bohr-Sommerfeld theory, modification to include uncertainty principle 2–55410
book, mathematical methods of quantum mechanics 2–41487
Born-von Karman boundary conditions, position operator 2–78829
bound systems, approx. perturbation theory for higher-order e.m. transitions 2–58747
charged particle transport in magnetic field 2–73492
classical approach, interaction of field of vacuum interpret. 2–76207
coherent states for arbitrary Lie group 2–41508
communication theory of quantum systems 2–41489
Copenhagen interpretation, logical basis 2–55409
correspondence principle, illustration by classical and quantum approach to harmonic oscillator problem 2–82215
Coulomb pot., attractive, with zero-radius hard core, energy eigenvalues 2–52076
cut-off potentials, scattering and bound states, energy power expansion of Green function and Pade approximation 2–45278
de Broglies book 'Research on quantum theory', translation into english of the first chapter 2–62996
de Sitter space-time and harmonic oscillator 2–63016
determinism of quantum-mechanical probability statements 2–82235
diffusivity mass and temp. depend., quantum and anharmonic effects 2–74806
Dirac delta function, integral representation 2–78735
dissipative systems, Darlington's method 2–45270
with distribution function non-negative in phase space 2–78812
dynamical proper time, nonrelativistic limit 2–62997
eikonal approximation, functional integration method 2–69600
Einstein Podolsky and Rosen paradox possible experimental test 2–73315
electron spin photon interaction, in presence of static magnetic field 2–52551
e.m. zero-point energy of cond. spherical shell 2–63166
equivalence of momentum operators in generalized coordinates 2–78811
essential self-adjointness for highly singular potentials 2–45264
expectation from the hypercharacteristic function 2–58755
expectation values, vibrational and vibrationally averaged structure 2–49999
exponential decay of excited state with memory 2–73327
Feynman's path integral 2–78817
Feynman path integrals, asymptotics, singular perturbations .2–41511
Fierz-Pauli equation for particles with spin 3/2 2–76214
fundamental concepts, review 2–44705
fundamentals, book 2–78830
gas atom scatt. by surface, one-phonon quantum theory 2–50423
generalized WKB method, soln. in form of sonverging series 2–82218
group algebras and tensor operators 2–58740
group velocity of wave packet, with extension to general cases 2–49003
Hamilton-Jacobi mechanics, validity in the mean 2–41497
Hamiltonian eigenvalues, Temple, Weinstein and Stevenson bounds 2–58739
Hamiltonian operators, q-equivalent, integral eqns. of motion 2–73328
harmonic oscillator, four-dimens., rel. to hydrogen atom bound states 2–42792
harmonic oscillator, free damped, soln. of eqn. of motion 2–78809
harmonic oscillator, one-dimens., with non-negative distrib. function in phase space 2–52074
harmonic oscillator energy levels described by dissipative and nonlinear model 2–49011
harmonic oscillator group, Clebsch-Gordan coefficients and special function identities 2–41513
harmonic oscillators, integral representation of Green's function 2–82232
hidden-variable theorems 2–58745
hidden-variables model and 2-dimensional Hilbert space 2–49002
hierarchies of density operator symmetry and interchangeable canonical pairs 2–63003
Hilbert space formalism, axioms 2–82236
homological foundation for scale problems, comment on paper by Atkin and Bastin, quantum logic framework 2–73313

Quantum theory continued
hypervirial theorem, transition moment integrals, application to harmonic oscillator 2−41484
infinite square-well potential, probability distribution of momenta 2−73281
interaction time meas. and causality 2−58744
intermediate Hamiltonian method, alternative formalism 2−66448
isolating integrals, stability, effect of perturbation in potential function 2−45263
Kallen-Pauli state vectors in $V\theta$ sector, algebraic solution by congruence transformation 2−45277
Kepler problem, generalised quantum mechanical, O(2, 1) × O(3) solution 2−58761
level spectrum of 3 resonantly interacting particles 2−82230
linear harmonic oscillator, Heisenberg indeterminacy relation for time and energy 2−66451
local potential energy eigenvalues calc. method 2−82224
Lorentz covariant anal. functions and scatt. functions 2−82648
macroscopic level of quantum mechanics 2−82231
many-body system theory, book 2−82240
many-electron wavefunction, probabilistic interpretation of cluster function series development 2−70554
many-particle reactions, quantum-mechanical description 2−82273
measurability of spin, reply to comments 2−82233
measurement, omission from basic postulates 2−73312
measurement procedures for case of nonapplicability of Von Neumann's projection axiom 2−63013
measurement theory formalism 2−69534
mechanical state preparation, simple model 2−73314
minimum principle for excited states, new proof 2−41498
modified perturbation expansion generalization for density matrix in path-integral formalism 2−78821
multiphonon quantum theory of adatom desorption 2−50523
N-body systems, continuum bound states and quantum mechanical virial theorem 2−41542
non-compact groups and harmonic oscillator 2−59909
non-normalizable eigenvectors and perturbations 2−41510
nonlinear Lagrangian theories and factor ordering problems, relativistically covariant formulation 2−45272
nonlinear oscillators, perturbation method 2−82225
nonorthogonality problem, perturbational treatment 2−62998
nonrelativistic mechanics, generaliz. 2−52064
operators in generalized coordinates 2−73277
particle represents. of canonical commutation relations 2−82237
particles of spin maximum 1, non-relativistic approx. 2−73320
Poincare group reduction with respect to Lorentz group 2−82649
point dynamic re-interpretation, eikonal eqn. for de Broglie waves 2−82214
polar systems, phenomenological theory 2−81147
potential energies for which particle motion is same in classical and quantum mechanics 2−78806
potential well, asymptotic expansion for eigenvalue density 2−73330
product-integral calculus formulation 2−62939
proposition systems, complete atomic lattice form. 2−52066
quantizable dynamical systems, topology and algebra of observables 2−55413
quantizable dynamical systems and homogeneous fibred systems 2−55414
quantum logic and ordering of propositions 2−41488
quantum mech. states, initial stationarity, stationary states criteria 2−66446
quantum mechanics, contour independent path integrals, barrier penetration and complex time 2−58741
quantum mechanics, hidden variable models 2−63008
quantum mechanics, implications of classical ergodicity, applic. to two-dimensional harmonic oscilator 2−41494
quantum mechanics, on multiply connected and homogeneous spaces 2−52065
quantum mechanics, principles and formalism, book 2−69585
quantum mechanics, probabilistic concepts 2−63000
quantum states, decay in exactly soluble models 2−45265
reduced density matrix eigenstruct. for canonical ensemble of free oscillators 2−82238
reduced density matrix eigenstruct. for ground-state of oscillator system 2−82239
relativistic, relation of space-time to internal symmetry 2−66440
relativistic, sign of static electric polarizability 2−78823
relativistic Coulomb Hamiltonian, approximate 2−55418
relativistic many-body, Riemannian space-time, applic. to superdense matter 2−66447
relativistic quantum mechanics, localization problem 2−63001
resonant scatt. of system with unstable discrete states 2−78820
Rutherford scattering amplitude, divergence in terms of Coulomb phase shifts 2−73331
scattering, high energy at backward angles, simple prescription 2−49020
scattering, into cones, generalization of Dollard's result 2−76203
scattering, nonspherical, semiclassical equivalence relations 2−78819
scattering, partial wave amplitudes, analyticity and conformal mapping methods 2−52080
scattering, quantum mechanical impact parameter operator 2−41521
scattering, repulsive singular potential, applic. of modified WKB approx. to solution 2−41519
scattering, three-body bound states in Amado's model 2−45280
scattering, time-dependent, relationship between time delay and phase shift operator 2−76204
scattering by charged centres, long-range Coulomb pot. 2−62976
scattering cross section, probabilistic interpretation 2−41518
scattering cross-section paradox, simplified resolution 2−49016
scattering of asymptotically Coulomb potentials, time-dependent and time-independent 2−45276
scattering of quantum mechanical wave packet, new definition of time delay 2−78822
scattering of well-localized wave packets by time dependent potential 2−63022
scattering processes, equivalence of local and nonlocal potentials 2−82936
Schrodinger operators of many-body systems with permutation and rotation symmetries, spectral theory 2−73318

Quantum theory continued
sets of automorphic structure, field eqns. and automorphic solns. 2−78827
simple harmonic oscillation, energy quantization 2−62943
singular oscillator, Green function and excitation 2−52075
solvable problems, algebraic structure 2−58743
space-time dynamics of interacting systems 2−55424
spheroidal bound states, rotationally invariant, zero-energy case 2−69599
spin space, drone fermion method generalization 2−58754
spin systems, loosely coupled, quantum mechanics 2−69590
spin-dependent operators in occupation- branching number representation, monoelectronic and bielectronic 2−41503
spin-exchange operator, algebraic derivation 2−78808
spinning particles, quantum-mechanical effect without force 2−76209
spontaneous decay in time dependent external field 2−41514
spontaneous emission theory, Wigner- Weisskopf, rotating wave and ladder approxs. 2−74209
square well, graphical solutions 2−55419
stability of systems with singular potentials 2−49013
Stefan-Boltzmann law illustration for students of quantum theory concepts 2−55349
stochastic quantum mechanics, derivation of diffusion coefficient 2−63009
Sturm-Liouville systems, asymptotic behaviour 2−41500
sum frequency amplification, quantum theoretical treatment 2−69888
symmetric top 2−41512
symmetry and degeneracy, particle is perturbed box, teaching techniques 2−82098
symmetry operation commutation with raising, simplified proof. 2−76208
teaching exercise, n.q.r. in solid nitrogen 2−55353
teaching text, college-level 2−62980
textbook, undergraduate level 2−45210
rel. to thermodynamics 2−41537
three body and three dimensional calc. reactive scattering, exact quantum mechanical 2−79867
three-body D-function, new parameterization 2−49012
three-body problem, quantum mechanical, complete set of functions 2−41490
three-particle systems, proof of Efimov effect 2−45281
two-body systems in fast motion, wave functions 2−82215
two-particle self-energy expansion, Green function method 2−52068
unitarity principle, distinction between consequences not directly required by probability conservation and others 2−45267
unstable particle, spin spectrum 2−42312
van der Waals forces calc. from dispersion relations 2−78816
Van Vleck relativistic ensembles, geometry 2−82270
variational trial functions, bound states of one and two particle systems 2−59937
variational trial functions, continuous spectrum of one and two particle systems 2−59938
vibrations, small, overdamped eigenvalue problem selfadjoint formulation 2−78866
von Neumann algebras, noncommutative probability 2−41486
wave mechanics, role of Louis de Broglie in founding it described by himself 2−58678
weakly coupled oscillators, diffusion equation 2−73329
Wigner coefficients, symmetries, three dimens. rotation group 2−41464
Wigner coeffs. of three-dimens. rot. group and Thomae-Whipple functions 2−78813
Zierler's axioms, elimination of lattice postulate 2−49001
H-Like atoms, exact, matrix elements and exact selection rules 2−42794
H atom, one dimens., repulsive core term in Coulomb pot., energy levels in strong mag. field 2−59940

application methods
anharmonic oscillator, centre-of- mass motion 2−73965
anharmonic oscillator model, hypervirial and Hellmann-Feynman theorems 2−64093
anisotropic cubic crystals, elastic displacement field of point defects by variational procedure 2−80697
anisotropic harmonic oscillator in magnetic field, calc. of energy spectrum and wave functions 2−76206
atom-heteronuclear diatom system, exact quantum reactive cross sections for three dimensional angle dependent model 2−44469
atomic and molecular variational wavefunctions, relativistic corrections 2−70557
atomic systems, quantum mechanical transport eqn. 2−46449
Bell's inequality and hidden-variable theories 2−73324
benzene, Urey-Bradley repulsive force const., quantum mech. estimation 2−83328
Bose liquids, variational wave function for ground state 2−45324
bound eigenstates of electron in exponential cosine screened Coulomb potential 2−69597
C*-algebra methods and their application 2−58756
comparison of Messmer and Rayleigh-Ritz variational methods for H atom 2−59942
convergence of lowest eigenvalue of real nearly-symmetric matrix, application to Boys' transcorrelated method 2−63011
Coulomb problem, Lie algebra and group theory, book 2−63017
D_2^+ double group, isomorphic to quaternion group, reln. to approx. eigenfunctions 2−63012
diagonalization of Hartree- Fock Hamiltonian for occupied states 2−45273
dipole coupling potential, Harris-Nesbet method 2−66449
eikonal approximation for coupled equations for multichannel scattering 2−52944
electron undergoing synchrotron radiation, quantum-mechanical treatment 2−49320
energy spectrum of potential well, graphical display 2−78810
Euler rotations, theorem 2−49048
exact treatment of spin-spin interaction and n.m.r. 2−77031
Fermion Green's functions, approximation by Ritz variational method 2−58807
Feynman path integrals 2−45268

Quantum theory continued
application methods continued
geminals, diagrammatical method based on second quantization formalism, Wick's theorem, Feynman-like diagrams 2−56081
geminals, diagrammatical method calc. of overlap and energy mean value expressions for wavefunctions 2−52894
Green's function, calc. for free electron in uniform. mag. field 2−55411
harmonic oscillator, relativistic formulation derivable from Lorentz-invariant variational principle 2−78798
harmonic oscillator, resonant modification and destruction of adiabatic invariants 2−52073
Hartree approx., variational principles for single-particle expectation values 2−66450
integral inequalities with mathematical structure of expectation values 2−76211
interaction operators, classification w.r.t. many-particle permutation symmetry 2−49008
irrotational dust cosmologies, quantum models for lowest-order velocity-dominated solution 2−55402
lanthanide $f \to f$ spectra, Judd-Ofelt parameters, effect of excluding hypersensitive transitions 2−83221
lattice electron behaviour in a uniform magnetic field 2−84231
Mathieu eqn. and anharmonic-oscillator eqn., continued fraction method of solution 2−73326
matrix elements evaluated for various potentials using correspondence principle, comparison with quantum mechanical results 2−56082
matrix method for eigenvalues of one-dimensional system 2−78727
molecular quantum mechanical calc., integral transformations 2−56146
molecular solids, quantum lattice dynamics for translational and vibrational modes 2−71703
Mossbauer hyperfine spectra, temp. depend. line shape, rel. to mag. order 2−75263
motion of body in ring-shaped potential 2−49014
multiatom multimode Hamiltonian, variational estimate of lowest eigenvalue 2−73538
multichannel Feshbach eqns. for scattering and rearrangement collisions, variational principles 2−52898
multipole operators from charge, current and moment operators as angular momentum recoupling problem 2−58757
n.m.r. spectra of AB spin system, calc. using analogue computer 2−66668
non linear Lagrangian, variations principle 2−45269
nuclear G-matrix eqns., projection-operator 2−79717
on- and off-shell T matrix, variational approach 2−73972
optimized pseudostates, rel. to intermediate energy electron-atom scatt. 2−67406
oscillator strength calculations in frozen core HF approx. length and velocity formulae 2−46408
Pariser-Pole- Pople method modification for qualitative interpretation of u.v. spectra of inorganic molecules 2−67471
potential model of ESCA shifts, near equivalence with thermochemical model 2−72535
projection operators, construction in semiclassical approx. based on Wigner transformation 2−52072
Raman scattering, polariton, in the vicinity of phonon resonance, fluctuation−dissipation theory 2−84496
reactive scattering calculations, exact method 2−69602
reduced rotation matrix elements, subprogram for calc. 2−66452
RPA eigenvalue problem, generalized, reduction 2−58758
RPA formalism, consistent derivation 2−58760
scattering of asymmetric molecules, interaction potential 2−53097
semipolar crysts. of NaCl-type, normalization integrals allowing for perturbations in ψ and ψ^* 2−57097
separable one-particle problems with cylinder symmetry, constants of motion 2−49015
Stark ladder for electron in electrified crystalline lattice, integral equation method 2−52077
Stark-broadening parameters for resonance lines of Ca^+ and Mg^+ calc. using theories of Barnes and Peach and of Bely and Griem 2−42727
three body problem treated by path integral approach of Feynman 2−41509
three body problems, approximate solutions 2−52081
three body rearrangements in reactive scattering, application of τ operator formalism 2−44467
transition density matrices, suggested calculations 2−59882
two interacting particles in potential hole, possibility of bineutron existence 2−67121
unidimensional motion in an electric nonhomogeneous field with Coulomb potential 2−76215
variation principle, time-dependent 2−41507
variational bounds for imaginary frequency polarizability and dispersion interaction constant 2−52943
variational principles and minimum entropy production 2−45318
H atom, energy level relativistic shift, operator domain paradox 2−63014
H atoms in plasma, time evolution operator in semiclassical theory of Stark-broadening 2−42793
H_2 ground-state energy calc. by new transcorrelated method, comparison with variational method 2−64134
Nb, diffusion of H and D, application to quantum theory 2−80718

many-particle systems *see Helium/liquid; Quantum fluids; Statistical mechanics/quantum; Superconductivity; Superfluidity*

quantization
see also Field theory,quantum/quantization
Dirac eqn. solution for new magnetic fields, energy levels 2−41502
dispersive media, wave quantiz., negative energy excitations 2−82223
electric field effects on quasibound states, integral equation method 2−52077
films, Raman scattering by size quantization levels 2−81394
general relativity, Einstein algebras 2−45258
generalized Hamiltonians, quantization scheme 2−41485
generalized Heisenberg relations 2−69591
hadron composite model, correlation effects 2−79511
Hamiltonian formalism for general Lagrangian with higher-order derivatives 2−69595
mass quantization of elementary particles 2−45860

Quantum theory continued
quantization continued
metal thin films in magnetic field, microwave absorption, quantization of electron momenta 2−80941
momentum operator in generalized coordinates 2−73323
orbital angular momentum, from harmonic oscill., Bargmann and Schrodinger representations 2−66453
relativistic quantization procedure for harmonic oscillator 2−78798
semantic foundation, rel. to development of quantum theory of gravitation 2−63002
structure with two point defect types, quantum states and energy spectrum 2−80998

wave equations
see also Dirac equation
− 2−67975
adiabatic invariants of quantized system perturbed by coherent wave 2−63005
adiabatic theorem for conservative systems 2−58748
atomic coherence effects illustration 2−59912
Born series convergence for nonrelativistic scatt. at all energies 2−82226
bound state wave functions for non-local potentials, prescence of anomalous nodes 2−55417
cholesteric liquid crystal, effect of a magnetic field on the optical transmission 2−84468
circular dichroism, semi- classical theory, time-dependent Schrodinger equation 2−52460
composite particles, relativistic wave functions 2−63007
condensed matter, multiple scatt. theory 2−58762
Coulomb wave functions, in Jacobi polynomial and hypergeom. functions 2−49006
diatomic molecules, vibrational- rotational Schrodinger eqn., numerical soln. 2−56142
DNA, simultaneous motion of protons in hydrogen bonds, Schrodinger eqn. soln. 2−70799
eigenvalue determination by hybrid computer 2−73334
eignvalues, computer-generated film 2−73272
electron wave functions in strong e.m. field, quantized dimensions 2−82219
formulation, simple concepts, education 2−82115
Gel'fand-Yaglom eqns. with charge or energy density of definite sign 2−73322
harmonic oscillator wave functions, algebraic derivation of generalized Talmi expansion 2−58753
Heitler London wavefunction, resonating, one and two particle reduced density matrices 2−52099
hydrogenic wave function for extended uniformly charged nucleus 2−49704
Kampe de Feriet expansion formulae evaluation of integrals for hydrogen like atoms 2−55373
Klein-Gordon and Dirac equations, superoperator theory, zitterbewegung as subdynamics 2−73321
Klein-Gordon eqn. factorization to an alternative to the Dirac eqn. 2−73753
Klein-Gordon equation, inverse problem of potential scattering 2−41495
macroscopic rotators, quantization, application to cosmology 2−75657
massive particle wave equations, multipole radiation solutions 2−41501
matrix elements of the Nilsson model Hamiltonian 2−79722
multip-particle Schrodinger Hamiltonians with weak pots., asymptotic completeness 2−58749
non-dispersive mirror wave-packets 2−62938
one-dimensional, soln. by resistance network 2−73319
one-dimensional Schrodinger equation computer solutions 2−73274
one-dimensional Schrodinger equations, numerical solutions 2−73279
paramagnetic resonance absorption of ultrasound by conduction electrons calc. using sodium wave functions 2−81464
perturbation theory, second-order, with exact zeroth-order Hamiltonian 2−76212
perturbed Schrodinger eqn. with odd perturbation, eigenvalues 2−82222
plasma, Schrodinger like equations for nonadiabatic escape of charged particles 2−56359
point dynamic model of wave mechanics 2−66441
positive energy relativistic equation 2−41504
radial equation in 3 dimensions, appl. of soln. to one-dimens. Schrodinger eqn. for arbitrary potential 2−84273
radial Schrodinger, derivation of phase shift for low-energy scattering by long range r^{-8} potential 2−69601
radial Schroedinger eqn., determination of potential strengths 2−66444
Rayleigh-Schrodinger perturbation theory, generalized equations 2−52071
relativistic equations for nonzero mass particles 2−58720
relativitic, particles with arbitrary spin 2−41505
scattering, abstract theory, scatt. states and wave operators 2−82241
scattering of wave packet by finite range potential calc. of time delay 2−82216
Schrodinger, bouncing ball as teaching tool 2−45207
Schrodinger, bound states in strong coupling limit 2−76210
Schrodinger, for electron in Hulthen potential, representation of SO(2,1) 2−69596
Schrodinger, in momentum representation, use to determ. classical limit of S matrix 2−69598
Schrodinger, numerical soln. 2−55415
Schrodinger, one-dimensional, new method for rapid numerical solution 2−82234
Schrodinger, solvable potentials, construction from Sharpe's, Hermite and Laguerre equations 2−41496
Schrodinger, symmetry props. of variational wavefunctions 2−78814
Schrodinger algebra, many-body realization 2−63006
Schrodinger eqn., in const. and homogeneous elec. and mag. fields, Green function 2−49007
Schrodinger eqn., one-dimens., analytic approx. method of soln. 2−58752

Quantum theory continued
wave equations continued
Schrodinger eqn., radial, SU(1,1) algebra determ. of eigenvalues 2—73317
schrodinger eqn., time depend., soln. by Laplace transform. method 2—73316
Schrodinger eqn., time-depend., integration rel. to two-level system 2—79862
Schrodinger eqn. approach to one and two body struct. in atomic nuclei 2—59662
Schrodinger eqn. integral form soln. for bound state atomic systems 2—70630
Schrodinger eqn. soln. for H atom in presence of arbitarily intense laser radiation, time-dependent approach 2—79955
Schrodinger eqn. soln. for James-Coolidge- Vernon pot. 2—67446
Schrodinger equation, nonlinear wave modulation, in collisionless plasma 2—53223
Schrodinger equation, perturbation by potentials with small support 2—66445
Schrodinger equation, plasma nonlinear wave modulation, Landau damping effects 2—53224
Schrodinger equation, point dynamic model 2—66441
Schrodinger equation, radial, program for numerical soln. 2—66442
Schrodinger equation, solution by unified algebraic method 2—45266
Schrodinger equation, steady-state, separation of variables 2—78818
Schrodinger equation, steady-state, separation of variables 2—78818
Schrodinger equation for electron in analytic spheroidal potential 2—73254
Schrodinger equation soln. at band edge in one-dimens. crystal 2—75019
Schrodinger equation with singular ptoential, approx. solution method 2—52069
Schrodinger Miller-Good method for approximating bound states 2—41499
Schrodinger theory, even and odd spectra of one-dimensional symmetrical potential 2—41492
Schrodinger-Langevin eqn. for Brownian particle interacting with thermal environment 2—82220
Schrodinger-like relativistic wave functions, position operator 2—63004
Schrodinger-Pauli-type eqn. for constant homogeneous electric and magnetic fields, Green's function 2—69589
Schroedinger, finite difference equation 2—52067
Schroedinger, in theory of electron- molecule collisions by frame transformations 2—50005
Schroedinger, invariants obtained using Lie's method 2—78825
Schroedinger, iterative nonperturbative method of solution 2—73326
Schroedinger determ. of invariants and dynamical groups of harmonic oscillator and hydrogenlike atom 2—78826
Schroedinger eqn., complete solution of inverse scattering problem at fixed energy 2—41520
Schroedinger eqn., finite difference method for one-dimensional eigenvalues, computer program 2—66443
Schroedinger eqn. for He atom unbound states solved by least squares variational method 2—56129
Schroedinger eqn. for motion of charged particle in magnetic field, Landau gauge soln. for wave packet motion 2—78807
Schroedinger eqn. with non-local potentials, technique for numerical solution 2—55416
Schroedinger N-particle eqn. construction of solution in spherical coordination, using group theory methods 2—52070
Schroedingers eqn. for charged particles in uniform magnetic field, geometrical relations 2—78761
semipolar crysts. of NaCl-type, normalization integrals allowing for perturbations in ψ and ψ^* 2—57097
spectral wave functions at very low energy 2—62999
spreading wave packets 2—41491
steady state syst., quasi-energy, wave functions, using perturb. theory 2—45271
SU(1,1) spinor algebra, spin coeffs. 2—82213
three-body problem in 1-d, with interacting, impenetrable particles 2—82228
two-component spin-1/2 wave equations 2—78824
two-component spin-${}^{1}._{2}$ wave equation, properties and connection with Dirac equation 2—59382
valence bond wavefunctions, reduced density matrices 2—49028
virial and hypervirial theory distrib. functions 2—58751
wavefunctions for exchange perturbations, optimization of treatment 2—49004
Cu angular dependence of Auger electron emission 2—84388
H_2^+, perturbed generalized eigenvalue equation 2—64128
^{2}H, relativistic wave function 2—49722
Ni, Kerr and magneto-optical effect meas., electronic structure 2—72265
Si, hybridization of wave function of Si atom near structural defect 2—81005

Quarks
3^- nonet and its coupling to lower-lying mesons, model 2—67038
— 2—66905
bound states, exchange forces, asymptotic behaviour of form factors 2—63554
conformal invariant theory two and three point function, construction 2—70163
in cosmic radiation with electric charge 1/3e and 2/3e, search at 2750 m altitude using scintillation counter telescope 2—76728
delayed shower particles at 70 m w.e. underground 2—46025
density, rel. to cosmologies 2—51683
diagrams for symmetry properties of composite object, rel. to hadronic internal symmetry groups 2—76637
diquarks with charge 4/3e, search at 2750 m altitude using scintillation counter telescope 2—76729
dual model developed from Venezians model by inclusion of Dirac spin 2—63530
dual models, diagrams, inclusion of spin, L-excitation and elimination of ghosts 2—59479
dual quark model 2—52569
dual quark models for high-energy forward, backward, and large-angle scattering 2—76642
dual quark theory as second quantiz. of Thirring model 2—66947

Quarks continued
dual quark-parton model for single-particle distribs. in deep elastic electroproduction 2—70160
electropeoduction of nucleon isobars in quark model 2—42423
existence, implication of quark model light-cone algebra 2—79513
flux loop representation 2—73772
hadron scattering, selection rule 2—49535
hadron spectra, quark-orbital Regge trajectories 2—76644
hadron strengths and currents, theory 2—52568
hadron structure 2—66951
hadron structure and 'wrong statistics' 2—73769
hadron weak interactions, $\Delta I = {}^{1}._{2}$ rule in paraquark model 2—59460
hadronic current products, short distance singularity estimate using free quark model 2—73801
hadronic symmetry, relation to leptonic symmetry 2—42332
harmonic-oscillator quark model for weak and electroproduction of N* 2—52647
helicity conservation from quark model and tensor coupling 2—70168
inclusive exchange region, symmetry considerations 2—79524
inner structure of hadrons, model employed 2—52565
L-excitation quark model in Y* spectroscopy 2—52648
light-cone current algebra of Fritzsch and Gell-Mann, implications for existence of quarks 2—59435
meson coupling const. calc. by four fermion model 2—49538
meson reson. photoproduction in backward direction cross sections prediction 2—63644
model, evaluation of SU(6) results using finite-energy and current algebra sum rules 2—63529
model showing mechanism for missing parity partners on baryon trajectories is different for N(938) an P_{33} resonance 2—63671
molecule, one-electron, energy and dipole moment 2—52985
multi-triplet quark models, breaking of scaling behaviour 2—66949
multiple scattering analysis of proton-proton scattering 2—52637
nonrelativistic harmonic oscillator model and reson electroprod. 2—59546
octet baryon nonleptonic decay mode in current-current quark model 2—76723
oscillator algebra represent., SO(3,2), applic. 2—66907
parton model, rel. to polarization effects in neutrino scatt. 2—66938
parton model and light cone current algebra relationships 2—70166
parton model of hadrons duality in dynamics of strong interactions 2—59441
parton model of Weinberg theory for lepton-nucleon scattering 2—45886
parton-quark field theory, perturbation series for dual amplitudes 2—73705
partons, energy and virtual photon mass parameters 2—70167
partons with integral charge 2—63528
photoproduction models, comparison of angular decay distribs. 2—55813
polarization in deep inelastic electron and neutrino scattering from light-cone quark algebra 2—52584
production in hadron collisions, modified peripheral model 2—82711
quark-boson model of internal structure of hadrons 2—66956
quark-gluon light cone, implications for neutrino scattering 2—42335
quark-gluon model, chiral symmetry realization 2—45897
quark-loop dynamics, application to meson decays 2—73770
quark-parton model and quark model with neutral gluons for determ. inequalities for structure functions of inelastic lepton-nucleon scattering 2—42329
quark-parton model for application of duality in deep inelastic electroproduction 2—59420
quartet model of hadrons leading to satisfactory theory of weak interactions 2—42349
relativistic charge ${}^{2}._{3}$e, search in cosmic radiation 2—59600
relativistic model, electromagnetic excitations of nucleon 2—55870
relativistic model, symmetries and nonsymmetries 2—79517
relativistic model with harmonic dynamics 2—63531
relativistic models based on Bethe-Salpeter equation 2—52566
relativistic oscillator model for light-cone expansion of commutators of bilocal currents 2—73706
review of quark model of hadron dynamics 2—59431
review of searches in air showers, terrestrial matter and stellar objects 2—59598
search, review of experiments on 70 GeV accelerator 2—52570
search for quarks at CERN intersection storage rings 2—66948
spin - ${}^{1}._{2}$, relation with lepton currents in $O_{4.2}$ current algebra 2—42330
standing-wave states concept and indefinite-metric theories 2—70107
SU(3) quarks, explanation of absence 2—52567
SU(4) weak interaction model modification 2—79531
SU(6) × O(3) quark model, diatomic-molecule type, for prediction of meson mass resonances in 1-3 GeV region 2—76690
symmetric model, radial excitation modes, SU(6) force and Roper resonance 2—76616
symmetry breaking for two-body processes energy dependence 2—79514
triplet models, distinguishing tests 2—59436
triplet quark model light-cone algebra of currents, lepton-nucleon scattering sum rules 2—76708
vector meson, photoprod. differential cross-sections, quark model 2—55864
vector meson photoproduction, and nucleon Compton scatt. amplitude, quark model 2—55865
vector meson production from γ-rays, quark model coupling constants 2—73834
vector mesons photoproduction, quark model predictions for angular decay distributions in inclusive processes 2—52624
vector-meson scattering, application of quark-model like results from duality 2—45984
weak and electromagnetic interactions, three-quark model 2—73750
weak and e.m. interaction symmetry 2—66933
weak interactions, scalar coupling and kaon decay parameters 2—59510
e-hadron scatt., quark-parton model 2—73787
$\gamma\gamma \to \pi^+\pi^-$, cross section determination using additive quark model 2—59410
$K_2^0 \to \gamma\gamma$, Steinberger fermion-loop model 2—52593

Quarks continued
N quark mass, pn bound state 2−73840
νN, νN interactions, cross-sections calc. from 3 quark boson-nucleon model 2−45876
Ω^- nonleptonic decay in current-current quark model 2−76723
πN scattering, Regge pole model with explicit quark spin applied to meson and baryon exchange 2−49572

Quartz
alpha, strained, acceleration wave obs. 2−45487
alpha-quartz, elastic props. based on interatomic force model 2−68854
atmospheric aerosol constituent, optical consts. 2−57946
balance, meas. of 10^{-12} g/s mass variations 2−52035
Brillouin spectra, calc. of polarization of back-scattered light relative to incident laser light 2−68667
capillary wicking of distilled water in quartz sand and cylindrical glass capillaries in magnetic fields 2−60402
crystal defects, obs. 2−69718
crystalline ceramics, precipitation 2−84063
crystals, use as oceanographic pressure sensor 2−44667
crystals, uses as current sensor in deep sea 2−44668
Dhanbad, quartz reefs, resistivity profiles 2−68850
diffusion and solubility of water, temp. depend. 2−50716
elastic wave propagation in crystal with surface film of Ge, electron microscope obs. 2−80732
elastic wave reflection from free surface 2−41681
elastic wave velocities and moduli, edge effect investigation in single crystal specimens 2−60854
electric breakdown field, dielec. dispersion analysis 2−61421
electro-optical effect, dispersion and temp. dependence in static fields 2−65224
electrolysis, i.r. spectra obs. and colour centres 2−74802
electrooptical effect, calc. from light wave intensity reduction 2−65222
emission polarization 2−72692
first and second sound velocity 2−71730
fused, ion-bombarded, refractive index and optical loss variations 2−50688
fused, longitudinal elastic constants, third and fourth order, det. by shock compression 2−47567
fused and crystalline, breakdown by mode-locked laser radiation, i.r. 2−79251
glass, integral normal emissivity meas. 2−54085
glass, tubular and bulk specimens, crystn., 1350-1550°C 2−64529
glass, with diminished heat flux, increased rate of ablation 2−73466
glassy sphere production from particles, by processing through plasma stream 2−56971
grinding, change to props. 2−68148
gyrotropy and asymmetric electro-optic properties, two beam refraction obs. 2−72269
highly strained, metastable growth of coesite in 2−65579
neutron irradiated, spin relax. rate depend. on static mag. field 2−57391
optical contacts, hardening by heat treatment 2−59252
plates, piezoelec. coupled vibrs. freq. temp. depend. 2−61437
preferred orientation in prograde metamorphic sequence 2−57766
purification, electrochem. method 2−61800
α-quartz, A_2 vibr. modes, i.r. lattice bands, classical oscill. model 2−74977
α-quartz, direct-recording electronograph in study of objects giving increased background 2−53639
α- quartz, Pockels effect 2−52461
quartz sand and sandstone recognition by two-channel i.r. imagery 2−65438
quartz-sand layers in N. Atlantic basin, with high thermal conductivity, heat flow obs. 2−65553
quartzite, static fatigue and creep mechanism 2−60898
radiation-induced diffusion of alkali ions and protons and formation of colour centres 2−71532
Raman scattering from polar phonons, forbidden A_2-like modes, α-modification 2−68655
Raman spectral line intensity changes in fast neutron irradiated α quartz 2−72373
Rayleigh wave electromechanical coupling constant, acoustic wave vel. obs. 2−43969
reflectance spectra, rel. to surface hydroxyl groups 2−48163
resonators, simultaneous obs. of thin film stress and mass change 2−50786
smoky, eval. of thermoluminescence dating technique 2−65570
static fatigue, earthquake phenomena 2−65499
strain-seismograph of Obnisk Central Seismological Observatory 2−72645
surface acoustic wave velocity meas. change caused by thin conducting film 2−51017
switching and steering of surface waves by nonlinear mixing in anisotropic media 2−51005
synthetic, Dauphine microtwins 2−68003
synthetic, hydro-thermal growth in Japan 2−74663
synthetic, loss at 1.06μ, rel. to fibre optic appl. 2−48136
synthetic, plasticity stages of single crysts. 2−56797
temperature field, effect of optical characteristics 2−68256
thermal fracture probability 2−50897
thermoluminescence, relative effects of α- and β-radiation 2−51379
thermoluminescence, thermal pretreatment, pre-irradiation, splitting mechanism 2−84720
thermoluminescence prod. by gamma rays determ. of geological origin 2−84709
time dependent crack growth, creep in rocks 2−65576
transducer, embedded, for internal dynamic stress obs. 2−56858
twinning, symmetry props. 2−77522
ultrahigh vacuum microbalance, evaporation rate and vapour pressure 2−85175
u.s. radiator, interference pattern visualization by optical illumination in direction of propagation 2−55547
X cur resonators, linear and nonlinear coeffs. 2−84362
X-cut, strain dependence of longitudinal piezoelectric, elastic and dielectric constants, det. by shock compression 2−51207
X-ray focusing monochromator using high-angle reflections from quartz crystal 2−85179

Quartz continued
YX and XY, Rayleigh wave reflection from electrically loaded interdigital transducers 2−51021
Hg arc lamp, far i.r. emission 2−55766
α-phase, photoelec. emission spectrum in neighbourhood of Si $L_{2,3}$ threshold 2−72094
SiO_2, quartz-coesite transition, effect of shear 2−77751
SiO_2, thermally grown, three terminal electron Hall mobility measurements 2−54178

Quartz resonators *see Piezoelectric oscillations; Resonators; Transducers*

Quasars
see also Cosmic radiations, radiofrequency; Cosmology; Galaxies; Stars
3C 273, mass distance and red shift 2−48738
3c 273, X-ray source 2−62597
— 2−62603
— 2−62602
activity, interpreted in terms of plasma processes 2−58220
activity, plasma MHD processes 2−58193
blue radiosources without u.v. excess identification with stellar objects 2−81878
4C 05.34, unidentified absorption features, rel. to multiple redshifts 2−51784
3 C 220.2, optical identification as QSO69117 2−69117
3C 273, brightness distribution and polarization of A and B components 2−73043
3C 273, brightness variation in small scale structure 2−75801
3C 273, circular polarization obs. 2−58405
3C 273, circular polarization of u.v. 2−81794
3C 273, electrographic UBV photometry of jet 2−44899
3C 273, periodicity from shot noise data 2−55081
3 C 273 and 3C 279, model to explain superlight velocity 2−58378
3C 279, brightness variation in small scale structure 2−75801
3C 323.1, association w.a rich cluster of galaxies 2−66125
3C quasi-stellar objects, correlation between positions and bright galaxies 2−48742
composite spectrum, redshift 2−75820
cosmological interpretation, interacting matter-radiation models 2−84931
cut-off at high redshift 2−75802
distances, redshift hypotheses 2−69118
distances rel. to expanding universe, Hubble constant and Friedmann time 2−69039
energy source for violent events, explosive phenomena 2−81865
Faraday depolarization rel. to cosmological redshift of quasars 2−73042
geometrical interpretation of luminosity distributions rel. to separate big bang 2−55079
gravitational collapse of massive body 2−58163
images of Seyfert nuclei rel. to quasars 2−69035
i.r. obs 2−58212
i.r. photometry 2−73051
kinematic quasi-stellar source model 2−58374
linear polarization of those with appreciable red shift 2−58376
luminosity, gravity generation of e.m. radiation 2−44890
luminosity, statistical evolution, appraisal of luminosity-volume test 2−51781
luminosity functions, rel. to galaxy evolution theory 2−51785
Markarian 205, evidence for physical connection with spiral galaxy NGC 4319 2−66058
model, stability of gas-star system 2−81895
NGC 520 chain, discrepant redshift of cluster galaxies 2−58375
optical circular polarization, search 2−75800
optical identifications of QSOs in the B2 catalogue of radiosources 2−62607
optical position meas. 2−81872
optical positions of 48 QSOs rel. to AGK3 and SAO stellar positions 2−69116
Parkes 0237-23, unidentified absorption features, multiple redshifts 2−51784
Parkes 2134 + 004, small-pitch-angle synchrotron radiation 2−58404
PHL 938, Fe abundance, det. from Fe I and Fe II resonance transitions in 2300 to 3050 Å region 2−58547
PHL 957, absorption line profiles 2−58373
PHL 957, unidentified absorption features, multiple redshifts 2−51784
photoionization models for emission line regions 2−69024
physical associations with galaxies 2−51782
PKS 0118 + 03, structure, from occultation observations 2−58383
polarization at 49 and 73 cms 2−58412
positions and brightness distributions by lunar occultation 2−66131
redshift, summary of evidence 2−81877
redshifts, power spectrum analysis 2−58377
redshifts and colours correlations 2−55080
role in observational cosmology 2−75804
rotation measures, redshift dependence 2−81871
Seyfert galaxies, structure and luminosity rel. to quasars 2−72974
source counts and evolution 2−62600
source counts and evolution 2−62598
spectra, excitation of CII line 2−44889
spectra, multiple redshift and very narrow absorption lines 2−81791
spectral energy distribution (rel. to Markarian 205) 2−73000
spectral index-luminosity relation for QSO and radiogalaxies 2−48741
spectroscopic observations, redshift, selection effects 2−66126
spinars, mass and angular momentum losses, temp. of corotating region 2−58371
Ton 1530, absorption lines 2−58372
Ton 1530, unidentified absorption features, multiple redshifts 2−51784
Ton 155 and 156, possibility of double system 2−58379
Ton 202, spectrum 2−51783
u.v. continuum, spectral and colour characteristics 2−69026

Quasi-particles
see also Crystal electron states/excitons; Crystal electron states/plasma; Crystal electron states/polarons; Helicons; Spin waves
electron-hole-phonon quasiparticle bound states in strong mag. fields 2−68302

Quasi-particles continued
- Fermi liquids, two-component, generalization of theory for zero-sound waves 2−71265
- Josephson junction, quasiparticle interference current 2−81040
- nonequilibrium, superconductors, photoexcitation of quasiparticles 2−77868
- phonon- impurity centre-exciton bound states, theory of dielec. modes 2−68303
- plasma, weakly turbulent, conservation 2−56372
- quantum electron-impurity transport, quasiparticle formulation 2−84240
- roton energy in liquid He, temp. depend. 2−80517
- small superconducting particles, quasiparticle contrib. to thermodynamic props. 2−64928
- in solid, interaction to form bound states which contrib. to nonlinear polarizability 2−84197
- superconductivity, rel. to Fermi liquid model of s-d electrons 2−71856
- superconductor, light scatt. with creation of 2 quasiparticles, temp. depend. calc. 2−65238
- superconductor, tunnelling detection of hole-electron imbalance 2−64926
- superconductor model, recombination time 2−47844
- type II superconductor in crossed electric and magnetic fields, coherent quasiparticle excitation 2−84307
- wave quantiz. in dispersive media, medium excitations description 2−82223
- NaI:Tl, recomb. luminesc. of crysts. excited in A-band by activator absorpt. 2−75334
- α'-$NaV_2O_{5-x}F_x$, $0\leqslant x\leqslant 1$, d electron distrib. on V atoms, from elec. and mag. props. 2−75080
- ^{121}Sn, 1 and 3 quasiparticle states, core-particle discription of low-lying levels 2−76798

Quenching, optical *see Luminescence*

Quenching, thermal *see Heat treatment*

Racah coefficients *see Quantum theory*

Radiation
- *see also Acoustic radiators; Bremsstrahlung; Cherenkov radiation; Electromagnetic waves; Electrons/radiation; Emissivity Radiative transfer; Stars/radiation; Sun/radiation; Sunlight*
- 10.6 mkm, modulation using Ge cryst. at 13 MHz u.s. 2−49201
- air plasma, 8000 to 12500 K, total radiant power det. 2−71061
- antenna, receivers, rad. pattern determ. by holography and optical processing 2−45623
- black body, application of theory of physical dimensions 2−41843
- black-body temp. 2.2K, theoretical 2−76392
- blackbody, stimulated emission and Bose-Einstein statistics 2−41838
- boundary-value problems in elasticity, radiation property 2−45411
- charge moving in field of arbitrary config., classical eval. 2−49315
- charged particle, in equal mutually perpendicular static elec. and mag. fields 2−63261
- charged particle, uniformly moving in time-dependent magnetoactive plasma 2−53180
- charged particle moving in helical path in crystal or hyperbolical path in vacuum 2−76416
- charged particle moving uniformly in cryst., soln. of field eqn. 2−82162
- coherent microwave, emission from relativistic electron beam propagating in modulated magnetic field 2−52313
- cone wall absorption of external radiant power 2−55569
- density distribution in scattering media with limited size source 2−66818
- Earth, atmosphere system, balance 2−48506
- earth-atmosphere system, determ. of total outgoing radiation 2−54810
- Einstein field equation with radiation energy transport, interior spherically symmetric solutions 2−69580
- e.m., due to point charges moving above ribbon diffraction grating 2−63173
- e.m. field of Gaussian beam with elliptical cross section 2−73597
- e.m. from loaded bodies of revolution 2−58996
- e.m. universal background radiation 2−69001
- emission and scattering at rough surface, geometrical optics theory, sea brightness temp. 2−44652
- exposure to terrestrial and cosmic radiation in United States 2−57803
- field, quantized, sum-frequency-amplification 2−69888
- fluxes during dust storm 2−48505
- gas laser, radiation field, characteristic function 2−41986
- gravitational, upper limit on X-ray flux 2−44826
- multipole, ultra high speed photography 2−45620
- multipole radiation source, exploding wire Sn 2−46441
- nonequilibrium optical field, temperature 2−69991
- nonstationary radiation field in semi-infinite media 2−58814
- nonthermal radiating systems, pseudothermodynamic model 2−58943
- oscillating charge crossing boundary between two dielectrics 2−69863
- polarized, nonconservative Rayleigh scatt., Milne problem 2−52459
- pulsars, from flares near magnetic poles 2−44901
- reflectance, average specular component eval. 2−45571
- relativistic particle anomalous motion in strong fields 2−55403
- scale of spectral irradiance, visible region 2−79449
- secondary standard with $\lambda=640.2$ nm for pyrometric obs. of plasma 2−45585
- source, propagation in space-time periodic media 2−52318
- sources, thin film production by radio frequency sputtering 2−74046
- Stefan-Boltzmann law illustration for students of quantum theory concepts 2−55349
- strong noise, effect on absorption line profile of atom 2−77002
- superradiance, radiative decay solutions 2−73260
- thermal, in finite cavities of various shapes second order corrections 2−76384
- total, from cylindrical volume of finite length 2−41841
- transition, generation by charged particle in waveguide 2−41930
- transition, in space-time periodic media 2−66657
- uniformly moving charged particle in random inhomogeneous medium, Cherenkov and transient radiation 2−52312

Radiation continued
- u.v., biomedical applications, review 2−85131
- ^{60}Co source with high output small diameter 2−69349
- OH maser source, astronomical, statistics 2−58368

heat
- – 2−67733
- – 2−68256
- – 2−60176
- absorbing emitting, isotropically scattering medium, simultaneous ablation and radiation studied by normal-mode-expansion technique 2−41854
- in annular channel, calcs. 2−66636
- automatic emissivity meas. apparatus 2−52264
- basin cooling in winter, radiation from snow covered mountains 2−75530
- black body source high frequency, as primary spectrometric standard 2−52266
- blackbodies, general analysis 2−78858
- blackbody radiation in small cavities, teaching paper 2−63140
- Comet Bennett nucleus, direct i.r. obs. 2−51836
- comparisons of International Pyrheliometric Scale with absolute radiation scale 2−73461
- Earth, radiation fluxes measured by Cosmos-320 satellite 2−61865
- emissivity meas. apparatus, high temp. 2−52265
- energy fluctuations formulae derivation 2−58816
- flux of surface in contact with hot radiating gas, during pulsed process 2−41842
- gases, nonhomogeneous, volume interchange factors rel. to radiative transfer 2−53335
- glass, molten, exptl. and analytical study 2−52270
- greenhouse effect on ambient air temperature distribution 2−72756
- heat evolving radiative systems, dependence of thermophysical props. on temperature 2−41840
- hot universe, non-existence of cosmic-ray cut-off around 10^{20}eV, choice of absolute reference system 2−72960
- interaction with diatomic gas, model kinetic eqn. for internal fluid 2−43263
- i.r., biomedical applications, review 2−85131
- i.r. radiometer, precision calibration and test 2−82387
- i.r. simulator for thermal vacuum testing of space vehicles 2−78415
- i.r. thermography of laminated materials, subsurface defect obs. 2−43767
- light-diffusing layer heating kinetics from radiant heat exchange calc. 2−82465
- Mars, Mariner orbiter mission (1971), i.r. radiometer experiment 2−85076
- moving radiometers, response when passing over field of varying emittance or reflectance 2−66637
- nongrey molecular gas, formulation in terms of slab band absorptance 2−77367
- opaque surfaces, influence of surface roughness 2−55574
- optical thick radiating gas flow, past smooth boundary, asymptotic theory 2−53279
- optical waveguide, temperature difference reduction in shielding pipes 2−76511
- pressurized water reactor, emergency cooling of 37-rod cluster by heat radiation following accident 2−79834
- scanning radiometer, for orbiting satellite 2−84865
- semiinfinite piezoelectric rod due to prescribed heat flux 2−41856
- simulation of exchange phenomena using electrical network 2−52263
- sky and earth thermal radiation field, spectral angular and height distribution 2−72798
- slab, absorbing, emitting, scattering, with reflecting boundaries 2−45580
- solar flux radiometer, economical design 2−65760
- spectral emissivity meas. on all nonmetallic materials at high temps. 2−55570
- sunlight, atmospheric radiative heating, effect of changing CO_2 concentration 2−72800
- thermal solar radiation reflected from ocean surfaces 2−65759
- thermophysical meas., optical utilization of redundant information 2−52290
- transfer, from internally heated slab, cylinder or sphere, exact steady state solutions 2−52284
- transfer, nonstationary, between simply shaped bodies and surrounding medium 2−41853
- transfer analysis, validity of simplified models 2−55578
- Wien's radiation law, determ. of constant 2−73462
- Al_2O_3-Cr_2O_3-P_2O_5 coating, radiative capacity rel. to struct., 600-2000K 2−57087
- Ar plasma, high-pressure thermal, use as high-radiance standard 2−46713

Radiation belts *see Atmosphere/radiation belts*

Radiation chemistry *see Chemical effects of radiations/ionizing radiations; Radiochemistry*

Radiation damage *see Physical effects of radiation*

Radiation detectors
- *see also Bolometers; Photometry; Radioactivity measurement*
- black body radiometer, self-calibrating, for use in u.v., i.r. and visible 2−66638
- Cd_3As_2-NiAs eutectic, Nernst effect based thermal detector 2−54246
- choice criteria and fundamental limits quality 2−41846
- displayed at 1972 Physics Exhibition 2−55899
- electrometric photocell compensator applics. 2−70302
- heterodyne detection of far i.r. radiation using Josephson junctions 2−41845
- heterojunction photodetectors, interface region struct. rel. to energy band profile 2−44181
- heterojunction photodetectors, review 2−44180
- i.r., electro-optical systems design conference 1971 West 2−82473
- i.r., heterodyne detectors for stellar interferometer 2−81975
- i.r., pyroelectric devices, review 2−69793
- i.r. detector parameter uniformity in alloy semiconductors 2−52274
- i.r. heterodyne solar radiometry 2−58549
- i.r. radiometer, Mars Mariner orbiter mission (1971) 2−85076
- i.r. radiometer, precision calibration and test 2−82387
- i.r. scanner, integrator, properties of output 2−76385
- i.r. thermal detectors, high speed 2−41839

Radiation detectors continued
i.r. thermometer with pyroelectric detector 2−55590
Josephson junction applics. 2−64956
laser beams, by current changes in gas laser discharge tube 2−42163
laser cone calorimeters, spectral response 2−73473
laser detector, frequency response of m.o.m. diodes at 1.15 μm radiation with a d.c. bias 2−45769
metal-$SiO_2(TiO_2)$- Si-$SiO_2(TiO_2)$-metal, for light signal amplification 2−45694
meteorological applications of Nimbus 4 temperature-humidity i.r. radiometer, 6.7 μm channel data 2−75487
mica, optical characts. 2−55754
microwave radiometer, theory and field tests for det. of sea ice thickness 2−44603
moving radiometers, response when passing over field of varying emittance or reflectance 2−66637
multipole, ultra high speed photography 2−45620
multiwire proportional chambers for X-ray transition radiation detection, use for relativistic particle separation 2−67081
nuclear reactor stochastic two-group model including neutron and gamma detection 2−83095
with optically corrected spectral sensitivity for photosynthetically effective radiations 2−42468
optimum radiation flux detection by zone plate disc sensor combinations 2−79364
photodetectors, obs. of spectral sensitivity 2−42470
photodiode-operational amplifier as relative-energy monitor for pulse laser systems 2−52441
photoelectrets as memory photon detectors 2−42219
photon counting system without amplifier for low radiation levels 2−52407
photonic standardized counting system for high resolving power applics. 2−63426
photons, conference Varna Bulgaria (1971) 2−42218
polyvinyl chloride, electrical response to i.r., preparation and use as sensor 2−47990
pulse shaper, anticoincidence circuits, resolving time, differentiating input 2−82803
pyranometers, Eppley model 6-90, sensitivity stability 2−63144
pyroelectric, noise sources 2−78944
radiation thermometry, compensatory techniques for unknown variations in emissivity 2−73467
radiometer, dual-channel polarizing, high-precision computer controlled, atmospheric use 2−62260
radiometer, microwave for meas. sea surface temp. 2−72721
radiometer system for spectral emittance obs. 2−58945
radiometers, electrically calibrated, NBS total irradiance scale 2−78950
radiometry, diffraction corrections 2−78951
scanning radiometer, for orbiting satellite 2−84865
selective chopper radiometer on Nimbus 4, meas. of CO_2 15 micron band emission 2−65660
short-lived activities produced in (n,γ) reactions, automatic irradiation apparatus with on-line mass system 2−79639
slow response, threshold sensitivity to pulsed and harmonic signals 2−59111
spectropyrometric apparatus for calibrating i.r. emitters 2−70078
SQUID freq. converter, resistive, design and h.f. response 2−44084
standard pyranometers, comparison on international basis 2−63141
thermal, film-type, use in radiative heat flux obs. during pulsed processes 2−41842
thermal, short time- constant, operating mechanism 2−41848
thermal image parametric upconversion, theory 2−69792
thermographic instrument with temp. standard 2−69791
thermography, integrated system of up to 64 units, applications 2−82378
transition counter for detection of radiation from ultrarelativistic charged particles 2−73946
X-ray, semiconductor type, low-noise amplifiers 2−52702
X-ray visualization and memorization device 2−76744
zone plate disk sensor combinations, chromatic properties 2−79432
Al_2O_3 thermoluminescence emission band at 4100 Å suitability as radiation detector 2−57376
CaF_2 dosimeter in sunburn range 2−85136
CaF_2 dosimeters, thermoluminescent, preparation and props. 2−82824
$CaSO_4$:Dy phosphor for meas. of u.v. irradiances 2−82561
$CaSO_4$:Tm phosphor for meas. of u.v. irradiances 2−82561
$CaWO_4$ scintillator, optical meas. in far u.v. 2−52689
CdS, neutron activated, for X-rays 2−42466
CdS, photoresistors, FSK-type, response to low-intensity modulated radiation 2−61452
CdS, sintered, for gamma detector 2−42469
Cu-constantan thermocouple with mica window 2−73472
Ge:Ga bolometer, construction and performance 2−41847
Ge:Hg photoresistor, heterodyne detection at high freq. 2−69986
Ge-Si heterojunction position sensitive photocell 2−44182
Ge(Li) coaxial detector, local efficiency variations 2−70301
$Hg_{1-x}Cd_xTe$ and InSb, comparison for low contrast target detection at 5 μm and 10 μm 2−63142
n-InSb, performance at 77K 2−78988
InSb and $Hg_{1-x}Cd_xTe$, comparison for low contrast target detection at 5 μm and 10 μm 2−63142
$KTa_xNb_{1-x}O_3$, pyroelectric, characteristics 2−73460
$Li_2B_4O_7$:Mn thermoluminescent dosimeter, energy response 2−58623
$LiTaO_3$, subnanosecond pyroelectric detector, for use with pulsed lasers 2−82466
PbS i.r., new material as window filter 2−58944
$PbTiO_3$, pyroelectric i.r. detector 2−55572
Si, obs. of average energy per electron-hole pair generation between 5 and 320K 2−70299
SrS:Ce,Sm luminescent i.r. sensors, preparation and properties 2−73463
T activity in ground and surface water obs. 2−72688
ZnCdS evaporated layers as photoresistors in u.v. 2−44179

Radiation effects *see Biological effects of radiations; Chemical effects of radiations; Physical effects of radiations*

Radiation monitoring
see also Dosimetry
γ-ray spectra obs. in reactor room 2−63983
air contamination with personal air samplers 2−58011
arc welding radiation meas. rel. to protective filter glass standardization 2−73668
digital multiplexing system for use near particle accelerator 2−49698
environmental monitors, optimal location and design 2−76957
by exoelectronemission 2−77974
fast neutron personnel monitoring by fission fragment registration in ^{237}Np 2−79676
gaseous effluents from nuclear facilities, meas. using high pressure ionization chambers 2−42690
in-pile calorimetry in Hungary, status report 2−63977
internal contamination by γ emitters, programme in use at INR, Warsaw 2−58629
internal contamination risk, influence on monitoring programmes 2−58628
ionisation chamber for controlling irradiation times in reactor pneumatic transport system 2−74189
ionization chamber for γ-ray energy deposition meas. in nuclear reactors 2−42699
neutron and γ-ray personnel dosimeters at critical assemblies, comparison 2−67368
nuclear bursts, measurement with detector having finite response time 2−63980
nuclear power plant following reactor accident 2−67370
nuclear reactor environment, instrumentation 2−82791
personnel, application of luminescence methods 2−69428
reactor accident, field radiological monitoring system 2−63979
thermoluminescent dosimetry, for automatic large-scale monitoring at Riso, Denmark 2−69433
$CaSO_4$:Dy thermoluminescence dosimeters for environmental monitoring 2−79675
I isotopes internal contamination in isotope production heat laboratory, Budapest 2−58632
^{131}I monitor for nuclear plants 2−67364
^{131}I production risks, routine thyroid monitoring 2−58631
^{90}Sr, internal contamination in isotope production heat laboratory, Budapest 2−58632

Radiation pressure
see also Acoustic streaming
acoustic wave elastic scattering, determ. of forces and torques 2−52235
averaged sound pressure in reverberation chamber, rotating vane effect 2−41693
cavitation bubble implosion pressure pulses and cavitation damage 2−56469
on dust, general relativity 2−58723
dye laser light, deflection of atomic beam 2−73624
effect on mobile charge carriers in semiconductor, photon drag detection 2−76465
efficiency factor for pressure on spherical particles of graphite and metallic materials 2−45772
induced, in pulsars, quasars, and galactic nuclei and maser type sources 2−62603
effect on infinitely small body in gravitational field of Earth and Sun, stability of motion 2−69012
laser light, review of expts. 2−42172
light press. acting on Echo-1 satellite, meas. 2−51675
light-pressure force moments det., photoelectric instrument 2−55725
satellite perturbed motion rel. to solar radiation pressure effects 2−84935
Saturn's rings formation 2−48778
solar, use in attitude and librational control of satellites 2−44802
around stars, effect on neutral atoms and dust grains 2−48730
C stars, stellar winds and mass loss resulting from radiation pressure 2−58269

Radiation protection
see also Radiation monitoring
— 2−63709
γ-ray and neutron distribution at large distances from source 2−63978
accident simulation with phantom, real neutron dose compared to badge meas. 2−52893
active X-ray shielding of viewing head of electron microscope 2−45201
arc welding, protective filter glass standardisation, radiation meas. 2−73668
arc welding radiation meas. rel. to protective filter glass standardization 2−73668
brachytherapy sources, recommendations 2−73190
bremsstrahlung from cylindrical beta sources 2−67191
children, gonad doses at X-ray examinations 2−69335
closed cycle water reactor, waste disposal systems 2−56075
contamination from operation of neutron generators 2−58603
contamination risk in laboratories using scaled radiation sources 2−58598
control of radiological hazards related to internal contamination by radionuclides 2−55220
criteria and recommendations 2−76082
in diagnostic radiology, review 2−69336
DNA, DPA, by sulphhydryl compounds 2−60094
dose albedos of intermediate energy bremsstrahlung on reactor shielding materials 2−76958
ear defender, amplitude sensitive 2−73219
ear protection in factory environment 2−73218
estimation of problem for high energy accelerators by calc. of hadronic cascade in matter 2−59643
eye, from i.r. laser radiation 2−76109
gamma-ray shielding calcs. eval. and parameters determ. with bremsstrahlung radiation 2−83156
gamma-ray source, visual control by luminesc. 2−85177
gamma-ray source containers, commercial aspects 2−70546
GeV range, from anal. of particles passing through thick layers 2−42692
health physics measures relating to radiation exposure of general public, from light-water-cooled nuclear power reactors 2−55243
health physics problems of instant contamination, 2nd European congress on radiation protection, Budapest (3-5 May 1972) 2−55219

Radiation protection continued
hearing protectors in industrial noise, variation with noise spectra and with people 2−73217
h.f. intensity meas. for radiation protection, accuracy limitation 2−78989
hot facilities, radiation safety 2−63985
h.v. vacuum interrupters, X-ray generation 2−82022
incorporation analysis in medical department of rotational centre for radiation protection of GDB 2−55245
instrumentation and applics. 2−70545
internal contamination hazard involved in industrial application of nuclear tracer technique 2−58599
internal contamination risk calc. for design and control of laboratories, modifying factors 2−58600
ionization chambers with air circulation, calibration, isotopes detection 2−70293
lead shielding, gas core nuclear rocket fission fragments 2−85127
light water power reactors, construction, operating experience in W. Germany 2−70521
limitation of release of radioactive material to environment, from nuclear power stations 2−70515
magnetized Fe muon shield for high energy neutrino laboratory, design 2−83157
microwaves, human exposure, potential hazards, safety standards 2−82025
modifying factors and dose equivalent 2−78646
natural uranium operation, assessment of radiation safety and efficiency of prophylactic measures 2−55241
neutron and γ radiation shielding by two types of concrete 2−79846
neutron dose, recommendations 2−70544
neutron radiation on human body, expt. with tissue equivalent substance 2−55239
neutron shielding calc., prep. of group consts. 2−42693
nuclear, ecology 2−49910
nuclear power field, safety aspects 2−67369
nuclear power stations, radioactive safety 2−63982
nuclear power stations, radiological safety for general public, health physics aspects 2−55226
nuclear reactor shielding, weight optimization using transmission matrix methods 2−76960
nuclear reactors, fission products retention 2−49880
nuclear reactors, methods for reducing release of ^{3}H to environment 2−52890
nuclear research centre, use of actual and model accidents for emergency planning 2−55244
nuclear star production by high energy hadrons 2−52891
pacemakers, safety aspects protection 2−51928
particle accelerator shielding, patent 2−82835
patients, conference, Copenhagen, (1972) 2−69347
personal protection facilities, methods of production and setting of working conditions in USSR 2−58602
prestressed concrete press. vessels for LWR's, safety survey 2−83143
quantities and units in health physics 2−58625
radioactive aerosols, estimation of risk from inhalation and appropriate protection meas. 2−55242
radioactive gases, safety measures required on work premises 2−58605
radioactive waste, treatment using local minerals 2−83158
radioactivity monitoring, nuclear reactor environment, instrumentation 2−82791
radiodiagnosis, analysis of risks 2−48881
radiodiagnosis, choice of dosemeter 2−48888
radiodiagnostic apparatus, technical aspects 2−48882
radioisotopic batteries, safety regulations and standards 2−49304
radiopharmaceutical dosimetry, pediatric 2−69379
radiopharmaceutical problems 2−73186
radioprotective effect of prostaglandin or mammalian cells in culture 2−73188
reactor accident, field radiological monitoring system 2−63979
reactor shield design with graphical assistance 2−42694
reactor shielding; γ-ray spectra obs. in reactor room 2−63983
reactor shielding materials from γ-ray deposition and penetration, benchmark source 2−46395
regulatory programs development under Radiation Control for Health and Safety Act of 1968 2−48879
research and measurement reactors at Braunschweig, during 1971 2−76935
research reactor, FRG, void coeff. of reactivity, expt. 2−49878
safety criteria for surface contamination by radioactive substances 2−58601
safety glasses, shielding ability in fluoroscopic exams 2−62857
sampling programme for control of persons working with open radioactive materials 2−52889
scanning electron microscope sample, handling 2−43560
shield for thermistor deployment in atmos. boundary layer 2−51579
shielding, determ. of photon differential albedo 2−76959
shielding, high energy neutrons, calc. of neutron density behind shield 2−42695
shielding for ultrarelativistic muons, calc. of survival probability by Monte Carlo method 2−79845
shielding Monte Carlo calcs. of high-energy nucleon-meson cascades in thick targets 2−79630
space vehicles, proton shielding 2−85065
standards, German regulations 2−45040
standards, review, book 2−59873
standards in Germany 2−49912
syringe radiation shield for short lived radionuclides 2−48861
testicles in X-ray examination 2−73185
thermoluminescent dosimeters in neutron dosimetry 2−69345
for underground uranium miners in USA, review of scientific basis for standard 2−55240
u.s. intensity measurements, Radiation Control for Health and Safety Act 2−45041
u.v. irradiated DNA, protective action of flavins 2−69346
in X-ray diagnosis, review 73183 2−73183
X-ray diffr. equipment, radiation hazards, safety suggestions 2−76081
X-ray diffraction and fluorescence analysis equipment, monitoring and dose limits 2−78657

Radiation protection continued
X-ray diffraction equipment, use of monitor 2−62855
X-ray diffraction shutter system, corrective action program for malfunctioning 2−62858
X-ray interlock system on Philips vertical diffraction unit 2−62856
x-ray machines, controlling and recording radiation exposure 2−58596
X-ray tube, diagnostic, inherent filtration, X-ray quality 2−69376
X-rays and γ-rays, instrument for calibration of monitoring instruments 2−69243
α particles from Pu in, implantable pacemakers, safety criteria, test results 2−51927
β particles from Pm in, implantable pacemakers, safety criteria, test results 2−51927
γ radioactivity in building materials, background reduction measures outside spectrometric facilities 2−56076
^{41}Ar release from Lowell Technological Institute reactor, environmental significance 2−59875
^{14}C labelled compounds, production control of surface and internal contamination 2−58604
Ce, series 100 glasses, spectral analysis, monitoring of radiation resistance 2−63981
^{252}Cf brachytherapy program 2−69381
^{3}H labelled compounds production control of surface and internal contamination 2−58604
I contamination of cyclotron workers 2−73189
^{131}I production laboratories, radiation monitoring and risk of internal contamination 2−58630
Pb sleeve-type screening on cylindrical scintillators, suitability for directional detection properties for γ-rays 2−59874
$^{147}Pm_2O_3$, thick cylindrical beta sources, bremsstrahlung 2−67191
RaA airborne atoms collection on wire gauze 2−69344
^{222}Rn short-lived daughters, maximum permissible doses by inhalation in mines and radon spas 2−55271
^{222}Rn short-lived daughters, recommendation of maximum permissible intake by inhalation 2−55270
^{90}Sr-$^{90}YTiO_3$, thick cylindrical beta sources, bremsstrahlung 2−67191
U concentrates, safety in operations and processes 2−83154
Radiative recombination *see Luminescence*
Radiative transfer
— 2−67697
Ambarzumian integral equation, initial value method 2−41550
in annular channel, calcs. 2−66636
astronomical, in line frequencies, approximate soln. 2−75702
atmosphere, inverse soln. by general relaxation method 2−62132
atmosphere, planetary, transfer with three-term phase function 2−58442
atmosphere-ocean system, Monte Carlo calcs. of flux 2−65627
atmosphere-ocean system, Monte Carlo calcs. of radiance 2−65628
atmospheric, by CO_2, spectral obs. 2−65770
atmospheric particulates composed of SiO_2, $CaCO_3$, H_2O, radiative properties in spectral interval 500-1500 cm^{-1} 2−54854
atmospheric radiation, conf., August 1972, Colorado 2−62248
coherence theory relation 2−78834
Compton and inverse Compton scattering 2−42325
β Cor Bor magnetic A star atmosphere, theory58289 2−58289
differentially expanding stellar atmospheres, transfer of resonance-line radiation 2−62522
differentially expanding stellar atmospheres, transfer of resonance-line radiation 2−62521
equation, eigenvalues and eigenvectors for solutions 2−69790
flows over convex and concave shapes 2−77337
gas, plane-parallel layer, radiative flux and flux divergence of Lorentz line 2−43271
gases, molecular band model formulation for large variation in temperature along optical path 2−43269
grey isothermal spherical layer, local flux 2−76221
heat, validity of simplified models 2−55578
heat exchanger, transient processes 2−58955
invariant imbedding and Chandrasekhar's planetary problem 2−58479
laminar flow of non-grey gases through circular tube 2−43228
laminar flows with radiative interaction using total band absorptance model 2−43229
linear, general theory of spherically symmetric boundary value problems 2−46361
linearity, applic. to source function determ. rel. to standard function 2−58815
Martian atmosphere, by CO_2 2−65770
matrix-operator theory for Rayleigh and maritime haze phase functions 2−76235
matrix-operator theory for realistic radiative transfer problems 2−76236
methods for e.m. reflection from turbulent plasma 2−80236
mineral, absorption spectra meas. at high shock press., apparatus design 2−61828
model atmospheres, homogeneous and inhomogeneous, synthetic absorption profile 2−66165
non-grey, semi-grey approximation, extension to arbitrary geometry 2−76237
nongrey, mathematical properties of $K_n(\tau)$ functions 2−76238
nonspherical thermal wave propag. 2−49177
nonstationary, between simply shaped bodies and surrounding medium 2−41853
piston movement in non-uniform medium, approximate analytic solutions 2−52261
planetary atmosphere with molecular anisotropy, soln. of auxilliary equation 2−62690
planetary atmospheres, line shape and band structure effects on temperatures 2−78516
planetary atmospheres, Mars and Venus 2−44946
radiation-matter interaction, steady state conditions and entropy role 2−76222
realistic atmospheres 2−65754
realistic gaseous atmospheres, transmission functions, calc. over inhomogeneous paths 2−65769
reflectance, average specular component eval. 2−45571
resonant line, in differentially expanding nebula 2−58250
through scattering absorbing layer, two-flux model 2−52115

Radiative transfer continued
scattering of line radiation in atmosphere, source function 2-41551
Scorpius X-1, transfer effects on X-ray lines of optically thick sources 2-84981
sea surface cooling mechanisms, surface stress 2-65593
semi-transparent clouds in thermal i.r. 2-65737
simplified theory, Kubelka-Munk 2-78859
solar corona, temperature-density structure, energy transport mechanisms 2-76031
solar irradiances penetrating through atmosphere and plant canopies 2-48475
stellar atmosphere, partially coherent scattering 2-41552
stellar envelope, spherically symmetric, numerical solution of equation 2-62557
between surfaces of solid materials 2-58946
theory, efficient stream distributions 2-79356
transfer of resonance radiation as process of photon random walks 2-82550
transient heat transfer in non-gray medium 2-58952
Venusian atmosphere, by CO_2 2-65770
Voigt line profile, rational approx. 2-41524
water, radiation energy transfer, local radiant flux, radiant energy loss or gain 2-67827
Ba cloud experiments rel. to mechanism of photoionization and radiative transfer problem in freely expanding gaseous clouds 2-46791
CCl_4 liquid, interactions of the radiation with conduction, analysis based on spectroscopic information 2-43346
O_2, compressed, 100 to 1000 K, total emissivity, total band absorptance, Planck mean absorption coeff. 2-76391

Radiators *see Electromagnetic waves/radiators; Transducers*

Radicals *see Free radicals*

Radioactive dating
— 2-62025
anticoincidence installation for internal counting counter 2-82814
apatite in Tatra Mountains, fission-track age determination 2-72661
Apollo 14 lunar rock samples, Rb-Sr data rel. to 4.3 aeon pre-Imbrium event 2-55119
Bjurbole chondrules, ^{129}I-^{129}Xe dating by neutron irradiation 2-69174
Black Sea, late Pleistocene and Holocene history 2-65451
fission method, expt. factors leading to modification of age results 2-48409
granitic rocks in Cape Breton Island, Nova Scotia 2-81592
igneous rocks from ophiolitic complexes, paleozoic ages 2-62002
Lewisian basement gneisses from Scotland, discordant zircon age patterns 2-61997
Lower Triassic rocks in central Nevada, fission track age 2-57927
lunar Apollo 14 and 15 samples, ^{40}Ar-^{39}Ar ages 2-62668
lunar petrogenesis, Sr isotope ages 2-62684
lunar rocks, Apollo 15 samples, ^{40}Ar-^{39}Ar ages 2-62667
marine sediments, dating by gamma ray spectrometry 2-57854
metamorphosed belt-series sediments, discordant radiometric ages 2-61999
meteorite Kiffa, exposition age determ. 2-55153
mica pairs, coexisting, K-Ar ages 2-62001
Mountsche Toundra Pluton, USSR, secular evolution limits of ^{87}Sr/^{86}Sr in mantle 2-62000
paragneisses, polymetamorphic and anatectic, zircon ages interpret. 2-61998
Precambrian rocks, Northern New Mexico, Rb-Sr geochronology 2-61995
S. Kenya, K/Ar determinations on rift volcanics 2-61993
sylvite from W. Germany, K-Ca age determ. 2-81638
techniques, biological applic., book 2-73177
thermoluminescence, of pottery circumventing natural radioactivity problem 2-84763
thermoluminescent dating of objects at Riso, 4000 B.C.-A.D. 1600 2-84762
thermoluminescent dating of pottery, predose method 2-84761
thermoluminescent dating of pottery, subtraction method 2-84760
volcanics of Southern High Plains, K-Ar dates and nature 2-62003
zircon U-Pb and whole rock Rb-Sr age lowering during metamorphism of Grenville Province 2-61996
^{40}Ar^{40}/^{39}Ar stepwise degassing technique, reappraisal 2-57806
^{14}C dating method employing emulsion 2-75438
^{14}C dating studies, report 2-63954
K/Ar data rel. to origin of feldspar megacrysts in alkali basalt 2-54729
K-Ar, origin of Hawaiian Ridge 2-57725
K-Ar ages, volcanic stratigraphy and geomagnetic polarity in Canary Islands, Tenerife, La Palma and Hierro 2-78220
K-Ar ages in Norwegian Caledonides, excess radiogenic Ar in metamorphis amphibotes and biotites 2-44601
K-Ar ages of feldspar megacrysts in basalt 2-61992
K-Ar ages of Gauss-Matuyama boundary 2-44600
K-Ar ages of pliocene volcanic rocks 2-57809
K-Ar ages of zenoliths from Tahiti 2-57808
K-Ar dating, orifice correction 2-59959
Rb-Sr ages of Middle Marker Horizon of Onverwacht Group 2-44599
Rb-Sr geochronolgy data, use of two-error linear regression treatments 2-61994
^{87}Sr/^{86}Sr, basalts from Nunivak Island 2-57807
^{87}Sr/^{86}Sr, det. of evolution of mantle beneath S. Pacific Basin 2-57730
U-Th-Pb ages of lunar rocks, discrepancies 2-44907

Radioactive tracers
application to determ. of Ag monolayers on Pt 2-71302
diffusion in solids, coeffs. calc. method 2-56749
electrolytic iodination of human serum albumin at alkaline pH 2-55213
helical scanning, computerized, location of radionuclides in human body 2-76099
insoluble monolayer leakage across movable barriers, radiotracer detection method 2-53416
lung scanning, ^{113m}In albumin aggregates 2-55251
material movement analysis, B tracer technique 2-65421
medicine, review 2-66253

Radioactive tracers continued
permeability meas. tech., applic. to H_2O vapour in coatings 2-80757
regional organ blood flow, mathematical model 2-78637
self-diffusion in Au films, $T<200$°C 2-56751
semiconductor surface contamination, quantitative assessment 2-54113
^{7}Be form. cross sections in ^{16}O by 135 and 550 MeV protons, radiochem. meas. 2-82961
^{10}Be form. cross sections in ^{16}O by 135 and 550 MeV protons, radiochem. meas. 2-82961
^{14}C labelled organic vapours, self-diffusion through polymer membrane obs. using radio tracer technique 2-71180
^{75}Se-selenourea, preparation 2-54527

Radioactivity
see also Alpha-particles; Atmosphere/radioactivity; Beta-decay theory;Beta-rays; Chemical effects of radiations/ionizing radiations; Fallout; Gamma-rays; Geophysical prospecting; Nuclear decay theory; Nuclear bombardment targets; Nuclear excitation; Nuclear reactions and scattering; Radiochemistry
α-decay of even-even nuclei $174 \leqslant A \leqslant 232$, absolute probabilities and superfluidity 2-82931
aeroradioactivity survey of Liberia, West Africa 2-78294
atomic recoil following alpha-decay, low energy electron spectrometry, book 2-41925
background radiation in USA, meas. with CaF_2:Dy thermoluminescent dosimeters 2-84859
Colorado, New Mexico, Texas, Utah and Wyoming, radioactive heat prod. 2-57486
decay curves, applic. of least squares method to anal. 2-63842
earth, induced by high energy electrons 2-52888
fractionation effect of fallout due to test explosion 2-79819
impact of advances in instrumentation 2-74044
muon capture reaction search, Cu(μ^-, e^+)Co 2-82935
natural, in soil, γ-spectroscopic obs. 2-72690
natural heavy nuclei, spontaneous α emission 2-52773
North Pacific Ocean, horizontal and vertical distributions of radionuclides 2-65598
odd-A nuclei, alpha intensities to rotational bands 2-49760
protection standards, German regulations 2-45040
recoil atom penetration into crysts., channelling pattern recording 2-54088
snow water equivalent meas. using attenuation of natural γ radiation emission from soil 2-54742
superheavy nuclei, half-lives calc. 2-76816
tracer field expts, stereo magnetic tape system 2-61987
$Z=59$ to 69, Q-values for α and β- decays 2-52743
α decay, influence of chemical environment 2-59728
α source plane, microstructure of dose 2-85134
β-decay of ^{235}U, ^{239}Pu fission fragments produced by thermal neutrons, bremsstrahlung, recoil radiation from 2-63843
γ-rays, computer code for searching attributions 2-82859
^{28}Al, n.m.r. from beta decay asymmetry 2-42500
AmO_2, thermal cond., self-irrad. effects 2-54078
^{74}As, decay to ^{74}Ge and ^{74}Se, energy level studies 2-49765
^{200}Au, beta-decay 2-79774
^{201}Au→^{201}Hg decay, low-lying levels of ^{201}Hg 2-63832
^{12}B→^{12}C 4.44 MeV excited states, β-γ coincidence meas. 2-82927
Bi neutron-deficient isotopes, α-decay parameters 2-76822
^{205}Bi→^{205}Pb decay, level scheme of ^{205}Pb 2-82928
β-source radiation dosages assessment 2-56073
^{9}C, β-delayed proton decay 2-63844
^{45}Ca in solid Xe, β-decay, optical excitation of the daughter atoms Sc. 2-84244
^{117}Cd and ^{117}Cd^{m} decay, energy levels of ^{117}In 2-76819
^{141}Ce, longitudinal polarization of β-particles 2-82933
^{36}Cl activity in meteorite 2-59753
^{38}Cl, n.m.r. from beta decay asymmetry 2-42500
^{54}Co→^{57}Fe in Xe, Mossbauer studies of ^{57}Fe atom 2-46426
^{58}Co, higher-order matrix elements in hindered-allowed β-decays 2-82921
^{60}Co, intensity ratio of 2158 keV and 2505 keV γ-rays 2-76811
^{60}Co source strength meas. using scintillation detectors and γ-γ coincidence, student expt. 2-78738
^{131}Cs decay, gamma gamma directional correl. meas. 2-46197
^{133}Cs, internal conversion electron studies 2-70422
^{137}Cs fallout in reservoir sediment 2-57802
^{153}Dy→^{153}Tb and ^{155}Dy→^{153}Tb decay, conversion electron data analysis 2-70421
^{158}Er→^{158}Ho and ^{161}Er→^{161}Ho decay, conversion electron data analysis 2-70421
^{152}Eu, decay to ^{152}Sm, monoenergetic positon line and positon distributions 2-52783
^{155}Eu→^{155}Gd, as source of X-radiation for subshell fluoresc. yield meas. on Gd 2-70581
^{152m}Eu→^{152}Sm decay, level scheme 2-59730
^{227}Fr isotope obs. in proton reactions on U 2-82925
^{228}Fr isotope obs. in proton reactions on U 2-82925
^{64}Ga ground state, isospin impurity 2-79771
^{154}Gd, internal conversion electron studies 2-70422
^{154}Gd, γ-transitions, angular correlation measurements 2-82919
^{160}Gd, neutron irrad., radiation characts. of ^{157}Sm 2-76820
^{64}Ge, β-decay systematics 2-55963
^{3}H, beta decay 2-67193
^{177m}Hf and ^{178m}Hf, γ-ray spectroscopic obs. using He jet recoil transport method 2-70290
$Hg \rightarrow Pt + p + e^+$, statistical calculation of p intensities, branching ratios to final levels and approx. spectral shapes 2-46194
^{181}Hg→^{180}Pt(158 keV state) coincidences between γ-rays and β-delayed protons 2-46193
^{203}Hg, nuclear matrix elements in first-forbidden beta-decay 2-46204
^{155}Ho→^{155}Dy decay, level scheme for ^{155}Dy 2-59716
^{131}I behaviour in types of soil found in Czechoslovakia 2-57804
^{116}In, n.m.r. from beta decay asymmetry 2-42500
^{124}In→^{124}Sn decay, E2-E1 transitions, energy levels 2-42520
^{187}Ir decay, investigation of ^{187}Os level structure 2-55966
K, drill core scanning by gamma-ray spectrometry 2-78293
^{36}K, decay props. from ^{36}Ar(p,n) and ^{36}Ar(^{3}He,t) 2-70387
^{36}K→^{36}Ar positron decay, excitation function, γ transitions 2-76817
^{48}K isotope obs. in proton reactions on U 2-82925

Radioactivity continued
^{49}K isotope obs. in proton reactions on U 2−82925
^{50}K isotope obs. in proton reactions on U 2−82925
^{73}Kr → ^{71}Se + p + e^{+}, beta-delayed proton emission obs. proton separation and electron capture energies 2−46187
^{131}La → ^{131}Ba and ^{132m}La → ^{132}Ba decay, conversion electron data analysis 2−70421
^{138}La decay obs. 2−46198
^{180}Lu, β- decay and half life 2−52786
Λ^{12}C → ^{1}H + Λ^{11}B, unstable resonant state of ^{12}C obs. 2−79732
Mg isotope during, rel. to properties of low lying levels of even mass Pt nuclei 2−49755
^{54}Mn, meas. of activity in source 2−55974
^{56}Mn, higher-order matrix elements in hindered-allowed β-decays 2−82921
^{101}Mo → ^{101}Tc β decay, low-energy transitions in ^{101}Tc 2−59705
^{101}Mo → ^{101}Tc decay, γ-ray spectra, energy levels of ^{101}Tc 2−74051
^{12}N → ^{12}C 4.44 MeV excited state, β-γ coincidence meas. 2−82927
^{16}N to high energy gamma-rays appl. in reactor shielding studies 2−46395
^{17}N → ^{17}O, energy distrib. of delayed neutrons 2−67194
^{20}Na, β^{+}-decay, anomalous fermi strength and minimum symmetry 2−59729
^{22}Na, higher-order matrix elements in hindered-allowed β-decays 2−82921
^{33}Na isotope obs. in proton reactions on U 2−82925
^{61}Ni, excited by (d,d') scatt., competition between gamma emission and neutron decay de-excitation process 2−70466
^{63}Ni, disintegration rate by 4π counting 2−79672
^{65}Ni, beta decay and K electrons from internal ionization, summing-energy spectrum 2−46186
^{32}P, higher-order matrix elements in hindered-allowed β-decays 2−82921
^{35}P β-decay to excited states in ^{35}S 2−74014
^{35}P → ^{35}S β-decay, ^{35}S level obs. and element assignment 2−74049
Pb neutron-deficient isotopes, α-decay parameters 2−76822
^{101}Pb, internal conversion and γ-ray intensities 2−49770
^{144}Pm → ^{144}Nd decay, triple coincidence meas., time spectra analysis 2−63815
^{148}Pm, β-γ circular polarization correl. 2−42547
^{148}Pm → ^{148}Sm β-decay mechanism 2−42525
PuO$_2$, thermal cond., self-irrad. effects 2−54078
^{239}Pu absolute meas. of α-activity by low- geometry method 2−63853
^{240}Pu, alpha particle emission energy meas. 2−76823
Rn, α-decay, exponential decay law deviation 2−59727
Rn(A = 220, 222) activity and potential alpha energy in different air atmospheres 2−56078
^{222}Rn and ^{220}Rn exhalation from ground, technique for meas. 2−65565
^{46}Sc source strength meas. using scintillation detectors and γ-γ coincidence, student expt. 2−78738
^{90}Sr, Great Lakes, sediments, diffusional transport 2−65564
T activity in ground and surface water, apparatus for obs. 2−72688
^{178}Ta → ^{178}Hf decay, γ-ray intensities and branchings in ^{178}Hf 2−76803
^{181}Ta, internal conversion electron studies 2−70422
^{182}Ta, higher-order matrix elements in hindered-allowed β-decays 2−82921
^{93}Tc β-decay, coincidence obs. of ^{93}Mo γ-decay 2−63805
^{101}Tc → ^{101}Ru decay, γ-ray spectra, energy levels of ^{101}Ru 2−74051
Th, drill core scanning by gamma-ray spectrometry 2−78293
Th daughter products, rel. to alpha spectroscopy, applic. to nuclear chemistry teaching 2−62931
^{228}Th radioactive decay simulations rel. to use of ThO$_2$ as theionic conversion heat source 2−52787
^{204}Tl, β-decay, internal bremsstrahlung spectral distrib. 2−42549
^{204}Tl, K-shell internal ionization accompanying β-decay, obs. 2−63850
^{165}Tm, level det. of ^{165}Er from decay 2−63821
^{170}Tm decay, first forbidden beta matrix elements 2−42548
U, drill core scanning by gamma-ray spectrometry 2−78293
U economic geology, radioactive series disequilibrium 2−61871
U fission products, behaviour in types of soil found in Czechoslovakia 2−57804
U well logging, pulsed neutron method 2−44598
^{232}U, alpha particle emission energy meas. 2−76823
^{236}U, specific activity 2−46206
^{188}W → ^{188}Re, forbidden $0^{+}\to 0^{+}$ β transition, quantitative interpretation 2−59731
Xe → Te + p + e^{+}, statistical calculation of p intensities, branching ratios to final levels and approx. spectral shapes 2−46194
^{115}Xe and neighbouring region, shell-model calc. of β^{+} strength 2−82922
^{115}Xe → ^{114}Te(709 keV state), coincidences between γ-rays and β-delayed protons 2−46193
^{117}Xe → ^{116}Te(679 keV state) coincidences between γ-rays and β-delayed protons 2−46193
^{90}Y, internal bremsstrahlung spectrum, contrib. of detour transitions 2−42542
Zn, A = 73, 74, decay characteristics, half-lives and Q-values 2−79746
dating *see Radioactive dating*
decay periods
beta decay, half-lives of exotic nuclei 2−79724
digital corrector for multichannel counting of short- and medium-lived nucleides 2−70284
half-lives of ^{33}P, ^{57}Co, ^{67}Cu, ^{85}Sr, ^{89}Sr, ^{113}Sn, ^{134}Cs, ^{192}Ir 2−52775
neutron, beta decay half life meas. 2−46006
odd nuclei, non-axial, β-transitions calcs. 2−55973
radionuclides, half-life determination 2−55972
α decay probability, half-lives and shell effect 2−79775
$^{143(m+g)}$Sm 2−46200
^{a}Cs, A = 117-120, half-lives determ. using on-line isotope separator techniques 2−42545
^{a}Ho, A = 164m, 164g, meas. of half-lives 2−52785
^{a}Sb, A = 110, 111, produced by (p,2n) and (p,3n) reactions on ^{112}Sn, meas. of half lives 2−46191
^{a}Sn, A = 129-132, half-lives determ. from X- and γ-ray emissions 2−46196

Radioactivity continued
decay periods continued
^{217}Ac, lifetime by in-beam α-spectroscopy 2−67199
^{240}Am electron capture decay, determ. of half-life 2−79770
^{241}Am, half-life determ. from metal sample using adiabatic microcalorimetric method 2−52789
^{34}Ar, Fermi β decay, mirror asymmetry 2−79772
^{36}Ar half-life determ. from position activity following ^{36}Ar(p,n)^{36}K reaction 2−70387
^{12}B, half-life determ. by Cerenkov counter and activation anal. 2−51488
^{10}Be, half-life meas. 2−63845
^{206}Bi, half-life decay times, int. conv. spectra and excitation functions detn. 2−67195
^{204m}Bi, half-life decay times, int. conv. spectra and excitation functions detn. 2−67195
^{96}Br → ^{86}Kr, average half-life determ. from direct measurement of half-life of transitions 2−46188
^{80g}Br, half-life determ. 2−70418
^{11}C 20.4 min, activity meas. 2−82969
^{113m}Cd, 14.6 ± 0.5 year half-life, decay data analyzed by least squares programme 2−46192
^{144}Ce, biological half-life in human chest determ. from in vivo meas. following accidental inhalation 2−55233
^{53m}Co, proton radioactivity, partial half-life determination 2−52776
^{141}Cs, direct meas. of half-life and gamma-ray energies 2−76812
^{64}Cu life-time variation and chemical state of (n, γ) recoil copper in α copper phtalocyanine crystals 2−72586
^{173}Er, 1.4 min beta decay 2−46202
^{78}Ga half-life, γ-ray energies and intensities 2−76814
^{64}Ge, attempted separation and half-life meas. 2−49766
^{79}Ge half-life, γ-ray energies and intensities 2−76814
^{80}Ge half-life, γ-ray energies and intensities 2−76814
^{81}Ge half-life, γ-ray energies and intensities 2−76814
^{82}Ge half-life, γ-ray energies and intensities 2−76814
^{83}Ge half-life, γ-ray energies and intensities 2−76814
^{84}Ge half-life, γ-ray energies and intensities 2−76814
Hf neutron deficient isotopes studied in ^{167}Hf-^{167}Lu-^{167}Yb decay chain 2−49771
^{164}Ho, 36.7 min half-life for isomeric state 2−46201
^{126}I, half-life measurement 2−52780
^{194}Ir → ^{194}Pt, half-life meas. 2−59732
Lu neutron deficient isotopes studied in ^{167}Hf-^{167}Lu^{167}Yb decay chain 2−49771
^{22}Mg, Fermi β decay, mirror asymmetry 2−79772
^{58}Mn 2−46290
^{32}Na half-life meas. after prod. in proton reactions on U 2−82925
^{18}Ne, Fermi β decay, mirror asymmetry 2−79772
^{236}Np long-lived isomer, determ. of partial negation half-life from growth of ^{235}Pu daughter 2−52788
^{14}O, half-life, beta decay coupling constant 2−74048
^{170}Os, alpha decay props. 2−49772
^{171}Os, alpha decay props. 2−49772
^{209}Pb, half-life of first forbidden beta decay 2−46205
^{142m}Pm, half-life decay times, int. conv. spectra and excitation functions detn. 2−67195
^{216}Ra, lifetime by in-beam α-spectroscopy 2−67199
^{214m}Ra, produced in (^{12}C, xn) reactions, meas. of half-life 2−55970
^{78}Rb, precision meas. of half-life, gamma transition energies 2−52778
^{78}Rb identification as source of 19 m activity following production of Rb and Sr isotopes 2−54563
^{83}Rb, half-life determ. 2−70419
^{87}Rb, half-life redetermined 2−46189
^{92}Ru, new neutron-deficient isotope, determ. of half-life 2−76813
^{92}Ru, separation and half-life meas. 2−49766
^{128}Sb isomers, half-lives 2−83036
^{129}Sb, half-life meas. 2−83036
^{130}Sb isomers, half-lives 2−83036
^{26}Si, Fermi β decay, mirror asymmetry 2−79772
^{140}Sm 2−46200
^{142}Sm 2−46200
^{141m}Sm 2−46200
^{129}Sn isomers, half-lives 2−83036
^{130}Sn, half-life meas. 2−83036
^{132}Sn doubly closed shell nucleus, β-decay, half-life determ. 2−82923
^{132}Sn half-life determ. following production in thermal neutron fission of $^{235,\,233}$U 2−52831
^{99}Tc, effect of high hydrostatic pressure (100 kbar) on decay constant 2−46190
^{206}Tl β-decay, half-life determ. 2−63851
^{236}U, half-life 2−46206
^{88m}Y, half-life decay times, int. conv. spectra and excitation functions detn. 2−67195
^{162}Yb, half-life and γ-ray spectra 2−67197
decay schemes
actinides, alpha decay and pairing vibrations 2−42540
exotic nuclei, prediction of new decay modes 2−79724
Pb (A = 202m, 204m), even-even isomers 2−49773
short-lived activities produced in (n,γ) reactions, automatic irradiation apparatus with on-line mass system 2−79639
α decay probability, shell effect 2−79775
^{113*}Tn (100 min) decay, internal conversion, M4, E5 character 2−74052
$^{143(m+g)}$Sm, positron emission and γ-transitions 2−46200
$^{93g+m}$Ru, produced by ^{92}Mo(^{3}He, xn), obs. of γ transitions 2−49768
^{a}Eu → ^{a}Gd, A = 156, 158, obs. of band mixing in ^{156,158}Gd 2−52766
^{a}Ho, A = 164m, 164g, decay to ^{164}Dy and ^{164}Er, meas. of energies and relative intensities of γ-rays and X-rays 2−52785
^{a}Sb, A = 110-114, production and decay constants of γ transition, β-γ, γ-γ coincidence meas. β spectra and point meas. 2−46191
^{110}Ag, study of γ-transitions to elucidate low-spin excited states in ^{110}Cd, determ. of log ft values of β decays 2−74035
^{24}Al → ^{24}Mg, investigation of energy levels in ^{24}Mg 2−52774
^{41}Ar → ^{41}K β-decay, study of nonconservation of P-parity in γ-decay of ^{41}K 2−49739
^{71}As → ^{71}Ge, γ-spectrum analysis 2−63848
^{81}As, partial scheme 2−76814
^{82}As, partial scheme 2−76814

Radioactivity continued
decay schemes continued
^{198}Au beta spectral shape, precision analysis 2−67198
^{198}Bi$\rightarrow$^{198}Pb, ^{200}Bi$\rightarrow$^{200}Pb, γ-ray and conversion electron spectra 2−46174
^{206}Bi, conveion-electron spectra, study of level structure of ^{206}Pb 2−70413
^{207}Bi electron capture-to-positron ratio 2−82930
^{78}Br, meas. of γ-ray spectrum following decay 2−74050
^{96}Br$\rightarrow$^{86}Kr, Ge(bi) detectors, assignment of transitions through half-life comparisons 2−46188
^{10}C$\rightarrow$^{10}B(2155 keV) β branch strength 2−46185
^{249}Cf$\rightarrow$^{245}Cm, γ decay, obs. of γ-γ coincidences, determ. total conversion coeff. of 54.7 and 66.7 keV transitions in first rotational band 2−52772
^{60}Co, weak intensities transitions of ^{60}Ni 2−52777
^{53m}Co, proton radioactivity, ratio of direct decay to ^{52}Fe* rel. to decay to ^{52}Fe 2−52776
^{122}Cs, positron decay 2−74037
^{124}Cs$\rightarrow$^{124}Xe, positron decay 2−74037
^{134}Cs β-decay, meas. of directional correlations of ^{134}Ba γ-rays 2−70404
^{134}Cs$\rightarrow$^{134}Ba, meas. of γ-γ coincidences 2−52781
^{137}Cs, internal bremsstrahlung spectrum of unique β-transition 2−82932
^{60}Cu(II) β^{+} decay, analysis of γ transitions between levels populated in ^{60}Ni 2−63846
^{173}Er, 1.4 min beta decay 2−46202
^{156}Eu$\rightarrow$^{156}Gd, from single and γ-γ coincidence meas. 2−49751
^{158}Eu$\rightarrow$^{158}Gd, from single and γ-γ coincidence meas. 2−49751
^{59}Fe$\rightarrow$^{59}Co β-decay, determ. of coincident intensity ratio for γ-rays and X-rays from K-electron conversion 2−79769
^{65}Ga, β-decay 2−63847
^{65}Ga, disintegration to ^{65}Zn, level scheme, γ-ray spectrum 2−49764
^{81}Ge, partial scheme 2−76814
^{3}H β-activity meas. for determ. of cross-sections of (n,t) reactions with 14 MeV neutrons 2−67257
^{5}He decay into $\alpha + n$ in spontaneous fission of ^{252}Cf 2−74125
^{8}He, evidence of production and subsequent disintegration in K^{-} interactions with nuclear emulsion nuclei 2−52736
Hf neutron deficient isotopes studied in ^{167}Hf-^{167}Lu-^{167}Yb decay chain 2−49771
^{173}Hf$\rightarrow$^{173}Lu, obs. of isomeric E1 transitions with $\Delta K = 0$ and lifetimes of states in ^{173}Lu 2−63823
^{164}Ho beta and electron capture, gamma and X-ray meas. 2−46201
^{126}I$\rightarrow$^{126}Te,^{126}Xe, energies and intensities of γ-rays meas. using Ge(Li) spectrometer 2−52780
^{107}In, β^{+}/EC decay, study of level scheme of ^{107}Cd by obs. of γ-rays 2−82934
^{112}In, 1+ ground state, beta decay 2−42544
^{112}In, study of γ-transitions to elucidate low-spin excited states in ^{112}Cd, determ. of log ft values of β decays 2−74035
^{192}Ir, γ-ray spectra, K-shell internal conversion coeffs. 2−70423
^{92}Kr, gamma ray study following beta decay 2−49767
^{92}Kr, γ-ray levels 2−70399
Lu neutron deficient isotopes studied in ^{167}Hf-^{167}Lu^{167}Yb decay chain 2−49771
^{24}Na, log ft values for second forbidden β-transitions 2−49762
^{97}Nb, γ-ray obs. 2−42543
^{23}Ne β-decay to levels in ^{23}Ne, meas. of γ radiation 2−79773
^{232}Np, determ. by gamma spectroscopy 2−82929
^{239}Np, polarized in ZrFe$_2$, γ-decay to levels of ^{239}Pu 2−46207
^{193}Os$\rightarrow$^{193}Ir, $+\beta$, energies and intensities of internal conversion lines 2−46173
^{28}P$\rightarrow$^{28}Si, investigation of energy levels in ^{28}Si 2−52774
^{230}Pa$\rightarrow$^{230}Th meas. of γ and electron singles-spectra and γ-γ coincidences, study of bands in ^{230}Th 2−70416
^{144}Pm$\rightarrow$^{144}Nd, electron capture decay obs. 2−67196
^{203}Po, internal conversion coeff. used to determine transition multipolarities 2−49774
^{205}Po, internal conversion coeff. used to determine transition multipolarities 2−49774
^{135}Pr$\rightarrow$^{135}Ce, excited states of ^{135}Ce 2−52782
^{224}Ra, ^{226}Ra, analysis of γ spectra in non-equilibrium with decay products, application to retention in mice 2−58615
^{224}Ra α decay, study of hyperfine interactions when implanted in Fe, Al, Cd, Bi, α-γ correlation meas. 2−81341
^{214m}Ra, photon spectrum, assignment of multipolarities, production in (^{12}C, xn) reactions 2−55970
^{92}Rb, gamma ray study following beta decay 2−49767
^{92}Rb, γ-ray levels 2−70399
^{190}Re, implications of allowed unhindered 3 min-β decay 2−46203
^{99}Rh$\rightarrow$^{99}Ru, new gamma-ray energy of 910.8 KeV 2−79740
^{101}Rh, levels with spin-parity assignments 2−49770
^{220}Rn α decay, study of hyperfine interactions when implanted in Fe, Al, Cd, Bi, α-γ correlation meas. 2−81341
^{222}Rn and daughters, detection of α-decay particles by triacetate cellulose foils for exposure evaluation 2−58618
^{92}Ru, 3.6 min produced by ^{92}Mo(^{3}He,xn), obs. of new weak γ transitions 2−49768
^{92}Ru$\rightarrow$^{92}Tc, new neutron- deficient isotope, meas. of energies and relative intensities of γ-rays 2−76813
^{110}Sb$\rightarrow$^{110}Sn, following Sn(p, xn) reactions 2−76818
^{111}Sb$\rightarrow$^{111}Sn, following Sn(p, xn) reactions 2−76818
^{112}Sb$\rightarrow$^{112}Sn, following Sn(p, xn) reactions 2−76818
^{113}Sb$\rightarrow$^{113}Sn, following Sn(p, xn) reactions 2−76818
^{114}Sb$\rightarrow$^{114}Sn, following Sn(p, xn) reactions 2−76818
^{125}Sb$\rightarrow$^{125}Te, γ:γ directional correlation expts. concerning negative and positive parity levels 2−46195
^{134}Sb β-decay to two-proton and proton-neutron states in doubly closed shell ^{132}Sn region 2−82895
^{78}Se, low lying levels, from ^{77}Se(n,γ) using thermal n 2−52779
^{140}Sm, positron emission and γ-transitions 2−46200
^{142}Sm, positron emission and γ-transitions 2−46200
^{141m}Sm, positron emission and γ-transitions 2−46200
^{132}Sn doubly closed shell nucleus, β-decay to proton-neutron-hole states in ^{132}Sb 2−82923
^{83}Sr, meas. of low-energy electron spectrum, obs. of 5.23 keV transition assigned to ^{83}Rb 2−55964
^{92}Sr, gamma ray study following beta decay 2−49767
^{92}Sr, γ-ray levels 2−70399
^{182}Ta, β- decay, population of K$^{\pi}$ = 2- octupole vibration band in ^{182}W 2−42533
^{154}Tb$\rightarrow$^{154}Gd, γ-ray, conversion electron and γ-γ coincidence spectra 2−52784
^{156}Tb$\rightarrow$^{156}Gd, study of levels in ^{156}Gd 2−46162
^{91}Tc, 3.2 min produced in ^{92}Mo(p,xn), obs. of γ transitions 2−49768
^{92}Tc, growth and decay of gamma-rays obs. following decay of ^{92}Ru neutron-deficient isotope 2−76813
^{99m}Tc, obs. of weak γ transition of 322 keV, determ. energy and intensity ratio to 140 keV transition 2−49769
^{227}Th, α-γ coincidence and directional correlation studies 2−63852
^{227}Th$\rightarrow$^{223}Ra, α-γ coincidence and directional correlation studies 2−49776
^{206}Tl β-decay, meas. of spectral shape and nuclear matrix elements 2−63851
^{138}Xe fission product, β- and γ-decay study using ARIEL on-line isotope separator, meas. of internal conversion and Auger L spectra 2−82924
^{97}Zr, γ-ray obs. 2−42543

electron capture
anticoincidence installation for internal counting counter 2−82814
polarized nuclei, ang. distrib. of K-electrons ejected during K-capture 2−64027
superheavy nuclei, half-lives calc. 2−76816
^{239}Am decaying to ^{239}Pu, study of levels in ^{239}Am 2−46179
^{240}Am$\rightarrow$^{240}Pu decay, meas. of γ-ray and conversion electron spectra, determ. of conversion coeffs. and multipolarities 2−79770
^{210}At$\rightarrow$^{210}Po, energy level studies in ^{210}Po 2−63836
^{7}Be$\rightarrow$^{7}Li radiative transition to first excited state, meas. of continuous photon spectrum 2−46184
^{207}Bi electron capture-to-position ratio 2−82930
^{109}Cd, mass spectrometer meas. of charge state of ions 2−79884
Co complex, diarsine complexes, Mossbauer emission spectra, after effects of electron capture decay 2−65233
Co complex, diarsine complexes, Mossbauer absorption spectra, after effects of electron capture decay 2−65232
^{131}Cs decay, double K-shell ionization 2−64028
^{64}Cu decay rate in α copper phtalocyanine crystals, comparison with rate for (n, γ) recoil copper 2−72586
^{161}Er$\rightarrow$^{161}Ho decay, level scheme of ^{161}Ho 2−76815
^{163}Er decay, determ. of ^{163}Ho level scheme from γ-radiation obs. 2−63820
^{185}Er decay, double K-shell ionization 2−64028
Fe complex, diarsine complexes, Mossbauer emission spectra, after effects of electron capture decay 2−65233
Fe complex, diarsine complexes, Mossbauer absorption spectra, after effects of electron capture decay 2−65232
^{55}Fe, orbital capture ratios 2−49763
^{164}Ho, gamma and X-ray meas. 2−46201
^{164g}Ho, branching ratio for electron capture decay to levels in ^{164}Dy 2−52785
^{73}Kr$\rightarrow$^{71}Se + p + e^{+}, beta-delayed proton emission obs. proton separation and electron capture energies 2−46187
^{170}Lu$\rightarrow$^{170}Yb decay, energy levels of ^{170}Yb 2−76821
^{140}Nd$\rightarrow$^{140}Pr, meas. of K-capture component, log β, energy of decay deduced 2−46199
^{19}Ne decay K electron capture/positron emission ratio 2−82926
^{235}Np, L-subshell fluorescence, Coster-Kronig yields 2−82918
^{185}Os decay, study of multipole mixing ratios of γ-transitions in ^{185}Re 2−67178
^{230}Pa$\rightarrow$^{230}Th decay meas. of γ and electron singles-spectra and γ-γ coincidences, study of bands in ^{230}Th 2−70416
^{144}Pm$\rightarrow$^{144}Nd, electron capture decay obs. 2−67196
^{143}Pr$\rightarrow$^{143}Nd, hindered $7/2^{+}\rightarrow 3/2^{-}$ decay 2−63849
^{211}Rn, decay to ^{211}At, energy levels 2−49775
^{169}Yb, energies and intensities of γ-rays, total internal conversion coeff. for 20.7 keV transition 2−79768

protection *see Radiation protection*

Radioactivity measurement
see also Dosimetry; Radiation monitoring; and the specific radiation, e.g. Gamma rays
airborne contamination near nuclear power station, use of tacky cloth collectors 2−58010
decaying radioactive source, device for maintaining constant detector counting rate 2−79647
flow rate determ., rel. to u.s. and thermodynamic methods 2−83760
gamma ray fluctuations, giving local nucl. reactor power 2−83102
gases, standard unit 2−55971
labelled aerosols, specific radioactivity measurements rel. to particle size 2−53464
low-activity samples, techniques and apparatus for γ, X-, α- and β-emitters 2−82818
low-geometry method used for absolute meas . of ^{239}Pu α-activity 2−63853
lunar soil, spectrometric obs., search for ^{210}Po activity 2−44910
nuclide activity, proportional counter, movable insulator 2−82797
sampling and dilution problems in gravimetic and volumetric techniques 2−74045
spring-waters in Hungary, dose originating from consumption 2−58634
whole-body counters and thyroid monitor for meas. of internal contamination by γ emitters 2−58629
α-activity in air near ground, meas. method and results 2−84850
^{14}C exhalation analysis, design of acclimation room 2−58597
^{14}C exhalation radiometry using CO$_2$-counter 2−58619
^{134}Cs released to water basins, meas. of accumulation in bed sediment 2−57833
^{3}H exhalation analysis, design of acclimation room 2−58597
^{222}Rn exhalation analysis, design of acclimation room 2−58597
^{85}Sr released to water basins, meas. of accumulation in bed sediment 2−57833
^{90}Sr concentration in human bones, ratio of spongious/compact bone in relation to age and time 2−58594
^{65}Zn released to water basins, meas. of accumulation in bed sediment 2−57833

Radioactivity measurement continued
apparatus
see also Particle detectors
automated atmospheric Rn sampling system, critique 2−62283
digital dual window for gamma radioactive decay meas. 2−46032
lifetimes of levels, apparatus for meas. 10^{-9}-10^{-12} sec 2−82794
low-activity samples, techniques and apparatus for γ, X-, α- and β-emitters 2−82818
radiation monitor capable of simultaneous meas. of direction and intensity 2−52664
Radioastronomy
see also Cosmic radiations, radiofrequency; Sun/radiation, radiofrequency
absolute radio brightness temperatures in Southern Sky 2−69115
antenna feed, dual polarized, applic. 2−73156
aperture synthesis telescope at 30 MHz, preliminary results in Southern Hemisphere 2−62815
Arecibo Observatory, radio-radar telescope 2−48818
baseline determination problems in 21-cm. H line observations 2−55193
Cambridge 5 km radio telescope 2−81969
computer techniques for mapping radio sources and searching for pulsars 2−81976
Culgoora radioheliograph, multiple frequency operation 2−69186
data acquisition and control system for 46 m radio telescope 2−45009
east west australian baseline interferometer obs. at 2.3 GHz 2−69198
electro-optical processing, for radio telescope array 2−62813
extragalactic radiosources, weak intensity variations due to interstellar scintillations 2−58382
interferometer, 136/138 MHz using steerable antennas 2−52321
interferometer, for long baselines, description 2−81965
interferometer expts., between US and USSR, observations of galaxies 2−58566
interferometer on super-long base line, sensitivity, signal freq. depend. rel. to digital information processing 2−81970
Io controlled Jovian decametric radiation, variation of highest cutoff 2−55141
Jovian decametric pulse distribution 2−75858
Jupiter, radio wave bursts and interaction of Io with magnetosphere 2−66174
Jupiter decametric radiation, two-dimensional probability and flux from 1957 to 1970 obs. 2−75862
linear polarization reduction at 1415 MHz and results for North Polar Spur 2−58387
long coherence intercontinental interferometry for detection of fine structure in compact radio sources 2−62814
Mars atmosphere meas. with Mariners 6 and 7 2−48767
meteor trails, radiowave reflection and detectability of radio meteors 2−73096
meteorites, radiolocation instruments 2−69173
Milky Way, spiral structure, theoretical 21 cm. line profiles 2−58186
millimetre wavelengths, observations of 3C273 Venus and Jupiter 2−66184
Moon, high resolution mapping 2−75936
motor drives and guidance of small radio telescopes 2−85066
new astronomy, conference, March 1972, Bloemfontein, S. Africa 2−66071
Ootacamund radiotelescope, system design 2−78633
Orion nebula, optical and radio observations interstellar absorption 2−72986
PSR 1749-28, accurate position from lunar occultations 2−66132
radar astrometry techniques applied to planets 2−76043
radio interferometer at K_u-band 2−55197
radiointerferometry signal processing with positive constraint 2−55198
radiometeors, selectivity effect on distribution of orbital parameters 2−75922
radiotelescope 25W 378 MHz local oscillator 2−81959
radiotelescope array for synoptic interplanetary scintillation obs. 2−62726
reflection of circularly polarized ultrashort radiowaves from celestial bodies 2−55196
spectral lines and information on interstellar and galactic matter 2−66124
stellar interferometer 2−69200
submillimetre background radiation, limit on energy density 2−75822
submillimetre radio telescopes, compensation method of earth's atmosphere radiation 2−58565
Sun, high resolution mapping 2−75936
techniques and objectives 2−76047
Venus, radar image and brightness map of surface 2−78504
Venus, radar interferometric observations, mapping of reflectivity features 2−81944
Venusian lower atm., model based on high resolution obs. 2−75914
very long baseline interferometry, mapping of radiosources 2−58564
NaBr, localized modes for H^- centre, calc. 2−74963
Radiocarbon dating *see Radioactive dating*
Radiochemistry
see also Chemical analysis/radioactive; Chemical effects of radiations/ ionizing radiations; Radioactive tracers
β-nuclide radioactivity meas. using Si detector with partially depleted surface barrier 2−49673
alkyl radical reaction products, chem. induced dynamic nucl. polarization 2−81540
angular correlation for γ cascade from nucleus bound to asymmetric-top molecule in soln., effect of molecular shape and flexibility 2−51474
book on basic principles 2−48351
nuclear polarization, chemical and non-equilib. magnetization for reactions in mag. field 2−78203
radioactive waste, treatment using local minerals 2−83158
radionuclide prod. thin-target cross sections determ. 2−82970
teaching, alpha spectroscopy using Th daughter products 2−62931
trapping of H atoms and electrons in acid glass 2−81535
^{7}Be and ^{10}Be form. cross sections meas. 2−82961
^{80}Br + CH$_3$Br, H and halogen displacement factors, survival probability of products 2−84664

Radiochemistry continued
^{38}Cd + CH$_3$Cl, H and halogen displacement factors, survival probability of products 2−84664
Cs compounds, production by 660 MeV proton irradiation of radioactive Sb and Te 2−68817
^{64}Cu life-time variation and chemical state of (n, γ) recoil copper in α copper phtalocyanine crystals 2−72586
H atoms in γ-irrad. aqueous solns., dynamic electron polarization 2−78204
Rb, Sr isotopes production in 19 min activity assigned to ^{78}Rb isomeric states 2−54563
^{181}Ta, He-ion induced fission at 41 and 65 MeV, radiochemical study of fission fragment mass distribution and total cross section 2−79810
Radiography
see also Luminescent devices; X-ray tubes
absorbed exit dose from patient radiation exposure, film techniques 2−69413
air gap technique, effect on detail and contrast 2−69250
alloy solidification, growth morphology obs. 2−47605
alveolar bone mineral content, in vivo measurement, monoenergetic attenuation technique 2−69314
angiography using slit diaphragm process 2−62869
automatic exposures with use of image intensifier method 2−76087
autoradiography, techniques and applics. 2−76072
body composition, dual photon radionuclide absorptiometry 2−69294
bone mineral content, in vivo measurement, scanning radiology 2−69313
calcipenic osteopathy, X-ray densitometry, computer evaluation 2−69374
cameras for single and serial exposures from X-ray image intensifiers, medical applications 2−73202
cell functional morphology, electron autoradiography 2−81999
cell processes studied with microautoradiography 2−73165
cinedensigraphic equipment, technical principles 2−69352
cineradiography, eval. and selection of optimum factors 2−69253
clinical radiation therapy in vivo thermoluminescent dosimetry 2−69415
combined liver-lung scanning, subdiaphragmatic abscess 2−58610
composite materials, metal matrix, radiography, review 2−43768
conference (Newton, Mass., USA, July 1972) 2−76068
dental, processing system 2−66274
diagnostic, e.s. imaging methods 2−69369
diagnostic, use of monochromatic radiation 2−69370
diagnostic X-ray tubes, focal spot analogue for det. focal spot distribution effects on image 2−78656
diagnostic X-ray tubes, kV measurement 2−69350
ear, tomography 2−62874
electron autoradiography, monolayer prep. technique 2−80616
experimental radiographs using 160 MeV protons 2−73204
film detail evaluation, significance of light density 2−73695
fluoroscopic, image enhancement, multiple image subtraction technique 2−69368
gamma, applications of linear accelerators, and non-destructive testing 2−70325
glass, entroradiographic obs. of water 2−53517
gynecologic radiation therapy, dose distrib. by meas. and computer 2−69411
hepatic mass lesions, blood pool scanning 2−58608
Hodgkin's disease, isotope scanning using ^{67}Ga citrate 2−55246
holography, biomedical applications 2−78662
image quality assessment 2−59346
image quality obs., systems and techniques for noise and modulation transfer function meas. 2−76090
imaging system for diagnostic radiography using pulse compression techniques 2−51930
infusion choledochography 2−55254
intensifier with improved picture quality 2−62909
intracranial aneurysms, electronic technique 2−69373
isotope imaging and counting, comparison of scintillation and semiconductor detectors 2−49643
line spread function sampling distance choice for MTF computation of radiographic screen film systems 2−78654
liver tumour detection with ^{67}Ga-citrate and scintillation camera, computer scintigraphy 2−73198
lung scanning, ^{113m}In albumin aggregates 2−55251
lung tomographic techniques 2−55255
lung tomography techniques 2−45045
magnification, advantages 2−69251
magnification, validity of MTF 2−76557
metal intensifying screens, for X-rays 2−45198
model diagnostic system, dependence on photon energy and exposure of X-ray pattern from phantom 2−69383
n.d.t. of adhesive bonded metal-to-metal joints 2−47674
neuroradiology, comparison with cerebral scanning 2−48887
neutron, converter thickness for optimum intensity 2−73902
neutron, creep of irradiated specimens measurement 2−82593
neutron, detection of H in cellulose acetate 2−65408
neutron, development of ^{252}Cf as source 2−55890
neutron, edge-spread function 2−67073
neutron, for creep meas. of irradiated specimens 2−71621
neutron, image quality, modulation transfer function, effective focal spot 2−52493
neutron, inspection techniques 2−73694
neutron, irrad. fuel rod investigation 2−83098
neutron, nondestructive testing, technique and applications 2−52515
neutron, review 2−63712
neutron imaging, Gd-exposure, role of internal conversion electrons 2−59638
neutron induced, bone containing ^{239}Pu 2−78660
neutron radiography in non-destructive testing of plate assemblies 2−53846
nuclear medicine, computer analysis 2−69323
nuclear medicine, diagnostic image quality using scintillation and semiconductor detectors 2−49645
pancreas scanning after ten years' experience 2−76086
proton, density profile and porosity meas. 2−60930
quantum noise, granularity and detail perceptibility 2−76088
radiodiagnosis, analysis of risks 2−48881

Radiography continued
radiodiagnosis, protection, choice of dosemeter 2−48888
radiodiagnostic apparatus, technical aspect, protection 2−48882
radiological treatment planning, compensation for tissue heterogeneity and contours 2−69414
radiology, autoactivation of accelerated N and O nuclei 2−69295
radionuclides for evaluation of pancreas and exocrine function 2−76085
reactor fuel, irrad. damage obs. 2−52856
reactor fuel elements, irrad., radiograph prod. and automatic meas. 2−42659
reactor fuel elements, post-irrad. radiographical exam: techniques 2−42660
screen-film system, truncation errors in calc. MTF from line spread function 2−42234
skeletal health, computer assessment, scanning of radiographic image 2−69375
soft tissue, placental localization 2−48859
stillborn infants, abnormalities and death causes obs. 2−48858
teleradiology, remote interpretation of roentgenograms 2−76091
thermal-neutron, using sealed-tube neutron generator and water moderator 2−42691
three dimensional density reconstruction from series of two dimensional projections 2−49047
tomography, variable depth display, holographic methods 2−69371
transuranium elements, biological implication, conference, Washington (1971) 2−78658
transuranium elements, interactions with cells and tissues 2−78659
u.s. cross sectional echography, diagnosis 2−76371
video roentgenography system, acquisition of quantitative data 2−69372
X-ray, calc. object pattern rel. to image intensity distrib. 2−69252
X-ray and holography for materials research 2−69970
X-ray examination of lumbago-sciatica syndrome 2−55253
X-ray fluoroscopy, dose reduction, use of scanning beams 2−69445
^{67}Ga scintillography, detection of metastatic lung tumours 2−48886
^{3}H autoradiography, obs. of behaviour of gas atoms in neutron irradiated Al-Li alloys 2−44009
^{131}I rose bengal imaging, differential diagnosis of jaundiced patients 2−58611
Si(Li) semiconductor probe for semi-microscanning device 2−55250
(U,Pu)O$_2$ microspheres and pellets, sol-gel derived, microstructure studied by α autoradiography 2−47610

Radiolysis *see Chemical effects of radiations/ionizing radiations*

Radiometer gauges *see Vacuum gauges*

Radiosondes *see Meteorological instruments*

Radiosources
108 between −33° and +27°, improved positions, some identifications 2−69119
3 138, compact source, circular polarization 2−58403
absolute and CKL flux density scale ratio at 408 MHZ 2−85064
Algol, radio flares 2−75821
B2 1212+30, i.r. obs. 2−69123
B2 1215+30 optical variations 2−73045
B2 catalogue, 408 MHz observations 2−78480
binary systems, variable emission 2−58389
BL Lac, coordinated multiwavelength obs. of intraday variability 2−75812
BL Lac, photographic UBV obs. 2−75809
BL Lac, radio and optical activity 2−75810
BL Lac optical circular polarization, search 2−75800
blue, without u.v. excess, identification with stellar objects 2−81878
3C273, asymmetries in compact source at 2298 MHz 2−55093
3C279, asymmetries in compact source at 2298 MHz 2−55093
3C279, quasi-stellar, evidence for non-superrelativistic model 2−48739
3C279 evidence for non-superrelativistic model 2−48739
3C391, continuum spectrum, effect of interstellar gas 2−58390
5 C3, near M31 and NGC 205, positions and flux density obs. at 1415 MHz 2−69121
3C454.3, asymmetries in compact source at 2298 MHz 2−55093
5C4 in Coma Cluster, identification 2−48748
3C 120, coordinated multiwavelength obs. of intraday variability 2−75812
30C 120, rapid expansion at 3.8 cm wavlength 2−58400
3 C 220.2, optical identification as QSO69117 2−69117
3C 225, fine structure, identification of components 2−58385
3C 270, linear polarization at 21 cm. 2−58380
3 C 272.1 associated with M84 elliptical galaxy obs. at 2.7 and 5.0 GHz 58409 2−58409
3C 273, electrographic UBV photometry of jet 2−44899
3 C 273, flux emission density at 2 and 8 mm wavelengths 2−66184
3C 273, search for hard X-ray emission 2−58432
3C 279, interplanetary scintillations, obs. of electron density irregularity in solar wind 2−58552
3C 279 sources, Doppler effects and hypervelocities 2−78482
3C 345, photographic UBV obs. 2−75809
3C 390.3, high resolution obs. at 2.7 and 5 GHz 2−62612
3C 391, supernova remnant, nature of low frequency absorption at 31.4 GHz 2−55085
3C 452, linear polarization at 21 cm. 2−58380
4C catalogue, obs. at 408 MHz in the declination range 20° to 0° 2−48740
3C quasi-stellar objects, correlation between positions and bright galaxies 2−48742
4C sources, identification with galaxies 2−81786
circular polarization meas. at 1.4 and 5 GHz 2−55096
compact, fine structure obs. using long coherence intercontinental interferometry 2−62814
compact, search for circular polarization at 9 mm wavelength 2−62604
compact, spatially independent outburst 2−55086
compact extragalactic radio sources rel. to radio cloud pairs 2−78485
continuum radiation at 820 MHz between declinations -7° and +85° 2−62606
cosmic plasma radio emission 2−85015
cosmological evolution of those of large angular extent 2−69124
counts, predictions of simple cosmological models 2−62611

Radiosources continued
counts of intense extragalactic sources at 1400 MHZ 2−55091
Crab nebula rel. to neutron star models 2−75692
CTA26, asymmetries in compact source at 2298 MHz 2−55093
CTA 102, compact source, circular polarization 2−58403
Cyg A, galaxy, emission-line spectrum 2−66060
Cyg X-3, 8 GHz emission during radio flare, absence of linear polarization 2−81886
Cyg X-3, detection of variable radio emission 2−55088
Cyg. X-3, distance det. by 21 cm absorption 2−81881
Cyg X-3, obs. at 15.5 GHz during radio flare 2−81885
Cyg X-3, obs. at 2.8 cms with 17 arc s beam 2−81882
Cyg X-3, obs. of outburst at 8 GHz 2−85020
Cyg X-3, radio obs. and of surrounding region 2−85024
Cyg X-3, X-ray obs. at time of radio flare 2−81883
Cyg X-3, X-ray obs. by Uhuru during radio flare 2−85021
Cyg X-3 flare, limits to circular polarization at 2695 MHz 2−85019
Cyg X-3 obs. at 3.3 mm at time of radio flare 2−85022
Cyg X-3 outburst, absence of recombination line emission 2−81884
Cyg. X-3 outburst, obs. at 408 MHz and angular size 2−81880
Cyg X-3 radio outburst spectrum and polarization 2−85023
Cygnus, search for visible counterpart of radio outburst 2−81890
Cygnus A, testing of theories 2−58397
Cygnus Loop, brightness and polarization meas. at 6-cm. wavelength 2−69017
Cygnus region in 20 to 300 keV, X-ray survey 2−69130
Cygnus X-1, 1415 MHz obs. 2−55092
Cygnus X-3, flux density obs. during outburst, in MHZ range 2−81889
Cygnus X-3, large outburst 2−81874
Cygnus X-3, obs. during Sept. 18-25 1972, following major radio event 2−81892
Cygnus X-3, outburst of radio emission rel. to possible superrova precursor 2−73056
Cygnus X-3 giant radio outburst, flux density and polarization meas. 2−81875
Cygnus X-3 outburst, 21 cm. and 18 cm. obs. 2−81888
Cygnus X-3 radio outburst, radiation mechanism 2−81879
Cygnus X-3 unusual radio events 2−81876
dark interstellar dust clouds, 21 cm line obs. 2−81826
decametric emission, identification of extragalactic X-ray source 2−48757
diffuse interstellar medium, giant H II regions 2−66068
discrete, obs. of H$_2$CO molecule at 4830 MHz 2−69109
discrete flux density and spectra obs. at 2.7 and 5 GHz 2−75806
double, energy source for violent events, explosive phenomena, gas dynamics 2−81865
double, extragalactic, preferred orientation 2−85011
electron diffusion, energy distribution of relativistic electrons with synchrotron or Compton radiation 2−55083
extended, scintillation for finite bandwidth receiver case 2−73047
extragalactic, circularly polarized radiation 2−62601
extragalactic, emission mechanisms 2−48754
extragalactic, flux densities meas. at 111.5 to 606 MHz 2−69125
extragalactic, polarization structure 2−58402
extragalactic, radio maps at 2.7 and 5.0 GHz 2−48747
extragalactic, source counts and evolution 2−62600
extragalactic, weak intensity variations due to interstellar scintillation 2−58382
Faraday depolarization of extragalactic radio sources 2−73042
flat spectra, cosmological implications 2−48751
flux densities, accurate, at 5009 MHz, 1007 sources 2−75803
flux densities at 3.5 cm. wavelength of 130 discrete radiosources 2−51790
G296.8-0.3, supernova remnant, association with pulsar PSR 1154-62 2−55098
galactic H II regions, radio emission at 1400 MHz from 130 areas 2−58252
galactic radio sources at metre wavelength and the galactic disc radiation 2−81898
Galactic supernova remnants, non thermal emission 2−78452
galaxies, dynamics of multiple explosions 2−58401
galaxies, interferometer expts., between US and USSR 2−58566
galaxies, luminosity-spectral index relationship 2−78481
galaxies, quasars and unidentified objects, rotation measures 2−81871
galaxies, redshift values 2−66061
galaxies and quasars, activity, plasma MHD processes 2−58193
galaxies and quasars, role in observational cosmology 2−75804
galaxies with radio trails in clusters, rel. to interacting galaxies hypothesis 2−51711
gravitationally interacting galaxies 2−84958
grouping in area of NGC 7331 and Stephan's quintet 2−75807
HB 21 supernova remnant, obs. at 4170 MHz 2−55056
HB-21, Hα obs. of area, interferometry of faint nebula 2−81809
He 2-53 planetary nebula, 100 micron flux density 2−55087
Hoffman i.r. sources, OH emission 2−81870
IC 10 heavily obscured galaxy. 21 cm line study 2−44896
IC 443 supernova remnant, obs. at 1.42 GHz 2−58328
IC 443 supernova remnant, obs. at 4170 MHz 2−55056
identifiable with compact X-ray sources 2−62608
identification with Uhuru extragalactic X-ray sources 2−55105
II Zw 40, neutral H study of compact galaxy 2−81793
immediate neighbourhood of galaxy 2−69032
intense sources at 1400 MHz, flux densities, positions and structure 2−69120
intensity and phase fluctuations, applic. as remote sensing probe for solar wind 2−62781
interplanetary scintillation, power spectrum, solar wind obs. 2−66205
interplanetary scintillation, theoretical study of higher moments 2−85029
interplanetary scintillation of radiosources rel. to enhanced density irregularities of solar wind 2−85058
interplanetary scintillations, higher moments, structure of source and interplanetary medium 2−85028
intrinsic radiopower correlation with spectral index for radiogalaxies 2−44895
Jupiter, decametric radio emission rel. to Great Red Spot 2−81903

Radiosources continued
Jupiter decametric radiation, two-dimensional probability and flux from 1957 to 1970 obs. 2−75862
BL Lacertae, i.r. obs. 2−69123
APLib., i.r. obs. 2−69123
linear polarization at 7.2 cm 2−66133
linear polarization of those with appreciable red shift 2−58376
M31, obs. at 1415 MHz 2−69031
in M51, structure at 2695 MHz72973 2−72973
M81, search for hard X-ray emission 2−58432
M87, search for hard X-ray emission 2−58432
map of galactic centre region, high resolution and sensitivity at 15.5 GHz 2−75818
mapping using computer techniques 2−81976
masers, instellar scattering effects on apparent size 2−75787
in nearby spiral galaxies, classification of observed spectra 2−73049
NGC 1275, galaxy, gas ejection from nucleus 2−48664
NGC 2024, det. of HNC line 2−58360
NGC 253, obs. at 80 MHz 2−81795
NGC 4486, galaxy, gas ejection and nuclei activity obs. 2−84963
NGC 4486, galaxy, gas ejection from nucleus 2−48664
NGC 5055, periodic light pulsations in supernova outburst 2−75761
NGC 5128, galaxy gas ejection from nucleus 2−48664
in NGC 7331, large Sb spiral58406 2−58406
NGC 7538 H II region microwave spectroscopic mapping 2−75696
North Polar Spur, reduction of linear polarization at 1415 MHz 2−58387
NRAO 140, compact source, circular polarization 2−58403
NRAO interferometric position accuracies for point sources 2−58391
OG + 003, small-pitch-angle synchrotron radiation 2−58404
Ohio sky survey statistics 2−55097
Ohio survey, optical identifications 2−75805
Ohio Survey and Zwicky's list of compact galaxies 2−51787
OJ287, circular polarization obs. 2−58405
OJ 287, BL Lac type, compact extragalactic nonthermal, spectral and photometric obs. 2−51788
OJ 287, circular polarization of u.v. 2−81794
OJ 287, coordinated multiwavelength obs. of intraday variability 2−75812
OJ 287, flux density and polarization variation at 8 GHz 2−75811
OJ 287, i.r. obs. 2−69123
OJ 287, optical variations 2−75813
OJ 287, photographic UBV obs. 2−75809
OJ 287 optical circular polarization, search 2−75800
OK 237, optical variations 2−75813
ON 231 = W Comae, optical variations 2−73045
ON 231, BL Lac type, compact extragalactic nonthermal, spectral and photometric obs. 2−51788
ON 231, i.r. obs. 2−69123
ON 231, optical variations 2−75813
ON 325, BL Lac type, compact extragalactic nonthermal, spectral and photometric obs. 2−51788
optical identifications of radiosources in the B2 catalogue 2−62607
optical position meas. 2−81872
OQ + 003, small-pitch-angle synchrotron radiation 2−58404
OQ 208, optical variations 2−75813
Ori A, detection of SiO at 87 GHz 2−48745
Orion A, det. of HNC line 2−58360
Orion Nebula, 85α radio recombination line survey 2−58245
Orion Nebula, 85α recombination line survey 2−81797
Orion nebula, emission in water vapour line 2−75823
P1127-14, asymmetries in compact source at 2298 MHz 2−55093
P 1127-14, compact source, circular polarization 2−58403
Parkes 0237-23, small-pitch-angle synchrotron radiation 2−58404
partially ionized interstellar cloud, microwave observations 2−81807
β Persei, eclipsing spectroscopic binary 2−62614
β- Persei, radio flare55066 2−55066
PKS 0118 + 03, structure, identified with QSO 2−58383
PKS 1514-24, BL Lac type, compact extragalactic nonthermal, spectral and photometric obs. 2−51788
PKS 2053-20, structure, identified with elliptical galaxy 2−58383
PKS 2057-17, structure identified with elliptical galaxy 2−58383
PKS 2204-54, new identification as object with u.v. excess 2−69122
planetary nebulae catalogue, radio observations of total fluxes, morphology and spectra 2−44845
polarization meas. at 9.55 mm wavelength 2−55082
polarization of extragalactic sources and quasars at 49 and 73 cms 2−58412
position determination 2−81868
positions and brightness distributions by lunar occultation 2−66131
positions and flux densities at 408 MHz 2−58411
PSR 1749-28, accurate position from lunar occultations 2−66132
pulsars, nature of emission 2−85012
pulsing X-ray source in Hercules, radio search 2−62605
quasi-stellar, statistical assoc. with rich clusters of galaxies 2−62609
radio galaxies, evolution and source counts 2−62599
radiogalaxies and QSOs, spectral index- luminosity relation 2−48741
rapidly varying, fruitless search 2−58384
RCW 38, RCW 49, RCW 57(b), RCW 74, H II regions, absorption profiles, 21 cm H I obs. 2−84949
rotation measures, interpretation 2−62602
Sagittarius B_2 complex, recombination line study 2−75814
Scd galaxies, HI distributions and rotation curves from obs. at 21 cms. 2−62464
scintillation spectra rel. to small-scale irregularities in interplanetary plasma 2−58408
Sgr A, 6 cm search for furan and imidazole 2−48725
Sgr A, det. of HNC line 2−58360
Sgr A, lunar occultation obs. at 327 MHz 2−73046
Sgr B2, 6 cm search for furan and imidazole 2−48725
Sgr B2, detection of SiO at 87 GHz 2−48745
Sgr B2, possible sites of star formation 2−69068
small-diameter, positions and flux densities at 408 MHz 2−51786
in solar corona, rel. to streamer struct. 2−62806
Stephan's Quintet, radio continuum emission at 21 cm 2−81806
in Stephan's Quintet area, mapping 2−58406

Radiosources continued
Sun, flux density obs. at 350 MHz 2−81949
supernova remnants, galactic, absorption of 80 MHz emission by interstellar medium 2−69089
supernovae remnants, polarization and total power emission at 2700 MHz 2−58316
supernovae remnants at 11 c.m., high resolution obs. 2−75759
supernovae remnants at 80MHz, high resolution obs. 2−75758
survey, NRAO 5 GHz, 140 ft strong, intermediate and deep source surveys 2−44892
survey at Molonglo, discovery of 3 pulsars 2−48750
survey using band-width synthesis interferometer 2−58388
variability rel. to redshift, spectral type, physical size and optical variability 2−58398
variable, extragalactic, expanding source model 2−75819
variations, rapid, search at 2.8 cm 2−58399
VRO 42.22.01, compact source, circular polarization 2−58403
VRO sources, extended observations at 750, 1400 and 2700 MHz 2−81866
W22, W37, H II regions, absorption profiles, 21 cm H I obs. 2−84949
W33, formaldehyde absorption 2−81869
W3, 21cm, atomic H absorption profile, Cnα recombination line and radial velocity 2−44897
W3, det. of HNC line 2−58360
W3, det. of new i.r. sources 2−58417
W3 OH source, variability in 1665 MHz spectrum 2−58413
W49, emission in water vapour line 2−75823
W49 H_2O vapour microwave sources 2−69114
W51, C248α transition 2−75815
W 44 supernova remnant, formaldehyde absorption 2−84983
water vapour in galactic sources microwave radiation obs. rel. to maser mechanism 2−69016
water vapour microwave emitters, from IR stars, time variations 2−58416
H I velocity-longitude diagram for southern Milky Way 2−84984
H self absorption in large region toward galactic centre 2−44885
HI 21-cm. line observations, low emission regions and baseline determination problems 2−55193
OH, new emission sources classification 2−44894
OH i.r. stars, maser emission at 1612 MHz 2−81830
OH maser, astronomical, statistics of radiation 2−58368
PKS 1514-24, diameter of compact component 2−55094

Radiostars *see Radiosources*

Radiotelescopes *see Radioastronomy*

Radiowave propagation *see Electromagnetic wave propagation*

Radiowave spectra *see Nuclear magnetic resonance and relaxation; Paramagnetic resonance and relaxation; Spectra*

Radium
abundance in seawater in-situ analysis using synthetic fibres 2−75469
dose calculations for linear Ra sources, simplified method 2−69423
Ra-A aerosol, filtration of 0.001 μ particles by wire screens 2−85159
Ra Crowe nasopharyngeal applicators, dose distributions 2−69436
^{228}Ra profile at Geosecs II in North Atlantic 2−75477

Radium compounds
No entries

Radium emanation *see Radon*

Radon
— 2−69344
atmospheric conc. correl. with airborne continental dust 2−62158
atmospheric concentrations of daughters by α-spectrometric extrapolation method 2−75615
automated atmospheric Rn sampling system, critique 2−62283
daughters, atmospheric, analysis methods, comparison using computer simulation 2−62288
diffusion in lunar regolith, model using random walk method 2−44921
exhalation from ground 2−61988
short-lived isotopes, e.m. separation 2−70647
whole-body radioactivity monitor, effect of deposited Rn daughter products on background count rate 2−69421
^{222}Rn, atmospheric, vertical distrib. up to 6 km 2−51594
^{222}Rn and ^{220}Rn exhalation from ground, technique for meas. 2−65565
^{222}Rn and daughters, captive balloon measurements 2−68923

Rain
see also Condensation; Snow
— 2−72795
Arizona cloud-seeding experiment, re-evaluation 2−62239
artificial stimulation in aid of Yugoslav water resources 2−44718
atmospheric attenuation compensation analysis rel. to radar meas. of rain rate 2−75501
attenuation meas. at 10 GHz using ADA 2−54865
attenuation of 10.6 and 0.63 μm laser radiation in 2−75611
attenuation on slant-path at 10 GHz, radar-derived statistics 2−54867
British Isles, westerly type rainfall and atmospheric mean sea level pressure 2−54842
Central America, rainy pentad distributions 2−65744
charge size meas. in warm rain 2−65740
cloud nuclei from September 1970-August 1971, automated obs. in Australia 2−78373
crosspolarisation of linearly and circularly polarised waves at microwaves 2−48514
rel. to cumulonimbus, breaking billows 2−84854
cumulus cloud seeding during 1971 south Florida drought 2−62225
depth duration studies of long period rainfall in India 2−62229
drizzle drops, effect of fluctuations in vertical acceleration on coalescence growth 2−48491
drop size changes inferred from underwater noise 2−57979
drop size distribution determ. by radar, errors rel. to vertical air motion 2−75592
drop size distribution in Florida summer showers, simultaneous radar reflectivity and rainfall data 2−62214
drop size distributions using 35 GHz Doppler radar 2−75591
drop size rel. to drop impaction 2−65714
droplets, evaporating, maximum relaxation times 2−43302

Rain continued
drought in northeast Brazil rel. to Northern Hemisphere general circulation 2−84849
electrical conductivity rel. to Cl^- content 2−65741
elevation effects on rainfall, stochastic model 2−57985
erosion, model, effect on supersonic flight 2−43252
fall during tropical thunderstorms 2−65784
fall rate-attenuation relationship, variability 2−75597
forecasting yield of principal crops in India on basis of weather regression analysis 2−62108
formation of water droplets and ice crystals in deep cloud cover 2−68875
freezing of drops with different solutes and anomalous ice concentrations in clouds 2−54843
frontal, halo phenomena 2−84853
gauge, capacitor type, with d.c. output and improved flow characteristics 2−65650
gauge catch variation due to airflow disturbances around gauge 2−78246
groundwater fluctuations in Delhi in relation to rainfall, mass-scale study 2−62261
major rainstorms in Tapi basin, evaluation of design storm 2−62232
Markov chain model fitting for daily rainfall data at Calcutta 2−62226
monsoon conditions, active and weak, streamline charts 2−62180
monsoon disturbances, vertical tilt 2−78372
monsoon period in S.W. India, rainfall and floods 2−62230
monsoons of southern Asia, review 2−48485
multiple input dynamic stochastic model of rainfall evapotranspiration - runoff process 2−54845
one minute rainfall, storms coefficient of variation probabilities, geographical distribution 2−84824
Peninsular Spain rainfall obs. 2−65752
radar and raingauge meas. of precipitation in Welsh hilly region 2−75589
radar echo from light rain, spectrum shape at 3.2 centimetre wavelength 2−81658
radar obs. of anisotropy of media 2−62238
radar raingauge accuracy rel. to drop size distribution and rainstorm type 2−75593
radar raingauge system for accurate precipitation measurements 2−75594
radioactive fallout measurement, Melbourne, (1958-1970) 2−72814
rainbow, colour and intensity, inhomogeneities 2−44733
raindrop size spectra, det. of parameters affecting shape 2−65751
rainfall and runoff data, conceptual anal. with hybrid computer 2−78302
rainfall anomalies in randomized seeding project 2−62222
rainfall augmentation via warm rain process 2−62205
rainfall events in convective storms, Z-R relationship for radar estimates 2−75571
rainfall rate and drop size distributions, simultaneous meas. using radar and raingauges 2−75590
rainfall rate-radar reflectivity relationships for individual storms 2−48494
reflectivity-attenuation obs. at altitudes below, within and above melting layer 2−75584
representative station rel. to river Tiber upper catchment area 2−54803
return period of intense rainfall, estimation using Alexander's technique 2−62227
satellite data rel. to precipitation estimates for hydrologic applications 2−84869
scanning f.m.-CW radar sounder, for structure obs. 2−84842
shower formation by AgI seeding, related calculations 2−65749
spectra determination at cloud base from ground spectra 2−72794
stochastic model of daily winter rainfall in North Santa Clara Valley 2−54844
storm, release of Li trace into cloud base, correlation with rainfall 2−57986
Sudan, power spectra analysis 2−62241
summer rainfall and temp., prediction for England and Wales from springtime anomalous atmospheric circulation 2−75518
terminal fallspeeds of raindrops 2−75603
time-dependent rain drop size distributions model 2−57930
Venezuela rainy season, precipitation characteristics 2−62242
Venezuelan rainstorms, radar obs. 2−62243
watershed, probabilistic simulation model development from rainfall runoff records 2−57984
winter rainfall and temp. for England and Wales, foreshadowing 2−44681
^{141}Ce-^{144}Ce isotopic activity ratios 2−62289
^{103}Ru-^{106}Ru isotopic activity ratios 2−62289

Raman spectra *see Scattering/light, Raman spectra*

Ramsauer effect *see Electron beams; Electrons/absorption; Energy loss of particles*

Random functions *see Random processes*

Random processes
see also Brownian motion; Fluctuations; Statistical analysis
buffered data resolving system, dead-time losses 2−79644
counters, Poisson distributed events, errors 2−49615
dispersion of material in slowly moving fluids, stochastic process 2−46664
Fermi stochastic particle acceleration mechanism 2−52710
flow, compounding of transmission probabilities for composite systems 2−67578
generalized Langevin eqn. for projections of n-dimensional Gaussian-Markov processes 2−66456
Hamiltonian oscillator system, stability of periodic orbits in regions exhibiting stochastic behaviour 2−41525
isomerization reactions, examination of underlying stochastic process 2−51426
kinoform, linear array, generation, random number generator 2−79283
Langevin eqn. for particle in general harmonic lattice 2−69610
lattice random variables, local theorems for nonidentical distributions 2−45294
multiplicative stochastic processes, dissipative behaviour 2−58773
neutron diffusion 2−63938

Random processes continued
nonfree random walk problem, relationship with phase separation line in two-dimensional Ising model 2−63028
nonstationary random vibration of nonlinear structures, random walk model 2−76347
packing of equal and unequal spheres in two and three dimensions, computer simulation 2−78838
polymer chain, span calculation 2−50120
propagation of disturbances from randomly moving sources, solution of 2-dimensional equation 2−45286
random vibration problems, applic. of theory of distribution of natural frequencies of elastic bodies 2−41656
random walk, continuous, method of characteristic event 2−76227
self-diffusion, simulation of obstruction effect by random walk methods 2−58777
spatially inhomogeneous system, structure propagation theorem 2−52083
stochastic, nonstationary spectral relationships for energy and power bounded functions 2−66457
stochastic instability of non-linear oscillations 2−66574
stochastic point processes in phase space 2−41532
stochastic space concept and phase fluctuations of propagating wave 2−78763
symmetry violating, in theory of irreversible processes 2−82379
system response to transient random excitation, smoothing mean square estimates 2−63051
temperature forecasts by numerical method using centred time-differences, growth of random errors 2−62107
transfer of resonance radiation as process of photon random walks 2−82550
unimolecular reactions stochastic model 2−84634

Range of particles *see Energy loss of particles*

Rapid recovery *see Recovery*

Rare earth compounds
see also the compounds of the individual metals; Ferrites
alloy, Ce-Ln, isomorphic transforms. 2−50959
alloy, dil., supercond., mag. phenomena, spin excitations and order 2−57162
alloy, rare earth-Ag, thermoelec. power, phonon drag and distrib. contribs., 1.6-6K 2−81160
alloy, X-ray spectra, 4f state distrib. 2−48209
aluminates, i.r. spectra and cryst. struct. 2−84489
arsenates, Jahn-Teller induced phase transitions, thermodynamic props. 2−64806
arsenates, low temp. phase transform., by Jahn-Teller effect 2−77746
binary, A_3B, A_2B and AB types, computer prediction of existence 2−74597
borates, vibrational spectra and structures 2−70727
carbonates, i.r. spectra 2−48186
chalcogenides, exchange interaction problems 2−54373
chalcogenides, thermophysical props. and electronic struct. 2−57053
chromates, $RCrO_3$ (R=Lu,Yb), flux growth 2−60717
cobalt intermetallics, 2-17 type, mag. characteriz. 2−61510
cobalt intermetallics, RCo_2 type, mag. behaviour in ordering region 2−44280
cobalt-hydrogen pseudo-binary system, mag. field influence on equil. press. 2−43498
cobaltides, Co atom paramagnetic moments 2−72116
complexes with acetylene bonds, fluoresc. 2−51373
conference, Blacksburg, USA [Oct. 1971] 2−47053
coordination compounds of lanthanide elements, angular parameters of overlap integrals of F-orbitals 2−77034
dicarbides, thermodynamic props. determ., solid state galvanic cell technique 2−43865
difluorides and trifluorides, electric deflection of molecular beams 2−42905
dihalides, cryst. struct. 2−47333
β-diketonate complexes, i.r. absorpt., vibr. modes 2−46577
dipolar-coupled spin systems, caloric and mag. obs. 2−68523
dodecaborides, electronic spectra and phys. props. 2−47838
double aluminates with Sr and Eu, cryst. struct. 2−56664
double nitrate, satellite lines, field perturbation energy 2−72345
double nitrate, satellite lines, Zeeman effect, field perturbation theory 2−72344
double nitrate, satellite lines from non-Kramers distorted trigonal lattice, calcs. 2−72343
ethyl sulphates, paramag. relax., interactions contrib. to sp. ht. 2−57314
fluorides, l.f. lattice vibrs. 2−43963
fluorozirconates, $LnZrF_7$, cryst. struct. 2−43581
gabbros in equatorial Mid-Atlantic Ridge, rare earth element distrib. 2−54676
gallium intermetallics, LnGa, magnetization and susceptibility, temp. depend. 2−72170
gallium intermetallics, mag. props. 2−48079
garnet, containing Fe ions, absorp. spectra 2−75305
garnet epitaxial film, effect of substrate defects on struct. 2−47092
garnets, LnAlG and LnGaG, phonon cond. 2−77786
garnets, with ions on dodecahedral and octahedral sites, mag. ordering 2−44226
gold intermetallics, mag. struct. 2−44308
hexaborides, nonstoichiometry 2−47183
hexaborides, stability 2−50965
hydrides, electronic props. review 2−77899
hydrides, mag. ordering, sensitivity to hydrogen conc. 2−77986
hydroxides, hydrothermal growth 2−47244
insulators, Gd^{3+} isotropic exchange interactions from e.p.r. measurement 2−72487
intermetallic, contribs. to low temp. heat capacity 2−51043
intermetallic, electronic struct., APW calcs. 2−54112
intermetallic with transition metals, Fe_3C struct. type., mag. props. and transition 2−61504
intermetallics, $R_2(C_{1-x}Fe_x)_{17}$ type, lattice consts. 2−50626
ion-aromatic acid complexes, rare consts. for intramol. energy transfer 2−72305
iron garnets, isomer shifts of ^{57}Fe 2−57333
iron garnets, mixed, easy magnetiz. direction, Mossbauer obs. 2−51314
iron garnets, physical props. near compensation temp 2−81286

Rare earth compounds continued
- Laves phase, $LnNi_2$, crystallographic, mag. and e.p.r. studies 2−81277
- Laves phases, $LnCo_2$, crystallographic, mag. and e.p.r. studies 2−81276
- lithium mixed oxides, luminesc. of Eu^{3+}, energy levels 2−48226
- luminescence relaxation time, probabilities of inter- and intra- molecular energy transfer 2−54449
- manganates RMn_2O_5 ($R=Er$ to Sm, and Y), $RMnO_3$ ($R=Er$ to Gd), flux growth 2−60717
- metal halides, variations of i.r. absorption spectra with nature and structure 2−78083
- misch metal, alloyed with Zn and Mg, struct. 2−50624
- molybdates, Ln_2MoO_6 type, prep. and cryst. struct. 2−74737
- monochalcogenide films, co-evap. and characteriz. 2−50502
- monochalcogenides, press. induced electronic collapse and struct. changes 2−68297
- monochalcogenides, press. induced struct. and electronic transform. 2−50948
- Mossbauer spectroscopy applics. to phys., chem. and metallurgy 2−51313
- nickel intermetallics, mag. struct. 2−48080
- ortho-ferrite, substituted, mag. non-equivalent states, Mossbauer obs. 2−61602
- orthochromites, i.r. spectra and cryst. struct. 2−84489
- orthochromites, n.m.r. of ^{53}Cr, h.f.s., mag. props. 2−48307
- orthoferrites, cryst. growth and phase relationships in R_2O_3-Fe_2O_3 melts 2−50601
- orthoferrites, possibility of intermediate state existence for first order phase transformation 2−81291
- orthoferrites and orthochromites, ang. depend. of superexchange interactions 2−68569
- oxide film, martensitic phase transformation 2−50949
- oxide systems, ThO_2-Ln_2O_3, phase equilib., 1250-2100°C 2−47718
- oxides, A-type, vibr. spectra and space groups 2−51355
- oxides, Eu^{3+} and Tb^{3+} doped, flame excited luminesc., temp. depend. 2−48270
- oxides, Ln_2O_3, L-series lines, multiplet struct., expt. and theory 2−81397
- oxides, Ln_2O_3, types of twinning process 2−53739
- oxides, temp. spikes following Coulomb excitation 2−71719
- oxybromides, R_3O_4Br type, cryst. struct. 2−47333
- oxyhalides, i.r. spectra, vibrs. assignments 2−57348
- oxyselenides, mag. props. 2−44228
- oxysulphide multilayer films, luminescent props. 2−48224
- phosphate RPo_4 ($R=Yb$ oGd), flux growth 2−60717
- phosphates, low temp. phase transform., by Jahn-Teller effect 2−77746
- phosphors, luminesc., quenching, energy transfer between unlike ions 2−54457
- physics and chemistry, conf., Blacksburg, USA [Oct. 1971] 2−47052
- platinum tin intermetallics, RPtSn type, crystallographic and Mossbauer study 2−50621
- pyrochlores, $Ln_2M_2O_7$, ($M=Ru,Ir,Os$), struct. and props. 2−60987
- rare earth ethyl sulphate: Gd^{3+}, e.s.r. obs. at room temp. and 77K 2−75349
- rare-earth fluoride crystals, vibronic spectra exam. 2−71705
- rare-earth pyrosilicates, vibrational spectra 2−72322
- sesquichalcogenides, Th_3P_4 struct., tetragonal struct. model for cationic vacancy ordering 2−74743
- sesquioxides, far-i.r. spectra, phonon excitation 2−51346
- silicates, apatite type struct., synthesis, cation distrib. 2−74742
- silicides, $LnAg_2Si$, prep. and cryst. struct. 2−74735
- silicides, struct., thermal expansion coeffs., transition products, 20-1200°C 2−68005
- solution energy transfer mechanism, role of electrostatic and covalent interactions 2−53440
- structure, related class of coordination polyhedra, genetic relationship with icosahedron 2−84094
- sulphides, L_2S_3 type, β-form, cryst. struct. and solid soln. mechanism 2−47345
- sulphotelluride solid solns., high temp. homogeneity regions 2−53905
- tetraborides, cryst. growth and struct. 2−43524
- tetraborides, mag. props. 2−81293
- tetraborides, thermal stability 2−53995
- titanates, $Ln_2Ti_2O_7$ type, cryst. struct. and press.-induced transform. 2−47344
- transition metal cpds., $CaCu_5$ type, valence bond form. 2−50559
- transition metal intermetallics, pulsed field magnetiz., critical phenomena 2−51261
- tricholorides, n.q.r., hydrostatic press. coeffs., soft sphere model 2−54519
- vanadate, crystal growth from the flux systems PbO-V_2O_5 and Bi_2O_3-V_2O_5 2−50589
- vanadates, cooperative Jahn-Teller distortions 2−43926
- vanadates, Jahn-Teller induced phase transitions, thermodynamic props. 2−64806
- vanadates, low temp. phase transform., by Jahn-Teller effect 2−77746
- zircon structure type, temp. dependence of lattice parameters 2−84215
- zirconium alloys, form. of metastable low temp. allotropic solid solns. 2−47646
- Co Laves phase, type RCo_2, e.p.r. obs. 2−51403
- Co rare earth compounds with $CaCu_5$ struct., stability 2−80796
- Fe garnet, damping of domain wall motion 2−57304
- $NaY(WO_4)_2$, single cryst. growth 2−74955
- Pd-rare earth dil. alloys, magnetiz., susceptibility, moments 2−44224
- Pd-rare earth intermetallic compound, electrical resistivity obs. 2−51102
- Tb_2O_3, effect of crystal field on direction of magnetic moments of ions in low site symmetry 2−65186

Rare earth metals
- *see also the individual metals*
- atom, diamag. susceptibility and nucl. mag. shielding const. 2 - 59918

Rare earth metals continued
- atom, relative energies of lowest levels of f^qds^2, f^qds^2, $f^{q+1}s^2$ electron configurations 2−49950
- atomic vapours, energy differences between electron configs. 2−46440
- atoms, 4f energy determination using X-ray and photoelectron spectroscopy 2−49926
- conference, Blacksburg, USA [Oct. 1971] 2−47053
- in dilute alloys, indirect exchange 2−44217
- dopant, in MgO, CaO, $CaCO_3$, X-ray excited optical fluorescence 2−61707
- doubly and triply ionized, ionization energies 2−79947
- effective f-f exchange interaction, temp. depend. 2−54317
- electrical resist. due to short range spin correls. 2−57272
- electronic properties, single electron energies, many electron effects, renormalized atom scheme 2−64875
- electronic struct. of hydrogen 2−77822
- heavy, energy band theory derived from group theory 2−57114
- heavy, lattice sums and ionic enhancement potentials 2−61566
- heavy, X-ray L-absorpt. spectra, white lines 2−78117
- helicoidal magnetic structure, pressure effects, temp. depend. 2−68542
- impurities in alkali earth fluorides possible existence of separate cubic symmetry 2−80705
- impurities in Fe, hyperfine fields 2−44322
- ion aqueous solns., fluoresc. quenching by vibrs. of solvents mols. 2−60481
- ion energy levels in cryst. hosts; for 10-μ quantum counter up-conversion 2−45704
- ions, effect of coordination polyhedra structure on 4f-shell energy level splitting 2−50051
- ions, effect of core polarization on f-f interactions 2−52929
- ions, electron excitation energy degradation 2−61678
- ions, electron transfer reactions and oxidation potential in aqueous soln., pulse radiolysis study 2−61815
- ions, in Y_2O_2S, La_2O_2S, Gd_2O_2S, X-ray excited optical fluoresc. 2−72418
- ions, trivalent in Y_2O_3, phonon assisted energy transfer 2−48234
- ions in combined mag. and hexagonal cryst. fields, energy levels and moments 2−72117
- ions in cryst. field, optical transitions, interference effects 2−84494
- ions in crystal matrices, moments of radial function distributions, dependence on calc. method 2−65199
- ions in metals, metal props. rel. to cryst. elec. field splitting 2−57315
- ions in single crysts., two-photon absorpt. and stimulated emission 2−48225
- isotopes, large single cryst. growth 2−47225
- Judd-Ofelt parameters, effect of excluding hypersensitive transitions 2−83221
- lanthanide ions in solution, pseudocontact contribution to n.m.r. shifts 2−80481
- lanthanides, mechanism of liver uptake 2−55225
- light, mag. props., neutron diffr. 2−61517
- lunar abundances and liquid type and solid type materials 2−55122
- in lunar igneous rocks from Apollo 15 mission 2−62669
- magnetic crit. scatt. role in elec. resist. 2−57271
- magnetic props., review 2−51239
- magnetic transition manifestations in thermal cond. and Lorenz functions 2−57311
- magnetism, orbital contribs. effects review 2−84392
- magnetoelastic effects, theory 2−75226
- magnon-phonon interaction in metals with helical spin struct. 2−75225
- Mossbauer spectroscopy applics. to phys., chem. and metallurgy 2−51313
- nucleus, M1-intranuclear conversion analysed on basis of Saxon-Woods potential 2−46089
- odd-mass nuclei, nonadiabatic treatment of rotation bands 2−49717
- overabundance in stellar systems and symmetric fission of superheavy nuclei 2−54998
- paramagnetic state, exchange anisotropy, variation with lattice parameters 2−51236
- paramagnetic susceptibility anisotropy, 5 to 750°C 2−44227
- physics and chemistry, conf., Blacksburg, USA [Oct. 1971] 2−47052
- rare earth:YLF solid laser, energy transfer and phonon interactions 2−42058
- solubility in $ZrSiO_4$, isomorphous substitution of Zr 2−74913
- in solution, transfer of electron excitation energy between ions, dependence on solvent nature 2−53442
- spin wave energy rel. to interatomic exchange Heisenberg parameters, exchange coupling 2−61505
- in steel, effect on mech. props. and microstruct. 2−53900
- systematics in relative energies of f-electron configurations 2−79937
- target fabrication, sample assay 2−57440
- trivalent ion-hydride complexes in CaF_2 2−47434
- X-ray emission spectra, h.f. satellite obs. 2−83190
- X-ray spectra, 4f state distrib. 2−48209
- C_2-exchange reactions of gaseous dicarbides of rare earth metals 2−65359
- $Ln_2O_3.4MoO_3$ type, synthesis and some properties of polymolybdates, classification into four structural groups 2−83838
- Na_2BeF_4-Rb_2BeF_4, phase diagram, struct. of phases 2−74957

Rare gases *see Inert gases*

Rayleigh scattering
- — 2−67976
- approximation, absorpt. and emission cross sections of nonspherical particles 2−64477
- atmospheric scattering data using large laser radar equipment 2−84867
- atomic two-level system, scattering of intense light studied using Green's function 2−49938
- benzene-nitroalkane solns., total intensity Rayleigh scatt. and depolarization at 546 nm and 30°C 2−64444
- chloroform, liquid, calc. of orientation correlation functions from depolarized Rayleigh wing scattering 2−43363
- conference, Washington, USA, Sept. (1971) 2−64475

Rayleigh scattering continued
- glass, optical grade, relative intensities of Rayleigh and Brillouin scatt. 2−57364
- n-hexane and nitrobenzene liquid system, linewidths 2−64445
- hyper, polarization phenomena in polar and nonpolar molecules 2−46515
- isobutyric acid-water solution, linewidth in critical region rel. to Kawasaki-Einstein-Stokes formula and dynamical scaling 2−46933
- of light pulse, theoretical considerations 2−79320
- liquid, binary mixture, Kawasaki mode-mode coupling theory nonlocal shear viscosity correction 2−67829
- liquid cryst., nematic, elec. field quenching of thermal fluctuations of orientation 2−43332
- liquid crystal, smectic-C, quasielec. scatt., twist mode obs. 2−67833
- 2,6-lutidine-water light scatt. and shear viscosity studies in critical region 2−50344
- magnetically ordered crystals, Mossbauer diffraction including Rayleigh dispersion 2−68610
- matrix-operator theory for Rayleigh and maritime haze phase functions 2−76235
- methyl iodide, liquid, calc. of orientation correlation functions from depolarized Rayleigh wing scattering 2−43363
- 3-methyl-pentane molecular liquid, influence of temperature on collisional wing 2−80471
- methylene chloride, liquid, calc. of orientation correlation functions from depolarized Rayleigh wing scattering 2−43363
- molecular liquid, influence of temperature on collisional wing 2−80471
- molecular optical anisotropy dispersion obs. 2−63394
- pivalic acid, plastic crystalline phase 2−44399
- polystyrene spheres suspended in water, line width, scatt. angle depend. 2−50381
- quinoline molecular liquid, influence of temperature on collisional wing 2−80471
- radiation, polarized, nonconservative Rayleigh scatt., Milne problem 2−52459
- stimulated scatt., investigation with picosecond laser pulses 2−63348
- Uranus limb and polar brightening at 8870 Å 2−73087
- CS_2 stimulated scattering in line wing with psec. extinction 2−81375
- D_2, compressed, Rayleigh-Brillouin scatt. and relaxing thermal cond. 2−56171
- D_2, Dicke narrowing and collision broadening of depolarized line 2−70700
- DBr, molecular motions, self-broadening and broadening in inert gases 2−46544
- DBr, molecular motions in liquid phase 2−46961
- DBr, molecular motions when dissolved in solvents 2−46962
- DCl, molecular motions, self-broadening and broadening in inert gases 2−46544
- DCl, molecular motions in liquid phase 2−46961
- DCl, molecular motions when dissolved in solvents 2−46962
- H_2, compressed, Rayleigh-Brillouin scatt. and relaxing thermal cond. 2−56171
- H_2, Dicke narrowing and collision broadening of depolarized line 2−70700
- H_2 in planetary atmosphere 2−58512
- HBr, molecular motions, self-broadening and broadening in inert gases 2−46544
- HBr, molecular motions in liquid phase 2−46961
- HBr, molecular motions when dissolved in solvents 2−46962
- HCl, molecular motions, self-broadening and broadening in inert gases 2−46544
- HCl, molecular motions in liquid phase 2−46961
- HCl, molecular motions when dissolved in solvents 2−46962
- HD, compressed, Rayleigh-Brillouin scatt. and relaxing thermal cond. 2−56171
- HD, Dicke narrowing and collision broadening of depolarized line 2−70700
- H_2O, cluster nucleation from vap. phase, exptl. obs. 2−64511
- SbSI, critical phenomena 2−61612

Rayleigh waves *see Elastic waves; Seismic waves*

Re(h)binder effect *see Mechanical strength; Surface phenomena*

Reaction kinetics
- *see also Catalysis; Chemical reactions; Exchanges, chemical; Explosions*
- 9-CN, 10-acetoxy anthracene dimers, thermal behaviour and monomerization kinetics in the solid state 2−57436
- 9-CNanthracene dimers, thermal behaviour and monomerization kinetics in the solid state 2−57436
- Arrhenius rate law, sufficient conditions for derivation 2−82383
- atomic vapour formation in hot hollow cathode 2−84641
- benzoyl peroxide, reaction with diphenyl amine and tetraphenyl hydrazine, reaction rate consts., chemilum. 2−78191
- bond entropy in activated complexes, calc. method 2−84638
- t- butyl ion-molecule reactions, charge recombination rate coeff. and absolute rate constants 2−68820
- chemical reactors with axial diffusion, variational solution of nonlinear boundary value problem 2−84633
- chemiluminescence, obs. using fibre optics 2−48319
- classical trajectory method of computer simulation, dynamical interpretation 2−44471
- closed uniform isochoric homogeneous isothermal systems, axiomatics 2−68770
- combustion, acoustic conductivity of burning surface of mixed solid fuel 2−44479
- continuous mixtures, lumping analysis 2−68764
- crossed molecular beam apparatus for meas. of differential elastic or reactive cross section, determ. of intermolecular potentials 2−64211
- crossed molecular beams, reactive scattering of atoms and molecules 2−44470
- cubic spline interpolation applic. to rate determ. 2−68767
- diatomic mol. thermal decomp. conjugate kinetic eqn. approach 2−78187
- DNA, electron correl. influence on physicochem. props. 2−77159
- electron transferr, nonadiabatic effects 2−81504
- e.s.r. studies, review 2−54569
- ethanol, pressure effects on reaction rates of solvated electrons 2−61812

Reaction kinetics continued
- fast, ultrasonic and relaxation spectroscopy, expression for C_p/C_v 2−81499
- formal, algebraic and analytical aspects 2−65364
- frequency modulation of laser by fluctuations in chemical reaction 2−41977
- generalized Enskog method, theory 2−84639
- graphite, isotropic nuclear and 'Poco' desorption and oxidation rel. to reactivity 2−59843
- hot atom system, scavenger competition effect, computer simulation 2−72542
- hot atom system, scavenger competition effect, kinetic theory correction 2−72541
- hot-atom reactions in dilute heat gas, time dependent theory 2−48317
- hydrated-electron reactions with H ion and organic liquids, specific rate determ. by pulse radiolysis 2−78210
- ion-molecule, surface crossing model 2−81498
- ion-molecule rate constants by ion cyclotron resonance mass spectrometry 2−61768
- ion-molecule reaction studies with quadrupole ion storage trap 2−83405
- isoleucine racemization in calcareous marine sediments kinetics and mechanism 2−48417
- mechanism obs. using electron microscope with gas reaction stage 2−65363
- methane-d_4 + silane ion molecule reactions, hydride ion transfer and isotope effects 2−68778
- molecular collisions, characterization of product energy distribs., information and entropy deficiency 2−54529
- noble metals, thin oxide formation in aqueous electrolyte solutions with anodic current 2−68784
- olefins, activation energies for addition of $O(^3P)$ 2−84621
- obs. using optical density rate of change, spectrophotometer attachment for recording 2−63436
- polymer crystal growth, fractionation effects 2−81501
- propylene, addition of $O(^3P)$ atoms by flash photolysis, absolute rate constants 2−44492
- quantum mech. formulation of reaction rates 2−61765
- siderite, thermal decomposition from mag. props. and Mossbauer effect 2−72666
- silane-methane mixtures, determ. of relative and absolute rate constants for ion-molecule reaction 2−68777
- sintering, modified equation 2−77695
- stability theory of complex homogeneous kinetics 2−54534
- three-dimensional chemical reactions, natural bifurcation coordinates 2−75363
- translational-vibrational energy transfer 2−75370
- unimolecular, expression for activation energy valid for all pressure regions 2−68768
- wustite, oxidation and reduction in H_2O vapour and H_2 mixtures, kinetics and mechanism 2−75381
- $2AgCl(g) + Pb(g) \rightarrow 2Ag(g) + PbCl_2(g)$ substitution reaction in hot hollow cathode 2−84641
- AgBr, sol, conversion to AgI; kinetics, turbidimetric obs. 2−81542
- AgCl photolysis, temp. depend., 77-400K 2−61803
- Ar-N_2, $-CO$ mixtures, heteronuclear associative ionization, formation of ArN_2^+, $ArCO^+$, Ar_2^+ following 30 eV electron impact 2−51430
- As_2S_3/Ag system, photochem. transformation rate temp. depend., ht. treatment and ageing effects 2−57433
- Ba oxidation, photoemission spectra of chemisorbed levels 2−51446
- $Ba + Cl_2 \rightarrow BaCl + Cl$ crossed beam reactions, primitive product ang. distrib. 2−81493
- $Ba + HI \rightarrow BaI + H$, meas. of angular distrib. of product, determ. of threshold kinetic energy limits on $D_0°$ 2−81494
- $Ba + NO_2 \rightarrow BaO + NO$ crossed beam reactions, primitive product ang. distribs. 2−81493
- Be^{2+}, meas. of termolecular association rate constants with Ar, O_2, N_2, CO, CO_2, N_2O, H_2O in flowing afterglow 2−48316
- C^+ reactions with ethane, ethylene and acetylene, behaviour of cross section as function of incident energy, 2-100 eV 2−57416
- $CH(^2\Pi)$, pulse radiolytically produced, reaction with methane, kinetics of ethylene production 2−48347
- CO fourth positive chemilum. excitation and quenching due to reactions involving C_2O 2−84628
- CO^+ reactions, with H_2, CO_2, CH_4, N_2O, SO_2, O_2, C_2H_2, COS, NO and rate constants 2−51434
- CS_2-O_2 CW chem. laser, reactions producing vibrationally excited CO 2−79202
- Ca^{2+}, meas. of termolecular association rate constants, with Ar, O_2, N_2, CO, CO_2, N_2O, H_2O in flowing afterglow 2−48316
- $Ca + HI \rightarrow CaI + H$, meas. of angular distrib. of product, determ. of threshold kinetic energy limits on $D_0°$ 2−81494
- $Cd(^3P_0) + NH_3 \rightarrow CdNH_3^*$ reaction kinetics, rate constant, excimer formation 2−81514
- $Cl_2^- + NO_2 \rightarrow Cl^- + NO_2Cl$, thermal energy rate consts. 2−68774
- DBr-Br_2 system, hot atom reaction rates 2−72549
- DF and DF-CO_2 chemical lasers, vibrational energy transfer processes 2−66751
- Eu^{2+}, gaseous ammoniation energies to form $Eu(NH_3)_6$ 2−61774
- $F + HCl \rightarrow HF + Cl$, effect of excess reagent vibr. excitation 2−84629
- $F + H_2$ laser oscillator, closed-form solution for rate equations 2−69922
- $F + H_2 \rightarrow HF + H$, Monte Carlo calcs. of reaction rates and energy distribs. among products 2−57410
- Fe, liquid, equilibrium between Mn and O_2 2−77676
- $Fe + O_2$, fast flow reactor for kinetic obs. 2−48318
- H_2-metal reactions, rate at reaction measurement 2−78190
- $H + H_2$ collinear reaction probability in threshold region, DWBA study 2−81489
- HBr-Br_2 system, hot atom reaction rates 2−72549
- HCl, thermal dissociation in shock waves, density gradient meas. 2−44473
- $HD + {}^{18}F$, classical dynamics of hot-atom reactions 2−81497
- HF and HF-CO_2 chemical lasers, vibrational energy transfer processes 2−66751
- HF laser rate eqns., closed-form soln. 2−82479
- $H_3O^+.H_2O$, rate constants and kinetic analysis for formation in inert gases 2−84622

Reaction kinetics continued
- H + formaldehyde, abs. rate constant, investigation using formaldehyde photolysis 2−54539
- $H_2 + Ar^+$, spin-orbit states of Ar^+, surface crossing model 2−81498
- $H_2 + CO_2$, $H_2 + CO$, $H_2 + N_2$ ion-molecule reaction rate constants by ion cyclotron resonance mass spectrometry 2−61768
- $H + CO + M$, rate consts., press. depend. and third body effects 2−84625
- $H_2 + D_2 \rightarrow 2HD$ four-centre exchange reaction ab initio calcs. of orbitals, contragradience and reaction surface 2−48323
- $H + H_2$, planar reactive collisions, classical trajectory studies 2−75373
- $H + H_2$ linear reactive collisions below the classical threshold complex-valued classical trajectories determ. from S-matrix theory 2−44474
- $H + H_2$ planar reaction, hindered rotor states, natural bifurcation coordinates 2−75372
- $H + H + OH \rightleftharpoons H_3O^+ + e^-$ reactions in flames, kinetics and heats of reactions 2−54541
- $H + NO + M$, rate consts., press. depend. and third body effects 2−84625
- $H + O_2 + M$, rate consts., press. depend. and third body effects 2−84625
- $He + H_2^+ \rightarrow HeH^+ + H$, reaction cross-section, statistical phase-space theory of nuclear spin 2−81500
- $He(2^3S) + CO \rightarrow (CO^+)^* + He + e[C^* + O + He]$, excitation transfer and Penning ionization reactions, determ. rate constants for production of excited products 2−54535
- K reaction with methyl iodide in crossed beams, energy dependence 2−68771
- KBr, vibrationally excited, inelastic scatt. by methanol 2−64220
- $K_2SO_4(c) \rightarrow 2K^+(g) + SO_4^{2-}(g)$, Madelung parameter and electrostatic energy charge, calc. based on Evald Bertaut method 2−47179
- $K + CCl_4$, dependence of reactivity on internal and translational energy 2−75374
- $K + SF_6$, dependence of reactivity on internal and translational energy 2−75374
- $K + SnCl_4$, dependence of reactivity on internal and translational energy 2−75374
- Mg^{2+}, meas. of termolecular association rate constants with Ar, O_2, N_2, CO, CO_2, N_2O, H_2O in flowing afterglow 2−48316
- mischmetal-Mg alloys, dilute, metallographic study of phase transformations 2−80794
- $MoO_3 + SrCO_3 \rightarrow SrMoO_4 + CO_2$, diffusion-type 2−54536
- N_2^+ reactions, with H_2, CO_2, CH_4, N_2O, SO_2, O_2, C_2H_2, COS, NO and rate constants 2−51434
- NO_2^-, NO_3^-, with HCl and HBr, rate const. meas. in flowing afterglow system 2−61775
- $NO_2^- + Cl_2 \rightarrow Cl_2^- + NO_2$, thermal energy rate consts. 2−68774
- $Na + O_2$, fast flow reactor for kinetic obs. 2−48318
- Ni olivine to Ni spinel, reaction rate of phase change, seismological implications 2−78270
- O_2-H_2O system, formation and decomposition of water cluster ions 2−57414
- O_2-S, on Ni surface, LEED obs. 2−78184
- $O^+ (^4S) + N_{2(v)}(^1\Sigma)$ crossed molecular beams, cross section for formation of NO^+ 2−54530
- $O_2 (^1\Delta_g) + O_3 \rightarrow 2O_2 + O$, rate const., activation energy 2−57413
- OH, kinetic behaviour in excess NO at 5-82 torr He 2−84666
- $OH + NO_2 + Ar \rightarrow HNO_3 + Ar$, rate const. determ. by u.v. fluorescent scatt. 2−81491
- OH reactions with H_2, D_2 and CO, pulsed vacuum u.v. obs. using reson. fluoresc. 2−84665
- $O(^3P) + CO \rightarrow CO_2$, rate coeffs., meas., 250-370K 2−51438
- $O(^3P)$ + benzene, rate constant meas. 2−61778
- $O(^1S)$, rate constant for quenching by $O(^3P)$ 2−49970
- $O^+ + N_2 \rightarrow NO^+ + N$, ab initio calculation of potential energy curves 2−44468
- $O + O_3$, rate constant and rate expression direct determination in flow system 2−61769
- $Rb + CH_3I \rightarrow RbI + CH_3$, 6-atom potential determ. using Monte Carlo trajectory methods, prediction of cross sections in 0-2 eV range 2−72553
- $RhC_{(2)}$, heats of atomization determ. by high temp. mass spectrometry 2−84623
- $SH^- + Cl_2 \rightarrow Cl_2^- + SH$, thermal energy rate consts. 2−68774
- $SH^- + NO_2 \rightarrow NO_2^- + SH$, thermal energy rate consts. 2−68774
- $S^- + NO_2 \rightarrow NO_2 - + S$, thermal energy rate consts. 2−68774
- SiH_4 reactions with Si^+, SiH^+, SiH_2^+, SiH_3^+, determ. of relative and absolute rate constants 2−51439
- Sr oxidation, photoemission spectra of chemisorbed levels 2−51446
- $Sr + HI \rightarrow SrI + H$, meas. of angular distrib. of product, determ. of threshold kinetic energy limits on $D_0°$ 2−81494
- $3Te + 4HNO_3 \rightarrow 4NO + 3TeO_2 + 2H_2O$, crystn. of TeO_2, rel. to conditions 2−56612
- TiC_2, heats of atomization determ. by high temp. mass spectrometry 2−84623
- U IV-U VI photosensitized electron exchange reaction in HCl 2−75365
- UO_2-C-N_2, 1695°C, carbonitride form. 2−54537
- $U^+ + O_2(N_2) \rightarrow UO^+ + O$, determ. of reaction rate from thermal energy to 5 eV using drift mobility-tube-mass spectrometer 2−68766
- W-halogen lamps, thermodynamic calc. 2−61764
- Yb^{2+}, gaseous ammoniation energies to form $Yb(NH_3)_6$ 2−61774
- ZnS-CdS solid-phase reactions, studied by diffuse reflection spectra 2−75332
- Zr oxidation, short-time O_2 exposure, 440- 850°C 2−51453

Reactors *see Nuclear reactors, fission; Nuclear reactors, fusion*

Recombination *see Ions, recombination; Semiconductors*

Recombination radiation *see Luminescence*

Recording
- automatic static deformation recorder 2−56854
- bioelectric potentials, bioelectrode systems, interface design 2−85085
- combustion curves when operating with an FES-1 steelometer 2−84682
- computer generated holograms 2−82498
- computer tape subjected to periodic motion, longitudinal motion in high performance tape drive 2−69685

Recording continued
- c.r.t. optical film recorder with optical feedback exposure control 2−42223
- derived thermograph from thermobalance and recorder 2−63159
- digital, mass spectra in geologic studies, using magnetic tape 2−72600
- digital, Raman spectra, using step by step scanned spectrometer with multichannel analyzer 2−42276
- digital of fast phenomena in pulse radiolysis 2−72582
- digital system, fast for use with photoelectric photometer and polarimeter 2−45005
- dilatometer, fast-acting, two-coordinate system 2−76150
- earthquakes, low power, low cost station 2−81575
- electron microscope, energy analysing, errors in single and double plate recording techniques 2−79015
- erasable holographic, optical information, patent 2−66793
- e.s.r. spectra, recording in digital form by remote computer 2−59010
- frequency, automatic plotting systems for frequency stability curves and discrete spectral density of frequency standards 2−78752
- Fuji CVR, new audio-visual system using single-8 film cartridges 2−52495
- head fluctuations, in turbulent flows 2−70854
- high velocity motion photographically, moire fringe method applic. 2−50788
- holographic materials, review 2−55716
- human voluntary muscles, temp. and action potentials 2−55210
- hysteresis curve of hard magnets, automatic apparatus 2−82427
- internal friction and elastic modulus, high temp. system for continuous recording 2−53852
- ionizing particles in photographic emulsion, effect of electric field 2−59642
- laser i.r. on Se films and magnetic films, comparison 2−69960
- magnetic, dynamic characteristics, hysteresis curves, apparatus, closed ferromagnetic cores 2−82426
- m.i.s. structures electrical characteristics 2−63214
- noninvasive pressure pulse recorder, clinical applications 2−69264
- ocean microstructure, using high speed digitizer 2−72728
- oceanographic data, instrumental system for multichannel recording 2−51566
- optical images on magnetic plate 2−52469
- optical memory matrices, resolution by focused laser beam 2−55710
- $Pb_xLa_{1-x}(Zr, Ti)O_3$ ceramics for selectively erasable image storage and display 2−79454
- sea surface temp. nonuniformity, automatic system 2−44644
- seismic response of Plowshare project, effect of source and recording site parameters 2−54625
- self-contained, for measuring electric field at ocean floor 2−68862
- sound tracks, in colour reversal film 2−76551
- sound-level measuring system 2−82361
- thermoplastic, local deformation of free emulsion surface 2−73235
- thermoplastic emulsion layers with regular image element structure, optimum resolution 2−73236
- time variation of weight, automatic recording balance for thermo-gravimetric meas. 2−69529
- track, electron-optical meas. of dynamic fields 2−63278
- video recording, colour, TV film, apparatus 2−76496
- video tape, influence of external magnetic field on ponderomotive forces causing surface deformation of carrier 2−73237
- X-ray scattering, photographically, pinhole systems efficiency comparison 2−73690
- $LiNbO_3$, doped, as erasable optical recording medium 2−73612

Recovery
- butyl rubber, temp. and extension time depend. of creep recovery 2−71555
- cement, hardened paste, short time creep recovery 2−80755
- cold worked solids, stress assisted diffusion to dislocations, theory 2−43652
- creep, primary recovery, physical basis 2−47508
- creep, recovery-work hardening theory 2−56799
- graphite, pyrolytic, electron irrad. at 5 K, resist. study 2−80659
- irradiated solids, stress assisted diffusion to dislocations, theory 2−43652
- metal, deformed, effect of impurity atoms on grain boundary motion 2−43785
- metal, strain-hardened, plastic flow theory 2−43684
- nylon 6 monofilament, model for deform. and fracture from creep and birefringence obs. 2−84022
- nylon 6 monofilament, model for deform. and fracture from creep and birefringence obs. 2−84021
- recovery-creep model with effective and internal stress evaluation 2−68087
- rutile powder, lattice distortion following impact 2−74831
- and shock compression in permanent property changes 2−68072
- steel, martensitic, low-C Mn, effect of Sb on high temp. tempering, recovery rates 2−56905
- Al, neutron irrad., void annealing 2−53705
- Al, polycrystalline, recovery of mech. props. after severe rolling 2−71633
- Al, quenched, annealing kinetics of point defects, resist. and magnetoresist. study 2−80680
- Au, plastically deformed after quenching, elec. resist. 2−56790
- CdS, electron irrad., stage III_n, activation energy 2−71455
- Cr, deformed at 77, 213, and 293K, resist. study 2−53805
- Cu-Al alloy, exo-electron emission, interdependence with annealing processes 2−48011
- Cu, cold worked at 200-300°C, creep and recovery 2−84163
- Cu, electron irrad., lattice parameter and resistivity changes 2−60777
- Cu, neutron irrad., impurity atom effects, elec. resistivity obs. 2−60964
- Cu, plastically deformed, rel. to specific dislocation energy determ. 2−53734
- Cu, polycrystalline, recovery of mech. props. after severe rolling 2−71633
- Fe:Sn, elastic recovery of micro-indentations rel. to grain-boundary hardening 2−60910
- Fe-C alloy, of internal friction after strain ageing 2−47481
- Fe-Co-V alloy, ordered and disordered, shocked and rolled 2−50804
- Fe-Mn alloy, b.c.c., shock deformed, flow stress and elec. resistivity 2−56912

Recovery continued
- Mo, deformed, Young's modulus and Poisson ratio, annealing time and temp. depend. 2−84054
- Mo, electron irrad. at 4.2K stage I recovery, resist. study 2−53718
- Mo, neutron irrad., stress-induced ordering of stage I defects 2−64654
- Nb, cold-worked or irrad., role of O and N impurities 2−47404
- Nb, cold-worked or neutron irrad., annealing, resist. study 2−64766
- Ni-Al alloy, flow-stress recovery 2−74888
- Ni-Al alloy, high temp. deformed, flow-stress recovery 2−74889
- Ni, after 300 kbar shock wave loading 2−56794
- Ni, electron-irrad., mag. after-effect and elec. resist. study 2−64655
- Ni, electron irradiated, rel. to ferromag. after effect at 55K 2−78026
- Pb-Ag alloys, ageing, softening mechanism and kinetics 2−43860
- Si, deform. behaviour, T > 850°C 2−56808
- p-Si, electron irrad. at 77K, Hall coeff. and cond. study 2−71944
- Si p-n diode, γ-irrad., photovolt. effect obs. 2−61358
- α-Sn, electron irrad., damage production and thermal annealing, resist. study 2−80682
- WC-Co cemented carbide, internal friction obs., dislocation config. 2−68070
- Zr-(1.5wt.%)Cr-(0.1wt.%)Fe tubing, heat-treated and hydrided 2−53918
- Zr, fault elimination by cold rolling, determ. by meas. elec. resist. 2−43797

Recrystallization (metals) *see Heat treatment*

Rectifiers
- *see also Electron tubes; Semiconducting devices*
- — 2−65032
- Schottky barriers between ZnTe and Au, Ni, Ta, Al, electrical properties, thermionic emission model, recombination current model 2−64962
- superconducting plants with inductive load, cryodiode behaviour 2−59037
- Nd:glass laser beam rectification by $LiTaO_3:Cu^{++}$ for electrical pulse generation 2−79268
- Se, electrical and photoelectric obs. of surface layers 2−44132

Red giants *see Stars*

Red shift
- 3C 273, mass and distance 2−48738
- astronomical spectra, interpret. 2−54993
- 3C 323.1, association w.a rich cluster of galaxies 2−66125
- CGCG 1622+4112 extremely compact galaxy 2−55018
- cluster galaxies in NGC 520 chain of quasars 2−58375
- Coma cluster, correlation with magnitude and morphology 2−51706
- Coma Cluster of galaxies 2−58224
- cosmological, effect on theory of X-ray background 2−48756
- distance redshift relation for universes with no intergalactic medium 2−75658
- 40 Eri B, DA white dwarf, gravitational redshift51749 2−51749
- expansion of the universe, review paper 2−62442
- Friedman universe, relation with luminosity 2−69003
- galactic anomalies, photon-photon inelastic interaction as explanation 2−48643
- galaxies, distant, diameter-redshift relationship 2−75690
- galaxies (near Abell 2147) 2−55009
- galaxies southern, with bright nuclei 2−58222
- gravitation theories rel. to redshift rocket probe experiment 2−69571
- gravitational, Newtonian, interaction with light 2−55383
- magnitude-redshift relation in Brans-Dicke cosmology 2−75659
- metagalactic background radiation, red shift losses 2−48649
- momentum balance in universe, effect on 2−69002
- non-Hubble or non-Doppler, occurrence in extragalactic objects 2−66058
- non-velocity redshifts of galaxies, systematic measurement errors 2−69036
- O type stars, individual reddening laws, computation method 2−84979
- quasar distances and redshift hypotheses 2−69118
- quasars, composite spectrum 2−75820
- quasars, correlation with colours 2−55080
- quasars, cosmological redshift rel. to obs. of Faraday depolarization 2−73042
- quasars, multiple, effect of intergalactic cloud 2−81791
- quasars, radio galaxies and unidentified sources, dependence of rotation measures 2−81871
- quasars, spectroscopic observations, selection effects 2−66126
- quasars, summary of arguments for and against cosmological redshift 2−81877
- quasars and emission line objects, power spectrum analysis 2−58377
- radio galaxies 2−66061
- solar limb effect, radial currents in atmosphere 2−66197
- supernovae, type I, determ. of Hubble constant 2−75765
- Ton 155 and 156, possibility of double quasar system 2−58379
- Zw Cl 0152+33, cluster of compact galaxies 2−66104
- $NaNd(WO_4)_2$, n.m.r. of ^{23}Na and mag. susceptibility detn. 4.2-300K 2−72513
- $NaPO_3$-$Co(PO_3)_2$ solid soln., phase diagrams, invariant points 2−74950
- Na_2WO_4-$Y_2(WO_4)_3$ solid soln., phase diagram 2−74955

Reflectance *see Electroreflectance; Magnetoreflectance; Piezoreflectance; Reflectivity; Thermoreflectance*

Reflection
- *see also Neutrons and antineutrons/reflection; X-ray reflection*
- acoustic gravity waves at density and velocity discontinuity 2−64226
- caustics of conic sections 2−79312
- elastic stress pulse reflection at interface between elastic rod and elastic half-space 2−73414
- elastic waves, micropolar elastic half space 2−41667
- elastic waves from free surface in quartz 2−41681
- emission of radiation by charged particles reflected from solid surfaces 2−54397
- inhomogeneous plane waves at interface between viscoelastic materials 2−57595
- MHD waves, incompressible, laws at fluid-solid interface 2−43104
- P_cP waves, vanishing reflection coeff. 2−78262
- plane longitudinal wave, from boundary of elastic half-space covered by particle layer 2−76359

Reflection continued
- rain, obs. at altitudes below, within and above melting layer 2−75584
- reflection density, multilayer colour prints, binder refractive index, colour gamut 2−82594
- seismic inner core reflections, nuclear explosions, diffraction 2−81580
- seismic waves, coefficients for gradient layer overlying homogeneous semisphere 2−44568
- seismic waves, primary and multiple reflections, intensities ratio 2−44570
- seismic waves, San Francisco Bay mud site 2−61906
- seismic waves in finely stratified multilayered media 2−61891
- shock waves, from permeable materials 2−69779
- shock waves, oblique, partly dispersed, from plane wall 2−78933
- shock waves of finite amplitude, in elastodynamics influence of non-linearity on reflection 2−52256
- shock waves on yawed wedge, supersonic outflow 2−76380
- solar radiation by cloud layers, Monte Carlo calc. 2−48486
- solids, surface plasmons, microscopic theory 2−84277
- surface elastic waves from edge of plate, generation of propagating acoustic diffraction field 2−55507
- total, electron beam at potential barrier, shift of beam position 2−69869
- water wave incident on 2 vertical parallel barriers, approx. soln. for coeff. 2−83737
- waves, by periodic medium 2−45244
- **acoustic waves**
  - *see also Echo; Reverberation*
  - atmosphere, stably stratified, sound beam zenith angle depend. 2−44742
  - broad-band trackchanging reflector using multistrip coupler 2−49172
  - channel with horizontal and vertical sound-speed gradients, reflected/refracted ray propagation 2−57841
  - coefficients for waves interacting with stratified media 2−45511
  - decay modes in exterior of reflecting body 2−82359
  - ferroelectric, at domain boundaries, influence of piezoelectric effect 2−74982
  - inhomogeneous layer with parallel surfaces 2−55531
  - interference pattern method for meas. reflection from uneven surfaces 2−69740
  - monostatic, by elastic spheres in water 2−43398
  - Rayleigh, Love surface waves at deformed boundaries and wedges 2−63113
  - Rayleigh wave reflection from electrically loaded interdigital transducers of YZ $LiNbO_3$, XY and YX quartz 2−51021
  - rough sea surface, acoustic field from source of arbitrary directivity 2−57837
  - shear discontinuity between hot and cold regions 2−78921
  - shock waves at boundary 2−55563
  - surface waves from transducer electrodes, meas. and modeling 2−49142
  - underwater acoustic surface- reflection channel characterization through impulse response measurements 2−45512
  - $LiNbO_3$, YZ, periodic arrays, elastic surface waves 2−51022
- **acoustic waves, ultrasonic**
  - average pressure response, piezoelectric circular transducer 2−69739
  - critical angle and Rayleigh angle incidence, radiated field 2−41731
  - crystal surface orientation meas. by u.s. beam displacement 2−56604
  - Rayleigh critical angle reflectivity, material properties influence 2−47740
  - water/Al interface, surface wave creation 2−64851
- **electromagnetic waves**
  - 10.6 mkm radiation, double reflection by Ge cryst. at 13 MHz u.s. modulation efficiency 2−49201
  - arbitrary wave incident on planar interface between dielectrics 2−78981
  - atmospheric layers, use as remote sensing technique 2−44738
  - circularly polarized ultrashort radiowaves from celestial bodies 2−55196
  - D-region, reflection coefficients, from thin parabolic layer 2−72889
  - D-region profiles from extraordinary component of partial reflections from lower ionosphere 2−84906
  - F2-layer, exptl. obs. 2−65980
  - F_2 layer, disturbances, strong spread reflections 2−72900
  - fading radio reflections from meteor tracks 2−81924
  - ground-wave propagation, Fresnel reflection coefficients, computational procedure 2−69825
  - inhomogeneous medium, TE-mode, coeff. calc. 2−59007
  - on inhomogeneous transmission line, nonlinear differential equation for reflection coefficient, linearization 2−69824
  - ionosphere, mode coupling, partial reflections, vertical incidence 2−41876
  - ionosphere, phase shift meas. 2−52319
  - from ionosphere, polarization of mean field 2−72860
  - ionosphere D-region, signal partial reflection, h.f. dynamic phase metering instrument 2−65967
  - ionospheric, ground pattern irregularities, obs. 2−78390
  - from ionospheric D-region, statistical characteristics 2−44754
  - lunar satellite propagated, lunar surface reflected e.m. waves 2−55600
  - meteoric for synchronizing frequency standards and relating time scales 2−58693
  - microwaves reflection in laboratory plasma 2−53192
  - mirrors, Fabry-Perot resonator, anisotropic medium 2−49210
  - by molecular beam using two-level medium as model of beam 2−82403
  - moving inhomogeneous plasma sheath, kinetic theory 2−74366
  - moving lossless inhomogeneous medium 2−82402
  - in nonhomogeneous isotropic medium 2−41877
  - nonlinear dielectric, const. amplitude plane wave phenomena 2−76415
  - obliquely incident on sinusoidally turbulent stratified half face 2−83536
  - from parallel grid of dielectric coated wires buried in earth 2−78957
  - plane, moving conducting medium, calc. 2−52310
  - plasma, comparison of random half- space and slab 2−64275

Reflection continued
electromagnetic waves continued
plasma, from moving front of ionization 2−46737
plasma half-space, normally incident wave 2−46739
plasma semi-bounded, resonance 2−56347
radio-wave reflection from inhomogeneous ionosphere, determ. of polarization using Stokes parameter 2−84904
radiowave reflection from meteor trails, detectability of radio meteors 2−73096
r.f., from time varying ionosphere irregularities 2−72856
SELFOC fibre, axial field component, multiple reflections 2−58988
on semi-infinite dielectric, exact solution of equations of molecular optics 2−73480
smooth brackish water, direct det. $10^8-4\times10^9$ Hz 2−72694
instratified turbulent magnetized plasma, e.m. wave reflection, transmission 2−77274
time domain reflection behaviour of transmission line partly filled with polar dielectric 2−63213
total internal, Maxwellian classical electrodynamics employed 2−55606
transient reflections, e.m. pulses, inhomogeneous and anisotropic media 2−58991
travelling ionospheric disturbances, rel. to amplitude probability distribution 2−48569
in turbulent plasma, radiative transfer methods 2−80236
uneven ground, reflecting power detn. knowing reflecting power of plane ground 2−76417
v.l.f., ionospheric, effect of positive ions 2−78393
InSe single crystals reflection and absorption in the i.r. region 2−81395
light
see also Films, solid/optical properties; Mirrors
absorbing multilayers, characteristics 2−66843
albedo of surfaces, as fn. of solar zenith angle 2−75485
alignment of planes and straight lines in space 2−70006
alkali halide, surface optical modes obs. 2−51344
alkali halide and oxide crystals, synchrotron radiation 2−47789
arsenate minerals and rocks, visible and near i.r. spectra 2−72672
asteroids, reflection, composition inferred 2−62714
asteroids, Vesta and others, reflection spectra 2−62713
attenuated total reflection spectroscopy applic. to industrial analytical chemistry 2−75404
borate minerals and rocks, visible and near i.r. spectra 2−72672
p-chlorobenzylidene-p-chloroaniline, conformation rel. to electronic structure, determination from solid-state reflection spectra 2−53051
coatings, deterioration by intermetallic diffusion, protection method 2−55764
coefficients meas. at low temp. using thermostated integrating sphere 2−57323
crystals, centrosymmetric and noncentrosymmetric, phonon spectra 2−68656
cube-corner reflector, treatment as linear operator 2−63371
cube-corner reflectors, testing method 2−66798
dielectrics, transparent, laser surface damage thresholds rel. to Fresnel reflections 2−79228
diffuse reflection technique for meas. on semiconductors, reflection peaks for Si, GaP and GaAs 2−75275
diffuse reflectors, effective reflection 2−52451
double pass catadioptric systems, mangin mirrors 2−69998
eruptive stars, reflection effect, optical properties of scattering medium 2−51759
feldspar, force field obs. 2−43955
film, metallic, optical consts., single refl. theory 2−48132
film with rough boundaries ellipsometric parameters 2−79328
GeS(Te), 1-12.5 eV, 73 and 293K 2−48161
ghosting of distant objects in twin-glazed windows, environmental effects 2−70005
group II-IV-V_2 compound, polarized reflectance spectra 2−61626
group III-V semiconductor, core levels detn. 2−65240
halide minearals and rocks, visible and near i.r. spectra 2−72672
ionic crystal plate, surface optical vibrations obs. 2−71704
laser beams, longitudinal displacements near total reflection, photon mass and new exptl. results 2−45759
liquid crystal, cholesteric mixtures, shear-induced struct. changes, refl. spectra obs. 2−64438
lunar dust layers, effect of fluidization on polarization 2−58453
l-menthol in nematic solvent, optical activity and circular dichroism 2−80442
metal, optical constant determ. by reflection method 2−78062
metal oxide film, reflection and emission coeff., thickness meas. 2−54398
meter, RCO type for measuring reflection ratio of flat, curved surfaces 2−66838
methanol-hexane solution, rel. to surface layer thickness meas. 2−60474
α-methylnaphthalene, liquid, specular reflection spectrum, obs. of excitons 2−80474
mica, characts. for radiation receivers 2−55754
mirror-prism systems, three dimensional problems, anomalous property 2−59210
mirrored surfaces, method of measuring coefficients 2−42181
multilayer coatings, graphical displays of complex reflectance based on circle diagrams 2−49439
nitrobenzene-hexane solution, rel. to surface layer thickness meas. 2−60474
noble metal, critical point detn., wavelength modulation derivative spectroscopy obs. 2−48160
noble metal-noble metal alloy, electronic struct. obs. 2−61174
ocular fundus reflectometer 2−66312
optical constants det. 2−42189
optically inhomogeneous layer, exact solutions for inverse boundary-value problem 2−59223
partially polarized light by dielectric plates 2−42188
particulate suspensions, interpretation of Kubelka-Munk coefficients 2−49426
phosphate minerals and rocks, visible and near i.r. spectra 2−72672
plane wave inhomogeneous field generated by total reflection on thin film system 2−52450

Reflection continued
light continued
by planetary atmosphere surface, numerical model 2−73078
planetary atmospheres, diffusely reflected photons rel. to absorption lines, probability distribution 2−78529
planetary emitted radiation and albedo simulator 2−78517
from plasma produced by nsec laser pulses 2−43177
polarization rotated, for travelling wave light intensity modulator 2−42158
powder, compressed pellets, i.r. refl. spectra rel. to struct. 2−68620
projection systems, optics 2−66875
quantized longitudinal and transverse shifts associated with total internal reflection 2−42213
quartz, reflectance spectra, rel. to surface hydroxyl groups 2−48163
reflectance model for mature corn, application to corn blight detection 2−78233
reflectometer, single beam single optical path for continuous meas. 2−49435
reflector surfaces for light collection in rectangular scintillation detectors 2−82807
relative derivative of reflectance with angle of incidence meas. and det. of optical constants 2−55730
sea water, space time structure of reflected light pulses 2−73633
semiconductor, critical point detn., wavelength modulation derivative spectroscopy obs. 2−48160
semiconductor, electronic transitions, opt. consts. evaluation, review 2−72291
semiconductor, lattice damage obs. due to ion implantation 2−47374
semiconductor, modulation of refl. of strong radiation, calc. 2−72257
semiconductor, wavelength modulated spectra, rel. to electronic structure calc. 2−81013
short pulse falling on linear dielectric medium, calc. of reflected wave 2−66809
silicate glass, corroded surface, i.r. spectra obs. 2−53541
space vehicle contaminant material optical constants det. by quartz microbalance and reflectometer 2−78418
spectra, lunar dust grains with amorphous coatings 2−85045
spectra at large angles of incidence, in vacuum u.v. 2−66855
spectrophotometer, split beam, for wavelength dependence meas. 2−55772
Sun-glitter pattern on sea rel. to roughness and surface wind measurements from spacecraft 2−84772
super-polished reflectors with low scatter, applics. 2−79429
thin film multilayer system, reflectance performance evaluation using computer 2−59222
total, inhomogeneous wave types at planar structures 2−63381
total Goos-Hanchen and Imbert effects splitting of polarization states 2−76514
total internal refl., transverse shift, quantization, circular polarization 2−70011
total internal reflection, plane wave analysis 2−49417
vanadate minerals and rocks, visible and near i.r. spectra 2−72672
vegetative canopies, azimuthal variations in directional reflectance 2−78232
veiling glare obs. in optical components and complete night vision systems 2−66810
water, disturbed surface, i.r. 2−48418
Ag cylinder, surface plasma wave study 2−61210
Al, u.v., rel. to LiF and MgF_2 films overcoating 2−79370
Al cylinder, surface plasma wave study 2−61210
AsS, refl. spectra, 100-800 nm, at 77K and 293K 2−75277
As_2S_3, refl. spectra, 100-800 nm, at 77K and 293K 2−75277
$As_2S_3(Se_3)$, amorphous, vibr. modes 2−61614
As_2Se_3, refl. spectra, 100-800 nm, at 77K and 293K 2−75277
As_2Te_3, refl. spectra, 100-800 nm, at 77K and 293K 2−75277
Au-Al, α-phase dil. alloy, 1.1-11.5 eV, rel. to band struct. determ. 2−75278
Au, 1.1-11.5 eV, rel. to band struct. determ. 2−75278
$Be_2Al_2Si_6O_{18}$, beryl, anharmonicity of i.r. vibration modes, reflectivity obs. 2−51317
C, glassy, optical consts., 0-82 eV, refl. meas. 2−61584
C black, tinting strength 2−75281
CO, adsorbed on Au, i.r. refl.-absorpt. spectra study 2−60676
CO, chemisorbed layer on W, vibr. freq. refl.-absorption i.r. spectra 2−47154
CO solid thin films, spectra of trapped atoms in vacuum ultra-violet 2−78096
CO_2, solid, in extreme u.v. 2−44365
CaF_2, surface optical modes obs. 2−51344
CdF_2, surface optical modes obs. 2−51344
$CdGeP_2$, zone recrystallised, coeff., spectral depend. 2−80595
$CdSe_xTe_{1-x}$, exciton reflection spectra obs. 2−84517
n-Cd_2SnO_4, Burnstein shifts, optical band gap 2−51137
Co, mag. permeability calc. from spectral meas. 2−65155
CoO, 3-27 eV, rel. to band struct. 2−84505
Cr_2O_3, wavelength modulated, rel. to absorp. of other Cr^{3+} containing insulators 2−65257
Cs thin films, 0.3 to 0.9 μ region 2−68597
$CsMnF_3$, perovskite, polarised i.r. refl. spectra, phonon dielec. dispersion 2−51319
$CsPbCl_3$, far i.r. refl. spectra, Kramers- Kronig analysis, optical lattice vibrs. 2−72300
CuI, low temp. spectra, excitonic transitions and levels 2−72302
$CuInTe_2$, 295K, 0.6−5.7 eV, rel. to band struct. determ. 2−78098
Cu_2O, electric field effects on excitons, electroreflectance obs. 2−51320
$Cu_{2-x}S$, 400-1200 nm 2−78085
CuTe, band struct. obs. 2−72301
Cu_2Te, carrier effective mass detn. 2−84520
DCN, spectra meas. in both crystalline phases 2−57351
Fe, mag. permeability calc. from spectral meas. 2−65155
Fe_3O_4, i.r. spectra, rel. to polaronic semicond. 2−61265
GaAs, polariton (n=1 exciton) spectra, temp. depend. 2−81400
Ga_2Se_3, i.r. refl. spectra at 290K, phonon freqs. and dielec. consts. 2−75279
a-Ge film, u.v. dielectric consts. detn. 2−61586
$GeS_2(Se_2)(Te_2)$, 1-12.5 eV, 73 and 293K 2−48161
GeTe, amorphous and polycryst., electronic struct. obs. 2−61465
HCN, spectra meas. in both crystalline phases 2−57351

Reflection continued
light continued
Hg vapour, selective refl., crossing effect between Zeeman sublevels of isotopes 2−79900
HgS, cinnabar, Kramers-Kronig inversion, optical const. obs. 2−61615
$HgS_{0.2}Se_{0.8}$ solid soln., plasma i.r. reflection at 100 and 300K 2−54404
InP-InAs solid solns., i.r. lattice vibrs. 2−47739
n-InSb mixed plasmon-phonon surface modes 2−81006
$In_2Se_{3x}Te_{3(1-x)}$ single crystal, optical props. detn. 2−54422
In_2Te, 1-12.5 eV, 73 and 293K 2−48161
KBr film, i.r., dielectric response obs. 2−72304
KCl, reflection spectra in vacuum u.v., investigation using synchrotron radiation 2−44367
KH_2PO_4 and KD_2PO_4, i.r. spectra obs. of high temp. phase transitions 2−71688
$K_2Pt(CN)_4Br_{0.3} \times 2.3H_2O$, reflection spectra rel. to one-dimensional metallic conductivity props. 2−68339
LiF film on Al, thickness monitoring by reflectance meas. using 1216 Å line of H 2−55733
LiF i.r. absorpt. and refl., breathing shell model 2−78102
MgF_2 film on Al, thickness monitoring by reflectance meas. using 1216 Å line of H 2−55733
$MgMoO_4$, i.r. reflection bands, shifts of polar phonon frequencies 2−81352
MnO, 3-27 eV, rel. to band struct. 2−84505
NaCl film, i.r., dielectric response obs. 2−72304
tris-$Nd_2(SO_4)_3$ diffuse reflectance spectrum, meas. of Slater-Condon, Racah, Lande, bonding and screening parameters, electronic energy states 2−61617
Ni, mag. permeability calc. from spectral meas. 2−65155
NiO, 3-27 eV, rel. to band struct. 2−84505
$PbCl_2$, optical consts. and exciton states 2−68625
PbI, band edge excitons study 2−68626
PbS, refl. spectra, X-ray photoemission, spin-orbit splitting 2−78092
n-PbSe, elec effective mass and relaxation time detn. 2−61651
PbSe, refl. spectra, X-ray photoemission, spin-orbit splitting 2−78092
PbTe, low temp. far i.r. spectra, TO lattice mode obs. 2−65265
PbTe, refl. spectra, X-ray photoemission, spin-orbit splitting 2−78092
$PdTe_2$, 1-12.5 eV, 73 and 293K 2−48161
Pt film, for u.v., optical props. 2−61653
RbH_2PO_4, i.r. spectra obs. of high temp. phase transitions 2−71688
Sb_2Se_3 film, amorphous, optical props. 2−61323
Si crystals, reflection spectra in vacuum u.v., investigation using synchrotron radiation 2−44367
SmS, metallic phase, 0.03-6 eV 2−80994
SmS, SmSe, SmTe, amorphous semicond., rel. to energy band struct. 2−61657
SnS(Se)(Te), 1-12.5 eV, 73 and 293K 2−48161
$SrB_2Si_2O_8$:Eu^{2+}, diffuse reflection spectrum 2−81420
$SrTiO_3$, differential spectra and band struct. 2−72307
TaS_2, two dimensional Van Hove singularity in band struct. obs. 2−81380
Te, thermomodulation, rel. to energy band models 2−65242
$Te_{81}Ge_{15}As_4$ glass, rel. to struct. of laser written lines 2−60600
TeO_2, lattice dynamics, i.r. study 2−71716
V_2O_3, absorpt. and refl. spectra in metal-semicond. transition 2−81407
V_2O_5, long wave vibrational spectrum obs. 2−68629
(Zn,Cd)S phosphors, diffuse reflection spectra for studying and controlling properties 2−75332
$ZnAs_2$, rel. to band struct. detn. 2−51326
$Zn_xCd_{1-x}Te$, band struct. obs. 2−78093
ZnP_2, rel. to band struct. detn. 2−51326
Reflectivity
see also Diffusion/light; Electroreflectance; Films, solid/optical properties; Magnetoreflectance; Modulation spectroscopy; Optical constants; Piezoreflectance; Thermoreflectance
absolute meas. in range 0.3 to 12 μ, apparatus 2−55755
albedo of interstellar particles det. from reflection nebulae 2−75794
albedo of sea surface 2−78318
clouds spectral albedo 1-6 μm 2−72790
diffuse from cloudy planetary atmospheres, lab. simulation 2−44933
directional spectral reflectance meas., response curve analysis 2−70079
double heterostructure injection laser cleaved facet, single mode operation 2−42076
Earth's surface, spectral solar u.v. radiation flux 2−62251
film, inhomogeneous dielectric, and transmission 2−54378
film at normal incidence, reflectances for optical constant determ. 2−78062
FN-85 photometer, reflectance and transmittance in 0.3 to 2.5 μm range 2−63435
group II-IV-V_2 chalcopyrite crysts., assignment of E_1 transitions 2−81384
hemispheric reflectance of plane water surface for atmospheric radiation 2−54853
instruments for measuring, calibration 2−66827
i.r., meas. at low temps. and high magnetic field 2−82569
lunar fines, Apollo 11 and 12 materials 2−78518
lunar highlands, high albedo central region observations and model 2−78519
lunar soil disturbance effect, rel. to changes in photometric function 2−44920
lunar soil samples rel. to telescopic spectral reflectivity measurements 2−78521
lunar surface rocks and fines 2−62652
Mars, u.v. observations from the OAO, albedo curves from 2000-3700 Angstroms 2−78555
Martian south polar cap, u.v. reflectance and 1971 dust cloud 2−75895
metals, at high temperatures 2−44344
meter, RCO type for measuring reflection ratio of flat, curved surfaces 2−66838
mirrors, reflection factor determination using a portable device, construction principles 2−45774
Reflectivity continued
Moon, albedo and linear polarization rel. to optical properties of igneous rocks in i.r. range 2−75846
Moon, spectral reflectivity properties, 0.3-1.1 μ 2−66153
Moon, telescopic spectral reflectivity rel. to four lunar spectral types and samples 2−78522
Moon albedo and temp. distribution at full moon 2−73065
planetary atm. and lunar soil, generalized Kirchhoff's law 2−75854
polarization effects on reflectance factor meas. 2−70010
powder, Kubelka-Munk diffuse reflectance remission function rel. to fund. optical parameters 2−79329
pyrolytic graphite, neutron, and use as analyzer and higher order filter in neutron scattering 2−55891
radar, clear air convection 2−75614
radar reflectivity factors in cloud model rel. to analyzed radar returns 2−75586
reflectance, average specular component eval. 2−45571
reflectance and transmittance of light by a thin inhomogeneous dielectric film, new formulae 2−54378
relative reflectance meas. using sliding mirrors and single beam reflectometer 2−82568
semiconductors class III-V, pressure depend. calc. of E_2 2−72297
surface film thickness determ. 2−79412
transparent film- absorbing substrate, reflection polarization 2−73644
water, temp effects on spectral reflectance 2−64461
$AgGaS_2$, i.r. in region 40 to 400 cm⁻¹ 2−44364
As_2Se_3, amorphous films, determination of optical constants 2−61620
Au-Zn dilute alloys, optical and piezo- optical properties from reflectivity measurements 2−68621
$Ba_2NaNb_5O_{15}$, far-i.r. dispersion, room temp. reflectivity spectrum analysis 2−68622
Bi:Te deposits, i.r. reflectance in 15-70μ region 2−75255
(C_3O_2)n polymer, u.v. and visible reflectivity rel. to colouring of Martian surface, laboratory studies 2−78542
$Cd_xHg_{1-x}Te$ mixed crysts., reststrahlen spectra, transverse optical modes 2−44366
$CdSiP_2$, i.r., characterization 2−80599
Co, calc. from optical constants and mag. permeability 2−65155
CuAu, Cu_3Au, effect of ordering on optical properties, reflectance measurements 2−72303
Fe, calc. from optical constants and mag. permeability 2−65155
GaAs, elec. field induced interference effects at ground exciton level 2−78084
GaAs, strain induced phonon line broadening observed by surface reflection Raman scattering 2−83858
GaSb, differential refl. in strong mag. field at E_1 and $E_1 + \Delta_1$ edges 2−68404
Ge, amorphous film, u.v. reflectance depend. on deposition temp. 2−54403
H_2O, reflectances in u.v. used to calc. optical constants 2−43361
Hg-In liquid alloy, meas. from 0.31 to 9 eV 2−64467
Hg, surface-induced vectorial optical props. 2−77436
Hg clouds in Venusian atm. 2−75915
HgTe, reststrahlen spectra, transverse optical modes 2−44366
InSb, differential refl. in strong mag. field at E_1 and $E_1 + \Delta_1$ edges 2−68404
K, obs. in 4-10.7 eV photon energy range 2−68593
$LiIO_3$, near and far i.r. investigations for α and β crystals 2−84511
MgF_2 multilayer, quarter wave as functions of angle of incidence 2−79410
$MoTe_2$, optical consts. Brillouin zone transitions 2−48162
NaCl aqueous solns. specular reflectance in i.r. 2−50362
$NaNO_3$, optical props. in vacuum u.v. region 2−84487
Ni, calc. from optical constants and mag. permeability 2−65155
Os film, in v.u.v. from 300 to 2000 Å 2−81336
$PbBr_2$ thin film, reflectivity spectrum calculation and measurement at 4.2K, 2-10 eV 2−57321
$Pb_{1-x}Sn_xTe$, optical props. determ. 2−48165
$Pb_{1-x}Sn_xTe$, i.r. plasma refl. study 2−84504
PbTe, optical props. determ. 2−48165
Re evaporated film, reflectance in v.u.v. from 300-2000 Å 2−44345
SF_6, extreme u.v. and soft X-ray region 2−42933
SbSI, far i.r. reflectivity, complex dielec. const. deriv., soft mode in paraelec. phase 2−61619
Sb_2Se_3, electron energy states for amorphous and cryst. material 2−68627
Se, amorphous films, determination of optical constants 2−61620
Si, irrad. with 400 eV ions, decrease in u.v. reflectivity 2−47081
Si, optically homogeneous, free carrier conc. determ. 2−54406
Si, surface oxide layer influence 2−51325
Si, wavelength modulated reflectivity spectrum in 3.4 eV region, piezo-optical evidence for λ transitions 2−75280
SiP_2 reflectance spectra, det. of band structure 2−72306
SmS, semicond.-to-metal transition under press., obs. 2−75098
SnTe, optical props. determ. 2−48165
W evaporated film, reflectance in v.u.v. from 300-2000 Å 2−44345
$ZnGeP_2$, i.r., characterization 2−80599
ZnS:Mn films, energy level scheme from reflectivity and transmission meas. 2−71799
ZnS multilayer, quarter wave as functions of angle of incidence 2−79410
$ZnS_{1-x}Se_x$ mixed crystals, optical, room temp., 2.5 to 9.5 eV range 2−54407
$ZnSe_xTe_{1-x}$, 2.0-6.6 eV, rel. to comp. depend. of energy gap 2−84500
$ZnSiP_2$, optical phonons, polaritons, mode freqs., strengths, damping factors 2−61621
Refraction
— 2−61906
fatigue testing 2−41593
film prep. using plasma jet in vacuo 2−83889
inhomogeneous plane waves at interface between viscoelastic materials 2−57595
MHD waves, incompressible, laws at fluid-solid interface 2−43104
seismic crustal refraction, New Britain 2−81599
seismic profile, sedimentary structure 2−81578

Refraction continued
seismic refraction mapping, Reframap Method, algorithm and procedure 2−57496
seismic refraction mapping, Reframap Method, model studies and performance 2−54624
seismic refraction measurements, crustal structure of Texas Gulf Coast area 2−54627

acoustic waves
see also Dispersion/acoustic
air jet as acoustic lens or waveguide 2−45508
channel with horizontal and vertical sound-speed gradients, reflected/refracted ray propagation 2−57841
cylindrical and annular ducts, attenuation 2−58917
h.f., by Earth's major crustal, upper mantle horizons 2−68842
normal waves in wedge lying on half space 2−72719
seismic, Lake Superior, delay-time function method of data analysis 2−68839

acoustic waves, ultrasonic
No entries

electromagnetic waves
see also Electromagnetic wave propagation
arbitrary wave incident on planar interface between dielectrics 2−78981
atmosphere, rocket tracking radar, corrections 2−78381
Einstein-de Sitter cosmology with plasma coupled to radiation at non-relativistic temperature 2−68997
gas prism resonator, toroidal as energy stores 2−71119
inhomogeneous medium, TE-mode, coeff. calc. 2−59007
nonlinear dielectric, const. amplitude plane wave phenomena 2−76415
r.f., from time varying ionosphere irregularities 2−72856
on semi-infinite dielectric, exact solution of equations of molecular optics 2−73480
spherical wave in statistically homogeneous and isotropic randomly-refracting medium 2−55607
stigmatic lens, near focus, utilization Fresnel formulae 2−69826
tropospheric radio-refractivity gradient over Japan, obs. 2−65803
u.h.f. radiowaves, biexponential model of ionosphere electron density profile 2−69840
whistler-mode wave refraction by large-scale gradients in middle-latitude ionosphere 2−84893

refraction
light
see also Double refraction
aromatic hydrocarbons, anisotropic polarizability eval. 2−80108
atmosphere, during total solar eclipse from Fresnel patterns 2−58001
atmosphere, sensing based on wave mechanics theory 2−44705
average field at superrefraction 2−79319
Cytherean atmosphere, rel. to phase anomaly 2−73089
differential refractometry with numerical reading 2−55731
double pass catadioptric systems, mangin mirrors 2−69998
Fresnel aether drag in transversely moving medium, direct observation 2−45773
glass, rel. to oxide content, computer calcs. 2−44500
inhomogeneous media in y-y diagram 2−79311
internal conical refraction, effects of optical activity of Faraday rotation 2−49430
laser beam bouncing in sugar soln., unusual effect 2−41435
mirror-prism systems, three dimensional problems, anomalous property 2−59210
optical free surface motion detector, use of He to eliminate refraction effects 2−45439
organic compounds, molar refraction, relationship with van der Waals constant 2−60119
polymer fracture surface layer, optical thickness determ. 2−70013
quartz, gyrotropy and asymmetric electro-optic props., two beam refraction obs. 2−72269
ray tracing in cylindrical gradient index media 2−42177
seawater, theory of meters of pulsations 2−51563
specific refractivities, atomic O and N, dual frequency laser interferometer 2−79902
starlight, effects on refractional and circumzenithal Talcott pairs, observations with ZTL-180 tube 2−48682
total reflection, inhomogeneous wave types at planar structures 2−63381
turbulent layer effects on point source image quality 2−70009
Ar singly ionized, specific refractivity 2−79903
$PbMg_{1/3}Nb_{2/3}O_3$ crystals, change in refractive index as function of electric field strength, use of prisms as light beam deflectors 2−42215
WSe_2, ellipsometric determ. 2−44383

Refractive index
atmosphere, effect of turbulence on radio waves 2−44705
binder, colour gamut, reflection density, multilayer colour prints 2−82594
Booker's theorem, generalization to wider range of profiles 2−54889
ionosphere, in vicinity of cross-over level and whistler propagation 2−72858
laser emission, effect of nonlinearity on dynamics 2−42079
Martian ionosphere, calc. 2−51828
Onsager reaction field as screened self-interaction in refractive index theory 2−59220
powder, Kubelka-Munk diffuse reflectance remission function rel. to fund. optical parameters 2−79329
semiconductor, amorphous, lone pair, press depend. 2−68594
thin films, determ. from X-ray specular reflection data 2−53563
tropospheric structure, remote sensing using ultrahigh resolution radar 2−44696
As_2S_3 crystals, massive and thin film, self-absorption edges 2−84479
Ge, X-ray interferometric determ. 2−72256
InSe single crystals reflection and absorption in the i.r. region 2−81395
$La_{2.97}In_{1.94}Ga_{3.09}O_{12}$ garnet, and spectral transmission 2−75300
$LiBaF_3$, elastic consts. 2−53781
Si, X-ray interferometric determ. 2−72256

Refractive index continued
light
see also Disperions, optical; Double refraction; Optical constants
aerosols, atmospheric, from 0.2 to 40 μm real and imaginary values 2−65773
antistatic agent film, on plastic, recovery, ellipsometry obs. 2−65073
atmosphere, airborne fly ash, laser radar and collection of particles 2−78376
atmosphere, scintillation obs. using ground-aircraft path 2−81682
atmosphere, scintillation of spherical and plane waves 2−81680
atmosphere, slant path scintillation in planetary boundary layer of laser beam 2−81675
atmospheric aerosol constituents 2−57946
atmospheric aerosol particles, relative humidity depend. 2−65780
atmospheric aerosols, meas. of complex index 2−62252
atmospheric aerosols of 800 nm to 1000 nm diam. 2−72802
atmospheric scintillation, turbulence profile correlation with stellar obs. 2−81683
atmospheric turbulence effects, and image deterioration of extraterrestrial objects 2−81677
barium behenate molec. film, ellipsometric study of optical constants and refractive index detn. 2−78064
barium margarate molec. film, ellipsometric study of optical constants and refractive index detn. 2−78064
benzene derivative crysts., index dispersion 2−54377
crystal, evaluation from excitonic spectra 2−72317
d-threonine crystals, nonlinear props. 2−55711
dielectric film, sputtered and evap., optical props. as function of deposition conditions 2−48131
dielectric films, determ. from reflectances 2−78062
dielectric thin film, interference method for meas. of dispersion in refractive index 2−44342
disperse system turbidity spectrum, determ. of size and refractive index of particles 2−43399
films, absorbing, det. from Brewster angle for film substrate interface 2−59224
fused quartz, ion-bombarded, refractive index and optical loss variations 2−50688
gases, wavelength dependence, non-linear optical obs. 2−71117
glass, change due to laser self-focusing damage 2−82501
glass fibre, effect on light propag. 2−42242
glass melt, striae solubility 2−59260
ice, broadband complex index between −20 and 0°C 2−64460
fromi.r. transmittance data, Kramers-Kronig dispersion anal. method 2−73643
liquid, gradients due to ultrashort laser pulses 2−43358
liquid crystal, nematic film polarimetry and interferometry studies 2−43329
liquids, close to cell wall, profile obs. using one-dimensional focusing critical angle refractometer 2−55760
measurement, by disturbance of total internal refl., accuracy 2−45781
measurement by interference microscopy and corrections for dispersion 2−70016
microcline, shock effects 2−61843
microscopic domain, using light interferometer 2−55736
mixed polymers of diethylene glycol- bis-allyl carbonate and isophthalic acid diallyl ester, with controlled optical refraction and dispersion 2−55752
nonlinear change, laser beam effect, self- focussing, trapping 2−79258
polymer in soln., index increments, conc. depend. 2−60520
propagation in random media, equivalence of Dyson and Bethe-Salpeter eqn. and Huygens-Fresnel principle 2−49414
scattering from inhomogeneous cylindrically symmetric lens with line infinity in refractive index 2−63374
semiconductor, amorphous, pressure effects rel. to band struct. 2−61333
spatial dependence, meas. with double exposure holograms 2−73616
strontium formate and strontium formate dihydrate, phase matchable optical nonlinearity 2−48124
three-dimensional field calc. using phase integrals 2−42196
transparent film- absorbing substrate, reflection polarization 2−73644
troposphere and turbulence profiles 2−65776
variations meas. using two beam interferometer 2−79354
water, temp. dependence calc. using two-state approach 2−60473
water broadband complex index between −20 and 50°C 2−64460
As-S-Ge glass film, laser induced changes 2−61583
As_2S_3, amorphous, press. depend. at 0.633 and 1.15 μ, one- oscillator model 2−54383
$3As_2Se_3.2Sb_2Se_3$ films, rel. to interband transition 2−54186
B glass, control by selective applic. of neutron irradiation 2−59226
B_2O_3 glasses, variation with hydrostatic press. up to 7 kbar, prep. history and structure 2−68595
C film, diamond-like props. characterization 2−56588
CO_2 TEA laser medium, interferometric obs. 2−49365
$CaSiO_3$-$NdSiO_5$ system, homogeneous phase 2−47707
$CdGeP_2$, dispersion of real and imag. parts and reln. to solid state phase change 2−72299
$CsBe_2(BO_3)F_2$ characterization 2−47210
Cu-Ni alloys, meas. in visible and ultraviolet spectral regions 2−81330
CuO film, wavelength depend., transmittance obs. 2−48135
$Cu_{2-x}S$, 400-1200 nm., refl. and absorpt. studies 2−78085
F_2, interferometric obs. rel. to wavelength 2−74488
GaSe, anisotropy near band edge 2−48178
$Gd_2O_3.GaO_2,Ge_2O_3.2GeO_2$, from phase diagram of Gd_2O_3-GeO_2 system 2−84097
Ge, pure, singly doped and compensated n-type, far i.r. props. 2−72384
HF, interferometric obs. rel. to wavelength 2−74488
$Hg_3Te_2Cl_2$, 5000-7000Å 2−71374
Ir, meas. in range 15-0.302 μm at 77 and 295 K 2−81359
K, determ. in 4-10.7 eV photon energy range 2−68593
$KBe_2(BO_3)F_2$ characterization 2−47210
$K(Ta,Nb)O_3$ crystals, paraelectric electro-optical, optical damage analysis 2−79226
$LiIO_3$, α and β forms compared 2−81326

Refractive index continued
light continued
Li_2O-B_2O_3-GeO_2 glass, rel. to struct. 2-47059
$LiTaO_3$ single crystal, temp. dependence 2-72008
MgO film, 0.22-8μ 2-79369
Mg_2SiO_4, forsterite, press. depend. 2-44350
$NaBe_2(BO_3)F_2$ characterization 2-47210
Nb_2O_5, anodic oxide film on Nb, ellipsometric obs. of field depend 2-44150
Nd:YAG laser material, holographic interferometry meas. of thermal refractive index coefficient 2-59174
Nd:YALO laser material, holographic interferometry meas. of thermal refracture index coefficient 2-59174
$PbMg_{1/3}Nb_{2/3}O_3$ crystals, change in refractive index as function of electric field strength, use of prisms as light beam deflectors 2-42215
PbO-RO-GeO_2, R=Mg, Ca, Sr, Ba, glass, rel. to structure 2-53540
Pt, 0.265-7 μ, 295 and 77K, rel. to band struct. 2-81358
$RbBe_2(BO_3)F_2$ characterization 2-47210
Sf_6, liquid-vapour coexistence curve, interferometric obs. 2-74591
Si, in 1.1 to 2.1 μ region of i.r. 2-72255
Si, ion irradiated, rel. to apparent damage induced absorp. 2-48158
Si, pure, singly doped and compensated n-type, far i.r. props. 2-72384
SiO, evaporated films, interference meas. 2-65212
SnF_2, soln. grown crysts. 2-47245
TiO_2 film, chemical vapour deposited, as function of processing temp. 2-50511
TiO_2 hydrosol, optical props. 2-74574
Ti(0001) single crystal, and polycrystalline, obs. as function of temp. 2-44341
Tl germanate glasses with high Tl_2O content, revised meas. 2-61585
Tl_3AsA_4 single crystal 2-48137
Tl_3AsS_3, nonlinear optical material 2-42243
Tl_3AsSe_3, phase matchable i.r. nonlinear material 2-48129
Tu_2O_5, anodic oxide film on Ta, ellipsometric obs. of field depend 2-44150
W_2O_5, anodic oxide film, on W, ellipsometric obs. of field depend 2-44150
W(110) single crystal and polycrystalline, obs. as function of temp. 2-44341
YVO_3:Eu, excitation induced anisotropy of local environment 2-81440
Refractive index measurement
atmosphere, laser beam scintillation meas. from 1.5 to 10.5 km altitude 2-81672
differential, construction of instrument from finished parts 2-42231
holographic interferometry, three-dimensional field 2-82582
optical glasses, non-immersion method 2-70048
$CaLaSi(PO_4)_2CaF_2$:Nd 2-49380
Refractometers
differential, construction of instrument from finished parts 2-42231
Refractories
alumino silicate refractory fibre, props. and applicatons 2-56953
arc furnace for thermal analysis of super-refractories 2-66363
basic raw materials, review 2-68165
b.c.c. metals, for thermionic nuclear reactor applications, effects of fast neutron irrad. 2-63229
carbide cemented alloys, carbide grain shape 2-53889
carbide/liquid metal contact interactions 2-68190
carbides, nitrides and borides, behaviour and properties, NASA research 2-64801
coating of materials, use of composite powders, new developments 2-61010
coatings, high temp., deposition from fused salts and by ion plating 2-50860
corrosion, wetting effects 2-43867
forging apparatus for temps. up to 1900°C under vacuum or inert atmospheres 2-58655
high alumina, relation of density, thermal shock resistance and hot modulus of rupture 2-56961
holder for preparation of sections 2-73238
metal, strength at elevated temp., vacuum technique obs. 2-77683
metals, thermophysical property meas. 2-57077
metals, zone decorations in field evaporated surface 2-53551
microstructure, optical and elec. microscope obs. 2-56955
nonmetallic, high temp. electrical insulator material, thermophysical props. 2-57079
oriented microsections of single crysts., prep. method 2-43534
oxide, oxide filament reinforced, characs. 2-56973
particle size distribution, effect on packing props. in high silica 'roseki' refractories 2-64786
periclase brick, microstruct. of hot fracture surface 2-77661
periclase-chrome brick, elec. probe microanalysis of chromite, empirical correction procedure 2-77663
powder metallurgy of high-temp. materials, conference, Tyrol, Austria, June 1971 2-53937
refractory oxides, bicrystals, growth by floating zone method 2-83898
scanning electron microscope applications 2-56956
single crystal metals, emitter and collector work function measurement 2-63234
targets, prep. by heavy ion sputtering 2-73911
ternary carbide, thermodynamic props. rel. to bonding and compressibility 2-71652
thermodynamic properties, enthalpy, heat and temp. of phase transitions 2-54036
Verneuil furnace lining, rel. to oxidation-reduction potential of environment 2-60705
Al_2O_3-ZrO_2-SiO_2 fused grain, rebonded, characteriz. 2-53926
Al_2O_3 based, stress-strain behaviour in torsion test 2-43687
B_2O_3-MgO, phase relations determined by quenching 2-74936
$CaZrO_3$-$CaHfO_3$ system solid solns., lattice parameters 2-43575
Cr carbides, nitrides and borides, atomic interactions 2-48206
CrSi, $CrSi_2$, Cr_3Si, Cr_5S_3, isobaric-isotherm. potl., entropy and heat of formation detn. by meas. galvanic e.m.f. 2-68246
$La_{1-x}Sr_xCrO_3$, volatile oxidation kinetics for optimum material characteriz. 2-50885
MgO-B_2O_3, phase relations determined by quenching 2-74936
MgO-B_2O_3, phase relations determined by quenching 2-74936
Refractories continued
MgO, effect of stress on grain growth 2-74915
Mo digermanide, reaction hot pressing from Mo and Ge powders 2-61001
Mo_2C, contact interaction with liquid Fe 2-77728
Na_2SO_4, volatile oxidation kinetics, 1173 to 1473K 2-50891
NbC_x, process for obtaining mat. in fluidized layer 2-68168
Si_3N_4-Cr_2O_3, thermal resistance, oxidizability, sintering, porosity and impact strength 2-68162
SiO_2, Si_3N_4 and SiC, interactions with metals at phase boundaries, thermodynamic analysis 2-84093
Ti carbides, nitrides and borides, atomic interactions 2-48206
TiB_2 coatings, electrodeposition and characteriz. 2-51460
Tic, surface struct., electron diffr. obs. in ultrahigh vacuum environment 2-43469
V carbides, nitrides and borides, atomic interactions 2-48206
$VC_x(O_x)(N_x)$, cryst. growth by floating zone technique 2-47277
W coating, deposited from the gaseous phase, grain size 2-84092
Zr containing, influence of gaseous medium on phase composition 2-84095
ZrO_2-Y_2O_3, elastic consts., current blackening effects, u.s. wave vel. obs. 2-43666
Refractory materials *see Refractories*
Refrigerators *see Low-temperature production*
Regge poles and trajectories
3^- nonet of states $\rho(1670)$, $\omega(1680)$, K*(1760), $\varphi(1820)$, Regge recurrences of 1^- nonet 2-67038
— 2-59480
ABFST model, relationship between Regge slopes and Lorentz poles 2-59497
baryon linear trajectory slope in GMO mass formula and (mass)^2 hypothesis 2-49587
baryon Regge pole models for single pion photoproduction and rhomeson production 2-52623
baryon resonances, correlations 2-59591
bi-Regge-pole duality 2-45926
biquark and triquark propagators in Reggeized supermultiplet theory, application to high-energy charge exchange reaction 2-52574
bootstrap mechanism for indefinitely rising trajectories 2-45905
charge exchange, model for relationship of fixed pole to shielding cut 2-49571
charge exchange reactions, inclusive single particle spectra using multi-Regge model 2-79560
Chew-Pignotti multi-Regge model, inclusion of charge 2-45902
coincidence electroproduction and scaling in the Regge region 2-63515
complex pole model and duality as basis for taking Regge cuts into account 2-66989
Compton amplitudes, fixed poles and Pomeranchukon coupling 2-49537
Compton and deep-inelastic, analysis of finite-energy sum rules using Regge-pole model including cuts 2-63494
coupling to photons, kinematics, applic. to pion photoproduction and charged Compton scatt. 2-63605
cut corrections to absorpt models from duality diagrams 2-79535
cut-to-cut extrapolations using Carleman-weighted dispersion relations 2-63570
cuts, generation of models, use when Regge pole model fails 2-59498
cuts, review of usefulness 2-45927
cuts from inclusive finite mass sum rules 2-67045
cuts in $\pi\pi \to NN$ amplitudes at T=0 2-42401
double Regge model, spin and parity analysis 2-49517
double resonance production, Regge pole model 2-45863
double-Regge vertex, singularity structure in nonplanar Veneziano model 2-82730
dual amplitudes satisfying the Mandelstam representation, Regge behaviour 2-76635
dual amplitudes with Mandelstam analyticity, asymptotic and Regge behaviour 2-66988
dual amplitudes with Mandelstam analyticity, asymptotic behaviour 2-70194
dual model, unitarization and absorpt. Regge cut 2-66981
dual model for unit Regge intercept, spectrum-generating algebra and no-ghost theorem 2-79515
duality, Regge description of scatt. amplitude 2-45913
duality props. of cuts 2-59488
eikonal model, application of unitarity sum rule, effect on moving pomeron trajectory 2-73793
electron scattering, Regge behaviour of Compton amplitudes 2-59426
exchange amplitude, ρ-P cut partial bootstrap and phenomenological pole 2-59496
exchange degeneracy and duality in generalized interference model 2-73792
finite energy sum rules unitarized by inclusion of Regge cuts, application to πN charge exchange 2-45921
Freund-Harari duality tests, evidence against resonance saturation in finite-energy sum rules 2-63568
functions of order p, Veneziano and Coon representations 2-79552
general consequences of Regge theory for Pomeranchukon-pole couplings 2-66985
geometrical Regge Model, in hadron- hadron scattering 2-45919
hadron dynamical parton model with independent tension 2-45895
hadron electroproduction, violation of scale invariance due to contribution of cuts 2-63534
hadron electroproduction distribution, one photon exchange part, Regge behaviour 2-70171
hadron interactions, Regge phenomenology of inclusive spectra in central region 2-59448
hadron interactions, triple Regge couplings and central region of inclusive distributions 2-59447
hadron multiplicity distrib., Regge branch ccts, high energies 2-66978
hadron spectra, quark-orbital Regge trajectories 2-76644
hadron-hadron scattering, eikonal model 2-82729
hadronic prod. in e^+e^- annihilation processes 2-63518
Harari-Freund theory, avoidance of factorization of Regge residues 2-70174
helicity pole location in terms of Regge poles 2-73795

Regge poles and trajectories continued
high energy scattering, unitary symmetry 2−42361
high-energy, pole positions for large coupling consts. 2−59500
high-energy, pole positions for large coupling consts. 2−59501
high-energy scatt. phenomenology 2−63566
inclusive processes, Regge behaviour for annihilation and decay 2−59492
inclusive reactions, Regge phenomenology, review 2−66967
inclusive reactions in Regge pole model and exotic resonances 2−45909
inclusive spectra in central region, Regge analysis 2−59481
inelastic scattering, role of lower lying exchanged trajectories studied in framework of two-fire-ball model 2−59482
KN scatt. amplitudes analysis in intermediate energy region 2−63596
light cone and multi-Regge theory for inclusive processes at large mass 2−73782
limiting fragmentation, double Regge boundary condition 2−49520
mass^2 operator representation of f and ρ trajectories 2−45924
meson reson. photoproduction in backward direction cross sections prediction 2−63644
Mueller's Regge hypothesis for high energy inclusive processes 2−59450
multi-Regge model of Chan, Loskiewicz and Allison, introduction of resonances for analysis of pp annihilation reaction 2−73845
multi-Reggeon vertex, factorization prop. 2−66982
multiperipheral dynamics, diffractive dissociation 2−73790
multiperipheral model and triplet Regge limit 2−63540
multiple-scattering Regge units, phase problem and signature rule 2−52589
new absorption model allowing for unequal absorption of rotating and non-rotating parts of exchange amplitude 2−73794
nonlinear fermion-field equation of motion, exact nonperturbative soln. with compounds lying on Regge trajectory 2−79467
nonsense wrong signature zeros used to explain $\gamma p \to \pi^0 p$, $\gamma n \to \pi^0 n$, $\gamma p \to np$, $\pi^0 p \to \rho^0 p$ 2−59529
in nuclear resonant reactions, solutions for spin 0-spin 0 and spin $^1/_2$-spin 0 scatt. 2−76825
optimized FESR for pole residue determ. 2−66980
P′ singularity, phenomenological anal. 2−79537
parity doublet elimination in Regge amplitudes 2−66990
photoproduction processes, high-energy quasi-inclusive, multi-Regge model applic. 2−52575
pole model, for particles with unequal masses or spins 2−42367
pole parameters, and pole residues determ. using optimized integral continuation methods 2−42314
Pomeranchon Regge trajectory, decoupling 2−82726
positronium trajectory, relation to mass formula in eikonal approx. 2−42304
quasi-eikonal approximation and scattering amplitudes 2−70134
reduced residues in large angle scattering 2−42366
Regge analysis and dual absorptive model, review 2−59451
Regge models and duality, review 2−63569
multi-Reggeon effects for inclusive reactions in pionization region 2−49536
Reggeon perturbation theory in Zachariasen-like model 2−52587
Reggeon-particle scattering, finite-energy sum rules 2−73849
residue functions eliminating all parity doublets in theory Reggeized baryon exchange 2−79605
residues, inhomogeneous relations obtained using nonlinear forms of average duality at intermediate energies 2−66986
review 2−76643
scaling function contributions from virtual $\gamma\gamma$ scatt. 2−82675
scattering amplitudes, corrective term to Regge model for real parts 2−59472
second trajectories and KN-KN charge-exchange cross-section difference 2−76658
signature multiplier parametrization, optical model 2−76645
single particle distributions near kinematical limits, phenomenological study 2−45904
single-particle inclusive cross sections, phenomenology of triple-Regge region 2−76628
single-particle inclusive reactions, triple- Regge phenomenology from finite-mass sum rules 2−76622
singularities, analyticity requirements 2−42367
spectra for fast π^+, π^-, K^+ secondaries in pp collisions in Reggeized forms with scaling 2−45953
strong interactions, application of ideas to deuteron stripping reaction at high energies 2−76633
symmetries of Regge-Regge cuts 2−59499
symmetries of Regge-Regge cuts in models incorporating Finkelstein's cut selection rule 2−59493
trajectories in relativistic quark model with harmonic dynamics 2−63531
triple Regge couplings, unitarity bound 2−59461
triple Regge vertex, eigenvalue integral equation 2−82724
triple Regge vertex, nonplanar couplings 2−45925
triple Reggeon graphs, mass dependence tested in single particle production 2−42353
triple-Regge amplitude 2−42368
triple-Regge formulae in photo and electroprod. 2−79494
two particle elastic scattering in presence of inelastic processes, form of complex separable interaction leading to linear Regge trajectories 2−52586
two-body scatt., Regge cuts, phenomenological description 2−63567
unequal-mass scatt. amplitude Reggeization 2−82720
ur-citon scheme, scatt. amplitude behaviour in high energy region 2−52582
vector meson dominance rel. to coupling of Reggeized ρ to 'charged' photons 2−79539
Veneziano-like represents. for scatt. amplitudes 2−59490
vertex strengths, graphical duality and algebra 2−70195
weak-cut-type models, reproduction of new pp scattering CERN data in 1000 GeV.c region 2−63660
Wick-Cutkosky model, Regge poles for large coupling constants 2−59350
$\Delta(1236)$ production reactions, application of Regge-pole model 2−73856

Regge poles and trajectories continued
eN deep inelastic scattering, interpretation of exptl. data in proton model, Regge pole analysis 2−59427
$ep \to ep +$ anything, t and q^2 dependence, triple-Regge formalism application 2−73757
η^0 production in $\pi^- p$ interactions at high energy and large momentum transfer, pole models 2−63575
γN deep inelastic scattering, Regge behaviour in Feynman diagram model 2−45872
$\gamma N \to \eta N$, Regge-pole Regge-cut analysis 2−63500
$\gamma N \to \pi^0 N$, Regge-pole Regge-cut analysis 2−63500
$\gamma p \to K^+ \Sigma^0$, strong cut Reggeized absorption model 2−70144
$\gamma p \to V^\circ p$, Regge pole model 2−67035
KN scatt., absorption model construction 2−63651
KN scatt. amplitudes analysis in intermediate energy region 2−63596
KN scattering, elastic and charge exchange, phenomenological analysis, Regge contributions 2−42400
$KN \to \pi[\Sigma,\Lambda]$, hypercharge exchange reaction, amplitude analysis 2−42389
NN, NN scattering, amplitude spin structure, partial analysis at high energy using Regge pole classification 2−45993
NN scatt., absorption model construction 2−63651
NN scatt., Regge cuts of pp and A_2A_2, sum rule calcs. 2−63652
NN scatt. amplitude behaviour at low energy 2−55873
np charge- exchange reaction, model for pion-Pomeranchon Regge cut 2−52640
pp scattering, pole scheme for polarization structure, differences in theory and expt. explained by exotic peripheral resonances 2−67056
pp scattering yields Λ,Σ hyperon- antihyperon, studied by absorbed Regge pole model with exchange degeneracy 2−42408
$pp \to \Delta^{++}(1236)\Delta^{++}(1236)$, Regge eikonal model calc. 2−70256
$pp \to X +$ anything ($X = \pi^\pm, K^\pm, p$), triplet Regge graph study 2−63656
$pp \to 2\pi^+ 2\pi^-$ annihilation process, 3.6 GeV/c, multi-peripheral model including reson. 2−59578
$pp \to p +$ anything, determination of triple Reggeon vertices 2−49594
$pp \to pp\pi^-\pi^+$, multi-Regge models analysis, 13.1 GeV/c 2−63655
$p\pi^-$ production, from interaction of 25-30 GeV/c neutrons with C, comparison with double Regge model 2−63670
π Compton scattering, low-energy theorem and threshold identity arguments for fixed pole 2−76671
π^0 photoprod., cut contribs. in dual cut model 2−55852
π^+ photoproduction on protons in backward direction, 0.7-8 GeV, comparison with Regge-pole analysis 2−63607
$\pi\eta \to \pi\eta, \pi\rho$, t-channel Regge amplitudes for local duality 2−63552
πK scattering, output K* and K** trajectories 2−45989
πN charge-exchange forward scattering, invariant amplitudes, energy dependence of ρ Regge-pole model 2−79579
πN interaction, short range P-wave interaction, comparison with high energy backward Regge models 2−70234
πN Regge pole exchange, multiple, consequence of crossing symmetry 2−79576
πN scatt., dual reson. model with Regge cut 2−55856
πN scatt., eikonal model for Regge cuts 2−59538
πN scatt., forward charge exchange, Regge cuts 2−59537
πN scatt., relativistic Regge-cut model for invariant functions 2−76667
πN scattering, elastic and charge exchange, phenomenological analysis, Regge contributions 2−42400
πN scattering, fixed-u finite energy sum rule calcs. using realistic spectral functions 2−63627
πN scattering, Regge pole model with explicit quark spin applied to meson and baryon exchange 2−49572
πN scattering amplitudes, energy dependence from finite energy sum rule Regge fits 2−82760
πN scattering at high-energy linear trajectory fits in simple Regge model 2−63623
πN short range P-wave scattering 2−79578
$\pi N \to K[\Sigma,\Lambda]$, hypercharge exchange reaction, amplitude analysis 2−42389
$\pi^- p$ elastic backward scattering, Regge pole analysis 2−63630
$\pi^- p \to K^0 \Lambda^0$ backward scattering at high energy, prediction of polarization sign 2−63628
$\pi^- p \to \pi^0 n$ (ηn), properties of polarization in forward direction determ. using Regge amplitudes 2−70237
$\pi^+ p$, 5.45 GeV/c, Deck type double Regge trajectory exchange amplitude for A_1^+ production 2−73838
$\pi^+ p$ backward scattering, simplified Regge analysis 2−79593
$\pi^\pm p \to A_1^\pm p$ at small momentum transfer, eikonal Regge model 2−45966
$\pi\pi$ scattering, continuous moment sum rules, estimation of Regge parameters of exchanged trajectories 2−55859
$\pi\pi$ scattering, Regge high-energy behaviour 2−70245
$\pi\pi$ scattering models, review 2−45978
ρ_{10} production in $KN \to K^*(890)N$, unnatural parity exchange 2−49586
$\rho\rho$ P triple-Regge vertex calc. from two-body scattering data assuming duality and f-coupled Pomeron 2−55842
V^0 photoproduction on protons studied in Regge pole model with cuts 2−49577
$K^\pm p$ scattering, Regge fit with Veneziano residues 2−52603

Relativity
aberration of light 2−73024
aether theory, determ. of fine struct. const. 2−82203
conference, Jerusalem, Israel (May 1972) 2−70340
conformally invariant equations of motion for massive particles and Maxwell equations 2−52308
dynamics of rigid test body in curved space-time 2−52050
Earth vel. rel. to absolute space, suggested meas. method 2−82204
e.m. wave propagation in nonuniformly moving medium, relativistic effects 2−63182
e.m. waves from charges in motion 2−82399
equations for nonzero mass particles 2−58720
group, single parameter, quasi-exchange, finite transforms 2−48982
law of conservation of angular momentum, some consequences rel. to relativity 2−45251
local equivalence and frame indifference generalizations 2−52056

Relativity continued
moving particle, relativistic kinetic temperatures 2–66474
photography of relativistically moving objects, apparently rotated image 2–55778
quantum mechanics, relativistic, relation of space-time to material symmetry 2–66440
teaching text, college-level 2–62980
time dilation and Doppler effect in space optics 2–79433
velocity of light postulate and Ritz emission theory 2–55378
wave equations, Lorentz tensors 2–41472
Weyl's lemma as transport and coupling rule 2–82185

general
see also Cosmology, Gravitation; Red shift; Space-time configurations
– 2–66433
– 2–66437
angular momentum and Kerr metric 2–73306
angular momentum conservation, description by pseudo-tensor technique 2–69002
asymptotically flat space-times, peeling 2–58980
axially symmetric distributions of matter 2–62994
axially symmetric interior solutions, new coordinate condition and elementary flatness 2–73303
Bianchi cosmologies, diagonal 2–66428
black holes, relativistic Roche problem 2–58161
black holes, time symmetric initial value problem 2–58726
black holes and temporal ordering 2–81764
Brans-Dicke theory, approx. solution for static spherically symmetric metric due to point charged mass 2–41478
Brans-Dicke theory test using cold neutron star model 2–73308
causality group in finite space-time 2–58730
clock paradox, experiments with atomic clocks, critique 2–62988
co-ordinate group symmetries 2–55399
conformal symmetry, spontaneous breaking and causality 2–58731
conformastat metric forms, soln. of vacuum field eqns. 2–76199
conservation of energy-momentum, in nonvacuum field eqns. 2–82200
continuous media, neighbourhood axiom and functional dependence of laws of relativistic mechanics 2–76192
cosmological model, generalized Taub solution 2–78428
cosmological spatial homogeneity criteria 2–66427
Cosserat continuum determ. of relativistic energy momentum tensor 2–69576
counter-rotating discs of matter surface stress-energy tensors, stability criteria and control red shift 2–55401
cross expts. and determ. of Riemannian curvature tensor 2–48994
curvature of physical space and difference between gravitational and inertial fields 2–78804
dimensionally dependent divergences 2–48995
Einstein's eqn. for energy density inside perfect fluid sphere, integration 2–82189
Einstein's field theory, use of Lorentz- covariant procedure for motion of particles interacting through gravitational field 2–49000
Einstein closed universe, electrodynamic Green functions 2–69562
Einstein effect, fourth, bending and retardation of light in a gravitational field 2–66426
Einstein equation, linearized, local and covariant quantization 2–59362
Einstein evolution equations as first-order quasi-linear symmetric hyperbolic system 2–78786
Einstein field eqns., in an ideal fluid, inner stationary axially symmetric solutions 2–69574
Einstein field equation, quadratic first integral for charged particle orbits in Kerr solution 2–73296
Einstein field equation with radiation energy transport, interior spherically symmetric solutions 2–69580
Einstein universe, propagators for arbitrary spin 2–52055
Einstein-Cartan equations 2–41470
Einstein-Cartan equations 2–73294
Einstein-Lorentz manifold, compact, consequences of vanishing Euler-Poincare characteristic 2–48990
electrodynamics, duality principle 2–76179
electrodynamics in expanding universe, co-determined Einstein-Maxwell equations, soln. 2–76193
electromagnetic field, geometrical theory, and gauge transformation 2–82198
elementary particle definition as irreducible unitary representations of group of asymptotically flat space-times in general relativity 2–73737
e.m. and gravit. wave, propag. of tensor discontinuities 2–78782
energy-momentum definition 2–52061
equations of motion, null tetrad formulation 2–66455
equations of motion in asymptotically flat empty spaces 2–66434
equivalence principle and curvature of spacetime metric rel. to redshift rocket probe experiment 2–69571
experimental tests and explanations 2–82205
experimental tests of gravity using radar and radio waves 2–76198
falling body problem 2–73273
field equations of high spin in curved spacetime, necessary integrability conditions 2–45257
finite amplitude sound equation for propagation, gravitational instability 2–52053
fluid, perfect, rotation with gravitational, electromagnetic and thermodynamic props. about fixed axis 2–69577
fluid electrically charged, some solns. to Einstein Maxwell equations 2–69563
free particle system, kinematical symmetry 2–82665
gauge group representation 2–76191
geometrodynamics, bubble-time canonical formalism 2–41480
gravitational absorption 2–51495
gravitational collapse, nonspherical perturbation in integer spin of zero-rest-mass fields treated in Newman-Penrose formalism 2–55387
gravitational collapse, nonspherical scalar of gravitational perturbations 2–55386
gravitational field, axially symmetric and the Kerr metric 2–82199
gravitational field eqns. approx solutions to describe clusters of galaxies 2–58197
gravitational field equations, Yang Mills type theory with SL(2,C) invariance 2–52049

Relativity continued
general continued
gravitational lens, uniform, transparent 2–58729
gravitational radiation from relativistic systems, calcs. for circular orbits and extreme hyperbolic trajectories 2–55390
gravity, compendium of metric theories and post Newtonian limits 2–62978
gyroscope equations of motion 2–69569
gyroscope expt., precession in Einstein and arbitrary theories of gravitation 2–76187
gyroscope expt. at arbitrary orbit inclinations, calc. of total precession and optimum orbit 2–66430
hadronic props. deduced, Yukawa potential 2–69564
Hamiltonian constraint, momentum constraints as integrability conditions 2–66432
higher spin rest-mass zero fields, properties 2–73304
inhomogeneous spacetime continuum, corresponding local pseudoeuclidian 4-dimensional tangent space construction by chronometric method in Hamiltonian space of special relativity 2–76180
initial-value problem, axially symmetric, applications of Regge calculus 2–48998
interacting particle system, asymptotic limit for speed of sound 2–66429
interior metric for stable static charged matter fluid with large e/m 2–48997
internally stressed body in gravitational field 2–78803
irrotational dust cosmologies, quantum models for lowest-order velocity-dominated solution 2–55402
Kepler problem with magnetic charges, quaternionic solutions 2–52060
Kerr geometry, solution of scalar wave equation by separation of variables 2–48999
Kerr metric, orbital and vortical motion 2–62990
Lorentz transformation from conservation of differential forms for action with invariance 2–58734
Lorentz variations, homothetic curvature of associated couples of hypersurfaces 2–45256
Lorentzian symmetric spaces 2–76185
Mach's principle, formulation and philosophical justification 2–76197
Mach's principle and cosmology 2–58735
Mach's principle and gauge freedom in Brans- Dicke theory 2–41477
Mach's principle rel. to gravitation theory 2–58736
Mach principle as feature of q-process theory of space-time 2–55424
macroscopic objects spinning on own axes, relativistic precessions 2–73305
magnetoelastic interaction, relativistic theory 2–41616
massive bodies, effects on static e.m. fields in general relativity 2–78799
matter-antimatter asymmetry and joining of two semiclosed worlds 2–62440
Maxwell-Dirac field in Coulomb gauge, covariant generalization of quantization 2–69578
Mercury, perihelion advance, radar determ., general relativity confirmed 2–51824
MHD, action principle 2–56316
neutrino field 2–69568
Newman-Penrose eqns., extension of asymptotic solns. using algebraic programming system FORMAC 2–76195
Newtonian gravitational theory, Poincares generalization 2–62946
Nordstrom scalar covariant theory of gravit. rel. to general relativity 2–76174
Oort-Schwarzschild formula, relativistic generalization 2–69573
oscillation of astrophysical fluid masses, exact hydrodynamical equation 2–58728
oscillatory behaviour of null geodesics, WKB approximation 2–62986
particle counts in relativistic revolutionary cosmos 2–48988
perfect fluids, Lagrangian density 2–82196
perohelic precession, contribution of spatial curvature 2–82191
principle of mass indifference, possible definition 2–73302
proton radius 2–76200
Ptolemy-Kopernik problem, reference frames and principle of nonholonomy 2–82212
quantization, Einstein algebras 2–45258
quantum many-body theory, Riemannian space-time, applic. to superdense matter 2–66447
radiating particle anomalous motion in strong fields 2–55403
radiation pressure on dust 2–58723
radius of elementary particles 2–69567
random unit vectors, averages of components 2–62979
relativistic perfect fluid, Einstein field equations, spherically symmetric solns. 2–56277
relativistic runaway problem of binary system with primary mass loss 2–72967
Robertson-Walker spaces, time-like geodesics from Hamiltonian viewpoint, characteristic function determ. 2–76194
rotating defects, exact equations for stationary equilib. in special comoving coord. system 2–78800
rotating stars, energy extremal properties 2–44851
scalar meson fields, axially symmetric massive, nonexistence 2–59359
Schwarzschild 2-particle metric superimposed on uniformly accelerated metric 2–69575
Schwarzschild background, meson e.m. and neutrino quantum fields, interactions 2–55406
Schwarzschild black hole, gravitational radiation pulses of particle falling radially 2–55405
Schwarzschild field, lightlike behaviour of particles 2–73309
Schwarzschild interior soln., conformally flat system 2–78429
Schwarzschild soln. interior, equation of state of static case 2–69579
second-order recurrent space-times 2–78790
single static zone planet, structure 2–69143
spheres, equation of state and adiabatic stability 2–48996
spherical shells of ideal gas in central gravitational field, motion 2–48984
spinning particles in gravitational and e.m. fields, canonical dynamics 2–41479

Relativity continued
- **general** continued
  - stability of axisymmetric systems to axisymmetric perturbations, instability onset in uniformly rotating configurations 2-62985
  - stability of axisymmetric systems to axisymmetric perturbed sytems, perturbations, equations governing nonstationary, stationary and perturbed systems 2-48989
  - static cosmological solns. of generalized field eqns. 2-69000
  - stationary black holes shown to be identical in general relativity and Brans Dicke theory 2-55385
  - symplectic mechanics, spin particle in gravitational and e.m. field 2-52059
  - synchrotron gravitational radiation, Regge-Wheeler formalism 2-44827
  - tachyon dust metric solutions to Einstein field equations 2-45259
  - tetrad field theory of gravitation conservation laws and identities 2-48993
  - Thomas precession and relativistic disc 2-52057
  - three-particle states, complete system 2-69572
  - time-delay expts., best-fit estimate of relativistic effects 2-66431
  - transformation formulae for accelerating frames of reference 2-78783
  - Trautman conservation law generator, Komar superpotential expression 2-78789
  - twisting null congruences is asymptotically flat space 2-62993
  - uniform fluid spheres surrounded by empty space, class of exact solutions 2-66425
  - variational principle, scalar-tensor formation 2-82208
  - Weyl equation solutions, neutrinos in spherically symmetric gravitational fields 2-58727
  - Weyl metric for 2 Schwarzschild particles superimposed on uniformly accelerated metric 2-69575
  - H atom, Dirac equation, formulation in Friedman universe 2-49972
- **special**
  - *see also Tachyons*
  - action and entropy equivalence, bicharacts. 2-62981
  - clock 'paradox', test of theory by around-world Cs beam atomic clocks 2-82210
  - clock 'paradox' test of theory by around-world Cs beams atomic clocks 2-82211
  - cosmic rays, ultra-high-energy, possible generalisation of relativistic theory 2-46023
  - Ehrenfest's paradox of relativistic rotating disc, application of Thomas precession to extended structures 2-76175
  - Einsteins approach to discovery 2-82093
  - elastic particle collisions, max. number under Newtonian and relativistic laws 2-82292
  - electron dynamics, Poincare's Rendiconti paper 2-41426
  - electron mass, meas. of increase with velocity., verification of special relativity predictions 2-55394
  - equilibrium concept, asynchronous formulation 2-58725
  - faster-than-light inertial frames and tachyons 2-78788
  - Fitzgerald-Lorentz contraction based on interactions with neutrino sea 2-82201
  - four-component hypermass eqn. from quarternion mass generalization, application to unstable neutrinos 2-78791
  - free tachyon fields in two dimensions, causal properties, calc. using Klein-Gordon eqn. and relativistic invariance 2-78801
  - general covariant observables, local Lorentz transforms., tetrad and general formalism 2-45255
  - geometrical exposition 2-82107
  - Hamiltonian for N-free relativistic particles, totally symmetric form 2-82188
  - harmonic oscillator, relativistic formulation derivable from Lorentz-invariant variational principle 2-78798
  - hot universe, non-existence of cosmic-ray cut-off around 10^{20}eV, choice of absolute reference system 2-72960
  - inertial frames of reference, relative velocities greater than c 2-45252
  - isotropy of C, expt. 2-78787
  - local pseudoeuclidian 4-dimensional tangent reference frame 2-76180
  - Lorentz group, homogeneous, unitary represents. in $O(1,1)\otimes O(2)$ basis 2-63024
  - Lorentz transformations, derivation of linearity and scale factor 2-62982
  - Lorentz transformations, teaching device 2-55351
  - Lorentz transformations and tachyons 2-41476
  - Lorentz transformations rel. to tachyons 2-45253
  - nonparallel convection of light, expts. to test relativistic velocity addition theorem 2-41474
  - nuclear Coulomb energy calc., relativistic corrections 2-46076
  - particle current and electric current concepts 2-55396
  - particle motion constant force and uniform gravitational field, student exercise 2-48966
  - problem for students 2-55395
  - pulsars, e.m. field, special relativistic treatment 2-58386
  - quantum theory, sign of static electric polarizability 2-78823
  - second-order Doppler-effect experiment 2-69561
  - and space-time absoluteness, experimentum Crucis 2-52058
  - space-time diagrams, teaching methods 2-78739
  - structure of relativity groups, class of equivalent reference frames in terms of kinematical characterization of free material point 2-41473
  - superdense stars, tachyon-like, matter implications 2-55397
  - superluminal frames and group of generalized Lorentz transforms. in four dimens. 2-58724
  - thermodynamics, co-moving, equivalence of two major formulations 2-41475
  - thermodynamics, formulation of second law 2-55567
  - Thomas precession and clock paradox 2-78781
  - three-dimensional elastic media, causality 2-78873
  - twin paradox, calc. in both frames 2-48987
  - twin-rod thought experiment, analysis 2-55393
  - velocity of light, meas. of first order effects 2-69560
  - wave equation for particles with arbitrary spin 2-41505
  - $NaClO_3$, irrad., double reson. obs. of mag. dipolar interaction 2-72534

Relativity continued
- **unified field theories**
  - axially symmetric interior solutions, new coordinate condition and elementary flatness 2-73303
  - Bonnor theory, static spherically symmetric solution 2-69583
  - Born-Infield nonlinear e.m. theory, Newman-Penrose conserved quantities 2-82163
  - charge production by coordinate transformation in five-dimensional Riemannian space 2-76178
  - construction and characterisation of gravitational fields 2-66437
  - Einstein's, external electrostatic field of axially symmetric localized charge 2-76202
  - Einstein's eqns., soln. for spatially flat field of e.m. origin 2-82193
  - Einstein's nonsymmetric theory, eqns of motion 2-82187
  - Einstein connection geodesics, rel. to charge paths in Lyttleton-Bondi electrodynamics 2-55795
  - Einstein equations, cylindrical symmetry 2-69582
  - Einstein-Kaufman nonsymmetric, static spherically symmetric solutions 2-55407
  - Einstein-Maxwell eqns., a class of non-spherically symmetric solutions 2-69584
  - Einstein-Maxwell eqns., soln. for static distrib. of massive charged particles 2-76196
  - Einstein-Maxwell equations, solutions of class of nonlinear coupled partial differential equations 2-58737
  - Einstein-Maxwell equations, stationary charged dust distribution 2-41483
  - Einstein-Maxwell null field, e.m. interpretation of Kerr-Vaidya metric 2-73297
  - Einstein-Maxwell space-time, symmetry 2-82197
  - Einsteins equations, solutions admitting 3-parameter group of isometries 2-66436
  - Einsteins nonsymmetric, relation of electromagnetic field to skew-symmetric part of fundamental tensor 2-69581
  - electro-gravitational matter 2-66439
  - electromagnetic field, geometrical theory, and gauge transformation 2-82198
  - electrovac fields with geodesic eigenrays 2-41471
  - e.m. field, generalized multipolar decomp., space-time multipolar sources 2-52530
  - e.m. field in presence of random sources, stationarity, homogeneity and isotropy 2-58738
  - e.m. field pot., multipolar represent. 2-45853
  - e.m. fields classification 2-82194
  - e.m.-gravitational field, uniform, coupled Einstein-Maxwell eqns. 2-45261
  - general-relativistic field equations solved for static charged matter fluid with large e/m 2-48997
  - geometrical formulation of gravitational and e.m. fields for systems of point mass charged particles 2-73310
  - gravitational field in unified spinor field theory 2-66438
  - isolated charge distribution, using Einstein's equations 2-66435
  - Newman-Penrose conserved quantities, conservation and existence 2-45262
  - physical laws invariance under space time depend. changes in unit of length 2-76176
  - simple coupling between e.m. and gravitational fields 2-73311
  - Weyl and Lyra manifolds, difference between geometries and relation to Reimannian geometry 2-45260

Relaxation
- *see also Acoustic wave propagation. Dielectric phenomena; Elastic relaxation; Ferroelectric phenomena; Ferromagnetic relaxation; Molecules/relaxation; Nuclear magnetic resonance and relaxation; Paramagnetic resonance and relaxation; Spin-lattice relaxation*
- air study of bound electron temperature and relaxation phenomena behind shock wave 2-54542
- beam-plasma system, instability control 2-74403
- chemical, as transport process 2-48315
- chemical, u.s. cavity resonator technique 2-76372
- defects, crystal lattice, diffusional relaxation, in the fields of local lattice disturbances 2-84000
- diatomic gas in shock front and wake, relaxation equations for vibrational and rotational energy including transport processes and chemical reactions 2-52966
- electromagnetic waves in resonant medium, frequency-dependent gain curves 2-82397
- excess electrons in polar solvent produced by photoionization 2-72568
- fluctuations, relaxation matrix for system with internal degrees of freedoms 2-45304
- ionization relaxation, direct absorpt. effect of transverse quanta of plasma oscills. 2-77296
- liquid droplets, evaporating, maximum relaxation times 2-43302
- liquid thermal relaxation times using improved rigid sphere equation of state rel. to sound absorption 2-56499
- liquid-bubble mixtures, shock wave propagation and relaxation effects 2-77453
- multilevel system, theory of spectrophone effect 2-80410
- neutron pulses, anisotropically scattered, relaxation times in decay 2-74138
- nonlinear mode coupling linearly unstable and stable waves, obs. of relaxation oscillations 2-83624
- optically pumped vapour, relaxation of electronic spin polarization by collisions with cell wall 2-76995
- polyethylene, linear, anomalous internal friction at low temps. 2-84107
- polymers, rigid dynamometer for obs. of stresses 2-43757
- polyurethane block polymers, meas. of stress and birefringence relaxation 2-74850
- rubber blocks, bonded, compressed, elastic stress strain eqns. dynamic relax. solns., Poissons ratio effects 2-66528
- shock relaxation in gas-dust medium 2-46834
- solid, effect on pressure pulse propagation 2-68074
- stress, equipment for testing at nonstationary temps. 2-68119
- stress, graph analytic method of evaluation of relationship with creep 2-64743
- ultrasonic in liquids and light scattering 2-50356
- ultrasonic of polystyrene in alcohol suspension 2-53462
- vibrational relaxation of anharmonic oscillators 2-66422

Relaxation continued
- viscoelastic in liquids, defect-diffusion model 2–64449
- weak shock waves propagation in relaxing gas 2–83653
- HF laser, transversely excited 2–45732
- ^{3}He fluid near critical point, meas. of thermal relaxation times 2–80514
- $KNbO_3$, ferroelectric single crystals, stress relaxation behaviour 2–80743
- $NaPO_4$ glasses, stress relaxation mechanism 2–77636
- Se, molten, ultrasonic absorption 2–43353
- Ti, stress relax., validity of modified Gilman's equation 2–80832

Remanence *see Magnetization state*

Renner effect *see Molecules*

Replica techniques *see Electron microscopy*

Reproduction *see Sound reproduction*

Resistance, electrical *see Conductivity, electrical*

Resistance thermometers *see Thermometers/resistance*

Resistivity *see Conductivity, electrical*

Resolving power, optics
- *see also Optical instrument testing*
- astronomical photographic degradation by atm., resolution enhancement by computer processing 2–76040
- circular aperture focusing system, nonuniform coherent illumination 2–59246
- electron microscopes with single-field condenser objective 2–79076
- electron microscopy, very thin specimens 2–79125
- Gaussian beam optics rel. to conventional optics 2–79296
- microscope, two-point resolution rel. to condenser obstruction 2–76525
- optical memory matrices, resolution by focused laser beam 2–55710
- photographic, of lenses, meas. from radial and line targets 2–59328
- photographic materials, determination by projection and interferometer methods 2–70095
- rate distortion fn., restoration 2–79306
- scanning, microscope, super resolution aperture 2–52464
- scanning electron microscope, image contrast effects from superimposed submicron structural networks 2–79127
- Selfoc lens, imaging properties 2–70003
- surface scanning electron microscope, low loss images 2–79126
- thermoplastic recording emulsion layers with regular image element structure 2–73236
- two point resolution in partial coherent light, microscopy 2–52457
- $Bi_{12}SiO_{20}$ electro-optic image modulator, sensitivity and resolution 2–79417

Resonance, elementary particles *see Baryons/resonances; Hyperons/resonances; Mesons/resonances*

Resonance, magnetic *see Magnetic resonance and relaxation*

Resonance spectra *see Spectra*

Resonators
- acoustic, with impedance wall 2–69777
- angle-tuned optical parametric oscillators, bandwidth and threshold calculations 2–59130
- beam modes, open resonators filled with anisotropic uniaxial crystals 2–45710
- cavity, emissivity det. by reflection meas. 2–41844
- cavity, freq. insensitive to axial elongation 2–69814
- cavity, reson. freq. shift of intense laser pulse 2–79180
- cavity pulling in passive frequency standards 2–63304
- characteristics rel. to polarization pulling in three level gas laser 2–66741
- confocal, output beam with pinhole for mode selection 2–69898
- c.w. dye lasers, improved astigmatically compensated resonator 2–59133
- CW gasdynamic laser with unstable resonator approximate theory 2–76471
- double heterostructure injection lasers, reflectivity of cleaved facet and single mode operation 2–42076
- E_{010} cavity, temp. variation of resonant frequency resonance curves 2–58985
- electron ring field 2–79703
- Fabry-Perot, diffraction props. of two closely-spaced apertures 2–58982
- Fabry-Perot, excitation of natural oscillations by laser beam 2–45711
- Fabry-Perot, line source illumination, resonances and resonant fields 2–45708
- Fabry-Perot, with annular output-coupling aperture, mode selection for CO_2 laser 2–73564
- gas laser, longitudinal elec. field rel. to internally modulated light beam 2–49367
- Helmholtz, resonant freq. calc., consideration of shape 2–78920
- h.f. modulation 2–49347
- injection pulse laser with adjustable combined resonator, characteristics 2–52409
- interaction of external radiation with a medium inside a cavity 2–66727
- laser, confocal spherical, excitation, theory 2–49346
- laser, effects on energy and time duration of self pulses 2–41962
- laser, equivalence relations with a lens-like medium, approx. from Huygens-Fresnel principle 2–69899
- laser, forced combination diffusion in benzene 2–41976
- laser, high power giant pulse, with unstable cavity 2–69934
- laser, kinetics of single pulse production and second harmonic conversion efficiency 2–66739
- laser, saturated optical absorption technique for meas. of optical resonances 2–79231
- laser multimode, cavity field, theory of wave packet 2–41967
- low loss, modes and losses, diffr. formulas 2–79375
- microwave cavity, for plasma diagnostics 2–77284
- microwave grating for masers, fabrication technology 2–41956
- modes, model for multimode solid state laser 2–76489
- noninstantaneous Q-switching for single pulse lasing 2–69902
- open resonators filled with inhomogeneous medium, integral equations 2–76468
- open with spherical mirrors, variational calc. of resonant microwave freq. to test beam-wave theory 2–58984
- optical, conical mode selector insert for radially polarized mode 2–69901

Resonators continued
- optical, three-mirror ring, with Gaussian diaphragm 2–59134
- optical, with inhomogeneous medium, equivalent parameters, quasi-geometric optics formulation 2–63316
- optical, with round spherical mirrors, diffraction loss of radiation 2–66738
- optical cavity, use in self synchronized laser, patent 2–66795
- particle accelerator low phase velocity supercon. resonant cavities, magnetic and electric fields meas. 2–49700
- passive auxiliary, returning by u.s., laser pulse modulation 2–69900
- quartz, simultaneous obs. of thin film stress and mass change 2–50786
- quartz, X cut resonators, linear and nonlinear coeffs. 2–84362
- ring, selection of principal transverse mode 2–41974
- ruby laser, scatt. in plane-parallel resonator 2–79179
- scanning Fabry-Perot, excitation resonance charact. 2–49449
- superconducting, harmonic generation 2–73485
- superconducting r.f. cavities, electron loading 2–59655
- three-mirrored, with Faraday element, frequency and polarization characteristics 2–52410
- transverse mode suppression using rimmed unstable resonators 2–41970
- transverse modes, diffractive calculations 2–82471
- tuned prismatic with active medium of $CO_2 + N_2 + HE$, selective properties 2–52411
- unstable, applications, review 2–41973
- unstable, scalar wave theory and experimental evaluation 2–41969
- unstable configuration for mode selectivity in TEA CO_2 volume excited laser 2–41991
- unstable modes, large Fresnel numbers 2–82470
- u.s., cavities, chemical relaxation studies 2–76372
- CO_2:N_2:H_2O c.w. gas dynamic laser, unstable resonator calculations 2–82483
- CO_2 unstable confocal ring laser 2–41992
- HCN resonant wavelength meas. at 311 and 337 μm using laser resonator interferometry 2–41985
- Hg spectral lamp in u.h.p. cavity, optical pumping 2–73550
- Ne absorption tube in alternating magnetic field in laser cavity as frequency standard 2–78757

acoustic *see Acoustic resonators*

electromagnetic *see Electromagnetic oscillations*

Reverberation
- *see also Architectural acoustics; Echo*
- acoustical design of synagogues in Israel 2–41828
- averaged sound pressure in reverberation chamber, rotating vane effect 2–41693
- degree of coherence of sound incident at different angles in reverberant chamber 2–52246
- diffuse sound field, reverberation time formulae 2–63115
- hall, light-construction, model obs. 2–45552
- helical spring for reverberation devices, propag. of struct. borne waves 2–45489
- industrial room models, noise propag. 2–45546
- integration time variance in reverberant room measurements 2–45526
- open plan offices, reverberation time measurement, equipment 2–58931
- panel, influence of measuring facility on measured sound insulating property 2–63131
- rooms, accuracy of sound power det. 2–41798
- rooms, effects on accuracy of sound power det. in 2–41811
- rooms, for sound power testing 2–41796
- rooms, noise obs. 2–41810
- rooms, qualification for det. of sound power 2–41795
- rooms, statistical behavior of source-receiver locations 2–41797
- simulated curves in rectangular rooms with diffuse sound field 2–55555
- sound field, effective modal density for finite sized sources 2–41799
- sound power level meas. in semireverberant rooms 2–41692
- spatial correlation of reverberant sound fields by k-transform technique 2–41687
- statistics of sound power radiation in reverberant room 2–41691
- synthetic sound fields, spatial distrib. of directions 2–52247
- volume reverberation, mathematical model 2–44665
- volume reverberation simulation 2–44666

Reviews
- — 2–74095
- — 2–70054
- — 2–73161
- acoustic holography 2–42153
- acoustic surface wave interdigital transducer theory 2–49140
- acoustics as physical science 2–41685
- acoustoelectronics in USSR 2–51029
- aerodynamics at National Physical Laboratory, 1917-70 period 2–67720
- aeroelasticity, trends and achievements 2–50254
- aerosol optical and dynamic props. 2–46998
- aerospace applics. of holography and optical data processing 2–48639
- alaryngeal speech, acoustical properties 2–45071
- alloy, supersaturated solid soln. decomp. 2–43928
- alloys, thermomechanical treatment 2–80854
- amorphous solids, opt. props. 2–72293
- Apollo 11 and 12 manned lunar landings 2–44931
- Apollo lunar spacecraft, equipment and instrumentation 2–51823
- applied acoustics and role in society 2–41686
- Arctic and Antarctic investigations during the Soviet Regime 2–62049
- artificial eye unit 2–51959
- atmospheres of very cool supergiants 2–62555
- atmospheric boundary layer descriptions 2–65694
- atmospheric waves and ionosphere 2–44671
- atomic collision processes, book 2–64049
- atomic fluorescence yields in K, L, and M shells, review of exptl. and theoretical techniques 2–42755
- atomic scattering, interference phenomena calc. 2–56113
- atomic shells, selection rules 2–49940
- atomic spectroscopy 2–46419

Reviews continued
auditory evoked potential in man, review 2−62875
Auger electron spectroscopy, principles and applications 2−77481
aurora, space-time regularities, electron fluxes, luminesc. 2−68944
auroral spectroscopy and excitation processes 2−48553
axiomatic quantum field theory, observables and fields 2−63476
band O stars spectra, theoretical interpretation 2−75740
benzene, radiative and nonradiative processes 2−60052
beta-ray spectrometers, magnetic prism 2−79670
bicrystal, epitaxial, interface struct., effect of misfit, bonding and cryst. dimens. 2−56690
biological macromolecules, biological, quasielastic light scattering 2−81991
biological molecules, structures, neutron diffraction 2−81994
biological systems, obs. of surface reactions by ellipsometry 2−69203
biomedical applications of i.r., visible and u.v. radiation 2−85131
biomedical technical equipment 2−85091
biophysics and bioengineering, book 2−81987
biopolymer molec. studies, flow dichroism spectra applic. 2−53089
blood flow measurement, technique and instruments 2−78645
boson spectroscopy, review of current exptl. problems 2−76647
β- brass type alloys, quenched, structure and microstructure 2−84106
breakwaters and transportable wave barriers 2−54747
broken symmetries, applic. of effective Lagrangians 2−63462
bubble chambers, current expts. and proposals for future expts. 2−76748
bubble dynamics 2−43304
bubbles, non-spherical oscillations, disintegration and surface instabilities 2−53372
BWR development in Germany 2−63949
capillarity, Young and Laplace eqns. 2−46903
cavity and wake flows, free-streamline theory 2−80205
celestial mechanics, present and future 2−81785
celestial mechanics in twentieth century 2−78443
ceramics, transparent, cryst., optical applications, prep. 2−60988
chalcogenide glass, elec. conductivity and electron transport processes, structural effects and physical mechanisms 2−61267
chalcopyrite semiconductors, linear and nonlinear optical props. 2−48126
chemical lasers 2−41981
chemisorption theory 2−48329
chromatography, applications in chemical practice 2−54565
collective ion acceleration by intense relativistic electron rings 2−55942
colour centres, electronic structure, theoretical developments 2−56746
colour instrumentation systems 2−70028
comet and meteoroid research 2−58524
comet astronomy in the USSR 2−75919
comets, formation, structure, and composition 2−44966
composite, fibre reinforced, strength 2−61009
composite materials, gradient 2−50914
composite materials, mechanical properties and structure 2−43901
compound nuclear reactions 2−82100
computer simulation of transport processes 2−82253
correlations between partial widths of different channels 2−46216
cosmic γ-rays and γ-astronomy 2−69010
cosmic background X-rays, observations of diffuse component 2−51695
creep, diffusional, grain boundary sliding 2−56730
crystal, interstitial atoms, radiation-induced 2−77577
crystal, opt. props. in excitonic region of spectrum 2−72317
crystal chemistry, hydrogen containing compounds by neutron diffr. obs. 2−74653
crystal dynamics, Raman theory 2−61054
crystal equil. forms 2−47189
crystal evap., model 2−47215
crystal growth, hydrodynamics and convection 2−47191
cutaneous perception of microwaves 2−55228
c.w. pumped dye lasers 2−63333
data processing for weather radar 2−75506
decoration and electron beam study of lattice structure and point defects 2−80604
defect evaluation by ultrasonics, work at German Federal Institute for Materials Testing 2−69756
delayed neutrons 2−83047
diffusion mechanisms in metals and alloys 2−68044
diffusion of hydrogen in metals 2−77604
direct electronography, astronomical objects 2−66243
disc lasers, developments and applics. 2−69933
dislocation thermal unpinning rel. to Hasiguti peaks of internal friction 2−68023
DNA, helix-coil transition 2−67526
doorway state phenomena and intermediate structure 2−46220
duality concept and development of Veneziano model 2−66975
dye lasers, c.w. and pulsed 2−55694
dynamic Jahn-Teller effect 2−77809
dynamics. classical nonlinear, recent progress 2−63059
ear protection in factory environment 2−73218
Earth, Moon and planets, dynamical properties and internal structures 2−51520
elastic stresses and deflections of flat square plate, under uniformly distributed normal press. 2−69675
elastic wave propagation, thermochemical effects 2−45481
electret transducers, operation and applics. 2−41758
electrets, electrostatic config. and characteristics 2−44168
electrical conduction in metallic, semiconducting and dielectric films 2−64907
electroluminescence, physical processes 2−65315
electroluminescence 2−48265
electron beam as multipurpose tool 2−59084
electron beam therapy techniques, megavolt 2−69318
electron bremsstrahlung interactions, 180-2000 keV on various atoms 2−64041
electron microscope in situ expts. 2−80620
electron microscopes advances 2−59096
electron microscopic image reconstruction methods 2−79149
electron microscopy, techniques and appls. 2−53638

Reviews continued
electron microscopy of crystn. mats., transmission and scanning 2−56700
electron multipliers, parallel plate, properties and development 2−49323
electron optics progress 2−79050
electron probe microanalysis, quantitative 2−48363
electron-molecule scattering, low-energy, resonance-type phenomena, extension of earlier review 2−74300
electron-optical methods of investigating inhomogeneities in rarefied gases 2−60343
electronic accessories, medical diagnostics and therapy, survey 2−81978
electrophotography, systems, materials, processing 2−70099
elementary atomic collision processes, simultaneous analysis of final charge states of both collision partners 2−42804
elementary particles, book 2−42310
elements, evolutionary mechanism 2−58159
e.m. universal background radiation 2−69001
embrittlement by neutron reaction-produced He in structural mats. at high temps. 2−68100
epitaxy process, transition layer structure and properties 2−47093
e.p.r., optical techniques 2−61729
equilibrium thermodynamics of critical points 2−41536
equipment for dielectrics obs. 2−71755
ESCA, u.v. photoexcitation 2−54567
ESCA, X-ray photoexcitation 2−54568
e.s.r., transition metal ions in liqs., equilibria of systs. 2−54569
eta mesons in pseudoscalar nonet 2−63574
exchange interaction measurement, e.s.r. and optical techniques 2−61730
exoelectron emission, thermally and optically stimulated, from insulating solids surfaces 2−84383
expansion of the universe 2−62442
experiments showing radiation pressure of laser light 2−42172
exponential absorption edge in solids, theory 2−78078
extensometry, optical, for elevated temperature fatigue testing 2−56871
F-region, nighttime maintenance, models 2−58093
fast heavy ions, charge states and charge changing cross sections for penetration through gaseous and solid media 2−60294
fast neutron personnel dosimetry, integral methods 2−85129
fast nuclear reactor fuel burn-up measurement methods 2−74188
fatigue crack initiation and propagation 2−60892
fatigue testing at elevated temperatures 2−56869
fatigue under combined stresses 2−47539
fatigue-crack propagation in metals and polymers 2−64728
Fennoscandia, structure and physical properties of Earth's crust 2−51511
Fermi surface of metals using photon annihilation spectrum 2−61171
ferromagnetic film, uniaxial unpinned, Green's function theory 2−78003
ferromagnetic films, electron microscopy of magnetic structure, review 2−84428
films, effects of ion bombardment and implantation 2−53568
final state interactions 2−63487
fission of heavy nuclei, Soviet work (1938 to 1971) 2−76887
flow, unsteady, in pipes, calc. by numerical methods 2−67752
flow metering, developments and prospects 2−83523
fluctuation dissipation theorems 2−58793
fluid, viscoelastic, non-viscometric flow 2−46659
fluid dynamics, techniques for numerical solution of problems 2−43056
fluid flow measurement, current industrial practice 2−83509
fluid line transients, survey of modelling techniques 2−67593
fluid mechanics, book 2−80200
Fourier transform spectroscopy, rapid scan i.r. 2−52486
fundamental dosimetry, current trends 2−69396
fusion, controlled, review article 2−79842
fusion with lasers 2−43175
galactic spiral arms, motion of stars and gas 2−58183
galaxies, spiral, internal motions, historical perspective of Adriaan van Maanen's work 2−55019
galaxy formation, evolution of expanding hot universe 2−51712
galaxy formation, from thermal instability in expanding universe 2−51714
gas, chemisorbed, thermal desorption kinetics 2−67918
gas cooled fast reactors, design and assessment studies, summary of performances 2−83090
gasdynamic flows in laser technique 2−73554
gasdynamics of detonations, blast wave and finite kinetic rate models 2−80378
gaseous turbulent jets, cryogenic discharges into gaseous medium 2−74460
geomagnetic field distortions rel. to radiation belt particles 2−62382
geomagnetic reversal chronology for Tertiary 2−58116
geometrical theory of measurement 2−52030
geometrically nonlinear structural analysis 2−41559
geostationary operational environmental satellite, state-of-the-art report 2−72746
giant resonances, neutron radiative capture, statistical theory 2−46095
glass laser technology 2−55701
global radiation and energy budget 2−61864
glow discharge sputtering systems for thin film production 2−71323
grain boundary migration, rel. to struct. 2−56728
gravitation, theoretical research 2−62992
gravitational collapse and black holes 2−78437
gravitational collapse from nebula to neutron star 2−84985
gravitational radiation, emission, propagation and absorption 2−76188
gravitational radiation, recent experiments, theoretical implications 2−78805
gravitational radiation detection 2−44823
gravity and magnetics, 1964-71, data processing and interpretation methods 2−78242
Great Lakes influence on weather 2−57935
Green function techniques, rel. to atomic and molec. physics 2−49919

Reviews continued
group III-V and II-VI compounds, negative differential mobility 2−44088
hadron interactions, leptonic weak processes 2−63553
hadron interactions, many-body, high energy 2−82717
hadron interactions, many-body problem 2−82719
hadron interactions, weak and e.m., theoretical aspects 2−49524
hadron reactions, phenomenology 2−66966
hadron scatt. amplitudes, rigorous constraints, bounds, analyticity 2−79551
hadron strong interactions, exptl. and theoretical aspects 2−49522
hadron-hadron interactions, two-body 2−82718
heat transfer, 1971 literature 2−76393
Hertzsprung-Russell diagrams, various forms 2−62511
heterojunction photodetectors, review 2−44180
h.f. levitation melting, prep. of targets 2−73906
high temp. plasma physics and fusion 2−77287
high-energy particle detectors, recent advances and developments 2−49610
high-energy scatt. phenomenology 2−63566
high-strain-rate investigations, stress/strain characts. 2−47489
high-temp. thermometry 2−52289
history of use of balloons in scientific experiments 2−72743
holographic information storage 2−63354
holographic magneto-optic memories, materials 2−63345
holographic recording in $LiNbO_3$ 2−63355
holographic recording materials 2−55716
holographic storage media, recyclable, performance parameters 2−63361
holography, biomedical applications 2−78662
holography (1948-1971) 2−79249
horizon sensors for geostationary satellites 2−44807
hot workability 2−50795
HTR, He quality control, gas circuit purification methods 2−42675
HTR core design in UK 2−42623
HTR reactor thermal insulation systems 2−42620
HTR refuelling sytems, on- and off-load 2−42648
human red blood cell, structure 2−69205
hurricane and tropical meteorology 2−75491
hydrogen bonded liquids, review of i.r. and Raman spectroscopy relating to structure properties 2−43315
hypernuclei spectroscopy 2−67139
hyperon-nucleon interactions 2−59587
ice, p.m.r. investigations 2−61746
ice particle growth in atmosphere from vapour and cloud drop accretion 2−54849
imperfections in metals 2−68012
inclusive reactions, kinematics and direct channel expansions in 1-particle and 2-particle processes 2−45862
inclusive reactions, Regge phenomenology 2−66967
injection laser diodes, future developments and applics. 2−69947
instrumentation and advances in fluid mechanics 2−77209
integrated optics, propagation of light in thin films 2−42190
interplanetary objects, statistics of masses and dynamics 2−75917
interstellar absorption, research development (1900-30 period) 2−81842
ion, with orbital ang. momentum, interactions in insulators 2−65112
ion bombardment effects on surface of metal crystals 2−74614
ion recombination, 3-body 2−74228
ion-atom collisions, inner shell ionization, X-ray production 2−83198
ion-phonon interactions in paramagnetic crystals 2−48117
ionosphere, propagation and application of waves 2−62352
ionosphere development in period (1925-1955) 2−68958
ionospheric cosmic radio noise absorption, riometry 2−84902
i.r. laser sources, tuning methods 2−76469
i.r. spectrometry, developments and digital computer control 2−70075
i.r. spectroscopy, 1970-71 2−52482
irregular wind induced waves, prediction methods 2−44641
Ising model, instabilities and phase transitions 2−63031
isotope separators, and design of RPI three stage separator 2−74249
Jovian atmosphere, physicochemical and meteorological explanation 2−44940
Kelvin equation 2−53512
large mass supergiant stars, structure and evolution 2−62514
laser beams for industrial appl. 2−82531
laser prod. plasmas, fusion, conditions expt. work, prospects 2−80299
lasers, pulsed gas-discharge 2−66742
lattice defect interaction with grain boundaries, review 2−68032
lattice vibrations of moelcular solids 2−61070
length standard 2−48972
lepton nonconservation in nuclear physics 2−46066
lepton-hadron scatt., high energy 2−82678
level spacings in complex nuclei, deviation from statistical distribution 2−46075
light instrumentation 2−55751
lighting technology 2−70067
limb darkening problem in eclipsing binaries 2−55063
linear conducting chains, elec. and mag. props. 2−61140
linear transmission systems, statistical hypotheses 2−78915
liquid chromatography, developments and applics. 2−44498
liquid crystal, role in inaminate and animate systems 2−53392
localized molec. orbitals 2−50008
loudspeaker horn theory, impedance concept 2−41762
loudspeaker horns, for sound reproduction 2−41763
lunar magnetism, origin theories 2−51807
lunar origin, evolution and present thermal state 2−85041
machine noise, measurement standards 2−41812
machine noise, sound field near array of noise sources 2−41813
machine windings, superconductor use 2−66686
macromolecules, natural org., review 2−83383
macrosonics, ultrasonic and macrosonic motors 2−41783
magnetic bubbles, properties, applications 2−78035
magnetic prism β spectrometer 2−73930
magnetic susceptibility, instrumentation and appls. 2−52381
magnetic treatment and structure of water 2−54521
magnetism in rare earth metals 2−51239
magneto-optical props. of solids 2−72294

Reviews continued
magnetosphere-ionosphere interactions, conference 2−48568
magnetospheric convection electric fields in high latitudes, satellite measurements 2−75626
many-particle production, review 2−66915
many-photon absorpt. in crystals and their applications 2−75282
Mars, Mariner 1969 obs. 2−44954
Mars, spacecraft observations, Mariner 9, Mars 2 and Mars 3 2−44947
Martian satellites Phobos, dynamical characteristics 2−62703
mass spectrometers, development and applications 2−59885
matter, extremal states under ultrahigh pressure or temperature 2−55342
Matthiessen's rule, deviations from, review and critical evaluation 2−71753
medical diagnosis photography 2−76075
medical radiobiology, modification of radiation response 2−69325
Mercury, structure and cartography 2−78502
meson spectroscopy, current problems and future directions, theory 2−73797
metal, gas chemisorption 2−50530
metal, grain boundary ordered struct., boundary dislocations, transmission electron microscopy 2−53651
metal, heat capacity at low temperature 2−47747
metal, opt. props. 2−72292
metal, vacancies and point defects clusters, nature and behaviour 2−43619
metal system, grain and particle size distrib. analysis 2−50817
metal vapour lasers, techniques and developments 2−42021
metal working plasticity, mechanics 2−71635
metallic electrons in magnetic fields 2−61155
metallurgy, physico-chemical, progress 1871-1971 2−47569
metals, mag. impurities, mag. hyperfine interaction studies 2−84397
metals, review of dislocation substructure strengthening and mechanical-thermal treatment 2−84099
metastable atoms and molecules, production and detection 2−64050
microdisplacement transducers 2−62957
microwave spectroscopy 2−52340
minerals Sn and W in Burma 2−48366
modulated reflectance 2−72298
molecular, u.v. photoabsorption cross sections, molecules of astrophysical and aeronomic interest 2−42838
molecular crystals, electron-vibrational spectra 2−57345
molecular diabatic states, quasistationary electronic states 2−50015
molecular spectroscopy 2−83233
molecular wave functions, calc. and applic. to atomic and molec. processes 2−50007
molecules in interstellar space, detection and meas. 2−75799
monomolecular films on Hg 2−74645
monsoons of southern Asia 2−48485
Moon paleocratering, post-Apollo data 2−85026
Mossbauer spectroscopy, 1970-71 2−52672
Mossbauer spectroscopy in rare earths 2−51313
multi-hadronic reactions at high energies 2−49521
multiband cameras for space missions, recent developments 2−82600
multispectral scanning from airborne stations and satellites, applics. in geophysics 2−75416
N-body problem, applic. of orthogonal and unitary group methods 2−58804
natural orbitals, properties and uses 2−59880
natural planetary satellites, physical properties 2−78530
negative electron affinity materials, in photomultipliers 2−49676
neutrino reactions at accelerator energies 2−59418
neutron cross section measurement and analysis technique 2−46282
neutron cross-sections, role of doorway states and intermediate structure 2−46268
neutron radiography, nondestructive testing technique 2−43765
neutron radiography 2−63712
neutron radiography nondestructive testing, technique and applications 2−52515
n.m.r., free precession and spin echo techniques 2−59020
n.m.r., high resolution, pulse Fourier transform method 2−66669
n.m.r., literature from July 1969 to July 1971 2−52342
n.m.r. at 220 MHz, applications 2−77030
noise sources in axial flow fans 2−41802
Nomarski differential interference contrast microscopy 2−52467
non-crystalline materials, theory of conduction 2−61143
nonlinear optics, picosecond laser pulse studies 2−63348
novae and supernovae, stellar outbursts of pretelescopic era 2−73022
nuclear charged particle cross-sections, fluctuations 2−46215
nuclear double resonance relaxation, techniques for solid state studies 2−61754
nuclear energy and public opinion in W. Germany 2−59821
nuclear fission, excitation energy dependence of shell effects 2−59794
nuclear fission, mass distributions and related phenomena 2−59803
nuclear fission, prompt neutrons and gamma rays 2−59805
nuclear fission, radiation emission 2−59798
nuclear fission models, barrier heights, energy release and fragment energy partition processes, review 2−59799
nuclear fuel and structural materials, IV international conference on nuclear energy, Geneva 1971 2−76908
nuclear fuel cycle, analytical methods 2−74161
nuclear fusion research, review 2−42611
nuclear instrumentation 2−82791
nuclear level density theories 2−46097
nuclear medicine and nuclear bioengineering 2−66253
nuclear physics, development at Radium Institute, USSR, (1922 to 1972) 2−76757
nuclear reaction models 2−46217
nuclear reactors in Germany 2−59820
nuclear resonance reaction theories 2−46213
nuclear structure and reactions, role of simple configurations 2−63732
nucleonic instrumentation in medicine 2−76092
objective lens design for transmission microscope 2−79063
ocean waves, deep, spectra, meas. 2−64416

Reviews continued
operational fast breeder reactor, continuous reactivity monitoring 2−46393
optical design and aberrations, part XXVIII 2−69999
optical diffraction in polycrystalline Raman theories 2−61594
optical filters review of some definitions 2−70038
optical spectroscopy and quantum electronics, Raman's contributions 2−59277
optical systems at Westinghouse Electric Corporation 2−42222
optical thin film applications, present and future 2−73660
optics in Du Pont 2−69990
optics work performed by Honeywell Corporation 2−79366
optimization problems, methods for solution 2−52116
optoelectronic semiconductor devices 2−51178
organic semiconductors, gas reactions, photoelectric detection method 2−72570
origin of the Earth 2−57448
paramagnetic resonance, electric effects 2−68728
parametric oscillators 2−42053
parametric transmitting arrays 2−41741
patient protection in X-ray diagnosis 2−73183
personnel dosimeters, present status 2−85125
perturbation theory, anomalies in quantum electrodynamics 2−63472
perturbation theory, time-dependent 2−58759
photodetachment cross sections and electron affinities for atoms and mols. 2−64035
photoelectric emission, electronic struct. 2−72088
photoelectron spectroscopy, applications 2−53862
photoelectron spectroscopy 2−68495
photofission at intermediate energies 2−70495
photoionization measurement methods including plasma arc spectroscopy 2−77301
photomultiplier developments 2−69881
photon-phonon interactions in solids 2−72318
photoproduction and electroproduction 2−82674
physics, current development areas 2−62911
plasma, linear transformation and absorption of e.m. waves 2−56352
plasma confinement, fast pinch experiments in UK (1956-1972) 2−53200
plasma flow effects on toroidal confinement 2−64285
plasma phenomenon, numerical simulation 2−80254
plasma physics, computer simulation, particle-in-cell model 2−80256
plasma wave attenuation, collisions, absorption and coupling 2−80340
plastic deformation, development of concepts 2−68078
plastic deformation of metallic crystals 2−68077
plastics, deformation to fracture 2−60863
plate tectonics, African Euler pole of rotation rel. to E. African rift system 2−61957
plate-tectonic theory, appl. to crustal rock mass history 2−61952
polarimeters, studying molecular structure of matter 2−59240
polarized orbital approximations for atomic electron scatt. 2−64039
polymer statistics and functional integrals 2−60102
polymer systems, conc., constitutive equations for nonlinear viscoelasticity 2−82316
polymers, solutions and melts, review of recent non-linear viscoelasticity expts. 2−83364
positron annihilation, appl. to struct. and props. determ. 2−47771
positron annihilation, fundamental ideas, measurement techniques and annihilation radiation 2−59428
precipitation 2−68187
precipitation in crystalline ceramics 2−84063
pressure meas. of liquids and gases 2−66410
pressure measurement, effect of hot filaments in vacuum systems 2−55332
proto-galaxy formation, from gravitational instability in expanding universe 2−51713
proton resonance reactions, high resolution on nuclei $40 \leqslant A \leqslant 64$ 2−46251
proton-neutron mass difference and related topics, report 2−49590
proustite, phase matched parametric upconversion, systems applications, review 2−79223
pseudopotentials, applic. to liquid metals 2−50311
pseudoscalar meson photoproduction, high energy models 2−59504
pulsars, survey of exptl. data and construction of theoretical models 2−44891
pulsed e.p.r. techniques 2−59012
pulsed nuclear double resonance, solids 2−61755
PWR development in Germany 2−63948
pyroelectric i.r. detectors 2−69793
quantum electrodynamics, comparison between theory and expt. 2−63471
quantum electrodynamics, for college teachers 2−73253
quantum field theory, GNS construction 2−63477
quantum field theory, local operator products and renormalization 2−63460
quantum theory fundamental concepts 2−44705
quark searches in air showers, terrestrial matter and stellar objects 2−59598
radar meteorology in Soviet Union during 1970 period 2−75488
radiation damage, primary recoil energy depend. 2−53691
radiation damage in diamond 2−47371
radiation damage in group III-V cpds. 2−47365
radiation involved brittle fracture in structural materials 2−68099
radiation protection standards, book 2−59873
radiation therapy at AAPM radiological physics center 2−69324
radiation thermometer 2−76386
radio aurora, caused by plasma instabilities 2−48555
radio recombination line observations, interpretations 2−48737
radioactivity, impact of advances in instrumentation 2−74044
radioastronomy techniques and objectives 2−76047
radiodiagnosis, analysis of risks 2−48881
radiodiagnostic apparatus, technical aspect, protection 2−48882
radiodiagnostics, image intensifiers and photography 2−70070
radioisotope power source development by AECL, MAPLE generators using ^{60}Co 2−49298
Raman spectrometry, from late 1969 to late 1970 2−52484
rapid cosmic processes, morphology 2−81749
rare earth metals, magnetism, orbital contribs. effects 2−84392

Reviews continued
reactor fuel performance models 2−52857
reactor physics expts., results, accuracies, using HTGR's 2−83068
Rebinder effect, applications 2−53869
refractories, basic raw materials 2−68165
Regge analysis and dual absorptive model 2−59451
Regge cuts, usefulness 2−45927
Regge models and duality, review 2−63569
relativity-gyroscope expt., precession in Einstein and arbitrary theories of gravitation 2−76187
rheology of monodisperse lattices 2−74565
rising cross-sections shrinking diffraction peaks and Pomeranchuk trajectories 2−45917
rocket astronomy, past 25 yrs. 2−62811
satellites of outer planets, spectrophotometric observations 2−78531
scanning electron microscope image contrast 2−82453
scanning high-energy electron diffraction, in materials science 2−74710
scattering, low energy electrons and atoms, from crystal surfaces 2−80555
Schwinger terms in equal time commutators of $SU(3) \times SU(3)$ charge densities 2−45859
science and society in USA, survey of 1960's 2−73259
science in today's universities 2−76144
scientific changes coherent social groups 2−82094
scientific satellites 2−48627
second order props. of solids 2−72250
seismic data processing methods 2−48393
semiconducting transducers, mechanical variable, physical principles 2−66627
semiconductor, hot electrons in quantizing magnetic fields 2−57182
semiconductor, opt. props. 2−72291
semiconductor detectors, new applications 2−55917
semiconductor devices for gamma X-ray and nuclear radiation detection 2−46043
semiconductors, amorphous liquid, conf., Ann Arbor, USA, Aug. (1971) 2−61259
semiconductors diamond-like 2−54158
ship hydrodynamics, theoretical models of flow 2−77379
shock waves in solar system 2−81899
SI units in nuclear engineering 2−49873
soft X-ray lasers, pumping methods 2−41960
solar and stellar abundance and spectra of iron 2−62748
solar chromosphere-corona transition region, physical properties 2−73148
solar structure and processes 2−62742
solid state array cameras 2−42289
solute-vacancy interaction energies, measurement methods 2−68019
South Carolina, historical seismic activity survey 2−72619
space investigations in 1966-70 period 2−58144
space shuttle, reusable space vehicle 2−72940
space shuttle thermal protection systems 2−44784
space vehicle nuclear power systems using ^{238}Pu, safety systems 2−51667
space vehicles observations, of Sun, Moon and planets 2−66164
spectra excitation by lasers 2−45818
spectrometry, emission 2−52481
spectrometry of soft γ and X-radiation using semiconductor detectors 2−70287
spectrophotometry, applics. 2−52483
spectroscopic light sources, for tunable wavelength high resolution techniques 2−55777
spectroscopy, double-wavelength 2−49448
spectroscopy, i.r., 1970-71 2−52482
spin-coupled wave functions, atoms and molecules 2−49918
sputter thinning of specimen foils for transmission electron microscopy 2−79101
star formation 2−66085
static deformation of elastic half space by surface pressure 2−75430
statistical theory of light propagation in turbulent medium 2−82553
stellar evolution for non-specialists 2−55034
stellar evolution toward main sequence 2−85007
stellar matter, various forms 2−55031
stochastic instability of non-linear oscillations 2−66574
strain anal. using gratings 2−66502
stress analysis, three dimensional, numerical methods applics. 2−41607
stress wave emission on material deformation 2−69745
sudden decrease of atmospherics at 5 kHz for 1962-1969 period 2−48515
superadditive black and white developing agents 2−59316
superalloy, chemical analysis of conjugate phases 2−77681
superconductivity and its appl. 2−77861
superheavy atoms, electronic structure 2−67385
surface phonons and magnons 2−50985
symmetries, dynnamic and algebraic 2−63485
talking computers, human speech generation 2−45052
temperature measurement systems 2−45600
thermal diffusion in multicomponent gaseous mixtures 2−56447
thermal ratcheting 2−56875
thermonuclear reactors, conditions for controlling 2−42645
thermoremanent magnetization rel. to single-domain particles 2−62399
thin layer chromatography apparatus 2−68822
three fragment fission 2−63929
time measurement, historical survey over 5000 years 2−45218
time measurement methods used in past and up to present day 2−62963
tinted ophthalmic lenses, function, evaluation and evaluation 2−62881
Townsend Huxley expt. lateral diffusion expt., theory and practice 2−69627
transplutonium series, number of secondary neutrons 2−56012
tropical storm development conditions 2−62188
tunable lasers, operation and applications 2−59127
turbulent boundary layers with mass transfer, data survey 2−43055
turbulent flows, experimental methods 2−77238
two dimensional crystallization and field emission microscopy 2−53622
TZM alloy, arc casted, props. and applications 2−53825

Reviews continued
- ultrasonic investigation methods for gases, liquids, solids, short review 2—60374
- underwater communication or navigation using e.m., conduction and magnetic induction techniques 2—81629
- unidirectional solidification 2—80850
- uniformly sheared turbulent flow 2—43078
- unstable resonators, applics. 2—41973
- upper atm. superrotation theories 2—75620
- u.s. cavitation 2—78925
- u.s. flaw detection methods 2—82362
- u.s. intensity measurements, Radiation Control for Health and Safety Act 2—45041
- u.s. metal removal, cutting, lathe turning, boring and twist drilling 2—41786
- u.s. transducers high power 2—69750
- vacuum deposition 2—66384
- vacuum industry 2—55330
- vapour-liquid equilibria, general correlations 2—84610
- vector mesons, photoproduction on protons, diffraction dissociation models 2—59551
- Veneziano formula, dynamical applications 2—63559
- virtual electronic levels, occurrence in molecules and crystals 2—59982
- viscoelastic theory for polymer melts 2—64708
- visual system and neuronal specificity 2—51958
- voids in irradiated metals 2—50635
- volumetric flow meas., u.s. methods 2—83514
- water waves, fairly-long 2—46896
- wave excitation in plasma 2—80335
- weak hadron interactions, CP violation, exptl. studies 2—49525
- weak interaction theories 2—42322
- weak interactions in particle physics, 1965-72 2—63491
- weather modification, USA and international activities 2—62104
- X-ray absorption and emission, review, 1969-1971 2—52901
- X-ray astronomy, survey of current developments 2—58423
- X-ray crystallography, its history and development 2—64612
- X-ray diffraction; instrumentation, appls., struct. anal. 2—53628
- X-ray diffraction, appl. to materials science 2—64744
- X-ray fluoresc. yields, Auger and Coster-Kronig transition probabilities 2—79923
- X-ray source, Scorpius X-1 2—51793
- X-ray sources, compact, theories 2—62622
- X-ray topography, transmission and reflection methods 2—60730
- γ-rays, perturbed angular distribution following nuclear reactions 2—67206
- $K^0{}_l N$, cross-sections and ang. distrib., compilation of 13 papers 2—82749
- K^-p interactions at 10 GeV/c 2—42377
- K^+p interactions in bubble chamber, resonance production 2—45941
- N, in pion photoproduction, polarization 2—45959
- n capture, single-particle effects 2—46267
- N*, scattering and photoproduction formalism, pion-nucleon 2-body reactions, pseudoscalar meson photoprod. 2—46016
- πN resonance, dynamics, review 2—46015
- πN scatt., value of sigma term 2—45929
- $\pi\pi$ scattering and related processes 2—82766
- $\pi\pi$ scattering models 2—45978
- $\rho\omega$ mixing 2—59552
- Ag halides, properties of holes 2—66863
- Al, diffusion 2—83992
- Al high purity and dil. alloys, deformation props. 2—68076
- Al thin films, hillock growth 2—77506
- Au, bicrystals, grain boundary dislocation behaviour, electron microscope obs. 2—56732
- B binary alloys, phase diagrams 2—50957
- Bi_2Te_3 and alloys, for Peltier cooling, thermoelec. props., 2—75160
- CO_2 lasers, high power, review 2—52419
- Co, single crystals, review 2—84008
- Cs arc mode thermionic convertor, low vapour pressures 2—52376
- Cu_2O, temp. depend. of electrical conductivity 2—75091
- n-GaAs, negative photocond. when illuminated with impurity absorbed light, recomb. mechanism 2—65083
- Gd^{3+}, e.p.r. spectra 2—72485
- Ge, low temp. irrad. and annealing, defect models 2—47375
- H bonded materials, proton migration studies, experimental methods, review 2—83998
- H maser physics 2—49342
- ^2H, low energy neutron scattering cross sections 2—55995
- He, solid, thermodynamic, elastic and mag. props. 2—80515
- He II, vortices, phenomenology 2—83831
- Hg, elec. props., evidence for pseudogap 2—77445
- ^{16}O structure, theory 2—52741
- U ores low grade, advances 2—61989
- U oxides reactor fuels, O/U ratio determ. methods 2—74155
- W, explosive compaction of powders by direct method, survey 2—61008

Reynolds number *see Flow; Hydrodynamics*

Rhenium
- — 2—72245
- electric quadrupole interaction of ^{181}Ta, Mossbauer obs. 2—61607
- evaporated film, reflectance in v.u.v. from 300-2000 Å 2—44345
- film, struct. and microhardness, condensation temp. effects 2—50501
- high melting point electrode materials, thermionic converters 2—54272
- interactions with O_2 2—51450
- LEED, averaging method for extraction of M-S data due to intralayer structure 2—71315
- metal, X-ray L_{III} absorption discontinuity, splitting and edge structure 2—61676
- photoelectron energy distribution and photocurrent meas. 2—72093
- shear wave attenuation, amplitude depend., near T_c 2—47745
- thermal conductivity, 1200-2500K 2—54080
- void form. on irrad., temp. effect 2—50642
- HFC-Re system, meas. of lattice consts., solubility relations and phase diagram 2—84096
- $LiNbO_3$:Rh, reversible holographic storage 2—69984
- Re-N target for DX-70 series X-ray tube 2—52022
- on W surface, interactions between atoms 2—50469

Rhenium compounds
- Cr-Re dil. alloys, single cryst., mag. struct., neutron diffr. exam. 2—61553
- Fe-Rh alloy, hyperfine field at Rh nuclei by Coulomb excitation 2—61572
- Mo-34%Re, deform. struct., twin and disloc. microstruct. 2—43624
- Mo-35%Re alloy, deform. twins, nucleation and growth 2—56720
- Mo-34%Re alloy, effect of dislocation tangles on supercond. props. 2—57167
- Nb-Re alloy single crystals thermally activated deformation 2—80823
- Ni-Re alloys, elimination of Barkhausen effect in electrodeposited films 2—72169
- Re-Al(Si)-B systems, phase equilib., X-ray study 2—64822
- Re-B system, phase diagram 2—50957
- Re-Mo film, A-15 struct., supercond. transition temp. 2—71867
- Re-N, nitrogen solubility as a function of pressure and degassing kinetics 2—60967
- Re-Pt alloy, strength, oxidation resist. 2—47533
- Re-W-ThO_2 alloy, creep, strength to rupture, 1800-2200°C 2—64719
- $ReBr_6{}^{2-}$ sharp-line luminesc. in Cs_2ZrB_6 2—57370
- $Re_2(CO)_{10}$ single crystal, broadline n.m.r., quadrupole coupling and anisotropic chemical shift 2—57397
- ReF_7, mol. consts., Raman and i.r. spectra 2—46576
- ReF_7, vibr. spectrum, normal coord. analysis, logarithmic steps methods 2—54024
- Re(I) complex, $K_5[Re(CN)_6]$, vibr. spectra and force consts. 2—77074
- $ReMn(CO)_{10}$ single crystal, broadline n.m.r., quadrupole coupling and anisotropic chemical shift 2—57397
- ReO_2, monoclinic to orthorhombic transition, electron microscope obs. 2—47695
- ReO_3, absorpt., 0.11-2.8 eV, rel. to band struct. 2—84499
- ReO_3, density of states by X-ray photoelectron spectroscopy 2—54111
- ReO_3, mag. susceptibility, 77-300K 2—75208
- $ReO_4{}^-$, dipole transition moments determ. by LCAO-MO calcs. in terms of ligand mixing coeff. 2—42928
- $ReXY_3$ C_{3v} ions, (X, Y=O, S, Se), assignments of electron charge transfer bands 2—80020
- W-Re alloys, carburized, work function in 1600- 1800 K range 2—54267

Rheology
- *see also Plasticity; Viscoelasticity*
- alkali borate glass, effects of water 2—53795
- alkali borate glass, high viscosity range 2—53794
- anomalous viscosity of disperse systems in shear stress zones 2—60515
- battened columns, out of plane buckling 2—69651
- bimodulus elastic materials, constitutive equations, model 2—45359
- blood, influences of red cells on anomalous flow, review 2—69205
- borate glass, separation of delayed elasticity from viscous flow 2—56781
- boric oxide glass, high viscosity range 2—53794
- cholesteric mesophases, normal stress effects 2—83770
- circular plate post buckling analysis 2—73357
- circular plates loaded beyond yield point 2—58841
- clamped circular plates with central blast loading, algorithm 2—73356
- compression of short cylinders with radial expansion constraint 2—76306
- conference, Nagoya, Japan, Oct. (1971) 2—82315
- constant shear modulus constitutive models 2—69635
- continuum materials, mechanical quantities and their relations 2—49062
- creep rupture of structures, failure times 2—69655
- cryorheology of reindeer blood 2—77419
- crystal, excitonic region, review 2—72317
- cumulative damage and strength 2—52136
- cylindrical beams, orthotropic and almost, Saint-Venant problem 2—49063
- cylindrical shell, optimization of torsional stiffness 2—73352
- cylindrical tube under pressure, elastic-plastic and thick-walled, effect of non-homogeneity on yield pressure 2—49064
- dilute suspensions, rheological properties in presence of rotary Brownian motion and external couples 2—50375
- discrete materials, mechanical quantities and their relations 2—49062
- disperse systems, role of particle interactions 2—64484
- dumbbell theory of dil. polymer solutions, anisotropic fluid theory 2—63075
- earthquakes, stress distribution beneath island arcs 2—81602
- equations from molecular network theories 2—63076
- essential features of inelastic behaviour, effects of geometry change 2—76295
- extrusion of polymer melts, computer aided rheology measurements and processing 2—64400
- flow stability of conducting fluid with power function rheological law in transverse field 2—60199
- formulation of rheological equations of structured systems rel. to fluids 2—58842
- free liquid films, rheological features of thinning process 2—60408
- fully stressed beams, effect of geometrical nonlinearity on minimum mass design 2—66524
- generalized isotropic yield criterion 2—66520
- geological massif, effect of rheological props. on stress concentration round supported elliptical tunnel 2—44590
- geometrically nonlinear shell theory anal. using method of asymptotic integration 2—76299
- holographic interferometric determ. of influence coeffs. for composite structures 2—82143
- imperfection sensitivity of wide integrally stiffened panel under compression 2—76305
- inextensible planes, spatial flows of incompressible media 2—45355
- infinite elastic plate with circular hole under normal loads on circumference, stress analysis 2—76277
- infinite elastic thick plate, load symmetrical to axis of revolution and middle plane, stress analysis 2—78887
- infinite plate of viscoelastic material, disturbances due to impulsive radial forces and twist on inner surface of circular hole 2—49060

Rheology continued
  initial yield surface of unidirectionally reinforced composite 2−66507
  laminated plate theories 2−66521
  load diffusion from bar embedded in semi infinite elastic medium 2−69653
  magneto and electro in dispersive systems 2−58854
  materials with memory, thermo-mechanical coupling 2−76291
  matrix displacement method for dynamic analysis with material and geometric non-linearities 2−58846
  molecules, particles, interfaces and continua 2−76280
  monodisperse lattices, review 2−74565
  multilayer shells, theory 2−63061
  non-Newtonian fluids, models under conditions of complex rheological behaviour 2−82302
  non-Newtonian fluids, time-dependent and time-independent, thermodynamic approach 2−67559
  non-Newtonian suspensions in water, rheological model 2−83823
  nonlinear buckling of cylindrical shells, numerical soln. 2−73360
  numerical analysis in fast computing of elastic structures symposium 2−41602
  numerical analysis of shells of revolution 2−41603
  photo-rheological method for stress analysis of bending 2−82318
  photo-rheological method of stress anal., similarity conditions 2−76298
  plate and shell analysis, finite element applics. 2−52169
  plates on a two parameter foundation model, finite element analysis 2−73359
  plates on linearly deformable bases 2−41592
  poly(vinyl chloride)-rubber system, rheological props. 2−83393
  polyethylene, high density melt rheology 2−83371
  polyethylene melt, low-density, branched rubber like liquid theory rel. to stress growth data for elongation 2−58871
  polystyrene-poly(2,6-dimethylphenylene oxide) freeze dried blends, viscoelastic response, rheological compatibility 2−83353
  pseudoplastic fluids, power requirements 2−83754
  Reiner fluid, yield value 2−76264
  rheo-mobility and structural creep 2−49058
  rheogram template for power law fluids, applic. to coaxial cylinder studies 2−53467
  rheoviscometer study of polymer solutions rel. to rheological properties and changes during two-phase separation 2−60392
  rocks, laboratory obs. at high temps. 2−57823
  rods with initial deflection, rheo-mobility effects in creep instability 2−49059
  rubber fluid storage bags, mech. behaviour, contact problem 2−66497
  sandwich panels analysis using triangular finite elements 2−41605
  sandwich structures, shear stiffness of honeycomb core, theory 2−63080
  sandwich type plates, two dimensional theory 2−55454
  sea ice, rel. to occurrence of surface tension cracks 2−65578
  shell analysis applic. of curved mixed finite elements 2−41604
  shells of revolution, geometrically nonlinear static and dynamic, numerical analysis 2−41606
  space eqn. of free surface of viscous and viscoelastic deformed layer 2−52194
  stress and stability problem of elastic transversely isotropic layered systems 2−58847
  suspension of nearly spherical particles, subject to Brownian rotations 2−83813
  suspension of small particles, phase interaction parameters 2−67843
  suspensions, rigid dumbbell, with Brownian motion modified Oldroyd model 2−60518
  symmetric structural systems, stability boundary 2−45362
  symmetrical bending of circular plates, finite element method 2−73358
  theory of shells, role of convergence 2−76300
  thermo-mechanical acceleration, in rheological material, analysis 2−63090
  thermo-mechanical acceleration, in rheological material with internal parameters 2−63091
  thermorheologically simple materials, identification problem 2−41567
  thin layer structure, spreading resistance det. 2−45402
  thin shell analysis, finite element applics. 2−52168
  thin shells, comparison of yield surfaces 2−69652
  thin shells analysis with doubly curved quadrilateral finite elements 2−73361
  viscoelastic continua, body-, space- and Cartesian space-tensor fields 2−63073
  viscoelastic continua, Oldroyd's 1950 formalism 2−63074
  viscoelastic fluids flowing through abrupt contraction 2−64406
  viscoelastic suspensions, rheological equation of state 2−83824
  viscoelasticity theory, nonlinear quasi-static problems 2−41636
  viscoplastic deposit formed in turbulent flow in pipes 2−83826
  Weissenberg rheogoniometer data rel. to viscoelastic liquids 2−77391
  B-epoxy laminated composite plates, holographic stress analysis 2−78895

Rhodium
  atom, e.u.v. spectra, energy levels 2−64001
  chemisorption of methane, activation mechanism 2−80577
  direct discharge neutron detector in thermal and epithermal regions 2−52699
  epitaxy by vapour deposition, low temp. 2−53575
  film electrodes on glass, deposition by sputtering 2−64573
  imaging of atoms with convention electron microscope 2−56665
  stopping power for protons and deuterons at same velocity 2−54098
  surface self-diffusion on Rh, low temp. 2−64555

Rhodium compounds
  $CeRh_xPd_x$ alloys electronic state, magnetic susceptibility and lattice spacings 2−81317
  Fe-Rh, Fe-Rh-Ir, magnetic contrib. to electronic sp. ht. 2−64856
  Fe-Rh alloy, f.c.c., Neel temp., Mossbauer study 2−78072
  Fe-Rh alloy, magnetoresist., temp. depend. 2−54330
  Ni-Rh disordered alloy, spin susceptibility calc. 2−65117
  Pd/Rh/H system, form. and decomp. equil. 2−77715
  Pd-Rh alloys, solubility of hydrogen, rel. to Fermi level position and clustering 2−77716

Rhodium compounds continued
  PdRhNi alloy, spin fluctuation resistivity 2−64916
  Rh-Fe, Coles alloy, temp. depend. of resist. due to localized spin fluctuations 2−75056
  Rh-Mn-Sb system, Cl_b type alloy, mag. props. and cryst. struct. 2−65156
  Rh-Pd alloy, low field Hall coeff., at 4.2K and 300K 2−61188
  Rh-Pd disordered alloy, spin susceptibility calc. 2−65117
  $RhC_{(2)}$, heats of atomization determ. by high temp. mass spectrometry 2−84623
  $RhCr_3N$, crystallographic parameters and struct. transforms. 2−60759
  Rh(III) triethylenediamine chloride, vibr. spectra analysis 2−72325

Riemann-Cristoffel tensors *see Relativity; Tensors*

Righi-Leduc effect *see Magnetothermal effects*

Ring currents *see Atmosphere; Ionosphere*

Riometers *see Ionosphere measuring apparatus*

Rochelle salt
  crystals grown from soln. size distribution 2−67939
  far i.r. spectra, using Fourier transform spectrometer 2−72319
  specific heat, ferroelec. contrib., two sublattice treatment 2−43990
  thermal cond., Curie pt. phenomena 2−44001
  triboluminescence, intensity obs. rel. to elastic const. detn. 2−51396
  u.s. anomalies, attenuation and ferroelectric anomalies 2−74988

Rock magnetism
  — 2−62024
  aboriginal fireplaces, evidence for geomagnetic reversal c.28000 BC 2−58133
  Africa, polar wander path det. for late precambrian 2−58128
  Aleutian Islands, Quarternary and late tertiary lava flows, geomag. field palaeosecular variation 2−62406
  Aleutian trench, config. of underthrust oceanic plate from anomalies 2−54687
  anisotropy, torsion balance for obs., calibration with conducting loop 2−66018
  anomalies along fracture zones 2−54942
  ash flows, upper cretaceous, evidence for magnetic reversal 2−54956
  astatic magnetometer with feedback for magnetized rock specimens 2−63259
  Australian-Antarctic continental drift, paleocirculation changes and oligocene deep sea erosion 2−78290
  basalt, lower tertiary, magnetic properties rel. to geomagnetic reversal investigation 2−54962
  basalt, susceptibility of deep drilled samples from Iceland 2−54963
  basalt, susceptibility of deep drilled samples from Iceland 2−54963
  basalt drill cores, from MAR median valley at 45°N 2−55443
  basaltic from Opole region, thermomagnetic analysis 20 to 600°C 2−51661
  basaltic rocks from Opole region, thermomagnetic analysis 20 to 600°C 2−51661
  basalts, from JOIDES programme in Atlantic Ocean 2−58135
  batholiths, cretaceous and miocene, evidence for plate tectonic evolution of West Central Cordillera (USA) 2−54955
  Bonito Canyon quartzite, micromagnetometer investigations of remanent magnetism 2−72923
  borehole sample, paleomagnetic orientation meas. methods 2−58134
  British Tertiary Igneous Province, Skye lavas exam 2−62404
  Brunhes epoch igneous rocks, applic. of magnetic data to secular variation and offset dipole models 2−54953
  Bukolan system, Tanzania, palaeomagnetic study 2−58099
  California, San Andreas fault, anomalies 2−65560
  chondrites, hysteresis properties 2−58473
  Cobb Seamount, field reversal and remanent magnetization obs. 2−44776
  Cretaceous sea-floor spreading from magnetic lineations in Pacific Ocean 2−66017
  Deccan trap lavas of Aurangabad region, remanent magnetic direction and tectonic significance 2−54946
  deep Pacific Ocean cores, geomag. reversal obs. 2−44763
  demagnetization apparatus using alternating magnetic field 2−51662
  demagnetization of heated rock sample using astatic magnetometer 2−66695
  applic. to earthquake phenomena 2−65514
  electric oven for studying 2−73241
  Et-Then Group, and Mackenzie diabase in Great Slave Lake Area 2−62400
  ferromanganese nodules, search for magnetic reversals 2−54951
  ferromanganese nodules, thermomagnetic behaviour 2−58142
  Frontenac Axis dikes 2−66016
  Gauss-Matuyama boundary, Kaena and Mammoth polarity reversal events 2−44600
  geomagnetic excursion 30000 b.p., aboriginal fireplace meas. 2−81743
  geomagnetic polarity in Canary Islands, Tenerife, La Palma and Hierro and K-Ar ages 2−78220
  Gila County, Arizona, Palaeomagnetism of 1140 to 1150 million year diabase sills 2−66021
  Giles Complex, Central Australia, stability tests 2−75638
  granite, precambrian, remanent magnetiz. obs. 2−62403
  granitic rock, magnetite bearing, complex magnetization 2−58140
  Gulf of Mexico, rel. to micropaleontological and tephrachronological studies 2−61968
  Honolulu volcanic series, palaeosecular variation 2−65997
  Icelandic lava flows, geomagnetic reversals and remanent magnetization 2−44777
  igneous rocks, blocking of TRM in small multidomain grains 2−54961
  igneous rocks from Indian and Atlantic Oceans, geomagnetic secular variations during Brunhes epoch 2−58104
  igneous rocks from Rockall Plateau 2−54677
  ilmenite-haematite solid solution, self- reversal and X-phase 2−54960
  impact glasses, remanence meas. 2−54967
  intrusive rocks of Western Siberian Platform, anisotropy 2−54938
  Jurassic Dufek intrusion, Antarctica, palaeomagnetism and magnetic polarity zones 2−58126

Rock magnetism continued
Kiaman magnetic interval lower boundary, palaeomagnetic and radiometric det. of age 2−48408
Kisii Series W. Kenya, palaeomagnetism 2−58127
lake sediments, geomagnetic secular variation recorded by remanent magnetization, applic. as chronological index 2−54954
Laschamp and Olby basalts, palaeomagnetic properties rel. to geomagnetic field reversal 2−54945
lava, lower cretaceous, evidence for geomagnetic reversal 2−58137
lava flows from Kauai, Hawaii 2−68986
l.f. e.m. fields, boundary equations 2−54940
lineated magnetic anomalies near sea floor rel. to geomagnetic chronology of Gilbert epoch 2−58125
lunar, effects of neutron irradiation on remanent magnetic properties of multidomain Fe 2−58458
lunar, rel. between magnetism and temp. 2−51818
lunar breccia and crystalline rocks 2−51809
lunar remanent magnetization rel. to solar wind perturbations 2−66150
lunar samples, hysteresis properties 2−58473
lunar samples, thermoremanent magnetization and NRM 2−58440
magnetic anomalies on Reykjanes Ridge 2−68988
magnetic viscosity of grains in magnetic fraction of basalts 2−54941
magnetite, blocking of TRM in small multidomain grains 2−54961
magnetite, magnetic and mineralogical changes associated with low-temp. oxidation 2−65571
magnetite dispersion, magnetic characteristics rel. to nature of remanence in rocks 2−58139
magnetization measurement, cryogenic magnetometer 2−54959
magnetotelluric method, petroleum exploration of sedimentary basins 2−44765
magnetotelluric method, transfer fns. with lateral variation of electrical conductivity 2−57788
marine pillow basalt, magnetic changes rel. to sea floor weathering 2−54966
metabasic dykes, Indian, natural remanent magnetization 2−75639
meteorites, natural remanent magnetization, possibility of external mechanisms 2−48787
Midway Atoll latitude of form. determ. from paleomag. meas. 2−57771
mineralogy of unheated and heated red sediments by coercivity spectrum analysis 2−51663
mineralogy of unheated and heated red sediments by coercivity spectrum analysis 2−51663
Mount Girnar, India, Deccan trap activity 2−81738
Mull regional dyke swarm, palaeomagnetic study 2−54937
natural remanent magnetization, stability obs. using method of rotationalmoments 2−48610
natural remanent magnetization of plunging fold, reduction to ancient coordinate system 2−78410
Northern Irish basalts, magnetization history 2−54936
Pacific Ocean, anisotropy of oceanic upper mantle 2−57540
Paganzo Basin, palaeomagnetic results 2−62402
palaeomagnetic latitudes, investigation using oceanic sediments of lower tertiary age 2−54952
palaeomagnetic poles from sea floor spreading anomalies 2−54948
palaeomagnetic stratigraphy, nomenclature problems 2−62398
palaeomagnetism of late Palaeozoic and early Mesozoic rocks of S. America 2−48607
palaeomagnetism rel. to geomagnetic field reversals and dipole characteristics 2−58132
palaeozoic sediments of northern Australia 2−68984
paleomagnetic differences between normal and reversed field sources, pole position problem 2−62405
paleomagnetic directions and pole positions, pole numbers 12/1 to 12/180 2−48608
paleomagnetic evidence for centred dipole source of geomagnetic field 2−58101
Pangea, assemblage and fragmentation, palaeomagnetic evidence 2−54695
pegmatites, palaeomagnetic and radiometric age det. 2−62401
Permian rocks of Black Forest 2−51664
pleistocene lake sediments, deep core, palaeomagnetic and palaeoclimatic implications 2−58136
pyroxenite, from Ontario, tectonic implications 2−58138
red beds, Mossbauer studies of magnetization affecting components 2−58141
remanence measurement, complete results magnetometer 2−54958
remanent demagnetization change under influence of mag. fields 2−54939
remanent magnetism, stability index 2−66019
remanent magnetization of long cores of sediment, rapid measurement 2−54944
Rogaland Precambrian (southwestern Norway) 2−44778
sandstone, lower Jurassic, evidence for geomagnetic reversal 2−54957
sandstones from India, pole positions 2−68985
seamounts, palaeomagnetism 2−54947
sedimentary cores, latest Pleistocene period, confirmatory evidence for Laschamp geomagnetic polarity event 2−54950
single-domain particles and thermoremanent magnetization 2−62399
submarine pillow basalt, remanent, induced and saturation magnetization in relation to titanomagnetic grains 2−68990
susceptibility anisotropy, significance in geophysics and geology 2−72924
synthetic magnetic anomaly curves, new interpretation technique 2−44779
taconites, discovery by natural remanent magnetism 2−68989
tektites, remanence meas. 2−54967
thermally activated magnetic viscosity in rocks 2−81739
titanomagnetite, effect of low temp. oxidation 2−54964
titanomagnetite, Mossbauer determination of cation distribution, geological significance 2−54965
titanomagnetite dispersion, magnetic characteristics rel. to nature of remanence in rocks 2−58139
titanomagnetites, cation deficient, spontaneous magnetization curve and Curie points 2−72925
titanomagnetites, effect of annealing on exchange anisotropy 2−72927
Tudor Gabbro, from Ontario, tectonic implications 2−58138

Rock magnetism continued
Twin Sisters dunite intrusion 2−58129
Upper Carboniferous to Eocene, polar wandering 2−54949
Utah, Permian Cutler and Elephant Canyon formation 2−66020
viscous magnetization, review of studies 2−78408
West Africa, palaeomagnetism of Gulf of Guinea volcanic province 2−72926
West Atlantic quiet zone, deep magnetic measurements 2−58131
Western Channel diabase, stable remanent magnetization rel. to polar wandering 2−75637
wurstite, increase in remanent magnetization during heating 2−62407
$(Fe_xMg_{1-x})_2SiO_4$, mag. transitions, comp. depend., 4-300K 2−68987
$0.35Fe_3O_4$-Fe_2TiO_4, self-reversal of thermoremanent magnetization 2−48609

Rockets
aerospace propulsion, conference Salt Lake City (1971) 2−62412
atomization and mixing of gas/liquid coaxial injector elements 2−62415
cold gas propulsion, optimum design parameters 2−62416
colloid core nuclear rocket, two component vortex flow studies 2−62414
Cosmos 307 rocket (1969-94b) orbit determination of mean rotational speed of atmosphere and density scale height 2−54989
damping of combustion instability oscillations by short nozzles 2−55516
Earth resource rockets, first firing in Australia using Skylark 2−75640
engines, high energy propellant, advanced materials for combustion chambers and nozzles 2−48619
exhaust plume/boundary layer interactions at supersonic speeds 2−56423
F-1 acoustic liner, little improvement in combustion stability 2−52234
flame autostabilization in combustion chamber of liq. rocket engine 2−52287
flight stability by SCO sensor 2−68991
gas core nuclear rocket radiation dose rate, fission fragments, lead shielding 2−85127
liquid, calc. of low frequency unsteady behaviour from droplet combustion parameters 2−54979
meteorological rocket data processor and results from 7 March 1970 solar eclipse 2−65648
meteorological soundings of upper atmosphere 2−65639
minimum time transfer between close coplanar orbits with thrust limited rocket 2−62417
missile propulsion project engineering for chemical engineers 2−44793
multistage, vertical motion, velocity components, mass distrib., number of stages selection 2−72930
nuclear, open cycle gaseous core, flow visualization studies 2−72932
nuclear coaxial jet, stability of u gas core 2−67733
particulate damping in solid propellant rockets 2−44792
plume induced boundary layer separation in rocket engines 2−53308
plumes, rarefaction effects 2−44790
propane, combustion, heat release in multistage reaction 2−58146
propulsion, travelling conduction waves for gas acceleration 2−44794
roll rate of launch vehicle rel. to random fin misalignments, statistical analysis 2−44791
solid Teflon pulsed plasma thruster, exhaust velocity studies 2−44811
sounding, aerodynamic heating effects 2−53309
sounding, for space astronomy, uses, applics. and future 2−81971
sounding, nonlinear aerodynamic characteristics 2−53312
sounding rocket, dynamics of ascending flight 2−80400
space shuttle, concept and implications 2−48618
space shuttle, economic evaluation 2−48621
space shuttle main engine 2−51674
supersonic nozzle flow, influence of contraction section shape and inlet flow direction 2−66023
tail groups, thin shaped, supersonic flow around edges 2−71096
thermonuclear, space propulsion 2−48617
turbopump inducers, internal steamliner flow analysis 2−43288

Rolling *see Forming processes*

Rotating bodies
see also Angular velocity measurement; Centrifuges; Earth/rotation; Gyroscopes
A-type stars, velocity determination 2−85004
aeolotropic elastic rotating disc, study of transverse vibrations 2−52204
American football to demonstrate top behaviour 2−62927
Ap stars, projected rotational velocities 2−51728
binary mixture on infinite rotating disk, barodiffusion isotope separation 2−77196
black hole, energy and angular momentum flow 2−78436
celestial, axial rotation, viscous friction effects 2−55006
circular plates with peripheral edge slots, vibrational stability control analysis by finite element procedure 2−76357
coherent states 2−45351
corrugated in incompressible viscous fluid 2−64249
cylinders, plastic collapse speeds 2−55473
disc, accelerating, displacements, closed form deform. solns. 2−66490
disk like stellar systems, constant models 2−81774
Ehrenfest's paradox of relativistic rotating disc, application of Thomas precession to extended structures 2−76175
elastic discs, stress analysis and optimum design, using dynamic programming 2−73373
elastic field of disc with eccentric elliptical insert 2−55465
containing elastic rods, dynamics 2−52123
ellipsoid, motion when filled with liquid 2−66486
energy, theory appl. to pulsars and active nebulae 2−85016
equilibrium configuration of slowly rotating liquid mass in poloidal magnetic field 2−77255
Euler rotations, theorem 2−49048
F-type metal deficient stars, luminosity and motion 2−51732
finite two body problem, common and individual rotation 2−81780
fixed reinforced shells, momentless stressed state 2−66487

Rotating bodies continued
fluid, perfect, rotation with gravitational, electromagnetic and thermodynamic props. about fixed axis 2−69577
fluid, viscous, oscillations of symmetric body, Coriolis force 2−46679
fluid, with finite resistivity, self-gravitat. instability 2−50167
fluid under weightless conditions, natural frequencies 2−77218
heat transfer between two rotating discs 2−76394
high speed fans, tone noise from rotor/stator interactions 2−82355
high-speed devices 2−58828
laminar boundary layer on rotating round-nosed blade 2−43062
macroscopic objects spinning on own axes, relativistic precessions 2−73305
magnetically suspended spheres, residual drag torque 2−73350
MG cylinder, stress and deflection meas. 2−43811
MHD boundary layer flow around oscillating axisymmetric body 2−60192
motion when filled with liquid 2−66486
orthogonal coordinate system, time dependence of effective axis and angle of rotation 2−55449
planets, Uranus and Neptune, moments of inertia 2−69142
potential development of smooth, dense rotating body rel. to planets 2−81757
relativistic, exact equations for stationary equilib. in special comoving coord. system 2−78800
relativistic rigid body motion, centre and axes of rotation defined by 6 parameter group of motion 2−63060
rigid body, angular velocity 2−58832
rolling contact between elastic bodies, dynamic response to random roughness 2−58829
satellites uniaxial, spinning, equations of motion, responding to magnetic and gravitational torques 2−44800
slender, aeroelastic equations 2−50257
spinning mass, exact soln. for gravitational field reducing to one of Weyl metrics at $J=0$ 2−82206
spiral galaxies, direction of winding of spiral arms 2−81811
stability analysis of force free spinning satellites with flexible appendages 2−51682
stability of systems with constraints and integrals of motion 2−76245
strain gauge current pickoff noise elimination 2−76436
Sun, Brans-Dicke theory 2−78430
Sun, circulation and differential rotation studies using similarity analysis 2−81954
Sun, linear velocity dependence of solar rotation on latitude and optical depth 2−44975
translatory-rotary motion of rigid bodies, first integrals of generalized problem 2−81751
triaxial rigid satellite in precessing elliptic orbit, effects of gravity-gradient torque on rotational motion 2−81752
vibrating uniform beam simply supported at one end, bounds to bending frequencies 2−73404
vibratory-rotational motion of free solid body carrying elastic elements 2−41654
viscous liquid flow on rotating disk, atomization effects 2−74509
whirling shaft, stability, material damping 2−52130

Rotation, molecular *see Molecules/rotation*

Rotatory power, dispersion *see Optical rotation*

RS coupling *see Atoms; Spectra/atoms*

Rubber
amorphous sodium-butadiene and butadiene-nitrile, stress effect study 2−60873
blocks, bonded, compressed, elastic stress strain eqns. dynamic relax. solns., Poissons ratio effects 2−66528
butyl, temp. and extension time depend. of creep recovery 2−71555
chloroprene, crystallization study by dielectric method 2−53544
crystallization of natural rubber at high pressures 2−60603
cylinder, swelling under torsion 2−60876
cylinder in torsion, swelling 2−60875
elastic behaviour and fracture of oil-extended SBR vulcanizates 2−84050
elastic behaviour under small uniaxial extension and compression 2−64705
elasticity on chemical relaxation 2−83378
elastomer, relationships between viscosity meas. at variable rates of shear and processing behaviour 2−53788
elastomers, electron microscope investigation of fatigue fractured surfaces 2−60899
elastomers, mechanical birefringence meas. by Hertzian waves 2−68601
elastomers, strength and toughness at low temperatures 2−60886
extension and compression behaviour 2−43681
fading memory materials, non-isothermal treatment 2−68056
fluid storage bags, mech. behaviour, contact problem 2−66497
molecular fracture during tensile testing at low temp. 2−43710
natural, cross-linked by dicumyl peroxide, exptl. obs. of creep modulus 2−50757
natural, in near molten state, morphology 2−60610
natural, multiple melting transitions 2−60545
oil-extended vulcanizates, SBR, dynamic props., principle of superposition of time, temp. and conc. 2−83367
poly(vinyl chloride)-rubber system, phys. props. 2−83393
cis-1,4-polybutadiene rubber vulcanizates, mechanical props., dynamic loading 2−60855
polychloroprene, gel fracture rate, crystallinity effects 2−47483
polyurethan, dynamic stress analysis, photoelastic studies 2−41613
rubber like materials, thermomech. behaviour, Valanis- Landel strain energy function 2−82312
rubberlike slightly compressible circular cylinders, finite torsion 2−76321
silicone based electrons, dynamic shear properties over wide temp. ranges 2−47488
styrene-butadiene, molecular orientation during stretching 2−56549
styrene-butadiene rubber mixture, electron microprobe study of chemical bond 2−64536
sytrene-butadiene, molecular weight and long-chain branching determination 2−43024
tearing energy detn. for estimation of fatigue life 2−68102
u.s. wave velocity as function of temp. 2−57048

Rubber continued
vulcanised, deformed, surface orientation obs. by polarization spectroscopy 2−84644
vulcanizates, SBR, temp. depend. of mech. props. under large deformation 2−83379
wear in liquids, testing apparatus 2−82128
Si rubber membranes as supporting medium for cells for electron microscopy 2−79097

Rubidium
adsorbed layer, on W(100), surface plasmon losses 2−64903
adsorption on Mo, LEED and Auger spectroscopy obs. 2−50540
atom, $6^2P_{1/2}$-$6^2P_{3/2}$ excitation transfer induced in noble gas collisions 2−74231
atom, cascade-decoupling meas. of excited S-state hyperfine structures 2−52922
atom, electron collisions, spin-exchange optical pumping expts., determ. of temperature dependence of cross sections 2−70615
atom, hyperfine structures of S and D excited states by cascade r.f. spectroscopy 2−70606
atom, reactive scattering on methyl iodide, determ. of potential and cross sections 2−72553
atom, Stark effect investigation of third excited $^2P_{3/2}$ levels in first spectrum, tensor polarizability determ. 2−70591
atomic, electronic g_j factors, natural lifetimes and electric quadrupole interaction for ^{87}Rb in $np^2P_{3/2}$ series of Rb I spectrum 2−46439
atomic spectra, self-broadening of principal series lines at high number densities 2−79930
coherently excited, spontaneous decay 2−67403
electrical resistivity, contribution of Umklapp processes 2−84293
film, photoemission, 3.7-21.2eV 2−54277
gas cell type atomic oscillator, optical pumping-optical detection system 2−77008
hyperfine structure of D_1 line, optical pumping 2−73670
K-absorption edge 2−72382
liquid, determ. of pseudo-Gruneisen parameters 2−74540
liquid, electron spectrum, calc. by cell method 2−83797
liquid, self-diffusion, 60 to 230°C 2−67817
liquid, sound velocity meas., 40-200°C, 0-20000 p.s.i. 2−71195
magnetometer, vector, operation and performance 2−73511
maser, atomic oscillator, fundamental characteristics and frequency stability 2−73544
maser, isotopic filter 2−59126
pliocene volcanic rock content det. 2−57809
resonance fluorescence 2−44328
surface diffusion near m.p. 2−60629
thermoelectric power rel. to Fermi surface shape and sample dimens. effects 2−68296
vapour, gas laser, phase matched, generation of u.v. radiation 2−42027
vapour, optically pumped, n.m.r., obs. of wiggles phenomena 2−74487
vapour, self defocusing of laser beam 2−43273
vapour, self-defocusing of laser light by adiabatic following 2−70608
vapour Q-switches for synchronizing mode-locked laser pulse trains with external events 2−73546
whisker growth from gas-phase 2−74639
βAl_2O_3, Rb substituted, mech. behaviour 2−56770
Cs-Rb differential Stark shift investigated using optically pumped atomic light modulation oscillators 2−46424
Rb/Sr radiometric dating of granitic rocks in Cape Breton Island, Nova Scotia 2−81592
Rb-Ar collisions at 100 torr, displacement of 7947 Å line of Rb 2−59933
Rb-Cs mixtures sorbed on graphite, vapour press. 2−53592
Rb-He collisions at 100 torr, displacement of 7947 Å line of Rb 2−59933
Rb-Kr collisions at 100 torr, displacement of 7947 Å line of Rb 2−59933
Rb-N_2 collisions at 100 torr, displacement of 7947 Å line of Rb 2−59933
Rb-Ne collisions at 100 torr, displacement of 7947 Å line of Rb 2−59933
Rb-Sr geochronolgy data, use of two-error linear regression treatments 2−61994
Rb-Sr isotope characts. of lunar soils 2−66139
Rb I, e.u.v. spectra, energy levels 2−64001
Rb^+, in CsBr, i.r. absorp. 2−61635
^{86}Rb, blood-tissue transport in dog gracilis muscle 2−62822
^{87}Rb-^{85}Rb D, line isotope shift, laser spectroscopic obs. 2−74222
^{87}Rb, h.f.s. separation of ground state, det. by optically pumped atomic beam resonator 2−79864

Rubidium compounds
CC RbF, surface phonon branch distrib., shell model 2−47734
K-absorption edge 2−72382
Cs-Rb alloy, Ashcroft's empty core model 2−74898
Cs-Rb alloy, heat of soln., pseudo alloy atom model 2−74897
K-Rb alloy, pseudopotential theory and Vegard's rule 2−67992
$K_xRb_{1-x}Cl$ solid solutions, linear thermal expansion coefficients and lattice parameters 2−64861
$K_{1-x}Rb_xI$, susceptibility and lattice const., comp. depend. 2−54289
$Li_2SO_4-Rb_2SO_4$ system, phase diagram 2−80527
$(NH_4,RB)_2CuBr_4.2H_2O$, mag. interactions 2−65144
Rb-Ar, Rb-Kr, Van der Waals molecules, action of r.f. field 2−56194
$RbAg_4I_5$ single crystals, Hall effect of Ag ions 2−77949
$RbAlF_6$, mag. susceptibility, temp. depend., 300-700K 2−72110
$RbBe_2(BO_3)F_2$, synthesis and physicochemical props. 2−47210
Rb_2BeF_4-Na_2BeF_4, phase diagram, struct. of phases 2−74957
$RbBiS_2$, cryst. struct., X-ray obs. 2−47342
$RbBiSe_2$, cryst. struct., X-ray obs. 2−47342
$RbBr:Ag^+$, static and dynamic paraelec. props., low temp., electrooptical study 2−61422
RbBr:OH, paraelastic alignment, optical absorp. pressure depend. obs. 2−61596
RbBr, gradient-elastic consts. determ. by n.m.r. 2−77637
RbBr, high temp. dielectric consts. meas. by standing wave technique 2−47968
RbBr, hysteresis and phase transformation under pressure 2−74940

Rubidium compounds continued
RbBr, reorientation rates of OH- defects, calc. from phonon spectra 2−61080
RbBr, thermal expansion and Debye temp. 2−61111
RbBr(Cl)(I), coherent neutron scatt. amplitudes from powders 2−53654
RbCL:RbOH, tunnelling levels, low temp., thermal cond. obs. 2−71758
$RbCaF_3$, Mossbauer effect of ^{57}Fe at substitution sites 2−81339
RbCl:Ag + , static and dynamic paraelec. props., low temp., electrooptical study 2−61422
RbCl:Na, F_b centres, absorpt. and emission study 2−64682
RbCl, anion self diffusion, tracer and sectioning technique 2−47471
RbCl, Arrhenius relax. of OH- ions, dielec. susceptibility study 2−65050
RbCl, Debye temp. 2−61111
RbCl, dielec. susceptibility of CN^- ions from 1 to 26 GHz 2−51192
RbCl, excited F-centres, emission mechanisms 2−80709
RbCl, F_a(Li) centre, a.c. photocond. study 2−71530
RbCl, gradient-elastic consts. determ. by n.m.r. 2−77637
RbCl, harmonic band parameters of NO_2^- and NO_3^-, high temp. 2−54410
RbCl, high temp. dielectric consts. meas. by standing wave technique 2−47968
RbCl, hysteresis and phase transformation under pressure 2−74940
RbCl, in sulfolane-water mixtures, conductance at 35°C 2−78199
RbCl, phonon dispersion relations, shell model calc. 2−61079
RbCl, surface phonon branch distrib., shell model 2−47734
RbCl, vibr. absorpt. spectrum of NO_2^- and NO_3^- 2−77769
$RbClO_3$, superiority to $KClO_3$ for n.q.r. thermometry 2−81477
Rb_2CoCl_4, crystal structure 2−83957
$RbCoF_3$, one- and two-magnon scatt. below Neel pt. 2−54435
Rb_2CoF_4, n.m.r. of ^{87}Rb, antiferromag. transition obs. 2−44458
Rb_xCrF_3, cryst. struct. 2−60760
RbF, excited F-centres, emission mechanisms 2−80709
RbF, Raman spectra, phonon modes 2−48196
$RbFeCl_3$, crystals growth and perfection 2−47224
$RbFeCl_3$, one-dimens. mag., Mossbauer obs. 2−72160
$RbFeF_4$, ferroelastic effect, spontaneous lattice strain 2−71571
$RbFeF_4$, two-dimens. antiferromag. ordering, susceptibility and neutron diffr. obs. 2−54363
RbH_2AsO_4, ferroelec. phase transition dynamics, spin-lattice relax. meas. by double reson. 2−84450
RbH_2AsO_4 ferroelectric, EPR and ENDOR 2−68734
RbH_2PO_4, ferroelectric, effect of deuteration, sound velocity obs. 2−74979
RbH_2PO_4, high temp. phase transitions 2−71688
RbH_2PO_4, light scatt. by elastic waves and rot. of polarisation plane 2−72358
$RbH_3(SeO_3)_2$, improper ferroelec. phase transition, group theoretical analysis 2−51197
RbI:K, additively coloured, colloidal absorption bands 2−47448
RbI:OH, paraelastic alignment, optical absorp. pressure depend. obs. 2−61596
RbI, Debye temp. 2−61111
RbI, diffusion coeff. of self-trapped holes and migration to thallium centres 2−68709
RbI, high temp. dielectric consts. meas. by standing wave technique 2−47968
RbI, hysteresis and phase transformation under pressure . 2−74940
RbI, magneto-reflectance of first exciton 2−51322
RbI, Rydberg series up to n=4 of Γ_1 exciton, thermoreflectance spectra at 90K 2−44363
RbI, V_k polaron, temp. dependence of jump frequency and diffusion constant 2−71813
RbI evaporated films, optical absorption spectra 1700-2500 Å, obs. of fine structure in exciton bands 2−44375
$RbICl_2$, vibr. spectra, cryst. symmetry 2−75313
α-$RbIO_3$ crystal struct. determ. 2−77548
$Rb_3Mn_2Cl_7$, crystal structure 2−83957
$RbMnF_3$, absorp. spectra 3900 Å region, exciton, magnon and phonon struct. 2−65266
$RbMnF_3$, critical neutron scatt., spin fluctuations 2−54361
$RbMnF_3$, e.p.r. linewidth, crit. point anomalies 2−78159
$RbMnF_3$, growth by Czochralski method, dislocation density determ. 2−53605
$RbMnF_3$, impure exchange-coupled, substitutions effect on e.p.r. linewidth and g-values 2−48292
$RbMnF_3$, mag. order-disorder transition phenomena, sound propag. 2−54026
$RbMnF_3$, n.m.r., spin-lattice and spin-spin relax. of ^{19}F and resonance of ^{87}Rb 2−72516
$RbMnF_3$, n.m.r. of ^{19}F, 1.5 to 300K, spin-lattice and spin-spin relax. 2−48113
$RbMnF_3$, spectrum uniaxial stress effects, Jahn-Teller effect in Mn^{2+} obs. 2−65268
$RbMnF_3$, spectrum uniaxial stress effects, Jahn-Teller effect in Mn^{2+} obs. 2−65267
$RbMnF_3$, temp. depend. oscill. strengths of optical absorp. 2−54428
$RbMnF_3$, temperature dependence of e.p.r. line width, room to liquid nitrogen temp., effect near Neel temp. 2−44440
$RbMnF_3$, two exciton transition, temp. depend. intensity calc. 2−61654
$RbMnF_3$, u.s. attenuation near Neel temp. 2−43975
$RbMnF_3$ antiferromagnet, magnetoelastic theory of ^{19}F nuclear acoustic resonance and lattice imperfection 2−51412
Rb_2MnF_4, quadratic layer antiferromagnet, e.p.r. linewidth temp. depend. 2−75345
Rb_2MoO_4-$Al_2(MoO_4)_3$ solid soln., phase diagram 2−57033
$RbNO_2$, phase diagrams, cryst. struct., to 40 kbar 2−74951
$RbNO_3$, molten, isotope effect of electromigration of Rb ions, temp. depend. 2−64457
$RbNiCl_3$, crystal growth and perfection 2−47224
$RbNiCl_3$, mag. struct. 2−48111
$RbNiCl_3$, one-dimens. antiferromag., spin-wave approach 2−54352
$RbNiCl_3$, one-dimens. mag., Mossbauer obs. 2−72160
$RbNiF_3$, crystal field theory of mag. anisotropy 2−61546
$RbNiF_3$, ferrimagnet, spin waves, neutron scatt. obs. 2−65171
RbO_2, magnetic properties, obs, of structural and magnetic transitions 2−65116

Rubidium compounds continued
RbO_2, Raman spectra, O_2^- and O_3^- ion props., solid-solid transition effects 2−81354
$RbPF_6$, solid, reorientation motions of PF_6^- ions 2−61562
Rb_2PO_3F, space groups and lattice parameters 2−83951
Rb_2PtCl_6, n.q.r., spin-lattice relax., rotary lattice mode freq. 2−77748
Rb_2SO_4, sound velocity, 1109 to 1191°C 2−71194
$Rb_2S_2O_6$, second harmonic generation 2−75248
$RbSbS_2$, cryst. growth, Bridgman method 2−47273
Rb_2SiF_6, press.-induced phase transform. 2−71677
$Rb_3UO_2F_5$, structure determ., X-ray examination of powder and twinned crystal samples 2−47343
$Rb_2UO_2F_4.H_2O$, space group, lattice parameters 2−68004

Ruby
absorption spectra, h.p., below elastic limit 2−61630
breakdown by mode-locked laser radiation, i.r. 2−79251
complex propagation constants, boundary considerations 2−82528
crossrelaxation, two step, freq. depend. susceptibility meas., generalized thermodynamics 2−61561
disk laser, optical distortion and depolarization effects 2−82489
energy levels of Cr^{3+} ions 2−68633
e.p.r., influence of lattice defects on e.p.r. line shapes 2−72468
e.p.r. instabilities, inc. ENDOR and n.m.r. obs. 2−44436
fluorescence, effect of magnetic field on intensity, decay time 2−72419
hydrothermal growth and G doping 2−47230
laser, high-repetition-rate continuously pumped 2−45748
laser, interferometric technique for obs. of coherence of single pulse 2−79348
laser, intracavity modulation with frequency close to difference frequency of neighbouring axial modes 2−59171
laser, mode-locked, applic. to holography 2−66781
laser, output energy, effect of Cr^{2+} conc. 2−59169
laser, picosecond pulse transient behaviour 2−69936
laser, scatt. in plane-parallel resonator 2−79179
laser, stimulated radiation props., γ-ray effects 2−73585
laser, TE and TM modes generation and self-focusing 2−42074
laser induced fluorescence line narrowing 2−48241
laser pulsed, beam parameter obs. using holographic interferometry 2−79218
laser stimulated emission when exposed to ^{60}Co gamma rays 2−69935
lasers, characterization of generation region with darkened solns. of phthalocyanines 2−49379
luminescence, quantum yield with u.v. excitation 2−61684
microhardness meas. by method of small penetration of indentor 2−47549
phase relaxation and self induced transparency 2−42118
photon echo-nuclear double reson., Cr-Al interaction parameters 2−81474
photon echo-nuclear double resonance 2−61733
Q-switched laser, fracture of nonlinear crystals 2−79254
quality estimation from e.p.r. line widths 2−54493
ruby: Cr^{3+}, spin-lattice relax. field effect obs., Van Vleck theory 2−65193
sharp-line luminescence employed in measurement of pressure in diamond-anvil high-pressure cell 2−58658
spin-echo modulation 2−47963
spin-lattice relax., Fe^{2+} ion obs. and cross relax. processes 2−51285
stream patterns, microscopic examination and associated microcracks 2−71424
TEM_{00}-mode mode-locked ruby laser triggering spark gap, switching jitter 2−74409
TW ring laser, passive non-reciprocal element 2−66764

Rupture *see Mechanical strength*

Russell-Saunders coupling
spin-dependent operators in occupation- branching number representation, monoelectronic and bielectronic 2−41503
Tm^{n+}, n=2,3, spin-orbit coupling consts. determ. from analytical SCF wave functions 2−46444
U complexes, insular uranyl complexes, test using equatorial ligation 2−60037

Ruthenium
atom, e.u.v. spectra, energy levels 2−64001
effect on ductility of nonsag W wire 2−43683
electric quadrupole interaction of ^{181}Ta, Mossbauer obs. 2−61607
galvanomagnetic properties and Fermi surface 2−51103
Hall constant and anisotropy of elec. resistance at low temps. 2−68333
Ru^{3+}, in Al^{3+}-substituted YIG, ferromag. reson. 2−81444
^{103}Ru-^{106}Ru, isotopic activity ratios in rainwater 2−62289
^{106}Ru accumulation in coastal sediments 2−62044

Ruthenium compounds
pyrochlores, $M_2Ru_2O_7$, (M=Ln,Bi,Pb,Tl), struct. and props. 2−60987
Mo-Ru alloy, microstruct., hardness and supercond. transition temp. 2−50840
Mo-Ru alloy, vapour deposited, struct., electron microscope obs. 2−60594
Ru-Cr alloy, absolute thermoelec. power, 350-1000K 2−68476
Ru-Pd alloy, low field Hall coeff., at 4.2K and 300K 2−61188
RuC spectrum in 4100-4800 Å region, determ of molecular consts., band analysis 2−77071
RuF_5 complexes with XeF_2, i.r. spectra 2−74279
RuO_2, elec. cond., temp. depend. 2−57145
RuO_2 film, 1-5 μm thick, prep., struct., and elec. props. 2−47123
RuO_4, LCAO MO calc. of dipole transition moment 2−77063
Ru^aO_4, A=16, 18, Raman and i.r. spectra, determ. of anharmonicity corrections, Coriolis constants, force field 2−46578
V-Ru alloys, Knight shift, relax. rate and lineshape, temp. and mag. field depend. 2−61753

Rutile *see Titanium compounds*

S-matrix theory
see also Dispersion relations
boundary condition constants of Lane-Robson theory 2−46212
classically forbidden processes, analytic continuation of classical mechanics 2−43029

S-matrix theory continued

- coupling of three or more positroniums, relativistic model, derivation of S-matrix elements 2−49508
- determinantal method and Pade approximants for S-matrix, comparison 2−70140
- Eckmann model, expression derived 2−76570
- elastic, of slow particles, due to long-range potential 2−76580
- existence of solns. to $\pi\mathfrak{R}$ static model, charged scalar model 2−79574
- Fourier transform of elements, effect of light cone singularities 2−82650
- gauge invariance of tree diagrams 2−73725
- Glauber's multiple diffraction theory, S-matrix approach 2−73746
- hadron dynamics interpret., composite theory 2−52576
- identical particle scattering, calc. of unitary S matrix from K-matrix soln. to inhomogeneous eqns. 2−63492
- Kadyshevsky momentum representation for boson- boson, bosn-photon interactions, regularization method 2−55789
- Lagrangian interaction choice, rel. to s-matrix for field-field interactions 2−66895
- leptons, high energy interactions, neutral current, and heavy lepton models 2−82641
- Lorentz noninvariance in covariant formulation of complex-ghost relativistic theory 2−49470
- molecular collision dynamics, classical theory 2−72551
- Mossbauer time-reversal studies, development of S-matrix formalism 2−46092
- nonlocal quantum electrodynamics, construction 2−52529
- nonrenormalizable quantum field theory, calc. of S-matrix elements as power series in symmetry violating mass difference 2−55782
- perturbation, for electromagnetic corrections in strong interactions and field-theoretic self-energy calculations 2−52518
- phase shift, numerical calculation, variable phase method 2−45869
- photon statistics of scattered light, calcs. 2−63308
- for photon-hadron interactions, analytic equivalence of Gupta-Bleuler formalism 2−52578
- potential scattering, semiclassical quantization condition for poles 2−49018
- potnetial scattering, pole trajectories in *N/D* approach 2−58764
- scalar boson trilinear coupling in small mass limit, S-matrix and field-theoretical arguments 2−59387
- scattering processes, equivalence of local and nonlocal potentials 2−82936
- spontaneously broken gauge symmetries, renormalizability 2−59371
- spontaneously broken gauge symmetries, S-matrix equivalence in R- and U-gauge formulations 2−59373
- state vectors with vanishing norm and probability distrib. 2−79471
- SU(2) × SU(2) chiral dynamics, invariant functional formulation 2−70127
- three-particle production, relation with coupling constant 2−52546
- time-dependent scattering including rearrangement processes, WKB approx. 2−69598
- unitarity breakdown in indefinite metric 2−70115
- unitarity effects on multiperipheral model 2−66972
- unitarity hyperon-nucleon interactions 2−79622
- K^0-K^0 states in K_l-K_s phenomenological S matrix 2−82745
- K^0 weak decay amplitudes, unitarity and CPT properties in S-matrix approach 2−70215
- K_s-K_l decay, equivalence with potential formalism 2−49547
- nd scattering, low-energy S-matrix theory, construction of sum rules 2−76758
- πN P-wave scattering amplitudes and their S-matrix calculations 2−45975
- πN S-wave analysis, low energy ambiguities of $\pi\pi$ isospin-zero S-wave on comparison 2−55861
- $\pi^0\pi^0$ S-wave amplitude improved constraints 2−45977
- $H + H_2$ linear reactive collisions below the classical threshold complex-valued classical trajectories determ. from S-matrix theory 2−44474
- N_2 low-energy electron scattering, calc. using pseudo-potential method, determ. of cross sections 2−70819

Safety precautions *see Radiation protection*

Sakata model *see Elementary particles*

Samarium

- astrophysical nucleosynthetic chronologies rel. to ^{146}Sm and p-process nucleosynthesis 2−51686
- atom, γ-ray scattering, incoherent, by K-shell electrons 2−59931
- electrical resist., thermoelec. power, anomalous behaviour, 300-1000K 2−54128
- isotopically enriched, electronic sp. h.t. 0.45-6K 2−68250
- in paramag. metals, giant, dwarf and negative moments 2−44222
- sunspot abundances, using high resolution spectra 2−73135
- Eu^{2+}-Sm^{2+} exchange coupling problems in chalcogenides 2−54373
- Eu^{3+}, luminescence in NaF, Ce^{3+} impurity effect 2−65295
- KCl:Sm^{2+}, impurity-vacancy dipole relax. and aggregation, and X-ray effects 2−83982
- $La_2Mg_2(NO_3)_{12}$:Sm, dynamic nuclear polarization 2−68590
- Sm^{2+}, in BaF_2, one phonon sideband fluoresc. theory 2−65304
- Sm^{2+} in alkali halide, Z-centres, optical absorpt. and e.p.r. at 77K 2−71526
- Sm^{3+}, in $PbCl_2$, luminesc. 2−54447
- Sm^{3+}, in phosphate glass, energy transfer with Eu^{3+} 2−48238
- Sm^{3+}, spin in SmF_3 2−84589
- ^{150}Sm, ranges and range straggling in Cu and Ag 2−68269
- ^{154}Sm, production and crystal growth, neutron diffraction expts. 2−74667

Samarium compounds

- complexes with β-diketones, Tb sensitized luminescence 2−74549
- ionic, semicond. and metallic cpds., Mossbauer isomer shifts 2−48154
- metallic ferromagnet, ordered moment estimated 2−61518
- monochalcogenides and monopnictides, band struct., press. effects 2−47915
- Co-Pr-Sm alloys, 10000 Oe B-coercive force magnet, props. optimization 2−44247
- Co-Sm permanent magnet alloy, sintering mechanisms 2−57289
- Sm-Au alloy system, phase diagram, intermetallic form. 2−50973
- Sm-Co alloys, comp. effect on mag. props. 2−51262
- Sm-Sn system, relative stability of intermetallics 2−47573

Samarium compounds continued

- $SmAg_2Si$, prep. and cryst. struct. 2−74735
- SmB_6, nonstoichiometry 2−47183
- SmC_x, chem., metallographic and X-ray characterization 2−71653
- $Sm_2(CO_3)_3.xH_2O$, standard heats of form. 2−43335
- $SmCo_5$, domain spacing at low temps. 2−51250
- $SmCo_5$, permanent mag. 2−52385
- $SmCo_5$, powder, coercive force rel. to sintering temp., decomposition stability 2−68511
- $SmCo_5$ magnet prod. using single phase sintering aid 2−43795
- $Sm_2(Co_{1-x}Fe_x)_{17}$, lattice consts. 2−50626
- SmF_3, anomalous ^{19}F n.m.r. shift 2−84589
- $Sm_3Fe_5O_{12}$, garnet, cell parameters, X-ray powder data 2−74745
- SmGa, magnetization and susceptibility, temp. depend. 2−72170
- $SmIn_3$ magnetic properties 2−72223
- Sm_3NbO_7, crystal structure 2−47346
- Sm_2O_3 molten, surface tension, density, volume change on melting 2−80465
- SmOBr(Cl), i.r. spectra, vibrs. assignments 2−57348
- $(Sm_{1-x}Pr_x)Co_5$, $0<x<1$, alloys, saturation magnetization, anisotropy field, coercive force 2−68510
- $SmRu_2$, high press. phase transition 2−71689
- SmS-SmSe system, metal-insulator behaviour 2−61190
- SmS, semicond.-metal transition, optical consts. and energy levels study 2−80994
- SmS, semicond.-to-metal transition under press., refl. study 2−75098
- SmS, SmSe, SmTe, amorphous semicond., optical absorp. 2−61657
- SmS(Se)(Te), press. induced electronic collapse and struct. changes 2−68297
- SmSe, press. depend. of optical absorpt. edge 2−75098
- SmSe film, prep., structure., optical and magneto-optical props. 2−81324
- SmSe(Te) films, co-evap. and characteriz. 2−50502
- SmTe, press. depend. of optical absorpt. edge 2−75098
- SmTe, press. induced struct. and electronic transform. 2−50948
- SmTe film, prep., struct., optical and magneto-optical props. 2−81324

Sampling *see Statistical analysis*

Sand

- acoustic props., elastic wave velocity and absorption, effect of grain size 2−84204
- capillary wicking of distilled water in quartz sand and cylindrical glass capillaries in magnetic fields 2−60402
- compressibility rel. to clays 2−62017
- eolian-modified craters, simulation 2−61844
- quartz sand and sandstone recognition by two-channel i.r. imagery 2−65438
- quartz-sand layers in N. Atlantic basin, with high thermal conductivity, heat flow obs. 2−65553
- seabed sand transport and whistling beaches 2−61959
- wet, near f.p., transient simultaneous measuring method for thermal prop. determ. 2−74989

Satellites, artificial

- aerodynamic forces, drag and lift, theoretical determination 2−62419
- Apollo 15 subsatellite, magnetic field of Moon 2−58472
- atmospheric pressure level determ. by two-satellite microwave occultation method 2−84858
- atmospheric temp. i.r. spectrometer data, insertion into forecasts 2−62139
- atmospheric temperature profile derived from satellite radiation meas. simulation of effect of varying atmospheric statistics 2−62138
- ATS 5, electrical charging in synchronous orbit rel. to magnetosphere 2−66025
- ATS III data on tropical waves and weak cyclones, intensity evaluation 2−57960
- attitude and librational control using solar radiation pressure 2−44802
- attitude of gravity oriented satellites, environmental forces effect 2−54980
- aurora, midday and polar cap, characts., satellite and airborne all-sky data 2−68945
- axisymmetric, in gravitational field, rapid-rotation stability 2−75648
- balloon, evolution of orbit. 2−62428
- circular orbit plane, bringing into specified positio, response time optimization 2−51677
- cloud motion and landmark registration, computer data processing applic. 2−48439
- compound pendulum and gyroscope motion in satellite 2−66489
- coordinate det. from wide angle ballistic camera installed in aeroplane 2−51865
- coordinate estimation, effect of interference parameters 2−75650
- cosmic triangulation by synchronous and quasi-synchronous straight lines 2−51680
- Cosmos 316 (1969-108 A), analysis of orbital changes for study of upper atmosphere winds 2−84927
- Cosmos 316 (1969-108A) orbit analysis rel. to zonal winds in upper atmosphere 2−51632
- data collection, from geostationary meteorological satellites 2−65652
- drag-free orbits, long-term development study using computer program PROD 2−68992
- Earth and lunar orbiters, higher order analysis of drag-free satellites 2−78423
- Earth and Moon mass, refinement from obs. of artificial satellite motion 2−55139
- earth resources, narrowband telemetry, S-band tracking, geology, agriculture 2−84929
- Earth resources satellites to rescue Earth from ecological disaster 2−62427
- Earth resources technology satellite 2−61841
- Earth Resources Technology Satellite data digital image processing 2−81641
- Earth Resources Technology Satellite model, testing 2−51676
- Echo-1, light press. meas. 2−51675
- elliptic orbits, Earth pointing attitude control 2−44809
- EOLE, developments 2−62425
- Eole programme for weather forecasts 2−68877

Satellites, artificial continued
- equilibrium potential of magnetospheric satellite in eclipse situation 2−72933
- Explorer 31, electron temperature enhancement in satellite wake 2−54899
- Explorer 34, meas. of magnetic noise in plasma sheet 2−62325
- Explorer 43 meas. of electric and magnetic field structure of magnetopause 2−62316
- free dual spin satellite, stability criteria 2−75641
- geopotential, evaluation of 15th order harmonics 2−58150
- GEOS, electric field perturbations caused by photoemission on sunlit side 2−54982
- geostationary, bolometric horizon sensors for, theory, technology, testing 2−44808
- geostationary, communication, horizon sensors, review 2−44807
- gravity-gradient momentum management 2−66026
- gyrostate, stability analysis for all possible equilibria under gravitational torques 2−62420
- international ultraviolet explorer, payload 2−62421
- ITOS-1, 2nd generation operational meteorological satellite, design and orbital performance 2−48630
- Kallisto, influence of Halileys satellites of jupiter on motion 2−58491
- loosely stabilized, orientation determination 2−75655
- low altitude controlled constellations, for required communications 2−44805
- lunar Explorer 35, upper limit determination of lunar atmosphere 2−58470
- magnetosphere satellite transmitting system design rel. to v.l.f./e.l.f. radiation patterns 2−68933
- magnetron press. gauge on O VI-15, adsorption/desorption press. effects 2−58148
- marine air air applications 2−48625
- Mariner 9, photographs of Mars 2−66177
- meteorological, reception 2−48443
- meteorological soundings of upper atmosphere 2−65639
- navigational algorithm from meas. of star position rel. to probe launched from satellite 2−72939
- Nimbus 2 high-resolution i.r. radiometer meas. for estimation of extratropical cyclone parameters 2−54840
- Nimbus 3 and 4, interrogation, recording and location system 2−66035
- Nimbus 3 and 4 flight missions 2−48629
- numerical artificial satellite theory using Picard iteration process 2−58149
- oceanographic survey operations, use of real-time satellite infrared data 2−57889
- optimally stable, generalization of Beletskij's concept, libration boundaries 2−44801
- orbit prediction, local gravitational anomalies in low orbits 2−72936
- orbital decay, atmospheric density variations at 140 km. from precise satellite radar tracking data 2−68926
- orbits rel. to tracking data accuracy 2−51679
- orientation, determ. from magnetometric measurements 2−75654
- perturbed motion rel. to solar radiation pressure effects 2−84935
- photographic obs. without using time recording arrangement 2−54981
- resonant attitude instabilities for symmetric satellite in circular orbit 2−72937
- resonant motion rel. to Moon and Sun, laser ranging and geodetic applications 2−81760
- rotation, vortex-type currents influence 2−85072
- scientific, developments and prospects review 2−48627
- SOLRAD, solar radiation meas. experiments 2−51844
- Soyuz 9, effects on human body of long term weightlessness 2−62424
- SPARCENT, Karachi, Pakistan, geodetic parameters determined by Doppler satellite geodesy 2−65441
- spinning drag-free, mass centre estimation 2−66036
- stability analysis of force free spinning satellites with flexible appendages 2−51682
- stability of earth-pointing satellite with multi-elastic domains 2−76251
- stability of motions of body of resolution in Newtonian field studied by Lyapunov methods 2−58176
- terrestrial magnetic field effect on satellite motion about its centre of gravity 2−72938
- tidal effects on artificial satellite motion 2−84933
- tracking of ATS-3 by v. long baseline interferometry 2−54988
- tracking using least squares estimation 2−41554
- TRANSIT navigational satellite, radioisotope thermoelectric generator using $^{238}PuO_2$ heat source 2−49296
- triaxial rigid satellite in precessing elliptic orbit, effects of gravity-gradient torque on rotational motion 2−81752
- two-body cluster, effect of atmosphere on relative motion 2−75649
- uniaxial, spinning, equations of motion, responding to magnetic and gravitational torques 2−44800

Saturn
- atmosphere, minor constituents, u.v. spectroscopy from Orbiting Astronomical Observatory 2−69140
- atmospheric investigations using Jupiter turbopause probe 2−78557
- atmospheric temp. sounding 2−78539
- circular polarization obs., polar scattering effect 2−75912
- comets, short period, effect of multiple encounters with Saturn on orbits 2−58523
- Iapetus, albedo, radius and temp. obs. 2−81905
- Iapetus, UBV photometry 2−75910
- Iapetus satellite, temp., radiometric measurement 2−58511
- i.r. spectrum rel. to Titan's spectrum 2−81906
- limb darkening and thermal props. of map at 10 and 20 μ 2−75911
- Phoebe (IX), photometric obs. 2−75859
- photographic astrometry of satellites rel. to mass and figure of Saturn 2−81901
- photometric characteristics of regions of disk in 0.33-0.48 microns region 2−58486
- Rhea, albedo, radius and temp. obs. 2−81905
- Rhea, satellite, temp., radiometric measurement 2−58511
- ring formation by solar radiation pressure and disruption of solid satellite 2−48778
- ring thickness from 1966 to edge-on observations 2−81934

Saturn continued
- rings, hypothesis on formation 2−73086
- rings, surface brightness as function of solar and terrestrial elevation angles 2−62708
- secular variations of asculating elements 2−62696
- thermal radio emission, model atm. 2−75882
- Titan, brightness temp. obs. at 20 microns 2−78487
- Titan, composition of atmosphere 2−69163
- Titan, i.r. spectrum, methane bands rel. to Saturn's spectrum 2−81906
- Titan, polarization obs., evidence for optically thick atm. 2−81907
- Titan's atm., greenhouse effect, evidence for H_2 content 2−78488
- Titan satellite, temp., radiometric measurement 2−58511
- u.v. absorption in continuous spectrum, time variations 2−75869
- H_2 absorption, quadrupole, spectral obs. 2−75872

SC (sudden commencement) *see Magnetic storms*

Scalers *see Counting circuits*

Scandium
- Compton profiles, electron momentum distrib. 2−78116
- deuteron bombarded, secondary electron emission 2−61468
- electron phonon enhancement factor, from specific heat data 2−64932
- film, elec. cond. and Hall const., size effect 2−81030
- film, optical sensitivity to energetic ions, tuning of ion microprobes 2−45691
- hyperfine field, in Fe matrix, spin echo obs. 2−72229
- ion, in $FeFe_{2-x}Sc_xO_4$, Sc-containing magnetite, K emission and absorp. spectra 2−44400
- Sc III, 50 new lines 2−79922
- Sc III ion, oscillator strengths 2−49934

Scandium compounds
- ferrite, struct. rel. to spectral props. 2−54440
- hydrides, empirically derived band diagrams 2−77833
- monoauride, dissociation energy rel. to bond energy calc. for Sc diatomic intermetallic 2−50557
- tritide film, ageing, bubble form. and rupture 2−43478
- LiO_2-Sc_2O_3-SiO_2-H_2O, hydrothermal crystallization 2−71383
- Sc-H, n.m.r. obs. Korringa product, diffusion parameters determ. 2−72517
- ScD_3, deuteron bombarded, secondary electron emission 2−61468
- ScF-TlF solid soln., phases, fusion diagram 2−53997
- $ScH_{1.99}$, acoustic velocity, limiting Debye temp. and elastic consts. detn. 2−57047
- Sc_3In, itinerant ferromagnet, theory of magnetic fluctuations 2−65157
- Sc_3In, magnetization, sound velocity and sp.ht. 2−81258
- $ScLiO_2$, luminesc. of Eu^{3+}, energy levels 2−48226
- ScN, epitaxial growth and elec. props. 2−50503
- Sc_2O_3-MgO solid soln., phase diagram, defects, disintegration, decomp. precip. 2−74906
- Sc_2O_3-V_2O_3 solid solution, mag. props., comp. depend. 2−48041
- ScO CNDO-II approx SCF molecular orbital method, levels calc. 2−83252
- Sc_2O_3, a.c. conductivity, hopping model 2−61324
- ScS, in solid Ar and He matrices, e.s.r. and i.r. spectra 2−46582
- Tb-Sc alloys, mag. characts. 2−68576

Scattering
- abstract theory, scatt. states and wave operators 2−82241
- Amado's model, three-body bound states 2−45280
- amplitude, geometrical interpretation of harmonic analysis 2−45275
- asymmetric molecules, quantum mechanical scattering, interaction potential 2−53097
- asymptotically Coulomb potentials, time-dependent and time-independent 2−45276
- bending waves, multiple scattering by random inhomogeneities 2−73416
- classical binary encounter approximation, derivation from Born approximation 2−41515
- condensed matter, multiple scatt. theory 2−58762
- into cones, generalization of Dollard's quantum mechanical result 2−76203
- conservative wave eqns. with single localised scatterer 2−58719
- cut-off potentials, energy power expansion of Green function and Pade approximation 2−45278
- deuteron beam, angular spreading in neutralizer cell 2−79697
- rel. to diffraction phenomena, theory 2−45246
- disordered systems, cluster effects 2−68270
- dissipative systems 2−49043
- elastic, integral approximation applied to Dirac equation 2−41522
- elastic waves, by moving objects 2−55514
- elastic waves, representation theorems and propagator matrices 2−78898
- Fredholm-Pade approximation for problems involving pair of coupled channels with square well potentials 2−76205
- gas-surface interactions, computation of scattering kernels, boundary-value problem 2−49042
- glory extrema in total scattering cross-section 2−49017
- gravity waves, by irregular bottom 2−54787
- high energy, at backward angles, simple prescription 2−49020
- interpolation of variationally obtained cross sections 2−63021
- inverse problem, free Riemann Green function 2−63019
- inverse problem, Riemann method 2−63018
- Kallen-Pauli state vectors in Vθ sector, algebraic solution by congruence transformation 2−45277
- Klein-Gordon equation, inverse problem of potential scattering 2−41495
- light field in scattering media a long time after illumination by pulse source 2−79321
- local potential energy eigenvalues calc. method 2−82224
- low-energy, by long range r^{-8} potential 2−69601
- momentum-space eqns., peaked potentials, numerical aspects 2−55421
- multichannel Feshbach eqns., variational principles 2−52898
- nonlinear, invariant embedding applics. 2−52048
- nonlocal potential matrix elements from scatter phases 2−52079
- nonspherical, semiclassical equivalence relations 2−78819
- optical potential calc. of absorption and elastic cross sections, computer program 2−52078

Scattering continued
partial wave amplitudes, analyticity and conformal mapping methods 2−52080
phase shifts, r^{-2n} potential scatt., Born approx. and applic. to dipole-quadrupole scatt. 2−58763
phase-shift formula for 3d problem derived from modified WKB approx. of Miller and Good 2−55422
phonon inelastic surface scatt., transition matrix for bound state interactions 2−83854
plasma, stability of monochromatic wave against induced scattering 2−74392
plasma waves by acoustic turbulence and type III solar radio bursts 2−62753
potential, comparison of plane-wave approximations 2−45274
potential, of well-localized wave packets, time-dependent aspects 2−63022
potential, resonance and phase shift calc. using Pade approximation theory 2−49019
potential, S-matrix pole trajectories in *N/D* approach 2−58764
potential, soft photon theorem for nonrelativistic bremsstrahlung 2−59412
potential, solution of standing wave integral equation 2−63020
potential scattering, reduction of semiclassical phase shifts to resonance form 2−49018
proton beam, angular spreading in neutralizer cell 2−79697
quantum cross section, probabilistic interpretation 2−41518
quantum mech. system with unstable discrete states, reson. scatt. theory 2−78820
quantum mechanical cross-section paradox, simplified resolution 2−49016
quantum mechanical representation, impact parameter operator 2−41521
of quantum mechanical wave packet, new definition of time delay 2−78822
quantum theory, time-dependent, relationship between time delay and phase shift operator 2−76204
quantum-mechanical wave packet by finite range potential, calc. of time delay 2−82216
radiation density distribution in scattering media with limited size source 2−66818
radiation from free electron interacting with circularly polarized laser pulse 2−78772
reactive, method for exact quantum mechanical calculations 2−69602
repulsive singular potential, applic. of modified WKB approx. to solution 2−41519
Rutherford amplitude, divergence in terms of Coulomb phase shifts 2−73331
seismic waves, by interface irregularities, unified treatment 2−61884
semiconductors, negative photoconductivity 2−81174
single channel, nonrelativistic time-dependent theory and von Neumann algebras 2−41517
soft sphere atom lattice, first approximation for normal incidence 2−55437
spheroidal bound states, rotationally invariant, zero-energy case 2−69599
sum frequency amplification, quantum theoretical treatment 2−69888
teleseismic P-waves, mechanism 2−57535
three body and three dimensional calc. reactive scattering, exact quantum mechanical 2−79867
three body break-up processes, Kohn variational principle 2−41516
three-body D-function, new parameterization 2−49012
three-body problem in 1-D, with interacting, impenetrable particles 2−82228
three-particle systems, proof of Efimov effect 2−45281
time-dependent theory including rearrangement processes, WKB approx. 2−69598
transfer problems in homogeneous cylindrical media, combined operations method 2−52040
transient stimulated thermal scattering, frequency response 2−41939
unstable states, theoretical approach 2−42551
waves, bending, diffr. and scatt. by mass impedance loadings of plane plate 2−63099
K atoms with methyl iodide, reaction in crossed beams 2−68771
acoustic waves
air bubbles in water, scattering strength meas. 2−74511
aircraft wake vortices, acoustic ray deflection 2−56430
backscattering from spherical and cylindrical shells, penetrability effects 2−41734
bistatic backscattering, from ocean surface, l.f. underwater sound 2−75479
Eastern Pacific Ocean, diurnal and seasonal variations in acoustic volume scattering meas. 2−62030
elastic body, determ. of radiation pressure forces and torques 2−52235
elastic cylinders, layered hollow 2−69744
elastic cylindrical shell, transient field 2−41732
elastic cylindrical shell surrounded by thermo-viscous media 2−66621
by elastic double cylindrical shell 2−58918
from expanding bubbles, velocity effects, underwater explosions 2−52237
from fluid-immersed elastic bodies, numerical solution 2−66622
fog, cloud, rain, snow, detection by acoustic echo sounding 2−62234
monochromatic point source, field in randomly inhomogeneous medium 2−69720
multiple spheres, interaction effects 2−55538
multiple surface reflection in linear gradient medium 2−44623
N-layer periodic grating, waveguide approach 2−78923
one dimensional nonlinear wave, in dissipative gas 2−52229
Philippine Sea, deep sound-scattering layers 2−57849
piezoelectric, stimulated combination scatt., theory 2−74981
planktonic animals in sea 2−78330
Rayleigh, Love surface waves at deformed boundaries and wedges 2−63113
rigid prolate spheroidal obstacle scattering in acoustical medium 2−73437

Scattering continued
acoustic waves continued
rigid sphere, separation and anal. of field 2−58916
rough surface, effect of beam width 2−44533
sea surface waves, rel. to underwater acoustic remote sensing 2−57886
sound-sound scatt. in water in presence of object 2−45515
in turbulent atmosphere 2−44705
underwater, surface backscatt. coeff. calc. from measured data 2−66625
underwater surface backscatter, of Doppler shift 2−55532
water tank meas. rel. to volume reverberations in ocean 2−53425
He, liquid, acoustic multiple beam scattering 2−83832
acoustic waves, ultrasonic
emulsions, characteristics 2−71251
polycrystalline materials, attenuation frequency dependence 2−69743
rough surfaces for forward specular and backscattering geometries 2−41735
from water surface, rough, Doppler frequency shift 2−68861
Al alloys, longitudinal ultrasonic plane waves, simulation 2−51023
electromagnetic waves
aerosols, atmospheric, aureole obs. 2−62267
anisotropic noncoherent scattering, redistribution function for frequency 2−55616
antiferromagnetic- ferromagnetic transition point, fluctuations and scatt. of slow neutrons and e.m. waves 2−72207
atmosphere-ocean system, multiple scattering calc. for solar radiation 2−65756
backscattering, by circular dielectric discs at X-band, modified Kirchhoff theory 2−49212
backscattering, Stokes parameter transformation 2−41879
backscattering from irregular thin lossy layer situated over lossy semi-infinite medium, acoustic simulation techniques 2−52329
black-hole bomb, floating orbits and superradiant scattering 2−62443
buried conductor effect rel. to subsurface fields 2−45612
circularly polarized e.m. waves, effective scattering area 2−45613
circularly polarized ultrashort radiowaves from celestial bodies 2−55196
conducting crystals, by sound, electron conc. wave contrib. 2−54396
by cross-junctions of oversized rectangular waveguides 2−59002
by cylindrically symmetrical objects, normal incidence, numerical solution, phase, multi-layer techniques 2−69833
dielectric ring, using integral- equation technique 2−52323
dielectric waveguides, propagation mode and scattering loss, gradual refractive index 2−49220
earth models, two- dimensional, finite element method 2−54717
elliptic cylinder, perfectly cond., inverse problem 2−76418
extinction theorems 2−78979
in flat waveguide containing magnetoactive plasma due to electron charge fluctuations 2−77275
hemispherical, from rough surfaces, intensity calc. 2−78978
human body in resonance region, rel. to admittance and radiation efficiency meas. in 30 to 70 MHz 2−49227
Huygen's principle, formulation for field strength's transverse components vanishing at infinity 2−82392
hydrodynamically turbulent systems, gases and plasmas 2−46860
incoherent, from high temp. plasma 2−64276
infinite plane grating with reflector, resonances near Rayleigh wavelengths 2−76411
interaction with irrotational fluids 2−41873
by ion acoustic wave, radially propagating in Hy positive column 2−74387
ionosphere, oblique sounding, mechanism of formation and form of scattered signal 2−72853
ionosphere, spread-F theory 2−48583
ionosphere characterization, using incoherent scatter sounder 2−78392
light detection and ranging, remote atmospheric probe 2−54802
by linear isotropic material of negative conductivity 2−41881
from loaded bodies of revolution 2−58996
lunar satellite propagated, lunar surface reflected e.m. waves 2−55600
magnetoactive plasma, induced wave scatt. 2−80347
magnetoplasma column moving in axial direction 2−49215
from moving cylindrical electron beam, velocity dependent scattering 2−52327
by moving target, quasi-ergodicity of dynamic scattering pattern 2−76419
nonforward differential cross section for waves in spherical gravity and spherical media 2−82401
oblique incident waves, by inhomogeneous fibres 2−78967
fromocean-like surfaces, numerical study 2−52328
optical, periodically modulated media 2−63380
plasma, oscillations, nonlinear scattering, harmonic cyclotron 2−64322
in plasma anisotropic, over conducting wedge 2−77273
by prolate spheroid, perfectly conducting, inverse problem 2−41878
radar backscatter along Earth-space paths, obs. 2−81652
radar properties of non-Rayleigh sea clutter 2−41880
radiosources, applic. as remote sensing probe for solar wind 2−62781
r.f., from random electron density fluctuations in cold magnetoplasma 2−63201
rotating, metal cylinder, monochromaticity 2−69834
rough cylindrical particles, scattering properties 2−52326
rough surface, Kirchhoff approach and small perturbation analysis relationship, comments 2−52325
solar radiobursts, coronal scattering at kilometer wavelengths 2−55172
sphere, transformed stochastic equation method 2−69832
stellar interiors, Thomson scattering 2−58271
symmetrical objects, zero polarization bases of one-position scattering matrix 2−55617
thin anisotropic near elliptical dielectric rod 2−55618
by thin elliptical rods in rectangular waveguide as function of rod position, orientation 2−63190

Scattering continued
electromagnetic waves continued
in troposphere, radiowave troposcatter time dependence over mountainous path, radiometeorological interpretations 2−68922
in turbulent atmosphere 2−44705
turbulent plasma, causing attenuation, phenomenological model 2−46740
turbulent plasma, criticism of theories 2−46742
two dimensional problem, optimal solution 2−52330
two-scale rough surfaces, bakscattering 2−41882
underdense plasmas, role of turbulence intermittency 2−50195
volume scatt. effects, surface roughness relations, depolarization 2−49427
wedge with rounded edge, comments 2−52324
light
see also Diffusion, light; Rayleigh scattering
ABA block copolymer films, anisotropic regions 2−44325
aerosol particle, measurement using Differential II 2−47000
aerosol particles, multiple scatt. 2−46998
aerosols and atmospheric particulates 2−72802
n- alkane gases, meas. of anisotropy and depolarization ratio by photon counting of scattered laser light 2−80083
angular from fibre waveguides with irregular core surfaces 2−79335
anisotropic elliptical objects, method of calc. for any desired dipole orientations 2−72289
antiferromagnetic insulator, phase transitions influence 2−54399
aqueous media, turbidity, frequency contrast characteristics 2−46991
atmosphere, from measured aerosol size distributions, six component log gaussian model 2−81688
atmosphere, noncoherent scattering problem, probabilistic formulation 2−57994
atmosphere, ocean colour determination 2−65587
atmosphere, simulated aerosols, effects of humidity and water droplet clouds 2−57991
atmosphere-ocean system, effects of aerosol variation on radiance 2−57990
atmospheric aerosol, particle size distrib., photometric obs. 2−75538
atmospheric aerosol light scattering from extinction measurements at remote clean air locations 2−51621
atmospheric aerosols, and absorbing props. 2−65780
atmospheric aerosols, effect on radiance and colour of twilight sky light 2−81690
atmospheric aerosols, size-altitude distrib. 2−65778
atmospheric extinction measurements, departures from Rayleigh scattering 2−54860
atmospheric ice clouds, scattering in visible and i.r. regions 2−58000
atmospheric pollution aerosol monitoring by scatter of Ar-ion laser beam, interferometry 2−51600
atmospheric scattering data using large laser radar equipment 2−84867
atmospheric turbidity meas. w. laser radar 2−62272
atmospheric turbidity rel. to aerosols above McCall glacier 2−62273
atomic vapour, resonance radiation scatt., linear systems analysis applic. 2−63999
backscatter of solar resonance radiation by interstellar Hi and HeI in solar system 2−55078
beam spreading in turbulent medium, calc. by modified von Karman spectrum 2−49415
benzene, second harmonic laser light scattering 2−43357
Bessel functions computation 2−70022
butyl alcohol aqueous solutions 2−74547
carbon tetrachloride and mixtures with cyclohexane, collision-induced scatt. 2−71202
chloroform, polycryst., low-freq. and intra- molecular vibrations obs. 2−57339
cirrus cloud layers 2−62253
clouds, backscattering, first and second order, illuminated by lidar beam 2−51610
clouds, effect on solar radiation absorption by atm. dust 2−84806
coherent, propagation in optically inhomogeneous medium 2−79253
coherent isotropic scattering in sphere with arbitrary source distribution 2−55734
coherently illuminated rough surface, structure of interference field 2−42207
by colloidal particles, application to study of turbulent flow, analysis 2−77216
Compton and inverse Compton, scattering centre motion effects 2−42325
conference, Washington, USA, Sept. (1971) 2−64475
correlation function approach to systems with nonrandom orientation correlations 2−64479
cyclohexane and mixtures with CCl_4, collision- induced scatt. 2−71202
data inversion, information theory 2−64476
deep scattering layers in Gulf of Mexico response to total solar eclipse 2−48416
dense dielectric media, dipole approx. and macropolarizability operator 2−79978
depolarized doublet spectra of liquid and shear retardation processes 2−53433
dielectric cryst., by entropy fluctuations, phonon transport theory 2−81327
by dielectric needles, finite, illuminated parallel to axis 2−79324
disperse system turbidity spectrum, determ. of size and refractive index of particles 2−43399
from E.coli cells, angular dependence and cell models 45017 2−45017
electrophoresis of particles and biological cells, det. from Doppler shift of scattered laser beams 2−79385
eruptive stars, reflection effect, optical properties of scattering medium 2−51759
f.c.c. cryst., antiferromag., by magnons 2−61550
ferroelectric ceramic, transparent, grain size and porosity effects 2−57244
ferromagnet, with weak antiferromagnetism, rel. to l-wave existence 2−78012
fluid, convective instability, spectral anal. study 2−67609
fluid layer, convective instability obs. 2−46660

Scattering continued
light continued
fluid with internal degrees of freedom, intensity and dispersion relations 2−64090
frequency modulation of laser by fluctuations in chemical reaction 2−41977
by gas, depolarization, rotating analyzer meas. and ratio method of analysis 2−64395
gas mixtures 2−67735
gaussian field production, amplitude correlation function obs. through joint photon-count distributions 2−41951
granulation around rough objects, linear systems 2−63391
gravitational wave detectors, use in 2−66424
heart conditions by photometry using whole blood 2−45023
holography through fog and image reconstruction 2−79259
homoform, polycryst., low-freq. and intra-molecular vibrations obs. 2−57339
from homogeneous sphere, internal and external light source 2−66816
from inhomogeneous cylindrically symmetric lens line infinity in refractive index 2−63374
inhomogeneous fluid, irradiance and spectral distrib. 2−79325
internal dust in nebulae, nonisotropic scattering 2−66067
ionic liquids, charge-induced anisotropy model 2−53432
laser, automated photometer, for particle size analysis 2−63307
laser, from cascaded arc, electron temp. and density meas. 2−53260
laser backscattering, optimal signal processing for det. of atmospheric irregularities structure 2−72801
laser beam from turbid water, depolarization 2−64486
laser beam scattering on polyethylene target, production of plasma instabilities 2−56366
laser beam technique for high-density plasma diagnostics 2−70924
laser beams by slowly varying leaky wave structures 2−79337
laser scattering from high density low temp. plasmas 2−67623
law of interstellar extinction, influence of surface roughness of grains 2−84972
lidar backscatter and extinction meas. of urban aerosols in atmosphere 2−51622
light-light and light-particle scatt., general relativity and quantum field theories 2−66433
liquid, fine structure in depolarized light scatt., use in calc. of stress-optical coeff. 2−50358
liquid, stimulated thermal scatt. of psec. laser pulses 2−67830
liquid compound of asymmetric top molecules, calc. of collective molecular orientation correlation functions 2−50313
liquid cryst., formation of nematic threads 2−67805
liquid cryst., nematic, dynamic scatt., effect of charge transfer acceptors, voltage transmission characts. 2−71201
liquid crystal, dynamic scatt. mode, rel. to matrix-addressed displays 2−52480
liquids, and ultrasonic relaxation 2−50356
Los Angeles smog, comparison of calculated and measured scatt. 2−51623
Los Angeles smog, comparison to light extinction by NO_2 2−51625
Los Angeles smog, correlation with size distrib. and vol. concentration 2−51624
loss in liquid and vitreous states in terms of fundamental material properties 2−50357
macromolecules, meas. of radii of gyration for particles ≈100Å 2−50117
macromolecules, transient scattering from absorbing solutions 2−50378
magnetoordered crystals with small exchange constant, spin waves and scatt. proc. of neutrons and light 2−72209
magnetoplasma, weakly ionized, incoherent scattering from charge density fluctuations 2−77267
mammalian cell identification, differential technique 2−66244
marcomolecule solutions, spectral analysis by analogue time correlation of scattered light 2−82585
matrix-operator theory for Rayleigh and maritime haze phase functions 2−76235
MBBA liq. cryst., dynamic scatt. in hydrodynamic regime, relax. time 2−77438
methanol-cyclohexane critical mixture, simultaneous meas. of viscosity and light scattering 2−71169
Mie scatt. by three polydispersions, atmos. aerosol. models 2−65779
Mie scatterers in stratosphere, inversion technique for obs. of characteristics 2−65768
molecular crystal, determination of general coupling parameters from classical theory of stimulated Stokes generation 2−51315
molecular portion of atmos., anomalous transparency effect 2−62268
Mossbauer diffraction in magnetically ordered crystals, kinematic theory including Rayleigh dispersion 2−68610
Mossbauer effect spectroscopy, backscatter detector 2−79659
multiple, of laser beams from turbid water 2−43391
multiple, synthetic foggy atmos., photometry, analog computation 2−64478
multiple, two-flux and many-flux eqns. 2−63393
multiple by inhomogeneities, application to ferroelectric display devices 2−79350
multiple diffusion, by assembly of spheres 2−70023
muscle proteins, effect of Ca^{2+} on dynamic props., quasielastic scatt. study 2−70798
nematic liquid crystal, surface tension and viscosity coeffs., detn. 2−56480
nematic liquid crystal, transient response caused by low freq. voltage pulse 2−53398
by nematic liquid crystals, comparison of rise and decay time for homeotropic, homogeneous boundary conditions 2−64442
nepheloid layer, correl. with suspended material analysis 2−57913
nephelometer, balloon-borne, for high altitude meas. 2−72805
nitrobenzene-n-hexane, crit. mixture, intensity and correlation length 2−80473
noncoherent, probabilitistic formulation 2−63392
noncoherent radiation transfer, across isothermic medium 2−66817
ocean colour from scattered sunlight meas. from spacecraft in noon orbit rel. to Earth resources studies 2−84773
by ocean particles, multi-component models 2−57894
optical heterodyne method for mixing spectroscopy 2−66820

Scattering continued
light continued
optimum collection of light scattered from plasma, optical system 2−56360
p-methoxybenzylidene-p′-amino phenyl acetate, nematic, dynamic scatt. life, current density effects 2−71203
parametric 4 photon exchange effect, spontaneous, theory 2−65236
particles, isotropic spherical, light scattering function calc. 2−50383
particulate suspensions, interpretation of Kubelka-Munk coefficients 2−49426
n-pentane-cyclopentane binary solution, height and temperature variations in scattering power near critical point of vaporization 2−43373
in periodically modulated media 2−63380
photochemical aerosol, mass concentration measurement 2−48511
photocounting receiver performance for detection of multimode laser or scattered radiation 2−41948
photoelastic scattering of light from a non-alkali alumino silicate glass 2−65226
photographic camera, quantitative determination of stray light 2−59327
photographic materials for holography 2−63438
in photographic phase holograms, technique for reduction 2−42149
photography of particle movement in flow system using scattered light at low levels of intensity 2−50376
photometer, using photographic film 2−73650
photon statistics, analysis of generalized birefringence expts. 2−63308
plane parallel purely scattering inhomogeneous atmosphere 2−48766
in plane parallel turbid media, equivalence of Kubelka-Munk and Chandrasekhar approaches 2−49416
planetary atmospheres, multiple scattering rel. to absorption lines, probability distribution 2−78529
planetary atmospheres with refraction, calculation of light scattering 2−81925
plasma, θ-pinch, laser-beam-scattering meas. of ion temperature 2−56364
plasma, ion-acoustic line profiles, Coulomb-collision corrected 2−67642
plasma, laser produced, spectral analysis of backscattered light 2−56355
plasma, Stokes line generation during laser irrad. due to Compton effect 2−74369
plasma dense, cold 2−60246
plasma lines, obs. of Landau and collisional damping 2−43143
plasma magnetic field meas. 2−64301
plasmodium actin polymers, dynamic properties obs. 2−60606
for point isotropic light sources in model atm. 2−81691
poly(ethylene terephthalate) light scattering study of spherulite evolution from rodlike nuclei in early stages of crystallization 2−64535
polycrystalline waveguides, from grain boundaries and surface defects 2−79336
polymer films dynamic light scattering study 2−83382
polymer latex, particle size analysis, angular scattering data 2−43411
polymer solution, determ. of press. and temp. depend. of thermodynamic props. 2−64446
polymer solution, wavelength dependence 2−64447
polyoxymethylene dioxide thin films, structure studies using small angle polarized light scattering 2−84526
polystyrene in ethyl acetate ethyl alcohol mixtures, diffusion meas. 2−60458
polystyrene latexes, multiple scattering, determ. of coeffs. of scattering and absorption 2−43400
polystyrene sphere solution, moments meas. 2−73541
polyvinyltriorganosilane solutions, relation between intrinsic viscosity and molecular weight 2−46997
in rabbit corneas 2−69477
random rough dielectric surface, depolarization props. 2−79309
remote sensing of atm. particulate pollutants 2−81693
resonant, by perturbed harmonic oscillator 2−66819
by rotating ground glass with surface inhomogeneities, statistical props. 2−79326
rough surfaces, circular polarization 2−63395
scattering media, light beam attenuation, exponential low limits, scatt. indicatrix 2−56527
sea water, axially symmetric submarine daylight field 2−65607
sea water, integral light scattering coeff. rel. to scattering coeff. in fixed direction 2−51564
seawater, intensity fluctuations 2−48419
seawater, Mie theory applic. to index calc. 2−57835
seawater, suspended matter in nepheloid layers 2−68870
seawater, volume scattering function rel. to axially symmetric light field 2−57892
semiconductor, degenerate, free carrier absorp., quantum theory 2−51329
simple gases, statistical mechanical description of depolarization and many body effects 2−53338
small-angle from anisotropic sphere, derivation of Mueller's phenomenological matrix 2−73642
small-angle multiple scatt. in iconal approx. 2−73621
solutions, scatt. by fluctuons 2−71151
by spherical particle of a short light pulse, theoretical considerations 2−79320
spherical particles, computer calculations 2−63396
statistics of non-Gaussian scattered light, for n-particle systems 2−73541
steel, cold-rolled, surface defect obs. 2−74871
stimulated elastic scattering, effect of coherence 2−42205
stimulated thermal, frequency response 2−59238
superconductor, with creation of 2 quasiparticle temp. depend. calc. 2−65238
surface diffusers' transmittance, design of near band limited binary diffusers 2−59237
surface flaw detection using oblique angle illumination 2−50415
suspension, seawater conc. determ. using total scatt. coeff. 2−62020
suspension of oriented particles, turbidity determ. from polarizability coeffs. 2−56532
Thompson, from coronal streamer models computer programme for numerical integration 2−76026
Thomson scattering, influence of radiation statistics 2−56348

Scattering continued
light continued
three-photon phenomena for randomly oriented molecules, polarization dependence 2−67441
transfer of resonance radiation as process of photon random walks 2−82550
triethylamine-water critical mixture, simultaneous meas. of viscosity and light scattering 2−71169
turbid media, low angle scatt. 2−77455
turbid medium, radiative transfer theory, efficient stream distributions 2−79356
turbidity in estuaries, spectrophotometric techniques 2−54797
under water, radiance distribution from collimated source 2−65590
upper atmosphere aerosol, rocket mounted laser radar obs. 2−54878
volume scatt. effects, surface roughness relations, depolarization 2−49427
waveguide's information carrying capacity, backscattering effects 2−49425
by weak acoustic waves, Huygens' expression for diffr. field 2−55742
Al_2O_3, light scatt. by elastic waves and rotation of polarisation plane 2−72358
Ar, compressed, complete spectrum of collision- induced light scattering analysed using Michelson interferometer 2−80408
Au black deposit, i.r., rel. to prep. conditions 2−57347
C arc, high current, electron temp. detn., Thompson scatt. obs. 2−64363
CS_2, second harmonic laser light scattering 2−43357
CdS, acoustoelectric instability, scattering of light by sound 2−71728
Cu_2O, normally forbidden transitions obs. 2−61636
Ge:Sn heavily doped, detection of Sn precipitates 2−77911
He II, by ultrasonic cavitation 2−43427
^3He-^4He liquid mixture, rel. to first and second sound detection 2−53481
^4He, liq., near λ line, intensity peak, rel. to isothermal compressibility 2−50391
^4He, superfluid, rel. to first and second sound detection 2−53481
n-InSb, stimulated spin-flip Raman scattering rel. to homogeneously broadened travelling-wave electronic Raman laser 2−42100
KCl spectrum, charge induced anisotropy model 2−53432
KH_2PO_4, light scatt. by elastic waves and rotation of polarisation plane 2−72358
KI:Cu, rel. to antiresonance phenomena in transmission spectra 2−54423
LiF:Mg, impurity associations decomp., light scatt. obs. 2−83983
$LiNbO_3$, light scatt. by elastic waves and rotation of polarisation plane 2−72358
$LiNbO_3$ spontaneous parameteric scattering, idler absorption and dispersion 2−44337
N_2 liquid, stimulated thermal scattering 2−46963
NO_2 atm. aerosol, fluorescence obs. 2−81692
NO_2 mol., inelastic photon scatt., of N_2, atmospheric pollutant monitoring 2−67496
Na, atom, resonance curve narrowing in forward scattering 2−56101
Na_2O-SiO_2 glass, with small additions of Al_2O_3 and Ga_2O_3, immiscibility temp. 2−53539
O_2 liquid, stimulated thermal scattering 2−46963
RbH_2PO_4, light scatt. by elastic waves and rotation of polarisation plane 2−72358
Rh(III) triethylenediamine chloride, vibr. spectra analysis 2−72325
Si, ion irradiated, apparent damage induced absorp., scatt. from defect zones 2−48158
SiO_3, light scatt. by elastic waves and rotation of polarisation plane 2−72358
ZnO:Li, light scatt., and photoconductivity, anisotropic 2−75317
ZnO, particle size determ., computer appl. to data processing 2−53942

light, Brillouin spectra
acoustically active crystals, calc. of polarization of scattered light relative to incident laser light 2−68667
alkali silicate glass, effect of conc. and density fluctuations 2−57365
anisotropic media, photoelastic tensor elements determ. 2−78114
benzene, u.s. attenuation meas. in 600-900 MHz range using Brillouin scattering techniques 2−71198
biophysical macromolecules, theory and applications 2−81991
as elastic and photoelastic consts. meas. tool 2−50731
electrolyte solutions, hypersonic velocity and absorption coefficients 2−43360
glass, optical grade, relative intensities of Rayleigh and Brillouin scatt. 2−57364
halobenzenes, Mandelstam-Brillouin components, 20−96°C, rel. to hypersonic props. determ. 2−77429
I_2-filter method 2−65274
ionic Brillouin effect, theory 2−84502
liquid crystal, Brillouin scattering study of propag. of hypersonic waves 2−80454
lithium acetate, elastic consts. meas. 2−50732
low temperature liquids, temp. dependence 2−64459
Mandel'shtam-Brillouin scatt., stimulated, wavefronts of reflected and exciting light 2−42123
metal, theory of scattering by long wavelength acoustic phonons 2−54438
microwave phonon bottleneck obs., rel. to optical techniques in e.p.r. 2−61729
nitrobenzene-n- hexane critical mixtures, investigation by interferometric technique 2−46965
parasitic light reduction using I_2 absorption filter 2−52471
Perspex, stimulated scatt., elastic const. variations with press. 2−47480
photoelastic parametric interactions in laser-pumped birefringent media 2−59121
pivalic acid, plastic, mol. symmetry effects 2−57366
pivalic acid, plastic crystalline phase 2−44399
plastic, stimulated scatt., phonon lifetime and gain determ. 2−68668
polyethylmethacrylate, molecular relaxation and hypersonic phonon waves 2−65284
polyethylmethacrylate, stimulated scattering, hypersonic vel. meas. 2−68669

Scattering continued
light, Brillouin spectra continued
polymethylacrylate, molecular relaxation and hypersonic phonon waves 2−65284
polymethylmethacrylate, stimulated scattering, hypersonic vel. meas. 2−68669
quartz, calc. of polarization of back-scattered light relative to incident laser light 2−68667
rare gas crystal, scatt. from transverse phonons 2−84509
stimulated backward Brillouin scattering in optical glass fibres 2−44398
$AgNO_3$, molten, hypersonic vel. dispersion obs. 2−77427
Ar, solid, stimulated scatt., elastic consts. detn. 2−68231
$CaCO_3$, photoelastic tensor elements determ. 2−78114
$Ca(NO_3)_2.4H_2O$, molten, hypersonic vel. dispersion obs. 2−77427
D_2, analysis of spectrum using kinetic model based on Wang Chang-Uhlenbeck eqn. 2−80409
D_2, compressed, Rayleigh-Brillouin scatt. and relaxing thermal cond. 2−56171
$DyVO_4$, elastic consts. determ., rel. to anomalies in Jahn-Teller phase transitions 2−71681
$DyVO_4$, obs. of elastic consts. anomalous behaviour at Jahn-Teller induced phase transition 2−84038
GaAs, dispersion, fast TA phonon cross section 2−61670
GaAs magnetic enhancement of acoustoelectric gain, obs. by Brillouin scattering 2−51034
H_2, analysis of spectrum using kinetic model based on Wang Chang-Uhlenbeck eqn. 2−80409
H_2, compressed, Rayleigh- Brillouin scatt. and relaxing thermal cond. 2−56171
HD, analysis of spectrum using kinetic model based on Wang Chang-Uhlenbeck eqn. 2−80409
HD, compressed, Rayleigh-Brillouin scatt. and relaxing thermal cond. 2−56171
^4He, solid, hypersonic phonons 2−43432
LiCl solutions, Brillouin scatt. 2−67835
$MgO:Ni^{2+}$, scatt. from microwave phonon bottleneck 2−65283
N_2, liq., effective stimulated scatt. in u.v. and gain dispersion in 1.06-0.26 band 2−46956
N_2 liquid, stimulated 2−46963
$(NH_4)_2SO_4$, elastic and photoelastic consts. determ. 2−43665
$NaNO_2$, piezoelectric and birefringent, at room temp. 2−48204
$NaNO_3$, molten, hypersonic vel. dispersion obs. 2−77427
O_2 liquid, stimulated 2−46963
$TbVO_4$, elastic consts. determ., rel. to anomalies in Jahn-Teller phase transitions 2−71681
$TbVO_4$ obs. of elastic consts. anomalous behaviour at Jahn-Teller induced phase transition 2−84038
Xe single cryst., elastic const. obs. 2−47737

light, Raman spectra
180°, industrial device for room and low temps. 2−42206
active spectroscopy using quasi-c.w. parametric light generator 2−66853
antiferromagnets, by four magnons, excited state exchange mechanism 2−65276
atmosphere, quantitative meas. of trace constituents 2−57941
atmospheric pollutants, applic. of N_2 TEA u.v. laser 2−42025
backscatter obs. of atmospheric temperature profiles 2−44691
band shapes rel. to molec. reorientation 2−59969
binary mixed liquids transient stimulated scattering 2−80472
corrosive melts up to 1100°C, reflective scattering arrangement 2−70083
crystal, first and second order ionic Raman effects 2−84503
crystal dynamics, review 2−61054
crystals, centrosymmetric and noncentrosymmetric, phonon spectra 2−68656
crystals, effects of external force gradients on i.r. and Raman activity of long wavelength optical phonons 2−84513
cubic crysts., localized polariton modes, continuum approx., variational approach 2−80885
degenerate Fermi systems, threshold anomaly 2−54432
difference spectroscopy technique 2−52487
difference spectroscopy using chopped laser beam 2−70072
digital recording using step by step scanned spectrometer with multi-channel analyzer 2−42276
DyAlG, resonant cancellation of Raman scattering from electronic levels 2−68657
ellipsoidal mirror system for increasing gain in Raman scattering 2−79414
enhanced by generalized polariton phase matching 2−42108
ethylenediamine and deutero derivative, gaseous state, laser spectrum 2−77106
films, Raman scattering by size quantization levels 2−81394
freons, cross sections normalized to N_2 2−80418
gas flow visualization 2−46824
gas temp. meas. applic. 2−50268
gases, use of Fabry-Perot interferometer for study under high resolution 2−74250
high temp., simple furnace 2−55775
hydrocarbons, cross sections normalized to N_2 2−80418
hydrogen bonded liquids, review of i.r. and Raman spectroscopy relating to structure properties 2−43315
hyper 4th order nonlinear optical process in polariton formalism 2−72361
hyper-Raman effect, polarization phenomena 2−46515
I_2-filter method 2−65274
induced Raman scattering excited by laser light 2−76517
i.r., from crystals, investigation of order-disorder phenomena 2−50991
isomorphous proustite pyrargyrite series, vibrational spectra 2−44387
laser beams self focusing, beam diameter limitation due to stimulated Raman scattering 2−42117
laser Raman spectroscopy, for small samples 2−61825
laser spectrometer, computer time averaging for matrix isolated species 2−66850
laser-excited spectroscopy, review 2−52967
in lattice vibration region, review 2−61070
light trapping cell for Raman spectra meas. 2−79380
liquid, intermol. interactions obs. 2−77431

Scattering continued
light, Raman spectra continued
lunar surface rocks and fines 2−62652
magnetically ordered crystal, morphic effects 2−72359
magnon-phonon interaction, microscopic theory of modifications caused by mag. ordering 2−72360
molecular crystal, rel. to molec. vibration studies 2−54012
molecular crystals, polarization effects 2−65275
molecular crystals, stationary Raman oscillators as special case 2−65273
in molecular crystals, stimulated, treatment as polariton scatt. 2−65272
molecular crystals, theory of stimulated Raman dispersion scattering 2−76499
molecular solids, vibrational spectra, librational, torsional and translational modes 2−72362
molecules in liquids, excitation of vibrations, meas. of lifetimes 2−42846
overlapping band separation, depolarization ratios determ., computer appl. 2−66849
parasitic light reduction using I_2 absorption filter 2−52471
pentafluorothiophenol liquid phase, vibrational assignments assuming C_{2v} symmetry 2−60078
from polar phonons, quantitative formulation 2−68655
by polaritons, anisotropy effect 2−44388
polaritons, giant, nonlinear theory of exciton-photon coupling 2−84241
prolate symmetric top mols., Coriolis constants from Raman band contours 2−70662
pulsed Raman technique, fluoresc. background reduction 2−79446
review, from late 1969 to late 1970 2−52484
semiconductor, conf., Warsaw, Poland, July (1972) 2−68384
semiconductor, scatt. from coupled LO-phonon-plasmon modes, theory 2−68663
semiconductors, unit 2−61348
shock wave tail, vibrational relaxation, anti-Stokes Raman scattering obs. 2−52970
solar Raman scattering, effect on distribution of molecules over vibrational levels 2−75940
spectrometer, highly efficient, using tunable laser 2−42270
spectroscopy, laser-excited 2−73261
spherical top molecules, type E and F_2 contour bands 2−46585
stimulated, with ultrashort light pulses, derivation of Baecklund transformations 2−82493
stimulated emission from bulk medium, theory of state of polarization of scattered radiation 2−63305
stimulated molecular relaxation and dispersion 2−41938
stimulated scatt., quantum theory 2−53434
stimulated spin flip, method for tuning i.r. light sources 2−76469
three-photon phenomena for randomly oriented molecules, polarization dependence 2−67441
transient effect and stimulated scatt., investigation with picosecond laser pulses 2−63348
tuned active Raman spectroscopy 2−42734
two-magnon Raman scatt., two-time Green function decoupling, heat-bath damping effects 2−68654
uniaxial crystal, oblique polaritons, freq. disperion 2−77770
vapour and dil. solution obs., applic. of semilongit. system for gases 2−64089
vibrational resonance, nonlinear spectroscopy 2−42269
vibrational spectroscopy, reorientation and vibrational relaxation as line broadening factors 2−79981
Ag_3AsS_3 single crystal, vibrational spectra 2−44387
BrO_3^-, vibrational spectra and force constants 2−59996
$Ca(OCl)_2.2Ca(OH)_2$, obs. of fundamental vibration of ClO^- anion, determ. of force constant and bond length 2−57341
$Ca(OCl)_2.4H_2O$, obs. of fundamental vibration of ClO^- anion, determ. of force constant and bond length 2−57341
CdS, resonant cancellation of Raman scattering from lattice vibrations 2−68657
CdS crystallites, surface modes 2−75311
ClO_3^-, vibrational spectra and force constants 2−59996
Ge III, vibrational properties 2−72372
H_2 coherently driven by light waves, obs. of anharmonic Raman scattering, determ. second order polarizability 2−42899
H_2 in planetary atmosphere 2−58512
He, 2^1S_0 metastable state, cross section for anti-stokes Raman scattering 2−46489
I_2 vapour excited by Ar ion laser, obs. of progressive change from resonance fluorescence to resonance Raman effect 2−56181
I_3^- Raman spectrum resonance laser excited spectrum 2−79998
IO_3^-, vibrational spectra and force constants 2−59996
$(Mn_{1-c}Zn_c)F_2$, two-magnon Raman scattering meas. 2−65261
N_2 liquid, stimulated 2−46963
NO, concentration determ. in water saturated N_2 2−70714
$NaBa_2Nb_5O_{15}$, polariton obs. 2−48202
O_2 liquid, stimulated 2−46963
Si III, vibrational properties 2−72372
SiC, scatt. from coupled LO-phonon-plasmon modes 2−68663
ZnS cubic structure anisotropy of intensities 2−65282

light, Raman spectra, inorganic
$A^IB^{III}O_2$ with rhombohedral α-$NaFeO_2$ structure 2−72321
$A^IB^{III}S_2$ with rhombohedral α-$NaFeO_2$ structure 2−72321
alkali fluorides, second order spectra, phonon modes 2−48196
alkali metal metavanadates, Raman modes and stimulated scatt. 2−47261
alkali metal superoxides and ozonides vibrs. of O_2^- and O_3^- ions, solid-solid transition effects 2−81354
alkaline earth fluorides, point defects vibr. spectra 2−71724
antiferromagnet, four-magnon excitation 2−54433
antiferromagnet, two- magnon scatt. at finite temps. 2−54431
chromates of divalent transition metal compounds, vibrational spectra, calc. of force constants 2−70678
colour centre behaviour and band modes in semiconductors and insulators 2−54448
cristobalite, α, β, fundamental optical modes from 77K to 538 K 2−81364
diatomic crystal, scatt. efficiency, calc. from dielec. theory 2−57357
diatomic mols., tunable Raman excitation and vibr. relax. 2−53023

Scattering continued
  light, Raman spectra, inorganic continued
    durene, phonon spectrum 2−54022
    group III-V compound, amorphous, phenomenological explanation 2−61665
    group III-V compound, amorphous, phonon density of states obs. 2−61664
    halogens, using tunable dye laser 2−42262
    minerals, rock forming, using tunable dye laser 2−42262
    molecular cryst., harmonic freqs. of vibr., harmonic intermol. pot. 2−81349
    molybdates of divalent transition metal compounds, vibrational spectra, calc. of force constants 2−70678
    phonon systems with disordered force constants, scattering cross section 2−43958
    polariton Raman scattering, in the vicinity of phonon resonance; fluctuation−dissipation theory 2−84496
    α-quartz, fast neutron irradiated, spectral line intensity changes 2−72373
    rare earth oxides, A-type, vibr. spectra and space groups 2−51355
    rare-earth borates, vibrational spectra and structures 2−70727
    ReF_7, mol. consts. 2−46576
    semiconductor, multiple spin-flip scatt., theory 2−57359
    semiconductor, stimulated emission and i.r. tunable light sources 2−78079
    semiconductors, obs. of surface space charge, Fermi level near band edges 2−47919
    spodiosite analogues, fund. modes, band assignments, Bravais unit cells 2−51318
    stimulated Raman gain in single mode glass waveguides 2−42130
    thiourea, above and below ferroelectric transition point, 169K, librational modes 2−75314
    vibrational amplitudes and Debye- Waller factors derivation 2−50983
    water, anomalous frequency broadening of ruby laser beam by self modulation 2−43362
    water, ground and upper state vibrational bands 2−46566
    AgI, wurtzite-type, fund. optic lattice modes 2−61662
    AlM_gBO_4 vibrational spectra, interpretation by factor group approx. calc. of force constants for BO_4 group 2−70728
    $Ar:OF_2$, vibrational assignments of mols. and free radicals 2−51466
    $Ar\text{-}O_2$ system, solid, $O_2\text{-}O_2$ pair vibrations obs. 2−75310
    Ar_2, Van der Waals dimers, pure rotation band 2−80050
    As_2S_3, vitreous, vibrational states density detn. 2−61663
    $As_2S_3(Se_3)$, amorphous, vibr. modes 2−61614
    As_2Se_3, vitreous and cryst., combination scatt. spectra, 5-1000 cm^{-1}, 100-300 K 2−84524
    B_2Cl_4 vapour, obs. of torsional mode in spectrum excited by Kr laser 2−52993
    Ba_2CaMO_6 ordered perovskites, M=Mo, Te, W, meas. of vibrational spectra, assignment of internal vibrations 2−81370
    BaF_2, second-order spectra, lattice dynamical analysis 2−57040
    Ba_2MgWO_6 ordered perovskite, meas. of vibrational spectra, assignment of internal vibrations 2−81370
    $Ba_2NaNb_5O_{15}$, vibr. props., characterization, 77-843K 2−72364
    $BaTiO_3$, line shape of soft E polariton mode 2−78112
    $BaTiO_3$ Raman cross sections, temp. dependence 2−84514
    $Ba_3(VO_4)_2$ 2−44382
    BeB_2H_8, BeB_2D_8, BeB_2HD_7, Raman spectra, frequency assignment and structure determination 2−52994
    BeF_2, vitreous, polycrystalline and molten, to 630°C 2−48197
    Bi powder, Raman effect 2−81383
    Br_2 vapour, reson. effect in absorpt. continuum, excitation freq. influence on line intensity 2−52996
    $BrNSF_2$ vibrational spectra, tentative assignment band shape and G-matrix elements calc. 2−70697
    CO and CO_2 scattering cross sections and depolarization ratio 2−53026
    CO_2, stimulated Raman scatt., time meas. for vibr.-trans. energy transfer 2−64118
    CO_2 transient stimulated Raman scatt., vibrational relax. detn. 2−56150
    CS_2, liquid effects of intermolecular interactions 2−71205
    C_3S_2, 77 K, assignment of bands to components of first overtone, crystalline structure study 2−51354
    CaF_2, second-order spectra, lattice dynamical analysis 2−57040
    $Ca_2[AsO_4B(OH)_4]$ vibrational spectra, interpretation by factor group approx. calc. of force constants for BO_4 group 2−70728
    Cd powder, Raman effect 2−81383
    $CdCl_2:Co^{2+}$, obs. of vibrational-electronic coupling in high resolution spectrum of spin forbidden band 2−81356
    CdS, anomalous double spin-flip scatt. 2−57358
    CdS, electron spin-flip Raman scattering, 70-100 KG at 4.2K 2−68658
    CdS, resonance Raman scattering by turnable dye laser 2−84486
    CdS, spin-flip scatt., linewidths and two-electron processes 2−84501
    CdS, spin-flip scattering from free and bound electrons 2−44389
    $CdS_{1-x}Se_x$, reson. Raman effect 2−72365
    CdS_xSe_{1-x} mixed crystal, study of lattice dynamics, phonon-phonon interactions 2−51353
    Cl_2, liq., fund. vibr. freqs. 2−43369
    Cl_2CNCl, vibrational assignments 2−70694
    $ClNSF_2$ vibrational spectra, tentative assignment band shape and G-matrix elements calc. 2−70697
    ClO_2, crystal structure determination 2−77561
    CoF_2, scatt. from high lying electronic excitations 2−44390
    Co(III) triethylenediamine chloride, vibr. spectra analysis 2−72325
    Cr complexes, Cr(III) dimethylsulfoxide compounds 2−51375
    Cr(III) triethylenediamine chloride, vibr. spectra analysis 2−72325
    Cr(III) triethylenediamine chloride, vibr. spectra analysis 2−72325
    CrO_2, phonon spectra rel. to VO_2 2−65277
    $CrO_4{}^{2-}$, resonance Raman spectra, analysis of ν_1 breathing mode 2−50054
    $CsICl_4$, normal modes of vibr. 2−71427
    CuCl, spectra interpretation 2−65278
    Cu_3MX_4 (M=V,Nb,Ta; X=S,Se) 2−42888
    Cu_2O, resonant scatt. near 1S exciton level 2−54434
    D_2, Dicke narrowing and collision broadening of depolarized Rayleigh and Raman line 2−70700

Scattering continued
  light, Raman spectra, inorganic continued
    D_2, effect of collisions on line profile 2−43039
    D_2 transient stimulated Raman scatt., vibrational relax. detn. 2−56150
    DBr, molecular motions, self-broadening and broadening in inert gases 2−46544
    DBr, molecular motions in liquid phase 2−46961
    DBr, molecular motions when dissolved in solvents 2−46962
    DCl, molecular motions, self-broadening and broadening in inert gases 2−46544
    DCl, molecular motions in liquid phase 2−46961
    DCl, molecular motions when dissolved in solvents 2−46962
    $DyAsO_4$, Jahn Teller induced phase trans., 12K 2−48198
    $DyVO_4$, Jahn Teller induced phase trans. 2−48198
    $EuAlO_3:Mn^{4+}$, Raman luminescence 2−44428
    F_2, liq., fund. vibr. freqs. 2−43369
    $FNSF_2$ vibrational spectra, tentative assignment band shape and G-matrix elements calc. 2−70697
    FeF_2, two-magnon Raman scatt., temp. depend., calc. 2−81304
    Fe(II) complexes, octahedral halogen-bridged 2−46558
    GaAs, strain induced phonon line broadening observed by surface reflection Raman scattering 2−83858
    GaAs and $GaAs_{1-x}P_x$, multiphonon scatt., i.r. 2−68659
    GaP, polariton scatt. phonon damping func. freq. depend. detn. 2−61076
    GaP, two phonon spectra, three independent components detn. 2−48156
    Gd_2MoO_4, det. of thickness of domain walls 2−72366
    $Gd_2(MoO_4)_3$, vibr. modes, group theoretical calc. 2−68660
    Ge, amorphous, phenomenological explanation 2−61665
    Ge, amorphous, phonon density of states obs. 2−61664
    Ge, tetrahedrally bonded, vibr. states from Keating model, Raman line intensity 2−68224
    Ge metastable polycryst III, photon Raman spectra 2−68664
    H_2, Dicke narrowing and collision broadening of depolarized Rayleigh and Raman line 2−70700
    H_2, Dicke narrowing of rotational Raman lines, anisotropy 2−42893
    H_2, effect of collisions on line profile 2−43039
    H_2, h.c.p., fund. and overtone vibr. transitions 2−61666
    H_2, line profile of $Q_{01}(1)$ vibr. resonance in Dicke narrowing zone 2−56176
    H_2, transient stimulated Raman scatt., vibrational relax. detn. 2−56150
    H_2, tunable stimulated Raman emission by dye laser 2−77078
    HBr, molecular motions, self-broadening and broadening in inert gases 2−46544
    HBr, molecular motions in liquid phase 2−46961
    HBr, molecular motions when dissolved in solvents 2−46962
    $HBr.4H_2O$, H-bonds 2−43314
    HCl, molecular motions, self-broadening and broadening in inert gases 2−46544
    HCl, molecular motions in liquid phase 2−46961
    HCl, molecular motions when dissolved in solvents 2−46962
    $HCl.2H_2O$, $H_5O_2{}^+$ ion vibrations 2−61667
    HD,Dicke narrowing and collision broadening of depolarized Rayleigh and Raman line 2−70700
    α-HIO_3, polariton Fermi resonance obs. 2−84493
    H_2O scattering cross sections and depolarization ratio 2−53026
    He liquid, by two roton bound states, roton binding energy 2−83828
    He liquid, modified Stephen's theory 2−80504
    Hg halides, in dioxane and benzene solutions, molec. bending determination 2−64463
    I_2, 5145Å excited anti-Stokes, vibrational-rotational structure 2−77086
    I_2, effect of excitation freq. on overtone intensities 2−56182
    I_2, vapour, reson. Raman scatt. change to reson. fluoresc., intensity distrib. 2−67485
    I_2 vapour, vibr.-Rot. struct. in reson. Raman effect 2−80037
    $I_3{}^-$, resonance Raman effect laser excited, vibration enhancement 2−80007
    IF_7, nonrigid D_{5h} molecule, vibrational assignment 2−42901
    InP, second order Raman spectrum and phonon frequencies detn. 2−81367
    InSb, from CO_2 i.r. laser, obs. 2−45730
    InSb, linewidth of spontaneous spin-flip scattering 2−48199
    InSb, reson. scatt. near E_1 transition 2−68661
    InSb, resonant far-i.r. generation theory 2−61579
    InSb spin flip Raman scatt., spin saturation and relax., rate eqn. technique 2−68662
    KBr, phonon energies at Van Hove crit. pts. 2−71712
    $KClO_3$, irrad., damage obs. 2−57361
    $KClO_3$, molten, vibr. bands and $ClO_3{}^-$ struct. 2−74545
    $KClO_3$, molten and aqueous, vibr. spectra 2−80475
    KD_2PO_4 solutions and crystals, group theoretical analysis, anomalous temperature dependence of low frequency lines 2−48200
    KH_2AsO_4 solutions and crystals, group theoretical analysis, anomalous temperature dependence of low frequency lines 2−48200
    KH_2PO_4, ferroelec., oscillatory intensity behaviour with temperature 2−65280
    KH_2PO_4, ferroelectric mode, proton-phonon coupling effects 2−65279
    KH_2PO_4, mode interactions 2−55680
    KH_2PO_4, tetragonal, phonon-tunnelling modes 2−72367
    KH_2PO_4 solutions and crystals, group theoretical analysis, anomalous temperature dependence of low frequency lines 2−48200
    K_2MgCl_4, pot. of average force, ion clusters 2−67797
    KN_3, Raman active librational modes, anharmonic self energy shift 2−71726
    $KNbO_3$, vibr. freqs. assignment 2−84476
    K_2OsBr_6, obs. of dynamic Jahn-Teller effects and quenching by charge transfer and spin-orbit coupling 2−72369
    K_2OsCl_6 obs. of dynamic Jahn-Teller effects, and quenching by charge transfer and spin-orbit coupling 2−72369
    K_2SO_4, laser spectra, lattice vibration modes 2−72368
    $KTa_xNb_{1-x}O_3$, lattice dynamics study 2−54425
    KYO_3, Raman modes and stimulated scatt. 2−47261
    $K+O_2$ reaction products, obs. in Ar matrix 2−61776
    La_2O_3, vibr. spectra and space groups 2−51355
    LiD:H, localized lattice vibrations and dynamics 2−61668

Scattering continued
light, Raman spectra, inorganic continued
$LiIO_3$, polariton dispersion, light scatt. associated with photons 2−68617
$LiNbO_3$, directional dispersion and assignment of optical phonons 2−77764
$LiNbO_3$, obs. of polaritons by photographic method 2−81374
$LiVO_3$, Raman modes and stimulated scatt. 2−47261
$LiIO_3$, oblique polaritons, freq. dispersion 2−77770
$MgMoO_4$, phonon spectra of single crystals 2−68656
MgO, second-order scatt. tensor calc. 2−71713
MgTe-CdTe mixed crystals, lattice vibrs. 2−71714
MnF_2, two-magnon Raman scatt., temp. depend., calc. 2−81304
Mn(I) complex, $K_5[Mn(CN)_6]$, vibr. spectra and force consts. 2−77074
Mn(II) complexes, octahedral halogen-bridged 2−46558
MnO_4-, resonance Raman spectra, analysis of ν_1 breathing mode 2−50054
MoO_2, phonon spectra rel. to VO_2 2−65277
$MoOS_3^{2-}$ and alkali metal salts in aqueous solution 2−46560
MoS_2, rigid layer lattice vibrations and van der Waals bonding 2−84194
MoS_4^{2-} and alkali metal salts in aqueous solution 2−46560
$MoSe_2$, laser induced, transverse optic lattice vibr. spectra 2−78105
N_2, ground and upper state vibrational bands 2−46566
N_2, liq., effective stimulated scatt. in u.v. and gain dispersion in 1.06-0.26 band 2−46956
N_2, rotational spectra, use of fixed path length etalon Fabry-Perot interferometer for meas. of wavelength of individual lines 2−74250
N_2, rotational temp. meas. using Raman spectroscopy 2−46857
N_2, tunable Raman excitation and vibr. relax. 2−53023
N_2 and NO scattering cross sections and depolarization ratio 2−53026
N_2 transient stimulated Raman scatt., vibrational relax. detn. 2−56150
NH_3-ND_3 mixtures, liq., vibr. freqs. assignment 2−77439
NH_3 and ND_3 crysts., metastable phase obs., lattice and internal modes 2−72370
NH_4Br, critical fluctuation enhanced scatt. by phonons 2−43956
NH_4Cl, system with disordered force constants, scattering cross section 2−43958
NH_4F II, l.f. obs., high pressure phase obtained at low temps. 2−57360
$NH_4H_2PO_4$, antiferroelectric, long-wavelength polarization fluctuations 2−78113
NO molecule, rotation-electronic spectrum 2−64166
NO_2, using tunable dye laser 2−42262
$NaBrO_3$, optical phonon spectrum by laser Raman spectroscopy 2−84495
$NaCl:Ag^+$, expt. and calc. 2−84508
NaCl, two-phonon Raman scattering and phonon-phonon interaction, nonlinear shell model 2−81368
$NaClO_3$, irrad., damage obs. 2−57361
$NaClO_3$, molten, vibr. bands and ClO_3^- struct. 2−74545
$NaClO_3$, molten and aqueous, vibr. spectra 2−80475
$NaNH_2$, solid and molten evidence for hindered rotation of NH_2- ion 2−60022
$NaNO_3$, scattering tensors, bond polarizabilities, force constants 2−75312
$NaVO_3$, Raman modes and stimulated scatt. 2−47261
$Na+O_2$ reaction products, obs. in Ar matrix 2−61776
$NdAlO_3$, scatt. by localized electronic excitations and cryst. field model 2−72371
Nd_2O_3, vibr. spectra and space groups 2−51355
Ni complexes, carbonyls 2−72363
Ni complexes, tetracoordinated trimethylphosphines Ni(II) 2−77091
$Ni(CO)_4$, type E and F_2 contour bands 2−46585
Ni(II) complexes, octahedral halogen-bridged 2−46558
O_2, ground and upper state vibrational bands 2−46566
O_2, tunable Raman excitation and vibr. relax. 2−53023
O_2 rotational spectra, use of fixed path length etalon Fabry-Perot interferometer for meas. of wavelength of individual lines 2−74250
O_2 scattering cross sections and depolarization ratio 2−53026
O_2 transient stimulated Raman scatt.,vibrational relax. detn. 2−56150
OF, vibrational assignments of mols. and free radicals 2−51466
$Os_4O_4(CO)_{12}$, vibr. spectrum, force consts. 2−56193
PH_4Cl, solid, vibrational modes 2−72362
$POBr_3$, crystal 2−44380
PbF_2, second-order spectra, lattice dynamical analysis 2−57040
$Pb_5Ge_3O_{11}$, ferroelec., soft optic phonon mode 2−43961
$5PbO.3GeO_2$, by ferroelec. modes 2−61669
PrF_3, matrix isolated, laser excited spectra, investigation of matrix effects on molec. structure 2−60031
$RbCoF_3$, one- and two-magnon scatt. below Neel pt. 2−54435
$RbICl_2$, vibr. spectra, cryst. symmetry 2−75313
Re(I) complex, $K_5[Re(CN)_6]$, vibr. spectra and force consts. 2−77074
Rh(III) triethylenediamine chloride, vibr. spectra analysis 2−72325
Ru^aO_4, A=16, 18, determ. of anharmonicity corrections, Coriolis constants, force field 2−46578
SCl_2, liquid and solid state, determination of crystal structure 2−77059
SF_4, solid at low temperature 2−44381
SO_2 scattering cross sections and depolarization ratio 2−53026
Sb, amorphous and cryst. 2−68665
Sb powder, Raman effect 2−81383
SbF_5, gaseous phase, evidence for trigonal bipyramidal shape of monomeric species 2−50067
SeO_2 soln. in aqueous HCl, effect of HCl conc. 2−50366
Si, multiphonon, phonon energy assignments 2−68221
Si, one and two phonon struct. obs. 2−61081
Si, stimulated Stokes and anti-Stokes emission by Nd glass laser 2−44391
Si, tetrahedrally bonded, vibr. states from Keating model, Raman line intensity 2−68224
Si, two phonon spectra, three independent compounds detn. 2−48156
Si amorphous, phenomenological explanation 2−61665
Si metastable polycryst III, photon Raman spectra 2−68664

Scattering continued
light, Raman spectra, inorganic continued
Si powder, Raman effect 2−81383
n-SiC:N, 6H polytype, electronic excitations 8K 2−44392
n-SiC, electronic excitations assignment 2−51356
SiF_4, type E and F_2 contour bands 2−46585
SiF_6, type E and F_2 contour bands 2−46585
SiO_2, vitreous, lattice vibrational spectra, pressure densification effects 2−74971
SnTe, amorphous and cryst. 2−68665
SrF_2, second-order spectra, lattice dynamical analysis 2−57040
SrO, second order spectrum 2−44393
$SrTiO_3$, two-phonon spectrum, from phonon freq. distrib. 2−77761
$SrTiO_3$ Raman cross sections, temp. dependence 2−84514
$Sr_3(VO_4)_2$, crystalline 2−44382
$TaBO_4$ vibrational spectra, interpretation by factor group approx. calc. of force constants for NO_4 group 2−70728
$TbVO_4$, Jahn Teller induced phase trans., 34K 2−48198
Tc(I) complex, $K_5[Tc(CN)_6]$, vibr. spectra and force consts. 2−77074
Te, amorphous, vibrational density of states detn. 2−65281
Te, extraordinary phonon Raman scatt. and reson. enhancement 2−84492
Te(IV) penta- and hexacoordinate mixed halide anions 2−77094
TeO_2, lattice dynamics 2−71716
TlN_3. low temp. phase transformation, i.r. absorption and Raman scatt. study 2−74944
$TmAs(V)O_4$, Jahn-Teller induced phase transitions, phonon excitations 2−54436
V_2O_5, long wave vibrational spectrum obs. 2−68629
WOS_3^{2-} and alkali metal salts in aqueous solution 2−46560
WS_4^{2-} and alkali metal salts in aqueous solution 2−46560
XeO_4 vibrational spectrum, determ. of Coriolis consts., isotopic freq. shift and force field 2−80023
YVO_4, phonon scatt., birefringent effects 2−48203
$Zn_xCd_{1-x}Se$ solid solution, phonons and structure 2−64837
$Zn_xCd_{1-x}Te$, luminesc. reson. Raman scatt., exciton transition 2−54437
$Zn(NO_3)_2$ aqueous solns., ion pairing 2−60475
$ZnO:Cu^{2+}$, spin-lattice relaxation process, 7-17 K, Raman process 2−65328
ZnO, resonance Raman scattering by turnable dye laser 2−84486
ZnS, polytypes, phonon spectra 2−61084
ZnS, spin-flip scattering from free and bound electrons 2−44389
ZnSe, spin-flip scatt., linewidths and two-electron processes 2−84501
ZnSe, spin-flip scattering from free and bound electrons 2−44389
$ZnSiP_2$, optical phonons, polaritons, mode freqs., strengths, damping factors 2−61621
$Zn(py)_2X_2$ complexes, py=pyradine, X-halogen, band assignments 2−70731

light, Raman spectra, organic
— 2−71447
acetone (-d_6), polycrystalline, assignment of methyl vibrations, determ. of torsional frequency splitting 2−72374
acetone oxime, obs. 70-4000 cm^{-1}, vibrational behaviour 2−50073
acetonitrile, meas. of correlation functions of rotation-vibration bands, determ. of relaxation characteristics 2−56474
acetyl fluoride liquid, assignment changes 2−83314
acetylene-d_0, d_1, d_2, high resolution analysis of Raman-active fundamental bands 2−64166
acetylenic derivatives of Si, Ge, Pb, P, As, Sb, vibr. assignment 2−56212
acridine and acridinium, vibr. assignment 2−60044
Al complex, AlX_3- dimethyl sulphoxide coordination compound (X=Cl, Br), vibrational analysis 2−52992
alkoxyazoxybenzenes, liquid cryst., conform. changes 2−81386
n-alkylbenzenes, l.f. vibr. spectra 2−56213
allyl chloride and bromide, rotational isomers 2−42952
amino acids, high resolution laser Raman spectra, study of S-S vibrations 2−83337
o-, m-, p-aminobenzaldehydes, vibr. assignments 2−56214
ammonium thiocyanate and ammonium thiocyanate-d_4, polycryatalline samples 2−48201
anisaldazine, liquid crystal, excitation by Ar laser 2−60476
anthracene, polarization effects 2−65275
cis-azobenzene, vibrational assignments 2−53048
azomethane, azomethane-d_6, liquid and solid samples, vibrational assignments and structure 2−42957
p-azoxyanisole, mol. conformations in nematic and isotropic states, Raman spectra 2−81382
4,4-azoxyanisole liquid crystal, excitation by Ar laser 2−60476
cis-azoxybenzene, vibrational assignments 2−53048
trans-azoxybenzene and isotopic derivatives, vibr. assignment 2−56217
bacteria suspensions 2−50374
benzene, self-focusing effect on stimulated Raman scattering 2−77437
benzene, toluene, liq., stimulated scatt., rel. to limiting diameters of self-focusing 2−67832
benzene and benzene-CCl_4 charge transfer complexes, l.f. spectra, assignments 2−81351
benzene chromium tricarbonyl-d_6, -h_6, low temp. study, vibrational spectrum 2−70752
benzene D_{2h}^{15}, spectral line strengths of lattice vibrations 2−44394
benzonitrile, meas. of correlation functions of rotation-vibration bands determ. of relaxation characteristics 2−56474
benzophenone, l.f. spectrum, 300 and 30K, librational motions 2−81355
biophysical macromolecules, theory and applications 2−81991
biphenyls, conjugation and angle of twist, determination by Raman intensity investigation 2−50086
bovine serum albumin, cryst., water content depend. 2−60092
bromoanisole, o- and m-, vibration frequency assignment 2−74283
butadienetricarbonyliron vibrational spectra in solution, liquid and solid phases, factor group analysis 2−70755
caesium methanesulphonate meas. of spectra in 4000-300 cm^{-1} range, correlation with crystal structure 2−72375
carbon tetrachloride, force field 2−74289

Scattering continued
light, Raman spectra, organic continued
carbon tetrachloride, self-focusing effect on stimulated Raman scattering 2—77437
carbon tetrafluoride, type E and F_2 contour bands 2—46585
carboxylic acid salts, vibr. assignment 2—60085
β carotene, using tunable dye laser 2—42262
chiral cpds., vibr. spectra and polymorphism 2—44396
3-chloro-1,2,5-thiadiazole 2—42968
p-chloroaniline $D_{2h}{}^{16}$, spectral line strengths of lattice vibrations 2—44394
chlorocyclobutane, ring-puckering vibrations 2—74287
chloroform, liq., ang. autocorrel. function determ. 2—71213
chlorophyll, using tunable dye laser 2—42262
α-chymotrypsin, conformationally dependent low-frequency motions 2—56268
cyclobutanecarboxylic acid, vibrational assignment 2—42973
cyclopentane-d_0 and -d_{10} cryst., vibr. assignment 2—84485
cyclopentene, ring puckering vibrations 2—43005
cyclopentene, ring- puckering vibr. freqs. 2—60058
dibenzanthracenes, vibr. analysis 2—53055
2,6-dibromoaniline 2—77145
1,4-dichloro-2-butyne, determ. of vibrational assignment and effect of free internal rotation 2—53059
p-dihalogenobenzenes, Davydov splitting, temp. and state of aggregation influence 2—68666
2,5-dihydrofuran, ring puckering vibrations 2—43005
2,5-dihydropyrrole, ring-puckering transitions 2—80084
o-dimethoxybenzene, u.v., vibration mode assignments 2—80081
dimethyl sulfates vibrational, spectra, i.r. and Raman 2—83317
1,1-dimethylhydrazine-monoborane, determ. of molecular structure, vibrational assignments 2—53057
dimethyliodoarsine, liq., normal modes of vibrs., freq. assignment 2—77141
dimethylphenols, 2,4- and 2,6-, vibrational assignment 2—74293
2, 3- and 3, 5- dimethylphenols, assignment of observed freqs. to modes of vibration 2—60059
p- dioxone, meas. of correlation functions of rotation-vibration bands, determ. of relaxation characteristics 2—56474
diphenyl mols., vibrational spectra 2—53056
enzymes high resolution laser Raman spectra, study of S-S vibrations 2—83337
1,2-ethane dithiol, investigation in liquid and solid state, determ. of rotational isomerism 2—53061
ethyl thiocyanate, vibrational assignment and conformation 2—42983
ethylamine, deuterated, analysis w.r.t. amino group vibrations 2—46610
ethylene oxide (-d_4 oxide), i.r. and Raman spectra, assignment of normal vibrations and normal coordinate analysis 2—42984
ethylenes, methyl substituted, gaseous and solid, torsional and internal rotation barriers 2—60067
fluorocyclobutane, ring-puckering vibrations 2—74287
fluoroperoxides, O-O stretching frequency identification 2—56232
formamide crystals, intermolecular interactions 2—44395
formamides, deuterated, vibrational assignment 2—50095
furane derivatives, 2-substituted 2—77146
hexamethyldisiloxane, isotopic shifts in vibrational spectra by CD_3 substitution, force constant calc. 2—46632
liquid, thermal periodicity of filament form. and elastic lattice vibrs. 2—50359
liquids, inverse Raman effect 2—71206
lithium acetate dihydrate, temp. dependence 2—72376
mercury(I), (II) acetate compounds, vibrational spectra, stretching frequencies determ. 2—46608
methane, scattering cross sections and depolarization ratio 2—53026
methane, vibrational band of Raman spectra, use of pressure-scanned Fabry-Perot interferometer for high resolution 2—74250
methanetellurol and isotopic species, vibr. spectra 2—83301
methanol, gain meas. of stimulated scattering using tunable dye laser 2—43375
methyl-substituted chloroaluminate ions, determ. of structure and bonding 2—77117
methylamine, deuterated and partially deuterated, analysis, w.r.t. amino group vibrations 2—46610
methylcyclobutane, ring-puckering vibrations 2—74287
methylpyridine, nonplanar vibrations, standard intensities and degrees of polarization of line widths 2—77152
monohalobenzene, monohalobenzene-d_5, calc. and interpretation of vibrational spectra 2—53066
monohalogeno(methyl)germanes, assignment of fundamental modes 2—46617
monophenyl mols., vibrational spectra 2—53056
naphthalene, exciton splittings and normal modes, heavily doped isotopic mixed crystal method 2—57362
naphthalene isotopic mixed crystals, Raman phonon spectra, exciton model and amalgamation limit 2—57363
oligopeptides, high resolution laser Raman spectra, study of S-S vibrations 2—83337
pentafluorobenzoylchloride, vibrational spectra 2—74285
pentafluorostyrene in liquid phase, vibrational assignments 2—50107
perfluorocyclohexane, vibrational assignments 2—46620
phenazine, vibrational assignments 2—46622
α-phenylethylamine, obs. of circular dichroism 2—64191
phenylsilane, normal vibrations and free rotation 2—46623
phospholipid-water mixtures 2—43374
polyester reserve, unsaturated, crosslinked with styrene, structure 2—44482
polyethylene, laser spectrum of different samples, sensitivity to crystallinity and impurities 2—44397
polyethylene, oriented samples assignment of laser-Raman spectrum for fundamental modes of vibration 2—70803
polymers, struct. characterization using laser-excited Raman spectroscopy 2—83343
polypeptides, high resolution laser Raman spectra, study of S-S vibrations 2—83337
polyphenyl derivatives, vibr. assignment 2—56255
2-propanol, meas. of correlation functions of bands, determ. of relaxation characteristics 2—56474

Scattering continued
light, Raman spectra, organic continued
propylamine, deuterated, analysis w.r.t. amino group vibrations 2—46610
pyrazine, vibronic coupling, prereson. effect 2—80066
pyridine, nonplanar vibrations, standard intensities and degrees of polarization of line widths 2—77152
pyridine solutions, stimulated Raman spectra, effect of intermolecular interaction 2—60477
pyrroles, liq., vibr. spectra 2—83306
1.4-selenoxan, i.r. spectra in vapour, liquid and crystal states, Raman spectra of liquid and solid 2—83315
semiconductors, cubic, stress dependence of the Raman frequencies and elastic constants 2—84497
sodium methanesulphonate meas. of spectra in 4000-300 cm^{-1} range, correlation with crystal structure 2—72375
stimulated Raman parameters for different types of substances, exptl. and theoretical substances 2—42944
strontium formate, anhydrous single crysts., fund. mode assignments 2—61661
succinyl chloride meas. of spectrum in solid and liquid states, determ. of rotational isomerism 2—53079
tetracyano-polymethine anions, using Ar laser excitation, 4880 Å 2—53081
1,1,2,2-tetrafluorocyclopane- d_0, d_1 and d_2, vibrational assignments 2—46629
tetramethylcyclobutane-1,3-dione 2—77155
tetramethylenecyclobutane-d_0 (-d_8), spectra meas for cooled soln. and solids below -150°, symmetry assignments 2—70792
1.4-thioselenan, i.r. spectra in vapour, liquid and crystal states, Raman spectra of liquid and solid 2—83315
toluene, liq., stimulated scatt., rel. to limiting diameters of self-focusing 2—67832
trans-3,4-dimethyl-2,2,5,5-tetradeuteriocyclopentanone, vibrational assignment and conformational studies 2—64189
trans-3,4-dimethylcyclopentanone, vibrational assignment and conformational studies 2—64189
tri(trifluoromethyl) arsenic, phosphorus and antimony, vibr. assignment 2—56262
triallyl amine 2—43012
triglycinefluoroberylate cryst., l.f. spectra, effect of temp. 2—51357
triglycineselenate cryst., l.f. spectra, −115 to 36°C 2—51357
triglycinesulphate cryst., l.f. spectra, effect of temp. 2—51357
1,1,1-trimethoxyethane, vibrational assignment 2—43013
trimethylchlorosilane, isotopic shifts in vibrational spectra by CD_3 substitution, force constant calc. 2—46632
trimethylene oxide and deuterated analogues, vapour phase Raman transitions and ring puckering vibr. 2—83278
trimethylene oxide deuterated analogues, ring-puckering vibr. 2—80095
trimethyleneimine, 1-d-, ring-puckering transitions 2—80084
trimethyloxysilane, isotopic shifts in vibrational spectra by CD_3 substitution, force constant calc. 2—46632
vegetable pigments in soln. and chloroplastic media, reson. Raman spectra 2—81977
vinyl trifluoroacetate, vibrational assignment depolarization ratios and configuration determ. 2—70797
X-rays *see X-ray scattering*
Scattering, elementary particles *see Elementary particles/scattering*
Scattering, nuclear *see Nuclear reactions and scattering*
Scattering, particles
see also Collision processes; Energy loss of particles; Field theory, quantum/interactions; Elementary particles/scattering; Nuclear forces; Nuclear reactions and scattering; Particle tracks; S-matrix theory; and under individual particles, e.g. Alpha-particles
amplitude for particles with various spins 2—55420
charged centres, long-range coulomb pot. 2—62976
differential cross section for scattering of non-parallel non-uniform beam 2—52668
eikonal approximation, functional integration method 2—69600
inverse problem at fixed energy for elastic scattering of a particle obeying the Schroedinger eqn., complete soln. 2—41520
multip-particle Schrodinger Hamiltonians with weak pots., asymptotic completeness 2—58749
multiple-scattering expansion and Glauber approximation 2—45279
one-dimensional system of three particles with pairwise interaction, solution of Faddeev equations 2—41543
plasma toroidal modes, resonant scattering of trapped ions 2—70918
quasi-potential amplitudes, high-energy approx. 2—58765
Rosenbluth-post convective loss-cone instability, scatt. calc. using slab model 2—53184
Sasakawa conversion of Faddeev eqns. into integral equations, 3-plate scatt. 2—79475
surface layers, analysis by elastic backscattering 2—80923
T-matrix for scattering of particle from bound state of two others, Pade approximant 2—52081
transmission secondary electron emitters resolution rel. to backscatter of electrons 2—81184
Schizons *see Elementary particles; Field theory, quantum/interactions, weak*
Schlieren systems
analytial ultracentrifuge, alignment with interference optical systems 2—61819
crystal surface orientation meas. by u.s. beam displacement 2—56604
fluidic logic study by optical visualization of attached flow 2—73664
laser interferometer, boundary layer study in fluids 2—59228
laser interferometer, design and performance 2—73635
polymers films characterization 2—56599
shock and detonation waves, local vel. meas. by Schlieren interferometry of Doppler shifted laser light 2—63138
technique for obs. of laminar boundary layer separation in water tunnel 2—67760
Schottky barriers *see Semiconductor-metal boundaries*
Schottky defects *see Crystal imperfections/vacancies*
Schottky effect (noise) *see Electron tubes; Noise/electrical; Semiconducting devices*
Schrodinger equation *see Quantum theory/wave equations*

Schwarzschild space *see Cosmology; Gravitation; Relativity/general*

Scintillation *see Luminescence*

Scintillation chambers *see Luminescence chambers*

Scintillation counters *see Counters/scintillation*

Seals
bellows seal superfluid value 2−85166
ceramic and ceramic-metal, fast-neutron irradiation effect 2−63227
cone, for high pressure systems 2−69494
electrical feedthrough, spherical, for high pressure vessels 2−62895
FEP teflon, for low temp., design 2−69486
ferromagnetic liquid, rotating lid vacuum chamber 2−66382
flange, bakeable, quick connect 2−52017
high pressure, self sealing, design calcs. 2−66374
high pressure container, duct seal break, reaction force calc. 2−62893
hydraulically actuated valve, for operation at very low temps. 2−58665
O-ring design 2−69495
rotatable, u.h.v. design configurations 2−48947
rotatable, u.h.v. design configurations 2−48947
space station design rel. to atmospheric leakage 2−44797
ultravacuum systems, production processes 2−85173
valve, 1 inch, with knife edge seal 2−76114
Al oxide-Nb metal seals, by solder glass in system CaO-Al_2O_3-SiO_2-MgO 2−66377
In, below 300°C, for joining pyrex to various materials 2−66385
NaCl vacuum seals and valves, review of scaling procedures and bibliography 2−69510
Si_3N_4, applic. in semicond. device manuf. 2−54221

Seawater
acoustic impedance, empirical equation 2−48423
acoustics, intensity range relations 2−72715
automatic spectrophotometry of dissolved carbohydrates 2−61824
Baltic, influence of suspended matter on transparency 2−78329
biogenic opal solution rate 2−72710
Black Sea, O_2-H_2O balance 2−44645
Black Sea temp. fields and salinity rel. to statistical structure analysis 2−81612
breakwaters and transportable wave barriers, review 2−54747
cabbeling instability analysis 2−57919
coastal, T levels near operating atomic power plants 2−62042
coastal upwelling region, automated NH_3 determ. 2−72708
deep scattering layers in Gulf of Mexico response to total solar eclipse 2−48416
diurnal temperature variations 2−62136
electrical conductivity conversion to salinity with digital temp.-salinity probe 2−54769
e.m. water-current velocity meter, oceanographic applications 2−71138
evaporation, migration of chemical components from ocean to atmosphere, ratios 2−62151
flow direction, speed and temp. meas. using thermistor and laser techniques 2−54775
foam, emissivity at microwave freq. 2−65602
freezing, interferometry meas. of convection currents 2−65601
freezing point, resolution of discrepancies in existing data 2−57896
high levels, in upper Pleistocene in mid-north Mediterranean 2−62018
ice stalactites growth 2−57915
integral light scattering coeff. rel. to scattering coeff. in fixed direction 2−51564
ion selective electrodes, properties and uses in seawater 2−54549
Levantine intermediate water, flow, salinity 2−72707
level at southern California, decadal fluctuation 2−81635
light propagation under water, radiance distribution 2−65590
light pulses, space time structure of reflected pulses 2−73633
light refraction coeffs., theory of meters of pulsations 2−51563
light scatt. index, Mie theory applic. 2−57835
light scattering, intensity fluctuations 2−48419
marine sediments, acoustic props. 2−57834
microwave brightness temp. of natural sea ice and salt water ice 2−84777
N. Atlantic deep sea sediments, Cd distrib. 2−81618
nepheloid layers, light scattering rel. to suspended matter 2−68870
North Atlantic Ocean, salinity, temperautre and o-profiles 2−75413
ocean colour from scattered sunlight meas. from spacecraft in noon orbit rel. to Earth resources studies 2−84773
optical meas. of seawater using two-detector integrating system 2−72699
optical properties, rel. to axially symmetric light field 2−57892
Pacific Ocean, propagation and absorption of sound 2−55530
pressure pulse generated by electric discharge, spectral characteristics 2−62056
propagation speed and attenuation coeff. of plane coherent acoustic waves 2−41721
quality survey vessel 2−72726
quark searches, review 2−59598
Red Sea hot brines, electrical resistivity probings of marine sediments 2−72729
sampling filter for drawing interstitial water from sediments 2−62086
Sargasso Sea, trace element profiles from Geosecs II test station 2−75471
sea surface cooling, evaporation, radiation and heat transfer 2−65593
Skagerrak, long-term variations of subsurface temperatures 2−48413
sound absorption, classical theory 2−51536
sound absorption, multistate dissociation 2−48434
specific gravity, instrumental obs. rel. to hydrographical tables 2−62022
speed of sound, measurement, at varying salinities 2−78317
surface, sound velocity, effect of increasing CO_2 conc. 2−65605
surface waves flow in deep turbulent boundary layer over water 2−84717
in suspended particles, conc. determ. using total scatt. coeff. 2−62020
swell-wave-tide u.s. analysis, industrial equipment 2−72731
temperature and salinity, vertical microstructure, San Diego trough high resolution probe obs. 2−62021

Seawater continued
temperature conductivity-depth survey equipment 2−72727
temperature meas. real time constant and salinity determ. reliability in ocean using temperature-conductivity probe 2−81611
thermohaline structure of western tropical Atlantic in Winter 2−78326
tidal resonance in Bay of Fundy/Gulf of Maine system 2−68872
underwater illumination, statistical characteristics rel. to sea roughness 2−81609
underwater light obs., data acquisition system 2−52005
wave data management 2−75484
wave generation by turbulent wind 2−44608
waves, sea waves, microwave emissivity calculation 2−72712
western Mediterranean Sea, inertial oscillations, circularly polarized currents 2−48414
Ba abundance profiles in Pacific and Mediterranean sea water 2−75467
Ba abundance profiles in southwest Pacific from Geosecs III station near Tonga 2−75466
^{7}Be concentrations in Atlantic Geosecs II water column rel. to oceanic circulation 2−75475
CO_2, total content in seawater at Geosecs II in North Atlantic Ocean 2−75470
^{13}C profiles in CO_2 total content in seawater at Geosecs II in North Atlantic Ocean 2−75470
^{144}Ce content, of fallout origin 2−62043
^{60}Co accumulation in coastal sediments 2−62044
^{137}Cs accumulation in coastal sediments 2−62044
^{137}Cs content, of fallout origin 2−62043
^{3}H abundance profile in Atlantic Ocean from Geosecs test cruise station 2−75474
^{3}He excess in Atlantic Ocean 2−75473
O_2 dissolved in seawater and ^{18}O profiles in dissolved O_2 at Geosecs II in North Atlantic Ocean 2−75470
^{18}O concentration, reef corals, temp. dependence 2−65592
Pu content, separation and anal. 2−62045
^{228}Ra profile at Geosecs II in North Atlantic 2−75477
^{106}Ru, accumulation in coastal sediments 2−62044
S isotope balance in oceans, model 2−57863
Si and trace elements in seawater, in-situ analysis using synthetic fibres 2−75469
Sr abundance distributions in seawater profiles at oceanographic test stations Geosecs I and II 2−75472
Sr abundance profiles in Pacific and Mediterranean sea water 2−75467
^{90}Sr content, fo fallout origin 2−62043
^{90}Sr in seawater from Geosecs II, shipboard analysis techniques 2−75476
^{95}Zr-^{95}Nb accumulation in coastal sediments 2−62044

Second sound
see also Helium/liquid, sound propagation
cubic crystals, velocity 2−61091
Heisenberg model, magnon relax. and second sound propag. 2−65129
weakly interacting Bose gas, transverse waves 2−41546
Bi, diffusive propagation of heat pulses 2−47762
He II, charged impurities conc. waves as type of second sound waves 2−53480
He II, entropy transport by vortices, and second sound vel. modifications 2−64500
He II, mutual friction force obs. 2−47018
He II, rel. to energy transfer from pulsed thermal source below 0.3K 2−71263
He II, under pressure and near superfluid transition, velocity, scaling and universality 2−43419
^{3}He-^{4}He liquid mixture, light scatt. study 2−53481
^{3}He-^{4}He mixture, second sound velocity and superfluid density near tricritical point 2−74578
^{3}He-^{4}He mixture, thermodynamic relationship between second sound velocity and osmotic pressure 2−64501
^{4}He, superfluid, light scatt. study 2−53481
^{4}He under press., superfluid density near λ point 2−43417
NaF, intrinsic anharmonic phonon-phonon interactions 2−68228

Secondary cells *see Electric cells*

Secondary electron emission *see Electron emission/secondary*

Sedimentation
blood tests, rate obs. 2−69223
Brownian particles, sedimentation rate, diffusion coeff., holographic interferometry 2−45767
clay-H_2O suspensions, flow behaviour 2−83816
Debye-Huckel theory, appl. to clay minerals 2−83809
gravimetric sedimentation method particle-size distribution of dust 2−78754
Lau Basin, accumulation of volcanic deposits 2−44610
Mid-Atlantic Ridge, age obs. 2−44611
particle size analysis by Sartorius sedimentation balance, correct end-weight determ. 2−43881
poly(vinyl cinnamate), hydrodynamic, optical props. 2−83388
red blood cells, in u.s. standing waves 2−81986
suspension, dil., conc. depend. of sedimentation rate 2−50379
ZnO, particle size determ., computer appl. to data processing 2−53942

Seebeck effect *see Thermoelectricity*

Seidel theory *see Aberrations, optical*

Seignette salt *see Rochelle salt*

Seignettoelectric materials *see Ferroelectric materials*

Seismic waves
see also Seismology
aftershock activity and aftershock risk in the area of Greece 2−44538
aftershocks of earthquake in northern Aegean Sea, time and magnitude distributions 2−51508
amomalous seismic *P.* travel times from Longshot, global tectonic implications 2−65500
amplification in sediments, det. of shear velocity using surface wave dispersion 2−57526
amplitude yield scaling for underground nuclear explosions 2−57568
antichannel propagation on two-dimensional models 2−72643
arriving between P and PP, array obs. of arrival times, slownesses and azimuths 2−48383

Seismic waves continued
Atlantic lithosphere, short period shear wave velocities 2−57460
attenuation and magnitude relations for eastern N. America 2−57624
attenuation in outer core 2−57537
Bahama platform, crustal structure from Rayleigh wave dispersion 2−65546
Bay of Biscay, mantle reflections 2−72621
Beaufort Sea, vel. analysis 2−78255
below Moho, P-wave velocity profile 2−72653
Birch-Murnaghan equation of state, test by longitudinal and transverse waves 2−61893
Bismarck-Solomon Seas region, crustal plates study 2−54709
body and surface waves and free oscillations, attenuation by mantle 2−57522
body wave directivity functions and kinematic parameters for deep focus earthquake 2−65495
body wave magnitude rel. to local magnitude, New Zealand earthquakes 2−44542
body wave magnitudes at 1 Hz and 2 Hz as short period discriminant between earthquakes and explosions 2−48385
body wave-surface wave discriminant for small events 2−57569
body waves, obs. of upper mantle structure in Western USA 2−57717
body waves, ray-theoretical spectral amplitudes from dislocation source in Earth 2−57510
boundary velocities det. in media with weak gradients 2−54634
Broach earthquake of March 23 1970 2−44546
broad band seismic signal recording using conventional long period seismometer 2−72651
Bulgaria, S.W. investigation of inter-mountain depressions 2−72620
Cagniard's progressive wave theory, physically operational formulation 2−78257
Canadian network, P- and Rayleigh amplitudes of nuclear explosions 2−57567
Cannikin explosion, T-phase signals 2−57593
coda waves, of microearthquakes, anal., Matsushiro rel. to California swarms 2−78275
common depth surface profiling from multiple reflections, statistical algorithm 2−44567
composite viscoelastic layer, propagation in magnetic field 2−55462
compressional wave velocity, dependence on porosity in unsaturated rocks 2−44555
core transition zone, vel. depth curves from PKP travel times 2−72658
crust, uppermost part, gradient layer as waveguide of body waves 2−54645
crustal refracton, applic. of simulated data obs. 2−68834
crustal structure beneath the seas and oceans 2−61894
decay of P waves, nuclear explosions, epicentral distance 2−81583
deep crustal seismic reflections, digital filtering 2−51498
Denver earthquakes, stresses and seismic efficiency 2−65489
depth limits in body wave inversions 2−68837
differential travel times use in sampling Earth structure 2−57696
dispersion of surface waves in ice cap 2−81573
disturbance due to point source in layered half space 2−75421
Earth model consistent with free oscillation and surface wave data 2−84726
earthquake bodywave and surface-wave magnitude relations rel. to source multiplicity 2−57504
earthquakes, nonlinear effects 2−71154
earthquakes and underground explosions, P-wave amplitude spectra 2−57566
elastic half-space, surface displacements due to surface dipole 2−58903
elastic half-space, vertical surface displacements due to buried dipole 2−58904
elastic waves from circular disc source, explosion inside oblate spheroidal and circular cylindrical cavities 2−51503
elastic waves in laterally inhomogeneous crustal structures 2−68844
elastic waves in laterally inhomogeneous media 2−54659
exploration system, patent 2−84759
explosions in northern Australia, S- and P-wave travel times and amplitudes 2−61883
extended distances, incidence angles of P waves 2−81568
Fennoscandia, P_n and S_n seismic phases 2−72652
fields, seismogram interpretation on basis of Huygens-Fresnel principle and wave equation 2−61898
finite propagating tensile fault, elastodynamic near field 2−72610
free oscillation spectral peaks, identification knowing earthquake source mechanism 2−57632
frequency-time analysis of surface and body seismic waves 2−84703
Great Circle Rayleigh waves and tectonic provinces 2−57534
holographic anal. to obtain energy distrib. and time variation 2−76502
horizontal acceleration components calc. from seismoscope data 2−61903
inhomogeneous, plane, reflection and refraction at interface between viscoelastic materials 2−57595
inhomogenous anisotropic media, intensities, numerical techniques 2−72635
isoseismal maps, rel. to accelerations calc. from specified earthquake sources 2−57628
Lamb's problem, leaking modes 2−44576
laterally inhomogeneous media, perturbation technique for obs. 2−48390
liquid core of Earth, dynamics 2−84724
locally generated body waves in short period noise 2−44543
long period signal enhancement by time varying adaptive filters 2−57616
long-period, mantle wave anal. by phase equalization and sum method 2−65457
long-period body waves, errors in spectral analysis 2−65507
long-period body-wave propagation from 4° to 13°, synthetic seismograms 2−48381
longitudinal from distant earthquakes, dynamic features of recordings 2−72642
longitudinal microseismic waves, origin 2−61888
Love type, propagation in infinite cylinder with rigidity and density varying linearly with radial distance 2−75418

Seismic waves continued
Love wave excitation by underground nuclear explosions 2−65491
Love wave propagation in spherically stratified internal layer, frequency equation 2−72609
Love waves, amplitude spectra, applic. of complex cepstrum technique 2−57638
Love waves dispersion, heterogeneous layer lying over homogeneous half space 2−72617
Love waves in crust and mantle, rel. to Rayleigh wave dispersion in inhomogeneous medium 2−73419
lunar surface scattering rel. to Earth 2−58475
magnitudes of surface and body waves from nuclear explosions and earthquakes 2−61877
marine refraction data near Kodiak Island, Alaska 2−78258
marine sediments, compressional wave attenuation 2−78256
marine seismic reflection data processing 2−48428
microbaroms on northern quarter of Earth's surface 2−65508
microseismic activity, comparison of Cuban and Central European stations 2−51507
microseisms associated with cyclonic winds 2−48377
microseisms from small closed basins and inland seas rel. to atmospheric pressure 2−44541
modelled as propagation along lumped-element transmission line, attenuation-dispersion pair 2−65476
on moon, duration, scattering and attenuation 2−73072
Moon, experiments on u.s. signals in steel balls 2−44927
effects on motion of massive rigid disc in infinite elastic medium 2−54639
multiple longitudinal waves from distant earthquakes in Earth's core structure investigations 2−44588
multiple wave arrival times of far Eastern earthquakes, statistical investigation 2−54640
New Britain - New Ireland, central refraction investigations 2−81599
New Madrid earthquakes, spectral classification 2−57637
nonstationary SH waves in elastic sphere with waveguide 2−61889
normal mode and body waves, Earth model 2−57533
North American upper mantle, seismic wave attenuation and partial melting 2−65527
nuclear reactor structures design earthquake response analysis and damping 2−59823
overtones with high radial order number 2−57631
P_cP waves, vanishing reflection coeff. 2−78262
P and S waves propag. rel. to rupture mechanism 2−81579
P wave rockburst location technique, error analysis 2−81581
P wave travel-time gradient meas. for Warramunga Seismic Array 2−57509
P- and S-waves from microearthquakes, directional variations of spectral shape 2−57636
p-travel time residuals from Cannikin explosion, tectonic implications 2−57590
P-wave amplitude spectra anal. from shallow earthquakes and underground explosions 2−65504
P-wave amplitudes, short-period, magnitude comput. 2−61872
P-wave amplitudes of intermediate focus earthquakes and shadows due to slabs 2−57623
P-wave propagation from Longshot nuclear explosion 2−68838
P-wave residuals at Iberic stations and deep structure of S-W Europe 2−44585
P-wave spectra, crustal model parameters 2−65458
P-wave spectra, refraction seismograms deconvolution, underwater explosions 2−65474
P-wave transmission, effect of dipping layer 2−48380
p-wave travel times, obs. of lithospheric tearing beneath Aleutian arc 2−44578
P-wave travel times, rel. to upper mantle velocity distribution 2−57519
P-wave velocities in mantle, continental array 2−44574
P-wave velocity, Rockall Plateau microcontinent, crustal structure obs. 2−48402
P-wave velocity in upper mantle in central USA 2−57445
P-waves, det. of small earthquake source dimensions 2−57556
P-waves, smoothed radiation patterns, calc. of distrib. of earthquake generating stresses 2−78274
P-waves, teleseismic, amplitudes for nuclear explosions 2−48382
P-waves, travel times, Swedish-Finnish network obs. 2−44573
P-waves det. of source parameters of nuclear explosions Milrow and Longshot from teleseismic P-waves 2−57444
PcP amplitude and first motion in distance range 22.5° to 70° 2−57536
Pg, Pn and Sg velocities, crustal anisotropy in N. Georgia 2−44545
PKP-amplitudes rel. to solidity of inner core 2−57650
Pn, travel time residuals and velocities, San Andreas seismograph network 2−44548
Pn arrival time obs. from Cannikin nuclear explosion 2−57592
power spectra of microseisms in north Pacific 2−51497
PP and precursors, vespagram anal. 2−57630
prestressed media, stress wave radiation from explosions 2−81604
principal waves generated by underground nuclear explosions 2−81576
propagation beneath and through lithosphere which descends under Tonga Island Arc 2−65486
propagation from cylindrical waves, effects of couple stresses 2−55508
propagation in anisotropic half-space 2−57506
propagation of vibrations near boundary of inhomogeneous elastic half space 2−54638
propagation with point source in stratified half space, numerical computation 2−54658
pseudo-aftershocks from underground nuclear explosions 2−57591
pseudo-aftershocks from underground nuclear explosions rel. to upper mantle and outer core 2−84728
pseudo-Stoneley waves, line source on a solid solid interface 2−81577
pulse propagation in layered sphere generalized ray theory 2−54629
Rayleigh, axial, in visco-elastic cylinder in mag. field 2−73417
Rayleigh, axial, on cylindrical surfaces of transversely isotropic material and varying density in mag. fields 2−73418
Rayleigh, caused by atmospheric explosions 2−65485
Rayleigh, interfering, large aperture seismic array obs. 2−65455
Rayleigh, numerical model for propagation around corners 2−57619

Seismic waves continued
Rayleigh, ocean, resonant coupling to Apollo rocket shock cones 2−57621
Rayleigh, surface, phase velocity and dispersion 2−57521
Rayleigh wave magnitude, distance corrections 2−57597
Rayleigh wave noise model, applic. to noise cancellation and signal enhancement 2−57611
Rayleigh wave phase vel. variations in regionalized Pacific 2−57656
Rayleigh wave radiation patterns, det. of focal mechanism of S.E. Missouri earthquakes 2−57554
Rayleigh waves, amplitude spectra, applic. of complex cepstrum technique 2−57638
Rayleigh waves, analysis 2−58900
Rayleigh waves, Earth flattening procedure for propagation in crust and mantle 2−57511
Rayleigh waves, isotropic half space, moving thrust fault 2−72613
Rayleigh waves from CANNIKIN and MILROW nuclear explosions 2−57551
Rayleigh waves from moving thrust fault 2−57558
Rayleigh waves on concave cylindrical surface, two-dimensional models 2−82337
Rayleigh-wave dispersion rel. to crustal and upper- mantle structure beneath Colorado Plateau 2−78278
reflected, in finely stratified multilayered media 2−61891
reflected, numerical processing using mathematical description of reconstructed wave field 2−84732
reflection, evidence supporting underthrusting beneath Aleutian arc near Amchitka Island 2−65487
reflection coefficient for gradient layer overlying homogeneous semi-sphere 2−44568
reflections, primary and multiple, intensities ratio, factors affecting 2−44570
refraction, Lake Superior, delay-time function method of anal. 2−68839
rock, undergoing phase transitions, det. of velocity and attenuation 2−57594
rocks under axial loading, wave velocities up to shear fracture 2−57654
rupture mechanism fault dislocation, propagation of P and S waves 2−81579
S waves incidence angles 2−81569
S-wave spectra analysis method rel. to layered structure inferences 2−78271
S-wave spectra rel. to structure studies in regions of Japan 2−78272
San Fernando earthquake aftershocks, spectra and source parameters 2−57557
San Francisco Bay mud site, reflection and refraction obs. 2−61906
scattering by interface irregularities, unified treatment 2−61884
seismic data from 12 nuclear explosions detonated underground 2−65525
seismic refraction mapping, Reframap Method, algorithm and procedure 2−57496
seismic refraction mapping, Reframap Method, model studies and performance 2−54624
seismic signal evaluation at teleseismic distance, P and Rayleigh wave seismograms 2−61885
seismoelectric effects in rocks, borehole and lab. studies 2−54641
semi-infinite heterogeneous media, disturbances due to torsional shocks 2−61878
SH, effect of simple topography 2−48379
SH, in inhomogeneous wedge, Green's function 2−73420
SH, incident plane, interaction of shear wall with soil 2−44547
SH and SV wave spectra, layered structure inferences 2−78276
SH reflection from core-mantle boundary, effect of magnetic field 2−72639
SH spectra from local earthquakes 2−61936
SH-wave propagation in anisotropic inhomogeneous crustal layer 2−51512
shear waves, tube wave velocity and resistivity logging, field expt. 2−78250
short period P- and S-waves attenuation in mantle, spectral analysis 2−78273
short period seismic discrimination between earthquakes and underground explosions 2−72650
short wave rel. to long wave velocities in layered medium 2−75419
signals from presumed atmospheric explosions 2−57633
soil stress meas. during transitory loads, errors 2−78277
solid earth tide and phase vel. variations 2−61979
source process of intermediate depth earthquakes from S and P waveforms 2−78266
source time function of propagating longitudinal-shear cracks 2−65493
spatial coherence and structure of propagating medium 2−55377
static correction determ. from reflection data 2−84733
statics and dynamics, interrelation 2−55448
surface, dispersion and crust-mantle structure of Indian Peninsula 2−65482
surface, in forest covered regions, dependence of intensity on depth, nature and weight of charges 2−65472
surface and ground from above-ground and underground explosions 2−81566
surface motion, topography effect for plane SH, P and SV waves 2−57652
surface wave anal. using residual dispersion measurement 2−44550
surface wave dispersion characteristics and Q for region in mid Atlantic ridge, relative event anal. 2−57622
surface wave magnitude, calc. of tsunami amplitudes 2−62061
surface wave radiation from buried volume relaxation source in multi-layered half-space 2−57639
surface wave spectra, det. of source parameters and focal depths of oceanic earthquakes 2−61912
surface waves, amplitude spectra, applic. of complex cepstrum technique 2−57638
synthetic seismogram computation and comparison using leaking modes and generalized ray theory 2−57505
T-phase refl. from underground exposions and earthquakes in Aleutians 2−57653
teleseismic beam formation by large arrays 2−65460
teleseismic detection between and below microseism peaks 2−54643

Seismic waves continued
teleseismic P-wave, synthesis from sources near transition zones 2−57564
teleseismic P-waves, scattering mechanism 2−57535
thin layers, reflected, transmitted and head waves, micromodelling data 2−54631
travel time measurement system for investigation of rock mass mechanical strength 2−51509
travel time obs. using deep earthquakes 2−61938
travel times, temporal change, generated by underground nuclear explosions 2−57629
two and three dimensional, transition between in seismic models 2−65459
two-dimensional half-space model of welded quarter- spaces, seismograms 2−65469
underground nuclear explosions, compressional wave arrivals 2−57565
upper mantle, vertical velocity gradient from DSS data 2−54633
upper mantle anisotropy from refraction meas. 2−72662
upper mantle anomalies velocities from P-wave residuals from Cannikin 2−57642
upper mantle velocities det. from local obs. of deep earthquakes 2−57643
Utah, crustal low velocity zone 2−57571
velocities in different rocks at high pressure and temp. up to 750°C 2−54644
velocities rel. to sea floor spreading and progressive alteration of basalts 2−72656
velocity filters, three-dimensional optimum multichannel 2−57498
velocity in lunar samples 2−66158
velocity in outer core 2−65464
velocity in rocks of troodos igneous complex 2−51501
velocity obs. using air gun as precise continuous monitor 2−61934
velocity profile for deep mantle, dT/dΔ in 35°-40° epicentral distance range 2−57532
velocity structure for New England 2−57644
velocity variations around Leduc reefs, Alberta 2−78254

Seismographs *see Seismology*

Seismology
see also Geophysical prospecting; Seismic waves
1969, February 28 earthquake, Azores-Gibraltar, aftershock sequence and focal parameters 2−72611
− 2−62059
accelerograms from four earthquakes in Central Italy, acceleration spectra 2−44540
accelerometer, wide band horizontal, with preliminary Earth normal mode and seismic band 2−48975
accelerometer instrument correction, strong motion accelerograms 2−48384
accelerometers, active notch filters for extending frequency response 2−61945
acoustical holography for underground objects identification 2−72655
active faults, master planning 2−61927
active faults, master planning to reduce risks 2−61909
activity on sinking edge of Nasca Plate rel. to spreading edge 2−57584
Adirondack earthquake swarm, tectonic stresses 2−57577
Adirondacks region, earthquake distribution 2−57604
Aegean region, morphology and activity of seismic zone 2−78229
aftershock activity and aftershock risk in the area of Greece 2−44538
aftershocks of earthquake in northern Aegean Sea, time and magnitude distributions 2−51508
airpulser as seismic energy source 2−57501
Alaska, Cook Inlet region, earthquakes survey 2−57580
Alaska-Aleutian earthquakes, focal dimensions and tsunami generation 2−61911
Alaskan earthquake, 1964 March 28, normal modes obs. 2−51502
Alaskan earthquake 1964, Chilean earthquake 1960, arc tectonics 2−68840
Aleutian arc, upper mantle from seismic data from nuclear explosions and earthquakes 2−61932
Aleutian Islands, large Earth strain episodes 2−57547
Aleutian trench, lithospheric normal faulting 2−57508
Aleutians, T-phase refl. from underground explosions and earthquakes 2−57653
the Alps, crustal structure, explosion seismology 2−81586
Amchitka, underground nuclear explosion, seismic effects 2−57548
amplifiers, phase characteristics with high-pass and low-pass filters 2−44566
analysis of microearthquakes and hazard function 2−81570
Anapa region, seismicity meas. rel. to instrument data 2−78227
anisotropy of lower oceanic crust 2−51519
Apollo 14 active seismic experiment 2−55132
Apollo lunar seismic experiment, results from seismic station network 2−44922
apparatus for seismographic geophyiscal exploration, h.f. filtering and nonlinear distortions 2−48394
Arizona, deeper crust obs. 2−57745
Armenia, seismotectonics 2−54642
array data, generalized linear filtering 2−57617
array design, noise reduction by beamforming 2−57615
array detection and location of core shadow events 2−44553
arrays, horizontal and vertical, at sea 2−81605
Asia, Eastern Central, activity 1907-, criteria 2−78252
ASPER system, complex crustal structure of South Fiji basin 2−57541
attenuation of ground accelerations in vicinity of faults 2−57530
autocorrelation function, time varying, estimation 2−61946
Azores-Gibraltar region, plate tectonics 2−57704
Baja earthquakes, regional variations of seismic source parameters 2−65492
basalts from East Pacific Rise, compressional and shear wave vels., 10 kbars 2−65481
basement anomaly, seismic, gravity and mag. surveys 2−57777
Beaufort Sea, velocity analysis 2−78255
below Moho, P-wave velocity profile 2−72653
Block Island Sound, geomagnetic and seismic measurements 2−57760

Seismology continued
Bristol Bay, Alaska, crustal lineations based on mag. and gravity surveys 2–57797
British Columbia and Alaska, earthquake survey 2–57579
Broach earthquake of March 23 1970 2–44546
broad band seismic signal recording using conventional long period seismometer 2–72651
Calavera's fault creep event 2–57599
calibrated model seismic system 2–65475
Californian coastal terraces, siting of nuclear power plants 2–57562
Calveras fault zone, travel time anomalies and distribution of small earthquakes 2–57572
Çanada, earthquake probability map, computation 2–61910
Cannikin, near field seismic motion 2–61937
Cannikin, strain and tilt records 2–61930
Cannikin, strain release characteristics and tectonic effects 2–61931
Cannikin nuclear explosion, reaction of shallow surface waters 2–57552
Cannikin nuclear explosion, seismic and acoustic signal obs. using l.f. sonobuoys in aircraft 2–57592
Cannikin strain and tilt steps, interpretations 2–61929
Cannikin underground nuclear explosion, seismic effects 2–57550
CANNIKIN underground nuclear explosion of 1971, seismic effects 2–57607
Cascade Mountains, quaternary andesitic volcanoes, coherent and divergent lava suites 2–57543
Castelgrande region, degree of risk of earthquakes for astronomical observatory 2–72648
Caucasian earthquakes, nomograms for determination of K value 2–72646
Caucasus, seismic activity and major earthquakes 2–78225
cavity resonance theory 2–57680
central Alaska, crustal morphology from earthquake data 2–57741
Central Aleutians, secular strain measurements 2–57546
Ceres, South Africa earthquake, aftershock obs. 2–68832
Challenger Plateau, continuous seismic profile 2–57538
Chilean earthquakes, focal mechanism and spatial distribution rel. to subduction of oceanic plate 2–57553
China, earthquake patterns 2–57657
common deep point method, use of inverse and fan filtering 2–84736
complex subsurface models, analysis 2–57665
computer applications 2–84712
computer mapping of seismic and velocity data in Australia 2–57497
computer-designed wavelet Wiener filters for seismic data 2–54623
continental shelf off southern Baffin Island, reflection seismic and magnetic profiles 2–57458
continental transform faults, sedimentation 2–61920
coupling analysis, energy approach 2–65505
crack, propagating in inifinite medium, exact solution for elastic displacements 2–61940
cracks, semi-infinite longitudinal-shear, stress concentration and rupture propagation 2–61939
crustal and upper-mantle-structure beneath Colorado Plateau, determ. from Rayleigh-wave dispersion 2–78278
crustal anisotropy in N. Georgia 2–44545
crustal movements in tectonic areas 2–65559
crustal refracton, applic. of simulated data obs. 2–68834
crustal structure beneath the seas and oceans 2–61894
crustal tilting prior to aftershock of earthquake 2–81571
data, frequency domain techniques 2–57687
data collection systems evaluation, signal-to-noise ratio 2–57660
data interpretation using interactive computer graphics 2–54649
data plotting system, high-speed, computer controlled 2–54648
data processing, digital, normal correction, interpolation procedures 2–44561
data processing by general reflection point method using digital computer 2–84734
data processing methods, review 2–48393
deep crust lateral continuity 2–61976
deep crustal seismic reflections, digital filtering 2–51498
deep focus earthquake, body wave directivity functions and kinematic parameters 2–65495
deep focus earthquake, characteristic periods of fundamental and overtone oscillations 2–48378
deep sounding reflection methods 2–65520
deformation of sea floor determ. by seismic reflection profiles from Tufts Abyssal Plain to Washington-Oregon coast 2–54646
delay-time-function method of analyzing refraction data, applic. to Lake Superior 2–68839
Denali Fault, Alaska, crustal deformation 2–65544
Denali fault, quarternary, movement 2–61918
density distrib. meas. near base of mantle and centre 2–72678
Denver earthquakes, stresses and seismic efficiency 2–65489
depth det. using wavefront reconstruction method 2–57685
derived velocities, weathering effects 2–57664
detector-amplifier-galvanometer channel, phase distortion 2–84731
differential travel times for gross earth studies 2–57651
digital data enhancement filters design using auto and cross-spectral estimation procedures 2–57689
digital instrumental and methodological development, concepts 2–44560
digital microbarography array data, frequency domain processing 2–65484
downhole seismometer array, results near San Francisco Bay 2–57525
Earth model consistent with free oscillation and surface wave data 2–84726
Earth model consistent with normal mode and body wave data 2–57533
Earth noise structure beyond 20 secs., window for earthquakes 2–44551
earthquake activity, effect on geyser activity 2–65572
earthquake activity during and after 1970 Hekla eruption 2–61944
earthquake activity rel. to crustal pressure of reservoirs 2–61881
earthquake and nuclear detonations, seismic signal comparison 2–57570
earthquake bodywave and surface-wave magnitude relations rel. to source multiplicity 2–57504

Seismology continued
earthquake displacement field, transformation for spherical earth-static case 2–65456
earthquake effects on ground, ground cracking, soil liquefaction and sliding of slopes 2–78279
earthquake effects on ground, ground motion and pore water pressure in soils 2–78280
earthquake focal mechanism, quantitative model, elastodynamic near field 2–65501
earthquake foci, det. of fault plane 2–61887
earthquake focus, characteristics from body-wave spectra 2–72641
earthquake forerunners, geodetic obs. 2–65511
earthquake frequency graph plotting, application to Western Tuva 2–54637
earthquake generating stresses, distrib., obtained by smoothing first motion patterns 2–78274
earthquake hazard reduction using master plan design 2–61908
earthquake in Burma-India border region, structural response results 2–44549
earthquake mechanism, kinematic models 2–57518
earthquake mechanism and implication for prediction and control program 2–61902
earthquake phenomena, applic. of tectonomagnetism 2–65514
earthquake prediction, dislocation approach 2–57618
earthquake prediction and control 2–65518
earthquake prediction and global tectonics 2–57516
earthquake prediction in Kamchatka 2–65515
earthquake records modification taking into account props. of rock motions 2–57531
earthquake relocation technique 2–57609
earthquake source parameters inferred from teleseismic body waves 2–65467
earthquake source time function scaling law 2–57640
earthquake stress, friction, heat generation and spectra 2–57544
earthquake swarms along spreading edges of Nasca Plate 2–57585
earthquake telemetering system using amplitude modulation 2–61886
earthquake volume det. from body wave strain 2–65519
earthquake-tide correlation 2–57503
earthquakes, anal. of P-wave amplitude spectra 2–65504
earthquakes, body wave magnitudes at 1 Hz and 2 Hz, discrimination from explosions 2–48385
earthquakes, body-wave spectra use in determ. of seismic-source parameters 2–61879
earthquakes, circum Pacific arcs, tsunamis and tectonic deformation 2–57545
earthquakes, deep, rel. to global tectonics 2–61942
earthquakes, fault rejuventation, destruction of Bahia Solano, Colombia 2–65463
earthquakes, fault stability and pore press. considerations 2–65471
earthquakes, higher seismic activity during night 2–61951
earthquakes, higher seismic activity during night 2–61950
earthquakes, higher seismic activity during night 2–61949
earthquakes, higher seismic activity during night 2–61948
earthquakes, Indian, focal mechanisms 2–61880
earthquakes, lab. obs. of stick-slip 2–65558
Earthquakes, rupture zones in South America 2–65498
earthquakes, solar activity effects 2–66226
earthquakes, source dimensions from P-wave data 2–57556
earthquakes, statistical anal. threat to telephone systems USA, design requirements 2–84708
earthquakes, stress distribution beneath island arcs 2–81602
earthquakes, submarine, amplitude patterns of tsunamis 2–65611
earthquakes and nucl. explosions, surface-wave and body-wave magnitudes 2–61877
earthquakes and underground explosions discrimination using improved M_s scale 2–68836
earthquakes at Rangely Oil Field 2–57658
Earthquakes in Amchitka Pass and Delarof Islands, fault motion and spatially bounded character 2–65496
earthquakes in New Zealand, relationship between teleseismic body wave magnitude and local magnitude 2–44542
earthquakes in Victoria, Australia, anal. for characteristics 2–81625
earthquakes of different strength, spatial and temporal distrib. of foci 2–78259
earthquakes rel. to tectonic processes, relation between Earth and Moon 2–48392
eastern Sierra Nevada region, seismic potential 2–57606
eigenfrequency perturbation of a cylinder due to ridge on surface 2–51505
elastodynamic representation theorems, propagator 2–78898
electro-spark pressure source in water, optimum depth 2–44572
electroprospecting by resistance method, inverse problem solution 2–84739
envelope of ground motions evaluation 2–61905
epicenter determination methods, comparison by analysis of residuals 2–57596
Excelsior Mountains, Nevada, microearthquakes, source mechanisms and stress drop 2–61915
excited vibs., effect of mechanical action parameters on ground surface on characteristics 2–84737
exploration, multi-channel, practical r.f. telemetry system 2–57672
exploration and prospecting of gently sloping structures with high-precision gravimetry 2–44524
exploration system, patent 2–84759
explosion seismology rel. to Upper Mantle Project 2–57515
explosive source parameters, multisite estimation 2–65494
Faeroe-Iceland-Greenland aseismic ridge 2–72649
Fairview Peak, Nevada, microearthquakes, spectral characteristics and stress drop 2–65483
fan filters, equiripple approximation 2–78253
fan-type seismo-probing, nature and aims 2–44571
fault detection by refraction method in Kopili hydroelectric project 2–54630
fault dimensions rel. to corner frequency 2–61916
fault plane determ. method rel. to earthquake focus of Hindukush zone 2–78226
Fennoscandia, P_n and S_n seismic phases 2–72652
Fennoscandia, structure and physical properties of Earth's crust 2–51511

Seismology continued
field variations near focal zones of Kamchatka 2−65516
Fiji-Tonga-Kermadec region, temporal and spatial aspects of seismicity 2−57581
focal mechanism, energy storage before crack growth 2−65529
forerunners to strong earthquakes, operational forecasting, prediction reliability 2−65517
foreshocks and earthquakes prediction 2−65512
free oscillations, nonlinear effects 2−81584
frequency sounding above electrical reference horizon of infinitely high resistance 2−84738
Galapos Islands, June 1968, earthquake swarm 2−57575
Gasbuggy seismic source measurements 2−54626
geoelectric sounding curves, multilayer, computer processing and representation 2−44562
geophone arrays, theoretical and practical design 2−57690
Georgia, crustal seismic anisotopy 2−57627
Geysers geothermal area, technique for det. of seismic noise 2−57598
granite, implications of stable sliding stick-slip transition 2−61941
ground motion induced by CANNIKIN and MILROW nuclear explosions 2−57551
ground velocity and dispersion computation from strong motion accelerograms 2−57529
groundwater research in Okanagan Valley, British Columbia 2−57682
Gulf of Alaska and Bering Sea areas development, model based on earth expansion 2−54716
Gulf of California, northern and central, tectonic elements obs. 2−57796
Gulf of Mexico, subsurface features, three dimensional method 2−57659
Hawaii from 1962 to 1970, earthquake distrib. 2−57574
h.f. acoustic and elastic wave propagation in Earth 2−68842
high seismicity areas det. by pattern recognition 2−57517
hodographs, directional summation of seismic data, effectiveness 2−61896
holography, underground objects, size and general shape det. 2−57679
hydrophone arrays for sea bed profiling, effects of noise 2−44621
hypocenter determination, prediction analysis using local array 2−72615
Imperial Valley earthquakes (1940), tectonic stress and source mechanism 2−61914
information processing and accumulation, cathode ray image storage tubes 2−84735
inner core reflections, nuclear explosions, diffraction 2−81580
intermediate depth earthquakes in southwest Pacific region, source process 2−78266
intermediate focus earthquakes and shadows due to slabs, p-wave amplitudes 2−57623
interpretation errors 2−54653
inverse problem, errors, resolution and separation of variables, application to mantle and crust in S. Africa and Scandinavia 2−48399
inverse problems, scheme for solution 2−57520
isochrons for three-dimensional seismic system 2−65480
isochrons for three-dimensional system displays 2−57684
Italy, seismicity, plate tectonics 2−81589
Japan, position for new crustal-deformation observatory 2−75423
JOIDES basalts, compressional and shear wave velocities 2−57539
Kamchatka, maps of frequency of earthquakes 2−54636
Karnaveh earthquake of 1970, July 30 in northeast Iran 2−44539
Kentucky lake project, seismic activity 2−57603
Kilauea shallow earthquake swarm, focal mechanisms 2−57586
Kilauea Volcano, contrasting rift zones 2−57831
Kilauea volcano, earthquake location using local seismic network and tripartite arrays 2−57608
Kilauea Volcano, Hawaii, earthquake locations using small tripartite arrays 2−57573
Kodiak Island, Alaska, marine refraction data 2−78258
Koyna earthquake, December 11, 1967, accelerogram 2−48386
Krisuvik geothermal area, Iceland, microearthquake study 2−57605
Kurobe dam, Japan, seismic activity associated with filling of reservoir 2−75435
large aperture seismic array, teleseismic residuals, crust and upper mantle structure 2−65528
large earthquakes, melting on fault planes 2−72637
lateral structure-foundation interaction of structures with base masses 2−61873
layered media, behaviour during earthquake by feed-back theory 2−51510
layering in intrusive rocks, effects of earth tremors and convection currents 2−75436
Leduc reefs, Alberta, seismic wave vel. variation 2−78254
Lesser Antilles earthquakes, distribution and number of epicentres variation with depth 2−48395
Lipari arc, deep structure det. from S-wave attenuation of deep focus earthquakes 2−75433
lithology from true amplitude data in Gulf of Mexico 2−54651
local earthquake phases, originating near Afar triple junction 2−65465
local earthquakes, shear wave spectrum obs. 2−61936
long period seismic background noise obs. 2−57613
longitudinal waves from distant earthquakes, dynamic features of recordings 2−72642
Love wave excitation by underground nuclear explosions 2−65491
Love wave propagation in spherically stratified internal layer, frequency equation 2−72609
low power, low cost station for seismic signals 2−81575
lower mantle, shear vels., S and ScS obs. 2−57649
lower mantle inhomogeneities 2−72680
lunar, Apollo 14 expt. 2−48764
lunar, Q and structure 2−62659
lunar, structure and composition of crust 2−55125
lunar, velocity structure of crust 2−62663
magnetotelluric soundings, smoothing of results 2−61892
mantle P-waves, dT/dΔ measurements 2−48388
marine exploration radio refraction buoy 2−57662
marine prospecting, energy sources 2−84753

Seismology continued
marine sediments, compressional wave attenuation 2−78256
marine seismic refraction system using single ship for shooting, recoverable sonobuoys 2−68843
marine sparker seismic data, characteristics 2−68835
Matsushiro earthquakes, acceleration data anal. for det. of envelope of ground motions 2−61905
maximum entropy spectra and maximum likelihood spectra relationship 2−54628
Mendocino escarpments, obs. from ocean bottom seismic data 2−57578
micro earthquakes, directional variations of spectral shape 2−57636
microearthquake at Geysers geothermal area, California 2−65497
microearthquakes, crustal model, glaciation 2−81582
microearthquakes in underground mines, source mechanisms 2−57555
microseism generation by atmospheric coupling 2−72654
microseismic activity, comparison of Cuban and Central European stations 2−51507
microseisms, origin rel. to that of microbaroms 2−57612
microseisms from small closed basins and inland seas rel. to atmospheric pressure 2−44541
microseisms in small closed basins, meteorological perturbation effects 2−48376
microtremors and seismic damage, technique for categorizing ground sites 2−57527
Middle East, focal mechanism of earthquakes, plate tectonics 2−72618
migration, linear and spatial 2−54664
MILROW underground nuclear explosion of 1969, seismic effects 2−57607
Mississippi Valley earthquakes 1811-1812, seismic risk problem in eastern N.America 2−61907
model earthquake sequence, stochastic analysis 2−81600
model for det. of principle anisotropic direction 2−57620
model for determ. of principal anisotropic direction 2−65503
modelling, structure of Earth's crust 2−61963
modelling, two-dimensional, influence of layer thickness and velocity configuration 2−57663
models and velocity analyses 2−57666
Mojave desert, young structure model 2−61926
Moon, ringing, experimental study 2−44926
moonquakes, tidal cycles 2−58471
moveout corrected seismograms, downward continuation 2−54656
Nasca Plate, crustal struct. obs. 2−57795
Nevada, Fairview Park, microearthquake clustering 2−57576
New Britain - New Ireland, central refraction investigations 2−81599
New Guinea-Solomon Islands area, crustal structure and tectonics 2−57542
New Madrid earthquakes, spectral classification 2−57637
noise analysis generated by secondary sources 2−57686
noise in arrays, autocorrelation function rel. to cross correlation function 2−57614
noise meas. in geothermal area 2−57499
noise reduction method applied to long-period oscillations from Alaskan earthquake 2−61874
normal moveout techniques, correlation analysis 2−57677
north circum Pacific belt, earthquake probability analysis 2−57549
north Pacific, rotated power spectra of microseisms 2−51497
North West Passage, marine seismic exploration 2−54647
NOS and USSR magnitudes, comparison 2−51499
nuclear explosion, stress changes in nearby rock 2−65468
NW Turkey, seismo-magnetic effect 2−58107
oceanic crust, geologic model, rel. to compressional wave velocities of dredged samples 2−57899
oceanic earthquakes, source parameters and focal depths from surface wave spectra 2−61912
oceanic mantle phase studies in Northwestern Pacific 2−65470
offshore refraction, field and data processing techniques 2−54665
optical processing in seismic data, description 2−72622
P-coda recording of Leduc crustal structure in Canada 2−68845
Pacific catastrophy and ocean floor convergence considerations 2−57489
Pacific Ocean, anisotropy of oceanic upper mantle 2−57540
Pacific-North American state boundary, seismic observations and tectonic implications 2−61933
Peru earthquakes of 1966 and 1970, mechanisms and tectonic implications 2−84727
phase converter for seismic signals 2−61897
plane Lamb's problem line load suddenly applied in a magnetoelastic initially stressed conducting half-space 2−51504
Plowshare project, effect of source and recording site parameters on seismic response 2−54625
predictive deconvolution, long range seismic refraction observations 2−57513
prestressed media, stress wave radiation from explosions 2−81604
processing hardware design, vendor and user responsibility 2−54650
pseudo-aftershocks from underground nuclear explosions rel. to upper mantle and outer core 2−84728
quartz, static fatigue, earthquake phenomena 2−65499
quartz linear strain-seismograph of Obnisk Central Seismological Observatory 2−72645
Queen Charlotte Fault zero, seismic profiles 2−61919
random seismic field, statistical frequency spectrum and wave number meas. 2−78260
rapakivi pyterlite outcrops, Deep Creek, Salmon river mountains, tectonism 2−61928
ray tracing in three dimensions 2−54660
recording channel, frequency and phase characteristics, with optimal choice of input and output parameters 2−61895
refined hypocenter computation, correction of station arrival times 2−57610
reflection, deterministic estimation applic. 2−48391
reflection amplitudes in layered earth model, divergence compensation 2−54652
reflection data, automatic X^2-T^2 velocity analysis 2−57674
reflection data, maximum likelihood filtering 2−57688
reflection picking in time, moveout and dip space, automated 2−54662

Seismology continued
reflection seismic profiles and gravimetric, combined interpretation 2−57691
reflections from inhomogeneous layers with gradually changing velocity 2−54764
refraction modelling by computer 2−54657
refraction profile, sedimentary structure 2−81578
refraction profile in western Canada 2−81593
relative location of seismic events using surface waves 2−44559
reservoir-associated earthquake sequences, common universal behaviour 2−61875
reservoir-associated earthquake sequences, discriminatory characts. 2−61876
response effects on embedded structures 2−44552
Reykjanes Ridge, seismic reflection survey of oblique aseismic basement trend 2−65526
Rincon field, South Texas geoseismic history and development 2−57668
Rinconada fault in southern coastal ranges, California 2−61925
Rockall Plateau microcontinent, crustal structure obs. 2−48402
rocks, stressed, elastic shock activity during injection of water 2−55510
rupture velocities and seismic source mechanisms 2−61917
S-wave spectra analysis method rel. to layered structure inferences 2−78271
S-wave spectra rel. to structure studies in regions of Japan 2−78272
San Andreas fault, rel. to boundary between Pacific and N. American plates 2−61921
San Andreas fault, water level fluctuations and creep 2−57635
San Andreas fault zone, postulated offsets of Eocene strata 2−61923
San Andreas fault zone in Southwest Sonora, right lateral displacement 2−61924
San Fernando earthquake, faulting, anal. of aftershocks 2−61935
San Fernando earthquake, February 9, 1971, stress estimates 2−72612
San Fernando earthquake, gravity changes 2−57471
San Fernando earthquake, identification of initial rupture and breakout phases 2−57634
San Fernando earthquake, static and dynamic obs. of source mechanism 2−65502
San Fernando earthquake, strong motion data 2−57524
San Fernando earthquake aftershocks, spectra and source parameters 2−57557
San Fernando earthquake afterslip on Sylmar fault segment 2−57601
San Francisco Bay area, crustal models from transfer function ratios 2−57740
Santa Barbara Channel, California, seismic and aseismic horizontal strain 2−57699
saturation velocity analysis, computer picking 2−57673
S.E. Missouri earthquake, focal mechanism det. from Rayleigh wave radiation patterns 2−57554
sedimentation models for sandstone and shale, seismic signatures 2−44557
seismic data recording, recommended standards for digital tape formats 2−44556
seismic energy, effect of stress drop 2−65488
seismic records evaluation by automatic equipment 2−44564
seismic refraction mapping, Reframap Method, algorithm and procedure 2−57496
seismic refraction mapping, Reframap Method, model studies and performance 2−54624
seismic refraction measurements, crustal structure of Texas Gulf Coast area 2−54627
seismic signal evaluation at teleseismic distance, P and Rayleigh wave seismograms 2−61885
seismic waves, operational frequency analysis, infrasonic spectrometer-analyzer 2−57507
seismograms, numerical synthesis 2−54654
seismograms of reflected waves in gradient layer overlying homogeneous semisphere 2−44568
seismomagnetic effect, possibility of using magnetic methods to study tectonic processes 2−65513
seismovac monopulse pneumatic rebound seismic source 2−44558
SH-wave propagation in anisotropic inhomogeneous crustal layer 2−51512
shallow earthquakes, detection thresholds, using high-gain long-period seismograph stations 2−57625
shallow earthquakes, precision of different methods of magnitude calculation 2−72616
shallow earthquakes, wide scattering in continents 2−57512
shallow faulting model 2−57559
shallow water, primary frequency microseisms, theoretical model 2−48389
short period P- and S-waves attenuation in mantle, spectral analysis 2−78273
short period seismic discrimination between earthquakes and underground explosions 2−72650
Sierra Madre fault zone, obs. and engineering consequences of recent activity 2−57588
signal distortion due to dynamic corrections 2−72632
site and propagation effects on earthquake motion 2−81572
solid earth tide and phase vel. variations 2−61979
Solomon Sea Junction, tsunamigenic earthquakes, seismotectonics 2−57582
SOSIE method application to land seismic 2−57671
source, electroacoustic boomer for underwater sound generators 2−57661
source mechanism, dynamic features det. 2−57560
source parameters of nuclear explosions Milrow and Longshot from teleseismic P-waves 2−57444
source summary for U.S. underground nuclear explosions (1961-1970) 2−65466
source time function, propagation of longitudinal shear cracks 2−57561
source time function of propagating longitudinal-shear cracks 2−65493
South America, seismicity and Q-structure 2−57645
South America deep earthquakes, stress release 2−65490
South Australian earthquakes, frequency depth relation 2−72638
South Carolina, historical seismic activity survey 2−72619

Seismology continued
southern Nevada, regional secular strain fields 2−48404
southern Rocky Mountain region, geochemistry of Sr isotopes 2−57698
southern Rocky Mountain region, upper Cenozoic basalts 2−57693
southwestern New Mexico, midtertiary Mogollon Datil volcanic province, volcano tectonic timing 2−57692
southwestern New Mexico, Mogollon Datil volcanic province, petrology and petrogenesis 2−57694
spatial filters effects on signal 2−61947
spheroidal and toroidal vibrations of Earth for order numbers higher than 50 from earthquakes 2−84704
stable sliding preceding stick-slip, lab. expts. with granite 2−57589
stacking weights, optimum det. 2−54663
static correction determ. from reflection data 2−84733
step location determination with single transverse hodograph of seismic head waves 2−48387
strain and pendulum seismographs 2−57626
strong earthquake, rel. to electrotelluric field 2−78264
strong earthquake ground motions, local distribution 2−57523
strong motion accelerometer, effect of large off- axis accelerations on response 2−61904
strong motion earthquake and microtremor spectra obs. 2−57528
subsidence earthquakes, source mechanisms for Wilmington Oil field 2−61913
subterranean cavity det. and delineation by seismic resonance 2−57681
summing tapes, complexity evaluation 2−44569
superficial noises, anomalous potentials using Grandinetti's type soundings 2−81585
supersonic faulting, far-field radiation 2−65461
surface source systems analysis 2−57669
surface wave propagation, guided by ridges calc. by finite element technique 2−76335
Sweden, short period microseisms, power spectra and geographical distrib. 2−44575
Swedish-Finnish network, travel times of P-waves 2−44573
synthetic seismogram computation and comparison using leaking modes and generalized ray theory 2−57505
synthetic seismograms for long spread of seismometer stations 2−54655
synthetic seismograms obtained by eikonal method series developments convergence 2−94711
Takabayama tunnel, Japan, landslide microtremors and vibration of underground structure 2−81615
tectonic stress, great earthquakes earthquake swarm relationships, model for Philippine Sea plate 2−48396
teleseismic array evidence for lower mantle inhomogeneities and origin of Hawaiian Islands 2−81622
teleseismic ray data, inversion and interference 2−57648
Tennessee Sandstone, exptl. investigation of stick-slip 2−62089
Tennessee Sandstone, influence of surface roughness and gouge on frictional sliding 2−65521
three-dimensional dynamic display technique for presenting data 2−65473
three-dimensional model expts. 2−78267
tilts associated with small and medium size earthquakes 2−78269
Tonankai and Nankaido earthquakes, tectonic implications, focal mechanism 2−44565
Tonga, volcanic island, submarine eruptions 2−65545
Tonga-Fiji region, zone of low vel. in uppermost mantle, Pn and Sn travel times 2−57655
Tottori earthquake of 1943, determ. of effective tectonic stress rel. to earthquake faulting 2−84730
transducer improvements 2−72640
transform fault system, tectonic evolution of crustal wedge 2−61922
travel time curve, triplication obs. at 35° 2−57647
Triassic basement of North-Western Pre-Caucasian region, wave propagation peculiarities 2−54632
Troodos Massif, Cyprus, reversed seismic refraction line 2−68841
true ground motion determ. from termwise integration of seismogram 2−78263
underground ducts longitudinal displacements 2−84715
underground explosion waves, propagation in nearly elastic range 2−57641
underground nuclear explosions, source energies 2−72614
underwater explosions, deconvolution of refraction seismograms 2−65474
upper mantle, mineralogy rel. to seismic properties 2−57695
upper mantle anisotropy from refraction meas. 2−72662
upper mantle beneath USA, seismic Q estimation from Pn amplitudes 2−57646
upper mantle in western Europe, study using long-range seismic refraction 2−84705
upper mantle zone of low Q 2−65509
USA, western, space-time patterns in seismicity, obs. using interactive computer-generated graphics display technique 2−57583
velocity analysis, resolution studies 2−57676
velocity and density profiles, lattice dynamics of MgO, Al_2MgO_4 and Mg_2SiO_4 spinel 2−72636
velocity profile for deep mantle, dT/dΔ in 35°-40° epicentral distance range 2−57532
velocity spectra displays interpretation through adaptive modelling strategy 2−57667
velocity variations around Leduc reefs, Alberta, Canada 2−57678
velocity-dip spectrum 2−57675
Vibroseis application to engineering work in urban area 2−57683
VIBROSEIS base plate distortion effects, reduction 2−57670
Virginia earthquakes, macroseismic effects 2−65462
volcano Aso, P-wave apparent azimuths, structural model 2−78251
Vrancea region, stochastic seismic model, magnitude-frequency relation 2−75420
Wasatch fault, Utah, earthquake correlation with strain and tilt changes 2−57600
wave propagation with point source in stratified half space, numerical computation 2−54658
wavelet processing, computer program 2−54661
well-to-well obs., iterative ray tracing technique for anal. 2−65477
Western Port earthquake, 6th July 1971, anal. 2−81626
worldwide 1971 earthquake activity 2−61882

Seismology continued
- Yellowknife seismic array and regional seismicity, detection statistics 2−68833
- Zagreb earthquakes in 1869-1968 period statistical information 2−51506
- NH$_4$F, shock generation accompanying pressure-induced phase change, earthquake initiation 2−78268
- Ni olivine to Ni spinel, reaction rate of phase change, earthquake generation 2−78270

Selenium
- — 2−67970
- adsorption on Ni, surface reconstruction, Madelung potential 2−47162
- amorphous, crystn., effect of alternating elec. field 2−60565
- amorphous, field dependent mobility, validity of model 2−61286
- amorphous, i.r. absorpt. obs.of ring-chain-struct. 2−78088
- amorphous, kinematics of deep trapping 2−61344
- amorphous, structure of three forms 2−43451
- amorphous, threshold and memory switching effects 2−57196
- amorphous, u.s. propagation, vel., Young's, rigidity moduli, 0-60°C 2−57051
- amorphous, valence band density of states, vacuum photoemission study 2−84258
- amorphous and cryst., diamag. mag. susceptibility, 40-300K 2−77988
- amorphous film, a.c. cond., temp. depend. 2−68392
- amorphous film, carrier lifetime determ. 2−81088
- amorphous film, one- and two-carrier space-charge-limited currents 2−75097
- amorphous film, optical const. determination from reflectivity spectra 2−61620
- amorphous layers, photo-effect 2−84374
- amorphous state, different forms 2−60578
- atom, forbidden transitions in the ground configuration 2−74224
- atom, positron scattering, 100, 200 keV, diff. cross-sections 2−79877
- chemisorption on Ni, bonding, orbital electron energy spectra 2−48328
- compressed, crystn., photocurrent and thermally stimulated current obs. 2−64533
- crystallization in quinoline, pyridine, diethyl amine, thermal effects 2−53619
- density changes of solid and molten state at elevated temps. 2−64699
- diffusion of Tl, 60-210°C, and TlSe formation 2−53771
- dislocation networks, in vapour grown crystals, X-ray topography obs. 2−50676
- field effect rel. to temp., field mobility, surface cond. 2−71933
- film, amorphous, thermally stimulated cond. 2−57189
- film, crystalline and amorphous, ion bombardment effects 2−60646
- film, rolling texture, X-ray and elec. resist. study 2−64574
- film, semiconducting on metal, substrate stress effect on elec. parameters 2−71966
- hole photoemission into S, 2.11 to 3.54 eV 2−84265
- liquid, polymerization parameters, calc. method 2−57418
- liquid, switching and anomalous magnetoresistance 2−60505
- liquid, switching effect 2−60503
- liquid, switching phenomena 2−60504
- liquid and solid, thermal cond. 2−64865
- liquid semiconductor, switching, thermal breakdown mechanism 2−81096
- magnetic susceptibility, low temp, glassy and crystalline state 2−61477
- molten, relaxational ultrasonic absorption 2−43353
- monoclinic, excitons and direct gap, optical absorp. obs. 2−68648
- n.m.r., anisotropic chem. shift 2−44459
- non-crystalline, impurity effects on struct. and elec. props. 2−61326
- photocell, temperature dependence of relative spectral sensitivity 2−44186
- photocell effects of polarization on performance 2−44185
- photoemission, effects of cryst. disorder on electronic struct. obs. 2−61466
- rectifier, electrical and photoelectric obs. of surface layers 2−44132
- surface, circular microdisc patterns 2−60630
- thin films, application as recording materials for i.r. laser radiation 2−69960
- trigonal, lattice dynamics, modified valence force field approach 2−57041
- vitreous, anomalous sp. ht. below 1 K 2−43987
- vitreous, hole drift mobility 2−61327
- vitreous film, trap-limited processes 2−61325
- Al-Se-Ag structure, electro-physical characteristics 2−71987
- Au-lacquer-Se structure, current passage mechanism 2−84348
- Cd-Se rectifier, I-V and C-V characts., rel. to existence of CdSe interface layer 2−54219
- GaAs:Se, donor self-compensation 2−75110
- GaAs$_{1-x}$P$_x$:Se, donor self-compensation 2−75110
- Ge-Se system (4-16.7 at.% Ge), glasses, temp. depend. of density and thermal expansion 2−84209
- He-Se vapour laser, role of thermal energy-charge exchange 2−42019
- Se: Cl, As film, vacuum evap., transport props., time resolved drift technique 2−44104
- Se-CdS(Se) heterojunction electrolum. 2−54481
- Se-CdSe p-n heterojunction, diffusion potential determ. 2−47942
- Se-polyvinylcarbazole multi-layer photoreceptor for electrophotography 2−59293
- Se, trigonal crystals, transmission e. microscopy obs. of dislocations after chem. polishing 2−64668
- Se IV spectrum, levels and lines classif., 2400-420 Å 2−74223
- SeI, newly observed lines in PbS region 2−79939
- ^{75}Se, imaging agent, dynamic vascular scintiphotography of liver 2−58609
- ZnS$_{1-x}$Se$_x$ mixed crystals, optical reflectivity and band structure 2−54407

Selenium compounds
- poly(N-vinyl carbazole) film, transient space charge perturbed current 2−57229
- selenides, mol. transform. rel. to elec. resist. 2−47900
- As-Se-Ge glass film, amorphous to crystalline state conversion by light irradiation 2−75077

Selenium compounds continued
- As-Se-Te, vitreous semicond., γ-ray induced cond. 2−54252
- As-Se amorphous layers, carrier lifetime determ. 2−81088
- As-Se glass, Ag doped, elec. props. 2−64975
- As-Te-Ge-Se glass switching device, small signal behaviour 2−61376
- Bi-Se system, phase separation 2−60591
- Co-Se system, nonstoichiometric phases, thermodynamic props. 2−43829
- CsI:SeO$^{2-}{}_4$, i.r. absorpt. 2−78086
- Cu-As-Se compositions, voltage controlled switching 2−67886
- Cu-Se, extension of equilibrium diagram 2−64812
- Ge-As-Se-Pd(Cd) glass, microstruct. and immiscibility temp. 2−56561
- Ge-As-Se glass chalcogenide system, atomic distribution and coordination numbers 2−56559
- Ge-Se-Te-As system, amorphous bulk and thin film, composition and physical props. 2−60573
- Sb-Se-I-R-H$_2$O system, R = solvent = HI, HCl, Na$_2$Se, hydrothermal crystn. process, 300-450°C 2−74682
- Sb-Se system, phase separation 2−60591
- Se-As glasses, thermal characteristics near glass transformation point 2−61104
- Se-Sn-Ge-As glass, Mossbauer effect, isomeric shift, quadrupole splitting, phase diagram 2−75267
- Se-Te alloy, acoustoelec. phenomena relating to two carriers 2−80908
- Se-Te alloy, liq., semicond., n.m.r. 2−61752
- Se-Te alloy, noncrystalline, n.m.r. at 1.3 K 2−61751
- Se-Te alloy, u.s. amplification, room temp. 2−51041
- Se-Te alloys, liquid, switching phenomena 2−60504
- Se-Te melt, electronic transport behaviour, switching, optical gap 2−60502
- Se complex, Se(II) diethyl dithiocarbamate, three-dimensional X-ray investigation 2−56666
- SeF, electron resonance spectra in J = 5/2 rotational levels 2−46530
- SeF$_4$, matrix isolated vibrational spectra, C$_{2v}$ symmetry, assignment of frequencies, axial and equatorial bonds 2−83265
- SeH-, photodetachment of electron determ. of electron affinity and spin-orbit coupling constant of SeH 2−46583
- SeO, ground state dissociation energy estimation 2−46581
- SeO$_2$ soln. in aqueous HCl, effect of HCl conc. on Raman spectra 2−50366
- Se$_x$Te$_{1-x}$, synchrotron radiation absorp., d level spin orbit splitting obs. 2−81401
- ^{75}Se- selenomethionine uptake for diagnosis of hepatoma 2−66281
- Te-Se-Ge and Te-Se-Sb glasses, thermal effects 2−71917
- Te$_{60}$As$_{25}$Ge$_{13}$Se$_x$, chalcogenide glass, interdepend. between switching, memory, and thermal behaviour 2−47901
- WSe$_2$-NbSe$_2$ alloys, antifriction and elec. props., comp. depend. 2−68115

Self-diffusion *see Diffusion in gases, in liquids, in solids*

Semi-insulating materials (high-resistivity semiconductors) *see Semiconducting materials*

Semiconducting devices
- *see also Counters/semiconductor; Lasers/semiconductor; Masers*
- amorphous chalcogenide threshold and memory devices, preswitching props., forming and switching 2−77920
- bolometers on quartz substrate, time and mechanical stress stability 2−55571
- breakdown voltage meas. apparatus 2−82423
- carrier conc. in transient conditions, two-dimensional model 2−54210
- chalcogenide glass threshold switch, time-delay 2−61273
- crystalline chalcogenide device, threshold and memory switching 2−77883
- drift field induced carrier inhomogeneities in low conductivity accumulation layer surface wave amplifiers 2−51030
- electron bombarded, ThO$_2$ on Ir cathodes as electron emitter 2−65099
- electron microscopy applic. to characterization 2−61372
- gamma ray spectrometer, Compton scattering suppression guard scintillator, pulse shape discriminator, isotope determination 2−82796
- glass controllable switch, based on lateral expansion of conducting channel 2−61274
- graphite-Ge switch, asymmetric, and light sensitivity 2−61272
- liquid N$_2$ level indicator, semiconductor detectors 2−85164
- magnetosensitive injection-field effect 2−44090
- materials and devices, a close interactive system 2−83890
- measurement methods for semiconductor materials, process control and devices 2−77908
- memory device, amorphous film, radiation effects 2−61365
- memory materials and devices, conference (Princeton, 1 May, 1972) 2−69478
- microwave, frequency variable semiconductor oscillator 2−73479
- optoelectronic, review 2−51178
- Ovonic Read-Mostly memory array, conducting filaments, scanning elec. microscope obs. 2−61367
- photo-etching techniques 2−71301
- pressure transducer, patent 2−82138
- solid state and quantum electronics, book 2−57092
- surface wave filters in integrated circuits 2−49112
- switching, thermal, current-voltage characts., temp., elec. field, current density distribs. 2−71953
- switching amorphous film morphology exam. by scanning electron microscopy 2−44129
- temperature measuring for surface transients 2−58972
- temperature sensing by liquid crystal probes 2−69804
- thermal switching, static I-V characts., calc. for cylindrical symmetry 2−54207
- thermistor, radiation shield, for deployment in atmos. boundary layer 2−51579
- thermistor array for flow direction, speed and temp. meas. in geophys. fluid dynamics expts. 2−54775
- thermistors, calibration over temp. range 0-30°C 2−41867
- thermistors, midget disk, effects of static mag. field at 77 K 2−49186
- thermistors, positive temp. coeff., sensitivity and appls. for temp. meas. 2−82385

Semiconducting devices continued
- thermoresistors, volt-ampere characts. for different velocities and flux temps. 2−55589
- threshold switch devices, strain sensitive props. 2−61364
- thyristors, p-n-p-n structure, electron emission microscope study 2−81113
- transducers, mechanical variable, physical principles 2−66627
- two-stage diffusion, layer parameters calc. allowing for evaporation 2−71512
- ultrasonic amplification by piezoelectric semiconductors, space charge effects on attenuation symmetry 2−51031
- As-Te-Ge-Se glass switching device, small signal behaviour 2−61376
- As_2Se_2Te film switching and memory device, inc. neutron irrad. effects 2−61373
- As_2Te_3-Si glass threshold switch, electronically assisted thermal breakdown 2−61276
- C film, diamond-like props. characterization rel. to technology applics. 2−56588
- CdSe-electrolyte blocking contact, photosensitivity and noise 2−72079
- GaAs-$Al_xGa_{1-x}As$ p-n heterojunction, current flow during electrolum. 2−72438
- n- GaAs Gunn oscillators, hot electron microwave mobility 2−51139
- GaAs high resistivity oscillator, characteristic operation 2−44137
- GaN, fabrication, electrolytic etching 2−71365
- Ge, manufacture, single crystal ribbon growth from melt 2−60725
- $Ge_{15}Te_{81}X_4$, amorphous, memory device model 2−61375
- $Pb_{1-y}Sn_ySe$, thin films i.r. photoconductors 2−64999
- $Pb_{1-x}Sn_xTe$ thin film i.r. photoconductors 2−64999
- Se rectifier, electrical and photoelectric obs. of surface layers 2−44132
- Si wafer characteriz., generation of stacking faults and dislocation loops 2−51179
- Si_3N_4 protective layer, high prod. system for deposition 2−71952
- SnO_2-CdS-Au, polarised memory device, photovoltage obs. 2−61381
- VO_2 switching device, influence of high-conducting bubble 2−54208
- VO_2 threshold switching device, capacitance discharge 2−54211
- **diodes**
  - — 2−65028
  - — 2−65029
  - — 2−65031
  - anthracene, double injection electrolum., and carrier injection props. of C fibres 2−75338
  - avalanche photodiodes, temp. dependence and stabilization 2−68485
  - avalanching and second breakdown in silicon-on-sapphire diodes 2−57216
  - breakdown voltage measurement, instrumentation 2−82423
  - bridge silicon and partial mag. diodes, volt-tesla and volt-amp characts. 2−82416
  - electroluminescent, Avzel effect fluoresc, process, visualisation applications 2−84530
  - energy source for photoelectric indicating instruments 2−61900
  - Gunn, construction, v.h.f. power generation 2−47943
  - Gunn, switching behaviour interpret. rel. to instabilities 2−54166
  - Gunn devices, impact ionization, high field domain 2−65034
  - Gunn diode, instability characteristics for negative differential conductivity 2−71982
  - Gunn effect, GaAs epitaxial type, coaxial resonant cavity mounted, low temperature characteristics 2−71983
  - IMPATT, basic phys. principles of operation 2−71971
  - IMPATT oscillator, tunnelling effects, calcs. 2−71980
  - light emitting, efficiency, carrier diffusion length, absorpt., auto-photovoltaic meas. 2−61451
  - light emitting, response time 2−51385
  - as magnetic probe for transistorized gaussmeter 2−55643
  - m.a.o.s., cond.-voltage characts. 2−61400
  - m.a.s., shifting characts. of flat band voltage, X-ray effects 2−57220
  - mesa, ion implantation technology, measurement techniques 2−71970
  - metal oxide layer on metal, semiconducting parameters, effect of substrate stress state 2−71966
  - noise, 1/f, variance fluctuations 2−51177
  - overcompensated semiconductor, analytic expressions for IV characs. 2−75129
  - Ovonic, S-shaped meg. differential cond., current instabilities 2−61368
  - p^+-n, terminal noise at high injection, theory 2−54218
  - p-n junction, effects of recombinations in base contact and on surface 2−54217
  - p-n junction avalanche, analytical determ. of small-signal impedance 2−68444
  - p-n junction current change, reverse biased, in diodes after storage at elevated temps. 2−61386
  - photodiode assembly, high speed 2−57215
  - planar, ion implantation technology, measurement techniques 2−71970
  - planar, with gate, electrical characts. rel. to fabrication conditions 2−71965
  - pnpn, S-shaped neg. differential cond., current instabilities 2−61368
  - Q-switched junction diode laser, fabrication, patent 2−82487
  - Schottky, cond. mechanism, diffusion and thermionic emission theories, quasi-Fermi levels 2−75128
  - Schottky barrier, for det. of donor density profile in semiconductors 2−75127
  - semiconductor-insulator-semiconductor, surface states, impurity effects, freq. depend. complex admittance 2−61385
  - semiinsulator long diode, S-type current-voltage characts. when illum., photosensitivity 2−65094
  - Si, arrays in camera tube, inspection by optical intensity spatial filtering 2−79424
  - single injection diode, generalized expression for small sig. impedance, inc. space charge effects 2−44134
  - s.i.s. using Si, admittance meas. 2−61388
  - solid state light sources, review in book 2−55700
  - thermionic injection, operation in transit mode 2−77926

Semiconducting devices continued
- **diodes** continued
  - tunnel diode comparator, fast recovery, high input impedance 2−73951
  - $Al_xGa_{1-x}As$ grown- diffused electroluminescent planar monolithic diodes 2−51386
  - $Al_xGa_{1-x}As$ heterojunction, electroluminescence characs. 2−81431
  - Au-n^+-GaAs, Schottky, hole diffusion contrib. to photocurrent, temp. depend. 2−44178
  - Au−n-GaP, surface barrier diode, photosensitivity, 1.4-5.2 eV spectral range 2−75182
  - Cd-Se rectifier, I-V and C-V characts., rel. to existence of CdSe interface layer 2−54219
  - (Ga, Al)As/GaAs, epitaxial luminesc. diodes, emission delay time between elec. and optical signals 2−72401
  - $Ga_{1-x}Al_xAs$:Si, electrolum., substrate orientation depend. 2−51153
  - $Ga_{1-x}Al_xAs$, light emitting, epitaxial growth on GaP substrates 2−51388
  - $Ga_{1-x}Al_xAs$ alloyed p-n tunnel diodes, resonant impurity- assisted tunnelling 2−71981
  - GaAs:Cr, p-i-n, nonadditive photocond. under combined excitation conditions 2−72080
  - GaAs, electrolum., electron diffusion length, internal quantum efficiency, temp. depend. 2−61725
  - GaAs, electrolum. diode, sinusoidal modulated, recomb. emission phase shifts rel. to injection levels 2−72400
  - n-GaAs, high-resist., current oscillation and photoresponse 2−54220
  - GaAs, high-resistivity double-injection devices, conditions for recombinative space-charge injection 2−68445
  - GaAs, Si-doped, infrared light emitting diode 2−65030
  - n-GaAs, surface barrier diode, hole diffusion length 2−61387
  - GaAs, transmission photocathode, prep. and characts. 2−75185
  - GaAs diodes, power and radiation pattern meas. 2−51369
  - GaAs Gunn device, degradation by dislocations induced during thermocompression bonding 2−68446
  - GaAs IMPATT, intrinsic response time of semicond. avalanches, carrier diffusion influence 2−61384
  - GaAs metal-semiconductor barriers, cascade frequency multipliers microwaves 2−84350
  - GaAs photodiode with anti-Stokes luminors 2−77967
  - GaAs photodiodes, feasibility of epitaxial production on single crystal strip of Ge 2−54260
  - GaAs varactor, p-n junction location using conductive mode amplifier and s.e.m. 2−55639
  - $GaAs_{1-x}P_x$, light emitting, characteristics, applications 2−44422
  - $GaAs_{1-x}P_x$, light emitting, reliability 2−44423
  - $GaAs_{1-x}P_x$, light emitting 2−44421
  - $GaAs_{1-x}P_x$ alloyed p-n tunnel diodes, resonant impurity- assisted tunnelling 2−71981
  - GaN:Mg, electrolum., fabrication, props. 2−72387
  - GaN, m.i.s. devices, radiative recombination due to electric field polarity reversal 2−71990
  - GaP:Zn, electrolum., red., prep. 2−44424
  - GaP:Zn, O, light emitting diode, efficiency shift under forward bias 2−75181
  - GaP, electroluminescent, etching phenomena, scanning elec. microscope obs. 2−71972
  - GaP, light emitting physics of radiative centres 2−61724
  - GaP, red-emitting, scanning electron microscope characteriz. 2−51389
  - GaP green emitting diode fabrication by double- bin liquid-phase epitaxy 2−72437
  - GaP light emitting, props. for green and red emission, quantum efficiencies 2−44418
  - GaP p-n-p-n, green light emitting, fabrication and characts. 2−72436
  - GaP p-n junction, electroluminescent with nonuniform distribution of isoelectronic N_2 traps, patent 2−54485
  - GaP red-emitting diode manufacture, cryst. growth technique 2−60711
  - Ge:As tunnel diode, mag. kondo scatt. 2−71973
  - Ge:Au, fabrication, double injection negative differential resist. 2−71974
  - Ge:Cu $P^+-\pi-N^+$ structures, negative resistance and magnetic sensitivity 2−75130
  - Ge IMPATT, intrinsic response time of semicond. avalanches, carrier diffusion influence 2−61384
  - Ge(Li) counters, trapping parameters, chemical impurities effect 2−49666
  - $In_xGa_{1-x}As$, p-n, electroluminescent, with efficient 1.06 μm emission 2−61726
  - $In_xGa_{1-x}As$ prep. and props. rel. to electroluminescent diodes 2−68708
  - $In_{1-x}Ga_xP$, vapour grown p-n junc., bright electroluminesc. and orange laser emission 2−49386
  - $In_{1-x}Ga_xP$ alloyed p-n tunnel diodes, resonant impurity-assisted tunnelling 2−71981
  - Nb-Nb_2O_5- metal, switching obs. 2−54223
  - p^+-GaAs-nZnSe, C-V, I-V, photovoltaic properties 2−53573
  - $Pb_{1-x}Sn_xTe$, photodiode, prep. and props. 2−75183
  - PbTe epitaxial thin film, evaporated, injection luminesc. and laser action 2−57382
  - PtSi-Al Schottky diode, barrier height rel. to heat treatment 2−75131
  - Se-CdS(Se) heterojunction electrolum. 2−54481
  - Se parameters, effect of substrate stress state 2−71966
  - p^+-n Si:Au, current filament behaviour in mag. field 2−71975
  - Si:Au, thermally-stimulated current from deep-lying trapping levels 2−68419
  - Si:Au, thermally stimulated current from deep-lying trapping levels 2−68419
  - Si:B, current-voltage characteristics 2−71969
  - Si:GaAs light emitting diode MV-50 fast luminescent decay meas. 2−45812
  - p-Si-i-nSi, admittance meas. 2−61388
  - Si, formed by gas doped epitaxial film 2−50690
  - Si, mesa type, reversely biased, effect of p-n junction size on thermal resistance 2−71967
  - Si, n^+-p, fast electron irrad., capacitance 2−71978
  - Si, p-n, γ-irrad., impurity effects, photovolt. effect obs. 2−61358
  - Si, p^+-n and n^+-p, with Au impurity in base, barrier capacitance 2−71979

Semiconducting devices continued
diodes continued
Si, square-law 'punch-through', application as high-level parabolic detectors 2−44135
Si, temperature measurement system 2−45600
Si avalanche photodiode, photomultiplication factor obs. 2−71968
Si IMPATT, intrinsic response time of semicond. avalanches, carrier diffusion influence 2−61384
Si junction diode sensor for electronic thermometer 2−55591
Si on sapphire, avalanching, second-breakdown phenomena, study based on local temperature induced changes in optical absorption 2−47945
Si on sapphire diodes as switching elements for surface wave devices, 60 to 100 MHz range 2−49126
Si p-n junction photodiode, spectral characts., effect of strong elec. fields 2−75184
Si planar diode, elec. props. rel. to lattice defects, X-ray obs. 2−47944
Si power devices, diodes and thyristors, carrier lifetimes, meas. 2−71977
Si single crystal point contact, polarized memory effect mechanism 2−61389
Si stack diodes, extremely high voltage, for colour TV receivers 2−65032
Si X-band double-drift IMPATT diode fabrication by consecutive epitaxy 2−71976
Ti-TiO_2-Au film, I-V characts., negative resist. 2−61390
$ZnSe_xTe_{1-x}$ p-n junction diodes, struct., props., electron microscope and cathodolum. obs., 77-300K 2−81118
ZnTe-InAs heterojunction, prep. by liq. phase epitaxy, optical and elec. props. 2−57213
ZnTe Schottky barrier, admittance spectroscopy of deep impurity levels 2−61391

junctions
— 2−71973
p-Cu_2Se-n-CdSe hterojunctions, Zener breakdown by tunnelling electrons 2−68442
diffused, capacitance, C^{-3} vs. U intercept with U axis, computer calcs. 2−81115
heterojunction, graded, electronic props., one band one dimens. model 2−68441
heterojunction solar cells, ZnSe-GaAs, characteristics 2−63253
heterosystems and nonheterosystems, polarized memory effects 2−61380
metal-GaAs (110) contact, Schottky barrier height 2−54214
mim structure, electrical pulse regime and switching study 2−77917
multiplication factor analysis 2−51180
n-p, series-connected, S-curves, switching rel. to amorphous semicond. 2−68381
n-p(n-i-p) nuclear particle detectors, space charge layer polarization during irradiation 2−65023
n-p-i structs., current-voltage characts., S and N type negative resist. regions 2−65022
p^+-n diode, terminal noise at high injection, theory 2−54218
p^+-n-n^+ struct., I-V characts., deep impurity centre effects 2−77923
p^+n junctions, SiO coated, degradation 2−44130
p^+nn^+, development of S-type negative resistance region 2−54213
p^+nn^+, negative resistance, obs. 2−47940
p^+np^+ structs., current transport mechanism, thermionic injection, space charge limited currents 2−61377
p-i-n junction anodic film on Ti 2−47138
p-n, breakdown, inhomogeneities effect 2−51182
p-n, C-V characteristic method with feedback for carrier distrib. determ. 2−68440
p-n, current determination using function of charge carrier energy distrib. 2−61378
p-n, diffused, with deep impurity centres, struct. and capacitance 2−75122
p-n, directly polarized, photoresist. effect 2−48006
p-n, electrical characts. rel. to surface conditions and oxide film fabrication 2−71965
p-n, heavily doped n-type region, current-voltage characts. 2−65024
p-n, III-V cpds., vapour phase growth system 2−43511
p-n, photoluminesc., quenching by elec. field in space charge region 2−65290
p-n, reverse characts. determ. using elec. field induced light scatt. in liq. cryst. 2−77918
p-n avalanche diode, analytical determ. of small-signal impedance 2−68444
p-n junction current change, reverse biased, in diodes after storage at elevated temps. 2−61386
p-n junction location in GaAs varactor diode using conductive mode amplifier and s.e.m. 2−55639
p-n junction photographic system, resolving power enhancement in magnetic field 2−75123
p-n junction space charge region, differential d.c. conductance, calc. 2−57212
p-n junctions, transmission electron microscope imaging of electric fields 2−79134
p-n junctions, X-ray image of internal structure 2−81112
p-n thermoelement, effect of switching layer resistance on transient cooling 2−65079
p-n-p-n, four-layer structure, static VI characteristic at two-collector inclusion under low level injection 2−54212
photodetectors, heterojunction, interface region struct. rel. to energy band profile 2−44181
photodetectors, heterojunction, review 2−44180
semiconductor-insulator-semiconductor structure, with electron-hole pairing, Josephson effect analogue 2−81124
small molecules, i.r. matrix isolation spectra, isotopic shift and structure determ. 2−70708
surface replication, polymeric, modulation by surface mag. and elec. fields 2−64539
temperature distrib., in crystals with junctions, obs. 2−51364
transient space-charge flow under ionizing radiation 2−71954
wavelength converter, i.r. region, antiStokes mechanism, heterojunction structure 2−66848
$Al_xGa_{1-x}As$-GaAs-$Al_yGa_{1-y}As$, double heterostruct., differential I/V correlating with laser threshold 2−66769
AlGaAs GaAs heterojunctions, band filling process 2−47941

Semiconducting devices continued
junctions continued
$Al_xGa_{1-x}As$-GaAs, prep. by multiple layer liq. phase epitaxy 2−50482
$Al_xGa_{1-x}As$-GaAs heterojunctions, elec. props., photoresponse, graded gap model, laser operation 2−81117
$Al_yGa_{1-y}As_xSb_{1-x}$-$GaAs_xSb_{1-x}$ double heterojunction laser, prep. and emission spectra 2−59184
Bi-Te, diffusion of Cd and In, creation of p-n junction 2−83991
n-CdS−p-Cu_2S film heterojunction, rectification, photosensitivity and tunnelling 2−71955
CdTe b-n, formation by natural doping 2−84349
Cu_2S-CdS heterojunction, photocapacitance effects 2−51221
Cu_2S-CdS heterojunction, prep. and photoelectronic props. 2−72056
Cu_xS-CdS photovoltaic cell, model 2−54261
Cu_2S-CdTe film heterojunction, photovoltaic effect 2−81123
$Ga_xAl_{1-x}As$-GaAs, p-n, field effect of GaAs photolum. 2−72399
$Ga_{1-x}Al_xAs$ epitaxial layer growth 2−47288
GaAs:Ge p-n junction, Zn- diffused, photolum., 8100-8500 Å 2−72404
GaAs:Si, p-n, reverse branch of I-V characts. and breakdown 2−71959
GaAs-CdS heterojunction, isotypic, prep. and photosensitive props. 2−71956
GaAs-GaP, prep. by multiple layer liq. phase epitaxy 2−50482
GaAs-(AlGa)As heterojunction cold cathode, factors affecting extended operation 2−48012
GaAs, $n^+/n^-/n^+$ pulse generating, interfacial defect obs., high voltage electron microscopy 2−54215
GaAs, p-n junctions, barrier capacitance, obs. 2−44131
GaAs p-n junction, insulation by proton irradiation 2−84353
$GaAs_{1-x}P_x$, electrolum. diode, Zn diffusion in open-tube system 2−75126
GaP: Zn, Al, p-n, electrolum., 1.7 to 2.3eV 2−75321
GaP:O p-n junction, deep double electron O trap transitions, photocapacitance obs. 2−75013
GaP-GaAs, p-n, field effect of GaAs photolum. 2−72399
GaP-Si heterojunction, liquid phase epitaxial growth 2−71957
GaP, melt-grown, S-pit correl. with reduced luminesc. efficiencies 2−50595
GaP, p-n, growth by liq. phase epitaxy 2−47287
GaP p-n-p-n green light emitting diode, fabrication and characts. 2−72436
Ge-GaAs heterojunction, liquid phase epitaxial growth 2−71957
Ge-Si heterojunction, pulse characts. 2−71961
p-Ge-n-CdS_xSe_{1-x} epitaxial heterojunction 2−77924
p-Ge-n-CdS_xSe_{1-x} epitaxial heterojunction, prep., struct. and elec. props. 2−77924
Ge, p-n, bistable state of microplasmas 2−71963
Ge, p-n junc., microplasma turn-on voltage, illumination effect 2−75124
p-nGe, secondary breakdown formation 2−71962
Ge p-n junction, IV characts. of microplasma 2−75125
Ge p-n junction, γ-ray detector, space charge region polarization, impurity centre charge exchange 2−65026
Ge p-n junction, microplasma turn-on delay time rel. to trapping levels, 77K 2−65025
H_2 on ferromagnetic catalyst, ortho-para conversion, surface magnetization orientation effect 2−71342
$Hg_{1-x}Cd_xTe$, n-p junction, absence of surface effects 2−57194
$In_{1-x}Ga_xP$ p-n junction, bright yellow emission 2−44425
InSb p-n junction, minority carrier diffusion across, electron beam study 2−81111
InSb tunnel junction, Cd diffused, I-V characts. and magnetotunnelling 2−54216
Se-CdS(Se) diode, electrolum. 2−54481
Se-CdSe p-n heterojunction, diffusion potential determ. 2−47942
Si:Au, with two Schottky contacts, low freq. current oscillations 2−61383
Si-CdSe, p-n heterojunctions vacuum deposition preparation and properties 2−77925
Si-Ge heterojunction position sensitive photocell 2−44182
Si-Ge p^+-n alloyed heterojunction, V-I characts., uniaxial stress effect 2−81120
Si, oxidized surfaces, contact pot. difference meas. 2−77914
Si, p-n, minority charge carrier diffusion length meas. by electron beam microprobe 2−44133
Si, pn junc., proton irrad., deep centre spatial distrib., from capacitance meas. 2−68443
Si, recombination centre parameters of irradiated p-n junctions, determ. 2−61382
Si, surface state density distrib. rel. to diffusion induced disloc. near junc. formed by P diffusion 2−44038
Si, thermally diffused, avalanche multiplication rel. to dislocation lines 2−65027
Si diode, p^+-n and n^+-p, with Au impurity in base, barrier capacitance 2−71979
Si hyperabrupt p-n, breakdown voltage 2−84347
Si n^+-p diode, fast electron irrad., capacitance 2−71978
Si p-n diode, γ-irrad., impurity effects, photovolt. effect obs. 2−61358
Si p-n junction, microplasma optical interactions 2−65021
Si p-n junction, protection by SiO_2 film prep. by oxygen bombardment 2−51176
Si p-n junction, reactor irrad., broadening of Zn and Ga impurity profiles 2−84355
SiC:B, p-n junc., impurity distrib. obs. 2−74797
SiC, phonon spedtra from tunnelling characts. of p-n junctions 2−57042
SiO_2 film, dielec., defects, local junction form 2−71964
SnO_2-SbSI, dielec.-semiond. thin film junc., memory and switching effects 2−61366
ZnCdS evaporated layers as photoresistors in u.v. 2−44179
ZnS-CdS, evaporated layers, mosaic heterojunction photo-emf 2−77970
n-ZnS-pGaP heterojunctions, growth, electrical properties 2−80596
ZnS electroluminescent p-n junction, electronic behaviour obs. 2−68711
n-ZnSe-pGaP heterojunctions, growth, electrical properties 2−80596

Semiconducting devices continued
junctions continued
ZnSe$_x$Te$_{1-x}$ p-n junction diodes, struct., props., electron microscope and cathodolum. obs., 77-300K 2—81118
ZnTe-InAs, prep. by liq. phase epitaxy, optical and elec. props. 2—57213
ZnTe, alloyed heterojunctions with InAs, GaSb, InSb, single carrier space charge limited current flow model 2—64962
transistors
alloyed junction, high level infection, determ. of emitter-base cut-off voltage 2—47947
DSA-MOS, using preferential etching charact. of Si with water-amine solution 2—71316
f.e.t., noise at long time constants 2—44136
m.o.s., differential charge pumping effect 2—44145
m.o.s., meas. of drain-source conductance in saturated current region 2—63211
m.o.s., transconductance meas. using differential amplifier 2—63210
p-n-p-n, four-layer structure, static VI characteristic at two-collector inclusion under low level injection 2—54212
p-type impurity distribs., anomalous base regions 2—71504
photomultiplier, pulsed blocking 2—59108
phototransistor, overcompensated semiconductor, mechanisms of decreased differential photosensitivity 2—75129
physical principles and circuit properties, book 2—84356
thin film, polarizability of bias- temperature drifted species 2—47946
GaP, switches, p-n-p-n, controlled rectifiers, blocking voltages, electrolum., $0 \leqslant T \leqslant 500C$ 2—61392
Ge alloy and drift, influence of biasing conditions and power dissipated on permanent radiation damage 2—75133
Si:As by evacuated capsule method 2—71518
Si-Ge alloy oxide layer etched away, reoxidation, production of MOS transistors 2—75132
Si, n-channel junction f.e.t., neutron damage annealing 2—51181
Si, npn planar, encapsulation 2—54221
tunnel and interface devices
see also Metal-insulator-metal structures and devices; Metal-insulator-semiconductor structures and devices; Tunnelling
diode comparator, fast recovery, high input impedance 2—73951
glass-semiconductor-LiNbO$_3$ structures, acoustoelectric dispersive surface wave amplification 2—49129
m.o.s. capacitors, fast surface states 2—68457
Schottky barrier tunnel diode, noise spectrum bias dependence 2—47789
Al-CdS-In thin film struct., memory effect, switching characts. 2—44139
Ga$_{1-x}$Al$_x$As alloyed p-n tunnel diodes, resonant impurity- assisted tunnelling 2—71981
GaAs Schottky-barrier diode preparation for differential capacitance meas. rel. to dopant conc. profile determ. 2—83905
GaAs$_{1-x}$P$_x$ alloyed p-n tunnel diodes, resonant impurity- assisted tunnelling 2—71981
In$_{1-x}$Ga$_x$P alloyed p-n tunnel diodes, resonant impurity-assisted tunnelling 2—71981
Si-Si$_3$N$_4$-SiO$_2$-Si structure, elec. characts., annealing and impurity effects 2—71984
Semiconducting materials
see also Ion implantation; Magnetoelectric effects; Photoconductivity; Photovoltaic effects; Semimetals
— 2—68259
— 2—61690
— 2—61319
A^{2}B^{4}C$_2^5$ type semiconductors lowest conduction band minima 2—80983
A$^{\text{III}}$B$^{\text{V}}$ compounds, nonlinear quadratic polarizability due to shallow impurity levels 2—64998
alloy, degenerate, e.s.r. obs. 2—48273
alloy, doped, supercond. transition temp. rel. to ferroelec. Curie temp. 2—44071
amorphous, avalanche ionization, Shockley hot-electron model 2—61287
amorphous, elec. instabilities of mixed electronic and thermal origin, theory 2—61285
amorphous, electronic, photovoltaic optical and e.s.r. props. 2—47789
amorphous, electrothermal switching, models 2—61284
amorphous, field dependent mobility, model 2—61286
amorphous, film morphology exam. by scanning electron microscopy 2—44129
amorphous, Hall mobilities, meas. by Corbino disc 2—68426
amorphous, modelled by fast-neutron- compensated n-Ge 2—68429
amorphous, radiation stability, effects of microstruct. 2—60567
amorphous, reversible optical effects, laser induced 2—60569
amorphous, trap levels, thermally stimulated capacitor discharge study 2—54188
amorphous, trapping mechanism, cavity perturbation study 2—61443
amorphous, with undulatorily-graded band edges, props., prediction 2—61282
amorphous chalcogenide threshold and memory devices, preswitching props., forming and switching 2—77920
amorphous film, interaction of electron beam, read and write processes 2—61260
amorphous film, ohmic and non-ohmic cond. 2—61289
amorphous organic, elec. cond., press. depend., random field model 2—44108
anthracene, deuterated, isotope effect in carrier mobility 2—47906
anthracene, electrons and holes interaction 2—80982
anthracene, evolution of space charge limited currents 2—75105
anthracene, freq. depend. cond. in single cryst. with monopolar injection 2—64993
anthracene, quenching of triplet excitons by trapped carriers used to determ. charge density gradient 2—47907
anthracene diode, double injection electrolum., and carrier injection props. of C fibres 2—75338
anthracene films and crystals current/voltage charact. rel. to thickness, temperature and light emission 2—57201
anthracene single crystal irradiated by electron beam, hole trap 2—51126

Semiconducting materials continued
anthracene transient photoinjection current 2—57200
band structure, critical point detn., wavelength modulation derivative spectroscopy obs. 2—48160
band structure, using generalized symmetrical Wannier functions 2—64889
benzene, solid and liquid, electron and hole mobilities 2—51146
bulk negative resistance, superlattice portion, spatial periodic variations, patent 2—84341
C$_{6v}$ class crystal, piezoelec. interaction of transverse u.s. waves with charge carriers 2—54030
β-carotene, elec. cond., photocond., and optical absorpt. 2—72072
β-carotene glass, photocond. transients 2—48003
β-carotene glass, photoconduction 2—48002
chalcogenide, amorphous, photocond. and photoluminesc., review 2—61445
chalcogenide, amorphous film, thermally stimulated cond. 2—57189
chalcogenide alloy, amorphous, photocond. model 2—61446
chalcogenide alloy amorphous film, sputtered, thermally stimulated Ar release study 2—43472
chalcogenide film, electronic transport, heterogeneous materials 2—64959
chalcogenide film, on SnO$_2$ coated glass, polarized memory effect 2—64971
chalcogenide glass, elec. conductivity and electron transport processes, structural effects and physical mechanisms 2—61267
chalcogenide glass, Mn^{2+}-, Fe^{3+}-, or Gd^{3+}-doped, e.p.r., fine struct. 2—72476
chalcogenide glass, states in the gap, expt. evidence 2—61334
chalcogenide glass, threshold and memory types, thermal effects 2—71917
chalcogenide glass film, switching behaviour 2—81071
chalcogenide glasses, elec. changes in surface region 2—54190
chalcogenide-glass switches, preswitching behaviour in terms of space charge injection mechanism 2—68379
collagen, elec. props., effect of adsorbed water 2—47908
conductivity and Hall coeff., meas. by four-probe method 2—54191
crystal growth, temp. profile calc. for complex shapes 2—53602
cubic, stress dependence of the Raman frequencies and elastic constants 2—84497
diamond, heavily doped with B, Al and Ti, resistivity 2—68396
diffused mixed single crystal waveguides on II-VI compound substrates 2—42240
diphenylpolyene film, elec. cond. temp. depend. 2—84338
disordered systems, model of conductivity in dense metallic vapours 2—54183
drift mobility detn. using Shockley-Haynes pulse method 2—68380
epitaxial layers, steady state surface photovolt., interpretation 2—75177
EuO, ferromag. semicond., Redfield technique detn. of Hall mobility of photoelectrons 2—81060
excitonic phase, thermoelec. power calc. 2—65077
Fe$_{1-x}$S, semicond. uniaxial ferroelec. qualitative model 2—77956
ferromagnetic, spin wave-helicon wave interactions 2—51122
film, magnetoresist. and Hall coeff., calc. 2—71892
film, nonlinear h.f. conductivity 2—44089
film, single crystal, electrical conductivity and adsorption, combined meas. 2—71932
furan quinone pigments, DFC and DF, photoinjection and photoemission, energy levels 2—54256
furan-quinone pigment, DFC, charge transport props. 2—51219
glass, a.c. conductivity, atomic and electronic hopping 2—47881
glass, chalcogenide, threshold switching, time delay 2—61273
glass, chalcogenide, threshold switching mechanisms 2—61272
glass, endotherm in switch-on process 2—64964
glass, endotherm in switch-on process 2—64965
glass, field effect in m.i.s. type struct. 2—65042
glass, mag. susceptibility, temp. and comp. depend. 2—61480
glass, perturbed bands, model 2—61335
glass, switching, lateral expansion of conducting channel 2—61274
glass chalcogenide, switching behaviour between Ge electrodes, firing 2—81074
glass films, thermally switching, pulse response of cond. channel 2—51129
glasses, pseudobinary section P$_2$Se$_3$—As$_2$Se$_3$, n.m.r. of ^{31}P, comp. depend. of width of spectral lines, second moment and chemical shift 2—84584
graphite, band struct., secondary electron emission study 2—51150
graphite, galvanomag. props., rel. to struct. imperfections 2—57190
graphite, I-V characts., in transverse mag. field, multiple kink effect 2—44093
graphite, thermomagnetic effects, coupled Boltzmann eqn. 2—54243
group I-III-VI$_2$, galvanomag. and thermomag. effects 2—71886
group I-III-VI$_2$, i.r. transmission cut-off 2—78058
group I-III-VI$_2$ cpds., s-d hybridization of valence bands 2—44112
group II-IV-V$_2$, i.r. transmission cut-off 2—78058
group II-IV-V$_2$ chalcopyrite crysts., assignment of E$_1$ transitions 2—81384
group II-IV-V$_2$ compound, single cryst. surface energy estimate 2—74615
group II-VI, deep Cu impurity, e.s.r. and optical spectra, dynamical Jahn-Teller interaction 2—80954
group II-VI, thermal cond. and phonon scatt. by Fe^{2+} impurities 2—84213
group II-VI compound film, epitaxial, struct., composition and elec. props. 2—56582
group II-VI compounds, excited state laser spectroscopy of impurities 2—64997
group II-VI cpds., deviations from stoichiometry 2—50657
group II-VI cpds., radiation damage 2—47366
group II-VI cpds., radiation induced and growth defect obs. 2—47372
group II-VI cpds., vapour growth, donor and acceptor identification 2—50573
group II-VI film, epitaxy by decomp. of group II metalorganic 2—47091
group IIB-VIA compounds, X-ray induced electron emission, electron energy levels detn. 2—48019
group III-V, band gap, temp. depend., calc. 2—68415

Semiconducting materials continued
group III-V, hot electron magnetophonon reson., theory 2−68386
group III-V, transition metal doped, anomalous elec. and mag. props. 2−68405
group III-V and II-VI compounds, negative differential mobility 2−44088
group III-V compound, X-ray photoemission, outermost core d and p electrons obs. 2−81195
group III-V compounds, amorphous, static electronic dielectric constant 2−51300
group III-V compounds, core levels obs. 2−65240
group III-V compounds, excited state laser spectroscopy of impurities 2−64997
group III-V cpds., pressure depend. of E_2 reflectivity peak and dielectric constant 2−72297
group III-V cpds., radiation damage, review 2−47365
group III-V film, epitaxy by decomp. of group III metalorganic 2−47091
group IV-VI chalcogenide, transverse Nernst-Ettingshausen effect, hydrostatic compression effects 2−75159
group V_2-VI_3 compound, Mossbauer effect of ^{121}Sb and ^{125}Te 2−75274
group V-VI-VII compound, Mossbauer effect of ^{121}Sb and ^{125}Te 2−75274
group VI chalcogenides, layer struct., optical props. 2−81334
hot electrons, effects of quantizing magnetic fields 2−57182
i.r. detector parameter uniformity in alloy semiconductors 2−52274
IV-IV cubic homopolar, magnitude of integrated i.r. absorption coeff. 2−75284
for light sources, incandescent and electroluminescent, electronic parameters 2−68439
liquids Hall effect, method of determ. 2−64469
magnetoresistance, longit., nonparabolicity contrib. at quantum mag. fields 2−64966
measurement methods for semiconductor materials, process control and devices 2−77908
melts, thermal cond., band struct. 2−60466
metal oxides, elec. cond. characts., classification 2−57106
micro and macrostructures, imperfections 2−61257
microwave magneto-Kerr effect 2−65215
mixed group III-V compounds, X-gap, nonlinear depend. on composition 2−61337
multilayer film, transport phenomena 2−51054
naphthalene electrons and holes interaction 2−80982
noncrystalline min. metallic cond., calc. 2−77888
organic, carrier drift mobility meas. 2−47905
organic, d.c. cond. mechanism 2−47904
organic, with narrow conduction based, soln. of kinetic eqn. 2−81011
organic, with narrow conductivity zones, electron-phonon interaction 2−77810
organic solid, density of states in bandgap 2−47916
phenol formaldehyde resin, thermal degraded, a.c. and d.c. cond. 2−47903
photography, appl. of semicond.-dielec. electrophotographic system 2−70090
piezoelectric, acoustoelec. effects at large sound intensities 2−61098
poly-N-vinylcarbazole complexed with trinitrofluorenone film, bulk recomb. of charge carriers 2−72073
polyazophenylenes, conductivity meas. 2−44118
polymers, Co chelate, of dihydroxyquinones, mag. moment and elec. resist., meas. 2−80815
polyphenylacetylene, electrical conductivity and ESR absorption 2−51127
polyvinylcarbazole, carrier drift mobility meas. 2−47905
precious metal pyrochlores, crystallographic, elec. and mag. props. 2−60987
profiled single crystals, instrument for meas. of specific resistivity with automatic compensation for geometrical factors 2−51158
pseudobinary alloy, phase diagrams and cryst. growth 2−47702
pyrene, photoelectret effect 2−81131
quinolinium $(TCNQ)_2^-$, electron localization 2−44110
radiation effects, conf. Albany, (1970) 2−47877
radiation effects, conf. opening address Albany, (1970) 2−47878
rare earth hydrides, electronic props. review 2−77899
rhodamine 6G amorphous film, carrier trapping, thermostimulated cond. study 2−54180
selenides, mol. transform. rel. to elec. resist. 2−47900
steel oxide layers, electronic props. rel. to substrate pitting susceptibility 2−57422
stilbene, elec. cond. in weak and strong elec. fields 2−77901
surface contamination, obs. 2−53748
switching phenomenon, contrib. of lateral thermal instability 2−61283
TCNQ complexes, hopping cond. 2−44109
TCNQ complexes, with quinolinium and triethylammonium, i.r. spectra, vibronic effects 2−81387
TCNQ salts, role of disorder rel. to electronic props. 2−64920
ternary group III-V compound, composition from surface photovoltage obs. 2−51220
tetracene, carrier drift mobility meas. 2−47905
tetracene, photovolt. current, anomalous temp. depend. 2−72075
tetracene films, investigation high and low conductivity stable states and switching 2−54181
thin bar, β-conductive signal, effect of surface recomb. velocity 2−51130
transition metal cpds., prep. and characteriz. 2−50571
transition metal germanide, elec. resistivity, temp. depend. 2−57175
triethylammonium-$(TCNQ)_2$ elec. cond., 77-355K, and metal-insulator transition 2−68410
trisiloxane film, electron beam polymerized, conductivity, photocond., and dielec. const. 2−47909
ZnSe, differential absorption spectrum on adsorption of molecules of donor-acceptor type 2−68651
Ag-naphthalene-Ag structures, electronic conduction in dark 2−57199
Ag halides, semiconducting analogues 2−81103
$AgGaS_2(Se_2)$, band struct., electrorefl. and absorpt. studies 2−75276

Semiconducting materials continued
$AgPO_3-X^{n+}(PO_3)_n$, $X^{n+}=Mg^{2+}$, Ca^{2+}, Sr^{2+}, Ba^{2+}, Pb^{2+}, Al^{3+} use for multichannel image convertors and amp. 2−68501
$Ag_2S(Se)$, efficiency criterion for thermogenerators 2−75158
Ag_2Se thin films, determ. of thermal activation energy for semiconducting phase, 40-120°C 2−53570
Ag_2Te, Hall coeff., elec. resist., thermoelec. power, at m.p. and to 1500 K 2−60495
n-Ag_2Te, Lorenz number, electron scatt. inelasticity obs. 2−84337
AlAs, cryst. growth, vapour phase 2−43511
AlAs, energy bands, relativistic APW calc. 2−81014
AlAs epitaxial layer, on GaAs, elec. props. and optical absorp. 2−71881
AlGaAs-GaAs heterojunctions, band filling process 2−47941
$Al_xGa_{1-x}As$-GaAs heterojunction, prep. by multiple layer liq. phase epitaxy 2−50482
$Al_xGa_{1-x}As$-GaAs n-p heterojunction, current flow during electrolum. 2−72438
$Al_{1-x}Ga_xAs$, optical electron-nuclear reson. 2−61695
AlGaAsP, solution growth, luminescence, stimulated emission, laser operation 2−45747
$Al_yGa_{1-y}As_xSb_{1-x}$-$GaAs_xSb_{1-x}$ double heterojunction laser, prep. and emission spectra 2−59184
$Al_{1-x}In_xP$, cryst. growth, vapour phase 2−43511
AlN, band struct. calc. 2−71925
AlSb, i.r. dispersion of second order electric susceptibilities 2−61581
AlSb band struct., critical point detn., wavelength modulation derivative spectroscopy obs. 2−48160
As-S-Te, vitreous, γ-ray induced cond. 2−54252
As-Se-Ge glass film, amorphous to crystalline state conversion by light irradiation 2−75077
As-Se-Te, vitreous, γ-ray induced cond. 2−54252
As-Se amorphous layers, carrier lifetime determ. 2−81088
As-Se glass, Ag doped, elec. props. 2−64975
As-Te-Ge-Se glass switching device, small signal behaviour 2−61376
As-Te-Ge-Si glass, thermal breakdown 2−61298
$As_xIn_{1-x}SeI$ vitreous compounds, x=1.00, 0.95, 0.90, 0.80, i.r. absorption, determ. of energy structure 2−78095
As_2S_3, amorphous, photoelastic consts. freq. depend., one-oscillator model 2−54383
As_2S_3, amorphous, refl. spectra, vibr., modes 2−61614
As_2S_3, vitreous, localized state distrib., Fermi level analysis from transient photocond. obs. 2−47913
As_2S_3 and As_4S_4 amorphous films, a.c. cond., temp. depend. 2−68392
$As_xSb_{2-x}Se_3$, amorphous and crysts., threshold and memory switching 2−77883
As_2Se_3-$As_2Te_3(Tl_2Se)(Sb_2Se_3)(As_2S_3)$ glass, e.s.r. and X-ray studies 2−61734
As_2Se_3, amorphous, a.c. cond, 30Hz-10.3GHz, ~180-500°C 2−81070
As_2Se_3, amorphous, refl. spectra, vibr. modes 2−61614
As_2Se_3, amorphous, Urbach tail in optical absorpt. edge 2−68641
As_2Se_3, glassy, high field cond. 2−68394
As_2Se_3, Hall mobility meas. by double a.c. technique 2−82415
As_2Se_3, liquid, switching, thermal breakdown mechanism 2−81096
As_2Se_3, vitreous, effects of group III A element dopant on physical props. 2−61300
As_2Se_3, vitreous, low temp. mag. susceptibility 2−54293
As_2Se_3, vitreous, polymeric struct. and energy spectrum 2−60590
As_2Se_3, vitreous, recombination centre nature 2−61686
As_2Se_3, vitreous and crystalline, electron energy spectrum, modulation spectroscopy obs. 2−61631
As_2Se_3, vitreous and monocryst., recomb. radiation mechanism 2−54451
As_2Se_3 amorphous film, a.c. cond., temp. depend. 2−68392
As_2Se_3 film, amorphous, charge transport, photocond. and dark current obs. 2−68393
As_2Se_3 films, amorphous, dark discharges 2−49458
As_2Se_3 glass, high field conductivity 2−51134
As_2Se_3 layers, carrier lifetime determ. 2−81088
$AsSe_{1.5}Sn_{0.28}$, pyroceramic, elec. cond. mechanism, 285-385K 2−75089
As_2Se_2Te film, switching and memory device, inc. neutron irrad. effects 2−61373
$As_2Se_3(Te_3)$ film, amorphous, trap-limited processes 2−61325
$As_2Se_3-xAs_2Te_3$, amorphous, elec. cond., Hall effect, and thermopower 2−77893
$3As_2Se_3.2Sb_2Se_3$ films, amorphous, elec. props., band struct. 2−54187
$3As_2Se_3.2Sb_2Se_3$ films, amorphous, band. struct., optical props. 2−54186
$1-xAs_2Se_3.xSb_2Se_3$ system, devitrification charact. 2−71286
As_2Te_3-As_2Se_3 glass, elec. cond. and switching 2−61299
As_2Te_3-Si glass system, electronically assisted thermal breakdown 2−61276
As_2Te_3, polycryst., threshold and memory switching 2−77883
As_2Te_3 film, amorphous, a.c. cond. rel. to localized tail states 2−61288
$As_{38}Te_{55}Ge_4Si_3$, $2As_2Se_3.As_2Te_3$, amorphous, minor switching and r.f. oscillations 2−61275
AsTeI glass, electronic transport 2−61296
As_2Te_2Se, thermalization in energy band tails 2−61685
B, crystalline, mag. suscept., comparison with amorphous like crystalline semicond. 2−77987
β-B, rhombohedral, carrier mobility in intrinsic cond. region 2−75090
BN, band struct. and optical props., pseudopotential calc. 2−61345
BN, energy spectrum and cryst. fine struct., X-ray studies 2−75026
BP, band struct. and optical props., pseudopotential calc. 2−61345
BP layers, vapour growth using open and closed tube processes 2−50486
$Ba(Ce_{1-x}Ta_x)O_3$ ion pair valency at high and low temps., structure mag. and electrical obs. 2−75203
BaO powder, recomb. luminesc., 103-423 K 2−61687
$Ba_xSr_{1-x}Nb_2O_6$, high 1/f noise anomaly 2−47888
$Ba_{1-x}Sr_xTiO_3$, mobility, gravimetric determ. 2−81086

Semiconducting materials continued
$BaTiO_3$-Bi_2O_3, La doped composite ceramic, two-step anomalous resistivity increase 2−68395
$BaTiO_3$, hopping model of d.c. elec. conductivity 2−68468
$BaTiO_3$, La doped, Bi_2O_3 grain boundary element, non-linear characts. 2−84366
Bi-Sb alloy, 5-100% Sb, Mossbauer effect of ^{121}Sb, 80K 2−81345
Bi-Sb alloy, band edge parameters, calc. 2−75027
Bi-Sb alloy, for magneto-thermoelec. and thermomag. cooling, props. 2−75161
Bi-Sb alloy, transport effects, effects of Ag, In and Pt addition 2−71896
Bi film, magnetoresistance as function of thickness 2−84332
BiI_3-Bi solutions, cond. mechanism 2−64472
BiI_3, localized states and electron-hole processes, photopolariz. and photoluminesc. obs. 2−61706
Bi_2S_3:Pb, capture level parameters, thermo-stimulated cond. study 2−71923
n-Bi_2S_3, Hall coeff. temp. depend. 2−44092
$Bi_{1-x}Sb_x$:Cd(In)(Sn), elec. props., (x=0-0.2), 180-420K 2−61301
BiSb, narrow band emission, nuclear electric quadrupole radiative transitions 2−78118
BiSb alloy, interband breakdown, voltage instabilities in electron-hole plasma 2−81095
$Bi_{92}Sb_{08}$, dc-pumped, line narrowing of microwave radiation caused by nuclear electric quadrupole transition in ^{209}Bi 2−44403
p-Bi_2Se_3, Hall and cond. mobilities, carrier compensation, galvanomag. effects, 4.2-300K 2−81076
Bi_2Te_3-Bi_2Se_3(Sb_2Te_3), efficiency criterion for thermogenerators 2−75158
p-Bi_2Te_3, low- and high-field galvanomag. props. 2−51135
p-Bi_2Te_3, second valence band, magneto-Seebeck and Shubnikov-de Haas obs. 2−61339
p-Bi_2Te_3, valence band struct., Shubnikov-de Haas oscills. of magnetoresist. 2−77805
p-Bi_2Te_3, valence bands, saturation and quantum oscill. in magneto-Seebeck effect obs. 2−81159
Bi_2Te_3 and alloys, for Peltier cooling, thermoelec. props., review 2−75160
C, soft pregraphitic, Hall coeff. depend. on heat treatment and doping 2−44113
C film, amorphous, elec. and optical props., and struct 2−61302
Cd_3As_2-2CdTe system, phase diagram 2−47708
$CdCr_2S_4$, red shift peak in absorpt. band, mag. F′ centre model 2−80712
n-$CdCr_2Se_4$:Ga, h.f. cond., freq. dispersion, Curie pt. phenomena 2−44095
$CdCr_2Se_4$ film, deposition and mag. props. 2−60649
CdF_2:Na^+(Ag^+)(Li^+)(La^{3+})(In^{3+})(Gd^{3+}), ionic thermocurrents, temp. depend. 2−81089
$CdGeAs_2$, liq., elec. cond., thermopower 2−60496
$CdGeAs_2$(P_2), i.r birefr. and optical activity 2−72261
$CdGeP_{2x}As_{2-2x}$, prep., struct., hardness and m.p. 2−47616
$CdGe_xSi_{1-x}P_2$, prep., struct., hardness and m.p. 2−47616
$Cd_{0.20}Hg_{0.80}Te$, photocond. oscillations in a magnetic field and photomagnetic effects 2−75169
$CdIn_2S_4$:Cr, cryst. growth, vapour transport method 2−71369
$CdIn_2S_4$, intrinsic and Co^{2+} doped, effect of S vacancies 2−68735
$CdIn_2S_4$ single crystal, photocurrent oscillations 2−75170
CdO electron concentration determ. using T activity 2−71934
CdO microcrystals, coupled surface phonon-surface plasmon modes, i.r. absorpt. 2−84263
Cd_3P_2-2CdSe system, phase diagram 2−47708
CdP_2, cathodolum. and photolum., recomb. mechanisms 2−72394
$Cd_xPb_{1-x}Se$ alloy, Hall coeff., Hall mobility, thermoelec. power, optical energy gap, 77-450 K 2−64977
CdS:Ag(Al), field quenching, influence of doping 2−54170
CdS:Cu, trapping parameters, photocond. response, i.r. quenching, photochem. effects 2−65000
CdS:In laser, spin flip, visible, operation at liq. He temps. 2−66768
CdS, acoustic wave attenuation, non-electronic lattice losses 2−43974
CdS, acoustoelectronic effects at large acoustic intensities 2−80915
CdS, bound-to-bound emission at 510 nm 2−61691
CdS, conductivity changes, O_2 chemisorption induced 2−47886
CdS, cyclotron reson. of piezoelec. polarons, far i.r. 2−71924
CdS, donor-acceptor luminesc., temp. depend. 2−48261
CdS, doped, 2.0 eV luminesc. band, donor-acceptor recomb. model 2−84539
CdS, electron-phonon interactions and current stabilization 2−47891
CdS, electron beam pumped laser, photon loss and gain 2−42077
CdS, electron concentration determ. using T activity 2−71934
CdS, electron energy loss spectra, rel. to interband transitions, bulk and surface plasmons 2−68318
CdS, electron irrad., stage III$_n$ recovery, activation energy 2−71455
CdS, electron spin-flip Raman scatt., 70-100KG at 4.2K 2−68658
CdS, exciton-impurity complex, optical absorp. anomalous intensity 2−72324
CdS, fast electron excitation, phonon assisted exciton recombination 2−48240
CdS, h.f. domain propagation, two-dimensional charact. 2−51156
CdS, in m.i.s.m. and m.s.i.m. structures, electron emission 2−57218
CdS, induced optical absorption by strong excitation 2−78097
CdS, mobility, maximum absorpt. freq. eval. expression 2−57176
CdS, multistep current saturation 2−75078
CdS, neutron activated, X-ray detector 2−42466
CdS, optical absorp., rel. to optical modulation due to moving acoustic domains 2−54418
CdS, optical modulation by acoustic phonon flux 2−61088
CdS, optical waveguide fabrication by Se diffusion 2−66842
CdS, paramag. surface centre density, e.p.r. obs. 2−65334
CdS, photocond., effects of 10 MeV electron irradiation 2−57254
CdS, photocond. spectrum, anisotropy 2−72060
CdS, photoconducting, acoustoelec. current, theory and expt. 2−54171
CdS, piezoelec. semicond., sound amplification threshold field non-monotonic cond. depend., 5-120 MHz 2−77783
CdS, Poisson and transport equations, high field domain solns. 2−54167

Semiconducting materials continued
CdS, production of super radiant light sources by electron beam pumping 2−79215
CdS, radiation from donor- acceptor pairs and phonic recurrence 2−72395
CdS, recomb. luminesc., effect of absorpt., recomb. and field mechanisms 2−78128
CdS, relax. oscill. induced by laser irrad. 2−64979
CdS, resonant interaction of LO phonon and donor electron 2−68278
CdS, self-diffusion of Cd, radiotracer study 2−83993
CdS, slow traps, optically pumped differential absorption apparatus 2−68427
CdS, spin-flip Raman scatt., linewidths and two-electron processes 2−84501
CdS, spin-flip scattering from free and bound electrons 2−44389
CdS, strain splitting of bound excitons 2−68678
CdS, temp. quenching of photocond., thermoelec. skin effect in presence of shallow levels 2−81171
CdS, thermal neutron damage, photolum. and elec. resist. 2−48219
CdS, u.s. absorption and dispersion, role of hopping conductivity 2−71733
CdS, valence band energy levels, Γ-point, from emission spectra due to A- and B-band excitons 2−68289
CdS, with Ag, Cu and In impurities, photocond., spectral sensitivity curves 2−72059
CdS acoustic wave mixing and amplitude dependent phase velocity 2−51032
CdS anode, electron injection 2−61797
CdS epitaxial film, optimum growth conditions 2−47105
CdS film, c-axis orientation modification, evaporation by reflection 2−50487
CdS film, electron mobility and scatt. rel. to grain boundaries and surfaces 2−61149
CdS film, electron scatt. by stacking faults rel. to elec. props. 2−61150
CdS film, Hall mobility, thickness depend., effects of Cu impurity 2−77894
CdS film, in polarized memory device, photovoltage obs. 2−61381
CdS film, liquid phase epitaxy 2−47104
CdS film, photocond., prolonged relax. of dark current after illumination 2−81173
CdS film, photocond. with gain in through thickness operation 2−44173
CdS film, photoelectret state formation and temp. depend. 2−77939
CdS film, photorectification in longitudinal quasi unipolar photocond. with non uniform illumination 2−81172
CdS film, sputter deposition and photocond. 2−53571
CdS films, shift in lux-ampere and I-V characts. due to photoelectret effect 2−81170
CdS high-field domains, propagation characteristics 2−61099
CdS phosphor, microwave photocond. and luminescence 2−51213
CdS photocell with non-linear characteristics, obs. of relative spectral sensitivity 2−42463
CdS platelets, drift meas., Schottky contact effects 2−77884
CdS semiconductors, dipole active exciton absorption, nonlinearity 2−44333
$CdS_{1-x}Se_x$:Mn, Mn^{2+} conc., e.p.r. determ. 2−72481
$CdS_{1-x}Se_x$:Mn^{2+}, hyperfine interaction const., temp. and comp. depend., e.p.r. study 2−81456
CdS(Se), hole photoemission into S, 2.11-3.54 eV 2−84265
CdS(Se), spontaneous and stimulated emission, exciton interactions 2−68677
CdS(Se), vapour growth, donor and acceptor identification 2−50573
$CdS_{1-x}Se_x$, reson. Raman effect 2−72365
CdS_xSe_{1-x} film, transmission, 7000-21000 cm^{-1}, band gap calc. 2−61633
CdS_xSe_{1-x} selective photoresistors for visible region 2−44172
CdS_xSe_{1-x}, free carrier optical absorption 2−75288
CdS(Se)(Te) films, a.c. photocond. on excitation with intensity-modulated light, trapping levels 2−57255
$CdS_{1-x}Zn_xS$:Mn, Mn^{2+} conc., e.p.r. determ. 2−72481
CdSb:Te, elec. cond. and Hall const., 78-293K 2−61307
CdSb, elec. props., effect of evaporation of Cd atoms 2−47890
p- CdSb, photoelectric props., conductivity anisotropy effects 2−57257
CdSe:Ag, impurity levels 2−51151
CdSe:Cu, a.c. photocond. in negative photocond. region 2−65081
CdSe-CdS film photoresistor, role of activating powder 2−65096
CdSe-Se n-p heterojunction, diffusion potential determ. 2−47942
CdSe-electrolyte blocking contact, photosensitivity and noise 2−72079
CdSe, conductivity changes, O_2 chemisorption induced 2−47886
CdSe, cryst. growth, static sublimation method 2−47217
CdSe, eff. of real growth on elec. and photoelec. props. 2−71419
CdSe, elec. behaviour between room temp. and 600C 2−61305
CdSe, elec. field distrib., subjected to 0-600 V applied voltages 2−64960
CdSe, electron energy loss spectra, rel. to interband transitions, bulk and surface plasmons 2−68318
CdSe, emission spectra under laser excitation, exciton interactions, exciton molecules formation 2−77840
CdSe, exciton-ionized donor complex, binding energy, theory and expt. 2−84266
CdSe, exciton bound to ionized centre, magneto-optical obs. 2−68636
CdSe, exciton scatt. by dislocations, absorpt. study 2−81007
CdSe, impure, multiphoton luminesc. satellites in strong e.m. field 2−61679
CdSe, l.f. noise, obs. 2−51136
n-CdSe, magnetophonon spectroscopy study 2−68385
CdSe, memory and photocond., 77 and 300K 2−75168
CdSe, paramag. surface centre density, e.p.r. obs. 2−65334
CdSe, photocond., undamped oscillations 2−54253
CdSe, photoconducting, effect of traps on acoustoelec. props. 2−61100
CdSe, resonant interaction of LO phonon and donor electron 2−68278
CdSe, room temp. hole and electron drift velocity, time of flight obs. 2−61306

Semiconducting materials continued
CdSe, temp. quenching of photocond., thermoelec. skin effect in presence of shallow levels 2−81171
CdSe anode, electron injection 2−61797
CdSe film, effect of O_2 and N_2 on Hall and field effect mobilities 2−57191
CdSe film, elec. props. rel. to substrate temp., 25-200°C 2−64980
CdSe film, photoelec. props. 2−57253
CdSe film, photoelectronic props. 2−51212
CdSe films, influence of Se vapour annealing on electrical conductivity 2−44094
CdSe films vacuum deposited, Hall mobility 2−83868
CdSe laser crystal, electron excited, photocurrent and light emission obs. 2−77965
CdSe powders, Cu, Cl_2 impurities, negative resistance behaviour, effects of light intensity, frequency variations 2−71919
CdSe(Te), high temp. defect equilib., elec. transport props. 2−44096
$CdSe_xTe_{1-x}$, exciton reflection spectra and absorp. edge obs. 2−84517
$CdSiAs_2$, i.r. birefr. and optical activity 2−72261
$CdSi_xGe_{1-x}As$, glassy, photocond. and elec. cond., rel. to band struct. determ. 2−61448
$CdSiP_2$, cryst. growth and struct., optical props. and energy gap 2−80599
$CdSnAs_2$, $CdSnP_2$, band structure, electroreflectance spectra obs. 2−81404
n-Cd_2SnO_4, optical and elec. props. 2−51137
$CdSnP_2$:Ag(Cu), spontaneous- and stimulated- emission spectra 2−51365
$CdSnP_2$, current controlled negative resist. due to Gunn effect 2−61304
$CdSnP_2$, photocunductivity spectra in extrinsic (impurity) range, and effects of doping 2−57256
$CdSnP_2$, stimulated emission, Coulomb interaction 2−61681
CdTe:In, Cu, high temp. cond., impurity effects 2−61303
CdTe:In, self-compensation calc. assuming Cd vacancies and impurity-vacancy complexes 2−47889
CdTe:Li, self-compensation and interaction of Li with defects 2−75107
CdTe, absorpt. spectra, direct exciton transitions 2−65255
p-CdTe, annealing effect on conductivity and photoconductivity, obs. 2−61263
n-CdTe, bending producing 60° dislocations, effect on conductivity and photoconductivity 2−61264
CdTe, compensation by intrinsic point defects, elec. cond. obs. 2−84334
CdTe, electroabsorpt., light quanta with energy less than forbidden bandwidth 2−78059
CdTe, electron energy loss spectra, rel. to interband transitions, bulk and surface plasmons 2−68318
CdTe, electron radiation damage and cathodolum. edge emission 2−48254
CdTe, epitaxial growth, on CdS, closed-tube chem. transport technique 2−77498
CdTe, growth from soln. melts, elec. props. 2−74677
CdTe, hole transport, taking into account polar scatt., Monte Carlo study 2−64968
CdTe, i.r. absorpt. spectra, shallow donor impurity transitions, polaron Zeeman effect 2−61634
CdTe, ion implantation doping 2−74790
CdTe, mag. susceptibility of defects, 4.2-290K 2−77980
CdTe, phase equil. considerations in prep. and props. 2−50593
CdTe, Poole-Frenkel effect of holes 2−44119
CdTe, radiation effects, carrier conc., Hall mobility, photocond. 2−47892
CdTe, thermal cond. and phonon scatt. by Fe^{2+} impurities 2−84213
CdTe, thermal neutron damage, photolum. and elec. resist. 2−48219
CdTe epitaxial film, optimum growth conditions 2−47105
p-CdTe film, photolum. and photocond. 2−48217
CdTe film, with anomalously high photovolt., photomag. effect 2−75178
CdTe room-temperature radiation detector possibilities 2−52692
CdYe, naturally doped p-n structs. 2−84349
$Cd_{2.8}Zn_{0.2}As$, high mobility, scattering, galvanomagnetic effects study 2−81090
$Cd_{1-x}Zn_xS:Mn^{2+}$, hyperfine interaction const., temp. and comp. depend., e.p.r. study 2−81456
$Cd_xZn_{1-x}S$ film, prep. and comp. depend. of energy gap and resist. 2−54169
Cds, cathodolum., donor-acceptor pair emission, electron irrad. damage effects 2−54478
$CoCr_2S_4$, cryst. growth, by chem. vapour transport 2−71371
CoP_2, high-press. synthesis and props. 2−83899
CrSi, energetic electron band and parameter calc. for normal and narrow band models 2−77797
$CrSi_2$ thermoelectric props. and crystal growth 2−84370
CuBr, X-ray K emission bands, valence electron obs. 2−68672
$CuCr_2Se_4$, galvanomag. props., 100-650K 2−81091
$CuGa_{1-x}In_xS_2$, soln. growth using In solvent 2−74679
$CuGaS_2$, soln. growth using In solvent 2−74679
CuI, emission under high density excitation 2−72397
$CuInSe_2$, transitions from Cu of levels in valence band 2−80974
$CuInTe_2$, band struct., refl., absorpt. and theoretical studies 2−78098
CuO, electronic prop. rel. to catalytic activity 2−75093
Cu_2O, 1s exciton state in green series 2−72327
Cu_2O, elec. cond. and photomemory effects 2−75091
Cu_2O, elec. conductivity, relationship in samples annealed at various temp. to activation energy 2−75092
Cu_2O, exciton luminesc., effect of absorpt., surface annihilation of excitons 2−78129
Cu_2O, near i.r. absorpt. and photocond., band scheme interpretation 2−54420
Cu_2O, photocond., spectral depend., oscills., up to 180 K 2−77963
Cu_2S-CdS heterojunction, photocapacitance effects 2−51221
Cu_xS-CdS photovoltaic cell, model 2−54261
CuS, supercond. transition temp. obs. 2−51112
$Cu_{2-x}S$, refl. and absorpt., 400-1200 nm 2−78085
$Cu_{2-x}S$ film, on NaCl, deposition and phase struct. 2−60653

Semiconducting materials continued
$Cu_2S(Se)(Te)(Te_xS_{1-x})$, efficiency criterion for thermogenerators 2−75158
Cu_2Se, $\alpha \rightarrow \beta$ phase transform 2−64811
Cu_2Te-Ag_2Te systems, regions of metallic, semimetallic and semiconducting behaviour 2−84323
CuTe, band struct., reflection spectra obs. 2−72301
Cu_2Te, carrier effective mass, reflection spectra obs. 2−84520
Cu_xTe, thermal e.m.f., electronic and ionic cond. at 400°C, composition 2−54247
diode, vapour grown, bright electroluminesc. and orange laser emission 2−49386
$Eu_{1-x}Gd_xO$, metal-nonmetal transition 2−71899
EuO:Gd, bidirectional threshold and memory type switching 2−81081
EuO:Gd, plasma resonance and lattice vibrations, dopant mechanism 2−68397
EuO, doped, metal-semiconductor transition 2−77842
EuO, insulator-metal transition and bound mag. polarons 2−80975
n-EuS, elec. resist. and Hall effect, 140 kOe, Curie pt. phenomena 2−47895
EuS, slightly Eu rich, systematics of conduction in band tail 2−75094
Eu_3SiO_5, prep. and phys. props. 2−48173
55Fe-45P_2O_5 glass, a.c. and d.c. characteristics, correlation with structure 2−81142
$FeAs_2$, diamag. semicond., band gap, band model 2−61340
$FeCr_2S_4$, cryst. growth, by chem. vapour transport 2−71371
α-Fe_2O_3, d.c. cond. and Fe diffusion, high temp. 2−51138
Fe_3O_4, high temp. polaronic semicond. i.r. reflectivity obs. 2−61265
$Fe_{1-x}S$, semicond. uniaxial ferroelectric, phase diagram 2−77957
$FeSb_2$, and mag. props., band model 2−61340
FeSi, energetic electron band and parameter calc. for normal and narrow band models 2−77797
$Ga_xAl_{1-x}As$-GaAs p-n heterojunction, field effect of GaAs photolum. 2−72399
GaAlAs, close confinement laser diodes using, structure, performance, applications 2−82490
GaAlAs injection laser materials, application to moderate power i.r. laser diode array light sources 2−82491
$Ga_{1-x}Al_xAs$, indirect gap, direct band recombination, electroluminesc. obs. 2−75337
n-$Ga_{1-x}Al_xAs$, metal-semicond. surface barrier struct., energy band diagram 2−75134
$Ga_{1-x}Al_xAs$, pseudobinary system, solidus boundary, thermodynamic analysis 2−50968
$Ga_{1-x}Al_xAs$ alloys, resonant impurity-assisted tunnelling 2−71981
n-$Ga_{1-x}Al_xAs$ epitaxial film, edge photoluminesce, free exciton annihilation contrib. 2−81432
$Ga_{1-x}Al_xAs$ light emitting diode, epitaxial growth on GaP substrates 2−51388
$Ga_xAl_{1-x}As$ heterostructure injection laser, construction and performance 2−42094
GaAs/GaAlAs, mesa stripe geometry double heterostruct. injection laser, very low current operation 2−42093
GaAs-AlAs, solid solution heterojunction injection laser, 7400-9000 Å range 2−73596
GaAs-$Ga_{1-x}Al_x$ single heterostructure laser, interferometric obs. of thermal elongation 2−42095
GaAs-GaAlAs layered structs., current-voltage characts., transport props. 2−68399
GaAs-(AlGa)As cold cathode, structure, factors affecting extended operation 2−48012
GaAs, layer compound, valence electron density and band struct. 2−81016
GaAs laser, injection future prospects 2−42099
$GaAs_{1-x}P_x$:SeTe, donor self- compensation 2−75110
GaAsP wafers, photoluminescence obs. using scanned laser microscope 2−55706
$GaAs_{1-x}P_x$, p- and n-type, direct and indirect gap, photoluminesc. spectra 2−84538
$GaAs_{1-x}P_x$ alloys, resonant impurity-assisted tunnelling 2−71981
$Ga_{0.6}In_{0.4}As$/Cs, photoemissive yield, phonon energy loss effects 2−61460
n-$Ga_xIn_{1-x}As$ alloy, effective mass compositional depend., sub mm. cyclotron resonance obs. 2−64982
$Ga_{1-x}In_xN$, fundamental absorpt. edge and energy gap 2−72329
$Ga_xIn_{1-x}P$ alloy, band structure, electroreflectance obs. 2−61641
$GaInS_3$, thermally stimulated cond., dark current, capture levels 2−75162
$Ga_{2x}In_{2(1-x)}S_3$ thermostimulated cond. 100-350K 2−84317
GaN, band struct. calc. 2−71925
GaN, conductivity type determ. using rectifying contacts 2−68428
GaN, cryst. growth, vapour phase 2−43511
GaN, fundamental absorpt. edge and energy gap 2−72329
GaN epitaxial layers, carrier conc., electron mobility 2−50495
GaP: Zn, Al, photolum. and electrolum., 1.7 to 2.3eV 2−75321
p-GaP:Cu,O, bound exciton luminesc., emission and excitation spectra 2−78131
GaP:Ge, e.p.r., linewidth and g-value 2−72484
GaP:N, null field splitting of B-line 2−61692
GaP:N(Bi), exciton binding to impurities, uniaxial stress effects 2−75108
GaP:O p-n junction, deep double electron O trap transitions, photocapacitance obs. 2−75013
GaP:Sb, recomb. radiation involving isoelectronic centres 2−72407
GaP:Sn, strain-depend. e.p.r. and spin-valley coupling of donors 2−84570
n-GaP:Te,Zn,O, electrolum., mean electron conc., influence of Te content 2−57381
GaP:Zn, O, light emitting diode, efficiency shift under forward bias 2−75181
GaP:Zn, red electrolum. diode, prep. 2−44424
p-GaP:Zn,O, donor electron capture cross sections, rel. to quantum efficiency limits 2−68681
GaP:Zn,O, luminesc. time response rel. to multiple trapping at Zn-O impurity centres, 4-120K 2−61696
p-GaP:Zn,O, photolum. efficiency and kinetics of Zn-O complex formation 2−51368

Semiconducting materials continued
p-GaP:Zn,O, recomb. of electrons bound to deep neutral donors and acceptors 2−68682
GaP-GaAs alloy, epitaxial growth on GaAs, by pyrolysis of $Ga(CH_3)_3$, AsH_3 and PH_3 2−50496
GaP-GaAs film, comp., effects of deposition conditions 2−60657
GaP-GaAs heterojunction, prep. by multiple layer liq. phase epitaxy 2−50482
GaP-GaAs mixed crystal, multiphonon Raman scatt. 2−68659
GaP-GaAs p-n heterojunction, field effect of GaAs photolum. 2−72399
GaP-ZnSe alloy, cond. hopping contrib., ionized impurity scatt., electrolum. and cathodolum. 2−81415
GaP, amorphous, absorption edge temp. depend. 2−75293
GaP, amorphous, band struct., optical props. pressure effects obs. 2−61333
GaP, band struct., X-ray photoemission study 2−84387
GaP, bond struct., critical point detn., wavelength modulation derivative spectroscopy obs. 2−48160
GaP, chem. shift in binding energies of Zn and Cd 2−65001
GaP, conductivity type determ. using rectifying contacts 2−68428
GaP, core levels, spectral obs. 2−65240
GaP, crystal growth, open flow quartz systems, Si contamination 2−43529
GaP, cyclotron resonance of holes 2−75041
GaP, diffuse reflection spectra, energies of E_1, E_0' and E_2 peaks 2−75275
GaP, donor-acceptor pairs, config. interaction 2−84260
GaP, electrically active background impurities, energy conc. and distrib. determ. by thermal release of space charge 2−80939
GaP, electron-hole pair form. by irrad. with α-particles, form. energy 2−71808
GaP, electron mobility theoretical calc. 2−77889
GaP, energy gap, temp. depend., calc. using Brooks-Yu theory 2−68415
GaP, epitaxial growth and electrical props. 2−47111
GaP, green electrolum. efficiency, weak photolum. band 2−84548
GaP, growth defects, S-pits, luminesc. efficiency 2−50595
GaP, i.r. dispersion of second order elec. susceptibilities 2−61581
GaP, impact ionization of carriers, energy conservation considerations 2−75081
GaP, ion implantation of S, junction form. 2−47429
GaP, ionicity, dispersion, and optical spectra 2−44374
GaP, liq. encapsulated growth from non-stoichiometric melts 2−47268
n-GaP, metal-semicond. barrier obs., surface levels detn. 2−84352
GaP, pair photolum., peak energy, excitation intensity depend. 2−75318
GaP, physics of radiative centres 2−61724
GaP, soln. growth, for red emitting diode manufacture 2−60711
GaP, switches, p-n-p-n, controlled rectifiers, blocking voltages, electrolum., $0 \leqslant T \leqslant 500C$ 2−61392
GaP, wavelength modulated refl. spectra, band struct. 2−61616
GaP evaporation by laser, mass-spectrometric analysis of ions in vapour 2−75409
GaP light emitting diode, props. for green and red emission, quantum efficiencies 2−44418
GaP p-n-p-n green light emitting diode, fabrication and characts. 2−72436
GaP p-n junction growth by liq. phase epitaxy 2−47287
GaP red-emitting diodes, scanning electron microscope characteriz. 2−51389
GaP(Cs) dynode photomultipliers, electron optics and time broadening 2−49677
GaP(Cs) dynodes photomultipliers, performance and characteristics 2−49678
p-GaP(Zn,O), p-GaP(N), minority carrier lifetime, luminesc. decay time obs. 2−48221
GaS, direct interband transitions, low energy photoemission spectra 2−51225
GaS, surface electronic props. detn. 2−65106
β-Ga_2S_3, photolum. and photocond. 2−84532
GaSb:Te, lightly doped, photolum. at high excitation levels 2−72402
GaSb:Te, segregation coeff. of Te 2−74798
GaSb:Te,Zn, thermal e.m.f. rel. to carrier conc., 300K 2−54248
GaSb:Te(Zn)(Te + Zn), heavily doped, photolum. at high excitation levels 2−72403
GaSb/Cs-O, photoemissivity yield, energy distrib. 2−44205
GaSb/Cs, photoemissive yield, phonon energy loss effects 2−61460
GaSb-GaAs system, phase diagram, thermodynamic analysis 2−44086
n-GaSb-Pb contact, tunnelling spectroscopy and band struct. press. effects 2−84351
p-GaSb, Auger recomb. of excess carriers, spin split off band effect 2−81067
GaSb, band struct., critical point detn., wavelength modulation derivative spectroscopy obs. 2−48160
n-GaSb, cond. band parameters from high-temp. transport meas. 2−57206
n-GaSb, conduction band minima energy separation temp. depend., p-n junc. tunnelling current obs. 2−75109
GaSb, core levels, spectral obs. 2−65240
GaSb, diffusion of Zn, temp. and cond. depend., radioactive tracer obs. 2−74799
p-GaSb, doped, heavy/light hole mobility ratio 2−81063
GaSb, doped with nonmag. impurities, negative magnetoresist. 2−68323
GaSb, energy gap, temp. depend., calc. using Brooks-Yu theory 2−68415
GaSb, heavily doped, phonon scatt., thermal cond. obs. 2−47765
GaSb, i.r. dispersion of second order electric susceptibilities 2−61581
GaSb, Landau levels at saddle point, diff. reflectivity in mag. field obs. 2−71795
GaSb, Landau transition at E_1 edges, excitonic effects 2−68404
GaSb, photoelectromag. effect in quantizing mag. field 2−68484
GaSb, piezoemission, stress effects on impurity and bound exciton lines 2−48179
GaSb, radiation damage, review 2−47365

Semiconducting materials continued
GaSb, transition metal doped, anomalous elec. and mag. props. 2−68405
p-GaSb, undoped, acceptor states and excitons, photocond. and photoluminesc. obs. 2−61708
GaSb, variation of energy bands with hydrostatic pressure 2−61393
n-GaSb(Te), galvanomag. props. rel. to hydrostatic press. at 4.2K 2−68400
GaSe, band struct., pseudopot. calc. 2−61341
GaSe, exciton absorpt. peak shift and phase change induced by hydrostatic press. 2−72330
GaSe, Faraday effect in exciton absorpt. region 2−72263
GaSe, interband Faraday effect 2−72262
GaSe, luminesc. of free and bound excitons, 4.2 and 1.8K 2−72406
GaSe, optical consts. anisotropy near band edge 2−48178
GaSe, surface electronic props. detn. 2−65106
GaSe, under two-photon excitation, stimulated emission 2−72405
GaSe, vapour growth and morphology 2−50574
Ga_2Se_3, i.r. refl. spectra at 290K, phonon freqs. and dielec. consts. 2−75279
Ga_2Te_3-Cu system, phase diagram and elec. props. 2−47715
GaTe, forbidden band width and exciton binding energy, optical absorp. obs. 2−75294
GaTe, surface electronic props. detn. 2−65106
$Ga_{1-x}Te_x$ alloy, liq., n.m.r., Knight shift, mag. relax., quadrupole relax., Fermi level 2−60512
Ga_2Te_3, radiation stability as result of stoichiometric vacancies 2−71906
A-Gd_2S_3, crystal growth from gaseous phase, physical properties 2−53607
Ge-Cr film, amorphous, hopping cond. 2−61313
Ge-Se-Sn system glasses, chem. comp., struct. units, Mossbauer obs. 2−43452
Ge-Se glass, microphase separation effect on elec. conductivity 2−60592
Ge-Te-As glass, high current density path shape 2−57193
$Ge_{10}As_{20}Te_{70}$, amorphous, electrical/thermal/optical properties 2−61262
dualGe(Li)-dual NaI(Tl) gamma ray spectrometer 2−63688
GeO, layers, defective, hopping cond., elec. cond., 77-453 K, 20-100 MHz 2−54173
$GeS_2(Se_2)(Te_2)$, refl., 1-12.5 eV, rel. to band struct. calc. 2−48161
GeS(Te), refl., 1-12.5 eV, rel. to band struct. calc. 2−48161
GeSe, liq., Hall effect 2−60498
$GeSe_2$, cryst. growth, Czochralski pulling 2−50597
$GeSe_2$, liquid, switching, thermal breakdown mechanism 2−81096
$Ge_{15}Se_{85}$ Hall mobility meas. by double a.c. technique 2−82415
$GeSe_{(2)}$(Te), cryst. growth and morphology 2−50575
$Ge_{1-x}Si_x$, indirect phononless optical transitions, wavelength modulated absorp. obs. 2−68640
GeTe-SnTe alloy, epitaxial film, twinning faults 2−53574
GeTe, amorphous, Urbach tail in optical absorpt. edge 2−68641
GeTe, amorphous and polycryst., electronic struct., photoemission and reflectivity obs. 2−61465
GeTe, efficiency criterion for thermogenerators 2−75158
GeTe, supercond props. 2−51114
GeTe epitaxial film, twinning faults 2−53574
Ge_xTe_{1-x} alloy, amorphous, energy level scheme, optical and electrical obs. 2−77904
$Ge_{15}Te_{80}As_5$ glasses, thermally induced surface and bulk electrical effects 2−68401
$Ge_{15}Te_{81}X_4$, amorphous, memory device model 2−61375
$Ge_{15}Te_{81}X_4$, X=Ga, P, As, switching glass, n.m.r. 2−61752
p-$Hg_{1-x}Cd_xTe$, carrier freeze-out and acceptor energies determ. 2−57194
$Hg_{1-x}Cd_xTe$, sweep out of minority carrier holes 2−54255
HgI_2 room-temperature radiation detector possibilities 2−52692
HgI_2 single crystal, tetragonal, exciton luminesc., temp. depend. 2−84541
HgS, hole photoemission into S, 2.11-3.54 eV 2−84265
$HgS_{0.2}Se_{0.8}$ solid soln., plasma i.r. reflection at 100 and 300K 2−54404
HgSe, HgSe-HgS solid solution, optical absorption, energy band struct. obs. 2−84522
HgSe, $\Lambda_3-\Lambda_1$ transition, electrorefl. 2−68624
HgSe, Shubnikov-de Haas effect, effect of uniaxial stress 2−68402
Hg_3Te_3-Ge_2Te_3 alloy, transport processes, Hall mobilities, near semimetal-semicond. transition at high press. 2−68406
Hg_3Te_3-In_2Te_3 alloys, h.p. phases, cond. types, band struct. 2−54175
HgTe, galvanomag. props. in high mag. field, 4.2, 77 and 300 K 2−64988
HgTe, Hall coeff. and self-conc. of carriers 2−61314
n-HgTe, pure, i.r. and magnetooptical absorp. 2−78101
HgTe films, temp. dependence of Hall coeff. and electrical conductivity 2−54174
In-Te alloy, molten, elec. cond. and thermoelec. power 2−77446
In-Te system, films, phase comp. and band struct of In_2Te_3 2−60662
InAs-ZnTe heterojuction, prep. by liq. phase epitaxy, optical and elec. props. 2−57213
p-InAs, ang. distrib. of photoemitted electrons, mag. field determ. 2−51226
p-InAs, Auger recomb. of excess carriers, spin split off band effect 2−81067
InAs, band struct., X-ray photoemission study 2−84387
n-InAs, compensated, absorpt. edge obs. 2−75297
InAs, core levels, spectral obs. 2−65240
InAs, energy gap, temp. depend., calc. using Brooks-Yu theory 2−68415
n-InAs, heavily doped, impact ionization, elec. field depend. 2−81087
InAs, helicon wave propagation in magnetic fields up to 200 kG 2−47910
InAs, i.r. dispersion of second order elec. susceptibilities 2−61581
n-InAs, photolum., 77-200K, temp. effects 2−72412
n-InAs, thermoelec. power in quantizing mag. fields 2−84372
$InAs_{0.4}P_{0.6}$/Cs-O i.r. photocathode, wavelength depend. of Cs-O optimum thickness 2−68498

Semiconducting materials continued
$InAs_{0.4}P_{0.6}$, cathode, negative electron affinity, photoemission rel. to Cs-O layers thickness 2−75194
$In_xGa_{1-x}As$, vapour growth, equilib. calc. 2−47222
$In_{1-x}Ga_xP$, solution growth, luminescence, stimulated emission laser operation 2−45747
$In_{1-x}Ga_xP$ p-n junction, bright yellow luminesc. 2−44425
$In_{1-x}Ga_xP$, cryst. growth, vapour phase 2−43511
$In_{1-x}Ga_xP$ alloys, resonant impurity-assisted tunnelling 2−71981
$In_xGa_{1-x}P$, vapour growth, equilib. calc. 2−50576
InN, fundamental absorpt. edge and energy gap 2−72329
InP, [110] surface Brillouin zone, intrinsic localized states, calc. 2−65007
p-InP, Auger recomb. of excess carriers, spin split off band effect 2−81067
InP, band struct., critical point detn., wavelength modulation derivative spectroscopy obs. 2−48160
InP, bound exciton photoluminescence spectra 2−57373
InP, core levels, spectral obs. 2−65240
InP, electron transfer 2−61315
InP, energy gap, temp. depend., calc. using Brooks-Yu theory 2−68415
InP, excitonic recomb. and photocond. 2−72410
InP, free and bound electron transitions to acceptors, 1.3776 eV emission 2−72411
InP, group IV doped, cryst. growth, luminesc., donor and acceptor levels 2−47272
InP, high resistance, doped with Cu, Fe or Cr, preparation aid props. 2−83895
n-InP, high resistivity, i.r. quenching of photocond. 2−75173
InP, i.r. dispersion of second order elec. susceptibilities 2−61581
InP, impure, multiphoton luminesc. satellites in strong e.m. field 2−61679
n-InP, magnetophonon spectroscopy study 2−68385
InP, n-type, electroreflection spectrum under depletion and enhancement conditions in surface layer 2−81433
InP, photoluminesc. of bound excitons 2−68685
InP, photoluminesc. of excitons bound to neutral acceptors, strain effects 2−48223
n-InP, photon replicas in the induced luminescence spectra under the conditions of two photon excitation 2−81429
n-InP, velocity-field charact., calc. 2−71912
InP, wavelength modulated refl. spectra, band struct. 2−61616
In_2S_3, thermostimulated cond. 100-300K 2−84317
n-InSb, uniaxial stress, obs. of tunable component in spectrum 2−82488
In_2Se_3-Sb_2Te_3 system, phase diagram, intermediate cpd. formation 2−61048
InSe, absorpt., 300K and 70K, 2.3 to 3.0 eV, hyperbolic excitons 2−81398
InSe, exciton-phonon interaction, absorption edge obs. 2−84518
n-InSe, rapid recomb. centres, during laser beam excitation 2−72063
$In_2Se(Te)$, molten, elec. cond. and thermoelec. power, temp. depend. 2−67837
In_2Te_3-Cu system, phase diagram and elec. props. 2−47715
In_2Te_3-Hg_3Te_3 alloy, negative magnetoresist., 77-400K 2−44102
InTe, supercond. props. 2−51114
In_2Te, refl., 1-12.5 eV, rel. to band struct. calc. 2−48161
In_2Te_3, radiation stability as result of stoichiometric vacancies 2−71906
$InTe_{0.5}Se_{0.5}$, molten, elec. cond. and thermoelec. power, temp. depend. 2−67837
InTlSe(Te), molten, elec. cond. and thermoelec. power, temp. depend. 2−67837
InaS, band struct., critical point detn., wavelength modulation derivative spectroscopy obs. 2−48160
K complex, $K_2Pt(CN)_4Br_{0.3}.xH_2O$, electron localization 2−44110
$K_{0.3}MoO_3$, blue phase, semicond. to metal transition, elec. cond. 2−61151
$K_2Pt(CN)_4Br_{0.3}\times 2.3H_2O$, one-dimensional conductivity, defect effects 2−68339
La_3Se_4, supercond props. 2−51114
Li alloy, liq., e.s.r., spin flip processes 2−60510
$Li(NH_3)_4$, carrier mobility, Hall effect, magnetoresist., thermoelec. power obs. 2−47894
Mg-Bi amorphous alloy, exciton screening 2−78115
Mg-Sb amorphous alloy, exciton screening 2−78115
n-Mg_2Ge, Hall mobility, magnetoresist., transport mechanisms 2−51143
MgO, elec. cond. and migrational polarization, 800-1300°C 2−81065
$Mg_xPb_{1-x}Se$ alloy, Hall coeff., Hall mobility, thermoelec. power, optical energy gap, 77-450 K 2−64977
Mg_2Sn pressure dependence of electrical resistance 2−84326
n-MgTe, interband magnetoabsorpt., $\Gamma_6\rightarrow\Gamma_8$, transmission obs. at 4.4K 2−68644
MnO:Li, electro-transmission in visible and near i.r., charge carrier obs. 2−51323
MnS, photocond. spectrum, room temp. 2−68480
α-MnS from sulphurization of Mn in H_2S-H_2 gas mixtures at 550° to 711°C, elec. cond. and thermoelec. power, obs. 2−75079
MnSi energetic electron band and parameter calc. for normal and narrow band models 2−77797
MnTe, cryst. growth from nonstoichiometric melts by liq. encapsulation 2−50598
MoO_3, ion bombardment enhanced elec. cond. 2−68408
MoS_2, composite exciton absorpt. spectrum, optical phonon effects 2−44377
MoS_2, layer-type 2H-polytype, electronic band struct. 2−47914
MoS_2, layer semicond., magneto-optical interband absorp., energy band model 2−81333
MoS_2 layer struct., contact annealing effect on Hall data 2−54177
MoS_2 layer structures, a.c. conductivity in high and low frequency limit 2−81062
$MoTe_2$, composite exciton absorpt. spectrum, optical phonon effects 2−44377
$MoTe_2$, reflectivity, optical consts. Brillouin zone transitions 2−48162
NaI(Tl) scintillation detector, 6″×4″, empirical formulae for calc. of full energy peak efficiency 2−42458

Semiconducting materials continued
NaI(Tl) thin crystals, Monte Carlo calc. of pulse height response to protons of energy less than 100 keV 2−49686
$Na_xV_2O_5$, elec. cond., n-type semicond. and ionic cond. props. 2−83795
α'-$NaV_2O_{5-x}F_x$, $0\leqslant x\leqslant 1$, d electron distrib. on V atoms, from elec. and mag. props. 2−75080
$NbSe_2$, 2H-type, Fermi surface 2−65002
Nd_2O_3, p- and n-type behaviour rel. to press. 2−44103
$Ni_{0.6}Mn_{2.4}O_4$, elec.-field-depend. cond. for hopping-type charge transport 2−81082
NiO:Li, electro-transmission in visible and near i.r., charge carrier obs. 2−51323
NiO, bound polaron hopping 2−47899
NiO, high temp. transport props. 2−84314
NiO, thermoreflectance, band transition assignment 2−44368
NiS, hexagonal, heat capacity and metal-nonmetal transition 2−47754
NiS_2, band model, opt. absorpt. and elec. conductivity obs. 2−68417
NiS_2, conductivity and optical absorp. obs. 2−81020
Pb-Sb-S system, amorphous like crystalline semicond., mag. suscept., comparison with B 2−77987
$PbBr_2$, pure and doped, hole cond., defect chem. 2−61322
$PbCrO_3$, perovskite, struct., elec. resist., mag. susceptibility 77-550K 2−61321
$Pb_{1-x}Ge_xTe$, lattice const., and phase transform. 2−84108
PbI_2, band edge excitons, refl. study 2−68626
PbI_2, band struct. computation and optical absorp. spectra 2−68418
PbI_2, conductivity changes, O_2 chemisorption induced 2−47886
PbO-Al_2O_3-SiO_2-B_2O_3 glass, between metal electrodes, memory effect 2−71915
PbO, autocompensated photoconductor, inversion of the sign of conductivity 2−44175
PbS, paramag. surface centre density, e.p.r. obs. 2−65334
PbS quantum yield of internal photoelec. effect and impact ioniz. 2−72065
PbS(Se)(Te), mech. props., carrier conc. effect 2−50784
PbSe, band struct., absorp. edge and intraband transition region obs. 2−81402
N-PbSe, elec. effective mass and relaxation time, reflectivity and magnetoreflectivity obs. 2−61651
PbSe, Faraday effect, free carrier dependence 2−84469
PbSe, solid and liq. thermal cond. up to 1500K 2−68259
PbSe expitaxial films on NaCl substrate, effect of ambient gases on electrical properties 2−65008
PbSe n and p type anisotropy of cyclotron and spin mass 2−80984
n-PbSe(Te), hot-electron cond., velocity-field characts., 77 and 4.2K 2−68407
$Pb_{0.8}Sn_{0.2}Te$, epitaxial film, photocond. 2−65085
n-$Pb_{1-x}Sn_xTe$, hot-electron cond., velocity-field characts., 77 and 4.2K 2−68407
$Pb_{1-x}Sn_xTe$, i.r. plasma refl. study 2−84504
$Pb_{1-x}Sn_xTe$, reflectivity, optical consts., energy band struct. 2−48164
$Pb_{1-x}Sn_xTe$ alloy, crystal growth, carrier conc. 2−53618
PbTe:In, donor level above the bottom of the cond. band 2−84281
p-PbTe-PbSe alloys, thermoelec. props., temp. depend. 2−75164
PbTe-UTe system, phase diagram 2−47717
PbTe, efficiency criterion for thermogenerators 2−75158
PbTe, electronic charge density 2−44121
PbTe, epitaxial film, photocond. 2−65085
p-PbTe, high field transport, current-field curves, mixed scatt. by phonons 2−81068
PbTe, mag. susceptibility calc. 2−68519
PbTe, paramag. surface centre density, e.p.r. obs. 2−65334
PbTe, thermoelec. props. rel. to partial substitution of Pb by Ga, In, Th 2−72053
PbTe epitaxial thin film, evaporated, diode struct., injection luminesc. and laser action 2−57382
PbTe film, effect of O_2 and N_2 on Hall and field effect mobilities 2−57191
PbTe film, optical and elec. props. 2−57172
p-PbTe room temp. transport props., scattering mechanisms, relative importance 2−54161
$PbTiO_3$, conversion to semicond. state by doping resist. positive temp. coeff. 2−81098
$PdTe_2$, refl., 1-12.5 eV, rel. to band struct. calc. 2−48161
Sb_2S_3, liquid, switching, thermal breakdown mechanism 2−81096
Sb_2S_3, liquid, switching effect 2−60503
Sb_2S_3 film, single cryst., optical absorp. edge obs. 2−81390
SbSBr, i.r. transmission, indirect transitions and band gap determ. 2−72346
SbSI, ferroelec., trapping levels, thermally stimulated photocurrents obs. 2−75154
SbSI, ferroelec. semicond., influence of nonequilib. carriers on domain struct. 2−72036
SbSI, ferroelec. semicond., photoluminescence of single crystals 2−72443
SbSI, paraelec. region, voltage-current characts., illumination effects 2−81163
SbSI, thermal currents induced by light 2−72039
Sb_2Se_3, electron energy states for amorphous and cryst. material 2−68627
Sb_2Se_3, liq., Hall effect 2−60498
Sb_2Se_3, polycryst., threshold and memory switching 2−77883
Sb_2Se_3, Sb_2Se_3-Bi_2S_3 alloy, switching behaviour 2−75096
Sb_2Se_3 film, amorphous, optical and transport props. 2−61323
Sb_2Se_3 film, amorphous, optical props. 2−53576
Sb_2Te_3-Bi_2Te_3, efficiency criterion for thermogenerators 2−75158
^{a}Sb, A=121, 123, nuclear electric quadrupole radiative transitions in InSb, explanation of microwave emission 2−44404
ScN, epitaxial growth and elec. props. 2−50503
Sc_2O_3 film, a.c. conductivity, hopping model 2−61324
Se: Cl, As film, vacuum evap., transport props., time resolved drift technique 2−44104
Se(:As), amorphous, Urbach tail in optical absorpt. edge 2−68641
Se-CdS(Se) heterojunction electrolum. 2−54481
Se-CdSe p-n heterojunction, diffusion potential determ. 2−47942
Se-Te alloy, acoustoelec. phenomena relating to two carriers 2−80908

Semiconducting materials continued
Se-Te alloy, liq., semicond., n.m.r. 2−61752
Se-Te alloy, liquid, switching phenomena 2−60504
Se-Te alloy, u.s. amplification, room temp. 2−51041
Se-Te melt, electronic transport behaviour, switching, optical gap 2−60502
Se, amorphous, crystn., effect of alternating elec. field. 2−60565
Se, amorphous, kinematics of deep trapping 2−61344
Se, amorphous, threshold and memory switching effects 2−57196
Se, amorphous, valence band density of states, vacuum photoemission study 2−84258
Se, current flow in Cd-Se rectifier diode 2−54219
Se, diffusion of Tl, 60-210°C, and TlSe formation 2−53771
Se, effects of cryst. disorder on electronic struct., photoemission obs. 2−61466
Se, field effect rel. to temp., field mobility, surface cond. 2−71933
Se, hole photoemission into S, 2.11-3.54 eV 2−84265
Se, in Al-Se-Ag structure, electro- physical characteristics 2−71987
Se, liquid, switching, thermal breakdown mechanism 2−81096
Se, liquid, switching and anomalous magnetoresistance 2−60505
Se, liquid, switching effect 2−60503
Se, liquid, switching phenomena 2−60504
Se, non-crystalline, impurity effects on struct. and elec. props. 2−61326
Se, vitreous, hole drift mobility 2−61327
Se amorphous film, a.c. cond., temp. depend. 2−68392
Se amorphous film, one- and two-carrier space-charge-limited currents 2−75097
Se amorphous layers, carrier lifetime determ. 2−81088
Se film, vitreous, trap-limited processes 2−61325
Se photocell, temperature dependence of relative spectral sensitivity 2−44186
Se reactor irradiation effect on the optical transitions 2−83976
Se rectifier, electrical and photoelectric obs. of surface layers 2−44132
Se_xTe_{1-x}, synchrotron radiation absorp., d level spin orbit splitting obs. 2−81401
Si-As-Te, energy gap depend. on glass transition and softening temp. 2−61346
Si-As-te, amorphous, relation between band gap and density 2−65003
Si-CdSe, p-n heterojunctions vacuum deposition preparation and properties 2−77925
Si-Ge alloy thermocouples, precip. of dopants 2−51210
Si-$ZnSiP_2$ solid solution, epitaxial growth on Si 2−60665
SiC:H(D), implanted, recomb. radiation of excitons and vibr. spectrum 2−68688
3C-SiC, band struct. and optical props., pseudopotential calc. 2−61345
SiC, defects, electron microscope obs. 2−47423
SiC, diffusion of B, distributions, elec. cond. and p-n junc. obs. 2−74797
β-SiC, electron irrad. effects on luminesc. 2−48232
SiC, impurity solubility, autoradiographic variant of activation analysis 2−72595
α-SiC, influence of struct. defects 2−71774
SiC, luminesc., Zeeman splittings, bound excitons 2−48227
SiC, Raman scatt. from coupled LO-phonon-plasmon modes 2−68663
n-SiC, Raman scatt. from electronic transitions 2−51356
α-SiC, residual lattice disorder due to ion bombardment 2−47391
SiC layers, system for chem. vapour deposition 2−50507
SiO_2, thin layer on Si, hot electron energy losses, photoemission obs. 2−81061
SiO_2 film, dielec., defects, local junction form 2−71964
Sm, monochalcogenides and monopnictides, band struct., press. effects 2−47915
SmS, semicond.-metal transition, optical consts. and energy levels study 2−80994
SmS, semicond.-to-metal transition under press., refl. study 2−75098
SmS, SmSe, SmTe, amorphous, optical absorption obs. 2−61657
SmSe, press. depend. of optical. absorpt. edge 2−75098
SmTe, press. depend. of optical absorpt. edge 2−75098
α-Sn, electron irrad., damage production and thermal annealing, resist. study 2−80682
SnS_2, band struct., pseudopotential calc. 2−44116
SnS_2, hopping conduction, a.c. conductivity meas., −100°C to 120°C 2−84290
SnSSe, vapour transport method 2−67937
$SnS_2(Se_2)$, cryst. growth and photocond. 2−67937
SnS(Se)(Te), refl., 1-12.5 eV, rel. to band struct. calc. 2−48161
SnTe-UTe system, phase diagram 2−47717
SnTe, efficiency criterion for thermogenerators 2−75158
SnTe, Fermi surface, de Haas-van Alphen and Shubnikov-de Haas study 2−68420
SnTe, supercond. props. 2−51114
SnTe film, epitaxial, carrier conc. and mobility, effect of atomic H 2−54179
SnTe polycrystalline film, electrical props., temp. depend. 2−71916
$SrTiO_3$, degenerate, u.s. propagation, effects of longitudinal mag. field 2−71731
$SrTiO_3$, mobility, gravimetric determ. 2−81086
$SrTiO_3$, supercond. props. 2−51114
TaS_2, 1S polymorph, cryst. growth and props. 2−47226
Te-As-Ge-S glass films, four-element quantitative analysis 2−72593
Te-As-Ge amorphous alloy, negative differential capacitance 2−64961
Te-As-Ge amorphous alloy, negative differential capacitance 2−64961
Te-As-Si-Ge film, amorphous, a.c. cond. rel. to localized tail states 2−61288
Te-Ge based memory glass film, thermal crystn. 2−47128
Te-SiO, in m.i.s. struct., flat band voltage temp. depend., interface states obs. 2−77930
Te-Tl, liquid, Hall mobility, electronic struct., two band model 2−60506

Semiconducting materials continued
Te, acceptor ground state under hydrostatic pressure, variational calc. 2−61192
Te, acoustomagnetoelectric effect 2−74986
Te, band structure, k.p perturbation theory calc. 2−81018
Te, CO_2 laser induced photoeffects 2−81178
Te, effects of cryst. disorder on electronic struct., photoemission obs. 2−61466
Te, electron irrad. damage, resist., Hall mobility 2−47392
Te, energy band models, thermomodulation of optical parameters obs. 2−65242
Te, extraordinary phonon Raman scatt. and reson. enhancement 2−84492
Te, liquid effective interionic pair potentials, calc. from structural diffraction data 2−50312
Te, mag. susceptibility anisotropy of holes, calc. 2−81214
p-Te, magnetophonon spectroscopy study 2−68385
Te, piezoelec., dislocations 2−60805
Te, second harmonic generation phase matching, laser-induced change 2−44338
Te, valence band Landau levels, cyclotron resonance obs. 2−81019
Te, valence band Landau levels, cyclotron resonance obs. 2−81017
Te film, on glass, elec. cond., temp. depend. below 300 K 2−75099
Te film, polycryst., on mica elec. transport props. 2−61330
Te films, amorphous, localized states, photoemission quantum yield 2−68422
Te films on uhv-cleaved TGS, aftereffects in field eff. at large gate charges 2−77900
Te valence band structure from Shubnikov-de Haas expts. 2−84245
$Te_{60}As_{25}Ge_{13}M_x$, M=S, Se, chalcogenide glass, interdepend. between, switching memory and thermal behaviour 2−47901
TeAsGeS glass, structural and electrical props. 2−61329
TeI_4-Te solutions, cond. mechanism 2−64472
TiO_2:Li,V,Cr,Mn,Fe, transition metal impurity levels, esr determ. 2−44117
TiO_2, AC Hall effect meas., polaron mass 2−57174
TiO_2, doped and undoped, frequency dependence of conductivity and adsorption of CO 2−77906
Ti_4O_7, metal-insulator transitions, charge localization, crystallographic evidence 2−44087
$Ti_xTa_{1-x}S_2$ $(0.1 \leqslant x \leqslant 0.9)$ solid solutions, resistivity, magnetic susceptibility and thermoelectric power 2−61266
Tl-Te alloy, amorphous film, cond., band struct. model 2−61328
$TlBiTe_2$, struct. and elec. props. 2−51144
TlI, photoconductivity, influence of polymorphic transitions 2−75174
$TlInSe_2$:Cu,Sn, cryst. and film, photosensitivity, optical absorpt., dark cond., forbidden band width 2−57197
$Tl_2SeAs_2Te_3$ glass, switching rel. to radiation emission 2−64981
$Tl_2Se.As_2Te_3$, amorphous, Hall coeff. and magnetoresistance 2−61331
$Tl_{1-x}Te_x$ alloy, liq., n.m.r., Knight shift, mag. relax., quadrupole relax., Fermi level 2−60512
Tl_2Te single crystal, growth and elec. cond. 2−64990
V_3Au, transition temp. rel. to ordering, rel. to phonons and electronic density of states 2−84308
$V_{1-x}Nb_xO_2$, metal-insulator transition, theory 2−75103
$V_{1-x}Nb_xO_2$, metal-insulator transition, crystallographic and transport props. study 2−75101
$V_{1-x}Nb_xO_2$, metal-insulator transition, mag. props. and n.m.r. studies 2−75102
VO_2, metal-insulator transition and phonon softening 2−51152
VO_2, semicond.-metal transition, rel. to struct. of $V_{0.95}Cr_{0.05}O_2$ 2−43592
VO_2 switching device, influence of high-conducting bubble 2−54208
VO_x, elec. props. and defect states 2−64991
V_2O_3, VO_2, V_2O_5 films, prep. by pyrolysis, temp. depend. of resistance 2−44106
V_2O_5, ion bombardment enhanced elec. cond. 2−68408
V_2O_5, liq., elec. cond., temp. and oxygen partial press. depend. n-type semicond. 2−83794
V_4O_7, metal-insulator transitions, charge localization, crystallographic evidence 2−44087
V_nO_{2n-1}, ^{57}Fe Mossbauer study 2−72286
V_nO_{2n-1} (n=3,4, ..., 8) single cryst., growth, temp. depend. of resist., susceptibility and thermoelec. power 2−43509
Vo_x, $1<x<1.3$, charge carrier freeze-out effects 2−65004
WO_3, elec. cond., temp. depend., four probe method and reflected microwave current obs. 2−71914
WSe_2, exciton spectrum, transmission obs. 2−81403
WSe_2, optical response in excitonic region 2−44383
Zn-In-S system polytypes, vapour growth 2−50579
$Zn_{1-x}Cd_xS$, melt-grown single crysts., struct. 2−64646
$Zn_xCd_{1-x}Te$, luminesc. reson. Raman scatt., exciton transition 2−54437
$Zn_xCd_{1-x}Te$, reflectivity spectra, band struct. obs. 2−78093
$Zn_{1-x}Cu_xCr_2Se_4$, magnetization and susceptibility, 4.2-900 K 2−44311
$ZnGeP_2$, cryst. growth and struct., optical props. and energy gap 2−80599
$ZnGeP_2$, i.r. birefr. and optical activity 2−72261
$Zn_xHg_{1-x}Te$ solid soln., light-hole band rel. to transport phenomena 2−64992
$Zn_2In_2S_5$ single crystal, photocond. relax. 2−75175
ZnO:Cu film, amorphous, band struct. and impurity state energy spectrum 2−68421
ZnO/O absorbed layers, sensitizing action of chlorophyll to corono discharge 2−44176
ZnO-Bi_2O_3 ceramic, elec. props. 2−57198
ZnO, (0001) surface, field emission and surface states 2−54271
ZnO, absorbed Hg excited atoms and molecules, interaction, elec. cond. study 2−47175
n-ZnO, acoustoelec. oscills. 2−61332
ZnO, band struct., photoemission study 2−75196
ZnO, cryst. growth, inversion twin obs. 2−50581
ZnO, crystal growth and semicond. props. 2−43516
ZnO, differential absorption spectrum on adsorption of molecules of donor-acceptor type 2−68651
ZnO, electron concentration determ. using T activity 2−71934

Semiconducting materials continued
ZnO, pure and doped single crysts., vapour phase growth 2−50580
ZnO anode, electron injection 2−61797
ZnO film, Burstein-Moss effect obs. 2−51350
ZnO(S)(Se)(Te), thermal cond. and phonon scatt. by Fe^{2+} impurities 2−84213
ZnS:B, luminesc., 400-800 nm, 110, 295 and 430K 2−75322
ZnS:Cl, quenching of photolum. by elec. field 2−72416
ZnS:Cl film, photovolt, polarity reversal by excess Zn 2−51222
ZnS:Cu, surface, volume, and contact components of current 2−71918
ZnS:Ni,O, photocond., spectral response interpret. 2−57258
ZnS, differential absorption spectrum on adsorption of molecules of donor-acceptor type 2−68651
ZnS, electron electron loss spectra 2−75111
ZnS, epitaxial on Si by forced vapour transort 2−50514
ZnS, many-photon absorption, carrier generation obs. 2−84519
ZnS, melt grown hexagonal, stabilization by donor impurity doping 2−47279
ZnS, photolum. and electrolum., temp. depend. 2−48267
ZnS, spin-flip scattering from free and bound electrons 2−44389
ZnS, Stark ladder levels 2−68276
ZnS, two photon photoconductivity 2−61450
ZnS epitaxial film, on GaAs, struct. 2−71339
ZnS phosphor, microwave photocond. and luminescence 2−51213
ZnS single crystal, homogeneous, wide-gap, electrical and electronic behaviour 2−68712
$ZnS_{1-x}Se_x$, stimulated cond. with persistent memory 2−75104
ZnSe:Ag, impurity levels 2−51151
ZnSe-CdTe system, miscibility 2−77464
ZnSe, dielec. function, freq.- and wave-vector-depend., calc. 2−84262
ZnSe, dislocation etch bits 2−50677
ZnSe, electron energy loss spectra 2−75111
ZnSe, many-photon absorption, carrier generation obs. 2−84519
ZnSe, optical props. of subsitutional donors 2−51372
ZnSe, pair photolum., peak energy, excitation intensity depend. 2−75318
ZnSe, self-consistent local orbitals 2−75031
ZnSe, spin-flip Raman scatt., linewidths and two-electron processes 2−84501
ZnSe, spin-flip scattering from free and bound electrons 2−44389
ZnSe, time of flight mobility, and trapping 2−44107
ZnSe, vapour growth, donor and acceptor identification 2−50573
ZnSe, vapour phase cryst. growth under controlled partial press. 2−64594
ZnSe, X-ray K emission bands, valence electron obs. 2−68672
n-ZnSe(Cu,Ga) film, photolum., photocurrent oscills., 80-220K, luminesc. field quenching 2−81168
$ZnSe_xTe_{1-x}$, refl., 2.0-6.6 eV, rel. to comp. depend. of energy gap 2−84500
$ZnSiP_2$, optical phonons, polaritons, mode freqs., strengths, damping factors 2−61621
$ZnSnAs_2$, $ZnSnP_2$, band structure, electroreflectance spectra obs. 2−81404
ZnSr, paramag. surface centre density, e.p.r. obs. 2−65334
ZnTe:Al, high temp. defect equilib., elec. transport props. 2−44096
ZnTe:Al, high temp. elec. props., self-compensation model 2−51128
ZnTe-InAs heterojunction, prep. by liq. phase epitaxy, optical and elec. props. 2−57213
ZnTe, absorpt. due to acceptor levels 2−57353
ZnTe, double-acceptor cathodolum. 2−54480
ZnTe, electron energy loss spectra 2−75111
p-ZnTe, high photosensitivity 2−72071
ZnTe, impure, multiphoton luminesc. satellites in strong e.m. field 2−61679
ZnTe, physical properties, device applications 2−64962
ZnTe epitaxial film, optimum growth conditions 2−47105
ZnTe film, on Ge, epitaxial growth and struct. 2−50515
ZnTe Schottky barrier, admittance spectroscopy of deep impurity levels 2−61391

gallium arsenide
acoustic amplification, surface shear wave mode characts., bulk wave theory incl. trapping effects 2−68241
acousto-electric domains, origin and properties 2−54034
acoustoelectric domains, elec. and optical props. 2−80912
amorphous, absorption edge temp. depend. 2−75293
amorphous, band struct., optical props. pressure effects obs. 2−61333
amorphous, field depend. of elec. cond. 2−77896
amorphous, thermoelec. power, cond., hopping cond., annealing effects 2−61312
band structure, critical point detn., wavelength modulation derivative spectroscopy obs. 2−48160
band structure, X-ray photoemission study 2−84387
bound exciton photoluminescence spectra 2−57373
Brillouin scattering, dispersion, fast TA phonon cross section 2−61670
bulk element, static negative resistance due to geometrical effect, computer analysis 2−84320
cathode, negative electron affinity, photoemission rel. to Cs-O layers thickness 2−75194
chemical shift in binding energies of Zn and Cd 2−65001
compensated, negative magnetoresist. temp. depend., influence of mag. field 2−71900
conductivity type determ. using rectifying contacts 2−68428
controlled sectioning by anodic oxidation and removal of oxide layer 2−64544
core levels, spectral obs. 2−65240
crystal growth, open flow quartz systems, Si contamination 2−43529
crystal growth, temp. fluctuation effect on nonuniformities 2−47267
current instability rel. to mag. field, negative resist 2−64984
Czochralski growth, temp. profile and thermal stress effects on dislocation structure formation 2−53615
dielectric function, freq.- and wave-vector-depend., calc. 2−84262
dielectric-surface-loaded elements, high field domain propagation 2−51141

Semiconducting materials continued
gallium arsenide continued
diffuse reflection spectra, energies of E_1, $E_1 + A_1$, E_0' and E_2 peaks 2−75275
diffusion, of Sn, effect of mask edges 2−54205
diffusion profile of Zn, anal. 2−47464
diode, high-resist. n-type, current oscillation and photoresponse 2−54220
diode, in cascade freq. multipliers, microwave 2−84350
diode, power and radiation pattern meas. 2−51369
double heterostructure, injection laser, gradual degradation 2−42086
electric field induced interference effects at ground exciton level 2−78084
electroabsorption, impurity levels obs. 2−65258
electroluminescent diode, electron diffusion length, internal quantum efficiency, temp. depend. 2−61725
electroluminescent diode, sinusoidal modulated, recomb. emission phase shifts rel. to injection levels 2−72400
electron and neutron irrad., i.r. absorpt. band obs. 2−48180
electron density ratio in valleys, elec. field depend. in presence of Gunn effect 2−81093
electron drift velocity meas. technique 2−54172
electron irradiated, asymmetric damage regions, elec. props. obs. 2−74759
electron irradiated n- and p-type, defect levels, Hall effect and resist. study 2−80992
electron mobility meas. 2−64969
electron transfer, and velocity-field characts., mag. field effect 2−44100
electron-hole pair energy for alpha particles and conversion electrons 2−49667
electroreflectance spectrum 1.2-5.3 eV photon energy range 2−68619
energy gap, temp. depend., calc. using Brooks-Yu theory 2−68415
energy gap, temperature dependence 2−80964
epitaxial, microwave meas. of velocity-elec. field charact. 2−51140
epitaxial, near band-edge optical absorpt. rel. to excitons 2−84516
epitaxial, photolum., 8250-8450Å 2−61694
epitaxial film, cathodolum., carrier mobility effects 2−72434
epitaxial film, doping lefel and impurity distrib., substrate orientation effects 2−47436
epitaxial growth 2−71386
epitaxial growth from vapour phase 2−83891
epitaxial growth on ZnSe from Ga, Sn solutions, properties 2−53573
epitaxial layer, electrical props. 2−71882
epitaxial layer, optical properties by photoluminescence method 2−72442
epitaxial layer, origin of high resistance region at substrate interface 2−71883
epitaxial layers, free carrier conc. and mobility 2−50492
etching, anisotropic behaviour of etchants 2−74660
evaporation by laser, mass-spectrometric analysis of ions in vapour 2−75409
exciton absorpt. meas. method 2−44373
exciton structure of fundamental absorption edge and oscillatory magnetoabsorption 2−72331
exciton-phonon coupling, optical absorp. obs. 2−61642
film, epitaxial, guiding and electrooptic modulation of light 2−68608
film, liq. phase epitaxy on ZnSe, elec. characts. rel. growth conditions 2−67910
film, magnetoresist. and Hall coeff., calc. and expt. 2−71892
GaAs:Te, heavily-doped, nature of defects, photolum. and internal friction study 2−71926
gamma ray detector, crystal growth and material quality obs. 2−46052
growth, impurity incorporation, effect of surface space charge layer 2−47428
Gruneisen parameter determ. at low temps. from elastic consts. 2−71752
Gunn diode, degradation by dislocations induced during thermocompression bonding 2−68446
heat treated, acceptor centres, Hall effect and photoluminesc. obs. 2−61343
heavily doped, absorp. edge at low temp. 2−65247
heavily doped, localization of band tail states, elec. cond. study 2−71922
helicon wave propagation in magnetic fields up to 200 kG 2−47910
heterojunction solar cells, ZnSe-GaAs, characteristics 2−63253
high-resistivity double-injection devices, conditions for recombinative space-charge injection 2−68445
hole transport, taking into account polar scatt., Monte Carlo study 2−64968
hot electron properties, rel. to Gunn effect bulk instabilities 2−57184
impact ionization of charge carriers, energy conservation considerations 2−75081
implantation with Cd, residual bombardment disorder and atom location 2−60813
impurity diffusion, technological aspects 2−71514
interfacial defect obs., high voltage electron microscopy, device manuf. considerations 2−54215
intrinsic localized surface states, [110] surface Brillouin zone, calc. 2−65007
intrinsic surface states, densities, photoemission densities 2−44207
ion implantation, lattice damage prod. 2−47374
ion implantation of S, junction form. 2−47429
ionicity, dispersion, and optical spectra 2−44374
i.r. absorpt., impurity induced, calc. by Green's function technique 2−61639
i.r. dispersion of second order electric susceptibilities 2−61581
junction laser, spontaneous emission behaviour across threshold 2−66766
laser, applic. in optical communications using glass fibre waveguide 2−42102
laser, double heterostruct., threshold current rel. to press., light polarization flip 2−69949
laser, electron beam pumped, generation of controllable light pulses by spatial scanning of beam 2−42090
laser, freq. time shift for short current pulses 2−82485

Semiconducting materials continued
- **gallium arsenide** continued
  - laser, high radiance, room temp. with controlled radiation in single transverse mode 2−45754
  - laser, optical filament formation theory 2−42098
  - laser, single heterojunction, injection, dependence of spectral mode frequencies on currents 2−42097
  - laser irrad., 0.694- 1.06μ, surface damage 2−61574
  - lasing characts., doping effect, double heterostruct. laser obs. 2−49384
  - layer compound, valence electron density and band structure 2−75081
  - light beam guidance and control in epitaxial films 2−42236
  - luminescence, exciton-exciton and electron-exciton interactions in highly excited material 2−78132
  - luminescence, obs. 2−54479
  - luminescence from LPE-grown crysts., shallow acceptor identification 2−54454
  - magnetic enhancement of acoustoelectric gain, obs. by Brillouin scattering 2−51034
  - magnetic susceptibility, calc. and expt. 2−71928
  - magnetophonon effect, oscill. struct., transverse config. 2−57179
  - many-photon absorption, carrier generation obs. 2−84519
  - metal-GaAs (110) contact, Schottky barrier height 2−54214
  - multiphonon Raman scattering 2−68659
  - n-type, γ-irrad. effects on current instabilities caused by recomb. centres 2−81092
  - n-type, acoustoelec. current oscill., temp. depend. 2−51040
  - n-type, acoustoelectricity, ultrasonics, Gunn diode, bulk diode, surface wave detection 2−77774
  - n-type, anisotropy of the submillimeter conductivity of warm carriers 2−84330
  - n-type, diffusion of Fe and Co, temp. depend. 2−47463
  - n-type, effective electron mass, pressure depend. 2−44098
  - n-type, electron drift velocity, Monte Carlo calc. 2−71901
  - n-type, electron irrad., annealing behaviour of elec. props. and photolum. 2−47918
  - n-type, epitaxial, Hall coeff. and mobility 300-800 K, valley energy separation 2−68398
  - n-type, flatband electrorefl. spectra, elec. field modulation 2−68623
  - n-type, frequency tripling employing electron heating effect by microwave field 2−71903
  - n-type, heavily doped, band-to-band recomb., quantum efficiency, lifetime, rel. to impurity conc. 2−61697
  - n-type, heavily-doped, gradual mobility transition in band tails 2−61342
  - n-type, hot electrons heated by high microwave fields 2−77897
  - n-type, impurity distrib. coeff. anisotropy, elec. props. study 2−47437
  - n-type, low field galvanomag. transport, Boltzmann eqn. soln. in mag. field, 77-300K 2−71902
  - n-type, luminesc. from implanted Zn ions 2−48222
  - n-type, mag. field effect on impurity cond. 2−81085
  - n-type, negative photocond. when illuminated with impurity absorbed light, recomb. mechanism 2−65083
  - n-type, optical waveguiding by proton implantation 2−66841
  - n-type, surface barrier diode, hole diffusion length 2−61387
  - n-type acoustoelectric amplification of injected coherent ultrasonic shear waves, small, large signal conditions 2−64847
  - n-type bulk element, static electric field distribution 2−84315
  - neutron irrad., tunnel assisted hopping via defect energy levels 2−51157
  - noise, 1/f, due to free surface 2−81079
  - optical absorption spectrum, resolved free-exciton transitions 2−84259
  - optical and dielec. props. 2−48189
  - oscillator, high resistivity, characteristic operation 2−44137
  - p-n jjnction, insulation by proton irradiation 2−84353
  - p-n junctions, barrier capacitance, obs. 2−44131
  - p-si-n structure, electroabsorption, polarization effects 2−70666
  - p-type, absorpt. saturation intensity at 10.6 μm 2−79227
  - p-type, Auger recomb. of excess carriers, spin split off band effect 2−81067
  - p-type, electron beam excited, internal quantum efficiency of spontaneous emission, effect of beam voltage increase 2−72433
  - p-type, magnetophonon spectroscopy study 2−68385
  - p-type, photocond. and photovolt. effect, surface effects 2−54254
  - p-type, secondary electron emission, refl. mode gains escape depth, photoresponse 2−75200
  - p-type, thermo. e.m.f., Hall effect, cond., effect of pressure, 10000 kg/cm^2 2−44099
  - photocathode, transmission, prep. and characts. 2−75185
  - photodiode, feasibility of epitaxial production on single crystal strip of Ge 2−54260
  - photodiode with anti-Stokes luminors 2−77967
  - photoelectric emission, electronic struct. 2−72088
  - photoemission spectroscopy, using synchrotron radiation, valence band and surface states obs. 2−81194
  - photoluminescence, nonequilib. carriers strong interaction, 77K 2−68680
  - photoluminescence meas., bulk effects 2−72391
  - polariton (n=1 exciton) spectra, transmittance and reflectance temp. depend. 2−81400
  - polishing by gaseous etching, during growth from gas phase in chloride system 2−83853
  - positron lifetime spectra, temp. depend. 2−75003
  - preferential etching using Br_2-CH_3OH system 2−71311
  - proton irradiated, absorpt. spectra 2−48177
  - radiation damage, review 2−47365
  - radiative recombination of screened excitons 2−72408
  - reactor irradiation effect on the optical transitions 2−83976
  - room-temperature radiation detector possibilities 2−52692
  - Schottky barrier height, temp. depend. 2−71958
  - Schottky diodes, hole diffusion contrib. to photocurrent, temp. depend. 2−44178
  - selective photoetching, surface photovoltaic effect 2−71364
  - semiconductor, electron diffusion, in high electric fields 2−57177
  - shallow donors, photothermal ionization, photocond. obs. 2−81177

Semiconducting materials continued
- **gallium arsenide** continued
  - solar cells, efficiency comparison with Si cells on spacecraft, 0.2 to 10 a.u. 2−49306
  - split, negative differential cond., i.r. emission 2−61311
  - stimulated emission, Coulomb interaction 2−61681
  - stimulated emission, optically pumped, mag. field shift 2−61698
  - substrate, film meas. using split-beam ellipsometer 2−71329
  - surface, Cs adsorption kinetics, photoyield, work function 2−53595
  - surface barrier diodes for X and alpha ray spectrometers 2−49628
  - transition metal doped, anomalous elec. and mag. props. 2−68405
  - two-photon conductivity, nanosec. and picosec. light pulses 2−47995
  - undoped, point defect conc. effects on props. 2−71905
  - work function, effect of light at low temps. on single crystals 2−75188
  - X-ray K emission bands, valence electron obs. 2−68672
  - $Al_xGa_{1-x}As$-GaAs-$Al_xGa_{1-x}As$ heterojunction laser, radiation spectral distrib. and polarization 2−63342
  - $Al_xGa_{1-x}As$-GaAs heterojunction, prep. by multiple layer liq. phase epitaxy 2−50482
  - $Al_xGa_{1-x}As$ grown- diffused electroluminescent planar monolithic diodes 2−51386
  - C ion implanted p-type, carrier conc. and Hall mobility obs. 2−64986
  - CaAs:Sn, photoluminescence props. 2−44427
  - $Ga_{1-x}Al_xAs$:Si layer growth, Al conc. effect on amphoteric behaviour of Si 2−51153
  - $Ga_{1-x}Al_xAs$, epitaxial layer growth, junction form. 2−47288
  - $Ga_{1-x}Al_xAs$, superlattice surface laser applics. 2−69945
  - $Ga_xAl_{1-x}As$, optical electron-nuclear reson. 2−61695
  - GaAs:Cr, deep levels and radiative recomb., photolum. and photocond. study 2−71927
  - GaAs:Cr, instability of recomb. radiation and photocurrent 2−84540
  - GaAs:Cr p-i-n diode, nonadditive photocond. under combined excitation conditions 2−72080
  - GaAs:Cu, behaviour in strong elec. field 2−71904
  - GaAs:Cu, elec. props., impurity centre form., conditions and mechanism 2−64985
  - n-GaAs:Cu film, epitaxial, carrier mobility, impurity effects, scatt. by space charge centres 2−64983
  - n-GaAs:Ge film, epitaxial, degenerate, forbidden gap, traps 2−44114
  - GaAs:Ge p-n junction, Zn- diffused, photolum., 8100-8500 Å 2−72404
  - GaAs:Mg-Li, i.r. absorpt. due to pair defects, absorpt. cross section 2−81360
  - n-GaAs:O, piezoelectric stiffening of active bulk modes and increase in velocity of 30 MHz shear wave 2−51204
  - GaAs:Se, donor self-compensation 2−75110
  - GaAs:Si laser, double heterostruct. diode, laser action 9100-9500 Å, threshold current conversion efficiencies 2−73591
  - GaAs:Si p-n junction, reverse branch of I-V characts. and breakdown 2−71959
  - GaAs:Si(Te), electron irrad., carrier removal, mobility changes, annealing characts. 2−47917
  - GaAs:Zn(Si)(Te), impurity effects on dislocation velocity 2−68028
  - GaAs/Cs, photoemissive yield, phonon energy loss effects, band-theoretic model 2−61460
  - GaAs/GaAlAs, mesa stripe geometry double heterostruct. injection laser, very low current operation 2−42093
  - GaAs-$Al_xGa_{1-x}As$ double heterostruct. laser diodes, reproducible liq. phase epitaxial growth 2−49385
  - GaAs-$Al_xGa_{1-x}As$ p-n heterojunction, current flow during electrolum. 2−72438
  - GaAs-CdS heterojunction, isotypic, prep. and photosensitive props. 2−71956
  - GaAs-Cu in supersaturated solid solution, differences in laws of decomposition 2−83836
  - GaAs-$Ga_{1-x}Al_xAs$ double heterostructure laser, lasing characteristics of optical guides 2−42092
  - GaAs-$Ga_xAl_{1-x}As$ heterojunction injection laser, time characteristics 2−42091
  - GaAs-$Ga_xAl_{1-x}As$ n-p heterojunction, field effect of GaAs photolum. 2−72399
  - GaAs-GaP heterojunction, prep. by multiple layer liq. phase epitaxy 2−50482
  - GaAs-GaP n-p heterojunction, field effect of GaAs photolum. 2−72399
  - GaAs-(AlGa)As cold cathode, structure, factors affecting extended operation 2−48012
  - GaAs-electrolyte contact, differential capacitance, Mott-Schottky relation 2−51174
  - GaAs-polyethylene system, use in long-wave semicond. photography 2−70090
  - GaAs, layers, influence of gas phase comp. on electrical properties 2−83893
  - GaAs, piezoelectric amplification of acoustic waves abrupt decrease in gain at quantum limit 2−51033
  - p-GaAs epitaxial layer, gas transport deposition, orientation effects 2−71387
  - GaAs interface, n-type, small-signal admittance meas. 2−65039
  - $GaAs_{1-x}P_x$:N, photoluminescence, spontaneous and stimulated, from N A-line and NN pair, transitions 2−81414
  - $GaAs_{1-x}P_x$, epitaxial growth on GaAs by pyrolysis on $Ga(CH_3)_3$, AsH_3 and PH_3 2−50496
  - $GaAs_{1-x}P_x$ film, comp., effects of deposition conditions 2−60657
  - $GaAs_{1-x}P_x$, epitaxial growth 2−43528
  - $GaAs_{1-x}P_x$, melt-growth under controlled vapour pressure 2−56611
  - $GaAs_{1-x}P_x$, multiphonon Raman scatt. 2−68659
  - $GaAs_xSb_{1-x}$-$Al_yGa_{1-y}As_xSb_{1-x}$ double heterojunction laser, prep. and emission spectra 2−59184
  - $GaAs_{1-x}Sb$, cryst. growth, vapour phase 2−43511
  - $Ga_{1-x}In_xAs$, vapour growth, equilib. calc. 2−47222
  - GaSb-GaAs system, phase diagram, thermodynamic analysis 2−44086
  - $In_xGa_{1-x}As$ prep. and props. rel. to electroluminescent diodes 2−68708
  - n-type, Gunn oscillators, hot electron microwave mobility 2−51139

Semiconducting materials continued
gallium arsenide continued
Pb-GaAs Schottky barrier tunnel junction, zero bias anomaly, irrad. effects 2-71960
S ion implanted n-type, carrier conc. and Hall mobility obs. 2-64986
Si-doped infrared light emitting diode 2-65030
Si ion implanted n-type, carrier conc. and Hall mobility obs. 2-64986
Si_3N_4-GaAs interface, deposition and surface state density obs. 2-65040
Si_3N_4-GaAs interface, surface states and insulator traps, m.i.s. cond. study 2-77919
SiO_2-GaAs interface, deposition and surface state density obs. 2-65040
Sn diffused, for N^+ layer formation 2-71515
Zn-diffused light emitting diodes 2-65031

germanium
— 2-71973
— 2-61183
acceptor states, Zeeman effect, group theoretical study 2-84264
acoustoelectric effects, quadrupole and octupole electron phonon coupling 2-61101
amorphous, absorption edge temp. depend. 2-75293
amorphous, band struct., optical props., pressure effect obs. 2-61333
amorphous, bridge method of measuring magnetoresistance 2-44122
amorphous, dark-field electron microscope obs. 2-60593
amorphous, electronic spectrum, variational LCAO method 2-61184
amorphous, obs. of electron tunnelling between metal electrodes, determ. tunnelling phonon density of states 2-44125
amorphous, photoelectron energy distrib. curve obs. 2-61464
amorphous, thermoelec. power, cond., hopping cond., annealing effects 2-61312
amorphous, transport model 2-61352
amorphous, unannealed, residual cond. at 77K 2-47926
amorphous, Urbach tail in optical absorpt. edge 2-68641
amorphous and crystalline, density of states, photoelectron and secondary electron emission obs. 2-77977
amorphous and crystalline polytypes, electronic struct. calc. 2-68431
amorphous film, ohmic and non-ohmic cond. 2-61289
amorphous film, u.v. reflectance depend. on deposition temp. 2-54403
band struct. rel. to struct. in tetrahedrally bonded and amorphous states 2-68436
band structure, critical point detn., wavelength modulation derivative spectroscopy obs. 2-48160
birefringence, infrared, on hot electrons in n-type Ge 2-81328
bound exciton luminescence 2-68692
characterization for detector fabrication, effects of Si and O impurities, smooth pits and trapping 2-49652
coaxial γ-ray detectors, efficiency instability problem 2-49671
condensed electron-hole state, temp. depend. props. 2-68683
conductivity, density depend. 2-54101
conductivity type determ. using rectifying contacts 2-68428
creep, and stress effects 2-84040
crystal growth, Stepanov method, effect of dopant conc. 2-47270
crystals, temperature distrib., obs. 2-51364
cylindrical crystal, contactless method for measurement of volume distribution of resistivity 2-51159
detector rise time gated leading edge trigger for improved timing of monoenergetic gamma rays 2-63703
detectors, coaxial and planar, space charge effects on fields and charge collection 2-49661
detectors, performance improvement 2-49660
dielectric function, freq.- and wave-vector-depend., calc. 2-84262
diffusion, of Sb, influence of In concentration gradient 2-71516
diffusion length of excess minority carriers generated by pulsed electron beam, freq. depend 2-51165
divacancy-donor complexes, in O-free γ-irrad. samples 2-71943
donor-vacancy complexes, γ-irrad. prod. kinetics and energy spectrum 2-47382
doping influence on dislocation velocity, electron trapping during kink nucleation 2-50674
electrical cond. when in contact with electrolyte, shunting effect, pot. distrib. 2-65016
electrical conductivity and work function, surface orientation effects 2-71935
electrical conductivity meas. in powerful electric fields by contactless method 2-61350
electrode, equilibrium and nonequilibrium effect near semiconductor-electrolyte boundary 2-61798
electrode surface, electrooptical method for determ. of recombination rate and term distribution 2-68423
electron bombarded, pair-prod. energy for free carriers 2-61351
electron irrad., changes in length and elec. resist. 2-68016
electron irradiated, 8.5 MeV, high field domain instability 2-57208
electron irradiated, asymmetric damage regions, elec. props. obs. 2-74759
electron mobility, theoretical calc. 2-77889
electron spectroscopy of amorphous film at energy losses below 1 eV 2-80934
electron-hole drops 2-68432
electron-hole plasma conductivity, plasma density depend. 2-61212
electroreflectance, curve fitting using one-electron theory 2-78091
electroreflectance of heavily doped n- and p-type near direct energy gap 2-51321
emission band, two electron band-to-band transitions, excitation intensity 2-61699
epitaxy, thermodynamic calc. of the Ge-H-Cl system 2-53623
evaluation by pulse meas. on guard ring radiation detectors 2-49653
exciton and electron-hole drop absorption, far i.r. obs. 2-78100
exciton condensation, ground state energy calc. using improved RPA approx. 2-71809
exciton ground state, exciton line broadening by elec. field 2-77841

Semiconducting materials continued
germanium continued
Faraday rotation in n-type effect of ionized impurity scattering 2-51302
field effect, effect of surface treatment and relief 2-57211
field-emission cathode, preparation technique 2-82433
film, amorphous, anisotropy in resist. 2-68430
film, amorphous, secondary electron emission spectrum obs. 2-61353
film, amorphous, substrate temp. effects on elec. props. 2-64987
film, elec. cond. and Hall effect, thickness depend. 2-54192
galvanomagneto-recombination effect kinetics rel. to elec. and mag. fields 2-65015
graphite-Ge switch, asymmetric, and light sensitivity 2-61272
Gruneisen parameter determ. at low temps. from elastic consts. 2-71752
heavily doped, absorp. edge at low temp. 2-65247
heavily doped, elec. cond. and Hall effect 2-81109
helicon wave propagation in mag. fields up to 200 kG 2-47910
high resolution counter, using radiation defect compensation 2-82815
hole scattering by neutral acceptors 2-71941
hopping cond. rel. to temp., doping, uniaxial compression 2-65013
hot electron capture by cu^{2-} centres 2-71936
impact ionization of charge carriers, energy conservation considerations 2-75081
impurities Au and Sb, absorption and movement of melted zone in the solid phase 2-83892
intrinsic surface states, densities, photoemission densities 2-44207
ion implantation of S, junction form. 2-47429
i.r. Faraday effect, hot electron transfer between equivalent valleys obs. 2-78067
irradiation damage, electrons and γ-rays, Mossbauer type photoluminesc. spectra obs. 2-48243
magneto-microwave free- carrier absorpt. in Faraday config. 2-68605
magnetoresistance, microwave field depend. 2-77909
metal-insulator transition, d.c. and microwave photocond. obs. 2-77829
metastable polycryst III, photon Raman spectra 2-68664
microwave absorpt., by electron-hole drops 2-57209
microwave Faraday effect, multiple reflections and lattice and impurity scatt. effects 2-75257
minority carrier mobility, influence of majority carriers in pulsed electric field 2-75114
minority hole mobility, on interaction with electrons, high microwave field effects 2-75116
n-type, γ-ray irrad., recombination parameters 2-47929
n-type, absolute negative cond., current instability, Erlbach effect 2-68433
n-type, cyclotron reson. linewidth in quantizing mag. field 2-71942
n-type, Debye temp. rel. to carrier conc. 2-77772
n-type, degenerate, epitaxial growth on GaAs 2-47115
n-type, disordered region prod. by 28 MeV electrons 2-47931
n-type, doped with nonmag. impurities, negative magnetoresist. 2-68323
n-type, effect of higher energy states on acoustic attenuation 2-74987
n-type, electron irrad., annealing kinetics 2-47380
n-type, electron irrad., impurity depend. of annealing, vacancy-interstitial pair effects 2-47379
n-type, electron irrad., impurity depend. of low temp. annealing 2-47376
n-type, even and odd Hall effect in strong electric fields 2-81108
n-type, fast-neutron- compensated, model for amorphous semiconductors 2-68429
n-type, Hall constant measurement by cubic type high-pressure multianvil apparatus 2-76431
n-type, hot electron charact., high-field scatt. mech. 2-61354
n-type, hot electron effects, calc. method 2-54193
n-type, hot electron instabilities, Monte Carlo calc. and neg. diff. cond. obs. 2-77912
n-type, impurity breakdown, size effects, at 4.2K 2-65014
n-type, laser generated carrier mobility, transient behaviour 2-47925
n-type, light modulation by non-equilib. optical phonons in pulsed elec. fields 2-78069
n-type, magnetoresist., transverse and longit., of hot electrons 2-65012
n-type, negative absolute resist. 2-71937
n-type, nonstationary elec. cond., momentum relax. time 2-68435
n-type, phenomenological energy relax. time, elec. field depend., 77K 2-65010
n-type, resist. below 1K, anomalous temp. depend. 2-57210
n-type, resist. rel. to donor spin reson., spin energy transfer model, 4K 2-68434
n-type, slow surface state relax., point contact diode, microwave e.m.f., contact potential pressure depend. obs. 2-84283
n-type, thermal magnetocond., electrn-phonon scatt., doping effects 2-81084
n-type, transverse magnetoresist. in quantizing mag. fields, calc. 2-71939
optical and dielec. props. 2-48189
p-n, secondary breakdown formation 2-71962
p-n junction, bistable state of microplasmas 2-71963
p-type, absorpt. saturation intensity at 10.6 μm 2-79227
p-type, anisotropic photon drag effect 2-75165
p-type, electron irrad., low temp. annealing 2-47378
p-type, electron irrad. defect prod., annealing and cond. obs. 2-47377
p-type, field emission obs. in impulse and stationary conditions 2-61458
p-type, galvanomag. effects, theory extended to include optical phonon scatt. 2-65011
p-type, hot electron population inversion in crossed electric and mag. fields 2-77817
p-type, impurity scatt. of warm holes 2-44124
p-type, low temp. elec. irrad., point defect annealing, Hall coeff. and cond. obs. 2-47381
p-type, low temp. electron irrad., 220K defect, resistivity and Hall obs. 2-47928

Semiconducting materials continued
germanium continued
p-type, magnetophonon spectroscopy study 2−68385
p-type, neutron irrad. effects, 77K 2−47930
p-type, photon-induced hopping on acceptors, theory 2−47923
p-type, radiation defect annihilation centre, photocond. obs. 2−83978
p-type, trapping parameters, chemical impurities effect 2−49666
p-type and intrinsic monocrystals, quality control of γ-radiation detectors 2−46044
particle detector, high purity ion implantation and glow discharge methods for contacts 2−49655
particle detectors, high purity operating temp. limitations 2−49656
particle detectors high purity, p type, grooving for fabrication 2−49654
phonon induced quadrupole potential 2−71772
phonon-assisted tunnelling in n-type, impurity dependence 2−54195
photoconducting for wide range of band bending near surface 2−72062
photoconductivity, surface excitation by Nd laser pulse, surface transport props. obs. 2−84379
photodiode detecting head for YAG laser 2−66761
photoelectromagnetic effect, oscillatory spectral distrib., rel. to direct interband transitions 2−65093
photoemission spectroscopy, using synchrotron radiation, valence band and surface states obs. 2−81194
plasma, screw instability in strong mag. fields 2−77844
polytype, density of states and optical props. 2−61185
quadratic Zeeman effect of donor lines 2−57350
quantum effic. of int. photoelec. eff. and impact ioniz. 2−71907
radiation defect form. and annealing 2−47383
radiation detectors, high-purity, characteristics analysis and obs. 2−52695
radiation effects, defect models, review 2−47375
radiative recombination, 2-77K, effect of electron-phonon interaction 2−68684
radiative recombination, during electron-hole condensation in pure and doped material 2−78133
radiative recombination of biexcitons 2−78134
reactor irradiation effect on the optical transitions 2−83976
resistivity distribution in longitudinal and transverse specimens, investigation by single probe method 2−51163
resistivity meas. by spreading resistance technique 2−54194
single crystal ribbon growth from melt, commercial scale processes, equipment development 2−60725
solubility and diffusion of Cu, temp. depend. 2−77613
surface, monomolecular layers exam. using ellipsometry 2−56601
surface charge, slow relax., surface cond. and contact potential studies 2−81105
surface electrical properties, effect tetragonal GeO_2 layer 2−47939
surface reaction, with O_2, LEED and conductivity obs. 2−50448
surface recombination, effects of chemisorption and sulphidization 2−71938
surface state density, Green function calc. 2−51164
tetrahedrally bonded, vibr. states from Keating model, Raman line intensity 2−68224
thermophotoelectric effect due to hot carriers, 300 and 77K 2−72057
X-ray K emission bands, valence electron obs. 2−68672
Zeeman effect, donor excited states, photocond. spectra obs. 2−75172
γ-ray detector using very pure Ge 2−52694
Al-Ge, contact, slow states activation energy, barrier height temp. depend 2−75135
n-GaAs:Ge film, epitaxial, degenerate, forbidden gap, traps 2−44114
Ge:As, far i.r. absorpt., impurity conc. and compensation effects 2−68642
p-Ge:Au, photocond., electron capture coeff., excess free carrier distrib., surface recomb. effects 2−81164
Ge:Au, photoconductivity theory and obs. rel. to multi-level impurities 2−54251
Ge:Au diode, fabrication, double injection negative-differential resist. 2−71974
Ge:Cu, donor compensation density determ. by Hall and mobility analysis 2−51166
Ge:Cu, heated by h.f. elec. field., hot electron recomb., electron capture 2−64972
Ge:Cu, recomb. cross section for holes at singly ionized impurity 2−51215
Ge:Cu $P^+-\pi-N^+$ structures, negative resistance and magnetic sensitivity 2−75130
p-Ge:Cu thermalization time of hot photoexcited holes 2−51214
Ge:Ga bolometer, construction and performance 2−41847
Ge:Hg photoresistor, heterodyne detection at high freq. 2−69986
Ge:Li, electron irrad., Hall effect and minority carrier diffusion length obs. 2−47927
Ge:Mn, nonlinear IV characts., exclusion and charge exchange between impurity levels 2−75115
Ge:Ni, electron and hole capture rates, photomagnetoelec. and photocond. studies 2−75171
n-Ge:O, γ-irrad., Hall mobility, anisotropy 2−54196
Ge:P, electron irrad., bombardment induced interstitial P, e.p.r. obs. 2−48279
n-Ge:P(As), resist. decrease due to donor spin reson. 2−81106
Ge:Sb, electron irrad., phonon scatt. and induced energy levels, thermal cond. obs. 2−47766
Ge:Sb, photocond., monochromatic submillimeter radiation 2−81180
Ge:Sb(P)(As), heavily doped, temp. depend. of resist. 2−71940
Ge:Sn, heavily doped, absorption spectrum, Sn precipitation and Hall mobility 2−77911
Ge/Cs, photoemissive yields, phonon energy loss effects 2−61460
Ge/YFe garnet interface, interaction of surface magnetostatic waves with carriers 2−84420
Ge-Si heterojunction, pulse characts. 2−71961
Ge-Si heterojunction position sensitive photocell 2−44182
Ge III band structure 2−80980
Ge surfaces, heat-treated in various atmospheres, e.s.r. obs. 2−72488

Semiconducting materials continued
germanium continued
Ge(Li), coaxial, gamma ray camera for medical use, computerised display 2−51936
Ge(Li) coaxial detector, local efficiency variations 2−70301
Ge(Li) coaxial detectors used as spectrometer, pulse shape analysis 2−46054
Ge(Li) coincidence spectrometer system for simultaneous spectroscopy of charge 1 and 2 particles, 1 to 60 MeV 2−49633
Ge(Li) counters for detection and energy det. of high energy protons 2−46055
Ge(Li) detector, pulse shape from gamma photon 2−42465
Ge(Li) detector, reactivation technique, using reverse bias clean up 2−49664
Ge(Li) detector, timing system for coincidence and nuclear lifetime obs. 2−49662
Ge(Li) detector, timing system 2−73942
Ge(Li) detectors, absolute γ-ray efficiencies for thermal neutron capture studies 2−67256
Ge(Li) detectors, side entry and thin contact types, dead layer effects for α- and β-particles 2−49663
Ge(Li) detectors, with highly compensated intrinsic regions 2−46050
Ge(Li) γ-ray detectors, evaluation procedures 2−55919
Ge(Li) particle detector, fast neutron flux meas. 2−63704
Ge(Li) spectroscopy, use of single escape peak 2−46036
Ge(Li) total absorption spectrometer for (n, xγ) cross section meas. 2−46039
Li compensated γ spectrometer 2−52678
Si-Ge alloy, oxide layer etched away reoxidation, production of MOS transistors 2−75132
Si-Ge p^+-n alloyed heterojunction, V-I characts., uniaxial stress effect 2−81120

indium antimonide
acousto-electric domains, origin and properties 2−54034
anodic dissolution potentials and activation energies in HCl 2−71366
band structure, critical point detn., wavelength modulation derivative spectroscopy obs. 2−48160
band structure, X-ray photoemission study 2−84387
band-structure, deformation potentials, from Shubnikov-de Haas measurements 2−68416
conversion of low voltage electric current 2−45634
core levels, spectral obs. 2−65240
crystal growth rate, effect on impurity distrib. 2−47209
density of states in impurity bands 2−80961
effective mass of conduction electrons det. from magnetophonon effect, undergrad. expt. 2−65009
electron lifetime, dHvA effect obs. 2−71909
electron-hole plasma in mag. field, carrier wave growth 2−61316
electronic structure study by a microwave beat method 2−84246
e.m. wave scatt. by sound, electron conc. wave contrib. 2−54396
energy gap, temp. depend., calc. using Brooks-Yu theory 2−68415
exciton-hole plasma prod. by laser irrad., two-photon absorpt., direct recomb., 77K 2−80972
film, Hall electron mobility parameters 2−54176
film, thickness dependence of electron mobility, model based on surface accumulation layer 2−68403
forbidden gap, pressure coeff. under uniaxial deform. 2−84284
Gruneisen parameter determ. at low temps. from elastic consts. 2−71752
heat treatment effects, field effect and elec. cond. obs. 2−64989
helicon wave propagation in magnetic fields up to 200 kG 2−47910
hot electron absorption of millimeter and submillimeter waves 2−78119
impact ionized excess carriers recomb., direct lifetimes obs. at 77 K 2−71910
i.r. detector, comparison with $Hg_{1-x}Cd_xTe$ for low contrast targets at 5 μm and 10 μm 2−63142
i.r. dispersion of second order electric susceptibilities 2−61581
Landau levels, at saddle point, diff. reflectivity in mag. field obs. 2−71795
Landau transitions at E_1 edges, excitonic effects 2−68404
magnetophonon spectroscopy study 2−68385
microwave emission, contact effect 2−47897
microwave radiation, acoustoelectric amplification 2−54159
microwave self- focusing, phenomenology 2−68591
mobility, maximum absorpt. freq. eval. expression 2−57176
n-type, acoustic gain parameter meas. 2−68243
n-type, acoustoelectricity, ultrasonic, amplification of surface waves 2−77774
n-type, anisotropic complex small signal cond. of hot electrons at 84K and 134 GHz 2−61318
n-type, effect of stress on frequency of magnetophonon oscillations 2−47571
n-type, elec. fields, current, charge densities, impact ionization phenomena, mag. field effects 2−61317
n-type, electric field modulated laser cyclotron resonance, impurity and cond. electron resonance obs. 2−81021
n-type, electron energy dissipation in high mag. fields, phonon heating effects 2−77898
n-type, electron-hole plasma form. rel. to current and voltage instabilities 2−57137
n-type, e.m. surface waves 2−44120
n-type, Faraday and Kerr effects of hot electrons in i.r. 2−57326
n-type, film, transport phenomena, 20-100 K and 300-500 K 2−71911
n-type, Gunn effect threshold in transverse mag. field, travelling domain form. 2−71908
n-type, heavily doped, impact ionization, elec. field depend. 2−81087
n-type, hot electron Kerr effect, birefringence phase shift calc. 2−51303
n-type, impurity band and shallow donors, far i.r. absorp. obs. 2−81389
n-type, in waveguide, effect of mag. field on microwave propagation 2−82395
n-type, Knight shift in the extreme quantum limit 2−84597
n-type, large amplitude current and voltage oscills. 2−57180
n-type, l.f. current noise, electron plasma critical fluctuations, 4.5-12 K 2−68319

Semiconducting materials continued
indium antimonide continued
n-type, magnetoacoustoelectric effect, acoustoelec. domain form. and instabilities 2-64850
n-type, nonlinear optical susceptibility dispersion in mag. field, band model calc. 2-51299
n-type, nonlinear transport props., hot electron cyclotron resonance obs. 2-77845
n-type, nonlinear transport props. of hot electrons in strong mag. field 2-47896
n-type, plasma echo oscillations 2-57195
n-type, quenching of sound amplification and e.m. wave radiation by holes 2-71929
n-type, recomb. radiation from impact-ionized shallow donors 2-68707
n-type, sound amplification 2-68238
n-type, surface plasmon-phonon interaction 2-71930
n-type, time and spatial distrib. of amplified acoustic flux 2-68242
n-type, transport coeffs. at high temp., degeneracy and screening effects 2-68378
n-type, uniaxial stress effect on magnetophonon effect 2-44115
n-type, u.s. second harmonic generation 2-51039
narrow band emission, nuclear electric quadrupole radiative transitions 2-78118
optical nonlinearity dispersion near band gap 2-48127
p-n junction, minority carrier diffusion across electron beam study 2-81111
p-type, anisotropic photon drag effect 2-75165
p-type, i.r. absorpt. rel. to hole and plasma currents 2-72335
p-type, lightly doped, radiative recomb. parameters temp. depend., 10-400K 2-65293
photoconductivity, effect of light and X-rays at 77K 2-47996
radiation damage, review 2-47365
Raman scattering, linewidth in spontaneous spin-flip 2-48199
recombination rate rel. to elec. field, drifted Maxwellians approx. 2-81077
resonant far-i.r. generation theory 2-61579
resonant optical nonlinearity due to cond. electron spins 2-65208
spheres, small, cyclotron reson. type absorpt. due to induced mag. moment at 35 GHz and 77K 2-68326
spin flip Raman scatt., spin saturation and relax., rate eqn. technique 2-68662
spin-flip Raman laser cavity, modes, transition schemes, gain, loss mechanisms 2-66770
stimulated spin-flip Raman scattering rel. to homogeneously broadened travelling-wave electronic Raman laser 2-42100
thermal etch pattern form. during diffusion 2-47440
transition metal doped, anomalous elec. and mag. props. 2-68405
tunnel junction, Cd diffused, I-V characts. and magnetotunnelling 2-54216
wave function, direct meas. from Knight shift in extreme quantum limit 2-68746
InSb:Fe, crystallisation features rel. to dopant, hole and acceptor distribution 2-53604
p-InSb:Ge, electrical instability in presence of elec. field 2-71884
InSb:Te, Zn, carrier distrib., thermal e.m.f., degree of compensation 2-44101
InSb:Zn,Ge, energy levels of shallow acceptors, far i.r. absorp. obs. 2-75296
InSb, magnetophonon mass change in drifting hot carriers 2-68389
n-InSb mixed plasmon-phonon surface modes 2-81006
n-InSb radiation detector, performance at 77K 2-78988
n-type, Corbino disc in mag. field, r.f. wave generation 2-84333
silicon
— 2-72499
acceptor states, Zeeman effect, group theoretical study 2-84264
acoustoelectric effects, quadrupole and octupole electron phonon coupling 2-61101
amorphous, absorption edge temp. depend. 2-75293
amorphous, band struct., optical props., pressure effect obs. 2-61333
amorphous, cryst. polytypes, electronic struct., pseudopot. and tight binding models 2-71946
amorphous, dark-field electron microscope obs. 2-60593
amorphous, electron emission, electronic struct. obs. 2-61454
amorphous, electron tunnelling through oxide barrier 2-61359
amorphous, field depend. of elec. cond. 2-77896
amorphous, photoelectron energy distrib. curve obs. 2-61464
amorphous, temp. depend. tunnelling, m.o.s. obs., density of states 2-47952
amorphous, the case for sharp band edges 2-61183
amorphous film, elec. cond., 77-3000K, annealing effects 2-61360
amorphous film localized state distrib., field effect study 2-68437
amorphous-crystalline junction, high photovoltages obs. 2-48005
anisotropy and hot electron effects, 1-300 K 2-84342
avalanche breakdown, statistical theory based on Boltzmann transport equation, scattering mechanisms 2-54202
avalanching and second breakdown in silicon-on-sapphire diodes 2-57216
average energy per electron-hole pair generation between 5 and 320K 2-70299
band edge position, under uniaxial pressure, Schottky barrier obs. 2-51167
band struct. rel. to struct. in tetrahedrally bonded and amorphous states 2-68436
band structure, critical point detn., wavelength modulation derivative spectroscopy obs. 2-48160
carrier concentration, determ. from refl. in optically homogeneous samples 2-54406
conduction band, deform. potential const. from piezospectroscopy of donors 2-68438
conductivity type determ. using rectifying contacts 2-68428
contact, Si-Si, symmetrical, thermal effects 2-61379
contact potential difference measurements on oxidised Si surfaces 2-77914
crystal growth, pedestal technique using electron beam heating 2-43512
crystals, temperature distrib., obs. 2-51364
cyclotron resonance of electrons generated by impurity excitation with CO_2 laser 2-71947

Semiconducting materials continued
silicon continued
detector, coaxial, tissue equivalent, for in-vivo dosimetry 2-46049
detector, pb, diffused, energy resolution, charge collection from entrance windows 2-49665
detector with partially depleted surface barrier for meas. of low-energy β-nuclide radioactivity 2-49673
detectors, p + n, low noise oxide passivated, fabrication and electrical props. 2-46048
dielectric matrix and phonon frequencies computed 2-47933
diffuse reflection spectra, energies of E_1, E_2 and E_1' peaks 2-75275
diffused impurities, As, Sb, Au, investigation of concentrations, lattice locations using He-Ion backscattering technique 2-64675
diffusion, of B, effect of mask edges 2-54205
diffusion of Au at 1000°C, rel. to dislocations, reaction rate limited 2-60833
diffusion of B, Si-B phase influence 2-77523
diode, p^+-n and n^+-p, with Au impurity in base, barrier capacitance 2-71979
diodes, square-law 'punch-through', application as high-level parabolic detectors 2-44135
donor states, group V and VI, multivalley effective mass approx. 2-54204
doping influence on dislocation velocity, electron trapping during kink nucleation 2-50674
doping inhomogeneities, obs. by electroreflectance 2-71510
drift detector, effective thickness of dead layer 2-42467
electroabsorption, split-off exciton and phonon-depend. lineshape 2-72349
electrode, equilibrium and nonequilibrium effect near semiconductor-electrolyte boundary 2-61798
electron beam monitor, surface barrier detector 2-63723
electron bombarded, pair-prod. energy for free carriers 2-61351
electron irrad., recomb. luminesc., annealing and impurity effects 2-48231
electron irrad., recomb. luminesc. mechanism 2-48230
electron irradiated, asymmetric damage regions, elec. props. obs. 2-74759
electron irradiation defects, liquid He temp., a.c. hopping cond. obs. 2-47936
electron mobility, theoretical calc. 2-77889
electron momentum distribution, Compton profile obs. 2-57128
electron spectroscopy of amorphous film at energy losses below 1 eV 2-80934
electron-electron interactions continuously variable in range $2.1>r_s>0.9$ 2-57134
electronic properties of surfaces and atomic structure, effect of annealing 2-72095
electrons, holes, transport properties in surface inversion layer 2-75117
emission band, two electron band-to-band transitions, excitation intensity 2-61699
energy bands, muffin tin potential calc. in open struct. 2-75032
epitaxial film, nonequilibrium carrier lifetime, photoelectric obs. 2-84331
epitaxial film growth using SiH_4-H_2 system 2-71335
epitaxial manufacturing at low temp., using HI-H_2 vapour etch technique 2-83852
epitaxial n-n^+ and n-n^+-p structures, metallurgical boundary det. 2-61356
exciton condensation, ground state energy calc. using improved RPA approx. 2-71809
exciton recomb. luminesc., 20-77K 2-78138
field-emission cathode, preparation technique 2-82433
film, amorphous, effects of thermal neutron irrad. 2-60666
film, amorphous, optical absorp. and photocond. spectra obs. 2-61655
film, epitaxial, gas doping during deposition 2-50690
film, prep. using plasma source 2-67912
film and bulk, electron irrad., defect prod., resist. change 2-80655
film on sapphire, elec. prop. determ. using m.o.s. Hall technique 2-51169
free hot carrier impact ionization obs. 2-54203
Gruneisen parameter determ. at low temps. from elastic consts. 2-71752
helicon wave propagation in mag. fields up to 200 kG 2-47910
high resistivity, space-charge- limited minority hole flow 2-75118
hole drift velocity rel. to band struct., elec. field effects, at 5 K 2-81107
impact ionization coefficient, Schottky barrier obs. 2-44091
impact ionization of charge carriers, energy conservation considerations 2-75081
implantation of B and P, channelling and anomalous diffusion effects on charge carrier distrib. 2-47432
intrinsic surface states, densities, photoemission densities 2-44207
inversion layer, quantum galvanomagnetic effects 2-68387
invivo particle detectors, medical and biological applications 2-51938
ion implantation technology 2-53747
ion irradiated, divacancy formation and annealing, i.r. absorpt. study 2-71457
ion-implanted, radiation damage under channelling conditions 2-68017
irradiated, multiple vacancy centres, e.p.r. obs. 2-48283
irradiation defects, concepts and correlations 2-47387
isolated vacancy, elec. struct., many electron molecular orbital method 2-47935
junction, thermally diffused, avalanche multiplication rel. to dislocation lines 2-65027
junction diode sensor for electronic thermometer 2-55591
low concentration diffusion in Si, under sealed tube conditions 2-74792
metastable polycryst III, photon Raman spectra 2-68664
microwave absorpt., by electron-hole drops 2-57209
microwave absorpt. spectra anisotropy hole reson. rel. to wave vector 2-71822
minority carrier lifetime and surface recombination velocity, m.o.s. transient response obs. 2-65017
m.i.s., inversion layer, hole field effect mobility rel. to dielec. charge 2-71992

Semiconducting materials continued
  silicon continued
    m.i.s. structure, using Al_2O_3 films, characts. 2−71997
    m.o.s. capacitor, current and capacitance transients, theory and applic. to initially depleted surface 2−47957
    m.o.s. structure, surface barrier electroreflectance obs. 2−65241
    n-channel junction f.e.t., neutron damage annealing 2−51181
    n-channel m.o.s.f.e.t., electron mobility, electron surfon interact. calc. 2−51172
    n-type, (111) surface, LEED and Auger spectroscopy obs. 2−50464
    n-type, Cd-compensated, current oscills. 2−71949
    n-type, degenerate, e.s.r. obs. 2−48273
    n-type, degenerate, transverse magnetoresist., low temp. 2−84344
    n-type, elasto-electronic effects 2−65020
    n-type, fast electron irrad., vacancy capture and transfer between defect complexes 2−80694
    n-type, heavily doped, under uniaxial stress, elastic consts. 2−68066
    n-type, hot electron instabilities, Monte Carlo calc. and neg. diff. cond. obs. 2−77912
    n-type, inversion layers, self-consistent calcs. 2−47934
    n-type, i.r. free carrier absorpt. consts. 2−81408
    n-type, microwave Faraday effect measurement 2−61591
    n-type, phenomenological energy relax. time, elec. field depend., 77K 2−65010
    n-type, proton bombardment induced shallow donors, elec. props. 2−61355
    n-type, radiation induced defect, photoconductivity obs. 2−72066
    n-type, resist. rel. to donor spin reson., spin energy transfer model, 4K 2−68434
    n-type, stress induced electric fields 2−44127
    n-type, surface states, energy distribution of photoemitted electrons 2−44208
    n-type, transverse magnetoresist., mag. field strength depend. 2−65018
    n-type, weak cond. anisotropy in static mag. field, e.m. propag. obs. 2−84343
    n-type doped, microwave propag., transverse static mag. field effect 2−54197
    neutron irrad., divacancies, i.r. absorpt. and photocond. 2−48194
    neutron irrad., space-charge- limited current obs. of electron trapping 2−51168
    neutron irradiated, space charge limited currents, fitting expt. data, third side of Lampert triangle 2−84328
    neutron irradiated, space charge limited currents, fitting expt. data, third side of Lampert triangle 2−84328
    neutron irradiated, traps-filled- limit region, third side of Lampert triangle 2−84329
    neutron irradiation damage, Mossbauer effect obs. 2−48153
    neutron irradition damage, piezospectroscopic obs. 2−48193
    optical and dielec. props. 2−48189
    optical constants, disturbed internal reflection method, electronic props. detn. 2−72253
    oxidized surface, orientation effects on electron and hole transport props. 2−51173
    p,n, impurity concentration meas. by mercury probe 2−71509
    p-channel charge coupled devices, resistive gate structure 2−61398
    p-n diode, γ-irrad., impurity effects, photovolt. effect obs. 2−61358
    p-n hyperabrupt junction, breakdown voltage 2−84347
    p-type, (001) inversion layer, continuously voltage tuneable line absorp. in surface quantization 2−47997
    p-type, absorpt. saturation intensity at 10.6 μm 2−79227
    p-type, electron irrad., hole emission rates, activation energy and annealing of defects 2−54199
    p-type, electron irrad., low temp. photocond. 2−47999
    p-type, field emission, temp. depend for various volume doping 2−57260
    p-type, Hall coeff. and elec. cond., electron irrad. effects 2−71944
    p-type, Hall effect and elec. cond., electron irrad. effects 2−54201
    p-type, impurity scatt. of warm holes 2−44124
    p-type, inversion layer, band structure, piezoresistance and mobility obs. 2−51171
    p-type, i.r. absorpt. by free carriers 2−48190
    p-type, role of surface states in auto-photoelectric emission 2−44199
    p-type epitaxial film, dual rate deposition on spinel, hole mobilities detn. 2−43482
    particle detector, simple multicounter system 2−55918
    photocell, temperature dependence of relative spectral sensitivity 2−44186
    photocell and phototransistor, with non-linear characteristics, obs. of relative spectral sensitivity 2−42463
    photocell effects of polarization on performance 2−44185
    photoconducting for wide range of band bending near surface 2−72062
    photoconductivity, intrinsic, spectral depend. 2−47998
    photodiodes as dosimeters for fast neutrons 2−46057
    photoelectric solar cells, crystals obtained by Stepanov method 2−45660
    photoemission spectroscopy, using synchrotron radiation, valence band and surface states obs. 2−81194
    photon emission line from condensed phase of nonequilibrium carriers 2−51370
    photovoltage, photocond., spectral and field depend. 2−65086
    photovoltage, photocond., under different bulk and surface recomb. characts. 2−65087
    planar diode, elec. props. rel. to lattice defects, X-ray obs. 2−47944
    point arrays, photosensitive field emission, quantum efficiencies 2−81186
    polytype, density of states and optical props. 2−61185
    positron annihilation rate, enhancement in periodic fields 2−77801
    positron lifetime spectra, temp. depend. 2−75003
    preferential etching charact. using water-ethylene-diamine-pyrocatechol solution 2−71316
    quadratic Zeeman effect of donor lines 2−57350
    radiation defects, recomb. processes, Fermi level obs. 2−47937
    radiation defects, theory of vacancies 2−47364
    radiation detectors, high-purity, characteristics analysis 2−52695
    radiative recombination, during electron-hole condensation in pure and doped material 2−78133
    radiative recombination rate, 300K, carrier conc. depend. 2−81430

Semiconducting materials continued
  silicon continued
    radiative two-electron transitions, in the electron-hole plasma 2−78139
    recombination centre parameters of irradiated p-n junctions, determ. 2−61382
    recombination radiation, spectrum and decay, laser excited 2−61700
    semiconductor, electron diffusion, in high electric fields 2−57177
    shallow donor electrons, ground-state wave function 2−61361
    single crystal point contact diode, polarized memory effect mechanism 2−61389
    single crystal substrate, Au covered, SiO_2 formation 2−67911
    single crystal substrate, Pt metallization, PtSi film formation and thermal stability 2−71334
    solar cells, efficiency comparison with GaAs cells on spacecrfat, 0.2 to 10 a.u. 2−49306
    solar cells, short-circuit current rel. to minority carrier diffusion length 2−59060
    spin dependent mobility 2−71778
    spreading resistance measurement, contact resistance temp. depend. 2−51161
    stack diodes, extremely high voltage, for colour TV receivers 2−65032
    stimulated Stokes and anti-Stokes emission by Nd glass laser 2−44391
    substrate, impurity adsorption, effect on epitaxial layers 2−74647
    surface, monomolecular layers exam. using ellipsometry 2−56601
    surface, spin-depend. recomb. of photocreated excess carriers 2−51217
    surface barrier detector, low-cost fabrication for laboratory use, characteristics 2−78731
    surface barrier detector, radiation damage effects from 2 MeV protons 2−46056
    surface barrier detectors, derivation of fast time marking signals 2−46051
    surface cleaning, H_2O_2 soln., HEED and Auger electron spectroscopy obs. 2−53555
    surface impedance, due to generation of unbalanced charge carriers 2−54200
    surface state density distribution, rel. to diffusion induced disloc. near junc. formed by P diffusion 2−44038
    surface states, e.p.r. data, correlation with Hubbard model 2−51154
    surface states, three parameter local pseudopot. method calc. 2−57131
    surface states rel. to photocond. obs. 2−47932
    surface struct. rel. to surface states, surface cond., LEED 2−77800
    surface wave filters in integrated circuits 2−49112
    tetrahedrally bonded, vibr. states from Keating model, Raman line intensity 2−68224
    two-stage diffusion, layer parameters calc. allowing for evaporation 2−71512
    u.s. attenuation stress depend., bound hole model, p-type mat. 2−54031
    wafer, device-processed, generation of stacking faults and dislocation loops 2−51179
    wafer, surface defect generation on reoxidation in H_2O vapour during B diffusion 2−64672
    wafers, thickness determ. using optical method 2−67902
    X-band double-drift IMPATT diode fabrication by consecutive epitaxy 2−71976
    X-ray spectrometer, lithium compensated 2−49650
    Al-Si contacts, electromigration failure 2−50706
    Al-SiO_2-Si, m.o.s., transport props. in inversion region, 123-573 K 2−47954
    B predeposition, using B_2H_6 2−71503
    fast neutron radiation damage, e.p.r. obs. 2−48282
    in $Ga_{1-x}Al_xAs$ layers, Al conc. effect on amphoteric behaviour of Si 2−51153
    GaAs:Si laser, double heterostruct. diode, laser action 9100-9500 Å, threshold current conversion efficiencies 2−73591
    Ge-Si heterojunction, pulse characts. 2−71961
    $LiNbO_3$-Si layered structure, transverse acoustoelectric effect obs. using capacity probes 2−51038
    n^+-p diode, fast electron irrad., cappacitance 2−71978
    n-type, inversion layer, two dimensional impurity states 2−51170
    Pt-Si contacts, solid-solid reactions 2−50715
    Si:Ag, deep impurity properties, photoconductivity decay, and TSC obs. 2−61363
    Si:As, evacuated capsule method, appl. to microwave transistor 2−71518
    Si:As, P, Sb, ground state wavefunctions of shallow donor electrons, Fermi contact consts. 2−71950
    Si:Au, Ag, Co, trapped minority carrier thermal emission rates, meas. technique 2−71784
    Si:Au, m.o.s. capacitance meas. of Au levels 2−61362
    Si:Au, near i.r. absorpt. 2−72348
    Si:Au, with two Schottky contacts, low freq. current oscillations 2−61383
    p^+-n Si:Au diode, current filament behaviour in mag. field 2−71975
    Si:Au diode, thermally-stimulated current from deep-lying trapping levels 2−68419
    Si:B, implantation profiles determ. by secondary ion mass spectrometry 2−74794
    Si:B, impurity profiling, techniques 2−71505
    Si:B, ion implanted, conc. distrib. by (n,^{4}He) nuclear reaction 2−56743
    Si:B, lateral spread of implanted ions, obs. by junction delineation 2−71508
    p-Si:B, Li-compensation influence on irrad. defect form. 2−47390
    Si:B, low temp. B diffusion using B_2H_6-CO_2 system 2−43645
    Si:B, shear deform. pot. consts. of B acceptors ground state, piezospectroscopy obs. 2−75306
    Si:B implanted, photocond. obs. 2−44126
    Si:B impurity enhanced diffusion 2−50693
    Si:B(As), diffusion by using emulsion type doped oxide 2−71517
    p-Si:Be, hole transport, piezoresist. gauge factor 2−54198
    Si:C, low temp. electron irrad. damage, i.r. absorp. obs. 2−48191
    Si:GaAs light emitting diode MV-50 fast luminescent decay meas. 2−45812

Semiconducting materials continued
- silicon continued
  - Si:Ge, O, C, low temp. electron irrad. damage, i.r. obs. 2−48192
  - Si:In, ion implanted, photoelectromag. effect rel. to dose and annealing 2−72077
  - Si:In, spectral depend. of extrinsic photocond. 2−51216
  - Si:K, doped surface layers, donor props. and diffusion 2−65019
  - n-Si:Li, impurity role in irrad. defect prod. 2−47385
  - Si:Mg, donor levels, excitation spectra 2−72351
  - Si:Na(K), elec. props., impurity atomic radius effects 2−71948
  - Si:Ni, photocond., thermal and field quenching by impurity electron capture 2−65088
  - Si:P, absorpt. due to transitions to cond. band edge region 2−72347
  - Si:P, diffused, impurity profile kink form. mechanism 2−56742
  - Si:P, electron drag rel. to impurity centre photoionization, photo-e.m.f. 2−65089
  - Si:P, epitaxial, doping during growth 2−47431
  - Si:P, heavily doped, e.s.r. linewidth, temp. depend. 2−72500
  - Si:P, heavily doped, temp. depend. of resist. 2−71940
  - Si:P, implantation damage annealing, resist. and electron microscope study 2−64678
  - Si:P, implanted, annealing characts. 2−77594
  - Si:P, implanted, carrier density and mobility, depth distrib. 2−80993
  - Si:P, intermediate region of impurity cond., e.s.r., effect on resist. 2−72498
  - Si:P, phonon and electric field influence on extrinsic photocond. 2−81179
  - n-Si:P, piezoresist. and piezo-Hall effect, 4.2, 77 and 300K 2−71945
  - Si:P, spin susceptibility of impurity band electrons, correl. effects 2−68520
  - n-Si:P epitaxial layer, on MgO.Al$_2$O$_3$, elec. and optical props. 2−77910
  - Si:P impurity enhanced diffusion 2−50693
  - Si:P thermometers, implanted, for 10 mK to 20 K 2−48938
  - Si:P thermometers, implanted, for 10 mK to 20 K 2−48938
  - Si:P(As) radiation-induced infrared absorption bands, piezospectroscopic studies 2−68650
  - Si:S, deep donor levels, pressure depend. 2−80962
  - Si:Zn, many-band pseudopotential calc. of photoioniz. 2−61357
  - n-Si:Zn, photoelectronic props. of Zn centres, Zn^{2-} energy level, centre density 2−61449
  - Si/Pt interface-state density, photoelectric measurement 2−44128
  - Si/SiO$_2$ interface, hot electron energy losses, photoemission obs. 2−81061
  - Si-AlN interface, in m.i.s. struct., elec. props. 2−54225
  - Si-CrSi$_2$, CrSi$_2$ fibres in Si matrix, anisotropy columnar structs., resist. anisotropy 2−74920
  - Si-Ge alloy, oxide layer etched away reoxidation, production of MOS transistors 2−75132
  - Si-Ge heterojunction position sensitive photocell 2−44182
  - Si-Ge p$^+$-n alloyed heterojunction, V-I characts., uniaxial stress effect 2−81120
  - Si-PZT coupled system, acoustic surface wave convolution by 14.5 MHz Bleustein-Gulyaev waves 2−71742
  - Si-Si$_3$N$_4$-SiO$_2$-Si structure, elec. characts., annealing and impurity effects 2−71984
  - Si-SiO$_2$-metal, m.o.s., potentials and d.c. rel. to oxide thickness and interface states 2−61406
  - Si-SiO$_2$ capacitor, frequency response of interface states 2−61404
  - Si-SiO$_2$ interface, effects of illumination on electrical properties 2−44147
  - Si-SiO$_2$ interface, fixed charge behaviour, rel. to growth conditions 2−54227
  - Si-SiO$_2$ interface, photoemission from Si to SiO$_2$ during laser irrad., photocurrents 2−81119
  - Si-SiO$_2$ interface, scatt. of conduction electrons by surface oxide charge 2−72000
  - Si-SiO$_2$ interface, surface state distrib., m.o.s. characs. obs. 2−47956
  - Si-SiO$_2$ m.o.s. structure, tunnel conductance, interface states obs. 2−68459
  - Si-SiO$_2$ system, diffusion of B 2−68037
  - Si, pn junction, proton irrad., deep centre spatial distrib. from capacitance meas. 2−68443
  - Si III band structure 2−80980
  - Si transmissive mode field emission array photoemitter, photosensitivity 2−81187
  - 4π- Si(Li)-β-spectrometer, reproduction of monoenergetic electron lines using coincidence method 2−63689
  - Si(Li) detectors, timing behaviour, comparison of methods for det. 2−49674
  - Si(Li) detectors side entry and thin contact types, dead layer effects for α- and β- particles 2−49663
  - Si(Li) miniaturized detector for β and γ meas. in superficial and deep parts of living tissue 2−55252
  - Si(Li) nuclear radiation detector, damage by thermal neutrons 2−76732
  - Si(Li) semictor adaptation for X-ray diffractometer 2−47298

Semiconductor lasers *see Lasers/semiconductor*

Semiconductor-metal boundaries
- amorphous chalcogenide, low resistance contacts 2−75121
- blocking contact, influence of Schottky effect applied voltage distrib. on depletion layer and V-I characs. 2−61369
- contact, semicond. base region, overheating mechanism rel. to negative resist. 2−65035
- contact, surface elec. field, determ. by differential electroabsorpt. 2−65036
- contact region, electrostatic potential distrib. during injection into blocking contact due to illumination 2−68447
- current transport, unified approach 2−51175
- Fowler universal photoemission curve, operational equivalent 2−72087
- many-body problems at metal- semicond. junctions, surface plasmons and e-e screened interac. 2−75119
- metal-GaAs (110) contact, Schottky barrier height 2−54214
- photodiodes, quantum yield inversion region effects 2−81116
- Schottky barrier, capacitance rel. to freq., deep level impurity effects 2−44138

Semiconductor-metal boundaries continued
- Schottky barrier on GaP, obs. of elec. active background impurities 2−80939
- solid surfaces, conference, Boston Mass., USA, Oct. (1971) 2−47070
- substrate stress effects on semicond. parameters 2−71966
- tunnelling characteristics, variation with hydrostatic pressure 2−61393
- Al-Ge, contact, slow states activation energy, barrier height temp. depend 2−75135
- Al-Si contacts, electromigration failure 2−50706
- Al-n-Si Schottky barrier structures, effects of Au doping on pressure sensitivity, boundary characteristics 2−65038
- Au−n-GaP, surface barrier diode, photosensitivity, 1.4-5.2 eV spectral range 2−75182
- CdS-Au, study of anode hole injection 2−84346
- CdS platelets, drift meas., Schottky contact effects 2−77884
- n-Ga$_{1-x}$Al$_x$As, surface barrier struct., energy band diagram 2−75134
- GaAs, Schottky barrier height, temp. depend. 2−71958
- n-GaP, surface barrier props., surface levels detn. 2−84352
- n-GaSb-Pb contact, tunnelling spectroscopy and band struct. press. effects 2−84351
- Ge$_{16}$As$_{35}$Te$_{28}$S$_{21}$, amorphous, photovoltaic effect and space charge capacitance 2−61374
- MoO$_3$ film, Schottky barrier obs. rel. to elec. behaviour under d.c. bias 2−68454
- MoO$_3$ film, Schottky barrier obs. using dielectric relax. currents in Al-MoO$_3$-Al structures 2−68453
- Pb-GaAs Schottky barrier tunnel junction, zero bias anomaly, irrad. effects 2−71960
- Pt-Si contacts, solid-solid reactions 2−50715
- PtSi-Al Schottky diode, barrier height rel. to heat treatment 2−75131
- Se on metal substrate, stress effects on semicond. parameters 2−71966
- Si Schottky barrier, band edge position under uniaxial pressure detn. 2−51167
- SiGe/W film, interface reactions, effects of p- or n-type substrates, ion backscattering analysis 2−71951
- SiO$_2$, interface states and potential barriers 2−65043
- SrTiO$_3$/Au(Pd), barrier props. 2−71985
- ZnO/Au(Pd), barrier props. 2−71985
- ZnTe with Au, Ni, Ta, Al, electrical properties, thermionic emission model, recombination current model 2−64962

Semiconductors
- *see also Crystal electron states; Ion implantation; Magnetoelectric effects; Photoconductivity; Photovoltaic effects*
- acoustoelectric effect, carrier trapping effects 2−47746
- adsorption,physical at semiconducting surfaces 2−47147
- alloy, substitutional, nonexistence of localized tail states 2−64996
- alloyed, absorption coeff. in ω>Eq region in presence of resonant scattering 2−72316
- ambipolar diffusion noise spectrum when ambipolar drift is negligible, mag. field effects 2−61269
- amorphous, band struct., optical props., pressure effect obs. 2−61333
- amorphous, band struct., tight-binding Hamiltonian 2−84274
- amorphous, bridge method of measuring magnetoresistance 2−44122
- amorphous, charge controlled switching effect 2−61271
- amorphous, conducting filament rel. to electrotransport in liquid alloys 2−60455
- amorphous, contace and surfact photovoltage, surface props. and chemisorption obs. 2−77969
- amorphous, d.c. hopping conduction, percolation treatment 2−68273
- amorphous, diamag. enhancement of susceptibility, mechanisms 2−44219
- amorphous, electronic struct., LCAO calc. 2−68414
- amorphous, Hall cond., random phase model 2−61277
- amorphous, localized state density energy depend. determ. using field effect 2−47911
- amorphous, lone pair, refr. index press depend. 2−68594
- amorphous, long range order, short range order and energy gaps 2−61158
- amorphous, modelled by fast-neutron- compensated n-Ge 2−68429
- amorphous, optical properties 2−61573
- amorphous, photocond. response characts., obs. with photocond. ccts. 2−84375
- amorphous, reversible elec. and optical memory effects, rel. to phase transition 2−57185
- amorphous, statistics, recomb. processes and photocond. 2−61290
- amorphous, steady state photocond. theory 2−61447
- amorphous, struct. modelling 2−67881
- amorphous, structural models 2−60566
- amorphous, switching mechanism 2−68381
- amorphous, tetrahedrally bonded, electronic density of states theory 2−61159
- amorphous, theory and band models 2−47879
- amorphous, tight-binding model 2−84275
- amorphous, Urbach tail in optical absorpt. edge 2−68641
- amorphous, with globular inhomogeneities, interglobular electronic transport 2−68390
- amorphous and liquid, conf., Ann Arbor, USA, Aug. (1971) 2−61258
- amorphous and liquid, conf., Ann Arbor, USA, Aug. (1971) 2−61259
- amorphous semicond. films, physical background of applic. 2−77885
- anisotropy and spin effects of electrons and holes on phonon instability in a magnetic field 2−84180
- antiferromagnetism, canted, magnetization curve, s-d model 2−81309
- Auger recombination determ. from impact ionization data 2−84385
- band extrema at Brillouin zone centre, interband optical transitions 2−65250
- band struct., survey of calc. methods, results, binding and transport props. 2−81012
- band structure, model for covalent semicond. with topological disorder 2−51149
- bound excitons, exchange interactions 2−81009

Semiconductors continued
bulk 1/f noise, exptl. evidence for existence 2−47938
carrier diffusion, effect of h.f. electric field 2−84335
carrier distribution determ., p-n junction C-V characteristic method with feedback 2−68440
carrier distribution function, high-field, calc. 2−61292
carrier mobility measurement, high ohmic layers, van Heek method 2−57207
carrier waves, with velocity distributions 2−84324
chalcopyrite, linear and nonlinear optical props. 2−48126
compensated, metal-nonmetal transition, theory 2−68412
compensated, thermal current instability 2−75088
conductivity, microwave-induced anisotropy, for semiconductors in quantizing magnetic field 2−71893
contacting bands, dielec. function, transverse and longit., RPA approx. 2−77941
contacting bands, transversal dielec. function in mag. field, RPA approx. 2−77942
contactless resistivity measurement 2−47922
covalent, with topological disorder, LCAO energies and wave functions 2−57096
crystal defects and strain 2−75076
cubic, anisotropic magneto- microwave Kerr effect in Voigt config. 2−68603
cubic, Debye temp. and energy band gap 2−51147
cubic, nonpolar-lattice scattering effect on Ohmic conductivity of holes 2−51131
cubic, polaron Hall mobility calc. 2−68383
cubic, spectral depend. of electro-optic coeffs. calc. 2−81335
cyclotron resonance harmonics, electron-plasmon coupling 2−54409
cyclotron resonance linewidth, mag. field dependence in quantum limit 2−51148
degenerate, accumulation layer, surface bound state energy, mag. field effects 2−51124
degenerate, free carrier absorp., quantum theory 2−51329
degenerate, magnetoplasma surface waves 2−44042
degenerate bands, direct exciton energy levels 2−61199
degenerate Fermi systems, threshold anomaly 2−54432
diamagnetic susceptibility enhancement of disordered or highly compensated crystalline semiconductors 2−81206
diamond structure classification, crystal chemistry 2−54158
diamond-like, ternary, vitrification 2−53522
dielectric constant, third moment of imaginary part, AB type mats. 2−68461
dielectric matrix computed in pseudopotential scheme 2−47933
dielectric screening, correction due to nonlinear term in charge density expansion 2−61217
diffused, electrostatic field gradient theory 2−61261
diffusivity-mobility ratio, in high mag. field, doping depend. 2−57181
dimerized one quarter filled band Hubbard chain, antiferromag. semicond. behaviour 2−61177
direct gap, exciton absorpt. meas. method 2−44373
discrete lattices, non-steady-state diffusion currents in large elec. fields 2−51066
disordered, discrete levels in band gap 2−77802
disordered, hopping conductivity theory 2−61279
disordered, problems arising from energy spectrum and change carrier kinetics theory 2−68391
disordered, theory of electroabsorption 2−51330
disordered binary alloy, two band model in CPA 2−61162
disordered system, Hall coeff. in narrow band, random phase model 2−75008
domain, electric, nL criterion 2−51133
donor density profile det. using Schottky barrier diodes 2−75127
donor-acceptor emission energy shift on varying the excitation intensity 2−72388
donor-acceptor pairs, config. interaction 2−84260
doped, heat treatment and properties of doping element 2−84321
doped, localization of electrons, Anderson's probabilistic approach 2−64880
doped, space-time distribution of excess carriers and their space charge 2−54163
double injection, in semiconductors with deep impurities 2−77923
drift mobility detn. using Shockley-Haynes pulse method 2−68380
electrical conductivity, of semicond. with non-standard zone, in alternating mag. field 2−84318
electrical conductivity anisotropy, semicond. plate in magnetic field 2−75087
electrical conductivity due to variable range hopping in nonuniform density of states 2−81104
electro-transmission in visible and near i.r., charge carrier obs. 2−51323
electrode surface, electrooptical method for determ. of recombination rate and term distribution 2−68423
electron diffusion, in high electric fields 2−57177
electron gas, field free heating, expressions for vel., pressure and temp. 2−51089
electron temp. and second amplification 2−51121
electron-electron interactions continuously variable in range $2.1>r_s>0.9$ 2−57134
electron-hole plasma, eddy currents in oscill. mag. field 2−80995
electron-hole plasma, surface generation of current carriers during Θ pinch 2−61294
electron-phonon coupled system evolution in strong elec. field 2−61291
electronic correlation, field-theoretic model 2−68411
electronic polarons, correl. formulae 2−51086
electronic structure, pseudopotential method calc. 2−81013
electroreflectance line shapes, local-field effects, contact exciton effects 2−68618
elementary excitations, book 2−71806
e.m. wave propagation, space charge waves and progressive amplification 2−55599
e.m. wave propagation and eigenoscillations, band struct. and elec. field effects 2−77892
energy states, occupancy probability, recombination rate theory 2−47875
equilibrium space-charge distribs., calcs., priority of report 2−71888

Semiconductors continued
exciton bound to neutral impurities complex binding energy and stability 2−77835
exciton complexes binding energies, exciton neutral donor complex 2−80970
exciton luminesc., effect of absorpt., surface annihilation of excitons 2−78129
exciton states, 2p, in materials with degenerate bands 2−84261
exponential absorp. edge, theory review 2−78078
extrinsic, nondegenerate, magnetoacoustic amplification 2−80906
extrinsic, nondegenerate, with high cond. electron concs., thermodynamic and kinetic props. 2−77890
ferrite/semiconductor interface, interaction of surface magnetostatic waves with carriers 2−84420
ferromagnetic, coupled helicon-magnon wave, neutron and electron scatt. 2−68314
film, impurity conc. determ. 2−71931
film, kinetics of small charge currents and carrier lifetime determ., from time depend. of photocurrent 2−81088
film, transport coeffs. rel. to surface states, Hall and Seebeck coeffs. 2−47884
film, transverse quantum galvanomag. effects rel. to elastic scatt. by optical phonons 2−64973
films, review of conducting props. 2−64907
films, thin, electrical conductivity for high electrical fields 2−64558
group III to V, transport properties 2−54162
Gunn effect, bulk instabilities, book contrib. 2−57184
Hall effect, anomalous, in ferromagnetic semiconductors with strong s-d coupling 2−71879
heavily doped, absorp. edge at low temp. 2−65247
heavily doped, localization of band tail states, elec. cond. study 2−71922
heavily doped, magnetoresistance at low temps. and weak mag. field, calc. 2−51132
heavily doped, temp. effects on two-band model for neg. magnetoresistance 2−64970
heterogeneous, carrier Hall mobility measurement 2−54164
high resistivity, Hall field determination 2−47883
high-resistivity compensated, impurity photocond. kinetics 2−72058
hopping cond., freq. depend. 2−61270
hot carrier instabilities, in strong mag. field 2−75106
hot electron cyclotron resonance, recomb. effects on line profile 2−84282
hot electron effects, calc. method 2−54193
hot electron magnetophonon resonance, theory 2−68386
hot electron population inversion in crossed electric and mag. fields 2−77817
hot electron recomb. when heated by h.f. elec. field 2−64972
hot electrons, interaction with optical phonons, distrib. func. and energy losses 2−71894
impact ionization coefficient, Schottky barrier obs. 2−44091
impact ionization of charge carriers, energy conservation considerations 2−75081
impedance, waveguide probe meas., effects of e.m. wave front curvilinearity 2−49240
impure, band tail investigations 2−61338
impurity band density of states, tight binding approx. 2−68413
impurity centre scatt. at low temp., transport coeffs. calc. 2−47885
impurity conc. profiles and site distrib. determ. using i.r localized vibr. modes 2−47433
impurity distribution, soln. of Poisson's equation 2−60816
impurity level activation energy, Hall effect determ. 2−80958
impurity profile, limitation of pulsed capacitance obs. 2−71506
impurity profiles, capacitance-voltage meas. 2−64673
impurity solubility, autoradiographic variant of activation analysis 2−72595
impurity states, kq representation 2−77902
incompletely ordered, exciton light absorpt. 2−78094
indirect interaction of nuclear spins through electrons in valence zones of semicond. 2−76760
indirect many-photon transitions, in quantizing mag. field, in Ge- and GaP-type crysts. 2−71920
induction cyclotron resonance 2−71820
inhomogeneous, universal mechanism of excess noise generation 2−75085
instabilities in materials with negative differential mobility 2−54166
instability due to forbidden band thermal deform. 2−54185
insulator, thermal switching behaviour 2−61268
interband transitions, magneto-optical obs., review 2−72294
intermediately bound exciton states, calc. by integral equation method 2−68309
inversion layer, theory of quantum galvanomagnetic effects 2−68387
ion implantation, lattice damage prod. 2−47374
ion implantation induced lattice disorder 2−47367
ionic, ground state energy for polaron bound to Coulomb potential 2−47821
ionic doping, simple ion gun 2−60812
isotropic, biexciton binding energy 2−57132
laser induced transmittance and emission phenomena in polycrysts. 2−61575
layered structs., h.f. surface wave amplification, rel. to carrier density, drift vel. 2−65006
liquid, heat transfer mechanisms, elec. and thermal cond. obs. 2−81094
low mobility, current produced by high elec. field, Poole-Frenkel cond. mechanism 2−77887
magnetic, band structure, survey 2−84226
magnetic, magnon drag effect 2−54165
magneto-optical properties, electron-phonon resonance, many-body theory 2−68604
magnetoactive plasma, overheat instability of drifting waves, theory 2−61293
magnetooptical transitions, plasmon assisted, cyclotron reson., lineshape calcs. 2−68320
magnetophonon spectroscopy, appl. to transport studies 2−68385
magnetoresistance, anomalies due to surface effect, freq. response and carrier lifetime 2−65005
magnetoresistance, in strong electric fields 2−75086
magnetoresistance, low temp. longit., intense mag. fields 2−68388

Semiconductors continued

- magnetosensitive injection-field effect 2-44090
- many photon absorption, by carriers, inc. electron-phonon interaction 2-84521
- many valley cubic, conduction anisotropies detn. 2-68382
- many-valley, n-type, effects of light pumping on conductivity 2-57204
- metal-insulator phase transitions, model 2-57119
- metal-insulator phase transitions, science and technology 2-57205
- microwave conductivity, in heating fields and in presence of electron-hole interaction 2-75084
- microwave field parameters, depend. on semicond. layer resistivity and thickness 2-49207
- minority carrier lifetime meas. by photocond. method 2-75179
- multi-level impurities, photoconductivity theory and obs. 2-54251
- multi-valley, discontinuities in V/I and lux-ampere characts. 2-71895
- multiphoton interband transition, electron- hole pair multiphoton excitation probability 2-77837
- multiphoton luminescence satellites, impure cryst. in strong e.m. field 2-61679
- n-type, heavily doped, model 2-61347
- n-type, quantum transport theory inc. higher order scattering effects 2-47887
- n-type, thermally produced current-voltage characts. 2-71891
- narrow band, current rel. to elec. field 2-77891
- Nernst-Ettingshausen coeff., rel. to nondegeneracy transition at low temps. in strong mag. field 2-71890
- nipi superstructure, critical and electrical props. 2-65237
- nipi superstructure, crystal electron states 2-61336
- non-crystalline, bond theory approach 2-57173
- non-degenerate single-valley, a.c. and d.c. conductivities 2-66454
- non-equilibrium chrage carrier condensation and recombination radiation 2-54184
- noncrystalline system, min. metallic cond., calc. 2-77888
- nonlinear forward drift of electrons in a laser beam 2-57252
- nonlinear optical susceptibilities, Miller's rule, freq. depend. 2-51297
- nonparabolic band, theory of light absorp. by free carriers 2-75285
- nonparabolic energy bands, mag. susceptibility calc. 2-71928
- nonpolar, longitudinal magnetoresist., magnetophonon struct. 2-84327
- one-carrier with variable doping, space charge waves excitation at doping density step 2-81066
- optical constants, disturbed internal reflection method, electronic props. detn. 2-72253
- optical detection of dynamic polarization of nuclei 2-44323
- optically pumped, instability in strong mag. field 2-71889
- organic, applic. 2-75075
- organic, photoelectric method for detecting reactions with gases 2-72570
- p-type, recomb. of excitons bound to deep neutral donors and acceptors 2-68682
- paramagnetic, magnetic polaron props. 2-47880
- photoconduction, anisotropy in persistent internal polarization 2-81176
- photoconductivity, meas. of dark current using electron beam contact 2-75166
- photoconductivity, negative 2-81174
- photodielectric effect, instrument for obs. 2-77907
- photoelectric emission, electronic struct. 2-72088
- photoemissive yield, phonon energy loss effects, band-theoretic model 2-61460
- photomagnetoelectric circulating current, spectral distrib. determ. 2-68483
- physics, conf., Warsaw, Poland, July (1972) 2-68384
- piezoelectric, elastomagnetic waves, coupled e.m. and lattice oscills. 2-64848
- piezoelectric, fluctuating elec. field and Franz-Keldysh effect inside acoustoelec. domains 2-54033
- piezoelectric, impurity, diffusion coefficients, ultrasonic meas. method 2-50691
- piezoelectric, moving acoustoelectric domain nucleation 2-68237
- piezoelectric, narrow propagating domains of acoustic flux, prod. method 2-43978
- piezoelectric, u.s. second harmonic generation 2-51039
- piezoelectric, u.s. second harmonic generation in mag. field 2-68239
- piezoelectric, u.s. wave propagation, effect of weak inhomogeneity in carrier density 2-74984
- piezoelectric, waveguide effect of surface domains 2-54029
- planar structures, thermal resistance 2-51125
- plasma waves, optically induced instabilities 2-61209
- plasmons, recombination by excitation 2-81083
- plates photoconductivity for microwave antenna near field amplitude-phase meas. 2-55624
- Poisson and transport equations, high field domain solns. 2-54167
- polar, electron-hole interaction, effective mass eqn., optical phonon effects 2-68306
- polar, electron-hole interaction, optical phonon interactions 2-68305
- polar, exciton-phonon interactions, Urbach's rule 2-44369
- polar, Hall effect, AC meas. apparatus 2-57174
- polar, hole transport props., Monte Carlo study 2-64968
- polar, in quantizing mag. field, electron momentum distrib. function 2-64967
- polar, magnetoplasmon surface waves, retardation effects 2-68377
- polar, oscill. struct. of magnetophonon effect, transverse config. 2-57179
- preparation, cryst. growth, props., bibliography 2-71880
- pulsed electron beam excited, β-conductive signal 2-71887
- quantum efficiency, threshold current density, effect on laser properties 2-79217
- quantum theory, introduction, book 2-47876
- Raman light-scattering spectra unit 2-61348
- Raman scattering from coupled LO-phonon-plasmon modes 2-68663
- Raman scattering from electronic levels, identification of Raman active photons 2-68657
- Raman-Nath diffraction, theory 2-54396

Semiconductors continued

- recombination luminesc. rel. to absorption, recomb. and field mechanisms 2-78128
- reflection of strong radiation, modulation, calc. 2-72257
- secondary ions from polycrystalline targets, energy distribution and mean energy, Ar^+ ion bombardment 2-61470
- secondary school approach 2-69525
- Seebeck coefficient and electrical conductivity at high temperatures 2-44123
- self-oscillation, in d.c. circuit due to recombinational instability 2-49231
- single crystal, apparatus for automatic resistivity obs. 2-61349
- solid surfaces, conference, Boston Mass,, USA, Oct. (1971) 2-47070
- sound absorption and amplification and nonlinear electron-sound interactions 2-51029
- space-charge factor and equivalent Llewellyn-Peterson equations 2-75082
- sphalerite, group III-V, charact. temps. 2-54013
- spin susceptibility of impurity band electrons, correl. effects 2-68520
- spin-electromagnetic waves in ferromag. semicond. and metals, theory 2-81225
- spin-flip Raman scatt., theory 2-57359
- spreading resistance correction factor, calc. 2-51162
- stimulated effects in radiative recomb. from electron-hole liq. 2-65289
- stimulated emission Coulomb interaction 2-61681
- stimulated Raman emission, and i.r. tunable light sources 2-78079
- stoichiometry departures determ. by chemico-analytical methods 2-43503
- strongly doped, model interpret. of thermodynamic props. and cond. 2-77880
- superconductivity, rel. to state mixing between bands due to e.m. field 2-77872
- superlattice struct., transport props., h.f. cond., e.m. wave amplification 2-64974
- surface electron states 2-75112
- surface layer on metal, semiconducting parameters, effect of substrate stress state 2-71966
- surface magnetoplasmons, theory 2-47920
- surface magnetovoltaic effect, in Hall effect measurements 2-68424
- surface quantization and surface transport, in inversion and accumulation layers 2-51123
- surface space charge, Fermi level near band edges, Raman scatt. obs. 2-47919
- surface states, Hubbard model, correlation with e.p.r. data 2-51154
- surface states photoemission obs. technique 2-48018
- temperature sensing by liquid crystal probes 2-69804
- tetrahedral, temp.-pressure phase diagram, scaling theory calc. from optical spectra 2-80528
- thermal conductivity, measurement in thermic non-stationary regime 2-47758
- thermal ionization of deep centers in the space charge of semicond. 2-71921
- thermoelectric for electrical measurement 2-76432
- three phonon processes in acoustoelectric interaction 2-84181
- transient space charge limited current on voltage removal 2-84336
- transmission electron microscope obs., at high voltage 2-56631
- transparency, self-induced 2-44111
- transport processes under external electric fields, magnetic fields and temperature gradients 2-47912
- transport props. in strong elec. and mag. fields, nonparabolic bands 2-81101
- trapping centres, defect related luminesc., two centre model 2-61680
- two-photon interband transitions in arbitrary elec. field 2-61623
- zincblende, band gap temp. depend. and Debye- Waller factors 2-84199
- zincblende crystal, excitation energy, self-consistent relativistic OPW calc. 2-81015
- WSe_2, exciton mechanism for superconductivity and nonequilibrium systems of excited excitons 2-71868

Semimetals

- anisotropy and spin effects of electrons and holes on phonon instability in a magnetic field 2-84180
- electronic struct., monotonic behaviour in strong mag. fields 2-44025
- e.m. excitation of sound, quantum effects 2-81010
- etch pit orientation determination 2-47187
- excitonic phase, investigation using strong electron-phonon interaction term 2-64897
- excitonic-insulator, intraband and interband scattering in mag. field 2-81003
- group V, magneto-optical transitions, energy band struct. model 2-68285
- indirect exchange interactions, interband susceptibility calc. 2-75022
- interband interactions, effect on critical temp. of supercond. transition temp. 2-71842
- intraband transitions, collective plasmic excitations, magneto-optical obs. 2-72294
- mixed phase, e.m. responses 2-64898
- sound and quantum waves, in strong mag. field, theory 2-81008
- sound propagation, e.m. excitation in moderatley strong mag. fields 2-71727
- Bi, Alfven wave amplitude and carrier relax. times 2-51092
- Bi, dispersion relation for holes 2-61223
- Bi, e.m. generation of u.s. waves 2-43967
- Bi, magnetoresistivity and thermoelectric power, frozen-in defects 2-68336
- Bi, magnetoresistivity coeffs, electron and hole transport, low field galvanomag. tensors, 77-300K 2-84233
- Bi, phonon drag thermomag. at low temps. 2-54244
- Cu_2Te-Ag_2Te systems, regions of metallic, semimetallic and semiconducting behaviour 2-84323
- PbTe, mag. susceptibility calc. 2-68519
- SiP_2 reflectance spectra, det. of band structure 2-72306
- TlTe, mobility temp. depend. obs. 2-51144
- YbB_{12}, electronic spectra 2-47838

Series
- Born series convergence for nonrelativistic scatt. at all energies 2−82226
- Cauchy problems soln. using reproducing kernel method 2−58709
- expansions in lattice statistics, new recurrence relation method for analysing singular behaviour 2−66458
- Fourier, absolute Norlund summability 2−69542
- Fourier, harmonic summation 2−69543
- Fourier, theory of meas. systems with periodic conversion function 2−76148
- hyperspherical harmonics, one-to-one correspondence with real analytic functions on hypersphere 2−45236
- Lie series treatment of boundary value problems in optically thick media 2−83112
- power series soln. for 3D unsteady compressible boundary layer eqns. 2−83680
- unbalanced angle-ply rectangular plates under transverse normal loading, analytical solution by Fourier series 2−82305

Sferics *see Atmospherics*

Shadow universe *see Cosmology; Elementary particles*

Shear strength *see Mechanical strength/shear*

Shell model *see Nucleus/models*

Shielding *see Radiation protection*

Shock tubes
- benzene, ${}^1B_{2u} \rightarrow {}^1A_{1g}$ emission in Ar afterglow 2−70747
- calorimeter for dissoc. energy determ. of mol. F_2 2−83253
- conical, boundary layer closure 2−55561
- contact surface 2−50252
- double ended diaphragm tube for colliding shocks 2−82371
- electrical with curved end wall, shock waves propagation in He and Ne 2−77356
- heating of driven gas, high stagnation temperatures 2−56403
- with imploding detonation drivers, performance and limitations 2−69778
- in line high vacuum conductance valve 2−48946
- in line high vacuum conductance valve 2−48946
- instrumentation problems due to high power and temp., techniques 2−83685
- laser, total temp. meas. using fine-wire thermocouple 2−49350
- Mach 3 windtunnel, design criteria 2−77360
- magnetically driven, steady-state current sheet speed obs. 2−52253
- as plasma flow source for MHD expts. 2−60252
- time-of-flight mass spectrometer with shock tube coupled through molecular beam 2−71107

Shock waves
- *see also Detonation; Explosions; Plasma/shock waves; Supersonic flow*
- − 2−64270
- acceleration in gas with decreasing density 2−60358
- acceleration in gas with density gradient 2−64386
- acceleration in shock tube, diaphragm opening time depend. 2−52254
- acceleration wave propagation in anisotropic hyperelastic materials 2−78911
- acoustic, reflection and transmission at boundary 2−55563
- acoustic shock pulses for meas. of stress-strain relationships in solids, application to Al 2−43777
- analog analysis of shock pulses 2−45564
- Apollo rocket shock cone, resonant coupling to ocean Rayleigh waves 2−57621
- arrival times, calc. of trajectory of object 2−45352
- atmosphere airblast overpressure decay at long ranges 2−65812
- atmospheric attenuation 2−65811
- attenuation by air bubbles in water, bubble screen design 2−80438
- blast wave studies in propulsion 2−44789
- blasts in medium with variable density, variable counter-pressure effects 2−82369
- bubbly liquids, one-dimensional flow, dynamic props. 2−80436
- capture area ratio effect on a propagating shock into a flowing duct 2−41835
- Chapman Jouguet surface in multiheaded gaseous detonation 2−83648
- Chapman-Jouguet detonation, self-similar blast waves 2−80392
- collision, investigation using X-ray flash tube 2−85181
- compressed gas volume expansion, two-dimensional unsteady problem 2−77325
- conbustible gas, propagation of blast waves 2−80380
- conditions and time of formation, nonlinear theories of elasticity and thermoelasticity 2−76340
- converging spherical and cylindrical, zero temp. gradient in rear flow field 2−52257
- curved, in nonequilibrium dissociative gas flow 2−46821
- density profiles during non-regular reflection from plexi-glass cylinders 2−66570
- detonation, cylindrical and spherical, for Mach stem induced detonation 2−80379
- detonation, transient studies 2−82368
- diamond shock pattern, decay 2−77355
- diffraction by sharp edge, semiempirical formulation 2−58933
- dynamics of low density heated fluid element, shock induced 2−50259
- Earth's bow shock, determ. of perturbation vectors of waves up and downstream from region of maximum compression 2−62320
- EHD, shock wave structure 2−77254
- in elastic materials, one-dimensional, amplitude governing equation 2−52221
- elastically nonlinear body, forced longit. oscillations 2−78901
- e.m. discontinuity, propagation in nonlinear isotropic material 2−58990
- exothermic hypersonic flows about blunt projectiles, periodicity 2−83650
- finite amplitude in elastodynamics influence of non- linearity on reflection 2−52256
- flow field, numerical calc., particle in cell method 2−49173
- fluids, inhomogeneous, propagation and growth 2−56314
- focused supersonic booms in turning flight, elimination 2−74479
- front, and contact front, resolution of arrival in time and space in shock tube 2−50252
- galactic, Perseus spiral arm, dynamical model 2−58231

Shock waves continued
- galactic dynamical model with 3 kpc, arm rel. to density and galactic shock waves 2−58184
- galactic nuclei violent events, model based on blast waves in rotating media in gravitational field 2−55014
- gas filled elastic tube, propagation effects 2−76381
- gas-dust medium, shock relaxation 2−46834
- gasdynamics, conference (Marseille, France, Sept. 1971) 2−80375
- gaseous free detonations, quasi one-dimensional analysis 2−52259
- geophysics, prestressed media, stress wave radiation from explosions 2−81604
- in glass due to internal focusing of laser beam 2−42124
- gravitational, energy considerations 2−62987
- high-speed impacts in solids and induced shock waves, theoretical model 2−41836
- hydraulic, in liquid in closed reservoirs 2−43294
- hydromagnetic, reflection from boundary shock 2−71067
- hyperelastic media, laminated, control vol. approach to propagating shock front 2−47486
- hypersonic flow, stagnation point, heat transfer, CO_2-N_2 mixture 2−82250
- hypersonic flow of ionized gas around blunt ended bodies and leading radiation 2−77347
- hypersonic model flow with strong shock waves, boundary layer method 2−83686
- hypersonic nose and loading edge shapes, minimum energy 2−43250
- initiation in fuel droplets, chemical aspects 2−83724
- interaction with boundary layers, effects of transition 2−43053
- interplanetary, flare generated effect of interplanetary mag. field on propagation 2−66119
- interplanetary, interaction with Earth's bow shock 2−62294
- interplanetary, Pioneer 8 obs. near 1 a.u., interpretation 2−62735
- interplanetary, rel. to closed mag. structs. in solar wind 2−66219
- interplanetary, solar-flare associated, fine structure obs. 2−62736
- interplanetary, thermal anisotropy influence on best-fit estimates of normals 2−62739
- interplanetary, thickness 2−62734
- interplanetary ensemble caused by solar flare 2−69177
- ionizing cylindrical symmetric strong shock in gas, study of self similar flow patterns 2−45563
- isolators for shock effects reduction 2−45496
- isopropyl nitrate, effect of confinement on detonation 2−80422
- laminar compressible boundary layers behind shock 2−46673
- laser radiation absorption by methane 2−64396
- linear visco-elastic inhomogeneous medium, propagation 2−66571
- liquid, high speed photography of laser-induced breakdown, bubbles obs. 2−56470
- liquid films in supersonic streams, nonlinear stability 2−78934
- local vel. meas. by Schlieren interferometry of Doppler shifted laser light 2−63138
- locally nonsimilar solutions for radiating shock layer about smooth axisymmetric bodies 2−69781
- magnetized low-β plasma, influence of reflected ions on magnetic structure of collisionless shock front 2−60226
- in magnetosphere tail, as reason for active phase of substorm 2−72824
- Mercury, unipolar interaction with solar wind, steady state bow shock problem 2−69145
- metal powders, occurrence during high-speed pressing 2−43885
- methane, 3.39 μ resonance line absorption 2−83275
- MHD, Petschek's mechanism, modification and criticism 2−81762
- moire fringe method for meas. 2−50788
- monoatomic gas, impurity effects on ionization zone behind strong normal shock waves 2−50239
- on moon, duration, scattering and attenuation 2−73072
- Mooney Rivlin material in state of arbitrary homogeneous strain 2−55562
- multidimensional gas dynamics, boundaries characteristics, in time dependent finite difference analysis 2−74478
- multitube multishroud supersonic jet noise suppressor 2−43233
- nitromethane, divergent cylindrical detonation 2−83722
- nitromethane, effect of confinement on detonation 2−80422
- non-steady, propag. in metals with phase transitions, hardening by explosion 2−80725
- non-uniform in quasi one-dimensional non-steady oblique field magnetogasdynamics 2−43101
- nonlinear, in one-dimens. lattice, perturbation soln. 2−80737
- nonlinear magnetic sound in gravitational field, shock wave formation 2−80302
- nonlinear model Boltzmann eqns. for shock wave structure in monatomic gas nonlinear model Boltzmann eqns. 2−50258
- nonlinear theory of resonance in continuous system with damping 2−77327
- nuclear explosion waves, surface and body 2−61877
- oblique, partly dispersed, reflection from plane wall 2−78933
- oblique, weak, propagation through diffusing gas mixtures 2−43241
- oblique hydromagnetic shocks, instability of whistler structure 2−80326
- one-dimensional, thermodynamic influences on growth in materials with memory 2−58932
- one-dimensional EHD flow with variable mobility coeff. 2−83528
- oscillatory MHD flow, possible shock waves 2−46708
- photoionization of impurity gas in inert gas, precursor shape and intensity 2−56381
- piston movement in non-uniform medium, approximate analytic solutions 2−52261
- plane wave refl. at free surface of water 2−83746
- plane-stress-wave propagation in solids, studies using laser interferometry 2−59233
- plasma, radiant energy absorption and thermonuclear reaction 2−70909
- point explosion problem, evolution of discontinuity in self-similar flows 2−73458
- propagation in compressible medium, hydrodynamics theory and scheme for incompressibility 2−82370
- propagation in gases with discrete velocity distribution 2−53301
- propagation of cylindrical magnetogasdynamic shock in nongravitating system 2−53185
- propagation speeds in gaseous mixtures 2−83647

Shock waves continued
- propagation through solar corona, responsible for type II radio bursts 2—81952
- propagation through two-phase medium 2—83656
- propagation toward Earth and reflection, from meteor explosions 2—81900
- radiative, propagation in inhomogeneous cosmic medium 2—68995
- radiative blast wave due to sudden explosion in stellar interiors 2—69049
- reaction zone behind, i.r. techniques for obs. 2—82562
- real gas flow, numerical soln. procedure 2—71078
- reflection and diffraction by interaction with yawed wedges, supersonic outflow 2—76380
- reflection form permeable materials 2—69779
- self-gravitating gas spheres, propag. in, rel. to stellar models 2—84987
- shape near body of rotation during hypersonic gas injection 2—56419
- shell motion subsequent to detonation, numerical soln. 2—76383
- slow, MHD shock wave propag. 2—80223
- solar system, role of gasdynamic processes in transfer of solar material 2—81899
- in solar wind, indication from decametric radio emission from Jupiter 2—48801
- sonic boom of hypersonic vehicles 2—46813
- sonic boom signatures by bicharacteristic method 2—83668
- sonic booms of supersonic flight, meteorological problems 2—78344
- in steady transonic flows, calc. using small disturbance theory 2—80402
- stochastically nonuniform elastic medium, propagation 2—52255
- straight oblique shock waves in radiating gases 2—46837
- streaming plasma interaction w. mag. mirror 2—64286
- strong diffraction at wall surface, pressure and temp. change 2—83655
- structure, effct of radiation on amplitude of isothermal discontinuity 2—69780
- supernova envelopes, e.m. pulses 2—62567
- supersonic nonequilibrium airflow, blunt bodies 2—83678
- switched Shuman filters, for numerical calculation 2—45561
- tail, vibrational relaxation, anti-Stokes Raman scattering obs. 2—52970
- travelling, obs. of boundary layer effects 2—80211
- turbulence, statistical mechanics of Burgers model 2—83462
- turbulent boundary layer interactions on blunted compression surface 2—53315
- underwater, diffraction by semi-infinite plane 2—56465
- underwater explosions, intense, model 2—78930
- underwater pressures from small detonators 2—46899
- volume thermal shock in a plate, determ. of eqns. for elastic potentials 2—82327
- weak, propag. analysis 2—66417
- weak waves propagation in relaxing gas 2—83653
- wedges and cones, hypersonic leading edge 2—83663
- Al, acoustic shock pulse generation, nonlinear elastic behaviour obs. 2—64842
- Al, appl. as impact energy absorber 2—66632
- Al_2O_3, shock impedance, rel. to viscosity and loss angle of Young's modulus calc. 2—84055
- H_2, normal and para, low temp. waves 30K min. 2—46550
- H_2, normal ionizing, press. jump 2—67721
- He, downstream propagation in electrical shock tube with curved end wall 2—77356
- Hg, partially ionized, boundary layer growth in shock tube flow 2—64389
- NH_4F, accompanying pressure-induced phase change, seismological implications 2—78268
- NaCl, porous, explosion of spherical charge, shock wave parameters 2—58936
- Ne, downstream propagation in electrical shock tube with curved end wall 2—77356
- **effects**
  - air bubble pulsation in water 2—80438
  - air study of bound electron temperature and relaxation phenomena behind shock wave 2—54542
  - Alfianello meteorite, shock metamorphism and dynamic deformation 2—44970
  - aquifer systems, response to explosions 2—57826
  - bimetallic junction, e.m.f. generated by shock wave propag. 2—75010
  - blunt bodies, transonic region 2—77329
  - breakup of liquid droplet columns 2—83806
  - breccia, lunar and terrestrial minerals, deform. substruct. 2—62688
  - Cannikin nuclear explosion, reaction of shallow surface waters 2—57552
  - cumulative fatigue failure, ballistic impact 2—60939
  - cylindrical elastic shell, with liquid, motion under axial shock loadings 2—73385
  - cylindrical flare bodies, bundary layer effects, in supersonic flow 2—77359
  - detonation initiation mechanically inhomogeneous explosives 2—73453
  - detonation of explosive substances, electrical conductivity 2—63139
  - diatomic gas, relaxation equations for vibrational and rotational energy including transport processes and chemical reactions 2—52966
  - e.m. T tubes, precursor ionization 2—78932
  - fracture of lucite cones 2—68055
  - fracture of triangular plaster of Paris plates due to contact explosive pressure 2—53793
  - graphite single crystal, compression, X-ray diffr. obs. 2—56646
  - heating of driven gas, in shock tube, high stagnation temperatures 2—56403
  - hybrid schemes, self-adjusting, for shock computations 2—55560
  - hydraulic shock in liquid confined in cylindrical shell determ. of transients and magnitude of hydraulic pressure 2—83743
  - instabilities in reaction zones of detonation waves 2—83646
  - interstellar medium, two component, structure and stability of shocks 2—75797
  - ionization behind shock waves in N_2-O_2 mixtures 2—77302
  - laser-generated shock waves for detonation of insensitive explosives and testing reliability of printed circuits 2—49174

Shock waves continued
- **effects** continued
  - liquid-bubble mixtures, shock wave propagation and relaxation effects 2—77453
  - lunar regolith and role of shock metamorphism 2—78511
  - metal, effect on microstruct. and mech. props. 2—68073
  - metal, shock spallation, appl. of phonon theory of brittle fracture 2—80747
  - MHD boundary layers 2—50174
  - microcline, deform. structs. 2—61843
  - nonisothermal plasma, turbulent heating by collisionless shock wave 2—56345
  - in nonlinear viscoelastic materials for prediction of acceleration waves response 2—49080
  - parametric acoustic array, analytical model using shock waves 2—76373
  - particle motion behind oblique shock in two-phase supersonic flow past a wedge 2—60145
  - plasma, blast waves generation, by pulsed electric discharges 2—74360
  - polarization of dielectrics, effects of non-uniform dynamic loading of test piece 2—76382
  - polytetrafluorethylene, shock compression, acoustic velocity behind stress wave front 2—77781
  - pressure by wire explosion in water under impulse heavy current 2—73452
  - pressure distribution on yawed wedge interacting with oblique shock waves 2—69689
  - pressure fluctuation, interactions with turbulent boundary layer 2—43257
  - quartz, X-cut, strain dependence of longitudinal piezoelectric, elastic and dielectric constants det. by shock compression 2—51207
  - rutile powder subjected to impact X-ray line profile analysis of particle size and strain 2—74831
  - shattering of supercooled water drops, freezing 2—47037
  - shock-induced flow in Ar, acceleration measurements 2—53297
  - solar H_α flares rel. to chromospheric response to downward propagating shock waves 2—78620
  - solid, compression, appl. of fourth-order anharmonic theory 2—84188
  - solid propellant, simulated, low-cycle dynamic fatigue-curve for dynamic shock wave loading 2—84027
  - sonic boom, far-field, non-asymptotic effects 2—53318
  - sonic boom, policy considerations 2—76379
  - sonic boom, UK research review 2—45534
  - sonic boom damage to large windows 2—55564
  - sonic boom focus 2—58015
  - sonic boom startle, field study in West Germany 2—85137
  - steel, carbon, dynamic strengthening singularities 2—84075
  - steel, stainless, struct., effect of explosive load 2—43836
  - turbulence in acoustic waves 2—66633
  - vibrations of circular elastic plates, due to sonic boom 2—55491
  - vortices and unsteady flow, meas. by hot wire anemometer 2—77242
  - window response to sonic boom, acoustic coupling of rooms 2—45562
  - yielding, hardness, stresss relief and permanent property changes 2—68072
  - Al, 7075, laser-induced, microstructural and mech. prop. changes 2—68075
  - Al, compression, X-ray Debyegram recording 2—84045
  - Al single crystal, compression, X-ray diffr. obs. 2—56646
  - Ar, atoms, multi-level initial ionization behind strong shocks and average atom-atom cross sections for excitation and ionization 2—67398
  - Ar, shock-heated, ionization relax. time calc. 2—70978
  - B_2O_3 glasses, photo- and X-ray luminescence, effects on intensity 2—84547
  - Bi, electron diffusion through shock wave front 2—71771
  - CO oxidation in shock waves, catalytic effect of $Fe(CO)_5$ 2—57417
  - $CaF_2:Tb^{3+}$ photo- and X-ray luminescence, effects on intensity 2—84547
  - Cs vapour, acoustic radiation from shock front 2—71115
  - Cu, dynamic strengthening singularities 2—84075
  - F_2, shock tube calorimeter studies of dissoc. energy 2—83253
  - Fe-(30 wt.%)Mn alloy, austenitic, strengthening by shock loading 2—43841
  - Fe, dynamic strengthening singularities 2—84075
  - H_2/air and H_2/O_2 combustion with spherical projectile 2—83651
  - HCl thermal dissociation density gradient meas. 2—44473
  - I_2-He mixture, interaction of dissoc. and vibr. relax. behind shock wave 2—77168
  - LiF single crystal, compression, X-ray diffr. obs. 2—56646
  - NH_3-N_2O population inversion in exothermal decomposition reactions on shock 2—73553
  - NH_3, decomposition behind reflected shock waves 2000-4500K, obs. of i.r. emission 2—48324
  - Ni, dynamic strengthening singularities 2—84075
  - Ni, recovery after 300 kbar shock wave loading 2—56794
  - Sb, electron diffusion through shock wave front 2—71771
  - Ti, dynamic strengthening singularities 2—84075
  - Xe, shock-heated, ionization relax. time calc. 2—70978
  - YIG demagnetization, method for investigation 2—48081
  - ZrO_2, monoclinic-tetragonal inversion 2—74946

Shot noise *see Noise/electrical*

Showers *see Cosmic rays/showers and bursts*

Shubnikov-de Haas effect *see Magnetoresistance*

Silicon
- *see also Semiconducting devices; Semiconducting materials/silicon*
- 2 electron transitions at liquid He temp., emission line obs. 2—51370
- abundance in powdered lunar soil samples, L16/O78, nondestructive neutron activation analysis 2—85043
- abundance in seawater in-situ analysis using synthetic fibres 2—75469
- adsorption of O_2, comments on expts. 2—47165
- adsorption of O_2 2—47164
- inAl-6.8% Zn alloy, effect on diffusion 2—56753
- amorphous, atomic arrangement, computer simulation 2—60574
- amorphous, Raman scatt., phenomological explanation 2—61665

Silicon continued
- amorphous films, density detn. by backscattering of 2500 keV alpha parts. 2−80559
- amorphous layer prod. by ion bombardment 2−71456
- amorphous region form. by neutron irrad. or ion bombardment 2−47384
- atom, far-u.v. absorpt. spectra analysis 2−67388
- Auger electron signals of P surface impurity as function of coverage 2−47080
- avalanche photodiode, photomultiplication factor obs. 2−71968
- bicrystal, Moire fringes, visibility improvement using parallel X-ray beam 2−71404
- binding effect due to K electrons, Compton profile obs. 2−83882
- bonding electrons, anharmonicity, and temp. depend. of forbidden (442) refl. 2−83885
- brittle-fracture and crack propag., atomistic computer simulation 2−84036
- channel-to-random transition meas. on single crystal overlaid with amorphous layer 2−61127
- channelling, energy spectra of back-scattered protons, variations 2−54093
- channelling of ions in crysts. overlaid with Al and Au films 2−54094
- channelling pattern recording using radioactive recoil atoms 2−54088
- chemisorbed O_2, on (111) surface, electron bombardment surface ion desorption study 2−71351
- clean and doped, mean square atomic displacement study by LEED 2−71318
- correlated successive collisions of 5-30 keV Ar ions, ion scatt. processes 2−47775
- covalent-metallic phase transition under pressure 2−83886
- crack structure, atomistic study 2−56831
- creep, recovery, deform. behaviour, $T>850°C$ 2−56808
- crystal growth, e.m. field in system inductor-concentrator- pedestal 2−47275
- crystal growth from pedestal, adaptations using combined heating 2−53601
- crystal growth from solution, 2-dimensional nucleation and corner growth 2−74684
- dechannelling of 0.3-1.5 MeV protons, Lindhard's multiple scatt. 2−47788
- dechannelling of 7.15 MeV He ions 2−61120
- defect struct. induced by localized B diffusion, X-ray diffraction topography 2−77567
- defects, identification of chem. constituents 2−77913
- diffusion as As, from arsenosilicate glass source, 1000-1200°C 2−83980
- diffusion in β-Co, internal oxidation studies 2−74811
- diffusion in M_5Si_3, M=Nb, Ta, Mo, W, at 1700°C 2−53769
- diffusion of As, props. of SiO_2:As and Ge/SiO_2:As diffusion sources 2−83979
- diffusion of Au, cpd. formation, refl. electron diffr. obs. 2−50463
- diffusion of B, from localized surface source 2−56739
- diffusion of B impurities 2−56745
- diffusion of P, coeff. determ. by Boltzmann-Matano method 2−71540
- diffusion of Sb and P, enhancement by proton irrad., dose rate effects 2−80707
- diode sensor, temperature measurement system 2−45600
- dislocation etch, for (100) planes 2−71495
- dislocation etch pits shapes rel. to mech. stress 2−80553
- dislocation structure, hydrostatic press. effect 2−47419
- dislocation velocity, dopant influences 2−50674
- dislocations, moving, obs. by X-ray topography 2−77585
- dislocations, screw and 60°, velocities 2−80678
- dislocations, X-ray topography, high resolution video display 2−83922
- dopant profile obs. using neutron activation anal. 2−56738
- doping, during whisker growth by gas transport 2−47430
- doping inhomogeneities, obs. by electroreflectance 2−71510
- elastic wave damping, effective anharmonicity consts. 2−80913
- electron beam irradiation induced defects, electron microscope investigation 2−64656
- electron diffraction, Kikuchi band and abnormal absorpt., exchange effects, calc. 2−64631
- electron energy loss functions, determination of optical props. 2−71769
- electron irrad., e.p.r. obs. of Li-defect interactions 2−48293
- electron momentum distribution, Compton profile obs. 2−57128
- electronic scattering in planar dechannelling, protons and deuterons 2−61128
- epitaxial film, diffusion of Sb, temp. and dislocation density depend. 2−74816
- epitaxial film, lattice resolution e. microscopy obs. of struct. of twin boundaries, faults and dislocats. 2−74779
- epitaxial growth, from dichlorosilane 2−71389
- epitaxial growth, rate calc. for barrel reactor 2−71388
- epitaxy, using hydrogen reduction in $SiCl_4$, two-dimensional growth 2−47125
- fast neutron irradiated, number of Frenkel defects, calc. 2−71458
- film, amorphous, characteriz. as function of decreasing spin conc., e.p.r. obs. 2−78162
- film, amorphous, metal contact induced crystalliz. 2−56590
- film, amorphous, microcrystallite struct. 2−43479
- film, amorphous struct., elec. microscope obs. 2−50479
- film, oriented growth on ZnS single crystal 2−56597
- film, prep. using plasma source 2−67912
- film and bulk, electron irrad., defect prod., resist. change 2−80655
- fracture speed meas. using u.s. fractography 2−82123
- in graphite, effect on ordering process 2−50829
- growth twins grown by pulling method 2−74688
- high-resistive floating-zone, striations revealed by preferential etching 2−74787
- implantation of B ions, channelling, depth distrib., computer simulation 2−47439
- impurity atom diffusion enhancement by light ion implantation 2−60814
- impurity content, O and C detn., i.r. and activation analysis 2−71502

Silicon continued
- interstellar, abundance det. from u.v. stellar spectra 2−58359
- ion damage obs., high resolution replica technique for electron microscope obs. 2−56629
- ion implantation, crit. amorphizing dose, mass depend., calc. 2−56677
- ion implantation damage and impurity location, channelling obs. 2−71511
- ion implantation profile of ^{10}B, calc. 2−74795
- ion implanted, lateral strains, X-ray topographic obs. 2−80704
- ion implanted, radiation hardening of thermal oxides by displacement damage 2−50689
- ion radiation damage, apparent optical absorp., scatt. from defect zones 2−48158
- irradiated, multiple vacancy centres, e.p.r. obs. 2−48283
- irradiated by C^+ ions, prod. of SiC heterostruct. films 2−50504
- irradiation defects, concepts and correlations 2−47387
- Kikuchi patterns, displaced lines 2−53636
- lattice defects, comparative study of X-ray topographic methods 2−47405
- lattice distortions due to scratching 2−43626
- lattice dynamics, Keating's model calcs. 2−71708
- layers, homoepitaxial, influence of substrate on interface props. 2−77495
- liquid, kinetics of polycryst. SiC in soln. 2−56487
- melt spreading over graphite surfaces 2−67814
- metal silicide formation, from thin metal films 2−43861
- metastable polycryst III, photon Raman spectra 2−68664
- Mossbauer effect of ^{57}Fe 2−48152
- n-type, (111) surface, LEED and Auger spectroscopy obs. 2−50464
- neutron irrad., divacancies, i.r. absorpt. and photocond. 2−48194
- neutron irrad. induced defect clusters, edge absorpt. obs. 2−47389
- neutron irradiation damage, Mossbauer effect obs. 2−48153
- neutron irradition damage, piezospectroscopic obs. 2−48193
- neutron Pendellosung fringe patterns, perfect crystals possess curved distortion 2−74744
- optical props., surface oxide layer influence 2−51325
- optical structure at 3.4 eV, piezo-optical evidence for Λ transitions 2−75280
- p-type, photoelectric charact. of photofield emission 2−84389
- phonon dispersion relations, homology with Ge 2−84190
- phonon energy assignments, multiphonon Raman spectra obs. 2−68221
- photocathode, emission on illumination from reverse side 2−44209
- photodiode operational amplifier combination, noise and frequency response 2−57214
- photoelectric emission under influence of external accelerating electric field 2−68499
- photoemission processes analysis and band bending profiles as a function of caesium coverage 2−72082
- point defects, investigation by non-irrad. techniques 2−47399
- powder, Raman effect 2−81383
- pure, singly doped and compensated n-type, far i.r. props. 2−72384
- Raman scattering, one and two phonon struct. obs. 2−61081
- reflection spectra in vacuum u.v., investigation using synchrotron radiation 2−44367
- refractive index, X-ray interferometric determ. 2−72256
- refractive index in 1.1 to 2.1 μ region of i.r. 2−72255
- ribbons, growth by edge-defined film-fed growth technique 2−71381
- secondary electron emission anisotropy, raster method with modulation and deflection 2−81198
- Si-SiO_2 interface, e. scatt. by surf. oxide charges and lattice vibrat. 2−71317
- single crystal, H_2^+ ion bombarded, bicrystal formation, X-ray obs. 2−47386
- single crystals, anisotropic thermal conduction at low temperatures 2−68260
- single-crystal cathode, thermionic emission anisotropy obs. 2−65101
- slice, spontaneous change in radius of curvature on plastic deformation 2−68083
- slip system, effects of crystal anisotropy and cryst. struct. 2−71577
- solar cell, effect of series resistance on power output at low intensities 2−73505
- solar cell, encapsulated in fluorinated ethylene propylene, effect of simulated micrometeoroid exposure 2−52380
- solar cell, series resistance methods of determ. 2−66692
- solar cells, 1 MeV electron radiation of TiO_x and SiO_x antireflective coatings 2−59056
- solar cells, performance improvement using passivated Ti(Pd)Ag contacts 2−59057
- solar flares, 1971, January and September, composition and energy spectra of heavy nuclei, 0.5 to 40 MeV per nucleon 2−58556
- solar overabundance, accelerated by solar flares 2−76001
- surface, (111), lattice vibrs. 2−43467
- surface, (111), Ni adsorp. and condensation, mass spectrometer obs. 2−50499
- surface, Auger electron spectroscopy and electron impact desorpt. combined studies 2−64556
- surface, cleaning by ion irrad., ellipsometric obs. 2−47082
- surface, Cs-O negative-electron-affinity surfaces, photoemission meas. 2−81185
- surface, monomolecular layers exam. using ellipsometry 2−56601
- surface, sputtered atom ejection and ion bombardment induced disorder 2−43466
- surface (111) chemical reaction with bromine studies using He^+ and Ne^+ ion scattering 2−50416
- surface barrier semiconductor detector temp. response, used in clinical dosimetry 2−69399
- surface cleaning, H_2O_2 soln., HEED and Auger electron spectroscopy obs. 2−53555
- surface constraints meas. 2−53545
- surface diffusion, on W, field emission obs. 2−47085
- surface impurities and disorder, detect. by $^4He^+$ and H^+ ion beams backscatt. 2−77485
- surface phonon, (111) surface, low energy electron spectroscopy obs. 2−50987
- surface states, three parameter local pseudopot. method calc. 2−57131
- surface struct. rel. to surface states, surface cond., LEED 2−77800

Silicon continued
thermal conductivity, phonon boundary scatt. after neutron irrad. 2−80917
thermal expansion, single cryst. X-ray obs. 2−47757
thermally oxidized, stacking faults, effect of impurities 2−60809
thermally oxidized, X-ray topographic study of small dislocation loops 2−64669
transmission electron diffraction, contrast reversal of Kikuchi bands 2−83921
two phonon Raman spectra 2−48156
vacancy equilibrium configuration, computer calc. 2−71467
vacancy mobility and conc., high-temp. behaviour 2−64659
vibronic spectra of γ-irrad. crysts., temp. depend. 2−48262
voids, small spherical, electron diffr. contrast profile, calc. 2−77571
W substrate, adsorbate induced work function changes 2−72084
X-ray absorption spectra, core excitons 2−81385
X-ray anomalous transmission for crystals containing dislocations 2−71496
X-ray diffraction, asymmetric, effects of lattice distortion on equal inclination fringes 2−77532
X-ray emission spectra, satellites, rel. to double ionization theory 2−72381
X-ray L emission band, short-wave satellites 2−51361
X-ray linear absorption coefficient, 78-292 K 2−80610
X-ray photoelectron spectra of valence bands 2−81191
X-ray spectra, mol. orbital model interpret. 2−48210
yield spectroscopy, fine struct. of 4d excitations 2−61675
zone melting, with temp. gradient, crystn. rate determ. 2−47253
BeO:Si, for environmental and personnel dosimetry in tropical countries 2−85133
in $CdFe_2O_4$, magnetic behaviour influenceb by Si from glass of reaction vessel 2−84432
fast neutron radiation damage, e.p.r. obs. 2−48282
GaAs:Si, impurity effects on dislocation velocity 2−68028
GaAs:Si p-n junction, reverse branch of I-V characts. and breakdown 2−71959
in GaAs, amphoteric impurity distrib. equilib. calc. 2−83981
He^+ irradiated, atomic displacements, Rutherford scatt. obs. 2−47388
in n-type radiation induced defects obs., photoconductivity obs. 2−72066
Li drift and precipitation in crystals grown and/or annealed in different ways 2−50692
$LiNbO_3$-Si layered structure, transverse acoustoelectric effect obs. using capacity probes 2−51038
Pb-Si solid structure, etching technique for macrostructure obs. 2−56607
Si:As, He ion min. backscatt. yield variation obs. 2−60820
Si:As, impurity distrib., determ. by He ion channeling obs. 2−60818
Si:B, implantation profiles determ. by secondary ion mass spectrometry 2−74794
Si:B, impurity lattice location, He^+ ion channelling obs. 2−60819
Si:B, ion implanted lattice disorder distributions, channelling effect analysis 2−68036
Si:B, ion microprobe analysis of implanted ion distribs. 2−64674
Si:B, lateral spread of implanted ions, obs. by junction delineation 2−71508
Si:B, shear deform. pot. consts. of B acceptors ground state, piezospectroscopy obs. 2−75306
Si:B diodes, current-voltage characteristics 2−71969
Si:C, low temp. electron irrad. damage, i.r. absorp. obs. 2−48191
Si:Ge, O, C, low temp. electron irrad. damage, i.r. obs. 2−48192
Si:In, ion implanted, photoelectromag. effect rel. to dose and annealing 2−72077
Si:Li, electron irrad., luminesc., annealing and Li impurity effects 2−48229
Si:O, lattice damage due to ion implantation, e.p.r. obs. 2−60780
Si:P, diffused, impurity profile kink form. mechanism 2−56742
Si:P, implantation damage annealing, resist. and electron microscope study 2−64678
Si:P, Knoop hardness and hardness anisotropy, impurity conc. effects 2−71604
Si:P quadratic Zeeman effect of donor lines in photoexcitation spectrum, transverse effective mass 2−81348
Si:P(As) radiation-induced infrared absorption bands, piezospectroscopic studies 2−68650
Si-Ar^+ collisions, 25 to 200 keV, noncharacteristic X-ray bands 2−56116
Si-Ar^{++} collisions, K X-ray yields of Si, double-scattering mechanism 2−42786
Si-CdSe, p-n heterojunctions vacuum deposition preparation and properties 2−77925
Si-Fe textured sheet, permeability, eddy current loss, angle and field depend. rel. to domains 2−65153
Si-$LiNbO_3$, convolution and correlation by nonlinear interactions between sonic induced space charge and field waves 2−51015
Si-N-O, free energies of form. of α and β silicon nitride and silicon oxynitride, 1200-1350°C 2−61037
Si-Sb compressed composite, obs. of neutron energies in range 13-15 MeV 2−59633
Si-SiO_2 interface, ion implanted, deep energy level detn. by m.o.s. technique 2−80938
Si, B diffusion from doped oxide layers 2−64677
Si, hybridization of atomic orbitals at structural defects 2−81005
Si II, Si III, vacuum u.v. absorption meas. using new continuum light source 2−77001
Si II, Stark broadening of 6347.4 and 6347.1 Å spectral lines 2−56097
Si II profiles in 56 Ari, Si Ap variable star 2−81853
Si III, polymorphs, Raman scattering from phonons 2−72372
Si XIII in solar flares, calc. of wavelengths in X-ray region 2−85050
Si^{4+}, self-diffusion in K_2O-SrO-SiO_2 glass 2−53765
Si(Li) detector, dead-time corrections for X-ray intensity obs. 2−73943
Si(Li) X-ray detection systems, pulse pile-up rejection 2−73944
SiXii, electron excitation cross sections for 2s-np ns-n'd, 2p-nd, 3s-np transitions calc. by Coulomb-Born method 2−56109
^{235}U fission fragment range 2−61125

Silicon continued
YIG:Si, magnetiz. switching by i.r. irrad., linear dichroism obs. 2−68599
YIG:Si, photoinduced dichroism, model 2−72260
YIG:Si^{4+},Ca^{2+} magnetostriction rel. to mag. field inclination to crystallographic axes at 4.2K, 77K and room temp. obs. 2−84437
YIG-Si, thermally induced negative resistance 2−51145

Silicon compounds
see also Quartz
binary arsenosilicate glass film, diffusion source, thermal stresses 2−71325
binary arsenosilicate glass film, vapour deposition for diffusion source 2−71324
borosilicate films, current-voltage characts. 2−47950
cristobalite, α, β, Raman spectra from 77 to 538K 2−81364
fayalite-forsterite solid solution between 900-1300°C at low pressures 2−65538
fused silica, effect of simulated space radiation 2−49440
illite, microstructure and chemical comp. 2−84710
interstellar reddening curve, absorption feature at 2200 angstroms for model silicate grains 2−55071
metal/SiO_2 cermet film, produced by recoil atom implantation 2−53578
methane-d_4 + silane ion molecule reactions, hydride ion transfer and isotope effects 2−68778
β-Nb-Al-Si alloys, superconducting critical temp. detn. 2−71869
olivine, dislocation mechanisms rel. to upper mantle flow 2−65533
olivine electrical conductivity rel. to temperature profile of lunar interior 2−66142
sapphire, ion beam polished, increased laser surface damage threshold obs. 2−57317
Si-SiO_2 interface, e. scatt. by surf. oxide charges and lattice vibrat. 2−71317
silica, fused, optical waveguide fabrication, ion implantation through electron resist masks 2−59268
silica, fused, thermophysical props. at high temps. 2−54069
silica, ionic transport 2−64696
silica, surface effects on self-diffusion of adsorbed H_2O layer 2−60686
silica, vitreous, structure, neutron and X-ray diffr. obs. 2−53534
silica, vitreous, thermal conductivity, hot wire method 2−51055
silica gel, absorpt. of electron pair donors, H bonding 2−77515
silica glass, anomalous properties, interpretation 2−67884
silica suspension in water, freezing using temp. gradient microscope stage 2−74585
silicate glass, binary, structure of corroded surface 2−53541
silicate glass, hydrogen-alkali exchange with aqueous solutions, theory 2−53518
silicate melts, interionic distance rel. to temp., stratification, 800-1900K 2−56563
silicate rocks, spectral compositional imaging 2−65548
silicates, liq., wetting of Pt, effect of oxides 2−67782
silicates, luminesc. of Eu^{3+}, spectral characts. and quantum efficiencies 2−48233
silicone lubricants, testing by ball and peg machine 2−68123
silicone oil, laser induced breakdown, high speed photography of cavitation and bubbles 2−56470
silicone oil, Rayleigh convection, roll diameter dependence and effect on heat flux 2−60370
$nSiO_2$-$1Al_2O_3$, isopaustic glasses, u.s. delay lines 2−78928
terrestrial planets, metal/silicate fractionation rel. to solar nebula 2−66166
tetrahedral oxy-compounds, force constants and regularities of chemical bonding 2−70725
tetraphenyl silicon, defect struct. determ. 2−53731
X-ray spectra, mol. orbital model interpret. 2−48210
zeolite, Y-type, e.p.r. study of Cu^{2+} pairs 2−75343
zeolites, noncooled, vacuum tests, trapping and pumping props. 2−76131
Ag-Si alloy, deformed by tension and rolling, X-ray diffr. 2−80845
Al-Mg-Si alloy, structure of metastable precipitates formed during ageing 2−56909
Al-Mg-Si alloys, quenched-in defect elimination mechanism 2−84149
Al-Si, solidification in shell mould, and effects of additional elements 2−84134
Al-Si dilute alloy fiom, Si precip., resist. study 2−50825
Al-Si liquid alloy, Cr or Mn impurity, susceptibility near nonmag.-mag. transition 2−80486
Al-pyrolytic SiO_2-Si system, effect of heat treatment on density of fast surface states 2−77915
As-Te-Ge-Si glass, thermal breakdown 2−61298
As_2Te_3-Si glass, electronically assisted thermal breakdown 2−61276
Au-SiO cermet film, post-deposition resistance changes 2−61222
3BaO-$5SiO_2$ glass, controlled spherulitic crystallization, 800-950°C 2−80530
3BaO.$5SiO_2$ glass-ceramic, mechanical props. 2−53930
C-Si alloys, co-deposited, high-fluence irrad.-induced dimens. changes 2−53776
C-Si alloys, dimensional changes and creep during neutron irradiation 2−76917
Ca-Si system, phase equilib., existence of silicides 2−71700
CaO-Nb_2O_5-TiO_2-SiO_2 system, liquidus temps. 2−43436
CaSi system, temp. vs. comp. and press. vs. temp. diagrams, correl. 2−71699
Cd-Si-As system, glass-forming region determ. by differential thermal analysis 2−74599
CdSe-SiO_x, electron transport study in space charge layer of vacuum-deposited film 2−77852
$CdSi_xGe_{1-x}As$, glassy, photocond. and elec. cond., rel. to band struct. determ. 2−61448
CoO-Al_2O_3-SiO_2 glass system, low field mag. suscept. 2−65178
Cr-Mo-Si system constitution diagram 2−50961
Cu-Si single crystal, tensile deformation 2−50743
Fe-Fe_3C-Si, phase diagram, white cast iron and carbon equivalent 2−74954
Fe-Ni-Si alloy, temper brittleness development, grain boundary adsorption of P, internal friction study 2−80767
Fe-(3(wt.%)Si, grain-oriented strips, saturation approach law of longitudinal magnetostriction 2−54335

Silicon compounds continued
Fe-Si, dislocation, dynamics on plastic deformation, high voltage electron microscope obs. 2−56785
Fe-Si, domain width, sample thickness and cryst. orientation depend. 2−48061
Fe-Si, elastic props. and model atomic interactions 2−74818
Fe-Si, magnetization and mag. reversals mag. texture effect 2−51252
Fe-Si, mech. props., influence of microstruct. 2−80778
Fe-Si, Neel lines, magnetooptic Kerr effect obs. 2−78014
Fe-Si, obs. of domain changes under cyclic tensile loading for specimens in remanent cond. 2−65147
Fe-Si, temp. depend. of specific energy loss during remagnetization 2−48069
Fe-Si alloy, phase stability and high temp. elastic consts. 2−71546
Fe-Si alloys, remagnetization specific energy losses rel. to specimen thickness and mag. induction amplitude 2−72163
Fe-Si dil. alloy, ave.-moment-internal field variations 2−78008
Fe-Si sheet, grain oriented, magnetostriction meas. by optical lever method 2−65160
Fe-Si single crystal, slip and hardening, effect of dimensional factors 2−71568
Fe-Si single crystals deformed by tensile forces, slip polygonization 2−84060
Fe-Si solid solns., b.c.c., ordered atomic configs. 2−47326
Fe-Si solid solns., ordering reactions and meas. of specific heat capac. 2−71745
Fe-2.89%Si (100) face, surface composition rel. to photoelec. work function 2−61463
Fe-(3 wt.%)Si alloy, surface films influence on effectiveness of thermomag. treatment44261 2−44261
Fe-Ti-Si alloy, age hardening, precipitation and yield stress 2−43806
Fe-3%Si foil specimens, low temp. tensile tests, h.v. electron microscope obs. 2−80872
Fe-3.1 wt.%Si, electrodiffusion activation energy of polygonization substruct. 2−53764
FeSi, two-dimensional ferromagnetic domain walls electron images 2−51247
FeSi films, e microprobe analysis 2−77509
Ge_x-Si_{1-x}, mixed crystals, photoelectric emission 2−72092
K_2O-SiO_2 glass, cond. and dielec. relax. as function of thermal history 2−54229
K_2O-SrO-SiO_2 glass, cation self-diffusion coeffs. 2−53765
Li_2O-Al_2O_3-SiO_2 glass-ceramic, strength and microstruct. 2−53931
LiO_2-Fe_2O_3-SiO_2 system, dielec. and magnetic props. 2−54333
LiO_2-Sc_2O_3-SiO_2-H_2O, hydrothermal crystallization 2−71383
Li_2O-SiO_2 glass, phase separation and crystn., X-ray obs. 2−56560
Li_4SiO_4-Zn_2SiO_4-Mg_2SiO_4-SiO_2 glass, phase equilibria and crystallization 2−64520
MgO-SiO_2-Al_2O_3, pressure sintered specimens, phase composition and dielectric constants 2−57226
MgO.Al_2O_3.SiO_2 glass-ceramic, ZrO_2-nucleated, phase transitions 2−47691
Na_2O-Al_2O_3-SiO_2, glass, X-ray diffraction study 2−60585
Na_2O-K_2O-SiO_2 glass, Na and K self diffusion, rel. to internal friction 2−50712
Na_2O-SiO_2 glass, dielectric loss and phase separation 2−54230
Na_2O-SiO_2 glass, elastic moduli and i.r. absorp. spectra, pressure depend. 2−53782
Na_2O-SiO_2 glass, immiscibility temp., effect of small additions of Al_2O_3 and Ga_2O_3 2−53539
Na_2O-SiO_2 glass, morphological changes produced by amorphous phase decomp. 2−47060
Na_2O-SiO_2 glass, nucleation process in the metastable region 2−60584
Na_2O-TiO_2-SiO_2 glasses press. and temp. depend. of elastic moduli, ultrasonic interferom. meas. 2−80741
$Na_2O.2SiO_2$ glass, annealing atmosphere effects on Na diffusion 2−53767
$NiSiO_2$ cermet films, granular, microstruct. 2−50498
PbO-Al_2O_3-SiO_2-B_2O_3 glass, between metal electrodes, memory effect 2−71915
Pt/SiO cermet films, elec. resist. in a.c. 2−75095
PtSi, nuclear resonance and susceptibility 2−65348
SIo_2 film, on Si, Fowler-Nordheim tunnelling and dielec. breakdown 2−47955
Si-Al-Cu-Mg-Mn-Fe-Ni-Zr-Ti alloy, D16T, cryst. and uncryst. struct., fracture under static and cyclic conditions 2−47527
Si-Al-Mg-Fe-Cu-Mn, alloy, AK6, ageing, temp.-time ranges 2−50802
Si-Al-Mg alloy, strength rel. to dislocation motion and GP zones 2−56717
Si-Al-N-O, new ceramic materials 2−60990
Si-Al-O glass, prep. and processing, i.r. spectra, crystn. products, mineral species form. 2−56557
Si-As-Te, amorphous semicond., energy gap depend. on glass transition and softening temp. 2−61346
Si-As-Te amorphous semiconductor, relation between band gap and density 2−65003
Si-Au, mixed phase formation at interface, Auger electron spectroscopy, 100-300C 2−74619
Si-B system, phase diagram 2−50957
Si-Fe alloy, ferromag. domain spatial replication, anisotropic decomp. struct. 2−72149
Si-Fe laminations, dynamic ferromag. domain wall response to a.f. field, rel. to eddy current losses 2−48062
Si-Ge-As-Te glass, comp. vs. glass transition temp. 2−60597
Si-Ge, single crysts., epitaxial growth from vapour phase 2−64599
Si-Ge alloy, He^+ irradiated, atomic displacements, Rutherford scatt. obs. 2−47388
Si-Ge alloy, oxide layer etched away reoxidation, production of MOS transistors 2−75132
Si-Ge alloy thermocouples, precip. of dopants 2−51210
Si-SiO_2 capacitor, frequency response of interface states 2−61404
Si-SiO_2 interface, fixed charge behaviour, rel. to growth conditions 2−54227
Si-SiO_2 interface, scatt. of conduction electrons by surface oxide charge 2−72000
Si-SiO_2 interface, surface state distrib., m.o.s. characs. obs. 2−47956

Silicon compounds continued
19 at.%Si-Te alloy, amorphous, struct. 2−53515
Si-$ZnSiP_2$ solid solution, epitaxial growth on Si 2−60665
$(Si,Al)(N,O)_4$ tetrahedral structure 2−60997
Si rubber membranes as supporting medium for cells for electron microscopy 2−79097
SiBr, emission spectrum, B-X system analysis 2−77060
SiC:H(D), implanted, recomb. radiation of excitons and vibr. spectrum 2−68688
n-SiC:N, 6H polytype, Raman spectra, electronic excitations, 8K 2−44392
SiC/W laser composites, thermal cond. and diffusivity 2−47768
SiC/graphite composite, thermal expansion, 300 to 800 K 2−54057
SiC-B alloy, phase composition rel. to press., 50-60 kbar 2−53996
SiC, 6H electroabsorption due to indirect excitons 2−81331
SiC, absolute signs of second harmonic generation coeffs. 2−44332
SiC, and base composites, impact strengths, 72-2400°F 2−60885
SiC, α-β polymorphic transformation 2−74941
3C-SiC, band struct. and optical props., pseudopotential calc. 2−61345
SiC, C-free crysts., synthesis 2−47212
SiC, defects, electron microscope obs. 2−47423
SiC, diffusion of B, distribution, elec. cond. and p-n junc. obs. 2−74797
β-SiC, electron irrad. effects on luminesc. 2−48232
SiC, filaments, high temp. testing of strength 2−60956
SiC, fracture energy relation, thermal shock behaviour, acoustic damping 2−60890
SiC, H- and D-implanted, CH and CD bond-stretching modes 2−65296
α-SiC, i.r. absorpt. spectra due to electron transitions in deep impurity centres 2−78106
SiC, impurity solubility, autoradiographic variant of activation analysis 2−72595
α-SiC, influence of struct. defects on elec. props. and luminescence 2−71774
SiC, interactions with metals at phase boundaries, thermodynamic analysis 2−84093
α-SiC, irrad. effects on e.p.r. and i.r. absorpt. 2−48294
SiC, luminesc., Zeeman splittings, bound excitons 2−48227
SiC, phonon spedtra from tunnelling characts. of p-n junctions 2−57042
SiC, polycryst., soln. in liquid Si, kinetics 2−56487
SiC, Raman scatt. from coupled LO-phonon-plasmon modes 2−68663
n-SiC, Raman scatt. from electronic transitions 2−51356
α-SiC, residual lattice disorder due to ion bombardment 2−47391
SiC, rigidity and limiting strength, comparative estimates 2−47475
SiC, self-bonded, texture and strength detn. to 1300°C in air and to 1750°C in argon 2−71393
SiC, strength, strength oxidation resist., thermal shock resist. 2−60882
SiC 2-stage decoration method, for surface struct. determ. 2−80539
SiC 2H, low temp. phase transformations 2−71695
SiC 6H cryst., absorption edge struct. at 9K 2−68649
SiC ceramic, resistance to dynamic fatigue at room temp. in air 2−80761
SiC fibre, rel. to composite material technology 2−47663
SiC film, heterostruct., prod. by irrad. of Si by C^+ ions 2−50504
β-SiC layer, on Si substrate, chemical conversion with hydrocarbon, growth mechanisms 2−60663
SiC layers, system for chem. vapour deposition 2−50507
SiC polycryst., effect of crystallite size on physical props. 2−56774
SiC polytypes, determ. of Madelung potentials by rule of thumb up to six figures 2−80589
SiC single crystals, monitoring gas medium during growth 2−60704
SiC system, phase relations, X-ray obs. 2−50972
SiC whiskers, twin morphology 2−53581
n-SiC(6H), impurity absorpt. of i.r. rad., high-temp. meas. 2−72350
$SiCl_4$, exact force field determ. from ^{35}Cl and ^{37}Cl isotope shift and analysis of vibrational spectra 2−42936
SiF_2, vacuum u.v. spectra, vibr. assignments 2−80040
SiF_4, fluorescence surrounding CO_2 laser induced sparks 2−74440
SiF_4, nucl. spin relax. obs. of spin-rot. interaction 2−56199
SiF_4, SiF_6, E and F_2 type Raman contour bands 2−46585
$Si_{1-x}Ge_x$ solid soln., film, photoelec. props. 2−65090
SiH^+, interstellar abundance discussed with reference to Franck-Condon factor measurements 2−44887
SiH_2, ab initio calcs. for potential curves, description of geometry and electronic spectrum 2−46584
SiH_4, absorption in extreme u.v. 2−46586
Si_2H_6, molecular structure determ. by electron diffraction 2−42937
SiH_3CN, molec. force fields detn. by kinetic methods 2−70776
$SiH_4 + H(CH_3)$ reaction, intermediate SiH_5 radical obs. 2−57415
SiI, absorption and emission spectra in 4200-4900 Å region, obs. of A $^2\Sigma^+$-X $^2\Pi_{1/2}$ transition, determ. of vibrational consts. 2−70726
Si_3N_4-AlN-Al_2O_3 system, solid solution, X-ray diffr. obs. 2−43823
Si_3N_4-Cr_2O_3, refractories, thermal resistance, oxidizability, sintering, porosity and impact strength 2−68162
Si_3N_4-GaAs interface, deposition and surface state density obs. 2−65040
Si_3N_4-GaAs interface, surface states and insulator traps, m.i.s. cond. study 2−77919
Si_3N_4, and base composites, impact strengths, 72-2400°F 2−60885
Si_3N_4, applic. in semicond. device manuf. 2−54221
Si_3N_4, ceramic, high density, fatigue behaviour, 250-1200°C 2−60897
Si_3N_4, ceramic, hot pressed, fracture energy at high temps. 2−60907
Si_3N_4, ceramic, hot pressed, strength fracture energy, microstruct relationships 2−60883
Si_3N_4, in m.i.s. struct., tunnelling with valence band as barrier 2−71993
Si_3N_4, in s.n.o.s. struct., elec. characts. 2−71984
Si_3N_4, interactions with metals at phase boundaries, thermodynamic analysis 2−84093
Si_3N_4, microstruct., transmission high-voltage electron microscope obs. 2−60998
Si_3N_4 ceramic, hot pressed, high temp. strength 2−60884
Si_3N_4 film, chemical vapour deposited on Si, dislocation generation 2−68031

Silicon compounds continued
- Si_3N_4 film, detection of silicon oxynitride layers on surface by Auger elec. emission 2−50506
- Si_3N_4 film, for semicond. devices, high prod. system for deposition 2−71952
- Si_3N_4 film, reactively sputtered onto Cu substrate 2−43481
- Si_3N_4 film, suppression of ionic contamination during deposition, rel. to m.n.o.s. struct. 2−71336
- Si_3N_4 film on Si substrate, ammonia free, props. at low temps. 2−74633
- Si_3N_4 films on Si, interface states, effect of ambient annealing 2−61397
- Si_3N_4 whiskers, Ni-coated, high temp. stability, gaseous environment effects 2−74640
- SiO_2:Au ion implanted, carrier transport and charge storage rel. to floating gate devices 2−68458
- SiO_2:C, amorphous, in m.i.m. tunnel cathode, threshold emission and elec. switching 2−81122
- SiO_2-Al_2O_3-CaO melt, dynamic viscosity, effect of CO_2, 1400−1700°C 2−74527
- SiO_2-Al_2O_3-K_2O-Na_2O glasses, thermal expansion and formation of leucite 2−74994
- SiO_2-Al_2O_3-Na_2O-K_2O-CaO-MgO glass, viscosity-temp. relations 2−67883
- SiO_2-Al_2O_3-R_xO glass, struct. state of Al ion, complex stability 2−56556
- SiO_2-Al_2O_3 glass, crystallization, DTA, elec. microscope and X-diffr. obs. 2−53542
- SiO_2-Au film, cermet, struct., elec. props., rel. to deposition condition 2−64976
- SiO_2-Au r.f. cosputtered films, combined electron microscopy X-ray microanalysis obs., and preparation 2−80576
- SiO_2-B_2O_3-Na_2O-Al_2O_3 system, comp. fluctuation and phase decomp. 2−53543
- SiO_2-CaO-Al_2O_3 glass, stratification, liquation, opalescence 2−56564
- SiO_2-CaO-MgO-Na_2O-AlF_3:Dy^{3+} glass syst., luminesc., effect of heat treatment 2−48228
- SiO_2-GaAs interface, deposition and surface state density obs. 2−65040
- SiO-K_2O system, binary interdiffusion coeffs. and O_2 self-diffusion 2−53772
- SiO_2-MgO-FeO system in mantle minerals, phase equilibria and elastic properties 2−57711
- SiO_2-Na_2O-CaO-MgO glass, phase equilib. in glass forming region 2−57023
- SiO_2-Na_2O system, binary interdiffusion coeffs. and O_2 self- diffusion 2−53772
- SiO_2-Nb_2O_5-ZnO, ternary system, phase relations at liquidus and subsolidus temps. 2−68203
- SiO_2-Si_3N_4 film, phase composition and thickness determ. by spectrophotometry 2−47086
- SiO-SiO_2, film, thickness and compositon, nondestructive meas. 2−50508
- SiO_2-SrO-K_2O, interdiffusion coeffs. matrix 2−80724
- SiO-Te, in m.i.s. struct., flat band voltage temp. depend., interface state obs. 2−77930
- SiO_2-TiO_2-Al_2O_3-Li_2O-MgO, glass-ceramic, crystn., microstruct., indentation hardness 2−80535
- SiO_2-graphite system, phase equilib. 2−43930
- SiO, A→X band system, vibr.-rot. analysis 2−83248
- SiO, amorphous, trap levels, thermally stimulated capacitor discharge study 2−54188
- SiO, dissoc. energy determ. from $Ge + SiO \rightleftharpoons GeO + Si$ study 2−72548
- SiO, evaporated films, interference meas. of refractive index 2−65212
- SiO, in Sgr B2 and Ori A, at 87 GHz 2−48745
- SiO, interstellar, detection of $J=2\rightarrow1$ rotational transition 2−58358
- SiO, matrix elements of dipole moment of bands in the system $A^1\Pi$ to $X^1\Sigma^+$ 2−67500
- SiO, Se, in Ag-SiO, Se-Al struct., electrophysical characteristics 2−71988
- SiO, substrate for Pb film, sticking coeff. effect of water vapour 2−64572
- SiO, transition probabilities for vibration- rotation bands 2−48696
- SiO film, dielec. props., moisture stability 2−72015
- SiO film, electron diffr. radial distrib. analysis 2−53577
- SiO films, electron-beam-evaporated, microwave relax. phenomena 2−54231
- SiO films, evaporated, i.r. spectra 2−50505
- SiO layer, between ferromag. films, hysteresis loop 2−48087
- SiO lines in interstellar spectrum of ξ Persei 2−81836
- SiO molecular lines in interstellar spectrum of Ophiuchi, expected equivalent width calculations 2−55072
- SiO vacuum evaporation on thin plastic films 2−69515
- SiO^+ electronic spectrum, vibr. and rot. anal. 2−77056
- SiO_2, acoustic birefringence under strong uniaxial compression 2−54028
- SiO_2, adsorption-desorption of CO_2, u.h.v. studies 2−71353
- SiO_2, adsorption of polystyrenes, competitive effects 2−60684
- SiO_2, adsorption of water, effect of surface acidity 2−53597
- SiO_2, channelling pattern recording using radioactive recoil atoms 2−54088
- SiO_2, crystalline and amorphous, structure-property relations, molecular orbital cluster calcs. 2−53516
- SiO_2, fused, development of new variety 2−70046
- SiO_2, fused, e.p.r. of transition metal ions struct. obs. 2−65338
- SiO_2, fused fibres, nonlinear elasticity at room temp. 2−60847
- SiO_2, glass-forming, He migration 2−50707
- SiO_2, HCl grown, Na^+ ion neutralization, m.o.s. obs. 2−51187
- SiO_2, in Al-SiO_2-Si struct., IV characs., breakdown, and switching 2−71996
- SiO_2, in m.o.s. struct., interface states and potential barriers 2−65043
- SiO_2, interactions with metals at phase boundaries, thermodynamic analysis 2−84093
- SiO_2, noncrystalline, Raman spectra 2−81364
- SiO_2, on planar struct., flower-like defects 2−47124

Silicon compounds continued
- SiO_2, partial volume determination, influence of composition for solid solution glass ceramics 2−56562
- SiO_2, photoinjection over interface barrier, exponential charging profiles effect on photocurrent 2−54226
- SiO_2, quartz-coesite transition, effect of shear 2−77751
- SiO_2, r.f. sputter deposited, electrical characteristics uniformity 2−61407
- SiO_2, silica, mechanically crushed, paramag. centres, e.p.r. obs. 2−67888
- SiO_2, steam grown on Si, cation transport 2−61405
- SiO_2, stishovite, elastic consts., rel. to upper mantle comp. 2−61980
- SiO_2, thermally grown, three terminal electron Hall mobility measurements 2−54178
- SiO_2, tridymite, growth from Li_2MoO_4-MoO_3 flux 2−77529
- SiO_2, vitreous, induced birefringence, nonlinear variation with uniaxial stress to 7 kbar 2−68600
- SiO_2, vitreous, lattice vibrational spectra, pressure densification effects 2−74971
- SiO_2, vitreous, phonon scatt., low temp., elec. and mag. field depend. 2−51056
- SiO_2, vitreous, radiation compaction mechanism 2−50410
- SiO_2, vitreous, struct., at. motions, neutron scatt. obs. 2−47061
- SiO_2, vitreous, struct., random network theory validity 2−47054
- SiO_2, X-ray emission and absorpt., bond breaking, point defect prod., model 2−80656
- SiO_2 adsorption of CO_2, e.s.r. obs., E'_s dangling bonds 2−71352
- SiO_2 and diatomite suspension in kerosene, mechanical behaviour during shearing in electric field 2−60531
- SiO_2 and $Si_{1-x}Ge_xO_2$, recrystn. in hydrothermal fluoride solns. 2−47285
- SiO_2 atmospheric particulates, radiative properties in spectral internal 500-1500 cm^{-1} 2−54854
- SiO_2 colloidal suspensions, electron density of particles, X-ray study under different collimation conditions 2−71285
- SiO_2 excesses of circumstellar shells, 10 micron spectroscopy 2−58294
- SiO_2 film, amorphous struct., elec. microscope obs. 2−50479
- SiO_2 film, dielec. props., moisture stability 2−72015
- SiO_2 film, grown by oxidation of silane, struct., electron diffr. and i.r. absorp. obs. 2−60664
- SiO_2 film, Na^+ ion transport, m.o.s. C-V characts. study 2−77936
- SiO_2 film, on Si by tetraethoxysilane oxidation 2−47126
- SiO_2 film, prep. by oxygen bombardment of Si, use in p-n junc. protection 2−51176
- SiO_2 film, pyrolytic, struct., electron diffr. obs. 2−80571
- SiO_2 film, pyrolytic decomposition of silicon compounds 2−74632
- SiO_2 film, r.f. sputtering, effects of substrate temp. on optical and chem. props., and re-emission coeff. 2−83865
- SiO_2 film, thermally grown, struct., i.r. absorpt. study 2−53579
- SiO_2 film thickness effect on MAOS charact. 2−71997
- SiO_2 films, growth and sputtering in low pressure glow discharge 2−74634
- SiO_2 films, study of transparency by luminescent method 2−44340
- SiO_2 films on Si, interface states, effect of ambient annealing 2−61397
- SiO_2 formation over Au layer on Si substrates 2−67911
- SiO_2 glass, ion irrad., surface topography 2−50462
- SiO_2 in m.o.s. struct., induced surface charge on oxidized surfaces 2−77916
- SiO_2 layers for compensation of Fabry Perot surface defects 2−70017
- SiO_2 layers on Si, ion implant and annealing effects, ir abs. and ellipsometric meas. 2−74791
- SiO_2 noncryst., defect struct. 2−60596
- SiO_2 on Ge, deposition and post-deposition treatments, interface C-U characts. 2−61402
- SiO_2 particles in α-brass, dislocation generation during plastic deform. 2−56708
- SiO_2 positive charge distribution meas. by channel conductance and step etching methods 2−71998
- SiO_2 thermally grown film, breakdown voltage and m.o.s. diode capacitance rel. to fabrication conditions 2−71999
- SiO_2 thin films, atomic structure 2−74623
- SiO_2 ultra thin layer, kinetics of thermal growth on Si 2−71337
- SiO_3, light scatt. by elastic waves and rot. of polarisation plane 2−72358
- SiO_3 excess in circumstellar shells, i.r. spectra 2−51742
- SiO_4^{4-}, in KBr and CsI, i.r. absorpt. 2−54424
- SiO_x, non crystalline, optical and bonding model 2−61656
- SiO_x, stoichiometric analysis by obs. of (d,p) reactions on Si and O 2−61835
- SiO_x antireflective coatings for Si solar cells, effects of electron irradiation 2−59056
- SiO_x film, r.f. sputtered in Ar-O_2, optical and elec. props., O_2 conc. effects 2−60667
- Si_2O_3, elemental anal. using neutron capture γ-rays 2−44513
- SiO_xN_y, non crystalline, optical and bonding model 2−61656
- SiP_{22}, det. of band structure from reflectance spectra 2−72306
- $^{28}SiH_3D$, ground state rotational constants determ. from high resolution i.r. spectra 2−64157
- $^{28}SiH_4$, high resolution i.r. meas. on ν_3 vibr.-rot. band 2−80039
- Te-As-Si-Ge film, amorphous, a.c. cond. rel. to localized tail states 2−61288
- TiO_2-SiO_2 glass, He migration 2−50718
- $Y_3Al_5O_{12}$:SiO_2 garnet, grown from melt, habit modification by doping 2−74751
- $Y_3Fe_5O_{12}$:SiO_2 garnet, grown from melt, habit modification by doping 2−74751
- $Y_3Ga_5O_{12}$:SiO_2 garnet, grown from melt, habit modification by doping 2−74751
- ZnO-Al_2O_3-SiO_2 glass-ceramics, dielec. props. and effects of adding (CaO, SrO, BaO) 2−65045
- ZrO_2-SiO_2-TiO_2 system, phase relations, 1050-1600°C 2−47722

Silver
- — 2−61690
- activated chemisorption and oxygen coverage 2−78192
- activated phosphate glasses, radiation induced photoluminescence, laser pulse excitation 2−68713
- adsorption of O_2, e.p.r. obs. 2−50531

Silver continued
  adsorption of oxygen, slow irreversible processes, work function depend., LEED pattern changes 2–60675
  adsorption on W, field emission microscope obs. 2–60690
  inAl-6.8%Zn alloy, effect on diffusion 2–56753
  atom, γ-ray scattering, incoherent, by K-shell electrons 2–59931
  atom, absolute total cross section for K-shell ionization by electron impact, 30-140 keV 2–46458
  atom, e.u.v. spectra, energy levels 2–64001
  atom, K-shell ionization by electron impact, absolute cross- sections 2–79931
  atom, L-series X-ray spectrum, calc. of relative intensities using radiative transition rates 2–42724
  Auger spectroscopy, quantitative, and electron ranges 2–71304
  band structure, crit. point detn., wavelength mod. derivative spectroscopy obs. 2–48160
  band structure, critical point determ., wavelength modulation derivative spectroscopy obs. 2–48160
  bulk modulus and internal friction, influence of neutron irrad. 2–77642
  channelling of 21.6 MeV I ions, axial channelling phenomenon 2–44007
  chemisorption of O_2, rel. to surface struct. LEED and secondary electron spectroscopy 2–51442
  clusters, electronic props., mol. orbital calc. 2–81026
  complexation by S_2O_3- SCN- during photographic fixing 2–59314
  Compton effect scatt. power, thermal vibr. freqs. 2–68213
  concentration meas. under variable exposure for latex, nitrocellulose, polyvinyl butyryl, rel. to optical density 2–52500
  conduction electron mean free path determ. from size effect of thin films 2–75012
  conduction electron optical mass 2–44029
  crack formation, in situ obs. in 500 kV electron microscope 2–80853
  crystal, t.e.m. specimen prep. using electrolytic technique 2–80619
  cylinder, surface plasma waves, optical refl. study 2–61210
  dendrites on amorphous substrates, disclinations 2–53582
  density changes of solid and molten state at elevated temps. 2–64699
  desorption, thermal, mass changes and gases evolved 2–47151
  development, non exposed grains, fogging, reactivity, oxidation 2–84672
  diffusion, in molten Ag-In alloy, capillary reservoir technique 2–56491
  diffusion in Al, interpreted using oscill. form of inter-ion potential 2–64691
  diffusion in Cd, tracer diffusion 2–56755
  diffusion in Pb, isotope effect in dissociative mechanism 2–68044
  diffusion in Pb-Sn alloy 2–56763
  diffusion of Co and Cd, 375-650°C, near-surface effects 2–68049
  direct discharge neutron detector in thermal and epithermal regions 2–52699
  disk, electron time-of-flight effects in skin-layers 2–44045
  dislocation etchants, use of H_2CrO_4 2–71363
  dispersion hardened, recryst. temp. rel. to particle vol. fraction, separation deform. 2–56900
  dye bleach colour copy materials 2–59320
  elastic constants, high pressure effects, meas. using torsional oscillatory method 2–68061
  electrical resistivity, evidence of phonon drag 2–64909
  electrochemical anal. in various stages of oxidation, paste electrodes 2–65384
  electrode with one crystallographic plane only, prep. 2–48337
  electrodes, sintered, morphology, electrical characteristics, KOH concentration effects 2–84654
  electromigration in Au-Ag alloy 2–83996
  epitaxial electrodeposition, computer simulation 2–71320
  epitaxial growth on substrates, various modes 2–77530
  equation of state, based on elastic and cohesive props. 2–68063
  fallout patterns from seeded convective storms 2–62220
  Fermi surface, de Haas-van Alphen meas., infinite field phases 2–61182
  Fermi surface, phase shift parametrization 2–44030
  Fermi surface orbits, integral calc. method 2–44028
  fibrous growth using solid-state ionics technique 2–80601
  filament formation, redox potential, development, catalysis 2–84673
  filament growth, from Ag compounds, solid state ionics technique 2–47133
  filament growth rate and photographic emulsion thickness 2–59313
  film, annealed, hillock and island form. by surface diffusion 2–67896
  film, Debye characteristic temp. 2–61102
  film, dielectric const. changes, piezoreflectivity obs. 2–54382
  film, growth processes on alkali halides, elec. microscope obs. 2–47096
  film, in Pb-Ag-Pb struct., heat capacity at ^{3}He temps., proximity effect obs. 2–81041
  film, induced supercond., energy gap and electron-electron interaction 2–44072
  film, on mica, oriented recrystallization on annealing 2–47097
  film, oriented growth on muscovite, intermediate C layer effect 2–74626
  film, piezorefl. and piezotransmission, rel. to electron states 2–81366
  film, Poissons ratio, X-ray obs. 2–67904
  film, significance of electric field on growth 2–60634
  film, single crystal, prep. and characterization 2–56586
  film, size effect on strain coefficient of resistance 2–57151
  film, vacuum deposition on Ni, secondary ion- ion emission obs. 2–50481
  film charact. and preparation, single crystal 2–74627
  film on mica, modulation of conductance due to changing interface, metallic field effect 2–75047
  films, epitaxial, temp. coefficient of resistance 2–61221
  films, indentation and impact studies of loading 2–77708
  films on mica substrates, exam. of internal stresses 2–77650
  films on W, work function determ. by employing retarding-field diode technique 2–72083
  fine particles in glass matrix, prep. and optical props. 2–54412
  fracture, high voltage electron microscope obs. 2–56825
  gamma-irradiated, recrystn., internal friction obs. 2–64758

Silver continued
  grain boundary self-diffusion, isotope effects, correl. effects vacancy model 2–56752
  Hall and Righi-Leduc coeffs., 4-125 K, Weidemann- Franz law 2–61224
  hyperchannelling of ^{127}I and ^{4}He ions, orientation rel. to intensity and energy loss 2–47778
  impurity in Ge(Li) detector, trap parameters 2–46045
  ion sources, laboratory, low intensity 2–55672
  L-subshell fluorescence yields 2–79905
  lattice dynamics, phonon dispersion curves 2–80900
  LEED from {001} surface, expt. and theory 2–50428
  liquid, surface tension, effect of dissolved O_2, sessile drop dimens., change method 2–43340
  liquid, thermotransport of Co, heat of transport 2–53414
  liquid, wetting of TaC 2–43468
  microsection preparation, electrochemical technique 2–50429
  monolayer on Pt, detection using tracers 2–71302
  optical props. and interband transitions, review 2–72292
  partial free enthalpies of form. determ. in galvanic cells 2–64887
  phonon dispersion curve, psuedopotential calc. 2–57039
  photoelectric emission, electronic struct. 2–72088
  photographic dye-bleach processing, printing 2–73687
  in photographic products, precision routine analysis 2–59332
  porous, physical adsorption of Ar, onset of Henry's law 2–60674
  powder, compaction process 2–50909
  quadrupole interaction of ^{111}Cd, time-differential perturbed ang. correl. obs. 2–57316
  radiation damage, nature and annealing characts. 2–47368
  radiation damage, proton, deuteron and He-ion, energy depend. 2–50643
  ranges and range straggling of ^{150}Sm 2–68269
  recrystallization, on annealing, internal friction and modulus anomaly obs. 2–47577
  rolling texture form. mechanism 2–60972
  secondary electron spectrum, charact. energy loss and gain, Auger peaks, fine struct. 2–54280
  shock waves, and temp. derivation along Hugoniot curves, appl. of fourth-order anharmonic theory 2–84188
  solar abundance, spectral scan of resonance lines 2–75949
  solar photospheric abundance det. from spectrum synthesis 2–58554
  steel, spectrographic determination 2–57443
  stopping power for 25-250 keV H ions 2–47774
  stopping power for protons and deuterons at same velocity 2–54098
  stopping powers for 30-90 MeV ^{238}U ions 2–47773
  stopping powers for ^{4}He, ^{16}O, ^{35}Cl at 1 to 3 MeV 2–80921
  stresses in vacuum evaporated films 2–80569
  surface, acid-treated, secondary ion yield 2–61471
  surface, inelastic scatt. of He atoms, 0.01 eV 2–50430
  surface diffusion on Cu (100), (111) and (110) planes 2–60626
  surface plasmon excitation by subwaves produced by gratings 2–64905
  surface plasmons, radiative decay from spherical particles 2–51332
  thermal resistivity, high temp., and electron-phonon interaction 2–68258
  thermoelectric power rel. to Fermi surface shape and sample dimens. effects 2–68296
  thick target, energy loss of scatt. protons 2–80928
  thin film atomic oxygen sensors 2–65403
  total energy, pseudopot. theory 2–61137
  u.s. attenuation, Gruneisen mode and const., phonon viscosity and thermoelastic effects 2–68234
  valence band density of states, X-ray photoemission spectroscopy obs. 2–65104
  vapour, high-current hollow cathode discharge, radiation, effect of reson. and recomb. 2–74423
  whisker growth and dissolution 2–50517
  work hardened, anelastic phenomena at low temp. 2–60848
  Ag/As_2S_3 system, photochem. transformation rate temp. depend., ht. treatment and ageing effects 2–57433
  Ag-Pd powder, soln.-precip. sintering in presence of reactive glass 2–80878
  Ag-naphthalene-Ag structures, electronic conduction in dark 2–57199
  Ag- centres, non-cubic, in mixed crystals of alkali halides 2–44370
  Ag I spectral lines, oscillator strengths 2–64011
  Ag on NaCl surface, decoration with anthraquinone, information microstructure 2–71305
  Ag sound tracks, in colour reversal film 2–76551
  Ag^- centres, in KCl(Br)(I), polarization and decay time of luminesc. 2–80710
  Ag^+, in RbCl and RbBr, paraelec. props. 2–61422
  Ag^+, interdiffusion coeff. in molten nitrates 2–65383
  Ag^+ in alkali halides, resonant phonon modes 2–54018
  Ag^+ in K halides, reson. phonon modes 2–50994
  Ag^{2+} e.p.r. in $SrCl_2$, conform. instability in hexagonal sites 2–84579
  As-Se glass, Ag doped, elec. props. 2–64975
  CdF_2:Ag^+, ionic thermocurrents, temp. depend. 2–81089
  CdF_2:Er^{3+}, Ag^+, correlated e.p.r. and optical study 2–78164
  CdS:Ag, field quenching, influence of doping 2–54170
  CdS:Ag, photosensitive material, spectral characts. 2–72059
  Fe-base alloys, spectrographic determination 2–57443
  KCl:Ag, colour centre form. by X-ray irrad., e.p.r. and optical obs. 2–80713
  KCl:Ag thermostimulated electron emission, retarding field depend. 2–54274
  NaCl:Ag^+, Raman scatt. and far i.r. absorpt., expt. and calc. 2–84508
  in Nb-Sn sinter material, supercond., effect on screening behaviour 2–75061
  Pb, Ag-doped, pore formation on annealing 2–71665
  Pd 24% Ag-H foils, electron microscope examination 2–56948
  Si:Au, Ag, Co, trapped minority carrier thermal emission rates, meas. technique 2–71784
  Ti(Pd)Ag passivated contacts, use with Si solar cells 2–59057
  ZnS:Ag,Mn,Cl phosphors, mechanism of activator interactions 2–84551

Silver compounds
  $Ag_2S-In_2S_3$ solid soln., coprecip. diagram 2–53901

Silver compounds continued
alloy, β-brass type, lattice vibrs. rel. to martensite struct. 2−56930
alloy, cold worked, X-ray line profile analysis, instrumental broadening correction 2−64636
alloys, soln. hardening, stress equivalence 2−80834
halide, adsorpt. states of gelatin and photographic stabilizers 2−80584
halide, energy bands, depend. on lattice const. and halogen 2−64886
halide, liquid particle growth rates in alkali alumino borosilicate glass 2−77478
halide, spectral sensitization by trapping of dye mobile positive holes 2−81552
halides, adsorption of 1,1-diethyl-2,2′-cyanine, J-aggregates props. 2−81027
halides, emulsion size distribs., meas. by electrolytic reduction 2−80499
halides, grains, photographic sensitizing and desensitizing by electron traps 2−81023
halides, lattice props., calc. using ionic Rydberg function 2−47727
halides, optical transitions, localized electron states, self-bound and impurity trapped excitons 2−81025
halides, photographic process, initial chem. develpment reaction 2−81547
halides, physics and chem., conf., Montreal, Canada, Aug. (1972) 2−81541
halides, rigid lattice band mass of electron, Feynman's polaron theory 2−61202
halides, semiconducting analogues 2−81103
halides, space charge due to Frenkel defects at surface 2−81022
halides, thermolum. and photocond., trap levels, meas. apparatus and technique 2−79389
halogenides, nucleation structure and primary photochemical process 2−49455
trifluoroacetate, ^{19}F shielding tensors of trifluoromethyl group 2−68751
$2AgCl(g) + Pb(g) \rightarrow 2Ag(g) + PbCl_2(g)$ substitution reaction in hot hollow cathode 2−84641
$[Ag_4Te][ClO_4]_2$, cryst. struct. 2−53653
Ag-15% Ge alloy, splat-cooled, martensitic transformation of structure 2−56921
Ag-Al alloy, thermal expansion, 10-300K 2−43992
β-Ag-Al alloys, splat quenched, martensitic transform 2−71672
Ag-Au-Cu alloy, sp. ht. and residual resist. 2−75051
Ag-Au alloy, effects of pressure on resistivity 2−51097
Ag-Au alloy, electronic struct., reflectance obs. 2−61174
Ag-Au alloy, impurity scatt., electron lifetimes, Fermi surface, de Haas-van Alphen meas. 2−61148
Ag-Au alloy, sp. ht. and residual resist. 2−75051
Ag-Au alloys, vacancy flow, effect and Kirkendall shift meas. 2−74809
Ag-Au system, coherent pseudopotential model 2−75025
Ag-(28 at.%) Au thermocouple wire, Standard Reference Material 733, thermoelec. voltage comparison with common materials, 4 to 273K obs. 2−65080
Ag-Au(Cd)(In) dilute alloy, Righi-Leduc and Hall coeff., 2.5-120 K 2−75050
Ag-Cd alloy, application of Lindemann's rule for melting 2−74582
Ag-Cd alloy, impurity scatt., electron lifetimes, Fermi surface, de Haas-van Alphen meas. 2−61148
β-Ag-Cd alloy, operative slip systems 2−60874
Ag-Cd alloys, solubility of hydrogen, rel. to Fermi level position and clustering 2−77716
Ag-Cd(Zn) alloys, stress corrosion sensitivity in $FeCl_3$ and $Fe_2(SO_4)_3$ solns. 2−64733
Ag-Cu alloy, 7.5 wt% Cu, discontinuous precip. kinetics, 200-500°C 2−80856
Ag-Cu alloy, eutectic, freezing and melting point determ. 2−53486
Ag-Cu alloy, rapid cooling by laser melt quenching 2−56897
Ag-Cu alloy, weakening resist. rel. to deform., heating time and temp. 2−50764
Ag-Er alloy, dilute, exchange interact. with cond. electrons, e.p.r. obs. 2−72467
Ag-Ga alloy, liquid, free enthalpy of mixing 2−53422
Ag-Ga(In)(Ge)(Sn) solid solns., partial free enthalpies of form. determ. in galvanic cells 2−64887
Ag-GaO_x alloy, dispersion strengthened, creep 2−53814
Ag-Ge alloy, impurity scatt., electron lifetimes, Fermi surface, de Haas-van Alphen meas. 2−61148
Ag-Ge alloy, laser irrad., metastable phase formation 2−50929
Ag-Ge alloy, liquid, free enthalpy of mixing 2−53422
Ag-Hg amalgam whisker, growth on Hg surface from aqueous solns. 2−60669
Ag-In alloy, liquid, free enthalpy of mixing 2−53422
Ag-In molten alloy, diffusion of Ag, capillary reservoir technique 2−56491
Ag-In solid solution, Zener relaxation 2−47453
Ag-Mg alloy, application of Lindemann's rule for melting 2−74582
Ag-Mn-Al alloy, high coercivity, struct. of ferromag. precip. 2−43821
Ag-Mn dilute alloys, s-d exchange interaction constant from electrical resistivity measurements 2−44214
Ag-Pd-H system, phase diagram 2−74953
Ag-Pd alloy, low field Hall coeff. at 4.2K and 300K 2−61188
Ag-Si alloy, deformed by tension and rolling, X-ray diffr. 2−80845
Ag-Sn alloy, impurity scatt., electron lifetimes, Fermi surface, de Haas-van Alphen meas. 2−61148
Ag-Sn alloy, liq., determ. of interdiffusion coeffs. 2−53415
Ag-Sn alloys, stacking faults, X-ray diffr. data interpret. 2−50678
Ag-Sn melt, electrotransport, current density effects 2−50348
Ag-Yb dil. alloys, perturbed ang. correl. on ^{169}Tm, h.f.s. 2−72247
Ag-Zn-Al alloy, transition from internal to external oxidation 2−48331
Ag-Zn, electrical conductivity, temp. depend. in range, melting pt. to 1100°C 2−71826
Ag-Zn alloy, application of Lindemann's rule for melting 2−74582
β-Ag-Zn alloy, operative slip systems 2−60874
Ag-Zn crystals, ion beam thinning 2−79103
Ag-Zn(41 at%) alloy, deform. induced martensite, X-ray diffr. obs. 2−80846

Silver compounds continued
Ag-rare earth alloy, thermoelec. power, phonon drag and distrib. contribs., 1.6-6K 2−81160
Ag complex, $[C_5H_5NH]Ag_5I_6$, cryst. struct. and cond., −30-125°C 2−43574
Ag complex, Ag di-isopropyldithiocarbamate, e.s.r. spectra, evidence for spin-spin and spin-orbit interaction 2−44443
Ag halides, photochemically dyed, absorption spectra 2−75392
Ag halides, photographic emulsions, response to low intensity illumination, hole trapping mechanism 2−66871
Ag I, thermoelectric power 2−77961
Ag solder alloy, superconducting transition at 64.4 mK 2−75058
Ag_3AsS_3, proustite, synthetic, low-temp. transform., spectral detect. 2−50930
AgBr:Ti^{3+}, V^{3+}, Cr^{3+}, charge transfer spectra 2−51333
AgBr, adsorpt. of dye aggregates, struct. and spectra 2−80557
AgBr, AgCl, sensitized photo-protective glasses, spectral properties 2−52503
AgBr, anharmonicity, far i.r. dielec. response study 2−61071
AgBr, chemical sensitization by doping, electronic mechanisms 2−81545
AgBr, coating, spectrally sensitized low intensity desensitization effect 2−81549
AgBr, emulsion, Ag formation in single emulsion grains 2−81546
AgBr, emulsions and crysts., red luminesc. at 77K, electron-hole recomb. 2−81438
AgBr, energy bands, depend. on lattice const. 2−64886
AgBr, heat of adsorption of photographic S sensitizers 2−73686
AgBr, impurity ions and vacancies interaction, diffusion mechanism 2−80699
AgBr, localized polariton modes, i.r. transmission obs. 2−80885
AgBr, molten, Hall effect 2−67839
AgBr, monodisperse photographic emulsions, r.m.s. granularity 2−66869
AgBr, nuclear track emulsion, track formation, analog theory 2−81543
AgBr, photocarrier mobility, electron-lattice interaction effects 2−81181
AgBr, photocond., photographic sensitivity, effect of sensitizing dyes 2−81550
AgBr, photographic sensitivity, impurity effects 2−81544
AgBr, positron decay rates, trapping at extended defects 2−81024
AgBr, positron lifetime, illumination effects, at 300 and 77 K 2−77808
AgBr, sol, conversion to AgI; kinetics, turbidimetric obs. 2−81542
AgBr, spectral sensitization by cyanine dye monolayer 2−81551
AgBr crystals, obs. of primary photographic process using transient photocharge obs. 2−66864
AgBr crystals, outer shell overlap integrals 2−50558
AgBr emulsion, latent image centres displacement 2−80723
AgBr grains, effects of metal ions on photographic and emission processes 2−59305
AgBr monodisperse photographic emulsions, development, fixing rate measurements 2−66870
AgBr phase holograms, dye induced desensitization to Ar laser light 2−42132
AgBr photographic development rate and emulsion thickness 2−59313
AgBr photographic emulsions, quantum sensitivity, absorption coefficient 2−59303
AgBr photographic films, photoconductivity obs. at 77 K with microwave methods 2−66867
AgBr reduction sensitization, effect of electron and positive hole traps 2−66862
AgBrI:Br^-, NH_3, cryst. morphology rel. to impurities 2−80648
AgBrI, photographic emulsion coatings, luminesc. spectra at 77K 2−81437
(AgBr + AgCl (5%)):$C^{5+}(N^{5+})$ $(O^{6+})(S^{6+})$ high energy implantations, Doppler broadening of positron annihilation photons 2−71507
AgCl:$C^{5+}(N^{5+})(O^{6+})(S^{6+})$ high energy implantations, Doppler broadening of positron annihilation photons 2−71507
AgCl:Cd, crysts., nuclear particle track detectors, development and props. 2−79687
AgCl:I-, decay mechanism of bound exciton, luminesc., 4.2-80K 2−72392
AgCl:Ni^{2+}, thermal cond., relaxation time approx. analysis 2−51057
AgCl:Ti^{3+}, V^{3+}, Cr^{3+}, charge transfer spectra 2−51333
AgCl, anharmonicity, far i.r. dielec. response study 2−61071
AgCl, energy bands, depend. on lattice const. 2−64886
AgCl, Frenkel defects, equilib. conc. perturbation by microwave pulse, ionic cond. change 2−80698
AgCl, heat of adsorption of photographic S sensitizers 2−73686
AgCl, impurity ions and vacancies interaction, diffusion mechanism 2−80699
AgCl, molten, Hall effect 2−67839
AgCl, photocarrier mobility, electron-lattice interaction effects 2−81181
AgCl, photographic coating, with adsorbed sensitizing and desensitizing dyes, photocurrents 2−81183
AgCl, polycryst., dislocation dynamics, thermally, activated deform., flow stress, 77-400K 2−77589
AgCl, positron decay rates, trapping at extended defects 2−81024
AgCl, positron lifetime, illumination effects, at 300 and 77 K 2−77808
AgCl, pure and doped, thermal cond., transverse phonon contrib. 2−77789
AgCl aerosol, scavenging by falling water droplet, particle size effect 2−75599
AgCl crystals, outer shell overlap integrals 2−50558
AgCl electron impact ionisation species, and dissociation energies 2−50021
AgCl emulsion microcrystals dichroism, spectral reversal 2−84470
AgCl photolysis, temp. depend., 77-400K 2−61803
AgF, energy bands, depend. on lattice const. 2−64886
AgF, photocarrier mobility, electron-lattice interaction effects 2−81181
AgF crystals, outer shell overlap integrals 2−50558

Silver compounds continued

- Ag_2F, estimation of work function from threshold value of photoelectric emission and by photoelectron spectroscopical method 2–72089
- δ-$AgFeO_2$, cryst., struct. 2–53652
- $AgGaS_2$, absolute signs of second harmonic generation coeffs. 2–44332
- $AgGaS_2$, birefringence, direct obs. using fringe technique 2–75259
- $AgGaS_2$ i.r. reflectivity and det. of optical constants mode frequencies and strengths and damping 2–44364
- $AgGaS_2(Se_2)$, band struct., electrorefl. and absorpt. studies 2–75276
- $AgGaS_2(Se_2)$, i.r. transmission cut-off 2–78058
- $Ag_2H_3IO_6$, ferroelec. phase transition dynamics, spin-lattice relax. meas. by double reson. 2–84450
- AgI-NaI-H_2O, aerosol-cloud interactions, parcel model 2–60527
- AgI-NaI-H_2O system, hydrous phase structs. 2–47314
- AgI-NaI aerosols, complexing, rel. to cloud seeding 2–62247
- AgI-NaI compared to AgI-NH_4I in cloud seeding, hail suppression program 2–62194
- AgI, exciton absorption spectrum detn. 2–68310
- AgI, optical constants of thin films in exciton band region, meas. 2–65209
- AgI, particle size and nucleating ability 2–48459
- AgI, rate of soln. of ice nuclei in water drops, nucleation 2–75600
- AgI, solubility in NaI and KI solutions, significance to cloud seeding 2–51595
- AgI, wurtzite-type, fund. optic lattice modes, Raman scatt. 2–61662
- AgI as contact or sublimation nucleus, electron microscope obs., cloud seeding 2–62190
- β-AgI crystal shapes rel. to ice nucleation properties 2–64589
- AgI freezing nuclei, behaviour during repeated freezing 2–48500
- AgI ice nucleation mechanisms 2–62192
- AgI particle in H_2O drop, contrib. of diffusion and interfacial kinetics to rate of solution 2–60434
- AgI particles, γ-irradiated, ice forming activity 2–48498
- AgI particles in seeded hail, simple technique for locating in nucleus 2–65747
- AgI seeded convective cloud, radar echoes, height temperature NaCl 2–84829
- AgI seeding, rain shower formation 2–65749
- α-AgI solid electrolyte, ionic Hall effect 2–83988
- $Ag_7I_4PO_4$, high cond. solid electrolyte from AgI-Ag_3PO_4 system 2–44152
- $AgInS_2$, i.r. transmission cut-off 2–78058
- $AgMo_4S_5$, superconducting properties, heat capacity, Debye temp. 2–81051
- $AgNO_3$, molten, hypersonic vel. dispersion obs. by Brillouin spectroscopy 2–77427
- $AgNO_3$ cryst. growth morphology at polymorphic transforms. 2–50945
- Ag_7NO_{11}, precise determ. of R factor and position of NO_3^- from diffractometer data 2–77557
- $AgNa(NO_2)_2$, crit. slowing down of dielec. relax., thermal noise study 2–72029
- $AgNa(NO_2)_2$, dielec. relax. time, temp. depend., press. effects 2–77955
- $AgNa(NO_2)_2$, ferroelec., spontaneous polariz., pyroelec. obs. 2–54235
- $AgNa(NO_2)_2$, hydrostatic pressure effects on ferroelectric transition 2–61426
- $AgNa(NO_2)_2$, hysteresis loop in quasi-static elec. field 2–72030
- Ag_2O-B_2O_3 glass system, n.m.r., B sites obs. 2–65342
- $Ag_{19}O_{15}P_2O_7$, high cond. solid electrolyte from, AgI-$Ag_4P_2O_7$ system 2–44152
- $AgPO_3-X^{n+}(PO_3)_n$, $X^{n+}=Mg^{2+}, Ca^{2+}, Sr^{2+}, Ba^{2+}, Pb^{2+}, Al^{3+}$ use for multichannel image convertors and amp. 2–68501
- AgPd system, density of states, X-ray photoemission obs. 2–61179
- Ag_4RbI_5, solubility and diffusion of I_2, electrochemical cell obs. 2–84657
- Ag_2S, (31-34 at.% S), molten comp. and temp. depend. of elec. cond., change of sign of temp. coeff. with increasing S conc. 2–83798
- Ag_2S, heat of adsorption of photographic S sensitizers 2–73686
- Ag_2S, phase II existence region determ. from electronic props. 2–47703
- Ag_2S epitaxial thin films, electrical and optical properties 2–53567
- $Ag_2S(Se)$, efficiency criterion for thermogenerators 2–75158
- AgSb mol., visible emission spectrum, assignment 2–64113
- Ag_2Se, polymorphic transitions, X-ray obs. 2–64809
- Ag_2Se thin films, formation and electrical properties, effect of heat treatment 2–53570
- Ag_3Sn, preparation of electrodeposits 2–53569
- Ag_2Te, Hall coeff., elec. resist., thermoelec. power, at m.p. and to 1500 K 2–60495
- n-Ag_2Te, Lorenz number, electron scatt. inelasticity obs. 2–84337
- Ag_3TlTe_2, crystal structure, electron diffraction obs. 2–74722
- Al-Ag alloy, effect of coherency strain field on disloc. struct. 2–56702
- Al-Ag alloy, pre-precip., elec. resist. and Hall coeff. variations 2–77692
- Al-Ag alloy, precipitation process study 2–84133
- Al-Ag alloys, supercond., pre-precip. state props. 2–64944
- Al-Ag liquid alloy, Cr or Mn impurity, susceptibility near nonmag.-mag. transition 2–80486
- Al-Ag system, discontinuous precipitation reactions and ternary component influence 2–71674
- Al-Ag type alloy, GP zone composition by relative intensities of diffuse effects 2–68035
- Au-Ag alloy, electromigration of Au and Ag 2–83996
- Bi-Ag alloy, thermomag. props., rel. to device appl. 2–59064
- Bi-Ag eutectic alloy, morphology, electron diffr. obs. 2–60976
- Bi-Ag eutectic alloy, surface damage after polishing, e. microscope study 2–67898
- Cu-Ag alloy, electronic struct., reflectance obs. 2–61174
- Cu-Be-Ag alloys, structural states in decomposition process, e. diffr., e. micro. and microhardness exam. 2–80782
- Cu-Be-Ag and Cu-Be-Ti, decomposition of solid solns., phase transformations 2–68194
- $CuAgTe_2$, synthesis and struct. detn. 2–71431

Silver compounds continued

- NaCl vacuum seals and valves, review of scaling procedures and bibliography 2–69510
- Pb-Ag alloys, ageing, softening mechanism and kinetics 2–43860
- Pd/Ag/H system, form. and decomp. equil. 2–77715
- Pd-Ag alloys, diffusion of H, coeff. meas. by electrochem. methods 2–77602
- Pd-Ag alloys, diffusive motions of hydrogen 2–77618
- Pd-Ag alloys, solubility and electromigration of H_2 and D_2 2–83990
- Pd-Ag alloys, solubility of hydrogen, rel. to Fermi level position and clustering 2–77716
- SgCl, ionic cond. up to 25°C below m.p. 2–68050
- Sn-Ag alloys, liq., interdiffusion coeffs. 2–50349
- Tm-Ag alloy, h.f. n.m.r. at 4.2 degrees K 2–72518

Sinanoglu's theory *see Atoms/structure*

Sintering

- alloys containing ZrC_x and HfC_x, effects of protective atmos. 2–77721
- amorphous spheres, kinetics 2–50907
- breccia, lunar and terrestrial minerals, deform. substruct. 2–62688
- bronze powders with spherical particles, kinetics 2–43890
- ceramic, corundum base, rel. to elec. cond. 2–53927
- ceramic alloy, B2Zh, prep. and mech. characterization 2–77720
- ceramics, at const. heating rate, kinetics 2–47652
- ceramics, rel. to wetting phenomena 2–43867
- cermet, Fe-based, antifriction props. rel. to sintering in various protective atmospheres 2–77727
- cermet, Fe-based, effects of protective sintering atmos. on physiomech. props. 2–68166
- cermet, in container with melting closure 2–50882
- cermet. ZHGp1.5D2.5, effects of cooling after sintering on struct. and mech. properties 2–77722
- clay, fusible, ceramic prep. by calcining 2–64784
- coagulation, closely located non-isomeric pores and gas filled cavities 2–53976
- diamond-metal system, compaction during liq.-phase sintering 2–80829
- diffusion models for initial sintering, effect of particle size distrib. 2–50904
- dynamic pressing, compaction process, fine structure and preps. of pressed parts 2–53879
- electron microscope obs., method of obs. without use of substrate 2–43879
- glass, metal-containing, phase comp., sintering temp. depend. 2–50862
- glass filaments, orientated, densification in hot pressing 2–77703
- glass powders, modelling of Fra Mauro breccias form. 2–62671
- graphite, Cu plated, cermet on Fe base 2–53863
- isostatic procedures for metal and ceramic powders 2–50859
- loosely packed and cold pressed powders, role of dislocations 2–61002
- metal, rate reduction by oxide dispersions 2–47512
- metal powder, on the possibility of thermal explosion 2–61003
- metal powder, spark isostatic pressing 2–68129
- metal powders, at different pressing rates and temps. 2–77697
- metal-carbide systems in solid state 2–77696
- mullite, densification kinetics and mechanism 2–50874
- mullite, stoichiometric, synthesis 2–50873
- nichrome thin films, elec. resist. obs. 2–68151
- oxide fuel struct. evolution, modelling using BEHAVE-2 code 2–52858
- powder, initial combined sintering analysis 2–50903
- powder metallurgy of high-temp. materials, conference, Tyrol, Austria, June 1971 2–53937
- reaction kinetics, modified equation 2–77695
- reactor fuel, 90% dense, fabrication for irrad. testing 2–53924
- reactor fuel, irrad., neutron radiography obs. 2–52856
- steatite materials, effect of modifying agents on structure and electromechanical properties 2–53933
- steel, dense struct. form. in the powder during stationary hot pressing in Cr steel 2–77698
- steel, martensite ageing, prep. by powder metallurgy 2–43892
- steel, stainless, in container with melting closure 2–50882
- superalloy, powder, elec. discharge activated press. sintering, composite struct. bonding 2–53938
- transition metal nitrides, hot pressing, compaction kinetics 2–47661
- two-phase systems, shrinkage rel. to conc. 2–43886
- Yttralox ceramic, Th-doped, processing 2–50900
- Ag-Pd powder, soln.-precip. sintering in presence of reactive glass 2–80878
- Al powder, effect of oxide film 2–43888
- AlN-Al_2O_3-Mo cermet, prep. by sintering 2–43869
- AlN-Y_2O_3, sintered, with fibrous struct., textural determ. 2–47666
- β-Al_2O_3, alumina, hot pressing and characteriz. 2–50875
- Al_2O_3, fine grained, rate controlled 2–77660
- Al_2O_3, kinetics, effect of iron oxide 2–50865
- Al_2O_3, powder, initial sintering rel. to surface diffusion, neck growth obs. 2–43887
- Al_2O_3, rapid sintering by glow-discharge apparatus 2–80804
- Al_2O_3, surface area and pore-size distrib. obs. 2–50866
- Al_2O_3, translucent alumina prep. and characteriz. 2–50863
- Ba formates, formation and surf. props. of electron emissive coatings 2–65365
- $BaFe_{12}O_{19}$, props, during sintering 2–77738
- $Ba_2NaNb_5O_{15}$ ceramic, scanning elec. microscope obs. 2–53929
- $BaTiO_3$ ceramic, dielec. props., sintering parameter effects 2–57241
- Bi_2O_3-SrO(CaO)(La_2O_3) sintered system, and ion transference no. determ. 2–61418
- CaF_2, effect of additives, reply to comments 2–80876
- CaF_2 effect of additives, comments 2–77723
- CaF_2 powder, sintering activity, effect of calcination 2–61004
- CdSb:Ag pressed powders, effect on elec. cond. 2–64906
- CeO_2, effect of TiO_2 addition on grain growth 2–47655
- Co-Cu-Fe-Ce alloy, permanent magnet prep. 2–50910
- Co-Sm permanent magnet alloy 2–57289
- CoO, comp. depend., volume diffusion mechanism 2–50878
- CoO, pure and Li-doped, final stage densification kinetics 2–50879
- Cu, internal porosity removal on sintering, effects of hydrostatic pressure 2–68130

Sintering continued
Cu powder, by electrolytic heating 2−74891
Fe, fine powder, density and shrinkage 2−61000
Fe green bodies, porous and sintered parts, polished metallographic specimen production 2−60933
Fe_2O_3, at const. heating rate, kinetics 2−47652
formates, formation and surf. props. of electron emissive coatings 2−65365
$GdCo_5$, powder, coercive force rel. to sintering temp., decomp. stability 2−68511
$Li_{0.93}Na_{0.07}Fe_5O_8$, effect of conditions on density and particle size 2−64790
$MgAl_2O_4$ polycryst. ceramic prep. and characteriz. 2−50887
MgO-SiO_2-Al_2O_3, pressure sintered specimens, phase composition and dielectric constants 2−57226
MgO, influence of inclusions 2−56964
MgO, surface area and pore-size distrib. obs. 2−50866
MgO refractories, effect of stress on grain growth 2−74915
Mn-Zn ferrite powders, core prod., crack reduction by pre-calcination 2−68163
Mo alloy TZM, sintered compact production, solid state reactions 2−56906
Mo powder, mechanism, mass transfer by diffusion- viscous flow 2−53941
Mo powder creep during hot pressing with and without addition of oxides 2−77694
Ni-Zn ferrite powder, hot-pressing and densification 2−43893
Ni particles, obs. using new hot stage in scanning electron microscope 2−56641
Ni powder, creep during hot pressing with and without addition of oxides 2−77694
NiO, at const. heating rate, kinetics 2−47652
$Ni_{1-x}O$, effect of O partial press. 2−61005
$(Pb,La)(Zr,Ti)O_3$, electrooptic ceramic, fabrication by atm. sintering 2−56967
$Pb(Mn_xNb_{1-x})O_3$ perovskites, synthesis and characteriz. 2−50893
$Pb(Ti,Zr)O_3$ and $(Pb,La)(Zr,Ti)O_3$, low temp. densification 2−50892
$Pb(Zn_{0.33}Nb_{0.67})O_3$ ceramic, electrooptical props. rel. to sintering conditions 2−65223
$PrCo_5$ magnets with Sm-Co additive 2−50797
Pt black, low temperature, mechanism 2−43894
$^{238}PuO_2$ fuel fabrication by hot pressing 2−53932
Si_3N_4-Cr_2O_3 refractories 2−68162
Sm-Co alloys, effect on mag. props. 2−51262
$SmCo_5$, powder, coercive force rel. to sintering temp., decomposition stability 2−68511
$SmCo_5$ magnet prod. using single phase sintering aid 2−43795
Sr formates, formation and surf. props. of electron emissive coatings 2−65365
TaC-Co alloy, oversaturated, microstruct. and reaction behaviour 2−64775
ThO_2 powder compacts, desintering 2−50898
TiB_2, effect of particle size 2−61006
TiC-Co alloy, oversaturated, microstruct. and reaction behaviour 2−64775
TiC-Nb cermet, hot pressing kinetics 2−56914
TiO_2 powder compact, abrupt shrinkage, SEM obs. 2−43895
UN, density increases, NASA study 2−64801
UO_2-PuO_2, mixed fuel, control and behaviour of O/M, offgas and moisture during fabrication 2−53934
UO_2, fission sintering and irrad. induced diffusion 2−52855
UO_2 pellets, prep. by sintering of $(NH_4)_2U_2O_7$ 2−80800
UO_2 sintered bodies, open pore distrib. 2−61025
W powder, with Ni additive, modified model 2−43897
W powder creep during hot pressing with and without addition of oxides 2−77694
W powders, activation by Ni and Fe, mechanism 2−50899
WC-Co alloy, oversaturated, microstruct. and reaction behaviour 2−64775
WC-Co hard metals, mixed milling effect on sintering, electron microscope investigation 2−56899
WC-Nb cermet, hot pressing kinetics 2−56914
ZnO, at const. heating rate, kinetics 2−47652
ZnO, effects of O_2 press. 2−74916

Skin effect
computation for laminar boundary layer without pressure gradient 2−53129
low frequencies, electrodynamic force moment, effect of a non-magnetic conducting cylindrical case 2−59026
metal, effect on n.m.r. Bloch decay 2−78171
metal, influence on amplitude and phase of pulsed n.m.r. signals 2−84608
metal, rel. to electron mean free path detn. 2−71829
metal film, anomalous effect 2−54121
metal film, surface impedance under anomalous skin effect conditions 2−51096
plasma, mechanism for anomalous current penetration 2−46721
Tokamaks, suppression in large devices 2−46753
transient, within nonlinear conductor 2−73493
Ag disk, electron time-of-flight effects in skin-layers 2−44045
CdS, temp. quenching of photocond., thermoelec. skin effect in presence of shallow levels 2−81171
CdSe, temp. quenching of photocond., thermoelec. skin effect in presence of shallow levels 2−81171
Sn, anamolous, d.c. cond., m.f.p., reflectivity factor 2−68341

Sky brightness
see also Airglow; Twilight
day sky brightness phase function rel. to optical thickness of atmosphere 2−62274
daylight, spectral irradiance for air mass 2 2−72799
light scattering and size-altitude distrib. of atmos. aerosols 2−65778
Olber's paradox rel. to evolutionary cosmology 2−72948
portable night sky photometer 2−69199
radiative properties of particulates composed of SiO_2, $CaCO_3$, H_2O, in spectral interval 500-1500 cm^{-1} 2−54854
spectral irradiance at Pretoria 2−62263
twilight, effect of aerosols on radiance and colour 2−81690
twilight sky, atmospheric scattering rel. to meas. of light polarization 2−81657

Sky brightness continued
zenith brightness temp. at 2.66 GHz 2−84810

Sliderules *see Calculating apparatus*

Slip
— 2−57589
adhesive wear, sliding model 2−68110
alloy, equil. configs. of passing dislocations on parallel slip planes 2−50665
boundary sliding, atomistic aspects, dislocations 2−56729
brass, fatigue cracking, effects of grain and twin boundaries, slip mode behaviour 2−71598
$\alpha+\beta$ brass, superplasticity 2−64714
ceramic, role in plastic deform. 2−47493
creep, diffusional, grain boundary sliding 2−56730
creep, recovery-work hardening theory 2−56799
creep kinetics, dislocation glide and viscous bowing, modified Orowan eqn. 2−56694
cross slip, model, screw dislocation shape calc. 2−60795
crustal deformation due to dislocation in multi-layered medium 2−78284
cyclic straining, subgrain formation 2−80763
diamond, framesite, microstructural aspects 2−50877
dislocation motion, activation area 2−47407
dislocations in non-parallel slip planes, elastic interaction 2−71479
electron emission microscope obs. of slip lines in cold deformation 2−43779
enstatite, X-ray topographic studies of natural and deformed crystals 2−61970
fatigue, high temperature phenomenological mechanisms 2−56818
feldspar, rel. to axial growth of inclined en echelon cleavage cracks during compression 2−61972
flaws, inherent, effect of microstruct. on stress to propagate at room temp. 2−68096
gravitational instability, Jean's criterion, slipping motion effect 2−84930
limestone, lightly loaded, stick-slip 2−72669
metal, strain-hardened, plastic flow theory 2−43684
in plasticity theory, macrohomogeneous model of continuum 2−77640
polyethylene, crysts., slip traces, dislocation motion 2−83847
polymers, high, extrusion and plastic deformation in solid state 2−84051
progressive failure of clay slopes, growth of slip surfaces 2−78238
quartz in prograde metamorphic sequence, rel. to preferred orientation 2−57766
rolling contact, surface roughness effects 2−68116
sheet drawing, effect of friction 2−60913
softened media theory, stress/strain relations 2−80735
soil slopes, effect of earthquakes 2−78279
steel, annealed low carbon, dislocation movement on slip planes to explain delayed yielding time 2−80813
steel, austenitic, surface slip lines and incipient cracks, during reverse bending 2−53837
steel, low-C, bending fatigue tests, Wohler curves, slip lines 2−50979
steel, slip lines in plastic flow 2−80831
steel, stainless, cross slip in fatigue deformation, elec. microscope obs. 2−77686
stick-slip, lab. obs. and applic. to earthquakes 2−65558
stress wave emission, review 2−69745
Udimet 500, rel. to low cycle fatigue 2−56820
velocity, calculation for binary gas mixtures 2−53273
Zircaloy-4, deform. mechanism 2−50747
B-Ag-Cd alloy, operative slip systems 2−60874
β-Ag-Zn alloy, operative slip systems 2−60874
Al-Mg alloy, slip struct. and crack growth during fatigue 2−47519
Al-(3 at.%)Mg alloy, high temp. deformation, lattice rotation, dislocation dragging 2−74835
Al, cross slip in fatigue deformation, elec. microscope obs. 2−77686
Al, evidence of glide on {110} plane 2−50760
Al, rel. to dislocation arrangement in surface layer 2−43465
Al, slip struct. and crack growth during fatigue 2−47519
Al, sub-grain boundary migration 2−80824
Al single crystal, influence of anodic coating 2−71576
Al single crystal, rel. to rolling texture and deformation banding 2−56788
Al_2O_3, rel. to microstruct. change on high temp. creep 2−71574
α-Al_2O_3, rel. to plastic deform., 1650-2000°C 2−53804
Be, basal slip effects on fracture 2−64753
Be, rel. to anisotropy of deform. after programmed loading 2−80775
C, diamond cubic struct., effects of crystal anisotropy and crystal struct. 2−71577
CsI, secondary slip generated by point load 2−74849
Cu-7.5 at.%Al alloy, deformed in tension, dislocations, etch pit obs.64664 2−64664
Cu, fatigue cracking, effects of grain and twin boundaries, slip mode behaviour 2−71598
Cu, neutron irradiated, surface slip steps, correl. with cleared channels 2−50761
Cu and Cu-Zn alloys, development of texture 2−80849
Cu whiskers, stress-strain diagram 2−56810
Fe-30% Ni alloy, martensitic transform. plasticity 2−68197
Fe-Cr-Ni, low temp. deform. characts. 2−43693
Fe-Cu alloy, dispersion strengthening model, slip dislocation precipitate interaction 2−50744
Fe-Si single crystal, effect of dimensional factors 2−71568
Fe-Si single crystals deformed by tensile forces, slip polygonization 2−84060
Ge, diamond cubic struct., effects of crystal anisotropy and crystal struct. 2−71577
$KNbO_3$, slip bands rel. to investigation of relation between surface deformation and ferroelectric domain structure 2−61429
Mg, plane strain extrusions, texture control and yield anisotropy 2−80848
Mg, pyramidal slip, dislocation configs. 2−47420
Mg substitutional soln. hardening 2−43855
Mo-Ru alloy, rel. to deform. mechanism 2−50840
Mo, plastic deform. under compression 2−53806
Mo single crystals, stress anal. for high temp.-creep and slip 2−84012

Slip continued
NaCl, creep at high temps., compression tests, stress dependence, creep mechanism 2−77651
NaCl, crystals, velocity of slip bands as a function of stress with respect to (100) [110] and (110) [110] systems 2−71578
NaCl, mech. props. and disloc. struct. 2−71579
NaCl, plastically deformed, X-ray and electron microscope obs. 2−53807
NaCl, single slip and double slip, electron microscope obs. 2−80749
NaF, mech. props and disloc. struct. 2−71579
Ni-Ni$_3$Nb, directionally solidified eutectic alloy, and mech. twinning 2−56796
Ni base superalloy Mar-M200, yield, orientation and temp. depend. 2−56795
Si, diamond cubic struct., effects of crystal anisotropy and crystal struct. 2−71577
SiC 2H, mechanisms for low temp. phase transformations 2−71695
Ta, deform. mechanism, orientation depend., 4.2-450K 2−50679
Tan-N, interstitial effects on geometry 2−74844
Ti, deformation kinetics for {1010}{1120} slip in single crystals below 0.4 T_m 2−64720
U, β phase, microstress behaviour during quenching, relaxation 2−77659
W, asymmetry, role of dislocations 2−56811
WC-Co cermets, electron microscope obs. 2−47505
Zn-0.1%Cd single crystal, deformed, elec. microscope obs. 2−47421
Zr alloys, anisotropic creep behaviour under fast neutron flux 2−50756
α-Zr. grain size depend. of deform. behaviour 2−50748

Smectic phase *see Liquid crystals*

Smokes *see Aerosols*

Snoek effect *see Crystal imperfections/interstitials; Elastic relaxation*

Snow
Antarctic, particulate matter 2−51526
Antarctica, local surface energy balance and surface regime 2−68851
atmospheric turbulent flux measurement over 2−72737
attenuation of 10.6 and 0.63 μm laser radiation in 2−75611
basin cooling in winter, radiation from snow covered mountains 2−75530
course in forested subalpine watersheds, areal water equiv. estimates, statistical analysis 2−68853
crystal growth, mechanisms 2−47207
deposited, measurement of specific surface 2−75441
detection by acoustic echo sounding 2−62234
dielectric constants, frequency dependence and relaxation times 2−53466
drifting, development and movement of wavy features 2−75442
fall rate obs. by radar 2−57974
flakes, methyl 2-cyanoacrylate replicas, electric field and symmetry 2−62245
formation of water droplets and ice crystals in deep cloud cover 2−68875
free water content determ., dilatometer for volume difference method 2−75440
hardness, temperature dependence 2−74865
hourly accumulation estimation from intensity or visibility obs. 2−51615
Lake Superior region, snowmelt energy exchange 2−57811
l.f. Young's modulus, using double pendulum 2−74878
melt, runoff and heat balance in small drainage area 2−75444
melt flood discharge in mountainous catchment, northern Iran 2−68856
meltwater, in snow cover, flow measurement 2−75443
mountain snow cover, displacement, strain and glide 2−75450
mountain snow cover, strains and strain rates 2−75449
project Snowman evaluation 2−62199
radar echo from snowfalls, spectrum shape at 3.2 centimetre wavelength 2−81658
radiowave attenuation at centimetre and millimetre wavelengths 2−51628
satellite data rel. to precipitation estimates for hydrologic applications 2−84869
storm, Great Lakes, Lavoie model 2−62102
water equivalent meas. using attenuation of natural γ radiation emission from soil 2−54742
weather map system, snow producing, and snowfall prediction 2−62122

Sodium
adlayer on W, K shell total electron impact ionization cross sections, Auger spectra 2−64579
adsorbed layer, on Ni (001), specular electron refl. 2−50544
adsorption on Mo, LEED and Auger spectroscopy obs. 2−50540
anomalous infra-red absorption and collective oscillations in small metal particles 2−65210
atmospheric layer, daytime laser radar obs. 2−81703
atom, D_1 line excited in N_2 afterglow, Doppler temp. meas. 2−49951
atom, D-doublet, temperature dependence of quenching cross section by N_2 and H_2O flames of 1500-2500 K 2−46454
atom, D-line radiation excited in collisions of atoms with vibrationally excited H_2, D_2, N_2 2−70627
atom, differential and total cross sections for elastic and inelastic electron scattering at 2.104 eV 2−79881
atom, elastic electron scatt., differential cross section calc. 2−79883
atom, electron excitation of D lines meas. from threshold to 1000 eV, determ. cross section, polarization 2−49959
atom, electron scatt., four state exchange close coupling eqns. 2−64042
atom, electronic energy levels, emission spectrum 2−45206
atom, equivalent D_1 linewidth in homogeneous magnetic field 2−46435
atom, low energy electron scatt., 0.5-20 eV, cross-section meas. 2−64022
atom, optically orientated, spin exchange with colliding buffer gas atom 2−79901
atom, optically pumped, obs. of maser transitions between Paschen-Back levels of ground state 2−52935
atom, resonance curve narrowing in forward scattering 2−56101

Sodium continued
atom, scattering from methane, methanol, methyl chloride, trimethylmethane, study of glory undulations 2−70821
atom, spectrum in premixed H_2-O_2-N_2 flame, emission noise spectrum 2−49952
atom, valence electron magnetic moment, rel. to free electron moment 2−42744
atom adsorbed on W surface, backscattering cross sections for K-shell ionization by electron impact 2−79919
atom depolarization cross-sections of D lines during collision with He 2−59957
atomic beam, deflection by radiation pressure of cw dye laser light 2−73624
atomic resonance excitation by tunable dye laser 2−59920
atoms, photoionization, pseudopotential calculation of cross-section 2−46448
Auger spectra, relative intensities determ. and interpret. 2−65111
in benzene-d_6 and mixed crysts. with benzene, absorpt. spectra 2−68653
bond disruption by gas bubbles in fast breeder reactor 2−49888
chemiluminescent excitation by active N_2, interferometric obs. of D-line profiles 2−81492
D-line emission from the atmosphere, solar eclipse effects 2−65885
desorption of submonolayer from Ge(100) substrate 2−67921
diamagnetism of free and Bloch electrons, many-body effects 2−68518
diffusion, in $Na_2O.3SiO_2$ glass, effects of annealing atmosphere 2−53767
diffusion in d.c. arc plasma, obs. using intensity distrib. of emitted light 2−60211
disordered overlayers, on Ni(001), specular electron refl. 2−60681
electrical and thermal cond., 40 to 360K 2−57086
electrical resistivity, contribution of Umklapp processes 2−84293
electrical resistivity, temp. and volume depend., 50K-m.p. 2−84296
electron-electron interaction and spin diffusion length, conduction e.s.r. study 2−48288
fast breeder reactor coolant, growth of single Na bubble, safety factors 2−74143
film, Xe adsorp., roughness and surface potential 2−50556
flowing, nonisothermal, ^{60}Co transport processes, corrosion and deposition rates 2−67344
impurity in KCl, effects on colorability 2−77595
ions, range-energy relations in air, 0.3-2.0 MeV 2−79917
laser action between $3^2P_{1/2}$ and $3^2S_{1/2}$ levels of optically pumped vapour 2−73555
liquid, compressibility, statistical mechanical perturbation theory calc. 2−80461
liquid, corrosion deposits in reactor cooling systems, effect on heat transfer coeffs. 2−83117
liquid, density response function from Mori's generalized Langevin eqn. 2−83776
liquid, determ. of pseudo-Gruneisen parameters 2−74540
liquid, effective pair pots. 2−50317
liquid, electron spectrum, calc. by cell method 2−83707
liquid, self-diffusion, 102-284°C, capillary method 2−67817
liquid, solubility, of inert gases, 600 degrees C rel. to reactor coolant behaviour 2−56041
liquid, structure factor, expt. and theoretical 2−50314
liquid, with small O content, oxidation of UC 2−51452
liquid, X-ray scattering, static structure function and atomic density distribution 2−47301
liquid cooling problems of fast breeder reactor 2−52843
metallic, Kohn-Sham self-consistent calc. of structure 2−60698
metallic, rigid neutral atom density, selfconsistent calc., auxiliary neutral atom model 2−71787
nuclear contact densities for electrons 2−61569
optical conductivity, interband, calcs. 2−68616
optical props. and surface plasmon states 2−71819
reactor coolant corrosion and mass transfer analysis using ion probe mass spectrometer 2−83118
in rocket vapour trail, neutral wind meas., daytime thermosphere 2−84886
self-diffusion in Na_2O-K_2O-SiO_2 glass, rel. to internal friction 2−50712
shock waves, and temp. derivation along Hugoniot curves, appl. of fourth-order anharmonic theory 2−84188
solar D line profiles, space and time variations 2−62746
solar spectrum, broadening coefficients of D-lines 2−55169
Stark effect in resonance lines, study by atomic beam method 2−74218
thermal conductivity, and elec. cond., 35°C-m.p. 2−84211
upper atmospheric, abundances, absorption meas. 2−65831
upper atmospheric abundance and stratospheric warmings 2−78385
vapour, forces of oscillators, meas. by more sensitive method of 'hooks' 2−49928
vapour, gas laser, phase matched, generation of u.v. radiation 2−42027
vapour discharge, high pressure, radial temp. distribution 2−71065
vapour discharge, high pressure, radiance at centre of D-lines, obs. value rel. to calc. value 2−71019
X-ray Compton profiles, theory and expt. 2−84255
X-ray emission spectra, satellites, rel. to double ionization theory 2−72381
X-ray L emission band, short-wave satellites 2−51361
β-Al_2O_3, Na and Na-K substituted, mech. behaviour 2−56770
CdF_2:Er^{3+}, Na^+, correlated e.p.r. and optical study 2−78164
CdF_2:Na^+, ionic thermocurrents, temp. depend. 2−81089
KCl:Na^+, X-ray irrad., hole centres, conversion and struct., optical absorpt. 2−84523
$Li + Na^+ \rightarrow Li^+ + Na$, nonresonant charge-transfer, multistate mol. wave-function approach 2−76980
$Li^+ + Na$ asymmetric nonresonant charge transfer, theoretical description by two-state approx. 2−70626
N_2-Na vibrational relaxation times in rapid expansion interpretation of Na line-reversal meas. 2−53102
Na/Cl secondary cell with inorganic electrolyte 2−66689
Na/NH_3 frozen solution, supercond., libron induced interelectron interaction calc. 2−64941
Na/S secondary cell with inorganic electrolyte 2−66689

Sodium continued

- Na-Ar liquid gas system, influence of gas on nucleation in sinusoidal pressure field 2−46893
- Na-He collision depolarization cross-sections for D lines 2−83169
- Na-He collisions, broadening of D lines and relaxation of resonance levels of Na 2−42784
- Na-He collisions, broadening of D_2 line at high temp. 2−74237
- Na^+-K^+ ion exchange, in Na borosilicate glass 2−53537
- Na-ammonia solution relaxation times and Overhauser enhancements for protons obs. 2−46988
- Na D_2 sunspot umbral line profile, photoelectric measurement 2−44989
- Na I, elec. quadrupole transitions, multiplet strengths 2−56102
- Na I, interstellar line in supernova spectrum in NGC 5253 2−81828
- Na II, spectrum between 350 and 9000 Å, term system revision 2−70589
- Na III, 180-380 Å, 90 lines meas. 2−79921
- Na III, 2500-1300 Å, $2p^43s$, 3d, 3p and 4s configurations 2−83196
- Na^-, continuous absorption coeff., contribs. from bound-free and free-free transitions 2−70586
- Na^+, heat of hydration, SCF Dirac-Slater calcs. 2−53403
- Na^+, hydrated binding energy calc. by ab initio, semi-empirical MO and classical methods 2−50030
- Na^+, in CsBr, i.r. absorp. 2−61635
- Na^+, in RbCl, KCl, and KBr, absorpt. and emission of F_b centres 2−64682
- Na^+, transport in SiO_2 films, m.o.s. C-V characts. study 2−77936
- Na^+ ion, neutralization in HCl grown SiO_2, m.a.s. obs. 2−51187
- Na_2, meas. of asymmetries in cross section for collision-induced rotational transitions in $B^1\Pi_g$ state 2−56274
- Na_2 mols., collision-induced rot. and vibrs. energy transfer, laser-induced fluoresc. obs. 2−83412
- Na_2 type diatomic molecule, application of model potential for valence electrons, determ. of terms 2−77072
- Na_3, Na_3^+, dissociation energies and equilibrium geometries, pseudo Hamiltonian model 2−56190
- Na°/Ca^+ ratio in interstellar medium, model of clouds 2−75785
- $NaOH$-H_2O solutions frozen, photoelectron emission spectra of ferrocyanide 2−44210
- ^{22}Na, blood-tissue transport in dog gracilis muscle 2−62822
- ^{22}Na diffusion in Pb meas. by sectioning diffusion couples, 249-313°C, vacancy mechanism 2−77600
- ^{24}Na, cosmogenic radionuclides, model for in-cloud scavenging 2−65808
- ^{24}Na labelled Na_2CO_3 solution for column flow obs. 2−56456
- $Na + O_2$ reaction in Ar matrix, Raman spectra of products 2−61776
- $Na^+ + O^-$, mutual neutralization rates, ionospheric D-region 2−65969
- Si:Na, elec. props., impurity atomic radius effects 2−71948

Sodium compounds

- ammonium tartrate, ferroelec. phase transition mechanism 2−81139
- benzene, u.v. spectrum, vibrational structuring of magnetic circular dichroism 2−70751
- n-butyrate and isovalerate mesophases, struct. behaviour 2−71158
- carbamate, solid, i.r. spectra 2−84527
- laser heating, for spherical wave, fusion energy taken into consideration 2−71554
- methylammonium tungstovanadate, VO^{2+} doped, e.p.r., ^{51}V quadrupole moment obs. 2−61741
- montmorillonite, isolation moncrystalline particles, selected area electron diffraction patterns 2−68001
- oxalate, monohydrate, crystal struct. by method of rhombs 2−74755
- silicate glass, γ-irrad., thermolum. 2−81410
- soda-lime, substrate for Au discontinuous film, ion drift rel. to film resist. 2−47833
- sodalite, synthetic, photolum. of O_2^- and S_2^- ion impurities, 4.2-300 K 2−81422
- synthetic sodium-containing adsorbants, NH_3 adsorption, temp. and press. depend. 2−47160
- zeolite, cation-exchanged, Mossbauer effect of Fe^0-atoms 2−54390
- AgI-NaI-H_2O, aerosol-cloud interactions, parcel model 2−60527
- AgI-NaI-H_2O system, hydrous phase structs. 2−47314
- AgI-NaI aerosols, complexing, rel. to cloud seeding 2−62247
- $AgNa(NO_2)_2$, crit. slowing down of dielec. relax., thermal noise study 2−72029
- $AgNa(NO_2)_2$, dielec. relax. time, temp. depend., press. effects 2−77955
- $Ba_2NaNb_5O_{15}$, Gd, substituted, thermal expansion 2−51048
- $Ba_2NaNb_5O_{15}$, temp. of phase synchronization for two wave freq. addition 2−48128
- $BaNaP_3O_9$, space group. cell constants 2−67987
- $CuNa_2(PO_3)_4$ crystal struct. determ. 2−77546
- Ge-Na liquid solution, thermodynamic props., e.m.f. cell obs. 2−71183
- Li-Na alloys, liq., immiscibility 2−53404
- $Li_{0.93}Na_{0.07}Fe_5O_8$, sintering, effect of conditions on density and particle size 2−64790
- $Li_2SO_4-Na_2SO_4$ system, phase diagram 2−80527
- Na-Au(Cd)(In)(Pb)(Sn) dilute alloy, liq., compressibility determ. 2−77415
- Na_2-CaO-MgO-Sio_2 glass, phase equilib. in glass forming region 2−57023
- Na-Cs alloys, liq., elec. resist., temp. depend. 2−64471
- Na-Cs alloys, molten, electric transport, electrical resistance and density of electron states 2−60497
- Na-Hg alloy, liq., compressibility determ. 2−77415
- Na-Hg melt, electrotransfer and elec. resist. 2−56517
- Na-K, eutectic, liquidus curves from conformal solution theory 2−83842
- Na-K alloys, liq., zero wave vector partial struct. factors 2−43318
- Na-NH_3, density of states, Mott g ratios, self consistence, significance in MNM transition 2−44033
- Na-Sn silicate glasses, elec. props., appl. of Mossbauer effect 2−47055
- Na-Ta-O-F, pseudoquaternary, struct. of new phases 2−53674
- Na-β-Al_2O_3 phases formation and area of existence 2−84066
- Na borosilicate, glass, boron coordination det. by n.m.r. 2−60586
- Na borosilicate glass, Na^+-K^+ ion exchange 2−53537
- Na silicate glass, surface stabilization by ion exchange and chemical vapour deposition 2−53538

Sodium compounds continued

- Na_3AlF_6-ZnS multilayer system, optical props. calc. 2−45810
- $NaAlSi_3O_8$:Fe^{3+}, site assignment of Fe^{3+} based on fourth-order spin Hamiltonian constants 2−44439
- $Na_8Al_6Si_6O_{24}X_2$ sodalite (X=Cl, Br, I), cathodochromism, elucidation of damage mechanism by ESCA 2−47447
- $Na_4As_2O_7$, i.r. spectra and normal coordinate analysis 2−77079
- $NaBO_2$, evaporation, mass spectrometer obs. 2−64512
- $Na_2B_4O_6(OH)_2.3h_2O$, kernite, charge distribution from analysis of X-ray data 2−50560
- $NaBa_2Nb_5O_{15}$, forward Raman scattering obs. 2−48202
- $NaBe_2(BO_3)F_2$, synthesis and physicochemical props. 2−47210
- γ-Na_2BeF_4, high temp. thermal expansion, bonding, struct. refinement 2−61109
- NaBr, higher anharmonic contribs. to diffuse X-ray scatt. 2−61059
- NaBr, ionic cond., press. depend. 2−44154
- NaBr, l.f. dielec. consts., press. and temp. derivatives 2−51188
- NaBr, local and gap modes due to substitutional impurity 2−47731
- NaBr, pure and doped, hardness, yield strength, Young's modulus 2−56835
- NaBr, resonant phonon modes of Ag^+ and Au^+ 2−54018
- NaBr, sputtering, positive ion ejection patterns 2−44008
- NaBr evaporated films, optical absorption spectra 1700-2500 Å, obs. of fine structure in exciton bands 2−44375
- $NaBrO_3$, optical phonon spectrum by laser Raman spectroscopy 2−84495
- NaCN, single cryst. growth 2−67944
- Na_2CO_3 solution, ^{24}Na labelled, for column flow obs. 2−56456
- $Na_2CO_3.H_2O$, hydrogen atom positions and hydrogen bonds prediction 2−47312
- $Na_2Cd(SO_4)_2.2H_2O$ vibrational frequencies assigned, Jahn-Teller effect obs. 2−83270
- NaCl:Cd^{2+}. dissolution of precipitates study 2−83844
- $NaClO_4$-H_2O, saturated solution, meas. of i.r. absorption spectra 2−46932
- $NaClO_3$, ClO_3 centres formed by low temp. X-irradiation, e.s.r. study 2−51407
- $NaClO_3$, collision breeding of cryst. nuclei 2−50608
- $NaClO_3$, cryst. growth from soln. 2−47240
- $NaClO_3$, ferroelectric phase transition, relation to phonon structure 2−61431
- $NaClO_3$, growth from supersaturated soln., contact nucleation mechanism 2−50585
- $NaClO_3$, irrad., radiation damage, Raman spectra obs. 2−57361
- $NaClO_3$, molten, Raman spectra 2−74545
- $NaClO_3$, molten and aqueous, vibr. spectra 2−80475
- $NaClO_3$, n.m.r., acoustic excitation 2−78166
- $NaClO_3$, n.q.r. of Cl, press. depend. to 20 kbar 2−51419
- $NaClO_3$ seeded solns., secondary nucleation 2−47283
- $NaCo_3$ molten, production of C-H-O fuels for high temp. fuel cells 2−59042
- $Na_5Co_3F_{14}$, chiolite type phase, ferrimag. props. 2−72199
- β-$Na_2Cr_2O_7$, cryst. struct. 2−43585
- $Na_2Cr(SO_4)_2.2H_2O$ vibrational frequencies assigned, Jahn-Teller effect obs. 2−83270
- $NaCsCr_2O_7$ crystal struct. determ. 2−77551
- NaF: $Eu^{3+}(Sm^{3+})$, Ce^{3+} impurity effect on $Eu^{3+}(Sm^{3+})$ luminescence 2−65295
- NaF:Eu crystals grown by Czochralski method, luminescence, absorption and excitation spectra 2−68686
- NaF:Ni^{2+}, visible and i.r. absorpt., 300K and 80K 2−84490
- NaF, convergence of reciprocal-lattice expansions and self-consistent energy bands 2−84269
- NaF, elastic wave damping, effective anharmonicity consts. 2−80913
- NaF, excited F-centres, emission mechanisms 2−80709
- NaF, Hartree-Fock band structure 2−61172
- NaF, higher anharmonic contribs. to diffuse X-ray scatt. 2−61059
- NaF, impurity sensitive etching 2−67934
- NaF, intrinsic anharmonic phonon-phonon interactions, second sound, low temp. thermal cond. obs. 2−68228
- NaF, l.f. dielec. consts., press. and temp. derivatives 2−51188
- NaF, M centre, optical props. and reorientation 2−51343
- NaF, nuclear acoustic resonance of ^{23}Na, pulse method obs. 2−78170
- NaF, Raman spectra, phonon modes 2−48196
- NaF, single slip, mech. props. and disloc. struct. 2−71579
- NaF, thin layers and plates, thermal cond. and Poiseuille flow of phonons 2−61058
- NaF, third-order elastic consts., u.s. determ. 2−60844
- NaF slabs, for-i.r. emission assignment 2−61649
- $Na_4Fe(CN)_6$, resonant γ-ray nuclear Bragg reflection, azimuthal depend. elec. field determ. 2−81342
- $NaFe(CrO_4)_2.2H_2O$, low temp. i.r. vibr. spectra 2−48175
- $Na_5Fe_3F_{14}$ and $Na_5Fe_2CoF_{14}$, chiolite type phase, ferrimag. props. 2−72199
- $Na_2Fe(SO_4)_2$ vibrational frequencies assigned 2−83271
- $Na_2Ga(NH_2)_5$, prep. and characteriz. 2−47340
- $NaHF_2$, neutron diffraction data refined, location of H, thermal motion and F-F distance 2−77087
- $Na_2H_2P_2O_6$, $Na_2H_2P_2O_6.6H_2O$, i.r. spectra C_{2v} configuration of $H_2P_2O_6^{2-}$ 2−83267
- $Na_2HPO_4.12H_2O$, rates of growth in aqueous solutions and kinetics of crystallization 2−71376
- NaI:Tl, fluorescence intensity changes during X-ray dynamical diffr. 2−65301
- NaI-AgI compared to AgI-NH_4I in cloud seeding hail suppression program 2−62194
- NaI, diffusion coeff. of self-trapped holes and migration to thallium centres 2−68709
- NaI, resonant phonon modes of Ag^+ and Au^+ 2−54018
- NaI, sputtering, positive ion ejection patterns 2−44008
- NaI, X-ray, u.v. and visible spectra, adsorbed O effects 2−81399
- NaI, X-ray diffuse scattering, higher anharmonic contribs. 2−61059
- NaI evaporated films, optical absorption spectra 1700-2500 Å, obs. of fine structure in exciton bands 2−44375
- NaI scintillation detectors, response functions for γ-rays 2−79668
- NaI solution, solubility of AgI particles in, significance to cloud seeding 2−51595
- $NaICl_4.2H_2O$, n.q.r. of Cl 2−84590

Sodium compounds continued
NaI(Tl)-CsI(Tl) scintillation detector, thin layer, low background, for soft protons 2−59622
dual NaI(Tl)-dual Ge(Li) gamma ray spectrometer 2−63688
NaI(Tl), ^{16}O ion beam bombardment at intermed. velocities, track-account theory 2−70316
NaI(Tl), scintillating phosphor in radioactive reference lights, transient temp. dependence 2−49443
NaI(Tl) cryst., elongated, scintillation counter 2−42456
NaI(Tl) good-geometry large volume detector, response function to γ-ray cascade 2−79665
NaI(Tl) scintillation detector, 6″ × 4″, empirical formulae for calc. of full energy peak efficiency 2−42458
NaI(Tl) thin crystals, Monte Carlo calc. of pulse height response to protons of energy less than 100 keV 2−49686
NaI(Tl) total absorption spectrometer, properties and applications 2−49630
$NaI.PbI_2.4H_2O$, luminescence, absorption and emission spectra 2−54456
$NaIn(WO_4)_2$, prep. and struct. 2−43586
NaK molecule, laser-induced resonance fluorescence, rotational and vibrational consts. determ. 2−64149
NaLi, electric resonance spectrum 2−53029
NaLi, fluoresc. obs., heat-pipe oven applic. 2−49453
$Na_2LiBe_2F_7$, cryst. struct. 2−71438
$Na_2M(SeO_4)_2.2H_2O$, M = Mg, Mn, Fe, Co, Ni, Cu, Zn, Cd, struct. 2−53673
$Na_2Mg(SO_4)_2$ vibrational frequencies assigned 2−83271
$NaMnF_3$, absorption spectra at 300K and 80K, vibration frequency determination 2−65262
$NaMnF_3$, powder, weak ferromag. props. 2−48098
$Na_2Mn(SO_4)_2.2H_2O$ vibrational frequencies assigned Jahn-Teller effect obs. 2−83270
NaN_3, rhombohedral, lattice dynamics 2−43957
$NaNH_2$, solid and molten, evidence for hindered rotation of NH_2- ion from laser Raman spectra 2−60022
$NaNH_4SeO_4.2H_2O$, ferroelec. temp. depend. of electro-pt. coeffs. 2−72268
$NaNH_4SeO_4.2H_2O$, prep. and analysis 2−43521
$NaNO_3$:Ca, specific heat, diffusivity and conductivity near transition point 2−60542
$NaNO_2$, ferroelec., modulation of millimeter wave absorp. by polariz. reversal 2−48212
$NaNO_2$, ferroelec. order- disorder transition 2−61432
$NaNO_2$, piezoelec, and birefringent, Brillouin scatt. at room temp. 2−48204
$NaNO_2$, polarization in reversal of applied field, 10^{-2} to 10^7 V/cm.sec 2−65064
$NaNO_3$, atmospheric aerosol constituent, optical consts. 2−57946
$NaNO_3$, crystal struct., order-disorder transforms, neutron diffraction obs., 20-290°C 2−77758
$NaNO_3$, molten, hypersonic vel. dispersion obs. by Brillouin spectroscopy 2−77427
$NaNO_3$, molten, interdiffusion coeff. of Ag^+ 2−65383
$NaNO_3$, n.m.r. of ^{123}Na, intensity variations under u.s. stimulating quadrupole transitions 2−81483
$NaNO_3$, optical props. in vacuum u.v. region 2−84487
$NaNO_3$, phase transition, X-ray diffr. obs. 2−65048
$NaNO_3$, Raman scattering tensors 2−75312
$NaNO_3$, thermal cond. and diffusivity, critical parameters 2−57052
$NaNO_3$, thermoluminesc. glow curves, capture cross-sections and trap. parameters detn. 2−48257
$NaNbO_3$, cryst. struct., 480-575°C, rel. to soft phonon modes 2−80649
$NaNbO_3$, dielectric const. changes after electron or gamma irrad., X-ray study 2−65047
$NaNbO_3$, flux growth 2−60717
$Na_{0.5}Nd_{0.5}TiO_3$, perovskite, prep., mag. susceptibility, cryst. field effects, 2-600K 2−54294
$Na_2Ni(SO_4)_2$ vibrational frequencies assigned 2−83271
Na_2O-Al_2O_3-SiO_2, glass, X-ray diffraction study 2−60585
Na_2O-B_2O_3-Al_2O_3, nabal glass, self-diffusion of Na ions and interdiffusion coeffs. 2−60832
Na_2O-B_2O_3-SiO_2 system glasses, struct. 2−43454
Na_2O-B_2O_3 glass, stratification effects on comp. depend. of elasticity modulus 2−47478
Na_2O-B_2O_3 system, glassy and crystalline compounds, n.m.r. spectra, structural obs. 2−48301
Na_2O-K_2O-SiO_2 glass, Na and K self diffusion, rel. to internal friction 2−50712
Na_2O-P_2O_5, glass, containing metal ion impurities, u.v. transparency 2−65225
Na_2O-SiO_2 glass, dielectric loss and phase separation 2−54230
Na_2O-SiO_2 glass, elastic moduli and i.r. absorp. spectra, pressure depend. 2−53782
Na_2O-SiO_2 glass, immiscibility temp., effect of small additions of Al_2O_3 and Ga_2O_3 2−53539
Na_2O-SiO_2 glass, ion exchanged, internal friction, effect of water 2−53791
Na_2O-SiO_2 glass, morphological changes produced by amorphous phase decomp. 2−47060
Na_2O-SiO_2 glass, nucleation process in the metastable region 2−60584
Na_2O-TiO_2-SiO_2 glasses press. and temp. depend. of elastic moduli, ultrasonic interferom. meas. 2−80741
NaO_2, magnetic properties, obs. of structural and magnetic transitions 2−65116
NaO_2, Raman spectra, O_2^- and O_3^- ions props., solid- solid transition effects 2−81354
NaOH environment for alloyed steel, stress corrosion cracking 2−68789
NaOH ice glass at 77K, matrix ENDOR linewidth of trapped electrons 2−57402
$Na_2O.2SiO_2$ glass, annealing atmosphere effects on Na diffusion 2−53767
β-$Na_2O.3B_2O_3$, cryst. struct. 2−47338
$NaPF_6$ in H_2O and D_2O solns., spin-lattice relaxation of ^{19}F, ^{31}P, ^1H, ^2H 2−50372
$Na_4P_2O_7$, cryst. struct., 22°C 2−77565

Sodium compounds continued
$Na_3PO_3CO_2.6H_2O$, systematic error differences between two refined sets of position coordinates 2−77554
Na_2PO_3F in H_2O and D_2O solns., spin-lattice relaxation of ^{19}F, ^{31}P, ^1H, ^2H 2−50372
$Na_5P_3O_{10}.6H_2O$, cryst. growth rate from soln. 2−47241
$NaRbCr_2O_7$ crystal struct. determ. 2−77551
Na_2S_x, molten, thermodynamic props., phase diagram, open circuit voltage obs. 2−71185
Na_2SO_4, coherent neutron scatt. amplitudes from powders 2−53654
Na_2SO_4, sound velocity, 947 to 1161°C 2−71194
Na_2SO_4, volatile oxidation kinetics, 1173 to 1473K 2−50891
$Na_2S_2O_4$, powder diffr. diagram 2−53672
$Na_2S_2O_3.5H_2O$, hydrogen atom positions and hydrogen bonds prediction 2−47312
$Na_2{}^{75}Se$ disappearance rate in rat's eye, comparison of meas. with CdTe and Si(Li) probes 2−51992
Na_2SiO_3, acoustic bonding material for u.s. delay line, high temp. characs. 2−77777
$NaTh_2(PO_4)_3$, ferroelec. props., rel. to struct. 2−54237
$Na_5V_3F_{14}$, chiolite type phase, ferrimag. props. 2−72199
$NaVO_3$, cryst. growth and characteriz. 2−47261
$Na_xV_2O_5$, elec. cond., n-type semicond. and ionic cond. props. 2−83795
Na_xWO_4, cryst. growth by fused salt electrolysis 2−48341
NaX synthetic zeolites, preferred rotation of adsorbed ClO_2 molecules 2−80579
NaX zeolites, H_2O, proton magnetic relaxation meas. used to determ. structure and dynamic properties of adsorbed phases 2−54515
$NaYF_4$:Yb, Er, phosphor, upconversion, i.r.-pumped visible luminesc. 2−72413
Na_2ZnGeO_4, solubility and crystn. kinetics under hydrothermal conditions 2−47242
$Na_2Zn(SO_4)_2$ vibrational frequencies assigned 2−83271
Na_2ZrSiO_5:Eu^{3+}, cryst. struct. and luminesc. 2−72414
$Na_3[Fe(CN)_5H_2O]$ and $Na_3[Fe(CN)_5 NH_3]$ in aqueous soln., photoelectron emission spectroscopy 2−68808
Pb-Na alloy, superconducting, heterogeneous, anisotropic crit. currents 2−77864
Pb-Na liquid solution, thermodynamic props., e.m.f. cell obs. 2−71183
SiO_2-Al_2O_3-Na_2O-K_2O-CaO-MgO glass, viscosity-temp. relations 2−67883
SiO_2-B_2O_3-Na_2O-Al_2O_3 system, comp. fluctuation and phase decomp. 2−53543
SiO_2-CaO-MgO-Na_2O-AlF_3:Dy^{3+} glass system, luminesc., effect of heat treatment 2−48228
SiO_2-Na_2O system, binary interdiffusion coeffs. and O_2 self-diffusion 2−53772
Sn-Na liquid solution, thermodynamic props., e.m.f. cell obs. 2−71184
SnS_2-Na_2S system phases, crystallographic parameters 2−83952
V_2O_5-Na_2O-Fe_2O_3 system, liq., n-type semicond. and ionic cond. props. 2−83796

sodium chloride
aerosols formed by condensation, density distrib. 2−60530
anharmonic contribs. to one-phonon Green function and dielec. props. 2−50996
aqueous soln., freezing using temp. gradient microscope stage 2−74585
aqueous solns., optical constants in i.r. 2−50362
cavitation erosion mechanism 2−71606
cleavage, electrical processes occurring at moment of cleavage 2−74659
cleavage, selective dissolution, complexes responsible for etching 2−74658
coacervate formation by aerosol OT with NaCl 2−74570
coherent neutron scatt. amplitudes from powders 2−53654
colour centres, electron microscope obs. in cathode luminescence mode 2−80708
colour centres, electronic struct. calc. and electronic polarization fields 2−71520
colour centres, plastic deformation effects on F-aggregates, optical absorp. obs. 2−53755
colour centres, thermal decoloration, mutual dependence of ε and p_0 in thermal excitation function 2−50697
creep at high temps, compression tests, stress dependence, creep mechanism 2−77651
crystal growth, from soln., evidence for spiral mechanism 2−50586
crystals, velocity of slip bands as a function of stress with respect to (100) [110] and (110) [110] systems 2−71578
dielectric breakdown, polarity effect 2−72021
dielectric consts., l.f., press. and temp. derivatives 2−51188
diffusion of Mn^{2+}, coeff. meas. using e.p.r. 2−50700
dislocation generation, grain boundary mechanism, expt obs. in single and polycrystalline mat. 2−68029
dislocation mobility obs. on (001) face, effects of H_2O adsorption 2−43627
dislocation-phonon interaction, 70-300K 2−83975
dynamic compression, porosity effect 2−53800
elastic constants, third order, measurement, new inertial loading technique 2−71551
elastic props. based on interatomic force model 2−68854
electric field gradient using molecular wavefunctions 2−80973
electrical conductivity and dielectric loss factor when doped with Bi^{3+} 2−51191
electron scattering in single crystals 2−57091
energy level structure, excited particle velocity spectrum on Ar-ion bombardment 2−48030
equation of state, 0-8kbar, 300-800K, u.s. determ. 2−68065
F→X-centre conversion, lattice and disloc. mechanism 2−50698
F-centres, excited, emission mechanisms 2−80709
film, dielectric response, i.r. reflectivity obs. 2−72304
gamma-irrad., d.c. conductivity obs., room temp. −70°C, electronic and ionic contribs. and Ca doping effects 2−57231
Hartree-Fock band structure 2−61172
ideal tensile and shear strengths computer calc. 2−77630
ideal tensile strength, relationship to surf. energy, expt. 2−64721
ion beam induced damage, backscatt. obs. 2−43611
ionic cond., press. depend. 2−44154

Sodium compounds continued
- **sodium chloride** continued
  - ionic conduction with temperature 2−44156
  - irradiated, electron concentration determ. using T activity 2−71934
  - kinetics of dislocation, influence of placing dislocations at starting positions 2−71493
  - laser induced breakdown 2−54376
  - lattice dynamics, resonant phonon modes of Ag^+ and Au^+ 2−54018
  - limiting optical frequency, temp. variation calc. 2−72311
  - local and gap modes due to substitutional impurity 2−47731
  - localized modes for H^- centre, calc. 2−74963
  - luminescence, fast recomb. transition lifetimes 2−54450
  - luminescence max. at 330 K, decay of f_2 centres 2−51380
  - multiphonon i.r. absorption spectra, effects of melting 2−68220
  - neutron irrad. induced dislocation pinning points 2−43638
  - plastically deformed, dislocations, X-ray and electron microscope obs. 2−53807
  - porous, explosion of spherical charge, shock wave parameters 2−58936
  - pure and doped, hardness, yield strength, Young's modulus 2−56835
  - quenched, X-irrad., cry. lattice defects and near surface props. 2−71477
  - rock salt crystal, uniform press. effects on plasticity 2−56793
  - rotating frame nuclear double resonance, non resonant oscill. field, energy matching condition modification 2−81473
  - saline aqueous frozen solns., permittivity obs. of cooperative phenomena 2−75139
  - seeded convective clouds, radar echoes, height, temperature AgI 2−84829
  - single slip, mech. props. and disloc. struct. 2−71579
  - single slip and double slip, electron microscope obs. 2−80749
  - sputtering, positive ion ejection patterns 2−44008
  - stability and mode of fracture of highly stressed ideal crystal 2−77631
  - Stark effect of M- and N-centres 2−61624
  - substrate, for Cr condensation, nucleation sites 2−50488
  - surface, before and after Cu vapour deposition, ion scatt. study 2−71314
  - surface, mean-square amplitudes of vibr. 2−50454
  - surface, polygonization, produced by electron bombardment and illumination 2−50457
  - surface, vibr. modes in rigid-ion model 2−50455
  - surface contamination, O ion induced X-rays from La obs. 2−60628
  - thermal conductivity, temp. depend., role of longitudinal and transverse phonons 2−84214
  - thermoluminescence rel. to alkali stoichiometric excess, glow peak due to F' centres, 77 K 2−81423
  - two-electron U-centres, point-ion models 2−83987
  - two-phonon Raman scattering and phonon-phonon interaction, nonlinear shell model 2−81368
  - u.s. waves, phonon absorp., relax. theory 2−68233
  - vacancy-divalent impurity complex, slow motion, press. effects, in n.m.r. study 2−72514
  - whiskers inelastic phenomena 2−80575
  - X-ray diffuse scattering, higher anharmonic contribs. 2−61059
  - X-ray K_β emission and K absorpt. spectra, rel. to density of states 2−72380
  - X-ray spectra, $K\beta$ emission and K absorp. of Cl- obs. 2−65288
  - Bryan field, sediment cored anticline 2−44584
  - C creep at high temp., creep substruct., tilt walls around parallelipipedic blocks 2−77579
  - CsCl-NaCl and CsCl-KCl-NaCl systems, m.p. and phase transform. 2−43932
  - KCl:NaCl, symmetry of far i.r. resonant-pair mode 2−84507
  - KCl-NaCl mixed single crystals, phase separation during heat treatment 2−74884
  - $NaCl:Ag^+$, Raman scatt. and far i.r. absorpt., exptl. and calc. 2−84508
  - $NaCl:Co(CN)_6{}^{3-}$, vibr. and electronic props. 2−54413
  - NaCl:Cu, one electron energy levels, charge consistent extended Huckel approach 2−77831
  - NaCl:Cu, X-ray coloured, Cu activated thermolum., 300-510K 2−78122
  - NaCl:NaOH, tunnelling levels, low temp. thermal cond. obs. 2−71758
  - NaCl:Pb, polarized luminesc. and dipolar relax. of Pb-vacancy complexes 2−72424
  - $NaCl:Sr^{2+}$, Z_1 generation, kinetics 2−84515
  - NaCl:Tl, X-irrad., traps responsible for 360 and 390 K glow peaks 2−54476
  - NaCl-KCl, solid solns., supersaturated, decomp. 2−43921
  - NaCl-KCl mixed crystal, with and without colour centres, spectra 2−74801
  - NaCl crystals containing colour centres, flow stress spectroscopy 2−81396
  - NaCl laser beam optical probing for sound intensity distribution 2−51026
  - Pb/NaCl-UCl_3 molten metal/fused salt system, surface and interfacial energy 2−52874

Sofar *see Sound ranging*

Sogicons *see Semiconducting devices*

Soil
- — 2−72716
- alluvial, simulation mathematical models for water tables 2−84714
- Cache Valley, ground-water potential rel. to integrated geophysical study 2−81642
- density obs. using X-rays, models 2−61964
- frozen, u.s. velocity of dilatational and shear waves 2−78306
- inhomogeneous, anisotropic, Darcy's law, tensor form transform. 2−67770
- land subsidence in Venice, subsoil one dimensional model 2−57817
- lateral structure-foundation interaction of structures with base masses 2−61873
- liquefaction, effect of earthquakes 2−78279
- lunar, α-radioactivity obs., ^{210}Po activity search 2−44910
- lunar, Apollo 14 and 15 samples, inorg. gas release obs. 2−62672
- lunar fines, spectral reflectance and emittance 2−78518
- lunar glasses, effect on spectrum of moon 2−58464

Soil continued
- lunar soil disturbance effect, rel. to changes in photometric function 2−44920
- lunar surface comp. mapping using mid-i.r. spectroscopic remote sensing 2−58463
- Mars, analytical instrumentation of Viking spacecraft for life detection 2−54977
- Mars, gas chromatography/mass spectrometry for life detection by Viking spacecraft 2−55147
- microscopic study 2−65585
- natural radioactivity, γ-spectroscopic obs. 2−72690
- physics, liquid flow in porous media, theoretical mechanics 2−77383
- pore-water pressure, effect of earthquakes 2−78280
- radionuclide behaviour in types of soil found in Czechoslovakia 2−57804
- reconnaissance using colour aerial photography 2−44535
- remote sensing of moisture of specular soils with multifrequency microwave radiometry 2−84778
- sandy, circular edge dislocation loop 2−44591
- sandy subsoil, model loading tests 2−44605
- specific electrical conductivity along power transmission lines 2−61985
- subsurface pollution, waste disposal sites 2−62005
- urban growth area, micrometeorological observations, soil heat fluxes 2−44685
- wind erosion, aerosol size, distribution, vertical flux, jet impactors 2−84827
- Pu content, separation and anal. 2−62045
- Rn exhalation from ground 2−61988
- S abundance and crop yields 2−78301
- Th exhalation from ground 2−61988

Solar activity
- 11-year cycle rel. to variations in ionospheric potential and thunderstorm activity 2−65961
- 80 to 90 year cycle of activity as a pseudo- harmonic oscillation 2−48806
- 1964-6 chromosphere observations in $H\alpha$ light 2−78622
- 1965 observations of sunspots and faculae and group evolution 2−78609
- α-effect dynamos by the Bullard-Gellman formalism 2−55160
- active longitudes rel. to activity centres and 11-year cycle 2−48807
- effect on atmospheric N and No content at 100-250 km height 2−48528
- August 1972, geophysical effects 2−81955
- chromospheric features rel. to photospheric magnetic fields 2−66234
- circular polarization associated with active regions at 2800 MHz and 13500 MHz 2−75987
- coronal lines, 5303Å and 6374Å, reduced intensities 2−73110
- coronal regions, equatorial sidereal rotation velocity obs. 2−76035
- correlation of activity with tidal effects of planets during 200 year period 2−75984
- cycle, effect on electron drifts over magnetic equator 2−44757
- cycle 20, coronal helmet evolution during ascending phase 2−78624
- cycles, rel. to processes in Sun-Earth space 2−66226
- delays, effect on solar terrestrial space processes 2−85031
- equatorial coronal arches, K-coronameter obs. 2−76032
- eruption observed on 13 Dec 1971, OSO-7 spacecraft 2−51854
- event of 18 November 1968, onset 2−75990
- exciter of type III bursts and coronal temp., time profiles and decay time const. 2−69193
- filament disintegration and associated activities 2−55177
- flare producing regions, statistical analysis of relationship to geomagnetic storms, Forbush decreases and SC + SI events 2−54925
- flares, rel. to sporadic geomag. storms 2−75634
- geomagnetic field variations as function of solar activity 2−44774
- geomagnetic field variations at Potsdam, Seddin and Niemegk 2−44770
- geomagnetic variations, lunar diurnal harmonic components and effect of solar activity 2−66013
- great flares (Aug. 1972) 2−81956
- height and temp. variations of F_2-region max. as function 2−48591
- high energy gamma-rays, search for radiation from flare regions 2−44995
- indices, rel. to cosmic ray intensity 2−48805
- individual regions, X-ray line emission 2−75952
- interplanetary cosmic-ray electron flux, solar activity rel. to temporal variations 2−66192
- ionization equilibrium and line radiation, under flarelike conditions 2−51857
- ionospheric electron content dependence 2−54894
- lower troposphere, potential gradient and air earth current 2−44735
- macrostructure distribution, photographic method 2−69191
- magnetic configurations and magnetic energy release from active regions 2−75998
- microwave bursts of different types in relation to optical flares and other allied events 2−62794
- neutron flux, satellite obs. and correlation with solar activity 2−66222
- observations in 1970 period 2−73136
- past activity, implications from obs. of ultrathin amorphous coatings on lunar dust grains 2−44929
- photo-electron energy distrib. and its variation with sunspot activity in F-region of ionosphere 2−65984
- photospheric, variation of geomagnetic K_p index 2−75992
- photospheric activity centres, early stages of development from photoheliograms 2−48804
- plages, vel. fields in active regions 2−62790
- rel.to planetary resonances classification 2−73079
- polarization scans of active regions at 3.8 cm 2−78599
- powerspectrum, 5-minute photospheric resonance oscillations 2−55178
- prediction formulae analysis 2−73141
- quiet Sun model from radio observations 2−78623
- quiet time meas. of interplanetary solar wind electrons 2−75967
- role of force-free mag. field structures 2−75985
- rel. to Schumann resonance frequency variation and Pc 1 occurrence58006 2−58006
- solar structure and processes, review 2−62742

Solar activity continued
- structure of transition zone in active region 2−73137
- sunrise, effects in low ionosphere 2−68959
- sunrise and sunset, effects on processes in Sun-Earth space 2−65763
- sunspot cycle, effect on Earth's mag. field variations 2−75633
- sunspot cycle obs. for forecasting rules 2−62791
- surges, motion rel. to magnetic field 2−51861
- synoptic chart, Hα patrol films 2−75991
- type III acceleration mechanism, source volume establishment 2−73122
- Type IV radio burst-active centres, temporal distribution over solar cycle 2−62763
- U shaped type IV bursts and l.f. radiation from relativistic electrons in magnetoplasma 2−75959
- X-ray emission in 1-55 Angstrom region from active limb prominence 2−48794
- X-ray flux, apparent control of D-region A_t absorption 2−58078
- X-rays from coronal condensations and development of active regions 2−76038
- yellow coronal line at Lomnicky Stit 2−73109
- young region, dynamics of mag. flux 2−75972
- H_α mottles 2−66201
- He solar wind relative abundance ratio rel. to solar activity 2−75975
- O^+ production rate dependence 2−48464

Solar batteries *see Electricity, direct conversion*

Solar cells *see Electricity, direct conversion/solar cells*

Solar constant *see Sunlight*

Solar corona *see Sun/corona*

Solar corpuscular streams *see Sun/radiation corpuscular*

Solar eclipses *see Sun/eclipses*

Solar flares *see Sun/flares*

Solar furnaces *see Heating; High-temperature phenomena and effects*

Solar noise *see Sun/radiation, radiofrequency*

Solar prominences *see Sun/prominences*

Solar system
- *see also Planets, etc.*
- AFCRL bibliography, 1971, first quarter 2−75842
- AFCRL bibliography, 1971, second quarter 2−75843
- astronomical and geodynamical constants, reevaluation from space tracking data 2−58441
- asymmetrically rotating fluid disc model 2−56279
- dynamic astronomy, meeting (College Park, USA, March 1972) 2−58166
- early, accretionary processes 2−85044
- early, evidence for objects of lunar mass 2−62655
- evolution from proto-Sun stage to planet forming stages 2−78494
- formation, Kant and Laplace's nebular hypothesis 2−48670
- geodynamic and astronical research in France (CERGA) 2−62641
- gravitational constant, possible anisotropy effects solar system orbits 2−81755
- inhomogeneous planetary accretion hypothesis, cosmogony implications 2−44934
- interstellar Hi and HeI in solar system, backscatter of solar resonance radiation 2−55078
- jet stream formation rel. to solar system development and Bode's Law 2−66140
- jetstreams, numerical simulation 2−85027
- law of planetary distances 2−75844
- light elements prod. rel. to early history 2−66141
- lunar composition rel. to early history of solar system 2−78501
- metal/silicate fractionation of terrestrial planets rel. to solar nebula 2−66166
- meteorite origin hypotheses rel. to asteroid parent body break-up 2−78514
- nebular hypothesis of Isaac Orr, historical aspects 2−81926
- new astronomy, conference, March 1972, Bloemfontein, S. Africa 2−66071
- origin, evolution, investigation of asteroids, space missions to asteroids 2−51835
- origin, secular rotation, geological evidence 2−85038
- origin and early development of planets rel. to primitive solar nebula 2−78500
- origin of satellites by accumulation of lunar mass objects present in system 2−58445
- planetary evolution from dust 2−69144
- planetary formation from solar nebula 2−66168
- planetary sciences, symposia (Hawaii, USA, March 1972) 2−75841
- planetology congress (Montreal, September, 1972) 2−78499
- pole of the ecliptic, position from improved values of reciprocal planetary masses 2−58172
- quiet-time electron increases as measure of outer Solar System conditions 2−75933
- quiet-time electron increases rel. to outer solar system modulating mechanism 2−66193
- research activities, probes and sampling 2−44904
- resonances in rotations of celestial bodies and Cassini's laws 2−78498
- restricted three-body problem periodic perturbation of libration points 2−78427
- shock waves, role of gasdynamic processes in transfer of solar material 2−81899
- solar nebula, low temp. condensation accretion procews rel. to planetary formation 2−44903
- space missions to comets and asteroids rel. to understanding of solar system 2−78411
- star-Sun-comet system using restricted hyperbolic three-body problem 2−85032
- superheavy nuclei, evidence for previous existence 2−62643
- terrestrial planets, structure and composition rel. to solar nebula 2−81939
- NH_4SH reflectivity studies rel. to structure of bodies in outer solar system 2−78525

Solar wind *see Sun/radiation, corpuscular*

Solid solutions
- *see also Alloys; and under compounds of the individual elements. Solid solutions such as Au-Cu, Au-Cu-Zn are indexed under compounds of the named elements, i.e. 'Gold compounds', 'Copper alloys', 'Zinc compounds' in these examples*
- alloys, body centred cubic, theory of solid solution hardening 2−77691
- ceramic systems, A_uX_v-B_uY_v type, ideal soln. behaviour 2−50852
- crack propag. growth and rate meas. 2−43729
- defective, cluster model 2−71637
- defective MA_xB_y type, ordering, cluster model 2−74892
- eutectoid decomp., lamellar eutectoid growth, stepwise growth model 2−50814
- ferroelectric, thermodynamic theory 2−61424
- fluorescence spectra fine structure obs., solvent selection for laser excitation conditions 2−68693
- hardening, Fleischer and Labusch theories 2−47591
- hardening, statistical theories 2−50813
- III-V compound, quasi-binary phase diagram, excess free energy 2−74948
- ilmenite-haematite, self-reversal and X-phase rel. to palaeomagnetic investigations 2−54960
- metal/hydrogen systems, conf., Julich, Germany (Mar 1972) 2−77713
- metal/hydrogen systems, h.p. thermodynamics 2−77715
- metal/hydrogen systems, non-ideal soln. behaviour 2−77716
- metal/hydrogen systems, thermodynamics, review 2−77714
- metallic, application of Lindemann's rule for melting 2−74582
- mixed growth, influence of kinetic order-disorder phase transitions 2−50816
- modulated struct. orientation in rhombohedral system 2−50853
- ordered, B2 and $L1_2$ superstruct., superdislocation-antiphase boundary interactions 2−47416
- ordered, B2 and $L1_2$ superstruct., superdislocations and antiphase boundaries 2−47417
- Pb-Si, etching technique for macrostructure obs. 2−56607
- polar substances in n-pentane, struct., dielectric. meas. 2−72016
- precipitation, investig. by lattice parameter method 2−61027
- random binary, X-ray diffr. and model of interatomic force equil. 2−74965
- random binary, X-ray diffr. and model of rigid atoms in closed-packed arrangement 2−77768
- rare earth sulphides, L_2S_3 type, β-form, mechanism 2−47345
- rare earth sulphotellurides, high temp. homogeneity regions 2−53905
- rare earth-zirconium system, form. of metastable low temp. allotropic solns. 2−47646
- rare gas binary mixtures, films, electron diffr. study 2−80573
- refractory carbide/liquid metal contact interactions 2−68190
- single phase, X-ray determ. of composition profiles and diffusion generated substructure 2−74696
- solvent self diffusion in dilute b.c.c. solid solns., calc. of partial correlation factors 2−80717
- supersaturated, decomp., review 2−43928
- ternary, diffusion of C, C conc. curve, at interface 2−47454
- thin films, thickness measurement X-ray diffraction 2−82125
- transition metal hydrides, interstitial atom interaction role in solid soln. form. 2−77733
- transition metal hydrides, struct. problems, review 2−77731
- transition metal oxides, chem. vapour transport 2−50587
- X-ray fluorescence analysis, quantitative, influence of quality of primary radiation 2−51485
- X-ray fluorescence analysis, quantitative, using solid solution specimens, influence of quality of primary radiation 2−51486
- X-ray fluorescence analysis, theory of double concentration method 2−51487
- Ag-Ga(In)(Ge)(Sn), partial free enthalpies of form. determ. in galvanic cells 2−64887
- Ag-In, Zener relaxation 2−47453
- Al-Ag system, discontinuous precipitation reactions and ternary component influence 2−71674
- Al-Mo, binary phase diagram, obs. 2−50955
- Al_2O_3, alumina, coupled solute solid soln. softening with MgO and TiO_2 2−47653
- Au-Sn, dil., correl. factor and self-diffusion 2−64693
- α-Fe-Sn, precip. of FeSn by dislocations, effect of third component on morphology and kinetics 2−80812
- B:Fe, crystallographic positions of Fe, isomer shifts, Mossbauer obs. 2−51305
- BaF_2-SrF_2, subsolidus formation and lattice parameter study 2−64772
- BaF_2-YF_3, phase relations 2−74922
- $Ba(Fe_{0.35}Al_{0.65})_2O_4$, disordered solid solution, blocking temps. of mag. random clusters from Mossbauer spectra 2−57309
- $BaSO_4$-$SrSO_4$, subsolidus formation and lattice parameter study 2−64772
- $Ba_{1-x}Sr_xTiO_3$, flux-grown, dielectric props., 4.2-600K 2−47966
- Be-(1 wt.%)Fe, supersaturated, precip. on thermal treatment, Mossbauer obs., mechanism 2−50931
- CaH_2-LaH_3 system, dissoc. press. and thermodynamic props. 2−50958
- $CdSe_xTe_{1-x}$, n-type solid soln. photoelec. props. and recombination diagram 2−72061
- $Ce_xY_{1-x}Sb$, $Ce_xLa_{1-x}Sb$, antiferromagnetically ordered, Neel temp. dependence on lattice constants 2−72212
- Co-Al alloy, disintegration of solid solution under hardening and cooling 2−60977
- Co-C interstitial solid solution, sat. magnetiz. and high field suscept. 2−81249
- Cu-Be-Ag alloys, structural states in decomposition process, e. diffr., e. micro. and microhardness exam. 2−80782
- Cu-Be-Ag and Cu-Be-Ti, decomposition of solid solns., phase transformations 2−68194
- Cu-Zr, dil. alloys., softening resistance mechanism 2−56709
- Cu alloys, determ. of partial free enthalpy of formation thermodynamic investigation 2−80811
- Cu base, grain boundary strengthening 2−53891
- $Eu_{1-x}Ca_xO$, magnetic props. exchange interactions, temp. depend. of magnetization 2−68545

Solid solutions continued
  Fe-N, rel. to ductile-brittle transition in nitrided zone refined Fe 2−47629
  Fe-Ni films, thermal evaporation prepn., detn. of lattice parameters and mag. props., 0-100% Ni 2−77496
  Fe-Si solid solns., ordering reactions and meas. of specific heat capac. 2−71745
  Fe-rich solid solutions, summary of magnetic properties 2−81243
  Fe solid solns., serrated yielding between 500 and 775 K 2−74839
  FeSi-CoSi system, itinerant ferromag., ^{59}Co n.m.r. obs. 2−61745
  $(Fe_2TiO_4)_c(NiFe_2O_4)_{1-c}$, $O \leqslant C \leqslant 1$, effect of comp., lattice parameter, saturation mag. moment and Curie temp. 2−83840
  GaAs-Cu, supersaturated, differences in laws of decomposition 2−83836
  GaSs-GaP pseudobinary, phase diagram, solidus boundary 2−83841
  KBr-KI single crystal, elastic consts. and Debye temp., u.s. pulse method obs. 2−71550
  KCl:Ba, two temp. regions of decomposition 2−80526
  KCl-H_2O frozen solns., permittivity discontinuities at crit. pt. 2−53499
  KCl-KBr positronium formation 2−80988
  KNO_3-bivalent metal nitrate, form. by precip. 2−56942
  Mg-Zn and Mg-Zn-Zr dendritic and nondendritic structs., soln. kinetics of secondary phases 2−47640
  Mg substitutional soln. hardening 2−43855
  $MgAl_2O_4$-Al_2O_3 system, spinel solid soln. form. 2−50971
  $(Mn, Fe)_3O_4$, i.r. absorp. spectra obs. 2−61648
  $Mn_xHg_{1-x}Te$ films, Hall coeff., Hall mobility and electrical condutivity 2−71885
  MnO-MgO, dense solid soln., preparation for testing 2−74907
  Mo_2C-$Fe_{(l)}$ contact zone obs., formation 2−77728
  NH_4Cl-H_2O frozen solns., permittivity discontinuities at crit. pt. 2−53499
  alpha-Nb-Mo-N ternary solid solution, equilibrium N concentration and thermodynamic behaviour 2−60983
  Nb-N, interstitial soln., mech. props. depend. on conc. and temp. 2−84009
  Nb-O, interstitial soln., mech. props. depend. on conc. and temp. 2−84009
  Ne-p-H_2, Ne-n-D_2, density obs., low temps. 2−57027
  Ni-C interstitial solid solution, sat. magnetiz. and high field suscept. 2−81249
  $NiFe_2O_4$-Fe_3O_4-Fe_2TiO_4, effect of lattice parameter on solubility 2−83840
  $(Ni_2TiO_4)_c(Fe_3O_4)_{1-c}$, $O \leqslant C \leqslant 1$, effect of comp., lattice parameter, saturation mag. moment and Curie temp. 2−83840
  PbF_2-BaF_2, subsolidus formation and lattice parameter study 2−64772
  PbF_2-SrF_2, subsolidus formation and lattice parameter study 2−64772
  $PbSO_4$-$BaSO_4$, subsolidus formation and lattice parameter study 2−64772
  $PbSO_4$-$SrSO_4$, subsolidus formation and lattice parameter study 2−64772
  Pd-H and Pd 24% Ag-H foils, electron microscope examination 2−56948
  Pd-H system, isotope equilib., 77K 2−68154
  Sc-H, n.m.r. obs. Korringa product, diffusion parameters determ. 2−72517
  Si_3N_4-AlN-Al_2O_3 system, X-ray diffraction obs. 2−43823
  Ti, dislocation structure effects in interstitial solute hardening 2−56714
  $(U,Pu)O_2$ microspheres and pellets, sol-gel derived, microstructure 2−47610
  UO_2-ThO_2, non-stoichiometric, thermodynamic props., e.m.f. obs. 2−64782
  $YbMnO_3$-$YbCrO_3$, $YbMnO_3$-$YbFeO_3$, extent of solid solns., mag. and elec. props. 2−51235
  (Zn,Cd)S phosphors, diffuse reflection spectra for studying and controlling properties 2−75332
  $Zn_xCd_{1-x}Se$, phonons and struct., Raman scatt. obs. 2−64837
  $Zn_xCd_{1-x}Te$ crystals, spontaneous luminescence and lum. spectra detn. 2−72417
  $Zn_xCd_{1-x}Te$ solid solution, phonon freq. detn. from reflection spectra 2−72308
  (ZnO-MgO):Fe,O photoconductor transient effect 2−84377
  Zr-Cr alloys, thermodynamic props. 2−74912
  ZrC-NbC, solid solution, creep in compression, temp. range 2600-3150 K 2−84033
  $(ZrO_2$-$CeO_2) + Cr_2O_3$ formation of cubic solid soln. $CeCrO_3$ on calcining in vacuum 2−84095

Solidification *see Freezing*

Solids
  see also Crystals; Films, solid; Metals; Plastics; Powders; Semiconductors; Vitreous state
  condensed matter physics, conf., Fribourg, Switzerland [Sept. 1972] 2−60563
  European Phys. Soc. conf., Wiesbaden, Germany (Oct. 1972) 2−76139
  high pressure studies 2−85171
  n.m.r.-pulse expts., method for calculating signals 2−81476
  u.s. methods of investigation, short review 2−60374
  van der Waal's force between curved mica 2−82169

 structure
  see also Crystal structure; Crystals; Electron diffraction examination of materials; Electron microscope examination of materials; Films, solid; Granular structure; Hartree-Fock method; Lattice energy; Metals; Neutron diffraction examination of materials; Plastics; Powders; X-ray examination of materials
  Atomix teaching model, atomic structs. of liqs. and solids 2−45205
  linear analysis, methods for edge error correction 2−64519
  polyethylene, crystallite size and lattice distortion, nitration effects 2−60612
  polystyrene, structure in glassy state determ. by fluorescence depolarization 2−60615
  polyvinyl chloride, wide mol. wt. range, struct. formation 2−83386
  polyvinylchloride, drawn samples, molec. orientation determ. by broad line p.m.r. 2−51417
  striae in glass, optical microscope system for obs. 2−59253

Solids continued
 structure continued
  systems with coincident buckling loads influence of imperfections 2−55452
  CO crystal, α phase, librational motion by linear spin-wave theory 2−80588
  $CaCO_3$, Madelung parameters and electrostatic energies for calcite, aragonite and vaterite and charge distrib. on CO_3^{2-} ion 2−43500
  $K_2SO_4(c) \rightarrow 2K^+(g) + SO_4^{2-}(g)$, Madelung parameter and electrostatic energy charge, calc. based on Evald Bertaut method 2−47179
  N_2 crystal, α phase, librational motion by linear spin-wave theory 2−80588
  Ni-P chemically deposited films, structure in relation to elec. conductivity 2−77510
  SiC polytypes, determ. of Madelung potentials by rule of thumb up to six figures 2−80589
  ZnS polytypes, determ. of Madelung potentials by rule of thumb up to six figures 2−80589

 theory
  Coulomb correlation effects and the exchange correlation energy, atomic and band struct. calc. 2−61157
  cubic lattices, electronic surface states calc. 2−47815
  dielectric theory, appl. to Raman scatt. efficiency calc. for diatomic cryst. 2−57357
  disordered system, many site theory 2−47723
  elastic cylinder, Somigliani type dislocations 2−52159
  elementary excitations, book 2−71806
  ferromagnetic alloys, coherent potential approximation, application 2−61500
  gas atom scatt., one-phonon quantum theory 2−50423
  heterophase systems, phase nucleation, internal stress relax., coherent loss, thermodynamics 2−60859
  hindered rotation, in various fields of cubic symmetry, Devonshire model 2−60564
  molecular rotational motion, random reorientation, influence of molecule symmetry 2−67880
  molecular rotational transitions, possible laser action, rot. damping 2−54446
  neopentane, plastic crysts., mol. rot. motion 2−53513
  plasmons, surface, microscopic theory 2−84277
  simple, isotropy group exponential form 2−47050
  statistical mechs. when under compression or tension, Hamiltonian modification 2−58789
  two-dimensional systems, long range order and metastability 2−50407
  van der Waals attraction between cylindrical solids 2−71282

Solions *see Transducers*

Sols
  see also Colloids; Sedimentation
  anomalous water regarded as silica sol 2−46921
  Sn-Pd, Mossbauer meas. in which core and stabilizing double layer distinguished 2−80491
  TiO_2 hydrosol, optical properties, turbidity and refractive index 2−74574

Solubility
  see also Phase equilibrium
  acetone-cyclohexane, excess volume meas. at 25°C 2−53408
  acetone-methanol, excess volume meas. at 25°C 2−53408
  alloy, binary, heat of soln. at infinite dilution, pseudopotential perturbation method 2−56495
  carbon tetrachloride-gas mixtures at high pressures, second cross virial coeffs. determ. from solubilities 2−43262
  crystal dissolution velocity in waves 2−74650
  gas bubble rising in water 2−46907
  glass-forming oxides, He migration 2−50707
  ice nuclei in water drops, nucleation 2−75600
  immiscible polymers, interface theory 2−60441
  liquids, of gases 2−53405
  metal, of hydrogen, non-ideal soln. behaviour 2−77716
  methanol-cyclohexane, excess volume meas. from 25 to 50°C 2−53408
  methanol-cyclohexane-acetone, excess volume meas. at 25°C 2−53408
  Mo-N, nitrogen solubility as a function of pressure and degassing kinetics 2−60967
  optical glass melt, striae solubility 2−59260
  quartz, of water, temp. depend. 2−50716
  rare earth-zirconium alloys, form. of metastable low temp. allotropic solid solns. 2−47646
  semiconductor, impurity solubility, autoradiographic variant of activation analysis 2−72595
  semiconductors, heat treatment and props. of doping element 2−84321
  steel, austenite, of NbC and NbN 2−74902
  water, of $LiIO_3$, rel. to cryst. growth process 2−50584
  water, solubility relationships for non-polar gases 2−56485
  Ag_4RbI_5, of I_2, electrochemical cell obs. 2−84657
  $BaTiO_3$-$BaGeO_3$ system phase equilibrium 2−84105
  CdSe, of Cd and Se mass-spectrometry study, homogeneity regions 2−83837
  Co-C solid solution, C solubility limit 2−50830
  Co-Cr-C solid soln., of C, 950-1200°C 2−56925
  Cr, O-enriched, of Ce, Pr, and Nd 2−43830
  Cr_2O_3-TiO_2 system, rutile struct. solid soln., interdiffusion and solubility limits 2−47618
  Cu-Zn and Cu-Zn-Al, of As, solid soln. equil. limit 2−47619
  Cu, of O_2, single cryst. obs., 350-1000°C 2−56926
  Fe-Ni-Al-Cu alloys, of In and Ga 2−43845
  Fe-Sn system, phase boundaries of γ-loop 2−47712
  Ge, of Cu, temp. depend. 2−77613
  Ge, of Li, hydrostatic press. effect 2−47443
  GeTe−Bi solid soln., regions of existence at 250, 400, 500 and 600°C 2−53888
  HFC-Re system, determ. of solubility relations and phase diagram of eutectic type 2−84096
  I_2 in benzene-cyclohexane mixtures, saturation solubility 2−43333
  KBr, of He, permeation, gas release and ion implantation studies 2−84002
  KI solution, of AgI particles, significance to cloud seeding 2−51595

Solubility continued
Li-Bi liquid alloy, of Nd and Th 2–43334
Mo, of H, 905-1521°C 2–50841
Na, liq., of inert gases, 600 degrees C, rel. to reactor coolant behaviour 2–56041
NaI solution, of AgI particles, significance to cloud seeding 2–51595
Na_2ZnGeO_4, under hydrothermal conditions 2–47242
Nb-O alloys with Zr and Hf additions, electron microscope obs. 2–43857
Nb, of H, phase equil. and evolution kinetics of dil. solns. 2–53903
Ni, of U, low limit. determ. from heterodiffusion coeffs. 2–43654
$NiFe_2O_4$-Fe_3O_4-Fe_2TiO_4, ternary solid soln., unlimited mutual solubility of components 2–83840
O_2 in organic electrolytes, rel. to air electrode feasibility for energy conversion 2–84652
Pb-Bi alloys, nonequilib. freezing, quantitative predic. by classical eqn. 2–47032
Pb, anodic dissolution in H_2SO_4 2–84658
Pd-Ag alloys, of H_2 and D_2, heat of soln. 2–83990
Pd-V system, solid solubility and phase studies 2–53770
Re-N, nitrogen solubility as a function of pressure and degassing kinetics 2–60967
Si, liquid, of polycryst. Si, kinetics 2–56487
Si, of Au, enhanced by P impurity, mechanisms 2–64675
SiC, impurity solubility, autoradiographic variant of activation analysis 2–72595
SnI_4 in benzene-cyclohexane mixtures, saturation solubility 2–43333
Ta-H alloy, quenching at liq. He temps. 2–56907
Ta, oxygen solid solubility limit, 1100-2500°C 2–50975
Th-Ln-Bi soln., Ln=La, Eu, Nd, mutual solubilities, 350-700°C 2–67809
Ti/Al chem. diffusion couple, Al_3Ti growth and solubility limits 2–53757
β-Ti and binary alloys, alloying element effect 2–74909
TiO_2-Cr_2O_3 system, solid solubility of $Ti_2Cr_2O_7$ 2–47719
UN, of O_2, 1600-1900°C 2–71649
W-N, nitrogen solubility as a function of pressure and degassing kinetics 2–60967
ZnSe-CdTe system, miscibility 2–77464
$ZrSiO_4$, of rare earths, isomorphous substitution of Zr 2–74913

Solution energy *see Heat of solution*

Solutions
see also Heat of solution; Liquids; Solid solutions
acetic acid/acetone mixtures, H bond formation causing ultrasonic relaxation, two state model 2–43322
alkane monoiodide solutions, X-ray diffraction study, quasiliquid crystal form 2–50318
alkanes in cyclane solvents, orientated mol. interactions 2–50340
aminoacids, aqueous solutions, u.s. velocity measurements using conventional flaw detector 2–60467
aqueous, of protonated amines, i.r. investig. of strongly polarizable hydrogen bonds 2–68652
benzene-nitroalkane solns., total intensity Rayleigh scatt. and depolarization at 546 nm and 30°C 2–64444
binary, light scattering study of thermodynamic functions near critical point of vaporization 2–43373
binary molten salt mixtures with common cation or anion, stat. model 2–84616
binary molten salt mixtures with common cation or anion, stat. model 2–84615
binary systems, free excess enthalpy represent. by mol. distrib. consts. 2–84613
butyl alcohol, aqueous, light scattering and phase transitions 2–74547
chlorobenzol-n-butanol system, microwave absorpt. and complexing 2–67810
complex molecules, effect of solvent on electronic vibrational spectra 2–74253
cytochrome c, electron transfer between molecules obs. by pulsed Fourier transform n.m.r. 2–56267
Debye-Huckel theory, extended, approximate individual ion values for aqueous solutions at 298.15K 2–77420
detergent, dye-aggregation 2–78202
dielectric constants, high specific electrical samples 2–71218
DNA, aqueous, u.s. absorption 2–80116
electrolyte, charged particle system, statistical theory, osmotic model 2–51459
electrolyte, compressibility conc. depend., ion-dipole free energy 2–50342
electrolyte, $LiClO_4$ with dimethylformamide, thinning of Mg-Li alloy Foils 2–80548
electrolyte, Rayleigh and Brillouin scattering studies 2–43360
electrolyte, thermodynamic properties, calc. using modified Poisson-Boltzmann equation 2–50355
electrolyte solutions, limitations of analogy with point defects in ionic crystals 2–64657
electrolytes, higher terms in concentration dependence of self-diffusion coeffs. 2–72563
electrolytes, van der Waals forces 2–51458
electrolytic, with temperature gradient, stability of laminar flow 2–67758
electron transfer reactions using Kubo linear response theory 2–84648
for electropoloshing, with universal appl., with props. of oxidation, depassivation and diffusion control 2–80547
energy transfer from excited donor molecule to acceptor molecule, Forster-Dexter theory 2–53093
energy transfer mechanism, role of electrostatic and covalent interactions 2–53440
ethanol solution, addition of anthracene, effect of triplet-triplet transfer on lasing threshold 2–76488
flowing, continuous neutron activation anal., optimal measuring conditions 2–72596
glasses, binary, effect of a third component upon the immiscibility 2–60607
hydrostatic effect in obs. of ultrasound velocity in critical region 2–43354
ion in dielectric medium, SCF Dirac-Slater calcs. 2–53403

Solutions continued
isobutyric acid-water, Rayleigh linewidth in critical region rel. to Kawasaki-Einstein-Stokes formula and dynamical scaling 2–46933
liquids, determination of excess Gibbs function from total vapour pressure measurements 2–81485
luminescence, quenching by electrostatic interaction of particles 2–60479
2,6-lutidine-water, crit. binary mixture, light scatt., shear viscosity 2–50344
2,6-lutidine-water, crit. binary mixture, transport props. 2–46941
macromolecular, electric birefringence, relaxation spectrum, decay curve, numerical method 2–74543
metal (K,Li, Na, Ca)-ammonia relaxation times and Overhauser enhancements for protons obs. 2–46988
metal-electrolyte solution interface, electron photoemission 2–68496
metal-NHz solns., transport props. in the non-metal-metal transition range 2–80484
methane, methane-d_4, in liquid Ar, system dynamics investigation via collision induced far i.r. spectra 2–43372
methyl cellulose aqueous soln., viscoelastic props. 2–83380
mixed solvent systems, solubility parameter theory 2–43333
multicomponent, Gibbs adsorption equation 2–83874
multicomponent, Gibbs adsorption equation 2–83873
multicomponent, hyperfiltration, extended Nernst-Planck eqns., integration method 2–53418
multicomponent, intermolecular effects in n.m.r. studies 2–56520
n-hexane-nitrobenzene, mode-mode coupling and nonlocal shear viscosity near consolute point 2–64445
n-octyl bromide in decalin, short range ordering, relative permittivity measurements 2–56476
nitrobenzene-n-hexane, crit. mixture, light scatt. intensity and correlation length 2–80473
non-electrolytes, binary, viscosity measurements 2–46940
optimized cluster expansion calc. for ionic solutions and atomic liquids 2–74513
organic dyes, flashlamp for pumping 2–76466
n-pentane-cyclopentane binary solution, height and temperature variations in scattering power near critical point of vaporization 2–43373
perylene radical cation in H_2SO_4 or HSO_3F, solvation shell relaxation and ion-electron recombination 2–46934
photoelectric emission, energy distrib. curves of emitted photoelectrons 2–81189
poly-4-vinylpyridine in solution, hydrodynamic and optical props. 2–60452
poly-γ-benzyl-L-glutamate conc. solns., local viscosity meas. by rotational diffusion of diphenylanthracene 2–60451
polydimethylsiloxanes in n-heptane-tetralin mixtures, surface tension calcs. and expts. 2–74535
polyisobutylene solns. obs. of spin-spin and spin-lattice n.m.r., relationship to viscosity 2–60513
polyisobutylenes in n-heptane-tetralin mixtures, surface tension calcs. and expts. 2–74535
polymer, atomization by grooved-core nozzle, mean drop size 2–50377
polymer, dil., excluded vol. effects and binary cluster integrals 2–60440
polymer, dil., thermodynamic interactions, virial coeffs. 2–60437
polymer, dilute, dumbbell theory 2–63075
polymer, dilute, laser velocimeter obs. of Reynolds stress and turbulence 2–71128
polymer, dilute, mutual diffusivity of liq. solutes, conc. depend. 2–53411
polymer, elongational flow of 100 segment chain 2–46870
polymer, free energy constitutive equation from dumbbell model 2–67811
polymer, interaction thermodynamics, symposium, Prague, Czechoslovakia (Aug-Sep 1971) 2–60435
polymer, laminar and turbulent entry flow 2–46884
polymer, light scatt. wavelength depend. 2–64447
polymer, suitability of eqns. for viscosity correlation over entire concentration range 2–60444
polymer, surface tension of three-component mixtures 2–74535
polymer, thermodynamic prop. depend. on mol. props. 2–60438
polymer, thermodynamics, free vol. role 2–60436
polymer, thermodynamics as functions of pressure and temp. 2–64446
polymer solutions, concentration depend. of steady state compliance 2–83373
polymer-binary solvent system, occurrence and character of inversion in preferential sorption 2–75375
polymer-binary solvent system, occurrence of maxima and minima in curve of total sorption 2–75376
polymers, drag-reducing, degradation 2–53351
polymers, solutions and melts, review of recent non-linear viscoelasticity expts. 2–83364
polymers, ultrasound attenuation, frequency behaviour 2–56503
polymers, u.s. sound abs., effect of conc., relax. processes 2–46954
polymethylmethacrylates, intramolecular mobility in solutions, solvent effects 2–43337
polystyrene in cyclohexane soln., conc. fluctuation dynamics near critical pt. 2–46996
isotactic polystyrene in toluene temperature dependence of confirmation 2–74522
polystyrene soln., neutron small angle scatt., obs. 2–50341
polystyrene sphere solution, moments meas. 2–73541
polystyrene-anisole, temp. depend. of spin- lattice relaxation obs., study of molecular mobility 2–60514
polystyrenes, star-shaped, concentrated solutions, viscoelastic props. 2–83369
polyvinyl acetate solution in toluene u.s. absorption and dielectric dispersion 2–83376
pure fluids, conformal solution theory 2–46650
purine aqueous, i.r. spectra study of formation of strong polarizable H bonds with increasing protonation 2–50112
rheoviscometer study of polymer solutions rel. to rheological properties and changes during two-phase separation 2–60392
salt, linearly stratified, laminar wake obs. 2–67751
seawater, rate of dissolution of biogenic opal 2–72710
sorption systems, mol. clustering and segregation 2–60439
statistical theory of salts in solvents with low dielect. const. 2–84617

Solutions continued
thianthrene complexes in solution, fluorescence study, enthalpies 2−84637
vapour pressure meas. using all-glass-mercury static equilibrium still 2−53511
water and solute, flow in extracellular channels with filtration, osmosis and active transport 2−46879
water-like particles in two dimensions, statistical mechanics of two-component system, hydrophobic interaction 2−80450
wave scattering by fluctuons 2−71151
X-ray fluorescence analysis, theory of double concentration method 2−51487
AgI particle in H_2O drop, contrib. of diffusion and interfacial kinetics to rate of solution 2−60434
$CdCl_2$, adiabatic compressibility and sound propag. speed, reln. to molec. struct. 2−72564
$CoCl_2$, adiabatic compressibility and sound propag. speed, reln. to molec. struct. 2−72564
Cs-NH_3, velocity of 10 MHz waves on function of temp. and metal concentration, structural changes 2−43352
Eu^{3+} fluorescence in organic solvents subject to quenching 2−50369
Fe(II) salt solutions, frozen at normal pressure 2−78178
Ge-Na liquid, thermodynamic props., e.m.f. cell obs. 2−71183
H-bonded solvents, lattice models 2−41526
H_2O, in relatively nonpolar organic solvents and in $NaClO_4$, meas. of i.r. absorption spectra 2−46932
Li-Na alloys, immiscibility 2−53404
LiCl heated hygrometer, phase transition between solid hydrate and saturated soln. 2−56486
LiCl solutions, Brillouin scatt. 2−67835
$MgCl_2$, adiabatc compressibility and sound propag. speed, reln. to molec. struct. 2−72564
NaOH-H_2O solutions frozen, photoelectron emission spectra of ferrocyanide 2−44210
Nd(III) complexes with N-donor ligands, solvent and complex formation defects on spectra 2−46569
$NiCl_2$, adiabatic compressibility and sound propag. speed, reln. to molec. struct. 2−72564
$O_2(^1\Delta_g)$ lifetime in solution, study of bimolecular loss processes 2−51464
Pb-Na liquid, thermodynamic props., e.m.f. cell obs. 2−71183
Si, liquid, of polycryst. Si, kinetics 2−56487
Sn-Na liquid, thermodynamic props., e.m.f. cell obs. 2−71184
$Y_3Fe_5O_{12}$-BaO-B_2O_3-Fe_2O_3 melt, for $Y_3Fe_5O_{12}$ cryst. growth, viscosity and density 2−60713
$Zn(NO_3)_2$, aqueous, ion pairing, Raman spectra obs. 2−60475
Sonar *see Sound ranging*
Sonic boom *see Aerodynamics; Shock waves/effects*
Sonoluminescence *see Luminescence/liquids and solutions*
Soret effect *see Diffusion in liquids, thermal*
Sorption
see also Adsorption; Chemisorption; Desorption
gas-surface interactions, accommodation coeffs., Devonshire theory rejection 2−80578
isotherms shapes and kinetics on porous solids 2−47140
poly-n-butylmethacrylate, effects of equilibrium vapour sorption on tensile creep 2−50758
polymer-binary solvent system, occurrence and character of inversion in preferential sorption 2−75375
polymer-binary solvent system, occurrence of maxima and minima in curve of total sorption 2−75376
rare earth cobalt-hydrogen pseudo-binary system, mag. field influence on equil. press. 2−43498
solids without resonant nuclei, with sorbed gas, susceptibility n.m.r. determ. 2−60671
solution, rel. to mol. clustering and segregation 2−60439
zeolite/methane system, static mag. susceptibility, n.m.r. determ. 2−60671
n-CdS, thin compound semicond., sorption-induced conductivity changes 2−77886
CeO_2, of oxygen, e.s.r. study 2−47156
Er films, maximum sorption capacities and gettering action 2−43495
H_2-metal reactions, rate at reaction measurement 2−78190
LiF, compressed, surface thermolum. after immersion in boiling water 2−48256
Ta filament in CO atmosphere, exam. using omegatron 2−77519
Ta getter, of residual gases in evacuated valve, mass spectrometer obs. 2−76130
Ti films, maximum sorption capacities and gettering action 2−43495
W, sorption of O, investig. by ioniz. of molec. beams 2−71357
Sound *see Acoustics*
Sound field *see Acoustic radiators; Acoustics; Intensity measurement/acoustics*
Sound ranging
— 2−68873
active sonar signal design problems rel. to range-estimation accuracy 2−45522
Arctic SOFAR propagation, effect of ice layer 2−41787
bats, echolocating and target-ranging rel. to sonar receiver 2−55546
code design for transmit beam scanning sonar 2−41792
directivity of sonar receiving arrays, nonomnidirectional case 2−41701
fishing sonar with advanced design 2−69764
marine frequency soundings, apparent resistivity curves in wave zone 2−72700
marine frequency soundings, problems with transmitting-measuring systems 2−72701
mirror sonar with 30° sector coverage, experimental equipment 2−69769
Northwest Pacific, shallow depth explosions, long range detection 2−72702
oceanographic, intensity range relations 2−72715
orientation of animals and insects on sensory basis, conference, N.Y., USA (1971) 2−58646
parametric sonar, use in marine archeology 2−41781
passive sonar performance, detection probability 2−41790
Sound ranging continued
scanning sonars, generation of modulation frequencies and phase stability 2−49169
sonar, side scan, long range, development and use 2−41789
sonar, submarine, Arctic ice pack under surface profile, automatic data processing 2−44602
sonar, surface backscatt. calc. method for performance prediction 2−66625
sonar design, effect of ferroelectric nonlinearities 2−49156
sonar equipment, using nonlinear projector 2−41782
sonar signal processing, off-line digital techniques 2−57901
synthetic aperture sonar, principles and performance 2−73444
underwater, bottom mounted tracking hydrophones 2−58925
underwater, geodetic positioning 2−62088
underwater, source to detector ranges, traveltime of multiply reflected sound waves 2−44614
Sound recording *see Recording*
Sound reproduction
see also Acoustic radiators; Recording; Transducers
in head localization of sound source rel. to headphones and loudspeakers 2−55540
optical sound tracks on super-8-films, test film 2−59341
sound effects equipment for film production, Rotophone CR-4E 2−66628
Space charge
channel electron multipliers, saturation current rel. to applied voltage, space charge saturation 2−74609
circular waveguide, relativistic dispersion eqn. for rotating tubular beam 2−82396
electron beam, effect on freq. shift of axial oscillations in cyclotron 2−70330
electron guns problems of computation and design 2−76454
electron microscopy, correction of spherical aberration 2−79075
electron stream, confined by magnetic field in waveguide 2−73484
electron tube, space charge flow with unrestricted variation of current density and energy range 2−49324
ionization chamber, rel. to voltage pulse profile of pulsed ioniz. chamber 2−52686
liquid crystal, nematic, rel. to instabilities in elec. fields 2−56477
semiconductor, surface space charge, Fermi level near band edges, Raman scatt. obs. 2−47919
wave systems with transverse magnetiz., quasi static approx., validity 2−55597
Cs vapour ionization by method of space charge amplifications 2−70603
Ge, electron irrad., 8.5MeV, high field domain instability 2−57208
[illegible]
arc, stationary atomic distribution in column with axial plasma injection 2−74447
atmosphere ionization in air traffic control laboratory personnel performance 2−75612
Ne, a.c. breakdown in cells with external electrodes, Townsend avalanche model 2−50234
solid
anisotropic conductor, role in Hall coeff. determ. 2−51065
anthracene, evolution of space charge limited currents 2−75105
anthracene films and crystals current/voltage charact. rel. to thickness, temperature and light emission 2−57201
biacetyl, triplet-singlet emission analysis 2−72574
β-carotene glass, resulting in photocond. transients 2−48003
chalcogenide-glass switches, preswitching behaviour in terms of space charge injection mechanism 2−68379
electron-donor acceptor complexes, formation of phosphorescent state from excited Franck-Condon state 2−72577
ice, ferroelec., polariz. and depolariz. current obs. at low temp. 2−57242
ice I_h, effect of space-charge pile-up on dielectric relaxation spectra 2−72013
insulator with nonconst. mobility and deep trapping, surface charge decay 2−51193
m.i.m. structure, space charge limited to electrode limited current transition theory 2−47949
n-p(n-i-p) nuclear particle detectors, space charge layer polarization during irradiation 2−65023
naphthalene crystals, space-charge limited cond., trap density calc. 2−84325
nonstationary current transfer at switch off 2−47976
nylon 66, hexamethylene adipamide, relaxation and Maxwell-Wagner effect 2−65051
p^+np^+ structs., current transport mechanism, thermionic injection, space charge limited currents 2−61377
p-n junction space charge region, differential d.c. conductance, calc. 2−57212
photoconductor, illuminated, electrostatic potentials across space charge layer in an illuminated photoconductor 2−51211
piezoelectric semiconductor ultrasonic amplification, effects on attenuation symmetry 2−51031
poly(N-vinyl carbazole) film, transient current 2−57229
semiconductor, amorphous, rel. to contact photovoltage obs. 2−77969
semiconductor, doped, space-time distribution of excess carriers and their space charge 2−54163
semiconductor, equilib. distrib., calcs., priority of report 2−71888
semiconductor, rel. to Gunn effect bulk instabilities 2−57184
semiconductor, simulation of transient space-charge flow under ionizing radiation 2−71954
semiconductor, space charge waves and progressive amplification 2−55599
semiconductor, transient space charge limited current on voltage removal 2−84336
semiconductors, effect of injected space-charge on equivalent Llewellyn-Peterson equations 2−75082
semiconductors, one-carrier, with variable doping, wave excitation at doping density step 2−81066
solid state single injection diode, generalized expression for small sig. impedance, space charge effects 2−44134
space charge limited current, with coulombic trapping, trap filled limit 2−57183

Space charge continued
 solid continued
  space charge limited currents, fitting expt. data, third side of Lampert triangle 2−84328
  space charge limited currents, third side of Lampert triangle 2−84329
  s-tetracyanobenzene complexes formation of phosphorescent state from excited Franck-Condon state 2−72577
  thermal ionization of deep centers in the space charge of semicond. 2−71921
  triethylammonium-(TCNQ)$_2$, rel. to majority carrier mobility determ. 2−68410
  Ag halides, space charge due to Frenkel defects at surface 2−81022
  Al-Al$_2$O$_3$-Al, space charge dependence of barrier height on insulator thickness 2−51185
  As$_2$Se$_3$ glass, rel. to high field conductivity 2−51134
  Au-lacquer-Se structure, rel. to current passage mechanism 2−84348
  CdS-LiNbO$_3$, convolution and correlation by nonlinear interactions between sonic induced space charge and field waves 2−51015
  CdSe-SiO$_x$, electron transport study in space charge layer of vacuum-deposited film 2−77852
  CdSe film, space charge limited current, rel. to photoelec. props. 2−51212
  n-GaAs:Cu film, epitaxial, carrier mobility, impurity effects, scatt. by space charge centres 2−64983
  GaAs, growth, impurity incorporation, effect of surface space charge layer 2−47428
  GaAs, high-resistivity double-injection devices, conditions for recombinative space-charge injection 2−68445
  n-GaAs diodes, high-resist., high-field domain propag. 2−54220
  GaP, electrically active background impurities, energy conc. and distrib. determ. by thermal release of space charge 2−80939
  Ge detectors, effect on fields and charge collection 2−49661
  Ge p-n junction, γ-ray detector, space charge region polarization, impurity centre charge exchange 2−65026
  Ge$_{16}$As$_{35}$Te$_{28}$S$_{21}$, amorphous, semiconductor- metal contact, space charge capacitance 2−61374
  PbBr$_2$, elec. cond. in cell arrangement, space charge effects, elec. polarization 2−61420
  Pb(Zr,Ti)O$_3$-Si-LiNbO$_3$, convolution and correlation by nonlinear interactions between sonic induced space charge and field waves 2−51015
  Se amorphous film, one- and two-carrier space-charge-limited currents 2−75097
  Si-LiNbO$_3$, convolution and correlation by nonlinear interactions between sonic induced space charge and field waves 2−51015
  Si, high resistivity, space-charge-limited minority hole flow 2−75118
  Si, neutron irrad., space-charge-limited current obs. of electron trapping 2−51168
  (ZnO-MgO):Fe,O photoconductor, transient effects 2−84377
  ZnTe-InAs heterojunction diode, space charge limited current 2−57213
Space groups
  coprime multiplicities of space-group point-positions 2−56614
  crystal structure determ., application of rigid group concepts 2−67974
  d_{6h} class, representations of double space groups 2−47290
  Fermi surface, tabulation and procedure to determine point symmetry of positions in Brillouin zone 2−47798
  Klassengleichen supergroup-subgroup relationships 2−83910
  magnetic structures, exchange interaction of electric and magnetic polarizations 2−81212
  molecular arrangement in crystals, classification using theory of space groups 2−67952
  noncentrosymmetric, with translational elements of symmetry, phase relationships 2−83907
  P2$_1$2$_1$2$_1$, one-dimens. phases expression 2−67951
  rare earth, heavy, rel. to energy band theory derived from group theory 2−57114
  rare earth oxides, A-type, centrosymmetric groups 2−51355
  spinel structure compounds, off centre ions, model for local distortions 2−80646
  symmetry, of ideal crystal, use for surf. struct. 2−71298
  symmetry labelling of electron and phonon states, orientation depend. 2−61134
  symmetry rel. to Σ_2 formula, non-centrosymmetric struct. determ. 2−67969
  symmetry rel. to props. of direct solns. based on Σ_2-relation 2−56615
  tetramethylcyclobutane-1,3-dione 2−77155
  zellengleichen supergroups of 230 Fedorov space groups 2−83909
  Al-Mg alloys, β, γ phases 2−71642
  CdI$_2$ polytypes, twelve-layered 2−43577
  ClO$_2$, from i.r. and Raman spectra 2−77561
  CsCoCl$_3$, mag. struct. 2−72213
  LiFe$_2$F$_6$, trirutile, mag. struct. 2−72220
  Pt complex, bis(triphenylphosphine)(ethylene)platinum 2−43587
  Rb$_2$CoCl$_4$ 2−83957
  Se complex, Se(II) diethyl dithiocarbamate, three-dimensional X-ray investigation 2−56666
  V$_{0.95}$Cr$_{0.05}$O$_2$, orthorhombic phase 2−43592
Space research
  see also Atmosphere
  — 2−72941
  — 2−72942
  acceleration effects on organisms using zero g and hyper-g 2−45025
  aerospace propulsion, conference Salt Lake City (1971) 2−62412
  aerospace sciences progress, theory and experimental techniques, book 2−81748
  Apollo 16, first report 2−62665
  Apollo rocket triggering of lightning 2−62278
  astronomy, problems 2−55195
  atmospheric re-entry, numerical treatment 2−53320
  comet exploration, utilization of Jupiter swingby trajectories 2−54975
  comet Halley rendezvous and outerplanet missions using thermionic reactor spacecraft 2−66032
  computing methods 2−82284
  contaminant material optical constants det. by quartz microbalance and reflectometer 2−78418

Space research continued
  contamination in space environmental test chambers, real time detection 2−78417
  cosmic apparatus interception 2−62408
  crater shape dependence on particle velocity and material of target and particle 2−54974
  directional molecular flow analysis and leak detection using rotatable gas analyzer, space simulation 2−78706
  Earth resources satellites, ERTS and Skylab programmes 2−48612
  electric propulsion employing thermionic reactor power systems 2−66033
  electric propulsion missions employing nuclear reactor power systems 2−66031
  France, VI-th plan 2−68993
  fuel element development for in-core thermionic reactor for space applications 2−49263
  gas injection into vac., fast ionisation gauge 2−84928
  geology, photography 2−84750
  GEOS-2 spacecraft, Goddard Range and Range rate system 2−54985
  holography and optical data processing applics., review 2−48639
  image processing on Mariner 9 2−78412
  impulsive rendezvous trajectories and optimality 2−48631
  in core thermionic reactors, applications to space and underwater technologies 2−49269
  interstellar navigation 2−66030
  investigations in 1966-1970 period, review 2−58144
  i.r. simulator for thermal vacuum testing of space vehicles 2−78415
  Jupiter, atmospheric entry probe missions, scientific objectives 2−75871
  Jupiter mission and launch vehicles 2−85049
  laser instrumentation in test facilities 2−46848
  manned space station, utilization planning 2−44787
  manned space station experiment modules, design and use 2−44786
  manned space station program information management 2−44788
  Mariner 1973 rel. to exploration of Mercury, mission objectives 2−78503
  Mariner-Mars 1971, unified S-band tracking and calibration expt. 2−54984
  Mars, exploration beyond Viking 1975 project 2−78543
  Mars, Viking '75 mission to examine possible life 2−75647
  Martian gravity simulator for Viking landing tests 2−78420
  mass loss from thin liquid surface films exposed to re-entry heating and shear 2−54976
  materials science and manufacturing in space 2−48626
  microparticle impacts, position sensing and momentum evaluation 2−66022
  microwave radiometry applics. 2−48616
  mission to asteroids, solar system origin and evolution 2−51835
  missions to Jupiter as part of Pioneer series 2−72935
  nuclear MHD electric power system 2−59050
  orbital eccentricity and angular momentum management scheme stability 2−48632
  orbiting astronomical observatory, analysis of u.v. data 2−81850
  orbiting astronomical observatory using 20 Ah Ni-Cd cell 2−85075
  orbiting gravity gradiometer, satellite requirements 2−54986
  orientation angle meas. with inertial sensors 2−54973
  performance optimization technique for Mars Viking lander 2−62422
  Phobos and Deimos, space missions for exploration of Martian satellites 2−78528
  planetary emitted radiation and albedo simulator 2−78517
  Planetary Explorer probe studies of Venus' atmosphere 2−75643
  planetary extreme enviornment simulation 2−78569
  plasma accelerator for ionospheric simulation 2−77280
  point position solutions for geoceiver stations in the US 2−54987
  probability characteristics of initial elements in virtually circular orbits 2−54978
  propulsion, blast wave studies 2−44789
  radiation exposure in manned spaceflight 2−51947
  re-entry electrical phenomena simulation using hotshot wind tunnel 2−72931
  simulation, conference New York (1972) 2−78413
  space missions to comets and asteroids rel. to understanding of solar system 2−78411
  space shuttle, economic evaluation 2−48621
  spacecraft thermal vacuum testing 2−78419
  spaced bumper systems, effects of material phase transformation effects 2−62413
  technology spin off to terrestrial problems 2−78421
  thruster system using anhydrous N$_2$H$_4$ ahd Shell 405 catalyst 2−84632
  vehicle entry simulation, arc-heated duct facilities for turbulent flow 2−66028
  Viking Project, martian ionospheric meas. during atmospheric entry phase 2−75890
  Ar arc lamp 400 KW for solar simulation 2−78414
  Nb, Nb alloys, evaluation for nuclear power systems 2−76938
  Xe radiation source, short arc, high reliability and power or solar simulation 2−76535
Space-time configurations
  asymmetric nonstatic deviation introduced in Minkowski metric 2−41469
  asymptotically flat empty spaces, soln. of Newman-Penrose eqns., application to metrics, geodesic rays 2−76195
  cellular structure, observer dependence 2−55382
  class one, perfect fluid distributions 2−76183
  conformal group approach for four and five dimens. 2−58722
  covariant chronogeometrical space time model and extreme distance 2−44816
  cresyl violet dye, laser and spectral props. 2−73578
  curved background manifold, gravitational waves dispersion 2−73295
  de Sitter group and harmonic oscillator 2−63016
  dynamics of rigid test body in curved space-time 2−52050
  Einstein's eqns., soln. for spatially flat field of e.m. origin 2−82193
  Einstein-Maxwell space-time, symmetry 2−82197

Space-time configurations continued
- elementary particle definition as irreducible unitary representations of group of asymptotically flat space-times in general relativity 2−73737
- equivalence principle and curvature of spacetime metric rel. to redshift rocket probe experiment 2−69571
- field equations of high spin in curved spacetime, necessary integrability conditions 2−45257
- gravitational field structure in asymptotic limit at spatial infinity 2−45248
- homogeneity axiom and structure of relativity groups 2−41473
- interacting systems, quantum concept. of space-time dynamics 2−55424
- Kerr Vaidya metric, e.m. interpretation 2−73297
- light cone singularities, effect on Fourier integral asymptotic expansion 2−82650
- light-like geodesics, study by WKB approximation 2−62986
- local pseudoeuclidian 4-dimensional tangent reference frame 2−76180
- Loedal diagram, equivalence to special case of Minkowski diagrams, use in teaching relativistic kinematics 2−78739
- Lorentzian symmetric spaces 2−76185
- Mach's principle and gauge freedom in Brans- Dicke theory 2−41477
- metric of astronomical defect in Lyttleton-Bondi theory 2−75660
- metric-space formulation of Newtonian fields 2−73298
- Minkowski space, Zeeman-order topology 2−73292
- Minkowski space-time, 2-dimens. V^2 types 2−55398
- model universe, 5-dimensional, elementary spinorial excitations 2−41455
- multipolar sources associated with generalized multipolar decomp. of e.m. field 2−52530
- Newtonian, associative and non-associative automorphism 2−73301
- nonmetrical specification and conservation of energy-momentum 2−82200
- physical laws invariance under space time depend. changes in unit of length 2−76176
- Prolemy-Kopernik problem, reference frames and principle of non-holonomy 2−82212
- pseudo-Euclidean, conformal covariant prescription for Wilson's operator product expansion 2−73719
- quantum mechanics, relativistic, relation of space-time to material symmetry 2−66440
- Riemann spaces, filled with matter, mean curvature 2−78767
- Riemann V4, symmetry properties, constancy of particle counts in general relativity 2−48988
- Riemannian, relativistic quantum many-body theory, applic. to super-dense matter 2−66447
- Riemannian space, compact orientable, with positive definite Ricci curvature 2−76201
- Riemannian space, pseudo-geodesic and pseudo-Riemannian coordinate systems 2−55380
- Riemannian spaces, five-dimensional, charge production by coordinate transformation 2−76178
- Robertson-Walker space-time, expansion-induced backscatt. of e.m. waves 2−55392
- Robertson-Walker spaces, time-like geodesics from Hamiltonian view-point, characteristic function determ. 2−76194
- second-order recurrent, in general relativity 2−78790
- seismicity of western USA, obs. using interactive computer-generated graphics display technique 2−57583
- space-time absoluteness, experimentum crucis with special relativity 2−52058
- surface-of-resolution cosmology, connection to real universe 2−66038
- symmetry of space, group representation 2−69549
- time-delay expts., best-fit estimate of relativistic effects 2−66431
- Weyl's lemma as transport and coupling rule 2−82185
- Weyl metrics, horizons exhibiting extra symmetries 2−76181
- zero dimensional, solns. for linear approx. 2−82634

Space vehicles
- *see also Rockets; Satellites, artificial*
- advanced spacecraft, dual bumper wall construction 2−66029
- analytical guidance in neighbourhood of optimal multi-impulse trajectories 2−62410
- Apollo lunar spacecraft, systems description 2−72934
- Apollo spacecraft guidance and navigation systems, performance 2−48624
- artificial gravity, centrifugally obtained, kinematics 2−62423
- for astronomy programme, ultraviolet 2−44857
- atmospheric re-entry at hyperbolic velocity, long-range trajectory 2−51678
- attenuation of communicating signal to reentering spacecraft 2−43137
- cold gas propulsion, optimum design parameters 2−62416
- collisionless plasma flow over conducting spheres rel. to spacecraft water 2−83543
- computing methods 2−82284
- coordinate estimation, effect of interference parameters 2−75650
- Delta and Thor/Agena launch vehicles for scientific and applications satellites 2−48628
- design, industrial and university approaches to teaching 2−48620
- design, small scale wind shear definition 2−44798
- Earth surface to orbit shuttle, design considerations 2−44781
- electric propulsion employing thermionic reactor, power conditioner design 2−66034
- geodetic latitude and altitude from geocentric coords. 2−62411
- guidance trajectory, optimal correction 2−51669
- interceptors, minimum energy intercept of deorbiting target 2−48633
- interplanetary flight trajectories, single impulse, energy optimum characteristics, variation 2−51668
- ion propulsion systems, missions and technology 2−44795
- Jupiter, mission 2−85049
- Jupiter entry probe rel. to atmospheric measurements 2−75642
- Jupiter turbopause probe, applicability to Saturn atmospheric investigations 2−78557
- low altitude controlled constellations, for required communications 2−44805
- low thrust outer planet orbiter, three body numerical solutions 2−54992

Space vehicles continued
- Mariner 9, map of Mars 2−69158
- Mariner 9 mission, scientific objectives rel. to Mariner Mars 1971 Project 2−75645
- Mars Viking lander, performance optimization technique 2−62422
- matrix transformations for spacecraft attitude determination 2−82171
- meteorite collision, crater shape dependence on particle velocity and material of target and particle 2−54974
- minimum time transfer between close coplanar orbits with thrust limited rocket 2−62417
- Mission Analysis and Trajectory Simulation, gravity model 2−54990
- moments of forces, in magnetic field 2−75646
- nose shape change obs. during re-entry, ablation transducer 2−48622
- nuclear and electrical propulsion, containment problems 2−44796
- nuclear power systems, advances in safety, review 2−51667
- on-orbit configurations, operation and integration aspects of sensors 2−48615
- optimal atmospheric entry trajectories 2−53310
- optimal deterministic guidance for bounded-thrust spacecraft 2−62409
- optimal reentry control problem, perturbation technique 2−60350
- optimal trajectories with delta velocity constraints 2−44803
- Pioneer, Jupiter project 2−48771
- Planetary Explorer probe studies of Venus' atmosphere 2−75643
- planetary quarantine constraint, optimum aim point biasing, unsterile spacecraft 2−44804
- propellant optimal guidance law on multiimpulse trajectories 2−48635
- propulsion, controlled thermonuclear fusion 2−51673
- propulsion, proposed use of cosmic plasmas 2−51672
- radio signals from Venera-7 spacecraft during descent to surface of Venus, digital computer analysis 2−73088
- radioisotope thermoelectric generator systems, safety aspects 2−51681
- ramjet, using interstellar medium as fuel 2−48613
- rate of descent in planetary atmosphere rel. to thermodynamic parameters 2−73074
- re-entry, lifting-body model 2−44785
- re-entry, rolling nonlinear anal. 2−78422
- re-entry vehicle dynamic stability, effect of lagging pitching moment 2−66027
- re-entry vehicles, optimal three dimensional motion 2−77331
- re-usable, atmospheric braking on returning to low orbit 2−44783
- reentry, descent control algorithm 2−54971
- reentry, navigation problem, algorithm 2−54969
- reentry stabilization, one-parameter multistep algorithm 2−54970
- reentry with parabolic velocity, navigational algorithm 2−54972
- rudder or sail, stabilizing efficiency 2−51671
- shielding against Van Allen belt and solar flare protons 2−85065
- shuttle, reusable space vehicle, review 2−72940
- shuttle, thermal protection systems, review 2−44784
- shuttle, transfer between low and stationary orbits 2−44806
- shuttle, U.S. space program 2−44780
- shuttles, surface oilflow patterns, aerodynamic heating 2−83679
- single stage re-usable ballistic space shuttle 2−44782
- singular control in flight mechanics with limited power and energy storage 2−51670
- Skylab contamination ground test, particle size distribution and velocities 2−78416
- solar probe, HELIOS, design and development 2−48789
- solar sail and electric propulsion systems compared 2−72929
- Soyuz, new generation of Soviet spacecraft 2−58143
- Soyuz 9, effects on human body of long term weightlessness 2−62424
- space shuttle, optimal transition from entry to cruising flight 2−53311
- space shuttle main engine 2−51674
- space station design rel. to atmospheric leakage 2−44797
- sterilization, stochastic bioburden model 2−62426
- structural optimization in random vibration environment 2−48611
- thermal vacuum testing 2−78419
- transfer from high elliptic to circular orbits using successive breakings in planetary atmospheres 2−48634
- transient flow field produced by secondary injection, numerical solution 2−43255
- Turbopause Probe for Jupiter, atmospheric experiments 2−75644
- Venus planetology mission based on planetary explorer space craft 2−55152
- Viking lander, martian atmospheric structure meas. during entry phase 2−75891
- Viking Project, martian ionospheric meas. during atmospheric entry phase 2−75890
- window for photographic studies, characteristics, structure, testing and thermal effects 2−79391
- H-He plasmas, thermodynamic properties for stagnation shock layer of spacecraft entering atmosphere of Jupiter 2−46718
- ZrO_2, stable white pigment, radiation stability 2−44799

instrumentation
- *see also Langmuir probes*
- — 2−72941
- — 2−72942
- all reflective linear image space scanner 2−79390
- altimeter-airspeed and Mach number transducers 2−48640
- altimeters, errors caused by atmospheric temp. deviations from International Standard 2−48638
- Apollo lunar craft, review 2−51823
- automatic mass trim system for spinning spacecraft 2−78424
- bolometric horizon sensors for geostationary satellites 2−44808
- camera system for Viking lander, Mars remote exploration 2−85077
- conference, Las Vegas, Nev., USA (1971) 2−48636
- Earth pointing attitude control, for elliptic orbits 2−44809
- electrically supported gyro, active damping at solid spherical rotor 2−44813
- EOLE, location and data collection, meteorological applications 2−65651
- Fabry Perot modulator, for visible and i.r. radiation 2−72945
- h.v. pulse generator for spark chambers 2−55933
- Intercosmos-3, recording of l.f. signals 2−75651
- isotensoid flywheels, applic. to spacecraft energy ang. momentum storage 2−72928

Space vehicles continued
instrumentation continued
life detection on Mars, computer-controlled analytical instrumentation of Viking spacecraft 2−54977
life detection on Mars, soil gas chromatography/mass spectrometry by Viking spacecraft 2−55147
loosely stabilized, orientation determination 2−75655
magnetron press. gauge on O VI-15, adsorption/desorption press. effects 2−58148
Mariner 9 Mars TV experiment, observations and results 2−75892
mass centre estimation in spinning drag-free satellites 2−66036
meteoroid detection panels 2−54983
multimagnetometer system, positioning optimisation 2−62418
multimagnetometer system, use in determining spacecraft fields 2−66024
neutron dosimetry by Ir and Ta foils 2−58147
Nimbus 3 and 4, interrogation, recording and location system 2−66035
Nimbus 4, selective chopper radiometer 2−65660
nuclear electric power systems, states review 2−58151
on-board weighing system for centre of gravity det. 2−48614
optical systems, all-metal, ultra-light-weight 2−73658
orientation, determ. from magnetometric measurements 2−75654
OSO-5 dim light monitor 2−72943
photomultiplier, open channel, performance obs. 2−45690
Pioneer Jupiter spacecraft, conical scanning system 2−44810
Planetary Atmosphere Experiments Test Project, spacecraft description 2−75652
plasma, particle and field detectors for atmos. 2−72745
proportional control using auxiliary jet engines 2−72944
proportional counters, self pressure regulating 2−42453
radiometer, microwave for meas. sea surface temp. 2−72721
rake probes, h.f., for inflight intake airflow distortion obs. 2−48637
satellite instrument for proton obs. in energy range 0.1 MeV to 6 MeV 2−65923
solar batteries, efficiency of GaAs and Si cells in range o.2 to 10 a.u. 2−49306
solar cells, thin films, state of the art and space applications 2−59059
solar electric propulsion, integration of broadboard power conditioner with ion thruster 2−44812
solid Teflon pulsed plasma thruster, exhaust velocity studies 2−44811
spectroheliographs, extreme u.v. and X-ray, applic. to solar corona meas. 2−62808
Viking entry mass spectrometer rel. to obs. of martian upper atmosphere 2−75653
Viking landing vehicle, biological instrumentation for examination of Mars surface 2−75647
Cs, thermionic energy converters, pole measurements 2−54991

Spallation *see Nuclear spallation*

Spark chambers
automatic, as magnetic spectrometer, with sonic and magnetostrictive readout 2−67101
automatic chamber system, with sonic and magnetostrictive read-out 2−79667
current limited, anomalous effects and general properties 2−73956
cylindrical wide gap and streamer, construction, operation and response 2−42478
cylindrical wire system, meas. of K^0 decay 2−55935
detector in multiparticle spectrometer for very high intensity charged particle beams 2−76738
film photographic variables optimization for automatic meas. 2−59641
h.v. pulse generator, use in space 2−55933
hybrid chamber, proportional chamber with gated spark readout 2−55904
interactive computer graphics system in spark chamber events display 2−48936
interactive computer graphics system in spark chamber events display 2−48936
liquid argon combined with spark chamber for particle track recording 2−73955
magneto-, sparko, and thermo-strictive phenomena in thin wires 2−73954
massless, plates of expanded polystyrene sandwiched between Al foils 2−52705
multiparticle wide aperture spectrometers with spark chambers, analysis of systems and use in particle spectroscopy 2−76737
optical, spatial Spark jitter measurements of highly charged nuclei 2−67100
scintillation counter combination, 1.5 m, high aperture ratio spectrometer 2−59621
single gap, breakdown development, phenomenological model 2−70315
spark drift in magnetic field 2−73937
spin rotation meas. at high energies of π-p scattering apparatus 2−73901
streamer chamber technique for triplet production meas. near threshold, results 2−76751
streamer chambers, pulse generator, pulse stabilization, transit time, spark gaps 2−82826
telescope for underground meas. of muon component in EAS 2−73876
time resolution improvement 2−55934
wide gap, obs. of performance 2−76750
wire, γ-ray imaging system for biomedical use 2−69290
π, secondary, due to cosmic ray interactions, detection 2−73899

Spark counters *see Counters/spark*

Sparks, electric
see also Breakdown, electric; Lightning
air, dry, sparking potentials in crossed electric and magnetic fields 2−74445
air, long gaps, 50 Hz sparkover characteristics 2−74438
air-gaps, prebreakdown current meas. 2−43216
breakdown mechanism in N_2, O_2 and Sf_6 2−60318
breakdown triggering of vacuum spark gap 2−71027

Sparks, electric continued
carbon tetrafluoride, CO_2 laser induced, fluorescence surrounding 2−74440
corona, power transmission lines, equivalent parameters 2−60317
dichlorodifluoromethane, CO_2 laser induced, fluorescence surrounding 2−74440
discharge light sources, multiple system 2−56397
high-frequency generators of condensed sparks, electrical processes 2−53258
h.v. spark pulse generator for quantitative spectrochemical analysis 2−60316
hydrocarbons, CO_2 laser induced, fluorescence surrounding 2−74440
laser beam triggering of spark gap 2−74406
metal powder, use in isostatic pressing to destroy oxide layers 2−68129
parallel, non-decoupled, ignition characteristics 2−71045
point-plate spark gap, flashover voltage, obs. 2−60315
repetition rate increase in 50-500 Hz for decreasing analysis time for optical emission spectroscopy 2−84694
spark gap operation by transmission-line circuit 2−66684
stabilized, formation and growth 2−56395
underwater, resistance and internal energy of discharge channel 2−64358
vacuum gap conditioning 2−67694
water droplets, interactions with positive corona streamers, atmospheric significance 2−64489
Ar, Townsend mechanism, effect of cathode 2−71047
Ar low-voltage spark discharge plasma, space and time distribution of temperature 2−70881
BF_3, CO_2 laser induced, fluorescence surrounding 2−74440
N_2, breakdown at high pressure 2−71043
N_2, thermalisation of spark channels 2−71046
SiF_4, CO_2 laser induced, fluorescence surrounding 2−74440

Specific heat
see also Debye temperature; Gruneisen relation; Thermodynamic properties
anharmonic chain, computer experiments 2−58787
fast reactions, ultrasonic and relaxation spectroscopy, expression for C_p/C_v 2−81499
heat capacity calorimeter for small sample 2−52303
heat receivers for pulse meas. of thermophysical properties, effects of heat capacity on pulse length 2−63155
Ising spin system, sp. ht. density 2−61486
Ising system, three-dimens., sp. ht. density asymptotic behaviour for $T \gg T_c$ 2−61487
at low temperatures, apparatus for obs. 2−58652
measurement, heat pulse methods, apparatus, 20- 300°C 2−55573
measurement at high-temps., fast system 2−52299
measurement at low temp., small samples 2−41868
polymers, automatic adiabatic calorimeter for meas. in temp. range −180 to +270°C 2−63165
pulse method of meas. 2−63163
pulsed electron beam measurement 2−54039
thermophysical properties at high temperatures, conf., Turin, June (1972) 2−54035
zeolite, molar heat of adsorption of water, 90-300K 2−60694
$FeBr_2$, meas. between 4 and 70 K 2−64852
$FeCl_2$, meas. between 4 and 70 K 2−64852
$SOBr_2$, mol. parameters 2−56169

gases
— 2−67870
dichlorofluoramine, calc. from spectroscopic data 2−60372
difluorocyanamide, calc. 2−71114
difluorocyanamide gas, heat content, heat capacity, entropy and free energy 2−71114
dimethylphenols, 2,3, 2,5 and 3,5, u.v. spectra, vibrational analyses 2−74294
CO_2, N isobaric, carbon dioxide with nitrogen impurity, supercritical pressures, flow type adiabatic calorimetry 2−83712
^3He-^4He mixture, study of specific heat near gas- liquid critical point 2−71255
Ne, specific heat at constant volume and critical point determination 2−71113
XeF_4, 5 to 350K, heat capacity, thermodynamic functions, entropy 2−80411

liquids
carbon tetrachloride, enthalpy of transition and heat capac. for metastable fcc to stable rhombohedral transform. 2−77754
critical mixtures, vacuum adiabatic calorimeter design 2−49191
2,2-dichloropropane, heat capacity detn. by adiabatic calorimeter 2−76406
$Ge_xAs_{40-x}S_{60}$ pseudobinary system 2−51045
n-heptane, heat capacity detn. by adiabatic calorimeter 2−76406
n-heptane, isobaric heat capacity along boundary curve 2−64458
n-hexane, isobaric heat capacity along boundary curve 2−64458
from isobaric ensemble formalism in Monte Carlo calcs. 2−64428
metal, ion-ion potentials, effective interaction, hard sphere dias., sp. ht., entropies 2−60415
p-methoxy benzylidene p-n butylaniline, liq. cryst., nematic-isotropic liq. phase transition, sp. ht. obs. 2−74523
n-octane, isobaric heat capacity along boundary curve 2−64458
n-pentane, isobaric heat capacity along boundary curve 2−64458
pulsed-adiabatic method for meas. heat capacity 2−43345
water, near freezing point, Ornstein-Zernike fluctuation corrections 2−60541
water calc. using hydro-polyhydrol model 2−43317
Al_2O_3, alumina, near melting point 2−54044
BeO, determination by mixing method 2−56496
Ga-Hg alloy, anomaly near phase separation critical pt. 2−50354
HF, heat capacity 2−60465
He II, heat capacity at const. vol. near λ pt. 2−47012
He II, phonon spectrum, thermodynamic evidence against quadratic term 2−77456
^3He-^4He mixture, study of specific heat near gas- liquid critical point 2−71255
^3He, singularity near critical point 2−47004
$^3He+{}^4He$ solutions, below λ temp. 2−52108
^4He, phonon dispersion and contribution to heat capacity 2−47001

Specific heat continued
liquids continued
Kr liquid 145-240 K sound velocity adiabatic compressibility and specific heats 2−83790
Mo, temp. dependence near melting point 2−57066
Ne, Cp determ. from sound velocity measurements 2−46950
Pb, 300-850K 2−54050
W, temp. dependence near melting point 2−57066
solids
84035
biphenyl crystal, 80-340K, specific heat formula 2−57043
capacity, analysis of low temp. data rel. to teaching 2−55352
carbons, soft and neutron-irrad. graphite, low temp. obs. rel. to heat treatment 2−54045
cerium ethyl sulphate, heat capacity below 1K, mag. behaviour 2−68551
cerium ethyl sulphate, low temp. heat capacity 2−44229
crystals, investigation of order-disorder transitions 2−50991
cubic monatomic lattice, surface mode dispersion relations and surface sp. ht. 2−77487
diatomic molecular crystal, calc. using lattice vibr. model 2−43960
dilute quantum crystal alloys, mass-defect induced changes 2−43948
electrically conducting, simultaneous obs. of thermophysical props. at high temp. 2−57078
electron gas, degenerate, Sommerfeld method applic. to grand partition function 2−57102
erbium ethyl sulphate, low temp. heat capacity 2−44229
ferroelectric solid solution, thermodynamic theory 2−61424
ferroelectric solid solutions, first-order phase transition characts. 2−65057
ferromagnetics near T_k, heat capacity and magnetocaloric effect 2−72158
films, Heisenberg ferromagnet, magnon specific heat 2−51263
glass, calc. from enthalpy meas. 2−74992
granular materials, by continuous flow Callendar and Barnes method 2−57057
graphite, neutron irrad., 0.6-5 K 2−57062
graphite, neutron irrad., 1.4-4.4 K, strong mag. field effects 2−57063
graphite, pyrolytic, meas. over wide temp. range 2−84208
harmonic solid, least-upper and greatest-lower bounds 2−74964
high temperature, one dimensional anharmonic lattice model 2−57058
high temperature measurement techniques 2−71616
hot powders, meas. of heat capacity 2−58971
inert gas, anharmonic corrections at high temp. 2−68247
insulators and structural materials, near room temp. 2−57080
ionic crystal with paraelectric dipolar impurities for $E\|[100]$, [110] and [111], E=applied field 2−57221
Ising ferromagnet, one-dimensional with single ion anisotropy 2−57274
lunar rocks, breccias and fines from Apollo missions 2−62661
magnesium highpolyphosphate glass, and crystallization 2−83851
magnetic system, low temp. anomalies due to simultaneous effects of exchange and mag. fields 2−57308
metal, influence of point defects at high temp. 2−54040
metal, low temp. ht. capacity, review 2−47747
metal, refractory, high temp. measurement 2−57077
metal systems, data compilation, NBS Permuted Materials Index 2−68155
metal/hydrogen systems, rel. to clustering model 2−77716
metallic glass, at low temperature 2−54021
nickel acetate tetrahydrate, 0.43-10.73 K, Schottky anomaly 2−78040
organic glasses, influence of annealing on thermal behaviour in glass transition region 2−71744
poly-L-alanine, low temp., one-, two- and three-dimensional models 2−47755
polychloroprene-rubber, recrystalliz. and reorganization processes, calorimetric obs. 2−71289
polyethylenes, chlorinated, differential scanning calorimetry 2−50400
polymers, linear in amorphous state, method of estimation 2−61106
polystyrene, from 4.2°K to room temperature, effect of divinylbenzene 2−71732
rare earth ethyl sulphates, mag. interactions contrib. 2−57314
rare earth intermetallic compounds, contribs. to low temp. heat capacity 2−51043
rare earth ionic cpds. with mag. dipole-dipole interaction, caloric and mag. obs. 2−68523
re-entry materials, carbon, thermal props. 2−56981
Rochelle salt, ferroelec. contrib., two sublattice treatment 2−43990
semiconductor, strongly doped, model interpret. 2−77880
semimetal, monotonic behaviour in strong mag. fields 2−44025
silica glass, anomalous properties, interpretation 2−67884
sphalerite semiconductors, group III-V, charact. temps. 2−54013
steel, 1Kh18N9T, between 300 and 900 K 2−57065
superconducting A15 cpds., anomalies interpret. 2−77877
superconducting alloys with paramag. impurities and local states in gap 2−71857
superconductor, calc. from Ginsburg-Landau theory of fluctuations 2−75067
superconductor, inclueence of mag. impurities, Kondo effect 2−64929
superconductor, peak, prediction from selfconsistent treatment of fluctuations 2−75065
Tarasov specific heat model, evaluation method 2−43979
TCNQ cpds., low temp., ionic binding contrib. 2−54052
transition metal, supercond. with non-mag. impurities, Green's function theory calc. 2−44061
transition metal alloys, 3d anomaly rel. to mag. phase changes 2−54332
transition metal binary alloys, low-temp, sp. Lt. parameters γ and θ_d, inverse scaling, rel. to phase stability 2−68248
transition metal carbides and borides 2−54043
1,2,3-trichloro-4,5,6-trimethylbenzene, heat capacity determination by adiabatic calorimetry, 30-300K 2−57070
wet porous materials near f.p., transient simultaneous measuring method 2−74989

Specific heat continued
solids continued
ytterbium ethylsulphate, Schottky specific heat, rel. to mag. props. 2−51241
Ag-Au-Cu alloy, meas. and theory 2−75051
Ag-Au alloy, calc. using coherent potential model 2−75025
Ag-Au alloy, meas. and theory 2−75051
$AgMo_4S_5$, superconducting properties, heat capacity 2−81051
Al-Al_2O_3 granular films, superconducting, T_c enhancement 2−77878
Al, α-irrad., low-temp. obs. of He bubble form. 2−50644
Al_2O_3, alumina, condensed phase near melting point 2−54044
α-Al_2O_3, anharmonic coeffs. 2−51047
Au, and lattice dynamics 2−61074
$AuCu_3$, ordered and disordered, effects of ordering 2−57060
$BaFe_{12}O_{19}$, ferrite, high temp. obs. 2−54049
$BaFe_2O_4$, ferrite, high temp. obs. 2−54049
$BaTiO_3$, ferroelec., a.c. calorimetry obs. near T_c 2−64853
BeO, determination by mixing method 2−56496
Bi, below 30 K, analysis using magnetically smoothed temp. scale 2−68249
C, 0.5-5 K, effect of heat treatments at 600-1600°C 2−57061
C, non-cryst., strong mag. field obs., 1.3 to 4.3 K 2−43980
C, non-crystalline, rel. to Curie paramagnetism 2−65123
CO crystal, calc. using lattice vibr. model 2−43960
Ca, molar heat content, electrical resistance, meas. by pulse method 2−64914
Cd, below 30 K, analysis using magnetically smoothed temp. scale 2−68249
CdO(c), drop calorimetry and diff. scanning calorimetry 2−54047
β-Ce and Ce-Y alloys, low temp. heat capacity and mag. ordering 2−47748
CeB_2, exchange interactoon and fluctuation effects 2−54339
$Ce_{1-x}Gd_x(Tb_x)Ru_2$, mag. ordering and supercond. coexistence 2−43981
$Ce_xLa_{1-x}Pd_3$ alloy, heat capacity rel. to Kondo effect 2−51098
$CeNi_2$, $CeCo_2$, electronic contrib. 2−57064
$CeRu_2$, $CeRu_{2-x}Pt_x$, superconductors, low temp. ht. capacity 2−77879
$CoCl_2.6H_2O$, antiferromag. spin wave theory calc. 2−54351
$(CoO)_{1.4}.P_2O_5$, glasses, antiferromag. interactions 2−75237
CoSi, near-stoichiometric, comp. effects 2−68521
Cr, 280-330K, rel. to antiferromag.-paramag. transition 2−75238
$(Cr_{1-x}Mn_x)Be_2$ meas. at 1-4 Kelvin 2−57059
$Cr_2(SO_4)_3$, $(CH_3NH_3)_2SO_4$, $24H_2O$, calc. above crit. temp. 2−48105
Cs, calc. using lattice dynamical model of Sharma and Joshi 2−47749
Cs, lattice vibration based on Toya's electron-phonon interaction 2−64834
α-Cu-Au alloys, low temp., conc. depend. 2−51044
Cu-Sn alloys, α-phase, low temp. electronic sp. ht. 2−43982
Cu-Zr-Cr alloy, rel. to precip. processes 2−50933
Cu, 1-30 K, effect of temp. scale differences on anal. of heat capacity data 2−47751
Cu, between 300 and 900 K 2−57065
Cu, high purity, 2-1357K 2−54048
Cu_3Au, low temp. electronic sp. ht., ordering influence 2−47750
$Cu(NH_3)_4SO_4.NH_3$, exchange integral variation with lattice spacing obs. 2−54353
^{63}Cu crystals, anharmonicity manifestations in comparison with phonon model 2−64855
DyAl garnet, mag. sp. ht. 2−43983
F_2 crystal, calc. using lattice vibr. model 2−43960
Fe-Al alloy, diffuse X-ray scatt. and temp. depend. of sp. ht. 2−56654
Fe-Al system, β-solid solns., order-disorder processes obs. 2−54002
Fe-Rh, Fe-Rh-Ir alloys, electronic sp. ht., magnetic contrib. 2−64856
Fe-Si solid solns., ordering reactions and meas. of specific heat capac. 2−71745
Fe and Fe-Cr alloys, mag. crit. pt. phenomena 2−57290
Fe(II) complex, $Fe(phen)_2(NCS)_2$, due to low spin $^1A_1 \rightleftharpoons$ high spin $^5T_2$ transition 2−75240
$Fe(NH_4SO_4)_2.6H_2O$, thermal variation, ligand field energy pattern 2−54292
α-Fe_2O_3 and natural haematite, true heat capacity, mag. component 2−43984
$(Fe_2O_3)_{0.79}.P_2O_5$, glasses, antiferromag. interactions 2−75237
$Fe_{1-x}Ti_{1\|x}$, rel. to resist. minimum 2−44252
GaAs, below 30 K, analysis using magnetically smoothed temp. scale 2−68249
$Ga_2O_3(c)$, drop calorimetry and diff. scanning calorimetry 2−54047
GaSb, below 30 K, analysis using magnetically smoothed temp. scale 2−68249
Gd, Curie pt. anomaly 2−57291
GdIG, temp. depend., in mag. field, rel. to sublattic rotation 2−61508
β-Gd_2MoO_4, from 0.4 to 4.2K along b crystal axis 2−51277
β-$Gd_2(MoO_4)_3$, electrically polarized 0.4 to 4.2K, up to 90 kG along a crystal axis, and entropy 2−44290
$Gd(OH)_2$, magnetic specific heat, and ac susceptibility measurements using a r.f. tunnel diode oscillator 2−68513
Ge, angular force model 2−74969
Ge, rel. to homology with Si 2−84190
$Ge_xAs_{40-x}S_{60}$ glass 2−51045
$GeMnO_3$, Neel pt. phenomena 2−44300
H_2, D_2, and H_2-D_2 system, Debye temp. and EQQ interactions 2−43985
He, submonolayer on Ar and Ne, two phase model 2−80581
^3He, λ transition to ordered antiferromag. phase 2−56537
^3He, review 2−80515
^4He, submonolayer on Cu and Ar and Ne monolayers on Cu, two dimensional Debye behaviour 2−80580
InSb, below 30 K, analysis using magnetically smoothed temp. scale 2−68249
K_2CuF_4, two-dimens. ferromagnet 2−81239
KH_2AsO_4 and KD_2AsO_4, rel. to ferroelec. transitions 2−47985
$KH_{2(1-x)}D_{2x}PO_4$, ferroelectric crystal, excess thermal capacity above transition temp. with high D conc. 2−84364
$KMnF_3$, 70-210K, anomalies and phase transitions 2−71747

Specific heat continued
  solids continued
    $KNiF_3$, Neel point determ., elastic, magneto-optical and heat capacity meas. 2−72219
    $K_2Pt(CN)_4Cl_{0.3}.n(H_2O)$, one-dimensional, low temp. sp. ht. 2−71746
    $LaAl_2$, Laves, phase, electronic contrib. 2−57067
    $LaRu_2$, superconductor, low temp. ht. capacity 2−77879
    La_3X, (X=Al, Ga, In, Tl, Sn, Pb), rel. to supercond. behaviour 2−61244
    Li, b.c.c., from Krasko-Gurskii model 2−68227
    LiCl, heat capacity, size-disparity anharmonicity 2−71748
    LiF, deformable shell model studies 2−50995
    $LiYF_4:Er^{3+}$, Schottky specific heat calc. 2−51240
    $Li_{1-x}Zn_{2x}Fe_{5-x}O_8$, ferrite, high temp. obs. 2−54049
    Mg-Cd and h.c.p. alloys, electronic sp. ht. 2−47859
    $(Mn_{1-x}Fe_x)Be_2$ meas. at 1-4 Kelvin 2−57059
    Mo, temp. dependence near melting point 2−57066
    Mo alloys, A15 type, rel. to supercond. transition temp. and cryst. order 2−61245
    N_2 crystal, calc. using lattice vibr. model 2−43960
    $NaNO_3$:Ca, near critical point, obs. 2−60542
    Nb, temp. depend. derived 2−54038
    $NdNi_2$, $NdAl_2$, $NcDo_2$, Laves phases, hyperfine contrib., cryst. field and exchange effect model 2−57067
    40 at.% Ni alloy, below 3K, effect of clusters and quenching 61103 2−61103
    $Ni(NH_3)_2.Ni(CN)_4.2C_6H_6$, rel. to mag. susceptibility, 1.2-4.2K 2−75241
    $Ni(NO_3)_26NH_3$, antiferromag. transition obs. 2−65185
    $Ni(NO_3)_26NH_3$, order-disorder transition pt. anomaly 2−61036
    NiS, hexagonal, heat capacity and metal-nonmetal transition 2−47754
    $NiSnCl_6.6H_2O$, mag. heat capacity, 0.35-4.2 K 2−78039
    $Ni_{3\pm x}Te_2$, temp. range 298-900K, including transition behaviour 2−57068
    $Ni_{1-x}Zn_xFe_2O_4$, ferrite, high temp. obs. 2−54049
    O_2 crystal, calc. using lattice vibr. model 2−43960
    Pb-Ag-Pb layers, heat capacity at ^3He temps., proximity effect obs. 2−81041
    Pb-Mn alloy, 0-300°C, determ. by monotonic heating method 2−51046
    Pb-Sn alloy, eutectic, lamellar, proximity effects, sp. ht. obs. 1.25-8 K 2−68369
    Pb, 0-300°C, determ. by monotonic heating method 2−51046
    Pb, Cp to Cv conversion, using dilation correction 2−54050
    Pb, molar heat content, electrical resistance, meas. by pulse method 2−64914
    $PbMo_6S_7$, superconducting properties, heat capacity 2−81051
    Pd-Co(Fe)(Mn) dil. alloys, mag. ordering obs. 2−81246
    Pd, supercond., rel. to electron-phonon enhancement factor detn. 2−64932
    $Pd_{0.775}Cu_{0.06}Si_{0.165}$ glassy alloy, electronic and lattice contribs. to sp. ht., excess, 2-18K 2−80916
    Pr, hyperfine sp. ht., mag.-ground-state props. of single crysts. 2−48078
    Pr, nuclear heat capacity, magnetic properties 2−65121
    $PrCu_2$, spontaneous mag. order, 54 mK 2−44225
    Pr_3Tl and $(Pr_{1-x}La_x)_3Tl$, induced-moment system, anomalies at Curie temp. 2−72154
    Pr_3X, (X=Al, Ga, In, Tl, Sn, Pb), rel. to supercond. behaviour 2−61244
    Pt-Co dil. alloys, nucl. sp. ht., low temp. 2−43986
    Pt, supercond., rel. to electron-phonon enhancement factor detn. 2−64932
    Pt pulsed electron beam measurement 2−54039
    Sc, supercond., rel. to electron-phonon enhancement factor detn. 2−64932
    Sc_3In, zero field and 1.3 kOe 2−81258
    Se-As glaases, obs. near glass transformation point 2−61104
    Se, vitreous, anomalous sp. ht. below 1 K 2−43987
    Si, rel. to homology with Ge 2−84190
    SiO_2, vitreous, heat capacity rel. to struct. props. 2−47061
    Sm, isotopically enriched, electronic sp. h.t. 0.45-6K 2−68250
    Sn, below 30 K, analysis using magnetically smoothed temp. scale 2−68249
    $SnCl_2.2H_2O$ and $2D_2O$, anomalous behaviour at phase transition, 155K 2−84212
    $SnMo_4S_6$, heat capacity 2−81051
    $SnNbS_3$, at low temp., supercond. 2−68371
    $SnNbSe_3$, at low temp., supercond. 2−68371
    $SnTaS_3$, at low temp., supercond. 2−68371
    $SrMoO_4:Er^{3+}$, Schottky specific heat calc. 2−51240
    $SrTiO_3$, from phoon freq. distrib. 2−77761
    Ta-10%W alloy, pulse heating obs., 1500-3200K 2−57069
    Ta, pulsed electron beam murement 2−54039
    $Tb(OH)_2$, magnetic specific heat, and ac susceptibility measurements using a r.f. tunnel diode oscillator 2−68513
    $TbPO_4$, low temp. mag. props. study 2−78046
    Th_4H_{15}, rel. to superconductivity 2−54143
    ThN, mag. sp. ht., 7 to 300K 2−43988
    TiC_xO_{1-x} solid solns., low temp. heat capacity 2−43989
    $Tl_2O_3(c)$, drop calorimetry and diff. scanning calorimetry 2−54047
    $TmAsO_4$, near Jahn-Teller transition, evidence of low lying excited state 2−61105
    $Tm_2(SO_4)_3.8H_2O$, heat capacity 0.08-20K, exchange induced magnetiz. obs. 2−64857
    $U(C_{1-x}N_x)$, rel. to electronic props. 2−57268
    $UO_{2\|x}$, high temp. data interpreted 2−54051
    V, supercond., rel. to electron-phonon enhancement factor detn. 2−64932
    V_3Au, origin of cryst. order effect on supercond. T_c 2−64952
    VC_x, rel. to vacancy ordering 2−54004
    W, high temp., calorimetry and rapid transient technique obs. 2−54083
    W, temp. dependence near melting point 2−57066
    XeF_4, 5 to 350K, heat capacity, thermodynamic functions, entropy 2−80411
    Y, supercond., rel. to electron-phonon enhancement factor detn. 2−64932

Specific heat continued
  solids continued
    Zn, below 30 K, analysis using magnetically smoothed temp. scale 2−68249
    ZnO(c), drop calorimetry and diff. scanning calorimetry 2−54047
    $ZrC_{0.95}$, low temp., differences from Debye model 2−80920

Spectra
    see also Absorption/light; Astronomical spectra; Atmospheric spectra; Chemical shift; Colour; Isotope shift; Mass spectra; Scattering/light, Raman spectra; Spectrochemical analysis; Spectroscopy; Stark effect; X-ray spectra; Zeeman effect
  absorption, derivation by wavelength modulation method 2−75283
  analysis by iterative deconvolution, FORTRAN computer program 2−63054
  beam, modulated by circular aperture, Fourier spectra 2−79315
  boundary conditions in exciton absorption region 2−65244
  continuous use of impulse source, calibration of luminosity in vac. U.V. 2−45827
  cross-relaxation, in spectrally inhomogeneous system, equations 2−64899
  cross-relaxation due to resonance transmission of excitations in spectral-inhomogeneous medium of imputiry centres 2−84525
  crystals, centrosymmetric and noncentrosymmetric, optical phonon spectra 2−68656
  disperse systems, link with solid-state spectra through weak absorption 2−53460
  electron microscope, energy analysing, superposition effects 2−79015
  electroreflectance line-shape analysis 2−78090
  emission of radiation by charged particles reflected from solid surfaces 2−54397
  equivalent line width and absorption coefficients, expression derived 2−42265
  estimator class, nonlinear functions of covariance matrix 2−63050
  even and odd, Dirac theory of one-dimensional symmetrical potential 2−41493
  even and odd, Schrodinger theory of one-dimensional symmetrical potential 2−41492
  fine structure constant, mathematical description in terms of group theory 2−78779
  fluid, convective instability, light scatt. study 2−67609
  gases, absorption, in 5-6 μm range with tunable spin flip Raman source 2−42264
  hydrogen bonded liquids, review of i.r. and Raman spectroscopy relating to structure properties 2−43315
  inhomogeneous absorber, photon-electron conversion during bremsstrahlung irradiation 2−44018
  insulating materials, i.r. absorption, application to aging processes measurement 2−68827
  ionic crystals, fine structure, exciton zones by exciton echo method 2−54395
  ions in laser-produced plasma, energy spectra 2−80253
  i.r. in lattice vibration region 2−61070
  lamps, emission spectra, chemical actinometer for u.v. region 2−51462
  laser, saturated optical absorption technique for meas. of optical resonances 2−79231
  laser excitation, pulse and continuous operation, review 2−45818
  liquid, intermol. interactions obs. 2−77431
  many-photon absorpt. in crystals and their applications, review 2−75282
  microwave double resonance, signal saturation phenomena 2−63204
  microwave frequency spectrum emitted by relativistic electron moving in spatially modulated magnetic field 2−66703
  molecular crystal, excitation spectra of charge-transfer complexes 2−68631
  molecular crystal with 2 exciton state regions, absorption spectrum 2−72310
  molecular crystals, electron-vibrational spectra, review 2−57345
  molecular crystals, fine structure, exciton zones by exciton echo method 2−54395
  molecular crystals, singlet spectrum coupling to 2-particle excitations 2−51327
  molecular crystals, substitutionally disordered 2−48157
  molecular crystals, temp. depend. of absorpt. bands intensities at Fermi resonance 2−81373
  moving particle, emission and absorption, relativistic kinetic temperature 2−66474
  natural vibr. of a shell of revolution 2−45456
  non-uniform broadening of spectral lines, effect on formation process of boson avalanches 2−66906
  optical absorption band shapes of Jahn-Teller systems with orbital doublet, path integration method 2−65198
  optical absorption band shapes of Jahn-Teller systems with orbital doublet, semiclassical approx. 2−65197
  paramagnet, van Vleck, excitation spectrum 2−61479
  phonon-induced shift of spectral lines, Jahn-Teller splittings 2−75245
  photo-protective glasses sensitized by AgCl and AgBr 2−52503
  plasma, determ. of radial distribution of intensity of lines 2−60239
  plasma, high temperature, continuum emission in vacuum u.v. 2−53196
  plasma, line oscillator strengths of spectral lines which are not optically thin 2−60242
  plasma, Stokes line generation during laser irrad. due to Compton effect 2−74369
  plasma, turbulent, interpret. by Blokhintsev theory 2−64061
  plasma spectral intensities and their interpretation 2−74370
  pulse discharge in cylindrical magnetron diode 2−60299
  radiation multipole, ultra high speed photography 2−45620
  Rayleigh approx., absorption and emission cross sections of nonspherical particles 2−64477
  red highway flares, luminous power spectrum 2−59270
  reflection, at large angles of incidence, in vacuum u.v. 2−66855
  reflection for det. of optical constants 2−42189
  Renner systems, optical lines and spectral curves 2−81393
  Renner-type system, with strong vibr. coupling, optical absorpt. band shape determ. 2−65248
  semiconductor, electronic transitions, opt. consts. evaluation, review 2−72291

Spectra continued
semiconductor, nonparabolic band, free carrier light absorp. theory 2−75285
semiconductors class III−V, pressure depend. calc. of E_2 reflectivity 2−72297
shaping with parity sequences, digitally generated holographic memories 2−66782
smog and synthetic smog, comparison of i.r. spectra 2−51620
solid, photon-phonon interactions 2−72318
solids, exchange interaction meas. technique 2−61730
solids, optical versus thermal transitions at high pressure 2−51328
solids and surfaces, data logging using spectrophotometer interfaced to minicomputer 2−58945
solvated electrons, absorpt. spectrum resolution, band shapes 2−67831
terrestrial, computer applications 2−84712
trace element analysis in arc plasma, spectral line intensity depend. on magnetic field 2−48356
transition radiation, integral equation approach 2−81439
trapped electrons in spherical pots., photodetachment spectra 2−53435
two photon absorption by a crystal in elec. field 2−65243
Voigt line profile, rational approx. 2−41524
ionizingH plasma, continuum emission in visible and u.v. 2−80247
H plasma, Stark broadening of Balmer lines 2−64278
Li plasma, recombination continuum 2−53197
W, standard for spectral emissivity 2−54087

atoms
see also Atoms/excitation; Atoms/structure; Auger effect; Russell-Saunders coupling
absorption, computer programs for calc. position and optical density of each band 2−46418
absorption due to transitions between weak monochromatic waves in presence of strong nonmonochromatic field 2−83202
absorption line profile of atom in field of strong noise radiation 2−77002
absorption spectroscopy in flame, population of atomic levels determ. 2−49939
alkali ground-state atoms, fine and hyperfine structure in laser saturation spectroscopy 2−46411
alkali metal, transition probabilities between hyperfine levels 2−56088
alkali metals, calc. of absorption line profiles and satellite bands caused by inert gas perturbing atom 2−70568
alkalies in inert gas atmospheres, quadratic hyperfine pressure shift 2−77013
antiprotonic, strong-interaction effects 2−79965
astrophysical plasma and the interpretation of stellar spectra 2−75703
atomic spectroscopy, review 2−46419
Auger and X-ray transition probabilities calc. for elements Z=4-54, Hartree-Fock model 2−64008
Auger lines, X-ray photoelectron spectrometry 2−52937
beam-foil spectroscopy, modulated decays, zero-field oscillation obs. 2−59895
beam-foil spectroscopy, velocity dispersion and steepest slope theorem 2−70574
bibliography on energy levels and spectra, Jul 1968 to Jun 1971 2−83206
calculation, applic. of molec. wave functions, review 2−50007
canonical bases of Lie groups, use in atomic spectroscopy theory 2−79935
cascade, polarization correlations of emitted photons, exptl. limitations to validity of semiclassical radiation theories 2−46415
coherent radiation, renormalized frequency shift 2−46417
collision broadening of spectral lines, long-range and short-range potentials 2−42839
decay curve analysis, upper bound on mean lives 2−70573
double resonance, rel. to coherence effects 2−59912
double-photon transitions in microwave spectroscopy 2−70657
electron, low energy, book 2−41925
electron impact excited, line radiation polarization variation with scattering angle 2−46457
electron-atom collisions, Stark broadening, one- electron approximation 2−42757
electronic struct. comparison in X-ray and electron spectroscopy 2−46455
electrons ejected from atoms by protons, character of interference of resonances with continuum 2−70618
emission, spectral data review 2−52481
energy flow from atomic dipole in classical electrodynamics 2−79942
fifth period elements, e.u.v. spectra, energy levels 2−64001
forces of oscillators, meas. by more sensitive method of 'hooks' 2−49928
frequency pulling between two spectral lines, calc. 2−46410
gaseous, correlation with absorption spectra of atoms isolated in noble gas matrices 2−52902
gases influence of elastic collisions on broadening 2−83418
glow discharges in air, obs. of near i.r. emission spectrum 2−46798
Hartree Fock Slater model nonrelativistic, Auger and X-ray transition probabilities 2−64008
highly ionized, spectra and lifetimes studied by vacancy cascade spectroscopy 2−42722
hyperfine structure, spectroscopy 2−52490
inert gases, correlation effects in Auger spectrum 2−46456
interactions between generating lines in a cascade 2−66735
ions, optically pumped, study of r.f. spectra 2−77009
ions, vacuum u.v. absorption meas. using new continuum light source 2−77001
ions in laser produced plasma, spatial distrib. determ. from spectral line emission 2−80272
Kr, relative transition probabilities 2−63996
L X-ray transition probabilities, tabulation 2−46406
Lamb shift, displacement of atomic levels, i.r. divergences and computational problems 2−64009
laser saturation spectroscopy, theory 2−79907
laser saturation spectroscopy of alkali ground-state atoms, fine and hyperfine structure 2−46411
laser spectroscopy applics., high precision techniques 2−77004

Spectra continued
atoms continued
level broadening due to absorption of radiation 2−42716
level crossings, vanishing of dipole matrix elements 2−46414
lifetime studies, using beam-foil light source 2−63994
lifetimes of states excited by electrons, system for direct meas. 2−52926
light elements, algorithms for continuous opacities 2−56089
line broadening, convergent theory in impact approximation 2−52918
line shift, forced transitions induced by collision with fast charged particle 2−52905
many-electron system, lower bounds for energies 2−56099
mean lives and g values of beam-foil excited levels, suppression of optical cascading effects 2−79910
metals, X-ray absorption edges, chemical shifts and effective nuclear charge 2−74208
muonium hyperfine splitting in low-pressure Ar determ. from field independent Zeeman transitions 2−42822
muonium hyperfine structure interval at strong magnetic field, discussion of errors and theory of resonance line shape 2−42821
muonium in inert gas atmospheres, quadratic hyperfine pressure shift 2−77013
noble gas mixtures, glow discharge emission in short wavelength vacuum region 2−83642
optical coherence phenomena, macroscopic, rel. to n.m.r. studies 2−59907
optical line modulation, ion acoustic waves in plasma 2−70956
overlapping spectral lines, criterion 2−52903
photoelectron, chemical effects on linewidths 2−70597
photon exit probability distribs. 2−59900
two photon spectroscopy, improved calc. method 2−49010
positronium, fine-structure interval of ground state 2−79964
pressure broadening, unified quantum statistical formulation 2−67382
pressure broadening as example of relaxation using cumulant expansions 2−76987
radiative transitions, low-energy free-free cross section, polarizability effect 2−59901
rare earths, 4f energy determination using X-ray and photoelectron spectroscopy 2−49926
relativistic effects in transition probabilities, hyperfine structures and isotope mass shifts 2−77005
resonance excitation diffusion, stimulated emission effect 2−59903
resonance radiation scatt., linear systems analysis applic. 2−63999
selective excitation, laser diagnostics of K plasma 2−70928
sorption effects in presence of strong wall interaction 2−46409
spin-flip resonance, theoretical refinements 2−46447
spontaneous emission by excited system, interference between different channels 2−79886
Stark broadening, electron correlations in unified model 2−42720
stripping, for study of impulse plasma accelerator 2−46768
three energy level system, density of excited states with repeated passage of light 2−52910
transient phenomena, detection by optical methods 2−59906
transition probabilities, bibliography 2−42721
transition probabilities and line shapes, meas. 2−70080
transition probabilities in collisions using Landau-Zener model 2−49967
with tunable dye lasers, pulsed and c.w. 2−79941
two level atom, incoherent source model 2−79895
two-electron ions, fine struct. singlet-triplet correction 2−83210
two-level system, scattering of intense light studied using Green's function 2−49938
two-level system, spontaneous emission analysis in rot. wave approx. 2−82460
two-level system, spontaneous emission analysis in rot. wave approx. 2−82461
two-level system, theory of saturated-absorption line shapes 2−70569
u.v. absorption spectroscopy using synchrotron light source 2−76549
Voigt profile, speed dependent, including shift parameters 2−67380
wavelengths and classification of emission lines due to $3s^23p^n$-$3s3p^{n+1}$, $3s^23p^n$-$3s^23p^{n-1}3d$ and other n=3-3 transitions 2−42729
X-ray, characteristic emission in O ion collisions with atoms with $13\leqslant Z\leqslant 79$ at 7 to 40 MeV 2−70629
X-ray, ultrasoft reflection and refraction in 100 to 1000 eV region 2−46416
Z=12 to 21, electronic correls. effect on KLL Auger lines 2−52938
Z=35-85, calc. of Auger group rates and fluorescence yields for vacancy in 3p or 3d shell using nonrelativistic HFS model 2−70572
Z=62-92, meas. of LX-ray transition probabilities, comparison with results calc. using RHFS and RCS potential 2−42718
Zeeman spectroscopy utilizing laser in mag. field 2−63428
Ag I lines, oscillator strengths 2−64011
Ag vapour, high-current hollow cathode discharge, radiation, effect of reson. and recomb. 2−74423
Al, far-u.v. absorpt., discrete features identification 2−67388
Al, h.f.s. in ground multiplets, mag. dipole radial parameters 2−70576
Al, plasma, laser produced, IV spectra, line identification 2−74212
Al III, elec. quadrupole transitions, multiplet strengths 2−56102
Ar-Ne discharge detection of Penning ionization by laser perturbation spectroscopy 2−80373
Ar-O_2 mixture, proton bombardment, dependence on energy 2−74235
Ar, absorption coeff., in wall stabilized arc at atmos. press. 2−70575
Ar, $L_{2,3}$ X-ray emission spectrum, satellite spectrum 2−74214
Ar, plasma, electrodeless discharge, high frequency, high press., line profile 2−46423
Ar, proton bombardment, dependence on energy 2−74235
Ar, pulsed plasma, containing 1-2% H_2, particle conc. and temp. determ. 2−49941
Ar, relative transition probabilities meas. by optical absorption 2−64012
Ar, small angle electron impact spectra, optical sums 2−70612
Ar electrodeless discharge 2−50228
Ar I, relative transition probabilities, optical absorpt. determ. 2−70582

Spectra continued
atoms continued
Ar I isoelectronic sequence, Hartree Fock predictions of ^1P term in p^5d configurations 2−46422
Ar I line halfwidths in wall-stabilized cascade arc 2−67387
Ar II-Ar VIII, excited lifetimes, beam foil spectra radiative decay times 2−79873
Ar II, excitation mechanisms at near laser conditions 2−77308
Ar II, transition branching ratios 2−83194
Ar I(II) radiative lifetimes meas. in electron tube using oscillograph method of delayed coincidences 2−77006
Ar thermal excitation functions of intense spectral lines in three different regions of spectrum 2−52911
Ar XVII, lifetime of 2^1S_0 state 2−42809
Ar$^+$ ion beam, optical spectra Zeeman splitting 2−70577
Ar(II), calc. of transition probabilities and lifetimes for radiative transitions using multi-configuration model 2−64004
Au, L X-ray production by 0.5-3.0 MeV protons, relativistic effects 2−52913
Au vapour, high-current hollow cathode discharge, radiation, effect of reson. and recomb. 2−74423
B, far-u.v. absorpt., discrete features identification 2−67388
B. h.f.s. in ground multiplets, mag. dipole radial parameters 2−70576
Ba, oscillator strengths for resonance transitions 2−79875
Ba I, auto-ionization resonance structures, high resolution photometry 2−79943
Ba plasma, laser-generated, spectral line parameters 2−67643
Be, far-u.v. absorpt., discrete features identification 2−67388
Be, polarization of dipole radiation emitted by electron impact double excited states 2−70607
Be I, configuration-interaction calcs. on 2sns ^1S and 2p3p $^{3,1}P$ series 2−70578
Be III, term system 2−42806
Bi I, radiative lifetimes 2−63997
Bi I, radiative lifetimes of excited levels belonging to $6p^27s$ and $6p^26d$ configurations by Hanle method 2−49942
Br isoelectronic sequence, anal. 2−79933
C, d.c. arc, in ext. mag. field, electron temp. rel. to line intensities 2−50238
C, far-u.v. absorpt., discrete features identification 2−67388
C, linewidths of 1s photoelectron energy spectra 2−70602
C, of d.c. arc, effect of mag. field on line intensity 2−49943
C, reson. line attenuation identification of atoms produced in nitrogen + org. gas reactions 2−61767
C I 2478 line, Stark half-width estimation 2−59916
C II, vacuum u.v. absorption meas. using new continuum light source 2−77001
C ions, radiative lifetimes for u.v. transitions by pulse decay method 2−46413
C^{5+}, Lamb shift studied via motional electric field quenching of $2^2S_{1/2}$ state 2−70633
C248α transition in W51 radio source 2−75815
Ca, matrix isolated, absorption spectrum 2−49944
Ca, oscillator strengths for resonance transitions 2−79875
Ca, polarization of dipole radiation emitted by electron impact double excited states 2−70607
Ca II plasma, Stark broadening and shift of lines 2−60245
Ca$^+$, measurement and calculation of Stark broadening parameters for resonance lines 2−42727
Ca$^+$ reson. lines, electron impact broadening 2−59914
Cd-Ar vapour, phase-matched, vacuum u.v. radiation generation 2−79904
Cd, L-shell photoelec. cross sections of gamma-rays 2−76967
Cd, magnetic depolarization of fluorescence lines, Hanle effect 2−79860
Cd, relative isotope shift (112-114)/(110-112) of 4416Å spectral line 2−64016
Ce isotopes, arc and spark spectra, ^{140}Ce-^{142}Ce shifts 2−79893
Ce isotopes, arc and spark spectra, isotope shifts 2−79892
Ce^{3+}, analytical SCF wavefunctions for ground and some excited states, calc. of oscillator strengths for optical transitions 2−52915
CeI and CeII, infrared spectra between 0.8 and 2.4 μm 2−76969
Cl II, new wavelengths and energy levels 2−79946
Co, highly-ionized, far u.v. spectra, rel. to solar lines 2−83189
Co, resonance lines, intensities using different spectral lamps 2−52492
Co I, hyperfine structure and hyperfine broadening 2−79940
Co XVII, multiplet strengths for electric quadrupole transitions calc. using HF orbital wave functions 2−42728
Cr, highly ionized, for u.v. spectra, rel. to solar lines 2−83189
Cs, 7 $^2P_{1/2}$ hyperfine structure, core polarization, optical double resonance obs. 2−74213
Cs, cascade-decoupling meas. of excited S-state hyperfine structures 2−52922
Cs, determ. of g_j factor in $7^2P_{3/2}$ state by optical double resonance in strong magnetic field 2−52916
Cs, emission profiles of resonance lines broadened by collisions with inert gases, extreme-wing line broadening, adiabatic potentials 2−70622
Cs, ionized vapour, electron density determ. from spectral line mixing 2−46792
Cs level population determ. using flame atomic absorption spectroscopy 2−49939
Cs$^-$, continuous absorption coeff. contribs. from bound-free and free-free transitions 2−70586
CsI, investigation of $np^2P_{3/2}$ level sequence by level crossing spectroscopy 2−79920
^{113}Cs, Stark effect investigation of third excited $^2P_{3/2}$ levels in first spectrum, tensor polarizability determ. 2−70591
^{133}Cs, phase destruction detection of ground state hyperfine transitions and population inversion with GaAs lasers 2−70599
Cu, d.c. arc effect of mag. field on line intensity, 230-790 Oe 2−49943
Cu, gaseous, correlation with absorption spectra of atoms isolated in noble gas matrices 2−52902
Cu, resonance lines, intensities using different spectral lamps 2−52492
Cu arc, free burning with 1-15A current, atom population and electron concentration 2−71064

Spectra continued
atoms continued
Cu I lines, oscillator strengths 2−64011
Cu vapour, high-current hollow cathode discharge, radiation, effect of reson. and recomb. 2−74423
Cu^{2+}, analytical SCF wavefunctions for ground and some excited states, calc. of oscillator strengths for optical transitions 2−52915
D, trapped atoms, interpretation of microwave power dependence of differential saturation of hyperfine components 2−49946
Dy II, classification of even levels 2−67390
Dy II, classification of odd levels 2−67389
Er, photoabsorption in vicinity of 3d edges 2−76988
Er, relative isotope shifts in u.v. region, determ. of coeff. of nuclear deformation and internal quadrupole moment 2−49947
Er III, emission spectrum analysis 2−70580
F, Li-like, classification of spectra of autoionization electrons 2−49953
Fe, beam-foil spectrum, hydrogenic transitions in multiply charged ions 2−67391
Fe, resonance lines, intensities using different spectral lamps 2−52492
Fe emission line wavelengths, and solar far u.v. spectrum and forbidden line identity 2−42729
Fe group, spin-dependent interactions in $3d^n$ configurations of third spectra 2−46427
Fe I, Fe II resonance transitions, radiative lifetimes, applic. to Fe abundance det. in sun and QSO PHL 938 2−58547
Fe I ionization and excitation equilibrium in solar atmosphere 2−58559
Fe IX to XVI, classification of transitions 2−49948
Fe XV, solar e.u.v. spectrum rel. to theory and collisional excitation 2−78586
Fe XVI, multiplet strengths for electric quadrupole transitions calc. using HF orbital wave functions 2−42728
H-Like atoms, exact, matrix elements and exact selection rules 2−42794
H- calc. of low-lying resonance in 2^1P state 2−46476
H, 1s-2s and 1s-2p transitions, cross section calc. in adiabatic approx. 2−46481
H, adiabatic theory of Stark broadening used to describe transitional frequency band between impact and quasi-static limits 2−46474
H, collisions with electrons, Stark broadening, one-electron approximation 2−42757
H, emission, in rotating electric field 2−59941
H, emission spectra of electronic energy levels 2−45206
H, in plasma, line broadening, quasistatic and impact approx. 2−52948
H, linear Stark effect due to resonant interactions of static and dynamic fields 2−64061
H, Lyman-α line profile meas. in arc experiment 2−74243
H, multiphoton transitions between 1S and 2P levels 2−67418
H, n=3 state, r.f. spectroscopy meas. of resonance narrowed Lamb shift 2−52947
H, spectrum generating current including spin-orbit and Lamb shift 2−59943
H, Stark broadened Lyman-α lines, electronic shifts 2−64059
H, Stark profile of Ly-α line in the region of transition from impact to quasi-static broadening 2−46475
H, time-dependent theory of Stark quenching of 2S states (cc He, time-dependent theory of Stark quenching of 2S states 2−49974
H, wings of Stark-broadened lines, Holtsmark's 5/2 power law 2−74242
H $\alpha^2\ln\alpha^1$ recoil correction to hyperfine splitting of ground state, estimation of proton polarizability 2−83214
H beam-foil excited, obs. of fine structure interference effects in Lyman β radiation 2−64062
H glow discharge columns, spectral line intensity in mag. field 2−52919
H in plasma, time evolution operator in semiclassical theory of Stark-broadening 2−42793
H line electron broadening, boundary of quasistatic region 2−77022
H plasma, dense, Lyman-α line asymmetry 2−70635
H plasma, expanding, population inversion of excited atomic levels 2−46709
H plasma, observed discrepancies in central region of Hβ profile at low electron densities 2−70631
H plasma, population inversion 2−49973
H$_\alpha$, optical resolution of fine structure and obs. of Lamb shift by laser saturation spectroscopy 2−52946
H(2p) vacuum u.v. excitation by electron impact on H_2, polarization free meas. of Lyman α radiation 2−80120
Hα,β and γ spectral line profiles of solar chromospheric lines on the disk 2−48810
He-Ar mixtures, collision induced- absorpt. near $\lambda = 1$ mm 2−77084
He-CO_2-N_2 deexcited plasma, quantitative emission spectroscopy 2−79206
He-Cd laser, determ. of wavelength for centre of Lamb dip 2−66754
He-like ions, observability of hyperfine structure and Lamb, nuclear-volume shifts in 1snl-1snl′ transitions 2−52952
He, 1S-2^3S transition, cross section calc. in adiabatic approx. 2−46481
He, 2 ^3P fine-structure splittings 2−52951
He, 44 71.48 Å line, plasma broadened, distant electron collisions effects 2−67429
He, atmospheric arc, determ. of thermal conditions in asymptotic region 2−77317
He, beam-foil excited, 40 keV, meas. of relative level populations 2−52955
He, excitation of $1'S \rightarrow 1'S$, $2'S$ and $2'P$ transition by electron collisions, application of second Born approx. 2−56132
He, fine-struct. splittings, nucl.-motion corrections 2−77020
He, fine structure splitting of deepest triplet P state, quantum-electrodynamical corrections 2−42810
He, quench radiation in const. elec. field 2−77025
He, relative absorpt. of 3889 and 10830 Å lines 2−59949
He, singlet + triplet mixing in n=3 states excited by proton impact 2−56130
He, Stark profiles of forbidden and allowed transitions in dense, laser produced plasma 2−42805

Spectra continued
- **atoms** continued
  - He arc at atmospheric pressure, spectroscopic intensity measurement 2−43225
  - He glow discharge columns, spectral line intensity in mag. field 2−52919
  - He I, energies and lifetimes of doubly excited states meas. using beam-foil technique 2−52954
  - He I line widths and shifts, line broadening calculations 2−52918
  - He II, improved Stark profile calc. for lines between 256 and 4686 Å 2−46477
  - He isoelectronic sequence, dynamic polarizabilities and mean excitation potentials 2−77026
  - He isoelectronic sequence, oscillator strengths 2−56126
  - He isoelectronic sequence, oscillator strength for allowed nd-n′f transitions 2−56125
  - He$^+$, intensity decay curves, cascade-induced alignment changes 2−42753
  - He$^+$, meas. of rate coeff. for recombination with electrons in pulsed afterglow 2−70643
  - ^{4}He$^-$, r.f. reson. obs. of fine struct. transitions 2−67428
  - He$^+$ + H_2 collisions, low-energy, Lyman and Balmer lines, emission cross sections 2−67436
  - Hg, self broadening of Hanle signals, backscattered light obs. 2−59932
  - Hg glow discharge columns, spectral line intensity in mag. field 2−52919
  - Hg vapour, absorpt. coeff. meas. in reson. region 2−46428
  - Hg vapour, selective refl., crossing effect between Zeeman sublevels of isotopes 2−79900
  - Ho, arc spectrum, configs. determ. 2−64015
  - Ho, u.v. absorpt. and i.r. emission, classification 2−52920
  - In spectral lines temperature effects in pressure broadening in flames 2−67413
  - K-Cs, broadening of principal series lines 2−56117
  - K-K collisions, broadening of principal series lines 2−56117
  - K, cascade-decoupling meas. of excited S-state hyperfine structures 2−52922
  - K, in premixed H_2-O_2-N_2 flame, emission noise spectrum 2−49952
  - K I, natural lifetimes and hyperfine structure for ^{39}K in 5p $^2P_{3/2}$ and 6p $^2P_{3/2}$ levels by resonant light scattering 2−46430
  - K$^-$, continuous absorption coeff. contribs. from bound-free and free-free transitions 2−70586
  - K$^+$ energy spectra, laser-produced ions 2−52921
  - KI, variations in relative intensities of lines in 4p-3d transition in i.r. region using hollow-cathode discharge 2−70585
  - Kr, absorption in range 330 to 600Å 2−49949
  - Kr electrodeless discharge 2−50228
  - Kr I isoelectronic sequence, Hartree Fock predictions of ^1P term in p^5d configurations 2−46422
  - Kr multi-charge ions moving in an impulse discharge 2−50223
  - La, photoabsorption in vicinity of 3d edges 2−76988
  - La IV, Hartree-Fock calc. for $4d^95s^25p^64f$ configuration 2−46431
  - Li-, photodetachment cross section of Li- 2−49984
  - Li, beam-foil excited, 40 keV, meas. of relative level populations 2−52955
  - Li, polarization of dipole radiation emitted by electron impact double excited states 2−70607
  - Li, radial, lower bounds for energies 2−56099
  - Li I, doubly excited states, energies and lifetimes 2−42735
  - Li II, obs. of transition between doubly excited state using beam-foil technique 2−52954
  - Li transitions, model pot. calcs. 2−76976
  - Li$^-$, continuous absorption coeffs. contribs. from bound-free and free-free transitions 2−70586
  - Li$^-$ ion, continuous absorpt. coeff. rel. to temp. and wavelength 2−70583
  - Li$^+$, intensity decay curves, cascade-induced alignment changes 2−42753
  - Li$^+$, Li^{2+} ions, beam foil excited, u.v. spectra, radiative mean lives 2−67420
  - Lu I, absorp. line series, u.v. region 2−56100
  - Lu I, theoretical study of odd configurations $5d6s6p + 6s^27p + 5f6s^2 + 5d^26p$ 2−64018
  - Mg, 1s-2p transitions during bombardment with 21 MeV O ions 2−46469
  - Mg, broadening and shift of lines by van der Waals interaction with Ar atoms 2−70588
  - Mg, far-u.v. absorpt., discrete features identification 2−67388
  - Mg, oscillator strengths for resonance transitions 2−79875
  - Mg, polarization of dipole radiation emitted by electron impact double excited states 2−70607
  - Mg II, elec. quadrupole transitions, multiplet strengths 2−56102
  - Mg IV, radial integrals and level assignments, 90-2100 Å 2−59899
  - Mg$^+$, measurement and calculation of Stark broadening parameters for resonance lines 2−42727
  - Mg$^+$ reson. lines, electron impact broadening 2−59914
  - Mn I, e^6D-y^6P multiplet lines, hyperfine structure, solar spectrum 2−48790
  - Mn I, relative oscillator strengths, precision obs. 2−55040
  - Mn VIII to XV, classification of transitions 2−49948
  - MnI, mag. dipolar h.f.s. of e^6D-y^6P multiplet 2−79894
  - Mo, emissive props., 1000 to 2000K 2−64019
  - Mo VIII, rel. to YV, ZrVI and Nb VII 2−74217
  - N, beam-foil lifetime meas. of excited levels 2−79890
  - N, doubly ionized by slow proton impact, Auger spectra, intense satellite lines 2−83195
  - N, far-u.v. absorpt., discrete features identification 2−67388
  - N, fine-structure density shift 2−79964
  - N arcs, cylindrical, radiative energy balance 2−67697
  - N IV, V, VI, VII, energy levels and multiplet tables 2−46434
  - N ions, radiative lifetimes for u.v. transitions by pulse decay method 2−46413
  - N linewidths of 1s photoelectron energy spectra 2−70602
  - NII, mean lives of excited levels, beam foil study 2−64020
  - Na-He collision depolarization cross-sections for D lines 2−83169
  - Na-He collisions, broadening of D_2 line at high temp. 2−74237
  - Na, broadening of D lines and relaxation of resonance levels during Na-He collisions 2−42784
  - Na, D_1 line excited in N_2 afterglow Doppler temp. meas. 2−49951

Spectra continued
- **atoms** continued
  - Na, emission spectra of electronic energy levels 2−45206
  - Na, equivalent D_1 linewidth in homogeneous magnetic field 2−46435
  - Na, in premixed H_2-O_2-N_2 flame, emission noise spectrum 2−49952
  - Na, resonance curve narrowing in forward scattering 2−56101
  - Na D-doublet, temperature dependence of quenching cross section by N_2 and H_2O in flames of 1500-2500K 2−46454
  - Na D-line radiation excited in collisions of atoms with vibrationally excited H_2, D_2, N_2 2−70627
  - Na D lines, depolarization cross sections during collisions with He 2−59957
  - Na I, elec. quadrupole transitions, multiplet strengths 2−56102
  - Na II, 350 to 9000 Å, term system revision 2−70589
  - Na III, 180-380 Å, 90 lines meas. 2−79921
  - Na III, 2500-1300 Å, $2p^43s$, 3d, 3p and 4s configurations 2−83196
  - Na optically pumped, obs. of maser transitions between Paschen-Back levels of ground state 2−52935
  - Na resonance excitation by tunable dye laser 2−59920
  - Na$^-$, continuous absorption coeff. contribs. from bound-free and free-free transitions 2−70586
  - Nb, absorpt. spectra in rare gas matrix at 14 degrees K, 500 50 50000 cm^1 2−83178
  - Nb VII, configurations and levels determ. 2−74219
  - NbVII, rel. to YV, ZrVI and MoVIII 2−74217
  - Nd, A=143, 145, hyperfine structure const. 2−76990
  - Nd, absorption, computer program for calc. position and optical density of each band 2−46418
  - Nd^{3+}, analytical SCF wavefunctions for ground and some excited states, calc. of oscillator strengths for optical transitions 2−52915
  - Ne-Ar discharge detection of Penning ionization by laser perturbation spectroscopy 2−80373
  - Ne, excitation of 2p-3s lines in He-Ne mixture 2−42742
  - Ne, He as standard for unknown transition 2−59915
  - Ne, Lande-factor of $2p_4$ level meas. with He-Ne laser 2−63428
  - Ne, line strengths and transition probabilities, obs. and theory 2−70590
  - Ne, pionic, strong interaction effects in 2p-1s transition 2−59964
  - Ne, polarization of light emitted on de-excitation under H ion impact 2−42736
  - Ne, Zeeman splitting in superradiance at 6143Å 2−46437
  - Ne discharge in hollow cathode, effect of nonlinear absorption at 0.63 m wavelength 2−83641
  - Ne excited levels, transition probabilities and collision induced transitions 2−63995
  - Ne gas discharge in magnetic field, optical pumping with multimode laser, saturation resonances by magnetic mode crossing 2−46436
  - Ne II, transition branching ratios 2−83194
  - Ne^{8+}, obs. of 2 quantum processes 2−64279
  - NeI, specific isotope shift of 1s-2p and 2p-2s lines, calc. 2−77007
  - NeV, NeVI, NeVII, NeVIII, new lines in 50-2000 angstrons range 2−74220
  - NeVII, experimental oscillator strengths, mean life meas. 2−64017
  - Ni, beam-foil spectrum, hydrogenic transitions in multiply charged ions 2−67391
  - Ni emission line wavelengths, and solar far u.v. spectrum and forbidden line identity 2−42729
  - Ni highly-ionized, far u.v. spectra rel. to solar lines 2−83189
  - Ni XVIII, multiplet strengths for electric quadrupole transitions calc. using HF orbital wave functions 2−42728
  - Np IV, V absorption, computer program for calc. position and optical density of each band 2−46418
  - ^{237}Np, hyperfine structure patterns A and B factors and nuclear magnetic moments 2−79938
  - O, Li-like, classification of spectra of autoionization electrons 2−49953
  - O atom excitation to S^1 state during aurora borealis 2−44745
  - O II, 3p and 3p′ level radiative lifetimes 2−76985
  - O II, mean lives and g values of beam-foil excited levels, suppression of optical cascading effects 2−79910
  - O IV-Vi, lifetime determ. in u.v., beam foil technique 2−56096
  - O ions, radiative lifetimes for u.v. transitions by pulse decay method 2−46413
  - O linewidths of 1s photoelectron energy spectra 2−70602
  - O nightglow emission at 5577 Angstroms during 1958-67 period above Ashkhabad 2−84881
  - O nighttime 6300 Angstroms airglow emission at magnetic equator rel. to ionospheric anomaly 2−84880
  - O$^+$ ion beam, optical spectra Zeeman splitting 2−70577
  - OI 5577 Å line emission at auroral zone latitude rel. to O concentrations 2−84890
  - OI 6300 Angstroms airglow emission, predawn enhancement above Abastumani 2−84883
  - O^{1}S atoms in pulsating aurora, 5577 and 4278 Å lines rel. to production process 2−84888
  - ^{16}O^{7+}, Lamb shift meas. for n=2 state 2−49975
  - ^{16}O^{7+}, meas. of Lamb shift 2−49976
  - O(2^1D_2), electronically excited, kinetic study by time-resolved atomic absorption spectroscopy in vacuum u.v. 2−83168
  - ^{206}Pb muonic atom, analysis of muonic X-rays in terms of equivalent radius 2−59963
  - ^{208}Pb muonic, energies and relative intensities of transitions to and from 2s level 2−42823
  - Pb(6^1D_2) electronically excited, atomic absorption spectroscopy using attenuation of resonance radiation 2−79859
  - Pm II, anal. in 3100 to 10000 Å region 2−79945
  - Pr^{3+}, analytical SCF wavefunctions for ground and some excited states, calc. of oscillator strength for optical transitions 2−52915
  - Pt, 3064.71 Å line, effect of ext. mag. field on intensity 2−49954
  - Pt, gaseous, correlation with absorption spectra of atoms isolated in noble gas matrices 2−52902
  - Rb, cascade-decoupling meas. of excited S-state hyperfine structures 2−52922
  - Rb, displacement of 7947 Å line by foreign gases 2−59933
  - Rb, hyperfine structures of S and D excited states by cascade r.f. spectroscopy 2−70606
  - Rb, self-broadening of principal series lines at high number densities 2−79930

Spectra continued
atoms continued
Rb I, electronic g_J factors, natural lifetimes and electric quadrupole interaction for ^{87}Rb in $np^2P_{3/2}$ series 2−46439
Rb$^-$, continuous absorption coeff. contribs. from bound-free and free-free transitions 2−70586
^{87}Rb-^{85}Rb D, line isotope shift, laser spectroscopic obs. 2−74222
^{87}Rb, h.f.s. separation of ground state, det. by optically pumped atomic beam resonator 2−79864
^{87}Rb, Stark effect investigation of third excited $^2P_{3/2}$ levels in first spectrum, tensor polarizability determ. 2−70591
^{87}Rb hyperfine structure of D_1 line, optical pumping 2−73670
Sc III, 50 new lines 2−79922
Sc III ion, oscillator strengths 2−49934
Se, forbidden transitions in the ground configuration 2−74224
Se I, newly observed lines in PbS region 2−79939
Se IV, levels and lines classif., 2400-420 Å 2−74223
Si, far-u.v. absorpt., discrete features identification 2−67388
Si II, Si III, vacuum u.v. absorption meas. using new continuum light source 2−77001
Si II, Stark broadening of 6347.4 and 6347.1 Å spectral lines 2−56097
SiXii, electron excitation cross sections for 2s-np ns-n′d, 2p-nd, 3s-np transitions calc. by Coulomb-Born method 2−56109
Sn I, multipole radiation excitation 2−46441
Sn I, natural radiative lifetimes of $5p6s^1P_1$, $5p6s^3P_{1,2}$ and $5p5d^3D_{1,2,3}$ levels by zero field level crossing spectroscopy 2−70592
Sn I, radiative lifetimes 2−63997
Sr, excited atoms 2−42715
Sr, oscillator strengths for resonance transitions 2−79875
Sr, quenching of fluorescence in H flames 2−42715
Sr III spectra from sliding spark discharge in 9800-350 Å range, obs. of even and odd energy levels 2−76997
Tb III, odd and even levels analysis 2−67392
TeI, investigation of hyperfine structure of ^{125}Te in $5p^36s$ $^5S_2$ level by optical double resonance and level crossing spectroscopy 2−76998
Ti I, Ti II, oscillator strength obs. 2−56103
Tl, $7^2S_{1/2}$ state, level-crossing spectroscopy, theory of self-broadening and Tl*-Tl-foreign gas collisions 2−49956
Tl lifetime, coherence narrowing, collision broadening, buffer-gas effects on $7^2S_{1/2}$ state studied by level-crossing spectroscopy 2−49955
Tm, photoabsorption in vicinity of 3d edges 2−76988
Tm II, electronic configurations $4f^{12}(5d+6s)^2+4f^{13}6p$ 2−46442
Tm II, odd excited configurations $4f^{12}(5d+6s)6p$ and $4f^{13}7s$ 2−46443
^{169}Tm, K-shell perturbations caused by static nuclear quadrupole moment 2−42738
UI and UII, emission spectrum between 19080 and 30261 cm^{-1} 2−79944
V, highly ionized, far u.v. spectra rel. to solar lines 2−83189
Xe, absorption in range 330 to 600Å 2−49949
Xe, dependence of deexcitation time of slow component on pressure 2−59616
Xe, laser action on unclassified transitions in highly ionized plasma 2−59142
Xe, plasma, electrodeless discharge, high frequency, high press., line profile 2−46423
Xe, pulse discharge radiation, space-time distrib. 2−56389
Xe, upper level lifetimes of high gain laser transitions 2−42740
Xe, vacuum u.v. spectra in solid carbon tetrafluoride 2−49957
Xe, vacuum u.v. stimulated emission, high current relativistic electron beam excitation 2−70584
Xe electrodeless discharge 2−50228
Xe multi-charge ions moving in an impulse discharge 2−50223
Xe plasma, Stark coeffs. determ. 2−67393
XeI, Hanle effect and radiative lifetimes of 2p levels 2−67394
Y IV, anal. of spectrum in 300 to 5200 Å range 2−79948
YV, rel. to ZrVI, NbVII and MoVIII 2−74217
ZrVI, configurations and levels determ. 2−74225
ZrVI, rel. to YV, NbVII and MoViii 2−74217

inorganic liquids and solutions
depolarized doublet spectra of light scattering and shear retardation processes 2−53433
electrolyte solns., aqueous, i.r. spectra, frequency shifts 2−46959
energy transfer mechanism, role of electrostatic and covalent interactions 2−53440
iodide, charge-transfer- to-solvent absorpt. bands in far-u.v. 2−56505
Kerr liq., spectral broadening of light filament, meas. with laser pulses 2−71204
sea water, shallow spectra 2−65608
transparent, dielec., ultrashort pulse spectra superbroadening 2−43368
water, influence of effective field of n light wave on observed spctrum in 4000-0.01 cm^{-1} range 2−67834
water, near i.r. studies of structure in mixed solvent systems 2−50316
water, optical absorption in vacuum u.v. meas. 2−50361
water, spectral reflectance, effects of temp. 2−64461
CCl_4 radiative transfer analysis based on spectroscopic information 2−43346
Cu complexes in solutions, study of metal-ligand bonding, magnetic susceptibility and moment of Cu(II) ion 2−64473
Cu(II) complexes in aqueous solutions, pressure, temp. and conc. effects 2−46960
DCN, i.r. absorption spectrum 2−57351
Eu^{3+}, in organic solvents, abs. and emission quenching effect of →C-H and -O-H groups 2−53436
$HBr.4H_2O$, Raman and i.r., H-bonds 2−43314
HCN, i.r. absorption spectrum 2−57351
H_2O and D_2O, correspondence of fundamental and combination bands in i.r. spectra 2−50365
Hg halides, in dioxane and benzene solutions, molec. bending determination from i.r. spectra 2−64463
HgX_2, (X=halogen), u.v. absorption spectra in aromatic solvents 2−43370
KBr, effect of melting on multiphonon i.r. absorp. 2−68220
LiF, effect of melting on multiphonon i.r. absorp. 2−68220

Spectra continued
inorganic liquids and solutions continued
NH_3, absorption, configuration diagram of solvated electron 2−71225
$(NO)_2$ dimer, low temperature liquid 2−67495
NaCl, effect of melting on multiphonon i.r. absorp. 2−68220
SCl_2, Raman and infrared, vibrational spectra 2−77059

inorganic molecules
see also Molecules
atmospheric mols., absorpt. cross sections, 100-600 Å 2−80057
atmospheric mols., including N_2, O_2 and CO_2, 304 Å photoelectron spectra 2−80058
lanthanides, Judd-Ofelt parameters, effect of excluding hypersensitive transitions 2−83221
monochloroamine, molec. structure and quadrupole coupling constants from microwave spectra data 2−46615
N_2, atmospheric arc, determ. of thermal conditions in asymptotic region 2−77317
Co compounds, chemical bonding study using X-ray photoelectron spectroscopy 2−53002
Cr compounds, chemical bonding study using X-ray photoelectron spectroscopy 2−53002
Cu compounds and complexes, X-ray photoelectron spectroscopy, study of satellite lines 2−80047
Fe compounds, chemical bonding study using X-ray photoelectron spectroscopy 2−53002
Mn compounds, chemical bonding study using X-ray photoelectron spectroscopy 2−53002
N_2O absorption lines, collisional broadening 2−80056
PbF, rotational analysis of (1,0), (0,0) and (0,1) bands of $B-X_2$ system 2−79994
V II, III, IV, V, i.r. spectra resolution into bands, transitions, charge transfer 2−83268

inorganic molecules, diatomic
alkali halides, u.v. absorption cross sections, potential curves and excited state radiative lifetimes 2−70738
electron-vibratory band, Ludenburg-Levy function analogue 2−70661
environmental monitoring 2−73676
multiplet struct. and centrifugal distortions, rot. energy levels 2−79991
NO absorption, in region 1890-1835 cm^{-1} with tunable spin flip Raman source 2−42264
vibration-rotation intensities calc. by factorization method 2−64109
vibration-rotation interaction effect on spectral line intensities, semi-classical treatment 2−70677
AgSb, visible emission, assignment 2−64113
Al, adsorption of Cl, Auger spectrosc., ellipsometry and surface potl. meas. of clean films 2−71345
AlH in solar sunspot spectrum, 4900-6441 Angstrom range 2−62743
AlN, emission spectrum, rotational analyses and isotopic studies 2−42868
AlO $^2\Sigma^+-x^2\Sigma^2$ band system, calc. of Franck-Condon factors and r centroids using RKR potentials 2−70679
AlO band system, Morse Franck-Condon factors and r-centroids 2−67467
Ar_2*, temp. dependence of vacuum u.v. emission spectra in gas and liquid phases 2−70680
AsF, near vacuum u.v. and near i.r., vibr. and rot. analysis, transitions 2−56154
AsO radical, rot. analysis of $C^2\Delta$ and $D^2\Sigma^-$ states, C-state perturbations 2−74255
AsS, $A'^2\pi_{3/2}-X^2\pi_{3/2}$ band system, vibrational analysis and rotational constants 2−77080
Au_2, Franck-Condon factors for AO_u^+-XO_g^+ system 2−56155
AuBe band system, Morse Franck-Condon factors and re-centroids 2−67467
BaI, obs. of new band system in 4481-4300 Å region, study of electronic transitions, vibrational analysis 2−70685
BaO, microwave rotational transition in short lived state obs. 2−67468
BeH(D) λ doubling variation with rot. quantum no. 2−83261
BeI, first excited state 2−42872
BeO, radiative lifetimes of excited vibrational states 2−46528
BiCl, rotational analysis of A-X band system 2−50024
BiO band system, Morse Franck-Condon factors and r-centroids 2−67467
Br_2^{79} and Br_2^{81} hyperfine structure near 6328 Angstroms by laser saturated absorption spectroscopy 2−46554
BrO, electron resonance spectra in J=5/2 rotational levels 2−46530
C_2, Franck-Condon factors of Morse oscillator when $\Delta S>0$ 2−60017
CL_2, pure, and mixtures with Ar and He, self induced transparency 2−46534
CN, calc. of Franck-Condon factors and R centroids for $B^2\Sigma\rightarrow A^2\Pi$ band system, validity of Morse potential 2−46535
CN, true pot. energy curves, Morse r-centroids and Franck-Condon factors for $E^2\Sigma^+$-$X^2\Sigma^+$ band system 2−42880
CN in solar sunspot spectra, 4900-6441 Angstrom range 2−62743
CN radical, level anticrossing 2−42878
CN red band system, shock tube determ. of electronic transition moment 2−77083
CO, a $^3\Pi$ state at 5 to 1000 MHz, fine structure, dipole moment and perturbation analysis 2−50026
CO, C X-ray emission spectra, obs. by grazing incidence grating spectrometer 2−74260
CO, electron impact excitation of vacuum u.v. radiation, threshold studies 2−80141
CO, Franck-Condon factors of Morse oscillator when $\Delta S>0$ 2−60017
CO, half-widths of lines in fundamental and first overtone bands broadened by CO_2 and air calc. using Anderson-Tsao- Curnutte theory 2−53105
CO, i.r. absorption coeff. 2−56156
CO, i.r. vibr.-rot. spectra, approx. calcs. of abs. coeff., 300 and 1200 K 2−46534
CO, intensity meas. of $d^3\Delta\rightarrow a^3\Pi$ emission system, determ. of relative electronic transition moments 2−80035
CO, photoelectron spectra, search for core electron satellites 2−42876

Spectra continued
inorganic molecules, diatomic continued
CO, solar, calc. of vibration-rotation line profiles and equivalent widths 2−73147
CO A $^{1}\Pi$ state, zero-field level crossing spectrosopy, obs. of fluorescence of resolved rotational features 2−70691
CO laser, frequency gain profile obs. using tunable semiconductor laser 2−45718
CO^+, comet tail system, electronic transition moment 2−50029
CO^+, electronic transition moments for $A \rightarrow X$, $B \rightarrow X$, $B \rightarrow A$ transitions, abs. absorption cross sections 2−52998
CO^+, emissions produced by $A \rightarrow X$ transitions, meas. of lifetimes, cross section for excitation of comet-tails 2−46563
CO^+, radiative lifetimes of $A^2\Pi$ state 2−74259
$CO \rightarrow CO^+$ system, electronic transition moments for $A \leftarrow X$ $B \leftarrow X$ transitions, abs. absorption cross sections 2−52998
CS, Hanle effect measurement of the lifetime of the $A^1\Pi$ vibration-rotation levels 2−42885
$^{13}C^{16}O$, $^{12}C^{18}O$, weak angstrom bands obs. 2−56157
CaH, in solar sunspot spectrum, 4900-6441 Angstrom range 2−62743
^{35}ClF, hyperfine structure constants in $J=1$, $J=2$ rotational states using molecular beam electric resonance spectroscopy 2−74261
CsI, quadrupole h.f.s. on rot. transition, ^{127}I coupling consts. 2−53003
$^{133}Cs^{23}Na$, molec. beam elec. resonance spectra, determination of molec. props. 2−64140
CuS, rot. consts. of (0,0) band in A-system 2−42887
D_2 hyperfine temp. shift in Ne and Ar buffer gas 2−50033
D_2 vibrational linewidths due to predissociation 2−79999
F_2, vacuum u.v. absorption spectrum, determ. of dissociation energy and ionization potential 2−70696
FeO, absorption coeff. for i.r. vibration-rotation spectrum 2−42890
FeO chemiluminescence and resonance fluorescence on release of $Fe(CO)_5$ in upper atm. 2−65825
GaCl, hyperfine structure in rotational spectrum 2−46540
GeH, multiplet struct. and centrifugal distortions, rot. energy levels 2−79991
H_2, collision induced- absorpt. near $\lambda = 1$ mm 2−77084
H_2, Dicke narrowing of rotational Raman lines, anisotropy 2−42893
H_2, Lyman band absorptions, equivalent widths 2−56170
H_2, microwave absorpt., at high press., Uranus atmos. obs. 2−55150
H_2, tunable stimulated Raman emission by dye laser 2−77078
H_2 hyperfine structure of $N=1$ rotational state of $^3\Pi_u$ electronic state 2−64137
H_2 vibrational linewidths due to predissociation 2−79999
HBr in condensed phases, first harmonic of vibration-rotation spectrum 2−53014
HBr in condensed phases, spectra of vibration rotation fundamental 2−53013
HBr in condensed phases, second harmonic of vibration rotation spectrum 2−53015
HCl, absorption in extreme u.v. 2−46586
HCl, in SF_6 solution, i.r. absorption bands, effect of vibration-rotation interaction 2−42841
HCl in condensed phases, first harmonic of vibration-rotation spectrum 2−53014
HCl in condensed phases, spectra of vibration rotation fundamental 2−53013
HCl in condensed phases, second harmonic of vibration rotation spectrum 2−53015
HCl vibrational fluorescence from $V=2$ to $V=1$ 2−83256
HD, absorption spectrum in vac. u.v., Rydberg states 2−50038
HD* colliding with HD or He, collision-broadened cross-sections from peak-absorbancy meas. 2−67479
HF, perturbed by compressed gases, rot. line broadening 2−53006
HF, polarizability anisotropy from Stark coefficient 2−42907
HF optical pumping of low-pressure gas sample, laser-induced line narrowing spectroscopy 2−45819
He-Kr mixtures, i.r. absorption spectrum, temp. dependence, determination of intermolecular potentials 2−50131
He-Xe mixtures, i.r. absorption spectrum, temp. dependence, determination of intermolecular potentials 2−50131
HeH, mol. with just H atom in ground state, translational absorption spectrum 2−74266
HeH^+, electron correl. influence 2−64139
HeNe absorption in vacuum u.v. region, obs. of band systems 2−77090
HfO, electronic band spectra interpret. 2−77069
Hg_2, fluoresc., transitions between vibr. levels and ground state 2−53020
$HgAr^+$, rotational analysis of u.v. emission spectrum 2−46553
$HgAr^+$, rotational energy levels, example of Hund's coupling case (c) 2−50048
I_2, rot. Lande factors in $B^3\Pi_{0(g)(u)}$ state 2−50049
I_2, saturation microscopy by intermodulated fluorescence 2−67502
I_2 fluorescence, laser induced line narrowing 2−74267
I_2 laser-induced fluorescence line narrowing 2−48241
I_2 molecular beam spectra excited by 5145 Å Ar ion laser 2−67486
I_2 vapour, absorption spectra teaching to sixth form students 2−76147
I_2^+, photoelectron spectrum, spin-orbit coupling 2−70709
I_2^{127} and I_2^{129} hyperfine structure near 6328 Angstroms by laser saturated absorption spectroscopy 2−46554
ICl, $J=2 \leftarrow 1$ microwave spectra for $v=0$ and $v=1$ levels 2−42902
ICl interhalogen, vacuum u.v. spectrum 160-130 nm obs. of Rydberg transitions 2−83272
IO, electron resonance spectra in $J=5/2$ rotational levels 2−46530
$^{127}I_2$, $^{129}I_2$, hyperfine interactions in optical transitions 2−50050
InBr photoelectron spectra, bonding in group III monohalides 2−80027
InCl photoelectron spectra, bonding in group III monohalides 2−80027
InF band systems, vibr. transition probabilities and r-centroids 2−60006
InI photoelectron spectra, bonding in group III monohalides 2−80027
IrO, 4200 to 6400 Å, band spectrum, rotational and vibrational analysis 2−77065

Spectra continued
inorganic molecules, diatomic continued
$^{39}K^7Li$, $^{39}K^{23}Na$, molec. beam elec. resonance spectra, determination of molec. props. 2−64140
$La^{18}O$ emission spectrum at 5600 Å, determ. of rotational constants of $B-X$ band system 2−80019
LiCl, hyperfine spectra in zero magnetic and low electric fields using new electric resonance molecular beam apparatus 2−46557
LiI, emission spectrum, line profiles, plasma parameters 2−60247
$(LiNa)^+$, charged transfer, transition, dipole moment, cross sections of vibr. levels 2−60009
LuD, obs. of new electronic system in 4000-8000 Å region, determ. of molecular consts. 2−70711
LuF, new electronic spectrum obs. in 3000-8000 Å region, determ. of molecular constants 2−70712
LuH, electronic band systems analysis, 4200 and 5000 Å 2−74268
LuH, obs. of new electronic system in 4000-8000 Å region, determ. of molecular consts. 2−70711
Mg_2, Franck-Condon factors in A-X system, rot. depend. 2−64141
Mg_2, matrix-isolated, absorpt. peaks 3540-3700, absence of optical pumping 2−80041
MgH in solar sunspot spectra, 4900-6441 Angstrom range 2−62743
MgO in solar sunspot spectra, 4900-6441 Angstrom range 2−62743
$^{24}MgH^+$, $^{25}MgH^+$, $^{26}MgH^+$, rot. analysis of $A^1\Sigma^+ \rightarrow X^1\Sigma^+$ and $B^1\Pi \rightarrow X^1\Sigma^+$ systems 2−56184
N_2, active, vacuum u.v. emission from levels of forbidden B-X transition, $N_2(B'^3\Sigma_u^-)$ kinetic behaviour 2−70719
N_2, active, vacuum u.v. emission, absolute population rates of $N_2(a^1\Pi_g)$ and $CO(A^1\Pi)$ 2−70718
N_2, active, vacuum u.v. emission, form. and removal of $N_2(a^1\Pi_g)$ 2−70716
N_2, $c_n\ ^1\Pi_u$ and $c_n'\ ^1\Sigma_u^+$ Rydberg states, high resolution studies 2−64145
N_2, excitation in $Ar + N_2$ high-frequency discharge obs. of) band structure 2−43041
N_2, Gaydon- Herman green system, rot. analysis 2−64146
N_2, new Rydberg bands in visible and identification of lowest $^1\Sigma_g^+$ Rydberg state 2−42915
N_2, rate constants for deactivation of $B^3\Pi_g$ and $A'^1\Sigma_u^-$ states 2−80125
N_2, reabsorption, $B^3\Pi g$ vibratory state conc. detn. 2−70715
N_2, rotational temp. meas. using Raman spectroscopy 2−46857
N_2, translational spectra due to overlap moments induced by collisions with He 2−50129
N_2, vibration-rotation interaction in calculated band strengths 2−46571
N_2, vibrational Raman scattering 2−46566
N_2 active, vacuum u.v. emission, excitation of singlet and triplet states of CO 2−70717
N_2 electron impact excitation, emission cross section for second positive system bands 2−46564
N_2 i.r. emission spectra in auroral excitation conditions 2−84873
N_2 plasma, h.p., spectral intensity, equil. radiation 2−60248
N_2 positive and N_2^+ band systems rel. to energy spectra of auroral electrons 2−54884
N_2 spectrum in i.r. range 6500-11500 Angstroms rel. to auroral spectra 2−84874
N_2^+, anomalous excitation in seeded Ar free plasma jet 2−42916
N_2^+, emission produced by $A \rightarrow X$ transitions, meas. of lifetimes, cross section for excitation of Meinel bands 2−46563
N_2^+ 4278 Å intensity in auroral energy spectra rel. to precipitating electrons 2−65914
N_2^+ radiative lifetimes of a $A^2\ PO_u$ vibr. levels 2−83257
NBr, $^1\Sigma^+$-$^3\Sigma^-$ system, Franck-Condon factors 2−53024
NO-$\gamma(A^2\Sigma$-$X^2\pi)$ system, oscillator strength of (0,0) band 2−50062
NO, concentration determ. in water saturated N_2 2−70714
NO, Franck-Condon factors of Morse oscillator when $\Delta S > 0$ 2−60017
NO, high resolution i.r. spectroscopy using tunable PbSSe laser 2−42922
NO, i.r. absorption coeff. 2−56156
NO, NO^+ configuration interaction studies, comparison with photoelectron spectra 2−83254
NO, obs. of Λ-doubling and Zeeman splitting in fundamental i.r. absorption band 2−46561
NO, Rydberg series of bands in 680−560 Å region, ionization of σ^*2s orbital 2−74271
NO^-, laser photodetachment and photoelectron spectrometry, determ. of molecular constants and electron affinity of NO 2−53027
NS, microwave spectra, transitions 2−76542
Na_2, meas. of asymmetries in cross section for collision-induced rotational transitions in $B^1\Pi_g$ state 2−56274
NaLi, $\Delta M_J = \pm 1$ transitions from rotational states obs. by molecular beam electric resonance method 2−53029
NaLi, heat-pipe oven applic. 2−49453
NbO band systems, vibr. transition probabilities and r-centroids 2−60006
Ne, absorption in vacuum u.v. region, obs. of band systems 2−77090
No, i.r. vibr.-rot. absorpt., nucl. hyperfine splitting 2−64143
O_2-Ar compressed mixtures, meas. of microwave absorption in 48-81 GHz region using Fabry-Perot interferometer 2−74273
O_2-N_2 compressed mixtures, meas. of microwave absorption in 48-81 GHz region using Fabry-Perot interferometer 2−74273
O_2, detect. on Mars 2−85047
O_2, dissociative excitation of vacuum u.v. emission by electron impact, cross section meas. 2−42900
O_2, fine struct. parameters of $B_3\Sigma_u^-$ state 2−64150
O_2, impact line shift in 0.762 μ band 2−77092
O_2, spin-orbit contribution to zero-field splitting 2−42925
O_2, u.v. photolysis, optical emission from $O(^1D)$ and $O_2(b^1\Sigma_g)$ 2−61801
O_2, vibrational Raman scattering 2−46566
O_2 7620 Angstroms A-band observations of Mars during and after 1971 dust storm 2−78549
O_2 7635 Angstroms band observations in atmospheres of Mars and Venus 2−78548
O_2 A-band absorption lines at different pressures, equivalent widths 2−46570

Spectra continued
inorganic molecules, diatomic continued
O_2 compressed meas. of microwave absorption in 48-81 GHz region using Fabry-Perot interferometer 2−74273
O_2 excitation cross sections and intensity ratios in auroral conditions 2−84872
O_2 in polystyrene, contact charge transfer complexing 2−72580
O_2 in solar sunspot spectrum, 4900-6441 Angstrom range 2−62743
O_2-, laser photodetachment and photoelectron spectroscopy determ. of structure of O_2^- and electron affinity of O_2 2−53028
O_2^+, spin-orbit coupling const. in $A^2\Pi_u$ state determ. from rotational term values of 1-7 and 0-8 bands 2−70721
OD, wavenumbers of $A^2\Sigma \rightarrow X^2\Pi$ (0, 0) and (1, 0) bands 2−67497
OH, intensity variations, vibrational and rotational temps. 2−46572
OH, microwave spectra, transitions 2−76542
OH, OD free radicals, laser oscill. in pure rot. transitions 2−56192
OH, u.v. 2−64152
OH, vibration-rotation interaction in calculated band strengths 2−46571
OH, wavenumbers of $A^2\Sigma \rightarrow X^2\Pi$ (0, 0) and (1, 0) bands 2−67497
OH nightglow emissions, spectrophotometric study 2−48546
OH rot. temp. in nightglow 2−54882
PO, analysis of some bands of β system 2−42931
PO, emission spectrum, red region analysis 2−60028
PO, vibrational and rotational analysis of emission spectrum in 1850-2350 Å region, $C^2\Sigma$--$X^2\Pi_r$ transition 2−46573
PO band systems, vibr. transition probabilities and r-centroids 2−60006
PO γ-system, localization of rot. perturbations in first vibr. levels 2−79995
$P^{16}O$, and $P^{18}O$, rot. analyses and deperturbations of visible systems 2−79996
$^{31}P^{14}N$, millimetre wave rotational spectrum, molec. constants 2−60029
Rb^7Li, $Rb^{23}Na$, molec. beam elec. resonance spectra, determination of molec. props. 2−64140
RuC, in 4100-4800 Å region, determ. of molecular consts., band analysis 2−77071
SO, $b^1\Sigma^+ - X^3\Sigma^-$ transition, rotational band structure 2−70724
SO, microwave spectra, transitions 2−76542
SO $A^3\Pi$-$X^3\Sigma^-$ band systems, oscillator strengths 2−56195
Sb_2, vibrational and rotational analysis of $B \rightarrow X$ system 2−50068
ScS, in solid Ar and He matrices, e.s.r. and i.r. spectra 2−46582
SeF, electron resonance spectra in $J=5/2$ rotational levels 2−46530
SeH, spin orbit coupling const. determ. following photodetachment of electron from SeH- 2−46583
SiBr, B-X system analysis 2−77060
SiI, absorption and emission spectra in 4200-4900 Å region, obs. of A $^2\Sigma^+$-X $^2\Pi_{1/2}$ transition, determ. of vibrational consts. 2−70726
SiO, $A \rightarrow X$ band system, vibr.-rot. analysis 2−83248
SiO^+ electronic spectrum, vibr. and rot. anal. 2−77056
SnF, rotational structure and isotopic shift in (1,0) band of $(A-X)$ system 2−77093
SnH(D), multiplet struct. and centrifugal distortions, rot. energy levels 2−79991
SnI emission band spectrum, isotope effect 2−53037
TeS, gaseous, electronic spectrum, rot. struct. of bands 2−64158
ThO, electronic band spectra interpret. 2−77069
TiO, α-system, perturbations 2−50070
TiO, electronic band spectra interpret. 2−77069
TiO, electronic chemiluminescence, emission spectrum 2−77068
TiO, u.v. bands, vibr.-rot. consts. 2−80042
TiO β system, Einstein coeffs. and oscillator strengths of excited levels 2−60036
TiO in solar sunspot spectrum, 4900-6441 Angstrom range 2−62743
Xe_2^*, temp. dependence of vacuum u.v. emission spectra in gas and liquid phases 2−70680
YO, $B^2\Sigma$-$X^2\Sigma$ system electron transition moment variation with internucl. distance and vibr. temp. 2−56203
YS, in solid Ar and He matrices, e.s.r. and i.r. spectra 2−46582

inorganic molecules, polyatomic
83271
chromates of divalent transition metal compounds, i.r. vibrational spectra, calc. of force constants 2−70678
group VI B metal carbonyls, cis-subst. derivatives, CO stretching spectra and force constants 2−80043
halogenosilane bis-pyridine and o-phenanthroline complexes, vibr. spectra 2−77081
HCN, investigation of bands at 14 μ 2−50042
holographic Fourier transform spectroscopy, Moire technique for hologram recording 2−73614
molybdates of divalent transition metal compounds, i.r. vibrational spectra, calc. of force constants 2−70678
rare earth β-diketonate complexes, i.r. absorpt., vibr. modes 2−46577
rare-earth borates, vibrational spectra and structures 2−70727
rare-earth pyrosilicates, vibrational spectra 2−72322
sulphuryl compounds, photoelectron spectra 2−64156
thionyl compounds, photoelectron specta 2−64156
transition metal complexes, revised INDO calc. of charge transfer spectra and sequence of metal and ligand orbitals 2−67472
transition metal halide complexes valence regions by X-ray photoelectron spectroscopy 2−83247
water, vibrational Raman scattering 2−46566
$[X_2O_7]^{n-}$ anions, vibr. spectra assignments 2−56153
$[C_nO_n]^{-2}$ dianions, u.v. absorpt., CNDO-CI calc. 2−70689
$[PtCl_4]^{2-}$ type planar square complexes, absorpt. band lineshape, electron-vibr. interaction 2−80054
Al complex, AlX_3-dimethyl sulphoxide coordination compound ($X=Cl$, Br), vibrational spectra 2−52992
$AlMgBO_4$ vibrational spectra, interpretation by factor group approx. calc. of force constants for BO_4 group 2−70728
BF_3 i.r. spectra, obs. of l-type resonances in Q branches of ν_4 bands, determ. of cubic potential consts. 2−70682
$B_3N_3H_6$, symmetry-forbidden $^1A_2'$-$^1A_1'$ transition analysis 2−70684
BO_2, fluorescent band enhancement, chemiluminescent reaction of O with triethyl boron 2−44475
BeB_2H_8, BeB_2D_8, BeB_2HD_7, i.r. spectra, frequency assignment and structure determination 2−52994
$BkCl_3$, low temp. absorption spectra, obs. 2−64116

Spectra continued
inorganic molecules, polyatomic continued
$BrNSF_2$ vibrational spectra, tentative assignment band shape and G-matrix elements calc. 2−70697
BrO_3^-, vibrational spectra and force constants 2−59996
CO_2, ^{18}O enriched, high resolution study of near i.r. bands 2−70693
CO_2, atmospheric radiative transfer 2−65770
CO_2, dissociative excitation by electron impact of vacuum u.v. emission features 2−50027
CO_2, i.r. absorption coeff. 2−56156
CO_2, i.r. spectral emissivity data, comparison with total emissivity charts 2−83702
CO_2, i.r. vibr.-rot. spectra, approx. calcs. of abs. coeffs., 300 and 1200 K 2−46534
CO_2, laser source obs, of 00^01-$(10^00$-$02^00)_1$ band 2−74257
CO_2, line broadening of $00°1$-$(10°0\ 02°0)_1$ transition perturbed by N_2, laser source spectroscopy 2−79993
CO_2, press.- induced absorpt., ν_1 band, density and temp. depend. of intensity, crit. phenomena 2−56158
CO_2, semi-empirical analysis of electronic spectra 2−42891
CO_2, translational spectra due to overlap moments induced by collisions with He 2−50129
CO_2, u.v. photolysis, optical emission from $O(^1D)$ and $O_2(b^1\Sigma_g)$ 2−61801
CO_2 laser, spectrum generated at reduced pressure of working mixture 2−73566
CO_2 molecular velocity distribution effect on the shape of spectral line wings 2−64119
CO_2 plasma, atmospheric pressure, 6500 to 9500 K, emission capacity in visible spectral range 2−43155
CO_2^-, $^2A_1$ and $^2B_1$ states 2−42874
CO_2^+, branching ratios det. from photoelectron spectroscopy 2−50032
CO_2^+, relative intensity meas. on Fox-Duffendack-Barker ($A^2\Pi_u$-$X^2\Pi_g$) and u.v. doublet ($B^2\Sigma_u^+$-$X^2\Pi_g$) band systems 2−56162
$(C_3O_2)n$ polymer, spectral analysis rel. to colouring of Martian surface, laboratory studies 2−78542
CS_2, u.v. absorpt. near N_2 laser wavelengths, excited states population 2−80014
CS_2, X-ray absorption spectra, comparison with MO LCAO-CNDO calc. 2−60034
C_3S_2, visible and near u.v. spectra, vibrational analysis 2−42877
$CSCl_2$, vibrational intensities from i.r. spectra 2−46533
CSF_2, vibrational intensities from i.r.spectra 2−46533
$Ca_3Al_2[SiO_4]_3:Fe^{3+}$, optical spectra calc. 2−72295
$Ca_3Fe_2[SiO_4]_3:Fe^{3+}$, optical spectra calc. 2−72295
$Ca_2[AsO_4B(OH)_4]$ vibrational spectra, interpretation by factor group approx. calc. of force constants for BO_4 group 2−70728
$Cd(^3P_0) + NH_3 \rightarrow CdNH_3^*$ reaction kinetics, rate constant, excimer formation 2−81514
$CfCl_3$ low temp. absorption spectra, obs. 2−64116
Cl_2CNCl, i.r. and Raman, vibrational assignments 2−70694
$ClNSF_2$ vibrational spectra, tentative assignments band shape and G-matrix elements calc. 2−70697
ClO_3^-, vibrational spectra and force constants 2−59996
ClO_3F, photoelectron spectrum determ. of vertical and adiabatic ionization potentials 2−46587
Co complex, acetylacetonate, u.v. and visible spectra calc. using MO LCAO method 2−83326
Co complex, Co(III) triethylenediamine chloride, vibr. spectral analysis 2−72325
Co complex, trisethylenediamine cobalt(III) thiophosphate, i.r. spectra 2−46537
Co_2, continuous, calculation of absorption coeffs. over temp. range 20000-100000°K 2−70692
Co(II) complexes with N,N′-ethylenebis(acetylacetoneimine), i.r. spectra, normal coordinate analysis 2−70695
Cr(III) thiacyanate complex in dimethyl-sulfoxide, phosphorescence spectra 77-150 K 2−83269
CrO_4^{2-}, valence region X-ray photoelectron spectra, energy spread of ioniz. pots. 2−80004
Cu complex, copper hydroxyquinolinate, d-d transitions, influence of host lattice 2−81455
Cu complex, copper picolinate, d-d transitions, influence of host lattice 2−81455
Cu^{2+} complexes, magnetic circular dichroism spectra of vibronically allowed d-d transitions 2−64124
Cu(II) complex, interpretation of u.v. spectrum using modified Pariser-Pople method 2−67471
Cu(II) complexes, chromophore trans- CuN_2S_2, covalent bonding, e.s.r. and electronic spectra 2−46539
Cu_3MX_4 ($M=V,Nb,Ta$; $X=S,Se$), i.r. 2−42888
D_2-Ne Van der Waals complexes in collision-induced fund. bands of deuterium 2−64127
D_2O, dipole moment determ. from Stark effect spectroscopy using HCN laser 2−80045
DOF, vibr.-rot. analysis 2−77062
$Er_2O_3:Er^{3+}$, electronic excitation, far i.r. and optical spectrosc. obs. 2−81369
$FNSF_2$ vibrational spectra, tentative assignment band shape and G-matrix elements calc. 2−70697
$Fe(CO)_5$, vibrational spectra of isotopic species, potential constants 2−67473
Fe(II) complexes, octahedral halogen-bridged, far i.r. spectra 2−46558
GeF_2, vacuum u.v. spectra, vibr. assignments 2−80040
GeH_2Br and GeHBr, fund. vibr. freqs., bonding 2−61804
GeH_3F, GeD_3F, microwave spectrum, molec. properties 2−60001
H_2-Ne Van der Waals complexes in collision-induced fund. bands of hydrogen 2−64127
H_3^+, observability of fundamental spectrum, comment on paper by Kawaoka and Borkman (1971) 2−70705
HCN, i.r. matrix islation spectra 2−70708
HCN, semi-empirical analysis of electronic spectra 2−42891
HCN hypersonic beam, electric resonance spectrography 2−67478
HCP, Zeeman effect in 2782Å band 2−70699
HDO, structural model for effect of perchlorates on i.r. bands, assignment of stretching bands 2−53016
HNCS, u.v., vibr. analysis 2−56175
HNO, microwave obs. 2−50034

Spectra continued
inorganic molecules, polyatomic continued
HNO_3 u.v. absorption intensity at 22°C 2−64135
HO_2 radical, vibr. funds., electronic struct. 2−56174
H_2O, calc. of half-widths of lines in ν_2-fundamental using Anderson-Tsao-Curnutte theory 2−53105
H_2O, in relatively nonpolar organic solvents and in $NaClO_4$, meas. of i.r. absorption spectra 2−46932
H_2O, valency oscill. bands, intensity by electrooptical parameters 2−46548
H_2O 8200 Angstroms band in Martian atmosphere, ground based photoelectric observations during Mariner 9 mission 2−78551
H_2O 8200 Angstroms band studies in Martian atmosphere with gound-based Varo image tube 2−78552
H_2O dimer, in CCl_4 soln., i.r. spectrum and structure 2−50043
H_2O vapour, absorption lines in ν_1-band, collisional narrowing 2−79992
H_2O vapour, calculation of intensities using vibrational rotational interaction data 2−74265
H_2O vapour, i.r. spectral emissivity data, comparison with total emissivity charts 2−83702
HOF, vibr.-rot. analysis 2−77062
H_2S, absorption in extreme u.v. 2−46586
H_2S, i.r. absorption coeff. 2−56156
H_2S, X-ray absorption spectra, comparison with MO LCAO-CNDO calc. 2−60034
H_2S and D_2S, i.r. matrix isolation spectra 2−70708
HSSH, direct obs. of anomalous K doubling caused by centrifugal distortion 2−64131
HTO, ν_1 and ν_3 levels determ. by i.r. spectrum, rot. consts. of fund. state 2−79997
I_3^-, resonance Raman effect laser excited, vibration enhancement 2−80007
IF_7, nonrigid D_{5h} molecule, vibrational assignment from i.r. and Raman spectra 2−42901
IO_3^-, vibrational spectra and force constants 2−59996
K complex, pentacyanonitrosylchromate, i.r. spectrum, normal coordinate analysis for $[Cr(CN)_5NO]^{-3}$ anion 2−60008
$KFe(CrO_4)_2.2H_2O$, low temp. i.r. vibrs. 2−48175
$K_2H_2P_2O_6$, $K_2H_2P_2O_6.3H_2O$, i.r. spectra C_{2h} configuration of $H!_2O_6$ 2−83267
$Mg(NH_3)_6Cl_2$ and $Mg(ND_3)_6Cl_2$, i.r. active vibr. freqs. assignment 2−77058
$Mn(CO)_5H$ and $Mn(CO)_5CH_3$ photoelectron spectra, ab initio SCF MO calcs. of electronic structure 2−70713
$Mn(CO)_4NO$ complex, i.r. spectra meas. in vapour phase and in solution, assignment of structure and fundamental modes 2−42909
Mn(I) complex, $K_5[Mn(CN)_6]$, vibr. spectra and force consts. 2−77074
Mn(II) complex, tetrahalogenomangonates, structure obs. in diffuse reflectance and phosphorescence excitation spectra at 77K 2−67488
Mn(II) complexes, octahedral halogen-bridged, far i.r. spectra 2−46558
MnO_4^-, valence region X-ray photoelectron spectra, energy spread of ioniz. pots. 2−80004
$MoOS_3^{2-}$ and alkali metal salts, i.r. and Raman spectra in aqueous solution 2−46560
MoS_4^{2-} and alkali metal salts, i.r. and Raman spectra in aqueous solution 2−46560
NF_2SO_3F, vibration spectra, C_s symmetry 2−42917
NH_3, i.r. absorption in spectral band 0.8-2.5 microns 2−46562
NH_3, i.r. emission obs. during dissociation behind reflected shock wave 2−48324
NH_3, intensities of i.r. spectra deduced from dipole moment derivatives calc. using Fock-Roothaan wave function 2−42921
NH_3, inversion spectrum, rotational structure 2−80033
NH_3, use for calibrating i.r. spectrometers 2−73681
NH_3 lines, collision-broadened by hydrogen, shapes and widths 2−67493
N_1(II) mandalate complex, i.r. spectrum 2−50065
NO_{-3}, matrix-isolated, i.r. spectra, 4000-400 cm^{-1} region 2−67492
NO_2, dynamics of electronic states excited by tunable dye laser 2−50059
NO_2, i.r. absorption coeff. 2−56156
NO_2, inelastic photon scatt., of N_2, atmospheric pollutant monitoring 2−67496
NO_2, laser magnetic resonance at 311 and 337 μm 2−42912
$(NO)_2$ dimer, low temperature vibrational and electronic bands 2−67495
N_2O, calc. of rotational half-widths for air broadened absorption lines by Anderson-Tsao-Curnutte theory 2−53105
N_2O, forbidden character of 2000 Å transitions 2−56186
N_2O, line parameters near 4.5 μm determ. from absorption spectra with Fabry-Perot interferometer 2−46568
N_2O, matrix isolated i.r. spectrum, temp. depend. 2−74269
N_2O, vibration bands when absorbed in cavities of zeolite NaA 2−46565
N_2O band intensities and half-width of N-broadened lines rotational lines in ν_3 fundamental meas. near 4.5 μ 2−42923
N_2O optical absorption and electron scattering spectra, obs. of resonant phenomena in B region at 6.8 eV 2−77061
NSF, photoelectron spectrum 2−42946
$^{14}NH_3$, $^{15}NH_3$, inverse Lamb dip for i.r.-microwave two photon transitions 2−60024
$^{14}NH_3$ and $^{15}NH_3$, i.r. vibration-rotation spectra, 2-photon spectroscopy 2−42920
$Na_2Cd(SO_4)_2.2H_2O$ vibrational frequencies assigned 2−83270
$NaCd(SeO_4)_2.2H_2O$ vibrational frequencies assigned 2−83270
$Na_2Co(SO_4)_2.H_2O$ vibrational frequencies assigned 2−83271
$Na_2Cr(SO_4)_2.2H_2O$ vibrational frequencies assigned 2−83270
$NaFe(CrO_4)_2.2H_2O$, low temp. i.r. vibrs. 2−48175
$Na_2Mg(SO_4)_2.4H_2O$ vibrational frequencies assigned 2−83271
$Na_2Mn(SO_4)_2.2H_2O$ vibrational frequencies assigned 2−83270
$NaMn(SeO_4)_2.2H_2O$ vibrational frequencies assigned 2−83270
$Na_2Ni(SO_42.H_2O$ vibrational frequencies assigned 2−83271
$Na_2Zn(SO_4)_2.H_2O$ vibrational frequencies assigned 2−83271
NbF_5, matrix isolated and gas phase, obs. of i.r. spectra, C_{4v} monomeric structure active frequencies 2−42918

Spectra continued
inorganic molecules, polyatomic continued
Nd(III) complexes with N-donor ligands, solvent and complex formation defects on spectra 2−46569
Ni complexes, tetracoordinated trimethylphosphines Ni(II) 2−77091
Ni II complexes, low-spin trigonal bipyramidal, electronic spectra, temp. dependence of lowest energy ligand field band 2−53031
Ni(II) complexes, octahedral halogen-bridged, far i.r. spectra 2−46558
Ni(II) complexes with N,N′-ethylenebis(acetylacetoneimine), i.r. spectra, normal coordinate analysis 2−70695
O_3, analysis of $(\nu_1+\nu_2+\nu_3)$ combination band 2−64153
O_3^- and $_4^-$ anions in Ar matrix, absorpt. assignment 2−56191
O_3^- anion isolated in Ar matrix, vibrational and electronic spectra, 5100-3700 Å, determ of ν_3 2−70720
OBF, infrared matrix isolation spectrum 2−64151
OCS, elec. dipole and mag. moments, determ. by mol. beam-electric resonance method 2−83245
OCS, forbidden character of 2000 Å transitions 2−56186
Os complex, tris(2,2′-bipyridine) osmium (II), singlet triplet charge transfer absorption spectrum 2−68632
$Os_4O_4(CO)_{12}$, vibr. spectrum, force consts. 2−56193
PH_2, A^2A_1-X^2B_1 transition, rotational analysis of bands 2−83241
PH_3, absorption in extreme u.v. 2−46586
Pd II complexes, low-spin trigonal bipyramidal, electrònic spectra, temp. dependence of lowest energy ligand field band 2−53031
Pd(II) complexes with N,N′-ethylenebis(acetylacetoneimine), i.r. spectra, normal coordinate analysis 2−70695
Pt II complexes, low-spin trigonal bipyramidal, electronic spectra, temp. dependence of lowest energy ligand field band 2−53031
ReF_7, mol. consts. i.r. spectra 2−46576
Re(I) complex, $K_5[Re(CN)_6]$, vibr. spectra and force consts. 2−77074
RuF_5 complexes with XeF_2, i.r. spectra 2−74279
Ru^aO_4, A=16, 18, i.r. spectrum, determ. of anharmonicity corrections, Coriolis constants, force field 2−46578
S_3, S_4, vibrational analysis of visible spectrum, correlation with photolysis reactions of S_3Cl_2 and S_4Cl_2 2−50069
SCl_2, Raman and infrared, vibrational spectra 2−77059
SF_6, inverted Lamb dip spectroscopy 2−63326
SF_6, saturation behaviour at high pressure and laser intensity 2−74277
SF_6 electronic structure, optical spectra of gas and solid in extreme u.v. and soft X-ray region 2−42933
SF_4O, microwave study of S-O bond distance 2−70723
SO_2, i.r., for det. of pollutants, using current tunable semiconductor laser 2−57940
SO_2, i.r. absorption coeff. 2−56156
SO_2, ν_1 band, tunable laser spectroscopy 2−42938
SO_2, π^*-π (2350 Å) band system analysis 2−64155
SO_2, tunable-laser spectroscopy of vibr.-rot. band transitions 2−60033
SO_2, X-ray absorption spectra, comparison with MO LCAO-CNDO calc. 2−60034
SOF_2, upper stage transitions in i.r. spectra 2−46580
SO_2F_2, photoelectron spectrum determ. of vertical and adiabatic ionization potentials 2−46587
SO_2F_2, upper stage transitions in i.r. spectra 2−46580
SeF_4 matrix isolated vibrational spectra, C_{2v} symmetry assignment of frequencies axial and equatorial bonds 2−83265
$SiCl_4$, exact force field determ. from ^{35}Cl and ^{37}Cl isotope shift and analysis of vibrational spectra 2−42936
SiF_2, vacuum u.v. spectra, vibr. assignments 2−80040
SiH_4, absorption in extreme u.v. 2−46586
$^{28}SiH_3D$, ground state rotational constants determ. from high resolution i.r. spectra 2−64157
$^{28}SiH_4$, high resolution i.r. meas. on ν_3 vibr.-rot. band 2−80039
$TaBO_4$ vibrational spectra, interpretation by factor group approx. calc. of force constants for BO_4 group 2−70728
Tc(I) complex, $K_5[Tc(CN)_6]$, vibr. spectra and force consts. 2−77074
TcO_3Cl, vibrational spectra 2−77067
TeF_4 matrix isolated vibrational spectra, C_{2v} symmetry, assignment of frequencies axial and equatorial bonds 2−83265
Te(IV) penta- and hexacoordinate mixed halide anions, i.r. spectra 2−77094
TeO_2, matrix isolated, thermodynamic functions and i.r. spectrum 2−56202
$TlFe(CrO_4)_2.2H_2O$, low temp. i.r. vibrs. 2−48175
UO_2F_2, for i.r. spectrum determ. of frequencies of i.r. active bands 2−60038
W complex, hexamethyl tungsten, photoelectron spectrum and electronic struct. 2−64160
WOS_3^{2-} and alkali metal salts, i.r. and Raman spectra in aqueous solution 2−46560
WS_3^{2-} and alkali metal salts, i.r. and Raman spectra in aqueous solution 2−46560
XeF_2 complexes with RuF_5, i.r. spectra 2−74279
XeO_4 i.r. vibrational spectrum, determ. of Coriolis consts., isotopic freq. shift and force field 2−80023
$Zn(py)_2X_2$, complexes py=pyradine, X=halogen, band assignments 2−70731

inorganic molecules, polyatomic, radiofrequency
see also Nuclear magnetic resonance and relaxation; Paramagnetic resonance and relaxation
BCl_3, i.r. double resonance 2−46526
ClNCO, rot. consts., inertial defects, centrifugal distortion consts., nucl. quad. coupling consts. 2−56165
D_2O, dipole moment determ. from Stark effect meas. on microwave transitions 2−80045
GeF_2 microwave spectrum, determ. of nuclear quadrupole coupling consts., and effect of centrifugal distortion 2−70698
HDO, rotational dependence of dipole moment determ. from Stark effect meas. on microwave transitions 2−80045
$(HF)_n$, microwave spectrum in X- and K-band at 70C 2−56177
$H_2{}^{18}O$, rotational spectrum in ground vibrational state, study by submillimeter microwave spectroscopy 2−70706
HTO, microwave spectrum, rot. consts. of fund. state 2−83242
NCN_3, microwave spectrum., struct., dipole moment 2−60014

Spectra continued
inorganic molecules, polyatomic, radiofrequency continued
NCNNN, microwave spectrum rot. analysis, electronic struct., dipole moments 2−64142
NH_3, press. induced shifts of (J,K)=(12,12) inversion line 2−50061
NH_3, transient-nutation effects in time- resolved i.r.-microwave double resonance 2−64147
NH_3, transient Stark effects on microwave line 2−42911
NH_2CN, microwave spectra, structural parameters 2−77066
$^{14}NH_3$ and $^{15}NH_3$ mol. beam h.f.s. data interpret. 2−83258
PH_3, ν_2 transition, r.f./i.r. double resonance 2−42930
$SO^{35}Cl^{37}Cl$, rot. and centrifugal distortion consts. 2−60032
SOF_2, microwave spectrum and harmonic force field 2−80036
T_2O, microwave spectrum, rot. consts. of fund. state 2−83242

inorganic solids
— 2−68427
$A^IB^{III}O_2$ with rhombohedral α-$NaFeO_2$ structure, Raman and i.r. spectra 2−72321
$A^IB^{III}S_2$ with rhombohedral α-$NaFeO_2$ structure, Raman and i.r. spectra 2−72321
alkali borate glasses, Ni^{2+}-containing, absorpt. anomalies, ligand field approach 2−75303
alkali halide, Stark effect of M and N colour centres 2−61624
alkali halide, surface optical modes obs. 2−51344
alkali halide crystals, limiting optical freq. calc. and temp. variation 2−72311
alkali halide phosphors, lineshpaes of C-bands by method of moments 2−57346
alkali halides: CrO_4^{2-}, optical and i.r. vibrational absorption spectra used to study defects in the host crystal 2−48171
alkali halides, absorpt., reson. of electronic polaron 2−72313
alkali halides, $Co(CN)_6^{3-}$ doped, vibr. and electronic props. 2−54413
alkali halides, coloured, spin-orbit effects in F- and K-bands 2−51335
alkali halides, F, F_{a1}, F_{a2}, U centres, temp. dependence of peak position of absorption and emission bands 2−75298
alkali halides, harmonic band parameters of NO_2^- and NO_3^-, high temp. 2−54410
alkali halides, tunnelling motions of impurities from Stark modulated microwave spectra 2−70739
alkali halides doped with Ni^{2+} 2−44379
alkali metals, interband absorpt., plasmon sidebands 2−51334
alkali silicate glass, Er^{3+} sites, absorpt. study 2−54429
alloy, virtual bound state, absorption model 2−65245
alloyed semiconductor, absorption coeff. in $\omega > Eq$ region in presence of resonant scattering 2−72316
amorphous, interband transitions, review 2−72293
antiferrodielectric, effective electrodipole transitions, optical and spin excited states 2−72290
antiferromagnetic insulator, magnon induced sidebands in optical transitions 2−54408
arsenates, near and i.r. spectra 2−72672
borates, near and i.r. spectra 2−72672
α-brass, optical transitions 2−44362
celites, i.r. spectra and crystal structure 2−65254
chalcogenide glass, parasitic absorpt. bands elimination 2−54411
colour centre behaviour and band modes in semiconductors and insulators 2−54448
diamond, irradiated, absorp. obs. of N impurity effects on annealing 2−71453
diatomic molecular crystal, calc. from lattice vibr. model 2−43959
exciton absorption lines, at high exciton conc., theory 2−71807
exponential absorption edge, theory review 2−78078
F-centres, higher absorp. bands, calc., review 2−56746
feldspar, force field obs. 2−43955
fluorides, $MeF_2:Ce^{3+}$(II), optical properties, of quasi-tetragonal Ce centres 2−61646
fluorophlogopite, Ti and V impurities, absorption spectra and e.p.r., levels of Ti^{2+} and Ti^{3+} ions 2−84562
garnet, almandine, optical absorpt spectra of Fe, cubic field approx. 2−72328
glass:Nd, absorpt., effect of phase separation 2−57372
glass, chalcogenide, i.r. cond., 10^9-10^{13}Hz 2−61638
glass, chalcogenide, solid and liq., struct., n.m.r. and i.r. vibr. spectra obs. 2−60595
glass, ultrashort pulse spectra superbroadening 2−43368
glass Ti , resolution of ^{47}Ti and ^{49}Ti hyperfine lines 2−84571
glasses, binary borosilicate, vapour-deposited films, infrared absorption vibrational spectra 2−48169
glasses and melts, systems $Co(PO_3)_2$-$NaPO_3$ and $Co(PO_3)_2$-KPO_3, absorption spectra 2−84481
graphite, magnetoreflectance at high fields 2−57340
group II-IV-V_2 chalcopyrite crysts., assignment of E_1 transitions 2−81384
group II-IV-V_2 compound, polarized reflectance 2−61626
group III-V semiconductor, core levels detn. 2−65240
group VI chalcogenides, layer semicond., excitonic structure 2−81334
halides, near and i.r. spectra 2−72672
HCN, i.r. and reflection, determ. of longitudinal freqs. of fundamental vibrations and dipole derivatives 2−57351
hydroxyapatites, OH ions i.r. spectra, stretching and librational modes, H-bonding 2−61650
ice, trapped electron, optical absorption spectra 2−75295
III-V compounds, dominant second order dipole moment contribution two two-phonon sidebands in i.r. absorption 2−75284
impurity centre, Stark effect by method of average moments 2−65246
insulating crystal, magnetic side bands induced by zero point motion 2−81376
interzone transitions in b.c.c. pentavalent metals, detn. of freq. and intensities 2−80946
1-iodoalkanes, far u.v. spectra, obs. of Rydberg series leading to one of first two ionization potentials 2−74292
i.r., calibration of apparatus in 450-750 cm^{-1} range using NH_3 spectrum 2−73681
isomorphous proustite pyrargyrite series, vibrational spectra 2−44387
Kramers Kronig analysis 2−61610

Spectra continued
inorganic solids continued
lunar pyroxenes and olivines, polarized absorption spectra 2−51812
lunar surface rocks and fines, i.r. 2−62652
lunar surface rocks and fines 2−62652
magnetically ordered crystal, i.r. absorp., morphic effects 2−72359
many exciton system, optical response 2−65249
$Me^{II}Me^{VI}O_4$:U single crystals with scheelite structure, Me^{II}=Ca, Sr, Ba, Me^{VI}=Mo, W, absorption and luminescence spectra 2−68676
metal, electronic transitions, opt. const. evaluation, review 2−72292
metal, i.r. divergence, electron-phonon interaction 2−48167
metal targets, electron bremsstrahlung cross-sections 2−44361
metals, antiferromagnetic, study of coupled oscillations of mag. moments 2−84443
metals, i.r. study of chemical forms when intruded in silica framework 2−72312
metals, soft X-ray emission, core hole lifetime effects studied by nonequilibrium quantum statistical mechanics 2−48205
mica, thermally modulated absorption of Fe^{2+} ions 2−61637
micas, i.r. abs., OH vibr. region, effect of Fe conc. 2−48168
mineral, absorption spectra meas. at high shock press., apparatus design 2−61828
molecular crystal, i.r. spectra rel. to molec. vibration studies 2−54012
molecular solids, vibrational spectra, librational, torsional and translational modes 2−72362
noble metal, critical point detn., wavelength modulation derivative spectroscopy obs. 2−48160
noble metal-noble metal alloy, electronic struct., reflectance obs. 2−61174
olivine, thermally modulated absorption of Fe^{2+} ions 2−61637
optical absorpt. spectra, 4d→4f transition, 4d level binding energy 2−75301
oxide glass, alkali metal cation vibrs., far i.r. spectra study 2−71284
paramagnetic crystal, one-phonon absorpt. by impurity ions, intensity calc. 2−51331
phosphates, near and i.r. spectra 2−72672
powder, compressed pellets, i.r. refl. spectra rel. to struct. 2−68620
quartz, i.r., rel. to electrolysis in air and vacuum 2−74802
quartz, reflectance spectra, rel. to surface hydroxyl groups 2−48163
quartz glass, integral normal emissivity meas. 2−54085
rare earth aluminates and orthochromites, correls. with cryst. struct. 2−84489
rare earth and actinide ions in single crysts., two-photon absorpt. and stimulated emission 2−48225
rare earth carbonates, i.r. 2−48186
rare earth double nitrate, satellite lines, field perturbation energy 2−72345
rare earth double nitrate, satellite lines, Zeeman effect, field perturbation energy 2−72344
rare earth double nitrate, satellite lines from non-Kramers distorted trigonal lattice, calcs. 2−72343
rare earth fluorides, l.f. lattice vibrs. 2−43963
rare earth ions in cryst. field, optical transitions, interference effects 2−84494
rare earth metal garnet, containing Fe ion, absorp. 2−75305
rare earth metal halides, variation of i.r. absorption spectra with nature and structure 2−78083
rare earth oxide systems, far-i.r. absorpt., phonon excitation 2−51346
rare earth oxides, A-type, vibr. spectra and space groups 2−51355
rare earth oxyhalides, vibrs. assignments 2−57348
rare-earth pyrosilicates, vibrational spectra 2−72322
Rochelle salt, far i.r., using Fourier transform spectrometer 2−72319
ruby, h.p. absorpt. below elastic limit 2−61630
ν Scorpii, close approach of Neptune (1972) 2−73085
semiconductor, amorphous, absorption edge temp. depend. 2−75293
semiconductor, amorphous, Urbach tail in optical absorpt. edge 2−68641
semiconductor, critical point detn., wavelength modulation derivative spectroscopy obs. 2−48160
semiconductor, degenerate, free carrier absorp., quantum theory 2−51329
semiconductor, direct gap, exciton absorpt. meas. method 2−44373
semiconductor, disordered, optical absorp. edge, effective impurity model 2−61169
semiconductor, disordered, theory of electroabsorption 2−51330
semiconductor, electro-transmission in visible and near i.r., charge carrier obs. 2−51323
semiconductor, electroreflectance, effective mass eqn. for Wannier exciton examined 2−72320
semiconductor, heavily doped, absorp. edge at low temp. 2−65247
semiconductor, II-IV-V_2 and I-III-VI_2, i.r. transmission cut-off 2−78058
semiconductor, incompletely ordered, exciton light absorpt. 2−78094
semiconductor, multiphoton interband transitions, electron-hole pair multiphoton excitation probability 2−77837
semiconductor, plasmon-assisted i.r. absorpt., cyclotron resonance harmonics 2−54409
semiconductor, rel. to electronic structure calc. 2−81013
semiconductor, tetrahedral, rel. to scaling theory calc. of temp.-pressure phase diagram 2−80528
semiconductors, II-VI, deep Cu impurity, absorpt., dynamical Jahn-Teller interaction 2−80954
silicate glass, binary, corroded surface, i.r. reflection obs. 2−53541
silicate glass, ligand field spectra of Ni^{2+} and struct. 2−50409
small polaron absorption, in high electric fields 2−57344
soda glass:Tb^{3+}, excitation, absorp. and luminesc. 2−57374
spinels, II-IV, i.r. absorpt. spectra, ionic ordering 2−72342
spodiosite analogues, fund. modes, band assignments, Bravais unit cells 2−51318
sprayed metal films, absorption spectra 2−75392
transition metal complexes, trigonally distorted, theoretical investigation of electronic spectra of d^1, d^3, d^8, d^9 complexes 2−44372
transition metal dichalcogenide layers, exciton peaks, press. to 6Kbars, 80-295K 2−44378
triglycine sulphate, forbidden band width determ. 2−77932
u.v. absorption spectroscopy using synchrotron light source 2−76549

Spectra continued
inorganic solids continued
vanadates, near and i.r. spectra 2–72672
vivianite, thermally modulated absorption of Fe^{2+} ions 2–61637
wolframites, i.r. spectra and crystal structure 2–65254
Ag, spherical particles, radiative decay of surface plasmons 2–51332
Ag halides, photochemically dyed, absorption spectra 2–75392
Ag particles in glass matrix, absorpt., particle size effects 2–54412
Ag_3AsS_3, proustite, synthetic, low-temp. transform., spectral detect. 2–50930
Ag_3AsS_3 single crystal, vibrational spectra 2–44387
$AgBr:Ti^{3+}$, V^{3+}, Cr^{3+}, charge transfer spectra 2–51333
$AgCl:Ti^{3+}$, V^{3+}, Cr^{3+}, charge transfer spectra 2–51333
AgCl(Br), anharmonicity, far i.r. dielec. response study 2–61071
$AgGaS_2(Se_2)$, band struct., electrorefl. and absorpt. studies 2–75276
Al-Si-O glass, prep. and processing, i.r. spectra, crystn. products, mineral species form. 2–56557
$(Al,Cr)(ur)_6(ClO_4)_3$ low temp. polarized absorption spectrum, 7500-3500 Å, Jahn-Teller distortion 2–51289
$(Al,Ti)(ur)_6X_3$, X=Cl, Br, I, low temp. polarized absorption spectrum, 7500-3500 Å, Jahn-Teller distortion 2–51289
Al, absorpt. peak temp. shift 2–54414
Al film, struct. change effects on opt. absorpt. 2–54415
AlAs epitaxial layer, on GaAs, absorp. 2–71881
AlN_x films, preparation by reactive r.f. sputtering, absorption spectra 2–77507
α-Al_2O_3:Fe, α-Al_2O_3, Ti and α-Al_2O_3(Fe,Ti), polarized and high resolution UV, visible and IR spectra, e.s.r. spectra 2–78082
Al_2O_3/Al ribbon system, thermal spectral radiation 2–61629
Al_2O_3, ruby, far i.r. absorp., energy levels of Cr^{3+} pairs 2–68633
Ar-Xe solid solution, absorpt., 8-10.5 eV, rel. to exciton studies 2–68634
$As_xIn_{1-x}SeI$ vitreous compounds, x=1.00, 0.95, 0.90, 0.80, i.r. absorption, determ. of energy structure 2–78095
AsS, refl. spectra, 100-800 nm, at 77K and 293K 2–75277
As_2S_3, refl. spectra, 100-800 nm, at 77K and 293K 2–75277
As_2S_3, vitreous, vibrational, computer generated 2–74966
β As_4S_4 far i.r. ^{75}As nuclear quadrupole resonance 2–84595
$As_2S_3(Se_3)$, amorphous, refl. spectra, vibr. modes 2–61614
As_2Se_3, refl. spectra, 100-800 nm, at 77K and 293K 2–75277
As_2Se_3, vitreous, i.r. absorp., effects of group III A element dopant 2–61300
As_2Se_3, vitreous, vibrational, computer generated 2–74966
As_2Se_3, vitreous and crystalline, modulated absorp., electron energy spectrum obs. 2–61631
As_2Se_3 film, crystalline and amorphous, ion bombardment effects on absorp. spectrum 2–60646
$3As_2Se_3.2Sb_2Se_3$, films, amorphous, band struct. obs. 2–54186
As_2Te_3, glassy, absorp. rel. to electronic props. 2–61297
As_2Te_3, refl. spectra, 100-800 nm, at 77K and 293K 2–75277
AsTeI glass, absorp. rel. to electronic transport props. 2–61296
Au/CO adsorbed layer, i.r. refl.- absorpt. spectra study 2–60676
Au-Al, α-phase dil. alloy, refl., 1.1-11.5 eV, rel. to band struct. determ. 2–75278
Au-Cr(V) alloy systems, band struct. obs. 2–44371
Au-Zn dil. alloys, reflectivity, 2.0- 6.2 eV, transitions 2–68621
Au, refl., 1.1-11.5 eV, rel. to band struct. determ. 2–75278
Au black deposit, i.r. transmission, rel. to prep. conditions 2–57347
BN, optical transitions, pseudopotential calc. 2–61345
BP, optical transitions, pseudopotential calc. 2–61345
$BaBr_2$, F-centre absorp. 2–51336
Ba_2CaMO_6 ordered perovskites, M=Mo, Te, W, meas. of i.r. spectra, assignment of internal vibrations 2–81370
$Ba(Ce_{1-x}Ta_x)O_3$, absorption and electronic transition at $Ta^{4+}(5d^1)$ 2–75203
$BaCl_2$, F-centre absorp. 2–51336
$Ba(ClO_4)_2.3H_2O/Ba(MnO_4)_2.3H_2O$ mixed crystal, effect of uniaxial pressure on absorption spectra, confirmation of red band system of MnO_4^- as $^1T_1 \leftarrow {}^1A_1$ 2–81372
$BaCl_2.2H_2O$, i.r. spectra of H_2O in crystals 2–48170
BaF_2, absorp., low temp. plasma produced radiational defects obs. 2–71452
BaF_2, colour centres, high temp. absorpt. study 2–77597
BaFCl, X-irrad. and additively coloured, F-centres, absorpt. 2–64680
Ba_2MgWO_6 ordered perovskite, meas. of i.r. spectra, assignment of internal vibrations 2–81370
$Ba_2NaNb_5O_{15}$, far-i.r. dispersion, room temp. reflectivity spectrum analysis 2–68622
BaO, F and F^+ centres, and free carrier absorp. 2–74803
$BaSO_4:MnO_4^{2-}$, polarized optical absorption and e.s.r. spectra, crystal field transition e-t_2 assignment 2–48274
$Ba_3(VO_4)_2$ 2–44382
$Ba_2ZnGe_2O_7:Nd^{3+}$, absorpt. and fluorescence spectra, Nd^{3+} stimulated emission and laser action 2–61705
Be film, on dielec. substrate, elec. resist., supercond. transition temp., absorpt. spectra 2–72323
$Be_2Al_2Si_6O_{18}$, beryl, anharmonicity of i.r. vibration modes, reflectivity obs. 2–51317
BeF_2, vitreous, i.r. at 25°C 2–48197
Bi single crystal piezoreflectance obs. and rel. to optical interband transitions 2–65213
BiOBr(Cl)(F)(I), vibrs. assignments 2–57348
BiOI, BiOBr, BiOCl, fundamental absorp. edge, band struct. effects on laminarity 2–75287
C film, amorphous, absorpt. 2–61302
C film, amorphous, change on graphitization by light pulses 2–61030
C films, turbostratic, effects of thermal treatment, comparison with graphite 2–78080
CO, chemisorbed layer on W, vibr. freq. refl.-absorption i.r. spectra 2–47154
CO, matrix-isolated, i.r. obs. at cryogenic temps., interactions 2–68638
CO, optical spectra of trapped atoms, importance of intermolecular interactions of excited species 2–78096
CO_2, (ν_1, $2\nu_2$) vibron-phonon infrared absorption band in temp. range 88-160 K 2–81347
CO_2, electronic excitation in extreme u.v. 2–44365

Spectra continued
inorganic solids continued
$CO_2Fe(CN)_5NO.2H_2O$, i.r. spectra, cryst. chem. 2–78081
CaF_2:Eu, and g-values rel. to electronic coupling in $4f^6$ 5d config. 2–72237
CaF_2:H-, local modes studied with intense CO_2 laser 2–61632
CaF_2:La,Ce, uncoloured and X-irrad., optical absorpt., charge transfer processes 2–65253
$CaF_2:Tm^{2+}$, mechanisms effecting optical spectra of $4f^{13}$ ions 2–61625
$CaF_2:Tu^{2+}$ crystal, Stark structure of ground state of Tu^{2+} 2–61611
CaF_2, absorp., low temp. plasma produced radiational defects 2–71452
CaF_2, absorp. band growth on proton irrad. 2–71454
CaF_2, absorp. superposition due to ⟨100⟩ and ⟨110⟩ oriented F_2-centres 2–53751
CaF_2, colour centres, high temp. absorpt. study 2–77597
CaF_2, coloured, zero-phonon lines 2–53752
CaF_2, ionicity, rel. to dispersion and absorpt. energies 2–44374
CaF_2, low symmetry complexes involving hydride ions paired with rare earth ions 2–47434
CaF_2, optical absorption following intense γ- irradiation 2–84529
CaF_2, surface optical modes obs. 2–51344
CaF_2 film, emission by polaritons, 400-1100 cm^{-1} 2–65252
$CaF_2.3Ca_3(PO_4)_2:Nd^{3+}$, M-, N-, P_1- and P_2-centres absorpt. 2–64681
$CaGeO_3$-$Sr(Ba)GeO_3$ solid solutions, i.r. 2–65251
CaO, F^+ and F' absorpt. bands 2–71523
CaO, Jahn-Teller coupling in excited level of F^+ centre, uniaxial stress effects 2–68635
CaO, neutron irrad., $F_a{}^+$ centre, absorp. band obs. 2–71522
$Ca(OCl)_2.2Ca(OH)_2$, i.r. study of fundamental vibration of ClO^- anion, determ. of force constant and bond length 2–57341
$Ca(OCl)_2.4H_2O$, i.r. study of fundamental vibration of ClO— anion, determ. of force constant and bond length 2–57341
$CaO.Al_2O_3.CaF_2$, glasses, i.r. spectra rel. to coordination number determination 2–64587
CaS phosphor, activator and co-activator absorp. spectra 2–48239
$Ca_3(VO_4)_2$, luminescence, wavelength range 300-700 nm, energy levels from diffuse reflection spectra 2–84534
CaX_2 absorption in e.u.v. 25 to 72 eV 2–42882
$CdAs_2$ glass, i.r. spectra in range 2 to 25 mk 2–61627
$CdCl_2:Co^{2+}$, obs. of vibrational-electronic coupling in high resolution spectrum of spin forbidden band 2–81356
$CdCr_2S_4$, red shift peak in absorpt. band, mag. F′ centre model 2–80712
$CdF_2:Er^+$, C_{2v} local-site symmetry, absorpt. 2–78164
CdF_2, absorpt. of Er^{3+}, ion site obs. 2–54416
CdF_2, absorption spectra of Co^{2+}, V^{3+} and Cr^{3+} impurities 2–54417
CdF_2, surface optical modes obs. 2–51344
$CdGeAs_2$, $CdGeP_2$, glass, i.r. spectra in range 2 to 25 mk 2–61627
$CdGeP_2$, i.r. reflection spectra, 2-100 μ, for crystalline and vitreous state 2–72299
$CdGeP_2$, reflection coeff., spectral depend. 2–80595
$Cd_xHg_{1-x}Te$ mixed crysts., reststrahlen spectra, transverse optic modes 2–44366
CdO microcrystals, coupled surface phonon-surface plasmon modes, i.r. absorpt. 2–84263
CdP_2 glass, i.r. spectra in range 2 to 25 mk 2–61627
$CdS:Yb^{3+}$, mechanisms effecting optical spectra of $4f^{13}$ ions 2–61625
CdS, absorp. rel. to optical modulation due to moving acoustic domains 2–54418
CdS, absorption induced by strong excitation 2–78097
CdS, anomalous intensity of exciton- impurity absorp. 2–72324
CdS, at 4.2K, localized exciton struct. 2–51366
CdS, cyclotron reson. of piezoelec. polarons, far i.r. transmission 2–71924
CdS, two-phonon sidebands in i.r. absorption due to third order potential 2–75284
CdS, valence band energy levels, Γ-point, from emission spectra due to A- and B-band excitons 2–68289
CdS film, optical absorpt. edges, rel. to pot. barriers at microcryst. boundaries 2–65256
CdS single crystal, analysis using principal exciton absorption bands 2–80999
CdS_xSe_{1-x} film, transmission, 7000-21000 cm^{-1}, band gap calc. 2–61633
CdS_xSe_{1-x}, free carrier absorption 2–75288
CdSe:S, local impurity and lattice vibrs., Fermi reson., absorpt. spectra obs. 2–80895
CdSe, exciton scatt. by dislocations, absorpt. study 2–81007
CdSe, magnetooptical absorp., exciton bound to ionized centre 2–68636
$CdSe_xTe_{1-x}$, exciton reflection spectra and absorp. edge obs. 2–84517
$CdSnAs_2$, $CdSnP_2$, electroreflectance, band struct. obs. 2–81404
n-Cd_2SnO_4, Burnstein shifts, optical band gap 2–51137
CdTe, absorpt. spectra, direct exciton transitions 2–65255
CdTe, i.r. absorpt. spectra, shallow donor impurity transitions, polaron Zeeman effect 2–61634
CdTe, resonant exciton absorpt. structures 2–61200
$CeSiP_2$, i.r. transmission, refl., and absorpt. 2–80599
Cl_2, i.r.-active intermol. translational band intensities, intermol. bonding obs. 2–74967
ClO_2, i.r., crystal structure determination 2–77561
Co, mag. permeability calc. from spectral meas. 2–65155
CoO, refl., 3-27 eV, and thermorefl., 4-8 eV 2–84505
Cr complexes, Cr(III) dimethylsulfoxide compounds, i.r. and far i.r. spectra 2–51375
Cr complexes, tris sulphur chelates chromium (III), electronic absorption 2–65306
Cr III complexes, polarized crystal spectra, comparison with theoretical investigation of electronic spectra of trigonally distorted complexes 2–44372
CrB_2, electronic spectra, MOLKAO method calc. 2–71792
$Cr(III)S_6$ trigonal systems, electronic structures and MCD spectra 2–59997
Cr_2O_3, wavelength modulated reflectivity, rel. to absorp. of other Cr^{3+} containing insulators 2–65257

Spectra continued
inorganic solids continued
$Cr(ur)_6I_3$, $^4A_2 \rightarrow {}^2E$ transition, spin-orbit interaction and Jahn-Teller distortion effects in calc. of vibronic spectra 2−51291
$Cr(ur)_6I_3$ low temp. polarized absorption spectrum, 7500-3500 Å, Jahn-Teller distortion 2−51289
Cs optical constants in liquid and solid, 0.3 to 2.5 μ region, dependence on temp. 2−68596
$CsBe_2(BO_3)F_2$, i.r. 2−47210
CsBr:K, non-cubic Ag- centres in mixed crystals 2−44370
CsBr, cation impurity, i.r. absorp. 2−61635
CsBr, electric field effects on F-band 2−51347
CsBr, X-irrad. at cryogenic temps., I-, α-, H, H′ and V_4 centres 2−68038
$CsCl:K^+$ (Rb^+), impurity-induced i.r. absorpt. calcs., lattice dynamical model 2−54419
CsCl, U band shape from first electronic transition of H- and D-substitutional impurities 2−47446
CsCl(Br)(I), vibr. absorpt. spectrum of NO_2^- and NO_3^- 2−77769
$CsCrCl_3$ single crystal polarized absorption spectra, ligand field interpretation 2−81363
$CsCr(SO_4)_2.12H_2O/D_2O$, Cr^{3+} obs., trigonal field splitting 2−54400
$CsI:PO_4^{3-}(SiO_4^{4-})$, i.r. absorpt. 2−54424
$CsI:SO^{2-}{}_4$, $CrO^{2-}{}_4$, $SeO^{2-}{}_4$, i.r. absorpt. by impurity anions 2−78086
$CsMgBr_3$:Ni polarized spectra, near i.r. and visible, ligand field model interpretation 2−84483
$CsMgCl_3:CsCrCl_3$, single crystal polarized absorption spectra, ligand field interpretation 2−81363
$CsMgCl_3$:Ni polarized spectra near i.r. and visible, ligand field model interpretation 2−84483
$CsMnF_3$, perovskite, polarised i.r. refl. spectra, phonon dielec. dispersion 2−51319
$CsNiBr_3$ polarized spectra, near i.r. and visible, ligand field model interpretation 2−84483
$CsNiCl_3$ polarized spectra, near i.r. and visible, ligand field model interpretation 2−84483
$CsPbCl_3$, far i.r. refl. spectra, Kramers- Kronig analysis, optical lattice vibrs. 2−72300
Cs_2UBr_6, Zeeman effect of vibronic transitions 2−84528
$Cs_2ZrCl_6:Ir^{4+}$, high resolution MCD, and absorption spectra 2−57342
$Cs_2ZrCl_6:U^{4+}$, Zeeman effect of vibronic transitions 2−84528
Cs_2ZrCl_2, high resolution absorpt. and mag. circular dischroism spectra analysis 2−75289
Cu-Al alloy, α-phase, Fermi surface obs. 2−64888
Cu-Ni alloys, optical properties in visible and ultraviolet spectral regions 2−81330
Cu-Pd alloy, disordered and ordered, band struct., absorpt. study 2−84237
Cu, i.r. absorption of adsorbed CO 2−50537
Cu films, far-i.r. transmission, surface plasma oscillation obs. 2−54401
CuCl, electrolytic coloration, absorpt. study 2−83985
CuCl, u.v. absorption, confirmation of calc. band struct. 2−71793
CuCl and CuBr, anomalous thermal expansion with i.r. spectroscopy 2−43993
CuCl with point defects associated with impurities, absorption spectra and e.p.r. 2−75290
CuCl(Br), absorpt., 3-30 eV 2−72326
$Cu_2Fe(CN)_5NO.2H_2O$, i.r. spectra, cryst. chem. 2−78081
CuI, low temp. reflection, excitonic transitions and levels 2−72302
γ-CuI thin film, piezo-optical effect at 77K in fundamental absorption band region 2−48172
$CuInTe_2$, refl. and absorpt., rel. to band struct. determ. 2−78098
CuNi dilute alloy, induced absorptivity at 4K, virtual-bound-state obs. 2−51337
Cu_2O, 1s exciton state in green series 2−72327
Cu_2O, electric field effects on excitons, electroreflectance obs. 2−51320
Cu_2O, i.r. absorp., normally forbidden transitions obs. 2−61636
Cu_2O, $\Gamma^+{}_5$ exciton quadrupole transition rel. to static elec. field, Stark splitting 2−81406
Cu_2O, near i.r. absorpt., rel. to band scheme 2−54420
$Cu_{2-x}S$, refl. and absorpt., 400-1200 nm 2−78085
CuTe, reflection spectra, band struct. obs. 2−72301
Cu_2Te, carrier effective mass, reflection spectra obs. 2−84520
D_2:Xe, vacuum u.v. study of Wannier states, obs. of host isotope effect on linewidth 2−51341
DBr, matrix-isolated, i.r. obs. at cryogenic temp., hindered rotation 2−68637
DBr(I), matrix-isolated, i.r. obs. at cryogenic temps., interactions 2−68638
DCN, i.r. and reflection, determ. of longitudinal freqs. of fundamental vibrations and dipole derivatives 2−57351
D_2O, pulse radiolysis at -150°C, optical absorption spectrum of trapped electrons, visible and i.r. 2−48348
$DyVO_4$, uniaxial stress effects on absorp. spectra 2−51338
Er^{3+} glass, stimulated emission cross section, relative gain coeff., absorpt. and fluorescence spectra obs. 2−75323
Er^{3+} in phosphate and borate glasses, emission and absorpt. cryst. field effects, luminesc. efficiency 2−75307
Er^{3+} ions in silicate glass, photoinduced absorption spectra 2−75291
$ErCl_3.6H_2O$, optical absorption, J-level structure 2−51340
Er_2O_2S: Er^{3+}, absorp., energy levels and crystal field splittings detn. 2−51339
Eu compounds with aromatic acids, i.r. spectra 2−75324
EuO film, transparent, prep. by oxid. of Eu film, absorp. obs. 2−64568
Eu_3SiO_5, absorpt. edge shifts rel. to Curie temp. 2−48173
F_2, i.r., calc. from lattice vibr. model 2−43959
Fe-Au alloy, intraband absorpt., anomalous temp. depend. 2−81388
Fe, mag. permeability calc. from spectral meas. 2−65155
$FeBO_3$, i.r. absorpt. spectra 2−75292
$Fe_3(CN)_5NO.2H_2O$, i.r. spectra, cryst. chem. 2−78081
Fe(III) complexes, magnetic circular dichroism of d-d transition, ligand field theory analysis 2−48176
Fe(III) complexes with oxyacids, low temperature photolysis 2−75393

Spectra continued
inorganic solids continued
Fe_xO-MnO solid solns., absorpt. edge, cryst. field transitions 2−48174
Fe_3O_4, i.r. reflectivity rel. to polaronic semicond. 2−61265
Fe_2SiO_4, olivine and spinel forms, pressure- induced red shift in absorption rel. to elec. conductivity increase 2−54421
GaAs:Mg-Li, i.r. absorpt. due to pair defects, absorpt. cross section 2−81360
GaAs:Si, boatgrown and pulled, B impurity, i.r. local mode absorption spectra, comparison 2−61640
GaAs-GaP alloys, i.r. lattice absorpt., thermodynamic props. detn. 2−57074
GaAs, 5 MeV proton irrad., absorpt. 2−48177
GaAs, absorp., exciton-phonon coupling obs. 2−61642
GaAs, absorpt. spectrum, resolved free-exciton transitions 2−84259
GaAs, diffuse reflection spectra, energies of E_1, $E_1 + \Delta_1$, E_0' and E_2 peaks 2−75275
GaAs, elec. field induced interference effects at ground exciton level 2−78084
GaAs, electron and neutron irrad., i.r. absorpt. 2−72332
GaAs, eletron, and neutron irrad., i.r. absorpt. band obs. 2−48180
GaAs, exciton absorpt. meas. method 2−44373
n-GaAs, flatband electrorefl. spectra, elec. field modulation 2−68623
GaAs, i.r. lattice absorpt., thermodynamic props. detn. 2−57074
GaAs, impurity electroabsorption 2−65258
GaAs, impurity induced i.r. absorpt., calc. by Green's function technique 2−61639
GaAs, polariton (n=1 exciton) transmittance and reflectance, temp. depend. 2−81400
GaAs, two-wave and three-wave mixing in far i.r 2−48189
GaAs(P), ionicity, rel. to dispersion and absorpt. energies 2−44374
$Ga_{1-x}In_xN$, fundamental absorpt. edge and energy gap 2−72329
$Ga_xIn_{1-x}P$ alloy, electroreflectance, band struct. 2−61641
GaN, fundamental absorpt. edge and energy gap 2−72329
GaP:B, i.r., localized mode frequencies and gap mode vibrations 2−80883
p-GaP:Cu,O, bound exciton luminesc., emission and excitation spectra 2−78131
GaP:N, i.r. absorp., localized vibr. modes due to N isotopes 2−68639
GaP, diffuse reflection spectra, energies of E_1, E_0, and E_2 peaks 2−75275
GaP, polariton dispersion and damping temp. depend. from k vector space non-linear spectra 2−71710
GaP, wavelength modulated refl. spectra, band struct. 2−61616
GaP i.r. lattice absorpt., thermodynamic props. detn. 2−57074
GaSb, differential reflectivity in mag. field, Landau levels obs. 2−71795
GaSb, excitonic effects in Landau transitions at E_1 edges 2−68404
GaSb, piezoemission, stress effects on impurity and bound exciton lines 2−48179
GaSe, exciton absorpt. peak shift and phase change induced by hydrostatic press. 2−72330
GaSe, linear electro-opt. eff. at room temp., photon energy 1.25-1.96eV 2−72270
GaSe crystals, reflection, wavelength range 100-750 nm, similarity with zone structure 2−84480
GaSe single crystal, anomalous light dispersion in exciton line 2−78099
Ga_2Se_3, i.r. refl. spectra at 290K, phonon freqs. and dielec. consts. 2−75279
GaTe, absorp., forbidden band width and exciton binding energy detn. 2−75294
$GdAlO_3$:Er, Zeeman absorp., Er^{3+}-Gd^{3+} exchange interaction obs. 2−57349
$GdCl_3$, single-ion-induced absorpt. lineshapes, magnon and exciton states dispersion 2−48181
$Gd(OH)_3$, single-ion-induced absorpt. lineshapes, magnon and exciton states dispersion 2−48181
Ge:As, far i.r. absorpt., impurity conc. and compensation effects 2−68642
Ge:Sn heavily doped, absorption, temp. and concentration effects, direct and indirect transitions 2−77911
p-Ge, absorpt., photon-induced hopping on acceptors, theory 2−47923
Ge, absorption edge under pressure, high resolution meas. 2−48182
Ge, amorphous film, u.v. reflectance depend. on deposition temp. 2−54403
Ge, direct-edge electrorefl., curve fitting using one-electron theory 2−78091
Ge, electroabsorpt. edge, exciton effects 2−48189
Ge, electromodulation study of forbidden indirect transitions 2−72333
Ge, electroreflectance of heavily doped n- and p-type near direct energy gap 2−51321
Ge, far i.r. exciton and electron-hole drop absorp. 2−78100
Ge, g-factors of B impurity 2−54402
Ge, indirect exciton ground state, exciton line broadening by elec. field 2−77841
Ge, pure, singly doped and compensated p-type, far i.r. props. 2−72384
Ge electrode, determ. of recombination rate and term distribution at surface by meas. of i.r. absorption of free charge carriers 2−68423
Ge polytype, density of states and optical props. 2−61185
$GeS_2(Se_2)(Te_2)$, refl., 1-12.5 eV, 73 and 293 K 2−48161
GeS(Te), refl., 1-12.5 eV, 73 and 293 K 2−48161
$Ge_{1-x}Si_x$, wavelength modulated absorp., indirect phononless optical transitions obs. 2−68640
GeTe, amorphous and polycryst., reflectivity, electronic struct. obs. 2−61465
Ge_xTe_{1-x} alloy, amorphous, absorp. spectra, band struct. obs. 2−77904
H_2:Xe, vacuum u.v. study of Wannier states, obs. of host isotope effect on linewidths 2−51341
H_2, ortho-enriched, fundamental i.r. absorption band meas. above and below order-disorder phase transition 2−81346
H_2 ortho, absorpt. spectra rel. to libron-libron interactions 2−74975
$HBr.4H_2O$, Raman and i.r., H-bonds 2−43314

Spectra continued
inorganic solids continued
$HCl.2H_2O$, i.r. spectra, $H_5O_2^+$ ion vibrations 2−61667
Hg-Xe layer, insulator-metal transition, Wannier exciton disappearance, u.v. spectra obs. 2−51079
HgO, i.r. absorption, reln. to colour and structure changes 2−68643
HgS, cinnabar, Kramers-Kronig inversion, optical const. obs. 2−61615
$HgS_{0.2}Se_{0.8}$ solid soln., plasma i.r. reflection at 100 and 300K 2−54404
HgSe, HgSe-HgS solid solution, absorp. rel. to energy band struct. 2−84522
HgSe, $\Lambda_3-\Lambda_1$ transition, electrorefl. 2−68624
n-HgTe, pure, i.r. and magnetooptical absorp. 2−78101
HgTe, reststrahlen spectra, transverse optic modes 2−44366
In-Te system, film, band gap determ. for In_2Te_3 phase 2−60662
In film, absorp., ellipsometry obs. rel. to electronic struct. 2−72334
n-InAs, compensated, absorpt. edge obs. 2−75297
$InBO_3$, i.r. absorpt. spectra 2−75292
InN, fundamental absorpt. edge and energy gap 2−72329
InP-InAs solid solns., i.r. lattice vibrs. 2−47739
InP, electroreflection spectrum shape under depletion and enhancement conditions in surface layer 2−81433
InP, wavelength modulated refl. spectra, band struct. 2−61616
InSb:Zn,Ge, far i.r. absorp., energy levels of shallow acceptors detn. 2−75296
InSb, differential reflectivity in mag. field, Landau levels obs. 2−71795
InSb, excitonic effects in Landau transitions at E_1 edges 2−68404
n-InSb, far i.r. absorption, impurity band and shallow donors obs. 2−81389
p-InSb, i.r. absorpt. rel. to hole and plasma currents 2−72335
InSe, absorpt., 300K and 70K, 2.3 to 3.0 eV, hyperbolic excitons 2−81398
InSe, exciton-phonon interaction, absorption edge obs. 2−84518
InSe crystals, reflection, wavelength range 100-750 nm, similarity with zone structure 2−84480
$In_2Se_{3x}Te_{3(1-x)}$ single crystal, optical props. detn. 2−54422
In_2Te, refl., 1-12.5 eV, 73 and 293 K 2−48161
Ir-Pt/CO chemisorbed layer, i.r. 2−68645
K, and opt. consts. determ. in 4-10.7 eV photon energy range 2−68593
K, anomalous i.r. absorpt. and collective oscills. in small metal particles 2−65210
K, interband opt. conductivity calcs. 2−68616
$K_4As_2O_7$, i.r., normal coordinate analysis 2−77079
$KBe_2(BO_3)F_2$, i.r. 2−47210
KBr:Na, F_b centres, absorpt. 2−64682
KBr:PO_4^{3-}(SiO_4^{4-}), i.r. absorpt. 2−54424
KBr:SH^-(SD^-), i.r., expt. and interpretation 2−84491
KBr-KCl mixed crystal, with and without colour centres, spectra 2−74801
KBr, absorp., colour centre transient form., pulsed electron beam 2−53753
KBr, analysis of R_2 absorp. struct 2−51342
KBr, effect of melting on multiphonon i.r. absorp. 2−68220
KBr, i.r., molecular CO^{2-}_3 centres obs. 2−71350
KBr evaporated films, optical absorption spectra 1700-2500 Å, obs. of fine structure in exciton bands 2−44375
KBr film, i.r. reflectivity, dielectric response obs. 2−72304
KBr(Cl)(F)(I), ionicity, rel. to dispersion and absorpt. energies 2−44374
KCl:Br-, with low Br- conc., optical absorpt., 77K 2−65259
KCl:Ca, Sr, X-irradiated, thermal annealing of defects, absorp. bands obs. 2−50696
KCl:$Co(CN)_6^{3-}$, vibr. and electronic props. 2−54413
KCl:Li^+, reorientation motions of H_a-centre 2−43648
KCl:Na, absorption, coloration, Na impurity effects 2−77595
KCl:Na, F_b centres, absorpt. 2−64682
KCl:Na, non-cubic Ag- centre in mixed crystals 2−44370
KCl:Na^+, X-ray irrad., hole centres, conversion and struct., optical absorpt. 2−84523
KCl:NaCl, symmetry of far i.r. resonant-pair mode 2−84507
KCl:Pb, rapidly grown from melt, absorpt. 2−50649
KCl:SH^-(SD^-), i.r., expt. and interpretation 2−84491
KCl:SO_4^{2-}, anion vacancy trapping, i.r. absorpt. study 2−43620
KCl:Sr, X-ray induced defects, thermal annealing, absorp. obs. 2−64684
KCl:Tl, electron pulse irrad., absorpt., rel. to colour centre formation 2−71524
KCl:Tl, luminesc. excitation spectra in the region of fundamental absorpt. 2−48244
KCl:Tl, room temperature absorption 2−75333
KCl, absorption changes during flash light excitation, F-centre transformations 2−43649
KCl, analysis of R_2 absorp. struct. 2−51342
KCl, i.r., molecular CO^{2-}_3 centres obs. 2−71350
KCl, γ-irrad. at liq. N_2 temp., hardening, H_a band obs. 2−53754
KCl, reflection spectra in vacuum u.v., investigation using synchrotron radiation 2−44367
KCl crystals, absorption band spectra obs. of quasimetallic centres 2−72338
$KCl.SnCl_2.H_2O$, luminescence, absorption and emission 2−54456
2 $KCl.SnCl_2.2H_2O$, luminescence, absorption and emission 2−54456
$KFe(CrO_4)_2.2H_2O$, low temp. i.r. vibrs. 2−48175
KH_2PO_4 and KD_2PO_4, i.r. refl. obs. of high temp. phase transitions 2−71688
KI:Cu, anomalous transmission, 300-450 nm 2−72337
KI:Cu, antiresonance phenomena in transmission spectra 2−54423
KI:K, additively coloured, colloidal absorption bands 2−47448
KI:SH^-(SD^-), i.r., expt. and interpretation 2−84491
KI:Tl covalency, overlap calcs. absorption spectra 2−61643
KI-SH-, phonon sideband struct. in i.r. absorpt. spectrum 2−48185
KI, magneto-reflectance of first exciton 2−51322
KI evaporated films, optical absorption spectra 1700-2500 Å, obs. of fine structure in exciton bands 2−44375
KIO_3, crystal struct. exam. and vibrat. struct. detn. 2−71435
$KI.PbI_2.2H_2O$, luminescence, absorption and emission 2−54456

Spectra continued
inorganic solids continued
$KMgF_3$-$KMnF_3$ mixed crysts., electron irrad., single defect involving F-centre, prod. mechanism 2−68040
KN_3, i.r. absorpt., selection rules and internal ± internal and internal ± external mode absorpts. 2−72336
KN_3, u.v. irrad., absorpt. bands identification 2−75299
$KNbO_3$, i.r. absorpt., vibr. freqs. assignment 2−84476
$K_2Pt(CN)_4Br_{0.3} \times 2.3H_2O$, reflection and transmission spectra rel. to one-dimensional metallic conductivity props. 2−68339
$KTa_xNb_{1-x}O_3$, conduction band edge splitting, absorpt. study 2−54425
$KTa_xNb_{1-x}O_3$, absorpt. edge splitting, paraelec. and ferroelec. phases 2−48184
$KTaO_3$, Urbach's tail behaviour, unified mechanism 2−54430
$K[PtCl_3NH_3].H_2O$, vibr. spectra 2−48183
La, optical absorpt. spectra, 4d→4f transition, 4d level binding energy 2−75301
La complex, lanthanide (III) tropolonates, crystal field effects in i.r. spectra 2−61644
$LaAlO_3$:Nd^{3+} laser crystal, absorpt. 2−75302
$LaCl_3$:Pm^{3+}, absorption spectrum in 12000 to 28000 cm^{-1} range 2−81405
LaF_3:Er^{3+}, optical absorption, J-level structure 2−51340
$La_{2.97}In_{1.94}Ga_{3.09}O_{12}$, garnet, spectral transmission and refractive index 2−75300
La_2O_3, vibr. spectra and space groups 2−51355
Li films, absorption and structure 2−65260
$LiClO_3.3H_2O/LiMnO_4.3H_2O$ mixed crystal, effect of uniaxial pressure on absorption spectra, confirmation of red band system of MnO_4^- as $^1T_1 \leftarrow {}^1A_1$ 2−81372
LiF:Mg, thermoluminescence variation with impurity distribution 2−84552
LiF, analysis of R_2 absorp. struct. 2−51342
LiF, assignments of two-phonon i.r. absorpt. spectrum 2−61645
LiF, effect of melting on multiphonon i.r. absorp. 2−68220
LiF, isotope-induced one-phonon i.r. absorpt. 2−78103
LiF, R-centre states in the region of F and M bands 2−47445
LiF i.r. absorpt. and refl., breathing shell model 2−78102
LiF;Ti thermoluminescence variation with impurity distribution 2−84552
LiH activated by Hg-like elements, luminescence and excitation spectra 2−78137
LiH crystal, Mg-activated, photocond. excitation spectra meas. 2−77799
$LiIO_3$, near and far i.r. investigations for α and β crystals 2−84511
Li_2O-B_2O_3-GeO_2 glass, i.r. absorpt. rel. to struct. 2−47059
$LiTmF_4$:Ho^{3+}, optical absorpt., emission and excitation spectra 2−81418
Mg-Bi amorphous alloy, exciton screening 2−78115
Mg-Sb amorphous alloy, exciton screening 2−78115
MgF_2:CO(Mn)(Ni), impurity-ion spin-forbidden absorpt. enhancement by colour centres 2−78104
MgF_2, refl., emission, transmission 2−72381
$MgMoO_4$, i.r. reflection bands, shifts of polar phonon frequencies 2−81352
MgO:Co^{2+}, i.r. magnetic circular dichroism, study of first ^2E_g excited state 2−81365
MgO:Cr^{3+}, phonon sideband of R line 2−48187
MgO:Fe^{3+}, charge transfer bands, magneto-opt. struct. 2−72339
MgO:V optical absorption and magnetic circular dichroism of impurity 2−68646
MgO, ionicity, rel. to dispersion and absorpt. energies 2−44374
MgO, MeV Ne^+ irrad., F-type centre prod., absorpt. band obs. 2−68042
MgO, radiation-induced $[Na]^0$ centres 2−43651
MgO, refl., emission, transmission 2−72381
MgO, V_{oh} centre obs. from absorpt. at 2.21 eV 2−54426
MgO film, emission by polaritons, 400-1300 cm^{-1} 2−65252
$MgO.Al_2O_3$, substrate for epitaxial Si, 0.2-300 μm 2−77910
$MgO.Al_2O_3$, substrate for epitaxial Si, transmission and refl. 2−77910
$Mg_2P_2O_7$, i.r., normal coordinate analysis 2−77079
$(Mn, Fe)_3O_4$, i.r. absorp. and cation distrib. 2−61648
MnF_2:Fe^{2+}, exchange field obs. under press. 2−44304
MnF_2:Fe^{2+}, far i.r., exchange polariz. in superexchange interactions 2−81297
MnF_2, far i.r., exchange polariz. in superexchange interactions 2−81297
MnF_2, magnon sideband intensity 2−61647
MnF_2, temp. depend. absorp. intensity, two exciton transition 2−61654
MnF_2, temp. depend. oscill. strengths of optical absorp. 2−54428
MnF_2, two-magnon absorpt., spin-flop transition effects 2−54358
MnF_2, zero field circular dichroism, uniaxial stress depend. 2−44376
$MnKH(SO_4)_2.2H_2O$, Zeeman decomp. of visible absorpt. lines 2−54427
MnO:Li, electro-transmission in visible and near i.r., charge carrier obs. 2−51323
MnO, far i.r., exchange polariz. in superexchange interactions 2−81297
MnO, refl., 3-27 eV, and thermorefl., 4-8 eV 2−84505
$(Mn_{1-c}Zn_c)F_2$, i.r. absorption meas. 2−65261
MoS_2, composite exciton absorpt. spectrum, optical phonon effects 2−44377
MoS_2, layer semicond., magneto-optical interband absorp., energy band model 2−81333
$MoSe_2$, i.r. absorpt. spectra, transverse optic lattice vibr. freq. 2−78105
$MoTe_2$, composite exciton absorpt. spectrum, optical phonon effects 2−44377
$MoTe_2$, reflectivity, optical consts. Brillouin zone transitions 2−48162
n-GaAs, electroreflectance in 1.2-5.3eV photon energy range 2−68619
N_2, emission spectra of trapped atoms, obs. of vibron- and phonon-induced dipole radiation of forbidden lines 2−78096
N_2, i.r., calc. from lattice vibr. model 2−43959
NH_4HCO_3, i.r. spectrum 2−84527

- **Spectra** continued
  - **inorganic solids** continued
    - $(NO)_2$ dimer, low temperature 2−67495
    - Na, anomalous i.r. absorpt. and collective oscills. in small metal particles 2−65210
    - Na, interband opt. conductivity calcs. 2−68616
    - $Na_2As_2O_7$, i.r., normal coordinate analysis 2−77079
    - $NaBe_2(BO_3)F_2$, i.r. 2−47210
    - NaBr evaporated films, optical absorption spectra 1700-2500 Å, obs. of fine structure in exciton bands 2−44375
    - $NaCl:Ag^+$, far i.r. absorpt., expt. and calc. 2−84508
    - $NaCl:Co(CN)_6^{3-}$, vibr. and electronic props. 2−54413
    - NaCl:Tl, X-irrad., absorpt. rel. to traps responsible for 360 and 390 K glow peaks 2−54476
    - NaCl-KCl mixed crystal, with and without colour centres, spectra 2−74801
    - NaCl, effect of melting on multiphonon i.r. absorp. 2−68220
    - NaCl, F→X-centre conversion, lattice and disloc. mechanism 2−50698
    - NaCl, γ-irrad., plastic deform. effect on F-aggregate colour centres 2−53755
    - NaCl film, i.r. reflectivity, dielectric response obs. 2−72304
    - NaF:Eu crystals grown by Czochralski method, luminescence, absorption and excitation spectra 2−68686
    - $NaF:Ni^{2+}$, visible and i.r. absorpt., 300K and 80K 2−84490
    - NaF, M centre optical props. 2−51343
    - NaF slabs, for-i.r. emission assignment 2−61649
    - $NaFe(CrO_4)_2.2H_2O$, low temp. i.r. vibrs. 2−48175
    - NaI, absorpt., adsorbed O effects 2−81399
    - NaI evaporated films, optical absorption spectra 1700-2500 Å, obs. of fine structure in exciton bands 2−44375
    - $NaI.PbI_2.4H_2O$, luminescence, absorption and emission 2−54456
    - $NaMnF_3$, absorption spectra of 300K and 80K, vibration frequency determination 2−65262
    - Na_2O-SiO_2 glass, i.r. absorp., pressure depend. 2−53782
    - Nd_2O_3, vibr. spectra and space groups 2−51355
    - Nd_2O_2S, absorp. and crystal field parameters of Nd^{3+} ion 2−65263
    - tris-$Nd_2(SO_4)_3$ diffuse reflectance spectrum, meas. of Slater-Condon, Racah, Lande, bonding and screening parameters, electronic energy states 2−61617
    - $Ne:NH_3$, i.r. spectra, fine struct., rot. and inversion obs. 2−72340
    - Ni, i.r. resonance, exchange energy detn. 2−65264
    - Ni, mag. permeability calc. from spectral meas. 2−65155
    - Ni alloys, binary, optical obs. of indirect transitions from ground-state to impurity bands 2−71796
    - Ni complex, high-spin NiN_3O_2 chromophore, polarized single-cryst. electronic spectrum 2−57337
    - Ni II complexes, polarized crystal spectra, comparison with theoretical investigation of electronic spectra of trigonally distorted complexes 2−44372
    - Ni^{2+} in alkali halide lattices 2−44379
    - $NiBr_2(Cl_2)$, electronic absorpt., cryst. field parameters, phonon and magnon sidebands 2−51345
    - $Ni_2Fe(CN)_5NO.2H_2O$, i.r. spectra, cryst. chem. 2−78081
    - $Ni_{1-x-y}Fe_x{}^{2+}Zn_yFe_2{}^{3+}O_4$ ferrite, spinel, Fe^{2+} cation distrib., i.r. spectra and Mossbauer obs. 2−72341
    - NiO:Li, electro-transmission in visible and near i.r., charge carrier obs. 2−51323
    - NiO, refl., 3-27 eV, and thermorefl., 4-8eV 2−84505
    - NiO, thermoreflectance, band transition assignment 2−44368
    - NiO films, optical consts., electrochem. deposition conditions depend. 2−61618
    - $Ni_2P_2O_7$, i.r., normal coordinate analysis 2−77079
    - NiS_2, absorption, energy gap obs. 2−81020
    - NiS_2 semiconducting, absorpt. and conductivity obs., rel. to band model 2−68417
    - $NiSO_4.6H_2O$ optical activity, calc. of rotatory strengths and dipole strengths associated with electronic transitions 2−57325
    - O_2, i.r., calc. from lattice vibr. model 2−43959
    - PH_4Cl, far i.r. spectra, vibrational modes 2−72362
    - $POBr_3$, i.r. 2−44380
    - Pb halides, energy level splitting, effective Hamiltonian theory 2−44319
    - $PbBr_2$ thin films, absorpt. and reflectivity opt. const. determ., exciton stress 2−57321
    - $PbCl_2$, obs. of Fano effect in exciton spectrum 2−68647
    - $PbCl_2$, optical consts. and exciton states 2−68625
    - PbI_2, absorp. spectra rel. to band struct. calc. 2−68418
    - PbI_2, band-edge excitons model, repulsive control cell correction 2−51324
    - PbI_2, band edge excitons, refl. study 2−68626
    - PbI_2 thin film, influence of nature of substrate and preparation conditions on exciton spectrum 2−48188
    - $PbMoO_4$:Cu, Gd site occupancies of dopant and trace impurity 2−68739
    - PbO film, absorp. characs. detn. 2−57352
    - PbS, refl. spectra, X-ray photoemission, spin-orbit splitting 2−78092
    - PbS film, prep. by chem. precip., transmission spectra, optimum prep. conditions 2−75304
    - PbSe, absorp. edge and intraband transition region 2−81402
    - PbSe, refl. spectra, X-ray photoemission, spin-orbit splitting 2−78092
    - n-PbSe, reflectivity and magnetoreflectivity 2−61651
    - $Pb_{1-x}Sn_xTe$, i.r. plasma refl. study 2−84504
    - $Pb_{1-x}Sn_xTe$, optical props., refl. meas., Kramers-Kronig analysis 2−48165
    - $Pb_{1-x}Sn_xTe$, reflectivity, optical consts., energy band struct. 2−48164
    - PbTe, low temp. far i.r. reflectance, TO lattice mode obs. 2−65265
    - PbTe, optical props., refl. meas., Kramers-Kronig analysis 2−48165
    - PbTe, refl. spectra, X-ray photoemission, spin-orbit splitting 2−78092
    - $PdTe_2$, refl., 1-12.5 eV, 73 and 293 K 2−48161
    - $Pr_2Zn_{3c}Mg_{3(1-c)}(NO_3)_{12}.24H_2O$, satellite lines, field perturbation energy 2−72345
    - $Pr_2Zn_{3c}Mg_{3(1-c)}(NO_3)_{12}.24H_2O$, satellite lines, Zeeman effect, field perturbation 2−72344
    - Pt, 0.265-7 μ, 295 and 77K, rel. to band struct. 2−81358

- **Spectra** continued
  - **inorganic solids** continued
    - Pt film, for u.v. reflectance 2−61653
    - $RbBe_2(BO_3)F_2$, i.r. 2−47210
    - RbCl:Na, F_b centres, absorpt. 2−64682
    - RbCl, vibr. absorpt. spectrum of NO_2^- and NO_3^- 2−77769
    - RbH_2PO_4, i.r. refl. obs. of high temp. phase transitions 2−71688
    - RbI:K, additively coloured, colloidal absorption bands 2−47448
    - RbI, magneto-reflectance of first exciton 2−51322
    - RbI evaporated films, optical absorption spectra 1700-2500 Å, obs. of fine structure in exciton bands 2−44375
    - $RbICl_2$, vibr. spectra, cryst. symmetry 2−75313
    - $RbMnF_3$, absorp. in 3900 Å region, exciton, magnon and phonon struct. 2−65266
    - $RbMnF_3$, temp. depend. absorpt. intensity, two exciton transition 2−61654
    - $RbMnF_3$, temp. depend. oscill. strengths of optical absorp. 2−54428
    - $RbMnF_3$, uniaxial stress effects, Jahn-Teller effect in Mn^{2+} obs. 2−65268
    - $RbMnF_3$, uniaxial stress effects, Jahn-Teller effect in Mn^{2+} obs. 2−65267
    - ReO_3, absorpt., 0.11-2.8 eV, rel. to band struct. 2−84499
    - SCl_2, Raman and infrared, vibrational spectra 2−77059
    - SF_4, i.r., at low temperature 2−44381
    - SF_6 electronic structure, extreme u.v. and soft X-ray region 2−42933
    - Sb-Bi alloys, band struct., magnetoreflection obs. 2−54405
    - Sb single crystal piezoreflectance obs. and rel. to optical interband transitions 2−65213
    - Sb_2S_3 film, single cryst., optical absorp. edge obs. 2−81390
    - SbSBr, i.r. transmission, indirect transitions and band gap determ. 2−72346
    - SbSI, electro-optic effects on absorp. edge 2−81379
    - SbSI, far i.r. reflectivity, complex dielec. const. deriv., soft mode in paraelec. phase 2−61619
    - Sb_2Se_3, electron energy states for amorphous and cryst. material 2−68627
    - Sb_2Se_3 film, amorphous, absorp. and reflectivity 2−61323
    - Sc ferrite, rel. to struct. 2−54440
    - Se, amorphous, i.r. absorpt. obs. of ring-chain-struct. 2−78088
    - Se, monoclinic, excitons and direct gap, absorp. obs. 2−68648
    - Se film, crystalline and amorphous, ion bombardment effects on absorp. spectrum 2−60646
    - Se_xTe_{1-x}, synchrotron radiation absorp., d level spin orbit splitting obs. 2−81401
    - Si:Au, near i.r. absorpt. 2−72348
    - Si:B, shear deform. pot. consts. of B acceptors ground state, piezospectroscopy obs. 2−75306
    - Si:C, low temp. electron irrad., i.r. absorp. obs. 2−48191
    - Si:Ge, O, C, low temp. electron irrad. damage, i.r. obs. 2−48192
    - Si:P, absorpt. due to transitions to cond. band edge region 2−72347
    - n-Si:P epitaxial film, on $MgO.Al_2O_3$, transmission and refl. 2−77910
    - Si:P quadratic Zeeman effect of donor lines in photoexcitation spectrum, transverse effective mass 2−81348
    - Si:P(As) radiation-induced infrared absorption bands, piezospectroscopic studies 2−68650
    - Si, 2 electron transitions at liquid He temp., emission line obs. 2−51370
    - Si, cond. band. deform. potential const. from piezospectroscopy of donors 2−68438
    - Si, diffuse reflection spectra, energies of E_1, E_2 and E_1' peaks 2−75275
    - Si, electroabsorpt. edge, exciton effects 2−48189
    - Si, i.r. absorp., O and C impurities detn. 2−71502
    - p-Si, i.r. absorpt. by free carriers 2−48190
    - Si, in m.o.s. struct., surface barrier electroreflectance obs. 2−65241
    - Si, ion irrad., divacancy formation and annealing, i.r. absorpt. study 2−71457
    - Si, low field electroabsorpt., split-off exciton and phonon-depend. lineshape 2−72349
    - Si, Mg donor levels, excitation spectra 2−72351
    - Si, neutron irrad., absorp. bands, piezospectroscopic obs. 2−48193
    - Si, neutron irrad., divacancy obs. 2−48194
    - Si, neutron irrad. induced defect clusters, edge absorpt. obs. 2−47389
    - Si, optically homogeneous, refl., free carrier conc. determ. 2−54406
    - Si, pure, singly doped and compensated n-type, far i.r. props. 2−72384
    - Si, wavelength modulated reflectivity spectrum in 3.4 eV region, piezo-optical evidence for λ transitions 2−75280
    - Si crystals, reflection spectra in vacuum u.v., investigation using synchrotron radiation 2−44367
    - Si film, amorphous, absorp. and photocond. rel. to band struct. 2−61655
    - n-Si i.r. free carrier absorpt. consts. 2−81408
    - Si polytype, density of states and optical props. 2−61185
    - SiC, 6H exciton electroabsorption, exciton binding energy from optical transition spectrum 2−81331
    - α-SiC, i.r. absorpt. spectra due to electron transitions in deep impurity centres 2−78106
    - 3C-SiC, optical transitions, pseudopotential calc. 2−61345
    - SiC 6H cryst., absorption edge struct. at 9K 2−68649
    - n-SiC(6H), impurity absorpt. of i.r. rad., high-temp. meas. 2−72350
    - SiO films, evaporated, i.r. spectra 2−50505
    - SiO_2, vitreous, lattice vibrational spectra, pressure densification effects, ir. absorp. obs. 2−74971
    - SiO_2 film, r.f. sputtered, i.r. absorpt., effect of substrate temp. 2−83865
    - SiO_2 film, thermally grown, struct., i.r. absorpt. study 2−53579
    - SiO_2 films, study of transparency by luminescent method 2−44340
    - SiO_x, non crystalline, optical and bonding model 2−61656
    - SiO_x film, r.f. sputtered in Ar-O_2, i.r. absorp., O_2 conc. effects 2−60667
    - SiO_xN_y, non crystalline, optical and bonding model 2−61656
    - SmS, absorpt., rel. to semicond.-metal transition 2−80994
    - SmS, semicond.-to-metal transition under press., refl. study 2−75098

Spectra continued
inorganic solids continued
SmS, SmSe, SmTe, amorphous semicond., absorp. and diffusive reflection 2−61657
SmSe, press. depend. of optical absorpt. edge 2−75098
SmSe film, absorpt. spectra, resolution using mag. circular dichroism 2−81324
SmTe, press. depend. of optical absorpt. edge 2−75098
SmTe film, absorpt. spectra, resolution using mag. circular dischroism 2−81324
SnS(Se)(Te), refl., 1-12.5 eV, 73 and 293 K 2−48161
SnTe, optical props., refl. meas., Kramers-Kronig analysis 2−48165
$SrAlF_5$, pure and Eu^{2+}-doped, characterization 2−60726
$SrCl_2$, U-centres obs. 2−71531
SrF_2:La,Ce, uncoloured and X-irrad., optical absorpt., charge transfer processes 2−65253
SrF_2, absorp., low temp. plasma produced radiational defects obs. 2−71452
SrF_2, absorp. superposition due to ⟨100⟩ and ⟨110⟩ oriented F_2-centres 2−53751
SrF_2, colour centres, high temp. absorpt. study 2−77597
SrF_2, coloured, zero-phonon lines 2−53752
$SrGeO_3$-$BaGeO_3$ solid solutions, i.r. 2−65251
SrO, radiation-induced $[Na]^0$ centres 2−43651
$SrTiO_3$, fundamental absorpt. edge, 6-300K 2−78107
$SrTiO_3$, Urbach's tail behaviour, unified mechanism 2−54430
$SrTiO_3$, wavelength modulated absorp., rel. to phase transition 2−51348
$Sr_3(VO_4)_2$, i.r. 2−44382
TaS_2, two dimensional Van Hove singularity in band struct., reflectivity obs. 2−81380
Te, absorp. and reflection, thermomodulation rel. to energy band models 2−65242
Te, amorphous, tight binding model calc. of optical props. 2−61658
TeO_2, amorphous and cryst., electronic bonding of Cu^{2+} 2−72501
TiB_2, electronic spectra, MOLKAO method calc. 2−71792
TiC-TiN solid solution, dispersion and absorpt., band struct. determ. 2−51080
TiO_2 amorphous film, absorpt., room temp. 2−72068
TlBr(Cl), ionicity, rel. to dispersion and absorpt. energies 2−44374
TlCl, X-point direct exciton, magnetoabsorp. obs. 2−72352
TlCl(Br), anharmonicity, far i.r. dielec. response study 2−61071
$TlFe(CrO_4)_2.2H_2O$, low temp. i.r. vibrs. 2−48175
TlN_3. low temp. phase transformation, i.r. absorption and Raman scatt. study 2−74944
Tm^{3+} in phosphate and borate glasses, emission and absorpt. cryst. field effects, luminesc. efficiency 2−75307
$TmVO_4$, Jahn-Teller induced magnon sidebands 2−81377
$TmVO_4$, optical obs. spectrum obs. of cooperative Jahn-Teller transition 2−65269
U III, prep. and absorption spectra in acid solutions 2−75367
$UO_2(NO_3)_3$ crystals, anisotropy of i.r. absorption spectra 2−75308
VB_2, electronic spectra, MOLKAO method calc. 2−71792
V_2O_3, absorpt. and refl. spectra in metal-semicond. transition 2−81407
V_2O_5, reflection and transmission, long wave vibrational spectrum obs. 2−68629
W, absorpt., n and k dispersion, interband transitions 2−72353
W, emission spectra by Fourier transform spectroscopy, 1000-2300°C 2−54086
WSe_2, exciton spectrum, transmission obs. 2−81403
WSe_2, line shape of electroreflectance spectra 2−84510
WSe_2, optical response in excitonic region 2−44383
Xe, vacuum u.v. absorpt., temp. depend. 2−81371
Y-Fe garnet, effect of magnetic ordering on optical absorption spectrum 2−81392
$Y_3Al_5O_{12}$:Pr(Tb)(Eu)(Yb) colour centre investigation during γ-irradiation 2−80714
$YAlO_3$, exchange coupled Cr^{3+} pair obs. 2−72415
Y_2O_3 phosphor, effect of Eu^{3+} and Tb^{3+} concentration 2−48235
$Y_2O_2S:Er^{3+}$, absorp., energy levels and crystal field splittings detn. 2−51339
Y_2O_2S phosphor, effect of Eu^{3+} and Tb^{3+} concentration 2−48235
$Y_2SiO_5:Nd^{3+}$, absorpt., 4.2, 77 and 290K 2−78123
(Zn,Cd)S phosphors, diffuse reflection spectra for studying and controlling properties 2−75332
Zn film, on dielec. substrate, elec. resist., supercond. transition temp., absorpt. spectra 2−72323
$ZnAs_2$, edge absorp. and reflection, band structure detn. 2−51326
$Zn_xCd_{1-x}Te$, reflectivity spectra, band struct. obs. 2−78093
$Zn_xCd_{1-x}Te$ solid solution, phonon freq. detn. from reflection spectra 2−72308
$Zn_2Fe(CN)_5NO.2H_2O$, i.r. spectra, cryst. chem. 2−78081
$ZnGeP_2$, i.r. transmission, refl., and absorpt. 2−80599
ZnO:Cu film, amorphous, absorp., band struct. detn. 2−68421
ZnO:Li, light scatt., and photoconductivity, anisotropic 2−75317
(ZnO-MgO):Fe,O photoconductor transient effect, shallow trap obs. 2−84377
ZnO, two-phonon sidebands in i.r. absorption due to third order potential 2−75284
ZnO, Zeeman splitting, anomalous shallow bound states 2−51349
ZnO Electrofax layers, effect of emission on print quality 2−66883
ZnO film, Burstein-Moss effect obs. 2−51350
ZnP_2, edge absorp. and reflection, band structure detn. 2−51326
ZnS:Al,Co^{2+}, grown from melt, struct. rel. to Al additions, Co^{2+} spectra obs. 2−77559
ZnS:Be, i.r. lattice absorption, localized mode sidebands obs. 2−72385
ZnS:Co with stacking faults, piezospectroscopic effect on group of zero-phonon lines associated with centres 2−44384
ZnS, differential absorption spectrum on adsorption of molecules of donor-acceptor type 2−68651
ZnS, disappearance of electron traps under influence of pressure 2−61722
$ZnS_{1-x}Se_x$ mixed crystals, reflectivity obs., band struct. determ. 2−54407
$ZnSe:Cr^{2+}$, absorp., Jahn-Teller splitting obs. 2−65270
ZnSe, ionicity, rel. to dispersion and absorpt. energies 2−44374

Spectra continued
inorganic solids continued
$ZnSe_xTe_{1-x}$, refl., 2.0-6.6 eV, rel. to comp. depend. of energy gap 2−84500
$ZnSnAs_2$, $ZnSnP_2$, electroreflectance, band struct. obs. 2−81404
ZnTe, absorpt. due to acceptor levels 2−57353
ZnTe, resonant exciton absorpt. structures 2−61200
inorganic solids, radiofrequency
see also Nuclear magnetic resonance and relaxation; Paramagnetic resonance and relaxation
$Bi_{92}Sb_{08}$, dc-pumped, line narrowing of microwave radiation caused by nuclear electric quadrupole transition in ^{209}Bi 2−44403
InSb microwave emission explained in terms of nuclear electric quadrupole radiative transitions of ^{121,123}Sb 2−44404
Tb films, phonon emission at 15 GHz, dynamic magnetoelastic coupling obs. 2−68562
molecules
π-electron molecule, geometry influence on excited state electron structure and transitions 2−52986
asymmetric rotator, sum rules 2−42840
asymmetric rotor, rot. consts., vibr. contrib. 2−56144
asymmetric rotor rot. spectra, internal rot.-quadrupole interaction 2−56143
band intensity, fringe shift and fringe slope band analysis procedures 2−49992
calculation, applic. of molec. wave functions, review 2−50007
complex molecules, effect of solvent on electronic vibrational spectra 2−74253
diatomic, compilation of measured lifetimes 2−46502
diatomic, vibr.-rot. spectrum in perturbation theory for Morse oscillator 2−67446
double resonance, i.r.-microwave 2−42835
double-photon transitions in microwave spectroscopy 2−70657
electron transitions of dissolved molecules in solution mixtures 2−56149
equilibrium system, internal rot. effect on band contours in oscillation spectra 2−83239
forbidden transitions between rotational levels of molecule, observational possibility 2−64104
gases influence of elastic collisions on broadening 2−83418
glow discharges in air, obs. of near i.r. emission spectrum 2−46798
highly ionized, spectra and lifetimes studied by vacancy cascade spectroscopy 2−42722
integrated absorption, asymmetry effect on intensity and half width 2−52969
interpretation of vibrational spectra of polyatomic molecules 2−70665
interstellar, in dense clouds of H_2, emission and absorption of spectral lines, numbers, densities, isotopic abundances 2−75799
isotopically substituted molecules, effect of inaccurate assignments, by least squares method 2−46500
laser spectroscopy applics., high precision techniques 2−77004
lifetimes of states excited by electrons, system for direct meas. 2−52926
light absorption by two-zone molecular crystal and absorption band spectra 2−72315
linear molecules in nonpolar buffer gas, collisional broadening of rotational absorption spectrum 2−67535
linear mols., photoioniz. cross sections in valence electron approx., photoelectron spectra intensities 2−79976
microwave double reson. line intensities for pump freqs. far from reson. 2−79984
microwave spectroscopy, time dependence of saturation 2−83226
multiphoton absorption cross sections, exptl., determ. of correction factor for distrib. of laser intensity 2−49990
optical line shape of resonance of large molecules, effect of intramolecular electronic relaxation 2−64088
optical lineshapes, effects of vibrational relaxation 2−70658
optical nutation and free induction decay, Stark shifted molecular levels 2−42834
photo-electron, study of chemical effects on inner shell 2−50014
two photon spectroscopy, improved calc. method 2−49010
polar, Kerr effect and dielec. saturation formulation 2−52971
polyatomic, absorpt. and luminesc. relationship in four-level system of electronic states 2−64087
polyatomic, complex computer program for treatment of i.r. spectra 2−52968
polyatomic, intramol. interactions and vibronic spectra, electronic rearrangments and four level scheme 2−67447
polyatomic, mechanisms for internal- conversion and line broadening processes 2−49989
polyatomic, role of vibrational relaxations in formation of diffuse and complex configuration spectra 2−77045
radiative transition probabilities, electronic correls. effect 2−64086
resonance fluorescence, cross sections and quantum yields, general expressions 2−74251
RKR Frank-Condon factors for blue and u.v. transitions of molecules of astrophysical interest 2−44887
rotational lines, integral criterion of non-overlapping lines 2−56139
spin-orbit coupling in doublet states, CNDO calcs. 2−67442
spontaneous emission from driven Doppler line 2−42833
structure, review 2−83233
symmetric-top, dipolar absorption in microwave and far i.r. region 2−70655
temperature distributions in planetary atmospheres from reflected sunlight 2−62711
tetrahedral mols., microwave transitions in vibronic ground state 2−64096
triplet state geometry studied by phosphorescence microwave double resonance spectroscopy 2−50010
with tunable dye lasers, pulsed and c.w. 2−79941
u.v. absorption spectroscopy using synchrotron light source 2−76549
u.v. photoabsorption cross sections, molecules of astrophysical and aeronomic interest, critical review 2−42838
vibration-rotation interaction effect on i.r. spectra 2−42841
vibrational, effect of introducing small asymmetry into symmetric double minimum potential 2−52975
vibrational spectroscopy, reorientation and vibrational relaxation as line broadening factors 2−79981

Spectra continued
  molecules continued
    vibronic interactions in doubly degenerate electron states 2−49991
    XY_2 type, vibr. spectra freqs. and intensities calc. by method of partial oscillations 2−67448
    CH, oscillator strength of $A^2\Delta$-$X^2\Pi$ electron transition 2−59993
    CO_2-N_2-He deexcited plasma, quantitative emission spectroscopy 2−79206
    CO, vibrational-rotational band, total band absorptance and absorption coefficient 2−56140

  organic molecules and substances
    see also Molecules
    acenaphthene in stretched PVA sheets, polarized absorpt. spectra, electronic transitions 2−83276
    acenaphthene-h_{10}, d_{10}, u.v. absorption spectra 2−74282
    acenaphthenequinone, near-u.v. and visible absorpt. spectra analysis 2−70784
    acetic acid, O−H overtone bands and pot. energy curves 2−56211
    acetone, in trialkylphosphines and CCl_4 mixtures, study of intermol. interac. 2−46647
    acetophenone crystal, Zeeman splitting pattern obs., assignment of lowest triplet state 2−80061
    acetylene, vacuum u.v. spectra in solid carbon tetrafluoride 2−49957
    acetylene-d_2 in CS_2 soln., ν_3 band profile analysis, temp. depend. 2−77135
    alcohol-tetraalkylphosphorus salt, H-bond strength determination 2−53044
    alcohols, of OH band, rel. to ionization potential of H bonds 2−50076
    alkanes, halogen substituted branched chain, obs. of far u.v. spectra, conjugative effects 2−80100
    alkanes, x-ray excited fluorescence, lifetime meas. 2−42951
    alkyl benzenes, pulsed radiolysis, transitory species obs. 2−57435
    alkyl isocyanates, integrated intensity of valence vibrations 2−74290
    alternation effect in electronic spectra of organic compounds containing methylene chains 2−53040
    aniline derivatives, u.v. absorpt., temp. effect, conform. change 2−68812
    aniline vapour, vibrational analysis of absorption bands in resonance fluorescence spectra 2−70742
    anthracene, auto-association of frozen solns., absorption spectra 2−54557
    anthracene, photoelectron spectra 2−60048
    anthracene addition to ethanol solns., triplet-triplet transfer 2−76488
    anthracene crystal, reflection and luminescence spectra, evidence for surface states 2−44408
    anthracene crystals and molecules in solution, two-photon absorption spectra meas. using dye lasers 2−72354
    aromatic and hetoroaromatic, meas. of fluorescence of phosphorescence quantum yields, study of radiative and radiationless transitions 2−53039
    aromatic hydrocarbons, photoelectron spectra 2−60048
    aromatic molecules adsorbed on MgO surface, photoactivation by u.v. radiation, electronic absorption spectra 2−78206
    aromatic molecules in gaseous and condensed state, bibliography 2−48159
    aromatic mols., isotropic shifts of electronic origins and ring vibrs. 2−56207
    aromatic mols., vibronic coupling in emission spectra revealed by crystal field distortion 2−75243
    aryl isocyanates, integrated intensity of valence vibrations 2−74290
    azabenzenes rot. mixing of excited electronic states 2−80099
    azobenzene and substituted derivatives, reversible orientational photodichroism and photoisomerization in viscous solutions 2−42959
    azomethines with fluorine-containing substituents 2−75326
    azulene in frozen n-pentane, quasilinear vibrational structure of second electronic transition in absorption spectrum 2−50079
    azulene in gas phase, laser excited emission of two lowest singlet states 2−42956
    benzaldehyde environmental effects on assignment and geometry of triplet state 2−61806
    benzaldehyde vapour, active out-of-plane modes in $^1A''(n\pi^*) \leftarrow S_0$ 2−80097
    benzene, calc. of relative strengths of vibrational structure lines of $^1A_{1g} \rightarrow {}^1B_{2u}$ band in absorption spectrum 2−42962
    benzene, elec. field perturbation of A-B transition, in-plane polarisability 2−80068
    benzene, liquid, meas. of absorption spectra in u.v. region in room temp. to freezing point range 2−71208
    benzene and hexadeuterobenzene impurity, absorption spectra and exciton-phonon interaction 2−71717
    benzene molecules, substituted, shift in lowest π-electron singlet excited state 2−70748
    benzene mono-substituted derivatives, calc. of single transition energies by Pariser-Parr-Pople method 2−46594
    benzene mono-substituted derivatives, calc. of singlet energies, polarization direction, band intensities by Pariser-Parr-Pople method 2−46593
    benzene single crystal, first $\pi^* \leftarrow \pi$ transition in polarized light 2−57354
    benzene vapour, u.s. excited shift in u.v. absorption band, sound velocity dispersion curve obs. 2−56218
    benzene-d_6 and mixed crysts. with benzene, isolated Na atom absorpt., interactions 2−68653
    benzenes, dihydroxy- and diamino-substituted, electronic absorpt. spectra and struct. 2−70749
    benzenes, fluorinated, X-ray photoelectron spectra, binding energy shifts 2−83289
    benzenes, substituted, high resolution electronic spectra, rotational analyses and Stark effects 2−67509
    benzol crystal with impurities, low-temperature spectral investigations of formation of local exciton states 2−54464
    benzophenone, prompt and delayed fluorescence 2−50081
    benzoquinoline, 7,8- and 5,6-, dipole moments in ground and fluorescent states 2−74281
    p- benzoquinone, electronic transitions involved in visible and near u.v. 2−42961
    benzoxazolyl-substituted aromatic hydrocarbons, absorption and fluorescence 2−57375

Spectra continued
  organic molecules and substances continued
    benzylamine, near u.v. absorption spectrum 2−74286
    biphenyl, influence of chloro substitution on electronic spectra 2−46595
    biphenyl derivatives in dibenzofuran single crystal, e.s.r. spectra of triplet state 2−64170
    o,o′-bridged biphenyl derivatives in frozen ethanol, e.s.r. spectra, determ. electronic structure 2−64170
    biphenylene, photoelectron spectra 2−60048
    borazine, gaseous, 2000Å absorpt. system, vibronic analysis, electronic transition 2−80090
    2- and 4-bromo-pyridine quadrupole hyperfine structure in rotational spectrum 2−70754
    3,3,bromomethyl d-$_3$-diazirine, vibrational analysis of $\pi^* \leftarrow n$ transitions 2−50087
    bromothiophene, high resolution photoelectron spectra 2−60087
    butadiene, SCF and CI calcs. of electronic spectrum 2−80069
    1,3-butadienes, 1-substituted and 1,4-disubstituted, electronic spectra, comparisons between geometric isomers 2−42965
    β-carotene, absorpt., 5000-25000Å 2−72072
    β-carotene film, solid, gas adsorption effect on absorpt. spectra 2−57355
    charge transfer complexes, photoelectron energy spectra 2−64163
    chlorobenzene, u.s. excited shift in u.v. absorption curve and sound velocity dispersion curve 2−56224
    3,3-chloromethyl-d_3-diazirine, vibrational analysis of $\pi^* \leftarrow n$ transitions 2−50087
    p-chlorostyrene, electronic absorption spectrum in 2961-2743 Å range, assignment of bonds 2−64173
    chlorostyrene, ortho and meta, electronic absorption spectra 2−46597
    clathrate, possible transitions between rot. sublevels 2−54446
    cobaltocene, optical spectroscopy at 77°K, determ. of electronic structure 2−56226
    coronene ions, magnetic circular dichroism meas. 2−80089
    cyanine dyes, regularities in radiating transitions from second excited singlet state, polarization characteristics of absorption band 2−53054
    cyanoacetylene, vacuum u.v. spectrum, calc. of ionization potential 2−46600
    1,4-cyclohexadienes, 3,6 bridged, photoelectric assignment of states 2−77051
    cyclopropane, photoelectron spectra, orbital structs. 2−64175
    cyclopropylketones, u.v. spectra, electronic transitions 2−77122
    cytochrome c, absorption in presence of magnetic field, magnetic circular dichroism 2−50118
    decacyclene, absorption spectra meas., comparison with LCAO SCF MO calc. in Pariser-Parr-Popl approx. 2−42976
    1,4-diazabicyclo (2.2.2) octane and methyl analogue, struct. effects on photophys. processes 2−81512
    diazines, symmetric, of $n \rightarrow \pi^*$ transitions, expt. and theory 2−53060
    diazirine and difluordiazirine, photoelectron spectra, orbital structs. 2−64175
    p-dibromobenzene, coupling of optical phonons to $T_1 \leftarrow S_0$ transition 2−81362
    p-dibromobenzene, vibr. analysis of 2800 Å band system 2−56228
    1,4-dibromonaphthalene absorption and emission study of triplet exciton state band structure 2−47820
    dichlorobenzophenone crystal, optical and electric field effects in singlet and triplet states 2−44385
    diethylamine phosphor activated by TlCl, excitation and emission spectra of exposure to u.v. radiation 2−54484
    1,1-difluoro-2, 2-dichloroethane, proton spin echo n.m.r. spectra, subspectral analysis 2−42977
    2,3-difluoroaniline, u.v. absorption spectrum, vapour phase 2−77100
    o-dimethoxybenzene, u.v., vibration mode assignments 2−80081
    4-N-dimethylaminopyridine, EPA solution, flash photolysis, triplet-triplet absorption 2−74548
    2,3-dimethylaquinoxaline, polarization of triplet-triplet absorption spectrum 2−42979
    3,4-dimethylenecyclobutene, valence shell CNDO, INDO and CNDO-CI calculations 2−60063
    dimethyloxalate, electronic states from absorption spectra 2−42980
    dimethylsulphide-d_6, rot. Zeeman effect 2−64177
    diphenyl acetylene, photoelectron spectra 2−60048
    diphenyl crystal, absorp. rel. to luminesc. and electron excitation energy migration 2−72425
    α,ω- diphenyloctatetraene solutions in bibenzyl and n-paraffins, low-lying weak transition obs. in optical spectra 2−50121
    Drosophila melanogaster visual screening pigments in situ absorption spectra 2−69472
    dye molecules in solid lipid layers, effect of electric field on absorption spectrum 2−68801
    dye solutions, absorption and fluorescence spectra in far anti-Stokes region 2−74546
    electron absorption spectra at u.v. and visible range for computer search system 2−79969
    ethane, saturated absorption heterodyne spectroscopy 2−46609
    ethane, translational spectra due to overlap moments induced by collisions with He 2−50129
    ethanol glass, optical absorption meas. of electron trapping and solvation at 4K 2−61810
    ethyl isocyanate, emission spectra in high frequency discharge 2−42990
    ethyl pyridines, substituted, near u.v. absorption 2−53071
    ethylamine phosphor activated by TlCl, excitation and emission spectra on exposure to u.v. radiation 2−54484
    ethylene in liquid and solid rare gas matrices, absorption spectra spectroscopic study 2−46603
    europium dibenzoylmethide chelate, electronic transitions 2−65239
    fatty acid molecules, monomolecular layers, improved resolution technique 2−55765
    fine structure obs. in fluorescence spectra of laser-excited complex molecules, solid solvent selection 2−68693
    formaldehyde, double resonance of 3.5 μm He-Xe laser radiation 2−46607
    formaldehyde, isotopic separation of H and D by photopredissociation 2−67438

Spectra continued
organic molecules and substances continued
formaldehyde, semi-empirical analysis of electronic-spectrum 2−42986
formic acid, emission spectra in high frequency discharge 2−42990
formic acid, O-H overtone bands and pot. energy curves 2−56211
fulminic acid, u.v. absorpt. spectrum, gas phase, ground-excited state transition 2−80098
furazan, u.v. absorpt., non-planar state obs. and barrier to planarity 2−70768
glasses, electronic spectra of trapped electrons 2−81516
cis-glyoxal microwave spectrum in range 18-40 GHz 2−83300
grating, role of first-order autocorrelation function 2−73678
hemoprotein derivatives, circular dichroism in visible region, nonlinear iron-ligand bonds 2−64197
heterocyclic, 5-membered saturated ring, combination scatt. spectra 2−46591
heterocyclics, six-membered with O and N, AVE CI SCF calculation 2−56204
hexamethylbenzene, absorption spectra, vibronic bands 2−51351
hydrocarbon ions, closed shell, electronic absorption spectra calc. 2−42991
hydrocarbons, interpretation of photoelectron spectra using SPINDO calc. 2−77114
hydroquinone solutions, intermediate products of pulse photolysis 2−75391
impure crysts., temp. broadening and shift of phonon-free lines 2−61613
iodo-alkenes, branched chain, for u.v. spectra, effect of fluorine substitution and conjugative effects 2−80100
iodoacetylene, far-u.v. spectrum, band assignments, electronic transitions 2−80072
isocyanates, integrated intensity of valence vibrations 2−74290
isoquinoline, photoelectron spectra, perfluoro effect 2−70790
isothiazole and derivatives, photoelectron and mass spectra obs. of ioniz. pots. 2−83305
liquid crystal, cholesteric mixtures, shear-induced struct. changes, refl. spectra obs. 2−64438
macromolecule, fluorescence polarization dynamics 2−56266
macromolecules in soln., polarized luminescence for investigation of intramolecular mobility 2−60090
metallocenes, electron spectra, electronic configs. 2−64187
methane, absorption line profile using laser tuned by magnetic field 2−60076
methane, saturated absorption heterodyne spectroscopy 2−46609
methane, translational spectra due to overlap moments induced by collisions with He 2−50129
methane $^{12}CH_4$, interpretation of the F_2 sub-level of the $2\nu_3$ harmonic band 2−64188
methane absorption at 3.39 μ, effect of pressure and temp. on half-width studied using He-Ne laser 2−42998
methane in atmosphere of Jupiter, computation of transmission profiles in ν_4 band 2−48769
methane spectral line equivalent widths in Jovian atmosphere rel. to absorption line formation models 2−78535
methanol, in trialkylphosphines and CCl_4 mixtures, study of intermol. interac. 2−46647
m-, p- methoxyphenyl thioethers, u.v. absorpt., steric interactions 2−56247
methyl alcohol, saturated absorption heterodyne spectroscopy 2−46609
methyl halides, saturated absorption heterodyne spectroscopy 2−46609
methyl iodide, vacuum u.v. spectra in solid carbon tetrafluorides 2−49957
methyl pyrazines, absorption spectrum in region of $n\pi^*$ transition, evidence for second electronic state 2−46624
methyl pyridines, substituted, near u.v. absorption. 2−53071
methyl thiophenols, isomeric, electronic spectra 2−56239
methyl-substituted chloroaluminate ions, i.r. spectra, bonding 2−77117
3-methyldiazirine and 3-methyl-d_3- diazirine, electronic absorption spectra 2−56250
10-methylene anthrone, polarizations of low energy $S_n \leftarrow S_0$ transitions 2−60080
α-methylnaphthalene, liquid, specular reflection spectrum, obs. of excitons 2−80474
methylphenylsilanes, electronic-vibrational absorption spectra 2−50111
4-methylumbelliferone, acidified solutions, influence of excitation intensity on laser spectra 2−77433
micelle solns., electron excitation energy transfer and conc. phenomena 2−60523
mixed ligand metal chelates, abs. and emission spectra, lifetimes and quantum yields 2−68630
molecular cryst., biexciton spectra 2−57338
molecular cryst., impurity one-phonon spectra, mirror symmetry breakdown 2−65271
molecular crysts., dilute mixed, multicomponent cluster states, Frenkel excitons 2−84228
molecular crysts., spectroscopy, bibliography for 1970 2−48159
naphthalene, in stretched PVA sheets, polarized absorpt. spectra, electronic transitions 2−83276
naphthalene Rydberg spectrum, analysis of antiresonances 2−70783
naphthalene vapour, electron energy-loss spectroscopy 2−80131
naphthalene vapour, vacuum u.v. absorption spectrum, Rydberg series assigned 2−80064
naphthalene with indol impurity, fine structure in absorption spectra 2−54466
α-naphthol in pure and mixed crysts., electronic singlet-singlet absorpt. 2−65395
α-naphthoquinone, near. u.v. and visible absorpt. spectra analysis 2−70784
neutron, detection 2−73006
nitrobenzene, and $-d_5$, electronic structure determ. using photoelectron spectroscopy 2−56251
nitromethane, and $-d_3$, electronic structure determ. using photoelectron spectroscopy 2−56251
1-nitronaphthalene, electronic spectra and intramolec. energy transfer 2−46619

Spectra continued
organic molecules and substances continued
oligo nuclear compounds, spectra calc. by summation of spectra corresponding nitrophenols 2−83320
organic dye solutions, frequency of electronic transitions, determ. method 2−50367
organoluminor solution, absorption and fluorescence spectra, obs. of stimulated emission by exciplexes 2−67836
organotin isocyanate, integrated intensity of valence vibrations 2−74290
oxacarbocyanine, excimer and related emission at low temp. 2−66861
oxalic acid, electronic states from absorption spectra 2−42980
2(2'-oxyphenyl)-benztriazole derivatives, electronic absorpt. spectra analysis 2−83334
paraffin crysts., temp. broadening and shift of phonon-free lines 2−61613
paraffin hydrocarbons, absorption spectrum in vacuum u.v., comparison with photoelectron and electron loss spectra 2−43004
in paraffins, broadening and shift of non-phonic lines in lower Debye temp. range 2−72296
phenanthrene, photoelectron spectra 2−60048
phenanthrene, polarized absorpt. edge and exciton-photon interaction 2−44386
phenanthrenequinone, near-u.v. and visible absorpt. spectra analysis 2−70784
phenanthrenes, aryl substituted, triplet-triplet absorpt. analysis 2−65396
phenylsilane, electronic-vibrational absorption spectra 2−50111
phosgene, photoelectron spectra 2−43006
phthalaldehyde, polarizations of low energy $S_n \leftarrow S_0$ transitions 2−60080
phthalic acid, methylsubstituted, u.v. spectra, obs. of bathochromic shift of short wave bands 2−83330
phthalocyanine solns., absorpt. from excited singlet states 2−84677
phthalocyanine solns., characterization of generation region of ruby lasers 2−49379
picene, triplet-triplet absorption spectrum 3750 to 15800 Å region 2−83281
PMMA, γ-irrad., absorpt. spectrum, optical density increment, u.v. filter 2−72357
poly-N-vinylcarbazole films, doped, spectral response and sensitometric curves, positive and negative modes 2−66884
polyenes and related molecules, origin of low-lying forbidden transition 2−50119
polymer latex, particle size analysis, angular light scattering data 2−43411
polymer solutions, concentration depend. of steady state compliance 2−83373
polymethine dye, triplet state absorption and relaxation 2−77443
polymethylene dyes, stimulated emission by laser pulses 2−49377
polypeptides, α-helical, in soln., oriented circular dichroism spectrum 2−80117
polypropionic acid solutions, absorption spectra, energy transfer mechanism 2−71209
polystyrene, absorpt. spectra of O_2, contact charge transfer complexing 2−72580
polyvinylalcohol films irradiated by ^{60}Co γ-rays, trapped radicals in u.v. and visible absorption spectra 2−57437
pyrazine, absorption spectrum in region of $n\pi^*$ transition, evidence for second electronic state 2−46624
pyrazine, polarized single-crystal absorption spectra 2−78111
pyrene, Davydov splitting of first triplet state 2−61660
pyrene crystal, calc. of Davydov splitting 2−51352
pyridine, 2875 Å band system, demonstration of quasiplanarity in first excited singlet state 2−46625
pyridine, 2,4,6 tri-substituted, shift in lowest π-electron singlet excited state 2−70748
pyrimidine crystals, emission and absorption at 4.2K 2−44412
pyrimidine nucleosides, electronic spectra from circular dichroism data 2−74299
quinoline, photoelectron spectra, perfluoro effect 2−70790
quinoline in durene, triplet absorption detection of magnetic resonance 2−50114
rhodamin B molecules in cadmium arachidate multilayers in thin capacitors, electrochromic spectra 2−68802
Rhodamine 6G, excited state obs. of absorpt. and luminesc. 2−60484
rhodamine 6G, triplet state, absorpt. spectra obs. 2−46628
rhodamine 6J solutions, intermediate products of pulse photolysis 2−75391
rhodamine B, in aqueous soln., absorp. excitation spectra 2−64465
rhodamine solutions, u.v. absorption spectra in 220 to 400 nm region 2−64466
scintillators, broad absorption bandwidth, almost degenerate transitions 2−76484
selenacarbocyanine, excimer and related emission at low temp. 2−66861
spiropyrans, 2 photon excitation of molecule under laser radiation 2−78208
cis-stilbene, electronic absorp. spectra calc. 2−56259
trans-stilbene, electronic absorp. spectra calc. 2−56259
sulphuryl compounds, photoelectron spectra 2−64156
s-tetracyanobenzene complexes, electronic spectra in phosphorescent state 2−72578
s- tetracyanobenzene-benzene complex, ionic dissociation from excited Franck-Condon state 2−72579
tetracyanoquinodimethane and its mono- and di-valent anion, u.v.spectra, comparison with SCMO CI calcs. 2−70791
tetramethylpyrazine, polarized single-crystal absorption spectra 2−78111
tetrapyrole, intramolecular transitions and energy, influence of structural factors 2−53078
thiacarbocyanine, excimer and related emission at low temp. 2−66861
thiacarbocyanine dyes with different substituents in meso position, absorption spectra of solutions 2−61701
thiazyl fluoride, photoelectron spectra, vibr. analysis, comparison with LCAO calcs. 2−53083

- **Spectra** continued
  - **organic molecules and substances** continued
    - thioformaldehyde, pyrolysis products of dimethyldisulphide, photoelectron spectrum 2—72538
    - thionyl compounds, photoelectron spectra 2—64156
    - thiophene, high resolution photoelectron spectra 2—60087
    - thiophosgene, photoelectron spectra 2—43006
    - thymine and other mols., ESCA spectra, assignments and interpretation 2—77156
    - toluene, electronic structure photoelectron spectrum and SPINDO calculation 2—70793
    - toluqinone single cryst., excitonic and zero-field splittings of first triplet state 2—78209
    - s-triazine absorption spectra, obs. of Jahn-Teller distortion in lowest excited singlet state 2—46631
    - S-triazine triplet state at 3455 Å, Stark effect meas, vibronic origin of state 2—83280
    - triethylamine phosphor activated by TlCl, excitation and emission spectra on exposure to u.v. radiation 2—54484
    - triphenylamine light-induced conversion to excited triplet state of 11,12-dihydrocarbazole 2—57431
    - triphenylenes, aryl substituted, triplet-triplet absorpt. analysis 2—65396
    - triphenylmethane, exciton splitting in electronic spectra 2—81523
    - tropolone, near u.v. spectrum rel. to molec. structure, rotational band contour analysis 2—53085
    - two-photon absorption cross sections, method 2—41952
    - u.v. absorption spectroscopy using synchrotron light source 2—76549
    - vibronic spectra of absorption and luminescence, distortion of mirror symmetry 2—78108
    - 1-vinylpyrene and poly(1-vinylpyrene), photophys. processes 2—65400
    - p-xylene, relative intensities of vibr.-struct. lines in absorpt. spectrum 2—67525
    - zinc porphin, polarized sharp line absorption spectra 2—64196
  - **organic molecules and substances, infrared**
    - 3,3-bromomethyldiazirine, absorption spectra, vibrational analysis 2—50089
    - 3,3-chloromethyldiazirine, absorption spectra, vibrational analysis 2—50089
    - — 2—71447
    - — 2—80950
    - absorption bands, temp. depend. of half-band widths 2—71207
    - acenaphthene-d_{10}, vibrational assignments 2—60043
    - acenaphthene-h_{10}, vibrational assignments 2—60043
    - acenaphthylene, vibrational assignments 2—60043
    - acetone oxime, obs. 70-4000 cm^{-1}, vibrational behaviour 2—50073
    - acetonitrile, study of rotational diffusion and intermolecular interactions in liquid 2—83323
    - acetonitrile-chloroform mixtures, complex form., solid phase 2—60042
    - acetyl fluoride vibrational spectra in-phase and our-of-phase stretches 2—83314
    - acetylene-d_2, vibrational assignment of spectrum near 18.6 μm 2—46592
    - acetylenic derivatives of Si, Ge, Pb, P, As, Sb, vibr. assignment 2—56212
    - acridine and acridinium, vibr. assignment 2—60044
    - acrylonitrile-styrene copolymers, sequence distribution of acrylonitrile units 2—67528
    - acyl peroxides, depend. of C—O—O—C chain vibrs. on mol. spatial struct. 2—83327
    - aliphatic alcohols, far i.r. group frequencies 2—50075
    - alkenoxyderivatives of silicon, frequencies and intensities of C=C vibrational bands 2—53045
    - n-alkylbenzenes, l.f. vibr. spectra 2—56213
    - allyl chloride and bromide, rotational isomers 2—42952
    - amines, protonated, in aqueous solns., i.r. investig. of polarizable hydrogen bonds and pKa depend. 2—68652
    - o-, m-, p-aminobenzaldehydes, vibr. assignments 2—56214
    - m- aminobenzotrifluoride, fund. vibr. assignment 2—56215
    - ammonium carbamate, solid, room temp. spectra 2—84527
    - ammonium citrate, 700 to 4000 cm^{-1} 2—72356
    - ammonium thiocyanate and ammonium thiocyanate-d_4, thin polycrystalline films 2—48201
    - aromatic acid halides, stretching frequencies 2—70743
    - azines, triplet-triplet and singlet-singlet absorpt. band intensities, electronic transitions 2—77138
    - cis-azobenzene, vibrational assignments 2—53048
    - azolidones, i.r. absorpt. spectra rel. to H bonding and mol struct. 2—56216
    - azomethane, azomethane-d_6, gaseous and polycrystalline samples, vibrational assignments and structure 2—42957
    - n-azoxyanisole, polarization of spectra in liq. cryst. and solid states 2—82588
    - cis-azoxybenzene, vibrational assignments 2—53048
    - trans-azoxybenzene and isotopic derivatives, vibr. assignment 2—56217
    - azulene, isotopic species, vibrationally excited states 2—70746
    - benzene, i.r. dispersion study of absolute integrated absorption intensity 2—64464
    - benzene, pure and isotropic mixed crystals, absorption spectroscopic study of isotope effects intermolecular interactions 2—81357
    - benzene chromium tricarbonyl-d_6, -h_6, low temp. study, vibrational spectrum 2—70752
    - benzene single crystal, polarized light, assignment of exciton components 2—51316
    - benzoyloxyimino-4 tetrahydroquinazolines and hexahydropyrimidines, vibr. band obs. 2—53049
    - bromoacetyl bromide, energy differences between rotational isomers by absolute i.r. intensity method 2—46598
    - bromoanisole, o- and m-, vibration frequency assignment 2—74283
    - butadienetricarbonyliron vibrational spectra in gaseous, solution, liquid and solid phases, factor group analysis 2—70755
    - butyl hydroperoxides, H bonding, effect of solvent 2—46964
    - caesium methanesulphonate meas. of spectra in 4000- 300 cm^{-1} range, correlation with crystal structure 2—72375
    - camphor in polar solvents, vibrational spectroscopy study of molecular dynamics 2—70757

- **Spectra** continued
  - **organic molecules and substances, infrared** continued
    - carbonyl group, theory of valence vibration spectrum 2—60056
    - carboxylic acid hydrazides valence oscillations of N-H group 2—42967
    - carboxylic acid salts, vibr. assignment 2—60085
    - carboxylic acids, alkoxy substituted, intramol. hydrogen bonding effect on i.r. bands 2—67510
    - β-carotene, absorpt., 5000-25000Å 2—72072
    - chemical structure search by molecular spectroscopy, on computer 2—79968
    - chiral cpds., vibr. spectra and polymorphism 2—44396
    - 3-chloro-1,2,5-thiadiazole 2—42968
    - chloroacetyl chloride, energy differences between rotational isomers by absolute i.r. intensity method 2—46598
    - chloroform, cryst. films, polarization depend. components assignments, vibrs. 2—84484
    - chlorostyrenes, absorpt. bands, vibr. assignment 2—56225
    - clathrates of Ni(4-methylpyridine)$_4$(NCS)$_2$ complex study of splitting of out-of-plane CH vibration band 2—53053
    - coumarins, protonated complexes, 1400-1800 cm^{-1} 2—46599
    - crotonaldehyde 2—67503
    - cumene hydroperoxides, H bonding, effect of solvent 2—46964
    - cyclobutanecarboxylic acid, vibrational assignment 2—42973
    - cyclobutanes, substituted, i.r. spectra-structure correlations 2—56227
    - cyclohexyl hydroperoxide, with bases, OH valency oscill. band 2—46601
    - B-decachlorocarboranes, C-H valency oscill. band 2—46602
    - diacetyl 2—67503
    - dialkylureas, determ. of molecular configurations from vibrational band assignments 2—70766
    - dibenzanthracenes, vibr. analysis 2—53055
    - dibenzo[a,e,]cyclooctatetraene, spectral discrepancies rel. to synthesis 2—77099
    - 2,6-dibromoaniline 2—77145
    - dichloracetyl chloride, energy differences between rotational isomers by absolute i.r. intensity method 2—46598
    - 1,4-dichloro-2-butyne, determ. of vibrational assignment and effect of free internal rotation 2—53059
    - o-dimethoxybenzene, vibration mode assignments 2—80081
    - dimethyl sulfates vibrational, spectra, i.r. and Raman 2—83317
    - 1,1-dimethylhydrazine-monoborane, determ. of molecular structure, vibrational assignments 2—53057
    - dimethyliodoarsine, liq., normal modes of vibrs., freq. assignment 2—77141
    - 2,5-dimethylphenol 2—77101
    - dimethylphenols, 2,4- and 2,6-, vibrational assignment 2—74293
    - 2, 3- and 3, 5- dimethylphenols, assignment of observed freqs. to modes of vibration 2—60059
    - dioxan mixtures with halogens and related molecules, v.l.f. far i.r. spectra 2—83322
    - diphenyl mols., vibrational spectra 2—53056
    - diphenylamine systems, effect of H bonding 2—74280
    - ethanes, halogen substituted, barriers to internal rotation 2—50092
    - ethanol, ethanol-d_1, ethanol-He, microwave double resonance studies of collision-induced transitions 2—60118
    - ethyl thiocyanate, vibrational assignment and conformation 2—42983
    - ethylene, absorption coeffs. 2—56156
    - ethylene, high resolution spectrum, determination of rotational constants and Coriolis interactions 2—50093
    - ethylene oxide (-d_4 oxide), i.r. and Raman spectra, assignment of normal vibrations and normal coordinate analysis 2—42984
    - ethylene-d_2(-d_4), ground state rot. consts. 2—56229
    - ethylene-vinyl acetate copolymers, liquid lattice type absorption for far i.r. and millimetre waves 2—53437
    - ethylenediamine and deutero derivative, gas, liquid, solid states 2—77106
    - ethylenes, methyl substituted, gaseous and solid, torsional and internal rotation barriers 2—60067
    - fluoromethane, solid, vibr. modes, site symmetry 2—57356
    - formamide crystals, i.r. and Raman vibrational spectra 2—44395
    - formyl-2(3) furan and thiophene, valence vibr. band, splitting obs. 2—83283
    - furan, solid phase, fund. vibrs. assignment 2—72355
    - furane derivatives, 2-substituted 2—77146
    - furocoumarins, in conc. H_2SO_4, protonated complexes, 1400-1800 cm^{-1} 2—46599
    - germanium (IV)-mandelic acid coordinated cpds., absorpt. lines 2—83332
    - heterocyclic, 5-membered saturated ring, vibr. spectrum 2—46589
    - heterocyclic five membered ring compounds, solns. vibr. freq. and intensity 2—83284
    - hexamethyldisiloxane, isotopic shifts in vibrational spectra by CD_3 substitution, force constant calc. 2—46632
    - ketene, ground state rot. and centrifugal distortion consts. 2—56238
    - lanthanum ethyl sulphate:Dy^{3+}, crystal field energy levels and Zeeman spectra 2—80951
    - lithium acetate dihydrate, 20 to 3500 cm^{-1}, temp. dependence 2—72376
    - lithium citrate tetrahydrate, in mull and KBr matrix, assignment 2—60073
    - mercury(I), (II) acetate compounds, vibrational spectra, stretching frequencies determ. 2—46608
    - methane, absorption coeffs. 2—56156
    - methane, calc. of half-widths of rotational lines in ν_3-band using Anderson-Tsao-Curnutte theory 2—53105
    - methane, methane-d_4 solutions in liquid Ar, collision induced far i.r. spectra, system dynamics investigation 2—43372
    - methane, mol. rot. of dissolved CH_3D, in liq. and plastic phases 2—80586
    - methane, shocked, 3.39 μ resonance line absorption 2—83275
    - methane, studies on collision-broadened rotational lines in ν_4-fundamental 2—42999
    - methane-d_1, ground state rotational constants, perturbation allowed transitions 2—77119
    - methane-d_1, resonances and doublings 2—77118
    - methane-d_3, force constants 2—67515
    - methanetellurol and isotopic species, vibr. spectra 2—83301
    - methanol, isotopic, torsion-rotation spectra, moments of inertia, barrier heights, Kirtman perturbation constants 2—77124

Spectra continued
organic molecules and substances, infrared continued
methanol and deuterated derivs., analysis of torsion-rotation spectra 2−67518
methyl acetylene investigation of vibration-rotation bands in near infrared 2−70781
methyl bromide, pressure broadening, Stark and double-resonance spectroscopy 2−42993
methyl cyanide and isocyanide in solid Ar, matrix isolation studies 2−56246
methyl fluoride, nonlinear laser spectroscopy, elec. dipole moments 2−53063
methyl fluoride, vibr. band analysis, general harmonic force field 2−77150
methyl group stretching and bending vibrs., substituent effect on absorpt. intensities 2−56245
methyl iodide, ν_4 band, spectroscopic consts. detn. 2−60077
methyl iodide, equilibrium structure determ. from rotation-vibration interaction constants from i.r. spectra 2−42995
methyl iodide, vibrational bands 2−46611
methyl iodide crysts., harmonic vibr. freqs., harmonic intermol. pot. 2−81350
methyl iodide-d_3, assignment of overtone and combination bands in vibrational spectrum 2−70782
methyl iodide-d_3, perpendicular bands ν_5 and ν_6 2−46613
methyl iodide-d_3, vibrational fundamentals 2−46612
methyl isocyanide of d_3-derivative, vibr.-rot. band analysis 2−70780
methyl nitrite isomers 2−77149
methyl radical, vibrational frequency assignments, study by rapid scan spectroscopy 2−83299
methyl sulphite isomers 2−77149
methyl-2-propanol-1, vibrational spectra of OH groups 2−70740
methylamine, force constant determination using ^{15}N isotope shifts 2−60075
methylamine, partially deuterated, analysis w.r.t. amino group vibrations 2−46610
N-methylaniline, dissolved, low temp. i.r. study of self-association by H bonds 2−54540
methylthiophene, in CS_2 solution, out-of-plane vibrations 2−77120
molecular crystal, rel. to molec. vibration studies 2−54012
molecular solids, vibrational spectra, librational, torsional and translational modes 2−72362
monoalkylbenzenes, rel. to conformational structure determination 2−42953
monohalobenzene, monohalobenzene-d_5, calc. and interpretation of vibrational spectra 2−53066
monohalogeno(methyl)germanes, assignment of fundamental modes 2−46617
mononitro alcohols, vibrational spectra of OH groups 2−70740
monophenyl mols., vibrational spectra 2−53056
nickel (II) oxalate complexes, resolution of structure 2−61659
nitrile group, MMO LCAO investigation of conjugated nitrile structure influence on absorption band intensity 2−50104
p-nitroaniline single crystals, hydrogen bonding study, effect of temp. on band posit. and dichroic ratios 2−78110
p-nitrobenzoic acid crystals, 17 bands, assignments to vibration modes 2−78167
oxalic acid derivatives 2−67503
oxamides and thio-oxamides, hydrogen bonding obs. 2−56252
paraffins, liq., two-phonon absorpt. processes 2−74550
pentafluorostyrene in liquid phase, vibrational assignments 2−50107
pentafluorothiophenol liquid phase, vibrational assignments assuming C_{2v} symmetry 2−60078
perfluorocyclohexane, vibrational assignments 2−46620
phenazine, vibrational assignments 2−46622
phenylacetylene systems, effect of H bonding 2−74280
phenylsilane, normal vibrations and free rotation 2−46623
phospholipid-water mixtures 2−43374
polar liquids, far-i.r. and microwave absorpt., theory 2−77434
poly-γ-benzyl- L-glutamate solns., elec. dichroism 2−60083
polyimide films, uniaxially drawn, study of orientation 2−43677
polymers, method for finding effect of inelastic deformation on hydrogen bonds 2−80119
polyphenyl derivatives, vibr. assignment 2−56255
polystyrene, isotactic, crystallization from solution 2−43456
polytetrafluorethylene, low temp. lattice bands in far i.r. 2−81353
polyurethanes OH and NH absorption bands 2−53092
polyvinylidene fluoride film, far i.r. spectral investigations of structural conformations rel. to piezoelectric props. 2−61438
potassium, carbamate, solid, room temp. spectra 2−84527
propionitrile-chloroform mixtures, complex form., solid phase 2−60042
purine aqueous solutions, formation of strong polarizable H bonds with increasing protonation 2−50112
pyridine, effect of organic and inorganic electron acceptors on abs. spectra 2−46626
pyrroles, liq., vibr. spectra 2−83306
quinoline, effect of organic and inorganic electron acceptors on abs. spectra 2−46626
rotation-vibration bands, determ. of relaxation characteristics 2−56474
1.4-selenoxan, i.r. spectra in vapour, liquid and crystal states, Raman spectra of liquid and solid 2−83315
sodium carbamate, solid, room temp. spectra 2−84527
sodium citrate pentahydrate, 700 to 4000 cm^{-1} 2−72356
sodium methanesulphonate meas. of spectra in 4000-300 cm^{-1} range, correlation with crystal structure 2−72375
spectral atlas 2−64164
strontium formate, anhydrous single crysts., fund. mode assignments 2−61661
structure recognition automation by computer 2−79967
sulphalane, doublet struct. of $\nu_{as}(SO_2)$ band 2−83331
TCNQ complexes, with quinolinium and triethylammonium, vibronic effects 2−81387
tetracyano-polymethine anions, far i.r. 2−53081
1,1,2,2- tetrafluorocyclopane-d_0, d_1 and d_2, vibrational assignments 2−46629
tetrafluoroethylene oxide vibrational assignments 2−46630
tetramethylcyclobutane-1,3-dione 2−77155

Spectra continued
organic molecules and substances, infrared continued
tetramethylenecyclobutane-d_0 (-d_8), spectra meas. for vapours and solids below -190°C, symmetry assignments 2−70792
tetrolaldehyde, internal rot. effects on band contours 2−80093
thiazanes, i.r. absorpt. spectra rel. to H-bonding and mol. struct. 2−56261
thioamides, heterocyclic H-bonding formation of cyclic dimers 2−83318
thioamides, NH stretching frequencies 2−43011
thiophene, -D, in CS_2 solution, out-of-plane vibrations 2−77120
1.4-thioselenan, i.r. spectra in vapour, liquid and crystal states, Raman spectra of liquid and solid 2−83315
thiourea, ferroelec. and paraelec. phases, absorpt. 2−75309
trans-3,4-dimethyl-2,2,5,5-tetradeuteriocyclopentanone, vibrational assignment and conformational studies 2−64189
trans-3,4-dimethylcyclopentanone, vibrational assignment and conformational studies 2−64189
tri(trifluoromethyl) arsenic, phosphorus and antimony, vibr. assignment 2−56262
triallyl amine 2−43012
triaryl 1,3,5-trivinylbenzene derivatives, charact. absorpt. band obs. 2−83333
trifluorochloroethylene, absorption saturation and optical strength for CO_2 laser pulses 2−67523
1,1,1-trimethoxyethane, vibrational assignment 2−43013
trimethylchlorosilane, isotopic shifts in vibrational spectra by CD_3 substitution, force constant calc. 2−46632
trimethylene oxide and deuterated analogues, i.r. band progressions and ring puckering vibr. 2−83277
trimethylene oxide deuterated analogs, far i.r. spectra and ring puckering vibr. 2−80094
trimethyloxysilane, isotopic shifts in vibrational spectra by CD_3 substitution, force constant calc. 2−46632
vinyl trifluoroacetate, vibrational assignment depolarization ratios and configuration determ. 2−70797
1,2-dibromoethane, i.r. spectra study of medium effect on rotational equilibria 2−78109
2,3-dihydropyran, hindered pseudorotation, estimation of barrier height for half-chair inversion 2−70764
1,4-dioxene, hindered pseudorotation, estimation of barrier height for half-chair inversion 2−70764

organic molecules and substances, radiofrequency
see also Nuclear magnetic resonance and relaxation; Paramagnetic resonance and relaxation
acetyl bromide and chloride, zero-point average structures determination 2−77136
2-aminopyridine, normal and deuterated, microwave spectrum studies 2−50077
aromatic carbonyl molecules, π-π^* triplet state, steady state and transient phosphorescence microwave double resonance studies 2−42966
1- azabicyclo[2.2.2]octane, torsional oscill. from microwave spectrum 2−42958
azulene, rotational microwave spectra of ground and vibrationally excited states 2−70744
benzene in cyclohexane matrix, sensitivity of pseudo-Jahn-Teller distortion to host lattice 2−80952
benzvalene 2−77139
bicyclo[2.1.1]hexan-5-one, microwave spectrum and dipole moment 2−42964
chlorobenzol-n-butanol system, microwave absorpt. and complexing 2−67810
o- chloropyridine, microwave rot. spectrum, h.f.s., quad. coupling consts. 2−53052
cyanamide, analysis of microwave spectrum by rotation-inversion theory 2−80103
2-Cyanopyridines, microwave spectra, ring distortion 2−74295
cyclopentadienylberyllium chloride, microwave spectrum analysis 2−70763
cyclopentanone, microwave- optical double reson. of triplet state 2−80065
p-dichlorobenzene, phosphorescence microwave double resonance studies of $^3\pi\pi^*$ state 2−60060
2,3-dihydrofuran, microwave spectrum 12.4-40 GHz, Q- and R-branch assignments for ground and excited states of ring-puckering mode 2−42978
dimethylnitrosamine, microwave spectrum and dipole moment 2−80107
1,3-dioxane, microwave spectrum, rot. consts. of vibr. states, dipole moment 2−64178
electron spin echoes in photo-excited triplet states in zero field 2−54556
epoxybutyne, microwave spectrum, structure and dipole moment 2−80088
ethyl alcohol, gauche, microwave rotational spectrum 2−80092
ethylene oxide, collision broadening of rot. lines by polar mols. 2−77115
ethylene sulphone, microwave rotational spectra, structure and dipole moment determination 2−60065
2-fluoropyridines, microwave spectra, ring distortion 2−74295
fulvene, microwave spectrum and struct., bond lengths and angles 2−80096
hydroxylamine, microwave, rot. consts. and molecular structure detn. 2−56234
ketene, ground state rot. and centrifugal distortion consts. 2−56238
methane, microwave transitions in vibronic ground state 2−64096
methanol, microwave spectrum, methanol, barrier height in excited vibrational state 2−56248
methanol in excited CO stretching state, microwave spectrum, torsion-vibration-rotation interaction 2−67517
methanol-d_4, microwave spectrum, torsion-vibration-rotation interactions 2−50100
2-methoxyethanol, microwave spectrum, minimum energy conformation and molec. properties 2−50098
methyl bromide, isotopic splitting in pure rot. spectrum 2−70777
methyl isocyanide, rotational spectrum, hyperfine structure, high resolution meas. 2−56249
methyl silane microwave spectrum, vibration-internal rotation- overall rotation interactions for symmetric-top molecules 2−70779

Spectra continued
organic molecules and substances, radiofrequency continued
methylbromoform, microwave spectrum, disubstitution method for struct. determ. 2−56243
methylchlorosilane, microwave spectrum, rot., centrifugal distortion and nucl. coupling consts. 2−64190
methylene difluoride self-broadening of rotational lines meas. on double modulation microwave spectrograph 2−56242
methylenecyclopentane, microwave spectrum 2−67516
methyleneimine, mol. transient, microwave spectrum analysis 2−64186
N- methylethylidenimine, microwave spectrum, internal rot. motions 2−64183
3- methylthiophene, microwave spectrum, barrier height to internal rotation of methyl group and dipole moment 2−42997
microwave absorption lines, barriers to internal rotation from relative intensity meas. of temp. 2−42943
nitrocyclopropane, microwave spectrum 2−70786
1,3,4-oxadiazoles, isotopic species 2−43003
3- oxetanone, microwave spectrum and ring-bending vibr. 2−70787
trans 3-penten-1-yne, barrier to internal rotation and dipole moment, determination from microwave spectrum 2−50108
phosphabenzene, microwave spectrum, dipole moment and l.f. vibr. states 2−56254
polar liquids, far-i.r. and microwave absorpt., theory 2−77434
propiolic acid, microwave spectrum, conform. and dipole moment 2−56256
pyrazine-d_4 2−60084
salicyl aldehyde, structure of H bond from microwave spectra 2−43008
1,2,4,5-tetrachlorobenzene in durene, zero-field parameter signs from MODR spectra 2−65398
thioformaldehyde, microwave generation and characterization from rotational spectrum, detection in space 2−44888
thiophene, dipole moment from microwave spectra 2−42997
trifluoro(trifluoromethyl)-silane, microwave spectrum and internal rot. barrier 2−83296
trimethyl silyl isocyanate, microwave spectrum analysis 2−80076
1-chloro-3,3,3-trifluoropropyne, microwave spectra analysis 2−70759
tertiary butyl chloride, absorption spectra, concentration dependence, obs. 2−50088

Spectral line breadth
see also Doppler effect; Stark effect; Zeeman effect
— 2−67493
— 2−67387
AM stars in clusters, equivalent width data 2−58283
α-amino isobutyric acid, p.m.r. study of line widths and second moments 2−68748
astronomical spectra, resolution enhancement technique 2−85059
atomic, coherence narrowing during multiple scattering of resonance radiation, general polarization 2−42714
atomic, criterion for overlapping 2−52903
atomic level broadening due to absorption of radiation 2−42716
atomic system, Voigt profile, speed dependent, including shift parameters 2−67380
atomic two-level system, theory of saturated- absorption line shapes 2−70569
atoms in plasma study by two-particle self-energy expansion 2−56091
Born lineshift integral, second order, closed form 2−79855
broadening, of light on filament induced by moving focus 2−42115
collision broadening of spectral lines, long-range and short-range potentials 2−42839
contour of optical transition at resonance with strong field on adjacent transition 2−49343
convergent theory of spectral line broadening in impact approximation 2−52918
diatomic molecules, perturbed by linear mols. with high moment of inertia, rotational lines 2−50011
Doppler broadening of spectral lines as indication of temp. of upper atmos. 2−72816
dye laser, flashlamp pumped, spectral narrowing and freq. tuning 2−76486
elastic collisions, influence on broadening of spectral lines in a gas 2−83418
ENDOR, mechanism applicable to homogeneously broadened lines 2−55629
equivalent line width and absorption coefficients, expression derived 2−42265
ethylene oxide, collision broadening of rot. lines by polar mols. 2−77115
fast beam spectral lines, broadening due to diffraction at spectrometer entrance slit 2−45816
gas, kinetic theory, transition between Doppler and collision broadening 2−64091
gaseous nebulae recombination spectra, pressure broadening of radio recombination lines 2−75693
glass: Nd, laser induced fluorescence line narrowing spectroscopy 2−48247
glass:Nd, ion-ion energy transfer temp. depend., laser induced line narrowing obs. 2−65307
isobutyric acid-water solution, Rayleigh linewidth in critical region rel. to Kawasaki-Einstein-Stokes formula and dynamical scaling 2−46933
large molecules, effect of intramolecular electronic relaxation on optical line shape 2−64088
laser, fine struct. in homogeneous line width limit 2−55678
laser, kinetic theory for spectrally heterogeneous medium 2−55679
laser linewidth due to quantum phase and quantum amplitude noise above and below threshold 2−49396
laser-induced fluorescence line narrowing in gases and solids 2−48241
laser-induced line narrowing spectroscopy, optical pumping of low-pressure HF gas sample 2−45819
linear molecules in nonpolar buffer gas, collisional broadening of rotational absorption spectrum 2−67535
Lyman-α interstellar equivalent widths in OB-stars, Mariner 9 observations 2−58362

Spectral line breadth continued
methane, calc. of half-widths of rotational lines in ν_3-band using Anderson-Tsao-Curnutte theory 2−53105
methane, studies on collision-broadened rotational lines in ν_4-fundamental 2−42999
methane absorption at 3.39 μ, effect of pressure and temp. on half-width studied using He-Ne laser 2−42998
methyl bromide, collision broadening of 0,0→1,0 rotational line by polar molecules 2−42996
methyl bromide, pressure broadening, Stark and double-resonance spectroscopy 2−42993
methyl bromide collision broadening of o,o, rh 1.0 rot. lines 2−83303
methylene difluoride self-broadening of rotational lines meas. on double modulation microwave spectrograph 2−56242
microwave double reson. line intensities for pump freqs. far from reson. 2−79984
molecular absorption spectra, asymmetry effect on intensity and half width 2−52969
molecular laser, c.w., pressure broadened lines, obs. technique 2−73574
molecule, photoelectron bandshapes depend. on ionizing radiation freq. 2−67440
Mossbauer line shape in coupled hyperfine interactions 2−75264
Mossbauer spectra of impurity atoms in crystals, correlation influence in diffusion 2−65228
n.m.r., effect of dipolar interaction between non-equivalent nuclei 2−72505
n.m.r., sixth moment of resonance line shape, theory 2−65340
n.m.r., sixth months of dipolar broadened line shapes, theory 2−65339
non-uniform broadening of spectral lines, effect on formation process of boson avalanches 2−66906
organic crysts., impure, temp. broadening and shift of phonon-free lines 2−61613
overlapping profiles, mathematical separation 2−42260
paraffin crysts., temp. broadening and shift of phonon-free lines 2−61613
photoelectron spectra, chemical effects on linewidths 2−70597
planetary absorption line profiles and equivalent widths in spectra from two model atmospheres 2−81930
plasma, electron impact broadening of isolated spectral lines of heavy elements 2−60244
plasma, laser produced, spectral analysis of backscattered light 2−56355
plasma lines, Landau and collisional damping, numerical computation of linewidths and intensities 2−43143
polyatomic gas undergoing pulsed discharge influence of dissociative recombination on spectral sharpness 2−60297
real contour parameters determ. from observed contour for instruments with periodic instrument function 2−66836
solar Fraunhofer spectrum lines, photographic factors influencing intensities and line widths 2−48791
solid, motionally narrowed n.m.r. spectrum, use second moment for studying kinetics of nuclear motion 2−84592
Stark broadening, electron correlations in unified model 2−42720
statistical accuracy of measurements, effect of heterodyne detection 2−42263
strongly coupled two-spin system relaxed by external catalyst, determ. of relaxation parameters by line-shape analysis 2−83231
thiourea, Raman spectra above and below 169K, librational modes 2−75314
Tl, $7^2S_{1/2}$ state, self-broadening theory rel. to level crossing spectroscopy 2−49956
vibrational spectroscopy, reorientation and vibrational relaxation as line broadening function 2−79981
Ar plasma electrodeless discharge, high freq., high press., Stark widening 2−46423
^{198}Au beta spectral shape, precision analysis 2−67198
Ba plasma, laser-generated, combined electron impact and Doppler widths 2−67643
CO, half-widths of lines in fundamental and first overtone bands broadened by CO_2 and air calc. using Anderson-Tsao-Curnutte theory 2−53105
CO, solar, calc. of vibration-rotation line profiles and equivalent widths 2−73147
CO laser, gain line shape measurement using tunable semicond. laser 2−45728
CO_2 laser, spectrum generated at reduced pressure of working mixture 2−73566
CO_2 line broadening of $00^\circ1$-$(10^\circ0, 02^\circ0)_I$ transition perturbed by N_2, laser source spectroscopy 2−79993
CO_2 molecular, inclusion of velocity distribution effect 2−64119
Ca^+, measurement and calculation of Stark broadening parameters for resonance lines 2−42727
Ca^+, reson. lines, electron impact broadening 2−59914
Co I, hyperfine structure and hyperfine broadening 2−79940
Cs, emission profiles of resonance lines broadened by collisions with inert gases, extreme-wing line broadening, adiabatic potentials 2−70622
D_2, Dicke narrowing and collision broadening of depolarized Rayleigh and Raman line 2−70700
D_2, effect of collisions on Raman line profile 2−43039
D_2 vibrational level linewidths due to predissociation 2−79999
Fe-Ni, ferromagnetic resonance line width, effect of Ni content after quenching or annealing 2−72174
H, in plasma, line broadening, quasistatic and impact approx. 2−52948
H, Stark broadened Lyman-α lines, electronic shifts 2−64059
H, wings of Stark-broadened lines, Holtsmark's 5/2 power law 2−74242
H plasma line electron broadening, boundary of quasistatic region 2−77022
H_2, Dicke narrowing and collision broadening of depolarized Rayleigh and Raman line 2−70700
H_2, effect of collision Raman line profile 2−43039
H_2, line profile of $Q_{01}(1)$ vibr. resonance in Dicke narrowing zone 2−56176
H_2, rotational Raman lines, anisotropy of Dicke narrowing 2−42893
H_2, vibrational level linewidths due to predissociation 2−79999

Spectral line breadth continued
HCl in CO_2 atmosphere, line shape parameters 2−42879
HD, Dicke narrowing and collision broadening of depolarized Rayleigh and Raman line 2−70700
HD* colliding with HD or He, collision-broadened cross-sections from peak-absorbancy meas. 2−67479
HF, perturbed by compressed gases, rot. line broadening 2−53006
HF in CO_2 atmosphere, line shape parameters 2−42879
H_2O, calc. of half-widths of lines in ν_2-fundamental using Anderson-Tsao-Curnutte theory 2−53105
H_2O vapour, absorption lines in ν_1-band, collisional narrowing 2−79992
$H\alpha,\beta$ and γ spectral line profiles of solar chromospheric lines on the disk 2−48810
He, 44 71.48 Å line, plasma broadened, distant electron collisions effects 2−67429
He II, improved Stark profile calc. for lines between 256 and 4686 Å 2−46477
Hg, self broadening of Hanle signals, backscattered light obs. 2−59932
$H\gamma$ and δ equivalent widths measurement for det. absolute magnitudes of young stars 2−48701
I_2 fluorescence, laser induced line narrowing 2−74267
In spectral lines temperature effects in pressure broadening in flames 2−67413
InSb, spontaneous spin-flip Raman scattering 2−48199
K-Cs, broadening of principal series lines 2−56117
K-K collisions, broadening of principal series lines 2−56117
Mg, broadening by van der Waals interaction with Ar atoms and micro fields 2−70588
Mg II in Vega spectra, u.v. absorption lines 2−81831
Mg^+, measurement and calculation of Stark broadening parameters for resonance lines 2−42727
Mg^+ reson. lines, electron impact broadening 2−59914
N_2 laser, 337 nm pulses, coherence props. and saturation broadening 2−73570
NH_3, microwave, press. induced shifts of (J,K)=(12,12) inversion line 2−50061
N_2O, calc. of rotational half-widths for air broadened absorption lines by Anderson-Tsao-Curnutte theory 2−53105
N_2O, collisional broadening of absorption lines 2−80056
N_2O, line parameters near 4.5 μm determ. from absorption spectra with Fabry-Perot interferometer 2−46568
N_2O band intensities and half-width of N-broadened lines rotational lines in ν_3 fundamental meas. near 4.5 μ 2−42923
Na-He collisions, broadening of D_2 line at high temp. 2−74237
Na, D-line broadening during Na-He collisions 2−42784
Na, equivalent D_1 linewidth in homogeneous magnetic field 2−46435
Na atom, resonance curve narrowing in forward scattering 2−56101
Na D-lines in solar spectrum, broadening coefficients 2−55169
Nd^{3+}:$POCl_3$-$ZrCl_4$ laser, line broadening of spectrum of Nd^{3+} ion in solution, stimulated emission cross section 2−42037
O_2 A-band absorption lines at different pressures, equivalent widths 2−46570
α-$Pb(N_3)_2$:Mn^{2+}, temp. dependence of e.s.r. linewidth 2−44447
Rb, self-broadening of principal series lines at high number densities 2−79930
SO_2, tunable-laser spectroscopy of vibr.-rot. band transitions 2−60033
Si II, Stark broadening of 6347.4 and 6347.1 Å spectral lines 2−56097
Tl, resonance broadening of $7^2S_{1/2}$ state studied by level-crossing spectroscopy 2−49955
Xe plasmas electrodeless discharge, high freq., high press., Stark widening 2−46423

Spectrochemical analysis
see also Chemical analysis/by mass spectrometry; Spectroscopy
83199
aerosol production and transplant optimization for introduction of analytic materials into plasmas 2−84692
atmosphere, gas trace detection spectroscopy 2−65664
atmospheric particulates, i.r. spectra monitoring method 2−68885
atomic absorption, use of graphitic cell for laser-produced sample 2−54571
atomic absorption flame spectrometry, use of oscillating Fabry-Perot interferometer 2−84693
atomic fluorescence spectrometry, combined hollow cathode and h.f. discharge as excitation source 2−72589
Auger electron spectroscopy, applic. to surface chemistry 2−48357
Auger electron spectroscopy, general topics 2−57264
Auger spectroscopy in emission electron microscope 2−81196
borate glasses, non-destructive method for ceric/cerous ratio determ. 2−48362
carbene anthronylidene, e.p.r. spectrum 2−44496
carbohydrates in sea water, automatic spectrophotometry 2−61824
cataphoresis separation, review of uses 2−84645
chemisorbed mols. on silica; surface-chlorosilane interactions 2−84643
condensed spark discharge, spectra excitation using shunting capacitor 2−65414
differential passage spectra, low temp. calc. methods 2−65415
dual wavelength mode spectrophotometry obs. of small amounts in dense materials 2−42275
electron absorption spectra at u.v. and visible range for computer search system 2−79969
emission analysis, concentration determination precision 2−84698
emission analysis, definition of limit of determination 2−84697
emission spectra interpretation using organic liquid laser based on Rhodamine 6J 2−84702
ESCA, appl. to nitroso rubbers 2−83350
ESCA, u.v. photoexcitation, review 2−54567
ESCA, X-ray photoexcitation, review 2−54568
e.s.r. applic., review 2−54569
flame atomic absorption spectroscopy, impulse evaporation method, increased sensitivity using microprobe 2−54570
flame photometry, book on laboratory practice 2−48359
flame photometry, effects of rate of entry and composition of soln. 2−48358
flame photometry, TV recording methods 2−57442

Spectrochemical analysis continued
flame spectrometry, use of novel sample modulation technique 2−84696
flame temp. meas. by atomic fluoresc. spectrometry 2−84691
glass, corrosion, automatic analysis 2−65379
Hg, cold vapour fluorescence detector 2−75405
high temperature reactor fuel cycle, burn-up determ. 2−74184
h.v. spark pulse generator 2−60316
impurity determination in C arc, effect of easily ionized major components on sensitivity 2−65413
industrial, applic. of attenuated total reflection 2−75404
kinetic curves obs. using optical density rate of change, spectrophotometer attachment recording 2−63436
laser beam spectroscopy 2−79447
laser microprobe, background and energy corrections, statistical evaluation 2−68826
laser Raman spectroscopy, for small samples 2−61825
laser torch, use as light source for spectral isotopic determ. of gases in metals 2−84701
lunar plagioclases, e.p.r., Ti^{3+}, Fe^{3+} and Mn^{2+} obs. 2−62686
lunar surface comp. mapping using mid-i.r. spectroscopic remote sensing 2−58463
metal, partial press. and evap. rate meas. 2−50406
metals, effect of heat on O_2 determination 2−72590
metals, i.r. study of chemical forms when intruded in silica framework 2−72312
meteorite PAWEL, using laser microspectral 2−48786
methyl iodide fixation by silver zeolites 2−84640
microwave, spectrometer design 2−55626
mineral, absorption spectra meas. at high shock press., apparatus design 2−61828
mixing of fine powders for spectral anal. 2−65406
molecules structure and properties from spectra, automation by computer 2−79967
non destructive techniques for nuclear fuels 2−74174
norbornadiene, ESCA spectrum of core and valency shell electrons 2−70785
nuclear fuels, total fissile content and isotopic anal. using γ-ray spectrometry 2−74175
nuclear sample assay 2−75406
nucleotides, spectrophotometry of very small volumes using TLC method 2−75410
optical emission analysis, time decrease by increasing spark source repetition rate 2−84694
organic structure by molecular spectroscopy on computer 2−79968
photoelectron spectrometry of low concentration samples, measurement method 2−84695
photoplates, increased light sensitivity by preliminary hypersensitization, effect on spectral analysis 2−84675
pig iron, antimony content, neutron activation analysis 2−78215
plasma spectroscopy, single-spike laser-generated plasma 2−60241
pollutant gases, i.r. absorption coeffs. rel. to quantitative analysis 2−56156
pollution aerosols, by neutron and gamma ray spectrometry 2−48360
polyester resins, unsaturated, crosslinked with styrene, structure, Raman spectroscopy 2−44482
powdered samples, evaporation temp. in arc discharge 2−53508
of power station boiler flue gas, dispersive spectroscopy technique 2−48361
quantitative, description of 10 ml cell for use in Cary 81 spectrometer 2−72588
reactor fuel burn-up determ. by gamma and mass spectrometric methods 2−75408
review 2−52481
rubber, vulcanised, deformed, surface orientation obs. by polarization spectroscopy 2−84644
sample preparation variables, X-ray analysis 2−65416
single-beam u.v. gas and liq. analyzer 2−61827
spectrophotometric analysis 2−81558
steel, diffusion layer, C distrib. by local anal. method 2−47435
steel, residual contents of Ce and Ca 2−54572
steel, spectrographic determination of Ag 2−57443
steel, trace impurities, effect of alkali metal carriers 2−51479
steel and Fe alloys, of trace nonferrous metals, effect of sample particle size 2−51476
surface comp., determ. by impact radiation analysis 2−84636
thermochemical model of ESCA shifts, near equivalence of quantum mechanical potential model 2−72535
trace analysis in arc plasmas, use of external magnetic fields 2−51477
trace element analysis in arc plasma, spectral line intensity depend. on magnetic field 2−48356
u.h.f. torch spectra-scan, water quality analysers 2−44502
vacuum X-ray automation using process control computer 2−58822
X-ray fluorescence, theory of double concentration method for liquid and solid solutions 2−51487
X-ray fluorescence, using solid solution specimens, influence of quality of primary radiation 2−51486
X-ray fluorescence, using solid solution specimens, influence of quality of primary radiation 2−51485
X-ray fluorescence analyzer VRA 2, VA-W-03 single-channel analyzer 2−81557
X-ray fluorescence analyzer VRA-2, automatic 2−81556
X-ray reduction of matrix influences by means of braking continuum 2−51484
Ba, flame spectrometric determ. in presence of excess Co using phototransistors as detection devices 2−68486
Ca line intensities, effect of HCl, H_3PO_4 and $AlCl_3$ in arc and flame 2−51478
CaO-Al_2O_3-SiO_2 glasses, i.r. spectra, struct. study 2−47057
Fe-base alloys, spectrographic determination of Ag 2−57443
KCl:Pb^{2+}, grown from soln., inhomogeneous impurity distrib., spectrophotometric obs. 2−74796
NO pollution monitor, laser device based on Zeeman modulation of absorption 2−61826
NO_2 mol., inelastic photon scatt., of N_2, atmospheric pollutant monitoring 2−67496
$Na_8Al_6Si_6O_{24}X_2$ sodalite (X=Cl, Br, I), cathodochromism, elucidation of damage mechanism by ESCA 2−47447

Spectrochemical analysis continued
- $OH + NO_2 + Ar \rightarrow HNO_3 + Ar$ reaction rate const. determ. by u.v. fluorescent scatt. 2−81491
- PuO_2-UO_2 fuels, determ. of non-metallic specification impurities 2−74177
- PuO_2 nuclear reactor fuel, analysis of Pu content and impurities 2−74163
- SiO_2-Si_3N_4 film, phase composition, by spectrophotometry 2−47086
- Sn-Pb alloy, rapid detn. of Sb, Pb, Sn and Cu by atomic absorp. spectroscopy 2−78218
- Ti alloys, standard samples for determination of H_2 2−72592
- U check specimens for spectrographic analysis of nuclear fuels 2−75407
- V, Auger electron spectroscopy of surface chem. comp., chem. shift and peak intensity anal. 2−51480
- $VO_{0.92}$, Auger electron spectroscopy of surface chem. comp., chem. shift and peak intensity anal. 2−51480
- VO_2, Auger electron spectroscopy of surface chem. comp., chem. shift and peak intensity anal. 2−51480
- V_2O_3, Auger electron spectroscopy of surface chem. comp., chem. shift and peak intensity anal. 2−51480
- $ZnWO_4:Cr^{3+}$, impurity conc. determ. 2−78157
- Zr concentrates, determination of impurities 2−72591

Spectrometers
- *see also Mass spectrometers; Monochromators; Particle spectrometers; Spectrophotometers; X-ray spectrometers*
- aerosol beam, focusing and spectrometry 2−85158
- complex permittivity meas. using unbalanced a.c. bridge and chart recorder 2−82419
- computer controlled, at McDonald observatory 2−45010
- Coude spectrograph, Kitt Peak, calibration curves for various emulsions 2−76041
- coude spectrograph system, astronomical 2−58573
- densitometer attachment, for gel electrophoretic meas. for Unicam SP800 spectrophotometer 2−73680
- DFS-12, standard illuminator, effect of refractive index on intensity 2−45826
- double, optimum slit settings at high grating angles 2−79441
- double beam, technique to meas. i.r. dichroism, stress, strain of elongated polymers 2−84465
- Echelle spectrograph for use in image tube, optimization of optics 2−76543
- electron, low energy, book 2−41925
- electron bombardment surface ion desorption apparatus 2−43491
- Fabry-Perot, adjustment for compensation of Doppler shift from rapidly rotating and flowing sources 2−70081
- Fabry-Perot, with stepwise automatic scanning 2−42273
- Fabry-Perot interferometer, obs. of weak signals by press. scanning 2−79437
- Fourier, diaphragm geometry effect on instrumental function 2−59284
- Fourier transform, using all reflection interferometer 2−59282
- Fresnel zone plate, with central stop 2−59283
- grating, concave toroidal, for spectrographs using Iglya scheme 2−73679
- grating, polarization calibration 2−63430
- grating, principle of operation, role of first-order autocorrelation function 2−73678
- imaging spectral radiometer, optical design for Earth resources applications 2−84775
- interference, with selective modulation 2−42268
- i.r., calibration in 450-750 cm^{-1} range using NH_3 spectrum 2−73681
- i.r., method for spectral purity determ. 2−82587
- i.r., using m.o.s. elements, patent 2−82590
- i.r. diffractional spectrometer, estimates of efficiency 2−45821
- i.r. Fourier transform interferometer with 500-5000 cm^{-1} bandwidth 2−62818
- laser, for use with optical-acoustic method 2−42259
- microspectrofluorimeter, automatic digital data logging 2−76548
- microspectrofluorimeter, intensity excitation and absorption spectra measurement 2−63434
- multichannel solar spectrometer at Sacramento Peak Observatory 2−76051
- neutron and gamma ray, inorganic analysis of pollution aerosols 2−48360
- nonlinear, using tunable lasers 2−45820
- optical array, for liquid water content obs. 2−57975
- particle size, electro-optical technique, meas. from aircraft 2−82579
- phosphoroscopes, disc, for phosphorescence decay meas. 2−79440
- pseudo-double beam atomic absorption, capable of compensating for nonspecific absorption 2−59287
- pulse, low-noise, non-stationary noise obs. 2−70303
- Raman, highly efficient, using tunable laser 2−42270
- Raman, laser light source 2−59291
- reflective scattering arrangement for obtaining laser Raman spectra of corrosive melts up to 1100°C 2−70083
- remote sensing of Earth resources with solid state multispectral imager 2−84776
- scanning, wavelength calibration by three shared system 2−52488
- scanning electron microscope-probe analyser combination, use in examination and anal. of ceramics 2−71414
- scanning Fabry-Perot, excitation resonance charact. 2−49449
- seismic waves, operational frequency analysis, infrasonic spectrometer-analyzer 2−57507
- sensitivity in optical region 2−42470
- single beam with internal reference 2−82583
- spectroradiometer, integrating-sphere 2−79442
- standard illuminator, of DFS-12 spectrometer, effect of refractive index on intensity 2−45826
- step by step scanned, digital recording of Raman spectra 2−42276
- TV recording of spectrum 2−55774
- two-mirror, plane-grating spectrograph, theory and aberrations 2−42271
- ultravariable resolution single interferometer echelle scanner 2−42266
- wavelength independent transmission grating spectrometer 2−42277
- X-ray fluorescence analyzer VRA 2, VA-W-03 single-channel analyzer 2−81557

Spectrometers continued
- X-ray fluorescence analyzer VRA-2, automatic spectrochemical analysis 2−81556
- Zeeman, utilizing laser in mag. field 2−63428
- Al single crystals, possibility of use of oscillating film spectrometer for detn. of dislocation density homogeneity 2−77582
- NO_2 photometric measurements in atmosphere using Fabry-Perot filters 2−54827
- NaI(Tl), non-linear energy response, correction, matrix method 2−55900
- **accessories**
  - automatic balanced bridge for e.p.r. spectrometer 2−66665
  - Cary 81, description of 10 ml cell for use in quantitative analysis 2−72588
  - cell, i.r.-u.v.-visible, high pressure, high temp., for in situ catalyst obs. 2−59290
  - Coude spectrograph of 188 cm reflector, high resolution scanning equipment 2−48824
  - Czerny-Turner 10m spectrograph, performance assessment 2−70693
  - dewar insert for Gigahertz- ultrasonics and ultrasonic paramagnetic resonance obs. 2−63203
  - differential absorption, optically pumped, slow traps in insulators 2−68427
  - double monochromator with two diffraction gratings 2−59285
  - Ebert, u.v., exit slit mirrors 2−70085
  - echelle, calibration and wavelength calculation 2−42280
  - far i.r. echelette gratings, obs. and production 2−42282
  - furnace for obtaining high temp. Raman spectra 2−55775
  - gradientless temp. cell for optical study of cpds. in elec. fields 2−82588
  - grille densitometer for photographic spectrograph 2−42281
  - heat-pipe oven for homogeneous mixtures of saturated and unsaturated vapours 2−49453
  - IKS-14A spectrophotometer attachment for specular-reflection spectra meas. 2−59288
  - multichannel emission spectrometry use of photodiodes and phototransistors as detection devices 2−68486
  - n.m.r., Varian HA-100, automatic lock holder 2−66671
  - n.m.r. superconducting solenoid mag. field nonuniformity compensators 2−61250
  - optical cell, high pressure, for biochemical solution obs. 2−45825
  - optical cell, high pressure for obs. in temp. range 77 to 500 K 2−66856
  - optical cryostat for two-beam spectrophotometers 2−73682
  - pulse photolysis apparatus 2−75391
  - quartz microcells 2−75410
  - RE-1301 radio spectrometer, mag. field intensity marker pickup circuit 2−59009
  - ruling engine, 750 mm, for producing large gratings and echelles 2−42221
  - for spectrograph DFS-5, use in meas. of vacuum u.v. reflection spectra meas. at large angles of incidence 2−66855
  - spectrophotometer attachment for recording kinetic curves 2−63436
  - spectrophotometers, SF-10 and SF-14, automatic recording of optical characteristics variations of sample 2−59289
  - vacuum u.v. spectrograph, for low temp. study of crystals 2−49454

Spectrometers, radiofrequency
- *see also Nuclear magnetic resonance and relaxation/measurement; Paramagnetic resonance and relaxation/measurement*
- double nuclear resonant, patent 2−78986
- electron double paramagnetic resonance spectrometer with cylindrical bimodal cavity 2−73489
- ENDOR, experimental techniques 2−63205
- ENDOR, show wave resonance system 2−82411
- ENDOR equipment, description 2−82408
- ENDOR high pressure cavity, F centre hyperfine interactions 2−82412
- e.p.r., sensitivity cals. noise performance 2−55627
- e.p.r. and mag. circular dichroism spectrometer 2−78983
- e.s.r., broadband low-field 2−78985
- e.s.r., fast-sampling, time resolved for photoflash expts. with gases 2−66663
- with frequency modulation, use of receiver with follow-up heterodyne 2−76422
- Hertzian, for free radical studies 2−76542
- high resolution magnetic spectrometer for energy selecting electron microscope 2−82431
- microwave, design for chemical anal. 2−55626
- microwave X-band, dewar insert for Gigahertz-ultrasonics and ultrasonic paramagnetic resonance obs. 2−63203
- n.m.r., autodyne, attenuation of modulation noise 2−76427
- n.m.r., electromagnet current stabilizer 2−76424
- n.m.r., lock channel modification allowing obs. of variety of nuclei 2−63208
- n.m.r., low-level for in situ magnetic field obs. at low temps. 2−63209
- n.m.r., multiple pulse, low power 2−66675
- n.m.r., phase transient obs. 2−45628
- n.m.r., pulse generator design 2−63207
- n.m.r., R22, high resolution 2−41893
- n.m.r., R-24, high resolution 2−41894
- n.m.r., Varian HA-100, automatic lock holder 2−66671
- n.m.r. apparatus, patent 2−73491
- n.m.r. probe, crossed-coil, high sensitivity low-temp. meas. 2−82410
- n.m.r. probe, for operation at v. low temps. 2−55635
- n.m.r. spectrometer, low level, for in situ obs. at low temps. 2−63209
- n.m.r. wide-line spectrometer, applications and production details 2−55634
- n.q.r., induction, frequency swept, injection locked, with signal averaging 2−45629
- PKW marginal oscillator, performance improvement 2−73500
- RE-1301, mag. field intensity marker pickup circuit 2−59009
- Stark microwave cavity, Q-pulling effect, error compensation 2−66662
- submillimetre, power stabilization 2−76423

Spectrophotometers
- accessories, dichroic mirror using interference layers to split light into predominantly green, red beams 2−42279

Spectrophotometers continued
atomic absorption, conversion to measure absorption in solution 2−63424
attachment for recording kinetic curves 2−63436
automatic, dissolved carbohydrate determ. in sea water 2−61824
automatic digitalized system 2−63433
cell, i.r.-u.v.-visible, high pressure, high temp., for in situ catalyst obs. 2−59290
30-inch coude spectrograph, instrumental profile 2−51876
densitometer attachment for Unicam SP800 for gel electrophoretic meas. 2−73680
design, three-dimensional optical diffusion theory 2−45824
differential, dual wavelength, theory and construction 2−42275
Dobson, atmospheric O_3 content, circuit modification 2−75539
double prism monochromator, automatic, wavelength setting by prepunched paper tape 2−66852
electronic scanning phototransducer for investigation of rapid processes 2−42278
flame emission, Quantacon-Foto-Multiplier, for increased sensitivity 2−66854
IKS-14A spectrophotometer attachment for specular-reflection spectra meas. 2−59288
impulse differential, high time resolution 2−52491
i.r., two beam, obs. of atmospheric transmission 2−48508
microspectrofluorimeter, intensity excitation and absorption spectra measurement of small samples 2−63434
nonlinearity correction determ. by double aperture method 2−79373
optical cryostat for two-beam spectrophotometers 2−73682
photoelectric stellar spectrophotometer with pressure scanned Fabry-Perot etalon and echelle grating 2−73162
polarization, spectral analysis of small single crystals at low temps. 2−42272
rapid scan microspectrophotometer, for monitoring intracellular pigment kinetics 2−48866
recording microspectrophotometer 2−70084
semi-automatic, point-by-point, for transmission and reflection meas. 2−42274
SF-10 and SF-14, automatic recording of optical characteristics variations of sample 2−59289
spectrophotofluorometer, computerized data acquisition system 2−82584
split beam for wavelength dependence of transmissivity or reflectivity 2−55772
standardization and calibration 2−63432
stellar, orbiting S59, u.v. MgII line profiles of β Aur 2−55044
teaching astronomical spectrophotometer for use at Cassegrain focus of telescopes 2−78635
u.v.-visible, design and performance 2−49451

Spectrophotometry
see also Colorimetry
absorption, hollow cathode spectral sources 2−76544
black body source high frequency, as primary spectrometric standard 2−52266
brightness outside instrumental range, statistical estimation 2−76547
calibration standards development, application 2−73677
CIE colour and solar energy transmittance and reflectance values, automatic computation 2−63431
derivative absorption and emission, comments 2−55769
Earth, from manned spacecraft 2−48373
Fabry-Perot etalon use for weak line profile investigations with spectrophotometer 2−76546
flame, use of jets with heating chambers 2−44503
flame photometry, TV recording methods 2−57442
FM-85, reflectance and transmittance in 0.3 to 2.5 μm range 2−63435
glass, alkali borate, containing nickel oxide, spectrophotometric studies rel. to struct. 2−67885
I_0 subtraction unit for use with pulsed or d.c. light sources, application to pulse radiolysis 2−45801
nucleotides, using TLC method for very small volumes 2−75410
photon counting technique 2−63367
photonic standardized counting system for high resolving power applics. 2−63426
precision measurement and calibration 2−82560
review, applics. 2−52483
spectrochemical analysis 2−81558
stars, weak and strong CN line G8 III type 2−55057
turbidity in estuaries, instrumentation development 2−54797
Ar-He discharge, cataphoresis separation of constituents 2−77313
$BaCO_3$ diffusion screens for u.v. radiation 2−45823
CO_2 microwave discharge, emission obs. 2−77303
Hg lines, relative sensitivities of 184.9 and 253.7 n.m. lines in atomic absorption 2−52489
N_2 afterglow, O_2 and temp. effect on first positive bands 2−77304

Spectroscopy
see also Modulation spectroscopy; Spectra; Spectrometers; Spectrophotometry
absorption hygrometry, atmospheric water vapour measurement, models 2−84864
activated ferroelectric study 2−72028
arcs high current, in narrow tube, obs. 2−74414
atomic, use of optical pumping 2−64007
atomic absorption spectroscopy in flame, population of atomic levels determ. 2−49939
atomic and molecular, using tunable dye lasers 2−79941
atomic spectra analysis 2−52490
atomic spectroscopy, review 2−46419
Auger, secondary emission analogue for improved spectroscopy with retarding potential analyzers 2−59923
Auger electron, for det. of element profiles across oxide films 2−56580
Auger electron, principles and applications, review 2−77481
automated scanning spectroradiometer applying computer analysis of spectral data 2−42258
camera-attachment to SL-11 styloscope and ST-7-stylometer 2−49457
canonical bases of Lie groups, use in atomic spectroscopy theory 2−79935
mini-computer, time shared, inexpensive system 2−70086
computer analysis by deconvolution 2−70073

Spectroscopy continued
computer-aided visual spectrum anal. 2−55768
correction technique, applic. to aerospace monitoring of earth resources and pollution 2−62159
correlation processing of isolated peaks on multichannel spectra 2−70282
coude spectrograph meas. of radial velocities for Large Magellanic Cloud Supergiants 2−69078
data processing of spectroscopic measurements 2−76545
derivative, determination of extrema of spectral profile 2−45822
directional spectral reflectance meas., response curve analysis 2−70079
double-wavelength, reviews 2−49448
electron, and Auger electron spectroscopy, review in relation to vacuum technique 2−59924
electron, low energy, book 2−41925
electron, surface vibration studies 2−50987
electron, using monochromatized X-rays for chemical analysis 2−54573
electron spectroscope, patent 2−82816
electron transmission 2−59088
emission, review 2−52481
equivalent line width and absorption coefficients, expression derived 2−42265
ESCA, principle of energy analysis by grid and cylindrical analysis, obs. of Auger spectra 2−84382
fast beam spectral line broadening, due to diffraction at spectrometer entrance slit 2−45816
fluorescence decay time meas. rel. to physical limitations of observation region 2−79435
Fourier, digital data handling of spectra 2−52485
Fourier, with Fabry-Perot interferometer 2−49450
Fourier transform, high resolution 2−63429
Fourier transform, rapid scan i.r. techniques and applications, review 2−52486
Fourier transform, submillimeter wavelength measurements 2−79171
Fourier transform, using Michelson interferometer 2−55344
Fourier transform, using Michelson interferometer 2−55771
Fourier transform spectrometry, interface effects 2−70074
gas velocity meas. technique 2−83690
glow discharge, transition probabilities and lines shapes, meas. 2−70080
grating synthesis 2−42267
heterodyne, saturated absorption, molecular constants det. 2−46609
high-resolution, use of mag. field tuned semicond. laser 2−70082
interferometric spectropolarimetry determ. of intensity and state of polarization 2−79436
i.r., absorpt. cell, image slicer, achromatic doublet lenses 2−79439
i.r., digital computer control, review 2−70075
i.r., for tin 2−82589
i.r., high resolution, techniques for gas obs. 2−42261
i.r., review, 1970-1971 2−52482
i.r. absorption, application to insulating materials testing, aging processes 2−68827
Kramers Kronig analysis 2−61610
laser, applic. to elastic scatt. cross section determ. in gases, Lamb dip features 2−83414
laser, excitation of spectra, review 2−45818
laser applications and developments 2−70076
laser beam, for high precision atomic and mol. investigs. 2−77004
laser perturbation, and detection of Penning ionization 2−80373
laser saturation, det. of fine structure and Lamb shift of H_α line 2−52946
laser saturation spectroscopy, theory 2−79907
laser saturation spectroscopy of alkali ground-state atoms, fine and hyperfine structure 2−46411
limitations and present state-of-art 2−71409
marcomolecule solutions, spectral analysis by analogue time correlation of scattered light 2−82585
matrix isolation, i.r. and Raman, high temp. species, deposition rate monitoring 2−69512
mixing, remote sensing of atm. particulate pollutants 2−81693
Mossbauer, in-beam system for use in backscattering geometry 2−63685
multiscanner spectral data processing, suitability of normal density assumption 2−81608
nonlinear, vibrational Raman resonance 2−42269
nonlinear and active, with tunable parametric oscillators 2−42734
ocean remote spectroscopy from high altitude, effect of atmospheric backscatter on reflection spectra 2−84774
optical, nongaussian signals, correlation of scaled photon-counting fluctuations 2−73542
optical, Raman's contributions, review 2−59277
optical bench, simple versatile construction 2−66851
optics course for engineers and scientists, book 2−69992
overlapping profiles, mathematical separation 2−42260
photoelectron, det. of branching ratios and transition probabilities 2−50032
photoelectron, electron-molecule interactions 2−83402
two photon, improved analytical method 2−49010
photon correlation spectroscopy using digital PDP-9 computer 2−79443
planetary nebulae, spatial spectroscopic diagnostic using synthetic approach 2−69041
planetary nebulae, spatial spectroscopic diagnostics, analytical approach using inverse integral equations 2−72982
plasma arc for photoionization meas. 2−77301
plasma temperature meas. 2−43171
plasma temperature measurement, optical method 2−43172
quality enhancement of data 2−59278
Raman, laser-excited, review 2−52967
Raman, method using quasi-c.w. parametric light generator 2−66853
Raman, overlapping band separation, depolarization ratios, computer appl. 2−66849
Raman, technique for obs. of polycrystalline high pressure phases 2−57360
Raman and Brillouin, reduction of parasitic light by I_2 absorption filter 2−52471

Spectroscopy continued
Raman difference, technique 2−52487
Raman difference spectroscopy using chopped laser beam 2−70072
Raman spectra by pulsed Raman technique, fluoresc. background reduction 2−79446
Raman spectroscopy, introductory presentation 2−73261
rapid scan, i.r. spectrum of methyl radical 2−83299
scale of spectral irradiance, visible region 2−79449
spectral plates, blackening distribution under various development conditions 2−59286
spectral selection, Pontryagin maximum principle 2−59280
spectrometry, high speed, in presence of absorption nonlinearity 2−63427
spectropyrometric apparatus for calibrating i.r. emitters 2−70078
storage vidicon electrophotographic spectrum imager for visible spectrum 2−59345
stray light effects 2−63425
transient absorbing species produced by radiation, techniques 2−59279
transient coherent emission, precision molecular spectroscopy applications 2−45817
HF optical pumping of low-pressure gas sample, laser-induced line narrowing spectroscopy 2−45819
HF pulsed chemical laser, using i.r. vidicon camera tube 2−59140
S, electron and Auger electron spectroscopy, review in relation to vacuum technique 2−59924
W, as spectral emissivity standard 2−54087
light sources
anthracene and 9-methyl-anthracene in ethanol as actinometer for u.v. region of impulse lamps 2−51462
emission, high-intensity and twin- discharge multielement lamps, comparative study for atomic absorption analyses 2−52492
frequency tunable i.r. source, nonlinear mixing of lasers 2−73599
hollow cathode and h.f. discharge combined 2−72589
impulse source, for continuous spectra, calibration of luminosity in vac. u.v. 2−45827
lamps, for tunable wavelength high-resolution techniques 2−55777
laser beams, developments 2−79447
laser saturated atomic reson. fluoresc. non-quenching collisions influence 2−83199
microplasma generated by laser beam impact, far-u.v. source 2−70088
monopolarised impulse generator 2−63437
pulse source for photolysis spectra 2−75391
raster theoretic problems for random slits distribution 2−79448
rhodamine 6G dye laser as tunable source of coherent u.v. radiation 2−79444
semiconductor and spin-flip Raman tunable lasers 2−42283
spectral radiance from highly symmetric cavities, S/N ratio advantages 2−79452
synchrotron radiation, use in u.v. absorption spectroscopy of atoms, molecules and solids 2−76549
tunable spin flip Raman source application to absorption spectra of gases meas. from 5-6μm 2−42264
CO$_2$ lasers, inverted Lamb dip in spectroscopy and laser stabilisation 2−63326
D lamp, lowering of ignition voltage by addition of Ne and He 2−42284
D$_2$ arc lamp, recalibration of spectral radiance in near u.v. 2−79450
H lamp, lowering of ignition voltage by addition of Ne and He 2−42284
He-Ne laser, output power intensity dips, use in Zeeman spectroscopy 2−66857
Hg discharge lamp, recalibration of spectral radiance in near u.v. 2−79450
Hg illuminator, with mixtures of K, Na and Rb, at ultra-high pressure, working model 2−45828
Hg lamp, use as intense pulsed source of near i.r. line spectrum 2−59292
I$_2$ vapour source, photon no. and lifetime 2−55776
W lamps, gas filled, reproducibility of output of visible radiation 2−79451
Spectroscopy, radiofrequency
see also Nuclear magnetic resonance and relaxation; Paramagnetic resonance and relaxation; Spectrometers, radiofrequency
e.p.r., meas. and data processing developments 2−73488
e.p.r., specimen orientation instrument 2−73487
filter distortion of spectral lines 2−52339
Lorentzian curve line parameters under conditions of combined modulation and saturation distortion 2−66661
magnetic double resonance Overhauser and solid state effect in methods of high frequency spectroscopy 2−54516
microwave, review 2−52340
molecular, time dependence of saturation 2−83226
n.m.r., Fourier, pulse and stochastic excitation cooled by computer 2−45627
n.m.r. 220 MHz, review of applications 2−77030
side band method for multiple nuclear magnetic resonance, density matrix analysis 2−55636
spin polarization detection, of free trapped electrons 2−79898
^{29}Si Fourier transform n.m.r., exptl. techniques 2−65355
Speech
see also Hearing
acoustic shape recognition 2−45506
alaryngeal, acoustical properties 2−45071
analysis and recognition, zero-crossing obs. 2−48894
analysis and recognition by computer, using zero crossing information 2−58635
analysis and synthesis on basis of sound microunits 2−52239
analysis for laryngeal disorder detection 2−45072
animal vocalizations and human speech 2−76102
articulatory movements for bilabials in normal and cleft palate speakers, electromyographic obs. 2−45059
basic frequency determ. by computer 2−66288
bilabial closure durations for p, b, and m in voiced and whispered vowel environments 2−48893
Chinese, acoustical features and perceptual cues of four tones 2−45065
communication interference rel. to noise levels on aircraft carrier flight decks 2−41825

Speech continued
communication quality, intelligibility over intefering background 2−45062
computer analysis technique 2−55304
consistency of hearing for speech across diverse listening conditions 2−55314
correlation with emotions 2−78918
deaf adults, acoustic and electromyographic investigation of consonant vowel transitions 2−45074
deaf children, acoustic and perceptual characteristics 2−45073
delayed auditory feedback and what the subject is asked to say 2−48896
female voices, text-independent speaker recognition experiment 2−45079
formant parameters of vocal tract, digital computer determination 2−73213
fundamental frequency rel. to chronological age in males 2−55307
German consonants, automatic recognition of spectrum features 2−58639
human, response of primary auditory neuron 2−45103
human auditory system modelling 2−76105
identification and temporal lobectomy patient 2−66289
infrasounds generated by human vocal apparatus 2−73214
intelligibility, human ear channel capacity 2−69451
intelligibility, in high pressure He-O$_2$ medium 2−73212
intelligibility, Russian male voices, formant distribution 2−73211
intelligibility in reverberant hall 2−45557
intonation display system, for deaf people 2−55303
intonation of special questions in stress and tone languages 2−76101
laryngeal control, thyrometer for obs. 2−45056
laryngeal control in speech, obs. using thyrometer 2−73210
linguistic vowel duration, physical analysis 2−66291
noncontextual, interruption effects 2−45076
normal and nasalized vowels, ultrasonic obs. of vocal fold vibration 2−45060
perceived pitch of prevocalic consonants 2−45067
perception of vowels and C-V syllables segmented from corrected speech 2−73209
perception under conditions of spectral transformation, phonetic characteristics 2−55305
phonation correction for deaf children, pitch stress indicator 2−82057
phonetic structure of voiced-unvoiced utterances 2−55302
processing, perceptual mechanisms 2−45053
pulse register phonation (vocal fry), laminagraphic obs. 2−45055
register equalization in singing 2−45070
response contingent neutral stimuli effects on normal speech disfluency 2−55306
rule synthesis of simple English sentences 2−45066
Russian phonology, transformational rule 2−69450
singing, simulated vocal chord motions 2−45054
Spanish stop consonants, voice timing perception 2−45078
speaker verification, implementation of on-line scheme 2−48897
spectral effects of subglottal cavity system 2−45064
spectral energy spectrum, effect of long term variations on talker recognition 2−78926
statistical characteristics of voice fundamental frequency 2−45069
stimulus bandwidth effects on listener judgements of vocal loudness and effort 2−66290
stop consonants in various phonetic environments, intraoral air pressure obs. 2−45058
stress patterns, obs. of perceptual errors 2−45090
stressed syllables, effects of diffusing sentence frames 2−45063
stuttered, acoustic aspects 2−45075
syllable production, lip and tongue pressure patterns 2−45057
talking computers, human speech generation 2−45052
temporal processing 2−45077
temporal structure of spoken utterances, effect of morphological and syntactic boundaries 2−48892
time domain techniques for pitch extraction 2−45068
timed correct sound production task, effects on carryover to conversational speech 2−55308
timing perception, word boundary effect 2−48895
transitional sounds of German as link elements for speech synthesis 2−58637
transmission channels evaluation by using artificial signals 2−58636
transmission equipment, intelligibility rating 2−69448
vocal tract X-rays anal. using interactive computer graphics 2−69449
vowel duration in polysyllabic words in American-English 2−45061
He speech convertor operating in time domain 2−73215
Spherical aberration *see Aberrations, optical*
Spicules *see Sun/prominences*
Spin *see Elementary particles; Hyperons/spin and parity; Mesons/spin and parity; Nucleus/spin and parity; Rotating bodies*
Spin echo *see Nuclear magnetic resonance and relaxation*
Spin-lattice relaxation
acetylene cryst., mol. motions, plastic behaviour 2−83881
adamantane, solid, proton relax., press. depend., mol. rot. 2−61563
aniline in solution ^{13}C spin-lattice relaxation and intermolecular interactions 2−80482
p-azoxyanisole, strong collision relaxation in rotating frame 2−61747
benzene, solid, anisotropic relax. of ^{13}C, chem. shielding 2−81310
beryllium oxyacetate, dipole-dipole reservoir, slow motion, n.m.r. obs. 2−72525
beryllium oxyacetate, molecular dynamics in -196°C to 286.7°C range, relation to polymorphism 2−57399
2-, 3- bromothiophenes, meas. of proton spin-lattice relaxation times in 300-450°K range using spin-echo spectrometer 2−77116
CaF$_2$:Dy^{3+}, temp. depend. 2−84198
carboxymioglobine aqueous soln., effect of hydration on relax. time from n.m.r. meas. 2−50373
chloroform, ^{13}C spin-lattice and spin- spin relaxation rates 2−56525
cubic crystal, theory 2−65192
cyclohexane, nitroxide radical doped, plastic phase, spin diffusion 2−72526
DDPH dil. benzene solns., proton relax. times 2−42960
1,4dibromo-naphthalene, e.s.r. of triplet excitons, optical detection 2−81522

Spin-lattice relaxation continued
- dicalcium lead propionate, near crit. point 2−65196
- N,N′-dimethyl-piperazine, ^{14}N quadrupole interaction, mol. motions 2−84603
- diphenylsilane, ^{29}Si Fourier transform n.m.r. study 2−65355
- dipolar relax. rates of quadrupole interacting spin system 2−84452
- e.s.r. dispersion signals on rapid transit, relax. time determ. from saturation curves 2−77053
- ferroelectric, double reson. applic. to order-disorder studies 2−81481
- ferroelectric systems, nucl. double reson. meas., phase transition dynamics 2−84450
- formic acid, ^{13}C relax. time 2−60069
- hydrides, n.m.r. analysis of hydrogen diffusion 2−54369
- ice, strong collision relaxation in rotating frame 2−61747
- lanthanum ethyl sulphate, of Nd^{3+} and Er^{3+} at zero mag. field 2−65194
- lattice resonant mode effects 2−51284
- liquid crystal, intermol. and intramol. contribs. to proton spin-lattice relax. 2−64440
- malonic acid, irradiated, electron spin- lattice relaxation 2−44442
- MBBA, nematic liquid crystals, proton spin-lattice relaxation mechanisms 2−84596
- measurement, adaptive n.m.r. method 2−55633
- measurement, microwave diode switch 2−76421
- measurement, of long periods, by autogenerator 2−49229
- measurement by Fourier transform proton n.m.r. in aqueous solution 2−77448
- methane, solid, γ-irrad., spin species conversion by paramag. impurities 2−84446
- methane adsorbed on graphite, n.m.r. obs. of barrier to rot. 2−67925
- methane adsorbed on MgO, microdynamics, n.m.r. relax. obs. 2−83875
- p-methoxybenzylidene p-n butylaniline, dynamical behaviour above nematic-isotropic transition 2−71160
- nematic liquid crystalline phase, proton spin-lattice relaxation 2−56524
- n.m.r. investigation, system AB of slowly interconverting nuclei, exchange rate effect 2−46520
- nuclear dipolar energy, expression for relaxation through dipole-dipole interaction 2−65191
- nuclear relax., n.m.r. bandshape studies 2−59983
- nuclear relax. recovery laws and exptl. condition for exponential decay 2−84451
- nuclear spin-lattice relaxation due to the orbital interaction 2−84585
- octamethylcyclotetrasiloxane, ^{29}Si Fourier transform n.m.r. study 2−65355
- paramagnet, perturbed γ-γ angular correl. eff. of spin-lattice relaxation and ultrasound 2−72241
- paramagnetic ion pair, $S=1/2$, coherence effect 2−54366
- paramagnetic relax. time calc., with allowance for spin-spin interaction 2−81312
- paramagnetic relax. times rel. to phys. processes characteriz. 2−84454
- paramagnetic spin systems, internucl. Overhauser effect, theory 2−59984
- phase transition phenomena, struct. and mag., review 2−84599
- phenol in solution, ^{13}C spin-lattice relaxation and intermolecular interactions 2−80482
- poly-γ-methyl-L-glutamate in soln., spin-lattice relaxation time meas. 2−66672
- polyisobutylene solns. obs. of spin-spin and spin-lattice n.m.r., relationship to viscosity 2−60513
- polymer, irrad., proton relax. times 2−84449
- polystyrene-anisole solution, temp. depend. of spin-lattice relaxation obs., study of molecular mobility 2−60514
- pyrazine-d_4, triplet state, Zeeman effects 2−60084
- pyrene-d-10, temperature dependent saturation meas. in photo-excited triplet state 2−84567
- quadrupolar relax. times, double reson. meas. 2−81315
- Raman, anharmonic, rel. to localized and quasilocalized vibrs. due to paramag. impurities 2−80896
- rare spins in solids, high resolution n.m.r. 2−81479
- ruby: Cr^{3+}, field effect obs., Van Vleck theory 2−65193
- ruby, crossrelaxation, two step, freq. depend. susceptibility meas., generalized thermodynamics 2−61561
- ruby, Fe^{2+} ion obs. and cross relax. processes 2−51285
- saturation recovery method for high resolution meas. using on line computer 2−66672
- spherical top mols., nucl. relax. of ^{19}F, spin-rot. interaction obs. 2−56199
- squalane, meas. as a function of temp. 2−46987
- squalene, meas. as a function of temp. 2−46987
- superconducting layered compounds, relax. due to fluctuations 2−71841
- symmetric top mols., nucl. relax. of ^{19}F, spin rot. interaction obs. 2−56200
- T_1 measurement, effects of H_1 inhomogeneity 2−59016
- 5,5,11,11-tetramethylhexadecane, spin-lattice relaxation rates meas., cf. with viscoelastic relaxation 2−46987
- β-tetramethylsilane, 77−174K, p spin-lattice relaxation 77−174K 2−75242
- tetramethylsiloxane, ^{29}Si Fourier transform n.m.r. study 2−65355
- thulium ethyl sulphate, of rare earth ions 2−78051
- time of conduction electrons in Li, Na, Al, Cu, Rb, improved average nuclear contact density 2−54372
- transition metals, n.m.r. obs. of hydrogen diffusion 2−77622
- 1,3,5 trinitrobenzene charge transfer complexes, mol. movements, proton mag. reson. 2−48308
- π-tropyliumvanadium tricarbonyl, ^{51}V quadrupole relax., coupling const. 2−84453
- Tutton salts, spin system dynamics obs. 2−84445
- viscous liquid, pulse n.m.r. meas. rel. to self-diffusion determination 2−60453
- yttrium ethyl sulphate; Yb^{3+}, Dy^{3+}, proton polarization and relaxation by rotational cooling 2−48122
- Al, solid and liq., n.m.r. obs., room temp.-1100°C 2−54503
- Al_2O_3-Fe_2O_3 solid solns., impurity ion effects on spin relax. time of ferric ions 2−54368

Spin-lattice relaxation continued
- n-B_9H_{15}, resolution enhancement in partially relaxed Fourier transform ^{11}B n.m.r. 2−56521
- BaF_2:Er, of ^{19}F in laboratory frame and rot. frame 2−68582
- BaF_2:Eu^{2+}, diffusion vanishing relax. of ^{19}F 2−44315
- ^{13}C relax. meas. under proton coupled and decoupled conditions 2−67462
- $CaCO_3$:Fe^{3+}, X-band pulse recovery and spectral line broadening obs. 2−65177
- CaF_2:Ce^{3+}, paramag. relax. due to flux jumping, nonequilib. spin distribs. 2−72231
- CaF_2:Gd^{3+}, second order spin-lattice coeffs., temp. depend., e.p.r. obs. 2−80890
- CaF_2:Gd^{3+}, spin-lattice coeffs. calc. 2−51286
- CaF_2:Tm^{2+}, Kramers doublets with hyperfine coupling, meas. 2−78048
- CaO:Gd^{3+}, spin-lattice coeffs. calc. 2−51286
- CaO:Mn^{2+}(Fe^{3+}), spin-lattice coeffs., relativistic cryst. field contrib. 2−65203
- CdF_2:Gd^{3+}, second order spin-lattice coeffs., temp. depend., e.p.r. obs. 2−80890
- CdS:Co^{2+}, Orbach process, Debye temp. 2−54367
- CeO_2:Gd^{3+}, spin-lattice coeffs. calc. 2−51286
- Cl_2, liq. and solid, temp. depend. 2−72507
- $CoCl_2.6H_2O$, proton relax. time, 1.12−4.18 K 2−78050
- Cr(III) cpds. in soln., temp. and mag. field depend. 2−77447
- Cs_2PtCl_6, of ^{35}Cl, rotary lattice mode freq., temp. depend. 2−77748
- $Cs_2SO_4.Cr_2(SO_4)_3.24H_2O$ alum., paramag. spin-lattice relax. times of Cr^{3+} 2−84444
- Cu-Mn dilute alloy, thin film, e.s.r. study 2−44446
- Cu, mechanism importance in nuclear refrigeration, by adiabatic demagnetization 2−66364
- Cu nucl. spin-lattice relax. of Zeeman and spin-spin systems, 1 to 17 mK 2−68581
- $CuCl_2.2H_2O$, proton relax. time, 1.12−4.18 K 2−78050
- $CuCs_2(SO_4)_2.6H_2O$, electron spin- lattice relax. of Zeeman and interaction systems 2−68580
- $Cu(NO)_3)_2.2^1/_2H_2O$, energy levels and relaxation effects 2−48106
- D_2O ice, ^{2}H n.m.r. 2−61744
- Fe-Co very dilute alloy, of ^{60}Co at 25 mK, field depend. 2−72232
- $Fe^{60}Co$, single- passage resonance obs. by β-emission and spin-lattice relax. meas. 2−72508
- $Ga(ClO_4)_3$ aqueous solns., relax. rates of ^{69}Ga and ^{71}Ga 2−77449
- H, effects on e.p.r. spectrum 2−79950
- H_2, solid, nucl. spin-lattice relax., temp. depend., 0.075-1.5K 2−68583
- He, liquid, acoustic multiple beam scattering 2−83832
- ^{3}He adsorbed monolayer on Vycor glass, config. and mobility obs. 2−80509
- HfH_x, rel. to electron-nuclear interactions 2−78047
- Ho^{3+} in yttrium ethyl sulphate, electron paramagnetic resonance techniques 2−68584
- In-Bi(Pb)(Tl) alloys, liq., longit. spin relax. of ^{115}In 2−50370
- InSb spin flip Raman scatt., spin saturation and relax., rate eqn. technique 2−68662
- $KAu(CN)_2$, of ^{197}Au, from time depend. of Mossbauer spectra asymmetry 2−44355
- $K_4Fe(CN)_6.3H_2O$, anomalous, by quasi-spin waves 2−75152
- $K_2Ir(Pd)(Pt)Cl_6$, incipient phase transitions 2−77748
- KPF_6, solid, reorientation motions of PF_6^- ions 2−61562
- K_2PtBr_6, rotary lattice mode softening obs. 2−61756
- $LaCl_3$, of Nd^{3+} and Er^{3+} at zero mag. field 2−65194
- $La_{1-x}Gd_xAl_2$, of ^{27}Al and ^{139}La 2−54370
- $LaIn_3$, n.m.r. obs. 2−65346
- $La_2Mg_3(NO_3)_2.24H_2O$:Ce^{3+},Pr^{3+}, e.p.r. obs. 2−44316
- $La_2Mg_3(NO_3)_{12}.24H_2O$:Nd, spin diffusion props. from spin heat bath relax. time 2−78049
- $La_2Mg_3(NO_3)_{12}.24H_2O$, spin system dynamics obs. 2−84445
- $LaPb_3$, ^{139}La n.m.r. obs. 2−65346
- $LiNbO_3$, relaxation times determ. by tone-bursting technique in quadrupole nuclei 2−48312
- $LiTaO_3$, relaxation times determ. by tone-bursting technique in quadrupole nuclei 2−48312
- MgO:Mn^{2+}(Fe^{3+}), spin-lattice coeffs., relativistic cryst., field contrib. 2−65203
- MgO:Ni^{2+} microwave phonon bottleneck, Brillouin spectra obs. 2−65283
- MgO, effect of anharmonic interactions of Cr^{3+} and Ni^{2+} ions 2−65195
- MgO, Raman relax. of Ni^{2+}, Cr^{3+} and V^{2+} ions, substitutional effects 2−48114
- $MnBr_2.4H_2O$, proton relax. time, 1.12−4.18 K 2−78050
- NH_4Cl, low temp. relax. time of hindered ions 2−84447
- NH_4Cl, of nucl. dipolar energy, temp. and orientation depend. 2−81314
- NH_4Cl, proton relaxation times meas. at 18 MHz by pulse technique, study of order-disorder transition 2−57401
- NH_4ClO_4, solid, spin-rot. relax. for protons 2−54371
- NH_4SnCl_3, proton relax. of ammonium ion undergoing hindered rot., cross correl. effect 2−84448
- $(NH_4)_2SnCl_6$, low temp. relax. time of hindered ions 2−84447
- NH_4X (X = halogen), spin-lattice relaxation of nuclear dipolar energy through dipole-dipole interaction 2−65191
- ^{15}N in organic compounds, interactions at high and low temperatures 2−57400
- $^{15}NH_3$, $^{15}ND_3$, liquid, ^{15}N relaxation meas. 2−50371
- NaF, nuclear acoustic resonance of ^{23}Na obs. 2−78170
- $NaNO_3$, mixed from ^{23}Na n.m.r. intensity variations under u.s. stimulating quadrupole transitions 2−81483
- $NaPF_6$ in D_2O and H_2O solns., ^{19}F, ^{31}P, ^{1}H and ^{2}H 2−50372
- Na_2PO_3F in D_2O and H_2O solns., ^{19}F, ^{31}P, ^{1}H and ^{2}H 2−50372
- β-NbH, proton jump rate determ. 2−77614
- $Nd_2Mg_3(NO_3)_{12}.24H_2O$, external mag. field depend., 1.5-2.0K 2−48115
- Ne, solid and liquid, pulsed n.m.r. of ^{21}Ne obs. 2−65347
- $NiCl_2.6H_2O$, proton relax. time, 1.12−4.18 K 2−78050
- $Pr_2(SO_4)_3.8H_2O$, of rare earth ions 2−78051
- PtSi, n.m.r. obs. 2−65348
- $RbMnF_3$, n.m.r. of ^{19}F in antiferromag. region 2−48113
- $RbMnF_3$, of ^{19}F, n.m.r. obs. 2−72516

Spin-lattice relaxation continued
$RbPF_6$, solid, reorientation motions of PF_6^- ions 2−61562
Rb_2PtCl_6, of ^{35}Cl, rotary lattice mode freq., temp. depend. 2−77748
SF_6 clathrate deuterate, ^{19}F spin-lattice relaxation meas. in 40-250 K range 2−72531
Sc-H solid solution, Korringa product, diffusion parameters determ. 2−72517
Si, relax. time of recomb. centres 2−51217
SnH_4, solid, proton relax., phase, transition obs. 2−48116
SrF_2:Tm^{2+}, Kramers doublets with hyperfine coupling, meas. 2−78048
Te, liquid, temp. depend. obs. rel. to electronic transport behaviour 2−71237
ThO_2:Gd^{3+}, spin-lattice coeffs. calc. 2−51286
ThO_2, e.s.r. absorpt. spectrum of monovalent iron 2−48296
ThO_2, of Fe^+, temp. depend., Debye temp. obs. 2−84581
Ti hydrides, ternary and binary, temp. and freq. depend. of proton spin relax. 2−78052
TiH_x, rel. to electron-nuclear interactions 2−78047
TlCl, pulse n.m.r. investigation of vacancy and interstitial diffusion 2−71471
$V_{1-x}Cr_xBe_2$, ^{51}V and ^9Be n.m.r. 2−72520
YIG, spin relaxation near Curie temp. studied by high frequency magnetic susceptibility 2−84417
ZnO:Cu^{2+} 7-17 K, Raman process 2−65328
$ZnSiF_6.6H_2O$ of Cu^{2+} phonon assisted tunnelling contrib. 2−84456
$ZnWO_4$:Co^{2+}, relaxation and time constant meas. 2−81311
ZrH_x, rel. to electron-nuclear interactions 2−78047
$Zr_{1-x}Ti_x(Hf_x)Zn_2$, e.p.r. linewidth behaviour 2−72173

Spin-spin relaxation
beryllium oxyacetate, molecular dynamics in -196°C to 286.7°C range, relation to polymorphism 2−57399
chloroform, ^{13}C spin-lattice and spin- spin relaxation rates 2−56525
coupling consts., review 2−52342
cross-relaxation between paramagnetic ions in crystals 2−68578
gaseous mixtures, nucl. relax. times, density depend. 2−79973
liquids, influence of molecular translations 2−74536
metal, retardation effects in longitudinal spin relaxation 2−65190
methane adsorbed on graphite, n.m.r. obs. of barrier to rot. 2−67925
4-methyl 2,6 ditertiarybutylphenol, proton dipole-dipole relax. rel. to quantum tunnelling 2−81472
molecular cryst., electron spin echoes in photo-excited triplet states in zero field 2−54556
n.m.r., error compensation in Carr-Purcell spin echo expt. 2−59017
nuclear relax., n.m.r. bandshape studies 2−59983
paramagnetic relax. times rel. to phys. processes characteriz. 2−84454
polyisobutylene solns. obs. of spin-spin and spin-lattice n.m.r., relationship to viscosity 2−60513
pyrene-d-10, temperature dependent saturation meas. in photo-excited triplet state 2−84567
yttrium ethyl sulphate: Yb, nuclear spin refrigeration rel. to electron spin-spin interaction 2−72246
Ag complex, Ag di-isopropyldithiocarbamate, e.s.r. spectra, evidence for spin-spin and spin-orbit interaction 2−44443
$CuCl_2.2H_2O$, rel. to antisymmetric exchange interactions 2−68579
EuO, of ^{151}Eu and ^{153}Eu, field depend. relax. rates 2−72230
H_2, low-density, nuclear-spin relaxation at room temperature 2−70707
^3He, solid, transverse relax. time, low temp. 2−47026
^3He adsorbed monolayer on Vycor glass, config. and mobility obs. 2−80509
In-Bi(Pb)(Tl) alloys, liq., longit. spin relax. of ^{115}In 2−50370
^{14}N in liquid organic nitrogen compounds 2−56523
Na atom, optically orientated, spin exchange with colliding buffer gas atom 2−79901
Ne, solid, pulsed n.m.r. of ^{21}Ne obs. 2−65347
$RbMnF_3$, n.m.r. of ^{19}F below 30 K 2−48113
$RbMnF_3$, of ^{19}F, n.m.r. obs. 2−72516

Spin waves
see also Ferromagnetism/spin wave theory
— 2−72462
antiferrodielectric, effective electrodipole transitions, optical and spin excited states 2−72290
antiferromagnet, critical condition for magnon localization found for all impurity concentrations 2−44284
antiferromagnet, density of states singularities 2−51276
antiferromagnet, easy plane anisotropy, additional absorpt. and parallel pumping 2−81308
antiferromagnet, Heisenberg model, principal susceptibilities, spin wave theory 2−65172
antiferromagnet, impurity effects on excitation spectra 2−44282
antiferromagnet, magnetic impurity atom located between magnetic sublattices, effects 2−72458
antiferromagnet, one-band model, spin waves in spin density wave ground state 2−68563
antiferromagnetic crysts., magnons and excitons 2−48159
antiferromagnetic insulator, light scatt. spectrum, magnon behaviour 2−54399
antiferromagnetic insulator, magnon induced sidebands in optical transitions 2−54408
antiferromagnetism, magnon model 2−75236
antiferromagnets, anisotropic, study of spectrum and correlation functions 2−81305
antiferromagnets, Heisenberg, evaluation of generalized susceptibilities 2−44269
antiferromagnets, Raman scatt. by four magnons, excited state exchange mechanism 2−65276
biaxial antiferromagnet, coupled spin waves and magnon-magnon resonances 2−72457
Bloch walls, cold neutron diffraction, nonelastic scatt., macroscopic anal. 2−51248
bound, in Heisenberg ferromagnet and antiferromagnet 2−44234
coherent magnon states, elementary excitations and order phenomena 2−77762
copper formate tetrahydrate, thermal cond., magnon contrib. 2−72226
dielectric layered struct., magnetostatic propag. 2−51268
excitation spectrum of antiferromagnetic hamiltonian 2−81295
excitation threshold anisotropy, ferromag. resonance 2−72448

Spin waves continued
f.c.c. cryst., antiferromag., magnons, light scatt., dispersion and absorpt. 2−61550
Fermi liquids, two component, study of paramag. reson. and excitation 2−81000
ferrimagnets, Heisenberg, evaluation of generalized susceptibilities 2−44269
ferrite/semiconductor interface, interaction of surface magnetostatic waves with carriers 2−84420
ferrites with planar anisotropy under perpendicular pumping, first-order instability 2−51269
ferro- and antiferromagnets, algebraic realization 2−44237
ferromagnet, amorphous susceptibility and Curie temp. rel. to spin-fluctuations 2−57277
ferromagnet, energy width due to exchange scatt. of magnons in mag. field 2−65139
ferromagnet, itinerant, electron-magnon interaction, energy and lifetime 2−48056
ferromagnet, itinerant, spin wave energy temp. depend., electron-phonon interact. influence 2−61498
ferromagnet, with weak antiferromagnetism, neutron and light scatt. study 2−78012
ferromagnetic film, band periodic domain struct., spin wave spectrum 2−72183
ferromagnetic film, surface spin-wave excitation 2−68716
ferromagnetic insulators, acoustic attenuation and frequency shift for 2 magnon-one phonon processes 2−80907
film, ferromagnetic, with periodic banded domain structure, spin wave spectrum 2−68553
fluorite-type crystals, doped spin- phonon interaction 2−72235
Heisenberg and Ising models, spin-spin correl. function, eqn. of state, droplet model 2−77991
Heisenberg antiferromagnet, two-magnon Raman scatt. at finite temp. 2−54431
Heisenberg ferromagnet with antiferromag. impurity spin, localized magnons 2−84424
Heisenberg ferromagnetic alloys, CPA approx. with random off-diagonal elements 2−78004
magnetic insulators, coupling to e.m. waves 2−72191
magnetic materials, surface dynamics and waves 2−68527
magnetoordered crystals with small exchange constant, spin waves and scatt. proc. of neutrons and light 2−72209
magnetostatic echo analysis 2−57313
magnetostatic mode pattern and mode spectrum analysis, in finite ferromag. circular disc 2−48053
magnon dispersion relations, accurate determ. by neutron scattering, corrections to integrated intensity 2−47311
magnons, elementary excitations, book 2−71806
metal, coupled helicon-magnon wave, neutron and electron scatt. 2−68314
metal alloys, local spin fluctuations, renormalized theory 2−61492
metals, antiferromagnetic, particle scattering by coupled electromagnetic-magnon waves 2−84443
metals, indirect exchange and s-d model, dispersion and attenuation of spin waves, effect of e.m. wave 2−72132
molecular crystals, triplet exciton-magnon coupling 2−51327
neutron mag. scatt. in critical region, magnetization waves rel. to Brillouin-Mandelstam doublet 2−75214
non-Heisenberg magnet, exchange interaction effects 2−72133
nonferromagnetic metals, quantum-mech. theory 2−75206
paramagnetic cryst., energy spectrum of elementary excitations 2−65118
parametrically excited, system transient behaviour 2−81263
particle detector, metal, using generation of, for ultrahigh energy particles 2−73941
Permalloy film, 0.8-16 GHz, below saturation magnetization 2−78034
permalloy films epitaxially grown on fcc metals, structural and standing spin wave resonance props. 2−78149
rare earth metals, with helical spin struct., magnon- phonon interaction 2−75225
rare earths, spin wave energy rel. to interatomic exchange Heisenberg parameters, exchange coupling 2−61505
s-band models, absence of complete ferromagnetism 2−72126
semiconductor, ferromagnetic, coupled helicon-magnon wave, neutron and electron scatt. 2−68314
semiconductor, magnetic, magnon drag effect 2−54165
solid state physics, an overview 2−57093
solid surfaces, conference, Boston Mass., USA, Oct. (1971) 2−47070
spectrum, crystal with helical mag. structure in external mag. field 2−57278
spin-electromagnetic waves in antiferromagnetic with small exchange constants 2−81290
spin-electromagnetic waves in ferromag. semicond. and metals, theory 2−81225
surface phonons and magnons, review 2−50985
two-dimensional magnet, spin-wave spectrum, temp. depend. 2−44240
two-magnon Raman scatt., two-time Green function decoupling, heat-bath damping effects 2−68654
CO crystal, α phase, librational motion by linear spin-wave theory 2−80588
$CoCl_2.6H_2O$, antiferromag. spin wave theory 2−54351
$Co_xZn_{1-x}Fe_2O_4$, ferrite, Fe^{3+} spin fluctuations mag. hyperfine splitting, relax. effects, Mossbauer spectra 2−81287
Cr, magnetic generalized spin susceptibility, interband contribs., Lindhard expression 2−61554
Cr, magnon-phonon interaction 2−48109
Cr, spin wave theory 2−61555
$CsNiCl_3$, one-dimens. antiferromag., spin-wave approach 2−54352
Dy, lattice excitation and magnon spectra, magnetoelastic effects 2−65141
EuS film, rel. to determination of effective exchange parameters 2−68532
Fe-Ni alloy, magnon heat conduction and scattering processes 2−65142
Fe, small-angle magnon scatt. collapse 2−44242
Fe group ion in a tetrahedral field mixing of 3d and excited orbitals, effect on orbital momentum and spin-orbit coupling coeff. 2−80981

Spin waves continued
$FeCO_3$, Ising behaviour, magnon-phonon coupling 2−44297
FeF_2, magnon-phonon interaction 2−44298
FeF_2, magnon-phonon interactions, coupling, spin Hamiltonian 2−80886
FeF_2, two-magnon Raman scatt., temp. depend., calc. 2−81304
α-Fe_2O_3, haematite, magnon energy of optic mode, Morin transition 2−51278
$GdAlO_3$, obs. of u.s. attenuation in high magnetic field, spin wave interactions 2−54348
$GdCl_3$, ferromag., magnon spectrum, dipole-dipole interact. theory 2−68534
$GdCl_3$, magnon dispersion and effect on single-ion-induced absorpt. lineshapes 2−48181
$Gd(OH)_3$, magnon dispersion and effect on single-ion-induced absorpt. lineshapes 2−48181
$K(Mn_{1-c}Co_c)F_3$, antiferromagnetic, critical condition for magnon localization found for all impurity concentrations 2−44284
$KMn_{1-x}Co_xF_3$, spin waves theory and coherent potl. approx. applic. to mag. excitations 2−78044
Mg-ferrite, spin-wave instability, obs. 2−78151
Mn complex, $(CH_3)_4NMnCl_3$, direct process n.m.r. relaxation in one dimensional antiferromagnet 2−51414
$Mn_{1-x}Co_xF_2$, spin waves theory and coherent potl. approx. applic. to mag. excitations 2−78044
MnF_2, magnon sideband intensity 2−61647
MnF_2, two-magnon absorpt., spin-flop transition effects 2−54358
MnF_2, two-magnon Raman scatt., temp. depend., calc. 2−81304
MnF_2, zero field circular dichroism in magnon sideband region 2−44376
$MnFe_2O_4$, acoustic magnon dispersion, neutron diffr. obs. 2−61544
MnO, antiferromag., inelastic neutron scatt. obs. 2−61558
N_2 crystal, α phase, librational motion by linear spin-wave theory 2−80588
$Nd_{1-x}Ho_xCo_3$, mag. moments, Curie temps., spin polarization effects 2−68535
Ni-Fe alloy, spinwave dispersion coeff. in the Invar region, compositional depend. 2−48077
Ni single crystal film, rel. to ripple magnetiz. effects in ferromag. resonance 2−65317
$NiBr_2(Cl_2)$, electronic absorpt. spectra, magnon sidebands 2−51345
NiO, spin wave dispersion, inelastic neutron scatt. study 2−81303
Pd-Ni alloy, magnetoresist., due to scatt. by spin fluctuations 2−48058
Pd, thermal expansion and elec. cond., 77-300K, effect of paramagnons 2−61226
Pd_3Fe, dispersion relation, neutron scatt. obs. 2−61503
$RbCoF_3$, one- and two-magnon scatt. below Neel pt. 2−54435
$RbMnF_3$, antiferromag., magnon struct. of absorp. spectra in 3900 Å region 2−65266
$RbNiCl_3$, one-dimens. antiferromag., spin-wave approach 2−54352
$RbNiF_3$, ferrimagnet, neutron scatt. obs. 2−65171
Tb, lattice excitation and magnon spectra, magnetoelastic effects 2−65141
Tb, meachnism for mixing of acoustic magnons and optic phonons propagating along c axis 2−75227
Tc, hexagonal symmetry, anisotropic behaviour of magnetic properties 2−71864
$Y_{3-x}Ca_xFe_{5-x}Sn_xO_{12}$ garnet, noncolinear spin config., Mossbauer spectra obs. 2−54344
YIG/dielectric/conductive plane, magnetostatic propag. 2−51268
YIG, parallel pump spin wave instab., discrete magnon resonances 2−48271
YIG, polycryst., spin wave transit time, limitation by pores 2−75232
YIG, surface spin wave propagation in inhomogeneous fields 2−78037
YIG cylindrical rod, mode separation 2−59005
YIG discs, epitaxial, anisotropy effects on magnetostatic modes 2−44432
YIG epitaxial film, coupling between dipole and exchange dominated spin waves 2−72189
YIG thin film disks, anisotropic excitations of magnetostatic modes 2−44434
Spinors *see Quantum theory/wave equations*
Spions (pions with spin) *see Pions*
Spirality *see Elementary particles; Field theory, quantum*
Sporadic-E *see Ionosphere/E-region*
Sprays
see also Aerosols; Drops; Jets
liquid-liquid spray column, dense packing of drops, influence of viscosities of liquids 2−43280
reacting liquid, in-line holography 2−83755
viscous liquid flow on rotating disk, atomization effects 2−74509
Spurions *see Elementary particles*
Sputtering
a.c., asymmetric, film deposition on cylindrical substrates 2−80600
alkali halides, positive ion ejection patterns 2−44008
application in industry 2−52019
cathode, automatic self-cleaning of transducers, in locking vacuum gauge 2−48944
cathode, automatic self-cleaning of transducers, in locking vacuum gauge 2−48944
cathode during discharge with oscillating electrons investigation using vacuum micro-balance 2−85176
cathodic, description of apparatus 2−54089
charged particle, trajectory distortion by incident beam field 2−57088
cylinder-type system with large deposition rates 2−60643
d.c. for NbN films preparation 2−84311
d.c. glow discharge energy transport and plasma diagnostic props. 2−50230
d.c. system, cathode dark-space meas. and Ta film deposition 2−50226
deposition, focussing effects 2−60642
deposition rate, effects of pressure in r.f. processes 2−62905
dielectric thin films, characteristics of deposited films 2−60638
ejection from surfaces by energetic atoms 2−74765
electron microscope specimen prep. 2−80617
energy analysis of particles on substrate in deposition 2−61118

Sputtering continued
fusion reactor wall erosion 2−46376
glass, optical finishing by ion-beam sputtering machining 2−82571
glow discharge sputtering systems for thin film production 2−71323
glow discharges, plasma diagnostics, obs. 2−53214
graphite, electron beam deposition, sublimation energies 2−60644
heavy ion, prep. of isotope targets 2−73911
heavy ion, prep. of isotope targets 2−49622
h.f., deposition of metal and dielectric films 2−78695
h.f., for film deposition, power supply unit 2−78696
inert gas ions on glass, 5.6 keV 2−61123
ion beam, application to production of insulators and semiconductor layers in microelectronics 2−58667
ion beams, substrate currents 2−58668
ion impact, for etching, in solid state device manuf. 2−43458
using ion microprobe, means for obtaining uniformity 2−71300
isolated and cooled, targets, for cathodic sputtering devices 2−45189
isotopic accelerator target prep. techniques 2−73962
metallic surfaces, 'cleaning' by Ar ions in ESCA studies 2−52018
noncrystalline film prep. 2−47114
permalloy films, thin, influence of plasma and cathode sputtering on struct. elec. and mag. props. 2−84410
power arcing, contact materials in switching devices 2−74454
protective layer in d.c. diode sputtering 2−60643
radiofrequency, thin film radiation source production 2−74046
reactive, preparation of MoO_2 films 2−55335
reactor fuel particles, coated, fission products distrib. determ. 2−46390
r.f., preparation of thin film radiation sources 2−49334
r.f., target etching and film growth, target processes 2−60640
r.f., target etching and film growth, transport and deposition processes 2−60641
r.f. for thin film $BaTiO_3$ on Si substrate 2−75148
r.f. systems, bombardment phenomena at substrate surface, origins 2−61119
r.p. sputtered glass film for light guide 2−44013
secondary ions from insulating materials, analysis 2−84687
stimulated emission contributions to a cathodic cavity plasma 2−82477
surface analysis, by mass spectrometry of sputtered neutrals 2−64541
surface comp. determ. by impact radiation analysis 2−84636
tetrode plasma, method for magnetostrictive thin film prep. 2−43473
thinning of specimen foils for transmission electron microscopy 2−79101
vacuum unit for coating deposition 2−62903
Al, Ar^+ ion bombardment, transmission sputtering and recoil implantation 2−54090
Al, electron beam deposition, sublimation energies 2−60644
AlN, deposition on Si, m.i.s. struct. prep. 2−54225
AlN_x, preparation by reactive r.f. sputtering 2−77507
Au, temp. rise during film deposition as a function of applied power 2−67913
Au {100} surface, focusing 2−64542
b.c.c. lattice, computer simulation 2−71763
Be film production and struct., effects on secondary electron emission 2−57265
Bi_2O_3, amorphous and polycrystalline film prep. by cathode reactive sputtering 2−80594
CdS, prep. by reactive sputtering, photocond. props. 2−65082
CdS film deposition method 2−53571
CdS films, r.f. sputtering in Ar, effects on photoconductive characteristics 2−68479
Cr film, sputtered, supercond. props. rel. to deposition conditions 2−81045
Cs^+ ion source, for mass spectrometer 2−69885
Cu-Au film, epitaxial growth by r.f. sputtering, microstruct. 2−67908
Cu-Ni alloy, surface composition, Auger spectroscopy obs. 2−50440
Cu, valence states produced by ion-sputtering reduction, X-ray photoelectron spectroscopic obs. 2−57263
Cu Ar^+ and Ne^+, angular and temp. depend. 2−51064
Cu film, r.f. deposition, film thickness distrib. 2−60651
Cu^+, from Cu source, energy spectrum 2−47783
Fe, valence states produced by ion-sputtering reduction, X-ray photoelectron spectroscopic obs. 2−57263
GaN film, prep. by cathode sputtering 2−56589
Ge film production and struct., effects on secondary electron emission 2−57265
Ge surface, sputtered atom ejection patterns indicative of cryst. order 2−43466
InSb surface, sputtered atom ejection patterns indicative of cryst. order 2−43466
KBr, ion bombardment, mass spectrometer obs. of sputtering and ion emission 2−71765
Mo, deposition and sputter removal from W, Cu, Al and Au, Auger spectroscopy 2−50520
NbN films, reactive high-vacuum codeposition and characteriz. 2−50497
Pd, temp. rise during film deposition as a function of applied power 2−67913
Rh film electrodes on glass, deposition by sputtering 2−64573
Sc thin film targets, relative rates for various ion beam types and energies 2−45691
Si single crystal substrate, by Pt, thin PtSi film formation and thermal stability 2−71334
Si surface, sputtered atom ejection patterns indicative of cryst. order 2−43466
SiO_2 dielectric films in low pressure glow discharge 2−74634
SiO_2 film, r.f., effects of substrate temp. on optical and chem. props., and re-emission coeff. 2−83865
Ta, temp. rise during film deposition as a function of applied power 2−67913
Ta, triode config. with rotary base and no mag. field 2−78694
Ta film with uniform thickness 2−47127
Ti-Zr-Al-N film, prep., struct., elec. resist. props. 2−47130
TiO_2 thin films, study of optimal conditions by γ-ray spectroscopy 2−45197
U alloy, ion etching and scanning electron microscopy 2−56578

Sputtering continued
  W-Mo alloy, energy spectra of W$^+$ and Mo$^+$ ions 2−68263
  ZnO, r.f. sputtered onto sapphire, u.s. transducers at microwave frequencies 2−52243
Stacking faults
  2−56591
  Au, tetrahedra formation, models 2−60808
  continuum theory of high-speed propagation, dynamic singularity 2−50680
  electron microscopy, weak beam method 2−80630
  electrons micrograph image contrast, effects of anomalous absorption, computer simulation 2−43551
  energy, deduction by anisotropic elastic theory, suitability of theory 2−60802
  enstatite, X-ray topographic studies of natural and deformed crystals 2−61970
  film, epitaxial, f.c.c., energy determ. 2−77588
  graphite, interactions with halogen impurities 2−53738
  interaction with grain boundaries, review 2−68032
  intersecting, electron diffraction contrast, intersecting overlapping stacking faults, computer simulation method display 2−80625
  metal, f.c.c., rel. to hexagonal Frank loop energy 2−50667
  metal, role in brittle fracture 2−43730
  metals, eigen-frequency of extended disloc., stacking fault energy depend. 2−60796
  quantitative defectoscopy, and computer-simulation of images 2−60745
  scanning electron microscope backscattered electron contrast, dynamical theory 2−56628
  steel, high-C martensitic, electron diffr. obs. 2−56934
  thick crysts., electron diffr., contrast at high voltages, Bloch wave interactions 2−71407
  transition metals, b.c.c., electronic and elastic contribs. to energy 2−43726
  transmission electron microscopy, complementary images 2−77541
  Ag-15% Ge alloy, splat-cooled, martensitic transformation of structure 2−56921
  Ag-Sn alloys, X-ray diffr. data interpret. 2−50678
  Al-Cu alloy, Frank loop nucleation on screw dislocations 2−50670
  Al-Mg alloy, stacking fault energy, rel. to high temp. creep mechanism 2−68089
  Al, rel. to n-value 2−53737
  Al single crystal, programme toughened, rel. to crit. sliding stress temp. depend. 2−71582
  Au, energy from Shockley partial dislocations separation meas. 2−77591
  Au, formed by elimination of vacancy clusters on quenching 2−71630
  Au, quenched, tetrahedra growth and annealing 2−77590
  CdI$_2$, growth characts., stacking faults distrib. and stability, polytypism 2−74781
  CdI$_2$, polytypes, rearrangement of faults as transform. mechanism 2−77745
  CdI$_2$ polytypes, rel. to occurrence of Zhdanov numbers 1,2, and 3 2−83945
  CdS film, scatt. of electrons, rel. to elec. props. 2−61150
  CdS powder, rel. to electroluminesc. brightness 2−61716
  CdS single crystals, stacking faults, polytypic growth, electron microscope study 2−60769
  CdSe$_x$Te$_{1-x}$, rel. to structure on absorp. edge obs. 2−84517
  Co film, effect on n.m.r. 2−81471
  Cu-Al alloy, conc. heterogeneities on faults 2−50681
  α-Cu-Al alloy, energy detn., electron microscope obs. 2−50682
  Cu-Al alloys, additives influence on stacking fault energy 2−77665
  Cu, rel. to n-value 2−53737
  Cu alloy, rel. to n-value 2−53737
  Cu film, condensed in presence of residual gases, rel. to oxidation 2−71328
  Cu single crystal, programme toughened, rel. to crit. sliding stress temp. depend. 2−71582
  GaAs, X-ray obs. in single crysts. and epitaxial layers 2−74767
  HgS single crystals, stacking faults, polytypic growth, electron microscope study 2−60769
  KCuF$_3$, stacking disorder, X-ray diffr. obs. 2−77569
  Mg, neutron irrad., rel. to damage production and annealing 2−80683
  MoC, foil, electron diffr. obs. 2−43641
  MoSe$_2$, deformed, anomalous X-ray line broadening obs. 2−60807
  Ni, low impurity conc. influence on energy 2−43642
  Ni stacking fault propagation from a coherent twin boundary 2−80670
  Si, thermally oxidized, effect of doping impurities 2−60809
  Si wafer, device-processed, due to thermal oxidation 2−51179
  SiC, transmission electron microscope obs. 2−47423
  TaC$_{1-x}$, energy rel. to C content on plastic deformation 2−60869
  Ti-Al alloy, cold-worked, X-ray diffr. study 2−80860
  V-C ordered alloys, fault vector analysis 2−71378
  ZnS:Co piezospectroscopic effect on group of zero- phonon lines associated with centres 2−44384
  ZnS, exciton piezoreflectance, exciton states exchange splitting by stacking faults 2−81391
  ZnS, melt grown, hexagonal, defect elimination by donor impurity doping 2−47279
  ZnS, stacking order, X-ray obs. 2−47213
  ZnTe epitaxial film, on Ge substrate 2−50515
  Zr-Al dilute alloy, ordering and stacking faults 2−47354
Standards
  see also Constants; Units
  2e/h, as-maintained voltage standards, international comparisons 2−78748
  acoustic noise reference source 2−45537
  arc welding radiation meas. rel. to protective filter glass standardization 2−73668
  astronomical absolute flux meas., errors in standard star Vega 2−81974
  atomic frequency, physical basis, H maser, Cs beam and Rb gas cell considered 2−41453
  average wavelength parameter for surface metrology 2−45212
  black body source high frequency, as primary spectrometric standard 2−52266

Standards continued
  calibration methods for gas humidity analysers 2−82135
  chemiluminescence intensity, NO/O gas phase and luminol oxidation in liquid phase 2−65372
  comparisons of International Pyrheliometric Scale with absolute radiation scale 2−73461
  dimensions and decibels 2−41444
  exposed dose units for X and gamma radiation, USSR state primary standard 2−76734
  freons, Raman spectra as internal standards for mass meas. 2−80418
  frequency, 3.39μ, He-Ne laser with internal nonlinearly absorbing methane cell 2−59158
  frequency, automatic plotting systems for frequency stability curves and dicrete spectral density 2−78752
  frequency, cavity pulling in masers and lasers 2−63304
  frequency and time measurement and standards, report 2−76158
  health care standardization 2−66255
  heats of reaction, 20°C 2−48314
  Hg, vapour pressure, supplement to water is comparative ebulliometric meas. 2−67877
  high-radiance, use of high pressure thermal Ar plasma 2−46713
  international atomic time scale 2−78750
  International Geomagnetic Reference Field, derivation 2−72903
  International Practical Temperature Scale, 1968, calibration of Pt resistance thermometers to 2−66653
  ionization vacuum gauge, secondary measuring standard 2−66381
  kilogram, primary state standard of USSR 2−69531
  laser, ring, freq. stabilization, as optical freq. standard 2−69906
  length, review 2−48972
  of light, NBS, luminous emissivity, effect of ceramic spectral emissivity variations 2−45808
  line standards subdivisions length meas., temp. errors of comparator method 2−76153
  luminol oxidation in liquid phase and NO/O oxidation gas phase, chemiluminescence intensity 2−65372
  magnetic flux, primary state standard in USSR system 2−76440
  melting point of eutectics as secondary temp. standards above 2327 K 2−53489
  microwave noise, hot and cold, in UK 2−78753
  neutron radiation on human body, expt. with tissue equivalent substance 2−55239
  noise annoyance sensitivity scale 2−73223
  nondestructive testing, of aluminium pressure vessels 2−62896
  nuclear fuel cycle, reference materials for accurate determ. of U, Pu and Th 2−74160
  nuclear timing system calibration using ^{85}Rb and ^{237}Np level halflives 2−79750
  ohm, state primary standard of unit of electric resistance 2−58682
  paramagnetic salt temperature scale for 0.9 to 18 K range 2−55586
  pascal, unit of sound pressure, in pneumatic medium 2−55369
  photometry for development of calibration standards 2−73677
  polarization in nuclear reactions, determ. using p polarization 2−74072
  primary electrical units, measurement techniques in Netherlands 2−78745
  pyranometers, international comparison of working standards 2−63141
  radiation, secondary, with $\lambda=640.2$ nm, for pyrometric obs. of plasma 2−45585
  radiation for solar constant and solar spectral irradiance 2−78579
  radiation protection, book 2−59873
  radiation protection, in Germany 2−49912
  radioisotopic batteries, safety regulations 2−49304
  radionuclide activity in gases 2−55971
  reactance, calculable cross capacitor 2−82119
  resistance thermometers, calibration in 4-90 K range 2−85163
  scale of hardness for Rockwell Superficial HR 30T test 2−43771
  sealed metal freezing point cell for thermometer calibration 2−45599
  secondary, reproduction of unit of length 2−58689
  secondary, therapy-level X-ray exposure meter 2−76149
  secondary standard instrument for protection level dose rates 2−69243
  SI system, development, units, definitions 2−48971
  solar constant and air mass zero solar spectral irradiance specifications 2−78580
  standard free air chamber effect of beam path length on photon scatter correction in low-energy X-radiation meas. 2−55907
  temperature, melting point of Mo as secondary fixed point 2−53493
  temperature conversion, international scale 2−41443
  temperature scales, effect of differences in anal. of heat capacity data 2−47751
  thermal expansion meas. at high-temps. by dilatometer reference materials 2−57071
  thermal neutron flux standard facility, construction and calibration 2−63942
  thermal noise, WR15 2−78760
  time, atomic unit adoption 2−55363
  time and frequency, tutorial introduction 2−76159
  time scales and frequency standard synchronization by meteoric reflection of radio waves 2−58693
  ultra high vacuum, H-Nb system equilibrium pressures as secondary standard 2−78692
  unified time-frequency-length standard using constancy of speed of light and optical frequencies 2−63370
  u.v. intensity, use of relative cross section meas. for simultaneous excitation and ionization of He 4^2S and 4^2P states 2−64076
  vacuum ionization gauge, hot filament, control calibration, American Vacuum Society standard 2−52012
  viscosity index, repeatability and reproducibility 2−60448
  viscosity units, state primary standard 2−58683
  volt, state primary standard of unit of e.m.f. 2−58688
  voltage, a.c. Josephson effect 2−78746
  voltage, Weston cell, 2e/h measurement, a.c. Josephson effect 2−78747
  Weston cell, with Cd-Pb amalgam electrodes 2−82118
  Ag-Cu alloy, eutectic, temp. standard, freezing and melting point determ. 2−53486
  CdSO$_4$, ‘acid’ standard cell, e.m.f.-temp. coeff., 15° to 40°C 2−82130
  Er-H system, gas pressure standard 2−52016

Standards continued
^{56}Fe, for atomic masses 2−73282
He-Ne laser, frequency stabilization by Ne absorption tube in laser cavity in alternating magnetic field 2−78757
Mg$_2$SiO$_4$ with Mn impurity as e.p.r. field marker and intensity reference 2−66664
NO/O gas phase and luminol oxidation in liquid phase, chemiluminescence intensity 2−65372
Pu metal, reference specimens for determ. amount of Pu and impurities in reactor fuels 2−75399
PuO$_2$, reference specimens for determ. of impurities in reactor fuels 2−74158
Rb frequency generator, phase tuned, r.m.s. fluctuations 2−82122
U/Pu oxide fuel, reference material for chemical specification analysis 2−74159
U check specimens for spectrographic analysis of nuclear fuels 2−75407
W, for spectral emissivity 2−54087

Stark effect
— 2−67387
alkali halide, of M and N colour centres 2−61624
2-aminopyridine, normal and deuterated, dipole moment from Stark effect meas. in microwave spectrum 2−50077
atom, decaying two-level, interaction with linearly polarized oscillating field 2−79879
atomic spectra, one-electron approx. for broadening by electron-atom collisions 2−42757
azines, of $n\pi^*$ and $\pi\pi^*$ states 2−77138
benzenes, substituted 2−67509
finite crystal, Stark ladder existence in electronic state spectrum 2−68281
hexamethylenetetramine, ^{14}N n.q.r. in axially symmetric field gradient 2−61757
impurity centre, method of average moments 2−65246
ladder from quantization of Bloch oscillations in strong elec. fields 2−61147
line broadening electron correlations in unified model 2−42720
line contour splitting in absorption in strong nonmonochromatic field 2−83202
longitudinal optical phonon, coupled with Stark ladder electron, current charact. 2−68276
methlenecyclopentane, dipole moment 2−67516
methyl bromide, pressure broadening, Stark and double-resonance spectroscopy 2−42993
microwave cavity spectrometer, Q-pulling effect, error compensation 2−66662
nuclear quadrupole resonance, polarizability of single bonds 2−52984
3-oxetanone, dipole moment determ. 2−70787
plasma, electron impact broadening of isolated spectral lines of heavy elements 2−60244
plasma arc, magnetized, h.f oscills., obs. using h.f. Stark effect 2−70942
polyatomic T_d molecules, rotational spectra 2−42844
rigid symmetric rotor, Stark perturbed rotational energy levels 2−77028
shifted molecular levels, optical nutation and free induction decay 2−42834
in superradiant two-level system 2−45702
symmetric top molecules, perturbation theory of higher-order effects 2−42836
S-triazine triplet state at 3455 Å, Stark effect meas, vibronic origin of state 2−83280
triethylenediamine, ^{14}N n.q.r. in axially symmetric field gradient 2−61757
two-level system, representation as linear oscillator 2−49927
Ar electrodeless discharge, radial distrib. of density of electrons 2−50228
Ar plasma, electrodeless discharge, high freq., high press., Stark widening of lines 2−46423
Ar plasma, laser perturbed, transient light emissions 2−80231
BeO, Stark shift of nuclear spin levels of ^{9}Be, n.m.r. obs. 2−44453
C I 2478 line, Stark half-width estimation 2−59916
C^{5+}, Lamb shift studied via motional electric field quenching of $2^2S_{1/2}$ state 2−70633
CO, spectrum of $a^3\Pi$ state at 5 to 1000 MHz, fine structure, dipole moment and perturbation analysis 2−50026
Ca II, Stark broadening and shift of lines 2−60245
Ca$^+$, measurement and calculation of Stark broadening parameters for resonance lines 2−42727
CaF$_2$:Nd$_2$O$_3$ (NdOF), optical spectra of Nd^{3+} 2−61702
CaF$_2$:Tu^{2+}, crystal, structure of ground state of Tu^{2+} 2−61611
CaF$_2$-YF$_3$:Er^{3+}, spectroscopic study of stimulated radiation 2−61689
CaF$_2$, coloured, linear effect in zero phonon lines 2−53751
CaF$_2$, coloured, zero-phonon lines 2−53752
CdF$_2$:Er^{3+}, i.r. transitions, Stark dissoc. by cryst. field 2−65305
Cs-Rb differential Stark shift investigated using optically pumped atomic light modulation oscillators 2−46424
Cs, ionized vapour, electron density determ. from spectral line mixing 2−46792
^{133}Cs, investigation of third excited $^2P_{3/2}$ levels in first spectrum, tensor polarizability determ. 2−70591
Cu$_2$O, Γ^+_5 exciton quadrupole transition rel. to static elec. field, Stark splitting 2−81406
D$_2$O, dipole moment determ. from Stark effect meas. on microwave transitions 2−80045
Er$_2$O$_2$S: Er^{3+}, energy levels and crystal field splittings detn. 2−51339
H, adiabatic theory of Stark broadening used to describe transitional frequency band between impact and quasi-static limits 2−46474
H, in plasma, line broadening, quasistatic and impact approx. 2−52948
H, one electron approx. for broadening by electron-atom collisions 2−42757
H, quenching of 2S states, time-dependent theory 2−49974
H, Stark broadened Lyman-α lines, electronic shifts 2−64059
H, Stark profile of Ly-α line in the region of transition from impact to quasi-static broadening 2−46475
H, wings of Stark-broadened lines, Holtsmark's 5/2 power law 2−74242

Stark effect continued
H atom, linear effect due to resonant interactions of static and dynamic fields 2−64061
H atoms in plasma, time evolution operator in semiclassical theory of Stark-broadening 2−42793
H plasma, broadening of Balmer lines 2−64278
HCP, dipole moments of $^1A''$ and $^3\Delta_1$ states 2−42897
HDO, rotational dependence of dipole moment determ. from Stark effect meas. on microwave transitions 2−80045
HF, polarizability anisotropy 2−42907
He, forbidden and allowed transitions in dense, laser produced plasma 2−42805
He, quenching of 2S states, time-dependent theory 2−49974
He, Stark splitting between Zeeman sub-levels, atomic beam mag. reson. obs. 2−83215
He II, improved Stark profile calc. for lines between 256 and 4686 Å 2−46477
He thermal plasma, absorption and emission line shapes for HeII resonance line 2−79952
ICl, dipole moment meas. 2−42902
InCl, electric dipole moment, Stark effect measurement 2−46555
Kr electrodeless discharge, radial distrib. of density of electrons 2−50228
Mg, line broadening by microfields of ions and electrons 2−70588
Mg$^+$, measurement and calculation of Stark broadening parameters for resonance lines 2−42727
NCN$_3$, dipole moment components determ. 2−60014
NH$_3$, transient effects on microwave line 2−42911
^{14}N nuclear quadrupole resonance in asymmetric field gradient 2−44462
^{14}N nuclear quadrupole resonance in asymmetric field gradient 2−44463
Na resonance lines, study by atomic beam method 2−74218
Na$_2$ArSiO$_5$:Eu^{3+}, luminesc. 2−72414
NaLi, ground vibronic Stark coeff. in electric resonance spectrum 2−53029
^{87}Rb, investigation of third excited $^2P_{3/2}$ levels in first spectrum, tensor polarizability determ. 2−70591
Si II, broadening of 6371.4 and 6347.1 Å spectral lines 2−56097
SrF$_2$, coloured, linear effect in zero phonon lines 2−53751
SrF$_2$, coloured, zero-phonon lines 2−53752
Xe, 2p$_2$, 2p$_7$, 3p$_6$, 3p$_7$ and 5d$_3$ levels 2−70594
Xe, 4300-5000 Å 2−70593
Xe electrodeless discharge, radial distrib. of density of electrons 2−50228
Xe plasma, electrodeless discharge, high freq., high press., Stark widening of lines 2−46423
Xe spectral line coeffs. determ. 2−67393
Y$_2$O$_2$S:Er^{3+}, energy levels and crystal field splittings detn. 2−51339

Stars
see also Multiple stars, Nebulae; Novae; Planetary nebulae; Stellar atmospheres; Sun; Variable stars
absolute declinations from measured differences of zenith distances 2−48815
angular diameters, est., independent of luminosity and reddening 2−62493
astrometry, effect of error in plate reduction 2−58259
atomic processes in astrophysical plasma 2−75703
baryonic, superdense, as nuclear energy sources 2−81854
black holes, colliding, computer solution 2−69006
blue globular clusters in LMC, spectral obs. 2−81804
TU Cas, mass determined from temp. and period ratio 2−58258
catalogue corrections from satellite obs. 2−62479
Cen X-3, optical search, not LR Cen or Wray 795 2−58421
ω Centauri, globular cluster, early- type C stars, objective-prism studies 2−75773
Cep OB 3 association, internal motions 2−75771
chemical reactions, influence of excited states of target nuclei in vicinity of Fe peak 2−62507
chromosphere, two-quantum photon-plasmon $2S_{1/2}-1S_{1/2}$ transition 2−79962
clusters, reddening and u.v. excess det. from UBV obs. of red giants 2−44862
compact, rotating in thermal plasma, angular momentum and energy loss 2−73055
constant of aberration and short-period terms of nutation from Pulkovo polar tube observations 2−51722
convection envelope response to tidal variation of gravitation field 2−85008
coordinate det. from wide angle ballistic camera installed in aeroplane 2−51865
R Coronae Australis and surrounding young stellar group, i.r. and optical obs. 2−78468
differentially rotating, models, binding energy calc. 2−58265
diffusion processes 2−51731
distance determination, trigonometric parallax, errors 2−69055
dynamic astronomy, meeting (College Park, USA, March 1972) 2−58166
dynamics connection with Markov processes, calc. of relaxation and evaporation times, quasisteady distributions 2−44853
early type, identification by i.r. photometry and spectroscopy 2−75824
early type, search for in anomalously excited H II regions 2−58253
early-type, radio obs., superbright radio knots 2−81825
encounter with cometary orbits 2−69171
energy source, popular article 2−81860
energy-loss rates for neutrino pair production mechanisms calc. in Weinberg's theory 2−69071
faint, immediate neighbourhood of galaxy 2−69032
faint M type, kinematics and mass density 2−55030
field, near M35 open cluster, secular parallaxes and luminosity functions 2−48685
field stars, simulation in numerical experiments 2−69105
fields, absolute calibration of objective prism plates for computer reduction 2−75698
FK4 system, right ascension by meridian observation with the Dollen method 2−69052
G 87-25, parallax determination 2−69102

Stars continued
galactic clusters, ratio of total to selective absorption, kinematic det. 2−62553
Galactic Globular Clusters, luminosity function, clustering properties 2−51772
galactic halo in direction of SA 71, star density, 3 colour photometric obs. 2−62461
galactic kinematic parameters from star clusters rel. to galactocentric distance to Sun 2−84959
Galaxy and the distance scale, Woolley symposium, Herstmonceaux, Aug (1972) 2−69015
galaxy population synthesis, quadratic programming 2−81799
globular cluster, with nonzero angular momentum, gravitational instability 2−55070
globular clusters, horizontal branch, core He burning, models 2−84966
globular clusters, NGC 2257, in Magellanic clouds, electronographic photometry 2−48722
globular clusters, Population II stars, electron-neutrino weak interactions 2−78459
globular clusters, pseudo colour-magnitude diagrams 2−44882
globular clusters, R-method for He abundance 2−81808
globular clusters, RV Tauri, photoelectric observations 2−58323
globular clusters, search for UV-bright stars, post- horizontal branch evolution 2−55062
Globular Clusters, space distribution, Palomar Sky Survey 2−51773
globular clusters, upper limits on atomic H I abundance 2−75783
globular clusters 10 colour photometry 2−58216
globular clusters and Hartwick's two-dimensional classification 2−75781
globular clusters and the distance scale 2−75780
Gould Belt, OB stars, distance moduli, proper motions and radial velocities 2−58267
gravitational collapse, nonspherical perturbation in integer spin of zero-rest-mass fields treated in Newman-Penrose formalism 2−55387
gravitational collapse, nonspherical scalar of gravitational perturbations 2−55386
GX3+1, search for optical stellar counterpart of X-ray source 2−51796
GX 340+0, hot neutron star 2−62639
HD 148937, peculiar O6f star, symmetrically surrounding nebulae (NGC 6164-5) 2−66066
HD 168785, surface gravity det. from forbidden He I 4045 Angstroms line 2−55027
HD 87634, associated nebula 2−85005
HD 96446, surface gravity det. from forbidden He I 4045 Angstroms line 2−55027
hot, acceleration of matter by absorption in spectral lines 2−69072
Humason-Mayall-Sandage clusters, velocity distance relation 2−58346
Hyades, region, trigonometric parallaxes using Schmidt telescope 2−66070
Hyades cluster, mass-luminosity relationship, unevolved stars 2−48724
Hyades group, identification of red giants 2−62530
hydrostatic O burning at balanced power 2−51736
IC 2602 open cluster, H-R diagram 2−75728
IC 4651 cluster, spectral class, slit spectra, UBV photometry 2−84955
image instability, experiments with bichromatic double- channel TV system 2−48675
intermediate age galactic population stars, kinematics near North Galactic Pole 2−58182
K and M dwarfs, wide moving pairs 2−75752
kinematics, statistical analysis 2−72995
KSZ stars, re-reduction of 107 additional objects in northern sky galaxy areas 2−48681
large-scale TV images, statistical analysis of form variations 2−48676
latitude observations rel. to declination errors in various star catalogues 2−51724
latitude observations with prismatic astrolabe at Pulkovo Observatory 2−51723
limiting magnitudes of visual observations of stars 2−48677
limiting stellar magnitudes in observations with visual telescopes 2−48678
local Population II density, upper limit 2−51745
lunar occultation near-elliptic bright stars 2−85063
in M31 galactic nucleus, velocity dispersion 2−75682
M4, globular cluster, structure, spatial distrib. of stars 2−84948
M67 cluster, Ba II- and R-type stars in old disc population 2−81844
M-type, field in Pleiades region, proper motions 2−69065
M-type giants, classification, statistical investigation of galactic structure 2−66092
massive, fundamental data rel. to theoretical models 2−51726
massive main sequence stars, effective temperatures 2−66075
in Milky Way, southern, atlas 75669 2−75669
Mira, rotational temp. at maximum light 2−58300
models, computer generated relation to reality 2−84932
Monoceros field, O-F7 type stars, space distrib., obscuring matter 2−78473
motions in galactic spiral arms, review 2−58183
neutron, accretion disc model for X-ray sources 2−85014
neutron, anisotropic superfluid matter, Ginzburg-Landau theory 2−51755
neutron, Brans-Dicke theory test using cold neutron star model 2−73308
neutron, cooling rel. to π^- condensation, independent particle model 2−75751
neutron, crystallization of matter 2−55049
neutron, degenerate electron gas magnetic props., Landau orbital ferromagnetic states 2−47823
neutron, development of stable states of matter, review 2−55034
neutron, energy shifts of excited nucleons 2−58313
neutron, equation of state, equilibrium configuration, transport props. 2−44866
neutron, equation of state of matter at subnuclear densities 2−66096
neutron, isolated, upper mass limit for pulsars 2−44893
neutron, mass accretion in binary system 2−58312

Stars continued
neutron, matter at extremely high temp. and pressure 2−62912
neutron, microquakes and macroquakes 2−55048
neutron, nonstationary hydrodynamical accretion 2−81852
neutron, nuclear forces, compressibility of neutron matter and maximum mass 2−44864
neutron, phys. props. of matter in superstrong mag. field 2−81858
neutron, relativistic, connection between amplitudes of scattered gravitational waves and nonradial vibrational modes 2−69088
neutron, rotating, as energy source in Crab and Vela nebulae 2−62471
neutron, rotating, physics of pulsars, book 2−73050
neutron, rotating in thermal plasma, angular momentum and energy loss 2−73055
neutron, star spot formation, possible pulsar emission mechanism 2−55050
neutron, superdense matter, condensed π^- phase 2−63727
neutron, superdense matter, condensed π^- phase 2−63726
neutron, superfluid, cooling rates 2−66127
neutron, superfluid props., Ginzburg-Landau eqn. for $^3P_2$ pairing 2−76234
neutron, superfluidity, BCS theory applic. 2−48703
neutron models rel. to Crab nebula e.m. radiation 2−75692
new astronomy, conference, March 1972, Bloemfontein, S. Africa 2−66071
NGC 1662, distance and B-V colour excess, UBV photometric obs. 2−51771
NGC 1893, open cluster, radial velocities of some stars 2−62589
NGC 2141, open star cluster, photometric observations 2−81789
NGC 2168, open cluster, secular parallaxes and luminosity functions 2−48685
NGC 2232, open cluster, photometric obs. 2−66105
NGC 2264, young cluster, effect of D_2 burning on pulsational stability 2−62505
NGC 2818, open cluster containing planetary nebula 2−62585
NGC 6352, globular cluster, metal abundance obs. 2−58339
NGC 6374, open cluster, catalogue and identification maps 2−44878
NGC 6383, open cluster, catalogue and identification maps 2−44878
NGC 6405, open cluster, catalogue and identification maps 2−44878
NGc 6416, open cluster, catalogue and identification maps 2−44878
NGC 6530, extremely young open cluster, membership obs. 2−81798
NGC 6530 cluster and association with M8 nebula 2−75772
NGC 6819, open cluster, probabilities of membership from relative proper motions 2−62582
NGC 6866, open cluster, catalogue of proper motions for 2036 stars 2−48720
NGC 6913, cluster hot stars, colour excess variations 2−81857
NGC 6981, globular cluster, colour-magnitude diagram 2−55041
NGC 6981, globular cluster, photometry of RR Lyrae variables 2−62571
NGC 7099, globular cluster, colour magnitude diagram 2−55042
NGC 752 galactic cluster, reddening, distance modulus, chemical composition and age 2−48723
nuclear reaction processes, He burning 2−69086
nuclear reactions in degenerate electron nuclear plasma 2−58256
nuclei, threshold of disintegration in degenerate electron neutron gas 2−58255
OB types, bright southern, distance moduli, proper motions and radial velocities 2−58267
observations using the Cerro-Calan Observatory meridian circle, value of screw of ocular micrometer 2−51874
occultations, study of terrestrial atmospheric composition 2−54877
occultations by planets, satellites and asteroids, predictions and observations 2−78515
occultations by planets, satellites and asteroids 2−48768
Ohio survey radiosources, optical identifications 2−75805
one dimensional system, double water Bag model, stability 2−75708
open clusters, catalogue and identification maps 2−44878
open clusters, velocity variation of star as discontinuous random process 2−69099
open clusters in Milky Way, southern atlas 2−75669
open star clusters, mean absolute magnitudes and colour indices of red giants 2−81812
Oph., wavelength dependence of interstellar polarization in that direction 2−58366
orbits, variations in collapsing galaxy 2−81784
overabundance of rare earths and symmetric fission of superheavy nuclei 2−54998
parallax, first measurements 2−69521
α Persei cluster, space-density curves from proper motion survey 2−81813
h and χ Persei double cluster, possible existence of different populations51769 2−51769
phase mixing of second kind 2−58257
photometer, with Cassegrainian optical system, for 1300-2000 Å region 2−69050
planetary occultation data rel. to vertical number density profile of atmosphere gases 2−84839
plasma gravitational instability and frictional effects with neutrals 2−66073
Pleiades field obs., photographic image calibration with 45° second surface reflector plate 2−75700
Pleides, rotational velocities rel. to transition from shallow to deep convection zones 2−81824
polariscope program for obs. in 0.2-0.3 μm range 2−72988
population in nuclear bulge of Galaxy 2−44839
positions using GALAXY-machine meas. of Schmidt plate 2−45001
Praesepe field obs., photographic image calibration with 45° second surface reflector plate 2−75700
proper motions, contrib. of Danjon's astrolabe to study 2−66069
proper motions rel. to galactic rotation constants 2−69021
Pulkovo catalogues of declinations Pu$_{50}$F and Pu$_{50}$Z 2−51721
Pulkovo ZTL-180 tube, ocular micrometer screw rotation value, observations of wide scale pairs 2−48827
radial oscillations, perturbation by magnetic field 2−75705

Stars continued
radial velocities of members of Large Magellanic cloud 2−62548
radial velocity evaluations using standard wavelengths of Fe spectrum 2−48687
radial velocity tables with heliocentric reductions 2−48686
rapidly rotating, detection of gravity darkening and axial inclination from photographic line profiles 2−75745
reaction rates for $^{12}C+^{12}C$, $^{12}C+^{16}O$, and $^{16}O+^{16}O$ reactions 2−51737
red, luminosity and temp., kinematics, distance scale 2−69056
reference catalogue system influence on coords. of stars det. in zonal meridian obs. 2−51866
refractional and circumzenithal Talcott pairs, observations with ZTL-180 tube 2−48682
relativistic, slowly rotating, stability of quasi radial modes 2−58264
right ascension, corrections to FK4 catalogue, meridian circle observations 2−48680
right ascension observations rel. to the Toepfer meridian circle, contact micrometer screw rotation effects 2−51873
Ross 986, parallax determination and possible binary orbital motion 2−69102
rotating, energy extremal properties in general relativity 2−44851
rotating, gravitational collapse approx. 2−62495
rotation and simulation of intensity interferometer 2−58270
rotational speeds rel. to Kant and Laplace's hypothesis 2−48670
SAO 076152, occultation, fading rather than abrupt cut off 2−62478
β Sco, occultation by Jupiter, flashing phenomena66171 2−66171
23 Sextantis, HD90386 as comparison star 84997 2−84997
single, lunar occultation, catalogue of diffraction patterns 2−75701
solar neighbourhood, hidden mass 2−84971
southern B-stars, associated with H II regions, radial velocities 2−62492
southern open clusters, UBV-$H\beta$ photometry, galactic structure 2−84954
stability of adiabatic l.f. nonradial oscillations of gravitating configuration with internal toroidal mag. field 2−81855
stellar encounters, new treatment in computation of N-body systems 2−58170
stellar interferometer 2−69200
superconducting neutron star matter, thermodynamic crit. field 2−73008
superdense, tachyon-like matter implications 2−55397
supergiant stars, colloquium (Trieste, Italy, Sept. 1971) 2−58262
supergiants, loop formation, homology relations 2−62519
supergiants, luminosity functions for 16 associations in Large Magellanic Cloud 2−58307
supergiants, results of observations 2−62482
supergiants, secular instabilities 2−62483
surfaces, spallation processes, anomalous He ratios 2−48692
Talcott pairs, working ephemerides for latitudes 0-15 degrees N 2−76046
telescopic images, random wave-front perturbations 2−62480
Terzan 5 system, identity and aliases 2−62583
transit measurements, accuracy using zenith telescope and transit instrum. 2−72987
TV microphotometry of photographic images 2−76045
Uhuru X-ray sources, association with bright stars 2−58422
UV Ceti, photometric studies, flare observations 2−78461
u.v. obs. by Apollo 16 from moon 2−75699
van Wijk sequence in Large Magellanic Cloud, UBV photometry obs. 2−69033
vertex deviation 2−44849
water bag model in cylindrical two dimensional stellar system 2−44850
winds and breezes, radial flow of inviscid heat conducting gas with gravitational effect 2−62527
Wolf 630 Group, Ba II- and R-type stars in old disc population 2−81844
young, motion rel. to gas in H II regions 2−44848
ZC.3091, grazing occultation Moon during eclipse 2−81927
zero-points of catalogues, application of obs. of Moon to improvement 2−76044
AP Lib, diameter of compact component 2−55094
B supergiant in peculiar eclipsing system, N_2 enhanced 2−73029
Cr-Sr, high mag. field strength 2−81839
He-weak, search in very young clusters 2−69053
$Me_{50}1(\delta)$ declination catalogue rel. to FK4 and N30 catalogues 2−48679
Mn, low mag. field strength 2−81839

composition
see also Elements/origin
η Aquilae, light variations for CO, CN, C_2, CH, OH and NH 81840 2−81840
V553 Centauri, type II Cepheid, overabundance of C66102 2−66102
3 Centauri A, ^3He-^4He ratio, spallation processes at surface 2−48692
Cepheids in SMC, distance determ. 2−69038
cool supergiant stars, model atmospheres, compositions 2−66074
cool supergiants, dissociation equilibrium and convection 2−62499
NML Cygnus, OH i.r. emission 2−55045
extreme Population I matter, noble gas abundance rel. to Sun 2−81838
F131 in galactic cluster M67, metal deficiency and reddening 2−84991
F90, in galactic cluster M67, metal deficiency and reddening 2−84991
forms of matter, review 2−55031
globular cluster, M92, He content from subgiant luminosity function 2−55065
grains in the atmosphere of late type irregular and semi-regular giants and supergiants 2−69084
HD 25354, Ap type, abundance of transuranium elements 2−72994
HD 33579, A3Ia-O supergiant, in LMC, model atmos. anal. 2−75727
HD 7583, supergiant in Small Magellanic Cloud, coarse analysis 2−69054
HD 86986, HD 109995, HD 161817 oxygen abundance 2−66095
HR 4072, double lined binary Hg type, Am stars as companions, abundance anal. 2−58340
HR 465, Ap stars, model atmosphere anal., abundance obs. 2−66076

Stars continued
composition continued
HR 465, Pm identification 2−51741
HR 465, proposed identification of Pm 2−51727
HR 465, search for Pm II lines, comments 2−66081
HR 465, search for Pm II lines 2−62501
HR 5447, element abundances and model atmosphere 2−78464
HR 6290, element abundances and model atmosphere 2−78464
HR 6596, element abundances and model atmosphere 2−78464
HR 6917, element abundances and model atmosphere 2−78464
HR 7061, element abundances and model atmosphere 2−78464
K giant, metal abundances from synthetic stellar spectra calc. using computer 2−69083
late-type giants, metal abundances detn. from narrow band photometry 2−69051
χ Lupi, double lined binary Hg type, Am stars as companions, abundance anal.58340 2−58340
M67, galactic cluster, metallicity meas. from dwarfs and subgiants 2−78469
neutron star matter, binding energy 2−81841
neutron stars, densities 2−69085
NGC 6352, globular cluster, metal abundance obs. 2−58339
NGC 7006, variation of N abundance among population II objects 2−69080
NGC 752 galactic cluster, reddening, distance modulus, chemical composition and age 2−48723
ε Pegasi spectra, chemical composition using atmosphere model 72993 2−72993
quark searches, review 2−59598
studies elliptical galaxies, multiple systems, photometric 2−69040
C star near cluster M37, evidence for extreme rotation 2−78457
Ca surface abundance in high velocity A-stars, from Ca II 3933 Angstrom line 2−48702
Fe/H ratio F1-F5 stars, by model atmos. 2−66077
Fe I, curves of growth, effect of systematic gf-value errors 2−66079
He abundance in horizontal branch 2−75714
He abundance in young O and B stars rel. to old hot subdwarfs in galactic halo and nebulae 2−81859
He abundance main sequence B-stars 2−62488
He abundances, globular clusters, R-method 2−81808
He core types equilibrium, multiple solutions 2−72990
Hg syndrome HR 4072 and chi Lupi, equivalent width meas. 2−69108

evolution
: 2−81873
− 2−62586
A- and F-type stars, rotation of evolving stars rel. to metal abundance 2−55029
A-stars, rotation and turbulent mixing due to meridional circulation velocity field 2−62503
apparent mass gap in 3-4.2 $M_\odot$ region 2−58278
B subdwarfs, extended horizontal branch loci 2−78450
binary systems, distrib. of semimajor axes and eccentricities after rapid mass loss. 2−44877
black holes, gravitational collapse 2−44828
blue horizontal branch stars, mixed models 2−62489
Centaurus X-3, reactivation of old neutron star by mass exchange in close binary 2−78479
centred difference equations and numerical instability 2−58275
β Cephei, spectral classification, location on theoretical HR diagram 2−58324
Cepheids in SMC, distance determ. 2−69038
chemically homogeneous main-sequence stars, structure and compositions 2−84990
close binary systems, with intermediate initial mass ratio 2−66082
computing experiments on dynamical evolution of stellar clusters, application of direct integration 2−78471
contact binaries, mass flow and period changes 2−69104
core He burning, models 2−84966
R Coronae Australis and surrounding young stellar group rel. to Taurus clouds 2−78468
curves of growth, effect of systematic gf-value errors 2−66079
RS CVn type binaries, models44870 2−44870
WWCygni, eclipsing binary, no pre-main-sequence contraction 2−84998
efficient star formation rel. to gas density of external galaxies 2−58230
endpoints, discussion of various possibilities and relation to phenomena of high energy astrophysics 2−78460
equations of stellar structure for a Giant envelope, multiple solutions 2−69063
extreme Population I, effect of D_2 burning on pulsational stability 2−62505
formation, influence of local conditions in interstellar medium 2−58279
formation, review of theories 2−66085
formation and dynamics of self gravitating magnetized cylinders 2−66072
formation rate formulae 2−69067
formation sites in Sgr B2 2−69068
globular clusters, dynamical relaxation process 2−69069
globular clusters, evolution dynamical relaxation process 2−69069
gravitational contraction and main-sequence phase, secular stability of 1.1 $M_\odot$ star 2−48693
Hertzsprung-Russell diagrams, various forms 2−62511
homogeneous stellar models, conditions for having real secular eigenvalues 2−78451
hydrodynamic events, numerical method of computation 2−51733
interior, physical state 2−58271
from interstellar gas, models for galactic evolution 2−78453
isochrones for disk population stars 2−75710
K3-M2 main sequence stars, variations with space motions 2−75719
large mass supergiant stars, review 2−62514
M4, globular cluster, structure, spatial distrib. of stars 2−84948
Magellanic clouds, properties of developing stellar systems 2−66062
main sequence to He exhaustion phase, 15 $M_\odot$ and 11 $M_\odot$ types 2−51738
mass loss, dynamical effects on diffuse nebulae 2−72984
massive stars, and mass loss 2−48690
massive stars, C burning 2−66087

Stars continued

- **evolution** continued
  - massive stars, He burning 2−66086
  - massive stars, shell H burning and core He burning 2−62518
  - Mira variables, S-type stars 2−62581
  - N-type semiregular variables, possible evolution constraints 2−75717
  - neutrino energy-loss rate due to electron-nucleus neutrino bremsstrahlung 2−49785
  - neutron star gravitational collapse from nebula, review 2−84985
  - nuclear laboratory expts. 2−48695
  - nucleosynthesis and formation of superheavy elements 2−84947
  - nucleosynthesis by slow neutrons 2−67281
  - nucleosynthesis of light elements 2−62508
  - old disc population, red-giant branch rel. to Ba II- and R-type stars 2−81844
  - Oorts constant, kinematic method of det. 2−62553
  - open star clusters, zero-age main-sequence from studies of red giants 2−81812
  - planetary nebulae formation analysis 2−72981
  - population I 8 $M_\odot$ star, during central He burning, computational technique 2−62506
  - population II star, 0.5$M_\odot$ sequence 2−62510
  - Population II type in horizontal branch, effects of semiconvection 2−81835
  - post-main sequence, semi-convective mixing 2−58277
  - pre-main sequence stellar evolution and circumstellar envelopes 2−75718
  - pre-main-sequence, evolution phases 2−85007
  - quasars, and radio source counts 2−62598
  - radiative blast wave due to sudden explosion in stellar interiors 2−69049
  - rapidly rotating types, viscous evolution 2−58276
  - red giant phase, mass loss due to stellar wind 2−69070
  - red giants and supergiants, effect of rotation 2−62502
  - red supergiants, superadiabacity effects in convective envelope 2−62513
  - relaxation oscillations in envelopes of luminous red giants 2−62484
  - rotation and evolution interacting, models and photometric obs. 2−55026
  - rotation of stars rel. to transition from shallow to deep convection zones 2−81824
  - S and N envelopes, chemical evolution model 2−62490
  - s-process neutron capture time determ. 2−75722
  - self accretion of matter, red subluminous stars and early evolution of low mass stars 2−48691
  - self gravitating cylindrical polytrope, struct. 2−84988
  - shock wave propag. in self-gravitating gas spheres rel. to novae 2−84987
  - spherical protostars with masses 0.25 to 10 $M_\odot$, newly-formed stars 2−48694
  - stable states of matter, review 2−55034
  - static stellar models, opacity changes effect 2−72991
  - stellar matter, black hole and expanding universe 2−66042
  - stellar nucleosynthesis relative abundances of elements 2−66084
  - supergiants, luminosity functions for 16 associations in Large Magellanic Cloud 2−58307
  - supergiants, ratio of blue to red 2−62516
  - supergiants, spectroscopic binaries 2−62515
  - supergiants, supernova explosions, Crab pulsar 2−62560
  - supergiants, surface enrichment from interior burning 2−62517
  - supermassive nonrotating $0.75 \times 10^6 M_\odot$ star, hydrodynamic model calc. for collapse to black hole 2−44821
  - synthesis of superheavy elements and termination of r-process 2−69093
  - synthetic clusters with finite formation times, main sequences, colour-magnitude diagrams 2−75767
  - thermonuclear reaction rates at high temps. 2−62509
  - thermonuclear reaction theory, modes of H burning with respective energy output 2−75723
  - tidal evolution of close binary systems 2−84969
  - u.v. stars and effects on interstellar medium 2−75716
  - UV-bright stars in 27 globular clusters, post-horizontal branch evolution 2−55062
  - virial theorem and linear, standard, boiling point, and uniformly distributed energy model calculations 2−66083
  - white dwarfs, with accretion of H rich envelope 2−69066
  - zero age main sequence, redetermination 2−69107
  - C ignition in degenerate cores 2−48689
  - C star of 0.8 $M_\odot$, evolution and secular stability 2−55033
  - D burning main sequence stars, low mass limit rel. to stellar models 2−75720
  - He abundances, globular clusters, R-method 2−81808
  - He burning of solar mass stars 2−75721
  - He shell-burning, thermal pulses, calc. including neutrino energy losses 2−62512
  - He stars, numerical models 2−66078
- **magnetism**
  - *see also Sun/magnetism*
  - UU Comae Berenicis, photoelectric observations of magnetic star 81819 2−81819
  - 21 Comae Berenicis, photoelectric observations of magnetic star 2−81819
  - β Cor Bor, magnetic A star 2−58289
  - β Coronae Borealis, field variations from det. of Zeeman effect in spectra 2−62520
  - Cr-Sr stars, high field strength 2−81839
  - β CrB, variations det. from Zeeman effect obs. 2−58288
  - 73 Dra, variations det. from Zeeman effect obs. 2−58288
  - 73 Draconis, field variations from det. of Zeeman effect in spectra 2−62520
  - dynamics, theories 2−75713
  - field enhancement due to optokinetic effects via optoelectrical effect 2−66656
  - HD 188041, periodic magnetic variable, magnetic intensification and starspots 2−75747
  - HD 24712, Ap type, variations 2−51740
  - β Lyrae, underluminosity and magnetic fields 2−58349
  - main-sequence, effects of uniform rotation and strong dipolar magnetic fields on structure and properties 2−84986

Stars continued

- **magnetism** continued
  - neutron stars 2−69085
  - oblique rotator model, internal dynamics 2−48688
  - spherical fluid model with convection zone 2−75715
  - 41 Tauri, photoelectric observations of magnetic star 2−81819
  - toroidal fields, effects of additional poloidal field on stability 2−62496
  - 78 Vir, variations det. from Zeeman effect obs. 2−58288
  - 78 virginis, field variations from det. of Zeeman effect in spectra 2−62520
  - white dwarfs, Landau Orbital ferromagnetism LOFER theory 2−62494
  - Mn stars, low field strength 2−81839
- **radiation**
  - *see also Cosmic radiations, radiofrequency; Sun/radiation*
  - V 1057 Cygni, far-infrared and four-colour photometry 2−73012
  - A0 types, four colour and Hβ photometry 2−58284
  - A-F supergiants in Geneva observatory photometric system 2−62551
  - absolute magnitude determinations for young stars using H lines 2−48701
  - absolute magnitudes of A and F supergiants 2−62536
  - o Andromedae shell star, eclipsing binary, 253 UBV photometry 2−73028
  - atmospheric monochromatic extinction from UBV photometry of stars 2−54864
  - ε Aur, eclipsing binary, light curve, secondary fluctuations 2−73026
  - εAurigae, intrinsic polarization in atmosphere of supergiant star 2−62545
  - B-stars, non LTE effects on continuum and H_2 line parameters 2−58281
  - black holes, gravitational wave radiation, review 2−48652
  - blue Ap stars, far u.v. photometry 2−75731
  - bright southern types, four-colour and Hβ photometry 2−69081
  - 3C58, supernova remnant, brightness obs. at 2.8 cm 2−75757
  - AS Cam, eclipsing binary, photometry 55039 2−55039
  - RU Cam, two colour photoelectric light curve, period variation obs. 2−48706
  - 20.08.01 Cancri, optical variability 2−55043
  - S Car, mira variable, photoelectric obs. 2−62565
  - η Car, short period optical oscillations 2−55046
  - α Car (Canopus), absolute flux obs. 2−75746
  - Y Carinae, photoelectric observations of beat period cepheid 2−48712
  - η- Carinae, X-ray emission 2−55108
  - TW Cas, photoelectric light curves 2−73016
  - T Cen, meas. of UBVRI photometry 62575 2−62575
  - LR Cen, not optical counterpart of Cen X-3 55101 2−55101
  - Cen X-3, search for optical counterpart 2−62576
  - SV Centauri, eclipsing and double lined spectroscopic binary 58347 2−58347
  - 14Cephei, spectroscopic binary, light variations 2−85000
  - cepheid variables, pulsation amplitudes 2−75756
  - Cepheids in Magellanic Clouds, photometry 2−62580
  - Cepheids in small magellanic cloud, influence of metal lines on colours 2−81823
  - colour excess variations of hot stars in cluster NGC 6913 2−81857
  - colour indices of F-, G- and K-type stars rel. to colour indices for the Sun 2−85056
  - 21 Comae Berenicis, photoelectric observations of magnetic star 2−81819
  - UU Comae Berenicis, photoelectric observations of magnetic star 81819 2−81819
  - SW Cygni, UBV photometry of ring 2−84999
  - Cygnus, search for visible counterpart of radio outburst 2−81890
  - cygnus OB2 association, rear i.r., photographic survey 2−58303
  - differentially expanding atmospheres, transfer of resonance-line radiation 2−62522
  - differentially expanding atmospheres, transfer of resonance-line radiation 2−62521
  - diffusion, stellar shell expanding with constant velocity 2−69073
  - early-type field stars, UBV and Hγ obs. 2−51747
  - eclipsing binary system with extensive atmosphere, information available from monocolour brightness loss curves 2−48717
  - elliptical polarization search 2−75724
  - F and G supergiants in Large Magellanic Cloud, six colour photometry 2−62549
  - F-type metal deficient stars, luminosity and motion 2−51732
  - far u.v. observations of stars in Orion-Monoceros-Canis Major region 2−44863
  - flare stars, X-ray emission flux calculations 2−55113
  - globular cluster, M92, He content from subgiant luminosity function 2−55065
  - gravitational radiation from binary systems, pointless limits 2−58345
  - Haro-Chavira i.r. stars, photometry 0.7 to 34 μm 2−51746
  - HBV 475, i.r. photometry 2−69126
  - HD 154445, early type, interstellar circular polarization 2−73002
  - HD 208095, spectroscopic binary, light variations 2−85000
  - HD 217312, spectroscopic binary, light variations 2−85000
  - HD 59643, photometric and spectrophotometric obs. 2−51753
  - AKHerculis, eclipsing binary, photoelectric light curves 2−85001
  - HR 5171, highly reddened supergiant, photoelectric photometry 2−73004
  - HR 6611, eclipsing binary, photoelectric obs. 2−75769
  - Hyades cluster, mass-luminosity relationship, unevolved stars 2−48724
  - IC 410, linear filaments of diffuse nebulosity rel. to stellar winds 2−58363
  - IC 443, supernova remnant, brightness obs. at 2.8 cm 2−75757
  - interstellar reddening law, wavelength dependence in u.v. 2−58292
  - intrinsic polarization in atmosphere of supergiant stars 2−62545
  - in Large Magellanic Cloud, photometry48697 2−48697
  - Large Magellanic Cloud, supergiants and galactic foreground stars 2−66059
  - limb darkening for B-type main sequence stars in i.r. 2−55037
  - luminosity variation in one zone Cepheid model 2−84977
  - RRLyrae, masses, radii, and luminosities 2−69094
  - β- Lyrae, radio variations55067 2−55067
  - β Lyrae, underluminosity and magnetic fields 2−58349

Stars continued
radiation continued
RR Lyrae types in globular cluster NGC 6981, photometry 2−62571
M supergiants, 8 colour narrow band i.r. photometry, CN and TiO obs. 2−62552
Markarian 205, Stromgren photometry 2−73000
mass-luminosity ratio for eclipsing and visual binaries 2−84968
mean absolute magnitudes and colour indices of red giants in open star clusters 2−81812
AX Monocerotis, symbiotic stars, UBV obs. 84996 2−84996
neutron, thermal emission and universal X-ray background 2−55884
neutron star, v.h.f. gravitational radiation 2−73007
neutron star crustars radiating as soft X-ray black bodies 2−58433
NGC 2232, open cluster, photometric obs. 2−66105
NGC 2257, cluster in Magellanic Clouds, electronographic photometry 2−48722
NGC 3201, four-colour photometry of blue horizontal-branch stars 2−75738
NGC 419, cluster in Small Magellanic Cloud, colour-magnitude diagram 2−81803
NGC 7226, star cluster, distance determ. using UBV and RGU photometry 2−78472
NGC 7245 star cluster, distance determ. using UBV and RGU photometry 2−78472
NGC 752, galactic cluster, uvby β theoretical colour analysis 2−48723
O type, individual reddening laws, computation method 2−84979
o Velorum, βCMa type, period brightness and velocities 2−44867
O-B supergiants in Large Magellanic Cloud, UBV photoelectric photometry of 160 objects 2−62546
O-stars, non LTE effects on continuum and H$_2$ line parameters 2−58281
OB stars, calibration of luminosities and magnitudes rel. to determination of galactic distances 2−69057
OB stars, southern, polarization 2−62524
OB stars in Norma Milky Way region, UBV and Hβ photometry 2−69075
optical flares, nonthermal bremsstrahlung of fast electrons comparison with inverse Compton radiation 2−72999
α Orionis, emergent fluxes and circumstellar reddening58293 2−58293
AG Pegasi, symbiotic stars, UBV obs. 2−84996
h and χ Per, search for short period light variability62577 2−62577
δ Per, u.v. observations from Mariner 9 2−58320
β- Persei, radio flare55066 2−55066
β- Persei, radio variations 2−55067
AX Persei, symbiotic stars, UBV obs. 2−84996
photometric observations rel. to galactic spiral and halo structure 2−69020
polarized 10μ radiation from cool stars with circumstellar shells 2−51743
Proxima Centauri, M dwarf, multicolour photometry 2−85002
pulsars, model involving relativistic beaming of rotating light source 2−58410
radiative transfer with partially coherent scattering 2−41552
red giants, reddening and u.v. excess det. of clusters from UBV obs. 2−44862
reddening effects of interstellar medium near North Galactic Pole, observations of B-, A-, and F-type stars 2−84993
reflection effect in eruptive stars, optical properties of scattering medium 2−51759
RGU and UBV colour system transformations rel. to application of synthetic spectra 2−81967
o Sco, early type, interstellar circular polarization 73002 2−73002
σ Sco, early type, interstellar circular polarization 73002 2−73002
β Sco, occultation by Jupiter75863 . 2−75863
Sco X-1, photometric props., colour- magnitude relation 2−58306
Sco X-1, search for optical circular polarization 2→73001
Sco X-1, simultaneous hard X-ray and optical observations 2−55110
β Scorpii, occultation on 1971, May 13-14, by Jupiter and its satellite Io 44879 2−44879
β Scorpii C, occultation by Io 2−75866
β Scorpii C occultation by Io, determ. of satellite's triaxial figure and apparent equatorial radius 2−78536
Scorpio-Centaurus association, A- and F-type stars as possible members of Upper Centaurus subgroup 2−69100
Sh2-157-1, central star of diffuse nebular, excitation and spectra of bright knot 2−55020
southern stars, UBV obs. 2−73003
supergiants, blue to red ratio dependence on stellar mass and neutrino induced reactions and emission 2−51735
supergiants, recalibration of visual absolute magnitudes 2−62528
supergiants in Large Magellanic Cloud, M$_{bol}$- log Te diagram 2−62547
supernova 1968 in M83, photometry 2−62564
IKTauri, period and near i.r. variability 2−75762
41 Tauri, photoelectric observations of magnetic star 2−81819
HL Tauri-76, white dwarf with multiple periodicities in light curve 2−81846
thermal waves, energy transfer 2−75726
UBV, photographic and photoelectric systems rel. to synthetic spectra of dwarf stars 2−81968
UBV colours, microturbulence effects 2−51752
UBV photometry of members of Large Magellanic Cloud 2−62548
UV Ceti flare star, obs. of flares 2−58309
u.v. Ceti type, flares, theoretical light curves 2−69074
V504 Sgr, eclipsing binary, UBV photometry 2−58342
Vega, errors flux standard and absolute flux meas. 2−81974
AX Velorum, photoelectric evidence of beat period cepheid48711 2−48711
AH Vir, eclipsing binary, time of minimum light 2−66110
W28, supernova remnant, brightness obs. at 2.8 cm 2−75757
W 44, supernova remnant, brightness obs. at 2.8 cm 2−75757
weak G-band stars, Stromgren photometry 2−75730
white dwarf G195-19, circular polarization and ephemeris 2−55035
white dwarfs, pulsed and continuous radiation in X-ray region 2−84967
wind, injection of relativistic particles into pulsar wave zone 2−58381
Wolf-Rayet types, northern, i.r. photometry 2−81833

Stars continued
radiation continued
X-ray stars, plasma phenomena 2−78432
Ba II- and R-type stars, UBVRI photometry and spectra 2−81844
Ba stars, absolute magnitudes 2−51748
C stars, stellar winds and mass loss resulting from radiation pressure 2−58269
He shell-burning, thermal pulses, calc. including neutrino energy losses 2−62512
Mg II resonance doublet, balloon borne spectrophotometry 2−58282
spectra
32 Cygni, atmospheric eclipse, preliminary analysis 2−55059
— 2−69196
— 2−62586
A0-stars and meas. of reddening within 200 pc of Sun 2−69112
A and B type supergiants, spectrum variability 2−58311
A-F supergiants in Geneva observatory photometric system 2−62551
A-type, MK spectral types of southern stars 2−85004
A-type supergiants, line intensity changes caused by variable velocity fields in atmos. 2−62556
A-type supergiants, microturbulence and radial velocity from metallic lines 2−62497
A-type supergiants, Ti/Fe ratio, turbulence and radial velocity 2−62537
AM types in clusters, equivalent width data 2−58283
analysis, Minnaert formula and spectrum calculation using model atmosphere 2−75743
Ap stars, projected rotational velocities 2−51728
Ap-type stars, two dimensional quantitative spectral classification from analysis of He, Fe and H lines 2−51751
108Aqr, Ap Si 4200 star, variations of Ti II lines 2−58317
Aquila stellar ring, analysis of spectrograms rel. to structure 2−84960
η Aquilae, light variations for CO, CN, C$_2$, CH, OH and NH 81840 2−81840
Arcturus, line blanketing, statistical description 2−58298
56 Ari, Si Ap variable, Si II and He I 2−81853
56 Arietis, variations in H, Mg and Ca lines44860 2−44860
astrophysical plasma and the interpretation of stellar spectra 2−75703
atmospheres, hydrodynamic characteristics of microturbulence 2−58310
β Aur, u.v. profiles of MgII lines 55044 2−55044
B stars, influence of u.v. line blanketing on He I triplet lines 2−84976
B-type, u.v. flux envelopes 2−58291
B-type stars spectral classification and search for He-weak stars in young clusters 2−69053
B-type stars with discrepant colours, model atmosphere analysis 2−81862
B-type supergiants, He I lines at 8776.74 and 8582.65Å 2−69077
B-type supergiants, temperature scale from Balmer jumps 2−58273
band O stars, theoretical interpretation 2−75740
BD + 56° 595, M supergiant, Hα characteristics 2−62550
BD-7°3007, peculiar blue variable, h.f. stellar oscillations 2−66097
BD-7°3007, unusual hot star, continuous spectrum 2−62566
binaries, Mv(K) dependence on Fe/H ratio in late-type giants 2−73036
bright B-type subdwarf, UBV photometry 2−62529
BW Vul, β CMa star, spectral variations 2−58325
AScamelopardalis, eclipsing binary, spectroscopic study 2−84994
β Canis Majoris, spectral classif., in HR diagram 2−48698
YCanum Venaticorum, C star, observed and computed spectra 6700-6712 Angstroms 2−75735
γ Cap, visible region, quantitative anal. 81832 2−81832
η Car, short period optical oscillations 2−55046
Cassiopeia, photoelectric UBV photometry of 74 stars 2−58285
WZ Cassiopeiae, C star, observed and computed spectra 6700-6712 Angstroms 2−75735
CD-42° 14462, evidence for rotating white dwarf 2−66093
β Cen, energy distrib. obs. at 2000-3800 Å 2−73005
SV Centauri, eclipsing and double lined spectroscopic binary 58347 2−58347
V553 Centauri, type II Cepheid, overabundance of C66102 2−66102
VV Cephei, BD + 54° 2698 and BD + 63°3 2−62525
β Cephei, spectral classification, location on theoretical HR diagram 2−58324
Cepheids in small magellanic cloud, influence of metal lines on lines 2−81823
IIICepheus, spectroscopic and astrometric study of the OB association 2−81863
o Ceti, variable, line identification in near i.r. spectrum 2−58327
circumstellar gas emission, pre-main sequence stars in Ic Orionis and NGC 2264 2−66116
classification of members of Large Magellanic Cloud 2−62548
close groups, classification with objective prism camera of very low dispersion 2−75749
colourimetric systems for bright stars, comparison of several systems rel. to automatic guiding of large telescopes 2−48700
β Cor Bor, magnetic A star 2−58289
β Coronae Borealis, magnetic field variations from det. of Zeeman effect in spectra 62520 2−62520
coude spectrograph meas. of radial velocities for Large Magellanic Cloud Supergiants 2−69078
CPD-31°1701, He-rich, subluminous o-type 2−75734
β CrB, Zeeman effect58288 2−58288
α Cyg, line intensity changes caused by variable velocity fields in atmos.62556 2−62556
Cyg OB3, obs. of diffuse interstellar absorption bands 2−58361
α Cygni, A-type super giant, coupling between mass loss and turbulence 2−75732
CY Cygni, irregular variable, spectrum and element abundances78465 2−78465
BF Cygni, symbiotic, interpret. 2−62526
NML Cygnus, OH i.r. emission 2−55045
Cygnus, photoelectric UBV photometry of 39 stars 2−58285
diffuse interstellar absorption feature, λ4430, polarization obs. 2−44854
diffuse interstellar features in stars with circumstellar dust shells 2−84992

Stars continued
spectra continued
double stars of equal components, spectral evidence of binary nature 2−55061
73 Dra, Zeeman effect 58288 2−58288
Draconis, estimates of radius and mass from spectral analysis 2−75750
38Draconis, peculiar B star in old disk population 2−66089
dwarf K- and M-type stars in Southern Hemisphere 2−69076
early type, Mariner 9 u.v. spectrometer obs. 2−58286
40 Eri B, DA white dwarf, gravitational redshift51749 2−51749
F0-K5 supergiants, spectral line variations rel. to atmospheres 2−62540
F and G-type dwarfs, UBV photographic and photoelectric systems rel. to synthetic spectra 2−81968
F- and G-type dwarf stars, synthetic spectra using RGU and UBV colour systems 2−81967
Fe abundances in evolved stars, det. from narrow band indices 2−66090
G8 III type, weak and strong CN line, photometric study 2−55057
G-K giants, calibration rel. to K-line luminosities 2−69082
G-type dwarfs and subgiants, H_α profiles 2−84978
G-type stars near North Galactic Pole spectral analysis rel. to dwarf hypothesis 2−58304
galactic clusters, ratio of total to selective absorption, kinematic det. 2−62553
HD 103877, possible Fm-type star, atmosphere rel. to spectral studies 2−81847
HD 111133 peculiar A star, periodic variability 2−62563
HD 117688, Wolf Rayet type 2−62532
HD 1273, possible astrometric spectroscopic binary, orbital elements 2−84989
HD 161227, double lined binary 2−44880
HD 163181, peculiar spectroscopic eclipsing binary, N_2 enhanced, absorption line 2−73029
HD 164402, B-type supergiant fine analysis rel. to τ Scorpii 2−62541
HD 188041, periodic magnetic variable, magnetic intensification and starspots 2−75747
HD 198478(55 Cygni), rapid variations in spectrum 2−62539
HD 201626, search for C_2^- radical 2−44861
HD 217050, Be type, time variations, Hβ line profiles, radial velocity determ. 2−62523
HD 24712, Ap type, variations 2−51740
HD 25354, Ap type, abundance of transuranium elements 2−72994
HD 33579, A3Ia-O supergiant, in LMC, model atmos. anal. 2−75727
HD 4180, Hγ, Hδ, Hε equivalent widths variations, comparison to Be stars with small extent envelopes 2−44856
HD 59643, spectrophotometric obs. 2−51753
HD 90657, Wolf Rayet type 2−62532
HD 96248, B-type supergiant fine analysis rel. to τ Scorpii 2−62541
high velocity A-stars, effective temperature and surface gravity det., Ca surface abundance 2−48702
highly reddened relatively bright O and B stars behind dense interstellar clouds 2−58302
hot stars, emission lines 2−62534
HR 2142, periodic shell variable 2−44871
HR 465, identification of trace elements in Ap stars 2−75733
HR 465, search for Pm II lines, comments 2−66081
HR 465, search for Pm II lines 2−62501
HR 7774, unresolved double lined binary, metallicism 2−66106
HV 12842, HV 5637, R Coronae Borealis type, in Large Magellanic Cloud 66099 2−66099
IC 2602 open cluster, H-R diagram 2−75728
i.r. astronomy and stellar observations 2−66136
i.r. of circumstellar shells, 10 micron SiO_2 excesses 2−58294
i.r. of circumstellar shells with SiO_3 excesses 2−51742
IRC+10216 polarization in K band 2−58280
IRC 10216, search for microwave HCN emission 2−58301
IRC 30219, search for microwave HCN emission 2−58301
irregular variables, intermittent photometric observations, interpretation 2−75755
Jefferies' eqns. for grand source function, soln. by kernel approximation 2−55047
K giant, metal abundances from synthetic stellar spectra calc. using computer 2−69083
K- and M-type stars, correlation coefficients for micron colour and band intensities 2−75737
K-type, super metal rich dwarfs and giants, model atmosphere anal. 2−58287
Large Magellanic Cloud, spectroscopic study of blue globular clusters 2−81804
α Leonis (Regulus), estimates of radius and mass from spectral analysis 2−75750
line intensity anomalies, laser action as explanation 2−48699
LR Cen, eclipsing binary, primary spectrum 2−58331
luminous late types, Hα characteristics 2−62550
LY Aur binary, u.v. photometry for OAO-2 2−75778
Lyman α absorption influence of hot star circumstellar envelopes 2−62559
α Lyra, energy distrib. obs. at 2000-3800 Å 73005 2−73005
M supergiants, 8 colour narrow band i.r. photometry, CN and TiO obs. 2−62552
M-dwarfs, absorption band at 5500-5560Å attributed to CaOH 2−75729
m-type variables, minimum light spectra 2−62531
main sequence, line broadening by macroturbulence 2−75741
main sequence types in NGC 330 cluster in SMC, Hα emission survey 2−69106
W Men, R Coronae Borealis type, in Large Magellanic Clou66099 2−66099
metallic line stars, narrow passing band photometry obs. 2−75748
MWC 56, analysis of peculiar spectrum rel. to structure 2−84995
NGC 3201, globular cluster, pseudo colour-magnitude diagrams 2−44882
NGC 330, large rich cluster in SMC, Hα emission in main sequence stars 2−69106

Stars continued
spectra continued
NGC 5138, 6134, 6208, clusters, spectral class, slit spectra, UBV photometry 2−84955
NGC 5927, globular cluster, pseudo colour-magnitude diagrams 2−44882
NGC 6388, globular cluster, pseudo colour-magnitude diagrams 2−44882
NGC 6981, globular cluster, colour-magnitude diagram 2−55041
NGc 7006, variation of N abundance among population II objects 2−69080
NGC 7099, globular cluster, colour magnitude diagram 2−55042
NML Cyg, polarimetric and photometric study in optical and i.r. regions, variability 2−58280
NML Tau, polarization in optical and i.r. regions 2−58280
Nova Cephei 1971, u.v. to near i.r., blue region obs. 2−55038
Nova Cephei 1971 2−58319
nova Delphini, metallic absorption lines before Dec. 1967 maximum 2−48707
Nova Delphini 1967, high dispersion spectra during nebular stage 2−58240
Nova Vulpeculae 1968 N. 1, photoelectric light curves 2−73010
novae, circumstellar envelope, formation of coronal lines 2−75766
O stars, N III and He II lines, spectrophotometric luminosity criteria 2−58290
OB association III Cepheus, spectroscopic and astrometric study 2−81863
OB stars in both hemispheres, classification and absolute magnitude calibration 2−44855
ob-stars, Lyman-α interstellar equivalent widths, Mariner 9 observations 2−58362
OB-type, search technique for faint stars 2−76039
Of stars, N III λλ4640, 4097 lines 2−55036
open clusters, slit spectra, UBV photometry 2−84955
Ophiuchi, detection of interstellar CN and 1.32 mm cosmic background radiation48736 2−48736
Ophiuchi, equivalent width of interstellar molecular lines 2−55072
Ophiuchi u.v. spectrum, interstellar lines 2−66088
θ Ori C, variable inverse P Cygni profile 2−58296
εOrionis, B-type supergiant, analysis of visual spectrum 2−62542
δ Orionis, spectroscopic binary, apsidal motion, orbital elements 62584 2−62584
βOrionis, supergiant, differential shifts in He I lines, atmospheric motion 2−62538
ε Orionis, supergiant, equivalent widths, line profiles 2−78462
peculiar types, A-type, metallic line and B-type 2−66094
EQ Peg, double flare star48714 2−48714
AT Peg, eclipsing binary, orbital elements 2−66109
ε Pegasi, chemical composition using atmosphere model 72993 2−72993
AG Pegasi, symbiotic, velocity obs. and spectrophotometry44859 2−44859
α Per, model atmosphere and continuum observations62500 2−62500
ξ Persei, CO, SiO, CS, H_2 and HD lines in interstellar spectrum 81836 2−81836
h Persei, early-type supergiant preliminary studies62543 2−62543
χ Persei, early-type supergiant preliminary studies 2−62543
β Persei, eclipsing spectroscopic binary, radiosource and probable X-ray star62614 2−62614
X Persei, evidence for assoc. with X-ray source 2U 0352+30 44858 2−44858
19Piscium, C star, observed and computed spectra 6700-6712 Angstroms 2−75735
radiative transfer in line frequencies, approximate soln. 2−75702
radiosources, in nearby spiral galaxies 2−73049
red giants in Hyades group 2−62530
red variables, in globular clusters, galactic centre, solar neighbourhood 2−73019
reddened B supergiants, obs. of diffuse interstellar absorption bands 2−58361
relative oscillator strengths, precision obs. 2−55040
RGU and UBV colour system transformations rel. to application of synthetic spectra 2−81967
RR Telescopii, Fe lines and model 2−58297
SC-type stars, image-tube spectrograms of 51 stars 2−78463
o Sco, circular polarization, interstellar origin 2−51750
Sco X-1, Balmer H line profiles in spectrum 2−58431
Scorpius X-1, high resolution search for Fe XXV line emission 2−85013
Scorpius X-1, transfer effects on X-ray lines of optically thick sources 2−84981
Sculptoris cluster, emission line stars 85003 2−85003
β Sextantis, estimates of radius and mass from spectral analysis 2−75750
RY Sgr, pulsating R Coronae Borealis type variable66098 2−66098
SRa variables, minimum light spectra 2−62531
subgiants, H_α profiles 2−84978
supergiants, effect of atmos. curvature on profiles formed in extended atmos. 2−62557
supergiants, luminosity functions for 16 associations in Large Magellanic Cloud 2−58307
supergiants, ratio of total to selective absorption, kinematic det. 2−62553
superluminous emission line stars, spectral analysis 2−62558
supernovae, type I, spectra and Hubble constant 2−75765
supernovae, type I 2−73011
supernovae, type II, absorption spectra 2−66100
suspected supergiant M stars, i.r. survey 2−66134
T-Tauri stars, CaII-FeI resonance 2−75744
type I supernovae, expansion envelope after maximum light 2−73021
UBV, photographic and photoelectric systems rel. to synthetic spectra of dwarf stars 2−81968
UBV photometry, very bright stars 2−66091
Upgren's G5-G7 unclassified stars, spectra rel. to densities of G-type dwarfs 2−81820
u.v., 2800 Å Mg feature, equiv. width 2−62533
u.v., det. of abundance of C, O_2 and Si in interstellar medium 2−58359

Stars continued
spectra continued
u.v. analysis of data collected by second orbiting astronomical observatory 2−81850
u.v. emission, space obs. 2−44857
u.v intrinsic colours, spectral classification 2−75739
V771 Sagittani, Be star, photoelectric obs. 2−58308
Vega, u.v. absorption lines 2−81831
velocity of light meas. from stellar spectrograms, experiment for students 2−78716
R Vir, variable, minimum light spectra62531 2−62531
78 Vir, Zeeman effect 58288 2−58288
78 Virginis, magnetic field variations from det. of Zeeman effect in spectra 2−62520
73 Virginis, magnetic field variations from det. of Zeeman effect in spectra 2−62520
ϵ Virginis (HD 113226), line blanketed model atmosphere 78458 2−78458
α Virginis (Spica), search for telluric NO_2 2−51601
VY CMa, polarization and position angle in optical and i.r. regions 2−58280
weak G-band stars, CH and CN absorption bands 2−75730
young Am stars in Orion 1c association, metallicism 2−51756
Ba II- and R-type stars, UBVRI photometry and spectra 2−81844
C stars, micron colour indices rel. to colour temp. and spectral type determ. 2−75736
C stars, search for microwave HCN emission 2−58301
C stars of early type in globular cluster ω Centauri, objective-prism studies 2−75773
CIII λ5696 line, recomb. spectrum struct. 2−85009
CN stars in solar neighbourhood, rel. to radial composition gradient in galactic disk 2−58181
Cepheids, ratio of total to selective absorption, kinematic det. 2−62553
Fe spectral line identification and abundance 2−62748
H lines, highly excited, gas density determ. 2−75725
H lines, Lorentz broadening, overestimation of gas densities 2−75742
H observations rel. to redetermination of zero age main sequence 2−69107
H_2 deficient, UBV photon 2−62529
Hα emission stars in the Large Magellanic Cloud 2−58204
He abundance main sequence B-stars 2−62488
He I D_3 line obs. in stellar chromospheres 2−58295
He I spectral lines, new identifications in i.r. spectra of B-type supergiants 2−62544
He II λ10124 line obs. in O and Of stars 2−51744
He line spectrum in large mag. fields 2−62535
He weak types, characteristics 2−51739
Mn I, relative oscillator strengths, precision obs. 2−55040
OH emission spectra rel. to laser and maser mechanisms 2−51754
OH i.r. stars, maser emission at 1612 MHz 2−81830
SiO band identification 2−48696
structure
A- and F-type stars, rotation of evolving stars rel. to metal abundance 2−55029
A-type, rotational velocities 2−85004
A-type supergiants, microturbulence and radial velocity from metallic lines 2−62497
Aquila stellar ring, analysis of spectrograms rel. to structure 2−84960
binary components with convective outer layers, mass loss 2−48716
3 Cen A, ^{3}He abundance, diffusion 2−58266
βCephei, determination of mean radius, spectrophotometric temperature and mass 2−48708
chemically homogeneous main-sequence stars, structure and compositions 2−84990
circumstellar shells with SiO_3 excesses, i.r. spectra 2−51742
critical luminosity in stellar interiors 2−78456
SW Cygni, UBV photometry of ring 2−84999
degenerate massive fluid spheres, minimal properties 2−58272
differentially rotating models, general relativistic analysis of linear pulsations and stability 2−72989
differentially rotating models, Newtonian analysis of linear pulsations and stability 2−75704
Draconis, estimates of radius and mass from spectral analysis 2−75750
equations of stellar structure for a Giant envelope, multiple solutions 2−69063
Eta Carinae, core 2−66080
extreme rotating star near cluster M37, carbon star evidence 2−78457
hadronic equilibrium concentrations for relativistic spheres for zero total baryon number 2−69060
hot stars, mass outflow 2−51730
HR 5986, model atmosphere 2−78464
IC 2944, young star cluster, i.r. studies rel. to circumstellar envelopes 2−75774
interior, physical state 2−58271
large mass supergiant stars, review 2−62514
α Leonis (Regulus), estimates of radius and mass from spectral analysis 2−75750
17 Leporis, i.r. shell star? 2−55068
lower H_2 burning main sequence, secular stability 2−62486
main-sequence, effects of uniform rotation and strong dipolar magnetic fields on structure and properties 2−84986
neutron, density region $3.1\times10^{11}-2\times10^{15}$ g/cm^3, study using Thomas-Fermi theory and new nuclear matter energy model 2−69087
neutron matter model 2−63043
neutron star matter, binding energy 2−81841
neutron star matter, density region where $^3P_2$ gap exists 2−73009
NGC 6530 young star cluster, i.r. studies rel. to circumstellar envelopes 2−75774
NGC 6611, young star cluster, i.r. studies rel. to circumstellar envelopes 2−75774
nonrotating baryon stars, atmosphere model 2−69058
Orion 1, young star cluster, i.r. studies rel. to circumstellar envelopes 2−75774
polytrope, oscillations with toroidal magnetic field 2−75706

Stars continued
structure continued
polytropes, resonance effects and anharmonic pulsational amplitudes 2−84973
Procyon, model chromosphere 2−75712
pulsating X-ray sources rel. to stars with high central densities 2−51799
pure He stars, secular stability, models 2−62487
quasistationary spherical system differing in mass, structural model 2−72997
red giants, dynamic instabilities when luminosity exceeds limiting value 2−51734
relaxation oscillations in envelopes of luminous red giants 2−62484
rotating non-mag. interiors, slow rot. with meridional circulation case 2−62485
rotation and evolution interacting, models and photometric obs. 2−55026
rotation of stars rel. to transition from shallow to deep convection zones 2−81824
β Sextantis, estimates of radius and mass from spectral analysis 2−75750
spherical fluid model, internal motions with convection zone 2−75715
spherical systems, phase mixing of second kind 2−69059
stellar stability using local Vogt-Russell theorem 2−72992
surface gravity of early-type stars from forbidden He I 4045 Angstroms line 2−55027
vibrational stability and non radial oscillations of star with 0.5 $M_\odot$ 2−55028
ϵ Virginis (HD 113226), line blanketed model atmosphere 78458 2−78458
zero temperature, mass-radius relation and energy 2−51725
CO cooling effect in atmospheres of red giants 2−75709
He core types equilibrium, multiple solutions 2−72990
He stars, numerical models 2−66078
Stars (nuclear) *see Particle track visualisation*
Statistical analysis
see also Measurement/errors; Probability; Random processes
conservation of information, energy storage 2−69552
data representation by analytic function, extrapolation methods 2−78860
dielectric relax., dipole-dipole interaction effects, model, Monte Carlo method 2−77943
edge errors in size distribution measurements with linear scanning instruments, a new formula 2−55356
electron microprobe, error calc. by Castaing's First approximation 2−82083
fitting theoretical expressions to statistical distributions, computer program suite 2−66483
G-factorial states generalization of positive ergodic measurements to noncommutative C* algebras 2−82155
least squares adjustment, multidimensional, point and interval estimations, especially point error 2−63049
luminescence kinetics, analysis of main errors in statistical determ. 2−83238
lunar regolith evolution mechanisms from impact experiments and computer simulations using Monte Carlo methods 2−81943
Markov's processes, theory, appl. to mechanically agitated systems 2−83753
Markov random process rel. to light beam displacement in turbulent medium 2−79317
matrix language applic. 2−82274
maximum likelihood estimators for generalized chi square parameters 2−82254
model earthquake sequence, stochastic analysis 2−81600
modularity of decision effects, symmetry of physical probability 2−82158
Monte Carlo calc. of thermodynamic properties of binary mixtures of Lennard-Jones (12-6) liquids 2−71182
Monte Carlo calcs. of survival probability of muon in shielding material 2−79845
Monte Carlo calculation of low energy spectra of transmitted γ radiation 2−80927
Monte Carlo simulation, sample size determination 2−78835
Monte-Carlo simulation, transformation of random numbers, systematic sampling, fast electron and photon transport 2−80926
sample size estimation and statistical filtering of on-line measurements 2−76151
scanning electron microscopy, electron probe microanalyzer, fund. phenomena Monte Carlo technique 2−80608
statistical linearization of systems of stochastic differential equations 2−58707
Steck's determinantal expressions for probabilities in Kolmogorov and Smirnov tests, simple proofs 2−82243
stochastic transmission system diffusion function 2−78915
system response to transient random excitation, smoothing mean square estimates 2−63051
teaching students statistics, a demonstrative experiment 2−63048
truncated sinusoids, maximum entropy power spectrum 2−63047
CdS hot electron mobility 2−84276
$He+H_2^+\rightarrow HeH^++H$, reaction cross-section, statistical phase-space theory of nuclear spin 2−81500
applications
see also Counters/statistical analysis
acoustic field, Monte Carlo analysis 2−41689
acoustic multipath transmission of finite bandwidth signals 2−55545
activation analysis, self- consistent deciphering of spectra 2−72594
Alexander's technique for estimation of return period of intense rainfall 2−62227
algorithm for profiling common depth surface from multiple reflections of seismic waves 2−44567
astronomical masers, search for departure of radiation from Gaussian statistics 2−73048
atmospheric pollutants conc. rel. to averaging time, statistical principles 2−68887
Bayesian statistics, applic. to Poisson and other distributions, introduction for physicists 2−66401
Black Sea temp. fields and salinity rel. to statistical structure analysis 2−81612

Statistical analysis continued
applications continued
blackbody radiation, stimulated emission and Bose-Einstein statistics 2−41838
boiling water reactor at Lingen, analysis of space dependent neutron flux density fluctuations by stochastic methods 2−79830
ceramic system, wetting angle, statistical interpretation 2−60970
charged particle beams, analysis of internal structure of nonlaminar beams 2−49317
chemical reactions in steady state nonisothermal low pressure plasma, statistical model 2−57411
classical one-component plasma, crystallization, Monte Carlo equations of state calc. 2−78843
conditional sampling analysis of turbulence near wall 2−83430
counters, random events, Poisson distributed, errors 2−49615
counting statistics of mixed modulated coherent and partially polarized chaotic light 2−69993
crystal structure refinement 2−50617
crystallization, nucleation, Monte Carlo simulation 2−47192
Denmark Strait, bottomside sea ice features 2−57885
diffusion modelling and control 2−73344
directional spectral reflectance meas., response curve analysis 2−70079
discriminant analysis of visually encoded e.e.g. data 2−45026
earthquake activity in USA, threat to telephone systems, design requirements 2−84708
EAS, 10^{11}-10^{12} eV, Monte Carlo calc. of time dependence of isophotes and multiple pulses in Cherenkov light 2−52657
eclipsing binaries, rate of period changes 2−73025
electrodeless discharge lamp, device for temperature control 2−82586
electrolyte, charged particle system, statistical theory, osmotic model 2−51459
electron energy loss spectrum meas. by electron microscopy and energy analyser, statistical analysis of errors 2−73524
elevation effects on rainfall, stochastic model 2−57985
excited nuclei, pairing fluctuations in nuclear gap parameter, absence of second order phase transition 2−49715
fatigue under variable stress amplitude, theory of successive stochastic processes 2−73393
filter geophysical obs. series using white noise as basis 2−54577
FLARE Monte Carlo procedure for scattering calc. for point isotropic light sources in model atm. 2−81691
free fermion model, combinatorial soln. 2−78844
gas lasers, intensity fluctuation meas. threshold oscillations 2−63320
geology, nonuniform density of data points in three variable closed array 2−81594
geophysics, biophysics, meteorology, stochastic processes, periodicities 2−52084
geophysics, Monte Carlo inversion, statistical estimation procedure 2−57446
geophysics and meteorology, statistical test methods and effective number of independent sample values 2−54576
grained solid, grains/unit volume, determ. from theory of stochastic processes 2−43877
hadron interactions, new treatment based on analogies with nuclei, Ericson fluctuations and Bohr model 2−82702
high-energy scattering exclusive and inclusive cross sections, interrelations investigated by efficiency matrices 2−59443
interactions, 25-10000 GeV, studied with multiplate cloud chamber using Monte Carlo simulations for energy calibration 2−42436
interplanetary mag. field, statistical properties of MHD discontinuities 2−62738
interplanetary objects, statistics of masses and dynamics 2−75917
Knudsen cell orifices, conical, divergent particulate fluxes, Monte Carlo analysis 2−50136
Lac St. Jean, Quebec, analysis of vertical crust movement 2−81595
laser microprobe analysis, background and energy corrections evaluation 2−68826
lasers, mode-locked, dynamics, statistical model 2−41972
least squares method generalization for adjustment of free networks 2−65429
least squares method treatment of measurements 2−55355
light plane wave propagation in randomly inhomogeneous medium, geometrical optics and Markov's process approximation 2−55726
light propagation in turbulent medium, review of statistical theory 2−82553
linear systems analysis applic. to reson. radiation scatt. by atomic vapour 2−63999
liquids, Metropolis Monte Carlo method in isobaric and canonical ensemble formalisms 2−64428
luminescent radiance, method for recording irregularities 2−63310
magnetization in harmonic oscillator assemblies, ergodic properties 2−49023
Markoffian model of hadrons, and solution of basic Kolmogorov's eqn. 2−73773
Markov chain model fitting for daily rainfall data at Calcutta 2−62226
Markov chain model of chemical reactions, comparison with ordinary differential equation model 2−75364
Markov processes connection with stellar dynamics calc. of relaxation and evaporation times, quasisteady distributions 2−44853
maximum likelihood estimation for depth to magnetic layer from aeromagnetic fields spectrum 2−51522
medical patient identification and disease categorization using discriminant and cluster analyses 2−69361
meteorological predictability 2−62114
methods in experimental physics, books 2−45337
microearthquakes in New Mexico 2−81570
molecular-statistical treatment of diffusion consts. in liquids 2−74536
Monte Carlo calc. of recoil spectra in ^{4}He proportional counters 2−42454
Monte Carlo calc. of reflection and absorption by cloud layers 2−48486
Monte Carlo calcs., on polypeptide chains 2−60103
Monte Carlo calcs. of elastic consts. of solid Ar, Kr and Xe 2−68062
Monte Carlo calcs. of excess thermodynamic properties of binary mixtures of Lennard-Jones liquids 2−74539

Statistical analysis continued
applications continued
Monte Carlo calcs. of $F + H_2 \rightarrow HF + H$ reaction rates and energy distribs. among products 2−57410
Monte Carlo calcs. of high-energy nucleon-meson cascades in thick targets 2−79630
Monte Carlo Calcs. of radiative transfer in atmosphere-ocean system 2−65627
Monte Carlo calcs. of radiative transfer in atmosphere-ocean system 2−65628
Monte Carlo calcs. on polypeptide chains 2−64202
Monte Carlo calcs. on polypeptide chains 2−64201
Monte Carlo calculation, nematic liquid crystal order 2−50331
Monte Carlo method, applic. to remote sensing systems 2−44751
Monte Carlo method, statistical mechanics of parallel hard squares in canonical ensemble 2−41528
Monte Carlo method, threshold reactions for det. of fast neutron streams in experimental channels of MR-reactor 2−42677
Monte Carlo method for anal. of transfer of resonant line radiation in differential expanding nebula 2−58250
Monte Carlo method for obs. of kinetics of homogeneous condensation 2−43445
Monte Carlo method for particle transport problems 2−63046
Monte Carlo methods, correlation energy of electron gas 2−49041
Monte Carlo neutron transport codes specification and testing 2−83061
Monte Carlo program, response of NaI counter to monoenergetic γ-rays 2−79651
Monte Carlo sampling with continuously varying cross-sections along flight paths 2−70508
Monte Carlo simulation of backscattering of electrons in Ar 2−70892
Monte Carlo simulation of electron scatt., applic. to quantitative microanalysis of alloys 2−68830
Monte Carlo simulation of low-density polyethylene struct. 2−83344
Monte Carlo simulation of weakly ionized gas 2−70891
Monte Carlo technique for response function to γ-ray cascade in NaI(Tl) detector 2−79665
Monte Carlo trajectory calcs. of three-body recomb. and dissoc. of diatomic mols. 2−64108
Monte Carlo treatment of thermal neutron scattering 2−63943
multiple input dynamic stochastic model of rainfall evapotranspiration - runoff process 2−54845
multivariate, application to medical research 2−78650
neutron scattering, Monte Carlo evaluation of multiple scatt. and resolution effects in double differential cross section meas. 2−56024
non-local modelling of crystals, channelling and shadow theories 2−84225
nuclear reactor, critical time step approach to Monte Carlo reliability calculation 2−56038
nuclear reactor cores, estimation of temp. limits 2−83083
nuclear reactor optimization, by modal analysis 2−42638
pacemakers, ^{238}Pu demand, statistical analysis 2−51912
particle combustion characteristics, error in statistical determination from particle characteristics 2−61786
polymer conformation, computer program for Monte Carlo calculations 2−70801
precipitable water meas. w. SIRS-b radiation profiles 2−62258
random data analysis procedures, book 2−66482
range pair counting method application to oxidation in combustion chamber exhaust gases 2−57421
reactor core thermal design, hot spot expectation 2−76921
reactor fuel materials, statistically designed program for sampling and chemical analysis 2−74156
reactor noise analysis, statistical accuracy 2−70542
resonance spectra fitting by linear combination of Lorentzian and Gaussian profiles 2−52662
reversing tidal current, vel. field 2−78324
rocks, theory of polyaxial compressive strength 2−72670
roll rate of rocket rel. to random fin misalignments 2−44791
sample size determination for log normal distribution 2−58817
self-consistent Monte Carlo method for thermodynamic properties of Heisenberg ferromagnet 2−68530
simplex method, appl. to adsorption for multicomponent systems 2−47141
solar activity prediction 2−73141
solid solutions, hardening, statistical theories 2−50813
spectral brightness outside instrumental range, statistical estimation 2−76547
spectral density, disperse systems, concentration fluctuations 2−83810
spectral estimator class, nonlinear functions of covariance matrix 2−63050
stability criterion for hydrodynamical transport states 2−49044
statistical mechanics, equilibrium properties numerical expts. 2−82245
stellar kinematics, least squares method, weighting and maximum likelihood principle 2−72995
stellar systems, dynamical evolution 2−78471
stochastic bioburden model for spacecraft stabilization 2−62426
stochastic model of daily winter rainfall in North Santa Clara Valley 2−54844
thickness profile, thin fluid films, electrical contact method 2−83733
Thomas-Fermi description of nuclear systems including spin-orbit interaction 2−42489
timing walk and time resolution estimation by least squares fitting technique 2−52665
turbulence models, conference, San Diego, California (1971) 2−43052
two band, transition temp. and energy gaps rel. to Fermi surface topology change under press. 2−75068
type II, structure and compositions of materials 2−75071
vapour deposition, computer simulation, Monte Carlo method 2−50476
water-like particles in two dimensions, statistical mechanics of one-component systems 2−80449
water-like particles in two dimensions, statistical mechanics of two-component system, hydrophobic interaction 2−80450
Ag solder alloy, superconducting transition at 64.4 mK 2−75058

Statistical analysis continued
  applications continued
    Ar, Monte Carlo calculations along solid-vapour coexistence curve 2−57055
    n-GaAs electron drift velocity, Monte Carlo calc. 2−71901
    He cloud diffusion, neutral turbulent boundary layer, simulated point-source, downstream cross sections, statistical parameters, concentration 2−84825
    ^{3}He, solid, exchange, Monte Carlo calc. 2−53484
    ^{4}He, liquid, Monte Carlo calculation for ground-state energy, liquid structure function 2−80506
    In$_2$Bi, magnetic properties, deduced to be intrinsic type II superconductor 2−75072
    (La,Ce)Al$_2$, Kondo system, re-entrant supercond.−normal phase boundary obs. 2−75060
    La$_3$Tl-Pr$_3$Tl, induced moment system, superconductivity and mag. props. in paramagnetic region 2−72115
    Mg, transition temp. from obs. of Mg-Cd alloy 2−75073
    NaI scintillation detectors, response functions for γ-rays 2−79668
    NaI(Tl) detector, Monte Carlo technique for response function to γ-ray cascade 2−79665
    Nb-Sn sinter material, screening behaviour on addition of Cu, Ag or Au 2−75061
    NbSn$_2$, transition temp. and crit. mag. field 2−75063
    Ta, press. depend. of transition temp. 2−75064
Statistical mechanics
    see also Heisenberg model; Lattices, theory and statistics; Quantum fluids
    − 2−66479
    − 2−58781
    activity expansions for lattice gases, radius of convergence 2−69612
    algebraic methods, textbook 2−45336
    anharmonic crystal interacting with ideal gas, dynamical study using computer expts. 2−58787
    Ashkin-Teller and eight-vertex model, duality relation 2−45288
    Ashkin-Teller and eight-vertex models, symmetry props. 2−52092
    atomic response to external disturbance 2−70600
    autocorrelation and memory functions, behaviour as $t\to\infty$ 2−69618
    Bogoliubov's functional assumption, math. validity 2−76223
    Boltzmann statistics for fermions 2−73339
    book, problems in thermodynamics and statistical physics 2−45282
    book 2−58795
    classical gas dynamics, new set of axioms 2−60364
    classical many-body systems, decay of order 2−52096
    classical many-body systems, decay of order 2−52095
    condensed phases, physicochemical props., anal. 2−41540
    correlation decay, necessary and sufficient conditions 2−41544
    correlation functions, time dependence of fluctuations 2−45315
    critical phenomena, conf., New York, USA (June 1970) 2−52102
    critical phenomena, scaling theory for finite size effects 2−45303
    dense gases, electromagnetic properties 2−71118
    depolarization of light by simple gases, contrib. of many-body effects 2−53338
    disordered system, low temp. thermodynamics, van Vleck like paramag. 2−69614
    disordered systems, generalized cumulent average, expansion 2−82261
    dynamical spherical model, phase transitions 2−52104
    electrical resistivity, general expression derived using projection techniques with Liouville equation 2−55423
    Enskog dense gas theory, self-consistency 2−56434
    entropy, comparison with thermodynamic entropy 2−45310
    entropy and normal states 2−73335
    entropy density of large system at low temperatures, lower limits 2−55429
    ergodic and non-ergodic systems, crit. slowing down, nonlinear dynamical response 2−54310
    ergodic theory, dissipative properties of quantum systems 2−55431
    ergodic theory, H-theorems, recurrence problems 2−45317
    Feynmann fluid analogy for high energy multi-particle production processes 2−66914
    fluctuation-regression hypothesis for one- dimensional system of hard rods 2−69621
    fluctuations, relaxation matrix for system with internal degrees of freedoms 2−45304
    fluid, dense classical, projection operators and interaction representation 2−55438
    fluids with nonspherical molecules, Ornstein-Zernike equation and mean spherical model 2−66466
    functional integration applic. to thermal situations equil. 2−58800
    Gaussian molecule mixture, correlation functions 2−64205
    generalized homogeneous function, appl. to static scaling, dynamic scaling and universality 2−76225
    Gibbs ensemble formalism, applic. to synchrony loss in cell colonies 2−69620
    Ginzburg-Landau field, one-dimens., real, complex and phase-only fields 2−78853
    Glansdorff and Prigogine's stability theory, ambiguities in entropy production 2−69617
    grain boundary, entropy, Einstein cryst. model and Morse pot., computer calcs. 2−56727
    Green function methods 2−45283
    H-theorems, ergodic theory and recurrence problems 2−45317
    hard parallel spheres, mol. dynamics 2−66478
    hard sphere fluid, inverse power pots., radial distrib. functions, virial coeffs. 2−73341
    hard sphere fluids, distrib. functions, theorem 2−73342
    hard sphere gas, hydrodynamic disturbances, nonanalytic dispersion relations 2−66477
    hard-sphere gas, thermal fluctuations 2−76224
    harmonic chains, isotopically disordered, spectral theory of difference eqns. 2−66470
    ideal systems 2−45311
    infinite systems, equil. phenomena 2−58797
    infinite systems, functional analysis methods 2−58796
    inverse-12 fluids, radial distrib. functions 2−82275
    irreversible processes, non-equilibrium statistical operators and quasi-averaging 2−82379
    itinerant ferromagnet, theory of magnetic fluctuations 2−65157
Statistical mechanics continued
    kinetic equation of one-particle distrib. function for rarefied system 2−69619
    lattice models for H-bonded solvents 2−41526
    light elements at high pressure, H-He mixtures in Jupiter's core 2−58779
    light scattering from n-particle system non-Gaussian 2−73541
    liquid, binary collision model of vibrational relaxation 2−53388
    macroscopic linear laws, conditions for derivation from microscopic law 2−49025
    Maxwell-Boltzmann distribution, different proof 2−62941
    Maxwell-Boltzmann distributions of defect pairs in alkali halides 2−83971
    mean spherical model equations, nonexistence of solidlike solutions 2−63034
    memory function, low density, props. 2−41534
    metal, liquid, perturbation theory, structure and mech. props. calc. 2−80461
    molecular model, asymptotic behaviour of wormlike chains 2−74296
    molecular model, stiff chains with excluded volume 2−74297
    molecular randomicity propagation 2−58780
    Monte Carlo method application to equilib. properties and molecules dynamics computer method for non-equilibrium properties 2−82245
    non-equilibrium states, projection operators 2−49035
    non-linear systems and fluctuation-dissipation theorem 2−69615
    nonequilibrium, conceptual foundation using multiplicative stochastic processes 2−58773
    nonequilibrium C*-algebraic theory, dynamics of open and mechanically driven systems 2−58784
    nonequilibrium systs., statistical and dynamical correlations 2−45308
    nonergodicity of spin systems 2−54311
    nonideal solutions, entropy of mixing 2−45305
    nonlinear BGK model 2−73336
    nucleation theory, thermodynamics of cluster formation 2−43435
    Nyquists theorem and its generalizations 2−45630
    one-dimensional lattice gas, phase transitions, transfer-matrix approach 2−61489
    Onsager relations 2−45316
    Onsager systems, linear phenomenological fluctuation 2−49037
    Onsager systems, linear phenomenological response 2−45309
    Onsanger relations, calc. of kinetic coeffs. when carriers and phonons participate symmetrically in transport phenomena 2−47792
    pair correlation decays in 3-dimensional systems 2−41533
    parallel hard squares, canonical ensemble, Monte Carlo analysis 2−41528
    phase transitions, decoupled-mode dynamic scaling theory 2−52103
    phase transitions, gases and solids, F-ensemble and quantum mech. calc. 2−45321
    phase transitions, models 2−58799
    plasma, neutral, application of effective potential method 2−64257
    plasma, relativistic 2−70876
    polar fluids, comparison of two-particle distribution function theories 2−43045
    polymer conformational thermodynamics, computer simulation 2−70801
    power spectra, time dependence of fluctuations 2−45315
    power-series density expansion of general canonical statistical-mechanical average 2−66467
    probabilistic concepts 2−63000
    quasi-equilibrium systems, covariant description 2−45300
    quasi-spin model, positive interactions, Thirring Hamiltonian, free energy 2−82266
    reacting systems, generalized extrapolation relation 2−49021
    recurrence problems, H-theorems, ergodic theory 2−45317
    relativistic kinetic theory, lecture notes 2−52101
    response theories including Kubo theory of linear response, Zwanzig projection techniques 2−45319
    rigid disks, extension of scaled particle theory 2−78836
    rigid particle fluids 2−41549
    self-diffusion coefficient, force correlation function representation 2−49046
    semiconductor, n-type, transport theory inc. higher order scattering effects 2−47887
    soft sphere fluid, inverse-12 potential, radial distribution functions 2−49039
    solid, statistical mechs. when under compression or tension, Hamiltonian modification 2−58789
    solutions, salts in solvents with low dielect. const., statistical theory 2−84617
    spin system, concept of negative temp. and population inversion 2−45313
    stochastic point processes in phase space 2−41532
    surfaces, thermodynamic properties, Gibbs model 2−45312
    thermodynamics, equations of motion for highly nonequilibrium systems 2−58794
    thermodynamics, Grand-canonical distribution and inhomogeneities 2−52098
    tricritical exponents and scaling fields for two-component systems 2−63035
    tricritical point, Landau theory 2−55430
    turbulence models, conference, San Diego, California (1971) 2−43052
    Ursell-Mayer functions, functional calculus approach 2−41530
    Van der Waals gas, thermodynamic rel. to dynamic stability 2−49034
    Van Vleck relativistic ensembles, geometry 2−82270
    variational method for time development of phase functions 2−82260
    velocity autocorrelation function, extension of hydrodynamics to binary dynamics 2−43278
    virial expansion, new derivation 2−73269
    virial expansion for non-ideal reference system, compared with perturbation theory 2−45298
    weak-scaling correls. characteriz. 2−45307
    Wiener-Khintchine relations, time dependence of fluctuations 2−45315
    X-Y-Z model, low-lying excitations at zero temp. 2−66463
    XY chain, excitations of single spin 2−77997

Statistical mechanics continued
- **quantum**
  - δ-function interaction model, one-dimensional, exact results for ground state energy of fermion-boson mixture, equilib. thermodynamics of fermions 2−45320
  - anharmonic oscillator, thermodynamic perturbation theory 2−66471
  - book, applic. to nuclear physics, liquid helium, neutron matter and superconductors 2−82240
  - boson fluid, spinless, stongly interacting, statistical thermodynamics, surface energy and tension 2−82267
  - C*-algebra methods and their application 2−58756
  - charged Bose gas, excitation spectrum, Jastrow theory versus correlated basis functions 2−41545
  - collision operator for exactly soluble models 2−78842
  - critical behaviour rel. to dimensionality, scaling theory 2−78849
  - density matrix, N-representable reduced 2-matrices, convex struct. 2−82229
  - density operator, product-integral calculus formulation 2−62939
  - double exchange ferromagnets, quantum theory 2−54295
  - dynamically coupled systems, Kubo's response theory 2−63033
  - electromagnetically interacting many-particle system, new theory of matter 2−55433
  - elementary particle collisions, statistical quantities defined using analogy between phase-space integral in multiparticle collisions and in relativistic quantum statistics 2−42320
  - energy and number of particles in system, fluctuations 2−45314
  - energy levels in modified quantum statistical potentials 2−59881
  - equilibrium states, structure of Choquet simplexes 2−58785
  - feedback model systems obeying quantum statistical mechanics 2−41531
  - fluctuation-dissipation theorems, review 2−58793
  - harmonic oscillator chain, dynamic and ergodic props. of impurity 2−66469
  - ideal gases, special class, fundamental properties 2−62944
  - imperfect gas, equation of state 2−45326
  - infinite systems, equil. phenomena 2−58797
  - Ising and Heisenberg models, cooperative phenomena 2−45295
  - Kando Hamiltonian, pseudo-fermion Hamiltonian representation 2−73340
  - kinetic equation of one-particle distrib. function for rarefied system 2−69619
  - kinetics of charge transfer on electrodes 2−65385
  - magneto-active plasma, formulation in framework of irreversible statistical mechanics 2−52113
  - Markovian processes 2−69613
  - measurement theory formalism 2−69534
  - metals, effects of lifetime of core hole in X-ray emission spectra studied by nonequilibrium methods 2−48205
  - non-equilibrium processes and quasi-averaging concept, boundary conditions for statistical operators 2−82246
  - nonequilibrium, superoperator theory, zitterbewegung as subdynamics 2−73321
  - nonlinear interactions of waves in weakly turbulent plasma 2−43186
  - parafermi statistics of given order, algebraic identities 2−45329
  - perfect boson gas, Einstein condensation 2−45327
  - phase transitions near 0K, quantum kinetics 2−78857
  - photodetection 2−41953
  - Planck law, classical derivation of Bose 2−62916
  - power-series density expansion of general canonical statistical-mechanical average 2−66467
  - radiating particles, pressure broadening, BBGKY technique 2−67382
  - real symmetric matrices class, eigenvalue distrib. 2−58791
  - real symmetric matrices class, Monte Carlo calcs. of eigenvalues 2−58790
  - self-interacting fermion systems, perturbation theory for grand canonical Gibbs states 2−45328
  - semiconductor, introduction, book 2−47876
  - solid, metastable state lifetime, effect of quantum fluctuations 2−84154
  - solutions, sine-Gordon eqn. for multiple collisions, exact solution 2−82259
  - spherical model, critical indices from conformal covarient self consistency conditions 2−78847
  - transformation theory, applic. to soluble model 2−58792
  - two-level magnetic system damped by interaction with bosons, transverse susceptibility 2−49022
  - two-level system damped by boson interaction, excitation, stationary populations 2−45299
  - variational principles and minimum entropy production 2−45318
  - XY model ground state equivalence to free fermion model 2−45330

Statistical thermodynamics *see Statistical mechanics*

Steady-state theory *see Cosmology*

Steam
- condensation heat transfer under stratified flow condiyions, empirical correlation 2−83670
- critical point thermodynamic anomalies 2−67870
- discharged from geothermal ground, physical properties 2−78247
- Joule-Thomson coeff. meas. by throttling element for radial flow of fluid 2−67825
- steam-air system, aerosol transport in naturally convected boundary layer 2−67786

Steel
- 34KhN3GSV, plastic deformation effects on kinetics of bainitic transf. 2−84077
- AISI 304 and 316, substructure correlation with elevated temperature low cycle fatigue 2−56819
- AISI type 310, transformation characteristics for ferrite, sigma phase and carbides, e. microscope study 2−68189
- AISI type 316, transformation characteristics for ferrite, sigma phase and carbides, e. microscope study 2−68189
- alloys, fracture mechanics of crack growth at elevated temperatures 2−56867
- alloys, high strain rate effect on room temperature strength and ductility 2−60877
- annealed low carbon, cyclic stress-strain relation 2−84124
- annealed low carbon, dislocation model for delayed yielding phenomenon 2−80813
- arc welding, mechanical strength, obs. 2−56919

Steel continued
- athermal martensitic morphology, arrow-like formations 2−67980
- ausformed by extrusion, mech. props. and form. of struct. 2−47327
- austenite, isothermal pearlitic transform. kinetics, plastic deform. effect 2−50939
- austenite, solubility of NbC and NbN 2−74902
- austenite, static recrystalliz. between intervals of hot working 2−47575
- austenite, transform., isothermal phase diagrams 2−47690
- austenite phase, transformation obs. using high-speed dilatometer 2−57008
- austenite-ferrite mixture, determ. of relative phase vol. by X-ray diffr. 2−71641
- austenitic, $Cr_{23}C_6$ precip., effect of Ni 2−47622
- austenitic, creep, rel. to shape and dimens. of particles 2−50656
- austenitic, creep behaviour, obs. 2−56920
- austenitic, fatigue crack growth at high temperatures for types 304, 316, 321 and 348 2−56864
- austenitic, grain coarsening temp., hot rolling effects 2−47582
- austenitic, high Mn, microhardness determ. 2−71638
- austenitic, irradiated, nucleation of voids 2−71466
- austenitic, neutron-induced mechanical property changes, damage function analysis 2−77718
- austenitic, stainless, grain boundary penetration by Cs-O solutions and caesium oxide, out-of-reactor study 2−67356
- austenitic, stainless, intergranular corrosion in sensitized or solution annealed condition, potentiokinetic polarization 2−68791
- austenitic, stainless, mech. props. rel. to Co content 2−47474
- austenitic, stainless, stress corrosion testing, mech. behaviour 2−50765
- austenitic, stainless, susceptibility to stress corrosion cracking, evaluation by chemical, electrochemical methods 2−68104
- austenitic, strengthening by ageing 2−53876
- austenitic, strengthening during ageing due to VC precip. 2−47636
- austenitic, substruct., effect of deform., temp. during thermomech. treatment 2−80770
- austenitic, surface slip lines and incipient cracks, during reverse bending 2−53837
- austenitic Cr-Mn, intergranular corrosion susceptibility 2−71646
- austenitic manganese, struct. stability 2−43848
- austenitic stainless, containing delta ferrite, solidification, segregation and homogenization 2−43847
- austenitic stainless, dynamic recrystallization 2−68133
- austenitic stainless, effect of neutron irradiation on tensile and creep-rupture ductility 2−77719
- austenitic stainless, in acid media, cold plastic deformation effect on corrosion 2−68790
- austenitic stainless, precip. at twin boundaries 2−43850
- austenitic stainless, segregation and effects of B 2−47623
- austenitic vanadium nitrogen type, fine precipitates struct. 2−53893
- austentic stainless, ferrite phase determ. using magnetic balance 2−44245
- ball bearing, rolling fatigue life, retained austenite effects 2−64764
- ballistic behaviour of targets, effect of metallurgical factors and mech. props. 2−60980
- Bauschinger effect on initial yield stress for design tests in high-yield pipes 2−60867
- brittle fracture, theory 2−43720
- brittle fracture susceptibility, effect of V alloying 2−53896
- ε- carbide, Curie temp. determ. 2−72165
- carbide formation, during low temp. isothermal drawing 2−43810
- ε-carbide phase form. and struct. 2−43844
- 1% carbon, fatigue crack propagation, stress intensity and microstruct. effects71645 2−71645
- carbon, volume fraction of retained austenite, X-ray obs. 2−56645
- carbon strain energy during rotatory bending fatigue, effect of pearlite patches 2−84125
- cavitation erosion mechanism 2−71606
- cementite, Ostwald ripening, alloying additions effects 2−50936
- cermet, dynamic hot pressing, thermal treatment effects on struct. and mech. props. 2−84146
- Charpy specimens, precracked, dynamic fracture toughness from impact hammer tests 2−71609
- chemical polishing technique for prepn. of thin foils for e. microscopy 2−67963
- chromized C type, elastic and relax. characts. 2−53780
- cladding on $(U, Pu)O_2$ fuel rods, plastic deformation 2−76944
- cladding/fuel interface, steel/$UO_{2\pm x}$-$PuO_{2\pm x}$, reaction 2−52875
- coatings, high temp., deposition from fused salts and by ion plating 2−50860
- composite steel concrete beams with welded stud shear connectors, behaviour under sinusoidal bending deformation 2−58836
- constructional, heat treatment effect of hydrogen permeability and diffusion 2−64757
- contact-free stimulation of waves in steel plates 2−78914
- control rods of ^{10}B-stainless steel, effect of B concentration gradient on thermal reactor performance 2−76948
- corrosion of austenitic stainless steel, microstructure determ. of oxide film 2−81505
- cost structure, effect of induced fluid flow 2−47620
- $^{1}/_{2}$Cr-Mo-V steels, high-strain fatigue properties 2−60948
- crack formation in heat affected zones of welded joints during heat treatment 2−71596
- crack propagation resistance, tempering temp. effects 2−53838
- cracking, stresses at start and finish 2−56832
- cracks, estimating work done in development 2−53834
- creep characteristics at ambient temp. 2−64747
- creep resistivity improvement by stabilized recovery induced substruct. 2−56913
- creep strain delay, at transition temp. 2−74846
- critical pts. and linear expansion coeff., additive effects 2−47686
- damping characteristics of certain steels 2−69703
- deformation at high strain rates of annealed low C steel 2−71565
- deformation temp. effect on changes of the mech. props. of α-Fe and low C steels 2−84159
- deformed by reverse bending, fatigue behaviour 2−50769
- demagnetizing field frequency, rel. to domain struct. for Fe-Si steels 2−84412
- diffusion in steel/Al solid/liquid system 2−80715
- diffusion layer, C distrib., study by spectroscopy 2−47435

Steel continued
diffusion of hydrogen at low-temps., effect of grain boundaries 2−68047
dislocation arrangement changes in low C steel during fatigue process 2−84162
dislocation-additive interaction during tempering 2−43790
drops, solidification in oil 2−43440
ductile-brittle transition, deform. mode influence 2−43694
dynamic strengthening singularities under infl. of shock waves 2−84075
effect of cyclic bending on strength and plasticity 2−84080
elastic stresses around nonmetallic inclusions 2−53725
electrochemical studies concerning caustic stress corrosion cracking 2−68789
embrittlement, effect of microstructure in low C steel 2−84158
embrittlement by hydrogen, mechanistic model 2−77653
En 24, soln. between microstructure and fracture toughness 2−71586
eutectoid, mech. props., effect of directional growth of pearlite and rolling 2−47529
eutectoid carbon, upper bainite and isothermal pearlite transform., effect of austenitizing cond. 2−50941
fatigue, impact, of C steels, effect on microstructure 2−80809
fatigue, low-cycle in hydrogen atmosphere or vacuum 2−60891
fatigue, thermal and low-cycle, effect on microstructure 2−60894
fatigue crack growth, threshold at 300°C 2−56863
fatigue damage, steel and cast-iron, microhardness method 2−77670
fatigue failure kinetics 2−53828
fatigue life, tests involving simulation of infrequent cycling 2−71593
fatigue lifetime and Wohler curves, statistical study 2−43714
fatigue stability tests, sensitivity estimates for asymmetrical loading cycles from strain diagrams 2−56840
fatigue strength of thick-walled cylinders 2−64781
fatigue-crack growth, effects of oxygen, water-vapour and hydrogen 2−68067
ferritic, irrad. embrittlement 2−43854
ferritic phase, electron microscope contrast of dislocations 2−80873
ferritic-austenitic transform., stored deform. energy influence 2−43918
fibre, stainless, in Sn-Pb alloy matrix, fracture behaviour 2−50921
fibre-reinforced Al, thermal and elec. cond. 2−53946
film, high tensile strength, chemical grinding prep. 2−71636
fine grained, structural, effect of welding conditions on microstructural region in weld transition area 2−50808
flaw formation in castings 2−68149
flow stress meas. using torsional split Hopkinson bar 2−68124
forge quenching treatment effects on mech. props., in med. C steel 2−80806
fractography in fatigue fracture of low-carbon steel 2−84126
fracture, high temp., influence of annealing twins 2−56833
fracture strength, low temp., notched specimens preloaded at room temp. 2−64783
grain size, dependence on cooling velocity 2−84122
Hadfield, recovered, shock stress amplitude and duration effects on residual hardness 2−68072
hardening depth in rolls, ultrasonic device for measurement 2−60928
heat capacity of 1Kh18N9T between 300 and 900 K 2−57065
heat treated, cyclic strain softening at various hydrostatic pressures 2−68142
heat treatment effect on mech. props. 2−60962
high C, low temp. tempering, retained austenite, X-ray obs. 2−74883
high carbon, workhardened, recovery and ageing 2−47597
high Ni content, austenite stabilization rel. to reverse transformation 2−74930
high strength, slow crack growth in H_2 and H_2S gas environments 2−71599
high temperature behaviour in He coolant gas and impurities 2−42673
high-alloy, suppression of pitting in phase analysis 2−57423
high-C martensitic, fine struct. singularities 2−56934
high-C martensitic, tempering, carbide precip. 2−64761
high-C martensitic, tempering, carbide precip. 2−64762
high-N content, formed by melting under high press., metallography 2−50812
high-speed, thermal expansion, partial coeffs. of MC, M_6C, and α and γ phases 2−54059
high-speed deformed low-C, dilatometric behaviour 2−43839
high-speed W-Mo, struct. and mech. props., effects of Co 2−53992
holder for preparation of sections 2−73238
hot pressed, C diffusion, dislocations, internal stresses, mosaic struct. 2−43793
hot-worked austenitic and ferritic, recrystn. during continuous cooling 2−53873
hyper-eutectoid, graphitization, effect of Ca and Ba, 550-700°C 2−47583
hypereutectoid, low carbon martensite struct., prod. by heat treatment 2−47585
impact props., rel. to FeO type inclusions 2−47530
impact strength and ductile-brittle transition, effect of cold rolling and heat treatment 2−80777
impact strength variation during heat treatment, role of cryst. distortions 2−43792
inclusions, stress fields rel. to mech. props. 2−47491
inoxidizable, passivation film study rel. to stress corrosion cracking 2−54547
isothermal coalescence of dispersed phase, kinetics 2−47611
Kh18N10T, fine structure changes for degree of deformation in creep 2−83956
laminate stacks, heat flow, surface texture effects 2−49180
LEED vacuum chamber of stainless steel and molec. beam assembly, H and N desorption phenomena 2−67922
liquid, degassing and refining by vacuum techniques 2−62904
loading, dynamic, effect of C steel structures on mech. props. 2−84161
low alloy, creep rupture strength, microstruct. depend. 2−77685
low alloy, fully heat treated, effects of sulphide morphology on impact props. 2−56908
low alloy, microduplex processing effects on strength-toughness 2−43835

Steel continued
low carbon, influence of vacuum annealing on dislocation structure and hydrogen saturation 2−60958
low carbon, microstructure and embrittlement 2−43783
low-alloy, mech. props. and brittle fracture, effect of Ce addition 2−53831
low-alloy, structural behaviour during controlled rolling 2−64778
low-alloy, temper-brittle fracture and grain boundary segregation 2−47624
low-C, bending fatigue tests, Wohler curves, slip lines, cracks 2−50979
low-C, dynamic strain aged, work softening 2−80837
low-C, fracture rel. to microstruct., embrittlement, bend tests 2−56823
low-C, low-alloy, AlN precip. 2−50833
low-C, plastic instability 2−43695
low-C, surface plastic deform., X-ray obs. 2−80769
low-C and low-alloy, neutron irrad., radiation- and anneal-hardening 2−80681
low-C low-alloy, fine struct. and phase comp. at elevated temps. 2−53898
low-C low-alloy pipe, formation of abnormal struct. 2−53897
low-C martensite,austenite stability and mech. props. 2−50834
lubricated friction against Al, oxidation influence 2−53844
manganin pressure transducers, influence of high pressure H_2 on electrical resistance, compared with Au-Cr alloy 2−76122
maraging, plane strain fracture toughness tests 2−60979
maraging weldments, sustained load failures 2−71590
maraging with 18%Ni, flow behaviour 2−84068
martensite, diffusion of C interacting with dislocations 2−56758
martensite, effect of lath boundary precip. on fracture toughness 2−57018
martensite, fine struct. field ion microscope obs. 2−64779
martensite, ordering temp. 2−57026
α- martensite, second stage of decomp., X-ray obs. 2−50938
martensite ageing, prep. by powder metallurgy 2−43892
martensite formation in Re steels, mechanism and kinetics 2−43917
α- martensite lattice orientation 2−43843
martensite transform. study using X-ray camera and He cryostat 2−43546
martensitic, Fe-plated fracture edge, elec. microscope obs. 2−56940
martensitic, intercryst. fracture mechanism, incompat form. 2−56815
martensitic, low-C Mn, effect of Sb on high temp. tempering 2−56905
martensitic, tempered, crack initiation and propag., plastic replication and electron microscope obs. 2−43734
martensitic, X-ray microstruct. rel. to low-cycle fatigue 2−43715
martensitic stainless, ageing, phase transforms. and mech. props. 2−53989
martensitic transform. activation by stimulated emission of phonons 2−43909
mechanical properties and microstructure, effect of rare earth alloying 2−53900
mechanical properties and microstructure, u.s. vibr. effects 2−53877
mechanical props. and short term fracture at elevated temps. and pressures 2−60917
melting in Fe-C melts, heat and mass transfer obs. 2−43438
microalloyed, KIDUR 60, precip. of plane carbides of Ti and Nb 2−47631
microhardness meas. by method of small penetration of indentor 2−47549
mild, acoustic emission and energy transfer during crack propag., instrum. for detectn. 2−69767
mild, annealed, effect of upper yield stress on torsion and bending 2−43685
mild, Bauschinger effect and discontinuous yielding 2−64716
mild, deformation layers in spark machined and mechanically sectioned steel 2−74879
mild, detonative loading, breakage and stress waves 2−84048
mild, dissolved oxygen influence on struct. and toughness 2−47628
mild, effect of high energy ultrasonic waves on structure and hardness 2−77673
mild, fatigue cracking, initiation, growth, rel. to thickness 2−53833
mild, scratch and indentation hardness 2−53841
mild, strain profile of propagating Luders front 2−47494
mild, thermal activation parameters during non-uniform and uniform deformation 2−80814
mild steel plates, automatic welding, plastic deformation kinetics 2−69481
multilayer, strength, rel. to soft steel percentage 2−53824
nitriding, by N-ion bombardment 2−56935
notched parts with compressive mean load, fatigue crack growth 2−47543
pearlite, strength and brittleness 2−43724
pearlitic, deform. influence on lowering of critical pts. 2−53986
peritectic transformation 2−61034
phase state determ. method of stainless steels at rolling temps. 2−84091
phase transformation, $\alpha \rightarrow \gamma$, singularities, rel. to initial state 2−80764
phase transformations during laser beam heating, effect of original struct. 2−53990
phosphide eutectic classification 2−47633
plastic anisotropy of low carbon deep drawing sheet steels, method for determ. 2−64710
plastically deformed, austenite form., kinetics and morphology 2−57014
plates in Fe-C melts, melting problem, numerical solution 2−60543
polymer friction, anomalous low level upon helium atom irradiation 2−56837
polymer-solid adhesion breakdown rel. to radio emission parameters 2−52314
pressure vessel, biaxially stressed, crack tolerating factor 2−50835
pressure vessel material, time-depend. embrittlement phenomena 2−59849
pressure vessel type, radiation sensitivity, effect of impurities 2−53895
quenched, aged, cooled, dislocation substruct. rel. to fracture behaviour 2−47413

Steel continued
quenched, cooling rate rel. to struct. and mech. props. 2−47587
quenched, quench-aged, fatigue behaviour rel. to microstruct. instability 2−50768
quenched, tempered, resist. to plastic deform. and cold brittle faulure 2−47502
quenching temperature, influence on γ'-phase precip. 2−80768
radiation damage data correl. using activation fluences and irrad. temp. 2−83131
radiation-induced swelling implications in fast reactor design 2−49900
reactor cladding and struct. materials, irrad. induced void form. 2−49901
reactor core material, swelling induced deform. problems 2−59863
reactor core material, swelling induced problems, metallurgical parameters 2−59864
reinforced Al tubes, bursting strength and toughness 2−71660
reinforced Al tubes, bursting under biaxial tension stresses 2−71661
retained austenite developed during surface grinding of carbon steel, exptl. obs. 2−74880
retarding recrystn. during thermomech. treatment at high temp. 2−60961
rolled plate, anisotropy of fatigue limit 2−74872
rolling conditions, heat affected zone properties 2−68132
shear, fracture, during heavy forming operations 2−53823
sheet, acoustic anisotropy obs. by pulse resonance method 2−64773
sheet, cold rolled, annealed, grain growth, X-ray obs. 2−47621
siliconized coated, voids in diffusion layer, holding time and content effects 2−47635
sintered, dense struct. form. in the powder during stationary hot pressing, in Cr steel 2−77698
sintered, for fuel element jackets, processing and mech. characterization 2−76951
sintered, mechanical behaviour model to explain behaviour of elastic moduli 2−84128
slip lines in plastic flow 2−80831
spectra of trace impurities, effect of alkali metal carriers 2−51479
spectral analysis by optical emission, time decrease by increasing spark source repetition rate 2−84694
spectral analysis of residual contents of Ce and Ca 2−54572
spectrographic determination of Ag 2−57443
spheroidization of cementite by plastic deform. at subcritical temp. 2−43840
stability of FeC at 700°C 2−50944
stainless, 18−8, cross slip in fatigue deformation electron microscope obs. 2−77686
stainless, 18% Cr ferritic, stress corrosion cracking 74901 2−74901
stainless, 18-10, electrochemical study for compounds which inhibit stress corrosion 2−65381
stainless, 18-8, carbide precip. rel. to creep rupture strength 2−77684
stainless, 18-8, flow stress, effect of high hydrostatic pressure 2−56936
stainless, 18-8 fatigue props. at cryogenic temp. 2−56939
stainless, 18/8 type, damage induced by high energy electron channelling 2−53713
stainless, 19Cr-9Ni, effects of alloying elements on stress corrosion cracking 2−77656
stainless, 20%Cr 25%Ni austenitic, tertiary creep processes 2−47514
stainless, 304L, surface characterization by proton induced X-rays 2−50832
stainless, annealed type 316, effect of fast reactor radiation on creep behaviour 2−83123
stainless, austenitic, Al_2O_3 dispersoid, prep. of thin foils for transmission electron microscopy 2−80549
stainless, austenitic, effect of creep and fatigue loading at high temps. 2−60946
stainless, austenitic, stress corrosion cracking under pulsating load 2−53836
stainless, cladding for fast reactor fuel elements, review of properties 2−59846
stainless, cold rolled and annealed sheets, ridging phenomenon 2−68131
stainless, Cr depletion of surface by vacuum annealing 2−47075
stainless, crack formation, in situ obs. in 500 kV electron microscope 2−80853
stainless, deuteron generated void form., in-reactor damage simulation 2−53714
stainless, dislocation dipole, electron microscope obs. 2−80666
stainless, Doppler effect due to structural material for fast reactor systems 2−83104
stainless, electrodes, fatigue strength 2−80762
stainless, electrodes, subjected to very high positive and negative voltages, struct. 2−71042
stainless, ferritic sheet, texture development 2−77701
stainless, fibres, tensile strength 2−77742
stainless, foil prep., for electron microscopy, electrolytic jet thinning procedures 2−71415
stainless, fracture, high voltage electron microscope obs. 2−56825
stainless, He migration and release after implantation 2−50639
stainless, He prod. rel. to LMFBR development 2−49902
stainless, high cycle fatigue properties at elevated temperatures 2−60951
stainless, high-tensile, containing Be, cryst. struct. determ. 2−77672
stainless, hot dip Al coated, alloy layer struct. and composition 2−56937
stainless, irrad., cold work effects on void form. 2−50646
stainless, irrad., fluence and temp. depend. of void form. 2−50647
stainless, low-cycle fatigue and stress relaxation at elevated temps. 2−60947
stainless, managing, high-strength, struct., props., optimum comp. 2−60881
stainless, material properties control of fatigue failure at elevated temperatures 2−60893
stainless, melted by different methods, struct. and props. 2−53899
stainless, neutron damage simulation by ion bombardment, void form. 2−53692
stainless, neutron displacement cross sections, based on Lindhard model 2−83053
stainless, neutron irrad., void form. and growth, theory 2−53701

Steel continued
stainless, permeation of hydrogen, surface effects 2−77608
stainless, pitting, intergranular corrosion and stress corrosion cracking, significance of protection potential 2−68787
stainless, proton irrad., swelling, displacement damage depend. 2−53716
stainless, proton- and nickel-irrad., void form. 2−53715
stainless, sensitized ferritic, pitting corrosion 2−78193
stainless, sintering, in container with melting closure 2−50882
stainless, stress corrosion crack propagation, film rupture mechanism 2−43727
stainless, struct., effect of explosive load 2−43836
stainless, suppression of void form. 2−50648
stainless, surface, energy spectrum of slow monoenergetic reflected electrons 2−50441
stainless, susceptibility to intergranular corrosion by potentiodynamic polarization 2−68788
stainless, swelling data analysis using displacement rates from Lindhard model 2−52880
stainless, thermal diffusivity, thickness effects 2−57085
stainless, type 304, passivity, effect of plastic deformation 2−78195
stainless, type 304, pitting susceptibility relative to semiconducting surface film 2−57422
stainless, type 304, ratchetting, parametric study for design curves and design rules 2−56895
stainless, type 304L, in-reactor creep 2−46382
stainless, type 403, influence of NaCl in steam on v.h.f. high- cycle fatigue 2−60955
stainless, type AISI 304, accelerated intergranular stress corrosion cracking tests using potentiostatic polarization 2−68105
stainless, types 301 and 304, different strain rates and tensile properties 2−64746
stainless, types 304, 316 estimates of creep- fatigue interaction in irradiated and unirradiated samples 2−83121
stainless, types 304 and 316, ^3H diffusion, 25-222°C 2−47458
stainless, types 316 and 304, Mo surface conc., Auger electron spectroscopy obs. 2−50442
stainless, void form. on quenching 2−53717
stainless, void nucleation and growth during fast neutron irrad. 2−50645
stainless, void nucleation and growth obs. using h.v. electron microscope irrad. 2−53694
stainless 20% cold-worked Type 316, fatigue- crack growth at elevated temps. 2−84141
stainless steel, types 304 and 316 low-cycle fatigue behaviour at LMFBR operating temps. 2−60945
stainless tubes, fast neutron irrad. effect 2−83085
stainless type 304, effect of irradiation on strain rate dependence of mechanical properties 2−83122
stainless types 304, 316 time-dependent deformation behaviour, elevated temp. design criteria 2−83119
stainless weldments, type 304, fatigue crack growth at elevated temperatures 2−56865
steel, austenitic, type 316, creep-rupture behaviour relative to boron content 2−60872
steel, low-C, hot-rolled, quenched, transformation effects on microstruct. and mech. props. 2−57017
steel, stainless, AISI 304, low-cycle fatigue, effect of strain rate and hold periods 2−60954
steel, stainless, solution treated type 304, empirical representation of irradiation-induced swelling 2−43609
strain-ageing resistance 2−43800
strength and ductility, hot impact tension tests 2−60978
strength and plasticity, effect of isothermal treatment 2−53874
strengthening and roughness of rubbing surfaces, effect on wear and bearing capacity 2−60916
stress concentration, dynamic, of mild steel notched strips 2−80807
stress corrosion cracking, cathodic protection and hydrogen 2−78194
stress-strain diagram parameter det. in temp. range 196-25°C 2−56843
structural, austenite grain growth 2−53988
structural, effect of C, Mn and Si on austenite content 2−74875
structural, fracture behaviour rel. to inclusion orientation and shape 2−43713
structural, single crystal temper brittleness 2−60982
structural, transmission electron microscope obs. 2−56631
surface defect obs. in cold-rolled strip using light scattering 2−74871
surface oxidation during annealing, obs. 2−67899
swelling, fast neutron induced 2−63969
technical, electronic grain-size analyser 2−60969
temperature monitoring during heating using thermopencils 2−63158
temperature obs. from self radiation applic. of computers 2−58973
tempering, anal. of stressed and strained states in surfaced components 2−71607
tempering, Ostwald ripening obs., grouping errors in data analysis 2−60942
tempering, transform. of retained austenite 2−47689
tempering behaviour of ausforming Mn-Cr-B spring steel 2−77688
tensile creep under transient stress, in 11% Cr steel, elevated temp. 71575 2−71575
thermomechanical treatment effect on mech. props. after ausforming 2−43801
thick walled cylinder failure test-machine using fracture mechanics on pressure cycling 2−69501
thick-walled cylinders, microstrain obs. under internal pressure up to 6 kbar 2−68156
transformer, dislocation density, X-ray diffr. obs. 2−43636
transformer, effect of induced magnetic anisotropy on magnetic properties and domain structure 2−68539
transformer, hot rolling, effect of S content on recrystn. 2−47586
transformer, precip. at grain boundaries, rel. to coercive force 2−47632
transformer steel, e. micro and e. diffr. exam. of disperse nonmetallic phase 2−84074
transition layer in electrolytically deposited Cu-Sn alloy 2−47683
transition temp. calc. and phonon vertex 2−71876
type, common or low alloy, thermoelectric method of determination 2−80784
type 304 stainless, prediction of in-pile behaviour using SCIM, theory based computer code 2−76939

Steel continued
  untempered, low-alloy, segregation effects and toughness 2–80822
  untempered ultrahigh strength steels of high fracture toughness 2–53872
  u.s. attenuation and velocity meas. at 1200°C using momentary contact method 2–74978
  u.s. properties during solidification 2–71669
  u.s. wave propagation, lunar seismic signals 2–44927
  vessels, welded, internal pressure tests 2–68153
  visualization of defects by three-dimensional imaging of ultrasound 2–76378
  wear behaviour of sapphire 2–74867
  welded joints, crack formation in stress relieving annealing 2–64759
  welded pressure vessels, loading capacity, stressed at high temps. 2–64771
  welding, restraint stress effect on delayed cracks 2–77711
  welding and hardfacing, with twin plasma jets 2–68147
  wire, annealing struct. of heavily drawn pearlite 2–64760
  wire reinforced polyester resin, fracture toughness 2–47528
  X-ray metallography 2–53892
  yielding, effect of electric strain rate and temperature 2–47524
  yielding and fatigue reln. under static and dynamic loading in low-c steel 2–84023
  C, weldability to Cr-Ni steel, gas pressure process 2–68146
  0.55% C steel, cracks, propagation under varying load conditions 2–43733
  Cr-Mn-Mo-Ti type, carbides identification 2–47627
  Cr-Mo-V steels, constitution diagrams for service lifetimes 2–60838
  Cr-Ni, weldability to C steels, gas pressure process 2–68146
  Cr-Ni steels, austenitic, stabilisation of resistance to intercrystalline corrosion 2–65380
  2-$^{1}/_{4}$ Cr-1 Mo steel, effect of carbon content on high temperature properties 2–60880
  2$^{1}/_{4}$Cr-1Mo ferritic steel high cycle fatigue properties at elevated temperatures 2–60951
  Cr, creep, tensile and compressive, at constant stress 2–68091
  CrV steels, free energy changes and boundary segregation of Sn and Sb 2–71309
  Fe-Cr, embrittlement at 475°C, ordering, decomp. of ferrite 2–47634
  Fe-Nb-Al bearing steel, dynamic strain ageing 2–47598
  Fe-Ni-Al, martensite transform, effect of disperse particles 2–50942
  Fe-Ni-Co-Mo, maraging alloy, coherent precip. electron microscope obs. 2–57019
  Fe-V-C steel, fibrous vanadium carbide occurrences after thermal or continuous cooling transformation 2–61033
  Fe and Cr simultaneous estimation in stainless steel by polarographic method 2–48352
  Fe loss due to rotating magnetic field in cold rolled Si steel plates 2–84422
  H content determination, using diffusion kinetics 2–64780
  MnS inclusion size, effect of solidification rate and S content 2–43852
  Mo-Cr-alloyed or unalloyed case hardened steel, residual stresses in carbonized layers for different thermal treatments 2–56931
  MoS$_2$ coating applied by detonation, heat and friction resist. 2–43744
  Ni-Cr, effect of Cu additive on tempering 2–60957
  Ni steels, 40N25, 60N20 and 80N15, amplitude-dependence of int. frict. 2–84076
  O$_2$ content, spectrochemical determination, effect of heat 2–72590
Stellar atmospheres
  A-type supergiants, line intensity changes caused by variable velocity fields in atmos. 2–62556
  A-type supergiants, microturbulence and radial velocity from metallic lines 2–62497
  A-type supergiants, Ti/Fe ratio, turbulence and radial velocity 2–62537
  A-type supergiants comparison to α-Cygni 2–69061
  absorption lines, effect of stochastic magnetic fields 2–48684
  abundances, analysis, Minnaert formula and spectrum calculation using model atmosphere 2–75743
  angular momentum, variance analysis 2–55032
  atomic processes in astrophysical plasma 2–75703
  B-type, u.v. flux envelopes 2–58291
  B-type stars with discrepant colours, model atmosphere analysis 2–81862
  band O stars, light ion spectra 2–75740
  Be stars, envelopes, temporal variations of flow parameters 2–75711
  blanketed model atmospheres for cool hydrogen-rich white dwarfs 2–69079
  V553 Centauri, type II Cepheid, overabundance of C66102 2–66102
  Cepheid envelopes, multiple solutions 2–58322
  chromospheres, obs. of He I D$_3$ line 2–58295
  close binaries, F-, G- and K-type components, transport mechanism in envelopes 2–78470
  CNO abundances, hydrodynamic models of nova outburst 2–58315
  convective envelopes, fluid dynamics 2–62477
  cool supergiant stars, model atmospheres, compositions 2–66074
  β Cor Bor, magnetic A star 2–58289
  curvature, effect on spectral line profiles formed in extended stellar atmos. 2–62557
  α Cyg, line intensity changes caused by variable velocity fields in atmos.62556 2–62556
  DA and DB white dwarfs, model 2–69064
  differentially expanding atmospheres, transfer of resonance-line radiation 2–62522
  differentially expanding atmospheres, transfer of resonance-line radiation 2–62521
  dispersion, gravitational instability of interface separating two streams 2–84930
  envelopes, thermal diffusion rel. to secular time scales 2–62504
  F0-K5 supergiants, spectral line variations rel. to atmospheres 2–62540
  G supergiants, microturbulence 2–58299
  grains in the atmosphere of late type irregular and semi-regular giants and supergiants 2–69084
  HD 103877, possible Fm-type star, atmosphere rel. to spectral studies 2–81847
Stellar atmospheres continued
  hot star circumstellar envelopes, Lyman α absorption 2–62559
  HR 465, Ap stars, model atmosphere anal., abundance obs. 2–66076
  hydrodynamic motions in stratified convective zones 2–78455
  Ic Orionis, pre-main sequence stars, circumstellar gas emission 2–66116
  limb darkening for B-type main sequence stars in i.r. 2–55037
  M-dwarfs, absorption band at 5500-5560Å attributed to CaOH 2–75729
  magnetic neutron stars and pulsars 2–44865
  magnetic stars, possible separation of elements 2–62498
  massive red supergiants, convective envelopes and radial pulsation 2–51729
  NGC 2264, pre-rain sequence stars, circumstellar gas emission 2–66116
  nonrotating baryon stars, model 2–69058
  novae, circumstellar envelope, formation of coronal lines 2–75766
  βOrionis, supergiant, differential shifts in He I lines, atmospheric motion 2–62538
  ϵ Pegasi spectra, chemical composition using atmosphere model 72993 2–72993
  α Per, model atmosphere and continuum observations62500 2–62500
  pulsars, ground state binding energies and bound free cross sections in pulsar atmospheres 2–58407
  radiation field effects on heating cooling and momentum transfer 2–58268
  radiation heat exchange in polytropic atmospheres 2–58263
  radiation pressure, effect on neutral atoms and dust grains 2–48730
  rotating, interacting with evolution, models and photometric obs. 2–55026
  S and N envelopes, chemical evolution model 2–62490
  spectra, line intensity anomalies, laser action as explanation 2–48699
  supergiant stars, colloquium (Trieste, Italy, Sept. 1971) 2–58262
  supergiants, loop formation, homology relations 2–62519
  very cool supergiants, review 2–62555
  ϵ Virginis (HD 113226), line blanketed model atmosphere 78458 2–78458
  white dwarfs, evolution, with accretion of H rich envelope 2–69066
  white dwarfs with convection, model 2–75707
  winds and breezes, relationship, effect of corona temp. and particle density 2–48683
  Wolf-Rayet type, chromospheric heating by radiation driven sound waves 2–69062
  CO cooling effect in atmospheres of red giants 2–75709
  Fe/H ratio in F1-F5 stars, by model atmos. anal. 2–66077
  Fe spectral line identification and abundance 2–62748
Stellar clusters *see Stars*
Stellar composition *see Stars/composition*
Stellar evolution *see Stars/evolution*
Stellar motion *see Celestial mechanics; Stars*
Stellar structure *see Stars/structure*
Stellarators
  convective motions due to trapped particles in field 2–43162
  diverter, ion and electron energy distributions 2–70890
  drift wave growth, effect of mag. shear on temporal damping 2–70946
  excitation system for h.f. plasma heating 2–43156
  high-β, toroidal, ISAR T 1, dynamical phase obs. 2–83562
  injector for transverse injection into linear stellarator like field 2–43163
  injector-diverter, purification of H plasmoids by mag. field 2–80298
  L-1, nonstationary phenomena in plasma decay 2–67670
  stability of finite β, l=2 stellerator 2–83569
  toroidal plasma, with helical mag. field, stationary equilib. and diffusion 2–77278
  transverse injection into linear stellarator like magnetic field 2–80289
  viscosity damping of convective cells 2–80276
Stereoisomerism *see Isomerism*
Stereophonic sound *see Acoustics*
Steroscopy *see Vision*
Stimulated emission
  see also Lasers; Luminescence, Masers
  anthracene as active laser element 2–78144
  astronomical masers, interstellar scattering effects on apparent size 2–75787
  atom, macroscopic optical coherence phenomena rel. to n.m.r. studies 2–59907
  atomic system, superradiance rel. to coherence effects 2–59912
  blackbody radiation, Bose-Einstein statistics 2–41838
  cathodic cavity plasma 2–82477
  composite system factorization 2–73543
  dyes, organic, degree of polarization 2–49375
  electron in strong wave field causing amplification of weak e.m. wave 2–63311
  glass:Nd, lasing efficiency, effect of phase separation 2–57372
  laser, X-ray, soft, rel. to ionization, inversion, stimulated emission and Auger effect 2–79209
  masers, steady state emission, spectral power distrib. for multisublevel system 2–45706
  metastable one-electron atom, interaction with e.m. radiation, calc. for second-order radiative processes 2–46488
  methanol, gain meas. of stimulated Raman scattering using tunable dye laser 2–43375
  molecular crystals, theory of stimulated Raman dispersion scattering 2–76499
  organoluminor solutions, obs. of emission by exciplexes 2–67836
  phonon maser effect in ferrous alloys 2–43909
  photon emission by atomic beam 2–45700
  polymethylene dyes, resonant combination laser pulse dispersion 2–49377
  Raman gain in single mode glass waveguides 2–42130
  Raman scattering, molecular relaxation and dispersion 2–41938
  Raman scattering from bulk medium, theory of polarization state 2–63305

- **Stimulated emission** continued
  - rare earth and actinide ions in single crysts., two-photon absorpt. 2−48225
  - rel. to resonance excitation diffusion in gas 2−59903
  - rhodamine 6G dye laser, transistory absorption meas. and stimulated emission 2−42044
  - ruby laser, stimulated emission when exposed to ^{60}Co gamma rays 2−69935
  - semiconductor, optical gain process 2−61681
  - semiconductor, Raman emission and i.r. tunable light sources 2−78079
  - semiconductor, stimulated effects in radiative recomb. from electron-hole liq. 2−65289
  - semiconductor lasers, assoc. with band-to-band transition, excitons, review 2−79217
  - singly ionized laser, optimum conditions for emission of 5208.3 Å, 5681.9 Å and 6470.9 Å lines 2−42023
  - stellar atmospheres, laser action 2−48699
  - superradiance from samples small rel. to wavelength, damping 2−66728
  - toluene and polymeric solutions of derivatives of oxazoles and oxadiazoles, stimulated emission 2−59164
  - transient stimulated thermal scattering, frequency response 2−41939
  - v.u.v. and soft X-ray emission from optical transitions of multiionized atoms in high current density discharges 2−41961
  - xanthene dye laser, effect of triplet levels on energy characteristics when pumped with mode-locked laser 2−66759
  - AlGaAsP, solution growth, luminescence, laser operation 2−45747
  - Ar laser, oscill. quenching model, collisional and deexcitation processes 2−59143
  - Ar plasma, laser perturbed, transient light emissions 2−80231
  - Ar^+ ion laser, properties of emission spectrum 2−41989
  - $Ba_2NaNb_5O_{15}$, stimulated parametric fluorescence induced by psec. pump pulses 2−69889
  - $Ba_2ZnGe_2O_7$:Nd^{3+}, by Nd^{3+}, laser action 2−61705
  - BiSb, narrow band emission, nuclear electric quadrupole radiative transitions 2−78118
  - C, atom, pulsed stimulated emission 2−79194
  - CO_2 laser, electrically excited, temp. and press. dependence 2−59151
  - CdS(Se), 2-100K, exciton interactions 2−68677
  - CdS_xSe_{1-x}, graded band gap crysts., tunable laser emission by two photon excitation 2−69948
  - CdSe, spontaneous and stimulated luminescence by high-density excitations in 77 to 300 K range 2−44406
  - $CdSnP_2$:Ag(Cu), band-edge photolum. obs. 2−51365
  - Cl atom, pulsed stimulated emission 2−79194
  - Er^{3+}:BaY_2F_8, laser emission in the visible 2−61704
  - Er^{3+}:$LiYF_4$ pulsed laser operation at 0.85 μm at room temperature 2−42062
  - Er^{3+} glass, cross section, relative gain coeff., absorpt. and fluorescence spectra obs. 2−75323
  - F, atom, pulsed stimulated emission 2−79194
  - GaAs, high purity, optically pumped, magnetic field shift 2−61698
  - GaSe, under two-photon excitation 2−72405
  - H, third harmonic generation coeff. calc. using sturmian function 2−46478
  - H_2, tunable stimulated Raman emission by dye laser 2−77078
  - H_2, Werner band, v.u.v. radiation 2−42013
  - H_2 labile negative ion, transference of attached electron between molecules with same rotational angular momentum 2−74264
  - H_2 laser theory, Lyman and Werner band v.u.v. emission 2−42014
  - H_2 Werner band, v.u.v. radiation 2−42012
  - HCl chem. lasers with $SOCl_2$, SO_2Cl_2, Cl_2CNCl and ClCN, pumping mechanisms 2−79192
  - HF anisotropic ultrahigh gain emission in rotational transitions, optical pumping 2−50047
  - He, 2^1S_0 metastable state, cross section for singly stimulated two-photon emission 2−46489
  - I_2 molecular vapour, optically pumped 2−49369
  - I_2 vapour, optically pumped 2−42022
  - $In_{1-x}Ga_xP$, solution growth, luminescence, laser operation 2−45747
  - InSb, narrow band emission, nuclear electric quadrupole radiative transitions 2−78118
  - N, atom, pulsed stimulated emission 2−79194
  - Nd^{3+}: $CaO.2Al_2O_3$, cross section calcs. 2−54452
  - Nd:$CaNb_2O_6$, CW operation 2−50592
  - Nd^{3+}:$LiGd(MoO_4)$, crystal laser 2−69938
  - Nd^{3+}:$POCl_3$-$ZrCl_4$ laser, line broadening of spectrum of Nd^{3+} ion in solution, stimulated emission cross section 2−42037
  - Nd^{3+}:phosphate glasses, time development of wide-band generation spectra in resonator with diffusion 2−42073
  - Nd laser frequency depend. of spatial synchronism of emission harmonics 2−76491
  - Nd^{3+}; yttrofluorite crystals, time development of wide-band generation spectra in resonator with diffusion 2−42073
  - Ne, excitation of 2p-3s lines in He-Ne mixture 2−42742
  - O_2 doped spherical laser plasmas, high intensity X-ray spectra 2−74378
  - O_2 labile negative ion, transference of attached electron between molecules with same rotational angular momentum 2−74264
  - O_2^- labile ions, vibration and rotation during d.c. discharge 2−46793
  - OH, OD free radicals, laser oscill. in pure rot. transitions 2−56192
  - OH interstellar molecule, pumping by polarized i.r. radiation, maser emission 2−81851
  - OH spectra rel. to laser and maser mechanisms 2−51754
  - Si, Stokes and anti-Stokes emission, by Nd glass laser 2−44391
  - Te in He or Ne buffer gas, cw laser action 2−56098
  - Xe, vacuum u.v., high current relativistic electron beam excitation 2−70584
  - Y_2SiO_5:nd^{3+}, room temp. and 77K 2−78123
  - ZnS:Ag phosphors, characteristics 2−65297
- **Stimulated Raman scattering** *see Lasers; Scattering/light, Raman spectra*
- **Stochastic processes** *see Probability; Random processes; Statistical analysis*
- **Stokes flow** *see Flow; Hydrodynamics*
- **Stokes law, fluids** *see Flow; Viscosity*
- **Stokes law, optical** *see Luminescence*
- **Stokes lines** *see Luminescence; Scattering/light, Raman spectra; Spectra/ molecules*
- **Stopping power** *see Energy loss of particles*
- **Storage devices**
  - amorphous chalcogenide devices, preswitching props., forming and switching 2−77920
  - amorphous material, imaging by structural alteration 2−60568
  - ferrite memory cores, strength rel. to water environment, comments 2−80756
  - ferrite memory cores, strength rel. to water environment 2−77652
  - ferroelectric/photoconductor, switching and remanence 2−47982
  - garnet mag. films, domain interaction with laser beams, domain writing 2−75230
  - heterosystems and nonheterosystems, polarized memory effects 2−61380
  - high density, dynamic holograph system 2−79257
  - image storage targets, F-centre photoelectric materials 2−48023
  - inductive store for 20MJ, construction and operation 2−59021
  - inhibited cathodoluminescence, using elec. irrad. defects 2−57379
  - magnetic implosion system, energy transfer efficiency 2−69853
  - memory device, amorphous film, radiation effects 2−61365
  - memory materials and devices, conference (Princeton, 1 May, 1972) 2−69478
  - metal-ZnTe-metal device, switching and memory props. 2−44142
  - m.i.s.i.m., pre-breakdown region operation, light pulse memory action 2−75137
  - M.N.O.S., max. tunnelling distance, theory 2−47953
  - optical memories, laser beam hole ('bit') creation, physical processes, occurring in Al 2−69989
  - optical memories for computers 2−79219
  - Ovonic Read-Mostly memory array, conducting filaments, scanning elec. microscope obs. 2−61367
  - Permalloy field access bubble domain drive ccts., magnetostatic pot. wells, drive fields, meas. technique 2−73507
  - piezoelectric crystal, charge storage of acoustic r.f. signals 2−61085
  - vidicon electrophotographic spectrum imager for visible spectrum 2−59345
  - As_2Se_2Te film switching and memory device, inc. neutron irrad. effects 2−61373
  - Cr_2O_3 magnetic tape, pulse recording and FM applications, thermoremanent duplication 2−66701
  - GdIG, substituted, compensation temp., applic. to beam- addressable magneto-optic memory 2−72193
  - $Ge_{15}Te_{81}X_4$, amorphous, memory device model 2−61375
  - KD_2PO_4 electro-optic light valve device 2−66847
  - Mn-permalloy, film, exchange anisotropy, ferromag. to antiferromag., thermomag. recording 2−57286
  - SiO_2:Au ion implanted, charge storage rel. to floating gate devices 2−68458
  - SnO_2-CdS-Au, polarized memory device, photovoltage obs. 2−61381
  - SnO_2-SbSI, dielec.-semicond. thin film junc. 2−61366
- **Storage rings**
  - CERN intersecting proton storage rings, description, performance 2−49699
  - CERN intersecting storage rings for protons, vacuum system description 2−69505
  - dose estimates outside shielding, CERN intersecting storage rings, Moyer method 2−59877
  - electron-positron, investigation of $\pi^0\gamma\gamma$, $\eta\gamma\gamma$ and $\eta'\gamma\gamma$ vertices 2−49496
  - electron-positron, investigation of $\pi^0\gamma\gamma$, $\eta\gamma\gamma$ and $\eta'\gamma\gamma$ vertices 2−49497
  - electrons, radiative polarization 2−70338
  - intersecting, at CERN, design of multiwire proportional chamber in split field spectrometer 2−76740
  - intersecting, at CERN, experiments in progress 2−76755
  - intersecting, colliding proton beam experiments at CERN 2−42409
  - intersecting, programs, CERN annual report 2−67109
  - intersecting at CERN, search for quarks 2−66948
  - Orsay, hadronic production by e^+e^- collisions at energy 990 MeV 2−66943
- **Storms** *see Atmosphere/movements; Magnetic storms; Thunderstorms*
- **Strain effects** *see Deformation; Elastic deformation; Plastic deformation*
- **Strain gauges**
  - AIMA-5-1 testing machine, automated strain measurements in creep studies 2−53859
  - balance, oscillating, five component, dynamic characteristics 2−45215
  - balance suspension applics. 2−66407
  - bridge voltages 2−41597
  - capacitive, for elevated temp., patent 2−82139
  - cermets, thin film, strain gauge factor study 2−77710
  - det of crack growth rate in fatigue testing of Al alloys 2−60934
  - Earth strainmeter transducer, interferometric calibration 2−65530
  - extensometry, optical, for elevated temperature fatigue testing, survey 2−56871
  - high temperature extensometering 2−58687
  - holographic interferometric meas. 2−73609
  - laser interferometer for strain amplitude meas. in internal friction exprts. 2−73395
  - laser strainmeter, methane absorption stabilized, design and operation 2−65439
  - load cells, design, manufacture and use 2−41452
  - mechanical, electronic and photoelastic, accuracy in sub-surface obs. 2−74873
  - photoelastic load gauge, incorporating glass element transducers, theory and design 2−53860
  - for photographic films, humidity and temp. dependent internal stress and strain 2−52497
  - piezoresistive transducers using Yb for in-situ field meas. 2−61943
  - quartz, behaviour, when inhomogeneously strained 2−45487
  - rate meter, remote sensing, based on Doppler shift of laser light 2−84148
  - resistance wire strain gauges, method for testing 2−82126
  - resistive, use in magnetostriction obs. in pulsed mag. fields 2−45667

Strain gauges continued
soil stress meas. during transitory loads, errors 2−78277
steel strips, notched, dynamic stress concentration 2−80807
strain distrib., interaction with substratum 2−66527
teaching device 2−48965
tensiometric, elimination of current pickoff noise 2−76436
tensioned-wire Earth strainmeters 2−81603
unit for determining the elastic limit in pure bending under the action of surface and corrosion active media 2−85156
volume change obs. on polymorphic transitions under pressure 2−47678
wide range, for static strain obs. 2−60929
Pt-W, temp. dependence of gauge factor and magnetoresistance 2−68121
p-Si:Be, piezoresist. gauge factor 2−54198
Ta, low density, strain gauge factor study 2−77710

Strain hardening *see Work hardening*

Strange particles
bubble chamber exprt. as teaching demonstration 2−52025
production in π^-p interactions at 1.69 GeV/c 2−46018
$\gamma N \rightarrow \Lambda(\Sigma)K$, photoproduction near the threshold, amplitudes and cross-sections 2−66929
pp interactions 24.9, 28.6 GeV/c, strange particle production, obs. 2−67053
Ξ^+, Ξ-, Ω^+ production in K^+p reactions at 10 GeV/c 2−63668

Strangeness *see Elementary particles; Field theory, quantum*

Stratosphere *see Atmosphere*

Streamers *see Discharges, electric*

Strength *see Electric strength; Mechanical strength*

Stress analysis
see also Bending; Photoelasticity; Strain gauges; Torsion
— 2−66568
— 2−60178
— 2−58884
— 2−59265
acrylonitrile butadiene styrene, Poisson's ratio and temp. dependence of tensile properties 2−53784
alpha-constant stiffness method for analysis of nonlinear problems 2−58850
anisotropic cylindrical shells, pure bending, stretching and twisting 2−45374
anisotropic plasticity, equivalent stress and plastic strain rate 2−41633
anisotropic rectangular plates, double Fourier series soln. of maximum deflection and bending moments 2−69669
anisotropic shells, concentrated forces effects 2−78883
anisotropic tapered elements using displacement models, FORTRAN IV subroutines 2−58849
annular disk, stresses and strains due to radial temperature variation 2−69680
anomalous viscosity of disperse systems in shear stress zones 2−60515
arbitrarily loaded shells of revolution, geometrically nonlinear analysis, computer program 2−66562
axially symmetric shells, numerical soln. of static boundary problem, reduction to Cauchy problems 2−52152
axisymmetric shells, mixed finite element method 2−45368
axisymmetric solids, with asymmetric properties, finite element analysis 2−69638
ball indentation analysis, elastic-plastic soln., finite element method 2−66496
band with circular hole, approx. method of determ. stressed state 2−69640
Bauschinger effect, kinematical strain hardening 2−55453
beam, Euler-Bernoulli, on elastic foundations, dynamical problem, perturbation soln. 2−66498
beam cantilever, Saint-Venant bending, closed form elasticity solns. 2−66505
beams subjected to combined direct load and cylindrically varying curvature 2−41586
bending and vibration of multilayered sandwich plates, analysis by finite strip method 2−58889
bending around elliptic hole in cylindrical shell 2−45365
bending process, 2 dimensional, photo-rheological method 2−82318
biaxial stress fields, transverse sensitivity errors 2−69660
bifurcation buckling as approximations of collapse load for general shells 2−45357
bimetal, individual det. of residual and reactive internal stresses 2−43752
bimetallic orthotropic media, elastic interaction of screw dislocation with interface micro crack 2−76279
bonded materials with perpendicular crack at interface 2−60901
bone model, two phase poroelastic material 2−41571
brittle body with disc-like crack, limiting equil. under force and temp. fields 2−45403
buckling, prebuckling and postbuckling, geometrical nonlinear analysis by finite elements method 2−52149
buckling and post buckling behaviour of shallow spherical and conical sandwich shells 2−45375
buckling stresses of axially compressed cylinders with localized or random axisymmetric imperfections, asymptotic formulae 2−45377
cantilever beams, collapse loads under end shear 2−41568
cantilever plates, numerical methods 2−73362
circular and ring plates, extension deformed, limiting equilibrium 2−63085
circular annulus, depression due to load uniformly distributed 2−52156
circular conical orthotropic shells of linearly variable thickness, strength analysis, elastic equilibrium 2−52157
circular conical orthotropic shells with linearly varying thickness, stress states, elastic equilibrium 2−52155
circular cylinder containing symmetric array of edge cracks, analysis under torsion 2−66538
circular cylindrical shell with circular cutouts 2−78874
circular cylindrical shells, differential equations reduction 2−58848
circular cylindrical shells axially compressed 2−52160
circular disc, Fourier series soln. 2−52135
circular plates loaded beyond yield point 2−58841

Stress analysis continued
circumferential crack extension force, normal anisotropic elastic body 2−41612
circumferential forces and moments in edge loaded conical shell elements 2−45385
clamped plastic circular plates, dynamics 2−52139
complex elastic contact surface integration, finite element analysis 2−73383
complex stress intensity factors at bifurcated cracks in perspex 2−71597
composite, fibre-reinforced, shrinkage stresses- near discontinuity 2−71659
composite, fibre-reinforced, stress boundary value problem for plane strain deform. 2−58868
composite, two dimensional plane stress configuration, matrix stress conc. factor 2−61012
composite beams of arbitrary cross-section, bounds on thermal stresses 2−45430
composite material, layered, continuum model 2−66533
compressed circular plates, load carrying capacity 2−66492
compressible isotropic elastic circular cylinder nearly isochoric finite torsion 2−41569
of compressible viscoelastic solids 2−63086
compression-release, plate impact expts. 2−66508
concrete tunnel surround, method of small perturbations 2−66499
contact problem, axisymmetric, for elastic half-space with cylindrical hole 2−58843
contact stresses at contacts between conical bodies, calc. 2−66532
continuum gas flows, thermostress and concentration stress convection 2−80403
crack energy release rates and stress-intensity factors, by finite-element method 2−66531
crack initiation and propagation analysis using finite element methods 2−52165
crack originating at edge of circular hole, stress intensity factor 2−82336
crack propag. in elastic material strips under plane extension 2−45407
crack stability of adhesive layer 2−55458
crack tip diffraction of tension stress wave and fracture 2−69654
cracked anisotropic finite elements, Lekhnitskii-Savin complex stress function approach 2−76285
cracking stress of glass fibre reinforced inorganic cement, use of fracture mechanics 2−64726
cracks, axial, in pressurized circular cylindrical shell, perturbation solutions of stresses 2−82307
cracks, circumferential and axial, anal. at tip 2−45365
cracks, elastic, parallel, noncoplanar, interaction, narrow spacing case 2−43731
cracks, penny shaped, between two bonded dissimilar materials 2−45390
cracks, photoelastic detn. of mixed mode stress intensity factors 2−69650
cracks, radial, in a circular ring, elastic anal. and comparison to internally pressurized cylinders 2−69647
cracks, radial, in a circular ring, elastic analysis and modified mapping-collocation technique 2−69646
cracks, radial in finite rotating discs, stress intensity factors 2−58844
cracks subjected to tension, torsion, flexure, stress intensity factor evaluation, numerical technique 2−66504
creep buckling analysis incorporating elastic deformation and time-hardening creep 2−58863
crippling and buckling of corrugated ring stiffened cylinders 2−58852
critical buckling load and deflection of beams, det. by three unknowns method 2−41580
critical points and stability boundary determination for nonlinear structural systems undergoing loading 2−52151
crystals, inelastic strain gradients rel. to equivalent body forces 2−73382
curved cylindrical shell finite element 2−41585
curved strip under pure bending, optimum thickness variation 2−58840
cylinder, glass and plastic, contact stresses, lubrication, stress distrib. 2−47559
cylinder, long circular and of isotropic material, thermal stresses when curved surface exposed to Suns rays 2−52199
cylindrical configurations, elastic analysis with stress singularities 2−66515
cylindrical shell, optimization of torsional stiffness 2−73352
cylindrical shell finite element based on independent strain functions 2−49067
cylindrical shell stressed by internal pressure optimal thickness 2−82324
cylindrical shell supported on elastic base, stability under axial compression 2−41589
cylindrical shell with reinforced openings, distribution of stress 2−63069
cylindrical shells, dynamic responses to concentrated radial loads 2−55457
cylindrical shells with arbitrary closed periphery 2−63072
cylindrical shells with circular cutout or crack, applic. of mixed finite element methods 2−73355
cylindrical stress waves generated by exploding wires 2−41600
cylindrical tube under pressure, elastic-plastic and thick-walled, effect of non-homogeneity on yield pressure 2−49064
deformation analysis, finite element method 2−45429
deformation and restraint stress of steel beam column connection due to welding 2−58855
dilational strain and strain probability distribution in dislocated materials 2−60794
disc, with couple stresses, stress functions 2−41618
disc shaped as circular ring 2−63064
disc shaped as plane with circular hole, Green's function methods 2−41579
disc shaped at semi-infinite plate with half-elliptic edge section, stretching 2−76271
disc with diametral crack, stress state 2−45404
disc with elliptic aperture, versatile stretching 2−76270

Stress analysis continued
discs, blocks, point loaded, plain stress, plane strain elasticity, numerical approx. method 2—66526
displacement and strain fields of nonuniform dislocations 2—57727
dome fastened rigidly on edge, stability under uniform external pressure 2—55461
double diffraction parameters, determination by photoelasticity method 2—82331
doubly folded plate, elastic model 2—41578
doubly-folded plate, fractured 2—41610
dynamic, photoelastic studies 2—41613
dynamic biaxial loading in plate testing 2—64750
dynamic forms of loss of stability in intense loading over finite time interval 2—76325
dynamic loading of fluid filled spherical shell 2—73363
dynamic response of pressurized cylindrical shells subjected to moving loads 2—45382
Earth, multilayered sphere model, static deformation by internal sources 2—51492
Earth-model with a rigid core, deformation and stresses 2—51521
earthquakes, stress distribution beneath island arcs 2—81602
eigenvalues of boundary-value problems for regions of complex form 2—41591
elastic and plastic strains, using symmetrical telecentric lens 2—45784
elastic bar, optimal nonhomogeneity, optimal problem of torsion 2—45353
elastic core, parametrical obs. of notch stresses 2—41572
elastic Cosserat layer, indentations by moving punches 2—58875
elastic cylinder, Somigliani type dislocations 2—52159
elastic equilibrium of circular conical orthotropic shells of linearly variable thickness 2—49061
elastic half space, due to surface loads progressing at speed of Rayleigh wave 2—66509
elastic half-space, plate contact problem 2—78884
elastic helicoidal shells, spirally sinusoidal stress distribution 2—52182
elastic layer weakened by circular slot, stress conc. 2—45406
elastic plate structures, finite element method, ZPLATE computer program 2—73384
elastic plate with part-through surface crack, tensile stretching and bending 2—45378
elastic plates, accurate practical theories 2—52176
elastic rotating discs, optimum design, using dynamic programming 2—73373
elastic spherical shells, numerical soln. of deformation problems 2—58861
elastic stability of hyperboloidal shell of revolution 2—66550
elastic-Earth models, Galerkin representation of plain strain with hydrostatic initial stress field 2—84718
elastic-plastic systems, shakedown theorem under dynamic loadings 2—66511
elastic/plastic compressed plate, buckling stress, yield surface 2—76301
elastically supported circular plates, dynamic response to general surface load 2—58838
elasto-plastic, numerical iterative procedure applic. 2—73388
elastoplastic material, eqn. of state 2—82300
elastoplastic medium, numerical solution of axially symm. problem of pressing a stamp 2—49055
elastoplastic thick-walled cylinder 2—55469
electromagnets, design principles relating to strength and structure 2—59072
elliptic notch with collinear cracks at tip, stress intensity factor during longit. shear 2—73392
elliptic opening in elastoplastic body, stress conc. 2—52154
elliptical discontinuity in elastic medium, dynamic stresses 2—45485
environmental dependent viscoelastic materials, constitutive relation for linear aging 2—41634
equipment for stress relaxation tests at nonstationary temps. 2—68119
fatigue failure obs. of materials under broad band random vibrations 2—77707
fatigue-crack initiation from flaws using fracture mechanics theory 2—69649
femur, determ. of individual load and diagram of forces at proximal part 2—69218
fibre reinforced plates, optimum design 2—55456
films, obs. using quartz resonators 2—50786
finite crack opened out by tractions 2—45366
finite deformation of rigid thick walled spherical shells under hydrostatic pressure 2—78897
finite element, teaching examples for one-dimensional beam 2—52029
finite element analysis of thin elastic shells of revolution 2—58837
finite element method 2—69662
finite element model for shells by discrete Kirchhoff hypothesis 2—73367
Flamant solution for loading on edge of semi- infinite half plane 2—45389
flat laminated plate, residual stress determ. 2—45372
flat plates, sectional stress distribution due to surface couples 2—52158
flat specimen with circular hole, plastic deformation of polycrystalline metals 2—45420
flat square plate, under uniformly distributed normal press. 2—69675
force balance in plasma sheet on closed field lines of magnetosphere 2—62322
fracture, crack tip singularity calc., geometrical-optic method of caustics 2—52161
free shape problem for closed ring under two opposing point loads 2—45354
frictionless elastic contact, minimum principle, with applic. to non-Hertzian half-space contact problems 2—45408
fully stressed beams, effect of geometrical nonlinearity on minimum mass design 2—66524
gelatin, stress frozen, photoelastic analysis for gravity stresses 2—41628

Stress analysis continued
girders, thin walled and various cross-sections, stability to central compression 2—63071
glass reinforced plastics, stress distribs., debonding, stress concentrators effects, microdamage effects 2—64724
Griffith crack, li.f. diffr. of elastic waves 2—49068
hexagonal cryst., anisotropic elasticity of prismatic dislocation loop 2—47408
hexagonal grid work of straight elastic rods, soln., digital computer application 2—45371
hollow nonhomogeneous cone, axial impact 2—45388
hollow notched bars and hydrogen embrittled specimens, stress-intensity factors 2—60857
hollow sphere subjected to dynamic pressure on inner or outer surface 2—73380
holographic interferometry application to anisotropic composite plates 2—41598
holographic strain anal. using spline functions 2—82142
holographic strain obs. on tensile specimen 2—82144
homogeneous prestressed cylinders, stability under small twist 2—52138
hull structure design, finite element method 2—73371
human intervertebral disk in pre compression, stress distribution 2—55217
hyperbolic paraboloid shells, stiffness matrix, using lumped parameter elements 2—45367
idealized elastoplastic column, effect of external load nonconservativeness of stability 2—82330
imperfection sensitivity of wide integrally stiffened panel under compression 2—76305
impulsive loading analysis of rigid plastic structures, quadratic programming approach 2—52150
inertialess finite rigid cylinder clamped in circular borehole 2—69702
infinite disc with circular hole, stress conc. coeffs. 2—45370
infinite elastic plate with circular hole under normal load on circumference 2—76277
infinite elastic thick plate, load symmetrical to axis of revolution and middle plane 2—78887
infinite elastic thick plate, subjected to axisymmetrical loads 2—41582
infinite plate with crack along circular arc, mixed boundary value problem of elasticity 2—52172
inhomogeneous elastic media, method of small perturbations 2—66499
initial postbuckling behaviour of optimally designed columns and plates 2—76287
intensity factors for cracked bodies from Buekner's formulation 2—84015
isotropic layer with shear stresses in contact region, punch problem 2—76319
isotropic plastic solids, geometric instabilities under uniaxial compression 2—66513
kinetic forming of billets 2—52141
laminated arch under mech. and thermal action 2—76324
laminated fibre-reinforced plates, plane strain bending 2—66543
large deflection of plates 2—41577
laser generated stress waves in circular elastic ring 2—45436
l.f. biaxial loads effects on stress concentration factors in plates 2—41599
lifetime predictions in turbine blades, stress calc. 2—56890
limitations on hexahedron finite elements with derivative degrees of freedom 2—73369
linear and nonlinear theories of elastic slender curved rods 2—76289
load diffusion from bar embedded in semi infinite elastic medium 2—69653
Luders front geometry, application of continuum dislocation theory 2—52144
magnetic coils, high field, uniform current density, stress calcs., computer program 2—73519
marble blocks, method of small perturbations 2—66499
matrix displacement analysis of shells and plates including transverse shear effects 2—52137
matrix method of vibrational analysis of framed structures 2—76355
maximum stress in twisted angle or channel 2—73365
membrane, thick, behaviour under static loading 2—45441
membrane stress, analysis of open noncircular cylindrical shells 2—58857
metal, f.c.c. and h.c.p., stress relax. analysis 2—71558
MG cylinder, stress and deflection meas. 2—43811
micromechanics, applications 2—58877
mild steel and plexiglass, detonative loading, waves and breakage patterns 2—84048
minimum weight beams and frames under random loading 2—58853
model preparation for thermal stresses investigation by restrained shrinkage method 2—53849
multilayer elastic media, contact problem 2—78889
multilayer media, impact and contact stress analysis in classical electricity theory, computer calcs. 2—82304
multilayered systems 2—73374
necking in circular cylindrical bar, numerical study 2—52148
non-circular stiffened cylindrical shells, dynamics 2—69657
non-selfadjoint mechanical systems, stability theory 2—73353
non-viscous stress, rate-depend., isotropic nonpolar contribs. 2—49071
nonlinear membrane shell, applic. to noncircular cylinders 2—45364
nonlinear membranes subjected to internal pressure 2—76312
nonlinear structures, model technique for meas. of stress resultants and displacements 2—58859
nonlinear theory of arches with transverse shear deformation and rotary inertia 2—73372
nonlinear viscoelastic rubber like material, creep and cylinder problem 2—52192
nonsymmetrically loaded spherical shells, limit analysis 2—66512
nonuniform layer on elastic half-space, stress state 2—41621
notch root radius effects on fatigue crack propagation and initiation 2—69648
nozzle to cylinder connections for small diameter ratios 2—55459
nuclear reactor building aseismic design 2—59824

Stress analysis continued
nuclear reactor piping system, obs. of dynamic response to multi-inputs 2−70540
numerically integrated stiffness matrices computation 2−73368
oblique holes in thick plates and cylinders 2−69676
orthotropic bodies, three-dimensional, stability of equilibrium with small deformations 2−41619
orthotropic photoelastic analysis of residual stresses in filament wound composite material rings 2−41601
panel arrays, vibr. characts. 2−69715
parametric stability of thin-walled beams of open section under axial load 2−45380
peeble bed reactor, shell thermal stress distrib. in loose-kernel spherical fuel element 2−49890
penny-shaped crack on interface 2−66542
perfectly locking bodies, limit displacements and solids parameters optimization 2−45393
perforated plates, complex variable method with point matching 2−49065
Perspex plates, array of collinear equal cracks, effects of loading 2−41583
photo-rheological method, similarity conditions 2−76298
photoelastic analysis using polarization holography 2−82148
photoelasticity appl. 2−58876
pipe bends, multi-mitred, subject to internal pressure and external loading, stress and flexibility factors 2−66530
plane strain consolidation in saturated clays, finite element method 2−76314
plane strain of plastic material, effects of anisotropy and hydrostatic stress 2−69656
plane stress shakedown analysis by finite elements 2−73366
plane stress structure design, inverse method in two- dimensional elasticity 2−76327
plastic anisotropy in linear transverse strains, calc. 2−64712
plastic flow with Coulomb friction, equilib. method and upper bound theorem in plane problems 2−45419
plastic strains associated with torsion of noncircular bars 2−45423
plastic structures design in plane stress, finite element approach to optimal design 2−63082
plastics, dimensioning of cyclically and multiaxially stressed structures 2−64711
plate, elastic, infinite mixed boundary value problem 2−41617
plate, isotropic, twisted by rigid circular stamp, mixed problem 2−45410
plate bending, convergence of finite element solutions represented by non-conforming basis 2−69658
plate dynamic response analysis, time dependent boundary conditions 2−58869
plate on elastic foundation with vertical periodic load, plate-foundation interaction 2−76309
plate with circular holes, dynamic stresses 2−45484
plates, boundary problems in Vekua theory including second order moments 2−41595
plates, circular, flat, creep rel. to geometry changes during deform. 2−66555
plates, circular with limited thickness, minimum weight design 2−76311
plates, elastic-plastic and eccentrically stiffened, finite element analyses 2−66561
plates, limit analysis, simple loading problem involving complex exact solution 2−55460
plates and shells, law of thickness variation for stationary value of stiffness functional 2−41596
plates and shells, static stability 2−52153
plates of arbitrary planform, bending, analysis using triangular, rectangular finite elements based on hybrid formulation 2−66495
plates on a two parameter foundation model, finite element analysis 2−73359
plates with curvilinear openings, concentration of stresses, Reissner's theory analysis 2−63070
plexiglass plate cracks, interferometric determination of opening and edge sliding mode stress-intensity factors 2−47544
polycrystals, Hill's stress rate 2−71564
polyethylene, molten, flow through parallel slit, flow birefringence obs. 2−71142
polyethylene melts, time dependent stress, review of viscoelastic theory 2−64708
polymers, dilute solutions, flowing in curved pipe, det. of normal stress coefficients 2−60385
polymers, relaxation stresses, rigid dynamometer for obs. 2−43757
polypropylene sandwich mouldings, deflection during bending, stress function solns. 2−43663
polystyrene melts, time dependent stress, review of viscoelastic theory 2−64708
polyurethane block polymers, meas. of stress relaxation 2−74850
post yield fracture mechanics, crack model for high and low strength materials 2−64727
precise theory of sandwich plates and shells 2−78890
pressure distribution in powders, theory 2−84129
pressure distribution in powders filled in a conical vessel, theory 2−84130
pressure vessels of pressurized water reactors at start up 2−59829
printer type piece deformation due to impact of print hammer, holographic interferometry applications 2−69666
prismatic plate assemblies, computation of natural frequencies and initial buckling stresses 2−41588
PVC, stress cracking and crazing in hexane and hexane/toluene environments 2−50779
radial stress release phenomena in plate impact expts. 2−66508
random eigenvalue problems in structural analysis, computerized Monte Carlo simulation 2−45356
reactor fuel element, cylindrical oxide rod, rel. to unsteady state fuel restructuring in fast reactors 2−49887
recovery-creep model with effective and internal stress evaluation 2−68087
rectangular plate, orthotropic, centrally placed crack, stress intensity factors 2−66525
rectangular plate problems, finite element method, general linear geometric matrix 2−45360

Stress analysis continued
rectangular plates with unsupported edges, large deflection 2−69661
reduced integration and isoparametric elements 2−73370
reinforced axially symmetric shells; momentless stressed state 2−66487
response of infinite strip to fluctuating pressure fields 2−41565
review of various methods and experimental techniques 2−66503
rigid body motions and strain displacement eqns. of curved shell finite elements 2−73364
rigid displacement condition for finite element analysis of structures with little rigidity 2−58851
rigid footing bonded to elastic half space, dynamic response 2−66518
rigid plastic material with entrapped viscous lubricant on platen face, plane strain compression 2−55467
ring inclusion, effect of couple stresses on stress concentration 2−69637
ring reinforced cylindrical shell, dynamic response to axisymmetric step pulse 2−66517
rock, brittle, crack propagation 2−75457
rocks, effect of triaxial stress system on fracture and flow 2−72679
rotating cylinder, effects of non-homogeneity 2−73377
rotating disc with hyperbolic thickness profile, radial-displacement soln. 2−69659
rubber blocks, bonded, compressed, elastic stress strain eqns. dynamic relax. solns., Poissons ratio effects 2−66528
rubber cylinder, swelling under torsion 2−60875
rubber cylinder, swelling under torsion 2−60876
rubber fluid storage bags, mech. behaviour, contact problem 2−66497
running crack arrest in elastic plates for transverse loading 2−69645
sandy subsoil, model loading tests 2−44605
second order stress in dense gas 2−71081
semiinfinite body containing spherical cavity, subjected to uniform pressure 2−41581
shaft torsion problem, Moire fringe method and membrane analogy 2−49056
shallow notched bar, three point loading, slip line field relations 2−41632
shear stress distribs. in transpired turbulent boundary layer 2−46688
shell, closed, cylindrical, with crack, determ. of stressed state 2−69641
shell, shallow and strongly buckling, crit. loads for loss of stability, asymptotic method 2−82323
shell, thin, with inner constraints, conformation field represent. 2−78885
shells of constant strength 2−69636
shells of resolution, simplification of relationships for total energy 2−41590
shells of revolution, stability and post-buckling equilibrium under axial compression 2−45392
shells of slowly varying curvatures, equations 2−52162
single underground opening in layered medium under gravity loading 2−75459
single underground opening near traction free surface 2−75458
solid cylinder compressed between rough rigid stamps 2−52143
solid sphere of isotropic material, thermal stresses due to const. temp. and normal pressure over band along equator 2−52198
spherical shells, stress fields, plastic limit 2−58870
spherical shells supported by three oblique planed edge arches 2−41573
spheroidal inclusion, (measuring slab) embedded in a thermoelastic medium, state of stress and strain 2−82333
spot welded joints between Al alloy sheets, using photoelastic coating technique 2−68143
square plate with hole of arbitrary shape, stress concentration 2−76313
steel, cracking, stresses at start and finish 2−56832
steel press. vessel, biaxially stressed, crack tolerating factor 2−50835
strain, holographic using millisecond pulsed laser 2−79277
strain, use of gratings, review 2−66502
strain gauge, strain distrib., interaction with substratum 2−66527
strain hardening material, temp. stress distribution due to uniform heat source 2−45384
strength of anisotropic materials under combined loading 2−45358
stress intensity factors determ. by numerical methods 2−66506
stretched circular plates, load carrying capacity 2−66492
structural elements of complex shape, limit analysis and plastic design 2−78888
supports of cylindrical shell produced by lateral pressure pulse 2−45373
surface cracks, infinite solid, stress intensity factors 2−45379
surfaced components after high temperature tempering 2−71607
suspension of drops in elec. field, stress system 2−83819
switching stresses in bimetal disks, used for thermostatic control 2−63067
symmetric structural systems, stability boundary 2−45362
systems with coincident buckling loads influence of imperfections 2−55452
tensile strip with large circular hole, stress conc. factors 2−58858
test specimens, variable modulus of elasticity 2−78755
thermal, examination by numerical methods 2−58880
thermal stresses in rods, due to distributed time dependent heat sources 2−45427
thermal stresses in thin circular disk of orthotropic material due to instantaneous point heat source 2−41637
thick sandwich conical shell, exact analysis by forward integration 2−66514
thick walled cylinder, plain strain fracture toughness test method 2−60937
thick-walled vessels, finite element analysis of threaded end closures 2−69496
thin circular plate of variable thickness, buckling under uniform compression 2−63066
thin conical shells, response to dynamically applied axial force 2−45363
thin plates, annular segment finite element 2−76315
thin shells, asymptotic solutions for stress concentrations 2−76294

Stress analysis continued
- thin shells, comparison of yield surfaces 2−69652
- three dimensional, numerical methods applics., review 2−41607
- three-dimensional body, static and dynamic analysis of stress and strain tensors 2−76336
- time-variable deformation of viscoelastic materials of rate type 2−66563
- Timoshenko type shells, deformation due to transverse displacements 2−66500
- transient, for torque applied to surface of penny shaped crack in infinite elastic body 2−66510
- transversely isotropic semi-infinite medium, thermal indentation 2−58879
- tube, thick walled with step change in thermal expansion 2−52201
- tubular manufacture stiffened by convolutions 2−83066
- turbulent boundary layer, incompressible, shear stress distrib., in air flow 2−60333
- twist disclination loop elastic behaviour near free surface 2−50664
- twisting of non-homogeneous sphere, using surface couple 2−73376
- two dimensional plane-wave propagation, calc. using dynamic scattered light photoelasticity 2−66519
- two-dimensional solids, determ. of elastic stresses at notches and corners by integral equations 2−82306
- U-notched plates, symmetrical, comparison of formulae and experimental stress-concentration factors 2−66529
- uniaxial stress apparatus, design and construction 2−47571
- unsymmetrical cross-ply rectangular plates 2−66522
- variable rectangular profile shell, influence of end plate and bulkhead on torsion and bending 2−78876
- wall shear, embedded hot wire method of obs. 2−45369
- wave propagation in cylindrical shells, perturbation analysis 2−66607
- waves, finite amplitude in rods, subject to impact loading, Bell's parabolic law study 2−58901
- welded joints, finite element method of strength assessment 2−63065
- Al, super-pure, hydrostatically extruded, substruct. and flow stress detn. 2−74876
- Al alloy, NS.5, effect of preferred orientation on X-ray stress meas. 2−71643
- B-epoxy laminated composite plates, holographic technique 2−78895
- Be, temp. depend. of friction stress for basal dislocations, 300-500K 2−64753
- Cu, single cryst., depend. of deform.-resist. on rate and temp. of prev. loading 2−84010
- Cu surface stress, strain produced by He bubbles elec. resistivity obs. 2−43678
- Ge, film, deposition and annealing parameters, influence on strain sensitivity 2−77709
- Mo-Cr-alloyed or unalloyed case hardened steel, residual stresses in carbonized layers for different thermal treatments 2−56931
- Mo single crystals, stress anal. for high temp.-creep and slip 2−84012
- Ni alloy, relative abilities of time-temperature parameters to correlate and extrapolate stress- rupture data 2−47608
- Ti, variation of r-value with increasing strain 2−41584
- WC-Co hard metal, X-ray stress meas. at carbide phase 2−74910
- Zn-Al alloys, strain-rate depend. of deform. mechanism and texture form. 2−84011

Stress effects
- − 2−57151
- adiabatic plastic bands, formation in thin tube submitted to dynamic torsion 2−69679
- alloy, light, s.c.c., microstruct. effects 2−56826
- alloy 800, low-cycle fatigue and stress relaxation at elevated temps. 2−60947
- austenitic stainless steels, susceptibility to stress corrosion cracking, evaluation by chemical, electrochemical methods 2−68104
- β-brass, stress corrosion cracking obs. by optical microscopy 2−84132
- α-brass, stress corrosion sensitivity in $FeCl_3$ and $Fe_2(SO_4)_3$ solns. 2−64733
- α-brass, tarnish films and stress corrosion cracking, theory 2−64734
- brittle materials, stress corrosion failure under dynamic loading conditions 2−50771
- California, southern, strain obs. 2−78288
- Coconino sandstone, fracture under confining pressure, effects of pore-fluid chemistry, temperature 2−68858
- corrosion cracking, catalytic dissociation as primary process in hydrogen embrittlement and s.c.c. 2−84020
- corrosion cracking, cathodic protection, hydrogen permeation 2−78194
- crack at elastic half-space rigid foundation interface, effect of shear, stress field 2−73387
- crystals, dislocation accumulation in stress fields, initial stage of plastic deformation 2−80696
- cubic cryst., linear dichroism due to stress induced mixing of electronic states of anisotropic centres 2−84462
- cylindrical shell stressed by internal pressure optimal thickness 2−82324
- cylindrical stress waves generated by exploding wires 2−41600
- delayed cracks in steel welding 2−77711
- dislocation first contribution to the flow stress 2−83974
- domain boundary displacement under deformation, effect of dislocations 2−72143
- Earth's interior, stress concentration and rupture propagation for semi-infinite longitudinal-shear cracks 2−61939
- elastic wave propagation in circular cylinder when torsional shear stress is applied to end surface 2−52220
- elastic-Earth models, Galerkin representation of plain strain with hydrostatic initial stress field 2−84718
- fatigue under combined stresses, review 2−47539
- ferrite, ferromag. reson. linewidth 2−68720
- ferromagnetic materials, stress depend. damping at stresses to fatigue limit 2−74826
- flow induced by thermal stress in rarefied gas 2−53277
- glass, acoustic birefringence under strong uniaxial compression 2−54028

Stress effects continued
- glass reinforced plastics, debonding and cracking under tensile and fatigue loading 2−64725
- glass reinforced plastics, stress distribs., debonding, stress concentrators effects, microdamage effects 2−64724
- hydrostatic, on void growth during irradiation, appl. to reactor core 2−76940
- ice, recrystallization under mechanical strain 2−74691
- in interface, dislocations, between two isotropic phases, stress fields and strain energies 2−80668
- laminated composite, thermally induced stress waves 2−47665
- laser surface damage and electric surface stress 2−59191
- liquid crystal, cholesteric mixtures, shear-induced struct. changes, refl. spectra obs. 2−64438
- Lower Devonian sandstone, effect on strength, deformation and fracture props. 2−54735
- martensitic transformation, stress-induced, and shape- memory effect 2−68185
- metal, on wear 2−53851
- metal-environment systems, stress-corrosion cracking, study using transient straining electrodes 2−68103
- metal-H system, applied stress field effects, thermodynamic analysis 2−71640
- metals, review of dislocation substructure strengthening and mechanical-thermal treatment 2−84099
- metals, strengthening, under variable stress 2−53812
- metals and alloys, stress corrosion cracking, significance of protection potential 2−68787
- mountain snow cover, strains and strain rates 2−75449
- moving loads in initially stressed conducting medium 2−41622
- necking in circular cylindrical bar, numerical study 2−52148
- Nimonic 90, tensile creep under transient stresses, elevated temp. 2−71575
- nondestructive crack detection method using liquid crysts. 2−43760
- nylon 66, monofilament, macroscopic failure and molecular bond rupture 2−60858
- nylon 6 fibres, bond rupture, reaction rate model of fracture 2−74854
- Permalloy thin wires, domain wall behaviour, Bitter pattern obs. 2−61535
- plastic solids, stress corrosion cracking, role of H environment 2−77654
- polyethylene films, nonlinear viscoelastic behaviour 2−83375
- polymeric glass, environmental crazing mechanics and mechanism 2−64735
- polyolefins, variation in sound velocity rel. to deformation 2−80750
- polystyrene, crazing in sample containing two rubber balls, model for ABS plastics 2−60909
- PVA, uniaxially stretched film, mechanical anisotropy 2−83365
- PVC, stress cracking and crazing in hexane and hexane/toluene environments 2−50779
- radiation-induced void growth 2−53704
- ratcheting under cyclic axial strain with torsional stress 2−56876
- relaxation behaviour for plastic deformation during supercond. transition 2−71843
- resistance to fracture of materials, particularly metal alloys, physical and technological significance 2−71580
- rocks, effect of stress gradient on brittle fracture initiation 2−72667
- rocks, statistical theory of polyaxial compressive strength 2−72670
- rubber, amorphous sodium-butadiene and butadiene-nitrile 2−60873
- rubber, relationships between viscosity meas. at variable rates of shear and processing behaviour 2−53788
- sandy soil, circular edge dislocation loop 2−44591
- semiconductors, cubic, stress dependence of the Raman frequencies and elastic constants 2−84497
- snow on mountain, displacement, strain and glide 2−75450
- Solenhofen limestone, creep testing at constant stress 2−62008
- spherical shell compressed between rigid plates, axisymmetric post-buckling and nonsymmetric buckling 2−45376
- stainless steel, type AISI 304, accelerated intergranular stress corrosion cracking tests using potentiostatic polarization 2−68105
- steel, 11% Cr, tensile creep under transient stresses, elevated temp. 2−71575
- steel, 1%C, fatigue crack propagation, stress intensity effect 2−71645
- steel, annealed low carbon, dislocation model for delayed yielding time 2−80813
- steel, annealed mild, effect of upper yield stress on bending and torsion 2−43685
- steel, carbon strain energy during rotatory bending fatigue, effect of pearlite patches 2−84125
- steel, cracking, stresses at start and finish 2−56832
- steel, inoxidizable, passivation film study rel. to stress corrosion cracking 2−54547
- steel, mild, thermal activation parameters during non-uniform and uniform deformation 2−80814
- steel, sintered, model to explain behaviour of elastic moduli 2−84128
- steel, stainless, 19Cr-9Ni, effects of alloying elements on stress corrosion cracking 2−77656
- steel, stainless, low-cycle fatigue and stress relaxation at elevated temps. 2−60947
- steel in caustic environment, corrosion cracking 2−68789
- strain energy function rel. to boundary value problems 2−73381
- strainrange partitioning approach for creep fatigue analysis 2−56889
- stress corrosion cracking, capillary model, test using pressure effects 2−74857
- styrene-butadiene-styrene block copolymer cast from organic solvents, time-temperature superposition 2−74829
- surface layer on metal, semiconducting parameters, effect of substrate stress state 2−71966
- Tennessee Sandstone, exptl. investigation of stick-slip 2−62089
- thermal ratcheting, review 2−56875
- thermoplastics, amorphous, hydrogen bonding influence on stress crazing and cracking 2−60908
- threshold switch devices, strain sensitive props. 2−61364
- tubes, under uniform pressure and steady temp., thermo-elastic-plastic transition 2−49083
- ultrasonic attenuation measurements, evidence against multiple energy gaps 2−75070

Stress effects continued
welded pressure vessels, loading capacity, stressed at high temps. 2−64771
Zircaloy-2, stress orientation and circumferential ductility, thermal cycling effect 2−53914
Ag-Cd(Zn) alloys, stress corrosion sensitivity in $FeCl_3$ and $Fe_2(SO_4)_3$ solns. 2−64733
Al-Zn-Mg alloy, stress corrosion crack paths 2−43732
Al, dislocation multiplication mechanism 2−80679
Al, on resist./strain relation 2−64700
Al, rel. to Fermi surface 2−68286
Al alloy, multiphase, creep tested under stress, study of microstructure 2−80820
Al alloy hand forgings, fracture toughness and stress corrosion cracking 2−60906
Al alloy hand forgings, fracture toughness and stress corrosion cracking 2−60905
Al alloys, acoustic emission due to low level periodic stress 2−51012
Al alloys, constructional materials, life, effect of low level of service load range 2−43750
Al alloys, fatigue damage at high temps. 2−80808
Al_2O_3, high temp. strength improvement by surface prestressing 2−50870
Al_2O_3, polycrystalline, stress corrosion in moist air and toluene, time-dependent failure characteristics 2−84039
$BaTiO_3$, light emission due to uniaxial stress pulses 2−72440
C fibre-epoxy composite, acoustic emission during continuous tensile cycling 2−56986
Cu, cold worked at 200-300°C, creep and recovery 2−84163
Cu, contact potential, compressionally induced change 2−75187
Cu_6Sn_5 fibres, brittle fracture surface morphologies 2−80744
Fe-Cr-Al alloy, potentiodynamic curves as function of tensile stress 2−44488
Fe-Mo solid solution, creep type, variation with applied stress 2−43703
Fe-Ni alloy film, crit. fields, effect of elastic stresses 2−51264
Fe-Ni and Fe-Ni-C martensitic alloys, delayed fracture formation during cathodic charging under static stress 2−64731
Fe alloy, rel. to martensitic transform. 2−50943
GaP:N(Bi), exciton binding to impurities, uniaxial stress effects 2−75108
Ge, hopping cond. rel. to temp., doping, uniaxial compression 2−65013
n-InSb, frequency of magnetophonon oscillations 2−47571
KD_2PO_4, u.s. stress wave interaction with domain walls 2−71740
KH_2PO_4, dense domain structure at ferroelectric transition, stress-induced birefringence 2−75260
$KNbO_3$, ferroelectric single crystals, deformation and stress relaxation behaviour 2−80743
LiF bicrystal, interaction of stress waves with a boundary 2−84061
Mg, plane strain extrusions, texture control and yield anisotropy 2−80848
MgO refractories, effect of stress on grain growth 2−74915
Mo, neutron irrad., stress induced ordering of stage I defects 2−64654
NH_4Br, l.f. soft vibrational modes 2−71696
$NaPO_4$ glasses, stress relaxation mechanism 2−77636
Nb, on oxidation process, oxide wedge formation 2−43736
Nb, stressed, dislocation struct. form. mechanism 2−71494
SbSI, ferroelectric, one dimensional mech. stress effect on phase transition, permittivity obs. 2−75155
Si-Ge p^+-n alloyed heterojunction, V-I characts., uniaxial stress effect 2−81120
Si, dislocation etch pits shapes rel. to mech. stress 2−80553
n-Si, stress induced electric fields 2−44127
Si, velocities of screw and 60° dislocations 2−80678
SiO_2, acoustic birefringence under strong uniaxial compression 2−54028
$SrTiO_3$, l.f. soft vibrational modes 2−71696
$SrTiO_3$, uniaxially stressed, domain struct. at 2K 2−61433
Ta, slip, orientation depend., deform. mechanism, 4.2-450K 2−50679
Ti-8% Al-1% Mo-1%V, accelerated stress-corrosion cracking in presence of hydrogen recombination poison 2−68107
α-Ti, torsional and longitudinal plastic waves 2−77638
U-Mo alloy, stress corrosion cracking in humid aid, C content effects 2−53839
U-Nb alloy, stress corrosion cracking, metallic protective coating 2−53911
V internal stress, during stress relax., rel. to dislocation generation and immobilization 2−43680
V_3Si change in soft mode sound velocity under shear strain 2−74980
W, stress induced growth irradiated at low temp. 2−60781
YIG, effect of tensile stresses generated by polishing on mag. anisotropy 2−81266
ZnS:Mn^{2+}, ^4E level, uniaxial stress effects, absorpt. study 2−84506
Zr alloy, stress corrosion cracking in Hg, fracture surface study 2−43737
Zr alloys, high-strength, characteriz. for press. tubes 2−53921
Zr alloys, strain-induced phase transforms., microstruct. exam. 2−54000

Stress measurement *see Strain gauges*

Stress/strain relations
see also Elastic constants
alloy, two-phase, effects of coherency strain fields on dislocations struct. 2−56702
α-brass, Portevin-le Chatelier effect and vacancies production during cyclic straining 2−74828
α-brass, Portevin-le Chatelier effect and vacancies production during cyclic stressing 2−74827
ceramic composites with alumina matrix, impact strength and dynamic loading 2−80758
elastic anisotropic bodies in cylindrical and polar co-ordinates 2−52171
elastoplastic wave propag. in bar for nonlinear stress/strain case 2−82345
fatigue stability tests, sensitivity estimates for asymmetrical loading cycles from strain diagrams 2−56840
ferrous alloys, nonlinearities at high elastic strains rel. to strength-differential effect 2−74853

Stress/strain relations continued
fibre composite, containing discont. fibres, theory for steady state creep 2−47510
filamentary specimens, tensile testing machine 2−43759
granite, low porosity, biaxial compression test implications 2−57765
graph analytic method of evaluation of relationship with creep 2−64743
high pressure effects on single crysts. 2−68080
high-strain-rate investigations, review 2−47489
2-hydroxyethyl methacrylate networks in dry and swollen states, effect of crosslinking density and dilution 2−56782
linear shell theory, pointwise displacement errors due to errors in stress/strain relations 2−82335
liquid in container, subject to periodic heating, temp. fluctuations 2−71181
magnesia, polycrystalline, deformation in compression, 1100-1750°C 2−68167
measurement using acoustic shock pulses, results for Al 2−43777
Nimonic 90, derived from creep equation 2−71575
nonlinear viscoelastic solid, single integral constitutive law 2−76332
norite, post-failure stress strain path dependence 2−62009
organic glasses, influence of annealing on thermal behaviour in glass transition region 2−71744
oxide fuel struct. evolution, modelling using BEHAVE-2 code 2−52858
plastic torsional straining of hollow cylinder, anisotropy theory 2−47497
polyethylene filled with randomly oriented glass fibres 2−77690
polyimide, aromatic, secondary dynamic dispersions 2−83366
polymer cryst., morphology influence 2−60860
polymer film, rel. to electromechanical model for capacitance effects 2−57228
polymeric rod, influence of cold working on tensile true stress-true strain curve 2−80810
polymers, crystalline undergoing plastic deformation, generalized equation formulation 2−56783
polymers, real stress diagram classification 2−56780
polystyrene, crazing behaviour 2−64736
Portevin-Le Chatelier effect, and density and activation entropy of moving dislocations 2−80748
Portevin-Le Chatelier effect, mathematical solutions for tensile specimen 2−73354
quartz, synthetic, plasticity stages of single crysts. 2−56797
reactor fuel particles, irrad., rupture stress, meas. device 2−43772
reactor fuel pins, irrad., automated meas. of induced strain 2−42657
rock deformation, volume changes at high pressure 2−62006
rocks, fracture and flow 2−57822
rubber blocks, bonded, compressed, elastic stress strain eqns. dynamic relax. solns., Poissons ratio effects 2−66528
rubberlike materials, stored energy function derived from simple tensile data 2−53787
shell, shallow and strongly buckling, crit. loads for loss of stability, asymptotic method 2−82323
snow and ice, l.f. Young's modulus, using double pendulum 2−74878
softened media, two-dimens. model 2−80735
Solenhofen limestone, effects of strain rate changes on strength and ductility 2−62007
statically loaded plane frames, nonlinear analysis 2−66535
steel, 11% Cr, derived from creep equation 2−71575
steel, annealed low carbon, cyclic straining 2−84124
steel, low-C, plastic instability 2−43695
steel, mild, rel. to Bauschinger effect and discontinuous yielding 2−64716
steel, stainless types 304, 316 time-dependent deformation behaviour, elevated temp. design criteria 2−83119
steel, true hardening curve between −196 and +25°C 2−56843
steel alloys, high strain rate effect on room temperature strength and ductility 2−60877
stress-strain-temperature behaviour of fatigue prone structure, model 2−56887
tensile and compressive strain obs., wide range strain gauge device 2−60929
thermal, thermoelastic effect caused by longitudinal collision of two bars 2−78877
thermoviscoelasticity, linearized theory, calc. of stressed strain states 2−69683
tube welds, stress relief by low-temp. heat treatment 2−71629
tuff, high porosity, biaxial compression test implications 2−57765
vulcanizates, oil-extended SBR, large elastic behaviour and fracture 2−84050
Zircaloy-4, neutron irrad., deform. parameters, 300°C 2−50749
Al-Mg alloy, Portevin-Le Chatelier effect, role of vacancies 2−47490
Al-Mg single crystals, infl. of strain rate and temp. on Portevin-Le Chatelier effect 2−71560
Al, plane shock structs., strain rate functions 2−60800
Al bar, annealed, containing a circumferential semicircular notch 2−77689
Al bar, elastic strain waves on centre line, resulting from impact, expt. and numerical obs. 2−66605
Al_2O_3 based refractories, torsion test 2−43687
Ar cryst. stability and mode of fracture of highly stressed ideal crystal 2−77631
BeO high pressure effects on single crysts. and polycrystalline mat. 2−68082
Cu-Si single crystal, tensile deform., Portevin-Lechatelier effect 2−50743
Cu whiskers, ductility determ. 2−56810
Fe-Ni-C alloy, rel. to deform.-induced martensitic reaction kinetics 2−80833
Fe-Si sheet Goss-oriented, magnetostriction effect 2−53778
Fe, cast, damping capacity 2−77674
Fe high strain rate behaviour using split Hopkinson bar method 2−53796
NaCl, stability and mode of fracture of highly stressed ideal crystal 2−77631
Nb-Mo alloy single crystals thermally activated deformation 2−80823

Stress/strain relations continued
Nb-Re alloy single crystals thermally activated deformation 2—80823
Ni-Fe, powder compact, struct. charact. compressive relationships 2—56946
Ni, powder compact, struct. charact. compressive relationships 2—56946
Ni high strain rate behaviour using split Hopkinson bar method 2—53796
Pb-Sn alloy, superplastically deformed, const. stress creep and strain rate tensile tests 2—47504
α-Ti, rel. to cyclic work softening 2—80835
Ti in shear, meas. using torsional split Hopkinson pressure-far and pneumatic-mechanical torsion testing machine 2—53797
WC-Co composite, microstruct. interpretation of non-elastic behaviour 2—47670
Zn-Al eutectic alloy, cold-rolled, rel. to superplastic deform. characts. 2—43701
Zr alloys, anisotropic creep behaviour under fast neutron flux 2—50756
Zr and Zr-Nb alloy, strain rate depend. hardening 2—50847

Stresses, internal
accuracy of mechanical, electronic and photoelastic strain gauges 2—74873
aerodynamic heating stresses of solid isotropic sphere, transient axi-symmetric thermoelastic problem, two-temperature theory 2—45433
Ag vacuum evaporated films 2—80569
cermet. ZHGp1.5D2.5, effects of cooling after sintering on struct. and mech. properties 2—77722
classical elastic sphere problems, numerical solution by integral equations 2—45383
coherent precipitates in elastically anisotropic mats., diffraction constant 2—80671
composite, fibre-reinforced, shrinkage stresses near discontinuity 2—71659
crack tip, finite deformation analysis of elastostatic stresses 2—77639
crystal class 6m2, standard choice of axes 2—68474
crystals, inelastic strain gradients rel. to equivalent body forces 2—73382
de Haas-van Alphen oscills. amplitude reduction by signal dephasing by strain fields round impurities 2—77846
diorites, effects of specimen size 2—57820
dislocation cell stresses 2—56698
dislocations, continuously distributed aggregate, equilib. config. from energy principle 2—74771
dynamic, obs. with embedded quartz crystal transducer 2—56858
epitaxial island alignment rel. to misfit dislocations, misfit strain 2—56697
epitaxial islands, equilib. elastic strains, misfit dislocations, size dependence 2—56696
ferrous alloys, effective modulus effects rel. to strength-differential effect 2—74853
ferrous metals, determ. by Mossbauer spectroscopy 2—51312
flat laminated plate, residual stress determ. 2—45372
forces on internal stress sources, elastic chemical potentials 2—71561
fracture toughness, fatigue cracks in zone of stress concentrators 2—80787
Gilsocarbon, generation rel. to high temp. reactor design 2—52871
glass, crystallizing, frozen elastic stresses 2—56784
glass, tempered, residual stresses 2—77648
glass-reinforced plastics, behaviour in water under high stress 2—84083
heterophase systems, phase nucleation, internal stress relax., coherent loss, thermodynamics 2—60859
hexagonal cryst., anisotropic elasticity of prismatic dislocation loop 2—47408
hexagonal cryst., elliptical dislocations loops pileups, elastic energy, tip stress 2—60791
hollow circular disk with heated stamps on external surface, stress relief through creep 2—66558
interfacial stress, at incoherent particles during coarsening 2—53798
interphase interfaces, strain fields, epitaxial dislocations, steps, electron diffr. contrast 2—56625
line forces, line force dipoles, displacement fields, anisotropic elastic solns. 2—56695
liquid, internal press., rel. to viscosity calc. 2—46937
metal, long-range stresses generated by solute segregation around voids 2—53697
metal, role in brittleness 2—43719
metal, stress relax. process 2—47507
metal powder, contact stresses, electron microscope obs. 2—56970
metal-matrix composite materials, development 2—43900
microhardness load dependence, microstresses and effects, tests on glasses and other non-metals 2—74864
motion through a dislocation array, model 2—71486
oblique holes in thick plates and cylinders 2—69676
organosilicon polymers, strongly cross-linked 2—71562
Orowan creep eqn., modified, form for internal stress due to dislocation interactions 2—74847
oscillating, effect on dislocation pile-ups. props. 2—77580
permalloy film electrodeposited on Cu wire, and e.m. props. 2—77990
Permalloy films, electrodeposited, comp. and depositing current effects 2—57302
plastic, fibre reinforced, stress distrib. in brittle matrix surrounding woven or crimped fibres 2—71657
plastic materials, hardening, accompanying deformation 2—80863
plate, prestressed, buckling under compressive stresses 2—78886
polyethylene, amorphous crosslinked, stress, strain meas. 2—84466
quasidislocations in magnetoelasticity 2—61519
Rangely anticline, northwestern Colorado, absolute meas. 2—72671
residual, measurement by bending of strips, effect of paint coatings 2—80788
residual and reactive, individual det. in bimetal 2—43752
residual stress det. for 2-10 mm zone, application to weld joints in steam pipes 2—53850
Reynolds, polymer solutions, dilute, laser velocimeter obs. of Reynolds stress and turbulence 2—71128

Stresses, internal continued
Reynolds stress, laser velocimeter for meas. 2—70838
rock burst mechanics study 2—72696
shear, in a laminar boundary-layer without pressure gradient, computation 2—53129
sphere, thermal stress at its boundary surface 2—78878
steel, due to inclusions, rel. to mech. props. 2—47491
steel, elastic stresses around nonmetallic inclusions 2—53725
steel, heat treatment depend. 2—60962
steel, low-C martensitic, stress relax. during heating 2—50834
steel, mild, rel. to Bauschinger effect and discontinuous yielding 2—64716
steel, rel. to hot pressing conditions 2—43793
steel, rel. to martensite ordering temp. 2—57026
steel thick-walled cylinders, microstrain obs. under internal pressure up to 6 kbar 2—68156
strain patterns around fold hinge zones 2—54680
thermal, in elastic beams 2—45431
thermal interphase microstresses, X-ray determination 2—43908
thermal microstresses of multiphase alloy, direct x-ray photography method 2—53884
thermal stresses in an orthotropic elastic semispace with plane strain 2—45434
thermoelastic, distribs. in vicinity of external crack in infinite medium 2—82308
time-hardening media, viscoelasticity theory 2—77706
two phase materials, circular disclination, elastic fields, interface effects 2—76272
vacancy and interstitial supersaturations, chemical stress concept 2—56688
volume dilatation caused by dislocations 2—50660
volume thermal shock in a plate, stresses described by damped harmonic vibrations 2—82327
wave propagation in nonpolar and Cosserat elastic rods 2—41679
Ag films on mica substrates, exam. 2—77650
Al, sub-grain boundary migration 2—80824
Al alloy, NS.5, effect of preferred orientation on X-ray stress meas. 2—71643
Al multilayer film structures, X-ray and Newton's rings obs. 2—43475
Al_2O_3 ceramics, quenched, residual stress determ. from mirror dimens. 2—50869
Au films, internal strain and crystallite size rel. to spitaxial growth and X-ray diffraction 2—50485
Be, rel. to increase of microplastic deform. resist. by thermocyclic treatment 2—53871
C, neutron irrad. at high-temp., mech. interactions among crystallites 2—56679
C fibre reinforced chem. vap. deposited C composites 2—53955
CaF_2, stress induced birefringence, dependence on growth technique 2—47396
CaO-ZrO_2 ceramic, substruct., stress relieving mechanism 2—43876
Cr, electrodeposited 2—64565
CrH_x, electrodeposited, f.c.c., h.c.p.→b.c.c. transform., domain size changes 2—47682
CrH_x, electrodeposited, f.c.c., h.c.p.→b.c.c. transform., micro-strain changes 2—47682
Cu-10at.%Al alloy, deformed neutron irrad., dislocation strain fields, low temp. lattice thermal cond. obs. 2—71498
Cu-16%Al alloy, rel. to sigmoidal transient creep 2—53816
Cu-Au alloy, melting, strain energy effects 2—53492
Cu-7at.%Ge alloy, deformed, neutron irrad., dislocation strain fields, low temp. lattice thermal cond. obs. 2—71498
Cu, plastically deformed, rel. to specific dislocation energy determ. 2—53734
Cu, rel. to influence of point defects on fatigue hardening 2—53724
α-Fe, cube edge dislocations, strain displacement field, linear elastic Volterra soln. 2—77568
α-Fe, edge dislocation, elastic field, computer simulation 2—56710
α-Fe, high temp., dislocation struct. and stresses 2—43637
Fe single crystal, latent hardening with 110 extension axis 2—43799
In, flow stress meas. in normal and superconducting state 2—47857
KCl-KBr solid solution, at Luders band front 2—84043
$KNbO_3$, ferroelec., mech. switching of domain walls 2—44160
LiF:Mg thermal-activation analysis study of impurity hardening 2—71491
Mg alloy, superplastic, rate controlling mechanism 2—74841
$MgO:V^{3+}$, effect of random static strains on e.p.r., model 2—72495
MgO, hot-pressed, annealing effect on elastic props. 2—50888
Mo, microdeform. under dynamic loading, temp. and impurities influence 2—43696
Nb, oxidized, annealing flexure obs. 2—43735
Ni film, induced mag. anisotropy 2—48095
Ni film, origins of stress interference obs. 2—43679
Ni films, intrinsic stress obs. by optical interference method 2—77649
RbCl, effect on dielec. susceptibility of CN^- ions 2—51192
Si_3N_4 film, chemical vapour deposited on Si, rel. to dislocation generation 2—68031
SiO_2, on planar struct., rel. to formation of flower-like defects 2—47124
Ti, diffusional saturation with O_2, residual stresses introduced 2—56949
Ti alloys, plastic defomration peculiarities in planar stress state 2—43698
U, β phase microstress behaviour during quenching cycles 2—77659
V, during stress relax., rel. to dislocation generation and immobilization 2—43680

Striations *see Discharges, electric*

Stripping reactions
deuteron, or deformed nuclei, two-step processes 2—63910
deuteron, rel. to investigation of intermediate nuclear structure 2—70347
deuteron deform. by Coulomb field 2—63906
DWBA model for stripping to unbound states 2—46209
form factors, Sturmian function applic. in calculations 2—46308
Hilbert-Schmidt integral equations, Pauli term isolation 2—67318
isobaric analog resonances, form factor for stripping DWBA amplitude 2—63861

Stripping reactions continued
- neutron, relation of cross section with off-shell neutron scattering cross section 2–67319
- proton polarization from (d, p) reactions 2–59779
- resonant state, modified distorted wave method 2–46310
- two-nucleon transfer reactions, noncentral effects 2–74107
- wet porous materials near f.p., transient simultaneous measuring method 2–74989
- (d,p), analytic expression for proton polarization 2–46311
- (d,p), on spherical and deformed nuclei, multistage effects 2–46306
- (d,p), three body model 2–49826
- (t,p), repulsive core effects 2–49818
- d, at high energies, application of hadron strong interaction theories 2–76633
- d, DWBA validity and three-body model 2–59780
- p stripping in d reaction on photoemulsion nuclei, 2.43 GeV/c 2–63909
- ^{40}Ar(τ,t)^{40}K, 35 and 18 MeV, pickup- stripping reaction mechanism contrib. to cross section 2–79799
- ^{9}Be(d,p), angular distributions analysed using DWBA and optical model 2–49820
- ^{9}Be(p,π^-)^{10}C, 600 MeV, cross-section for π^- production 2–67222
- ^{12}C(^{6}Li,d)^{16}O, use of Eckhart interactions in DWBA 2–46223
- ^{12}C(d,n)^{13}N, weakly bound projectile model calcs. of spectroscopic factors 2–67325
- ^{12}C(d,p)^{13}C, weakly bound projectile model calcs. of spectroscopic factors 2–67325
- ^{12}C(t, n)^{14}N, 8.0 MeV, meas. and comparison with double stripping theory 2–76874
- ^{44}Ca/^{3}He,d) ^{45}Sc, 24 MeV, transition strength to $d_{3/2}$ hole state 2–82854
- ^{40}Cu(α,p)^{43}Sc, $E_\alpha = 28.5$ MeV, stripping rel. to knockout mechanism 2–76871
- ^{101}Mo spectroscopy by sub-Coulomb stripping 2–76797
- ^{15}N(d,p)^{16}N(unbound), parallelism between proton spectra and off-energy-shell n-^{15}N total cross section 2–42585
- ^{20}Ne(d, n)^{21}Na, 3.6-6 MeV, meas. of angular distribs., excitation energies, stripping patterns 2–74005
- ^{62}Ni(d,p)^{63}Ni, 4.45, 5.12 MeV, meas. of absolute differential cross sections, determ. of spectroscopic factors, DWBA analysis 2–79794
- ^{28}Si(d,p)^{29}Si, Ej = 10 MeV, energy levels of ^{29}Si 2–82887
- ^{116}Sn(d,p)^{117}Sn, 4.35-5.55 MeV, Coulomb stripping to states in ^{117}Sn 2–67331
- ^{122}Sn(d,p)^{123}Sn, 4.35-5.55 MeV, Coulomb stripping to states in ^{123}Sn 2–67331
- ^{124}Sn(d,p)^{125}Sn, 4.35-5.55 MeV, Coulomb stripping to states in ^{125}Sn 2–67331
- ^{46}Ti(d, p)^{47}Ti, 5 MeV, study of spin-dependent reaction mechanism from pγ correlation 2–63919
- ^{90}Zr(d, n)^{91}Nb, energy level properties in ^{91}Nb 2–63922
- ^{96}Zr(d, n)^{97}Nb, energy level properties in ^{97}Nb 2–63922

Stroboscopes
- acoustic wave visualization by acoustic stroboscopy 2–78927

Strong interactions *see Elementary particles / interactions, strong; Field theory, quantum / interactions, strong*

Strontium
- abundance distributions in seawater profiles at oceanographic test stations Geosecs I and II 2–75472
- abundance profiles in Pacific and Mediterranean sea water 2–75467
- atom, oscillator strengths for resonance transitions 2–79875
- atomic, quenching of a fluorescence in H flames 2–42715
- oxidation, u.v. photoelectron spectroscopy obs. 2–72557
- oxidation kinetics, photoemission spectra of chemisorbed levels 2–51446
- pliocene volcanic rock content det. 2–57809
- thermal expansion, 1.5-30K, 55-90K and room temp. 2–74993
- KCl:Sr, X-ray induced defects, thermal annealing, absorp. and luminesc. obs. 2–64684
- NaCl:Sr^{2+}, Z_1 generation, kinetics 2–84515
- Rb-Sr geochronolgy data, use of two-error linear regression treatments 2–61994
- Sr-Rb isotope characts. of lunar soils 2–66139
- Sr I, e.u.v. spectra, energy levels 2–64001
- Sr III spectra from sliding spark discharge in 9800-350 Å range, obs. of even and odd energy levels 2–76997
- Sr^{2+}, self-diffusion in K_2O-SrO-SiO_2 glass 2–53765
- ^{87}Sr/^{86}Sr, det. of evolution of mantle beneath S. Pacific Basin 2–57730
- ^{87}Sr/^{86}Sr, in Cenozoic basalts of southern Rocky Mountain region 2–57698
- ^{87}Sr/^{86}Sr abundance ratio in fresh South African kimberlites 2–75452
- ^{87}Sr/^{86}Sr geochemistry of lherzolite inclusions and host basaltic rocks 2–57827
- ^{87}Sr/^{86}Sr ratio in lherzolites from Puerco necks, New Mexico 2–65537
- ^{90}Sr, Great Lakes, sediments, diffusional transport 2–65564
- ^{90}Sr, seawater content, of fallout origin 2–62043
- ^{90}Sr and ^{89}Sr fallout from Chinese nuclear tests 2–62285
- ^{90}Sr fallout, bearing on weather conditions 2–62286
- ^{90}Sr in Great Lakes, concentration time model 2–65615
- ^{90}Sr in seawater from Geosecs II, shipboard analysis techniques 2–75476
- ^{90}Sr nasopharyngeal applicators, dose distributions 2–69436
- ^{90}Sr nasopharyngeal applicator, photographic determ. of dose rate distribution 2–69435
- ^{90}Sr thermoelectric generator TRISTAN 2–49293
- ^{87m}Sr radiation dose calculation, evidence for calculation errors 2–76096
- Sr + HI → SrI + H, meas. of angular distrib. of product, determ. limits on $D_0°$ 2–81494

Strontium compounds
- borate glasses, struct. changes, e.p.r. 2–54496
- fluorophosphate, Mn^{2+} doped, optical excitation and fluoresc. spectra of Mn^{2+} 2–81421
- formate, anhydrous, i.r. and Raman spectra 2–61661
- vanadates, bonds, struct., dielec. const. 2–43589

Strontium compounds continued
- BaF_2-SrF_2, solid solutions, theoretical study 2–64772
- $BaSO_4$-$SrSO_4$, solid solutions, theoretical study 2–64772
- $Ba_{0.5}Sr_{0.5}Nb_2O_6$, absolute signs of second harmonic generation coeffs. 2–44332
- $Ba_{0.5}Sr_{0.5}Nb_2O_6$, cryst. growth rate variation with supersaturation in fluxed melts 2–47255
- $Ba_4SrNb_{10}O_{30}$, solidification structs. 2–47654
- $Ba_xSr_{1-x}Nb_2O_6$, semicond., high 1/f noise anomaly 2–47888
- $Ba_{1-x}Sr_xTiO_3$, mobility, gravimetric determ. 2–81086
- $Ba_xSr_{1-x}ZrO_3$ dielectrics, high-permittivity temp.-stable, low microwave loss 2–51190
- Ge-Sr system, phase diagram 2–47714
- K_2O-SrO-SiO_2 glass, cation self-diffusion coeffs. 2–53765
- KPO_3-$Sr(PO_3)_2$ system, phase diagram 2–43935
- $MoO_3 + SrCO_3 \rightarrow SrMoO_4 + CO_2$ reaction kinetics 2–54536
- $Na_{2x}Sr_{1-x}Pb(OH)_6$, nonstoichiometric, struct. 2–71437
- PbF_2-SrF_2, solid solutions, theoretical study 2–64772
- PbO-SrO-GeO_2 glass, structure and properties 2–53540
- $PbSO_4$-$SrSO_4$, solid solutions, theoretical study 2–64772
- $SiTiO_3$, critical asymmetry in local fluctuations for $T \rightarrow T_c^-$ 2–72472
- Sr formates, formation and surf. props. of electron emissive coatings 2–65365
- $SrAlF_5$, pure and Eu^{2+}-doped, cryst. growth and characterization 2–60726
- $SrAl_2SiO_8$-$BaAl_2SiO_8$ solid soln., isomorphism, phase diagram 2–54009
- $Sr_2B_5O_9Br(Cl)$, cryst. struct. 2–53657
- $SrB_2Si_2O_8$:Eu^{2+}, meas. of diffuse reflection, excitation and emission spectrum 2–81420
- $SrCaAlF_7$:Eu^{2+}, three polymorphs., luminesc. 2–72420
- $SrCaKnB_5O_{15}$, crystallographic, dielec. and nonlinear optical props. 2–75251
- $SrCl_2$:Cm^{3+}, e.p.r. investigations of zero-field splittings 2–44449
- $SrCl_2$:$^{151}Eu^{2+}$, $^{153}Eu^{2+}$, hyperfine interactions, temp. dependence, e.p.r. obs. 2–72471
- $SrCl_2$:$K^+(Na^+)$, dielec. const., loss angle, cond., Frenkel defect form. 2–47969
- $SrCl_2$:Ti^{2+}, e.p.r. investigation, obs. of double quantum transitions, determ. of spin- Hamiltonian parameters 2–81454
- $SrCl_2$, e.p.r. of Ag^{2+}, conform. instability in hexagonal sites 2–84579
- $SrCl_2$, mag. circular dichroism on F-centre absorpt. band, $g_{orbital}$ factor 2–74805
- $SrCl_2$, U- and U_2-centres, absorpt. spectra and e.p.r. 2–71531
- $SrCo_{1-x}Fe_xO_{3-y}$, Curie temp. and magnetization 2–81238
- $SrCoO_{2.5}$, mag. struct., neutron diffr. obs. 2–81294
- SrF_2: Gd^{3+}, Ce^{3+}, Ce^{3+} codopant effect on Gd^{3+} e.p.r. spectrum at room temp. 2–61737
- SrF_2:$Cm^{3+}(Am^{2+})$, e.p.r. investigations of zero-field splittings 2–44449
- SrF_2:Dy, Tb, Nd, axial distrib. of impurities, neutron activation analysis 2–56744
- SrF_2:La,Ce, uncoloured and X-irrad., optical absorpt., charge transfer processes 2–65253
- SrF_2:Tm^{2+}, Kramers doublets with hyperfine coupling, meas. 2–78048
- SrF_6:Tm^{2+}, crystal field splitting and g values within $(TmF_8)^{6-}$ cluster framework 2–78054
- SrF_2, colour centres, high temp. absorpt. study 2–77597
- SrF_2, ENDOR spectrum of U^{3+}-F- 2–84607
- SrF_2, e.p.r., linear elec. field effects for Ce^{3+}-F^- tetragonal sites 2–48285
- SrF_2, elastic wave damping, effective anharmonicity consts. 2–80913
- SrF_2, F-centres, zero-phonon line obs. 2–53752
- SrF_2, F_2-centres, ⟨100⟩ and ⟨110⟩ oriented, spectral obs. 2–53751
- SrF_2, l.f. dielec. consts., temp. and press. derivatives 2–51189
- SrF_2, low temp. plasma produced radiational defects 2–71452
- SrF_2, phonon dispersion curves, harmonic vibr. props. 2–77760
- SrF_2, Raman spectra, lattice dynamics 2–57040
- SrF_2, thermal expansion, shell model calcs. 2–84216
- SrF_2, trigonal Gd^{3+} e.s.r. centres produced by hydrolysis reaction 2–84582
- SrF_2, two-electron U-centres, point-ion models 2–83987
- SrF_2 colour centre interconversion induced by electron irradiation 2–77598
- SrF_2 force fields, contrib. of three-body overlap effects 2–77765
- $SrFeO_3$, mag. struct., neutron diffr. obs. 2–81282
- $SrFe_{12}O_{19}$, ferrite, crystallized from B_2O_3-SrO-Fe_2O_3 glasses 2–54345
- $SrFe_{12}O_{19}$, saturation magnetization, reduced temp. depend. by As or P substitution 2–78019
- $SrGeO_3$-$Ca(Ba)GeO_3$ solid solutions, struct., i.r. spectra study 2–65251
- $Sr^{181}HfO_3$, perovskite-type, nucl. quadrupole interactions, perturbed-angular-correlation meas. 2–72244
- SrI, produced in Sr + HI reaction, determ. of lower bound for $D_0°$ 2–81494
- $Sr_2KNb_5O_{15}$, crystallographic, dielec. and nonlinear optical props. 2–75251
- $Sr_2KNb_5O_{15}$, Ta-substitution influence on crystallographic and dielec. props. 2–47315
- $Sr_{2-x}K_{1+x}Nb_5O_{15-x}F_x$, synthesis, struct. and ferroelec. props. 2–51198
- $SrLiTa_2O_6F$, spontaneous crystalliz. and pyrochlore struct. obs. 2–74689
- $SrLn(AlO_4)$, (Ln = La, Ce, Pr, Nd, Sm, Eu, Gd), cryst. struct. 2–56664
- $Sr_\alpha(MO)_\beta MO_3$(M = Ta,W and Nb,W), structural evolution as a function of α 2–83958
- $SrMe^{VI}O_4$:U, single crystals with scheelite structure, Me^{VI} = Mo, W luminescence and absorption spectra between 300K and 4.2K 2–68676
- $Sr_{2.96}MgSi_2O_8$:Eu^{2+}, luminescent props., prep. depend. 2–84550
- $SrMoO_4$:Er^{3+}, crystal parameters verified 2–51240
- $SrMoO_4$, elastic consts., u.s. determ. 2–77773
- $Sr(NO_3)_2$, precip. in KNO_3, solid soln. form. 2–56942

Strontium compounds continued
$Sr_2NaNb_5O_{15}$, crystallographic, dielec. and nonlinear optical props. 2−75251
$Sr_2Nb_2O_7$, cryst. growth by floating zone technique 2−47276
$SrO:Ce^{3+}$, cubic sites, EPR investigations, g values 2−54491
$SrO-SiO_2-K_2O$, interdiffusion coeffs. matrix 2−80724
$SrO-ZrO_2-SiO_2$ 2−75320
SrO, dissoc. energy from crossed beam expt. 2−80002
SrO, elastic consts., temp. depend. 2−74823
SrO, Gruneisen parameter and thermal expansion 2−47756
SrO, radiation-induced $[Na]^0$ centres 2−43651
SrO, Raman scatt. spectrum 2−44393
SrO in Bi_2O_3, ion conduction obs. 2−61418
$SrO(6-x)Fe_2O_3xAl_2O_3$, influence of thermal history on Mossbauer spectra 2−48144
$SrO.2Al_2O_3$, refined cryst. struct. 2−68007
$SrO.xB_2O_3$, glass and cpds., n.m.r. of ^{11}B, struct. 2−54504
$SrPd_2H$, prep., struct., and elec. resist. 2−47347
Sr_2PdH_4, prep., struct., and elec. resist. 2−47347
$SrRuO_3$, orthorhombic perovskites, metallic elec. props. of single crystals 2−84291
SrS:Ce,Sm luminescent i.r. sensors, preparation and properties 2−73463
SrS:Mn, Zr phosphors decay study 2−75330
SrS phosphors, activated by Zr, Sn, Pb and Th 2−61713
SrS phosphors activated by Zr, Sn, Pb and Th, thermoluminescence and phosphorescence decay 2−65314
$SrSO_4$, crystal growth from silica gels 2−43519
$SrS_2O_6.4H_2O$, second harmonic generation 2−75248
$SrSi_2$, cryst. struct., space group, cryst. class O(432) 2−68006
$SrTeO_3$, ferroelectric, growth, structure and dielec. props. 2−68472
$SrTiO_3$, anomalous reson. in permittivity on cooling in elec. field 2−77935
$SrTiO_3$, antiferrodistortive transition, fluctuation phenomena, e.p.r. obs. 2−84574
$SrTiO_3$, band struct., self-consistent- field tight-binding calc. 2−61191
$SrTiO_3$, degenerate semicond., u.s. propagation, effects of longitudinal mag. field 2−71731
$SrTiO_3$, dielec. props. at low temps. explained by ferroelectric mode model 2−81152
$SrTiO_3$, dielectric const. changes after electron or gamma irrad., X-ray study 2−65047
$SrTiO_3$, differential optical spectra and band struct. 2−72307
$SrTiO_3$, displacive transition phenomena, sound propag. 2−54026
$SrTiO_3$, doubly ionized oxygen vacancy obs. 2−47403
$SrTiO_3$, dynamics of structural transitions 2−65065
$SrTiO_3$, e.p.r. of Mo^{5+}, dynamic Jahn-Teller effect 2−48295
$SrTiO_3$, electric polarization of crystals by inertial forces 2−54238
$SrTiO_3$, electrostatic potentials, calc. 2−60700
$SrTiO_3$, fundamental absorpt. edge, 6-300K 2−78107
$SrTiO_3$, l.f. soft vibrational modes under stress 2−71696
$SrTiO_3$, lattice dynamics, normal mode freqs., harmonic models, calc. of props. 2−77761
$SrTiO_3$, mobility, gravimetric determ. 2−81086
$SrTiO_3$, photochromic crystals, erase-mode optical recording characteristics 2−63422
$SrTiO_3$, response function of soft zone boundary phonon, microscopic calc. 2−61082
$SrTiO_3$, self consistent lattice dynamical theory of structural phase transitions 2−77767
$SrTiO_3$, semiconductor/metal barrier props. 2−71985
$SrTiO_3$, static and dynamic crit. phenomena near struct. phase transitions, e.p.r. 2−81465
$SrTiO_3$, uniaxially stressed, domain struct. at 2K 2−61433
$SrTiO_3$, Urbach's tail behaviour, unified mechanism 2−54430
$SrTiO_3$, wavelength modulated absorp. spectra, rel. to phase transition 2−51348
$SrTiO_3$ Raman cross sections, temp. dependence 2−84514
$SrUO_4$, X-ray examination using Hagg-Guinier camera, analogy with $BaUO_4$, calc. of interatomic distances 2−77558
$Sr_3(VO_4)_2$, vibrational spectra 2−44382
$Sr(Zr,Ti)O_3$ dielectrics, high-permittivity temp.-stable, low microwave loss 2−51190
$SrZrO_3$, creep, 1160-1275°C 2−43705

Structure factors *see Crystal structure, atomic; X-ray crystallography*

Structure of matter *see Crystal structure; Liquids/structure; Solids/structure*

SU(3) group theory *see SU(n) theory*

SU(n) theory
— 2−66952
σ model in tree approx., analytic properties of symmetry-breaking 2−79466
(3.3+) + (3+.3) symmetry breaking model in pole-dominance approximation 2−82710
chiral SU(2) × SU(2), σ term in (N/2, N/2) representation in πN scattering 2−79590
chiral SU(3) × SU(3) algebra, hadrons currents and Cabibbo angle 2−63533
chiral SU(3) × SU(3) canonical second rank tensor 2−42311
chiral SU(3) × SU(3) mass breaking, effect of 'weighted' linear transforms 2−49480
chiral SU(3) × SU(3) symmetry, test of (3,3) breaking via σ term of KN scattering 2−63598
fermion pair creation in alternating external field, SU(2N) group 2−52540
generalized exchange operators 2−82647
generic vector, matrix and tensor construction 2−52538
invariant operator eigenvalues 2−41461
invariant operators, true values 2−69551
meson-baryon resonances and high energy forward scattering, SU(3) 2−42404
Nevue-Schwarz dual model, axial currents which satisfy local SU mult SU algebra 2−82615
nonlinear realization and associated invariant Lagrangian 2−76561
parametrization and invariant volume element 2−82645
pseudo SU(3), validity for A=59,60 nuclei 2−52750
quark-gluon model, chiral symmetry realization 2−45897
relativistic SU(3), mass splitting 2−76584

SU(n) theory continued
renormalizable theories of weak and e.m. interactions, mixing angle 2−49486
renormalized linear SU(2) × SU(2) σ model, hypothesis of threshold dominance 2−66912
Schrodinger eqn., radial, SU(1,1) algebra determ. of eigenvalues 2−73317
Schwinger terms in equal time commutators of SU(3) × SU(3) charge densities 2−45859
$SU_{1,1}$ dynamical group for strongly interacting particles with identical quantum numbers 2−73741
SU_2 and SU_2 mult SU_2 in canonical representation of theory of currents Lagrangian solution82659 2−82659
SU_3 model consistency and core polarization effective charge 2−49709
SU(12) broken symmetry formalism for spin and internal symmetry in dual resonance model 2−63560
SU(1,1) spinor algebra, spin coeffs. 2−82213
SU(2,2), nondegenerate complementary series of representations 2−62975
$SU(2)_l \times U(1)$ symmetry of weak and e.m. interactions 2−66933
SU(2) × SU(2) breaking and effective Lagrangian of pionic processes 2−82603
SU(2) × SU(2) chiral dynamics, invariant functional formulation 2−70127
SU(2) × SU(2) chiral invariant pion-nuclear interaction, matrix superpropagator 2−73820
SU(2) × SU(2) dynamics, study of $\pi^+p \rightarrow \rho^0\Delta_{1236}{}^{++}$ near threshold 2−67025
SU(2) × SU(2) equal-time time component current algebra, construction of axial vector current 2−76579
SU(2) × SU(2) representation of Regge couplings 2−45924
SU(2) × SU(2) symmetry, chiral, and PCAC 2−79478
SU(2) × SU(3) quark representation with non-violation of Pauli principle 2−73772
SU(2) × U(1), models of weak and e.m. interactions based on spontaneously broken gauge 2−79476
SU(3), invariant tensors constructed in terms of λ matrices 2−49479
SU(3), phys. basis and E2-transition probability 2−59680
SU(3), singlet and octet, $^1{}_2{}^+$ baryon poles, interpretation of Λ, Ξ decay 2−70266
SU(3) × SU(3), (8, 8) chiral symmetry breaking representation 2−63484
SU(3) × SU(3), chiral, limit of no explicit breaking 2−63532
SU(3) × SU(3), linear and non-linear realizations 2−73774
SU(3) × SU(3), non-linear chiral dynamics, violated Lagrangian 2−63573
SU(3) × SU(3) (1,8) representation of chiral tensors, commutation with axial charge 2−76585
SU(3) × SU(3) broken nonlinear chiral dynamics, study of photoproduction of vector and axial vector resonances 2−59547
SU(3) × SU(3) chiral symmetry, approach to study of strong interactions 2−63489
SU(3) × SU(3) field algebra amplitudes, unitarization 2−73720
SU(3) × SU(3) invariance, scale and chiral, realisation with Goldstone bosons and broken SU(3) coupling constants 2−59386
SU(3) × SU(3) light cone commutators and K_{l3} decay 2−79558
SU(3) × SU(3) nonlinear models, scalar mesons and symmetry breaking 2−79479
SU(3) × SU(3) spontaneous breaking, mass relations and particle mixings 2−66910
SU(3) × SU(3) symmetry, model of spontaneous breakdown 2−66953
SU(3) × SU(3) symmetry breaking and mass-dispersion relations 2−66911
SU(3) × SU(3) symmetry breaking Lagrangian, restrictions imposed by W-invariance and octet dominance 2−66909
SU(3) × SU(3) symmetry breaking Lagrangian, W-parity, octet dominance 2−73739
SU(3) × SU(3) symmetry violations in electromagnetic and weak interactions 2−76590
SU(3) σ model for calc. of symmetry-breaking corrections to current algebra formulas for K pionic decays 2−52595
SU(3) σ model of $0^{\pm}$ fields, effects of adding $1^{\pm}$ gauge fields, chiral and scale symmetry breaking 2−79469
SU(3) and Σ(1385) π decay mode of D_{03} resonances 2−42426
SU(3) and SU(2) multiplets in baryon excited states, infinite-component wave eqns. and mass splittings 2−52630
SU(3) and SU(6) breaking in differential cross sections for charge exchange reactions with t-dependent residues 2−52574
SU(3) and SU(6) symmetry models for statistical weight of n-particle system 2−59385
SU(3) asymptotic algebraic realization, baryon classification, $g_a(0)$ and D/F ratio 2−52629
SU(3) basis of representation for Faddeev eqns. for three particles, application to nd scattering 2−76722
SU(3) boson families, review 2−76647
SU(3) breaking for baryon reson. decay rates 2−76726
SU(3) equalities for strong, e.m. and weak inclusive processes 2−49484
SU(3) exact symmetry limit calc. of KN scattering cross section 2−67012
Su(3) group, finite transforms. in arbitrary irreducible represent. 2−58713
SU(3) groups, irreducible representations spanned by wave functions of non-normal parity states of A=14, 15 nuclei 2−42498
SU(3) incorporation in parton dual reson. model 2−59478
SU(3) lagrangian for meson decays 2−63634
SU(3) mass differences, rel. to medium mass splittings for pseudoscalar and vector mesons and spin 3/2 baryons 2−70204
SU(3) mass splittings of 0^- octet and 1^- nonet in meson decays, quark-loop dynamics 2−73770
SU(3) octet currents, generalized 'similarity' relation 2−70126
SU(3) prediction for $(\eta \rightarrow \gamma\gamma)/(\pi^0 \rightarrow \gamma\gamma)$ decay width ratio 2−79553
SU(3) predictions in inclusive exchange region 2−79524
SU(3) predictions or cross sections, introduction of angular momentum barrier penetration coeffs. 2−59556
SU(3) quarks, explanation of absence 2−52567
SU(3) rotation applied in FESR analysis of $K^-n \rightarrow \pi^-\Lambda$ 2−42351

- **SU(n) theory** continued
  - SU(3) symmetric interaction of scalar meson and two pseudo-scalar mesons 2−66995
  - SU(3) symmetry breaking, Sakata-Taketani field assoc. with Kemmer field 2−66897
  - SU(3) symmetry breaking and slopes of baryon linear trajectories 2−49587
  - SU(3) symmetry breaking for $\Lambda \rightarrow pe^- \nu_e$ decay 2−79624
  - Su(3) symmetry for hyperon-nucleon interactions 2−79622
  - SU(3) symmetry for nuclei in ds-shell 2−82853
  - SU(3) symmetry of 3^- nonet and its couplings to lower-lying mesons 2−67038
  - SU(3) symmetry of Regge residues, symmetries of Regge-Regge cuts 2−59493
  - SU(3) symmetry used in calcs. on η four-body decay 2−52590
  - SU(3) unitary representations, algebraic method with Bose operators 2−45858
  - SU(3) x SU(3) irreducible representations, breaking of hadronic internal symmetry 2−63535
  - SU(4) bilocal current algebra, application to inclusive reactions 2−73756
  - SU(4) weak interaction quark model modification 2−79531
  - $SU(6)_w$, test for basic violations using resonance decays involving two partial waves 2−63642
  - $SU(6) \times O(3)$ quark model, diatomic-molecule type, for prediction of meson mass resonances in 1-3 GeV region 2−76690
  - SU(6) and low mass of Roper resonance 2−76616
  - SU(6) results derived using finite-energy and current algebra sum rules 2−63529
  - $SU(n) \times SU(n)$ chiral interaction and localizability for $n \geqslant 3$ 2−79474
  - Wigner supermultiplet scheme, construction of basis states 2−52537
  - Wigner supermultiplet scheme, derivation of coupling coeffs. 2−45846
  - $[SU(3)]^4$ group model for gauge theory of weak and electromagnetic interaction of leptons and hadrons 2−42332
  - $\eta \rightarrow \pi^0\pi^0\pi^0$, $SU(3) \times SU(3)$ broken symmetry model 2−70206
  - ^{24}Mg, SU(3) calculations 2−46121
- **Sublimation**
  - *see also Heat of sublimation; Vaporization*
  - dielectric thin films, characteristics of deposited films 2−60638
  - fluoranthene crystal, purity determ. by spectral depend. of fluorescence lifetime 2−84536
  - graphite, bulk, effect of microstruct. on characts. 2−60560
  - graphite, electron beam deposition, sublimation energies 2−60644
  - ionic crystals, influence of surface charge and surface structure 2−60561
  - kinetics of vac. evaporation of solids 2−77465
  - nichrome, film, prod. by multiple sublimation, vacuum system, props. 2−47121
  - Al, electron beam deposition, sublimation energies 2−60644
  - As(111) crystal, evaporating molecule speed and spatial distributions 2−67879
  - CdSe, solid-gas phase equilibria and thermodynamic props. 2−71368
  - CuO, single cryst. prep. 2−74678
  - GaS, growth from vapour phase 2−71373
  - HgI_2, red tetragonal phase, sublimation growth in vacuum 2−74671
  - HgSe, partial press. of Hg and Se, equilib. total dissociation press. 2−74596
  - Kr, activation energy, cryst. thickness depend. 2−60562
  - TeI_4, and $TeI_4 \rightarrow TeI_2 + I_2$ reaction, 300-900 K 2−54526
  - $ZnSiP_2$, crystal growth technique 2−64593
- **Sudden commencement** *see Magnetic storms*
- **Suhl effect** *see Hall effect; Semiconductors*
- **Sulphur**
  - — 2−68774
  - adlayer on Ni, electron energy loss spectra, electronic transition characts. 2−47079
  - adsorbed layer, on Cu, phase transitions 2−50535
  - adsorbed on Ni(110), electron energy loss spectra, elastic scatt. 2−84222
  - adsorption on Ni, surface reconstruction, Madelung potential 2−47162
  - air and soil abundance and crop yields 2−78301
  - atmosphere, budget over N. Europe, emission and deposition 2−54824
  - band structure, from hole photoemission from CdS(Se), HgS and Se into S 2−84265
  - chemisorption on metal, thermodynamic and struct. aspects 2−50530
  - chemisorption on Ni, bonding, orbital electron energy spectra 2−48328
  - decarburizing of cast Fe with graphite, struct. effects 2−43837
  - diffusion in Fe, effective radii of diffusing particles, diffusion mechanisms 2−50709
  - diffusion in Fe, solid and liq. states 2−43661
  - diffusion in ZnS single cryst. 2−56764
  - electron and Auger electron spectroscopy, review in reln. to vacuum technique 2−59924
  - high pressure, phases I and III, indexing powder patterns 2−53679
  - ion implantation into GaAs, GaP and Ge 2−47429
  - isotope balance in oceans, model 2−57863
  - liquid, polymerization parameters, calc. method 2−57418
  - lunar and terrestrial basalt composition 2−58457
  - magnetic susceptibility, low temp, glassy and crystalline state 2−61477
  - innuclear fuels, chemical anal. 2−74176
  - particulate borne, long distance transport in Sweden Sept.-Dec. 1969 2−72766
  - Pasadena smog, chemical states, photoelectron spectroscopy obs. 2−51602
  - reaction with O on Ni surface 2−78184
  - sensitization mechanism, photographic 2−59304
  - solar overabundance, accelerated by solar flares 2−76001
  - surface impurity on Th, bulk to surface equilib. 2−50465
  - vapour pressures and densities up to 800°C, apparatus for obs. 2−47045
  - X-ray absorption spectra in SO_2, H_2S and CS_2 molecules 2−42939
  - in C fibre, effect on mech. and crystallographic props. 2−50913
- **Sulphur** continued
  - CdSe:S, local impurity and lattice vibrs., Fermi reson., absorpt. spectra obs. 2−80895
  - GaP:Mn,S, Mn-S nearest neighbour complex, e.s.r. obs. 2−75344
  - Li/S secondary cell with inorganic electrolyte 2−66689
  - Li/S secondary cells 2−66687
  - Na/S secondary cell with inorganic electrolyte 2−66689
  - S II lines in crab Nebula spectra, det. of interstellar reddening 2−58247
  - S_2, ground state dissociation energy estimation 2−46581
  - $S_2{}^-$ ion, in synthetic sodalite, photolum. spectra, 4.2-300 K, fine struct., multiband spectra 2−81422
  - S_3, S_4, vibrational analysis of visible spectrum, correlation with photolysis reactions of S_3Cl_2 and S_4Cl_2 2−50069
  - S_8 orthorhombic mol. orbital interpret. of valence X-ray emission 2−84488
  - SIII forbidden lines in diffuse nebulae spectra 2−58242
  - Si:S, deep donor levels, pressure depend. 2−80962
- **Sulphur compounds**
  - — 2−68774
  - — 2−67686
  - $A^IB^{III}S_2$ with rhombohedral α-$NaFeO_2$ structure, Raman and i.r. spectra 2−72321
  - acid hydrates, hydronium ion struct. and dynamics 2−84601
  - molecular electronic struct., ^{33}S n.m.r. spectroscopy 2−83290
  - photographic sensitizers, heat of adsorption to AgBr, AgCl and Ag_2S 2−73686
  - solid solutions with Fe, Co and Ni, thermodynamic props. 2−50837
  - sulphuryl molecules, photoelectron spectra 2−64156
  - tetrahedral oxy-compounds, force constants and regularities of chemical bonding 2−70725
  - thionyl molecules, photoelectron spectra 2−64156
  - As-S-Ge glass film, laser induced refractive index changes 2−61583
  - As-S-Te, vitreous semicond., γ-ray induced cond. 2−54252
  - As-S glass, mechanism of hologram formation 2−59204
  - $CsI:SO^{2-}{}_4$, i.r. absorpt. 2−78086
  - $Ge_{16}As_{35}Te_{28}S_{21}$, amorphous, semicond-metal contact, photovoltaic effect and space charge capacitance 2−61374
  - glass, As-S, As-S-I, As-S-Tl viscosity in transition region 2−84049
  - H_2SO_4 anodic oxidation of binary compounds 2−61790
  - He-SF_6 system, binary diffusion coeffs. conc. depend. 2−67737
  - $KCl:SO_4{}^{2-}$-, anion vacancy trapping, i.r. absorpt. study 2−43620
  - S-Sb-Ge-I glass system, glass forming regions 2−80533
  - SCl_2, Raman and infrared, vibrational spectra 2−77059
  - S_3Cl_2, S_4Cl_2, photolysis reactions, correlation with vibrational analysis of S_3 and S_4 visible spectra 2−50069
  - SD^-, in KCl(Br)(I), i.r. spectra 2−84491
  - SF_4, vibrational spectra and structure of solid 2−44381
  - SF_6, adsorption on Cd and Zn, stepwise isotherms 2−77518
  - SF_6, atmospheric, detection, test of airborne gas chromatography 2−48467
  - SF_6, breakdown, electrode surface conditions and dust particle effects 2−74439
  - SF_6, compressed, electrical breakdown and prebreakdown dark current 2−71035
  - SF_6, compressed, surface flashover on solid insulation 2−71040
  - SF_6, compressed discharge, voltage time characteristics 2−70998
  - SF_6, d.c. electrical breakdown at e.h.v. in coaxial systems, similarity law 2−74432
  - SF_6, edge breakdown between uniform field electrodes 2−71033
  - SF_6, electron diffusion and drift 2−43202
  - SF_6, gas-blasted in nozzle, arc voltage distribution 2−71066
  - SF_6, gaseous, sulphur K and L and fluorine K X-ray emission and absorption spectra 2−56197
  - SF_6, inverted Lamb dip spectroscopy 2−63326
  - SF_6, ionization and breakdown obs. 2−71039
  - SF_6, nucl. spin relax. obs. of spin-rot. interaction 2−56199
  - SF_6, photoabsorpt. cross sections in soft and ultrasoft X-ray range in ioniz. threshold region 2−67499
  - SF_6, saturation behaviour at high pressure and laser intensity 2−74277
  - SF_6, X-ray absorption spectra, MO LCAO interpretation 2−56196
  - SF_6 and SF_6-air mixtures, pressure dependence of resonance fluorescence lifetimes 2−42932
  - SF_6 clathrate deuterate, ^{19}F spin-lattice relaxation meas. in 40-250 K range 2−72531
  - SF_6 discharge, mechanism of spark breakdown 2−60318
  - SF_6 electronic structure, optical spectra of gas and solid in extreme u.v. and soft X-ray region 2−42933
  - SF_6 gas-air tracer in following atmospheric dispersion of effluents 2−62095
  - SF_6 gas, frequency-dependent thermal conductivity, two-temp. hydrodynamic theory 2−60371
  - SF_6 gas flow, temp. profile around arc column 2−71049
  - SF_6 liquid-vapour transition, interferometric meas. of isotherms in critical region 2−80519
  - SF_6 static-breakdown voltage measurements at h.v. 2−56394
  - SF_6 vibrational relaxation in HCN hypersonic molecular beam 2−67478
  - SF_4O, S-O distance by microwave studies 2−70723
  - SF_6 + K reaction, dependence of reactivity on internal and translational energy 2−75374
  - SF6 decomposition, current interruption, gas circuit breakers 2−74489
  - SH, second rotational level, Λ-doubling transition frequencies 2−46579
  - SH^-, in KCl(Br)(I), i.r. spectra 2−84491
  - $SH^- + NO_2 \rightarrow NO_2{}^- + SH$, thermal energy rate consts. 2−68774
  - SO_2-Pt system, thermal cond., accommodation effect 2−67734
  - SO, $b^1\Sigma^+ - X^3\Sigma^-$ transition, rotational band structure 2−70724
  - SO, ground state dissociation energy estimation 2−46581
  - SO, microwave spectra, transitions 2−76542
  - SO $A^3\Pi$-$X^3\Sigma^-$ band systems, oscillator strengths 2−56195
  - SO_2, heat of adsorption on MgO at 423K 2−83871
  - SO_2, i.r. absorption coeffs. 2−56156
  - SO_2, ionization and dissociation attachment cross-sections by electron collision 2−60035
  - SO_2, MO LCAO-CNDO calc. of electronic structure, comparison with X-ray spectra 2−60034

Sulphur compounds continued
  SO_2, Martian atmosphere, minor constituents, Mariner borne i.r. spectrometer 2−69156
  SO_2, ν_1 band, tunable laser spectroscopy 2−42938
  SO_2, oxidation, rel. to photolysis of atmospheric gaseous impurities 2−51586
  SO_2, π^*-π (2350 Å) band system analysis 2−64155
  SO_2, solubility in liqs. 2−53405
  SO_2, tunable-laser spectroscopy of vibr.-rot. band transitions 2−60033
  SO_2 atmospheric distribution over Hungary, obs. 2−54819
  SO_2 atmospheric pollution in Los Angeles 2−57944
  SO_2 clustering to NO^+ 2−61762
  SO_2 concentrations, remote sensing of ambient air quality and gaseous pollutant flow 2−84870
  SO_2 emission to atmosphere estimated from airborne meas. 2−62143
  SO_2 fine structure of ultrasoft X-ray absorption spectra of S in 160-210 eV range 2−42939
  SO_2 pollutants, detection using current tunable $Pb_{1-x}Sn_xTe$ diode lasers 2−57940
  SO_2 Raman scattering cross sections and depolarization ratio 2−53026
  SO_4^{2-}, localized orbital calc. of bonding 2−67498
  $SOBr_2$, pot. energy consts., vibr. amplitudes, Corriolis coupling consts., rot. distortion, thermodynamic props. 2−56169
  $SOCl_2$, localized orbital calc. of bonding 2−67498
  $SO^{35}Cl^{37}Cl$, rot. spectrum analysis 2−60032
  SOF_2, microwave spectrum and harmonic force field 2−80036
  SOF_2, upper stage transition in i.r. spectra 2−46580
  SO_2F_2, localized orbital calc. of bonding 2−67498
  SO_2F_2, upper stage transitions in i.r. spectra 2−46580
  SO_2F_2 electronic structure, exptl. and theoretical study 2−46587
  $SPCl_3$, valence force constants, molecular polarizabilities 2−74276
  SPF_3, valence force constants, molecular polarizabilities 2−74276
  $^{16}SO_2$, $^{18}SO_2$, molecules, second order anharmonic potential function 2−56201
  $^{35}SO_2$, determ. of average concentration in air, method based on selective absorption in oxident soln. 2−58013
  Sf_6, liquid-vapour coexistence curve, interferometric obs. 2−74591
  So_3F radical, and anion, normal coordinate analysis in Urey-Bradley force field 2−56198
  Te-As-Ge-S glass films, four-element quantitative analysis 2−72593
  $Te_{60}As_{25}Ge_{13}S_x$, chalcogenide glass, interdepend. between switching, memory, and thermal behaviour 2−47901
  Ti-Ce-S system, struct. and phase equilib. 2−43943
  $Ti_xTa_{1-x}S_2$ $(0.1 \leqslant x \leqslant 0.9)$ solid solutions, resistivity, magnetic susceptibility, thermoelectric power 2−61266

Sum rules
  Adler, infinite-momentum derivation for forward inelastic scattering of neutrinos 2−66936
  Adler, with crossing properties in bound-state formulation of physical nucleon 2−45991
  Adler rule for inelastic lepton-hadron processes 2−82642
  axial charge commutation with axial divergence decuplet contribution to sum rules 2−73766
  Bell-Steinberger, overlapping resonance scattering, exact formalism 2−70249
  Cabibbo-Radicati, high energy contrib. calc. 2−79539
  charged-particle multiplicity distributions, predictions for higher moments 2−70128
  cluster decomposition approach to phenomenology of high energy inclusive and exclusive processes 2−42355
  Compton scattering, photonlike particles in dual resonance models 2−59469
  continuous moment, for $\pi\pi$ scattering 2−55859
  current algebra, by hard-meson technique 2−70123
  current algebra, in two-particle bases and single- particle inclusive processes 2−49514
  deep inelastic electroproduction 2−70158
  Drell-Hearn, derivation from light-cone current commutators 2−73841
  Drell-Hearn, rel. to photon lepton scatt. 2−59408
  electron Compton scattering, tests of complex scaling 2−59426
  electron scattering, elastic and inelastic, from nucleons 2−70162
  electroproduction, model independent deep inelastic 2−55821
  electroproduction, nonforward fixed mass sum rules 2−52559
  Fermi liquids, and Landau theory 2−45331
  Finite Energy, for process $\rho\rho \rightarrow \pi\sigma$ 2−63552
  finite energy sum rules and light cone dominance 2−70188
  finite energy sum rules from light cone commutators 2−63557
  finite-energy, current commutators near light-cone 2−70122
  finite-energy, in Compton and deep-inelastic scattering, analysis using Regge-pole model including cuts 2−63494
  finite-energy, inclusive reactions, Reggeon-particle scattering amplitudes 2−73849
  finite-energy, modification due to piecewise-analytic scattering amplitude of indefinite-metric quantum field theory 2−63457
  finite-energy, of non-Pomeranchukon amplitudes, evidence against resonance saturation 2−63568
  finite-energy, use of inelastic ep scattering at small four-momentum transfers as test 2−45883
  finite-energy for inclusive reactions, φ^3 analyticity 2−66960
  finite-energy pi-pomeron proton scattering, estimation of η_p associated with triple-pomeron vertex 2−42364
  finite-mass, in single-particle inclusive reactions, triple-Regge phenomenology 2−76622
  fixed-mass, derivation from light-cone commutators 2−82663
  fixed-mass, derivation using canonical light-core commutators 2−59397
  generalized and Bloom-Gilman, derivation from null-plane commutators 2−52536
  generalized moments and Kramers-Kronig relations 2−82646
  hadron scatt., connecting low and high energy behaviour 2−42361
  hadron scattering coupling parameters, unitarization of dual models and bootstrap 2−55834
  inclusive, diagonalization using multidimensional Laplace transforms 2−66992
  inclusive, for isotopic spin 2−66958

Sum rules continued
  inclusive cross-section, derivation from charge and strangeness conservation 2−70172
  inclusive cross-section, for various kinds of particles in final state 2−49483
  inclusive processes, derivation of general properties of correlation functions 2−63538
  inclusive processes in hadronic reactions 2−45910
  inclusive reactions, finite mass sum rules 2−49516
  inclusive reactions analogues of superconvergence relations for two-body reactions 2−63550
  isospin, for inclusive cross-sections 2−66968
  lepton-nucleon scatt. linked by sum rule to baryon mass splitting D/F ratio 2−70153
  lepton-nucleon scattering, triplet quark model light-cone algebra of currents 2−76708
  light nuclei, for two-nucleon transfer 2−42553
  light-cone rules rel. to parton dual reson. model 2−59478
  many-particle matrix elements in seniority scheme 2−55949
  mass relations and particle mixings in SU(3) × SU(3) symmetry breaking 2−66910
  meson-baryon elastic scatt. amplitudes 2−70242
  multi-particle reactions, partial wave amplitudes, sum rules from crossing symmetry 2−66977
  neutrinoproduction, nonforward fixed mass sum rules 2−52559
  pairing plus quadrupole-quadrupole interaction for single j level of deformed nucleus 2−73986
  physical-mass, effect of 'weighted' linear transformations on chiral SU(3) × SU(3) mass breaking 2−49480
  Pomeranchukon-pole couplings, general consequences of Regge theory 2−66985
  pseudoscalar meson prod. in νN collisons 2−76724
  Regge cuts from inclusive finite mass sum rules 2−67045
  Regge cuts of pp and A_2A_2 from inclusive finite rules 2−63652
  scattering, constraints of helicity amplitudes from analyticity, crossing symmetry, unitarity 2−52545
  spectra-function, for (8, 8) representation of SU(3) × SU(3) symmetry breaking 2−63484
  spontaneously broken continuous symmetries in an effective-Lagrangian framework 2−55785
  static model for πN, $\pi\Delta$ elastic scattering 2−42399
  for structure functions for polarization in deep inelastic scattering 2−52584
  symmetry point, applic. to $\pi^- p \rightarrow \eta n$ reaction 2−49566
  two-nucleon transfer reactions 2−79781
  unitarity, application to Regge eikonal model, effect on moving pomeron trajectory 2−73793
  unitarized finite energy, application to πN change exchange 2−45921
  weak, e.m. and strong interaction processes 2−79498
  Weinberg's first sum rule, current algebra in broken chiral symmetry 2−73736
  ep scattering, Callan-Gross sum rule, rederivation from light-cone commutator 2−45889
  ep scattering sum rule connecting resonance region of virtual Compton amplitude to deep inelastic region 2−70161
  $\gamma N \rightarrow \pi N$, sum rules relating p and n mag. moments to amplitudes 2−82670
  $K \rightarrow \pi\mu(e)\nu$, form factors determ. from current algebra sum rules using Veneziano model 2−73802
  $K \rightarrow \pi\mu(e)\nu$, sum-rule from SU(3) × SU(3) light cone commutators 2−79558
  $K^\circ \rightarrow \pi^\mp e^\pm \nu$, test of $\Delta S = \Delta Q$ rule in heavy liquid bubble chamber expt. 2−63588
  $K^\circ \rightarrow \pi\mu\nu$, test of $\Delta S = \Delta Q$ selection rule and CP symmetry 2−45940
  $N^{**} \rightarrow N^*\gamma$, sum rules for isovector e.m. transition moments, derivation using combined back and forward dispersion relations 2−49601
  nd scattering, low-energy S-matrix theory, construction of sum rules 2−76758
  ν scattering, current algebra sum rules and scale dimension of chiral symmetry breaking Hamiltonian 2−55818
  ν scattering, inelastic, light-cone behaviour 2−82681
  νN, Adler's sum rule for W_3 from time-space ETC 2−70154
  νN, from low energy theorems 2−42337
  π production, relation of inverse square of π decay const. to integral of scaling function 2−45954
  $\pi K \rightarrow \omega K$, finite-energy rules 2−63635
  $\pi K \rightarrow \varphi K$, finite-energy rules 2−63635
  πN scatt., forward charge exchange, finite energy sum rules 2−59537
  πN scattering, fixed-u finite energy sum rule calcs. using realistic spectral functions 2−63627
  πN scattering length, derivation using broken scale invariance and mass-dispersion relations 2−66911
  $\pi\pi$ scattering in physical region, desication from crossing symmetry 2−70245

Sun
  see also Chromosphere; Photosphere; Solar activity; Sunspots
  α-effect dynamos by the Bullard-Gellman formalism 2−55160
  atmosphere, field of velocities and brightness 2−51862
  atmosphere, minimum temp., model anal. 2−76011
  atmosphere, plasma turbulence in upper layers 2−62801
  atmosphere, upper bound of longitudinal MHD wave frequency 2−74347
  atmospheric five minute oscillations, horizontal propag. 2−81946
  Brans-Dicke theory, general relativity, fast rotating core oblateness, rotation, Li and Be on surface gravitation 2−78430
  brightness temp. determ. using atmospheric attenuation of 4.3 mm waves 2−68914
  circulation and differential rotation studies using similarity analysis 2−81954
  convection zone and sunspot depth 2−55180
  convection zone model, derivation of temperature profile from finite-amplitude convection theory 2−62741
  convective layer, effect of a magnetic field on finite amplitude convection 2−58961
  Culgoora solar magnetograph, image motion due to vibr. 2−85071
  curve of growth for Fe and abundance 2−44974
  differential rotation, unstable Hough modes in tidal equation with negative equivalent depth 2−58544

Sun continued
distance from galactic centre using exponential disc models 2−72972
evolution of solar inner rotation by Eddington-Sweet circulation, solar wind torque 2−55161
fluctuating atm., regression anal. and calibration of multi-channel obs. 2−76017
galactocentric distance to Sun from kinematic parameters from star clusters 2−84959
gravitational field, obs. using twin probe method 2−85052
inert gas abundance rel. to extreme Population I matter 2−81838
inner solar nebula, physical conditions 2−81948
interaction contributions to solar p-p reaction 2−75934
i.r. heterodyne radiometry 2−58549
light deflection, velocity and wavelength changes, wave theory 2−45247
linear velocity dependence of solar rotation on latitude and optical depth 2−44975
metric continuum noise sources, active longitude persistence rel. to solar and interplanetary mag. fields 2−58545
molecules, effects in solar phenomena 2−78584
new astronomy, conference, March 1972, Bloemfontein, S. Africa 2−66071
nonlinear dynamo waves for solar cycles 2−73134
oblateness measurement, nonimaging instrument 2−75939
observation, influence of psychological factors 2−69197
oscillations, five-minute, spatial properties 2−73105
parhelion, origin, 'sun-dog' obs. 2−66196
photographic degradation by atm., resolution enhancement by digital computer processing 2−76040
physics, conference (College Park, Md., USA, April 1972) 2−75935
plasma, cloud, dynamic form. of striations 2−60218
powerspectrum, 5-minute photospheric resonance oscillations 2−55178
quiet, OSO for 1 arc sec. obs. 2−58541
radio mapping, high resolution 2−75936
right ascension, systematic errors in astronomical ephemerides 2−48788
rotation rate from EUV spectroheliograms 2−78583
solar nebula, low temp. condensation accretion process rel. to planetary formation 2−44903
solar-oblateness signal fluctuation rel. to density fluctuations above radiative zone 2−62788
space vehicles observations, reviews 2−66164
stability of magnetic baroclinic flow of unbounded fluid with linear velocity profile 2−78585
structure and processes, review 2−62742
thermal convection, effect of rotation on total heat transport 2−58960
velocity oscillations in atm. 2−73106
P effect on D-region rel. to riometer absorption during polar cap absorption events 2−48575
^{35}Cl abundance from i.r. umbral spectrum 2−55163
Fe abundance, deduced from particle obs. made with nuclear emulsions 2−62745
^{3}He, primordial reduction of neutrino flux 2−81947

corona
abundances and quiet Sun model from radio observations 2−78623
active region models and relative abundances rel. to soft X-ray emission and continuum fluxes 2−78628
chromosphere-corona transition region, structure and energy balance 2−44998
chromospheric and coronal networks, correlation between intensity fields 2−76021
coronal hole, properties from e.u.v. observations 2−62804
corpuscular radiation source, isolated with enhanced velocity 2−62783
current dissipation rel. to energy of solar flares 2−62800
electron density, from occultations of pulsar NP 0532 2−51863
electron density distrib. from K-coronameter data 2−55192
electron density distrib. from K-coronameter data 2−76025
emission line polarization rel. to magnetic field and temperature and density structure 2−48811
enhanced region, temp. and density structure 2−73150
equatorial arches, K-coronameter 2−76032
eruptive phenomena, radial vel. meas. 2−73152
e.u.v. and X-ray spectroheliograms 2−76030
e.u.v. spectroheliograms, temp. gradient and electron density maps 2−76022
exciter of type III bursts and coronal temp., time profiles and decay time const. 2−69193
F and K components rel. to electrons and dust densities in solar system 2−62803
Faraday rotation of Crab radiowaves and local structure in corona 2−66236
form change between 7 March and 7 June 1970, coronameter obs. 2−78625
gyro-synchrotron radiation from plasma, temperature effects 2−81950
HELIOS probe, design and development 2−48789
helmet evolution during solar cycle 20 ascending phase 2−78624
hole, properties, e.u.v. observations 2−76029
inner, white light, obs. for compressional waves during solar eclipse 2−76033
ion-sound current instability, turbulent resistivity 2−78616
magnetic field, practical representation 2−76023
magnetic field configs. of field-aligned particle events 2−62774
magnetic field strengths, direct measurement from type IV burst 2−76037
magnetic fields, atlas 2−73151
magnetic struct. evolution, Hα photographs obs. 2−62807
mathematical analysis and interpretation, separation into electronic and dust scattered components 2−73153
model for drift pair and hook burst emission from corona 2−62805
moving type IV disturbance, brightness variation 2−76034
NE, streamer during 7th March, 1970, eclipse, hydrodynamical equation 2−76036
origin of flares, following collapse of streamer 2−75997
outer coronal forms obs. 2−76028
phenomena associated with proton flares, solar activity 2−44997
phenomena during proton flares 2−44996

Sun continued
corona continued
Pioneer IV, solar occultation, transformation of signal polarization angle to plane of ecliptic 2−44999
plasma, electron impact excitation of ions, interpolation formulae 2−74244
polarigraphic observations of white light corona during 1970, March 7 total eclipse 2−78576
prominences and filaments, e.u.v. spectra 2−76002
radiation distribution, meas. using extreme u.v. and X-ray spectroheliographs 2−62808
radio emission, source of slowly varying component at cm. and mm. wavelengths 2−76020
radio obs. of plasmoids and shocks, rel. to mag. fields 2−62806
radiobursts, coronal scattering at hectometer and kilometer wavelengths 2−55172
rocks, in uniaxial strain 2−75454
rotation of active regions 2−76035
rotation rate of material across disc from EUV spectroheliograms 2−78583
shock wave propag. responsible for type II radio bursts 2−81952
spatial structure, effect of photospheric- chromospheric mag. field networks 2−78604
spectral green line intensity, rel. to limiting primary rigidity of solar diurnal anisotropy of cosmic rays 2−62744
stable coronal magnetic field configurations rel. to structure of solar continuum radio bursts 2−62761
streamer models, computer programme from numerical integration of Thompson scattering 2−76026
streamers, current sheets, Pneuman's model 2−81945
streamers, photometric and polarimetric analysis during 1970, March 7 Mexican eclipse 2−78575
talc, rel. to appl. as press. transmitting medium at low temp. 2−73248
teflon, rel. to appl. as press. transmitting medium at low temp. 2−73248
temperature-density structure, energy transport mechanisms 2−76031
three channel SEC vidicon system for photometric obs. 2−76024
transition region with chromosphere, review of physical properties 2−73148
transport of cosmic rays, in corona rel. to photospheric granular cell boundaries 2−44984
transport of scatter-free electrons rel. to associated flares 2−78629
type III burst, coronal site, source of interplanetary electrons 2−62758
type III radio bursts rel. to neutralization and stabilization of particle streams in corona 2−48798
type IV emissions, pulsating modulations and peculiar absorptions 2−62754
white light, movement of bright source 2−78627
X-ray, surrounding quiescent filaments, structure 2−78626
X-ray structure 2−75953
X-rays from condensations and development of active regions 2−76038
C, O_2, Ne density dependent ionization balance 2−66231
Ca/H abundance ratio from observations of Ca Xv lines 2−55159
CrTe, anomalies near Curie temp. 2−72148
Fe abundance and electron temperature meas. during 1966, November 12 eclipse 2−76027
Fe spectral line identification and abundance 2−62748

eclipses
7 March 1970, continuum emission obs. in chromosphere 2−66233
1019, April 8, from al-Biruni's solar data, det. of lunar acceleration 2−65427
1966, November 12, meas. of coronal Fe abundance and electron temperature 2−76027
1970, March, hydrodynamics of large NE coronal streamer 2−76036
1970, March 7, atmospheric pressure and temperature changes during totality 2−57937
1970, March 7, effect on 3-50 eV photoelectron flux in lower ionosphere 2−65948
1970, March 7, effect on Na D-line emission from the atmosphere 2−65885
1970, March 7, Gulf of Mexico, response of deep scattering layers in sea 2−48416
1970, March 7, meteorological rocket data 2−65648
1970, March 7, photometric and polarimetric analysis of coronal streamers 2−78575
1970, March 7, polarigraphic observations of white light corona 2−78576
1971, Feb. 25, partial, time of contact determ. 2−73104
1972, July 10, site surveys in North America 2−44976
effect on sporadic-E ionization 2−65972
July 10th 1972, obs. in North America 2−73107
recurrence of solar and lunar eclipses 2−73102
total, Fresnel diffraction patterns for time element correlation 2−58001

flares
1968-71 cosmic ray events flare location 2−62770
1970, August 12, soft X-ray flare at limb 2−78611
1971, Jan 24., composition and energy spectra of heavy nuclei 2−78600
1971, January and September, composition and energy spectra of heavy nuclei 2−58556
1972 August, resurgence of solar activity 2−81956
acceleration of electrons and emitted radiation 2−75999
activity rel. to sporadic geomag. storms 2−75634
August 1972, geophysical effects 2−81955
chromospheric, motion rel. to magnetic field 2−51861
chromospheric flare activity rel. to atmospheric electrical elements in lower troposphere 2−65797
chromospheric knots, motion of details 2−51860
coronal origin, following collapse of streamer 2−75997
coronal transport of scatter-free electrons rel. to associated flares 2−78629
current interruption electrostatic discharge model 2−78613
current limitation, ion-sound current instability, current dissipation 2−62800

Sun continued
flares continued
c.u.v. flares rel. to −F subflares and X-ray, $H\alpha$ and radio correlations 2−62798
development with time, initial, explosive and decay phases 2−62793
discharge plasma comparison, X-ray spectra and microwave emission 2−76000
E-layer recombination coeff. meas., solar flares 2−44756
electron acceleration region and ion density in X-ray source region 2−55188
energetic solar particle events, international cooperative survey 2−78610
e.u.v. and X-ray spectroheliograph for obs. 2−78578
e.u.v. emissions of solar flares, sudden frequency deviations rel. to OSO-6 obs. 2−78589
e.u.v. flare emission rel. to OSO 4 and 6 observations 2−78619
e.u.v. flares rel. to X-ray and microwave bursts 2−62799
e.u.v. obs. with rocket borne SEC vidicon system 2−44990
filament disintegration and associated activities 2−55177
flare producing regions, statistical analysis of relationship to geomagnetic storms, Forbush decreases and SC + SI events 2−54925
gamma rays between 50 and 500 MeV, satellite meas. 2−73142
geomagnetic storms of September and June 1963, correlation 2−51658
high energy electrons from flares rel. to propagation conditions in interplanetary space 2−55190
high energy gamma-rays, search for radiation from flare regions 2−44995
ion-sound current instability, turbulent resistivity 2−78616
ionization equilibrium and line radiation, under flarelike conditions 2−51857
ionospheric response obs. 2−75954
i.r. emission 2−75945
magnetic boundary morphology, flare generation 2−76008
magnetic configurations and magnetic energy release from active regions 2−75998
magnetic field configurations associated with flares 2−55186
matched patrol telescope systems 2−78614
MHD, Petschek's mechanism, modification and criticism 2−81762
microwave bursts, free-free absorption of gyrosynchrotron radiation 2−75995
microwave bursts of different types in relation to optical flares and other allied events 2−62794
multiple components in impulsive phase of flares 2−78617
neutron burst, effect on radiation belt protons 2−62348
optical, latitudinal distribution and nature of occurrence 2−58557
particulate, satellite obs. of composition in $6\leqslant Z\leqslant 26$ charge range 2−78601
Petschek's mechanism, variations along current sheet 2−76004
photospheric magnetic fields, longitudinal component 2−76009
physical mechanism for production rel. to energy requirements 2−44994
plage activity and small flares at 10830Å 2−81957
plasma arcs and loops, trapping in cosmic atm. 2−78577
plasma heating by high energy electrons and non-thermal X-ray emission 2−81951
plasma phenomena in high energy, astrophysics 2−78432
production of flares rel. to dynamo action 2−78618
proton, near limb, development and spatial structure 2−44996
proton, near limb, development and spatial structure (from Nov. 1969) 2−44997
proton and non-proton, comparison of physical conditions 2−51859
proton events, high energy, forecasting method 2−62771
proton events, variations in X-ray flux 2−44978
proton flare, near limb, development and spatial structure (from Nov 1969) 2−44997
proton flares production from sunspot groups, magnetic polarities 2−44993
proton shielding of space vehicles 2−85065
proton to alpha particle ratios change during storm particle event 2−73132
relativistic electrons, acceleration from keV electrons 2−73143
rotational motion of prominence ejected from rotating flare 2−44992
shock wave production, fine structure obs. 2−62736
soft X-ray and microwave observations of hot regions in solar flares 2−48795
spectra, location of continuous emission regions 2−51858
spectral analysis of highly inhomogeneous chromospheric flares, radiation dilution 2−62797
stimulation of free oscillations of Sun 2−66227
subflares, hard X-ray emission, detection using ionospheric D region 2−66228
very heavy nuclei, overabundance, meas. by OGO 5 2−76001
white light, association with $H\alpha$ flares and sudden freq. deviations 2−55187
white-light, thick-target processes 2−73146
X-ray, effect on ionospheric electron density 2−72879
X-ray, polarization obs. 2−73121
X-ray and microwave bursts, correlation 2−51848
X-ray effects on 164 kHz, radio-wave propagation 2−81736
X-ray emission, 10-20 keV, during initial stage 2−85051
X-ray emission from thermal and non-thermal flares, OSO-7 observations 2−78590
X-ray periodic heating mechanism 2−62749
X-ray polarization meas. of Intercosmos-4 rel. to OSO-5 meas. 2−78591
X-rays and limits on gamma line emission from November 1971 flare 2−78592
XUV and radio emission of 24 October, 1969 event 2−76005
Ar XII-XVI lines in e.u.v. spectra of flare 2−58546
Ca XIV-XVIII lines in e.u.v. spectra of flare 2−58546
Fe XIV, XV, XXIV lines in e.u.v. spectra of flare 2−58546
H_α flares rel. to chromospheric response to downward propagating shock waves 2−78620
He D_3 emission obs. using narrow band filtergrams 2−62795
He enrichments rel. to solar wind, He/H relative abundance measurements 2−55189
SI XIII, Ca XIX, Fe XXV, calc. of wavelengths in X-ray region 2−85050

Sun continued
magnetism
activity correl. with gravitational signals in Weber's expt. 2−44824
chromosphere, force free field configurations 2−76014
chromosphere and lower corona magnetic field, practical representation 2−76023
chromospheric fields, analogue model 2−76010
corona, atlas of fields 2−73151
coronal field configs. of field-aligned particle events 2−62774
coronal fields, rel. to plasmoids and shocks 2−62806
coronal magnetic field strength, direct measurement from type IV burst 2−76037
coronal struct. evolution, $H\alpha$ photographs obs. 2−62807
diffusion of fields in weak plage regions 2−78605
dynamical behaviour of force-free field, nonlinear study 2−78582
dynamo based on horizontal shear 2−58542
evolution over 11 year period, distrib. of sunspots, faculae and prominences 2−55181
field, rel. to active longitude persistence for metric continuum noise sources 2−58545
field enhancement due to optokinetic effects via optoelectrical effect 2−66656
fields derived from $H\alpha$ filtergrams 2−75938
flare, mag. field immediately before and after, polarimetry 2−62796
flare generation, magnetic boundary morphology 2−76008
flare generation, photospheric magnetic field variations 2−76009
flares and magnetic configurations and magnetic energy release from active regions 2−75998
force-free mag. field structures, role in solar activity 2−75985
inferred interplanetary magnetic field variations with solar magnetic cycle 2−78572
line formation, mean depth 2−73112
mean field rel. to interplanetary field (1969) 2−75937
meridional circulation of field 2−58543
microwave burst generating region, mag. field decay 2−48796
Petschek's mechanism, variations along current sheet 2−76004
photosphere, rel. to chromospheric features 2−66234
photospheric fields, flare-associated, real-time anal. 2−75980
photospheric fields, latitude distrib. rel. to temp. distrib. 2−75976
photospheric mag. fields, meas. 2−62789
photospheric velocity field surrounding sunspots 2−75981
polar magnetic field, variations (1960-1971) 2−75941
polarity of sunspot groups rel. to production of solar proton flares 2−44993
quiscent prominences, two-dimensional model 2−73145
small scale fields, energy spectral analyses 2−76015
solar corona, det. from Faraday rotation of Crab radiowaves 2−66236
solar flares, associated magnetic field configurations 2−55186
spherical fluid model with convection zone 2−75715
sunspot, splitting of π-component in spectra 2−73138
sunspot fields, measurement methods 2−78602
sunspot formation from mag. flux concentration 2−75994
sunspot rel. to moving magnetic features 2−78608
transverse field, rel. to chromospheric flares and surges 2−51861
young active region, dynamics of mag. flux 2−75972
He-D_3 spectroheliograms, distrib. of photospheric mag. field 2−73103

prominences
absorption features, observation at 3.5 mm wavelength 2−76007
active, formation of condensations, density and intensity variations 2−55185
bright arch of April 24 1971, $H\alpha$ spectra and radio emission 2−55182
filaments, rel. to H_α loops 2−66203
flare, mag. field immediately before and after, polarimetry 2−62796
formation of prominences, theoretical study 2−78621
line intensity ratios, $E(H\alpha)/E(\text{He D3})$ and $E(H\beta)/E(\text{He D3})$ 2−76006
loop stability compared to M82 galactic prominences 2−55011
macroscopic velocity fields, spectra and monochromatic images 2−55183
quiescent, electric current calc. method 2−73145
quiescent, hydrodynamics of formation 2−78615
quiescent, internal motion, fine structure wavelength shift 2−55184
quiescent, response of the triplet radiation to increase in u.v. flux from flares 2−75996
quiescent, temperature-density structure, energy transport mechanisms 2−76031
rotational motion of prominence ejected from rotating flare 2−44992
solar magnetic field, evolution over 11 year period 2−55181
u.e.v. spectra, quiet corona 2−76002
X-ray activity 2−73116
X-ray emission in 1-55 Angstrom region from active limb prominence 2−48794
Zeeman splitting 2−44991
He, ionized, in quiscent and loop 2−73144
He I and H lines intensity ratio in prominence and chromosphere 2−66229

radiation
see also Sunlight
automated solar seeing measurements 2−78581
backscatter of solar resonance radiation by interstellar gas in direction of solar apex 2−85006
backscatter of solar resonance radiation by interstellar Hi and HeI in solar system 2−55078
coronal X-ray structure 2−75953
cosmic ray spectrum, integral production multiplicities for computing 2−73131
cosmic rays, diurnal anisotropy, limiting primary rigidity rel. to coronal green line intensity 2−62744
cosmic-ray diurnal intensity variation during Forbush decreases between 2 and 20 GV, diffusion processes 2−73860
Earth atmosphere turbulent elements, size distribution using solar scintillation meas. 2−62171
e.m. wave conversion from electron plasma waves 2−69185

Sun continued
radiation continued
e.u.v. heating in upper atmosphere, annual and sub-annual effects 2−84840
e.u.v. heating of atmosphere, annual and sub-annual effects rel. to density variations 2−84841
excess oblateness signal, relation to photospheric faculae 2−51856
flares, and acceleration of electrons 2−75999
gamma ray flux and energy spectrum 2−62750
gyro-synchrotron from coronal plasma, temperature effects 2−81950
hard X-ray bursts, models, decay characteristics 2−75955
high energy gamma-rays, search for radiation from flare regions 2−44995
intensity rel. to weather pattern 2−68878
i.r., 110-500μ region, brightness obs. 2−75956
irradiance meas. rel. to comparisons of International Pyrheliometric Scale with absolute radiation scale 2−73461
limb darkening in the forbidden MgI λ4571 line 2−45000
Lyman α radiation, resonant scattering by interstellar hydrogen 2−78433
microwave burst thick-target processes for electrons in flares 2−73146
neutrino absorpt., ^{37}Cl cross section eval. 2−67212
neutrino flux, existence of reson. in ^{3}He + ^{3}He system 2−69188
neutrino flux calc. of effect of dilaton theory of gravity 2−79632
neutrino-producing reactions, resonant energy depend. of ^{3}He + ^{3}He 2−82990
nuclear gamma rays associated with class M X-rays, OSO-7 obs. 2−62751
oblateness signal, relation to photospheric faculae 2−51855
penetration through atmosphere and plant canopies 2−48475
radiometer meas. discrepancy and aperture geometry 2−51846
Raman scattering, effect on distribution of molecules over vibrational levels 2−75940
reflection and absorption by cloud layers 2−48486
resonance scattering from Ba ion cloud released at 31000 km 2−62303
soft X-rays, type III acceleration mechanism, source volume establishment 2−73122
solar constant and air mass zero solar spectral irradiance specifications 2−78580
solar constant and solar spectral irradiance, radiation scales 2−78579
solar flux and equatorial electrojet effects on diurnal development of total electron content of equatorial anomaly 2−65921
solar flux radiometer, economical design 2−65760
solar soft X-radiation photometry with broad band detectors for signal-energy conversion function 2−73117
sunlight, energy and spectral distribution from high- altitude observations 2−75605
thermal solar radiation reflected from ocean surfaces 2−65759
transfer equation integration, choice of boundary conditions 2−62740
type-III radiation, transformation of electrostatic waves in cold magnetized plasma, nonlinear interaction of plasma waves 2−46782
u.v., effect on selected optical materials, simulation 2−49440
u.v., upward and downward flux atmos. 2−62251
wind, anisotropy, thermal, due to binary encounters 2−73128
wind enhanced density irregularities rel. to interplanetary scintillation of radiosources 2−85058
X-radiation, hard, from subflares, detection using ionospheric D region 2−66228
X-ray burst, spectral characteristics of primary and Earth albedo X-rays 2−62752
X-ray burst, spectral development 2−58550
X-ray burst, thick-target processes for electrons in flares 2−73146
X-ray effects on 164 kHz, radio-wave propagation 2−81736
X-ray emission in 1-55 Angstrom region from active limb prominence 2−48794
X-ray emission in solar atmosphere, height distribution, satellite obs. 2−69184
X-ray flare, 24 October, 1969 obs. 2−76005
X-ray flux, apparent control of D-region A$_1$ absorption 2−58078
X-ray flux, applic. to sudden ionospheric disturbance interpretation 2−75954
X-ray flux, variations during proton events 2−44978
X-ray photographs 2−73116
X-ray polarization meas. of Intercosmos-4 rel. to OSO-5 meas. 2−78591
X-ray spectra of flares, comparison with laboratory discharge plasma 2−76000
X-rays, hard, scintillation detector obs. 2−62631
X-rays and limits on gamma line emission from November 1971 flare 2−78592
X-rays from coronal condensations and development of active regions 2−76038
XUV fluxes, Solrad 10 obs. from July-Dec (1971) 2−73120
Ar arc lamp 400 KW for solar simulation 2−78414
He triplet radiation in prominences response to increase in u.v. flux from flares 2−75996

radiation, corpuscular
acceleration time of particles in solar atmosphere 2−66206
alpha particles, 17th Dec. 1971 event, ang. distrib. meas. 2−62769
alpha particles, 17th Dec. 1971 event, flux and spectra obs. 2−62768
composition meas. with nuclear emulsions flown on sounding rockets 2−78597
coronal streamer obs. during 7th March, 1970 eclipse 2−76036
cosmic ray activity, post solar maximum, 1968-71 2−62770
cosmic ray events, riometer absorpt. meas. 2−62765
cosmic ray generation, rel. to microwave type IV bursts 2−75962
cosmic rays, acceleration, rel. to microwave type IV radio bursts 2−85025
cosmic rays, effect on reson. freqs. of earth-ionosphere cavity resonator 2−62353
cosmic rays, identification with solid dielec. track detectors 2−63714
cosmic rays, rel. to light elements prod. and solar system origin 2−66141
cosmic-ray electrons in 3 to 12 MeV range, temporal variations 2−66192

Sun continued
radiation, corpuscular continued
cutoff rigidity during polar cap absorption event at commencement of geomagnetic disturbance 2−48802
diffusion model of solar cosmic radiation through interplanetary medium 2−75974
electrons and protons, rapid access to polar caps 2−65842
energetic electron emission, associated with radio bursts 2−75957
energetic solar particle events, international cooperative survey 2−78610
energetic solar particles, observations during solar cosmic ray events 2−85054
energetic storm particle event, change in proton to alpha particle ratios 2−73132
flare accelerated particles, satellite obs. of composition in $6 \leqslant Z \leqslant 26$ charge range 2−78601
heavy nuclei, composition and energy spectra 2−78600
ionospheric D-region, ionization in central latitudes 2−51650
lunar photon albedo from galactic and solar proton bombardment 2−66148
lunar wake in solar wind flow, magnetic-field anomalies 2−69134
magnetosphere, solar particle event effects on energetic particle population 2−68941
neutral sheets in solar wind, structure and dynamics 2−48803
neutrino, discpreancy between astrophysical predictions and terrestrial exptl. obs. 2−44979
neutrino capture rate in ^{37}Cl 2−55960
neutrino emission rel. to nuclear physics and theoretical solar structure and evolution 2−58553
neutrino flux, reduction by primordial ^{3}He in Sun 2−81947
neutrino-photon interaction, effect on solar neutrino flux 2−85055
neutron burst, effect on radiation belt protons 2−62348
neutron flux, 1-20 MeV, upper limit 2−62775
neutron flux, satellite obs. and correlation with solar activity 2−66222
neutrons, detection, balloon and satellite expts., Max-Planck Inst. 2−51692
neutrons, large area detector for search in 2-100 MeV range 2−72818
particle events, Fe abundance obs. 2−62745
particle flux rel. to dayside limit of closed geomagnetic field lines 2−68982
pitch angle distribution of energetic solar particles 2−75968
positrons, low energy unstable CNO emitters 2−66214
proton access effects during interplanetary field sector boundary crossing 2−62767
proton event, O$_3$ obs. in mesosphere 2−84803
proton events, end prediction from real-time data obs. 2−62772
proton events, high energy, forecasting method 2−62771
proton flux propag. over polar caps, uneven illumination analysis 2−65878
protons, 17th Dec. 1971 event, ang. distrib. meas. 2−62769
protons, 17th Dec. 1971 event, flux and spectra obs. 2−62768
protons, entry into magnetosphere, polar cap structures 2−65857
protons, interaction with Moon 2−66149
protons, obs. from widely separated spacecraft 2−75970
protons, penetration into magnetosphere, electrostatic field 2−62316
protons, polar cap. structs. during passage of interplanetary discontinuities 2−62766
protons injection onto interplanetary field lines, relation to times and positions of solar radio bursts 2−62759
quiet-time electron increases rel. to outer solar system modulating mechanism 2−66193
reconnection rate of geomagnetic field meas. using interplanetary solar particle discontinuities 2−62727
relativistic electrons associated with solar flares 2−73143
response of lower atm. pressure 2−84811
search for neutrons of solar origin using balloon borne detectors 2−73133
solar flare characteristics and magnitude of solar cosmic ray increase 2−75969
solar protons, absorpt. in Earth's atmosphere, solar proton event, Nov. 18, (1968) 2−58123
terrestrial noctilucent clouds, heavy metal particles, possible solar origin 2−65888
transport of cosmic rays, in corona rel. to photospheric granular cell boundaries 2−44984
type III bursts at 23.5 and 30 MHz, relative polarization 2−81953
above vertical geomagnetic cutoff, >75 GeV 2−55175
wind, adiabatic cooling of protons for spiral interplanetary mag. field case 2−73127
wind, boundary with magnetosphere, wave coupling at collisionless plasma discontinuity 2−83615
wind, closed mag. structures assoc. with interplanetary shock waves 2−66219
wind, collisionless protons, comparison of kinetic and hydrodynamic descriptions 2−62785
wind, component in low latitude magnetic daily variation 2−44768
wind, compressions and rarefactions, stream dynamics 2−62776
wind, concentration averaged in time and space 2−62782
wind, corotating structures models 2−66218
wind, correlation between local plasma density fluctuations and oblique nonlinear MHD waves 2−62784
wind, correlation of fluctuations with solar and terrestrial events 2−78387
wind, darkening of lunar surface 2−66154
wind, discrete wave packet theory 2−66213
wind, electron density irregularity spectrum 2−58552
wind, excitation and propagation of upstreaming e.m. wave 2−66211
wind, Explorer 35 obs. of electron density, temp. and anisotropy 2−66215
wind, extended power spectra of ion charge flux 2−62777
wind, flow past planets Earth, Mars and Venus 2−78574
wind, geometry nonlinear interaction with galactic cosmic rays 2−48653
wind, He abundance variations 2−62780
wind, He relative abundance ratio rel. to solar activity 2−75975
wind, heating, review of models 2−69187

Sun continued
radiation, corpuscular continued
wind, high velocity fluxes and shock waves, indication from decametric radio emission from Jupiter 2-48801
wind, identification of tangential discontinuities 2-75973
wind, implantation of ions in lunar dust grains as explanation of ultrathin amorphous coatings 2-44929
wind, interaction with interstellar medium, model 2-51853
wind, interpenetrating ion beams 2-66221
wind, interplanetary solar electrons, meas. during solar quiet times 2-75967
wind, isolated coronal sources of enhanced velocity 2-62783
wind, lunar response, investigation of differences in e.m. transfer function 2-62683
wind, lunar wake in magnetohydrodynamic model, numerical calc. 2-58454
wind, multispacecraft data rel. to mapping of large-scale interplanetary mag. field 2-62729
wind, obs. using power spectrum of interplanetary scintillation of radio sources 2-66205
wind, perturbations by Moon rel. to anomalies in interplanetary mag. field 2-62730
wind, radio scattering obs. as remote sensing probe technique 2-62781
wind, relative role of limiting factors 2-73129
wind, rotational discontinuities 2-69189
wind, spatial disturbances of plasma parameters 2-73130
wind, speed variations, 1964- 1967, autocorrelation anal. 2-66208
wind, tangential discontinuities 2-69190
wind, thermal properties 2-44983
wind, three-dimensional model 2-66212
wind, time series data and power spectral analyses of high speed streams 2-62786
wind, twenty seven day recurrences in speed, Mariner 2 obs. 2-66217
wind, two-fluid model including spiral structure of interplanetary mag. field 2-66207
wind, unipolar interaction with Mercury, steady state bow shock problem 2-69145
wind, unipolar interaction with planet Mercury, steady state bow shock problem 2-44955
wind, velocity and flux dependence of He abundance 2-62779
wind, velocity changes, relationship with atmos. circulation 2-44704
wind discontinuities, double structure, dissipation mechanisms 2-66216
wind discontinuities, effect on magnetosphere, space-time correlations 2-72823
wind electrons, heat cond. in turbulent mag. field 2-66220
wind fluctuations rel. to natural oscillations of type-I comet tails 2-81937
wind interaction fronts, structure and orientations, Pioneer 6 data 2-66209
wind meas. for lunar atmosphere upper limit 2-58470
wind model including latitude effects 2-78603
wind models, amplitude of equatorial convergence 2-62787
wind observations on lunar surface with Apollo-12 alsep 2-85057
wind particle distrib. in aurora 2-65909
wind perturbations rel. to lunar remanent magnetization 2-66150
wind plasma, interaction with Earth's mag. field 2-80225
wind plasma, rotational discontinuities closed system of hydrodynamic equations 2-48800
wind plasma, spherically symmetric outflow 2-48799
wind plasma interaction with moon Apollo 15 subsatellite 2-55129
wind rotational discontinuity, magnetic effect upon Earth's field 2-72922
wind structure determ. by corotating coronal inhomogeneities, arbitrary perturbations 2-66210
wind temperature, macroscale relation with bulk velocity 2-62778
wind torque effects on evolution of solar inner rotation, calc. by Eddington-Sweet circulation 2-55161
H, ^{2}H, ^{3}He abundances in solar wind and sun comparison with ratios on Earth and meteorites 2-44982
H and He bulk speeds in solar wind, interplanetary shocks 2-62764
He enrichments in major flares rel. to solar wind, He/H relative abundance measurements 2-55189
He in cosmic rays, relative abundance 2-75971
He$^+$ ion flux in solar wind rel. to intensity of resonantly backscattered HeII solar radiation at 304 angstroms 2-55157
Hi atoms flux in solar wind rel. to intensity of resonantly backscattered Lyman α radiation 2-55157

radiation, radiofrequency
active regions, polarization at 9.5 mm 2-66204
bright arch prominence of April 24 1971, thermal emission 2-55182
brightness temperatures and frequency spectra of local sources in 8 to 16 mm wavelength range 2-51851
burst, Faraday rot. and tangled mag. fields 2-62806
bursts, 3 cm, obs. of electron temp. 2-73126
bursts, correlation with sudden increases in total electron content of ionosphere 2-51648
bursts, distrib. of peak flux- density spectra 2-75958
bursts, large amplitude plasma waves, Rayleigh and Raman scattering 2-75961
bursts, microwave and X-ray, correlation studies 2-51848
bursts, spectra characteristics associated with energetic electron emission 2-75957
bursts in decametre range, type III, obs. 2-69193
bursts relation of time sequence and position to those where protons were injected onto interplanetary field lines 2-62759
chromosphere, chromosphere-corona transition and corona, source of slowly varying component at cm. and mm. wavelengths 2-76020
chromospheric inhomogeneities, quiet Sun brightness distribs. at millimeter wavelengths 2-85053
circular polarization of 3.15 cm radio emission of local sources and bursts 2-51849
continuum and type III bursts, simultaneous, at decametric wavelengths 2-58551
coronal abundances and quiet sun model from radio observations 2-78623
Culgoora radioheliograph, multiple frequency operation 2-69186

Sun continued
radiation, radiofrequency continued
c.u.v. flares rel. to $-$F subflares and X-ray, Hα and radio correlations 2-62798
decameter bursts, frequency drift and time splitting 2-48797
e.u.v. flares rel. to X-ray and microwave bursts 2-62799
flare, 24 October, 1969 obs. 2-76005
flare, mag. field immediately before and after, polarimetry 2-62796
flux density obs. at 350 MHz 2-81949
frequency separation in structure of solar continuum radio bursts 2-62761
local sources of radio emission in 0.9 to 1.5 mm wavelength range 2-51852
microwave burst generating region, mag. field decay 2-48796
microwave bursts, free-free absorption of gyrosynchrotron radiation 2-75995
microwave bursts of different types in relation to optical flares and other allied events 2-62794
microwave emission of flares, X-ray spectra of flares, comparison with laboratory discharge plasma 2-76000
microwave flux, effect on reson. freqs. of earth-ionosphere cavity resonator 2-62353
microwave type IV bursts, characteristics and generation of solar cosmic rays 2-75962
microwave type IV radio bursts and acceleration of solar cosmic rays 2-85025
moving type IV bursts, isolated, model of evolution of flux density and polarization 2-62755
moving type IV disturbance, brightness variation in corona 2-76034
non-thermal emission in absence of flares 2-55174
proton flare radio burst characts. 2-62771
proton fluxes, solar and interplanetary configs. of field-aligned events 2-62774
proton streams rel. to large scale wind structs. 2-62773
quasiperiodic pulsations, d.m. wavelengths 2-75966
radio bursts, temperature and emission measure of three events 2-44980
radio emission at metre wavelengths, spectra and polarization during noise storms 2-62762
radio emission at microwaves, long-period oscillations in bursts 2-44981
radiobursts, coronal scattering at hectometer and kilometer wavelengths 2-55172
reflected from Earth's surface, effect of haze layers on obs. 2-62269
scattering and refraction effects on observable source properties at 80 MHz 2-62756
slowly varying component at mm wavelengths 2-62760
soft X-ray and microwave observations of hot regions in solar flares 2-48795
solar microwave at 2800 MHz and burst characteristics 2-78594
steady state, linearized, inhomogeneous solar wind flow problem, critical point regularity conditions, asymptotic solutions 2-44985
temperature depressions on brightness-temperature contour maps at 3.3 mm wavelength 2-78596
time profile comparisons of type IV bursts at 1.5 metres with total flux of Hα emission 2-51850
type II bursts, shock wave propag. through corona 2-81952
type II meter bursts, heating of solar plasma 2-75963
type III burst, coronal site, source of interplanetary electrons 2-62758
type III bursts, electron excitation 2-75960
type III bursts, relative positions of fundamental and second harmonic 2-62757
type III bursts and simultaneous continuum position obs. at decametric wavelengths 2-78595
type III noise bursts, below 100 KHz, OGO 3 2-75964
type III radio bursts, dynamic theory 2-73124
type III radio bursts, possible mechanisms for emission at frequencies much higher than the plasma frequency 2-55173
type III radio bursts and scattering of beam of plasma waves by acoustic turbulence 2-62753
type III radio bursts rel. to neutralization and stabilization of particle streams in corona 2-48798
type IIIb burst, precursor of decametre type III burst 2-73123
type IV burst, direct meas. of coronal magnetic field strength 2-76037
type IV bursts, time behaviour of continua during initial stage 2-73125
type IV emissions, pulsating modulations and peculiar absorptions from corona 2-62754
type IV outburst of March 1970, absorption and emission microstructures 2-75965
Type IV radio burst-active centres, temporal distribution over solar cycle 2-62763
U shaped type IV bursts and l.f. radiation from relativistic electrons in magnetoplasma 2-75959
X-ray burst, associated with v.l.f. disturbances 2-73119

spectra
see also Sun/corona; Sun/flares; Sun/prominences
alpha particles, during 17th Dec. 1971 event 2-62768
atmosphere, transition zone, structure in active regions 2-73137
bright arch prominence of April 24 1971, Hα spectra 2-55182
chromosphere continuum emission obs. at 7 March 1970 total eclipse 2-66233
chromosphere continuum obs. at eclipse and model of low chromosphere 2-66232
chromospheric short-lived brightening observed in Hα and Ca II K-line 2-78612
colour indices for the Sun derived from stellar and Uranus observations 2-85056
coronal green line intensity, rel. to limiting primary rigidity of solar diurnal anisotropy of cosmic rays 2-62744
coronal lines, 5303 Å and 6374 Å, reduced intensities 2-73110
coronal visible lines, electron temperature and emission measure 2-73149
cosmic rays, integral production multiplicities for computing 2-73131

Sun continued
spectra continued
c.u.v. flares rel. to −F subflares and X-ray, Hα and radio correlations 2−62798
daylight irradiance for air mass 2 2−72799
diatomic molecular lines in sunspot spectra, 4900-6441 Angstrom range 2−62743
disk chromosphere, fine structures, high resolution spectroscopy 2−76018
Doppler spectroheliograms, horizontal velocity field, surrounding sunspots 2−75993
e.u.v., prominences and filaments 2−76002
e.u.v. 60 to 385Å, wavelengths and identification 2−51845
e.u.v. and X-ray spectroheliograms, obs. of corona 2−76030
e.u.v. emissions of solar flares, sudden frequency deviations rel. to OSO-6 obs. 2−78589
e.u.v. flares rel. to X-ray and microwave bursts 2−62799
e.u.v. obs. of chromospheric network 2−66235
e.u.v. quiet solar spectrum, emission measure and relative abundances 2−75943
e.u.v. solar flare emission rel. to OSO 4 and 6 observations 2−78619
e.u.v. spectroheliograms, temp. gradient and electron density maps 2−76022
flares, location of continuous emission regions 2−51858
Fraunhofer lines, intensity fluctuations rel. to contribution functions 2−48792
interferometry applied to small scale visible features 2−55164
i.r., 110-500μ region, brightness obs. 2−75956
i.r., Arizona atlas, 21492-25583 Å 2−69182
i.r., Arizona NASA atlas, 12187-17731 Å 2−69179
i.r., Arizona NASA atlas, 19374-20930 Å 2−69181
i.r., Arizona NASA atlas, 25583-30920 Å 2−69183
i.r., Arizona NASA atlas, 4 m spectrometer 2−69180
i.r., Arizona-NASA atlas, 1.4 μ H_2O band 2−69178
i.r. emission from flares 2−75945
i.r. umbral spectrum, HCl fundamental vibration rotation bands and ^{35}Cl abundance 2−55163
limb effect, radial currents in atmosphere 2−66197
line formation, mean depth in a magnetic field 2−73112
line intensity ratios, E(Hα)/E(He D3) and E(Hβ)/E(He D3) 2−76006
Lyman α radiation distribution 2−62731
Lyman continuum, difference between poles and equator in region of formation 2−78588
molecular lines, obs. of sunspot umbral velocity oscillations 2−75988
multichannel solar spectrometer at Sacramento Peak Observatory 2−76051
new lines obs. during total eclipse, 3600-6650 Å region 2−73115
nonlocal thermodynamic equilibria, empirical analysis 2−55165
photographic factors influencing the intensities of Fraunhofer spectrum lines 2−48791
photosphere, synthesis for heavier element abundance det. 2−58554
photosphere-chromosphere transition region, brightness temperature minimum 2−62802
photospheric abundances, spectrum synthesis 2−69192
photospheric fluctuations, coherence and phase spectra, radial velocity 2−75950
photospheric light, polarization near solar limb 2−66223
profiles of chromospheric lines, relation to intensity gradients 2−48809
prominences, absorption features, observation at 3.5 mm wavelength 2−76007
proton flare characts. 2−62771
protons, during 17th Dec. 1971 event 2−62768
quiescent prominences, fine structure wavelength shift, internal motion 2−55184
quietness and sharpness of image, dependence on Earth's atmos. circulation 2−73111
radio bursts, distrib. of peak flux-density spectra 2−75958
radio emission at metre wavelengths, spectra and polarization during noise storms 2−62762
small scale magnetic fields, energy spectral analyses 2−76015
solar short period oscillations, photospheric velocity field at disk centre 2−55176
solar soft X-radiation photometry with broad band detectors for signal-energy conversion function 2−73117
spectral line profiles of chromospheric H lines on the disk 2−48810
sunlight, energy and spectral distribution from high- altitude observations 2−75605
sunspot umbra, comparison of magnetically non-split line profile predictions by models 2−66225
sunspot umbra, splitting of π-component 2−73138
sunspot umbral spectra, photoelectric line profiles of Hα, Na D_2 and He I λ10830 lines 2−44989
sunspots, profiles of magnetically split lines 2−44987
sunspots line profiles 2−44986
synoptic chart, Hα patrol films 2−75991
transition elements classif. far u.v. emission 2−83189
umbral, Fraunhofer lines of singly-ionized metals 2−48808
u.v., absolute intensity in 1200-1790 Å region 2−75942
u.v., balloon borne u.v. Fabry-Perot spectrograph 2−66198
velocity spectrum, photospheric microturbulence and macroturbulence 2−75982
X-ray, e.u.v. and Hα, obs. of flares 2−78593
X-ray, improved wavelengths and lne identifications from 60-385 Å 2−75951
X-ray, proportional counter expt., resultant ionization in mesosphere 2−73118
X-ray, satellite lines of He like Mg 2−55171
X-ray burst, spectral development 2−58550
X-ray emission from thermal and non-thermal flares, OSO-7 observations 2−78590
X-ray line emission from individual active regions 2−75952
x.u.v., rocket measurements, Li like ions, O VI, Ne VIII, Mg X 2−55167
XUV and radio emission of flare, 1969 obs. 2−76005
XUV-region photographs 2−73116
yellow coronal line at Lomnicky Stit 2−73109

Sun continued
spectra continued
Z-dependence of level intervals in $2s^22p^2$, $2s^22p^3$ and $2s^22p^4$ 2−73114
Zeeman lines, detection of blending within large umbra 2−55166
Zeeman splitting in bright prominences 2−44991
Ag, abundance, spectral scan of resonance lines 2−75949
Ar XII-XVI lines in e.u.v. spectra of flare 2−58546
Au/H abundance ratio from spectral synthesis of λ3123 AuI line 2−44977
C II and C III, u.v. line anal., statistical equilibrium and radiative transfer equations 2−51847
C_2 in sunspot umbras 2−73140
C_2 lines in sunspot spectra 2−73139
C_2^- radical, search for rotational lines 2−44861
CO line, thermal oscillations in high photosphere 2−66224
CO vibration rotation, line profiles and equivalent widths 2−73147
Ca/H abundance ratio in solar corona from observations of Ca XV lines 2−55159
Ca I and Ca II lines, collision broadening by H, solar abundance 2−75948
Ca II, H and K emissions, disk chromosphere spectroscopy 2−76019
Ca II K-line profiles in quiet sun 2−73113
Ca II K_{2v} spectral features in non-magnetic regions, temporal behaviour 2−55170
Ca II line profiles in plages, chromosphere and sunspots 2−75947
Ca K line obs. in chromospheric and coronal networks, correlation between intensity fields 2−76021
Ca XIV-XVIII lines in e.u.v. spectra of flare 2−58546
Ca^+, H and K lines, determination of continuum 2−58548
Dy II identification 2−66200
Eu abundances in sunspots 2−73135
Fe abundance, det. from Fe I and Fe II resonance transitions in 2300 to 3050 Å region 2−58547
Fe abundance det. from weak Fe I line λ5127.7 2−75944
Fe and Ni emission line wavelengths, and solar u.v. spectrum and forbidden line identity 2−42729
Fe I, first order analysis of variations of limb darkening and shapes for Fraunhofer lines 2−66199
Fe I 5250.216 Angstroms line profiles rel. to sunspot models 2−75989
Fe I ionization and excitation equilibrium in atmosphere 2−66230
Fe I ionization and excitation equilibrium in atmosphere 2−58559
Fe I lines rel. to saturation of Fraunhofer lines 2−78587
Fe spectral line identification and abundance 2−62748
Fe XIII ion, intensity ratios of i.r. lines 2−55168
Fe XIII line in corona, Fe abundance and electron temperature meas. during 1966, November 12 eclipse 2−76027
Fe XIV, XV, XXIV lines in e.u.v. spectra of flare 2−58546
Fe XV e.u.v. spectrum rel. to theory and collisional excitation 2−78586
Ga, abundance, spectrum synthesis 2−75946
H_α fine structure, intensity oscill. 2−66202
H_α loops, rel. to filaments 2−66203
H_α mottles 2−66201
Hα, chromospheric observations in 1964-6 period 2−78622
Hα emission, total flux, rel. to type IV bursts at 1.5 metres, time profile comparisons 2−51850
Hα filtergrams, mag. field distrib. and polarity obs. 2−75938
He-D_3 spectroheliograms, distrib. of photospheric mag. field 2−73103
He emission regions, temp. in atmosphere 2−62747
He_{II} 4686 in quiescent and loop prominences and in chromosphere 2−73144
La abundances in sunspots 2−73135
Mg I 4571 Å, determ. of minimum temp. of atmos. 2−76011
Mg II emission line profiles obs. 2−43200
Mg II u.v. line anal., statistical equilibrium and radiative transfer equations 2−51847
MgI, λ4571 forbidden line, measurements of limb darkening 2−45000
MgI b_1 λ5183.6 line from photosphere, residual intensity fluctuation measurements in wings 2−48793
MgII and CaII H and K resonance lines, compact grating spectroheliograph 2−45014
Mn I, e^6D-y^6P multiplet lines, hyperfine structure 2−48790
Mn solar abundance determinations 2−55158
Na D-lines, broadening coefficients 2−55169
Na D line profiles, space and time variations 2−62746
Ni abundance in coronal enhanced region 2−73150
O I u.v. line anal., statistical equilibrium and radiative transfer equations 2−51847
Sm abundances in sunspots 2−73135

Sunlight
see also Sky brightness
— 2−63141
absorption by atmospheric aerosols, coefficient measurement methods 2−51617
absorption in stratified Rayleigh atmosphere, numerical model 2−73078
albedo of surfaces, as fn. of solar zenith angle 2−75485
atmospheric aerosols effects 2−81689
atmospheric radiative heating, effect of changing CO_2 concentration 2−72800
daylight observations of comets, Venus and Mercury when close to the Sun 2−48781
e.u.v. heating in upper atmosphere, annual and sub-annual effects 2−84840
e.u.v. heating of atmosphere, annual and sub-annual effects rel. to density variations 2−84841
GEOS satellite, electric field perturbations caused by photoemission on sunlit side 2−54982
intensity rel. to weather pattern 2−68878
natural underwater light field, dependence of radiance fluctuations on statistical characteristics of rough sea surface 2−44616
ocean colour from scattered sunlight meas. from spacecraft in noon orbit rel. to Earth resources studies 2−84773
particulate extinction in near i.r. spectrum of sun 2−57999
penetration through atmosphere and plant canopies 2−48475
potential energy in atmosphere, theoretical calculation 2−57989

Sunlight continued
radiation balance at tropical station 2−68908
over snowfield at elevated site, radiation meas. 2−65761
solar energy and spectral distribution from high- altitude observations 2−75605
solar flux radiometer, economical design 2−65760
solar irradiance meas. rel. to comparisons of International Pyrheliometric Scale with absolute radiation scale 2−73461
submarine daylight field, axially symmetric 2−65607
Sun-glitter pattern on sea rel. to roughness and surface wind measurements from spacecraft 2−84772
sunrise and sunset, effects on processes in Sun-Earth space 2−65763
temperature distributions in planetary atmospheres from reflected sunlight 2−62711
thermal solar radiation reflected from ocean surfaces 2−65759
u.v. radiation flux, Earth's surface reflectivity 2−62251
O_3, atmospheric, biological screen, history of life 2−78348

Sunspots
80 to 90 year cycle of activity as a pseudo- harmonic oscillation 2−48806
1965 observations of sunspots and faculae and group evolution 2−78609
activity centres, early stages of development from photoheliograms 2−48804
area, east west asymmetry, faculae 2−55179
area to number ratio changes, associated sub-auroral geomagnetic activity 2−62792
bright running penumbral waves obs. 2−78598
cycle, effect on Earth's mag. field variations 2−75633
cycle obs. for forecasting rules 2−62791
depth and thin solar convection zone 2−55180
diatomic molecular lines in sunspot spectra, 4900-6441 Angstrom range 2−62743
force-free mag. field, non-linearity of dynamical behaviour 2−78582
formation from mag. flux concentration 2−75994
geomagnetic field variations at Potsdam, Seddin and Niemegk 2−44770
horizontal velocity field, near solar limb 2−75993
interferometric obs. of small continuum features 2−81958
i.r. umbral spectrum, HCl fundamental vibration rotation bands and ^{35}Cl abundance 2−55163
line profiles 2−44986
magnetic fields, measurement methods 2−78602
moving magnetic features rel. to decay 2−78608
neutral sheet between sunspots of opposite polarity, charged particle acceleration 2−44988
number prediction analysis 2−73141
photospheric velocity field surrounding 2−75981
profiles of magnetically split lines 2−44987
solar magnetic field, evolution over 11 year period, distrib. of sunspots 2−55181
solar proton flares production from sunspot groups, magnetic polarities 2−44993
splitting of π-component in umbra spectrum 2−73138
umbrae, vertical velocity oscillations 2−75986
umbrae, working model 2−66225
umbral model atm. derived from i.r. obs. 2−78607
umbral spectra, Fraunhofer lines of singly-ionized metals 2−48808
umbral spectra, photoelectric line profiles of Hα, Na D_2 and He I λ10830 lines 2−44989
umbral velocity oscillations, obs. using molecular lines 2−75988
Wolf number, correlation with ionosphere parameter variations 2−48560
young active region, dynamics of mag. flux 2−75972
C_2 in spectra of umbra 2−73140
C_2 lines in spectra 2−73139
Ca II line profiles in plages, chromosphere and sunspots 2−75947
Eu abundances, spectra high resolution 2−73135
Fe I 5250.216 Angstroms line profiles rel. to sunspot models 2−75989
La abundances, spectra, high resolution 2−73135
Sm abundances, spectra, high resolution 2−73135

Superconducting devices
a.c. Josephson effect, 2e/h measurement, Weston cell voltage standard 2−78747
a.c. Josephson effect, calibration as voltage standard 2−78746
bridge, Sn film superimposed with ferromag. Ni 2−54154
capacitive weak links and finite load lines 2−51119
coaxial line, Q-factor det. using inductive coupling 2−64922
complex solenoid with external superconductor 250 kG 2−73517
cryogenic power transmission lines for mag. suspended high speed train 2−61255
d.c. ratio transformer, standardisation and current detection 2−82421
double Josephson junction, crit. current temp. depend. 2−57171
electron lenses, shielding and rings 2−79064
forced cooled superconducting systems, cryogenic problems 2−66365
heterodyne detection of far i.r. radiation using Josephson junctions 2−41845
Josephson contacts, direct voltage characteristics, mixing of microwaves 2−54153
Josephson junction, quasiparticle interference current 2−81040
Josephson junction, subharmonic steps in V-I curves on microwave irrad. analog computer studies 2−81046
Josephson junction applics. in radiation detection 2−64956
Josephson junction interferometers, critical current periodicity, interf. patterns, mag. field effects 2−61254
Josephson junction magnetometer detection of n.m.r. 2−66674
Josephson junction with normal metal barrier, thermodynamic properties 2−47873
Josephson junctions, double, quantum interference props. 2−54157
Josephson junctions with semicond. barriers 2−64957
Josephson point contact, intrinsic steps on VI characs. 2−68374
Josephson point contacts, response to external h.f.currents 2−61252
Josephson tunnelling, thin polymer insulator synthesis and deposition 2−71877
junction, supercond.-insulator-supercond., barrier region tunnelling, paramag. impurity effects 2−61256

Superconducting devices continued
junctions, one electron and Josephson, tunnelling phenomena 2−51120
lenses, electron optics, book 2−66715
lumped parameter circuit, temp. dependence of resonance freq. 2−63216
machine windings, developments, review 2−66686
magnetic flux exclusion tube for particle physics expts. 2−76446
magnetically doped tunnel junctions, mag. interactions 2−68449
memory materials and devices, conference (Princeton, 1 May, 1972) 2−69478
metal filled supercond. multifilamentary braids, pulsed field losses 2−61253
microbridge, two-fluid model applic. 2−44083
m.i.m. junction, nonequil. phenomena in electron tunnelling 2−68373
monograph on superconductivity 2−47841
multiply-connected, phase transition 2−68353
objective lens, phase contrast transfer functions 2−52393
particle accelerator low phase velocity supercon. resonant cavities, magnetic and electric field meas. 2−49700
point contact quantum interference device, model for operation 2−82554
point contacts, static and microwave props. 2−81054
point junctions, fluctuation spectrum calcs. 2−68372
quantum flux detector, intrinsic fluctuations 2−54156
rectifier plants with inductive load, cryodiode behaviour 2−59037
resonators, harmonic generation 2−73485
review in book 2−57154
r.f. cavities for accelerators, surface condition of Nb 2−70337
r.f. cavities of accelerator, electron loading 2−59655
S-N-S structures, dependence of supercurrent on normal layer thickness 2−64953
shielding lens for electron microscope 2−41922
solenoid, magnetic field monitoring using ^{133}Cs n.m.r. 2−66700
SQUID, applic. to magnetic susceptibility obs. 2−52384
SQUID freq. converter, resistive, design and h.f. response 2−44084
synchrotron extension, high β insertions 2−42486
three Josephson junction interferometer, mag. field sensitivity and amplitude deviation 2−51118
tunnel junction, microwave assisted tunnelling 2−47848
tunnel junction bolometer for heat-pulse determ. of acoustic wave dispersion in InSb 2−80911
tunnel junctions, phonon generation 2−47735
weak link, current-phase relationships and fluctuations 2−44085
weak link point contacts, thermal effects 2−47874
Al-Al$_2$O$_3$-M tunnel junction, M=Fe, Co, Ni, Gd, electron spin polariz. detn. 2−64958
Al-insulator-Al junction, tunnelling results with interacting mag. impurities 2−61243
KTa$_x$Nb$_{1-x}$O$_3$, pyroelectric detectors, characteristics 2−73460
Nb-Nb point contact, I-V characts. 2−47863
Nb helix resfnator cavity, suitable for heavy ion accelerator 2−70321
NbTi filaments, operating conditions for use as liquid He level sensors 2−66368
Nb+Ti alloy, multiple strand composition 2−64955
Pb-Al$_2$O$_3$-Al junction, electric depend. of paraconductivity 2−54155
Pb-Al$_2$O$_3$-Al junction, impurity assisted tunnelling, 4.2-148 K 2−44140
Pb, tunnel junctions, single particle tunnelling in mag. field 2−54149
Pb Josephson junction, microwave- induced constant voltage steps 2−71878
Sn-CdSe-Sn, tunnel junctions, fabrication and props. 2−81039
Sn-In microbridge, transition from bulk like behaviour to Josephson junction like behaviour 2−64951
Sn-Sn tunnelling junction, on Si, in liq. He, phonon emission 2−84304
Sn-SnO-Sn Josephson junctions, critical currents near BCS value 2−81043
Sn-SnO-Sn Josephson tunnel junction, Josephson and quasiparticle currents, microwave radiation effects 2−68375
Sn Josephson junction, microwave-induced constant voltage steps 2−71878
Sn microbridge, transition from bulk like behaviour to Josephson junction like behaviour 2−64951

Superconducting magnets
40 kG saddle-shaped 2−41915
coil moving over cond. surface, lift and drag forces 2−41914
construction and design for $40\sim60$ kOe field production 2−59076
electron lens testing using 400 kV electron optical system 2−79070
electron lenses 2−79064
filamentary composites for pulsed operation 2−63257
large, applications in research and technology 2−52386
levitation systems for high-speed transportation 2−49310
objective lens for 300 kV microscope, properties and applications 2−79069
for proton synchrotron, design 2−45670
solenoid, 28 koe with 20 cm working aperture diameter 2−64954
solenoid, mag. field nonuniformity compensators 2−61250
solenoid field monitoring using ^{133}Cs n.m.r. 2−66700
solenoid system, 1/H drive circuit for magnetic field sweeping 2−45650
solenoid with transverse working gap and field up to 90 kOe 2−61251
theory, production, future applications 2−45671
toroidal, quantization of trapped flux 2−76445

Superconducting materials
A15 cpds., nucl. spin relax., order parameter fluctuations influence 2−68355
A15 cpds., transition temp. and lattice instabilities 2−77877
A15 cpds. with paramag. impurities, compensation effect 2−64947
a.c. loss obs. by boil-off method 2−54131
alloy, mag., localized bound state and impurity band props. 2−77873
alloy with paramag. impurity and local states in gap. crit. field order parameter. sp. ht. 2−71857
alloys with mag. impurities, coherent potential approx. corrections to transition temp. 2−84312
basic phenomena 2−47839

Superconducting materials continued
- C16-type compounds and pseudobinary alloys, transition temps. 2−51104
- UV Ceti, photometric studies, flare obs. 71876 2−71876
- cylinders, multiply connected, magnetic flux quantization 2−47847
- elemental, critical-mag.-field curve, anisotropy and strong-coupling effects 2−54137
- film, thermal cond., mag. field depend. 2−68344
- Kondo alloys, critical field and temp. behaviour below 0.1K 2−44082
- layered compounds, spin-lattice relax. due to fluctuations 2−71841
- light scatt. from surface with creation of 2 quasiparticles, temp. depend. calc. 2−65238
- low temperature prod. for material utilization at 1.8 to 5K 2−64491
- metal, simple, mag. phenomena, spin excitations and order 2−57162
- molecular cryst., existence of supercond. 2−44039
- monograph on superconductivity 2−47841
- multifilamentary composites, degradation and losses 2−64935
- β-Nb-Al-Si alloys, superconducting critical temp. detn. 2−71869
- nonequilibrium, photoexcitation of quasiparticles 2−77868
- optical props. and electronic transitions, review 2−72292
- organic, operative at room temperatures, possibilities 2−45671
- Pb-In alloys, surface resistance variations with applied field 2−64942
- properties review rel. to future applics. 2−64934
- rare earth dil. alloys, mag. phenomena, spin excitations and order 2−57162
- semiconducting alloy, doped, transition temp. rel. to ferroelec. Curie temp. 2−44071
- single crystal, ultrasonic velocity obs. using digital averaging technique 2−61090
- three kinds, results of relevant theories, magnetic properties and phenomena 2−84300
- transition metal, dirty, thermal conductivity near upper crit. field 2−77876
- transition metal, dirty two-band, mixed state transport coeffs. near H_{c2} 2−47871
- transition metal, with non-mag. impurities, specific heat calc. 2−44061
- transition metals, applic. of self-consistent electron-phonon coupling 2−57098
- transition metals and alloys, mag. phenomena, spin excitations and order 2−57162
- transition metals containing nonmagnetic impurities, thermal conductivity in two-band model 2−71874
- type II, Q-factor det. using inductive coupling 2−64922
- type II, vortex relation, filamentary layer model 2−47851
- vortices in flux lines, comparison with other physical systems 2−60122
- wire immersed in He II bath, thermal resists. 2−64498
- wires made of alloys Nb+Zr+Ti and N+Ti, properties of welded joints 2−61227
- Ag film, induced supercond. energy gap and electron-electron interaction 2−44072
- $AgMo_4S_5$, heat capacity, Debye temp. 2−81051
- Al-Ag alloys, pre-precip. state props. 2−64944
- Al-Al_2O_3 granular films, sp. ht. obs., T_c enhancement 2−77878
- Al, transition temp., electrostatic charging effects 2−71845
- Al, u.s. attenuation, electron- phonon interaction const. 2−81049
- Al film, density of states change due adsorbed molecular oxygen, tunnel diode obs. 2−51111
- Al film, thermodynamic fluctuations in resistive transition 2−71858
- Al film, transition temp. depression by noble gas overlayers 2−61228
- AlMn, supercond. transition temp., 0-20 kbar press., Mn impurity effect 2−47870
- As, high press. supercond. phase 2−44058
- Bi-Pb alloy, under high press., supercond. transition 2−47868
- Bi, high press. supercond. phase 2−44058
- Bi, high pressure phases up to 30kbar 2−68357
- Bi film, disordered, supercond. transition temp. and normal state cond., effects of surface charge 2−44070
- Bi film, transition temp. change due to noble gas adsorption 2−47856
- Cd film, disordered, supercond. energy gap and transition temp. 2−54134
- Ce, α-α' phase transition, model 2−84309
- $Ce_{1-x}Gd_xRu_2$ alloys, magnetiz. curves, temp. depend. 2−44073
- $Ce_{1-x}Gd_x(Tb_x)Ru_2$, mag. ordering and supercond. coexistence 2−43981
- $CeRu_2$:Gd^{3+} transition temp. rel. to Gd^{3+} conc. 2−84302
- $CeRu_2$, $CeRu_{2-x}Pt_x$, low temp. ht. capacity 2−77879
- Cr film, sputtered, supercond. props. rel. to deposition conditions 2−81045
- CuS semiconducting film, transition temp. obs. 2−51112
- Ga, amorphous, strong coupling superconductor, crit. mag. field temp. variation 2−68356
- Ga, energy gap, expt. orientation depend., tunnel junc. obs. 2−68358
- Ga film, disordered, supercond. transition temp. and normal state cond., effects of surface charge 2−44070
- Ga film, transition temp. change due to noble gas adsorption 2−47856
- Ga single crystals, anisotropy in crystal length change at superconducting transitions 2−71846
- Ge-Au films, quench- condensed, energy gap meas. by tunnelling 2−51115
- GeTe, and semicond. props. 2−51114
- Hf-Ta alloys, superconductivity under pressure 2−81058
- HfV_2, lattice transition, supercond., cryst. struct., alloying effects 2−71865
- Hg, aligned mag. inclusions effects 2−64945
- Hg filaments in chrysotile asbestos, supercond. rel. to external mag. field 2−84313
- Hg_3Te_3-In_2Te_3 alloy rocksalt phase, low temp. supercond. 2−54175
- In-Bi alloys, flux flow state props. 2−44074
- In-Cd alloy, type II supercond. and mag. hysteresis 2−71863
- In-Cd dilute alloy, pressure and strain derivatives of transition temp., Fermi surface topology effects 2−71859

Superconducting materials continued
- In-Hg-Pb alloy, thermodynamics, role of electron scatt. 2−81038
- In-Hg alloy, thermodynamics, role of electron scatt. 2−81038
- In-Mn alloys, thin film, electronic thermal conductivity 2−68352
- In, flow stress meas., comparison with normal state 2−47857
- In cylindrical layers, crit. mag. field 2−84299
- In film, intermediate state struct., magneto-optical study 2−81050
- In films, e.m. generation of transverse acoustic waves, transition temp., penetration depth 2−71866
- In films, noise props., r.f. generation 2−68348
- In films, penetration depth and flux creep 2−68345
- In fine particles, magnetization study 2−71847
- In thin film, electronic thermal conductivity 2−68352
- In_5Bi_3 phase, thermodynamic props. 2−71687
- InSb, crit. temp. determ. 2−71848
- InTe, and semicond. props. 2−51114
- La-Ce(Gd) dil. alloys, temp.-depend. pair breaking, impurity interactions 2−54144
- La film superconducting, phonon structure in tunnelling density of states 2−75059
- $(La_{1-x}Ce_x)Al_2$, Kondo supercond., anomalous crit. field curves 2−61238
- $(La_{1-x}Ce_x)Al_2$ alloys, supercond. vanishing below second transition pt. due to Kondo effect 2−44075
- $La_{3-x}Ce_xIn$ alloys, crit. temp. and field behaviour, conc. depend. 2−64946
- $La_{1-x}Gd_xRu_2$, mixed cryst., supercond. and mag. props., T_c depression 2−68549
- $La_{3-x}InCe_x$, supercond. and magnetic props., conc. depend. 2−47854
- $La_{1-x}Pr_xRu_2$, mixed cryst., supercond. and mag. props., T_c depression 2−68549
- $LaRu_2$, low temp. ht. capacity 2−77879
- La_3Se_4, and semicond. props. 2−51114
- La_3X, (X=Al, Ga, In, Tl, Sn, Pb), mag. props. sp. ht., cryst. field states 2−61244
- $Li_xTi_{1.1}S_2$, $0.1<x\leqslant0.3$, high transition temp. compounds 2−47858
- Mg-Cd alloy, transition temp., determ. of Mg T_c by extrapolation 2−75073
- Mg-Cd alloys, transition temp., electronic sp. ht., Debye temp. 2−47859
- Mg alloys, h.c.p., transition temp., electronic sp. ht., Debye temp. 2−47859
- Mo:C film, supercond. transition temp., struct. 2−57169
- Mo:C film, supercond. transition temp. effect of C coating 2−54145
- Mo-Pt system, identification of supercond. phases 2−61239
- Mo-Pt system, phase diagram, transition temp., conc. depend. 2−61246
- Mo-Re film, A-15 struct., supercond. transition temp. 2−71867
- Mo-34%Re alloy, effect of dislocation tangles on supercond. props. 2−57167
- Mo-Ru alloy, microstruct., hardness and supercond. transition temp. 2−50840
- Mo, experimental obs. discussed in terms of band models 2−47832
- Mo alloys, A15 type, low temp. sp. ht., transition temp. and cryst. order 2−61245
- Mo ternary sulphides, crystallographic instability 2−71691
- $Mo_{6-x}A_xS_6$ (A=Cu, Zn, Mg, Ag, Cd, Sn or Pb), high-temp ternary system 2−51105
- $Mo_{1-x}M_xGa_4$, M=Nb, Ru, Mn, Fe, Co, exchange field due to paramagnet impurities 2−77862
- $Mo_{75}Os_{25-x}Fe_x$, compensation effect 2−64947
- NA/NH_3 frozen solution, libron induced interelectron interaction calc. 2−64941
- Nb-40% Ti alloy, mag. irreversibility and microstruct. 2−47855
- Nb-Al-Ge system, phase equilib. and supercond. props. 2−43936
- Nb-Al alloy, heat treatments rel. to transition temp. 2−47589
- Nb-(38 at.%)Hf alloy, fluxoid pinning rel. to precipitate dispersion 44076 2−44076
- Nb-Mo alloy, properties, u.s. technique, investigation 2−47862
- Nb-Sn alloys, vacuum deposited, characteristics 2−68365
- Nb-Ta alloy, microwave surface resist. 2−54133
- Nb-Ti alloy, mag. instabilities 2−64948
- Nb-Ti and Nb-Ti-Zr alloys, wire, crit. current, mag. field intensity depend. 2−75062
- Nb-Zr-Ti alloy, struct. 2−50842
- Nb-(40 wt.%)Zr alloy, metallurgical variables influence on T_c and crit. current 2−47861
- Nb-(25 wt.%)Zr wire, macroscopic quantum effect in meas. of current threshold57166 2−57166
- Nb_3(Al-Ge) compound tapes, prep. and props. 2−64949
- Nb_3Al, crit. temp. variation, density of states variation, positron annihilation obs. 2−47860
- Nb_3Al, critical current variation, a.c. current obs. 2−61240
- $Nb_2Al_xGe_{1-x}$, crit. temp. variation, density of states variation, positron annihilation obs. 2−47860
- NbC_{1-x}, transition temp., rel. to band struct. determ. 2−81055
- Nb_3Ga, annealed, transition temp. obs. 2−43937
- $Nb_{85}Mo_{15}$, energy gap field depend. from vortex entropy in low-field limit 2−57170
- NbN, bulk and films, lower crit. field meas. 2−54146
- NbN film, crit. current anisotropies rel. to columnar structure 2−68366
- NbN film, photolum. spectra, freq. shift gap struct. 2−68687
- NbN films, reactive high-vacuum codeposition and characteriz. 2−50497
- NbN films, superconductive critical field 2−84310
- NbN films prepared by d.c. sputtering, props. 2−84311
- NbN type cpds., RY, R=Ti, Zr, Hf, V, Nb, Ta, Y=C, N, O, transition temp., phonon spectra 2−61247
- $NbS_2(Se_2)$, transition temp., press. depend. 2−54147
- $NbSe_2$/organo intercalation compounds, electron microscope examination of lattice, and superconductivity 2−53676
- $NbSe_2$, discontinuous flux flow 2−61241
- $NbSe_2$, lamellar, pressure effect on transition temp. 2−71860
- $NbSe_2$, low-temp. cryst. modification and transition temp. 2−81052
- $NbSe_2$, resist. anisotropy with press. 2−51116
- $NbSe_2$, supercond. transition temp., press. depend., 1.5-6.5kbar 2−68346

Superconducting materials continued
NbSe$_2$, transition temp., pressure depend. to 140 kbar 2−68359
Nb$_3$Sn-type cpds., lattice dynamics theory 2−84187
Nb$_3$Sn, elastic moduli and mag. susceptibility 2−51117
Nb$_3$Sn, high-T$_c$ superconductor, tunnelling, phonon spectrum 2−81048
Nb$_3$Sn, Mossbauer recoil-free fraction and Debye-Waller factors 2−44357
Nb$_3$Sn, multifilamentary composite in ductile matrix 2−51113
Nb$_3$Sn, photolum. spectra, freq. shift gap struct. 2−68687
Nb$_3$Sn, vapour deposited, crit. current, effect of impurity gas additions 2−51109
NbTi filaments of round composite structures, anisotropy of critical current density 2−71870
Nb$_{0.88}$Ti$_{0.12}$N film, fluctuation broadening of supercond. transition 2−71850
Nb + Ti alloy, multiple strand composition 2−64955
Pb-Ag-Pb layers, heat capacity at ^{3}He temps., proximity effect obs. 2−81041
Pb-In-Sn ternary alloy wire, magnetic properties, flux flow voltages 2−81037
Pb-In, strong coupling, mag. meas. 2−64950
Pb-In alloy, electronic thermal conductivity, temp. and mag. field depend. 2−47867
Pb-In alloy, microwave surface resist. 2−54133
Pb-In alloy, phonon spectrum, hydrostatic pressure effects, electron tunnelling obs. 2−64936
Pb-In alloy, thermodynamic critical field deviation from parabolic law 2−84303
Pb-In alloy film, electronic thermal cond. 2−81042
Pb-In alloys, thermal conductivity, temp. and mag. field depend. 2−71872
Pb-In alloys, thermal Hall effect and the Righi-Leduc angle, observations 2−68370
Pb-In dilute alloy, phonon spectra, electron tunnelling obs. 2−54142
Pb-Mn films, tunnelling conductance curves 2−71851
Pb-Na alloy, heterogeneous, anisotropic crit. currents 2−77864
Pb-(40 at.%)Tl alloy, force free mag. fields, solns. for spherical geometry 2−44067
Pb-(40 at.%)Tl alloy, force free mag. fields, solns., for cylindrical geometry 2−44066
Pb-Tl alloy, Ginzburg-Landau parameters, temp. depend. 2−64921
PbBi film, thermal cond. 2−68344
Pb$_{0.9}$Bi$_{0.1}$ alloy, strong coupling superconductor, crit. mag. field temp. variation 2−68356
Pb$_{1-2x}$Bi$_x$Tl$_x$, strong coupling, mag. meas. 2−64950
PbMo$_6$S$_7$, heat capacity, Debye temp. 2−81051
Pb$_{0.5}$Tl$_{0.5}$ films, phonon generation 2−47735
Pd-H system, elec. resist. study 2−54135
Pd-Ni-H system, elec. resist. study 2−54135
Pd, electron phonon enhancement factor, from specific heat data 2−64932
Pr$_3$X, (X = Al, Ga, In, Tl, Sn, Pb), mag. props. sp. ht., cryst. field states 2−61244
Pt, electron phonon enhancement factor, from specific heat data 2−64932
Re-Mo film, A-15 struct., supercond. transition temp. 2−71867
Sb, high press. supercond. phase 2−44058
Sc, electron-phonon enhancement factor, from specific heat data 2−64932
Sn-In alloys, flux-trapping, structural sensitivity 2−54152
Sn-Mn film, magnetic state of Mn 2−68512
Sn, current-carrying one-dimens., instabilities in transition curve 2−44079
Sn, effect of strain on u.s. attenuation 2−51106
Sn, finely dispersed, crit. temp., particle size and oxidation effects 2−61230
Sn, phonon excitation spectra, junc. tunnelling obs., effects of material props. 2−68360
Sn, phonon generation 2−47735
Sn, supercond. bridge superimposed with ferromag. Ni 2−54154
Sn cylinders, a.c. behaviour in transition region 2−44080
Sn film, crit. temp. oscillatory depend. on thickness 2−57164
Sn film, cylindrical, supercurrent stability 2−47850
Sn film, Josephson effect 2−61248
Sn film, mag. flux penetration depth 2−71871
Sn film, nonlinear flux flow resistivity 2−47849
Sn film, transition temp. change due to noble gas adsorption 2−47856
Sn film, transition temp. depression by noble gas overlayers 2−61228
Sn films, noise props., r.f. generation 2−68348
Sn fine particles, mag. susceptibility, temp. depend. 2−71852
Sn whisker, mech. twinning rel. to supercond. behaviour 2−47869
SnMo$_5$S$_6$, heat capacity, Debye temp. 2−81051
SnNbS$_3$, crystallographic data and ions temp. sp.ht. meas. 2−68371
SnNbSe$_3$, crystallographic data and low temp. sp.ht. meas. 2−68371
SnTaS$_3$, crystallographic data and low temp. sp.ht. meas. 2−68371
SnTe, and semicond. props. 2−51114
SrTiO$_3$, and semicond. props. 2−51114
Ta-Nb alloys, sp. ht. and mag. meas. 2−71875
Ta-W alloys, superconductivity under pressure 2−81058
TaC$_{1-x}$, transition temp., rel. to band struct. determ. 2−81055
TaC$_x$, lattice instability effects on supercond. props. 2−68349
Ta$_{0.96}$Nb$_{0.04}$ alloy, surface pinning of fluxoids 2−44064
TaS$_2$/organo intercalation compounds, electron microscope examination of lattice, and superconductivity 2−53676
Tc-40 at% Mo alloy, A-15 type II superconductor, cryst. struct. 2−80647
Te-Ge-As system, supercond. and structural features 2−61242
Th-H, Th-D systems, composition effect on transition temp. 2−54143
ThCe, supercond. transition temp., 0-20 kbar press., Ce impurity effect 2−47870
Th$_4$H$_{15}$, transition temp., diamag. suscept and specific heat 2−54143
ThU, supercond. transition temp., 0-20 kbar press., U impurity effect 2−47870
Tl, phonon spectrum, supercond. tunnelling and neutron scatt. data, discrepancy 2−84189

Superconducting materials continued
Tl film, transition temp. change due to noble gas adsorption 2−47856
TlBiTe$_2$, struct. and elec. props. 2−51144
V-Ga-Al alloy, A15 struct., crit. temp. and current density 2−57168
V, electron phonon enhancement factor, from specific heat data 2−64932
V, flux line lattice obs. 2−47872
V, magnetization curve, 0K, calc. 2−61233
V, press. depend. of transition temp. 2−75064
V, transition temp. calc. and phonon vertex 2−71876
V$_3$Au, transition temp., effect of cryst. order 2−64952
(V$_{1-x}$Cr$_x$)$_3$Si, ternary alloys, physical props. and electron struct. and transition temp. 2−68514
V$_3$Ga formation by a new diffusion process 2−84301
V$_3$Si, elastic softening phenomena at T$_c$ 2−44081
V$_3$Si, lattice stablization in high magnetic fields 2−77869
V$_3$Si, superconduct. cpds. formation by a new diffusion process 2−84301
Y, electron phonon enhancement factor, from specific heat data 2−64932
Zn-Cr(Mn) Kondo alloys, critical field and temp. behaviour below 0.1K 2−44082
Zn film, disordered, supercond. energy gap and transition temp. 2−54134
Zr-Nb alloy, transition temp., consitution and microstruct. effects 2−51107

lead
critical magnetic field, temp. variation for strong coupling supercond. 2−68356
density of states enhancements and suppressions in tunnel junctions due to asymmetry effects 2−54150
destruction of superconductivity, current induced 2−54139
dilute alloy, phonon spectra and supercond. parameters 2−47865
film, 9.4 GHz u.s. attenuation 2−61229
film, current-induced intermediate state mag. struct., magneto-optical obs. 2−54151
film, disordered, supercond. transition temp. and normal state cond., effects of surface charge 2−44070
film, mag. flux penetration depth 2−71871
film, transition temp. change due to noble gas adsorption 2−47856
flux-flow props. under press. 2−44078
fountain effect, crit. current asymmetry obs. in point contact 2−68368
intermediate state, isotropic and anisotropic galvanomag. props. 2−47866
intermediate state, path- depend. mag. struct. 2−47864
Josephson junction, microwave- induced constant voltage steps 2−71878
Landau domain struct., motion induced by electric transport current 2−75074
Meissner state energy loss, transition state-intermediate state, loss down to 10^{-15} watts/cm^2 2−71873
phonon excitation spectra, junc. tunnelling obs., effects of material props. 2−68360
photocurrent temperature dependence due to superconducting energy gap, 2.5 to 12°K 2−68354
surface supercond. anisotropy, electron m.f.p., surface resist. obs. 2−68367
tunnel junctions, single particle tunnelling in mag. field 2−54149
Pb-Al$_2$O$_3$-Al junction, impurity assisted tunnelling, 4.2-148 K 2−44140
Pb-Bi alloy, under high press., supercond. transition 2−47868
Pb-In alloy, m sheath state, flux motion in surface investigated 2−64943
Pb-Ir-Pb structure, BCS interaction parameter determ. for normal state Ir 2−71849
Pb-Sn alloy, eutectic, lamellar, proximity effects, sp. ht. obs. 1.25-8 K 2−68369

niobium
critical current rel. to radiation induced defects 2−81053
helix resonator cavity, suitable for heavy ion accelerator 2−70321
interfaced with Cu, thermal conductance measurements between 1.4 and 5°K 2−54141
internal friction, Young's modulus, when in normal and supercond. states 2−77635
local magnetic field distributions at 4.2 K by neutron diffraction 2−57155
longitudinal u.s. absorption, 2-band character 2−68347
properties, u.s. technique, investigation 2−47862
residual resist. and upper crit. field, influence of Al$_2$O$_3$ additions 2−44077
surface pinning by defects, expt. evidence 2−77866
thermal cond., 0.03 to 4K, phonon scatt. 2−47767
vortex entropy in low-field limit 2−57170
vortex lattice spacing and attractive interaction 2−54148
Nb-Nb point contact, I-V characts. 2−47863
Nb, superconducting point contacts, static and microwave properties 2−81054

Superconductivity
see also BCS theory
— 2−64898
A15 cpds., phonon linewidths, Kohn anomaly 2−43951
a.c. Josephson effect measurement of 2e/h 2−69532
basic phenomena 2−47839
BCS system, struct. of Cooper pairs 2−61232
Bose-Einstein and Fermi-Dirac systems supporting normal superfluid and superconducting components, unified theory 2−66476
boson method, application to study of Josephson effect 2−54136
bridge and layer compounds, microscopic model, comparison of maximum superconducting transition temperatures 2−44054
closeness of states as a function of energy level in a two zone system 2−68343
conference, Aussois, France [Mar. 1972] 2−64923
critical anomalies in external fields, nonperturbational calc. 2−61235
critical fluctuations in zero-dimens. systems 2−47843
critical phenomena, functional integral method 2−68351
critical phenomena in zero-dimens. system, functional integral method 2−77874

Superconductivity continued
cylinder, thin-film, phase transition in mag. field, angular depend. 2−71855
in cylinders, multiply connected, magnetic flux quantization 2−47847
detecting microwave transitions, phase sensitive method 2−61249
dilute magnetic impurity system, electronic struct. 2−71854
energy gap, bound states due to reson. scatt. 2−57159
Fermi liquid model of s-d electrons 2−71856
fermion gas system, condensated, gapless excitations 2−58808
ferromagnetic superconductor, micromagnetic theory 2−77870
film, phase reversal and modulated flux motion 2−54138
films, metastable, surface resistance meas. 2−64924
flat coil, between halves of infinite cylinder, in periodic mag. field, pick-up voltage 2−77863
flow voltages and critical currents, effect of superimposed a.c. magnetic field 2−81059
fluctuations, selfconsistent treatment, beyond Hartree approx. 2−75065
flux exclusion, He liquid cooled stage for scanning electron microscope 2−82439
flux quantization, teaching demonstration 2−41432
fluxons, possibility of transmission electron microscope obs. 2−77867
fountain effect, crit. current asymmetry obs. in point contact 2−68368
gap, equilib. value, rel. to weak alternating fields 2−57157
de Gennes' equations for Bogoliubov amplitudes solved for inhomogeneous case 51108 2−51108
Ginsburg-Landau theory of fluctuations in small size samples 2−75067
Ginzburg-Landau eqn., time-dependent determ. using methods of thermodynamics of irreversible processes 2−77865
Ginzburg-Landau field, one-dimens., statistical mechanics 2−78853
Ginzburg-Landau theory of anisotropic superfluid neutron star matter 2−51755
h.f. surface conductivity, contrib. of mag. field induced surface states 2−51083
induced voltages in absence of transport currents 2−57161
inhomogeneous, application of Eilenberger theory to penetration of weak magnetic field 2−54132
inhomogeneous, self-consistent pair potential 2−51108
interband interactions, effect on critical temp. of supercond. transition temp. in semimetal 2−71842
isolated flux line core, gap parameter $T \geqslant 0.7\ T_c$, BCS value 2−75069
Josephson effect, 2e/h, as-maintained voltage standards, international comparisons 2−78748
Josephson effect, quantum mech. model 2−61231
Landau diamagnetic and spin paramagnetic susceptibility for electrons 2−47842
localized magnetic states, s-d exchange model with generalized Hartree-Fock approximation 2−47840
Luttingers mechanism 2−71853
metal, phenomenological model of electron- phonon interactions 2−57160
metal filled supercond. multifilamentary braids, pulsed field losses 2−61253
model with external pair breaking influence 2−47844
monograph 2−47841
neutron scattering spectral function and phonon modes, electron-phonon interactions 2−71861
nonequilibrium, pair-quasiparticle potential difference 2−44056
nonequilibrium, pair-quasiparticle potential difference 2−44055
nonlocal electrodynamics in spatially varying gap parameter care 2−44060
rel. to nuclear level density calc. 2−59681
one dimens. supercond., excess cond. near transition point, fluctuation rel. to inhomogeneity broadening 2−81044
optical cooling of conduction electrons as means of raising superconducting temp. 2−81004
pairing tendency in nearly-ferromag. systems 2−57163
phase transitions, D-dimensional, self consistent theory 2−64931
phonon bremsstrahlung, sharp edge isolated by modulation 2−47732
phonon spectra, determ. by computer from tunnelling effect 2−81056
resonance state, spun potential mechanism 2−81047
review 2−77861
review in book 2−57154
ring cct. inductively L-C coupled, analog computer simulation 2−71844
second order phase transition size effects 2−83869
semiconductor, rel. to state mixing between bands due to e.m. field 2−77872
semimetal, excitonic phase, investigation using strong electron-phonon interaction term 2−64897
semimetals, excitonic-insulator phase, Meissner effect and interband scattering 2−81003
shielded film, current distribution 2−81057
small particles, thermodynamic props., static approx. 2−64928
smectic A conform. analogy 2−43331
solid state and quantum electronics, book 2−57092
solid state physics, an overview 2−57093
specific heat, influence of mag. impurities, Kondo effect 2−64929
stability aspects of composite superconductors 2−44057
strong coupling superconductor, crit. mag. field temp. variation 2−68356
superconducting transition temperature, press. depend. 2−75064
superconductor, two band, transition temp. and energy gaps rel. to Fermi surface topology change under press. 2−75068
surface energies in pure system, theory 2−47845
suspension of a permanent magnet over a superconductor, expt. 2−59069
theory, applications 2−45671
thermopower in plasmon-coupled superconductor near transition temp. 2−75057
three kinds of superconductors, results of relevant theories, magnetic properties and phenomena 2−84300
time dependent. and quantum dissipation, theory 2−64925

Superconductivity continued
transition, effect on macroscopic properties of plastic deformation 2−71843
transition in multiply-connected superconductors 2−68353
transition temp., influence of ferromagnetic and antiferromagnetic spin correlations 2−44059
transition temp., quasifield, under nonequilib. conditions 2−68350
transition temperature, influence of lattice defects 2−57156
transition temperature, rel. to energy gap, for strong electron-phonon coupling 2−57158
transport equations, in slowly varying elec. field, thermodynamic Green's function methods 2−71779
tunnelling, generation, relax., and hole-electron imbalance detection 2−64926
type I, surface excitations in static magnetic field 2−61236
voltage pulses produced by vortex motion, calc. 2−75066
vortex entropy in low-field limit 2−57170
vortices, dynamic struct. for $H \ll H_{c2}$ 2−47846
vortices, dynamic structure 2−64933
weakly connected granular superconductors, phase coherence and noise resistivity 2−64930
weakly-coupled systems, time-depend. phenomena 2−61234
AlMn, transition temp., Mn impurity effect, 0-20 kbar press. 2−47870
Be film, on dielec. substrate, elec. resist., supercond. transition temp., absorpt. spectra 2−72323
$CeRu_2$:Gd^{3+} transition temp. rel. to Gd^{3+} conc. 2−84302
He II, fluctuations and a.c. Josephson effect 2−64499
HfV_2, transition temp., effect of alloying 2−71865
$La_{1-x}Gd_xRu_2$, mixed cryst., supercond. and mag. props., T_c depression 2−68549
$La_{1-x}Pr_xRu_2$, mixed cryst., supercond. and mag. props., T_c depression 2−68549
Mg-Cd alloy, transition temp., determ. of Mg T_c by extrapolation 2−75073
Mg, transition temp. from obs. of Mg-Cd alloy 2−75073
Mo:C film, supercond. transition temp. effect of C coating 2−54145
Mo-Re film, A-15 struct., supercond. transition temp. 2−71867
MoS_2, exciton mechanism for superconductivity and nonequilibrium systems of excited excitons 2−71868
Nb-Al alloy, transition temp. rel. to heat treatment 2−47589
Nb-Mo alloy, props., u.s. technique investigation 2−47862
Nb, props., u.s. technique investigation 2−47862
Nb, supercond., critical current rel. to radiation induced defects 2−81053
Nb_3Al, crit. temp. variation rel. to density of states variation, strong bond model 2−47860
$Nb_3Al_xGe_{1-x}$, crit. temp. variation rel. to density of states variation, strong bond model 2−47860
NbN films, superconductive critical field 2−84310
NbN type cpds., RY, R=Ti, Zr, Hf, V, Nb, Ta, Y=C, N, O, transition temp., phonon spectra 2−61247
Nb_3Sn, phonon linewidths, Kohn anomaly 2−43951
Pb-Bi alloy, supercond. under high press., supercond. transition 2−47868
Pb-In alloy, thermodynamic critical field deviation from parabolic law 2−84303
Pb-Sn alloy, eutectic, lamellar, proximity effects, sp. ht. obs. 1.25-8 K 2−68369
Pb, surface anisotropy, electron m.f.p., surface resist. obs. 2−68367
Pb, type I, Meissner state energy loss, transition state-intermediate state, loss down to 10^{-15} watts/cm^2 2−71873
Pb Landau domain struct., motion induced by electric transport current 2−75074
Sn-SnO-Sn Josephson junctions, critical currents near BCS value 2−81043
$SnNbS_3$, crystallographic data and low temp. sp.ht. meas. 2−68371
$SnNbSe_3$, crystallographic data and low temp. sp.ht. meas. 2−68371
$SnTaS_3$, crystallographic data and low temp. sp.ht. meas. 2−68371
ThCe, transition temp., Ce impurity effect, 0-20 kbar press. 2−47870
ThU, transition temp., U impurity effect, 0-20 kbar press. 2−47870
WSe_2, exciton mechanism for superconductivity and nonequilibrium systems of excited excitons 2−71868
Zn film, on dielec. substrate, elec. resist., supercond. transition temp., absorpt. spectra 2−72323

type II
coherent quasiparticle excitation in crossed electric and magnetic fields 2−84307
dirty, thermal conductivity in transition metals near upper critical field 2−77876
dirty superconductors, higher order corrections due to order parameter to flux flow conductivity 2−47852
Eliashbergs theory 2−68362
filamentary layer model, vortex relation 2−47851
flux flow noise, study with pick-up coils 2−71862
flux jumps, limited, model 2−64939
flux line, isolated, mag. field at finite temp. 2−44062
flux lines, attractive interactions, generalized Neumann Tewordt functional 2−77871
fluxons, viscous forces under a.c. conditions 2−54140
force free fields, critical current determ. 2−68361
force free mag. fields, solns., for cylindrical geometry 2−44066
force free mag. fields, solns. for spherical geometry 2−44067
hardening, statistical problem, flux line motion and pinning 2−68125
isolated vortices, numerical consts. derived 2−64927
low temp. physics, conf., Freudenstadt, Germany (Apr. 1972) 2−45183
macroscopic quantum effect in meas. of current threshold 2−57166
magnetic field distribution calculations 2−61237
magnetic hysteresis 2−68363
magnetization, hysteretic model for hard supercond. 2−68364
mixed state transition, order parameter perturbation, flux lines 2−44065
nonideal, flux flow, generalized time-depend. Ginzburg-Landau equations 2−64937
nonideal, local model, flow cond. determ. 2−51110

Superconductivity continued
type II continued
nonlinear props. of fluxoids in high-speed flux-flow state 2−47853
Pb-In alloys, surface resistance variations with applied field 2−64942
pinning centres, alternating current obs. 2−44068
pinning sites, alternating current obs. 2−44069
quasiperfect crystal of vortex lines observed 2−44063
in semiconductors 2−51114
in sheath state flux motion in surface investigated 2−64943
structure and compositions of materials 2−75071
surface flux line pinning, model 2−77875
surface pinning of fluxoids 2−44064
viscous vortex motion, friction coeff., effect of paramag. centres 2−57165
vortex lattice pinning energy and proximity effects 2−64940
vortex line pinning models 2−64938
Hg filaments in chrysotile asbestos, supercond. rel. to external mag. field 2−84313
In_2Bi, intrinsic behaviour deduced from mag. props. 2−75072
In_2Bi, magnetic properties, deduced to be intrinsic type II superconductor 2−75072
$La_3In:Gd$, e.s.r. obs. 2−72475
Nb/Cu metal interface, thermal conductance measurements between 1.4 and 5°K 2−54141

Supercooling
cholesteryl derivatives, crystal nucleation in supercooled mesomorphic phases 2−77414
liquid metals, homogeneous nucleation study 2−71275
metal, spherical cryst. dendritic growth from highly supercooled liq. metals 2−60966
steel drops, solidification in oil 2−43440
water, nucleus formation and crystallization 2−74588
Al drops, effect of Cu inclusions 2−43441
Bi-Sb alloy system, cryst. growth rate, diffusional supercooling theory 2−53613
Fe drops, solidification in oil 2−43440
Fe(II) salt solutions, frozen at normal pressure 2−78178
H_2O in clouds, acceleration of ice phase 2−62236

Superexchange *see Antiferromagnetism; Exchange interactions*

Superfluidity
see also Helium/liquid; Quantum fluids
α-decay of even-even nuclei $174 \leqslant A \leqslant 232$, absolute probabilities and superfluidity 2−82931
bellows seal superfluid value 2−85166
Bose system, condensed, microscopic theory 2−45322
Bose-Einstein and Fermi-Dirac systems supporting normal superfluid and superconducting components, unified theory 2−66476
boson system, superfluid density determ. 2−41541
charged Bose gas, density-temp. diagram 2−78851
fermion system, Ginzburg-Landau eqn. for $^3P_2$ pairing 2−76234
fermion systems, ground state model wave junction of BCS type 2−63043
film, size effects near second order phase transition 2−83869
hadron matter, derivation of critical temp. for superfluid phase 2−59434
hadronic matter 2−73775
neutron star, Ginzburg-Landau eqn. for $^3P_2$ pairing 2−76234
neutron star matter, anisotropic, Ginzburg- Landau theory 2−51755
neutron star matter, density region where $^3P_2$ gap exists 2−73009
neutron stars, BCS theory applic. 2−48703
ordered phase, point and planar singularities 2−78831
phase transitions, decoupled-mode dynamic scaling theory 2−52103
quantum mechanics, superfluid density determ. 2−58805
roton lifetime theory, inclusion of two-roton resonances in final-state interaction 2−71262
two-dimensional systems, long range order and metastability 2−50407
vortices in He II, phenomenology, review 2−83831
H_2 liquid, possibility 2−53470
He/metallic layer/He bath system, energy flux eval. 2−53474
He/metallic layer/He bath system, energy flux calc. 2−47010
He, application of equation-to-motion method to two-branch excitation spectrum 2−71261
He, application of equation-of-motion method to two-branch excitation spectrum 2−71260
He, dissipative flow theory 2−71257
He, flow channel, extrinsic dissipation mechanism 2−56535
He, force exerted by charged vortex rings 2−80508
He, hydrodynamic approx. approach to charge carrier scatt. by phonons 2−77459
He, phonon emission and absorpt. due to rotons 2−64495
He, quantized charged vortex rings, electromagnetic field dependence 2−74577
He, superfluid vortices and turbulence as ultrasonic cavitation nucleation mechanism 2−43426
He baths counted through a small hole, oscillations 2−47014
He II, boundary pressures and forces generated by moving vortices 2−47016
He II, charged impurities conc. waves as type of second sound waves 2−53480
He II, critical flow through holes 2−47020
He II, critical heat flux density and thermal quenching in long channels 2−47021
He II, emission and absorpt. of phonons by rotons 2−43425
He II, entropy transport by vortices, and second sound vel. modifications 2−64500
He II, flow in restricted geometries 2−47013
He II, fluctuations and a.c. Josephson effect 2−64499
He II, forces in superfluid flow 2−80501
He II, growing collective modes in vortex rings 2−53477
He II, h.f. u.s. attenuation, press. depend. of phonon dispersion 2−47025
He II, heat capacity at const. vol. near λ pt. 2−47012
He II, interaction of charged vortex rings with superfluid surface 2−50392
He II, laminar and turbulent flow 2−47017
He II, Landau parameters for rotons 2−43418

Superfluidity continued
He II, liquid, superfluid, thermohydrodynamic conditions at peak flux of horizontal heaters 2−67859
He II, low temp. superfluid density in restricted geometries 2−47019
He II, negative charge carriers 2−47024
He II, phase analysis of evaporation spectrum 2−50390
He II, phonon emission rate of rotons 2−47011
He II, phonon spectrum, thermodynamic evidence against quadratic term 2−77456
He II, positive impurity ion mobility 2−60535
He II, pressurized turbulent, escapt of negative ions and vortex annihilation model 2−67857
He II, relaxation phenomena at rotation acceleration in spherical vessel, rel. to pulsar relaxation 2−81893
He II, second sound, mutual friction force obs. 2−47018
He II, thermally excited sound waves 2−47023
He II, turbulence, stabilization by flow modulation 2−43421
He II, two-roton bound states 2−50393
He II, under pressure and near superfluid transition, second sound velocity, scaling and universality 2−43419
He II film, rotating, thickness changes 2−64496
He II film flow transfer over Plexiglas ampoules, singularities 2−67856
He II in rotating bucket, origin of quantized vortices 2−67858
He II superflow, saturated dissipation 2−53475
He mixtures, transition temp. gradient with heat flow 2−43424
He superflow, model 2−44085
HeII, counter flow, onset of turbulence 2−43420
HeII, persistent currents, linear velocities and role of vortex lines 2−47015
^3He-^4He mixture superfluid density near tricritical point 2−74578
^4He, ^3He limited drift of charge carriers 2−77458
^4He, eqn. of state in λ transition region 2−80502
^4He, ionic mobilities, λ point phenomena 2−47007
^4He, phonon spectrum, self-energy 2−71258
^4He, thermally driven film, saturation of fluctuation dissipation in flow 2−80507
^4He calc. of roton-limited mobility of ions at temps. below 1.7 K 2−71259
^4He film, adosrbed, quartz microbalance obs. 2−64497
^4He under press., superfluid density near λ point 2−43417

Superlattice structure *see Alloys; Crystal structure, atomic; Solid solutions*

Supernovae *see Novae*

Superparamagnetism
critical superparamagnetism 2−61513
B_2O_3-BaO-Fe_2O_3 glass, rel. to microstruct. 2−56558
2 at.%Co-Cu alloy, superparamag. relax. time rel. to Co precip. particle size 2−48067
Fe film, u.h.v. Mossbauer emission spectra, mag. behaviour rel. to particle size 2−72284
$FeClO_4$, frozen solns., Fe^{3+} ion behaviour, Mossbauer effect 2−78070
γ-Fe_2O_3, magnetiz. and Mossbauer obs. 2−48038
$Fe_{1-x}Ti_{1\|x}$, rel. to resist. minimum 2−44252
Ni, rel. to loss mechanism at low freq. 2−78024

Supersonic flow
see also Shock waves
aerodynamic heating of shell in supersonic turbulent flow 2−60368
air stream, wave resistance of thin spindle 2−83645
asymmetrical triangular plate with blunt edges 2−56414
axisymmetric body, rain erosion model 2−43252
axisymmetric hypersonic flow, subsonic and supersonic regions 2−60346
beam continuum model, over flat plate at zero angle of incidence 2−43231
blunt bodies, transonic region, shock waves 2−77329
boundary layer, three dimensional with heat transfer, iterative calculation 2−53275
boundary layer flow past wavy wall 2−56408
cascade, stationary and rotating channels 2−53291
chemically reacting gas, over base 2−43240
closed channel, temp. influence on burning characteristics of diffusion H_2 flame 2−67703
combustion gases, elec. conductivity, nonequilibrium phenomena, calc. 2−80261
compressible turbulent mixing layers, shock tube expt. 2−71102
compressible unsteady boundary layer eqns., 3D soln. 2−83680
conical nose shape effects on drag and static stability at Mach 10 2−43251
over convex and concave shapes, with radiation and ablation effects 2−77337
corner of intersecting wedges at high Reynolds number 2−56410
cylindrical flare bodies, boundary layer effects 2−77359
degree of combustion calc. methods 2−61788
delta wing, symmetrically deformed influence of vortices on aerodynamic characteristics 2−50261
dissociated gas, over flat plate 2−43239
ethanol drops, homogeneous nucleation and growth 2−80393
exhaust plume/boundary layer interactions 2−56423
exothermic hypersonic flows about blunt projectiles, periodicity 2−83650
far field sonic boom approach, non-asymptotic effects 2−53318
film cooling effectiveness and skin friction in hypersonic turbulent flow 2−93666
flap turbulent heating, skin friction and pressure data from hypersonic shock tunnel 2−53314
flat plate boundary-layer transition in supersonic wind tunnels 2−43248
flight test base pressure data results at hypersonic Mach numbers in turbulent flow 2−43247
flowfield meas. using total temperature probe at Mach numbers 2, 6 and 25 2−43234
free air jets, velocity and temperature 2−77352
gas, round body of rotation with injection from ring slot 2−56419
gas flow through entrance region of cooled tube, computer solution for heat transfer at v. high temp. 2−46818

Supersonic flow continued

- h.f. discharges, breakdown voltage and electric field strength 2−74418
- hypersonic bodies, maximum drag for reentry vehicles 2−60360
- hypersonic boundary-layer transition obs. using hot wire anemometry 2−60328
- hypersonic flow, internal, inviscid, about unyawed cones, closed form solutions 2−56428
- hypersonic flow, shock waves, stagnation point, heat transfer, CO_2-N_2 mixture 2−82250
- hypersonic low-density cone drag 2−56421
- hypersonic meas. techniques, recent progress 2−80399
- hypersonic nose and loading edge shapes, minimum energy 2−43250
- hypersonic of ionized gas around blunt ended bodies and leading radiation 2−77347
- hypersonic past wedge, effects of upstream unsteadiness 2−74466
- hypersonic projectile wake, electron density fluctuation meas. 2−60352
- hypersonic rarefied, over sharp slender cones drag, heat transfer and number flux measurements 2−74470
- hypersonic transitional boundary layers, space-time correlation meas. 2−60329
- hypersonic turbulent boundary layers structure 2−50247
- hypersonic unsteady compressible boundary layer depend. on Prandtl number 2−56416
- hypersonic wake in ballistic apparatus, conductivity measurement 2−74480
- hypersonic wind tunnel, flow nonuniformities effect 2−83692
- hypersonic wings, thin shock layer approx. applic. to non-conical shapes 2−64371
- hypersonic with massive blow in, asymptotic theory 2−77328
- injected gas filament diffusion in supersonic free jet 2−74457
- internal conical flow past wedge 2−60326
- internal over blunt leading edges and two blunt bodies, numerical method 2−56407
- inviscid, over blunt delta wing, space shuttle reentry 2−71093
- ion, in low pressure plasma, exptl. evidence 2−53181
- ionosphere, topside plasma flow inside and outside of plasmasphere 2−58095
- jet, discrete tone radiation 2−46841
- jet, free and emitted in wake of cyclinder parallel to hypersonic flow, comparative study 2−83669
- jets, effects of nozzle plenum pressure fluctuations on noise 2−69771
- jets, incompletely expanded, form of boundaries 2−64388
- laminar boundary layer equations from differential- difference method 2−80398
- laminar hypersonic interacting boundary layers, subcrit. branching in strong interaction regime 2−83691
- Laval type nozzles, non-symmetric flow 2−83684
- lifting aerofoils and slender bodies, computation 2−71092
- liquid films in supersonic streams, nonlinear stability 2−78934
- low density aerodynamic tube, cryogenic pump calc. 2−82078
- magnetogasdynamic channel, current and heat dissipation 2−53186
- MHD boundary layers, interaction with weak shock waves 2−50174
- multitube multishroud jet noise suppressor 2−43233
- near wake of a slender body, decay rate of boundary layer turbulence 2−56411
- noise field of Mach 1.5 cold model jet 2−41801
- about nonaxial symmetric bodies 2−53327
- nonequilibrium condensation with gas flow in supersonic nozzles and jets 2−60331
- nonequilibrium flow, blunt body, shock layer boundaries 2−83678
- nonlinear panel response, turbulent boundary layer 2−71090
- nonuniform freestreams, blunt cones, inviscid aerodynamics, wakes 2−83675
- nozzle, turbulent boundary layer meas. with and without wall cooling 2−53287
- nozzle flow, influence of contraction section shape and inlet flow direction 2−66023
- nozzle wall boundary layers, at high Mach numbers 2−71069
- nozzles and channels of variable cross section, 3-dimens. subsonic and supersonic flow 2−74468
- ogive-cylinder bodies at high angles of attack, side forces in transonic flow 2−64383
- oil flow photographs, aerodynamic heating, space shuttle vehicle 2−83679
- parabolic wing, transition from laminar to turbulent boundary layer 2−64376
- particle motion behind oblique shock in two-phase supersonic flow past a wedge 2−60145
- past wing, unified area rule 2−71094
- plane symmetrical gaseous mol. beam, vel. distrib. and Mach no. 2−53302
- plasma, in combustion MHD generator, obs. 2−80257
- plasma, interaction w. mag. mirror 2−64286
- plasma ions rel. to neutrals and ensuring dissipative instability 2−74399
- polytropic, velocity coefficient, with friction and heat transfer 2−74344
- pressure and temperature behind blunt bodies in supersonic flow with supply of inert and reacting gases to base region 2−60332
- pressure gradient, effects on hypersonic turbulent skin friction 2−83662
- rarefied large scale from molecular jets effusing from perforated boundary 2−77335
- rarefied slightly ionized, flow field diagnostics 2−50245
- rarified, hypersonic, delta wings with trailing edge spoilers 2−71091
- r.f. preionization in transversely excited supersonic flow CO_2 laser 2−59146
- secondary injection ratio supersonic stream application to thrust vector control 2−60339
- separated, finite span, with turbulent boundary layer 2−46814
- separated turbulent flows 2−77336
- sharp cones at angle of attack, hypersonic characteristics 2−53307
- sonic transverse jet, viscous interaction 2−71089
- spherical source with finite back pressure 2−80395
- static aerodynamic characts. of bulbous base cones 2−71105

Supersonic flow continued

- suddenly fitted plate, flow field calc. using method of characteristics 2−74469
- surface jet, hypersonic flow interaction with axial symmetry 2−56424
- surface pressure meas. in low-density flow 2−83665
- Taylor-Maccoll, theorems 2−67598
- around thin shaped tail group edges 2−71096
- thin wing, Baranoff's analytical form of kernal of Possio's integral eqn. 2−53323
- three-dimensional, in nozzles and channels of variable cross section 2−53285
- transonic, Laval type nozzles, non-symmetric flow 2−83684
- transonic, two-dimensional and axisymmetric stability, nonlinear approximation of hyperbolic system near bicharacteristic curve 2−53283
- turbulent, hypersonic, construction of hot-wire anemometer 2−64373
- turbulent boundary layer, impact probe displacement 2−46815
- turbulent boundary layer, incipient separation, heat transfer 2−71070
- turbulent boundary layer in adverse pressure gradient, data analysis 2−56426
- turbulent boundary layer in adverse pressure gradient 2−46806
- turbulent boundary layers in nozzles 2−71071
- turbulent jet, reattachment to ejector shroud 2−50256
- turbulent mixing layer between streams of gases 2−80208
- underexpanded exhaust plumes, flowfield interactions 2−43232
- unseeded supersonic airflow meas. using a laser anemometer 2−83682
- pastunyawed semiinfinite circular cone with attached shock wave, theorems 2−67598
- uplift flow, drag on aeroplanes with three pointed edges 2−67723
- velocity measurement of supersonic gas flow 2−77342
- viscous fluid pass parabolic obstacle, numerical calc. 2−60163
- viscous interaction over concave and convex surfaces at hypersonic speeds 2−77357
- visualization at weak inhomogeneities, with holograph interferometer 2−64374
- wave patterns near sonic line in non-homentropic flow 2−60355
- wedges and cones, hypersonic leading edge 2−83663
- wind tunnel models design for aeroelastic studies in transonic flow 2−46838
- in wind tunnels, holographic interferometer and fringe analyser 2−46836
- CO_2-N_2-H_2O arc-driven laser operating in gas-dynamic mode, numerical analysis 2−49359
- Cs plasma, in magnetic de Laval nozzle, characteristics 2−50203
- H_2/air and H_2/O_2 combustion, shock-induced 2−83651
- N rotational temp. in rarefied supersonic flow in glowing-discharge 2−60311
- NO_2-N_2O_4-N_2-Al_2O_3, powder reactive nozzle flow 2−83660

Supersonics *see Ultrasonics*

Surface diffusion *see Diffusion in liquids; Diffusion in solids; Surface phenomena*

Surface energy

- *see also Crystal electron states/surface*
- alkali metals, rel. to bulk density of lattice energy 2−77493
- anisotropic surfaces, vector thermodynamics, plane surface junctions 2−56570
- anisotropy data analysis using lattice harmonics 2−43460
- atomic He scattering and diffraction, surface potential depend. 2−67889
- boson fluid, spinless, stongly interacting, statistical thermodynamics, surface energy and tension 2−82267
- carbides, wetting by liq. metals 2−50427
- CC Cu-W composite, fracture 2−55475
- Coconino sandstone, reduction by dilute $AlCl_3$, $FeCl_3$ solutions, hydrolysis of Si-O surface bonds 2−68858
- composite, glass fibre reinforced polyester, fracture surface energy determ. 2−50780
- crystal/melt interface, free energy calc. from radial distrib. function 2−43463
- cubic monatomic lattice, surface mode dispersion relations and surface sp. ht. 2−77487
- rel. to dislocation mobility, in cryst. with high Peierls barrier 2−71482
- of domain boundary, antiferromagnet in tilted mag. field 2−81306
- ferromagnetic film, surface free-energy for spin-wave and molecular field models 2−75229
- graphite, pyrolytic, spreading critical surface energy, from liq. metal wetting obs. 2−80558
- group II-IV-V_2 semiconductor single crystal, estimate from melt surface energy 2−74615
- liquid metal-ceramic systems, critical surface energy of spreading 2−50425
- metal, collective modes contribs. 2−56568
- metal, of brittle fracture, from phonon freqs. 2−60902
- metal, plasmon theory 2−64893
- naphthalene crysts., determ. by cleavage method 2−80543
- polyethylene, low mol. wt. crysts., interfacial free energy 2−60633
- polyvinylidene fluoride electret. depolarization current and surface potential decay 2−51208
- powdered metals, e. microscopy study of contact zones 2−64789
- rare earth orthoferrites, surf. energy of phase boundaries for phase transform. 2−81291
- steel, rel. to kinetics of isothermal coalescence of dispersed phase 2−47611
- superconductor, planar phase boundary, theory 2−47845
- transition metal, plasmon theory 2−64894
- variational formulation of crystal surface equilibrium 2−47069
- wetting, spreading kinetics, driving forces 2−74506
- zero creep condition, grain boundary term 2−56569
- Al-Mg alloy, rel. to kinetics of isothermal coalescence of dispersed phase 2−47611
- α-Al_2O_3, spreading critical surface energy, from liq. metal wetting obs. 2−80558
- Ar, ideal tensile strength, relationship to surf. energy, expt. 2−64721
- Au film, on amorphous C, oriented crystn. mechanism, rel. to interaction forces at interface 2−77502
- Cr interfacial free energies meas. 2−80795

Surface energy continued
CrV steels, free energy changes and boundary segregation of Sn and Sb 2−71309
Cu, surface potential, weak adsorp. of CO and H_2 obs. 2−50537
Cu film, Xe adsorp., surface potential 2−50556
Fe film, Xe adsorp., surface potential 2−50556
He liquid, electron transport, non-ohmic, in image-potential-induced surface states 2−56534
He monolayer adsorbed on Ar, correlation energy 2−74644
LiF surface-gas atom potentials 2−50450
Mo, cathode, flashing effect, surface atom migration, field ion microscopy 2−53557
Mo interfacial free energies meas. 2−80795
Na film, Xe adsorp., surface potential 2−50556
NaCl, ideal tensile strength, relationship to surf. energy, expt. 2−64721
Ni, and grain boundary free energy obs. using electron microscopy 2−56576
Ni film, surface potential of adsorbed Xe, photoelec. emission obs. 2−47163
Pb/NaCl-UCl_3 molten metal/fused salt system, surface and interfacial energy 2−52874
PbTe, free energies, calc., reply to comments 2−77491
PbTe, free energy, calc., comments 2−77490
TaC, estimation from obs. of wetting by liq. Ag and liq. Cu 2−43468
Tc, polycrystalline, derivation from accurate estimation of work function 2−71319
VC_x, fracture surface energy determ. 2−50776
W, cathode, flashing effect, surface atom migration, field ion microscopy 2−53557
W interfacial free energies meas. 2−80795
W single crystal, rel. to {110} cleavage in ⟨110⟩ axis 2−56606
Surface ionization *see Ionization, surface*
Surface measurement
see also Area measurement
absolute flatness det, by combination of standard and compensating hologram 2−79244
acoustic wave velocity meas. change caused by thin conducting film 2−51017
adatom position in surface from fluoresc., adsorbed atoms determ. 2−77488
analysis, by mass spectrometry of sputtered neutrals 2−64541
appearance potential spectroscopy 2−81361
area determination from stepwise adsorption isotherms 2−77518
area using N adsorption and Harkins and Jura isotherm 2−58686
aspherical surface inspection using correction plates made by vacuum deposition of aspherizing layers 2−59262
atomic and molecular scatt. 2−50422
Auger electron spectroscopy rel. to appearance pot. spectroscopy 2−47071
automatic inspection, metal polygon mirror, lapping technique 2−79386
average wavelength parameter 2−45212
billets, surface inspection, Billetscan eddy current device 2−43764
chemical anal. using Auger electron spectroscopy 2−48357
displacement, by double exposure laser photographs 2−52032
elastic surface wave probe, waveform distortion meas. 2−49170
elastic waves, velocity meas., coherent pulse superposition technique 2−49108
field ion microscopy, development, applications to metallurgy, image form., construction operation 2−56643
film surface density meas. by proton excited X-rays, Fredholm expression 2−80542
flatness, broad source interference method rel. to mechanical face seal meas. 2−66405
flaws, non-destructive testing by surface wave coupling 2−50417
geology, airborne resistivity mapping using E-PHASE 2−54727
graphite, surface study of gases prod. by thermal decomposition from acidic surface oxides 2−64551
ion scattering, spectroscopic tool for study of outermost atomic layer of solid surface 2−50416
LEED, electron dynamical scatt. problem soln. 2−56624
LEED intensities, effects of deviation from Bethe model, investigation for exactly soluble one-dimensional model 2−50419
metal single crysts., low energy ion refl., energy and angular distribs. 2−67895
Moon, selenodetic nets of coordinates, relative deformations, comparison of catalogues 2−44916
noble gas ion probe technique for surf. anal. and struct. exam. 2−71297
nuclear density, isotopic tracing by charged particle beams, review 2−80556
optical component parallelism using c.w. gas laser 2−82532
optical surface microtopography measurement and/or automatic focusing 2−73655
photoelectron spectroscopy, applications 2−53862
photoemission obs. technique 2−48018
polymer shavings, apparatus 2−50471
powder, by nitrogen desorption, appartus 2−56969
PZT-5, surface wave velocity depend. on degree of poling 2−51202
reconstruction of surface profiles from diffraction spectra 2−55732
replica techniques for scanning microscopes 2−64622
scattering of low energy ions, surface analysis technique 2−47072
snow, specific surface 2−75441
structure and props. of grain boundaries and interfaces, conference, Yorktown Heights, N.Y., USA, Aug (1971) 2−56722
temperature in incandescent range, opaque, translucent and transparent surfaces, thermoprobe 2−63160
thermal transients meas. technique 2−58972
topografiner, non-contacting instrument 2−60622
wave filters in integrated circuits 2−49112
wave velocity using coherent pulse superposition 2−49127
Al, adsorption of Cl, Auger spectrosc., ellipsometry and surface potl. meas. of clean films 2−71345
γ-Al_2O_3, specific surface area meas. 2−64548
Cu:S, Bragg peaks, temp. effects 2−71310
Cu-Ni alloy, surface composition after annealing and sputtering, Auger spectroscopy obs. 2−50440
GaAs obs., by Rutherford scatt., and channelling 2−64553
$LiNbO_3$, rotated Y cuts, leaky wave attenuation 2−51025
Surface measurement continued
$LiTaO_3$ acoustic wave velocity temp. depend. 2−51019
Ni:Pb, Bragg peaks, temp. effects 2−71310
Pt, detection of Ag monolayers using tracers 2−71302
Si, Auger electron signals of P surface impurity as function of coverage 2−47080
Si, Auger electron spectroscopy and electron impact desorpt. combined studies 2−64556
W electrostatic cathode lens, temp. det. in electrostatic field of immersion objective 2−41923
Surface phenomena
see also Adsorption; Capillarity; Catalysis; Electron emission; Films; Interface phenomena; Ionization, surface; Liquid waves/surface; Sorption
acoustic surface wave steering by nonlinear mixing 2−80903
acoustic wave interactions, nonlinear 2−69735
acoustic wave transducer, grating array 2−49153
acoustic waveguide excitation using wedge transducers 2−49131
acoustic waveguides and components, properties and applications 2−49120
acoustic waves, ridge waveguides 2−49121
acoustic waves on impedance bodies of resolution 2−52226
Ag, activated chemisorption and oxygen coverage 2−78192
alloy, binary, molten, electric charge rel. to thermodynamic props. 2−56515
alloy, surface reconstruction due to chemisorption 2−50524
atom-crystal interaction, energy exchange, role of phonons 2−80537
atomic and molecular scatt. 2−50422
atomic He scattering and diffraction 2−67889
ATR spectroscopy 2−65360
biological systems, obs. of surface reactions by ellipsometry, review 2−69203
boiling water, bubble motion in annular channel 2−74592
carbon blacks, surface oxygen complexes, effect on selective adsorption of non electrolytes from mixtures 2−64552
ceramic system, wetting angle, statistical interpretation 2−60970
chalcogenide glasses, cond. skin form. mechanism 2−54190
charged particle emission during heterogeneous chem. reaction of atom recomb. 2−48269
cubic crystal, crystal face growth kinetics, computer simulation 2−60703
cubic crystals, shear horizontal surface waves on (001) face 2−80745
cubic monatomic lattice, surface mode dispersion relations and surface sp. ht. 2−77487
diamond, activation energies of {110} and {111} surfaces during graphitization 2−47677
diatomic linear lattice, local and gap modes due to surface 2−74963
dickite ground, negative surface charges 2−78235
diffusion, pore migration and coalescence, rel. to swelling during postirrad. annealing 2−53548
diffusion rates, determ. from thermal transpiration meas. 2−83719
discharge current impulse rel. to applied voltage and specific capacitance, obs. 2−71017
discharge growth on polluted insulating surfaces, theor. anal. 2−83635
effects on exptally. determined value of elastic limit 2−43675
electrical flashover characts. 2−74407
electron backscattering by solid targets, 0.5-10 keV, rel. to angle of incidence 2−83855
electron bombardment surface ion desorption apparatus 2−43491
electrons near solid surfaces, quantum mechanics of infinite chain of atoms 2−84286
emission of radiation by charged particles reflected from solid surfaces 2−54397
equilibrium, generalisation of variational formulation 2−50418
evaporation of moisture from wet surface, determ. of flux of vapour 2−83833
f.c.c. crystal, (110) interface, surface diffusion 2−50426
ferromagnet, Heisenberg, long wavelength surface spin waves, effect on mag. props. 2−44231
ferromagnetic film, surface spin-wave excitation 2−68716
flow across gas dynamic discontinuity, vorticity and cureent density jump 2−83644
gas atom scatt., one-phonon quantum theory 2−50423
gas surface interaction, effects of roughness 2−77363
gas-solid interactions, development of very sensitive vibrating quartz balance 2−69538
gas-surface interactions, accommodation coeffs., Devonshire theory rejection 2−80578
GaSb and GaSb:Cs, electronic properties of surface, exam. by photoemission meas. 2−71312
glass, laser damage rel. to surface film 2−82504
glass, optical finishing by ion-beam sputtering machining 2−82571
glass, soluble, surface stabilization by alkali ion exchange 2−53519
glass roughness factor changes with heating in vacuum 2−60618
gloss power measuring device, based on Schulz-Methke principle 2−63411
graphite, heats of immersion rel. to degassing behaviour 2−53549
graphite, surface polarity when covered by oxygen complexes, evaluation using heats of immersion 2−64550
heat transfer and pressure drop performance of roughened surfaces, used in nuclear reactors 2−59872
hot plasma, surface waves 2−53227
hydrophilic solid surface characterization technique 2−71174
hypervelocity model, surface erosion, laser photography obs. 2−82578
ice crystal growth from vapour phase study of abrupt habit changes as function of temperature 2−54847
inelastic atom-surface scattering, quantum theory 2−46465
interdigital surface wave, broadband coupling network 2−63121
ionic crystal, realistic models for surface phonons 2−50988
ionic crystal plate, surface optical vibrations 2−71704
ionic crystals, surface charge influence on sublimation 2−60561
kaolin structure, effect of surface-active substances studied by i.r. spectroscopic method 2−84642
kaolinite ground, negative surface charges 2−78235
layered structs., h.f. surface wave amplification, rel. to carrier density, drift vel. 2−65006
LEED intensity profiles rel. to spin-polarization, atomic core scatt., surface barrier struct. 2−77483

Surface phenomena continued

- Love wave, surface excitation 2−63111
- low energy electron inelastic scattering, by one phonon processes, theory 2−50986
- magnetic materials, surface dynamics and waves 2−68527
- mass spectrometer studies using ion-ion emission 2−61469
- mean square displacements of vol. and surf. atoms of fcc crystals, calc. 2−71307
- and mechanical properties, obs. using FIM and AES 2−56571
- metal, surface plasmons, collective mode excitation in electron and ion-solid scatt., theory 2−51087
- metal single crysts., low energy ion refl., energy and angular distribs. 2−67895
- metals, layer formation by anodic reaction within an electrolyte solution, thermodynamics 2−68781
- mica, surface conduction and surf. Hall coeff. dependence on temp. and mag. field 2−80541
- microtopography obs., non-contacting topografiner 2−60622
- mineral, hydrophilic character, determ. by N_2, Kr and H_2O adsorption 2−47155
- mixed surface waves at boundary between elastic medium and fluid 2−52216
- monolayer, partially ionized, surface press., from Vrij's formula 2−47144
- neutron total refl. and transmission, roughness effects 2−63946
- phonon inelastic surface scatt., transition matrix for bound state interactions 2−83854
- phonons and magnons, review 2−50985
- piezo-semiconductors, waveguide effect of acoustoelectric surface domains 2−54029
- piezoelectric waves, annular, transversely isotropic substrate, boundary value soln. 2−63112
- polymers, glassy, crazing in alcohols and hydrocarbons 2−83357
- polypeptide monolayer raft, non-Newtonian surface viscosity, flow equation derivation 2−74528
- polypeptide raft, non-Newtonian surface viscosity 2−74529
- polystyrene films, passage of transient currents along surface 2−72001
- polystyrene lattices, surface conductance, comparison of theory and expt. 2−60521
- pyrolytic graphite basal plane, reaction with modulated O_2 beam, study of surface chemistry 2−51447
- Rayleigh wave coupling, tunable matching 2−50417
- Rebinder effect, applications 2−53869
- sapphire, ion beam polished, increased laser surface damage threshold obs. 2−57317
- sapphire, relationship between laser induced surface damage and surface plasmas 2−60266
- semiconductor, amorphous, contact and surface photovoltage obs. of surface props. 2−77969
- semiconductor, contamination, radioactive tracers applic. 2−54113
- semiconductor, surface quantization and transport in inversion and accumulation layers 2−51123
- semiconductor electrodes on insulators, aftereffects 2−77905
- semiconductors, surface magnetoplasmons, theory 2−47920
- Si-SiO_2 interface, e. scatt. by surf. oxide charges and lattice vibrat. 2−71317
- solid surfaces, conference, Boston Mass., USA, Oct. (1971) 2−47070
- solids, surface plasmons, microscopic theory 2−84277
- steel, retained austenite developed during surface grinding of carbon steel, exptl. obs. 2−74880
- steel, surface oxidation during annealing, obs. 2−67899
- study, contribution made by vacuum technology 2−67892
- superconductors condensed on cold substrates, film, surface resistance meas. 2−64924
- surface impurities, bulk to surface equilib., Auger spectroscopy obs. 2−50465
- surface phonons and gas surface interactions 2−50522
- temperature fluctuations at air-water interface caused by surface waves 2−65616
- thermal expansion, calc. 2−50424
- transition metal surface, electronic density of states 2−75035
- u.h. vacuum system, oil pumped, surface contamination, ellipsometric obs. 2−48941
- u.h. vacuum system, oil pumped, surface contamination, ellipsometric obs. 2−48941
- Van der Waals attraction, role of surface plasmons 2−51088
- vibrational properties, perturb. by steps 2−57036
- vibrational spectra, inelastic law energy electron scatt. 2−71706
- vibrations, low energy electron spectroscopy obs. 2−50987
- water drop evaluation with monomolecular surface films 2−60557
- wave excitation by bulk-wave beam for high efficiency wedge transducers 2−49113
- X-ray anomalous reflection 2−67955
- zircaloy, in water cooled reactors, hydriding rel. to surface conditions 2−81502
- Ag, inelastic scatt. of He atoms, 0.01 eV 2−50430
- Ag halide, spectral sensitization by trapping of dye mobile positive holes 2−81552
- Ag halides, space charge due to Frenkel defects at surface 2−81022
- 6Al-4V-Ti, surface embrittlement charact. during diffusion bonding 2−68160
- Al (100) LEED, elastic and inelastic scatt., bulk and surface plasmon excitation 2−50434
- Al foil, h-pit production by hydrating and annealing 2−74616
- Al single crystals, cavitation in liquid oxygen, plastic deformation in metal surface layers 2−71306
- Al_2O_3, alumina, grain boundary grooving on single cryst. surfaces 2−50432
- As_2Se_3 films, amorphous, dark discharges 2−49458
- Au {100} surface, focusing in sputtering 2−64542
- Au boundary layers, transmission of struct. information 2−77494
- (Ba, Pb)TiO_3 ceramic, light emission by surface microplasma new Curie temp. 2−65303
- $Bi_{12}GeO_{20}$, propagation of Bleustein-mode piezoelectric surface wave 2−61095
- C, laser beam irrad., chaoite formation in craters 2−56574
- C fibre, area changes on outgassing 2−53951
- C fibres, gas chromatographic obs. of surface reactivity 2−60623

Surface phenomena continued

- CdS, paramag. surface centre density, e.p.r. obs. 2−65334
- CdS crystallites, Raman scattering from surface modes 2−75311
- CdS photoconductor, transverse surface wave depth penetration 2−84206
- CdSe, paramag. surface centre density, e.p.r. obs. 2−65334
- Cr, theory of surface atom mean square displacements 2−61075
- Cr (100), Debye-Waller factor and thermal exp. coeff., LEED obs. 2−50992
- Cu, diffusion of Ag on (100), (111) and (110) planes 2−60626
- Cu, oxide nucleation on (001) face, off angle effect 2−64566
- Cu, surface diffusion of Ni, 600 and 900°C 2−53761
- Cu, surface stress, strain produced by He bubbles, elec. resistivity obs. 2−43678
- EuS film, magnetic anisotropy 2−68532
- GaAs, cathode, negative electron affinity, photoemission rel. to Cs-O layers thickness 2−75194
- GaAs, controlled sectioning by anodic oxidation and removal of oxide layer 2−64544
- GaAs, mean square atomic displacement study by LEED 2−71318
- Ge, elec. props., effect of tetragonal GeO_2 layer 2−47939
- Ge powder, heat-treated in various atmospheres, e.s.r. obs. 2−72488
- Ge(Li) detectors, method for controlling surface properties 2−59625
- He liquid, cyclotron resonance of surface-bound electrons 2−80513
- Hg, surface-induced vectorial optical props. 2−77436
- $InAs_{0.4}P_{0.6}$, cathode, negative electron affinity, photoemission rel. to Cs-O layers thickness 2−75194
- Ir film, surface ionization of CsCl, effect of C adsorption on Ir (111) face 2−64543
- K anomalous infra-red absorption and collective oscillations in small metal particles 2−65210
- $KNbO_3$, ferroelec., surface change layers, obs. by AF electrolum. 2−75151
- LiF, scatt. of He atoms, one-phonon transitions 2−50451
- LiF_4, disloc. displacement mechanism during formation of small disloc. layer at cryst. surface 2−71492
- $LiNbO_3$, propagation of Rayleigh-mode piezoelectric surface wave 2−61095
- $LiNbO_3$ elastic waves, generation and detection, amplification 2−77774
- Mo, cathode, flashing effect, surface atom migration, field ion microscopy 2−53557
- Mo, interaction with H beams, scatt. chemisorption 2−50461
- Mo, single crystals, influence of surf. states and Ti coatings on disloc. struct. 2−83969
- Mo (100), Debye-Waller factor and thermal exp. coeff., LEED obs. 2−50992
- Na, anomalous infra-red absorption and collective oscillations in small metal particles 2−65210
- Na silicate glass, surface stabilization by ion exchange and chemical vapour deposition 2−53538
- Ni, backscatt. of Ne^+ 600 eV ions, chain effect 2−77484
- Ni, effects of surface preparation on oxidation 2−72559
- Ni, reaction of O_2 and S on surface, LEED obs. 2−78184
- Ni, surface reconstruction on absorption of O, S, Se, Madelung potential 2−47162
- Ni (111), charac. energy loss in Curie temp. region 2−51267
- Pb, supercond. surface anisotropy, electron m.f.p., surface resist. obs. 2−68367
- PbS, paramag. surface centre density, e.p.r. obs. 2−65334
- PbTe, paramag. surface centre density, e.p.r. obs. 2−65334
- Pt, interaction with H beams, scatt. chemisorption 2−50461
- Pt(110), CO catalytic oxidation, Auger spectroscopy obs. 2−51443
- Rb, surface diffusion near m.p. 2−60629
- Rh surface self-diffusion on Rh, low temp. 2−64555
- Se single crystals, circular microdisc patterns 2−60630
- Si, Au-diffused, cpd. formation, refl. electron diffr. obs. 2−50463
- Si, clean and doped, mean square atomic displacement study by LEED 2−71318
- Si, ion implanted, lateral strains, X-ray topographic obs. 2−80704
- UC, surface diffusion, rel. to surface smoothing kinetics 2−53556
- W, atomic and mol. scatt., effect of surface composition and cryst. orientation 2−47084
- W, cathode, flashing effect, surface atom migration, field ion microscopy 2−53557
- W, contrast patterns produced by self-interstitial ions in field ion microscope images 2−64625
- W, diffusion of Ni, coeff. determ., mass transfer method 2−50466
- W, flash and electron stimulated desorption of CO on (100) planes 2−71356
- W, interactions between Re atoms 2−50469
- W, surface diffusion Si, field emission obs. 2−47085
- W(112) single crystal, effect of O adsorption on scattering of He and Ar atoms 2−67894
- Zn single crystals, cavitation in liquid oxygen, plastic deformation in metal surface layers 2−71306
- ZnO film, d.c. triode sputtered, u.s. surface elastic waves, coupling factor phase velocity, propag. loss 2−80560
- ZnO film surface acoustic wave transducers, coupling constants and film thickness 2−49152
- ZnSr, paramag. surface centre density, e.p.r. obs. 2−65334
- Zr alloys, accelerated oxidation, significance of surface preparation 2−68786

Surface structure

- abrading surface shape, microscopic probability model 2−47562
- adatom position in surface from fluoresc., adsorbed atoms determ. 2−77488
- alloy, surface reconstruction due to chemisorption 2−50524
- aluminas, polycrystalline, influence of texture on mechanical props. 2−68093
- appearance potential spectroscopy 2−81361
- atomic He scattering and diffraction, surface struct. depend. 2−67889
- centred cubic, mean square displacement of atoms, simple conc. 2−57037
- ceramics, texture, examination by reflective replica technique 2−80869
- ceramics, texture with ref. to mech. props. 2−67949
- ceramics, textured studies by scanning electron microscopy, examples of use 2−71413

Surface structure continued
- ceramics for electronic device substrates, analysis, characterization techniques 2−80868
- chemical polishing technique for prepn. of thin foils for e. microscopy 2−67963
- chemisorption, struct. types, LEED obs. 2−56600
- computer simulation of crystal-fluid interface 2−50564
- crystals, low energy electron, atom scatt., review 2−80555
- crystals, single, facet size determ. by rel. between surface tension and curvature 2−80550
- decoration and electron beam study of lattice structure and point defects 2−80604
- diamond, ion machining 2−50811
- dispersion hardened materials prep. of thin foils by spark machining and electropolishing 2−80549
- dynamics, mean-square displacements of atoms in continuum approx. 2−43461
- elastomers, electron microscope investigation of fatigue fractured surfaces 2−60899
- electron microscope specimen preparation, polishing conditions 2−71415
- electron spectroscopy apparatus with monochromatized X-ray source 2−57261
- electropolishing procedure for Debye-Scherra camera specimen prep. 2−43544
- electropolishing soln., universal appl., with props. of oxidation, depassivation and diffusion control 2−80547
- element distribution, analyzing system using electron probe microanalyzer 2−65412
- epitaxial layers, surface quality improvement 2−60656
- epitaxial overgrowths of finite thickness, misfit dislocation energy 2−60798
- exam. using scanning electron microscope, magnification calibration technique 2−79013
- f.c.c. crystal, (110) interface 2−50426
- field ion microscope specimen, automatic electropolishing control unit 2−47309
- flaw detection using oblique angle illumination 2−50415
- friction, surface deform. and destruction, statistical model 2−43746
- glass, decoration effects using evap. gold film 2−64527
- glass, effect of high pressure organic impregnation, electron microscope obs. 2−53520
- glass, ion beam polishing 2−50444
- glass and electron microscope examination 2−60587
- graphite, detect. by $^4He^+$ and H^+ ion beams backscatt. 2−77485
- graphite, highly oriented pyrolytic, effects of oxidation on basal and edge surfaces 2−56572
- graphite, laser effects at mod. Ar press., crater formation 2−53552
- graphite, pyrolytic, effects of oxidation, electron microscope obs. 2−60620
- graphite, pyrolytic siliconated, fracture surface, electron microscope obs. 2−74861
- group $A^{II}B^{VI}$ cpds., ion etched, scanning electron microscope obs. 2−64540
- h.c.p. cryst., vibrs. calc. and behaviour 2−50456
- height and depth meas. using shadow casting and JEM/TEM 2−43564
- holographic automatic surface mapping, recording and image projection 2−79274
- interferometer systems for light microscopy 2−55736
- ionic crystals, influence on sublimation 2−60561
- kaolinite, Egyptian, radiation effects on surface structure 2−53550
- laser surface damage and electric surface stress 2−59191
- lattice deform. meas. method, applic. to Si 2−53545
- LEED, electron dynamical scatt. problem soln. 2−56624
- LEED determination, state-of-the-art 2−50420
- LEED intensities, Fourier analysis for determ. of struct. 2−47073
- LEED intensities reduction methods 2−53546
- LEED intensity profiles rel. to spin-polarization, atomic core scatt., surface barrier struct. 2−77483
- medium energy electron diffraction investigation, state-of-the-art 2−50421
- metal, asperities, single and multiple, deform., profilometric obs. 2−50452
- metal, f.c.c., {001} surface, LEED, expt. and theory 2−50428
- metal, field emission microscopy, defects produced by method of exam. 2−56567
- metal, kinematic LEED intensities extraction from averaged data 2−43462
- metal, roughness factor determ. method 2−47067
- metal crystals, effect of ion bombardment on surface roughness 2−74614
- metallic, conduction losses, surface roughness 2−53547
- m.i.m. structures, surface roughness, influence on emitted electron distributions 2−47948
- morphology study using new medium resolution scanning electron microscope 2−66720
- mullite, stoichiometric ceramic compact 2−50873
- optical surfaces, computer controlled ionic polishing 2−79434
- perforation-free polished specimen prep. for t.e.m. 2−79106
- polishing, thinning and cutting of disk specimens for electron microscopy 2−67957
- polishing, water soluble crystals, single lap apparatus 2−67893
- polymer replica modulation by surface electrical and magnetic fields 2−64539
- polymers, glassy, crazing in alcohols and hydrocarbons 2−83357
- polypropylene, changes during photooxidation, i.r. spectroscopic and electron microscopic studies 2−51472
- pore struct. analysis, computer program 2−47145
- porosity networks, determ. of infiltration of epoxy mixture 2−80819
- porous material, preparation for scanning electron microscope study 2−80540
- refractory metals, zone decorations in field evaporated surface 2−53551
- roughness, rel. to X-ray anomalous reflection 2−67955
- roughness, response of turbulent boundary layer to step change rough-to-smooth 2−50248
- roughness meas., pneumatic 2−60616
- roughness parameters, inclusion in adsorption isotherm 2−67919

Surface structure continued
- rubber, vulcanised, deformed, surface orientation obs. by polarization spectroscopy 2−84644
- scanning electron microscope exam. of hot and electron emitting surfaces, techniques 2−47305
- scanning electron microscope fractography as microstruct. determ. technique 2−56639
- scanning electron microscopy, electron channelling patterns 2−47074
- silicate glass, binary, corroded surface 2−53541
- space group symmetry of ideal crystal 2−71298
- sppectroscopic study by induced electron emission 2−67891
- sputter etching, r.f., target processes 2−60640
- sputter etching, r.f., transport and deposition processes 2−60641
- steel, 304L stainless, composition by proton induced X-rays 2−50832
- steel, cavitation erosion, pit form and struct. 2−71606
- steel, cold-rolled, surface defect obs. using light scatt. 2−74871
- steel, stainless, Cr depletion of surface by vacuum annealing 2−47075
- steel, stainless, electrodes subjected to very high positive and negative voltages 2−71042
- steel, stainless, energy spectrum of slow monoenergetic reflected electrons 2−50441
- steel, stainless, types 316 and 304, Mo conc., Auger electron spectroscopy obs. 2−50442
- steel, synthetic weld structure, mech. strength, obs. 2−56919
- step motion of growing crystal under electric fields 2−74613
- stepwise adsorption isotherms applied to study of surface phases 2−77518
- study, contribution made by vacuum technology 2−67892
- thin films, refractive indexes and thickness determ. from X-ray specular reflection data 2−53563
- topaz, prism face structure, development and growth mechanism 2−60702
- topography during ion bombardment computer simulation 2−60619
- two-dimensional nets, classification 2−71299
- vacuum decoration method, study of growth processes and defect structure 2−80538
- Ag, chemisorption of O_2, rel. to surface struct. LEED and secondary electron spectroscopy 2−51442
- Ag, microsection preparation, electrochemical technique 2−50429
- Ag film, annealed, hillock and island form, by surface diffusion 2−67896
- Ag on NaCl surface, decoration with anthraquinone, information microstructure 2−71305
- Al, expt. and theoretical LEED rotation diagrams 2−50433
- Al, kinematic LEED intensities extraction from averaged data 2−43462
- Al, plastically deformed, dislocations in surface layer, electron microscope obs. 2−43465
- Al, surface prep. by electrolytic etching and polishing, apparatus 2−50431
- Al, X-ray scatt. from surface rel. to polishing 2−74617
- Al (100) surface, LEED intensity profiles 2−50436
- Al {111} and {110} surfaces, LEED spectra, calc. 2−83857
- Al alloys, analysis by electron emission microscopy 2−80875
- Al sheet, rolling and annealing texture of outer layer 2−64756
- Al wires, cyclic textures 2−77700
- α-Al_2O_3, alumina, (0001) surface, LEED obs. 2−50435
- Al_2O_3, LEED, (0001) surface structure detn. 2−67897
- Al_2O_3, sapphire filaments, strength enhancement due to continuous flame polishing 2−80867
- Al_2O_3, thermal grooving and growth kinetics 2−80545
- Al_2O_3, transmission e. microscopy obs. of subsurface damage caused by mech. polishing and grinding 2−71418
- Al_2O_3 ceramic, fine grain, Cr_2O_3 additions effect 2−50867
- Au, 5 × 20 struct., RHEED obs. 2−77482
- Au, kinematic LEED intensities extraction from averaged data 2−43462
- Au boundary layers, transmission of struct. information 2−77494
- Au film, LEED, RHEED 2−77500
- $BaTiO_3$ surface domain reorientation prod. by abrasion and annealing, X-ray diffraction exam. 2−80544
- Be (0001), LEED beam intensities 2−50438
- Be cleaved surface, LEED intensity-energy curves 2−60625
- Bi-Ag eutectic alloy, surface damage after polishing, e. microscope study 2−67898
- C fibre and composites, topography, electron microscope exam. 2−53951
- CdS (0001), (00) LEED beam intensity at normal incidence 2−71308
- CdSb, Cd atom density at surface, effect on elec. props. 2−47890
- Cu-Ni alloy plates for relay thin leaf springs 2−80862
- Cu, (001) and (111), (00) LEED beam intensity at normal incidence 2−71308
- Cu, neutron irradiated, slip steps, correl. with cleared channels 2−50761
- Cu, plastically deformed, exo-emission rel. to surface struct. 2−77975
- Cu, punched-out dislocation rosettes 2−50439
- Cu (100), CO weak adsorp., LEED obs. 2−50538
- Cu film, lattice consts. of small nuclei, rel. to surface stress 2−60655
- Cu film, Xe adsorp., roughness and surface potential 2−50556
- Fe-2.89%Si (100) face, surface composition rel. to photoelec. work function 2−61463
- Fe, (100) surface, LEED and photoelec. work function study 2−50443
- Fe, cast, cavitation erosion, pit form and struct. 2−71606
- Fe, cast, with graphite, decarburizing, effect of S, Al, or Mg 2−43837
- Fe, single and polycrystals, secondary electron emission, rel. to rocking curves 2−54281
- Fe film, Xe adsorp., roughness and surface potential 2−50556
- Fe green bodies, porous and sintered parts, polished metallographic specimen production 2−60933
- Fe single crystal plates, tensile strength, surface orientation depend. 2−71583
- Ga, rel. to plastic deform. by unidirectional abrasion and rolling 2−83856

Surface structure continued
GaAs, epitaxial layers, surface quality improvement 2−60656
GaAs, etched surface morphology, elec. microscope obs. 2−56575
GaAs, laser irrad., 0.694-1.06μ surface damage 2−61574
GaAs, polishing by gaseous etching 2−83853
GaAs, strain induced phonon line broadening observed by surface reflection Raman scattering 2−83858
GaAs, surface vacancy model, LEED, HEED, Auger spectroscopy and molecular beam obs. 2−50445
GaAs obs., by Rutherford scatt., and channelling 2−64553
GaAs$_{1-x}$P$_x$ epitaxial layer, on GaAs, cross-hatch pattern due to misfit disloc array 2−47110
GaSe, LEED, photoemission, Auger spectroscopy obs. 2−48024
Gap, surface vacancy model, Leed, Heed, Auger spectroscopy and molecular beams obs. 2−50445
Ge, effect of treatment and relief on field effect 2−57211
Ge, etched surface, kinetics of development of first-order network 2−50447
Ge, field ion microscopy at 80K 2−64554
Ge, hexagonal pit growth on etching with water vapour 2−67933
Ge, sputtered atom ejection patterns indicative of cryst. order 2−43466
Ge, surface orientation effects on elec. cond. and work function 2−71935
Ge, surface reaction with O$_2$, LEED and conductivity obs. 2−50448
Ge, symmetry and form of etched pits on (111), (110) and (001) surfaces 2−50446
Ge profiled crystal, photogoniographic obs. 2−47076
Ge single crystal, rel. to adsorp. and nucleation of Cd 2−47158
InAs, LEED and Auger spectroscopy obs. 2−50449
InBi, morphology, effect of thermal cycling 2−51101
InSb, sputtered atom ejection patterns indicative of cryst. order 2−43466
KCl, growth spirals on crysts. grown from soln. 2−50586
KCl, polygonization, produced by electron bombardment and illumination 2−50457
KNO$_3$, aragonite- to calcite-type transform., surface effects 2−74932
KNbO$_3$, surface deformation rel. to feroelectric domain structure 2−61429
LiF, proton irrad., surface damage monitoring using (p,α) reaction 2−43610
LiH, LEED and Auger spectroscopy obs. 2−47078
LiNbO$_3$ single crystal, lapping characts. 2−71603
Mg-Li alloys, electropolishing bath for prep. of thin foils 2−80548
MgO, thermal grooving and growth kinetics 2−80545
MgO (001) single crystal with Fe deposit, LEED-AES system analysis 2−74612
MgSO$_4$.7H$_2$O, stepped relief of artificial vicinal faces 2−74680
Mo-Cu-Co cermet contact, elec. erosion characts. working surface struct., rel. to Co content 2−47659
Mo, electrode, in vacuum, elec. breakdown rel. to electrode surface finish 2−75190
Mo, ion irrad., surface damage, LEED obs. 2−50468
Mo, proton and electron excited Auger electron spectra, composition detn. 2−50453
Mo single crysts., surface orientation effects on yield 2−74842
Na film, Xe adsorp., roughness and surface potential 2−50556
NaCl, cavitation erosion, pit form and struct. 2−71606
NaCl, growth spirals on crysts. grown from soln. 2−50586
NaCl, La surface contamination, O ion induced X-rays obs. 2−60628
NaCl, mean-square amplitudes of vibr. 2−50454
NaCl, polygonization, produced by electron bombardment and illumination 2−50457
NaCl, vibr. modes in rigid-ion model 2−50455
NaCl before and after Cu vapour deposition, ion scatt. study 2−71314
Nb, backscatt. of He$^+$, Ne$^+$ and Ar$^+$ 2−50467
Ni-Fe-Mo alloys, thin strips, magnetic properties and texture 2−68509
Ni, (001) surfaces, absolute intensity energy LEED spectra 2−50459
Ni, (111) surface, averaged LEED intensities 2−50460
Ni, backscatt. of Ne$^+$ 600 eV ions, chain effect 2−77484
Ni, Ir, comparative interfacial structures, transmission electron-microscope obs. 2−56576
Ni, multiple scatt. of low energy noble gas ions 2−50458
Ni, preferential orientation of CO adsorp., extended Huckel calc. 2−50546
Ni, surface interplanar spacings, LEED, Bragg peak widths 2−77486
Ni, surface reconstruction on absorption of O, S, Se, Madelung potential 2−47162
Ni (111), (00) LEED beam intensity at normal incidence 2−71308
Ni(001), impurity segregation, work function and Auger electron spectroscopy obs. 2−53554
Pb(N$_3$)$_2$, polishing and cutting 2−83900
PbS film, epitaxial, struct. rel. to substrate surface struct. 2−64571
PbSe film, epitaxial, struct. rel. to substrate surface struct. 2−64571
Pb$_{1-x}$Sn$_x$Te, epitaxial layers, surface quality improvement 2−60656
PbTe film, epitaxial, struct. rel. to substrate surface struct. 2−64571
Pt film, lattice consts. of small nuclei, rel. to surface stress 2−60655
Se, trigonal crystals, transmission e. microscopy obs. of dislocations after chem. polishing 2−64668
Se single crystals, circular microdisc patterns 2−60630
Si, cleaning by ion irrad., ellipsometric obs. 2−47082
Si, constraints meas. 2−53545
Si, dislocation etch pits shapes rel. to mech. stress 2−80553
Si, H$_2$O$_2$ soln. cleaning, HEED and Auger electron spectroscopy obs. 2−53555
Si, impurities and disorder, detect. by ^{4}He$^+$ and H$^+$ ion beams backscatt. 2−77485
Si, irrad. with 400 eV ions, surface damage, change in optical consts., ellipsometric obs. 2−47081
Si, lattice vibrs. at ideal (111) surface 2−43467
Si, rel. to surface states, surface cond., LEED 2−77800
Si, sputtered atom ejection patterns indicative of cryst. order 2−43466
n-Si (111), LEED and Auger spectroscopy obs. 2−50464
Si oxidized surface, orientation effects on electron and hole transport props. 2−51173
SiC, 2-stage decoration method, for (0001) plane 2−80539

Surface structure continued
SiC, self-bonded, texture and strength detn. to 1300°C in air and to 1750°C in argon 2−71393
Si$_3$N$_4$ film, detection of silicon oxynitride layers on surface by Auger elec. emission 2−50506
SiO$_2$ glass, ion irrad., surface topography 2−50462
Sn, dislocation generation at single cryst. surface, X-ray obs. 2−47083
Th, surface impurities, bulk to surface equilib., Auger spectroscopy obs. 2−50465
TiC, 2-stage decoration method for (001) plane 2−80539
TiC, electron diffr. obs. in ultrahigh vacuum environment 2−43469
Ti(0001) single crystal and polycryst., cleaning process rel. to opt. const. meas. 2−44341
U, chem. shifts in Auger transitions 2−67901
U alloy, ion tched, scanning electron microscope obs. 2−56578
UC, kinetics of surface smoothing 2−53556
U$_3$Si, irradiated, effect of electropolishing on voids 2−67354
W, adsorption of N, surface crystallography effects 2−47168
W, alkalis, rare gases and H$_2$ adsorbate structure 2−50554
W, atomic and mol. scatt., effect of surface composition and cryst. orientation 2−47084
W, backscatt. of H$^+$, Ne$^+$ and Ar$^+$ 2−50467
W, ion irrad., surface damage, LEED obs. 2−50468
W, polycrystalline, crystal orientation distribution determination, colour etching process 2−64545
W, surface interplanar spacings, LEED, Bragg peak widths 2−77486
WC-(25 wt.%)Co alloy, surface finish effects on fatigue 2−43717
WO$_3$ cryst., photoemission microscopy obs. 2−60631
W(110) single crystal and polycryst., cleaning process rel. to opt. const. meas. 2−44341
Xe (111), LEED thermal scatt. obs. 2−50470
Xe (111), one phonon thermal diffuse scattering calc. 2−60632
Zn-Al alloys, strain-rate depend. of deform. mechanism and texture formation 2−84011
Zn, ductility, in presence of Hg, effect of surface layer defects 2−74830
Zn cleaved surface, LEED intensity-energy curves 2−60625
Zn single crystal, oriented, morphology developed during sublimation 2−53558
Zr alloy, stress corrosion cracking in Hg, fracture surface study 2−43737
Zr alloys, anisotropy of secondary in-reactor creep, relation to texture 2−67349

Surface tension
see also Capillarity
acetone-cyclohexane, meas. at 25°C 2−53408
acetone-methanol, meas. at 25°C 2−53408
binary mixtures of organic compounds at 15°C 2−53410
boson fluid, spinless, stongly interacting, statistical thermodynamics, surface energy and tension 2−82267
bubbles, computation for stretched regions of surface 2−64454
carbon tetrachloride-He system, press. depend., 1-71 atm., room temp. 2−64453
circular film, smallest stable radius rel. to contact angle and line tension 2−60412
crystal growth, effect of gradient in liquid column on crystal profile curve 2−47251
crystals, surface facet size determined by relation between surface curvature and tension 2−80550
curved surface, concave and convex, iteration method, rel. to v.p. 2−46943
dispersion contrib. and crit. surface tension of wetting of liquid substrate 2−74532
fluid interfaces near critical point, absolute value calc. 2−67813
forces in liquid film flow, effect on film acceleration 2−67793
gravity wave propagation, Fokker-Planck type eqn., third order approx. 2−50304
gravity-capillary wave spectra, nonlinear energy transfer 2−67778
hard square lattice gas 2−55426
interfacial layers, equidistant mol. plane model 2−84630
interfacial layers, equidistant mol. plane model 2−84631
liquid alkali metals, significant structure theory 2−50346
liquid bridges, effects of reduced pressures on tensile strength 2−71176
liquid-gas system, boundary surface tension 2−60550
low gravity environment, demonstration of convection driven by surface tension 2−58954
menisci, axisymmetric, tables of profiles 2−60413
meniscus, vel. profiles for plate withdrawal, Navier-Stokes eqns. 2−60383
methanol-cyclohexane, meas. from 25 to 50°C 2−53408
methanol-cyclohexane-acetone, meas. at 25°C 2−53408
methanol-cyclohexane-acetone, meas. at 25°C 2−53408
molecular liquids, rel. to positronium annihilation 2−43311
nematic liquid crystal, scattered light obs. 2−56480
non-ionic surfactants as drag reducing additives 2−71162
polyacrylamide solutions, effect of changes on normal force obs. with Weissenberg rheogoniometer 2−64455
polydimethylsiloxanes in n-heptane-tetralin mixtures, calcs. and expts. 2−74535
polyisobutylenes in n-heptane-tetralin mixtures, calcs. and expts. 2−74535
polymer solution, calcs. for three-component mixtures 2−74535
pyrolytic graphite, stress-annealed 2−60621
sessile drop profiles, derivation of corrected methods 2−83785
sessile drops and captive bubbles, interfacial tension 2−67789
sessile lenticular configs., translationally and rotationally symmetric lenses 2−74510
soap film, stabilised with ionic surfactants, impurity effects in meas. of very small contact angles 2−60410
soap film, transition regions, line tensions and contact angles 2−60409
surface active agent adsorption densities on interfaces in three-phase system 2−71173
water, contact angle rel. to drop size at b.p. for 50-760 Torr 2−77474
water, effect of changes on normal force obs. with Weissenberg rheogoniometer 2−64455
water, effect on cavitation threshold 2−43290
water, limiting shear stress measurement 2−64418

Surface tension continued
- water, molecular depression by dissolution of fatty acids 2−71172
- water on hydrophobic glass, determ. of smallest non-collapsing drop 2−77492
- welding slags, 1200 to 1700°C 2−71165
- rel. to wetting and wetting angle 2−43867
- Ag, effect of dissolved O_2, sessile drop dimens., change method 2−43340
- Al_2O_3, liq., correl. with covalent bonding 2−43338
- Al_2O_3 molten, from menisci profiles 2−80465
- Bi, 239°C, determ. using zero creep method 2−56577
- Cr_2O_3 molten, from menisci profiles 2−80465
- D_2O, at boiling point, contact angles on Cu and polytetrafluoroethylene surfaces, 10-770 torr 2−74533
- Fe, cast, melt, solidification, graphite spherulite formation 2−74881
- H_2O-He system, press. depend., 1-71 atm., room temp. 2−64453
- He II, electronic bubble surface tension, press. depend. 2−77463
- He II films, temp. depend., surface excitations contrib. 2−53473
- Hg, effect of base-metal impurities 2−74534
- Hg on glass, determ. of smallest non-collapsing drop. 2−77492
- Hg on polymer thin films, contact angle meas. using scanning electron microscope 2−46942
- I_2, liquid 2−71175
- In-Ga(Sn) alloys, comp. depend., 700K 2−67815
- In, 142°C, determ. using zero creep method 2−56577
- Pb-Sn liquid alloy, max. bubble pressure method 2−53409
- Pb,309°C, determ. using zero creep method 2−56577
- Sm_2O_3 molten, from menisci profiles 2−80465
- Sn, 215°C, determ. using zero creep method 2−56577
- Tl, 272°C, determ. using zero creep method 2−56577
- Zn-Bi alloy, 860-920K 2−43341

Surface tension measurement
- drop-weight (volume) technique, correction factors, applic. to high density liquids (metals) 2−74531
- liquid interface, dynamic meas. of dilational properties 2−50302
- microtensiometer for obs. of perilymph 2−45036
- molten glass, dipping cylinder method 2−83780
- molten metal pool in welding with cored electrode wire 2−71618
- polymeric solutions, gravitation sensitive gas phase device for obs. with viscosity 2−64452
- in saturated system or controlled atmosphere, obs. rel. to temp. 2−43342

Surface texture *see Surface structure*

Surveys *see Reviews*

Suspensions
- *see also Aerosols; Sedimentation; Sols*
- alumina, zero point of charge, temp. depend. 2−72567
- bacteria, Raman spectra 2−50374
- bentonite-water suspensions, flow behaviour for time-dependent non-Newtonian fluid 2−60159
- biological, rising velocity of bubbles in vertical columns 2−83825
- chlorophyll-a microcrystal, photoelectric response 2−51469
- clay-H_2O suspensions, flow behaviour 2−83816
- concentrated, discontinuous and dilatant viscosity behaviour, flow instability 2−64245
- convective diffusion for case of Stokes flow of fluid 2−64481
- Coulter counter analysis 2−64480
- dense particles in horizontally oscillating liquid, transitions between flow regimes 2−83741
- diffusion of small particles, electrostatic effects 2−71250
- dilute, rheological properties in presence of rotary Brownian motion and external couples 2−50375
- dilute, sedimentation rate, conc. depend. 2−50379
- drops in elc. field, stress system 2−83819
- electrokinetic movement of suspended colloids in flowing medium, expt. obs. 2−71127
- fibre, stock flow 2−77220
- flame propagation 2−48326
- gas-solids suspensions, turbulent pipe flow, particle slip velocity 2−53284
- Gouy magnetometer, lateral instability 2−73510
- light scatt., low angle, in turbid media 2−77455
- liquid and solid aerosols, acoustic dispersion and velocity 2−74569
- liquid drops in cylindrical tube, viscous flow 2−64419
- macroscopic, of elongated particles, significance of viscosity obs. 2−67845
- magnetite, zero point of charge, temp. depend. 2−72567
- mammalian cell identification, differential light scatt. 2−66244
- non-Newtonian, in water, rheological model 2−83823
- non-Newtonian fluids, best possible concentration in pipe flow 2−60143
- oriented particle, simultaneous obs. of birefringence, absorpt. dichroism and turbidity 2−56532
- particle counting, Coulter counter instrument settings, calc. 2−50380
- particle in electrolyte, proportional to voltage pulse meas. 2−44489
- particulate aerosol, acoustic streaming, agglomeration 2−43407
- phase interaction parameters in conc. mixtures of fluids with small particles 2−67843
- polydisperse crystal suspensions obeying McCabe's ΔL law, growth calc. 2−77524
- polystyrene in alcohol, ultrasonic relaxation 2−53462
- polystyrene spheres, in water, Rayleigh scatt. 2−50381
- PVC-filler composites, influence of fillers on dynamic mechanical props. 2−64792
- quick clays, Rosenqvist theory, liquid crystal dispersant 2−60517
- reflection, interpretation of Kubelka-Munk coefficients 2−49426
- rigid dumbbell, hydrodynamic interaction effects, steady shear flow 2−67738
- rigid dumbbell, with Brownian motion, modified Oldroyd model for rheological behaviour 2−60518
- rigid ellipsoids, theory of motion, stresses, viscosity and optical anisotropy 2−67844
- scattering media, light beam attenuation, exponential low limits, scatt. indicatrix 2−56527
- sea, light scattering rel. to suspended matter in nepheloid layers 2−68870
- seawater conc. determ. using total scatt. coeff. 2−62020

Suspensions continued
- silica, aqueous system, freezing using temp. gradient microscope stage 2−74585
- solid in non-Newtonian liquids, viscosity 2−83822
- solid particle in fluid, anomalous readings in Pitot tubes 2−53360
- solid-liquid, agitated, heat transfer 2−83827
- sound attenuation, theory and experiment 2−43395
- spherical particles, subject to Brownian rotations, rheology 2−83813
- spherical particles in isotropic matrix, elastic behaviour 2−53458
- transverse migration of particles, in turbulent flow 2−74571
- turbid water, depolarization of scattered laser light 2−64486
- turbulent drag reductions, of rigid particles, high Reynolds numbers, expt. 2−53373
- turbulent flow, agglomeration rate/deposition rate relationship 2−43396
- variable concentration, unsteady flow 2−77452
- viscoelastic, rheological equation of state 2−83824
- viscosicity props., for limiting conds. of turbulent drag reduction 2−53364
- viscosity for doublets of two equal sized spheres 2−74559
- Fe, finely divided, in toluene, magnetization, temp. depend., 20-105°C 2−77450
- $FeBO_3$, i.r. absorpt. spectra 2−75292
- SiO_2 and diatomite in kerosene, mechanical behaviour during shearing in electric field 2−60531
- ZnO in loose contact with electrode, photocurrents and photovoltages obs. 2−51218

Suzuki atmospheres *see Crystal imperfections/dislocations*

Switching time, ferroelectric *see Ferroelectric materials; Ferroelectric phenomena*

Switching time, ferromagnetic *see Ferromagnetism; Magnetic properties of substances/ferromagnetic*

Symbols *see Nomenclature and symbols*

Symmetry *see CPT conservation*

Synchrocyclotrons *see Particle accelerators/cyclotrons*

Synchrotron radiation
- electron, applic. to investigation of Si and KCl reflection spectra spectra in vacuum u.v. 2−44367
- electron, second-order correction to first-order quantum mechanical treatment 2−82617
- electron beam separation from other particles by synchrotron radiation, for 100 GeV beam 2−73959
- from electrons, 800 MeV, angular distrib. of polarization and intensity 2−45879
- electrons moving in weakly focusing magnetic field 2−58983
- Galactic Centre, e.m. spectrum as proton synchrotron emission 2−81796
- gravitational, Regge-Wheeler formalism 2−44827
- gravitational 2−58721
- gravitational synchrotron radiation, analysis in terms of Stokes parameters 2−72958
- gyro, from solar corona plasmas, temperature effects 2−81950
- gyrosynchrotron radiation, free-free absorption in solar microwave bursts 2−75995
- l.f. radiation from relativistic electrons in magnetoplasma and U shaped type IV solar bursts 2−75959
- light source for u.v. absorption spectroscopy of atoms, molecules and solids 2−76549
- NINA, additional project 2−52715
- OG + 003, small-pitch-angle radiation 2−58404
- OQ + 003, small-pitch-angle radiation 2−58404
- Parkes 0237-23, small-pitch-angle radiation 2−58404
- Parkes 2134 + 004, small-pitch-angle synchrotron radiation 2−58404
- Peres gravitational field effect 2−69823
- phase vibrations of electrons in synchrotrons, effect of synch. rad. 2−79689
- polarization, electron dynamic effects, expt. 2−42339
- power, from electron in uniform helical motion 2−45676
- Ritz emission theory and Einstein's postulate on the velocity of light 2−55378
- spatial time correlation of radiation field in synchrotrons 2−55941
- synchro-Compton radiation, polarisation 2−72983
- synchrotron instability of modulated beam of charged particles 2−78777

Synchrotrons *see Particle accelerators/synchrotrons*

Szilard-Chalmers reactions *see Radiochemistry*

Tables, mathematical
- symmetrized powers of group representations 2−52046

Tables, physical *see Collections of physical data*

Tachometers *see Angular velocity measurement*

Tachyons
- Cerenkov radiation 2−55408
- Cherenkov radiation, Lorentz-invariant formulation 2−69559
- dual-resonance model without tachyons 2−79512
- dust metric in general relativity 2−45259
- electron spin, semi-classical model 2−52052
- exchange in hadronic interactions, phenomenology of high-energy processes 2−63546
- field, commutator and anticommutator calc. using Klein-Gordon eqn. and relativistic invariance 2−73712
- free fields in two dimensions, causal properties, calc. using Klein-Gordon eqn. and relativistic invariance 2−78801
- Lorentz transformations 2−45253
- Lorentz transformations 2−41476
- monopols, searches in photoproduction reactions at 1 MeV, detection by emitted Cherenkov radiation 2−82638
- negative energy, limits on emission rate in $p \rightarrow p + t^0$ decay 2−45254
- one-dimensional causal theory 2−62983
- quantization of free fields 2−79464
- special relativistic treatment, interacting and non-interacting fields 2−78788
- superdense stars, tachyon-like, matter implications 2−55397
- theory and arrow of causality 2−82209
- in two-pion channels, decoupled, for arbitrary pion concept 2−66947

Tandel *see Dielectric devices*

Tantalum
- arodic sectioning technique 2−60817
- atom, γ-ray scattering, incoherent, by K-shell electrons 2−59931

Tantalum continued
- crystal, centred cubic, mean square displacement of atoms, simple calc. 2−57037
- electrical and thermal cond., 20 to 1200°C 2−47769
- film deposition, sputtering, triode config. with rotating base 2−78694
- film deposition by sputtering, temp. rise as a function of applied power 2−67913
- film deposition in d.c. sputtering system 2−50226
- film sputtering with uniform thickness 2−47127
- films, strain gauge factor study 2−77710
- getter, residual gas sorption in evacuated valve, mass spectrometer obs. 2−76130
- hyperfine field, in Fe matrix, spin echo obs. 2−72229
- neutron displacement cross sections, based on Lindhard model 2−83053
- photoactivation analysis in ores 2−65424
- photoelectric emission, two-photon photoelec. effect 2−48021
- photoelectron energy distribution and photocurrent meas. 2−72093
- proton motion, temp. depend. 2−43653
- single crystals, emitter and collector work functions, modified Shelton measurement method 2−63234
- slip, orientation depend., deform. mechanism, 4.2-450K 2−50679
- Snoek effect absence for H 2−77647
- sorption of filament in CO atmosphere, exam. using omegatron 2−77519
- spaceflight neutron dosimetry 2−58147
- specific heat, pulsed electron beam measurement 2−54039
- stopping power for 0.50-1.75 MeV protons meas. by backscattering method 2−64872
- stopping power for 28 MeV α-particles 2−54099
- substrate for TiC_x, chem. vap. deposition 2−80597
- superconducting transition temperature, press. depend. 2−75064
- thick target, energy loss of scatt. protons 2−80928
- Hf polycrystalline sample, influence of Zr on the quadrupole interaction of ^{181}Ta 2−84593
- Ta-Al anodic oxides, correlation between temp. coeff. of capac. and dielectric loss 2−77946
- Ta-N, interstitial effects on asymmetry of yield stress 2−74844
- Ta-W emitter, for plane parallel Cs diode 2−49287
- Ta anodic oxides, correlation between temp. coeff. of capac. and dielectric loss 2−77946
- Ta + Co, Laves phases and thermodynamic props., solid-electrolyte galvanic cell studies 2−77424

Tantalum compounds
- alloy, foil prep., for electron microscopy, electrolytic jet thinning procedures 2−71415
- hydrides, clustering model rel. to sp. ht. anomalies 2−77716
- tantalates, $M_4Ta_2O_9$, (M=Co, Mn), magneto-electric effect obs. 2−54359
- Fe-Ta alloy, ductility enhancement using allotropic phase change 2−57020
- Hf-Ta alloys, superconductivity under pressure 2−81058
- Nb-Ta alloy, superconductor, microwave surface resist. 2−54133
- $Nb_{1-x}Ta_x$ alloy, $0<x<0.25$, growth by electron beam float zoning 2−50599
- Ni-Ta-Al system, Ni_3Al-Ni_3Ta eutectic, directional solidification growth 2−47644
- Ni_8Ta, quenched, microstruct. aspects, cry. orientation and grain boundaries during deformation 2−64709
- Ta-B system, phase diagram 2−50957
- Ta-Cr-B alloy, phase equilibria, at 1400°C, X-ray obs. 2−43912
- Ta-H alloy, quenching at liq. He temps. 2−56907
- Ta-H system, ordering in β-Ta_2H 2−54003
- Ta-H system, resist. rel. to solute conc. 2−80857
- Ta-H systems, phase transitions due to elastic interaction 2−77744
- Ta-Nb alloys, superconducting, sp. ht. and mag. meas. 2−71875
- Ta-7.3 at.%Mo alloy, oxidation, 950°C 2−72560
- Ta-O system, high temp. solid solubility limit and phase studies 2−50975
- Ta-O thermionic emission constants and electron work function changes 2−54268
- Ta-Pt alloy, strength, oxidation resist. 2−47533
- Ta-W-Hf alloy, tensile props., effects of O contamination 2−43862
- Ta-W alloys, superconductivity under pressure 2−81058
- Ta-10%W alloy, heat capacity, elec. resistivity, thermal radiation props. 1500-3200K57069 2−57069
- TaB_x, thermionic emission, rel. to electronic struct. 2−48017
- $TaBO_4$ vibrational spectra, interpretation by factor group approx. calc. of force constants for BO_4 group 2−70728
- TaC-Co alloy, oversaturated, microstruct. and reaction behaviour 2−64775
- TaC, band struct. calc. 2−57126
- TaC, phonon anomalies 2−64836
- TaC, wetting by liq. Ag and liq. Cu, surface energy 2−43468
- TaC film, epitaxial growth by electron beam evap. 2−67916
- TaC neutron absorber rods, modelling of swelling and gas release 2−52861
- TaC_{1-x}, vacancy short range order, calc. 2−83966
- TaC_{1-x}, plastic deform. up to 2200°C 2−60869
- TaC_{1-x}, supercond. transition temp., rel. to band struct. determ. 2−81055
- TaC_x, lattice instability effects on supercond. and mechanical props. 2−68349
- TaC_x film, on needle-like W microcrysts., electron and field emission microscope obs. 2−50509
- $TaCl_6^-$, $TaBr_6^-$, Urey bradley force fields 2−42919
- Ta_4D_3, stepwise phase transitions, neutron diffr. obs. 2−74947
- TaH_x, quasielastic neutron scatt. obs. of hydrogen diffusion 2−77621
- TaN, microhardness and thermal expansion, 80-300K 2−61112
- TaN film, adhesion to ceramic, effect of substrate surface chem. 2−57005
- Ta_2N film resistor, relative nitrogen doping level by Seebeck effect 2−74793
- $Ta_{0.96}Nb_{0.04}$ alloy, surface pinning of fluxoids 2−44064
- Ta_2O_5, anodic oxide film, dielec. const. field depend., ellipsometric obs. 2−44150
- Ta_2O_5 film, anodic, precise sectioning method for conc. profiles 2−43483

Tantalum compounds continued
- Ta_2O_5 film, in m.i.m. struct., transients, capacitance variation with temp. 2−57219
- Ta_2P, metallic bonding, Brewer-Engel correl. 2−47180
- TaS_2, 1S and 2S polymorphs, cryst. growth and props. 2−47226
- TaS_2, two dimensional Van Hove singularity in band struct., reflectivity obs. 2−81380
- TaS_2 organo intercalation compounds, electron microscope examination of lattice and superconductivity 2−53676
- Ta_2S, metallic bonding, Brewer-Engel correl. 2−47180
- $TaSe_2$, growth by Br transport, and cryst. struct. 2−60707
- Ta_5Si_3, diffusion of Si, oxide coating form., 1700°C 2−53769
- Ti-Ta alloys, martensitic, precip. reactions 2−47697
- Ti-Ta alloys, martensitic transform. 2−47696
- $Ti_xTa_{1-x}S_2$ $(0.1\leqslant x\leqslant 0.9)$ solid solutions, resistivity, magnetic susceptibility, thermoelectric power 2−61266
- $(W, Ta)O_x$, cryst. shear struct., electron microscope obs. 2−47352
- $W_{1-x}Ta_xSe_2$, cell dimens. 2−43593
- $Zr_xTa_{1-x}Co_2$, Laves-phase compound, mag. susceptibility, temp. depend. 2−65128

Targets *see Nuclear bombardment targets*

Teaching
- 'A' level examinations, appraisal 2−48954
- algebraic methods in statistical mechanics and quantum field theory 2−45336
- astronomy for nonspecialist, topical rather than survey approach 2−78715
- atomic and molecular structure, book based on course for arts students 2−62954
- atomic physics, book 2−83203
- atomic physics, current developments and applications 2−82110
- atomic physics course on modified Keller plan 2−78719
- atomic theory, calculation of energy levels of light atoms 2−6294
- ballistic motion in gravitational field of rotating Earth, Coriolis deflection 2−73270
- Bayesian statistics, applic. to Poisson and other distributions, introduction for physicists 2−66401
- blackbody radiation in small cavities 2−63140
- Boltzmann eqn. for charge particle transport in magnetic field, simplified soln. 2−73492
- Bragg equation, shortcomings in simple derivations 2−62950
- calcite crystal, double refraction 2−82113
- Cerenkov radiation, teaching paper 2−82105
- chiral dynamics, book 2−82667
- coin spinning on table 2−73280
- compression heating of classical particles in ID box 2−62948
- Comptons scattering, X-ray 2−82114
- computer generated films for motion of electrons in periodic potentials 2−78729
- computer simulation of high school laborators experiments 2−78742
- continuing education program for IEEE nuclear science group 2−78740
- creative education of modern youth, reply to Kapitsa's essay, 'elitist' schools 2−82117
- crystallography of single crystals, UNESCO pilot project 2−69528
- current balance, classroom instrument 2−48962
- de Broglies book 'Research on quantum theory', translation into english of the first chapter 2−62996
- diffeomorphism generalization of Hopf bifurcation theorem 2−76170
- diffraction, spatial filtering, predictions of Fourier transformations and development of general transformations 2−79314
- diffraction theory, new emphasis 2−62945
- Dirac delta function, integral representation 2−78735
- double refraction in calcite crystal 2−82113
- electron linear accelerator, cheap, construction for students 2−78723
- elementary particles, semi-popular exposition 2−42308
- elements, new systematic table 2−57405
- end-weighted spring, comparison of normal modes for discrete od continuous mass distributions 2−78864
- energy, resources, production and environmental effects 2−41421
- equivalence of momentum operators in generalized coordinates 2−78811
- Euler rotations, theorem 2−49048
- experimental error treatment, simple approach 2−62952
- experimental physics course for prospective school teachers 2−78743
- Faraday's law paradoxes 2−49196
- finite element stress analysis, one-dimensional examples for a beam 2−52029
- Foucault pendulum, role of constraining force 2−48967
- Fourier analysis, discovery approach, use of computer as calculational aid 2−78734
- functional analysis, text book for first year graduate student 2−82182
- general relativity, experimental tests and explanations 2−82205
- general relativity, falling body problem 2−73273
- harmonic oscillator, free damped, soln. of eqn. of motion 2−78809
- heat capacity, analysis of low temp. data 2−55352
- Heisenberg ferromagnet, 2 spin 1/2, exact solution 2−78726
- humanistic science course 2−78721
- ideal quantum gases, special class, fundamental properties 2−62944
- illumination systems tutorial paper 2−66800
- individualized instruction course (without lectures) in physics 2−73257
- infinite square-well potential, probability distribution of momenta 2−73281
- information retrieval course for undergraduate 2−76141
- integrated course in physics and mathematics for A level biology and arts students 2−41430
- interference patterns as confocal conic sections 2−49418
- ionic thermoconductivity in dielectrics, undergraduate research project 2−41437
- Keller method of physics teaching, evaluation 2−62924
- kinetic theory, relativistic, lecture notes 2−52101
- laboratory, flexible scheme 2−73255
- laboratory course philosophy and objectives 2−78720
- laboratory expt. involving parallel LC circuit containing real inductor with non-zero resistance 2−78728
- LaCoste-Romberg gravimeter, simplified theory 2−48968

Teaching continued
Lagrange's equations, derivation from Newtons second by projection onto moving tangent 2–78724
Lagrangian, rapid determ using complex numbers 2–78725
lecture room audio equipment 2–45544
Legendre's eqn., simple proof for teaching 2–41438
Loedal diagram, equivalence to special case of Minkowski diagrams, use in teaching relativistic kinematics 2–78739
magnetic linkage 2–48970
magnetic susceptibility meas. on ferrimagnets, graphical analysis 2–81280
Mars, features explained in terms of elementary physics 2–78714
materials science, at McMaster University 2–43761
Maxwell's equations, a self-contained derivation of their invariance 2–49193
Maxwell-Boltzmann distribution, different proof 2–62941
Maxwells equations, Amperes law derivation and displacement current 2–49192
mechanics, new approach 2–73271
medical physics, course based on hospital field experience 2–55346
molecular energy levels, analytic independent particle model, quantum mechanical study 2–73254
neutron diffusion equation, solution by random walk technique 2–63938
non-destructive testing course 2–45204
non-Newtonian viscosity and lubrication 2–48969
nuclear chemistry, alpha spectroscopy using Th daughter products 2–62931
nuclear physics, book, elementary treatment of basic ideas 2–82838
nuclear physics textbook for final year undergraduate 2–62955
nuclear reactions due to neutrons, textbook for 1st yr. graduate student 2–52815
Nuffield A level physics, background for students entering university 2–41428
Nuffield O-level physics course, conceptual demands 2–76143
Nuffield physical science course, background in physics which students entering university will have 2–41429
one-dimensional Schrodinger equation computer solutions 2–73274
one-dimensional Schrodinger equations, numerical solutions 2–73279
optical aberrations and design 2–76506
optical design and aberrations, tutorial 2–49410
optical design and aberrations 2–73626
optical design and aberrations 2–73630
optical dispersion, classical theory recapitulated 2–73632
perturbation theory, stationary, ambiguities 2–73325
photon, limits on mass 2–82106
physical chemistry, computer programs for laboratory expts., classroom problems 2–82101
physical sciences, computer based methods 2–41440
physics, Advanced level course lasting few months 2–82103
physics, American college textbook 2–45209
physics, based upon sense impressions 2–82111
physics, computer applications 2–41441
physics, digital computer applications in A-level course 2–41442
physics, evaluation of nonlecture technique 2–55345
physics, transition from schools to universities 2–62921
physics for biology and medicine, book 2–45208
physics course, non-mathematical, for non-scientists 2–78717
physics course covering war, peace, science and technology 2–62919
physics education, use of computers 2–58679
physics education in Ghana 2–62920
physics in developing countries 2–82090
physics review course of theoretical physics at student level, book 2–82116
plane wave in spherical waves, derivation of expansion 2–73278
plasma waves, simulation in transmission line 2–73263
point charges, computer plotting of equipotential lines 2–78744
potential energies for which particle motion is same in classical and quantum mechanics 2–78806
programmed learning, group controlled audio-visual system 2–48956
project work, design of experiments and error estimation 2–62951
projectile kinematics, expt. using spring- gun portion of ballistic pendulum 2–78733
projectile range, effect of rotation of Earth 2–73276
protein mol. wt. by X-ray diffr. 2–82097
quantum electrodynamics, resource letters 2–73253
quantum field theory, book 2–82635
quantum mechanical cross-section paradox, simplified resolution 2–49016
quantum mechanical exercise, n.q.r. in solid nitrogen 2–55353
quantum mechanical one-dimensional system matrix method for eigenvalue determ. 2–78727
quantum mechanical operators in generalized coordinates 2–73277
quantum mechanical square well, graphical solutions 2–55419
quantum mechanical symmetry operation commutation with raising, simplified proof 2–76208
quantum mechanics, bouncing ball as wave packet 2–45207
quantum mechanics, computer-generated film of eigenvalues 2–73272
quantum mechanics, non-dispersive mirror wave-packets 2–62938
quantum mechanics, product-integral calculus formulation 2–62939
quantum mechanics, simple concepts 2–82115
quantum mechanics, undergraduate textbook 2–45210
quantum theory of many body problems and applications, book 2–82240
radioactive dating method, ^{14}C, employing nuclear emulsion 2–75438
Raman spectroscopy, introductory presentation 2–73261
ray diagrams for virtual objects 2–70007
reality in physics, a classroom dialogue 2–78718
reflection of light at a surface, total internal 2–49417
relativistic particle motion, constant force and uniform gravitational field 2–48966
relativistic rocket problem for students 2–55395
relativity, Poincares generalization of Newtonian gravitational theory 2–62946
relativity and quantum theory, college-level text-book 2–62980

Teaching continued
repetitive multiloop resistive circuits, solution by finite-difference equations 2–62942
Russian-English dictionary, book 2–52024
school physics, concepts 2–55343
school-industry cooperation for scientific and technological projects 2–76140
school-research laboratory liaison 2–82102
school-University physics interface project 2–48955
Schrodinger eqn., radial, SU(1,1) algebra determ. of eigenvalues 2–73317
science, criteria of assessment of progress 2–76142
science, in comprehensive schools in 1970s 2–76145
science, place in education 2–82109
science in junior forms of primary schools curriculum 2–69526
science skills, programmed approach 2–76146
second virial coefficients, undergraduate apparatus 2–52026
similarity transformation, examples for physics students 2–62965
simple harmonic motion, a teaching example 2–55445
simple harmonic oscillation, energy quantization 2–62943
solid state physics in secondary schools in Hungary 2–73258
solid state physics in the secondary school 2–69525
spacecraft design, industial and university approaches 2–48620
special relativity, device for illustrating Lorentz transformations 2–55351
special relativity, geometrical exposition 2–82107
special relativity, Thomas precession and clock paradox 2–78781
spin-exchange operator, algebraic derivation 2–78808
spin-flip probability calc., use of Sylvester's formula 2–41439
spontaneous magnetization by Peierls method 2–73275
stars, the source of their energy, popular article 2–81860
strain measurement, strain gauge device 2–48965
structural geology game 2–57455
superradiance, radiative decay solutions 2–73260
symmetry and degeneracy, particle is perturbed box 2–82098
symmetry principles in particle physics, book 2–82666
temperature, teaching of concept to school students 2–62953
thermodynamics undergraduate curriculum, inclusion of intrinsic disorder 2–62923
Thomson's e/m expt. using cathode ray tube 2–78730
time reversal in classical mechanics, a paradox 2–63055
total internal reflection, Maxwellian classical electrodynamics employed 2–55606
tutorial on optical design and aberrations 2–45775
tutorial on optical design and aberrations 2–49411
unique MS programme for graduates of four-year colleges 2–62922
videocassette for education, development and design 2–78741
virial expansion, new derivation 2–73269
waves, computer simulation 2–62947
Wigner-Witmer rules for electronic structure of diatomic molecules, elementary derivation 2–78732
X-ray structure determination, introductory lectures 2–48961
H atom, energy level relativistic shift, operator domain paradox 2–63014
I_2 vapour absorption spectrum to sixth form students 2–76147

demonstrations
air cushion expts. for teaching of school physics 2–62930
air table for basic dynamics 2–62932
air track photodiode timing gate 2–55347
alpha-particle energy loss in air, He and CO_2 2–56433
American football to demonstrate top behaviour 2–62927
Atomix teaching model, atomic structs. of liqs. and solids 2–45205
Boyle's law, on an air track 2–62949
Brownian motion 2–66400
bubble chamber exprt. on strange particles 2–52025
crystal growth movies, survey 2–50565
crystal struct. soln. by Patterson heavy atom technique, FORTRAN programs 2–73267
diffraction pattern reconstruction on closed circuit TV 2–78736
digital circuitry, simple units 2–82099
Doppler effect, simple experiment 2–82108
electromagnetic induction, computer-assisted experiment 2–62925
electron densities in atoms, percentage contour maps 2–48958
electron velocity in atoms, Compton effect demonstration for students 2–78722
e.m. induction, jumping ring expt. 2–48963
energy spectrum of potential well, graphical display 2–78810
exploratorium, museum combining perception and art in science educations 2–48953
Faraday's law coils 2–48960
ferrite rod, experimental determ. of relative permeability 2–41433
forced oscillation system, mechanical 2–62937
Fourier synthesizer, electromechanical 2–48957
Frank-Hertz experiment, using modified LM-2 manometer valve 2–69527
Frank-Hertz experiment using oscilloscope 2–82096
Fraunhofer diffraction studies in schools 2–62934
Fresnel diffraction using laser 2–62933
granular materials specific heat meas. by continuous flow Callendar and Barnes method 2–57057
gravity, using an elevator 2–55354
holographic reconstruction method of determ. location and magnification of images 2–63349
holography reconstruction of image of a plane object 2–66398
interference single-photon double-slit 2–48959
laser beam bouncing in sugar soln., unusual effect 2–41435
l.f. electrical oscillations 2–73265
light, velocity meas., expt. using laser Foucault's rotating mirror 2–41434
light velocity determ., experiment involving only distances and frequencies 2–82104
metallography, television use with metallurgical microscopes 2–55350
Mossbauer effect, linear air track demonstration 2–62926
optical bench, apparatus for making x and y adjustments 2–41436
phase diagrams, visual aid 2–48964
physics experiments for school teachers 2–52028
Ramsauer effect 2–67407
recording creep apparatus 2–52027
resolution of forces using a linear air track 2–55348

Teaching continued
demonstrations continued
Schottky barrier diodes for det. of donor density profile in semiconductors 2−75127
second-order Doppler-effect experiment in special theory of relativity 2−69561
signal averaging at modest cost 2−62918
sound speed in vibrating metal rods, simple electronic experiment 2−62928
standing microwaves by oblique incidence on mirror 2−41431
statistical error theory, expt. for students 2−63048
Stefan-Boltzmann law illustration for students of quantum theory concepts 2−55349
stereographic projection, closed circuit TV aid 2−66397
structure factor simulation and one-dimens. electron density calc., computer program 2−73268
students measuring apparatus 2−57385
superconductors, flux quantization 2−41432
television retinoscopy, teaching and research tool 2−45172
temperature-gradient microscope stage, aid in teaching solidification phenomena 2−58680
transient phenomena teaching using Heaviside operational calculus 2−59022
Vanderbilt planetarium, available facilities 2−66396
velocity of light meas. from stellar spectrograms 2−78716
wave optics using gas laser as light source 2−66399
weighing in the physics laboratory 2−62961
Cu wire conductivity at low temp. 2−73262
FeRh, first-order transition expt. 2−61476
Ge(Li)γ-ray detector for college laboratories, nonsensitive area determ. 2−62929
H, atomic energy levels, emission spectrum, measurement of lines 2−45206
InSb, n-type, effective mass of conduction electrons det. from magnetophonon effect, undergad. expt. 2−65009
$Li_{0.5}Cr_{1.25}Fe_{1.25}O_4$, thermal reversal of residual magnetization 2−61476
MnAs, first-order transition expt. 2−61476
Na, atomic energy levels, emission spectrum, measurement of lines 2−45206

Technetium
crystal structure, X-ray obs., 4.2-298 K 2−80647
generator for medical diagnosis 2−62859
superconductor hexagonal symmetry, anisotropic behaviour of magnetic properties 2−71864
work function of polycryst., accurate estimation and surface energy derivation 2−71319
$^{99}Tc^m$ thyroidal uptake, meas. by profile scanning 2−73191
^{99m}Tc, method of optimizing window of Anger camera for use with 2−48857
^{99m}Tc chelated complex, use in cisternography 2−66258
^{99m}Tc thyroidal uptake, area and profile scanning 2−69360

Technetium compounds
n-InP, high resistivity, i.r. quenching of photocond. 2−75173
Tc-40 at% Mo alloy, crystal structure, X-ray obs., 4.2-298 K 2−80647
Tc(I) complex, $K_5[Tc(CN)_6]$, vibr. spectra and force consts. 2−77074
TcO_4^-, LCAO MO calc. of dipole transition moment 2−77063
TcO_3Cl, vibrational spectra 2−77067

Tektites *see Meteorites*

Telescopes
deformational aberrations of main mirror, holographic correction 2−59251
astronomical
see also Radioastronomy
AFCRL 152 cm telescope, operational tests 2−58570
aperture synthesis telescope at 30 MHz, preliminary results in Southern Hemisphere 2−62815
automatic compensation of atmospheric dispersion 2−48825
automatic guiding of large telescopes using bright stars, comparison of several colourimetric systems 2−48700
Bamberg transit N. 1500 instrument, overhaul and first observations 2−51872
book on new techniques 2−58562
Cassegrain, 450 mm, Wollongong University, water cooled secondary mirror 2−73159
Cassegrain-Newtonian telescope, simplification rel. to Dall-Kirkham system 2−45004
clock drives for telescopes and cameras, invertor circuits and motors 2−45006
computer automated with on line data processing 2−45013
construction 2−58572
data acquisition, control, computer applications 2−85069
Fabry lens 2−66237
JOSO 71 site testing program at Tenerife, MTF for 3 telescopes 2−51868
large, autocorrelation methods to obtain diffraction limited resolution 2−66238
Leonard Extended Yolo All-Reflecting System 2−58569
mirror, spaceborne, evaluation of real-time figure control system 2−81973
mirror flexure, influence of cell deformation 2−48819
mirrors, method of determining thermal deformations 2−48820
modulation transfer function determ. in thermally turbulent atmos. 2−73160
motor drives and guidance of small radio telescopes 2−85066
muon, calibration during cosmic-ray obs. 2−70270
Ootacamund radiotelescope, system design 2−78633
optical, 7.6 meter equivalent, using array of 1.5 meter telescopes 2−58571
optical aberrations due to temperature deformations and convective fluxes, interferometric investigations 2−48821
orbiting, future of scientific satellites 2−48627
photographic refracting telescope at Torino Observatory 2−51871
radio, 46 m, data acquisition and control system 2−45009
radio-radar, at Arecibo Observatory 2−48818
radiotelescope array for synoptic interplanetary scintillation obs. 2−62726

Telescopes continued
astronomical continued
random perturbations induced in wavefronts in entry pupil, computational model 2−62480
188cm reflector, Coude spectrograph, high resolution scanning equipment 2−48824
188cm reflector of Okayama Observatory, reflectivity 2−48823
Ritchey-Chretien, extending stellar field of view 2−58567
RM-700 telescope, Coude focus adjustment using laser beam 2−48822
Schmidt corrector plates fabrication 2−58568
Schupmann medial, adaptation to large scale optical system 2−66242
six element multiple mirror 2−73157
solar, modulation transfer fn., atmospheric turbulence 2−76049
spherochromatic aberration correction in apochromatic objectives 2−73161
stellar image instability, experiments with bichromatic double-channel TV system 2−48675
submillimetre radio telescopes, compensation method of earth's atmosphere radiation 2−58565
two-element, high collecting efficiency, for submm. obs. 2−73158
u.v. sky scan, in TD1 satellite 2−58261

Tellurium
acceptor ground state, under hydrostatic pressure, variational calc. 2−61192
acoustomagnetoelectric effect 2−74986
amorphous, tight binding model calc. of optical props. 2−61658
amorphous, vibrational density of states, Raman spectra obs. 2−65281
band structure, k.p perturbation theory calc. 2−81018
crystal struct. of h.p. phase 2−47348
cyclotron resonance, valence band structure and transitions between Landau levels determ. 2−68321
Debye-Waller factors, 296 K 2−47736
electron irrad. damage, resist., Hall mobility 2−47392
epitaxial growth on alkali halides at 100°C 2−47120
extraordinary phonon Raman scattering and resonance enhancement 2−84492
film, amorphous, localized states, photoemission quantum yield 2−68422
film, large grained, prep. techniques 2−64575
film, on glass, elec. cond., temp. depend. below 300 K 2−75099
film, polycryst., on mica, elec. transport props. 2−61330
film, significance of electric field on growth 2−60634
film, thermoelectric power, Hall and Seebeck coeffs., resistivity 2−54249
films on uhv-cleaved TGS, aftereffects in field eff. at large gate charges 2−77900
GaAs:Te, heavily-doped, nature of defects, photolum. and internal friction study 2−71926
impurity, in $Bi_{88}Sb_{12}$, effect on mag. susceptibility 2−72109
impurity in Ge(Li) detector, trap parameters 2−46045
L-subshell fluorescence yields 2−79905
Landau levels in the valence band for mag. field at arbitrary angle, calc. 2−71797
liquid, effective interionic pair potentials, calc. from structural diffraction data 2−50312
liquid, n.m.r. obs. rel. to electronic transport behaviour 2−71237
liquid, structure, neutron scatt. obs., review 2−60423
magnetic susceptibility anisotropy of holes, calc. 2−81214
noncrystalline, n.m.r. at 1.3 K 2−61751
nuclear quadrupole diffr. of resonant γ-rays by ^{125}Te 2−57335
p-type, magnetophonon spectroscopy study 2−68385
photoeffects, CO_2 laser induced 2−81178
photoemission, effects of cryst. disorder on electronic struct. obs. 2−61466
piezoelectric semiconductor, dislocations 2−60805
radioactive Te produced in Cs compounds by 660 MeV p irradiation 2−68817
second harmonic generation phase matching, laser-induced change 2−44338
second harmonic generation with CO_2 Q-switched laser, 210-370K 2−79238
thermal expansion and Gruneisen relations, low temp. 2−68254
thermomodulation of optical parameters, rel. to energy band models 2−65242
valence band Landau levels, cyclotron resonance obs. 2−81019
valence band Landau levels, cyclotron resonance obs. 2−81017
valence band structure from Shubnikov-de Haas expts. 2−84245
vapour, cw laser action, He or Ne buffer gas 2−56098
whisker, vapour grown, morphology and dislocation structure 2−67915
Bi:Te deposits, optical and electrical props. 2−75255
CdSb:Te, elec. cond. and Hall const., 78-293K 2−61307
GaAs:Te, impurity effects on dislocation velocity 2−68028
GaAs:Te ion implanted, radiation damage, elec. microscope obs. 2−60821
$GaAs_{1-x}P_x$:Te, donor self-compensation 2−75110
n-GaP:Te,Zn,O, electrolum., mean electron conc., influence of Te content 2−57381
GaSb:Te, lightly doped, photolum. at high excitation levels 2−72402
GaSb:Te, segregation coeff. of Te 2−74798
GaSb:Te, thermal e.m.f. rel. to carrier conc., 300K 2−54248
GaSb:Te(Zn+Te), heavily doped, photolum. at high excitation levels 2−72403
inInSb, distrib. coeff., conc. depend. 2−47438
Te:Sb, single crystal, acoustoelectric effect 2−71828
Te-SiO, in m.i.s. struct., flat band voltage temp. depend., interface states obs. 2−77930
Te-Tl system, viscosity and density of melt 2−56490
p-Te, photon drag detector for CO_2 laser 2−79170
Te VIII, e.u.v. spectra, energy levels 2−64001
Te_2, ground state dissociation energy estimation 2−46581
TeI, investigation of hyperfine structure of ^{125}Te in $5p^36s\ ^5S_2$ level by optical double resonance and level crossing spectroscopy 2−76998

Tellurium compounds
− 2−61242
hexahalides, ^{125}Te Mossbauer isomer shifts and quadrupole splittings 2−61608

Tellurium compounds continued
TeO_2, monocryst., growth 2−71377
As-S-Te, vitreous semicond., γ-ray induced cond. 2−54252
As-Se-Te, vitreous semicond., γ-ray induced cond. 2−54252
As-Te-Ge-Se glass switching device, small signal behaviour 2−61376
As-Te-Ge-Si glass, thermal breakdown 2−61298
AsTeI glass, electronic transport props. 2−61296
Bi-Te unit crystals, determ. Sb diffusion rate on function of composition 2−68051
Co-Te system, nonstoichiometric phases, thermodynamic props. 2−43829
$CuAgTe_2$, synthesis and struct. detn. 2−71431
Ga-As-Te system, GaAs-Te polythermal section determ. 2−61047
Ge-Mn-Te alloy, degenerate semicond., e.s.r. obs. 2−48273
Ge-Se-Te-As system, amorphous bulk and thin film, composition and physical props. 2−60573
Ge-Te-As glass, high current density path shape 2−57193
Ge-Te alloy film, amorphous structure, elec. microscope obs. 2−50479
Ge-Te non-crystalline phases, structural differences 2−60577
Ge-Te system, noncrystalline film prep. by sputtering 2−47114
$Ge_{16}As_{35}Te_{28}S_{21}$, amorphous, semiconductor- metal contact, photovoltaic effect and space charge capacitance 2−61374
GeTe, amorphous and polycryst., electronic struct., photoemission and reflectivity obs. 2−61465
$Ge_{15}Te_{85}$, liquid, atomic transport 2−60457
$H_2Te_2O_6$ single crysts., cryst. struct. 2−74747
In-Te alloy, molten, elec. cond. and thermoelec. power 2−77446
In-Te system, films, phase comp. and band struct of In_2Te_3 2−60662
$Ni_{3\pm x}Te_2$, heat capacities and transition behaviour 2−57068
Se-Te alloy, acoustoelec. phenomena relating to two carriers 2−80908
Se-Te alloy, u.s. amplification, room temp. 2−51041
Se-Te alloys, liquid, switching phenomena 2−60504
Si-As-Te, amorphous semicond., energy gap depend. on glass transition and softening temp. 2−61346
Si-As-Te amorphous semiconductor, relation between band gap and density 2−65003
Te-As-Ge-S glass films, four-element quantitative analysis 2−72593
Te-As-Ge-Si, amorphous, trapping mechanism, cavity perturbation study 2−61443
Te-As-Ge, amorphous, cryst. layer form., effect of water during heat treatment 2−60571
Te-As-Ge amorphous alloy, negative differential capacitance 2−64961
Te-As-Si-Ge film, amorphous, a.c. cond. rel. to localized tail states 2−61288
Te-As, memory glass system, glass forming regions, transition temps., melt crystn. temps. 2−80805
Te-As system, vapour press. of Te_2, As_4, and As_2 over molten As_2Te_3 2−47046
Te-Ge, memory glass system, glass forming regions, transition temps., melt crystn. temps. 2−80805
Te-Ge based memory glass film, thermal crystn. 2−47128
Te-Se-Ge and Te-Se-Sb glasses, thermal effects 2−71917
Te-Se alloy, liq., semicond., n.m.r. 2−61752
Te-Se alloy, noncrystalline, n.m.r. at 1.3 K 2−61751
Te-Se melt, electronic transport behaviour, switching, optical gap 2−60502
Te-Si-Ge-As glass, comp. vs. glass transition temp. 2−60597
Te-19 at.%Si alloy, amorphous, struct. 2−53515
Te-Tl, liquid, semicond., Hall mobility, electronic struct., two band model 2−60506
Te based glass film, sputtered, thermal crystalliz. 2−60668
Te glass system, chemical aspects of glass formation 2−60599
$Te_{60}As_{25}Ge_{13}M_x$, M=S, Se, chalcogenide glass, interdepend. between, switching memory and thermal behaviour 2−47901
TeAsGeS glass, structural and electrical props. 2−61329
TeF_4 matrix violated vibrational spectra C_{2v} symmetry, assignment of frequencies, axial and equatorial bonds 2−83265
Te_xGa_{1-x} alloy, liq., n.m.r., Knight shift, mag. relax., quadrupole relax., Fermi level 2−60512
$Te_{85}Ge_{15}$, $Te_{81}Ge_{15}Sb_4$, $Te_{81}Ge_{15}As_4$ glasses, struct. and crystalliz. 2−60598
$Te_{15}Ge_3As_2$ glass, u.s. velocity, hydrostatic press. effects 2−47742
$Te_{81}Ge_{15}As_4$ glass, struct. of laser written lines, elec. microscope obs. 2−60600
TeI_4-Te solutions, semicond. behaviour 2−64472
TeI_4, sublimation and $TeI_4 \rightarrow TeI_2 + I_2$ reaction, 300-900 K 2−54526
Te(IV) penta- and hexacoordinate mixed halide anions, i.r. and Raman spectra and molec. structure 2−77094
TeO_2, acoustic attenuation coeffs. rel. to acousto-optic device applic. 2−51027
TeO_2, amorphous and cryst., electronic bonding of Cu^{2+} 2−72501
TeO_2, crystn. by $3Te + 4HNO_3 \rightarrow 4NO + 3TeO_2 + 2H_2O$ reaction 2−56612
TeO_2, lattice dynamics, i.r. refl. and Raman scatt. study 2−71716
TeO_2, matrix isolated, thermodynamic functions and i.r. spectrum 2−56202
TeO_2, optical activity, applic. in acoustooptic light deflector 2−45804
TeO_2 acoustooptic light deflector with 1000 spot capacity and 40 microsecond retrace time 2−51016
TeO_2 single crystal, acoustic and acousto-optical properties 2−77779
Te_4O_9 single crysts., cryst. struct. 2−74747
$TeO_2-V_2O_5-Fe_2O_3$, glass formation 2−64534
$TePb_{1-x}Sn_x$ diode laser, current tunable, detection of SO_2 pollution 2−57940
TeS, gaseous, electronic spectrum, rot. struct. of bands 2−64158
Te_xTl_{1-x} alloy, liq., n.m.r., Knight shift, mag. relax., quadrupole relax., Fermi level 2−60512
$TeVO_4$, synthesis, polymorphic transform., cryst. struct. of α form. 2−74748
Tl-Te alloy, amorphous film, cond., band struct. model 2−61328
$Tl_2Se-As_2Te_3$, vitreous, photocond kinetics, photoresponse 2−72067
Zn-Cd-Te, system, phase diagram, rel. to cryst. growth technique selection 2−47702

Tellurium compounds continued
$ZnO-TeO_2$, phase equilibrium 2−64504
Temperature
see also High-temperature phenomena and effects; Low-temperature production
cometary atmosphere, Tago-Sato-Kosaka and Bennett comets 2−58521
controller, programmable, inexpensive digital ramp 2−58976
converter, reciprocal, function generators for converting thermovoltages to temps. 2−66650
coronal enhanced region 2−73150
counting characteristics, fluorescence, scintillation counters, noise 2−82801
diurnal, use in short-range forecasting 2−72763
electronic linearization using dual element sensing technique 2−63161
influence on fracture strength of material 2−74852
lunar surface brightness, as measured by Apollo 15 heat flow experiment 2−62681
Moon subsurface, meas. from thermal radiation 2−58451
moving particle, relativistic kinetic temperatures 2−66474
oceanographic measurements in Block Island Sound, seasonal temp. variations 2−57872
paramagnetic salt temperature scale for 0.9 to 18 K range 2−55586
powdered samples, evaporation temp. in arc discharge 2−53508
stagnation temperature-temperature difference in natural convection flow 2−62137
switching stresses in bimetal disks, used for thermostatic control 2−63067
teaching of concept to school students 2−62953
transients, in cylinder, with varying heat transfer coeff. 2−42615
viscous incompressible fluid, unsteady flow between two parallel flat plates, temp. distribution 2−56304
Ar plasma, high-pressure thermal, use as high-radiance standard 2−46713
Fe, melting, thermodynamic properties, significant structure theory 2−56542
H_2S, solid, lower phase transition temp. 2−50398
Temperature control *see Cryostats; Thermostats*
Temperature distribution
— 2−66649
— 2−66648
air, flow in square channel with partially heated sides, temp. field 2−53336
ambient air, greenhouse effect on 2−72756
annular channel, and radiosity and transmission probabilities 2−66636
anode, porous, transpiration cooled, of electric arc 2−83634
antiradiation cell, emittance distrib. along walls 2−58969
Atlantic Ocean, surface temperature nonuniformities 2−44642
atmospheric fluctuations of temp. and wind, meas. instrument attached to captive balloon 2−81663
Bermuda slope, temp. and salinity microstructure rel. to mean flow pattern 2−84752
Black Sea temp. fields and salinity rel. to statistical structure analysis 2−81612
boundary layer, thermal laminar with arbitrary surface temp. distrib., exact solutions 2−60150
condenser cooling water discharge into adjacent water body 2−80201
conductor material, in d.c. heated conductors, calc. 2−57054
convection in horizontal fluid layer, volumetric energy sources 2−80429
experiment performed in Tuttle hydrothermal pressure vessel, errors 2−45597
flame front, analysis by method of spliced asymptotic expansions 2−82269
fluid flow along tube, applic. to reactor fuel element circulating system 2−52840
in gas laser 2−45715
Gaussian isotropic turbulent flow, velocity field and temperature distribution 2−74334
glass, Se-As, effect of opt. characts. 2−68256
heat eqn., semi-linear n-dimensional boundary-value problem, existence, uniqueness 2−76168
heated wire, response to unsteady surface cooling rates 2−52292
hot spot generation in lossy multilayer spheres, differential temp. rise obs. 2−49203
hot wires in high enthalpy, low density flows 2−66651
infinite plate, temp. distrib. heat source depend. on temp. 2−82255
Ionian Sea, surface temp., temporal and spatial variability 2−72704
Jupiter, adiabatic model for gaseous-liquid H and He, temperature distributions 2−81933
laminar boundary layer with continuous or local injection and variable wall temp., analytical soln. 2−83688
laminar boundary layer with large injections, eqn. soln. 2−83471
laser induced turbulence, spectral law of temp. fluctuations 2−82523
Mars top surface layer during 1971 opposition 2−73081
MEVARC, sready-state and post-arc spatial temp. distrib. obs. 2−71060
MHD Couette flow between cond. walls with heat transfer, effects of ext. circuit 2−46703
North Atlantic Ocean, salinity, temperautre and o-profiles 2−75413
nuclear fuel element with randomly dispersed discontinuous phase 2−49889
nuclear fuel elements, computer program THISTLE 2−83149
nuclear reactor active zone after brief cooling 2−42637
ocean surface, satellite obs. 2−44638
oceanic temperature gradient, fine structure of vertical component for San Diego Trough, Florida Current and central Pacific 2−68864
operational heat pipe, internal temp. distrib. 2−69802
Pacific, western equatorial, Reid's passage temp. profiles 2−57864
peeble bed reactor, shell thermal stress distrib. in loose-kernel spherical fuel element 2−49890
planetary atmosphere, temperature gradient detection by spectroscopic analysis 2−78561
plasma, finite-sized radiating, differential eqn. solns. 2−60285
prediction in rectangular wall cavity with turbulent flow 2−67596
pressure vessel internal loose-fill insulant 2−69498

Temperature distribution continued
quartz, effect of opt. characts. 2−68256
radial gradient, effect on stability of viscous flow between two rotating coaxial cylinders 2−67597
reactor fuel element, cylindrical oxide rod, rel. to unsteady state fuel restructuring in fast reactors 2−49887
sapphire, effect of opt. characts. 2−68256
sea water, San Diego trough, vertical microstructure, salinity fluctuations 2−62021
slab, appl. of sudden temp. field, thermoelastic stresses 2−49082
smooth cylindrical pipe, during turbulent flow 2−80160
solar photosphere, rel. to mag. field distrib. latitudinally 2−75976
solar temperature depressions on brightness- temperature contour maps at 3.3 mm wavelength 2−78596
solid, in high temp. gas flow, during initial heating, meas. 2−55566
in solids under laser irradiation, calc. using Carlslaw-Yaeger method 2−74990
stream in limited space, distribution of average temp. along the direct and reverse stream 2−46696
transient, prediction with embedded thermocouples 2−58968
tube systems with H-flow 2−71124
unsteady-state, in convecting fin of constant area 2−63154
viscous gravity flow of water in horizontal pipes 2−64402
welding torch flame, burning natural gas 2−69484
Ar low-voltage spark discharge plasma, space and time distribution of temperature 2−70881
LiBr, aqueous, equilibrium phases, entropy-temp. diagram 2−58942
Na vapour discharge, high pressure 2−71065
SF$_6$ gas flow, temp. profile around arc column 2−71049

Temperature measurement
see also Pyrometers; Thermocouples; Thermometers
— 2−62141
air, turbulent, meas. rel. to predictions 2−77323
atmosphere remote sensing of temp. profiles, optimization of spectral intervals 2−78339
atmospheric Arcasonde-1A temperatures, magnitudes and uncertainties of corrections 2−65818
atmospheric profiles, Raman backscatter 2−44691
atmospheric profiles, real-time retrieval from satellite obs. for dynamic forecasting 2−48449
automatic instruments, linearization of static characteristics 2−55587
Bermudan main thermodine; temperature fluctuation spectrum 2−81597
brightness temperature, thermal emission from a rough lunar surface, directionality 2−44915
clouds, using i.r. radiometry 2−44727
conversion, international scale 2−41443
c.w. molecular laser, obs. technique 2−73574
deep body temp. monitoring technique 2−69277
derived thermograph from thermobalance and recorder 2−63159
Earth's lower mantle, estimation 2−51496
electron microscope target, ultrathin Sn layers 2−71416
experiment performed in Tuttle hydrothermal pressure vessel, errors 2−45597
fixed point, melting point of Mo 2−53493
flame or hot gas flow, using β-radiation 2−58966
flowing gases, temp. sensor errors 2−69803
fuel rod, with time varying heat transfer coeff., calc. of temp. transients 2−42615
Galilean satellites, brightness temp. obs. at 20 microns 2−78487
gas, by Raman laser scattering 2−50268
gas in molecular laser, from thermal conductivity 2−45715
Geodyne model underwater sensor unit 2−72720
glass surface, elimination of effect of radiant heat transfer 2−55588
grounded thermocouples, errors due to improper grounds 2−66652
high temps., precise meas. apparatus 2−52291
high-temp. thermometry, review 2−52289
hot gases, up to 1600°C, using thermocouples 2−73471
of individual droplets in cloud of drops 2−67784
instrument for thermophysical investigation 2−63156
integral temp. over thickness of dielectric sensitivity and error of thermal fluctuation method 2−76403
ionospheric electron temp. meas. IC apparatus design 2−65966
i.r. system application 2−84764
linear system, Si diode sensor, review 2−45600
liquid crystal probes for semiconductor investig. 2−69804
low temp. meas. using thermal noise in Ge sensor 2−62889
low temperature (−45°C), thermography 2−84757
in low-temperature plasma 2−43171
melting point of eutectics as secondary temp. standards above 2327 K 2−53489
metal, during fatigue tests, radiation method 2−63157
neutron transmission temperature sensing 2−78942
nonisothermal flows, simultaneous measurement of temperature and velocity 2−74337
ocean microstructure obs. using high speed digitizer 2−72728
ocean temperature meas. real time constant and salinity determ. reliability using temperature-conductivity probe 2−81611
ocean temperature meter, self-contained integrating system 2−72732
planetary temperature meas. at 350 and 700 microns 2−78527
plasma, absorbing optically-non-thin, calc. of temperature profile using extension of brightness-emissivity method 2−46761
plasma, optical methods for plasma in MHD generator ducts and combustion chambers 2−43172
pulse method, effect of intrinsic heat capacity of heat receivers 2−63155
radar echoes, seeded convective clouds, height NaCl, AgI 2−84829
radiation thermometers, review 2−76386
radiation thermometry, compensatory techniques for unknown variations in emissivity 2−73467
radiation thermometry, physical basis 2−55585
radiometer, microwave for meas. sea surface temp. 2−72721
Rhea and Iapetus, brightness temp. 2−81905
satellite radiometric meas. of surface temperature, water vapour absorption problems 2−54821
sea surface, estimation from space 2−78231
sea surface, i.r. sensing factors affecting accuracy 2−44651
sea surface, using i.r. radiometry 2−44650
sea surface temp. nonuniformity, automatic recording device 2−44644
sea surface temperature, remote sensing from NOAA-I satellite, atmospheric effects 2−57888
sea surface temperature fluctuations, radiation thermometer meas. 2−57890
sea surface temperatures derived from direct readout i.r. data via APT satellite receiver 2−57887
self radiation from bodies, applic. of computers 2−58973
semiconducting thermoresistors, volt-ampere characts. for different velocities and flux temps. 2−55589
sensors, airborne, anal. of time responses 2−55815
sensors, linearity deviations det. using dual element sensing technique 2−63161
sheathed thermo-electric probes, mechanical, electrical and dynamic properties and applics. 2−73470
shock tube laser, fine-wire thermocouple applic. 2−49350
skin, contact probe 2−69233
solar atmosphere, minimum determ. using Mg I 4571 Å spectrum 2−76011
solar photosphere, variation with latitude 2−58555
stabilization of temp. of dilution refrigerator 2−82076
surface, surface temperature measurement, in ultrahigh vacuum 2−76387
surface in contact with hot radiating gas, during pulsed process 2−41842
techniques, limitations, n.q.r. 2−81477
thermistor and laser techniques for flow temp. meas. in geophys. fluid dynamics expts. 2−54775
thermistors, positive temp. coeff., sensitivity and appls. 2−82385
thermoindicators of melting, coloured, for monitoring heat regimes 2−82381
thermopencils for monitoring steel articles during heating 2−63158
thermoprobe for opaque, translucent and transparent surfaces in incandescent range 2−63160
thermoresistors, high temp., industrial temp. control 2−76405
Titan, brightness temp. obs. at 20 microns 2−78487
transient temps., metrological problems 2−45598
tumour, monitoring using implanted thermistors to det. optimum therapy for breast cancer 2−69241
Venus, at radiofrequencies 2−69165
Ar luminescent-arc discharge 2−43210
CO$_2$ laser 2−76473
Cu-constantan thermocouple with mica window, for detection of radiant energy 2−73472
H$_2$O, turbulent, meas. rel. to predictions 2−77323
Hg, turbulent, meas. rel. to predictions 2−77323
Kr pulsed discharge 2−43212
W electrostatic cathode lens, temp. det. in electrostatic field of immersion objective 2−41923

spectral methods
ethyl alcohol counterflow diffusion flame in transverse electric field, optical study of temperature profiles 2−83703
flame, by atomic fluoresc. spectrometry 2−84691
flames containing Al$_2$O$_3$ particles, meas. by i.r. emission 2−73468
Galilean satellites, Io and Ganymede, thermal properties from 20 μm eclipse radiometry 2−78538
microwave brightness temp. of natural sea ice and salt water ice 2−84777
Planck law for single- and two-colour temp. meas. in remote sensing 2−82388
pyrometry, colour, calibration equipment 2−52297
sea surface temp. determ. by multispectral technique using Nimbus 2 data 2−65621
surface thermal transients meas. technique 2−58972
temperature distributions in planetary atmospheres from reflected sunlight 2−62711
CO$_2$ gas laser, with N$_2$ and He mixtures, meas. from R-branch bands of N$_2$ 2−46769
Hg liquid flow in tube, temp. fluctuation spectra 2−64413
N rotational temp. in rarefied supersonic flow in glowing-discharge 2−60311
N$_2$, rotational temp. meas. using Raman spectroscopy 2−46857

Tensile strength *see Mechanical strength/tensile*

Tensors
body-, space- and Cartesian space-tensor fields, rheological props. of viscoelastic continua 2−63073
canonical second rank, for chiral SU(3) × SU(3) 2−42311
classical, e.m. energy transfer in material, Maxwell's tensor 2−63167
coaxial, dissimilar deviators relationship, rel. to plastic bodies 2−78769
conformal curvature type, for classification of e.m. fields 2−82194
Debye frequency tensor of single crystals 2−80891
e.m. and gravit. wave, propag. of tensor discontinuities 2−78782
energy, in bivectorial and spinorial fields 2−45832
equations with partial derivatives, pseudo true connexion 2−69544
irreducible, in terms of spherical functions 2−48981
irreducible, spinor equivalents under special Lorentz group 2−41458
Lorentz, relativistic wave equations 2−41472
operators, as symmetry adapted elements of group algebra 2−58740
oscillating electric field in absorbent dielectric medium, time-averaged Maxwell stress tensor 2−73495
permittivity, equivalent, calc. for parallel anisotropic homogeneous stratified media 2−80483
representing the observable props. of an aligned spin assembly undergoing mag. reson. 2−76978
scalar-tensor theory, formalism in general relativity theory 2−82208
skew symmetric, geometrical formulation of analytical mechanics 2−69550
Stokes flow, material tensors symmetries for a particle 2−67743
symmetry group O*, irreducible-tensor theory, V and W coeffs. 2−42830
three dimensional diffraction problems for plane semi-infinite impedance systems 2−55608

Terbium
— 2−57380
acoustic magnons and optic phonons propagating along c axis. mechanism for mixing 2−75227
elastic consts., 70-300K, u.s. wave vel. obs., Debye temp. 2−60846

Terbium continued
ferromagnetic reson. at 24 GHz, free lattice model behaviour 2−65318
film, phonon emission at 15 GHz, dynamic magnetoelastic coupling obs. 2−68562
Hall effect, elec. resist., galvanomag. effect of press., 77-400K 2−77858
Hall effect, pressure effect on single crystals 2−68547
lattice excitation and magnon spectra, magnetoelastic effects 2−65141
magnetic crit. scatt. role in elec. resist. 2−57271
paramagnetic susceptibility anisotropy, 5 to 750°C 2−44227
ultrasonic propagation, magnetic fields effects and temperature dependence 2−51036
SrF_2:Tb, axial distrib. of impurities, neutron activation analysis 2−56744
Tb III spectrum analysis 2−67392
Tb^{3+}, in $Ba_2MgGe_2O_7$ glass and crystal matrices, luminesc. props. 2−72423
Tb^{3+}, in $Tb_{1-x}Y_xPO_4$, luminesc. from strong selective excitation of $^5D_4$ 2−54469
Tb^{3+} activated $Ce_2Si_2O_7$, luminesc. 2−48220
Tb^{3+} in GdFe garnet, ferromag. reson. 2−72453
Tb^{3+} in rare earth oxides, flame excited luminesc., temp. depend. 2−48270
Tb^{3+} in soda glass, optical characts. 2−57374
Tb^{3+} in $Y_2O_2S:Eu^{3+}$, sensitization of luminesc. 2−51371
Tb^{3+} in YAG, luminesc. quenching by direct transfer and migration 2−54459
Tb^{4+}, mag. form factor in $BaTbO_3$ neutron diffr. detn. 2−81217
Y_2O_3 and Y_2O_2S phosphors, emission spectra rel. to Tb^{3+} conc. 2−48235

Terbium compounds
oxides, higher, cryst. growth and struct. 2−47243
Ho-50%Tb alloy, u.s. propagation 64843 2−64843
$La_{1-x-y}Ce_xTb_yPO_4$, fluoresc. quantum efficiency 2−48246
PrF_4, thermal decomp., elec. deflection study 2−51431
Tb-Sc alloys, mag. characts. 2−68576
Tb-Zr alloys, form. of low temp. metastable allotropic solid solns. 2−47646
Tb^{3+}, luminesc. quenching by dyes at 77 and 293 K 2−54460
$TbAl_2$, mag. struct., neutron diffr. study 2−75217
$Tb_3Al_5O_{12}$, luminesc. time depend., dipolar transfer 2−54459
$TbAsO_4$, crystallographic distortion at $T<26K$, transition, X-ray diffr. obs. 2−84142
$TbAsO_4$, magnetically controllable phase transition 2−78045
$TbAsO_4$, paramag. to antiferromag. transition, susceptibility study 2−65187
TbB_6, nonstoichiometry 2−47183
$TbCo_2$, Co atom paramagnetic moments 2−72116
$TbCo_2$, mag. behaviour in ordering region 2−44280
$TbCu_2$, mag. struct. and props. 2−44309
$Tb_{0.167}Fe_{0.633}Al_{0.20}$, Th_6Mn_{23} struct. type, X-ray powder diffr. obs. 2−64645
$TbFeO_3$, mag. struct., shape effects 2−61559
TbGa, mag. props. 2−48079
TbGa, magnetization and susceptibility, temp. depend. 2−72170
$Tb_xHO_{1-x}FeO_3$, magnetic properties, rare-earth grids, Neel temps. of sublattices, easy magnetization axis, rare earth ion interactions 2−65033
TbIG, high temp. high press. phase formation 2−57024
$Tb_2(MoO_4)_3$, ferroelectric phase transition, neutron scatt. obs. 2−65066
β-$Tb_2(MoO_4)_3$, second harmonic generation, pseudotetragonal symmetry effects 2−51298
$TbNbO_4$, crystal growth, from the flux systems PbO-V_2O_5 and Bi_2O_3-V_2O_5 2−50589
$TbNi_2$, magnetization mechanisms 2−72107
$TbNi_3$, mag. struct. 2−48080
$TbNi_{1-x}Cu_x$, sinusoidal wave mag. structs., stability, at 1.3 K 2−75216
TbO_2, antiferromagnet, mag. struct. 2−72224
TbO_2, Tb^{4+} e.p.r., comparison with computer-calculated spectrum 2−54494
Tb_2O_3, effect of crystal field on direction of magnetic moments of ions in low site symmetry 2−65186
Tb_4O_7, far-i.r. spectra, phonon excitation 2−51346
$Tb(OH)_2$, magnetic specific heat, and ac susceptibility measurements using a r.f. tunnel diode oscillator 2−68513
$Tb(OH)_3$, ferromag. relax. 2−54334
Tb_2O_2Se, mag. props. 2−44228
$TbPO_4$, low temp. mag. moment and sp. ht. anomalies 2−78046
$TbRu_2$, struct., high press. effects 2−71689
TbSb, magnet system with singlet ground state, excitations, pseudospin formalism 2−72233
$TbVO_4$, cooperative Jahn-Teller distortions 2−43926
$TbVO_4$, cryst. struct., refined 2−60756
$TbVO_4$, elastic consts. anomalous behaviour at Jahn-Teller induced phase transition 2−84038
$TbVO_4$, Jahn-Teller phase transitions, acoustic mode anomalies 2−71681
$TbVO_4$, Jahn Teller induced phase trans., Raman scatt. study, 34K 2−48198
$TbVO_4$, quadratic-orthorhombic transition 2−43915
$Tb_{1-x}Y_xPO_4$, luminesc. from strong selective excitation of $^5D_4$ of Tb^{3+} ion 2−54469

Terrestrial electricity *see Earth/electricity*

Terrestrial heat *see Earth/heat*

Terrestrial magnetism *see Earth/magnetic field; Magnetic storms*

Tetraneutrons *see Neutrons and antineutrons*

Texture *see Crystal structure/microstructure; Surface structure*

Thallium
atom, lifetime, coherence measuring, collision broadening, buffer-gas effects on $7^2S_{1/2}$ state studied by level-crossing spectroscopy 2−49955
atom, lifetime meas. using beam-foil technique 2−42730
atoms, $7^2S_{1/2}$ state, level-crossing spectroscopy, theory of self-broadening and Tl*-Tl-foreign gas collision 2−49956

Thallium continued
density of states, relativistic effects, mass velocity and Darwin terms 2−84242
diffusion in liquid metals 2−46945
diffusion in Se, 60-210°C and TlSe formation 2−53771
Fermi surface in basal plane, r.f. size effect technique 2−71798
film, supercond. transition temp. change due to noble gas adsorption 2−47856
KI:Tl, total emission spectra and energy transfer from excitons to activator 2−61710
liquid, struct. factor rel. to entropy of melting 2−64434
mathematical formulation for fibre 2−71405
muonic atoms, X-rays, nucl. γ-rays and μ-capture γ-rays analysis 2−59961
odd excited configurations $4f^{12}(5d+6s)6p$ and $4f^{13}7s$ 2−46443
phonon spectrum, supercond. tunnelling and neutron scatt. data, discrepancy 2−84189
surface tension, 272°C 2−56577
CsBr:Tl, luminesc. crystals, exciton and hole migration 2−48242
CsI:Tl, α-particle irrad., scintillation yield orientational depend. 2−81434
KBr:Tl, ionisation of Tl^+ centres by interstitial halogen atoms 2−81001
KCL;Tl, electron pulse irrad., colour centre formation 2−71524
KCl:Tl, ionisation of Tl^+ centres by interstitial halogen atoms 2−81001
KCl:Tl, luminesc. excitation spectra near fundamental absorpt. 2−48244
KCl:Tl, room temp. absorption and thermal glow 2−75333
KCl-KI:Tl, intracentre luminesc. 2−81425
KI:Tl, host-sensitized luminesc., elec. field effects 2−81419
KI:Tl, recomb. and capture probabilities of F-centre electrons 2−84285
NaCl:Tl, X-irrad., traps responsible for 360 and 390 K glow peaks 2−54476
NaI:Tl, fluorescence intensity changes during X-ray dynamical diffr. 2−65301
NaI:Tl, recomb. luminesc. of crysts. excited in A-band by activator absorpt. 2−75334
$PbBr_2:Tl^+$, vacancies, ionic cond. study 2−47401
Tl^+-Gd^{3+} energy transfer, in inorganic glasses, fluorescence obs. 2−61709
Tl-Ne collisions, excitation of metastable levels of Tl behind shock waves 2−79932
Tl-Te system, viscosity and density of melt 2−56490
Tl^+, in CsBr, i.r. absorp. 2−61635
Tl^+, in KBr, magneto-optical obs. of Jahn-Teller effect 2−68606
Tl^+ lifetime meas. using beam-foil technique 2−42730
Tl^{2+}, in K_2SO_4, g-factor, hyperfine interact., e.p.r. obs. 2−72470
^{189}Tl isotope, search for and energy levels 2−55967
^{203}Tl, muonic atom, energies of 5g to 4f X-rays, higher order vacuum polarization corrections 2−59962
^{204}Tl, K-shell internal ionization accompanying β-decay, obs. 2−63850

Thallium compounds
halides, lattice props., calc. using ionic Rydberg function 2−47727
pyrochlores, $Tl_2M_2O_7$, (M=Ru,Ir,Os), struct. and props. 2−60987
Tl_3AsS_4, single crystal, transparency, refractive index, optoacoustic props. 2−48137
As-Tl-X glass, (x=chalcogen), e.p.r., fine struct. 2−72476
Bi-Tl induced high press. phases, X-ray and specific volume studies 2−74926
Cd-In, binary liquid metals, electrotransport and elec. resist. detn. for density of states at Fermi level 2−80476
glass, As-S-Tl, viscosity in transition region 2−84049
Hg-Tl amalgam, dil., viscosity comp. depend., 0-100°C 2−64451
Hg-Tl liquid alloy, partial struct. factors and atomic distribs. 2−64437
Hg-Tl system, m.p. of Hg_5Tl_2, press. effects 2−71273
In-Tl alloys, liq., longit. spin relax. of ^{115}In 2−50370
Pb-(40 at.%)Tl alloy, force free mag. fields, solns., for cylindrical geometry 2−44066
Pb-(40 at.%)Tl alloy, force free mag. fields, solns. for spherical geometry 2−44067
Pb-Tl alloy, Ginzburg-Landau parameters, temp. depend. 2−64921
$Pb_{0.5}Tl_{0.5}$ films, supercond., phonon generation 2−47735
Tl-Te alloy, amorphous film, cond., band struct. model 2−61328
Tl-Te liquid, semicond., Hall mobility, electronic struct., two band model 2−60506
Tl_3AsS_3, nonlinear optical material, optical props. 2−42243
Tl_3AsS_4, optoacoustic props. 2−61597
Tl_3AsS_4 acousto-optic crystal, props. 2−76530
Tl_3AsSe_3, phase matchable i.r. nonlinear material 2−48129
Tl_3AsSe_3, pyroelec. effect obs. 2−72044
$TlBiTe_2$, struct. and elec. props. 2−51144
TlBr, anharmonicity, far i.r. dielec. response study 2−61071
TlBr, cyclotron reson., electron and hole resons., carrier mobilities 6.5-14K 2−68322
TlBr, cyclotron reson. of electrons and holes 2−47830
TlBr, electron energy loss spectra, optical consts. detn. 2−61129
TlBr, ionicity, dispersion, and optical spectra 2−44374
TlBr, TlCl, thermal expansion rel. to lattice dynamics 2−57076
TlBr(Cl)(I), coherent neutron scatt. amplitudes from powders 2−53654
$Tl_2Cd_2(SO_4)_3$ ferroelectric Langbeinite, optical and dielectric props. 2−51199
TlCl, anharmonicity, far i.r. dielec. response study 2−61071
TlCl, cyclotron reson. of electrons and holes 2−47830
TlCl, electron energy loss spectra, optical consts. detn. 2−61129
TlCl, ionicity, dispersion, and optical spectra 2−44374
TlCl, pulse n.m.r. investigation of vacancy and interstitial diffusion 2−71471
TlCl, valence and conduction band calc., Heine-Abarenkov model 2−75034
TlCl, X-point direct exciton, magnetoabsorp. obs. 2−72352
TlCl, X-ray $L_{2,3}$ valence band emission 2−72383
TlCl pressure dependence of elastic constants 2−84035
TlCl(Be,I) scintillator as a total absorption shower cascade detector 2−49646

Thallium compounds continued
TlCl(I,Be) scintillation crystals, response to energetic ionizing radiation 2-49649
Tl_2CrO_4, cryst. struct., X-ray obs. 2-60766
Tl_2CrO_4, struct., phase transform., thermal props. 2-53680
TlF-ScF solid soln., phases, fusion diagram 2-53997
$TlFe(CrO_4)_2.2H_2O$, low temp. i.r. vibr. spectra 2-48175
TlH, potential energy curves and dissociation energies 2-60000
TlH_2PO_4, lattice parameters 2-53682
TlI, electron energy loss spectra, optical consts. detn. 2-61129
TlI, photoconductivity, influence of polymorphic transitions 2-75174
$TlInSe_2$:Cu,Sn, cryst. and film, photosensitivity, optical absorpt., dark cond., forbidden band width 2-57197
Tl_2MoO_4, struct., phase transform., thermal props. 2-53680
$TlN_3:Mn^{2+}$, e.s.r., spin Hamiltonian parameters, temp. depend. 2-72502
$TlNO_3$, molten, interdiffusion coeff. of Ag^+ 2-65383
TlN_3. low temp. phase transformation, i.r. absorption and Raman scatt. study 2-74944
Tl_2O_3(c), heat capacity, drop calorimetry and diff. scanning calorimetry 2-54047
$TlSbS_2$, thin films on NaCl, determ. of cryst. struct. 2-80564
Tl_2Se-As_2Se_3 glass, e.s.r. and X-ray studies 2-61734
$Tl_2SeAs_2Te_3$, liquid and glassy, struct., n.m.r. and i.r. absorp. obs. 2-60420
Tl_2SeO_4, struct., phase transform., thermal props. 2-53680
$Tl_2Se.As_2Te_3$, amorphous, Hall coeff. and magnetoresistance 2-61331
TlTe, struct. and elec. props. 2-51144
$Tl_{1-x}Te_x$ alloy, liq., n.m.r., Knight shift, mag. relax., quadrupole relax., Fermi level 2-60512
Tl_5Te single crystal, growth and semicond. props. 2-64990
$TmAsO_4$, heat capacity, near Jahn-Teller transition, evidence of low-lying excited state 2-61105

Thermal conductivity *see Conductivity, thermal*

Thermal decomposition *see Chemical reactions*

Thermal diffusion *see Diffusion in gases/thermal; Diffusion in liquids/thermal; Diffusion in solids/thermal*

Thermal diffusion columns *see Diffusion in gases/thermal; Isotope separation*

Thermal diffusivity *see Conductivity, thermal; Heat conduction*

Thermal expansion
see also Gruneisen relations
alkali metals, calc. from Gruneisen parameters 2-74997
alloys and engineering materials, tabulation of quadratic function coeffs. 2-71639
benzene and benzene plus cyclohexane, dilution piezometer meas. at 298.15K 2-67823
carbon phenolic, two dimensionally reinforced, re-entry material, characterization 2-56980
composite, hemispherical laminar, linear coeffs., 300 to 800 K 2-54057
composite, thermally degrading organic matrix, theory 2-53963
composite struct., thermally stable 2-64794
cooperative meas., techniques, errors 2-54053
cyclohexane and benzene plus cyclohexane, dilution piezometer meas. at 298.15K 2-67823
diatomic molecular crystal, calc. using lattice vibr. model 2-43960
obs. using dilatometer using photoelectric recording of elongation 2-71749
drops, heating by internal heat sources 2-43300
eurocryptite, of lattice consts., 20-1100°C 2-54060
ferromagnetic metal, hyperfine field, magnetization, temp. depend. 2-48066
fibrous metallic composite, thermophysical characs. 2-54070
Gilsocarbon, neutron irrad. effects rel. to high temp. reactor design 2-52871
glass, rel. to frozen elastic stresses 2-56784
glass, rel. to oxide content, computer calcs. 2-44500
glasses, around 1K 2-61107
glasses, Se enriched, Ge-Se system, (4-16.7 at.% Ge), temp. depend. maximum of coeff. at 5 at.% G84209 2-84209
graphite, isotropic, and Young's modulus porosity depend. up to 1800°C 2-56772
graphite, nuclear, high fluence neutron irrad. behaviour, two-phase model 2-56048
graphite, parallel to basal plane, high temp. coeff. 2-57073
graphite, pyrolytic, highly oriented, high dose fast neutron effects 2-57072
graphite, pyrolytic, meas. over wide temp. range 2-84208
graphite, theory applied to basal planes 2-64859
graphite, theory applied to expansion coefficients, electronic contribution 2-64860
graphite, theory applied to hexagonal axis 2-68251
graphite fibre, transverse coeffs. 2-53954
graphite from isotruxene carbons 2-61023
graphite/SiC composite, linear coeffs., 300 to 800 K 2-54057
halides, heavier metal type, calc. using ionic Rydberg function 2-47727
high temperature measurement techniques 2-71616
Invar, thermal expansion, low temp., Fermi liquid props. 2-84217
Invar alloy, anomaly, localized moment collapse 2-53660
invars, neutron diffraction study of crystal structure 2-68002
Ising magnet, compressible, high temp. contrib. of spin-phonon interactions 2-72124
Lennard-Jones solid, high temp. coeffs. near surface 2-43991
linear lattice 2-64858
liquid, from isobaric ensemble formalism of Monte Carlo calcs. 2-64428
liquids, normal, at saturation states 2-56450
magnesium highpolyphosphate glass, and crystallization 2-83851
measurement, accuracy 2-52260
measurement, laser interferometer dilatometer 2-49183
measurement at high-temps., fast system 2-52299
measurement at high-temps. by dilatometer reference material 2-57071
metal, diffusion of hydrogen, by lattice expansion method 2-77606

Thermal expansion continued
metal, ferromag., effect on temp. depend. of magnetiz. and hyperfine field 2-54323
metal, influence of point defects at high temp. 2-54040
metal, positron annihilation and meas. of coeff. 2-81002
near solid surface, calc. 2-50424
nonmetallic refractory compound, high temp. electrical insulator material 2-57079
Pd, 77-300K, effect of paramagnons 2-61226
pentaerythritol, molecular crystal, X-ray obs. 2-74995
Perspex sheet, orientated, axial and transverse, 0-30°C 2-64862
polymers, relation between expansion coefficients and glass temperature 2-60604
pyrocarbons, lattice thermal expansion perpendic. to layer planes, depend. on struct. props. 2-68252
pyrofoil tape, production and characterisation for reactor use 2-56050
rare earth compounds with zircon struct., temp. dependence of lattice parameters 2-84215
rare earth intermetallics, $R_2(Co_{1-x}Fe_x)_{17}$ type, c-axis expansion 2-50626
rare earth silicides, 20-1200°C 2-68005
re-entry materials, carbon, thermal props. 2-56981
solid, high temperature, one dimensional anharmonic lattice model 2-57058
steel, high-speed, partial coeffs. of MC, M_6C, and α and γ phases 2-54059
steel, high-speed deformed low-C, dilatometric behaviour 2-43839
steel, linear expansion coeff., additive effects 2-47686
thermophysical properties at high temperatures, conf., Turin, June (1972) 2-54035
transition metal carbides and borides 2-54043
transition metal nitrides, 80-300K 2-61112
triglycine fluoroberyllate, in ferroelec. transition region 2-71751
triglycine selenate, temp. depend., deuteration effects 2-72042
triglycine sulphate, temp. depend., deuteration effects 2-72042
Vanadium Permendur, dimens. stability 2-43994
vapour bubbles, spherical expansion due to application of thermal impulse 2-46909
Ag-Al alloy, 10-300K 2-43992
Al, correl. with γ-ray irrad. induced point defects 2-43607
α-Al_2O_3, linear coeffs., 100-800K 2-51047
As, coeffs., anistropy, 2-30K, 55-90K, and at 283K, Gruneisen parameters 2-77784
Ba, 1.5-30K, 55-90K, and room temp. 2-74993
$Ba_2NaNb_5O_{15}$, Gd-substituted, c-axis contraction 2-51048
Bi-Pb alloy, meas. in room temp.-100°C range, applicability of rule of mixtures in two phase region 2-60975
Bi-Sn alloy, meas. in room temp.-100°C range, applicability of rule of mixtures in two phase region 2-60975
Bi, coeffs., anisotropy, 2-30K, 55-90K, and at 283K, Gruneisen parameters 2-77784
$BiFeO_3$, coeffs. determ. 2-47317
C, pyrolytic, depend. on struct. props. of coeff. perpendicular to layer planes 2-61108
C composite felt, neutron irrad., 20-1000°C 2-54055
C fibre, anisotropy effects on struct. and mech. strength 2-54054
C fibre, room temp. −1800°C, rel. to preferred orientation 2-53953
C fibres, neutron irrad. effects 2-56998
C glassy, to 2300°C 2-54056
CO crystal, calc. using lattice vibr. model 2-43960
Ca, 1.5-30K, 55-90K, and room temp. 2-74993
$CaCO_3$, determ. from generalized Gruneisen parameters 2-74996
CaO, press. depend. shell model calcs. 2-47756
$CaZrO_3$-$CaHfO_3$ system solid solns., lattice parameters 2-43575
Cd, Keating's approach 2-84182
$^{248}CmO_2$, linear coeff., 25°-450°C 2-84207
Cr, Invar effect 2-57269
Cr (100) surface, LEED obs. 2-50992
CrTe, anomalies near Curie temp. 2-72148
CsCl, effects of KCl and NaCl additions 2-43932
Cu, correl. with γ-ray irrad. induced point defects 2-43607
CuCl and CuBr, anomalous, i.r. spectroscopy data and anharmonic behaviour of lattice vibrations 2-43993
F_2 crystal, calc. using lattice vibr. model 2-43960
Fe/boride coating system, anisotropy 2-54058
Fe-Ni-Co alloys, dilatometric study of vol. exp. for fcc to bcc transformations 2-65146
Fe-Ni alloy, thermal stability of elastic modulus, contrib. of Invar anomaly and ΔE effect 2-50724
Fe, spheroidal graphite and common grade grey, hardness and dilatation 2-43739
Ga single crystals, anisotropy in crystal length change at superconducting transitions 2-71846
GaAs-GaP, i.r. lattice absorpt. obs. 2-57074
GaAs, i.r. lattice absorpt. obs. 2-57074
GaP, i.r. lattice absorpt. obs. 2-57074
Ge, rel. to differential expansion of epitaxial Ge on GaAs 2-57075
^3He, solid, review 2-80515
^4He, liq., 0.1 to 0.7K 2-47002
^4He, liq. 0.2 to 0.7 K 2-47009
InBi, rel. to thermal cycling effect on resist. and morphology 2-51101
$In_xGa_{1-x}P$ alloys coeff. temp. depend., 15-650°C 2-71750
Ir, high temp. obs. 2-51049
$K_xRb_{1-x}Cl$ solid solutions, linear coefficients, lattice parameters, 20 to 600°C range 2-64861
Li thermal expansion coefficient and Gruneisen parameter, lattice dynamical calculation 2-84179
$LiH_3(SeO_3)_2$, ferroelec., rel. to band arrangement, -150 to +25°C 2-68253
Li_2O-B_2O_3-GeO_2 glass, rel. to struct. 2-47059
Li_2O-MgO-Al_2O_3-SiO_2, F addition effects rel. to crystallization 2-47058
$LiTaO_3$ single crystal, temp. dependence 2-72008
Mn-Cu-Mo alloy, cold worked, heat treated 2-47476
Mn-Cu-W alloy, cold worked, heat treated 2-47477
Mn, α and γ phases, Invar effect 2-57269
Mo, correl. with γ-ray irrad. induced point defects 2-43607

Thermal expansion continued
Mo, meas. to 2550°C 2−54061
Mo (100) surface, LEED obs. 2−50992
N_2 crystal, calc. using lattice vibr. model 2−43960
γ-Na_2BeF_4, high-temp. X-ray diffr. obs. 2−61109
NaF, calc. from third-order elastic consts. 2−60844
Nb_2O_5, X-ray and dilatometric study 2−80803
Nd:YAG laser material, holographic interferometry meas. of expansion coefficient 2−59174
Nd:YALO laser material, holographic interferometry meas. of expansion coefficient 2−59174
Ne liquid, isotonic expansion, coefficient determ. from sound velocity measurements 2−46950
Ni/C fibre composite, high temp. deformation characts. 2−74919
$Ni_xZn_{1-x}Cr_2O_4$, cooperative Jahn-Teller phase transition obs. 2−71693
$Ni_xZn_{1-x}Fe_2O_4$, Curie pt. phenomena, conc. depend. 2−81281
O_2 crystal, calc. using lattice vibr. model 2−43960
Pb-Sb(8 to 17%) alloy, influence of annealing temp. 2−43995
PbF_2, from shell model calcs., rel. to phase transform. 2−84216
PbI_2, lattice parameters meas. by X-ray method in temp. range 25-114°C, evaluation of coeffs. of thermal expansion 2−61110
Rb, liquid, calc. using sound velocity data at high pressures 2−71195
RbBr, linear coeff. 2−61111
Sb, coeffs., anisotropy, 2-30K, 55-90K, and at 283K, Gruneisen parameters 2−77784
Si single crystal, X-ray obs. 2−47757
SiO_2-Al_2O_3-K_2O-Na_2O glasses, and formation of leucite 2−74994
SnF_2, soln. grown crysts. 2−47245
Sr, 1.5-30K, 55-90K, and room temp. 2−74993
SrF_2, shell model calcs. 2−84216
SrO, press. depend. shell model calcs. 2−47756
Tb-Sc alloys, and mag. characts. 2−68576
Tc-40 at% Mo alloy, struct., X-ray obs., 4.2-298 K 2−80647
Tc, struct., X-ray obs., 4.2-298 K 2−80647
Te, low temp., and Gruneisen relations 2−68254
TiS, 25-1300°C, X-ray obs. 2−54062
TlBr, TlCl, rel. to lattice dynamics 2−57076
UO_2 fuel elements, Zircaloy-sheathed, circumferential strain obs. 2−52879
V_2O_5-P_2O_5 glass, rel. to comp. 2−60601
W, high temp., vacancy equilibrium conc. detn. 2−68255
W, meas. to 3330°C 2−54061
W, to 1900K 2−54063
$YbAl_2$, $YbAl_3$ magnetic susceptibility and expansion coefficient 2−81218
Zn, activated vacancy, self-diffusion coefficients and thermal coeff. of expansion 2−68048
Zr, calc. using Keating's approach 2−43964
ZrO_2-Yb_2P_3 and ZrO_2-Yb_2O_3-Y_2O_3 solid solutions 2−47721
$ZrSiO_4$, anisotropy, X-ray obs. 2−54064

Thermal measurement
see also Calorimeters; Calorimetry; Conductivity, thermal/measurement; Temperature measurement; Vapour pressure measurement; Entries describing measurement methods for specific thermal quantities and effects may also be found listed under the various headings for the subjects concerned
9-CN, 10-acetoxy anthracene dimers, thermal behaviour and monomerization kinetics in the solid state 2−57436
9-CNanthracene dimers, thermal behaviour and monomerization kinetics in the solid state 2−57436
arc furnace for thermal analysis of super-refractories 2−66363
benzene and benzene plus cyclohexane, dilution piezometer meas. at 298.15K of excess compressibility 2−67823
bolometers and vacuum thermoelements, thin layer properties, selection and research properties 2−82377
conductivity and specific heat meas. by pulse method 2−63163
cross-inclined tube bundles, thermal performance meas. by transient method 2−55580
cyclohexane and benzene plus cyclohexane, dilution piezometer meas. at 298.15K of excess compressibility 2−67823
expansion, accuracy 2−52260
fluid flow during moving internal heat source 2−67819
Gardon heat flux sensors, finite thickness, temp. time response 2−52267
gases, accommodation coeffs. det. by temp. jump and free molecular flow methods 2−77368
heat pulse methods, apparatus, 20-300°C 2−55573
i.r. radiometer, precision calibration and test 2−82387
magnesium highpolyphosphate glass, and crystallization 2−83851
Moon, book 2−75853
permanent magnet, temperature coeff. meas. 2−59061
printed circuit boards, thermal analysis method 2−52354
pulsed-adiabatic method for meas. heat capacity of a liquid 2−43345
resins, heat deflection temp. meas. with automatic apparatus 2−52293
silicone liquids thermal breakdown under pulsed h.f. fields 2−56513
solids, simultaneous determination by periodic method 2−52304
specific heat of small samples at low temp. 2−41868
thermal resistance meas. of solid deposits on surface of working structures 2−69799
thermoacoustic fatigue testing of space shuttle thermal protection panels 2−56873
thermophysical meas., optical utilization of redundant information 2−52290
thermophysical quantities, meas., at high temps., fast system 2−52299
thin film resistance thermometer temperature fluctuations in turbulent wakes 2−77330
time of flight of heat pulses using supercond. tunnel function bolometer 2−80911
HFC-Re system, lattice consts., solubility relations and phase diagram 2−84096

Thermal properties of substances
see also Conductivity, thermal; Equations of state; Heat conduction; Specific heat; Thermal expansion; Thermodynamic properties
9-CN, 10-acetoxy anthracene dimers, thermal behaviour and monomerization kinetics in the solid state 2−57436

Thermal properties of substances continued
9-CNanthracene dimers, thermal behaviour and monomerization kinetics in the solid state 2−57436
ceramic, corundum based, thermal stability rel. to microstruct. 2−56959
creep in inert gases, expts. 2−74484
fibre composite, brittle matrix thermal shock resist. 2−53968
glass ceramics, workability and thermal props. 2−43868
lunar fines, Apollo 12 samples thermal radiation props. 2−51815
mica glass-ceramics, thermal shock-resistance rel. to microstruct. 2−60999
optimized cluster expansion calc. for ionic solutions and atomic liquids 2−74513
refractory, high alumina, thermal shock resistance 2−56961
rubber like materials, thermomech. behaviour, Valanis- Landel strain energy function 2−82312
solid state physics, an overview 2−57093
water boundary layer, temp. depend. 2−67739
Ba-mica/Al_2O_3 composite, shock resistance 2−56977
Bi, diffusive propagation of heat pulses, second sound 2−47762
C, glass like, thermal shock and crack propagation 2−56822
CdS temp. distribution, effect of optical characteristics 2−68256
$CsPr(MoO_4)_2$, stability and cryst. struct. 2−74729
CuO-Al_2O_3 solid soln., form. and stability of $CuAl_2O_4$ phase 2−74899
Cu_2O-Al_2O_3 solid soln., form. and stability of $Cu_2Al_2O_4$ phase 2−74899
^3He fluid near critical point, meas. of thermal relaxation times 2−80514
MgO-Fe_2O_3-CaO-Al_2O_3-SiO_2, charges caused by phase transformations during heating 2−83839
SiC, fracture energy relation, thermal shock behaviour, acoustic damping 2−60890
SiC, thermal shock resist. 2−60882
$Te_{60}As_{25}Ge_{13}M_x$, M=S, Se, chalcogenide glass, interdepend. between, switching memory and thermal behaviour 2−47901
W-HfO_2 composite, thermal shock resistance 2−56989
W-ZrO_2 composite, thermal shock resistance 2−56989

Thermal radiation *see Radiation/heat*

Thermal spikes *see Crystal imperfections; Physical effects of radiations*

Thermal transformations *see Boiling; Condensation; Crystallization; Freezing; Heat of transformation; Melting; Phase transformations; Sublimation; Vaporization*

Thermionic emission *see Electron emission/thermionic; Ion emission/thermionic; Ionization, surface*

Thermionic generators *see Electricity, direct conversion/thermionic; Electron tubes*

Thermionic tubes *see Electron tubes*

Thermistors *see Semiconducting devices*

Thermo-optical effects
see also Thermoluminescence; Thermoreflectance
dielectric cryst., light scatt. by entropy fluctuations, phonon transport theory 2−81327

Thermochemistry *see Heat of reaction, etc.*

Thermocouples
detector for fast neutral particles 2−59628
e.m.f., press. effect. meas. method 2−49190
fine-wire, applic. to total temp. meas. in shock-tube lasers 2−49350
general response in gases at low pressures 2−45601
high-temp. thermometry, review 2−52289
hot gas temperature measurement applic., up to 1600°C 2−73471
intrinsic, transient responses, accuracy 2−52300
using semiconductor thermoelectric materials, to replace metal branches in electrical measurement apparatus 2−76432
temperature control of electrodeless discharge lamp 2−82586
temperature measurement errors due to improper grounds 2−66652
thermoelectric generator, isotope powered, description 2−59046
thin films in isotopic thermoelectric battery for cardiac pacemakers 2−49290
u.s. meas. in liquid 2−69719
Au-Fe, Seebeck voltage rel. to KP, Ag, Cu, temp. range 4K-280K 2−81158
Bi_2Te_3, for nuclear batteries intended for cardiac pacemakers, new fabrication techniques 2−51907
Cu-constantan, effect of mag. field on Seebeck effect 2−63162
Cu-constantan, in linear direct reading thermometer 2−73469
Cu-constantan, with mica window, for detection of radiant energy 2−73472
Pt/Pt-Rh movable-junction stationary-lead 2−45602
Pt/Pt-10%Rh, method for control and measurement of wire temps. in preparatory anneals 2−45603
Pt-Mo, e.m.f. rel. to neutron irrad. 2−78940
Si-Ge alloys, precip. of dopants 2−51210
W-Re material, high temp. behaviour, report 2−84373

Thermodynamic properties
see also Critical constants, thermal; Entropy; Heat of reaction; Latent heat
— 2−67718
— 2−67870
air in bubble in water, shock excited pulsations 2−80438
alkali halide vapours, vapour pressures and enthalpies of vaporization, detn. 2−77473
alkali metal ammonia solns., solvation model 2−84614
alkali metals, molten, interionic interaction and thermodynamic potl., analysis 2−84650
alloy, binary, molten, surface electric charge obs. 2−56515
alloy, low melting, calorimetric investigations 2−57056
alloy, ternary, prediction from binary alloy data 2−43814
anharmonic lattices, stability 2−80882
antiferromagnetic chain, uniform, thermodynamic props. and magnetostriction 2−84439
B-2 type phase, activities, rel. to disorder 2−43819
Baxter model, spin $^1{}_{\cdot 2}$ lattice system, duality relation 2−78845
benzene-nitroalkane solns., excess Gibbs energy of mixing, from Rayleigh scatt. and depolarization obs. 2−64444
binary mixtures of Lennard-Jones (12-6) liquids, Monte Carlo calc. 2−71182

Thermodynamic properties continued
binary mixtures of Lennard-Jones liquids, Monte Carlo calcs. of excess thermodynamic properties 2−74539
binary mixtures of molecules interacting via Kihara potential, Percus-Yevick theory 2−67552
binary molten salt mixtures with common cation or anion, stat. model 2−84615
binary molten salt mixtures with common cation or anion, stat. model 2−84616
binary solutions light scattering study of thermodynamic functions near critical point of vaporization 2−43373
binary systems, free excess enthalpy represent. by mol. distrib. consts. 2−84613
BWR eqn. of state development and applic. for c.-a.d. of cryogenic plant 2−76121
carbon tetrachloride, enthalpy of transition and heat capac. for metastable fcc to stable rhombohedral transform. 2−77754
cholesteryl esters, effect of substituent location, entropy and temp. of transitions 2−80452
critical volume prediction, new correlation using parachor, application to organic compounds 2−50397
crystals, strongly anharmonic, under arbitrary external pressure 2−68208
crystals, strongly anharmonic, under arbitrary external pressure 2−68207
Debye-Huckel theory, extended, approximate individual ion values for aqueous solutions at 298.15K 2−77420
2,6-dibromoaniline 2−77145
α,ω-dichloroalkanes, rel. to dielec. relax. behaviour 2−60489
dichlorofluoramine, heat content, heat capacity, entropy, free energy determ. from spectroscopic data 2−60372
electrolyte solution, calc. using modified solution, calc. using modified Poisson-Boltzmann equation 2−50355
enthalpy of air-vapour mixture instructions and example 2−83710
eutectic solidification, stable steady state 2−47035
eutectics containing compound phases, correl. with morphology 2−47600
excess Gibbs function, determination from total vapour pressure measurements 2−81485
Fe_2Cl_6, calc. from spectroscopic data 2−42945
ferroelectric solid solutions, first-order phase transition 2−65057
ferromagnet, itinerant, electron model, behaviour thermodynamic quantities near critical point 2−84427
ferromagnet, one dimensional amorphous Ising model 2−57273
ferromagnetics near T_k, heat capacity and magnetocaloric effect 2−72158
fluid, perfect, rotation with gravitational, electromagnetic and thermodynamic props. about fixed axis 2−69577
gas, mixture, compressed, calc. 2−56441
gas-metal interaction, rel. to chemisorption 2−50530
gases, polyatomic, prediction from mol. struct. 2−83698
gases, thermally, radiating separated by vortex sheet, stability 2−67733
glass, meas. and calc. of sp. ht. 2−74992
grain boundaries, entropy, Einstein cryst. model and Morse pot., computer calcs. 2−56727
graphite, effect of porosity on evaporation 2−56545
graphite, heats of immersion rel. to degassing behaviour 2−53549
graphite, nuclear, production by mixing different cokes 2−68174
halobenzenes, significant struct. theory applic. 2−83778
heterogeneous mixture, partial functions 2−41538
Hubbard model, disordered four point, thermodynamic properties 2−81300
Hubbard model, metal-nonmetal transition 2−80965
III-V compound, quasi-binary solid solution, excess free energy 2−74948
interfacial layers, equidistant mol. plane model, surface tension 2−84631
interfacial layers, equidistant mol. plane model, surface tension 2−84630
Josephson junction with normal metal barrier, thermodynamic properties 2−47873
linear fracture thermodynamics of solids, convolution inverse variational principles applics. 2−55466
liquid, from isobaric ensemble formalism of Monte Carlo calcs. 2−64428
liquid, polar, partition function using Prigogine's cell theory 2−53421
liquid metal, ion-ion potentials, effective interaction, hard sphere dias., sp. ht., entropies 2−60415
liquid state, equilib. props. from interactions of walks 2−46948
liquids, binary mixtures, variational approach to prediction of excess props. 2−43312
liquids, significant structure, numerical methods 2−56475
liquids, superheat rel. to vaporization with and without solid surface 2−53505
magnetic relaxation, quasithermodynamics theory 2−51283
materials with memory, thermo-mechanical coupling 2−76291
metal, cold worked, pressure induced thermal activated processes, tensile strengths 2−43781
metal, gas containing void formation 2−50633
metal, liq., equilib. thermodynamic states, enthalpy meas. technique 2−46949
metal, liquid, temp. depend. hard sphere model 2−67824
metal, single-atomic, in liquid state 2−71152
metal chloride molecular discharges, thermodynamic and kinetic considerations 2−64354
metal melts, determ. by e.m.f. meas. 2−77421
metal-H system, thermodynamic analysis with applied stress field 2−71640
metal/hydrogen systems, h.p. props. 2−77715
metal/hydrogen systems, non-ideal soln. behaviour 2−77716
metal/hydrogen systems, review 2−77714
mysids, energy equivalents of body mass, respiration and calorific value 2−78639
naphthalene, enthalpy of sublimation, calorimetric detn. 2−77477
non-ideal reference system, virial expansion, chain approximations 2−55436
nonthermal radiating systems, pseudothermodynamic model 2−58943

Thermodynamic properties continued
normal liquids, internal energy 2−56450
nuclear fuel core exit, enthalpy distribution 2−76929
Pippard's relations applied to λ transitions in dielec. and mag. materials 2−61490
poly-kind particle systems, diffusion for gradient of vacancy conc. 2−64688
polyethylene oxide, data used to compute end interfacial free energy 2−71274
polymer soln. interactions, symposium, Prague, Czechoslovakia (Aug-Sep 1971) 2−60435
polymer solns., dil., excluded vol. effects and binary cluster integrals 2−60440
polymer solns., dil., virial coeffs. for interactions 2−60437
polymer solns., mol. props. depend. 2−60438
polymer solution, press. and temp. depend. 2−64446
polymers, automatic adiabatic calorimeter for enthalpy meas. in temp. range −180 to +270°C 2−63165
polypeptide chains, helix-coil transition parameters 2−60096
polyurethanes, influence of urethane groups 2−83389
porous materials with vacuous pores, thermodynamic model 2−50924
rare earth cpds., Jahn-Teller induced transitions 2−64806
rare earth dicarbides, solid state galvanic cell technique 2−43865
refractories, enthalpy, heat and temp. of phase transitions 2−54036
ruby, crossrelaxation, two step, freq. depend. susceptibility meas., generalized thermodynamics 2−61561
semiconductor, extrinsic, nondegenerate, with high cond. electron concs., thermodynamic and kinetic props. 2−77890
semiconductor, tetrahedral, scaling theory calc. from optical spectra 2−80528
simple substance, one parameter model 2−71743
small superconducting particles, static approx. 2−64928
small-crystal, number dependence of entropy on crystal size and shape 2−68245
small-crystal, number dependence of vibrational entropy 2−68244
steel, mild, resulting activation enthalpies for Luders band propagation and strain hardening 2−80814
structural phase transition, two-fluid model, heat diffusion mode 2−84185
surface layers on metals, formed by anodic reaction within an electrolyte solution 2−68781
ternary refractory carbide, rel. to bonding and compressibility 2−71652
thermal disequilibrium in vapours, laser- induced 2−77343
thermodynamics of crystals, book 2−43950
viscoelastic Maxwellian media, finitely deformed, evolutionary conditions for mechanics equations 2−52190
Ag-Ga alloy, liquid, free enthalpy of mixing 2−53422
Ag-Ge alloy, liquid, free enthalpy of mixing 2−53422
Ag-In alloy, liquid, free enthalpy of mixing 2−53422
Ag, lattice dynamics, phonon dispersion curves 2−80900
Al-Zn alloy, liq., Zn activity at 1053K, comp. depend., Krupkowski's eqn. 2−56498
Al_2Cl_6, calc. from spectroscopic data 2−42945
Al_2O_3, alumina, enthalpy, condensed phase near melting point 2−54044
α-Al_2O_3, corundum, enthalpy high temp. calorimeter obs. 2−53490
Ar solid, from Monte Carlo calculations along solid-vapour coexistence curve 2−57055
Ar solid, static lattice energies, PV relation, at T=0K 2−80889
Au-Ga alloy, liquid, free enthalpy of mixing 2−53422
Au-Ge alloy, liquid, free enthalpy of mixing 2−53422
Au-In alloy, liquid, free enthalpy of mixing 2−53422
$BaFe_{12}O_{19}$, high temp. enthalpy 2−54049
$BaFe_2O_4$, high temp. enthalpy 2−54049
Be, melting enthalpy 2−53491
BeO, determination of enthalpy between 2000 and 3200 K 2−56496
Bi-Sn(Pb)-Zn system, activity coeffs., calc. 2−43827
CO_2, liquid 2−69789
CaH_2-LaH_3 system, enthalpy and entropy of soln. 2−50958
Cd-Sn-Zn system, activity coeffs., calc. 2−43827
$CdCu_{1.5}Ga_{0.5}$, Laves phases, enthalpies of soln. and formation detn. 2−47692
CdSe, rel. to solid-gas phase equilibria 2−71368
Co-C system, rel. to Curie temp. depend. on C conc. 2−44246
Co-Cr-C solid soln., partial dissolving enthalpy and entropy of C, 950-1200°C 2−56925
Co-S solid solution, partial entropy and partial energy of soln. 2−50837
Co-Se(Te) system, nonstoichiometric phases 2−43829
Co alloy, h.c.p.→f.c.c. transform., enthalpy, transform. temp. 2−43913
CrSi, $CrSi_2$, Cr_3Si, Cr_5Si_3, isobaric-isotherm. potl., entropy and heat of formation detn. by meas. galvanic e.m.f. 2−68246
Cs plasma 2−56328
Cs vapour, by statistical theory 2−50264
CsCl-phases, thermodynamics and lattice disorder 2−80843
Cu alloys, determ. of partial free enthalpy of formation of α-Cu solid solns. 2−80811
Er-H system, rel. to gas pressure standards 2−52016
$EuCl_2$, third-law enthalpy calc. 2−64515
$Eu(NH_3)_6$, equilibrium pressure and standard enthalpy 2−61774
Fe-C-i-j-...-n multicomponent solid solution, rel. to diffusion coeff. 2−43662
Fe-Cr-Mn alloy, α-γ phase transform., Gibbs free energy 2−47687
Fe-Mg-O system, activities, calc. by Darken's method 2−43815
Fe-Mn-O system, activities, calc. by Darken's method 2−43815
Fe-S solid solution, partial entropy and partial energy of soln. 2−50837
Fe, liquid and Ni alloy, electromagnetic levitation melting in inert atmosphere 2−67871
Fe, melting, significant structure theory 2−56542
Fe alloy, of martensitic transform. 2−50943
Fe_2O_3-FeO-$Li_{0.5}Fe_{0.5}O$, coexisting phases equilibrium and thermodynamics, 900-1200°C 2−74931
Fe_2O_3, heat of transformation, decomposition temp. Gibbs free energy of formation determ. by EMF method 2−51425
GaN, heat and entropy of formation, rel. to equilib. pressure of N_2 over GaN 2−47049

Thermodynamic properties continued

- $GdCl_3$, ferromag., dipole-dipole interact. theory 2−68534
- β-Gd_2MoO_4, from 0.4 to 4.2 K along b crystal axis 2−51277
- $Ge/H_2O/H_2$ system, etching rate, average reaction enthalpy, 950-1200K 2−74661
- Ge-Na liquid solution, e.m.f. cell obs. 2−71183
- He II, liquid, superfluid, thermohydrodynamic conditions at peak flux of horizontal heaters 2−67859
- ^3He, b.c.c., ground state energy 2−71266
- ^3He, interaction energy and entropy 2−77462
- ^3He, solid, review 2−80515
- ^4He, interaction energy and entropy 2−77462
- In-Hg-Pb alloy, supercond., role of electron scatt. 2−81038
- In-Hg alloy, supercond., role of electron scatt. 2−81038
- In_5Bi_3 phase, calorimetric detn. and Wagner analysis 2−71687
- $InBr_2$, heterogeneous equilib. 750-1050 K, enthalpy, entropy of evaporation, boiling point 2−74593
- In_2S vapour, thermodynamic functions, electronic and i.r. spectra, heats of sublimation and formation, 273-2000 K 2−74485
- KH_2AsO_4 and KD_2AsO_4, rel. to ferroelec. transitions 2−47985
- Li-Bi liquid alloy, activity coeffs. of Nd and Th 2−43334
- Li-Na alloys, liq., immiscibility 2−53404
- LiH, enthalpy and heat of fusion meas. 2−64507
- $Li_{1-x}Zn_{2x}Fe_{5-x}O_8$, high temp. enthalpy 2−54049
- Mg-Cu-Ni, Mg-Zn-Ni, Laves phases, enthalpies of soln. and formation detn. 2−47692
- MgCuGa, Laves phases, enthalpies of soln. and formation detn. 2−47692
- $MnCl_2$-ACl, where A=Li, Na, K and Cs, e.m.f. meas. 2−77787
- Mo-N, nitrogen solubility as a function of pressure and degassing kinetics 2−60967
- NH_3, aqueous, enthalpy of ionization, by solution calorimetry 2−77423
- NH_3, enthalpies of solution and formation by direct solution calorimetry 2−77422
- N_2O_4, dissociated, surface metastable states 2−47041
- N_2O_4, liq., ioniz. enthalpy determ. from cond. and permittivity 2−84612
- NaCl:Cd^{2+}, determ. of dissolution enthalpy of precipitates 2−83844
- Na_2S_x, molten, open circuit voltage obs. 2−71185
- Nb-H dil. solns., phase equil. and evolution kinetics of dil. solns. 2−53903
- Nb-H solns., nondil., equil. press.- comp.-temp. relationships 2−50843
- Nb-Mo-N system, α solid soln. 2−43856
- alpha-Nb-Mo-N ternary solid solution, equilibrium N concentration and thermodynamic behaviour 2−60983
- Nb, liquid and solid state enthalpy 2−54038
- Nb_xH_y, impurity effects on stability 2−77729
- Ni-S solid solution, partial entropy and partial energy of soln. 2−50837
- Ni_2Si, rel. to solidification characts. 2−43924
- $Ni_{1-x}Zn_xFe_2O_4$, high temp. enthalpy 2−54049
- Pb-Na liquid solution, e.m.f. cell obs. 2−71183
- Pb-Sn, of melting, determ. of thermodynamics of Sn phase transform. 2−50950
- Pt, interaction with O_2, thermodynamic props. of volatile products, obs. method 2−65378
- Rb, liquid, internal energy and free energy change with temp. and pressure, calc. from PVT data 2−71195
- Re-N, nitrogen solubility as a function of pressure and degassing kinetics 2−60967
- $RhC_{(2)}$, heats of atomization determ. by high temp. mass spectrometry 2−84623
- $SOBr_2$, mol. parameters 2−56169
- Si-N-O, free energies of form. of α and β silicon nitride and silicon oxynitride, 1200-1350°C 2−61037
- Sm-Sn system, relative stability of intermetallics 2−47573
- Sn-Na liquid solution, e.m.f. cell obs. 2−71184
- Sn, phase transform., determ. by obs. of Pb-Sn alloy 2−50950
- Ta + Co, Laves phases and thermodynamic props., solid-electrolyte galvanic cell studies 2−77424
- TeO_2, matrix isolated, thermodynamic functions and i.r. spectrum 2−56202
- TiC_2, heats of atomization determ. by high temp. mass spectrometry 2−84623
- TiC_xO_{1-x} solid solns., low temp. obs. 2−43989
- Tl_2XO_4, X=Se, Cr, Mo, of phase transform and struct. 2−53680
- U-Sb alloys, liq., 1130°C parameters 2−56497
- U, melting and transformation enthalpies 2−53491
- UO_2-ThO_2 solid solution, non-stoichiometric, e.m.f. obs. 2−64782
- UO_{2-x}, 1600-1900°C 2−53935
- $UO_{2.25}$, enthalpy detn. by drop calorimetry, 800 to 1600 K 2−77425
- V_xH_y, impurity effects on stability 2−77729
- W-N, nitrogen solubility as a function of pressure and degassing kinetics 2−60967
- W-halogen lamps, thermodynamic study 2−61764
- Yb-Sn system, relative stability of intermetallics 2−47573
- $Yb(NH_3)_6$, equilibrium pressure and standard enthalpy 2−61774
- Zn-Sn-Cd-Bi liquid quaternary solution, e.m.f. method 2−71186
- Zr-Cr solid solutions, phase diagram and lattice parameter meas. 2−74912
- ZrO_2, nonstoichiometric, thermionic emission and cond. study 2−43506

Thermodynamics

see also Atmosphere/thermodynamics; Entropy; Equations of state; Statistical mechanics

- — 2−70208
- — 2−66478
- δ-function interaction model, one-dimensional, exact result for equilib. thermodynamics of fermions 2−45320
- λ transitions for mixtures, special thermodynamic relations for Curie and Neel points 2−52107
- λ transitions in mixtures, revised thermodynamic relations 2−52106
- amorphous polymers, cell model partition function for thermodynamic calc. 2−43457
- Ar fluid around critical point, density fluctuations in microscopic volumes 2−56539
- book, problems in thermodynamics and statistical physics 2−45282

Thermodynamics continued

- boson fluid, spinless, stongly interacting, statistical thermodynamics, surface energy and tension 2−82267
- boundary layers, curved, uni-phase, -component fluids, theory 2−82382
- Carnot efficiencies for moving reservoirs 2−73459
- central Sierra snowstorms, and cloud seeding potential 2−65731
- chemical equilibrium calculation 2−44465
- classical, axiomatic approach 2−55568
- classical fluid, optimized cluster expansions, variational formulation of mean spherical model and hard sphere Percus-Yevick eqns. 2−67553
- classical gas functions expressed as Wiener integrals 2−60364
- classical many-body systems, decay of order 2−52095
- classical many-body systems, decay of order 2−52096
- cloud glaciation 2−62211
- condensed phases, physiochemical props., statistical treatment 2−41540
- constant pressure systems, fluctuations of thermodynamic variables 2−45570
- in continuum mechanics 2−52191
- critical indices, thermodynamic method for obtaining equalities 2−49033
- critical phenomena, non-equilibrium, dynamical scaling and mode mode coupling theories 2−60539
- critical phenomena, static correl. function selfconsistent singularities 2−54296
- critical point exponents, inequalities for spin- spin and energy-energy correlation functions 2−63030
- crustal heat sources, statistical thermodynamic model for distribution 2−54678
- crystals, monatomic, entropy and free energy 2−53488
- dense medium, functions in model of higher order 2−49036
- diatomic lattice, diagrammatic method analysis, Helmholtz free energy 2−80888
- disordered system, low temp. thermodynamics, van Vleck like paramag. 2−69614
- distribution function of mixed hard spheres, perturbation calc. 2−78941
- effective critical exponents and confluent singularities, temperature-dependence 2−69616
- electron gas characts. in parallel elec. and mag. fields 2−45332
- elementary particle analogue quantities calc. for uncorrelated jet model 2−42320
- energy and number of particles in system, fluctuations 2−45314
- energy transformation, averaging process 2−52262
- entropy, comparison with statistical entropy 2−45310
- entropy and normal states 2−73335
- entropy density of large system at low temperatures, lower limits 2−55429
- entropy production in irreversible processes and Liapunov function method 2−76390
- equilibrium, of critical points, recent developments 2−41536
- excited hadron substance characteristics in multiparticle production processes 2−66965
- Fermion Green's functions, approximation by Ritz variational method 2−58807
- fermions with gravostatic and electrostatic interactions, thermodynamic functions 2−82244
- flow rate obs. rel. to radioactivity cloud and u.s. methods 2−83760
- fluid, two-dimensional model 2−46649
- free-energy and chemical potentials of regular multi-component systems with molecules of different sizes 2−78181
- freezing of small solution droplets containing insoluble particles 2−54841
- gas of hard discs at high density, investigation using De Boer cell-cluster theory 2−64391
- gases, neutral and ionized, study of transport phenomena 2−83701
- general classical mechanical variables, fluctuations under external force when system in contact with heat bath 2−45339
- Gibbs paradox 2−66472
- Glansdorff and Prigogine's stability theory, ambiguities in entropy production 2−69617
- hadron physics, limiting-temperature concept 2−76618
- hard sphere fluid, inverse power pots., radial distrib. functions, virial coeffs. 2−73341
- harmonic oscillator chain, dynamic and ergodic props. of impurity 2−66469
- Hartree-Fock Hamiltonian Green's function, occupation numbers computed 2−58788
- heat disposal from power generation 2−80201
- Heisenberg-Ising ring for $|\Delta| \geqslant 1$, low-temperature thermodynamics 2−69611
- Heisenburg-Ising ring, $|\Delta| < 1$, improved eqns. 2−69606
- heterophase systems, of coherent loss during relax. of internal stresses 2−60859
- homogeneous systems, dressed particle theory and reduced distrib. functions 2−63032
- ideal classical polyatomic gases 2−45567
- ideal relativistic classical and quantum gases 2−45325
- imperfect Boson gas, thermodynamic limit 2−78833
- imperfect classical gas, equation of state, virial theorem 2−45569
- interacting particle systems in presence of external macroscopic fields, partition function 2−58782
- internal combustion engines, thermodynamic cycles and efficiency 2−58939
- irreversibility, its origin, time anisotropy, thermodynamic foundations of natural sciences 2−54995
- irreversibility and second law, rel. to nature of entropy 2−78943
- irreversible, memory effects, corrected derivation of transport equations 2−41535
- irreversible, of coupled chemical reactions, rel. to interpretation of u.s. relaxation spectra 2−54532
- irreversible processes, application of second law in continuum theories of processes in matter 2−69787
- irreversible processes, determ. of time-dependent Ginzburg-Landau eqn. 2−77865
- irreversible processes, non-equilibrium statistical operators and quasi-averaging 2−82379
- Ising lattice, cubic, correl. functions near crit. temp. 2−78840

Thermodynamics continued
Ising model with long-range interactions, determ. of thermodynamic functions, diagram expansion of free energy 2–45296
isolated systems, fluctuations of thermodynamic variables 2–45570
lattice gas, cluster expansion, determination of first ten high temp. coeff. 2–45291
laws, mathematical formulation 2–45566
linear and nonlinear state-space eqns., Lagrange and Hamilton methods 2–53485
magnetoelastic interaction, relativistic theory 2–41616
many-body, exact dynamical basis for fluctuating cell model 2–63038
Martini perpetual motion machine 2–49051
mechanics, harmonic principal functions applic. 2–70826
metal surfaces covered by electropositive adsorbates, thermodynamic analysis 2–53588
minimum entropy production and variational principles 2–45318
moving reservoirs, Carnot efficiencies 2–73459
multi-component mixtures of hard spheres, determ. of pair distribution functions 2–69625
multicomponent system, Gibbs-Duhem eqn., integration along phase boundaries 2–72536
multicomponent systems, connection between magnitude of phase effects and location of isothermal-isobaric surfaces 2–76388
multicomponent systems, structure of correlation functions near critical point 2–45306
multiple-particle production, remarks on paper by Wayland 2–49482
myocardium, contractile state, thermodynamic characterization 2–62820
non-electrolyte liquids and solutions 2–46913
nonequilibrium, conceptual foundation using multiplicative stochastic processes 2–58773
nonequilibrium, current-affinity relations and thermokinetic potentials 2–49031
nonequilibrium systs., statistical and dynamical correlations 2–45308
nonlinear, rel. to polymer melt flow 2–83748
nonlinear BGK model 2–73336
nonlinear coupling among critical fluctuations, source of weak divergences at a critical point 2–66468
nonlinear Onsager theory of irreversibility 2–45301
nonuniform system under external pot., canonical enemble limit 2–58786
nucleus, density of particle-hole excited states in shell model 2–67128
one fluid theory of mixtures, variational properties 2–49032
Onsager relations 2–45316
order-parameter correlations within screening approximation 2–63036
pair correlation decays in 3-dimensional systems 2–41533
Percus-Yevick theory, critical pt. phenomena 2–66479
phase transitions, gases and solids, F-ensemble and quantum mech. calc. 2–45321
phase transitions, non-equil. props. 2–63037
phase transitions in model systems 2–58798
piston movement in non-uniform medium, approximate analytic solutions 2–52261
planetary atmosphere thermodynamics rel. to rate of descent of spacecraft by parachute 2–73074
plasma, two-dimens., canonical partition function stability 2–46715
trans-1,4-polyisoprene, equilib. melting temp. of two crystalline modifications 2–71292
polymer chain, Gibbs distrib., correl. functions for vel. and position 2–60100
potential well, hybrid computer determination of functions 2–73334
primary and secondary compressions, deviations of pressure-velocity adiabatics 2–64234
rel. to quantum mechanics 2–41537
quantum systems, continuum thermodynamic limit for master equation 2–58802
quantum-anharmonic oscillator, partition function and free energy 2–66471
radiation in finie cavities, Planck Weyl asymptotic density refined 2–76384
random system, critical conc. against interaction range 2–52089
reacting gas mixture, equilibrium distribution of chemical constituents 2–54525
reacting system, thermodynamic concentration fluctuations by fluorescence correlation spectroscopy 2–72540
reactive mixture, reciprocal relations in relativistic kinetic gas theory 2–64392
relativistic, co-moving, equivalence of two major formulations 2–41475
rigid disks, extension of scaled particle theory 2–78836
scaling laws and crit. phenomena, geometrical interpret. 2–72119
second law, formulation in special relativity for heat conduction between bodies in relative motion 2–55567
second law and black holes 2–72957
second laws, adiabatic unattainability of absolute zero 2–58941
second order differential operator with eigenvalue degeneracy 2–52100
self-interacting fermion systems, perturbation theory for grand canonical Gibbs states 2–45328
shock waves, one-dimensional, influences on growth in materials with memory 2–58932
simple materials, non equilibrium thermodynamic theory, single integral entropic functional 2–76257
simple materials with fading memory, book 2–69686
singulary and binary systems, stability 2–45568
solid, statistical mechs. when under compression or tension, Hamiltonian modification 2–58789
spin system, concept of negative temp. and population inversion 2–45313
statistical, equations of motion for highly nonequilibrium systems 2–58794
statistical, Grand-canonical distribution and inhomogeneities 2–52098
surface, anisotropic, vector thermodynamics, plane surface junctions 2–56570
surfaces, Gibbs model, statistical analysis 2–45312

Thermodynamics continued
thermo-hydrodynamical model of ocean circulation 2–62027
triangular well pot. at low densities, perturbational calcs. 2–58781
tricritical exponents and scaling fields for two-component systems 2–63035
two-dimensional systems, long range order and metastability 2–50407
two-phase fluid interface at equilibrium, continuum model 2–53109
two-species model, idealized properties 2–78946
undergraduate curriculum, inclusion of intrinsic disorder 2–62923
unilateral flows, nonlinear transfer eqns. 2–78945
Van der Waals gas, rel. to dynamic stability 2–49034
of variable mass systems 2–69788
variable units concept applics. 2–66635
virial expansion, new derivation 2–73269
weak-scaling correls. characteriz. 2–45307
CsBO$_2$, evaporation, mass spectrometric obs. 2–64512
^{3}He liquid-solid mixture, interpretation of NMR and thermodynamic data below 3 mK, new liquid phase 2–80511
KBO$_2$, evaporation, mass spectrometric obs. 2–64512
LiBo$_2$, evaporation, mass spectrometric obs. 2–64512
NaBO$_2$, evaporation, mass spectrometric obs. 2–64512
RbBO$_2$, evaporation, mass spectrometric obs. 2–64512
XeO$_4$ vapour, standard-state functions calc. in range 250-400K 2–80023

applications
adsorption from liq. mixtures on solids, excess props. and temp. coeffs. 2–53583
Biot's variational principle for Stefan problem with constant heat flux 2–43437
brittle fracture initiation triaxial stress conditions, Gibbs free energy 2–84016
diffusion of electrolyte, calc. by methods of irreversible processes 2–83782
electrocapillary phenomena and thin films 2–43344
expanding universe 2–44817
higher alkanes, meas. of acoustic nonlinearity parameter 2–71197
hyperfiltration of multicomponent solutions, extended Nernst-Planck eqns., integration method 2–53418
interstellar gas, third thermally stable phase 2–78475
irreversible processes, creep recovery of amorphous polymers 2–56809
materials with memory 2–52097
network, biological systems 2–48836
nonlinear solid mechanics, thermodynamic foundations 2–56766
porous medium, fluid-filled, nonequilib. thermodynamics 2–50137
porous medium containing filtering fluid, equations of behaviour, using thermodynamics principles 2–50286
pure fluids, conformal solution theory 2–46650
SiO$_2$, Si$_3$N$_4$ and SiC, interactions with metals at phase boundaries, thermodynamic analysis 2–84093

Thermoelasticity
— 2–60178
aerodynamic heating stresses of solid isotropic sphere, transient axisymmetric thermoelastic problem, two-temperature theory 2–45433
anisotropic plates, solution of wave equation and coupled thermoelastic problem 2–55506
cavities, thermoelastic wave propag., two-temp. theory, wave speeds, travelling discontinuities 2–58883
circular disc, stresses due to rotating heat source on surface 2–52195
classical boundary value problems of thermal stresses with piecewise continuous anisotropic bodies 2–58884
complex potentials for an infinite elastic medium in plane strain with an insulated cavity 2–82299
composite, fibre-reinforced, shrinkage stresses near discontinuity, photothermoelasticity study 2–71659
composite beams of arbitrary cross-section, bounds on thermal stresses 2–45430
cone, stresses investigated due to mixed thermal loading on surface 2–58881
coupled problem of elastic half-space with rigidly fixed plane boundary subjected to constant temperature 2–41640
coupled theory, det. of free vibration frequencies 2–55477
coupled thermoelastic waves in solids 2–43673
cylinder, long circular and of isotropic material stresses when curved surface exposed to Suns rays 2–52199
cylindrical shell under moving hot spot 2–41638
disc with elliptic aperture, versatile stretching 2–76270
elastic plate on viscoelastic foundation, deflection in variable temp. field 2–41639
electromagneto-thermoelastic plane waves in solids with thermal relaxation 2–45435
generalized, acceleration wave propag. 2–49081
graphite, phonon-drag thermoelectricity rel. to structural imperfections 2–57248
hollow circular disk with heated stamps on external surface, stress relief through creep 2–66558
infinite cylinder in mag. field, temp. due to line heat source 2–52197
infinite elastic solid, interactions due to concentrated heat sensor 2–69688
longitudinal collision of two bars 2–78877
magneto-thermo-elasto-statics, solution of plane problems 2–45432
mechanical problems, book 2–66569
new theory, plane wave propagation 2–73394
nonlinear heat-conducting viscoelastic fluid flow 2–67599
nonlinear Onsager theory of irreversibility 2–45301
nonlinear theory, containing hyperbolic type equation of heat conduction 2–76340
cis-polybutadiene, cross-linked in swollen state, thermoelastic behaviour 2–60835
polyethylene, linear, anomalous internal friction at low temps. 2–84107
potential function for integration of thermoelastic differential eqn. 2–69687
rock grinding model, thermal stresses in spheres 2–62010
rods, stresses due to distributed time dependent heat sources 2–45427

Thermoelasticity continued
slab, under contin. surface temp., transient thermal stresses 2—49082
solid sphere of isotropic material, stresses due to const. temp. and normal pressure over band along equator 2—52198
solid surface, thermoelastic deform. by laser beam 2—43459
sphere, thermal stress at its boundary surface 2—78878
spheroidal inclusion, (measuring slab) embedded in a thermoelastic medium, state of stress and strain 2—82333
stability criteria for perturbations of the gradient of deformation and temperature field of the fundamental state 2—52200
stress distribs. in vicinity of external crack in infinite medium 2—82308
stress waves, laser generated in circular elastic ring 2—45436
stresses, examination by numerical methods 2—58880
stresses in elastic beams 2—45431
thermodynamics of simple materials with fading memory, book 2—69686
thermoviscoelasticity, boundary problems, perturbation method 2—66564
thermoviscoelasticity, linearized theory 2—69683
thick rectangular plates and laminates, flexure with temp. variation across thickness 2—52196
thick welled tube with step change in thermal expansion, stress analysis 2—52201
thin circular cylindrical shells subjected to instantaneous line heat sources 2—66568
thin rod of finite length and heated by electric current with one end at constant temp. and other fixed and thermally insulated 2—63089
transient waves, in half-space with thermal relaxation 2—58905
transversely isotropic semi-infinite medium, thermal indentation 2—58879
tubes, under uniform pressure and steady temp., elastic-plastic transition 2—49083
two-dimensional infinite elastic medium weakened by two coplanar Griffith cracks 2—58882
vibrations, rectangular plate 2—41657
viscoelastic cylinder, longitudinal oscillations, thermomechanical coupling effects 2—76348
volume thermal shock in a plate, determ. of eqns. for elastic potentials 2—82327
wave diffr. at cylindrical cavities 2—76363
Ag, u.s. attenuation, thermoelastic effects 2—68234
n-Ag_2Te, thermoelec. power rel. to Lorenz number and electron scatt. in elasticity obs. 2—84337
Au, u.s. attenuation, thermoelastic effects 2—68234
Cu, u.s. attenuation, thermoelastic effects 2—68234
$LiBaF_3$, consts. meas. by u.s. vel. 2—53781
SnF_2, soln. grown crysts. 2—47245
W, sintered, porosity influence 2—84145

Thermoelectric conversion *see Electricity/direct conversion*

Thermoelectricity
see also Thermocouples
anisotropic media, piezothermoelec. effects 2—51209
antiferromagnetic alloy, e.m.f., effect of spin orbit interaction 2—57295
β-brass obs. in thermopower near order-disorder phase 2—84371
C16-type pseudobinary alloys, valence electron conc. depend. 2—51104
chalcogenide amorphous films, Seebeck coeff. 2—61442
chalcogenide glasses, Seebeck coeff. changes in surface region 2—54190
cylindrical surface, wave diffraction 2—55505
dilute magnetic alloys, thermoelectric power 2—54242
excitonic phase, thermoelec. power calc. 2—65077
ferromagnetic alloy, e.m.f., effect of spin orbit interaction 2—57295
film, semicond., transport coeffs. rel. to surface states, Hall and Seebeck coeffs. 2—47884
flowmeter, thermoelectric, rapid response and small sensor size 2—83758
graphite, and thermomagnetic effects 2—57249
graphite, phonon drag, low temp., rel. to struct. impefection 2—44170
graphite, thermopower, mag. field effect, coupled Boltzmann eqn. 2—54243
high-conductivity solid electrolytes, thermoelectric powers 2—77961
liquid binary alloys, absolute thermoelectromotive force 2—56518
maximum power mode, criterion for thermolec. materials 2—75158
metal, Seebeck coeff., influence of point defects at high temp. 2—54040
metal-NHz solns., transport props. in the non-metal-metal transition range 2—80484
metal-$PbTiO_3$-metal, Seebeck effect 2—44169
method to determine type of steel, metal part production 2—80784
MnSi, elec. cond., thermal e.m.f. and Hall coeff. detn. 2—77797
Ni:H, hydrogenated, thermo-e.m.f., 3d band shape 2—72052
p-n junction, effect of switching layer resistance on transient coding 2—65079
Peltier effect, applic. in thermal conductivity determ. by parallel flow sandwich technique 2—68257
Peltier elements, stress-free system for mounting 2—76117
polyvinyl fluoride, thermoelectric effect 2—64995
Seebeck coefficient, semiconductors at high temperatures 2—44123
Seebeck effect, Cu-constantan thermocouple, effect of mag. field 2—63162
Seebeck effect for determining relative nitrogen doping level in Ta_2N resistor film 2—74793
semiconductor, amorphous, thermoelec. switching model 2—61285
semiconductor, magnetic, thermopower, magnon drag effect 2—54165
semiconductor multilayer film, transport phenomena 2—51054
semiconductor thermoelectric materials for electrical obs. 2—76432
spherical surface, wave diffraction 2—55505
superconductor, plasmon-coupled, thermopower near transition temp. 2—75057
thermal conductivity measurement of thermoelectric materials 2—52276
thermoelectric generator, isotope powered, description 2—59046
thermoelectric materials, rapid meas. of temperature dependence of thermal e.m.f. and electrical conductivity 2—52351

Thermoelectricity continued
Ag-(28 at.%) Au thermocouple wire, Standard Reference Material 733, comparison with common materials, 4. to 273K obs. 2—65080
Ag-rare earth alloy, thermoelec. power, phonon drag and distrib. contribs., 1.6-6K 2—81160
Ag, power rel. to Fermi surface shape and sample dimens. 2—68296
Ag_2Te, thermoelec. power at m.p. and to 1500 K 2—60495
Al-Zn alloy, Seebeck coeff., comp. depend., 400°C 2—81162
$As_2Se_3-xAs_2Te_3$, amorphous, thermopower, as func. of temp. and subsequent annealing 2—77893
AsTeI glass, power, rel. to transport props. 2—61296
Au-V, Au-Cu-V dil. alloys, thermopower and resistivity obs, Kundo temp. determ. 2—71831
Au, power rel. to Fermi surface shape and sample dimens. 2—68296
Au film, thermoelec. power. rel. to surface scatt., Matthiessen's rule 2—64895
BN, hexagonal, due to paramag. centres 2—74804
Be, elec. resist., laser beam heating effects 2—81036
Bi:Te, effect of high hydrostatic pressures on props. 2—81102
Bi-Sb alloy, for cooling appl. 2—75161
Bi-Sb alloy, thermo e.m.f., effects of Ag, In and Pt addition 2—71896
Bi, quenched in liquid N_2, thermoelectric power and frozen in defects 2—68336
Bi, thermopower, low temp., sample dimens. influence 2—47992
Bi film, thermo-e.m.f. rel. to struct. 2—81161
Bi films, figure of merit experimental study 2—55642
$Bi_{1-x}Sb_x$:Cd(In)(Sn), (x=0-0.2), 180-420K 2—61301
BiSe and BiTe, single crystal plates, thermal e.m.f. 2—84322
BiSeI, thermo e.m.f., band struct. determ., 300—400 K 2—80997
BiTe, diffusion of Cd and In, effect of thermal e.m.f. 2—83991
p-Bi_2Te_3, magnet-Seebeck effect, saturation and quantum oscill. 2—81159
Bi_2Te_3, performance as solar thermoelectric generator material 2—59058
Bi_2Te_3 and alloys, for Peltier cooling, review 2—75160
C film, amorphous, temp. depend. 2—61302
Ca-NH_3, solution, 203-243K 2—46984
$CdGeAs_2$, thermopower 2—60496
$Cd_xPb_{1-x}Se$ alloy, Hall coeff., Hall mobility, thermoelec. power, optical energy gap, 77-450 K 2—64977
CdS, temp. quenching of photocond., thermoelec. skin effect in presence of shallow levels 2—81171
CdSe, temp. quenching of photocond., thermoelec. skin effect in presence of shallow levels 2—81171
Ce_3Se_4, thermo e.m.f., 80—680 K, complex cond. band 2—80918
Co single crystal, technique for low temp. obs. 2—65078
CoB, thermo-e.m.f., temp. depend., 100-1200°C 2—51099
Cr-Ru alloy, absolute thermoelec. power, 350-1000K 2—68476
Cr and alloys, excitonic phase, thermoelec. power calc. 2—65077
CrSi, elec. cond., thermal e.m.f.. and Hall coeff. detn. 2—77797
$CrSi_2$ thermoelectric props. and crystal growth 2—84370
Cs, power rel. to Fermi surface shape and sample dimens. 2—68296
Cu-Mn alloy, thermo-e.m.f., 4.2-250K 2—57250
Cu-Ni-Mn alloy, order-disorder transform study 2—54001
Cu-Ni alloy, power rel. to Fermi surface shape and sample dimens. 2—68296
Cu_x-Sn_{1-x} liquid alloy, thermopower computation, comparison with exptl. data 2—43387
Cu, power rel. to Fermi surface shape and sample dimens. 2—68296
Cu film, props. thermoelec., resist., cond. electron m.f.p. 2—68477
$CuCr_2Se_4$, temp. depend., 100-650K 2—81091
$Cu_4Mn_2Te_4$, Seebeck coeff. 2—84442
CuO, thermal e.m.f. temp. depend. during dissociation, 960-1330K 2—57251
Cu_xTe, thermal e.m.f., electronic and ionic cond. at 400°C, composition 2—54247
Fe and Fe-Cr alloys, thermopower near mag. crit. pts. 2—57290
FeSi, elec. cond., thermal e.m.f. and Hall coeff. detn. 2—77797
GaAs, amorphous, thermoelec. power, cond., hopping cond., annealing effects 2—61312
p-GaAs, differential thermo e.m.f., effect of pressure, 10000 kg/cm² 2—44099
n- GaAs, thermal e.m.f., pressure depend., rel. to effective electron mass. 2—44098
$GaAs_{1-x}P_x$:SeTe, donor self- compensation 2—75110
$GaInS_3$, thermally stimulated cond., dark current, capture levels 2—75162
GaSb:Te,Zn, thermal e.m.f. rel. to carrier conc., 300K 2—54248
$GdTiO_3$, Seebeck coeff., 77-1500 K 2—57144
Ge, amorphous, thermoelec. power, cond., hopping cond., annealing effects 2—61312
Ge, thermophotoelec. effect due to hot carriers, 300 and 77K 2—72057
GeTe-Bi_2Te solid soln., thermal e.m.f. 2—74903
Ge_xTe_{1-x} alloy, amorphous, Seebeck coeff., rel. to band struct. detn. 2—77904
Hg, crit. fluid, influence of metal- nonmental transition 2—60377
Hg, liq. and supercrit., absolute thermopower, density depend., metal-nonmetal transition 2—60499
In-Pb alloy, Seebeck coeff., comp. depend., 120°C 2—81162
In-Sn alloy, Seebeck coeff., comp. depend., 100°C 2—81162
In-Te alloy, molten, cond. and temp. depend. 2—77446
n-InAs, thermoelec. power in quantizing mag. fields 2—84372
InSb:Te, Zn, thermal e.m.f. 2—44101
In_2Se(Te), molten, temp. depend. 2—67837
$In_2Te_{0.5}Se_{0.5}$, molten, temp. depend. 2—67837
InTlSe(Te), molten, temp. depend. 2—67837
$IrB_{1.1}$, temp. depend. of thermal e.m.f. 2—47657
$Ir(CO_3)Br$, organometallic, thermoelec. analysis of elec. cond. 2—72055
K-NH_3, solution, 203-243K 2—46984
K, power rel. to Fermi surface shape and sample dimens. 2—68296
$K_2Pt(CN)_4Cl_{0.3}.xH_2O$, organometallic, thermoelec. analysis of elec. cond. 2—72055
$K_2Pt(N)_4Br_{0.3}.3H_2O$, quasi one dimensional conductor, anisotropic thermopower 2—64915
La_2Te_4, thermo e.m.f., 80—680 K, complex cond. band 2—80918
$LaTiO_3$, Seebeck coeff., 77-1500 K 2—57144
Li-NH_3, solution, 203-243K 2—46984

Thermoelectricity continued
$Li(NH_3)_4$, carrier mobility determ., thermoelec. power 4.2-100K 2−47894
$Mg_xPb_{1-x}Se$ alloy, Hall coeff., Hall mobility, thermoelec. power, optical energy gap, 77-450 K 2−64977
$MgSi_{1.72}$-$CrSi_2$ solid soln., prep., thermal e.m.f., elec. and thermal cond. 2−74905
$MgSi_{1.72}$-Ge solid soln., prep., thermal e.m.f., elec. and thermal cond. 2−74905
α-MnS from sulphurization of Mn in H_2S-H_2 gas mixtures at 550° to 711°C, obs. 2−75079
MnTe, mag. semicond., thermopower, magnon drag effect 2−54165
Na, thermopower, 40 to 360 K 2−57086
Nd_3S_4, thermo e.m.f., 80−680 K, complex cond. band 2−80918
Ni-Co alloy, thermo e.m.f., temp. depend. 2−72051
NiB, thermo-e.m.f., temp. depend., 100-1200°C 2−51099
Ni_3(Mn,Co) and Ni_3(Mn,Fe) alloys, electron and hole mobility obs. 2−47837
NiS, thermoelec. power, 80−400 K, semicond.- semimetal transition 2−81097
Pb, liq. elec. resist. and thermoelec. power temp. depend., models 2−60501
Pb, thermoelec. power, from electron-ion pseudopot. model 2−77812
PbO-Al_2O_3-SiO_2-B_2O_3 glass, between metal electrodes, rel. to memory effect 2−71915
p-PbTe-PbSe alloys, temp. depend. 2−75164
PbTe, performance as solar thermoelectric generator material 2−59058
p-PbTe, Seebeck coeff., rel. to room temp. transport props. 2−54161
PbTe, thermoelec. props. rel. to partial substitution of Pb by Ga, In, Th 2−72053
Pd_5B_2, Pd_3B, synthesis and thermal e.m.f. 2−72054
Pt-Mo, thermocouple, e.m.f. rel. to neutron irrad. 2−78940
Rb, power rel. to Fermi surface shape and sample dimens. 2−68296
Se-Te melt, electronic transport behaviour, thermopower 2−60502
Si-Ge alloy, Seebeck coeff., temp. depend. 2−51210
Si single crystal point contact diode, thermo e.m.f. obs. of polarized memory effect 2−61389
Sm, elec. resist., thermoelec. power, anomalous behaviour, 300-1000K 2−54128
Sn-Co soln., thermoelec. power 2−71227
Sn-Fe soln., thermoelec. power 2−71227
Sn-Ni soln., thermoelec. power 2−71227
SnTe polycrystalline film, thermo-e.m.f., temp. depend. 2−71916
Te film, thermoelectric power, Hall and Seebeck coeffs., resistivity 2−54249
TiO-MnO alloy, thermal e.m.f. 2−74908
TiO_2, rutile, powder in lightly pressed tablets, thermal e.m.f., 300-1300K 2−77821
$Ti_xTa_{1-x}S_2$ ($0.1\leqslant x\leqslant 0.9$) solid solutions, thermoelectric power 2−61266
$TlBiTe_2$, and TlTe, thermopower sign 2−51144
$UC_{1-x}N_x$, $0\leqslant x\leqslant 1$, meas. of resistivity and absolute Seebeck coeff. 2−44105
$V_{1-x}Nb_xO_2$, metal-insulator transition study 2−75101
$V_{1-x}Nb_xO_2$, metal-insulator transition, theory 2−75103
VO_x, thermal e.m.f., 80-1400K 2−64991
V_nO_{2n-1} (n=3,4, ..., 8) single cryst., temp. depend. of thermoelec. power 2−43509
W-Re thermocouple materials, high temp. behaviour, report 2−84373

Thermoluminescence
clinical dosimetry, experience gained at Radiumhemmet, Stockholm 2−69429
dating of objects at Riso, 4000 B.C.-A.D.1600 2−84762
dating of pottery, circumventing natural radioactivity problem 2−84763
dating of pottery by predose method 2−84761
dating of pottery by subtraction method 2−84760
dating technique, applic. to smoky quartz 2−65570
deformation, explosion and grinding effects 2−84554
dosimeter characts. as personnel monitor 2−70552
dosimeters, responses in D^+ on Be neutron fields 2−69391
dosimeters, uniform extremely thin, manufacture by liquid moulding technique 2−67086
dosimeters for environmental monitoring 2−79675
dosimetry, det. of atmospheric contamination 2−62291
dosimetry, in medical physics laboratory 2−73264
dosimetry, with photon counting 2−49340
dosimetry for clinical use in radiation therapy 2−69430
dosimetry in personnel monitoring 2−58620
dosimetry phosphors, 6, thermally stimulated exoelectron emission and thermoluminescence following β-irradiation 2−82821
fluorite, relative effects of α- and β-radiation 2−51379
glow curve differential equations, numerical solution using Runge-Kutta method 2−84535
hexachloroethane, γ-irrad., thermolum. and e.s.r. 2−48259
in vivo dosimetry, clinical radiation therapy 2−69415
kapis shells as possible thermoluminescent dosimeter 2−82823
lunar core material, temp. gradient obs. 2−62651
material evaluation for low-temperature dosimetry system 2−67085
non-linearity and LET effects of response, releasing probability change model 2−68697
phosphors with two captive levels, model 2−65313
quartz, irradiated by gamma rays, geological appl. 2−84709
quartz, relative effects of α- and β-radiation 2−51379
quartz, splitting mechanism 2−84720
quartz, thermal pretreatment, pre-irradiation, splitting mechanism 2−84720
appl.in radiation dosimetry 2−42696
radiothermoluminescence meas. of diffusion coeff. of O_2 in polypropylene and polyethylene 2−84004
squalane containing biphenyl, concentration effect 2−46969
teflon tape, adhesive tape 2−62872
thermoluminescent dosimeter with digital readout 2−55924
TMPD in hydrocarbon glass, rigid matrix photoioniz., anion form., bleaching kinetics 2−81511

Thermoluminescence continued
Ucera meteorite, determ. of differential atmospheric heating using natural thermoluminescence 2−75926
Ag halides, thermolum. and photocond., trap levels, meas. apparatus and technique 2−79389
Al_2O_3, absorption spectra and reln. between thermoluminescence and thermobleaching 2−71521
Al_2O_3, emission band at 4100 Å suitability as radiation detector 2−57376
BN, hexagonal, blue thermolum. emission, paramag. centre identification 2−72430
BN, hexagonal, due to paramag. centres 2−74804
BaF_2, due to low temp. plasma produced radiational defects 2−71452
CaF_2:Dy phosphor, thermoluminescent for thermal neutron dosimetry 2−83160
CaF_2:Dy thermoluminescence dosimeter meas. of background radiation in USA 2−84859
CaF_2:Gd^{3+}, glow curves, hole activation energies, 4.2 to 600K 2−57377
CaF_2:Mn, CaF_2:Tb relative effects of α- β-radiation 2−51379
CaF_2:Mn, trapping centres 2−68699
CaF_2:Mn dosimeters, influence of size on ^{60}Co γ-ray dosimetry in extended media 2−67088
CaF_2:Mn thermoluminescent γ-dosimeter, sensitivity to neutrons 2−82820
CaF_2, due to low temp. plasma produced radiational defects 2−71452
CaF_2, exposure to u.v. light 2−68700
CaF_2, natural phosphor, thermoluminescent for thermal neutron dosimetry 2−83160
CaF_2 dosimeter for meas. natural background radiation 2−42698
CaF_2 dosimeter in sunburn range 2−85136
CaF_2 dosimeters, thermoluminescent, preparation and props. 2−82824
CaS:Bi, Pd phosphors, kinetics 2−54475
CaS phosphors, self activated emission, study of trap depths and nature of trapping centres 2−54473
$CaSO_4$:Dy phosphor for meas. of u.v. irradiances 2−82561
$CaSO_4$:Dy phosphor thermoluminescent for thermal neutron dosimetry 2−83160
$CaSO_4$:Mn, dose relationship, energy reponse and rate dependence from 8 keV-30 MeV 2−68701
$CaSO_4$:Sm, Mn, role of activators 2−48255
$CaSO_4$:Tm phosphor for meas. of u.v. irradiances 2−82561
$CaSO_4$:Tm thermoluminescent dosimeter construction and characts. 2−55923
$CaSo_4$:Mn, relative effects of α- and β-radiation 2−51379
CsI:Na, mechanism of thermally stimulated afterglow in 60-90 K range 2−72431
KBr crystals, u.v. irrad. and colour centre prod. from exciton decay 2−71527
KCl:Tl, thermal glow traps responsible single negative ion vacancies 2−75333
$Li_2B_4O_7$:Mn, optimum properties for dosimetry applic. 2−49913
$Li_2B_4O_7$:Sm, Mn, role of activators 2−48255
LiF:Mg, sensitivity enhancement by Mn 2−44415
LiF:Mg, thermoluminescence variation with impurity distribution 2−84552
LiF:Mg^{2+}, depend. on state of aggregation of Mg^{2+} vacancy pairs 2−44416
LiF:Ti thermoluminescence variation with impurity distribution 2−84552
LiF-100 (-7), dose relationship, energy response and rate dependence from 8 keV-30 MeV 2−68701
LiF, compressed, surface thermolum. after immersion in boiling water 2−48256
LiF, dependence on 340 nm colour-centres 2−43650
LiF, dosimeter, radiation protection in radiodiagnosis 2−48888
LiF, dosimetry glow peaks, mechanism 2−61720
LiF, single crystal ribbon prod. by edge-defined film-fed growth technique 2−67943
LiF, X-irrad., temp. depend. 2−65313
LiF (TLD-100), at low and high exposures 2−44414
LiF detector, thermoluminescent, for neutron and gamma radiation 2−52691
LiF detector for meas. of close gradients at interfaces between different media 2−82822
LiF dosimeter, for obs. during radiotherapy 2−69400
LiF dosimeter, response to 1.7-3.7 MeV α and 2.4-13.3 MeV p 2−85135
LiF dosimeters, response to fast neutrons 2−79671
LiF dosimetric grade powders, influence of thermal and chemical treatment on properties 2−67090
LiF dosimetry grade 100 powder incorporated in silicone rubber, dependence of energy response on grain size 2−68702
LiF in teflon discs, consistency of dosimetric properties over repeated cycles of use 2−67087
LiF personal dosimeter system 2−69432
LiF phosphor, study of sensitivity factor mechanism 2−68698
LiF thermoluminescence following plastic deformation 2−61721
LiH:Pb, after X-irradiation 2−72422
MgO, $F^+\rightleftharpoons F$ centre conversion obs. 2−68043
MgO, u.v. excitation, glow peak assignment 2−57378
Mg_2SiO_4(Tb) phosphor, study of sensitivity factor mechanism 2−68698
NaCl:Cu, X-ray coloured, Cu activated thermolum., 300-510K 2−78122
NaCl:Tl, X-irrad., traps responsible for 360 and 390 K glow peaks 2−54476
NaCl, rel. to alkali stoichiometric excess, glow peak due to F′ centres, 77 K 2−81423
NaCl, temperature dependence of 330 K luminescence maximum 2−51380
NaI:Tl, recomb. luminesc. of crysts. excited in A-band by activator absorpt. 2−75334
$NaNO_3$, glow curves, capture cross-sections and trap. parameters detn. 2−48257
SrF_2, due to low temp. plasma produced radiational defects 2−71452
SrS phosphors activated by Zn, Sn, Pb and Th 2−65314

Thermoluminescence continued
- $Y_3Al_5O_4$:Ce(Pr)(Tb)Eu, characteristic spectra of activators in recombination processes after γ-irradiation 2−80714
- YBO_3:Ce, cathodic excitation, also dependence on Ni, Co and De impurities 2−54477
- ZnS:B, 100-400K 2−75322
- ZnS:Cu phosphors, extralinear effects 2−75335
- $ZnS_{1-x}Se_x$, rel. to stimulated cond. with persistent memory 2−75104
- Zn_2SiO_4:Mn, thermoluminesc., glow curves, impurity depend. 2−48258

Thermomagnetic effects *see Magnetothermal effects*

Thermometers
- *see also Pyrometers; Thermocouples*
- calibration, sealed metal freezing point cell 2−45599
- capacitance, glass-ceramic, low temp., thermometer equations 2−49187
- electronic, direct reading. portable, development 2−63161
- electronic, with Si junction diode sensor 2−55591
- glass-ceramic capacitance thermometer, performance in 0.007 to 0.040 K range 2−66371
- glass-ceramic capacitance thermometer for obs. in 1.7 to 300K range 2−76404
- ideal gas-calorimetric 2−58974
- i.r. thermometer with pyroelectric detector 2−55590
- linear, direct reading, using Cu-constantan thermocouples 2−73469
- noise, Josephson junction applics. 2−64956
- osmotic press. thermometry with dil. ^3He-^4He mixtures 2−45184
- radiation, review 2−76386
- U.S., construction, application, operation 2−52296
- u.s. attenuation and modulus, meas. in wires at elevated temp. 2−49189
- C, cryogenic, interpolation routines for calibration 2−52294
- $CeMgNO_3$, slurry type, rel. to Cu n.m.r. thermometer 2−49185
- Cu n.m.r. type, construction and use 2−49185
- Ge, cryogenic, interpolation routines for calibration 2−52294
- Hg and alcohol, thermostat for null-point checking 2−58975
- $Na_3[Ce(C_7H_3NO_4)_3].15H_2O$, for 2-20 mK range 2−82079
- Si:P implanted, for 10 mK to 20 K 2−48938

resistance
- calibration of resistance thermometers in 4-90 K range 2−85163
- general response in gases at low pressures 2−45601
- null-point checking, thermostat 2−58975
- thermistors, midget disk, effects of static mag. field at 77 K 2−49186
- thermoresistors, high temp., industrial temp. control 2−76405
- C, method of reducing effective magnetoresistance 2−52295
- C, time response and thermal diffusivity 2−49184
- GaAs, characteristics 2−49188
- Pt, calibration to new International Practical Temperature Scale, application techniques 2−66653
- Pt, effects of static mag. field at 77 K 2−49186

Thermonuclear devices *see Plasma/devices*

Thermonuclear reactions
- *see also Elements/origin; Nuclear fusion*

Elements/origin; Nuclear fusion
- θ-pinch deuterium plasma, laser-beam- scattering meas., obs. of neutron emission 2−56364
- conditions for quasi steady development of self sustaining nuclear reactions 2−63952
- controlled, ergonic fusion of D_2 and T_2, power production 2−70930
- controlled fusion, applications of laser compression of matter to super-high density 2−70487
- controlled fusion, plasma diagnostic techniques 2−53213
- controlled fusion, use of laser heating 2−70486
- fusion, controlled, for space propulsion 2−51673
- fusion by laser driven flame propagation in solid DT targets 2−64308
- galactic gas evolution, mixing time scale of newly made material, spatial inhomogeneities 2−66048
- Galaxy, heavy element synthesis, separation of r- and s-process abundances 2−66052
- high β fusion plasmas, formation by intense relativistic electron beams 2−83607
- high-altitude, fission fragment localization method 2−51630
- hot spot expansion and energy production 2−64309
- initiation by high current electron beams 2−46722
- in laser generated plasma, use of very powerful beams which could be developed in the foreseeable future 2−63313
- neutron prod., in exploding-wire discharges 2−67665
- neutron yields from spherical targets heated by spherically symmetric irrad. from multiple-beam laser 2−67339
- neutronic calc. for blanket assembly by discrete ordinates and Monte-Carlo methods 2−46369
- nucleosynthesis theory and formation of elements up to Fe group 2−72949
- plasma, non-equil., effect of modified Maxwell distrib. of ionic energies 2−56331
- plasma, triggered by laser beam absorption behind shock wave 2−70909
- plasma confinement, supersonic flow, high power electron beam 2−70914
- plasma production, laser radiation use 2−70931
- plasma stability in helical field 2−83552
- stars, nuclear laboratory expts. 2−48695
- stars, s-process neutron capture time determ. 2−75722
- in stars, theory including resonant and non-resonant reactions, rates and estimation of reaction 2−75723
- stellar, hydrostatic O burning at balanced power 2−51736
- stellar evolution, nucleosynthesis of light elements 2−62508
- stellar evolution, rates at high temps. 2−62509
- stellar nucleosynthesis relative abundances of elements 2−66084
- stellar reaction rates for $^{12}C + ^{12}C$, $^{12}C + ^{16}O$, and $^{16}O + ^{16}O$ reactions 2−51737
- superheavy elements, synthesis by r-process in supernovae 2−69093
- D burning main sequence stars, low mass limit rel. to stellar models 2−75720
- ^2H solid target, laser irradiation 2−43153

Thermopiles *see Thermocouples*

Thermoreflectance
- alkali halides, room temp. study 2−44363
- band struct. analysis, review 2−72298
- CoO, 4-8 eV, rel. to band struct. 2−84505
- MnO, 4-8 eV, rel. to band struct. 2−84505
- NiO, 4-8 eV, rel. to band struct. 2−84505
- NiO, band transition assignment 2−44368
- $SrTiO_3$, differential spectra and band struct. 2−72307
- WSe_2, rel. to optical consts. determ. 2−44383

Thermosphere *see Atmosphere/upper; Ionosphere*

Thermostats
- *see also Cryostats*
- automatic temperature stabilization, effect on ferroelec. oscillatory system 2−44157
- feedback temp. control system test for nucleate boiling heat transfer function 2−53506
- gas temp. of 220°C with 0.003° error 2−58971
- i.r. study of heating of sample using electrical analogy 2−52263
- fornull-point checking 2−58975
- transistorized temp. controller, thyristor as power switch 2−52301

Theta pinch *see Plasma/confinement*

Thickness measurement
- *see also Particle size*
- air, thin films, white light interferometry technique 2−70015
- alpha-particle gauge 2−41449
- Antarctic ice sheet, radio echo method of measuring thickness changes 2−84722
- bloom slabs by laser gauge, beam triangulation, CCTV scanning 2−82495
- cylindrical shells, by inductive method 2−76430
- dielectric layers with imposed spectral characts., control and preparation 2−63418
- electrical contact method, thin fluid films, hysteresis, statistical profile 2−83733
- film, by holographic interferometry 2−50477
- film, ellipsometric method 2−47095
- film, ellipsometry, calc. method 2−44339
- film, metal, on opaque substrate, thickness uniformity determ. by optical transmission microscopy 2−64560
- film, X-ray glassy halo obs. 2−64557
- film surface density meas. by proton excited X-rays, Fredholm expression 2−80542
- film thickness calc. from ellipsometric values and intensity meas. using Drude equations 2−56581
- film thickness uniformity on rotating substrates 2−67903
- films, electron backscattering 2−79116
- films, light absorbing, det. from reflectance and angle of incidence 2−59224
- films, solid, by elastic backscattering 2−80923
- films, vacuum deposition control using optical monitor 2−47094
- fluid film, by Moire fringe contouring 2−79371
- foil samples, X-ray transmission texture photography 2−41447
- ice, e.m. sounding 2−44604
- interferometric method of meas. optical thickness of layer 2−70013
- liquid solution surface layer meas., use of reflection coeff. 2−60474
- lubricated sliding point contacts, load, traction, film thickness meas. device 2−53864
- lubricating, insulating and protective coatings on metals and semiconductors 2−55357
- magnetic thin uniaxial films, and magnetization determ. method 2−68559
- metal and dielectric foils by electron backscattering 2−41921
- metal oxide film, from reflection and emission coeff. meas. 2−54398
- method for μm changes obs., isohypses tracing 2−84014
- non-destructive testing conference, London (1971) 2−43782
- nuclear targets, using charged particles 2−73924
- optical thin films, photoelectric monitoring 2−59225
- oral mucosa, u.s. echo ranging applic. 2−51945
- Permalloy film, X-ray meas., rel. to mag. moment and demag. field 2−61539
- polymer fracture surface layer, optical thickness determ. 2−70013
- recording thickness gauge using Instron universal testing machine 2−45214
- rigid surface films 2−53382
- sea ice, theory and field tests of microwave radiometer 2−44603
- targets, using α-particles 2−55897
- thin film deposition, meas. and control for coating different from $\lambda_0/4$ 2−80602
- thin films, solid solutions. X-ray diffraction 2−82125
- thin layer, X-ray fluorescence method 2−43470
- white light interferometric thickness gauge 2−70031
- Al film, comparison of optical and electromechanical methods 2−47118
- Au film, comparison of optical and electromechanical methods 2−47118
- CuO film, determ. by use of quartz cryst. oscill. 2−48135
- He liquid film, acoustic interference applic. 2−47008
- LiF on Al, monitoring by reflectance meas. using 1216 Å line of H 2−55733
- MgF_2 film, comparison of optical and electromechanical methods 2−47118
- MgF_2 on Al, monitoring by reflectance meas. using 1216 Å line of H 2−55733
- Si wafers, optical gauge 2−67902
- SiO_2-Si_3N_4 film, by spectrophotometry 2−47086
- SiO-SiO_2 film, nondestructive technique 2−50508
- UO_2 surface films, using reflectivity 2−79412

Thin film devices
- amorphous chalcogenide threshold and memory devices, preswitching props., forming and switching 2−77920
- atomic oxygen sensors for upper atmosphere 2−65403
- chalcogenide-glass switches, preswitching behaviour in terms of space charge injection mechanism 2−68379
- garnet mag. films, domain interaction with laser beams, domain writing 2−75230
- geodesic lens, for laser beam focusing in integrated optics 2−49393
- geodesic lenses for integrated optics 2−79401

Thin film devices continued
hard dielectric film optical waveguides dispersion and loss meas. 2−42238
i.r. thin film filters rel. to developments in optical equipment 2−73667
isotopic thermoelectric battery for cardiac pacemakers 2−49290
Josephson junctions with semicond. barriers 2−64957
memory device, amorphous film, radiation effects 2−61365
optical memories for computers 2−79219
optical waveguide, self-focusing, using nitrocellulose film 2−63412
optical waveguides, propagation characteristics 2−55762
organic dye lasers, expts. 2−42035
passive, stable layer systems, diffusion barrier arrangements, ageing, stability rel. to comp. 2−75120
periodic layered waveguide structure for distributed lasers 2−42051
quantum interference junction, desired characteristics 2−71844
shielded superconducting, current distribution 2−81057
surface layer on metal, semiconducting parameters, effect of substrate stress state 2−71966
surface wave deflection of optical guided wave and coupling in thin films 2−49431
temperature measuring for surface transients 2−58972
transistors, polarizability of bias- temperature drifted species 2−47946
Al-CdS-In, memory effect, switching characts. 2−44139
As-Te-Ge-Se glass switching device, small signal behaviour 2−61376
As_2Se_2Te switching and memory device, inc. neutron irrad. effects 2−61373
Au-SiO cermets, mechanisms of conduction, nucleation 2−54127
CdS, thin film solar cells, state of the art and space applications 2−59059
CdSe-CdS photoresistor, role of activating powder 2−65096
Cu_2S-CdTe heterojunction, photovoltaic effect 2−81123
GaAs-$Al_xGa_{1-x}As$ dielec. waveguide, fabrication by mol. beam epitaxy 2−80593
GaAs waveguide, phase matched parametric oscillation theory 2−73483
In superconducting thin films, penetration depth and flux creep 2−68345
M-CdS-I-M, electron emission 2−68450
Nd-glass thin film waveguide for amplification at 1.06 microns 2−42057
$Pb_{1-y}Sn_ySe$ i.r. photoconductors, properties 2−64999
$Pb_{1-x}Sn_xTe$ i.r. photoconductors, properties 2−64999
PbTe epitaxial diode, evaporated, injection luminesc. and laser action 2−57382
SnO_2-CdS-Au, polarised memory device, photovoltage obs. 2−61381
SnO_2-SbSI, dielec.-semicond. junc., memory and switching effects 2−61366
Ti-TiO_2-Au, diode, I-V characts., negative resist. 2−61390
ZnO optical waveguides, epitaxial, low losses, below 5dB/cm 2−79377
ZnO oxygen partial pressure sensor 2−41454
ZnO single crystal optical waveguides, sapphire substrate, properties, technology 2−52463

Thin films *see Films; Films, solid*

Thirring model *see Elementary particles; Field theory, quantum*

Thixotropy
viscoelastic medium, kinetic model 2−71242

Thomas-Fermi method *see Atoms/structure*

Thomson effect *see Thermoelectricity*

Thorium
abundance in seawater in-situ analysis using synthetic fibres 2−75469
in Ap star HD 25354, spectral obs. 2−72994
content in wind-borne Saharan dust over N.Atlantic Ocean 2−44583
drill core scanning by gamma ray spectrometry 2−78293
exhalation from ground 2−61988
ions, addition to reserpine, fluoresc. detection reaction sensitivity increase 2−71215
in Li-Bi liquid alloy, solubility and heat of soln. 2−43334
LWR fuel, replacement at UD_2 in PWR 2−42650
nuclear fuel cycle, reference materials for accurate determ. of U, Pu and Th 2−74160
in nuclear fuels, chemical analysis techniques 2−74168
quantitive det. in various matrices using nuclear track technique 2−48364
reactor fuel cycle utilization in HTGR 2−56065
solar photospheric abundance det. from spectrum synthesis 2−58554
surface impurities, bulk to surface equilib., Auger spectroscopy obs. 2−50465
I ion-Au, Th, U collisions, 10 to 60 MeV, X-ray spectra of temporarily formed superheavy quasiatoms 2−74236
Th, photon appearance potential spectroscopy on O_2 exposure 2−54441

Thorium compounds
Ce-Th alloy, isomorphic transforms. 2−50959
Gd-Th alloys, elec. resist., mag. ordering effects 2−84294
Mg-Th, Mg-Th-Mn alloys, precipitation processes, elec. microscope obs. 2−53993
Mg-Th and Mg-Th-Zr systems, e. microscopy exam. of precipitation 2−71690
$NaTh_2(PO_4)_3$, ferroelec. props., rel. to struct. 2−54237
Pr_xTh_{1-x}, h.f. n.m.r. at 4.2 degrees K 2−72518
TO_2 on Ir cathodes as electron emitter for electron bombarded semiconductor devices 2−65099
Th/U fuel elements with known irradiation data, actinide composition studies 2−75403
Th-Ce alloy, phase transition critical region, elec. resistivity obs. 2−50951
Th-H, Th-D systems, diamag. suscept. rel. to superconductivity 2−54143
Th-Ir system, 66-83% Ir, phase relations 2−50976
Th-Ln-Bi soln., Ln=La, Eu, Nd, mutual solubilities, 350-700°C 2−67809
Th-Ni system, 50-96% Ni, phase equilib., 1000-1500°C 2−74943

Thorium compounds continued
ThC_2-UC_2, ThO_2-UO_2 coated nuclear fuels for GCR, chemical analysis techniques 2−74169
ThC, ThS, crystal synthesis by electron beam melting 2−53620
ThCN, cryst. struct., X-ray and neutron powder diffr. 2−53681
ThCe, supercond. transition temp., 0-20 kbar press. 2−47870
Th_4H_{15} diamag. suscept., specific heat, rel. to superconductivity 2−54143
ThN-ThO_2-Th system, phase behaviour 2−50977
ThN, mag. sp. ht., 7 to 300K 2−43988
ThO_2:Cm^{3+}, e.p.r. investigations of zero- field splittings 2−44449
ThO_2:Gd^{3+}, spin-lattice coeffs. calc. 2−51286
ThO_2:Y_2O_3 ceramic, high optical quality, powder prep. and processing technique 2−77736
ThO_2-Ln_2O_3 system, phase equilib., 1250-2100°C 2−47718
ThO_2-W-Re alloy, creep, strength to rupture, 1800-2200°C 2−64719
ThO, electronic band spectra interpret. 2−77069
ThO_2, crystal growth, from the flux systems PbO-V_2O_5 and Bi_2O_3-V_2O_5 2−50589
ThO_2, e.s.r. absorpt. spectrum of monovalent iron 2−48296
ThO_2, effect of fluoride adsorp. on hot-pressed density 2−74648
ThO_2, spin-lattice relax. of Fe^+ amd hyperfine splitting of Gd^{3+}, Debye temp. obs. 2−84581
ThO_2, stimulated emission from rare earth and actinide ions 2−48225
ThO_2, thermal diffusivity, 900-2550°C 2−54081
ThO_2 and solid solns., electrolyte transport props. 2−65053
ThO_2 as heat source in thermionic conversion rel. to ^{228}Th radioactive decay simulations 2−52787
ThO_2 in Ni dispersion strengthening effects on hydrogen susceptibility, deformation and fracture 2−74862
ThO_2 powder compacts, desintering 2−50898
$(ThO_2)_{1-x}(YO_{1.5})_x$ solid soln., electronic contrib. to mixed conductivity 2−75100
$ThOs_2$-$ThIr_2$ system, comp. range of stability C15 phase 2−50976
$ThPbV_2O_8$, crystal growth, from the flux systems PbO-V_2O_5 and Bi_2O_3-V_2O_5 2−50589
$ThSiO_4$:M^{3+} (M=Er, Yb, Gd), e.s.r. spectra 2−48278
$ThSiO_4$, lattice constants 2−43590
$ThSiO_4$, X-ray powder study of crystal structure 2−68008
ThU, supercond. transition temp., 0-20 kbar press. 2−47870
$Th_{1-x}U_xO_2$, thermal diffusivity, 650-2700K 2−54082
UO_2-ThO_2, solid solution, non-stoichiometric, thermodynamic props., e.m.f. obs. 2−64782

Thulium
photoabsorption spectra in vicinity of 3d edges 2−76988
Tm^{3+}, spectra in phosphate and borate glasses, emission and absorpt., cryst. field effects, luminesc. 2−75307
X-ray emission spectra, h.f. satellite obs. 2−83190
$CaSO_4$:Tm thermoluminescent dosimeter construction and characts. 2−55923
Fe: ^{169}Tm, hyperfine field at Tm temp. depend. from perturbed angular correl. expts., 4.2-450K 2−81252
Tm:Cr:$YAlO_3$, laser, four-level operation at 2.35 microns 2−42075
Tm, Er, Ho, Yb:YAG laser, recirculating liquid N_2 system for cooling 2−63339
Tm, I, $4f^{13}5d6s$ and $4f^{12}6s^26p$ config., theory 2−56104
Tm II, electronic configurations $4f^{12}(5d+6s)^2+4f^{13}6p$ 2−46442
Tm^{2+}, in CaF_2, mechanisms effecting optical spectra of $4f^{13}$ ions 2−61625
Tm^{2+}, in SrF_6, crystal field splitting and g values within $(TmF_8)^{6-}$ cluster framework 2−78054
Tm^{3+}, electronic shielding in crysts., variational and outward integration calc. 2−81319
Tm^{3+}, splitting of $p_{3/2}$ core levels in thulium ethyl sulphate due to crystal field 2−44318
Tm^{n+}, n=2,3, calc. of analytical SCF wave functions for ground and excited states, free-ion energy levels, spin-orbit coupling consts. 2−46444
^{169}Tm atom, K-shell perturbations caused by static nuclear quadrupole moment 2−42738

Thulium compounds
ethyl sulphate, spin-lattice relax. of rare earth ions 2−78051
orthoferrite, Faraday effect, periodic stripe structure 2−54384
Tm-Ag alloy, h.f. n.m.r. at 4.2 degrees K 2−72518
$TmAl_2$, h.f. n.m.r. at 4.2 degrees K 2−72518
Tm_3Al_2, n.m.r. and Mossbauer spectra, quadrupole coupling, EFG tensor 2−48155
TmAs, h.f. n.m.r. at 4.2 degrees K 2−72518
$TmAsO_4$, Jahn Teller induced phase transitions, phonon excitations Raman scatt. 2−54436
TmBi, h.f. n.m.r. at 4.2 degrees K 2−72518
$TmFeO_3$, orthoferrite, domain struct., effect on mag. field 2−57306
$TmFeO_3$, spin reorientation, n.m.r. study 2−44460
TmGa, mag. props. 2−48079
$TmNi_3$, mag. struct. 2−48080
TmNiAl, mag. props., metamagnetism 2−72162
TmP, h.f. n.m.r. at 4.2 degrees K 2−72518
$TmRh_2$, h.f. n.m.r. at 4.2 degrees K 2−72518
$Tm_2(SO_4)_3.8H_2O$, heat capacity 0.08-20K, exchange induced magnetiz. obs. 2−64857
TmSb, anisotropic magnetiz. and ideal crystal field only behaviour 2−65127
TmSb, cryst. field effects in mag. form factor 2−81254
TmSb, h.f. n.m.r. at 4.2 degrees K 2−72518
$Tm_2Si_2O_7$, press. effect on $\beta \rightarrow \alpha$ transform. 2−71698
$TmSn_3$, h.f. n.m.r. at 4.2 degrees K 2−72518
TmTe, press. induced electronic collapse and struct. changes 2−68297
$TmTe_{3-x}S_x$ solid solns., high temp. homogeneity regions 2−53905
$TmVO_4$, cooperative Jahn-Teller distorsions 2−43926
$TmVO_4$, Jahn-Teller induced magnon sidebands 2−81377
$TmVO_4$, Jahn Teller induced phase transitions, phonon excitations 2−54436
$TmVO_4$, optical obs. spectrum obs. of cooperative Jahn-Teller transition 2−65269

Thunderstorms
see also Lightning
acoustics of thunder, phenomenological model obs. using computer 2−44741
activity variations rel. to 11-year solar cycle 2−65961

Thunderstorms continued
  airflow in weak echo regions, obs. using slowfall chaff 2−75565
  Alberta hailstorms, aircraft seeding using pyrotechnic flare system 2−65746
  convective, total liquid water mass estimation using digitized photographic data from 3 cm radar 2−75562
  convective, wind gradient obs. using Doppler radar 2−75560
  cumulonimbus anvil growth data rel. to thunderstorm circulation and severe local storms 2−84846
  electric field in ionosphere and magnetosphere due to thundercloud, calc. 2−62347
  electricity electrical shielding layer around charged clouds 2−84812
  e.m. fields, information about ore objects 2−72647
  flow round a storm, study of flow past smooth and rough cylinders as model 2−62185
  gravity waves from tropospheric winds, jet streams, weather fronts and thunderstorms 2−57955
  internal structure, non-tornadic, radar and radiosonde obs. 2−75567
  international lightning counter, construction, aims and results 2−62280
  lightning discharge mechanism and cylindrical cloud charge model 2−72807
  lightning triggering by small rockets 2−65792
  lower stratospheric water vapour concentrations, due to storms 2−54826
  northeastern Colorado, radar climatology 2−65702
  organized updrafts at thunderstorm bases, hail sizes 2−65748
  precipitation efficiency in high plains 2−62176
  radar echo distributions rel. to Arizona summer thunderstorm regime 2−65700
  rainfall events in convective storms, Z-R relationship for radar estimates 2−75571
  recorder for storms within a 200 km. radius 2−65710
  severe, detection and prediction using digital radar data 2−75564
  severe, high reflectivity cores, Doppler radar obs. 2−75559
  severe, locating organized updrafts 2−48483
  severe storms, digital radar data applics. 2−75495
  tornadic, morphology, surface, upper air and radar data 2−75568
  tropical, broad and extensive cloud band connections, autumnal build-up of planetary circulation 2−44725
  tropical, electric field, precipitation current, rainfall and wind obs. 2−65784
  ^{222}Rn daughter ions, numerical study of diffusion 2−62184

Thyratrons *see Gas-discharge tubes*

Tides *see Atmosphere/movements; Ionosphere; Oceanography*

Time interval measurement
  between consecutive detected photons, light coherence obs. 2−49337
  device for det. fluorescence lifetimes based on phase-shift technique 2−55366
  frequency and time measurement and standards, report 2−76158
  microwave correlometer for fast processes 2−55364
  microwave correlometer for precision meas. of time intervals having resolution of fractions of nanoseconds 2−55365
  nuclear timing system calibration using ^{85}Rb and ^{237}Np level halflives 2−79750
  pulse generator with exponentially decreasing repetition rate suitable for time marking 2−55640
  single photon detection, lunar laser ranging experiment 2−48973

Time measurement
  astronomy, universal and ephemeris time 2−62431
  atomic frequency standards, physical basis, H maser, Cs beam and Rb gas cell considered 2−41453
  atomic unit adoption 2−55363
  automated collection and processing system for controlling master clock system 2−78751
  clock comparison by Loran-C signals 2−45217
  frequency and time measurement and standards, report 2−76158
  historical survey over 5000 years 2−45218
  instantaneous and finite-duration pulses, influence on oscillations of time-measuring mechanisms 2−73284
  international atomic time scale 2−78750
  laser frequency meas., speed of light 2−78758
  optical frequency 2−69997
  optical frequency of 633 nm laser line, and speed of light 2−58694
  oscilloscope with digital counter, measurement of complex waveforms 2−45216
  picosecond light pulse duration, produced by mode-locked pulsed and c.w. lasers 2−76470
  remote clock synchronization using CS beam portable clocks, Loran-C transmissions and network TV broadcasts 2−55367
  review of methods used in past and up to present day 2−62963
  scintillation counter, using pulse height analyzer 2−49685
  standard time scales and frequency standard synchronization by meteoric reflection of radio waves 2−58693
  standards, time and frequency, tutorial introduction 2−76159
  two laser mixing and direct frequency meas. using m.i.m. point-contact diodes 2−45757
  unified time-frequency-length standard using constancy of speed of light and optical frequencies 2−63370
  Cs atomic time scales, generation dissemination stability and accuracy 2−78749
  He-Ne laser frequency measurement rel. to speed of light determination 2−48974

Tin
  amorphous state, Hall effect 2−75048
  atom, inner-shell ioniz. cross sections calc. 2−52936
  atom, K X-rays produced by heavy ions, energy shifts and relative intensities 2−64013
  atom, natural radiative lifetimes of $5p6s^1P_1$, $5p6s^3P_{1,2}$ and $5p5d^3D_{1,2,3}$ levels by zero field level crossing spectroscopy 2−70592
  covalent-metallic phase transition under pressure 2−83886
  density changes of solid and molten state at elevated temps. 2−64699
  diffusion, in GaAs, effect of mask edges 2−54205
  diffusion in GaAs for N^+ layer formation 2−71515
  diffusion of Hg, obs. and mechanism 2−68054
  diffusion width of wide-angle grain boundaries 2−47469
  dislocation generation at single crystal surface, X-ray obs. 2−47083
  elastic and plastic anisotropy 2−80726

Tin continued
  elastic consts., third-order, u.s. vel. obs. 2−50727
  elastic stiffness constants, room temp. to m.p., u.s. determ. 2−74822
  electron backscattering, spectral ang. distrib. meas. 2−84218
  EuS:Sn, nonmag. impurity effects, first and second neighbour exchange 2−65138
  film, cylindrical, supercurrent stability 2−47850
  film, deposition on NaCl, island density 2−43480
  film, Josephson effect 2−61248
  film, quantum oscill. amplitude, temp. depend. 2−71838
  film, quantum size effect and supercond. crit. temp., oscillatory depend. on thickness 2−57164
  film, significance of electric field on growth 2−60634
  film, supercond., nonlinear flux flow resistivity 2−47849
  film, supercond. transition temp. change due to noble gas adsorption 2−47856
  film, supercond. transition temp. depression by noble gas overlayers 2−61228
  film, vapour deposited, growth, nucleation rel. to thickness and substrate temp. 2−77512
  film on quartz, heat transport, phonon emission, low temp. 2−54084
  finely dispersed, supercond. crit. temp., particle size and oxidation effects 2−61230
  impurity, in $Bi_{88}Sb_{12}$, effect on mag. susceptibility 2−72109
  ingot, unidirectional solidification, uniaxed crystal origin 2−74882
  i.r. spectroscopy appl. 2−82589
  Josephson junction, microwave- induced constant voltage steps 2−71878
  liquid, diffusion of Tl 2−46945
  liquid, optical consts. 2−43359
  liquid, struct. factor, X-ray diffr. apparatus 2−74516
  liquid, struct. factor rel. to entropy of melting 2−64434
  liquid, u.s. velocity, theory and expt. 2−80469
  melt spreading over Ge surface 2−67814
  phase transform., determ. of thermodynamics by obs. of Pb-Sn alloy 2−50950
  phonon excitation spectra, junc. tunnelling obs., effects of material props. 2−68360
  skin effect, anamolous, d.c. cond., m.f.p., reflectivity factor 2−68341
  solution with Fe, Ni and Co, thermoelec. power 2−71227
  specific heat below 30 K 2−68249
  spectral analysis by X-rays, reduction of matrix influences by means of braking continuum 2−51484
  stopping power for 25-250 keV H ions 2−47774
  superconducting, current-carrying one-dimens., instabilities in transition curve 2−44079
  superconducting, effect of strain on u.s., attenuation 2−51106
  superconducting, phonon generation 2−47735
  superconducting bridge, superimposed with ferromag. Ni 2−54154
  superconducting cylinders, a.c. behaviour in transition region 2−44080
  superconducting film, mag. flux penetration 2−71871
  superconducting film, noise props., r.f. generation 2−68348
  superconducting fine particles, mag. susceptibility, temp. depend. 2−71852
  superconducting microbridge, transition from bulk like behaviour to Josephson junction like behaviour 2−64951
  surface tension, 215°C 2−56577
  thermal conductivity, above and below melting point, laser pulse technique 2−54041
  u.s. shear wave, circularly polarized, attenuation and vel. in magnetic field 2−47789
  whisker, deform. twinning, nucleation and propag. stresses 2−47424
  whisker, mech. twinning rel. to supercond. behaviour 2−47869
  white, Fermi surface cross sections stress derivatives 2−75033
  Bi:Sn, magnetoacoustic oscillations, with mag. field orthogonal to sound propagation 2−71738
  Bi-Sn, magnetoacoustic oscills. with mag. field orthogonal to sound propag. direct., fields to 100 kG 2−84203
  $Bi_{1-x}Sb_x$:Sn, elec. props., (x=0-0.2), 180-420K 2−61301
  in Fe-1%C alloy, effect on tempering stages 2−50796
  GaP:Sn, strain-depend. e.p.r. and spin-valley coupling of donors 2−84570
  Ni:Sn, plastically deformed, deviations from Matthiesen's rule 2−71837
  Sn-Pd sols, Mossbauer meas. in which core and stabilizing double layer distinguished 2−80491
  α-Sn, electron irrad., atomic displacement process evidence 2−53722
  α-Sn, electron irrad., damage production and thermal annealing, resist. study 2−80682
  Sn, superconducting point contacts, static and microwave properties 2−81054
  Sn I, multipole radiation excitation 2−46441
  Sn VI, e.u.v. spectra, energy levels 2−64001
  Sn(II) materials, lattice contribution to electric field gradient 2−65206
  $TlInSe_2$:Cu,Sn, cryst. and film, forbidden band width, elec. and photoelec., props. 2−57197

Tin compounds
  alloy, dilute, ^{119}Sn nuclei vibrations, Mossbauer obs. 2−71721
  bronze, ancient, rapid non-destructive analysis by X-ray fluorescence 2−44505
  bronze powder, spherical particles, sintering kinetics 2−43890
  halides, electronegativity correlations with ^{119}Sn Mossbauer shift 2−44360
  halides, Mulliken electronegativities rel. to ^{119}Sn Mossbauer shifts 2−44359
  Nb-Sn alloys, vacuum deposited, superconducting characteristics 2−68365
  solder, k-shell differential cross sections, effective atomic numbers 2−54439
  stress corrosion cracking, capillary model, test using pressure effects 2−74857
  tetraphenyl tin, defect struct. determ. 2−53731
  Ag-Sn alloys, stacking faults, X-ray diffr. data interpret. 2−50678
  Ag-Sn melt, electrotransport, current density effects 2−50348

Tin compounds continued
- Au-Sn alloy, Mossbauer oscills 2−51308
- Au-Sn solid solns., dil., correl. factor and self-diffusion 2−64693
- Bi-Sn-Zn system, activity coeffs., calc 2−43827
- Bi-Sn alloy, thermal expansion meas. in room temp.-100°C range, applicability of rule of mixtures 2−60975
- Bi-Sn induced high press. phases, X-ray and specific volume studies 2−74926
- Cd-Sn-Zn system, activity coeffs., calc. 2−43827
- $CeSn_3$ alloy, absence of magnetic ordering, n.m.r. obs. 2−84588
- Cu-Sn alloy, γ phase decomposition at lower temps. 2−71679
- Cu-Sn alloy, liquid, density, max. bubble pressure method 2−56488
- Cu-Sn alloys, α-phase, low temp. electronic sp. ht. 2−43982
- Cu-Sn alloys, liq., optical consts. 2−43359
- Cu-Sn alloys, martensitic transform., interphase boundary shifting 2−43910
- Cu-Sn alloys, unidirectionally solidified, columnar dendrite structure 2−74641
- Cu-Sn system, electrodeposited, phase diagram 2−84085
- Cu_x-Sn_{1-x} alloy, resistivity and thermopower computation, comparison with exptl. data 2−43387
- Cu(15.1 at.%)Sn alloy, β_1 phase stabilization mechanism47684 2−47684
- Cu_6Sn_5 fibres, brittle fracture surface morphologies 2−80744
- Fe-Sn-C system, formation and stability range of ternary cpds. 2−43933
- Fe-Sn system, phase boundaries of γ-loop 2−47712
- Ga-In-Sn alloy, field ion microscope obs. of liquid-solid interface in vacuum 2−67900
- GaAs-Sn quasi-binary system, phase diagram 2−43934
- GeTe-SnTe alloy, epitaxial film, twinning faults 2−53574
- Hg-Sn amalgam, dil., viscosity, comp. depend., 0-100°C 2−64451
- In-Sn alloy, Seebeck coeff., comp. depend., 100°C 2−81162
- In-Sn alloy, surface tension and density, comp. depend., 700K 2−67815
- Mg_2Sn pressure dependence of electrical resistance 2−84326
- MnSb-(Sb,Sn) eutectic, morphology, growth rate effects 2−47641
- Na-Sn dilute alloy, liq., compressibility determ. 2−77415
- Nb-Sn sinter material, supercond., screening behaviour on addition of Cu, Ag or Au 2−75061
- Nb_3Sn, vapour deposited supercond., crit. current, effect of impurity gas additions 2−51109
- Pb-Bi-Sn eutectic, superplasticity 2−80839
- Pb-Sb(8 to 17%) alloy, influence of annealing temp. on thermal expansion 43995 2−43995
- Pb-Sn alloy, dependence of γ ang. correlation of positron annihilation on composition 2−71766
- Pb-Sn alloy, superplastically deformed, const. stress creep and strain rate tensile tests 2−47504
- Pb-Sn liquid alloy, surface tension, max. bubble pressure method 2−53409
- $Pb_{1-x}Sn_xTe$, epitaxial growth from soln., surface quality improvement 2−60656
- n-$Pb_{1-x}Sn_xTe$, hot-electron cond., velocity-field characts., 77 and 4.2K 2−68407
- $Pb_{1-x}Sn_xTe$, i.r. plasma refl. study 2−84504
- $Pb_{1-x}Sn_xTe$, reflectivity, optical consts., energy band struct. 2−48164
- Sb-Sn-Zn system, heats of mixing, 650°C 2−43336
- Sm-Sn system, relative stability of intermetallics 2−47573
- Sn-Ag alloy, impurity scatt., electron lifetimes, Fermi surface, de Haas-van Alphen meas. 2−61148
- Sn-Ag alloy, liq., determ. of interdiffusion coeffs. 2−53415
- Sn-Ag alloys, liq., interdiffusion coeffs. 2−50349
- Sn-Bi-As system, Sn_4As_3-Bi-SnAs subsystem, phase equilib. 2−74942
- Sn-Cd dilute alloy, lattice thermal cond. and Matthiessen's rule deviations 2−84295
- Sn-Cu alloy, electrolytically deposited on steel 08kp, transition layer 2−47683
- Sn-Ga, liquid binary alloys, absolute thermoelectromotive force 2−56518
- Sn-Ge-Se-As glass, Mossbauer effect, isomeric shift, quadrupole splitting, phase diagram 2−75267
- Sn-Ge, saturated melt spreading over Ge surface 2−67814
- Sn-Ge alloy, Shubnikov-de Haas oscills. rel. to carrier heating in cond. band 2−81080
- Sn-In dil. alloy, third-order elastic consts., u.s. vel. obs. 2−50727
- Sn-In superconducting alloys, flux-trapping, structural sensitivity 2−54152
- Sn-In superconducting microbridge, transition from bulk like behaviour to Josephson junction like behaviour 2−64951
- Sn-Mg alloy, liquid, elec. resist., Faber-Ziman theory, partial interference functions 2−83799
- Sn-Mn alloy film, mag. state of Mn rel. to supercond. 2−68512
- Sn-Na liquid solution, thermodynamic props., e.m.f. cell obs. 2−71184
- Sn-Pb-Cd alloy, eutectic morphology, unidirectional solidification microstruct. 2−74895
- Sn-Pb-In ternary alloy superconducting wire, magnetic properties, flux flow voltages 2−81037
- Sn-Pb alloy, diffusion of Ag 2−56763
- Sn-Pb alloy, rapid detn. of Sb, Pb, Sn and Cu by atomic absorp. spectroscopy 2−78218
- Sn-Pb alloy, solder, interaction with NO_2, corrosion, humidity effects 2−65382
- Sn-Pb alloy, thermodynamics of melting, determ. of thermodynamics of Sn phase transform. 2−50950
- Sn-Pb alloy stainless steel fibre reinforced, fracture behaviour 2−50921
- Sn-Pb eutectic alloy reinforced by stainless steel fibres, tensile strength 2−77742
- Sn-Pb(Zn, Sb) alloys, unidirectional solidification, uniaxed crystal origin 2−74882
- Sn-Sb alloy, liq., determ. of interdiffusion coeffs. 2−53415
- Sn-Sb alloy, peritectic crystn., pore form. 2−53906
- Sn-Sb alloys, liq., interdiffusion coeffs. 2−50349
- Sn-W bronze alloy, struct. 2−71441
- Sn-Zn alloy, liq., elec. resist. at 500°C 2−60507

Tin compounds continued
- $SnCl_4$ + K reaction, dependence of reactivity on internal and translational energy 2−75374
- $SnCl_2.2H_2O$ and $2D_2O$, anomalous behaviour of sp ht at phase transition 2−84212
- $SnCr_3N$, crystallographic parameters and struct. transforms. 2−60759
- SnD, multiplet struct. and centrifugal distortions, rot. energy levels 2−79991
- SnF, rotational structure and isotopic shift in (1,0) band of (A−X) system 2−77093
- SnF_2, cryst. growth from soln., and phys. props. 2−47245
- SnH, multiplet struct. and centrifugal distortions, rot. energy levels 2−79991
- SnH_4, solid, proton spin-lattice relax., phase transition obs. 2−48116
- $Sn^{181}HfO_3$, perovskite-type, nucl. quadrupole interactions, perturbed-angular-correlation meas. 2−72244
- SnI emission band spectrum, isotope effect 2−53037
- SnI_4, saturation solubility in benzene- cyclohexane mixtures 2−43333
- $SnMo_5S_6$, superconducting properties, heat capacity Debye temp. 2−81051
- SnO_2:Ni, e.p.r. of Fe^{3+} centre 2−84564
- SnO_2/In_2O_3 film, transparent electrode for CdS 2−54209
- SnO_2-SbSI, dielec.semicond. junc., memory and switching effects 2−61366
- SnO_2-TiO_2 mixed crystals, exsolution obs. 2−74746
- SnO_2-TiO_2 solid soln., extent of miscibility gap region 2−77732
- SnO_2-TiO_2 system, two-phase region studies 2−50974
- SnO_2, band struct. calcs. using KKR method 2−54189
- SnO_2, e.p.r. and ENDOR meas. on Cr^{3+} and Fe^{3+} 2−48309
- Sn_2PO_4Cl, lattice parameters, space group, powder data 2−43588
- SnS_2-Na_2S system phases, crystallographic parameters 2−83952
- SnS_2, a.c. conductivity meas., −100°C to 120°C 2−84290
- SnS_2, band struct., pseudopotential calc. 2−44116
- SnSSe, vapour transport method 2−67937
- $SnS_2(Se_2)$, cryst. growth and photocond. 2−67937
- $SnS_2(Se_2)$, nearly perfect crysts., prep. and X-ray obs. 2−50577
- SnS_xSe_{2-x}, (x=0-1), cryst. growth by vapour transport 2−50577
- SnS(Se)(Te), refl., 1-12.5 eV, rel. to band struct. calc. 2−48161
- SnSe film, epitaxial on KCl, boundary struct., rotational Moire method obs. 2−74635
- SnTe-GeTe alloys, retaining metastable phases by quenching under pressure 2−84152
- SnTe-UTe system, phase diagram 2−47717
- SnTe, amorphous and cryst., Raman spectra 2−68665
- SnTe, efficiency criterion for thermogenerators 2−75158
- SnTe, Fermi surface, de Haas-van Alphen and Shubnikov-de Haas study 2−68420
- SnTe, Mossbauer effect, oxidation and chem. stability obs. 2−44485
- SnTe, optical props., refl. meas., Kramers-Kronig analysis 2−48165
- SnTe, retaining metastable phases by quenching under pressure 2−84152
- SnTe film, epitaxial, carrier conc. and mobility, effect of atomic H 2−54179
- SnTe polycrystalline film, elec. props., temp. depend. 2−71916
- V-Sn alloy, struct. and props., comp. depend. 2−53912
- Yb-Sn system, relative stability of intermetallics 2−47573
- Zn-Sn-Cd-Bi liquid quaternary solution, thermodynamic props., e.m.f. method 2−71186
- Zr-Sn alloys, solute strengthening at high temps. 2−50846

Titanium
- − 2−72272
- adsorbed on Ni, surface band struct., X-ray appearance pot. obs. 2−47816
- adsorption of Cs, ellipsometry, Auger spectra and surface pot. difference obs. 2−50550
- alloy, etching behaviour 2−50687
- alpha and beta phase stabilizers, segregation 2−64807
- anodic oxide film formed on Ti, effect of formation electrolyte on no. of imperfections 2−50518
- atomic mass determination for all stable isotopes 2−46470
- centres, induced in X-ray irrad. borate glasses, e.p.r. spectra 2−44450
- crystal growth, phase transform. technique 2−77526
- deformation kinetics for {1010}{1120} slip in single crystals below 0.4 T_m 2−64720
- diffusion mechanism in β-modification 2−68044
- diffusion of H, quantum interpret. 2−71537
- diffusional saturation with O_2, residual stresses introduced 2−56949
- dislocation struct. rel. to strength 2−56714
- dispersive particles, in coaxial high-temp. jet radiation, energy losses 2−80497
- doping of diamond, elec. resistivity obs. 2−68396
- dynamic mechanical behaviour in shear meas. using torsion apparatus 2−53797
- dynamic strengthening singularities under infl. of shock waves 2−84075
- electrical and thermal cond., 20 to 1200°C 2−47769
- energy level structure, excited particle velocity spectrum on Ar-ion bombardment 2−48030
- fatigue using high power ultrasonics 2−50794
- film, maximum sorption capacities and gettering action 2−43495
- flow stress, thermal and athermal components in zone refined sample 2−56798
- in fluorophlogopite, e.p.r. and optical absorption spectra, levels of Ti^{2+} and Ti^{3+} ions 2−84562
- in glass, resolution of ^{47}Ti and ^{49}Ti hyperfine lines 2−84571
- grain size distribution, recrystallized α-phase 2−56898
- ion-getter pump, investigation of ^3H contamination in neutron generator 2−58662
- ligand hyperfine interaction of Ti^{2+} in CdS and CdSe on sites with trigonal symmetry C_{3v} 2−80977
- p-i-n junction anodic film on Ti 2−47138
- phonon dispersion, Debye temp., noncentral force model 2−80887
- pitting, intergranular corrosion and stress corrosion cracking, significance of protection potential 2−68787
- r-value variation with increasing strain 2−41584

Titanium continued
single crystal and polycrystalline, optical constants as function of temp. 2—44341
sorbed gases, photoemission energy level meas. of sorbed gases 2—47166
sputter ion pumps, influence of asymmetry of magnetic and electric fields 2—62899
in steel, rel. to retarding recrystn. during thermomech. treatment at high temp. 2—60961
stopping power for 0.50-1.75 MeV protons meas. by backscattering method 2—64872
stress relaxation, validity of modified Gilman's equation 2—80832
sublimation as pump in high-speed economical ultrahigh vac. chamber 2—69507
surface adsorption of ^{19}F, time depend curve 2—83877
surface film, formation in water and methanol solns., ellipsometric-electrochemical cell obs. 2—50510
X-ray absorption, K-spectrum 2—44401
X-ray Kα and Kβ spectra, excited by protons, α-particles and O ions 2—57368
X-ray spectra, α- and proton-induced de-excitation 2—57367
X-ray spectra, K- and L-emission and K-absorp. 2—48195
Al-9.5 wt.%Mg:Ti alloy, mech. props., fracture toughness, cracking effect of alloy in additions 2—47546
α-Al_2O_3:Fe, α-Al_2O_3, Ti and α-Al_2O_3(Fe,Ti), polarized and high resolution UV, visible and IR spectra, e.s.r. spectra 2—78082
Fe/Ti diffusion couples, atomic mobility in Kirkendall plane 2—53763
MnZn ferrites, influence of Ti ions on magnetic properties 2—84405
Nb + Zr + Ti and Nb + Ti alloys, properties of welded joints 2—61227
in Ni_3Al, effect on hardness 2—43740
O_2 content, spectrochemical determination, effect of heat 2—72590
Ti/Al chem. diffusion couple, Al_3Ti growth and solubility limits 2—53757
Ti/Fe abundance ratio in A-type supergiant stars 2—62537
Ti-Gd alloy, thermal conductivity and electrical resistivity 2—64866
Ti-Nb-Zr alloy, Cu cladding bimetallic wire, solenoid, strong pulsed magnetic field 2—63255
α-Ti, cyclic work softening 2—80835
Ti, electron scattering mechanisms at high temps. rel. to kinetic properties 2—81035
α-Ti, hydride precip., resistometric obs. 2—64813
β-Ti, solubility of H_2, Sieverts meas. 2—74909
α:Ti, torsional and longitudinal plastic waves 2—77638
α-Ti, ultra-fast diffusion of ^{63}Ni 2—64697
Ti bioimplant interfaces, biological aspects 2—69293
Ti I, Ti II, oscillator strength obs. 2—56103
Ti II lines, variations in Ap star 108 Aqr 2—58317
Ti in LiF impurity distrib. effect on thermoluminescence 2—84552
Ti^{3+}, in AgCl and AgBr, charge transfer spectra 2—51333
Ti^{3+}, in Al_2O_3, corundum, e.p.r. g-value calc., Jahn-Teller theory 2—65331
Ti^{3+} in $[Al(ha)_6]Br$, luminesc., $^2E \rightarrow {}^2T_2$ transition mechanism 2—65302
Ti^{3+} in lunar plagioclases, e.p.r. obs. 2—62686
Ti(Pd)Ag passivated contacts, use with Si solar cells 2—59057

Titanium compounds
β—phase content of alloys, electrochemical and X-ray diffraction methods 2—77669
β Ti-V alloys, thermal etching and dislocations 2—80546
alloy, ω phase struct. symmetry 2—47349
alloy, b.c.c., struct. and decomp. 2—68204
alloy, b.c.c., superplasticity 2—50745
alloy, elec. resist., exponential temp. depend. 2—54129
alloy, foil prep., for electron microscopy, electrolytic jet thinning procedures 2—71415
alloy, gas saturation, effect on microstruct. and hardness 2—53909
alloy, grain boundary etching, grain surface etching 2—50686
alloy, martensitic transform., under isothermal conditions 2—43927
alloy, martensitic transforms., Burgers and Bogers-Burgers mechanisms 2—68182
alloy, orthorhombic martensites 2—71697
alloy, T-A6V6E2, struct. hardening, work hardening effects 2—60963
alloy OT4, influence of hydrogen on fracture structure 2—60888
alloys, plastic deformation peculiarities in planar stress state 2—43698
alloys, standard samples for spectrochemical determination of H_2 2—72592
anatase, molecular charge distribs. K X-ray emission obs. 2—67930
binary alloy, H_2 solubility, alloying elements effect, Sieverts meas. 2—74909
Co-Ni-Cr-Ti alloy, quench-ageing behaviour, 700-900°C 2—68138
$Fe_{36}Cr_{22-x}Ti_x$, χ-phase alloy, $8 < x < 10$, inversion domain obs. 2—64637
hydrides, ternary and binary, temp. and freq. depend. of proton spin relax. 2—78052
Mo-Ti(0.5%) alloy, transmission e. microscopy obs. of void superlattice after n. irradiation 2—64667
nimonic alloy, ageing, solid sln. decomp. and volume change 2—50805
refractories, atomic interactions 2—48206
rutile, molecular charge distribs. K X-ray emission obs. 2—67930
rutile, point defect effects on dielec. props. 2—61412
Ti alloy VT14, phase transf. during heating and cooling 2—68201
Ti-Mo binary alloys, phase separation processes in beta phase during aging 2—80816
titania, room-temp. strengths for various biaxial stress states 2—77677
titanomagnetite bearing rocks, piezomagnetic effects 2—68857
tritide film, ageing, bubble form. and rupture 2—43478
6Al-4V-Ti, surface embrittlement charact. during diffusion bonding 2—68160
$(Al,Ti)(ur)_6X_3$, X=Cl, Br, I, low-temp. polarized absorption spectra, determ. of cubic and trigonal parameters 2—51289
Al_2O_3-TiO_2 ceramic, sprayed layers, thermal. cond. 2—44000
Au-Ti dil. alloys, weak resist. minimum 2—44052
Au-Ti dilute alloys, deviation from Matthiessen's rule, 0.5-60 K 2—77854

Titanium compounds continued
Baf$_2$-TiO_2 system, $baTi_{1-x}{}^{4+}Ti_x{}^{3+}O_{3-x}F_x$ formation and props. 2—47705
CaO-Nb_2O_5-TiO_2-SiO_2 system, liquidus temps. 2—43436
Co-Ni-Ti system, decomp. and formation of modulated struct. in coherent phase zone of stability 2—57030
Co-Ti alloy, solid soln. decomp. 2—56933
Cr-Ti compounds phase transformations 2—80798
Cr_2O_3-TiO_2 system, rutile struct. solid soln., interdiffusion and solubility limits 2—47618
Cr_2O_3-Ti_2O_3 solid solution, mag. ordering, diffr. and e.s.r. obs. 2—48104
Cu-Be-Ag and Cu-Be-Ti, decomposition of solid solns., phase transformations 2—68194
Fe-Al-Ni-Co-Ti alloy, prod. by Magnicol process, reaction mechanisms 2—43834
Fe-Co(Ni)-Ti-Al alloy, solid soln. decomp. 2—56933
Fe-Mn-Ti alloys, ferritic and martensitic, hardening 2—47592
Fe-Ti-Si alloy, age hardening, precipitation and yield stress 2—43806
β-Fe-Ti alloy, diffusion of Fe, Mossbauer study 2—77612
$Fe_{1-x}Ti_{1+x}$, magnetization and sp. ht., rel. to resist. minimum 2—44252
Ge-Ti-O system, noncrystalline film prep. by sputtering 2—47114
Mn-Fe-Ti-O system ferrites, mag. props. and crystallochem. 2—44254
$Mn_{0.8}Ti_{0.2}Bi$ film, Curie-temp. writing 2—78032
Na_2O-TiO_2-SiO_2 glasses press. and temp. depend. of elastic moduli, ultrasonic interferom. meas. 2—80741
Nb-40% Ti alloy, supercond., mag. irreversibility and microstruct. 2—47855
Nb-Ti alloy, mag. instabilities 2—64948
Nb-Ti and Nb-Ti-Zr alloys, supercond. wire, crit. current, mag. field intensity depend. 2—75062
Nb-Zr-Ti alloy, supercond., struct. determ. 2—50842
NbTi filaments of round composite superconductors, anisotropy of critical current density 2—71870
$Nb_{0.88}Ti_{0.12}N$ film, fluctuation broadening of supercond. transition 2—71850
Nb + Ti alloy, multiple-strand composition superconductor 2—64955
Ni-Cr-Ti alloys, strengthening by precip. of intermetallic phases 2—43859
Ni-(46 wt.%) Ti alloy, martensite phase form., plastic deform. influence 2—43863
NiTi, non-stoichiometric, elec. resist., comp. and temp. depend. 2—74885
SnO_2-TiO_2 system, two-phase region studies 2—50974
TZM alloy, arc casted, props. and applications 2—53825
Ti-Al-Cu-Fe-Co-Ni, alloy, YuNDK42T8, homogenizing rel. to phase comp., mech. and mag. props. 2—47688
Ti-Al-Cu-Mg-Mn-Fe-Si-Ni-Zr alloy, D16T, recryst. and uncryst. struct., fracture under static and cyclic conditions 2—47527
Ti-Al-Mo-Zr alloy, ductility, influence of β-phase 2—50746
Ti-Al-V alloy, mill-annealed, fatigue crack growth, temp. effects 2—60904
Ti-Al-V brazed foils, scanning e. microscope metallographic study 2—68158
Ti-Al alloy, cold-worked, X-ray diffr. study 2—80860
Ti-Au film conductor stripes, electromigration damage rel. to pulsed d.c. powering 2—80940
Ti-C-N-O solid soln., phase diagram, form. of carbonitrides and oxycarbides 2—54010
Ti-Ce-S system, struct. and phase equilib. 2—43943
Ti-Cr alloy, fracture modes, effect of ω phase 2—47547
Ti-Mo alloy, anomalous resist, rel. to microstruct. 2—84297
Ti-Mo alloy, effect of deform. rate and temp. on ductility, mech. props. and struct. 2—47503
Ti-Mo base β-alloy, ageing characs. rel. to tensile props. and microstruct. 2—50807
Ti-Nb alloy, electronic struct., X-ray spectral study 2—44402
Ti-22at.%Nb alloy, ω-phase, electron diffr. obs.53908 2—53908
Ti-Ni-Cu-Al alloy, age hardening, precip. 2—53878
Ti-Ni-Cu homogeneity range by electron microprobe X-ray analysis 2—43858
Ti-Ni-H, intermetallic phase and absorption of hydrogen 2—71354
Ti-Ni alloy, near equiatomic, shape memory effect 2—77693
Ti-O system, saturated, residual stresses 2—56949
Ti-Pt alloy, strength, oxidation resist. 2—47533
Ti-Ta alloys, martensitic, precip. reactions 2—47697
Ti-Ta alloys, martensitic transform. 2—47696
Ti-V-O and Ti-V-Al-O solid solutions, charact. temp. and elasticity modulus 2—50844
Ti-W-Mo alloy, mech. and technological props. 2—47535
Ti-W-Zr alloy, mech. and technological props. 2—47535
Ti-W alloy, mech. and technological props. 2—47535
Ti-Zr-Al-N film, sputtered, struct., elec. resist. props 2—47130
Ti-8% Al-1% Mo-1%V, accelerated stress-corrosion cracking in presence of hydrogen recombination poison 2—68107
Ti alloy, fatigue stability tests, sensitivity estimates for asymmetrical loading cycles from strain diagrams 2—56840
Ti alloys, crack growth criteria in stress corrosion cracking for thin materials 2—71600
Ti martensite, effect of Si, Zr, Al and Mo on struct. and strength 2—64723
TiB and TiB_2, Compton profiles, electron momentum distrib. 2—48211
TiB_2, electronic spectra, MOLKAO method calc. 2—71792
TiB_2, sintering kinetics, particle size effects 2—61006
TiB_2, thermionic emission, rel. to electronic struct. 2—48017
TiB_2 coatings, electrodeposition and characteriz. 2—51460
$TiBr_4$, orbital valence force field consts. 2—77075
TiC-Co alloy, oversaturated, microstruct. and reaction behaviour 2—64775
TiC-Mo_2C-Ni alloy, rupture strength and hardness rel. to microstruct. 2—47538
TiC-Nb cermet, hot pressing kinetics 2—56914
TiC-Ni-Mo alloy, cermet, hardness, bending strength, wear resist. 2—47534
TiC-TiN solid solution, band struct., optical dispersion and absorpt. study 2—51080

Titanium compounds continued
TiC-WC, short-range order, heat treatment and quenching effects 2–84072
TiC, 2-stage decoration method, for surface struct. determ. 2–80539
TiC, band struct. calc. 2–57126
TiC, changes in microhardness, lattice parameters, electrical resistance following neutron irradiation 2–52848
TiC, heterogeneous nucleation of Al, orientation relations 2–47098
TiC, hot working and strength improvement, NASA research 2–64801
TiC, X-ray absorpt., K-spectrum 2–44401
TiC_2, heats of atomization determ. by high temp. mass spectrometry 2–84623
TiC_x, chemical vapour deposition on Ta substrates 2–80597
TiC_x, work function, correl. with surface recomb. of H atoms 2–50549
$TiC_{1-x}N_x$ in Ni binder, cermet hard alloy, prep. and props. 2–53945
TiC_xO_{1-x} solid solns., low temp. heat capacity, entropy and enthalpy 2–43989
TiC_xO_y solid soln., long range order parameters from cluster model 2–74892
$TiCl_4$, orbital valence force field consts. 2–77075
TiFe, electron energy spectrum, X-ray emission study 2–75316
TiH_x, electron-nuclear interactions rel. to spin- lattice relax. 2–78047
TiI_4, orbital valence force field consts. 2–77075
TiMo, TiZrMo alloys, radiation induced transformations in h.v. electron microscope 2–80874
TiN-MgO solid soln., solid phase interaction, diffusion of Ti, 1700-2000 K 2–53907
TiN-VN particles, nitriding and annealing effects 2–68202
TiN, powder production using s.h.f. discharge 2–43896
TiN, X-ray absorpt., K-spectrum 2–44401
TiN_{1-x}, vacancy short range order, calc. 2–83966
TiN_x, microhardness and thermal expansion, 80-300K 2–61112
TiN_x, X-ray spectra and electronic struct. 2–48195
$TiNb_{24}O_{62}$, electron microscopy using n-beam lattice images 2–56669
TiNi, electron energy spectrum, X-ray emission study 2–75316
TiNi, unique property changes related to martensitic transformation 2–68200
$TiNi_{1-x}$, vacancy short range order, electron diffr. obs. 2–83965
TiO_2:Cr, γ-irradiated, a.p.r., Cr^{3+} spin- phonon coupling constants detn. 2–51408
$TiO_2:Fe^{3+}$, hole trapping by surface ferric acceptor states, Mossbauer obs. 2–84236
$TiO_2:Fe^{3+}$, substitutional and charge compensated impurity in anatase, temp. depend. 2–68730
$TiO_2:Fe^{3+}$ spin- lattice relaxation mechanism 2–81459
TiO_2:Li,V,Cr,Mn,Fe, transition metal impurity levels, esr determ. 2–44117
TiO_2-Cr_2O_3 system, solid solns. and cryst. shear struct., electron microscope obs. 2–47406
TiO_2-Cr_2O_3 system, solid solubility of $Ti_2Cr_2O_7$ 2–47719
TiO_2-Fe_2O_3 solid soln., crystallographic shear structs., planar boundaries 2–74768
TiO_2-Ga_2O_3 solid soln., crystallographic shear structs., planar boundaries 2–74768
TiO-MnO alloy, synthesis, struct., density, elec. cond., mag. susceptibility, thermal e.m.f. 2–74908
TiO_2-SiO_2-Al_2O_3-Li_2O-MgO, glass-ceramic, crystn., microstruct., indentation hardness 2–80535
TiO_2-SiO_2 glass, He migration 2–50718
TiO_2-SnO_2 mixed crystals, exsolution obs. 2–74746
TiO_2-SnO_2 solid soln., extent of miscibility gap region 2–77732
TiO, α-system, perturbations 2–50070
TiO, CNDO-II approx. SCF molecular orbital method, levels calc. 2–83252
TiO, cation self-diffusion 2–50717
TiO, Compton profiles, scatt. factors, determ. of electron state 2–68628
TiO, electronic band spectra interpret. 2–77069
TiO, electronic chemiluminescence, emission spectrum 2–77068
TiO, in M supergiants, 8 colour narrow band i.r. photometry 2–62552
TiO, ion bombarded, electron yield 2–51228
TiO, u.v. bands, vibr.-rot. consts. 2–80042
TiO, X-ray absorpt., K-spectrum 2–44401
TiO β system, Einstein coeffs. and oscillator strengths of excited levels 2–60036
TiO film, amorphous, sputtered, dielec. props. equiv. elec. cct. 2–47970
TiO in solar sunspot spectrum, 4900- 6441 Angstrom range 2–62743
TiO_2, AC Hall effect meas., polaron mass 2–57174
TiO_2, adsorption and desorption of water 2–60688
TiO_2, anatase, e.p.r., g-tensor for Ti(III), parametric obs. 2–61739
TiO_2, anatase non porous particles, photoreduction under u.v. irrad. 2–48342
TiO_2, crystal growth, from the flux systems PbO-V_2O_5 and Bi_2O_3-V_2O_5 2–50589
TiO_2, doped and undoped, frequency dependence of conductivity and adsorption of CO 2–77906
TiO_2, e.p.r. of interstitial V^{4+}, thermal treatments effects 2–61738
TiO_2, effect on grain growth during CeO_2 sintering 2–47655
TiO_2, elastic consts., temp. depend., 4-583K 2–84042
TiO_2, in m.i.m. struct., bistable and threshold switching after forming process 2–44141
TiO_2, ion impact effects on electrical conductivity 2–60779
TiO_2, recrystn. in hydrothermal fluoride solns. 2–47285
TiO_2, reduced, bound polaron hopping and mag. impurity effects 2–47902
TiO_2, rutile, brookite and anatase, X-ray absorpt., K-spectrum 2–44401
TiO_2, rutile, dissolution forms of single crystal spheres 2–47197
TiO_2, rutile, friction and wear, fund. review 2–47554
TiO_2, rutile, powder in lightly pressed tablets elec. cond., thermal e.m.f., 300-1300K 2–77821
TiO_2, rutile, temp. dependent ultrasonic attenuation for 3GHz and 9GHz waves 2–51028

Titanium compounds continued
TiO_2, sputtering, study of optimal conditions by γ-ray spectroscopy 2–45197
TiO_2 amorphous film, photocond. and photolum., room temp. 2–72068
TiO_2 and MgO coupled solute solid soln. softening of alumina 2–47653
TiO_2 effect on sintering of Al_2O_3 and MgO 2–50866
TiO_2 film, chemical vapour deposited, properties as function of processing temp. 2–50511
TiO_2 film, crystallization, by electron beam irradiation 2–47129
TiO_2 film, in m.i.m. struct., transients, capacitance variation with temp. 2–57219
TiO_2 film, sputtered and evap., optical props. as function of deposition conditions 2–48131
TiO_2 hydrosol, optical properties, turbidity and refractive index 2–74574
TiO_2 powder compact, abrupt shrinkage on sintering, SEM obs. 2–43895
TiO_2 switching and steering of surface waves by nonlinear mixing in anisotropic media 2–51005
TiO_x, positron lifetime spectra, rel. to cond. and nonstoichiometry 2–71825
TiO_x antireflective coatings for Si solar cells, effects of electron irradiation 2–59056
Ti_2O_3, X-ray absorpt., K-spectrum 2–44401
Ti_4O_7 metal-instuator transitions, charge localization, crystallographic evidence 2–44087
Ti_xO_g, molar mag. susceptibility rel. to temp., effective mag. moment, mag. parameters 2–75221
Ti_xO_y, cryst. growth, controlled stoichiometry and order 2–50570
TiS, thermal expansion, 25-1300°C, X-ray obs. 2–54062
TiS_2, band struct., semi-empirical tight binding method 2–84232
TiS_2, nearly perfect cryst., growth and X-ray obs. 2–50577
$TiSe_2$, band struct., semi-empirical tight binding method 2–84232
$TiSe_2(Te_2)$, cryst. growth by vapour transport 2–50577
$TiSi_2$, formation on Si from Ti film 2–43861
Ti_3SiC, preparation from gaseous phase, chemical and physical properties 2–53580
TiT_x, size spectrum, T contamination determ. during neutron generator target replacement 2–83155
$Ti_xTa_{1-x}S_2$ $(0.1 \leqslant x \leqslant 0.9)$ solid solutions, resistivity, magnetic susceptibility, thermoelectric power 2–61266
$TiTe_2$, Auger electron spectroscopy investig. of adsorption anisotropy 2–60687
$TiTe_2$, band struct., semi-empirical tight binding method 2–84232
Ti(13 wt.%)V-(11 wt.%)Cr-(3 wt.%)Al beta alloy, mech. prop.-fracture-microstruct. relns. 56950 2–56950
Tic, surface struct., electron diffr. obs. in ultrahigh vacuum environment 2–43469
$Tn_xMn_{1-x}O$, $0.07 \leqslant x \leqslant 0.9$, mag. props., mag. susceptibility, struct., 100-1000 K 2–54364
V-Ti alloy, scavenging of interstitials, internal friction study 2–50845
V-Ti alloy, struct. and props., comp. depend. 2–53912
$ZrSiO_4$-TiO_2 system, phase relations, 1050-1600°C 2–47722
Torquemeters *see Mechanical measurement*
Torsion
see also Elastic constants; Stress analysis
apparatus for meas. of mechanical properties of materials at high shear-strain rates 2–53821
balance, effect of convection and nonequilibrium flow on motion 2–72605
balances, relative deflection meas. in 10^{-9} rad sensitivity range 2–82184
bar, prismatic, in steady creep, bounds for stiffness 2–45421
centre of twist 2–45340
circular cylinder containing symmetric array of edge cracks, analysis under torsion 2–66538
cracks, circular, propagation for tension and torsion 2–60900
cracks subjected to, stress intensity factor evaluation, numerical technique 2–66504
cylinder whose section is sector of a circle 2–45387
cylindrical shell, optimization of torsional stiffness 2–73352
cylindrical shell, twisted, composite, cylindrically aeolotropic material, torsional vibr. 2–45440
dynamical theory, rods, deduced from equations of linear elasticity 2–45397
elastic bar, optimal nonhomogeneity, optimal problem of torsion 2–45353
elastic-plastic, circular bars with variable diameter 2–45418
epoxy-diamine networks, glass transition temp. determ. using torsion pendulum 2–71287
finite, nearly isochoric, compressible isotropic elastic circular cylinder 2–41569
gravity meas. with noiseproof torsional system 2–76161
incompressible continuous media mechanics 2–76328
laminar composite debounded, analysis 2–50912
low-cycle, machine for testing 2–64740
metals, det. of plastic deformation at point of ultimate failure 2–56842
microhardness tester attachment for meas. of deformation of wire in coiling 2–82129
nematics, method for meas. twist elastic constant 2–50329
nylon 66, monofilament, effect of torsion on uniaxial bond rupture 2–60858
plastic, of hollow cylinder, anisotropy theory 2–47497
plate, isotropic, twisted by rigid circular stamp, mixed problem 2–45410
polyethylene oxide, mechanical damping index obs. with torsional braid analyser 2–71547
rubber cylinder, swelling 2–60875
rubber cylinder, swelling 2–60876
rubberlike slightly compressible circular cylinders, finite torsion 2–76321
shafts with elliptic inner boundaries by perturbation techniques 2–73351
steel, annealed mild, effect of upper yield stress 2–43685
torsional vibration of finite circular cylinder of non-homogeneous material by twist on one end plane 2–49099

Torsion continued
variable rectangular profile shell, influence of end plate and bulkhead 2−78876
wire testing, device for automatically plotting torsion diagrams 2−71612
Ti, dynamic mechanical behaviour in shear meas. using torsion apparatus 2−53797
Total cross-sections *see under individual particles, no subheading*
Townsend coefficient *see Ionization/gases*
Transducers
see also Acoustic generators; Acoustic receivers; Microphones; Sound reproduction
acoustic surface wave, grating array 2−49153
acoustic surface wave, hybrid junction interdigital 2−49154
acoustic surface wave filter analysis 2−49144
acoustic surface wave interdigital transducer theory 2−49140
acoustic surface wave reflections from electrodes, meas. and modeling 2−49142
acoustic surface waves, broad-band unidirectional transducer using multistrip coupler 2−49172
acoustic surface wedge waves, parametric interaction 2−66626
acoustic surface-wave filters 2−58924
acousto-optical deflector, high capacity composite 2−69753
amplitude frequency characteristics of discrete transducers, det. by subtraction circuit 2−69537
biomedical, biological and engineering constraints, applics. 2−73180
capacitative, for meas. of weak acoustic waves 2−41793
capped cylinder design of underwater transducer, USRD type F50 2−41755
ceramic, under mechanical load, meas. of clamped capacitance and electromechanical coupling coeffs. 2−52241
cermets and Ta films strain gauge factor study 2−77710
conducting polymer as fatigue damage indicator 2−53971
contactless vacuum thermal, for pressure obs. 2−58695
design, effect of ferroelectric nonlinearities 2−49156
dielectric, generation of ultrasound 2−55535
diffraction losses between input and output 2−49145
Doppler flow, for detection of bubbles in blood 2−66277
Earth strainmeter, interferometric calibration 2−65530
electret, characteristics and special applics. 2−41760
electret, operation and applics., review 2−41758
electro-osmotic energy conversion in glass/n-propanol system 2−66678
electronic tuning device for pianos 2−45523
electrostatic feedback, for meas. of low differential pressure 2−58697
e.m. generation of ultrasound in hot metals 2−69751
flat array for broad band acousto-optic deflector 2−79419
flow-rate, electrochemical 2−60384
frequency analysis technique using two transducers to characterize discontinuities 2−41791
glass element, in photoelastic load gauge, theory and design 2−53860
for head fluctuations recording in turbulent flows 2−70854
helical surface waves on cylindrical bodies from non-contacting electrodynamic transducers 2−78913
implantable biologic force transducer 2−51894
inductive transformer transducers of linear displacements 2−69536
interdigital, at surface-wave centre freq., excitation of shear waves 2−51008
interdigital, long surface wave, operation 2−49159
interdigital, surface wave, amplitude weighting by rotated electrodes, flat bypass response 2−73441
interdigital surface wave, broadband coupling network 2−63121
interdigital surface wave, impulse response model for input impedance 2−49141
interdigital surface wave grids, response 2−49143
IS, O-type and E-type, for inflight intake airflow distortion obs. 2−48637
kinematics, calibration by interferometric method 2−73634
layered plate, for microphones, sensitivity 2−49149
microdisplacement meas. 2−62957
nearfield calibration arrays of arbitrary configuration, design 2−41699
nondestructive testing, helical Rayleigh waves, excitation and reception on rods by contactless electrodynamic transducers 2−50634
optical polarization representation by bilinear transformation 2−73645
phase coded, experimental and theoretical analysis 2−49155
piezoelectric, circular, average pressure response, different reflecting objects 2−69739
piezoelectric, mechanical response to current flowing in semiconducting boundary layer having polarization gradient 2−54239
piezoelectric, mechanical response under influence of body force 2−69749
piezoelectric, nonuniformly irradiated interdigital, power transfer factors 2−63120
piezoelectric array, acoustic imaging sensor, characts. 2−63127
piezoelectric bar vibrating in compressional mode, response calc. 2−63118
piezoelectric composite, mechanical response in thermal field 2−41756
piezoelectric crystal, source detector system 2−41757
piezoelectric film on interdigital electrode structure, impedance and capacity for Rayleigh and SV modes 2−49151
piezoelectric film surface wave, coupling factor, capacitance and phase velocity 2−49111
piezoresistive, using Yb for in-situ field meas. 2−61943
piezoresistive acceleration, use in velocity measuring system 2−45221
piezotransducers, photoelectric stabilized interferometer for amplitude-frequency response obs. 2−76515
piston, pulsed operation, diffraction corrections 2−69754
plane circular displacement, with variable area 2−69535
point source simulation in h.f. acoustical system 2−52242
pressure, altitude and airspeed obs. 2−48640
pressure, applic. to obs. of buffet phenomena 2−46827
pressure, differential 2−45227
pressure, for intracranial pressure obs. 2−69296

Transducers continued
pressure, intravascular, materials for construction 2−69225
pressure, laser technique for study of thermal transients on performance characteristics 2−66413
pressure, miniature, for wind tunnel models 2−46828
pressure laser beam testing of temp. change effects 2−73286
quartz, YX and XY, Rayleigh wave reflection from electrically loaded interdigital transducers 2−51021
quartz crystal, embedded, for internal dynamic stress obs. 2−56858
radiation from transducer array on finite cylinder 2−41697
seismic, range extension 2−72640
semiconducting, mechanical variable, physical principles 2−66627
shape change ablation, for space vehicle nose cones during re-entry 2−48622
sinusoidal calibration of pressure transducer 2−66412
sonic, dynamic analysis, conference, Washington (1971) 2−41658
strain gauge, for three component dynamic wind tunnel balance design 2−46829
surface wave, apodized wideband, wavefront distortion meas. by electric probe 2−49138
surface wave, dispersive interdigital, design 2−49148
surface wave, interdigital, broadband coupling network 2−49147
surface wave, interdigital, eval. of nonideal performance 2−49146
surface wave, wideband unidirectional interdigital 2−49137
surface wave devices, second order effects 2−49136
thin film mosaic for bulk acoustic waves 2−49135
tilted, design, performance in multifinger surface wave lines 2−49160
ultrasonic flow, chronic respiratory monitoring 2−55247
ultrasonic pulse generation, intermediate layer of quarter wavelength, transient response analysis 2−41769
underwater, geodetic positioning 2−62088
u.s., graphical anal. 2−69752
u.s., Gunn oscillator-piezoelectric structures 2−84458
u.s., high power, review 2−69750
u.s., improvement by optical and acoustic holography, macrosonics 2−76497
U.S devices, h.f., review in book 2−57046
u.s. echo ranging applics. to oral mucosa 2−51945
u.s. transducer material fatigue testing of magneto- and electrostrictive materials 2−71625
vacuum gauge, cathode sputtering for automatic self-cleaning 2−48944
vacuum gauge, cathode sputtering for automatic self-cleaning 2−48944
vibration-frequency, errors resulting from elastic imperfections in their materials 2−58696
wedge, high efficiency, surface wave excitation by bulk-wave beam 2−49113
CdS, deposition, parameters controlling device usefulness 2−67906
CdS film shear mode, c-axis orientation modification, evaporation by reflection 2−50487
CdSe, thin film transducer, operation characteristics and anomalous behaviour 2−77922
$LiIO_3$, elastic surface wave props. and device applics. 2−77778
$LiNbO_3$, acoustic convolution and correl., nonlinearity parameters 2−51014
$LiNbO_3$, Y cut, parameter periodic coupling of volume acoustic modes 2−51003
$LiNbO_3$,YZ, Rayleigh wave reflection from electrically loaded interdigital transducers 2−51021
ZnO, r.f. sputtered onto sapphire, u.s. transducers at microwave frequencies 2−52243
ZnO film surface acoustic wave transducers, coupling constants and film thickness 2−49152
Transformations *see Phase transformations*
Transformations, mathematical
amplifications in earthquake motion 2−81572
approximate Z-transform technique, transient anal. of lumped and distributed parameter systems 2−55440
Baecklund transforms. and invariance props. of axially-symmetric flows 2−70833
bending of shallow hyperbolic paraboloidal shells, analysis using finite Fourier transformations 2−73375
canonical, for field variables, from generating functionals 2−66421
canonical, rel. to quadratic Hamiltonians 2−41456
canonical transformations, new proof of the conditions 2−78765
in celestial mechanics, applic. to power series solns. of differential eqns. of motion 2−62453
compressible boundary layer eqns., Stewartson type 2−80194
coordinate, in space variant image enhancement and restoration 2−79302
diffraction, spatial filtering, predictions of Fourier transformations and development of general transformations 2−79314
finite, of single parameter group of relativistic quasi-exchange 2−48982
finite integral, for unsteady heat conduction of solid 2−55582
Fourier, of two-centre Slater orbital products 2−52895
Fourier, use for resolution improvement technique in computer analysis of gamma-ray spectra 2−61564
Fourier integral asymptotic expansion, with light cone singularities 2−82650
generalized three-dimensional 2−66419
image filtering with fast Fourier transformation using digital computer 2−79142
integral, transform method for 2D and 3D neutron transport problems 2−70507
Laplace, for heat and mass transfer in porous plate in moving fluid 2−49176
Laplace and Hankel, for Cauchy-Poisson wave problem in rotating fluid 2−50149
Laplace transform, in ion neutralization theory, applic. to scavenging probability calc. in gamma radiolysis of dielectric liquids 2−44493
Laplace transform on Lorentz groups, quasiregular representations 2−82156
local potential energy eigenvalues calc. method 2−82224
Lorentz tensors, relativistic wave equations 2−41472
matrix transformations for spacecraft attitude determination 2−82171
nuclear medicine, nomenclature for Fourier transforms of spread functions of imaging systems 2−76065

Transformations, mathematical continued
- rainfall-runoff regression with logarithmic transforms and zero's in data 2−78375
- relativistic, transformation to accelerating frames of reference 2−78783
- shafts, transverse vibrations, step-wise linear transformations of the argument 2−82297
- similarity transformation, examples for physics students 2−62965
- Su(3) group, finite transforms. in arbitrary irreducible represent. 2−58713
- Van Vleck expansions, formulas in closed form 2−52042

Transistors *see Semiconducting devices/transistors*

Transition metal compounds
- actinide alloys, mag. susceptibility interpret., narrow band reson. model 2−54286
- alloy, 3d. mag. crit. point phenomena 2−54332
- alloy, antiferromagnetism, itinerant model 2−44286
- alloy, binary, low-temp. sp.LT. parameters γ and Θ_d, inverse scaling, rel. to phase stability 2−68248
- alloy, dil., Kondo effect in two-band model 2−61145
- alloy, dilute Al-transition metal, temp. depend. of charge perturbation, n.m.r. 2−44452
- alloy, localized mag. moments, generalization of Anderson model 2−68515
- alloy, supercond., mag. phenomena, spin excitations and order 2−57162
- 3d alloys, magnetization effect on lattice constants 2−53660
- arsenides, MM'As, metallic interactions, struct. evolution 2−71361
- binary, Mott insulation breakdown, Mott transition 2−57099
- borides, neutron irradiation swelling 2−77790
- borides, of IVA-VIA metals, thermionic emission, rel. to electronic struct. 2−48017
- borides, thermophysical props. 2−54043
- carbide systems in solid state, sintering phenomena 2−77696
- carbides, phonon anomalies 2−64836
- carbides, thermophysical props. 2−54043
- carbides of Gp IV and V, nonstoichiometry rel. to order-disorder changes 2−61029
- chalcogenides, TX_2 type, with pyrite marcasite, arsenopyrite structs., energy bands 2−61189
- chromates, i.r. vibrational spectra, calc. of force constants 2−70678
- Coles alloys, temp. depend. of resist. due to localized spin fluctuations 2−75056
- complexes, trigonally distorted, theoretical investigation of electronic spectra of d^1, d^3, d^8, d^9 complexes 2−44372
- coordination cpds., electronic struct., SSP MO LCAO method in p.p.d.p approx. 2−50020
- crystal growth and characteriz. 2−50571
- dichalcogenide layers, spectra, exciton peaks, band struct., press. to 6Kbars, 80-295K 2−44378
- difluorides, covalency parameters 2−77057
- germanide, elec. resistivity, temp. depend. 2−57175
- germanides, group IV-VI, microhardness, rel. to atomic volume change, structural loosening 2−74866
- halide complexes valence regions by X-ray photoelectron spectroscopy 2−83247
- halides, modified orbital valence force field, vibrational amplitudes 2−70729
- hydrides, energy band calcs., model obs. 2−61187
- hydrides, interstitial atom interaction role in solid soln. form. 2−77733
- hydrides, struct. problems, review 2−77731
- intermetallic with rare earth metals, Fe_3C struct. type., mag. props. and transitions 2−61504
- molecular orbital calculations, parameterized self-consistent-field theory 2−46525
- molybdates, i.r. vibrational spectra, calc. of force constants 2−70678
- monoxides, positron lifetime spectra, rel. to cond. and nonstoichiometry 2−71825
- Mott transition theory 2−57113
- nitrides, hot pressing, sintering, compaction kinetics, Hall coeff., elec. resist. 2−47661
- nitrides, microhardness and thermal expansion, 80-300K 2−61112
- nitrides, of Gp IV and V, monstoichiometry rel. to order-disorder changes 2−61029
- oxide scales, on Fe alloys, partitioning of transition metals, chem. diffusion model 2−78197
- oxide solid solns., chem. vapour transport 2−50587
- oxides, metal-insulator phase transitions, role of phonons 2−57120
- phosphides, MM'P, metallic interactions, struct. evolution 2−71361
- rare earth transition metal cpds., $CaCu_5$ type, valence bond form. 2−50559
- rare earth-transition metal intermetallics, pulsed field magnetiz., critical phenomena 2−51261
- TCNQ anion radical salts, mag. susceptibility Schottky type behaviour 2−68575
- tetranuclear systems, determ. of relative energies by irreducible tensor method 2−80044
- transition element oxide glasses, amorphous antiferromagnets, absence of ordering 2−81301
- transition metal complexes, revised INDO calc. of charge transfer spectra and sequence of metal and ligand orbitals 2−67472
- Al-3d transition metal dil. alloys, validity of Kondo model 2−81029
- Fe group ion in a tetrahedral field mixing of 3d and excited orbitals, effect on orbital momentum and spin-orbit coupling coeff. 2−80981
- ML_4 complexes, tetrahedral, tetragonally distorted, splitting of d^2-configuration in strong ligand fields of D_{2d} symmetry 2−80937

Transition metals
- 3d, L-shell X-ray appearance pot. spectra, spin orbit splittings, binding energies 2−61677
- 4d series, vapour deposited, struct., electron microscope obs. 2−60594
- additions to AL9V Al alloy, effect on ageing 2−47595
- adsorbed on transition metal surfaces, band struct., X-ray appearance pot. obs. 2−47816
- adsorption of alkali metal, atomic theory of work function variation 2−71343
- adsorption on transition metal, tight binding model 2−50527
- approximate analytical wavefunctions 2−49930

Transition metals continued
- atomic central-field models for open shells, SCF calcs. 2−64025
- atoms, energy interactions in $3d^n4s^0$ and $3d^n4s^2$ configuration excited states 2−76965
- b.c.c., cold brittleness 2−43726
- CNDO calculations using 3 sets of orbital exponents 2−83252
- diffusion of hydrogen, n.m.r. obs. 2−77622
- diffusion of hydrogen, quasielastic neutron scatt. obs. 2−77623
- diffusion of tritium, time-lag method obs. 2−77624
- electrical and thermal cond., 20 to 1200°C 2−47769
- electronic struct. of hydrogen 2−77822
- electronic wavefunctions, rapid calculation 2−75018
- ferromagnetic, magnetostriction, band model using spin- orbit term 2−48082
- ferromagnetic transition phenomena 2−77989
- film, amorphous, deposition and annealing resist. study 2−77499
- Hall resistivity, formal expression using nonequilib. statistical operator 2−71776
- h.c.p., phonon dispersion, Debye temp., noncentral force model 2−80887
- hyperfine field data on actinide impurities 2−68588
- impurities, in soda lime silicate, glass, analysis by neutron activation 2−60580
- ion, in liq. state, mag. props. by e.s.r., review 2−54569
- ions, core polarization, semiempirical law 2−84577
- ions, electron excitation energy degradation 2−61678
- ions, e.p.r. in fused silica 2−65338
- ions in aqueous solns., proton n.m.r. field shift 2−74558
- lattice dynamics, ang. force models 2−43945
- liquid, elec. resist., nearly free electron model, muffin tin potential 2−56514
- localized magnetic moments, generalization of Anderson model 2−68515
- magnetic properties, direct exchange interact. calc., generalized Heitler-London model 2−68529
- optical absorption, a model calc. 2−84498
- optical props. and interband transitions, review 2−72292
- paramagnetostriction, oscillatory magnetostriction, rel. to Fermi surface 2−54290
- effect on phase equilib., of Fe-Cr-Mn alloys 2−47687
- photoelectric emission, electronic struct. 2−72088
- semiconductor, III-V, transition metal doped, anomalous props. 2−68405
- in solution, const. of stability and specific mag. rotation determ. using Faraday effect 2−66823
- superconducting, dirty two-band, mixed state transport coeffs. near H_{c2} 2−47871
- superconducting, with non-mag. impurities, specific heat calc. 2−44061
- superconducting, with non-mag. impurities, thermal conductivity, two-band model 2−71874
- superconducting transition temp. calc. and phonon vertex 2−71876
- superconductivity, applic. of self-consistent electron-phonon coupling 2−57098
- superconductivity, mag. phenomena, spin excitations and order 2−57162
- superconductor, dirty, thermal conductivity near upper crit. field 2−77876
- surface density of electron states 2−75035
- surface energy, plasmon theory 2−64894
- trivalent ions, in interstellar dust 2−81848
- Fe group atoms, spin-dependent interactions in $3d^n$ configurations of third spectra 2−46427

Transmission
- multiphase mixtures, composition dependence of flux propagations 2−75252
- water wave transmission through small apertures 2−77393
- **acoustic waves**
  - *see also Acoustic wave propagation*
  - apparent gain, underwater explosive sources 2−41713
  - between rooms with interconnecting services, statistical energy analysis studies 2−41830
  - control and measurement in enclosed spaces 2−63135
  - curved partitions, due to resonant and non-resonant vibr. 2−45548
  - drill string, idealized, passbands 2−41704
  - ducts with thin shear layers, convergence to uniform flow case 2−55521
  - effect of absorption within cavity of timber stud/plasterboard partition 2−41726
  - in isospeed ocean channel with depth dependent current 2−44622
  - loss at lightweight concrete walls, effect of air flow resistance 2−41725
  - loss obs. for small dimension samples 2−52230
  - multipath, statistics of finite bandwidth signals 2−55545
  - outer-middle-ear complex in man and guinea pig 2−45147
  - plate with damping layer, transmission loss 2−45509
  - Rayleigh, Love surface waves at deformed boundaries and wedges 2−63113
  - into sea basin, with bigradient sound speed profile losses 2−44654
  - shear discontinuity between hot and cold regions 2−78921
  - shock waves at boundary 2−55563
  - sound in a duct with flow 2−66619
  - sound insulation at l.f., two rooms coupled by panel 2−41831
  - sound loss through deep apertures, tables of rectangular piston radiation impedance functions 2−45502
  - sound transmission from deep to shallow water 2−44658
  - stochastic transients, power moments spectra 2−58912
  - stochastic transmission system diffusion function 2−78915
  - water, deep saline, low-angle emission, layered temp. jump models 2−60471
- **acoustic waves, ultrasonic**
  - attenuation meas., beam divergence effect 2−73434
  - biological cell discrimination by ultrasonic probing 2−51880
  - freon, intensity variation with time at 22 kHz at atmos. and excess pressure 2−52232
  - perchloroethylene, intensity variation with time at 22 kHz at atmos. and excess pressure 2−52232
  - soft tissue visualization 2−69307
  - water, intensity variation with time at 22 kHz at atmos. and excess pressure 2−52232

Transmission continued
acoustic waves, ultrasonic continued
ZnO/Al_2O_3, heteroepitaxial layer structure, surface props. rel. to delay line fabrication and behaviour 2−68235
electromagnetic waves *see Electromagnetic wave propagation*
light
see also Absorption/light; Filters, optical
absorbing multilayers, characteristics 2−66843
atmosphere, absorption coeffs., realistic calc. 2−62271
atmosphere, dependence on temp., water vapour and O_3 distrib. 2−65771
atmosphere, in 0.76 microns O_2 band 2−44732
atmosphere, i.r., u.v., visible and X-ray, aeronomical balloon obs. 2−72769
atmosphere, i.r. attenuation, aerosol extinction contrib. 2−81647
atmosphere, non-homogeneous, Curtis-Godson approx. 2−84805
atmosphere, transmission functions, calc. over inhomogeneous paths 2−65769
atmospheric aerosol attenuation coefficient, vertical profile 2−57996
atmospheric laser radar transmission 2−62281
atmospheric spectral transparency, visible and i.r. region, apparatus and technique 2−54855
atmospheric transmission measurements in 0.35 to 1.6 μm spectral range, worldwide variations in 1902-50 period 2−54862
atmospheric turbulence, fluctuating properties of Gaussian light beam from viewpoint of mode conversion 2−46859
beam transmittance in turbid waters of Biscayne Bay, time series study 2−57893
cholesteric liquid crystal, effect of a magnetic field on the optical transmission 2−84468
cloud layers, water vapour bands 2−48486
clouds, angular transmittance props. 2−57977
clouds, semi-transparent, radiative transfer props. in thermal i.r. 2−65737
clouds, transmission functions for direct and reflected light 2−44731
coefficients meas. at low temp. using thermostated integrating sphere 2−57323
d-threonine crystals, nonlinear props. 2−55711
echelette high pass filters, optical props. 2−70063
film, inhomogeneous dielectric, and reflectance, formulae 2−54378
film, metal, on opaque substrate, thickness uniformity determ. by optical transmission microscopy 2−64560
filter, induced-transmission, symmetrical containing absorbing layers, equiv. layers concept 2−79445
filter multilayer, tandem arrays, radiant transmittance, attenuation optimization 2−79382
filters, for contrast enhancement of light sources 2−55763
fluorescent lamp glass, performance improvement by additives 2−52474
FN-85 photometer, reflectance and transmittance in 0.3 to 2.5 μm range 2−63435
fog element length, horizontal transmittance discontinuities 2−75602
gas, mean opacities measured using wide bandwidths and a number of path lengths 2−43270
glass, photochromic, containing AgCl, effects of heat treatment, u.v. irrad. and CuO additive 2−78065
glasses containing La and Ce, radiation and optical stability 2−70071
group VI chalcogenides, layer semicond., optical dielectric consts. obs. 2−81334
instruments for measuring, calibration 2−66827
i.r., atmosphere, two beam spectrophotometer obs. 2−48508
i.r., atmosphere universal representations for applic. to nonhomogeneous paths 2−62270
i.r., refractive index determ. using Kramers-Kronig dispersion anal. method 2−73643
laser propagation in turbulent weak drizzles, intensity fluctuations spectra 2−75607
lenslike medium, vector wave solution 2−76510
liquid and vitreous states, optical scatter loss formulated in terms of fundamental material properties 2−50357
liquid cryst., nematic, dynamic scatt., effect of charge transfer acceptors, voltage transmission characts. 2−71201
mica, characts. for radiation receivers 2−55754
modulated, information carrying, wave guides, optical circuits, design 2−82546
optical beamwaveguide, two-dimensional case 2−70008
optical waveguide, temperature difference reduction in shielding pipes 2−76511
partially polarized light by dielectric plates 2−42188
piezosemiconductor, modulation on passage of acoustoelec. domain 2−54033
polycrystals, polarization effects 2−81325
pulsed plasma arc lamps, transmittance measurements 2−83643
quartz, synthetic, loss at 1.06 μ, related to fibre optic appl. 2−48136
rare earth fluorides, l.f. lattice vibrs. 2−43963
semiconductor, II-IV-V_2 and I-III-VI_2, i.r. cut-off 2−78058
semiconductor, polycryst., laser-induced transmittance modulation 2−61575
semiconductor film/solid surface, as substrate thermal transients meas. technique 2−58972
smoke plumes, remote obs. using ruby lidar system 2−68910
space radiation effects on selected optical materials, simulated 2−49440
spectrophotometer, split beam, for wavelength dependence meas. 2−55772
stack polarizers, quarter-wave, radiant transmittance obs. 2−79411
surface optical waveguide, semiconductor 2−70014
target edge response viewed through atmospheric turbulence over water 2−81648
Al_2O_3, alumina, characteriz. 2−50863
Ar and Kr laser lights attenuation in water 2−76512
$3As_2Se_3.2Sb_2Se_3$, films, amorphous, band struct. obs. 2−54186
Au black deposit, i.r., rel. to prep. conditions 2−57347
Bi:Te deposits, optical constant determ. in 15-70μ region 2−75255
C film, amorphous, change on graphitization by light pulses 2−61030

Transmission continued
light continued
$CaWO_4:Nd^{3+}$, photon echoes, generation, detection, mag. field and temp. depend. 2−72251
CdS, cyclotron reson. of piezoelec. polarons, far i.r. 2−71924
CdS_xSe_{1-x} film, 7000-21000 cm^{-1}, band gap calc. 2−61633
$CdSiP_2$, i.r., characterization 2−80599
n-Cd_2SnO_4, Burnstein shifts, optical band gap 2−51137
Cs thin films, 0.3 to 0.9 μ region 2−68597
Cu films, far-i.r. transmission, surface plasma oscillation obs. 2−54401
CuO film, optical constas., wavelength depend., transmittance obs. 2−48135
GaAs, polariton (n=1 exciton) spectra, temp. depend. 2−81400
GaAs film, epitaxial, optical mode propag. cut-off effect 2−68608
K, obs. in 4-10.7 eV photon energy range 2−68593
K, vapour, reson. nonlinear susceptibility dispersion 2−43272
KI:Cu, anomalous spectra, 300-450 nm 2−72337
KI:Cu, antiresonance phenomena 2−54423
$K_2Pt(CN)_4Br_{0.3} \times 2.3H_2O$, transmission spectra rel. to one-dimensional metallic conductivity props. 2−68339
$La_{2.97}In_{1.94}Ga_{3.09}O_{12}$, garnet, spectral transmission and refractive index 2−75300
$LiIO_3$, α and β forms compared 2−81326
$MgAl_2O_4$ polycryst. ceramic characteriz. 2−50887
MgO coated integrating sphere, transmittance measurements 2−66840
MnO:Li, electro-transmission in visible and near i.r. charge carrier obs. 2−51323
$Na_2O-P_2O_5$, glass, containing metal ion impurities, u.v. transparency 2−65225
NiO:Li, electro-transmission in visible and near i.r. charge carrier obs. 2−51323
O_2 doped spherical laser plasmas, high intensity X-ray spectra and stimulated emission 2−74378
PbS film, prep. by chem. precip., transmission spectra, optimum prep. conditions 2−75304
Sb_3Se_3 film, amorphous 2−53576
$Te_{81}Ge_{15}As_4$ glass, rel. to struct. of laser written lines 2−60600
V_2O_5, long wave vibrational spectrum obs. 2−68629
WSe_2, exciton spectrum obs. 2−81403
$ZnGeP_2$, i.r., characterization 2−80599
ZnTe-InAs heterojunction 2−57213
Transmission lines, r.f. *see Electromagnetic wave propagation/guided waves*
Transparency
see also Optical constants; Transmission/light
alkali metal metavanadates, melt grown crysts. 2−47261
atmosphere, anomalous transparency effect, due to scattering by molecular portion of atmos. 2−62268
atmospheric transparency measurements, transmission measurements in 0.35 to 1.6 μm spectral range, worldwide variations in 1902-50 period 2−54862
Baltic seawater, influence of suspended matter on transparency 2−78329
coherent pulse chirping in self-induced transparency 2−59205
e.m. pulse undergoing self-induced transparency 2−52443
ferroelectric ceramic, grain size and porosity effects 2−57244
mineral, absorption spectra meas. at high shock press., apparatus design 2−61828
plasma, induced, e.m. wave barriers 2−53219
semiconductors, self-induced 2−44111
strontium formate and strontium formate dihydrate, phase matchable optical nonlinearity 2−48124
C film, diamond-like props. characterization 2−56588
CaF_2, effect of calcining temp. 2−61004
$Gd_2O_3:Eu^{3+}$ transparent phosphor, prep. and optical props. 2−72409
$Na_2O-P_2O_5$, glass, containing metal ion impurities, u.v. transparency 2−65225
$(Pb,La)(Zr,Ti)O_3$, prepared by atm. sintering 2−56967
SiO_2 films, study by luminescent method 2−44340
Tl_3AsA_4 single crystal 2−48137
Transport processes
see also Boltzmann equation; Diffusion; Kinetic theory; Liquids/theory; Mass transfer; Radiative transfer; Solids/theory; Statistical mechanics
— 2−67786
— 2−67786
air-water interface, wavy, energy and mass transfer 2−72748
anisole mols. in polystyrene, mobility study 2−83387
blood, primary hemostasis, convective transport theory anal. 2−48846
carbon tetrachloride, transport coeffs., density depend., rel. to hard sphere fluid model 2−74525
chemical relaxation due to bimolecular reaction time obtained from linearized Boltzmann equation 2−48315
classical fluids, diffusive and collective motion 2−74314
coefficient calc., comparison of Boltzman and Liouville approaches 2−45319
collision integrals $\Omega^{(l,s)*}$, empirical equations for calc. in Lennard-Jones (12-6) potential 2−58812
computer simulation, review 2−82253
convection and diffusion, upwind difference scheme for formulation 2−58811
correlation formula for volumetric viscosity 2−50275
dense fluids, application of modified Enskog theory 2−64227
dense gases, Greens function theory 2−43275
diatomic, rotational excitation, effect of generalized phase shift expansion terms on classical limit of gas transport coefficients 2−43030
diatomic gas in shock front and wake, relaxation equations for vibrational and rotational energy including transport processes and chemical reactions 2−52966
diffusion waves induced by high intensity sources 2−83699
dilute gas, collision integrals, FORTRAN IV program adapted to run on IBM computers 2−53340
distance to collision, Monte Carlo sampling with continuously varying cross-sections along flight paths 2−70508
electron, non-ohmic, in image-potential-induced surface states on liquid He surface 2−56534
electron current equations development 2−64878

Transport processes continued
- electron gas, Grad's thirteen moment method 2−41547
- electron group drift between plane parallel electrodes, in gases, mathematical model 2−83715
- electrons in gases, meas. methods for drift velocity 2−64397
- energy in electromagnetic fields 2−76410
- fluctuation-dissipation theorem in non-linear system, Langevin method 2−78850
- fluid, dense classical, projection operators and interaction representation 2−55438
- fluid containing high molecular weight polymer, non-Newtonian flow 2−50289
- fluids, Kubo integrands, low-frequency behaviour of transport coefficients 2−43048
- fluids of polyatomic molecules, transport equations of multicomponent systems 2−50135
- Fokker-Planck and master equations 2−45285
- gas of hard spheres, coefficients, first density corrections 2−46851
- gaseous mixtures with internal degrees of freedom, classical mech. calcs. 2−50281
- gases, mixtures, chem. reacting 2−48320
- gases, transport collision integral evaluation using rigid core model 2−60363
- gases of linear molecules in magnetic field, time correlation functions 2−46853
- interacting particles system, thermal and diffusion wave propag. 2−45334
- ion mobility in liquid, hydrodynamic determ. 2−71163
- irreversible thermodynamics, memory effects, corrected derivation of equations 2−41535
- isotropic, stationary gas, free path and displacement of foreign molecule 2−46854
- K ions in gases, apparent pressure dependence of reduced mobility 2−56448
- linear chain of r elements, transport properties and theorem of corresponding states 2−83342
- liquid crystals, nematic, study using noise meas. 2−83802
- liquid surface waves, evaporation at air- water interface 2−77395
- liquid surface waves, isothermal conditions, shear prediction methods 2−77394
- liquid system, vertical transport due to fingers in double diffusive convection 2−67826
- liquid waves, non-linear slowly varying, instabilities 2−50301
- in liquids, generalized Rice-Allnatt theory 2−74524
- mass, energy and momentum transfer problems, solving using vector maths. 2−82276
- master and Fokker-Planck equations 2−45285
- membrane, against external driving force due to mass transfer reaction coupling 2−56493
- membrane water transport across, study technique 2−69207
- membranes, preselective, ion and water movements, equilib. props. 2−60460
- molecular transmission probability of complex systems, computation 2−82268
- momentum transfer in horizontal liquid jet ejector 2−67781
- multicomponent system of polyatomic molecules, rotational coeffs. 2−50280
- multigroup theory, degenerate transfer kernel 2−58813
- multiphase mixtures, composition dependence of flux propagations 2−75252
- neutral and ionized gases, non-equilibrium thermodynamics and kinetic theory 2−83701
- nonpolar-polar gas mixtures, calc. of collision integrals required for evaluation of transport properties 2−80413
- one-dimensional crystal, velocity autocorrelation function determ. 2−49029
- oxide formation on Al 2−68798
- particle transport problems, boundary effect 2−63046
- Pauli master equation, weakly coupled quantum oscillators 2−73329
- plasma neutral component, macroscopic velocity obs. in crossed fields 2−70976
- polymeric mats., rel. to spatial gradients and applics. 2−61026
- porous medium, fluid-filled, nonequilib. thermodynamics 2−50137
- quantum systems, continuum thermodynamic limit for master equation 2−58802
- reactive mixture, reciprocal relations in relativistic kinetic gas theory 2−64392
- stability criterion for hydrodynamical transport states 2−49044
- stellar interiors 2−58271
- stochastic Ising model, computer simulation 2−45335
- thermionic convertors, transport phenomena in gaseous mixers and plasma, improved formalism 2−63248
- Townsend Huxley lateral diffusion expt., review 2−69627
- traffic flow, kinematic waves, analytical solns. 2−69626
- turbulent shear flow, local transport eqns., determ. of mean velocity, kinetic energy, shear stress 2−83468
- variational methods modification to approx. arbitrary functionals 2−66480
- Ar-K, flowing plasma, heat transfer between electrodes 2−60209
- Ar gas, electron momentum transfer cross section from Boltzmann eqn. 2−83708
- Cs arc mode theory, assumptions, parameters 2−63249
- Cs$^+$ ion transport of red blood cells of rats, comparison with k$^+$ by kinetic tracer model 2−55257
- GaP crystals grown by vapour transport, 780-935°C, thermodynamics, kinetics, rate of transport, nucleation and crystal size 2−71372
- H bonded solids, proton migration study, experimental methods, review 2−83998
- In-Bi liquid alloy, viscosity, density and autodiffusion 2−46939
- K$^+$ ion transport of red blood cells of rats, comparison with Cs$^+$ by kinetic tracer model 2−55257
- Ne, liquid, negative carrier mobility rel. to localized electrons 2−46916
- THO, transport kinetics in human body, use of compartment analysis 2−55290

Transport theory, neutron *see Neutron transport theory*

Trapped free radicals *see Free radicals*

Traps *see Crystal electron states/impurity states and effects; Crystal imperfections; Semiconductors*

Travelling wave tubes *see Electron tubes*

Triboelectric emission *see Electron emission*

Triboelectricity
- No entries

Triboluminescence *see Luminescence*

Trions (^{3}He, ^{3}H) *see Helium-3; Tritons*

Triple point *see Critical constants, thermal*

Tritium
- abundance profile in Atlantic Ocean from Geosecs test cruise station 2−75474
- application to determ. of electron concentration in semiconductor materials 2−71934
- atmosphere contamination, thermoluminescent dosimetry obs. 2−62291
- bubble chamber, deuterium, background due to tritium decay 2−79682
- chromatograms, thin-layer, det. using luminous Zn compounds 2−61832
- chromatograms, two-dimensional, automatic scintillation scanning unit 2−61831
- counting together with ^{14}C, optimization 2−59615
- D-T reactor, thermal stability of spatially non-uniform plasma 2−80309
- D-T reactors blanket chemistry 2−63953
- dating, low background proportional counter 2−52685
- detector, gas counting tube 2−70306
- diffusion in stainless steel, 25-222°C 2−47458
- diffusion in transition metals, time-lag method obs. 2−77624
- energy spectra, comparison of chemiluminescence and phosphorescence 2−59605
- ergonic fusion, controlled thermonuclear reactions, power production 2−70930
- in fuel pins, residual tritium determ. after irrad. 2−42663
- fusion by laser driven flame propagation in solid DT targets 2−64308
- gas, interference proportional tube filled with pentane for det. 2−55906
- ions acceleration on IPCR cyclotron, 13-24 MeV 2−70328
- isotope mixture separation using critical state method 2−56134
- isotopic H_2 molecules, gas chromatographic separation and quantitative det. 2−52956
- natural activity in ground and surface water, apparatus for obs. 2−72688
- neutron yield from Zr target fed with ^{3}H 2−42443
- neutrons precision monitoring from TD and DD reactions 2−70305
- nuclear targets, high-yield neutron generators 2−73923
- organic-bound, in mice as increasing tissue dose after single or daily administration of titiated water 2−55291
- penetration in Atlantic thermocline exchange coeffs., advection rules 2−72705
- produced in molten salt reactor, containment and disposal 2−46378
- in rainfall, Rhodesia, indicator of airmass source 2−72795
- sea water and river content near operating atomic power plants 2−62042
- substitution reactions, energy nonrandomized decomposition in spiropentane 2−81533
- T-D plasma, laser heating to thermonuclear temps., by ion-ion collisions 2−64289
- target, preparation techniques 2−49624
- water samples, meas. of T content using gas proportional counter 2−82808
- D-T fusion reactor review of recent progress in mag. confinement 2−79843
- ^{3}H for energy conversion 2−49247
- ^{3}H miniature batteries medical appl. 2−49248
- ^{3}He battery, for submicrowatt range 2−49245
- T(d,n) gas target source, cancer therapy 2−69340

Tritium compounds *see Hydrogen compounds*

Tritons
- *see also Nuclear reactions and scattering due to/tritons*
- binding energy by two-term nonlocal separable potentials 2−82845
- magnetic moments, quark model approach 2−82877
- **interactions**
  - No entries
- **scattering**
  - No entries

Troposphere *see Atmosphere*

Tungsten
- (100) surface, adsorption of Cs and O, work function 2−83878
- adlayers of Na, C, N, O, K shell total electron impact ionization cross sections, Auger spectra 2−64579
- adsorbant, D_2 and ethylene on polycrystalline substrate 2−44484
- adsorption, of CO, on (210) surface, binding states and work function 2−60692
- adsorption, of O, field emission microscope obs. 2−64580
- adsorption, simultaneous of Cs and Ba, work function and thermal stability obs. 2−67923
- adsorption and dissociation of CO, field emission microscope obs. 2−71355
- adsorption lifetime and desorption energy of O_2 as function of coverage 2−47171
- adsorption of Ag, field emission microscope obs. 2−60690
- adsorption of Cd, mol. beam technique 2−50534
- adsorption of Cl, field emission study 2−60693
- adsorption of CO_2, binding states 2−77513
- adsorption of Cs, atomic theory of work function variation 2−71343
- adsorption of Cs, ellipsometry, Auger spectra and surface pot. difference obs. 2−50550
- adsorption of Cs and o, LEED and work function obs. 2−47169
- adsorption of H_2 and D_2, field emitted electrons energy distrib. as function of coverage 2−48016
- adsorption of methane, ethane and propane onto (100) face 2−74642
- adsorption of methane, field ion microscopy obs. 2−64583
- adsorption of N_2O, binding states, LEED obs. 2−64581
- adsorption of N, surface crystallography effects 2−47168
- adsorption of O_2, atomic and electronic processes 2−74649
- adsorption of O_2, thermionic electron emission and work function obs. 2−47172

Tungsten continued
- adsorption of O, low coverage, at 78K, field ion microscopy 2−64584
- adsorption of O on surface, inhibition of reactions with H 2−71344
- annealing, before and after neutron irradiation, physical mechanical properties 2−53730
- in Ap star HD 25354, spectral obs. 2−72994
- atomic and mol. scatt., effect of surface composition and cryst. orientation 2−47084
- atomic surface potential, one dimensional, from (5,7) Mie potential 2−72101
- atoms, calc. of bremsstrahlung spectra from thick targets using thin-target formulas 2−42739
- bubble-forming impurities, identification in W rods doped with Al, K or Si 2−80792
- cathode, flashing effect, surface atom migration, field ion microscopy 2−53557
- cathode, in Cs plasma, electron emission rel. to temp. and current density 2−75191
- cathode, locally heated, in electron gun 2−79026
- cathode, O_2 pumping effect rel. to ionization gauges and mass spectrometers 2−48943
- cathode, O_2 pumping effect rel. to ionization gauges and mass spectrometers 2−48943
- cathode surface temp. det. in electrostatic field of immersion objective 2−41923
- chemical vapour deposition, for thermionic converters 2−53559
- chemisorption, of C, N and O, K shell ionization by electron impact 2−50553
- chemisorption, of CO, thermal desorp. spectra quantitative analysis 2−47173
- chemisorption of CO, refl.-absorption i.r. spectra 2−47154
- chemisorption of O, mass spectrometric obs. of desorption 2−48327
- cladding for Mo-UO_2 cermet fuel, neutron irradiation 2−52882
- cleavage, {110} in ⟨110⟩ axis 2−56606
- compatibility with buffered hyperstoichiometric UC alloys 2−63252
- composite, SiC/W layer, thermal cond. and diffusivity 2−47768
- contrast patterns produced by self-interstitial ions in field ion microscope images 2−64625
- creep during hot pressing with and without addition of oxides 2−77694
- crystal, centred cubic, mean square displacement of atoms, simple calc. 2−57037
- CVD coated Mo thermionic emitters, out of pile investigations 2−52370
- CVD films, formation of pores, interdiffusion in emitters of thermionic converters 2−53560
- density changes in single crystal induced by neutron irradiation 2−52849
- desorption and adsorption of CO, O_2, H_2 SIMS, EID, flash-filament obs. 2−47170
- desorption of CO, electron stimulated 2−47153
- desorption of Cs^+, mol. beam study 2−60691
- diffusion of Fe and Co along grain boundaries 2−47472
- diffusion width of wide-angle grain boundaries 2−47469
- elastic oscillations, damping, orientation depend. 2−43671
- electrical and thermal cond., 20 to 1200°C 2−47769
- electrical and thermal conductivity, high temp. 2−54130
- electrodes, heated, pre-breakdown phenomena 2−71028
- electron density distrib., neutron electron scatt. obs. 2−57138
- emitters, thermionic convertors 2−49289
- energy accommodation coeffs. for one-phonon inelastic scatt. of He 2−50528
- equilibrium Cs adsorption measurement, ellipsometry technique 2−63232
- evaporated film, reflectance in v.u.v. from 300-2000 Å 2−44345
- exploding wires in vacuo, X-ray production 2−76135
- fibre composite, UO_2/W system, eutectic structs., influence of growth parameters 2−53969
- field emission, modified pot. barrier effect 2−54270
- filament, high temp. mech. props. and struct., rel. to composite reinforcement 2−53970
- filament reinforced Ni-Cr base alloy, mech. props. 2−56988
- filament reinforced nichrome, filament-matrix interface struct. 2−53966
- filament reinforced nichrome, struct. and props. 2−53967
- film, chem. vapour deposition, substrate temp. and gas press. effects 2−47131
- film on SiGe, interface reactions, effects of p- or n-type substrates, ion backscattering analysis 2−71951
- film prep. using plasma jet in vacuo 2−83889
- films, 110 orientation, deposition using WCl_6 gas discharge 2−50512
- foil, 60 keV Au ion irrad., dislocation loop prod. 2−43615
- foil, Au ion irrad., vacancy-type dislocation loop prod. 2−43616
- free energies, interfacial meas. 2−80795
- grain size of W coating deposited from the gaseous phase 2−84092
- grain-size dependences of the failure mode and ductility transition temperatures 2−68098
- growth orifice, effects on use in sapphire filament growth 2−60720
- high melting point electrode materials, thermionic converters 2−54272
- high temperature strength, increase due to submicroscopic bubbles, mechanisms 2−71581
- ion backscattering, H^+, Ne^+ and Ar^+, energy and ang. distrib. 2−50467
- ion irradiated, He entrapment at vacancies 2−50651
- ion irradiated, surface damage, LEED obs. 2−50468
- lamps, gas filled, reproducibility of output of visible radiation 2−79451
- lattice damage, prod. by ion irrad., He interstitial diffusion 2−47394
- lattice dynamics 2−84178
- monocrystal, electrical characteristics, thermionic emitter 2−54275
- m.p. and electrical resistivity above 3600 K, determ. by pulse heating method 2−74584
- neutron irrad., void form. and ordering, alloying and purity effects 2−53719
- optical absorption, interband transitions 2−72353
- oxide form. at 1000 K, LEED obs. 2−78196
- oxides, formed on emitter, additive thermionic converters 2−49279

Tungsten continued
- particle absorber, ranges of ^{99}Mo and ^{132}Te fragments from fission of ^{235}U 2−47786
- photoelectric emission, two-photon photoelec. effect 2−48021
- photoelectron energy distribution and photocurrent meas. 2−72093
- photoemission, field effect, pot. barrier lowering 2−54279
- photoemission from surface state 2−75198
- photoemission obs. of surface state 2−75197
- polycrystalline, surface crystal orientation distribution determination, colour etching process 2−64545
- polycrystalline ribbon, with Ag film work function determ. by employing retarding-field diode technique 2−72083
- porous, shock response, Hugoniot elastic limits, model 2−61024
- powder, with Ni additive, sintering, modified model 2−43897
- powder sintering activation by Ni and Fe, mechanism 2−50899
- probe, rotating, for analysis of spatial current distrib. in particle beam 2−52388
- in rocks, rapid determ. using ^{183m}W 2−61834
- secondary electron emission, from (100) face, under action of slow electron beam 2−72100
- secondary electron emission by keV K^+ ions, sharp threshold obs. 2−54282
- single crystal and polycrystalline, optical constants as function of temp. 2−44341
- single crystals, emitter and collector work functions, modified Shelton measurement method 2−63234
- sintered, porosity influence on phys. and mech. props. 2−84145
- slip, asymmetrical, role of dislocations 2−56811
- spectra, emission, by Fourier transform spectroscopy, 1000-2300°C 2−54086
- spectral emissivity standard 2−54087
- stationary cathodic arcing in vacuum 2−43221
- stopping power for 0.50-1.75 MeV protons meas. by backscattering method 2−64872
- stress induced growth irradiated at low temp. 2−60781
- surface, (100), adsorp. state of hydrogen and flash desorp. spectrum 2−50555
- surface, (100), CO_2 decomposition, flash desorp. obs. 2−50551
- surface, (100), surface plasmon losses due to Rb and K adsorbed layers 2−64903
- surface, (110), polarizability of W adatoms, field ion microscope obs. 2−60689
- surface, adsorption and decomposition of ethylene 2−50552
- surface, alkalis, rare gases and H_2 adsorbate structure 2−50554
- surface, interactions between Re atoms 2−50469
- surface, low angle scatt. of 275 keV He^+ ions and surface channelling 2−80929
- surface, sputter deposition and sputter removal of Mo, Auger spectroscopy 2−50520
- surface (110) plasmon angular profiles, LEEDS obs. 2−51093
- surface diffusion of Ni, coeff. determ., mass transfer method 2−50466
- surface interplanar spacings, LEED, Bragg peak widths 2−77486
- surface self-diffusion rel. to C adsorpt., field emission obs. 2−64582
- surface states, interband transitions, at (110) surface 2−64896
- swaged and drawn, deform. textures 2−53868
- target, micrometeoroid simulation, Fe microparticles from Van de Graaff accelerator 2−66187
- thermal expansion, to 1900K 2−54063
- thermal expansion, to 3330°C 2−54061
- thermal expansion and vacancy equilibrium, at high temp. 2−68255
- thermal-field emission, meas. by probe hole FEM for micromonocrystals 2−72085
- thermophysical properties, high temperature obs. 2−54083
- thermophysical properties near melting point, electrical- explosion method 2−57066
- thick target, energy loss of scatt. protons and α- particles 2−80928
- wire, drawn, micropore pinning effect on grain boundary motion during recrystn. 2−47647
- wire, from powder metallurgical, pure, doped and thoriated material, high temp. creep 2−61007
- wire, nonsag, ductility, ruthenium effect 2−43683
- wires, anomalous electron emission, effect of surface contamination 2−65098
- work function, on needle-like microcrysts., coated with TaC_x film 2−50509
- work function change as function of Mo coverage of single crystal surface 2−54265
- work function change rel. to adsorption of O and Cs and O-Cs co-adsorption 2−54266
- work function changes in pure O_2, Cs vapour/O_2 mixtures, adsorption phenomenology, analytical model 2−63231
- work function dependence on orientation for planar single crystals 2−54264
- work function rel. to Cs adsorbed layer struct. 2−68487
- X-ray spectra, charact. L and K radiation emission from thick targets 2−51362
- A^IB^V coated W monocrystal, field emission microscopy 2−83872
- Au/W-SiO_2-Si, m.o.s. system, effect of bias-temp. treatments 2−84345
- Ba-W_{110} system, temperature dependence of work function 2−75186
- Cu/W composite, fibre reinforced, resist. 2−50915
- Cu-W composite, continuous-fibre metal-matrix, fracture surface energy det. 2−55475
- MgO, plastic yielding, high pressure effects 2−68081
- in Ni_3Al, effect on hardness 2−43740
- Pt-W strain gauge, temp. dependence of gauge factor and magnetoresistance 2−68121
- Si coated, surface diffusion, field emission obs. 2−47085
- UO_2/W composite, unidirectional solidification behaviour 2−47669
- W:K,Si,Al wire, incandescent lamp filament, working and process annealing 2−47590
- W:O, grain boundary segregation, field run microscopy obs. 2−53746
- W/Cs(Cs-O) work function theory 2−54262
- W-Nb, CVD, variable spacing converter, thermionic performance 2−59053
- W-Re target for DX-70 series X-ray tube 2−52022
- W-Ta emitter, for plane parallel Cs diode 2−49287

Tungsten continued
W-UC thermionic, fuel cladding systems, material development 2–52369
W-halogen lamps, thermodynamic study 2–61764
W, angular distrib. of inelastically reflected electrons 2–80551
W, explosive compaction of powders by direct method, survey 2–61008
W, field desorption of CO in FIM, image gas enhancement 2–60673
W, secondary emission of W^+ on irradiation by alkali metal ions 2–48031
W, sorption of O, investig. by ioniz. of molec. beams 2–71357
W foil, rolling and annealing textures 2–43796
W^+, ion energy spectra from W-Mo alloy sputtering 2–68263
^{186}W Mossbauer scattering obs. with in-beam system 2–63685
W(112) single crystal, effect of O adsorption on scattering of He and Ar atoms 2–67894

Tungsten compounds
alloy, foil prep., for electron microscopy, electrolytic jet thinning procedures 2–71415
alloy, T15K6, effect of tungsten prep. on props. 2–56916
complexes, polar and nonpolar in benzene and hexafluorobenzene, p.m.r. study of solvent induced shifts 2–83264
CW crystals in cobalt, kinetics of growth 2–64590
Co-(31.8 wt.%)W alloy, excess vacancy conc. effect on grain boundary diffusion 2–47455
Cr-1.6%W alloy, phonon freqs., neutron scatt. obs. 2–74973
Cu-W solid solns., binding energy of dislocations to impurities, internal friction obs. 2–43630
Fe-C-W alloy, precipitation of eutectic carbide, and microsegregation obs. 2–74929
Ni-Al-W alloy, γ' matrix, fatigue fracture 2–43716
Ni-Cr-Nb-W-Mo alloy, struct. and phase comp. 2–43941
Ni-Fe-W alloy, mag. props., magnetostriction and elec. resistivity 2–48076
Ni-(5wt.%)Fe-(5wt.%)W, powder composite, fracture micromechanism obs. 2–56947
Ni-W, alloy, ^{182}W Mossbauer effect, rel. to saturation magnetization 2–75273
Ta-W-Hf alloy, tensile props., effects of O contamination 2–43862
Ta-W alloys, superconductivity under pressure 2–81058
Ta-10%W alloy, heat capacity, elec. resistivity, thermal radiation props. 1500-3200K 2–57069
TiC-WC, short-range order, heat treatment and quenching effects 2–84072
U-Pu-W-C system, phase relations 2–54011
W-B system, phase diagram 2–50957
W-Cr alloy, dilute, phonon freqs. and widths rel. to force const. changes 2–68223
W-Cu-Mn alloy, cold worked, heat treated, Young's modulus, rigidity, hardness, thermal expansion 2–47477
W-Eu-O, subsolidus phase relations and cryst. chem., phase diagram 2–74952
W-HfO_2 composite, thermal shock resistance 2–56989
W-Mo-Ti alloy, mech. and technological props. 2–47535
W-Mo alloy, elec. and thermal cond., high temp. 2–54130
W-Mo alloy, sputtering, energy spectra of W^+ and Mo^+ ions 2–68263
W-N, nitrogen solubility as a function of pressure and degassing kinetics 2–60967
W-Pt alloy, strength, resist. to oxidation 2–47533
W-Re-ThO_2 alloy, creep, strength to rupture, 1800-2200°C 2–64719
W-Re alloys, carburized, work function in 1600- 1800 K range 2–54267
W-Re thermocouple materials, high temp. behaviour, report 2–84373
W-Sn bronze alloy, struct. 2–71441
W-Ti-Zr alloy, mech. and technological props. 2–47535
W-Ti alloy, mech. and technological props. 2–47535
W-Y_2O_3 two-phase system, black-body radiation and elec. resist. 2–43875
W-ZrC compounds, high temp. vacuum evaporation, from open surface and through W coating 2–73239
W-ZrO_2, composite, growth by unidirectional solidification of eutectic melt 2–64796
W-ZrO_2 composite, thermal shock resistance 2–56989
W complex, hexacarbonyl X-ray photoelectron spectra, multiple peak structure 2–46538
W complex, hexamethyl tungsten, photoelectron spectrum and electronic struct. 2–64160
WB_x, thermionic emission, rel. to electronic struct. 2–48017
WC-Co alloy, oversaturated, microstruct. and reaction behaviour 2–64775
WC-Co cemented carbide, internal friction recovery obs. 2–68070
WC-Co cemented carbides, effects of Cr and Ni additions on structure 2–43864
WC-Co cermets, plasticity, slip, grain boundary sliding 2–47505
WC-Co composite, microstruct. interpretation of stress-strain behaviour 2–47670
WC-Co hard metal, X-ray stress meas. at carbide phase 2–74910
WC-Co hard metals, mixed milling effect on sintering, electron microscope investigation 2–56899
WC-(25 wt.%)Co alloy, surface finish effects on fatigue 43717 2–43717
WC-Nb cermet, hot pressing kinetics 2–56914
WC dendrite, chemical vapour deposition 2–43487
$W_4Nb_{26}O_{77}$, electron microscopy using n-beam lattice images 2–56669
$W_xNb_{1-x}Se$, cryst. struct. 2–60767
WO_3-Dy_2O_3 solid soln., phase equilib., transform, phase diagram, densities, m.p. 2–57013
WO_3-P_4O_{10}-V_2O_5, elec. cond. and mag. resonances 2–54495
WO_3, elec. cond., temp. depend., four probe method and reflected microwave current obs. 2–71914
WO_3, ion bombardment-induced amorphization and mean damage rates determ. 2–77576
WO_3, monoclinic phase, domain struct. 2–77522
WO_3 cryst. surface, photoemission microscopy obs. 2–60631
WO_4^{2-}, dipole transition moments determ. by LCAO-MO calcs. in terms of ligand mixing coeff. 2–42928

Tungsten compounds continued
WO_x and $(W, M)O_x$, cryst. shear struct., (M=V, Nb, Ta, Mo) 2–47352
W_2O_5, anodic oxide film, dielec. const. field depend., ellipsometric obs. 2–44150
$WO_{3-x}F_x$, prep. and elec. props. 2–57146
WOS_3^{2-} and alkali metal salts, i.r. and Raman spectra in aqueous solution 2–46560
WS_4^{2-} and alkali metal salts, i.r. and Raman spectra in aqueous solution 2–46560
WSe_2-$NbSe_2$ alloys, antifriction and elec. props., comp. depend. 2–68115
WSe_2, exciton mechanism for superconductivity and nonequilibrium systems of excited excitons 2–71868
WSe_2, exciton spectrum, transmission obs. 2–81403
WSe_2, growth by direct vapour transport, and cryst. struct. 2–60707
WSe_2, line shape of electroreflectance spectra 2–84510
WSe_2, optical response in excitonic region 2–44383
W_5Si_3, diffusion of Si, oxide coating form., 1700°C 2–53769
$W_{1-x}Ta_xSe_2$, cell dimens. 2–43593
WTe_2, growth by Br transport, and cryst. struct. 2–60707
$(W_{0.2}V_{0.8})_3O_7$, synthesis and cryst. struct. 2–47351
WXY_3 C_{3v} ions, (X, Y=O, S, Se), assignments of electron charge transfer bands 2–80020
ZrC-W solid soln., interactions, isothermal sections struct. at 2200 and 2600°C 2–74911

Tuning forks *see Vibrating bodies*

Tunnel diodes *see Semiconducting devices/tunnel and interface devices*

Tunnelling
– 2–57150
– 2–71973
acoustic waves in elastic waveguide 2–52231
ammonium salts, p.m.r. lineshapes of ions undergoing quantum mech. tunnelling in solid state 2–81470
Cambridge surface states, tunnelling and electron field emission theory 2–47814
ceramic-metal systems, ion tunnelling 2–51183
disordered system, rel. to hopping conductivity theory 2–61279
electron, from metal electrodes to traps in dielectric near interface, dielectric loss model 2–47964
electron field emission rel. to multiple particle tunnelling 2–77976
electrostatically charge activated, mechanisms of conduction, nucleation in discontinuous thin metal films 2–54127
ferroelectric, H-bonded, harmonic generation, proton tunnelling model 2–44326
film, chalcogenide glass, between traps and valence and cond. bands 2–44097
furan-quinone pigment, DFC, charge transport props. 2–51219
graphite, Esaki effect, I-V characts. in mag. field 2–44093
graphite, tunnelling spectroscopy, state density near Fermi level 2–57122
IMPATT oscillator, effects on small-signal admittance, calcs. 2–71980
impurity-assisted, microscopic theory 2–47794
ion-dipole collisions, computer plotter studies of vibrational effects, classical tunnelling 2–46467
Josephson junction, rel. to capacitive weak links and finite load lines 2–51119
Josephson junctions with semicond. barriers 2–64957
junction, supercond.-insulator-supercond., barrier region tunnelling, paramag. impurity effects 2–61256
junctions, one electron and Josephson 2–51120
KH_2PO_4, tetragonal, Raman spectrum, phonon-tunnelling modes 2–72367
lithium ammonium tartrate, proton tunnelling, n.m.r. obs. 2–72527
magnetically doped tunnel junctions, mag. interactions 2–68449
4-methyl 2,6 ditertiarybutylphenol, proton dipole-dipole relax. rel. to quantum tunnelling 2–81472
methyl malonic acid, tunnelling sidebands of methyl group hyperfine structure, e.s.r. obs. 2–57389
microscopic theory, general theory and appl. to static impurity case 2–68275
m.i.m., band struct. effect on VI characs. 2–51184
m.i.m., paramagnetic impurity effects 2–47789
m.i.m. junction, nonequil. phenomena in electron tunnelling 2–68373
M.N.O.S., max. tunnelling distance, theory 2–47953
m.o.s. junctions, temp. depend. tunnelling into amorphous Si 2–47952
Schottky barrier diode, noise spectrum bias dependence 2–47789
semiconductor-insulator-semiconductor structure, with electron-hole pairing, Josephson effect analogue 2–81124
in semiconductor-metal boundaries, effects of hydrostatic pressure 2–61393
superconducting junction, microwave assisted tunnelling 2–47848
in superconducting semiconductors 2–51114
superconductor, generation, relax., and hole-electron imbalance detection 2–64926
superconductor, phonon spectra computation 2–81056
through thin adsorbed films in ion discharge at limiting current, determ. of potential barriers and analytic eqns. 2–57426
Al-Al_2O_3-Al struct, photosensitive tunnelling conductance 2–54222
Al-Al_2O_3-M superconducting junction, M=Fe, Co, Ni, Gd, electron spin polariz. detn. 2–64958
Al-Al_2O_3-Pb junction, impurity assisted tunnelling, 4.2-148 K 2–44140
Al-Si_3N_4-Si structure, insulator valence band as barrier 2–71993
Al-insulator-Al junction, tunnelling results with interacting mag. impurities 2–61243
Au island films on insulators magnetoresistance 2–84298
BaO, F centres reported, recombination by tunnelling 2–74803
n-CdS–p-Cu_2S film heterojunction, current passage mechanism 2–71955
Cu_2S-CdS heterojunction, tunnelling through cond. band spike of photoexcited electrons 2–51221
Ga-Ga_xO_y-Pb, Ga supercond. energy gap detn. as function of cryst. orientation 2–68358
$Ga_{1-x}Al_xAs$ alloyed p-n tunnel diodes, Zn doped 2–71981
GaAs-$Al_xGa_{1-x}As$ p-n heterojunction, current flow during electrolum. 2–72438

Tunnelling continued

GaAs, neutron irrad., tunnel assisted hopping via defect energy levels 2−51157
$GaAs_{1-x}P_x$ alloyed p-n tunnel diodes, Zn doped 2−71981
n-GaSb-Pb contact, tunnelling spectroscopy and band struct. press. effects 2−84351
n-GaSb, conduction band minima energy separation temp. depend., p-n junc. tunnelling current obs. 2−75109
Ge-Au films, quench-condensed, supercond. energy gap obs. 2−51115
n-Ge, phonon-assisted, impurity dependence 2−54195
Ge amorphous, obs. of electron tunnelling between metal electrodes, determ. tunnelling phonon density of states 2−44125
$In_{1-x}Ga_xP$ alloyed p-n tunnel diodes, Zn doped 2−71981
InSb junction, Cd diffused, I-V characts. and magnetotunnelling 2−54216
KCl, OH^- substituted, paraelectric centres with low zero field splitting 2−75147
KH_2PO_4, of protons, rel. to permittivity, 130-280K 2−77945
La film superconducting, phonon structure in tunnelling density of states 2−75059
ND_4^+ compounds, effect on deuteron mag. reson. 2−72512
Nb_3Sn, high-T_c superconductor, phonon spectrum 2−81048
Pb-GaAs Schottky barrier tunnel junction, zero bias anomaly, irrad. effects 2−71960
Pb-In dil. alloy, phonon spectra and supercond. parameters 2−47865
Pb-In dilute alloy, in thin film supercond. tunnelling junc., phonon spectra detn. 2−54142
Pb-In superconducting alloy, phonon spectrum, hydrostatic pressure effects obs. 2−64936
Pb-Mn superconducting films, tunnelling conductance curves 2−71851
Pb, density of states enhancements and suppressions in tunnel junctions due to asymmetry effects 2−54150
Pb, phonon excitation spectra, junc. tunnelling obs., effects of material props. 2−68360
Pb, tunnel junctions, single particle tunnelling in mag. field 2−54149
Pt film, cond., rel. to temp., 77-573 K, adsorpt. effects, tunnelling mechanism 2−64917
Pt film, discontinuous, rel. to current noise 2−68340
Pt island films on insulators magnetoresistance 2−84298
$RbBr:Ag^+$, paraelec. behaviour 2−61422
$RbCl:Ag^+$, paraelec. behaviour 2−61422
$Si-SiO_2$ m.o.s. structure, interface states obs. 2−68459
Si, amorphous, electron tunnelling through oxide barrier 2−61359
SiC, phonon spedtra from tunnelling characts. of p-n junctions 2−57042
Si_3N_4-GaAs interface, m.i.s. cond., tunnelling model 2−77919
SiO_2 film, in m.o.s. struct., Fowler-Nordheim tunnelling 2−47955
Sn-CdSe-Sn, tunnel junctions, fabrication and props. 2−81039
Sn, phonon excitation spectra, junc. tunnelling obs., effects of material props. 2−68360
Tl, phonon spectrum, supercond. tunnelling and neutron scatt. data, discrepancy 2−84189
$W-SiO_2$:C-Au tunnel cathode, using amorphous dielectric, threshold emission and elec. switching 2−81122
$ZnO-Bi_2O_3$ ceramic, cond. mechanism 2−57198
ZnS:Cu, green luminesc., recombination, tunnelling effects 2−48236
ZnS:Cu, rel. to surface, volume, and contact components of current 2−71918
$ZnSiF_6.6H_2$ spin-lattice relax. of Cu^{2+} phonon assisted tunnelling contrib. 2−84456

Turbidimetry *see Chemical analysis*

Turbidity *see Scattering/light; Suspensions*

Turbulence

see also Cavitation; Flow; Vortices
— 2−67609
— 2−60345
absolute intensity obs. using hot-wire anemometers calibration technique 2−43089
acoustic, scattering of beam of plasma waves and type III solar bursts 2−62753
acoustic wave phase, optical recording, for meas. turbulent props. of fluids 2−60123
acoustic waves, effect on weak shock waves 2−66633
aerodynamic heating of shell in supersonic turbulent flow 2−60368
aerodynamics, flight test base pressure data results at hypersonic Mach numbers in turbulent flow 2−43247
air, heat transfer to transpired boundary layer 2−45577
air, intensity and time-mean velocity distributions in low Reynolds number pipe flows 2−46832
air, small-scale structure, temp. obs. 2−77323
air and H_2 streams, optical method for concentration measurement 2−67704
air flow, plane deform. 2−80390
air flow in plain tube, heat and mass transfer 2−76397
air flow through porous tube with suction, friction factors 2−60338
air over heated horizontal plane, mixed convection 2−80391
air round raingauge causing catch variations 2−78246
amplifier, fluid mechanics for automation 2−74456
asymptotic theory, steady state turbulent flow of liquids with bubbles 2−43310
atmosphere, amplitude scintillations 2−65775
atmosphere, and dispersion parameters, direct determination 2−44701
atmosphere, associating fluctuations of submillimeter waves 2−51629
atmosphere, associating laser beam broadening along sloping traces 2−45756
atmosphere, associating light beam focussing, mean illumination and intensity fluctuations 2−49413
atmosphere, astronomical image aberrations and their removal by optical array technique 2−85074
atmosphere, causing e.m. wave distortions, h.f. plane wave filter function for folded path 2−75609
atmosphere, dynamic models 2−75555
atmosphere, effects on laser beam propagation, spot dancing 2−76500

Turbulence continued

atmosphere, effects on refractive index and image deterioration of extraterrestrial objects 2−81677
atmosphere, filtering, radar pulse volume 2−75549
atmosphere, focused irradiance fluctuations beyond turbulent layer 2−54856
atmosphere, incoherent radar meas. 2−75542
atmosphere, intensity within canopies with simple and complex roughness elements 2−72772
atmosphere, Kirchhoff-Fresnel diffraction fluctuations 2−45791
atmosphere, laser propagation in weak drizzles, intensity fluctuations spectra 2−75607
atmosphere, model choice and e.m. wave propagation 2−44736
atmosphere, near ground level, determ. from optical spherical wave propag. 2−81684
atmosphere, predictability calc., ω test field model 2−65682
atmosphere, rel. to air traffic control, laser beam detection 2−78337
atmosphere, resolution by line-of-sight microwave propagation expt. 2−68897
atmosphere, sensing based on wave mechanics theory 2−44705
atmosphere, small scale, optimal choice of parameters of airborne hot-wire anemometer for obs. 2−44680
atmosphere, temp. gradients 2−44703
atmosphere, vertical profile, correlation with stellar obs. 2−81683
atmosphere, vorticity flow, temperature stratification 2−72774
atmosphere, with laser beam propagated, field fluctuations 2−57995
atmosphere and multiwavelength scintillation phenomena 2−65774
atmosphere associating light beam propagating, correlation meas. of light gravity centres 2−48435
atmosphere flow, predictability 2−84795
atmosphere turbulence investigated by optical wave, criterion for choice of exposure time 2−81678
atmospheric, conference (Las Cruces, USA, Dec 1971) 2−62146
atmospheric, Doppler radar observations at vertical incidence 2−75550
atmospheric, effect on remote sensing of atm. particulate pollutants 2−81693
atmospheric, effects on laser beam propagation 2−84861
atmospheric, errors in optoelectronic angle sensors 2−58690
atmospheric, filtering of radar pulse volume measurements 2−75551
atmospheric, fluctuating properties of Gaussian light beam from viewpoint of mode conversion 2−46859
atmospheric, flux near ground, field measurements 2−78354
atmospheric, hybrid analogue data acquisition system 2−78353
atmospheric, intermittent, phase angle considerations in modelling 2−48479
atmospheric, kinetic energy, dissipation, aircraft measurements 2−68896
atmospheric, laser beam wander phenomenon due to. 2−84862
atmospheric, modulation transfer fn., solar telescope 2−76049
atmospheric, optical transfer function detn. averaging time depend. 2−57997
atmospheric, over snow 2−72737
atmospheric, radar meas. 2−75547
atmospheric, rel. to internal gravity waves 2−58038
atmospheric, spatially-bounded light beam propagation in, influence of initial diameter on beam axis intensity 2−44730
atmospheric, stability, heat and momentum fluxes, during dry unstable conditions 2−75529
atmospheric, veloc. field meas., by Doppler radar 2−75543
atmospheric flow system instabilities associated with clear air turbulence 2−72782
atmospheric gravity waves, nonlinear model of growth characts. 2−65689
atmospheric kinetic energy spectrum power laws using harmonic functions 2−75558
atmospheric model, scintillation of spherical and plane waves 2−81680
atmospheric Pasquill stability classes, turbulence intensity and stability ratio measurements 2−65692
atmospheric surface layer, cospectral similarity 2−68895
atmospheric surface layer, over water, instrumentation 2−68902
atmospheric surface layer, spectral characteristics 2−65696
atmospheric surface layer, structure modelling 2−62160
atmospheric surface layer, turbulent diffusion 2−62092
atmospheric surface layer over water, velocity and temp. fluctuations 2−68903
atmospheric transports, near ground, on-site data analysis 2−78352
atmospheric turbulence meas. instrument attached to captive balloon 2−81663
atmospheric turbulence structure function, radar measurements 2−75548
atmospheric turbulent Ekman boundary layer, laboratory study 2−54828
atmospheric type boundary layers with large Reynolds number 2−43235
axial flow turbomachines, annulus wall boundary layer development 2−77351
axisymmetric jets and wakes, implicit finite difference soln. 2−60325
axisymmetric turbulent boundary layers in zero pressure-gradient flows 2−46691
Batchelor's invariant, validity in incompressible magnetohydrodynamics 2−83529
beam spreading in turbulent medium, calc. by modified von Karman spectrum 2−49415
benzoic acid/water, mass transfer coeffs. on flat plate by parallel channel flow and turbulence promoter 2−67601
boundary layer, 3-dimensional, calc. by explicit finite-difference scheme 2−46661
boundary layer, air flow over sudden change of surface roughness, numerical computation 2−48480
boundary layer, discontinuity in wall temp. and concentration, heat and mass transfer 2−53274
boundary layer, effects of injection through porous surface 2−74458
boundary layer, free boundary obs. 2−83433
boundary layer, incompressible shear stress distrib., in air flow 2−60333

Turbulence continued
boundary layer, influence of uniformly sheared free stream 2–77353
boundary layer, intermittent phenomena, theory and analog computer obs. 2–43079
boundary layer, meas. of Reynolds shear stress fluctuations 2–64385
boundary layer, on flat plate, wall heat flux obs. 2–43082
boundary layer, separation influenced by blowing 2–46810
boundary layer, supersonic, impact probe displacement 2–46815
boundary layer, three-dimens., low-speed, flow characts. 2–70859
boundary layer, transition from laminar to turbulent flow at supersonic velocities over parabolic wing 2–64376
boundary layer calc. with foreign gas injection 2–67718
boundary layer flow, effects of strong axial pressure gradients 2–83481
boundary layer flow, memory effect due to axial variation of meas velocity gradient 2–77185
boundary layer flow, theory of small disturbances 2–77187
boundary layer flow over surface distorted by water waves 2–84717
boundary layer flow with heat transfer and press gradient using compressibility transform. 2–70864
boundary layer flow with heat transfer and press. gradient using compressibility transform. 2–70862
boundary layer interaction with shock wave on blunted compression surface 2–53315
boundary layer over sloping underlying surface 2–72785
boundary layer pressure excitation, response of finite periodic beam 2–76358
boundary layer response to step change in surface roughness, rough-to-smooth 2–50248
effects on boundary layer transition 2–50152
boundary layer with positive pressure gradient and injection 2–74328
boundary layers, anomalies in anemometer obs. 2–80406
boundary layers, at low Reynolds number 2–60126
boundary layers, development on circular cylinder, separation bubbles 2–80437
boundary layers, friction in gas saturated liquid 2–53375
boundary layers, highly nonequilibrium, velocity and shear stress obs. and calc. 2–80214
boundary layers, interactions of shock wave, pressure fluctuation 2–43257
boundary layers, intermittent structure of wall region 2–77181
boundary layers, large Reynolds number, asymptotic expansion of eqns. of motion 2–74330
boundary layers, on yawed flat plate 2–53319
boundary layers, separation in strong adverse pressure gradients with injection through porous flat plate 2–74317
boundary layers, three-dimens., behind yawed separation bubbles, flow props. 2–67699
boundary layers, time scales and correlations 2–64403
boundary layers, two dimensional, in increasingly adverse pressure gradients 2–43086
boundary layers, wake hypothesis 2–43083
boundary layers along curved surfaces, flow characts. 2–67602
boundary layers calc. 2–74305
boundary layers flow separation, model 2–43084
boundary layers in supersonic nozzles 2–71071
boundary layers uniform mass transfer including low Reynolds numbers 2–43064
boundary layers with mass transfer, data survey 2–43055
broad-band, conditions for vibrs. in hot-wire filaments 2–73405
bubbly two-phase flow, characteristics 2–80440
Burgers eqn. for turbulent flow, table of solns. 2–77179
Burgers model, statistical mechanics, random triangular shock waves 2–83462
CAT, detect using lidar 2–81649
cetyltrimethylammonium bromide, velocity profile in turbulent pipe flow 2–53350
Chandrasekhar's equation and correlation functions for isotropic turbulence, resolution of equation 2–70871
circular air jets, subsonic, pressure fluctuations, space correlations 2–71076
clean air turbulence, remote i.r. detection 2–84866
clear air, automated forecasting 2–72750
clear air, generation by nonlinear waves 2–54831
clear air, global dynamics, statistical self-similarity theory 2–68898
clear air, life cycle by mesoscale analysis 2–75544
clear air echoes, coexistent waves and turbulence, near marine inversion 2–75546
clear air turbulence, air motion meas. using high-power Doppler radar 2–78366
clear air turbulence, radar and radiosonde measurements 2–75545
cocurrent jets, isothermal and nonisothermal mixing 2–74462
colloidal dispersions, viscoplastic deposit formation in turbulent pipe flow 2–83826
column flow, obs. using ^{24}Na labelled Na_2CO_3 solution 2–56456
combustion process, acoustic noise generated by, analytical results 2–69774
complex and non-self-similar flow 2–77321
compressible boundary layer, calculation method with heat transfer 2–43061
compressible boundary layer heat transfer to rough surfaces in pressure gradient 2–56425
compressible nonadiabatic boundary layers calc. 2–70861
compressible subsonic separated jet flow, numerical method of description 2–83674
convective heat transfer of liquid in tube 2–60461
deformation of velocity profile in turbulent boundary layer in water and oil 2–74492
degeneration in wake of square mesh grids in wind tunnel 2–74459
density stratified fluids, heat transfer 2–77249
density stratified fluids, instrumentation for obs. 2–43081
developed, model, law of energy distrib. 2–77194
developing laminar and turbulent duct flow with chemical reactions 2–83658
diffusion, analogy with molecular diffusion, features of turbulent motion in sea 2–44629

Turbulence continued
diffusion, variational methods of quantum mechanics in theory 2–46677
diffusion across density interface in ocean, model 2–84706
diffusion flame in homologous turbulent shear flows 2–69786
diffusion in sea, use of tracers, dependence of eddy diffusion coefficients on scale of phenomena 2–44630
distortion approaching two-dimensional bluff body 2–46676
drag reduction in fluids rel. to wavelength of flow-oriented wall eddies 2–53172
early period decay process, Millionshtchikov's hypothesis, consequences 2–50235
Earth atmosphere turbulent elements, size distribution using solar scintillation meas. 2–62171
effects on point source image quality 2–70009
electron longitudinal temp., ion transverse temp., scatt. by elec. field pulsations 2–80306
e.m. propagation, beam shape effects on phase fluctuation, atmospheric application 2–44728
entrainment, across density discontinuities 2–77241
exhaust plume/boundary layer interactions at supersonic speeds 2–56423
flame struct., chemilum. meas. applic. 2–61780
flap turbulent heating, skin friction and pressure data from hypersonic shock tunnel 2–53314
flat plate boundary-layer transition in supersonic wind tunnels 2–43248
flow, axisymmetric, past a long cylinder, analysis using law-of-the-wall approach 2–46689
flow, conditional sampling 2–43080
flow, damping of precessing vortex cores in swirl generators by combustion 2–83427
flow, free shear, errors in intermittency obs. 2–46811
flow, heat transfer processes 2–77219
flow, homogeneous, statistical theory 2–70842
flow, in long, straight rectangular duct of high aspect ratio 2–43085
flow, in rotating cylinder cell, mass transfer 2–53347
flow, incompressible turbulent, resolution of split flows at thick bodies, numerical method for computer solution 2–64231
flow, intermittent nature 2–77183
flow, isotropic and Gaussian exact Gaussian soln. of passive scalar 2–70851
flow, kinetic theory 2–70853
flow, laser anemometer, tracer behaviour 2–43054
flow, model, laws for boundary layers and pipes 2–77190
flow, pressure fluctuations at boundary 2–74326
flow, shear, mechanics of controlled wave disturbances 2–60171
flow, shear, small amplitude wave disturbances, models rel. to expts. 2–60172
flow, time mean values, equations 2–56288
flow, time-interval and amplitude analyser, control of chronophotographic analyser 2–67708
flow, uniformly sheared, review 2–43078
flow, with shear, effect of mag. field 2–70873
flow around bluff bodies 2–77186
flow electro-diffusion method of meas. of spectral characteristics 2–77234
flow fluctuations near wall, mean period 2–83425
flow in heated channel, eddy conductivity 2–76396
flow in rough tubes, heat transfer 2–56282
flow instability on rotating disc, electrochemical obs. 2–67579
flow meas., three component dynamic wind tunnel balance design 2–46829
flow near rough surface 2–74324
flow over rigid half plane, sound radiation 2–74311
flow stability in M shaped velocity profiles and MHD 2–60206
flow through truncated sector ducts, momentum transfer coeffs. 2–83439
flow with weak drag reducing solution of polymers 2–77373
flowing liquids, in pipe, separation of binary mixtures by freezing 2–46878
flowmeters, float-area-type, characteristics for turbulent region 2–71134
flows, experimental methods, review 2–77238
flows of liquids in pipes, forced convection heat transfer 2–55577
fluid, buoyancy-surface tension instability due to internal heat source 2–64248
fluid flow, study using light dispersion techniques, evaluation 2–77216
fluid flow and heat transfer, conference (Lucas Heights, Australia Aug. 1971) 2–43077
fluid near wall, stat. analysis by conditional sampling 2–83430
fluid turbulent heat transfer near pseudo-critical temp. in supercritical pressure 2–74320
fluids, generation of thrust, continuum mechanics, book 2–70825
fluids, turbulent shear stress, calculation method 2–67588
formation of regular components in random field of turbulent fluctuations with unsteady growth of boundary layer 2–74327
free shear layers, instability considerations 2–80198
friction, effect of polymer additions in free flow of water in tubes 2–53361
friction, flow in tubes and channels 2–53124
fully developed turbulent air flow through concentric annuli 2–53280
G supergiant atmospheres, microturbulence 2–58299
gas, liquid droplet evaporation, impurities effect 2–71279
gas flow, hot wire anemometer corrections 2–64369
gas jets, cryogenic discharges into gaseous medium 2–74460
gas-solids suspensions, turbulent pipe flow, particle slip velocity 2–53284
Gaussian isotropic turbulent flow, velocity field and temperature distribution 2–74334
geostrophic, resolution implications 2–78363
glass particles in air flow, suspension trajectories, velocity of particles 2–76395
Hartman flow, hydrodynamic stability in two dimensional perturbations 2–50182
heat and mass transfer from large body of water 2–57891
heat island formation, numerical expt. 2–75527
heat transfer to non-Newtonian liquids 2–50297

Turbulence continued
high speed jets, acoustic noise 2−77350
homogeneous, decay, theory and expt. 2−46682
homogeneous, stationary, fluid line growth, simple proof 2−56306
homogeneous, two dimensional, relative dispersion in enstrophy-cascading inertial range 2−46669
homogeneous, two species isothermal reactions 2−83426
homogeneous associated with purely plane deformation, velocity- pressure correlations 2−56281
homogeneous with rot. anisotropy, eqns. for moments 2−46657
hot wire anemometers, spatial calibration properties in turbulent velocity fields 2−60341
hydraulics and fluid mechanics, conference, Melbourne Australia (1971) 2−77207
hydrodynamic systems, scattering of e.m. waves 2−46860
hydromagnetic, produced by momentary current in semi-infinite fluid 2−53171
hypersonic flow, construction of hot-wire anemometer 2−64373
hypersonic turbulent boundary layers structure 2−50247
incompressible flow, instabilities in limiting laminar layers 2−43069
incompressible fluid, homogeneous isotropic turbulence studies using eddy representation of Navier-Stokes equation 2−46697
incompressible fluid flow, turbulent wake behind plane plate 2−50144
incompressible fluid theory of homogeneous isotropic turbulence, eddy description of Navier-Stokes eqn. 2−77173
incompressible fluids, interaction of two flows in flat duct 2−77217
incompressible turbulent flow in permeable-walled duct 2−70856
incompressible two dimensional wall jet characts. 2−50158
induced secondary flow in square sectioned ducts 2−60156
instability pattern in pipe flow produced by turbulence promoter on viscous sublayer 2−43088
intermittency, qualitative model 2−56307
intermittency effect on e.m. wave scatt. by underdense plasmas 2−50195
intermittent in free atmosphere, energy budget 2−44702
intermittent small-scale structure of turbulence, data processing hazards 2−77261
inviscid fluid flow between rotating cylinders under circular magnetic field, stability of non-rotationally symmetric disturbances 2−43111
ionosphere, local turbulence stability criteria 2−58077
isotropic, angular dispersion of fluid line element 2−80170
isotropic, generated by mechanically agitated grid, decay 2−60389
isotropic, quasi-stable energy spectrum 2−80166
isotropic homogeneous, Reynolds tensors with pure deformation 2−60127
isotropic plasma, radiative transport analysis of e.m. propagation 2−64274
jet, circular, aerodynamic noise obs. 2−64387
jet, homogeneous free, turbulence characteristics meas., investigation of the peculiarities of the heat diffusion method 2−80196
jet, in cross flow, distribs. of vel., press., temp. and intensity 2−71084
jet, turbulent, pot. core, entrainment region, intrinsic struct. 2−64237
jet, two-phase, intensity determ. 2−46995
jet discharging horizontally into lake or river, heat transfer, diffusion and mixing 2−78304
jet flames, structure, effect of rotation 2−80376
laminar cross flow, turbulent plume growth and rise 2−67701
laminar pipe jet 2−83422
large eddies, calculation by extension of classical energy method for stability analysis 2−43286
laser anemometer, Doppler difference method, automatic data processing system 2−84789
laser Doppler vel. meter for charact. 2−69540
laser Doppler velocimeter, instantaneous turbulence velocity measurement 2−43230
laser Doppler velocimeter design for use in turbomachinery 2−46826
laser induced, spectral law of temp. fluctuations 2−82523
laser velocimeter for meas. 2−70838
lateral shearing interferometry data reduction, application to turbulent medium 2−79352
limiting layer, primary vel. distrib. in dihedron interior 2−50143
liquid, mass transfer coeffs. for gas absorption 2−50298
liquid films, vertical falling, classification of flow regimes 2−74490
liquid-filled, precessing spherical cavity, turbulent motion, rigid body approximations 2−46892
low speed wind tunnel, turbulent separated flow downstream of rearward-facing step, heat transfer 2−50242
lower atmosphere, effects of evaporation on stability, and radiation on temp. fluctuations 2−44699
lower atmosphere boundary layer, static pressure fluctuations measurement in, instrumentation 2−72755
macroturbulence, main sequence stars, line broadening 2−75741
magnetoplasma column, transverse Kelvin- Helmholtz turbulence 2−70933
magnetospheric processes, computer simulation 2−65867
Markov random process rel. to light beam displacement in turbulent medium 2−79317
mean velocity profile thick turbulent boundary layer, along circular cylinder 2−70835
measurement, in two-phase region of hydraulic jump 2−64235
measurement by laser anemometer measuring individual realizations 2−80182
measurement using Laser Doppler Velocimeter system 2−71087
mechanically agitated systems, applic. of theory of Markov's processes 2−83753
meteorology, computer applications 2−84787
MHD, effect of Alfven waves on struct. 2−50181
MHD, generation of sound 2−53170
MHD, Hall effect, effect of conductivity 2−43110
MHD disturbances due to sudden introduction of an oscillating dipole in a fluid of finite conductivity 2−67618
MHD plasma, nonlinear analysis 2−80258

Turbulence continued
microfluctuations of wind velocity derivative in surface layer 2−72786
Millionshtchikov's hypothesis of early period decay, consequences 2−50235
mixing, co-flowing streams, diffusion flames 2−77349
mixing free gas jets 2−74461
mixing layer between streams of gases 2−80208
mixing of different density jets, gas jet mixing with density differences 2−56404
naphthalene/air, mass transfer coeffs. on flat plate by parallel channel flow and turbulence promoter 2−67601
I-naphthol, velocity profile in turbulent pipe flow 2−53350
natural signals, for velocity and mass flow obs. 2−83762
near wake of a slender body, decay rate of boundary layer turbulence 2−56411
near-wall collateral flow in three-dimensional turbulent boundary layers 2−43063
neutral atmosphere, radio meteor method of observing winds and turbulence 2−48522
non-Newtonian liquids, heat transfer in agitated vessels 2−74538
non-Newtonian suspensions in water, flow 2−83823
nonequilibrium wakes, applic. of model Reynolds stress equation 2−56294
nonisothermal pipe flow, obs. behind attached ring-type turbulence promoter 2−43087
nonlinear panel response, turbulent boundary layer 2−71090
nonstationary flow in tubes, coefficient of frictional resistance 2−50148
North Atlantic Ocean, internal waves and turbulence 2−62040
nozzle, turbulent boundary layer meas. with and without wall cooling 2−53287
nuclear fuel rod assembly, utilizing helical wire wrap spacer, turbulent flow pressure drop model 2−76930
ocean, vertical exchange, effect of water stability 2−44637
ocean, vertical mixing, thermoclines 2−44609
ocean wave breaking, turbulent dissipation 2−57874
oceanic general circulation problem, turbulent equations 2−57836
oceanography, mixing in deep stratified ocean 2−78224
open channel flow, suspension wire-probe and hot film anemometer 2−77386
optical, in sea 2−84766
optical beam propagating in turbulent medium, mutual coherence function 2−49390
paradichlor benzene/air and ammonia/air, mass transfer coeffs. on flat plate by parallel channel flow and turbulence promoter 2−67601
partial differential equations, turbulence solutions 2−53118
passive scalar dispersion in non-uniform turbulent flow, Wiener-Hermite expansion 2−56325
persistent, intense, clear air turbulence in upper level frontal zone 2−57966
pipe and channel flow, eddy viscosity model 2−43065
pipe flow, burst signatures 2−77184
pipe flow, longitudinal velocity fluctuations 2−60125
plasma, book 2−83625
plasma, causing acceleration, momentum exchange between two plasmas in relative motion 2−50188
plasma, e.m. reflection 2−64275
plasma, e.m. scattering theories, criticism 2−46742
plasma, ion energy distribution resulting from turbulent heating 2−70927
plasma, ion wave lifetimes 2−80308
plasma, ion-sound instability, three-dimens. current-driven, computer simulation 2−53234
plasma, kinetic equations 2−53221
plasma, low β perpendicular MHD shock waves, exptl. study of turbulent resistivity 2−53187
plasma, magnetized, application of hierarchy of eqns. to resonant three wave interactions 2−43133
plasma, magnetized, hierarchy of eqns. 2−43132
plasma, nonlinear mechanics of unstable systems 2−83627
plasma, nonlinear theory of density fluctuations 2−56380
plasma, probabilistic models 2−56371
plasma, produced by electron cyclotron drift instability 2−46787
plasma, quasiparticle conservation 2−56372
plasma, solar atmosphere 2−62801
plasma, stimulation of optical transitions 2−43145
plasma, summary 2−80334
plasma, theories and expts. 2−80333
plasma, theta-pinch, with azimuthal mag. field, small-scale drift instability turbulence 2−67644
plasma, transport phenomena det. from e.m. waves interactions 2−70886
plasma, wave growth 2−70944
plasma, whistler disturbence, computer simulation 2−60283
plasma dense focus, model 2−83589
plasma direct and cross polarized radar backscatter power 2−74363
plasma of combustion products, conductivity and Hall parameter 2−64265
plasma phenomena in high energy, astrophysics 2−78432
plasma stationary turbulence, mechanism 2−77295
plasmas, nonlinear magnetosonic waves 2−60275
polyacrylamide aqueous soln., pulsation velocity in turbulent boundary layers 2−74491
polymer solutions, dilute laser velocimeter obs. 2−71128
polymer solutions, laminar and turbulent entry flow 2−46884
pregalactic, damping of eddy motion for model of hot expanding universe 2−81810
propagation speed and attenuation coeff. of plane coherent acoustic waves 2−41721
propane-air mixture, flow, burning stability 2−67702
random inhomogeneous media, amplitude-phase fluctuations of plane light wave in 2−48507
Reynolds stress near wall in turbulent boundary layer flow 2−77260
Richardson's criterion, determ. of new and less restrictive filter conditions 2−53145
rough and smooth wall boundary layers, statistical props. 2−77180
sea wave generation by turbulent wind 2−44608
separated turbulent supersonic flows 2−77336

Turbulence continued
- shallow rectangular cavity flow 2−60151
- shear flow, conditional sampling 2−70860
- shear flow, growth and maintenance of turbulence field 2−80181
- shear flow, local transport eqns., determ. of mean velocity, kinetic energy, shear stress 2−83468
- shear flow, model equation 2−64239
- shear flow in wall region 2−77203
- shear flows, burst rates 2−77384
- shear layer prediction on basis of transport equations for Reynolds stresses 2−77237
- ship hydrodynamics, theoretical models, review 2−77379
- ship resistance, Havelock-Oseen theory 2−77375
- skin-friction meas. in laminar and turbulent flows using heated thin film gauges 2−60138
- in smooth, rough pipes, Reynolds numbers from 30000 to 480000 2−67589
- smooth cylindrical pipe, temp. distrib. obs. 2−80160
- solar chromosphere, microturbulence and line profiles, generated by acoustic waves 2−76016
- space vehicle entry simulation, arc-heated duct facilities 2−66028
- spatially-bounded light beams in turbulent medium, correlation function of axial displacements in turbulent medium 2−44729
- spreading of disturbance 2−70829
- stars, UBV colours, microturbulence effects 2−51752
- statically stable parallel shear flow, coupled wave- turbulence system 2−68892
- statistical models, conference, San Diego, California (1971) 2−43052
- statistical theory of light propagation in turbulent medium, review 2−82553
- stellar and planetary atmospheres, hydrodynamic motions in stratified convective zones 2−78455
- stellar atmospheres, hydrodynamic characteristics 2−58310
- stellar atmospheres, mixing due to meridional circulation velocity field 2−62503
- stratified magnetized plasma, e.m. wave reflection, transmission 2−77274
- structure in rotating fluid 2−77202
- subsonic and supersonic boundary layer flow past wavy wall 2−56408
- supersonic boundary layer, in adverse pressure gradient, data analysis 2−56426
- supersonic boundary layer, incipient separation, heat transfer 2−71070
- supersonic boundary layer in adverse pressure gradient 2−46806
- supersonic compressible turbulent mixing layers, shock tube expt. 2−71102
- supersonic jet, aerodynamic study of two-stream propulsive systems 2−50256
- suppression by magnetic field 2−50184
- suspension, of rigid particles, high Reynolds number, drag reductions, expt. 2−53373
- suspension, viscosity props., in limit of drag reduction 2−53364
- suspensions, agglomeration rate/deposition rate relationship 2−43396
- swirling flow vel. profiles, fluid resist. in duct, expt. 2−80197
- thermal convection in horizontal fluid layer, volumetric energy sources 2−80429
- three dimensional disturbances in boundary layer along concave wall 2−74495
- three-dimensional boundary layers, hodograph models for cross flow velocity components 2−67587
- three-dimensional wall jet from circular orifice 2−64380
- toroidal hydromagnetic waves, in dipole field, asymmetry 2−65863
- transition from laminar to turbulent flow past sphere 2−67750
- transpired boundary layer velocity and shear stress distribs. 2−46688
- transport of solid particles by turbulent flows 2−74329
- troposphere, and refractive index structure coefficients 2−65776
- troposphere, Kelvin Helmholtz billows in upper tropospheric jet stream, radar Doppler meas. 2−75541
- troposphere, kinetic energy 2−72775
- two phase flow of liquids with bubbling, method of limited expansions 2−56462
- two-dimensional, lower order models 2−80177
- two-dimensional, statistically steady, numerical simulation studies 2−68893
- two-dimensional jet attachment on plane wall 2−83689
- two-dimensional separation, numerical experiment 2−70839
- two-dimensional unsteady flow, forced heat transfer from hot film 2−80431
- ultrasonic holography with large phase disturbances using stochastic processing 2−73607
- underwater, causing decay of surface capillary-gravity waves 2−53367
- upper atmosphere mixing, thermal effects of buoyancy forces 2−48530
- Venusian atmosphere, turbulence characteristics of atmosphere from Mariner V S-band occultation data 2−78568
- viscoelastic fluid layer, thermal instability 2−64225
- viscous sublayer, effect of drag-reducing polymers 2−46880
- viscous sublayer near plane wall 2−74325
- wake, asymmetrical, generated by pairs of cylinders, flow characteristics 2−50246
- wake, large scale instabilities 2−67771
- wakes, equilibrium and relaxation 2−56293
- wakes, flat plate in uniform flow, velocity fluctuations 2−80407
- wakes, temp. fluctuations, measurement by probe 2−77330
- wakes of cylinders in crossflow, sensitivity to freestream turbulence of heat transfer 2−55576
- wall jet interaction with shear flow, mixing flow 2−83482
- wall jets, three dimensional, growth 2−77200
- wall jets, turbulent kinetic energy prod., Reynolds numbers 2−83455
- water, bonded jet, mean flow properties 2−77396
- water, free jet flow, amplitude modulation of ultrasound 2−74494
- water, hot wire anemometer measurements 2−77385
- water, small-scale structure, temp. obs. 2−77323
- water, turbulent velocity fluctuation meas. using cell flowmeter based on variation of electrical resistance 2−71137

Turbulence continued
- wave breaking, wave generation by wind and momentum conversion to steady currents 2−78335
- waves in weakly ionized plasma 2−80312
- weirs and flumes, flow measurement 2−83756
- wind and temp. profiles, turbulence effects 2−62172
- wind structure in city environment 2−57964
- winds over open water, trivane measurements, tilt errors and precipitation effects 2−72783
- CO_2 electric discharge convection laser, electrical power deposition control 2−59152
- H_2O circular jet, energy spectrum and turbulent scales 2−46901
- He^+/Ar^+ plasma simultaneous ion heating in linear turbulent-heating expts., mass dependence 2−80288
- He, superfluid as ultrasonic cavitation nucleation mechanism 2−43426
- He II, forces in superfluid flow 2−80501
- He II, laminar and turbulent flow 2−47017
- He II, onset of turbulence for counter flow 2−43420
- He II, pressurized, escape of negative ions and vortex annihilation model 2−67857
- He II, superfluid, stabilization by flow modulation 2−43421
- Hg, small-scale structure, temp. obs. 2−77323
- Hg liquid flow in tube, temp. fluctuation spectra 2−64413
- Rn steady state diffusion in atm. 2−65669

Turbulent flow *see Flow*

Twilight
- *see also Atmospheric spectra; Zodiacal light*
- brightness of twilight sky, atmospheric scattering rel. to meas. of light polarization 2−81657
- circular polarization of scattered light 2−68911
- Orionid 1970 meteor shower, effect on optical properties of twilight sky 2−84781
- simultaneous photometric meas., 21 and 6 mb, aerosol obs. 2−75782
- sky, effect of aerosols on radiance and colour 2−81690
- thermospheric O_2 abundance obs. at 6300Å 2−58055
- vertical scatter distribution, free electrons and dust particles 2−72835
- visual observation from manned spacecraft 2−75624
- O $\lambda6300$ and $\lambda5577$ profiles, det. of neutral temp. in ionospheric F_2 and E-regions 2−65973
- O_2 $(^1\Delta_g)$ emission, altitude profile 2−58054

Twinning *see Crystals, twinning*

Twistors *see Calculating apparatus; Magnetic devices*

Two-phase flow *see Flow/two-phase*

Type II superconductors *see Superconductivity/type II*

Ultracentrifuges *see Centrifuges*

Ultrasonics
- *see also separate headings, e.g. Absorption/acoustic waves, ultrasonic*
- alloy production that are otherwise difficult to make 2−50820
- aortic diameter pulsatile variations meas. 2−51944
- arterial flow monitoring, u.s. Doppler probe 2−69367
- arteriography using phase locked echo tracking for meas. of arterial diameter changes 2−51932
- atomization of liquids 2−80495
- attenuation meas., beam divergence effect 2−73434
- B-scanning in differentiation of Baker's cyst and thrombophlebitis 2−78636
- basic theory 2−52225
- biomedical diagnosis, broad-band technique 2−45046
- biomedical techniques for differentiation between normal and infected myocardium 2−51889
- blood velocity profiles, real-time obs. using u.s. multigated pulsed Doppler velocimeter 2−69311
- blood vessel imaging 2−69310
- blood vessel imaging using Doppler effect 2−62828
- bolt clamped electrostrictive torsional vibrator for u.s. power applications 2−73412
- broad-band technique, specific acoustic impedance of human skull bone 2−48890
- bubble chamber 2−67099
- bulk modulus loss factor determ. of small specimens 2−71615
- cavitation, review 2−78925
- chemical relaxation studies, resonance technique 2−76372
- CHLF hamster cells resistance to 1.5 MHz ultrasonic radiation 2−48873
- chromosome aberration induction rel. to ultrasound intensity 2−48867
- chromosome damage at diagnostic power and frequency ranges 2−48870
- chromosome damage in Chinese hamster cells following high intensity pulsed ultrasound irradiation 2−48869
- chromosome damaging effects on human blood cells 2−48871
- cleaning process, efficiency and meas. of degree of cleaning 2−63130
- clinical safety of low megaHertz frequencies, production of haemorrhagic injury and paraplegia in rat spinal cord 2−48872
- crack depth obs. 2−71614
- cross sectional echography, medical diagnosis applications 2−76371
- cutting, of rock materials 2−41785
- defect evaluation, work at German Federal Institute for Materials Testing 2−69756
- delay line, 600 MHz acousto-optical deflector 2−51296
- delay lines, isopaustic glasses 2−78928
- delay lines, surface acoustic wave tapped, techniques for code changing 2−49125
- diagnostic, radiation therapy applics. 2−69303
- diagnostics, teratogenic effects 2−73203
- display of three dimensional u.s. data for medical diagnosis using computer 2−66273
- Doppler blood flowmeter, theory 2−85092
- Doppler flow transducers for detection of bubbles in blood 2−66277
- Doppler flowmeter, vol. blood flow meas. 2−51901
- Doppler probe for studying foetal cardiac activity 2−51939
- echo ranging applics. to oral mucosa 2−51945
- echoencephalography, u.s. tomogram 2−69366
- elastic property meas. method for solids under pressure 2−68060
- encephalographic system, patent 2−85093
- fibre reinforced composite, stress wave dispersion 2−47743

Ultrasonics continued
field meas. by liquid surface relief method 2−63110
flaw detection, grain size meas. strength and elasticity 2−64752
flow detection, electromagneto-acoustic n.d.t. in USSR 2−45524
flow detection in machine construction, review 2−82362
flow rate obs. rel. to radioactivity cloud and thermodynamic methods 2−83760
flow transducer for chronic respiratory monitoring 2−55247
flowmeter, meas. at variations in circulation 2−71136
flowmeter and applic. 2−76370
fluids, influence of non-uniformity of acoustical fields 2−82365
forging testing, fault position detn. 2−84156
fractional harmonic generation, in resonant wave system 2−58919
fracture speed meas. using u.s. fractography applic. to Si and Ge 2−82123
generator magnetically tunable with laminated Fe core 2−49132
guided waves in symmetric fluid-solid systems, normal modes 2−49123
heterodyning with noncritical angular alignment using pair of u.s. light modulators 2−79240
holographic imaging, synthetic aperture 2−82367
holographic multiplexing technique to construct 3-D images 2−79250
holography, methods and applications, book 2−63363
holography, real time image reconstruction techniques 2−49166
holography, underwater viewing system and acoustical hologram reconstruction 2−49165
holography, visualization of holograms using Pohlman cell 2−69976
holography, with large phase disturbances using styochastic processing 2−73607
horns, high power, for liquid processing 2−49139
hypersonic flow, internal, inviscid, about unyawed cones, closed form solutions 2−56428
imaging, with good lateral resolution, for medical diagnosis 2−51935
imaging system using optical pulse compression 2−73443
inspection equipment for reactor safety 2−59871
intensity measurements, Radiation Control for Health and Safety Act 2−45041
interference pattern visualization in front of radiating quartz by optical illumination in direction of propagation 2−55547
intracardiac scanner, circular array cathetertip 2−45044
intracranial pressure wave detection with ultrasound 2−69304
laminography of laryngeal tumours 2−69306
Langevin type electrostrictive torsional vibrator, bolt clamped 2−69725
lesion formation by high intensity ultrasound, relation of temperature 2−51917
light diffraction, data processor, high speed printer 2−76116
light diffractions for optical images of two-dimensional object 2−45790
liquid, meas. using thermocouple 2−69719
liquid atomization, mechanisms 2−60379
liquid crystal, study of propag. of hypersonic waves near cholesteric-isotropic transition 2−80454
liquid crystals, cholesteric nematic transition, ultrasonic pulse-echo attenuation meas. 2−80456
liquid level detection using flexural wave attenuation in tube 2−49168
liquids atomization 2−74507
liver scanning, A-scan obs. of normal and cirrhosis liver 2−45033
low temp. techniques especially for acoustic paramagnetic resonance, review
lymphocytes, chromosome aberrations, ultrasonic irradiation 2−48868
macrosonics, ultrasonic and macrosonic motors 2−41783
manometer column height obs. 2−45226
measurement, multiple crystal folder 2−82360
mechanical strength det. of brittle surface layers 2−56845
medical B scan examination difficulties 2−76083
metal crystal growth in macrosonic fields, dislocation structures 2−50590
metal fatigue studies 2−50794
metal removal, cutting, lathe turning, boring and twist drilling 2−41786
metal working processes, sonically assisted 2−41784
minerals, determ. of elastic props. 2−68848
mixing of fine powders for spectral anal. 2−65406
multiple gate pulse Doppler flowmeter for spatial velocity profiles in blood vessels 2−51934
multiple probe array 2−69760
n.d.t. of adhesive bonded metal-to-metal joints 2−47674
non-destructive testing applics., visualization methods 2−69758
non-destructive testing technique for multilayered media 2−69762
nondestructive monitoring for optimization of in-service performance tests 2−60924
nondestructive testing of materials 2−69757
ocean swell-wave-tide u.s. analysis, industrial equipment 2−72731
one path ultrasonic fluid flowmeter using electroacoustic feedback 2−55549
optical Bragg diffraction by standing ultrasonic waves with application to optical demultiplexing 2−49421
optical modulation, matched filter, using Raman-Nath diffraction 2−79285
paramagnet, perturbed γ-γ angular correl. eff. of spin-lattice relaxation and ultrasound 2−72241
paramagnetic resonance absorption of ultrasound by conduction electrons 2−81464
particle detector, metal, using generation of, for ultrahigh energy particles 2−73941
passive resonator returning, rel. to laser pulse modulation 2−69900
physiological diagnostic moving target indicator system 2−51931
piezoelectric crystals, scanned bulk waves, surface excitation 2−51201
piezoelectric semiconductors, impurity diffusion coefficients, ultrasonic meas. method 2−50691
piezosemiconductor, effect on polarization on ultra-sound amplification 2−84202
plastics molding and extrusion using high powered ultrasonics 2−50412

Ultrasonics continued
polycrystalline materials, scattering, attenuation frequency dependence 2−69743
power meas. by calorimetric meas., effects of thermal parameters 2−52245
power measurement, in microwatt-milliwatt range 2−41794
probes, standardization, factors affecting performance 2−69759
pulse echo investigation of solids, electronic equipment 2−73499
pulse echo visualization for clinical diagnosis 2−51942
pulse generation, transducer with intermediate layer of quarter wavelength, transient response analysis 2−41769
pulsed, applic. to phase transition studies 2−58927
pulsed Bragg diffraction method of ultrasonic visualization 2−49164
pulsed Bragg imaging, U.S. visualization 2−63126
pulsed Doppler velocity detector, evaluation 2−51933
radiator using standing wave formation 2−49133
review of methods used for solids, liquids and gases 2−60374
rotational fast scanner applic. to diagnosis 2−51943
scanner for two-dimensional instantaneous obs. of moving cardiac structures 2−69308
scanning, liver volume determ. 2−69348
scanning system for heart obs. 2−69309
segregation and sedimentation of red blood cells 2−81986
sheet steel inspection, acoustic anisotropy obs. by pulse resonance method 2−64773
solid state and quantum electronics, book 2−57092
spectrometric study of formation of seroalbumin polysaccharide complexes 2−73171
steel rolls hardening depth ultrasonic device for measurement 2−60928
stroboscopic visualiz. of u.s. waves in liq. media 2−82492
surface wedge waves, parametric interaction 2−66626
symposium, IEEE, Miami Beach (1971) 2−49119
systems for medical diagnostic visualization 2−69239
technique for determ. of piezoelectric and elastic constants of piezoelectric materials 2−65069
test device for steel tubes using electronically focused acoustic arrays 2−69761
therapeutical intensities, breakdown of calculi 2−69343
thermometer, construction, application, operation 2−52296
thermometry, attenuation and moduli meas. in wires at elevated temp. 2−49189
transducers, graphical anal. 2−69752
transducers, holography, optical and acoustic 2−76497
transmission u.s. soft tissue visualization 2−69307
Vicia faba roots, 1.5 MHz ultrasound effects on growth 2−48833
visualization of defects by three-dimensional imaging of ultrasound 2−76378
visualization of density gradients by schlieren-optical method 2−49433
vocal fold movement obs. 2−69305
volumetric flow meas. 2−83514
water droplet production applic. 2−71241
wave interaction with laser rel. to modulators and deflectors 2−55709
welding, electrical conductivity applications 2−45181
wire bonding device, motion, holographic interferometry 2−63128
ZnO acoustoelectric device, high and low field resistivity, uniaxial press. effect 2−63119

Ultraviolet detectors *see Radiation detectors*

Ultraviolet sources *see Light sources*

Umklapp process *see Crystals/lattice mechanics*

Uncertainty *see Indeterminacy; Probability*

Undor *see Electron theory; Field theory, quantum*

Unified field theory *see Relativity/unified field theories*

Unimolecular layers *see Adsorbed layers*

Units
see also Constants; Dimensions; Nomenclature and symbols
effective magnetic moment and Bohr magneton 2−82132
electronics, German regulations 2−45211
Gaussian to International System transformation, electrostatic and e.m. equations 2−45607
photometric, measuring techniques, apparatus 2−45797
physical quantities, mathematical theory of units and dimensions 2−62956
Rontgen unit determ., magnetic field chamber 2−58675
SI, in nuclear engineering, review 2−49873
SI system, development, units, definitions 2−48971
SI system, meteorological aspects 2−65638
time, atomic unit adoption 2−55363

Upper atmosphere *see Atmosphere/upper; Ionosphere*

Uranium
see also Nuclear fission/uranium
$(U,Pu)C$ and $(U,Pu)_2C_3$, distribution coeffs. of U and Pu, microprobe analysis 2−67352
albedo data rel. to atmosphere and cloud structure 2−78558
in Ap star HD 25354, spectral obs. 2−72994
assay in rocks, neutron activation method 2−84690
atmospheric temp. sounding 2−78539
atom, electron impact ionization cross-section 2−46588
atomic imaging with electron microscope by phase contrast, specimen preparation 2−80637
atomic imaging with electron microscope by phase contrast 2−80638
automatic analysis in solutions 2−75411
burning curve ignition, expt. confirmation of theory 2−46383
chromatographic determination 2−74165
colour indices for t Sun derived from stellar and Uranus observations 2−85056
concentrates of metal 2−83072
content determ., delayed neutron counting method 2−44512
content in wind-borne Saharan dust over N.Atlantic Ocean 2−44583
covalent model for nature of 5f bonding 2−84396
diffusion mechanism in gamma modification 2−68044
distribution in Mg-Be fuel jacket, study technique using fission particle track obs. 2−42679
drill core scanning by gamma ray spectrometry 2−78293
economic geology, radioactive series disequilibrium 2−61871
electron backscattering, spectral ang. distrib. meas. 2−84218

Uranium continued
electron beam straggling, calc. of range for energies up to 4 MeV 2–68266
enrichment status in Europe 2–56016
geometric albedo, calc. and obs. 2–58512
industry and nuclear fuel requirements in Portugal 2–56056
ions charge states in emergent beams from solid foils, 29.2 - 45.7 MeV 2–49971
isotope separation, power reactor applic. 2–63961
Kuiper bands rel. to laboratory spectra of methane 2–62709
limb and polar brightening at 8870 Å 2–73087
manufacture of metal and description of plant 2–83073
masses, densities and moments of inertia 2–69142
melting and transformation enthalpies 2–53491
microwave absorpt. of atmos. H_2 2–55150
minerals, preparation for X-ray fluorescence, pressed fused disc method 2–65586
miners, investigation of immunoglobin levels in blood serum after high exposure in ionizing radiation 2–55296
mines, assessment of radiation safety and efficiency of prophylactic measures 2–55241
mines, review of scientific basis for radiation standard in USA 2–55240
mixed oxide nuclear fuels, U-content and burn-up and isotopic distribution meas. 2–75401
nuclear fuel cycle, reference materials for accurate determ. of U, Pu and Th 2–74160
innuclear fuels, chemical anal. 2–74176
in nuclear fuels, chemical analysis techniques 2–74168
separation from nuclear fuels containing Th, hydrofluorination process 2–49886
nuclear reactor fuel, chemical analysis service of JEN for purification 2–83077
nuclear reactor fuel, manufacturing control of quality of U products 2–83078
nuclear reactor fuel, quality and specifications 2–83076
nuclear targets, electrodeposition methods of prep. for cross section obs. and accelerator bombardment 2–73919
ore processing 2–61990
ores low grade, advances in prospecting 2–61989
positional observations during 1919-67 period 2–48779
prospecting, well logging, pulsed neutron method 2–44598
quantitive det. in various matrices using nuclear track technique 2–48364
radiation protection in handling 2–83154
in Rapsodie fuel reprocessing, determ. using X-ray fluorescence 2–74173
recrystallization after annealing and cold rolling at room temp. 2–68141
rods, multiquenched, microstress behaviour 2–77659
secular variations of asculating elements 2–62696
solubility in Ni, low limit. determ. from heterodiffusion coeffs. 2–43654
spectrum in 8060-8360Å region, pressure induced absorption 2–75913
superplastic behaviour under tensile stress and temp. cycles 2–47516
surface, chem. shifts in Auger transitions 2–67901
target, preparation using tilt-pour and injection casting techniques 2–73907
targets, prep. techniques 2–73912
X-ray photoelectron spectra 2–54278
I ion-Au, Th, U collisions, 10 to 60 MeV, X-ray spectra of temporarily formed superheavy quasiatoms 2–74236
U-distribution in basaltic fragments of five lunar rock samples 2–75849
α-U, diffusion coeff. of Fe, 645°C 2–50719
α-U, radiation-induced size changes 2–52845
U check specimens for spectrographic analysis of nuclear fuels 2–75407
U enrichment, gas centrifuge method 2–70530
U III, prep. and absorption spectra in acid solutions 2–75367
U IV-U VI photosensitized electron exchange reaction in HCl, kinetics 2–75365
U_2 double scatt. investigated with Glauber theory 2–42831
U^{3+} in CaF_2 and SrF_2 ENDOR spectrum of U^{3+}-F- 2–84607
U^{4+} in Cs_2ZrCl_6, Zeeman effect of vibronic transitions 2–84528
UI and UII, emission spectrum between 19080 and 30261 cm^{-1} 2–79944
^{235}U fuel element, meas. of surface contamination by fission fragments 2–52846
$U + O_2 \rightarrow UO_2^+ + e$ chemi-ionization, determ. probability of occurrence 2–68766
$U^+ + O_2(N_2) \rightarrow UO^+ + O$, determ. of reaction rate from thermal energy to 5 eV using drift mobility-tube-mass spectrometer 2–68766
Uranium compounds
alloy, scanning electron microscope obs. of ion-etched sample 2–56578
luminescence spectra 2–54458
mixed-oxide fuel elements, performance in 11 at.% burnup 2–76943
mixed-oxide fuel pins, F3A series unencapsulated, examination following irradiation in EBR-II 2–76947
oxides, adsorption of chemically nonequivalent O atoms (ions) 2–47167
U_2C_3 mag. susceptibility, after neutron irradiation, anomalous behaviour 2–84398
$UO_2(NO_3)_2.6H_2O:VO^{2+}$, e.p.r., hindered motion obs., single crysts. 2–57392
uranyl complexes, electronic structure, equatorial ligation tests of coupling schemes 2–60037
uranyl compounds in solution, transfer of electron excitation energy between ions, dependence on solvent nature 2–53442
Mo/UO_2 thermionic conversion emitter-fuel system technology and test results 2–63251
Pb/NaCl-UCl_3 molten metal/fused salt system, surface and interfacial energy 2–52874
PuO_2-UO_2 fuel rods, foil handling technique for meas. of lattice parameters 2–70532
PuO_2-UO_2 in FFTF driver fuel assembly 2–63965
$Pu_xU_{1-x}O_2$, thermal cond., 673-1273K 2–54079
ThU, supercond. transition temp., 0-20 kbar press. 2–47870

Uranium compounds continued
$Th_{1-x}U_xO_2$, thermal diffusivity, 650-2700K 2–54082
U/Pu oxide fabrication process, sampling and analysis 2–74157
U/Pu oxide fuel, reference material for chemical specification analysis 2–74159
U/Pu oxide fuels, gravimetric methods of studying O/metal ratio 2–74152
U/Pu oxides reactor fuel, comparison of two methods of determ. of O/metal ratios 2–74153
U/Pu oxides reactor fuel, comparison of two methods of determ. of O/metal ratios 2–74153
U/Pu oxides reactor fuel, determ. of Pu content by calorimetry 2–74164
U/Pu oxides reactor fuel, measurement of O/heavy metal atom ratio 2–74154
U/Th fuel elements with known irradiation data, actinide composition studies 2–75403
U-Mo alloy, stress corrosion cracking in humid aid, C content effects 2–53839
U-Nb alloy, stress corrosion cracking, metallic protective coating 2–53911
U-Nb and U-Nb-Zr alloys, low temp. oxidation 2–48334
U-O system, oxidation equilib. study 2–44487
U-Pu-W-C system, phase relations 2–54011
U-Pu carbide nuclear fuel particles, preparation 2–56062
(U-Pu)C, two-phase mixed carbides, quantitative analysis by X-rays 2–64626
$(U\text{-}Pu)_2C_3$, two-phase mixed carbides, quantitative analysis by X-rays 2–64626
U-Sb alloys, liq., thermodynamic props., 1130°C 2–56497
U-9.5 wt %Nb alloy, gamma phase decomp., discontinuous precip., 450-600°C 2–80802
$(U, Pu)O_2$ fuel rods, cladding plastic deformation and swelling rate 2–76944
$(U, Pu)O_2$ mixed-oxide with initial addition of fission product elements, postirradiation obs. 2–76945
$(U,Pu)O_2$ fuel, U-Pu redistrib., transport model 2–52853
$(U,Pu)O_2$ fuel pin, porosity and actinide redistrib., grain growth and desintering 2–56043
$(U,Pu)O_2$ microspheres and pellets, sol-gel devised, microstructure 2–47610
$(U,Pu)O_{2-x}$fuel irrad., oxygen redistrib. 2–52868
U oxides reactor fuels, O/U ratio determ. methods, review and comparisons 2–74155
UAs-US system, magnetic phase diagram, neutron diffr. obs. 2–65188
$UAs_{1-x}S_x$ system, mag. phase diagram 2–44258
UAsS(Se, Te), magnetization rel. to temp. and mag. field, 3 K to Curie point, hysteresis loop, anisotropy 2–72172
UC_2-ThC_2, UO_2-ThO_2 coated fuels for GCR, chemical analysis techniques 2–74169
UC-UC_2 and UC_2 phases, U_2C_3 formation 2–47720
UC-UN, solid soln. formation mechanism 2–53910
UC-W and UO-W thermionic, fuel cladding systems, material development 2–52369
UC-ZrC solid solns., diffusion props. 2–71541
UC, kinetics of surface smoothing 2–53556
UC, mag. susceptibility, after neutron irradiation anomalous behaviour 2–84398
UC, nuclear fuel, swelling and fission gas release obs. 2–52877
UC, oxidation in liq. Na with small O content 2–51452
UC, polycrystalline, high-temp. deformation and yielding 2–67348
UC, US, crystal synthesis by electron beam melting 2–53620
UC alloys, hyperstoichiometric, compatibility with W 2–63252
UC fuel to simulate burn-up of 100000 MWd/t, thermodynamic study 2–67351
UC_{1-x}, estimation of electrical resistivity increase due to C deficients 2–43874
UC_2, decomp. to U_2C_3 2–46384
UC_2, mag. susceptibility, after neutron irradiation, anomalous behaviour 2–84398
UC_2 coated fuel, kernel migration in out-of-pile heating 2–83081
UC_x, high temp. deform., proportional limit 2–53809
UC_x, nuclear fuel, fission gas swelling, external diametrical swelling, $T \leqslant 1900$°C 2–43614
$UC_{1-x}N_x$, $O \leqslant 1$, meas. of electrical resistivity and absolute Seebeck coeff. 2–44105
$U(C_{1-x}N_x)$, electronic properties 2–57268
$UCl_{3(4)}$-LiCl systems, binary and ternary, melting point diags. 2–67873
UF_4, induction levitation melting, shaping and thermal reduction 2–50810
UF_4, nuclear reactor fuel, description of production operations 2–83075
UF_4, sample prep. by metallurigical methods 2–73906
UF_6, spark source mass spectrometric anal. of trace elements 2–74172
UF_6 MHD units, thermal efficiency 2–63964
UN, elastic consts., 278K, u.s. determ. 2–53783
UN, O_2 solubility, 1600-1900°C 2–71649
UN, sintering study of density increases, NASA research 2–64801
UN fueled converter, out of core evaluation 2–49265
UN_x, nuclear fuel, fission gas swelling, external diametrical swelling, $T \leqslant 1900$°C 2–43614
UNCl, Patterson function calc. 2–74749
UO_2/W composite, unidirectional solidification behaviour 2–47669
UO_2/W system, eutectic structs., influence of growth parameters 2–53969
UO_2-C-N_2 reaction kinetics, 1695°C, carbonitride form. 2–54537
UO_2-Mo, W clad cermet fuel, behaviour under neutron irradiation 2–52882
UO_2-Mo cermet, finely-dispersed, creep rate and particle growth 2–71650
UO_2-Mo cermets, reactor behaviour 2–52883
$UO_{2\pm x}$-$PuO_{2\pm x}$/steel fuel/cladding interface, reaction 2–52875
UO_2-PuO_2, irradiated, gas release and swelling, 1260-1900°C 2–80662
UO_2-PuO_2, mixed fuel, control and behaviour of O/M, offgas and moisture during fabrication 2–53934

Uranium compounds continued
- UO_2-PuO_2 fuel, temp. calc., use of GAPCON and HYBRID-SINTER programs 2−52854
- UO_2-PuO_2 fuel rods, ratios of effective cross sections from burnup data 2−59856
- UO_2-PuO_2 fuels, analysis techniques for process control, quality assurance and post-irradiation examination 2−74170
- UO_2-PuO_2 fuels, chemical analysis techniques 2−74171
- UO_2-PuO_2 fuels, determ. of non-metallic specification impurities 2−74177
- UO_2-PuO_2 fuels, simulated fission product transport 2−52867
- UO_2-PuO_2 mixed fuel, discrete PuO_2 particle behaviour during rapid power transients 2−59857
- UO_2-PuO_2 mixed fuel, plastic flow and stress relax. 2−53808
- UO_2-PuO_2 mixed fuel, radiation dose rates 2−59876
- UO_2-PuO_2 mixed fuel, thermal creep, 1300-1700°C 2−53818
- UO_2-PuO_2 mixed fuel irrad. performance in PRTR 2−59853
- UO_2-PuO_2 mixed fuels, Pu and fission product redistrib. during irrad. 2−59852
- UO_2-PuO_2 particulate fueled lattice, H_2O-moderated, neutron multiplication and relative reaction rates 2−59854
- UO_2-PuO_2 thermal reactor fuel, defect performance 2−59855
- UO_2-ThO_2, solid solution, non-stoichiometric, thermodynamic props., e.m.f. obs. 2−64782
- UO_2-Zircaloy-2 contacts, thermal conductivity 2−42655
- UO, UO_2, UO_3, electron impact ionization cross-sections and fragmentation 2−46588
- UO_{2-x}, thermodynamic props., 1600-1900°C 2−53935
- UO_2, entrapment of noble gas ions 2−60815
- UO_2, fission gas bubbles, nucleation and evolution, math. treatment 2−67358
- UO_2, fission sintering and irrad. induced diffusion 2−52855
- UO_2, irradiated, gas release and swelling, 1260-1900°C 2−80662
- UO_2, lenticular pore migration, impurity effects 2−74150
- UO_2, molten, for analysis of gross fuel movement 2−67353
- UO_2, molten, stoichiometry change 2−53621
- UO_2, neutron irrad., fission gas bubble nucleation and gas migration 2−63971
- UO_2, plastic deform., fracture, rel. to porosity 2−43699
- UO_2, polycryst., plasticity, 1400-2100°C 2−53810
- UO_2, simulation of gaseous fission products for nuclear fuels 2−79838
- UO_2, thermal diffusivity, 650-2700K 2−54082
- UO_2, thermal diffusivity, 750-2700°C 2−54081
- UO_2, U_3O_8, UO_3, X-ray photoelectron spectra 2−54278
- UO_2, UO_3, nuclear reactor fuel, description of production operations 2−83075
- UO_2 and UO_2/PuO_2 nuclear fuels, X-ray spectrometric obs. of impurities 2−74167
- UO_2 clad fuel element swelling at high temp., factors 2−63250
- UO_2 clusters, fast fission ratios meas. 2−42671
- UO_2 coated fuel, kernel migration in out-of-pile heating 2−83081
- UO_2 deposit thickness, effect on fission fragment double kinetic energy meas. 2−55895
- UO_2 dispersed through graphite, fission-gas release obs. 100-950°C 2−70534
- UO_2 fuel, bubble re-soln. and creep 2−52862
- UO_2 fuel coating failure analysis 2−52864
- UO_2 fuel elements, Zircaloy-sheathed, circumferential strain obs. 2−52879
- UO_2 fuel pins, irrad. Zircaloy clad, internal free vol. and press. meas. 2−42666
- UO_2 fuel rod, irrad., pore movement kinetics 2−52873
- UO_2 fuelled W coated Mo thermionic emitters, out of pile investigations 2−52370
- UO_2 pellets, grain growth, long term obs. under annealing 2−49898
- UO_2 pellets, prep. by sintering of $(NH_4)_2U_2O_7$ 2−80800
- UO_2 properties 2−49891
- UO_2 reactor fuel, burn-up meas. from mass spectrometry of stable fission-product Nd 2−74182
- UO_2 reactor fuel pellets technology 2−56061
- UO_2 single crystal, influence of stoichiometry on compression creep 2−67350
- UO_2 sintered bodies, open pore distrib. 2−61025
- UO_2 surface film thickness determ. using reflectivity 2−79412
- UO_2 unirradiated nuclear fuel, analytical methods for determ. of total U and impurities 2−74162
- UO_2 vipac and pellet fuels, transient behaviour 2−63970
- $UO_{2\|x}$, high temp. specific heat 2−54051
- $UO_{2\|x}$, redistribution of oxygen subject to temp. gradient 2−67359
- $UO_{2.25}$, enthalpy detn. by drop calorimetry, 800 to 1600 K 2−77425
- UO_x, nuclear fuel, fission gas swelling, external diametrical swelling, $T \leqslant 1900$°C 2−43614
- $(UO_2Cl_4)^{2-}$ and $(UO_2Br_4)^{2-}$ complexes, calculation of frequencies and normal vibrations 2−74278
- UO_2F_2, for i.r. spectrum determ. of frequencies of i.r. active bands 2−60038
- $(UO_2F_5)^{3-}$, frequencies and form of normal vibrations, interpretation of luminescence spectra 2−64159
- $UO_2(NO_3)_3$ crystals, anisotropy of i.r. absorption spectra 2−75308
- $UO_2(OH)_2$, $\beta \rightarrow \alpha$ transform., transition temp. and mechanism 2−74945
- UPb_3, mag. struct., neutron diffr. obs. 2−78041
- US, cubic ferromagnet, mag. moment distrib., polarized neutron diffr. obs. 2−72171
- US, mag. ordering, ordered mag. moments, neutron diffr. obs. 2−84418
- α-US_2, mag. props., magnetization, 4.2-1000K 2−72108
- USe, mag. ordering, ordered mag. moments, neutron diffr. obs. 2−84418
- α-USe_2, mag. props., magnetization, 4.2-1000K 2−72108
- U_3Se_5, cryst. struct., refined by Weissenberg method 2−53683
- U_3Si, in-pile irrad. effects, electron microscopy and diffr. 2−47393
- U_3Si, irradiated, effect of electropolishing on voids 2−67354
- UTe-SnTe(PbTe) system, up to 10 mol % UTe, phase diagram 2−47717
- UTe, mag. ordering, ordered mag. moments, neutron diffr. obs. 2−84418
- UTe, mag. ordering, ordered mag. moments, neutron diffr. obs. 2−84418

Uranium compounds continued
- U_3X_4 compounds, theory of noncollinear ferromagnetism 2−75222
- Uo_2-PuO_2 mixed fuels, advanced characteriz. 2−52870

Uranus
- No entries

Urey-Bradley forces *see Molecules/internal mechanics*

V-centres *see Colour centres*

V-particles *see Hyperons; Mesons*

Vacancies *see Crystal imperfections/vacancies*

Vacancy breakdown *see Diffusion in solids*

Vacuum apparatus
- *see also Seals*
- automatic pressure controller, closed loop servo system controls gas throughput 2−76113
- centrifugal high vacuum still 2−76132
- CERN intersecting storage rings for protons, vacuum system description 2−69505
- chamber, for obs. of luminescence emission from liquids and glasses following electron irradiation 2−58670
- combination foreline trap and valve 2−76133
- controllable bleeder, construction and operation 2−78709
- cryostats, super high vacuum, with self contained pump 2−66367
- cylindrical systems, gas flux patterns, gauge correction factors 2−52011
- for deposition of metal films 2−43476
- desorption phenomena for stainless steel LEED and molec. beam assembly 2−67922
- drive mechanism for exptal. apparatus in vacuum system 2−58666
- electron beam evaporator, multiple source 2−66376
- feedthroughs, doubly insulated, guarded ultrahigh resistance 2−62902
- flange, bakeable, quick connect 2−52017
- flanges production processes for ultravacuum 2−85173
- gaskets, joints, lubricants for ultrahigh vacuum equipment 2−69511
- gate valve for laboratory applics. 2−69514
- gate valve for ultrahigh vacuum use 2−58669
- heatable u.h.v. tight circulator 2−66383
- high-speed economical ultrahigh vac. chamber using Ti sublimation 2−69507
- h.v. feedthrough, 80 kV using compressing O-ring seal 2−69516
- h.v. interrupters, evaluation of radiation hazards 2−82022
- impurities, ionization, e.m. T tubes 2−78932
- in line conductance valve for shock tubes 2−48946
- in line conductance valve for shock tubes 2−48946
- interlock protection circuit for vacuum system 2−48945
- interlock protection circuit for vacuum system 2−48945
- leakage detection, modulation of gas flow 2−78710
- multipin electrical leadthrough 2−48948
- multipin electrical leadthrough 2−48948
- nichrome, film, prod. by multiple sublimation, vacuum system, props. 2−47121
- outgassing rate and ultimate pressure limitations in vac. systems 2−76126
- outgassing rate and ultimate pressure limitations of vac. systems 2−76125
- pressure regulator, automatic, within 10^{-3} to 10^{-7} torr 2−58659
- residual gas analyser, trace impurity analysis, impurity conc. 2−52015
- rotating lid vacuum chamber, ferromagnetic liquid seal 2−66382
- seal, rotatable, u.h.v., design configurations 2−48947
- seal, rotatable, u.h.v., design configurations 2−48947
- selective O_2 leak source using $Zr_{0.85}Ca_{0.15}O_{1.85}$ 2−85174
- servosystem for controlling pressures, design and performance 2−66386
- trap for oil-vapour evacuation system in MKh1307 chromato-mass spectrometer 2−56086
- u.h. vacuum system, oil pumped, surface contamination, ellipsometric obs. 2−48941
- u.h. vacuum system, oil pumped, surface contamination, ellipsometric obs. 2−48941
- ultra-high unit for achievement of vacuum of 10^{-11} to 10^{-13} torr 2−58661
- ultrahigh, for clean surface obs. of high resistivity photoconductors 2−69513
- URS-501M diffractometer for thin films, vacuum attachment 2−62907
- valve, 1 inch, with knife edge seal 2−76114
- zone refining apparatus, oil free pumping system 2−48949
- zone refining apparatus, oil free pumping system 2−48949

Vacuum gauges
- Bayard-Alpert type, characteristics 2−78703
- calibration, using Er-H system gas pressure standard 2−52016
- calibration, using H-Nb system equilibrium pressures as secondary standard 2−78692
- compression McLeod gauge using organic liquids 2−66380
- cylindrical systems, gas flux patterns, gauge correction factors 2−52011
- directional molecular flow analysis and leak detection using rotatable gas analyzer, space simulation 2−78706
- electronic injection into radial electrostatic field gauge 2−62901
- fast ionisation, quasisteady gas injection into Vac. 2−84928
- flow meter for calibration system 2−76129
- hot cathode ionization gauge, modified geometries 2−55334
- hot wire gauge, cylindrical, range extension to atmospheric pressure by natural convection 2−45195
- hot wires, effect in vacuum systems 2−55332
- ionisation, stabilised amplifier and pico-amperemeter 2−78699
- ionisation methods for high vacuum measurements 2−78698
- ionization, design for high and low vacuum measurements 2−78704
- ionization, hot filament, control calibration American Vacuum Society standard 2−52012
- ionization, W cathode O_2 pumping effect 2−48943
- ionization, W cathode O_2 pumping effect 2−48943
- Knudsen absolute manometer, modified, kinetic theory 2−76127
- locking, in 0.0133-133 Pa range, cathode sputtering for automatic transducer self-cleaning 2−48944
- locking, in 0.0133-133 Pa range, cathode sputtering for automatic transducer self-cleaning 2−48944

Vacuum gauges continued
master instruments, total and partial pressures, ultrahigh vacuum regions 2−58663
omegatron applic. to H content determ. in metal 2−53866
oscillator gauge, electron trajectories 2−76128
pressure gauges, total and partial, in ISR ultra-high vacuum system 2−55333
quartz crystal microbalance and mass spectrometers compared 2−78707
residual gas analyser, trace impurity analysis, impurity conc. 2−52015
thermoelectric, NiCr-constantan element in metal encapsulation, indication repeatability 2−78702
thermoelectric, readings stability to temp. change 2−62900
thermoelectric ionisation vacuum meter, for use with thermoelec. and ionisation gauges 2−78700
thermoelectric vacuum meter 2−78701
thermoemission ionization meter, secondary measuring standard 2−66381
triode ionization, for u.h. vacuum 2−69509

Vacuum polarization *see Quantum electrodynamics*

Vacuum pumps
absorbing-condensing, use in oil free zone refining apparatus 2−48949
absorbing-condensing, use in oil free zone refining apparatus 2−48949
circulating Roots type pump for ultrapure or toxic gases 2−66379
cryo pumps and diffusion pumps for 5×10^{-9} torr 2−85172
diffusion, oil and Hg, performance rel. to nozzle geometries 2−52013
diffusion pumps, two in tandem, bounded of a high resolution mass spectrometer 2−83166
electron microscope system, 10^{-8} to 10^{-9} mm Hg 2−79007
electronic injection into radial electrostatic field pump 2−62901
ion getter pump and oil diffusion pump comparison 2−76720
McLeod gauge, Hg contamination obs. 2−69508
perfluropolyether as vacuum pump fluid resistant to electron induced polymerization 2−58664
Sprengel-Babo pump, history and evolution 2−52014
sputter ion, high vapour pressure metal ion source 2−45193
sputter-ion 2−69506
sublimation 2−69506
turbomolecular for Siemens Elmiskop 101 electron microscope 2−45194
turbomolecular pumps application in electron microscopes 2−55331
zeolites, noncooled, trapping and pumping props. 2−76131
Ti ion-getter pump, investigation of ^{3}H contamination in neutron generator 2−58662
Ti sputter ion pumps, influence of asymmetry of magnetic and electric fields 2−62899
Ti sublimation, design and performance of high- speed economical ultrahigh vac. chamber 2−69507

Vacuum technique
see also Getters
Auger electron spectroscopy, review in relation to vacuum technique 2−59924
breakdown at pulsed voltage rel. to macroparticle detachment of electrode surface 2−62898
cathode sputtering, description of apparatus 2−54089
CERN intersecting storage rings for protons, vacuum system description 2−69505
conduction and breakdown, field emission 2−48942
conduction and breakdown, field emission 2−48942
cryopumping with liquid H_2, advantages over He refrigerator 2−78705
distillation devices, packings, comparative separation performance 2−45196
efficiency of absorbing structure in system with point gas source 2−73250
evacuation rate increase using high energy charged particle beams 2−78708
evaporation, isotope target preparation, stable and active 2−73909
evaporation, standard layer prep. for nuclear meas. 2−73913
evaporation rate and vapour pressure, quartz spring microbalance 2−85175
film deposition, review 2−66384
flanges production processes for ultravacuum systems 2−85173
freeze-drying, using homogeneous beds of sand and beef 2−73249
gettering action of evap. Ti and Er films 2−43495
high temperature species deposition rate monitoring by quartz crystal microbalance 2−69512
isotopic accelerator target prep. techniques 2−73962
mechanical strength measurement, at elevated temps. in vacuum 2−77683
metal film evaporation 2−47087
metal vapour, production of constant stream by control of electron emission 2−67890
metallurgy, melting and degrassing, activated reactive evaporation 2−55336
molecular, flow resistance concept in transmission probability 2−60344
outgassing rate and ultimate pressure limitations in vac. systems 2−76126
preparation of wall coated Cs vapour cells 2−69517
pumping by chemical means 2−69506
radiofrequency sputtering, thin film radiation source production 2−74046
residual gas analysis, during vapour deposition of CdSe 2−78697
review 2−55330
r.f. sputtering processes, deposition rate, effects of pressure 2−62905
spacecraft thermal vacuum testing 2−78419
sputtering, unit for coating deposition 2−62903
steelmaking, applications of technology 2−62904
surface structure study 2−67892
surface temperature measurement, in ultrahigh vacuum, by ellipsometry 2−76387
thin film deposition, technology and state of art 2−78693
ultravacuum using cryo pumps and diffusion pumps, 5×10^{-9} torr 2−85172

Vacuum technique continued
C thin film production using evaporation method 2−74629
In seals below 300°C, for joining pyrex to various materials 2−66385
SiO evaporation on thin plastic films 2−69515
ZrC-W compounds, high temp. evaporation from open surface and through W coating 2−73239

Vacuum tubes *see Electron tubes*

Valence bands *see Crystal electron states/band structure*

Valency
average valency V materials, trends in ionicity 2−83887
elements, atomic coordination valency 2−80591
molecular cryst., valence struct. from X-ray diffr. data 2−64610
XY_4 and XY_3 type mols., orbital valency force field, approx. to general valence force fields 2−70663
B_2H_6, B_4H_{10} B_5H_{11}, B_6H_{10} unique preferred localized valence structures 2−50023
$CeRh_xPd_x$ alloys electronic state, magnetic susceptibility and lattice spacings 2−81317
Cm 2−48037
Cu(I) and (II) complexes with sulphur ligands, K- absorpt. edge shift depend. 2−56167
Gd, electrotransport of C, N_2 and O_2 2−80716
KI:Tl covalency, overlap calcs. absorption spectra 2−61643
Pu in nuclear fuels, determ. following reprocessing 2−74178

Valves, thermionic *see Electron tubes*

Van Allen radiation *see Atmosphere/radiation belts*

Van de Graaff generators *see High voltage techniques; Particle accelerators/linear*

van der Waals forces *see Atoms; Kinetic theory; Molecules/intermolecular mechanics; Solids*

Vanadium
arodic sectioning technique 2−60817
atom, highly-ionized far u.v. spectra, rel. to solar lines 2−83189
atomic scatt. factor, determ. by vanishing Kikuchi line electron diffr. method 2−74750
Auger electron spectroscopy of surface chemical composition 2−51480
crystal, centred cubic, mean square displacement of atoms, simple calc. 2−57037
direct discharge neutron detector in thermal and epithermal regions 2−52699
electrical and thermal cond., 20 to 1200°C 2−47769
electron momentum distrib., Compton profile obs. 2−51081
electron phonon enhancement factor, from specific heat data 2−64932
in fluorophlogopite, e.p.r. and optical absorption spectra 2−84562
foil, quenched, vacancy detects, electron microscope obs. 2−71472
heat of fusion 2−47029
internal stress, during stress relax., rel. to dislocation generation and immobilization 2−43680
neutron irrad., activation volume rel. to dose and strain, interstitial impurity precip. 2−80663
neutron irrad., anneal and radiation hardening, tensile props. 2−80665
renormalized-free-atom model, and electron momentum distrib. 2−68670
solar overabundance, accelerated by solar flares 2−76001
in steel, effect on brittle fracture susceptibility 2−53896
steel, welded joints, crack formation in stress relieving annealing 2−64759
influence on strengthening of austenitic steel 2−47636
superconducting, flux line lattice obs. 2−47872
superconducting transition temp. calc. and phonon vertex 2−71876
superconducting transition temperature, press. depend. 2−75064
superconductor, magnetization curve, 0K, calc. 2−61233
surface, cleaned and oxidized, secondary ion yield 2−61471
vacancy condensate prod. by laser irrad. 2−53726
valence electron charge density, asphericity 2−80990
yield behaviour, effect of pre-strain 2−80752
Al_2O_3:V, before and after γ-irrad., phonon scatt., thermal cond. study 2−68214
GeO_2:V^{4+}, e.p.r., g and A tensors, orbital mixing parameter, radial average, core polarization 2−72503
$KZnF_3$:V^{2+}, e.p.r. and ^{19}F ENDOR study 2−75353
TiO_2:Li,V,Cr,Mn,Fe, transition metal impurity levels, esr determ. 2−44117
V II, III, IV, V, i.r. spectra resolution into bands, transitions, charge transfer 2−83268
V^{2+}, double chlorides, Ligand field theory 2−61567
V^{2+} in MgO, Raman relax. modifications due to substitutional effects 2−48114
V^{3+}, in AgCl and AgBr, charge transfer spectra 2−51333
V^{3+} in Al_2O_3, ground state study using phonon generation in Sn 2−47735
V^{3+} in Al_2O_3, phonon scatt. using superconducting tunnel junction source obs. 2−47732
V^{3+} in CdF_2, optical absorption bands due to photoionization 2−54417
V^{3+} in MgO, effect of random static strains on e.p.r., model 2−72495
V^{4+}, e.p.r. in TiO_2, thermal treatment effects 2−61738

Vanadium compounds
— 2−71831
alloys, oxidation in contact with mixed oxide nucl. fuel 2−83099
$^1/_2$Cr-Mo-V steels, high-strain fatigue properties 2−60948
dilute liquid alloy, V in Cu, CuZn, Zn, ZnGa, Ga, GaGe, GeAs, As, mag. susceptibility 2−80485
oxides, adsorption of chemically nonequivalent O atoms (ions) 2−47167
refractories, atomic interactions 2−48206
vanadate minerals and rocks, visible and near i.r. spectra 2−72672
Vanadium Permendur, dimens. stability 2−43994
VB_2, Hall coeff. and magnetoresistance one and two-zone model and measurements, comparison 2−77881
6Al-4V-Ti, surface embrittlement charact. during diffusion bonding 2−68160
Au-V alloy, dil., field depend. of mag. susceptibility 2−61475
Au-V alloy systems, optical absorpt., band struct. 2−44371

Vanadium compounds continued
Au-V dil. alloys, mag. susceptibility, 2-293K, local behaviour 2−68517
Bi_2O_3-V_2O_5 flux system, for oxide crystal growth 2−50589
Ca-Bi-V ferrite rods, excitation of longit. acoustic waves 2−43968
Co-V dilute alloy, n.m.r. and nuclear relaxation study of satellite lines 2−44454
Cr-Mo-V steels, constitution diagrams for service lifetimes 2−60838
Cr-V alloy system, melting equil. diagram 2−47709
Cr_2O_3-V_2O_3 mixtures, powder pattern detn. of Cr_2O_3 and V_2O_3 2−74728
Cr_2O_3-V_2O_3 solid solution, mag. ordering, diffr. and e.s.r. obs. 2−48104
CrV steels, free energy changes and boundary segregation of Sn and Sb 2−71309
Fe-Co-V, alloy, plastic deform. and brittleness 2−60868
Fe-V-C steel, fibrous vanadium carbide occurrences after thermal or continuous cooling transformation 2−61033
Fe-V-C system, phase diagram, pseudo-binary section at 0.5 wt-%V 2−47711
Fe-V-N system, abnormal Snoek peak 2−47482
Fe-V alloy, Fe-rich, ^{57}Fe n.m.r. 2−75355
Fe-V alloys, meas. of longitudinal and transverse magnetoresistance at 4.2K, 77K, 273K 2−48063
Fe-V σ-phase, atomic distrib. and mag. props., Mossbauer obs. 2−44253
Ni_2V alloy, ordering transformation for wide range of subcritical temps. 2−74938
PbO-V_2O_5 flux system, for oxide crystal growth 2−50589
Pd-V system, diffusion processes, phase obs. 2−53770
$RbBO_2$, evaporation, mass spectrometric obs. 2−64512
Sc_2O_3-V_2O_3 solid solution, mag. props., comp. depend. 2−48041
Ti-Al-Mo-V alloys, fatigue fracture behaviour in dry Ar environments 2−84118
Ti-Al-V alloy, mill-annealed, fatigue crack growth, temp. effects 2−60904
Ti-Al-V brazed foils, scanning e. microscope metallographic study 2−68158
Ti-V-O and Ti-V-Al-O solid solutions, charact. temp. and elasticity modulus 2−50844
Ti(13 wt.%)V-(11 wt.%)Cr-(3 wt.%)Al beta alloy, mech. prop.-fracture-microstruct. relns. 56950 2−56950
V-C alloys, ordering effects in struct. obs. comp. depend. 2−71378
σ-V-Co, n.m.r. of ^{51}V, quadrupole satellite intensity variation 2−72519
V-Fe-Co alloy, ordered and disordered, recovery behaviour 2−50804
V-Ga-Al alloy, A15 struct., superconducting crit. temp. and current density 2−57168
V-Ge-Al alloy, Knight shift meas. 2−57398
V-H system, low temp. phase transform. 2−53998
V-H systems, phase transitions due to elastic interaction 2−77744
V-H(D) systems, n.m.r., β- and δ-phase behaviour 2−78175
V-N system, V_3N phase, electron microscope obs. 2−50978
V-Ru alloys, Knight shift, relax. rate and lineshape, temp. and mag. field depend. 2−61753
V-Ti alloy, scavenging of interstitials, internal friction study 2−50845
V-Ti(Cr)(Sn)(Al) alloys, struct. and props., comp. depend. 2−53912
V complex, bipyramidal trigonal, computational errors in term energies 2−60025
V Ti-8% Al-1% Mo-1% alloy, accelerated stress-corrosion cracking in presence of hydrogen recombination poison 2−68107
V^{3+} complexes, trigonally distorted octahedral, lattice-ion interactions in the ligand field theory 2−81205
V_3Au, supercond. transition temp. rel. to ordering, rel. to phonons and electronic density of states 2−84308
V_3Au, supercond. transition temp., effect of cryst. order 2−64952
VB_2, electronic spectra, MOLKAO method calc. 2−71792
VB_x, thermionic emission, rel. to electronic struct. 2−48017
VC_x:B, precipitation and dislocation struct., electron microscope obs. 2−61038
VC, energy band structure calc. by quasi-self- consistent APW method 2−51082
VC, mixtures with Mn_6C and Cr_7C_3, X-ray analysis 2−44506
VC_{1-x}, vacancy short range order, calc. 2−83966
VC_x, cryst. growth by floating zone technique 2−47277
VC_x, fracture surface energy determ. 2−50776
VC_x, order-disorder transitions, elec. resist. and enthalpy changes 2−54004
V_6C_5, disordered, C self-diffusion 2−60834
V_6C_5, superlattice, C vacancy ordered distrib. 2−43621
$V_xCr_{1-x}B_2$, diluted, nuclear magnetic resonance study of antiferromagnetic transition 2−72521
$V_{1-x}Cr_xBe_2$, n.m.r. and mag. props. 2−72520
$V_{0.95}Cr_{0.05}O_2$, cryst. struct. 2−43592
$V_{2-x}Cr_xO_3$, domain form. during Mott metal-insulator transition, geometry and crystallography 2−71785
$V_{1-x}Cr_x)_3Si$, ternary alloys, physical props. and electron struct. 2−68514
V_3Ga, supercond., formation by a new diffusion process 2−84301
VH_x, quasielastic neutron scatt. obs. of hydrogen diffusion 2−77621
V_xH_y, impurity effects on stability 2−77729
$V_xH_y(D_y)$, ordering transitions at low temps. 2−77752
V_2MoO_8, cryst. shear struct., electron microscope obs. 2−47352
VN-TiN particles, nitriding and annealing effects on phase comp. 2−68202
$VN_{0.98}$, microhardness and thermal expansion, 80-300K 2−61112
VN_x, hexagonal, magnetic and Mossbauer obs. 2−54331
VN_x cryst. growth, by floating zone technique 2−47277
$V_{1-x}Nb_xO_2$, metal-insulator transition, mag. props. and n.m.r. studies 2−75102
$V_{1-x}Nb_xO_2$, metal-insulator transition, crystallographic and transport props. study 2−75101
$V_{1-x}Nb_xO_2$, metal-insulator transition, theory 2−75103
V_2O_5-Fe_2O_3 system, e.p.r. of Fe^{3+} 2−48297
V_2O_5-Na_2O-Fe_2O_3 system, liq., n-type semicond. and ionic cond. props. 2−83796
V_2O_5-P_2O_5 glass, microstruct., mag. ordering mag. props., e.s.r. 2−44310

Vanadium compounds continued
V_2O_5-P_2O_5 glass, struct., elec. resist., thermal expansion, rel. to comp. 2−60601
$VO_{0.79}$-$VO_{1.29}$, thermal conductivity, between 100 and 1000°K 2−64867
VO-doped triglycine sulphate, domain struct. changes, e.p.r. obs. 2−77937
VO, CNDO-II approx. SCF molecular orbital method, levels calc. 2−83252
VO, effusion mass spectrometric determination of heat of formation 2−44476
VO short range ordering of defects, electron diffraction study 2−80701
$VO_{0.92}$, Auger electron spectroscopy of surface chemical composition 2−51480
VO_2, Auger electron spectroscopy of surface chemical composition 2−51480
VO_2, effusion mass spectrometric determination of heat of formation 2−44476
VO_2, metal-insulator transition and phonon softening 2−51152
VO_2, semicond.-metal transition, rel. to struct. of $V_{0.95}Cr_{0.05}O_2$ 2−43592
VO_2, twinned crystal transformation to tetragonal phase, X-ray obs. 2−47698
VO_2 switching device, influence of high-conducting bubble 2−54208
VO_2 threshold switching device, capacitance discharge 2−54211
VO^{2+}, e.p.r. in $UO_2(NO_3)_2.6H_2O$ single crysts., hindered motion 2−57392
VO^{2+} e.p.r. in palladium benzoylacetonate, and sodium methylammonium tungstovanadate 2−61741
VO^{2+} impurity ions in α-amino acid crystals, e.p.r. 2−84566
$VO_4{}^{3-}$, ground states, SCF-MO calcs. and X-ray spectroscopy 2−77095
VO_x, cryst. growth, by floating zone technique 2−47277
VO_x, elec. props. and defect states 2−64991
VO_x, positron lifetime spectra, rel. to cond. and nonstoichiometry 2−71825
V_2O_3, absorpt. and refl. spectra in metal-semicond. transition 2−81407
V_2O_3, Auger electron spectroscopy of surface chemical composition 2−51480
V_2O_3, band struct. below Fermi level, X-ray photoelectron spectra obs. 2−61193
V_2O_3, model for metal-insulator transiton 2−72225
V_2O_3, VO_2, V_2O_3, prep. by pyrolysis temp. depend. of resistance 2−44106
V_2O_5, dielectric relaxation in large crystals 2−68463
V_2O_5, dislocations, X-ray diffr. obs. 2−56691
V_2O_5, ion bombardment enhanced elec. cond. 2−68408
V_2O_5, ion impact effect on electrical conductivity 2−60779
V_2O_5, liq., elec. cond., temp. and oxygen partial press. depend. n-type semicond. 2−83794
V_2O_5, long wave optical vibrational spectrum 2−68629
V_2O_5, molecular dimensions from light scattering in absorbing suspensions 2−50378
V_2O_5 bronzes, electrical conductivity in solid and liquid state 2−84339
V_4O_{10}, effusion mass spectrometric determination of heat of formation 2−44476
V_4O_7, cryst. struct. 2−47350
V_4O_7 metal-insulator transitions, charge localization, crystallographic evidence 2−44087
V_4O_8, effusion mass spectrometric determination of heat of formation 2−44476
V_nO_{2n-1}, ^{57}Fe Mossbauer study 2−72286
V_nO_{2n-1} (n=3,4, ..., 8) single cryst., growth, temp. depend. of resist., susceptibility and thermoelec. power 2−43509
$V_nO_{2n\|1}$, (n=3,4), electronic localization of d electrons 2−84239
$VO_{3-x}F_x$ 2−57146
$VOPO_4$, prep. and struct. props. 2−50627
V_7S_8, monoclinic, cryst. struct. 2−43591
$VSO_4.xH_2O$, prep. and struct. 2−50628
V_7Se_8, monoclinic, cryst. struct. 2−43591
V_3Si, anomalous Gruneisen consts. 2−74980
V_3Si, elastic softening and supercond. 2−44081
V_3Si, lattice stablization in high magnetic fields 2−77869
V_3Si, supercond. formation by a new diffusion process 2−84301
Vo_x, $1<x<1.3$, charge carrier freeze-out effects 2−65004
(W, V)O_x, cryst. shear struct., electron microscope obs. 2−47352
WO_3-P_4O_{10}-V_2O_5, elec. cond. and mag. resonances 2−54495
$(W_{0.2}V_{0.8})_3O_7$, synthesis and cryst. struct. 2−47351

Vaporization
see also Boiling; Condensation; Distillation; Evaporation; Heat of vaporization; Vapour pressure
alloy, binary, phase diagram 2−53509
forced convection droplet evaporation with finite vaporization kinetics and liquid heat transfer 2−77398
liquid superheat, with and without solid surface, theory 2−53505
lunar rocks and minerals, impact induced rel. to normal 2−51821
metal vapour escape from a droplet containing volatile solute 2−43447
multicomponent data predictions from binary isobaric data using single parameter Wilson equation 2−83835
under quenching conditions, effect of effusivity and thermal resistance of solid surface 2−60555
refractory carbides, nitrides and borides, NASA research 2−64801
thermal tube, length of zone 2−60553
within liquid of immiscible moving droplets 2−83834
As(111) crystal, evaporating molecule speed and spatial distributions 2−67879
KCl crystal, effect of $MnCl_2$ mol. beam 2−71281
$La_{1-x}Sr_xCrO_3$, volatile oxidation kinetics for optimum material characteriz. 2−50885
Lu-C system, Knudsen effusion mass spectrometry studies in temp. range 2100 to 2600K 2−64518
Na_2SO_4, volatile oxidation kinetics, 1173 to 1473K 2−50891
Sf_6, liquid-vapour coexistence curve, interferometric obs. 2−74591

Vapour density *see Density/gases*

Vapour pressure
see also Humidity; Vaporization
alkali halide vapours, vapour pressures and enthalpies of vaporization, detn. 2−77473
alkali metal ammonia solns., solvation model 2−84614
benzene + cyclohexane system, meas. using all-glass- mercury static equilibrium still 2−53511
curved surface, concave and convex, v.p. rel. to curvature and surface tension 2−46943
ethane, 80 to 135K 2−60559
ethylamine, effect of deuterium substitution 2−43450
Hg, ebulliometric meas. and variations with temp. 2−67877
Kelvin equation, review 2−53512
methylamine, effect of deuterium substitution 2−43450
partial pressure, computer calc. from total press. curve 2−43449
propylamine, effect of deuterium substitution 2−43450
rare earth cobalt-hydrogen pseudo-binary system, mag. field influence on equil. press. 2−43498
Redlich-Kwong equation of state, modified, determination of equilibrium constants 2−50265
water, equation for representation 2−77476
water under negative pressure, vapour pressure and bulk modulus 2−83734
CdO, dissociation and form. equilib. const. from saturation v.p. temp. depend. 2−75371
Cs-Rb mixtures sorbed on graphite 2−53592
$CsBO_2$, evaporation, mass spectrometric obs. 2−64512
H-Nb system, secondary standard for ultra high vacuum gauge calibration 2−78692
H_2, saturated, deviation from Clausius Clapeyron law, study using cryostat with optimization of low pressure condensation cryopumping 2−45190
^{3}He + ^{4}He solutions, saturated vapour pressure below λ temp. 2−52108
Hg-Bi-Pb liquid metal systems, effectiveness of boiling separation 2−74594
HgSe, sublimation, partial press. of Hg and Se, equilib. total dissociation press. 2−74596
KBO_2, evaporation, mass spectrometric obs. 2−64512
$LiBO_2$, evaporation, mass spectrometric obs. 2−64512
N_2, det. from equations of state representing all saturated state variables 2−53332
N_2, equilib. pressure over GaN 2−47049
$NaBo_2$, evaporation, mass spectrometric obs. 2−64512
Ne liquid, pressure coefficient at constant volume determ. from sound velocity measurements 2−46950
$RbBO_2$ evaporation, mass spectrometric obs. 2−64512
Sb_2S_3, mass spectrometric and thermogravimetric Knudsen effusion vaporization studies 2−74595
Te-As system, vapour press. of Te_2, As_4, and As_2 over molten As_2Te_3 2−47046

Vapour pressure measurement
Knudsen effusion method, modification 2−47048
Knudsen method, effusion of vapour molecules 2−82081
liquid mixtures, meas. using all- glass-mercury static equilibrium still 2−53511
metal, partial press. and evap. rate by atomic reson. absorption 2−50406
ultrahigh vacuum quartz spring microbalance 2−85175
vapour pressures, compensating technique using zero indicator 2−52036
S, apparatus for obs. 2−47045

Variable stars
V 1057 Cygni, far-infrared and four-colour photometry 2−73012 − 2−62577
A and B type supergiants, spectrum variability 2−58311
A-stars, rotation and turbulent mixing due to meridional circulation velocity field 2−62503
QS Agl, eclipsing binary photoelectric observations 2−58335
Algol, radio flares 2−75821
108Aqr, Ap Si 4200 star, variations of Ti II lines 2−58317
η Aquilae, light variations for CO, CN, C_2, CH, OH and NH 81840 2−81840
56 Ari, Si Ap type, spectral obs.81853 2−81853
σ Aurigae, eclipsing variable, mean spectral type, rotational velocity and absolute visual magnitude of components51766 2−51766
AR Aurigae, eclipsing variable, mean spectral type, rotational velocity and absolute visual magnitude of components 2−51766
BD-7°3007, peculiar blue, h.f. stellar oscillations 2−66097
BD-7°3007, unusual hot star, continuous spectrum 2−62566
binaries, X-ray spectra, and short period pulsations of Cen X-3 2−75776
binary double cepheid CE Cas, periods, photoelectric observations 2−75777
TZBootis, eclipsing variable, spectral classification determ. 2−81861
BW Vul, β CMa star, spectral variations 2−58325
RU Cam, two colour photoelectric light curve, period variation obs. 2−48706
AScamelopardalis, eclipsing binary, spectroscopic study 2−84994
WYCancri, eclipsing variable, spectral classification determ. 2−81861
20.08.01 Cancri, optical variability 2−55043
β Canis Majoris, spectral classif., in HR diagram 2−48698
YZ Canis Minoris, UV Ceti type flare star, rotational velocities 51760 2−51760
S Car, photoelectric obs. 62565 2−62565
η Car, short period optical oscillations 2−55046
Y Carinae, photoelectric observations of beat period cepheid 2−48712
TW Cas, photoelectric light curves 2−73016
Cassiopeia V418, possible point gamma ray source 2−75840
SX Cassiopeiae, analysis of giant binary system 2−69101
cataclysmic, high speed photometry 2−44872
T Cen, polarization and photometry meas. 2−62575
Cen X-3, search for optical counterpart 2−62576
cen X-3 X-ray source, possibility of being radially pulsating white dwarf 2−81867
V553 Centauri, type II Cepheid, overabundance of C66102 2−66102
ε Centauri new β Canis Majoris variable, period obs. 2−48713

Variable stars continued
Centaurus X-3, reactivation of old neutron star by mass exchange in close binary 2−78479
EG Cep, eclipsing binary photoelectric observations 2−58335
βCephei, determination of mean radius, spectrophotometric temperature and mass 2−48708
AH and CW Cephei, eclipsing variables, mean spectral type, rotational velocity and absolute visual magnitude of components 51766 2−51766
β Cephei, spectral classification, location on theoretical HR diagram 2−58324
W Cephei, VV Cephei-type star, weak i.r. excess84995 2−84995
β Cephei instability, strip, high-luminosity boundary 51757 2−51757
Cepheid envelopes, multiple solutions 2−58322
Cepheids, Magellanic Clouds, composition data 2−66103
cepheids, pulsation amplitudes 2−75756
Cepheids, ratio of total to selective absorption, kinematic det. 2−62553
Cepheids in Magellanic Clouds, photometry 2−62580
Cepheids in small magellanic cloud, influence of metal lines on colours 2−81823
Cepheids in SMC and distance determ. 2−69038
o Cet B, Mira companion, rapid blue, u.v. photoelectric photometry 2−69097
o Ceti, line identification in near i.r. spectrum 58327 2−58327
CH Cygni, photoelectric observations 2−51762
classical Cepheids, Wesselink radii, revision of conversion factor (24/17) 2−62554
classical Cepheids rel. to extragalactic distances determinations 2−69095
21 Comae Berenicis, photoelectric observations of magnetic star 2−81819
UU Comae Berenicis, photoelectric observations of magnetic star 81819 2−81819
R Coronae Borealis type, in Large Magellanic Cloud66099 2−66099
AM CVn, rapid blue, photometric obs.69098 2−69098
Cyg X-3, detection of variable radio emission 2−55088
α Cygni, A-type super giant, coupling between mass loss and turbulence 2−75732
YCygni, eclipsing binary photoelectric obs., (1959-61) 2−75770
Y Cygni, improvement of spectroscopic orbit, masses and radii of binary components51764 2−51764
CY Cygni, irregular variable, spectrum and element abundances78465 2−78465
V1016 Cygni, symbiotic star, prominent i.r. excess84995 2−84995
Eta Cygni field, 30 new stars 51763 2−51763
FZ Del, eclipsing binary photoelectric observations 2−58335
displacement potential technique in pulsational analysis, solution error 2−81843
eclipsing binaries, effect of time shift of secondary minimum 2−73035
eclipsing binaries, parallaxes 2−73037
eclipsing binary system with extensive atmosphere, information available from monocolour brightness loss curves 2−48717
γ Equ period weighting73014 2−73014
eruptive binaries, physical properties and outburst mechanisms 2−73034
EX Hydrae rapid blue variable, photometric obs. and identification with X-ray source 2ASE 1253-28 2−66101
flare star rotational velocities of UV Ceti type stars, YZ CMi, EV Lac, and AD Leo 2−51760
flare stars as possible source of soft X-ray background 2−55103
U Geminorum, eruptive binary, period variations 2−44883
U Geminorum type, cataclysmic, high speed photometry 2−44872
globular clusters and the distance scale 2−75780
HD 111133 peculiar A star, periodic variability 2−62563
HD 152667 2−85018
HD 175514, binary analysis of 1968 photoelectric light curve observations 2−51765
HD 188041, periodic magnetic variable, magnetic intensification and starspots 2−75747
HD 197481, 1uiescent light variations and enhanced u.v. activity at minimum, periodic dMe variable star 2−48704
HD 198478(55 Cygni), rapid variations in spectrum 2−62539
HD 218348 red variable, photoelectric obs. 2−58329
HD 25354, Ap type, abundance of transuranium elements 2−72994
HD 32633 Ap star, no changes in period 2−44868
HD 4180, Hγ, Hδ, Hε equivalent widths variations, comparison to Be stars with small extent envelopes 2−44856
HD 90386, short-period, comparison for 23 Sextantis 2−84997
LS Her, eclipsing binary photoelectric observations 2−58335
AK Her, eclipsing binary photoelectric observations 2−58335
88 Herculis, shell star, pulsating envelope or binary star 58318 2−58318
88Herculis, spectroscopic binary? shell star 2−73032
Herculis X-1, precessing binary pulsar model 2−81873
HR 2142, periodic shell variable, spectral obs. 2−44871
HR 465, Ap stars, model atmosphere anal., abundance obs. 2−66076
HR 465, proposed identification of Pm 2−51727
HR 5491, evidence for being pulsating Am star 2−62578
HV 12842, HV 5637, R Coronae Borealis type, in Large Magellanic Cloud 66099 2−66099
HZ 29, rapid blue, photometric 2−69098
interface for small computer allowing variable star data to be recorded 2−62481
irregular, intermittent photometric observations, interpretation 2−75755
in 1 Lac field, photographic obs. 2−73017
EV Lacertae, UV Ceti type flare star, rotational velocities 2−51760
U Lacertae, VV Cephei-type star, weak i.r. excess 2−84995
Large Magellanic Cloud, topography of 1830 variable stars 2−75691
AD Leonis, UV Ceti type flare star, rotational velocities 51760 2−51760
XY Leonis, W UMA-type eclipsing binary, period changes rel. to third mass55058 2−55058
luminosity variation in one zone Cepheid model 2−84977
δ Lup, new β Canis Majoris variable, period obs. 2−48713
LY Aur binary, u.v. photometry for OAO-2 2−75778
EW Lyr, eclipsing binary photoelectric observations 2−58335

Variable stars continued
  in Lyra field, photographic obs. 2−73017
  TZ Lyrae, light variation and orbital elements 2−75753
  RRLyrae, masses, radii, and luminosities 2−69094
  RR Lyrae type, influence of shock waves on light curves 2−58314
  RR Lyrae types in globular cluster NGC 6981, photometry 2−62571
  RRLyrae-type stars, motions and absolute magnitudes for 65 objects 2−78466
  M type SR variables, kinematics, radial velocities 2−62570
  m-type, minimum light spectra 2−62531
  main sequence pulsation in open clusters 2−62562
  massive, iterative nonlinear pulsations, terms to second order 2−84975
  massive, iterative nonlinear pulsations 2−84974
  W Men, R Coronae Borealis type, in Large Magellanic Clou66099 2−66099
  Mira companion, rapid blue, u.v. photoelectric photometry 2−69097
  Mira variables, S-type stars, evolution 2−62581
  T Monocerotis, spectral line variation of Hα absorption 62540 2−62540
  AX Monocerotis, symbiotic stars, UBV obs. 84996 2−84996
  N-type semiregular variables, possible evolution constraints 2−75717
  non-radial oscillations, tidal perturbations 2−73013
  o Velorum, βCMa type, period brightness and velocities 2−44867
  OB stars, small amplitude variations 2−81834
  U Ophiuchi, eclipsing variable, mean spectral type, rotational velocity and absolute visual magnitude of components 2−51766
  UPegasi, photoelectric obs. 2−44873
  AG Pegasi, symbiotic stars, UBV obs. 2−84996
  U Pegasi close binary system, light curve variations 2−81864
  U Pegasi close binary system, light curve variations 2−81864
  XPer, optical polarization, possibility of being X-ray source 2ASE 0352+30 2−44869
  δ Per, u.v. observations from Mariner 9 2−58320
  periodic pulsating binary X-ray source in Hercules 2−75829
  AG Persei, eclipsing variable, mean spectral type, rotational velocity and absolute visual magnitude of components 2−51766
  AX Persei, symbiotic stars, UBV obs. 2−84996
  photometric observations of four new variables near nova Vulpeculae 1968(1) 2−55051
  polytropes, resonance effects and anharmonic pulsational amplitudes 2−84973
  population I Cepheids, pulsation consts. 2−72996
  pulsating in Pleiades cluster 2−62561
  RX Puppis, symbiotic star, prominent i.r. excess 84995 2−84995
  quasi-periodic, periodogram anal. 2−75764
  radiosources, fruitless search 2−58384
  red, in globular clusters, galactic centre, solar neighbourhood 2−73019
  red supergiants of large amplitude in Small Magellanic Cloud 2−62579
  reflection effect in eruptive stars, optical properties of scattering medium 2−51759
  relaxation oscillations in envelopes of luminous red giants 2−62484
  RR Lyrae, survey at high galactic latitude 2−69096
  RR Telescopii, Fe lines in spectrum and model 2−58297
  RV Tauri, photoelectric observations 2−58323
  V505 Sagittarii, eclipsing binary system, UBV photoelectric observations 2−81821
  λ Sco and κ Sco, period obs.48713 2−48713
  Sco X-1, rapid blue, photometric obs. 2−48710
  Sco X-1, X-ray fluctuations 2−55111
  RY Scuti, symbolic star, weak i.r. excess84995 2−84995
  δ Scuti stars, rotation of evolving stars rel. to pulsational instability 55029 2−55029
  AU Serpentis, light variations and light curve obs. 2−75754
  RY Sgr, pulsating R Coronae Borealis type, spectral and photometric obs. 2−66098
  SRa type, minimum light spectra 2−62531
  supergiants, small amplitude variations 2−81834
  IKTauri, period and near i.r. variability 2−75762
  41 Tauri, photoelectric observations of magnetic star 2−81819
  T Tauri like, in eclipsing binary RS CVN 44870 2−44870
  HL Tauri-76, white dwarf with multiple periodicities in light curve 2−81846
  RW Trianguli, eruptive binary, period variations 44883 2−44883
  TX Cancri as test of theory of age zero contact binary systems 2−75763
  TX Cancri close binary, light curves and period change 2−55069
  UX Ursae Majoris, eclipsing binary, photoelectric photometry of rapid variations81845 2−81845
  TYUrsae Majoris, eclipsing variable, photoelectric observations 2−81861
  UX Ursae Majoris, eruptive binary, period variations44883 2−44883
  V42, W Virginis type in M5, long term investigation 2−58321
  V84, W Virginis type in M5, long term investigations 2−58321
  AX Velorum, photoelectric evidence of beat period cepheid48711 2−48711
  R Vir, minimum light spectra 2−62531
  AZVirginis, eclipsing variable, photoelectric observations and spectral classification determ. 2−81861
  W Virginis type, influence of shock waves on light curves 58314 2−58314
  VW Cephei, period changes, photoelectric obs. 2−51761
  VY Canis Major as multiple star 2−55054
  water vapour microwave emitters, from IR stars, time variations 2−58416
  white dwarf G195-19, circular polarization and ephemeris 2−55035
  white dwarf non-radial pulsations, oscillations rel. to dwarf novae and g-mode pulsations 2−73018
  white dwarf variables, model with non-radial oscillations of gravity modes 2−55055
  WRA 795 optical identification with Cen X-3 2−75828
  X-ray sources, pulsation mechanism 2−73057
  X-ray sources, search for h.f. optical variability 2−69092
  He pulsating star, instability strip for $2M_\odot$ model 2−48709
  He pulsating stars, instability strip in HR diagram 2−58326
Variational calculus *see Mathematics*
Variational method *see Quantum theory/application methods*
Vavilov-Cherenkov radiation *see Cherenkov radiation*
Vectons (vector mesons) *see Mesons*
Vectors
  Helmholtz wave eqn., Moseley's non-separable solutions 2−41466
  solenoidal field represent. by poloidal and toroidal. pots. 2−82179
  surface, anisotropic, vector thermodynamics, plane surface junctions 2−56570
Velocity
  angular, rigid body 2−58832
  elastic waves, in Indian rocks rel. to others 2−75453
  elastic waves, in saturated porous media, calc. using Frenkel-Biot theory 2−82343
  elastic waves, in solid granules, effect of grain size 2−84204
  fall of drop in pulsated medium 2−46904
  fall of drops in non-Newtonian media 2−46905
  granular solid, distrib. in gravity flow in inclined open channel 2−74338
  liquid, profile in tube flow 2−64407
  plasma, meas. using Doppler effect 2−64296
  seismic waves, short wave rel. to long wave in layered medium 2−75419
  Si, velocities of screw and 60° dislocations 2−80678
  acoustic waves
    see also Dispersion, acoustic; Helium/liquid, sound propagation; Shock waves
    —. 2−71693
    anharmonic metal, collision free regime 2−43966
    anharmonic metal, collision-dominated regime 2−43965
    benzene mono- and disubstituted derivatives, sound propagation rel. to H bonding analysis 2−56502
    critical region phenomena, intermediate and h.f. dispersion 2−54027
    cubic crystals, second sound velocities 2−61091
    dense gases, calc. 2−80386
    displacive and mag. order-disorder phase transition phenomena 2−54026
    electrolyte solutions, Rayleigh and Brillouin scattering studies 2−43360
    gas of Maxwell molecules, phase velocity 2−41707
    gaseous mixtures, dispersion obs., rel. to linearized Boltzmann eqns. 2−60375
    geoacoustics, WKB approximation, turning points and meas. of phase vel. 2−57840
    liquid, rel. to dynamical equation of state 2−46919
    liquid metals and alloys, speed of sound calc. 2−46952
    nomograph, for solid media 2−64844
    oceanographic applications, geometrical acoustics 2−44653
    plane coherent waves in turbulent medium 2−41721
    polymer films, determ. of mech. props. rel. to mol. orientation 2−47536
    polyolefins, variation in stressed specimens rel. to deformation 2−80750
    in polystyrene, longitudinal and transverse waves, from 4.2°K to room temperature 2−71732
    polytetrafluorethylene, shock compression, velocity behind stress wave front 2−77781
    porous materials with vacuous pores, thermodynamic model calcs. 2−50924
    relativistic interactng particle system, asymptotic limit for speed of sound 2−66429
    seawater, surface, effect of increasing CO_2 conc. 2−65605
    sound dispersion in mag. field at low temp., meas. 2−61092
    Al, directly generated standing sound wave dHvA effect influence 2−51018
    Al single crystal, along (110) direction; elastic behaviour detn. 2−60837
    Ar, solid, longitudinal sound vel. temp. depend., stimulated Brillouin scatt. obs. 2−68231
    $Ca(OH)_2:Mn^{2+}$, temp. depend. 2−78163
    $CdCl_2$, adiabatic compressibility and sound propag. speed, reln. to molec. struct. 2−72564
    $CoCl_2$, adiabatic compressibility and sound propag. speed, reln. to molec. struct. 2−72564
    CoO, sound velocity and acoustic absorption coefficients at room temp. 2−43971
    Cs_2SO_4, 1046 to 1156°C 2−71194
    D_2, solid, sound at 4.2K and pressures up to 200 bar 2−80910
    $ErH_{1.81}$, limiting Debye temp. and elastic consts. detn. 2−57047
    H_2, solid, sound at 4.2K and pressures up to 200 bar 2−80910
    He-Ar gaseous mixtures, dispersion obs., rel. to linearized Boltzmann eqns. 2−60375
    He, anisotropic h.c.p. solid 2−50394
    He, meas. at low frequency by resonance tube method 2−43265
    ^3He, solid, review 2−80515
    $KZnF_3$, reson. meas. of elastic consts. 2−84007
    Kr, liquid 145-240 K, PVT surfaces, adiabatic compressibilities derived 2−83790
    $LiTaO_3$, surface velocity, temp. depend. 2−51019
    $MgCl_2$, adiabatic compressibility and sound propag. speed, reln. to molec. struct. 2−72564
    MnO, sound velocity and acoustic absorption coefficients at room temp. 2−43971
    Na liquid alloy, 7.5 MHz rel. to compressibility determ. 2−77415
    Na_2SO_4, 947 to 1161°C 2−71194
    Ne liquid, meas. used to determ. thermodynamic properties 2−46950
    $NiCl_2$, adiabatic compressibility and sound propag. speed, reln. to molec. struct. 2−72564
    NiO, sound velocity and acoustic absorption coefficients at room temp. 2−43971
    Rb, liquid, 40-200°C, 0-20000 p.s.i. 2−71195
    RbH_2PO_4, longitudinal waves, effect of deuteration 2−74979
    Rb_2SO_4, 1109 to 1191°C 2−71194
    $ScH_{1.99}$, limiting Debye temp. and elastic consts. detn. 2−57047
    Se_3In, zero field, 1.5 and 4.2K, and field, depend., 1.5-300K 2−81258
    Tl_3AsA_4 single crystal 2−48137
    TlCl pressure dependence of elastic constants 2−84035
    V_3Si change in soft mode sound velocity under shear strain 2−74980
    $YH_{1.93}$, limiting Debye temp. and elastic consts. detn. 2−57047
    ZnO, epitaxial layers on Al_2O_3, surface wave acoustic props. 2−51020

Velocity continued

acoustic waves, ultrasonic

see also Dispersion, acoustic/ultrasonic

— 2–72462

alkali silicate glass, static longitudinal modulus determ. 2–56773

amino-compounds, organic liquids 2–53428

aniline binary mixtures, free length and collision factor theories 2–53424

benzene-cyclohexane system on saturation line 2–71199

carboxylic acid series, velocity dispersion 2–71192

chemical relaxation studies, resonance technique 2–76372

chlorobenzene, u.s. excited shift in u.v. absorption curve and sound velocity dispersion curve 2–56224

CW techniques for obs. 2–58914

diamond, elastic moduli determ. 2–50728

elastomers, vel. as function of temp. 2–57048

ethyl alcohol, dehydrated, hydrostatic effect in obs. in critical region 2–43354

ethyl esters of some carboxylic acids, temp. variation of u.s. velocity 2–74486

fatty acids, normal, chemical structure det. 2–56231

fibres and composites, elastic const. obs. 2–50723

frozen soils, dilatational and shear waves 2–78306

glycerin, as function of temperature and pressure 2–71193

granular rocks, wave vel. and compression simultaneous meas., porosity depend. 2–61982

halobenzenes, 20–96°C, hypersonic freq. 2–77429

iron, cast, during solidification 2–71669

liquid, phys. basis for Rao's and Wada's relations 2–71191

liquid crystal, Brillouin scatt. study of hypersonic waves at cholesteric-isotropic transition 2–80454

liquid metal, calc. 2–80469

liquids, u.s. velocimeter design 2–60470

N-p-methoxybenzylidine-p-butylaniline nematic liquid crystal, temp. dependence of velocity of longitudinal waves 2–46953

methyl alcohol, hydrostatic effect in obs. in critical region 2–43354

momentary contact method with pressure coupling for hot specimens rel. to u.s. velocity in steel at 1200°C 2–74978

nitro-compounds, organic liquids 2–53428

nitrobenzene-n-hexane binary mixture near critical point, dispersion meas. in 5-55 MHz range 2–71196

organic liquids, det. of molecular parameters 2–53429

pentaerythritol, high temp., phase, 30-200°C 2–57049

plastics, vel. as function of temp. 2–57048

polyethylmethacrylate, hypersonic phonon waves, Brillouin scattering 2–65284

polyethylmethacrylate, hypersonic vel. rel. to stimulated Brillouin scatt. 2–68669

polymer solutions, meas. at 23.6 and 50.96 MHz 2–46954

polymethyl siloxanes, as function of temperature and pressure 2–71193

polymethylacrylate, hypersonic phonon waves, Brillouin scattering 2–65284

polymethylmethacrylate, hypersonic rel. to stimulated Brillouin scatt. 2–68669

quartz, first and second sound velocity 2–71730

quartz, Rayleigh surface wave vel. change caused by cond. film, electromech. coupling const. detn. 2–43969

solids, digital averaging, pulse echo technique 2–61090

steel, cast, during solidification 2–71669

surface wave guidance by $(\Delta v/v)$ guidance structures 2–51010

syntactic foam, vel. as function of temp. 2–57048

triglycine sulphate, ferroelectric, rel. to electromech. coupling near T_c 2–68475

visualization of u.s. phase liquid, laser gratings 2–60469

$AgNO_3$, molten, hypersonic vel. dispersion obs. by Brillouin spectroscopy 2–77427

Au films, temp. depend. meas. by pulse-echo method 2–77780

Bi, adiabatic elastic stiffness consts. determ. 2–74822

$Bi_{12}GeO_{20}$, Rayleigh surface wave vel. change caused by cond. film, electromech. coupling const. detn. 2–43969

C composites, fibre reinforced resin matrix, elastic prop. meas. 2–53964

$Ca(NO_3)_2.4H_2O$, molten, hypersonic vel. dispersion obs. by Brillouin spectroscopy 2–77427

$Cs\text{-}NH_3$ solutions, velocity of 10 MHz waves on function of temp. and metal concentration, structural changes 2–43352

$Fe_{0.98}O$, wustite, elastic consts., rel. to upper mantle comp. 2–61980

Ga, elastic consts. determ. by u.s. pulse method 2–71549

n-GaAs:O, piezoelectric stiffening of active bulk modes and increase in velocity of 30 MHz shear waves 2–51204

^4He, liquid, 30 to 90 MHz 2–53469

$xK_2O(1-x)SiO_2$ glass, u.s. vel. and absorpt., meas. apparatus, 0–300K 2–74983

K_2SO_4, liq. 2–53426

Kr, solid, pulse echo obs. of elastic constants 2–50725

$LiBaF_3$, elastic and thermoelastic consts. 2–53781

$LiNbO_3$, Rayleigh surface wave vel. change caused by cond. film, electromech. coupling const. detn. 2–43969

$LiNbO_3$, surface wave device, laser beam probe obs. 2–68232

Li_2SO_4, liq. 2–53426

$LiTaO_3$, Rayleigh surface wave vel. change caused by cond. film, electromech. coupling const. detn. 2–43969

NaCl, rel. to equation state determ., 0-8kbar, 300-800K 2–68065

NaF, third-order elastic consts. determ. 2–60844

$NaNO_3$, molten, hypersonic vel. dispersion obs. by Brillouin spectroscopy 2–77427

$Pb_{1-3x/2}La_x(Zr_{0.65}Ti_{0.35})O_3$ ceramic, acoustic detection of ferroelectric phase changes 2–51196

Sb_2S_3, and absorpt. 2–80914

Se amorphous, Young's, rigidity moduli, 0-60°C 2–57051

n-Si, heavily doped, under uniaxial stress, elastic consts. determ. 2–68066

SiO_2, stishovite, elastic consts., rel. to upper mantle comp. 2–61980

Sn, adiabatic elastic stiffness consts. determ. 2–74822

Sn, and Sn-In dil. alloy, third-order elastic consts. 2–50727

$SrTiO_3$, degenerate semicond., effects of longitudinal mag. field 2–71731

Tb, determ. of elastic consts., 78-300K 2–60846

$Te_{15}Ge_3As_2$ glass, hydrostatic press. effects 2–47742

Velocity continued

acoustic waves, ultrasonic continued

UN, elastic consts. determ., 278K, pulse echo technique 2–53783

ZnO/Al_2O_3, heteroepitaxial layer structure, surface props. rel. to delay line fabrication and behaviour 2–68235

ZnO, Rayleigh surface wave vel. change caused by cond. film, electromech. coupling const. detn. 2–43969

$ZrO_2\text{-}Y_2O_3$, elastic consts., current blackening effects, u.s. wave vel. obs. 2–43666

light

constancy, establishment of unified time- frequency-length standard 2–63370

Einstein's postulate and Ritz emission theory 2–55378

Fresnel aether drag in transversely moving medium, direct observation 2–45773

isotropy of C, expt. 2–78787

measurement, by det. of laser radiation wavelengths 2–78759

measurement, laser frequency and wavelength meas. 2–78758

moving source, Lloyd mirror interferometer experiments 2–42174

He-Ne laser frequency measurement rel. to speed of light determination 2–48974

Velocity analysis, particles *see Particle velocity analysis*

Velocity measurement

see also Angular velocity measurement; Stroboscopes

anemometer, hot wire, reverse flow sensing 2–67707

atmospheric laser Doppler methods, performance analysis 2–62964

blood, in aortic arch, transcutaneous aortovelography 2–69312

blood, real-time obs. using u.s. multigated pulsed Doppler velocimeter 2–69311

e.m. water-current velocity meter, oceanographic applications 2–71138

gas flow, from Doppler shift of spectral line 2–83690

hot wire anemometer, calibration 2–67717

laser Doppler, noise-cancelling signal difference method 2–66772

laser Doppler, one-, two- and three- dimensional, self-aligning comparison beam method 2–66773

laser Doppler meter, application to turbulence charact. 2–69540

laser Doppler velocimeter, applic. to aerospace tests 2–46848

laser Doppler velocimeter, factors affecting accuracy 2–45220

laser Doppler velocimeter, fluid flow meas. 2–66408

laser Doppler velocimeter, for MHD boundary layer studies 2–80217

laser Doppler velocimeter design for use in turbomachinery 2–46826

laser Doppler velocimeters, unified analysis 2–62958

laser velocimeter, operation, accuracy and performance 2–66409

laser velocimeter, two dimensional, optical configuration 2–55368

light speed 2–58694

ocean current velocity meter, self- contained integrating system 2–72732

ocean currents, quartz crystal sensor 2–44668

oceanographic velocity microstructure, free fall probe for determining velocity and density gradients 2–48415

particles in fluid flow, optical methods 2–60165

piezoresistive acceleration-integration system 2–45221

radial velocities of several groups of galaxies 2–69029

speed of light, laser frequency and wavelength meas. 2–78758

squall line, Doppler velocity obs. 2–75561

supersonic gas flow 2–77342

terminal velocities of ice crystals in air, equivalent metal disk models 2–57972

u.s. velocimeter, for meas. in liquids 2–60470

vertical velocity of water surface, registration using e.m. induction method 2–72717

water flow velocity meas. using H_2 bubble apparatus 2–71135

wind, using pattern velocity computers 2–57968

He-Ne laser frequency measurement rel. to speed of light determination 2–48974

acoustic waves

castor oil, 0–40°C, 1 atmosphere–110 MPA 2–76375

liquid and solid aerosols 2–74569

ocean waters, coastal, sound-speed dispersion and fluctuations 2–44661

seawater, at varying salinities 2–78317

surface, change caused by thin conducting film 2–51017

surface waves using coherent pulse superposition 2–49127

vibrating metal rod, speed of sound determ. by simple electronic equipment, teaching experiment 2–62928

acoustic waves, ultrasonic

absolute accuracy of pulse-echo overlap and pulse-superposition methods 2–73431

Bragg diffraction imaging in plate-like elastic materials 2–43970

pulse echo system for obs. in megahertz region 2–55526

light

apparatus using stabilized CO_2 laser and Fabry-Perot interferometer 2–69539

closed-path interferometric experiments, test of Einstein's postulate 2–73285

experiment involving only distances and frequencies 2–82104

first order effects, new method of meas. 2–69560

laboratory experiment for students using stellar spectra 2–78716

using methane stabilized He-Ne laser 2–42018

precision obs. using simultaneous obs. of absolute frequency and wavelength obs. in i.r. 2–42173

school expt. using laser and Foucault's rotating mirror method 2–41434

technique and measuring errors 2–59209

techniques using krypton lamp 2–69997

Veneziano model

ABFST model with dual amplitudes applied to π^+p reactions 2–82750

current amplitude construction which satisfy local current algebra 2–55838

deep inelastic electroproduction application of duality through Veneziano-like amplitude 2–59420

dual Pomeron compatibility with unitarity, absence of ghosts 2–59491

dual quark model developed from Veneziano model by inclusion of Dirac spin 2–63530

dynamical applications, review 2–63559

Veneziano model continued
- exotic exchange reactions, insertion of total widths of baryon resonances into leading terms of model 2−66961
- functions of order p, Veneziano and Coon representations 2−79552
- generalized amplitudes, hypergeometric structure 2−59464
- generalized calc. compared with $K^0\pi^-n$ and $\Lambda\pi^-\pi^0$ channels in K^-d interactions at 4.9 GeV/c 2−42375
- generalized combination with U(6,6) symmetric kinematic factors, application to $K^-p\rightarrow K^{*-}\pi^+n$ 2−67010
- N-body inclusive reactions 2−70177
- N-particle amplitude, similarity of dual resonance loop amplitude structure in Mandelstam variables S_{ij} 2−45915
- n-point, Lorentz invariance and duality 2−70198
- n-point functions, recurrence formula 2−82721
- narrow resonance approx. for scattering amplitudes 2−76634
- nonplanar, singularity structure of double-Regge vertex 2−82730
- Regge trajectories behaviour 2−59490
- review of fundamental and characteristic features, consequences, agreement with exptl. data 2−66975
- spectrum of states in unit intercept model 2−63541
- string model, scatt. amplitude determ. 2−52581
- unified treatment of meson-meson, meson-baryon and baryon-baryon scattering 2−70190
- $\gamma N\rightarrow\pi N$, sum rules relating p and n mag. moments to amplitudes 2−82670
- K e.m. form factor in Veneziano-type represent. 2−63578
- $K\rightarrow\pi\mu(e)\nu$, form factors determ. from current algebra sum rules using Veneziano model 2−73802
- $K\text{-}n\rightarrow K^0\pi\text{-}n$ channel 2−70222
- $K^-p\rightarrow\Delta^{++}K^{*-}\pi^-$, production for quasi-three body final state 2−73808
- NN elastic scattering, one-boson exchange model with amplitudes constructed from Veneziano functions 2−45994
- $pn\rightarrow P^+\pi^-\pi^-$, 1.2 GeV, investigation using model with satellites 2−52636
- $pn\rightarrow\kappa\kappa\pi$, investigation at threshold 2−63552
- π electromagnetic form factor, unitarization in smoothed model 2−55850
- π form factor represent. 2−79594
- $\pi^-p\rightarrow\pi^+\pi^-n$, one pion exchange model developed using Veneziano five point function 2−52618
- $\pi\pi$, low energy final state interaction 2−55855
- $\pi\pi$ scattering models, review 2−45978
- $K^\pm p$ scattering, Regge fit with Veneziano residues 2−52603

Venus
- aeronomy of CO_2 atmospheres rel. to Mars and Venus 2−73075
- atmosphere, CO_2 emission behaviour 2−77303
- atmosphere, minor constituents, u.v. spectroscopy from Orbiting Astronomical Observatory 2−69140
- atmosphere, radio wave propagation, Venera-7 spaceprobe data 2−55151
- atmosphere, temp. and pressure distribution to surface, Venera-7 meas. 2−51831
- atmosphere, Venera 4, 5 and 6 probes obs. 2−44964
- atmosphere, water vapour evolution 2−44958
- atmosphere above cloud deck, radiative transfer, study of diurnal variations in atmospheric temperature profiles 2−44946
- atmosphere radiative transfer by CO_2 2−65770
- atmospheric thermal equilibrium 2−85030
- brightness temp. and radar cross section meas. 2−69165
- brightness temperature, at 2 and 8 mm wavelengths, comparison with Jupiter 2−66184
- brightness temperature, phase dependence of 2.7 cm wavelength radiation 2−44959
- cloud cover, atmos. circulation obs. 2−58513
- clouds, dirty hydrochloric acid model 2−44963
- clouds, spectroscopic evidence against pure H_2O ice particles 2−78564
- clouds of HCl containing dissolved Fe compounds 2−58514
- cloudy atm., spectral line formulation 2−62710
- daylight observations when close to inferior and superior conjunction 2−48781
- diameter meas. using double image micrometry 2−75916
- environmental simulation 2−78569
- far u.v. emission spectra and features rel. to Mars 2−78566
- far-u.v. spectrum, reson. line analysis 2−58515
- halo effect during 1970 inferior conjunction, photometric obs. 2−44960
- interferometric visibility at 11.1 cm wavelength 2−51830
- lower atm., model based on high resolution radio obs. 2−75914
- mesosphere, radiative equilibrium, temp. profile 2−66185
- microwave absorption in lower atmosphere of Venus 2−48780
- microwave spectrum in 18.5-24.0 GHz range 2−62712
- multiple exospheric temperatures 2−73090
- phase anomaly, atmosphere refraction effect 2−73089
- Planetary Explorer probe studies of Venus' atmosphere 2−75643
- planetology congress (Montreal, September, 1972) 2−78499
- planetology mission based on planetary explorer space craft 2−55152
- radar image and brightness map of surface 2−78504
- radar interferometric observations, mapping of reflectivity features 2−81944
- radar obs. processing using Venera 4, 5, 6 and 7 2−51832
- radio signals from Venera-7 during descent to surface, digital computer analysis 2−73088
- solar wind flow past planet, ionospheric interaction 2−78574
- surface and atmosphere, Venera entry probes and Mariner flyby 2−69164
- surface and atmospheric conditions meas. by microwave interferometry 2−51829
- surface height variations over equatorial region, radar echo-delay meas. 2−44962
- thermodynamic parameters from spacecraft descending by parachute, Venera-5 and 6 spacecraft 2−73074
- thermosphere comp. maintenance by large-scale circulation 2−58508
- turbulence characteristics of atmosphere from Mariner V S-band occultation data 2−78568
- u.v. and red light photographs, using T.V. device 2−51833
- u.v. observations during 1969 W. elongation, features and atmospheric rotation 2−44961

Venus continued
- CO_2 7820 Å band, temperature distributions from reflected sunlight 2−62711
- CO_2 8710 Å line profile meas. rel. to several atmospheric models 2−78560
- CO_2 band spectroscopic observations during 1971 superior conjunction 2−78565
- CO_2 clouds, variability and lateral inhomogeneity 2−78563
- CO_2 variations during 1971 superior conjunction, spectroscopic observations 2−78562
- ClOO radical in atm., structure and stability 2−78559
- Hg clouds in atmosphere 2−75915
- O I 1304 and 1356 Angstroms lines intensity rel. to O concentrations in upper atmosphere 2−78567
- O_2 7635 Angstroms band observations rel. to atmospheric composition 2−78548

Verdet constant *see Magneto-optical effects*

Verneuil process *see Crystals/growth*

Vertex functions *see Elementary particles; Field theory, quantum; Functions*

Vibrating bodies
- *see also Crystals/lattice mechanics; Elastic waves; Pendulums; Piezoelectric oscillations*
- aeolotropic elastic rotating disc, study of transverse vibrations 2−52204
- aero space vehicle, noise-induced structure vibrations 2−69714
- anisotropic rectangular plates, free vibrations 2−55494
- annular bar, disc and fibre, comparison of eigenvalues and natural vibration modes 2−82340
- annular plate with supporting edge beams, deflections 2−45442
- axisymmetric shells, free vibrations by finite difference method 2−41644
- bar, contactless parameter measurements of changes in length 2−52210
- bars and discs, elastic consts. meas. method 2−45464
- bars and plates with concentrated masses, forced vibrs. 2−45469
- bars and threads with concentrated masses 2−52214
- beam, transverse vibrations, calculation by slowly varying parameter method 2−63103
- beam under periodic excitation, nonlinear response 2−55488
- beam-slab type highway bridges, transverse free vibrs. 2−49092
- beams, nonlinear vibrations, matrix displacement method 2−41643
- beams and plates, statically deformed 2−41662
- beams with continuous mass distribution, effects of discrete masses and elastic supports on natural frequencies 2−69704
- beams with hysteresis damping, transient vibration problem 2−73400
- bolt clamped electrostrictive torsional vibrator for u.s. power applications 2−73412
- box-type structures, anal. of inplane vibs. by a finite element method 2−41653
- buckling and vibration analysis for stiffened orthotropic shells of revolution 2−69693
- cantilever cylindrical thin elastic shells, analysis by matrix progression method 2−58888
- cantilevered columns under periodic loads, stability and non-stationary vibration digital simulation 2−69705
- circular cylindrical shells under nonuniform initial stress, free vibrs. 2−45501
- circular elastic plates, due to sonic boom 2−55491
- circular plate, variable thickness, clamped and free 2−69706
- circular plate supported at several points, Lagrangian minimization analysis 2−76345
- circular plate with central hole, asymptotic solution for large deflection 2−55490
- circulator rings coupled first bending vibrations, effect of transverse shear and rotary inertia 2−45560
- combined cylindrical shell, displacement, bending moment and shearing force 2−76346
- composite circular and annular membranes, radiation of sound 2−66584
- composite circular plate with central hole, frequency equation 2−73409
- composite cylindrical shell, radial vibration in magnetic field 2−66581
- composite elastic sphere and cylinder 2−66583
- concentric cylindrical shells in acoustic fluids, forced harmonic and random vibrations 2−73398
- cored mirrors, holographic interferometric det. of vibratory mode shape patterns 2−52434
- coupled fluid/structural system, beam like vibrations 2−52217
- coupled non-linear system, natural modes 2−45443
- curved Bernoulli Euler beams, natural frequencies 2−55493
- curved partition sound transmission props. 2−45548
- curvilinear plate bending elements, possible loss of accuracy 2−73407
- cylinder in fluid, oscillatory damping 2−45473
- cylinders, axisymmetric vibrations, finite element analysis 2−58892
- cylindrical film equil. under hydrostatic press., axisymmetric problem 2−78903
- cylindrical panels, finite strip solns. for free vibrations 2−55499
- cylindrical shell, finitely deformed, stability 2−49069
- cylindrical shell, twisted, composite, cylindrically aeolotropic material, torsional vibr. 2−45440
- cylindrical shells, axially equispaced constraints, characteristics 2−78907
- cylindrical shells, energy transfer between flexural and extensional modes 2−66593
- damping characteristics of certain steels, cast irons and other metals 2−69703
- discrete symmetric structural systems, post flutter oscillations 2−69699
- double tapered cantilever beams, transverse vibrations 2−41648
- dynamical systems subjected to impulsive parametric excitation, theory 2−66587
- eigenfrequency perturbation of a cylinder due to ridge on surface 2−51505
- elastic layer, nonlinear, forced steady state vibration 2−49088

Vibrating bodies continued
elastic plate with random properties, eigenvalue problem, free vibrations 2−55497
elastic rod, stability of nonlinear oscillations 2−73399
elastic shells of different material, paradoxes in vibrations 2−52205
elastic sphere, horizontal heterogeneity effects on torsional oscillation 2−76354
elastic system, stationary vibrations in combined parametric resonance 2−41655
elastically supported sandwich plates, damping 2−78909
elastodynamic oscillations, Fredholm integral equation 2−45455
electrical machine, rot., vibr. admittances, eigenfreqs. and modes 2−45655
electrodynamic vibr. table design 2−45474
electromechanically excited bar, equivalent electrical circuit for longitudinal vibrations 2−78916
elliptical plate with simply supported edge, free flexural vibrations 2−73401
end-weighted spring, comparison of normal modes for discrete od continuous mass distributions 2−78864
extremum principles for rigid plastic dynamic loading problems 2−69681
flexible cable in uniform flow field, coupling of longitudinal and transverse matrices 2−55492
floor slabs, column-supported, finite element displacement analysis 2−49097
free flexural vibrations of damped plates 2−45463
free-free beams, sound radiation by resonance 2−55537
fuel rods in parallel flow, computer program for determ. characteristics 2−63973
gas-liquid cocurrent flow, backmixing effect in mass transfer charact. 2−67564
guitar, acoustical and hologram interferometric meas. of top plate vibrations 2−52244
heavy filament in satellite orbit, transverse oscillations 2−73349
holographic measurement 2−58897
hot wire anemometer filaments in air stream, aeroelastic behaviour 2−55498
hot-wire filaments, in broad band turbulence 2−73405
hydrofoil, circular in stream of ideal liquid, determ. of lifting force and longitudinal momentum 2−83744
inertial foundation, Pasternak-type dynamic analysis 2−49100
inertialess finite rigid cylinder clamped in circular borehole 2−69702
infinite Bernoulli-Euler beam, on elastic foundation, dynamic response 2−66585
initially stressed shells, theory of vibration 2−41646
kettledrum 2−41647
ladder frame work H type, calc. 2−63098
laminated anisotropic circular plate, elastic stability 2−41650
laminated composite materials, simple thickness modes 2−73438
laminated orthotropic plates, nonlinear oscillations 2−76349
laminated Reissner plates, bonded by thin adhesive layer 2−41649
Langevin type electrostrictive torsional vibrator, bolt clamped 2−69725
lifting rotors with feedback controls, random vibration statistics using shaping filters 2−45451
loudspeaker diaphragm, dynamic behaviour, holographic obs. 2−45519
lumped and continuous dynamic systems, bounds on motion 2−45459
marine engines, torsional vibrations calc. 2−41642
mass measurement by measuring frequencies of natural oscillations of body 2−66406
Maxwell solid body, generalized, free vibrs., internal friction limiting value 2−55487
mechano-acoustical networks, l.f. damping mechanisms 2−41652
membrane, clamped, isoperimetric inequality for first eigenfunction 2−58898
membrane, elastically supported, bounds for lowest eigenvalue 2−82346
membrane, natural freqs., estimation method 2−49093
membrane, thick, behaviour under small deflections, singular perturbation methods 2−45441
metal rod, speed of sound determ. by simple electronic equipment, teaching experiment 2−62928
multilayered sandwich plates, analysis by finite strip method 2−58889
multiple synchronization in system of weakly coupled objects with one degree of freedom 2−52211
multistory buildings, two-dimensional ambient vibration tests 2−58899
natural frequencies of thin circular rings, selection rules for splitting of degenerate doublets 2−55484
natural oscillations of a bar, suppression by dynamic vibfation absorbers 2−52203
non-linear travelling, string, determ of frequency of transverse vibration by Panavko's direct linearisation method 2−49089
noncircular elastic hinged arcs, fundamental frequencies 2−78905
noncircular elastic hinged arcs, fundamental frequency det. 2−41661
nonconservative problems, nature of instability 2−69696
nonhomogeneous isotropic hollow thick cylinder, torsional vibration 2−66579
nonlinear conservative vibrating systems, phase plane analysis 2−73408
nonlinear panel response, turbulent boundary layer 2−71090
nonlinear system with two degrees of freedom, effect of damping 2−55489
nonlinear systems with secondary generalized coordinates, resonant harmonic excitation, equivalence principle 2−66578
nonlinear vibration of rotary cantilever blades, treated by Ritz averaging process 2−78865
nonlinear vibrations of two degree of freedom systems with repeated linearized natural frequencies 2−45462
nonstationary random vibration of nonlinear structures 2−76347
numerical calculation method for transient responses of vibrating systems with collision 2−82291
oddly stiffened circular cylindrical shells 2−45452
orthotropic cylindrical shell, torsional vibrations, solution in terms of Bessel functions 2−73411

Vibrating bodies continued
orthotropic plates, free vibrations 2−73403
oscillators, weakly coupled, perturbation procedure 2−45444
periodic and transient deformations, study by double pulsed holographic interferometry 2−41665
periodic perturbation effects at resonance 2−55483
piezoceramic disk, equivalent circuit for radial vibrations 2−66617
piezoelectric bar vibrating in compressional mode, response calc. 2−63118
piezoelectric crystal plate, h.f. vibration, two-dimensional eqns. 2−59025
piezoelectric crystal plates, two-dimensional equations of motion 2−45445
pinned-end beam undergoing nonlinear free vibrations, stability analysis 2−55502
plate, algorithms of vibr. modes 2−45466
plate, boundary conditions 2−45470
plate, coupling of vibrs. with acoustic field in fluid 2−45472
plate, free vibrs. soln. in polar coords. 2−45498
plate, infinite, radiation relationships and mech. impedance 2−45476
plate, laminated, eqns. derivation 2−49095
plate, layer potentials applic. for vibr. problem soln. 2−45471
plate, rectangular, nonlinear dynamic lumped parameter model 2−49118
plate, thick layered rectangular, free vibr. by finite element method 2−52208
plate, unbounded, vibrs. in random force field 2−76356
plate dynamic response analysis, time dependent boundary conditions 2−58869
plate on elastic foundation with vertical periodic load, plate-foundation interaction 2−76309
plates, circular and annular, analysis using finite element method 2−45446
plates, flexural and longitudinal vibrations, random coupling 2−69710
plates, vibrations from layer potentials 2−63095
plates, with density and stiffness discontinuities 2−45450
polar orthotropic annular plates, axisymmetric vibration 2−76351
prismatic bars, viscous damping 2−76350
Rayleigh Ritz method modification for obtaining lower bounds to eigenvalues 2−52207
rectangular plate, orthotropic clamped, natural frequencies 2−41660
rectangular plate with mixed edge conditions, eigenvalue problems 2−66516
rectangular plates, subject to inplane loads, Ritz soln. 2−76353
reed, forced, linearized error analysis 2−63104
Reiss type viscoelastic rod, in magnetic field 2−66580
response of system of N-coupled elements 2−41666
rigid, on Kerr foundation, free vibrations 2−49102
rigid movable sphere, motion when struck by plane or spherical acoustical waves 2−73402
ring, stiffened, in-plane flexural vibr. 2−63100
rotating circular plates with peripheral edge slots, stability control analysis by finite element procedure 2−76357
rotating uniform beam simply supported at one end, bounds to bending frequencies 2−73404
rotational-vibratory motion of free solid body carrying elastic elements 2−41654
rough inclined plane, motion of body on surface 2−66575
sandwich beam, dynamic analysis by finite element method 2−49114
sandwich beams, flexural vibrations, eigenvalue boundary problems 2−69707
shafts, transverse vibrations, step-wise linear transformations of the argument 2−82297
shear wall structures, in plant vibration by finite element method 2−45449
shell, circular cylindrical, natural freqs. 2−49096
shells, eqns. for nonlinear vibration 2−69694
simple linear oscillator, stationariness, filtration, periodic nonstationary random process 2−73406
simple supported beam with time dependent material properties 2−78908
speaker vibrating at audio frequency, modes by holographic interferometry 2−52436
sphere in viscous fluid, high frequency oscillations 2−70866
spherically isotropic hollow sphere, free vibrations 2−63097
spinning membrane disc with central hub, coupled transverse vibrations 2−78904
stability of clamped skew plates 2−58886
straight beam, nonlinear response to narrow beam random excitation 2−55495
strain amplitudes meas. in internal friction expts. using laser interferometer 2−73395
string and membrane, eigenfrequency, numerical determination by simulation 2−45448
supporting surface, boundary value problems of vibration theory, reduction to integral equations 2−55486
symmetric spring mass networks, group representation theory 2−82290
symmetrically loaded ring, characteristic frequencies 2−55485
Takabayama tunnel, Japan, landslide microtremors and vibration of underground structure 2−81615
taut string, on elastic foundation, deflections under random loads 2−55478
telephone diaphragm, holographic obs. 2−45475
thermoelastic plates, coupled theory, det. of free vibration frequencies 2−55477
thick laminar cylinder of finite length, under various end conditions 2−76352
thick plate free vibration, convergence of eigenvalue solutions in finite element method 2−45447
thick spherical shell of isotropic non-homogeneous elastic material, rotatory vibrations, frequency equation 2−73410
thin beams, large flexural oscillations 2−66598
thin bounded plate in liquid, interaction of vibrational modes 2−69711
thin infinite fluid loaded plate 2−63096

Vibrating bodies continued
- thin plates subjected to complex middle-plane force systems, free vibrations finite element analysis 2—69700
- thin shells of rotation, distrib. of freq. 2—52212
- thin shells of rotation, self-oscillation freq. spectra 2—52213
- Timoshenko beam element, stiffness consistent mass matrices 2—63101
- Timoshenko beam under initial axial stress, eqns. of motion 2—45460
- Timoshenko beams, clamped and free, dynamic responses 2—82342
- torsional vibration of finite circular cylinder of non-homogeneous material by twist on one end plane 2—49099
- towers and overhead power conductors, aerodynamic forces, modelling 2—80384
- transversely isotropic finite cylindrical magnetic field 2—66582
- travelling strings, equations of motion of nonlinear vibrations 2—55496
- truncated conical shell, Ritz's method analysis 2—76344
- tuning fork, excitation of self-oscillation 2—58887
- tuning forks' eigenfrequencies, numerical determination 2—69698
- unsymmetrically laminated plates, nonlinear vibr. 2—82286
- variable curvature effects in mechanic behaviour of arc structures 2—41645
- vertical plate, effect of longitudinal vibrations on free convection from plate 2—45593
- vibratory-impact system, two degrees of freedom, eqns. of motion 2—45453
- viscoelastic cylinder, longitudinal oscillations, thermomechanical coupling effects 2—76348
- viscoelastic Timoshenko beams, isotropic and transversely isotropic, forced motion using measured material 2—69701
- vortex street in wake of vibrating cylinder 2—77228
- Ziegles model and cantilever beam, stability, external and internal damping effects 2—45454

Vibration, molecular *see Molecules/vibration*

Vibrations
- *see also Acoustics; Damping; Oscillations; Vibrating bodies; Waves*
- 3-layer plates, investigation of symmetric vibrations with respect to centre plate 2—82344
- active compensation multichannel systems for bounded structs. 2—45468
- amplitude-phase-frequency characteristics of vibrating system, dependence on dissipative properties 2—82296
- analysis by hologram interferometry 2—66576
- anharmonic oscillators, vibrational relaxation 2—66422
- anisotropic shallow shells 2—41659
- asymmetric buckling of spherical caps under uniform step pressures 2—45424
- automated modal vibration testing, MODAPS, instrumentation system 2—45491
- bars and threads with concentrated masses 2—52214
- basilar membrane, frequency response curve in living guinea pig 2—82035
- basilar membrane, fuzziness detection and anal. using laser light 2—82033
- basilar membrane, vibratory amplitude and phase pattern along membrane 2—82034
- beam, transverse vibrations, calculation by slowly varying parameter method 2—63103
- beam on elastic foundation subjected to follower force, stability 2—66596
- beam-columns, computer programs 2—66599
- beams and plates, thermally induced, ratio of maximum dynamic to static deflection 2—45437
- beams with hysteresis damping, transient vibration problem 2—73400
- bell tones, simulation with pipe-bells and keyboard sounds 2—63122
- bending waves, multiple scattering by random inhomogeneities 2—73416
- cantilever cylindrical thin elastic shells, analysis by matrix progression method 2—58888
- cat's tympanic membrane, obs. using time-averaged holography 2—51955
- cavitation erosion, determination of resistance of materials by magnetostrictive vibratory method 2—76115
- circular elastic plates, due to sonic boom 2—55491
- circular plate, rotating large-deflection waves 2—49087
- computer tape subjected to periodic motion, longitudinal motion in high performance tape drive 2—69685
- continuous systems under parametric excitation, Liapunov stability criteria 2—45458
- control, conference, Lafayette USA (1971) 2—52249
- coupled non-linear system, natural modes 2—45443
- cylindrical shell, response to random press. field 2—45499
- cylindrical shell, twisted, composite, cylindrically aeolotropic material, torsional vibr. 2—45440
- damped lateral, in axial creeping beam with random material parameters 2—41664
- damping, optimal control 2—82347
- deflections of taut string on elastic foundations under random load 2—55478
- discrete stratified fluid free oscillations, numerical weather prediction 2—62112
- distributed parameter systems, equivalence conditions 2—78868
- elastic bodies, distribution of natural frequencies, applic. to random vibration problems 2—41656
- elastic composite laminates in cylindrical bending, exact solution 2—66493
- elastic conical shell, fastened in screen, effect of sound press. wave 2—69712
- elastic layer, nonlinear, forced steady state vibration 2—49088
- elastic shells of different material, paradoxes 2—52205
- elastic stability, nonconservative problems, approximate methods 2—58893
- elastic string, nonlinear vibrations, investigation 2—55503
- elastic systems with discrete dynamic systems, free vibrs. 2—45500
- elastomechanics problems, bounds on field quantities 2—41609
- elliptical plate with simply supported edge, free flexural vibrations 2—73401

Vibrations continued
- equivalent electrical circuit for longitudinal vibrations in electromechanically excited bar 2—78916
- extensional, composite circular plate with central hole 2—73409
- finite element method in stress analysis 2—69662
- flexural and extensional modes, energy transfer between, cylindrical shells 2—66593
- flutter of thin cylindrical shells conveying fluid 2—58895
- forced normal mode, viscoelastic systems 2—66615
- fourth order nonlinear oscillations, normal forms 2—49084
- free, finite element plates subjected to complex middle plane force systems 2—69700
- free, for finite inhomogeneous elastic rods, asymptotic behaviour of eigenvalues 2—66592
- free, infinite isotropic magneto-thermo-elastic plate 2—69692
- free, noncircular elastic hinged arcs, fundamental frequency det. 2—41661
- free and forced, det. of rigid modulus of rectangular steel springs 2—63079
- free bending oscillations of array of strut-like members linking two beams 2—49098
- free transverse, of elastic plate with random properties, eigenvalue problem 2—55497
- free-free, rational reduction of large scale eigenvalue problems 2—69695
- hand-arm system, dynamic response to sinusoidal input 2—52209
- Helmholtz resonators, resonant freq. calc., consideration of shape 2—78920
- h.f., piezoelectric crystal plates 2—45445
- high speed fans, tone noise from rotor/stator interactions 2—82355
- holographic analysis of general displacement field 2—82541
- holographic applic. in studies, book 2—42154
- holographic vibration analysis, phase mapping 2—79281
- effects on human body, equal comfort contours for whole body vertical, pulsed sinusoidal vibrations, 4 to 80 Hz 2—73169
- hybrid cylindrical shell finite element 2—49105
- hybrid cylindrical shell finite element 2—49104
- infinite strip, variable thickness, effect of transverse shear and rotatory inertia 2—76334
- inplane, box-type structures, anal. by finite element method 2—41653
- isolators for vibr. effects reduction 2—45496
- isoparametric shell elements for numerical solution 2—73397
- laminar elastic systems, Trefftz-Fichera eigenvalue bounding methods for natural freq. 2—49101
- large amplitude, natural frequency, circular plate with concentric rigid mass 2—66591
- lateral, clamped rectangular membrane, influence of small bending stiffness 2—41641
- l.f. effects on man, human body-mechanical vibratory system analysis 2—62865
- linear system, mathematical smoothing of admittance obs. 2—69708
- linear system response to modulated sinusoidal inputs 2—49094
- linear systems subjected to nonwhite excitation, calc. of correlation matrices 2—66588
- matrices, stiffness and mass, extremal eigenvalue bounds 2—66577
- matrix method of vibrational analysis of framed structures 2—76355
- Maxwell solid body, generalized, free vibrs., internal friction limiting value 2—55487
- membrane, thick, behaviour under small deflections, singular perturbation methods 2—45441
- membrane freqs., stability of finite difference methods 2—63102
- metal, damping capacity meas. under direct cyclic stresses 2—53861
- modal characteristics of structure subjected to random excitation 2—69709
- modelling of dynamic systems with dry friction, analogue computer method 2—82287
- narrow band random, fatigue failure of materials 2—48623
- natural bending frequency rel. to rotational frequency in rotating cantilever beam 2—66594
- natural frequencies of clamped generally orthotropic rectangular plates 2—41660
- natural frequency, estimator for standard deviation, 9 degree-of-freedom system 2—66601
- natural frequency, estimator for standard deviation 2—66600
- natural oscillations of a bar, suppression by dynamic vibfation absorbers 2—52203
- neutralizers, Lanchester dampers and impact dampers, theory 2—66589
- non-linear, free, pinned-end beam, stability anal. 2—55502
- non-stationary and stability of columns under periodic loads 2—69705
- nonlinear, of rotating cantilever blades, treated by Ritz averaging process 2—78865
- nonlinear, two-degree-of-freedom systems, approximate method of treatment 2—66595
- nuclear reactor subassembly ducts, prismatic shells with hexagonal cross section 2—76932
- numerical eigenfrequency approx. by simulation 2—45448
- orthotropic skew plates, formulation using Ritz variational method 2—49090
- overdamped eigenvalue problem selfadjoint formulation 2—78866
- parametric amplifier for mechanical vibrations 2—55480
- parametric resonance of stiffened rectangular plates 2—45457
- plate deflections with point clamped constraints using Lagrange multipliers 2—45461
- plates, method of layer potentials 2—63095
- plates, thin elastic, anal. of vibrational modes, finite element method 2—82341
- point contact, theoretical response diagrams 2—58896
- polar orthotropic annular plates, axisymmetric vibration 2—76351
- powder layer, finely dispersed, vibration effects 2—43393
- propagation near boundary of inhomogeneous elastic half space 2—54638
- random, broad band, obs. of fatigue failure of materials 2—77707
- Rayleigh Ritz analysis, selection of significant eigenvalues 2—58891
- rectangular plate with mixed edge conditions, eigenvalue problems 2—66516

- **Vibrations** continued
  - resonances of treble viol plates, obs. by hologram interferometry, design of improved instrument 2−45520
  - rigid body on Kerr foundation, free vibrations 2−49102
  - ring, stiffened, in-plane flexural vibr. 2−63100
  - rotatory, thick spherical shell of isotropic non- homogeneous elastic material 2−73410
  - seismic effect of mechanical action parameters on ground surface on characteristics 2−84737
  - silicone based electrons, dynamic shear properties over wide temp. ranges 2−47488
  - sinusoidal, testing, use of programmable filters 2−45490
  - slender rotating beam with end masses, asymptotic theory 2−66590
  - sonic, in heated channels 2−58920
  - spectra of natural vibr. of a shell of revolution 2−45456
  - spherically isotropic hollow sphere, free vibrations 2−63097
  - static membrane deflections in capacitance-microphone nonlinear equations 2−73442
  - statically deformed beams and plates 2−41662
  - stationary, elastic system in combined parametric resonance 2−41655
  - stationary impact, mechanical system with two degrees of freedom 2−69697
  - stationary random response of nonlinear multidegree-of-freedom dynamical systems, applic. of statistical linearization techniques 2−66586
  - strings and membranes, direct and reverberant response to convecting random pressure fields 2−41663
  - synthesis of vibrating systems, conference, Washington (1971) 2−41658
  - thermoelastic, rectangular plate 2−41657
  - thick laminar cylinder of finite length, under various end conditions 2−76352
  - thin infinite fluid loaded plate 2−63096
  - thin shells of rotation, distrib. of freq. 2−52212
  - torsional, effect of deviations from spherical symmetry on frequency, rel. to Earth 2−61838
  - torsional, orthotropic cylindrical shell, solution in terms of Bessel functions 2−73411
  - torsional elastodynamic, solution with Fredholm integral equation 2−45455
  - transverse, class of orthotropic plates, fundamental and higher frequencies and mode shapes 2−66613
  - turbine disk, optimal mode det. using computer 2−41651
  - tympanic membrane of human cadaver ears, obs. by time-averaged holography 2−82052
  - underground workings, due to rail traffic, ballast and concrete supports comparison 2−45538
  - unsymmetrically laminated plates, nonlinear vibr. 2−82286
  - vibrodamping treatment distrib. on structs., optimization methods 2−45497
  - viscoelastic half-space, crit. vibrs. 2−66616
  - vocal folds in normal and nasalized vowels, ultrasonic obs. 2−45060
  - volume thermal shock in a plate, stresses described by damped harmonic vibrations 2−82327
  - of wall due to plane, P, S and Rayleigh waves, solution 2−58890
  - Al/resin/Al sandwich bar, complex dynamic modulus 2−80742
  - B-epoxy laminated composite plates, holographic stress analysis 2−78895
  - Nb, internal friction, vibr. freq., damping, β-process, 20-170°C 2−56778
  - **excitation**
    - beam under periodic excitation, nonlinear response 2−55488
    - circular arches, symmetrical and unsymmetrical forced excitation 2−49117
    - contact-free stimulation of waves in steel plates 2−78914
    - cylindrical shell, thin, longitudinal impact 2−66597
    - electrodynamic, new concepts in exciters 2−69713
    - linear systems, response to random impulses 2−78906
    - N-span, Bernoulli-Euler beam, response to turbulent boundary layer pressure excitation 2−76358
    - natural frequencies of thin circular rings, selection rules for splitting of degenerate doublets 2−55484
    - nonlinear, resonant, of infinitely long cylindrical shells 2−76343
    - nonlinear interactions in free-shear layer transitions 2−76338
    - nonlinear nonconservative systems, subject to step fn. excitation 2−58894
    - nonlinear systems with secondary generalized coordinates, resonant harmonic excitation, stability behaviour 2−66578
    - nuclear reactor fuel rod in vertical coolant tube, hydrodynamics, vibration and wear obs. 2−52844
    - panel arrays, normal mode characts. 2−69715
    - plates and shells, statistics of acoustically induced vibrs. 2−45465
    - straight beam, nonlinear response to narrow beam random excitation 2−55495
    - strings and thin plates, warble-tone excitation 2−78910
    - tuning fork, self-oscillation 2−58887
    - water surface waves, vibrating in bell mode 2−43296
  - **measurement**
    - *see also Seismology*
    - — 2−66788
    - — 2−58877
    - accelerometer for low-level building vibrs. 2−45467
    - cored mirrors, holographic interferometric det. of vibratory mode shape patterns 2−52434
    - damped oscillations, time average holographic interferometry 2−63094
    - dynamic stiffness and transmissibility of vibration isolating materials 2−49086
    - electrodynamic test vibration racks, technique in det. of characteristics 2−69691
    - frequency response testing, spectrally shaped transient forcing function 2−73396
    - guitar, acoustical and hologram interferometric meas. of top plate vibrations 2−52244
    - holographic interferometry, projected ruling Moire method 2−82149
    - holographic interferometry, supersonic vibrator 2−49103
    - holographic real-time/time averaged interferometry of solid surface 2−82147
    - holographic technique 2−58897

- **Vibrations** continued
  - **measurement** continued
    - holographic using millisecond pulsed laser 2−79277
    - holography, real time and time average methods, bibliography 2−58885
    - instrumentation system for PWR 2−74142
    - kinematics transducers calibration by interferometric method 2−73634
    - laminated honeycomb structures, adhesive layer, elastic properties 2−50927
    - laser-interferometry for calibration of detectors 2−55479
    - material integrity of mechanical structures by computer interpretation of vibration analysis 2−60925
    - natural oscillation magnitudes from dynamic response by harmonic excitation in one configuration 2−52202
    - optical free surface motion detector use of He to eliminate refraction effects 2−45439
    - paper loudspeaker cones, scanned holography 2−55541
    - segmented shells, holographic interferometry 2−82146
    - spheroidal and toroidal vibrations of Earth for order numbers higher than 50 from earthquakes 2−84704
    - super-high freq. apparatus, interference of standing e.m. waves 2−55482
    - telephone diaphragm, holographic obs. 2−45475
    - underwater, Michelson interferometer with laser light source 2−55481

- **Vibronic states** *see Molecules/electronic structure; Molecules/vibration*

- **Vidicons** *see Electron tubes*

- **Virial coefficients** *see Equations of state*

- **Virtuons (virtual phonons)** *see Crystals/lattice mechanics*

- **Viscoelasticity**
  - *see also Plasticity*
  - — 2−60518
  - belting, power-transmission, uniaxial tensile creep meas. 2−43702
  - bone model, two phase poroelastic material 2−41571
  - butadiene-styrene copolymer, nonlinear behaviour under constant strain rates 2−50733
  - butyl rubber, temp. and extension time depend. of creep recovery 2−71555
  - composite layer, disturbance propag. in mag. field 2−55462
  - composites, isotropic, improved bounds for real and imaginary parts of complex moduli 2−56776
  - compressible solids, stress analysis 2−63086
  - computer tape subjected to periodic motion, longitudinal motion in high performance tape drive 2−69685
  - concrete creep, nonlinear analysis of two-dimensional problems 2−66557
  - contact problem of rigid punch on viscoelastic beam 2−66565
  - continua, rheological props., body-, space- and Cartesian space-tensor fields 2−63073
  - continua, rheological props., Oldroyd's 1950 formalism 2−63074
  - converging flat plates, flow between, numerical analysis 2−67777
  - cracks, variational principle applied to theory 2−63088
  - cylinders rolling on viscoelastic plane, contact area rel. to vel. 2−66488
  - deformable solids, layered waveguide technique for determ. 2−64751
  - deformed solid, propagation of sinusoidal small amplitude waves 2−41705
  - disturbances on infinite plate due to impulsive radial forces and twist on inner surface of circular hole 2−49060
  - dynamic linear one-dimensional problem, iterative solution 2−45425
  - dynamic properties, mechanical impedance technique 2−74874
  - elastic plate on viscoelastic foundation, deflection in variable temp. field 2−41639
  - elastic waves, longitudinal, in linear material 2−58906
  - emulsions, semi-solid, viscoelastic props., dynamic measurement by Weissenberg rheogoniometer 2−83817
  - environmental dependent materials, constitutive relation for linear aging 2−41634
  - fading memory materials, non-isothermal treatment 2−68056
  - f.c.c. polycrystals, grains disorientation effects 2−53786
  - fibrin elongated, films, piezoelectricity and dielectricity 2−85087
  - filtration of nonlinear viscous liquids in porous viscoelastic-plastic media 2−53357
  - flow, in V-shaped duct, constitutive eqn. 2−43057
  - flow between 2 circular cylinders under periodic pressure gradient 2−53365
  - flow in disc and cylinder system, orthogonal collocation analysis 2−70857
  - flow of two immiscible Maxwell fluids with transient press. gradient through rectangular channel 2−50161
  - flow past infinite plane porous wall with time dependent suction 2−50160
  - fluid, flow stability 2−53143
  - fluid, generalized measures of deformation rates in secondary flows between rotating spheres 2−50147
  - fluid, horizontal layer, thermal instability 2−64225
  - fluid, stability in Couette flow 2−46871
  - fluid flow, unsteady, through circular, coaxial circular ducts, press. function of time 2−83451
  - fluid layer, thermal instability, effect of mag. field 2−80224
  - fluid layer, thermal instability, effect of rotation 2−70830
  - fluids, determ. of material parameters by rotational non-viscometric flows 2−50140
  - fluids, generalized measures of deformation rates in secondary flows between rotating spheres 2−50147
  - fluids, non-viscometric flows, review 2−46659
  - fluids flowing through abrupt contraction, rheological props. 2−64406
  - fracture, delayed, in solids, criteria and experimental verification 2−71585
  - glass, tempered, residual stresses 2−77648
  - glass fibre reinforced nylon 6, dynamic viscoelasticity temp. depend., two-phase blend system model applic. 2−71556
  - half-plane, Lambs problem 2−66573
  - half-space, crit. vibrs. 2−66616

Viscoelasticity continued

- 2-hydroxyethyl methacrylate networks in dry and swollen states, effect of crosslinking density and dilution 2−56782
- incompressible fluid, flow between 2 coaxial rot. cylinders different permeab. 2−83449
- ionic polymers in dilute solution, charged bead-spring models 2−53366
- laminar motion of Maxwell fluid near oscillating porous infinite plane 2−60154
- linearly viscoelastic shallow spherical shell, large deflections 2−66566
- liquid crystalline biological materials, viscoelastic props. in vicinity of isotropic-cholesteric phase transition 2−51881
- liquid flow in disc and cylinder, exp. 2−67754
- liquid flow in disc and cylinder 2−67753
- liquids, layered waveguide technique for determ. 2−64751
- liquids, linear stability of plane Poiseuille flow 2−67755
- liquids, nonlinear stability of plane Poiseuille flow 2−67756
- liquids, small disturbance stability of plane Poiseuille flow of Oldroyd fluid 2−50292
- Maxwell fluid, oscillatory motion in annular channel under periodic pressure gradient 2−74343
- methyl cellulose, aqueous soln. 2−83380
- micromorphic materials with memory, constitutive theory 2−49070
- nematic liquid crystals, optical method of obs. 2−71141
- network theory for nonlinear viscoelasticity for conc. polymer systems 2−83377
- Noll's fluid, flow between two infinite planes with suction, solution by method of singular perturbations 2−53126
- nonlinear, variational principles 2−52193
- nonlinear heat-conducting fluid flow 2−67599
- nonlinear materials, hysteresis effects 2−71552
- nonlinear materials, steady shock waves for prediction of acceleration waves response 2−49080
- nonlinear quasi-static, uniqueness of solution of first boundary-value problem 2−41635
- nonlinear rod of finite length, elastic pulse propagation 2−45482
- nonlinear solid mechanics, thermodynamic foundations 2−56766
- nonlinear solids, single integral constitutive law 2−76332
- nonlinear viscoelastic rubber like material, creep and cylinder problem 2−52192
- nylon-6, structure property, relationship from viscoelastic analysis 2−56775
- oil-extended vulcanizates, SBR, dynamic props., principle of superposition of time, temp. and conc. 2−83367
- plastic potential theory applied to viscoplasticity 2−55476
- plate, unbounded, vibrs. in random force field 2−76356
- poly sodium acrylate, shear stress and normal stress meas. on moderately concentrated solutions 2−60395
- polybutadienes, narrow distribution, dynamic shear modulus 2−60394
- poly(n-butyl acrylate) lightly crosslinked network, dynamic mechanical behaviour in rubberlike region 2−71544
- poly(n-butyl methacrylate) lightly crosslinked network, dynamic mechanical behaviour in rubberlike region 2−71544
- polydimethylsiloxanes, constants determ. using layered waveguide technique 2−64755
- polyethylene, high density melt rheology 2−83371
- polyethylene, molten, flow through parallel slit, flow birefringence obs. 2−71142
- polyethylene films, nonlinear viscoelastic behaviour 2−83375
- polyethylene terephthalate, non-linear viscoelastic behaviour 2−56777
- polyimide, aromatic, secondary dynamic dispersions 2−83366
- cis-1,4-polyisoprene, linear, nonlinear behaviour under constant strain rates 2−50734
- polyisoprenes, influence of entanglements 2−47484
- polyisoprenes, narrow distribution, dynamic shear modulus 2−60394
- polymer networks, Mooney's mol. theory, effect of chain dimens. 2−83356
- polymer systems, conc., constitutive equations for nonlinear viscoelasticity 2−82316
- polymers, solutions and melts, review of recent non-linear viscoelasticity expts. 2−83364
- polymers, undiluted linear narrow molecular weight distrib. samples in terminal zone 2−83336
- polymethyl methacrylate, epoxy formulations, u.s. dispersion, acoustic characterization 2−80905
- polymethylmethacrylate, dilatational response 2−64707
- polystyrene, three-dimensional damped Debye lattice model 2−60104
- polystyrene solution, constants determ. using layered waveguide technique 2−64755
- polystyrene solution and latex, nonlinear viscoelasticity 2−83368
- polystyrene-poly(2,6-dimethylphenylene oxide) freeze dried blends, viscoelastic response, rheological compatibility 2−83353
- polystyrenes, star-shaped, concentrated solutions, viscoelastic props. 2−83369
- pulsatile flow of fluids in elastico-viscous tubes 2−80167
- pulse propagation, numerical Laplace transform inversion of function 2−82313
- quasistatistical problems, principles of correspondence and of Volterra 2−82325
- Reiss type rod, disturbances in magnetic field 2−66580
- relaxation in liquids, defect-diffusion model 2−64449
- restricted nonisothermal theory 2−76308
- rheologic parameters in quasi-static problems 2−41636
- rheological approach to cumulative damage and strength 2−52136
- rheology, conference, Nagoya, Japan, Oct. (1971) 2−82315
- Rivlin-Ericksen fluids, channel bounded by 2 flat parallel plates, axial press. gradient 2−83448
- rolling contact of rigid cylinder over viscoelastic layer 2−41608
- rubber, relationships between viscosity meas. at variable rates of shear and processing behaviour 2−53788
- salt media, analysis of time-dependent deformations of openings 2−62012
- shallow spherical shell, large deflections 2−66566
- silicone based electrons, dynamic shear properties over wide temp. ranges 2−47488
- space eqn. of free surface of deformed layer 2−52194

Viscoelasticity continued

- spherical waves in viscoelastic media, numerical computation 2−66608
- squalane, relaxation study 2−46987
- squalene relaxation study 2−46987
- stability of plane Poiseuille flow to finite-amplitude perturbations 2−46666
- structure analysis, non-homogeneous linear visco-elastic material rel. to pressure vessels 2−76333
- styrene-butadiene-styrene block copolymer cast from organic solvents, time-temperature superposition 2−74829
- suspensions, rheological equation of state 2−83824
- 5,5,11,11-tetramethylhexadecane, spin-lattice relaxation rates meas., cf. with viscoelastic relaxation 2−46987
- theory for polymer melts, review 2−64708
- thermodynamic interpretation of evolutionary conditions for eqns. of mechanics of finitely deformed Maxwellian media 2−52190
- thermodynamics of simple materials with fading memory, book 2−69686
- thermomechanical coupling behaviour in viscoelastic medium 2−66567
- thermoviscoelasticity, boundary problems, perturbation method 2−66564
- thermoviscoelasticity, linearized theory 2−69683
- thin 3-parameter solid, quasi-static soln. 2−69684
- thin layers, damping, measurement techniques 2−76342
- thixotropy of viscoelastic medium, kinetic model 2−71242
- time-hardening media 2−77706
- time-variable, of viscoelastic materials of rate type 2−66563
- time-variable deformation of viscoelastic materials of rate type 2−66563
- Timoshenko beams, clamped and free, dynamic responses 2−82342
- transient pulse propagation from spherical cavity in viscoelastic medium 2−45426
- viscoelastic cylinder, thermomechanical coupling effects 2−76348
- Voigt fluid, sound propagation 2−60468
- Volterra integral equations linear and nonlinear, solution by power series 2−82310
- vulcanizates, oil-extended SBR, large elastic behaviour and fracture 2−84050
- waves in linear viscoelastic medium 2−66571
- whisker, viscoelastic parameters, effect of adhesive flow, viscoelastic three element elastic modes 2−63087

Viscometers

- capillary, for viscosity of water 2−46938
- capillary, for volatile liquids 2−43297
- concentric cylinder, with curvilinear flow patterns 2−71166
- cone and plate, with curvilinear flow patterns 2−71167
- for diluted solutions, small shear rate range 2−64450
- double-ring rotational-torsional surface viscometer, reduction of secondary flow effects 2−83781
- falling cylinders viscometer for gases 2−46864
- flow of viscoelastic medium in constant cross-section tubes, pressure drop 2−60128
- high viscosity mixing devices, evaluation methods 2−83787
- oscillation, double slit, for high molecular wt. polymers solutions 2−60445
- rheoviscometer study of polymer solutions rel. to rheological properties and changes during two-phase separation 2−60392
- rotating, modification for shear rate dependence meas. 2−60446
- torque on sphere inside rot. cylinder 2−83476

Viscoplasticity *see Plasticity*

Viscosity

- absolute measurements comparison of results using channel flow and torsional pendulum techniques 2−60132
- alkali borate glass, rheological props., effects of water 2−53795
- alkali borate glass, rheological props. 2−53794
- anomalous viscosity of disperse systems in shear stress zones 2−60515
- p-azoxyanisole anisotropic bulk and shear viscosity calc. from ultrasonic absorption data 2−50334
- p-azoxyphenetole anisotropic bulk and shear viscosity calc. from ultrasonic absorption data 2−50334
- binary mixture, asymptotic behaviour of Green Kubo integrands 2−74308
- borate glass, separation of delayed elasticity from viscous flow 2−56781
- boric oxide glass, rheological props. 2−53794
- cholesteric mesophases, normal stress effects 2−83770
- Earth's core, viscosity at boundary on inner and outer regime 2−65542
- eddy, planetary boundary layer, baroclinicity 2−84786
- flow, due to impulsive motion of flat plate 2−70847
- flow of viscoelastic medium in constant cross-section tubes, pressure drop in viscometers 2−60128
- fluids, Kubo integrands, low-frequency behaviour of transport coefficients 2−43048
- fluids, nonlocal shear, and order-parameter decay rate near critical point 2−53114
- freons, F-22, F-114, F-115, FC-318, isotherms, high pressures 2−83784
- glass, rel. to oxide content, computer calcs. 2−44500
- glass fibre, effect on light propag. 2−42242
- glass-ceramic, changes during nucleation and crystallization 2−53923
- incompressible fluid, effective turbulent viscosity description of small eddies 2−77173
- ion, effects on plasma stability 2−80351
- isotropic fluid systems of nonspherical mols., hydrodynamic eqns. and expressions 2−80178
- layered viscous fluids, accelerated motion of sphere 2−77248
- liquid crystal, nematic, coeff. determ. using alignment kinetics in mag. fields 2−53400
- liquid crystal, temp. depend., equations 2−80464
- liquid crystals, effect of mag. field 2−80463
- macroscopic suspensions of elongated particles 2−67845
- magnetic, of grains in magnetic fraction of basalts 2−54941
- MBBA anisotropic bulk and shear viscosity calc. from ultrasonic absorption data 2−50334
- nematics, method for meas. shear viscosity 2−50329

Viscosity continued
non-Newtonian, translating or rotating cylinder in lubricating oil and solid-in-liquid dispersions 2−71168
non-Newtonian fluids in coaxial cylinder, applic. of rheogram template 2−53467
plasma, flow characteristics in arc channel 2−64294
plasma, heavy component contribution in partially ionized gases 2−43122
plasma, resistive with flow, toroidally confined, effects on containment 2−46756
poly(dimethyl siloxane), in high shear rate region, relation between mol. wt. and viscosity 2−83374
polyethylene fractions, melt viscosity 2−83370
polyethylenes, linear, melt blended with atactic polystyrenes, microstructure 2−67848
polymers, narrow distribution, relation between mol. wt. and non Newtonian viscosity 2−83372
polystyrene, atactic, melt blended with linear polyethylenes 2−67848
rubber, amorphous sodium-butadiene and butadiene- nitrile, stress effect study of creep viscosity 2−60873
shear and bulk coeffs. eval. using perturbation theory 2−77213
steady two-dimensional viscous flow in jet due to point source 2−77229
Stokes formula, correction for oscillations of body in rotating fluid 2−46679
suspension, concentrated, discontinuous and dilatant viscosity behaviour, flow instability 2−64245
suspension, for limiting conds. of turbulent drag reduction 2−53364
suspension, of rigid particles, pipe flow, turbulent drag reductions, expt. 2−53373
suspension of solids in non-Newtonian liquids 2−83822
three-dimensional flow, numerical calculation application to hypersonic leading edge 2−46835
turbulent in incompressible fluid, describing influence of small eddies 2−46697
viscosity of suspension for doublets of two equal sized spheres 2−74559
Al-Mg alloys, viscous glide in solid solution, dislocation climb and Newtonian viscous deformation mechanisms 2−64718
Ar, calc. of coeffs. using modified Enskog theory over wide range of temperature and mass density 2−64227
p-H_2, calc. of coeffs. using modified Enskog theory over wide range of temperature and mass density 2−64227
O atoms, collision integrals 2−83184
O_2, calc. of coeffs. using modified Enskog theory over wide range of temperature and mass density 2−64227

gases
aircraft and missiles, three-dimensional flow separations 2−56422
atmospheric motion, long term prediction 2−62162
correlation formula, transport processes 2−50275
falling weight method, effect of local drag 2−46864
intermolecular potential energy functions determ. from viscosity meas. by new iterative method 2−64206
methanol-methane system at atmos. pressure 2−64398
mixtures, expression in terms of props. of pure components 2−53341
multicomponent system of polyatomic molecules rotation viscosity coeff. 2−50280
non-polar polyatomic, m-6-8 pot. analysis 2−77370
polar gases, viscosity dependence on pressure 2−56444
polar gases at atmospheric pressure, Stookmayer force consts. for viscosity 2−83716
rarefied flow through slits 2−71082
sonic transverse jet, interaction with supersonic external flows 2−71089
three-dimensional compressible flow 2−77322
vapour-gas systems at atmos. pressure 2−64398
velocity-correlation functions in two and three dimensions, low density limit 2−53329
viscous interaction over concave and convex surfaces at hypersonic speeds 2−77357
Ar, calc. of coeffs. using various interatomic potential models 2−64393
Ar, intermolecular potential energy functions determ. from viscosity meas. by new iterative method 2−64206
CO_2, m-6-8 pot. analysis 2−77370
H, calculations, comparison with exptl. results 2−50277
H, meas. in range 1 to 10^5K 2−50276
He-Ne mixtures, meas. in temp. range 25 to 700°C 2−50278
N_2-Ar mixture, temp. range 25 to 500°C 2−80419
N_2-Kr mixture, temp. range 25 to 500°C 2−80419
N_2, m-6-8 pot. analysis 2−77370
Ne-N_2 mixtures, meas. in temp. range 25 to 700°C 2−50278
Ne calc. using scattering potential of Siska 2−46863
O_2, m-6-8 pot. analysis 2−77370

liquids
see also Lubrication; Superfluidity
acetic acid/water, viscosity-pressure behaviour 2−60449
acetone-cyclohexane, meas. at 25°C 2−53408
acetone-methanol, meas. at 25°C 2−53408
acoustic attenuation due to viscous losses, calc. 2−46918
alkali metals, significant liquid-structure theory 2−56489
aqueous polymer solution, surface viscosity meas. using new double-ring rotational-torsional surface viscometer 2−83781
p-azoxyanisole nematic liquid crystal in Poiseuille flow, apparent viscosity calc. by continuum theory 2−50337
benzene-methanol mixtures, meas. in temp. range 10°-50°C 2−60450
binary mixture, Kawasaki mode-mode coupling theory nonlocal shear viscosity correction 2−67829
binary-liquid phase transition, critical viscosity 2−53407
carboxymethyl-cellulose dil. solns., in absence of neutral electrolytes 2−50343
chlorparaffin/paraffin-white oil, viscosity-pressure behaviour 2−60449
computer simulation and determ. under high shearing forces 2−60442
concentric cylinder viscometer with curvilinear flow patterns 2−71166
correlation formula, transport processes 2−50275

Viscosity continued
liquids continued
cryogenic fluids in saturated liquid state, calc. of kinematic viscosity 2−83732
cryorheology of reindeer blood 2−77419
α,ω-dichloroalkanes, rel. to molar activation energy for viscous flow 2−60489
DNA, dilute solution, viscometers 2−64450
drag on sphere, low Reynolds number expansion 2−67745
duct flow, formula for drag per unit length 2−43282
Earth's core, effect of mag. field on SH reflection 2−72639
eddy, in transient oceanic Rossby waves 2−57859
flow, free convective, of elastico-viscous liquid past infinite porous plate 2−46881
flow analysis, photoviscosity and double exposure bubble techniques 2−60393
flow into dense beds in liquid-liquid spray column, hydrodynamic study, influence of viscosities of liquids 2−43280
flow of viscous liquid on rotating disk, atomization effects 2−74509
fluid motion past impulsively started semi- infinite flat plate, numerical soln. 2−83459
fluorcarbon/paraffin-white oil, viscosity-pressure behaviour 2−60449
glass, molten, of mixed alkali $PbSiO_3$ 2−77416
glass, optical and window, melt, dynamic viscosity, effect of CO_2, 1400−1700°C 2−74527
glycerine-water system, influence of free radicals and paramagnetic ions 2−74530
n-hexane and nitrobenzene system, nonlocal shear viscosity and mode-mode coupling near consolute point 2−64445
immiscible mixtures, continuous and dispersed phases, nomogram 2−43392
internal pressure application to calculations 2−46937
internal waves generation, perturbation similarity solution 2−67744
isobutyric acid-water solns., supercrit. 2−53453
2,6-lutidine-water, shear viscosity obs. 2−46941
2,6-lutidine-water light scatt. and shear viscosity studies in critical region 2−50344
magmatic silicate liquids, viscosity prediction 2−78222
methanol-cyclohexane, meas. from 25 to 50°C 2−53408
methanol-cyclohexane critical mixture, simultaneous meas. of viscosity and light scattering 2−71169
methanol-cyclohexane-acetone, meas. at 25°C 2−53408
multicomponent mixing influence of feedpoint location and viscosity on mixing time 2−83493
nematic liquid crystal, scattered light obs. 2−56480
non-electrolytes, binary solutions, exptl. results compared with viscosity-composition relations 2−46940
non-ionic surfactants as drag reducing additives 2−71162
non-Newtonian, teaching course 2−48969
poly(vinyl cinnamate), hydrodynamic, optical props. 2−83388
poly-4-vinylpyridine in solution, hydrodynamic and optical props. 2−60452
poly-γ-benzyl-L-glutamate conc. solns., local viscosity meas. by rotational diffusion of diphenylanthracene 2−60451
polyisobutylene solns. obs. of spin-spin and spin-lattice n.m.r., relationship to viscosity 2−60513
polymer solution, time-dependent elongational viscosity calc. using elastic dumbbell model 2−71171
polymer solutions, suitability of eqns. for correlation over entire concentration range 2−60444
polymeric, pressure and temp. effects 2−60443
polymeric solutions, gravitation sensitive gas phase device for obs. with surface tension 2−64452
polymers, randomly crosslinked, with Schulz-Zimm primary distributions, intrinsic viscosity analysis 2−61818
polypeptide monolayer raft, non-Newtonian surface viscosity, flow equation derivation 2−74528
polypeptide monolayer raft, non-Newtonian surface viscosity 2−74529
polystyrene in N,N-dimethylformamide, intrinsic viscosity-molecular weight relationship 2−83359
polyvinyl alcohol-water mixtures, internal viscosity estimation from conductance meas. 2−50345
polyvinylcarbazole, dependence on shear rate, rotating viscometer meas. 2−60446
polyvinyltriorganosilane solutions, relation between intrinsic viscosity and molecular weight studied by light scattering and viscometry 2−46997
repeatability and reproducibility 2−60448
shear, method of evaluation, binary dense mixture with single-liquid model 2−77417
shear and bulk, for 6-12 Lennard Jones potential, determ. using generalized Rice Allnatt theory 2−74524
ship hydrodynamics, theoretical models, review 2−77379
single-component system, derived from mol. mechanical model 2−71187
state primary standard 2−58683
stirring with rotating agitator, radial component of vel. vector 2−60382
Stokes flow, material tensors symmetries for a particle 2−67743
suspension of liquid drops in cylindrical tube, viscous flow 2−64419
suspension of rigid ellipsoids 2−67844
triethylamine-water critical mixture, simultaneous meas. of viscosity and light scattering 2−71169
triphenylamine in alkane, effects on ion recombination rate 2−46968
water, crystal dissolution velocity 2−74650
water, dynamic viscosity at 250 to 375°C and up to 1000 bars 2−46938
water, open packed state mole fraction, adiabatic volume viscosities, press. depend., u.s. absorpt. obs. 2−60447
waves, due to moving oscillatory surface pressure, viscosity effects 2−60398
Weissenberg rheogoniometer data rel. to viscoelastic liquids 2−77391
welding slags, 1200 to 1700°C 2−71165
Al_2O_3, correl. with covalent bonding 2−43338
Ar, bulk viscosity, temp. depend. 2−74526

- **Viscosity** continued
  - **liquids** continued
    - Ar, temp. depend. of coeffs. on saturation line of liq. and vapour phases at const. density 2−71170
    - CaO-Al_2O_3-SiO_2 melt, dynamic viscosity, effect of CO_2, 1400−1700°C 2−74527
    - Co-Al melt, rel. to interatomic interaction energy determ. 2−71155
    - D_2O, u.s. structural absorption and adiabatic volume viscosity 2−56500
    - glass, As-S, As-S-I, As-S-Tl in transition region 2−84049
    - ^3He-^4He soln., dilute, 0.03-0.6K 2−71254
    - ^4He, temp. depend. above 4.2K 2−43415
    - Hg-Cd(Ga)(In)(Tl)(Sn)(Sb)(Bi) amalgams, dil., comp. depend., 0-100°C 2−64451
    - In-Bi alloy equi-atomic 2−46939
    - Kr, temp. depend. of coeffs. on saturation line of liq. and vapour phases at const. density 2−71170
    - Ne isotopes, shear viscosity 2−53406
    - SiO_2-Al_2O_3-Na_2O-K_2O-CaO-MgO glass, viscosity-temp. relations 2−67883
    - Tl-Te system, melting point to 1300 K 2−56490
    - UO_2, molten, for analysis of gross fuel movement 2−67353
    - Xe, temp. depend. of coeffs. on saturation line of liq. and vapour phases at const. density 2−71170
    - $Y_3Fe_5O_{12}$-BaO-B_2O_3-Fe_2O_3 melt, for $Y_3Fe_5O_{12}$ cryst. growth 2−60713
- **Visibility** *see Atmospheric optics*
- **Vision**
  - *see also Colour vision; Eye*
  - accessory optic endings in rat medial terminal nucleus, electron microscopy 2−78686
  - accommodation, model and equipment for meas. 2−73231
  - accommodation control circuit, continuous objective measurement 2−78674
  - accommodation simulation by image autocorrelations 2−73229
  - accommodative response times using histogram information 2−66378
  - acuity, analysis and synthesis in microscopic vision 2−66339
  - acuity, dynamic, effect of target contrast variation 2−66321
  - acuity of children from 1 to 5 yrs. of age 2−55319
  - acuity using binoculars 2−66333
  - adaptation and retinal photopigments photoproducts 2−51963
  - aircraft display element colour for minimum instrument reading errors 2−48922
  - aircraft display element colour for minimum instrument reading errors 2−48922
  - albino rat sensitivity to lights of different wavelength behavioural assessment 2−51993
  - albino rats, monkeys and man, isolated retinas, optical modulation 2−78684
  - ametropia, correction with high refractive index glasses of low dispersion 2−66329
  - analysis of spatio-temporal characteristics, retina, analogue simulation 2−85139
  - average cortical response evoked by sinusoidally modulated light, variability sources 2−51974
  - binocular, depth discrimination, target background luminance contrast effects 2−62883
  - binocular contour rivalry, monocular analogues 2−51977
  - binocular interaction and signal detection theory 2−66345
  - binoptic summation of liminal stimulation 2−66332
  - border discrimination in frog 2−78683
  - brightness, electrical filter model lateral facilitation and inhibitory feedback 2−66346
  - brightness changes due to border, meas. by compensation method 2−82061
  - cat, anaesthetized paralyzed, torsion meas. during receptive field studies 2−51997
  - cat, effect of X-rays on interaction of flash evoked cortical, potentials 2−45179
  - cat, light decrement perception, role of transient neural off response 2−66355
  - cat visual system, spatial organization, photic responses in cortex 2−48928
  - cat visual system, spatial organization, photic responses in cortex 2−48928
  - cat visual system, spatial organization, topology and interaction in geniculo-cortical projection 2−48929
  - cat visual system, spatial organization, topology and interaction in geniculo-cortical projection 2−48929
  - central and peripheral ganglion cells, differential effects of refractive errors and receptive field organization 2−69474
  - characteristics from lighting viewpoint 2−85154
  - contact lens, modulation transfer function as performance specification 2−55321
  - contact lens data rel. to pupil diameter role 2−55320
  - contact lens practice, luminance of fluorescein solns. 2−55318
  - contrast sensitivity, influence of reference cues 2−78678
  - cortical evoked potential from visual stimulus 2−62878
  - dark adaption, early phase, threshold rise after bleaching 2−51970
  - Disability Glare Factor meas., visibility meter 2−51973
  - disparity masking 2−51980
  - eccentric fixation in amblyopia ex anopsia, entoptic method 2−66313
  - e.m. radiation effects during welding 2−69461
  - entoptical phenomenon, conspicuity, modulation depth effect 2−51975
  - ethambutol hydrochloride causing visual loss and recovery of retinal sensitivity 2−82069
  - evoked cortical responses to dichoptically presented patterned light flashes, interocular interaction 2−69462
  - evoked responses and spontaneous brain activity as background noise 2−66311
  - evoked responses in visual pathway of cat with elevation of intraocular pressure 2−78685
  - evoked responses to coloured and patterned stimuli, analysis techniques 2−85149
  - experiments system 2−85090
  - eye-with-image intensifier, performance characts. 2−66337
  - field loss treatment with cemented prisms 2−55322
- **Vision** continued
  - fixation eye movements and visual information processing 2−66335
  - frog, retinal image contrast and acuity, effect of modulation transfer function 2−66354
  - frog, retinal response, linear-nonlinear-linear response as function of frog 2−66356
  - fusional information processing, disparity threshold for diplopia 2−51972
  - geometrical illusions, adaptation site shown in figural after effects 2−51987
  - geometrical illusions, adaptation site shown in figural after effects 2−51986
  - glass spectacle lenses with back surface vinyl membrane, fracturing and safety properties 2−70066
  - guidance and control displays, conference, Paris (1971) 2−48920
  - guidance and control displays, conference, Paris (1971) 2−48920
  - heredo-familial optic atrophies, diagnostic criteria 2−55317
  - Hering's law of equal innervation and position of binoculus 2−69465
  - hue shifts and phase induced modulation enhancement of flickering lights 2−62884
  - human visual evoked response, ensemble characteristics, periodic and random stimulation 2−81982
  - image detection, display signal-to-noise ratio requirements 2−82066
  - latencies as function of stimulus luminance and state of adaption, Pulfrich stereophenomenon 2−51978
  - limiting magnitudes of visual observations of stars 2−48677
  - limiting stellar magnitudes in observations with visual telescopes 2−48678
  - low illumination effects on galvanic skin response 2−73230
  - Mach bands meas. by compensation method 2−69464
  - mammals with all cone retinas, visual capacities 2−82072
  - meridional variation to vertical and horizontal gratings, signal detection analysis 2−85151
  - minimum brightness gain in viewers using image intensifiers 2−66338
  - monkeys, optokinetic thresholds 2−66359
  - monochromatic aberration, effect of spherical spectacle lenses 2−78676
  - movement perception, effect of stimulus orientation on phi phenomenon 2−51982
  - mudpuppy retina sensitization 2−82073
  - nervous system model 2−85141
  - neural mechanisms of contour and contrast 2−55324
  - night, quantitative performance meas. 2−66336
  - occipital spikes rel. to visual evoked responses in photosensitive epilepsy 2−45027
  - ocular interdependence studied by electroretinography 2−76108
  - oculomotor error signal in retina 2−51979
  - optical illusions, geometrical origin 2−45176
  - optics course for engineers and scientists, book 2−69992
  - orientation, optical and labyrinthean 2−66341
  - orientation of animals and insects on sensory basis, conference, N.Y., USA (1971) 2−58646
  - perceived light level calc., rel. to perceived sound 2−73221
  - perception of accelerated N nuclei interacting with human retina 2−76112
  - perception of real and apparent movement, neural mechanisms 2−51985
  - perception of real and apparent movement, neural mechanisms 2−51984
  - perceptual characteristic data for electronic flight display design 2−48921
  - perceptual characteristic data for electronic flight display design 2−48921
  - perceptual latency as function of stimulus onset and offset and retinal location 2−85148
  - photographic light sources, colour rendering index 2−82596
  - photopic, model for threshold detection 2−66331
  - pointing obs., systematic errors 2−66342
  - primary receptor cells, excitatory mechanisms 2−82064
  - psychological correlates digital simulation for transform model of human visual system 2−85155
  - psychophysical investigation of effect of controlled eye movements on movement detectors in humans 2−69463
  - Pulfrich pendulum, apparent orbit 2−66344
  - pupil light reflex, adaptation 2−51966
  - pupil light reflex., autonomic effector control loop, qualitative model 2−76107
  - range when observing aircraft with and without field glasses 2−66340
  - recognition and evaluation of faces, effect of angle of light 2−55323
  - relative luminous efficiencies for near i.r. and u.v. laser light 2−45175
  - response functions for sine and square wave modulations of disparity 2−51976
  - retina, diffusive properties, aberrations 2−78675
  - retina, visual acuity testing using Moire fringes 2−45171
  - retinal image and excitability of retinal ganglion cells, linear systems theory description 2−51981
  - rhythmic after activity to flashes, rel. to background alpha preceding and following photic stimuli 2−45018
  - rod and frame test in perception 2−66334
  - selective adaption effects on detection of parafoveal stimuli 2−66343
  - signal transfer functions in threshold 2−62882
  - simulation of ganglion cells, phemomena 2−69468
  - single binocular vision, Panum's limits, low scotopic luminance 2−78679
  - single stimulus and multiple stimulus threshold 2−69466
  - size perception, human sensory, learned and cognitive mechanisms 2−58648
  - soft contact lenses, visual acuity, astigmatism 2−66325
  - spatial frequency masking, critical bands and masking spread 2−76111
  - spatial interaction with different diameter stimuli matched on threshold luminance or total luminous flux 2−66326
  - squid, light evoked responses from extra-ocular photoreceptors 2−48931
  - squid, light evoked responses from extra-ocular photoreceptors 2−48931
  - star tracing, sex and eye-hand preferential difference 2−66315

Vision continued
suprathreshold contrast perception and its electrophysiological correlate 2−66330
temporal discrimination of two-pulse stimuli as function of psychophysical method and luminance 2−45174
tinted ophthalmic lenses, function, evaluation and evaluation 2−62881
tracking tests, self-adaptive props. of human operator 2−69467
Troxler's effect, total disappearance time in peripheral vision 2−78677
TV imagery detection, humans rel. to machines 2−45173
viewing stereoscopically through binocular optical systems 2−66328
visual receptive fields electronic model 2−78680
visual scotopic transmittance variability for red and blue filters 2−66324
whiteness contrast, simultaneous, relative contribs. of depth and directional adjacency 2−51983

Vitreous state
see also Glass
carbon, bulk resistivity and temp. coeff. 2−71827
ethanol, vitreous transition, fluoresc. depolarization obs. in soln. 2−60602
germania, structure, neutron and X-ray diffr. obs. 2−53534
noncrystalline solids, molecular dynamics, ENDOR and ELDOR obs. 2−65353
polymers, relation between expansion coefficients and glass temperature 2−60604
polystyrene, structure in glassy state determ. by fluorescence depolarization 2−60615
semiconductor, bond theory approach 2−57173
semiconductor, diamond-like, ternary, vitrification 2−53522
silica, structure, neutron and X-ray diffr. obs. 2−53534
silica glass, anomalous properties, interpretation 2−67884
sodium phosphate melt, condensed, vitrifaction, effect of cooling rates 2−77479
solutions doped with molecular anions, low temp. study of luminescence properties 2−54444
structure, contrib. of classical magnetic measurements 2−60581
structure, static magnetic and Mossbauer obs. 2−64526
vtrifaction of condensed sodium phosphate melts, effect of cooling rates 2−77479
As-S-Te, semicond., γ-ray induced cond. 2−54252
As-Se-Te, semicond., γ-ray induced cond. 2−54252
$As_xIn_{1-x}SeI$ vitreous compounds, x=1.00, 0.95, 0.90, 0.80, i.r. absorption, determ. of energy structure 2−78095
As_2S_3, local struct. order, ^{75}As n.q.r. obs. 2−57404
As_2S_3, localized state distrib., Fermi level analysis from transient photocond. obs. 2−47913
As_2S_3, Raman scatt., vibrational states density detn. 2−61663
As_2S_3, vibration spectra, computer generated 2−74966
AsSI and AsSeI, molten, temp. depend. of density mag. susceptibility and forbidden band width 2−84393
As_2Se_3, effects of group III A element dopant on physical props. 2−61300
As_2Se_3, high field cond. 2−68394
As_2Se_3, low temp. mag. susceptibility 2−54293
As_2Se_3, polymeric struct. and energy spectrum 2−60590
As_2Se_3, recomb. radiation mechanism 2−54451
As_2Se_3, vibration spectra, computer generated 2−74966
$1-xAs_2Se_3.xSb_2Se_3$ semiconductor system, devitrification characs. 2−71286
B_2O_3, glass-forming, He migration 2−50707
Bi-Se system, phase separation 2−60591
C, glassy, pore struct. 2−47056
C, glassy, struct., X-ray obs. 2−53531
C, glassy, struct. 2−53529
C, glassy, X-ray small-angle scatt. obs. 2−53530
C electrode material, electrochemical evidence for struct. 2−84649
$CdSi_xGe_{1-x}Ge$, photocond. and elec. cond., rel. to band struct. determ. 2−61448
GeO_2, glass-forming, He migration 2−50707
GeO_2, glassy, struct., small-angle X-ray scatt. obs. 2−43453
Ge_xS_{1-x} alloys, radial distrib. studies 2−53536
P_2O_5-LaF_3-RF_2, R=Ba, Mg, triangular diagrams, crystn. and vitrification regions 2−57035
Sb-Se system, phase separation 2−60591
Se, anomalous sp. ht. below 1 K 2−43987
Se film, trap-limited processes 2−61325
SiO_2, fused, e.p.r. of transition metal ions struct. obs. 2−65338
SiO_2, glass-forming, He migration 2−50707
SiO_2, phonon scatt., low temp., elec. and mag. field depend. 2−51056
SiO_2, radiation compaction mechanism 2−50410
SiO_2, random network theory validity 2−47054
SiO_2, struct., at. motions, neutron scatt. obs. 2−47061
SiO_2 defect struct. 2−60596
Tl_2Se-As_2Te_3 photocond. kinetics, photoresponse 2−72067

Vlasov equation *see Plasma*

Vocoders *see Speech*

Voigt effect *see Magneto-optical effects*

Volta effect *see Contacts, electrical*

Volume measurement
dilatometer, quartz, applic. to obs. of crystallization kinetics of polymers 2−56565
dilatometer for liquids, volume obs. as function of temp. 2−46935
expansion coefficient, use of hydrostatic microbalance 2−80785
liver, by u.s. scanning 2−69348
metal, liq., equilib. thermodynamic states, at high temp. and press. 2−46949
microvolumenometer for free volume determ. of coated fuel particles 2−42664
reactor fuel pins, irrad., internal free volume, meas. technique 2−42666
Bi polymorph III modification at 42 kbar and 20°C, volume change 2−74925

Vortices
see also Cavitation; Turbulence
— 2−67733
aerodynamic wing loads, vortex induced 2−71073

Vortices continued
alternative flow regimes in agitated vessels 2−53362
analogies in different physical systems, survey 2−60122
angular momentum exchange in rotating fluid 2−80430
annular flow with rotating core, frictional resistance 2−83750
anticyclonic, trapped above seamount, mechanism for generation 2−44627
asymmetrically rotating fluid disc, application to galaxies and solar system 2−56279
atmosphere, leeward of islands, velocity field 2−48481
atmosphere, vorticity flow, temperature stratification 2−72774
atmospheric, balance at 200 mb in tropics during northern Summer 2−84801
atmospheric boundary layer, vortex streets wind tunnel simulation 2−72771
atmospheric tropical cyclones, dynamics 2−78367
atmospheric vortex street phenomena, Lin parameter, obs. above Canary islands 2−44698
axial flow, motion of vortex filament 2−60361
axisymmetric potential flow past annular aerofoils and bodies of revolution 2−67577
binary mixture on infinite rotating disk, barodiffusion isotope separation 2−77196
boundary layer separation on slender cone at angle of attack 2−56409
boundary layer separation patterns over inclined body of revolution 2−77215
boundary vorticity for slightly viscous fluids 2−53135
breakdown, occurrence, position, forms and mechanism 2−80204
buoyant vortex rings and thermals, dynamics 2−77189
clouds, atmospheric structure, surface pressure anomaly patterns classification schemes, models 2−84822
columnar, concentrated, structure and dynamics 2−80156
computer simulations, process of vortex condensation 2−83440
core structure 2−64382
cyclone, intermediate scale, numerical simulation of development in moist model atm. 2−84793
cyclone waves, nonlinear waves 2−44708
in cylindrical shock tube, hot wire anemometer 2−77242
delta wing, symmetrically deformed influence of vortices on aerodynamic characteristics in supersonic flow 2−50261
distribution and cancellation in two dimensional incompressible periodic wake 2−77192
flow across gas dynamic discontinuity, vorticity and current density jump 2−83644
flow aeroelastic instability of hot-wire filaments 2−80406
flow near trailing edge of oscillating airfoil, visualization 2−80382
fluids, generation of thrust, continuum mechanics, book 2−70825
geostrophic adjustment rel. to conservation of potential vorticity of rotating homogeneous or stratified fluid 2−61861
Gosiewski's theorem, vorticity tensor, stretching tensor 2−46653
heat transfer with dissipation, vorticity effects 2−53125
helical vortex filament, stability 2−67772
hurricanes, role of warm currents in ocean in directing 2−44635
incompressible thin wing flow, vortex lattice numerical solution, accuracy 2−53271
interacting line, negative temp. instability for two-dimens. motions 2−53111
jet, turbulent, sound influence, vortex generation 2−46842
in jet due to subsonic cross flow 2−43067
jets, two-dimens., coalescing, vortex formation processes 2−67712
laminar wake, flat plate in shear flow 2−77245
longitudinal, development in boundary layers growing with time along concave walls 2−43059
MGD discontinuity, stationary, vorticity jump 2−53154
MHD in compressible, perfectly conducting fluid 2−64254
mixing between two parallel streams, vortex sheet model 2−80209
Navier-Stokes eqns., incompressible, exact vorticity solns. 2−83456
nonbuoyant vortex ring, hot wire anemometer meas. 2−77250
penetration of density interface by heavy vortex rings 2−77214
plane sheet, hydromag. stability, effect of discontinuity in density or cond. 2−53158
plasma, ball lightning, mechanism of formation, laser analogue 2−81665
plasma, toroidal vortices 2−83587
plasma focus, breakdown condition 2−83586
plasma focus, highly localized X-ray source 2−83585
prècessing cores, damping by combustion in swirl generators 2−83427
pressure driven Stewartson layers, rotating circular cylinder in viscous fluid 2−77198
propeller vortex noise with boundary layer control 2−41822
quasi-geostrophic flow, generalized potential vorticity equation 2−57857
radiation props. of semi infinite vortex sheet 2−77320
rate sensor, theoretical analysis of angular momentum conservation and signal transmission 2−60327
rectilinear, in plane flow, stationarity and stabilization 2−60141
ring, close to Hill's spherical vortex 2−60175
rings, buoyant, large scale, production and propagation 2−43098
rotating stratified fluid, flow due to point source 2−43099
semi-infinite vortex trails, rel. to oscillating airfoils 2−67580
shedding excited motion of cable stayed bridge, wind tunnel obs. 2−80384
sheets, definition of wakes and boundary layers 2−77239
slender wing in uniform stream, vortices over leading edge 2−77332
Southern Ocean cyclones, available sensible heating, generation by sensible heating 2−65695
spheroidal gas bubble rising in water, effect of periodic nature of drag, vortex structure 2−80425
stability of coaxial rotating jet and vortex of different densities 2−74336
standing, flow instability on rotating disc, electrochemical obs. 2−67579
starting-vortex length for circular cylinders, unsteady flows 2−53134
stationary spherical vortices in perfect fluid 2−83467
steady axisymmetric vortex flow 2−43071
Taylor, eccentric rotating cylinders 2−77240
Taylor, laminar axial flow, in annulus with rotating inner cylinders 2−43075

Vortices continued
Taylor, stability and growth, in flow between eccentric rotating cylinders 2—80210
tornadic storms, radio noise obs. 2—84813
tornado, effects of ground roughness, laboratory simulation 2—48482
tornado dynamics, obs. using lab. model 2—84809
tornado-like, simulated, velocity field meas. using three dimensional velocity probe 2—44712
tornadoes and hurricanes, steady and unsteady, fluid mechanics 2—81644
toroidal, structure of blunt base wakes in swirling flow 2—80157
trailing vortex wake downwind of external flow jet flap 2—80385
turbulence, two-dimensional, lower order models 2—80177
turbulence, with vortex character, eqns. for moments 2—46657
turbulent wakes, temp. fluctuations, measurement by probe 2—77330
two component vortex flow studies of colloid core nuclear rocket 2—62414
two dimensional flow, geometrical interpretation 2—53123
two-dimensional motion, negative temps. 2—50139
United States Midwest tornado wind records, geometrical analysis 2—75577
urban area, effect of temp. field on winds 2—75572
viscous fluid, transient and steady state vorticity generated by horizontal temp. gradients 2—67561
vortex excitation and galloping of rectangular block in uniform flow 2—53316
vortex street in wake of vibrating cylinder 2—77228
vortexline geometry of pseudostationary, inviscid, unsteady gas flows 2—56413
wake system, motion through stratified atmosphere 2—81670
wakes, behind two dimensional square cylinders, at low Reynolds numbers 2—77247
wakes, flat plate in uniform flow, velocity fluctuations 2—80407
wing-tip, dissipation and breakdown 2—83681
H_2O periodic cortex formation in rear of fixed plate, comparison with solution of Navier-Stokes equation 2—53348
He, liquid, collective modes in streams of charged vortex rings 2—53476
He, superfluid, force exerted by charged vortex rings 2—80508
He, superfluid as ultrasonic cavitation nucleation mechanism 2—43426
He, superfluid flow channel, extrinsic dissipation mechanism 2—56535
He II, boundary pressures and forces generated by moving vortices 2—47016
He II, growing collective modes in vortex rings 2—53477
He II, interaction of charged vortex rings with superfluid surface 2—50392
He II, liquid, charged vortex rings, focusing using electrostatic lenses 2—80503
He II, liquid, vorticity by obs. of current at a grid in an ion cell 2—83829
He II, phenomenology, review 2—83831
He II, pressurized turbulent, escapt of negative ions and vortex annihilation model 2—67857
He II, vortex core radius, temp. depend. 2—71264
He II film flow, thermally driven, 1.7-2.1 K, dissipation rel. to vortex ring production 2—67862
He II in rotating bucket, origin of quantized vortices 2—67858
He II rotating superfluid, obs. of single vortex lines, detection of trapped charge 2—53479
He liquid, expt. for detection at known location 2—67861
I ion-Au, Th, U collisions, 10 to 60 MeV, X-ray spectra of temporarily formed superheavy quasiatoms 2—74236

Water
see also Ice; Seawater; Steam
— 2—71276
— 2—67480
absorption of CO_2 2—67816
acoustic cavitation at 10 kHz 2—56464
acoustic communication channel, model capacity 2—49157
acoustic ray tracing, nonlinear velocity profiles 2—73432
acoustic scattering in water tank rel. to volume reverberations in ocean 2—53425
acoustic wave generation, normal mode, vertical array of projectors in shallow water 2—44660
adsorbed, environmental states, NMR of porous glass desalination membrane, function of external salt concentration 2—56522
adsorbed layer on silica, freezing process, n.m.r. linewidth obs. 2—53596
adsorbed layer on silica, self-diffusion obs. 2—60686
adsorbed on collagen, effect on elec. props. 2—47908
adsorbed on zeolite, molar heat, 90-300K 2—60694
adsorption and desorption on TiO_2 2—60688
adsorption on LiF and NaCl (001) faces, effect on dislocation mobility 2—43627
adsorption on SiO_2, effect of surface acidity 2—53597
aerosol, interactions with positive corona streamers, atmospheric significance 2—64489
aerosol droplets, capture by plane stellate crystalline obstacles 2—71247
aerosol particle counter, multichannel, choice design and performance 2—82075
air-water concurrent flow on flat plate, enhancement of heat transfer by waves 2—56494
air-water mixture in two-dimensional diffuser, pressure recovery performance 2—46910
air-water two-phase flow, horizontal, pressure as stochastic parameter 2—43096
air-water-glass bead three phase flow system, exptl. investigation of hold-up 2—67605
analysis, in borate glasses 2—56555
analytical flow nets in channel seepage 2—57825
anomalous, fabrication environment and impurities 2—53385
anomalous, regarded as silica sol 2—46921
anomalous frequency broadening of ruby laser beam by self modulation 2—43362
aquifer overlain by water table aquitard, numerical simulation of flow 2—78307

Water continued
arc plasma effect of reaction energies on radial temperature distribution 2—53261
atmosphere, ground-based cloud data for mesoscale analysis 2—65661
atmosphere, vertical water vapour flux, airborne measurements 2—78349
atmospheric, attenuation of 4.3 mm waves 2—68914
atmospheric content, absorption hygrometry measurement techniques, models 2—84864
atmospheric particulates, radiative properties in spectral interval 500-1500 cm^{-1} 2—54854
atmospheric water vapour absorption rel. to surface temperature determinations from satellite radiometric measurements 2—54821
autoradiography, water in glass obs. 2—53517
bentonite-water suspensions, flow behaviour for time-dependent non-Newtonian fluid 2—60159
boundary layers, mech. and thermal props., temp. depend. 2—67739
bounded turbulent jet, mean flow properties 2—77396
broadband complex refractive index between −20 and 50°C 2—64460
bubbles, planar, cylindrical and spherical, expansion and contraction 2—77405
Cache Valley, ground-water potential rel. to integrated geophysical study 2—81642
capillary wicking of distilled water in quartz sand and cylindrical glass capillaries in magnetic fields 2—60402
cavitation threshold, effects of surface tension 2—43290
charge deposition from high energy electron beam 2—55984
cloud content obs., conventional devices rel. to integrated optical devices 2—57975
clouds, evaporation accelerating the ice phase in supercooled water 2—62236
cometary atmosphere, Tago-Sato-Kosaka and Bennett comets 2—58521
condensation, cluster nucleation and growth, Rayleigh scatt. obs. 2—64511
contact angle rel. to drop size at b.p. for 50-760 Torr 2—77474
contact glow-discharge electrolysis, study in water containing various electrolytes 2—54551
convective heat transfer enhancement to water containing bubbles 2—60464
cool supergiant stars, model atmospheres, compositions 2—66074
corrosion by water in nuclear installations 2—59845
corrosion of austenitic stainless steel, microstructure determ. of oxide film 2—81505
crystalline layer form. on amorphous As-Te-Ge, effect of water 2—60571
deep saline, low-angle emission of sound rays, layered temp. jump models 2—60471
deformation of velocity profile in turbulent boundary layer 2—74492
dielectric absorption around 70 MHz, meas. of total impedance and phase angle 2—74552
dielectric const. to high temps. and press. from Mean Spherical Model 2—83793
dielectric props., use in megavolt energy concentrating device 2—46974
diffusion and solubility in quartz 2—50716
diffusion in KCl crysts., influence of OH^- ions 2—60831
diffusion into gelatin gels, interfacial contact resist. 2—60533
dimer, hydrogen-bond n.m.r. shift 2—60003
dimer, in CCl_4 soln., i.r. spectrum and structure 2—50043
dissolution velocity of crystals 2—74650
distilled, electric strength, for use in h.v. pulse generators 2—65055
distilled, rotating annulus, isothermal motion of O_2 bubbles 2—46912
distilled, turbulent, absorption of He, H_2, O_2, CO_2 gases 2—50298
disturbed surface, brightness, i.r., statistical characts. 2—48418
drop, AgI particle dissolving in, contrib. of diffusion and interfacial kinetics to rate of solution 2—60434
drop, stationary, in superheated vapour atmosphere, condensation characteristics 2—53500
drop response to sudden accelerations 2—83739
droplet, scavenging of aerosol by falling droplet, particle size effect 2—75599
droplets produced by u.s. 2—71241
drops, disruption by electric forces 2—64426
drops, formation in deep cloud cover 2—68875
drops, freely suspended, oscillation freq. 2—64427
drops, freely suspended supercooled, freezing by contact nucleation 2—47036
drops, heat transfer from small diameter channel in film boiling temp. range 2—53379
drops, in air and CO_2, evaporation rate meas., conditions of thermostatic drop surface 2—77406
drops, internal circulation for drops falling at terminal velocity in air 2—64414
drops, rate of soln. of ice nuclei, nucleation 2—75600
drops, supercooled shattered by shock waves, freezing 2—47037
drops on glass, determ. of smallest non-collapsing drop 2—77492
dynamic viscosity at 250 to 375°C and up to 1000 bars 2—46938
electrical probe characteristics, isothermal plasma model 2—74554
electrically suspended water droplets, wind correction to evaporation rate and Rayleigh instabilities 2—56531
electrochemical photolysis of water at semiconductor electrode 2—57428
e.m. reflection properties of smooth brackish water, direct det. $10^8-4\times10^9$ Hz 2—72694
e.m. water-current velocity meter, oceanographic applications 2—71138
emission sources in H II regions, interferometric positions 2—51719
emulsion, dipolar Debye type relax., −40 to −15 degrees C 2—43409
emulsion, dipolar type Debye relax. 2—43408
equation of state in metastable region, thermodynamic stability boundary 2—60418
equilibrium properties, Metropolis Monte Carlo method in isobaric and canonical ensemble formalisms 2—64428
evaporation of drops with monomolecular surface films 2—60557
excess u.s. absorption, evaluated from relaxation time and relaxing compressibility 2—74541

Water continued
explosive boiling, overheating, nuclear reactor coolants 2−42686
falling film, wave inception 2−50287
ferrite memory cores, strength rel. to water environment 2−77652
flow, air entrained, under reduced ambient pressure 2−77404
flow, cavity, unsteady, anal. using linearized free streamline theory within incompressible inviscid flow approx. 2−67759
flow, laminar, mixed convection 2−53343
flow, nonuniform, in rivers and estuaries, longit. dispersion 2−67747
flow, periodic cortex formation in rear of fixed plate, comparison with solution of Navier-Stokes equation 2−53348
flow behaviour of clay-H_2O suspensions 2−83816
flow rate obs., automatic device 2−50296
flow velocity meas. using H_2 bubble apparatus 2−71135
flowing, mass transfer of 2-naphthol particles 2−71129
force obs. with Weissenberg rheogoniometer, effect of changes of surface tension and contact angle 2−64455
freezing drops, ejection of microdroplets from surface 2−50401
freezing point lowering in porous glass 2−80880
galaxies microwave radiation obs. rel. to maser mechanism 2−69016
glass fibre/polyester resin composite, cracking and debonding on water uptake 2−61020
glycerine-water system, influence of free radicals and paramagnetic ions on viscosity 2−74530
glycerol-water mixture, heat transfer on boiling in trapezoidal channel 2−60556
gravity waves, nonlinear modulation, singular perturbation methods 2−71144
gravity waves, nonlinear modulation 2−77372
gravity waves of permanent form, conformal transformation 2−64417
growing water drop rel. to diffusion-kinetic approach 2−56471
heat transfer on boiling in trapezoidal channel 2−60556
heavy, H-D separation factor, current density, cathode material, temp. effects 2−42820
heavy, u.s. structural absorption and adiabatic volume viscosity 2−56500
hemispheric reflectance of plane water surface for atmospheric radiation 2−54853
hydrates of ions Li^+, Na^+, Be^{2+}, F^-, Cl^-, calc. by CNDO/2 method, determ. of H bond strength 2−50053
hydrogeological and engineering-geological possibilities for method of induced potentials 2−54721
ice water system, freezing, Stephan problem solution 2−77470
interface with Al, u.s. refl., surface wave creation 2−64851
i.r. absorption spectra in relatively non-polar organic solvents and in $NaClO_4$ 2−46932
isobutyric acid-water mixture near critical point, temperature dependence of electrical resistance 2−80525
isotope effects in hydrated solid and aqueous $CuSO_4$ 2−47324
jet, circular, energy spectrum and turbulent scales 2−46901
jet, heated, discharging into lake or river, turblent heat transfer, diffusion and mixing 2−78304
Joule-Thomson coeff. meas. by throttling element for radial flow of fluid 2−67825
laser induced breakdown, high speed photography of cavitation and bubbles 2−56470
light and heavy, positron lifetimes 2−54091
limiting shear stress measurement 2−64418
low pressure water vapour condensation and growth of ice on cold metal 2−53498
lunar experiments and results 2−44925
lunar surface, vapours detected by Apollo 14 SIDE mass spectrometer analysis 2−58468
magnetic treatment for purification and structure 2−54521
Mars, discrete white clouds, diurnal and seasonal behaviour 2−69152
Martian atmosphere, 8200 Angstroms band studies with ground-based Varo image tube 2−78552
Martian atmosphere 8200 Angstroms band, ground based photoelectric observations 2−78551
Martian surface, water of hydration, high altitude aircraft i.r. spectrometric observations 2−78553
Martian white clouds 2−66183
maser, at HII region boundaries, gain parameters 2−69047
mass and phase spectrometry of jet 2−49986
meltwater, in snow cover, flow measurement 2−75443
microscope, molecular, scanning 2−67465
mixture-model approach, two-structure model 2−83771
molecular dissociation, kinetic energy release 2−80028
molecular octopole moments calc. using semi-empirical wavefunctions 2−70701
molecular stretcjing frequency, bond angle change effect 2−83266
molecular structure, properties deduced 2−43317
molecule, 13 basis function calc. based on selection of proper canonical orbitals 2−67477
molecule, ab-initio bond-orbital calcs. 2−53018
molecule, CI expansion, large-scale method for coeffs. calc. 2−67451
molecule, dissoc. collision with metastable Ar, rotational excitation of $OH(A^2\Sigma^+, v'=0)$ 2−64215
molecule, electronic states of H_2O^+ produced by electron bombardment 2−42896
molecule, electrooptical parameters, H bond distortion 2−46548
molecule, second order props., perturbation theory 2−46541
molecule, self-consistent procedures for generalized valence bond wavefunctions 2−53012
molecule, slow neutron scattering, analytical improvement of Nelbin's formalism 2−49868
molecule, small angle electron diffr., chemical binding energy detn. 2−64133
molecule, statistical total energy in multiple scattering formalism 2−42828
molecule, strongly orthogonal geminal wavefunctions for lowest singlet states 2−70686
molecule, total nonrelativistic energy calc. using many-body perturbation theory 2−52914
molecules, quenching of Na D-doublet in flames of 1500-2500 K, temp. dependence of cross sections 2−46454

Water continued
molten metal explosive interaction 2−73457
monostatic reflection by elastic spheres 2−43398
under negative pressure, vapour pressure and bulk modulus 2−83734
neutralizer cell, angular spreading of low energy charged particle beams 2−79697
neutron collision rate in borated water 2−70501
n.m.r. field shift of protons due to addition of transition metal ions 2−74558
nonspherical vapour bubbles, dynamics 2−77407
nonsteady flow at high speeds 2−77371
nuclear reactor, nucleate and film boiling, heat transfer mechanisms 2−53510
nucleate boiling conditions at artificially active nuclei 2−50405
nucleation theory, props. of clathrate-like cluster structures 2−50404
open packed state mole fraction, adiabatic volume viscosities, press. depend., u.s. absorpt. obs. 2−60447
optical absorption in vacuum u.v. 2−50361
optical constants in the vacuum u.v. from reflectances 2−43361
optical det. of nonlinearity parameter 2−43351
outgassing role in evolving Martian atmosphere 2−58507
permeability of the vapour in films, measurement techniques 2−80757
plane shock wave refl. at free surface 2−83746
pole radiolysis, study of 'dry' electrons 2−61813
pollution monitoring using on-line computer 2−62091
polyacrylamide aqueous soln., pulsation velocity in turbulent boundary layers 2−74491
polywater, comparison with normal water 2−50307
polywater, existence and structure 2−53386
polywater, obs. on hydrogen bonded HBr 2−43314
pressure rel. to fission tracks in mica and volcanic glass, stability consideration 2−67097
quality data analysis using spectral analysis 2−78300
radiation energy transfer, local radiant flux, radiant energy loss or gain 2−67827
radio-emission at 1.35 cm., from W49 and Orion Nebula 2−75823
rain, electrical conductivity rel. to Cl^- content 2−65741
Rayleigh convection, roll diameter dependence and effect on heat flux 2−60370
refractive index, temp. dependence calc. using two-state approach 2−60473
resistivity under irradiation, applic. in dosimetry 2−69402
second order fluctuations in particle no., integration over X-ray scattering intensities 2−74517
seismoacoustic investigations, electro-spark pressure source, optimum depth 2−44572
shallow, acoustic wave propagation, normal mode amplitude functions 2−77428
shock wave pressures from small detonators underwater 2−46899
shock waves underwater, diffraction by semi-infinite plane 2−56465
slowing down spectra of secondary electrons 2−75006
small cloud droplets, collision efficiency 2−68906
snow course in forested subalpine watersheds, areal water equiv. estimates, statistical analysis 2−68853
solid-water system, moisture detn., n.m.r. obs. 2−48303
solubility relationships for non-polar gases 2−56485
solutions, flow in extracellular channels with filtration, osmosis and active transport 2−46879
sound pressure due to source in air 2−43348
specific heat near m.p. and Ornstein-Zernike corrections 2−60541
spectral reflectance, effects of temp. 2−64461
spectrum of liquid in 4000-0.01 cm^{-1} range, influence of effective field of a light wave 2−67834
steam bubbles in water, collapse of bubbles due to compression 2−43298
stratospheric water vapour content meas. 2−65665
structure, direct correl. function near triple pt. 2−74514
structure, near i.r. studies in mixed solvent systems 2−50316
structure and kinetics molec. dynamics study of temp. effects on structure and kinetics 2−60417
supercooled, nucleus formation and crystallization 2−74588
superheated to 279.5°C at atmospheric pressure 2−60558
surface tension molecular depression by dissolution of fatty acids 2−71172
surface waves, depths less than boundary layer thickness 2−74503
surface waves, interaction with acoustic fields, spatial resonance phenomena 2−43295
surface waves, vibrating in bell mode 2−43296
temperature distribution of viscous gravity flow in horizontal pipes 2−64402
theory of liquid structure 2−77413
thin films, flow and stability on rotating horizontal disc 2−43309
transmission of water waves through small apertures 2−77393
transport across biological membrane, molecules and ions 2−69207
triethylamine-water critical mixture, simultaneous meas. of viscosity and light scattering 2−71169
turbid, depolarization of scattered laser light 2−64486
turbulence, hot wire anemometer measurements 2−77385
turbulence, small-scale structure, temp. obs. 2−77323
turbulent free jet flow, amplitude modulation of ultrasound 2−74494
turbulent friction, effect of polymer additions in free flow 2−53361
turbulent velocity fluctuation meas. using cell flowmeter based on variation of electrical resistance 2−71137
unconfined aquifer, unsteady radial flow 2−78309
unconfined aquifers, flow theory considering delayed response of water table, model 2−78234
unsteady state transfer of solute across water-ethyl acetate interface, effect on Marangoni convection 2−77381
u.s. transmission intensity variation with time at 22 kHz at atmos. and excess pressure 2−52232
u.s. wave backscatter from rough water surface 2−68861
vapour, absorption lines in ν_1-band, collisional narrowing 2−79992
vapour, atmospheric, distrib. effects on transmittance 2−65771
vapour, atmospheric, effect on radiative equilibrium 2−62262
vapour, atmospheric, vertical sounding with Nimbus IV i.r. spectrometer expt. 2−48452

Water continued
vapour, atmospheric absorpt. lines, using tunable i.r. laser spectroscopy 2−84843
vapour, calc. of half-widths of lines in ν_2-fundamental using Anderson-Tsao-Curnutte theory 2−53105
vapour, calculation of spectral intensities using vibrational rotational interaction data 2−74265
vapour, effect on Pb-SiO sticking coeff. 2−64572
vapour, elec. discharge, formation of rotationally excited $OH(^2\Sigma^+)$ radicals 2−60027
vapour, electron impact cross sections, atmospheric applications 2−53019
vapour, eqn. of state from triplet point to critical point, droplet modes 2−67869
vapour, heterogeneous nucleation 2−47047
vapour, i.r. spectral emissivity data, comparison with total emissivity charts 2−83702
vapour absorption meas. using single frequency CO laser 2−82519
vapour bubble motion in annular channel 2−74592
vapour from aircraft rel. to pollutant effects on radiation budget of stratosphere 2−65663
vapour intracavity cell in CO laser to meas. absorptive losses, applic. to atmospheric transmission 2−82518
vapour laser, submillimeter wavelength measurements 2−79171
vapour mols., saturated and superheated, neutron inelastic scatt. 2−67539
vapour press. rel. to surface tension and surface curvature 2−46943
vapour pressure, equation for representation 2−77476
Venus atmosphere, Venera entry probes and Mariner flyby 2−69164
Venusian atmosphere, vapour evolution 2−44958
vibrational Raman scattering 2−46566
water-drop impacts, electro-acoustic meas. of drop size, shape and velocity 2−63129
water-ethanol liq. layer, heated from below, temp. field oscills. due to thermal diffusion 2−67821
water-Freon 113 system, direct contact heat transfer in stratified flow with simultaneous interfacial boiling 2−50285
water-polyvinyl alcohol mixtures, conductance meas., internal viscosity estimation 2−50345
watershed subsurface response, surface runoff rel. to subsurface flow, base flow contribs. 2−67761
waves, fairly-long, review 2−46896
waves, solitary, stability, anal. by Korteweg-de Vries eqn. 2−46898
wind-disturbed, curvature distrib. 2−57925
AgI-NaI-H_2O, aerosol-cloud interactions, parcel model 2−60527
Ar and Kr laser lights attenuation charact. 2−76512
Co_2:N_2:H_2O c.w. gas dynamic laser, unstable resonator calculations 2−82483
D_2O, at boiling point, contact angles on Cu and polytetrafluoroethylene surfaces, 10-770 torr 2−74533
D_2O liquid, atom pair correlation functions from neutron and X-ray diffraction 2−43323
Fe(II) salt solutions, frozen at normal pressure 2−78178
HDO, structural model for effect of perchlorates on i.r. bands, assignment of stretching bands 2−53016
$H^+(H_2O)_n$ cluster ions, in thermosphere and mesosphere 2−65829
H_2O:Tl, excitation luminescence spectra, effect of concentration of Tl ions 2−53441
H_2O-He system, surface tension, 1-71 atm., room temp. 2−64453
H_2O and D_2O, correspondence of fundamental and combination bands in i.r. spectra 2−50365
H_2O FIR pulse excited laser output, effects of microwave power 2−59155
H_2O^+ content of Japanese Paleozoic geosynclinal basalt, measure of hydration 2−65536
$H_2{}^{18}O$, rotational spectrum in ground vibrational state, study by submillimeter microwave spectroscopy 2−70706
H_3O, identification in aqueous solutions 2−72583
$H_3O^+.H_2O$, rate constants and kinetic analysis for formation in inert gases 2−84622
HTO mol., microwave spectrum, rot. consts. of fund. state 2−83242
HTO mol., ν_1 and ν_3 levels determ. by i.r. spectrum, rot consts. of fund. state 2−79997
in KCl, drop migration under various driving forces 2−47466
NH_3...H-OH mol., hydrogen bonding 2−67475
$NO^+ + H_2O$ reactions in photoioniz. mass spectrometer 2−68775
in Na_2O-SiO_2 glass, ion exchanged, effect on internal friction 2−53791
O_2-H_2O system, formation and decomposition of water cluster ions 2−57414
T content meas. of water samples using gas proportional counter 2−82808
T_2O mol., microwave spectrum, rot. consts. of fund. state 2−83242
Wave equations, quantum theory *see Quantum theory/ wave equations*
Wave functions *see Quantum theory/ wave equations*
Wave mechanics *see Quantum theory*
Wavefront-reconstruction imaging *see Diffraction/ light; Holography; Optical images*
Waveguides *see Electromagnetic wave propagation/ guided waves*
Waves
see also Acoustic waves; Elastic waves; Electromagnetic waves; Liquid waves; Magnetohydrodynamics; Seismic waves; Shock waves
acceleration, propagation in linear visco-elastic inhomogeneous medium 2−66571
acceleration waves of arbitrary shape, behaviour 2−45242
acoustic gravity, reflection and amplification at density and velocity discontinuity 2−64226
acoustic-gravity, from nuclear explosion, obs. using Hg tiltmeter 2−65810
asymptotic soln. for eqn. with variable vel. and boundary conditions 2−82176
atmosphere, Rossby and pure rotational 2−78362
atmosphere balancing and damping of gravitational oscillations for forecast models including orography 2−51571
atmospheric, internal gravity wave, self destructing 2−78355
atmospheric, large nighttime gravity wave at Arecibo 2−65687
atmospheric, planetary-scale travelling components estimated 2−62120
Waves continued
atmospheric gravity waves, nonlinear model of growth characts. 2−65689
atmospheric gravity waves, perturbation profiles in ionospheric F-region 2−65987
bar, incremental wave effects, effect of strain rate history 2−45477
bending, diffr. and scatt. by mass impedance loadings, of plane plate 2−63099
boundary-initial-value problems, semidiscrete approx. 2−63053
Cauchy-Poisson type, in rotating fluid, unsteady flow anal. 2−50149
clear air echoes, coexistent waves and turbulence, near marine inversion 2−75546
cnoidal, generated by moving pressure field 2−67610
in cochlea, and action in pitch feedback and lateralisation 2−58638
computer simulation 2−62947
density, M51 galaxy, spiral structure 2−58234
density, streaming, in spiral galaxies 2−58232
diffraction for oblique incidence on half-plane 2−73293
diffraction of plane waves by a strip, exact and asymptotic solns. 2−82177
diffusion, induced by high intensity sources 2−83699
dispersion, gravitational instability of interface separating two streams 2−84930
dispersive media, oscillatory solitary waves 2−52047
eigenvalues for motion in irregularly shaped regions 2−41467
elastic-plastic medium, propagation of two-dimensional waves 2−66572
electrohydrodynamics, propagating in nonhomogeneous unperturbed conditions 2−67608
equatorial stratospheric waves induced by diabatic heat sources 2−84802
expansion wave, Martin-Ludford gas into vacuum 2−80397
flow, unsteady, at branched duct junction, press. wave behaviour 2−67713
fluid, inviscid, incompressible, homogeneous, surface waves considered under magnetic and current fluids 2−50165
fluid, standing waves, parametric amplification 2−46839
fluid, steady capillary gravity waves, generated by press. periodically distrib. along flow surface 2−70867
fluid wave patterns produced by point disturbance, calc. 2−50153
fluids, internal gravity waves, convective instability 2−53146
generation and propagation in one-dimensional linear dispersive systems, application to oceanography 2−83725
generation of waves magnetically confined and field-permeated axisymmetric jet 2−77256
gravity, accompanying cyclogenesis on East Coast 2−65697
gravity, atmospheric, effect on ionospheric parameters determined during vertical sounding 2−72877
gravity, atmospheric, rel. to dynamics 2−72777
gravity, density variation from wind speed profiles 2−72762
gravity, field interaction with mean vel. and buoyancy field 2−54788
gravity, internal, nonlinear, in slowly varying medium 2−60131
gravity, internal, rel. to turbulence 2−58038
gravity, internal standing, breaking mechanism, in atmos. and ocean 2−72776
gravity, linear low-pass filter development 2−57903
gravity, neutral, magnetic storms 2−44772
gravity, scatt. by irregular bottom 2−54787
gravity, Stokes expansion by computer 2−77197
helical, motion of vortex filament with axial flow 2−60361
Helmholtz eqn., Moseley's non-separable solutions 2−41466
inertial foundation, Pasternak-type, travelling waves at metal surface 2−49100
interacting particles system, thermal and diffusion wave propag. 2−45334
internal, around body moving curved path 2−80216
internal, propagation in randomly stratified rotating fluid 2−80213
internal gravity wave spectra, wave number dependence 2−65690
interstellar spiral density waves, damping by induced shocks 2−81827
Kelvin waves on oceanic boundaries, effects of continental shelf and coastlines 2−78319
Lake Biwa-ko, seiche, numerical expt. 2−78316
linear theory, asymptotic expansion of integrals 2−82154
local storm area, wave field generated by variable wind 2−54744
marine breakwaters and transportable wave barriers, review 2−54747
matrices, stiffness and mass, extremal eigenvalue bounds 2−66577
modified Korteweg-de Vries equation, exact soln. 2−69553
N-dimensional travelling, in N-dimensional radial gas flow 2−56418
neutron, in cryst. media, effect of cold neutrons 2−83044
nonlinear, generation of clear air turbulence 2−54831
nonlinear, in dispersive media, stationary solutions and stability 2−82153
nonlinear, with dispersion, averaging of variational equation 2−69554
nonlinear dispersive, asymptotic method in theory 2−45243
nonlinear dispersive wave problems, approximate methods for obtaining multi-phase models 2−52037
nonlinear in Kelvin-Helmholtz flow 2−80171
nonlinear interaction between three waves, 1st initially absent. 2−83620
nonlinear interactions, gas dynamics 2−80405
nonlinear propagation, asymptotic theory 2−76169
nonlinear wave-wave interacting systems with well- defined phase description, bounds for solution 2−45241
nonlinear weakly dissipative, amplitude dispersion and stability 2−58715
packet propagation in baroclinic shear flow 2−62094
perfect gas, multidimensional simple wave flow 2−60342
periodic, stability in weakly dispersive media 2−53147
plane, expansion in spherical waves 2−73278
plane, in linear homogeneous media, solns. for first order propagation eqn. 2−58717
plane, in linear homogeneous media, solns. for second order propagation eqn. 2−58718
plane-parallel layer instability 2−67607

Waves continued
- planetary, in rotating global fluid shells 2−81745
- pressure, excitation by high speed drop impact 2−51890
- propagation in random media, function space integrals applic. 2−58716
- propagation of disturbances from randomly moving sources, solution of 2-dimensional equation 2−45286
- random lattice, coherent and mean wave propag. 2−63027
- reflecting body, modes of decay in exterior 2−82359
- reflection by periodic medium 2−45244
- scalar pulse, closed solutions for wedge diffraction 2−45245
- shear, in linearized stationary plane flow, perfect fluid 2−83457
- shellac wax thermoelectret behaviour under different humidity conditions 2−81145
- simple, in one-dimensional, unsteady, nonequilibrium dissociative, gasdynamics 2−46809
- solid, thermoelastic incompressible, discontinuity wave propag. 2−45478
- solitons, development on shelf, variable coefficient Korteweg-de Vries equation 2−56276
- spatial coherence and structure of propagating medium 2−55377
- standing periodic waves, existence in perfect inviscid incompressible fluid 2−56289
- steel strips, notched, dynamic stress concentration 2−80807
- steepening of long internal waves in stratified fluid influenced by vertical density profile curvature 2−53148
- stimulated emission due to electron moving in weak wave field 2−63311
- surface, nonlinear effects when resonantly driven 2−80161
- surface and space waves, transition radiation from boundary of plasma 2−80230
- surface waves on bubble, thresholds for acoustic excitation 2−43307
- thermal in nearshore environment 2−48429
- thermo-mechanical acceleration, in rheological material, analysis 2−63090
- thermo-mechanical acceleration, in rheological material with internal parameters 2−63091
- thermosphere dynamics, planetary waves 2−81701
- tidal, thermosphere dynamics 2−81700
- transverse, focused, propagation, induced by geometrical and physical nonlinearity 2−78893
- tropospheric, equatorial, induced by diabatic heat sources 2−78346
- tropospheric wave motions with baroclinic basic flow in equatorial latitudes 2−84847
- uniformly rotating fluid, propagation of surface and inertial waves 2−50164
- vibrations of wall due to plane, P, S and Rayleigh waves, solution 2−58890
- water, trapped shallow, for continuous bottom topographies 2−72698
- wind waves, frequency spectra of inner and outer structure at different development stages 2−81613
- zonal harmonic standing waves in Southern Hemisphere 2−65659

Waxes
- shellac, electret effect 2−61440
- sugarcane electrets, heterocharge mechanism 2−75157
- surface charge distributions in carnauba wax electrets 2−72046
- volume charge distributions in carnauba wax electrets 2−72046

Weak interactions *see Elementary particles/interactions, weak; Field theory, quantum/interactions, weak*

Wear
- abrading surface shape, microscopic probability model 2−47562
- adhesive, sliding model 2−68110
- AK-4 alloy, strengthening and roughness of rubbing surfaces, effect on wear and bearing capacity 2−60916
- apparatus for testing materials for wear in liquid and vaporised alkali metals at temps. up to 700°C 2−82127
- cathodic contact erosion due to gas breakdown arcs · 2−43223
- cavitation erosion, relax. hypothesis, proof of validity 2−71605
- ceramic, fund. review 2−47554
- ceramic alloy B2Zh, prep. and mech. characterization 2−77720
- ceramic and cermet characts. 2−47555
- ceramic coupled with surface-hardened metallic alloy 2−47556
- cermet, Fe-based, antifriction props. rel. to sintering in various protective atmospheres 2−77727
- cylinders rolling on viscoelastic plane, contact area rel. to vel. 2−66488
- diamond, abrasion resist. during polishing and grinding, microscopic cleavage mechanism 2−74868
- friction material, neutron activation analysis applic. 2−47551
- fusible material, with diminished heat flux, increased rate of ablation 2−73466
- graphite, anti-friction AG-T type, 150 to 600°C 2−43743
- Hertzian partial elastohydrodynamic contacts between real surfaces 2−68117
- lubrication ball and peg testing machine, wear monitoring 2−68123
- machine for testing 2−56849
- metal, internal friction, negative reversing effect, elimination 2−53789
- metal, stress effects 2−53851
- metals, methods of obs. and diagnostics 2−43754
- nuclear reactor fuel rod in vertical coolant tube, hydrodynamics, vibration and wear obs. 2−52844
- parameters rel. to Young's modulus to hardness ratio 2−68111
- polyfluoroethylene, filler content influence 2−47553
- polymethyl methacrylate in soln. containing solid phase, mech. destruction 2−47560
- rate of erosion, time dependence 2−68112
- rubbers, apparatus for testing for wear in liquids 2−82128
- sapphire sliding on steel 2−74867
- scanning electron microscope obs. 2−43741
- steel, 38KRM Yu A, strengthening and roughness of rubbing surfaces, effect on wear and bearing capacity 2−60916
- steel, cavitation erosion mechanism 2−71606
- steel, wear resist., effect of heat treatment temp. 2−53842
- surface deformation and destruction, statistical structural model 2−43746
- tester, for cast iron, obs. 2−50792
- vinyl chloride-acetate copolymer, wear resist. and frictional props. 2−47561

Wear continued
- Al, surface, impact effects, impingement erosion 2−68113
- Al_2O_3 and Al_2O_3/B fibre composites, high temp. bearing characts. 2−47558
- C-metal composite, high strength, evaluation as sliding material 2−61019
- C film, resist., diamond-like props. characterization 2−56588
- Co, porous, dry wear behaviour, rubbed against mild steel 2−60911
- Cu, influence of air, oxygen or vacuum on durability 2−60912
- Fe, cast, cavitation erosion mechanism 2−71606
- Fe, cast, nodular, 4-5% Si, high wear resistance 2−74869
- Fe, gray cast, rolling mild wear, Amsler machine obs. 2−56938
- HfN-ZrB_2 cutting tool materials characteriz. 2−50883
- NaCl, cavitation erosion mechanism 2−71606
- TiB_2 coatings characteriz. 2−51460
- TiC-Ni-Mo alloy, cermet, wear resist., Mo alloying effects 2−47534
- WSe_2-$NbSe_2$ alloys, antifriction and elec. props., comp. depend. 2−68115

Weather *see Meteorology*

Weighing *see Balances; Mechanical measurement*

Weissenberg cameras *see Cameras; X-ray crystallography/apparatus*

Welding *see Forming processes*

Wentzel-Kramers-Brillouin method *see Quantum theory*

Wertheim effect *see Magnetomechanical effects*

Wetting
- *see also Capillarity*
- rel. to bubble separation from horizontal surface 2−67791
- carbides, by liq. metals, relative surface energies 2−50427
- ceramic, solid, by liq. ceramic 2−43464
- ceramic system, wetting angle, statistical interpretation 2−60970
- rel. to ceramics sintering, refractory meterials corrosion 2−43867
- contact angle, effect of changes on normal force obs. with Weissenberg rheogoniometer 2−64455
- contact angles, solid-liquid, in saturated system or controlled atmosphere, obs. rel. to temp. 2−43342
- graphite, heats of immersion rel. to degassing behaviour 2−53549
- graphite, pyrolytic, spreading critical surface energy, from liq. metal wetting obs. 2−80558
- graphite/oil/water/air system, forced spreading 2−53380
- hydrophilic solid surface characterization technique 2−71174
- liquid metal-ceramic systems, critical surface energy of spreading 2−50425
- liquid substrate, crit. surface tension and dispersion contrib. of surface tension 2−74532
- metal melt spreading over hard surfaces, kinetics 2−67814
- polyethylene terephthalate, stressed, crack propag. in presence of org. liqs. 2−50781
- refractory carbides, by liquid metals, contact zone reactions 2−68190
- spreading kinetics, driving forces 2−74506
- W, by Ni, rel. to sintering of W/Ni powder 2−43897
- α-Al_2O_3, spreading critical surface energy, from liq. metal wetting obs. 2−80558
- C-graphite matrix composites, effect on mech. props. 2−61015
- C fibre wettability meas. 2−64802
- D_2O, at boiling point, contact angles on Cu and polytetrafluoroethylene surfaces, 10-770 torr 2−74533
- Pt, by silicate glass, contact angle meas. 2−53371
- Pt, by silicates, effect of oxides 2−67782
- TaC, by liq. Ag and liq. Cu, surface energy 2−43468

Whiskers *see Crystals/whiskers*

Whistlers *see Atmospherics; Ionosphere*

White dwarfs
- blanketed model atmospheres for cool hydrogen-rich white dwarfs 2−69079
- CD-42° 14462, rotating, spectral obs. 2−66093
- CNO abundances, hydrodynamic models of nova outburst 2−58315
- cosmic ray source, rel. to explanation of anisotropies 2−72961
- DA and DB, model atmospheres 2−69064
- degenerate electron gas magnetic props., Landau orbital ferromagnetic states 2−47823
- 40 Eri B, DA white dwarf, gravitational redshift51749 2−51749
- evolution, with accretion of H rich envelope 2−69066
- G-type, H_α profiles 2−84978
- G-type stars near North Galactic Pole spectral analysis rel. to dwarf hypothesis 2−58304
- H-rich material ejection from white dwarfs, computer calc., formation of planetary nebulae 2−72980
- hot, photoionization of intergalactic medium 2−81791
- HZ-22, old evolved binary, white dwarf secondary 2−58343
- Landau Orbital ferromagnetism, LOFER theory 2−62494
- magnetic, as source of cosmic rays in Galaxy 2−69007
- non-magnetic, in rapid differential rotation, viscous evolutions 2−58276
- non-radial oscillations of gravity modes to explain variable white dwarfs 2−55055
- non-radial pulsations, oscillations rel. to dwarf novae and g-mode pulsations 2−73018
- Proxima Centauri, M dwarf, multicolour photometry 2−85002
- pulsating X-ray sources rel. to stars with high central densities 2−51799
- pulsed and continuous radiation in X-ray region 2−84967
- radially pulsating, variable X-ray source cen X-3 model 2−81867
- Ross 640, model atmos. with convection 2−75707
- superdense, nuclear energy sources 2−81854
- HL Tauri-76, white dwarf with multiple periodicities in light curve 2−81846
- thermal imbalance, anal. of pulsation damping 2−58274
- Upgren's G5-G7 unclassified stars, spectra rel. to densities of G-type dwarfs 2−81820
- von Maanen 2, model atmos. with convection 2−75707

Wiedemann effect *see Magnetomechanical effects; Magnetostriction*

Wiedemann-Franz law *see Conductivity, electrical/solids; Conductivity, thermal/solids*

Wien effect *see Conductivity, electrical/liquids, electrolytic*

Wigner coefficients *see Quantum theory*

Wigner effect *see Physical effects of radiations*

Wilson cloud chambers *see Cloud chambers*

Wind
- airflow over arbitrary mountain ridge, diabatic heating and cooling 2−78364
- anemometer dynamics, error analysis 2−75573
- Antarctica, diurnal variations 2−68901
- atmospheric stagnation periods, simulation of wind conditions 2−75557
- atmospheric surface layer turbulence over water, instrumentation 2−68902
- atmospheric surface layer turbulence over water, velocity and temp. fluctuations 2−68903
- balance eqn., use for computation of geopotential in tropics 2−62179
- beach dynamics as function of prevailing wind direction and speed 2−57852
- boundary layer, atmospheric vortex streets, wind tunnel simulation 2−72771
- boundary-layer trade-wind profile and shearing stress on tropical windward coast 2−44706
- Caspian Sea oil field areas, maximum wave parameters computation 2−54762
- clear air turbulence, life cycle by mesoscale analysis 2−75544
- clear air turbulence, radar and radiosonde measurements 2−75545
- cloud free regions, isentropic analysis, temperature, water vapour, cloud tracking microwave 2−84834
- cloud motion meas. from geostationary satellite spin scan camera pictures 2−65716
- cloud motion vectors, computation of kinematic properties 2−65693
- coastline under hurricane action, computer simulation 2−57875
- computation by forced adjustment to height field 2−44714
- over continental shelf, comparison with current obs. 2−65612
- coupling with upper ocean currents 2−57921
- cross wind shear effects on atmospheric diffusion 2−57961
- cup anemometer, response to fluctuating wind speeds 2−75576
- cyclogeresis on East Coast, accompanying gravity wave phenomena 2−65697
- cyclone, Hamburg, Feb. 1962, available potential energy and transfer between zonal and eddy parts 2−54836
- cyclone parameters, extratropical, estimation from satellite radiation measurements 2−54840
- cyclone waves, nonlinear waves 2−44708
- cyclones, numerical study of effect of Great Lakes 2−62175
- direction, frequency distribution function 2−44701
- direction and speed meas. over ice drift during aerial photo survey 2−57967
- direction-insensitive static head sensor, wind-induced pressure in ambient air stream 2−82131
- diurnal variations over planetary boundary layer 2−78365
- Drake Passage, sealevel slope rel. to press. and wind half-yearly oscills. 2−72709
- driven ocean circulation and effects of latitudinally varying bottom topography 2−54774
- effect on d.c. transmission line corona, loss on monopolar lines 2−74441
- Ekman layer over St. Louis 2−75665
- energy spectra, scale representation in terms of degree of Legendre polynomial expansion 2−62182
- energy transfer to ocean waves 2−78315
- eolian-modified craters, simulation 2−61844
- equatorial stratosphere, diurnal variation 2−68883
- equatorial stratospheric, quasibiennial oscillations 2−44715
- erosion, atmospheric soil particles, aerosol size distributions, vertical fluxes, jet impactors 2−84827
- estuarine circulation, wind effects 2−57868
- field, adjustment to geopotential data in primitive equations model 2−84796
- field analysis using Nimbus 4 THIR 6.9 micrometer obs. 2−62257
- field structure in convective baroclinic planetary boundary layers 2−51609
- fluctuations, in atmospheric boundary shears, meas. by infra-sonic wave propagation expt. 2−54816
- fluctuations of wind and temp., meas. instrument attached to captive balloon 2−81663
- focused unstable laser beams, thermal distortion effects 2−82520
- forecast winds rel. to forecasting of cloud ceiling 2−65717
- generation of capillary waves and interaction with gravity waves 2−62084
- geostrophic equations, correlation functions for isobaric surfaces 2−44713
- Global Radio Meteor Wind Studies Project 2−58036
- gradients in convective storms, Doppler radar obs. 2−75560
- gravity waves from tropospheric winds, jet streams, weather fronts and thunderstorms 2−57955
- hemisphere zonal, effect on Earth's rotation rate 2−54584
- horizontal divergence, magnitude obs. 2−62181
- hurricane and tropical meteorology 2−75491
- hurricanes, asymmetrically rotating fluid disc model 2−56279
- hurricanes, energy control, cloud seeding applics. 2−62223
- hurricanes, role of warm currents in ocean in directing 2−44635
- hurricanes, unaccelerated drifting tropical, effective wind trajectories 2−51606
- hurricanes, unaccelerated drifting tropical, wind trajectories 2−51607
- inshore currents, wind-driven, trajectories 2−57877
- interhemispheric transport of radioactive debris, role of Indian monsoons 2−65807
- ionosphere, height structure of tidal winds, incoherent scatter obs. 2−72872
- ionospheric wind fields, vertical profiles 2−58077
- irregular variations between 50 and 200 km 2−72764
- jet stream over India and to its north in winter 2−62177
- Lake Erie, current mechanics 2−65609
- Lake Michigan, effect of cold water on wind profiles 2−65691
- land-sea breeze circulation system, rel. to diurnal variation in visually-observed breaking waves 2−57867
- land-sea breeze effects, evidence for in wave gauge data from Pt. Mugu, Calif. 2−57866
- large stratified lakes, response to wind stress 2−62031
- leeward of islands, velocity field 2−48481
- liquid surface waves, evaporation at air-water interface 2−77395

Wind continued
- liquid surface waves, transport phenomena, isothermal conditions, shear prediction methods 2−77394
- liquid waves, wind driven, waveheight probability structure 2−77392
- local storm area, wave field generated by variable wind 2−54744
- lower troposphere, velocity meas. by Doppler optical radar 2−78359
- Mars, aeolian deposition of dust, Mariner 9 photographs 2−66176
- Mediterranean Sea response 2−57922
- meteor wind radar meas. rel. to ionospheric drift 2−72870
- monsoon disturbances, vertical tilt 2−78372
- monsoons of southern Asia, review 2−48485
- mountain ranges, mathematical model for calculating non-linear effects on lee side 2−72784
- mountainous terrain, potential analysis 2−44690
- Natal, regional topographically-induced wind systems 2−65707
- national hurricane warning program 2−75492
- neutral atmosphere, radio meteor method of observing winds and turbulence 2−48522
- neutral wind charge, effect on low-latitude F-region 2−65989
- New York, vertical moisture content surface winds 2−75526
- North Africa, lower troposphere, easterly waves, origin and structure 2−44711
- numerical circulation model, use of satellite radiance meas. 2−62134
- over ocean, coastal upwelling, numerical model 2−62032
- over ocean, continuously stratified, steady coastal upwelling 2−62033
- ocean surface fields, remote passive microwave sensing 2−44648
- ocean wind waves, frequency spectra of inner and outer structure at different development stages 2−81613
- oceanic equatorial currents driven by eastern wind, nonlinear theory 2−68866
- potential energy in atmosphere, theoretical calculation 2−57989
- profile, surface boundary layer 2−84782
- profiles, dependence on weather conditions 2−72787
- rawin observations in Caribbean, observational accuracy and sampling resolution 2−65644
- recurved typhoon intensity rel. to reconnaissance aircraft measurements 2−65706
- regime characteristics in coastal area 2−44643
- rotation of direction with altitude, vapour trail obs. 2−65703
- Salt Lake Valley, surface wind flow during low visibility-ventilation episode 2−75575
- over sea ice surface roughness and resistance coeff. 2−65567
- sea level, derived from simulated obs. of satellite radar-radiometer data 2−57963
- sea surface, wind stress rel. to temperature fluctuations 2−57890
- sea wave generation, energy balance 2−78336
- sea wave generation by turbulent wind 2−44608
- sea waves generation rel. to microscale pressure fluctuations 2−68871
- sensor, spherical balloon, aerodynamic props. 2−57933
- severe storm, rotating updraft configuration, two dimensional model 2−72788
- shear fluctuations, probability distribution, mean wind profile, aerospace vehicles, stochastic process 2−83465
- small scale shear definition, aerospace vehicle design 2−44798
- snow drifting, development and movement of wavy features 2−75442
- south coast of England, sea breeze front 2−54838
- squall line, Doppler velocity obs. 2−75561
- squall line dynamics, diagnosis from rawinsonde obs. 2−62173
- in storm basin, technical and regime characteristics 2−44716
- stratospheric winds and winter warmings in Southern Hemisphere 2−65711
- stress fluctuations in continuously stratified ocean, quasi-geostrophic response 2−57906
- stress parameterization, barotropic planetary boundary layer, geostrophic drag coefficient variation, cross isobar angle variation 2−84785
- structure in city environment, turbulence obs. 2−57964
- Sun-glitter pattern on sea rel. to roughness and surface wind measurements from spacecraft 2−84772
- surface, adaptation of marine boundary layer model 2−65699
- surface wind fields and sea-level pressure, adjustment by variational matching 2−65705
- Texas coastline, surface roughness and internal boundary layer 2−65708
- thermosphere, daytime measurements, rocket vapour trail obs. 2−84886
- thermosphere, one- and three-dimens. model obs. 2−58039
- thermospheric, causing directional filtering of travelling ionospheric disturbances 2−54896
- thermospheric, from exptl. density data 2−58042
- tidal variations of components, 45-60 km up 2−62189
- tornado, 1955 Blackwell, Oklahoma, sferic rate azimuth profile 2−78368
- tornado, effects of ground roughness, laboratory simulation 2−48482
- tornado dynamics, obs. using lab. model 2−84809
- Tornado funnel, force field required to maintain dynamics and shape 2−62186
- tornado-like vortex, simulated, velocity field meas. using three-dimensional velocity probe 2−44712
- tornadoes, airborne seedings 2−65701
- tornadoes, radar and Nimbus 4 i.r. obs. 2−75569
- tornadoes and hurricanes, steady and unsteady, fluid mechanics 2−81644
- tropical cyclones, as origin of longitudinal microseismic waves 2−61888
- tropical cyclones Althea and Ada, radar estimation of max. wind speed 2−75570
- tropical depression analysis based on radar data 2−51578
- tropical hurricanes, unaccelerated drifting, eye effect and wind lengths 2−48484
- tropics, and reference pressure meas., numerical simulation of observing systems 2−54839
- tropics, general circulation, numerical simulation expts. 2−84797
- tunnel with laminar flow, sting-free meas. of sphere drag 2−67719
- turbulence effect on wind and temp. profiles 2−62172
- turbulent clear air, veloc. field meas., by Doppler radar 2−75543

Wind continued
turbulent fluxes over open water, trivane measurements, tilt errors and precipitation effects 2−72783
turbulent microfluctuations of wind velocity derivative in surface layer 2−72786
United States Midwest tornado wind records, geometrical analysis 2−75577
upper atm., smoke trail motion under constant vel. shear 2−65833
upper atmos., v.h.f. radar obs. 2−75618
upper atmosphere, monitoring using expanded synoptic network of infrasound recorders 2−44743
upper atmosphere, radar meteor trails and chem. release methods, comparison 2−58037
upper atmosphere, study by analysis of orbital changes of Cosmos 316 (1969-108 A) satellite 2−84927
upper atmosphere wind patterns, model calcs. 2−58040
upper atmosphere wind speed and direction, air density and temperatures up to 95 km, simultaneous meas. using chaff cloud sensors 2−54876
upper atmosphere zonal winds from orbit analysis of Cosmos 316 (1969-108A) 2−51632
upper tropospheric cold core cyclones, numerical model of parametrized i.r. cooling 2−68900
urban area, effect of temp. field 2−75572
urban meas., tower networks 2−75516
velocity, effect on heat and mass transfer from large body of water 2−57891
velocity, effect on remote sensing of atm. particulate pollutants 2−81693
velocity obs. using pattern velocity computers 2−57968
vertical, measuring instrument 2−62109
vertical shear, topographical effect, stratified flow over extended obstacles 2−62183
vertical structure, effect on aspects of convective activity at Bombay 2−62178
Wangara, west wind belts, vertical propagation of angular momentum 2−65712
waves, long dispersive, on a rotating ocean, generation by wind stress distribution 2−84716
wind profile development above locally adjusted sea surface 2−44707
windfield in northern hemisphere, zonal harmonic analysis, rel. to geostrophic flow pattern 2−48476

WKB method *see Quantum theory*

Wolfram *see Tungsten*

Wood
mechanical props., vibration method of det. 2−56844

Work function
see also Electron emission
additive thermionic convertors, emitters, formation and effects of metal oxides 2−63233
alloy, change due to chemisorption 2−50524
electron gas theory, effect of ferromagnetism 2−54118
electron work function from plasma immersion probe measurements 2−54263
measurement by obs. of contact pot. between emitting electrode and probe 2−74376
metal, change caused by adsorption of alkali atoms 2−48007
metal, of positrons 2−84243
metal, rel. to nonmetal to metal transition of adsorbed alkali metal layers 2−83870
Si, intrinsic, work function change analysis of photoemission processes as a function of caesium coverage 2−72082
surface ionization methods for measuring change 2−48028
thermionic emitter surface properties, measurement 2−75192
transition metal, variation on alkali metal adsorption, atomic theory 2−71343
transition metal borides, of IVA-VIA metals, 1300-2100K 2−48017
trialkali photocathode, thermionic emission 2−61459
Ag on W, employing retarding-field diode technique 2−72083
Ag_2F, estimation from threshold value of photoelectric emission and by photoelectron spectroscopical method 2−72089
Al, adsorpt. of O_2, work function changes obs. 2−77517
Al, adsorption of water, detn. by meas. of work function 2−71346
Au, adsorption of water, detn. by meas. of work function 2−71347
Au, elongated, rel. to exoemission 2−54269
B on W substrate, adsorbate induced work function changes 2−72084
Ba-W_{110} system, temperature dependence 2−75186
$BaTiO_3$, piezoeffect rel. to semicond. props. and work function 2−77959
BiI_3, thermionic work function, effect of adsorption 2−47993
C, variation with adsorption of H and H_2 2−60677
CO, change on absorpt of CO 2−71348
Ca films, photoelec. props., elec. field influence 2−81188
CrB, thermionic emission, calc. 2−44191
Cs-W electrode for thermionic convertor beneficial effects of O_2, statistical mechanical model 2−63230
Cs covered surfaces, with plane parallel Cs diode, technology 2−61455
Cs covered surfaces, with plane parallel Cs diode, physical basis 2−61456
Cu-Ni alloy, adsorption of CO and O_2, work function changes 2−50536
Cu, contact potential, compressionally induced change 2−75187
Fe-2.89%Si (100) face, photoelec., relation to surface composition 2−61463
Fe, (100) surface, LEED and photoelec. work function study 2−50443
Fe, change on absorpt. of CO 2−71348
GaAs, Cs adsorption effect 2−53595
GaAs single crystal, effect of light at low temp. 2−75188
GaS, surface electronic props. detn. 2−65106
GaSe, surface electronic props. detn. 2−65106
GaTe, surface electronic props. detn. 2−65106
Ge_x-Si_{1-x}, mixed crystals, photoelectric emission 2−72092
Ge, time depend., surface orientation effects 2−71935
$InAs_{0.4}P_{0.6}$/Cs-O low work function surface, wavelength depend. of Cs-O optimum thickness 2−68498

Work function continued
K_2CsSb photocathode, thermionic emission 2−61459
Mn, change on absorpt. of CO 2−71348
Mo, changes due to exposure to Co, N_2 and O_2, surface photoelectric yield obs. 2−51227
Mo(110), hot emitters, modified Shelton measurement method 2−63234
Nb-C system, electron emission pulsing voltage measurement technique 2−63235
Nb-C thermionic emission constants and electron work function changes 2−54268
Nb crystal surface, rel. to simultaneous adsorp. of Cs and Ba 2−67923
NbC_x, correl. with surface recomb. of H atoms 2−50549
Ni, change on chemisorption of S, Se, O, obs. of bonding 2−48328
Ni film, photoelec. emission obs., rel. to surface potential of adsorbed Xe 2−47163
NiO, true work function, A constant, normal energy distribution 2−44192
Ni(001), changes rel. to impurity segregation 2−53554
Pd, elongated, rel. to exoemission 2−54269
Pt, elongated, rel. to exoemission 2−54269
Pt, rel. to absorp. of Ba, field emission microscope obs. 2−67924
Si/Cs-O negative-electron-affinity surfaces, photoemission meas. 2−81185
Si on W substrate, adsorbate induced work function changes 2−72084
Si surface, effect of annealing 2−72095
Ta-O thermionic emission constants and electron work function changes 2−54268
Ta(110, 100), hot emitters, modified Shelton measurement method 2−63234
Tc, polycrystalline, accurate estimation, and surface energy derivation 2−71319
Ti, Ar-ion bombarded, excited particle velocity spectrum obs. 2−48030
TiC_x, correl. with surface recomb. of H atoms 2−50549
W/Cs(Cs-O) work function theory 2−54262
W-Re alloys, carburized, work function in 1600- 1800 K range 2−54267
W, (211) and (110) planes, Cl adsorption effects 2−60693
W, adsorption of Cs and O, double layer form., work function obs. 2−47169
W, adsorption of O_2, thermionic electron emission and work function obs. 2−47172
W, coated with Si, field emission obs. rel. to surface diffusion 2−47085
W, effect of Ag adsorption 2−60690
W, effect of CO adsorption on (210) surface 2−60692
W, effects of pure O_2, Cs vapour/O_2 mixtures, adsorption phenomenology, analytical model 2−63231
W, needle-like microcrysts., coated with TaC_x film 2−50509
W, rel. to Cs adsorbed layer struct. 2−68487
W crystal surface, rel. to simultaneous adsorp. of Cs and Ba 2−67923
W single crystal plane, rel. to O adsorption 2−64580
W single crystal surface work function change rel. to adsorption of O and Cs and O-Cs co-adsorption 2−54266
W single crystals, work function dependence on crystal orientation 2−54264
W work function change as function of Mo coverage of single crystal surface 2−54265
W(100) surface, adsorption of Cs and O 2−83878
W(110, 100, 111, 210), hot emitters, modified Shelton measurement method 2−63234
Zr-Nb-C system, electron emission, pulsing voltage measurement technique 2−63235
Zr-O (B)(C) thermionic emission constants and electron work function changes 2−54268
Zr-Ta-C system, electron emission 2−63235
Zr-Ta(Nb)-C thermionic emission constants and electron work function changes 2−54268

Work hardening
see also Cold working; Surface structure
anisotropic work hardening materials, elasto plastic analysis 2−76265
b.c.c. metals, disloc. distrib. 2−60799
brass, annealing after deform. 2−43789
creep, recovery-work hardening theory 2−56799
differential calorimetery applic. to process obs. in arbitrary real castings 2−47576
elastic viscoplastic medium, propagation of two dimensional strong discontinuity waves 2−76255
high pressure effects on single crysts. 2−68080
hot workability, review 2−50795
metal, at high strain, electron microscope exam. 2−56908
metal forming, upper bound approach for conical flows 2−46882
oscillating internal stresses and Lomer- Cottrell dislocations effects 2−77580
recrystallization, dynamic 2−68133
sandwich shells of revolution, large elastic plastic deflections 2−76266
solid solution, Fleischer and Labusch theories 2−47591
solid solutions, statistical theories 2−50813
statistical problem, dislocation, flux line and Bloch wall motion, pinning 2−68125
steel, austenitic, strengthening by ageing, optimal conditions 2−53876
steel, effect on mech. props. after ausforming 2−43801
steel, heat treated, cyclic strain softening at various hydrostatic pressures 2−68142
steel, mild, resulting activation enthalpies for strain hardening 2−80814
steel, spheroidization of cementite by plastic deform. at subcritical temp. 2−43840
steel, strain-ageing resistance 2−43800
steel, synthetic weld structure, obs. 2−56919
time dependent materials, plastic behaviour 2−76256
Ag, effect on anelastic phenomena at low temp. 2−60848

Work hardening continued
- Al-Mg-Si alloy, strengthening rel. to age hardening, thermally activated dislocation motion 2−56717
- Al-Ni-Cu-Ti alloy, age hardening, precip. 2−53878
- Al-Zn alloy, fatigue hardening 2−80840
- Al alloy, superstrength, by continuous cyclic thermomech. treatment 2−47614
- Al alloys, multiphase, strengthening by dislocation substructures 2−56706
- BeO high pressure effects on single crysts. and polycrystalline mat. 2−68082
- Co-Al alloy, disintegration of solid solution under hardening and cooling 2−60977
- Co alloys, metallurgical structure and properties 2−71667
- Cu-Co alloy f.c.c. single crystals, effect of coherent precip. 2−50798
- Cu-Cr alloy, rel. to dispersion struct. production 2−43832
- Cu, effect of initial disloc. density 2−64665
- Cu, point defect clusters, effect on fatigue hardening 2−53724
- Fe-Co-V alloy, ordered and disordered, recovery behaviour 2−50804
- Fe-Cu alloy, dispersion strengthening model, slip dislocation precipitate interaction 2−50744
- Fe-Mn-Ti alloys, ferritic and martensitic, low temp. 2−47592
- Fe-(30 wt.%)Mn alloy, austenitic, strengthening by shock loading 2−43841
- Fe-Ni alloy, hardening at high strain rates, rel. to microstruct. changes 2−47593
- Fe single crystal, latent hardening with 110 extension axis 2−43799
- Ni, double texture development 2−60985
- Ni, secondary recrystn. texture development 2−60986
- Ti-(13 wt.%)V-(11 wt.%)Cr-(3 wt.%)Al, deformation substructures rel. to strengthening56950 2−56950
- Ti, dislocation struct. effects in strain-, grain size− and interstitial solute hardening 2−56714
- Ti alloy, T-A6V5E2, struct. hardening 2−60963
- W:K,Si,Al wire, incandescent lamp filament, working and process annealing 2−47590
- Zn single crystal, crit. orientation for max. work hardening coeff. 2−71631
- Zr and Zr-Nb alloy, strain rate depend. hardening 2−50847
- α-Zr. grain size depend. of deform. behaviour 2−50748

X and gamma-ray astronomy
- 2U 0613+9, 1970 Sept. sky survey, locations 2−66137
- 2U 1908+0, 1970 Sept. sky survey, locations 2−66137
- 2U 1912-5, 1970 Sept. sky survey, locations 2−66137
- accretion disc model for X-ray sources 2−85014
- 2ASE 1253-28, identification with rapid blue variable EX Hydrae 2−66101
- background fluctuation analysis 2−55112
- background X-rays, observations of diffuse component 2−51695
- balloon observational techniques 2−73058
- binaries, X-ray spectra, and short period pulsations of Cen X-3 2−75776
- 3C 273, search for hard X-ray emission 2−58432
- η- Carinae, constraints on models 55108 2−55108
- Cas A, 1970 Sept. sky survey, locations 2−66137
- Cas A, low energy X-ray survey 2−84952
- celestial nuclear γ-ray monitoring from OSO-7 2−58438
- Cen X-3, anomalous minima, from rocket data 2−55114
- Cen X-3, mass limit, model 2−62618
- Cen X-3, optical counterpart is not LR Cen 2−55101
- Cen X-3, optical search, not LR Cen or Wray 795 2−58421
- Cen X-3, pulsating X-ray source, shape and energy spectrum 2−62632
- Cen X-3, search for optical counterpart 2−62576
- cen X-3, variable, possibility of being radially pulsating white dwarf 2−81867
- Cen X-3, X-ray obs. 2−58426
- Cen X-3 pulsar optical identification with WRA 795 2−75828
- Cen X-3 pulsing binary system, models 2−69103
- Cen X-3 system, X-ray flux and orbital elements 2−48758
- Centaurus X-3 and Roche limits of close binary systems 2−66138
- clusters of galaxies, relation between X-ray luminosity and velocity dispersion 2−58202
- Coma constellation, enhanced emission from balloon flights 2−55109
- compact galactic X-ray sources rel. to binary star model 2−58424
- cosmic γ-ray obs. above 250 MeV 2−62628
- cosmic X-ray background radiation, significance of small scale isotropy 2−62623
- Crab Nebula; cosmic γ-ray obs. above 250 MeV 2−62628
- Crab Nebula, detection of high energy γ-rays 2−58437
- Crab Nebula, low energy X-ray survey 2−84952
- crab nebula, pulsed X-radiation 2−55090
- Crab nebula rel. to neutron star models 2−75692
- Crab pulsar, γ-ray obs. with scintillation detectors 2−62631
- Cyg X-1, fluctuations in period 2−62635
- Cyg X-1, obs. of hard X-ray flare 2−62638
- Cyg X-1, search for h.f. optical variability 2−69092
- Cyg X-1, X-ray variability 2−58435
- Cyg X-2, low energy X-ray survey 2−84952
- Cyg X-3, obs. by Uhuru during radio flare 2−85021
- Cyg X-3, X-ray obs. at time of radio flare 2−81883
- Cyg XR-1, 1970 Sept. sky survey, locations 2−66137
- Cyg XR-2, 1970 Sept. sky survey, locations 2−66137
- Cyg XR-3, 1970 Sept. sky survey, locations 2−66137
- Cygnus, search for visible counterpart of radio outburst 2−81890
- Cygnus region in 20 to 300 keV 2−69130
- Cygnus X-1, correlation anal. of X-ray emission 2−75832
- Cygnus X-1, radiation model 2−55107
- Cygnus X-1 and X-2, soft X-rays, eclipse? 2−55100
- Cygnus X-3, flux density obs. during outburst, in MHZ range 2−81889
- Cygnus X-3, obs. during Sept. 18-25 1972, following major radio event 2−81892
- Cygnus X-3, obs., using Copernicus in range 1 to 3 angstroms 2−81891
- Cygnus X-3, OH and formaldehyde absorption obs. 2−81849
- Cygnus X-3, outburst of radio emission rel. to possible superrova precursor 2−73056

X and gamma-ray astronomy continued
- Cygnus X-3 outburst, 21 cm. and 18 cm. obs. 2−81888
- Cygnus-Cassiopeia region, high energy gamma radiation 2−55115
- Cygnus-X region, radio continuum search for ring of filaments around area 2−75827
- diffuse cosmic γ-rays in 30-50 MeV region 2−51800
- diffuse cosmic soft X-rays, origin, galactic component 2−51797
- diffuse cosmic X-rays, 30-250 KeV, OSO-5 obs. 2−62627
- diffuse soft cosmic X-rays, spatial distribution 2−62446
- diffuse X-ray background, contrib. of transition radiation from dust grains 2−51778
- discrete X-ray sources, obs. of diffuse galactic X-rays 2−51794
- extended X-ray source at galactic centre, models 2−69127
- extensive air showers, γ-ray point source search by registration of Cherenkov light 2−51801
- extragalactic sources, search for hard X-ray emission 2−58432
- extragalactic X-ray sources, Compton scattering of electrons and photons rel. to extended and compact sources 2−51798
- extragalactic X-ray sources, thermal bremsstrahlung and inverse Compton models 2−75835
- flare stars, X-ray emission flux calculations 2−55113
- flare stars as possible source of soft X-ray background 2−55103
- galactic gamma-radiation between 200 MeV and 10 GeV, balloon-borne observations 2−58439
- galactic origin of soft X-ray background 2−62617
- Galactic plane, cosmic γ-ray obs. above 250 MeV 2−62628
- galactic soft X-ray sources, diffuse component 2−75826
- galactic sources, diffuse flux 2−55104
- galactic wind X-rays 2−55106
- galactic X-ray sources, discrete, Uhuru obs. 2−62463
- galactic X-ray sources, distances and absolute luminosities 2−58429
- gamma-rays above 60 MeV in Northern Hemisphere, extraterrestrial, balloon search 2−73060
- GX3+1, search for optical stellar counterpart of X-ray source 2−51796
- GX 340+0, black-body X-ray source, crustar model 2−58433
- GX 340+0, hot neutron star 2−62639
- hard solar X-rays, scintillation detector obs. 2−62631
- Herculis X-1, precessing binary pulsar model 2−81873
- high energy, conference (San Juan, Puerto Rico, Dec 1971) 2−62620
- high energy γ-radiation from galactic centre region 2−62636
- infall of intergalactic matter in the Galaxy and soft X-ray emission 2−75666
- inner bremsstrahlung, X-ray background, steady state universe 2−58434
- Large Magellanic Cloud, X-ray observation 2−62467
- low energy γ-radiation from galactic centre 2−62629
- M81, search for hard X-ray emission 2−58432
- M87, search for hard X-ray emission 2−58432
- Magellanic Clouds gamma radiation flux rel. to metagalactic origin of primary component of cosmic rays 2−72959
- Mertz shadowgram reconstruction for X-ray source astronomy 2−66129
- metagalactic γ-rays from relativistic bremsstrahlung interactions 2−62634
- modulation collimator, variable spacing for X-ray astronomy .2−73053
- NGC 1275, 1970 Sept. sky survey, locations 2−66137
- nova IM Normae, possible X-ray source 2−55052
- NP 0532, low energy X-ray survey 2−84952
- number-intensity distrib. of X-ray sources 2−75830
- XPer, seach for h.f. optical variability 2−69092
- periodic pulsating binary X-ray source in Hercules 2−75829
- β Persei, eclipsing spectroscopic binary, evidence for X-ray star62614 2−62614
- X Persei, evidence for assoc. with X-ray source 2U 0352+30 44858 2−44858
- point contacts, static and microwave properties 2−73061
- point sources with energy $>10^{12}$eV in Cassiopeia and Cygnus regions 2−75840
- proportional counter for soft X-rays 2−70292
- PSR 0833-45, UHURU obs. 2−75834
- pulsar det. from γ-ray flux 2−51792
- pulsating X-ray sources rel. to stars with high central densities 2−51799
- pulsing X-ray binaries, models 2−69103
- pulsing X-ray source in Hercules, radio search 2−62605
- Pup A, UHURU obs. 2−75834
- γ-ray background flux, relativistic Bremsstrahlung as source 2−62626
- review of γ astronomy, cosmic-ray sources and production and propagation in interstellar and intergalactic space 2−69010
- review of current status, expt. results 2−81972
- rocket flight stability by SCO sensor 2−68991
- Sco X-1, absorption measure 2−58430
- Sco X-1, Balmer H line profiles in spectrum 2−58431
- Sco X-1, less prominent features in optical spectrum 2−58305
- Sco X-1, photographic obs. 2−73059
- Sco X-1, photometric props., colour- magnitude relation 2−58306
- Sco X-1, rapid blue variable, photometric obs. 2−48710
- Sco X-1, reality of 165-S period in variation 2−69129
- Sco X-1, search for h.f. optical variability 2−69092
- Sco X-1, search for optical circular polarization 2−73001
- Sco X-1, simultaneous hard X-ray and optical observations 2−55110
- Sco X-1, X-ray fluctuations 2−55111
- Scorpius X-1, high resolution search for Fe XXV line emission 2−85013
- Scorpius X-1, review 2−51793
- Scorpius X-1, transfer effects on X-ray lines of optically thick sources 2−84981
- SCOX-2 optical counterpart HD 152667 spectrosopic binary 2−85018
- Small Magellanic Cloud, search for absorption of soft X-ray diffuse flux 2−81816
- soft, 0.6 to 1.6 keV energy from Lupus Loop and supernova 2−58425
- soft diffuse X-ray flux near galactic plane 2−62619
- soft X-ray and microwave observations of hot regions in solar flares 2−48795

X and gamma-ray astronomy continued
soft X-ray distrib. in selected region of sky 2−75831
solar corona active region models and relative abundances rel. to soft X-ray emission and continuum fluxes 2−78628
solar corona X-ray structure 2−75953
solar flare X-rays, electron acceleration region and ion density in X-ray source region 2−55188
solar limb prominence, X-ray emission in 1-55 Angstrom region 2−48794
solar soft X-ray flare at limb 2−78611
solar X-ray emission from thermal and non-thermal flares, OSO-7 observations 2−78590
stellar evolution endpoints rel. to X-ray source phenomena 2−78460
stellar X-ray obs., graphite crystal polarimeter 2−62640
stellar X-ray sources, pulsation mechanism 2−73057
sun, height of emission in solar atmosphere, satellite obs. 2−69184
Sun, high energy gamma-rays, search for radiation from flare regions 2−44995
superheavy element det. 2−51687
supernova remnants as soft X-ray sources 2−44900
supernova remnants in Aquila, 2−20 keV X-rays search 2−75839
Tau X-1, obs. from 1 to 60 KeV 2−62625
Tau XR-1, 1970 Sept. sky survey, locations 2−66137
thermal X-ray sources, models in which energy is produced by rotation 2−73055
Tycho 1572 X-ray source, nature 2−62637
2U 1543-47, transient X-ray source, extraglactic origin 2−58420
UCSD X-ray obs. in galactic plane OSO-7 2−58428
Uhuru extragalactic X-ray sources, radio identification 2−55105
Uhuru X-ray sources, association with bright stars 2−58422
universal X-ray background, supernovae source, observational evidence 2−58419
Vela Puppis region, UHURU obs. of X-ray structure 2−75834
Vela region, UCSD X-ray obs. 2−58427
Vela XR-1, Vela X, UHURU obs. 2−75834
Vela-Puppis region, soft X-ray structure obs. with focussing collector 2−75833
Vir X-1, obs. from 1 to 60 KeV 2−62625
Virgo Cluster, spectrum of soft X-rays 2−62624
X-ray astronomy, survey of current developments 2−58423
X-ray attenuation in interstellar space 2−62594
X-ray background, line feature, effect of cosmological redshift and galactic evolution 2−48756
X-ray background radiation rel. to distributions and clustering of galaxies 2−58436
X-ray binary, 2U 1700-37, associated with O-type star HD 153919 2−75775
X-ray det. using atmospheric fluorescence as ground-based method 2−44902
X-ray emission, 10-20 keV, during initial stage of solar flare 2−85051
X-ray emission near galaxies from accretion of hot gas 2−66050
X-ray galaxies, possibility for high galactic latitude sources 2−75837
X-ray polarimeter, Thompson scattering, design 2−51795
X-ray pulsars, pulsed radiation, considerations as bremsstrahlung radiation from hot plasma 2−78478
X-ray pulsations of long-period in NPO527 region, search 2−75838
X-ray satellite UHURU obs., sources and diffuse background 2−62621
X-ray source 2U 1706 + 78, decametric radio identification 2−48757
X-ray source in Aries-Taurus region, cosmic soft X-ray obs. 2−85010
X-ray source in Virgo cluster, structure and time variability 2−62630
X-ray source studies, state-of-the-art 2−62597
X-ray sources, compact, theories, review 2−62622
X-ray sources, Compton scattering by thermal electrons 2−73040
X-ray sources, review of current theories 2−55102
X-ray sources, spatial coincidences with supernova remnants 2−69128
X-ray sources in clusters of galaxies rel. to isolated extragalactic sources, energy cut-off obs. 2−75836
X-ray sources near galactic centre from 1 to 60 keV 2−62633
X-rays from supernova remnants in Aquila 2−62569
Sco X-1, interaction with environment 2−73054

X-ray absorption
see also X-ray spectra/absorption
attenuation in interstellar space 2−62594
metal, hole correlation function, electron-phonon interaction 2−48167
nonlinear response of electrons in solid 2−61576
Ge-As solid soln., absorpt. and scatt. of X-rays by cluster defects and dislocation loops 2−77584
NaCl:Sr^{2+}. Z_1 generation, kinetics 2−84515
Si, perfect single cryst., linear absorpt. coeff., 78-292 K 2−80610

X-ray analysis *see Chemical analysis/X-ray; Crystal structure, atomic; X-ray crystallography*

X-ray astronomy *see X and gamma-ray astronomy*

X-ray characteristic temperature *see Specific heat*

X-ray crystallography
see also Debye-Waller factors
For results of structure analysis see Crystal structure, atomic
(hk) interferences linewidth, effects of preferred orientation 2−53627
absorption, statistical evaluation 2−83917
achondrites, Basaltic, diffraction analysis of pigeonites 2−58533
anomalous enhancement of transmitted intensity, asymmetric diffr. 2−53634
anti-phase domain mats., diffraction theory 2−67973
applications of recrystallized Al monocrystals 2−64611
automatic indexing by trial-and-error, method of X-ray powder patterns 2−64600
charge density determ. in crystals desirability of absolute scale 2−77535
crystal struct. analysis, mean squared atomic scatt. factors for all atoms, tables 2−53624
diffraction, appl. to materials science, review 2−64744
diffraction, review, (Jan 1070-Dec 1971' 2−53628
diffraction, solarisation phenomena 2−83911
diffraction in perfect single crysts., theory 2−67954

X-ray crystallography continued
dynamical theory of diffraction, equivalence of Darwin and Ewald-Laue methods 2−47294
heavy atom position determ., applic. to TMV 2−56621
history of development of direct methods 2−64612
intensity angular distrib. function, from size and form factors and Laue contrib. 2−74702
Laue diffraction in nearly perfect crysts., 111 and 440 reflections 2−71403
molecular cryst., valence struct. from diffr. data, phys. props. 2−64610
optical imaging description of process 2−77538
pole figures, theoretical model 2−67947
powder, granularity rel. to refl. X-ray intensity 2−74700
small angle X-ray scatt., absolute intensity meas., unified theory 2−74699
spot dimensions rel. to grain size of polycrystalline materials 2−71402
structure cosine seminvariants formulas for $\cos(\varphi+\varphi)$ 2−67950
structure factor detn. of single crystals with high secondary extinction 2−77534
teaching, introductory lectures 2−48961
tensor formulation and N-beam approx., dispersion surfaces and polarisation directions 2−67954
two-dimensional lattices, interference effects, preferred orientation influence 2−43541

apparatus
see also X-ray monochromators; X-ray spectrometers
alignment device for diffractometer and monochromator 2−47299
automated multiple specimens holder for X-ray powder diffractometer 2−83926
automated powder diffractometer, APD 3500 2−56622
automatic diffraction spectrograph for molecular biology 2−55201
baffle, low temp., for single crystal X-ray diffraction 2−58654
camera, convergence beam type, construction 2−74704
camera, high pressure, diffr. pattern recording, two film cassette 2−66872
camera, small angle, with glass blocks as monochromator and background radiation shield 2−60735
camera design for imperfections study 2−43545
cameras, precession, alignment fixtures 2−64608
camers, Supper and Stoe precession, consid. of optimum precession angle 2−64607
capillary support apparatus for use in glove bags and dry boxes 2−64604
collimation system, small-angle, role of Soller slits 2−64603
control system for step scanning powder diffractometer 2−43540
controlled humidity generator for X-ray struct. determ. of clay minerals 2−56623
cryostat for single cryst. analysis 2−43546
crystal cutting, error reduction method and apparatus 2−74705
Debyye-Scherrer and Guinier-de Wolff diffraction cameras, integrating 2−83925
diffraction patterns, device giving visual pictures 2−55337
diffractometer, Si(Li) semictor adaptation 2−47298
diffractometer attachment for elastic deform. obs. of polymers 2−43749
diffractometer attachment for high temp. obs. 2−77536
diffractometer attachment for rewinding wire specimens 2−43539
diffractormeter, liquid Na, static structure function and atomic density distribution 2−47301
display method contrast improvements for electron beam scanning system 2−63276
gas flame heating equipment producing temps. up to 2300°C for diffractometer 2−67800
goniometer, symmetrically moving θ-θ 2−53635
Guinier camera for single cryst. investigation, principles and applications 2−77539
heating stage for temps. 20-1000°C 2−60732
image intensifier for direct viewing and brief-time recording 2−56620
image intensifier for direct viewing and brief-time recording of crystallographic events 2−56620
for interatomic distance determ. from radial distrib. function, improvement 2−64605
powder diffractometer, computer controlled, on-line data processing 2−64609
proportional detector, position sensitive 2−80611
radiation hazards, safety suggestions 2−76081
retigraph, with pure precession motion 2−53631
review, Jan. 1970-Dec. 1971 2−53628
small-angle X-ray diffraction, optimal dimensions of pinholes 2−67953
URS-501M diffractometer for thin films, vacuum attachment 2−62907
URS-501M diffractometer for thin films, vacuum attachment 2−62907

calculation apparatus
computer applications 2−60748
pole figures, computer plotting using CDC 6600 and SC 4020 from X-ray crystal data 2−67978

calculation methods
83913
— 2−67970
— 2−67971
Σ_2 formula rel. to space group symmetry, non-centrosymmetric struct. determ. 2−67969
absorption correction by analytical method, algorithm improvement 2−67972
algorithmic language for intensity meas. 2−43569
atomic scattering factor, aspherical, computational aspects 2−77543
bis(picolinato)bis(allylthiourea)Cu(II), X-ray analysis and Patterson-Fourier and least-squares methods 2−71446
bis(picolinato)bis(thiourea)Cu(II), X-ray analysis and Patterson-Fourier and least-squares methods 2−71446
cell parameter determination from Debye photographs, choice of reflections 2−71421
computer program for symmetrified plane wave calc. 2−60747
counting time optimization in single crystal diffractometry, background counting, slewing times 2−67968

X-ray crystallography continued
- **calculation methods** continued
  - crystallite orientation distrib., refinement procedure, test. 2−80534
  - Debye-Scherrer lines of deformed crystals, profile analysis 2−53629
  - diffraction film indexing, applic. of reciprocal space lattice concept 2−50611
  - diffraction line deviation as measure of Scherrer eqn. broadening, curve fitting, computer program 2−77542
  - diffraction line profile correction, optimal soln. in deconvolution 2−67967
  - diffractometer data, optimization for min. average variance in electron density 2−83916
  - domains, one-dimensional antiphase, interpretation with non-integral half period, intensity calc. 2−53625
  - dynamical scattering amplitude of imperfect crystal equations 2−83912
  - fibre, mathematical problems 2−71405
  - fibrous systems, small-angle equatorial X-ray scattering, methods of extracting physical parameters 2−50616
  - Fourier analysis of line profiles for talc from sepiolite 2−64627
  - Fourier refinement methods 2−77531
  - Fourier series calcs., fast Fourier and trigonometric Fourier algorithms comparison 2−43570
  - fundamental system containing K-(poly)-gons, separation from vector set 2−53650
  - group concepts applied to simple organic structures 2−67974
  - indexing figure of merit definition 2−43543
  - inelastic scattering, from optically induced charge density oscills., calc. 2−83924
  - intensity angular distrib. function, from size and form factors and Laue contrib. 2−74702
  - intensity profile, harmonic analysis and doublet component extraction 2−74707
  - intensity profile, harmonic analysis and doublet component extraction 2−74707
  - for interatomic distance determ. from radial distrib. function, improvement 2−64605
  - lattice const. and error evaluation using Bragg-Brentano focussing diffractometer 2−47302
  - line broadening analysis, background separation, computer program 2−74714
  - martensite-austenite lattices, orientation relationships, application of statistical methods 2−43532
  - Olekhnovich polarization factor for mosaic crystals, comment 2−53633
  - oscillation type photographs, broadening of selective reflections 2−45199
  - Patterson function, probabilistic approach 2−53648
  - perpendicularity of X-ray beam and film, numerical method of checking 2−71401
  - phase determination, applic. of weighted phase sum formulas 2−53646
  - pole figures, computer plotting using CDC 6600 and SC 4020 from X-ray crystal data 2−67978
  - powder diffr. phase analysis, new algebraic conception 2−74715
  - probable reflection symmetry, determ. by counting statistics appl. to zeolite NaPl 2−83914
  - profile correction and calcs. before Fourier analysis, computer program 2−47303
  - silicate with complex cation, $4[Cu(NH_2CH_2CH_2NH_2)_2)_2]. Si_8O_{20}. 38H_2O$, 3-D Patterson synthesis 2−74753
  - small-angle X-ray scattering, numerical solution of integral equation applied to slit correction 2−56619
  - structure factor simulation and one-dimens. electron density calc., computer program 2−73268
  - structure soln. by Patterson heavy atom technique, FORTRAN programs 2−73267
  - thermal scattering, Model Q-function descrip., linear lattice approx. 2−53630
  - three dimensional density reconstruction from series of two dimensional projections 2−49047
  - variances and covariances of the anisotropic temperature parameters, derivation 2−56644
  - vector set analysis, peaks of arbitrary multiplicity, parallel vector method 2−53649
- **structures** *see Crystal structure, atomic*
- **technique**
  - alignment method for precession camera with monochromatic radiation 2−43548
  - anomalous transmission for dislocation obs., applic. to Si 2−71496
  - austenite-ferrite mixture, determ. of relative phase vol. by X-ray diffr. 2−71641
  - Buerger precession camera, alignment method and general eqns. describing the record 2−74701
  - convergence beam, advantages 2−74704
  - crystal cutting, error reduction method and apparatus 2−74705
  - crystal perfection, precise measurement 2−47297
  - dislocation Burgers vectors, interferometric determ. 2−77581
  - dislocation struct., studies by Borman topography 2−43631
  - doublet separation methods and influence on diffr. profiles 2−60734
  - extended X-ray absorption fine structure, appl. to amorphous struct. determ. 2−71283
  - fine crystalline structure from integral width of lines 2−56618
  - fine structure, limits on diffr. anal. 2−74697
  - grain size determ. in polycrystals, factors influencing diffraction patterns 2−60733
  - high resolution video display of topographs with divergent Laue method 2−83922
  - hot stage use with two-circle diffractometer for precise lattice parameter meas. 2−43542
  - Kossel line method, crystal fine structure 2−43536
  - Kossel method photographs, indexing, crystal lattice parameters 2−47296
  - lattice parameter meas. 2−47295
  - metal specimen prep. technique 2−43544
  - Moire fringes, visibility improvement using parallel X-ray beam 2−71404
  - order-disorder phenomena investigation, review 2−50991

X-ray crystallography continued
- **technique** continued
  - orientation sections in single crysts., prep. method 2−43547
  - orientations associated with sharp texture 2−43538
  - polarized hydrogen atom formalism use in refinement 2−43535
  - pole figures for crystallographic directions 2−43537
  - powder sample prep. in form of small diameter rod shaped specimen 2−74703
  - precession photography using monochromatic radiation, alignment technique 2−74698
  - review, Jan. 1970-Dec. 1971 2−53628
  - Schulz, for pole fig. determ., defocussing correction 2−50610
  - surface lattice deform. meas. using grazing incidence obs. 2−53545
  - topographic photography using conical cassette 2−43545
  - topography, applic. to diamond obs. 2−64613
  - topography studies of single crystals, transmission and reflection methods 2−60730
  - twin identification from intensity statistics 2−47184
  - twinning fault probability of metal coatings 2−50473
  - X-ray absorption edge, X-ray fluorescence and X-ray diffraction anal., computer applics. 2−64606
  - X-ray crystallographic, convergence beam type, construction 2−74704

X-ray diffraction
- *see also X-ray crystallography; X-ray scattering*
- amorphous system, static structure factor 2−61622
- anti-phase domain materials 2−67973
- asymmetric, equal inclination fringes, effects of lattice distortion, study on Si 2−77532
- balanced filter device, controllable attenuation, automatic beam stop 2−78711
- computer applics. at Oak Ridge National Laboratory 2−64606
- crystallographic events, image intensifier for direct viewing and brief-time recording 2−56620
- detector use, and kinetics of ordering of lipids in E. coli membranes, use of new detector 2−66251
- dynamic theory, for ideal cryst., equivalence of Darwin and Ewald-Laue methods 2−47294
- dynamical scattering amplitude of imperfect crystal equations 2−83912
- film indexing, applic. of reciprocal space lattice concept 2−50611
- gas flame heating equipment producing temps. up to 2300C for diffractometer 2−67800
- grain size determ. in polycrystals, factors influencing diffraction patterns 2−60733
- high pressure camera, diffraction pattern recording w. two film cassette 2−66872
- Kikuchi band detect and excess regions, calc. for Ni 2−60763
- line grating, possible violation of extinction law 2−52020
- line profile correction, optimal soln. in deconvolution 2−67967
- molecular force constants calculation from diffraction data 2−77043
- monitor methods, comparison of focusing and nonfocusing arrangements 2−83919
- multiple beam Borrmann effect, peculiarities in Ge 2−47330
- multiple Borrmann diffraction, excitation and absorption obs. in Ge 2−60736
- patterns, device giving visual pictures 2−55337
- review, instrumentation, appls. (Jan 1970-Dec 1971) 2−53628
- small angle, diffraction patterns, use of image converter for visualization 2−77537
- small-angle, optimal dimensions of pinholes 2−67953
- tensor formulation and N-beam approx., dispersion surfaces and polarization directions 2−67954
- URS-501M diffractometer for thin films, vacuum attachment 2−62907

X-ray diffractometers *see X-ray crystallography/apparatus*

X-ray examination of materials
- *see also Chemical analysis/X-ray; Radiography*
- − 2−56598
- − 2−71430
- − 2−60668
- alkali halide, higher anharmonic contribs. to diffuse X-ray scatt. 2−61059
- alkali halides, scatt. by F-centres, quantum theory 2−47444
- alloys, with different volume disparity between precip. phase and matrix, ageing 2−71634
- amorphous solid, binary, microsegregation 2−60570
- amorphous system, static structure factor 2−61622
- austenite-ferrite mixture, determ. of relative phase vol. 2−71641
- p-azoxyphenetole, oriented nematic phase, cylindrical atom distrib. 2−80441
- bis(2-imino-4-amino-4-methyl-pentane)nickel II bromide 2−71445
- bis(picolinato)bis(allylthiourea)Cu(II), X-ray analysis and Patterson-Fourier and least squares methods 2−71446
- bis(picolinato)bis(thiourea)Cu(II), X-ray analysis and Patterson-Fourier and least-squares methods 2−71446
- cantharidine, X-ray diffraction study, molecular bond lengths and conformation 2−68010
- carbonate crystals, natural rhombohedral, growth defects study by X-ray transmission topography 2−53732
- cellulose, cryst. state, effect of moisture 2−83962
- ceramics, texture and phases in spark plugs, e. probe anal. and X-ray diffr. study 2−71390
- chalcogenide glass, threshold and memory types, thermal effects 2−71917
- cholesteryl nonanoate and myristate in smectic-A, cholesteric and isotropic phases 2−67807
- colloidal suspensions and glasses, X-ray study under different collimation conditions 2−71285
- diamond, X-ray topographic studies 2−64613
- 2-dichloromethyl-4-(4- bromobenzyl)-5-(4-bromophenyl)-6-hydroxypyrimidine, cryst. struct. 2−64649
- 2-dichloromethyl-4-(4-chlorobenzyl)- 5-(4-chlorophenyl)-6-hydroxypyrimidine, crystallographic props. 2−64648
- diethyl ether, cryst. and mol. struct. at 128K 2−68011
- 2,3-dihydro-1,4-benzoxazepin-5(4H)-ones, cryst. struct. 2−56672
- DPPH film, organic free radical, vapour deposited 2−56598
- Ekco mineral analyser, radio-isotopic X-ray fluorescence, Cu and Zn in presence of Fe 2−81643

X-ray examination of materials continued
- estradiol-urea complex., struct. determ. by two-dimens. struct. invariants 2−53686
- film, thickness meas. glassy halo obs. 2−64557
- film surface density meas. by proton excited X-rays, Fredholm expression 2−80542
- garnet, bubble domain, epitaxial film, effect of substrate defects on struct. 2−47092
- GdB_6, polycrystalline, existence of single phase, of cubic symmetry 2−72486
- germania, vitreous, structure obs. 2−53534
- glass:Nd, phase separation degree, rel. to optical props. 2−57372
- glass, aluminoborosilicate, B coordination number, heat treatment effects, obs. 2−64528
- glass, metal-containing, phase comp., sintering temp. depend. 2−50862
- graphite, porous, crystallite size, interplanar spacing, and anisotropy 2−50926
- graphite single crystal, diffr. during shock wave compression 2−56646
- graphite-SiO_2 system, phase diagram determ. 2−43930
- growth defects characteriz. by topography 2−47216
- h.p. device for thermodynamic investig. of metal/hydrogen systems 2−77715
- HTR fuel elements, heavy metal particle distribution 2−67360
- ice, hoar crystals forming on cooling pipes, X-ray Laue examination 2−74732
- intensity angular distrib. function, from size and form factors and Laue contrib. 2−74702
- lattice vibrations, anharmonicity estimation from X-ray interference intensity coeff. 2−54017
- liquid crystal, A-type smectic, scatt. intensity analysis 2−43327
- liquid crystal, cylindrical distrib. functions 2−83765
- liquid crystal, smectic, polymorphism, D and E modifications 2−50327
- lumbago-sciatica syndrome 2−55253
- magnetite, crystalliz. from high Fe glass 2−54329
- MBBA, small angle scatt., near nematic-isotropic transition temp. 2−43328
- mercury picramate, cryst. data, orthorhombic cell dimens. 2−74754
- metal coating, twinning fault probability 2−50473
- metal spheres, internal displacements meas. method 2−77644
- N-methyl-4-brom- benzamide, crystal structure 2−64651
- minerals, grinding, change in props. 2−68148
- Moire fringes, visibility improvement using parallel X-ray beam 2−71404
- m-nitroaniline, crystal structure rel. to linear electro-optic props. 2−72271
- nondestructive monitoring for optimization of in-service performance tests 2−60924
- nylon, solution- grown crystals, combined wide-angle and low-angle X-ray diffraction patterns 2−50630
- nylon 6, crystallization from melt, X-ray diffraction study of α and γ forms 2−74605
- Olekhnovich polarization factor for mosaic crystals, comment 2−53633
- organic ionic salt mesophases, struct. behaviour 2−71158
- orthophenylene diamine dihydrochloride, structure study 2−71449
- p-n junctions, X-ray image of internal structure 2−81112
- particle size and X-ray diffraction profiles, application of Wilson's variance-range analysis 2−64601
- pentaerythritol, molecular crystal, thermal expansion obs. 2−74995
- Permalloy film, thickness meas., rel. to demag. field and mag. moment 2−61539
- phase comp. analysis by X-ray diffr., verification of Ordway elemental phase analysis theory 2−74725
- plagioclase, at. scatt. factor satellite intensities, reciprocal space distrib. 2−53678
- poly-N-methyllaurolactam, fully methylated nylon 12, crystallinity 2−83846
- polyamides, chain-folded lamellar crystals, structure analysis 2−47359
- polycrystalline metals, slow elastic plastic deformation with micro stresses 2−76260
- polyethyleneterephthalate fibres, determ. of degree of crystallinity by X-ray methods 2−74607
- polyimide, aromatic, secondary dynamic dispersions 2−83366
- polymer, submicroscopic crack formation, under load, small angle scatt. obs. 2−68108
- polymers, X-ray diffraction profiles, applic. of variance analysis 2−64602
- polytetrafluoroethylene, cryst. struct. at high press., transition at 4.5kbar 2−83849
- potassium biphthalate, lattice consts. and space group 2−47357
- powder, granularity rel. to refl. X-ray intensity 2−74700
- protein mol. wt. by X-ray diffr., teaching techniques 2−82097
- rare earth compounds with zircon struct.. temp. dependence of lattice parameters 2−84215
- rare earth monchalcogenides, compressibility determ., up to 300 kbar 2−68297
- rare earth silicides, struct., 20-1200°C 2−68005
- rare earth sulphotelluride solid solns., high temp. homogeneity regions 2−53905
- reference list, materials studied by anomalous X-ray scatt. 2−60749
- review, Jan. 1970-Dec. 1971 2−53628
- rutile powder X-ray line profile analysis of particle size and strain 2−74831
- seeding aerosol particle size distrib. determ. method 2−62246
- silica, vitreous, structure obs. 2−53534
- soil, density obs., models 2−61964
- solid solution film thickness determ. 2−82125
- solid solutions, random binary. diffr. intensity and model of interatomic force equil. 2−74965
- solid solutions, random binary, diffr. intensity and model of rigid atoms in close-packed arrangement 2−77768
- solutions, scatt. by fluctuons 2−71151
- spinel solid solution, scatt., calc. using method of cluster components 2−74719

- spinel solid solution, scatt., calc. using method of cluster components 2−74719

X-ray examination of materials continued
- steel, ε-carbide phase form. and struct. 2−43844
- steel, austenitic stainless, rel. to stress corrosion testing, mech. behaviour 2−50765
- steel, α- martensite decomp., second stage 2−50938
- steel, sheet, cold rolled, annealed, grain growth 2−47621
- steel, stainless, Cr depletion of surface by vacuum annealing 2−47075
- steel, stainless, hot dip Al coated, alloy layer struct. and composition 2−56937
- steel, transformer, hot rolling, effect of S content on recrystn. 2−47586
- steels, structural, effect of C, Mn and Si on austenite content 2−74875
- stress diagrams, residual stresses in test specimens 2−78755
- structure and dynamics of crystals, new exptl. methods 2−74706
- talc from sepiolite, Fourier analysis of line profiles 2−64627
- texture goniometer, adjustable specimen holder 2−83927
- texture transmission photographs, effective thickness of foil sample 2−41447
- thiourea, grown by evaporation, defect struct., X-ray topography obs. 2−74769
- Ti alloy VT14, phase transf. during heating and cooling 2−68201
- transmission topographic goniometer, improvement of translation stage 2−80612
- zeolite, NaPl, probable refl. symmetry, determ. by counting statistics 2−83914
- zirconia ceramics, phase analysis by X-ray analysis, matrix method, polymorph technique 2−80879
- Ag-Mn-Al alloy, high coercivity, struct. of ferromag. precip. 2−43821
- Ag-Zn(41 at%) alloy, deform. induced martensite 2−80846
- Ag, Compton effect scatt. power, thermal vibr. freqs. 2−68213
- Ag alloy, cold worked, X-ray line profile analysis, instrumental broadening correction 2−64636
- Ag film, Poissons ratio, X-ray obs. 2−67904
- AgI-NaI-H_2O system, hydrous phase structs. 2−47314
- Ag_2Se, polymorphic transitions 2−64809
- Al-4%Cu alloy, ageing, effects of additional elements56910 2−56910
- Al-Mg-Zn alloy, decomp., phase transform. 2−43911
- Al-(3 at.%)Mg alloy, high 2−74835
- Al, dislocations, multiplication mechanism, near surface, Lang X-ray obs. 2−43635
- Al, multilayer film structures, internal stresses obs. 2−43475
- Al, single crystal, diffr. during shock wave compression 2−56646
- Al, solid solubility and diffusion of Ga, 100−310°C 2−74810
- Al, thermal vibr. freqs., scatt. obs. 2−61073
- Al, X-ray scatt. from surface rel. to polishing 2−74617
- 9 Al_2O_3-AlN, periodic antiphase domain struct. 2−50618
- α-Al_2O_3, cleavage on $\{10\bar{1}1\}$ planes 2−74657
- Al_2O_3 amorphous anodic films, partial model for structure from X-ray scattering data 2−47100
- As_2Se_3-As_2Te_3(Tl_2Se)(Sb_3Se_3)(As_2S_3) glass, struct. rel. to e.s.r. 2−61734
- BN, wurtzite-like, fine struct. determ. 2−75026
- B_2O_3 glass, hydrostatically compacted, electron radial distrib. obs. 2−53527
- BP-P system, h.p. phase equil. 2−50956
- Ba_2MReO_6, (M=Mn,Re,Co,Ni), perovskites, characteriz. 2−50876
- $BaNaP_3O_9$, space group. cell constants 2−67987
- $BaTiO_3$, dielec. const. changes after electron or gamma irrad. 2−65047
- $BaTiO_3$, distortion of cry. lattice and effect of admixed nickel 2−71406
- Be, monocrystals, growth by Czochralski technique, obs. of cryst. perfection 2−47262
- Bi-In(Sn)(Tl) alloys, induced high press. phases 2−74926
- $BiFeO_3$, lattice parameters, thermal expansion, elec. Curie temp. 2−47317
- Bi_2Te_2Se, 7.5 MeV proton irrad. induced disorder 2−64653
- $Bi_4Ti_3O_{12}$, crystal struct. determ. 2−71425
- C, glassy, pore struct. 2−47056
- C, various forms, comparison of intensity ratios of 002 and 004 diffraction lines 2−64633
- C effective temperature factor 2−53655
- C fibre, PAN-based, fine struct. 2−53948
- C fibre, produced from lignin and PVA, void obs. 2−47667
- $(C_3O_2)n$ polymer, X-ray crystallographic examination rel. to colouring of Martian surface, laboratory studies 2−78542
- Ca-Si system, phase diagram determ. 2−71700
- $2CaO.Mn_xFe_{2-x}O_3$ ($O \leqslant x \leqslant 0.5$), lattice parameters, temp. depend. 2−43644
- Cd_3As_2-2CdTe system, phase diagram determ. 2−47708
- $Cd_2(Ge_2O_6)$, from hydrothermal synthesis, cryst. struct. 2−74687
- Cd_3P_2-2CdSe system, phase diagram determ. 2−47708
- CeS, product from $Ce_2S_3 + CeO_2$ + coke reaction 2−47656
- Ce_2Se_3-GeS_2 system, phase diagram determ. 2−61043
- $Ce_2Si_2O_7$, lattice parameters 2−48220
- Co-C solid solution, struct. determ. 2−50830
- Co-Ti alloy, solid soln. decomp., obs. 2−56933
- Co_2MnSn, Heusler ferromag. alloy, atomic struct. 2−48075
- Co_3Sn_2, superlattice struct. 2−47319
- Cr-I system, phase diagram and phase identification 2−71701
- Cr-Ni-B system, isothermal section at 800°C 2−61044
- Cr dendrites, galvanostatically obtained from CrO_3-H_2SO_4-dimethylsulphoxide-H_2O solution 2−47135
- CrH_x, electrodeposited, f.c.c., h.c.p. → b.c.c. transform., heating time and temp. effects 2−47682
- Cr_2O_3-Ti_2O_3 solid solution, mag. ordering study 2−48104
- Cr_2O_3-V_2O_3 mixtures, powder pattern detn. of Cr_2O_3 and V_2O_3 2−74728
- Cr_2O_3-V_2O_3 solid solution, mag. ordering study 2−48104
- CrP_4, cryst. struct., synthesis, props. 2−53659
- $CsFeF_4$, planar antiferromagnet, crystal struct. 2−65180
- γ-$CsHCO_3$, cryst. struct. 2−43579
- $CsICl_4$, lattice parameters 2−71427
- $CsPr(MoO_4)_2$, crystal struct. and thermal stability 2−74729
- Cu:S, Bragg peaks, temp. effects 2−71310

X-ray examination of materials continued
Cu-Au alloys, side bands of fundamental reflections and diffuse superstructure lines, detection 2−64614
Cu-Au bimetallic film, interdiffusion, X-ray obs. 2−60828
Cu-Ga alloy, cold-worked, defect obs. 2−80861
Cu-Ge alloy, liquid, struct. X-ray diffr. interference functions 2−83774
Cu-Ge solid soln. single crysts., growth and characteriz. 2−53614
Cu-In alloy, liquid, struct., X-ray diffr. interference functions, 700°C 2−83775
Cu-P-O system phase relations 2−50962
Cu-P system, constitution diagram determ. 2−61045
Cu-Zn-Mn system, rel. to phase diagram detn. 2−50963
α-Cu-16 at.%Al alloy, spherical single crysts., struct. anomalies 2−71429
Cu, charge density form factor determ. 2−84251
Cu, Ni diffusion coeffs. 2−53761
Cu, Pt diffusion study 2−56756
Cu alloy, cold worked, X-ray line profile analysis, instrumental broadening correction 2−64636
Cu film, electroplated and vapour deposited, struct. rel. to annealing 2−77497
Cu texture transition mechanism during rolling 2−47323
Cu wire specimens, plastic deformation and static lattice distortion determinations 2−53890
$CuAgTe_2$, synthesis and struct. detn. 2−71431
$Cu_{80}Au_{20}$, application of model of structure periodically modulated in three dimensions 2−50615
$CuFe_2O_4-CuGa_2O_4$ system, phase diagram 2−71702
$CuLi(PO_3)_3$, space group, lattice parameters 2−67989
Cu_2Se, $\alpha\rightarrow\beta$ phase transform 2−64811
$DyVO_4$, quadratic-orthorhombic transition 2−43915
Fe-Al-C alloy, martensite cryst. struct. change, −196 to 20°C 2−80766
Fe-Al alloy, diffuse X-ray scatt. and temp. depend. of sp. ht. 2−56654
Fe-Ca olivines, synthesised minerals 2−47325
Fe-Co(Ni)-Ti-Al alloy, solid soln. decomp., obs. 2−56933
Fe-Ga alloys, magnetic props, and Mossbauer investigations 2−84416
Fe-Pd-H system, phase diagram determ. 2−74953
Fe_2MoO_4, spinel, X-ray and neutron diffraction studies 2−84414
γ-Fe_2O_3, vacancy distrib. over tetrahedral and octahedral sites 2−60786
γ-FeOOH, lepidocrocite, crystal struct. and mag. props. at temp. of conversion to α-Fe_2O_3, hematite 2−57287
6α-fluorocortisol, struct. determ. by two- dimens. struct. invariants 2−53686
Ga-As-Te system, GaAs-Te polythermal section determ. 2−61047
Ga-As-Zn system, GaAs-Zn polythermal section determ. 2−61046
GaAs-As_2Te_3 system, rel. to phase diagram determ. 2−47713
GaAs, grown from gas phase, cryst. morphology 2−56656
GaP, characterization of epitaxial layers on insulating substrates 2−47111
Ga_2Te_3-As_2Te_3 system, rel. to phase diagram determ. 2−47713
Ge-Sr system, phase diagram determ. 2−47714
Ge, absorption and excitation in multiple Borrmann diffraction 2−60736
Ge, amorphous, struct., extended X-ray absorpt. fine struct. determ. 2−71283
Ge, anomalous transmission pattern, effect of simultaneous refl. 2−53662
Ge, Laue case of X-ray diffraction in nearly perfect crystals, 111 and 440 reflections 2−71403
Ge, liquid, structure 2−60424
Ge, peculiarities of multiple beam Borrmann effect 2−47330
Ge, refractive index, interferometric determ. 2−72256
Ge film, amorphous, small angle scatt., struct. obs. 2−60661
Ge films, total refl. meas. of density 2−74630
GeO_2, amorphous, struct., extended X-ray absorpt. fine struct. determ. 2−71283
GeO_2, glassy, struct., small-angle scatt. obs. 2−43453
Ge_xS_{1-x} alloys, radial distrib. studies 2−53536
GeSe, amorphous, struct., extended X-ray absorpt. fine struct. determ. 2−71283
$Ge_{0.17}Te_{0.83}$, amorphous, radial distrib. functions 2−56548
Ge_xTe_{1-x} alloy, amorphous, radial distrib., structure and bonding 2−60575
GeTe−Bi solid soln., regions of existence at 250, 400, 500 and 600°C 2−53888
^3He, b.c.c., thermal excitations 2−43434
Hf-Nb-B alloy, phase equilibria 2−43912
$HgCr_2Se_4$, spinel structure formation, X-ray diffract. study 2−77563
$Ho_3Fe_5O_{12}$ garnet, cell parameters, X-ray powder data 2−74745
KBr, scatt. from displacement field of point defects 2−60787
KCl, sylvite, thermal oscillation freqs., 295, 80 and 5K 2−64835
$KCuF_3$, stacking disorder obs. 2−77569
$KFe(CrO_4).2H_2O$, space group, lattice parameters 2−67991
$K_2H(IO)_3)_2Cl$, cryst. struct. 2−53665
$K_2SiF_6.Na_2SiF_6$, cryst. data 2−74734
$LaTaO_4$, cryst. struct. 2−53669
$LiAl_5O_8:Fe^{3+}$, powder diffraction studies of ordered and disordered phases 2−48253
LiF, neutron irrad., defect obs. 2−80660
LiF, spark discharge induced damage 2−68013
LiF single crystal, diffr. during shock wave compression 2−56646
$LiH_3(SeO_3)_2$, ferroelec., thermal expansion rel to band arrangement, -150 to +25°C 2−68253
$LiMn(PO_3)_3$, crystallographic data 2−64641
$Li_2Mn(PO_3)_4$, crystallographic data 2−64641
Li_2O-SiO_2 glass, phase separation and crystn. 2−56560
Li_2TiO_3 crystal struct. determ. 2−71425
Lu-H(D) system, α-phase characts. 2−77749
Mg-Mn ferrites, electronic struct. of Mn and Fe ions 2−47182
MgF_2, texture of KO-1 optical ceramic 2−70042
MgO, plastic deform. during cleavage fracture 2−71570
$6MgO.As_2O_5$, Mn activated phosphor, flux grown crystals, crystal struct. 2−43525
$MgSiF_6.6H_2O$, phase transition at 25°C, cryst. struct. of low temp. form 2−67996

X-ray examination of materials continued
$Mg_yU_{1-y}O_{2-x}$, structural analysis by X-ray and electron microscope meas. 2−47336
Mn-Zn system, phase diagram detn. 2−57032
MnBi film, props., struct., domain struct. 2−44263
$Mn_xHg_{1-x}Te$ films, Hall coeff., Hall mobility and electrical condutivity 2−71885
$Mn_2(PO_4)Cl$, cryst. struct. 2−67997
$Mn_2(PO_4)F$, cryst. struct. 2−67998
MoP_4, cryst. struct., synthesis, props. 2−53659
NH_4Br, allotropic transform. kinetics 2−54008
NH_4Br, diffr. pattern, diffuse rods 2−80893
NH_4Br, order-disorder transition, crit. scatt. obs. 2−47699
β-$NH_4Fe(CrO_4)_2$, space group, lattice parameters 2−68000
γ-Na_2BeF_4, struct. refinement, high temp. thermal expansion 2−61109
$NaCl:Cd^{2+}$. X-ray photographs for dissolution of precipitates study 2−83844
$NaNO_3$, phase transition, diffr. obs. 2−65048
$NaNbO_3$, anisotropic diffuse X-ray scatt. and phase transitions 2−71715
$NaNbO_3$, dielec. const. changes after electron or gamma irrad. 2−65047
Na_2O-Al_2O_3-SiO_2 glass, X-ray diffraction study 2−60585
$NaTh_2(PO_4)_3$, struct., rel. to ferroelec. props. 2−54237
Nb:H, X-ray diffr. pattern, anomalous line broadening due to H 2−64642
Nb-H system, phase diagram, 80-500 K 2−77756
Nb, deformed, angle and wave depend. of diffr. linewidth 2−43625
$Nd(BO_2)_3$, cryst. struct. 2−74738
Nd_2NiO_4, monoclinic to tetragonal transform. 2−77750
Ne, high purity crystalline, equilibrium vacancy formation and self-diffusion 2−71470
Ne, solid, Debye temp. 2−47753
Ni:Pb, Bragg peaks, temp. effects 2−71310
Ni, anomalous dispersion correlation close a K-absorption edge 2−60764
Ni, deformed, angle and wave depend. of diffr. linewidth 2−43625
Ni, Kikuchi band defect and excess regions calc. 2−60763
Ni hexamethylenedithiocarbamate with M-S bonds, X-ray struct. study 2−71448
$NiCr_xMn_{2-x}O_4$, spinel, atomic and cation distrib., lattice distortion 2−74740
Ni_3Fe, long range order parameter 2−60984
$NiFe_{0.8}Cr_{1.2}O_4$, ferrite, structural transition at mag. transformation obs. 2−72201
Ni_2MnSb, Ni_2MnSn, Heusler ferromag. alloys, atomic struct. 2−48075
NiO, mag. superlattice peaks 2−44307
$Ni(OH)_2$ powder, crystallite struct. from X-ray diffr. profiles 2−74739
$NpPd_3$, cubic and hexagonal phases, unit-cell and X-ray powder data 2−64644
$(Pb,La)(Zr,Ti)O_3$, phase boundary and defect struct. 2−56968
$Pb_{1-3x/2}La_xZr_{0.65}Ti_{0.35}O_3$, phase transitions 2−57245
$Pb(Mg_{1/3}Nb_{2/3})O_3$ rel. to formation processes in the solid state reaction 2−77560
PbTe-UTe system, phase diagram determ. 2−47717
$PbTiO_3$, dielec. const. changes after electron or gamma irrad. 2−65047
$PbZrO_3$, dielec. const. changes after electron or gamma irrad. 2−65047
β-Pu, oxidation hot-stage X-ray diffr., microtopography, and thermogravimetric obs. 2−54544
$Pu(MoO_4)_2$-$Na_2MoO_4(Li_2MoO_4)$ system, scheelite phase obs. 2−71694
rare earth elements, polymolybdates, $Ln_2O_3.4MoO_3$ type, classification into four structural groups 2−83838
RbBr(Cl)(I), thermal expansion and Debye temp. 2−61111
$Rb_3UO_2F_5$, structure determ., X-ray examination of powder and twinned crystal samples 2−47343
$Rb_2UO_2F_4.H_2O$, space group, lattice parameters 2−68004
Re-Al(Si)-B systems, phase diagram determ. 2−64822
Rh-Mn-Sb system, $C1_b$ type alloy, lattice parameters 2−65156
RuO_2 film 1-5 μm thick 2−47123
Se film, rolling texture determ. 2−64574
Si-C system, phase relations 2−50972
19 at.%Si-Te alloy, amorphous struct.53515 2−53515
Si, asymmetric diffr., effects of lattice distortion on equal inclination fringes 2−77532
Si, bonding electrons, anharmonicity, and temp. depend. of forbidden (442) refl. 2−83885
Si, dislocation struct., hydrostatic press. effect 2−47419
Si, dislocations, moving, obs. by X-ray topography 2−77585
Si, electron momentum distrib., Compton profile obs. 2−57128
Si, ion implanted, lateral strains, X-ray topographic obs. 2−80704
Si, lattice defects, comparative study of topographic methods 2−47405
Si, lattice distortions due to scratching 2−43626
Si, lattice parameters rel. to thermal expansion 2−47757
Si, refractive index, interferometric determ. 2−72256
Si, thermally oxidized, X-ray topographic study of small dislocation loops 2−64669
Si planar diodes, elec. props. rel. to lattice defects 2−47944
SiC-B alloy, phase composition rel. to press., 50-60 kbar 2−53996
Si_3N_4-AlN-Al_2O_3 system, solid soln. obs. 2−43823
SiO_2-Al_2O_3 glass, crystallization obs. 2−53542
SiO_2, vitreous, struct., random network theory validity 2−47054
SmC_x characterization 2−71653
$Sm_3Fe_5O_{12}$, garnet, cell parameters, X-ray powder data 2−74745
Sn-Bi-As system, Sn_4As_3-Bi-SnAs subsystem, phase equilib. 2−74942
Sn, dislocation generation at single cryst. surface 2−47083
SnO_2-TiO_2 mixed crystals, exsolution obs. 2−74746
Sn_2PO_4Cl, lattice parameters, space group, powder data 2−43588
SnS_2-Na_2S system phases, crystallographic parameters 2−83952
SnTe-UTe system, phase diagram determ. 2−47717
$Sr_{2-x}K_{1+x}Nb_5O_{15-x}F_x$, ferroelec. tungsten bronze struct. 2−51198
$SrLiTa_2O_6F$, pyrochlore struct. obs. 2−74689
$SrO.2Al_2O_3$, refined cryst. struct. 2−68007

X-ray examination of materials continued

- SrSi$_2$, cryst. struct., space group, cryst. class O(432) 2−68006
- SrTiO$_3$, dielec. const. changes after electron or gamma irrad. 2−65047
- SrUO$_4$ structure determ. using Hagg-Guinier camera, analogy with BaUO$_4$, calc. of interatomic distances 2−77558
- Ta-Cr-B alloy, phase equilibria 2−43912
- TbAsO$_4$, crystallographic distortion at T<26K, transition, X-ray diffr. obs. 2−84142
- Tb$_{0.167}$Fe$_{0.633}$Al$_{0.20}$, Th$_6$Mn$_{23}$ struct. type, X-ray powder diffr. obs. 2−64645
- TbVO$_4$, quadratic-orthorhombic transition 2−43915
- ThC, ThS, cleavage surface of crystals synthesised by electron beam melting 2−53620
- ThCN, cryst. struct., X-ray and neutron powder diffr. 2−53681
- ThN-ThO$_2$-Th system, phase behaviour 2−50977
- ThSiO$_4$, atomic positions 2−68008
- Ti-Al alloy, cold-worked 2−80860
- Ti alloys, β→ω phase transform. 2−68204
- TiC-WC, short-range order, heat treatment and quenching effects 2−84072
- TiS, thermal expansion, 25-1300°C, powder techniques 2−54062
- Tl-Se equimolar mixture, reactivity study 2−53771
- Tl$_2$CrO$_4$, cryst. struct. 2−60766
- U-O system, oxidation equilib. study 2−44487
- (U-Pu)C, two-phase mixed carbides, quantitative analysis by X-rays 2−64626
- (U-Pu)$_2$C$_3$, two-phase mixed carbides, quantitative analysis by X-rays 2−64626
- U minerals, preparation for fluorescence measurements, pressed fused disc method 2−65586
- UC, oxidation in liq. Na with small O content 2−51452
- UC, US, cleavage surface of crystals synthesised by electron beam melting 2−53620
- Uo$_2$-PuO$_2$ mixed fuels, advanced characteriz. 2−52870
- VO$_2$, twinned crystal transformation to tetragonal phase 2−47698
- V$_2$O$_3$, band struct. below Fermi level, X-ray photoelectron spectra obs. 2−61193
- VO$_2$−NbO$_2$ system, phase diagram determ. 2−75101
- YAlO$_3$:Nd^{3+}, high temp. phase instability 2−74958
- YD$_3$, crystal struct. obs. 2−74752
- Zn single crystal, oriented, surface morphology developed during sublimation 2−53558
- ZnS, hollow cryst., grown by pulling sealed tube method, polytypical struct. obs. 2−43527
- ZnS, polytypes, high-order, identification and reliability of results 2−56670
- ZnSO$_3$.2H$_2$O structure, Patterson and Fourier synthesis 2−60770
- ZnSe, grown from vapour phase under controlled partial press. 2−64594
- Zr-Al dilute alloy, ordering and stacking faults 2−47354
- Zr-O α solid solution, interstitial O atom arrangement 2−71443
- Zr alloys, β→ω phase transform. 2−68204
- ZrO$_2$-Y$_2$O$_3$ system, phase diagram above 2000°C 2−61049
- ZrO$_2$, calcia-stabilized, destabilization by ZrB$_2$ 2−50902
- ZrO$_2$, monoclinic-tetragonal inversion, effects of detonation shock wave 2−74946
- ZrSiO$_4$, thermal expansion anisotropy, compressibility anisotropy 2−54064
- Zr$_2$Si$_2$Se$_2$, nonstoichiometry obs. 2−43505
- ZrTe$_2$, nonstoichiometric phase, struct., homogeneous phase limit 2−60772

liquids

- alkane monoiodide solutions, quasiliquid crystal form 2−50318
- alloy, diffuse Laue-scatt. and prepeaks in partial struct. factors 2−53391
- bibliography to 1971, 900 refs. 2−64436
- dielectric, motion of condensed matter formed by electric spark 2−46876
- melt, binary, microsegregation 2−60570
- metal, struct., problems of investigation, short range order models 2−46923
- metals, X-ray diffr. apparatus 2−74516
- very high pressures, X-ray diffraction studies along melting curves 2−67799
- water, second order fluctuations in particle no., integration over X-ray scattering interactions 2−74517
- Al, ion-ion pot. calc. from diffr. data 2−50315
- Al$_2$O$_3$, molten, surface tension, density, volume change on melting 2−80465
- Cr$_2$O$_3$ molten, surface tension, density, volume change on melting 2−80465
- H$_2$SO$_4$ 100%, determ. of molecular density correlation function and mean amplitude variation, geometric model 2−67801
- Hg-In alloy, partial struct. factors and atomic distribs. 2−64437
- Hg-Tl alloy, partial struct. factors and atomic distribs. 2−64437
- Hg, interference functions temp. range 50-150C 2−67802
- Na, coherent X-ray diffraction patterns at very high pressures, along melting curve 2−67803
- Na, static structure function and atomic density distribution 2−47301
- Sm$_2$O$_3$ molten, surface tension, density, volume change on melting 2−80465

microstructures

see also Crystal structure/microstructure

- : 2−84096
- — 2−68027
- — 2−56591
- alkali borate glass containing Fe, struct. 2−65230
- anti-phase domain mats., diffraction theory 2−67973
- α-brass, recrystn. texture 2−68139
- carbons, isotruxene 2−61023
- co-existing phases, volume fraction detn. 2−56645
- deformation studies using a combination (synenergy) method 0f X-ray line profile topography and trans. e. microsc. 2−8242
- films, diffusion zones, composition profiles and diffusion generated substructure 2−56585
- fluorite, natural 2−80669
- grain size, very fine, diffracted power obs. 2−56958
- graphite, artificial, anisotropic and isotropic, struct. distrib. 2−53972

X-ray examination of materials continued

microstructures continued

- graphite from isotruxene carbons 2−61023
- Guinier Preston zone, size effect on X-ray diffusion near Bragg spots 2−47300
- metal fibre/refractory oxide matrix, composites, growth and characterization 2−56990
- metals, deformed polycrystalline, influence of hydrostatic pressure soaking on structural change 2−84127
- metals, polycrystalline and monocrystalline sheet specimens, changes in misorientation during plastic deformation 2−84046
- microcline, shock deform. struct. 2−61843
- naphthalene thermoelectrets, X-ray diffraction structural studies 2−65075
- periclase brick, hot fracture surface obs. 2−77661
- polyethylene, diffraction relaxation 2−43674
- polyethylene, injection moulded specimens, crystallite orientation determ. 2−64797
- polyethylene films, changes in crystal orientation with time following stretching 2−83381
- polyimide films, uniaxially drawn, study of orientation by X-ray diffraction analysis 2−43677
- polypropylene, drawn and annealed, determ. of crystallite size from breadth of equatorial X-ray reflections 2−71288
- polypropylene, effects of pre-melting conditions on crystalline form 2−47066
- polypropylene, quenched and annealed samples, wide-angle X-ray scattering in neck region 2−71572
- single crystal, containing additions, substructure obs. 2−71474
- single phase solid solution, determ. of composition profiles and diffusion generated substructure 2−74696
- steel, carbon fraction of retained austenite detn. 2−56645
- steel, high C, low temp. tempering, retained austenite 2−74883
- steel, high-carbon Mn type, lattice orientation of α-martensite 2−43843
- steel, low-C, martensite, surface plastic deform. 2−80769
- steel, martensitic, rel. to low-cycle fatigue 2−43715
- steel, metallography 2−53892
- steel, transformer dislocation density 2−43636
- steel stainless, high- tensile, cryst. struct. determ. 2−77672
- steel wire, annealing struct. of heavily drawn pearlite 2−64760
- steels, stainless, phase state determ. method at rolling temps. 2−84091
- tetraphenyl tin and isomorphs, defect struct. determ. 2−53731
- thermal interphase microstresses 2−43908
- thermal microstresses of multiphase alloy, direct x-ray photography method 2−53884
- Ag-Ge alloy, laser irrad., metastable phase formation 2−50929
- Ag-Si alloy, deformed by tension and rolling, diffr. obs. 2−80845
- Ag-Sn alloys, stacking fault probability and energy, diffr. data interpret. 2−50678
- Ag, rolling texture form. mechanism 2−60972
- Ag single crystal films, dislocation density 2−74627
- Al-Ag, Al-Zn type alloys, GP zone composition by relative intensitives of diffuse effects 2−68035
- Al-Ag alloy, precipitation process study 2−84133
- Al-Mg and Al-Mg-Zn alloys, preprecip. zone obs. 2−53885
- Al-Mn alloy, structural features of a plane strip obtained directly from melt by Stepanov method 2−50821
- Al-Zn alloys, X-ray central diffusion study of Guinier Preston zones after quenching 2−64632
- Al-6.8%Zn alloy, GP zones rel. to diffusion, and effects of Ag, Si, or Mg 2−56753
- Al, deformed, grain boundaries, rel. to resistivity changes 2−53744
- Al, diffusion, review 2−83992
- Al, dislocation multiplication mechanism 2−80679
- Al, low disloc. density crystal, anomalous X-ray transmission due to subtropographic defect clusters 2−47395
- Al, shock-wave compressed, X-ray Debyegram recording 2−84045
- Al alloy, NS.5, effect of preferred orientation on X-ray stress meas. 2−71643
- Al crystal, dislocation config. as result of thermal treatment 2−47411
- Al foil, mosaic block misorientation during creep 2−74848
- Al sheet, rolling and annealing texture of outer layer 2−64756
- Al$_2$O$_3$-ZrO$_2$-SiO$_2$ fused grain refractories, rebonded, characteriz. 2−53926
- αAl$_2$O$_3$, detn. in alumina crystallites 2−56647
- Al$_2$O$_3$, sapphire, dislocation tangle formation 2−80703
- As$_2$Se$_3$, vitreous, effects of group III A element dopant on physical props. 2−61300
- Au films, internal strain and crystallite size rel. to spitaxial 2−50485
- BaTiO$_3$-BaGeO$_3$ system phase equilibria 2−84105
- BaTiO$_3$ surface domain reorientation prod. by abrasion and annealing, X-ray diffraction exam. 2−80544
- Be, deformation obs. by synergy of TEM, selected area X-ray topography and line profile analysis 2−56791
- C, defect theory of struct. 2−53729
- C, glassy, small-angle scatt. obs. 2−53530
- C, glassy 2−53531
- C, porous, multiple X-ray small-angle scatt. 2−53978
- C, pyrolytic, highly graphitized, fault obs. 2−60752
- C, pyrolytic and fibre, (hk) interferences linewidth, effects of preferred orientation 2−53627
- C fibre reinforced, X-ray preferred orientation obs. 2−53949
- CaCO$_3$, synthetic calcite, dislocations obs. 2−47412
- CaSo$_4$2H$_2$O, symmetry of SO$_4$ ion 2−64635
- Cd$_3$Mg, two-phase region, morphology, habit planes and orientation relns. 2−61042
- CdS, quenching under pressure of metastable phases, low temp. high pressure X-ray camera 2−84152
- Cu-Al alloy, plastically deformed, conc. heterogeneities on stacking faults 2−50681
- Cu, Burgers vector rel. to external geometry at initial deform. stage 2−50673
- Cu, grain topography in early stage of plastic flow 2−47500
- Dy, recrystallization obs. 2−80773
- Fe-Ni-C alloy, martensite, surface plastic deform. 2−80769
- Fe-Ni alloys, deform. martensite obs. 2−43838

X-ray examination of materials continued
microstructures continued
Fe-Si single crystals deformed by tensile forces, slip polygonization 2—84060
Fe, foil, polycryst., plastic deform. structs. 2—71567
Fe single crystal, H induced plastic strain, divergent X-ray beam obs. 2—64715
GaAs, epitaxially grown, plane defect at interface and dislocations obs. 2—71488
GaAs, perfection of single crysts. and epitaxial layers 2—74767
$GaAs_{1-x}P_x$ epitaxial layer, on GaAs, surface struct., cross-hatch pattern due to misfit disloc. array 2—47110
Ge films, evaporated amorphous, anisotropy 2—47116
HfS_2, grown by vapour transport 2—50577
InSb, investigation of defects in longitudinal sections grown by Chokral'ski method 2—50675
LiF, extinction obs. in large crystals 2—67993
LiF, extinction obs. in spherical crystal, Zachariasen's theory 2—67994
$MgO-Al_2O_3-ZrO_2-SiO_2$ glass, complex particle growth, small-angle X-ray scatt. obs. 2—67887
$MgO-Fe_2O_3-CaO-Al_2O_3-SiO_2$, charges caused by phase transformations during heating 2—83839
Mg_2Sn quenching under pressure of metastable phases, low temp. high pressure x-ray camera 2—84152
$MoSe_2$, stacking faults 2—60807
NaCl, deformed, dislocation arrangement and glide 2—53807
Nb-40% Ti alloy, supercond., rel. to mag. irreversibility 2—47855
Nb-Zr-Ti alloy, supercond., struct. determ. 2—50842
Ni-P chemically deposited films, structure in relation to elec. conductivity 2—77510
Ni, work hardened in tension, double texture, twinned growth influence 2—60985
Se, vapour grown single cryst., dislocation networks obs. 2—50676
Si, defect struct. induced by localized B diffusion 2—77567
Si, dislocations, topography, high resolution video display 2—83922
Si, X-ray anomalous transmission for crystals containing dislocations 2—71496
Si monocrystal, H_2^+ ion bombarded, bicrystal formation 2—47386
Sn-Te, quenching under pressure of metastable phases, low temp. high pressure X-ray camera 2—84152
$SnS_2(Se_2)$, grown by vapour transport 2—50577
SnTe-GeTe alloys, quenching under pressure of metastable phases, low temp. high pressure X-ray camera 2—84152
Ti, Burgers vector of straight dislocations 2—77526
Ti alloys, β—phase content determ., comparison with electrochem. methods 2—77669
TiS_2, grown by vapour transport 2—50577
V_2O_5, dislocation density detn. 2—56691
WC-Co hard metal, stress meas. at carbide phase 2—74910
Yb-Al system eutectic transformations 2—80797
ZnS, stacking order, polytypic ordering and birefringent striations 2—47213
Zr and Zircaloy tubular materials, texture and anisotropy rel. to plastic deform. 2—53916
$ZrO_2-Y_2O_3$ system, tetragonal-cubic transform., lattice parameters of two phases 2—84098
ZrS_2, grown by vapour transport 2—50577
molecular structure
force constants, calculation from diffraction data 2—77043
organic, biological and crystalline materials 2—42861
phosvitin, beta-pleated-sheet structure 2—74298
polyethylene, oriented, struct. effect of annealing under high press. 2—83395
proteins, determ. of quaternary structure 2—77158
structure analysis of atomic and molecular level, role of computers in collection and pouring of data 2—83340
tobacco mosaic virus, heavy atom positions 2—56621
NH_4SCN, X-ray diffractometric refinement of struct. 2—71436
X-ray fluorescence
see also Fluorescence; X-ray spectra/emission
see also Fluorescence, X-ray spectra/emission
No entries
atomic K-, L- and M-shell yields and Coster-Kronig transitions, review 2—79923
cosmic ray det. using atmospheric fluorescence as ground-based method 2—44902
disperse systems, particle size determ. by sequential X-ray fluorescence 2—64485
monitor methods and meas. errors 2—84477
monitor methods and optimal working range 2—84478
spectrochemical analysis, VRA-2, VA-W-03 single- channel analyzer 2—81557
spectrochemical analysis, VRA-2 analyzer 2—81556
target chamber for charged particle induced fluorescence 2—73925
thin layer thickness determination 2—43470
voltage meas. of diagnostic X-ray tubes 2—66279
Ag, L-subshell fluorescence yields 2—79905
Cr carbides, nitrides and borides, atomic interactions 2—48206
Gd_2O_2S:Tb as phosphor for X-ray image intensifier screen 2—73251
Mn-Mg-Fe ferrite film, flash evaporated, chem. comp., X-ray fluoresc. obs. 2—71331
Pb, in paint, chem. analysis, instrument 2—65418
Te, L-subshell fluorescence yields 2—79905
Ti carbides, nitrides and borides, atomic interactions 2—48206
V carbides, nitrides and borides, atomic interactions 2—48206
X-ray measurement
see also Dosimetry
beam characteristics, meas. using portable microcalorimeter 2—85180
calorimeter, fluence and front surface dose, simultaneous obs. 2—58672
calorimeters, array, development 2—63708
camera monitor for recording small angle scattering 2—55894
depth dose calorimeter, for high intensity, l.v., flash X-ray machines 2—66285
detector, sealed Ti window proportional counter 2—55905
detectors, efficiency calibration for range 3-200 eV 2—46053
diffraction patterns, device giving visual pictures 2—55337
X-ray measurement continued
polar diagrams, graphical construction 2—45200
proportional counters, energy resolution, gas multiplication factor 2—82798
Rontgen unit determ., magnetic field chamber 2—58675
standard free air chamber effect of beam path length on photon scatter correction in low-energy X-radiation meas. 2—55907
Si(Li) detector meas. of X-ray peak intensities by integration over fixed energy range 2—82809
X-ray microscopes *see Microscopes*
X-ray monochromators
balanced filter device, controllable attenuation, automatic beam stop 2—78711
diagnostic radiology, improved contrast to noise ratio 2—69370
focusing monochromator using high-angle reflections from quartz crystal 2—85179
X-ray photoeffect *see Electron emission/photoelectric*
X-ray reflection
atom, ultrasoft reflection in 100 to 1000 eV region 2—46416
Bragg equation, shortcomings in simple derivations 2—62950
powder, granularity rel. to refl. X-ray intensity 2—74700
solid surface, conditions for anomalous reflection 2—67955
specular from thin films, calc. of refractive index and thickness 2—53563
total reflection measurement apparatus for a wide range of temp. 2—62908
X-ray scattering
see also Compton effect; X-ray diffraction
Brillouin, rel. to investigation of phonon phenomena 2—47725
collimation system, small-angle, role of Soller slits 2—64603
condensed matter, from electrons, theory 2—47293
Earth, spectral characteristics of albedo X-rays from hard solar burst 2—62752
usingglancing incidence telescope mirror and twelve optically flat samples 2—70148
hexamethylenetetramine, X-ray scattering and interpretation of the thermal scattering power 2—53632
metals, antiferromagnetic, scattering cross section by electromagnetic-magnon waves 2—84443
nonlinear, parametric conversion and mixing with laser beam 2—41937
oscillation type photographs, broadening of selective reflections 2—45199
polystyrene, low-angle X-ray scattering from crazes and fracture surfaces 2—74855
small angle, absolute intensity meas., unified theory 2—74699
small angle, diffraction patterns, use of image converter for visualization 2—77537
small angle, pinhole systems efficiency for photographically recording 2—73690
small angle, semiconductor detector obs. 2—59626
small-angle, numerical solution of integral equation applied to slit correction 2—56619
Ge-As solid soln., absorpt. and scatt. of X-rays by cluster defects and dislocation loops 2—77584
H_2, 5.41 keV, obs. of differential scattering cross-section 2—64138
H_2, photoelectric cross-section meas. at 5.41 keV 2—67483
He isoelectronic sequence, coherent atomic scatt. factor for ground state 2—64071
$Ne(^1S)$, determ. of coherent, incoherent and total scattering, importance of electronic correlations 2—79882
$SrTiO_3$, one-phonon scatt. intensity, from phonon freq. distrib. 2—77761
X-ray spectra
see also Atmospheric spectra; Chemical analysis/X-ray
alloy, disordered, interpretation of exptl. data 2—61671
antiprotonic atoms, optical pot. analysis 2—79965
antiprotonic atoms, strong interaction effects 2—79966
atom, ultrasoft reflection and refraction in 100 to 1000 eV region 2—46416
atoms, L X-ray transition probabilities, tabulation 2—46406
L, γ-transition multipolarity for ^{227}Th, ^{243}Am, and ^{249}Cf, coincidence obs. 2—74042
metal systems, data compilation, NBS Permuted Materials Index 2—68155
rare earth atoms, 4f energy determination 2—49926
rare earth metals and alloys, 4f state distrib 2—48209
solar, improved wavelengths and line identifications from 60-385 Å 2—75951
solar flares, OSO-7 obs. 2—78593
solder, k-shell differential cross sections, effective atomic numbers 2—54439
transition metal on transition metal surfaces, band struct., X-ray appearance pot. obs. 2—47816
Virgo Cluster, down to 1/4 keV 2—62624
Cu compounds and complexes, X-ray photoelectron spectroscopy, study of satellite lines 2—80047
D_2 focused plasma, X-ray fine sturcute in coaxial accelerator 2—80270
LiF X-ray Raman spectrum, peaks superimposed on Compton distrib. 2—72386
MnO Compton profiles, electron momentum distrib. 2—78116
Sc, Compton profiles, electron momentum distrib. 2—78116
Sc ferrite, rel. to struct. 2—54440
TiB and TiB_2, Compton profiles, electron momentum distrib. 2—48211
^{169}Tm atom, K-shell perturbations caused by static nuclear quadrupole moment 2—42738
absorption
alloy, disordered, intensity, Green's function method 2—51359
atom, electronic struct. comparison in X-ray and electron spectroscopy 2—46455
extended fine struct., electron shake off mechanism following photoionization 2—72377
metals, edge shifts, relation to effective nuclear charge and electronegativity 2—74208
rare earth metals, heavy, L-absorpt. spectra, white lines 2—78117
review, 1969-1971 2—52901
zinc acetate, study of K absorption edge of Zn atom 2—70595

X-ray spectra continued
absorption continued
$ZnCO_3$, study of K absorption edge of Zn atom 2−70595
Al, correlation with appearance potential spectra 2−81378
CS_2, comparison with MO LCAO-CNDO method 2−60034
CS_2, fine structure of ultrasoft $L_{II,III}$ spectra of S in 160-210 eV range 2−42939
CdI vapour, 30 μ, reson. identification 2−76996
$CoCl_2$, K absorpt. of Cl^- 2−65287
Cu-Ni alloy film, 50-90 eV, band struct. interpretation 2−65286
Cu-Ni alloys, d-band filling obs. 2−47809
Cu (II), (III) complexes involving oxygen ligands, meas. of edge-shift and edge-width of K-absorption of Cu 2−56166
CuCl, K absorpt. of Cl, rel. to band struct. 2−75315
Cu(I) and (II) complexes with sulphur ligands, K-absorpt. edge shift 2−56167
$FeCl_2$, K absorpt. of Cl 2−65287
$FeFe_{2-x}Sc_xO_4$, Sc-containing magnetite, K absorp. spectra 2−44400
$Fe_{3-x}Sc_xO_4$, electronic struct. of ions 2−48207
Ge, amorphous, structure by Fourier analysis of EXAFS 2−60576
GeO_2, amorphous, structure by Fourier analysis of EXAFS 2−60576
GeSe, amorphous, structure by Fourier analysis of EXAFS 2−60576
Ge_xTe_{1-x} alloy, amorphous, structure and bonding 2−60575
H_2S, comparison with MO LCAO-CNDO method 2−60034
H_2S, fine structure of ultrasoft $L_{II,III}$ spectra of S in 160-210 ev range 2−42939
K_2ReCl_6, Re L_{III} absorption discontinuity, splitting and edge structure 2−61676
$KReO_4$, Re L_{III} absorption discontinuity, splitting and edge structure 2−61676
$MnCl_2$, K absorpt. of Cl^- 2−65287
MnS, α-, β- and δ-forms, $K\beta$ emission and K absorpt. spectra 2−51358
NaCl, K absorp. of Cl-, rel. to energy band struct. 2−65288
NaCl, K spectra, rel. to density of states 2−72380
NaI, adsorbed O effects 2−81399
Nb and compounds, K-absorpt., fine struct. 2−68674
Ni, anomalous dispersion correlation close a K-absorption edge 2−60764
$NiCl_2$, K absorpt. of Cl^- 2−65287
Pr, fine structure of 4d excitations 2−61675
Rb and cpds., K-absorption edge 2−72382
Re metal, L_{III} absorption discontinuity, splitting and edge structure 2−61676
SF_6, gaseous, sulphur and fluorine K spectra 2−56197
SF_6, MO LCAO interpretation 2−56196
SF_6, photoabsorpt. cross sections in soft and ultrasoft range 2−67499
SF_6 electronic structure in solid and gas 2−42933
SO_2, comparison with MO LCAO-CNDO method 2−60034
SO_2, fine structure of ultrasoft $L_{II,III}$ spectra of S in 160-210 e range 2−42939
Si, fine structure of 2p excitations 2−61675
Si, photoabsorption coeff., core excitons 2−81385
SiO_2, and emission, model 2−80656
Ti, K-spectrum 2−48195
Ti, K-spectrum 2−44401
TiC, K-spectrum 2−44401
TiN, K-spectrum 2−44401
TiN_x, K-spectrum 2−48195
TiO, K-spectrum 2−44401
TiO_2, rutile, brookite and anatase, K-spectrum 2−44401
Ti_2O_3, K-spectrum 2−44401
Zn metallic, study of K absorption edge of Zn atom 2−70595
ZnO, study of K absorption edge of Zn atom 2−70595
$ZnSO_4$, study of K absorption edge of Zn atom 2−70595
emission
see also X-ray fluorescence
alloy, disordered, intensity, Green's function method 2−51359
amplifier design for population inversion in ion-atom collisions 2−82084
anatase, molecular charge distribs. K X-ray emission obs. 2−67930
appearance potential spectroscopy, meas. of surface props. 2−81361
atom, $13 \leqslant Z \leqslant 79$, characteristic emission ion collisions with O ions at 7 to 40 MeV 2−70629
atomic inner-shell deexcitation mechanism, combination with Auger electron emission 2−42745
atoms, characteristic X-ray production induced by heavy ion-atom collisions, total cross section determ. 2−42777
atoms, electron impact excitation of characteristic X radiation, polarization determ. 2−76975
atoms with $Z=62$-92, meas. of L X-ray transition probabilities, comparison with results calc. using RHFS and RCS potential 2−42718
covalent compounds, theoretical interpretation of fine structure of K lines 2−70654
escape peaks and internal fluorescence, Si(Li) detector obs. 2−67082
film surface density meas. by proton excited X-rays, Fredholm expression 2−80542
fluorescence, monitor methods and meas. errors 2−84477
fluorescence, monitor methods and optimal working range 2−84478
Group III-V cpds., observed structure due to K and L-emission bands 2−65285
laser beam scattering on polyethylene target, production of plasma instabilities 2−56366
metals, core hole lifetime effects studied by nonequilibrium quantum statistical mechanics 2−48205
rare earth metals, h.f. satellite obs. 2−83190
rare earth oxides, Ln_2O_3, L-series lines, multiplet struct., expt. and theory 2−81397
review, 1969-1971 2−52901
rutile, molecular charge distribs. K X-ray emission obs. 2−67930
scanning electron microscopy of metals, Lilienfeld radiation 2−79131
solar active regions 2−75952
solar corona, surrounding quiescent filament 2−78626
steel, 304l stainless, surface characterization by proton induced X-rays 2−50832
transition metals, 3d, L-shell appearance pot. spectra, spin orbit splittings, binding energies 2−61677

X-ray spectra continued
emission continued
$Z=35$-85, conversion of M-shell X-ray production cross section to M-shell vacancy production cross section using theoretical fluorescence yields 2−70572
^{a}Sn, $A=129$-132, half-lives determ. from X- and γ-ray emissions 2−46196
Ag, L-subshell fluorescence yields 2−79905
Ag L-series, calc. of relative intensities using radiative transition rates 2−42724
Al-Au alloy, rel. to electronic structure 2−68671
Al, appearance potential spectra, correlation with soft X-ray absorp. 2−81378
Al, $L_{2,3}$ band satellites, rel. to double ionization theory 2−72381
Al, L emission bands, short-wave satellites 2−51361
Al, noncharacteristic X-ray bands produced by collisions with Ar^+ at keV energies 2−56116
Al compound, bond type and crystal struct. influence on Al $K\alpha$-satellite 2−51360
Al_2O_3, Al $K\beta$ spectra, molecular struct. effects in proton and alpha particle excitation 2−81381
Ar, $L_{2,3}$ spectrum, satellite spectrum 2−74214
Ar, noncharacteristic X-ray bands produced by collisions with Ar^+ at keV energies 2−56116
Au, $L\alpha$, $L\beta$, $L\gamma$ peaks meas. as function of proton bombarding energy, 0.5-3.0 MeV, relativistic effects 2−52913
BN, wurtzite-like, energy spectrum determ. 2−75026
Be, K-shell ionization by protons and heavy ions
C, noncharacteristic X-ray bands produced by collisions with Ar^+ at keV energies 2−56116
C atom K-shell X-ray fluorescence, effect of molecular environment 2−49995
CO, C spectra, obs. by grazing incidence grating spectrometer 2−74260
^{252}Cf fission products, rel. to charge parity 2−70497
Co K X-rays produced by heavy ions, energy shifts and relative intensities 2−64013
Co_3B, Co K-emission obs., electron structure detn. 2−72379
$CoCl_2$, $K\beta$ emission of Cl^- 2−65287
Cr-Ni, Cr-Pd, Cr-Pt, structure of $K_{\beta 5}$ emission band 2−72378
Cr surface, appearance potential spectrum, L_3/L_2 intensity ratio 2−51230
CrO_4^{2-}, interpret. using SCF-MO calcs. 2−77095
Cu-Ni alloys, d-band filling obs. 2−47809
Cu, with V, Cr and Fe secondary anodes, K_α emission, primary and secondary excitation 2−61673
CuBr, K band, valence electron obs. 2−68672
CuCl, $K\beta$ emission of Cl, rel. to band struct. 2−75315
Fe, ferromagnetic, structural features within d bands 2−61672
Fe, K X-rays produced by heavy ions, energy shifts and relative intensities 2−64013
Fe, paramagnetic, structural features within d bands 2−61672
Fe XXV and Fe XXVI, high temp. obs. in minute plasma pts. 2−53179
Fe XXVI, highly ionized, linewidths 2−52917
$(Fe_{0.64}Mn_{0.36})_3C$, Mn K-emission obs., electron structure detn. 2−72379
Fe_3C, Fe K-emission obs., electron structure detn. 2−72379
$FeCl_2$, $K\beta$ emission of Cl^- 2−65287
$FeFe_{2-x}Sc_xO_4$, Sc-containing magnetite, K emission spectra 2−44400
GaAs, K band, valence electron obs. 2−68672
Ge, K_α X-ray prod., by 350 keV electron irrad. 2−48208
Ge, K band, valence electron obs. 2−68672
K_2SO_4, high-resolution sulphur $K\beta$ emission, symmetry assignment 2−60007
La contamination on NaCl surface, O ion induced 2−60628
LaF_3, X-ray luminesc. excitation efficiency of lanthanide ions 2−84549
Li, K emission band, short-wave satellites 2−51361
Mg, K-series X-ray valence band line, many body effects 2−68673
Mg, $L_{2,3}$ band satellites, rel. to double ionization theory 2−72381
Mg, L emission bands, short-wave satellites 2−51361
$MnCl_2$, $K\beta$ emission of Cl^- 2−65287
MnO_4^-, interpret. using SCF-MO calcs. 2−77095
MnS, α-, β- and δ-forms, $K\beta$ emission and K absorpt. spectra 2−51358
Mo, with Cr, Fe, Co, Ni and Cu secondary anodes, K_α emission, primary and secondary excitation 2−61673
Na, $L_{2,3}$ band satellites, rel. to double ionization theory 2−72381
Na, L emission bands, short-wave satellites 2−51361
NaCl, K_β spectra, rel. to density of states 2−72380
NaCl, $K\beta$ emission of Cl-, rel. to energy band struct. 2−65288
NaI, adsorbed O effects 2−81399
Ni-Cu alloys, appearance pot. spectra, density of states 2−61674
Ni XXVII, highly ionized, linewidths 2−52917
Ni_3B, Ni K-emission obs., electron structure detn. 2−72379
$NiCl_2$, $K\beta$ emission of Cl^- 2−65287
^{206}Pb muonic atom, analysis in terms of equivalent radius 2−59963
S_8 orthorhombic mol. orbital interpret. of valence X-ray emission 2−84488
SF_6, gaseous, sulphur K and L and fluorine K spectra 2−56197
Si, $L_{2,3}$ band satellites, rel. to double ionization theory 2−72381
Si, L emission bands, short-wave satellites 2−51361
Si, noncharacteristic X-ray bands produced by collisions with Ar^+ at keV energies 2−56116
Si and cpds., mol. orbital model interpret. 2−48210
SiO_2, and absorpt., model 2−80656
Sn, K X-rays produced by heavy ions, energy shifts and relative intensities 2−64013
Te, L-subshell fluorescence yields 2−79905
Th, photon appearance potential spectroscopy 2−54441
Ti-Nb alloy, electronic struct. 2−44402
Ti, α- and proton-induced de-excitation 2−57367
Ti, K- and L-spectra 2−48195
Ti, $K\alpha$ and $K\beta$ spectra, excited by protons, α-particles and O ions 2−57368
TiFe, electron energy spectrum determ. 2−75316
TiN_x, K- and L-spectra 2−48195
TiNi, electron energy spectrum determ. 2−75316
TlCl, $L_{2,3}$ valence band emission 2−72383

X-ray spectra continued
emission continued
VO_4^{3-}, interpret. using SCF-MO calcs. 2−77095
W thick target, calc. of bremsstrahlung spectra produced by electrons using thin-target formulas 2−42739
W thick targets, charact. L and K radiation emission 2−51362
ZnO:Li, light scatt., and photoconductivity, anisotropic 2−75317
ZnSe, K band, valence electron obs. 2−68672
ZnTe, electron energy loss spectra 2−75111
Zr, K X-rays produced by heavy ions, energy shifts and relative intensities 2−64013
Zr, L-emission interpret. 2−64037

X-ray spectrometers
see also Gamma-ray spectrometers; X-ray crystallography/apparatus
appearance pot. spectrometer 2−48950
appearance pot. spectrometer 2−48950
appearance potential, construction and performance 2−55902
automation and sample loading techniques 2−85182
Compton summing, improvement of accuracy 2−59632
electronically gated calibration scheme 2−52679
fluorescence spectrometers for trace element 2−48951
fluorescence spectrometers for trace element 2−48951
focussing vacuum spectrometer with automation 2−58671
grazing incidence grating spectrometer for ultra soft X-rays 2−74260
high-resolution, for mesonic X-rays and nucl. phys. meas. 2−66389
semiconductor, design and applications 2−46038
single axis 2-crystal for fluorescent X-ray analysis 2−44508
soft, using semiconductor detectors, review 2−70287
three crystal, high dispersion and resolution 2−52021
GaAs detector and two semiconductor thermoelements 2−49667
n- GaAs surface barrier diodes, high purity 2−49628
Si(Li) cooled detectors 2−49650

X-ray spectroscopy
see also X-ray crystallography; X-ray diffraction
atomic fluorescence yields in K, L, and M shells, detection 2−42755
microanalysis, electron probe, grazing incidence grating monochromator, description 2−63275
system performance, method for testing presented 2−62906

X-ray topography *see X-ray crystallography; X-ray examination of materials*

X-ray tubes
600 kV continuously pumped flash, characteristics 2−52023
anode current stabilizer using a triac 2−45652
camera, medical diagnostic applics. 2−48853
compact transportable design for 250-300 kV operation 2−55340
conical anode types, construction and application 2−58674
with controllable focal spot size, patent 2−55341
diagnostic, focal spot analogue for det. focal spot distribution effects on image 2−78656
diagnostic, kV measurement 2−69350
diagnostic, radiation protection, inherent filtration, X-ray quality 2−69376
diagnostic, scintillation counter for kilovoltage obs. 2−63700
diagnostic, voltage meas. using K-characteristic fluorescence 2−66279
emission current stabilizer, a.c. heated filaments 2−69518
fine-focus, construction and applications 2−55339
flash, for study of fast processes 2−85181
flash tube using laser-plasma 2−76134
focal spots, exptl. study of modulation transfer functions 2−66388
generating machine, patent 2−85185
high power, pulsed, laser driven 2−85183
high speed rotating anode X-ray tube unit for mammography 2−66387
Bi alloys for apertures, Cu K_α X-ray experiments 2−85184
Re-W target, graphite heat sink and integral heat exchanger, DX-70 series 2−52022

X-rays
see also Cosmic rays/X-rays; Gamma-rays
active shielding of viewing head of electron microscope 2−45201
close gradients at interfaces between different media, use of LiF detectors 2−82822
counting circuit used in electron microprobe anal., source and nature of deadtime 2−63706
d.c. beam, fiducial pulse generator for light-gas gun work 2−58673
electron microscope, scanning, with shadow image 2−79001
emission from laser plasma from high Z target 2−43151
emission from laser produced plasma 2−43165
gas proportional counters for localisation of ionizing radiation 2−73935
generating machine comprising X-ray tube and spiral generator power sources, patent 2−85185
generation by proton and heavy-ion bombardment, soft and ultrasoft X-rays 2−49964
generation rel. to geminate recombination of charge carriers 2−57187
generator for producing monoenergetic high intensity, soft X-rays 2−55338
from Jovian magnetosphere, survey 2−66173
laser, physical aspects 2−79209
laser production 2−66765
metal radiographic intensifying screens 2−45198
semiconductor detector in Kratky X-ray small angle scattering camera 2−59626
semiconductor devices for detection 2−46043
solar, soft, type III acceleration mechanism, source volume establishment 2−73122
solar burst, spectral development 2−58550
solar flares, periodic heating mechanism 2−62749
solar flares, polarization obs. 2−73121
solar flux, applic. to sudden ionospheric disturbance interpretation 2−75954
solar flux, variations during proton events 2−44978
topography, low cost ω axis and linear slide 2−66390
Cs plasma, obs. of shock waves by pulsed X-rays 2−64297
W exploding wires in vacuo, X-ray production 2−76135

X-rays continued
effects
see also Nuclear reactions and scattering due to/photons
biological, conference (Mishima, Japan, Nov. 1971) 2−62284
cat's visual pathways, interaction of flash evoked cortical potentials 2−45179
children, medical examinations 2−69335
eye, carotid angiography 2−69334
glass, borate, induced Ti centres, e.p.r. spectra 2−44450
kaolinite, Egyptian, radiation effects on surface structure 2−53550
malonamide, X-irradiated, confirmation of σ-radical, e.s.r. spectra obs. 2−64185
malonic acid, electron spin-lattice and cross relaxation 2−44442
mammalian cells, transient change in radioresistivity due to pre-irradiation culture conditions 2−62850
m.a.s. diode, irrad., shifting characts. of flat band voltage 2−57220
Moire patterns, dependence on wavelength 2−85178
monkeys, on blood flow, vascular resistance, blood pressure and heart rate obs. 2−69316
Mylar, elec. cond., pulsed X-ray irrad. induced 2−65091
nitella flexilis cells, membrane potential, membrane resistance and action potential 2−66268
organic aerosol production 2−46999
photoionization of Ne, Ar, Kr, relative abundances of multiply charged ions 2−53245
polytetrafluoroethylene, elec. cond., pulsed X-ray irrad. induced 2−65091
polythene, elec. cond., pulsed X-ray irrad. induced 2−65091
rabbit brain, change in specific gravity after high doses 2−62849
rare earth ions, in Y_2O_2S, La_2O_2S, Gd_2O_2S, X-ray excited optical fluoresc. 2−72418
rat, morphological changes in cortical medullary thymocytes 2−62848
rat femurs, early effect on mechanical properties 2−69228
rats, irradiation of subependymal plate, mitotic activity 2−55227
salivary gland growth in rat, local X-radiation 2−76078
semiconductor, amorphous, radiation stability, effects of microstruct. 2−60567
water phantom and tissue equivalent materials, calc. of dose distrib. for treatment planning 2−69406
BaFCl, irrad., F-centres 2−64680
Be_2SiO_4:Cr_2O_3, enhancement of e.s.r. of Cr^{5+} 2−72477
CaF_2:La,Çe, irrad., optical absorpt., charge transfer processes 2−65253
$CaWO_4$ following low temp. X-irradiation, photoconductivity 2−81175
$CdCl_2$ crystals, e.p.r. spectra of impurity ions at 5 eV, radiation effects 2−84475
CsBr, irrad. at cryogenic temps., I-, α-, H, H′ and V_4 centres 2−68038
InSb, photocond. rel. to X-ray irrad., at 77K 2−47996
KCl:Ag, colour centre form. by X-ray irrad., e.p.r. and optical obs. 2−80713
KCl:Br, irrad., $BrCl^- - V_k$ centre 2−81461
KCl:Ca, Sr, thermal annealing of defects produced by irradiation 2−50696
KCl:Eu^{2+}(Yb^{2+})(Sm^{2+}), impurity- vacancy dipole behaviour 2−83982
KCl:Na, effect of Na impurity, first stage colorability 2−77595
KCl:Na^+, X-ray irrad., hole centres, conversion and struct., optical absorpt. 2−84523
KCl:OH^-, irrad., temp. effect on F-centre formation 2−47449
$KClO_3$, radiation damage, Raman spectra obs. 2−57361
KH_2AsO_4 and KD_2AsO_4, X-irradiated, identification of Slater configurations of $(AsO_4)^{4-}$ radical by ESR 2−81453
KX-K_2O-B_2O_3 glass, (X=F,Cl,Br,I,O), irrad., colour centres, e.p.r. obs. 2−81463
LiF, irrad., thermolum., temp. depend. 2−65313
$NH_4H_2AsO_4$, $ND_4D_2AsO_4$, identification of Slater configurations of $(AsO_4)^{4-}$ radical by ESR 2−81453
NaCl:Cu, X-ray coloured, Cu activated thermolum., 300-510K 2−78122
$NaClO_3$, radiation damage, Raman spectra obs. 2−57361
SrF_2:La,Ce, irrad., optical absorpt., charge transfer processes 2−65253
protection *see Radiation protection*

Xenon
adsorption, on Cu, Fe, and Na films, roughness and surface potential 2−50556
adsorption, on graphite, LEED obs. 2−50533
adsorption, on Ni film, surface potential, photoelec. emission obs. 2−47163
adsorption on quartz glass, isotherms meas. 2−50529
arc lamp, 50 KW, in elliptical collector 2−76540
arc lamp, stability tests 2−45813
atom, absorption spectra in range 330 to 600Å 2−49949
atom, elastic reson. energy 2−74230
atom, excitation by collisions with metastable Kr atoms 2−59936
atom, ionization in slow collisions with He and He^+, meas. of energy spectra and angular distribs. of ejected electron 2−56119
atom, oscillator strengths for multiple ioniz. in outer and first inner shells 2−79891
atom, outer s shell role in single ioniz. by electron impact 2−67399
atom, upper level lifetimes of high gain laser transitions 2−42740
atom, vacuum u.v. spectra in solid carbon tetrafluoride 2−49957
atomic deexcitation time of slow component on pressure 2−59616
binary mixture with methane, ultrasonic absorption meas. of rotational relaxation time 2−64219
critical density, law of rectilinear diameter employed 2−53502
diffusion in CsI, calc. of activation energies 2−74812
discharge, radial distrib. of temp. and density of charged particles 2−50228
discharge plasma, electrical conductivity det. 2−56341
discharge pulsed, rel. between electrical conductivity and current density 2−60302
elastic scattering for slow positrons 2−70644
equation of state, improved, in vicinity of critical point 2−80522
film, on Ir substrate, use in obs. Ir surface struct., LEED 2−47077
follow spotlight 2−49445
high pressure discharge, initial stage 2−67691

Xenon continued
- ion penetration in Au 2−61124
- ion range in Cu 2−61126
- ions, three-body conversion to mol. ions 2−83188
- isotopic abundances, in terrestrial and extraterrestrial matter 2−66040
- laser, 3.5 μm superradiation, saturation effect 2−82482
- laser, pulsed, effect of axial mag. field on output power 2−73572
- laser action on unclassified transitions in highly ionized plasma 2−59142
- light distortion, freq. dependence 2−50273
- liquid, gamma emitting radioisotope camera for medical use 2−55249
- liquid, longitudinal phonons and the law of corresponding states 2−71156
- in lunar breccia, fission product from extinct ^{244}Pu 2−66145
- multi-charge ions moving in an impulse discharge, method of measuring velocity 2−50223
- natural, local magnetic field shift, n.m.r. obs. 2−65349
- plasma, afterglow, electron temp. lowering by diffusion cooling 2−70882
- plasma, continuum absorption coefficient 2−60243
- plasma, electron thermal conductivity temperature dependence 2−60263
- plasma, pulsed discharge, basic parameters, optical and electrical props. 2−74381
- plasma, spectral lines, Stark coeffs. determ. 2−67393
- precursor ionization, e.m. T tubes, Mach. 5 shocks 2−78932
- proportional counters, gas amplification factor 2−63697
- pulse discharge radiation, space-time distrib. 2−56389
- pulsed discharge, meas. of plasma temp. 2−56388
- pulsed discharge, parameter time depend. obs. 2−53254
- radiation source, short arc, high reliability and power for solar simulation 2−76535
- scattering of H atoms, absolute total cross sections, interatomic forces 2−67424
- shock-heated, ionization relax. time calc. 2−70978
- short-lived isotopes, e.m. separation 2−70647
- solid:^{45}Ca β-decay, optical excitation of the daughter atoms Sc 2−84244
- solid, adsorption of He and Ne, energy spectrum calculation method 2−43499
- solid, Ar atom adsorp. at crystal edges and vertices 2−47174
- solid, Brillouin spectra and elastic consts. 2−47737
- solid, elastic const. calcs. using Monte Carlo procedure 2−68062
- solid, photocond., energy gap, at 135K 2−72069
- solid, specific heat, anharmonic corrections at high temp. 2−68247
- solid, vacuum u.v. absorpt., temp. depend. 2−81371
- solidified, lattice dynamics 2−61083
- Stark effect, 4300-5000 Å 2−70593
- Stark splitting, $2p_2$, $2p_7$, $3p_6$, $3p_7$ and $5d_3$ levels 2−70594
- stimulated emission, in vacuum u.v., high current relativistic electron beam excitation 2−70584
- surface, (111), LEED thermal scatt. 2−50470
- surface, (111), one phonon thermal diffuse scattering calc. 2−60632
- third virial coeff. calc. at low temps. 2−56440
- viscosity, temp. depend. of coeffs. on saturation line of liq. and vapour phases at const. density 2−71170
- Ar-Xe laser, energy transfer as excitation mechanism 2−41988
- He-Xe laser 3.508 μ transition, freq. stabilization methods 2−63330
- He-Xe mixtures, i.r. absorption spectrum, temp. dependence, determination of intermolecular potentials 2−50131
- Hg-Xe layer, insulator-metal transition, Wannier exciton disappearance, u.v. spectra obs. 2−51079
- Xe:^{57}Co→^{57}Fe, Mossbauer study of atomic states of Fe 2−46426
- Xe-H^+ charge exchange collisions, 15 eV, three-state calcs. of spin polarization 2−79918
- Xe-Ne discharge gyroscopic effect in constricted discharge 2−74410
- Xe^+-Xe, charge transfer cross section and effect of initial J-states in ions 2−70624
- Xe I lines, Stark widening of h.f. electrodeless discharge 2−46423
- Xe_3, binding energies, calc. for Lennard-Jones 12-6 pair potentials 2−60023
- XeI, Hanle effect and radiative lifetimes of 2p levels 2−67394
- $Xe^{+}\,{}^2P_{3/2}$ and $^2P_{1/2}$ ions, in Xe and O_2, charge transfer cross section 2−70625
- ^{133}Xe used to determine rates of clearance in anterior tibial muscle 2−69359
- Xe^+ + Xe collision, charge transfer and fine struct., transitions 2−46462
- Xe_2*, temp. dependence of vacuum u.v. emission spectra in gas and liquid phases 2−70680
- ^{129}Xr, in stony meteorites, age of Solar System, Moon rocks and stony meteorites 2−66190

Xenon compounds
- Ar-Xe solid solution, absorpt., 8-10.5 eV, rel. to exciton studies 2−68634
- Xe-Ar(Kr) film, struct., 6K to sublimation temp., electron diffr. obs. 2−80573
- XeF_2 complexes with RuF_5, i.r. spectra 2−74279
- XeF_4, heat capacity, thermodynamic functions, entropy 2−80411
- XeF_6, electronic states and molecular geometry, electronic isomerism 2−42940
- XeO_4, vibr. props. 2−52991
- XeO_4 i.r. and Raman spectra, determ. Corilis consts., isotopic freq. shift and force field 2−80023

Xerography *see Photography*

Y-particles *see Hyperons/resonances*

Yield *see Elastic limit; Plastic deformation; Plastic flow*

Young's modulus *see Elastic constants*

Ytterbium
- film, condensed on glass, amorphous to cryst. transition temp. 2−43474
- film, phase transform. on annealing 2−50952
- piezoresistance, temp. and uniaxial stress dependence obs. 2−71840
- piezoresistive transducers for in-situ field meas. 2−61943
- solar photospheric abundance det. from spectrum synthesis 2−58554
- thick target, energy loss of scatt. protons 2−80928

Ytterbium continued
- KCl:Yb^{2+}, impurity-vacancy dipole relax. and aggregation, and X-ray effects 2−83982
- $NaYF_4$:Yb, Er, phosphor, upconversion, i.r.-pumped visible luminesc. 2−72413
- YF_3: Yb, Ho, diffusion and transfer of optical excitation 2−61714
- Yb, Er, Ho, Tm:YAG laser, recirculating liquid N_2 system for cooling 2−63339
- Yb III $4f^{13}6s$, $4f^{13}6p$, $4f^{13}5d$ configurations and effective magnetic operations for inequivalent electrons 2−79936
- Yb^{2+} in alkali halide, Z-centres, optical absorpt. and e.p.r. at 77K 2−71526
- Yb^{3+}, e.p.r. spectra, in $ZrSiO_4$, $HfSiO_4$ and $ThSiO_4$ hosts 2−48278
- Yb^{3+}, in CdS, mechanisms effecting optical spectra of $4f^{13}$ ions 2−61625
- Yb^{3+}, in glass, fluoresc. quenching by OH^- ions 2−54467
- Yb^{3+}, in $YAsO_4$, pair interaction and relax., e.p.r. obs. 2−65326
- Yb^{3+}, in YF_3, Y_3OCl_7 and YOCl, i.r. to visible conversion 2−54470
- Yb^{3+} doped oxides, visible luminesc., i.r. excited, effect of host lattice 2−78140
- Yb^{3+} e.s.r. in Cs_2HfCl_6 in octahedral cryst. field 2−72482
- $YbVO_4$, cryst. struct., refined 2−60756
- yttrium ethyl sulphate: Yb, nuclear spin refrigeration rel. to electron spin-spin interaction 2−72246

Ytterbium compounds
- YAG laser, Ge photodiode detecting head 2−66761
- Ag-Yb dil. alloys, perturbed ang. correl. on ^{169}Tm, h.f.s. 2−72247
- Au-Yb dilute alloy, localized moments, Mossbauer obs. 2−81210
- $(Y,Yb,Er)F_3$ phosphor., i.r. convertor, prep. by coprecipitation 2−48248
- Yb-Al system eutectic transformations 2−80797
- Yb-Sn system, relative stability of intermetallics 2−47573
- $YbAl_2$, $YbAl_3$ magnetic susceptibility and expansion coefficient 2−81218
- $YbAsO_4$, a.c. susceptibility, absence of phase transition down to 0.6K 2−65187
- YbB_{12}, electronic spectra and phys. props. 2−47838
- $YbCl_3$, n.q.r., hydrostatic press. coeffs., soft sphere model 2−54519
- $YbCu_{6.5}$, cryst. struct. determ. 2−43594
- YbFe garnet, Ca-Si substituted, flux growth and mag. characterization 2−47278
- YbFe garnet, perturbed ang. correl. on ^{169}Tm, h.f.s. 2−72247
- YbFe garnet, stat. mol. field interpret. of mag. props. 2−72205
- $YbMnO_3$-$YbCrO_3$, $YbMnO_3$-$YbreO_3$, extent of solid solns., mag. and elec. props. 2−51235
- $Yb(NH_3)_6$, thermodynamic properties and gaseous ammoniation energies of Yb^{2+} 2−61774
- $Yb(NO_3)_3$, aqueous solution at 25°C, u.s. relaxation 2−53427
- Yb_2O_3-BaO solid soln., phase diagram 2−54005
- Yb_2O_2Se, mag. props. and struct. 2−44228
- $YbPd_3$, mag. props., cryst. fields, Mossbauer obs. 2−54393
- YbSe(Te) films, co-evap. and characteriz. 2−50502
- YbTe, press. induced electronic collapse and struct. changes 2−68297
- YbTe, press. induced struct. and electronic transform. 2−50948
- ZrO_2-Yb_2O_3 and ZrO_2-Yb_2O_3-Y_2O_3 systems, solid soln. formation kinetics 2−47721

Yttrium
- adsorption of O_2, Auger spectrum chem. shift 2−51223
- electron phonon enhancement factor, from specific heat data 2−64932
- film, core level binding energies, X-ray photoelectron spectra study 2−72096
- film, elec. cond. and Hall const., size effect 2−81030
- phonon dispersion, Debye temp., noncentral force model 2−80887
- stopping powers for ^{4}He, ^{16}O, ^{35}Cl at 1 to 3 MeV 2−80921
- Y IV, anal. of spectrum in 300 to 5200 Å range 2−79948
- YV specrum rel. to ZrVI, NbVII and MoVIII 2−74217

Yttrium compounds
- ethyl sulphate: Yb, nuclear spin refrigeration rel. to electron spin-spin interaction 2−72246
- garnets, diamagnetically displaced, magneto-elastic bond 2−65161
- garnets, magneto-elastic bonding of Fe^{3+} and Cr^{3+} ions, EPR and FMR study 2−65321
- hydrides, empirically derived band diagrams 2−77833
- monoauride, dissociation energy rel. to bond energy calc. for Sc diatomic intermetallic 2−50557
- plastic deformation of alloy 2−68084
- tritide film, ageing, bubble form. and rupture 2−43478
- YIG sphere under parallel pumping condits., anisotropy of above-threshold susceptibility 2−72140
- yttralox, characteriz. as laser material 2−49381
- Yttralox ceramic, Th-doped, processing 2−50900
- yttrium ethyl sulphate:Yb^{3+}, phonon field contrib. to g shift 2−68586
- yttrofluorite crystals, Nd^{3+} doped, time development of wide-band generation spectra in resonator with diffusion 2−42073
- AlN-Y_2O_3, sintered, with fibrous struct., textural determ. 2−47666
- $Al_2O_3/ZrO_2/Y_2O_3$ eutectic, directionally solidified, mech. props. 2−47526
- $Al_2O_3/ZrO_2/Y_2O_3$ system eutectics, strength 2−47525
- Al_2O_3-Y_2O_3 system, noncrystalline film prep. by sputtering 2−47114
- CaF_3-YF_3:Er^{3+}, spectroscopic study of stimulated radiation 2−61689
- β-Ce-Y alloys, low temp. heat capacity and mag. ordering 2−47748
- CeO_2-ZrO_2-Y_2O_3 solid solns., electronic behaviour 2−47893
- $Ce_{0.25}(Y,La)_{9.75}Al_2$, inelastic neutron scatt. determination of cryst. field levels of Ce^{3+}, susceptibility calc. 2−72105
- $Ce_xY_{1-x}Sb$, antiferromagnetically ordered, Neel temp. dependence on lattice constants 2−72212
- $Er_xY_{1-x}Al_2$, mag. struct., neutron diffr. obs. 2−81275
- Gd-Y alloys, Hall effect, 4.2-340K 2−68332
- Gd_xY_{1-x}, e.p.r. of Gd, g-shift and linewidths 2−81462
- Mg-(10.8 at.%)Y alloy, thermomech. treatment for increased ductility and high strength 2−47588
- MgO-Y_2O_3 system, noncrystalline film prep. by sputtering 2−47114
- Nd:YAG new laser transitions $^4F_{3/2}$ to $^4I_{9/2}$ 2−42066
- Nd^{3+}:YAG intracavity phase modulated laser separation of mode locked states 2−42048

Yttrium compounds continued
Pr-γ alloy, h.f. n.m.r. at 4.2 degrees K 2−72518
$ThO_2:Y_2O_3$ ceramic, high optical quality, powder prep. and processing technique 2−77736
W-Y_2O_3 two-phase system, black-body radiation and elec. resist. 2−43875
Y-Ce alloy, Kondo effect under press. 2−71839
Y-Ce alloys, n.m.r. meas. 2−65350
Y-Co-Ni pseudobinary compounds, magnetization minima 2−75223
Y-Fe garnet, effect of magnetic ordering on optical absorption spectrum 2−81392
Y-Fe garnet, l.f. magnetization oscillations where absorption maximum coincides with ferromagnetic resonance 2−75340
$(Y,Yb,Er)F_3$ phosphor., i.r. convertor, prep. by coprecipitation 2−48248
Y complex, yttrium ethylsulphate: ^{166}Er, $\gamma\gamma$ cascade, crystal orientation effect 2−78053
Y orthoferrites and orthochromites, ang. depend. of superexchange interactions 2−68569
YAG:Nd, crystal growth, boule defects, and Nd distrib. obs. 2−47246
YAG:Nd, Q-switched laser, pumping CdSe i.r. parametric oscillator 2−42061
YAG:Nd electro-optically Q-switched laser, multipulsing behaviour 2−59173
YAG:Nd laser, CW pumped, output fluctuations 2−45751
YAG:Nd laser, diode-pump-modulated, response to pump intensity sinusoidal modulation 2−52427
YAG:Nd laser, harmonic mode locking 2−59172
YAG:Nd laser, meas. of start photon number 2−52428
YAG:Nd laser, props. rel. to Nd:YALO, Nd:Yttralox, Nd:apatites 2−63338
YAG:Nd laser, pulsed, organic dyes as filters 2−73588
YAG:Nd laser, single freq. travelling wave, output 2−73581
YAG:Nd laser, space qualified, design 2−69940
YAG:Nd laser material, holographic interferometry meas. of thermal refractive index and expansion coefficients 2−59174
YAG:Nd lasers bibliography 2−42065
YAG:Nd solid laser, pumping $LiIO_3$ internal parametric oscillator 2−45746
YAG:Nd^{3+}, random variation of static crystalline field, e.s.r. line width obs. 2−44441
YAG:Nd^{3+} laser, effect of pressure in Xe and Kr arc lamps on pumping efficiency 2−42072
YAG:Nd^{3+} laser, recirculating liquid N_2 system for cooling 2−63339
YAG:Nd^{3+} laser target designators and range finders 2−42064
YAG:Nd^{3+} quasicontinuous laser, spectral characts. and oscill. dynamics 2−79216
YAG:Nd^{3+} solid laser, generation of subnanosecond 10 μ pulses 2−42068
YAG:Pm laser, radiative transition probabilities rel. to YAG:Nd 2−59186
YAG:Tm, Ho, Er, Yb laser, recirculating liquid N_2 system for cooling 2−63339
YAG-YALO:Nd^{3+} laser, hybrid operation at 1.064 μ 2−69939
YAG, crystallization from PbO-YF_3-Al_2O_3 melts, det. of stability range for YAG 2−74692
YAG, luminesc. of Tb^{3+}, quenching by direct transfer and migration 2−54459
YAG films, Nd^{3+} site preferences for growth by liquid phase epitaxy, spin-reson. meas. 2−83867
YALO:Nd laser material, holographic interferometry meas. of thermal refractive index and expansion coefficients 2−59174
YAP, Nd doped, solid laser, polarization and crystal direction effects 2−42067
YAl_2:Gd, paramagnetic resonance meas., 5-70K, temp. and impurity depend. 2−65327
$YAlO_3$:Cr:Tm laser, four-level operation at 2.35 microns 2−42075
$YAlO_3:Ho^{3+}$, optical transition probabilities for Ho^{3+} 2−54468
$YAlO_3:Nd^{3+}$, high temp. phase instability 2−74958
$Y_3Al_5O_{12}$:Pr(Tb)(Eu)(Yb) colour centre investigation during γ-irradiation 2−80714
$Y_3Al_5O_{12}:SiO_2$ garnet, grown from melt, habit modification by doping 2−74751
$YAlO_3$, optical spectrum of exchange coupled Cr^{3+} pairs 2−72415
$YAlO_3$ laser, design, device parameter obs. 2−45752
$YAsO_4:Yb^{3+}$, pair interaction and relax., e.p.r. obs. 2−65326
YBO_3:Ce, thermoluminescence during cathodic excitation, also dependence on Ni, Co and Fe impurities 2−54477
$Y_{3-x}Ca_xFe_{5-x}Sn_xO_{12}$ garnet, noncollinear spin config., Mossbauer spectra obs. 2−54344
$Y_3Cd_4Zn_7$ crystallographic system, lattice parameter and space group determ. 2−80644
YCo_5-YFe_5 pseudobinary system, $CaCu_5$-type phase stability 2−43944
YCo_3-YNi_5 pseudobinary system, $CaCu_5$-type phase stability 2−43944
YCo_2, crystallographic, mag. and e.p.r. studies 2−81276
YCo_5, permanent mag. 2−52385
$Y_2(Co_{1-x}Fe_x)_{17}$, lattice consts. 2−50626
$YCrO_3$, n.m.r. of ^{53}Cr, h.f.s., mag. props. 2−48307
YCu intermetallic, electronic struct., APW calcs. 2−54112
YD_3, crystal struct., neutron and X-ray diffr. obs. 2−74752
$Y_{3-x}Eu_xAl_yFe_{5-y}O_{12}$ films, epitaxial, characteriz. for bubble devices 2−61541
YF_3: Yb, Ho, diffusion and transfer of optical excitation 2−61714
$YF_3:Er^{3+}$, Yb^{3+}, mechanisms and controlling factors of i.r. to visible conversion 2−54470
$YF_3:Yb^{3+}$-Ho^{3+}, anti-Stokes luminescence, spectrum and excitation energy dependence 2−61688
YF_3-BaF_2 system, phase relations 2−74922
YF_3-PbO-Al_2O_3 crystallization of YAG and det. of stability range 2−74692
$Y_3Fe_{5-(x\|y)}Al_xGa_yO_{12}$ ferrite garnet, magnetiz. and ferromag. resonance 2−72204
$YFe_{1-x}Al_xO_3$, local mag. field at ^{57}Fe, effect of Fe^{3+} exchange linkages, Mossbauer obs. 2−72288
$Y_3Fe_{5-x}Al_xO_{12}$, garnet, mag. anisotropy, natural ferromag. reson. obs. 2−78148

Yttrium compounds continued
$Y_3Fe_{5-x}Cr_xO_{12}$, crystal growth, fluxed melt technique 2−47289
$Y_3Fe_5O_{12}:Co^{2+}$, Mn^{3+}, anisotropy and magnetostriction consts. rel. to Co^{2+} and Mn^{3+} ion substitutions 2−75233
$Y_3Fe_5O_{12}:SiO_2$ garnet, grown from melt, habit modification by doping 2−74751
$YFeO_3$, cryst. growth and characteriz. 2−50605
$YFeO_3$, intrinsic domain-wall damping 2−65176
$YFeO_3$, with high coercivity surface layer, domain struct., magnetooptical study 2−81284
$Y_2Fe_5O_{12}$, grown from soln., dislocation density rel. to conditions 2−56715
$Y_3Fe_5O_{12}$ garnet, mag. phase transition, polarized neutrons and RF susceptibility obs. 2−57284
$Y_3Fe_5O_{12}$ garnet, ultrasound absorpt. in vicinity of mag. phase transition 2−71735
$YFeO_3$; ^{119}Sn, Mossbauer effect, eff. mag. fields and transfer of spin density to electronic shells 2−72287
$Y_3Ga_{1.1}Fe_{3.9}O_{12}$ layer, laser beam thermomagnetic recording 2−51273
$Y_3Ga_5O_{12}:SiO_2$ garnet, grown from melt, habit modification by doping 2−74751
$Y_{2.5}Gd_{0.5}Fe_4Ga_1O_{12}$ garnet, film, magnetization orient. depend., induced anisotropies, magnetooptic Faraday effect obs. 2−72188
$YH_{1.93}$, acoustic velocity, limiting Debye temp. and elastic consts. detn. 2−57047
YIG:Ru, magnetostriction consts. 2−44281
YIG:Si, magnetiz. switching by i.r. irrad., linear dichroism obs. 2−68599
YIG:Si, photoinduced dichroism, model 2−72260
YIG:Si^{4+},Ca^{2+} magnetostriction rel. to mag. field inclination to crystallographic axes at 4.2K, 77K and room temp. obs. 2−84437
YIG/Ge interface, interaction of surface magnetostatic waves with carriers 2−84420
YIG/dielectric/conductive plane, magnetostatic propag. 2−51268
YIG-Si, thermally induced negative resistance 2−51145
YIG, Al^{3+}-substituted, Ru^{3+}-doped, ferromag. reson. 2−81444
YIG, Ca-Si substituted, flux growth and mag. characterization 2−47278
YIG, cryst. growth, chem. transport 2−43513
YIG, cryst. growth, viscosity and density of melts 2−60713
YIG, crystal growth, fluxed melt method, effects of oxygen pressure 2−50603
YIG, d.c. magnetization produced by parallel optical pumping 2−72203
YIG, diamagnetically substituted, Mossbauer spectra in crit. region 2−78077
YIG, electrostatic forces, elec. field gradient, mol. orbitals construct. 2−68615
YIG, epitaxial film growth by chem. vapour deposition 2−47132
YIG, epitaxial magnetic film, prep. by chem. vapour deposition 2−77527
YIG, ferroacoustic surface wave resonance 2−51035
YIG, flux growth, local cooling and accelerated crucible rotation effects on quality 2−50602
YIG, heteroepitaxy, flux method and hydrothermal synthesis 2−50513
YIG, high temp. high press. phase formation 2−57024
YIG, hysteresis loop, wall displacement and bulging in magnetization mechanism 2−65167
YIG, light-induced Bloch wall pinning 2−48060
YIG, magnetocryst. anisotropy, reson. fields, iodine additive effects 2−44279
YIG, magnetooptical coeffs., temp. depend. 2−72266
YIG, magnetostriction consts., meas. by ferromag. reson. 2−72176
YIG, nonmag. ion substituted, polycryst., ferrimag. resonance obs. 2−61547
YIG, nucl. gamma reson. study of mag. anisotropy 2−81266
YIG, parallel pump spin wave instab., discrete magnon resonances 2−48271
YIG, photomechanical effect 2−81332
YIG, polycryst., spin wave transit time, limitation by pores 2−75232
YIG, reson. phenomena at moving domain boundaries 2−72456
YIG, shock induced demagnetization, method for investigation 2−48081
YIG, spin relaxation near Curie temp. studied by high frequency magnetic susceptibility 2−84417
YIG, substituted, ultra-low bandwidth, microwave loss 2−44435
YIG, substituted, ultralow-linewidth, microwave loss 2−51397
YIG, surface spin wave propagation in inhomogeneous fields 2−78037
YIG, tangentially magnetized substrate, magnetoelastic, Rayleigh type surface wave 2−43976
YIG cylindrical rod, mode separation of magnetostatic waves 2−59005
YIG discs, epitaxial, anisotropy effects on magnetostatic modes 2−44432
YIG domains, laser beam diffraction 2−44348
YIG epitaxial film, coupling between dipole and exchange dominated spin waves 2−72189
YIG film, chem. vapour deposited, substrate growth band and core struct. replication 2−71338
YIG film, chem. vapour deposited, comp. variation and magnetization 2−72202
YIG garnet, sound wave absorpt. effects, magnetoelasticity, domain wall motion 2−61097
YIG magnetostatic echo analysis 2−57313
YIG rod, internal field distrib., magnetoelastic reson. determ. 2−57285
YIG single cryst./polycryst. composites, amplified Hahn-type echoes 2−44270
YIG single crystal film, domain wall mobility meas. by light diffraction 2−84434
YIG thin film disks, anisotropic excitations of magnetostatic modes 2−44434
YIG thin single-crystal distrib., magnetoexchange branch repulsion 2−44433
YIG(Si), reversible photomagnetic effects, microscopic theory 2−54259

Yttrium compounds continued
YLF, rare earth doped, solid laser, energy transfer and phonon interactions 2−42058
$YLiO_2$, luminesc. of Eu^{3+}, energy levels 2−48226
YNi_2, crystallographic, mag. and e.p.r. studies 2−81277
Y_2O_3:Eu^{3+}(Tb^{3+}), flame excited luminesc., temp. depend. 2−48270
Y_2O_3-BaO solid soln., phase diagram 2−54005
Y_2O_3-ZrO_2, elastic consts., current blackening effects, u.s. wave vel. obs. 2−43666
YO, $B^2\Sigma$-$X^2\Sigma$ system, Einstein coefficients and oscillator strengths 2−64161
YO, $B^2\Sigma$-$X^2\Sigma$ system electron transition moment variation with internucl. distance and vibr. temp. 2−56203
Y_2O_3, fast neutron irradiation, thermionic reactor design 2−53707
Y_2O_3, low loss dielec. film, use of mag. fields in electron beam evaporation 2−77947
Y_2O_3, phonon-assisted energy transfer between Ln^{3+} ions 2−48234
Y_2O_3, stimulated emission from rare earth and actinide ions 2−48225
Y_2O_3 dispersion strengthing of Zircaloy-2 2−53917
Y_2O_3 particle growth in Ni ceramic, matrix density effects 2−68169
Y_2O_3 phosphor, emission spectrum rel. to Eu^{3+} or Tb^{3+} concentration 2−48235
Y_2O_3 seals, fast-neutron irradiation effect 2−63227
YOCl:Er^{3+}, Yb^{3+}, mechanisms and controlling factors of i.r. to visible conversion 2−54470
Y_3OCl_7:Er^{3+}, Yb^{3+}, mechanisms and controlling factors of i.r. to visible conversion 2−54470
$(Y_2O_3)_3(Fe_2O_3)_5$ ferrite garnet, photocond., 280-800 nm 2−84380
Y_2O_2S:Er^{3+}, energy levels and crystal field splittings detn. 2−51339
Y_2O_2S:Eu^{3+}, luminesc. sensitization by Pr^{3+} and Tb^{3+} 2−51371
Y_2O_2S phosphor, emission spectrum rel. to Eu^{3+} or Tb^{3+} concentration 2−48235
YS, in solid Ar and He matrices, e.s.r. and i.r. spectra 2−46582
Y_2SiO_5:Nd^{3+}, absorpt. and luminesc. spectra, and stimulated emission 2−78123
YVO_3:Eu, excitation induced anisotropy of local environment 2−81440
YVO_4, crystal growth, modified pulling method 2−50604
YVO_4, luminescence dependence on electronic transitions in VO_4^{3-} 2−65300
YVO_4, Raman scatt., phonons 2−48203
$Y_2(WO_4)_3$-Na_2WO_4 solid soln., phase diagram 2−74955
YZn intermetallic, electronic struct., APW calcs. 2−54112
$Y_3[Si_3O_{10}](OH)$, talenite, cryst. struct. 2−71442
$Y_{1-w}Th_wAl_2$, paramagnetic resonance meas., 5-70K, temp. and impurity depend. 2−65327
Zr-Y syst., H_2 diffusion through layers, calc. by eigenfunction method 2−50720
ZrO_2-Y_2O_3 system, effect of Y_2O_3 conc. on tetragonal-cubic transformation 2−84098
ZrO_2-Y_2O_3 system, phase diagram above 2000°C 2−61049
ZrO_2-Yb_2O_3-Y_2O_3 system, solid soln. formation kinetics 2−47721

Yukawa potential *see Field theory, quantum/meson field; Nuclear forces; Scattering*

Zeeman effect
acetophenone crystal, Zeeman splitting pattern obs., assignment of lowest triplet state 2−80061
atom, obs. in nonresonant e.m. field 2−59906
atomic system, double resonance, rel. to coherence effects 2−59912
chloroacetylene, mol. g-value, mag. susceptibility anisotropy, quadrupole and elec. dipole moments 2−70758
collisions between excited and ground state of atoms, mixing between Zeeman sublevels 2−42776
β CrB spectra, magnetic field variation obs. 58288 2−58288
dimethylsulphide-d_6, rot. spectrum 2−64177
73 Dra spectra, magnetic field variation obs. 2−58288
Fresnel evanescent wave, TEM case 2−73476
Fresnel evanescent wave, transverse mag. mode case 2−63306
g-values for various organic molecules from microwave Zeeman effect 2−70739
lanthanum ethyl sulphate:Dy^{3+}, crystal field energy levels and Zeeman spectra 2−80951
laser, monomode anisotropic, freq.-locking region obs. 2−52414
Mossbauer dipole transitions in magnetically ordered crystals 2−68610
muonium hyperfine splitting in low-pressure Ar determ. from field independent Zeeman transitions 2−42822
near-symmetric rotor, effect in doublet states 2−77064
n.m.r., Zeeman energy modification by non-resonating oscillation field in rot. frame 2−54501
in n.q.r., Hamiltonian, line splitting, mixed states 2−51418
nuclear spin-lattice relaxation due to the orbital interaction 2−84585
pollution monitor for NO, laser device based on Zeeman modulation of absorption 2−61826
pyrazine-d_4, triplet state 2−60084
rare earth double nitrate, satellite lines, Zeeman effect, field perturbation energy 2−72344
rare earth double nitrate, satellite lines from non-Kramers distorted trigonal lattice, calcs. 2−72343
scanning of optically pumped vapour for determ. h.f.s. 2−46429
solar line splitting in bright prominences 2−44991
spectroscopy, atomic, using He-Ne laser in mag. field 2−63428
Sun, detection of blending within large umbra 2−55166
thioformaldehyde, obs. of high-field rotational effect, determ. of molecular g values, magnetic susceptibilities, quadrupole moments 2−43010
toluqinone single cryst., exciton levels 2−78209
78 Vir spectra, magnetic field variation obs. 2−58288
Ar^+ ion beam, optical spectra Zeeman splitting 2−70577
CdSe, exciton bound to ionized centre 2−68636
CdTe, i.r. absorpt. spectra, shallow donor impurity transitions, polaron Zeeman effect 2−61634
ClO_2, ${}^2A_2 \leftarrow {}^2B_1$ transition, spin-rotation coupling constants 2−77064
Cr complex, di-μ-hydroxotetraglycinatodichromium(III), e.p.r. spectrum, zero-field splitting, domination by Zeeman interaction 2−80645
Cs_2UBr_6, vibronic transitions of uranium ion, Zeeman splitting 2−84528

Zeeman effect continued
Cs_2ZrCl_6:U^{4+}, vibronic transitions of uranium ion, Zeeman splitting 2−84528
Cu Kondo alloys, exchange splitting of electron spins 2−77848
Cu nucl. spin-lattice relax. of Zeeman and spin-spin systems, 1 to 17 mK 2−68581
$CuCs_2(SO_4)_2.6H_2O$, electron spin- lattice relax. of Zeeman and interaction systems 2−68580
GaP:N, on bound exciton-complex 2−61693
$GdAlO_3$:Er, absorp. spectra, Er^{3+}-Gd^{3+} exchange interaction obs. 2−57349
Ge, acceptor states, group theoretical study 2−84264
Ge, donor excited states, photocond. spectra obs. 2−75172
Ge, g-factors of B impurity 2−54402
Ge, quadratic splitting of donor lines 2−57350
HCP, 2782 Å band, excited state obs. 2−70699
He-Ne laser, effect of axial field on mode intensity spectrum and output power 2−79208
He, Stark splitting between Zeeman sub-levels, atomic beam mag. reson. obs. 2−83215
^{193}Hg 3.5h, h.f.s. and isotope shift, by new Zeeman-scanned optical pumping method 2−46429
^{165}Ho, transitions between Zeeman levels in ground state, rel. to magnetic dipole moment meas. 2−46167
I_2, rot. Lande factors in $B^3\Pi_{0(\|)(u)}$ state 2−50049
KI, magneto-reflectance of first exciton 2−51322
Mg, splitting of lines, in mag. field of discharge 2−70588
$MnKH(SO_4)_2.2H_2O$, Zeeman decomp. of visible absorpt. lines 2−54427
NO, obs. of Λ-doubling and Zeeman splitting in fundamental i.r. absorption band 2−46561
NO_2, laser magnetic resonance at 311 and 337 μm 2−42912
Ne, Zeeman splitting in superradiance at 6143 Å 2−46437
Ne gas discharge in magnetic field, optical pumping with multimode laser, saturation resonances by magnetic mode crossing 2−46436
O^+ ion beam, optical spectra Zeeman splitting 2−70577
Pb polarized metastable states, obs. of optical-pumping Zeeman resonances 2−42785
$Pr_2Zn_{3c}Mg_{3(1-c)}(NO_3)_{12}.24H_2O$, satellite lines, Zeeman effect, field perturbation 2−72344
RbI, magneto-reflectance of first exciton 2−51322
Si:P quadratic Zeeman effect of donor lines in photoexcitation spectrum, transverse effective mass 2−81348
Si, acceptor states, group theoretical study 2−84264
Si, quadratic splitting of donor lines 2−57350
SiC, luminesc., Zeeman splittings, bound excitons 2−48227
Zn complex, 2,6-pyridinedicarboxylate, Cu-doped, e.p.r. obs. 2−78155
ZnO, splitting of anomalous shallow bound states 2−51349
ZnSe, splitting of donor states, electron effective mass determ. 2−51372

Zener diodes *see Semiconducting devices/diodes*

Zener effect *see Metals; Semiconducting materials; Semiconductors*

Zero sound
see also Helium/liquid, sound propagation
Fermi liquids, two-component, generalization of theory for zero-sound waves 2−71265
^{3}He solid interface, Kapitza resist., single- particle vs zero-sound couplings 2−47006

Zeta-potential *see Electrokinetic effects*

Zinc
adsorption of SF_6, stepwise isotherms 2−77518
arc lamp for deep ocean water light source 2−49442
atom, study of X-ray K-absorption edge in metallic zinc and in compounds of zinc 2−70595
Auger spectra, LMM, fine struct., L-S coupling interpretation 2−61453
bombarded by C, N and O ions, 0.5-2 MeV, stopping power 2−47782
cavitation in liquid oxygen, plastic deformation in metal surface layers 2−71306
condensed particle size determ. using time discrete sampling apparatus 2−77454
deformation memory 2−71566
diffusion, in Cu and Cu-Zn solid solns., residual activity method 2−47457
diffusion, in Si p-n junction, profile broadening by reactor irrad. 2−84355
diffusion in Al, interpreted using oscill. form of inter-ion potential 2−64691
diffusion in Fe, determ. of Fe-Zn interdiffusion coeffs. 2−47459
diffusion profile, in GaAs, anal. 2−47464
dislocation formation, in single crysts. grown by Bridgeman method 2−77586
dislocation structure of the boundary blocks in the base plane of single crystals 2−60806
ductility, in presence of Hg, effect of surface layer defects 2−74830
Ekco mineral analyser, radio-isotopic X-ray fluorescence 2−81643
electron transmission, det. of lattice potentials 2−83942
exo-emission, threshold illumination intensity 2−44189
Fermi surface, stress depend., torque and magnetostriction obs. 2−61194
in ferromagnetic metal, effective mag. field 2−84404
film, disordered, supercond. energy gap and transition temp. 2−54134
film, on dielec. substrate, elec. resist., supercond. transition temp., absorpt. spectra 2−72323
fracture, large grain size specimens, 3 kbar range pressure effects 2−68097
GaAs:Zn, impurity effects on dislocation velocity 2−68028
grain boundary motion in bicrystals, expt. confirmation of theory 2−74786
h.c.p., non-relativistic electronic band struct., Korringa-Kohn-Rostoker method 2−68298
LEED intensities from cleaved surface 2−60625
liquid, diffusion of Tl 2−46945
liquid, next-neighbour distribs. 2−64432
liquid, struct. factor rel. to entropy of melting 2−64434
magnetic surface states 2−84254

Zinc continued
  magnetic susceptibility, steady, uniaxial stress depend. 2−81204
  melting energy from nonlocal pseudopotential theory 2−60544
  Mossbauer effect large anisotropy prediction 2−80891
  passivation mass transfer effect in flowing electrolyte 2−59039
  phonon limited resistivity, anisotropy 2−64919
  positron angular distributions using wavefunctions with proper crystal symmetry 2−80942
  secondary cell electrode active material migration obs. 2−65386
  secondary electrons, emission from surface bombarded with low-energy ions, energy spectrum structure 2−48027
  specific heat below 30 K 2−68249
  stretched, activated volume, deformation rate, dislocation struct. 2−43700
  superplastic behaviour under tensile stress and temp. cycles 2−47516
  surface morphology, developed during sublimation of oriented single cryst. 2−53558
  vacancy, activated, thermal expansion coefficients from high pressure self diffusion 2−68048
  whisker, deform. twinning, nucleation and propag. stresses 2−47424
  work hardening coefficient, crit. crystal orientation for max. value 2−71631
  X-ray fluorescence anal. in Fe-rich minerals radioisotope detector-radiator assembly 2−61821
  GaAs:Ge p-n junction, Zn- diffused, photolum., 8100-8500 Å 2−72404
  $GaAs_{1-x}P_x$:Zn, direct gap, acceptor levels rel. to photoluminesc. spectra 2−84538
  in GaAs(P), chem. shift in binding energies of Zn and Cd 2−65001
  GaN:Zn, acceptor site location and new emission band obs. 2−72398
  GaP: Zn, Al, photolum. and electrolum., 1.7 to 2.3eV 2−75321
  n-GaP:Te,Zn,O, electrolum., mean electron conc., influence of Te content 2−57381
  GaP:Zn, O, light emitting diode, efficiency shift under forward bias 2−75181
  GaP:Zn, red electrolum. diode, prep. 2−44424
  p-GaP:Zn,O, donor electron capture cross sections, rel. to quantum efficiency limits 2−68681
  GaP:Zn,O, luminesc. time response rel. to multiple trapping at Zn-O impurity centres, 4-120K 2−61696
  p-GaP:Zn,O, photolum. efficiency and kinetics of Zn-O complex formation 2−51368
  p-GaP:Zn,O, recomb. of electrons bound to deep neutral donors and acceptors 2−68682
  p-GaP(Zn,O), minority carrier lifetime, luminesc. decay time obs. 2−48221
  GaSb:Zn, thermal e.m.f. rel. to carrier conc., 300K 2−54248
  GaSb:Zn(Te + Zn), heavily doped, photolum. at high excitation levels 2−72403
  He-Zn vapour laser, role of thermal energy-charge exchange 2−42019
  $InAs_xP_{1-x}$:Zn, growth, laser diode fabrication, lasing action 2−59185
  $In_xGa_{1-x}As$:Zn, growth, laser diode fabrication, lasing action 2−59185
  InSb:Zn, energy level of shallow acceptors, far i.r. absorpt. obs. 2−75296
  inInSb, distrib. coeff., conc. depend. 2−47438
  n-Si:Zn, photoelectronic props. of Zn centres, Zn^{2-} energy level, centre density 2−61449
  Zn-He, gas mixture, glow discharge, laser action in Crookes region 2−79196
  ZnI, Hanle effect obs. of $4s4p\,^3P_1$ and $4s5s\,^3S_1$ levels 2−74232
  inZnS:Cl film, photovolt. polarity reversal by excess Zn 2−51222
Zinc compounds
  Al-Zn liquid alloy, Cr or Mn impurity, susceptibility near nonmag.-mag. transition 2−80486
  brass, annealing after work hardening 2−43789
  α-brass, containing SiO_2 particles, dislocation generation during plastic deform. 2−56708
  brass, elec. cond. meas. by inductive method 2−49239
  brass, extrusion behaviour rel. to solidification texture 2−43809
  α-brass, Fermi surface, positron annihilation study 2−80955
  α-brass, optical transitions 2−44362
  α-brass, recrystn. texture, X-ray obs. 2−68139
  α-brass, stress corrosion sensitivity in $FeCl_3$ and $Fe_2(SO_4)_3$ solns. 2−64733
  α + β brass, superplasticity 2−64714
  α-brass, tarnish films and stress corrosion cracking, theory 2−64734
  β-brass obs. of anomaly in thermopower near order-disorder transition 2−84371
  Electrofax layers, effect of emission on print quality 2−66883
  luminous for ^3H det. in thin-layer chromatograms by scintillations 2−61832
  phthalocyanine, fluoresc. and photocond. 2−72426
  ZnSe(Te), thermal cond. and phonon scatt. by Fe^{2+} impurities 2−84213
  Ag-Zn-Al alloy, transition from internal to external oxidation 2−48331
  Ag-Zn, electrical conductivity, temp. depend. in range, melting pt. to 1100°C 2−71826
  b-Ag-Zn alloy, operative slip systems 2−60874
  Ag-Zn alloy, stress corrosion sensitivity in $FeCl_3$ and $Fe_2(SO_4)_3$ solns. 2−64733
  Ag-Zn(41 at%) alloy, deform. induced martensite, X-ray diffr. obs. 2−80846
  Al-Mg-Zn alloy, decomposition, phase transform., influence of Zn 2−43911
  Al-Mg-Zn alloys, preprecip. zone obs. 2−53885
  Al-(1.7 at.%) Zn, vacancy-impurity binding energy, positron-annihilation study 2−53727
  Al-Zn-Mg-Cu-Mn forging alloy, fracture toughness rel. to microstructure 2−53826
  Al-Zn-Mg-Cu alloy, fatigue behaviour of bolted joints 2−71622
  Al-Zn-Mg alloy, ageing process after quenching and cold work, resistometric obs. 2−71632
  Al-Zn-Mg alloy, precipitate free zone, elec. microscope obs. 2−56902
Zinc compounds continued
  Al-Zn-Mg alloy, solute distrib. using electron probe analyzer EMMA-4 2−56924
  Al-Zn-Mg alloy, stress corrosion crack paths 2−43732
  Al-Zn, ageing and formation of GP zones, elec. resistivity obs. 2−50800
  Al-Zn alloy, effect of coherency strain field on disloc. struct. 2−56702
  Al-Zn alloy, Seebeck coeff., comp. depend., 400°C 2−81162
  Al-Zn alloys, morphology and crystal structure of a precipitate, Y-phase, exam. 2−67986
  Al-Zn alloys, X-ray central diffusion study of Guinier Preston zones after quenching 2−64632
  Al-Zn solid solution, miscibility gap, resist. study 2−50826
  Al-Zn type alloy, GP zone composition by relative intensities of diffuse effects 2−68035
  Al-6.8%Zn alloy, diffusion and effects of Ag, Si or Mg 2−56753
  Al-Zn(4at%) alloy, fatigue hardening 2−80840
  Au-Zn alloy, β′ phase, liquidus and solidus temps. 2−80838
  Au-Zn dilute alloys, optical and piezo- optical properties from reflectivity measurements 2−68621
  $Ba_2Zn_2Fe_{12}O_{22}$ crystal, grown by seeding, density and distribution of dislocations 2−68026
  $Ba_3Zn_2Fe_{24}O_{41}$, hexagonal, anisotropy, comparison with $BaMg_2Fe_{12}O_{22}$ 2−72451
  Bi-Pb-Zn system, activity coeffs., calc. 2−43827
  Bi-Sn-Zn system, activity coeffs., calc 2−43827
  Bi-Zn, liquid binary alloys, absolute thermoelectromotive force 2−56518
  Bi-Zn alloys density obs. between m.p. and 600°C 2−43339
  Bi-Zn eutectic alloy, morphology, electron diffr. obs. 2−60976
  Cd-Sn-Zn system, activity coeffs., calc. 2−43827
  Cd-Zn system, liq., elec. resist. 2−46981
  $Cd_{2.8}Zn_{0.2}As$, high mobility, scattering, galvanomagnetic effects study 2−81090
  Cu-Zn-Mn system, phase diagram 2−50963
  Cu-Zn, electrical conductivity, temp. depend. in range, melting pt. to 1100°C 2−71826
  Cu-(30 wt.%)Zn alloy, relax. of diffused Zn during short-range-ordering 2−77705
  Cu-Zn (10 wt.%) and Cu-Zn, (30 wt.%) alloys, development of texture 2−80849
  Cu-Zn alloy, martensite memory, shape recovery effect 2−50935
  Cu-Zn alloys, with tarnish film in stress corrosion environments, electrometric study 2−68785
  Cu-Zn and Cu-Zn-Al, solubility of As 2−47619
  Cu-Zn dil. alloys, vacancy-impurity complexes and positron annihilation 2−47398
  Cu-Zn solid solution, Zn diffusion, residual activity method 2−47457
  Cu-Zn system, deform. influence on diffusion processes during electron irrad. 2−47456
  Cu-Zn(40%) microduplex, metallographic study of superplasticity and cavitation 2−80738
  α-Fe-Zn solid solution, precip., influence of P 2−80855
  Fe-Zn system, influence of ultrasonic strains on diffusion growth of various phases 2−43655
  $(Fe,Zn)_2Mo_3O_8$, Mossbauer effect 2−75270
  Ga-As-Zn system, GaAs-Zn polythermal section determ. 2−61046
  In-Zn, liquid binary alloys, absolute thermoelectromotive force 2−56518
  Li_4SiO_4-Zn_2SiO_4-Mg_2SiO_4-SiO_2 glass, phase equilibria and crystallization 2−64520
  Mg-Zn-Ni alloy, Laves phases, enthalpies of soln. and formation detn. 2−47692
  Mg-Zn alloys, Ostwald ripening during solidification of nondendritic spherical structures, model 2−64508
  Mg-Zn and Mg-Zn-Zr dendritic and nondendritic structs., soln. kinetics of secondary phases 2−47640
  Mn-Zn ferrite powders, comp. effects on technological props. 2−68163
  Mn-Zn ferrite single crystal, signal processing technique to obtain Kerr-effect M-H loops 2−48064
  Mn-Zn system, phase diagram, X-ray and magnetic obs. 2−57032
  $Mn_{1-x}Zn_xFe_2O_4$, mag. order 2−78022
  Na_2ZnGeO_4, solubility and crystn. kinetics under hydrothermal conditions 2−47242
  $Na_2Zn[PO_4](OH)$, cryst. struct. determ. 2−71439
  Ni-Co-Zn ferrite, h.f. magnetic props., temp. depend. 2−68723
  Ni-Zn-Co ferrite film, anisotropy induced by thermomagnetic treatment 2−81228
  Ni-Zn ferrite powder, hot-pressing and densification 2−43893
  Ni-Zn ferrite powder, quality characterization 2−57312
  $Ni_xZn_{1-x}Fe_2O_4$, thermal expansion coeffs. at Curie pt., conc. depend. 2−81281
  Sb-Sn-Zn system, heats of mixing, 650°C 2−43336
  Si-$ZnSiP_2$ solid solution, epitaxial growth on Si 2−60665
  Sn-Zn alloy, unidirectional solidification, uniaxed crystal origin 2−74882
  $Y_3Cd_4Zn_7$ crystallographic system, lattice parameter and space group determ. 2−80644
  ZNO/O adsorbed layers, sensitizing action by chlorophyll to corona discharge 2−44176
  Zn-Ag alloy, application of Lindemann's rule for melting 2−74582
  Zn-Ag crystals, ion beam thinning 2−79103
  Zn-Al-Cu-Mg alloy, tensile deform. and high-temp. creep rel. to microstruct. 2−56800
  Zn-Al-Mg alloy, soln. softening effect of Zn additions at high temps. 2−47613
  Zn-Al alloy, liq., Zn activity at 1053K, comp. depend., Krupkowski's eqn. 2−56498
  Zn-Al alloy, solute distrib. using electron probe analyzer EMMA-4 2−56924
  29 at.%Zn-Al alloy, spinodal decomp., metastable rhombohedral form., elastic anisotropy effects 2−56923
  Zn-Al alloys, strain-rate depend. of deform. mechanism and texture form. 2−84011
  Zn-Al eutectic alloy, room-temp. deform. characts. rel. to superplasticity 2−43701
  Zn-Bi alloy, surface tension, 860-920K 2−43341

Zinc compounds continued
Zn-Cd-Te, system, phase diagram, rel. to cryst. growth technique selection 2–47702
Zn-Cd alloy, microsegregation of Cd during growth, partition coefficient 2–47648
Zn-Cd dilute alloy, dendrite growth and morphology 2–43488
Zn-0.1%Cd, single crystal, deformed, slip lines, elec. microscope obs. 2–47421
Zn-Cr alloy, dilute, elec. resist., $T<0.1K$ 2–68342
Zn-Cr Kondo alloys, supercond. below 0.1K 2–44082
Zn-Cu alloy, application of Lindemann's rule for melting 2–74582
Zn-Cu alloy, b.c.c., superplasticity 2–50745
Zn-Cu alloys, electrometric characterization of tarnish films 2–77717
Zn-Fe, interdiffusion coeffs. determ. 2–47459
Zn-Fe alloy, phase diagram, obs. of Fe rich side 2–50967
Zn-Ga, liquid binary alloys, absolute thermoelectromotive force 2–56518
Zn-In-S system polytypes, vapour growth 2–50579
Zn-M dilute alloy, M=Mn, Cr, Fe, Kondo effect and localized spin fluctuations 2–64918
Zn-Mg-Mn-Al alloy, strength rel. to rest between quenching and ageing, effect of additions 2–50803
Zn-Mg-misch metal alloy, struct. 2–50624
Zn-Mg misch metal alloy, struct. 2–50624
Zn-Mn alloy, dilute, elec. resist., $T<0.1K$ 2–68342
Zn-Mn Kondo alloys, supercond. below 0.1K 2–44082
Zn-Ni ferrites, mag. losses in h.f. fields 2–84435
Zn-Pb alloy, liq., elec. resist. at 500°C 2–60507
Zn-Sn-Cd-Bi liquid quaternary solution, thermodynamic props., e.m.f. method 2–71186
Zn-Sn alloy, liq., elec. resist. at 500°C 2–60507
Zn-Ti alloys, effect of cooling rate and composition on as cast microstructure 2–80818
Zn-V(Cr)(Mn)(Fe)(Co)(Ni) dilute liquid alloys, mag. susceptibility 2–80485
$(Zn, Mn, Fe)Ti_3O_7$, landauite, Baumhauer type twins 2–71499
Zn complex, 2,6-pyridinedicarboxylate, Cu-doped, e.p.r., mag. parameters 2–78155
Zn complexes, porphyrins, e.p.r. spectra, hyperfine structure 2–50071
$ZnAl_2O_4$, partial volume determination, influence of composition for solid solution glass ceramics 2–56562
$ZnAs_2$, optical spectra and band structure 2–51326
$ZnCO_3$, study of X-ray K absorption edge of Zn atom 2–70595
$Zn_xCd_{1-x}Se$ solid solution, phonons and struct., Raman scatt. obs. 2–64837
$Zn_xCd_{1-x}Te$, luminesc. reson. Raman scatt., exciton transition 2–54437
$Zn_xCd_{1-x}Te$, reflectivity spectra, band struct. obs. 2–78093
$Zn_xCd_{1-x}Te$ solid solution, phonon freq. detn. from reflection spectra 2–72308
$Zn_{1-x}Cu_xCr_2Se_4$, magnetization and susceptibility, 4.2-900 K 2–44311
$Zn_xCu_{(1-x)}Fe_x Mn_{(2-x)}O_4$, X-ray determ. of lattice parameters, assignment of crednerite and gahnite symmetries 2–60768
ZnF_2, ab initio SCF study, determ. of Walsh diagram and molecular orbitals 2–70730
ZnF_2, mag. hyperfine interactions of Fe^{2+} interpret. 2–61604
ZnFOH, ^{19}F and ^1H n.m.r. 2–84591
$Zn_2Fe(CN)_5NO.2H_2O$, i.r. spectra, cryst. chem. 2–78081
ZnGa-V(Cr)(Mn)(Fe)(Co)(Ni) dilute liquid alloys, mag. susceptibility 2–80485
$ZnGa_2O_4$, spinel, oxygen parameter determ. 2–47353
$ZnGeAs_2$, $ZnGeP_2$, sphalerite- chalcopyrite transition, struct. of phases, microhardness 2–57025
$ZnGeP_2$, absolute signs of second harmonic generation coeffs. 2–44332
$ZnGeP_2$, cryst. growth and struct., optical props. and energy gap 2–80599
$ZnGeP_2$, i.r. birefr. and optical activity 2–72261
$Zn_xHg_{1-x}Te$ solid soln., light-hole band rel. to transport phenomena 2–64992
$Zn_{1.685}In_{2.21}S_5$, $Zn_{4.37}In_{2.42}S_8$, $Zn_{6.18}In_{2.58}S_{10}$, cryst. struct. 2–60771
$Zn(NO_3)_2$, aqueous solns., ion pairing, Raman spectra obs. 2–60475
ZnO:Cu film, amorphous, band struct. and impurity state energy spectrum 2–68421
$ZnO:Cu^{2+}$ e.s.r. line width, doping and temp. depend., spin-lattice relaxation mechanism 7-17 K 2–65328
$ZnO:Nb^{2+}$, dynamic Jahn-Teller effect, e.s.r. obs. 2–48284
ZnO/Al_2O_3, heteroepitaxial layer structure, surface acoustic props. rel. to delay line behaviour 2–68235
$ZnO-Al_2O_3-SiO_2$ glass-ceramics, dielec. props. and effects of adding (CaO, SrO, BaO) 2–65045
$ZnO-Bi_2O_3$ ceramic, elec. props. 2–57198
(ZnO-MgO):Fe,O photoconductor, transient effects 2–84377
$ZnO-Nb_2O_5-SiO_2$, ternary system, phase relations at liquidus and subsolidus temps, 2–68203
$ZnO-TeO_2$, phase equilibrium 2–64504
ZnO-resin electrophotographic coating for positive charging 2–63452
ZnO, (0001) surface, field emission and surface states 2–54271
ZnO, absorbed Hg excited atoms and molecules, interaction, elec. cond. study 2–47175
n-ZnO, acoustoelec. oscills. 2–61332
ZnO, band struct., photoemission study 2–75196
ZnO, chemisorption of H_2, i.r. studies of isotope effects 2–65375
ZnO, cryst. growth, inversion twin obs. 2–50581
ZnO, decay of pyroelectrically induced polarization charges 2–54241
ZnO, electrode potential control, possible use as probe for electrochemical reactions 2–61717
ZnO, electron irrad., F^+ centre, e.p.r. obs. 2–47366
ZnO, epitaxial layer on Ge and GaAs, electron diffr. obs. 2–74636
ZnO, epitaxial layers on Al_2O_3, surface wave acoustic props. 2–51020
ZnO, experimental sintering kinetics, approx. equation 2–47652
ZnO. Fuchs Kliewer surface modes, low energy electron spectroscopy obs. 2–50987

Zinc compounds continued
ZnO, growth from vapour phase, influence of multicomponent conc. 2–43515
ZnO, morphology, physico-chem. conditions influence during growth 2–43514
ZnO, photovoltage inversion effect, surface states continuous spectrum 2–48000
ZnO, polycrystalline study of spectral, chemical sensitization centres of internal photo-effect, optical extinction method 2–75176
ZnO, pure and doped single crysts., vapour phase growth 2–50580
ZnO, r.f. sputtered onto sapphire, u.s. transducers at microwave frequencies 2–52243
ZnO, Rayleigh wave electromech. coupling const., acoustic wave vel. obs. 2–43969
ZnO, resonance Raman scattering bt turnable dye laser 2–84486
ZnO, sintering, effects of O_2 press. 2–74916
ZnO, study of X-ray K absorption edge of Zn atom 2–70595
ZnO, thermal cond. and phonon scatt. by Fe^{2+} impurities 2–84213
ZnO, two-phonon sidebands in i.r. absorption due to third-order potential 2–75284
ZnO, X-ray induced electron emission, core electron energy levels detn. 2–48019
ZnO, Zeeman splitting of anomalous shallow bound states 2–51349
ZnO acoustoelectric device, resistivity, threshold field, current oscills. 2–63119
ZnO anode, electron injection 2–61797
ZnO as low temp. photometer filter in 20 μ atmospheric window 2–63399
ZnO crystal, growth by chemical vapour transport and semicond. props. 2–43516
ZnO differential absorption spectra on adsorption of molecules of donor-acceptor type 2–68651
ZnO film, Burstein-Moss effect 2–51350
ZnO film, d.c. triode sputtered, u.s. surface elastic waves, coupling factor phase velocity, propag. loss 2–80560
ZnO film, surface states, thermally stimulated exo-emission obs. 2–48008
ZnO film surface acoustic wave transducers, coupling constants and film thickness 2–49152
ZnO luminescence, depend. on adsorbed gases 2–78121
ZnO plate, dispersion curves of flexural modes 2–84205
ZnO powder, particle size distrib. data processing, computer appl. 2–53942
ZnO semiconductor/metal barrier props. 2–71985
ZnO single crystal, hydrothermal growth rate and morphology 2–47247
ZnO suspension and film, photocurrents and photovoltages obs. 2–51218
ZnO thermal control coating pigment, u.v. irrad., e.s.r. of defects 2–81460
ZnO thin film oxygen partial pressure sensor 2–41454
ZnO(c), heat capacity, drop calorimetry and diff. scanning calorimetry 2–54047
ZnP_2, optical spectra and band structure 2–51326
ZnS:Cu, Al, Br film, temp. depend. of electrolum. and thermal quenching 2–84533
ZnS:Cu, Pb, Cl film, temp. depend. of electrolum. and thermal quenching 2–84533
$ZnS-CdS:Er^{3+}$ mixed fluorescent compounds, spectroscopic investigation 2–84545
ZnS, multilayer, quarter wave, generalized Brewster angle condits. at non-normal incidence 2–79410
$ZnSO_4$, study of X-ray K absorption edge of Zn atom 2–70595
$ZnSO_3.2H_2O$, X-ray single crystal analysis of structure, Patterson and Fourier synthesis 2–60770
$ZnSO_4.7H_2O-NiSO_4.7H_2O-CoSO_4.7H_2O$, isomorphous relationships, distribution coeff. 2–74959
$ZnS_{1-x}Se_x$, stimulated cond. with persistent memory 2–75104
$ZnS_{1-x}Se_x$ mixed crystals, optical reflectivity and band structure 2–54407
ZnSe:Ag, impurity levels 2–51151
$ZnSe:Co^{2+}$, ligand hyperfine struct., molecular orbital approx. calc. 2–51294
$ZnSe:Cr^{2+}$, Jahn-Teller splitting, optical absorp. spectrum obs. 2–65270
ZnSe:Ge, Pb, e.p.r. theory 2–51399
ZnSe:Mn, luminesc. enhancement by electric fields in polycryst. and crystalline samples 2–48249
ZnSe-CdTe system, miscibility 2–77464
ZnSe-GaP alloy, cond. hopping contrib., ionized impurity scatt., electrolum. and cathodolum. 2–81415
$XZnSe-Ge_{1.5}As_{0.5}Se_3$, pseudobinary system, glass formation 2–80531
ZnSe, chem. vapour deposition of transparent polycrysts. 2–50578
ZnSe, dielec. function, freq.- and wave-vector-depend., calc. 2–84262
ZnSe, dislocation etch pits 2–50677
ZnSe, donor-acceptor emission energy shift on varying the excitation intensity 2–72388
ZnSe, electron energy loss spectra 2–75111
ZnSe, electron irrad., cathodolum., Se atom displacement 2–61723
ZnSe, electron irrad., vacancy obs. 2–47366
ZnSe, ionicity, dispersion, and optical spectra 2–44374
ZnSe, many-photon absorp., carrier generation obs. 2–84519
ZnSe, optical props. of subsitutional donors 2–51372
ZnSe, pair photolum., peak energy, excitation intensity depend. 2–75318
ZnSe, self-consistent local orbitals 2–75031
ZnSe, spin-flip Raman scatt., linewidths and two-electron processes 2–84501
ZnSe, spin-flip scattering from free and bound electrons 2–44389
ZnSe, time of flight mobility, and trapping 2–44107
ZnSe, vapour growth, donor and acceptor identification 2–50573
ZnSe, vapour phase cryst. growth under controlled partial press. 2–64594
ZnSe, vapour phase deposition to improve contrast in metallographic obs. of transition zones 2–43780
n-ZnSe, vapour phase epitaxial growth on pGaP, electrical properties 2–80596
ZnSe, X-ray K emission bands, valence electron obs. 2–68672

Zinc compounds continued
  ZnSe (Cu, Ga), epitaxial thin films, photoluminescent, oscillations of photocurrent 2−78147
  ZnSe coatings on hard metals, metallographic production of phase pictures 2−56918
  ZnSe differential absorption spectra on adsorption of molecules of donor-acceptor type 2−68651
  ZnSe film, epitaxial, struct., composition and elec. props. 2−56582
  ZnSe X-ray induced electron emission, core electron energy levels detn. 2−48019
  ZnSe X-ray photoemission valence-band spectra, valence-band densities of states 2−81192
  n-ZnSe(Cu,Ga) film, photolum., photocurrent oscills., 80-220K, luminesc. field quenching 2−81168
  $ZnSe_xTe_{1-x}$, refl., 2.0-6.6 eV, rel. to comp. depend. of energy gap 2−84500
  $ZnSiAs_2$, polarized reflectance spectra 2−61626
  $ZnSiAs_2$, sphalerite-chalcopyrite transition, struct. of phases, microhardness 2−57025
  $ZnSiF_6.6H_2O$, n.m.r. study of internal motions 2−51415
  $ZnSiF_6.6H_2O$ spin-lattice relax. of Cu^{2+} phonon assisted tunnelling contrib. 2−84456
  Zn_2SiO_4:Mn, thermoluminesc., glow curves, impurity depend. 2−48258
  $Zn_2SiO_4:Mn^{2+}$, willemite, cathodoluminesc., electron microprobe obs. 2−51382
  $ZnSiP_2$, crystal growth, sublimation technique 2−64593
  $ZnSiP_2$, i.r. transmission cut-off 2−78058
  $ZnSiP_2$, optical phonons, polaritons, mode freqs., strengths, damping factors 2−61621
  $ZnSnAs_2$, $ZnSnP_2$, band structure, electroreflectance spectra obs. 2−81404
  $ZnSnAs_2$, $ZnSnP_2$, sphalerite-chalcopyrite transition, struct. of phases, microhardness 2−57025
  ZnTe:Al, high temp. elec. props., self-compensation model 2−51128
  ZnTe:Ge, Pb, e.p.r. theory 2−51399
  ZnTe-InAs heterojunction, prep. by liq. phase epitaxy, optical and elec. props. 2−57213
  ZnTe, absolute signs of second harmonic generation coeffs. 2−44332
  ZnTe, absorpt. due to acceptor levels 2−57353
  ZnTe, double-acceptor cathodolum. 2−54480
  ZnTe, heat and entropy of melting 2−47033
  ZnTe, high temp. defect. equilib., elec. transport props. 2−44096
  ZnTe, impure, multiphoton luminesc. satellites in strong e.m. field 2−61679
  ZnTe, physical properties, device applications 2−64962
  ZnTe, resonant exciton absorpt. structures 2−61200
  ZnTe, threshold energy for Te displacement, cathodoluminesc. obs. 2−68018
  ZnTe, X-ray induced electron emission, core electron energy levels detn. 2−48019
  ZnTe and $Zn_xCd_{1-x}Te$, spontaneous luminescence and lum. spectra detn. 2−72417
  ZnTe epitaxial film, optimum growth conditions 2−47105
  ZnTe film, on Ge, epitaxial growth and struct. 2−50515
  ZnTe film on NaCl, KCl, determ. migration length, 1.5 to 10 K 2−80563
  ZnTe Schottky barrier, admittance spectroscopy of deep impurity levels 2−61391
  Zn_2TiO_4, i.r. absorpt. spectra, ionic ordering 2−72342
  $ZnWO_4:Co^{2+}$, epr spectrum and interpretation 2−81457
  $ZnWO_4:Co^{2+}$, spin-lattice relaxation and time constant meas. 2−81311
  $ZnWO_4:Cr^{3+}$, impurity conc. determ., e.s.r. and optical emission studies 2−78157
  $ZnWO_4:Cr^{3+}$, temp. variation of e.p.r. line splitting by external electric field 2−72473
  $ZnWO_4:Fe^{3+}$, e.p.r., elec. field effect 2−48286
  $ZnWO_4$, effect of struct. charact. on penetration of Cr and Gd impurities 2−71542
  $Zn(py)_2X_2$ complexes, py = pyradine, X = halogen, band assignments from far i.r. and Raman spectra based on isotope shifts 2−70731
  Zr-Co alloy system, paramagnetic behaviour in non stoichiometric composition of the Laves phase compound 2−81220

zinc sulphide
  — 2−56582
  cathodoluminescence, rel. to S atom displacement by electron irrad. 2−48263
  core electron energy levels, X-ray induced electron emission obs. 2−48019
  crystal growth, vapour phase, polytype form. and perfection rel. to photovoltaic effect 2−47227
  crystal texture, stacking order, polytypic ordering and birefringent striations 2−47213
  cubic, anisotropy of Raman scatt. intensities 2−65282
  dielectric thin film, interference method for meas. of dispersion in refractive index 2−44342
  differential absorption spectra on adsorption of molecules of donor-acceptor type 2−68651
  diffusion of Mn, Au, and S 2−56764
  electroluminescence in homogeneous single crystal wide-gap semiconductor, electronic props. 2−68712
  electroluminescent p-n junction, electronic behaviour obs. 2−68711
  electron energy loss spectra, refl. technique 2−75111
  electron irrad., F^+ centre, e.p.r. obs. 2−47366
  epitaxial film, on GaAs, struct. 2−71339
  epitaxial growth on Si by forced vapour transport 2−50514
  exciton piezoreflectance, exciton states exchange splitting by stacking faults 2−81391
  exciton state excitation, spectroscopic investig. 2−71810
  film, amorphous, in m.i.m. structs., electroforming and elec. cond. props. 2−64978
  film, in electrolum. device, high field a.c. electrolum. rel. to field clamping 2−81412
  film, sputtered and evap., optical props. as function of deposition conditions 2−48131
  hexagonal modification, melt growth, defect elimination by donor impurity doping 2−47279

Zinc compounds continued
zinc sulphide continued
  hollow crystal, growth by pulling sealed tube method 2−43527
  inclusion identification by vapour phase deposited interference layers 2−56737
  luminescence extinction by electric field 2−75331
  luminescence obs. disappearance of electron traps under influence of pressure 2−61722
  luminophor, Gudden-Pohl effect, optical quenching 2−51393
  luminophors, prep., 36−180°C 2−78141
  many-photon absorption, carrier generation obs. 2−84519
  multilayer, quarter wave, generalised Brewster angle conditions at non-normal incidence 2−75175
  optically transparent polycryst. prep. by chem. vapour deposition 2−50578
  phosphor, microwave photocond. and luminesc. 2−51213
  phosphor, photolum. and electrolum., temp. depend. 2−48267
  phosphor electroluminescence abnormality due to variable d.c. bias, obs. 2−51392
  phosphor electroluminescence abnormality with variable impedance 2−48268
  photoconductivity, two-photon, linear behaviour 2−72070
  photoelectroluminescence following u.v. irradiation confliction with Fischer model 2−51391
  polytypes, determ. of Madelung potentials by rule of thumb up to six figures 2−80589
  polytypes, high-order, identification and reliability of results 2−56670
  polytypes, Raman scatt. obs. 2−61084
  polytypic growth of single crystals 2−60769
  polytypism, new polytypes of 28L family 2−68009
  scintillating phosphor in radioactive reference lights, transient temp. depend. 2−49443
  self-activated, excitation spectra of blue emission bands 2−61682
  spin-flip scattering from free and bound electrons 2−44389
  Stark ladder levels 2−68276
  thermal conductivity, and phonon scatt. by Fe^{2+} impurities 2−84213
  two photon photoconductivity 2−61450
  vapour phase epitaxial on pGaP, electrical properties 2−80596
  vibrational amplitudes and Debye- Waller factors from elastic consts. and Raman freqs. 2−50983
  $CdS_{1-x}Zn_xS:Mn$, Mn^{2+} conc., e.p.r. determ. 2−72481
  $Cd_{1-x}Zn_xS:Mn^{2+}$, hyperfine interaction const., temp. and comp. depend., e.p.r. study 2−81456
  $Cd_xZn_{1-x}S$ film, prep. and comp. depend. of energy gap and resist. 2−54169
  (Zn, Cd)S:Ag, Ni, fluorescence, efficiency curves, investigation of Klasens' simple thermal quenching theory 2−48250
  (Zn,Cd)S phosphors, diffuse reflection spectra for studying and controlling properties 2−75332
  (ZnCd)S:Cu,Cl phosphors, luminescence emission spectra and decay characteristics as a function of temperature 2−78120
  $Zn_xCd_{1-x}S$:Cu, Cl temp. and i.r. quenching of luminescence and photocond. 2−84543
  $Zn_{1-x}Cd_xS$, melt-grown single crysts., struct. 2−64646
  $ZnCd_{1-}S$, steeply graded, photoluminescence and growth 2−72444
  $Zn_xCd_{1-x}S$ evaporated layers as photoresistors in u.v. 2−44179
  ZnS:Ag,Mn,Cl phosphors, mechanism of activator interactions 2−84551
  ZnS:Ag phosphors, stimulated emission characteristics 2−65297
  $ZnS:Al,Co^{2+}$, grown from melt, struct. rel. to Al additions, Co^{2+} spectra obs. 2−77559
  ZnS:B, luminesc., 400-800 nm, 110, 295 and 430K 2−75322
  ZnS:Be, i.r. lattice absorption spectra, localized mode sidebands obs. 2−72385
  ZnS:Cl, quenching of photolum. by elec. field 2−72416
  ZnS:Cl film, photovolt, polarity reversal by excess Zn 2−51222
  ZnS:Co with stacking faults, piezospectroscopic effect on group of zero-phonon lines associated with centres 2−44384
  ZnS:Cu:Co,(O) photoconductor, existence of negative thermally stimulated current and transient effect 2−68481
  ZnS:Cu, Cl, changes in brightness wave during ageing 2−65316
  ZnS:Cu, recombination of green luminesc., tunnelling effects 2−48236
  ZnS:Cu, surface, volume, and contact components of current 2−71918
  ZnS:Cu phosphor particles with nonluminescent coatings, cathode-ray efficiency, voltage depend. 2−51383
  ZnS:Cu phosphors, extralinear effects in thermostimulated luminescence 2−75335
  $ZnS:Fe^{2+}$, crystal field splitting, effect of configuration interaction 2−51293
  ZnS:Mn films, energy level scheme from reflectivity and transmission meas. 2−71799
  ZnS:Mn laser, gain calcs. 2−79213
  $ZnS:Mn^{2+}$, ^4E level, uniaxial stress effects, absorpt. study 2−84506
  ZnS:Ni,O, photocond., spectral response interpret. 2−57258
  ZnS-CdS, evaporated layers, mosaic heterojunction photo-emf 2−77970
  ZnS-Cu,Co,Cl, differences between optical and thermal depths of electron traps 2−51395
  ZnS-Cu crystallites, centres of luminescence, radiation intensity, influence of milling 2−51390
  $ZnS-Na_3AlF_6$ multilayer system, optical props. calc. 2−45810
  ZnS with Cu and Cl impurities, photo- and electroluminescent props. 2−51394

Zirconium
  atom, K X-rays produced by heavy ions, energy shifts and relative intensities 2−64013
  de Haas-van Alphen effect, rel. to Fermi surface 2−84249
  diffusion mechanism in β-modification 2−68044
  diffusion of hydrogen, 275-700°C 2−53773
  electrical and thermal cond., 20 to 1200°C 2−47769
  fault elimination by cold rolling, determ. by meas. elec. resist. 2−43797
  Fermi surface, transverse magnetoresist. study 2−84248
  in graphite, effect on ordering process 2−50829
  impurities in concentrates, spectrochemical determination 2−72591
  lattice dynamics, elastic consts., and thermal expansion calc. 2−43964

Zirconium continued
neutron irrad., dislocation loops characteriz. 2−43639
neutron irrad. effects on aqueous oxidation, 290°C 2−44486
oxidation kinetics, short-time O_2 exposure, 440-850°C 2−51453
refractories, influence of gaseous medium on phase composition 2−84095
in steel, rel. to retarding recrystn. during thermomech. treatment at high temp. 2−60961
strain rate depend. hardening 2−50847
strain-ageing, internal friction and electron microscope obs. 2−47599
tubular materials, texture and anisotropy rel. to plastic deform. 2−53916
vacancies, formation energy, quenching obs. 2−53728
X-ray spectrum, L-emission interpret. 2−64037
zircaloy-2 with Y_2O_3 dispersed, prep. of thin foils for transmission electron microscopy 2−80549
α-Zr, ductile void growth and crack propag. 2−50778
inAl-Mg alloy, effect on stress corrosion cracking 2−50775
Al-9.5 wt.%Mg:Zr alloy, mech. props., fracture toughness, cracking effect of alloy in additions 2−47546
Hf polycrystalline sample, influence of Zr on the quadrupole interaction of ^{181}Ta 2−84593
Nb + Zr + Ti and Nb + Ti alloys, properties of welded joints 2−61227
SrS:Mn, Zr phosphors decay study 2−75330
Zr:Y_2O_3, dispersion-hardened, prep. of thin foils for transmission electron microscopy 2−80549
Zr-Nb-Ti alloy, Cu cladding bimetallic wire, solenoid, strong pulsed magnetic field 2−63255
α-Zr, bulk diffusion of ^{51}Cr 2−67357
α-Zr, diffusion of oxygen, coeff. variations 2−71543
Zr, electron scattering mechanisms at high temps. rel. to kinetic properties 2−81035
α-Zr, ultra-fast diffusion of ^{59}Fe, ^{60}Co, and ^{63}Ni 2−64697
Zr-^{3}H bombardment target, calc. of ^{2}H-^{3}H neutron yield 2−42443
ZrVI, spectral anal., configurations and levels determ. 2−74225
ZrVI, spectrum rel. to YV, NbVII and MoVIII 2−74217
^{95}Zr-^{95}Nb accumulation in coastal sediments 2−62044
^{95}ZrNb concentrations in Atlantic Geosecs II water column rel. to oceanic circulation 2−75475
α-Zr. grain size depend. of deform. behaviour 2−50748

Zirconium compounds
alloy, ω phase struct. symmetry 2−47349
alloy, anisotropic creep behaviour under fast neutron flux 2−50756
alloy, b.c.c., struct. and decomp. 2−68204
alloy, conference, Montreal, Canada (Aug. 1971) 2−50815
alloy, corrosion and hydriding behaviour in org. coolants 2−51454
alloy, corrosion resist. in steam, 400 to 500°C 2−51457
alloy, elec. resist., exponential temp. depend. 2−54129
alloy, foil prep., for electron microscopy, electrolytic jet thinning procedures 2−71415
alloy, high-strength, creep and stress-rupture 2−53921
alloy, high-strength, development 2−53920
alloy, in-flux corrosion in pressurized water loop 2−51455
alloy, nuclear fuel element sheath, F contamination, proton activation analysis 2−52876
alloy, strain-induced phase transforms., microstruct. exam. 2−54000
alloy, stress corrosion cracking, fracture surface study 2−43737
alloys, accelerated oxidation, significance of surface preparation 2−68786
alloys, anisotropy of secondary in-reactor creep, relation to texture 2−67349
ceramics, phase analysis by X-ray analysis, matrix method, polymorph technique 2−80879
composite material, graphite−ZrC_x(−Zr) systems, durability props. rel. to comp. and struct. 2−77741
rare earth-zirconium alloys, form. of metastable low temp. allotropic solid solns. 2−47646
tubing, method for determining pole figure 2−67979
zircaloy, for fuel cladding, properties 2−49893
zircaloy, in water cooled reactors, hydriding rel. to surface conditions 2−81502
Zircaloy, tubular materials, texture and anisotropy rel. to plastic deform. 2−53916
Zircaloy 37-rod cluster in pressurized water reactor, emergency cooling 2−79834
zircaloy cladding, rel. to corrosion and hydrogen pick up dependent on coolant 2−49892
Zircaloy cladding-fuel reaction 2−59853
Zircaloy tubing, mech. props., effect of oxygen and fabrication variables 2−53915
zircaloy-2, -4, tensile props. rel. to neutron irrad. 2−80664
Zircaloy-2, containing ZrH_x, fatigue, metallographic obs. 2−47649
Zircaloy-2, corrosion in steam-water mixture under reactor radiations 2−51456
Zircaloy-2, dispersion strengthening with yttria 2−53917
Zircaloy-2, irrad. and temp. effect on tensile and creep props. 2−43802
Zircaloy-2, low-cycle fatigue behaviour at 573 K 2−60943
Zircaloy-2, stress orientation and circumferential ductility, thermal cycling effect 2−53914
Zircaloy-2, thermal diffusivity, thickness effects 2−57085
zircaloy-2(-4), diffusion of hydrogen, 275-700°C 2−53773
Zircaloy-2 anodic oxide, in m.i.m. struct., pre-breakdown electrical switching 2−47951
Zircaloy-4, deform. and fracture 2−50747
Zircaloy-4, neutron irrad., deform. parameters, 300°C 2−50749
Zircaloy-4 tubing, yield loci, effect of texture variations 2−50850
zirconia electrolyte appl., oxygen ion conduction 2−49259
$Al_2O_3/ZrO_2/Y_2O_3$ eutectic, directionally solidified, mech. props. 2−47526
$Al_2O_3/ZrO_2/Y_2O_3$ system eutectics, strength 2−47525
CeO_2-ZrO_2-Y_2O_3 solid solns., electronic behaviour 2−47893
Cu-Zr-Cr, precip. processes, specific heat and resistivity obs. 2−50933
Cu-Zr, Cu-Zr-Cr alloys, precip. size effect on recrystalliz. temp. 2−56927
Cu-Zr, dil. alloys., softening resistance mechanism 2−56709
HfB_2-ZrN alloy, microhardness and resist., conc. depend. 2−47638

Zirconium compounds continued
Mg-Th and Mg-Th-Zr systems, e. microscopy exam. of precipitation 2−71690
Mg-Zn-Zr nondendritic structs., soln. kinetics of secondary phases 2−47640
Mg-Zr alloy, Ni diffusion and precip. formation 2−47467
Mg-Zr alloys, precipitation processes, elec. microscope obs. 2−53993
Mo-Zr alloy, vapour deposited, struct., electron microscope obs. 2−60594
Nb-Ti-Zr alloy, supercond. wire, crit. current, mag. field intensity depend. 2−75062
Nb-Zr-Ti alloy, supercond., struct. determ. 2−50842
Nb-(40 wt.%)Zr alloy, metallurgical variables influence on supercond. 2−47861
Nb-(25 wt.%)Zr wire, macroscopic quantum effect in meas. of current threshold 2−57166
Nb-Zr alloy, vapour deposited, struct., electron microscope obs. 2−60594
Nb-Zr alloys, internal friction peaks due to nitrogen impurity 2−60849
$POCl_3$:$ZrCl_4$:Nd^{3+} liquid laser, amplification of mode locked trains 2−59167
PrO_x-ZrO_2 ternary system, phase relationships, oxygen press. effect 2−47694
TZM alloy, arc casted, props. and applications 2−53825
Ti-Al-Mo-Zr alloy, ductility, influence of β-phase 2−50746
U-Nb-Zr alloy, low temp. oxidation 2−48334
UC-ZrC solid solns., diffusion props. 2−71541
UO_2-Zircaloy-2 contacts, thermal conductivity 2−42655
Zr-Al-Cu-Mg-Mn-Fe-Si-Ni-Ti alloy, D16T, recryst. and uncryst. struct., fracture under static and cyclic conditions 2−47527
Zr-Al dilute alloy, ordering and stacking faults 2−47354
Zr-B system, phase diagram 2−50957
Zr-C-N-O solid soln., phase diagram, form. of carbonitrides and oxycarbides 2−54010
Zr-C-O system study and formation of different composition zirconium oxycarbides, NASA research 2−64801
Zr-(2at.%)Cr-(0.16at.%)Fe alloy, precip. reactions rel. to corrosion resist. 2−53919
Zr-(1.5wt.%)Cr-(0.1wt.%)Fe tubing, hydrided, mech. props. and struct. 2−53918
Zr-Cr-Fe alloy, correl. of microstruct. with properties 2−53922
Zr-Cu alloy, weakening resist. rel. to deform., heating time and temp. 2−50764
Zr-H(O) dil. alloys, internal friction peaks 2−50737
Zr-Mo-Ti alloys, radiation induced transformations in h.v. electron microscope 2−80874
Zr-(2.5 wt.%) Nb press. tubes, heat-treated, embrittlement 2−50770
Zr-(2.5 wt.%) Nb press. tubing, hydriding, orientation and effect on tensile props. 2−50849
Zr-Nb-C, electron work function measurement, pulsing voltage procedure 2−63235
Zr-(2.5wt.%)Nb press. tubes, irrad., metallurgical props.53913 2−53913
Zr-Nb alloy, strain rate depend. hardening 2−50847
Zr-Nb alloy, supercond. transition temp., constitution and microstruct. effects 2−51107
Zr-Nb alloys, phase transforms. 2−53999
Zr-(2.5 wt%)Nb press, tubes, texture development 2−50848
Zr-O (B)(C) thermionic emission constants and electron work function changes 2−54268
Zr-O alloy, strain-ageing, internal friction and electron microscope obs. 2−47599
Zr-O α solid solution, cryst. struct., neutron and X-ray diffr. obs. 2−71443
Zr-O system, near $ZrO_{1/3}$, interstitial order-disorder transform. 2−68205
Zr-Sn alloys, solute strengthening at high temps. 2−50846
Zr-Ta-C, electron work function measurement, pulsing voltage procedure 2−63235
Zr-Ta(Nb)-C thermionic emission constants and electron work function changes 2−54268
Zr-Ti-Al-N film, sputtered, struct., elec. resist. props. 2−47130
Zr-W-Ti alloy, mech. and technological props. 2−47535
Zr-Y syst., H_2 diffusion through layers, calc. by eigenfunction method 2−50720
Zr-alloy reactor pressure tubes rel. to tube irradiation programme 2−76953
ZrB_{12}, electronic spectra and phys. props. 2−47838
ZrB_2, thermionic emission, rel. to electronic struct. 2−48017
ZrB_2 as grain growth inhibitor for HfN 2−50883
$ZrBr_4$, orbital valence force field consts. 2−77075
ZrC_x/C composite, vapour deposition by iodide process 2−50922
ZrC-C composites, vapour deposition by the chloride process 2−80793
ZrC-NbC, solid solution, creep in compression, temp. range 2600-3150 K 2−84033
ZrC-W compounds, high temp. vacuum evaporation 2−73239
ZrC-W solid soln., interactions, isothermal sections struct. at 2200 and 2600°C 2−74911
ZrC, thermal conductivity between 2100 and 3400 K 2−61117
$ZrC_{0.95}$, low temp. sp. ht., differences from Debye model 2−80920
ZrC_x fibres, physical and mech. props. detn. 2−68178
$Zr_{0.85}Ca_{0.15}O_{1.85}$, use as selective O_2 leak source in vacuum system 2−85174
$ZrCl_4$-$POCl_3$:Nd liquid laser, Q-switching parameters and energy scaling 2−59166
$ZrCl_4$, orbital valence force field consts. 2−77075
$ZrCr_xO_y$, lattice spacing rel. to O content 2−56671
$Zr_3Cu_4Si_2(Ge_2)$, cryst. struct. 2−43597
$ZrFe_2$:Np, hyperfine splitting of ^{239}Np 2−46207
ZrH_x, effect of H_2 chemical binding on effective cross sections and n spectra, calc. 2−56029
ZrH_x, electron-nuclear interactions rel. to spin-lattice relax. 2−78047
ZrI_4, orbital valence force field consts. 2−77075
ZrN_x, microhardness and thermal expansion, 80-300K 2−61112
Zr_2Ni_7, cryst. struct. 2−43596
ZrO_2-CaO ceramic, struct., thermomech. props. 2−43876

Zirconium compounds continued
  ZrO_2-Ce_2O_3, phase relation by quenching between 1350 and 1900°C 2−74935
  (ZrO_2-CeO_2) + Cr_2O_3 solid soln., formation of cubic solid soln. $CeCrO_3$ on calcining in vacuum 2−84095
  ZrO_2-W, composite, growth by unidirectional solidification of eutectic melt 2−64796
  ZrO_2-W composite, thermal shock resistance 2−56989
  ZrO_2-Y_2O_3, elastic consts., current blackening effects, u.s. wave vel. obs. 2−43666
  ZrO_2-Y_2O_3 system, phase diagram above 2000°C 2−61049
  ZrO_2-Y_2O_3 system, tetragonal-cubic transformation, X-ray exam. 2−84098
  ZrO_2-Yb_2O_3 and ZrO_2-Yb_2O_3-Y_2O_3 systems, solid soln. formation kinetics 2−47721
  ZrO_2-6 mol%CaO, castable, elec. cond., 900-1700K 53936 2−53936
  ZrO_2, calcia-stabilized, destabilization by ZrB_2 2−50902
  ZrO_2, calcia-stabilized, fracture toughness 2−50777
  ZrO_2, calcia stabilized, thermal stress induced microstruct. modifications 2−50901
  ZrO_2, elec. cond., 1600-1900K 2−54233
  ZrO_2, hydrothermal growth and etching in HF 2−50588
  ZrO_2, martensitic transform. struct. 2−50953
  ZrO_2, monoclinic-tetragonal transform., isothermal kinetics, burst phenomena, 850-1000°C 2−77753
  ZrO_2, monoclinic-tetragonal inversion, effects of detonation shock wave 2−74946
  ZrO_2, nonstoichiometric, microscopic thermodynamic props., rel. to macroscopic props. 2−43506
  ZrO_2, stable white pigment, for space environment 2−44799
  ZrO_2, Y_2O_3-stabilized, current blackening effects, defect struct. obs., e.s.r. spectra 2−61740
  ZrO_2,CeO_2 and Cr_2O_3 mixtures, formation of cubic solid soln. $Ce_2Zr_2O_7$-ZrO_2 on calcinating in vacuum 2−84095
  ZrO_2 amorphous, radiation induced thermal effects 2−64522
  ZrO_2 fibre-reinforced MgO, fabrication and mech. props. 2−50918
  ZrO_2 nucleated MgO.Al_2O_3.SiO_2 glass-ceramic, phase transitions 2−47691
  ZrO_2.CaO solid electrolyte, ion transport number 2−65054
  ZrS_2, nearly perfect cryst., growth and X-ray obs. 2−50577
  Zr_9S_2, cryst. struct. 2−43595
  $ZrSe_2$, cryst. growth by vapour transport 2−50577
  $ZrSiO_4$:M^{3+} (M = Er, Yb, Gd), e.s.r. spectra 2−48278
  $ZrSiO_4$-TiO_2 system, phase relations, 1050-1600°C 2−47722
  $ZrSiO_4$, solubility of rare earths, isomorphous substitution of Zr 2−74913
  $ZrSiO_4$, thermal expansion anisotropy, compressibility anisotropy 2−54064
  $ZrSiO_4$, zircon, hydrothermal and flux growth 2−47248
  $Zr_2Si_2Se_2$, nonstoichiometry, X-ray obs. 2−43505
  $Zr_xTa_{1-x}Co_2$, Laves-phase compound, mag. susceptibility, temp. depend. 2−65128
  $ZrTe_2$, nonstoichiometric phase, struct., homogeneous phase limit 2−60772
  $Zr_{1-x}Ti_x(Hf_x)Zn_2$, itinerant ferromag., e.p.r. obs. 2−72173

Zodiacal light
  amateur observations (1971) 2−72803
  circular polarisation measurement 2−73108
  night sky continuum, obs. in range 4100-8200 2−68942
  OSO-5 dim light monitor 2−72943
  surface photometry, from space vehicle, obs. procedures 2−45003
  OH airglow at 2.2 μ rel. to possibility of ground- based observations of zodiacal light 2−65886

Zonal heating *see Atmosphere/thermodynamics*

Zone melting and refining
  alloy, ternary, theory 2−47601
  fluoranthene crystal, purity determ. by spectral depend. of fluorescence lifetime 2−84536
  horizontal zone refiner for crystal growth of group V-VI compounds 2−67941
  metals, crystallization front shape 2−60718
  refractory oxides, bicrystals, growth by floating zone method 2−83898
  semiconductor pseudobinary alloy, soln. zoning for cryst. growth 2−47702
  with temperature gradient, crystn. rate determ. 2−47253
  vacuum apparatus, oil free pumping system 2−48949
  vacuum apparatus, oil free pumping system 2−48949
  Al_2O_3, ^{17}O enriched, growth by floating zone technique in image furnace 2−74686
  Bi-Sb alloy, preparation of single crystals antimony content by radiactivation determination 2−81554
  $CaCO_3$, calcite, travelling solvent zone melting 2−50591
  $CdGeP_2$ zone recrystallised, optical props. and energy zone calc. 2−80595
  Cu, growth of twin free crystals by secondary recrystn. and zone refining 2−47580
  Fe, high purity, prep. from re-electrolytic Fe, floating zone melting method 2−47266
  Fe, high purity, prep. from re-electrolytic Fe, floating zone melting method 2−47266
  Ge, Au and Sb impurities, absorption and movement in the solid phase 2−83892
  $Hg_{1-x}Cd_xTe$ alloy, cryst. growth using Te as solvent 2−47271
  KCN, single cryst. growth 2−67944
  KCl-KBr solid solution, for neutron monochromator appl. 2−47205
  NaCN, single cryst. growth 2−67944
  $Nb_{1-x}Ta_x$ alloy, $0 < x < 0.25$, growth by electron beam float zoning 2−50599
  Si, with temp. gradient, crystn. rate determ. 2−47253
  ZrO_2-W, composite, growth by unidirectional solidification of eutectic melt 2−64796

Zone plates *see Diffraction/light*

Zoology
  bats, echolocating and target-ranging rel. to sonar receiver 2−55546
  cerebral blood flow, sympathetic control in dogs 2−85122
  kapis shells as possible thermoluminescent dosimeter 2−82823

Zoology continued
  orientation of animals and insects on sensory basis, conference, N.Y., USA (1971) 2−58646
  submarine biological objects, acoustic characteristics of fish species 2−69763

CLASSIFIED LIST OF SUBJECT INDEX HEADINGS

The headings are grouped into sections on the same basis as the arrangement of the abstracts in the fortnightly issues of Physics Abstracts. A summary of the layout of these sections (these are actually further subdivided), is given below. Each section lists the headings which concern its subject and it follows that many of the headings are listed in several places.

SUBJECT SECTIONS

01.00	GENERAL
02.00	MATHEMATICAL PHYSICS
03.00	MECHANICS. ELASTICITY. VIBRATION. ACOUSTICS
04.00	HEAT. THERMODYNAMICS
05.00	ELECTROMAGNETISM
06.00	ELECTRODYNAMICS & PARTICLE OPTICS
07.00	QUANTUM ELECTRONICS. QUANTUM OPTICS
08.00	OPTICS
09.00	QUANTUM FIELD THEORY
10.00	ELEMENTARY PARTICLES
11.00	ELEMENTARY PARTICLE & NUCLEAR MEASUREMENT
12.00	NUCLEAR PHYSICS
13.00	ATOMIC & MOLECULAR PHYSICS
14.00	FLUIDS
15.00	CHANGE OF STATE
16.00	SOLID-STATE STRUCTURE & MECHANICAL PROPERTIES
17.00	SOLID-STATE ELECTRICAL & MAGNETIC PROPERTIES
18.00	SOLID-STATE SPECTROSCOPY & OPTICAL PROPERTIES
19.00	PHYSICAL CHEMISTRY
20.00	GEOPHYSICS
21.00	ASTROPHYSICS
22.00	BIOPHYSICS
23.00	LABORATORY & EXPERIMENTAL TECHNIQUES

01.00 GENERAL

Biographies
Collections of physical data
History

Laboratories
Laboratory apparatus and technique

Nomenclature and symbols
Physics

Physics fundamentals
Reviews

01.10 EDUCATION

Biographies
History
Laboratories

Laboratory apparatus and technique
Physics

Physics fundamentals
Reviews
Teaching demonstrations

01.20 UNITS. MEASUREMENT AND METROLOGY

Acceleration measurement
Anemometers
Angle measurement
Angular velocity measurement
Area measurement
Balances
Constants
Density measurement

Dimensions
Force measurement
Instruments
Interferometry
Length measurement
Manometers
Measurement errors
Mechanical measurement

Micrometry
Nomenclature and symbols
Particle size
Pressure measurement
Recording
Standards
Strain gauges
Stroboscopes

Surface measurement
Thickness measurement
Time interval measurement
Time measurement
Units
Vapour pressure measurement
Velocity measurement
Volume measurement

02.00 MATHEMATICAL PHYSICS

Algebra
Differential equations
Equations
Field theory, classical
Fluctuations
Fourier analysis
Functions

Geometry
Green's function methods
Group theory
Hysteresis
Information theory
Integral equations
Integrals

Mathematics
Matrices
Probability
Radiation
Relaxation
Series
Space-time configurations

Statistical analysis/applications
Tensors
Transformations, mathematical
Vectors
Waves

02.10 GRAVITATION AND RELATIVITY

Gravitation
Gravitational collapse
Gravitational waves
Red shift

Relativity/
  general
  special
  unified field theories
Space-time configurations
Tachyons

02.20 QUANTUM THEORY

Collision processes
Dispersion relations
Indeterminacy
Parity
Perturbation theory
Quantum electrodynamics

Quantum theory/
  application methods
  quantisation
  wave equations
Scattering

02.30 STATISTICAL PHYSICS

Boltzmann equation
Brownian motion
Electron gas
Fluctuations
Hysteresis
Information theory
Ising lattices and models

Kinetic theory
Lattices, theory and statistics
Many-body problems
Mass transfer
Probability
Quantum fluids/
  boson systems
  fermion systems

Quantum theory
Quasi-particles
Radiation
Radiative transfer
Random processes
Relaxation

Statistical analysis/applications
Statistical mechanics/
  quantum
Thermodynamics
Transport processes

02.40 MATHEMATICAL AND COMPUTATIONAL METHODS

Calculation
Computer applications
Graphs
Nomograms

Statistical analysis/applications
Tables, mathematical

03.00 MECHANICS. ELASTICITY. VIBRATION. ACOUSTICS

Oscillations
Vibrations
Waves

03.10 MECHANICS

Ballistics
Centrifuges
Dynamics
Friction
Gravitation
Gyroscopes
Impact
Kinematics

Mechanics
Pendulums
Pressure
Rockets
Rotating bodies
Torsion
Velocity

03.15 RHEOLOGY, ELASTICITY AND PLASTICITY

Bending
Compressibility
Damping
Deformation
Elastic deformation
Elasticity
Photoelasticity
Plastic deformation

Plasticity
Relaxation
Rheology
Stress analysis
Stresses, internal
Thermoelasticity
Viscoelasticity

03.30 VIBRATIONS AND ELASTIC WAVES

Damping
Elastic waves
Magnetoelastic waves
Membranes

Oscillations
Piezoelectric oscillations
Relaxation
Resonators

Seismic waves
Shock waves/
  effects
Vibrating bodies

Vibrations/
  excitation
  measurement
Waves

03.40 ACOUSTICS

- Absorption/
  - acoustic waves
  - acoustic waves, ultrasonic
- Acoustic analysis
- Acoustic generators
- Acoustic impedance
- Acoustic radiators
- Acoustic receivers
- Acoustic resonators
- Acoustic streaming
- Acoustic wave amplification
- Acoustic wave propagation/
  - ultrasonic
- Acoustic waves/
  - effects
- Acoustical laboratories
- Acoustical measurement
- Acoustics/
  - musical
- Acoustoelectric effects
- Architectural acoustics
- Atmospheric acoustics
- Biological effects of radiations
- Chemical effects of radiations/
  - acoustic waves
- Diffraction/
  - acoustic waves
  - acoustic waves, ultrasonic
- Diffusion/
  - acoustic waves
- Dispersion, acoustic/
  - ultrasonic
- Doppler effect
- Echo
- Helium/
  - liquid, sound propagation
- Holography
- Intensity measurement/
  - acoustics
- Interference/
  - acoustic waves
- Interferometers/
  - acoustic waves
- Interferometry/
  - acoustic waves
- Magnetoacoustic effects
- Microphones
- Musical instruments
- Noise/
  - acoustic
- Noise abatement
- Physical effects of radiations
- Radiation pressure
- Recording
- Reflection/
  - acoustic waves
  - acoustic waves, ultrasonic
- Refraction/
  - acoustic waves
  - acoustic waves, ultrasonic
- Refractories
- Reverberation
- Scattering/
  - acoustic waves
  - acoustic waves, ultrasonic
- Schlieren systems
- Sound ranging
- Sound reproduction
- Speech
- Stroboscopes
- Transducers
- Transmission/
  - acoustic waves
  - acoustic waves, ultrasonic
- Ultrasonics
- Velocity/
  - acoustic waves
  - acoustic waves, ultrasonic
- Velocity measurement/
  - acoustic waves
  - acoustic waves, ultrasonic

03.50 SHOCK WAVES

- Detonation
- Exploding wires
- Explosions/
  - nuclear
- Schlieren systems
- Shock tubes
- Shock waves/
  - effects
- Supersonic flow

04.00 HEAT. THERMODYNAMICS

- Annealing
- Bolometers
- Calorimeters
- Calorimetry
- Combustion
- Conductivity, thermal
- Convection
- Cooling
- Emissivity
- Entropy/
  - properties of substances
- Equations of state/
  - gases
  - liquids
  - solids
- Flames
- Heat
- Heat conduction
- Heat transfer
- Heat treatment
- Heating
- High-temperature phenomena and effects
- Joule-Thomson effect
- Latent heat
- Pyrometers
- Radiation/
  - heat
- Radiation detectors
- Radiation pressure
- Radiation transfer
- Specific heat
- Temperature
- Temperature distribution
- Temperature measurement/
  - spectral methods
- Thermal expansion
- Thermal measurement
- Thermocouples
- Thermodynamic properties
- Thermodynamics/
  - applications
- Thermometers/
  - resistance
- Thermostats

05.00 ELECTROMAGNETISM

- Eddy-currents
- Electromagnetism
- Electromagnetic fields
- Electromotive force
- Inductance

05.10 ELECTROMAGNETIC WAVES AND OSCILLATIONS

- Absorption/
  - electromagnetic waves
- Amplifiers
- Diffraction/
  - electromagnetic waves
- Diffusion/
  - electromagnetic waves
- Doppler effect
- Electromagnetic oscillations
- Electromagnetic wave propagation/
  - atmosphere
  - ionosphere
  - guided waves
- Electromagnetic waves/
  - radiators
- Interference/
  - electromagnetic waves
- Interferometers/
  - electromagnetic waves
- Interferometry/
  - electromagnetic waves
- Light/
  - electromagnetic theory
- Microwave techniques and devices
- Plasma/
  - electromagnetic wave propagation
- Radiation
- Reflection/
  - electromagnetic waves
- Refraction/
  - electromagnetic waves
- Scattering/
  - electromagnetic waves

05.20 RADIOFREQUENCY SPECTROSCOPY. MAGNETIC RESONANCES

- Acoustic paramagnetic resonance
- Antiferromagnetic resonance
- Cyclotron resonance
- ENDOR
- Ferrimagnetic resonance
- Ferroacoustic resonance
- Ferromagnetic relaxation
- Ferromagnetic resonance
- Magnetic resonance and relaxation
- Nuclear magnetic resonance and relaxation/
  - measurement
- Nuclear quadrupole resonance
- Paramagnetic resonance and relaxation/
  - measurement
- Spectra
- Spectrometers, radio frequency
- Spectroscopy, radio frequency

05.30 ELECTRICAL QUANTITIES AND THEIR MEASUREMENT. CIRCUITS

- Acoustoelectric effects
- Amplifiers
- Breakdown, electric
- Circuits
- Conductivity, electrical/
  - measurement
- Contacts, electrical
- Counting circuits
- Current, electrical
- Dielectric devices
- Dielectric measurement
- Dielectric phenomena
- Eddy-currents
- Electrets
- Electric charge
- Electric fields/
  - effects
- Electric strength
- Electrical machines
- Electrical measurement
- Electrical properties of substances
- Electrokinetic effects
- Electroluminescence
- Electromotive force
- Electron density
- Electron gas
- Electrons
- Electro-optical effects
- Electrophoresis
- Electrostatics
- Electrostriction
- Ferroelectric phenomena
- Fluctuations
- Hall effect
- High-voltage techniques
- Hysteresis
- Image convertors and amplifiers
- Inductance
- Magnetoelectric effects
- Magnetoresistance
- Noise, electrical
- Oscillators
- Permittivity
- Photoconductivity
- Photoelectricity
- Photoelectromagnetic effects
- Photovoltaic effects
- Piezoelectric oscillations
- Piezoelectricity
- Piezoresistance
- Plasma/
  - diagnostics
- Pyroelectricity
- Rectifiers
- Relaxation
- Semiconductors
- Skin effect
- Space charge
- Superconductivity
- Thermocouples
- Thermoelectricity
- Triboelectricity

05.35 DIRECT CONVERSION

- Electricity, direct conversion/
  - fuel cells
  - magnetohydrodynamics
  - solar cells
  - thermionic

05.40 MAGNETISM

- Antiferromagnetism
- Compasses
- de Haas-van Alphen effect
- Demagnetisation
- Diamagnetism
- Ferrimagnetism
- Ferromagnetism/
  - spin-wave theory
- Films, solid/
  - magnetic properties
- Gyromagnetic effect
- Gyromagnetic ratio
- Hall effect
- Magnetic devices
- Magnetic field measurement
- Magnetic fields/
  - effects
- Magnetic measurement
- Magnetic permeability
- Magnetic resonance and relaxation
- Magnetism
- Magnetisation process
- Magnetisation state
- Magnetoacoustic effects
- Magnetoelectric effects
- Magnetomechanical effects
- Magneto-optical effects
- Magnetoresistance
- Magnetostriction
- Magnetothermal effects
- Magnets
- Paramagnetism
- Storage devices

06.00 ELECTRODYNAMICS AND PARTICLE OPTICS

- Electrodynamics
- Electrohydrodynamics
- Energy loss of particles
- Particle beams
- Particle optics
- Particle velocity analysis
- Scattering, particles

06.10 ELECTRON BEAMS, ELECTRON OPTICS AND TUBES

- Anodes
- Electrodes
- Electron beams/
  - effects
- Electron density
- Electron diffraction
- Electron gas
- Electron lenses/
  - electrostatic
  - magnetic
- Electron microscopes
- Electron microscopy
- Electron optics
- Electron tubes
- Electrons/
  - absorption
  - ionisation
  - radiation
  - scattering
- Fluctuations
- Gas-discharge tubes
- Image convertors and amplifiers
- Noise, electrical
- Photomultipliers
- Space charge

06.20 ION BEAMS, ION OPTICS AND SOURCES

- Field ion microscopy
- Ion beams/
  - effects
- Ion microscopes
- Ion optics
- Ion sources
- Ion velocity
- Ions/
  - recombination
  - scattering
- Sputtering

07.00 QUANTUM ELECTRONICS. QUANTUM OPTICS

- Light/
  - coherence
- Optical pumping
- Photons
- Q-switching
- Quantum optics

07.10 MASERS

- Amplifiers
- Masers
- Optical pumping
- Q-switching

07.20 LASERS

- Amplifiers
- Lasers
- Light/
  - coherence
- Optical pumping
- Q-switching
- Resonators

07.23 Gas and Liquid Lasers

- Amplifiers
- Lasers/
  - gaseous
  - liquid
- Light/
  - coherence
- Optical pumping
- Q-switching

07.25 Solid Lasers

- Amplifiers
- Lasers/
    - semiconductor
    - solid
- Light/
    - coherence
- Optical pumping
- Q-switching

07.27 Laser Beam Optics. Holography

- Holography
- Laser beams/
    - applications
    - effects
- Light/
    - coherence
    - modulation
- Q-switching

08.00 OPTICS

- Doppler effect
- Electro-optical effects
- Light/
    - electromagnetic theory
    - modulation
- Light sources
- Nonlinear optics
- Optics
- Photons
- Photophoresis
- Radiation
- Radiation pressure
- Velocity/
    - light
- Velocity measurement/
    - light

08.10 GEOMETRICAL OPTICS

- Aberrations, optical
- Dispersion, optical
- Lenses/
    - aspherical
    - photographic
- Mirrors
- Optical images
- Optical systems
- Optics/
    - geometrical
- Prisms, optical
- Reflection/
    - light
- Refraction/
    - light
- Refractive index/
    - light
- Resolving power, optics
- Schlieren systems

08.20 PHYSICAL OPTICS

- Absorption/
    - light
- Diffraction/
    - light
- Diffraction gratings
- Diffusion/
    - light
- Dispersion, optical
- Doppler effect
- Double refraction/
    - flow
    - mechanical
- Electro-optical effects
- Ellipsometry
- Filters, optical
- Holography
- Interference/
    - light
- Interferometers/
    - light
- Interferometry/
    - light
- Magneto-optical effects
- Optical constants
- Optical films
- Optical pumping
- Optical rotation
- Photoelasticity
- Pleochroism
- Polarimeters
- Polarisation/
    - light
- Reflection/
    - light
- Reflectivity
- Refraction/
    - light
- Refractive index/
    - light
- Scattering/
    - light
- Thermo-optical effects
- Transmission/
    - light
- Transparency

08.30 PHOTOMETRY. CALORIMETRY

- Bolometers
- Brightness
- Colorimetry
- Colour
- Densitometry
- Emissivity
- Illumination
- Photometers
- Photometry/
    - light sources
- Pyrometers
- Radiation detectors

08.40 INSTRUMENTAL OPTICS

- Abberations, optical
- Dispersion, optical
- Fibres/
    - optical
- Films/
    - liquid
- Films, solid/
    - optical properties
- Filters, optical
- Glass
- Image convertors and amplifiers
- Lasers/
    - gaseous
    - solid
- Lenses/
    - aspherical
    - photographic
- Light sources
- Luminescent devices
- Microscopes
- Microscopy
- Mirrors
- Optical constants
- Optical images
- Optical instrument testing
- Optical instruments
- Optical materials
- Optical systems
- Prisms, optical
- Projectors, optical
- Quartz
- Reflection/
    - light
- Refraction/
    - light
- Refractive index/
    - light
- Refractive index measurement
- Refractometers
- Resolving power, optics
- Schlieren systems
- Stroboscopes
- Telescopes

08.45 Spectroscopy

- Astronomical spectra
- Atmospheric spectra
- Exploding wires
- Modulation spectroscopy
- Monochromators
- Spectral line breadth
- Spectrochemical analysis
- Spectrometers/
    - accessories
- Spectrophotometers
- Spectrophotometry
- Spectroscopy/
    - light sources
- Stark effect
- Temperature measurement/
    - spectral methods
- Zeeman effect

08.50 PHOTOGRAPHY

- Cameras
- Cinematography
- Densitometry
- Lenses/
    - photographic
- Light sources
- Nuclear track emulsions
- Photographic materials/
    - sensitivity
- Photographic process/
    - development
- Photography/
    - applications
    - colour
    - high-speed
- Radiography

09.00 QUANTUM FIELD THEORY

- Bethe-Salpeter equation
- Current algebra
- Dispersion relations
- Dual resonance model
- Field theory, quantum/
  - interactions
  - interactions, strong
  - interactions, weak
  - meson field
  - quantisation
  - scattering
- Lee model
- Nuclear forces
- Parity
- Quantum electrodynamics
- Quantum theory/
  - application methods
  - quantisation
  - wave equations
- S-matrix theory
- Scattering

10.00 ELEMENTARY PARTICLES

- Bosons
- Elementary particles
- Fermions
- Gravitons
- Parity
- Energy loss of particles
- Particle velocity analysis
- Quarks
- Strange particles
- Synchrotron radiation

10.10 ELEMENTARY PARTICLE THEORY

- Bootstrapping
- Bosons
- Chirality
- CPT conservation
- Current algebra
- Dirac equation
- Dispersion relations
- Elementary particles/
  - interactions
  - interactions, electromagnetic
  - interactions, strong
  - interactions, weak
  - scattering
  - symmetry
  - theory
- Fermions
- Form factors
- Magnetic monopoles
- Mass differences
- Mass formulae
- Nuclear forces
- Parity
- S-matrix theory
- Strange particles
- SU(n) theory
- Sum rules
- Tachyons

10.20 PHOTONS. GAMMA-RAYS. X-RAYS

- Bremsstrahlung
- Cherenkov radiation
- Compton effect
- Gamma-ray spectrometers
- Gamma-rays/
  - absorption
  - angular distribution
  - detection, measurement
  - effects
  - scattering
- Mössbauer effect
- Photons/
  - interactions
  - polarisation
  - scattering
- Synchrotron radiation
- X-ray absorption
- X-ray diffraction
- X-ray measurement
- X-ray reflection
- X-ray scattering
- X-rays/
  - effects

10.30 LEPTONS

- Leptons

10.33 Neutrinos

- Neutrinos and antineutrinos

10.35 Electrons

- Beta-ray spectra/
  - conversion electrons
- Beta-ray spectrometers
- Beta-rays/
  - absorption
  - angular distribution
  - detection, measurement
  - effects
  - polarisation
  - scattering
- Dirac equation
- Electron pairs/
  - annihilation
  - production
- Electron theory
- Electrons/
  - absorption
  - interactions
  - ionisation
  - radiation
  - scattering
  - scattering, electron-proton
- Positronium
- Positrons
- Synchrotron radiation

10.37 Muons

- Muons/
  - capture
  - decay
  - detection, measurement
- Muons/
  - interactions
  - production
  - scattering
- Muonium

10.40 HADRONS

- Hadrons/
  - current
  - decay
- Quarks

10.41 Hadron interactions

- Hadrons/
  - interactions

10.42 Hadron scattering

- Bootstrapping
- Dual resonance model
- Hadrons/
  - scattering
- Pomeranchuk poles and trajectories
- Regge poles and trajectories
- Veneziano model

10.45 Mesons

- Mesons/
  - absorption
  - capture
  - decay
  - detection, measurement
  - effects
- Mesons/
  - interactions
  - magnetic moment
  - mass
  - production
  - scattering
  - spin and parity

10.46 Kaons

- Kaons/
  - decay
  - interactions
- Kaons/
  - production
  - scattering

10.47 Pions

- Pions/
  - decay
  - interactions
  - interactions, pion-nucleon
  - interactions, pion-pion
  - interactions, pion-proton
- Pions/
  - production
  - scattering
  - scattering, pion-nucleon
  - scattering, pion-pion
  - scattering, pion-proton

10.48 Meson Resonances

- Intermediate bosons
- Mesons/
  - resonances

10.51 Baryons

- Baryons/
  - interactions
  - scattering

10.52 Nucleons

- Nuclear forces
- Nucleons and antinucleons/
  - antinucleons
  - interactions
  - interactions, nucleon-nucleon
  - scattering
  - scattering, nucleon-nucleon

10.53 Protons

- Proton spectra
- Protons and antiprotons/
  - absorption
  - angular distribution
  - antiprotons
  - detection, measurement
  - effects
  - interactions
  - interactions, proton-proton
  - magnetic moment
  - polarisation
  - production
  - scattering
  - scattering, proton-deuteron
  - scattering, proton-proton

10.54 Neutrons

- Neutron diffraction
- Neutron spectra
- Neutron spectrometers
- Neutrons and antineutrons/
  - absorption
  - angular distribution
  - detection, measurement
  - diffusion
  - effects
  - interactions
  - moderation
  - polarisation
  - production
  - reflection
  - scattering
  - scattering, neutron-proton

10.56 Hyperons

- Hypernuclei
- Hyperons/
  - absorption
  - capture
  - decay
  - detection, measurement
  - effects
  - interactions
  - magnetic moment
  - mass
  - production
  - resonances
  - scattering
  - spin and parity
- Strange particles

10.58 Baryon Resonances

- Baryons/
  - resonances
- Hyperons/
  - resonances
- Nucleons

10.60 COMPOSITE PARTICLES

- Composite particles

10.63 Deuterons

- Deuterons/
  - effects
  - interactions
  - photodisintegration
  - polarisation
  - scattering

10.65 Tritons

- Tritons/
  - interactions
  - scattering

10.67 Alpha-particles and He^3

- Alpha-particle spectrometers
- Alpha-particles/
  - absorption
  - angular distribution
  - detection, measurement
  - effects
  - interactions
  - scattering
- Helium-3
  - interactions
  - scattering

10.70 COSMIC RAYS

- Cosmic rays/
  - absorption
  - apparatus
  - alpha-particles and helium nuclei
  - composition
  - deuterons
  - effects and interactions
  - electrons
  - mesons
  - muons
  - neutrinos
  - neutrons
  - nucleons
  - origin
  - photons
  - primary
  - protons
  - showers and bursts
  - variations
  - X-rays

11.00 ELEMENTARY PARTICLE AND NUCLEAR MEASUREMENT

11.10 APPARATUS. DETECTORS AND DETECTOR CIRCUITS

- Alpha-particle spectrometers
- Amplifiers
- Beta-ray spectrometers
- Counters/
  - accessories
  - Cherenkov
  - crystal
  - Geiger
  - operation technique
  - proportional
  - scintillation
  - semiconductor
  - spark
  - statistical analysis
- Counting circuits
- Dosimetry
- Gamma-ray spectrometers
- Ionisation chambers
- Neutron spectrometers
- Nuclear bombardment targets
- Particle accelerators
- Particle detectors
- Particle optics
- Particle spectrometers
- Particle velocity analysis
- Photomultipliers
- Radioactivity measurement/
  - apparatus

11.15 Track Visualisation

- Bubble chambers
- Cloud chambers
- Energy loss of particles
- Luminescence chambers
- Nuclear track emulsions
- Particle tracks
- Particle track visualisation
- Spark chambers

11.20 PARTICLE ACCELERATORS

- High-voltage techniques
- Ion sources
- Particle accelerators/
  - accessories
  - betatrons
  - cyclotrons
  - linear
  - synchrotrons
- Storage rings

12.00 NUCLEAR PHYSICS

Nuclear physics

12.10 NUCLEAR STRUCTURE AND ENERGY LEVELS

- BCS theory
- Beta-ray spectra/
  - conversion electrons
- Gamma-ray spectra
- Gamma-rays/
  - angular distribution
  - internal conversion
- Gyromagnetic ratio
- Hypernuclei
- Isobaric analog states
- Mössbauer effect
- Nuclear excitation
- Nuclear forces
- Nuclear isomerism
- Nuclear magnetic resonance and relaxation
- Nuclear polarisation
- Nuclear structure
- Nuclei with $A < 5$
- Nuclei with $6 \leq A \leq 19$
- Nuclei with $20 \leq A \leq 49$
- Nuclei with $50 \leq A \leq 89$
- Nuclei with $90 \leq A \leq 149$
- Nuclei with $150 \leq A$
- Nucleus/
  - electric moment
  - energy level transitions
  - energy levels
  - magnetic moment
  - models
  - size
  - spin and parity
  - theory

12.20 NUCLEAR DECAY AND RADIOACTIVITY

- Alpha-particles
- Alpha-particle spectra
- Alpha-particle spectrometers
- Alpha-particles/
  - absorption
  - angular distribution
  - detection, measurement
  - effects
  - scattering
- Beta-decay theory
- Beta-ray spectra/
  - conversion electrons
- Beta-ray spectrometers
- Beta-rays/
  - absorption
  - angular distribution
  - detection, measurement
  - effects
  - polarisation
  - scattering
- Biological effects of radiations
- Chemical effects of radiations/
  - ionising radiations
- Dosimetry
- Fallout
- Gamma-ray spectra
- Gamma-ray spectrometers
- Gamma-rays/
  - absorption
  - angular distribution
  - detection, measurement
  - effects
  - internal conversion
  - scattering
- Nuclear decay theory
- Nuclear bombardment targets
- Physical effects of radiations
- Radiation monitoring
- Radiation protection
- Radioactive dating
- Radioactive tracers
- Radioactivity/
  - decay periods
  - decay schemes
  - electron capture
- Radioactivity measurement/
  - apparatus
- Radiochemistry

12.30 NUCLEAR REACTIONS AND SCATTERING

- Chemical analysis/
  - by nuclear reactions
- Collision processes
- Nuclear bombardment targets
- Nuclear excitation
- Nuclear forces
- Nuclear reactions and scattering/
  - chemical effects
  - high energy $\geq$ 1GeV
- Nuclear reactions and scattering due to/
  - alpha-particles
  - cosmic rays
  - deuterons
  - electrons
  - helium-3
  - hyperons
  - mesons
  - muons
  - neutrinos
  - neutrons
  - nuclei of $Z > 2$
  - nucleons
  - photons
  - protons
  - tritons
- Nuclear spallation
- Nuclei with $A \leq 5$
- Nuclei with $6 \leq A \leq 19$
- Nuclei with $20 \leq A \leq 49$
- Nuclei with $50 \leq A \leq 89$
- Nuclei with $90 \leq A \leq 149$
- Nuclei with $150 \leq A$
- Radiation monitoring
- Radiation protection
- Scattering, particles
- Stripping reactions

12.39 Nuclear fission and fusion

- Explosions/
  - nuclear
- Nuclear fission/
  - products
  - uranium
- Nuclear fusion
- Nucleons and antinucleons
- Photo fission
- Plasma
- Thermonuclear reactions

12.40 NUCLEAR POWER STUDIES

12.43 Neutron Physics

- Neutron transport theory
- Neutrons and antineutrons/
  - absorption
  - angular distribution
  - detection measurement
  - diffusion
  - effects
  - interactions
  - moderation
  - polarisation
  - production
  - reflection
  - scattering
- Nuclear fission/
  - products
  - uranium
- Nuclear fusion
- Nuclear reactions and scattering
- Thermonuclear reactions

12.47 Nuclear Reactors

- Biological effects of radiations
- Chemical analysis/
  - by nuclear reactions
- Chemical effects of radiations/
  - ionising radiations
- Dosimetry
- Nuclear fission/
  - products
  - uranium
- Nuclear fusion
- Nuclear reactions and scattering/
  - chemical effects
- Nuclear reactors, fission/
  - materials
  - operation
  - theory
- Nuclear reactors, fusion
- Physical effects of radiations
- Plasma/
  - devices
- Radiation monitoring
- Radiation protection
- Radiochemistry
- Thermonuclear reactions

12.50 RADIATION TECHNOLOGY

- Dosimetry
- Neutron transport theory
- Physical effects of radiation
- Radiation protection
- Nuclear reactors, fission/
  - operation
- Biological effects of radiation
- Particle accelerators/
  - betatrons
  - cyclotrons
  - linear
  - synchrotrons

13.00 ATOMIC AND MOLECULAR PHYSICS

- Collision processes
- Orbital calculation methods
- Quantum theory

13.10 MASS SPECTROMETERS

- Mass spectra
- Mass spectrometers/
  - accessories
  - applications

13.20 ATOMS

- Atomic beams
- Atomic mass and weight
- Atoms
  - electron scattering
  - excitation
  - magnetic moment
  - structure
- Auger effect
- Binding energy
- Charge exchange
- Collision processes/
  - atoms
- Electron emission
  - photoelectric
- Elements
  - origin
  - relative abundances
- Exchange interactions
- Gyromagnetic ratio
- Hartree-Fock method
- Helium/
  - gas
- Hydrogen/
  - ions
  - neutral atoms
- Ionisation potential
- Isotope shifts
- Luminescence
  - gases
- Optical pumping
- Orbital calculation methods
- Periodic system
- Polarisability
- Rayleigh scattering
- Red shift
- Russell-Saunders coupling
- Spectra
  - atoms
- Spectral line breadth
- Stark effect
- Stimulated emission
- X-ray spectra
  - absorption
  - emission
- Zeeman effect

13.25 Isotopes

- Isotope effects
- Isotope exchanges
- Isotope separation
- Isotopes
  - detection
  - relative abundances
- Mass spectra
- Mass spectrometers/
  - applications
- Radioactive dating
- Radioactive tracers
- Radiochemistry
- Tracers

13.27 Mesic and Muonic Atoms

- Atoms, mesic and muonic

13.30 MOLECULES

- Binding energy
- Bonds
- Chemical shift
- Chemical structure
- Exchange interactions
- Isomerism
- Jahn-Teller effect
- Luminescence/
  - gases
- LCAO calculations
- Magnetic resonance and relaxation
- Molecular weight
- Molecules/
  - configuration and dimensions
    - inorganic
    - organic
  - dissociation
  - dissociation energies
  - excitation
  - electron scattering
  - internal mechanics
  - electronic structure
  - electronic structure, inorganic
  - electronic structure, organic
  - excitation
  - intermolecular mechanics
  - internal mechanics
  - moments
  - nuclear coupling
  - relaxation
  - rotation
  - vibration
- Nuclear magnetic resonance and relaxation
- Nuclear quadrupole resonance
- Optical pumping
- Orbital calculation methods
- Paramagnetic resonance and relaxation
- Polarisability
- Rayleigh scattering
- Red shift
- Scattering/
  - light
  - light, Brillouin spectra
  - light, Raman spectra
  - light, Raman spectra, inorganic
  - light, Raman spectra, organic
- Spectra/
  - inorganic molecules
    - diatomic
    - diatomic, radiofrequency
    - polyatomic
    - polyatomic, radio-frequency
  - inorganic liquids and solutions
  - inorganic solids
    - radiofrequency
  - molecules
  - organic molecules and substances
    - infrared
    - radiofrequency
- Spectral line breadth
- Stark effect
- Stimulated emission
- Valency
- Zeeman effect

13.35 Macromolecules

- Association
- Heat of formation
- Isomerism
- Macromolecules
- Molecules/
  - configuration and dimensions, macromolecules
- Polymers
- Proteins

13.36 Mesic and Muonic Molecules

- Molecules, mesic and muonic

13.37 Intermolecular mechanics

- Charge exchange
- Collision processes/
  - molecules
- Molecular beams
- Molecules/
  - intermolecular mechanics

14.00 FLUIDS

- Boundary layers
- Flow/
  - two-phase
- Fluidised beds
- Fluids
- Hydrodynamics
- Hydrostatics
- Non-Newtonian fluids
- Oscillations
- Turbulence
- Viscosity
- Vortices
- Waves

14.10 MAGNETOHYDRODYNAMICS

Magnetohydrodynamics
Shock waves/
  effects
Turbulence

14.20 PLASMA

Discharges, electric/
  glows
  high-frequency
Electrohydrodynamics
Electrode density
Exploding wires
Nuclear fusion
Nuclear reactors, fusion

Plasma/
  collison processes
  electromagnetic waves
  magnetohydrodynamics
  production
  shock waves
  transport processes

Shock waves/
  effects
Space charge/
  gas
Thermonuclear reactions

14.24 Plasma Confinement, Devices and Measurements

Plasma/
  confinement
  devices
  diagnostics

Probes
Stellarators

14.26 Plasma Oscillations and Stability

Plasma/
  magnetohydrodynamics
  oscillations
  stability

14.30 IONISATION

Charge exchange
Dissociation
Ion velocity
Ionisation/
  gases

Ionisation potential
Ionisation, surface
Ions/
  recombination
  scattering
Magnetohydrodynamic waves

Photoionisation/
  gases
Shock waves/
  effects
Space charge/
  gas

14.40 ELECTRIC DISCHARGES

Arcs, electric
Breakdown, electric/
  gases
Corona, electric discharge

Discharges, electric/
  glows
  high frequency
Electron density

Gas-discharge tubes
Lightning
Sparks, electric
Sputtering

14.50 MECHANICS OF GASES

Acoustic streaming
Aerodynamics
Anemometers
Compressibility/
  gases
Condensation
Density/
  gases

Diffusion in gases/
  thermal
Flow/
  gases
  two-phase
Flowmeters
Gases
Humidity

Hygrometers
Jets
Manometers
Moisture
Pressure
Pumps
Radiation pressure
Supersonic flow

Turbulence
Viscometers
Viscosity
  gases
Vortices
Waves

14.60 GASEOUS STATE

Absorption/
  acoustic waves
  acoustic waves, ultrasonic
  electromagnetic waves
  light
Acoustic wave amplification
Association/
  gases
Breakdown, electric/
  gases
Conductivity, electrical/
  gases
  measurement
Conductivity, thermal/
  gases
  measurement
Dielectric properties of substances/
  gases
Diffraction/
  acoustic waves
  acoustic waves, ultrasonic
  electromagnetic waves
  light

Diffusion/
  acoustic waves
  electromagnetic waves
  light
Electrical properties of substances
Electroluminescence
Equations of state/
  gases
Fluorescence
Gases
Helium/
  gas
Interference/
  acoustic waves
Joule-Thomson effect
Kinetic theory/
  gases
Lasers/
  gaseous
Luminescence/
  gases
Magnetic resonance and relaxation

Molecules/
  intermolecular mechanics
Nuclear magnetic resonance and relaxation
Nuclear quadrupole resonance
Optical properties of substances
Paramagnetic resonance and relaxation
Permittivity
Phosphorescence
Rayleigh scattering
Reflection/
  acoustic waves
  acoustic waves, ultrasonic
  electromagnetic waves
  light
Refraction/
  acoustic waves
  acoustic waves, ultrasonic
  electromagnetic waves
  light

Scattering/
  acoustic waves
  acoustic waves, ultrasonic
  electromagnetic waves
  light
Sorption
Specific heat/
  gases
Spectra
Statistical mechanics
Thermoluminescence
Transmission/
  acoustic waves
  acoustic waves, ultrasonic
  light
Velocity/
  acoustic waves
  acoustic waves, ultrasonic
X-ray fluorescence

14.65 Viscosity and Diffusion of Gases

- Diffusion in gases/
  - thermal
- Transport processes
- Viscosity/
  - gases

14.70 MECHANICS OF LIQUIDS

- Acoustic streaming
- Bubbles
- Capillarity
- Cavitation
- Compressibility/
  - liquids
- Density/
  - liquids
- Diffusion in liquids
  - thermal
- Double refraction/
  - flow
- Drops
- Elasticity/
  - liquids
- Emulsions
- Films/
  - liquid
- Filters
- Flow/
  - liquids
  - two-phase
- Flowmeters
- Foams
- Hydrodynamics
- Hydrostatics
- Jets
- Liquid oscillations
- Liquid waves/
  - surface
- Lubrication
- Moisture
- Pressure
- Pumps
- Radiation pressure
- Rheology
- Schlieren systems
- Sprays
- Surface energy
- Surface tension
- Surface tension measurement
- Thixotropy
- Turbulence
- Viscometers
- Viscosity/
  - liquids
- Vortices
- Wetting

14.80 LIQUID STATE

- Liquids
- Liquid metals

14.82 Theory and Structure of Liquids and Solutions

- Association/
  - liquids
- Electron diffraction examination of materials
- Equations of state/
  - liquids
- Films/
  - liquid
- Heat of solution
- Liquid crystals
- Liquids/
  - structure
  - theory
- Neutron diffraction examination of materials
- Neutrons and antineutrons/
  - scattering
- Polymers
- Solubility
- Solutions
- X-ray examination of materials/
  - liquids

14.83 Viscosity, Surface tension and Diffusion

- Diffusion in liquids/
  - thermal
- Filters
- Membranes
- Osmosis
- Sorption
- Surface tension
- Surface tension measurement
- Transport processes
- Viscosity/
  - liquids

14.85 Thermal Properties of Liquids

- Conductivity, thermal/
  - liquids
  - measurement
- Heat of solution
- Specific heat/
  - liquids
- Thermal expansion
- Thermodynamic properties

14.86 Acoustical Properties of Liquids

- Absorption/
  - acoustic waves
  - acoustic waves, ultrasonic
- Acoustic wave amplification
- Acoustic wave propagation/
  - ultrasonic
- Diffraction/
  - acoustic waves
  - acoustic waves, ultrasonic
- Diffusion/
  - acoustic waves
- Interference/
  - acoustic waves
- Reflection/
  - acoustic waves
  - acoustic waves, ultrasonic
- Refraction/
  - acoustic waves
  - acoustic waves, ultrasonic
- Scattering/
  - acoustic waves
  - acoustic waves, ultrasonic
- Transmission/
  - acoustic waves
  - acoustic waves, ultrasonic
- Velocity/
  - acoustic waves
  - acoustic waves, ultrasonic

14.87 Optical Properties of Liquids

- Absorption/
  - electromagnetic waves
  - light
- Chemical shift
- Chemiluminescence
- Diffraction/
  - electromagnetic waves
  - light
- Diffusion/
  - electromagnetic waves
  - light
- Double refraction/
  - flow
- Electroluminescence
- Fluorescence
- Luminescence/
  - liquids and solutions
- Optical pumping
- Optical properties of substs.
- Phosphorescence
- Rayleigh scattering
- Reflection/
  - electromagnetic waves
  - light
- Refraction/
  - electromagnetic waves
  - light
- Scattering/
  - electromagnetic waves
  - light
  - light, Brillouin spectra
  - light, Raman spectra
  - light, Raman spectra, inorganic
  - light, Raman spectra, organic
- Spectra/
  - inorganic liquids and solutions
- Stimulated emission
- Thermoluminescence
- Transmission/
  - light
- X-ray fluorescence

14.88 Electrical and Magnetic Properties of Liquids

- Absorption/
  - electromagnetic waves
- Acoustic paramagnetic resonance
- Breakdown, electric/
  - liquids
- Conductivity, electrical/
  - liquids
  - liquids, electrolytic measurement
- Dielectric properties of substs./
  - liquids and solutions
- Electrical properties of substs.
- ENDOR
- Ferroacoustic resonance
- Ionisation, liquids
- Liquid metals
- Magnetic properties of substs.
- Magnetic resonance and relaxation
- Metals
- Nuclear acoustic resonance
- Nuclear magnetic resonance and relaxation
- Nuclear quadrupole resonance
- Paramagnetic resonance and relaxation
- Permittivity
- Proton magnetic resonance
- Semiconducting materials
- Semiconductors

14.90 DISPERSIONS AND COLLOIDS

- Aerosols
- Centrifuges
- Colloids
- Disperse systems
- Electrophoresis
- Emulsions
- Filters
- Foams
- Gels
- Heat of solution
- Membranes
- Osmosis
- Particle size
- Precipitation
- Sedimentation
- Sols
- Solubility
- Solutions
- Surface phenomena
- Suspensions
- Thixotropy

14.95 Liquid and solid helium

- Helium/
  - liquid
  - liquid, sound propagation
  - solid
- Quantum fluids/
  - boson systems
  - fermion systems
- Second sound
- Superfluidity
- Zero sound

15.00 CHANGE OF STATE

- Boiling
- Boiling point
- Condensation
- Critical constants, thermal
- Distillation
- Drying
- Equations of state
  - gases
  - liquids
  - solids
- Evaporation
- Freezing
- Heat of fusion
- Heat of sublimation
- Heat of transformation
- Heat of vaporisation
- Humidity
- Liquefaction, gases
- Melting
- Melting point
- Phase equilibrium
- Phase transformations
- Sublimation
- Supercooling
- Vapour pressure
- Vapour pressure measurement
- Vaporisation

16.00 SOLID STATE STRUCTURE AND MECHANICAL PROPERTIES

- Crystal properties
- Equations of state/
  - solids
- Solids/
  - structure
  - theory

16.10 NON-CRYSTALLINE STATE

- Amorphous state
- Glass
- Plastics
- Polymers
- Rubber
- Vitreous state
- Waxes

16.20 SURFACE AND INTERFACE PHENOMENA

- Ellipsometry
- Interface phenomena
- LEED
- Metallography
- Surface energy
- Surface measurement
- Surface phenomena
- Surface structure

16.23 Films. Whiskers. Dendrites

- Crystals/
  - growth
- Epitaxy
- Evaporation
- Films, solid/
  - electrical properties
  - magnetic properties
  - optical properties
- Sputtering
- Sublimation

16.25 Adsorption

- Adsorbed layers
- Adsorption
- Chemisorption
- Composite materials
- Desorption
- Heat of adsorption
- Sorption

16.30 CRYSTALLOGRAPHY

- Binding energy
- Bonds
- Charge compensation
- Cleavage
- Crystal chemistry
- Crystal morphology
- Crystal properties
- Crystallography
- Crystals/
  - etching
  - faces
  - orientation
  - twinning
- Debye-Waller factors
- Field ion microscopy
- Isomorphism
- Lattice energy
- Minerals
- Polymorphism
- Solids/
  - structure
- Surface structure

16.33 Crystal growth

- Crystal morphology
- Crystallisation
- Crystals/
  - growth
  - whiskers
- Dendrites
- Epitaxy
- Nucleation
- Zone melting and refining

16.35 Crystal Structures, Techniques and Apparatus

- Alloys
- Amorphous state
- Computer applications
- Crystal morphology
- Crystal structure/
  - microstructure
- Crystal structure, atomic/
  - alloys
  - elements
  - inorganic compounds
  - organic compounds
- Debye-Waller factors
- Density/
  - solids
- Electron diffraction crystallography
- Electron diffraction examination of materials
- Electron microscope examination of materials
- Electron microscopy
- Fibres
- Field ion microscopy
- Grain boundaries
- Granular structure
- Ion microscopes
- Metallography
- Metallurgy
- Microscopy
- Neutron diffraction crystallography
- Neutron diffraction examination of materials
- Particle size
- Polymers
- Porous materials
- Powders
- Radiography
- Space groups
- Surface structure
- X-ray absorption
- X-ray crystallography/
  - apparatus
  - calculation apparatus
  - calculation methods
  - technique
- X-ray diffraction
- X-ray examination of materials
  - microstructure
  - molecular structure
- X-ray measurement
- X-ray monochromators
- X-ray reflection
- X-ray scattering
- X-ray tubes

16.40 DEFECT PROPERTIES OF SOLIDS

- Cold working
- Creep
- Crystal imperfections
  - dislocations
  - impurities
  - interstitials
  - vacancies
- Crystal structure
- Crystals
  - etching
  - twinning
- Deformation
- Elastic deformation
- Electron diffraction examination of materials
- Electron microscope examination of materials
- Grain boundaries
- Heat treatment
  - alloys
- Internal friction
- Neutron diffraction examination of materials
- Plastic deformation
- Plastic flow
- Slip
- Stacking fault
- Stresses, internal
- Work hardening
- X-ray examination of materials/
  - microstructure

16.43 Crystal Impurities

- Crystal imperfections/
  - impurities
  - interstitials
- Ion implantation
- Physical effects of radiation

16.45 Colour centres

- Absorption/
  - light
- Colour centres
- F-centres
- X-rays/
  - effects

16.50 DIFFUSION IN SOLIDS

- Diffusion in solids/
  - thermal
- Permeability, mechanical

16.60 MECHANICAL PROPERTIES OF SOLIDS

- Abrasion
- Bending
- Brittleness
- Compressibility
- Cracks
- Creep
- Deformation
- Densification
- Density/
  - solids
- Elastic constants/
  - measurement
- Elastic deformation
- Elastic limit
- Elastic relaxation
- Elastic waves
- Elasticity/
  - fatigue
- Fracture
- Friction
- Hardness
- High-pressure phenomena and effects
- Hysteresis
- Impact
- Internal friction
- Lubrication
- Magnetoelastic waves
- Magnetomechanical effects
- Mechanical properties of substances
- Mechanical strength/
  - compressive
  - shear
  - tensile
- Photoelasticity·
- Plastic deformation
- Plastic flow
- Plasticity
- Rheology
- Slip
- Strain gauges
- Stress analysis
- Stress effects
- Stress/strain relations
- Stresses, internal
- Thermoelasticity
- Thixotropy
- Torsion
- Viscoelasticity
- Wear

16.65 Metallurgy. Materials Science. Phase Transformations

- Adhesion
- Aging
- Alloys
- Annealing
- Cold working
- Corrosion
- Densification
- Forming processes
- Granular structure
- Heat treatment/
  - alloys
- Metallurgy
- Order-disorder changes
- Phase equilibrium
- Particle size
- Phase transformations/
  - solid-state
- Physical effects of radiations
- Polymorphism
- Powders
- Precipitation
- Recovery
- Refractories
- Sintering
- Solid solutions
- Solubility
- Work hardening

16.70 LATTICE MECHANICS

- Crystals/
  - lattice mechanics
- Debye temperature
- Debye-Waller factors
- Mössbauer effect
- Phonons

16.80 ACOUSTICAL PROPERTIES OF SOLIDS

- Absorption/
  - acoustic waves
  - acoustic waves, ultrasonic
- Acoustic wave amplification
- Acoustic wave propagation/
  - ultrasonic
- Acoustoelectric effects
- Acousto-optical effects
- Diffraction/
  - acoustic waves
  - acoustic waves, ultrasonic
- Dispersion, acoustic/
  - ultrasonic
- Magnetoacoustic effects
- Reflection/
  - acoustic waves
  - acoustic waves, ultrasonic
- Refraction/
  - acoustic waves
  - acoustic waves, ultrasonic
- Scattering/
  - acoustic waves
  - acoustic waves, ultrasonic
- Transducers
- Transmission/
  - acoustic waves
  - acoustic waves, ultrasonic
- Velocity/
  - acoustic waves
  - acoustic waves, ultrasonic

16.90 THERMAL PROPERTIES OF SOLIDS

- Conductivity thermal/
  - measurement
  - solids
- Debye temperature
- Entropy/
  - properties of substances
- Equations of state/
  - solids
- Gruneisen relation
- Heat conduction
- Specific heat/
  - solids
- Thermal expansion
- Thermal properties of substances
- Thermodynamic properties

16.95 RADIATION INTERACTION WITH SOLIDS

- Acoustic waves/
  - effects
- Alpha-particles/
  - effects
- Beta-rays/
  - effects
- Channelling
- Deuterons/
  - effects
- Electron beams/
  - effects
- Energy loss of particles
- Gamma-rays/
  - effects
- Hyperons/
  - effects
- Ion beams/
  - effects
- Mesons/
  - effects
- Neutrons and antineutrons/
  - effects
- Physical effects of radiations
- Protons and antiprotons/
  - effects
- Sputtering
- X-rays/
  - effects

17.00 SOLID STATE ELECTRICAL AND MAGNETIC PROPERTIES

- Crystals/
  - internal fields

17.10 ELECTRON STATES IN SOLIDS

- Brillouin zones
- Crystal electron states
  - band structure
  - excitons
  - Fermi level
  - Fermi surface
  - impurity states and effects
  - plasma
  - polarons
  - surface
  - transport processes
- Crystal properties
- Cyclotron resonance
- de Haas-van Alphen effect
- Electron beams/
  - effects
- Electron density
- Electron gas
- Electron pairs/
  - annihilation
- Electron-phonon interactions
- Electron traps
- Electrons
  - absorption
  - radiation
  - scattering
- Hall effect
- Helicons
- Kondo effect
- Magnetoacoustic effects
- Magnetoresistance
- Metals/
  - theory
- Piezoresistance
- Pseudopotential methods
- Quasi-particles
- Skin effect
- Solids/
  - theory
- Surface phenomena
- Tunnelling
- Zero sound

17.20 ELECTRICAL PROPERTIES OF SOLIDS

- Acoustoelectric effects
- Conductivity, electrical/
  - measurement
  - solids
- Contacts, electrical
- Crystal electron states
- Eddy-currents
- Electrical properties of substs.
- Electron density
- Electron gas
- Electro-optical effects
- Films, solid/
  - electrical properties
- Fluctuations
- Hall effect
- Magnetoelectric effects
- Magnetoresistance
- Magnetothermal effects
- Noise, electrical
- Piezoelectricity
- Piezoresistance
- Space charge/
  - solid
- Thin film devices
- Tunnelling

17.22 Metallic Conducting Properties

- Electron gas
- Hall effect
- Magnetoelectric effects
- Magnetoresistance
- Metals/
  - theory
- Piezoresistance
- Semimetals
- Skin effect
- Thin film devices

17.24 Superconducting Properties

- BSC theory
- Galvanothermomagnetic effects
- Storage devices
- Superconducting devices
- Superconducting magnets
- Superconducting materials/
  - lead
  - niobium
- Superconductivity/
  - type II
- Thin film devices
- Tunnelling

17.26 Semiconducting Properties

- Acoustoelectric effects
- Contacts, electrical
- Electron gas
- Electro-optical effects
- Fluctuations
- Gunn effect
- Hall effect
- Ion implantation
- Magnetoelectric effects
- Magnetoresistance
- Magnetothermal effects
- Noise, electrical
- Piezoelectricity
- Piezoresistance
- Semiconductors
- Space charge/
  - solid
- Semiconducting materials/
  - gallium arsenide
  - germanium
  - indium antimonide
  - silicon
- Tunnelling

17.28 Semiconductor and Interface devices

- Gunn effect
- Ion implantation
- Metal-insulator-metal structures and devices
- Metal-insulator-semiconductor structures and devices
- Microwave techniques and devices
- Rectifiers
- Semiconductor devices/
  - diodes
  - junctions
  - transistors
  - tunnel and interface devices
- Semiconductor-metal boundaries
- Storage devices
- Thin film devices
- Tunnelling

17.29 Dielectric Properties

- Antiferroelectric materials
- Breakdown, electric/
  - solids
- Contacts, electrical
- Dielectric devices
- Dielectric measurement
- Dielectric phenomena
- Dielectric properties of substs./
  - solids
- Dielectric relaxation
- Domains
- Electrets
- Electric charge
- Electric fields
- Electric strength
- Electrostriction
- Ferroelectric materials/
  - barium titanate
- Ferroelectric phenomena
- Hysteresis
- Ionic conduction, solids
- Paraelectric resonance
- Permittivity
- Piezo-optical effects
- Piezoelectric oscillations
- Piezoelectricity
- Pyroelectricity
- Relaxation
- Rochelle salt
- Space charge/
  - solid
- Triboelectricity
- Tunnelling

17.40 THERMOELECTROMAGNETIC PROPERTIES

- Magnetoelectric effects
- Magnetothermal effects
- Thermocouples
- Thermoelectricity

17.50 PHOTOELECTRIC PROPERTIES

- Photoconducting devices
- Photoconductivity
- Photoelectricity
- Photoelectromagnetic effects
- Photovoltaic effects

17.52 ELECTRON AND ION EMISSION BY SOLIDS

- Cathodes/
  - oxide
- Electron emission
  - field emission
  - photoelectric
  - secondary
  - thermionic
- Ion emission/
  - secondary
  - thermionic
- Ionisation/
  - solids
- Ionisation, surface
- Work function

17.60 MAGNETIC PROPERTIES OF SOLIDS

- Antiferromagnetism
- de Haas-van Alphen effect
- Diamagnetism
- Demagnetisation
- Domains
- Electron diffraction examination of materials
- Electron microscope examination of materials
- Exchange interactions
- Ferrimagnetism
- Ferrites
- Ferromagnetism/
  - spin-wave theory
- Films, solid/
  - magnetic properties
- Gyromagnetic ratio
- Hall effect
- Hysteresis
- Kondo effect
- Magnetic devices
- Magnetic fields/
  - effects
- Magnetic anisotropy
- Magnetic permeability
- Magnetic properties of dilute systems
- Magnetic properties of substs.
  - antiferromagnetic
  - diamagnetic
  - ferrimagnetic
  - ferromagnetic
  - paramagnetic
  - transitions
- Magnetic structure
- Magnetism
- Magnetisation process
- Magnetoacoustic effects
- Magnetoelastic waves
- Magnetoelectric effects
- Magneto-optical effects
- Magnetoresistance
- Magnetostriction
- Magnetothermal effects
- Neutron diffraction examination of materials
- Paramagnetism
- Zeeman effect

17.62 Paramagnetic Properties

- Magnetic anisotropy
- Magnetic properties of substances/
  - paramagnetic
- Magnetic structure
- Paramagnetism

17.64 Ferromagnetic Properties

- Domains
- Exchange interactions
- Ferromagnetism/
  - spin-wave theory
- Films, solid/
  - magnetic properties
- Heisenberg model
- Helicons
- Hysteresis
- Ising lattices and models
- Magnetic anisotropy
- Magnetic devices
- Magnetic properties of substances/
  - ferromagnetic
- Magnetisation process
- Magnetic structure
- Metamagnetism
- Storage devices
- Superparamagnetism
- Spin waves
- Thin film devices

17.66 Ferrimagnetic Properties

- Domains
- Exchange interactions
- Ferrimagnetism
- Ferrites
- Films, solid/
  - magnetic properties
- Helicons
- Hysteresis
- Magnetic anisotropy
- Magnetic devices
- Magnetic properties of substances/
  - ferrimagnetic
- Magnetic structure
- Thin film devices
- Spin waves
- Storage devices

17.68 Antiferromagnetic Properties

- Antiferromagnetism
- Domains
- Exchange interactions
- Heisenberg model
- Magnetic anisotropy
- Magnetic properties of substances/
  - antiferromagnetic
- Magnetic structure
- Metamagnetism
- Spin waves

17.69 Magnetic Relaxation Phenomena

- Ferromagnetic relaxation
- Magnetic resonance and relaxation
- Nuclear magnetic resonance and relaxation
- Paramagnetic resonance and relaxation
- Spin lattice relaxation
- Spin-spin relaxation

18.00 SOLID STATE SPECTROSCOPY AND OPTICAL PROPERTIES

- Chemical shift
- Crystal field theory
- Crystals/
  - hyperfine field interactions
- Jahn-Teller effect
- Isomer shift
- Nuclear polarisation

18.10 OPTICAL PROPERTIES OF SOLIDS

- Absorption/
  - electromagnetic waves
  - light
- Acousto-optical effects
- Diffraction/
  - electromagnetic waves
  - light
- Diffusion/
  - electromagnetic waves
  - light
- Dispersion, optical
- Double refraction/
  - mechanical
- Electromagnetic wave propagation
- Electro-optical effects
- Electroreflectance
- Ellipsometry
- Emissivity
- Faraday effect
- Films, solid/
  - optical properties
- Interference/
  - light
- Isomer shift
- Lasers/
  - solid
- Magneto-optical effects
- Magnetoreflectance
- Nonlinear optics
- Optical constants
- Optical materials
- Optical properties of substances
- Optical pumping
- Optical rotation
- Photoelasticity
- Piezo-optical effects
- Piezoreflectance
- Pleochroism
- Polarisation/
  - light
- Reflection/
  - electromagnetic waves
  - light
- Reflectivity
- Refraction/
  - electromagnetic waves
  - light
- Refractive index/
  - light
- Scattering/
  - electromagnetic waves
  - light
- Thermo-optical effects
- Thermoreflectance
- Transmission/
  - light
- Transparency
- Velocity/
  - light

18.20 RESONANT GAMMA RAY INTERACTIONS. MÖSSBAUER EFFECT

- Chemical shift
- Crystals/
    - hyperfine field interactions
    - internal fields
- Isomer shift
- Magnetoreflectance
- Mössbauer effect

18.30 OPTICAL SPECTRA OF SOLIDS

- Crystals/
    - hyperfine field interactions
- Electroreflectance
- Isomer shift
- Magnetoreflectance
- Piezoreflectance
- Reflection/
    - electromagnetic waves
    - light
- Reflectivity
- Scattering/
    - electromagnetic waves
    - light
    - light, Brillouin spectra
    - light, Raman spectra
    - light, Raman spectra, inorganic
    - light, Raman spectra, organic
- Spectra/
    - inorganic solids
    - inorganic solids, radio frequency
    - organic molecules and substances
    - organic molecules and substances, infrared
    - organic molecules and substances, radio frequency
- Spectral line breadth
- Stark effect
- Stimulated emission
- Thermoreflectance
- X-ray spectra/
    - absorption
    - emission
- Zeeman effect

18.40 LUMINESCENCE SPECTRA OF SOLIDS

- Cathodoluminescence
- Chemiluminescence
- Colour centres
- Counters/
    - scintillation
- Electroluminescence
- Fluorescence
- Luminescence/
    - solids, inorganic
    - solids, organic
- Luminescent devices
- Phosphorescence
- Stimulated emission
- Thermoluminescence
- X-ray fluorescence

18.50 MAGNETIC RESONANCES IN SOLIDS

- Crystals/
    - hyperfine field interactions
- Antiferromagnetic resonance
- Cyclotron resonance
- Ferrimagnetic resonance
- Ferroacoustic resonance
- Ferromagnetic relaxation
- Ferromagnetic resonance
- Gyromagnetic ratio
- Magnetic resonance and relaxation
- Magnetoelastic waves
- Magnetomechanical effects
- Optical pumping

18.52 Paramagnetic Resonances and Relaxation

- Acoustic paramagnetic resonance
- Crystals/
    - hyperfine field interactions
- Gyromagnetic ratio
- Paramagnetic resonance and relaxation/
    - measurement

18.54 Nuclear Magnetic Resonance and Relaxation

- Chemical shift
- Crystals/
    - hyperfine field interactions
- ENDOR
- INDOR
- Knight shift
- Nuclear acoustic resonance
- Nuclear magnetic resonance and relaxation/
    - measurement
- Nuclear quadrupole resonance
- Proton magnetic resonance

19.00 PHYSICAL CHEMISTRY

- Atomic mass and weight
- Balances
- Bonds
- Centrifuges
- Chemical structure
- Chemical technology
- Distillation
- Elements/
    - origin
    - relative abundances
- Filters
- Isomerism
- Laboratory app. and technique
- Macromolecules
- Molecular weight
- Molecular weight determination
- Periodic system
- Physical chemistry
- Precipitation
- Pumps
- Quantum chemistry
- Sedimentation
- Valency

19.10 THERMOCHEMISTRY AND REACTIONS

- Association
    - gases
    - liquids
- Catalysis
- Chemical reactions
- Combustion
- Crystal chemistry
- Detonation
- Dissociation
- Exchanges, chemical
- Explosions
- Flames
- Heat of adsorption
- Heat of combination
- Heat of dissociation
- Heat of formation
- Heat of reaction
- Isotope exchanges
- Phase equilibrium
- Phase transformations
- Polymerisation
- Polymers
- Reaction kinetics
- Sorption

19.15 Oxidation and Corrosion

- Corrosion
- Oxidation

19.20 ELECTROCHEMISTRY

- Anodes
- Conductivity, electrical/
    - liquids, electrolytic
- Dissociation/
    - electrolytic
- Electric cells
- Electrochemistry
    - electrodes
- Electrokinetic effects
- Electrolysis
- Electrolytic deposition
- Electrophoresis
- Ion velocity/
    - electrolytic
- Ions, electrolytic

19.30 PHOTOCHEMISTRY AND RADIOCHEMISTRY

- Chemical effects of radiations/
  - acoustic waves
  - ionising radiations
- Nuclear reactions and scattering/
  - chemical effects
- Photochemistry
- Photochromism
- Radiochemistry

19.40 PHYSICAL METHODS OF CHEMICAL ANALYSIS

- Chemical analysis/
  - adsorption
  - by mass spectrometry
  - by nuclear reactions
  - electrochemical
  - radioactive
  - X-ray
- Chromatography
- Electron-pole analysis
- Probes
- Radioactive tracers
- Spectrochemical analysis
- Tracers

20.00 GEOPHYSICS

- Earth/
  - age
  - composition
  - electricity
  - heat
  - rotation
- Geodesy
- Geophysical prospecting
- Geophysics
- Glaciers
- Gravity
- Minerals
- Oceanography
- Radioactive dating
- Radioactivity
- Seawater
- Seismic waves
- Seismology
- Soil

20.10 ATMOSPHERE

- Anemometers
- Atmosphere/
  - composition
  - humidity
  - movements
  - precipitation
  - radioactivity
  - structure
  - temperature
  - thermodynamics
- Atmospheric acoustics
- Atmospheric electricity
- Atmospheric optics
- Atmospheric pressure and density
- Atmospheric spectra
- Atmospherics
- Clouds
- Condensation
- Electromagnetic wave propagation/
  - atmosphere
- Evaporation
- Fallout
- Fog
- Humidity
- Hygrometers
- Ice
- Lightning
- Meteorological instruments
- Meteorology
- Rain
- Rockets
- Satellites, artificial
- Sky brightness
- Snow
- Sunlight
- Thunderstorms
- Twilight
- Wind

20.20 UPPER ATMOSPHERE

- Airglow
- Atmosphere/
  - composition
  - movements
  - radiation belts
  - radioactivity
  - structure
  - temperature
  - thermodynamics
  - upper
- Atmospheric electricity
- Atmospheric optics
- Atmospheric pressure and density
- Atmospheric spectra
- Atmospherics
- Aurora
- Fallout
- Ionisation, atmosphere
- Magnetosphere
- Meteors
- Rockets
- Satellites, artificial
- Sky brightness
- Sunlight
- Twilight
- Zodiacal light

20.30 IONOSPHERE

- Atmospherics
- Aurora
- Electromagnetic wave propagation/
  - ionosphere
- Ionisation, atmosphere
- Ionosphere
- Ionosphere measuring apparatus

20.35 D, E and F-regions

- Ionosphere/
  - D-region
  - E-region
  - F-region

20.40 GEOMAGNETISM

- Compasses
- Earth/
  - magnetic field
  - magnetic field, variations
- Magnetic storms
- Micropulsations
- Rock magnetism

20.50 SPACE RESEARCH TECHNIQUES

- Rockets
- Satellites, artificial
- Space research
- Space vehicles/
  - instrumentation

21.00 ASTROPHYSICS

- Astronomical observations
- Astronomical spectra
- Astronomy and astrophysics
- Celestial mechanics
- Cosmic rays
- Cosmology
- Elements/
  - origin
  - relative abundances
- Gravitation
- Infrared astronomy
- Interstellar matter

21.10 GALAXIES

- Cosmic radiations, r.f.
- Galaxies/
  - the Galaxy
- H I regions
- H II regions
- Intergalactic matter
- Magnetohydrodynamics
- Nebulae
- Planetary nebulae

21.20 STARS

- Gravitational collapse
- Interstellar magnetic field
- Interstellar matter
- Magnetohydrodynamics
- Multiple stars
- Novae
- Stars/
  - composition
  - evolution
  - magnetism
  - radiation
  - spectra
  - structure
- Stellar atmospheres
- Thermonuclear reactions
- White dwarfs
- Variable stars

21.30 RADIOSOURCES, X-RAY AND GAMMA-RAY SOURCES

- Cosmic radiation, r.f.
- Pulsars
- Quasars
- Radio sources
- X- and gamma-ray astronomy

21.40 SOLAR SYSTEM

- Asteroids
- Comets
- Cosmic rays
- Earth/
  - rotation
- Gravitation
- Interplanetary magnetic field
- Interplanetary matter
- Jupiter
- Mars
- Mercury, planet
- Meteorites
- Meteors
- Moon
- Neptune
- Planetary atmospheres
- Planets
- Pluto
- Saturn
- Solar system
- Uranus
- Venus

21.45 Sun

- Chromosphere
- Cosmic rays
- Photosphere
- Solar activity
- Sun/
  - corona
  - eclipses
  - flares
  - magnetism
  - prominences
  - radiation
  - radiation, corpuscular
  - radiation, r.f.
  - spectra
- Sunspots
- Zodiacal light

21.60 ASTRONOMICAL TECHNIQUES

- Astronomical instruments
- Astronomical observations
- Astronomy and astrophysics
- Radioastronomy
- Telescopes/
  - astronomical

22.00 BIOPHYSICS

Biophysics

22.10 HEALTH AND MEDICAL PHYSICS

- Biological effects of radiations
- Biological technique and instruments
- Blood
- Dosimetry
- Medical science
- Physiology
- Proteins
- Radiation protection
- Radiography
- Zoology

22.20 HEARING AND SPEECH

- Ear
- Hearing
- Noise/
  - acoustic
- Speech

22.30 VISION

- Eye
- Colour vision
- Vision

23.00 LABORATORY AND EXPERIMENTAL TECHNIQUES

- Biological technique and instruments
- Calculating apparatus/
  - analogue apparatus
  - digital computers
  - digital computer programmes
- Chemical technology
- Heat treatment/
  - alloys
- Laboratory apparatus and technique
- Leak detection
- Materials
- Metallurgy
- Zone melting and refining

23.10 HIGH AND LOW TEMPERATURE TECHNIQUES

- Cryostats
- High-temperature phenomena and effects
- High-temperature techniques
- Joule-Thomson effect
- Liquefaction, gases
- Low-temperature phenomena
- Low-temperature production
- Low-temperature technique
- Magnetic cooling
- Refractories

23.20 HIGH PRESSURE TECHNIQUES

- Getters
- High-pressure phenomena and effects
- High-pressure techniques

23.30 VACUUM TECHNIQUES

- Leak detection
- Manometers
- Seals
- Sputtering
- Vacuum apparatus
- Vacuum gauges
- Vacuum pumps
- Vacuum technique

23.40 X-RAY TUBES AND TECHNIQUES

- Dosimetry
- High-voltage techniques
- Radiation monitoring
- Radiation protection
- Radiography
- X-ray absorption
- X-ray diffraction
- X-ray examination of materials
- X-ray measurement
- X-ray monochromators
- X-ray reflection
- X-ray scattering
- X-ray spectra/
  - absorption
  - emission
- X-ray spectrometers
- X-ray spectroscopy
- X-ray tubes
- X-rays/
  - effects

SUBSTANCES

Chemical elements and inorganic compounds

All the chemical elements are listed by name, followed by their compounds, e.g. "Cadmium, Cadmium compounds".

"Hydrogen" is subdivided by the subheadings "neutral atoms", "neutral molecules" and "ions". "Deuterium" and "Tritium" are independent headings. "Hydrogen compounds" is supplemented by "Ice", "Steam" and "Water".

"Oxygen" is supplemented by "Ozone" and "Carbon" is supplemented by "Diamonds" and "Graphite".

The following inorganic compounds are further subdivided by subheadings as shown:-

- Barium compounds/
  - barium titanate*
- Cadmium compounds/
  - cadmium sulphide
- Calcium compounds/
  - calcium fluoride
- Gallium compounds/
  - gallium arsenide†
- Indium compounds/
  - indium antimonide†
- Lithium compounds/
  - lithium fluoride
- Nitrogen compounds/
  - ammonia
  - ammonium compounds
- Potassium compounds/
  - potassium bromide
  - potassium chloride
- Sodium compounds/
  - sodium chloride
- Zinc compounds/
  - zinc sulphide

* Ferroelectric properties are listed under "Ferroelectric materials/barium titanate"

† Semiconducting properties are listed under the corresponding subheadings of "Semiconducting materials"

Organic compounds

Organic compounds are grouped under headings "Organic compounds", "Polymers", "Plastics", "Proteins". "Rochelle salt" is an independent heading.

Co-ordination compounds

Metallic co-ordination compounds are regarded as inorganic with a few exceptions and are indexed under the appropriate metallic compound heading (not under organic compounds), e.g. Ni complex, bis (dimethylglyoximato) nickel (II) under Nickel compounds.

Substance groups

In addition there are the following headings for groups of elements, compounds or substances:-

- Actinides
- Actinide compounds
- Alkali metals
- Alkali-metal compounds/
  - halides
- Alkaline-earth metals
- Alkaline-earth compounds
- Ferrites
- Ferroelectric materials/
  - barium titanate‡
- Garnets
- Halogens
- Inert gases
- Metals
- Minerals
- Rare-earth metals
- Rare-earth compounds
- Semiconductors
- Semiconducting materials/
  - gallium arsenide§
  - germanium§
  - indium antimonide§
  - silicon§
- Superconducting materials/
  - lead‖
  - niobium‖
- Transition metals
- Transition-metal compounds

‡ Used for ferroelectric properties only

§ Used for semiconducting properties only

‖ Used for superconducting properties only

Alloys

General papers on alloys are indexed under "Alloys". Alloys of specified composition are listed under, either

(i) special alloy headings (there are five of them: "Aluminium alloys", "Copper alloys", "Iron alloys", "Nickel alloys", "Steel"), e.g. Al-Ni alloys under "Aluminium alloys" and "Nickel alloys".

(ii) compounds of the named elements, e.g. Mn-Zn alloys under "Manganese compounds" and "Zinc compounds". Silicon-iron under "Iron alloys" and "Silicon compounds".

Special substances and materials

There are also the following special headings for certain common substances:-

- Air
- Blood
- Ceramics
- Clay
- Coal
- Concrete
- Fibres
- Gelatin
- Glass
- Mica
- Optical materials
- Paper
- Porous materials
- Powders
- Quartz
- Rubber
- Ruby
- Sand
- Seawater
- Soil
- Waxes
- Wood

ABSTRACTS AND CURRENT PAPERS JOURNALS

Three main subject areas are covered by INSPEC abstracts and current papers journals: physics, electrical and electronics engineering, and computer and control engineering. For each field an abstracts journal and a companion titles journal are published. The abstracts journals are intended as library tools for retrospective information retrieval, whereas the companion titles journals, which omit the abstracts and associated indexes, are intended as low-cost current-awareness tools for the individual.

SUBSCRIPTION PRICES

ABSTRACTS JOURNALS	Annual subscription Paper or microfiche	Annual subscription Combined paper and microfiche
Physics Abstracts (PA) Published every two weeks in conjunction with the American Institute of Physics, New York, and the Institute of Physics, London	£130	£195
Electrical & Electronics Abstracts (EEA) Published monthly jointly with the Institute of Electrical & Electronics Engineers Inc., New York	£105	£157
Computer & Control Abstracts (CCA) Published monthly jointly with the Institute of Electrical & Electronics Engineers Inc., New York	£55	£82
Combined Subscription to Electrical & Electronics Abstracts and Computer & Control Abstracts (EEA/CCA)	£135	£202

CURRENT PAPERS JOURNALS	Annual subscription IEE, AIP, IEEE, IOP, IERE members	Annual subscription Non-members
Current Papers in Physics (CPP) Published every two weeks in conjunction with the American Institute of Physics, New York, and the Institute of Physics, London	£7	£14
Current Papers in Electrical & Electronics Engineering (CPE) Published monthly jointly with the Institute of Electrical & Electronics Engineers Inc., New York	£7	£14
Current Papers on Computers & Control (CPC) Published monthly jointly with the Institute of Electrical & Electronics Engineers Inc., New York	£6	£12

CUMULATIVE INDEXES

Cumulative indexes are available for *Physics Abstracts*, *Electrical & Electronics Abstracts*, and *Computer & Control Abstracts*, for both authors and subjects. These cumulations generally cover a period of four years, with the exception of *Computer & Control Abstracts* where the initial volume covered the period 1966–68. The table below shows the prices and periods for the two types of cumulative index.

	Physics Abstracts		Electrical & Electronics Abstracts		Computer & Control Abstracts	
	Subject	Author	Subject	Author	Subject	Author
1955–59	£20	£20	£15	£20	—	—
1960–64	£40	£17	£20	£12	—	—
1965–68	£60	—	£35	£20	—	—
1966–68	—	—	—	—	£15 (combined)	

ORDERING PROCEDURE

AMERICAN SUBSCRIPTIONS

Physics Abstracts
Current Papers in Physics

For AIP members, wherever they reside, and from the public in the Americas, to the Subscription Department, American Institute of Physics, 335 East 45th Street, New York, NY 10017, USA. Please allow six weeks' notice for change of address, send both old and new addresses and include an address label from a recent issue.

Electrical & Electronics Abstracts
Computer & Control Abstracts and associated current papers journals in these fields

For IEEE members wherever they reside, and from the public in the Americas, to the Fulfillment Manager, Institute of Electrical & Electronics Engineers Inc., 345 East 47th Street, New York, NY 10017, USA.

REMAINDER OF THE WORLD

Abstracts Journals
Current Papers
Cumulative Indexes

For all remaining subscriptions, and for all cumulative indexes, to IEE, Savoy Place, London WC2R 0BL, England. Telephone 01-240 1871, Telex 261176, Telegrams Voltampere London WC2.

OTHER INSPEC SERVICES

SDI

(Selective Dissemination of Information.) This is a service individually tailored to the requirements and interests of the engineer or research worker. Details of information relevant to the interest profile of the individual subscriber are selected from the data being processed for the INSPEC database. Information is dispatched weekly on 150 mm × 100 mm (6″ × 4″) cards.

TOPICS

This is an SDI service based on standard profiles. There are 72 subjects covering high-activity areas of research and development. This is an inexpensive card service designed to alert engineers and researchers to the availability of literature within their subject area.

MAGNETIC TAPES

These are produced, containing all the information included in the INSPEC publications. They enable the larger research and development organisations to produce their own internal information and current-awareness services.

For more details of any of these services please write to:
INSPEC Marketing Department, The Institution of Electrical Engineers, Savoy Place, London WC2R 0BL, England

Cables Voltampere London WC2
Grams Voltampere London Telex

Telephone 01-240 1871
Telex 261176

inspec
The Institution of Electrical Engineers

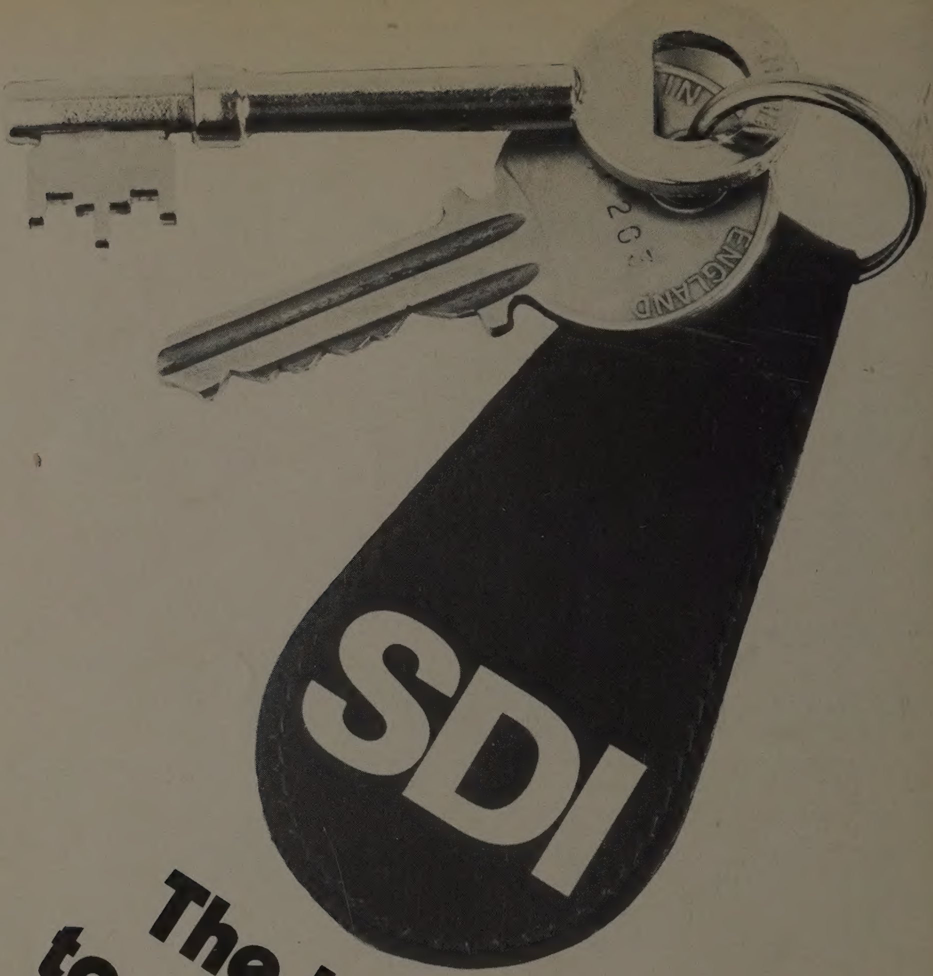

Your key to more effective Research and Development is INSPEC'S SDI: Selective Dissemination of Information.

When you join INSPEC'S SDI service, we hold your detailed information requirements in INSPEC'S computer system.

Each week we collate data from thousands of international documents collected worldwide.

Bearing your particular requirements in mind, we scan this data and send you details of the relevant documents.

The unique feature of INSPEC'S SDI service is the continuous monitoring and feedback facility that enables you to alter your information requirements to take advantage of the data we're sending you.

INSPEC'S SDI service operates in the fields of Physics, Electrotechnology, Computer and Control Engineering. Subscriptions to the service range from £65 per annum.

For more details of this service, contact INSPEC immediately.

INSPEC Marketing Department
The Institution of Electrical Engineers
Savoy Place, London WC2R 0BL
England

Telephone 01-240 1871

inspec
The Institution of Electrical Engineers